

ORGANOMETALLICS

Volume 14, Number 4, April 1995

© Copyright 1995
American Chemical Society

Communications

Oxidation of Coordinated Alkynes by Dimethyldioxirane. Conversion to α -Keto Carbene Complexes

Shouheng Sun, J. O. Edwards, and D. A. Sweigart*

Department of Chemistry, Brown University, Providence, Rhode Island 02912

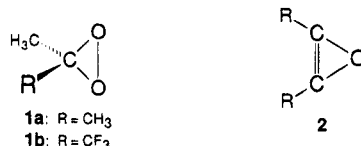
Lucia D'Accolti and Ruggero Curci*

CNR Centre MISO, Department of Chemistry, University of Bari,
Via Amendola 173, Bari, Italy 70126

Received November 28, 1994[®]

Summary: Dimethyldioxirane (DMDO) oxidizes the coordinated alkyne ligand in $(RCp)Mn(CO)_2$ (diarylalkyne) (**3**) to give moderate yields of the corresponding α -keto carbene complex $(RCp)Mn(CO)_2C(Ar)C(O)(Ar)$ (**5**), thus illustrating the synthetic potential of dioxiranes for the controlled oxidation of coordinated ligands. The transformation **3** \rightarrow **5** might involve initial alkyne epoxidation to give an intermediate containing a coordinated oxirene ligand.

Recent research has shown¹ that dioxiranes (**1**) rapidly oxidize a wide range of organic functionalities. Dimethyldioxirane (DMDO; **1a**), which can be easily prepared as a solution in acetone, and methyl(trifluoromethyl)dioxirane (**1b**) are the most commonly employed oxidants.² These reagents have been used in a variety of synthetic transformations, including the oxyfunctionalization of saturated hydrocarbons (C–H bond activation).^{2a,c} However, applications of these oxidants to inorganic and organometallic systems are quite limited to date. It is known that DMDO oxidizes Cp^*Re-



(CO)₃ to Cp^*ReO_3 and transfers an oxygen to certain metal(II) porphyrins to produce metal oxo species.³ It has been shown that DMDO oxidizes organometallic thiolates to sulfinato complexes⁴ and induces the oxidative decomplexation of the arene from (arene)Cr(CO)₃ and the carbene (as the ketone) from Fischer carbene complexes.⁵

In this paper we address the reaction of DMDO (**1a**) with alkynes coordinated to a manganese center. The oxidation of *free* alkynes $RC\equiv CR$ with DMDO⁶ and with

(3) (a) Herrmann, W. A.; Kiprof, P.; Rypdal, K.; Tremmel, J.; Blom, R.; Alberto, R.; Behm, J.; Albach, R. W.; Bock, H.; Solouki, B.; Mink, J.; Lichtenberger, D.; Gruhn, N. E. *J. Am. Chem. Soc.* **1991**, *113*, 6527. (b) Wolowicz, S.; Kochi, J. K. *Inorg. Chem.* **1991**, *30*, 1215.

(4) (a) Schenk, W. A.; Frisch, J.; Adam, W.; Prechtel, F. *Inorg. Chem.* **1992**, *31*, 3329. (b) Pérez-Encado, A.; Perrio, S.; Slawin, A. M. Z.; Thomas, S. E.; Wierzchlejski, A. T.; Williams, D. J. *J. Chem. Soc., Perkin Trans. 1* **1994**, 629.

(5) (a) Lluch, A.-M.; Sánchez-Baeza, F.; Camps, F.; Messegue, A. *Tetrahedron Lett.* **1991**, *32*, 5629. (b) Lluch, A.-M.; Jordi, L.; Sánchez-Baeza, F.; Ricart, S.; Camps, F.; Messegue, A.; Moretó, J. M. *Tetrahedron Lett.* **1992**, *33*, 3021.

(6) (a) Curci, R.; Fiorentino, M.; Fusco, C.; Mello, R.; Ballistreri, F. P.; Failla, S.; Tomaselli, G. A. *Tetrahedron Lett.* **1992**, *33*, 7929. (b) Murray, R. W.; Singh, M. *J. Org. Chem.* **1993**, *58*, 5076.

[®] Abstract published in *Advance ACS Abstracts*, March 15, 1995.

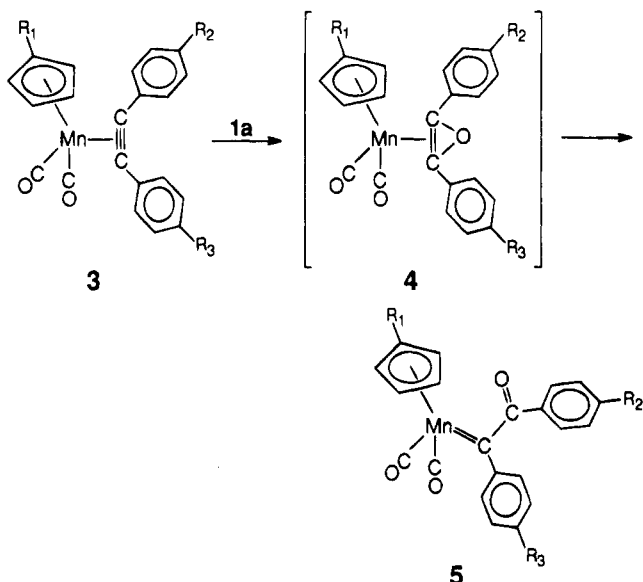
(1) (a) Adam, W.; Curci, R.; Edwards, J. O. *Acc. Chem. Res.* **1989**, *22*, 205. (b) Murray, R. W. *Chem. Rev.* **1989**, *89*, 1187. (c) Curci, R. In *Advances in Oxygenated Processes*; Baumstark, A. L., Ed.; JAI: Greenwich, CT, 1990; Vol. 2, Chapter 1.

(2) (a) Mello, R.; Fiorentino, M.; Fusco, C.; Curci, R. *J. Am. Chem. Soc.* **1989**, *111*, 6749. (b) Mello, R.; Cassidei, L.; Fiorentino, M.; Fusco, C.; Hümmel, W.; Jäger, V.; Curci, R. *J. Am. Chem. Soc.* **1991**, *113*, 2205. (c) Kuck, D.; Schuster, A.; Fusco, C.; Fiorentino, M.; Curci, R. *J. Am. Chem. Soc.* **1994**, *116*, 2375.

Table 1. Spectroscopic Data for α -Keto Carbene Complexes (**5**) Obtained by the Oxidation of Coordinated Alkynes with Dimethyldioxirane

R ₁	R ₂	R ₃	yield (%) ^a	ν_{CO} (cm ⁻¹) ^b	¹ H NMR (δ) ^c
H	H	H	30	1989, 1931, 1641	7.38–7.70 (m, Ph), 4.98 (s, Cp)
H	Me	Me	42	1985, 1929, 1642	7.15–7.63 (m, Ph), 4.94 (s, Cp), 2.35 (s, Me), 2.28 (s, Me)
Me	H	H	25	1985, 1927, 1641	7.31–7.75 (m, Ph), 4.78–4.90 (m, Cp), 1.81 (s, Me)
Me	Me	Me	41	1983, 1923, 1642	7.15–7.63 (m, Ph), 4.75–4.84 (m, Cp), 2.35 (s, Me), 2.28 (s, Me), 1.82 (s, Me)
Me	H	OMe	27 ^d	1983, 1925, 1640 ^d	6.80–8.10 (m, Ph), 4.71–4.78 (m, Cp), 3.81 (s, OMe), 1.81 (s, Me)
Me	OMe	H	<i>d</i>	<i>d</i>	6.80–8.10 (m, Ph), 4.81–4.87 (m, Cp), 3.83 (s, OMe), 1.83 (s, Me)
Me	Me	OMe	29 ^d	1977, 1919, 1638 ^d	6.83–7.74 (m, Ph), 4.70–4.85 (m, Cp), 3.81 (s, OMe), 2.35 (s, Me), 1.81 (s, Me)
Me	OMe	Me	<i>d</i>	<i>d</i>	6.83–7.74 (m, Ph), 4.70–4.85 (m, Cp), 3.83 (s, OMe), 2.28 (s, Me), 1.82 (s, Me)

^a Yield based on total amount of starting complex. ^b In hexanes. ^c In CD₂Cl₂. ^d Product consisted of a mixture of two isomers with R₂ and R₃ interchanged (see text).

Scheme 1

peroxyacids⁷ produces a variety of products which are believed to be derived from an oxirene intermediate (**2**) formed in an initial epoxidation step. The oxirene ring is a 4π antiaromatic system and is predicted⁸ theoretically to undergo facile ring opening to the α -keto carbene, which then undergoes subsequent reactions. Direct evidence for the existence of oxirene (**2** (R = CH₃, CF₃)) has resulted⁹ from trapping experiments using rare-gas matrices and from IR spectra of intermediates formed during the photolysis of α -diazo ketones. It occurred to us that *in situ* generation of a coordinated oxirene via epoxidation of a coordinated alkyne may provide the stability required for the generation of an oxirene complex (e.g., the transformation **3** \rightarrow **4**), which might then evolve to the α -keto carbene complex **5** (Scheme 1).

A series of alkyne complexes **3** were synthesized by published procedures.¹⁰ Reaction of **3** with DMDO typically proceeded as follows: under nitrogen, **3** (0.080

mmol) was dissolved in 10 mL of anhydrous HPLC grade methylene chloride and cooled to -20 °C. A solution of DMDO was prepared as previously described² and stored at -78 °C; assays showed that these solutions typically contained DMDO at 0.07 M. A volume of the DMDO solution containing 0.4 mmol (ca. 6 mL) was quickly added to the solution of **3**, and the reaction mixture was stirred for ca. 20 h at -20 °C. The solvent was then stripped to leave a viscous oil that was dissolved in benzene and chromatographed through deactivated neutral alumina. Hexanes eluant removed unreacted starting material, and hexanes/diethyl ether (4/1 to 10/1) removed the product as a yellow-green band.

IR and ¹H NMR spectra (Table 1) suggested that the products were α -keto carbene complexes (**5**). This was verified by obtaining the X-ray structure of one of the products (**5**; R₁ = R₂ = R₃ = Me), which is illustrated in Figure 1.¹¹ (Selected bond lengths and angles are provided in Figure 1.) The yields of **5** were modest (Table 1) and were found to depend markedly on the temperature and the molar ratio of DMDO to complex **3**. Along with product **5**, the final reaction mixture generally contained some starting material, unidentified insoluble brown metal-containing species (probably oxides), and α -diketones (from the further oxidation of **5**). It is likely that the reactions with DMDO could be optimized to provide better yields than have been obtained so far.¹² It is pertinent to note that an attempt to epoxidize **3** in CH₂Cl₂ with the common oxidant *m*-chloroperbenzoic acid led to rapid and complete decomposition, with no evidence for species **4** or **5**. In contrast, the dioxirane DMDO effected the *controlled* oxidation of the coordinated alkyne.

(10) (a) Strohmeier, W.; Laporte, H.; Hobe, D. V. *Chem. Ber.* **1962**, *95*, 455. (b) Strohmeier, W.; Hellmann, H. *Chem. Ber.* **1965**, *98*, 1598. (c) Butler, I. S.; Coville, N. J.; Cozak, D. J. *Organomet. Chem.* **1977**, *133*, 59. (d) Cash, G. G.; Pettersen, R. C. *J. Chem. Soc., Dalton Trans.* **1979**, 1630. (e) Caulton, K. G. *Coord. Chem. Rev.* **1981**, *38*, 1. (f) Alt, H. G.; Engelhardt, H. E. *J. Organomet. Chem.* **1988**, *342*, 235. (g) Coughlan, S. M.; Yang, G. K. *J. Organomet. Chem.* **1993**, *450*, 151.

(11) A single crystal of **5** (R₁ = R₂ = R₃ = Me) of dimensions 0.50 \times 0.44 \times 0.40 mm was grown by ether diffusion from a solution of **5** in pentane/ether (2/1). Crystal data: triclinic, space group *P* $\bar{1}$, with *a* = 8.071(2) Å, *b* = 8.373(2) Å, *c* = 15.909(3) Å, α = 77.64(3)°, β = 86.87°, γ = 72.25°, *V* = 1000.1(4) Å³, *Z* = 2, *D*_{calcd} = 1.369 g cm⁻³; data collected at 25 °C with Mo K α radiation, μ = 6.81 cm⁻¹, θ range 2.61–26.00°, 256 variables refined with 3905 independent reflections (*I* > 2 σ (*I*)) to *R* = 0.0427, *wR*₂ = 0.01114, and *GOF* = 0.981. Refinement based on *F*² was carried out using the SHELXL 93 package.

(12) The reaction of **3** with DMDO was attempted in three solvents (CH₂Cl₂, Me₂CO, C₆H₁₄), at five temperatures (-78 , -40 , -20 , 0 , 25 °C), and with six **3**/DMDO ratios (1.0, 0.50, 0.33, 0.25, 0.20, 0.10). The best results were obtained in CH₂Cl₂ at -20 °C with a **3**/DMDO ratio of 0.20. (Indenyl)Mn(CO)₂(alkyne) analogues of **3** were also found to react with DMDO to give α -keto carbene complexes, although the yields were low.

(7) For example, see: (a) Ciabattini, J.; Campbell, R. A.; Renner, C. A.; Concannon, P. W. *J. Am. Chem. Soc.* **1970**, *92*, 3826. (b) Ibne-Rasa, K. M.; Pater, R. H.; Ciabattini, J.; Edwards, J. O. *J. Am. Chem. Soc.* **1973**, *95*, 7894.

(8) (a) Strausz, O. P.; Gosavi, R. K.; Denes, A. S.; Csizmadia, I. G. *J. Am. Chem. Soc.* **1976**, *98*, 4784. (b) Strausz, O. P.; Gosavi, R. K.; Gunning, H. E. *J. Chem. Phys.* **1977**, *67*, 3057. (c) Fowler, J. E.; Galbraith, J. M.; Vacek, G.; Schaefer, H. F. *J. Am. Chem. Soc.* **1994**, *116*, 9311.

(9) (a) Debú, F.; Monnier, M.; Verlaque, P.; Davidovics, G.; Pourcin, J.; Bodot, H.; Aycard, J.-P. *C. R. Acad. Sci. Paris, Ser. 2* **1986**, *303*, 897. (b) Torres, M.; Bourdelande, J. L.; Clement, A.; Strausz, O. P. *J. Am. Chem. Soc.* **1983**, *105*, 1698.

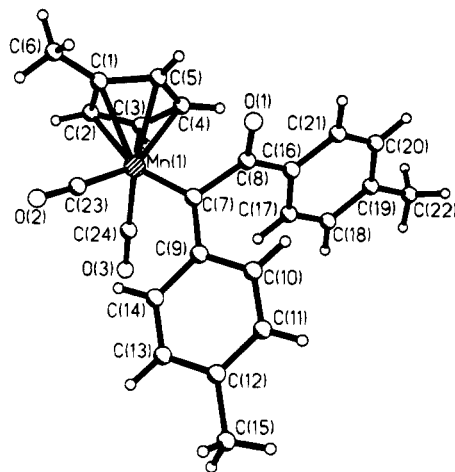


Figure 1. Molecular structure and labeling scheme for complex **5** ($R_1 = R_2 = R_3 = \text{Me}$). Selected bond lengths (\AA): Mn–C(7), 1.887(2); C(7)–C(8), 1.499(3); C(7)–C(9), 1.466(3); C(8)–O(1), 1.224(3); C(8)–C(16), 1.483(3). Selected bond angles (deg): Mn–C(7)–C(9), 132.2(2); Mn–C(7)–C(8), 114.9(2); C(9)–C(7)–C(8), 112.8(2); C(7)–C(8)–C(16), 118.4(2); C(7)–C(8)–O(1), 121.2(2); C(1)–C(8)–C(16), 120.6(2).

The α -keto carbene complex **5** ($R_1 = \text{Me}$, $R_2 = R_3 = \text{H}$) has been previously synthesized in 37% yield,^{13a} and a low-resolution X-ray structure of **5** ($R_1 = R_2 = R_3 = \text{H}$) has been described.^{13b} The reported synthesis of **5** consisted of the direct reaction of $(\text{MeCp})\text{Mn}(\text{CO})_2(\text{THF})$ with the appropriate α -diazo ketone carbene precursor (e.g., diazodeoxybenzoin). The reaction **3** \rightarrow **5** is fundamentally different in that carbene formation is the consequence of alkyne oxidation. It is quite likely that an intermediate oxirene complex **4** is formed, which rapidly undergoes ring opening to give **5**. When $R_2 \neq$

R_3 in **3**, oxidation with DMDO gave an isomeric mixture of **5** (as determined from ^1H NMR data). Thus, the isomers ($R_2 = \text{Me}$; $R_3 = \text{OMe}$) and ($R_2 = \text{OMe}$; $R_3 = \text{Me}$) were formed in a 1:1 ratio when **3** had the substituent set (Me, OMe) on the alkyne ligand. The isomeric ratio of **5** formed at -20 $^\circ\text{C}$ with the alkyne substituent set (H, OMe) was 4:1 in favor of the complex having ($R_2 = \text{OMe}$; $R_3 = \text{H}$); however, the isomer ratio was reversed at low temperatures. It might become possible to stabilize (and hence detect) an oxirene intermediate in the epoxidation of coordinated alkynes by increasing the barrier to metal slippage via increased rigidity at the metal–alkyne bond. Experiments along this line are planned using caged alkynes as well as alkynes anchored to the metal via appended phosphine ligands.

In conclusion, we have shown that dimethyldioxirane oxidizes the coordinated alkyne ligand in **3** to generate moderate yields of the corresponding α -keto carbene complex **5**. It is speculated that this reaction involves initial alkyne epoxidation to give an intermediate containing a coordinated oxirene ligand. Whether or not this is the case, the reaction **3** \rightarrow **5** illustrates that dioxiranes are potentially useful reagents for the controlled oxidation of coordinated ligands.

Acknowledgment. This work was supported by a grant from the National Science Foundation (Grant No. CHE-9400800) and by the CNR (Rome, Italy), Progetto Strategico "Tecnologie Chimiche Innovative". We are grateful to Professor G. B. Carpenter for valuable expert assistance with the X-ray structure determination.

Supplementary Material Available: Crystallographic data for complex **5**, including tables of atomic coordinates, bond lengths, bond angles, and anisotropic displacement coefficients and figures giving additional views of the structure (8 pages). Ordering information is given on any current masthead page.

(13) (a) Herrmann, W. A. *Angew. Chem.* **1974**, *86*, 556. (b) Redhouse, A. D. *J. Organomet. Chem.* **1975**, *99*, C29.

Synthesis of Azazirconacyclopropanes and Azazirconacyclopentenes from η^2 -Iminosilaacyl Complexes

Takahiro Honda,[†] Shun-ichi Satoh,[‡] and Miwako Mori^{*,†}

Faculty of Pharmaceutical Sciences, Hokkaido University, Sapporo 060, Japan, and
Institute for Drug Discovery Research, Yamanouchi Pharmaceutical Co. Ltd.,
21-Miyukigaoka, Tsukuba, Ibaraki 305, Japan

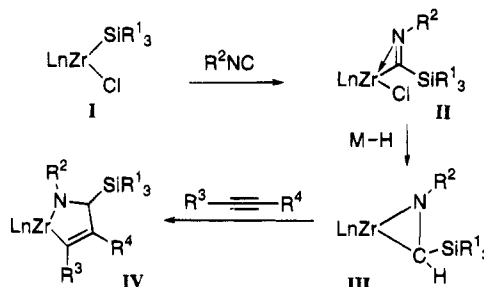
Received November 18, 1994[®]

Summary: Reaction of zirconium–silyl complex **1**, which was prepared from Cp_2ZrCl_2 and $\text{LiSi}^t\text{BuPh}_2$ in THF, with isonitriles **2** gave η^2 -iminosiacyl complexes **3** by a one-pot procedure in good to moderate yields. Treatment of complex **3a** with metal hydride and then addition of alkyne gave azazirconacyclopentene **11** via azazirconacyclopropane **7**. Hydrolysis of azazirconacyclopentenes **11** gave (α -silylallyl)amine **10**.

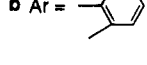
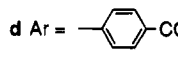
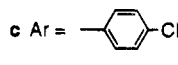
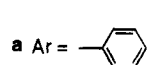
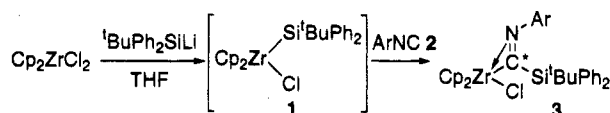
The reactivity of transition-metal–silyl complexes is quite interesting because an unsaturated bond can be inserted into the silyl–zirconium bond to provide an alternate organometallic complex which has metal–carbon and silyl–carbon bonds, further providing a new method for the carbon–carbon bond-forming reaction. A few zirconium–silyl complexes **1** are known, and they were prepared by the reaction of Cp_2ZrCl_2 with $\text{Al}(\text{SiMe}_3)_3$ ^{1a} or with corresponding LiSiR_3 ^{1b} and by oxidative addition of R_3SiH to Cp_2Zr coordinated by a butene ligand.^{1c} The insertion of carbon monoxide or an isonitrile into the zirconium–silyl bond provided a η^2 -silaacyl complex or an η^2 -iminosiacyl complex.^{1a,b} However, the reactivities of these complexes are not known. Here, we wish to report the syntheses and reactivities of zirconium–silyl complexes **1**, η^2 -iminosiacyl complexes **2**, azazirconacyclopropanes **3**, and azazirconacyclopentenes **4**. That is, the insertion of an isonitrile into the silyl–zirconium bond of **1** affords η^2 -iminosiacyl complexes **2**. Treatment of **2** with metal hydride affords the azazirconacyclopropane **3**. The insertion of alkyne into the carbon–zirconium bond of **3** gives azazirconacyclopentene **4**.

Zirconium–silyl complex **1** was prepared from Cp_2ZrCl_2 and $\text{LiSi}^t\text{BuPh}_2$ according to the modified Tilley procedure.^{1b} To a THF solution of $\text{LiSi}^t\text{BuPh}_2$ was added a THF solution of Cp_2ZrCl_2 at -78°C , and the solution was stirred at 0°C for 1 h. An orange Cp_2 -

Scheme 1



Scheme 2



δ -value of imino carbon
of **3** on ^{13}C -NMR (CDCl_3)

	yield (%)	δ (ppm) of C^*
3e	61	266.7
3a	71	269.7
3c	43	272.3
3d	53	274.2
3b	54	272.2

$\text{ZrSi}^t\text{BuPh}_2\text{Cl}$ (**1**) solution was obtained, but the isolation of zirconium–silyl complex **1** was unsuccessful because it was exceedingly sensitive to moisture. Thus, the insertion of an isonitrile into the zirconium–silyl bond of **1** was carried out *in situ*. To a THF solution of **1**, prepared from $\text{LiSi}^t\text{BuPh}_2$ and Cp_2ZrCl_2 , was added PhNC^3 (**2a**) in THF at -78°C , and then the solution was stirred at room temperature for 10 h. Aqueous NH_4Cl solution was added, and the aqueous layer was extracted with AcOEt . The organic layer was dried and concentrated. The air- and moisture-stable η^2 -iminosiacyl complex **3a** was obtained in 71% yield after column chromatography on silica gel (mp 193 – 194°C , from hexane– CH_2Cl_2). The structure of **3a** was determined by the X-ray diffraction method. Various η^2 -iminosiacyl complexes **3** were prepared. The chemical shifts of imino carbon atoms in the ^{13}C NMR spectra are shown in Scheme 2. Evidently, the chemical shifts of those complexes **3** having an electron-withdrawing group at the 4-position on the aromatic ring appear at lower field.

Monitoring the reaction of **3d** with dry HCl in C_6D_6 revealed that the Cp peak of **3d** (δ 5.81) gradually

[†] Hokkaido University.

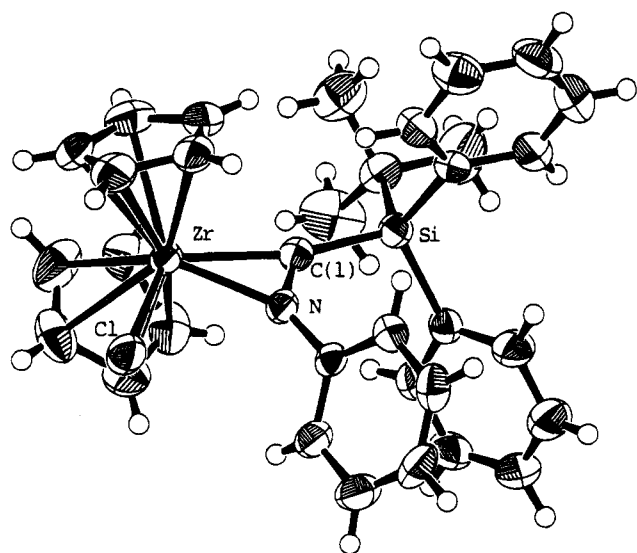
[‡] Yamanouchi Pharmaceutical Co. Ltd.

[®] Abstract published in *Advance ACS Abstracts*, March 1, 1995.

(1) (a) Tilley, T. D. *Organometallics* **1985**, *4*, 1452. Tilley, T. D. *J. Am. Chem. Soc.* **1985**, *107*, 4084. Elsner, F. H.; Woo, H.-G.; Tilley, T. D. *J. Am. Chem. Soc.* **1988**, *110*, 313. (b) Campion, B. K.; Falk, J.; Tilley, T. D. *J. Am. Chem. Soc.* **1987**, *109*, 2049. Elsner, F. H.; Tilley, T. D.; Rheingold, A. L.; Geib, S. J. *J. Organomet. Chem.* **1988**, *358*, 169. Heyn, R. H.; Tilley, T. D. *Inorg. Chem.* **1989**, *28*, 1768. Cardin, D. J.; Keppie, S. A.; Kingston, B. M.; Lappert, M. F. *J. Chem. Soc., Chem. Commun.* **1967**, 1035. Xue, Z.; Li, L.; Hoyt, L. K.; Diminnie, J. B.; Pollitte, J. L. *J. Am. Chem. Soc.* **1994**, *116*, 2169. Procopio, L. J.; Carroll, P. J.; Berry, D. H. *J. Am. Chem. Soc.* **1991**, *113*, 1870; *Organometallics* **1993**, *12*, 3087. (c) Takahashi, T.; Hasegawa, M.; Suzuki, N.; Saburi, M.; Rousset, C. J.; Fanwick, P. E.; Negishi, E. *J. Am. Chem. Soc.* **1991**, *113*, 8564. Kreutzer, K. A.; Fisher, R. A.; Davis, W. M.; Spaltenstein, E.; Buchwald, S. L. *Organometallics* **1991**, *10*, 4031.

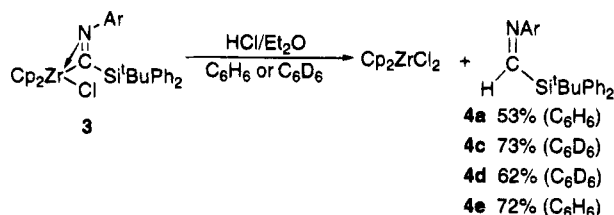
(2) Campion, B. K.; Heyn, R. H.; Tilley, T. D. *Organometallics* **1993**, *12*, 2584.

(3) Ugi, I.; Meyr, R. *Organic Synthesis*; Wiley: New York, 1973; Collect. Vol 5, p 1060.

Figure 1. ORTEP drawing of **3a**.Table 1. Selected Bond Distances and Angles for **3a**

Bond Distances (Å)			
Zr-Cl	2.57	N-C(1)	1.27
Zr-N	2.19	C(1)-Si	1.92
Zr-C(1)	2.28		
Bond Angles (deg)			
C(1)-Zr-N	33.1	Zr-C(1)-N	69.6
Zr-N-C(1)	77.3		

Scheme 3



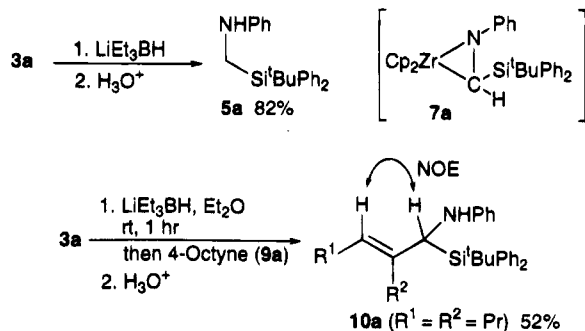
changed to that of Cp_2ZrCl_2 (δ 5.93). After the usual workup, formidoysilane **4d** was isolated in 62% yield. Other η^2 -iminosilaacyl complexes **3a,c,e** were treated with dry HCl in C_6D_6 , and the reactions were followed by NMR. The formidoysilanes **4a,c,e** were isolated in 53%, 73%, and 72% yields, respectively. However, formidoysilane **4b**⁴ was not obtained in a similar manner. Surprisingly, treatment of complex **3a** with aqueous 10% HCl did not afford the formidoysilane **4a**, and **3a** was completely recovered unchanged.

The various attempts to insert an unsaturated bond into the zirconium-carbon bond of **3** were unsuccessful. Thus, we examined the conversion of iminosilaacyl complex **3** into azazirconacyclopropane **7** and then the insertion of the unsaturated bond into the carbon-zirconium bond of **7**. Treatment of the η^2 -iminosilaacyl complex **3a** with LiEt_3BH (1.3 equiv) in THF at room temperature followed by hydrolysis gave (silylmethyl)aniline **5a** in 82% yield.⁵ The results indicate that azazirconacyclopropane **7a** was formed in this reaction. It is generally accepted that various unsaturated bonds can be inserted into the zirconium-carbon bond of

(4) Ito, Y.; Matsuura, T.; Murakami, M. *J. Am. Chem. Soc.* **1987**, *109*, 7888.

(5) Use of toluene instead of THF for this reaction gave a fair amount of formidoysilane **4a** (14% yield) along with **5a** (14% yield), and **3a** was recovered in 68% yield.

Scheme 4

Table 2. Insertion of Alkyne **9** into the C-Zr Bond of **3a**

run	alkyne 9 (2.0 eq.)	product 10	10 (%)	5a (%)
1	Pr-C≡C-Pr (9a)	R ₁ = R ₂ = Pr (10a)	A ^a) 52 B ^b) 73	48 27
2	TMS-C≡C-Me (9b)	R ₁ = TMS (10b) R ₂ = Me	A 58 B 72	21 12
3	TMS-C≡C-C ₅ H ₁₁ (9c)	R ₁ = TMS (10c) R ₂ = C ₅ H ₁₁	A 34 B 66	65 23
4	1-heptyne (9d)	R ₁ = C ₅ H ₁₁ (10d) R ₂ = H	A 37 B 22	48 20
5	ROCH ₂ -C≡C-CH ₂ OR (9e R = TBS)	R ₁ = CH ₂ OH (10e) R ₂ = CH ₂ OTBS	B 61	33
6	ROCH ₂ -C≡C-CH ₂ OR (9f R = Bn)	R ₁ = R ₂ = CH ₂ OBn (10f)	B 75	17

a) method A: **9** was added to the ethereal solution of **7a**, prepared from **3a** and LiEt_3BH in THF, and the solution was stirred at room temperature for 12 h. b) method B: To the solution of **3a** and **9** was added LiEt_3BH in THF at 0 °C and the solution was stirred at room temperature for 12 h.

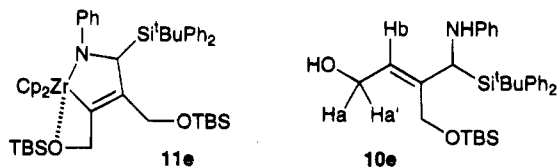


Figure 2.

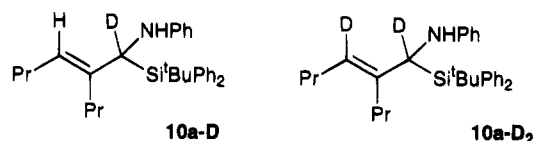
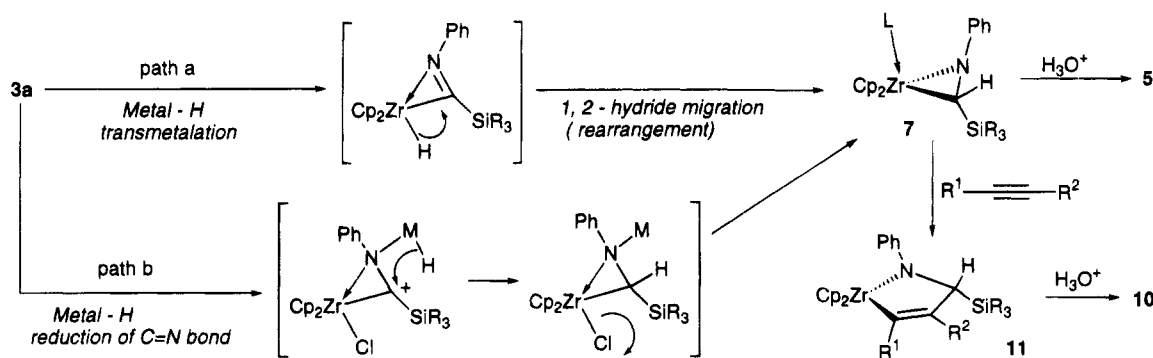


Figure 3.

azazirconacyclopropane.⁶ Thus, when 4-octyne (2.0 equiv) was added to the ethereal solution of azazirconacyclopropane **7a** at 0 °C, which was prepared from **3a** and LiEt_3BH in Et_2O , the yellow solution changed to red. The solution was further stirred at room temperature for 12 h. After the usual workup, (α -silylallyl)amine **10a** was obtained in 52% yield along with **5a** (48% yield).⁷ The structure of **10a** was determined by

(6) (a) Jensen, M.; Livinghouse, T. *J. Am. Chem. Soc.* **1989**, *111*, 4495. Ito, H.; Taguchi, T.; Hanzawa, Y. *Tetrahedron Lett.* **1992**, *33*, 4469. (b) Buchwald, S. L.; Watson, B. T.; Wannamaker, M. W.; Dawan, J. C. *J. Am. Chem. Soc.* **1989**, *111*, 4486. Buchwald, S. L.; Wannamaker, M. W.; Watson, B. T. *J. Am. Chem. Soc.* **1989**, *111*, 776. Grossman, R. B.; Davis, W. M.; Buchwald, S. L. *J. Am. Chem. Soc.* **1991**, *113*, 2321. Coles, N.; Whitby, R. J.; Blagg, J. *Synlett* **1990**, 271. Coles, N.; Harris, M. C. J.; Whitby, R. J.; Blagg, J. *Organometallics* **1994**, *13*, 190; *Tetrahedron Lett.* **1994**, *35*, 2431. (c) Davis, J. M.; Whitby, R. J.; Jaxa-Chamiec, A. *Tetrahedron Lett.* **1992**, *33*, 5655; **1994**, *35*, 1445; *Synlett* **1994**, 110. (d) Wolczanski, P. T.; Bercaw, J. E. *J. Am. Chem. Soc.* **1979**, *101*, 6450.

Scheme 5. Possible Reaction Course



spectral data and the NOE experiment. It was ascertained that the *E* isomer was formed in this reaction, which indicates that the insertion of alkyne into the C–Zr bond proceeds in a stereoselective manner and the product is obtained as a single isomer. Various alkynes **9** could be inserted into the zirconium–carbon bond (Table 2, method A). The yields were improved when LiEt_3BH was added to an ethereal solution of η^2 -iminosilaacyl complex **3** at 0 °C in the presence of alkyne **9** (method B). The reaction of **3a** with terminal alkyne **9d** afforded (α -silylallyl)amine **10d** in moderate yield (run 4). In the reaction of **3a** with **9e**, monosilylated product **10e** was obtained.⁸ Since the silyl group of **9e** would coordinate to zirconium of zirconacyclopentene **11e** (see Figure 2), the bond cleavage of the O–Si bond would occur during the aqueous workup to give **10e**.

To confirm the formation of azazirconacyclopropane **7**, treatment of **3a** with LiEt_3BD ⁹ in the presence of 4-octyne was carried out to give **10a-D** (D content ~100%) in 84% yield. Furthermore, when the same reaction was carried out and then the solution was treated with D_2O , **10a-D₂** (D content 86%) was obtained in quantitative yield. These results strongly suggest that azazirconacyclopropane **III** was formed. On the basis of these results, the possible reaction course is shown in Scheme 5. It was not clear¹⁰ whether azazirconacyclopropane **7** was formed by reduction of the C=N

bond with metal hydride or by transmetalation of **3a** with metal hydride followed by 1,2-hydride migration.

Although there have been a few reports on the formation of azazirconacyclopropane (reaction of imine with Cp_2ZrBu_2 ,^{6a} reaction of Cp_2ZrMeCl with lithium amide followed by β -elimination,^{6b} and insertion of isonitrile into zirconacyclopentene followed by rearrangement^{6c}), our method, which involves the reaction of η^2 -iminosilaacyl complex **3** with metal hydride, is different from the previous methods.

Further insertion reactions of unsaturated bonds into the azazirconacycles are now being investigated.

Supplementary Material Available: Text giving the general procedure for the synthesis of η^2 -iminosilaacyl complex **3** and formidoysilane **4**, typical procedures for the insertion of the C–Zr bond of **3a** into alkynes (methods A and B), and characterization data for **3b–e**, **4–e**, **5a**, **10a**, **10a-D**, **10a-D₂**, and **10b–f** and details of the X-ray structure determination of **3a**, including figures giving views of the structure, text giving data collection and refinement details, and tables giving atomic coordinates, thermal parameters, bond distances and angles, and torsion angles (35 pages). This material is contained in libraries on microfiche, immediately follows this article in the microfilm version of the journal, and can be ordered from the ACS; see any current masthead page for ordering information.

OM940878X

(7) For this reaction, DIBAH can be used; the use of THF as a solvent decreased the yield of desired product.

(8) The structure was confirmed by ^1H NMR ($\text{CDCl}_3\text{-D}_2\text{O}$). The vinylic proton H_b (δ 5.70 (dd, J = 7.0, 7.0 Hz, 1 H)) was coupled with allylic protons H_a (δ 4.00 (dd, J = 12.6, 7.0 Hz, 1 H)) and H_{a'} (δ 4.04 (dd, J = 12.6, 7.0 Hz, 1 H)).

(9) LiEt_3BD is commercially available (Aldrich).

(10) When the reaction of **3b** with LiEt_3BH was carried out in the presence of 4-octyne, the desired product was not obtained and **3b** was recovered (93%). This suggests that the reaction proceeds by reduction of the C=N bond by M–H because the nitrogen of **3b** could not coordinate to the metal of M–H, and the C=N bond could not be reduced by metal hydride in this case. Cf.: Waymouth, R. M.; Clauser, K. R.; Grubbs, R. H. *J. Am. Chem. Soc.* **1986**, *108*, 6385.

Synthesis and Reactivity of Cp₂ZrH(OSO₂CF₃), a Soluble Alternative for Schwartz's Reagent, and the Solid-State Structure of Its Dimer, [Cp₂Zr(OSO₂CF₃)(μ-H)]₂·0.5THF

Gerrit A. Luinstra,* Ursula Rief, and Marc H. Prosenec

Department of Chemistry, University of Konstanz, Postfach 5560 M738,
D-78643 Konstanz, Germany

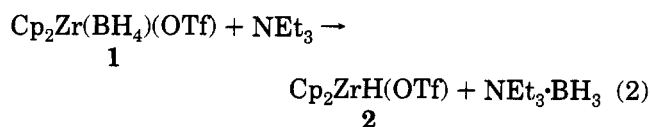
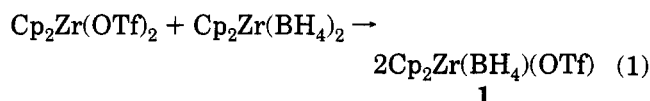
Received December 2, 1994[©]

Summary: Comproportionation of Cp₂Zr(OTf)₂ and Cp₂Zr(BH₄)₂ (Cp = C₅H₅; OTf = OSO₂CF₃) gives Cp₂ZrBH₄(OTf) (**1**). Reaction of **1** with NEt₃ yields Cp₂ZrH(OTf) (**2**), which was crystallized from THF to yield dimeric [Cp₂Zr(OSO₂CF₃)(μ-H)]₂·0.5THF (**2b**). The structure of **2b** was determined by X-ray methods. Reaction of **2** with hexene, (trimethylsilyl)acetylene, and ^tBuCN yields Cp₂Zr(hexyl)(OTf), Cp₂Zr[CH=CH(SiMe₃)](OTf), and Cp₂Zr[N=C(^tBu)H](OTf), respectively.

Schwartz's reagent, a polymer with the stoichiometry Cp₂ZrH(Cl) (Cp = C₅H₅), has proven to be very useful reagent. It has been applied extensively in both organometallic and organic research (e.g. hydrozirconation of olefins).¹ It is commercially available and easy to handle. However, it has one significant drawback in that it is poorly soluble in commonly used solvents such as toluene, THF, and dichloromethane, and purification is difficult, also because of disproportionations. The hydrozirconation mixture of Cp'₂ZrH₂ and Cp'₂ZrCl₂ (Cp' = C₅H₄Me), which is assumed to comproportionate to give the Cp' analog to Schwartz's reagent, Cp'₂ZrH(Cl), is more reactive,² but its solubility in THF is still marginal and the lower symmetry makes it less ideal for application in NMR studies. In our investigations on the hydrozirconation of metal-bonded vinyls, a soluble and monomeric hydride was needed. We concluded that substitution of the chloride in Schwartz's reagent by the larger triflate anion would obstruct the formation of larger polymeric structures, at the same time yielding a very reactive hydride by virtue of the weak coordination properties of the triflate anion.³

The borohydride complex Cp₂ZrBH₄(OTf) (**1**) is a convenient precursor for Cp₂ZrH(OTf) (**2**). The former was obtained almost quantitatively from the comproportionation of Cp₂Zr(OTf)₂⁴ and Cp₂Zr(BH₄)₂ (eq 1). The equilibrium lies totally to the right, and **1** can be isolated as a white microcrystalline solid by evaporation of the solvent.

Addition of 1 equiv of NEt₃ to a toluene solution of **1** results in the formation of [Cp₂ZrH(OTf)] (**2**; eq 2). It readily crystallizes from solution as large off-white needles. **2** is sparingly soluble in benzene and ether but



can be dissolved in THF (up to a concentration of about 0.10 mol/L), from which solvent it can be recrystallized. A Zr-H stretching vibration is assigned at 940 cm⁻¹ (685 cm⁻¹ in the deuterium analog Cp₂ZrD(OTf) (**2d**)), in the normal range for bridging zirconium hydrides.^{1c} This indicates that Cp₂ZrH(OTf) is not monomeric in the solid state. Complex **2** has one signal in the proton NMR for the Cp rings at 6.48 ppm (THF-*d*₈) and one for the hydride at 0.12 ppm. A mixture of **2** and SiMe₂(C₅H₄)₂ZrH(OTf) (**3**)⁵ in THF-*d*₈ gives three sets of resonances, assigned to the three possible dimers (Cp₂ZrOTf)₂(μ-H)₂ (**2**), [SiMe₂(C₅H₄)₂ZrOTf]₂(μ-H)₂ (**3**), and the mixed complex [SiMe₂(C₅H₄)₂ZrOTf][Cp₂ZrOTf](μ-H)₂, illustrating that these zirconocene triflate hydrides are probably dimeric in solution.⁶

The needles of **2** obtained from synthesis in toluene were structurally disordered and unsuitable for X-ray diffraction studies. However, single crystals of a closely related complex, [(Cp₂ZrOTf)₂(μ-H)₂]·0.5THF (**2b**), could be obtained by diffusing diethyl ether into a concentrated THF solution of **2**.⁷ The results of an X-ray structure determination are shown in Figure 1. Compound **2b** is a dimer of **2**, where two bent-zirconocene units are bridged by two hydride ligands. The triflates are η¹ coordinated. The hydride was located accurately from a difference Fourier map. The inversion symmetry operation of the space group places another hydride in the close vicinity of the metal center. In this way an asymmetric bridge is formed between two discrete Cp₂-

(5) **3** was prepared analogously to **2**. ¹H NMR (THF-*d*₈): 7.35 (m, 2H; Cp), 6.66 (m, 2H; Cp), 6.30 (m, 2H; Cp), 5.53 (m, 2H; Cp), 0.78 (s, 3H; Me), 0.64 (s, 3H; Me), 0.37 ppm (s, 1H; H).

(6) A molecular weight determination by ebulliometry of **2** in THF solution gives a molecular weight of 340, indicating that the triflate partly dissociates from **2**.

(7) Crystallographic data were collected using a Siemens R3m/V diffractometer with Mo Kα radiation (0.710 73 Å, μ = 3.7 cm⁻¹). The SHELXL93 program was used for structure solution and refinement. C₁₃H₁₅F₃O_{3.5}SZr: triclinic, P1̄ (a = 8.486(3) Å, b = 8.703(4) Å, c = 11.793(4) Å, α = 86.55(3)°, β = 72.40(3)°, γ = 66.55(3)°, Z = 2, V = 759.8(5) Å³). The intensity data were collected using a Wyckoff type scan over the range 3.6° < 2θ < 56°. The 3666 unique intensities collected were used in the least-squares full-matrix refinement on F² with anisotropic thermal parameters for all non-hydrogen atoms to converge at R_F = 0.0291 (R_w² = 0.0776) (T = 243 K). Cocrystallized THF is disordered.

* Abstract published in *Advance ACS Abstracts*, March 1, 1995.

(1) See e.g.: (a) Schwartz, J.; Labinger, J. A. *Angew. Chem., Int. Ed. Engl.* **1976**, *15*, 33. (b) Hart, J. W.; Schwartz, J. J. *Am. Chem. Soc.* **1974**, *96*, 8115. (c) Gibson, T. *Organometallics* **1987**, *6*, 918. (d) Wailes, P. C.; Weigold, H. J. *Organomet. Chem.* **1970**, *24*, 405. (e) Laycock, D. E.; Alper, H. J. *Org. Chem.* **1981**, *46*, 289. (f) Sorell, T. N. *Tetrahedron Lett.* **1978**, 4983. (g) Swanson, D. R.; Nguyen, T.; Noda, Y.; Negishi, E.-I. *J. Org. Chem.* **1991**, *56*, 2590.

(2) Erker, G.; Schlund, R.; Krüger, C. *Organometallics* **1989**, *8*, 2349.

(3) Cf.: (a) Lawrance, G. A. *Adv. Inorg. Chem.* **1989**, *34*, 145 and references cited therein. (b) Strauss, S. H. *Chem. Rev.* **1993**, *93*, 927. (c) Jordan, R. F. *Adv. Organomet. Chem.* **1991**, *32*, 325.

(4) Thewalt, U.; Lasser, W. Z. *Naturforsch., B* **1983**, *38B*, 1501.

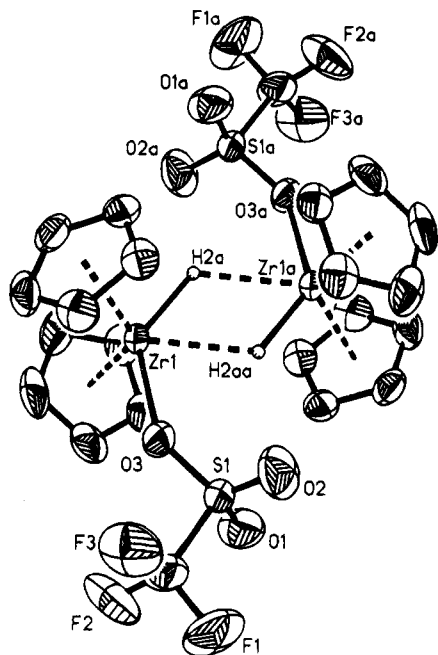


Figure 1. ORTEP drawing of **2b**, showing terminal ellipsoids (50% probability level). Selected bond lengths: Zr(1)–O(3), 2.205(2) Å, Zr(1)–H(2AA), 2.231(10) Å; Zr(1)–H(2A), 1.831(9) Å; Zr(1)–Zr(1A), 3.4865(14) Å. Selected bond angles: H(2AA)–Zr(1)–H(2A), 62.1(5)°; O(3)–Zr(1A)–H(2A), 134.8(3)°; CE(1)–Zr(1)–CE(2), 127.6°; Zr(1)–H(2A)–Zr(1A), 117.9(5)°.

ZrH(OTf) molecules, with alternating Zr–H distances Zr(1)–H(1A) = 1.831(9) Å and Zr(1A)–H(2AA) = 2.231(10) Å.

The $Zr_2(\mu-H)_2$ unit has been crystallographically characterized in a number of cases. Two types are found, those with two long bridges with characteristic Zr–H distances of about 2.0 Å (for example in the Cp_2 derivatives $[Cp_2Zr(SiPhMeH)]_2(\mu-H)_2$ at 1.94(10) and 1.95(10) Å,^{8a} in $[Cp_2Zr(SiPh_2H)]_2(\mu-H)_2$ at 2.01(2) and 1.96(3) Å,^{8b} in $(Cp'_2ZrH)_2(\mu-H)_2$ at 2.05(3) and 1.94(2) Å,^{8c} and in $[(tBuCp)_2ZrH]_2(\mu-H)_2$ at 2.012(7) and 1.999(4) Å,^{8d}) and those with one longer and one shorter Zr–H distance (as in $(C_8H_8ZrOAr)_2(\mu-H)_2$ (Ar = 2,6-di-*tert*-butylphenyl)^{9a} with Zr–H distances of 1.85(3) and 2.03(3) Å or in $[SiMe_2(C_5H_4)_2][CpZrCl(\mu-H)]_2$ ^{9b} with alter-

nating Zr–H distances of 1.75(4) and 2.05(4) Å). In our case, the long Zr–H bond of over 2.23 Å is significantly longer than observed in the complexes mentioned above, whereas the short bond is clearly in the range of terminal Zr–H bond lengths (bond lengths of about 1.8 Å are typical for terminal zirconium hydrides^{8c,d,10}). This suggests that no large reorganization of the geometry (and hence energy) would be necessary for dissociation to the monomer.

We find that **2** is very reactive; for example, it reacts instantaneously with 1-hexene to give the monoalkyl complex $Cp_2ZrC_6H_{13}(OTf)$. Terminal acetylenes are selectively hydrozirconated at room temperature; no acid–base reaction is observed. Addition of 1 equiv of (trimethylsilyl)acetylene to a THF solution of **2** quantitatively yields $Cp_2Zr[CH=CH(SiMe_3)](OTf)$ (by NMR, trans isomer only). Hetero unsaturated molecules react likewise quickly and selectively with **2**: addition of 1 equiv of $tBuC\equiv N$ gives the azomethine complex $Cp_2Zr[N=C(tBu)H](OTf)$.^{2,11} Thus, substitution of the chloride in Schwartz's reagent for triflate gives a well-defined, easily accessible hydrozirconation reagent. Studies of the reactivity of **2** toward other substrates (C=O) as well as convenient ways to prepare hydrozirconation reagents with other weakly coordinating anions are in progress.

Acknowledgment. Financial support for this work by the European Economic Community (Contract No. ERBCHICT930812) is gratefully acknowledged. We thank Prof. H. H. Brintzinger for useful discussions.

Supplementary Material Available: Full details of the X-ray structure of **2b**, including tables of atomic coordinates, bond lengths and angles, and anisotropic displacement coefficients and figures giving additional views of the structure, and text giving details on the synthesis and characterization of **1–3** and the reactivity of **2** toward 1-hexene, (trimethylsilyl)acetylene, and pivalonitrile (17 pages). Ordering information is given on any current masthead page.

OM9409229

(9) (a) Beerno, P.; Floriani, C.; Chiesi-Villa, A.; Guastini, G. *J. Chem. Soc., Chem. Commun.* **1991**, 109. (b) Reddy, K. P.; Petersen, J. L. *Organometallics* **1989**, *8*, 547.

(10) Cf.: (a) Kot, W. K.; Edelstein, N. M.; Zalkin, A. *Inorg. Chem.* **1987**, *26*, 1339. (b) Highcock, W. J.; Mills, R. M.; Spencer, J. L.; Woodward, P. *J. Chem. Soc., Chem. Commun.* **1986**, 821. (c) Erker, G.; Kropp, K.; Krüger, C.; Chiang, A.-P. *Chem. Ber.* **1982**, *115*, 2447.

(11) Cf.: (a) Bercaw, J. E.; Davies, D. L.; Wolczanski, P. T. *Organometallics* **1986**, *5*, 443. (b) Gambarotta, S.; Floriani, C.; Chiesi-Villa, A.; Guastini, G. *J. Am. Chem. Soc.* **1983**, *105*, 1690.

(8) (a) Mu, Y.; Aitken, C.; Cote, B.; Harrod, J. E. *Can. J. Chem.* **1991**, *69*, 264. (b) Takahashi, T.; Hasegawa, M.; Suzuki, N.; Saburi, M.; Rousset, C. J.; Fanwick, P. E.; Negishi, E.-I. *J. Am. Chem. Soc.* **1991**, *113*, 8564. (c) Choukroun, R.; Dahan, F.; Larsonneur, A.-M.; Samuel, E.; Petersen, J.; Meunier, P.; Sornay, C. *Organometallics* **1991**, *10*, 374. (d) Jones, S. B.; Petersen, J. L. *Inorg. Chem.* **1981**, *20*, 2889.

The Silolyl Anion $C_4H_4SiH^-$ is Aromatic and the Lithium Silolide C_4H_4SiHLi Even More So

Bernd Goldfuss, and Paul v. R. Schleyer

Organometallics, **1995**, 14 (4), 1553-1555 • DOI: 10.1021/om00004a004 • Publication Date (Web): 01 May 2002

Downloaded from <http://pubs.acs.org> on March 9, 2009

More About This Article

The permalink <http://dx.doi.org/10.1021/om00004a004> provides access to:

- Links to articles and content related to this article
- Copyright permission to reproduce figures and/or text from this article



The Silolyl Anion $C_4H_4SiH^-$ Is Aromatic and the Lithium Silolide C_4H_4SiHLi Even More So

Bernd Goldfuss and Paul von Ragué Schleyer*

Institut für Organische Chemie, Universität Erlangen-Nürnberg, Henkestrasse 42, D-91054 Erlangen, Germany

Received November 15, 1994[®]

Summary: The η^5 coordination of Li^+ in lithium silolide $Li^+(CH)_4SiH^-$ (**4**), increases the delocalization and aromaticity relative to $C_4H_4SiH^-$ (**1a**) strongly: **4** exhibits 80% of the stabilization energy of $Li^+C_5H_5^-$, decreased pyramidalicity of the silicon center, and increased CC bond length equalization. In addition, $\delta(^{29}Si)$ in **4** is shifted downfield, $\delta(^{13}C)$ is shifted upfield, and the diamagnetic susceptibility is exalted (Δ). Likewise, experimental X-ray data on $\{Cp^*Ru(H)[\eta^5-Me_4C_4SiSi(SiMe_3)_3]\}[BPh_4]$ (**2**) and NMR studies on lithium 1-*tert*-butyl-2,3,4,5-tetraphenylsilolide (**3**) suggest delocalized silole rings.

Why is the parent silolyl anion $C_4H_4SiH^-$ (**1**) still unknown, in contrast to the well-characterized cyclopentadienyl anion?¹ Could the lack of aromaticity or appreciate resonance stabilization in **1** be responsible? The available information is in disagreement. Gordon's early theoretical conclusion that **1** is "approximately 25% as aromatic as the cyclopentadienyl anion" was based on very low level (STO-2G) *ab initio* theory as well as an assumed planar geometry for **1**.^{2a} Damewood employed a better 6-31G* basis set (but one also lacking diffuse functions) which indicated that the silicon environment is nearly as pyramidal in **1** as in the parent silyl anion, SiH_3^- .^{2b} Although the inversion barrier in **1** (16.2 kcal/mol) was reduced relative to SiH_3^- (26.0 kcal/mol), he concluded that the ground state of **1** "has only ca. 3% of the resonance stabilization of $C_5H_5^-$ ". Damewood predicted "a significantly lower stability of η^5 -metal complexes than that found for the all-carbon analogues". Nevertheless, the first η^5 -silolyl complex, $\{Cp^*Ru(H)[\eta^5-Me_4C_4SiSi(SiMe_3)_3]\}[BPh_4]$ (**2**), was synthesized and characterized by X-ray and NMR recently.³ The planar silole ring and the bond length equalization in the butadiene moiety of **2** indicate delocalization. Furthermore, recent NMR investigations of a derivative of **1**, lithium 1-*tert*-butyl-2,3,4,5-tetraphenylsilolide (**3**),

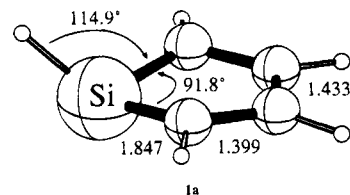


Figure 1. Silolyl anion **1a** (C_s , RMP2(fc)/6-31+G** level, bond length in Å).

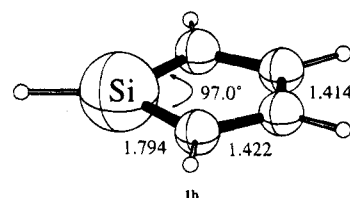
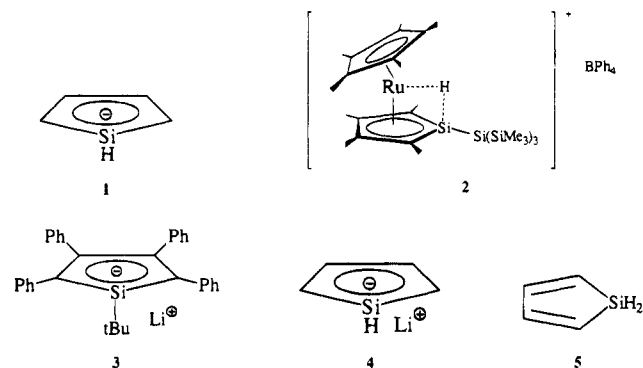


Figure 2. Silolyl anion **1b** (C_{2v} , RMP2(fc)/6-31+G** level, bond length in Å).

support "delocalization of the negative charge, justifying an aromatic resonance contributor".⁴



On the basis of the mutually related structural, energetic, and magnetic criteria for aromaticity,⁵ we now demonstrate that $(CH)_4SiH^-$ (**1**) exhibits a much higher degree of delocalization and aromaticity than has been deduced before.² This revises the conclusions of the previous theoretical studies.² Calculations on $Li^+C_4H_4SiH^-$ (**4**; a model system for **2** and **3**) reveal that the η^5 coordination of Li^+ in **4** is similar to that in $Li^+C_5H_5^-$. Moreover, we find that **4** is even more aromatic than **1**.

The $C_4H_4SiH^-$ ground state (C_s) **1a** (Figure 1) and the planar inversion transition structure (C_{2v}) **1b** (Figure 2) were optimized at the RMP2(fc)/6-31+G** level (GAUSSIAN 92)⁶ and characterized by frequency analy-

[®] Abstract published in *Advance ACS Abstracts*, March 1, 1995.

(1) (a) Paquette, L. A.; Bauer, W.; Sivik, M. R.; Bühl, M.; Feigel, M.; Schleyer, P. v. R. *J. Am. Chem. Soc.* **1990**, *112*, 8776 and references therein. (b) Bordwell, F. G.; Drucker, G. E.; Fried, H. E. *J. Org. Chem.* **1981**, *46*, 632. (c) Li, W. K.; Nobes, R. H.; Poppinger, D.; Radom, L. In *Comprehensive Carbanion Chemistry*; Bunzel, E., Durst, T., Eds.; Elsevier: Amsterdam, 1987; Vol. C and references therein. (d) Lambert, C.; Schleyer, P. v. R. *Angew. Chem., Int. Ed. Engl.* **1994**, *33*, 1129. (e) Lambert, C.; Schleyer, P. v. R. *Methoden Org. Chem. (Houben-Weyl)*, *4th Ed.*, 1952–1993, E19d, p 1.

(2) (a) Gordon, M. S.; Boudjouk, P.; Anwari, F. *J. Am. Chem. Soc.* **1983**, *105*, 4972. (b) Damewood, J. R., Jr. *J. Org. Chem.* **1986**, *51*, 5028. (3) Freeman, W. P.; Tilley, T. D.; Rheingold, A. L. *J. Am. Chem. Soc.* **1994**, *116*, 8428.

(4) Hong, J.-H.; Boudjouk, P. *J. Am. Chem. Soc.* **1993**, *115*, 5883. (5) (a) Schleyer, P. v. R.; Freeman, P. K.; Jiao, H.; Goldfuss, B. *Angew. Chem.* **1995**, *107*, 332; *Angew. Chem., Int. Ed. Engl.*, in press. (b) Grützmacher, H. *Angew. Chem.* **1995**, *107*, 323; *Angew. Chem., Int. Ed. Engl.*, in press. Compare: (c) Chesnut, D. B.; Quin, L. D. *J. Am. Chem. Soc.* **1994**, *116*, 9638. These authors also studied the aromaticity in a series of five- as well as six-membered heterocycles but did not include the silolyl anion.

(6) Frisch, M. J.; Trucks, G. W.; Schlegel, H. B.; Gill, P. M. W.; Johnson, B. G.; Wong, M. W.; Foresman, J. B.; Robb, M. A.; Head-Gordon, M.; Replogle, E. S.; Gomperts, R.; Andres, J. L.; Raghavachari, K.; Binkley, J. S.; Gonzalez, C.; Martin, R. L.; Fox, D. J.; Defrees, D. J.; Baker, J.; Stewart, J. J. P.; Pople, J. A. GAUSSIAN 92/DFT, Revision F.2; Gaussian, Inc., Pittsburgh, PA, 1993.

Table 1. Angle Sums ($\angle\Sigma$) at Silicon, Si-C $_{\alpha}$ Bond Lengths, C $_{\beta}$ C $_{\beta}$ -C $_{\alpha}$ C $_{\beta}$ Bond Length Differences, and Julg Parameters (Å)^a

	1a (C _s)	1b (C _{2v})	2 ^c	4 (C _s) ^f	5 (C _{2v}) ^b
$\angle\Sigma$ (Si) (deg)	321.6 ^b (293.8 ^c) (290.5 ^d)	360.0 ^b (360.0 ^c) (360.1 ^d)	355.1	340.2	
Si-C $_{\alpha}$ (Å)	1.847 ^b (1.916 ^c) (1.924 ^d)	1.794 ^b (1.787 ^c) (1.788 ^d)	1.830 (7)	1.823	1.875
C $_{\beta}$ C $_{\beta}$ -C $_{\alpha}$ C $_{\beta}$ (Å)	+0.034 ^b (+0.121 ^c) (+0.131 ^d)	-0.008 ^b (+0.001 ^c) (+0.004 ^d)	0.07 (2)	0.004	0.124
A	0.971 ^b (0.620 ^c) (0.552 ^d)	0.998 ^b (1.0 ^c) (0.9996 ^d)	0.874	0.9996	0.608

^a Reference 8. ^b RMP2(fc)/6-31+G** geometry. ^c RHF(fc)/6-31+G** geometry. ^d RHF/6-31G* geometry.^{2b} ^e Data were obtained from the X-ray structure of 2.³ ^f RMP2(fc)/6-31G** geometry.

Table 2. Calculated Total Energies and Zero-Point Energies (ZPE)

	1a (C _s) ^b	1b (C _{2v}) ^b	4 (C _s) ^c	5 (C _{2v}) ^b
ZPE (kcal/mol) ^a	42.2	41.6	45.1	49.1
tot. energy (au)	-443.89356	-443.88656	-451.37169	-444.47930
min		TS (-410 cm ⁻¹) ^d	min	min

^a Scaled by 0.94.¹⁹ ^b RMP2(fc)/6-31+G**//RMP2(fc)/6-31+G**. ^c RMP2(fc)/6-31G**//RMP2(fc)/6-31G*. ^d Value of the imaginary frequency.

Table 3. Aromatic Stabilization Energies (ASE; Eq 1) for C₅H₅⁻, C₄H₄SiH⁻, and Their Lithium Complexes

	ASE (kcal/mol)			
X = CH ⁻	6	7	8	
tot. energy (au) ^a	-193.9906	-195.15096	-192.86967	-23.6
ZPE (kcal/mol) ^b	60.0 (0)	73.9 (0)	47.2 (0)	
X = SiH ⁻	9	10	1a	
tot. energy (au) ^a	-445.02291	-446.21414	-443.85217	-12.9
ZPE (kcal/mol) ^b	56.2 (0)	69.9 (0)	42.5 (0)	
X = CHLi	11	12	13	
tot. energy (au) ^c	-201.47025	-202.64253	-200.36418	-40.2
ZPE (kcal/mol) ^d	62.9 (0)	76.8 (0)	50.3 (0)	
X = SiHLi	14	15	4	
tot. energy (au) ^c	-452.47673	-453.67380	-451.33142	-32.0
ZPE (kcal/mol) ^d	58.2 (0)	72.2 (0)	44.7 (0)	

^a RMP2(fc)/6-31+G**//RMP2(fc)/6-31+G*. ^b RHF(fc)/6-31+G**//RHF(fc)/6-31+G*, scaled by 0.89;¹⁹ number of imaginary frequencies in parentheses. ^c RMP2(fc)/6-31G**//RMP2(fc)/6-31G*. ^d RHF(fc)/6-31G**//RHF(fc)/6-31G*, scaled by 0.89;¹⁹ number of imaginary frequencies in parentheses.

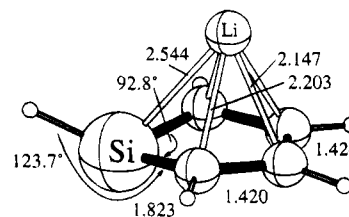
sis. In contrast to earlier RHF/6-31G* calculations,^{2b} **1a** has a strongly flattened pyramidal silicon center (angle sum 321.6°; Table 1) relative to SiH₃⁻ (C_{3v}, RMP2/6-31+G**, angle sum 289.3°).

Our 3.8 kcal/mol inversion barrier (**1a** → **1b**; Table 2) is much smaller than that computed previously (16.2 kcal/mol).^{2b} A correlation between such inversion barriers of silyl anions and the degree of planarization at silicon has been noted.⁷

The C $_{\beta}$ C $_{\beta}$ -C $_{\alpha}$ C $_{\beta}$ bond length difference in **1a** (0.034 Å) is reduced significantly relative to that in the neutral C₄H₄SiH₂ (**5**; 0.124 Å) (Table 1). In addition, **1a** exhibits a large Julg parameter (A = 0.971).⁸ While the C₄H₄SiH⁻ ground state **1a** is delocalized, the silicon lone pair is aligned optimally for conjugation with the hydrocarbon moiety in planar **1b** (Figure 2), which is even more aromatic. The Julg parameter (A = 0.998) is not only nearly unity, but **1b** also exhibits a C $_{\beta}$ C $_{\beta}$ distance which is shorter than the C $_{\alpha}$ C $_{\beta}$ bond length (-0.008 Å). The SiC $_{\alpha}$ bond distance in **1b** decreases to 1.794 Å.

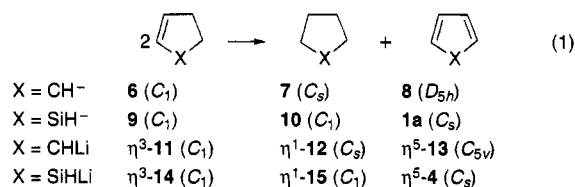
(7) Damewood, J. R., Jr.; Hadad, C. M. *J. Phys. Chem.* **1988**, *92*, 33.

(8) Julg's parameter (A) defines the degree of aromaticity in terms of deviations of (*n*) individual CC bond lengths (*r_i*) from the mean carbon bond length (*r*): A = 1 for benzene (D_{6h}) and A = 0 for Kekulé benzene (D_{3h}), assuming CC distances of 1.33 and 1.52 Å. A = 1 - (225/*n*) \sum (1 - *r_i*/*r*)². (a) Julg, A.; Francois, P. *Theor. Chim. Acta* **1967**, *7*, 249. (b) Kerk, S. M. v. d. *J. Organomet. Chem.* **1981**, *215*, 315.

**Figure 3.** Lithium silolide **4** (C_s, RMP2(fc)/6-31G** level, bond length in Å).

Li⁺ coordination influences these structures significantly. Optimization of Li⁺C₄H₄SiH⁻ at RMP2(fc)/6-31G** results in the η^5 complex **4** (Figure 3), which is characterized as a minimum (Table 2). The Si-H group is bent toward lithium. This preference for inverted coordination of silicon centers in alkali-metal silanides has precedents.⁹ The nonplanar silole rings in **4** and in **1a** differ significantly. Relative to the anion **1a**, the silicon environment in **4** is significantly less pyramidal (the angle sum at silicon increases by 18.6°), the SiC $_{\alpha}$ distance is shortened by 0.024 Å, and the CC bonds have nearly the same length (A = 0.9996) (Table 1). The increased delocalization due to lithium coordination is apparent. Although the silicon center in **4** is slightly less planar than that in **2** (note the angle sums in Table 1), bond length equalization is more pronounced in **4** than in **2**. As experimental evidence suggests, delocalization of electron density in the silole ring of **2** is enhanced when the hydride ligand on ruthenium is removed.³

We employ eq 1 to evaluate the aromatic stabilization energies (ASE) for the C₅H₅⁻ and the C₄H₄SiH⁻ anions as well as their lithium complexes (Table 3). The



reference carbocycles and silacarbocycles in eq 1 are calculated in their most stable conformations. In the (sila)cyclopentane, (sila)cyclopentene, and (sila)cyclopentadiene systems, the lithium ions are η^1 , η^3 , and η^5 coordinated, respectively. Whereas **1a** exhibits 55% of the ASE of for C₅H₅⁻ (similar results were obtained without diffuse functions),^{5a} the ASE in **4** increases to 80% of that computed for Li⁺C₅H₅⁻. The enhancement of ASE by Li⁺ coordination in both cases (Table 3) can

(9) (a) Pritzkow, H.; Lobreyer, T.; Sundermeyer, W.; Hommes, N. J. R. v. E.; Schleyer, P. v. R. *Angew. Chem., Int. Ed. Engl.* **1994**, *33*, 216. (b) Schleyer, P. v. R.; Clark, T. *J. Chem. Soc., Chem. Commun.* **1986**, 1371.

Table 4. NPA Charges,^a Chemical Shifts δ ,^b Magnetic Susceptibilities χ ^c and Susceptibility Exaltations Λ ^c

	Si charge	$\delta(\text{Si})$	C _{α} charge	$\delta(\text{C}_\alpha)$	C _{β} charge	$\delta(\text{C}_\beta)$	Li charge	$\delta(\text{Li})$	χ	Λ
1a	+0.618	-50.6	-0.755	+153.4	-0.335	+134.6			-72.3	-10.4
1b	+0.896	-6.6	-0.905	+100.5	-0.356	+121.1			-80.4	-18.5
2^{d,e}		-27.14		+74.36		+108.83				
3^{d,f}		+25.1		+139.51		+155.76				
4	+0.920	-22.4	-0.930	+123.6	-0.388	+130.0	+0.914	-6.2	-76.7	-14.1
5	+1.317	-42.0	-0.704	+136.2	-0.220	+163.2			-52.2	+4.8
16^{d,f}		+3.62		+144.77		+158.04				
C ₅ H ₅ ^{-g}			-0.397	+109.2	-0.397	+109.2			-67.8	-17.3
C ₅ H ₅ Li ^h			-0.423	+112.9	-0.423	+112.9	+0.912	-9.1 (-8.6) ^{d,i}	-65.7	-14.5

^a In au.¹⁴ ^b The IGLO (basis II)¹³ chemical shifts are relative to the absolute shielding constants (σ) of TMS (T_d , RMP2(fc)/6-31+G**) and Li(H₂O)₄⁺ (D_{2d} , RMP2(fc)/6-31+G*): $\sigma(\text{C}) = 197.5$, $\sigma(\text{Si}) = 379.4$, $\sigma(\text{Li}) = 92.1$. ^c χ and Λ (in ppm cgsu) are obtained from IGLO (basis II)¹³ calculations; see text. ^d Experimental result. ^e Reference 3. ^f Reference 4. ^g Optimized at the RMP2(fc)/6-31+G** level in D_{5h} symmetry. ^h Optimized at the RMP2(fc)/6-31G** level in C_{5v} symmetry. ⁱ Reference 1a.

be attributed to "aromaticity in three dimensions"¹⁰ and stabilization by the favorable polarization of the π electrons by the cation.¹¹ The Li⁺ coordination increases the ASE in C₄H₄SiHLi (**4**) even more than in Li⁺C₅H₅⁻.

Delocalization of the negative charge from silicon to the hydrocarbon moiety in **3** was suggested experimentally by an unusual downfield ²⁹Si NMR chemical shift (+25.10 ppm) and an upfield shift of the carbon signals in the butadiene moiety relative to the corresponding neutral disilole bis(1-*tert*-butyl-2,3,4,5-tetraphenylsilole) (**16**; $\delta(^{29}\text{Si}) = +3.62$).⁴ Compared to their neutral disilanes, only upfield shifts of ²⁹Si have been reported for silyl anions before.¹² A progression of $\delta(^{29}\text{Si})$ to lower fields has been noted in going from Me₄C₄Si(H)Si(SiMe₃)₃ ($\delta(^{29}\text{Si}) -32.68$) (precursor of **2**) to **2** ($\delta(^{29}\text{Si}) -27.14$ ppm) and then to -7.35 in {Cp**Ru*[\eta⁵-Me₄C₄-SiSi(SiMe₃)₃]} (the HBPh₄ elimination product of **2**).³ This suggests enhanced delocalization in the same order.³

The computed (IGLO) chemical shifts¹³ of **4** are consistent with these experimental NMR data (Table 4). Lithiation of **5** (**5** → **4**) and coordination of Li⁺ to **1a** (**1a** → **4**), both result in downfield $\delta(^{29}\text{Si})$ and $\delta(^{13}\text{C})$ upfield displacement (Table 4). In the latter case, this can be attributed to a partial electron transfer from silicon to the carbon atoms (note the NPA¹⁴ charges in Table 4). However, this charge-chemical shift relation-

ship is not general. Lithiation of **5** results in a $\delta(^{29}\text{Si})$ downfield shift, although the negative charge on silicon is increased.¹⁵

As in C₅H₅Li, the upfield $\delta(^7\text{Li})$ value in **4** (-6.2, Table 4) can be attributed to the aromatic ring current anisotropy.¹⁶ In contrast to σ -bonded lithium silanes,¹⁷ derivatives of **4** should exhibit a high-field $\delta(^7\text{Li})$ and, due to the ionic π -bonding,^{1d} no scalar lithium-silicon coupling.

The diamagnetic susceptibility exaltation Λ provides a good measure of aromaticity.^{5a,b,18} This parameter is calculated as the difference between the magnetic susceptibility of the system (χ_M) and the susceptibility estimated by an increment scheme for the hypothetical system without cyclic delocalization (χ_M'): $\Lambda = \chi_M - \chi_M'$. The negative Λ value of **4** (-14.1 ppm cgsu, Table 4) is nearly as large as that for Li⁺C₅H₅⁻ (-14.5 ppm cgsu). Whereas **1a** exhibits a less negative Λ value (-10.4 ppm cgsu) than C₅H₅⁻ (-17.3 ppm cgsu), Λ of **1b** is even more negative (-18.5 ppm cgsu). The magnetic criterion leads to the same conclusion as the structural and energetic criteria: Li⁺ coordination increases the aromaticity of **4** over that in **1a** strongly.

Hence, the structural, energetic, and magnetic criteria all agree that lithium silolide, C₄H₄SiHLi (**4**), is delocalized and shows significant aromatic character. These results are consistent with recent experimental conclusions on **2** and **3**, derivatives of **4**.^{3,4} The silolyl anion C₄H₄SiH⁻ (**1a**) exhibits at least moderate aromaticity, which is enhanced strongly by η^5 coordination of Li⁺.

Acknowledgment. This work was supported by the Fonds der Chemischen Industrie, the Stiftung Volkswagenwerk, Convex Computer Corp., and the Deutsche Forschungsgemeinschaft. B.G. thanks the Fonds der Chemischen Industrie for a scholarship and H. Jiao for helpful discussions.

OM9408627

(18) (a) Dauben, H. J.; Wilson, J. D.; Laity, J. L. *J. Am. Chem. Soc.* **1969**, *91*, 1991. (b) Jiao, H.; Schleyer, P. v. R. *Angew. Chem., Int. Ed. Engl.* **1993**, *32*, 1763 and references therein.

(19) Hehre, W. J.; Radom, L.; Schleyer, P. v. R.; Pople, J. A. *Ab Initio Molecular Theory*; Wiley: New York, 1985.

(10) Jemmis, E. D.; Schleyer, P. v. R. *J. Am. Chem. Soc.* **1982**, *104*, 4781.

(11) Jiao, H.; Schleyer, P. v. R. *Angew. Chem., Int. Ed. Engl.* **1993**, *32*, 1760.

(12) (a) Söllradl, H.; Hengge, E. *J. Organomet. Chem.* **1983**, *243*, 257. (b) Olah, G. A.; Hunadi, R. *J. Am. Chem. Soc.* **1980**, *102*, 6989.

(13) Kutzelnigg, W.; Schindler, M.; Fleischer, U. *NMR Basic Princ. Prog.* **1990**, *23*, 165.

(14) (a) Reed, A. E.; Curtiss, L. A.; Weinhold, F. *Chem. Rev.* **1988**, *88*, 899. (b) Reed, A. E.; Schleyer, P. v. R. *J. Am. Chem. Soc.* **1990**, *112*, 1434.

(15) For a discussion of $\delta(^{29}\text{Si})$ see for example: Williams, E. A. In *The Chemistry of Organic Silicon Compounds*; Patai, S., Rappoport, Z., Eds.; Wiley: New York, 1989; Chapter 8, p 511, and references therein.

(16) Fleischer, U.; Kutzelnigg, W.; Lazzeretti, P.; Mühlenkamp, V. *J. Am. Chem. Soc.* **1994**, *116*, 5298.

(17) (a) Heine, A.; Herbst-Irmer, R.; Sheldrick, G. M.; Stalke, D. *Inorg. Chem.* **1993**, *32*, 2694. (b) Edlund, U.; Lejon, T.; Pyykkö, P.; Venkatchalam, T. K.; Buncel, E. *J. Am. Chem. Soc.* **1987**, *109*, 5982. (c) Edlund, U.; Lejon, T. *J. Am. Chem. Soc.* **1985**, *107*, 6408.

Reaction of (Z)-(Phenylvinyl)acetylenes and (Z)-(Cyclopropylvinyl)acetylenes with Fischer Carbene-Chromium Complexes: An Alternative Approach to Benzannulation and Cyclopentannulation

James W. Herndon, and Anthony Hayford

Organometallics, 1995, 14 (4), 1556-1558 • DOI: 10.1021/om00004a005 • Publication Date (Web): 01 May 2002

Downloaded from <http://pubs.acs.org> on March 9, 2009

More About This Article

The permalink <http://dx.doi.org/10.1021/om00004a005> provides access to:

- Links to articles and content related to this article
- Copyright permission to reproduce figures and/or text from this article



ACS Publications
High quality. High impact.

Reaction of (*Z*)-(Phenylvinyl)acetylenes and (*Z*)-(Cyclopropylvinyl)acetylenes with Fischer Carbene–Chromium Complexes: An Alternative Approach to Benzannulation and Cyclopentannulation

James W. Herndon* and Anthony Hayford

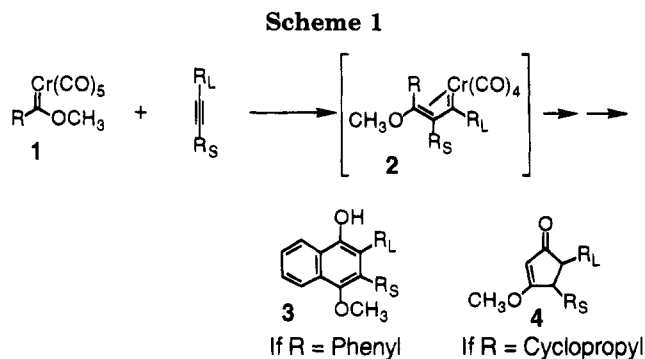
Department of Chemistry and Biochemistry, University of Maryland,
College Park, Maryland 20742-2021

Received December 20, 1994[⊗]

Summary: The reaction of (*Z*)-(phenylvinyl)acetylenes and carbene complexes provides benzannulation products in fair to good yields. Similarly, the reaction of (*Z*)-(cyclopropylvinyl)acetylenes and carbene complexes provides cyclopentenone derivatives. When the carbene complex is capable of further ring-forming reactions, subsequent ring-forming steps occur preferentially from the substituent on the enyne.

The reaction of α,β -unsaturated chromium carbene complexes (**1**; Scheme 1) and alkynes leads very reliably to hydroquinone derivatives (**3**) (the Dötz reaction),¹ while cyclopropylcarbene complexes and alkynes reliably afford cyclopentenone derivatives (**4**).² An essential intermediate common to both annulation reactions in Scheme 1 is vinylcarbene complex **2**, formed via a regioselective and stereoselective alkyne insertion reaction.³ The reaction of an appropriately substituted (*Z*)-vinylacetylene derivative (**5**; Scheme 2) and a simple carbene complex can also provide an intermediate having the essential structural features of intermediate **2** (**6**, **9**; Scheme 2).^{4,5} The first objective of the studies in this paper is to evaluate the efficacy of a mechanism-based alternative to the annulation processes in Scheme 1, which employs simple carbene complexes and (*Z*)-(phenylvinyl)acetylenes (**5**; $R_1 = \text{Ph}$) to effect benzannulation and (*Z*)-(cyclopropylvinyl)acetylenes (**5**; $R_1 = \text{cyclopropyl}$) to effect cyclopentannulation. The second objective is to determine the relative ability of carbene complex substituents and R_1 substituents of enynes to undergo subsequent annulation processes.

Initially, the reaction between (*Z*)-(phenylvinyl)acetylene **5A** and simple carbene complex **1A** was examined (Table 1, entry A). The expected benzannulation product, enol ether **7A**, was never observed; however, the ketal **8A** was obtained in 61% yield. Ketalization might occur during purification by chromatography on silica



gel. This reaction proceeded similarly for the internal alkyne **5B** (entry D) and less substituted enyne **5C** (entry E). The ability of (cyclopropylvinyl)acetylene **5D** to undergo cyclopentannulation reactions upon treatment with methylcarbene complex **1A** was then tested. From this reaction, cyclopentenone **11A** (45%) and the analogous trienone **12A** (5%) were obtained (entry F). Trienone **12A** presumably results from a competing vinylogous enolization of cyclopentadienone intermediate **10**. Predominantly the *E* enol ether was obtained for both **11A** and **12A**.

In the next phase of these studies, carbene complexes which can undergo competitive annulation processes were tested in their reactions with enynes **5A** and **5D**. As noted in entry C, exclusive benzannulation onto the enyne phenyl was observed from the reaction of phenylcarbene complex **1C** and (phenylvinyl)acetylene **5A**. In this case, the exclusive product of the reaction was

(5) For additional mechanism-based alternatives to the Dötz reaction, see: (a) Wulff, W. D.; Kaesler, R. W.; Peterson, G. A.; Tang, P.-C. *J. Am. Chem. Soc.* **1985**, *107*, 1060–1062. (b) Semmelhack, M. F.; Ho, S.; Steigerwald, M.; Lee, M. C. *J. Am. Chem. Soc.* **1987**, *109*, 4397–4399. (c) Merlic, C. A.; Xu, D.; Gladstone, B. G. *J. Org. Chem.* **1993**, *58*, 538–545. (d) Krysan, D. J.; Gurski, A.; Liebeskind, L. S. *J. Am. Chem. Soc.* **1992**, *114*, 1412–1418. (e) Danheiser, R. L.; Cha, D. D. *Tetrahedron Lett.* **1990**, *31*, 1527–1530. (f) Perri, S. T.; Moore, H. W. *J. Am. Chem. Soc.* **1990**, *112*, 1897–1905.

(6) **Procedure for Benzannulation:** Dioxane (20 mL) was heated to reflux under nitrogen in a flask fitted with a condenser and syringe port. To the dioxane was added a solution of alkyne **5A** (0.110 g, 0.604 mmol) and carbene complex **1A** (0.137 g, 0.549 mmol) in dioxane (10 mL). This solution was added dropwise via syringe pump over a 2-h period. The reaction mixture was heated for an additional 4 h, after which the solvent was evaporated. The residue was redissolved in ethyl acetate and the solution filtered through a pad of Celite. After removal of the solvent on a rotary evaporator, this residue was subjected to flash chromatography on silica gel. A single fraction identified as ketal **8A** (0.090 g, 61%) was obtained. **8A**: ¹H NMR (CDCl₃) δ 8.00–7.90 (m, 2 H), 7.45–7.35 (m, 2 H), 3.36 (s, 3 H), 3.32 (d, 1 H, *J* = 17.5 Hz), 3.16 (d, 1 H, *J* = 17.5 Hz), 3.09 (m, 2 H), 2.73 (m, 2 H), 1.95 (m, 4 H), 1.73 (s, 3 H); ¹³C NMR (CDCl₃) δ 151.3, 132.7, 131.4, 127.4, 125.5, 124.0, 123.1, 121.8, 119.0, 118.4, 112.2, 49.8, 40.0, 27.8, 25.5, 25.1, 23.2, 22.7; IR (CDCl₃) 3079 (w), 3019 (w), 2939 (s), 1600 (cm⁻¹); MS (EI) *m/e* 268 (M⁺, 100); HRMS calcd for C₁₅H₂₀O₂ 268.1463, found 268.1470.

[⊗] Abstract published in *Advance ACS Abstracts*, March 15, 1995.

(1) Wulff, W. D. In *Comprehensive Organic Synthesis*; Trost, B. M., Fleming, I., Paquette, L. A., Eds.; Pergamon: Oxford, U.K., 1991; Vol. 5, pp 1065–1113.

(2) Tumer, S. U.; Herndon, J. W.; McMullen, L. A. *J. Am. Chem. Soc.* **1992**, *114*, 8394–8404.

(3) (a) Bos, M. A.; Wulff, W. D.; Miller, R. A.; Chamberlain, S.; Brandvold, T. A. *J. Am. Chem. Soc.* **1991**, *113*, 9293–9319. (b) Anderson, B. A.; Wulff, W. D.; Rheingold, A. L. *J. Am. Chem. Soc.* **1990**, *112*, 8615–8617. (c) McCallum, J. S.; Kunng, F.-A.; Gilbertson, S. R.; Wulff, W. D. *Organometallics* **1988**, *7*, 2346–2360. (d) Hofmann, P.; Hämmerle, M.; Unfried, G. *New J. Chem.* **1991**, *15*, 769–789. (e) Barluenga, J.; Aznar, F.; Martín, A.; García-Granda, S.; Pérez-Carreño, E. *J. Am. Chem. Soc.* **1994**, *116*, 11191–11192. (f) Anderson, B. A.; Bao, J.; Brandvold, T. A.; Challener, C. A.; Wulff, W. D.; Xu, Y. C.; Rheingold, A. L. *J. Am. Chem. Soc.* **1993**, *115*, 10671–10687.

(4) In some cases, enynes are suitable substrates for the benzannulation reaction. Wulff, W. D.; Chan, K.-S.; Tang, P.-C. *J. Org. Chem.* **1984**, *49*, 2293–2295. See also ref 2.

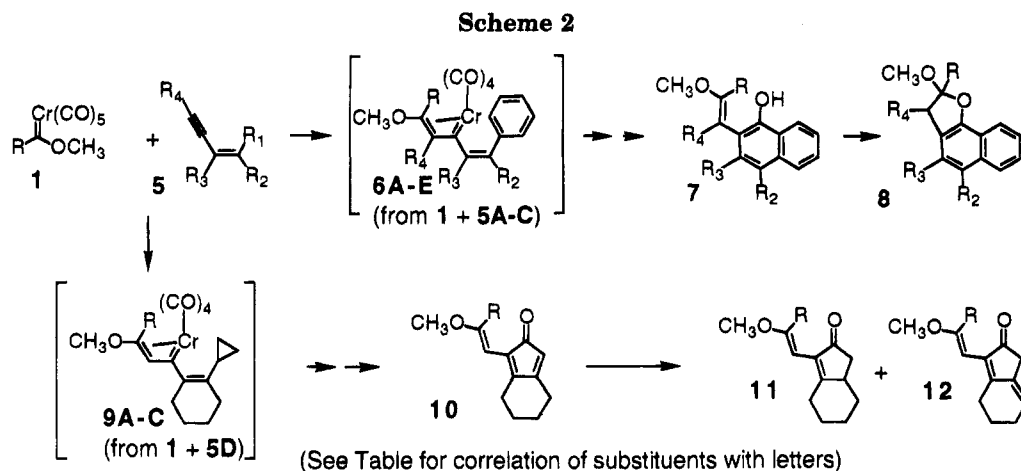


Table 1. Reaction of Conjugated Z Enynes with Carbene Complexes

Entry	Carbene Complex	Enyne	Product(s) and Yield ^a
A ^b			
B		5A	
C		5A	
D	1A		
E	1A		
F ^d	1A		
G	1B	5D	
H	1C	5D	

^a In all cases, the yield refers to isolated compounds which are pure by TLC and high-field NMR analysis, unless otherwise noted. ^b For a procedure, see ref 6. ^c Compound **8D** was very sensitive to air oxidation and could not be purified; the air oxidation products **8D-I** and **8D-II** were characterized. ^d For a procedure, see ref 7. ^e Obtained after exposure of the crude reaction mixture to aqueous acid. In separate experiments the enol ether isomers of **11** were isolated; however, higher yields of adduct could be obtained after hydrolysis. ^f Compound **11B** was obtained in a 6:1 *E:Z* ratio. ^g Compound **11C** was obtained in a 3:1 *E:Z* ratio; partial hydrolysis occurred during chromatographic purification. ^h The yield was determined by integration of the crude ¹H NMR spectrum.

benzofuran derivative **13**, and none of the product from benzannulation onto the carbene phenyl, **17** (Figure 1), was observed. As noted in entry G, exclusive cyclopentannulation onto the enyne cyclopropyl was observed from the reaction of cyclopropylcarbene complex **1B** and (phenylvinyl)acetylene **5D**; none of the product from annulation onto the carbene cyclopropyl, **18**, was observed. Benzannulation was the exclusive reaction

pathway observed from the reaction of cyclopropylcarbene complex **1B** and (phenylvinyl)acetylene **5A** (entry B); none of the expected cyclopentannulation product, **19**, was observed in this reaction. When the location of the cyclopropyl and phenyl groups was reversed (entry H), cyclopentannulation giving **11C** was the predominant reaction pathway. In this reaction, a sizable amount of benzannulation product **16** was

Scheme 3

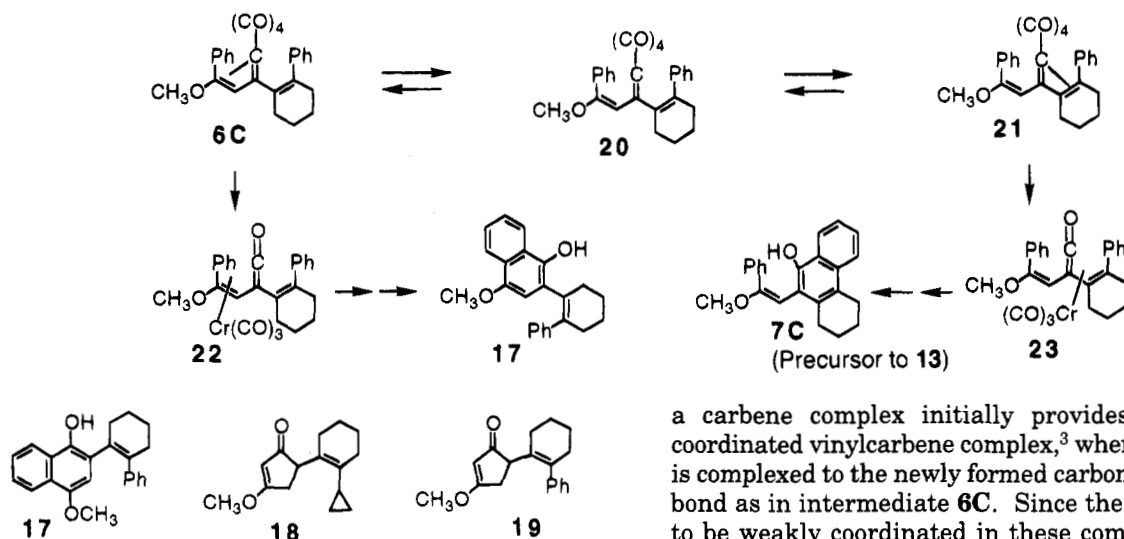


Figure 1. Hypothetical products predicted if annulation occurs at the carbene complex substituent.

observed. In all of the cases involving competing annulation reactions (entries B, C, G, and H), the predominant reaction pathway observed was annulation onto the R_1 substituent on the enyne.

The reason for preferential annulation onto the enyne substituent relative to the carbene complex substituent is not completely clear at present. A possible mechanistic rationale is depicted in Scheme 3. According to previous mechanistic studies, insertion of an alkyne into

a carbene complex initially provides an internally coordinated vinylcarbene complex,³ where the chromium is complexed to the newly formed carbon-carbon double bond as in intermediate **6C**. Since the alkene appears to be weakly coordinated in these complexes,^{3e} equilibration between vinylcarbene complexes **6C** and **21** and coordinatively unsaturated carbene complex **20** would be expected.⁸ Since electron-donor substituents suppress the CO-insertion step in vinylcarbene complexes,⁹ conversion of vinylcarbene complex **21** to vinylketene complex **23** should occur faster than the analogous conversion of **6C** to **22**. On the basis of the extremely facile conversion of chromium-complexed (*Z*)-(phenylvinyl)ketenes to naphthols,^{3c} vinylketene complex **23** is expected to provide naphthol **7C**, while complex **22** would provide naphthol **17**. The observed preferential annulation onto enyne cyclopropyl groups (entry G) is also predicted from this argument if vinylketene complexes are involved in the cyclopropane ring-opening step; however, mechanistic details of the cyclopentannulation process are not as clear.² Further examination of other enynes and evaluation of these reactivity trends are currently under investigation.

Acknowledgment. We thank the donors of the Petroleum Research Fund, administered by the American Chemical Society, for financial support of this research. We thank Mr. Christoph Müller and Dr. Metin Zora for some evaluation of synthetic routes to *Z* enynes. We are deeply indebted to the reviewers for their excellent mechanistic comments and suggestions.

Supplementary Material Available: Text giving spectral data for the compounds listed in Table 1 including ¹H NMR, ¹³C NMR, infrared, and mass spectral data (6 pages). Ordering information is given on any current masthead page.

OM940969U

(7) **Procedure for Cyclopentannulation:** Dioxane (20 mL) was heated to reflux under nitrogen in a flask fitted with a condenser and syringe port. To this mixture was added a solution of alkyne **5D** (0.094 g, 0.643 mmol) and carbene complex **1A** (0.162 g, 0.648 mmol) in dioxane (10 mL). This solution was added dropwise via syringe pump over a 2-h period. The reaction mixture was heated for an additional 6 h, after which the solvent was evaporated. The residue was redissolved in ethyl acetate and the solution filtered through a pad of Celite. After removal of the solvent of a rotary evaporator, this residue was subjected to flash chromatography on silica gel pretreated with triethylamine. The product in the first fraction was identified as a mixture of enol ether isomers **11A** (0.060 g, 45%). The product in the second fraction was identified as trienol **12A** (0.007 g, 5%). **11A**, *E* Isomer: ¹H NMR (CDCl₃) δ 4.84 (s, 1 H), 3.61 (s, 3 H), 2.71 (dt, 1 H, *J* = 10.4, 3.0 Hz), 2.61 (m, 1 H), 2.59 (dd, 1 H, *J* = 12.8, 5.2 Hz), 2.17 (br d, 1 H, *J* = 10.4 Hz), 2.06 (td, 1 H, *J* = 10.4, 4.4 Hz), 1.99 (dd, 1 H, *J* = 12.8, 4.0 Hz), 1.98 (m, 1 H), 1.83 (br d, 1 H, *J* = 10.8 Hz), 1.66 (s, 3 H), 1.49 (qt, 1 H, *J* = 10.4, 3.0 Hz), 1.33 (qt, 1 H, *J* = 10.4, 3.0 Hz), 1.09 (qd, 1 H, *J* = 10.4, 3.0 Hz); ¹³C NMR (CDCl₃) δ 208.0, 175.7, 157.9, 134.4, 87.5, 54.7, 41.6, 40.1, 35.1, 29.7, 26.3, 25.4, 18.2; IR (CDCl₃) 1700 (s), 1656 (s) cm⁻¹; MS (EI) *m/e* 206 (M⁺, 100); HRMS calcd for C₁₃H₁₈O₂ 206.1307, found 206.1310. Irradiation of the methyl group (δ 1.66) led to enhancement of the signal for the methoxy group (δ 3.61). Irradiation of the methoxy group (δ 3.61) led to enhancement of the signals for the vinylic hydrogen (δ 4.84) and the methyl group (δ 1.66). The enhancements were determined by subtraction of the original ¹H NMR spectrum. **11A**, *Z* Isomer: ¹H NMR (CDCl₃) δ 4.92 (s, 1 H), 3.56 (s, 3 H), 2.81 (br d, 1 H, *J* = 10.4 Hz), 2.60 (m, 2 H), 2.30–1.70 (m, 5 H), 1.97 (s, 3 H), 1.65–1.05 (m, 3 H). Extensive attempts to purify this compound resulted in no better than a 9:1 ratio of **11A-Z** to **11A-E**. **12A**: ¹H NMR (CDCl₃) δ 5.91 (br t, 1 H, *J* = 7.4 Hz), 4.96 (s, 1 H), 3.63 (s, 3 H), 2.92 (br s, 2 H), 2.51 (t, 2 H, *J* = 7.4 Hz), 2.27 (br q, 2 H, *J* = 7.4 Hz), 1.79 (quintet, 2 H, *J* = 7.4 Hz), 1.73 (s, 3 H); IR (CDCl₃) 1700 (s) cm⁻¹; MS (EI) *m/e* 204 (M⁺, 100); HRMS (EI) calcd for C₁₃H₁₆O₂ 204.1150, found 204.1169.

(8) A similar equilibrium has been proposed for vinylcarbene-titanium complexes: (a) Wallace, K. M.; Liu, A. H.; Davis, W. M.; Schrock, R. R. *Organometallics* **1989**, *8*, 644–654. (b) Doxsee, K. M.; Juliette, J. J. J.; Mouser, J. K. M.; Zientara, K. *Organometallics* **1993**, *12*, 4742–4744.

(9) Notable examples of this effect have been observed in the reaction of aminocarbene-chromium complexes with alkynes: (a) Grotjahn, D. B.; Kroll, F. E. K.; Schäfer, T.; Harms, K.; Dötz, K. H. *Organometallics* **1992**, *11*, 298–310. (b) Hoye, T. R.; Rehberg, G. M. *Organometallics* **1989**, *8*, 2071–2073. (c) Yamashita, A. *Tetrahedron Lett.* **1986**, *27*, 5915–5918.

η^2 -Thiophene Complexes of Pentaammineosmium(II) and Their Reversible Protonation To Form Novel η^2 -2H-Thiophenium Species

Michael L. Spera and W. Dean Harman*

Department of Chemistry, University of Virginia, Charlottesville, Virginia 22901

Received February 6, 1995*

Summary: A series of complexes of the type $[\text{Os}(\text{NH}_3)_5(4,5\text{-}\eta^2\text{-L})](\text{OTf})_2$ (where L = thiophene (**1a**), 2-methylthiophene (**1b**), 3-methylthiophene (**1c**), 2,5-dimethylthiophene (**1d**), 2-methoxythiophene (**1e**), 3-methoxythiophene (**1f**), and benzo[b]thiophene (**1g**)) were prepared and characterized by NMR and cyclic voltammetry (CV). Treatment of **1a–d** with 1 equiv of HOTf yields novel isolable 2H-thiophenium complexes with the osmium bound to C(5) and sulfur.

The development of hydrodesulfurization (HDS) technology has spawned considerable interest in the coordination chemistry of thiophenes.¹ Although a number of different bonding modes for thiophene complexes have now been identified, including η^1 , η^2 , η^3 , η^4 , and η^5 , remarkably little is known about η^2 -coordinated species, even though this form is often invoked as an intermediate in C–S bond activation.¹ Herein, we report the synthesis and characterization of a series of complexes of the type $[\text{Os}(\text{NH}_3)_5(4,5\text{-}\eta^2\text{-L})](\text{OTf})_2$ (where L = thiophene (**1a**),² 2-methylthiophene (**1b**),³ 3-methylthiophene (**1c**), 2,5-dimethylthiophene (**1d**), 2-methoxythiophene (**1e**), 3-methoxythiophene (**1f**), and benzo[b]thiophene (**1g**)). For complexes **1a–d,f**, treatment with triflic acid generates an unprecedented series of (1,5- η^2)-2H-thiophenium complexes, resulting from the direct protonation of an α -carbon.

Complexes **1a–g** were prepared in 85–95% yield from $\text{Os}(\text{NH}_3)_5(\text{OTf})_3$ by reducing the osmium(III) precursor (3.00 g, 4.16 mmol) in *N,N*-dimethylacetamide (2.12 g) with Mg^0 (1.84 g) in the presence of an excess of the desired thiophene (~3.5 g).² ¹H and ¹³C NMR spectra for the parent complex **1a** each show four well-resolved signals corresponding to the organic ligand, with the atoms associated with metal coordination significantly shifted upfield relative to those of the uncoordinated thiophene. In addition, widely spaced *cis* and *trans* ammine ¹H signals at 2.91 and 4.19 ppm (CD_3CN) and an oxidation wave in the cyclic voltammogram of **1a** at $E_{\text{p,a}} = 0.55$ V (NHE) are consistent with a pentaammine unit bound η^2 to an olefinic fragment.⁴ The similarity of these data to those of the analogous η^2 -pyrrole and η^2 -furan complexes confirms that the thiophene ligand of **1a** is bound across C(4) and C(5).⁵

Similar trends in ¹H and ¹³C data for the complexes **1a–f** (supplementary material) indicate that the η^2 -binding mode is present in all thiophenes investigated, even with the hindered 2,5-dimethylthiophene (**1d**). Except for benzo[b]thiophene (*vide infra*), a single regioisomer is observed for all thiophene complexes examined; when the heterocycle bears a single substituent, the osmium metal center is always located on the unsubstituted side of the ring. Showing remarkable thermal stability for a η^2 -coordinated aromatic system, compounds **1a–f** are stable at 120 °C in $\text{DMF-}d_7$ solution and show no signs of fluxional behavior by ¹H NMR (300 MHz).

In contrast to the simple thiophene ligands, the reaction of benzo[b]thiophene and pentaammineosmium(II) initially produces a 4:1:1 mixture of regioisomers thought to correspond to the 2,3- η^2 , 4,5- η^2 , and 6,7- η^2 isomers, respectively.⁶ Over time (36 h, 20 °C; 5 min, 80 °C) in CH_3CN , the mixture of isomers resolves into a single species, the 2,3- η^2 complex similar to that reported by Angelici et al. for $\text{ReCp}^*(\text{CO})_2(\eta^2\text{-benzothiophene})$.⁷

Owing to differences in the heteroatom, thiophene is considerably less basic than furan or pyrrole.⁸ However, the strong back-bonding interaction between osmium(II) and this ligand enhances the basicity of the heterocycle: the thiophene complexes **1a–d,f** are readily protonated with triflic acid in acetonitrile and isolated as their conjugate acids (**2a–d,f**; 80–90%, Figure 1).

(5) For crystal structures of these other η^2 -heterocycle complexes see the following. For **pyrrole**: Myers, W. H.; Sabat, M.; Harman, W. D. *J. Am. Chem. Soc.* **1991**, *113*, 6682. For **furan**: Chen, H.; Hodges, L. M.; Liu, R.; Stevens, W. C.; Sabat, M.; Harman, W. D. *J. Am. Chem. Soc.* **1994**, *116*, 5499.

(6) Two sets of *cis* and *trans* ammine resonances (2.89, 4.19 ppm and 2.77, 4.12 ppm) are observed in a 2:1 ratio, and six coordinated olefin signals are initially observed. A cyclic voltammogram shows two reversible oxidation waves at 0.37 and 0.51 V (NHE). Upon heating in acetonitrile (5 min, 80 °C), all signals vanish except for those assigned to **1g**. Characterization of **1g**: ¹H NMR (300 MHz, CD_3CN) δ 7.61 (m, 1H), 7.41 (m, 1H), 7.25 (m, 2H), 5.80 (d, $J = 5.8$ Hz, 1H), 5.43 (d, $J = 5.8$, 1H), 4.19 (br s, 3H), 2.89 (br s, 12H); ¹³C NMR (75 MHz, CD_3CN) δ 146.5 (C), 139.7 (C), 126.7 (CH), 125.8 (CH), 124.2 (CH), 123.1 (CH), 62.5 (CH), 55.6 (CH); CV ($\text{CH}_3\text{CN/TBAH}$; 100 mV/s) $E_{\text{p,a}} = 0.51$ V (NHE).

(7) Robertson, M. J.; Day, C. L.; Jacobson, R. A.; Angelici, R. J. *Organometallics* **1994**, *13*, 179.

(8) A ¹H NMR of a mixture of thiophene and an excess of HOTf in CD_3CN shows no reaction after 1 h.

(9) Synthesis and characterization of **2a**: A solution of 206 mg of HOTf in 120 mg of CH_3CN was added to a solution of **1a** (229 mg, 0.349 mmol) in 878 mg of CH_3CN . The resulting deep red solution was added to 150 mL of stirred diethyl ether and filtered through a 30 mL fine-porosity frit. The filter cake was washed with ether (3 \times 20 mL portions) and dried *in vacuo*, affording 257 mg (91%) of pink powder: ¹H NMR (CD_3CN , 300 MHz) δ 7.96 (s, 1H), 6.90 (dd, $J = 5.9$, 1.9 Hz, 1H), 6.76 (dd, $J = 5.9$, 1.9, 1H), 5.21 (br s, 3H), 3.71 (br s, 12H), 3.08 (dd, $J = 20.7$, 1.9, 1H), 2.62 (dd, $J = 20.7$, 1.9, 1H); ¹³C NMR (CD_3CN , 75 MHz) δ 136.81 (CH), 131.35 (CH), 71.29 (CH), 43.47 (CH₂); CV ($\text{CH}_3\text{CN/TBAH}$; 100 mV/s) $E_{\text{p,a}} = 1.59$ V, $E_{\text{p,c}} = 0.25$ V (NHE). Anal. Calcd for $\text{C}_7\text{H}_{20}\text{N}_5\text{O}_9\text{S}_4\text{F}_9\text{Os}$: C, 10.41; H, 2.50; N, 8.67. Found: C, 10.54; H, 2.73; N, 8.94.

* Abstract published in *Advance ACS Abstracts*, March 15, 1995.

(1) For comprehensive reviews of transition-metal thiophene chemistry see: Rauchfuss, T. B. *Prog. Inorg. Chem.* **1991**, *39*, 259. Angelici, R. J. *Coord. Chem. Rev.* **1990**, *105*, 61.

(2) Experimental values cited correspond to the preparation of **1b**. The synthesis of the parent thiophene complex $[\text{Os}(\text{NH}_3)_5(\eta^2\text{-thiophene})]^{2+}$ has been previously reported. See: Cordone, R.; Harman, W. D.; Taube, H. *J. Am. Chem. Soc.* **1989**, *111*, 5969.

(3) Numbering in **1a–g** is consistent with that for the uncoordinated ligand (Figure 1).

(4) E.g. the pentaammineosmium(II) complex of cyclohexene has an $E_{1/2} = 0.55$ V and ammine resonances at 3.95 and 2.88 ppm (CD_3CN). See: Harman, W. D.; Taube, H. *J. Am. Chem. Soc.* **1988**, *110*, 7906.

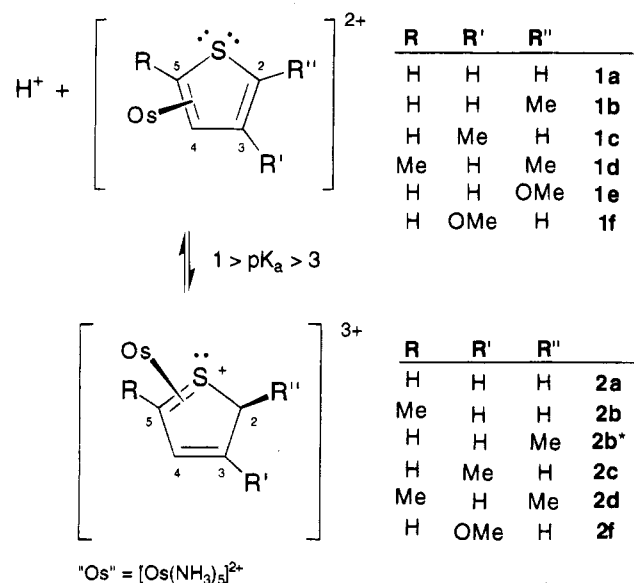


Figure 1. Reaction scheme for the η^2 -thiophene complexes **1a-f**.

2a,⁹ obtained from protonation of the thiophene complex **1a**, shows in its ¹H NMR spectrum *cis* and *trans* ammine resonances shifted downfield ca. 1 ppm from their original values, three methine resonances (7.96, 6.90, 6.76 ppm), and a pair of diastereotopic methylene signals (3.08, 2.61 ppm; *J* = 20.7 Hz).¹⁰ ¹³C NMR data indicate that only one of the ring carbons is coordinated to osmium.¹¹ An NOE enhancement is observed for the proton on C(5) (5.8%) and the *endo* proton (i.e. that pointing toward the metal) on C(2) (4.8%) upon irradiation of the *cis* amines, indicating their close proximity to the osmium (*vide infra*). Compound **2a** is stable in acetonitrile solution for about 1 day at 20 °C. The thiophenium complexes of 2-methylthiophene, 3-methylthiophene, and 2,5-dimethylthiophene (**2b-d**) show ¹H and ¹³C NMR spectra that are virtually identical with those of **2a**, except where a methyl group is substituted for a proton. Finally, treatment of any of the protonated thiophene products (**2a-d,f**) with 1 equiv of Hunig's base (*i*-Pr₃NEt) restores these compounds to their conjugate bases (i.e. **1a-d,f**). When they are taken together, these observations are consistent with protonation occurring at C(2) to give a 2*H*-thiophenium complex where the metal is coordinated across C(5) and sulfur (Figure 1). From ¹H/¹H coupling data and chemical shifts, the 2-methylated thiophene species **2b** protonates away from the methyl substituent while the 3-methylated species, **2c**, protonates adjacent to the alkyl substituent. For the latter compound, an analogous protonation and isomerization process has been observed for the pentaammineosmium(II) complex of 3-methylpyrrole.¹² For the 2,5-dimethylthiophenium

species (**2d**), an NOE interaction (3.4%) is observed between the C(2) methyl group and the *cis*-ammine protons, indicating that protonation occurs *anti* to the metal.¹³

In acetonitrile, treatment of the parent 2*H*-thiophenium complex **2a** with 1.2 equiv of 2,6-di-*tert*-butylpyridine (*pK_a* = 3) slowly generates the conjugate base **1a**, but no reaction is observed with the base diphenylamine (*pK_a* = 0.8).¹⁴ These experiments establish an approximate *pK_a* for the thiophenium complex of 1 < *pK_a* < 3.¹⁵ Remarkably, the 2*H*-thiophenium complexes **2a-c** are stable even in aqueous solution. In contrast, the 2,5-dimethylthiophene analog (**2d**) is considerably more acidic and rapidly deprotonates in solvents as weakly basic as diethyl ether; as a result, NMR characterization for this complex was carried out in acidic CD₃CN solution. Although the methyl groups of **1d** would be expected to make the heterocycle more electron-rich than the parent, protonation from the ring face opposite of metal coordination forces a methyl group into a severe steric interaction with the pentaammineosmium moiety,¹⁶ thereby making **2d** more susceptible to deprotonation than its analogs (**2a-c**). The case of the 5-methylthiophenium complex (**2b**) also deserves comment since its formation from **1b** requires that the metal isomerize from the 4,5- η^2 position to the 2,3- η^2 position. If the dominant isomer of **1b** (i.e. 4,5- η^2) was protonated at C(2) from the *exo* face (i.e. **2b*** in Figure 1), as is observed for the 2,5-dimethylthiophene analog **2d**, the methyl group again would be forced into a steric interaction with the ammine ligands. Thus, the hypothetical isomer **2b*** (not observed) resulting from direct protonation of **2a** is probably kinetically favored, yet is unstable relative to its linkage isomer **2b**.

Finally, in an attempt to observe a stable 3*H*-thiophenium complex, complexes of 2- and 3-methoxythiophene (**1e,f**) and benzo[*b*]thiophene (**1g**) were also exposed to acidic conditions. Of these, only the 3-methoxythiophene species gave rise to a stable protonated species, **2f**.¹⁷ On the basis of the strong correlation between the spectral data for **2f** and **2a-d**, we assign the former species as [Os(NH₃)₅((1,5- η^2)-3-methoxy-2*H*-thiophenium)]³⁺.

A transition-metal-assisted protonation of thiophene represents a potential mechanism for hydrogen transfer in the hydrodesulfurization (HDS) process.¹⁸ For comparison, the C(2) protonation of thiophene has also been reported for (C₆Me₆)Ru⁰(C₄H₄S).¹⁹ In contrast to our observations, this d⁸ system undergoes protonation initially at the metal. Such an action is followed by hydride transfer from ruthenium(II) to C(2) of the η^4 -thiophene ligand and results in an *endo* addition of

(14) Reaction conditions: [Os] = 0.13 M; [diphenylamine] = 0.51 M; no reaction observed over a period of 6 h at 20 °C.

(15) Given that protonation of **1a** in methanol (*pK_a* ≈ -2) is rapid and quantitative, it is unlikely that the inactivity of **2a** with Ph₂NH is a kinetic phenomenon.

(16) A similar steric interaction is observed for the 2,5-dimethyl-3-pyrroline complex of pentaammineosmium(II).¹²

(17) After 24 h, no reaction is observed for the benzo[*b*]thiophene complex in a 6 M HOTf solution of CH₃CN. Protonation of the 2-methoxythiophene complex **1e** resulted in an intractable mixture of paramagnetic materials.

(18) Gates, B. C. *Catalytic Chemistry*; Wiley: New York, 1991.

(19) Luo, S.; Rauchfuss, T. B.; Wilson, S. R. *J. Am. Chem. Soc.* **1992**, *114*, 8515.

(20) Although by convention one can describe the 2*H*-thiophenium species as Os(IV) complexes, we believe they are chemically and spectroscopically most similar to pentaammineosmium(II) complexes of electron-deficient olefins. Similar *exo* protonations have been observed for η^2 -pyrrole complexes of pentaammineosmium(II).^{12,13}

(10) Carbon multiplicities were determined by DEPT and proton-carbon assignments by ¹H-¹³C HETCOR.

(11) The possibility of an η^3 -allyl complex is ruled out on the basis of ¹³C NMR data; pentaammineosmium(II) complexes of η^3 -allyl cations have ¹³C resonances for the allyl group in the range of 70-85 ppm. Harman, W. D.; Taube, H. *Inorg. Chem.* **1991**, *30*, 453. Kopach, M. E.; Spera, M. L.; Winemiller, M. D.; Harman, W. D. Unpublished results.

(12) Hodges, L. M.; Gonzalez, J.; Koontz, J. I.; Myers, W. H.; Harman, W. D. *J. Org. Chem.*, in press.

(13) Protonation at C(2) *anti* to the metal has also been observed for the 2,5-dimethylpyrrole analog. See: Myers, W. H.; Koontz, J. I.; Harman, W. D. *J. Am. Chem. Soc.* **1992**, *114*, 5684.

hydrogen to the heterocycle. The protonations described herein for compounds **1a-f** are unique in that the d^6 metal activates the thiophene toward *direct protonation from the exo face* without a required change in metal oxidation state.²⁰ Studies are in progress to determine if the direct electrophilic addition to the C(2) carbon of thiophene is general and if the resulting *2H*-thiophenium species are susceptible to nucleophilic attack.

Acknowledgment is made to the donors of the Petroleum Research Fund, administered by the American Chemical Society (PRF#26027-AC), the Camille and

Henry Dreyfus Foundation, and the National Science Foundation (NSF Young Investigator program) for their generous support of this work.

Supplementary Material Available: Text and tables giving details on the synthesis and characterization of compounds **1a-g** and **2a-d,f** (5 pages). This material is contained in many libraries on microfiche, immediately follows this article in the microfilm version of the journal, and can be ordered from the ACS; see any current masthead page for ordering information.

OM950092E

Two Counterintuitive Routes to an Iron Alkylidyne Complex

Stephen Anderson and Anthony F. Hill*

Department of Chemistry, Imperial College of Science, Technology and Medicine,
London SW7 2AY, U.K.

Received December 20, 1994[®]

Summary: The cationic aminomethylidyne complex $[\text{Fe}(\equiv\text{CN}^i\text{Pr}_2)(\text{CO})_3(\text{PPh}_3)]^+$ has been prepared by two unexpected routes: (i) Iodination of the carbamoyl complex $[\text{Fe}(\eta^2\text{-OCN}^i\text{Pr}_2)(\text{CF}_3)(\text{CO})_2(\text{PPh}_3)]$ and (ii) *O*-trifluoroacetylation of the carbamoylate $[\text{Fe}\{\text{C}(=\text{O})\text{N}^i\text{Pr}_2\}(\text{CO})_4]\text{-Li}$, a reaction which shows an unusual solvent dependence.

Alkylidyne complexes of group 8¹ remain very rare, with only one example known for iron.² Recent advances in the chemistry of osmium³ in addition to Roper's studies on the complexes $[\text{M}(\equiv\text{CR})\text{Cl}(\text{CO})(\text{PPh}_3)_2]$ ^{4,5} would however suggest that there is nothing inherently unstable about late transition metal alkylidyne, merely that many of the synthetic routes used for groups 5–7 are not generally applicable to the later transition metals. We have been concerned recently with the preparation of alkylidyne complexes of iron. These efforts are based on the realization that if alkylidyne complexes are to have the extensive application to stoichiometric organic synthesis enjoyed by alkylidene complexes, economic and expedient synthetic strategies are required. We have previously attempted, unsuccessfully, to adapt Mayr's oxide-abstraction approach⁶ to iron(0) acylates.⁷ Our failure resulted from a generally encountered problem with the *O*-alkylation of acylate complexes of the form $[\text{Fe}\{\text{C}(=\text{O})\text{R}\}(\text{CO})_4]^-$, this being that the metal center offers an alternative site for electrophilic attack by any but the hardest of electrophiles. Thus the sequential treatment of $[\text{Fe}(\text{CO})_5]$ with LiN^iPr_2 , $(\text{CF}_3\text{CO})_2\text{O}$, and PPh_3 in diethyl ether provides $[\text{Fe}(\eta^2\text{-OCN}^i\text{Pr}_2)(\text{CF}_3)(\text{CO})_2(\text{PPh}_3)]$ (1)⁷ rather than the desired alkylidyne complex $[\text{Fe}(\equiv\text{CN}^i\text{Pr}_2)(\text{O}_2\text{CCF}_3)(\text{CO})_2(\text{PPh}_3)]$. Semmelhack has discussed the effect of solvent on the *O*- vs *Fe*-alkylation of acyl complexes of iron and shown that very hard electrophiles and strongly solvating solvents (thf, HMPA) favor attack at the oxygen atom of the acyl ligand and the formation of alkylidene complexes.⁸ In applying these ideas to the reaction of $[\text{Fe}\{\text{C}(=\text{O})\text{N}^i\text{Pr}_2\}(\text{CO})_4]^-$ (2) with

$(\text{CF}_3\text{CO})_2\text{O}/\text{PPh}_3$, we have met with comprehensive failure. For a variety of thf, Et_2O , and HMPA solvent combinations the only products observed were $[\text{Fe}(\text{CO})_3(\text{PPh}_3)_2]$ and $[\text{Fe}(\eta^2\text{-OCN}^i\text{Pr}_2)(\text{CF}_3)(\text{CO})_2(\text{PPh}_3)]$ (1). It was therefore with some surprise that we find that if the carbamoylate (2) (performed in diethyl ether) is dissolved in dichloromethane and treated with $(\text{CF}_3\text{CO})_2\text{O}$ and PPh_3 , the product isolated in moderate yield is the salt $[\text{Fe}(\equiv\text{CN}^i\text{Pr}_2)(\text{CO})_3(\text{PPh}_3)](\text{O}_2\text{CCF}_3)$ (3a) (13% based on 15 mmol of $[\text{Fe}(\text{CO})_5]$)^{9a} in addition to $[\text{Fe}(\eta^2\text{-OCN}^i\text{Pr}_2)(\text{CO})_2(\text{PPh}_3)_2](\text{O}_2\text{CCF}_3)$ (4a) (3%).¹⁰ The latter complex may be prepared independently, and in high yield, as the BF_4^- salt (4b) from the reaction of $[\text{Fe}(\eta^2\text{-OCN}^i\text{Pr}_2)(\text{CF}_3)(\text{CO})_2(\text{PPh}_3)]$ (1) with HBF_4 to provide $[\text{Fe}(\eta^2\text{-OCN}^i\text{Pr}_2)(\text{CO})_3(\text{PPh}_3)](\text{BF}_4)$ (5)¹¹ followed by treatment with PPh_3 which results in substitution of one carbonyl ligand. Alternatively reaction of 2 with iodine and triphenylphosphine provides the iodo complex $[\text{Fe}(\eta^2\text{-OCN}^i\text{Pr}_2)\text{I}(\text{CO})_2(\text{PPh}_3)]$ (6)¹² and the halide of this complex may be abstracted with AgBF_4 in the presence of CO to provide 5. The ultimate retention of the η^2 -

(9) (a) $[\text{Fe}(\equiv\text{CN}^i\text{Pr}_2)(\text{CO})_3(\text{PPh}_3)](\text{O}_2\text{CCF}_3)$ (3a): $[\text{Fe}(\text{CO})_5]$ (3.0 g, 15 mmol) was diluted in diethyl ether (50 cm³) under nitrogen and LiN^iPr_2 (10.2 cm³, 1.5 mol dm⁻³ in hexane, 15 mmol) added dropwise. The ether was removed in vacuo, the residue was redissolved in dry CH_2Cl_2 , the solution was cooled (dry ice/acetone), and a solution of $(\text{CF}_3\text{CO})_2\text{O}$ (2.4 cm³, 17 mmol) in ether (20 cm³) was added dropwise. After the solution was stirred for 15 min, PPh_3 (6.0 g, 23 mmol) was added and the mixture allowed to warm slowly to room temperature to provide an oily precipitate. Petroleum ether (40–60) (25 cm³) was added and the reaction mixture filtered through Celite. The filtrate was concentrated and cooled to -30°C to provide 4a [Yield: 0.24 g (2.5%)].¹⁰ The yellow precipitate remaining on the Celite was then eluted through with THF, diluted with petroleum ether, and cooled (-30°C) to provide 3a. Yield: 1.2 g (13%). (b) $[\text{Fe}(\equiv\text{CN}^i\text{Pr}_2)(\text{CO})_3(\text{PPh}_3)]\text{I}$ (3c): Iodine (0.17 g, 0.68 mmol) and 1 (0.39 g, 0.68 mmol) were combined under nitrogen. Diethyl ether (30 cm³) was then added and the mixture stirred for 3 h. The gray precipitate which formed was isolated and extracted into CH_2Cl_2 /petrol (2:1), and the extracts were filtered through Celite. On concentration of the solution under vacuum, the product crystallized. Yield: 0.16 g (36%). (c) Data for $[\text{Fe}(\equiv\text{CN}^i\text{Pr}_2)(\text{CO})_3(\text{PPh}_3)]\text{X}$ [X = CF_3CO_2 (3a), I (3c)] are as follows. IR: CH_2Cl_2 , 2083, 2034, 2012 (CO), 1664 cm⁻¹ (CN); Nujol, 2079, 2041, 1992 (CO), 1642 (CN) cm⁻¹. NMR [$(\text{CD}_3)_2\text{CO}$, 25°C]: ¹H, δ 1.17 [d, 12 H, CHMe_2 , $J(\text{HH})$ 6.3 Hz], 3.96 [h, 2 H, CHMe_2], 7.58–7.76 [m, 15 H, C_6H_5] ppm; ¹³C{¹H}, 266.5 [d, $\text{Fe}=\text{C}$, $J(\text{PC})$ 42.8 Hz], 206.5 [d, FeCO , $J(\text{PC})$ not resolved], 134.4–130.3 [C_6H_5], 58.5 [s, CHMe_2], 22.0 [s, CHMe_2] ppm; ³¹P{¹H}, 58.4 ppm. These data are essentially identical to those reported² for 3b. FAB-MS (nba matrix, correct isotope patterns): $m/z = 514$, [M]⁺, 486 [M – CO]⁺, 458 [M – 2(CO)]⁺, 318 [FePPh₃]⁺ (M refers to the cationic complex).

(10) $[\text{Fe}(\eta^2\text{-OCN}^i\text{Pr}_2)(\text{CO})_2(\text{PPh}_3)_2]\text{BF}_4$ (4): PPh_3 (0.13 g, 0.5 mmol) and 5¹¹ (0.20 g, 0.30 mmol) were heated in refluxing THF (20 cm³) for 1 h, and then the THF was removed under vacuum. The residue was titrated ultrasonically with diethyl ether (30 cm³) and the resulting yellow solid recrystallized from CH_2Cl_2 /petroleum ether. Yield: 0.16 g (58%). IR: CH_2Cl_2 , 2039, 1968 (CO), 1605 cm⁻¹ (NCO); Nujol, 2026, 1960 (CO), 1612 (NCO) cm⁻¹. NMR (CDCl_3 , 25°C): ¹H, δ 0.08, 1.03 [d × 2, 12 H, CHMe_2], 3.06, 5.16 [h × 2, 2 H, CHMe_2], 7.33–7.53 [m, 30 H, C_6H_5] ppm; ¹³C{¹H}, 214.0 [t, FeCO , $J(\text{PC})$ 30.1 Hz], 211.4 [t, FeCO , $J(\text{PC})$ 21.3 Hz], 184.0 [t, OCN, $J(\text{PC})$ 23.0 Hz], 133.6–129.4 [C_6H_5 , virtual triplet of $\text{C}(\text{C}_6\text{H}_5)$ confirms *trans* FeP_2], 56.2, 49.6 [CHMe₂], 21.5, 19.2 [CHMe₂] ppm; ³¹P{¹H}, 54.6 ppm. FAB-MS (nba matrix, correct isotope patterns): $m/z = 764$ [M]⁺, 708 [M – 2(CO)]⁺, 580 [FePPh₃]⁺ [M refers to complex cation].

* Abstract published in *Advance ACS Abstracts*, March 15, 1995.

(1) Gallop, M. A.; Roper, W. R. *Adv. Organomet. Chem.* **1986**, *25*, 121. For a recent review of group 8 alkylidyne complexes, see: Hill, A. F. In *Comprehensive Organometallic Chemistry II*; Abel, E. W., Stone, F. G. A., Wilkinson, G., Eds.; Pergamon Press: Oxford, U.K., 1995; Vol. 7.

(2) Fischer, E. O.; Schneider J.; Neugebauer, D. *Angew. Chem., Int. Ed. Engl.* **1984**, *23*, 1820.

(3) Hodges, L. H.; Sabat, M.; Harman, W. D. *Inorg. Chem.* **1993**, *32*, 37. Lapointe, A. M.; Schrock, R. R. *Organometallics* **1993**, *12*, 3379.

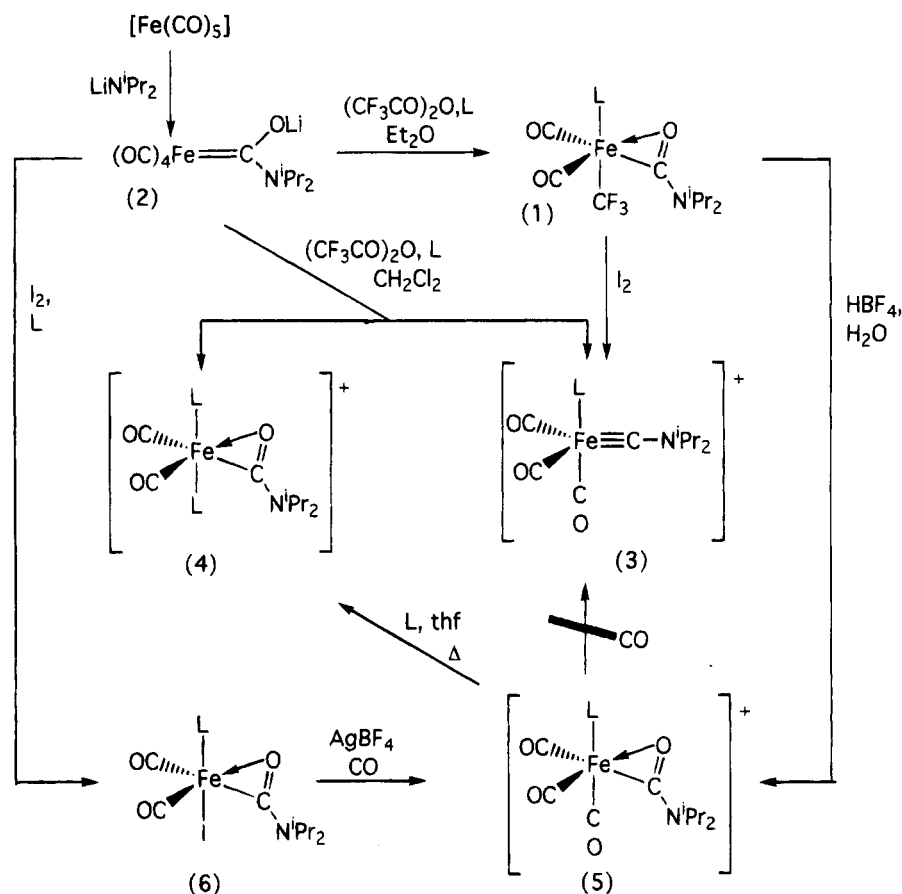
(4) Roper, W. R. *J. Organomet. Chem.* **1986**, *300*, 167.

(5) Roper, W. R. In *Transition Metal Carbonyl Complexes*; Kreissl, F. R., Ed.; Kluwer Academic Publishers: Dordrecht, The Netherlands, 1993; pp 155–168.

(6) Mayr, A.; McDermott, G. A. *J. Am. Chem. Soc.* **1986**, *108*, 458.

(7) Anderson, S.; Hill, A. F.; Clark, G. R. *Organometallics* **1992**, *11*, 2323.

(8) Semmelhack, M. F.; Tamura, R. J. *J. Am. Chem. Soc.* **1983**, *105*, 4099.

Scheme 1. Synthesis and Interconversion of Carbamoyl and Aminomethylidyne Complexes of Iron (L = PPh₃)


carbamoyl coordination mode in these transformations is noteworthy, although η^1 intermediates cannot yet be excluded.

The salt $[\text{Fe}(\equiv\text{CN}^i\text{Pr}_2)(\text{CO})_3(\text{PPh}_3)](\text{BCl}_4)$ (**3b**) has been reported by Fischer² as resulting from the reaction of $[\text{Fe}=\text{C}(\text{OEt})\text{N}^i\text{Pr}_2](\text{CO})_3(\text{PPh}_3)$ with BCl_3 . Fischer's multistep procedure requires comparatively sophisti-

cated synthetic techniques. Clearly the procedure described here offers considerable economy and expedience; however, we have subsequently found an even more convenient if somewhat more curious route to this complex. The carbamoyl complex $[\text{Fe}(\eta^2\text{-OCN}^i\text{Pr}_2)(\text{CF}_3)(\text{CO})_2(\text{PPh}_3)]$ (**1**) reacts cleanly with iodine to produce $[\text{Fe}(\equiv\text{CN}^i\text{Pr}_2)(\text{CO})_3(\text{PPh}_3)]\text{I}$ (**3c**) (Scheme 1)^{9b} (36% non-optimized yield based on 0.68 mmol of precursor). If the somewhat arbitrary description of an alkylidyne ligand as $[\text{CR}]^+$ (isobal with $[\text{NO}]^+$) is accepted, we are faced with a situation where iodine has acted *formally* as a reductant $[\text{Fe}(\text{II}) \rightarrow \text{Fe}(\text{0})]$.¹³ The nature of the salt **3c** was not initially appreciated, and so we can confidently say that it is stable in the solid state for up to 3 years.

We are still investigating and somewhat equivocal about the actual mechanism by which this unusual transformation takes place; however, the following observations should be noted: The trifluoromethyl group is of critical importance, since no **3c** is obtained from the reaction of $[\text{Fe}=\text{C}(\text{=O})\text{N}^i\text{Pr}_2](\text{CO})_4$ (**2**) with I_2 and PPh_3 , or preformed I_2PPh_3 , the sole product being the new complex $[\text{Fe}(\eta^2\text{-OCN}^i\text{Pr}_2)\text{I}(\text{CO})_2(\text{PPh}_3)]$ (**6**).¹² This is also the product of the reaction of $[\text{Fe}(\eta^2\text{-OCN}^i\text{Pr}_2)(\text{SnPh}_3)(\text{CO})_2(\text{PPh}_3)]$ ⁷ with iodine.¹⁴ Furthermore,

(13) The assignment of formal oxidation states for alkylidyne-carbyne complexes offers more debate than utility, with both extremes $[\equiv\text{CR}]^{3-}$ and $[\equiv\text{CR}]^+$ having their proponents. If infrared data of carbonyl coligands are taken as indicative of metal electron density, then the effect of an alkylidyne ligand on a metal center is most comparable to that of a linear nitrosyl, *i.e.*, $[\text{CR}]^+$ isobal with $[\text{NO}]^+$, *e.g.*, see ref 5. The alternative trianionic formulation would make the compound **3a** a somewhat implausible tricarbonyl derivative of tetravalent iron.

(11) $[\text{Fe}(\eta^2\text{-OCN}^i\text{Pr}_2)(\text{CO})_3(\text{PPh}_3)]\text{BF}_4$ (**5**): To 1 (1.00 g, 1.75 mmol) in diethyl ether (50 cm³) was added $\text{HBF}_4(\text{aq})$ (0.12 mL [wt/mL = 1.31 g], 1.75 mmol). A bright yellow precipitate slowly formed which was isolated and then recrystallized from CH_2Cl_2 /petroleum ether. Yield: 0.89 g (82%). IR: CH_2Cl_2 , 2102, 2058, 2023 cm⁻¹ (CO); 1650 cm⁻¹ (NCO); Nujol, 2099, 2053, 2011 cm⁻¹ (CO); 1652 cm⁻¹ (NCO). NMR (CDCl_3 , 25 °C): ¹H, δ 0.55, 1.24, 1.36, 1.45 [4 x d (br), 12H, CHMe_2], 3.64, 4.68 [2 x h, 2H, CHMe_2], 7.30, 7.53 [2 x m, 15H, C_6H_5]; ¹³C{¹H}, 206.6 [d, FeCO, $J(\text{PC})$ 31.4 Hz], 202.2 [d, FeCO, $J(\text{PC})$ 26.5 Hz], 197.1 [d, FeCO, $J(\text{PC})$ 51.0 Hz], 185.9 [d, OCN, $J(\text{PC})$ = 18.8 Hz], 133.2–127.5 [C_6H_5], 56.7, 50.3 [2 x s, CHMe_2], 21.8, 19.7, 19.4, 19.1 ppm [4 x s, CHMe_2]; ³¹P{¹H}, 22.4 ppm. FAB-MS: m/z = 530 [M^+], 502 [$\text{M}^+ - \text{CO}^+$], 474 [$\text{M}^+ - 2\text{CO}^+$], 446 [$\text{M}^+ - 3\text{CO}^+$], 318 [FePPh_3]⁺ [M refers to complex cation].

(12) $[\text{Fe}(\eta^2\text{-OCN}^i\text{Pr}_2)\text{I}(\text{CO})_2(\text{PPh}_3)]$ (**6**): To $[\text{Fe}(\text{CO})_5]$ (3.0 g, 15 mmol) in diethyl ether (50 cm³) was added LiN^iPr_2 (1.5 mol dm⁻³ in hexane, 10.2 cm³, 15 mmol) dropwise. The reaction mixture was cooled (dry ice/acetone) and I_2 (3.88 g, 15 mmol) added. When all the iodine had dissolved, PPh_3 (6.0 g, 23 mmol) was added, and the reaction was left to warm slowly to room temperature. The resulting purple precipitate was isolated and extracted with CH_2Cl_2 /petroleum ether (2:1). The combined extracts were filtered through Celite and chromatographed (silica gel, -40 °C). Concentration and cooling of the purple band eluted with CH_2Cl_2 provided **6**. Yield: 6.9 g (72%). Yield: 8.5 g (88%) using preformed I_2PPh_3 . IR: CH_2Cl_2 , 2017, 1958 (CO), 1634, 1614 cm⁻¹ (NCO); Nujol, 2012, 1964 (CO), 1634 (NCO) cm⁻¹. NMR (CDCl_3 , 25 °C): ¹H, δ 1.28, 1.41, 1.46, 1.53 [d x 4, 12H, CHMe_2], 3.87, 4.67 [h x 2, 2H, CHMe_2], 7.34–7.69 [m, 15H, C_6H_5] ppm; ¹³C{¹H}, 218.6 [d, FeCO, $J(\text{PC})$ 26.8 Hz], 210.4 [d, FeCO, $J(\text{PC})$ 21.4 Hz], 197.4, OCN, $J(\text{PC})$ 19.7 Hz], 134.2–127.4 [C_6H_5], 53.8, 49.5 [CHMe_2], 21.7, 21.4, 20.9, 20.7 [CHMe_2] ppm; ³¹P{¹H}, 78.5 ppm. FAB-MS (nba matrix, correct isotope patterns): m/z = 629 [M^+], 573 [$\text{M}^+ - 2(\text{CO})^+$], 445 [$\text{FeI}(\text{PPh}_3)$]⁺.

as the complexes **5** and **6** are isolable and indefinitely stable, they may be excluded as intermediates.

The two approaches to the synthesis of thermally stable iron alkylidyne complexes presented here, while surprising, do further illustrate that late transition metal alkylidynes can be easily prepared if suitable synthetic strategies can be found, which need not have precedent in the chemistry of groups 5–7. Furthermore, the expedient methods described do not require

sophisticated preparative techniques, are economic, and may be carried out on large scales using commercially available starting materials. We hope that these factors will facilitate the study of these complexes as synthons in organic synthesis, and we are currently exploring this avenue, in particular with respect to C–C bond-forming processes.

Acknowledgment. We are grateful to the SERC for the award of a post-graduate studentship (to S.A.).

OM940974Y

(14) Anderson, S.; Berridge, T.; Hill, A. F. Unpublished observations.

Protonation of Acyllithium Reagents by Dichloromethane and Dichloroarylmethane: A New Method for the Synthesis of α,α -Dichloro Alcohols

George W. Kabalka,* Nan-Sheng Li, and Su Yu

Departments of Chemistry and Radiology, The University of Tennessee,
Knoxville, Tennessee 37996-1600

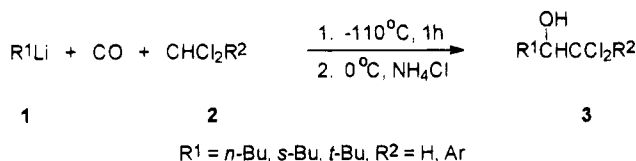
Received February 7, 1995[⊗]

Summary: The first example of the protonation of acyllithium reagents by dichloromethane and dichloroarylmethane is described. The reaction affords the corresponding α,α -dichloro alcohols in excellent yields.

Introduction. The transformation of organometallic reagents into useful synthetic intermediates has played an important role in organic chemistry for many years. Recently, studies involving acyl anion reagents generated via the carbonylation of organometallic reagents with carbon monoxide have proven to be an especially productive area of research.^{1–7}

Much attention has been focused on the nucleophilic acylation of electrophiles utilizing acyllithium reagents. For example, Seyferth reported that acyllithium reagents, generated *in situ* from an alkyllithium and carbon monoxide, react with aldehydes,¹ ketones,¹ esters,⁸ lactones,⁹ isocyanates,¹⁰ isothiocyanates,¹⁰ carbodiimides,¹¹ carbon disulfide,¹² carbonyl sulfide,¹² organic disulfides,¹³ and trimethylchlorosilanes¹⁴ to give acylated products. Nudelman found that the acyllithium generated from phenyllithium and carbon monoxide, in the presence of alkyl bromides at $-78\text{ }^\circ\text{C}$, gave diphenylalkylcarbinols.^{15,16} Although Seyferth predicted that nucleophilic acylation might also be applied in protonation and alkylation reactions to give aldehydes and ketones,³ no report on the protonation and alkylation of acyl anion reagents has appeared in the literature. Recently, we found that trialkylboranes reacted with acyllithium reagent to afford ketones in modest yields.¹⁷ During our investigation of this reaction, the acyllithium reagent was preformed from *n*-butyllithium and carbon

Scheme 1



monoxide according to Seyferth's method¹ and then equimolar quantities of a butylborane reagent in methylene chloride were added. After the reaction mixture was worked up oxidatively, we found that the reaction produced the desired ketone along with a significant quantity of 1,1-dichloro-2-hexanol. These results encouraged us to investigate the reaction of acyl anions with dichloromethane, and its derivatives, since α,α -dichloroalcohols are important synthetic intermediates, which can be transformed into substituted chloroethylene oxides or α -chlorocarbonyl compounds.^{18–22} The synthesis of α,α -dichloro alcohols is usually achieved via reduction of α,α -dichloro ketones^{18–20} or by the addition of the dichloromethyl anion to aldehydes or ketones.^{21,22} However, no general method exists for the synthesis of α,α -dichloro α -aryl alcohols.²³ We wish to report the preliminary results of a study involving the reaction of acyllithium reagents with dichloromethane (or dichloroarylmethane) to afford α,α -dichloro alcohols (Scheme 1).

Results and Discussion. The reactions are straightforward. Commercially available alkyllithium reagents (*n*-butyl-, *s*-butyl-, and *tert*-butyllithium) were utilized in this initial study. However, as demonstrated by Seyferth for the nucleophilic acylation of chlorosilane,¹⁴ other alkyllithium reagents may be used. The reaction is initiated by the slow addition of the alkyllithium reagent to a solution of dichloromethane (or a dichloroarylmethane) in a 4:4:1 (by volume) solvent system of THF–Et₂O–pentane saturated with carbon monoxide at $-110\text{ }^\circ\text{C}$. After the acyllithium is added, the reaction mixture is stirred at $-110\text{ }^\circ\text{C}$ for 1 h, and then the reaction mixture is hydrolyzed using saturated aqueous NH₄Cl at $0\text{ }^\circ\text{C}$. After separation of the organic layer, and silica gel column chromatography, pure products are obtained in excellent yields (Table 1).

[⊗] Abstract published in *Advance ACS Abstracts*, April 1, 1995.

(1) Seyferth, D.; Weinstein, R. M.; Hui, R. C.; Wang, W.-L.; Archer, C. M. *J. Org. Chem.* **1992**, *57*, 5620 and references cited therein.

(2) Orita, A.; Fukudome, M.; Ohe, K.; Murai, S. *J. Org. Chem.* **1994**, *59*, 477 and references cited therein.

(3) Seyferth, D.; Weinstein, R. M.; Wang, W.-L.; Hui, R. C.; Archer, C. M. *Isr. J. Chem.* **1984**, *24*, 167.

(4) Seyferth, D.; Hui, R. C.; Weinstein, R. M.; Wang, W.-L. *Nova Acta Leopold.* **1985**, *59*, 335; *Chem. Abstr.* **1988**, *108*, 6056t.

(5) Narayana, C.; Periasamy, M. *Synthesis* **1985**, 253.

(6) Wakefield, B. J. *Organolithium Methods*; Academic Press: London, 1988; pp 95–97.

(7) Hui, R. C.; Seyferth, D. *Org. Synth.* **1990**, *69*, 114.

(8) Seyferth, D.; Weinstein, R. M.; Hui, R. C.; Wang, W.-L.; Archer, C. M. *J. Org. Chem.* **1991**, *56*, 5768.

(9) Weinstein, R. M.; Wang, W.-L.; Seyferth, D. *J. Org. Chem.* **1983**, *48*, 3367.

(10) Seyferth, D.; Hui, R. C. *Tetrahedron Lett.* **1984**, *25*, 5251.

(11) Seyferth, D.; Hui, R. C. *J. Org. Chem.* **1985**, *50*, 1985.

(12) Seyferth, D.; Hui, R. C. *Tetrahedron Lett.* **1984**, *25*, 2623.

(13) Seyferth, D.; Hui, R. C. *Organometallics* **1984**, *3*, 327.

(14) Seyferth, D.; Weinstein, R. M. *J. Am. Chem. Soc.* **1982**, *104*, 5534.

(15) Nudelman, N. S.; Vitale, A. A. *J. Org. Chem.* **1981**, *46*, 4625.

(16) Vitale, A. A.; Doctorovich, F.; Nudelman, N. S. *J. Organomet. Chem.* **1987**, *332*, 9.

(17) Kabalka, G. W.; Gotsick, J. T.; Pace, R. D.; Li, N.-S. *Organometallics* **1994**, *13*, 5163.

(18) Kimpe, N. D.; Corte, B. D. *Tetrahedron* **1992**, *48*, 7345.

(19) Gralak, J.; Valnot, J.-Y. *Org. Prep. and Proced. Int.* **1979**, *11*, 107.

(20) Duhamet, P.; Duhamel, L.; Gralak, J. *Bull. Soc. Chim. Fr.* **1970**, 3641.

(21) Villieras, J.; Bacquet, C.; Normant, J. F. *J. Organomet. Chem.* **1975**, *97*, 325.

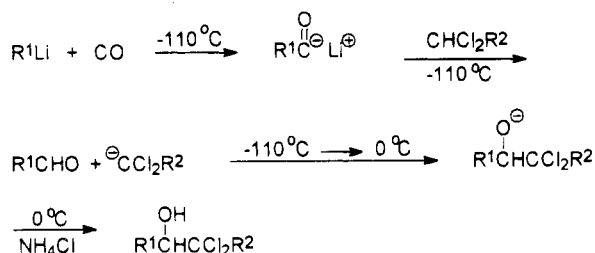
(22) Normant, H. J. *Organomet. Chem.* **1975**, *100*, 189.

(23) 1,1-Dichloro-1-phenyl-2-hexanol was prepared by cathodic addition of trichloromethylbenzene to pentanal in only 25% yield: Steiniger, M.; Schaefer, H. J. *Bull. Chem. Soc. Jpn.* **1988**, *61*, 125.

Table 1. Synthesis of α,α -Dichloro Alcohols

entry no. ^a	product ^b	R ¹	R ²	2:1 (molar equiv) ^c	yield (%) ^d
1	3a	<i>n</i> -Bu	H	15:1	81
2 ^e	3a	<i>n</i> -Bu	H	15:1	58
3	3a	<i>n</i> -Bu	H	6:1	84
4	3a	<i>n</i> -Bu	H	4:1	81
5 ^f	3a	<i>n</i> -Bu	H	4:1	59
6	3a	<i>n</i> -Bu	H	2:1	74
7	3a	<i>n</i> -Bu	H	1:1	62
8	3b	<i>s</i> -Bu	H	6:1	23
9	3b	<i>s</i> -Bu	H	4:1	34
10	3c	<i>t</i> -Bu	H	15:1	32
11	3c	<i>t</i> -Bu	H	6:1	40
12	3c	<i>t</i> -Bu	H	4:1	36
13	3d	<i>n</i> -Bu	Ph	2:1	97
14	3d	<i>n</i> -Bu	Ph	1:1	89
15	3e	<i>n</i> -Bu	α -naphthyl	2:1	90
16	3e	<i>n</i> -Bu	α -naphthyl	1:1	87
17	3f	<i>n</i> -Bu	<i>p</i> -CH ₃ C ₆ H ₄	2:1	74
18	3f	<i>n</i> -Bu	<i>p</i> -CH ₃ C ₆ H ₄	1:1	62
19	3g	<i>n</i> -Bu	<i>p</i> -ClC ₆ H ₄	2:1	90
20	3g	<i>n</i> -Bu	<i>p</i> -ClC ₆ H ₄	1:1	80
21	3h	<i>n</i> -Bu	<i>p</i> -BrC ₆ H ₄	2:1	90
22	3h	<i>n</i> -Bu	<i>p</i> -BrC ₆ H ₄	1:1	86

^a Acyllithium reagents were generated in the presence of the dichloro compounds at -110°C in all experiments except where noted. ^b All new products were characterized by appropriate spectral and elemental analyses. All known compounds were characterized by comparing their spectral and physical properties with those in the literature. ^c Ratio of dichloro compound **2** to acyllithium **1**. ^d Isolated yields based on acyllithium reagent. ^e Acyllithium reagent was generated prior to the addition of dichloromethane. ^f Experiment was carried out at -78°C .

Scheme 2

The reaction presumably occurs via the intermediate formation of an aldehyde generated by proton abstraction from the dichloro reagent by the initially formed acyl anion. The aldehyde then reacts with the chlorine-stabilized anion as outlined in Scheme 2.

As shown in Table 1, generation of the acyllithium in the presence of dichloromethane (Table 1, entry 1) was more efficient than generating the acyllithium prior to the addition of dichloromethane (Table 1, entry 2). In addition, product yields decreased when higher temperatures (-78°C) were used (Table 1, entry 5). In most

cases, excess dichloro reagent (**2**) resulted in an increased product yield; however, a large excess was not required. The reaction of a stoichiometric quantity of the dichloro compound (**2**) and the acyllithium also gave α,α -dichloro alcohols in good yields (Table 1, entries 7, 14, 16, 18, 20, and 22). The reaction is most efficient when R is a primary alkyl group. Acyl anion reagents generated from secondary or tertiary acyllithium reagents react with dichloromethane to give α,α -dichloro alcohols in modest yields (Table 1, entries 8–12). The lower yields observed with secondary and tertiary acyllithium reagents may be due to the steric interactions between the bulkier aldehyde intermediates and the chlorinated anion.

The preparation of 1,1-dichloro-1-phenyl-2-hexanol (**3d**) is representative: in a three-necked, 250 mL, round-bottomed flask equipped with magnetic stirrer, glass-enclosed thermocouple probe, and a fritted-glass gas dispersion tube were added α,α -dichlorotoluene (1.61 g, 10.0 mmol) and 150 mL of a 4:4:1 (by volume) mixture of THF, diethyl ether, and pentane. The solution was cooled to -110°C by means of a low-temperature bath. Carbon monoxide was then continuously bubbled into the solution. After 30 min of carbon monoxide addition, *n*-butyllithium (5.0 mmol, 3.1 mL of a 1.6 M solution, in hexane) was added slowly via syringe over a period of approximately 45 min, forming a pale yellow solution. After the addition was complete, the reaction mixture was stirred at -110°C for 1 h and warmed to 0°C . Hydrolysis was achieved by adding saturated aqueous ammonium chloride (40 mL). The two phases were separated, and the aqueous phase was extracted with diethyl ether (3×20 mL). The organic phases were combined, washed with a saturated NaCl solution (20 mL), and then dried over anhydrous MgSO₄. The solvent was removed under reduced pressure, and the residue was isolated by silica gel chromatography (9:1 hexane–ethyl acetate (v/v) as eluent) to give **3d**²³ (1.195 g, 97% (Table 1, entry 13)).

The reaction described in this communication provides a useful, one-pot synthesis of primary alkyl-(dichloroalkyl)carbinols and is the first example of acyllithium reagents being protonated to form aldehydes which further react with anions to afford alcohols. Further examination of the scope of this reaction is in progress.

Acknowledgment. We wish to thank the Department of Energy and the Robert H. Cole Foundation for support of this research.

OM950099W

Articles

Synthesis and Reactivity of Tris(pyrazolyl)borate-Stabilized Molybdenum Imido Alkylidene Complexes

William M. Vaughan, Khalil A. Abboud, and James M. Boncella*

Department of Chemistry and Center for Catalysis, University of Florida,
Gainesville, Florida 32611

Received October 19, 1994[⊗]

The addition of LiCH_3 to $\text{TpMo}(\text{CHR})(\text{NAr})(\text{OTf})$ (**1**; Tp = hydridotris(1-pyrazolyl)borate; R = $\text{C}(\text{CH}_3)_2\text{Ph}$; Ar = 2,6-*i*-Pr- C_6H_3 ; OTf = $\text{OSO}_2(\text{CF}_3)$) gave $\text{TpMo}(\text{CHR})(\text{NAr})(\text{CH}_3)$ (**2**). Compound **2** was used to prepare several solvent-bound, cationic complexes by abstracting the methyl ligand. The addition of tetrakis(3,5-bis(trifluoromethyl)phenyl)boric acid to **2** in Et_2O gave $[\text{TpMo}(\text{CHR})(\text{NAr})(\text{Et}_2\text{O})][\text{BAR}'_4]$ (**3**; Ar' = 3,5- $\text{C}_6\text{H}_3(\text{CF}_3)_2$) and CH_4 . The reaction of **2** and trityl tetrakis(pentafluorophenyl)borate in the presence of excess acetonitrile gave $[\text{TpMo}(\text{CHR})(\text{NAr})(\text{NCCH}_3)][\text{B}(\text{C}_6\text{F}_5)_4]$ (**4**) and Ph_3CCH_3 . The Lewis acid $\text{B}(\text{C}_6\text{F}_5)_3$ abstracted the methyl ligand of **2** in the presence of acetonitrile or tetrahydrofuran to give the compounds $[\text{TpMo}(\text{CHR})(\text{NAr})(\text{S})][\text{B}(\text{CH}_3)(\text{C}_6\text{F}_5)_3]$ (**5**, S = NCCH_3 ; **6**, S = THF). The triflate ligand of **1** was displaced by trimethylphosphine to give $[\text{TpMo}(\text{CHR})(\text{NAr})(\text{P}(\text{CH}_3)_3)]\text{[OTf]}$ (**7**). Stirring **1** in the presence of methanol and Florisil gave $\text{TpMo}(\text{CHR})(\text{NAr})(\text{OCH}_3)$ (**8**). The addition of excess potassium methoxide to **1** gave $\text{TpMo}(\text{CR})(\text{NHAr})(\text{OCH}_3)$ (**9**). Attempts to convert **8** to **9** by heating, photolysis, and the addition of NEt_3 or PMe_3 were unsuccessful. Since only excess methoxide converts **8** to **9**, a methoxide-mediated proton transfer mechanism is proposed. X-ray structures of *syn*-**8** ($P2_12_12_1$, $a = 12.620(2) \text{ \AA}$, $b = 13.492(2) \text{ \AA}$, $c = 19.682(2) \text{ \AA}$, $Z = 4$, $V = 3351.3(7) \text{ \AA}^3$, $M_r = 647.48$, $d_{\text{calc}} = 1.283 \text{ g/cm}^3$, $R = 6.00\%$, $R_w = 5.89\%$) and *syn*-**9** ($P\bar{1}$, $a = 10.624(2) \text{ \AA}$, $b = 11.766(2) \text{ \AA}$, $c = 13.980(2) \text{ \AA}$, $\alpha = 86.96(2)^\circ$, $\beta = 86.54(2)^\circ$, $\gamma = 67.77(2)^\circ$, $Z = 2$, $V = 1635.8(7) \text{ \AA}^3$, $M_r = 647.48$, $d_{\text{calc}} = 1.283 \text{ g/cm}^3$, $R = 4.84\%$, $R_w = 4.87\%$) were obtained, and a *trans*-influence series has been established for several ligands. Rotational isomers due to rotation about the Mo–alkylidene bond were observed for all compounds, and marked differences in rates of rotamer interconversion are observed for **1**, **2**, and **8**. Compounds **1** and **2** in the presence of AlCl_3 successfully catalyzed the ring-opening metathesis polymerization of cyclooctene and norbornylene and the oligomerization of 1,9-decadiene via acyclic diene metathesis polymerization.

Introduction

The chemistry of transition-metal–ligand multiple bonds is widely encountered throughout the literature, especially concerning high-oxidation-state metal alkylidene complexes and their role in olefin metathesis reactions.^{1–4} Our efforts have focused on developing and studying metal alkylidene compounds employing ancillary chelating ligands. Previous communications

from our group have described the function of hydridotris(pyrazolyl)borate (Tp) ligands⁵ in the stabilization of tungsten(VI) alkylidene complexes. The Tp ligand, serving as a template to bind and stabilize the metal center, has led to the development of neutral and cationic tungsten alkylidene complexes.^{6–8} These compounds serve as precursors to ring-opening metathesis polymerization (ROMP) and acyclic diene metathesis (ADMET)^{9,10} oligomerization catalysts in the presence of Lewis acid cocatalysts.

[⊗] Abstract published in *Advance ACS Abstracts*, March 1, 1995.

(1) Nugent, W. A.; Mayer, J. M. *Metal-Ligand Multiple Bonds*; Wiley-Interscience: New York, 1988.

(2) (a) Feldman, J.; Schrock, R. R. *Prog. Inorg. Chem.* **1991**, *39*, 1.
(b) Schrock, R. R. *J. Organomet. Chem.* **1986**, *300*, 249.

(3) Schrock, R. R.; Murdzek, J. S.; Bazan, G. C.; Robbins, J.; DiMare, M.; O'Regan, M. *J. Am. Chem. Soc.* **1990**, *112*, 3875.

(4) Schrock, R. R.; DePue, R. T.; Feldman, J.; Yap, K. B.; Yang, D. C.; Davis, W. M.; Park, L.; DiMare, M.; Schofield, M.; Anhaus, J.; Walborsky, E.; Evitt, E.; Kruger, C.; Betz, P. *Organometallics* **1990**, *9*, 2262.

(5) Trofimenko, S. *Acc. Chem. Res.* **1971**, *4*, 17.

(6) Blosch, L. L.; Abboud, K.; Boncella, J. M. *J. Am. Chem. Soc.* **1991**, *113*, 7066.

(7) Blosch, L. L.; Gamble, A. S.; Abboud, K.; Boncella, J. M. *Organometallics* **1992**, *11*, 2342.

(8) Gamble, A. S.; Boncella, J. M. *Organometallics* **1993**, *12*, 2814.

(9) Wagener, K. B.; Boncella, J. M.; Nel, J. G.; Duttweiler, R. P.; Hillmyer, M. A. *Makromol. Chem.* **1990**, *191*, 365.

(10) Wagener, K. B.; Boncella, J. M.; Nel, J. G. *Macromolecules* **1991**, *24*, 2649.

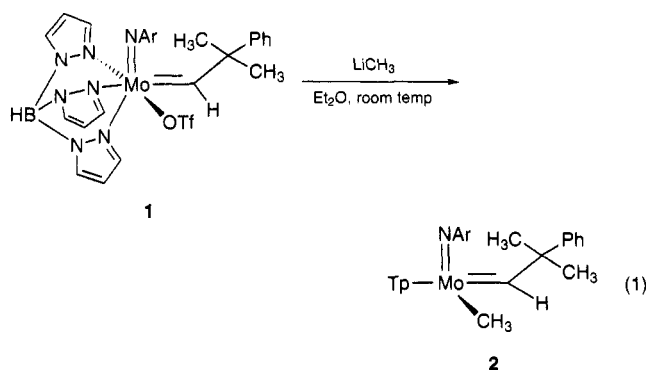
Recently we reported the synthesis, characterization, and crystal structure of a new molybdenum imido alkylidene complex, $\text{TpMo}(\text{CHC}(\text{CH}_3)_2\text{Ph})(\text{NAr})(\text{OTf})$ (**1**; Ar = 2,6-*i*-Pr-C₆H₃).^{11,12} Compound **1** has been a useful starting material for the synthesis of several neutral and cationic alkylidene complexes. These compounds are synthesized by displacing the triflate ligand to give compounds of the general formula $\text{TpMo}(\text{CHC}(\text{Me})_2\text{Ph})(\text{NAr})(\text{X})$.

In this paper, we report the synthesis of $\text{TpMo}(\text{CHC}(\text{CH}_3)_2\text{Ph})(\text{NAr})(\text{CH}_3)$ (**2**) by the alkylation of **1**. The methyl ligand of **2** can be abstracted by several methods to give solvent-bound, cationic alkylidene complexes with noncoordinating anions. Also, we report the direct formation of a cationic complex from the displacement of the triflate ligand of **1** by phosphine to give $[\text{TpMo}(\text{CHC}(\text{CH}_3)_2\text{Ph})(\text{NAr})(\text{P}(\text{CH}_3)_3)]^+[\text{OTf}]^-$ (**7**). Substitution of the electron-withdrawing triflate ligand with the π -donating methoxide ligand gives the alkylidene complex $\text{TpMo}(\text{CHC}(\text{CH}_3)_2\text{Ph})(\text{NAr})(\text{OCH}_3)$ (**8**) or the alkylidyne complex $\text{TpMo}(\text{CC}(\text{CH}_3)_2\text{Ph})(\text{NAr})(\text{OCH}_3)$ (**9**), depending on the method of preparation. The crystal structures of the related tautomers, compounds **8** and **9**, are presented. Rotational isomers arising from rotation about the metal-carbon double bond are observed for many of the reported alkylidene complexes. Also, the metathesis activity of compounds **1**, **2**, and the cationic alkylidenes is reported herein.

Results and Discussion

The stability imposed at the molybdenum metal center by the tridentate Tp ligand enables the modification of the $\text{TpMo}(\text{CHC}(\text{CH}_3)_2\text{Ph})(\text{NAr})$ template by varying the ligand in the sixth coordination site. Thus, we have prepared a number of new molybdenum imido alkylidene compounds from the parent compound **1** by displacing the labile triflate ligand. One goal of this research was to prepare cationic molybdenum alkylidenes and to observe how the increased electrophilicity of the metal center modifies the properties of these compounds. The general scheme that was employed for such a transformation was to abstract an alkyl group from a complex of the type $\text{TpMo}(\text{CHC}(\text{CH}_3)_2\text{Ph})(\text{NAr})(\text{alkyl})$ in the absence of a coordinating anion to give the desired cationic metal complex. By employing large, noncoordinating counterions, the open coordination site of the cationic complex should readily bind olefin substrates or coordinating solvent molecules. Similar schemes have been successful in preparing and isolating cationic catalysts for olefin-insertion polymerizations.^{13,14} Cationic tungsten alkylidenes have been prepared by using Brønsted acids of noncoordinating anions to protonate the complex followed by loss of the alkyl ligand.⁸

Synthesis and Characterization of $\text{TpMo}(\text{CHC}(\text{CH}_3)_2\text{Ph})(\text{NAr})(\text{CH}_3)$ (2**).** For the purposes of eventually preparing cationic alkylidenes, the alkylation of **1** with a methyl group proved to be the most facile route. The transmetalation of **1** with a moderate excess of methyl lithium in Et₂O at ambient temperature gave $\text{TpMo}(\text{CHC}(\text{CH}_3)_2\text{Ph})(\text{NAr})(\text{CH}_3)$ (**2**; eq 1) in good yield. Compound **2** exhibits marked air and moisture stability.



Compound **2** can be purified over neutral alumina and is stable as a solid in air indefinitely. Stirring **2** in THF with 1 equiv of H₂O showed no reaction. In *d*₈-toluene at 80 °C over 3.5 h, compound **2** decomposes, forming unidentified products.

The ¹H NMR spectrum of **2** at 22 °C is complicated by the chirality of the compound, resulting in nine distinct pyrazolyl ring proton resonances and diastereotopic neophyl methyl resonances. The alkylidene proton resonance is shifted upfield from that of **1** at 14.73 ppm to 13.11 ppm, and the ¹J_{CH} value observed in the ¹³C{¹H} spectrum is reduced slightly to 115 Hz. The methyl proton signal at 1.29 ppm is a sharp singlet, and the methyl carbon resonance at 18.0 ppm in the ¹³C NMR has a ¹J_{CH} value of 123 Hz. This ¹H-¹³C coupling constant is normal for sp³ C centers¹⁵ and does not suggest any interaction of the C-H σ bond with the metal center as is expected for a coordinatively and electronically saturated metal complex.¹⁶ The proton signals for the isopropyl groups of the arylimido ligand are broadened and occur in a 6:3:3 ratio, suggesting sterically hindered rotation about the carbon-nitrogen bond. Hindered rotation has been observed in other Tp arylimido alkylidenes.^{7,11}

Protonation of **2** with 1 equiv of triflic acid in C₆D₆ resulted in a quantitative conversion to $\text{TpMo}(\text{CHC}(\text{CH}_3)_2\text{Ph})(\text{NAr})(\text{OTf})$ (**1**) and methane. Addition of a second equivalent of triflic acid causes loss of the alkylidene proton resonance and formation of unidentified decomposition products. In the presence of 1 equiv of H₂O, treatment of **2** with triflic acid in Et₂O only yielded **1**.

Synthesis of Cationic Molybdenum Alkylidene Complexes. Removing the methyl group from compound **2** led to several cationic molybdenum alkylidene complexes. Three methods were successfully employed to remove the methyl ligand: protonation by the acid of a noncoordinating anion, abstraction by the trityl cation, and abstraction by a boron-containing Lewis acid. The anions used were fluorinated aryl borates that have been used as noncoordinating anions to stabilize group 4 metallocene cations.^{13,14}

The addition of tetrakis(3,5-bis(trifluoromethyl)phenyl)boric acid (HBAr'₄·2Et₂O, Ar' = 3,5-C₆H₃(CF₃)₂)¹⁷ to a Et₂O solution of **2** at -78 °C gave the thermally un-

(13) Chien, J. C. W.; Tsai, W.-M.; Rausch, M. D. *J. Am. Chem. Soc.* **1991**, *113*, 8570.

(14) Yang, X.; Stern, C. L.; Marks, T. J. *J. Am. Chem. Soc.* **1991**, *113*, 3623.

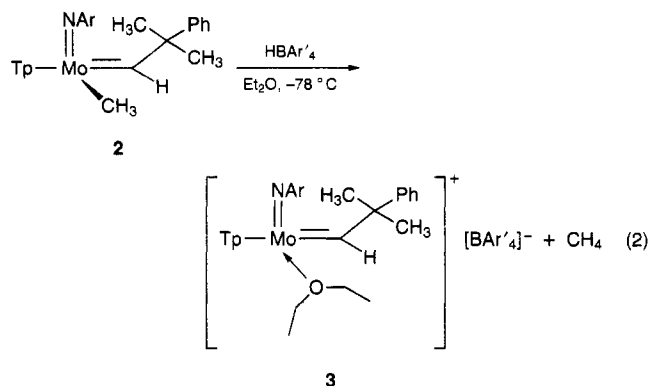
(15) Silverstein, R. M.; Bassler, G. C. *Spectrometric Identification of Organic Compounds*; Wiley: New York, 1981.

(16) Collman, J. P.; Hegedus, L. S.; Norton, J. R.; Finke, R. G. *Principles and Applications of Organotransition Metal Chemistry*, 2nd ed.; University Science Books: Mill Valley, CA, 1987; p 989.

(11) Vaughan, W. M.; Abboud, K. A.; Boncella, J. M. *J. Organomet. Chem.* **1995**, *485*, 37.

(12) Vaughan, W. M.; Boncella, J. M.; Abboud, K. A. *Acta. Crystallogr., Sect. C* in press.

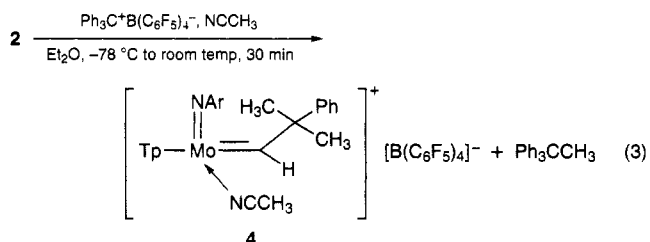
stable cation $[\text{TpMo}(\text{CHC}(\text{CH}_3)_2\text{Ph})(\text{NAr})(\text{Et}_2\text{O})][\text{BAR}'_4]$ (**3**; eq 2) as a brown oily solid and methane. Compound



3 is insoluble in hydrocarbons and benzene, and the cation decomposes within hours at room temperature in CD_2Cl_2 .

The ^1H NMR spectrum of **3** indicates the highly electrophilic nature of this cationic complex. The chemical shift of the alkylidene proton is at δ 14.79 and is shifted significantly downfield from that of compound **2**. A diethyl ether molecule is tightly bound to the metal center, as indicated by the ABX_3 coupling pattern for the methylene protons. The ether molecule freely rotates on the NMR time scale, interchanging the two sets of diastereotopic methylene protons. At room temperature, four doublets and two septets are observed for the isopropyl groups of the arylimido ring, indicating that the C–N bond of the arylimido group does not rotate on the NMR time scale.

Using the trityl cation to abstract the methyl ligand,¹³ the reaction of **2** and trityl tetrakis(pentafluorophenyl)borate in the presence of excess acetonitrile gave $[\text{TpMo}(\text{CHC}(\text{CH}_3)_2\text{Ph})(\text{NAr})(\text{NCCH}_3)][\text{B}(\text{C}_6\text{F}_5)_4]$ (**4**; eq 3) and

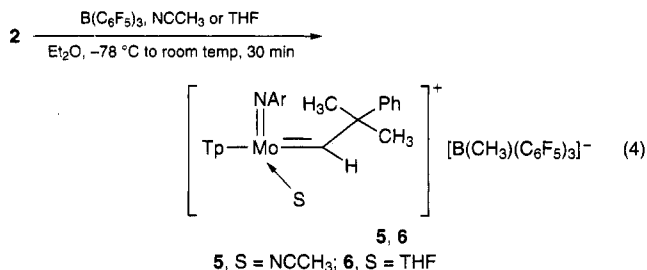


Ph_3CCH_3 . The cationic product was obtained as a yellow-brown solid which was insoluble in benzene and saturated hydrocarbons. Efforts to obtain crystals of **4** failed, but precipitation from Et_2O afforded an analytically pure solid.

The ^1H NMR spectrum of **4** at -40.0°C shows two distinct alkylidene rotamers in equilibrium which is *ca.* 10% in the minor isomer. The chemical shifts of the alkylidene protons of the major and minor isomers are shifted downfield relative to the neutral complexes and occur at δ 14.47 and 15.28, respectively. The presence of the tetrakis(pentafluorophenyl)borate anion is confirmed by its broad doublets in the ^{13}C NMR spectrum. The ^1H and ^{13}C NMR resonances of the Tp, arylimido, and alkylidene ligands are similar to those observed in the parent compounds, and the new resonance for the acetonitrile ligand is prominent at 2.35 ppm in the proton spectrum.

(17) Brookhart, M.; Grabt, B.; Volpe, A. F., Jr. *Organometallics* **1992**, *11*, 3920.

The Lewis acid tris(pentafluorophenyl)boron, $\text{B}(\text{C}_6\text{F}_5)_3$, has been shown to abstract alkyl ligands, forming cationic metal complexes.¹⁴ The addition of $\text{B}(\text{C}_6\text{F}_5)_3$ to an Et_2O solution of **2** in the presence of acetonitrile gives the compound $[\text{TpMo}(\text{CHC}(\text{CH}_3)_2\text{Ph})(\text{NAr})(\text{NCCH}_3)][\text{B}(\text{CH}_3)(\text{C}_6\text{F}_5)_3]$ (**5**; eq 4), in which the Lewis acid

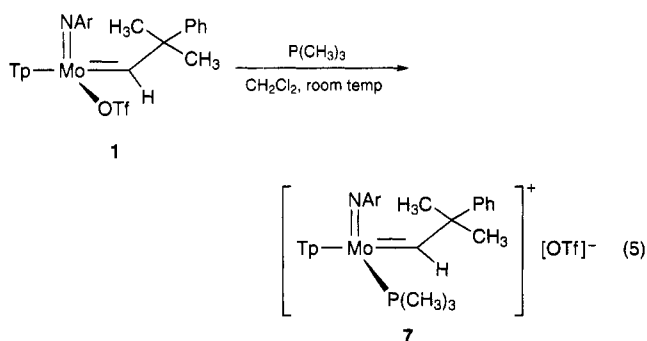


abstracts the methyl ligand to give methyltris(pentafluorophenyl)borate as the noncoordinating anion. The cationic product was obtained as a yellow-brown solid which was insoluble in hydrocarbons. Efforts to obtain crystals of **5** failed, but precipitation from Et_2O afforded an analytically pure solid.

Similar to **4**, compound **5** is a mixture of two rotamers which is composed of *ca.* 10% of the minor rotamer. The alkylidene proton resonances are deshielded with respect to the neutral complexes and occur at δ 14.53 and 15.32 for the major and minor rotamers, respectively. The resonance of the methyl protons of the borate anion is a broad singlet at 0.47 ppm. The remaining NMR spectral data for **5** are similar to those data for **4**. This is not surprising, since the only difference between **4** and **5** is the substitution of a methyl group for a perfluorophenyl group on the borate anion.

The THF-coordinated analogue of **5**, $[\text{TpMo}(\text{CHC}(\text{CH}_3)_2\text{Ph})(\text{NAr})(\text{THF})][\text{B}(\text{CH}_3)(\text{C}_6\text{F}_5)_3]$ (**6**; eq 4), was also prepared and isolated as was compound **5**. NMR spectral data of **6** are similar to those of **5**, and the coordinated THF ligand is observed to be rotating slowly on the NMR time scale, showing two sets of diastereotopic methylene proton triplets at δ 3.65 and 3.55.

We later found that a cationic complex, $[\text{TpMo}(\text{CHC}(\text{CH}_3)_2\text{Ph})(\text{NAr})(\text{P}(\text{CH}_3)_3)][\text{OTf}]$ (**7**; eq 5), could be prepared directly from compound **1** in quantitative yield by the addition of trimethylphosphine at room temperature. Compound **7** is isolated as a pale yellow powder,



and it is soluble in methylene chloride and insoluble in pentane and benzene.

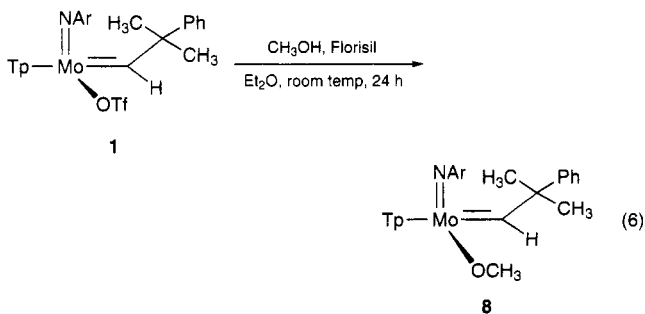
The ^1H NMR spectrum of **7** in CD_2Cl_2 at -20°C is comparable to those of its parent compound **1** and the other cationic complexes **3–6**. The distinctive feature of the ^1H NMR spectrum of **7** is the $^3J_{\text{PH}}$ coupling to the bound phosphine observed for the alkylidene protons of the two rotamers. The chemical shifts for the

alkylidene proton for the major rotamer (δ 14.51, 5.4 Hz, 84%) and the minor rotamer (δ 14.73, 6.2 Hz, 16%) are shifted slightly downfield from that of **1** (δ 14.44). The ^{13}C resonance for the alkylidene α -carbon of the major rotamer is also a doublet (δ 335.9, $^2J_{\text{PC}} = 17.6$ Hz). The ^{31}P NMR signals for the coordinated phosphine ligand are observed at -2.83 and -7.81 ppm for the major and minor rotamers, respectively. The ^{19}F signal for the ionic triflate (δ -78.8 vs H_3PO_4) is slightly upfield from the signal for the covalently bound triflate ligand of **1** (δ -77.7 vs CFCl_3).¹⁸ Evidence for an ionic triflate species in **7** is best seen by a comparison of its vibrational spectrum with that of **1**.¹⁹ The S=O stretching frequency of the free triflate anion of **7** (1268 cm^{-1}) is split into two observable stretching modes in **1** (1332 , 1202 cm^{-1}). Also, a S=O stretch at 1048 cm^{-1} for **7** is shifted to 1011 cm^{-1} for **1**.²⁰

Obviously, the ability of the triflate ligand of **1** to be displaced by trimethylphosphine suggests that the triflate ligand is not as tightly bound as originally considered, and possibly an equilibrium exists between the bound triflate complex (**1**) and a base-free, ionic triflate complex. Such an equilibrium would lie markedly toward the coordinatively and electronically saturated complex **1**, but in the presence of the strongly coordinating phosphine ligand, the base-free cationic complex is consumed to give **7**. Attempts to observe adducts analogous to **7** in CD_2Cl_2 by ^1H NMR by mixing **1** with 30 equiv of ethylene or 50 equiv of phenylacetylene were unsuccessful, showing only unreacted **1**.

Synthesis and Characterization of $\text{TpMo}(\text{CHC}(\text{CH}_3)_2\text{Ph})(\text{NAr})(\text{OCH}_3)$ (8**).** So far, the compounds of the general formula $\text{TpM}(\text{CHC}(\text{CH}_3)_2\text{R})(\text{NAr})(\text{X})$ ($\text{M} = \text{Mo}, \text{W}$; $\text{R} = \text{CH}_3, \text{C}_6\text{H}_5$; $\text{X} = \text{Cl}, \text{Br}, \text{OTf}, \text{pyrazolide}, \text{alkyl}$) described in this paper and elsewhere have X being electron-withdrawing substituents and/or poor π donors.^{6-8,11,21} We were interested in replacing the triflate ligand in compound **1** with a better π -donating substituent, namely methoxide, to observe how this substitution would effect the chemistry of these molecules.

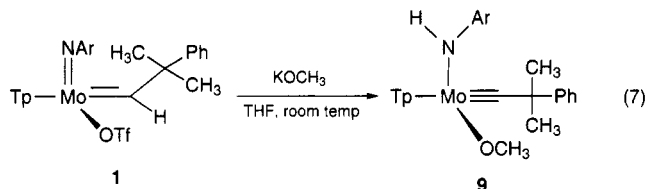
Similar to the hydrolysis of **1** to give $\text{TpMo}(\text{CH}_2\text{C}(\text{CH}_3)_2\text{Ph})(\text{NAr})(\text{O})$,¹¹ $\text{TpMo}(\text{CHC}(\text{CH}_3)_2\text{Ph})(\text{NAr})(\text{OCH}_3)$ (**8**; eq 6) was prepared by the methanolysis of **1** stirred in the presence of Florisil. Extraction and



recrystallization of **8** afforded yellow crystals. An unidentified insoluble white powder remained from the pentane extraction; however, a low-resolution mass spectrum indicated the presence of molybdenum.

The ^1H NMR spectrum of compound **8** at $22\text{ }^\circ\text{C}$ is comparable to that of its parent compound. The spectrum has nine distinct pyrazole proton resonances and diastereotopic methyl groups for the neophylidene ligand and isopropyl groups of the arylimido ligand. The broadening of the isopropyl group proton resonances suggests hindered rotation about the nitrogen-aryl bond due to the steric demands of the Tp ligand. The chemical shift of the alkylidene proton is δ 13.14. This is one of the highest field shifts for these molybdenum alkylidene compounds, indicating a more electron-rich metal center. The new resonance corresponding to the methyl protons of the methoxide ligand is found at δ 4.60. Absorptions due to the methoxide ligand are also observed in the IR spectrum at 2778.2 and 1081.8 cm^{-1} , corresponding to the methoxy C-H and C-O stretches, respectively.

Synthesis and Characterization of $\text{TpMo}(\text{CC}(\text{CH}_3)_2\text{Ph})(\text{NAr})(\text{OCH}_3)$ (9**).** In a separate attempt to prepare $\text{TpMo}(\text{CHC}(\text{CH}_3)_2\text{Ph})(\text{NAr})(\text{OCH}_3)$, compound **1** was allowed to react with 1 equiv of potassium methoxide in THF at room temperature. The solution color changed from yellow to red-orange, and recrystallization of the product from pentane gave orange crystals. A ^1H NMR spectrum of the product showed loss of the alkylidene resonance and the appearance of two broad singlets at δ 9.55 and 10.26 and two methoxide singlets at δ 5.11 and 4.98. A ^{13}C $\{^1\text{H}\}$ NMR spectrum confirmed the presence of sp-hybridized alkylidyne carbons at δ 301.7 and 298.7, and the structure was determined to be the major and minor rotamers of $\text{TpMo}(\text{CC}(\text{CH}_3)_2\text{Ph})(\text{NAr})(\text{OCH}_3)$ (**9**; eq 7). This mo-



lybdenum amido alkylidyne complex is formally the tautomer of **8**. The major and minor isomers arise from rotational isomers of the molybdenum-amide bond. Variable-temperature ^1H NMR experiments showed that the two amide proton resonances coalesce at $65\text{ }^\circ\text{C}$. This corresponds to an activation energy, ΔG^\ddagger , of 15.7 kcal/mol. Cooling the solution to room temperature reestablishes the same equilibrium ratio of rotamers and shows that ΔG° for the two rotamers is 0.8 kcal/mol. The IR spectrum of **9** reveals a single sharp absorption at 3308.7 cm^{-1} for the N-H stretch of the amido ligand.

Since compounds **8** and **9** are formally related by transfer of the alkylidene proton to the nitrogen of the imido ligand, we tried to convert **8** to **9**. Compound **8** was stable toward tautomerization for 1 week in d_8 -toluene. Photolysis, continued heating at $110\text{ }^\circ\text{C}$, and addition of Lewis bases (NEt_3 , $\text{P}(\text{CH}_3)_3$) did not cause tautomerization of **8** to give **9**. Only the addition of excess potassium methoxide caused the proton to transfer from the alkylidene to the imido ligand. To avoid adding excess methoxide, a THF solution of 0.9 equiv of potassium methoxide was added dropwise to **1**. However, only **9** resulted from this method of addition.

The experimental results concerning the formation of **9** and orbital considerations suggest that the mechanism

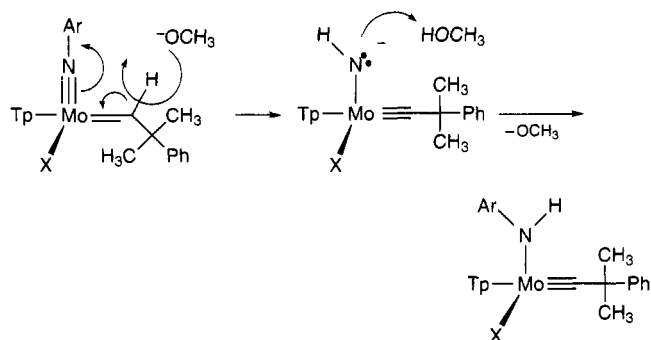
(18) Wu, T. K.; Pruckmayr, G. *Macromolecules* **1975**, *8*, 77.

(19) Lawrence, G. *Chem. Rev.* **1986**, *86*, 17.

(20) Schnabel, R. C.; Roddick, D. M. *Organometallics* **1993**, *12*, 704.

(21) Blossch, L. L.; Gamble, A. S.; Boncella, J. M. *J. Mol. Catal.* **1992**, *76*, 229.

Scheme 1



for the formation of **9** involves a methoxide-mediated proton transfer.

In Scheme 1, a methoxide anion deprotonates the alkylidene ligand of either the starting material **1** or compound **8**, forming an anionic molybdenum species with the negative charge localized on the imido nitrogen. Following this step is a reprotonation of the metal complex at the nitrogen by methanol. The reverse reaction to deprotonate the amido ligand and re-form the alkylidene is less likely due to the stability of the strong metal-carbon triple bond. Also, the amide would be expected to be less acidic in complexes with good π donors versus those with electron-withdrawing triflates. The conversion of **8** to **9** is the reverse of the proton transfer reaction observed by Schrock and co-workers for the NEt_3 -catalyzed conversion of $\text{M}(\text{NHAr})(\text{C}-t\text{-Bu})(\text{dme})\text{Cl}_2$ to $\text{M}(\text{NAr})(\text{CH}-t\text{-Bu})(\text{dme})\text{Cl}_2$ ($\text{M} = \text{W}, \text{Mo}$). They observed that the same reaction was impossible when the chlorides of the metal amido alkylidyne complexes were replaced with hexafluoro-*tert*-butoxide ligands.^{3,4,22}

Attempts to isolate derivatives of **8** with the stoichiometry $\text{TpMo}(\text{CC}(\text{CH}_3)_2\text{Ph})(\text{NHAr})(\text{X})$ ($\text{X} = \text{N}(\text{CH}_3)_2$, *O-p*-tol, *OPh*) were unsuccessful, giving complex mixtures of imido-alkylidene, amido-alkylidyne, and other species which have proven impossible to separate.

Crystal Structure Determination of 8 and 9. The structure of compound **8** was determined by X-ray diffraction methods, and a thermal ellipsoid plot is found in Figure 1. Selected bond distances and angles are given in Table 1. The structure consists of well-separated molecules with the coordination geometry around the molybdenum atom in **8** being a distorted octahedron. The geometric constraints of the facially bound Tp ligand force the alkylidene, imido, and methoxide ligands to be mutually *cis*.²³ The N-Mo bond lengths of the chelating pyrazole rings range from 2.327(10) to 2.232(8) Å and are consistent with the decreasing *trans* influence of the ligands imido > alkylidene > methoxide.¹

The *cis* orientation of the arylimido ligand and alkylidene ligand allows for maximum $d\pi$ - $p\pi$ bonding between the molybdenum and the multiply bonded ligands.¹ The Mo-N1 bond length of 1.741(9) Å and Mo-N1-C11 bond angle of 169.7(8)° are within normal ranges for molybdenum imido complexes in which the molybdenum-nitrogen bond can be considered to be triply bound with the lone pair of the nitrogen donating

Table 1. Bond Lengths (Å) and Angles (deg) for the Non-H Atoms of Compound **8**

1	2	3	1-2	1-2-3
O1	Mo	N1	1.960(7)	100.6(4)
O1	Mo	N2		155.1(4)
O1	Mo	N4		81.7(3)
O1	Mo	N6		84.9(3)
N1	Mo	N2	1.741(9)	99.2(4)
N1	Mo	N4		168.5(4)
N1	Mo	N6		90.9(4)
N1	Mo	C1		102.1(5)
N2	Mo	N4	2.232(8)	76.0(4)
N2	Mo	N6		79.8(3)
N2	Mo	C1		90.5(4)
N4	Mo	N6	2.327(10)	78.0(3)
N4	Mo	C1		88.5(5)
N6	Mo	C1	2.295(8)	165.0(4)
C1	Mo	O1	1.963(10)	100.0(4)
C32	O1	Mo	1.37(2)	130.1(7)
C11	N1	Mo	1.390(14)	169.7(8)
C4	C1	Mo	1.56(2)	136.8(10)

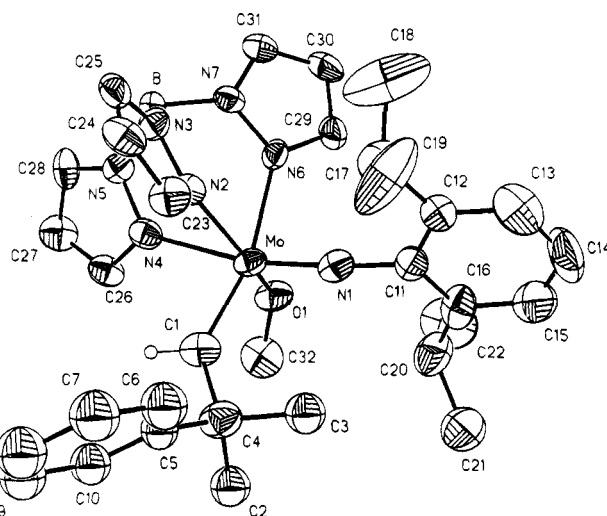


Figure 1. Molecular structure of **8**, showing 50% thermal ellipsoids and the atomic labeling scheme.

to an empty $d\pi$ orbital of the d^0 molybdenum atom. The Mo-C1 bond length, 1.963(10) Å, lies within the expected range for molybdenum-carbon double bonds, and the $-\text{C}(\text{CH}_3)_2\text{Ph}$ group of the alkylidene is in the *syn*, or *s-cis*, orientation with respect to the imido ligand. The steric requirements of the bulky arylimido group force the Mo-C1-C4 angle to open to 136.8(10)°. The *syn* orientation is preferred to the *anti* orientation due to the apparently unfavorable steric interaction of wedging the $-\text{C}(\text{CH}_3)_2\text{Ph}$ group between two pyrazole rings of the Tp ligand.

The crystal structure of compound **9** was also determined by X-ray diffraction methods, and a thermal ellipsoid plot is found in Figure 2. Selected bond distances and angles are given in Table 2. Similar to **8**, the geometry around the molybdenum is a distorted octahedron dictated by the geometric and electronic constraints of the Tp ligand. The N-Mo bond lengths of the chelating pyrazole rings range from 2.386(4) to 2.235(4) Å and are also consistent with the decreasing *trans* influence of the ligands alkylidyne > amido > methoxide.¹ The Mo-C1 bond length and angle (1.765(4) Å, 177.2(4)°) are within accepted ranges for d^0 molybdenum-alkylidyne bonds, and the sp -hybridized alkylidyne carbon donates to two metal d orbitals of π symmetry. Thus, compound **9** is formally a 16-electron

(22) Schrock, R. R.; DePue, R. T.; Feldman, J.; Schaverien, C. J.; Dewan, J. C.; Liu, A. H. *J. Am. Chem. Soc.* **1988**, *110*, 1423.

(23) Hinkle, R. J.; Stang, P. J.; Arif, A. M. *Organometallics* **1993**, *12*, 3510.

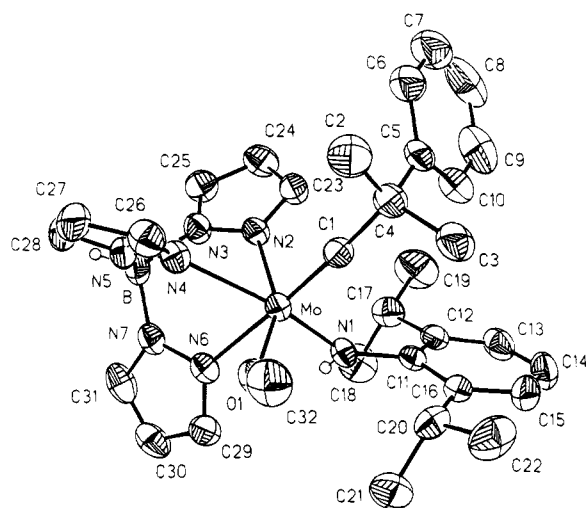


Figure 2. Molecular structure of **9**, showing 50% thermal ellipsoids and the atomic labeling scheme.

Table 2. Selected Bond Lengths (Å) and Angles (deg) for the Non-H Atoms of Compound **9**

1	2	3	1-2	1-2-3
O1	Mo	N1	1.928(3)	102.9(2)
O1	Mo	N2		155.46(12)
O1	Mo	N4		83.56(14)
O1	Mo	N6		85.36(14)
N1	Mo	N2	1.952(3)	94.2(2)
N1	Mo	N4		160.7(2)
N1	Mo	N6		80.48(14)
N1	Mo	C1		97.6(2)
N2	Mo	N4	2.235(4)	74.87(13)
N2	Mo	N6		80.24(14)
N2	Mo	C1		93.7(2)
N4	Mo	N6	2.265(3)	81.95(12)
N4	Mo	C1		99.0(2)
N6	Mo	C1	2.386(4)	173.5(2)
C1	Mo	O1	1.765(4)	101.2(2)
C32	O1	Mo	1.398(7)	131.7(3)
C11	N1	Mo	1.419(5)	141.1(3)
C4	C1	Mo	1.510(6)	177.2(4)
H1	N1	C11	0.76(4)	109(3)
H1	N1	Mo		109(3)

complex with one $d\pi$ metal orbital available for electron donation from the arylimido and/or methoxide ligands.

The molybdenum–arylamido bond length and the Mo–N–C angle (1.952(3) Å, 141.1(3)°) differ markedly from the triply bound and linear arylimido ligand of **8**. The amido proton was located for compound **9**, and the geometry about the amido nitrogen is essentially planar. This planar geometry is consistent with the lone pair of the nitrogen being donated to the empty metal $d\pi$ orbital, making compound **9** an 18-electron complex. Notably, the orientation of the arylimido ring is that of the *syn* rotamer in the solid-state structure with the ring situated toward the alkylidyne ligand, though in solution both rotamers are present. The *syn* rotamer is assumed to be the major rotamer in solution. The molybdenum–methoxide bond in compound **9** is slightly shorter than the Mo–O bond of compound **8** by 0.032 Å and may indicate a higher degree of π bonding between the oxygen atom in **9** versus **8**. However, as evidenced by the geometry about the nitrogen and the respective *trans* influence of the amido and the methoxide ligands, the amide is a better π donor than the methoxide.

The values for the molybdenum–pyrazole bond distances in these two compounds in addition to the values from other related Tp molybdenum compounds pub-

lished elsewhere^{11,12} make it possible to rank a number of ligands with respect to their *trans* influence: alkylidyne \approx oxo $>$ imido \approx alkylidene $>$ amido $>$ alkoxy $>$ alkyl \approx μ -oxo $>$ triflate.

Rotational Isomerism of the Molybdenum–Alkylidene Bond. Rotational isomers are observed for many of the compounds reported in this paper. These isomers arise from restricted rotation about the molybdenum–alkylidene double bond and result in *syn* and *anti* rotamers with the neophyl group oriented toward and away from the imido ligand, respectively. Rotational studies for other metal–alkylidene complexes have also been reported in the literature, and electronic effects and orbital considerations best describe the energetic differences between the related *syn* and *anti* rotamers.^{24–27} Interestingly, it has been reported that the different alkylidene orientations of Mo(ChC(CH₃)₂Ph)(NAr)(OC(CH₃)(CF₃)₂)₂ can have profound effects on the rates of olefin metathesis.^{25,26} Due to the unique stabilizing ability of the Tp ligand versus the more active alkylidene complexes reported, extensive kinetic studies have been possible for a number of tungsten alkylidene complexes.²⁸ Here we report preliminary studies and evidence for rotational isomerism in several Tp molybdenum alkylidenes.

Irradiating TpMo(ChC(CH₃)₂Ph)(NAr)(OTf) (**1**) with a sun lamp at -50 °C for 1 h generated a minor rotamer in a 1:4 ratio with the major rotamer. The alkylidene proton signal for this minor rotamer was observed at δ 14.82, which is 0.09 ppm downfield from the major rotamer. The $^1J_{CH}$ value of the minor rotamer is 126 Hz, compared to 120 Hz for the major rotamer. Large coupling constants (145–155 Hz) have been observed for the *anti* rotamers of four-coordinate alkylidene complexes, and differences in $^1J_{CH}$ values have been used to assign *syn/anti* orientations.^{25,26} The electronically and coordinatively saturated nature of **1** minimizes interaction of the alkylidene C–H bond with the metal center that would give rise to large differences in coupling constants for the two rotamers. The major rotamer was determined to be the *syn* rotamer by 1H NOE differences spectroscopy. The rates of thermal conversion of the *anti* rotamer to the *syn* rotamer were measured from $+40.0$ to $+60.0$ °C. The activation parameters for this unimolecular process were determined to be $\Delta H^\ddagger = +21.5 \pm 0.3$ kcal/mol and $\Delta S^\ddagger = -8.9 \pm 0.8$ eu. The reduction of entropy in the transition state is consistent with restriction of ancillary bond rotation during alkylidene rotation.

For TpMo(ChC(CH₃)₂Ph)(NAr)(CH₃) (**2**), only one rotamer is observed at room temperature. Irradiation of **2** in *d*₈-toluene by a sun lamp at -50 °C generated a new rotamer, observed in the low-temperature 1H NMR spectrum at δ 13.78, downfield from the major rotamer at δ 13.04. The rate of thermal conversion of the minor rotamer to the major rotamer is 3.7×10^{-4} s⁻¹ at -20.0 °C. Similar rates were found for **1** at higher temperatures of $+40.0$ and $+50.0$ °C.

The cationic molybdenum alkylidene complexes, compounds **4**–**7**, each have two rotamers present at equi-

(24) Schrock, R. R.; Crowe, W. E.; Bazaz, G. C.; DiMare, M.; O'Regan, M. B.; Schofield, M. H. *Organometallics* **1991**, *10*, 1832.

(25) Oskam, J. H.; Schrock, R. R. *J. Am. Chem. Soc.* **1992**, *114*, 7588.

(26) Oskam, J. H.; Schrock, R. R. *J. Am. Chem. Soc.* **1993**, *115*, 11831.

(27) Cundari, T. R.; Gordon, M. S. *Organometallics* **1992**, *11*, 55.

(28) Bloesch, L. L. Ph.D. Thesis, University of Florida, 1993.

librium at ambient temperatures. The irradiation of $[\text{TpMo}(\text{CHC}(\text{CH}_3)_2\text{Ph})(\text{NAr})(\text{NCCH}_3)][\text{B}(\text{C}_6\text{F}_5)_4]$ (**4**) by a sun lamp at -40°C increased the population of the minor rotamer to 32%, enabling ^1H NMR peak assignments for both isomers. The most notable difference between the spectra of the two rotamers is the 0.8 ppm downfield shift for the alkylidene proton resonance of the minor rotamer versus that of the major rotamer. The rotamer distribution of **4** returned to equilibrium over time upon warming the sample. Irradiation of compounds **3**, **5**, **6**, and **7** was not performed.

Rotamers for $\text{TpMo}(\text{CHC}(\text{CH}_3)_2\text{Ph})(\text{NAr})(\text{OCH}_3)$ (**8**) were not observed at room temperature. Photolysis at -50°C for 90 min in *d*₈-toluene using a sun lamp generated a minor rotamer (δ 13.44, 12.5%) which isomerizes thermally to the major rotamer very rapidly. The rate of thermal conversion of the minor rotamer to the major rotamer was measured at -40.0°C with $k = 3.7 \times 10^{-4} \text{ s}^{-1}$. From the crystal structure of **8** discussed above, the major rotamer in solution is reasoned to be the syn rotamer. This rate compares with the anti to syn thermal isomerization rate of compound **1** at $+40.0^\circ\text{C}$, where $k = 8.2 \times 10^{-5} \text{ s}^{-1}$. The extremely fast rates of the alkylidene rotation of **8** made repeated rate measurements at low temperatures difficult, and thus activation parameters were not determined for the compound.

The marked difference in the rates of alkylidene rotation for compounds **1**, **2**, and **8** is best understood by considering the competition for the empty $d\pi$ orbitals of molybdenum by the $p\pi$ orbitals of the alkylidene, imido, and X groups, where X is a triflate, methyl, or methoxide ligand, respectively. In the ground state, the alkylidene carbon p_y orbital interacts with the metal d_{xy} orbital, and the p_x and p_y orbitals of the imido ligand interact with the metal d_{xz} and d_{yz} orbitals, respectively. In the transition state, where the alkylidene ligand is rotated 90° , the carbon $p\pi$ orbital is of the appropriate symmetry to compete with the imido p_x orbital for the metal d_{xz} orbital. Rehybridization of the nitrogen atom allows the filled alkylidene $p\pi$ orbital to fully donate to the empty d_{xz} orbital, thus lowering the barrier to the transition state. Such a scheme has been proposed and supported by *ab initio* calculations for four-coordinate tungsten and molybdenum imido alkylidenes.^{24,27}

The Tp ligand system employed in compounds **1**, **2**, and **8** force the alkylidene, imido, and X ligands to be oriented mutually *cis*. For ligands X with π -donor capabilities, the bonding situation described above is further complicated. Considering **8**, when X is a π -donating methoxide, a $p\pi$ orbital of oxygen can interact with either the d_{yz} or the d_{xy} orbitals, but not the d_{xz} orbital. Interaction of the oxygen p_z orbital with the d_{yz} orbital competes only with a metal-imido π -bond, a bond that is unaffected during alkylidene rotation. Shown in Figure 3, interaction of the oxygen p_x orbital with the d_{xy} orbital competes directly with the metal-alkylidene π bond in the ground state. Such an interaction should raise the ground-state energy of the metal-alkylidene bond, resulting in a decrease in the barrier for alkylidene rotation. The kinetic data for alkylidene rotation in **8** versus that in **1** and **2** support this argument. A similar explanation was offered to describe changes in activation barriers for alkylidene rotation due to changes in the ancillary ligands for d^0 ,

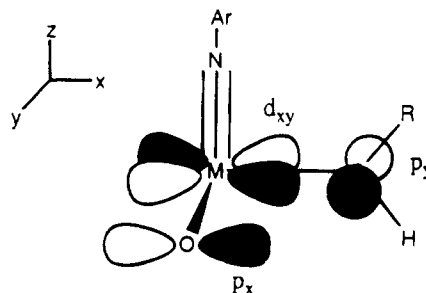


Figure 3. Orbital diagram showing competitive donation to the metal d_{xy} orbital by the alkylidene and methoxide π electrons.

five-coordinate $\text{W}(\text{CHR})(\text{OCH}_2-t\text{-Bu})_n\text{X}_{4-n}$ complexes.²⁹ Other reports regarding alkylidene rotation rates for molybdenum arylimido neopentylidenes also show increased rotational rates as alkoxide substituents become more electron donating, as in the series $\text{OR} = \text{OC}(\text{CH}_3)_3 > \text{OC}(\text{CH}_3)_2(\text{CF}_3) > \text{OC}(\text{CH}_3)(\text{CF}_3)_2 > \text{OC}(\text{CF}_3)_2(\text{CF}_2\text{CF}_2\text{CF}_3)$.^{25,26} Such a relationship is consistent with our finding for the relative rates of rotation for the series $\text{X} = \text{OCH}_3 > \text{CH}_3 > \text{OSO}_2\text{CF}_3$.

Polymerization Studies. Compound **1** is inert toward the metathesis of neat cyclooctene or 1,9-decadiene, and no polymerization was observed for **1** and 500 equiv of norbornylene in *o*-dichlorobenzene at 80°C . However, in the presence of the Lewis acid AlCl_3 , **1** quantitatively catalyzed the ring-opening metathesis polymerization of cyclooctene. With a 1:6:500 mixture of **1**, AlCl_3 , and neat cyclooctene, poly(octenamer) ($M_n = 57\,000$, $M_w/M_n = 1.30$) was formed. This result compares with that for the tungsten analogue of **1**, which quantitatively polymerizes cyclooctene in the presence of a Lewis acid.⁷

A mixture of **1**, AlCl_3 , and 1,9-decadiene at 90°C under static vacuum only dimerized a small fraction of the monomer to give a degree of polymerization of 2.3 before the catalyst became inactive. The stepwise fashion of ADMET condensation polymerizations require quantitative conversion ($>99\%$) of end groups to achieve high polymer. The tungsten analogue of **1** shows very little conversion of 1,9-decadiene to dimer. This result that molybdenum is more active than tungsten for the metathesis of terminal olefins agrees with other reports.^{3,7,22,30,31}

Compound **2** in the presence of AlCl_3 polymerized norbornylene to give a quantitative yield of poly(norbornylene) in toluene at room temperature. With a 1:7:500 mixture of **2**, AlCl_3 , and neat norbornylene, poly(norbornylene) with $M_n = 75\,000$ and $M_w/M_n = 1.8$ was formed. A related compound, $\text{TpW}(\text{CHC}(\text{CH}_3)_3)(\text{NAr})(\text{CH}_2\text{C}(\text{CH}_3)_3)$, also catalyzes the ROMP of cyclooctene under similar conditions.⁸

As with **1**, compound **2** and AlCl_3 did not successfully polymerize 1,9-decadiene via ADMET. With a 1:5:500 mixture of **2**, AlCl_3 , and neat 1,9-decadiene, only 7% of the monomer was converted to dimer during 8 h of stirring under static vacuum.

Attempts to trap and isolate any unsaturated metal complex from the catalytic mixture of **1** or **2** and AlCl_3

(29) Kress, J.; Osborn, J. A. *J. Am. Chem. Soc.* **1987**, *109*, 3953.

(30) Patton, J. T.; Boncella, J. M.; Wagener, K. B. *Macromolecules* **1992**, *25*, 3862.

(31) Wagener, K. B.; Patton, J. T. *Macromolecules* **1993**, *26*, 249.

with $P(CH_3)_3$ were unsuccessful. Observation of **1** or **2** with $AlCl_3$ in C_6D_6 by 1H NMR initially gave a complex mixture, and after several days free pyrazole was observed.

Lewis acids are proposed to play a role in generating a four-coordinate cationic active catalyst in $W(CHR)(OCH_2R)_2X_2/Al_2X_6$ metathesis systems.^{32,33} Also, $W(O)(CHC(CH_3)_3)(PEt_3)_2Cl_2/AlCl_3$ metathesizes olefins while the five-coordinate, neutral complex $W(O)(CHC(CH_3)_3)(PEt_3)Cl_2$ is an active catalyst in the absence of a Lewis acid.³⁴ In contrast to a mechanism involving the Lewis acid simply removing the triflate or methyl ligand of **2** or **3** to generate a five-coordinate, cationic active catalyst, no metathesis activity is seen for the solvent-bound, cationic complexes **3** and **4**. Contributing to the inactivity of the cationic complexes, the high electrophilicity of the metal center does not allow dissociation of the bound solvent molecule to open a coordination site on these electronically and coordinatively saturated compounds. Heating a CD_2Cl_2 solution of **4** pressurized with ethylene at 60 °C for 24 h showed no reaction or loss of acetonitrile.

Though five-coordinate metathesis catalysts are known,^{32,34} other reported five-coordinate complexes have coordinated bases that are most likely lost to give four-coordinate, active catalytic species.^{35,36} We propose that though the role of the Lewis acid may include abstraction of a triflate or methyl ligand to give a five-coordinate, cationic complex, the Lewis acid also reacts with the Tp ligand system and removes a pyrazole ring from the coordination sphere of molybdenum. This would result in a four-coordinate, 14-electron, cationic complex in which the Tp ligand is bound to the metal center by only two pyrazolyl rings.

Indirect evidence for this proposal is the production of free pyrazole from **1** and **2** in the presence of $AlCl_3$ mentioned above and the observation that $[TpMo(CHC(CH_3)_2Ph)(NAr)(THF)][B(CH_3)(C_6F_5)_3]$ (**6**) and 2 equiv of $AlCl_3$ in toluene quantitatively polymerizes 500 equiv of norbornylene. Further indirect evidence includes the observation that the closely related complex $[TpW(NPh)(CHCMe_3)(i-Pr_2O)][BAR'_4]$ does not initiate the polymerization of norbornylene, even though the diisopropyl ether ligand readily dissociates and is displaced by other Lewis bases such as diethyl ether and acetonitrile.⁸

Experimental Section

Materials and Methods. All syntheses were performed under a dry argon atmosphere using standard Schlenk techniques. Tetrahydrofuran (THF), diethyl ether (Et_2O), toluene, and pentane were distilled from sodium benzophenone ketyl; dichloromethane (CH_2Cl_2) was distilled from P_2O_5 . Methanol and acetonitrile were dried over 3 Å molecular sieves. $Mo(CHC(CH_3)_2Ph)(NAr)(OTf)_2(DME)^3$ ($NAr = 2,6-i-Pr_2-C_6H_3$, $Ph = C_6H_5$, $OTf = OSO_2CF_3$, $DME = CH_3OCH_2CH_2OCH_3$), $TpMo(CHC(CH_3)_2Ph)(NAr)(OTf)$ (**1**),¹¹ potassium hydridotris-

(1-pyrazolyl)borate (KTp),⁵ and $HBAR'_4 \cdot Et_2O$ ($Ar' = 3,5-C_6H_3-(CF_3)_2$,¹⁷ trityl tetrakis(pentafluorophenyl)borate,¹³ and tris(pentafluorophenyl)boron³⁷) were prepared according to literature methods.

1H and ^{13}C NMR spectra were recorded on a Varian VXR-300 (300 MHz) or a General Electric QE-300 (300 MHz) spectrometer. Elemental analyses were performed by the University of Florida Analytical Services. IR spectra were recorded on a Perkin-Elmer 1200 series spectrometer, and the samples were prepared as KBr pellets unless otherwise noted. GPC analyses were carried out with the use of Phenomenex Phenogel 5 500 Å and 5000 Å coupled columns, a Waters Associates differential refractometer, and a Perkin-Elmer LC-75 spectrophotometric detector on polymer samples 0.1–0.3% (w/v) in THF. The GPC columns were calibrated versus commercially available 1,4-polybutadiene standards ranging from 430 to 25 000 g/mol.

$TpMo(CHC(CH_3)_2Ph)(NAr)(CH_3)$ (2**).** To a stirred solution of **1** (0.39 g, 0.51 mmol) in 50 mL of Et_2O was added an ether solution of CH_3Li (0.6 mL, 1.4 M, 0.84 mmol) at room temperature under argon. A yellowish brown solution resulted after 3 h, and the solvent was removed under reduced pressure. The residue was extracted with pentane (2×10 mL), and the combined extracts were passed through Celite. Removal of the solvent yielded oily, yellowish brown solids. Extracting the solids in Et_2O and filtering through a column of neutral alumina resulted in a yellow solution. Removal of the solvent gave the product as a yellow solid (0.24 g, 0.38 mmol, 74.5% yield). The product can be recrystallized from Et_2O . 1H NMR data (300 MHz, C_6D_6 , 22 °C; δ): 13.11 (s, 1H, $CHC(CH_3)_2Ph$); 8.00, 7.62, 7.45, 7.36, 7.32, 7.23 (each a d, 1 H each, Tp ring H's, 3,5-positions); 7.54 (d, 2 H, ortho H's of neophylidene phenyl); 7.25 (t, 2 H, meta H's of neophylidene phenyl); 7.12–6.85 (m, 4 H, para H of neophylidene, phenyl, meta, and para H's of arylimido); 5.78, 5.76, 5.74 (each a t, 1 H each, Tp ring H's, 4-position); 4.54, 3.28 (each a broad sept, 1 H each, $CH(CH_3)_2$); 1.95, 1.78, 1.29 (each a s, 3 H each, $CHC(CH_3)_2Ph$, CH_3); 1.42, 1.02, 0.29 (each a broad d, 6:3:3 H, $CH(CH_3)_2$). ^{13}C NMR data (75 MHz, C_6D_6 , 22 °C; δ): 302.5 ($^1J_{CH} = 115$ Hz, $CHC(CH_3)_2Ph$); 148.4, 146.8, 142.3, 142.1, 135.5, 134.4, 127.0, 126.5, 125.8, 124.0, 123.3, 105.9, 105.2 (Tp, Ph, Ar); 53.7 ($CHC(CH_3)_2Ph$); 32.0, 30.9, 27.9, 26.7, 24.0, 23.7, 22.9, ($CH(CH_3)_2$, $CHC(CH_3)_2Ph$); 18.0 ($^1J_{CH} = 123$ Hz, CH_3). Anal. Calcd for $C_{32}H_{42}BMoN_7$: C, 60.86; H, 6.70; N, 15.53. Found: C, 60.94; H, 6.87; N, 15.55. IR: $\nu_{BH} = 2484$ cm^{-1} .

Reaction of $TpMo(CHC(CH_3)_2Ph)(NAr)(CH_3)$ (2**) with HOTf.** Compound **2** (0.023 g, 0.036 mmol) was dissolved in C_6D_6 in an NMR tube under nitrogen. HOTf (3.3 μ L, 0.037 mmol) was added by syringe. After 10 min, a 1H NMR spectrum of the reaction mixture showed that **2** was completely converted to **1**. The formation of CH_4 was observed as a singlet at δ 0.20.

$[TpMo(CHC(CH_3)_2Ph)(NAr)(Et_2O)][BAR'_4]$ (3**).** A 10 mL Et_2O solution of $HBAR'_4 \cdot 2Et_2O$ (0.16 g, 0.16 mmol) and a 10 mL ethereal solution of **2** (0.10 g, 0.16 mmol) were each cooled to -78 °C. The two solutions were mixed and stirred for 12 h under argon at -78 °C. The solvent was removed under reduced pressure at -78 °C; the brown solids were washed with pentane at -78 °C. The residual product was dried under reduced pressure to give oily brown solids. 1H NMR data for **3** (CD_2Cl_2 , 22 °C; δ): 14.79 (s, 1 H, $CHC(CH_3)_2Ph$); 8.28, 7.89, 7.82, 7.77, 7.48, 6.62 (each a d, 1 H each, Tp ring H's, 3,5-positions); 7.83 (s, 8 H, *o*-Ar'); 7.64 (s, 4 H, *p*-Ar'); 7.60–7.18 (m, 8 H, Ph, Ar); 6.51, 6.28, 6.12 (t, 1 H each, Tp ring H's, 4-position); 3.93, 3.60 (each an ABX_3 m, 2 H each, $O(CH_2CH_3)_2$); 4.03, 2.50 (each a broad sept, 1 H each, $CH(CH_3)_2$); 2.01, 1.99 (each a s, 3 H each, $CHC(CH_3)_2Ph$); 1.62, 1.48, 0.92, -0.08 (each a broad d, 3 H each, $CH(CH_3)_2$); 0.89 (t, 6 H, $O(CH_2CH_3)_2$). ^{13}C NMR data for **3** (CD_2Cl_2 , 22 °C; δ): 337.4 ($CHC(CH_3)_2Ph$); 162.2 ($^1J_{BC} = 50$ Hz, ipso-Ar' carbon); 153.0–

(32) (a) Kress, J.; Agüero, A.; Osborn, J. A. *J. Mol. Catal.* **1986**, *36*, 1. (b) Kress, J.; Osborn, J. A. *J. Am. Chem. Soc.* **1983**, *105*, 6346.

(33) Kress, J.; Osborn, J. A.; Greene, R. M. E.; Ivin, K. J.; Rooney, J. J. *J. Am. Chem. Soc.* **1987**, *109*, 899.

(34) Wengrovius, J. H.; Schrock, R. R.; Churchill, M. R.; Missert, J. R.; Youngs, W. J. *J. Am. Chem. Soc.* **1980**, *102*, 4515.

(35) Schrock, R. R.; Luo, S.; Zanetti, N. C.; Fox, H. H. *Organometallics* **1994**, *13*, 3396.

(36) VanderLende, D. D.; Abboud, K. A.; Boncella, J. M. *Organometallics* **1994**, *13*, 3378.

(37) Massey, A. G.; Park, J. J. *Organomet. Chem.* **1964**, *2*, 245.

107.0 (23 resonances, Ph, Ar', Tp); 125.2 ($^1J_{FC} = 270$ Hz, CF₃); 76.9 (O(CH₂CH₃)₂); 30.8, 30.6 (CHC(CH₃)₂Ph); 28.8, 28.6 (CH(CH₃)₂); 25.2, 25.0, 23.4, 22.6 (CH(CH₃)₂); 12.5 (O(CH₂CH₃)₂).

[TpMo(CHC(CH₃)₂Ph)(NAr)(NCCH₃)] [B(C₆F₅)₄] (4). Compound **2** (0.331 g, 0.524 mmol) and trityl tetrakis(pentafluorophenyl)borate (0.515 g, 0.558 mmol) were dissolved separately in Et₂O at -78 °C and mixed to give a yellow solution. The solution was stirred and warmed to room temperature over 30 min to give a yellow-brown solution. A 5 mL portion of acetonitrile was transferred to the reaction mixture, which was then recooled to -78 °C and stirred for 1 h. The solvent was removed under reduced pressure, and the oily brown residue was washed with pentane. Attempts to recrystallize the product from Et₂O were unsuccessful, but evaporation of an ethereal solution results in an analytically pure solid. The yield is essentially quantitative. ¹H NMR data for major rotamer (CD₂Cl₂, -40.0 °C; δ): 14.47 (s, 1H, CHC(CH₃)₂Ph); 7.94, 7.88, 7.82, 7.80, 7.73, 6.94 (each as d, 1 H each, Tp ring protons, 3,5-positions); 7.38-7.09 (m, 8 H, Ph, Ar); 6.36, 6.27, 6.20 (each a t, 1 H each, Tp ring protons, 4-position); 3.96, 2.40 (sept, 1 H each, CH(CH₃)₂); 2.35 (s, 3H, NCCH₃); 1.89, 1.81 (each a s, 3H each, CHC(CH₃)₂Ph); 1.49, 1.30, 0.81, -0.02 (each a d, 3 H each, CH(CH₃)₂). ¹³C NMR data (δ): 340.6 ($^1J_{CH} = 124.3$ Hz), 148.6, 138.6, 136.7 (br d, $^1J_{CF} = 244.4-238.8$ Hz), 149.7, 148.2, 148.0, 146.4, 142.2, 142.1, 141.7, 138.8, 137.1, 136.7, 135.5, 130.5, 129.2, 127.3, 126.5, 124.6, 107.2, 106.8, 106.7, 57.9, 30.1, 29.6, 29.1, 28.4, 26.3, 23.8, 23.4, 22.3, 4.0. Anal. Calcd for C₅₇H₄₂B₂F₂₀MoN₈: C, 51.22; H, 3.17; N, 8.38. Found: C, 50.81; H, 2.95; N, 7.69. ¹H NMR data for minor rotamer (CD₂Cl₂, -40.0 °C; δ): 15.28 (s, 1H, CHC(CH₃)₂Ph); 7.98, 7.65, 7.52, 7.30, 7.03, 6.01 (each as d, 1 H each, Tp ring protons, 3,5-positions); 6.45, 6.20, 6.07 (each a t, 1 H each, Tp ring protons, 4-position); 2.32 (s, 3H, NCCH₃); 1.93, 1.87 (each a s, 3H each, CHC(CH₃)₂Ph); Ar, Ph, and *i*-Pr resonances are not distinguishable in the spectrum.

[TpMo(CHC(CH₃)₂Ph)(NAr)(NCCH₃)] [B(CH₃)(C₆F₅)₃] (5). Compound **2** (0.153 g, 0.242 mmol) and tris(pentafluorophenyl)boron (0.124 g, 0.242 mmol) were dissolved separately in Et₂O at -78 °C and warmed to room temperature over 30 min to give a yellow-brown solution. A 5 mL portion of acetonitrile was transferred to the reaction mixture, which was then recooled to -78 °C and stirred for 1 h. The solvent was removed under reduced pressure, and the oily brown residue was washed with pentane. Attempts to recrystallize the product from Et₂O were unsuccessful, but evaporation of an ethereal solution results in an analytically pure solid. The yield is essentially quantitative. ¹H NMR data for major rotamer (CD₂Cl₂, 22 °C; δ): 14.53 (s, 1H, CHC(CH₃)₂Ph); 7.94, 7.90, 7.84, 7.82, 7.33, 7.12 (each as d, 1 H each, Tp ring protons, 3,5-positions); 7.40-7.07 (m, 8 H, Ph, Ar); 6.41, 6.34, 6.32 (each a t, 1 H each, Tp ring protons, 4-position); 3.98, 2.46 (sept, 1 H each, CH(CH₃)₂); 2.34 (s, 3H, NCCH₃); 1.97, 1.81 (each a s, 3H each, CHC(CH₃)₂Ph); 1.52, 1.35, 0.87, 0.08 (each a d, 3 H each, CH(CH₃)₂); 0.47 (br s, 3 H, BCH₃). ¹³C NMR data (δ): 340.9 ($^1J_{CH} = 125.9$ Hz), 148.6, 138.6, 136.7 (br d, $^1J_{CF} = 244.4-238.8$ Hz), 149.6, 148.1, 148.0, 146.3, 142.13, 142.07, 141.7, 138.8, 137.0, 136.7, 135.4, 130.5, 129.2, 128.8, 127.3, 126.4, 124.6, 107.2, 106.8, 58.0, 30.1, 29.8, 29.1, 28.4, 26.3, 25.2, 23.8, 23.4, 22.3, 4.2. Anal. Calcd for C₅₂H₄₅B₂F₁₅MoN₈: C, 52.73; H, 3.83; N, 9.46. Found: C, 53.09; H, 3.59; N, 9.14.

[TpMo(CHC(CH₃)₂Ph)(NAr)(THF)] [B(CH₃)(C₆F₅)₃] (6). Compound **2** (0.084 g, 0.133 mmol) and tris(pentafluorophenyl)boron (0.068 g, 0.134 mmol) were dissolved separately in Et₂O at -78 °C and warmed to room temperature over 30 min to give a yellow-brown solution. A 5 mL portion of THF was transferred to the reaction mixture, which was then recooled to -78 °C and stirred for 1 h. The solvent was removed under reduced pressure, and the oily brown residue was washed with pentane. Attempts to recrystallize the product from Et₂O were unsuccessful, but evaporation of an ethereal solution results in an analytically pure solid. The yield is essentially quantitative. ¹H NMR data for major

rotamer (CD₂Cl₂, 22 °C; δ): 14.46 (s, 1H, CHC(CH₃)₂Ph); 8.00, 7.90, 7.85, 7.78, 6.46 (each as d, 1 H each, Tp ring protons, 3,5-positions); 7.46-7.04 (m, 9 H, Ph, Ar, one Tp ring proton); 6.51, 6.23, 6.11 (each a t, 1 H each, Tp ring protons, 4-position); 3.81, 2.48 (sept, 1 H each, CH(CH₃)₂); 3.65, 3.55, 1.82 (t:t:t, 2:2:4, THF); 1.98, 1.91 (each a s, 3H each, CHC(CH₃)₂Ph); 1.58; 1.39, 0.94, -0.12 (each a d, 3 H each, CH(CH₃)₂); 0.47 (br s, 3 H, BCH₃). ¹³C NMR data (δ): 336.4, 148.8, 138.6, 136.7 (three br d, $^1J_{CF} = 244-240$ Hz), 148.4, 146.2, 144.2, 142.6, 140.5, 138.8, 137.4, 136.2, 133.6, 129.6, 128.2, 126.6, 125.7, 124.6, 123.6, 107.9, 107.5, 107.1, 106.9, 106.3, 82.9, 57.5, 31.8, 30.7, 30.3, 28.9, 28.4, 26.9, 25.9, 25.4, 24.4, 22.7. Anal. Calcd for C₅₄H₅₀B₂F₁₅MoN₇O: C, 53.36; H, 4.15; N, 8.07. Found: C, 52.95; H, 4.26; N, 7.81.

[TpMo(CHC(CH₃)₂Ph)(NAr)(P(CH₃)₃)] [OSO₂CF₃] (7). A 0.5 mL amount of a 0.17 M P(CH₃)₃ solution in C₆D₆ (0.085 mmol of P(CH₃)₃) was added to **1** (0.032 g, 0.042 mmol) in a sealable NMR tube. Pale yellow solids formed over 2 h, the C₆D₆ was removed under reduced pressure, and the resulting solids were dissolved in CD₂Cl₂. The yield was quantitative by ¹H NMR. ¹H NMR data for major rotamer (CD₂Cl₂, -20 °C; δ): 14.51 (d, 1H, CHC(CH₃)₂Ph, $^3J_{PH} = 5.4$ Hz); 8.23, 7.99, 7.88, 7.85, 7.38, 7.28 (each as d, 1 H each, Tp ring protons, 3,5-positions); 7.45-7.06 (m, 8 H, Ph, Ar); 6.48, 6.38, 6.25 (each a t, 1 H each, Tp ring protons, 4-positions); 3.74, 2.23 (sept, 1 H each, CH(CH₃)₂); 2.03, 1.86 (each a s, 3H each, CHC(CH₃)₂-Ph); 1.60, 1.42, 0.59, 0.31 (each a br d, 3 H each, CH(CH₃)₂); 1.12 (d, 9H, P(CH₃)₃, $^2J_{PH} = 9.9$ Hz). ¹³C NMR data (CD₂Cl₂, 22 °C; δ): 335.9 ($^1J_{CH} = 122.1$ Hz, $^2J_{PC} = 17.6$ Hz), 147.7, 147.2, 143.9, 143.1, 138.2, 137.9, 137.8, 130.2, 129.4, 127.3, 126.2, 125.0, 123.7, 119.4, 107.9, 107.1, 107.0, 57.0, 31.6, 30.2, 28.3, 26.2, 24.9, 17.6 ($^1J_{PC} = 30.2$ Hz). ¹⁹F NMR data (282 MHz, vs CFC1₃; δ): -78.75. ³¹P NMR data (121 MHz, vs H₃PO₄; δ): -2.83. Anal. Calcd for C₃₅H₄₃BF₃MoN₇O₂PS: C, 49.95; H, 5.75; N, 11.65. Found: C, 49.58; H, 5.68; N, 11.25. IR (CD₂-Cl₂ film): 1268, 1048 cm⁻¹ (S=O).

TpMo(CHC(CH₃)₂Ph)(NAr)(OCH₃) (8). A 5 g amount of Florisil was slurried for 1 h in dry methanol. Compound **1** (0.475 g, 0.620 mmol) was dissolved in 3 mL of Et₂O and transferred to the Florisil slurry, giving a faint yellow solution. After it was stirred at room temperature for 24 h, the mixture was filtered and the methanol solution was reduced to dryness under reduced pressure. The yellow solids were extracted with pentane, leaving a white powder. Concentration of the pentane solution gave yellow microcrystals, which were determined to be a mixture of **1** (10%) and **8**. Further recrystallizations of the product from pentane gave 0.163 g (0.252 mmol, 40.5% yield) of **8**. ¹H NMR data (δ): 13.14 (s, 1H, CHC(CH₃)₂-Ph), 8.24, 7.62, 7.32, 7.30, 7.28, 6.99 (each as d, 1 H each, Tp ring protons, 3,5-positions); 7.4-6.8 (m, 8 H, Ph, Ar); 5.90, 5.71, 5.64 (each a t, 1 H each, Tp ring protons, 4-position); 4.82, 3.42 (br m, 1 H each, CH(CH₃)₂); 4.60 (s, 3H, OCH₃); 2.02, 1.79 (each a s, 3H each, CHC(CH₃)₂Ph); 1.59, 1.00, 0.14 (each a br d, 6:3:3 H, CH(CH₃)₂). ¹³C NMR data (δ): 302.2 ($^1J_{CH} = 121$ Hz, CHC(CH₃)₂Ph), 151.3, 150.6, 146.6, 141.2, 139.9, 135.5, 134.4, 133.8, 128.6, 127.3, 127.0, 126.6, 125.8, 123.9, 123.0, 105.4, 105.0, 104.8, 72.7 (OCH₃, $^1J_{CH} = 137.3$ Hz), 53.7, 33.1, 31.5, 28.2, 27.4, 25.7, 24.3, 23.0. Anal. Calcd for C₃₂H₄₂-BMoN₇O: C, 59.36; H, 6.54; N, 15.14. Found: C, 59.36; H, 6.58; N, 15.13. IR: $\nu_{OMe} 2778.2$ cm⁻¹, $\nu_{BH} 2472.6$ cm⁻¹, $\nu_{OMe} 1081.8$ cm⁻¹.

TpMo(CC(CH₃)₂Ph)(NHAr)(OCH₃) (9). Compound **1** (0.664 g, 0.867 mmol) and an excess of potassium methoxide (0.300 g, 4.28 mmol) were dissolved in THF at -78 °C to give a yellow slurry. The mixture was warmed to room temperature, and stirring continued for 24 h. The solution became red-orange, and the white solids remained. The THF was removed under reduced pressure, and the residue was extracted with Et₂O. Concentration of the Et₂O extract and cooling to -20 °C gave orange crystals of the product **9**. Two further crops of crystals were obtained to give a combined yield of 78% (0.439 g, 0.678 mmol). ¹H NMR data of major rotamer

(CD₂Cl₂, -40.0 °C; δ): 9.55 (br s, 1 H, NH); 8.06, 7.72, 7.71, 7.69, 7.60, 6.19 (each as d, 1 H each, Tp ring protons, 3,5-positions); 7.38, 7.19, 7.09 (t:d:d, 1:1:1 H, Ar ring protons); 6.61, 7.01, 5.98 (d:t:t, 2:2:1 H, Ph ring protons); 6.30, 6.24, 5.81 (each a t, 1 H each, Tp ring protons, 4-position); 5.11 (s, 3H, OCH₃); 4.79, 2.13 (sept, 1 H each, CH(CH₃)₂); 4.52 (br s, 1 H, HB); 1.49, 1.38 (each a s, 3H each, CHC(CH₃)₂Ph); 1.56, 1.20, 0.96, 0.60 (each a d, 3 H each, CH(CH₃)₂). ¹³C NMR data (δ): 301.3, 155.2, 145.2, 144.9, 142.6, 142.4, 139.7, 139.3, 135.4, 135.0, 134.9, 128.3, 126.2, 125.8, 123.8, 123.2, 121.8, 105.5, 105.1, 103.9, 73.7, 57.6, 30.8, 28.0, 27.0, 26.4, 24.7, 24.0, 21.5, 21.0. Anal. Calcd for C₃₂H₄₂BMoN₇O: C, 59.36; H, 6.54; N, 15.14. Found: C, 59.30; H, 6.57; N, 15.11. IR: ν_{NH} 3308.7 cm⁻¹, ν_{OMe} 2781 cm⁻¹, ν_{BH} 2472.9 cm⁻¹, ν_{OMe} 1083.9 cm⁻¹. ¹H NMR data of minor rotamer (CD₂Cl₂, -40.0 °C; δ): 10.26 (br s, 1 H, NH), 8.08, 7.76, 7.66, 7.54, 7.45, 6.63 (each as d, 1 H each, Tp ring protons, 3,5-positions); 6.29, 6.23, 5.66 (each a t, 1 H each, Tp ring protons, 4-position); 4.98 (s, 3H, OCH₃); 3.68, 2.90 (sept, 1 H each, CH(CH₃)₂); 1.73, 1.53 (each a s, 3H each, CHC(CH₃)₂Ph); 1.31, 0.96, 0.44, -0.28 (each a d, 3 H each, CH(CH₃)₂); Ar and Ph protons of minor isomer not discernible. ¹³C NMR data (δ): 298.7, 149.0, 145.4, 144.8, 144.7, 142.0, 141.4, 135.6, 134.4, 133.8, 129.0, 126.4, 126.0, 124.8, 122.6, 122.2, 122.1, 105.2, 103.8, 72.4, 57.4, 31.1, 27.7, 26.7, 25.3, 24.1, 22.7, 22.2, 20.0.

X-ray Data Collection and Structure Refinement.

Compound **8**: C₃₂H₄₂BN₇OMo, *M_r* = 647.48, orthorhombic, *P*2₁2₁2₁, *a* = 12.620(2) Å, *b* = 13.492(2) Å, *c* = 19.682(2) Å, *V* = 3351.3(7) Å³, *Z* = 4, *d*_{calc} = 1.283 g cm⁻³, Mo Kα (λ = 0.710 73 Å), *T* = 298 K. Compound **9**: C₃₂H₄₂BN₇OMo, *M_r* = 647.48, triclinic, *P*1, *a* = 10.624(2) Å, *b* = 11.766(3) Å, *c* = 13.980(3) Å, α = 86.96(2)°, β = 86.54(2)°, γ = 67.77(2)°, *V* = 1635.8(7) Å³, *Z* = 2, *d*_{calc} = 1.315 g cm⁻³, Mo Kα (λ = 0.710 73 Å), *T* = 298 K. Data were collected at room temperature on a Siemens R3m/V diffractometer equipped with a graphite monochromator utilizing Mo Kα radiation (λ = 0.710 73 Å); 32 reflections from each structure with 20.0° ≤ 2θ ≤ 22.0° were used to refine the cell parameters. Totals of 4317 and 6094 reflections, for **8** and **9**, respectively, were collected using the ω-scan method (**8**, 2θ range 3–55°, 1.2° scan range, and 3–6° min⁻¹ scan speed depending on intensity; **9**, 2θ range 3–50°, 1.2° scan range, and 3–6° min⁻¹ scan speed depending on intensity). Four reflections from each data set were measured every 96 reflections to monitor instrument and crystal stability (maximum corrections on *I* were <1% and 4%, respectively). Absorption corrections were applied based on the basis of measured crystal faces using SHELXTL plus.³⁸ Absorption coefficients: **8**, μ = 0.43 mm⁻¹ (minimum and maximum transmission factors are 0.928 and 0.950, respectively); **9**, μ = 0.44 mm⁻¹ (minimum and maximum transmission factors are 0.850 and 0.948, respectively).

The structures were solved by the heavy-atom method in SHELXTL plus, from which the positions of the Mo atoms were obtained. The rest of the non-H atoms were obtained from subsequent difference Fourier maps. The structures were refined in SHELXTL plus using full-matrix least squares. In **8**, the alkylidene ligand was found to be disordered by a 20° rotation around the C1–C4 bond. The site occupation value for one partial moiety was refined to 0.69(1); thus, the other part of the disordered moiety had a site occupation value of 0.31(1). All of the non-H atoms were refined with anisotropic thermal parameters except the disordered atoms (C2, C3, C5 to C10 and C2', C3', C5' to C10'). All of the H atoms were calculated in idealized positions, and their thermal parameters were fixed (the boron H atom was located from a difference Fourier map and was refined without any constraints). In **9**, all of the non-H atoms were refined with anisotropic thermal parameters. The H atoms were calculated in idealized positions, and their thermal parameters were fixed; the boron H atom was located from a difference Fourier map and was refined without any constraints. Totals of 352 and 463

Table 3. Fractional Coordinates and Equivalent Isotropic Thermal Parameters (Å²) for the Non-H Atoms of Compound **8**

atom	<i>x</i>	<i>y</i>	<i>z</i>	<i>U</i>
Mo	0.38168(8)	0.95336(7)	0.35907(5)	0.0408(3)
O1	0.4455(6)	1.0699(5)	0.4022(4)	0.055(3)
N1	0.2483(7)	0.9862(6)	0.3612(5)	0.049(3)
N2	0.3733(9)	0.8293(6)	0.2843(4)	0.042(3)
N3	0.4306(7)	0.8260(7)	0.2250(5)	0.043(3)
N4	0.5582(8)	0.9199(7)	0.3336(5)	0.049(4)
N5	0.5958(8)	0.9067(6)	0.2690(5)	0.042(3)
N6	0.4048(7)	1.0395(7)	0.2596(4)	0.042(3)
N7	0.4606(7)	1.0051(7)	0.2057(4)	0.042(3)
B	0.5158(11)	0.9041(11)	0.2090(7)	0.043(5)
C11	0.1481(9)	1.0289(7)	0.3587(7)	0.052(4)
C12	0.0756(12)	0.9985(10)	0.3097(7)	0.061(5)
C13	-0.0213(12)	1.0449(14)	0.3077(8)	0.087(6)
C14	-0.0456(14)	1.1189(13)	0.3515(11)	0.102(8)
C15	0.027(2)	1.1496(11)	0.3993(8)	0.088(7)
C16	0.1276(13)	1.1079(8)	0.4044(7)	0.065(5)
C17	0.1007(13)	0.9153(12)	0.2624(7)	0.083(6)
C18	0.113(2)	0.942(2)	0.1917(8)	0.199(14)
C19	0.029(2)	0.8323(13)	0.2702(11)	0.159(12)
C20	0.2030(13)	1.1446(12)	0.4555(8)	0.083(7)
C21	0.1561(13)	1.1495(12)	0.5265(7)	0.107(8)
C22	0.248(2)	1.2434(11)	0.4357(10)	0.137(10)
C23	0.3208(11)	0.7432(9)	0.2860(7)	0.057(5)
C24	0.3398(10)	0.6852(10)	0.2332(7)	0.057(5)
C25	0.4123(11)	0.7379(9)	0.1944(6)	0.056(5)
C26	0.6449(9)	0.9177(8)	0.3724(6)	0.053(4)
C27	0.7347(11)	0.9056(10)	0.3355(7)	0.062(5)
C28	0.6999(10)	0.8972(8)	0.2697(8)	0.053(5)
C29	0.3685(10)	1.1282(8)	0.2419(6)	0.051(4)
C30	0.4030(11)	1.1548(9)	0.1778(6)	0.055(5)
C31	0.4612(9)	1.0754(8)	0.1574(6)	0.050(4)
C32	0.4851(11)	1.0819(10)	0.4666(7)	0.081(6)
C1	0.3915(11)	0.8580(8)	0.4341(5)	0.052(4)
C4	0.3162(12)	0.8165(10)	0.4902(6)	0.065(5)
C2	0.346(2)	0.8606(14)	0.5584(9)	0.069(6)
C3	0.1932(15)	0.8515(14)	0.4810(10)	0.064(6)
C5	0.3198(12)	0.7056(8)	0.4875(8)	0.053(6)
C6	0.2454(12)	0.6455(8)	0.4551(8)	0.078(7)
C7	0.2597(12)	0.5430(8)	0.4533(8)	0.085(7)
C8	0.3486(12)	0.5006(8)	0.4838(8)	0.089(7)
C9	0.4230(12)	0.5607(8)	0.5162(8)	0.082(7)
C10	0.4087(12)	0.6631(8)	0.5181(8)	0.065(6)
C2'	0.250(3)	0.879(3)	0.512(2)	0.063(13)
C3'	0.409(3)	0.805(3)	0.556(2)	0.054(12)
C5'	0.287(2)	0.711(2)	0.471(2)	0.041(10)
C6'	0.191(2)	0.706(2)	0.437(2)	0.061(12)
C7'	0.152(2)	0.615(2)	0.415(2)	0.10(2)
C8'	0.209(2)	0.528(2)	0.428(2)	0.11(2)
C9'	0.306(2)	0.533(2)	0.462(2)	0.059(12)
C10'	0.345(2)	0.625(2)	0.484(2)	0.10(2)

^a For anisotropic atoms, the *U* value is *U*_{eq}, calculated as *U*_{eq} = 1/3 Σ_j Σ_i U_{ij} a_i^{*} a_j A_{ij}, where A_{ij} is the dot product of the *i*th and *j*th direct space unit cell vectors.

parameters for **8** and **9**, respectively, were refined, and Σw(|*F*_o| - |*F*_c|)² was minimized: *w* = 1/(σ(*F*_o))², σ(*F*_o) = 0.5 *kI*^{-1/2}{σ(*I*)² + (0.02*I*)²}^{1/2}, *I*(intensity) = (*I*_{peak} - *I*_{background})(scan rate), and σ(*I*) = (*I*_{peak} + *I*_{background})^{1/2}(scan rate), where *k* is the correction due to decay and Lp effects, 0.02 is a factor used to downweight intense reflections and to account for instrument instability. *R* = 0.0600 and *R*_w = 0.0589 for **8**, and *R* = 0.0484 and *R*_w = 0.0487 for **9**, in the last cycle of refinement using 2298 (with *I* > 3σ(*I*)) and 4596 (with *I* > 2σ(*I*)) reflections for **8** and **9**, respectively. Fractional coordinates for the atoms of compounds **8** and **9** are given in Tables 3 and 4, respectively.

Determination of Activation Parameters for the Thermal Isomerization of the anti to the syn Rotamer of 1. An NOE difference study of the major isomer of **1** indicated it to be the *syn* rotamer. Irradiation of the alkylidene proton showed 0% enhancement of the methine proton of the isopropyl groups. Irradiation of the methyl groups of the alkylidene ligand caused a 8.7% enhancement of the methine protons. To determine the rotational rates of conversion for the minor

Table 4. Fractional Coordinates and Equivalent Isotropic Thermal Parameters (\AA^2) for the Non-H Atoms of Compound 9

atom	x	y	z	U
Mo	0.25571(4)	0.14529(3)	0.23974(3)	0.02951(13)
O1	0.4338(3)	0.1543(3)	0.2327(2)	0.0427(12)
N1	0.1497(3)	0.2966(3)	0.1754(3)	0.0328(14)
N2	0.1026(3)	0.0567(3)	0.2267(2)	0.0334(13)
N3	0.1241(4)	-0.0406(3)	0.1712(3)	0.0407(15)
N4	0.3664(3)	-0.0550(3)	0.2681(3)	0.0397(14)
N5	0.3645(4)	-0.1398(3)	0.2060(3)	0.0408(15)
N6	0.3021(4)	0.0860(3)	0.0771(3)	0.0391(15)
N7	0.3009(4)	-0.0230(3)	0.0504(3)	0.0398(15)
B	0.2631(6)	-0.1069(5)	0.1243(4)	0.045(2)
C1	0.2030(4)	0.1884(4)	0.3587(3)	0.035(2)
C2	0.2391(6)	0.1188(5)	0.5263(3)	0.063(2)
C3	0.1776(6)	0.3385(5)	0.4847(3)	0.056(2)
C4	0.1541(5)	0.2212(4)	0.4607(3)	0.043(2)
C5	0.0040(5)	0.2406(4)	0.4707(3)	0.043(2)
C6	-0.0472(7)	0.1667(6)	0.5294(4)	0.063(3)
C7	-0.1827(9)	0.1855(8)	0.5345(6)	0.084(4)
C8	-0.2695(9)	0.2756(10)	0.4832(6)	0.091(4)
C9	-0.2205(7)	0.3513(7)	0.4242(5)	0.077(3)
C10	-0.0855(6)	0.3330(5)	0.4195(4)	0.054(2)
C11	0.0628(4)	0.4157(4)	0.1957(3)	0.032(2)
C12	-0.0722(4)	0.4537(4)	0.1689(3)	0.037(2)
C13	-0.1535(5)	0.5720(5)	0.1882(4)	0.050(2)
C14	-0.1056(6)	0.6499(5)	0.2310(4)	0.058(2)
C15	0.0255(6)	0.6126(5)	0.2557(4)	0.050(2)
C16	0.1135(5)	0.4961(4)	0.2373(3)	0.037(2)
C17	-0.1223(5)	0.3683(5)	0.1189(4)	0.046(2)
C18	-0.0861(6)	0.3680(6)	0.0118(4)	0.070(3)
C19	-0.2724(5)	0.3912(6)	0.1351(5)	0.081(3)
C20	0.2616(5)	0.4601(5)	0.2558(4)	0.045(2)
C21	0.3449(5)	0.4549(5)	0.1618(4)	0.061(2)
C22	0.2953(6)	0.5389(5)	0.3267(4)	0.070(3)
C23	-0.0243(5)	0.0860(5)	0.2612(3)	0.041(2)
C24	-0.0846(5)	0.0102(5)	0.2285(4)	0.050(2)
C25	0.0123(5)	-0.0690(5)	0.1720(4)	0.049(2)
C26	0.4600(5)	-0.1120(5)	0.3296(4)	0.048(2)
C27	0.5189(6)	-0.2321(5)	0.3088(5)	0.058(2)
C28	0.4561(5)	-0.2465(5)	0.2304(4)	0.052(2)
C29	0.3360(5)	0.1392(5)	-0.0025(3)	0.046(2)
C30	0.3583(5)	0.0655(5)	-0.0801(4)	0.053(2)
C31	0.3359(5)	-0.0357(6)	-0.0441(4)	0.053(2)
C32	0.5146(5)	0.1679(5)	0.3034(4)	0.062(2)

^a For anisotropic atoms, the U value is U_{eq} , calculated as $U_{eq} = 1/3 \sum_i \sum_j U_{ij} a_i^* a_j^* A_{ij}$, where A_{ij} is the dot product of the i th and j th direct space unit cell vectors.

anti rotamer to the major *syn* rotamer, 0.02 g of **1** was dissolved in approximately 1 mL of d_8 -toluene and the solution sealed in an NMR tube. The NMR tube was placed in a Pyrex beaker containing dry ice/isopropyl alcohol as a coolant and irradiated by a 275 W tungsten lamp for 1 h to give a *syn:anti* rotamer ratio of approximately 4:1. A temperature of $-50\text{ }^\circ\text{C}$ was typically employed. The alkylidene proton signal for the

minor isomer is δ 14.82. The thermal isomerization of the *anti* to the *syn* rotamer was followed by ^1H NMR at 40.0, 50.0, and 60.0 $^\circ\text{C}$ by integration of the alkylidene resonances for a minimum of 3 half-lives. Rates were also determined by this method for **2** and **8**. Decomposition of **1** was determined to be less than 1% by summing the integration of the *syn* and *anti* rotamers over time. The rate constants k were determined by plotting the natural logarithm of the integral of the *anti* rotamer versus time. The rate constants were $(8.2 \pm 0.1) \times 10^{-5}$, $(2.4 \pm 0.1) \times 10^{-4}$, and $(7.0 \pm 0.1) \times 10^{-4} \text{ s}^{-1}$ for 40.0, 50.0, and 60.0 $^\circ\text{C}$, respectively. A ΔH^\ddagger value of $+21.5 \pm 0.3 \text{ kcal/mol}$ and a ΔS^\ddagger value of $-8.9 \pm 0.8 \text{ eu}$ were determined from a plot of $\ln(k/T)$ vs $1/T$.

ROMP Reactions by 1 and 2 with AlCl_3 . In a typical reaction, recrystallized **1** or **2** was dissolved in 500 equiv of neat cyclooctene or norbornylene. An excess of AlCl_3 (6 equiv) was added, and a red solution immediately formed. The solution became viscous, and stirring ceased within 10 min. The polymer was dissolved in 10 mL of toluene, and the viscosity increased over 24 h. The polymer was precipitated in methanol with 20 mg of BHT (three times), filtered, and dried under reduced pressure to yield a white solid. Molecular weights were determined by GPC and reported relative to poly-(1,4-butadiene) standards. For **1**, poly(octenamer) of $M_n = 57\ 000$ and $M_w/M_n = 1.3$ was obtained. For **2**, poly(norbornylene) of $M_n = 75\ 000$ and $M_w/M_n = 1.8$ was obtained. Polymer yields were greater than 90%. No vinyl addition products were evident by the ^{13}C NMR attached proton test (APT).

Oligomerization of 1,9-Decadiene by 1 and 2 with AlCl_3 . In a typical reaction, compounds **1** or **2** and 5 equiv of AlCl_3 were dissolved in 500 equiv of neat 1,9-decadiene. The solution was stirred at ambient temperature under static vacuum for 12 h with no obvious change. The excess monomer was removed under reduced pressure, leaving a brown gum. ^1H NMR in CDCl_3 showed the gum to be only dimer by integration of internal versus terminal olefinic protons. ^{13}C NMR of the product showed both *cis* and *trans* internal olefins. No vinyl addition products were evident by the ^{13}C NMR attached proton test (APT). The yields of these reactions were less than 10% dimer relative to monomer.

Acknowledgment. We acknowledge the National Science Foundation (Grant No. DMR-9207358) for the support of this research.

Supplementary Material Available: Details of the X-ray crystal structure determinations of **8** and **9**, including tables of atomic coordinates for hydrogen atoms, thermal parameters, and bond distances and angles (16 pages). Ordering information is given on any current masthead page.

OM9408066

π -Coordination of Arenes to Phosphorus: Models of Stable π -Complex Intermediates in Electrophilic Aromatic Substitution

Neil Burford,* Jason A. C. Clyburne, Pradip K. Bakshi, and T. Stanley Cameron*

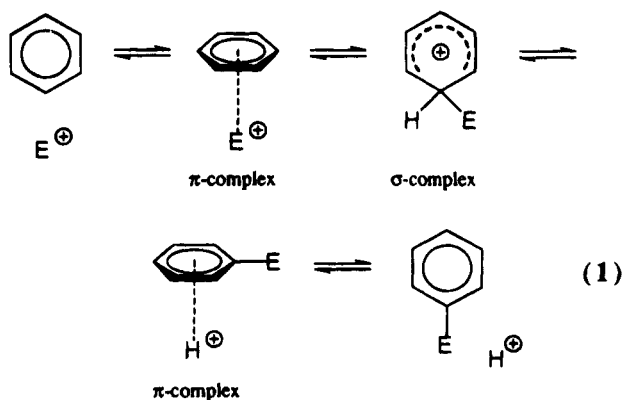
Department of Chemistry, Dalhousie University, Halifax, Nova Scotia B3H 4J3, Canada

Received November 8, 1994[®]

A series of salts containing cations of the form $[\text{Mes}^*\text{NP}(\text{arene})]^+$ (arene = benzene, toluene, mesitylene) have been isolated and structurally characterized, representing the first arene π -complexes of phosphorus. X-ray crystal structures reveal hexahapto association of the arene to the phosphorus center in all cases with the distance between phosphorus and the centroid of the arene decreasing from benzene [P -benzene_{centroid}, 2.820(4) Å] to toluene [P -toluene_{centroid}, 2.767(7) Å] to mesitylene [P -mesitylene_{centroid}, 2.687(4) Å] in the hepta-chlorodigallate (Ga_2Cl_7^-) salts {crystal data: $[\text{Mes}^*\text{NP}(\text{benzene})][\text{GaCl}_4]$, $Pbca$, $a = 24.948(4)$ Å, $b = 20.195(4)$ Å, $c = 11.953(3)$ Å, $V = 6022(4)$ Å³, $Z = 8$, $D_c = 1.279(1)$ Mg m⁻³, $R = 0.0419$, $R_w = 0.0419$; $[\text{Mes}^*\text{NP}(\text{toluene})][\text{GaCl}_4]$, $Pbca$, $a = 25.006(9)$ Å, $b = 20.358(8)$ Å, $c = 12.126(5)$ Å, $V = 6173(8)$ Å³, $Z = 8$, $D_c = 1.278(2)$ Mg m⁻³, $R = 0.0760$, $R_w = 0.0760$; $[\text{Mes}^*\text{NP}(\text{benzene})][\text{Ga}_2\text{Cl}_7]$, $P\bar{1}$, $a = 11.579(2)$ Å, $b = 16.350(3)$ Å, $c = 11.085(3)$ Å, $\alpha = 90.74(2)^\circ$, $\beta = 118.00(2)^\circ$, $\gamma = 73.53(2)^\circ$, $V = 1559(1)$ Å³, $Z = 2$, $D_c = 1.428(1)$ Mg m⁻³, $R = 0.0386$, $R_w = 0.0386$; $[\text{Mes}^*\text{NP}(\text{toluene})][\text{Ga}_2\text{Cl}_7]$, $P\bar{1}$, $a = 11.571(4)$ Å, $b = 16.335(5)$ Å, $c = 11.326(3)$ Å, $\alpha = 91.47(4)^\circ$, $\beta = 117.87(2)^\circ$, $\gamma = 105.34(3)^\circ$, $V = 1797(1)$ Å³, $Z = 2$, $D_c = 1.423(1)$ Mg m⁻³, $R = 0.0464$, $R_w = 0.0464$; $[\text{Mes}^*\text{NP}(\text{mesitylene})][\text{Ga}_2\text{Cl}_7]$, $P\bar{1}$, $a = 12.119(3)$ Å, $b = 16.575(4)$ Å, $c = 11.309(3)$ Å, $\alpha = 93.22(2)^\circ$, $\beta = 115.62(2)^\circ$, $\gamma = 107.64(2)^\circ$, $V = 1905(1)$ Å³, $Z = 2$, $D_c = 1.391(1)$ Mg m⁻³, $R = 0.0420$, $R_w = 0.0450$ }. In the solid state and in dichloromethane solution, the ¹³C and ¹H NMR chemical shifts for the arene units of the complexes are significantly deshielded with respect to those for the corresponding free arene. In addition, there are notable differences in the positions of characteristic combination bands in the IR spectra (1700–2000 cm⁻¹). The new cations are viewed as models for π -complex intermediates of electrophilic aromatic substitution.

Introduction

The electrophilic aromatic substitution reaction (1) and its mechanism have fascinated chemists for decades.¹ Kinetic studies first revealed the σ -complex



intermediate (most commonly referred to as the Wheland intermediate²), and numerous examples of stable

σ -complexes have been characterized spectroscopically.³ More recently, two σ -arene complexes **1** ($\text{E} = \text{Et}_3\text{Si}^+$)^{4–6} and **2** (Cl^+)⁷ have been isolated and X-ray crystal structures provide unambiguous support for such species (the drawings indicate the observed long E–C bond). Furthermore, Olah et al. have shown that derivatives of these silicon cations ultimately transform into the phenylsilanes, products of electrophilic aromatic substitution.⁵

A π -complex intermediate was proposed for the electrophilic aromatic substitution reaction by Dewar,⁸ and kinetic data were provided by Olah who defined the complex as “an electrophile interacting with the aromatic substrate with little deformation of the latter in

(3) See for example: Olah, G. A.; Lin, H. C.; Mo, Y. K. *J. Am. Chem. Soc.* **1972**, *94*, 3667–3669. Olah, G. A.; Schlosberg, R. H.; Porter, R. D.; Mo, Y. K.; Kelly, D. P.; Mateescu, G. D. *J. Am. Chem. Soc.* **1972**, *94*, 2034–2043.

(4) Lambert, J. B.; Zhang, S.; Stern, C. L.; Huffman, J. C. *Science* **1993**, *260*, 1917–1918. Lambert, J. B.; Zhang, S. *J. Chem. Soc., Chem. Commun.* **1993**, 383–384. See also: Pauling, L. *Science* **1994**, *263*, 983. Lambert, J. B.; Zhang, S. *Science* **1994**, *263*, 984. Reed, C.; Xie, Z. *Science* **1994**, *263*, 985.

(5) Olah, G. A.; Rasul, G.; Li, X.; Buchholz, H. A.; Sandford, G.; Prakash, G. K. S. *Science* **1994**, *263*, 983.

(6) Lambert, J. B.; Zhang, S.; Ciro, S. M. *Organometallics* **1994**, *13*, 2430–2443.

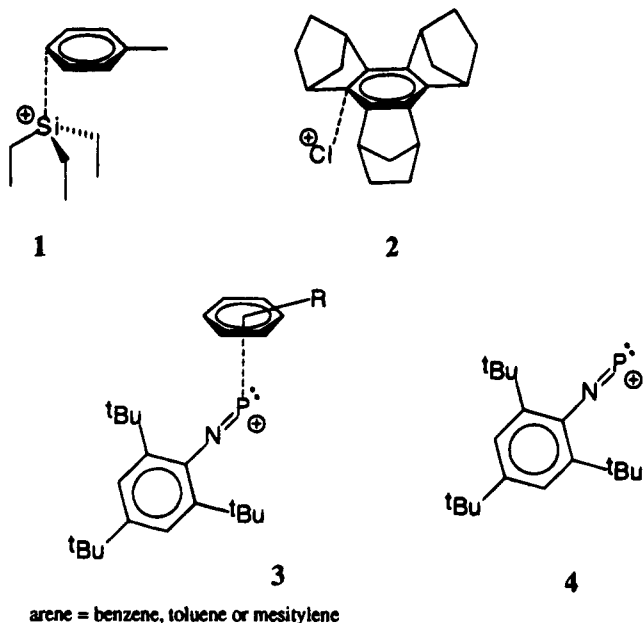
(7) Rathore, R.; Loyd, S. H.; Kochi, J. K. *J. Am. Chem. Soc.* **1994**, *116*, 8414–8415.

(8) Dewar, M. J. S. *J. Chem. Soc.* **1946**, 406–408, 777–781; *Nature* **1945**, *176*, 784.

[®] Abstract published in *Advance ACS Abstracts*, February 15, 1995.

(1) Taylor, R. *Electrophilic Aromatic Substitution*; John Wiley and Sons: New York, 1990.

(2) Wheland, G. W. *J. Am. Chem. Soc.* **1942**, *64*, 900–908.



the transition state".⁹ A rate determining formation of π -complex intermediates has been contested,¹⁰ and evidence for such systems is limited.

Here we report the isolation and comprehensive characterization of the first arene (benzene, toluene, and mesitylene) complexes **3** of a phosphoazonium **4** cation^{11,12} (cation **4**, also called an iminophosphenium cation,¹³ can be considered a phosphorus analogue of the diazonium cation). The new complexes **3** involve a hexahapto (η^6) association of the arene with the phosphorus center and represent models of π -complex intermediates in electrophilic aromatic substitution. In addition, we relate other known structures which have perhaps been overlooked in the context of this important reaction.

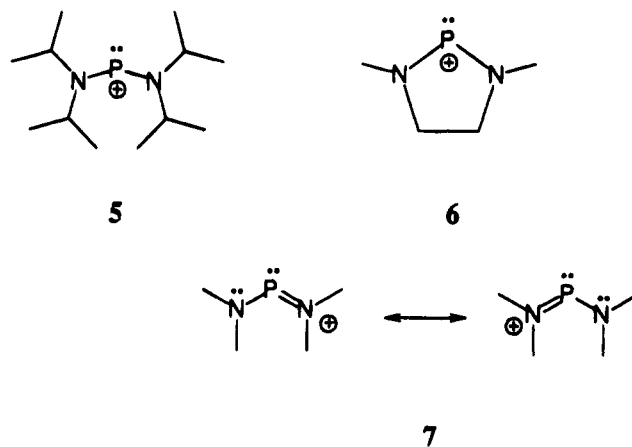
Results and Discussion

Reactions of [(2,4,6-tri-*tert*-butylphenyl)imino]chlorophosphine (Mes^*NPCl)¹³ and GaCl_3 in three arene solvents (benzene, toluene, or mesitylene) produce salts of the form $[\text{Mes}^*\text{NP-arene}][\text{anion}]$. Observation of a single signal in the ³¹P NMR spectra of the reaction mixtures indicates a quantitative reaction in each case. The salts contain either the GaCl_4^- (gallate) or the Ga_2Cl_7^- (digallate) anion which are obtained on the basis of the selected stoichiometry. Reaction mixtures generally separate into oily layers or produce oils upon removal of solvent *in vacuo*, but crystalline materials have been obtained in good yield by redissolution and recrystallization from various solvents, as described in the experimental section. The gallate salts are suscep-

tible to loss of the arene from the solid,¹⁴ and under dynamic vacuum (24 h at 10^{-3} Torr) benzene and toluene can be quantitatively removed from the respective salts. In contrast, the digallate salts remain unchanged under vacuum over long periods of time (>60 h).

Solid State Structures. Five salts of the general formula $[\text{Mes}^*\text{NP(arene)}][\text{anion}]$ have been isolated and comprehensively characterized, including X-ray crystal structures. The crystal data are presented in Table 1, atomic positional parameters are listed in Tables 2–6, and selected bond lengths and angles are compared in Table 7. Table 8 lists pertinent structural features, solid state and solution NMR data, and IR data for the five salts in comparison to data obtained for the material from which the arene has been removed *in vacuo* (containing the uncomplexed cation, Mes^*NP^+), as well as literature data for the free arenes.

Each salt is composed of discrete ions with a typical tetrahedral geometry observed for GaCl_4^- anions and predictable structural parameters for Ga_2Cl_7^- anions.¹⁵ Nevertheless, there are a number of close contacts evident. In the gallate salts the cation engages two anions with phosphorus to chlorine contacts (P...Cl) as short as 3.083(4) Å. The digallate salts adopt an ion pair arrangement with the closest contacts (P...Cl) at 3.395(3) Å (see Table 7 for a complete listing of ion contacts). The contacts are all substantially longer than a typical covalent P–Cl bond (PCl_3 , 2.043 Å; PCl_6^- , 2.14 Å)¹⁶ or than in the covalent compounds Mes^*NPCl [2.142(4) Å]¹³ and $\text{Mes}^*\text{NPCl}_3$ [2.017(1) and 2.004(1) Å].¹⁷ The interactions are, however, significantly shorter than the interior contacts observed in other salts of phosphorus cations. For example, the closest P...Cl contacts for the diaminophosphenium cations **5** and **6**



are 3.867(6) and 3.548(1) Å, respectively.¹⁸ Such cation–anion contacts are routinely observed in salts of non-metal cations and have been interpreted as donations from anion to cation;¹⁹ however, they do not appear to

(9) Olah, G. A. *Acc. Chem. Res.* **1971**, *4*, 240–248.

(10) Caille, S. Y.; Corriu, R. J. P. *Tetrahedron* **1989**, *25*, 2005–2022. Christy, P. F.; Ridd, J. H.; Stears, N. D. *J. Chem. Soc. B* **1970**, 797–801. Ridd, J. H. *Acc. Chem. Res.* **1971**, *4*, 248–253. Taylor, R.; Tewson, T. J. *J. Chem. Soc., Chem. Commun.* **1973**, 836.

(11) Preliminary communication: Burford, N.; Clyburne, J. A. C.; Bakshi, P. K.; Cameron, T. S. *J. Am. Chem. Soc.* **1993**, *115*, 8829–8830.

(12) Curtis, J. M.; Burford, N.; Parks, T. M. *Org. Mass Spectrom.* **1994**, *29*, 414–418.

(13) Niecke, E.; Nieger, M.; Reichert, F. *Angew. Chem., Int. Ed. Engl.* **1988**, *27*, 1715–1716.

(14) As previously noted for the AlCl_4 salt by: Curtis, R. D.; Schriver, M. J.; Wasylishen, R. E. *J. Am. Chem. Soc.* **1991**, *113*, 1493–1498.

(15) Klinzing, P.; Willing, W.; Müller, U.; Dehnicke, K. *Z. Anorg. Allg. Chem.* **1985**, *520*, 35–45.

(16) Corbridge, D. E. C. *Phosphorus*; Elsevier: Amsterdam, 1990.

(17) Burford, N.; Clyburne, J. A. C.; Gates, D. P.; Schriver, M. J.; Richardson, J. F. *J. Chem. Soc., Dalton Trans.* **1994**, 997–1001.

(18) Burford, N.; Losier, P.; Macdonald, C.; Kyrimis, V.; Bakshi, P. K.; Cameron, T. S. *Inorg. Chem.* **1994**, *33*, 1434–1439.

(19) Bader, R. F. W.; Gillespie, R. J.; MacDougall, P. J. In *From Atoms to Polymers; Molecular Structure and Energetics*; Liebman, J.; Greenberg, A., Eds.; VCH: New York, 1989; Vol. 11, p 1.

Table 1. Crystallographic Data

compd	[Mes*NP(benzene)]-[GaCl ₄]	[Mes*NP(toluene)]-[GaCl ₄]	[Mes*NP(benzene)]-[Ga ₂ Cl ₇]	[Mes*NP(toluene)]-[Ga ₂ Cl ₇]	[Mes*NP(mesitylene)]-[Ga ₂ Cl ₇]
formula	C ₂₄ H ₃₅ NPCL ₄ Ga	C ₂₅ H ₃₇ NPCL ₄ Ga	C ₂₄ H ₃₅ NPGa ₂ Cl ₇	C ₂₅ H ₃₇ NPGa ₂ Cl ₇	C ₂₇ H ₄₁ NPGa ₂ Cl ₇
crystl size (mm ³)	0.20 × 0.25 × 0.35	0.5 × 0.25 × 0.10	0.50 × 0.45 × 0.35	0.40 × 0.15 × 0.35	0.20 × 0.30 × 0.40
system	orthorhombic	orthorhombic	triclinic	triclinic	triclinic
space group	<i>Pbca</i> (No. 61)	<i>Pbca</i> (No. 61)	<i>P1</i> (No. 2)	<i>P1</i> (No. 2)	<i>P1</i> (No. 2)
<i>a</i> (Å)	24.948(4)	25.006(9)	11.579(2)	11.571(4)	12.119(3)
<i>b</i> (Å)	20.195(4)	20.358(8)	16.350(3)	16.335(5)	16.575(4)
<i>c</i> (Å)	11.953(3)	12.126(5)	11.085(3)	11.326(3)	11.309(3)
α (deg)	90	90	90.74(2)	91.47(4)	93.22(2)
β (deg)	90	90	118.00(2)	117.87(2)	115.62(2)
γ (deg)	90	90	73.53(2)	105.34(3)	107.64(2)
<i>V</i> (Å ³)	6022(4)	6173(8)	1759(1)	1797(1)	1905(1)
<i>Z</i>	8	8	2	2	2
<i>D_c</i> (Mg m ⁻³)	1.279(1)	1.278(2)	1.428(1)	1.423(1)	1.391(1)
<i>F</i> (000)	2400	2464	764	780	812
μ (cm ⁻¹)	13.32	13.01	21.23	20.80	19.64
no. of measd rflns	5002	3719	5175	4807	7068
no. of unique rflns	1463	1136	3338	2416	3009
100 <i>R</i> merg			2.00	4.70	4.60
no. of obsd rflns [<i>I</i> > 3σ(<i>I</i>)]	1463	1136	3338	2416	3009
no. of params refined	280	289	377	391	343
transm factors (min, max)	0.61:1.00	0.56:1	0.70:1.0	0.59:1.0	
weighting scheme	unit	2.444/σ ² (<i>F</i>) + 0.0038 <i>F</i> ²	unit	unit	unit
100 <i>R</i>	4.19	7.60	3.86	4.64	4.20
100 <i>R_w</i>	4.19	7.60	3.86	4.64	4.50
goodness of fit	3.28	2.17	1.31	2.11	2.43
residual electron density (min, max) (e/Å ⁻³)	-0.26, 0.28	-0.58, 0.69	-0.33, 0.41	-0.41, 0.50	-0.38, 0.54

Table 2. Fractional Atomic Positional Parameters and Equivalent Isotropic Temperature Factors (Å²) for [Mes*NP(benzene)][GaCl₄]

atom	<i>x/a</i>	<i>y/b</i>	<i>z/c</i>	<i>U_{eq}</i>
Ga(1)	0.3182(0)	0.0637(0)	0.0986(1)	0.0670
Cl(1)	0.2933(1)	0.0394(1)	-0.0718(2)	0.0970
Cl(2)	0.2504(1)	0.1072(1)	0.1840(2)	0.0933
Cl(3)	0.3417(1)	-0.0275(1)	0.1796(2)	0.1005
Cl(4)	0.3831(1)	0.1328(1)	0.0950(3)	0.1130
P(1)	0.6989(1)	0.1126(1)	0.0538(2)	0.0749
N(1)	0.6490(2)	0.1448(3)	0.0942(6)	0.0521
C(1)	0.6047(3)	0.1794(4)	0.1336(6)	0.0491
C(2)	0.5638(3)	0.1434(4)	0.1878(7)	0.0516
C(3)	0.5229(3)	0.1800(4)	0.2342(7)	0.0548
C(4)	0.5214(3)	0.2500(4)	0.2322(7)	0.0563
C(5)	0.5613(3)	0.2819(4)	0.1727(7)	0.0574
C(6)	0.6039(3)	0.2503(4)	0.1221(6)	0.0499
C(7)	0.5612(3)	0.0668(4)	0.1942(7)	0.0589
C(8)	0.5086(4)	0.0417(4)	0.2488(10)	0.0945
C(9)	0.5608(3)	0.0369(4)	0.0752(8)	0.0771
C(10)	0.6069(3)	0.0386(4)	0.2657(7)	0.0700
C(11)	0.4778(3)	0.2894(4)	0.2902(8)	0.0737
C(12)	0.5023(4)	0.3387(5)	0.3704(10)	0.1161
C(13)	0.4376(5)	0.2482(6)	0.3531(13)	0.1665
C(14)	0.4459(5)	0.3286(7)	0.2027(11)	0.1538
C(15)	0.6458(3)	0.2892(3)	0.0572(6)	0.0519
C(16)	0.6503(3)	0.2638(4)	-0.0641(6)	0.0667
C(17)	0.6308(3)	0.3632(4)	0.0498(8)	0.0845
C(18)	0.6995(3)	0.2872(4)	0.1205(7)	0.0704
C(19)	0.8019(4)	0.0746(6)	0.9029(13)	0.1189
C(20)	0.7893(4)	0.1331(9)	0.8532(9)	0.1148
C(21)	0.7934(5)	0.1904(6)	0.9118(14)	0.1288
C(22)	0.8145(5)	0.1883(7)	1.0171(14)	0.1276
C(23)	0.8305(5)	0.1300(9)	1.0648(9)	0.1321
C(24)	0.8259(5)	0.0719(7)	1.0062(14)	0.1360

Table 3. Fractional Atomic Positional Parameters and Equivalent Isotropic Temperature Factors (Å²) for [Mes*NP(benzene)][GaCl₄]

atom	<i>x/a</i>	<i>y/b</i>	<i>z/c</i>	<i>U_{eq}</i>
Ga(1)	0.31653(9)	0.55624(9)	0.09355(17)	0.0531
Cl(1)	0.3397(2)	0.4620(2)	0.1650(4)	0.0804
Cl(2)	0.2898(2)	0.5350(3)	-0.0743(4)	0.1009
Cl(3)	0.3819(2)	0.6220(3)	0.0899(6)	0.1090
Cl(4)	0.2502(2)	0.5991(2)	0.1842(4)	0.0807
P(1)	0.3011(2)	0.3820(2)	-0.0516(5)	0.0624
N(1)	0.3526(5)	0.3495(6)	-0.0922(10)	0.0425
C(1)	0.3981(7)	0.3200(8)	-0.1345(13)	0.0458
C(2)	0.4389(6)	0.3552(7)	-0.1853(13)	0.0307
C(3)	0.4782(6)	0.3196(7)	-0.2359(14)	0.0449
C(4)	0.4806(7)	0.2503(8)	-0.23069(14)	0.0588
C(5)	0.4410(7)	0.2184(8)	-0.1701(15)	0.0585
C(6)	0.3983(6)	0.2513(9)	-0.1197(12)	0.0419
C(7)	0.4370(8)	0.4316(7)	-0.1941(17)	0.0597
C(8)	0.4892(10)	0.4555(8)	-0.2496(19)	0.0850
C(9)	0.4396(8)	0.4621(8)	-0.0755(16)	0.0681
C(10)	0.3917(8)	0.4595(7)	-0.2614(15)	0.0511
C(11)	0.5244(7)	0.2141(8)	-0.29199(17)	0.0835
C(12)	0.4997(9)	0.1584(10)	-0.3634(22)	0.1321
C(13)	0.5612(12)	0.1782(16)	-0.2077(23)	0.2399
C(14)	0.5598(11)	0.2562(11)	-0.3650(26)	0.1939
C(15)	0.3584(6)	0.2080(7)	-0.0561(14)	0.0552
C(16)	0.3762(8)	0.1356(7)	-0.0459(17)	0.0744
C(17)	0.3035(6)	0.2093(10)	-0.1159(14)	0.0818
C(18)	0.3520(7)	0.2331(9)	0.0638(13)	0.0738
C(19)	0.6716(8)	0.0979(14)	0.0094(20)	0.1118
C(20)	0.6741(10)	0.1573(16)	0.0645(23)	0.1368
C(21)	0.6952(11)	0.2019(13)	-0.0103(28)	0.1412
C(22)	0.7189(13)	0.2055(15)	-0.1138(30)	0.1744
C(23)	0.7111(9)	0.1430(16)	-0.1506(24)	0.1461
C(24)	0.6926(8)	0.0892(12)	-0.0959(20)	0.0938
C(25)	0.6461(14)	0.0362(14)	0.0617(26)	0.1894

affect the structural features of the cation.²⁰ We interpret these significant differences in contact distance in terms of the relative acidic character of the phosphorus centers, which is likely mediated more effectively in the diamminophosphonium cations (such as **5** and **6**) by virtue of π-resonance of positive charge over

three atomic centers, **7**. All structures consist of the novel [Mes*NP(arene)]⁺ cation in which the arene is best described as hexahapto bound (η⁶) to the phosphorus center. A crystallographic view of the mesitylene derivative [Mes*NP(mesitylene)]⁺ is shown in Figure 1. The arene carbon atoms for all salts are essentially equidistant from the phosphorus center, and the largest angle deviation from 90° between the phosphorus center, the arene centroid, and a carbon

(20) See, for example: Burford, N.; Mason, S.; Spence, R. E. v. H.; Whalen, J. M.; Richardson, J. F.; Rogers, R. D. *Organometallics* **1992**, *11*, 2241-2250.

Table 4. Fractional Atomic Positional Parameters and Equivalent Isotropic Temperature Factors (\AA^2) for [Mes*NP(benzene)][Ga₂Cl₇]

atom	<i>x/a</i>	<i>y/b</i>	<i>z/c</i>	<i>U</i> _{eq}
Ga(1)	0.10912(7)	0.78079(4)	0.28540(7)	0.0613
Ga(2)	-0.25324(7)	0.78813(4)	0.18563(7)	0.0569
Cl(1)	-0.0116(1)	0.8899(0)	0.1258(1)	0.0759
Cl(2)	0.2737(2)	0.8053(1)	0.4611(2)	0.1245
Cl(3)	0.1660(2)	0.6641(1)	0.2094(2)	0.1050
Cl(4)	-0.0308(1)	0.7591(1)	0.3686(1)	0.0719
Cl(5)	-0.3418(2)	0.9236(1)	0.1496(2)	0.1022
Cl(6)	-0.3446(1)	0.7243(1)	0.2661(1)	0.0934
Cl(7)	-0.2306(1)	0.7315(1)	0.0191(1)	0.0771
P(1)	0.0959(1)	0.1948(0)	0.1742(1)	0.0604
N(1)	-0.0187(3)	0.2511(2)	0.1888(3)	0.0442
C(1)	-0.1261(4)	0.3040(2)	0.2066(4)	0.0387
C(2)	-0.1252(4)	0.3880(2)	0.2384(4)	0.0387
C(3)	-0.2345(5)	0.4374(3)	0.2552(4)	0.0468
C(4)	-0.3410(4)	0.4084(3)	0.2428(4)	0.0446
C(5)	-0.3354(4)	0.3250(3)	0.2133(4)	0.0464
C(6)	-0.2320(4)	0.2708(2)	0.1937(4)	0.0423
C(7)	-0.0101(5)	0.4248(3)	0.2543(5)	0.0505
C(8)	-0.0361(6)	0.5176(3)	0.2907(7)	0.0787
C(9)	-0.0056(6)	0.4299(4)	0.1186(6)	0.0778
C(10)	0.1295(5)	0.3714(3)	0.3747(6)	0.0723
C(11)	-0.4584(5)	0.4678(3)	0.2601(5)	0.0529
C(12)	-0.4019(6)	0.5061(4)	0.3944(6)	0.0875
C(13)	-0.5394(6)	0.5436(4)	0.1422(6)	0.1004
C(14)	-0.5554(6)	0.4243(4)	0.2607(8)	0.1097
C(15)	-0.2344(5)	0.1789(3)	0.1599(6)	0.0583
C(16)	-0.2413(6)	0.1666(4)	0.0190(6)	0.0884
C(17)	-0.1085(6)	0.1111(3)	0.2768(7)	0.0808
C(18)	-0.3624(5)	0.1628(3)	0.1502	0.0810
C(19)	0.4111(6)	0.1094(6)	0.2955(9)	0.1465
C(20)	0.3629(7)	0.0454(5)	0.2319(7)	0.1349
C(21)	0.2960(8)	0.0094(4)	0.2762(8)	0.1310
C(22)	0.2790(7)	0.0355(5)	0.3835(8)	0.1159
C(23)	0.3259(7)	0.0981(5)	0.4475(6)	0.1233
C(24)	0.3920(7)	0.1355(5)	0.4042(8)	0.1464

center of the arene is 6.2(8)°. Therefore, the phosphorus center represents a perpendicular projection from the centroid of the arene. Although there are clear differences between gallate and digallate salts, the decreasing P- -arene_{centroid} distance for the three digallate salts (benzene > toluene > mesitylene) is in accord with the π -donor capabilities of the arene. The benzene units in [Mes*NP(benzene)][GaCl₄] and [Mes*NP(benzene)][Ga₂Cl₇] are each structurally identical to free benzene,²¹ and there are no obvious distortions from planarity of the arene in any of the structures {maximum deviations (\AA) from planarity: benzene [GaCl₄], 0.0029; benzene [Ga₂Cl₇], 0.005; toluene [GaCl₄], 0.033; toluene [Ga₂Cl₇], 0.028; mesitylene [Ga₂Cl₇], 0.014}. Nonetheless, it is interesting to note that the P- -Cl contacts increase in length as the P- -arene_{centroid} distances decrease.

The N-P bond lengths in the new cations are predictably short and are comparable to the shortest yet reported in the trihaloiminophosphoranes [Mes*NP(Cl)₃, 1.467(4) \AA ;¹⁷ (CF₃)₃CN(P(Cl)₃, 1.504(2) \AA ;²² (CCl₃)₂(Cl)-CN(P(Cl)₃, 1.505(3) \AA ;²³], which are themselves substantially shorter than typically observed in monomeric iminophosphoranes [PhNPPPh₃, 1.602(3) \AA ;²⁴ PyNPPPh₃,

Table 5. Fractional Atomic Positional Parameters and Equivalent Isotropic Temperature Factors (\AA^2) for [Mes*NP(toluene)][Ga₂Cl₇]

atom	<i>x/a</i>	<i>y/b</i>	<i>z/c</i>	<i>U</i> _{eq}
Ga(1)	0.88762(14)	0.27725(9)	0.22694(13)	0.0710
Ga(2)	1.25120(14)	0.28186(8)	0.33209(13)	0.0665
Cl(1)	0.7243(4)	0.2973(3)	0.0506(3)	0.1385
Cl(2)	0.8300(4)	0.1622(2)	0.2986(4)	0.1230
Cl(3)	1.0042(3)	0.3886(2)	0.3841(3)	0.0923
Cl(4)	1.0309(3)	0.2539(2)	0.1500(2)	0.0791
Cl(5)	1.2260(3)	0.2244(1)	0.4899(3)	0.0873
Cl(6)	1.3435(3)	0.2180	0.2506(3)	0.1069
Cl(7)	1.3412(3)	0.4179(1)	0.3799(3)	0.1020
P(1)	0.9051(3)	0.6955(1)	0.3165(3)	0.0711
N(1)	1.0188(7)	0.7500(4)	0.3018(7)	0.0486
C(1)	1.1250(9)	0.8014(5)	0.2846(8)	0.0448
C(2)	1.1241(9)	0.8858(5)	0.2553(8)	0.0447
C(3)	1.2340(9)	0.9343(6)	0.2424(9)	0.0541
C(4)	1.3405(9)	0.9056(6)	0.2534(9)	0.0523
C(5)	1.3347(9)	0.8220(6)	0.2794(9)	0.0532
C(6)	1.2312(9)	0.7686(5)	0.2960(9)	0.0502
C(7)	1.0074(10)	0.9232(6)	0.2403(9)	0.0552
C(8)	1.0322(11)	1.0145(6)	0.2063(12)	0.0823
C(9)	0.8672(10)	0.8684(7)	0.1235(10)	0.0811
C(10)	1.0043(12)	0.9300(7)	0.3740(10)	0.0830
C(11)	1.4571(10)	0.9644(6)	0.2396(10)	0.0604
C(12)	1.4027(12)	1.0037(8)	0.1111(12)	0.0988
C(13)	1.5532(12)	0.9201(8)	0.2369(14)	0.1119
C(14)	1.5366(12)	1.0389(7)	0.3571(12)	0.1001
C(15)	1.2336(10)	0.6776(6)	0.3247(11)	0.0702
C(16)	1.3605(11)	0.6596(7)	0.3297(13)	0.0952
C(17)	1.2453(12)	0.6668(8)	0.4645(12)	0.1036
C(18)	1.1078(11)	0.6088(6)	0.2105(13)	0.0946
C(19)	0.3864(13)	0.4240(9)	0.7470(14)	0.1434
C(20)	0.3251(13)	0.4848(10)	0.7532(14)	0.1474
C(21)	0.2788(14)	0.4819(8)	0.8464(14)	0.1382
C(22)	0.3100(12)	0.4222(9)	0.9294(12)	0.1203
C(23)	0.3748(12)	0.3616(9)	0.9344(14)	0.1329
C(24)	0.4093(13)	0.3661(10)	0.8343(14)	0.1494
C(25)	0.2683(17)	0.4243(13)	1.0342(15)	0.2565

1.574(2) \AA ;²⁵ NC(NMe₂)NC(Cl)NCNPPPh₃, 1.622(5) \AA ;²⁶]. The original report of **4** revealed a N-P bond length of 1.475(8) \AA ,¹³ which was considered a triple NP bond, and this model is supported by theoretical modeling.²⁷

The CP/MAS solid state ³¹P NMR spectra reveal a significant shielding (15 ppm) of the phosphorus center after removal of the arene from solid [Mes*NP(toluene)][GaCl₄] *in vacuo*. CP/MAS solid state ¹³C NMR data for [Mes*NP(benzene)][Ga₂Cl₇] and [Mes*NP(toluene)][Ga₂Cl₇] show shifts to higher frequency as large as 5 ppm relative to the values for pure liquid arene, and the values are consistent with the data observed in dichloromethane solution (see below).

The FT-infrared spectra of the salts are complex; nonetheless, overtone and combination bands in the 2000-1750 cm⁻¹ region corresponding to the C-H out-of-plane deformations²⁸ are well separated from other bands in the spectra. These bands are distinctive for the arene (Table 8), and their significant shift to higher energy with respect to those of the pure (free) arene is further evidence of interaction between the arene and the phosphorus center.

(25) Kulpe, S.; Seidel, I.; Bodeker, J.; Kockritz, P. *Cryst. Res. Technol.* **1984**, *19*, 649-654.

(26) Cameron, T. S.; Mannan, K.; Biddlestone, M.; Shaw, R. A. *Z. Naturforsch.* **1975**, *30B*, 973-974.

(27) Glaser, R.; Horan, C. J.; Haney, P. E. *J. Phys. Chem.* **1993**, *97*, 1835-1844. Glaser, R.; Horan, C. J.; Choy, G. S.-C.; Harris, B. L. *J. Phys. Chem.* **1992**, *96*, 3689-3697. Bunker, R. J.; Bruna, P. J.; Peyerimhoff, S. D. *Isr. J. Chem.* **1980**, *19*, 309-316.

(28) Bellamy, L. J. *The Infrared Spectra of Complex Molecules*; Chapman and Hall: London, 1975; p 75. Socrates, G. *Infrared Characteristic Group Frequencies*; Wiley and Sons: New York, 1980; p 85.

(21) Cameron, T. S.; Borecka, B.; Kwiatkowski, W. *J. Am. Chem. Soc.* **1994**, *116*, 1211-1219.

(22) Antipin, M. Y.; Struchkov, Y. T.; Yurchenko, V. M.; Kozlov, E. S. *J. Struct. Chem.* **1982**, *227*. Antipin, M. Y.; Struchkov, Y. T.; Kozlov, E. S. *J. Struct. Chem.* **1986**, *575*.

(23) Müller, U. Z. *Anorg. Allg. Chem.* **1980**, *463*, 117.

(24) Böhm, E.; Dehnicke, K.; Maurer, A.; Fenske, D. *Z. Naturforsch.* **1988**, *43B*, 138-144.

Table 6. Fractional Atomic Positional Parameters and Equivalent Isotropic Temperature Factors (\AA^2) for $[\text{Mes}^*\text{NP}(\text{mesitylene})][\text{Ga}_2\text{Cl}_7]$

atom	x	y	z	B_{eq}
Ga(1)	0.26421(9)	0.27867(6)	0.3570(1)	4.69(3)
Ga(2)	-0.08402(9)	0.27402(6)	0.2463(1)	5.18(4)
Cl(1)	0.3541(2)	0.4159(1)	0.4131(3)	7.4(1)
Cl(2)	0.2358(3)	0.2200(2)	0.5104(2)	7.1(1)
Cl(3)	0.3495(2)	0.2205(2)	0.2625(3)	7.2(1)
Cl(4)	0.0568(2)	0.2460(1)	0.1784(2)	5.23(8)
Cl(5)	-0.1606(3)	0.1577(2)	0.3045(4)	10.6(2)
Cl(6)	0.0270(3)	0.3845(2)	0.4110(3)	7.6(1)
Cl(7)	-0.2188(3)	0.2971(3)	0.0691(3)	11.6(2)
P(1)	-1.0978(2)	-0.3095(1)	0.2899(2)	4.05(7)
N(1)	-0.9797(5)	-0.2498(3)	0.2904(6)	3.5(2)
C(1)	-0.8721(6)	-0.1956(4)	0.2805(7)	3.2(2)
C(2)	-0.8718(6)	-0.1125(4)	0.2523(7)	3.3(2)
C(3)	-0.7636(7)	-0.0620(4)	0.2401(7)	3.8(3)
C(4)	-0.6622(7)	-0.0889(5)	0.2519(7)	4.0(3)
C(5)	-0.6671(7)	-0.1701(5)	0.2799(7)	4.0(3)
C(6)	-0.7695(7)	-0.2255(4)	-0.2956(7)	3.5(2)
C(7)	-0.9798(7)	-0.0780(4)	0.2385(8)	3.9(3)
C(8)	-0.992(1)	-0.0726(6)	0.370(1)	6.3(4)
C(9)	-1.114(8)	-0.1330(5)	0.1158(9)	5.7(3)
C(10)	-0.9494(9)	0.0147(5)	0.212(1)	6.1(4)
C(11)	-0.5464(8)	-0.0284(5)	0.236(1)	5.1(3)
C(12)	-0.600(1)	0.0076(8)	0.110(1)	9.3(5)
C(13)	-0.469(1)	0.0482(7)	0.354(1)	8.7(5)
C(14)	-0.462(1)	-0.0732(7)	0.222(2)	10.7(6)
C(15)	-0.7647(7)	-0.3129(5)	0.331(8)	4.5(3)
C(16)	-0.6412(9)	-0.3267(6)	0.343(1)	6.6(4)
C(17)	-0.8839(9)	-0.3902(5)	0.223(1)	6.2(4)
C(18)	-0.760(1)	-0.3144(6)	0.472(1)	6.6(4)
C(19)	0.6623(8)	0.5188(5)	0.2059(8)	4.9(3)
C(20)	0.6083(7)	0.5818(6)	0.1984(9)	5.2(3)
C(21)	0.6132(8)	0.6385(5)	0.112(1)	5.1(3)
C(22)	0.6710(8)	0.6291(5)	0.0321(8)	4.7(3)
C(23)	0.7254(8)	0.5656(5)	0.0369(8)	4.8(3)
C(24)	0.7217(8)	0.5120(5)	0.1276(8)	4.7(3)
C(25)	0.654(1)	0.4562(6)	0.297(1)	7.4(4)
C(26)	0.555(1)	0.7076(7)	0.102(1)	8.7(5)
C(27)	0.783(1)	0.5521(7)	-0.054(1)	7.9(5)

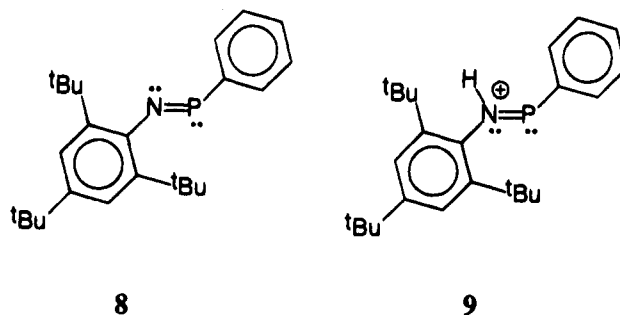
Solution Features. Solution NMR data have been obtained for all salts both in the corresponding arene and in CD_2Cl_2 . ^{31}P NMR chemical shifts for the salts seem to be independent of the type of arene solvent, but there is a significant chemical shift difference (as large as 15 ppm) between the gallate and digallate salts. In general, the solution chemical shifts are consistent with those observed in the solid state. The arene free salt $[\text{Mes}^*\text{NP}][\text{GaCl}_4]$ reacts slowly with dichloromethane; however, spectra obtained within minutes of sample preparation reveal a ^{31}P chemical shift (76 ppm) identical to those of the benzene and toluene complexes. This is in contrast to the 15 ppm difference observed between $[\text{Mes}^*\text{NP}][\text{GaCl}_4]$ and $[\text{Mes}^*\text{NP}(\text{toluene})][\text{GaCl}_4]$ in the solid state spectra, and we conclude that solvation of the arene free salt involves a significant interaction with dichloromethane which has an affect comparable to that of the coordinated arene. It is interesting to note that the nature of the anion has a more dramatic effect on the ^{31}P chemical shift, thus supporting the existence of substantial ion pairing in solution.¹⁸

The arene units of the salts in dichloromethane solution exhibit a significant deshielding of the ^{13}C and ^1H nuclei with respect to those of the pure arene, and the data are consistent with the solid state NMR spectra. Most importantly, the observed deshielding of resonances due to the arene confirms retention of the P--arene interaction in CD_2Cl_2 solution.

Isolable π -Complexes as Models for Intermediates in Electrophilic Aromatic Substitution. The

extensive and diverse coordination chemistry that has been established for metal elements, including those from the s and p block, represent an enormous component of our understanding of inorganic chemistry. The non-metal elements of the p block are rarely considered in this context, except in the typical adducts of boranes. A rich and diverse coordination chemistry of the non-metal elements is in fact demonstrated by compounds such as I_3^- , SF_5^- , and PCl_6^- , which represent σ -complexes of halide ions coordinated to non-metal acids (I_2 , SF_4 , PCl_5). Non-metals are also observed to accommodate π -ligands such as cyclopentadienide,²⁹ as in Cp^*As^+ ,³⁰ which may be considered a non-metal analogue of the metallocenes. Examples of η^6 -arene complexation to the heavier p-block metals and metalloids are also well established,³¹ including a series of complexes involving benzenes coordinated to group 15 trihalides (EX_3 : E = As, Sb, Bi; X = Cl, Br, I)³² and cationic centers such as $\text{Ga}(\text{I})$,³³ $\text{In}(\text{I})$,³⁴ and $\text{Sn}(\text{II})$.³⁵ The classical benzene--dihalogen complexes,³⁶ referred to as charge transfer complexes, represent examples of π -complexation to neutral non-metal elements. Most fascinating are the arene π -complexes of NO^+ which are reported to have much greater stability³⁷ than the group 15 trihalide complexes. Interestingly, these complexes have not been discussed in the context of the electrophilic aromatic substitution reaction despite being obvious examples of stable models for the π -complex intermediate (where E = NO^+).

The arene-phosphaazonium complexes **3** described in this report are also examples of stable π -complex intermediates in electrophilic aromatic substitution. The kinetic stability for the derivatives of **3** is implied by the fact that reaction of the phenyliminophosphine **8**³⁸



with triflic acid (HSO_3CF_3) quantitatively generates a compound with a ^{31}P NMR shift of 187 ppm, which we assign to the aminophenylphosphenium cation **9**, dem-

(29) Jutzli, P. *J. Organomet. Chem.* **1990**, *400*, 1-17; *Chem. Rev.* **1986**, *86*, 983-996.

(30) Jutzli, P.; Wippermann, T.; Krüger, C.; Kraus, H. *J. Angew. Chem., Int. Ed. Engl.* **1983**, *22*, 250-251.

(31) See, for example, Maslowsky, E. *J. Chem. Educ.* **1993**, *70*, 980-984.

(32) Schmidbaur, H.; Nowak, R.; Steigelmann, O.; Müller, G. *Chem. Ber.* **1990**, *123*, 1221-1226. Schmidbaur, H.; Nowak, R.; Steigelmann, O.; Müller, G. *Chem. Ber.* **1990**, *123*, 19-22. Probst, T.; Steigelmann, O.; Riede, J.; Schmidbaur, H. *Chem. Ber.* **1991**, *124*, 1089-1093. Schmidbaur, H.; Bublak, W.; Huber, B.; Müller, G. *Angew. Chem., Int. Ed. Engl.* **1987**, *26*, 234-236.

(33) See, for example: Schmidbaur, H. *Angew. Chem., Int. Ed. Engl.* **1985**, *24*, 893-1008. Schmidbaur, H.; Bublack, W.; Huber, B.; Müller, G. *Organometallics* **1986**, *5*, 1647-1651. Schmidbaur, H.; Thewalt, U.; Zafropoulos, T. *Angew. Chem., Int. Ed. Engl.* **1984**, *23*, 76-77. Schmidbaur, H.; Thewalt, U.; Zafropoulos, T. *Organometallics* **1983**, *2*, 1550-1554.

(34) Ebenhöch, J.; Müller, G.; Riede, J.; Schmidbaur, H. *Angew. Chem., Int. Ed. Engl.* **1984**, *23*, 386-388.

Table 7. Selected Bond Lengths (Å) and Angles (deg)

	[Mes*NP(benzene)]- [GaCl ₄]	[Mes*NP(toluene)]- [GaCl ₄]	[Mes*NP(benzene)]- [Ga ₂ Cl ₇]	[Mes*NP(toluene)]- [Ga ₂ Cl ₇]	[Mes*NP(mesitylene)]- [Ga ₂ Cl ₇]
P-N	1.484(7)	1.529(15)	1.463(5)	1.464(9)	1.471(6)
N-C _{Mes*}	1.391(11)	1.39(2)	1.396(7)	1.393(13)	1.395(8)
C _{Mes*} -N-P	175.5(7)	177.0(13)	178.5(4)	178.7(8)	175.7(5)
P ₁ -C ₁₉	3.232(14)	3.31(3)	3.102(10)	3.201(3)	3.122(7)
P ₁ -C ₂₀	3.318(14)	3.28(3)	3.135(9)	3.144(3)	3.117(8)
P ₁ -C ₂₁	3.30(2)	3.24(3)	3.079(9)	3.021(3)	2.989(8)
P ₁ -C ₂₂	3.30(2)	3.38(4)	3.011(9)	2.956(3)	2.874(7)
P ₁ -C ₂₃	3.306(15)	3.37(3)	2.989(9)	3.017(30)	2.899(8)
P ₁ -C ₂₄	3.32(2)	3.30(3)	3.028(9)	3.140(3)	2.983(8)
P--arene _{centroid}	3.0012(6)	3.038(13)	2.820(4)	2.767(7)	2.687(7)
P ₁ -C _{centroid} -C ₁₉ ^a	87.3(6)	90.8(13)	87.5(4)	91.7(7)	94.2(7)
P ₁ -C _{centroid} -C ₂₀	91.7(7)	86.9(13)	89.7(4)	93.4(7)	93.4(7)
P ₁ -C _{centroid} -C ₂₁	90.3(7)	88(2)	88.6(4)	87.3(7)	87.6(7)
P ₁ -C _{centroid} -C ₂₂	89.4(7)	87.1(13)	86.0(4)	83.8(8)	83.5(7)
P ₁ -C _{centroid} -C ₂₃	88.9(6)	91.4(13)	84.0(4)	85.0(7)	84.6(7)
P ₁ -C _{centroid} -C ₂₄	89.6(7)	90.0(12)	84.7(4)	87.7(7)	89.0(7)
P--Cl _{anion}	3.083(4)	3.139(9)	3.395(3)	3.487(4)	3.513(4)
P--Cl _{anion}	3.389(4)	3.237(9)	3.570(3)	3.584(4)	3.805(4)
P--Cl _{anion}	3.429(4)	3.474(8)			

^a Note: C19-C24 are the aromatic carbons of the coordinated arene (benzene, toluene, or mesitylene).

Table 8. Selected Bond Lengths (Å) and Angles (deg)

	[Mes*NP]- [GaCl ₄]	[Mes*NP- benzene]- [GaCl ₄]	[Mes*NP- toluene]- [GaCl ₄]	[Mes*NP- benzene]- [Ga ₂ Cl ₇]	[Mes*NP- toluene]- [Ga ₂ Cl ₇]	[Mes*NP- mesitylene]- [Ga ₂ Cl ₇]	benzene	toluene	mesitylene
P-arene _{centroid} (Å)		3.0012(6)	3.038(13)	2.820(4)	2.767(7)	2.687(4)			
³¹ P NMR (ppm, H ₃ PO ₄)									
in arene		71	78	93	91	91			
in CD ₂ Cl ₂	76	76	76	93	95	91			
in solid	63 ^a	c	79 ^b	90 ^a	89 ^a	c			
	65 ^b								
¹³ C NMR, arene only (ppm, TMS)									
in CD ₂ Cl ₂		128.7	C ₂ 132.4 C ₃ 131.4 C ₄ 128.1 CH ₃ 22.0	132.6	C ₂ 134.4 C ₃ 133.1 C ₄ 130.0 CH ₃ 22.3	131.1 CH ₃ 21.6	128.5 ^d	C ₂ 129.3 ^d C ₃ 128.5 C ₄ 125.7 CH ₃ 21.4	127.4 ^d CH ₃ 21.2
in solid				129.4			120		
¹ H NMR in CD ₂ Cl ₂ (ppm, TMS)									
arene only		7.38	7.56-7.47 (m) 7.49 _{max} CH ₃ 2.48	7.80	7.76-7.66 (m) 7.69 _{max} CH ₃ 2.56	7.21 2.42	7.23 ^e	7.04 _{max} ^e 2.29	6.69 ^e CH ₃ 2.23
IR _{Nujol} mult (cm ⁻¹)									
arene only		1979 1842	w and br	1981 1849	1971 1892 1842 1787	1813 1784 1759	1960 ^f 1815	1943 ^f 1860 1803 1735	1759 ^f 1713
mp (°C)	> 100 dec	90 dec	157-160	78-81	87-89	105-107			

^a This work. ^b See ref 14. ^c Not obtained. ^d Kalinowski, H. O.; Berger, S.; Braun, S. *Carbon-13 NMR Spectroscopy*; Wiley: New York, 1981. ^e Simons, W. W. Ed. *The Sadtler Handbook of Proton NMR Spectra*; Sadtler Research Laboratories: Philadelphia, 1978. ^f *Aldrich Library of Infrared Spectra*; Nicolet Instrument Corp.: Madison, WI, 1988.

onstrating the relative thermodynamic stability of **9** with respect to **3** or other possible structural arrangements. We are currently investigating the conditions

(35) See, for example: Weininger, M. S.; Rodesiler, P. F.; Amma, E. L. *Inorg. Chem.* **1979**, *18*, 751-755. Lefferts, J. L.; Hossain, M. B.; Molloy, K. C.; van der Helm, D.; Zuckerman, J. J. *Angew. Chem., Int. Ed. Engl.* **1980**, *19*, 309-310. Schmidbauer, H.; Probst, T.; Huber, B.; Müller, G.; C. Krüger, C. *J. Organomet. Chem.* **1989**, *365*, 53-60. Probst, T.; Steigelmann, O.; Riede, J.; Schmidbauer, H. *Angew. Chem., Int. Ed. Engl.* **1990**, *29*, 1397-1398. Luth, H.; Amma, E. L. *J. Am. Chem. Soc.* **1969**, *91*, 7515-7516. Weininger, M. S.; Rodesiler, P. F.; Gash, A. G.; Amma, E. L. *J. Am. Chem. Soc.* **1972**, *94*, 2135-2136. Rodesiler, P. F.; Auel, Th.; Amma, E. L. *J. Am. Chem. Soc.* **1975**, *97*, 7405-7410.

(36) Hassel, O.; Strømme, K. O. *Acta Scand.* **1958**, *12*, 1146-1147; **1959**, *13*, 1781-1786.

(37) Brownstein, S.; Gabe, E. J.; Lee, F.; Tan, L. *J. Chem. Soc., Chem. Commun.* **1984**, 1566-1568. Brownstein, S.; Morrison, A.; Tan, L. *Can. J. Chem.* **1986**, *64*, 265-269. Brownstein, S.; Gabe, E. J.; Lee, F.; Piotrowski, A. *Can. J. Chem.* **1986**, *64*, 1661-1667.

(38) Prepared *in situ* as alluded to by: Niecke, E.; Nixon, J. F.; Wenderoth, P.; Trigo Passos, B. F.; Nieger, M. *J. Chem. Soc., Chem. Commun.* **1993**, 846-848.

under which **3** is transformed into **9** in order to confirm the intermediacy of **3**.

The new phosphorus complexes **3** offer important comparisons with the recently reported silicon complex **1**. The novel salt [Et₃Si(toluene)][B(C₆F₅)₄]^{4,6} contains a formally cationic silicon center bound to a toluene molecule in an η^1 π -coordination **1**,³⁹ or as a σ -complex,⁴⁰ and is viewed as an example of a stabilized *Wheland intermediate* (where E = Et₃Si⁺).³⁹ The dramatic differences in coordinative strength and hapticity {E-arene distance, Si--C = 2.18 Å in [Et₃Si(η^1 -toluene)]^{4,6}; P--C_{avg} = 3.31(3) Å for [Mes*NP(η^6 -toluene)][GaCl₄]; P--C_{av} = 3.080(3) Å for [Mes*NP(η^6 -toluene)][Ga₂Cl₇]} are related to the relative acidities of the cationic centers. While the Si center of Et₃Si⁺ is

(39) Reed, C. A.; Xie, Z.; Bau, R.; Benesi, A. *Science* **1993**, *262*, 402-404.

(40) Schleyer, P. v. R.; Buzek, P.; Müller, T.; Apeloig, T.; Siehl, H. U. *Angew. Chem., Int. Ed. Engl.* **1993**, *32*, 1471-1473.

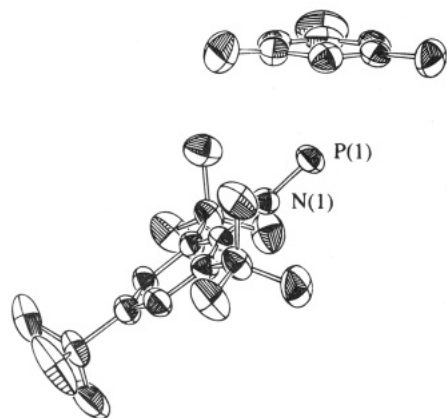
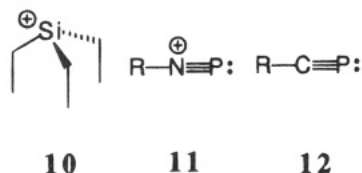


Figure 1. Crystallographic view of the cation in $[\text{Mes}^*\text{NP-mesitylene}][\text{Ga}_2\text{Cl}_7]$.

truly electron deficient, **10**, Mes^*NP^+ can be described



as an iminiophosphine, **11**, isoelectronic to the phosphalkynes **12**.⁴¹ In view of the significantly shorter Si...toluene interaction observed in the crystal structure of $[\text{Et}_3\text{Si}(\text{toluene})][\text{B}(\text{C}_6\text{F}_5)_4]$,^{4,6} we expect more pronounced spectroscopic features for the coordinated arene in the solid state than observed for salts of $[\text{Mes}^*\text{NP}(\text{arene})]^+$. More importantly, the $[\text{Et}_3\text{Si-toluene}]^+$ complex should remain intact in other solvents, such as dichloromethane, as observed for the $[\text{Mes}^*\text{NP}(\text{arene})]^+$ salts. We anticipate the discovery of numerous σ -arene and π -arene cationic complexes as kinetically stable species in suitable environments.

Experimental Section

$\text{Mes}^*\text{NP}(\text{Cl})$ was prepared following the literature procedure.⁴² GaCl_3 was sublimed under vacuum before use. Benzene, toluene, and mesitylene were dried over sodium/benzophenone. Hexanes were dried over CaH_2 . NaBPh_4 and HSO_3CF_3 were used as received from Aldrich. Solids were handled in a Vacuum Atmospheres nitrogen-filled drybox. Reactions were performed in an evacuated (10^{-3} Torr) reactor,⁴³ and all glassware was flame-dried under vacuum before use. Melting points were recorded on a Fisher-Johns apparatus and are uncorrected. Elemental analyses were performed by Beller Laboratories, Göttingen, Germany. Infrared spectra were recorded as Nujol mulls on CsI plates on a Nicolet 510P spectrometer. Solution NMR spectra were recorded on a Bruker AC-250 spectrometer in 5 mm flame-sealed Pyrex tubes. Solid state ^{31}P NMR spectra were obtained on a Bruker AMX 400 spectrometer and spin speeds are reported in hertz. All chemical shifts are reported in ppm referenced to external standards, 85% H_3PO_4 for ^{31}P , and TMS for ^1H and ^{13}C .

$[\text{Mes}^*\text{NP}(\text{benzene})][\text{GaCl}_4]$. A solution of GaCl_3 (0.21 g, 1.2 mmol) in benzene (≈ 15 mL) was added over a period of ≈ 5 min to a stirred solution of $\text{Mes}^*\text{NP}(\text{Cl})$ (0.38 g, 1.2 mmol) in benzene (≈ 15 mL), giving a bright yellow solution [^{31}P NMR

spectrum of the reaction mixture, 71 ppm]. Solvent was removed *in vacuo* overnight to yield a yellow powder which was characterized as $[\text{Mes}^*\text{NP}][\text{GaCl}_4]$. Recrystallization from benzene through repeated cycles of warming to ≈ 60 °C and slow cooling to room temperature gave $[\text{Mes}^*\text{NPC}_6\text{H}_6][\text{GaCl}_4]$, $\text{dp} \approx 90$ °C. Elemental analysis was not obtained. NMR (CD_2Cl_2): ^{31}P , 76 ppm; ^1H , 7.47 (d, $^5J_{\text{PH}} = 2$ Hz, 2 H), 1.56 (s, 18 H), 1.33 (s, 9 H) [Mes^*], 7.38 ppm (s, 6 H) [benzene]; ^{13}C , 123.8 (d, $^4J_{\text{PC}} = 3$ Hz), 30.9 (s), 30.1 (d, $^5J_{\text{PC}} = 2$ Hz) [Mes^*], 128.7 ppm (s) [benzene], quaternary carbon nuclei not observed. IR: 1979 (w), 1842 (w), 1597 (s), 1267 (m), 1245 (m), 1134 (m), 1066 (m), 1033 (m), 927 (w), 886 (s), 764 (m), 699 (s), 674 (s), 393 (s), 361 (s), 263 (m) cm^{-1} .

Benzene is quantitatively removed from the crystals under dynamic vacuum for 24 h to give $[\text{Mes}^*\text{NP}][\text{GaCl}_4]$, as characterized by IR and elemental analysis, $\text{dp} 122\text{--}123.5$ °C.

Anal. Calcd: C, 43.07; H, 5.82; N, 2.79. Found: C, 43.02; H, 5.79; N, 2.97. ^{31}P NMR (CH_2Cl_2): 76 ppm. IR: 1594 (s), 928 (m), 885 (m), 842 (m), 763 (m), 693 (m), 650 (w), 474 (w), 464 (m), 401 (s), 373 (s), 360 (s), 261 (m) cm^{-1} . ^{31}P CP/MAS NMR: 63 ppm (4000, 7000 Hz).

$[\text{Mes}^*\text{NP}(\text{toluene})][\text{GaCl}_4]$. A solution of GaCl_3 (0.08 g, 0.47 mmol) in toluene (≈ 2 mL) was added over ≈ 5 min to a stirred solution of $\text{Mes}^*\text{NP}(\text{Cl})$ (0.15 g, 0.47 mmol) in toluene (≈ 2 mL), giving a yellow solution [^{31}P NMR, 78 ppm]. Solvent was removed *in vacuo* to give a yellow powder which was recrystallized from a minimum amount of toluene to give $[\text{Mes}^*\text{NPC}_7\text{H}_8][\text{GaCl}_4]$ (0.13 g, 0.21 mmol, $\approx 50\%$), $\text{dp} 157\text{--}160$ °C. Elemental analysis was not obtained. NMR (CD_2Cl_2): ^{31}P , 76 ppm; ^1H , 7.36 (s, 2 H), 1.45 (s, 18 H), 1.28 (s, 9 H) [Mes^*], 7.56–7.47 (multiplet, 5 H), 2.48 ppm (s, 3 H) [toluene]; ^{13}C , 123.7 (d, $^5J_{\text{PC}} = 3$ Hz), 30.6, 29.4 [Mes^*], 132.4, 131.4, 128.1, 22.0 ppm [toluene], quaternary carbon nuclei not observed. IR: 1594 (w), 1267 (m), 1243 (w), 1133 (m), 886 (m), 762 (w), 722 (m), 699 (m), 674 (w), 400 (s), 368 (s), 266 (s) cm^{-1} .

Toluene is quantitatively removed from the crystals under dynamic vacuum for 24 h to give $[\text{Mes}^*\text{NP}][\text{GaCl}_4]$. IR: 1596 (s), 928 (m), 887 (m), 842 (m), 764 (m), 694 (m), 464 (m), 402 (s), 373 (s), 362 (s) cm^{-1} .

$[\text{Mes}^*\text{NP}(\text{benzene})][\text{Ga}_2\text{Cl}_7]$. A solution of GaCl_3 (0.41 g, 2.3 mmol) in benzene (≈ 10 mL) was added over a period of ≈ 5 min to a stirred solution of $\text{Mes}^*\text{NP}(\text{Cl})$ (0.38 g, 1.2 mmol) in benzene (≈ 10 mL). Upon standing for ≈ 5 min, a small amount of yellow oil formed under a bright yellow solution [^{31}P NMR: 93 ppm]. Solvent was removed *in vacuo* to yield a yellow powder which was recrystallized from benzene in hexane (75% v/v) with repeated cycles of warming to ≈ 60 °C and slow cooling to room temperature to give $[\text{Mes}^*\text{NPC}_6\text{H}_6][\text{Ga}_2\text{Cl}_7]$ (0.71 g, 0.95 mmol, 82%), $\text{mp} 78\text{--}81$ °C. Anal. Calcd: C, 38.12; H, 4.67; N, 1.85%. Found: C, 37.97; H, 4.47; N, 1.89. NMR (CD_2Cl_2): ^{31}P , 93 ppm; ^1H , 7.40 (s, 2 H), 1.48 (s, 18 H), 1.30 (s, 9 H) [Mes^*], 7.80 ppm (s, 6 H) [benzene]; ^{13}C , 124.0, 30.6, 29.3 [Mes^*], 132.6 ppm [benzene], quaternary carbon nuclei not observed. IR: 1981 (w), 1849 (w), 1597 (m), 1268 (m), 1135 (m), 1068 (m), 1025 (w), 986 (w), 929 (w), 887 (m), 763 (w), 700 (s), 400 (s), 367 (s), 265 (s) cm^{-1} . ^{31}P CP/MAS NMR: 90.0 ppm (3000, 7000 Hz).

$[\text{Mes}^*\text{NP}(\text{toluene})][\text{Ga}_2\text{Cl}_7]$. $\text{Mes}^*\text{NP}(\text{Cl})$ (0.34 g, 1.1 mmol) in toluene (≈ 30 mL) was added over a period of ≈ 5 min to a stirred solution of GaCl_3 (0.38 g, 2.1 mmol) in toluene (≈ 30 mL) [^{31}P NMR: 91 ppm]. An orange oil formed on removal of the solvent *in vacuo*. Fresh toluene (≈ 25 mL) was distilled onto this oil, and yellow orange crystals formed upon standing overnight. Solvent was decanted from the crystalline material which was washed with hexanes and characterized as $[\text{Mes}^*\text{NPC}_7\text{H}_8][\text{Ga}_2\text{Cl}_7]$ (0.65 g, 80%), $\text{mp} 87.5\text{--}89$ °C. Anal. Calcd: C, 38.99; H, 4.84; N, 1.82. Found: C, 38.72; H, 5.01; N, 1.81. NMR (CD_2Cl_2): ^{31}P , 95 ppm; ^1H , 7.42 (s, 2 H), 1.50 (s, 18 H), 1.31 (s, 9 H) [Mes^*], 7.76–7.66 (multiplet, 5 H), 2.56 ppm (s, 3 H) [toluene]; ^{13}C , 124.0, 30.6, 29.4 [Mes^*], 134.2, 133.1, 130.0, 22.3 ppm [toluene], quaternary carbon nuclei not observed. IR: 1971 (w), 1892 (w), 1842 (w), 1787 (w), 1594

(41) Regitz, M. *Chem. Rev.* **1990**, *90*, 191–213.

(42) Burford, N.; Clyburne, J. A. C.; Losier, P.; Parks, T. M. *Handbuch der Preparativen Anorganischen Chemie*, English ed., in press.

(43) Burford, N.; Müller, J.; Parks, T. M. *J. Chem. Educ.* **1993**, *71*, 807–809.

(m), 1266 (s), 1244 (m), 1134 (m), 1067 (m), 887 (s), 764 (m), 419 (s), 401 (s), 362 (s), 263 (s) cm^{-1} . ^{31}P CP/MAS NMR: 98.4 ppm (3137, 4045 Hz).

[Mes*NP(mesitylene)][Ga₂Cl₇]. Mes*NPCl (0.35 g, 1.1 mmol) in mesitylene (≈ 7 mL) was added to a solution of GaCl₃ (0.38 g, 2.2 mmol) in mesitylene (≈ 3 mL), and a yellow oil formed under a clear yellow solution [^{31}P NMR: 91 ppm]. Hexanes (≈ 10 mL) were distilled onto this solution giving a light yellow precipitate, which was isolated by decantation and recrystallized from a warm solution of hexane/mesitylene (20/80). Two crops of crystals were isolated and characterized as [Mes*NP(mesitylene)][Ga₂Cl₇] (total yield 0.76 g, 0.97 mmol, 90%), mp 105–107 °C. Anal. Calcd: C, 40.63; H, 5.18; N, 1.75. Found: C, 38.38; H, 5.54; N, 1.71. NMR (CD₂Cl₂): ^{31}P , 91 ppm; ^1H , 7.41 (d, $^5J_{\text{PH}} = 2$ Hz, 2 H), 1.50 (s, 18 H), 1.30 (s, 9 H) [Mes*], 7.21 (s, 3 H), 2.42 ppm (s, 9 H) [mesitylene]; ^{13}C , 123.8 (s), 31.0 (s), 30.3 (s) [Mes*], 131.1 (s), 21.6 ppm (s) [mesitylene], quaternary carbons not reported. IR: 1813 (w), 1784 (w), 1759 (w), 1589 (m), 1302 (m), 1265 (m), 1243 (m), 1219 (m), 1194 (m), 1134 (m), 885 (m), 856 (m), 762 (m), 676 (m), 407 (s), 367 (m), 360 (m), 265 (m) cm^{-1} .

Protonation Reaction of Mes*NPPH. A blue solution of Mes*NPPH (0.61 mmol), prepared in situ by the reaction of Mes*NPCl with NaBPh₄ in CH₂Cl₂ (≈ 10 mL), was added to a solution of HSO₃CF₃ (0.61 mmol) in CH₂Cl₂ (≈ 10 mL). A ^{31}P NMR spectrum of the yellow reaction mixture showed a single signal at 187 ppm assigned to [Mes*N(H)PPh][SO₃CF₃].

X-ray Crystallography. Crystals suitable for crystallography were obtained as described above and were selected and mounted in Pyrex capillaries in the drybox. Unit cell parameters were obtained from the setting angles of a minimum of 16 carefully centered reflections having $2\theta > 20^\circ$; the choice of space groups was based on systematically absent reflections and confirmed by the successful solution and refinement of the structures. All pertinent crystallographic data are summarized in Table 2.

Data were collected at room temperature (18 ± 1 °C) on a Rigaku AFC5R diffractometer (Mo K α radiation, $\lambda = 0.71069$ Å) using the ω - 2θ scan technique, and the stability of the crystals was monitored using three standard reflections; no significant decay was observed. Data were corrected for Lorentz and polarization effects. An empirical absorption correction was applied using ψ -scan corrections.⁴⁴

Structures were solved by direct methods which revealed

the positions of all non-hydrogen atoms. The non-hydrogen atoms were refined anisotropically. All of the hydrogen atoms were placed in geometrically calculated positions with a C–H distance of 108 pm. Their positions were not refined and they were assigned fixed isotropic temperature factors with a value of $1.2\beta_{\text{eq}}$ of the atom to which it was bonded. Neutral atom scattering factors for non-hydrogen atoms were taken from Cromer and Waber,⁴⁵ and the scattering factors for hydrogen atoms were taken from Stewart, Davidson, and Simpson.⁴⁶ Anomalous dispersion effects were included in F_o ,⁴⁷ the values for $\Delta f'$ were those of Cromer.⁴⁸ All calculations were performed using the TEXSAN/SHELX 93.⁴⁹

Acknowledgment. This work has been funded by the Natural Sciences and Engineering Research Council of Canada. Solid state NMR data were obtained by Gang Wu at the Atlantic Region Magnetic Resonance Center. We thank Profs. J. S. Grossert and J. A. Pincock for valuable discussions.

Supplementary Material Available: Tables of positional parameters, anisotropic thermal parameters, intramolecular bond distances and angles, and intermolecular bond distances involving non-hydrogen atoms for [Mes*NP(mesitylene)][Ga₂Cl₇] (7 pages). Ordering information is given on any current masthead page. Crystallographic data for the other structures described in this article, [Mes*NP(benzene)][GaCl₄], [Mes*NP(toluene)][GaCl₄], [Mes*NP(benzene)][Ga₂Cl₇] and [Mes*NP(toluene)][Ga₂Cl₇], have been previously deposited.

OM940848U

(44) TEXSAN-TEXRAY Single Crystal Structure Analysis Package, version 5.0; Molecular Structure Corp., The Woodlands, TX 1989.

(45) Cromer, D. T.; Waber, J. T. *International Tables for X-ray Crystallography*; The Kynoch Press: Birmingham, England (present distributor, Kluwer Academic Publishers: Dordrecht, The Netherlands): 1974; Vol. IV, Table 2.2A, pp 71–98.

(46) Stewart, R. F.; Davidson, E. R.; Simpson, W. T. *J. Chem. Phys.* **1965**, *42*, 3175–3187.

(47) Ibers, J. A.; Hamilton, W. C. *Acta Crystallogr.* **1964**, *17*, 781–782.

(48) Cromer, D. T.; Ibers, J. A. *International Tables for X-ray Crystallography*; The Kynoch Press: Birmingham, England (present distributor, Kluwer Academic Publishers: Dordrecht, The Netherlands), 1974; Vol. IV, Table 2.3.1, pp 149–150.

(49) Sheldrick, G. M. *SHELX-93: A program for crystal structure determination*; Institut für Anorganische Chemie: Göttingen, Germany, 1993.

Reactions of Tricarbonyl(vinylketene)iron(0) Complexes with Imines

Ana C. Reduto dos Reis and Louis S. Hegedus*

Department of Chemistry, Colorado State University, Fort Collins, Colorado 80523

Received October 19, 1994[®]

Tricarbonyl(vinylketene)iron(0) complex **1** underwent reaction with a variety of imines to produce η^3 -allyl- η^1 -alkyl iron complexes **4**–**7**, resulting from insertion of the imine into an iron–acyl carbonyl bond. Complex **4** was characterized by X-ray crystallography, confirming the proposed structure: monoclinic, space group $P2_1/n$, $a = 11.098(2)$ Å, $b = 9.837(2)$ Å, $c = 16.531(3)$ Å, $\beta = 108.67(3)$ Å, $Z = 4$, $R = 0.0443$, and $R_w = 0.0669$ for the 2862 reflections observed. Oxidative degradation of these complexes with I_2/Me_3NO produced 2-pyridones or unsaturated δ -lactams, along with minor amounts of β -lactams.

Introduction

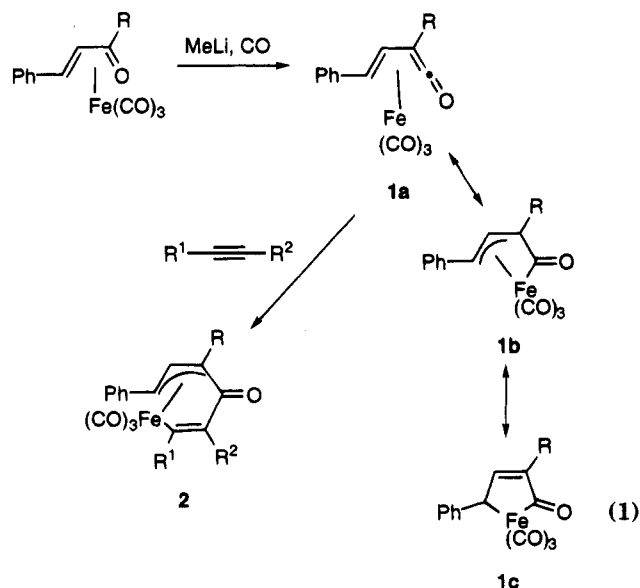
Over the last decade, transition metal complexes of vinylketenes have been proposed as key intermediates in a wide range of transition metal mediated organic reactions.¹ In addition, a number of stable vinylketene complexes, including those of chromium,² cobalt,³ and iron,⁴ have been isolated and characterized, and their reaction chemistry has been extensively developed. The reactions of the η^4 -vinylketene iron complexes, **1**, synthesized by the reaction of the corresponding η^4 -vinylketene iron complexes with organolithium reagents, under an atmosphere of carbon monoxide,⁵ have been particularly well developed.

reactivity of these complexes suggest that the η^3 -allyl- η^1 -acyl resonance form **1b** is an important contributor to the description of the $Fe(CO)_3$ -bound vinylketenes. For example, complexes **1** insert alkynes into the iron–acyl carbon bond to produce η^3 -allyl- η^1 -alkenyl iron complexes **2**⁴ and undergo attack at the iron acyl group by ylides to give η^4 -vinylallene complexes.⁶

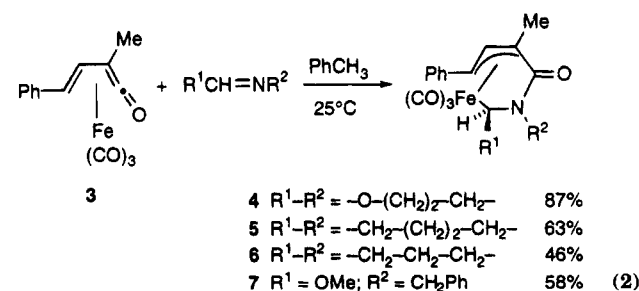
These laboratories have had a long-standing interest in the reactions of chromium ketene⁷ and chromium vinylketene^{1d} complexes with imines, the former providing efficient routes to β -lactams.⁸ Herein we describe the reactions of η^4 -vinylketene iron complexes **1** with imines.

Results and Discussion

The methyl-substituted tricarbonyl(vinylketene)iron(0) **3**⁵ was treated with a variety of imines (2.5 equiv) in toluene at room temperature to produce tricarbonyl- $(\eta^3$ -allyl- η^1 -alkyl)iron(0) complexes **4**–**7**, resulting from formal insertion of the imine into the iron–acyl carbon bond (or, alternatively, by nucleophilic attack of the imine nitrogen on the ketene carbonyl group) (eq 2).



Although usually represented as the η^4 -vinylketene species **1a**, both the X-ray crystal structure⁵ and the



These compounds were stable yellow crystalline solids, with physical data consistent with the assigned struc-

[®] Abstract published in *Advance ACS Abstracts*, February 15, 1995.
 (1) The most prominent of these is the Dötz benzannulation reaction. For reviews, see: (a) Dötz, K. H. *Angew. Chem., Int. Ed. Engl.* **1984**, *23*, 587. (b) Wulff, W. D. Metal Carbene Cycloadditions. In *Comprehensive Organic Synthesis*; Trost, B. M., ed.; Pergamon: London, 1991; Vol. 5, pp 1065–1113. For other classes of transformations proposed to involve metal–vinylketene complexes, see the following: (c) Semmelhack, M. F.; Tamura, R.; Schnatter, W.; Springer, J. *J. Am. Chem. Soc.* **1984**, *106*, 5363 (pyrones). (d) Hegedus, L. S.; Miller, D. B. *J. Org. Chem.* **1989**, *54*, 1241 (bicyclo[3.1.0]lactams). (e) Hoye, T. R.; Rehberg, G. M. *J. Am. Chem. Soc.* **1990**, *112*, 2841 (butenolides). (f) Cho, S. H.; Liebeskind, L. S. *J. Org. Chem.* **1987**, *52*, 2631 (phenols, pyrones).

(2) (a) Anderson, B. A.; Wulff, W. D.; Rheingold, A. L. *J. Am. Chem. Soc.* **1990**, *112*, 8615. (b) Anderson, B. A.; Bao, J.; Branvold, T. A.; Challenger, C. A.; Wulff, W. D.; Xu, Y.-C.; Rheingold, A. L. *J. Am. Chem. Soc.* **1993**, *115*, 10671.
 (3) (a) Wulff, W. D.; Gilbertson, S. R.; Springer, J. P. *J. Am. Chem. Soc.* **1986**, *108*, 520. (b) Huffman, M. A.; Liebeskind, L. S.; Pennington, W. T. *Organometallics* **1992**, *11*, 255, and references therein.
 (4) Morris, K. G.; Saberi, S. P.; Salter, M. M.; Thomas, S. E.; Ward, M. F.; Slawin, A. M. Z.; Williams, D. J. *Tetrahedron* **1993**, *49*, 5617, and references therein.
 (5) Alcock, N. W.; Richards, C. J.; Thomas, S. E. *Organometallics* **1991**, *10*, 231.

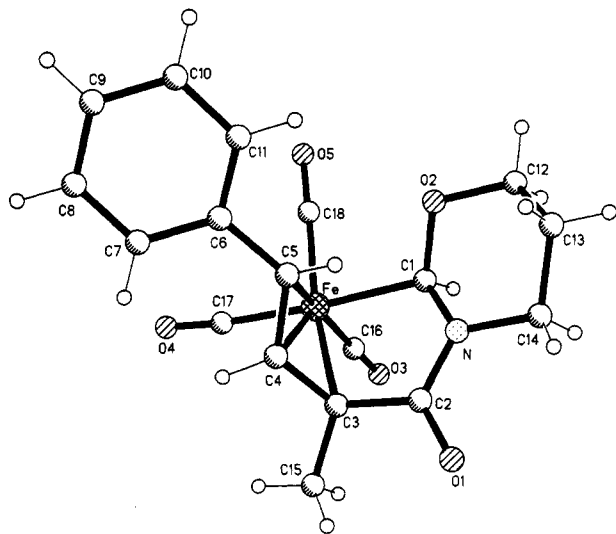


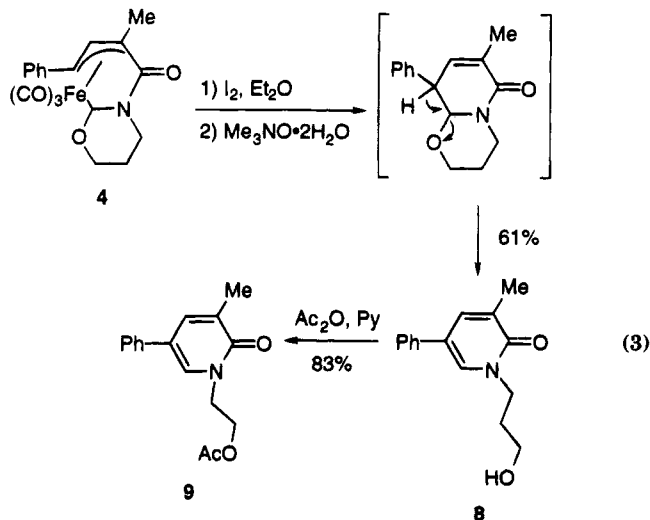
Figure 1.

Table 1. Selected Bond Lengths (Å) and Angles (deg) in Complex 4

Bond Lengths					
Fe-C(5)	2.189 (2)	N-C(1)	1.454 (3)	C(3)-C(4)	1.424 (4)
Fe-C(4)	2.071 (2)	N-C(2)	1.342 (3)	C(4)-C(5)	1.400 (4)
Fe-C(3)	2.134 (3)	C(2)-C(3)	1.510 (3)	O(1)-C(2)	1.230 (3)
Fe-C(1)	2.060 (2)				
Bond Angles					
C(1)-Fe-C(3)	82.3 (1)	C(3)-C(4)-C(5)	123.4 (2)		
C(3)-Fe-C(4)	39.5 (1)	C(16)-Fe-C(18)	102.6 (1)		
C(4)-Fe-C(5)	38.3 (1)	C(17)-Fe-C(18)	90.0 (1)		

ture. Complex 4 was further characterized by X-ray crystallography (Figure 1), which confirmed the assigned structure. Selected bond lengths and angles are collected in Table 1, and non-H atomic coordinates are reported in Table 2. The structure is quite comparable to those resulting from the insertion of alkynes into the iron-acyl bond (2),⁴ with the η^3 -allyl fragments having similar bond distances and bond angles, and the other structural features being very similar. The regiochemistry of insertion is that expected from a process involving nucleophilic attack of the imine nitrogen on the electrophilic η^4 -vinylketene carbonyl group, although the mechanism of insertion is not known.

A number of imines failed to react cleanly with complex 3 to produce insertion complexes. Although 5,6-dihydro-4*H*-1,3-oxazine was the most efficient imine studied for insertion complex formation (to give 4), the five-membered analog 2*H*-2-oxazoline failed to insert under mild conditions and led to decomposition under more severe conditions. (Oxazolines similarly fail to efficiently trap photogenerated chromium ketene complexes,⁹ while oxazines are among the most efficient in this process.) The simple 2*H*-2-thiazoline reacted with complex 3 at room temperature to give an intractable mixture of organic and organometallic compounds, while at -78 °C, the β -lactone resulting from dimerization of the vinylketene ligand was obtained. In this instance,



This reaction is likely to proceed by oxidatively driven reductive elimination (coupling) to form the six-membered lactam, followed by elimination of the attached alkoxy group. Complex 7, from addition of an imidate, underwent a similar cleavage producing pyridone 10 in modest yield (eq 4). Complexes 5 and 6, produced from

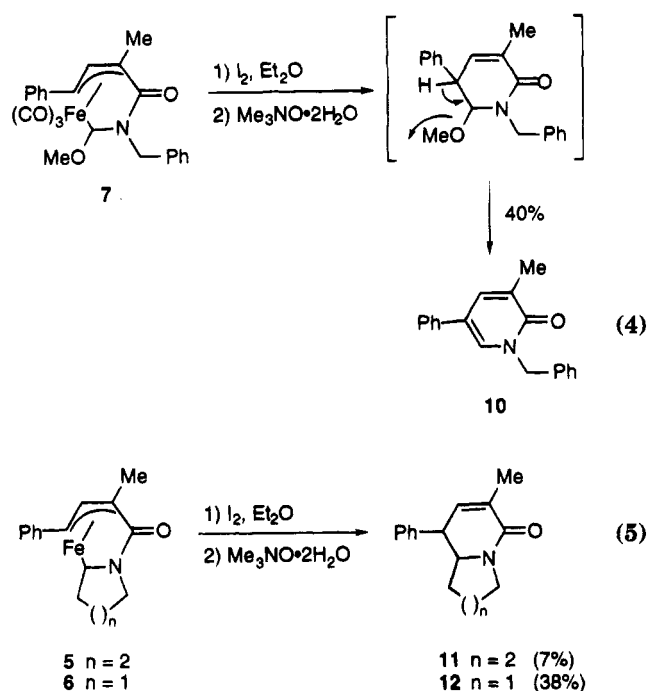
(6) Saberi, S. P.; Thomas, S. E. *J. Chem. Soc., Perkin Trans. 1* **1992**, 259.

(7) Hegedus, L. S.; deWeck, G.; D'Andrea, S. *J. Am. Chem. Soc.* **1988**, *110*, 2122.

(8) Narukawa, Y.; Juneau, K.; Snustad, D.; Miller, D. B.; Hegedus, L. S. *J. Org. Chem.* **1992**, *57*, 5453, and references therein.

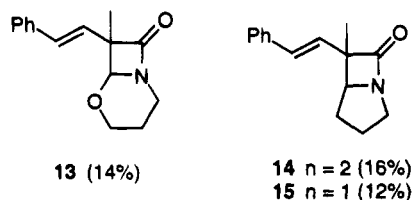
(9) Hegedus, L. S.; Schultze, L. M.; Toro, J.; Chen, Y. *Tetrahedron* **1985**, *41*, 5833.

(10) For the production of β -lactones and β -lactams from oxidative decomposition of "ferrilactone" and "ferrilactam" η^3 -allyl- η^1 -acyl iron complexes see: (a) Ley, S. V. *Philos. Trans., R. Soc. London A* **1988**, *326*, 633. (b) Annis, G. D.; Hebblethwaite, E. M.; Hodgson, S. T.; Hollingshead, D. M.; Ley, S. V. *J. Chem. Soc., Perkin Trans. 1* **1983**, 2851.



carbocyclic imines, lack a leaving group α to the amide nitrogen, and cleavage of these complexes under the above conditions produced δ -lactams **11** and **12** in poor to modest yield (eq 5), as single diastereoisomers (relative stereochemistry unknown).

Compounds **8**–**12** all resulted from reductive elimination between the η^1 -alkyl group and the γ -terminus of the η^3 -allyl system, producing six-membered lactams. A careful examination of the oxidative cleavage products from complexes **4**–**6** led to isolation of small amounts of β -lactams **13**–**15**, respectively, resulting from reduc-



tive elimination between the η^1 -alkyl group and the α -terminus of the η^3 -allyl system. These had characteristic infrared absorptions for the strained lactam carbonyl group (1746 and 1735 cm^{-1} , respectively). 1H NMR spectra and mass spectra were also consistent with the assignment. (Both compounds were obtained as single diastereoisomers whose relative configurations could not be assigned.) Studies to expand the range of imines that insert into η^4 -vinyketene iron complexes and procedures to control the site of reductive elimination are ongoing.

Experimental Section

General Procedures. All reactions involving metal complexes were performed using standard vacuum line techniques¹¹ under an atmosphere of argon.

Melting points were taken on a Mel-Temp apparatus and are uncorrected. The 300 MHz 1H NMR and 75 MHz ^{13}C NMR spectra were obtained with a Bruker AC-300P NMR spectrom-

Table 2. Atomic Coordinates ($\times 10^5$) and Equivalent Isotropic Displacement Coefficients ($\text{\AA}^2 \times 10^4$)

	x	y	z	U(eq)
Fe(1)	95403(3)	20716(3)	18104(2)	213(2)
N(1)	102142(19)	46975(19)	12750(11)	235(6)
O(1)	89676(23)	9917(21)	765(12)	520(8)
O(2)	98640(21)	-6335(18)	26335(14)	517(8)
O(3)	70397(18)	22125(19)	20676(12)	371(7)
O(4)	123021(17)	45798(18)	13743(11)	357(6)
O(5)	82583(15)	46960(15)	15398(9)	250(5)
C(1)	91851(24)	13906(24)	7612(16)	314(8)
C(2)	79927(25)	21600(23)	19496(14)	264(8)
C(3)	97978(25)	2943(23)	23196(16)	325(8)
C(4)	101223(23)	30335(21)	37700(14)	220(7)
C(5)	103864(21)	32992(24)	29572(14)	223(7)
C(6)	112777(21)	25595(24)	26982(14)	224(7)
C(7)	114141(23)	26822(24)	18735(14)	239(7)
C(8)	113484(22)	40752(23)	14778(13)	240(7)
C(9)	100518(26)	60848(23)	9320(16)	312(8)
C(10)	90554(28)	68231(23)	12198(16)	326(9)
C(11)	79026(25)	59491(24)	10795(15)	311(8)
C(12)	90717(21)	39191(22)	12033(13)	227(7)
C(13)	123241(26)	17087(28)	16570(17)	353(9)
C(14)	107151(24)	19892(23)	43361(15)	260(8)
C(15)	104320(25)	18191(26)	50954(15)	314(8)
C(16)	95791(26)	26684(27)	52960(15)	325(9)
C(17)	89803(24)	36924(25)	47395(16)	310(8)
C(18)	92604(23)	38763(23)	39765(14)	268(7)

eter. All chemical shifts are quoted in ppm relative to Me_4Si (δ 0.0, 1H) or $CDCl_3$ (δ 77.23, ^{13}C). IR spectra were recorded on a Perkin-Elmer 1600 FTIR spectrometer and mass spectra were obtained on a V. G. Micromass Ltd. Model 16F spectrometer.

Elemental analyses were performed by M-H-W Laboratories, Phoenix, AZ.

Materials. Tetrahydrofuran and diethyl ether were pre-dried over CaH_2 and distilled from benzophenone ketyl under a nitrogen atmosphere just prior to use. Toluene was dried over sodium wire, distilled over CaH_2 , and stored over 4 \AA molecular sieves. Hexane was distilled at atmospheric pressure.

Tricarbonyl(3-methyl-5-phenyl-1-oxapenta-1,2,4-triene)iron(0) (**1**) was prepared according to a reported procedure.⁵ Methyl lithium (1.4 M in diethyl ether) was purchased from Aldrich and its concentration checked by titration against diphenylacetic acid.¹² 5,6-Dihydro-4*H*-1,3-oxazine,¹³ 3,4,5,6-tetrahydropyridine,¹⁴ 3,4-dihydro-2*H*-pyrrole,¹⁵ and methyl *N*-benzylformimidate¹⁶ were prepared according to literature procedures. All other chemicals were used as obtained from commercial sources. Nonacarbonyldiiron was prepared by a published procedure.¹⁷

Column chromatography was performed on Merck silica gel (230–400 mesh). The alumina used for filtrations was deactivated with H_2O (Brockmann grade 4, $Al_2O_3:H_2O = 10:1$ w/w). For Celite filtrations, Celite 545 from Fischer Chemicals was used.

General Procedure for the Reaction of Tricarbonyl(3-methyl-5-phenyl-1-oxapenta-1,2,4-triene)iron(0) (1**) with Imines.** The vinyketene complex **1** was dissolved in dry toluene (25 mL/g) under an argon atmosphere. A solution of the imine (2.5 equiv) in dry toluene (6 mL/g) was then added dropwise and the reaction mixture was stirred at room temperature, under argon, for 18–24 h. The resultant brown reaction mixture was filtered through a small plug of Celite, using diethyl ether as eluent. The yellow/orange solution

(12) Kofron, W. G.; Baclawski, L. M. *J. Org. Chem.* **1976**, *41*, 1879.

(13) Ito, Y.; Inubushi, Y.; Zenbayashi, S. T.; Saegusa, T. *J. Am. Chem. Soc.* **1973**, *95*, 4447.

(14) Quick, J.; Oilrson, R. *Synthesis* **1976**, 745.

(15) Nomura, Y.; Ogawa, K.; Takeuchi, Y.; Tomoda, S. *Chem. Lett.* **1977**, 693.

(16) Guzman, A.; Muchowski, J. M.; Naal, N. T. *J. Org. Chem.* **1981**, *46*, 1224.

(17) Bray, E. H.; Hubel, W. *Inorg. Synth.* **1966**, *8*, 178.

obtained was evaporated under vacuum to give an orange oil. Column chromatography on silica gel, followed by crystallization, yielded the η^1, η^3 -tricarbonyl(amide)iron(0) adducts 4–7 as yellow crystalline solids.

Synthesis of Adduct 4. A solution of 5,6-dihydro-4H-1,3-oxazine (0.265 g, 3.11 mmol) in toluene (1.5 mL) was added to a solution of vinylketene complex 1 (0.355 g, 1.19 mmol) in toluene (9 mL) and the reaction mixture was stirred at room temperature, under argon, for 18 h. Filtration through Celite followed by evaporation of solvent gave a "foamy" orange oil. Crystallization from hexanes/diethyl ether (1:1) yielded the adduct 4 as a yellow crystalline solid (0.40 g, 87%): mp 128–130 °C; $^1\text{H NMR}$ δ 1.51 (m, 1H, OCH_2CH_2), 1.74–1.85 (m, 1H, OCH_2CH_2), 2.11 (s, 3H, Me), 2.92 (dt, $J = 4.0$ and 12.9 Hz, 1H, NCH_2), 3.65 (dt, $J = 2.0$ and 12.0 Hz, 1H, OCH_2), 4.11 (m, 2H, $\text{NCH}_2\text{CH}_2\text{CH}_2\text{O}$), 4.92 (d, $J = 12.8$ Hz, 1H, PhCH), 4.99 (s, 1H, OCHN), 5.58 (d, $J = 12.8$ Hz, 1H, PhCHCH), 7.22–7.44 (m, 5H, Ph); $^{13}\text{C NMR}$ (75.5 MHz, CDCl_3) δ 24.2 (Me), 25.2 (OCH_2CH_2), 43.5 (NCH_2), 71.1 (OCH_2), 78.2 (PhCH), 83.1 (CMe), 86.8 (OCHN), 92.8 (PhCHCH), 126.1 (Ph, *meta*), 128.1 (Ph, *para*), 129.3 (Ph, *ortho*), 138.5 (Ph, *ipso*), 169.0 (C=O), 204.7, 207.6 and 211.2 (C \equiv O); IR (C_6H_{12}) 2070, 2014 and 1995 (vs, C \equiv O), 1666 (s, C=O) cm^{-1} ; MS (EI) m/z 384 (MH^+ , 0.05), 355 (2.7, $\text{M}^+ - \text{CO}$), 327 (43.2, $\text{M}^+ - 2\text{CO}$), 299 (29.5, $\text{M}^+ - 3\text{CO}$), 242 (20.6, $\text{M}^+ - \text{Fe}(\text{CO})_3 - \text{H}$), 214 (56.5, $\text{M}^+ - 3\text{CO} - \text{OCH}_2\text{CH}_2\text{CH}_2\text{NCH}$), 186 (75.3, $\text{M}^+ - 3\text{CO} - \text{OCH}_2\text{CH}_2\text{CH}_2\text{NCHCO}$), 184 (100, $\text{M}^+ - 2\text{H} - 3\text{CO} - \text{OCH}_2\text{CH}_2\text{CH}_2\text{NCHCO}$), 128 (48.6, PhCH=CHCMe - 2H); MS (CI, NH_3) m/z 384 (MH^+ , 100). Anal. Calcd for $\text{C}_{18}\text{H}_{17}\text{FeNO}_5$: C, 56.42; H, 4.47; N, 3.66. Found: C, 56.51; H, 4.56; N, 3.72.

X-ray Crystallographic Analysis of Adduct 4. Crystal Data. Single crystals of 4 suitable for X-ray crystallography were grown from hexanes/diethyl ether. $\text{C}_{18}\text{H}_{17}\text{FeNO}_5$, $M = 383.2$, monoclinic, $a = 11.098(2)$, $b = 9.837(2)$, $c = 16.531(3)$ Å, $\beta = 108.67(3)^\circ$, $U = 1710$ Å 3 , space group $P2_1/n$, $Z = 4$, $D_c = 1.49$ g/cm 3 ; yellow air-stable plates, dimensions $0.04 \times 0.20 \times 0.44$, $\mu(\text{MoK}\alpha) = 9.10$ cm $^{-1}$, and $F(000) = 792$. A total of 3167 independent measured reflections were collected on a Siemens P4/IRIS diffractometer, ω -scan method, ($4 \leq 2\theta \leq 50^\circ$), graphite monochromated $\text{MoK}\alpha$ radiation ($\lambda = 0.71073$ Å) with 2862 observed [$|F_o| > 2.5\sigma(|F_o|)$] and corrected for Lorentz and polarization factors. No absorption corrections were applied. The structure was solved by direct methods, and the non-hydrogen atoms were refined anisotropically. The hydrogen atoms were idealized (C–H = 0.96 Å), assigned isotropic thermal parameters $U(\text{H}) = 0.08$, and allowed to ride on their parent carbons. Refinement was by full-matrix least-squares analysis to give $R = 0.0443$, $R_w = 0.0669$ for all data ($\omega^{-1} = \sigma^2(F) + 0.0018F^2$). The maximum residual electron density in the final ΔF maps was 0.52 e/Å 3 , and the mean and maximum shift/error in the final refinement cycle were 0.006 and 0.033, respectively. Computations were carried out on an Silicon Graphics 4D35 using the SHELXTL PLUS (UNIX) program system.¹⁸ Atom coordinates, bond lengths and angles, and thermal parameters have been deposited at the Cambridge Crystallographic Data Center.

Synthesis of adduct 5. A solution of 3,4,5,6-tetrahydro-pyridine (0.316 g, 3.80 mmol) in toluene (2 mL) was added to a solution of vinylketene complex 1 (0.435 g, 1.46 mmol) in toluene (11 mL), and the reaction mixture was stirred at room temperature, under argon, for 24 h. The reaction mixture was then filtered through Celite, and the yellow solution obtained was evaporated under vacuum to give a dark yellow oil. Column chromatography on SiO_2 , 5% EtOAc/hexanes, followed by crystallization from hexanes/diethyl ether (1:1) yielded the adduct 5 as a yellow crystalline solid (0.100 g, 32%): mp 120–122 °C; $^1\text{H NMR}$ δ 1.21–1.37 (m, 1H, NCH_2CH_2), 1.41–1.58 (m, 1H, NCH_2CH_2), 1.62–1.72 (m, 1H, NCH_2CH_2), 1.74–1.96 (m, 2H, NCH_2CH_2), 2.08–2.18 (m, 1H, NCH_2), 2.13

(s, 3H, Me), 2.64 (dt, $J = 3.3$ and 12.9 Hz, 1H), 3.25 (dd, $J = 3.3$ and 11.7 Hz, 1H), 3.73 (d, $J = 12.0$ Hz, 1H, PhCH), 4.04 (dq, $J = 2.2$ and 13.0 Hz, 1H), 5.56 (d, $J = 12.0$ Hz, 1H, PhCHCH), 7.22–7.39 (m, 5H, Ph); $^{13}\text{C NMR}$ δ 24.3 (Me), 24.8 (NCH_2CH_2), 28.6 (NCH_2CH_2), 38.0 (NCH_2CH_2), 44.6 (NCH_2), 46.7 (NCH), 76.9 (PhCH), 83.8 (CMe), 92.2 (PhCHCH), 125.9 (Ph, *meta*), 128.2 (Ph, *para*), 129.5 (Ph, *ortho*), 138.3 (Ph, *ipso*), 170.5 (C=O), 205.0, 210.1 and 212.0 (C \equiv O), ^{13}C assignments were confirmed by a DEPT experiment; IR (C_6H_{12}) 2059, 2001 and 1993 (vs, C \equiv O), 1656 (s, C=O) cm^{-1} ; MS (EI) m/z 325 ($\text{M}^+ - 2\text{CO}$, 0.4), 297 (0.6, $\text{M}^+ - 3\text{CO}$), 241 (7.6, $\text{M}^+ - \text{Fe}(\text{CO})_3$), 158 (40.9, PhCHCHCMeCO), 129 (43.7, PhCHCHCMe - H), 128 (51.4, PhCHCHCMe - 2H), 115 (61.0, PhCHCHC), 91 (100, PhCH $_2$); MS (FAB, MNBA) m/z 382 (MH^+ , 100), 354 (26.1, $\text{MH}^+ - \text{CO}$), 325 (59.4, $\text{M}^+ - 2\text{CO}$), 297 (27.9, $\text{M}^+ - 3\text{CO}$). Anal. Calcd for $\text{C}_{19}\text{H}_{19}\text{FeNO}_4$: C, 59.86; H, 5.02; N, 3.68. Found: C, 60.00; H, 5.16; N, 3.60.

Synthesis of Adduct 6. A solution of 3,4-dihydro-2H-pyrrole (0.084 g, 1.22 mmol) in toluene (0.5 mL) was added to a solution of vinylketene complex 1 (0.140 g, 0.47 mmol) in toluene (3.5 mL), and the reaction mixture was stirred at room temperature, under argon, for 19 h. The reaction mixture was then filtered through Celite, and the yellow solution obtained was evaporated under vacuum to give an orange oil. Column chromatography on SiO_2 , 5% MeOH/ CH_2Cl_2 , followed by crystallization from hexanes/diethyl ether (1:1) yielded the adduct 6 as a yellow crystalline solid (0.060 g, 43%): mp 134–136 °C; $^1\text{H NMR}$ δ 1.58–1.72 (m, 1H, NCH_2CH_2), 1.74–1.93 (m, 1H, NCH_2CH_2), 1.94–2.06 (m, 1H, NCH_2CH_2), 2.17–2.28 (m, 1H, NCH_2CH_2), 2.19 (s, 3H, Me), 2.74 (d, $J = 12.0$ Hz, 1H, PhCH), 3.18–3.43 (m, 3H, NCH and NCH_2), 5.53 (d, $J = 12.0$ Hz, 1H, PhCHCH), 7.19–7.32 (m, 5H, Ph); $^{13}\text{C NMR}$ δ 23.2 (Me), 23.8 (NCH_2CH_2), 34.7 (NCH_2CH_2), 42.8 (NCH), 44.8 (NCH_2), 72.8 (PhCH), 88.3 (CMe), 90.3 (PhCHCH), 125.5 (Ph, *meta*), 127.7 (Ph, *para*), 129.2 (Ph, *ortho*), 138.0 (Ph, *ipso*), 167.6 (C=O), 205.2, 210.6 and 211.0 (C \equiv O), ^{13}C assignments were confirmed by a DEPT experiment; IR (C_6H_{12}) 2059, 2002 and 1994 (vs, C \equiv O), 1660 (s, C=O) cm^{-1} ; MS (EI) m/z 339 ($\text{M}^+ - \text{CO}$, 3.7), 311 (29.4, $\text{M}^+ - 2\text{CO}$), 283 (40.3, $\text{M}^+ - 3\text{CO}$), 214 (30.8, $\text{M}^+ - 3\text{CO} - \text{CH}_2\text{CH}_2\text{CH}_2\text{CHN}$), 186 (46.0, $\text{M}^+ - 3\text{CO} - \text{CH}_2\text{CH}_2\text{CH}_2\text{CHNCO}$), 184 (100, $\text{M}^+ - 2\text{H} - 3\text{CO} - \text{CH}_2\text{CH}_2\text{CH}_2\text{CHNCO}$), 128 (68.3, PhCHCHCMe - 2H), 115 (82.1, PhCHCHC); MS (CI, NH_3) m/z 227 ($\text{M}^+ - \text{Fe}(\text{CO})_3$, 71.8); MS (FAB, MNBA) m/z 368 (MH^+ , 49.4), 311 (15.9, $\text{M}^+ - 2\text{CO}$), 283 (10.4, $\text{M}^+ - 3\text{CO}$). Anal. Calcd for $\text{C}_{18}\text{H}_{17}\text{FeNO}_4$: C, 58.90; H, 4.67; N, 3.82. Found: C, 59.04; H, 4.60; N, 3.80.

Synthesis of Adduct 7. A solution of *N*-benzylformimidate (0.089 g, 0.596 mmol) in toluene (0.4 mL) was added to a solution of vinylketene complex 1 (0.069 g, 0.23 mmol) in toluene (1.7 mL), and the reaction mixture was stirred at room temperature, under argon, for 3.5 days. Filtration through neutral alumina followed by evaporation of solvent yielded crude adduct 7 as a yellow oil (0.060 g, 58%): $^1\text{H NMR}$ δ 2.19 (s, 3H, Me), 3.36 (s, 3H, OMe), 4.14 (d, $J = 12.1$ Hz, 1H, PhCH), 4.73 (s, 1H, NCHOMe), 4.77 (d, $J = 14.8$ Hz, 1H, NCH_2Ph), 4.80 (d, $J = 14.8$ Hz, 1H, NCH_2Ph), 5.63 (d, $J = 12.1$ Hz, 1H, PhCHCH), 7.18–7.43 (m, 10H, Ph); $^{13}\text{C NMR}$ 27.1 (Me), 48.2 (NCH_2Ph), 59.8 (OMe), 78.9 (PhCH), 81.2 (CMe), 89.4 (NCHOMe), 92.8 (PhCHCH), 126.1 (CHPh, *meta*), 127.4 (NCH_2Ph , *meta*), 127.9 (NCH_2Ph , *para*), 128.1 (CHPh, *para*), 128.7 (NCH_2Ph , *ortho*), 129.3 (CHPh, *ortho*), 137.2 (NCH_2Ph , *ipso*), 138.4 (CHPh, *ipso*), 170.1 (C=O), 204.2, 207.9 and 211.6 (C \equiv O); IR (C_6H_{12}) 2062, 2004 and 1993 (vs, C \equiv O), 1662 (s, C=O) cm^{-1} . This complex lacked sufficient stability for further characterization.

General Procedure for the Oxidation of Tricarbonyl(η^3 -allyl- η^1 -alkyl)iron(0) complexes 4–7 by Iodine/Tri-methylamine *N*-Oxide. To a stirred solution of iodine (4 equiv) in anhydrous, deoxygenated diethyl ether (30 mL/g), at room temperature, was added under argon a solution of the tricarbonyl(η^3 -allyl- η^1 -alkyl)iron complex in diethyl ether (150 mL/g). The reaction was monitored by infrared spectroscopy.

(18) Sheldrick, G. M. SHELXTL PC Rev. 4.2, PLUS version, Siemens Analytical X-Ray Instruments Inc., Madison, WI, 1990.

When all the starting material complex was consumed, trimethylamine *N*-oxide dihydrate (5 equiv) was added and the reaction mixture stirred at room temperature for 18 h. The mixture was then poured into water and extracted with diethyl ether. The combined organic extracts were washed with aqueous sodium thiosulfate saturated solution and then with water, dried (MgSO₄), and evaporated to give crude product, which was purified by column chromatography on silica gel.

Synthesis of 3-Methyl-5-phenyl-1-(3-hydroxypropyl)-2-pyridone (8). A solution of the amide complex **4** (0.390 g, 1.02 mmol) in diethyl ether (40 mL) was added to a solution of iodine (1.03 g, 4.06 mmol) in diethyl ether (27 mL). After 5 h, no iron tricarbonyl absorptions corresponding to complex **4** were detected by infrared spectroscopy. Trimethylamine *N*-oxide dihydrate (0.578 g, 5.10 mmol) was then added and the reaction mixture stirred at room temperature for 16 h. Workup followed by column chromatography on silica gel (1:9 MeOH/CH₂Cl₂) yielded the title pyridone **8** as a white solid (0.618 g, 61%): mp 90–92 °C; ¹H NMR δ 1.88–1.96 (m, 2H, NCH₂CH₂), 2.18 (s, 3H, Me), 3.51 (t, *J* = 5.6 Hz, 2H, NCH₂), 4.14 (t, *J* = 6.3 Hz, 2H, HOCH₂), 4.3–5.1 (v br s, 1H, OH), 7.22–7.28 (m, 1H, CMeCH), 7.29–7.38 (m, 5H, Ph), 7.49 (m, 1H, NCH); ¹³C NMR δ 17.7 (Me), 32.7 (NCH₂CH₂), 46.4 (NCH₂), 57.8 (HOCH₂), 121.1 (CMe), 126.0 (Ph, *meta*), 127.5 (Ph, *para*), 129.2 (Ph, *ortho*), 129.8 (CPh), 132.3 (NCH), 136.7 (Ph, *ipso*), 137.4 (CMeCH), 163.3 (C=O), ¹³C assignments were confirmed by a DEPT experiment; IR (C₆H₁₂) 3444 (w, OH), 1658 (s, C=O), 1612 and 1601 (m, C=C) cm⁻¹; MS (EI) *m/z* 244 (MH⁺, 6.5), 243 (35.9, M⁺), 226 (29.7, M⁺ - OH), 199 (100, MH⁺ - (CH₂)₂OH), 185 (54.1, MH⁺ - (CH₂)₃OH), 156 (30.5, M⁺ - CH₂N(CH₂)₃OH), 128 (32.5, PhCCHCMe - H). This compound was converted to its acetate **9** for further characterization.

The pyridone **8** (0.046, 0.19 mmol) was converted to the corresponding acetate **9** by reaction with acetic anhydride (0.54 g, 5.30 mmol) in dry pyridine (1.8 mL). The reaction mixture was stirred at room temperature, under argon, for 19 h and then poured into water (5 mL) and extracted with diethyl ether (3 × 5 mL). The combined organic extracts were dried (MgSO₄), and the solvent was evaporated to give a light yellow oil. Purification by column chromatography on silica gel (1:9 MeOH/CH₂Cl₂) yielded 1-(acetoxypentyl)-3-methyl-5-phenyl-2-pyridone (**9**) as a colorless, clear oil (0.045 g, 83%): ¹H NMR δ 2.04 (s, 3H, MeCO₂), 2.10–2.18 (m, 2H, NCH₂CH₂), 2.19 (s, 3H, Me), 4.07 (t, *J* = 7.2 Hz, 2H, NCH₂), 4.13 (t, *J* = 6.0 Hz, 2H, AcOCH₂), 7.30 (m, 1H, CHCMe), 7.33–7.59 (m, 5H, Ph), 7.50 (m, 1H, NCH); ¹³C NMR δ 17.5 (Me), 21.0 (MeCO₂), 28.2 (NCH₂CH₂), 48.0 (NCH₂), 61.7 (AcOCH₂), 120.2 (CMe), 126.0 (Ph, *meta*), 127.4 (Ph, *para*), 129.2 (Ph, *ortho*), 130.1 (CPh), 132.5 (NCH), 136.9 (Ph, *ipso*), 137.0 (CMeCH), 162.4 (NC=O), 171.1 (AcC=O), ¹³C assignments were confirmed by a DEPT experiment; IR (C₆H₁₂) 1752 (s, MeOC=O), 1664 (NC=O), 1624 and 1602 (C=C) cm⁻¹; MS (EI) *m/z* 286 (MH⁺, 8.8), 285 (46.1, M⁺), 226 (66.7, M⁺ - OAc), 199 (86.1, MH⁺ - (CH₂)₂OAc), 185 (64.1, MH⁺ - (CH₂)₃OAc), 156 (44.2, M⁺ - CH₂N(CH₂)₃OAc), 128 (65.8, PhCCHCMe - H). Anal. Calcd for C₁₇H₁₉NO₃: C, 71.56; H, 6.71; N, 4.91. Found: C, 71.49; H, 6.56; N, 4.86.

Synthesis of 1-Benzyl-3-methyl-5-phenyl-2-pyridone (10). A solution of complex **7** (0.060 g, 0.134 mmol) in diethyl ether (5 mL) was added to a solution of iodine (0.136 g, 0.537 mmol) in diethyl ether (4 mL), under argon. After 3 h, no starting complex **7** could be detected by infrared spectroscopy. Trimethylamine *N*-oxide dihydrate (0.076 g, 0.670 mmol) was then added and the reaction mixture stirred at room temperature for 22 h. Workup followed by column chromatography on silica gel (1:1.8 Et₂O/hexanes/CH₂Cl₂) yielded the title pyridone **10** as a white crystalline solid (0.015 g, 40%): mp 129–130 °C; ¹H NMR δ 2.24 (s, 3H, Me), 5.20 (s, 2H, CH₂Ph), 7.25–7.39 (m, 11H, CHCPh and CH₂Ph), 7.48–7.50 (m, 1H, NCHCPh); ¹³C NMR δ 17.8 (Me), 52.8 (CH₂Ph), 120.2 (CMe),

126.0 (CH₂Ph, *meta*), 127.4 (Ph, *meta*), 128.2 (CH₂Ph, *para*), 128.4 (Ph, *para*), 129.1 (CH₂Ph, *ortho*), 129.2 (Ph, *ortho*), 130.3 (NCHCPh), 132.1 (NCH), 136.7 (CH₂Ph, *ipso*), 136.9 (CMeCH), 137.1 (Ph, *ipso*), 162.2 (C=O), ¹³C assignments were confirmed by a DEPT experiment; IR (C₆H₁₂) 1664 (s, C=O), 1624 (m, C=C), 1602 (w, C=C) cm⁻¹; MS (EI) *m/z* 275 (M⁺, 82.6), 198 (8.9, M⁺ - Ph), 184 (22.9, M⁺ - CH₂Ph), 169 (16.5, M⁺ - CH₂-Ph - N), 128 (8.7, PhCCHCMe - H). Anal. Calcd for C₁₉H₁₇NO: C, 82.88; H, 6.22; N, 5.09. Found: C, 82.69; H, 5.98; N, 4.96.

Synthesis of 5,6,7,8,9,10-Hexahydro-3-methyl-5-phenyl-2-quinolizone (11). A solution of the amide complex **5** (0.245 g, 0.64 mmol) in diethyl ether (24 mL) was added to a solution of iodine (0.652 g, 2.57 mmol) in diethyl ether (18 mL). After 11 days, all the starting material complex **5** had been consumed according to the infrared spectrum of the reaction mixture. Trimethylamine *N*-oxide dihydrate (0.36 g, 3.21 mmol) was added, and the reaction mixture was stirred at room temperature for 24 h. Workup followed by column chromatography on silica gel (1:9 MeOH/CH₂Cl₂) gave the title compound **11** as a colorless oil (0.010 g, 7%): ¹H NMR δ 1.23–1.33 (m, 1H, CH₂), 1.42–1.51 (m, 2H, CH₂), 1.61–1.72 (m, 3H, CH₂), 1.91 (s, 3H, CH₃), 2.49 (dt, *J* = 3.3, 12.9 Hz, 1H, CH₂N), 3.37 (m, 2H, CHN, CHPh), 4.54 (m, 1H), 6.15 (m, 1H, HC=N), 7.17–7.35 (m, 5H, Ph); ¹³C NMR δ 17.8, 24.2, 25.3, 33.1, 43.9, 48.0, 62.6, 127.6, 128.6, 129.1, 136.6, 142.5, 166.4. IR (C₆H₁₂) 1679, 1644 (C=O) cm⁻¹. MS (FAB, MNBA) *m/z* 242 (MH⁺, 100). In addition, β-lactam **14** was obtained (0.025 g, 16%): ¹H NMR δ 1.28–1.50 (m, 2H, CH₂), 1.49 (s, 3H, CH₃), 1.60–1.70 (m, 2H, CH₂), 1.92 (m, 1H, CH₂), 2.24 (m, 1H, CH₂), 2.78 (dt, *J* = 2.6, 11.7 Hz, 1H, CH₂N), 4.16 (m, 1H), 5.05 (m, 1H), 6.36 (d, *J* = 17.0 Hz, PhCH=CH), 6.75 (d, *J* = 17.0 Hz, 1H, PhCH=C), 7.16–7.46 (m, 5H, Ph). IR (C₆H₁₂) ν 1725 (CO) cm⁻¹. MS (FAB, MNBA) *m/z* 242 (MH⁺, 100).

Synthesis of 3-Methyl-5,6,7,8,9-pentahydro-5-phenyl-2-indolizone (12). A solution of the amide complex **6** (0.309 g, 0.84 mmol) in diethyl ether (27 mL) was added to a solution of iodine (0.854 g, 3.37 mmol) in diethyl ether (26 mL). After 18 h, all the starting complex **6** had been consumed according to the infrared spectrum of the reaction mixture. Trimethylamine *N*-oxide dihydrate (0.477 g, 4.21 mmol) was then added and the reaction mixture stirred at room temperature for 18 h. Workup followed by column chromatography on silica gel (1:9 MeOH/CH₂Cl₂) yielded the title indolizone **12** as a white solid (0.072 g, 38%): mp 108–109 °C; ¹H NMR δ 1.58–1.69 (m, 2H, NCH₂CH₂CH₂), 1.79–1.88 (m, 1H, NCH₂-CH₂CH₂), 1.89–1.98 (m, 1H, NCH₂CH₂), 1.92 (s, 3H, Me), 3.40–3.53 (m, 2H, NCH₂ and PhCH), 3.59–3.69 (m, 2H, NCH₂ and NCHCH₂), 6.16 (s, 1H, CMeCH), 7.12–7.34 (m, 5H, Ph), ¹H assignments were confirmed by ¹H-¹H DQF COSY and ¹H-¹³C HETCOR experiments; ¹³C NMR δ 16.8 (Me), 22.9 (NCH₂CH₂), 32.7 (NCH₂CH₂CH₂), 44.9 (NCH₂), 48.8 (PhCH), 63.9 (NCHCH₂), 127.4 (Ph, *meta*), 128.2 (Ph, *para*), 128.9 (Ph, *ortho*), 132.9 (CMe), 137.5 (CMeCH), 141.2 (Ph, *ipso*), 164.3 (C=O), ¹³C assignments were confirmed by a DEPT experiment; IR (C₆H₁₂) 1672 (s, C=O), 1634 (m, C=C) cm⁻¹; MS (EI) *m/z* 226 (M⁺ - H, 12.7), 225 (70.2, M⁺ - 2H), 224 (60.9, M⁺ - 3H), 212 (15.6, M⁺ - Me), 196 (35.8, M⁺ - Me - O), 182 (17.9, M⁺ - Me - O - CH₂), 174 (22.7, PhCHCH=CMeCON + 2H), 158 (16.8, PhCHCH=CMeCO + 2H), 128 (24.4, PhCHCH=CMe), 115 (27.3, PhCHCH=C), 105 (35.9, PhCHCH + 2H), 77 (48.4, Ph), 67 (100, COCMe=C), 57 (47.6, COCMe + 2H); MS (FAB, glycerol) *m/z* 228 (MH⁺, 100). Anal. Calcd for C₁₅H₁₇NO: C, 79.26; H, 7.54; N, 6.16. Found: C, 78.92; H, 7.68; N, 6.43.

Data for β-Lactam 13. **13** was obtained as a side product in the synthesis of pyridone **8**, purified by column chromatography on silica gel (1:9 MeOH/CH₂Cl): clear, colorless oil (0.035 g, 14%); ¹H NMR δ 1.75 (s, 3H, Me), 1.8–1.9 (m, 2H, NCH₂CH₂), 3.62 (m, 2H, NCH₂), 3.73 (m, 2H, OCH₂), 6.23 (d, *J* = 16.1 Hz, PhCH), 6.79 (d, *J* = 16.1 Hz, PhCH), 7.28–7.42 (m, 5H, Ph); IR (C₆H₁₂) 1747 (NC=O) cm⁻¹; MS (EI) *m/z*

242 ($M^+ - H$, 3.0), 186 (6.4, $M^+ - O(CH_2)_3$), 171 (16.8, $M^+ - O(CH_2)_3N$), 158 (52.2, $PhCH=CHCMeCO - H$), 131 (100, $PhCH=CHCMeH$), 115 (79.9, $PhCH=CHC$), 103 (38.8, $PhCH=CH$).

In addition, small amounts of β -lactam **15**, purified by column chromatography on silica gel (1:9 MeOH/ CH_2Cl_2 ; $R_f = 0.76$) were obtained: clear, colorless oil (0.022 g, 12%); 1H NMR δ 1.53 (s, Me), 1.4–2.2 (m, $NCH_2CH_2CH_2$), 3.0–3.2 (m, CONCH and CMeCHN), 3.5–3.9 (m, CONCH), 6.23 (d, $J = 17$ Hz, PhCHCH), 6.72 (d, $J = 17$ Hz, PhCHCH), 7.1–7.5 (m, Ph); IR (C_6H_{12}) 1734 (NC=O) cm^{-1} .

Support for this research by National Science Foundation Grant CHE-9224489 is gratefully acknowledged. A.C.R.R.

thanks the Portuguese–American Foundation (FLAD) and the Junta Nacional de Investigaç o Cient fica e Tecnol gica (JNICT) for their support in the form of fellowships.

Supplementary Material Available: Structure determination summary, tables of atomic coordinates, all bond distances and angles, anisotropic displacements, and H atom coordinates and isotropic displacement coefficients for **4** (5 pages). Ordering information is given on any current masthead page.

OM940805D

Ethylene Insertion into a Ruthenium-Phenyl Bond of a Chiral Lewis Acid. A Facile Method of Preparing Olefin-Hydride Complexes. Crystal Structure of [CyRuH(C₂H₃Ph)(PPh₃)]SbF₆·CH₂Cl₂

J. W. Faller* and Kevin J. Chase

Department of Chemistry, Yale University, P.O. Box 208107,
New Haven, Connecticut 06520-8107

Received June 29, 1994[®]

Treatment of CyRuPR₃Cl₂ (Cy = η⁶-cymene, *p*-isopropyltoluene; R = Ph or OMe) with PhMgBr gave the racemic ruthenium complexes CyRuBrPh(PPh₃) (**3**) and CyRuClPh(P(OMe)₃) (**4**). Reaction of **3** or **4** with AgSbF₆ in the presence of 1 atm of ethylene at ambient temperature or below leads to the styrene-hydride complexes [CyRuH(C₂H₃Ph)(PR₃)]SbF₆ (**5** (R = Ph) and **6** (R = OMe)). NMR and chemical studies of both **5** and **6** showed that they exist as two diastereomers in solution. Only one rotamer of each diastereomer is present in significant concentrations, and rotational averaging of the resonances from this process is essentially complete at ambient temperatures. Hydrogen exchange between the olefin and hydride causes averaging at higher temperatures than olefin rotation and also provides a route for interconversion of the diastereomers. A significant feature of the insertion process is that the formation of a secondary alkyl, α-phenethyl, is more facile than that of the primary alkyl, β-phenethyl. An X-ray crystal structure determination of **5** shows a classical olefin-hydride structure rather than an agostic Ru-H-C interaction. Racemic **5** crystallizes in the monoclinic space group P2₁/n with cell parameters of *a* = 10.49 Å, *b* = 15.24(1) Å, *c* = 24.015(4) Å, β = 101.94(3)°, *V* = 3755(9) Å³, *Z* = 4. The reaction of **3** with AgSbF₆ in the presence of carbon monoxide gives [CyRu(CO)Ph(PPh₃)]SbF₆ (**7**).

Introduction

The insertion of an olefin into a transition metal-aryl bond is of significance in many catalytic reactions. This is a critical step in the Heck reaction, the Pd-catalyzed arylation of olefins.¹ The recently reported catalytic addition of olefins to substituted arenes also involves this path.² Previous results with related transition metal-alkyl complexes have shown that there is a high kinetic barrier to olefin insertion in d^{*n*} systems where *n* > 0,³⁻⁵ even though this is a critical and necessary step in the Cossee-Arlman mechanism in the Ziegler-Natta polymerization of olefins.⁶ Insertion of an olefin into a metal-aryl bond apparently has a somewhat lower barrier than insertion into a metal-alkyl bond,^{7,8} although at this point, the evidence is sparse. In contrast, the insertion of an olefin into a transition metal-hydride bond usually has a much lower barrier.^{3,4} Consequently, the number of reported R-M-olefin complexes is relatively high compared to the number of H-M-olefin complexes. Recently, however, there have been a number of reports of stable

olefin-hydride complexes, including many that contain the olefin and hydride *cis* to each other. These include complexes of Mo, Co, Rh, Ir, Ru, Nb, and Ta.^{3,4,7,9-16} Most of these complexes are fluxional and undergo reversible migratory insertion and β-hydride elimination, as shown by variable-temperature NMR and isotopic labeling studies. Some complexes contain a three-center two-electron C-H-M bond; i.e., they exhibit an "agostic" interaction,¹¹ and a few have been shown to be catalysts in olefin polymerization^{3,10} and dimerization reactions.^{4,17}

We report here a novel preparation of styrene-hydride complexes via the reaction of ethylene with the organometallic Lewis acids, [CyRu(Ph)PR₃]⁺ (Cy = η⁶-cymene, *p*-isopropyltoluene), which were prepared *in situ*. This process presumably involves the insertion of

(9) Osborn, J. A.; Byrne, J. W.; Blaser, H. U. *J. Am. Chem. Soc.* **1975**, *97*, 3871.

(10) Schmidt, G. F.; Brookhart, M. *J. Am. Chem. Soc.* **1985**, *107*, 1443.

(11) (a) Cracknell, R. B.; Orpen, A. G.; Spencer, J. L. *J. Chem. Soc., Chem. Commun.* **1984**, 326. (b) Brookhart, M.; Lincoln, D. M. *J. Am. Chem. Soc.* **1988**, *110*, 8719.

(12) (a) Werner, H.; Feser, R. *J. Organomet. Chem.* **1982**, *232*, 351. (b) Werner, H.; Keltzin, H.; Höhn, A.; Paul, W.; Knaup, W.; Ziegler, M. L.; Serhadli, O. *J. Organomet. Chem.* **1986**, *306*, 227. (c) Werner, R.; Werner, H. *Chem. Ber.* **1983**, *116*, 2064. (d) Werner, H.; Werner, R. *J. Organomet. Chem.* **1979**, *174*, C63.

(13) Klein, H. F.; Hammer, R.; Gross, J.; Schubert, U. *Angew. Chem., Int. Ed. Engl.* **1980**, *19*, 809.

(14) Green, M. L. H.; Sella, A.; Wong, L.-L. *Organometallics* **1992**, *11*, 2650.

(15) Doherty, N. M.; Bercaw, J. E. *J. Am. Chem. Soc.* **1985**, *107*, 2670.

(16) Burger, B. J.; Santarsiero, B. D.; Trimmer, M. S.; Bercaw, J. E. *J. Am. Chem. Soc.* **1988**, *110*, 3134.

(17) Bennett, M. A.; Smith, A. K. *J. Chem. Soc., Dalton Trans.* **1974**, 233.

[®] Abstract published in *Advance ACS Abstracts*, March 1, 1995.

(1) Heck, R. F. *Org. React. (N.Y.)* **1982**, *27*, 345.

(2) Murai, S.; Kakiuchi, F.; Sekine, S.; Tanaka, Y.; Kamatani, A.; Sonoda, M.; Chatani, N. *Nature* **1993**, *366*, 529.

(3) Brookhart, M.; Volpe, A. F.; Lincoln, D. M.; Horvath, I. T.; Millar, J. M. *J. Am. Chem. Soc.* **1990**, *112*, 5634.

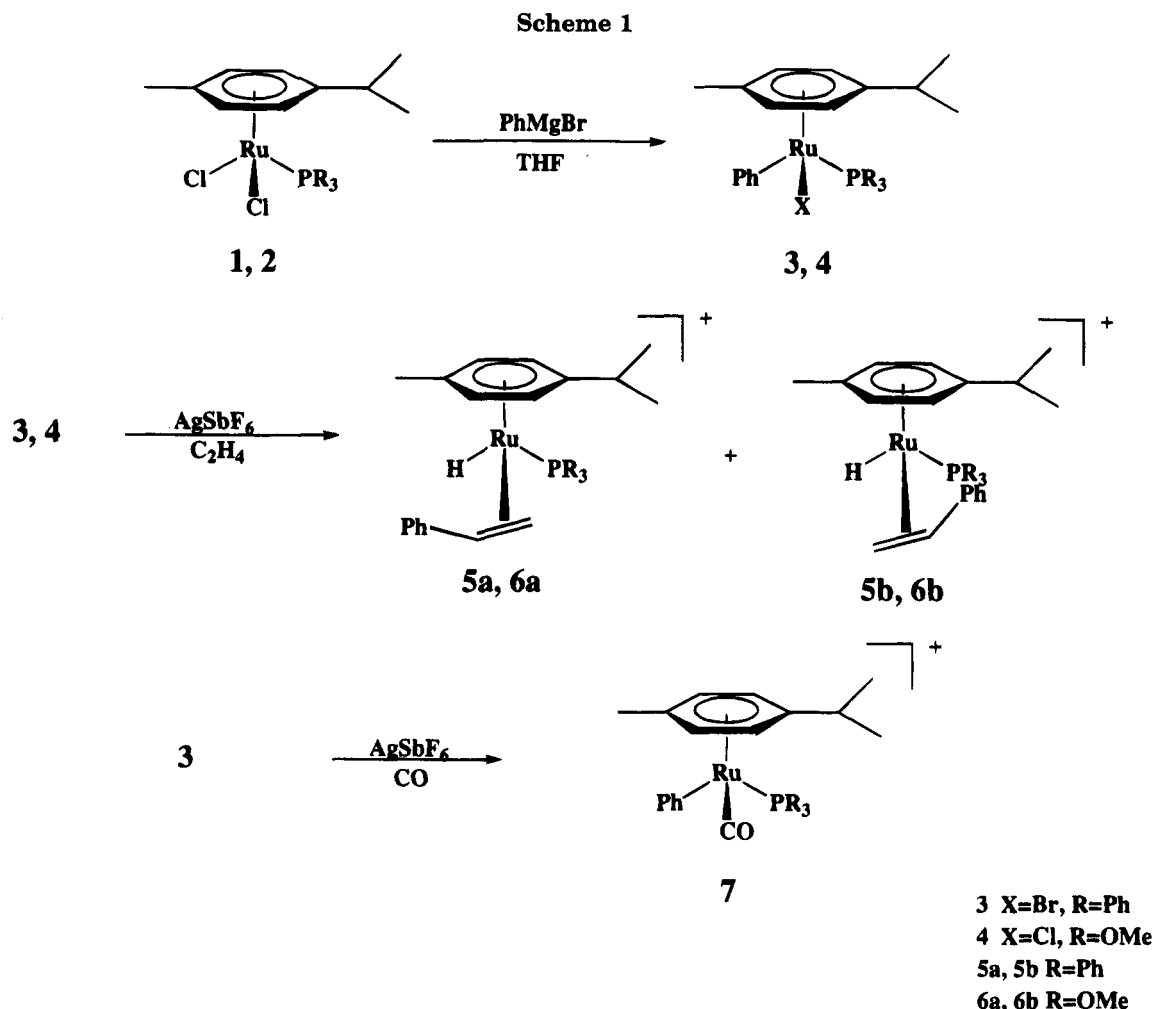
(4) Brookhart, M.; Hauptmann, E.; Lincoln, D. M. *J. Am. Chem. Soc.* **1992**, *114*, 10394.

(5) Flood, T. C.; Wang, L. *J. Am. Chem. Soc.* **1992**, *114*, 3169.

(6) Jolly, C. A.; Marynick, D. S. *J. Am. Chem. Soc.* **1989**, *111*, 7968, and references therein.

(7) Lehmkuhl, H.; Grundke, J.; Schroth, G.; Bann, R. *Z. Naturforsch.* **1984**, *39B*, 1052.

(8) Lehmkuhl, H. *Pure Appl. Chem.* **1990**, *62*, 731.



ethylene into a phenyl-Ru bond, followed by β -hydride elimination, which provides excellent yields of the moderately stable olefin hydride complexes $[\text{CyRuH}(\text{C}_2\text{H}_3\text{Ph})\text{PR}_3]^+$ at ambient temperatures and pressures.

Results and Discussion

Synthesis of Phenyl-Halide, Styrene-Hydride, and Carbonyl Complexes. These syntheses are summarized in Scheme 1. Treatment of the dimer $[\text{CyRuCl}_2]_2$ with triphenylphosphine or trimethyl phosphite gave the monomeric $\text{CyRuPR}_3\text{Cl}_2$ derivatives **1** and **2**.¹⁷ The reaction of **1** or **2** with excess PhMgBr in THF at room temperature, followed by chromatography on silica gel, gives the air-stable complexes $\text{CyRuBrPh}(\text{PPh}_3)$ (**3**) and $\text{CyRuClPh}(\text{P}(\text{OMe})_3)$ (**4**) in about 90% yield. Complex **3** was formed by apparent Br/Cl exchange, either in the reaction or in the workup. Repeated attempts to prepare the related chloride complex using PhMgCl led to the formation of $\text{CyRuPh}_2\text{PPh}_3$. Complex **4** surprisingly does not undergo Br/Cl exchange. The ^1H NMR spectrum of **3** exhibits a very broad peak in the phenyl region at 20 °C, as well as a multiplet at δ 6.8. The broad peak in **3** can be ascribed to a high barrier to rotation arising from a large steric interaction between the triphenylphosphine and the phenyl ligand. Complex **4** in contrast, with a less bulky phosphine, exhibits a sharp multiplet at δ 6.8 and a doublet at δ 7.69. The chemical shifts of the phenyl peaks are consistent with the shifts reported for analogous compounds of rhodium.¹⁸

The styrene-hydride complexes **5** and **6** were prepared by the reaction of **3** and **4** with AgSbF_6 in the presence of ethylene at ambient temperature and pressure. After 20 to 30 min, the reaction mixture was filtered through Celite, and the filtrate was evaporated and washed with heptane, giving the olefin-hydrides **5** and **6** in high yield as pale yellow solids. Complex **5** was found to be stable up to 90 °C in CD_3NO_2 , but **6** decomposed very slowly (over several hours) in solution at room temperature. A similar reaction was reported by Lehmkühl,⁷ in which ethylene inserted into the Ru-Ph bond of a coordinatively unsaturated CpRuPhPPh_3 intermediate, followed by β -hydride elimination to give the corresponding olefin-hydride complex. However, severe conditions (70–100 °C, 50–150 bar) were needed to carry out this transformation. Another related reaction has been reported in which ethylene inserts into the Ru-aryl bond of a proposed orthometalated intermediate $[\text{C}_6\text{Me}_6\text{Ru}(\text{C}_6\text{H}_4\text{PPh}_2)]^+$ to yield a derivative of $[\text{C}_6\text{Me}_6\text{Ru}(\text{H}_2\text{C}=\text{CHC}_6\text{H}_4\text{PPh}_2)]^+$.¹⁸

Usually the insertion of an olefin into an aryl-metal bond is followed by β -hydride elimination and loss of the arylated olefin, as found for insertions of olefins into Pd-phenyl bonds via the Heck reaction.¹ These reactions yield Pd-hydride intermediates, but there is no observation of an olefin-hydride complex; although as a five-coordinate Pd(II) species, the olefin-hydride would not be expected to be stable. The formation of **5** and **6** is very similar to the Heck reaction, except that

(18) Kletzin, H.; Werner, H. *J. Organomet. Chem.* **1985**, 291, 213.

it does not proceed all the way to give the free styrene but rather yields what may be considered an intermediate in the catalytic cycle of the Heck reaction. What is remarkable is that there seems to be no tendency for the olefin-hydride complexes **5** and **6**, under conditions of excess olefin, to undergo irreversible migratory insertion of the styrene into the ruthenium-hydride bond to give a stable alkyl-olefin complex, which occurs in the closely related $[\text{CpRhH}(\text{C}_2\text{H}_4)\text{PR}_3]^+$ complexes ($\text{R} = \text{Me}, \text{OMe}$).⁴

An alkyl analogue, $[\text{C}_6\text{H}_6\text{RuCH}_3(\text{C}_2\text{H}_4)\text{PMe}_3]^+$, has been reported by Werner^{12d} but shows no tendency to undergo olefin insertion into the Ru-CH₃ bond, as addition of PMe_3 gives instead $[\text{C}_6\text{H}_6\text{RuCH}_3(\text{C}_2\text{H}_4\text{PMe}_3)\text{PMe}_3]^+$. It is not clear why the olefin inserts into the Ru-Ph bond but not the Ru-Me bond. Considering the fact that a M-phenyl bond is more stable than an M-methyl bond,^{19,20} one might have expected insertion into a M-Ph bond to be less facile than insertion into a M-CH₃ bond. Comparative data on these insertions are relatively limited, although this trend was also observed by Lehmkuhl in CpRu complexes under extreme conditions.⁷

Removal of bromide from **3** and treatment with CO instead of ethylene did not yield a benzoyl-Ru-carbonyl complex, as one might have anticipated from insertion into the ruthenium-phenyl bond, but rather gave the phenyl carbonyl complex **7**. This is shown clearly by the infrared spectrum, where only a single carbonyl stretching band at 1998 cm^{-1} was observed. The ¹H NMR of **7** also shows the presence of a σ -bound phenyl group, as peaks are observed at less than δ 7.

Characterization of the Olefin-Hydride Complexes 5 and 6. These complexes were characterized by ¹H and ¹³C NMR spectra, and in one case by an X-ray crystal structure determination. In both **5** and **6**, two isomers were detected in solution. The solid state structure of **5** provides a secure point of departure for discussion of the isomerism. Since there is a chiral metal center and styrene is prochiral, different diastereomers can be formed depending upon which face of the styrene binds to the ruthenium. The crystal contains a racemic mixture of the *RR* and *SS* diastereomers

Diastereomers:

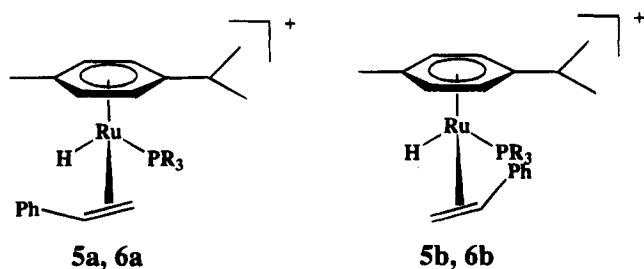
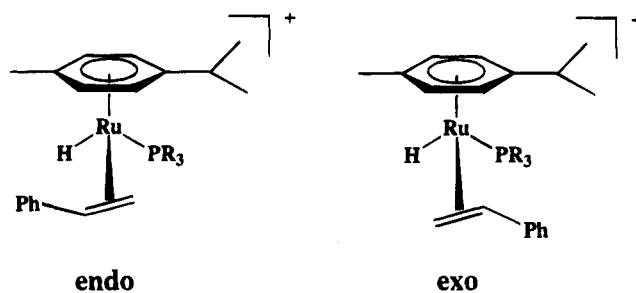


(Figure 1 shows only the *R*_{Ru} metal center, which will be shown in the figures and sketches that follow). η^2 -Olefins generally have barriers to rotation which allow observation of conformers or rotamers by variable-

Rotamers:



temperature NMR.²¹⁻²⁴ In the solid, the *RR*, *SS* diastereomer exists as the endo conformer. On the basis of analogues,^{3,4,7} one would expect that these rotamers should be interconverting rapidly enough at room temperature that the resonances would be averaged at 20 °C. Resonances for both rotamers were not observed in any of the complexes, even at low temperature. There is apparently a pathway for isomerization of the diastereomers in solution. In both **5** and **6**, the *RR*, *SS* and *RS*, *SR* diastereomers were observed by ¹H NMR, one with very sharp olefin resonances at 20 °C and one with broad resonances at 20 °C.

The isomerization path will be discussed below in connection with NMR data; however, the X-ray structure provides some further structural features of note for **5**. Although one should regard the accuracy of metal hydride position determinations by X-ray methods with some suspicion, the hydride is found at a substantial distance, 2.23(7) Å, from the α -carbon of the styrene. Thus it appears that there is no evidence in the solid for an agostic interaction between the hydride and the η^2 -olefin. The electronic difference between hydride and phosphine causes a tilting of the olefin^{21,22} so that it tends to align with the metal-hydride bond. This tilting alleviates some of the steric repulsion that would otherwise occur between the phenyl of the styrene and the cymene ring and which might ordinarily be expected to destabilize the endo conformation (see Figure 2). The correlation of structural data is discussed below, but briefly summarized in Table 1. This structure is similar to the ethylene analogue $[(\text{C}_6\text{Me}_6)\text{RuH}(\text{C}_2\text{H}_4)(\text{PPh}_3)]^+$, which also shows the olefin tilting and was reported by Werner et al.^{12b}

[CyRuH(C₂H₃Ph)PPh₃]⁺ (5**).** The 300 MHz ¹H NMR spectrum of **5** at 20 °C revealed the presence of two diastereomers in a ratio of 8.2:1. The major diastereomer **5a** exhibits sharp resonances corresponding to the olefin protons at δ 3.84 (dd, $J = 12.6, 8.1$ Hz), 3.64 (d, $J = 12.6$ Hz), and 1.70 (dd, $J = 8.1, 6.8$ Hz). Homonuclear decoupling experiments verified the assignments as in Figure 1. The extra coupling exhibited at δ 1.70 is from coupling to phosphorus, observed for analogous CpRh complexes.⁴ The hydride resonance is observed at δ -9.00 as a doublet ($J_{\text{P-H}} = 35.4$ Hz), and

(21) For a recent discussion of olefin rotation in diastereomeric organometallics, see: Pu, J.; Peng, T.-S.; Mayne, C. L.; Arif, A. M.; Gladysz, J. A. *Organometallics* **1993**, *12*, 2686.

(22) For a recent review, see: Faller, J. W. Stereochemical Nonrigidity of Organometallic Complexes. In *Encyclopedia of Inorganic Chemistry*; King, R. B., Ed.; Wiley: New York, 1994; pp 3914-3933.

(23) Faller, J. W.; Johnson, B. V.; Schaeffer, C. D. *J. Am. Chem. Soc.* **1976**, *98*, 1395.

(24) Alt, H.; Herberhold, M.; Kreiter, C. G.; Strack, H. *J. Organomet. Chem.* **1975**, *102*, 491.

(19) Connor, J. A.; Zafarani-Moattar, M. T.; Bikerton, J.; Saied, N. I.; Suradi, S.; Carson, R.; G. A.; Skinner, H. A. *Organometallics* **1982**, *1*, 1166.

(20) Bruno, J. W.; Marks, T. J.; Morss, L. R. *J. Am. Chem. Soc.* **1983**, *105*, 6824.

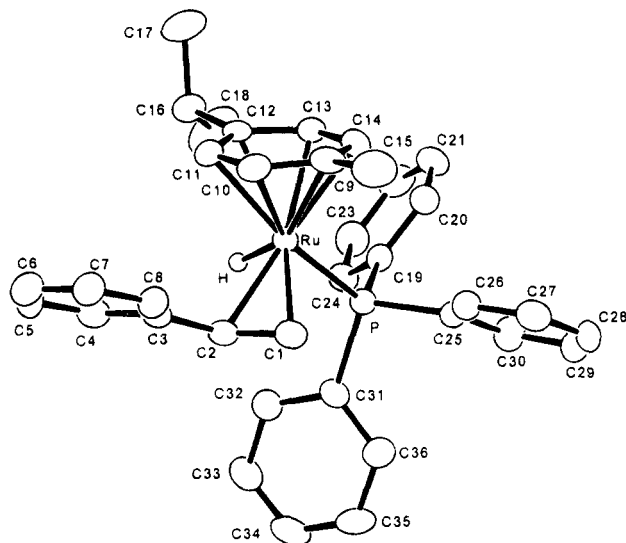


Figure 1. ORTEP view of **5** demonstrating that in the solid the endo rotamer is favored and the *RR*, *SS* diastereomer crystallizes. (*RR*)-**5a** is shown. Hydrogen atoms are omitted for clarity, except for H(40), the metal hydride. Significant bond lengths are as follows: Ru-H, 1.44(7) Å; Ru-P, 2.297(7) Å; C(1)-C(2), 1.397(8) Å; Ru-C(1), 2.195(6) Å; Ru-C(2), 2.216(6) Å. Significant bond angles are as follows: P-Ru-C(1), 84.1(2)°; P-Ru-C(2), 97.3(2)°; P-Ru-H, 80(3)°; H-Ru-C(2), 71(3)°.

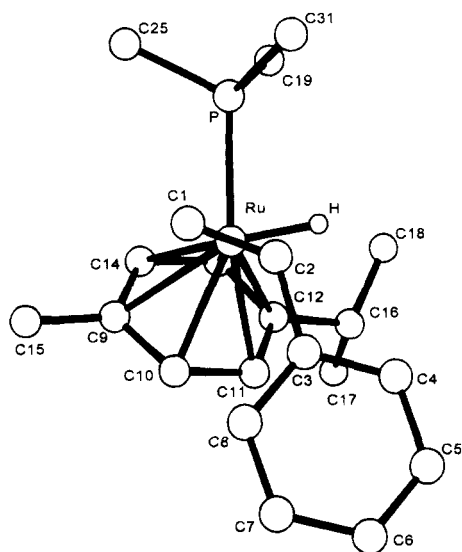


Figure 2. PLUTO view of (*RR*)-**5a** looking from the C(1)-C(2) midpoint toward the Ru.

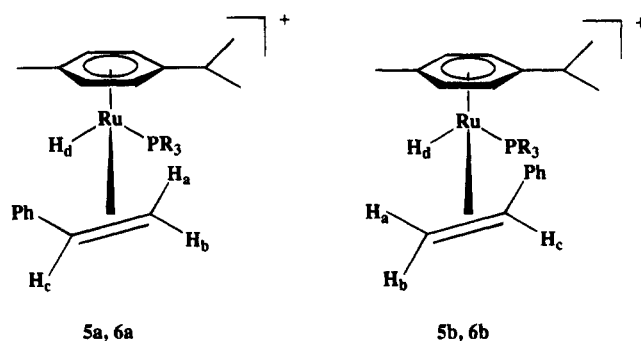
the coupling constant is well within the range of a "classical" olefin-hydride complex. This is confirmed by the ^1H -coupled ^{13}C NMR spectrum, where the methine carbon appears as a doublet at δ 62.01 ($J_{\text{C-H}} = 161$ Hz), and the methylene carbon is a triplet at δ 37.57 ($J_{\text{C-H}} = 159$ Hz). There is little, if any, coupling of the hydride to either carbon, in contrast to that found in agostic olefin-hydride complexes, where the hydride-carbon coupling can be substantial. The major conformation of **5a** was confirmed by difference NOE experiments, as there is a substantial NOE to the methine proton upon saturation of the hydride resonance at δ -9.00. Upon irradiation of the methine proton, the cymene ring protons did not show a NOE. One would expect that the most likely structure for **5a** would be that found in the solid (*vide infra*). The NOE experi-

ment confirms the proximity of the methine proton to the hydride required for this diastereomer and the endo rotamer. (Note that this "endo-exo" terminology denotes the positions of olefin substituents relative to the cymene ring, whereas a similar nomenclature^{15,16} for $\text{Cp}^*\text{M}(\text{H})$ - (styrene) systems denotes positions relative to the hydride.)

The minor diastereomer **5b** exhibited two broad olefin resonances at δ 3.40 and 3.30, as well as a hydride resonance that appeared as a broad doublet at δ -9.96 ($^2J_{\text{P-H}} = 43.2$ Hz). The third olefin resonance was not observed and was presumably buried under other signals. variable-temperature ^1H NMR spectra (-70 to $+40$ °C and 0 - 90 °C) in CD_2Cl_2 and CD_3NO_2 reveal information regarding the rotamer population of the two diastereomers. The resonances assigned to diastereomer **5a** exhibit little, if any, noticeable change within the entire temperature range. The spectra of diastereomer **5b**, however, indicate significant activity. The low concentration of **5b**, variations of δ with temperature, and decomposition at high temperatures make observations difficult. Heating the sample causes the olefin (especially the δ 3.30 resonance) and hydride resonances of **5b** to broaden between 0 and 50 °C. Cooling the sample to -70 °C in CD_2Cl_2 sharpened the broad peaks of **5b** considerably, and a resonance at δ 3.22 became a broad doublet ($J = 12.9$ Hz). This doublet is assigned to the terminal methylene proton *cis* to the phenyl ring on the styrene. The resonances shift with temperature, and δ 3.22 at -70 °C correlates with the room-temperature δ 3.30 resonance. The other olefin proton was not observed at -70 °C either. At low temperature, the lack of new peaks that can be assigned to rotational isomers, and the lack of broadening of the hydride resonance of **5a** at any temperature, suggest that **5a** and **5b** exist predominantly as single rotamers.

The hydride resonance of **5b** broadens into the baseline at higher temperatures. The crucial experiments for analyzing the process, however, are saturation transfer experiments at 10 °C on **5b**, which confirm the presence of exchange between the hydride and the terminal olefin proton at δ 3.30. Saturation of the hydride resonance at δ -9.96 causes the resonance at δ 3.30 to decrease drastically in intensity, while the δ 3.40 resonance is essentially unaffected. Both peaks are broad and they overlap. Irradiation at δ 3.30 also results in an intensity decrease in the hydride resonance. It would seem reasonable that this exchange would most readily be effected if the methylene were adjacent to the hydride in the principal rotamer. This would then require that the phenyl ring of the styrene oriented toward the cymene ring in the principal rotamer of **5b** and it would be assigned as the endo rotamer. Although one could imagine a scenario where a major exo rotamer rotated to a less populated endo form to allow the exchange, it seems more likely that endo-**5b** would be the predominant form. These interpretations for **5b** are somewhat tenuous owing to the low concentration of the minor isomer and overlapping peaks. The observations of saturation transfer and the analogous assignments in **6** are much more straightforward owing to the greater concentration of the minor isomer and ease of observation.

[CyRuH(C₂H₅Ph)P(OMe)₃]⁺ (6**).** The ^1H NMR spectrum of **6** at 20 °C shows the presence of two diaster-

Table 1. ^1H NMR Assignments of Olefin and Hydride Resonances for Complexes **5** and **6**^a

complex	H _a	H _b	H _c	H _d
5a	3.64, d (12.6)	1.70, dd (8.1, 6.8)	3.84, dd (12.6, 8.1)	-9.00, d (35.4)
5b	3.30 ^b	<i>c</i>	3.40	-9.96, d (43.2)
6a	3.66, d (12.3)	2.25, dd (9.0, 6.9)	4.48, dd (12.3, 9.0)	-9.27, d (31.2)
6b	3.24, d (12)	2.60 m ^d	4.46 ^d	-10.97, d (30.6)

^a Chemical shifts in ppm downfield from TMS in CD_2Cl_2 . Numbers in parentheses denote coupling constants (in Hz). d, doublet; dd, doublet of doublets.
^b Observed at δ 3.22 (12.9) at -70°C . ^c Obscured by other resonances. ^d Partially overlapped by other resonances.

Table 2. Crystallographic Data for X-ray Diffraction Studies of $[\text{C}_y\text{RuH}(\text{C}_2\text{H}_3\text{Ph})(\text{PPh}_3)] \text{SbF}_6 \cdot \text{CH}_2\text{Cl}_2$

(A) Crystal Parameters at $-103 \pm 2^\circ\text{C}$	
formula	$\text{RuPC}_{38}\text{H}_{28}\text{SbF}_6 \cdot \text{CH}_2\text{Cl}_2$
space group	$P2_1/n$ (No. 14)
<i>a</i> , Å	10.49(1)
<i>b</i> , Å	15.24(1)
<i>c</i> , Å	24.015(4)
β , deg	101.94(3)
<i>V</i> , Å ³	3755(9)
FW	923.41
ρ_{calcd} , g/cm ³	1.633 (<i>Z</i> = 4)
abs coeff, cm ⁻¹	13.58
cryst dimens, mm	$0.22 \times 0.22 \times 0.45$
(B) Intensity Measurements	
diffractometer	Rigaku AFC5S
monochromator	graphite
radiation	Mo K α (0.710 69 Å)
scan type	$\omega-2\theta$
no. of reflectns measd	$+h, +k, \pm l$
max 2θ , deg	60
no. of unique reflectns measd	9483
(C) Solution and Refinement	
data used, $F^2 > 3\sigma(F^2)$	5539
params refined	553
abs correctn	empirical (0.81-1.16)
<i>R</i> factor	0.02
final residuals <i>R</i> , <i>R_w</i>	0.046, 0.050
convergence, largest shift/error	0.00
GOF	1.83
largest $\Delta(\rho)$ e ⁻ /Å ³	1.09

omers in the ratio of 2.6:1. The olefin protons of the major isomer **6a** appear as a doublet of doublets at δ 4.48 ($J = 12.3, 9.0$ Hz), a doublet at δ 3.66 ($J = 12.3$ Hz), and a doublet of doublets at δ 2.25 ($J = 9.0, 6.9$ Hz). The hydride appears at δ -9.27 as a doublet ($J_{\text{P-H}} = 31.2$ Hz). As with **3**, the large P-H coupling constant, as well as the ^1H -coupled ^{13}C spectrum show that this is a "traditional" olefin-hydride complex. Homonuclear decoupling experiments clearly assign the δ 4.48 resonances as belonging to the methine proton. The preferred conformation of **6a** was determined by the large NOE found between the methine proton and the hydride from NOE difference experiments.

The minor isomer **6b** displays olefin resonances at δ 4.46 (partially masked by the δ 4.48 resonance of **6a**), δ 3.24, a broad doublet ($J = 12$ Hz), and δ 2.60, which is partially obscured by the cymene $\text{CH}(\text{Me})_2$ septet. The

hydride is observed as a doublet at δ -10.97 ($J_{\text{P-H}} = 30.6$ Hz). Saturation transfer experiments at 20°C on **6b** show that there is exchange between the hydride and the protons corresponding to the doublet at δ 3.24 and the resonance at δ 2.60. Irradiation of the hydride resonance at δ -10.97 severely diminishes the intensity of the δ 3.24 and 2.60 resonances, while the δ 4.46 resonance was unaffected. Difference NOE experiments on **6b** show that the resonance at δ 4.46 only exhibits a NOE to the $\text{P}(\text{OMe})_3$ and the styrene phenyl, and not to the cymene ring. Both the NOE and the saturation transfer experiments are good evidence that the δ 4.46 resonance belongs to the methine proton and that it is oriented away from the cymene ring in the predominant (endo) rotamer.

Variable-temperature NMR of **6** (-90 to $+20^\circ\text{C}$) reveals the olefin rotation of the minor isomer **6b**. At -50°C , there is broadening of the δ -10.97 resonance, and at -60°C , the signal is very broad. Cooling to -90°C shows a resharping of the peak, but no new hydride resonances are observed. At -60°C , there is slight broadening of the **6a** hydride peak, and it sharpens up again by -90°C . This indicates that both of these diastereomers must have very small populations (<5%) of the exo rotamers. It is interesting to note that the slowed olefin rotation of **6a** and **6b** is observed at -50°C , while for **5a** and **5b** there is no such observation to -70°C . It is not clear whether the absence of broadening the **5** is a consequence of lower barriers or extremely low populations of exo rotamers. Brookhart observed that the more donating phosphorus-containing ligand, Me_3P vs $\text{P}(\text{OMe})_3$, correlates with the larger the barrier of rotation for similar CpRh complexes.⁴

Since we know the geometry of **6a** and we also know from the saturation transfer experiment on **6b** that *two* hydrogens are exchanging with the hydride, it follows that both diastereomers probably exist predominantly as endo rotamers with the phenyl ring oriented toward the cymene.

Reactions of 5 and 6. Complexes **5** and **6**, upon reaction with excess pyridine in CD_2Cl_2 , slowly yield styrene as one of the products. Reaction of **5** with excess CH_3CN yielded free styrene, but the reaction was very

Table 3. Positional Parameters and $B(\text{eq})$ for $[\text{CyRu}(\text{PPh}_3)(\text{H})(\text{styrene})]\text{SbF}_6\cdot\text{CH}_2\text{Cl}_2$

atom	x	y	z	$B(\text{eq})$	atom	x	y	z	$B(\text{eq})$
Sb	0.49295(5)	0.03049(3)	0.12971(2)	3.74(2)	C(34)	0.3712(7)	0.4118(5)	0.0938(3)	3.4(3)
Ru	0.04563(4)	0.20436(3)	0.22272(2)	1.75(2)	C(35)	0.2614(7)	0.4604(4)	0.0916(3)	3.4(3)
Cl(1)	0.0246(2)	0.1947(2)	0.4712(1)	6.3(1)	C(36)	0.1511(6)	0.4216(4)	0.1050(3)	2.6(2)
Cl(2)	-0.2430(2)	0.2513(2)	0.4535(1)	6.6(1)	C(37)	-0.080(1)	0.2826(6)	0.4745(4)	5.4(4)
P	0.0093(1)	0.27991(9)	0.13816(6)	1.83(5)	H(1)	0.093(7)	0.342(5)	0.286(3)	5.0
F(1)	0.4300(4)	-0.0837(3)	0.1180(2)	5.1(2)	H(2)	0.123(7)	0.383(4)	0.234(3)	5.0
F(2)	0.5624(5)	0.1427(3)	0.1369(3)	10.0(3)	H(3)	0.279(7)	0.275(4)	0.231(3)	5.0
F(3)	0.5929(8)	-0.0011(4)	0.1969(3)	11.9(4)	H(4)	0.407(7)	0.152(5)	0.278(3)	5.0
F(4)	0.629(1)	-0.0035(6)	0.1002(5)	18.2(7)	H(5)	0.545(7)	0.087(5)	0.352(3)	5.0
F(5)	0.3640(8)	0.0588(6)	0.1611(6)	20.7(8)	H(6)	0.531(7)	0.120(4)	0.449(3)	5.0
F(6)	0.389(1)	0.0640(5)	0.0654(4)	21.5(7)	H(7)	0.349(7)	0.219(5)	0.450(3)	5.0
C(1)	0.1319(6)	0.3284(4)	0.2588(3)	2.4(2)	H(8)	0.228(7)	0.289(4)	0.374(3)	5.0
C(2)	0.2330(6)	0.2678(4)	0.2619(2)	2.2(2)	H(9)	0.030(7)	0.179(5)	0.340(3)	5.0
C(3)	0.3059(6)	0.2244(3)	0.3143(2)	2.3(2)	H(10)	0.131(7)	0.067(5)	0.305(3)	5.0
C(4)	0.4024(7)	0.1626(4)	0.3101(3)	2.8(3)	H(11)	-0.146(7)	0.086(5)	0.161(3)	5.0
C(5)	0.4779(7)	0.1252(4)	0.3585(3)	3.7(3)	H(12)	-0.247(7)	0.199(4)	0.200(3)	5.0
C(6)	0.4592(7)	0.1464(4)	0.4118(3)	3.6(3)	H(13)	-0.120(7)	0.304(5)	0.329(3)	5.0
C(7)	0.3639(7)	0.2065(4)	0.4168(3)	3.1(3)	H(14)	-0.233(7)	0.305(5)	0.278(3)	5.0
C(8)	0.2883(6)	0.2458(4)	0.3690(3)	2.7(2)	H(15)	-0.237(7)	0.249(5)	0.327(3)	5.0
C(9)	-0.1153(6)	0.1999(4)	0.2775(3)	2.7(2)	H(16)	0.145(7)	-0.028(4)	0.225(3)	5.0
C(10)	0.0006(6)	0.1607(4)	0.3066(3)	2.5(2)	H(17)	-0.112(7)	-0.092(5)	0.197(3)	5.0
C(11)	0.0579(6)	0.0891(4)	0.2836(3)	2.5(2)	H(18)	-0.002(7)	-0.153(5)	0.206(3)	5.0
C(12)	0.0007(5)	0.0562(3)	0.2285(2)	2.1(2)	H(19)	-0.035(7)	-0.116(5)	0.254(3)	5.0
C(13)	-0.1087(6)	0.1011(4)	0.1973(3)	2.2(2)	H(20)	0.076(8)	0.017(5)	0.127(3)	5.0
C(14)	-0.1665(6)	0.1719(4)	0.2228(3)	2.4(2)	H(21)	0.095(7)	-0.075(5)	0.131(3)	5.0
C(15)	-0.1820(9)	0.2698(5)	0.3051(4)	4.3(4)	H(22)	-0.049(7)	-0.015(5)	0.122(3)	5.0
C(16)	0.0541(6)	-0.0254(4)	0.2062(3)	3.0(3)	H(23)	-0.246(7)	0.212(4)	0.084(3)	5.0
C(17)	-0.027(1)	-0.1016(5)	0.2197(4)	4.8(4)	H(24)	-0.304(7)	0.113(5)	0.014(3)	5.0
C(18)	0.052(1)	-0.0224(6)	0.1436(4)	5.7(5)	H(25)	-0.179(7)	0.048(4)	-0.038(3)	5.0
C(19)	-0.0518(5)	0.2098(3)	0.0765(2)	2.1(2)	H(26)	0.046(7)	0.093(5)	-0.017(3)	5.0
C(20)	-0.1821(6)	0.1847(4)	0.0650(3)	2.5(2)	H(27)	0.117(7)	0.190(4)	0.051(3)	5.0
C(21)	-0.2276(6)	0.1241(4)	0.0219(3)	2.8(3)	H(28)	-0.108(7)	0.378(4)	0.212(3)	5.0
C(22)	-0.1453(7)	0.0896(4)	-0.0098(3)	3.1(3)	H(29)	-0.265(7)	0.494(5)	0.197(3)	5.0
C(23)	-0.0173(7)	0.1149(4)	0.0007(3)	2.9(3)	H(30)	-0.351(7)	0.548(4)	0.113(3)	5.0
C(24)	0.0307(6)	0.1742(4)	0.0437(3)	2.5(2)	H(31)	-0.286(7)	0.497(4)	0.036(3)	5.0
C(25)	-0.1135(5)	0.3680(3)	0.1297(2)	2.1(2)	H(32)	-0.146(7)	0.379(5)	0.047(3)	5.0
C(26)	-0.1519(6)	0.4031(4)	0.1769(3)	2.4(2)	H(33)	0.276(7)	0.235(4)	0.134(3)	5.0
C(27)	-0.2419(6)	0.4703(4)	0.1706(3)	3.0(3)	H(34)	0.452(7)	0.296(4)	0.118(3)	5.0
C(28)	-0.2944(6)	0.5049(4)	0.1172(3)	2.9(3)	H(35)	0.438(7)	0.437(5)	0.089(3)	5.0
C(29)	-0.2560(6)	0.4706(4)	0.0703(3)	3.1(3)	H(36)	0.262(7)	0.516(5)	0.080(3)	5.0
C(30)	-0.1678(6)	0.4024(4)	0.0757(3)	2.8(3)	H(37)	0.073(7)	0.463(4)	0.103(3)	5.0
C(31)	0.1530(6)	0.3334(4)	0.1214(2)	2.2(2)	H(38)	-0.072(7)	0.303(5)	0.508(3)	5.0
C(32)	0.2677(6)	0.2865(4)	0.1253(3)	2.6(2)	H(39)	-0.068(7)	0.331(5)	0.452(3)	5.0
C(33)	0.3753(6)	0.3254(5)	0.1113(3)	3.0(3)	H(40)	0.147(6)	0.167(4)	0.198(3)	5.0

sluggish, taking several hours to go to completion. The introduction of CO to **5** at ambient pressure and temperature did not result in substitution of the styrene ligand or the β -phenethyl-carbonyl complex, as no reaction occurred. As was noted previously, complexes **5** and **6** were prepared under conditions of excess ethylene and did not produce the β -phenethyl-ethylene complex in either case. These reactions also demonstrate that the styrene ligand is not especially labile.

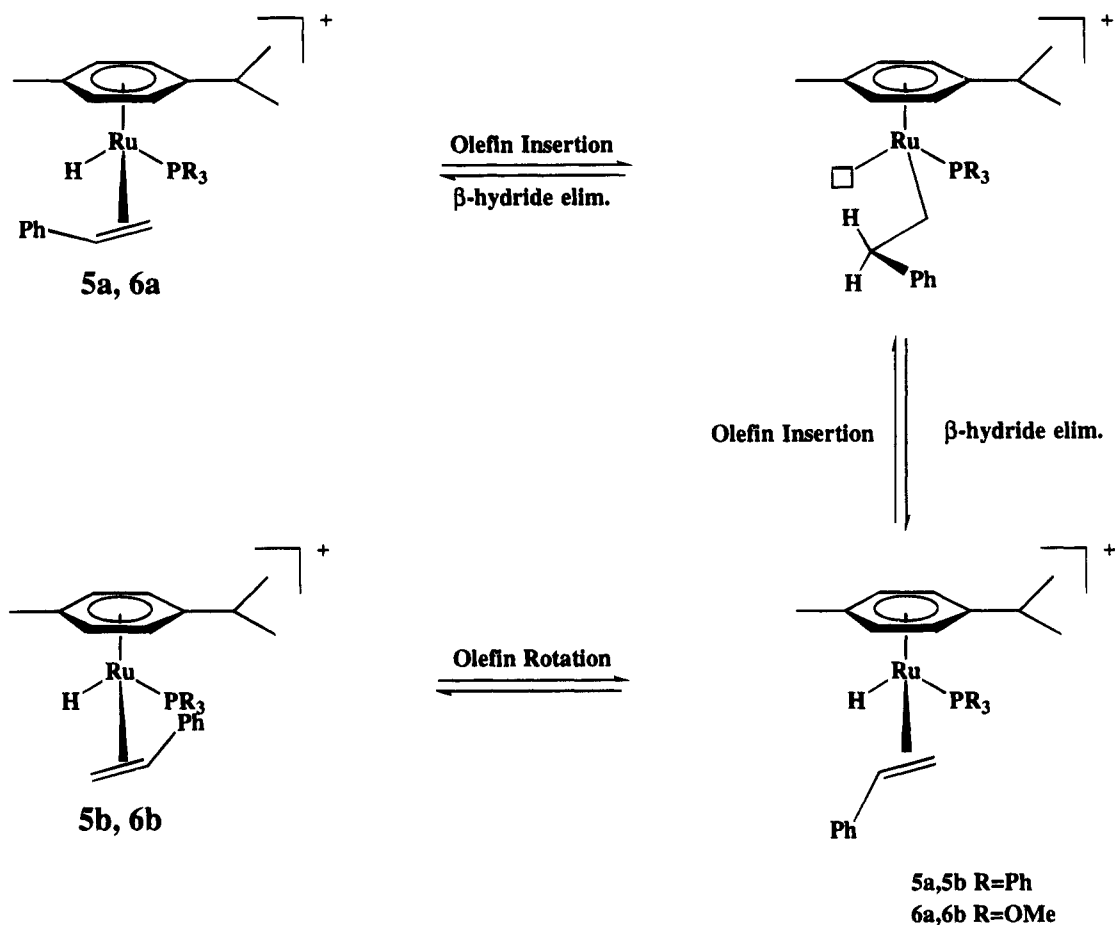
Proposed Mechanism of Isomerization. The single crystal used for the X-ray analysis, shown to be **5a**, was placed in an NMR tube with CD_2Cl_2 , and a ^1H NMR spectrum was taken as rapidly as possible. The total time from dissolving the crystal to final acquisition of the data was less than 15 min. The spectrum clearly showed the two isomers **5a** and **5b** in a ratio of 8.2:1, the same ratio as observed at much longer times. This demonstrates that there is an equilibrium between these diastereomers, and that it takes much less than 15 min to achieve equilibrium, but that the equilibration is relatively slow on the NMR time scale. It was shown previously (*vide supra*) that **5a** and **5b** are not rotational isomers, so another mechanism must account for this isomerization. A dissociation-recombination mechanism, where the styrene dissociates from the ruthenium and then binds with the other enantioface, can be dis-

counted owing to the rapid isomerization of the complex and the sluggish reactivity of **5** in substitution reactions.

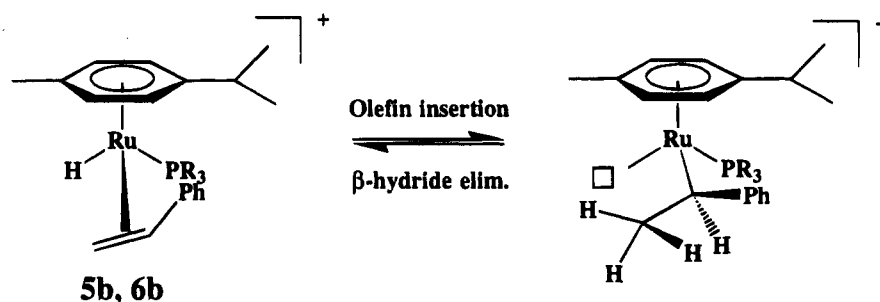
The proposed mechanism for interconversion of **5a** and **5b** (Scheme 2) involves hydrogen exchange between the metal-hydride and the methine hydrogen. This exchange occurs on a time scale that is effectively slower than the NMR experiment at room temperature. This process for **5a**, followed by fast olefin rotation, will give **5b**. The **b** diastereomers also undergo a three-site exchange mechanism between the two methylene hydrogens and the metal-hydride, a process observed for both **5b** and **6b** (Scheme 3). This is in agreement with the results obtained by Bercaw for $\text{Cp}_2\text{NbH}(\text{C}_2\text{H}_5\text{Ph})$,¹⁶ where the methine-hydride exchange is slower than the methylene-hydride exchange by 1–2 orders of magnitude.

In summary, we conclude that olefin insertion into the Ph-Ru bond occurs rapidly in the $[\text{CyRu}(\text{ethylene})(\text{Ph})\text{PR}_3]^+$ intermediate formed by addition of ethylene to the species formed by removal of halide from $\text{CyRu}(\text{Ph})\text{PR}_3\text{X}$. β -Hydride elimination from the coordinatively unsaturated $\text{RuCH}_2\text{CH}_2\text{Ph}$ intermediate gives the styrene-hydride complexes **5** and **6**. NMR studies suggest that hydride-olefin insertion occurs rapidly to yield unobserved transient phenethyl intermediates. Hydride-olefin insertion occurs rapidly and reversibly

Scheme 2



Scheme 3



in the styrene hydrides and produces unobserved transient phenethyl intermediates. A significant feature of the relative rates of these hydride-olefin insertion processes is that the formation of a secondary alkyl, α -phenethyl, is more facile than that of a primary alkyl, β -phenethyl.

Experimental Section

All reagents were purchased from Aldrich. $[\text{CyRuCl}_2]_2$,²⁵ $\text{CyRuCl}_2\text{PPh}_3$, and $\text{CyRuCl}_2\text{P(OMe)}_3$ ¹⁷ were prepared as in the literature. NMR spectra were recorded on GE-QE 300 or Yale 490 MHz instruments. AgSbF_6 was stored and manipulated in a nitrogen atmosphere glovebox. CO (Linde) and ethylene (Cryodyne) were used as received.

Preparation of $[\text{CyRuBr(Ph)PPh}_3]$ (3). 3 was prepared by a method similar to Jones' preparation of analogous Rh complexes.²⁶ 1 (1.007 g, 1.77 mmol) was added to 50 mL of

dry THF under nitrogen. The solution was cooled to -78°C , and a 3-fold excess of 3 M PhMgBr in ether (1.77 mL, 5.32 mmol) was added via syringe. The reaction was slowly warmed to room temperature and stirred for 30 min. Wet THF was carefully added by pipet to deactivate unreacted PhMgBr . The mixture was opened to the air, and the solvent was removed by rotary evaporation. The residue was then dissolved in CH_2Cl_2 and washed through silica gel, followed by chromatography (silica gel/ CH_2Cl_2) to give a single yellow-orange band, found to be pure 3 (1.000 g, 0.153 mmol, 86%): $^1\text{H NMR}$ (CD_2Cl_2 , 20°C) δ 7.8–6.8 (vbr, 17H, Ph), 6.71 (m, 3H, Ph), 5.37 (d, 1H, Cy-H), 5.13 (d, 1H, Cy-H), 5.07 (d, 1H, Cy-H), 4.97 (d, 1H, Cy-H), 2.08 (septet, 1H, $\text{CH}(\text{CH}_3)_2$), 1.53 (s, 3H, Cy- CH_3), 1.05 (d, 3H, $\text{CH}(\text{CH}_3)_2$), 0.92 (d, 3H, $\text{CH}(\text{CH}_3)_2$). Anal. Calcd for $\text{C}_{34}\text{H}_{34}\text{BrP}_1\text{Ru}_1$: (C, 62.39; H, 5.24. Found: C, 62.64; H, 5.30. This compound crystallizes in the monoclinic space group $P2_1/c$ (No. 14) with $a = 9.683(4)\text{ \AA}$, $b = 15.480(5)\text{ \AA}$, $c = 19.758(4)\text{ \AA}$, $\beta = 103.15(2)^\circ$; $V = 2884(1)\text{ \AA}^3$, $Z = 4$. The structure, which will be published elsewhere,

(25) Bennett, M. A.; Huang, T-N; Matheson, T. W.; Smith, A. K. *Inorg. Synth.* **1982**, *21*, 75.

(26) Jones, W. D.; Kuyendall, V. L. *Inorg. Chem.* **1991**, *30*, 2615.

is fully consistent with the complex being the bromide with a Ru-Br bond length of 2.556(3) Å and a normal thermal parameter for the Br of $B_{eq} = 3.8(1) \text{ \AA}^2$.

Preparation of [CyRuCl(Ph)P(OMe)₃] (4). **4** was prepared similarly to **3**. Amounts used: 0.104 g (0.24 mmol) of **4**; 0.24 mL (0.72 mmol) of 3 M PhMgBr in 25 mL of dry THF; yield, 0.099 g, 0.21 mmol, 86%. ¹H NMR (CD₂Cl₂, 20 °C) δ 7.69 (d, 2H, Ph), 6.86 (d, 3H, Ph), 5.43 (d, 1H, Cy-H), 5.32 (d, 1H, Cy-H), 5.19 (d, 2H, Cy-H), 3.45 (d, 9H, P(OCH₃)₃), 2.68 (septet, 1H, CH(CH₃)₂), 1.94 (s, 3H, Cy-CH₃), 1.18 (d, 3H, CH(CH₃)₂), 1.14 (d, 3H, CH(CH₃)₂). Anal. Calcd for C₁₉H₂₈Cl₁O₃P₁Ru₁: C, 48.36; H, 5.98. Found: C, 48.97; H, 6.01.

Preparation of [CyRuH(C₂H₃Ph)PPh₃]SbF₆ (5). Under nitrogen, **3** (0.124 g, 0.19 mmol) was placed in a 100 mL Schlenk flask equipped with a stirring bar, and 25 mL of freshly distilled CH₂Cl₂ was added via cannula. The orange solution was then purged for 10 min with ethylene, and AgSbF₆ (0.070 g, 0.20 mmol) was added with stirring under an ethylene stream. The color of the solution changed almost immediately to a very pale yellow color, and a colorless solid, presumably AgCl, precipitated. After 20–30 min of stirring, the pale yellow color remained, and the mixture was filtered through Celite to remove the AgCl. The filtrate was collected and partially evaporated by a nitrogen stream, and dry *n*-heptane was added to initiate precipitation. The mother liquor was removed via cannula, and the pale yellow solid was washed twice times with *n*-heptane, dried under high vacuum, and then placed into a drybox, giving 0.145 g (0.17 mmol, 89%) of **5**. NMR samples were prepared by adding the solid into a screw-cap NMR tube, removing to a high vacuum line, and distilling in dry solvent (CD₂Cl₂ or CD₃NO₂). The NMR samples were stable for many weeks under these conditions. **5** was found to be moderately air stable as a solid, but is air-sensitive in solution. ¹H NMR (CD₂Cl₂, 20 °C): Major isomer **5a**, δ 7.7–7.2 (m, 20H, Ph), 5.73 (d, Cy-H), 4.89 (d, Cy-H), 4.66 (d, Cy-H), 4.40 (d, Cy-H), 3.84 (d, 1H, CH₂CH, *J* = 12.6, 8.1 Hz), 3.64 (d, 1H, CHHCH, *J* = 12.6 Hz), 2.61 (s, 3H, Cy-CH₃), 2.55 (septet, 1H, CH(CH₃)₂), 1.70 (dd, 1H, CHHCH, *J* = 8.1, 6.8 Hz), 1.23 (d, 3H, CH(CH₃)₂), 1.08 (d, 3H, CH(CH₃)₂), -9.00 (d, 1H, RuH, *J*_{P-H} = 35.4 Hz). Minor isomer **5b**, δ 7.7–7.2 (m, 20H, Ph), 6.08 (d, 1H, Cy-H), 5.86 (d, 1H, Cy-H), 4.80 (d, 1H, Cy-H), 4.55 (d, 1H, Cy-H), 3.40 (br, 1H, CH₂C-H), 3.30 (br, 1H, CHHCH), 2.61 (s, 3H, Cy-CH₃), 2.56 (septet, 1H, CH(CH₃)₂), 1.18 (d, 3H, CH(CH₃)₂), 1.13 (d, 3H, CH(CH₃)₂), -10.98 (d, 1H, RuH, *J*_{P-H} = 43.2 Hz). ¹³C NMR (CD₂Cl₂, 20 °C): Major isomer **5a**, δ 142.58 (s, Cy-CR), 135–125 (P(C₆H₅)₃, C₂H₃(C₆H₅)), 116.70 (s, Cy-CR), 103.84 (d, Cy-CH), 100.52 (d, Cy-CH), 97.98 (d, Cy-CH), 91.15 (d, Cy-CH), 62.01 (d, CH₂CHPh, *J*_{C-H} = 161 Hz), 37.57 (t, CH₂CHPh, *J*_{C-H} = 159 Hz), 32.29 (d, C(CH₃)₂), 23.56 (q, C(CH₃)(CH₃)), 23.40 (q, C(CH₃)(CH₃)), 19.64 (q, Cy-CH₃). Minor isomer **5b**, δ 136.61 (s, Cy-CR), 135–125 (P(C₆H₅)₃, C₂H₃(C₆H₅)), 118.50 (s, Cy-CR), 91.59 (d, Cy-CH), 90.11 (d, Cy-CH), 90.00 (d, Cy-CH), 89.44 (d, Cy-CH), 70.16 (d, CH₂CHPh, *J*_{C-H} = 165 Hz), 50.18 (t, CH₂CHPh, *J*_{C-H} = 162 Hz), 39.52 (d, CH(CH₃)₂), 22.88 (q, CH₃), 17.41 (q, CH₃), 16.96 (q, CH₃). Anal. Calcd for C₃₆H₃₈F₆O₁P₁Ru₁Sb₁·0.5CH₂Cl₂: C, 49.76; H, 4.46. Found: C, 49.34; H, 4.50. (The amount of CH₂Cl₂ incorporation was variable and depended upon the workup of the complex, as shown by ¹H NMR in CD₃NO₂, which always showed <1 equiv of CH₂Cl₂ present in several samples. Concentrations of CH₂Cl₂ varied between 0.5 and 1 equiv of CH₂Cl₂.)

Preparation of [CyRuH(C₂H₃Ph)P(OMe)₃]SbF₆ (6). **6** was prepared in essentially the same manner as **5**. Due to the slight thermal instability of **6** at 20 °C, the reaction was performed at 0 °C and stored in the cold (-25 °C). The NMR samples were quickly prepared at room temperature under a nitrogen stream using dry CD₂Cl₂ as solvent. Neither the solid nor the NMR samples decomposed at -25 °C over several weeks. ¹H NMR (CD₂Cl₂, 20 °C): Major isomer **6a**, δ 7.5–7.2 (5H, Ph), 5.86 (d, 1H, Cy-H), 5.58 (d, 1H, Cy-H), 5.44 (d, 1H, Cy-H), 5.01 (d, 1H, Cy-H), 4.48 (dd, 1H, PhCHCH₂, *J* = 12.3,

9.0 Hz), 3.69 (d, 9H, P(OCH₃)₃, *J* = 12.0 Hz), 3.66 (d, 1H, *J* = 12.3), 2.58 (septet, 1H, CH(CH₃)₂), 2.44 (s, 3H, Cy-CH₃), 2.25 (dd, 1H, *J* = 9.0, 6.9 Hz, PhCHCH₂), 1.29 (d, 3H, CH(CH₃)(CH₃)), 1.27 (d, 3H, CH(CH₃)(CH₃)), -9.27 (d, 1H, RuH, *J*_{P-H} = 31.2 Hz). Minor isomer **6b**, δ 7.5–7.2 (5H, Ph), 6.11 (d, 1H, Cy-H), 6.02 (d, 1H, Cy-H), 5.60 (d, 1H, Cy-H), 5.17 (d, 1H, Cy-H), 4.46 (br, 1H, PhCHCH₂), 3.64 (d, 9H, P(OCH₃)₃, *J* = 12.3 Hz), 3.24 (d (br), 1H, *trans*-PhCHCH₂, *J* = 12 Hz), 2.72 (septet, 1H, CH(CH₃)₂), 2.60 (br, 1H, *cis*-PhCHCH₂), 1.97 (s, 3H, Cy-CH₃), 1.36 (d, 3H, CH(CH₃)(CH₃)), 1.34 (d, 3H, CH(CH₃)(CH₃)), -10.97 (1H, d, RuH, *J*_{P-H} = 30.6 Hz). ¹³C NMR (CD₂Cl₂, -10 °C): Major isomer **6a**, δ 143.51 (s, Ph), 128.26 (d, Ph), 126.64 (d, Ph), 126.20 (d, Ph), 117.47 (s, Cy-CR), 116.65 (s, Cy-CR), 103.37 (d, Cy-CH), 100.31 (d, Cy-CH), 99.51 (d, Cy-CH), 91.87 (d, Cy-CH), 60.41 (d, PhCHCH₂, *J*_{C-H} = 160 Hz), 53.67 (q, P(OCH₃)₃), 35.20 (d, PhCHCH₂, *J*_{C-H} = 163, 144 Hz), 32.35 (d, CH(CH₃)₂), 23.44 (q, CH₃), 19.83 (q, CH₃). Minor isomer **6b**, δ 143.10 (s, Ph), 110.30 (s, Cy-CR), 116.56 (s, Cy-CR), 98.22 (d, Cy-CH), 96.40 (d, Cy-CH), 92.68 (d, Cy-CH), 89.50 (d, Cy-CH), 59.39 (d, PhCHCH₂, *J*_{C-H} = 162 Hz), 48.91 (t, PhCHCH₂, *J*_{C-H} = 172 Hz), 42.71 (d, CH(CH₃)₂), 22.76 (q, CH₃), 18.43 (q, CH₃). Some peaks corresponding to the phenyl carbons in **6b** were obscured by peaks from the major isomer. No elemental analysis was performed, owing to the thermal instability of the complex.

Preparation of [CyRu(CO)(Ph)PPh₃]SbF₆ (7). The preparation of **7** followed that of **5**, except that CO was substituted for ethylene. To 0.1536 g (0.23 mmol) of **3** in 25 mL of CH₂Cl₂ was added 0.0870 g (0.25 mmol) of AgSbF₆ under a CO atmosphere. The color of the solution became yellow over a period of 1 min, with concomitant precipitation of AgBr. The reaction was stirred for 30 min, then the mixture was washed through Celite, and *n*-heptane was added to the yellow filtrate to initiate precipitation. The precipitate was washed twice with *n*-heptane and dried under high vacuum to give 0.1533 g (0.18 mmol, 78%) of pure **7**: ¹H NMR (CD₂Cl₂, 20 °C) δ 7.56 (m, 3H, Ph), 7.45 (m (br), 6H, Ph), 7.13 (m (br), 6H, Ph), 6.94 (m, 3H, Ph), 6.85 (m, 2H, Ph), 6.48 (d, 1H, Cy-H), 6.38 (d, 1H, Cy-H), 6.25 (d, 1H, Cy-H), 6.17 (d, 1H, Cy-H), 2.10 (septet, 1H, CH(CH₃)₂), 1.68 (s, 3H, Cy-CH₃), 1.16 (d, 3H, CH(CH₃)₂), 1.01 (d, 3H, CH(CH₃)₂). IR (CH₂Cl₂) 1998 cm⁻¹. Anal. Calcd for C₃₅H₃₄F₆O₁P₁Ru₁Sb₁: C, 50.14; H, 4.09. Found: C, 49.85; H, 4.10.

Crystallographic Analysis. Crystals of **5** were grown from CH₂Cl₂/*n*-heptane at -25 °C. The crystal used was cut from a larger needle and mounted on a glass fiber. Diffraction measurements were made on a Rigaku AFC5S fully automated four-circle diffractometer using graphite-monochromated Mo K α radiation at -103 °C. Cell constants and an orientation matrix for data collection were obtained from a least-squares refinement using the setting angles of 24 carefully centered reflections in the range 20.90 < 2 θ < 29.46°. Data processing was performed on a Digital Equipment Corp. Vaxstation 4000 computer using the TEXSAN crystallographic software package of Molecular Structure Corp. Neutral atom scattering factors were calculated using standard procedures.²⁷ Anomalous dispersion effects were applied to all non-hydrogen atoms.²⁸ The data were corrected for Lorentz and polarization effects. An empirical absorption correction using the program DIFABS²⁹ was applied. Full-matrix least-squares refinements minimized the function $\sum w(|F_o| - |F_c|)^2$, where $w = 4F_o^2/\sigma^2(F_o^2)$, $\sigma^2(F_o^2) = [(I_{raw}^2 + (pI_{net}^2)^2)/Lp]^2$, Lp is the Lorentz polarization factor, and p is the p factor, 0.02.

5 crystallized in the monoclinic crystal system. The space group P2₁/n for **5** was determined from the systematic absences, and the structure was solved by a combination of the

(27) Cromer, D. T.; Waber, J. T. *International Tables for X-ray Crystallography*; The Kynoch Press: Birmingham, England, 1974; Vol. IV, Table 2.2 A.

(28) Cromer, D. T. *International Tables for X-ray Crystallography*; The Kynoch Press: Birmingham, England, 1974; Vol. IV, Table 2.3.1.

(29) Walker, N.; Stuart, D. *Acta Crystallogr.* **1983**, *A39*, 158.

Patterson methods to find the heavy atoms, direct methods (DIRDIF), and difference Fourier syntheses. The positions of the hydrogen atoms *including the one attached to the ruthenium atom* were located by difference Fourier syntheses, and their positions were refined with isotropic thermal parameters fixed at 5.0 Å². All non-hydrogen atoms were refined with anisotropic thermal parameters. Crystallographic data are listed in Table 2. Selected bond distances and angles are given in the caption for Figure 1.

Acknowledgment. These studies were supported by the National Science Foundation.

Supplementary Material Available: Tables of anisotropic thermal parameters, bond distances and angles, atomic coordinates, and torsion angles for **5** (17 pages). Ordering information is given on any current masthead page.

OM940512K

Selenolates of Aluminum and Gallium. Synthesis and Molecular Structures of $[\text{Me}_2\text{Al}(\mu\text{-SeMe})]_2$, $[\text{Ph}_2\text{Ga}(\mu\text{-SeMe})]_2$, and $[\text{Me}_2(\text{PhSe})\text{Al}\cdot\text{PPh}_3]$

Rajesh Kumar, David G. Dick, Shahid U. Ghazi, Majid Taghiof, Mary Jane Heeg, and John P. Oliver*

Department of Chemistry, Wayne State University, Detroit, Michigan 48202

Received August 18, 1994[®]

The reaction of triorganoaluminum and -gallium derivatives, R_3M , ($\text{M} = \text{Al}$, $\text{R} = \text{Me}$, Mes ; $\text{M} = \text{Ga}$, $\text{R} = \text{Ph}$) with the diselenide, $\text{R}'_2\text{Se}_2$ ($\text{R}' = \text{Me}$, Ph) yields $[\text{R}_2\text{M}(\mu\text{-SeR}')_n]$, ($\text{M} = \text{Al}$, $\text{R} = \text{Me}$, $\text{R}' = \text{Me}$, **1**; $\text{R} = \text{Me}$, $\text{R}' = \text{Ph}$, **2**; $\text{R} = \text{Mes}$, $\text{R}' = \text{Me}$, **3**; $\text{M} = \text{Ga}$, $\text{R} = \text{Ph}$, $\text{R}' = \text{Me}$, **4**) and the corresponding selenoether RSeR' . **1** is also prepared by a simple insertion reaction of elemental grey selenium into the Al–C bond of trimethylaluminum. **1** reacts with 4-picoline to give the addition compound, $\text{Me}_2(\text{MeSe})\text{Al}\cdot\text{Pic}$, **6**. **2** reacts with PPh_3 to yield $\text{Me}_2(\text{PhSe})\text{Al}\cdot\text{PPh}_3$, **5**, with benzaldehyde to yield $\{\text{Me}_2\text{Al}[\mu\text{-OC}(\text{H})(\text{SePh})\text{Ph}]\}_n$, **7**, and with methyl benzoate to give the selenoester $\text{PhC}(\text{O})\text{SePh}$. The resulting derivatives have been characterized by ^1H , ^{13}C , ^{31}P , and ^{77}Se NMR spectroscopy and by chemical analyses. The structures of **3**, **4**, and **5** were determined by single crystal X-ray diffraction techniques. The crystal structure parameters of **3** are as follows: orthorhombic, space group $Cmca$ (No. 64); cell constants $a = 23.419(3)$ Å; $b = 14.830(2)$ Å; $c = 12.020(2)$ Å; and $Z = 8$; $R = 5.3\%$, $R_w = 4.7\%$ based on 996 ($I > 2.0\sigma(I)$) observed reflections. The $(\text{AlSe})_2$ core is planar, and the aluminum center is in a pseudotetrahedral environment with an Al–Se bond distance of 2.519(2) Å. **4** crystallizes in the monoclinic space group $P2_1/c$ (No. 14); cell constants $a = 11.170(1)$ Å; $b = 13.637(3)$ Å; $c = 18.311(2)$ Å; $\beta = 96.52(1)^\circ$; $Z = 4$; and $R = 3.0\%$, $R_w = 6.0\%$ based on 2205 ($I > 2.0\sigma(I)$) observed reflections. The central $(\text{GaSe})_2$ ring of the dimer is planar with a Ga–Se bond distance of 2.509(1) Å. The unit cell parameters of **5** are as follows: triclinic space group $P\bar{1}$ (No. 2); cell constants $a = 9.777(2)$ Å; $b = 9.817(3)$ Å; $c = 14.125(3)$ Å; $\alpha = 82.84(2)^\circ$; $\beta = 77.53(2)^\circ$; $\gamma = 66.40(2)^\circ$; and $Z = 2$; $R = 4.0\%$, $R_w = 3.4\%$ based on 3292 ($I > 2.0\sigma(I)$) observed reflections. The aluminum center is in a pseudotetrahedral environment with an Al–Se bond distance of 2.394(1) Å and an Al–P bond distance of 2.517(1) Å.

Introduction

The current interest in the preparation of III–V, III–VI (13–15, 13–16), and more complex films by the MOCVD method has led to a resurgence in the organometallic chemistry of group 13/16 derivatives. A number of reports have appeared on aluminum–sulfur compounds,^{1–6} and a single paper on $[\text{Np}_2\text{Ga}(\mu\text{-TePh})]_2$ ⁷ has appeared, but only two compounds, $\text{Cl}_3\text{Al}\cdot\text{SePPh}_3$ ⁸ and $\text{K}^+[\text{MeSe}(\text{AlMe}_3)_3]^-$,⁹ have been reported that contain direct Se–Al bonds. No neutral species with Al–Se bonds have been described. Gallium compounds that contain direct Ga–Se bonds include the monomeric species $\text{Ga}[\text{Se}(2,4,6\text{-t-Bu}_3\text{C}_6\text{H}_2)]_3$ ¹⁰ and $[\text{t-BuGaSe}]_4$ with

a cubane structure.^{11,12} Barron and co-workers prepared the dimeric indium thiolate $[(\text{t-Bu})_2\text{In}(\mu\text{-S-t-Bu})]_2$, which decomposes under APMOCVD conditions to give thin films of polycrystalline tetragonal InS .^{13,14} Similarly, the cubane derivatives of gallium, $[(\text{t-Bu})\text{GaS}]_4$, give highly oriented thin films of GaS .¹⁵ Gysling et al. showed that the indium selenolates, $\text{R}_{3-n}\text{In}(\text{SeR}')_n$, serve as molecular precursors in the control of phase and stoichiometry in In_xSe_y films,¹⁶ and Beachley reported a mixed bridged species, $\text{Np}_2\text{In}[\mu\text{-SePh}, \mu\text{-P}(\text{t-Bu})_2\text{-InNp}_2]$.¹⁷ We have also found that $\text{In}(\text{ER})_3$ ($\text{E} = \text{S}, \text{Se}$) complexes serve as precursors to previously unidentified phases of In_xE_y materials.¹⁸ Recently, we reported the syntheses and X-ray studies of precursors to ternary compounds such as $[\text{R}_2\text{M}(\mu\text{-ESnR}_3)]_2$ ($\text{M} = \text{Al}, \text{Ga}, \text{In}$;

[®] Abstract published in *Advance ACS Abstracts*, February 15, 1995.

- (1) Brauer, D. J.; Stucky, G. D. *J. Am. Chem. Soc.* **1969**, *91*, 5462.
- (2) Haaland, A.; Stokkeland, O.; Weidlein, J. *J. Organomet. Chem.* **1975**, *94*, 353.
- (3) de Mel, V. S. J.; Kumar, R.; Oliver, J. P. *Organometallics* **1990**, *9*, 1303.
- (4) Kumar, R.; de Mel, V. S. J.; Oliver, J. P. *Organometallics* **1989**, *8*, 2488.
- (5) Boardman, A.; Small, R. W. H.; Worrall, I. J. *Inorg. Chim. Acta* **1986**, *120*, L23.
- (6) Ruhlandt-Senge, K.; Power, P. P. *Inorg. Chem.* **1991**, *30*, 2633.
- (7) Banks, M. A.; Beachley, O. T., Jr.; Gysling, H. J.; Luss, H. R. *Organometallics* **1990**, *9*, 1979.
- (8) Burford, N.; Royan, B. W.; Spence, R. E. v. H.; Rogers, R. D. *J. Chem. Soc., Dalton Trans.* **1990**, 2111.
- (9) Atwood, J. L.; Seale, S. K. *J. Organomet. Chem.* **1976**, *114*, 107.

- (10) Ruhlandt-Senge, K.; Power, P. P. *Inorg. Chem.* **1991**, *30*, 3683.
- (11) Cowley, A. H.; Jones, R. A.; Harris, P. R.; Atwood, D. A.; Contreras, L.; Burek, C. J. *Angew. Chem., Int. Ed. Engl.* **1991**, *30*, 1143.
- (12) Power, M. B.; Ziller, J. W.; Tyler, A. N.; Barron, A. R. *Organometallics* **1992**, *11*, 1055.
- (13) MacInnes, A. N.; Cleaver, W. M.; Barron, A. R.; Power, M. B.; Hepp, A. F. *Adv. Mater. Opt. Electron.* **1992**, *1*, 229.
- (14) MacInnes, A. N.; Power, M. B.; Hepp, A. F.; Barron, A. R. *J. Organomet. Chem.* **1993**, *449*, 95.
- (15) MacInnes, A. N.; Power, M. B.; Barron, A. R. *Chem. Mater.* **1992**, *4*, 11.
- (16) Gysling, H. J.; Wernberg, A. A.; Blanton, T. N. *Chem. Mater.* **1992**, *4*, 900.
- (17) Beachley, O. T., Jr.; Chao, S.-H. L.; Churchill, M. R.; Lake, C. H. *Organometallics* **1993**, *12*, 5025.
- (18) Kumar, R.; Narula, C.; Oliver, J. P., unpublished results.

E = O, S, Se).^{19,20} As a continuation of our studies on group 13/16 chemistry,^{21,22} we now report the synthesis and characterization of selenolato complexes, $[\text{R}_2\text{M}(\mu\text{-ER}')_n]$, formed by the interaction of the diselenide $\text{R}'_2\text{Se}_2$ with trimesitylaluminum, trimethylaluminum, and triphenylgallium. The first crystal structures of neutral selenolato derivatives of aluminum and gallium, $[\text{Me}_3\text{Al}(\mu\text{-SeMe})_2]$, $[\text{Ph}_2\text{Ga}(\mu\text{-SeMe})_2]$, and $[\text{Me}_2(\text{PhSe})\text{Al}\cdot\text{PPh}_3]$, are described.

Experimental Section

General Experimental Procedures. All solvents were purified and dried by standard techniques.²³ Argon gas was purified by passing it through a series of columns containing Deox catalyst (Alfa), phosphorus pentoxide, and calcium sulfate. Trimethylaluminum (Aldrich; Me_3Al , 2 M solution in toluene), grey selenium, dimethyl diselenide, dimesityl diselenide (Alfa), diphenyl diselenide, triphenylphosphine, benzaldehyde, methyl benzoate, and 4-picoline (Aldrich) were used as received. Ph_3Ga ²⁴ and Me_3Al ²⁵ were prepared as described previously. All of the glassware used in the synthetic work was oven-dried. The compounds are both oxygen and water sensitive so standard Schlenk line and drybox techniques were employed for all reactions and transfers. ^1H and ^{13}C NMR spectra were recorded on a General Electric QE-300 NMR, a GN-300 NMR, or a Varian-U500 NMR spectrometer. The chemical shifts were referenced to the residual proton line from benzene- d_6 ($\delta = 7.15$ ppm for ^1H ; $\delta = 128.0$ ppm for ^{13}C). The ^{77}Se (57.23 MHz, external reference Me_2Se in CDCl_3) and ^{31}P (121.47 MHz, external reference 85% H_3PO_4) NMR spectra were recorded in benzene- d_6 at ambient temperature. Mass spectra were obtained on a MS-80 Autoconsole (Kratos Analytical Instruments) mass spectrometer in the EI or CI mode. Chemical analyses were carried out by Galbraith Laboratories, Knoxville, TN.

Preparation of $[\text{Me}_2\text{Al}(\mu\text{-SeMe})_n]$ (1). Me_3Al , 40 mmol (20 mL of 2.0 M solution in toluene), was added to 3.15 g (40 mmol) of grey selenium in ca. 50 mL of benzene. The mixture was refluxed for a period of 24 h to give a colorless solution. The volatile materials were removed under vacuum, leaving a white solid. The solid was sublimed (65–70 °C/0.01 mmHg), affording the complex formulated as $[\text{Me}_2\text{Al}(\mu\text{-SeMe})_n]$ on the basis of elemental analyses and NMR spectroscopic data. **1** is quite soluble in aromatic solvents at room temperature but has limited solubility in saturated hydrocarbons such as hexane at room temperature. Yield: 85%. mp: 111 °C. Anal. Calcd (Found) for $\text{C}_3\text{H}_9\text{AlSe}$: C, 23.86 (23.72); H, 6.01 (6.09); Se, 52.28 (52.91). ^1H NMR (C_6D_6 , δ , ppm): -0.31 (dimer), -0.26 (trimer) (s, 6H, *AlMe*), 1.48, $^2J_{\text{Se-H}} = 7.3$ Hz (dimer), 1.53 (trimer) (3H, *SeMe*). $^{13}\text{C}\{^1\text{H}\}$ NMR (C_6D_6 , δ , ppm): -0.3 , $^1J_{\text{C-Se}} = 188$ Hz (dimer), -0.7 (trimer) (*SeMe*); -9.0 (dimer), -7.5 (trimer) (*AlMe*). ^{77}Se NMR (C_6D_6 , δ , ppm): -232 . No ^{77}Se signal was observed for the trimer because of low concentration, nor was ^1H - ^{77}Se coupling observed for the trimer. The equilibrium between trimer and dimer, $K_{32} = 230$, will be discussed elsewhere.²⁶ The CI mass spectra showed the following ions [*m/e* (relative abundance)] associated with

the fragments indicated: 591 (0.5) $\text{Me}_{11}\text{Al}_4\text{Se}_4^{4+}$, 519 (2.3) $\text{Me}_6\text{Al}_4\text{Se}_4^{4+}$, 489 (0.3), 487 (0.4), 485 (0.6) $\text{Me}_4\text{Al}_4\text{Se}_4^{4+}$, 455 (0.5) $\text{Me}_3\text{Al}_3\text{Se}_3^{3+}$, 439 (37.5), 438 (13.8), 437 (29.7), 436 (11.3), 435 (17.2) $\text{Me}_6\text{Al}_3\text{Se}_3$, $\text{Me}_6\text{Al}_4\text{Se}_3^{3+}$, 367 (12.4), 365 (12.9), 363 (10.1) $\text{Me}_3\text{Al}_3\text{Se}_3^{3+}$ and other ions, 305 (10.9), 303 (10.5) $\text{Me}_6\text{Al}_2\text{Se}_2$.

Synthesis of **1 via the Reaction of Trimethylaluminum with Dimethyl Diselenide.** Dimethyl diselenide was reacted with a 2-fold excess of trimethylaluminum in benzene- d_6 in a 5 mm NMR tube at room temperature and monitored over a period of 2 h. The yellow color of the diselenide faded, giving a colorless solution. The ^1H NMR spectrum of the resulting solution showed that the formation of **1** and Me_2Se was quantitative. No attempt was made to repeat this reaction on the synthetic scale.

Attempted Synthesis of $[\text{Mes}_2\text{Al}(\mu\text{-SeMes})_n]$. The reaction of Mes_3Al (1.00 g, 2.6 mmol) with selenium (0.21 g, 2.6 mmol) was studied using the reaction conditions described for **1**. Removal of the solvent followed by sublimation of the residue gave Mes_2Se_2 and a white product that was insoluble in hydrocarbon solvents. This product was not characterized further. Spectral data for the sublimed product, Mes_2Se_2 , are as follows. ^1H NMR (C_6D_6 , δ , ppm) (authentic sample of Mes_2Se_2): 2.02 (2.02) (s, 3H, *p-Me* of *Mes*), 2.31 (2.32) (s, 6H, 2,6-*Me_2* of *Mes*), 6.67 (6.67) (s, 2H, aryl of *Mes*). ^{77}Se NMR (C_6D_6 , δ , ppm): 372 (372).

Preparation of $[\text{Me}_2\text{Al}(\mu\text{-SePh})_n]$ (2). Diphenyl diselenide (1.0 g, 3.20 mmol) was stirred in pentane (ca. 60 mL), and Me_3Al (1.60 mL, 3.20 mmol) was added over a period of 5 min. The reaction mixture was stirred for 3 days, during which time the solution lost color. The solution was separated by cannula from traces of a yellow precipitate, and the solvent was removed under vacuum. The residue was stirred in ca. 50 mL of pentane for 2 h. The white solid was isolated and washed with 10–15 mL of very cold pentane and dried under vacuum. The solid was identified from its ^1H and ^{13}C NMR spectra as $[\text{Me}_2\text{Al}(\mu\text{-SePh})_n]$ (**2**). Yield: 90%. mp: 141–144 °C. Anal. Calcd (Found) for $\text{C}_8\text{H}_{11}\text{AlSe}$: C, 45.09 (46.00); H, 5.20 (5.39). ^1H NMR (C_6D_6 , δ , ppm): -0.16 (dimer); -0.05 (trimer) (s, *AlMe*); 6.78–6.88, 7.29–7.30, 7.55–7.56 (m, Ph). $^{13}\text{C}\{^1\text{H}\}$ NMR: -6.2 , -6.9 (*AlMe*); 127.5, 129.5, 129.9, 134.6, 135.0 (Ph). ^{77}Se NMR (C_6D_6 , δ , ppm): 46.3, 26.6. The equilibrium constant between monomer and dimer as a function of concentration and temperature, $K_{32} \sim 2.5$, has been determined. Details of this study will be described elsewhere.²⁷ Mass spectra obtained using CI and EI modes showed the following ions [*m/e* ratio (relative abundance)] associated with the fragments indicated. MS (CI mode): 625 (1.6) $(\text{Me}_2\text{AlSePh})_3\text{-Me}^+$, 553 (4.6) $\text{Me}_4\text{Al}_2\text{Se}(\text{SePh})_2^{2+}$, 489 (0.8) $\text{Me}_6\text{Al}_3\text{Se}_2\text{SePh}^+$, 471 (0.5) $\text{Me}_5\text{Al}_3(\text{SePh})_2^{2+}$, 413 (21.2) $\text{Me}_3\text{Al}_2(\text{SePh})_2^+$, 371 (3.5) $\text{Me}_2\text{Al}(\text{SePh})_2^{2+}$, $\text{Me}_2\text{Al}_2\text{Se}(\text{SePh})^{2+}$, PhSeSePh^+ , $\text{Me}_4\text{Al}_2\text{SePh}^+$, $\text{Me}_2\text{AlSePhH}^+$, MeAlSePh^+ , Me_2AlSe^+ , PhH^+ . MS (EI mode): 552 (0.3) $\text{Al}_3(\text{SePh})_3^{3+}$, 486 (0.3) $\text{Me}_6\text{Al}_3(\text{SePh})_2^{2+}$, 471 (1) $\text{Me}_5\text{Al}_3(\text{SePh})_2^{2+}$, 413 (4.6) $\text{Me}_3\text{Al}_2(\text{SePh})_2^{2+}$, 356 (1.1) $\text{MeAl}(\text{SePh})_2^{2+}$, 341 (0.4) $\text{Al}(\text{SePh})_2^{2+}$, 314 (8.8) PhSeSePh^+ , 271 (2.1) $\text{Me}_4\text{Al}_2\text{SePh}^+$, 234 (5.1) PhSePh^+ , 214 (14.5) $\text{Me}_2\text{AlSePh}^+$, 199 (63) MeAlSePh^+ , 157 (25.2) PhSe^+ , 78 (49.9) PhH^+ .

A mixture of Me_3Al and diphenyl diselenide in 20 mL of toluene was monitored by ^{77}Se NMR. After 14 h, the solution showed resonances at 203 ppm (intense and sharp) and at 34 ppm (broad). The resonance at 34 ppm is assigned to Me_2AlSePh and the one at 203 ppm to MeSePh . The ^1H NMR of this solution showed resonances at 6.93 (m, *SePh*), 1.86 (s, *SeMe*), and -0.24 ppm (s, *AlMe*).

Preparation of $[\text{Mes}_2\text{Al}(\mu\text{-SeMe})_2]$ (3). Trimesitylaluminum and dimethyl diselenide (1:1.5) were placed in an NMR tube containing C_6D_6 , and the tube was flame sealed. No reaction was observed after 24 h at room temperature. The tube was heated to 100 °C, and the reaction was monitored at

(19) Ghazi, S. U.; Kumar, R.; Heeg, M. J.; Oliver, J. P. *Inorg. Chem.* **1994**, *33*, 411.

(20) Ghazi, S. U.; Heeg, M. J.; Oliver, J. P. *Inorg. Chem.* **1994**, *33*, 4517.

(21) Oliver, J. P.; Kumar, R. *Polyhedron* **1990**, *9*, 409.

(22) Oliver, J. P.; Kumar, R.; Taghiof, M. In *Coordination Chemistry of Aluminum*; Robinson, G. H., Ed.; VCH: New York, 1993; pp 167–195.

(23) Shriver, D. F.; Drezzdon, M. A. *The Manipulation of Air-Sensitive Compounds*; John Wiley & Sons: New York, 1986.

(24) Miller, S. B.; Jelus, B. L.; Smith, J. H.; Munson, B.; Brill, T. B. *J. Organomet. Chem.* **1979**, *170*, 9.

(25) De Mel, V. S. J.; Oliver, J. P. *Organometallics* **1989**, *8*, 827.

(26) Kumar, R.; Bailey, M.; Barber, M.; Hendershot, D. G.; Taghiof, M.; Rahbarnoohi, H.; Dick, D. G.; Oliver, J. P., work to be published.

(27) Taghiof, M.; Heeg, M. J.; Bailey, M.; Dick, D. G.; Kumar, R.; Hendershot, D. G.; Rahbarnoohi, H.; Oliver, J. P., work to be published.

regular intervals. After 100 h, the tube was slowly cooled to room temperature, resulting in the formation of X-ray-quality crystals of $[\text{Mes}_2\text{Al}(\mu\text{-SeMe})_2]$. The crystals are slightly soluble in benzene at room temperature. A second reaction on a large scale was carried out in toluene under the same conditions. Yield: 66%. mp: 248–249 °C (no decomposition). Anal. Calcd (Found) for $\text{C}_{19}\text{H}_{25}\text{AlSe}$: C, 63.59 (64.74); H, 7.01 (7.29). (Note that the sample sent for analysis was evacuated, removing some but not all of the toluene of crystallization.) Integrated intensities of the ^1H NMR spectrum showed $1/2$ mol of toluene remained/dimer. Anal. Calcd (Found) for $\text{C}_{83}\text{H}_{108}\text{Al}_4\text{Se}_4$: C, 64.99 (64.74); H, 7.10 (7.29). ^1H NMR (C_6D_6 , δ , ppm): 1.25 (s, 3H, *SeMe*), 2.14 (s, 6H, *p*-Me of Mes), 2.68 (s, 12H, *o*-Me of Mes), 6.72 (s, 4H, aryl of Mes), 2.10 (s, 1.5H, Me of Tol), 6.9–7.1 (m, aryl of Tol). $^{13}\text{C}\{^1\text{H}\}$ partial NMR (C_6D_6 , δ , ppm): 21.2 (*p*-Me of Mes), 25.8 (*o*-Me of Mes). The mass spectral data obtained using the CI mode showed the following ions [m/e (relative abundance)] associated with the fragments indicated. No significant fragments were observed above 309 (0.3), 307 (0.3) 265 (6.5), and 264 (3.2) Mes_2Al . Most ion current was associated with fragments 121 (33.8), 120 (21.7), 119 (7.8) and below which are primarily organic species.

Preparation of $[\text{Ph}_2\text{Ga}(\mu\text{-SeMe})_2]$ (4). Ph_3Ga , 1.59 mmol (0.48 g), was added to a solution of 0.30 g (1.59 mmol) of Me_2Se_2 in ca. 70 mL of pentane. The mixture was stirred for approximately 24 h, at which time all the Ph_3Ga had reacted and a solution formed. At -10 °C overnight, the solution deposited colorless crystals which were isolated, washed with pentane, and dried under vacuum. The product was formulated as $[\text{Ph}_2\text{Ga}(\mu\text{-SeMe})_2]$ on the basis of its NMR spectroscopic data and X-ray crystallography. Yield: 70%. mp: 213 °C. Anal. Calcd (Found) for $\text{C}_{13}\text{H}_{13}\text{GaSe}$: C, 49.11 (48.32); H, 4.12 (4.25). ^1H NMR (C_6D_6 , δ , ppm): 1.36 (s, 3H, *SeMe*), 7.15–7.66 (m, 10H, *GaPh*). $^{13}\text{C}\{^1\text{H}\}$ NMR (C_6D_6 , δ , ppm): 3.01 (*SeMe*); 141.5, 136.8, 128.9, 128.4 (*GaPh*). ^{77}Se NMR (C_6D_6 , δ , ppm): –247. Mass spectral data obtained using the CI mode showed the following ions [m/e (relative abundance)] associated with the fragments indicated: 563 (2.1), 561 (5), 559 (6.2), 557 (4.8) $\text{Ph}_3\text{Ga}_2\text{Se}_2\text{Me}_2^{+}$, 545 (5.6), 543 (13.9), 541 (13.9), 539 (6) $\text{Ph}_4\text{Ga}_2\text{SeMe}^{+}$, 320 (3.5), 319 (9.5), 317 (4.8) $\text{Ph}_2\text{-GaSeMe}^{+}$, 241 (13.2), 239 (6.1) PhGaSeMe^{+} , and 223 (75.4) Ph_2Ga^{+} .

Preparation of $[\text{Me}_2(\text{PhSe})\text{Al}(\text{PPh}_3)]$ (5). The synthesis of **5** proceeded as described for **2** up to the final workup; then 0.84 g (3.20 mmol) of triphenylphosphine was added, and the mixture was allowed to stir for 2 h. The solution was decanted to remove traces of yellow solid. The product was crystallized at -20 °C. The crystals were isolated at dry ice–acetone bath temperature, washed with pentane (10 mL), and dried under vacuum. The product was identified as $[\text{Me}_2(\text{PhSe})\text{Al}(\text{PPh}_3)]$ by NMR spectral data and X-ray crystallography. Yield: 95%. mp: 108–110 °C. Anal. Calcd (Found) for $\text{C}_{26}\text{H}_{26}\text{AlSeP}$: C, 65.69 (65.73); H, 5.51 (5.43). ^1H NMR (C_6D_6 , δ , ppm): –0.09 (s, 6H, *AlMe*), 6.83–7.51 (m, 20H, PPh_3 + *SePh*). $^{13}\text{C}\{^1\text{H}\}$ NMR (C_6D_6 , δ , ppm): –6.9 (*AlMe*); 135.8, 134.2, 134.0, 129.9, 129.2, 129.1, 129.0, 126.6 (PPh_3 + *SePh*). ^{77}Se NMR (C_6D_6 , δ , ppm): 42.1; ^{31}P NMR (C_6D_6 , δ , ppm): –5.5.

Preparation of $[\text{Me}_2(\text{MeSe})\text{Al}(4\text{-picoline})]$ (6). 4-Picoline, 0.89 mL (9.13 mmol), was added to a solution of 1.38 g (9.13 mmol) of $[\text{Me}_2\text{AlSeMe}]_n$ in ca. 200 mL of pentane. The solution was stirred at room temperature for 15 min. Colorless crystals were obtained by cooling the solution at ca. 0 °C. The product was isolated at 0 °C, washed with cooled pentane (dry ice–acetone), and dried under stream of argon, followed by vacuum. The complex showed solubility in benzene and toluene and was slightly soluble in pentane. mp: 53 °C. Anal. Calcd (Found) for $\text{C}_9\text{H}_{16}\text{AlNSe}$: C, 44.26 (45.29); H, 6.55 (7.61); N, 5.73 (5.40). ^1H NMR (C_6D_6 , δ , ppm): –0.09 (s, 6H, *AlMe*), 1.52 (s, 3H, *SeMe*), 1.91 (s, 3H, *Me*-picoline), 6.23–6.25; 8.28–8.29 (4H, 4-picoline). $^{13}\text{C}\{^1\text{H}\}$ NMR (C_6D_6 , δ , ppm): –6.5 (*SeMe*); –8.5 (*AlMe*), 20.5 (*Me*-picoline), 125.7, 146.6, 152.6 (4-picoline). ^{77}Se NMR (C_6D_6 , δ , ppm): –300.

Preparation of $\{\text{Me}_2\text{Al}[\mu\text{-OC}(\text{H})(\text{SePh})\text{Ph}]\}_n$ (7). The synthesis of **7** followed the general procedure described for **2** up to the final workup; then 0.33 mL of benzaldehyde was added, and the mixture was stirred for 2 h. The solution was decanted to remove traces of yellow solid. The product was crystallized at -20 °C. The crystals were isolated at dry ice–acetone bath temperature, washed with pentane (10 mL), and dried under vacuum. The product was identified as $\{\text{Me}_2\text{Al}[\mu\text{-OC}(\text{H})(\text{SePh})\text{Ph}]\}_n$ by NMR spectral data. mp: 125–136 °C. ^1H NMR (C_6D_6 , δ , ppm): –0.377(2), –0.383(1), –0.390(1) (s, 6H, *AlMe*), 6.53, 6.56 (*OC}(\text{H})(\text{SePh})\text{Ph}*); 6.88–7.37 (m, H, *OC}(\text{H})(\text{SePh})\text{Ph}*). $^{13}\text{C}\{^1\text{H}\}$ NMR (C_6D_6 , δ , ppm): –8.4 (1), –8.1 (2), –7.9 (1) (*AlMe*); 79.4 (*OC}(\text{H})(\text{SePh})\text{Ph}*); 126.6, 126.8, 127.7, 128.48, 128.51, 128.8, 128.89, 128.93, 129.21, 129.24, 135.4, 135.7, 140.6, 140.7 (*OC}(\text{H})(\text{SePh})\text{Ph}*). ^{77}Se NMR (C_6D_6 + 4-picoline, δ , ppm): 601. Mass spectral data showed the following fragments [m/e (relative abundance)]. MS (CI mode): 289 (0.2) $\text{AlOC}(\text{SePh})\text{Ph}^{+}$, 247 (14) $\text{C}(\text{H})(\text{SePh})\text{Ph}^{+}$, 167 (4.8) $\text{C}(\text{H})(\text{Ph})\text{Ph}^{+}$, 158 (1.8) SePhH^{+} , 107 (12.5) $\text{OC}(\text{H})\text{-PhH}^{+}$, 91 (2.6) $\text{C}(\text{H})\text{PH}^{+}$, 78 (2.1) PhH^{+} . MS (EI mode): 392 (0.8) $\text{Me}_4\text{Al}_2\text{O}_2\text{C}(\text{H})(\text{SePh})\text{Ph}^{+}$, 314 (61.3) PhSeSePh^{+} , 234 (18.8) PhSePh^{+} , 157 (92.5) SePh^{+} , 105 (18.7) OCPh^{+} , 77 (100) Ph^{+} .

Preparation of Selenoester $\text{PhC}(\text{O})\text{SePh}$. The synthesis of $\text{PhC}(\text{O})\text{SePh}$ was attempted by the same general procedure as described for the synthesis of $[\text{Me}_2\text{Al}(\mu\text{-SePh})]_n$ up to the final workup; then 0.436 g (0.40 mL) of methyl benzoate was added, and the mixture was allowed to stir for 2 h. The solution was decanted to remove traces of yellow solid. The solvent was completely removed under vacuum. The residue was redissolved in pentane (ca. 30 mL) and crystallized at -20 °C. The crystals were isolated at dry ice–acetone bath temperature, washed with pentane (10 mL), and dried under vacuum. The product was identified as $\text{PhC}(\text{O})\text{SePh}$. Yield: 85%. mp: 36–37 (lit.²⁸ mp 35–37 °C). ^1H NMR (C_6D_6 , δ , ppm): 7.41 – 7.95 (m, 10H, C_6H_5). Mass spectral data (EI mode): peaks at 262 (molecular ion) $\text{PhC}(\text{O})\text{SePh}^{+}$, 312 (the recombination species) $(\text{C}_6\text{H}_5)_2\text{Se}_2^{+}$, and fragments at 224, 157, 105, and 77 corresponding to the ions $(\text{C}_6\text{H}_5)_2\text{Se}^{+}$, $\text{C}_6\text{H}_5\text{Se}^{+}$, $\text{PhC}(\text{O})^{+}$, C_6H_5^{+} were observed.

X-ray Structure Determination of $[\text{Mes}_2\text{Al}(\mu\text{-SeMe})_2]$, C_6D_6 (3), $[\text{Ph}_2\text{Ga}(\mu\text{-SeMe})_2]$ (4), and $[\text{Me}_2(\text{PhSe})\text{Al}(\text{PPh}_3)]$ (5). X-ray-quality crystals of **3**, **4**, and **5** were grown as described in the Experimental Section. In each case, a crystal suitable for X-ray diffraction studies was mounted in a thin-walled capillary tube in a drybox. The capillaries were plugged with grease, removed from the drybox, flame sealed, mounted on a goniometer head, and placed on a Nicolet P3/V (4) or P2₁ (3 and 5) diffractometer for data collection. Selected crystal structure parameters are presented in Table 1.

The crystals are orthorhombic (3), monoclinic (4), and triclinic (5). Lattice constants were verified by axial photographs. **3** has two possible space groups, *Cmca* (No. 64) and *C2cb* (No. 41), on the basis of systematic absences and was assigned to the former based on its successful refinement. **4** was assigned to *P2₁/c* (No. 14) on the basis of systematic absences. The initial data indicated that **5** may be assigned to space group *P1* (No. 1) or *P $\bar{1}$* (No. 2); it was assigned to *P $\bar{1}$* based on successful refinement of the structure. Data reduction and calculations for **4** were carried out using the SHELXTL program.²⁹ Structure solution and refinement were carried out using SHELXS-86³⁰ and SHELXL-93.³¹ No correction for secondary extinction was made. Absorption corrections were semiempirical from ψ scans. Data reduction,

(28) Back, T. G.; Collins, S.; Kerr, R. G. *J. Org. Chem.* **1981**, *46*, 1564.

(29) Sheldrick, G. M. *SHELXTL*; University of Göttingen: Göttingen, Federal Republic of Germany, 1978.

(30) Sheldrick, G. M. *SHELXL-86*; University of Göttingen: Göttingen, Federal Republic of Germany, 1986.

(31) Sheldrick, G. M. *SHELXL-93*; University of Göttingen: Federal Republic of Germany, 1993.

Table 1. Selected Experimental Parameters for the X-ray Diffraction Study of Compounds, [Me₂Al(μ-SeMe)]₂·C₆D₆ (3), [Ph₂Ga(μ-SeMe)]₂ (4), and [Me₂(SePh)Al·PPh₃] (5)

compd	3	4	5
empirical formula	C ₂₂ H ₂₈ SeAl	C ₁₃ H ₁₃ SeGa	C ₂₆ H ₂₆ AlSeP
mol wt (amu)	802.99	635.83	475.41
cryst syst	orthorhombic	monoclinic	triclinic
space group	<i>Cmca</i> (No. 64)	<i>P2₁/c</i> (No. 14)	<i>P1̄</i> (No. 2)
<i>a</i> (Å)	23.419(3)	11.170(1)	9.777(2)
<i>b</i> (Å)	14.830(2)	13.637(3)	9.817(3)
<i>c</i> (Å)	12.020(2)	18.311(2)	14.125(3)
α (deg)			82.84(2)
β (deg)		96.52(1)	77.53(2)
γ (deg)			66.40(2)
vol (Å ³)	4174.5(9)	1257.8(4)	1212.0(1)
Z	8	4	2
<i>d</i> _{calc} (g/cm ³)	1.28	1.68	1.30
<i>F</i> (000)	1656	624	488
temp (°C)	20	22	20
no. of obsd reflns	996 with (<i>I</i> ≥ 2.0σ(<i>I</i>))	2205 with (<i>I</i> ≥ 2.0σ(<i>I</i>))	3292 with (<i>I</i> ≥ 2.0σ(<i>I</i>))
linear absn coeff (μ) (cm ⁻¹)	18.41	50.46	16.59
abs corr	none applied	ψ scans	none applied
no. of params refined	119	137	262
obsd/param ratio	8.4:1	16.09:1	12.6:1
$R = \sum(F_o - F_c) / \sum F_o $	5.3	3.0	4.0
$R_w = [\sum_w(F_o - F_c)^2 / \sum_w F_o ^2]^{1/2}$	4.7	6.0	3.4
$w^{-1} = \sigma^2(F_o) + g(F_o)^2$			
goodness of fit	2.17	1.02	2.53
largest difference peak (e/Å ³)	0.76	0.474	0.51
largest difference hole (e/Å ³)	-0.55	-0.237	-0.48

Table 2. Atomic Coordinates (×10⁴) and Isotropic Thermal Parameters (×10³) for the Non-Hydrogen Atoms of [Me₂Al(μ-SeMe)]₂·C₆D₆ (3)

atom	X	Y	Z	<i>U</i> _{eq} ^a
Se(1)	5000	118(1)	11482(1)	52(1)
Al(1)	4243(1)	0	10000	38(1)
C(1)	3811(3)	1142(4)	10143(7)	38(3)
C(2)	3811(3)	1898(5)	9422(7)	51(3)
C(3)	3506(3)	2673(5)	9653(7)	57(4)
C(4)	3188(3)	2752(6)	10596(9)	59(4)
C(5)	3164(3)	2020(7)	11322(7)	60(3)
C(6)	3455(3)	1239(5)	11106(6)	46(3)
C(7)	4145(3)	1854(5)	8330(8)	85(4)
C(8)	2876(3)	3642(6)	10855(8)	84(4)
C(9)	3395(3)	478(5)	11932(6)	66(3)
C(10)	5000	1403(8)	11733(15)	126(9)
C(20) (benzene)	5571(7)	5000	0	137(10)
C(21) (benzene)	4701(4)	4230(7)	321(9)	113(6)

$$^a U_{eq} = 1/3 \sum_i \sum_j U_{ij} a_i a_j^* \bar{a}_i \bar{a}_j$$

structure solution, and refinement for **3** and **5** were carried out using the SHELXTL PC programs.³² The direct method routines produced acceptable solutions for the structures, yielding positions for most non-hydrogen atoms with the remaining heavy atoms located during subsequent refinement. No correction for secondary extinction was made. In **3**, **4**, and **5**, hydrogen atom positions were calculated and riding on the carbon atoms to which they were bound (*d*_{CH} = 0.96 Å). In **3** the benzene molecule was located and refined. Atomic coordinates and isotropic thermal parameters for the non-hydrogen atoms of **3**–**5** are presented in Tables 2–4.

Results and Discussion

Compounds that have direct Al–Se bonds can be prepared in several ways. These include the insertion of selenium into the M–C bond in R₃M derivatives,^{12,33} the reaction of R₃M with R'₂Se₂ to yield R₂MSeR' and RSeR',³⁴ and the reaction of M'SeR with R₂MX deriva-

Table 3. Atomic Coordinates (×10⁴) and Isotropic Thermal Parameters (×10³) for the Non-Hydrogen Atoms of [Ph₂Ga(μ-SeMe)]₂ (4)

atom	X	Y	Z	<i>U</i> _{eq} ^a
Se(1)	9809(1)	8813(1)	1074(1)	43(1)
Ga(1)	11483(1)	9921(1)	429(1)	38(1)
C(1)	12250(3)	10535(3)	2413(4)	37(1)
C(2)	12240(3)	11536(3)	2663(5)	47(1)
C(3)	12850(4)	11963(3)	4020(5)	58(1)
C(4)	13470(4)	11392(3)	5172(5)	58(1)
C(5)	13476(4)	10392(4)	4986(5)	61(1)
C(6)	12877(4)	9977(3)	3611(5)	52(1)
C(7)	12405(3)	9157(3)	-995(4)	38(1)
C(8)	13656(3)	9175(3)	-736(5)	47(1)
C(9)	14347(4)	8612(3)	-1656(5)	58(1)
C(10)	13808(4)	8022(3)	-2832(6)	63(1)
C(11)	12582(4)	7984(3)	-3121(5)	62(1)
C(12)	11890(4)	8549(3)	-2207(5)	51(1)
C(13)	9677(4)	9118(4)	3336(5)	66(1)

$$^a U_{eq} = 1/3 \sum_i \sum_j U_{ij} a_i a_j^* \bar{a}_i \bar{a}_j$$

tives.^{6,7,10} The advantages of the first process are that all of the R groups bound to M are used and that Se, rather than a volatile organoselenium derivative, is used. The second process makes it possible to prepare species with R ≠ R' but does require use of the diselenides. The third process requires use of the mixed diorganometallic halide and the use of a metal selenolate. In the present work, the first two methods have been used to prepare several new organoaluminum selenolates which have been characterized by NMR spectroscopy, elemental analysis, X-ray diffraction, and chemical reactions. The compounds are colorless crystalline solids that decompose on contact with moisture. They have moderate solubility in hydrocarbon solvents.

The reaction of Me₃Al with selenium powder in refluxing benzene yields a product formulated as [Me₂-Al(μ-SeMe)]_n (**1**). **1** was also obtained quantitatively by reaction of Me₃Al with Me₂Se₂. Elemental analysis confirms the stoichiometric formula of the compound. The ¹H, ¹³C, and ⁷⁷Se NMR data are consistent with the stoichiometry of the products but at high concentration indicate formation of a second species which has been

(32) SHELXTL PC; Siemens Analytical X-Ray Instruments, Inc.: Madison, WI, 1990.

(33) Kozikowski, A. P.; Ames, A. *J. Org. Chem.* **1978**, *43*, 2735–2737.

(34) Kumar, R.; Mabrouk, H. E.; Tuck, D. G. *J. Chem. Soc., Dalton Trans.* **1988**, 1045.

Table 4. Atomic Coordinates ($\times 10^4$) and Isotropic Thermal Parameters ($\times 10^3$) for the Non-Hydrogen Atoms of $[\text{Me}_2(\text{PhSe})\text{AlCPPh}_3]$ (5)

atom	X	Y	Z	U_{eq}^a
Se(1)	3729(1)	3106(1)	3020(1)	59(1)
P(1)	8166(1)	1925(1)	2299(1)	38(1)
Al(1)	5719(1)	2995(1)	1665(1)	44(1)
C(1)	3755(1)	1125(1)	3202(1)	51(1)
C(2)	3687(1)	468(1)	4125(1)	75(1)
C(3)	3718(1)	-961(1)	4263(1)	103(1)
C(4)	3865(1)	-1751(1)	3485(1)	102(1)
C(5)	3924(1)	-1111(1)	2589(1)	80(1)
C(6)	3857(1)	318(1)	2433(1)	61(1)
C(7)	8211(1)	2648(1)	3415(1)	40(1)
C(8)	7100(1)	3983(1)	3722(1)	48(1)
C(9)	7180(1)	4613(1)	4533(1)	56(1)
C(10)	8359(1)	3904(1)	5014(1)	63(1)
C(11)	9462(1)	2562(1)	4712(1)	72(1)
C(12)	9399(1)	1924(1)	3912(1)	60(1)
C(13)	9596(1)	2329(1)	1401(1)	39(1)
C(14)	9860(1)	1882(1)	454(1)	58(1)
C(15)	10885(1)	2207(1)	-266(1)	65(1)
C(16)	11656(1)	3004(1)	-70(1)	66(1)
C(17)	11402(1)	3472(1)	843(1)	71(1)
C(18)	10394(1)	3127(1)	1577(1)	55(1)
C(19)	8875(1)	-83(1)	2496(1)	37(1)
C(20)	7850(1)	-713(1)	2931(1)	50(1)
C(21)	8323(1)	-2234(1)	3107(1)	61(1)
C(22)	9810(1)	-3136(1)	2844(1)	60(1)
C(23)	10837(1)	-2529(1)	2409(1)	64(1)
C(24)	10387(1)	-1007(1)	2223(1)	52(1)
C(25)	6094(1)	1691(1)	615(1)	62(1)
C(26)	5522(1)	5047(1)	1320(1)	75(1)

$$^a U_{\text{eq}} = \frac{1}{3} \sum_i \sum_j U_{ij} a_i^* a_j^* \bar{a}_i \bar{a}_j.$$

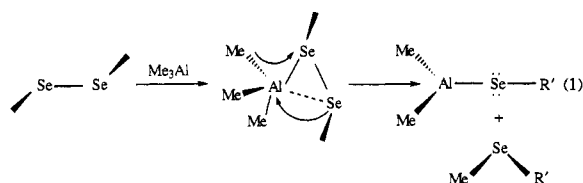
formulated as a trimer, $[\text{Me}_2\text{Al}(\mu\text{-SeMe})]_3$. A full discussion of the concentration and temperature dependence of the equilibria involved will be presented elsewhere.²⁶ The solubility and behavior in solution are similar to those observed for $[\text{Me}_2\text{Al}(\mu\text{-SMe})]_n$ which is polymeric in the solid state¹ but rearranges to give a dimer in the gas phase² and also has been shown to have an equilibrium between dimer and trimer in solution.²⁶ This behavior is consistent with a polymeric structure in the solid state, but to this time we have been unable to obtain crystals suitable for X-ray diffraction studies.

The mass spectra of 1–4 have all been obtained by chemical ionization. The spectrum of 2 was obtained also by electron ionization techniques. The fragments produced are listed in the Experimental Section. 1 shows major fragments corresponding to the following species: $\text{Me}_{11}\text{Al}_4\text{Se}_4$, $\text{Me}_6\text{Al}_4\text{Se}_4$, $\text{Me}_8\text{Al}_3\text{Se}_3$, $\text{Me}_3\text{Al}_3\text{Se}_3$, $\text{Me}_6\text{Al}_2\text{Se}_2$, $\text{Me}_5\text{Al}_2\text{Se}_2$, and many additional fragments of lower molecular weight. 2 shows low concentrations of high-mass fragments corresponding to $\text{Me}_5\text{Al}_3\text{Se}_3\text{Ph}_3$, $\text{Ph}_3\text{Al}_3\text{Se}_3$, with most of the ion current carried by the dimeric fragment, $\text{Me}_3\text{Al}_2\text{Se}_2\text{Ph}_2$, and the smaller ions, Me_2AlSePh and MeAlSePh derived from the monomer. 3 shows no heavier fragments. It is dominated by ions associated with the monomeric unit, Me_3AlSeMe , with the major peak the ion associated with the Me_2Al moiety. 4 shows major fragments associated with the dimer, including $\text{Ph}_3\text{Ga}_2\text{Se}_2\text{Me}_2$ and $\text{Ph}_4\text{Ga}_2\text{SeMe}$, and the monomeric species, including Ph_2GaSeMe and PhGaSeMe . A large ion current is carried by Ph_2Ga . For 1, these studies strongly support some form of higher aggregate in the solid state such as a polymer, $[\text{Me}_2\text{Al}(\mu\text{-SeMe})]_n$, similar to that observed for $[\text{Me}_2\text{Al}(\mu\text{-SMe})]_n$.¹ The mass spectra of $[\text{Me}_2\text{Al}(\mu\text{-SePh})]_2$, using CI and EI modes, also show trimeric aggregates in addition to the dimeric species observed in the solid

state. These observations, the large fragments observed in the gas phase, and the decomposition patterns are consistent with the known properties of these compounds, including formation of trimers and higher aggregates and low temperature decomposition which yields cubanes and larger clusters.

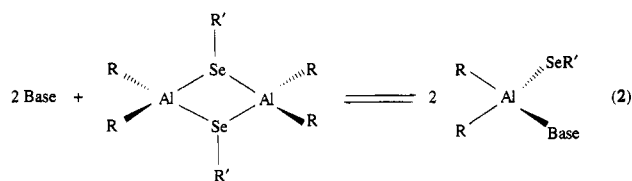
The reaction of Me_3Al with elemental selenium under conditions similar to those used for the preparation of 1 gave insoluble, unidentified white solid and yellow microcrystalline Me_2Se_2 . This implies that the selenium inserts into the M–C bond in Me_3Al but, under the reaction conditions, undergoes further reaction/decomposition to yield the diselenide and a second product still under investigation.

The second process described, the reaction of R_3M with $\text{R}'_2\text{Se}_2$, was used to prepare compounds 1–4 (M = Al, R = R' = Me, 1; R = Me, R' = Ph, 2; R = Mes, R' = Me, 3; M = Ga, R = Ph, R' = Me, 4). The reaction is thought to proceed by initial formation of the diselenide adducts followed by elimination of the selenoether and the formation of the product.³⁵ This process is depicted in eq 1. The selenoethers from these reactions were not



separated due to their inherent toxicity and foul smell but were identified from their ^1H , ^{13}C , and ^{77}Se NMR spectra. The resonance at 481 ppm of Ph_2Se_2 was replaced by two resonances at 203 (sharp) and 34 ppm (broad). The former resonance is typical of selenoether, and the latter may be assigned to the selenolato complex of aluminum, $[\text{Me}_2\text{Al}(\mu\text{-SePh})]_n$ (2).

The Al–Se–Al bridge bond is relatively weak and may undergo dissociation with formation of monomers or be displaced by a Lewis base with the formation of an addition compound. This process may also serve as the initial step in more complex reaction schemes for these species. The formation of addition compounds has been studied by reaction of 1 with 4-picoline to yield 6 and of 2 with PPh_3 to yield 5. This is illustrated in eq 2. In each case the stoichiometry of the addition com-

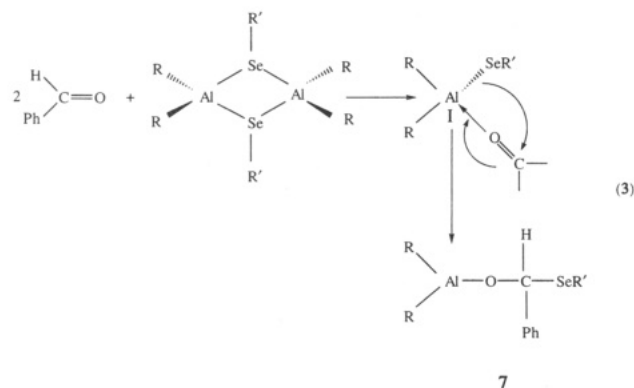


pound has been established by integration of the NMR spectrum and, for 5, by single crystal X-ray diffraction.

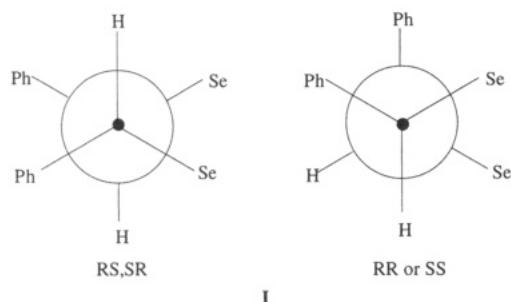
When 2 is added to benzaldehyde, it presumably forms an adduct which rapidly undergoes a migration of the phenylselenolato ligand to give the alkoxide, 7. A possible reaction path (eq 3) is similar to that proposed by Inoue et al.³⁶ for the reaction of $(i\text{-Bu})_2\text{AlTe}(n\text{-Bu})$ with esters. We were unable to isolate the

(35) Woodard, C. M.; Brown, D. S.; Lee, J. D.; Massey, A. G. *J. Organomet. Chem.* **1976**, *121*, 333.

(36) Inoue, T.; Takeda, T.; Kambe, N.; Ogawa, A.; Ryu, I.; Sonoda, N. *Organometallics* **1994**, *13*, 4543.

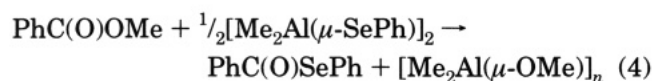


adduct, but a number of such adducts have been isolated in the solid state and characterized by X-ray crystallography.^{37–40} The reduction of the aldehyde to the alkoxide was confirmed from the ¹H and ¹³C NMR spectra of the isolated product. The groups were present in the appropriate ratios, and the aldehyde resonance at 192 ppm was replaced by a new resonance at 79.4 ppm. The latter resonance is typical of tertiary carbon of the alkoxide ligand. The ¹H and ¹³C NMR spectra show complex patterns for this molecule as a result of the stereochemistry at the tertiary carbon. Newman projections viewed along the C–O–O–C vector of the possible products are shown in I. It is assumed



that the central core of this molecule, (AlO)₂, is planar based on earlier observations.^{21,22,41} The methyl groups attached to the Al atom in the *RR* or *SS* form can be made equivalent with rotation about the C–O single bond; in the *RS,SR* form, the Al–methyl groups will be nonequivalent. This is shown in the NMR spectra, and the two diastereomers are also shown to be present in equal amounts for the integrated ¹H NMR spectra obtained at 500 MHz.

2 also reacts with methyl benzoate. However, in this case, the reaction proceeds beyond the alkoxide stage by ligand rearrangement to give the selenoester in excellent yield. This reaction to produce selenoesters, described in eq 4, is simple and economical, gives better



yield, and may be a preferred route over the literature methods.²⁸

(37) Shreve, A. P.; Mulhaupt, R.; Fultz, W.; Calabrese, J.; Robbins, W.; Ittel, S. D. *Organometallics* **1988**, *7*, 409.

(38) Power, M. B.; Bott, S. G.; Clark, D. L.; Atwood, J. L.; Barron, A. R. *Organometallics* **1990**, *9*, 3086.

(39) Power, M. B.; Barron, A. R. *Polyhedron* **1990**, *9*, 233.

(40) Power, M. B.; Bott, S. G.; Atwood, J. L.; Barron, A. R. *J. Am. Chem. Soc.* **1990**, *112*, 3446.

(41) Haaland, A. In *Coordination Chemistry of Aluminum*; Robinson, G. H., Ed.; VCH: New York, 1993; pp 1–51.

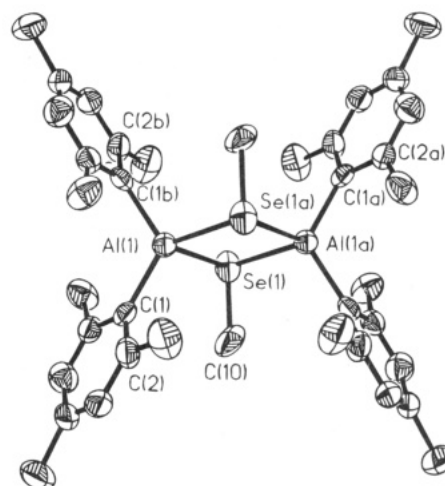
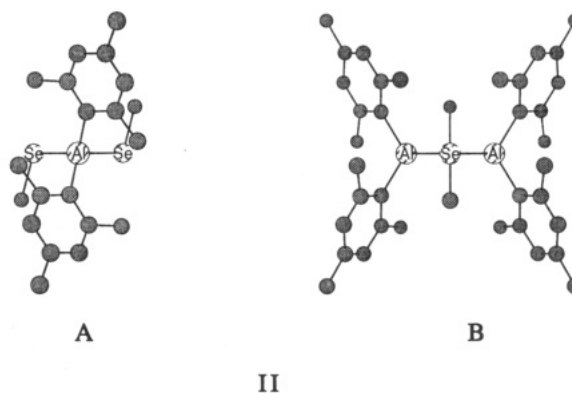


Figure 1. ORTEP diagram (50% thermal ellipsoids) of [Mes₂Al(μ-SeMe)]₂ (**3**), showing the atom labeling scheme. Hydrogen atoms have been omitted for clarity.

Structures of [Mes₂Al(μ-SeMe)]₂ (3**) and [Ph₂Ga(μ-SeMe)]₂ (**4**).** The structures of these compounds are shown in Figures 1 and 2. Each has a central (MSe)₂ ring with the methyl substituent on the selenium in the *anti* conformation. The core of the dimer in **3** is composed of an (AlSe)₂ ring that is strictly planar as required by the symmetry of the space group *Cmca* (No. 64). In **4**, the central ring is also required to be planar by symmetry. The gross features of the molecular structures are similar to those of related organoaluminum and organogallium alkyl- and arylthiolates. Each metal atom has a quasi-tetrahedral geometry. Selected bond distances and bond angles are presented in Table 5. The Al–Se bond distance (2.519 Å) is shorter than in the “ate” anion⁹ but substantially longer than in the addition compound **5**. The average Al–C bond distance and the exocyclic C–Al–C angle are also in the normal range for such complexes.^{21,22} The view along the Al–Al axis (IIA) shows that the two SeMe groups are *trans*



to each other. This orientation of the mesityl groups minimizes methyl–methyl interactions (IIB) between Mes-*o*-CH₃ and bridging SeMe groups. The Ga–Se bond distance (2.509 Å) is slightly longer than those found in the cubane [(*t*-Bu)GaSe]₄¹² and much longer than the Ga–Se distance observed in planar, neutral three-coordinate gallium selenolate, Ga[Se(2,4,6-*t*-Bu₃C₆H₂)]₃,¹⁰ and in Ga₂Se₃.⁴² The average Ga–C bond distance and the exocyclic C–Ga–C angle are in the normal

(42) Hahn, V. H.; Klingler, W. Z. *Anorg. Allg. Chem.* **1949**, *259*, 135.

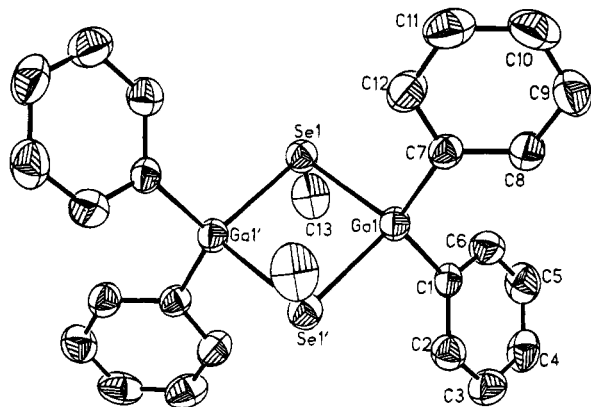


Figure 2. ORTEP diagram (50% thermal ellipsoids) of $[\text{Ph}_2\text{Ga}(\mu\text{-SeMe})_2]_2$ (**4**), showing the atom labeling scheme. Hydrogen atoms have been omitted for clarity.

Table 5. Selected Bond Distances (Å) and Angles (deg) for $[\text{Me}_3\text{Al}(\mu\text{-SeMe})_2\text{C}_6\text{D}_6]$ (**3**) and $[\text{Ph}_2\text{Ga}(\mu\text{-SeMe})_2]$ (**4**)

3		4	
Bond Distances			
Se(1)–Al(1)	2.519(2)	Se(1)–C(13)	1.947(4)
Se(1)–C(10)	1.930(12)	Se(1)–Ga(1)	2.493(1)
Se(1)–Al(1A)	2.519(2)	Se(1)–Ga(1)	2.509(1)
Al(1)–C(1)	1.981(7)	Ga(1)–C(7)	1.955(3)
		Ga(1)–C(1)	1.958(3)
Bond Angles			
Al(1)–Se(1)–Al(1A)	89.4(1)	Ga(1)–Se(1)–Ga(1)	83.07(2)
Se(1)–Al(1)–Se(1A)	90.6(1)	C(7)–Ga(1)–C(1)	121.8(2)
C(1)–Al(1)–C(1A)	118.4(4)	Se(1)–Ga(1)–Se(1)	96.93(2)
C(1)–Al(1)–Se(1A)	118.7(2)		

range.^{11,43,44} The selenium atom is pyramidal in **3** and **4** (Σ angle at Se = 290° in **3** and 289° in **4**) with C–Se bond distances of 1.930 Å for **3** and 1.947 Å for **4**, which are similar to the distances found in two- or three-coordinate bridging selenium atoms in organoselenolates.⁴⁵

Structure and Bonding in $[\text{Me}_2(\text{PhSe})\text{Al}(\text{PPh}_3)]$ (5**).** An ORTEP diagram of **5** is shown in Figure 3. Selected bond distances and angles are listed in Table 6. The structure is typical of organoaluminum addition compounds with the aluminum bonded to two methyl groups, a phosphorus atom and a selenium atom. The Al–C bond distances of 1.959 and 1.953 Å are comparable to those found in related organoaluminum compounds.^{21,22} The Al–Se bond distance is 2.394 Å, and it appears to be the first such distance to be reported in a neutral complex of this type. This distance is slightly longer than the 2.37 Å observed in Al_2Se_3 ⁴⁶ but substantially shorter than a similar distance of 2.578 Å observed in the “ate” anion.⁹ This distance is also less than the Al–Se distance observed in the selenium addition compound, $\text{Cl}_3\text{Al}(\text{Se}=\text{PPh}_3)$.⁸ The large variation observed in the Al–Se distance may be due to

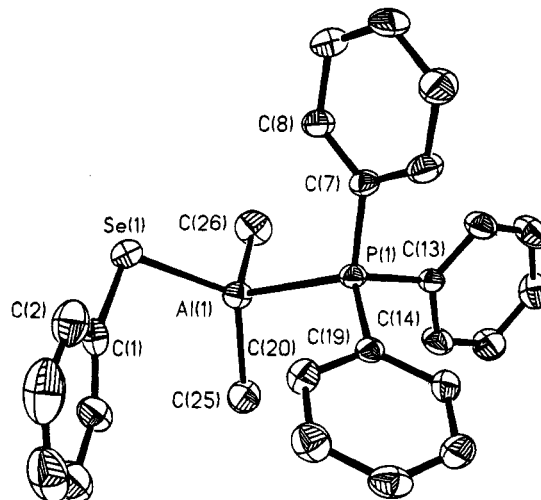


Figure 3. ORTEP diagram (50% thermal ellipsoids) of $[\text{Me}_2(\text{PhSe})\text{Al}(\text{PPh}_3)]$ (**5**), showing the atom labeling scheme. Hydrogen atoms have been omitted for clarity.

Table 6. Selected Bond Distances (Å) and Angles (deg) for $[\text{Me}_2(\text{PhSe})\text{Al}(\text{PPh}_3)]$ (**5**)

Bond Distance			
Se(1)–Al(1)	2.394(1)	Al(1)–C(26)	1.953(1)
Al(1)–C(25)	1.959(1)	P(1)–Al(1)	2.517(1)
Bond Angle			
Al(1)–Se(1)–C(1)	104.9(1)	Se(1)–Al(1)–C(26)	106.3(1)
Se(1)–Al(1)–P(1)	107.1(1)	P(1)–Al(1)–C(26)	102.0(1)
Se(1)–Al(1)–C(25)	118.4(1)	C(25)–Al(1)–C(26)	118.0(1)
P(1)–Al(1)–C(25)	103.2(1)		

mixing of “normal” and “dative” bonds.⁴⁷ The Al–P bond distance of 2.517 Å is slightly shorter than that observed in phosphorus addition compounds, $(\text{Me}_3\text{Al})_2(\text{Ph}_2\text{PCH}_2)_2$,⁴⁸ $\text{Me}_3\text{Al}(\text{PR}_3)$ (R = Me, Ph, *o*-tolyl),⁴⁹ and $\text{R}_n(\text{Cl})_{3-n}\text{Al}(\text{P}(\text{SiMe}_3)_3)$ (R = Et, $n = 1$; R = *i*-Bu, $n = 2$).⁵⁰ Other structural features such as P–C distances and the geometry around the phosphorus atoms are normal for such complexes. The selenium atom is two-coordinate, and the geometry around it is bent with a C(1)–Se(1)–Al(1) angle of 104.9° . The magnitude of this angle is typical of neutral two-coordinate selenium. The Se(1)–C(1) bond distance of 1.918 Å is similar to that observed in Ph_2Se_2 and $(\text{C}_6\text{F}_5)_2\text{Se}_2$.³⁵

Acknowledgment. Acknowledgement is made to the donors of the Petroleum Research Fund administered by the American Chemical Society for the support of this research.

Supplementary Material Available: Complete listings of crystal and X-ray data collection parameters, bond distances and bond angles, anisotropic thermal parameters for the heavy atoms, and hydrogen atom coordinates and isotropic thermal parameters (17 pages). Ordering information is given on any current masthead page.

OM940662V

(43) Cowley, A. H.; Jones, R. A. *Angew. Chem., Int. Ed. Engl.* **1989**, *28*, 1208.

(44) Wells, R. L.; Aubuchon, S. R.; Self, M. F.; Jasinski, J. P.; Woudenberg, R. C.; Butcher, R. J. *Organometallics* **1992**, *11*, 3370.

(45) Beachley, O. T., Jr.; Lee, J. C., Jr.; Gysling, H. J.; Chao, S.-H. L.; Churchill, M. R.; Lake, C. H. *Organometallics* **1992**, *11*, 3144.

(46) Schneider, V. A.; Gattow, G. Z. *Anorg. Allg. Chem.* **1954**, *277*, 49.

(47) Haaland, A. *Angew. Chem., Int. Ed. Engl.* **1989**, *28*, 992.

(48) Robinson, G. H.; Self, M. F.; Sangokoya, S. A.; Pennington, W. T. *J. Crystallogr. Spectrosc. Res.* **1988**, *18*, 285.

(49) Wierda, D. A.; Barron, A. R. *Polyhedron* **1989**, *8*, 831.

(50) Wells, R. L.; McPhail, A. T.; Self, M. F.; Laske, J. A. *Organometallics* **1993**, *12*, 3333.

Palladium-Catalyzed Reductive Couplings of Organic Halides with 7-Heteroatom Norbornadienes. New Synthetic Methods for Substituted Aryls and *cis*-1,2-Dihydro-1-naphthyl Alcohols and Carbamates

Jiun-Pey Duan and Chien-Hong Cheng*

Department of Chemistry, National Tsing Hua University,
Hsinchu, Taiwan 300, Republic of China

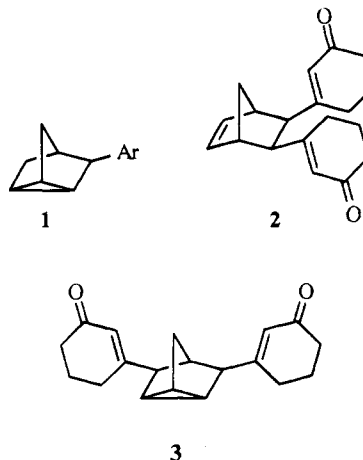
Received November 1, 1994[®]

$\text{PdCl}_2(\text{PPh}_3)_2$ in the presence of zinc metal powder and triethylamine catalyzes coupling reactions of 7-aza- and 7-oxanorbornadienes, dimethyl 7-carbomethoxy-7-azabicyclo[2.2.1]-2,5-heptadiene-2,3-dicarboxylate (**4a**) and dimethyl 7-oxabicyclo[2.2.1]-2,5-heptadiene-2,3-dicarboxylate (**4b**), with organic iodides (RI) to give the substituted aryls 1,2-(MeO_2C)₂-4- RC_6H_3 (**5**) in fair to good yields. Under similar reaction conditions, 7-carbomethoxy-7-azabenzonorbornadiene (**4c**) and 1,4-epoxy-1,4-dihydronaphthalene (**4d**) react with organic iodides to afford the 2-substituted naphthalenes 2- RC_{10}H_7 (**7**) and the *cis*-dihydro products methyl *N*-(*cis*-1,2-dihydro-1-naphthyl)carbamate (*cis*-1,2- H_2 -1-(MeO_2CHN)-2- RC_{10}H_6 , (**8**)) and *cis*-1,2-dihydro-1-naphthol (*cis*-1,2- H_2 -1-(OH)-2- RC_{10}H_6 , (**9**)), respectively. To improve the product yields of the last two *cis*-dihydro compounds, a modified system, $\text{Pd}(\text{PPh}_3)_2\text{Cl}_2\text{-ZnCl}_2\text{-Et}_3\text{N-Zn}$, was used to catalyze the reactions of **4c,d**, 1,4-dihydro-5,8-dimethoxy-1,4-epoxynaphthalene (**4e**), and 1,4-dihydro-5,8-dimethoxy-1-methyl-1,4-epoxynaphthalene (**4f**) with organic halides. These catalytic reactions produce the corresponding derivatives of **8** and **9** *cis*-1,2- H_2 -1-(OH)-2-R-5,8-(MeO)₂ C_{10}H_4 (**11**) and *cis*-1,2- H_2 -1-(OH)-2-R-4-Me-5,8-(MeO)₂ C_{10}H_3 (**12**) stereo- and regioselectively in high yields. A mechanism is proposed to account for the observed catalytic reactions.

Introduction

Insertion of an alkene into a palladium-carbon bond and subsequent elimination of a β -hydrogen are the two key steps in palladium-catalyzed Heck type reactions.¹ In order for the elimination to proceed, the β -hydrogen should be syn to the palladium center.² In some cases, the β -hydrogen is not suitable for elimination after insertion of the alkene into a palladium-carbon bond; instances of such alkenes are norbornadiene, norbornene, and their derivatives.^{3–5} Either *exo* or *endo* addition of a palladium-carbon bond to these alkenes would produce intermediates in which a bridgehead hydrogen of the norbornadiene or norbornene fragment is at a β -position relative to the palladium center. This β -hydrogen cannot undergo elimination to give a cyclic olefin due to the great angle strain of the resulting organic product. In addition to the bridgehead hydrogen, the bridging methylene group of the norbornadiene or norbornene fragment is at a β -position. However, it

is difficult to eliminate a β -carbon group under normal conditions for Heck type reactions. Thus, several products which do not involve the step of β -hydride elimination were observed from the reaction of norbornadiene and organic halide.^{3–6} We reported a palladium-catalyzed reaction of norbornadiene with aryl halide to give the three-membered aryl-substituted nortricyclenes **1** in the presence of a palladium(II)



complex and zinc metal.⁵ Under similar reaction conditions, different types of products were observed for the reaction of norbornadiene with 3-iodo-2-cyclohexen-1-one. The reaction may selectively lead to the *cis,exo*-2,3-disubstituted norbornene **2**⁷ or to the 3,5-disubsti-

(6) Larock, R. C.; Johnson, P. L. *J. Chem. Soc., Chem. Commun.* **1989**, 1368.

[®] Abstract published in *Advance ACS Abstracts*, March 1, 1995.

(1) Heck, R. F. *Acc. Chem. Res.* **1979**, *12*, 146.
 (2) Dieck, H. A.; Heck, R. F. *J. Am. Chem. Soc.* **1974**, *96*, 1133.
 (3) (a) Catellani, M.; Chiusoli, G. P. *J. Organomet. Chem.* **1982**, *233*, C21–C24. (b) Catellani, M.; Chiusoli, G. P. *J. Organomet. Chem.* **1982**, *239*, C35–C37. (c) Sgarabotto, P.; Catellani, M.; Chiusoli, G. P. *J. Organomet. Chem.* **1982**, *240*, 311. (d) Catellani, M.; Chiusoli, G. P. *J. Organomet. Chem.* **1983**, *250*, 509. (e) Catellani, M.; Chiusoli, G. P. *J. Organomet. Chem.* **1983**, *247*, C59–C62. (f) Amari, E.; Catellani, M.; Chiusoli, G. P. *J. Organomet. Chem.* **1985**, *285*, 383. (g) Catellani, M.; Chiusoli, G. P.; Concaro, S. *Tetrahedron Lett.* **1989**, *45*, 5263. (h) Catellani, M.; Chiusoli, G. P.; Costa, M. *Pure Appl. Chem.* **1990**, *623*.
 (4) Kosugi, M.; Tamura, H.; Sano, H.; Migita, T. *Chem. Lett.* **1987**, 193.
 (5) Li, C.-S.; Cheng, C.-H.; Cheng, S.-S.; Shaw, J.-S. *J. Chem. Soc., Chem. Commun.* **1990**, 1774.

Table 1. Addition of Organic Iodides to Substrates 4a–d in the Presence of PdCl₂(PPh₃)₂–Et₃N–Zn

entry no.	substrate	RI	reacn time (h)	product (amt, %) ^a
1	4a	C ₆ H ₅ I	22	5a (55)
2	4a	<i>p</i> -CH ₃ C ₆ H ₄ I	17	5b (53)
3	4a	<i>m</i> -CH ₃ OC ₆ H ₄ I	25	5c (63)
4	4a	<i>p</i> -CH ₃ OC ₆ H ₄ I	89	5d (37)
5	4a	<i>p</i> -O ₂ NC ₆ H ₄ I	22	5e (61)
6	4a	1-iodonaphthalene	36	5f (37), 6 (17)
7	4a	2-iodothiophene	34	5g (59)
8	4a	3-iodo-2-cyclohexen-1-one	34	5h (44)
9	4b	<i>p</i> -CH ₃ C ₆ H ₄ I	25	5b (37)
10	4c	<i>p</i> -CH ₃ C ₆ H ₄ I	34	7a (15), 8a (79)
11	4c	<i>p</i> -CH ₃ OC ₆ H ₄ I	21.5	7b (12), 8b (70)
12	4c	C ₆ H ₅ I	31	7e (15), 8c (66)
13	4c	<i>p</i> -CH ₃ COC ₆ H ₄ I	21	7f (25)
14	4c	3-iodo-2-cyclohexen-1-one	26	7g (62)
15	4c	5,5-dimethyl-3-iodo-2-cyclohexen-1-one	27	7h (77)
16	4d	<i>p</i> -CH ₃ C ₆ H ₄ I	22.5	7a (18), 9a (57)
17	4d	<i>p</i> -CH ₃ OC ₆ H ₄ I	14.5	7b (13), 9b (67)
18	4d	<i>m</i> -CH ₃ OC ₆ H ₄ I	13	7c (24), 9c (64)
19	4d	<i>m</i> -CH ₃ C ₆ H ₄ I	12	7d (16), 9d (66)
20	4d	C ₆ H ₅ I	7	7e (12), 9e (70)
21	4d	3-iodo-2-cyclohexen-1-one	18.5	7g (64)

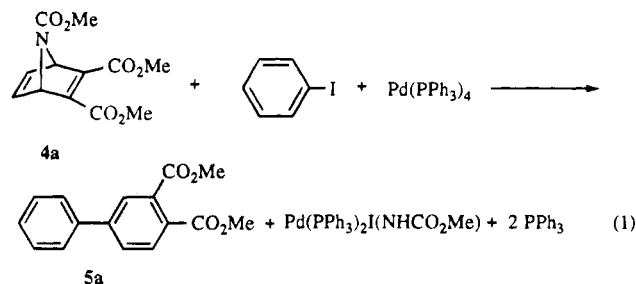
^a Isolated yield.

tuted nortricyclene **3**⁸ on adjusting the reaction conditions. In all these reactions, exo addition of the palladium–aryl bond to norbornadiene was found.

If the bridging methylene group in norbornadiene or norbornene is replaced by a heteroatom, insertion of a carbon–carbon double bond of these compounds into a palladium–carbon bond would yield palladium intermediates in which a heteroatom group is at a β -position relative to the palladium center. It is of interest to see whether β -heteroatom elimination takes place. To the best of our knowledge, few examples of β -heteroatom elimination have appeared in the literature.⁹ We report here palladium-catalyzed reactions of organic halides with norbornadiene derivatives containing a heteroatom at the bridging position to give highly substituted aryl products or to afford *cis*-1,2-dihydro-1-naphthyl derivatives stereoselectively, depending on the reaction conditions. These catalytic reactions not only provide novel methods for the preparation of these organic products but also involve a mechanism in which β -heteroatom elimination is a key step. The results have appeared in part in a communication.¹⁰

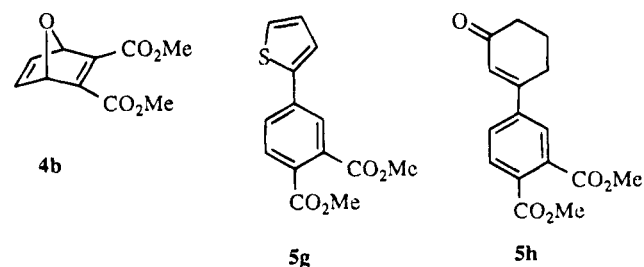
Results and Discussion

Reactions of 7-Azanorbornadiene and 7-Oxanorbornadiene with Organic Halides in the Presence of PdCl₂(PPh₃)₂–Et₃N–Zn. Heating 7-azanorbornadiene **4a** with 1 equiv of iodobenzene and Pd(PPh₃)₄ (5%) in THF at 55 °C for 10 h gave the biaryl species **5a** in 60% yield. Stoichiometrically, this product may be considered to result from addition of a phenyl group to the unsubstituted double bond in **4a**, followed by extrusion of a HNCO₂Me fragment. A rational stoichiometry for this reaction is shown in eq 1, in which Pd(PPh₃)₄ was oxidized to a Pd(II) species at the end of



the reaction. In order to make the reaction catalytic, a reducing agent is necessary to reduce Pd(II) back to the Pd(0) species; the use of zinc metal powder as a reducing agent appears to meet the requirement. Thus, heating **4a** with iodobenzene in the presence of excess zinc powder and a catalytic amount of PdCl₂(PPh₃)₂ in toluene at 80 °C led to the formation of **5a**. Control reactions indicate that in the absence of Pd species no desired product was observed, whereas the omission of zinc and Et₃N afforded only a trace of the expected product.

Under similar conditions, the PdCl₂(PPh₃)₂–Zn–Et₃N system also catalyzes coupling reactions of **4a** with *p*-iodotoluene, *m*-iodoanisole, *p*-iodoanisole, *p*-iodonitrobenzene, and 1-iodonaphthalene to give the corresponding biaryls **5b–f** in 37–63% yields. The reaction conditions and results are presented in Table 1. In addition to aryl iodides, 2-iodothiophene and 3-iodo-2-cyclohexen-1-one also react with **4a** in the presence of PdCl₂(PPh₃)₂ and zinc powder to yield the highly substituted arenes **5g** and **5h**, respectively. In general,



aryl bromides and chlorides did not react with **4a** to

(7) Li, C.-S.; Jou, D.-C.; Cheng, C.-H.; Liao, F.-L.; Wang, S.-L. *Organometallics* **1993**, *12*, 3553.

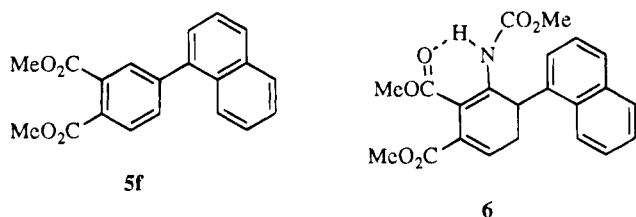
(8) Li, C.-S.; Jou, D.-C.; Cheng, C.-H. *Organometallics* **1993**, *12*, 3945.

(9) (a) Hacksell, U.; Daves, G. D., Jr. *Organometallics* **1983**, *2*, 772. (b) Cohen, H.; Meyerstein, D.; Shusterman, A. J.; Weiss, M. *J. Am. Chem. Soc.* **1984**, *106*, 1876. (c) Sorek, Y.; Cohen, H.; Meyerstein, D. *J. Chem. Soc., Faraday Trans. 1* **1989**, *85*, 1169.

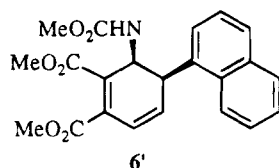
(10) Duan, J.-P.; Cheng, C.-H. *Tetrahedron Lett.* **1993**, *34*, 4019.

afford the expected biaryls in the presence of $\text{PdCl}_2(\text{PPh}_3)_2\text{-Zn-Et}_3\text{N}$, even though reaction temperatures higher than those for the corresponding aryl iodides were employed. Similar to **4a**, the 7-oxanorbornadiene **4b** reacted with *p*-iodotoluene in the presence of $\text{PdCl}_2(\text{PPh}_3)_2$, zinc powder, and Et_3N to give the corresponding biaryl **5b**. Aryl iodides with either electron-withdrawing or -donating substituents react with **4a** or **4b** to give unsymmetrical biaryls. One example that deserves notice is the reaction of *p*-iodonitrobenzene with **4a** to afford the corresponding biaryl product **5e**. In a previous report, *p*-iodonitrobenzene and norbornadiene in the presence of $\text{PdCl}_2(\text{PPh}_3)_2$ and zinc powder did not lead to the expected substituted nortricyclene.⁵

For the reaction of **4a** with 1-iodonaphthalene in the presence of the $\text{PdCl}_2(\text{PPh}_3)_2\text{-Zn-Et}_3\text{N}$ system, the new product **6** was isolated in 17% yield in addition to the aryl compound **5f**. Compound **6**, a cyclic enamine, is



characterized on the basis of its NMR and mass spectral data. In contrast to the spectra for **5f**, which consist of only two methoxy groups, there are three methoxy signals in the ^1H and ^{13}C NMR spectra of **6**. The presence of a methylene group in the cyclohexadiene ring is evidenced by the AB type proton resonances at δ 2.61 (ddd) and 2.83 (ddd) and the ^{13}C signal of the methylene carbon at δ 29.43. An unusual downfield signal for the proton attached to the nitrogen on NHCO_2Me was observed at δ 10.68, presumably due to an enamine type resonance and hydrogen bonding between N-H and one ester group as shown in the structure. The hydrogen bonding likely stabilizes **6** and enabled the isolation of this species. It is expected that the precursor for **6** is **6'**, which is also an intermediate for



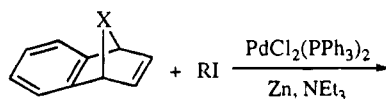
5. Deamination of **6'** affords **5** (*vide infra*), while a hydrogen shift of **6'** from the carbon to which the NHCO_2Me group is attached to the olefin carbon next to the naphthyl group gives the enamine **6**.

Due to the instability of **4a** and **4b**, which undergo retro-Diels-Alder reactions under conditions for the catalysis of eq 1, the product yields for reactions of **4a** and **4b** with organic iodides are in the range 37–63%. Several products related to the retro-Diels-Alder reaction of **4a** were found in the catalytic reactions; they are *N*-carbomethoxypyrrole, *cis*- and *trans*- $\text{CH}_3\text{O}_2\text{CCH}=\text{CHCO}_2\text{CH}_3$, and $\text{CH}_3\text{O}_2\text{CCH}_2\text{CH}_2\text{CO}_2\text{CH}_3$, with the last three from hydrogenation of the retro-Diels-Alder reaction product $\text{CH}_3\text{O}_2\text{CC}=\text{CCO}_2\text{CH}_3$. In the reaction of bromobenzene with **4a** in the presence of the $\text{PdCl}_2(\text{PPh}_3)_2\text{-Zn-Et}_3\text{N}$ system, monitoring of the re-

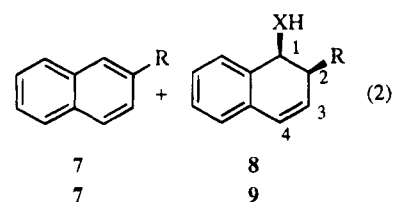
acting solution by ^1H NMR showed that **4a** decomposed to give products resulting from the retro-Diels-Alder reaction of **4a**, but the concentration of bromobenzene remained essentially unchanged. This observation indicates that the reaction of bromobenzene with palladium is slower than the decomposition of **4a** and explains why no biaryl products were detected from aryl bromides and **4a**.

The structures of products **5** from the reactions of **4** with organic iodides were determined according to their spectral data as well as the results of elementary analysis. Using **5a** as an example, there are six resonances (δ 7.41 (t, 1 H), 7.47 (t, 2 H), 7.61 (dd, 2 H), 7.74 (dd, 1 H), 7.84 (d, 1 H), and 7.91 (d, 1 H)) in the aromatic region and two methoxy resonances at δ 3.93 (s) and 3.94 (s) in its ^1H NMR spectrum. The ^{13}C NMR spectrum includes two quartets, six doublets, and six singlets. Both ^1H and ^{13}C NMR spectra completely agree with the proposed structure. In addition, the mass spectrum also supports the proposed chemical formula. Satisfactory analytical data and spectral data were obtained for other similar products in Table 1. The formation of **5** from **4** involves both addition of an organic group and heteroatom extrusion. Nitrene and oxo extrusions of 7-azanorbornadiene and 7-oxanorbornadiene, respectively, mediated by metal complexes and by acids have been rather extensively investigated,^{11–14} but there is no example known in the literature that undergoes addition and extrusion together.

Reactions of 7-Azabenzonorbornadiene and 7-Oxabenzonorbornadiene with Organic Halides in the Presence of $\text{PdCl}_2(\text{PPh}_3)_2\text{-Et}_3\text{N-Zn}$. The reaction of 7-azabenzonorbornadiene **4c** with aryl iodide in the presence of the $\text{PdCl}_2(\text{PPh}_3)_2\text{-Zn-Et}_3\text{N}$ system gave a mixture of 2-substituted naphthalene **7** and methyl *N*-(*cis*-1,2-dihydro-1-naphthyl)carbamate derivative **8** (eq 2). For iodobenzene, *p*-iodotoluene, and *p*-iodoani-



X = NCO_2Me **4c**
X = O **4d**



sole, the corresponding carbamate **8** is the major product, but for *p*-iodoacetophenone, only the biaryl product **7** was observed (run 13), albeit in low yield.

- (11) (a) Sun, C.-H.; Chow, T. J. *J. Organomet. Chem.* **1987**, 333, C21.
(b) Sun, C.-H.; Chow, T. J.; Liu, L.-K. *Organometallics* **1990**, 9, 560.
(12) (a) Wong, H. N. C.; Ng, T.-K.; Wong, T.-Y. *Heterocycles* **1983**, 20, 1815. (b) Wong, H. N. C. *Acc. Chem. Res.* **1989**, 22, 145.
(13) (a) Huang, N.-Z.; Xing, Y.-D.; Ye, D.-Y. *Synthesis* **1982**, 1041.
(b) Xing, Y.-D.; Huang, N.-Z. *J. Org. Chem.* **1982**, 47, 140.
(14) (a) Polovsky, S. B.; Franck, R. W. *J. Org. Chem.* **1974**, 39, 3010.
(b) Hart, H.; Nwokogu, G. *J. Org. Chem.* **1981**, 46, 1251. (c) Best, W. H.; Collins, P. A.; McCulloch, R. K.; Wege, D. *Aust. J. Chem.* **1982**, 35, 843. (d) Gribble, G. W.; Kelly, W. J.; Sibi, M. P. *Synthesis* **1982**, 143.
(e) Jung, K.-Y.; Koreeda, M. *J. Org. Chem.* **1989**, 54, 5667.

Similarly to *p*-iodoacetophenone, 3-iodo-2-cyclohexen-1-one and 5,5-dimethyl-3-iodo-2-cyclohexen-1-one react with **4c** to afford the corresponding naphthalene derivatives in 62 and 77% yield (runs 14 and 15), respectively. The products from reaction of 7-oxabenzonorbornadiene (**4d**) with organic iodides in the presence of PdCl₂(PPh₃)₂-Zn-Et₃N are analogous to those from **4c** and the corresponding organic iodides. For instance, treatment of **4d** and *p*-iodotoluene gave a mixture of the *cis*-1,2-dihydro-1-naphthol derivative **9a** and 2-(4-methylphenyl)naphthalene **7a**. For the reactions shown in eq 2, all the dihydronaphthalene products **8** and **9** exhibit *cis* stereochemistry (*vide infra*). No corresponding *trans* product was detected by GC-MS at the end of the reactions.

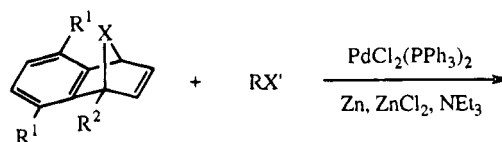
Products **8** and **9** were characterized according to their spectral and elemental analysis data (see Experimental Section) and X-ray analysis of one of these compounds. Both **8** and **9** exhibit characteristic proton resonances in the range 5.5–7.0 ppm for olefin protons and 2.7–5.5 ppm for protons attached to C-1 and C-2. For example, the corresponding olefin resonances of product **8a** appear at δ 6.18 (H-3, dd) and 6.73 (H-4, d), and the resonances of H-1 and H-2 come at δ 5.40 and 3.84, respectively. The presence of a carbamate group was evident from the observation of a N-H resonance at δ 4.75 (d) and methoxy signal at δ 3.70, while the *cis* stereochemistry of carbamate and tolyl substituents was established on the basis of the crystal structure of this compound determined by X-ray diffraction. The crystal structure results and the observed coupling constants of *ca.* 8 Hz between H-1 and H-2 of all products **8** suggest a *cis* stereochemistry at C-1 and C-2 for these compounds. The proton-proton coupling constants between H-1 and H-2 for products **9** are *ca.* 5.0 Hz, in accordance with the values of compounds having similar structure and stereochemistry reported previously.¹⁵

Analysis of the product distribution for reactions of **4** with organic halides RI reveals that electron-withdrawing substituents on substrate **4** and on the organic halide favor formation of deamination or dehydration product **5** or **7**, while electron-donating groups facilitate nonelimination products. In reactions using **4a** and **4b** as substrates which consist of two electron-withdrawing ester groups, only the corresponding aryl products **5** were isolated for all organic halides except 1-iodonaphthalene (*vide supra*). On the other hand, for the less electron-withdrawing substrates **4c** and **4d**, both products, **7** and **8** (or **9**), were detected. For reactions of **4c** and **4d** with an electron-withdrawing organic halide such as 3-iodo-2-cyclohexen-1-one, naphthalene derivatives **7** were the major products, but when electron-rich iodoanisole was employed, **8** or **9** was the favored product.

Both *cis*-1,2-dihydro-1-naphthyl derivatives **8** and **9** are thermodynamically unstable relative to corresponding deamination or dehydration product **7**. We may view **8** and **9** as resulting from *trans* addition of a water and a carbamate NH₂COOMe molecule, respectively, to 2-substituted naphthalenes. Due to loss of aromaticity and the great energy required to break an O-H or N-H bond, the addition reaction is expected to be an unfavor-

able process. Under the present catalytic conditions, carbamates **8** and *cis*-1,2-dihydro-1-naphthol derivatives **9** were converted slowly to corresponding aryl products. In basic or neutral solution, **8** and **9** are stable to more than 100 °C. However, in the presence of acid, they undergo deamination or dehydration to give the corresponding aryl products **7** in quantitative yield.

Reactions of 7-Oxabenzonorbornadiene and 7-Azabenzonorbornadiene with Organic Halides in the Presence of the PdCl₂(PPh₃)₂-Et₃N-ZnCl₂-Zn System. The observation of *cis*-dihydro products **8** and **9** from eq 2 led us to search for more suitable catalytic conditions for the preparation of these compounds. An effective catalytic system is obtained from a modification of the reaction conditions for eq 2 by including ZnCl₂ in addition to Et₃N, Pd(PPh₃)₂Cl₂, and zinc powder. For a millimolar scale synthesis of **8** and **9**, the optimal molar ratios of **4**, RX', Et₃N, Pd(PPh₃)₂Cl₂, ZnCl₂, and zinc powder are 1.5:1:8:0.02:0.5:10. Treatment of *p*-CH₃OC₆H₄I with 7-oxabenzonorbornadiene (**4d**) in the presence of Et₃N, Pd(PPh₃)₂Cl₂, and zinc powder at 60 °C in THF for 6 h gave the corresponding *cis*-1,2-dihydro-1-naphthol derivative **9b** in 95% yield (Table 2 and eq 3). The omission of ZnCl₂

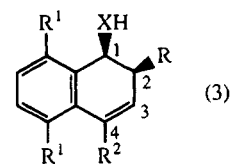


4c: X = NCO₂Me, R¹ = R² = H

4d: X = O, R¹ = R² = H

4e: X = O, R¹ = OCH₃, R² = H

4f: X = O, R¹ = OCH₃, R² = CH₃



8

9

11

12

from the reaction at 60 °C yielded a trace of product **9b**. As shown in Table 1, the use of PdCl₂(PPh₃)₂-Et₃N-Zn as a catalyst system for the reaction of *p*-CH₃OC₆H₄I with **4d** requires higher temperature (100 °C), prolonged reaction time (14.5 h), and a higher molar ratio of catalyst to substrate yet affords a lower yield (67%) of **9b**. One disadvantage of the presence of ZnCl₂ is the promotion of ring opening of **4d** under the reaction conditions to give 1-naphthol (**10**). The addition of Et₃N

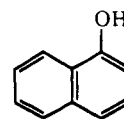
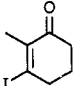


Table 2. Product Numbers, Yields, and Reaction Times of the Reactions of 4c–f with Organic Halides Catalyzed by the PdCl₂(PPh₃)₂–Et₃N–ZnCl₂–Zn System

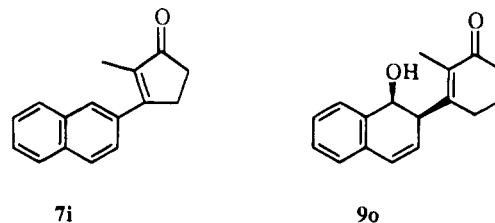
RX'	4d	4e	4f	4c
<i>p</i> -CH ₃ C ₆ H ₄ I	9a (85%, 9 h)		12a (85%, 10 h)	8a (80%, 8 h)
<i>p</i> -CH ₃ OC ₆ H ₄ I	9b (95%, 6 h)	11a (81%, 13 h)		8b (87%, 11 h)
<i>m</i> -CH ₃ OC ₆ H ₄ I	9c (92%, 4 h)	11b (94%, 10 h)		
<i>m</i> -CH ₃ C ₆ H ₄ I	9d (95%, 8 h)			
C ₆ H ₅ I	9e (86%, 4 h)			8c (63%, 5 h)
<i>o</i> -CH ₃ C ₆ H ₄ I	9f (98%, 11 h)			
<i>p</i> -HOC ₆ H ₄ I	9g (94%, 8 h)			
<i>m</i> -ClC ₆ H ₄ I	9h (87%, 8 h)			
<i>p</i> -CH ₃ COC ₆ H ₄ I	9i (10%, 13 h)	11c (26%, 11.5 h)		
1-iodonaphthalene	9j (94%, 10 h)		12b (90%, 12 h)	
2-iodothiophene	9k (71%, 37 h) ^a			
C ₆ H ₅ CH ₂ Br	9l (99%, 11 h) ^a			8d (60%, 2.5 h) ^a
β -bromostyrene	9m (52%, 14 h) ^a			
CH ₃ I	9n (38%, 12 h) ^a		12c (90%, 12 h)	8e (92%, 9 h)
	9o (83%, 9 h)	11d (71%, 12 h)		

^a NEt₃ was not added to the catalytic system.

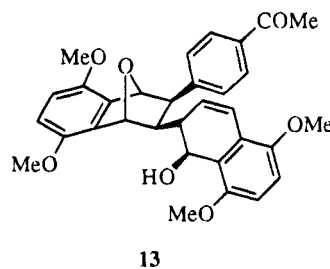
appears to suppress the Lewis acidity of ZnCl₂ and to inhibit formation of 1-naphthol. For comparison, when the catalytic reaction of *p*-CH₃OC₆H₄I with 7-oxabenzonorbornadiene was carried out in the absence of Et₃N, the yield of 9b was down to 49%.

The Pd(PPh₃)₂Cl₂–ZnCl₂–Et₃N–Zn catalyst system shows high activity and selectivity also for the reactions of 4d with a vast number of aryl iodides and 3-iodo-2-methyl-2-cyclohexen-1-one to give the *cis*-1,2-dihydro-1-naphthol derivatives 9 in high yields (Table 2). Iodothiophene, benzyl bromide, methyl iodide, and β -bromostyrene react with 4d to afford the corresponding products 9, but unlike most aryl iodides, the yields for products 9 are higher in the absence of Et₃N (Table 2) than in its presence. The facile reactions of Et₃N with benzyl bromide and methyl iodide account for the low yields of products 9 in the presence of Et₃N. However, the reason for low yields of products 9 for iodothiophene and β -bromostyrene remains unknown. In a comparison of the results in Tables 1 and 2, it is clear that addition of ZnCl₂ to the Pd(PPh₃)₂Cl₂–Et₃N–Zn system greatly facilitates formation of products 9 from 4d and most organic halides and shortens the duration required for reaction. Nevertheless, exceptions were observed for the electron-withdrawing organic halides 3-iodo-2-cyclohexen-1-one, 5,5-dimethyl-3-iodo-2-cyclohexen-1-one, 3-iodo-2-methyl-2-cyclopenten-1-one, and *p*-iodoacetophenone; the major addition products are the corresponding substituted aryls 7g (15%), 7h (34%), 7i (81%), and 7f (70%), respectively. It is interesting to note that, of the several cyclic 3-iodo enones tested, only 3-iodo-2-methyl-2-cyclohexen-1-one reacted with 4d selectively to give the *cis* stereo product 9o. All other cyclic 3-iodoenones afforded the corresponding 2-naphthalene derivatives without detectable corresponding product 9. We are unable to explain these observations at present.

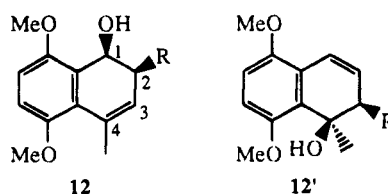
In the presence of the Pd(PPh₃)₂Cl₂–ZnCl₂–Et₃N system and Zn metal, substituted 7-oxabenzonorbornadienes 4e and 4f reacted with aryl iodides and 3-iodo-2-methyl-2-cyclohexen-1-one also to afford the expected *cis*-1,2-dihydro-1-naphthol derivatives 11 and 12, re-



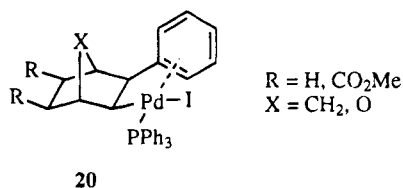
spectively, in good to excellent yields (Table 2). For the reaction of 4e with *p*-iodoacetophenone, the corresponding biaryl was observed as the major product (58%) and the *cis*-1,2-dihydro-1-naphthol derivative 11c was a minor product. In addition, the side product 13, resulting originally from two 4e and one acetophenone molecule, was isolated. This side product was appar-



ently obtained from two consecutive insertions of 4e into the Pd–C₆H₄–*p*-COCH₃ bond, followed by ring opening and protonation. The addition of an organic group to the carbon–carbon double bond of 4f, in which a methyl is attached to one of the bridgehead carbons, occurred regioselectively. There are two possible *cis*-1,2-dihydro-1-naphthol products 12 and 12' from reaction of an



observation that reaction of $\text{Pd}(\text{PPh}_3)_2\text{ArI}$ with norbornadiene or norbornene yielded the Pd complex **20**, in



which the aryl group and the Pd center are all at exo positions.¹⁶ Moreover, the *cis* stereochemistry of product **18** can be explained only by exo addition of R-Pd to the carbon-carbon double bond of **4**.

There are two possible roles of ZnCl_2 which on addition to the reaction solution enhance the activity of catalyst system. One possibility is that ZnCl_2 acts as a Lewis acid associated with the bridging oxygen atom or nitrogen atom of **16**, facilitating β -heteroatom elimination of **16**. The other possible role is attachment of ZnCl_2 to the coordinated iodide of $\text{Pd}(\text{PPh}_3)_2\text{ArI}$, assisting the removal of this ligand and enhancing coordination of **4** to the palladium center and insertion of **4** into the R-Pd bond. Since the observed rate-determining step of these catalytic reactions is insertion of **4** into the R-Pd bond, the role of ZnCl_2 is more likely to assist removal of iodide and to enhance the rate of the insertion.

Conclusion

In this report, we have demonstrated novel methods for the transformations of 7-heteroatom norbornadienes to substituted aryls, biaryl, *cis*-1,2-dihydro-1-naphthols, and *N*-(*cis*-1,2-dihydro-1-naphthyl)carbamates using the $\text{PdCl}_2(\text{PPh}_3)_2\text{-Et}_3\text{N-Zn}$ or $\text{Pd}(\text{PPh}_3)_2\text{Cl}_2\text{-ZnCl}_2\text{-Et}_3\text{N-Zn}$ system as the catalyst. The catalytic reactions to give *cis*-1,2-dihydro-1-naphthols and *N*-(*cis*-1,2-dihydro-1-naphthyl)carbamates occur stereo- and regioselectively. Both products are interesting classes of organic compounds that may be viewed as addition products of H_2O and $\text{NH}_2\text{CO}_2\text{CH}_3$ molecules to a substituted naphthalene, respectively. Although these compounds are thermodynamically unstable, they are kinetically stable to 100 °C in the absence of acid. The formation of substituted aryls and biaryl in the present work, involving both addition of an organic group to a carbon-carbon double bond of a 7-heteroatom norbornadiene and extrusion of the heteroatom group, is different in mechanism from metal-mediated nitrene and oxo extrusion of 7-heteroatom norbornadienes to aryls.

Experimental Section

All reactions were performed under dry nitrogen, and all solvents were dried by standard methods. ¹H and ¹³C NMR experiments were performed on a Varian Gemini 300 instrument at 300 MHz or a Varian Unity 400 at 400 MHz. Infrared spectra were obtained on a Bomem MB-100 spectrometer. Mass spectra at low and high resolutions were recorded on JEOL JMS-D100 and JMS-HX110 instruments, respectively. Melting point measurements were carried out on a Mel-Temp apparatus and are uncorrected. Microanalytical data were obtained on a CHN-O-RAPID instrument.

Iodobenzene, *p*-iodoanisole, *p*-iodonitrobenzene, 1-iodonaphthalene, and 1,4-epoxy-1,4-dihydronaphthalene (**4d**) (Janssen), *p*-iodotoluene, 2-iodothiophene, and *p*-bromotoluene (Aldrich), *m*-iodoanisole (TCI), Zn (<60 μm) and NEt_3 (Merck), and ZnCl_2 (Wako) were used as purchased. Dimethyl 7-carbomethoxy-7-azabicyclo[2.2.1]-2,5-heptadiene-2,3-dicarboxylate (**4a**), dimethyl 7-oxabicyclo[2.2.1]-2,5-heptadiene-2,3-dicarboxylate (**4b**), 7-carbomethoxy-7-aza-2,3-benzonorbornadiene (**4c**), 1,4-dihydro-5,8-dimethoxy-1,4-epoxynaphthalene (**4e**), 1,4-dihydro-5,8-dimethoxy-1-methyl-1,4-epoxynaphthalene (**4f**), 1,4-dihydro-5-methoxy-1,4-epoxynaphthalene (**4g**), 5,5-dimethyl-3-iodo-2-cyclohexen-1-one, 3-iodo-2-methyl-2-cyclohexen-1-one, 3-iodo-2-methyl-2-cyclopenten-1-one, and 3-iodo-2-cyclohexen-1-one were prepared according to reported methods.¹⁷⁻²¹

General Procedure for the Addition of Organic Iodides to Dimethyl 7-Carbomethoxy-7-azabicyclo[2.2.1]-2,5-heptadiene-2,3-dicarboxylate (4a). To a mixture of $\text{Pd}(\text{PPh}_3)_2\text{Cl}_2$ (0.0175 g, 0.025 mmol), zinc powder (0.3270 g, 5.0 mmol), and toluene (10 mL) was added organic iodide (0.50 mmol), **4a** (0.1335 g, 0.50 mmol), and NEt_3 (0.70 mL, 5.00 mmol). The system was heated under nitrogen with stirring at 80 °C for several hours until **4a** was completely consumed, as indicated in the ¹H NMR spectrum of the solution. Upon completion of the reaction, the solution was filtered through Celite. The filtrate was concentrated and separated on a silica gel column using ethyl acetate/hexane as the eluent to give the desired product **5**. When 1-iodonaphthalene was used as the organic iodide, both **5f** and **6** were isolated.

Compounds **5a-h** and **6** were prepared according to this method. While the reaction conditions and the yields of products for each reaction are listed in Table 1, important spectral data of these compounds are listed below.

Dimethyl 1,1'-biphenyl-3,4-dicarboxylate (5a): ¹H NMR (400 MHz, CDCl_3) δ 3.93 (s, OCH₃, 3 H), 3.94 (s, OCH₃, 3 H), 7.41 (t, $J = 7.1$ Hz, 1 H), 7.47 (t, $J = 7.6$ Hz, 2 H), 7.61 (dd, $J = 7.3$ Hz, $J = 1.7$ Hz, 2 H), 7.74 (dd, $J = 8.1$ Hz, $J = 1.8$ Hz, 1 H), 7.84 (d, $J = 8.1$ Hz, 1 H), 7.91 (d, $J = 1.8$ Hz, 1 H); ¹³C-{¹H} NMR (75 MHz, CDCl_3) δ 52.47 (OCH₃), 52.56 (OCH₃), 127.31, 127.46, 128.58, 129.14, 129.41, 129.83, 130.02, 133.22, 139.12, 144.51, 167.91 (COO), 168.61 (COO); IR (neat) 3040, 2944, 1728 ($\nu(\text{C=O})$), 1606, 1434, 1277, 1128, 1075, 757, 697, 668 cm^{-1} ; HRMS calcd for $\text{C}_{16}\text{H}_{14}\text{O}_4$ 270.0893, found 270.0884.

Dimethyl 4'-methyl-1,1'-biphenyl-3,4-dicarboxylate (5b): ¹H NMR (400 MHz, CDCl_3) δ 2.40 (s, CH₃, 3 H), 3.92 (s, OCH₃, 3 H), 3.94 (s, OCH₃, 3 H), 7.27 (d, $J = 8.1$ Hz, 2 H), 7.51 (d, $J = 8.1$ Hz, 2 H), 7.72 (dd, $J = 8.1$ Hz, $J = 2.0$ Hz, 1 H), 7.83 (d, $J = 8.1$ Hz, 1 H), 7.88 (d, $J = 2.0$ Hz, 1 H); ¹³C-{¹H} NMR (75 MHz, CDCl_3) δ 20.80 (CH₃), 52.35 (OCH₃), 52.47 (OCH₃), 127.07, 129.03, 129.82, 133.26, 136.11, 138.58, 144.40, 167.82 (COO), 168.67 (COO); IR (neat) 3040, 2951, 1731 ($\nu(\text{C=O})$), 1607, 1435, 1280, 1129, 1075, 817, 772 cm^{-1} ; HRMS calcd for $\text{C}_{17}\text{H}_{16}\text{O}_4$ 284.1050, found 284.1075.

Dimethyl 3'-methoxy-1,1'-biphenyl-3,4-dicarboxylate (5c): ¹H NMR (400 MHz, CDCl_3) δ 3.85 (s, OCH₃, 3 H), 3.91 (s, OCH₃, 3 H), 3.92 (s, OCH₃, 3 H), 6.94 (dd, $J = 8.2$ Hz, $J = 2.6$ Hz, 1 H), 7.11 (t, $J = 2.1$ Hz, 1 H), 7.17 (dt, $J = 7.6$ Hz, $J = 0.9$ Hz, 1 H), 7.37 (t, $J = 7.9$ Hz, 1 H), 7.72 (dd, $J = 8.1$ Hz, $J = 1.8$ Hz, 1 H), 7.81 (d, $J = 8.1$ Hz, 1 H), 7.88 (d, $J = 1.8$ Hz, 1 H); ¹³C-{¹H} NMR (75 MHz, CDCl_3) δ 52.45 (OCH₃), 52.56 (OCH₃), 55.21 (OCH₃), 113.00, 113.93, 119.74, 127.50, 129.47, 129.80, 130.15, 130.20, 133.19, 140.60, 144.38, 160.35, 167.86 (COO), 168.58 (COO); IR (neat) 3008, 2951, 1729 ($\nu(\text{C=O})$), 1598, 1439, 1284, 1215, 1129, 1075, 774 cm^{-1} ; HRMS calcd for $\text{C}_{17}\text{H}_{16}\text{O}_5$ 300.0999, found 300.1008.

(17) Bansal, R. C.; McCulloch, A. W.; McInnes, A. G. *Can. J. Chem.* **1969**, *47*, 2391.

(18) Xing, Y.-D.; Huang, N.-Z. *J. Org. Chem.* **1982**, *47*, 140.

(19) Piers, E.; Grierson, J. R.; Lau, C. K.; Nagakura, I. *Can. J. Chem.* **1982**, *60*, 210.

(20) Anteunis, M. J. O.; Borremans, F. A. M.; Gelan, J.; Marchand, A. P.; Allen, R. W. *J. Am. Chem. Soc.* **1978**, *100*, 4050.

(21) Cragg, G. M. L.; Giles, R. G. F.; Roos, G. H. P. *J. Chem. Soc., Perkin Trans. 1* **1975**, 1339.

(16) (a) Li, C.-S.; Cheng, C.-H.; Liao, F.-L.; Wang, S.-L. *J. Chem. Soc., Chem. Commun.* **1991**, 710. (b) Duan, J.-P.; Cheng, C.-H. *J. Chin. Chem. Soc.* **1994**, *41*, 749.

Dimethyl 4'-methoxy-1,1'-biphenyl-3,4-dicarboxylate (5d): $^1\text{H NMR}$ (400 MHz, CDCl_3) δ 3.86 (s, OCH_3 , 3 H), 3.92 (s, OCH_3 , 3 H), 3.93 (s, OCH_3 , 3 H), 6.99 (d, $J = 8.5$ Hz, 2 H), 7.56 (d, $J = 8.5$ Hz, 2 H), 7.69 (dd, $J = 8.1$ Hz, $J = 1.9$ Hz, 1 H), 7.82 (d, $J = 8.1$ Hz, 1 H), 7.84 (d, $J = 1.9$ Hz, 1 H); $^{13}\text{C}\{^1\text{H}\}$ NMR (100 MHz, CDCl_3) δ 52.54 (OCH_3), 52.68 (OCH_3), 55.34 (OCH_3), 114.42, 126.63, 128.30, 128.56, 128.91, 129.74, 131.28, 133.22, 143.95, 160.02, 167.55 (COO), 168.53 (COO); IR (neat) 3040, 2992, 2952, 1728 ($\nu(\text{C}=\text{O})$), 1605, 1521, 1436, 1276, 1185, 1129, 1076, 1044, 829, 773 cm^{-1} ; HRMS calcd for $\text{C}_{17}\text{H}_{16}\text{O}_5$ 300.0999, found 300.1006.

Dimethyl 4'-nitro-1,1'-biphenyl-3,4-dicarboxylate (5e): mp 118–120 °C dec; $^1\text{H NMR}$ (400 MHz, CDCl_3) δ 3.93 (s, OCH_3 , 3 H), 3.94 (s, OCH_3 , 3 H), 7.76 (d, $J = 8.8$ Hz, 2 H), 7.77–7.79 (m, 1 H), 7.87 (d, $J = 8.3$ Hz, 1 H), 7.94 (d, $J = 2.0$ Hz, 1 H), 8.33 (d, $J = 8.8$ Hz, 2 H); $^{13}\text{C}\{^1\text{H}\}$ NMR (75 MHz, CDCl_3) δ 52.69 (OCH_3), 52.76 (OCH_3), 124.44, 127.93, 128.25, 129.86, 130.10, 131.91, 133.34, 141.87, 145.46, 148.05, 167.64 (COO), 167.97 (COO); IR (KBr) 3069, 2951, 2444, 1726 ($\nu(\text{C}=\text{O})$), 1653, 1601, 1514, 1440, 1296, 1129, 1074, 957, 865, 845, 782, 748, 697 cm^{-1} ; HRMS calcd for $\text{C}_{16}\text{H}_{13}\text{NO}_6$ 315.0742, found 315.0738. Anal. Calcd for $\text{C}_{16}\text{H}_{13}\text{NO}_6$: C, 60.95; H, 4.16; N, 4.44. Found: C, 60.01; H, 4.11; N, 4.46.

Dimethyl 4-naphthylbenzene-1,2-dicarboxylate (5f): $^1\text{H NMR}$ (400 MHz, CDCl_3) δ 3.91 (s, OCH_3 , 3 H), 3.95 (s, OCH_3 , 3 H), 7.40–7.92 (m, 10 H); $^{13}\text{C}\{^1\text{H}\}$ NMR (75 MHz, CDCl_3) δ 52.54 (OCH_3), 52.62 (OCH_3), 125.45, 126.24, 126.75, 127.24, 128.60, 128.78, 129.25, 130.48, 131.24, 131.29, 132.56, 132.71, 133.90, 138.16, 144.34, 168.16 (COO), 168.14 (COO); IR (neat) 3056, 3002, 2951, 1732 ($\nu(\text{C}=\text{O})$), 1636, 1435, 1278, 1195, 1127, 1073, 782 cm^{-1} ; HRMS calcd for $\text{C}_{20}\text{H}_{16}\text{O}_4$ 320.1049, found 320.1061.

2-[3,4-Bis(methoxycarbonyl)phenyl]thiophene (5g): $^1\text{H NMR}$ (400 MHz, CDCl_3) δ 3.91 (s, OCH_3 , 3 H), 3.93 (s, OCH_3 , 3 H), 7.11 (dd, $J = 5.2$ Hz, $J = 3.6$ Hz, 1 H), 7.37 (dd, $J = 5.2$ Hz, $J = 1.2$ Hz, 1 H), 7.42 (dd, $J = 3.6$ Hz, $J = 1.2$ Hz, 1 H), 7.73 (dd, $J = 7.9$ Hz, $J = 1.9$ Hz, 1 H), 7.79 (d, $J = 7.9$ Hz, 1 H), 7.87 (d, $J = 1.9$ Hz, 1 H); $^{13}\text{C}\{^1\text{H}\}$ NMR (100 MHz, CDCl_3) δ 52.57 (OCH_3), 52.75 (OCH_3), 124.87, 125.56, 126.66, 127.48, 128.35, 129.23, 129.96, 133.55, 137.51, 141.81, 167.16 (COO), 168.24 (COO); IR (neat) 3120, 3008, 2951, 1729 ($\nu(\text{C}=\text{O})$), 1685, 1435, 1292, 1246, 1204, 1129, 1072, 702, 669 cm^{-1} ; HRMS calcd for $\text{C}_{14}\text{H}_{12}\text{O}_4\text{S}$ 276.0456, found 276.0445.

3-[3,4-Bis(methoxycarbonyl)phenyl]-2-cyclohexen-1-one (5h): $^1\text{H NMR}$ (400 MHz, CDCl_3) δ 2.16–2.19 (m, 2 H), 2.50 (t, $J = 6.8$ Hz, 2 H), 2.77 (td, $J = 6.0$ Hz, $J = 1.2$ Hz, 2 H), 3.92 (s, OCH_3 , 3 H), 3.93 (s, OCH_3 , 3 H), 6.44 (t, $J = 1.3$ Hz, 1 H), 7.67 (dd, $J = 8.2$ Hz, $J = 2.0$ Hz, 1 H), 7.77 (d, $J = 8.2$ Hz, 1 H), 7.85 (d, $J = 2.0$ Hz, 1 H); $^{13}\text{C}\{^1\text{H}\}$ NMR (100 MHz, CDCl_3) δ 22.50 (CH_2), 27.81 (CH_2), 37.01 (CH_2), 52.67 (OCH_3), 52.72 (OCH_3), 126.39, 126.91, 126.93, 128.30, 129.33, 132.43, 141.65, 157.11, 167.18 (COO), 167.39 (COO), 199.15 (CO); IR (neat) 2992, 2938, 1730 ($\nu(\text{C}=\text{O})$), 1669 ($\nu(\text{C}=\text{O})$), 1606, 1583, 1439, 1277, 1131, 1073, 965, 893, 827, 771, 704 cm^{-1} ; HRMS calcd for $\text{C}_{16}\text{H}_{16}\text{O}_5$ 288.0998, found 288.0975.

Methyl N-[2,3-bis(methoxycarbonyl)-6-naphthyl-1,3-cyclohexadienyl]carbamate (6): $^1\text{H NMR}$ (400 MHz, CDCl_3) δ 2.61 (ddd, $J = 16.9$ Hz, $J = 7.1$ Hz, $J = 1.1$ Hz, 1 H), 2.83 (ddd, $J = 16.9$ Hz, $J = 8.5$ Hz, $J = 2.0$ Hz, 1 H), 3.54 (s, OCH_3 , 3 H), 3.75 (s, OCH_3 , 3 H), 3.79 (s, OCH_3 , 3 H), 6.11 (dd, $J = 7.1$ Hz, $J = 3.0$ Hz, 1 H), 6.15 (dd, $J = 8.5$ Hz, $J = 1.1$ Hz, 1 H), 7.21 (d, $J = 6.9$ Hz, 1 H), 7.33 (t, $J = 7.7$ Hz, 1 H), 7.49 (t, $J = 7.4$ Hz, 1 H), 7.56–7.60 (m, 1 H), 7.73 (d, $J = 8.2$ Hz, 1 H), 7.86 (d, $J = 7.6$ Hz, 1 H), 8.12 (d, $J = 8.5$ Hz, 1 H), 10.68 (s, NH, 1 H); $^{13}\text{C}\{^1\text{H}\}$ NMR (100 MHz, CDCl_3) δ 29.43 (CH_2), 33.44, 51.79 (OCH_3), 51.94 (OCH_3), 52.62 (OCH_3), 105.18, 122.92, 124.06, 125.25, 125.28, 125.50, 126.48, 127.87, 129.09, 129.22, 130.32, 130.73, 132.30, 134.47, 152.76 (COO), 167.80 (COO), 168.10 (COO); IR (neat) 3244, 3008, 2953, 1738 ($\nu(\text{C}=\text{O})$), 1684 ($\nu(\text{C}=\text{O})$), 1597, 1463, 1261, 1204, 1159, 1089, 1002, 789, 669 cm^{-1} ; HRMS calcd for $\text{C}_{22}\text{H}_{21}\text{NO}_6$ 395.1369, found 395.1380.

Isolation of Dimethyl 4'-Methyl-1,1'-biphenyl-3,4-dicarboxylate (5b) from Dimethyl 7-oxabicyclo[2.2.1]-2,5-heptadiene-2,3-dicarboxylate (4b) and *p*-Iodotoluene. To a mixture of $\text{Pd}(\text{PPh}_3)_2\text{Cl}_2$ (0.0175 g, 0.025 mmol), zinc powder (0.327 g, 5.00 mmol), and DMF (10 mL) were added *p*-iodotoluene (0.109 g, 0.500 mmol), **4b** (0.2102 g, 1.00 mmol), and NEt_3 (0.70 mL, 5.00 mmol). The system was heated under nitrogen with stirring at 100 °C for 25 h. The solution was filtered through Celite, and to the filtrate was added water (10 mL). The mixture was extracted with ether (10 mL) three times. The ether solution was dried over magnesium sulfate and concentrated on a rotary evaporator. Separation on a silica gel column using ethyl acetate/hexane as the eluent gave **5b** (0.0525 g) in 37% yield.

Addition of Organic Iodides to 4c and 4d in the Presence of $\text{PdCl}_2(\text{PPh}_3)_2\text{-Et}_3\text{N-Zn}$. Isolation of Compounds **7a–h**, **8a–c**, and **9a–e**. Compounds **7a–h**, **8a–c**, and **9a–e** were prepared from reactions of **4c** and **4d** with the corresponding organic iodides. Reaction conditions and isolation methods were similar to those for the reaction of **4a** with organic iodides (*vide supra*), except that the reaction temperature is 100 °C. The yields of these compounds and reaction conditions are presented in Table 1, while important spectral data of these compounds are listed below. 2-Phenyl-naphthalene (**7e**) was prepared and characterized previously.²² The observed spectral data are in agreement with those reported in the literature.

2-(4-Methylphenyl)naphthalene (7a): mp 73–75 °C; $^1\text{H NMR}$ (400 MHz, CDCl_3) δ 2.41 (s, CH_3 , 3 H), 7.28 (d, $J = 8.1$ Hz, 2 H), 7.45–7.49 (m, 2 H), 7.61 (d, $J = 8.1$ Hz, 2 H), 7.73 (dd, $J = 8.6$ Hz, $J = 1.7$ Hz, 1 H), 7.83–7.90 (m, 3 H), 8.01 (d, $J = 1.7$ Hz, 1 H); $^{13}\text{C}\{^1\text{H}\}$ NMR (100 MHz, CDCl_3) δ 21.09 (CH_3), 125.37, 125.49, 125.71, 126.17, 127.21, 127.59, 128.10, 128.31, 129.54, 132.46, 133.69, 137.05, 138.15, 138.41; IR (KBr) 3051, 2918, 1684, 1654, 1559, 1499, 1437, 893, 810, 745, 669 cm^{-1} ; HRMS calcd for $\text{C}_{17}\text{H}_{14}$ 218.1095, found 218.1111.

2-(4-Methoxyphenyl)naphthalene (7b): mp 138–140 °C; $^1\text{H NMR}$ (300 MHz, CDCl_3) δ 3.93 (s, OCH_3 , 3 H), 7.08 (d, $J = 8.7$ Hz, 2 H), 7.50–7.55 (m, 2 H), 7.72 (d, $J = 8.7$ Hz, 2 H), 7.77 (dd, $J = 8.4$ Hz, $J = 1.8$ Hz, 1 H), 7.89–7.96 (m, 3 H), 8.05 (d, $J = 1.8$ Hz, 1 H); $^{13}\text{C}\{^1\text{H}\}$ NMR (100 MHz, CDCl_3) δ 55.38 (OCH_3), 114.31, 125.02, 125.43, 125.65, 126.22, 127.61, 128.04, 128.33, 128.42, 132.30, 133.62, 133.74, 138.14, 159.23; IR (KBr) 3040, 2950, 1606, 1563, 1282, 1253, 1183, 1038, 1023, 831, 813, 714 cm^{-1} ; HRMS calcd for $\text{C}_{17}\text{H}_{14}\text{O}$ 234.1045, found 234.1056.

2-(3-Methoxyphenyl)naphthalene (7c): $^1\text{H NMR}$ (400 MHz, CDCl_3) δ 3.90 (s, OCH_3 , 3 H), 6.93 (dd, $J = 8.0$ Hz, $J = 2.4$ Hz, 1 H), 7.26 (s, 1 H), 7.31 (d, $J = 8.0$ Hz, 1 H), 7.40 (t, $J = 7.8$ Hz, 1 H), 7.46–7.53 (m, 2 H), 7.74 (dd, $J = 8.6$ Hz, $J = 1.7$ Hz, 1 H), 7.85–7.92 (m, 3 H), 8.04 (d, $J = 1.7$ Hz, 1 H); $^{13}\text{C}\{^1\text{H}\}$ NMR (75 MHz, CDCl_3) δ 55.22 (OCH_3), 112.86, 113.27, 120.08, 125.74, 126.01, 126.12, 126.45, 127.80, 128.37, 128.55, 130.02, 132.89, 133.81, 138.61, 142.87, 160.32; IR (neat) 3043, 2833, 1592, 1467, 1291, 1034, 854, 782, 747, 696 cm^{-1} ; HRMS calcd for $\text{C}_{17}\text{H}_{14}\text{O}$ 234.1045, found 234.1041.

2-(3-Methylphenyl)naphthalene (7d): $^1\text{H NMR}$ (400 MHz, CDCl_3) δ 2.50 (s, CH_3 , 3 H), 7.24 (d, $J = 7.6$ Hz, 1 H), 7.42 (t, $J = 7.6$ Hz, 1 H), 7.51–7.59 (m, 4 H), 7.78 (dd, $J = 8.6$ Hz, $J = 1.7$ Hz, 1 H), 7.89–7.95 (m, 3 H), 8.08 (d, $J = 1.7$ Hz, 1 H); $^{13}\text{C}\{^1\text{H}\}$ NMR (75 MHz, CDCl_3) δ 21.36 (CH_3), 124.70, 125.83, 125.91, 126.01, 126.39, 127.80, 128.28, 128.35, 128.38, 128.50, 128.94, 132.79, 133.88, 138.64, 138.89, 141.33; IR (neat) 3049, 2918, 1599, 1493, 856, 785, 700 cm^{-1} ; HRMS calcd for $\text{C}_{17}\text{H}_{14}$ 218.1095, found 218.1108.

2-(4-Acetylphenyl)naphthalene (7f): $^1\text{H NMR}$ (400 MHz, CDCl_3) δ 2.66 (s, CH_3 , 3 H), 7.52–7.54 (m, 2 H), 7.77 (dd, $J = 8.6$ Hz, $J = 1.8$ Hz, 1 H), 7.83 (d, $J = 8.8$ Hz, 2 H), 7.88–7.96 (m, 3 H), 8.07–8.10 (m, 3 H); $^{13}\text{C}\{^1\text{H}\}$ NMR (75 MHz, CDCl_3) δ 26.42 (CH_3), 125.28, 126.50, 126.62, 126.70, 127.57, 127.83,

128.50, 128.85, 129.12, 133.18, 133.72, 136.03, 137.29, 145.85, 197.57 (CO); IR (KBr) 3057, 1733, 1700, 1677 ($\nu(\text{C}=\text{O})$), 1653, 1559, 1265, 821, 754 cm^{-1} ; HRMS calcd for $\text{C}_{18}\text{H}_{14}\text{O}$ 246.1045, found 246.1058.

3-(2-Naphthyl)-2-cyclohexen-1-one (7g): mp 100–102 °C; ^1H NMR (400 MHz, CDCl_3) δ 2.20–2.23 (m, CH_2 , 2 H), 2.53 (t, CH_2 , $J = 6.7$ Hz, 2 H), 2.91 (td, CH_2 , $J = 6.0$ Hz, $J = 1.5$ Hz, 2 H), 6.57 (t, $J = 1.5$ Hz, 1 H), 7.52–7.54 (m, 2 H), 7.66 (dd, $J = 8.5$ Hz, $J = 2.0$ Hz, 1 H), 7.86–7.88 (m, 3 H), 8.01 (d, $J = 2.0$ Hz, 1 H); $^{13}\text{C}\{^1\text{H}\}$ NMR (100 MHz, CDCl_3) δ 22.67 (CH_2), 27.86 (CH_2), 37.17 (CH_2), 123.09, 125.51, 125.97, 126.56, 127.05, 127.51, 128.31, 128.54, 132.90, 133.79, 135.71, 159.25, 199.74 (CO); IR (KBr) 3056, 2944, 1657 ($\nu(\text{C}=\text{O})$), 1602, 1358, 1252, 1192, 1137, 962, 870, 819, 760, 669 cm^{-1} ; HRMS calcd for $\text{C}_{16}\text{H}_{14}\text{O}$ 222.1045, found 222.1059. Anal. Calcd for $\text{C}_{16}\text{H}_{14}\text{O}$: C, 86.45; H, 6.35. Found: C, 85.73; H, 6.42.

5,5-Dimethyl-3-(2-naphthyl)-2-cyclohexen-1-one (7h): mp 82–84 °C; ^1H NMR (400 MHz, CDCl_3) δ 1.17 (s, 2 CH_3 , 6 H), 2.38 (s, CH_2 , 2 H), 2.78 (d, CH_2 , $J = 1.5$ Hz, 2 H), 6.56 (t, $J = 1.5$ Hz, 1 H), 7.51–7.53 (m, 2 H), 7.65 (dd, $J = 8.7$ Hz, $J = 1.6$ Hz, 1 H), 7.83–7.89 (m, 3 H), 8.00 (d, $J = 1.6$ Hz, 1 H); $^{13}\text{C}\{^1\text{H}\}$ NMR (100 MHz, CDCl_3) δ 28.31 (2 CH_3), 33.61, 42.04 (CH_2), 50.83 (CH_2), 123.24, 124.46, 125.96, 126.57, 127.04, 127.51, 128.32, 128.51, 132.91, 133.76, 135.96, 157.02, 199.88 (CO); IR (KBr) 3040, 2951, 1655 ($\nu(\text{C}=\text{O})$), 1599, 1503, 1462, 1367, 1285, 1265, 904, 814, 750 cm^{-1} ; HRMS calcd for $\text{C}_{18}\text{H}_{18}\text{O}$ 250.1358, found 250.1368. Anal. Calcd for $\text{C}_{18}\text{H}_{18}\text{O}$: C, 86.36; H, 7.25. Found: C, 85.94; H, 7.30.

Methyl N-[cis-1,2-dihydro-2-(4-methylphenyl)-1-naphthyl]carbamate (8a): mp 104–106 °C; ^1H NMR (300 MHz, CDCl_3) δ 2.32 (s, CH_3 , 3 H), 3.70 (s, OCH_3 , 3 H), 3.84 (dd, $J = 8.3$ Hz, $J = 5.5$ Hz, 1 H), 4.75 (d, NH, $J = 10.1$ Hz, 1 H), 5.40 (dd, $J = 10.1$ Hz, $J = 8.3$ Hz, 1 H), 6.18 (dd, $J = 9.4$ Hz, $J = 5.5$ Hz, 1 H), 6.73 (d, $J = 9.4$ Hz, 1 H), 7.01 (d, $J = 8.1$ Hz, 2 H), 7.08 (d, $J = 8.1$ Hz, 2 H), 7.18–7.31 (m, 4 H); $^{13}\text{C}\{^1\text{H}\}$ NMR (75 MHz, CDCl_3) δ 20.70 (CH_3), 44.17, 52.04 (OCH_3), 52.63, 125.35, 126.43, 127.82, 128.17, 128.25, 128.97, 129.34, 130.57, 133.41, 134.01, 134.68, 137.14, 156.90 (COO); IR (KBr) 3287, 3024, 2944, 2901, 1727, 1694 ($\nu(\text{C}=\text{O})$), 1653, 1548, 1507, 1260, 1057, 789 cm^{-1} ; HRMS calcd for $\text{C}_{19}\text{H}_{19}\text{NO}_2$ 293.1416, found 293.1415. Anal. Calcd for $\text{C}_{19}\text{H}_{19}\text{NO}_2$: C, 77.79; H, 6.53; N, 4.77. Found: C, 77.72; H, 6.58; N, 4.85.

Methyl N-[cis-1,2-dihydro-2-(4-methoxyphenyl)-1-naphthyl]carbamate (8b): mp 126–128 °C; ^1H NMR (300 MHz, CDCl_3) δ 3.68 (s, OCH_3 , 3 H), 3.77 (s, OCH_3 , 3 H), 3.81–3.84 (m, 1 H), 4.71 (d, NH, $J = 9.5$ Hz, 1 H), 5.37 (dd, $J = 9.5$ Hz, $J = 8.3$ Hz, 1 H), 6.15 (dd, $J = 9.8$ Hz, $J = 5.3$ Hz, 1 H), 6.69 (d, $J = 9.8$ Hz, 1 H), 6.78 (d, $J = 8.7$ Hz, 2 H), 7.02 (d, $J = 8.7$ Hz, 2 H), 7.16–7.26 (m, 4 H); $^{13}\text{C}\{^1\text{H}\}$ NMR (100 MHz, CDCl_3) δ 43.83, 52.12 (OCH_3), 52.75, 55.03 (OCH_3), 113.81, 125.13, 126.21, 127.60, 127.90, 127.96, 128.69, 129.89, 130.50, 133.20, 134.41, 156.59, 158.81 (COO); IR (KBr) 3368, 2970, 1718 ($\nu(\text{C}=\text{O})$), 1608, 1511, 1339, 1245, 1179, 1045, 837, 792, 755 cm^{-1} ; HRMS calcd for $\text{C}_{19}\text{H}_{19}\text{NO}_3$ 309.1365, found 309.1354. Anal. Calcd for $\text{C}_{19}\text{H}_{19}\text{NO}_3$: C, 73.77; H, 6.19; N, 4.53. Found: C, 73.02; H, 6.19; N, 4.46.

Methyl N-[cis-1,2-dihydro-2-phenyl-1-naphthyl]carbamate (8c): ^1H NMR (300 MHz, CDCl_3) δ 3.67 (s, OCH_3 , 3 H), 3.88 (dd, $J = 8.0$ Hz, $J = 5.3$ Hz, 1 H), 4.74 (d, NH, $J = 10.1$ Hz, 1 H), 5.40 (dd, $J = 10.1$ Hz, $J = 8.0$ Hz, 1 H), 6.18 (dd, $J = 9.6$ Hz, $J = 5.3$ Hz, 1 H), 6.73 (d, $J = 9.6$ Hz, 1 H), 7.11–7.28 (m, 9 H); $^{13}\text{C}\{^1\text{H}\}$ NMR (75 MHz, CDCl_3) δ 44.60, 52.01 (OCH_3), 52.63, 125.46, 126.48, 127.48, 127.89, 128.22, 128.42, 128.59, 129.08, 130.30, 133.31, 134.59, 137.35, 156.85 (COO); IR (neat) 3317, 3038, 2944, 1715 ($\nu(\text{C}=\text{O})$), 1511, 1451, 1342, 1236, 1062, 825, 796, 763, 703, 668 cm^{-1} ; HRMS calcd for $\text{C}_{18}\text{H}_{17}\text{NO}_2$ 279.1259, found 279.1259.

cis-1,2-Dihydro-2-(4-methylphenyl)-1-naphthol (9a): ^1H NMR (400 MHz, CDCl_3) δ 1.45 (s, OH, 1 H), 2.30 (s, CH_3 , 3 H), 3.82 (ddd, $J = 6.0$ Hz, $J = 4.1$ Hz, $J = 2.0$ Hz, 1 H), 4.90 (d, $J = 6.0$ Hz, 1 H), 6.09 (dd, $J = 9.9$ Hz, $J = 4.1$ Hz, 1 H), 6.67 (dd, $J = 9.9$ Hz, $J = 2.0$ Hz, 1 H), 7.08–7.33 (m, 8 H);

$^{13}\text{C}\{^1\text{H}\}$ NMR (100 MHz, CDCl_3) δ 20.97 (CH_3), 46.77, 71.21, 126.21, 126.55, 127.86, 127.97, 128.10, 129.05, 129.15, 129.27, 132.60, 134.30, 136.08, 136.94; IR (neat) 3413, 3034, 2917, 1638, 1512, 1452, 1381, 1073, 838, 783, 694 cm^{-1} ; HRMS calcd for $\text{C}_{17}\text{H}_{16}\text{O}$ 236.1201, found 236.1210.

cis-1,2-Dihydro-2-(4-methoxyphenyl)-1-naphthol (9b): ^1H NMR (400 MHz, CDCl_3) δ 1.64 (s, OH, 1 H), 3.80 (s, OCH_3 , 3 H), 3.83 (ddd, $J = 6.0$ Hz, $J = 4.2$ Hz, $J = 1.9$ Hz, 1 H), 4.95 (br, 1 H), 6.13 (dd, $J = 9.5$ Hz, $J = 4.2$ Hz, 1 H), 6.70 (dd, $J = 9.5$ Hz, $J = 1.9$ Hz, 1 H), 6.86 (d, $J = 8.6$ Hz, 2 H), 7.18 (d, $J = 8.6$ Hz, 2 H + 1 H), 7.25–7.38 (m, 3 H); $^{13}\text{C}\{^1\text{H}\}$ NMR (100 MHz, CDCl_3) δ 46.26, 55.09 (OCH_3), 71.14, 113.93, 126.15, 126.38, 127.87, 128.03, 129.06, 130.02, 130.20, 132.59, 136.17, 158.81; IR (neat) 3452, 3060, 3036, 2944, 2897, 2836, 1693, 1603, 1511, 1302, 1258, 1179, 1032, 837, 806 cm^{-1} ; HRMS calcd for $\text{C}_{17}\text{H}_{16}\text{O}_2$ 252.1150, found 252.1149.

cis-1,2-Dihydro-2-(3-methoxyphenyl)-1-naphthol (9c): ^1H NMR (400 MHz, CDCl_3) δ 1.61 (d, OH, $J = 7.2$ Hz, 1 H), 3.70 (s, OCH_3 , 3 H), 3.81 (ddd, $J = 6.0$ Hz, $J = 4.0$ Hz, $J = 2.0$ Hz, 1 H), 4.89 (t, $J = 6.8$ Hz, 1 H), 6.09 (dd, $J = 9.8$ Hz, $J = 4.0$ Hz, 1 H), 6.67 (dd, $J = 9.8$ Hz, $J = 2.0$ Hz, 1 H), 6.78–6.85 (m, 3 H), 7.14 (dd, $J = 7.2$ Hz, $J = 1.2$ Hz, 1 H), 7.18–7.33 (m, 4 H); $^{13}\text{C}\{^1\text{H}\}$ NMR (100 MHz, CDCl_3) δ 47.21, 54.96 (OCH_3), 71.12, 112.68, 114.72, 121.42, 126.22, 126.57, 127.87, 128.08, 128.14, 129.45, 129.50, 132.51, 136.01, 139.28, 159.61; IR (neat) 3526, 3456, 3034, 2930, 2034, 1595, 1489, 1285, 1263, 1157, 1055, 782 cm^{-1} ; HRMS calcd for $\text{C}_{17}\text{H}_{16}\text{O}_2$ 252.1150, found 252.1146.

cis-1,2-Dihydro-2-(3-methylphenyl)-1-naphthol (9d): ^1H NMR (400 MHz, CDCl_3) δ 1.50 (br, OH, 1 H), 2.32 (s, CH_3 , 3 H), 3.83 (ddd, $J = 5.7$ Hz, $J = 3.8$ Hz, $J = 2.3$ Hz, 1 H), 4.89 (br t, $J = 4.6$ Hz, 1 H), 6.11 (dd, $J = 9.5$ Hz, $J = 3.8$ Hz, 1 H), 6.69 (dd, $J = 9.5$ Hz, $J = 2.3$ Hz, 1 H), 7.05–7.35 (m, 8 H); $^{13}\text{C}\{^1\text{H}\}$ NMR (75 MHz, CDCl_3) δ 21.10 (CH_3), 47.02, 71.05, 126.22, 126.37, 126.89, 127.96, 128.11, 128.16, 128.29, 128.56, 129.84, 130.12, 132.71, 136.17, 137.94, 138.23; IR (neat) 3542, 3447, 3036, 2911, 2859, 1605, 1486, 1456, 1073, 781, 701 cm^{-1} ; HRMS calcd for $\text{C}_{17}\text{H}_{16}\text{O}$ 236.1201, found 236.1202.

cis-1,2-Dihydro-2-phenyl-1-naphthol (9e): ^1H NMR (400 MHz, CDCl_3) δ 1.53 (s, OH, 1 H), 3.86 (ddd, $J = 5.8$ Hz, $J = 4.2$ Hz, $J = 2.0$ Hz, 1 H), 4.92 (d, $J = 5.8$ Hz, 1 H), 6.12 (dd, $J = 9.7$ Hz, $J = 4.2$ Hz, 1 H), 6.69 (dd, $J = 9.7$ Hz, $J = 2.0$ Hz, 1 H), 7.16 (dd, $J = 7.1$ Hz, $J = 1.4$ Hz, 1 H), 7.24–7.34 (m, 8 H); $^{13}\text{C}\{^1\text{H}\}$ NMR (75 MHz, CDCl_3) δ 47.05, 71.07, 126.39, 126.76, 127.38, 128.03, 128.21, 128.29, 128.64, 129.36, 129.81, 132.71, 136.20, 137.92; IR (neat) 3538, 3441, 3059, 3039, 2896, 2831, 1491, 1451, 1071, 768, 700 cm^{-1} ; HRMS calcd for $\text{C}_{16}\text{H}_{14}\text{O}$ 222.1045, found 222.1059.

General Procedure for the Addition of Organic Iodides to 4c–f in the Presence of $\text{PdCl}_2(\text{PPh}_3)_2$ – Et_3N – ZnCl_2 – Zn . A mixture of $\text{Pd}(\text{PPh}_3)_2\text{Cl}_2$ (0.014 g, 0.020 mmol), zinc powder (0.654 g, 10.0 mmol), ZnCl_2 (0.0681 g, 0.500 mmol), and **4** (1.50 mmol) in a side-arm flask was purged with nitrogen gas three times. To the system were added THF (20 mL), organic halide (1.00 mmol), and NEt_3 (1.12 mL, 8.00 mmol). The system was further purged with nitrogen gas three times and was heated with stirring at 60 °C for several hours until the organic halide was completely consumed, as indicated by TLC analysis of the solution. The mixture was filtered through silica gel and Celite. The filtrate was concentrated and separated on a silica gel column using ethyl acetate/hexane as the eluent to give the desired product.

Compounds **7i**, **8**, **9** and **11–15** were prepared according to this method. While the reaction times and yields of products of each reaction are listed in Table 2, important spectral data for these products (**8d,e**, **9f–m,o**, **11a–d**, **12a–c**, and **13–15**) are listed below. *cis*-1,2-Dihydro-2-methyl-1-naphthol (**9n**) was prepared and characterized previously.¹⁵ The observed spectral data are in agreement with those reported.

2-Methyl-3-(2-naphthyl)-2-cyclopenten-1-one (7i): ^1H NMR (400 MHz, CDCl_3) δ 2.03 (t, CH_3 , $J = 2.0$ Hz, 3 H), 2.57–2.60 (m, CH_2 , 2 H), 3.01–3.03 (m, CH_2 , 2 H), 7.52–7.54

(m, 2 H), 7.63 (dd, $J = 8.6$ Hz, $J = 1.7$ Hz, 1 H), 7.85–7.91 (m, 3 H), 7.98 (d, $J = 1.7$ Hz, 1 H); $^{13}\text{C}\{^1\text{H}\}$ NMR (75 MHz, CDCl_3): δ 9.95 (CH_3), 29.17 (CH_2), 33.89 (CH_2), 124.70, 126.52, 127.00, 127.22, 127.55, 128.06, 128.41, 132.83, 133.35, 133.67, 136.58, 166.27, 209.60 (CO); IR (neat) 3059, 2922, 1682 ($\nu(\text{C}=\text{O})$), 1613, 1317, 819, 746 cm^{-1} ; HRMS calcd for $\text{C}_{16}\text{H}_{14}\text{O}$ 222.1045, found 222.1048.

Methyl *N*-(*cis*-1,2-dihydro-2-benzyl-1-naphthyl)carbamate (8d): ^1H NMR (400 MHz, CDCl_3) δ 2.71 (dd, $J = 13.2$ Hz, $J = 9.6$ Hz, 1 H), 2.93–2.96 (m, 1 H), 3.01 (dd, $J = 13.2$ Hz, $J = 6.4$ Hz, 1 H), 3.66 (s, OCH_3 , 3 H), 4.86 (dd, $J = 10.0$ Hz, $J = 5.2$ Hz, 1 H), 5.15 (d, NH, $J = 10.0$ Hz, 1 H), 5.76 (dd, $J = 9.4$ Hz, $J = 2.2$ Hz, 1 H), 6.52 (dd, $J = 9.4$ Hz, $J = 2.2$ Hz, 1 H), 7.09 (d, $J = 7.2$ Hz, 1 H), 7.21–7.36 (m, 8 H); $^{13}\text{C}\{^1\text{H}\}$ NMR (100 MHz, CDCl_3) δ 35.01 (CH_2), 40.06, 51.25, 51.54 (OCH_3), 125.78, 125.96, 126.69, 127.37, 127.44, 127.61, 128.00, 128.75, 129.64, 132.18, 135.21, 139.12, 156.18 (COO); IR (neat) 3037, 2953, 1708 ($\nu(\text{C}=\text{O})$), 1601, 1511, 1446, 1341, 1250, 1088, 772, 698 cm^{-1} ; HRMS calcd for $\text{C}_{19}\text{H}_{19}\text{NO}_2$ 293.1416, found 293.1425.

Methyl *N*-(*cis*-1,2-dihydro-2-(1-oxo-2-methyl-2-cyclohexen-3-yl)-1-naphthyl)carbamate (8e): ^1H NMR (400 MHz, CDCl_3) δ 1.75–1.82 (m, 2 H), 1.89 (t, CH_3 , $J = 1.4$ Hz, 3 H), 1.90–2.00 (m, 1 H), 2.33–2.39 (m, 3 H), 3.66 (s, OCH_3 , 3 H), 3.97 (ddd, $J = 7.2$ Hz, $J = 4.5$ Hz, $J = 2.0$ Hz, 1 H), 4.84 (d, NH, $J = 10.0$ Hz, 1 H), 5.30 (dd, $J = 10.0$ Hz, $J = 7.2$ Hz, 1 H), 5.91 (dd, $J = 9.7$ Hz, $J = 4.5$ Hz, 1 H), 6.66 (dd, $J = 9.7$ Hz, $J = 2.0$ Hz, 1 H), 7.11 (dd, $J = 6.8$ Hz, $J = 1.6$ Hz, 1 H), 7.26–7.27 (m, 3 H); $^{13}\text{C}\{^1\text{H}\}$ NMR (75 MHz, CDCl_3) δ 10.90 (CH_3), 22.31 (CH_2), 28.14 (CH_2), 37.58 (CH_2), 42.59, 50.81, 51.99 (OCH_3), 124.89, 126.37, 126.71, 127.74, 128.10, 128.80, 132.35, 133.53, 134.20, 154.75, 156.35 (COO), 198.81 (CO); IR (neat) 3312, 2947, 1701 ($\nu(\text{C}=\text{O})$), 1659 ($\nu(\text{C}=\text{O})$), 1528, 1248, 1054, 792 cm^{-1} ; HRMS calcd for $\text{C}_{19}\text{H}_{21}\text{NO}_3$ 311.1521, found 311.1523.

***cis*-1,2-Dihydro-2-(2-methylphenyl)-1-naphthol (9f):** ^1H NMR (400 MHz, CDCl_3) δ 1.53 (s, OH, 1 H), 2.43 (s, CH_3 , 3 H), 4.20 (ddd, $J = 5.2$ Hz, $J = 3.2$ Hz, $J = 2.2$ Hz, 1 H), 4.82 (d, $J = 5.2$ Hz, 1 H), 6.07 (dd, $J = 9.7$ Hz, $J = 3.2$ Hz, 1 H), 6.71 (dd, $J = 9.7$ Hz, $J = 2.2$ Hz, 1 H), 7.16–7.36 (m, 8 H); $^{13}\text{C}\{^1\text{H}\}$ NMR (100 MHz, CDCl_3) δ 19.65 (CH_3), 42.96, 69.45, 126.14, 126.35, 127.05, 127.47, 127.75, 128.42, 129.22, 130.32, 130.43, 132.35, 135.22, 136.41, 136.63; IR (neat) 3560, 3539, 3449, 3057, 3022, 2944, 2863, 1488, 1380, 1197, 1088, 759 cm^{-1} ; HRMS calcd for $\text{C}_{17}\text{H}_{16}\text{O}$ 236.1201, found 236.1202.

***cis*-1,2-Dihydro-2-(4-hydroxyphenyl)-1-naphthol (9g):** ^1H NMR (400 MHz, d_6 -acetone) δ 3.65 (d, OH, $J = 6.8$ Hz, 1 H), 3.69–3.72 (m, 1 H), 4.93 (t, $J = 6.4$ Hz, 1 H), 6.08 (dd, $J = 9.6$ Hz, $J = 4.4$ Hz, 1 H), 6.66 (dd, $J = 9.6$ Hz, $J = 2.0$ Hz, 1 H), 6.68 (d, $J = 8.4$ Hz, 2 H), 7.03 (d, $J = 8.4$ Hz, 2 H), 7.14–7.24 (m, 3 H), 7.35 (dd, $J = 8.0$ Hz, $J = 0.8$ Hz, 1 H), 8.11 (br s, OH, 1 H); $^{13}\text{C}\{^1\text{H}\}$ NMR (100 MHz, d_6 -acetone) δ 46.49, 70.88, 114.85, 125.86, 126.26, 127.46, 127.49, 127.52, 129.10, 130.50, 131.12, 133.11, 137.59, 156.26; IR (KBr) 3427, 3195, 1597, 1512, 1451, 1376, 1227, 1068, 946, 845, 807, 761, 690 cm^{-1} ; HRMS calcd for $\text{C}_{16}\text{H}_{14}\text{O}_2$ 238.0993, found 238.1006.

***cis*-1,2-Dihydro-2-(3-chlorophenyl)-1-naphthol (9h):** ^1H NMR (400 MHz, CDCl_3) δ 1.50 (s, OH, 1 H), 3.82 (ddd, $J = 5.7$ Hz, $J = 3.8$ Hz, $J = 2.1$ Hz, 1 H), 4.88 (d, $J = 5.7$ Hz, 1 H), 6.06 (dd, $J = 9.5$ Hz, $J = 3.8$ Hz, 1 H), 6.70 (dd, $J = 9.5$ Hz, $J = 2.1$ Hz, 1 H), 7.13–7.18 (m, 2 H), 7.22–7.34 (m, 6 H); $^{13}\text{C}\{^1\text{H}\}$ NMR (100 MHz, CDCl_3) δ 46.84, 70.87, 126.32, 126.62, 127.19, 127.26, 127.96, 128.27, 128.29, 128.74, 129.29, 129.50, 132.13, 134.01, 135.57, 140.33; IR (neat) 3431, 3040, 2891, 2838, 1583, 1437, 1082, 763, 668 cm^{-1} ; HRMS calcd for $\text{C}_{16}\text{H}_{13}\text{OCl}$ 256.0655, found 256.0648.

***cis*-1,2-Dihydro-2-(4-acetylphenyl)-1-naphthol (9i):** ^1H NMR (400 MHz, CDCl_3) δ 1.58 (s, OH, 1 H), 2.58 (s, CH_3 , 3 H), 3.94 (ddd, $J = 5.6$ Hz, $J = 3.8$ Hz, $J = 2.0$ Hz, 1 H), 4.94 (d, $J = 5.6$ Hz, 1 H), 6.11 (dd, $J = 9.7$ Hz, $J = 3.8$ Hz, 1 H), 6.75 (dd, $J = 9.7$ Hz, $J = 2.0$ Hz, 1 H), 7.19 (d, $J = 6.4$ Hz, 1 H), 7.26–7.40 (m, 5 H), 7.91 (dd, $J = 8.2$ Hz, $J = 1.4$ Hz, 2 H);

$^{13}\text{C}\{^1\text{H}\}$ NMR (75 MHz, CDCl_3) δ 26.55 (CH_3), 47.35, 71.24, 126.56, 126.64, 128.20, 128.52, 128.61, 128.74, 129.48, 132.34, 135.84, 136.15, 143.97, 197.77 (CO); IR (neat) 3434, 3046, 3032, 2918, 1676 ($\nu(\text{C}=\text{O})$), 1604, 1359, 1270, 1074, 803 cm^{-1} ; HRMS calcd for $\text{C}_{18}\text{H}_{16}\text{O}_2$ 264.1150, found 264.1141.

***cis*-1,2-Dihydro-2-naphthyl-1-naphthol (9j):** ^1H NMR (400 MHz, CDCl_3) δ 1.45 (s, OH, 1 H), 4.82 (dt, $J = 4.8$ Hz, $J = 2.8$ Hz, 1 H), 4.94 (d, $J = 4.8$ Hz, 1 H), 6.20 (dd, $J = 9.6$ Hz, $J = 2.8$ Hz, 1 H), 6.81 (dd, $J = 9.6$ Hz, $J = 2.8$ Hz, 1 H), 7.23–7.37 (m, 4 H), 7.45–7.58 (m, 4 H), 7.82 (d, $J = 8.4$ Hz, 1 H), 7.90 (dd, $J = 8.0$ Hz, $J = 1.2$ Hz, 1 H), 8.16 (d, $J = 8.0$ Hz, 1 H); $^{13}\text{C}\{^1\text{H}\}$ NMR (75 MHz, CDCl_3) δ 42.68, 70.20, 123.04, 125.49, 125.62, 126.27, 126.63, 126.89, 127.83, 127.91, 127.99, 128.16, 128.73, 129.07, 130.21, 131.84, 132.48, 134.02, 134.65, 135.11; IR (neat) 3537, 3410, 3050, 2893, 1691, 1664, 1390, 1256, 1026, 772, 741 cm^{-1} ; HRMS calcd for $\text{C}_{20}\text{H}_{16}\text{O}$ 272.1201, found 272.1183.

***cis*-1,2-Dihydro-2-(2-thienyl)-1-naphthol (9k):** ^1H NMR (400 MHz, CDCl_3) δ 1.77 (d, OH, $J = 7.2$ Hz, 1 H), 4.13 (ddd, $J = 6.2$ Hz, $J = 4.6$ Hz, $J = 1.7$ Hz, 1 H), 5.00 (t, $J = 6.0$ Hz, 1 H), 6.14 (dd, $J = 9.7$ Hz, $J = 4.6$ Hz, 1 H), 6.63 (dd, $J = 9.7$ Hz, $J = 1.7$ Hz, 1 H), 6.94–6.96 (m, 2 H), 7.14–7.16 (m, 2 H), 7.25–7.29 (m, 2 H), 7.37–7.39 (m, 1 H); $^{13}\text{C}\{^1\text{H}\}$ NMR (75 MHz, CDCl_3) δ 42.45, 71.03, 125.32, 126.38, 126.59, 126.66, 127.12, 128.30, 128.40, 128.44, 129.70, 132.61, 136.42, 140.20; HRMS calcd for $\text{C}_{14}\text{H}_{12}\text{OS}$ 228.0609, found 228.0603.

***cis*-1,2-Dihydro-2-benzyl-1-naphthol (9l):** mp 64–66 °C; ^1H NMR (400 MHz, CDCl_3) δ 1.58 (s, OH, 1 H), 2.77–2.83 (m, 1 H), 2.88 (dd, $J = 13.0$ Hz, $J = 8.2$ Hz, 1 H), 3.15 (dd, $J = 13.0$ Hz, $J = 8.2$ Hz, 1 H), 4.47 (d, $J = 4.0$ Hz, 1 H), 5.80 (ddd, $J = 9.6$ Hz, $J = 2.6$ Hz, $J = 1.2$ Hz, 1 H), 6.57 (dd, $J = 9.6$ Hz, $J = 2.6$ Hz, 1 H), 7.13 (d, $J = 6.8$ Hz, 1 H), 7.21–7.35 (m, 8 H); $^{13}\text{C}\{^1\text{H}\}$ NMR (75 MHz, CDCl_3) δ 35.06 (CH_2), 42.27, 69.40, 125.94, 126.35, 126.90, 127.45, 128.24, 128.35, 129.14, 130.23, 132.47, 136.36, 140.00; IR (neat) 3413, 3028, 2918, 1601, 1453, 1073, 791, 701 cm^{-1} ; HRMS calcd for $\text{C}_{17}\text{H}_{16}\text{O}$ 236.1201, found 236.1200. Anal. Calcd for $\text{C}_{17}\text{H}_{16}\text{O}$: C, 86.41; H, 6.82. Found: C, 86.44; H, 6.84.

(*E*)-1-(*cis*-1,2-Dihydro-1-hydroxynaphth-2-yl)-2-phenylethylene (9m): ^1H NMR (400 MHz, CDCl_3) δ 1.78 (s, OH, 1 H), 3.33 (ddd, $J = 8.8$ Hz, $J = 5.6$ Hz, $J = 4.4$ Hz, 1 H), 4.90 (d, $J = 5.6$ Hz, 1 H), 5.99 (dd, $J = 9.6$ Hz, $J = 4.4$ Hz, 1 H), 6.13 (dd, $J = 16.2$ Hz, $J = 8.8$ Hz, 1 H), 6.55 (d, $J = 9.6$ Hz, 1 H), 6.64 (d, $J = 16.2$ Hz, 1 H), 7.10–7.45 (m, 9 H); $^{13}\text{C}\{^1\text{H}\}$ NMR (75 MHz, CDCl_3) δ 45.10, 70.60, 125.82, 125.85, 126.25, 127.47, 127.51, 127.83, 127.91, 128.39, 128.85, 132.42, 133.99, 136.69, 136.78; IR (neat) 3394, 3034, 1599, 1449, 969, 790, 694 cm^{-1} ; HRMS calcd for $\text{C}_{18}\text{H}_{16}\text{O}$ 248.1201, found 248.1205.

2-Methyl-3-(*cis*-1,2-dihydro-1-hydroxynaphth-2-yl)-2-cyclohexen-1-one (9o): mp 118–120 °C; ^1H NMR (400 MHz, CDCl_3) δ 1.65 (s, OH, 1 H), 1.86–1.93 (m, 5 H), 2.40–2.46 (m, 4 H), 3.89 (ddd, $J = 5.6$ Hz, $J = 3.2$ Hz, $J = 2.4$ Hz, 1 H), 4.88 (d, $J = 5.6$ Hz, 1 H), 5.93 (dd, $J = 9.6$ Hz, $J = 3.2$ Hz, 1 H), 6.67 (dd, $J = 9.6$ Hz, $J = 2.4$ Hz, 1 H), 7.16 (dd, $J = 7.0$ Hz, $J = 1.8$ Hz, 1 H), 7.26–7.39 (m, 3 H); $^{13}\text{C}\{^1\text{H}\}$ NMR (100 MHz, CDCl_3) δ 10.72 (CH_3), 22.41 (CH_2), 29.08 (CH_2), 37.63 (CH_2), 44.85, 69.60, 126.10, 126.23, 126.45, 126.48, 127.88, 127.99, 131.77, 132.05, 136.12, 158.09, 199.67 (CO); IR (neat) 3410, 3033, 2940, 2860, 1659 ($\nu(\text{C}=\text{O})$), 1640, 1609, 1355, 1306, 1067, 696 cm^{-1} ; HRMS calcd for $\text{C}_{17}\text{H}_{18}\text{O}_2$ 254.1307, found 254.1303. Anal. Calcd for $\text{C}_{17}\text{H}_{18}\text{O}_2$: C, 80.28; H, 7.13. Found: C, 80.14; H, 7.17.

***cis*-1,2-Dihydro-5,8-dimethoxy-2-(4-methoxyphenyl)-1-naphthol (11a):** ^1H NMR (400 MHz, CDCl_3) δ 1.58 (s, OH, 1 H), 3.74–3.77 (m, 1 H), 3.82 (s, OCH_3 , 3 H), 3.83 (s, 2 OCH_3 , 6 H), 5.05 (d, $J = 4.4$ Hz, 1 H), 6.11 (dd, $J = 9.9$ Hz, $J = 1.4$ Hz, 1 H), 6.80 (d, $J = 9.2$ Hz, 1 H), 6.83 (d, $J = 9.2$ Hz, 1 H), 6.94 (d, $J = 8.4$ Hz, 2 H), 7.07 (dd, $J = 9.9$ Hz, $J = 3.2$ Hz, 1 H), 7.35 (d, $J = 8.4$ Hz, 2 H); $^{13}\text{C}\{^1\text{H}\}$ NMR (100 MHz, CDCl_3) δ 46.07, 54.84 (OCH_3), 55.75 (2 OCH_3), 63.96, 110.58, 110.97, 113.57, 121.61, 122.14, 124.21, 129.05, 129.72, 132.10, 149.26,

150.38, 158.21; IR (neat) 3359, 2938, 2835, 1604, 1519, 1456, 1272, 1243, 1098, 1041, 813, 721 cm^{-1} ; HRMS calcd for $\text{C}_{19}\text{H}_{20}\text{O}_4$ 312.1361, found 312.1344.

cis-1,2-Dihydro-5,8-dimethoxy-2-(3-methoxyphenyl)-1-naphthol (11b): ^1H NMR (400 MHz, CDCl_3) δ 1.64 (br, OH, 1 H), 3.74–3.77 (m, 1 H), 3.80 (s, OCH_3 , 3 H), 3.81 (s, OCH_3 , 3 H), 3.82 (s, OCH_3 , 3 H), 5.08 (t, $J = 4.0$ Hz, 1 H), 6.12 (dt, $J = 10.0$ Hz, $J = 1.9$ Hz, 1 H), 6.77 (d, $J = 9.2$ Hz, 1 H), 6.81 (d, $J = 9.2$ Hz, 1 H), 6.84 (dd, $J = 8.6$ Hz, $J = 2.6$ Hz, 1 H), 6.98 (d, $J = 2.4$ Hz, 1 H), 7.01 (d, $J = 7.6$ Hz, 1 H), 7.08 (dd, $J = 10.0$ Hz, $J = 3.2$ Hz, 1 H), 7.29 (t, $J = 8.0$ Hz, 1 H); $^{13}\text{C}\{^1\text{H}\}$ NMR (100 MHz, CDCl_3) δ 47.23, 55.12 (OCH_3), 56.12 (2 OCH_3), 64.19, 110.87, 111.38, 112.35, 114.72, 121.30, 121.97, 122.43, 124.19, 128.65, 129.44, 141.97, 149.59, 150.65, 159.72; IR (neat) 3505, 2941, 2835, 1595, 1475, 1262, 1087, 790, 690 cm^{-1} ; HRMS calcd for $\text{C}_{19}\text{H}_{20}\text{O}_4$ 312.1361, found 312.1367.

cis-1,2-Dihydro-5,8-dimethoxy-2-(4-acetylphenyl)-1-naphthol (11c): ^1H NMR (400 MHz, CDCl_3) δ 1.60 (s, OH, 1 H), 2.61 (s, CH_3 , 3 H), 3.81–3.85 (2 OCH_3 + 1 H, 7 H), 5.10–5.12 (m, 1 H), 6.11 (dt, $J = 9.9$ Hz, $J = 1.8$ Hz, 1 H), 6.80 (d, $J = 9.0$ Hz, 1 H), 6.84 (d, $J = 9.0$ Hz, 1 H), 7.11 (dd, $J = 9.9$ Hz, $J = 3.0$ Hz, 1 H), 7.52 (d, $J = 8.4$ Hz, 2 H), 7.98 (d, $J = 8.4$ Hz, 2 H); $^{13}\text{C}\{^1\text{H}\}$ NMR (100 MHz, CDCl_3) δ 26.50 (CH_3), 47.17, 56.03 (OCH_3), 56.12 (OCH_3), 64.16, 111.02, 111.44, 122.13, 122.31, 124.22, 127.80, 128.41, 129.35, 135.75, 146.43, 149.62, 150.47, 197.78 (CO); IR (neat) 3470, 2943, 2835, 1676 ($\nu(\text{C}=\text{O})$), 1605, 1483, 1263, 1085, 804, 716 cm^{-1} ; HRMS calcd for $\text{C}_{20}\text{H}_{20}\text{O}_4$ 324.1361, found 324.1365.

2-Methyl-3-(cis-1,2-dihydro-1-hydroxy-5,8-dimethoxynaphth-2-yl)-2-cyclohexen-1-one (11d): ^1H NMR (300 MHz, CDCl_3) δ 1.80 (br s, OH, 1 H), 1.92 (t, CH_3 , $J = 1.6$ Hz, 3 H), 1.97–2.06 (m, 2 H), 2.40–2.65 (m, 4 H), 3.74–3.77 (m, 1 H), 3.86 (s, OCH_3 , 3 H), 3.88 (s, OCH_3 , 3 H), 5.20 (d, $J = 4.2$ Hz, 1 H), 6.02 (ddd, $J = 9.9$ Hz, $J = 2.8$ Hz, $J = 1.4$ Hz, 1 H), 6.83 (d, $J = 9.0$ Hz, 1 H), 6.87 (d, $J = 9.0$ Hz, 1 H), 7.08 (dd, $J = 9.9$ Hz, $J = 3.1$ Hz, 1 H); $^{13}\text{C}\{^1\text{H}\}$ NMR (100 MHz, CDCl_3) δ 10.57 (CH_3), 22.71 (CH_2), 30.72 (CH_2), 37.82 (CH_2), 44.83, 55.73 (OCH_3), 55.88 (OCH_3), 62.92, 110.53, 111.11, 120.94, 121.64, 124.13, 126.22, 131.99, 149.22, 150.07, 158.84, 199.24 (CO); IR (neat) 3443, 2941, 1654 ($\nu(\text{C}=\text{O})$), 1482, 1260, 1087, 957, 804, 728 cm^{-1} ; HRMS calcd for $\text{C}_{19}\text{H}_{22}\text{O}_4$ 314.1518, found 314.1520.

cis-1,2-Dihydro-5,8-dimethoxy-4-methyl-2-(4-methoxyphenyl)-1-naphthol (12a): ^1H NMR (400 MHz, CDCl_3) δ 1.58 (s, OH, 1 H), 2.34 (dd, CH_3 , $J = 2.8$ Hz, $J = 1.6$ Hz, 3 H), 3.61–3.65 (m, 1 H), 3.80 (s, OCH_3 , 3 H), 3.82 (s, OCH_3 , 3 H), 3.83 (s, OCH_3 , 3 H), 4.99 (dd, $J = 4.0$ Hz, $J = 1.6$ Hz, 1 H), 5.83 (dq, $J = 4.2$ Hz, $J = 1.4$ Hz, 1 H), 6.84 (d, $J = 9.0$ Hz, 1 H), 6.89 (d, $J = 9.0$ Hz, 1 H), 6.93 (d, $J = 8.8$ Hz, 2 H), 7.36 (d, $J = 8.8$ Hz, 2 H); $^{13}\text{C}\{^1\text{H}\}$ NMR (75 MHz, CDCl_3) δ 23.24 (CH_3), 46.04, 55.14 (OCH_3), 56.16 (OCH_3), 56.28 (OCH_3), 64.57, 111.26, 113.22, 113.80, 124.34, 126.50, 127.87, 129.84, 132.83, 133.16, 150.62, 151.52, 158.40; IR (neat) 3508, 2942, 2835, 1601, 1512, 1472, 1249, 1041, 819, 723 cm^{-1} ; HRMS calcd for $\text{C}_{20}\text{H}_{22}\text{O}_4$ 326.1518, found 326.1533.

cis-1,2-Dihydro-5,8-dimethoxy-4-methyl-2-naphthyl-1-naphthol (12b): ^1H NMR (400 MHz, CDCl_3) δ 1.59 (s, OH, 1 H), 2.40 (dd, CH_3 , $J = 2.4$ Hz, $J = 1.6$ Hz, 3 H), 3.82 (s, OCH_3 , 3 H), 3.85 (s, OCH_3 , 3 H), 4.53–4.55 (m, 1 H), 5.22 (dd, $J = 3.6$ Hz, $J = 1.6$ Hz, 1 H), 5.96–5.97 (m, 1 H), 6.87 (d, $J = 9.0$ Hz, 1 H), 6.93 (d, $J = 9.0$ Hz, 1 H), 7.49–7.56 (m, 3 H), 7.77 (d, $J = 6.4$ Hz, 1 H), 7.82 (d, $J = 8.4$ Hz, 1 H), 7.91 (dd, $J = 8.2$ Hz, $J = 2.0$ Hz, 1 H), 8.09 (dd, $J = 8.4$ Hz, $J = 2.4$ Hz, 1

H); $^{13}\text{C}\{^1\text{H}\}$ NMR (100 MHz, CDCl_3) δ 23.13 (CH_3), 41.77, 55.87 (OCH_3), 55.96 (OCH_3), 62.80, 111.11, 112.97, 122.77, 124.11, 125.06, 125.15, 125.71, 126.19, 126.38, 127.08, 127.95, 128.71, 131.42, 132.64, 133.68, 136.41, 150.42, 151.30; IR (neat) 3499, 2944, 2834, 1587, 1479, 1256, 1048, 785, 728 cm^{-1} ; HRMS calcd for $\text{C}_{23}\text{H}_{22}\text{O}_3$ 346.1569, found 346.1562.

2-Methyl-3-(cis-1,2-dihydro-1-hydroxy-5,8-dimethoxy-4-methyl-1-naphth-2-yl)-2-cyclohexen-1-one (12c): ^1H NMR (400 MHz, CDCl_3) δ 1.75 (br s, OH, 1 H), 1.84 (t, CH_3 , $J = 1.8$ Hz, 3 H), 1.95–2.02 (m, 2 H), 2.32 (dd, CH_3 , $J = 3.0$ Hz, $J = 1.4$ Hz, 3 H), 2.38–2.54 (m, 2 H), 2.57–2.71 (m, 2 H), 3.60–3.63 (m, 1 H), 3.79 (s, OCH_3 , 3 H), 3.84 (s, OCH_3 , 3 H), 5.07 (br d, $J = 2.8$ Hz, 1 H), 5.71 (d, $J = 1.6$ Hz, 1 H), 6.84 (d, $J = 9.2$ Hz, 1 H), 6.89 (d, $J = 9.2$ Hz, 1 H); $^{13}\text{C}\{^1\text{H}\}$ NMR (100 MHz, CDCl_3) δ 10.46 (CH_3), 22.75 (CH_2), 23.13 (CH_3), 30.47 (CH_2), 37.83 (CH_2), 44.53, 55.86 (OCH_3), 56.09 (OCH_3), 63.47, 110.96, 113.06, 123.49, 124.31, 126.14, 131.76, 132.16, 150.01, 151.21, 159.47, 199.28 (CO); IR (neat) 3431, 2941, 1651 ($\nu(\text{C}=\text{O})$), 1476, 1354, 1267, 1060, 1048, 797, 734 cm^{-1} ; HRMS calcd for $\text{C}_{20}\text{H}_{24}\text{O}_4$ 328.1674, found 328.1673.

Compound 13: ^1H NMR (400 MHz, CDCl_3) δ 1.85 (brs, OH, 1 H), 2.37–2.40 (m, 1 H), 2.55 (s, CH_3 , 3 H), 2.68 (dd, $J = 12.0$ Hz, $J = 8.8$ Hz, 1 H), 3.35 (d, $J = 8.8$ Hz, 1 H), 3.69 (s, OCH_3 , 3 H), 3.78 (s, OCH_3 , 3 H), 3.85 (s, 2 OCH_3 , 6 H), 5.21 (dt, $J = 9.9$ Hz, $J = 1.8$ Hz, 1 H), 5.40 (br, 1 H), 5.51 (s, 1 H), 6.02 (s, 1 H), 6.51 (dd, $J = 9.9$ Hz, $J = 3.0$ Hz, 1 H), 6.67–6.74 (m, 4 H), 7.54 (d, $J = 8.0$ Hz, 2 H), 7.83 (d, $J = 8.8$ Hz, 2 H); $^{13}\text{C}\{^1\text{H}\}$ NMR (100 MHz, CDCl_3) δ 26.47 (CH_3), 38.43, 46.17, 48.78, 55.85 (OCH_3), 55.97 (OCH_3), 56.76 (OCH_3), 61.83, 78.79, 84.50, 110.11, 111.02, 111.20, 112.54, 120.33, 122.31, 124.70, 128.22, 128.74, 129.95, 134.32, 135.36, 136.08, 146.55, 146.83, 147.46, 149.13, 150.29, 197.81 (CO); IR (neat) 3483, 2943, 2835, 1678 ($\nu(\text{C}=\text{O})$), 1603, 1499, 1260, 1083, 797 cm^{-1} ; HRMS calcd for $\text{C}_{32}\text{H}_{32}\text{O}_7$ 528.2148, found 528.2173.

cis-1,2-Dihydro-5-methoxy-2-(4-methoxyphenyl)-1-naphthol (14): ^1H NMR (400 MHz, CDCl_3) δ 1.47 (d, OH, $J = 8.4$ Hz, 1 H), 3.77–3.80 (m, OCH_3 + 1 H, 4 H), 3.87 (s, OCH_3 , 3 H), 4.86 (t, $J = 6.4$ Hz, 1 H), 6.08 (dd, $J = 9.8$ Hz, $J = 4.2$ Hz, 1 H), 6.82–6.85 (m, 3 H), 6.96 (d, $J = 7.6$ Hz, 1 H), 7.06 (dd, $J = 9.8$ Hz, $J = 2.2$ Hz, 1 H), 7.16–7.25 (m, 3 H); $^{13}\text{C}\{^1\text{H}\}$ NMR (100 MHz, CDCl_3) δ 45.90, 55.03 (OCH_3), 55.49 (OCH_3), 71.27, 110.29, 113.84, 118.82, 121.15, 121.70, 128.44, 128.80, 129.38, 130.17, 137.51, 154.57, 158.69; IR (neat) 3442, 2929, 2836, 1609, 1511, 1470, 1256, 1032, 762, 668 cm^{-1} ; HRMS calcd for $\text{C}_{18}\text{H}_{18}\text{O}_3$ 282.1256, found 282.1255.

cis-1,2-Dihydro-8-methoxy-2-(4-methoxyphenyl)-1-naphthol (15): ^1H NMR (400 MHz, CDCl_3) δ 1.57 (s, OH, 1 H), 3.77–3.79 (m, 1 H), 3.83 (s, OCH_3 , 3 H), 3.86 (s, OCH_3 , 3 H), 5.10 (dd, $J = 4.8$ Hz, $J = 1.2$ Hz, 1 H), 6.11 (dt, $J = 9.6$ Hz, $J = 2.0$ Hz, 1 H), 6.69 (dd, $J = 9.6$ Hz, $J = 3.2$ Hz, 1 H), 6.68 (d, $J = 8.0$ Hz, 1 H), 6.85 (d, $J = 8.0$ Hz, 1 H), 6.95 (d, $J = 8.8$ Hz, 2 H), 7.29 (t, $J = 7.6$ Hz, 1 H), 7.35 (d, $J = 8.8$ Hz, 2 H); $^{13}\text{C}\{^1\text{H}\}$ NMR (100 MHz, CDCl_3) δ 46.71, 55.27 (OCH_3), 55.64 (OCH_3), 64.04, 110.50, 114.02, 119.61, 122.98, 127.98, 129.44, 130.02, 130.17, 132.17, 133.57, 156.69, 158.66; IR (neat) 3400, 3070, 2958, 1611, 1512, 1472, 1257, 1180, 1080, 816 cm^{-1} ; HRMS calcd for $\text{C}_{18}\text{H}_{18}\text{O}_3$ 282.1256, found 282.1255.

Acknowledgment. We thank the National Science Council of the Republic of China (Grant No. NSC 81-0228-M-007-72) for support of this research.

OM940831B

Utilization of Molybdenum–Allyl Compounds for Synthesis of α -Methylenebutyrolactones

Shie-Hsiung Lin,[†] Chi-Chung Chen,[†] Wen-Jung Vong,[‡] and Rai-Shung Liu^{*,†}

Department of Chemistry, National Tsing-Hua University, Hsinchu 30043, Taiwan, Republic of China, and Chia-Nan Junior College of Pharmacy, Tainan 10764, Taiwan, Republic of China

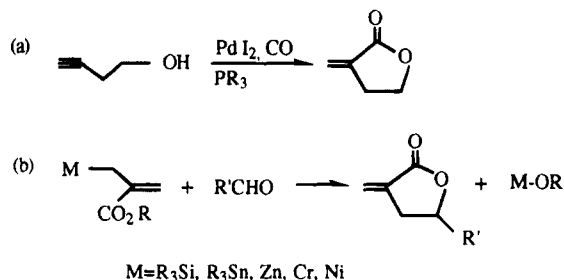
Received October 24, 1994[®]

Syntheses of *anti* (**1a**) and *syn* (**1b**) isomers of $\text{CpMo}(\text{CO})_2(\eta^3\text{-1-methyl-2-(methoxycarbonyl)-allyl})$ are described. Sequential addition of NOBF_4 and LiCl to **1a** or **1b** at -40°C preferentially produced $\text{CpMo}(\text{NO})\text{Cl}(\eta^3\text{-1-anti-methyl-2-(methoxycarbonyl)allyl})$ (**3a**) or $\text{CpMo}(\text{NO})\text{Cl}(\eta^3\text{-1-syn-methyl-2-(methoxycarbonyl)allyl})$ (**3b**), respectively. The variable-temperature ^1H NMR spectra (CDCl_3 , -60°C) of **3b** show the presence of *endo* and *exo* conformers, between which mutual exchange was observed. Stirring mixtures of **3a** and **3b** (**3a/3b** = 85/15 to 11/89) with PhCHO in $\text{CH}_2\text{Cl}_2/\text{CH}_3\text{OH}$ (20°C , 24 h) gave *trans*-2-methylene-3-methyl-4-phenylbutyrolactone (**4a**) as the major product in addition to (1*S**,2*R**)-1-phenyl-2-methyl-3-(methoxycarbonyl)-3-buten-1-ol (**4b**). Compound **4b** was converted to a *cis*- α -methylene butyrolactone quantitatively with *p*-toluenesulfonic acid. Utilization of $\text{CpMo}(\text{CO})_3(\eta^1\text{-vinylpropargyl})$ (**5**) for the synthesis of $\text{CpMo}(\text{NO})\text{Cl}(\eta^3\text{-}(3*R*^*,4*R*^*)\text{-CH}_2\text{CCHCH}(\text{Me})\text{OC=O})$ (**8**) is described; reaction of **8** with RCHO ($\text{R} = \text{Ph}, \text{Me}_2\text{CH}$) in $\text{CH}_2\text{Cl}_2/\text{CH}_3\text{OH}$ gave (1*S**,3*R**,4*S**)-2-methylene-3-(α -hydroxybenzyl)-4-methylbutyrolactone (**9**; 52%) and (1*S**,3*R**,4*S**)-2-methylene-3-(1-hydroxy-2-methylpropyl)butyrolactone (**10**; 50%), respectively. The stereochemistry of **9** and **10** was elucidated.

Introduction

α -Methylenebutyrolactone is an important structural unit¹ in many naturally occurring compounds, and the importance of its activity in biological metabolism is well recognized. Transition-metal-mediated synthesis of α -methylenebutyrolactone from common organic chemicals is well developed in both catalytic and stoichiometric reactions. In the former, the palladium-catalyzed cyclocarbonylation of homopropargyl alcohol² is particularly attractive because of the easily accessible starting material and mild operating conditions. Stoichiometrically, the most convenient one-step synthesis of α -methylenebutyrolactone involves reactions of aldehydes with 2-(alkoxycarbonyl)allylic zinc,^{1a,3} nickel,⁴ chromium,⁵ tin⁶ and silanes⁷ as depicted in Scheme 1. Although some of the reactions above proceed with high diastereoselectivities, few^{1c} of them deal with the ste-

Scheme 1



reoselective synthesis of complex α -methylenebutyrolactones.

$\text{CpMo}(\text{CO})_2(\pi\text{-allyl})$ ⁸ is useful for organic synthesis because it can be easily converted to $\text{CpMo}(\text{NO})\text{CO}(\pi\text{-allyl})^+$, which functions as an allyl cation.^{9a-c} Halide substitution of the remaining carbonyl group of $\text{CpMo}(\text{NO})\text{CO}(\pi\text{-allyl})^+$ produces $\text{CpMo}(\text{NO})\text{X}(\pi\text{-allyl})$ ^{9d,e} ($\text{X} = \text{halide}$), which can be regarded as an allyl anion. Faller reported¹⁰ that reactions of $\text{CpMo}(\text{NO})\text{Cl}(\pi\text{-crotyl})$ with aldehydes gave homoallylic alcohols with excellent diastereoselectivities. Enantiomerically pure $\text{CpMo}(\text{NO})\text{X}(\pi\text{-allyl})$ ($\text{X} = \text{halide}$) complexes of several types¹¹ were prepared to provide chiral homoallylic alcohols

[†] National Tsing-Hua University.

[‡] Chia-Nan Junior College of Pharmacy.

[®] Abstract published in *Advance ACS Abstracts*, February 15, 1995.

(1) For reviews of the synthesis of α -methylenebutyrolactones see: (a) Hoffman, H. M. R.; Rabe, J. *Angew. Chem., Int. Ed. Engl.* **1985**, *24*, 94. (b) Grieco, P. A. *Synthesis* **1975**, 67. (c) Sidduri, A. R.; Knochel, P. *J. Am. Chem. Soc.* **1992**, *114*, 7579 and references therein.

(2) (a) Murray, T. F.; Norton, J. R. *J. Am. Chem. Soc.* **1979**, *101*, 4107. (b) Tsuji, Y.; Kondo, T.; Watanabe, Y. *J. Mol. Catal.* **1987**, *40*, 295. (c) Martin, L. D.; Stille, J. K. *J. Org. Chem.* **1982**, *47*, 3603. (d) Matsuda, I.; Ogiso, A.; Sato, S. *J. Am. Chem. Soc.* **1990**, *112*, 6120.

(3) (a) Matles, H.; Senerra, C. *Tetrahedron Lett.* **1985**, *26*, 5697. (b) Rao, S. A.; Knochel, P. *J. Am. Chem. Soc.* **1991**, *113*, 5735. (c) Still, I. W. J.; Drewery, M. J. *J. Org. Chem.* **1989**, *54*, 290.

(4) Hegedus, L. S.; Wagner, S. D.; Waterman, E. L.; Siirala-Hansen, K. S. *J. Org. Chem.* **1975**, *40*, 593.

(5) Drewes, S. E.; Hoole, R. F. A. *Synth. Commun.* **1975**, *5*, 245.

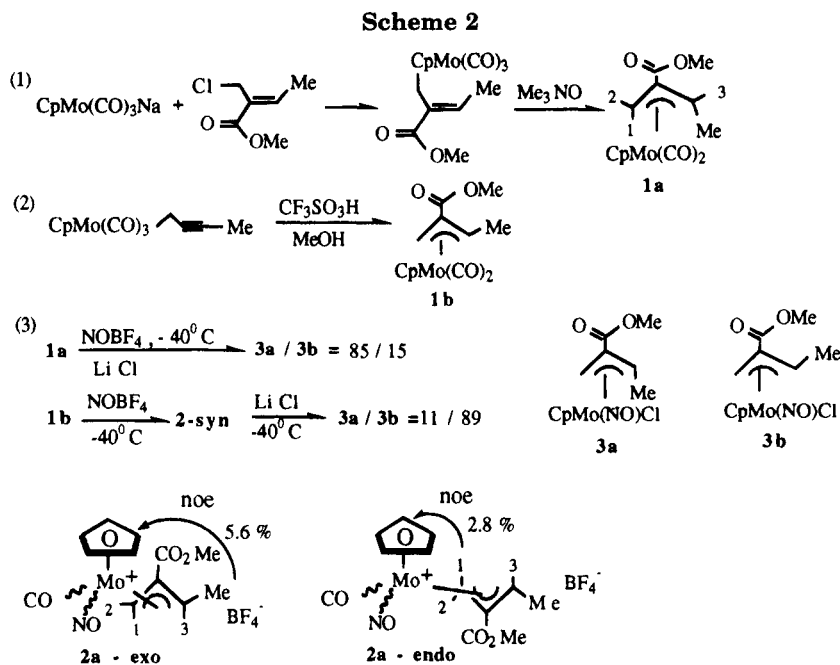
(6) (a) Balwin, J. E.; Aldington, R. M.; Sweeney, J. B. *Tetrahedron Lett.* **1986**, *27*, 5423. (b) Tanaka, K.; Yoda, H.; Isobe, Y.; Kaji, A. *Tetrahedron Lett.* **1985**, *27*, 5423.

(7) (a) Hosomi, A.; Hashimoto, H.; Sakurai, H. *Tetrahedron Lett.* **1980**, *21*, 951. (b) Itoh, K.; Yogo, T.; Ishii, Y. *Chem. Lett.* **1977**, 103.

(8) (a) Pearson, A. J. *Synlett* **1990**, 10. (b) Pearson, A. J. In *Advances in Metal-Organic Chemistry*; Liebeskind, L. S., Ed.; JAI Press: London, 1989; Vol. 1, Chapter 1, p 1.

(9) (a) Adams, R. D.; Chodosh, D. F.; Faller, J. W.; Rosan, A. M. *J. Am. Chem. Soc.* **1979**, *101*, 2570. (b) Cosford, N. D. P.; Liebeskind, L. S. *Organometallics* **1994**, *13*, 1498. (c) Pearson, A. J.; Khan, M. N. I. *J. Org. Chem.* **1985**, *50*, 5276. (d) Faller, J. W.; Shvo, Y. *J. Am. Chem. Soc.* **1980**, *102*, 5398. (e) Faller, J. W.; Shvo, Y.; Chao, K. H.; Marray, H. H. *J. Organomet. Chem.* **1982**, *226*, 251.

(10) (a) Faller, J. W.; John, J. A.; Mazziari, M. R. *Tetrahedron Lett.* **1989**, 1769. (b) Faller, J. W.; DiVerdi, M. J.; John, J. A. *Tetrahedron Lett.* **1991**, *32*, 1271.



with high ee values. We also applied this reaction to the stereoselective synthesis of 1,3-diols and 1,3,5-triols.¹² To expand the scope of this reaction, we herein report the utilization of compounds of the type CpMo(NO)Cl(π -2-(methoxycarbonyl)allyl) for synthesis of complex α -methylenebutyrolactones.

Results and Discussion

To achieve stereoselective synthesis of various lactones, we prepared *anti* and *syn* isomers of η^3 -1-methyl-2-(methoxycarbonyl)allyl complexes **1a** and **1b** according to the literature procedure.^{13,14} The overall synthetic scheme is provided in Scheme 2. Treatment of **1b** with NOBF₄ in cold CH₃CN (−40 °C) followed by precipitation with anhydrous ether afforded a yellow precipitate of **2-syn**. ¹H NMR spectra (CDCl₃, 23 °C) of **2-syn** showed the presence of *exo* and *endo* conformers with a ratio *exo/endo* = 2/1. ¹H NMR signal assignment of the two conformers relied on proton-NOE results as depicted in Scheme 2. The methyl group signal (δ 2.33 ppm) of the *exo* isomer and the H¹ proton signal (δ 3.35 ppm) of the *endo* isomer exerted NOE enhancement on their cyclopentadienyl signals by 5.6% and 2.8%, respectively. For **1a**, attempts to obtain the corresponding nitrosyl salt **2-anti** in pure form were not successful due to some impurity which could not be removed by fractional crystallization. Preparation of the key CpMo(Cl)NO derivative of **1a** was achieved by sequential addition of NOBF₄ and LiCl (Scheme 2), which produced a diastereomeric mixture of **3a**(*anti*) and **3b**(*syn*) that were inseparable by either column chromatography or fractional crystallization. The presence of **3b** showed the existence of *syn-anti* isomerization. To minimize this isomerization, we performed the reaction at −40 °C, followed by column chromatography at −20 °C; in this manner the

product ratio **3a/3b** = 85/15 (84% yield) was obtained according to ¹H NMR spectra (−40 °C, CD₂Cl₂). When the NMR sample was left at 20 °C for 4 h, the equilibrium ratio **3a/3b** = 25/75 was obtained but with small decomposition (ca. 5–10%) to an unknown precipitate. The compounds **3a** and **3b** are stable in solution only below 20 °C; the same ratio **3a/3b** = 25/75 was attained if the NMR sample was kept at 0 °C for 24 h to reach the equilibrium state. Figure 1 shows variable-temperature spectra of **3a** and **3b** in CD₃CN that contained the ratio **3a/3b** = 71/29 at −60 °C. The proton NMR resonances were broad at 20 °C but became well resolved at −60 °C to show the presence of four isomers, labeled **3a'**, **3a''**, **3b'**, and **3b''**. All ¹H NMR signals of the four isomers are assigned clearly and labeled in the figure. On the basis of the proton-NOE effect (Chart 1), **3a'/3a''** are assigned as *endo/exo* conformers of the *anti* isomer and **3b'/3b''** are assigned as the *exo/endo* conformers of the *syn* isomer. For example, irradiation of the H¹ signal (δ 2.21 ppm) of **3b'** caused an intensity increase in the H³ proton (δ 5.12 ppm) signal of 3.8%, whereas irradiation of the H¹ proton signal (δ 2.98 ppm) of **3a'** caused an intensity increase in the methyl (δ 1.87 ppm) signal of 2.8%. We assign the major species **3a'** and **3b'** as *endo* and *exo* conformers, respectively, because their methyl signals exert NOE enhancement on the corresponding cyclopentadienyl signals as shown in Chart 1. As shown in Figure 1, the NMR signals of **3a'** and **3a''** became broad at 0 °C, whereas those of **3b'** and **3b''** remained unaltered at this temperature. As the temperature was raised to 20 °C, the NMR signals of **3a'** and **3a''** coalesced, whereas the signals of **3b'** and **3b''** began to broaden. At this temperature, the four H¹ and H² signals of **3a'** and **3a''** coalesced to one broad resonance at δ 3.21 ppm. Attempts to record NMR spectra at 30 °C led to rapid decomposition of the sample, and the signals of the four isomers became very weak. On the basis of the coalescence temperatures, *endo/exo* isomerization of the *anti* isomer proceeds more rapidly than that of the *syn* isomer. This phenomenon is reasonable because the *syn* isomer is the more stable form according to the equilibrium ratio *anti/syn* = 25/75, which requires higher activation energy if the

(11) (a) Faller, J. W.; Nguyen, J. T.; Ellis, W.; Mazzieri, M. R. *Organometallics* **1993**, *12*, 1434. (b) Faller, J. W.; Linebarrier, D. L. *J. Am. Chem. Soc.* **1989**, *111*, 1937.

(12) Vong, W.-J.; Peng, S. M.; Lin, S.-H.; Lin, W.-J.; Liu, R.-S. *J. Am. Chem. Soc.* **1991**, *113*, 573.

(13) Yang, G.-M.; Su, G.-M.; Liu, R.-S. *Organometallics* **1992**, *10*, 3444.

(14) (a) Charrier, C.; Collin, J.; Merour, J. Y.; Roustan, J. L. *J. Organomet. Chem.* **1978**, *162*, 57.

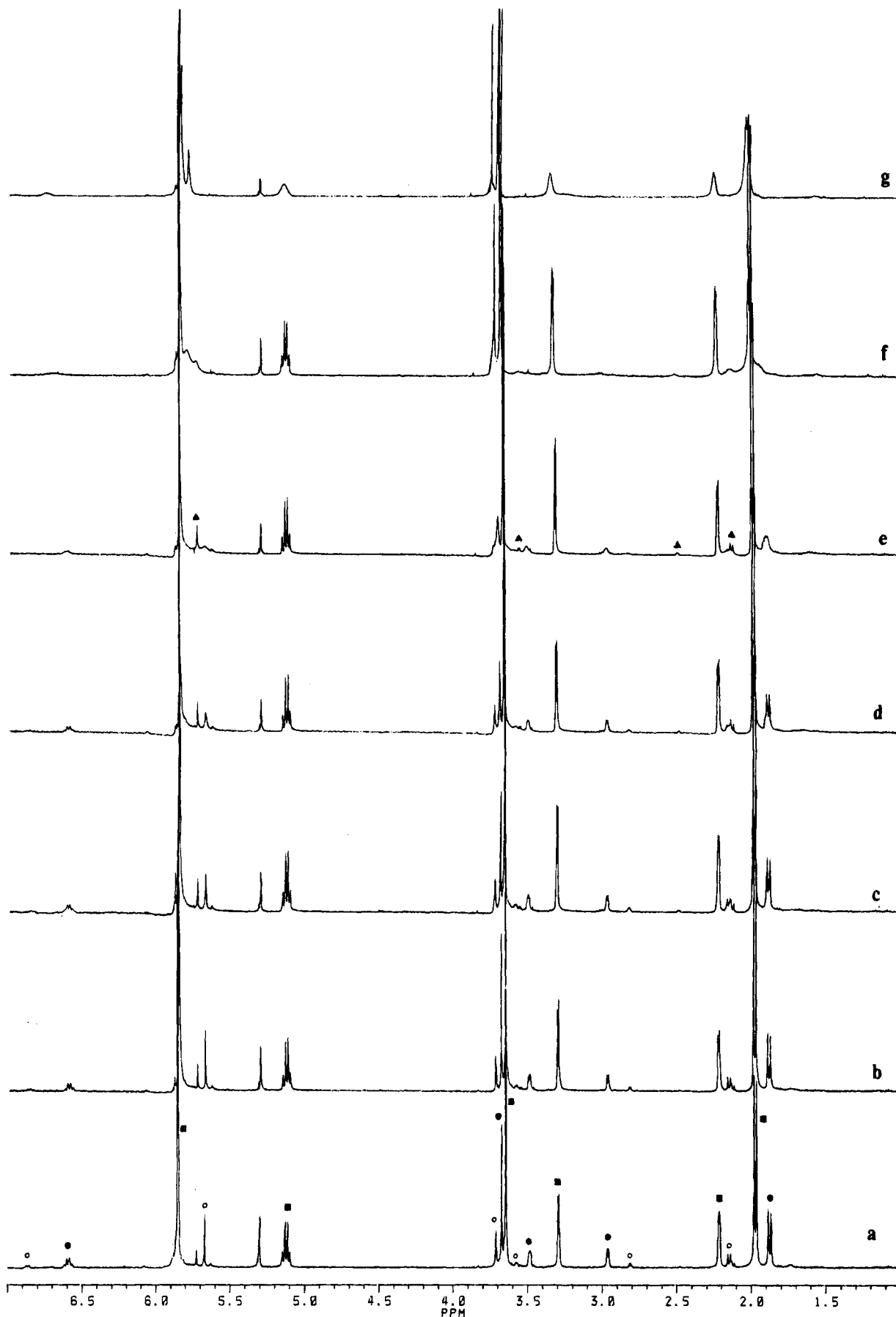
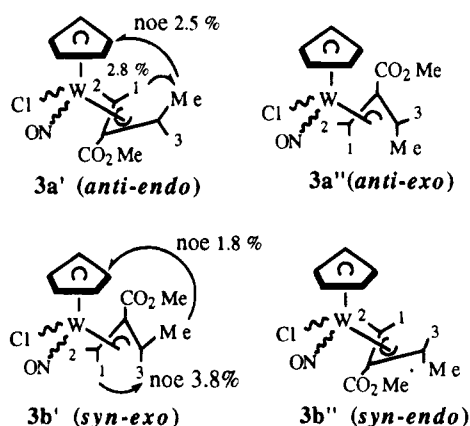


Figure 1. Variable-temperature NMR spectra of **3** in CD_2Cl_2 (δ 5.32 ppm): (●) **3a'**(*anti-endo*); (○) **3a''**(*anti-exo*); (■) **3b'**(*syn-exo*); (▲) **3b''**(*syn-endo*). **a-g** represent the temperatures: (a) -60 °C; (b) -40 °C; (c) -20 °C; (d) -10 °C; (e) 0 °C; (f) 10 °C; (g) 20 °C.

intermediates of *exo/endo* isomerization of the two isomers are alike, i.e. η^1 -allyl species (*vide infra*). The

NMR results represent a general feature of $\text{CpMo}(\text{NO})\text{-Cl}(\pi\text{-allyl})$,^{10,15} in which *endo-exo* isomerization is

Chart 1



much more feasible than *anti-syn* isomerization. The mechanism of isomerization of **3a'**/**3a''** and **3b'**/**3b''** is likely to follow $\eta^3-\eta^1-\eta^3$ allyl slippage rather than rotation of the metal- π -allyl bond. The $\eta^3-\eta^1-\eta^3$ allyl slippage process is suggested by the variable-temperature ^1H NMR spectra, in which the four H^1 and H^2 signals of **3a'** and **3a''** were averaged to a broad resonance at 20 °C. Rotation of the metal-allyl group is commonly observed for $\text{CpMo}(\text{CO})_2(\pi\text{-allyl})$ compounds.¹⁶ As pointed out by Faller,^{10,16} metal-allyl bonding of $\text{CpMo}(\text{NO})\text{Cl}(\pi\text{-allyl})$ is dissymmetric because of the differential acceptor characters of NO and Cl, and the allyl carbon terminus trans to NO tends to dissociate to induce a $\eta^3-\eta^1$ allyl slippage.

Sequential treatment of **1b** with $\text{NOBF}_4/\text{LiCl}$ (-40 °C), followed by purification through a silica column (-20 °C), also produced a mixture of **3a'**, **3a''**, **3b'**, and **3b''** with $(\mathbf{3a}' + \mathbf{3a}'')/(\mathbf{3b}' + \mathbf{3b}'') = 11/89$ ($\mathbf{3a} = \mathbf{3a}' + \mathbf{3a}''$, $\mathbf{3b} = \mathbf{3b}' + \mathbf{3b}''$) according to NMR spectra (-40 °C, CD_2Cl_2). Likewise, an equilibrium state with $\mathbf{3a}/\mathbf{3b} = 25/75$ was attained when the NMR sample was kept at 20 °C for 4 h. This *syn-anti* isomerization seemed much more rapid than that of $\text{CpMo}(\text{NO})\text{Cl}(\pi\text{-crotlyl})$.¹⁰

Despite the presence of two diastereomers, we treated **3a/3b** composed of varying ratios with PhCHO in CH_2Cl_2 in the presence of CH_3OH (8 equiv) at 20 °C. After the mixture was stirred for 24 h, the reaction was complete, producing the two new organic compounds **4a** and **4b**, which were separated by preparative TLC. The selectivities and combined yields are presented in Scheme 3. The ^1H NMR results indicate that **4b** is a homoallylic alcohol rather than an α -methylenebutyrolactone as found for **4a**. Compound **4b** was subsequently converted to **4c** in 95% yield in CH_2Cl_2 (23 °C, 8 h) in the presence of *p*-toluenesulfonic acid catalyst (5%) and was found to be a distinct isomer of **4a**. On the basis of the ^1H -NOE results of **4a** and **4c** as shown in Chart 2, we assign a *trans* structure to the former and a *cis* structure to the latter. Regardless of the ratios of starting material $\mathbf{3a}/\mathbf{3b} = 85/15$ to $11/89$, *trans*-lactone **4a** is the major reaction product, indicative of *anti* selectivity in the formation of a homoallylic alcohol. We attribute the *anti* selectivity to rapid isomerization of **3a** to **3b** under the reaction conditions. With the reaction ($\mathbf{3a}/\mathbf{3b} = 85/15$) monitored by ^1H NMR spectra,

Scheme 3

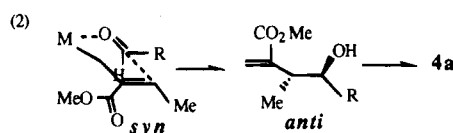
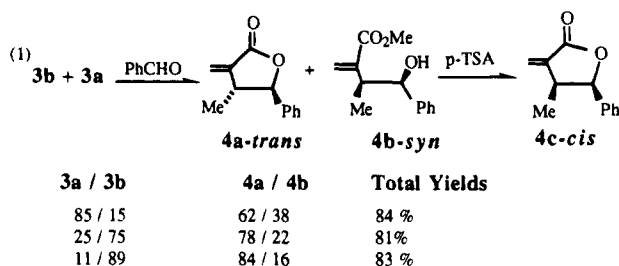
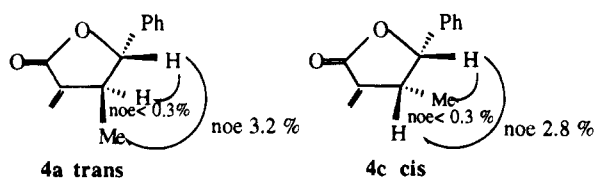


Chart 2

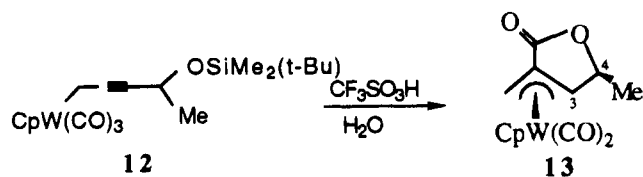


3a and **3b** attained an equilibrium ratio $\mathbf{3a}/\mathbf{3b} = 25/75$ within 4 h at 20 °C at ca. 25% conversion. In Scheme 3, the fact that the product ratios **4a/4b** increase with decreasing $\mathbf{3a}/\mathbf{3b}$ ratios is basically compatible with the model that *syn*-allyl isomer **3b** produces an *anti*-homoallylic alcohol^{9a} (Scheme 3, eq 2).

In continued efforts toward stereoselective synthesis of complex α -methylene butyrolactones, compound **6** was synthesized in one step by acidification of **5** with $\text{CF}_3\text{SO}_3\text{H}$ (2.5 equiv) in the presence of MeOH (1.5 equiv) in cold diethyl ether (-40 °C), followed by addition of excess H_2O ; only one diastereomer was obtained in 83% yield. According to the same chemistry of tungsten analogues reported earlier,¹⁷ formation of **6** is envisaged by sequential generation of the two intermediates **A** and **B**, depicted in Scheme 4. Subsequent treatment of **6** with NaH induced cyclization to give the η^3 -($3R^*$, $4S^*$)-lactonylallyl compound **7** in 96% yield. The structures of **7** and **8** are proposed on the basis of comparison of NMR data with those of their tungsten analogues.¹⁷ In the case of **8**, the magnitude of the proton coupling constant $J_{34} = 0$ Hz is identical with that reported for its tungsten analogue. The other diastereomer with methyl lying on the same face with the metal, i.e. the $3R^*$, $4S^*$ isomer, is expected to have the coupling constant $J_{34} = 3-4$ Hz.¹⁸ According to the above $\text{NOBF}_4/\text{LiCl}$ method, **7** was converted to **8** in 54%

(17) Cheng, M.-H.; Ho, Y.-H.; Lee, G.-H.; Peng, S.-M.; Liu, R.-S. *Organometallics* **1991**, *10*, 3600.

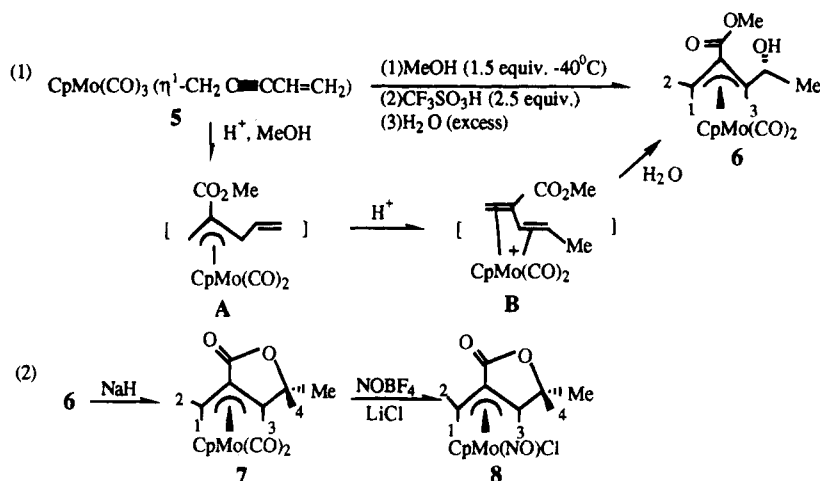
(18) The tungsten η^3 -($3R^*$, $4S^*$)-lactonyl compound **13** was synthesized by acidification of **12** with $\text{CF}_3\text{SO}_3\text{H}$ in CH_2Cl_2 (-40 °C), and the mechanism of this cyclization is under investigation: Cheng, C.-C.; Fang, J.-S.; Lee, G.-H.; Peng, S.-M.; Wang, S.-L.; Liu, R.-S. *J. Am. Chem. Soc.*, in press. Before this work, we attempted synthesis of α -methylene lactone compounds from the tungsten analogue of **8**, but we were unsuccessful in preparing the corresponding $\text{CpW}(\text{NO})\text{Cl}$ derivative.



(15) (a) Faller, J. W.; Shvo, Y.; Chao, K.; Murray, H. H. *J. Organomet. Chem.* **1982**, *226*, 251. (b) Faller, J. W.; Chodosh, D. F.; Katahira, D. *J. Organomet. Chem.* **1980**, *187*, 227.

(16) Faller, J. W.; Chen, C. C.; Mattina, M. J.; Jabukowski, A. *J. Organomet. Chem.* **1973**, *52*, 361.

Scheme 4



yield. No CpMoNO(Cl) compound of **6** was prepared, as a possible rapid *syn-anti* isomerization of this derivative would ruin the stereoselectivity. $^1\text{H NMR}$ (CDCl_3) spectra of **8** revealed the presence of two isomers in the ratio 2.5:1, and both have the same coupling constant $J_{34} = 0$ Hz. This information indicates that the methyl groups of both isomers lie on the nonmetal face as for **7**.¹⁷ Here, the major isomer has an *endo* configuration because the H^1 proton signal (δ 2.78 ppm) caused NOE enhancement on the Cp signal by 1.8%. We were unable to determine the conformation of the minor isomer by proton NOE spectra. Attempts to grow crystals of **8** for X-ray structural determination were unsuccessful due to poor crystal quality. The two isomers underwent no isomerization in the temperature range -60 to $+20$ $^\circ\text{C}$, and it is unclear whether the two isomers are related to each other by an *exo-endo* structural relationship.

Despite the presence of two isomers, condensation of **8** with aldehydes RCHO ($\text{R} = \text{Ph}, \text{Me}_2\text{CH}$) in $\text{CH}_2\text{Cl}_2/\text{CH}_3\text{OH}$ (20 $^\circ\text{C}$, 12 h) afforded **9** (52% yield) and **10** (50% yield) as single diastereomers after isolation on a preparative TLC plate. Both **9** and **10** are *trans*- α -methylenebutyrolactones according to the proton NOE effect. Irradiation of the H^1 proton signal (δ 2.76 ppm) of **10** caused an intensity increase of the methyl signal (δ 1.45 ppm) by 3.37%, whereas the H^2 signal (δ 4.48 ppm) was unaffected. Likewise, irradiation of the H^2 proton signal (δ 4.48 ppm) of **10** led to an intensity increase of the CH(OH) proton (δ 3.30 ppm) signal by 2.84%, whereas the H^1 signal (δ 2.76 ppm) was unaffected. Although the NOE results of **9** and **10** clearly establish the *trans*-butyrolactone structure, the stereochemistry of CH(OH)R relative to lactone remains unclear. To solve this problem, we treated **10** with *p*-toluenesulfonic acid (5 mol %) in CH_2Cl_2 (23 $^\circ\text{C}$, 2 h) to yield the new lactone **11**, which equilibrated with **10** in the ratio $\text{11/10} = 4/1$. Pure **11**, obtained in 65% yield by subsequent isolation on a preparative SiO_2 plate, like **9** and **10** showed a $\nu(\text{CO})$ absorption (1765 cm^{-1}) characteristic of organic lactones. In the proton NOE experiment, the H^1 (δ 2.78 ppm) proton signals of **11** exerted no Overhauser effects on H^2 (δ 4.21 ppm) proton signals but showed 3.1% enhancement on the CHMe (δ 1.80 ppm) protons. Likewise, irradiation of the H^2 proton signal of **11** caused an intensity increase of the CH(OH) (δ 3.82 ppm) by 2.1%, whereas the signal of

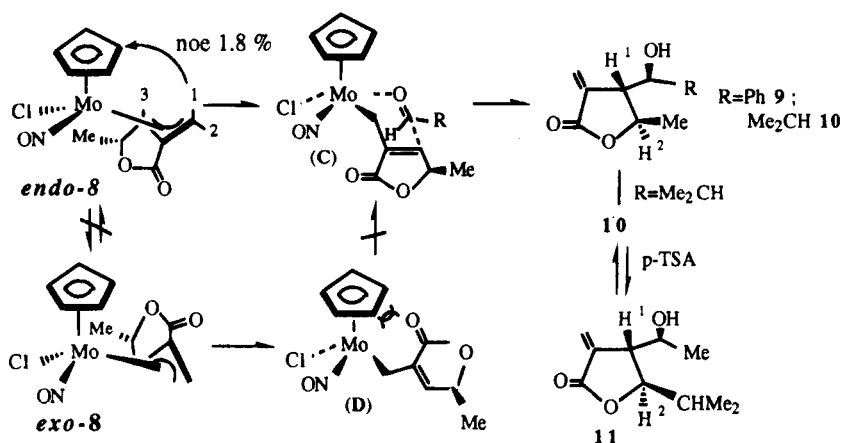
the H^1 proton is unaffected. These NMR data suggest a *trans*-butyrolactone structure for **11**.

The minor isomer of **8** is virtually inactive toward aldehyde. In the above reactions, we recovered the minor isomer exclusively during workup. To clarify the reaction roles of the two isomers, we monitored the reaction by an *in situ* NMR experiment containing **8** and PhCHO (2.0 equiv each) in $\text{CD}_2\text{Cl}_2/\text{CD}_3\text{OD}$. After an 18 h period of reaction, the NMR spectra showed that in addition to features due to **9** and unreacted aldehydes, the signals of the major isomer completely disappeared, whereas the signals of the minor isomer remained at ca. 75% of the original intensity. Here the intensity decrease of the minor isomer likely arose from its intrinsic instability under the reaction conditions. No attempts were made to characterize the decomposition product of the minor isomer.

To elucidate the stereochemical outcome of **9** and **10**, we propose a plausible mechanism in Scheme 5 based on Faller's model.¹⁰ Presumably the stereochemistry of the major isomer of **8** is the same as that of $\text{CpMo(NO-Cl)(}\pi\text{-crotyl)}$;¹⁰ the allyl CH_2 terminus of **8** becomes *cis* to NO and *trans* to chloride in both *endo* and *exo* conformations, as depicted in Scheme 5. In the *endo* conformation, after an $\eta^3\text{-}\eta^1$ allyl slippage, the aldehyde coordinates to the empty site *trans* to NO with its carbonyl in an antiperiplanar conformation relative to the Mo-Cp group and its hydrogen is situated in a pseudoaxial position to minimize interligand steric hindrance. These steric factors generate the chairlike transition state **C**, which has the methyl group lying on the face opposite to aldehyde. Subsequent addition of η^1 -lactonylallyl to the *re* face of the aldehyde produces the observed homoallylic alcohols **9** and **10**.

It is of interest to examine the stereochemical course of the *exo* isomer. With the same lactonyl stereochemistry, the *exo* isomer depicted in Scheme 5 will not produce **9** and **10** according to this model. Here, an $\eta^3\text{-}\eta^1$ allyl slippage of the *exo* isomer produces conformation **D**, which is unstable due to strong interaction with the Cp and lactonyl groups. Further rotation of the σ Mo-C bond of this intermediate fails to produce **C** because the C(OH)HMe stereochemistry is reverse. Addition of aldehydes to **D** encounters a higher energy barrier than for **C** because of increasing steric hindrance, and the product was not observed in our case. Isomerization of these two isomers cannot be achieved by an $\eta^3\text{-}\eta^1\text{-}\eta^3$ allyl slippage.

Scheme 5



Experimental Section

All operations were carried out under argon in a Schlenk apparatus or in a glovebox. The solvents benzene, diethyl ether, tetrahydrofuran, and hexane were dried with sodium benzophenone and distilled before use. Dichloromethane was dried over calcium hydride and distilled. Compounds **1a**,¹³ CpMo(CO)₃(η¹-methylpropargyl),¹⁴ and **5**¹⁹ were prepared according to the procedures in our previous papers.

All ¹H NMR (400 and 300 MHz) and ¹³C NMR (75 MHz) spectra were obtained on either a Bruker AM-400 or a Varian Gemini-300 spectrometer; the chemical shifts of ¹H and ¹³C NMR were reported relative to TMS. NMR spectra were recorded at 23 °C unless otherwise specified. Elemental analyses were performed at the National Cheng Kung University, Tainan, Taiwan. Infrared spectra were recorded on a Perkin-Elmer 781 spectrometer. High-resolution mass spectra were recorded on a JEOL HX 110 spectrometer.

(a) Synthesis of CpMo(CO)₂(η³-1-syn-methyl-2-(methoxycarbonyl)allyl) (1b). To CpMo(CO)₃(η¹-methylpropargyl) (3.0 g, 10 mmol) in diethyl ether (15 mL) was added methanol (5 mL) at -40 °C, and the mixture was stirred for 2 h before addition of CF₃SO₃H (1.65 g, 11 mmol). After stirring for 1 h at -40 °C, the solution was added to a saturated NaHCO₃ solution (10 mL), warmed to 23 °C, and extracted with diethyl ether (3 × 20 mL). After removal of solvent, the solution was eluted through a silica column (diethyl ether/hexane=1/1) to produce a yellow band (R_f=0.73) of **2** as a yellow oil (2.96 g, 0.89 mmol). IR (Nujol, cm⁻¹): ν(CO) 1964(vs), 1887(vs) and 1665(s). ¹H NMR (400 MHz, CDCl₃, -40 °C): *exo* isomer (60%), δ, 0.49 (1H, d, *J* = 1.8 Hz, H¹), 1.41 (1H, q, *J* = 6.8 Hz, H³), 2.11 (3H, d, *J* = 6.8 Hz, Me), 3.13 (1H, d, *J* = 1.8 Hz, H²), 3.78 (3H, s, OMe) 5.30 (5H, s, Cp); *endo* isomer (40%), 2.11 (1H, s, H¹), 1.96 (3H, d, *J* = 6.8 Hz, Me), 2.54 (1H, q, *J* = 6.8 Hz, H³), 2.97 (1H, s, H²), 3.62 (3H, s, OMe), 5.11 (5H, s, Cp). ¹³C NMR (100 MHz, CDCl₃, -40 °C): δ, *exo* isomer, 18.5 (Me), 38.4 (CH¹H²), 52.4 (OMe), 63.6 (CH³), 68.4 (C-CO), 94.4 (Cp), 170.9 (CO), 235.1 and 236.9 (2 Mo-CO); *endo* isomer, 18.6 (Me), 31.9 ((CH¹H²), 51.1 (OMe), 58.2 (CH³), 83.4 (C-CO), 89.9 (Cp), 170.9 (CO), 231.9 and 236.4 (2 Mo-CO). Mass (12 eV): 332 (M⁺). Anal. Calcd. for C₁₃H₁₄MoO₄: C, 47.29; H, 4.27. Found: C, 47.12; H, 4.41.

(b) Synthesis of [CpMo(NO)CO(η³-1-syn-methyl-2-(methoxycarbonyl)allyl)]BF₄ (2-syn). To **1b** (0.50 g, 1.50 mmol) in CH₃CN (3 mL) at -40 °C was added NOBF₄ (0.17 g, 1.43 mmol), and the solution was stirred for 1 h. To the resulting dark yellow solution was added diethyl ether (20 mL), to yield a yellow precipitate which was collected by filtration. Further recrystallization from a saturated CH₂Cl₂/diethyl ether solution gave **2-syn** as a dark orange crystalline solid (0.49 g, 1.16 mmol, 81%). IR (Nujol, cm⁻¹): ν(CO) 2109 (s), 1708 (s); ν(NO) 1720 (s). ¹H NMR (400 MHz, CDCl₃ δ): *exo*

isomer (78%), 2.33 (d, *J* = 6.6 Hz, 3H, Me), 3.15 (d, *J* = 2.7 Hz, 1H, H¹), 3.81 (s, 3H, OMe), 4.76 (q, 1H, *J* = 6.6 Hz, 1H, H³), 5.05 (d, *J* = 2.7 Hz, 1H, H²), 6.26 (q, 5H, Cp); *endo* isomer (22%), 2.66 (d, *J* = 6.5 Hz, 3H, Me), 3.35 (d, 1H, *J* = 1.7 Hz, H¹), 3.79 (s, 3H, OMe), 4.19 (d, *J* = 1.7 Hz, 1H, H²), 4.47 (1H, q, *J* = 6.5 Hz, H³), 6.24 (s, 5H, Cp). ¹³C NMR (100 MHz, CDCl₃, δ): 17.3 (Me), 52.9 (OMe), 62.9 (CH¹H²), 79.9 (CH³), 102.0 (Cp), 113.7 (C-CO), 162.9 (CO), 206.9 (Mo-CO). Anal. Calcd for C₁₂H₁₄MoNO₄BF₄: C, 34.20; H, 3.35; N, 3.33. Found: C, 34.14; H, 3.42; N, 3.11.

(c) Synthesis of CpMo(NO)Cl(η³-1-anti-methyl-2-(methoxycarbonyl)allyl) (3a) and CpMo(NO)Cl(η³-1-syn-methyl-2-(methoxycarbonyl)allyl) (3b). **Method A.** To **1a** (1.00 g, 3.03 mmol) in CH₃CN (10 mL) was added NOBF₄ (0.38 g, 3.20 mmol) at -40 °C, and liberation of CO started immediately. Stirring was continued for 30 min before addition of excess precooled diethyl ether 150 mL, -40 °C) to produce a yellow solid. Diethyl ether was decanted away to leave a yellow solid that was washed twice with cold diethyl ether (-40 °C) before being dissolved in acetone at -40 °C. LiCl (0.15 g, 3.50 mmol) was added to the acetone solution, and stirring of the mixture continued for 1 h, gradually resulting in evolution CO. The solvent was removed in vacuo (-20 °C), and the residues were washed with hexane/diethyl ether (1/1, 5 mL). Flash chromatography through a short silica column (-20 °C) with CH₂Cl₂ gave an orange solid (0.80 g, 2.36 mmol, 78%) with **3a**(*anti*)/**3b**(*syn*) = 85/15. IR (Nujol, cm⁻¹): ν(NO) 1652. ¹H NMR (400 MHz, CD₂Cl₂, -40 °C, δ): **3a'**, *anti-endo*, 1.87 (3H, d, *J* = 7.5 Hz, Me), 2.98 (1H, d, *J* = 3.2 Hz, H¹), 3.48 (1H, d, *J* = 3.2 Hz, H²), 3.65 (3H, s, OMe), 5.86 (5H, s, Cp), 6.58 (1H, q, *J* = 7.5 Hz, H³); **3a''**, *anti-exo*, 2.13 (3H, d, *J* = 7.5 Hz, Me), 2.82 (1H, d, *J* = 3.4 Hz, H¹), 3.58 (1H, d, *J* = 3.4 Hz, H²), 5.68 (5H, s, Cp), 6.86 (1H, q, *J* = 7.5 Hz, H³); **3b'**, *syn-exo*, 1.97 (3H, d, *J* = 7.5 Hz, Me), 2.21 (1H, d, *J* = 3.2 Hz, H¹), 3.29 (1H, d, *J* = 3.4 Hz, H²), 5.12 (1H, q, *J* = 7.5 Hz, H³), 5.86 (5H, s, Cp); **3b''**, *syn-endo*, 2.15 (3H, d, *J* = 7.5 Hz), 2.82 (1H, d, *J* = 3.1 Hz, H¹), 3.58 (1H, d, *J* = 3.1 Hz, H²), 5.71 (5H, s, Cp), the remaining resonances were masked by the signals of the other three isomers. ¹³C NMR (100 MHz, CDCl₃, -40 °C, δ): **3a'**, *anti-endo*, 18.7 (Me), 40.4 (CH¹H²), 52.1 (OMe), 105.1 (Cp), 111.9 (C-CO), 135.4 (CH³), 164.9 (CO); **3b'**, *syn-exo*, 16.0 (Me), 45.3 (CH¹H²), 51.8 (OMe), 102.6 (Cp), 111.0 (C-CO), 115.0 (CH³), 164.9 (CO). Mass (Nujol, *m/e*): 341 (M⁺). Anal. Calcd for C₁₁H₁₄MoNO₃Cl: C, 38.90; H, 4.16; N, 4.12. Found: C, 38.50; H, 4.18; N, 4.11.

Method B. Compounds **3a** and **3b** were also prepared from **1b** in the procedure described in method A, and the combined yields were 83% with the ratio **3a/3b** = 11/89.

(d) Synthesis of trans-2-Methylene-3-methyl-4-phenylbutyrolactone (4a) and (1S*,2R*)-1-Phenyl-2-methyl-3-(methoxycarbonyl)-3-buten-1-ol (4b). **Method A.** To a mixture of **3a/3b** (0.180 g, 0.52 mmol, **3a/3b** = 85/15) in CH₂Cl₂ (5 mL) was added PhCHO (0.12 g, 1.11 mmol) and CH₃OH (0.12 g, 3.75 mmol) at 20 °C; the mixture was stirred for

(19) Cheng, M.-H.; Lee, H.-H.; Peng, S.-M.; Liu, R.-S. *Organometallics* **1991**, *10*, 3600.

24 h. The solution was evaporated to dryness, extracted with diethyl ether (2×10 mL), and concentrated in vacuo. Elution on a preparative TLC plate (diethyl ether/hexane = 1/1) provided the two organic components **4a** (R_f 0.69; 51 mg, 0.27 mmol, 52%) and **4b** (R_f 0.38; 35.2 mg, 0.16 mmol, 31%). **4a**: IR (neat, cm^{-1}) $\nu(\text{CO})$ 1760 (s), $\nu(\text{C}=\text{C})$ 1653 (m), 1602 (w); ^1H NMR (400 MHz, CDCl_3 , δ) 1.30 (3H, d, $J = 6.7$ Hz, Me), 2.88 (1H, dq, $J = 7.7, 6.7$ Hz, CHMe), 4.84 (1H, d, $J = 7.7$ Hz, CH Ph), 5.52 (1H, s = CHH'), 6.24 (1H, s = CHH'), 7.36–7.20 (5H, m, Ph); ^{13}C NMR (75 MHz, CDCl_3 , δ) 15.6 (Me), 43.3 (CHMe), 85.9 (CHPh), 121.1 (=CHH'), 126.0 (Ph), 126.4 (Ph), 129.0 (Ph), 138.6 and 140.7 (C=CH₂ + Ph), 170.4 (CO); HRMS calcd for C₁₂H₁₂O₂ 188.0838, found 188.0832. **4b**: IR (neat, cm^{-1}) $\nu(\text{OH})$ 3465 (s), $\nu(\text{CO})$ 1711 (s), $\nu(\text{C}=\text{C})$ 1628 (m), 1605 (w); ^1H NMR (400 MHz, δ) 0.79 (3H, d, $J = 7.2$ Hz, Me), 3.07 (1H, dq, $J = 7.2, 3.8$ Hz, CHMe), 3.69 (3H, s, OMe), 4.81 (1H, d, $J = 3.8$ Hz, CHPh), 5.50 (1H, d, $J = 1.4$ Hz, =CHH'), 6.18 (1H, d, $J = 1.4$ Hz, CHH'), 7.17–7.29 (5H, m, Ph); ^{13}C NMR (75 MHz, CDCl_3) 12.5 (Me), 42.4 (CHMe), 51.9 (OMe), 75.5 (CHPh), 121.8 (=CHH'), 126.0 (Ph), 127.3 (Ph), 128.1 (Ph), 142.7 and 142.8 (Ph + C=CH₂), 168.4 (CO); HRMS calcd for C₁₃H₁₆O₃ 220.1099, found 220.1093.

Method B. **4a** and **4b** were also prepared from a mixture of **3a** and **3b** with the ratio **3a/3b** = 11/98, and the yields of **4a** and **4b** were 70% and 13%, respectively.

(e) Synthesis of cis-2-Methylene-3-methyl-4-phenylbutyrolactone (4c). To **4b** (35 mg, 0.16 mmol) in CH_2Cl_2 (2 mL) was added *p*-toluenesulfonic acid (0.85 mg, 5×10^{-3} mmol), and the mixture was stirred for 2 h. The solution was chromatographed through a short silica column and concentrated to yield **4c** (28 mg, 0.15 mmol) as an oil. IR (neat, cm^{-1}): $\nu(\text{CO})$ 1762 (s); $\nu(\text{C}=\text{C})$ 1662 (m), 1605 (w). ^1H NMR (400 MHz, CDCl_3 , δ): 0.77 (3H, d, $J = 7.1$ Hz, Me), 3.43 (1H, dq, $J = 8.0, 7.2$ Hz, CHMe), 5.55 (1H, d, $J = 2.7$ Hz, =CHH'), 5.60 (1H, d, $J = 8.0$ Hz, CHPh), 6.31 (1H, d, $J = 2.7$ Hz, =CHH'), 7.14–7.36 (5H, m, Ph). ^{13}C NMR (100 MHz, CDCl_3 , δ): 16.6 (Me), 44.3 (CHMe), 82.9 (CHPh), 124.1 (=CHH'), 125.0 (Ph), 127.4 (Ph), 130.0 (Ph), 139.7 and 140.7 (C=CH₂ + Ph), 171.2 (CO). HRMS: calcd for C₁₂H₁₂O₂ 188.0838, found 188.0838.

(f) Synthesis of CpMo(CO)₂[η^3 -(3R*,4R*)-2-(methoxycarbonyl)-4-hydroxy-3-penten-1-yl] (6). To CpMo(CO)₃(η^3 -vinylpropargyl) (**5**); 0.50 g, 1.58 mmol) in diethyl ether (20 mL, -40 °C) was added CH_3OH (0.79 g, 2.46 mmol) and then $\text{CF}_3\text{SO}_3\text{H}$ (0.42 mL, 4.34 mmol); stirring was continued for 1 h at the same temperature to produce a heavy yellow precipitate. To the solution was added a mixture of H_2O (10 mL) and THF (10 mL), and the mixture was brought to 23 °C. After addition of a saturated Na_2CO_3 solution (5 mL), the organic layer was extracted with diethyl ether, dried over MgSO_4 , and evaporated to dryness. The residues were chromatographed through a silica column (diethyl ether/hexane = 2/1) to produce a yellow band (R_f 0.45) of **6** as a yellow solid (0.48 g, 1.32 mmol, 83%). IR (Nujol, cm^{-1}): $\nu(\text{CO})$ 1965 (vs), 1890 (vs), 1684 (s). ^1H NMR (300 MHz, CDCl_3 , δ): 1.28 (3H, d, $J = 6.3$ Hz, Me), 1.48 (1H, s, H¹), 2.29 (1H, d, $J = 9.4$ Hz, H³), 3.00 (1H, s, H²), 3.67 (s, 3H, OMe), 4.63 (1H, dq, $J = 9.4, 6.3$ Hz, CH(OH)), 5.20 (5H, s, Cp). ^{13}C NMR (75 MHz, CDCl_3 , δ): 22.9 (Me), 33.9 (CH¹H²), 51.6 (OMe), 64.7 (CH³), 68.7 (CHOH), 88.3 (C–CO), 90.2 (Cp), 172.5 (COOMe), 234.3 and 235.5 (2 Mo–CO). Mass (12 eV, *m/e*): 344 (M⁺ – 18). Anal. Calcd for C₁₄H₁₆MoO₅: C, 46.68; H, 4.48. Found: C, 46.72; H, 4.65.

(g) Synthesis of CpMo(CO)₂[η^3 -(3R*,4R*)-CH₂CCHCH(Me)OC=O (7). To **6** (0.60 g, 1.64 mmol) in diethyl ether (30 mL) was added NaH (50 wt %, 0.20 g, 4.16 mmol), and the solution was stirred for 1 h at 23 °C before addition of water (10 mL). The organic layer was extracted with diethyl ether (2×10 mL), dried over MgSO_4 , and finally evaporated to dryness. The residues were eluted through a silica column to produce a yellow band (R_f 0.52) of **7** (0.52 g, 1.62 mmol, 96%) as a yellow solid. IR (Nujol, cm^{-1}): $\nu(\text{CO})$ 1960 (vs), 1886 (vs), 1759 (s). ^1H NMR (400 MHz, CDCl_3 , δ): 1.43 (1H, d, $J = 2.4$ Hz, H¹), 1.60 (3H, d, $J = 6.6$ Hz, Me), 2.77 (1H, s, $J = 2.4$

H²), 3.29 (1H, s, H³), 4.81 (1H, q, $J = 6.6$ Hz, H⁴), 5.20 (5H, s, Cp). ^{13}C NMR (75 MHz, CDCl_3 , δ): 24.0 (Me), 30.2 (CH¹H²), 75.5 (C–CO), 77.2 (CH⁴), 80.1 (CH³), 95.0 (Cp), 176.5 (CO₂-Me), 232.7 and 237.5 (2 Mo–CO). Mass (12 eV, *m/e*): 330 (M⁺). Anal. Calcd for C₁₃H₁₂MoO₄: C, 47.58; H, 3.69. Found: C, 47.65; H, 3.84.

(h) Synthesis of CpMo(NO)Cl(η^3 -(3R*,4R*)-CH₂CCHCH-

(Me)OC=O (8). This compound was similarly prepared from NOBF_4 and LiCl by following a procedure identical with that described in section b. The yield of **8** was 54% with the presence of two isomers in the ratio 2.5/1. IR (Nujol, cm^{-1}): $\nu(\text{CO})$ 1757 (s); $\nu(\text{NO})$ 1652 cm^{-1} . ^1H NMR (400 MHz, CD_2Cl_2 , δ): major isomer, 1.58 (3H, d, $J = 6.9$ Hz, Me), 2.78 (1H, d, $J = 3.2$ Hz, H¹), 3.41 (1H, d, $J = 3.2$ Hz, H²), 5.03 (1H, q, $J = 6.9$ Hz, H⁴), 5.92 (5H, s, Cp), 6.45 (1H, s, H³); minor isomer, 1.63 (3H, d, $J = 6.8$ Hz, Me), 3.02 (1H, d, $J = 3.8$ Hz, H¹), 3.63 (1H, d, $J = 3.8$ Hz, H²), 5.23 (1H, q, $J = 6.8$ Hz, H⁴), 5.74 (5H, s, Cp), 6.71 (1H, s, H³). ^{13}C NMR (100 MHz, CDCl_3 , δ): major isomer, 19.3 (Me), 37.8 (CH¹H²), 77.1 (CH⁴), 103.2 (Cp), 110.9 (C–CO), 124.2 (CH³), 170.1 (CO); minor isomer, 19.6 (Me), 38.5 (CH¹H²), 78.9 (CH⁴), 104.4 (Cp), 110.9 (C–CO), 133.8 (CH³), 171.8 (CO). Anal. Calcd for C₁₁H₁₂MoNO₃Cl: C, 38.94; H, 3.57; N, 4.13. Found: C, 39.12; H, 3.66; N, 4.32.

(i) Synthesis of (1'S*,3R*,4S*)-2-Methylene-3-(α -hydroxybenzyl)-4-methylbutyrolactone (9). This compound was synthesized from **8**, PhCHO, and CH_3OH in CH_2Cl_2 according to the method described in section c. The yield of **9** was 52% as a single diastereomer. IR (neat, cm^{-1}): $\nu(\text{OH})$ 3437 (s); $\nu(\text{CO})$ 1758 (s); $\nu(\text{C}=\text{C})$ 1657 (m), 1608 (w). ^1H NMR (400 MHz, CDCl_3 , δ): 1.07 (3H, d, $J = 6.4$ Hz, Me), 2.94 (1H, dd, $J = 7.8, 3.8$ Hz, H¹), 4.32 (1H, qd, $J = 6.4, 3.8$ Hz, H²), 4.66 (1H, d, $J = 7.8$ Hz, CHPh), 5.80 (1H, d, $J = 2.3$ Hz, =CHH'), 6.36 (1H, d, $J = 2.3$ Hz, CHH'), 7.24–7.42 (5H, m, Ph). ^{13}C NMR (75 MHz, CDCl_3 , δ): 21.4 (Me), 52.8 (CH¹), 75.4 and 76.1 (CH² and CHPh), 126.1 (=CHH'), 126.8 (Ph), 128.9 (Ph), 129.0 (Ph), 135.9 and 141.0 (Ph and C=CHH'), 170.4 (CO). HRMS: calcd for C₁₃H₁₄O₃ 218.0943, found 218.0945.

(j) Synthesis of (1'R*,3R*,4S*)-2-Methylene-3-(1-hydroxy-2-methylpropyl)-4-methylbutyrolactone (10). This compound was synthesized from **8**, Me₂CHCHO, and CH_3OH in CH_2Cl_2 according to the method described in section c; the yield of **10** was 50%. IR (neat, cm^{-1}): $\nu(\text{OH})$ 3445 (s); $\nu(\text{CO})$ 1761 (s); $\nu(\text{C}=\text{C})$ 1651 (m), 1608 (w). ^1H NMR (400 MHz, CDCl_3 , δ): 0.96 (3H, d, $J = 6.6$ Hz, Me), 1.00 (3H, d, $J = 6.6$ Hz, Me), 1.45 (3H, d, $J = 6.5$ Hz, Me), 1.77 (1H, m, CHMe₂), 1.89 (1H, br s, OH), 2.76 (1H, ddd, $J = 6.5, 3.2, 2.1$ Hz, H¹), 3.30 (1H, q, $J = 6.5$ Hz, CH(OH)), 4.48 (1H, dq, $J = 6.5, 3.2$ Hz, H²), 5.77 (1H, d, $J = 2.1, 1.8$ Hz, =CHH'), 6.37 (1H, d, $J = 1.8$ Hz, =CHH'). ^{13}C NMR (100 MHz, CDCl_3 , δ): 16.7 (Me), 19.9 (Me), 21.8 (Me), 30.4 (CHMe), 49.1 (CH¹), 77.1 and 77.4 (CH¹ + CH(OH)), 125.2 (=CHH'), 135.5 (C=CHH'), 170.3 (CO). HRMS: calcd for C₁₀H₁₆O₃ 185.1178, found 185.1179.

(k) Synthesis of (1'R*,3R*,4S*)-2-Methylene-3-(1-hydroxyethyl)-4-isopropylbutyrolactone (11). To **10** (92 mg, 0.49 mmol) was added *p*-toluenesulfonic acid (1.70 mg, 1.0×10^{-2} mmol) in CH_2Cl_2 , and the mixture was stirred for 4 h at 23 °C. The solution was filtered through a short-bed silica column and then eluted through a preparative SiO₂ TLC plate to produce two organic bands. Collection of the major band afforded **11** as an oil (59 mg, 0.32 mmol). IR (neat, cm^{-1}): $\nu(\text{OH})$ 3454 (s); $\nu(\text{CO})$ 1765 (s); $\nu(\text{C}=\text{C})$ 1648 (m), 1600 (w). ^1H NMR (400 MHz, δ): 0.90 (3H, d, $J = 5.0$ Hz, Me), 0.91 (3H, d, $J = 5.0$ Hz, Me), 1.18 (3H, d, $J = 6.3$ Hz, Me), 1.80 (1H, m, CHMe₂), 2.79 (1H, ddd, $J = 6.2, 2.3, 1.8$ Hz, H¹), 3.82 (1H, dq, $J = 6.3, 6.2$ Hz, CH(OH)), 4.21 (1H, dd, $J = 5.6, 2.3$ Hz, H²), 5.69 (1H, d, $J = 2.1, 1.8$ Hz, =CHH'), 6.29 (1H, d, $J = 2.1$ Hz, =CHH'). ^{13}C NMR (100 MHz, CDCl_3 , δ): 16.8 (Me), 18.6 (Me), 19.4 (Me), 33.2 (CHMe₂), 48.5 (CH¹), 69.2 (CH¹), 84.2 (CH²), 124.2 (=CHH'), 136.0 (C=CHH'), 170.5 (CO). HRMS: calcd for C₁₀H₁₆O₃ 185.1178, found 185.1179.

OM940814M

Transition-Metal-Substituted Acylphosphanes and Phosphaalkenes. 27.¹ Synthesis and Structure of $\eta^1:\eta^2$ -Metallophosphaalkene Complexes $(\eta^5\text{-C}_5\text{H}_5)_2(\text{CO})_2\text{Fe}_2[(\eta^5\text{-C}_5\text{Me}_4\text{R})(\text{CO})\text{LM-P=CHSMe}]$ ($\text{M} = \text{Fe, Ru, Mn}$; $\text{L} = \text{CO, NO}$; $\text{R} = \text{Me, Et}$)

Lothar Weber,* Iris Schumann, Hans-Georg Stammer, and Beate Neumann

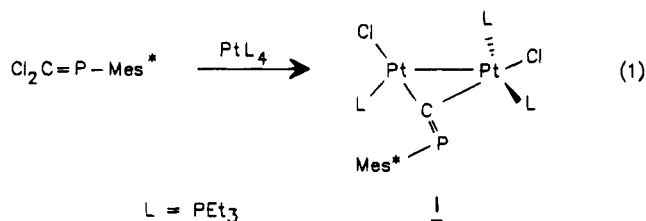
Fakultät für Chemie der Universität Bielefeld, Universitätsstrasse 25,
D-33615 Bielefeld, Germany

Received March 28, 1994[®]

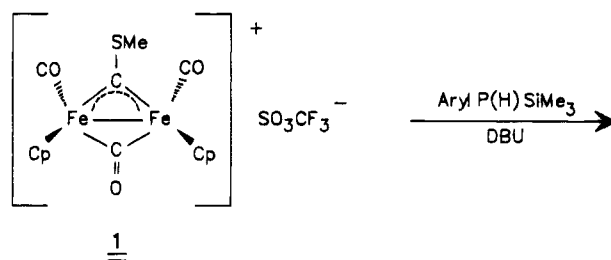
The condensation of the μ -carbyne complex $[(\eta^5\text{-C}_5\text{H}_5)_2(\text{CO})_2(\mu\text{-CO})(\mu\text{-CSMe})\text{Fe}_2](\text{SO}_3\text{CF}_3)$ (**1**) with metallobis(trimethylsilyl)phosphanes $[\text{M}]\text{-P}(\text{SiMe}_3)_2$ (**2** (**2a**, $[\text{M}] = (\eta^5\text{-C}_5\text{Me}_5)(\text{CO})_2\text{Fe}$; **2b**, $[\text{M}] = (\eta^5\text{-C}_5\text{Me}_5)(\text{CO})_2\text{Ru}$; **2c**, $(\eta^5\text{-C}_5\text{Me}_5)(\text{CO})(\text{NO})\text{Mn}$; **2d**, $(\eta^5\text{-C}_5\text{Me}_4\text{Et})(\text{CO})_2\text{Fe}$) in acetonitrile afforded $\mu(\eta^1:\eta^2)$ -metallophosphaalkene complexes $(\eta^5\text{-C}_5\text{H}_5)(\text{CO})_2\text{Fe}_2\{[\text{M}]\text{-P=CHSMe}\}$ (**3a–d**). Similarly **3a** results from the reaction of **1** and the complex $(\eta^5\text{-C}_5\text{Me}_5)(\text{CO})_2\text{Fe-PH}_2$. The compounds **3a–d** were characterized by spectroscopic methods (IR, ^1H , ^{13}C , ^{31}P NMR, mass spectroscopy). The solid state structure of **3a** was determined by a single crystal X-ray diffraction analysis ($P\bar{1}$, $a = 9.445(5)$ Å, $b = 11.654(6)$ Å, $c = 15.732(9)$ Å, $\alpha = 99.93(4)^\circ$, $\beta = 103.09(4)^\circ$, $\gamma = 105.58(4)^\circ$).

Introduction

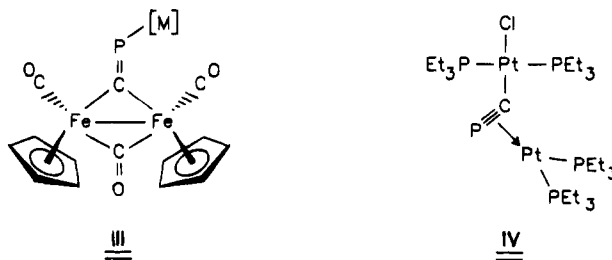
Theoretical calculations² and experimental evidence³ underline the pronounced instability of isophosphaalkynes $\text{R-P}\equiv\text{C}$ (isocyaphides) with respect to the more familiar phosphaalkynes $\text{R-C}\equiv\text{P}$.⁴ Recently Angelici et al. succeeded in the preparation of a first diplatinum complex **I** featuring a semibridging supermesitylisophosphaalkyne (supermesitylisocyaphide) ligand (eq 1).⁵ More recently we described an alterna-



tive and complementary approach to μ -isophosphaalkyne complexes which was based on the condensation of the (μ -carbyne)diiron complex **I** with aryl(silyl)phosphanes (eq 2).⁶ The employment of metallobis(trimethylsilyl)phosphanes instead of aryl(silyl)phosphanes should provide a synthetic access to compounds **III** exhibiting the $\text{C}\equiv\text{P}$



ligand in a novel mode of coordination. Two years ago the first cyaphide complex **IV** with a $\mu(\eta^1:\eta^2)$ ligand arrangement was reported by Angelici et al.⁷



Experimental Section

General Information. Standard inert-atmosphere techniques were used for the manipulation of all reagents and reaction products. Infrared spectra were recorded on a Perkin-

(7) Jun, H.; Young, V. G., Jr.; Angelici, R. J. *J. Am. Chem. Soc.* **1992**, *114*, 10064.

[®] Abstract published in *Advance ACS Abstracts*, February 15, 1995.
(1) Part 26: Weber, L.; Kaminski, O.; Stammer, H.-G.; Neumann, B. *Organometallics* **1995**, *14*, 581.

(2) (a) Lehmann, K. K.; Ross, S. C.; Lohr, L. L. *J. Chem. Phys.* **1985**, *82*, 4460. (b) Nguyen, M. T.; Ha, T.-K.; *J. Mol. Struct. (Theochem)* **1986**, *139*, 145.

(3) (a) Goede, S. J.; Bickelhaupt, F. *Chem. Ber.* **1991**, *124*, 2677. (b) Yoshifuji, M.; Niitsu, T.; Inamoto, N. *Chem. Lett.* **1988**, 1733. (c) Markovskii, L. N.; Koidan, G. N.; Marchenko, A. P.; Romanenko, V. D.; Povolotskii, M. I.; Pinchuk, A. M. *Zh. Obshch. Khim.* **1988**, *59*, 2133.

(4) (a) Becker, G.; Gresser, G.; Uhl, W. *Z. Naturforsch.* **1981**, *36b*, 16. (b) Regitz, M. *Chem. Rev.* **1990**, *90*, 191. (c) Regitz, M.; Binger, P.; *Angew. Chem.* **1988**, *100*, 1541; *Angew. Chem., Int. Ed. Engl.* **1988**, *27*, 1484. (d) Regitz, M. In *Multiple Bonds and Low Coordination in Phosphorus Chemistry*; Regitz, M., Scherer, O. J., Eds.; Thieme: Stuttgart, Germany, 1990; p 58.

(5) Jun, H.; Young, V. G.; Angelici, R. J. *J. Am. Chem. Soc.* **1991**, *113*, 9379. Jun, H.; Angelici, R. J. *Organometallics* **1994**, *13*, 2454.

(6) Weber, L.; Schumann, I.; Schmidt, T.; Stammer, H.-G.; Neumann, B.; *Z. Anorg. Allg. Chem.* **1993**, *619*, 1759.

Elmer Model 580 spectrometer. UV/vis spectra were obtained with a modified Omega UV/vis spectrometer. ^1H , ^{13}C , and ^{31}P NMR spectra were taken on a Bruker AM 400, Bruker AM 300, or Bruker AC 100 spectrometer in C_6D_6 solution at room temperature. Mass spectra were measured on a Finnigan MAT MS 311A (EI-mode, 80 eV).

Materials. All solvents were rigorously dried with an appropriate drying agent and distilled before use (e.g. CH_3CN according to ref 8). The metallophosphanes ($\eta^5\text{-C}_5\text{Me}_5(\text{CO})_2\text{FeP}(\text{SiMe}_3)_2$),⁹ ($\eta^5\text{-C}_5\text{Me}_5(\text{CO})_2\text{RuP}(\text{SiMe}_3)_2$),¹⁰ ($\eta^5\text{-C}_5\text{Me}_5(\text{CO})\text{(NO)MnP}(\text{SiMe}_3)_2$),¹¹ ($\eta^5\text{-C}_5\text{EtMe}_4(\text{CO})_2\text{FeP}(\text{SiMe}_3)_2$),¹² and ($\eta^5\text{-C}_5\text{Me}_5(\text{CO})_2\text{FePH}_2$)¹³ and the carbyne complex [$(\eta^5\text{-C}_5\text{H}_5)_2(\text{CO})_2\text{Fe}(\mu\text{-CO})(\mu\text{-CSMe})$] $^+\text{SO}_3\text{CF}_3$ ⁻¹⁴ were prepared as described in the literature. 1,8-Diazabicyclo[5.4.0]undec-7-ene (DBU) and silica gel 60, silanized, 70–230 mesh ASTM (Merck), were obtained commercially.

Preparation of Compounds: ($\eta^5\text{-C}_5\text{H}_5$)₂(CO)₂Fe₂[($\eta^5\text{-C}_5\text{Me}_5$)(CO)₂Fe–P=CHSMe] (3a). Path A. A sample of 0.46 g (1.09 mmol) of solid **2a** was added to a solution of 0.58 g (1.09 mmol) of **1** in 30 mL of acetonitrile at 0 °C. After the solution was stirred for 15 min at 0 °C, 0.23 g (1.52 mmol) of DBU was added, whereupon the color of the mixture immediately changed to reddish-brown. Stirring was continued at ambient temperature for another 3 h. After evaporation to dryness the oily brown residue was chromatographed on silanized silica gel. The product was eluted as a dark red zone with a hexane/ether mixture (1:5). The elute was freed from volatiles, and the residue was crystallized from toluene/cyclopentane at –30 °C. After 24 h 0.20 g (28%) of deep-red crystalline **3a** was isolated.

Path B. A sample of 0.51 g (1.82 mmol) of ($\eta^5\text{-C}_5\text{Me}_5(\text{CO})_2\text{Fe}–\text{PH}_2$) was added to a solution of 0.97 g (1.82 mmol) of **1** in 30 mL of acetonitrile at 0 °C. After stirring of the solution for 10 min at 0 °C, 0.39 g (2.55 mmol) of DBU was added, where upon the color of the mixture changed from red to reddish-brown. An analogous workup led to the isolation of 0.45 g (39%) of **3a**.

IR (KBr, cm^{-1}): 2963 m, 2909 m, 1997 s [$\nu(\text{CO})$], 1952 s [$\nu(\text{CO})$], 1917 s [$\nu(\text{CO})$], 1762 s [$\nu(\text{CO})$], 1429 m, 1379 m, 1262 m, 1129 m, 1025 m, 816 m, 668 m, 580 s, 501 m. IR (toluene, cm^{-1}): 2002 s, 1955 s, 1920 s, 1783 s. UV/vis (toluene) [λ_{max} (log ϵ): 339 (3.97), 430 (3.56) nm. ^1H NMR (C_6D_6): δ 1.38 (d, $^2J_{\text{PH}} = 1.6$ Hz, 1H, CH), 1.50 (d, $^4J_{\text{PH}} = 1.0$ Hz, 15H, $\text{C}_5(\text{CH}_3)_5$), 1.83 (d, $^4J_{\text{PH}} = 1.5$ Hz, 3H, SCH_3), 4.37 (d, $^3J_{\text{PH}} = 1.0$ Hz, 5H, C_5H_5), 4.74 (d, $^3J_{\text{PH}} = 0.5$ Hz, 5H, C_5H_5). $^{13}\text{C}\{^1\text{H}\}$ NMR (C_6D_6): δ 9.5 (d, $^3J_{\text{PC}} = 2$ Hz, $\text{C}_5(\text{CH}_3)_5$), 20.6 (d, $^3J_{\text{PC}} = 5$ Hz, SCH_3), 55.6 (d, $^1J_{\text{PC}} = 49$ Hz, P=C), 81.7 (s, C_5H_5), 84.4 (s, C_5H_5), 98.1 (s, $\text{C}_5(\text{CH}_3)_5$), 215.0 (d, $^2J_{\text{PC}} = 13$ Hz, Cp^*FeCO), 216.3 (d, $^2J_{\text{PC}} = 18$ Hz, Cp^*FeCO), 219.6 (d, $^2J_{\text{PC}} = 25$ Hz, CpFeCO), 257.3 (s, $\mu\text{-CO}$). $^{31}\text{P}\{^1\text{H}\}$ NMR (C_6D_6): δ 301.7 s. MS: m/e 636 (M^+), 608 ($\text{M}^+ - \text{CO}$), 580 ($\text{M}^+ - 2\text{CO}$), 537 ($\text{M}^+ - 3\text{CO} - \text{CH}_3$), 509 ($\text{M}^+ - 4\text{CO} - \text{CH}_3$), 186 (Cp_2Fe^+), 121 (CpFe^+). Anal. Calcd for $\text{C}_{26}\text{H}_{29}\text{Fe}_3\text{O}_4\text{PS}$ (636.09): C, 49.09; H, 4.60; Fe, 26.34. Found: C, 48.95; H, 4.82; Fe, 27.02.

($\eta^5\text{-C}_5\text{H}_5$)₂(CO)₂Fe₂[($\eta^5\text{-C}_5\text{Me}_5$)(CO)₂Ru–P=CHSMe] (3b). The solution of 0.46 g (0.97 mmol) of **2b** and 0.52 g (0.97 mmol) of **1** in 30 mL of acetonitrile was stirred at ambient temperature for 30 min. Then 0.20 g (1.36 mmol) of DBU was added. After 3 h of stirring the mixture was freed from volatiles to give a greenish brown residue. Column chromatography on silanized silica gel with hexane/ether (5:1) and hexane/ether (1:1) as eluents furnished a green fraction, from which 0.20 g

(30%) of dark-green microcrystalline **3b** was obtained as described before.

IR (KBr, cm^{-1}): ν 2981 w, 2912 m, 2013 s [$\nu(\text{CO})$], 1960 s [$\nu(\text{CO})$], 1920 s [$\nu(\text{CO})$], 1754 s [$\nu(\text{CO})$], 1698 w, 1631 m, 1487 w, 1456 w, 1422 w, 1385 m, 1364 w, 1307 w, 1158 w, 1112 w, 1073 m, 1028 m, 957 s, 848 w, 818 w, 668 w, 630 w, 582 m, 556 s, 538 s, 522 s, 504 s, 474 m. IR (toluene, cm^{-1}): ν 2016 s, 1965 s, 1919 s, 1783 s. UV/vis (toluene) [λ_{max} (log ϵ): 370 (3.89), 550 (2.50) nm. ^1H NMR (C_6D_6): δ 1.40 (s, 1H, CH), 1.59 (d, $^4J_{\text{PH}} = 1.9$ Hz, 15H, $\text{C}_5(\text{CH}_3)_5$), 1.83 (d, $^4J_{\text{PH}} = 1.4$ Hz, SCH_3), 4.34 (d, $^3J_{\text{PH}} = 1.3$ Hz, 5H, C_5H_5), 4.73 (d, $^3J_{\text{PH}} = 0.6$ Hz, 5H, C_5H_5). $^{13}\text{C}\{^1\text{H}\}$ NMR (C_6D_6): δ 9.6 (s, $\text{C}_5(\text{CH}_3)_5$), 20.4 (d, $^3J_{\text{PC}} = 6$ Hz, SCH_3), 50.2 (d, $^1J_{\text{PC}} = 43$ Hz, P=C), 81.6 (s, C_5H_5), 83.7 (s, C_5H_5), 101.4 (s, $\text{C}_5(\text{CH}_3)_5$), 200.8 (s, Cp^*RuCO), 201.7 (d, $^2J_{\text{PC}} = 11$ Hz, Cp^*RuCO), 219.8 (d, $^2J_{\text{PC}} = 24$ Hz, CpFeCO), 257.6 (s, $\mu\text{-CO}$). $^{31}\text{P}\{^1\text{H}\}$ NMR (C_6D_6): δ 264.0 s. MS: m/e 682 (M^+), 654 ($\text{M}^+ - \text{CO}$), 626 ($\text{M}^+ - 2\text{CO}$), 583 ($\text{M}^+ - 3\text{CO} - \text{CH}_3$), 555 ($\text{M}^+ - 4\text{CO} - \text{CH}_3$), 186 (Cp_2Fe^+), 121 (CpFe^+). Anal. Calcd for $\text{C}_{26}\text{H}_{29}\text{Fe}_2\text{O}_4\text{PRuS}$ (681.32): C, 45.84; H, 4.29. Found: C, 45.57; H, 4.20.

($\eta^5\text{-C}_5\text{H}_5$)₂(CO)₂Fe₂[($\eta^5\text{-C}_5\text{Me}_5$)(CO)(NO)Mn–P=CHSMe] (3c). Analogously, 0.10 g (30%) of microcrystalline red-brown **3c** was synthesized from 0.24 g (0.56 mmol) of **1**, 0.30 g (0.56 mmol) of **2c**, and 0.12 g (0.79 mmol) of DBU in 20 mL of acetonitrile.

IR (KBr, cm^{-1}): 2962 m, 2920 m, 1984 s [$\nu(\text{CO})$], 1925 sh [$\nu(\text{CO})$], 1748 s, br [$\nu(\text{CO})$, $\nu(\text{NO})$], 1630 m, 1429 m, 1384 m, 1269 m, 1015 m, 961 m, 842 m, 672 m, 579 m. IR (toluene, cm^{-1}): 1994 s, 1919 s, 1783 s [$\nu(\text{CO})$], 1734 s, [$\nu(\text{NO})$]. UV/vis (toluene): λ_{max} (log ϵ): 328 (4.00) nm. ^1H NMR (C_6D_6): δ 1.37 (d, $^2J_{\text{PH}} = 1.2$ Hz, 1H, CH), 1.53 (d, $^4J_{\text{PH}} = 0.5$ Hz, 15H, $\text{C}_5(\text{CH}_3)_5$), 1.80 (d, $^4J_{\text{PH}} = 1.5$ Hz, 3H, SCH_3), 4.40 (d, $^3J_{\text{PH}} = 1.1$ Hz, 5H, C_5H_5), 4.82 (d, $^3J_{\text{PH}} = 0.3$ Hz, 5H, C_5H_5). $^{13}\text{C}\{^1\text{H}\}$ NMR (C_6D_6): δ 9.7 (s, $\text{C}_5(\text{CH}_3)_5$), 20.8 (s, br, SCH_3), 55.8 (d, $^3J_{\text{PC}} = 49$ Hz, P=C), 81.6 (s, C_5H_5), 84.5 (s, C_5H_5), 104.4 (s, $\text{C}_5(\text{CH}_3)_5$), 219.7 (d, $^2J_{\text{PC}} = 23$ Hz, CpFeCO), 233.1 (s, br, Cp^*MnCO), 257.2 (s, $\mu\text{-CO}$). ^{31}P NMR (C_6D_6): δ 312.0 s. MS/FD: m/e 637 (M^+). Anal. Calcd for $\text{C}_{25}\text{H}_{29}\text{Fe}_2\text{MnNO}_4\text{PS}$ (637.18): C, 47.13; H, 4.59; N, 2.20. Found: C, 46.87; H, 4.95; N, 2.47.

($\eta^5\text{-C}_5\text{H}_5$)₂(CO)₂Fe₂[($\eta^5\text{-C}_5\text{Me}_4\text{Et}$)(CO)₂Fe–P=CHSMe] (3d). Analogously to the synthesis of **3a**, 0.14 g (35%) of microcrystalline brown **3d** was prepared from 0.33 g (0.62 mmol) of **1**, 0.27 g (0.62 mmol) of **2d**, and 0.13 (0.86 mmol) of DBU in 20 mL of acetonitrile.

IR (KBr, cm^{-1}): 2966 m, 2914 m, 1998 s [$\nu(\text{CO})$], 1956 s [$\nu(\text{CO})$], 1920 sh [$\nu(\text{CO})$], 1768 s [$\nu(\text{CO})$], 1631 m, 1457 m, 1429 m, 1383 m, 1308 m, 1261 m, 1012 m, 813 m, 671 m, 580 s. IR (toluene, cm^{-1}): 2002 s, 1955 s, 1920 s, 1782 s. UV/vis (toluene) [λ_{max} (log ϵ): 315 (4.06), 400 (3.69) nm. ^1H NMR (C_6D_6): δ 0.75 (t, $^3J_{\text{HH}} = 7.6$ Hz, 3 H, CH_2CH_3), 1.39 (d, $^2J_{\text{PH}} = 1.2$ Hz, 1H, CH), 1.51 (d, $^4J_{\text{PH}} = 0.6$ Hz, 3H, CH_3 -3 or 4), 1.53 (s, 3H, CH_3 -3 or 4), 1.56 (s, 3H, CH_3 -2 or 5), 1.58 (s, 3H, CH_3 -2 or 5), 1.83 (d, $^4J_{\text{PH}} = 1.3$ Hz, 3H, SCH_3), 2.11 (qd, $^3J_{\text{HH}} = 7.5$ Hz, $^4J_{\text{PH}} = 1.2$ Hz, 2H, CH_2CH_3), 4.38 (d, $^3J_{\text{PH}} = 0.5$ Hz, 5H, C_5H_5), 4.74 (s, 5H, C_5H_5). $^{13}\text{C}\{^1\text{H}\}$ NMR (C_6D_6): δ 9.3 (s, CH_3 -3,4), 9.5 (s, CH_3 -2,5), 14.3 (d, $^4J_{\text{PC}} = 8$ Hz, CH_2CH_3), 18.4 (s, CH_2CH_3), 20.7 (d, $^3J_{\text{PC}} = 4$ Hz, SCH_3), 55.8 (d, $^1J_{\text{PC}} = 49$ Hz, P=C), 81.8 (s, C_5H_5), 84.5 (s, C_5H_5), 97.5 (s, $\text{C}_5(\text{CH}_3)_5$ -3 or 4), 97.6 (s, $\text{C}_5(\text{CH}_3)_5$ -3 or 4), 98.6 (s, $\text{C}_5(\text{CH}_3)_5$ -2 or 5), 99.0 (s, $\text{C}_5(\text{CH}_3)_5$ -2 or 5), 102.5 (s, $\text{C}_5(\text{C}_2\text{H}_5)_5$), 215.0 (d, $^2J_{\text{PC}} = 13$ Hz, $(\text{C}_5\text{EtMe}_4)\text{FeCO}$), 216.3 (d, $^2J_{\text{PC}} = 18$ Hz, $(\text{C}_5\text{EtMe}_4)\text{FeCO}$), 219.9 (d, $^2J_{\text{PC}} = 24$ Hz, CpFeCO), 258.1 (s, $\mu\text{-CO}$). $^{31}\text{P}\{^1\text{H}\}$ NMR (C_6D_6): δ 300.0 s. MS: m/e 650 (M^+), 622 ($\text{M}^+ - \text{CO}$), 594 ($\text{M}^+ - 2\text{CO}$), 551 ($\text{M}^+ - 3\text{CO} - \text{CH}_3$), 523 ($\text{M}^+ - 4\text{CO} - \text{CH}_3$), 186 (Cp_2Fe^+), 121 (CpFe^+). Anal. Calcd for $\text{C}_{27}\text{H}_{31}\text{Fe}_3\text{O}_4\text{PS}$ (650.12): C, 49.88; H, 4.81; Fe, 25.77. Found: C, 50.06; H, 4.88; Fe, 25.84.

X-ray Structure Determination of 3a. Dark red crystals of **3a** were grown from a solution in toluene/cyclopentane at –40 °C. An irregularly shaped crystal of the approximate dimensions 0.60 × 0.15 × 0.10 mm was coated with a layer of

(8) Christe, K. O.; Dixon, D. A.; Mahjoub, A. R.; Mercier, H. P. A.; Sanders, J. C. P.; Seppelt, K.; Schrobilgen, G. J.; Wilson, W. W. *J. Am. Chem. Soc.* **1993**, *115*, 2696.

(9) Weber, L.; Reizig, K.; Boese, R. *Chem. Ber.* **1985**, *118*, 1193.

(10) Weber, L.; Reizig, K.; Boese, R.; *Organometallics* **1985**, *4*, 2097.

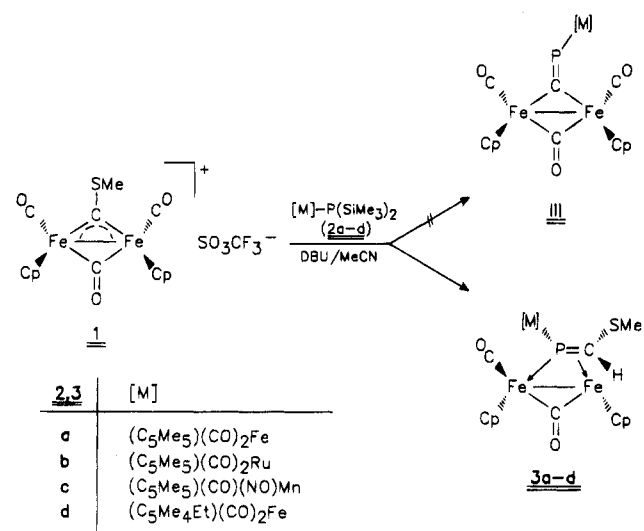
(11) Weber, L.; Meine, G.; *Chem. Ber.* **1987**, *120*, 457.

(12) Weber, L.; Schumann, I.; Stammler, H.-G.; Neumann, B. Z. *Naturforsch.* **1992**, *47b*, 1134.

(13) Weber, L.; Kirchoff, R.; Stammler, H.-G.; Neumann, B. *Chem. Ber.* **1992**, *125*, 1553.

(14) Quick, M. H.; Angelici, R. J. *Inorg. Chem.* **1981**, *20*, 1123.

Scheme 1



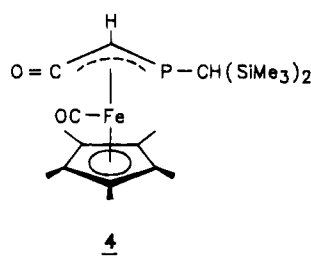
hydrocarbon oil, attached to a glass fiber, cooled to 173 K for data collection, and mounted on a Siemens P2₁ four-circle diffractometer (Mo K α radiation, graphite monochromator, $\lambda = 0.71073$ Å). The cell dimensions were determined by refinement of the setting angles of 30 reflections ($4^\circ < 2\theta < 25^\circ$): $a = 9.445(5)$ Å, $b = 11.654(6)$ Å, $c = 15.732(9)$ Å, $\alpha = 99.93(4)^\circ$, $\beta = 103.09^\circ$, $\gamma = 105.58^\circ$, $V = 1537(2)$ Å³. The space group was established to be $P\bar{1}$ ($Z = 2$, $D_{\text{calc}} = 1537$ mg/m³, $\mu = 1.518$ mm⁻¹) with ω -scan data collection of 7225 independent intensities ($3^\circ < 2\theta < 55^\circ$). The structure was solved by direct methods, successive difference Fourier maps, and full-matrix least-squares cycles. The crystallographic programs applied were SHELXS-86/SHELXL-93 using intrinsic scattering factors. All non-hydrogen atoms were given anisotropic displacement parameters; all the hydrogen atoms were fixed at calculated positions. The R values based on the final model refined with 379 parameters were $R_F = \sum(|F_o| - |F_c|)/\sum(|F_o|) = 0.0949$ and $R_{wF^2} = [\sum w(F_o^2 - F_c^2)^2/\sum F_o^2]^{1/2} = 0.2253$, based on 4185 reflections with $F_o > 4\sigma(F_o)$. The maximum residual electron density was 1.4 e/Å³, 1.03 Å from Fe(3).

Results and Discussion

The reaction of the μ -carbyne complex **1** with equimolar amounts of the metallodisilylphosphanes **2a-d** in the presence of DBU afforded microcrystalline deeply colored solids, which were isolated by column chromatography and subsequent crystallization (Scheme 1).

The course of the reaction was conveniently monitored by ³¹P NMR spectroscopy. The high-field singlets of **2a-d** ($\delta -202.9$ to -219.9) were replaced by singlets at $\delta 264.0$ – 312.0 . These resonances compare well with

the ³¹P NMR data of the arylisophosphaalkyne complex **II** ($\delta 249.3$ – 258.0)⁶ and would be consistent with the anticipated formation of **III**. On the grounds of ¹H and ¹³C NMR evidence, however, this assumption had to be discarded. Doublets which would correspond to the carbon atom of the C=P moiety of hypothetical **III** were absent in the low-field region of the spectra (in **II** they were registered at $\delta 333.8$ – 345.8). Instead doublets at $\delta 50.2$ – 55.8 ($^1J_{\text{PC}} = 43$ – 49 Hz) in the J -modulated ¹³C NMR spectra are in agreement with the situation of a π -bonded P=CH unit. As later confirmed by an X-ray study of **3a** the dinuclear iron complexes **3a-d** were formed, displaying μ -(η^1 : η^2)-ligated metallophosphaalkenes of the type [M]–P=CHSMe. With respect to the low-field ³¹P-resonances of related metallophosphaalkenes such as (η^5 -C₅Me₅)(CO)₂Fe–P=C(SiMe₃)₂ ($\delta = 641.5$),¹⁵ (η^5 -C₅Me₅)(CO)₂Fe–P=C(Ph)SiMe₃ ($\delta = 520.0$),¹⁶ and (η^5 -C₅Me₅)(CO)₂Fe–P=C(SSiMe₃)₂ ($\delta = 503.8$)¹⁷ (the free metallophosphaalkenes [M]–P=CHSMe are unknown), the ³¹P NMR data of **3a-d** are also in accord with an η^2 -phosphaalkene ligand featuring the familiar high-field shifts upon π -coordination. The $^2J_{\text{PC}}$ couplings (23–25 Hz) of the remaining terminal carbonyl ligand at the CpFe building block ($\delta 219.6$ – 219.9) indicate an intense Fe–P interaction. In **II** the terminal CO groups gave rise to absorptions at much higher field ($\delta(^{13}\text{C}) 209.9$ – 211.0). This observation is in accord with a considerable charge transfer from the metallophosphaalkene to the Cp(CO)Fe unit in **3a-d**. Singlets at $\delta 257.2$ – 258.1 were attributed to the μ -CO ligand. These signal are markedly shielded as compared to the related resonances in **II** ($\delta(^{13}\text{C}) 269.2$ – 270.8). The carbonyl resonances of the ligands incorporated in the fragment [M] in **3a-d** are well comparable with the corresponding absorptions in the metallodiphosphenes Cp*(CO)₂Fe–P=P–Mes* [$\delta = 216.3$ (d, $^2J_{\text{PC}} = 11.9$ Hz)],¹⁸ Cp*(CO)₂Ru–P=P–Mes* [$\delta = 202.1$ (d, $^2J_{\text{PC}} = 13.9$ Hz)],¹⁸ and Cp*(CO)(NO)Mn–P=P–Mes* ($\delta = 233.4$ m).¹¹ The presence of the S–CH₃ group in **3a,b,d** is ascertained by doublets at $\delta(^{13}\text{C}) 20.4$ – 20.7 ($^3J_{\text{PC}} = 4$ – 6 Hz) and a broad singlet at $\delta(^{13}\text{C}) 20.8$ for **3c**. The ¹H NMR spectrum shows doublets at $\delta 1.80$ – 1.83 ($^4J_{\text{PH}} = 1.3$ – 1.5 Hz) for this functionality. The proton at the C=P bond in **3a,c,d** is detected as a doublet at $\delta 1.37$ – 1.39 ($^2J_{\text{PH}} = 1.2$ – 1.6 Hz) and as a singlet at $\delta = 1.40$ in **3b**. In complex **4** a doublet at δ



(15) Gudat, D.; Niecke, E.; Arif, A. M.; Cowley, A. H.; Quashie, S. *Organometallics* **1986**, *5*, 593.

(16) Niecke, E.; Metternich, H.-J.; Nieger, M.; Gudat, D.; Wenderoth, P.; Malisch, W.; Hahner, C.; Reich, W. *Chem. Ber.* **1993**, *126*, 1299.

(17) Weber, L.; Torwiehe, B. Unpublished results.

(18) Weber, L.; Reizig, K.; Bungardt, D.; Boese, R. *Organometallics* **1987**, *6*, 110.

(19) Weber, L.; Lücke, E.; Boese, R.; *Chem. Ber.* **1990**, *123*, 23.

(20) Appel, R.; Casser, C.; Knoch, F. *J. Organomet. Chem.* **1985**, *293*, 213.

(21) Holand, S.; Charrier, C.; Mathey, F.; Fischer, J.; Mitschler, A. *J. Am. Chem. Soc.* **1984**, *106*, 826.

(22) Knoll, K.; Huttner, G.; Wasciucione, M.; Zsolnai, L. *Angew. Chem.* **1984**, *96*, 708; *Angew. Chem., Int. Ed. Engl.* **1984**, *23*, 739.

(23) Adelt, S.; Bitterer, F.; Fischer, J.; Rothe, J.; Stelzer, O.; Sheldrick, W. S. *Chem. Ber.* **1992**, *125*, 1999.

(24) Williams, G. D.; Geoffrey, G. L.; Whittle, R. R.; Rheingold, A. L.; *J. Am. Chem. Soc.* **1985**, *107*, 729.

(25) Appel, R.; Krieger, L. *J. Organomet. Chem.* **1988**, *354*, 309.

(26) Niecke, E.; Leuer, M.; Nieger, M. *Chem. Ber.* **1989**, *122*, 453.

(27) Karsch, H. H. Personal communication.

0.35 ($^2J_{\text{PH}} = 2.5$ Hz) accounts for the proton at the π -bonded organophosphorus ligand.¹⁹ In the IR spectra of the complexes **3a,b,d** (toluene solution) the carbonyl stretching vibrations give rise to three intense bands at 2013 – 1919 cm⁻¹ for the terminal CO groups and one intense band at 1792 – 1783 cm⁻¹ for the bridging carbonyl. In **3c** the NO stretching vibration is assigned to a strong absorption at 1734 cm⁻¹.

X-ray Structure Analysis of 3a. Single crystals of **3a** suitable for an X-ray analysis were grown from

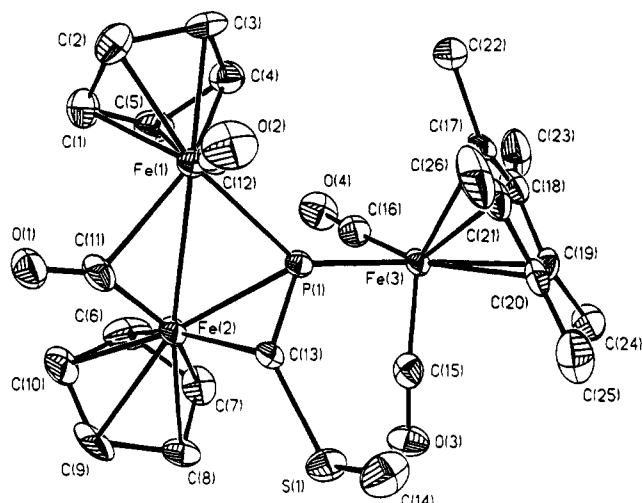


Figure 1.

Table 1. Atomic Coordinates ($\times 10^4$) and Equivalent Isotropic Displacement Parameters $U(\text{iso})$ or $U(\text{eq})^a$ ($\text{\AA}^2 \times 10^3$) for 3a

	x	y	z	$U(\text{eq})$
Fe(1)	1850(1)	2432(1)	7102(1)	22(1)
Fe(2)	4275(1)	2502(1)	6548(1)	21(1)
Fe(3)	3937(1)	5933(1)	6931(1)	20(1)
S(1)	7351(3)	4626(2)	8040(2)	29(1)
P(1)	3801(2)	4084(2)	7233(1)	19(1)
O(1)	3322(8)	493(6)	7370(5)	33(2)
O(2)	2766(9)	2697(7)	9029(5)	43(2)
O(3)	6805(8)	6232(6)	6459(5)	35(2)
O(4)	1896(9)	4710(7)	5109(5)	41(2)
C(1)	148(12)	920(9)	6144(7)	42(3)
C(2)	-305(11)	1193(9)	6921(7)	32(2)
C(3)	-397(9)	2399(9)	7026(6)	29(2)
C(4)	0(10)	2845(9)	6302(6)	29(2)
C(5)	352(11)	1939(9)	5768(6)	32(2)
C(6)	3577(12)	1990(11)	5103(6)	40(3)
C(7)	4821(11)	3079(9)	5417(6)	30(2)
C(8)	6092(11)	2885(9)	5971(6)	28(2)
C(9)	5688(13)	1645(10)	6015(7)	39(3)
C(10)	4133(13)	1089(9)	5488(7)	40(3)
C(11)	3418(11)	1379(8)	7110(6)	27(2)
C(12)	2468(11)	2622(8)	8283(6)	28(2)
C(13)	5429(10)	3710(7)	7828(6)	23(2)
C(14)	7976(12)	5110(10)	9259(6)	39(2)
C(15)	5657(11)	6052(8)	6655(6)	27(2)
C(16)	2711(11)	5179(8)	5823(6)	29(2)
C(17)	2423(11)	6543(8)	7556(7)	35(2)
C(18)	2895(11)	7332(8)	6983(6)	29(2)
C(19)	4502(11)	7858(7)	7321(6)	27(2)
C(20)	5011(11)	7406(8)	8094(6)	26(2)
C(21)	3701(12)	6606(8)	8228(6)	32(2)
C(22)	771(14)	5912(11)	7508(11)	66(4)
C(23)	1883(14)	7596(10)	6208(8)	51(3)
C(24)	5492(12)	8793(9)	6973(7)	35(2)
C(25)	6605(14)	7835(10)	8700(7)	47(3)
C(26)	3682(17)	6001(10)	8991(7)	53(3)
C(27)	8393(14)	1111(9)	10531(7)	40(2)
C(28)	6877(13)	1056(10)	10216(8)	47(3)
C(29)	6329(14)	1320(11)	9410(9)	51(3)
C(30)	7289(16)	1677(10)	8900(8)	50(3)
C(31)	8768(14)	1731(12)	9168(7)	52(3)
C(32)	9334(13)	1459(12)	9976(8)	52(3)
C(33)	9030(16)	784(11)	11399(8)	54(3)

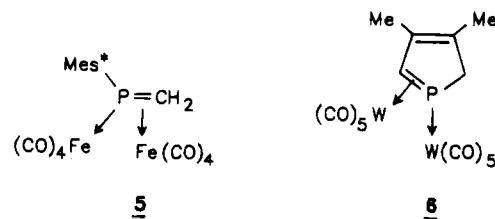
^a $U(\text{eq})$ is defined as one-third of the trace of the orthogonalized U_{ij} tensor.

toluene/cyclopentane solutions at -40°C . The analysis displays the picture of a metallophosphaalkene which serves as a bridging $\eta^1:\eta^2$ -ligand toward the $\text{Cp}_2(\text{CO})_2\text{-Fe}_2$ moiety (Figure 1; Tables 1 and 2). Such a coordination mode of metallophosphaalkenes is novel. Metal-free phosphoalkenes may well interact as μ -($\eta^1:\eta^2$)-

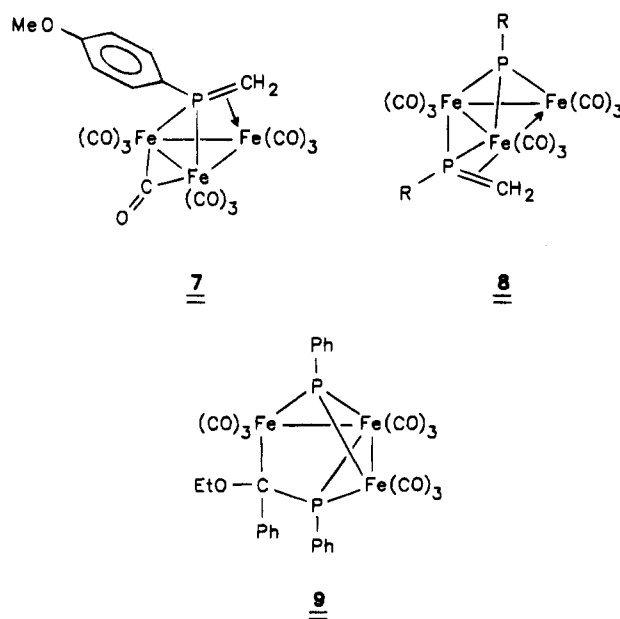
Table 2. Selected Bond Lengths (\AA) and Angles (deg) for 3a

Fe(1)–C(12)	1.771(10)	C(12)–Fe(1)–C(11)	82.7(4)
Fe(1)–C(2)	2.080(10)	C(12)–Fe(1)–P(1)	89.3(3)
Fe(1)–C(3)	2.088(9)	C(11)–Fe(1)–P(1)	87.9(3)
Fe(1)–C(1)	2.104(10)	C(12)–Fe(1)–Fe(2)	105.7(3)
Fe(1)–C(4)	2.129(9)	C(11)–Fe(1)–Fe(2)	43.5(2)
Fe(1)–C(5)	2.130(10)	P(1)–Fe(1)–Fe(2)	52.74(7)
Fe(1)–C(11)	2.162(9)	C(11)–Fe(2)–P(1)	98.8(3)
Fe(1)–P(1)	2.221(3)	C(13)–Fe(2)–P(1)	50.0(2)
Fe(1)–Fe(2)	2.616(2)	C(11)–Fe(2)–Fe(1)	54.9(3)
Fe(2)–C(11)	1.818(9)	C(13)–Fe(2)–Fe(1)	82.9(2)
Fe(2)–C(9)	2.101(9)	P(1)–Fe(2)–Fe(1)	54.27(7)
Fe(2)–C(10)	2.085(9)	C(15)–Fe(3)–C(16)	95.8(4)
Fe(2)–C(13)	2.104(9)	C(13)–S(1)–C(14)	101.8(5)
Fe(2)–C(8)	2.098(8)	C(13)–P(1)–C(12)	62.9(3)
Fe(2)–C(6)	2.144(10)	C(13)–P(1)–Fe(1)	102.2(3)
Fe(2)–C(7)	2.128(8)	Fe(2)–P(1)–Fe(1)	72.98(9)
Fe(2)–P(1)	2.177(3)	C(13)–P(1)–Fe(3)	124.3(3)
Fe(3)–C(15)	1.752(9)	Fe(2)–P(1)–Fe(3)	131.65(11)
Fe(3)–C(16)	1.778(10)	Fe(1)–P(1)–Fe(3)	133.06(11)
Fe(3)–C(19)	2.105(8)	O(1)–C(11)–Fe(2)	152.3(7)
Fe(3)–C(17)	2.111(8)	O(1)–C(11)–Fe(1)	125.8(7)
Fe(3)–C(20)	2.113(9)	Fe(2)–C(11)–Fe(1)	81.7(3)
Fe(3)–C(18)	2.118(9)	O(2)–C(12)–Fe(1)	175.5(9)
Fe(3)–C(21)	2.138(9)	S(1)–C(13)–P(1)	123.5(5)
Fe(3)–P(1)	2.261(3)	S(1)–C(13)–Fe(2)	118.9(4)
S(1)–C(13)	1.764(9)	P(1)–C(13)–Fe(2)	67.1(3)
S(1)–C(14)	1.811(10)	O(3)–C(15)–Fe(3)	174.1(8)
P(1)–C(13)	1.812(9)	O(4)–C(16)–Fe(3)	178.3(8)
O(1)–C(11)	1.163(10)		
O(2)–C(12)	1.126(11)		
O(3)–C(15)	1.168(11)		
O(4)–C(16)	1.150(11)		

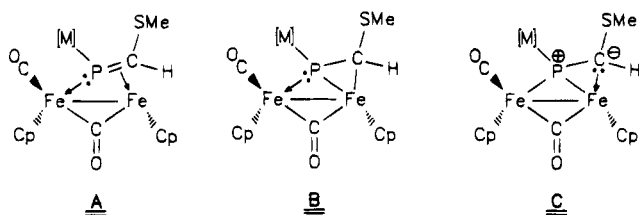
ligands in dinuclear complexes (e.g. in **5**²⁰ and **6**²¹).



Here, however, unlike in **3a–d** a direct metal–metal linkage is absent. In cluster-stabilized phosphoalkenes **7**²² and **8**,²³ the phosphorus atom also bridges two metal centres, whereas the P=C π -bond interacts with a third iron atom.

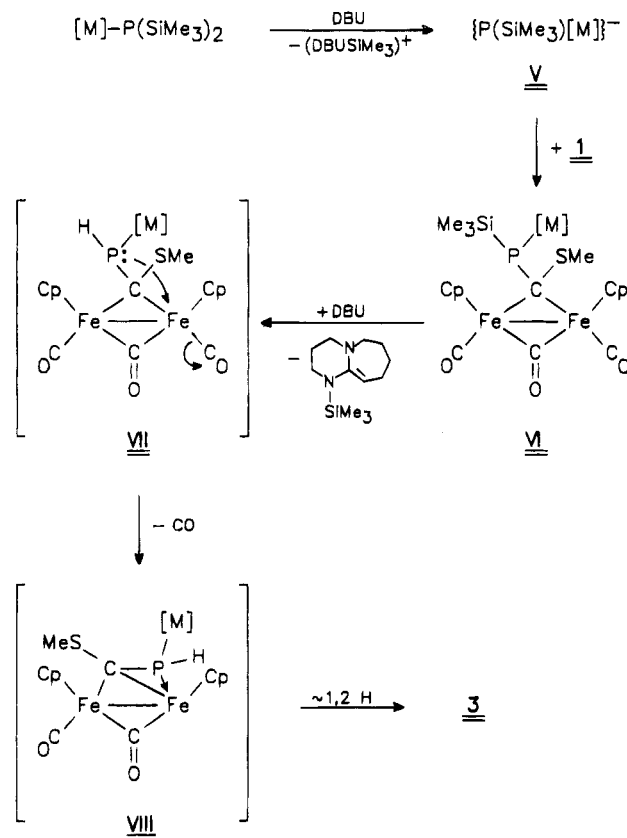


Two different iron–phosphorus bonds [Fe(1)–P(1) = 2.221(3), Fe(2)–P(1) = 2.177(3) Å] and an iron–carbon bond [Fe(2)–C(13) = 2.104(9) Å] underline the unsymmetrical ligation of the P=C moiety of the metallophosphaalkene to the Fe–Fe unit. The σ/π coordination is accompanied by an elongation of the P=C bond to 1.812(9) Å. In free phosphoalkenes P=C double bonds range from 1.65 to 1.72 Å, whereas P=C distances in **5** and **7–9**²⁴ amount to 1.737(6), 1.76(1), 1.772(4), and 1.800(6) Å, respectively. The Fe–Fe bond in **1** [2.616(2) Å] is similar to the metal–metal separation in **1** (SET instead of SMe) [2.510(2) Å]¹⁴ or **II** [2.527(5) Å]⁶ and those found in clusters **8** and **9** [2.671(2)–2.750(1) Å]. The (*Z*)-configured organophosphorus ligand is distorted from planarity as evidenced by the torsion angle Fe(3)–P(1)–C(13)–S(1) [–13.3°]. The Cp₂Fe₂ unit possesses a nearly linear terminal CO ligand at Fe(1) [Fe(1)–C(12) = 1.771(10) Å, Fe(1)–C(12)–O(2) = 175.5(9)°], whereas the second ligand is a semibridging one with a short Fe(2)–C(11) contact [1.818(9) Å] and a markedly longer Fe(1)–C(11) bond [2.162(9) Å]. In keeping with this, the bond angles Fe(2)–C(11)–O(1) = 152.3(7)° and Fe(1)–C(11)–O(1) = 125.8(7)° differ significantly. Both cyclopentadienyl rings are *syn*-configured. The metric parameters of the (C₅Me₅)(CO)₂Fe fragment which is linked to P(1) via a Fe–P single bond [2.261(3) Å] are as expected. With respect to the spectroscopic and structural data the bonding situation in **3a** may be described by the canonical structures **A–C**.

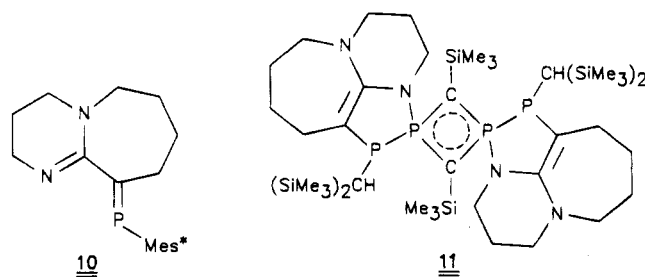


Discussion. It is conceivable that the formation of compounds **3** is initiated by the nucleophilic attack of metallo(silyl)phosphide {P(SiMe₃)[M]}[–] (**V**) at the carbyne bridge of **1** to give the μ -alkylidene complex **VI** (Scheme 2). Compounds such as **VI** were detected as intermediates during the formation of **II**. The replacement of the Me₃Si group at phosphorus in **VI** by hydrogen was unexpected. Hydrolysis by traces of moisture can be excluded as the reaction vessels were flame-dried. The acetonitrile and trideuterioacetonitrile used as solvents were dried by refluxing over P₄O₁₀ as described by Christe et al.⁸ With CD₃CN as a solvent no incorporation of deuterium in **3a** was observed. DBU was treated with potassium metal before use. Thus the source of the hydrogen may be DBU itself. This is in line with findings where the acidic methylene group in the α -position of the imino carbon of DBU was involved in a condensation reaction with Mes*PCl₂ to give **10**.²⁵ Moreover one of these α -hydrogens of DBU was substituted by a phosphiranyl group when treated with ClPC(SiMe₃)₂CHSiMe₃.²⁶ The attempted dehydrochlorination of (Me₃Si)₂CHPCl₂ by means of DBU surpris-

Scheme 2



ingly afforded the condensation product **11**.²⁷ Thus it is reasonable that **VI** is desilylated by DBU and that the cation [DBU–SiMe₃]⁺ is deprotonated by the generated metallophosphide. An intramolecular replacement of CO by the phosphine function results in **VIII**. A 1,2 hydrogen shift and a second Fe–P contact leads to the final product. It is worth mentioning that the formation of **3** failed when NEt₃ was used instead of DBU.



In a control experiment **1**, (η^5 -C₅Me₅)(CO)₂Fe–PH₂ and DBU afforded **3a** in a slightly better yield (39% instead of 28%). The difference in the reactivity of arylPH–(SiMe₃) or arylPH₂ and [M]–PH(SiMe₃) or [M]–PH₂ towards **1** may be rationalized by regarding the common intermediate **VI**. Obviously activation by the aryl group at phosphorus promotes 1,2 elimination of Me₃SiSMe or HSMMe to give **II**, whereas the electron donating metal group enhances the phosphane nucleophilicity facilitating intramolecular CO displacement instead of 1,2-elimination. In **VIII** the P–H bond at the tetracoordinate phosphorus atom is acidified enough to allow the

1,2 H-shift from phosphorus to carbon yielding μ -(η^1 : η^2)-metallophosphaalkene complexes **3a-d** as final products.

Acknowledgment. This work was generously supported by the Deutsche Forschungsgemeinschaft, Bonn, the Fonds der Chemischen Industrie, Frankfurt, the

BASF AG, Ludwigshafen, and the DEGUSSA AG, Hanau, which is gratefully acknowledged.

Supplementary Material Available: Tables of crystallographic data collection parameters, bond lengths and angles, anisotropic thermal parameters, and H coordinates and U values (7 pages). Ordering information is given on any current masthead page.

OM940245I

Ionic Titanocene(IV) α -Amino Acid Complexes of DL-Phenylalanine and DL-4-Fluorophenylalanine: Synthesis, Characterization, and Investigation of the Antimicrobial Behavior toward *Escherichia coli*

Inis C. Tornieporth-Oetting*

Institut für Anorganische und Analytische Chemie, Technische Universität Berlin,
Strasse des 17 Juni 135, Sekr. C2, D-10623 Berlin, Germany

Peter S. White

Department of Chemistry, University of North Carolina, Chapel Hill, North Carolina 27599

Received October 24, 1994[®]

Antitumor-active titanocene dichloride (Cp_2TiCl_2 ; $\text{Cp} = \eta^5\text{-C}_5\text{H}_5$) reacts with α -amino acids (aa) in methanol to give the titanium(IV) amino acid complexes $[\text{Cp}_2\text{Ti}(\text{aa})_2]^{2+}[\text{Cl}]_2^-$ (aa = DL-phenylalanine, **1**; DL-4-fluorophenylalanine, **2**). Metathetical reactions of **1** and **2** with 2 equiv of AgAsF_6 yielded the ionic complexes $[\text{Cp}_2\text{Ti}(\text{DL-Phe})_2]^{2+}[\text{AsF}_6]_2^-$ (**3**) and $[\text{Cp}_2\text{Ti}(\text{DL-4-F-Phe})_2]^{2+}[\text{AsF}_6]_2^-$ (**4**). All complexes have been characterized by chemical analyses (C/H/N) and NMR (^1H , ^{14}N , ^{19}F), infrared, and Raman spectroscopy. Preliminary structural data of complex **4** are also presented: monoclinic, $P2_1/c$; $a = 11.751(3)$, $b = 20.257(3)$, $c = 16.080(4)$ Å; $\beta = 110.01(0)^\circ$; $Z = 4$. In addition, the antimicrobial behavior (against *E. coli*) of all complexes was determined and is discussed in comparison with the free amino acids. It was established that not only DL-4-fluorophenylalanine but also the titanocene complex **2** and, to some minor extent, also **3** and **4** cause elongation of *E. coli*.

Introduction

Recently we became interested in the coordination behavior of the cytostatic active titanocene dichloride toward α -amino acids in order to synthesize titanium model complexes containing biologically important ligands. All reactions of Cp_2TiCl_2 with glycine, L-alanine, and 2-methylalanine were carried out in aqueous methanol.^{1,2} The synthesized complexes, which are stable toward air and moisture, were fully characterized, and it was shown by vibrational spectroscopy and X-ray structure determination that the amino acids are bound to titanium exclusively via the oxygen of the carboxylate group.^{1,2} Continuing these studies, we became interested in complexes containing essential amino acids such as phenylalanine. Moreover, especially fluorine-substituted analogues of the naturally occurring amino acids and nucleic acids have become established as antiviral, antitumor, and antifungal agents, and a number of potential drugs in which fluorine substitution is a key to biological activity are under intensive study.³ In these instances, the electronic or polar effects of the fluorine substituent must play a significant role in the expression of biological activity.³ Therefore, we also included one (artificial) fluorine analogue of DL-phenylalanine, *p*-fluorophenylalanine, in the present study. In previous studies by other investigators it was established that peptides accessible to phenylalanine during normal biosynthesis are also accessible to *p*-fluorophenylalanine and that there is some suppression of protein

synthesis by the F analogue.^{4,5} Moreover, it has been pointed out that labile proteins are of general importance in controlling cell division and that the fundamental chemical events which regulate cell division are similar in higher organisms and in bacteria.^{4,6} Therefore, we became interested not only in the syntheses of these complexes but also in the investigation of the biological properties toward *Escherichia coli*.

Experimental Section

General Techniques. All reactions were carried out using Schlenk technique under argon atmosphere or were carried out in SO_2 atmosphere in a two-bulb glass vessel equipped with PTFE valves.⁷ Titanocene dichloride (Cp_2TiCl_2) was prepared by literature methods.⁸ The amino acids (aa) DL-phenylalanine (DL-Phe) and DL-4-fluorophenylalanine (DL-4-F-Phe) were used as commercially available without further purification (Aldrich). Methanol (Merck) and Freon-11 (CFCl_3 , Merck) were used as supplied. Infrared spectra were recorded using a Perkin-Elmer 580 B instrument, and Raman spectra were measured with a Jobin Yvon Ramanor U 1000 spectrometer, equipped with a Spectra Physics Kr laser ($\lambda = 647.09$ nm) or a Bruker FT-IR/Raman spectrometer (IFS 66/FRA 106), equipped with a Nd-YAG laser (1060 nm). ^1H NMR and ^{19}F NMR spectra were obtained from a Bruker ARX200 instrument (200 MHz, ^1H ; 188 MHz, ^{19}F) and were referred to TMS or CFCl_3 , respectively. ^{14}N NMR spectra were recorded using a Bruker ARX400 instrument operating at 28.901 MHz and were referred to external CH_3NO_2 . Elemental analyses were performed by the TU Berlin service.

[®] Abstract published in *Advance ACS Abstracts*, March 1, 1995.

(1) Klapötke, T. M.; Köpf, H.; Tornieporth-Oetting, I. C.; White, P. S. *Angew. Chem.* **1994**, *106*, 1587-1589; *Angew. Chem., Int. Ed. Engl.* **1994**, *33*, 1518-1519.

(2) Klapötke, T. M.; Köpf, H.; Tornieporth-Oetting, I. C.; White, P. S. *Organometallics* **1994**, *13*, 3628-3633.

(3) Bergstrom, D. E.; Swartling, D. J. In *Fluorine-Containing Molecules*; Liebman, J. F., Greenberg, A., Dolbier, W. R., Jr., Eds.; VCH Publishers: New York, 1988; pp 259-308, and references therein.

(4) Wheatley, D. N.; Henderson, J. Y. *Nature* **1974**, *247*, 281-283, and references therein.

(5) Richmond, M. H. *J. Mol. Biol.* **1963**, *6*, 284-294.

(6) Smith, H. S.; Pardee, A. B. *J. Bacteriol.* **1970**, *101*, 901-909.

(7) Woollins, J. D. *Inorganic Experiments*; VCH: Weinheim, New York, 1994; pp 217-219.

(8) Wilkinson, G.; Birmingham, J. M. *J. Am. Chem. Soc.* **1954**, *76*, 4281-4284.

Synthesis of 1. Cp₂TiCl₂ (0.75 g, 3.0 mmol) and DL-Phe (1.00 g, 6.0 mmol) were stirred in 10 mL of CH₃OH at room temperature. After 20 min the precipitated light orange solid was filtered off, washed several times with CFCl₃, and dried in vacuo (94%, T_{dec} > 140 °C). Anal. Calcd for C₂₈H₃₂Cl₂N₂O₄Ti (579.36): C, 58.1; H, 5.6; N, 4.8. Found: C, 57.2; H, 5.5; N, 4.8. ¹H NMR (D₂O, relative to D₂O int): δ 7.25–7.12 (m, C₆H₅, 10H), 6.41/6.31 (Cp, 10H), 3.93–4.03 (m, CH, 2H), 3.20–2.90 (m, CH₂, 4H). ¹⁴N NMR (D₂O): δ –340.4 (s, NH₃⁺). IR (KBr, cm⁻¹): 3450 (ms, br), 3030 (s), 2925 (s, br, sh), 2860 (s, br, sh), 2716 (ms, sh), 2640 (ms), 2495 (m), 1665 (s), 1605 (m, sh), 1594 (ms), 1530 (ms), 1515 (ms), 1496 (ms), 1455 (m), 1438 (ms), 1378 (s), 1352 (ms), 1312 (s), 1272 (s), 1210 (ms), 1132 (ms), 1080 (m), 1028 (ms), 1015 (m), 827 (s), 810 (ms), 760 (m), 745 (ms), 702 (s), 615 (ms), 590 (m), 541 (ms), 482 (m), 442 (m), 423 (ms). Raman (647 nm, 22 °C, 20 mW, 8 scans, cm⁻¹): 3120 (<1), 3068 (<1), 2934 (<1), 2330 (<1), 1738 (1), 1664 (1), 1608 (1), 1529 (1), 1445 (1), 1133 (5), 1002 (5), 811 (1), 761 (1), 623 (1), 422 (2), 381 (2), 354 (3), 296 (3), 260 (10), 147 (1).

Synthesis of 2. Cp₂TiCl₂ (1.05 g, 4.2 mmol) and DL-4-F-Phe (1.55 g, 8.5 mmol) were reacted at room temperature for 30 min as described above and yielded an orange solid (83%, T_{dec} > 140 °C). Anal. Calcd for C₂₈H₃₀Cl₂F₂N₂O₄Ti (615.34): C, 54.7; H, 4.9; N, 4.6. Found: C, 54.1; H, 4.9; N, 4.3. ¹H NMR (D₂O, rel to D₂O int): δ 7.18–6.93 (m, C₆H₄F, 8H), 6.43/6.34 (Cp, 10H), 4.03–3.96 (m, CH, 2H), 3.18–2.94 (m, CH₂, 4H). ¹⁴N NMR (D₂O): δ –340.2 (s, NH₃⁺). ¹⁹F NMR (D₂O): δ –117.3 to –117.5 (m, C₆H₄F). ¹⁹F{¹H} NMR (D₂O): δ –117.4 (s, C₆H₄F). IR (KBr, cm⁻¹): 3436 (ms, br), 3130 (s, br), 3092 (s, br), 3025 (s, br), 2926 (s, br), 2867 (s, br), 2716 (ms), 2643 (ms), 2626 (m), 2560 (m), 2492 (m), 1660 (vs), 1605 (ms), 1593 (ms), 1583 (ms), 1530 (ms), 1510 (vs), 1447 (ms), 1438 (ms), 1420 (m), 1377 (vs), 1352 (s), 1325 (vs), 1313 (vs), 1294 (s), 1275 (vs), 1224 (s), 1215 (vs), 1198 (m), 1168 (m), 1165 (m), 1160 (m), 1131 (m), 1101 (m), 1096 (m), 1045 (m), 1028 (m), 1016 (m), 880 (m), 856 (ms), 840 (ms), 830 (vs), 790 (ms), 725 (ms), 708 (m), 638 (m), 625 (ms), 614 (s), 595 (m), 570 (m), 541 (ms), 500 (m), 436 (ms). Raman (647 nm, 22 °C, 50 mW, 8 scans, cm⁻¹): 3193 (<1), 2940 (<1), 2872 (<1), 1981 (<1), 1663 (<1), 1600 (<1), 1438 (<1), 1364 (<1), 1215 (<1), 1200 (<1), 1162 (<1), 1134 (3), 1072 (<1), 977 (<1), 822 (2), 638 (1), 438 (2), 374 (1), 357 (3), 336 (<1), 294 (2), 261 (10), 241 (2), 189 (1), 124 (1).

Synthesis of 3. **1** (1.31 g, 2.3 mmol) and AgAsF₆ (1.35 g, 4.6 mmol) were reacted at room temperature in SO₂ solution for 30 min during which AgCl precipitated and the solution turned into light red. The crude product was isolated in the drybox and filled in an extraction vessel and orange **3** was separated from insoluble AgCl by extraction with SO₂ (77%, T_{dec} > 60 °C). Anal. Calcd for C₂₈H₃₂As₂F₁₂N₂O₄Ti (886.28): C, 38.0; H, 3.6; N, 3.2. Found: C, 37.0; H, 3.4; N, 3.1. ¹H NMR (CD₃CN, rel to TMS ext.): δ 7.41–7.30 (m, C₆H₅, 10H), 6.57/6.55 (Cp, 10H), 4.28–4.22 (m, CH, 2H), 3.39–3.11 (m, CH₂, 4H). ¹⁴N NMR (SO₂): δ –338.8 (s, NH₃⁺). ¹⁹F NMR (SO₂): δ –67.6 (q, AsF₆⁻, ¹J_{AsF} = 932 Hz). IR (KBr, cm⁻¹): 3630 (m), 3570 (m), 3430 (ms, br), 3260 (ms), 3120 (m), 3030 (m), 2930 (m, br), 1740 (m, br), 1655 (s, br), 1615 (ms, br, sh), 1498 (s), 1456 (m), 1445 (m), 1390 (ms, br), 1332 (ms, br, sh), 1232 (w), 1210 (w), 1132 (m), 1075 (w), 1030 (m), 1018 (m), 950 (w), 920 (w), 835 (s), 745 (s), 700 (vs), 675 (s, sh), 585 (m), 552 (m), 540 (m, sh), 483 (m), 395 (vs). Raman (1064 nm, 22 °C, 180 mW, 1024 scans, cm⁻¹): 1133 (5), 1004 (4), 679 (3), 264 (10).

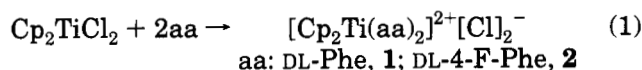
Synthesis of 4. **2** (1.40 g, 2.3 mmol) and AgAsF₆ (1.35 g, 4.6 mmol) were reacted in the way described above (59%, T_{dec} > 68 °C). **4** was redissolved in SO₂, and slow evaporation of the solvent yielded red crystals which were suitable for X-ray structure determinations. Anal. Calcd for C₂₈H₃₀As₂F₁₄N₂O₄Ti (922.26): C, 36.5; H, 3.3; N, 3.0. Found: C, 35.9; H, 3.1; N, 3.1. ¹H NMR (CD₃CN, rel to TMS ext.): δ 7.37–7.10 (m, C₆H₄F, 8H), 6.60/6.58 (Cp, 10H), 4.16–4.09 (m, CH, 2H), 3.38–3.09 (m, CH₂, 4H). ¹⁴N NMR (SO₂): δ –338.2 (s, NH₃⁺). ¹⁹F

NMR (SO₂): δ –67.6 (q, AsF₆⁻, 6F, ¹J_{AsF} = 928 Hz), –118.2 (s, C₆H₄F, 2F). ¹⁹F NMR (CD₃CN): δ –67.5 (q, AsF₆⁻, 6F, ¹J_{AsF} = 930 Hz), –118.3 (s, C₆H₄F, 2F). IR (KBr, cm⁻¹): 3630 (m), 3555 (m), 3300 (s), 3265 (s), 3240 (s), 3118 (s), 3060 (s, br), 2960 (s, br), 1950 (m), 1650 (vs, br), 1605 (s, br), 1510 (vs), 1485 (s), 1445 (s), 1400 (vs), 1345 (s), 1328 (vs), 1265 (s), 1222 (vs), 1160 (s), 1140 (m), 1125 (m), 1100 (ms), 1070 (ms), 1020 (ms), 950 (m), 935 (m), 920 (m), 860 (s), 838 (vs), 822 (s), 795 (ms), 695 (vs, br), 625 (m), 585 (ms), 568 (s), 530 (s), 492 (s), 485 (ms), 425 (ms), 395 (vs), 350 (ms). Raman (1064 nm, 22 °C, 180 mW, 1024 scans, cm⁻¹): 1445 (1), 1203 (1), 1163 (1), 1134 (8), 1074 (1), 826 (2), 679 (5), 433 (3), 264 (10), 109 (1).

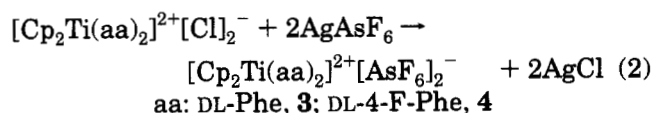
Antimicrobial Studies. *Escherichia coli* strain DSM 498 (Deutsche Sammlung von Mikroorganismen, Braunschweig, Germany) was used throughout these experiments. The bacteria were grown aerobically in a gyratory shaker at 37 °C in an M-9 broth modified according to literature procedures:⁶ 7 g of Na₂HPO₄, 3 g of KH₂PO₄, 0.5 g of NaCl, 1 g of NH₄Cl, 0.2 g of MgSO₄·7H₂O, and 4 g of glucose as carbon source per liter of distilled water. After addition of 1.2% agar (Unipath, UK) and appropriate amounts of the bactericides (**1**–**4**; DL-Phe; DL-4-F-Phe) to the bouillon, 10 mL of these media was transferred into each culture disk and inoculated with different concentrations of *E. coli* in the exponential phase. After incubation at 37 °C for 72 h, the colonies were counted.

Results and Discussion

Chemical Aspects. The new complexes containing the aromatic amino acids phenylalanine and 4-fluorophenylalanine were synthesized in high yields from Cp₂TiCl₂ in methanol at room temperature according to eq 1. The solid orange compounds **1** and **2** are stable



at room temperature and are nonsensitive toward air and moisture. They are insoluble in most organic solvents such as dichloromethane, tetrahydrofuran, toluene, ethanol, or diethyl ether but can be dissolved in water. Metathetical reactions of **1** or **2** with 2 equiv of AgAsF₆ in SO₂ solution led to the formation of the corresponding AsF₆⁻ salts **3** and **4** of the titanocene amino acid complexes (eq 2). These AsF₆⁻ salts are of



lower thermal stability and are insoluble in water, but dissolve in SO₂ or acetonitrile. In contrast to **1** and **2**, complexes **3** and **4** decompose slowly in air but can be stored under argon atmosphere. All compounds (**1**–**4**) gave reasonable microanalytical data (C/H/N; see Experimental Section).

The ¹H NMR spectra (see Experimental Section) of the titanocene amino acid complexes **1**–**4** clearly show two sharp resonances in the Cp region indicative for the presence of the DD, LL (not resolved, same resonance frequency), and DL isomers. This result can easily be understood since we started with a racemic mixture of D- and L-amino acids. For all compounds, the ¹⁴N NMR spectra show resonances in agreement with the ionic ammonium (NH₃⁺) structures (relative to MeNO₂: **1**, –340 ppm; **2**, –340 ppm; **3**, –339 ppm; **4**, –338 ppm; cf. ⁻O₂CCH(NH₃⁺)CH₂C₆H₅, –338 ppm; ⁻O₂CCH(NH₃⁺)CH₂C₆H₄F, –338 ppm). Whereas the ¹⁹F{¹H} NMR

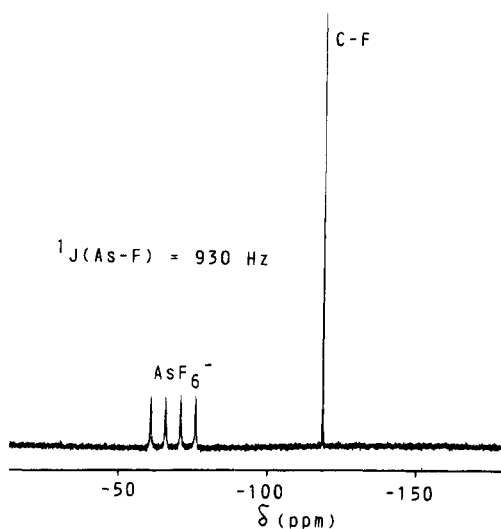


Figure 1. $^{19}\text{F}\{^1\text{H}\}$ NMR spectrum of **4** (188 MHz, 20 °C SO_2 , rel to CFCl_3).

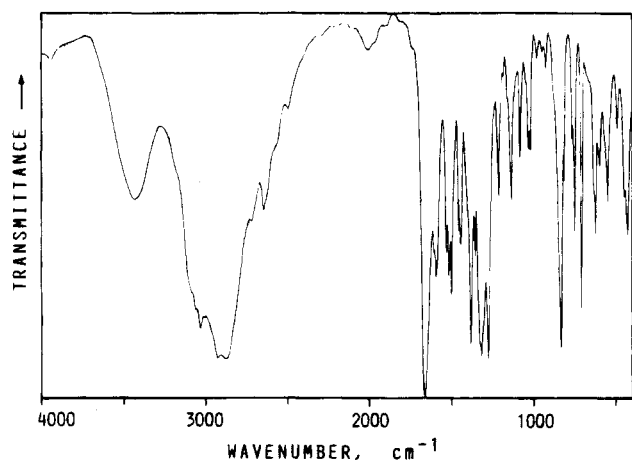


Figure 2. IR spectrum of **1** (KBr disk, 22 °C).

spectrum of **2** shows only one sharp resonance at -117.4 ppm (rel to CFCl_3), the $^{19}\text{F}\{^1\text{H}\}$ NMR spectra of **3** (-67.6 ppm, q, $^1J_{\text{AsF}} = 932$ Hz) and **4** (-118.2 ppm, s; -67.6 ppm, q, $^1J_{\text{AsF}} = 928$ Hz) (Figure 1) clearly show the presence of free octahedral AsF_6^- ions.

The infrared spectra of **1–4** show very strong absorptions due to the asymmetric $\nu(\text{COO})$ stretching mode (1665 ± 10 cm^{-1}) and a strong band that can be assigned to the symmetric $\nu(\text{COO})$ stretching mode (1350 ± 50 cm^{-1}) (Figure 2) (for assignment cf. ref 2).

Raman spectra of all complexes **1–4** were also recorded. Since the AsF_6^- salts **3** and **4** show strong fluorescence when the 647 nm excitation line was used, the Raman spectra of these compounds were obtained with an infrared Nd–YAG laser (1060 nm). In agreement with earlier studies,^{1,2} a strong peak at 1133 ± 1 cm^{-1} ($\delta(\text{CH})$, Cp; $\rho(\text{NH}_3^+)$) could be observed for all compounds (Figure 3). In addition, an intense peak at 262 ± 2 cm^{-1} that is characteristic for these titanocene amino acid complexes was detected in all cases (**1–4**).

In earlier studies, we established that ionic titanocene amino acid complexes of the type $[\text{Cp}_2\text{Ti}(\text{aa})][\text{Cl}]_2$ have strong cation–anion interactions in the solid state.² In such chloride complexes, all hydrogen atoms of the NH_3^+ groups have contacts to chloride ions and the mean N–Cl distances of 3.2 Å are substantially shorter than the sum of the van der Waals radii of N, H, and Cl (4.27

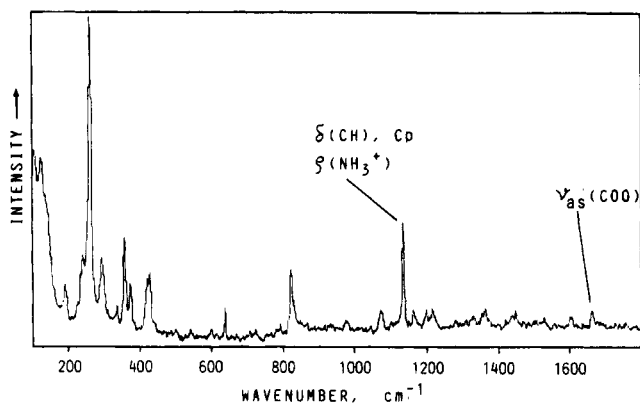


Figure 3. Raman spectrum of **2** (647.09 nm, 22 °C, 50 mW).

Å)⁹ (cf. sum of covalent radii of N, H, and Cl, 2.06 Å).¹⁰ In the present study, we now replaced the Cl^- ions in **1** and **2** in a metathetical reaction by the large and very weakly basic AsF_6^- ions (eq 2; **3** and **4**). Since the ^{19}F NMR data already indicated the presence of free AsF_6^- ions in solution (see above), we became interested in the solid state structures of **3** and **4**. In contrast to the chloride complexes **1** and **2**, the AsF_6^- compounds **3** and **4** are not water soluble. The decreased solubility of **3** and **4** vs **1** and **2** is a nice example of the low solubility of large cation, large anion salts in water.¹¹ However, **3** and **4** dissolve nicely in SO_2 and acetonitrile. Whereas we have so far been unable to grow crystals from CH_3CN solution (only oils were recovered after recrystallization), **3** and **4** slowly decompose in liquid SO_2 and crystals have to be grown within hours. This explains the poor quality of the crystalline material we obtained from SO_2 solution. However, we have been able to subject five different crystals of **4** to an X-ray diffraction analysis¹² and the *still preliminary data* clearly confirm the ionic structure of **4** in the solid state¹³ with no significant cation–anion interactions (Figure 4) and regularly octahedral AsF_6^- ions ($d_{\text{As–F}} = 1.62(4)$ Å). The appearance of only the DD isomer in the crystals investigated might be coincidence since the NMR data show the presence of all expected isomers. The prepa-

(9) Bondi, A. J. *Phys. Chem.* **1964**, *68*, 441–451.

(10) Greenwood, N. N.; Earnshaw, A. *Chemistry of the Elements*; Pergamon: Oxford, New York, 1984.

(11) Shriver, D. F.; Atkins, P. W.; Langford, C. H. *Inorganic Chemistry*, 2nd ed.; Oxford University Press: Oxford, U.K., 1994; Chapter 4.8.

(12) **Work in Progress.** Crystal data: **4**, $\text{C}_{28}\text{H}_{30}\text{AsF}_{14}\text{N}_2\text{O}_4\text{Ti}$, $M = 922.27$, monoclinic, space group $P2_1/c$; $a = 11.751(3)$, $b = 20.257(3)$, $c = 16.080(4)$ Å; $b = 110.01(0)^\circ$; $U = 3596.8(14)$ Å³; $Z = 4$; $D_{\text{calc}} = 1.703$ g cm^{-3} ; $F(000) = 1834.43$. Red crystal, dimensions $0.20 \times 0.20 \times 0.20$ mm; $\mu(\text{Mo K}\alpha) = 0.27$ mm^{-1} ; $\lambda(\text{Mo K}\alpha) = 0.709$ 30 Å. Data collection and processing: Rigaku AFC6S diffractometer using the routine DIFRAC,^{10a,b} θ – 2θ scan mode ($2\theta_{\text{max}} = 44.9^\circ$, $T = 22$ °C, graphite-monochromated Mo K α radiation; 4676 unique reflections measured, 1525 with $I_{\text{net}} > 2.5\sigma(I_{\text{net}})$ used for calculations; absorption correction was made using DIFABS.^{10a,b} Structure analysis and refinement: The structure was solved and refined with 82 atoms, 208 parameters, and 1525 of the 4676 independent reflections with use of NRCVAX^{10a,b} to residuals of $R_F = 0.151$ and $R_W = 0.180$. All non-hydrogen atoms were anisotropically refined. (a) Gabe, E. J.; Le Page, Y.; Charland, J.-P.; Lee, F. L.; White, P. S. *J. Appl. Crystallogr.* **1989**, *22*, 384–387. (b) Le Page, Y. *J. Appl. Crystallogr.* **1988**, *21*, 983–984.

(13) Bond lengths: Ti1–O1 1.89(3), Ti1–O3 1.96(3), O1–C1 1.32(7), C1–O2 1.18(7), C1–C2 1.61(8), C2–N1 1.40(7), C2–C3 1.35(9), C3–C4 1.45(7), C5–F1 1.33(4), and C10–F2 1.33(3) Å. Bond angles: O1–Ti1–O3 88.0(13), O1–C1–O2 128(5), O2–C1–C2 119(5), C1–C2–N1 105(4), C1–C2–C3 (117(5), N1–C2–C3 121(5), and C2–C3–C4 118(5)°.

(14) Motherwell, S. *University Chemical Laboratory, Cambridge, U.K.*, 1978.

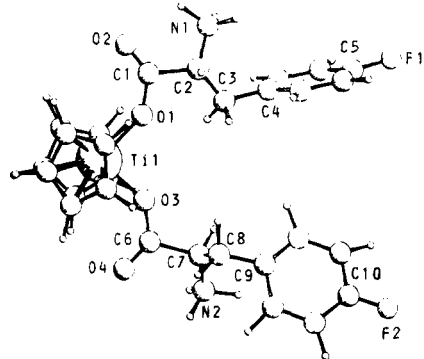


Figure 4. Structure of the dication in **4** (PLUTO plot).¹⁴

Table 1. Microbiological Activity of Ionic Titanocene Amino Acid Complexes

compd	MIC/g·g ⁻¹ ^b	$\kappa_{10^{-3}}$ ^a	κ_i ^a	$i/g\cdot g^{-1}$ ^b	max elong ^c
1	10 ⁻²	4	4	10 ⁻³	4
2	10 ⁻³	10 ⁴	4	10 ⁻⁵	30
3	10 ⁻⁵	∞	1.5	10 ⁻⁶	4
4	10 ⁻⁵	∞	4	10 ⁻⁶	10
DL-Phe	10 ⁻²	4	4	10 ⁻³	2
DL-4-F-Phe	10 ⁻⁴	10 ⁴	10	10 ⁻⁶	6
Cp_2TiCl_2 ²¹	> 10 ⁻²	1.2	1.2	10 ⁻³	
KAsF ₆ ²¹	> 10 ⁻²	1.3	1.3	10 ⁻³	

^a κ_i = bacterial count ($c = 0$)/bacterial count ($c = i$); c , bactericide content/g·g⁻¹. ^b The unit g·g⁻¹ means grams of solid per grams of solution. ^c Elongation of *E. coli* relative to the blind sample after 72 h incubation time and $c(\text{bactericide}) = 0.1$ MIC.

ration of **4** starting with enantiomerically pure amino acid led only to the formation of oily products. We are still trying to get better crystals of either **3** or **4**; however, with these compounds slowly decomposing in SO₂ a better solvent is still yet to be found and is likely not possible as **3** and **4** are insoluble in methanol and most of the organic solvents (including hydrocarbons, halocarbons, alcohols, ether, tetrahydrofuran, and benzene).

Microbiological Aspects. Table 1 summarizes the results from the microbiological studies and gives the minimum inhibitory concentrations (MIC) as well as the κ values for bactericide contents of 10⁻³ (0.1%, $\kappa_{10^{-3}}$) and the κ values for the lowest bactericide content i with significant inhibition (κ_i). For comparison, the literature data obtained for Cp_2TiCl_2 and KAsF₆ have also been included.

Whereas neither Cp_2TiCl_2 nor KAsF₆ shows strong bactericide activity compounds **1** and DL-Phe are somewhat active, but high concentrations of the bactericide are needed to get significant inhibition of the bacterial growth. Compounds **2** and DL-4-F-Phe on the other hand have strong biological activity that was again substantially exceeded by complexes **3** and **4**. It follows from these experiments, therefore, that the combination of the well-known bactericide DL-4-F-Phe with the antitumor drug Cp_2TiCl_2 , which does not show strong bactericide behavior, results in a complex (**2**) that is as active as the free fluoro amino acid is. Moreover, the metathetical exchange of the chloride counterions in **1** and **2** by the very large and weakly basic octahedral AsF₆⁻ ions afforded the ionic titanocene complexes **3** and **4**, which are highly active bactericides. (N.B. Neither KAsF₆ nor free DL-phenylalanine shows strong inhibition of bacterial growth.)

In previous studies (protein synthesis) by other investigators it has been established that peptides accessible to phenylalanine during normal biosynthesis are also accessible to *p*-fluorophenylalanine and that there is some suppression of protein synthesis by the F analogue.^{4,5} Moreover, it has been pointed out that labile proteins are of general importance in controlling cell division and that the fundamental chemical events that regulate cell division are similar in higher organisms and in bacteria.^{4,6} In this context, it is very interesting that the coordination of DL-4-fluorophenylalanine to the titanocene fragment Cp_2Ti , which is supposed to be the antiproliferative active moiety in antitumor titanocene complexes,¹⁵ results in a complex (**2**) that also displays strong bactericide properties. Moreover, the replacement of the chloride ions in **2** by weakly basic AsF₆⁻ anions in **4** greatly enhanced the bacteriocidal activity. Whereas in the solid state of titanocene amino acid complexes of the type $[Cp_2Ti(aa)_2][Cl]_2$ there are strong cation–anion interactions with contacts of all hydrogen atoms of the NH₃⁺ groups to chloride ions,^{1,2} the related AsF₆⁻ salts $[Cp_2Ti(aa)_2][AsF_6]_2$ do not show significant cation–anion interactions. This is probably due to the extremely low basicity of the AsF₆⁻ ions (which is only exceeded by “superanions” like $[(OTeF_5)_6E]^-$, E = As, Sb, Bi)¹⁶ and may very well explain the different biological behavior of **1** vs **3** and **2** vs **4**, respectively.

The finding of elongation of *E. coli* by Rosenberg et al.¹⁷ was the first hint to the biological activity of inorganic platinum complexes (cisplatin) and led to the detection of pronounced antitumor effectivity against animal and human tumors.¹⁸ It was also noticed that under treatment of *E. coli* with organobismuth compounds the bacteria became elongated, and eventually, the antiproliferative activity of this class of compounds was established.¹⁹ DL-4-F-Phe, when added to cultures of *E. coli* in the exponential phase, was also reported to cause a transformation of exponential into linear growth.²⁰ With the present study we confirm these observations. Moreover, we have been able to show that not only DL-4-F-Phe but also the titanocene complex **2** and, to some minor extent, **3** and **4** cause elongation of *E. coli* (Table 1). Elongation is generally interpreted as evidence that the agents are effecting cell division and DNA replication. Therefore, further investigations of the coordination behavior of these complexes to DNA is desirable and should be done in future studies.

Summary

This study allows the following conclusions to be drawn: (i) the reaction of Cp_2TiCl_2 with DL-Phe and DL-

(15) Köpf-Maier, P. In *Metal Complexes in Cancer Chemotherapy*; Keppler, B. K., Ed.; VCH: Weinheim, New York, 1993; pp 259–296, and references therein.

(16) Mercier, H. P. A.; Sanders, J. S. P.; Schrobilgen, G. J. *J. Am. Chem. Soc.* **1994**, *116*, 2921–2937.

(17) Rosenberg, B.; Camp, L.; Krigas, T. *Nature* **1965**, *205*, 698–699. Rosenberg, B.; Camp, L.; Grimley, E. B.; Thomson, A. J. *J. Biol. Chem.* **1967**, *242*, 1347. Rosenberg, B.; Renshaw, E.; Camp, L.; Hartwick, J.; Drobuik, J. *J. Bacteriol.* **1967**, *93*, 716.

(18) Rosenberg, B.; Camp, L.; Trosko, J. E.; Mansour, V. H. *Nature* **1969**, *222*, 385–386. Rosenberg, B. *Cancer* **1985**, *55*, 2303.

(19) Klapötke, T. M. *Biol. Met.* **1988**, *1*, 69–76, and references therein.

(20) Cohen, G. N.; Munier, R. *Biochim. Biophys. Acta* **1959**, *31*, 347–356.

(21) Gowik, P.; Klapötke, T. M. *Monatsh. Chem.* **1989**, *120*, 711–714.

4-F-Phe led to the preparation of the first titanocene complexes (**1**, **2**) containing essential amino acids; (ii) the metathetical reaction of **1** and **2** with AgAsF_6 yielded the corresponding titanocene amino acid hexafluoroarsenate salts **3** and **4**, which unlike all known chloride complexes contain both in solution and in the solid state "free" $[\text{Cp}_2\text{Ti}(\text{aa})_2]^{2+}$ cations with no significant cation-anion interactions; (iii) for all new complexes **1**–**4** the bactericide activity toward *E. coli* was established and increases in the order $1 < 2 \ll 3 \approx 4$; (iv) it was also established that the titanocene complex **2** and, to some minor extent, **3** and **4** also cause elongation of *E. coli*.

Since the finding of elongation of *E. coli* was the first hint to the biological activity of cisplatin and eventually led to the detection of the cytostatic activity of this

compound, we are now going to investigate in collaboration with other groups the antiproliferative activity of this new class of titanocene amino acid complexes by in vivo and in vitro experiments.

Acknowledgment. We gratefully acknowledge continuous financial support by the Deutsche Forschungsgemeinschaft, the Fonds der Chemischen Industrie, and the North Atlantic Treaty Organization (CRG 920034). We thank Dipl.-Chem. Rodion Kopitzky for recording the FT-Raman spectra and Prof. Dr. Dieter Knorr and Martin Bunzeit for supporting the microbiological studies. We are also indebted to Prof. Dr. Thomas M. Klapötke for his support of this work.

OM940811+

Multinuclear NMR Studies and Reaction with *tert*-Butyl Isocyanide of Dinuclear Tungsten– or Molybdenum–Palladium μ -Alkylidene Complexes. X-ray Structure of [PdI{ μ -C(*p*-tolyl)dmba}{ μ -CO}Mo(Cp)(CN-*t*-Bu)₂]

Alceo Macchioni and Paul S. Pregosin*

Laboratorium für Anorganische Chemie, ETH Zentrum, Zürich, 8092 Switzerland

Philippus F. Engel, Stefan Mecking, and Michel Pfeffer*

Laboratoire de Synthèses Métallo-induites (URA 416 du CNRS), 4, rue Blaise Pascal, 6F-7070 Strasbourg Cédex, France

Jean-Claude Daran and Jacqueline Vaissermann

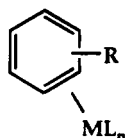
Laboratoire de Chimie des Métaux de Transition (URA 419 du CNRS), Université Pierre et Marie Curie, F-75230 Paris Cédex 05, France

Received November 9, 1994[®]

The ¹H, ¹³C, and ¹⁸³W NMR characteristics for a series of dinuclear complexes containing a W-(μ -CR¹R²)-Pd moiety are reported. These compounds, derived from the reaction of the carbyne complex (Cp)(CO)₂M(\equiv CR), M = Mo, W, R = cyclopentenyl or *p*-tolyl, with a dinuclear cyclopalladated complex are shown to possess an η^2 -bond from the cyclopentenyl or *p*-tolyl fragment to the metal, thus attaining an 18-electron configuration at M. The bridging carbon has its ¹³C absorption at δ = 142.4–155.1. Reaction of a Mo derivative with 2 equiv of *t*-BuNC displaces the η^2 -bond and affords a new complex, [PdI{ μ -C(*p*-tolyl)-dmba}{ μ -CO}Mo(Cp)(*t*-BuNC)₂], whose structure in the solid state was determined by X-ray diffraction. The solution NMR data for this complex clearly show that the η^2 -bond is no longer present.

Introduction

The organometallic chemistry of olefin complexes remains a field of active research.¹ One rather special subclass concerns the chemistry of η^2 -aromatic complexes, which, although rare, are increasingly recognized.^{2,3}



fragment showing an η^2 -aromatic complex

Recently,⁴ some of us have been involved in the preparation and characterization of the unusual dinuclear complexes that can be prepared from the reaction of several different halogen-bridged cyclometalated com-

plexes of Pd(II) with the tungsten carbyne complex W(Cp)(CO)₂(\equiv CR), where R is the cyclopentenyl fragment C₅H₇ or the *p*-tolyl fragment C₇H₇. Examples of these products are 1–4, with 4 having been characterized by X-ray crystallography. Analogous Mo complexes exist as well.

The immediate nature of the formerly carbyne carbon in 1–4 is not obvious. One can consider this bridging carbon ligand as formally a dianion, i.e., an [R¹R²C]²⁻-type donor, in which case the carbon might approach sp³ hybridization. This formalism would result in the assignment of Pd(II) and W(II) as the appropriate oxidation states for the metals. The observation of a quaternary ¹³C signal at ~100 ppm seemed consistent with this approach.⁵

We report here ¹H, ¹³C, ¹⁸³W, and NOESY NMR results which suggest that the above structures should be modified to include coordination of the double bond of the C₅H₇ or one of the C₇H₇ double bonds, thereby producing a complex whose structure contains an η^2 -olefin moiety.

Results and Discussion

Chart 1 shows the complexes studied, and Table 1 shows selected ¹³C and ¹⁸³W NMR data. We give full ¹H and ¹³C data for 1, 2, 10, and 13a in Tables 2 and 3.

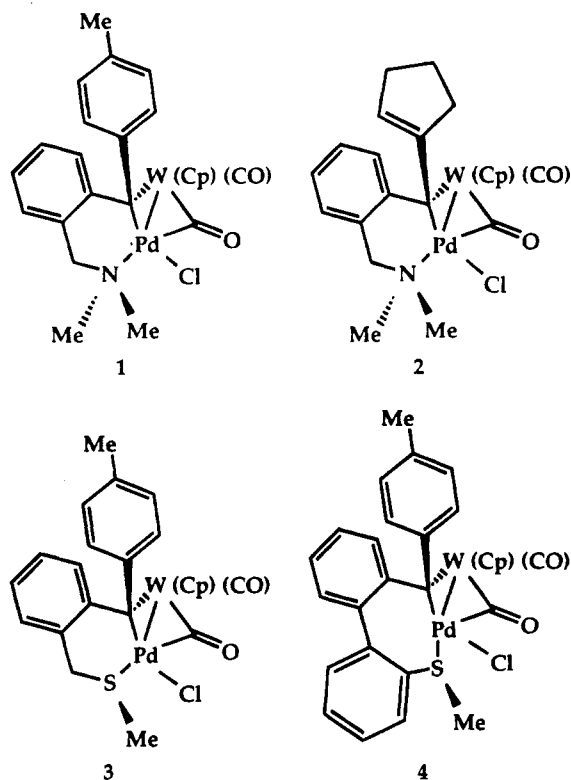
(5) (a) Herrmann, W. A. *Adv. Organometallic Chem.* **1982**, *20*, 159. (b) Ashworth, T. V.; Howard, J. A. K.; Laguna, M.; Stone, F. G. A. *J. Chem. Soc., Dalton Trans.* **1980**, 1593.

[®] Abstract published in *Advance ACS Abstracts*, March 1, 1995.
(1) Parshall, G. W.; Ittel, S. D. *Homogeneous Catalysis*, 2nd ed.; John Wiley and Sons, Inc.: New York, 1992.

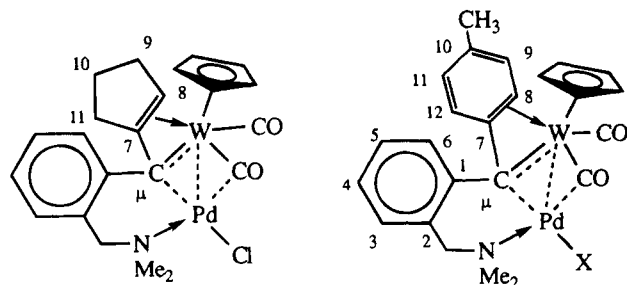
(2) Chin, R. M.; Dong, L.; Duckett, S. B.; Jones, W. D. *Organometallics* **1992**, *11*, 871. Belt, S. T.; Dong, L.; Duckett, S. B.; Jones, W. D.; Partridge, M. G.; Perutz, R. N. *J. Chem. Soc., Chem. Commun.* **1991**, 266. Jones, W. D.; Dong, L. *J. Am. Chem. Soc.* **1989**, *111*, 8722. Osson, H.; Pfeffer, M.; Jastrzebski, J. T. B. H.; Stam, C. H. *Inorg. Chem.* **1987**, *26*, 1169.

(3) (a) Kopach, M. E.; Hipple, W. G.; Harman, W. D. *J. Am. Chem. Soc.* **1992**, *114*, 1736. (b) Li, C.; Cheng, C.; Liao, F.; Wang, S. *J. Chem. Soc., Chem. Commun.* **1991**, 710.

(4) Engel, P. F.; Pfeffer, M.; Fischer, J. *Organometallics* **1994**, *13*, 4751.



Modified View of the Bonding in 1–10. We became aware of a possible η^2 -interaction involving the double bond of the cyclopentenyl group in **2** via a 2-D ^1H NOESY spectrum, a section of which is shown in Figure 1. An analysis of the cross-peaks reveals face-selective NOEs which arise from the two distinct faces of this C_5H_7 ligand when coordinated. A similar selectivity was also found to be present for the *p*-tolyl complexes. Indeed, inspection of the ^1H and ^{13}C spectra for these *p*-tolyl compounds reveals four ^1H and six ^{13}C *p*-tolyl signals, so that here, as well, there is restricted rotation about the $\mu\text{-C}-\text{C}(7)$ bond. In addition, the 2-D ^1H NOESY spectrum proved valuable in the assignment of the aromatic protons and, subsequently, via a ^{13}C , ^1H correlation, the pertinent ^{13}C signals.



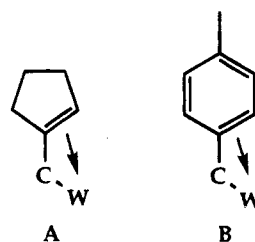
A routine ^{13}C , ^1H correlation for **2**, shown in Figure 2, revealed that the ^{13}C resonance for the protonated olefinic carbon appeared at $\delta = 60.8$, a much lower frequency than is expected if the double bond were not coordinated, but normal⁶ for a W(II) olefin complex. The assignment of the quaternary $\mu\text{-C}$ and C(7) resonances followed from a long-range ^{13}C , ^1H correlation, a section of which is also reproduced in Figure 2. From the observed two- (and the more reliable) three-bond

(6) Johnson, L. K.; Grubbs, R. H.; Ziller, J. W. *J. Am. Chem. Soc.* **1993**, *115*, 8131.

$J(^{13}\text{C}, ^1\text{H})$ -values,⁷ we see that the $\mu\text{-C}$ resonance appears at 147.6 ppm (the total range for our complexes is 142.4–155.1 ppm) whereas C(7) is at 109.7 ppm. Consequently, the signal at ~ 100 ppm, mentioned above, is C(7) and not the bridging carbon. Similar ^{13}C results were found for the *p*-tolyl complexes **1** and **3–9** (see Table 1). We note that the $\mu\text{-}^{13}\text{C}$ signal for **6** ($\delta = 155.1$), which has a terminal PMe_2Ph on Pd(II) in pseudo trans position to the $\mu\text{-C}$ atom, appears as a doublet, $^2J(^{31}\text{P}, ^{13}\text{C})_{\text{trans}} = 56.4$ Hz. Adams et al.⁸ reported ^{13}C shifts of 98.5, 80.2 and 52.1 ppm for the coordinated allyl carbons in the η^3 -benzyl complex $\text{CpW}\{\eta^3\text{-C}_6\text{H}_5\text{CH}(\text{OEt})\}(\text{CO})_2$, with the 98.5 ppm value for the ipso carbon. Further, Su and Wojcicki⁹ give ^{13}C shifts of 61.1 and 90.7 ppm for the two aromatic carbons of the η^3 -benzyl derivative $\text{CpW}(\text{CO})_2(\eta^3\text{-CH}(\text{CH}_3)\text{Ph})$. On the basis of our $\mu\text{-C}$ ^{13}C data, we do not believe that we have an η^3 -complex; however, we consider our aromatic ^{13}C chemical shift data to be in good agreement with what one would expect for two coordinated aryl carbons in a tungsten(II) complex.

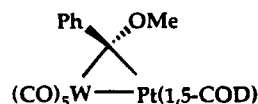
Interestingly, the olefinic CH proton, H(8), in **2**, $\delta = 5.26$, is only moderately shifted away from its position, e.g., in cyclopentene, $\delta = 5.60$, and qualitatively, the same modest change is observed for the aromatic ortho proton of the coordinated double bond, $\delta = 6.72$ in **1**.

Our ^{13}C assignments require that, relative to the sketches **1–4**, the bonding for both the double bond and the bridging carbon atom be reconsidered. We suggest η^2 -interactions of the following type:



Coordination of the appropriate double bond leads to 18-electron configurations at the tungsten atoms and, of course, restricted rotation about the $\mu\text{-C}-\text{C}(7)$ bond. It is pertinent that, in their discussion of the reactive species $\text{Cp}(\text{CO})_2\text{W}(\text{CH}=\text{Tol})^+$, which arises from the protonation of the analogous carbyne complex, Garrett et al.¹⁰ mentioned an η^3 -carbene as a structural possibility but offered no proof of its existence.

The exact nature of the bridging carbon atom in **1–10** remains open. In the absence of evidence to the contrary, we consider this atom as having some bridging carbene character, in analogy with the literature.⁵ For the dinuclear bridging carbene complex



Ashworth et al.^{5b} found the bridging carbene ^{13}C signal

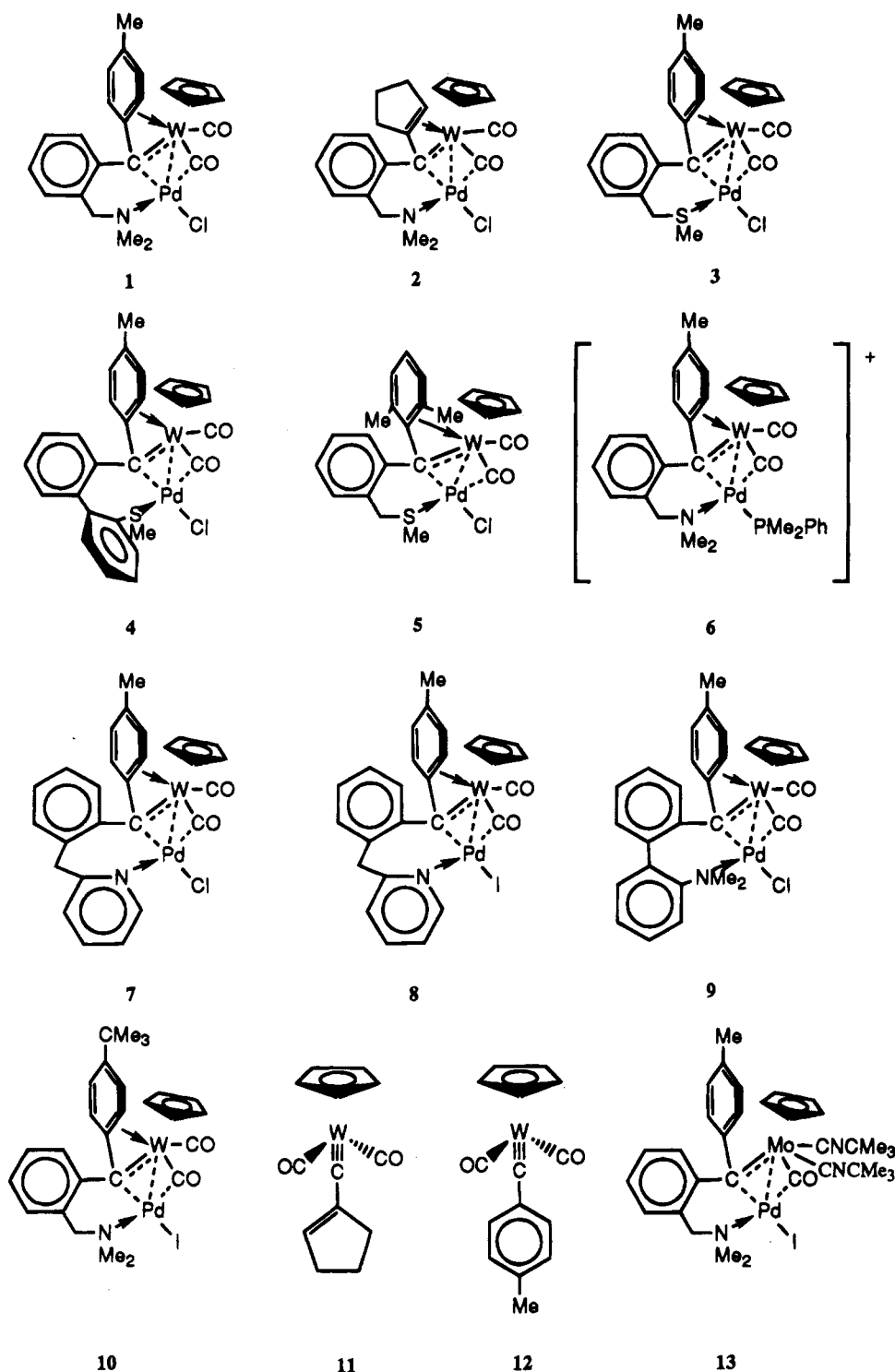
(7) Kalinowski, H.; Berger, S.; Braun, S. *^{13}C -NMR Spektroskopie*; Georg Thieme Verlag: Stuttgart, 1984; pp 461–490.

(8) Adams, H.; Bailey, N. A.; Winter, M.; Woodward, S. *J. Organomet. Chem.* **1991**, *418*, C39.

(9) Su, S. H.; Wojcicki, A. *Organometallics* **1983**, *2*, 1296.

(10) Garrett, K. E.; Sheridan, J. B.; Pourreau, D. B.; Feng, W. C.; Geoffroy, G. L.; Staley, D. L.; Rheingold, A. L. *J. Am. Chem. Soc.* **1989**, *111*, 8383.

Chart 1



at 197 ppm, too high a frequency for a simple sp^3 carbon. Our μ - ^{13}C chemical shifts are not consistent with the ^{13}C characteristics for an η^3 -benzyl-type ligand in that they come at too high a frequency.^{11,12} However, these same δ values are too low in frequency for normal tungsten-carbene complexes.¹³

Further, in the X-ray structure⁴ for 4, the W-(μ -C) separation is 2.158(4) Å and the Pd-(μ -C) separation is 2.024(4) Å. The former is not suggestive of W=C character, but is somewhat short for a W-C single bond,¹⁰ and the latter is quite reasonable for a Pd-C σ -bond.

(11) Mann, B. E.; Keasey, A.; Sonoda, A.; Maitlis, P. J. *Chem. Soc., Dalton Trans.* **1979**, 338. Sonoda, A.; Bailey, P. M.; Maitlis, P. J. *Chem. Soc., Dalton Trans.* **1979**, 346.

(12) Brookhart, M.; Buck, R. C.; Danielson, E. J. *Am. Chem. Soc.* **1989**, *111*, 567.

(13) Mayr, A.; Asaro, M. F.; Glines, T.; J.; van Engen, D.; Tripp, G. M. *J. Am. Chem. Soc.* **1993**, *115*, 8187.

(14) Templeton, J. L.; Philipp, C. C.; Pregosin, P. S.; Rügger, H. *Magn. Reson. Chem.* **1993**, *31*, 58. Pregosin, P. S.; Macchioni, A.; Templeton, J. L.; White, P. S.; Feng, S. *Magn. Reson. Chem.* **1994**, *32*, 415.

(15) Macchioni, A.; Pregosin, P. S.; Rügger, H.; Van Koten, G.; van der Schaff, P. A.; Abbenhuis, A. T. M. *Magn. Reson. Chem.* **1994**, *32*, 235.

Table 1. ^{183}W and Relevant ^{13}C NMR Data

	$\delta^{183}\text{W}$ (ppm)	$\delta^{13}\text{C}^a$ (ppm)		
		$\mu\text{-C}$	C(7)	C(8)
1	-1877	142.4	101.8	76.5
2	-2244	147.6	109.7	60.8
3	-1880	144.3	103.2	77.7
4	-1836	144.8 ^b	100.6	80.1
5	-1925	146.4 ^b	100.4	83.7
6	-1893	155.1	100.2	78.9
7	-2033	145.2	101.3	75.3
8	-1975	na ^d	102.7	90.5 ^{b,c}
9	-1825	na	100	78 ^b
10	-1852	145.4	101.3	74.6
11	-1921			
12	-1950			
13		148.7	158.2	122.1

^a CDCl_3 . ^b Tentative assignment from Ph.D. Thesis of P.F.E. ^c CD_2Cl_2 . ^d na, not assigned.

Table 2. ^{13}C NMR Data^a (ppm) for 1, 2, 10, and 13a

	1	2	10	13a
C(1)	146.2	145.4	145.8	159.4
C(2)	136.6	135.1	136.8	136.1
C(3)	130.8	130.3	130.8	130.2
C(4)	126.5	126.4	126.6	124.1
C(5)	129.6	129.6	129.7	127.4
C(6)	128.3	126.3	128.4	133.1
C(7)	101.8	109.7	101.3	158.2
C(8)	76.5	60.8	74.6	122.1
C(9)	132.0	31.8	127.8	127.4
C(10)	137.5	22.1	150.7	132.1
C(11)	133.9	33.2	130.9	128.2
C(12)	127.2		127.1	129.1
CH ₃	21.4			20.8
C(CH ₃) ₃			30.8	
CMe ₃			35.1	
$\mu\text{-C}$	142.4	147.6	145.4	148.7
CH ₂	68.3	68.6	68.1	66.1
NMe ₂	47.3	47.3	49.5	49.5
	51.1	51.3	52.5	52.4
Cp	91.6	90.7	91.8	91.9
CO	215.6	212.2	215.3	249.4
	222.0	221.4	221.3	
CNCMe ₃				162.8
				160.4
CNCMe ₃				57.2
				58.4
CNCMe ₃				30.2
				30.9

^a CDCl_3 .

^{183}W NMR. The ^{183}W literature is relatively sparse,¹⁴⁻²⁷ however, we recently suggested^{14,15} that inverse detection methodology readily allows access to

(16) McFarlane, H. C. E.; McFarlane, W.; Rycroft, D. S. *J. Chem. Soc., Dalton Trans.* **1976**, 1616.

(17) Andrews, G. T.; Colquhoun, I., J.; McFarlane, W.; Grim, S. O. *J. Chem. Soc., Dalton Trans.* **1982**, 2353.

(18) *NMR and the Periodic Table*; Harris, R. K., Mann, B. E., Eds.; Academic Press: New York, 1978; p 214. Santure, D. J.; McLaughlin, K. W.; Huffman, J. C.; Sattelberger, A. P. *Inorg. Chem.* **1983**, *22*, 1877.

(19) Brevard, C.; Schimpf, R.; *J. Magn. Reson.* **1982**, *47*, 528.

(20) Benn, R.; Brenneke, H.; Heck, J.; Rufinska, A. *Inorg. Chem.* **1987**, *26*, 2826.

(21) Benn, R.; Brevard, C.; Rufinska, A.; Schroth G. *Organometallics* **1987**, *6*, 938.

(22) Benn, R.; Rufinska, A. *Magn. Reson. Chem.* **1988**, *26*, 895.

(23) Ma, Y.; Demou, P.; Faller, J. W. *Inorg. Chem.* **1991**, *30*, 62.

(24) van der Zeijden, A. A. H.; Sontag, C.; Bosch, H. W.; Shklover, V.; Berke, H.; Nanz, D.; von Philipsborn, W.; *Helv. Chim. Acta* **1991**, *74*, 1194.

(25) Clegg, W.; Errington, R. J.; Kraxner, P.; Redshaw, C. *J. Chem. Soc., Dalton Trans.* **1992**, 1431.

(26) Kraatz, H. B.; Aramini, J. M.; Gao, X.; Boorman, P. M.; Vogel, H. J. *Inorg. Chem.* **1994**, *32*, 3976.

(27) Sekino, M.; Sato, M.; Nagasawa, A.; Kikuchi, K. *Organometallics* **1994**, *13*, 1451.

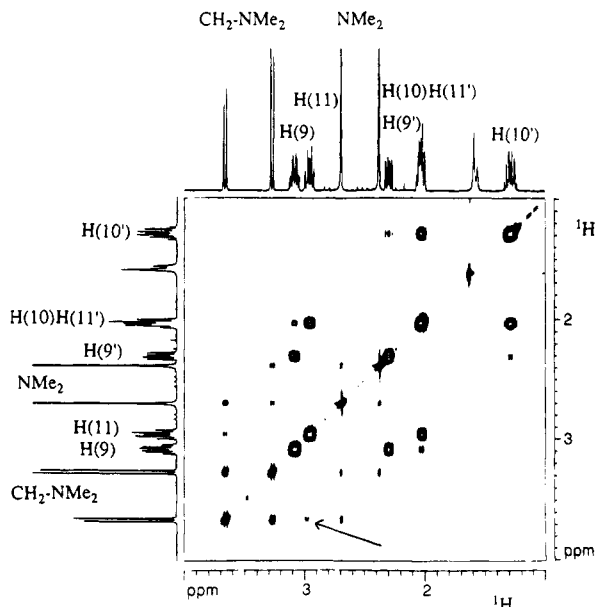


Figure 1. Section of the 2-D ^1H NOESY spectrum for **2**, showing the six nonequivalent protons on C(9)–C(11) of the cyclopentenyl fragment. The primed protons face tungsten. Note the weak cross-peak (arrow) from the nonprimed proton H(11) to one of the NCH_2 protons, thus assigning the two faces.

Table 3. ^1H NMR Data^a (ppm) for 1, 2, 10, and 13a

	1	2	10	13a
H(3)	7.29	7.28	7.31	6.98
H(4)	7.29	7.22	7.30	7.05
H(5)	7.43	7.32	7.44	7.24
H(6)	7.05	6.86	7.07	7.19
H(8)	7.46	5.26	7.46	6.02
H(9)	7.14	3.08	7.27	6.61
H(9')		2.30		
H(10)		2.02		
H(10')		1.28		
H(11)	6.95	2.95	7.21	7.02
H(11')		2.03		
H(12)	6.73		6.74	8.22
CH ₃	2.32			2.15
CMe ₃			1.29	
CH ₂	3.28	3.66	3.37	3.24
	3.11	3.27	3.15	2.65
NMe ₂	2.52	2.69	2.59	2.97
	2.38	2.38	2.43	2.43
Cp	4.70	5.34	4.67	4.60
CNCMe ₃				1.58
				1.16

^a CDCl_3 .

the ^{183}W metal resonances for a variety of organometallic tungsten complexes and show such a spectrum for **2** in Figure 3. Specifically, we have been able to obtain chemical shift data for Cp, Tp'(= 3,5-dimethyltris(pyrazolyl)borate), allyl, acetylene, and imido ($\equiv\text{NPh}$) tungsten complexes, among others.^{14,15} Table 1 also shows ^{183}W chemical shifts for the binuclear complexes **1–10** as well as data for the model carbyne complexes **11** and **12**.

There are several interesting points concerned with these ^{183}W chemical shifts:

(1) All of the chemical shifts come at relatively low frequency, in the range -1825 to -2244 ppm relative to WF_6 . The resonance positions for the coordinatively saturated W(0) complexes $\text{W}(\text{Cp})(\text{CO})_3^-$,^{14a} $\text{WH}(\text{NO})(\text{CO})_2(\text{PET}_3)_2$,²⁴ and $\text{W}(\text{CO})_6$ ¹⁸ are -2298 , -1441 , and -2340 ppm, respectively, i.e., in the same region.

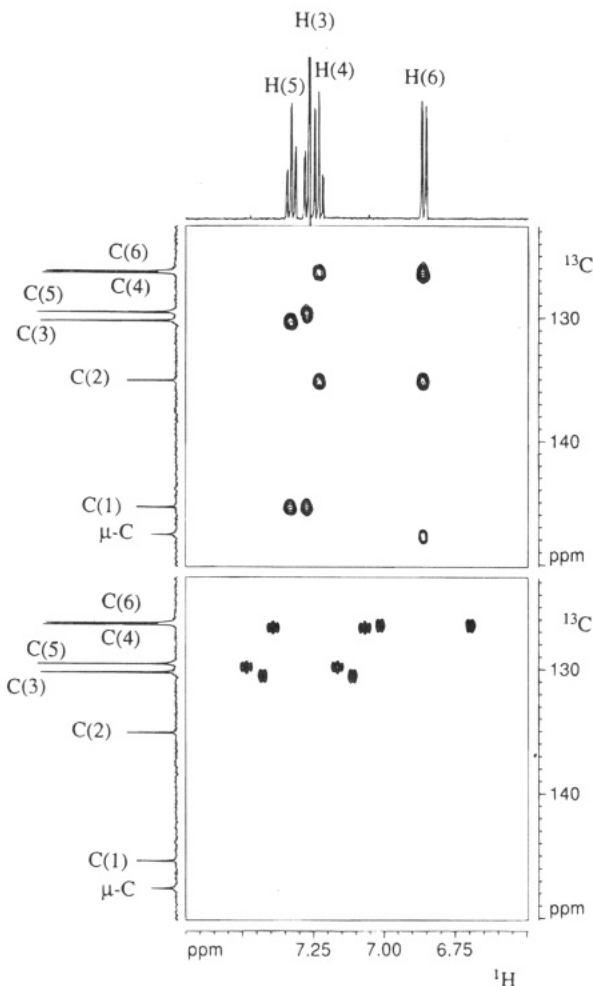


Figure 2. Section from (a) the long-range ^{13}C - ^1H inverse correlation (upper part) and (b) the conventional ^{13}C - ^1H inverse correlation (lower part) for **2**. Note the correlation of the bridging carbon ^{13}C signal to H(6), in the upper spectrum, thereby helping to identify this resonance. The ipso carbon C(1) correlates to both H(3) and H(5).

Further, the coordinatively saturated compounds, $\text{W}(\text{Et})(\text{Cp})(\text{CO})_3$,¹⁶ and $\text{W}(\eta^3\text{-C}_3\text{H}_5)_4$,²¹ have their absorptions at $\delta = -2358$ and -2069 , also relatively close to those we find. The model carbyne complexes $\text{W}(\text{Cp})(\equiv\text{CR})(\text{CO})_2$, $\delta = -1921$ and -1950 , for $\text{R} = \text{C}_5\text{H}_7$ and *p*-tolyl, **11** and **12**, respectively, fall in the range found for **1–10**. The various observed differences between **1–12** are modest given that the total range of ^{183}W chemical shifts is $\sim 11\,000$ ppm.^{16–27} We consider our ^{183}W chemical shifts for **1–10** to be consistent with an 18-electron, coordinatively saturated, electronic structure, i.e., having an additional double bond donor and possessing a relatively large HOMO–LUMO gap, such that the $1/(E_i - E_j)$ term in the paramagnetic shielding expression is relatively large. Assuming¹⁷ the ^{183}W resonance frequency ν to be

$$\nu = \infty (1 - \sigma_p)$$

$$\sigma_p = \infty - \sum (E_i - E_j)^{-1}$$

then a relatively large $(E_i - E_j)$ affords a low-frequency position. Coordinatively unsaturated complexes afford much higher frequency ^{183}W absorptions, e.g., for $\text{W}_2(\text{CF}_3\text{CO}_2)_4$,^{18b} $\delta = +5643$, for $\text{W}(\text{NEt})\text{Cl}_4(\text{Et}_2\text{O})$,¹⁴ $\delta = +2382$,

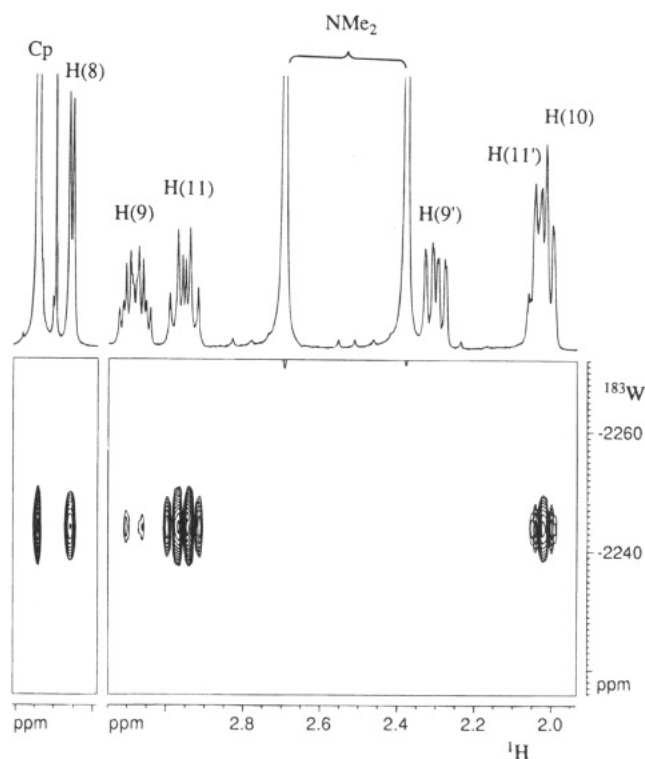


Figure 3. Proton–tungsten correlation for **2**, showing interactions of the ^{183}W with the Cp protons, H(8), H(11), and presumably H(10). All of these $^nJ(^{183}\text{W}, ^1\text{H})$ values are not visible in the 1-D spectrum.

Table 4. Selected Bond Distances (Å) and Angles (deg) for **13a**

Bond Distances			
Pd(2)–I(1)	2.737 (2)	C(6)–C(17)	1.53 (2)
Pd(2)–C(4)	2.12 (2)	C(24)–N(25)	1.19 (2)
Pd(2)–N(14)	2.20 (1)	Pd(2)–Mo(3)	2.692 (2)
Mo(3)–C(24)	2.06 (2)	Pd(2)–C(6)	2.02 (2)
Mo(3)–C(30)	2.14 (2)	Mo(3)–C(4)	1.98 (2)
Mo(3)–C(6)	2.21 (1)	C(4)–O(5)	1.18(2)
C(6)–C(7)	1.51 (2)	C(30)–N(31)	1.11 (2)

Bond Angles			
N(14)–Pd(2)–I(1)	118.94 (7)	N(14)–Pd(2)–C(4)	161.4 (6)
C(4)–Pd(2)–I(1)	90.1 (5)	C(6)–Pd(2)–I(1)	172.5 (4)
C(6)–Pd(2)–C(4)	83.6 (6)	C(6)–Mo(3)–C(4)	82.4 (6)
N(14)–Pd(2)–C(6)	93.5 (5)	C(24)–Mo(3)–C(6)	134.9 (6)
C(24)–Mo(3)–C(4)	80.1 (7)	C(30)–Mo(3)–C(4)	120.9 (7)
C(7)–C(6)–Mo(3)	120.8 (11)	C(30)–Mo(3)–C(24)	73.8 (7)
C(17)–C(6)–Mo(3)	119.2 (10)	O(5)–C(4)–Mo(3)	154.4 (11)
C(7)–C(6)–Pd(2)	114.3 (10)	C(17)–C(6)–Pd(2)	115.7 (10)
C(17)–C(6)–C(7)	106.1 (12)	N(25)–C(24)–Mo(3)	175.8 (15)
N(31)–C(30)–Mo(3)	172.5 (17)	C(32)–N(31)–C(30)	171.2 (20)

and for $\text{W}(\text{Cp}^*)(=\text{O})_2\text{Me}$, $\delta = +464.9$,²³ i.e., thousands of ppm to higher frequency.

(2) The small-to-modest changes in the ^{183}W chemical shifts for **1–10** support the formulation of these complexes as structurally similar with respect to the tungsten coordination sphere; i.e., the different halogens (or phosphine or cyclometalated N-donor, etc.) are indeed on palladium and not on tungsten.

(3) Complex **2** has the lowest metal resonance frequency, $\delta = -2244$. We believe this arises due to a stronger interaction of the double bond in **2**, relative to the corresponding interaction in the *p*-tolyl complexes. We note in this connection that the ^{13}C position for C(8) in **2** is also at the lowest frequency.

A Molybdenum Derivative. Since we postulate an interaction between a double bond of the *p*-tolyl group and the tungsten (and by analogy, an η^2 -bond to the molybdenum⁴), we considered a reaction to disrupt this

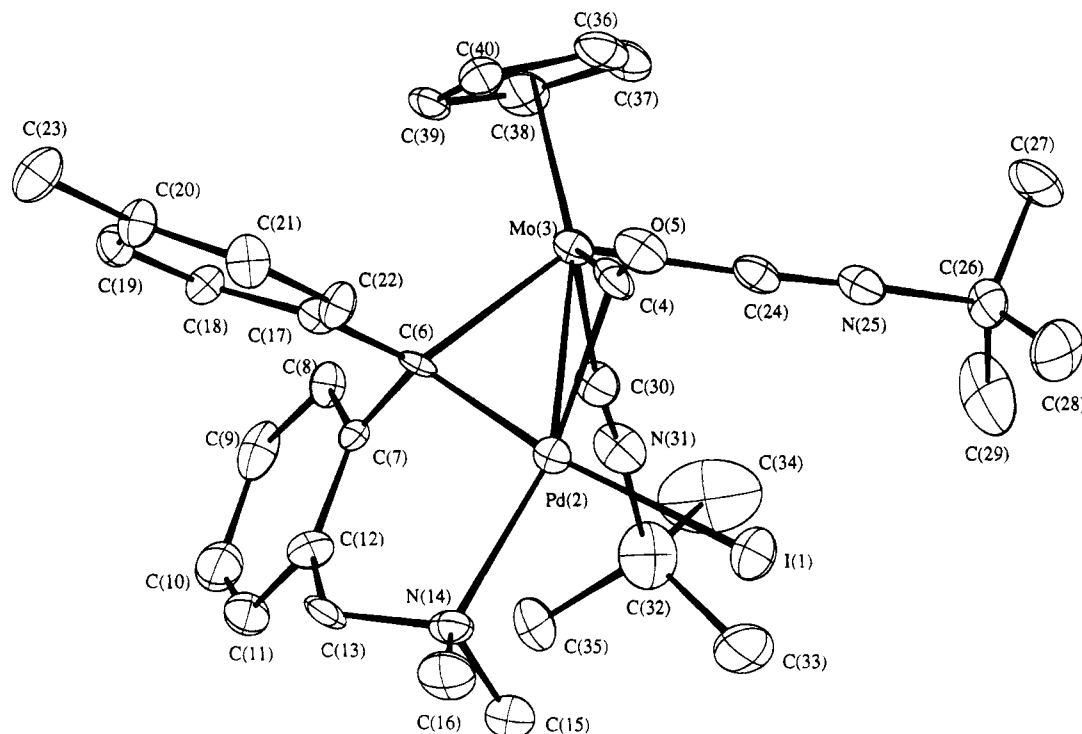
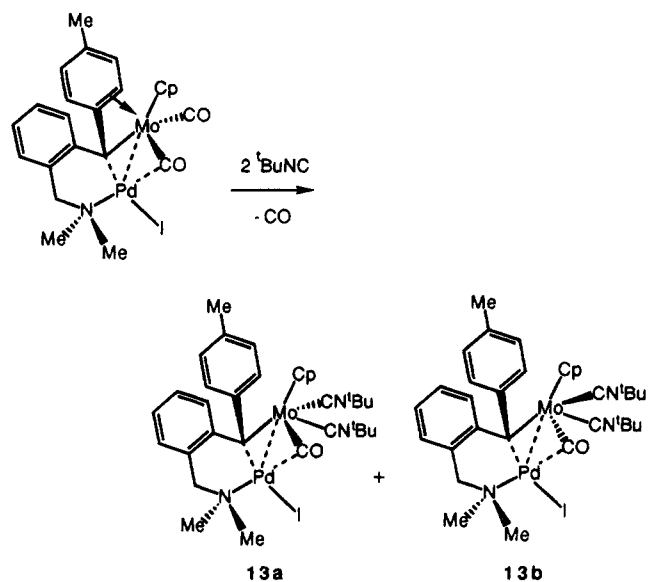


Figure 4. Cameron view for **13a**.

bond and decided on the isocyanide chemistry, shown:



The addition of an excess of *t*-BuNC to the Mo-Pd analog, shown above, gave high yields of a mixture of two compounds after 2 days at room temperature (the analogous tungsten reaction was slow, leading to mixtures of mono- and di-*t*-BuNC adducts which were difficult to separate). **13a** and **13b** result from the addition of two isocyanide ligands and the displacement of one CO and were shown by ¹H NMR and infrared spectroscopy to be closely related, thus suggesting isomers. However, only **13a** could be obtained in a pure form by fractional crystallization as single crystals suitable for X-ray diffraction analysis. Complex **13b** was always contaminated by variable amounts of **13a**. Consequently, we have fully characterized **13a** and assign **13b** to a geometric isomer by comparison.

Table 5. Crystallographic Data for **13a**

chemical formula	PdMoC ₃₃ H ₄₂ ON ₃
fw	825.96
crystal system	monoclinic
space group	<i>P2₁/a</i>
Z	4
<i>a</i> , Å	18.091(4)
<i>b</i> , Å	10.928(7)
<i>c</i> , Å	16.970(3)
β, deg	95.61(1)
<i>V</i> , Å ³	3339
<i>F</i> (000)	1640
<i>ρ</i> (calcd), g cm ⁻³	1.64
μ(Mo Kα), cm ⁻¹	18.41
cryst size, mm	0.2 × 0.24 × 0.36
diffractometer	Philips PW1100
monochromator	graphite
radiation	Mo Kα (0.710 70)
temperature °C	20
scan type	ω/2θ
scan range θ, deg	1.10 + 0.34 tan θ
2θ range, deg	4–45
no. of reflctns collected	3693
no. of reflctn used (criteria)	2046 (<i>I</i> > 3σ(<i>I</i>))
<i>R</i>	0.048
<i>R</i> _w ^a	0.054
absorptn corr ^b	min 0.78, max 1.09
weighting scheme	unit weights
rms (shift/esd)	0.16
ls params	362
residual electron dens, e Å ⁻³	0.69

^a $R_w = [\sum w_i(F_o - F_c)^2 / \sum w_i F_o^2]^{1/2}$. ^b Difabs: Walker, N.; Stuart, D. *Acta Crystallogr.* **1983**, *A39*, 159.

The ORTEP plot of **13a** is given in Figure 4; selected bond lengths and bond angles are given in Table 4, crystallographic data in Table 5, and fractional parameters in Table 6.

If one neglects the Pd-Mo interaction (which at 2.692(2) Å, is ~0.1 Å shorter than in a number of Mo-

(28) Bender, R.; Braunstein, P.; Jud, J.; Dusausoy, Y. *Inorg. Chem.* **1983**, *22*, 3394.

(29) Kläui, W.; Hamers, H.; Pfeffer, M.; de Cian, A.; Fischer, J. *J. Organomet. Chem.* **1990**, *394*, 213.

Table 6. Fractional Parameters for PdMoC₃₃H₄₂ON₃

atom	<i>x/a</i>	<i>y/b</i>	<i>z/c</i>	<i>U(eq)</i>
I(1)	0.80131(8)	0.0317(2)	0.70692(9)	0.0790
Pd(2)	0.94326(7)	0.0969(1)	0.76128(7)	0.0384
Mo(3)	1.03525(9)	0.1778(1)	0.65711(9)	0.0385
C(4)	0.983(1)	0.019(2)	0.6589(9)	0.0481
O(5)	0.9702(7)	-0.083(1)	0.6385(7)	0.0549
C(6)	1.0503(9)	0.148(1)	0.7863(8)	0.0284
C(7)	1.0614(8)	0.255(2)	0.8430(9)	0.0373
C(8)	1.1081(9)	0.356(1)	0.829(1)	0.0402
C(9)	1.121(1)	0.446(2)	0.887(1)	0.0579
C(10)	1.088(1)	0.443(2)	0.956(1)	0.0775
C(11)	1.043(1)	0.350(2)	0.968(1)	0.0577
C(12)	1.0301(9)	0.252(2)	0.914(1)	0.0409
C(13)	0.983(1)	0.147(2)	0.9385(9)	0.0432
N(14)	0.9167(8)	0.122(1)	0.8838(8)	0.0480
C(15)	0.864(1)	0.222(2)	0.888(1)	0.0797
C(16)	0.883(1)	0.007(2)	0.913(1)	0.0719
C(17)	1.1033(9)	0.047(1)	0.8200(9)	0.0377
C(18)	1.1707(8)	0.070(1)	0.8618(9)	0.0366
C(19)	1.2161(9)	-0.020(2)	0.8935(9)	0.0468
C(20)	1.201(1)	-0.143(1)	0.879(1)	0.0449
C(21)	1.132(1)	-0.165(2)	0.842(1)	0.0454
C(22)	1.0832(9)	-0.077(2)	0.812(1)	0.0428
C(23)	1.254(1)	-0.242(2)	0.913(1)	0.0678
C(24)	0.946(1)	0.213(2)	0.576(1)	0.0459
N(25)	0.8968(9)	0.239(1)	0.5266(8)	0.0578
C(26)	0.839(1)	0.292(2)	0.469(1)	0.0520
C(27)	0.872(1)	0.310(3)	0.392(1)	0.0802
C(28)	0.775(1)	0.201(2)	0.460(1)	0.0911
C(29)	0.815(2)	0.413(2)	0.502(1)	0.0947
C(30)	0.985(1)	0.342(2)	0.696(1)	0.0546
N(31)	0.958(1)	0.430(1)	0.7077(9)	0.0601
C(32)	0.913(1)	0.543(2)	0.734(1)	0.0931
C(33)	0.829(1)	0.539(3)	0.726(1)	0.0980
C(34)	0.924(2)	0.644(3)	0.672(2)	0.1298
C(35)	0.944(1)	0.616(4)	0.815(1)	0.1105
C(36)	1.097(1)	0.090(2)	0.563(1)	0.0593
C(37)	1.098(1)	0.217(2)	0.548(1)	0.0569
C(38)	1.138(1)	0.273(2)	0.611(1)	0.0627
C(39)	1.1636(9)	0.182(2)	0.6668(9)	0.0479
C(40)	1.138(1)	0.074(2)	0.635(1)	0.0502

Pd complexes^{28,29}) then one can consider the palladium atom as being in a distorted square-planar environment defined by I(1), N(14), C(6), and C(4). The two isocyanide ligands are complexed to Mo, which is heptacoordinated (again neglecting the metal-metal bond). The geometry around this Mo atom is close to that of a four-legged piano stool. The interactions between the three atoms C(6), Mo(3), C(4) and the Pd(2) atom are similar to those found in a closely related dinuclear Pd-Mo complex, **14**, in which the Cp has been substituted by the tripod ligand, CpCo{P(OMe)₂O}₃.²⁹ The Pd(2)-Mo(3) distance in **13a**, 2.2692(2) Å is shorter by 0.14 Å than that found for the CpCo{P(OMe)₂O}₃⁻ analog. However, the Mo(3)-C(6) bond in **13a**, 2.21(1) Å, is longer by ~0.1 Å, than that found in **14**, 2.118(7) Å, with the former value being close to that of a normal Mo-C single bond, 2.24-2.41 Å.³⁰ The two isocyanides have a cis geometry (the C(24)-Mo-C(30) angle is 73.8(7)°), and the semibridging carbonyl group, C(4)O(5) is in a syn position with respect to the *p*-tolyl unit.

Given the local geometry at molybdenum, one can imagine an alternative geometric isomer in which the carbonyl C(4)O(5) and the isocyanide *t*-BuN(31)C(30) have exchanged positions. This would place the CO in a position anti to the *p*-tolyl unit, and this is our suggestion for the structure of **13b**. From the ¹H NMR

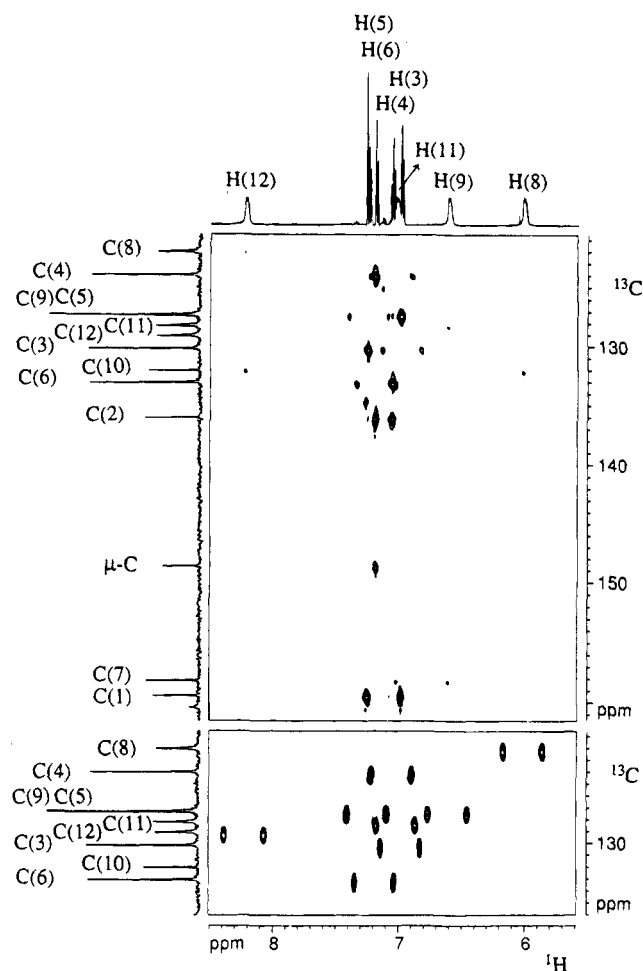


Figure 5. Section from (a) the long-range ¹³C-¹H inverse correlation (upper part) and (b) the conventional ¹³C-¹H inverse correlation (lower part) for the Mo complex, **13a**. Note that there are four, broad, *p*-tolyl protons, and that the μ -C carbon signal (upper trace, lower center) correlates to H(6). The four *p*-tolyl protons correlate to four normal protonated aromatic ¹³C signals, C(8,9) C(11,12), with chemical shifts between 122 and 129 ppm.

of **13b** it may be seen that the signals of the tolyl protons are dramatically shifted as compared to those of **13a**. This could arise because of some steric hindrance between the *t*-BuNC and the *p*-tolyl.

Since the solid-state structure for **13a** is known, we measured its ¹H NOESY and ¹³C, ¹H correlations and show the latter in Figure 5. From these spectra it is clear that (1) there are four (definitely broad) *p*-tolyl proton signals. These four protons exchange pairwise (based on the positive cross-peaks observed in the phase-sensitive NOESY). (2) The four *p*-tolyl protons correlate to four normal protonated aromatic ¹³C signals, with chemical shifts between 122 and 129 ppm. (3) ³J(C,H) can be used to identify all the important quaternary carbons: μ -C(bridging) C(1), C(2), C(7), and C(10). (4) The bridging carbon resonance, at 148.7 ppm, is in the same region as in **1-10**.

From point 2 we conclude that the η^2 -bond in **13a** has been displaced in that the ¹³C chemical shifts for the aromatic carbons are no longer indicative of complexation, and from point 4 we see that the position of the bridging carbon absorption is not dependent upon the presence of the η^2 -bond, in keeping with our discussion above. It is interesting that there is still restricted

(30) Guzman, E. C.; Wilkinson, G.; Rogers, R. D.; Hunter, W.; Zaworotko, M. J.; Atwood, J. L. *J. Chem. Soc., Dalton Trans.* **1980**, 229.

rotation about the μ -C-C(7) bond. Obviously, the complex is relatively crowded in the region of the *p*-tolyl aromatic moiety; however, based on the proton line widths, the barrier is lower for the Mo complex than for the tungsten complexes, although these complexes are not strictly comparable.

In summary, we conclude that the complexes 1–10 are best thought of as containing an η^2 -olefin bond from the *p*-tolyl (or C_5H_7) moiety to the tungsten, with the driving force most likely the desire for an 18-electron configuration. The bridging carbon seems to be a compromise between a carbene and an sp^3 carbon, in that its chemical shift falls between the two expected positions.

Experimental Section

All compounds except **13a** and **13b** were synthesized according to literature procedures.⁴

Synthesis of 13a and 13b. To a stirred solution of [Cp(CO)(μ -CO)Mo][μ -C(4-tolyl)(dmba)][Pd(I)] (150 mg, 0.25 mmol) in dichloromethane (20 mL) was added *tert*-butyl isocyanide (1 mL) at room temperature. The deep red color of the solution became slightly lighter red and gas evolved. After being stirred for 48 h, the solution was filtered through an alumina column (2 \times 5 cm). Elution with pure acetone afforded a red orange band. Evaporating the solvent gave an oily residue which was washed with *n*-hexane (2 \times 10 mL) and then redissolved in dichloromethane (10 mL). Addition of *n*-hexane (30 mL) to this solution and cooling at -20°C afforded, after 24 h, 160 mg (78%) of orange crystals which are a mixture of **13b/13a** in the ratio 3/1. Redissolution of this mixture in dichloromethane layered with *n*-hexane afforded deep red crystals of **13a** (20 mg). All efforts to purify **13b** via fractional crystallization were unsuccessful. Anal. Calcd (Found) for $C_{33}H_{42}IMoN_3OPd$ (MW = 825.98) (+0.25 CH_2Cl_2): C, 47.13 (47.11); H, 5.07 (4.77); N, 4.96 (5.02). 1H NMR ($CDCl_3$): **13a**, δ 8.22 (d, 1 H arom, $^3J_{HH} = 8.2$), 7.22–6.96 (m, 5 H arom), 6.61 (d, 1 H arom, $^3J_{HH} = 7.7$), 6.01 (d, 1 H arom, $^3J_{HH} = 8.2$), 4.59 (s, 5 H, Cp), 3.23, 2.64 (AB pattern, 2 H, CH_2 , $^2J_{HH} = 11.5$), 2.97, 2.43, 2.15 (3 s, 9 H, NMe_2 and 4-Me), 1.57, 1.15 (2s, 18 H, *t*-Bu); **13b**, δ 7.37–6.92 (m, 8H, *p*-tolyl + dmba), 4.74 (s, 5 H, Cp), 3.04 and 2.68 (AB pattern, 2 H, CH_2 , $^2J_{HH} = 11.7$), 2.81, 2.31, 2.16 (3 s, 9 H, NMe_2 and 4-Me), 1.61, 1.17 (2s, 18 H, *t*-Bu). ^{13}C NMR ($CDCl_3$): **13a**, δ 249.0 (CO), 162.8, 160.4 (*t*-BuNC), 159.3, 158.1, 148.4 (μ -C), 135.9, 133.0, 131.9, 130.0, 129.0, 127.3, 123.9, 121.9 (C arom), 91.7 (Cp), 66.0 (NCH_2), 58.2, 57.1 (CMe_3), 52.2, 49.4 (NMe_2), 30.8, 30.3 (CMe_3), 20.7 (4-Me); IR (cm^{-1}): ν_{CN} 2150, 2138; ν_{CO} 1797.

X-ray Study of 13a. Intensity data were collected at room temperature on a Philips PW 1100 diffractometer using Mo $K\alpha$ radiation. Accurate cell dimensions and orientation matrix were obtained from least-squares refinement of the setting angles of 25 well-defined reflections. No decay in the intensities of two standard reflections was observed during the course of data collection. This compound crystallizes in the monoclinic space group $P2_1/a$ with $Z = 4$. Complete crystal data, collection parameters, and other significant details are listed in Table 5. The usual corrections for Lorentz and polarization effects were applied. Computations were performed by using CRYSTALS.³¹ Scattering factors and corrections for anomalous dispersion were taken from the literature.³² The structure was resolved by direct methods (Shelxs 86³³) and refined by least squares with anisotropic thermal parameters for all non-

hydrogen atoms. Hydrogen atoms were introduced as fixed contributors in theoretical positions, and their coordinates were recalculated after each refinement. The structure was refined to $R = 0.048$ with the use of 2046 reflections for 362 least-squares parameters.

NMR measurements were performed on $CDCl_3$ solutions (20–30 mg of compound in 0.6 mL of solvent) using a Bruker AMX-500 instrument operating at 500.13, 202.5, 125.8, and 20.8 MHz for 1H , ^{31}P , ^{13}C , and ^{183}W , respectively. Referencing is relative to internal TMS and external 85% H_3PO_4 for 1H , ^{13}C , and ^{31}P , respectively. Chemical shifts are given relative to WF_6 for ^{183}W .

^{183}W - 1H Long-Range Correlations. The heteronuclear shift correlation experiments were performed using the HMQC sequence³⁴ $\pi/2(^1H) - \Delta - \pi/2(^{183}W) - t_1/2 - \pi(^1H) - t_1/2 - \pi/2(^{183}W) - \text{acquisition}(^1H)$. The defocusing delay Δ was deliberately set to 100 ms, which, given the natural abundance of 14.4% for ^{183}W , allows detection of $^nJ(^{183}W, ^1H)$ interactions in the range of 0.5–9.5 Hz with a sensitivity analogous or better than for a corresponding ^{13}C - 1H correlation. Absorption mode data in the tungsten dimension were obtained using the TPPI³⁵ method. Processing involved zero filling and apodization with cosine windows in both dimensions prior to double Fourier transformation, phase correction in ω_1 , and magnitude calculation³⁶ in ω_2 . For 1H NOESY, the phase-sensitive NOESY spectra were obtained with a mixing time of 800 ms using standard techniques as described previously.³⁷

^{13}C - 1H Long-Range Correlations. The heteronuclear shift correlation experiments were performed using the HMQC sequence³⁴ $^1H, 90^\circ_x - \Delta_1 - \Delta_2 - t_1/2 - 180^\circ_x - t_1/2 - \text{Acq}(t_2)$; $^{13}C, 90^\circ_y, 90^\circ_x$.

The delays $\Delta_1 = 1/(2^1J_{CH})$ and Δ_2 were set to 3.2 and 50 ms, respectively. Processing involved zero filling and apodization with cosine windows in both dimensions prior to double Fourier transformation, absolute value mode representation in ω_1 , and magnitude calculation in ω_2 .

^{13}C - 1H Routine Correlations. The heteronuclear correlation experiments were performed using the HMQC sequence³⁴ $^1H, 90^\circ - \Delta - 180^\circ - \Delta - 90^\circ - t_1/2 - 180^\circ - t_1/2 - \text{Acq}(t_2)$; $^{13}C, 180^\circ, 90^\circ, 90^\circ$.

The delay $\Delta = 1/(4^1J_{CH})$ was set to 1.8 ms. The processing parameters are the same used for the ^{183}W - 1H long-range correlations.

The following are comments on the individual measurements:

Complex 1. For ^{183}W - 1H , there are correlations between tungsten and H-11, H-12, and the Cp protons. The ^{13}C - 1H inverse long-range shift correlation shows a weak correlation between the carbonyl resonances at 215.6 ppm and H(8) that supports the η^2 -interaction ($^3J_{C-H}$ instead of $^5J_{C-H}$ is the active coupling constant). From the $^{13}C\{^1H\}$ spectrum the $^1J(^{183}W, ^{13}C)$ is 40 Hz for the μ -C.

Complex 2. For ^{183}W - 1H , there are correlations between tungsten and H(8), H(9), H(11), H(10), and/or H(11'), and the Cp protons. It is interesting to note that there is correlation of the ^{183}W to one face only of the cyclopentene ring. From the $^{13}C\{^1H\}$ spectrum, the $^1J(^{183}W, ^{13}C)$ values are 166 and 150 Hz for the two CO groups at 212.2 and 221.5 ppm, respectively.

(34) Summers, M. F.; Marzilli, L. G.; Bax, A. *J. Am. Chem. Soc.* **1986**, *108*, 4285.

(35) Marion, D.; Wüthrich, K., *Biochem. Biophys. Res. Commun.* **1983**, *113*, 967.

(36) Bax, A.; Marion, D., *J. Magn. Reson.* **1988**, *78*, 186.

(37) (a) Pregosin, P. S.; Rügger, H.; Salzmänn, R.; Albinati, A.; Lianza, F.; Kunz, R. W. *Organometallics* **1994**, *13*, 83. (b) Breutel, C.; Pregosin, P. S.; Salzmänn, R.; Togni, A. *J. Am. Chem. Soc.* **1994**, *116*, 4067. (c) Pregosin, P. S.; Salzmänn, R. *Magn. Reson. Chem.* **1994**, *32*, 128. (d) Ammann, C. J.; Pregosin, P. S.; Rügger, H.; Albinati, A.; Lianza, F.; Kunz, R. W. *J. Organomet. Chem.* **1992**, *423*, 415. (e) Rügger, H.; Kunz, R. W.; Ammann, C. J.; Pregosin, P. S. *Magn. Reson. Chem.* **1992**, *29*, 197. (f) Albinati, A.; Kunz, R. W.; Ammann, C. J.; Pregosin, P. S. *Organometallics* **1991**, *10*, 1800. (g) Albinati, A.; Ammann, C.; Pregosin, P. S.; Rügger, H. *Organometallics* **1990**, *9*, 1826.

(31) Watkin, D. J.; Carruthers, J. R.; Betteridge, P. W. *Crystals User Guide*; Chemical Crystallography Laboratory: University of Oxford, Oxford, U.K., 1988.

(32) *International Tables for X-ray Crystallography*; Kynoch Press: Birmingham, U.K., 1974; Vol. IV.

(33) Sheldrick, G. M. *Shelxs-86, Program for Crystal Structure Solution*; University of Göttingen, 1986.

Complex 3. $^{183}\text{W}-^1\text{H}$, there are correlations between tungsten and H(11), H(12), and the Cp protons.

Complexes 4 and 7-9. The correlations are as for 3.

Complex 5. For $^{183}\text{W}-^1\text{H}$, there are correlations between tungsten and H(9), H(11), CH_3 in the 8 and 12 positions, and the Cp protons.

Complex 6. For $^{183}\text{W}-^1\text{H}$, there are correlations between tungsten and H(11), H(12), and the Cp protons. The $^{31}\text{P}\{^1\text{H}\}$ shows a singlet at -13.6 ppm and the satellites due to the tungsten: $^1J(^{183}\text{W}, ^{31}\text{P}) = 17.3$ Hz. From the $^{13}\text{C}\{^1\text{H}\}$ spectrum the $^1J(^{183}\text{W}, ^{13}\text{C})$ values are 164 and 165 Hz for the two CO groups at 223.3 and 215.9 ppm, respectively. $^2J(^{13}\text{C}, ^{31}\text{P})$ for the μ -C is 56.4 Hz.

Complex 10. For $^{183}\text{W}-^1\text{H}$, there are correlations between tungsten and H(11), H(12), and the Cp protons. From the $^{13}\text{C}\{^1\text{H}\}$ spectrum the $^1J(^{183}\text{W}, ^{13}\text{C})$ value is 39 Hz for the μ -C.

Complex 11. For $^{183}\text{W}-^1\text{H}$, there are correlations between tungsten and H(2), H(4), and the Cp protons. From the $^{13}\text{C}\{^1\text{H}\}$ spectrum the $^1J(^{183}\text{W}, ^{13}\text{C})$ values are 204 and 196 Hz for the carbyne ($\delta = 295.9$ ppm) and the CO ($\delta = 220.4$ ppm) carbons, respectively.

Complex 12. The $^{183}\text{W}-^1\text{H}$ correlation recorded with $\Delta = 150$ ms shows correlations between the tungsten and *all* the protons of the molecule, although several of these are quite weak. Quite surprising is the correlation between the tungsten and the para CH_3 group that occurs via the $^2J(^{183}\text{W}, ^1\text{H})$ coupling constant.

Complex 13a. The 2-D ^1H NOESY spectrum shows that the protons 8 and 9 are exchanging with 12 and 11, respectively, indicating that there is restricted rotation of the tolyl group. The carbon-proton correlations allow the complete assignment of the resonances and, in particular, show that carbons 7 and 8 fall in the "normal" aromatic range. These facts indicate that there is no η^2 -interaction.

Acknowledgment. P.S.P. thanks the Swiss National Science Foundation as well as the ETH for support and the Johnson-Matthey Research Foundation, Reading, England, for the loan of precious metals. A.M. thanks the CNR (Consiglio Nazionale delle Ricerche, Italy) for a grant. P.F.E. thanks the Commission of European Communities (Science Program, Contract SC1-0319-C(GDF)) for a grant.

Supplementary Material Available: Tables of anisotropic thermal parameters (S1), interatomic distances (S2), and bond angles (S3) for **13a** (3 pages). Ordering information is given on any current masthead page.

OM940849M

Base Stabilization of Functionalized Silylene Transition Metal Complexes

Robert J. P. Corriu,* Bhanu P. S. Chauhan, and Gérard F. Lanneau*

Laboratoire des Précurseurs Organométalliques de Matériaux, UMR 44-Université Montpellier II, Case 007, Place Eugène Bataillon, 34095 Montpellier Cedex 05, France

Received December 9, 1994[®]

The dehydrogenative coupling reaction of primary silanes ArSiH_3 [$\text{Ar} = [2-(\text{Me}_2\text{NCH}_2)\text{C}_6\text{H}_4]$, $[8-(\text{Me}_2\text{NCH}_2)\text{C}_{10}\text{H}_6]$, $[8-(\text{Me}_2\text{N})\text{C}_6\text{H}_4]$] with $\text{Fe}(\text{CO})_5$, $\text{Cr}(\text{CO})_6$, $\text{CpCo}(\text{CO})_2$, and $\text{RCpMn}(\text{CO})_3$ ($\text{R} = \text{H}, \text{CH}_3$) under photolytic conditions affords an effective access to intramolecular base-stabilized functionalized silanediyl-transition metal complexes of general formula $[\text{ArHSi}=\text{ML}_n]$. ²⁹Si-NMR investigations of the photochemical reaction of PhSiH_3 with $\text{Fe}(\text{CO})_5$ in the presence of 1,3-dimethyl-2-imidazolidinone (DMI) or hexamethylphosphoric triamide indicates a two-step mechanism for the formation of base-stabilized silanediyl-transition metal complexes. The carbonyl displacement reactions of the complex $[2-(\text{Me}_2\text{NCH}_2)\text{C}_6\text{H}_4]\text{HSi}=\text{Cr}(\text{CO})_5$ in the presence of PPh_3 or $\text{P}(\text{OMe})_3$ lead to the formation of *trans*- $(\text{PPh}_3)_2\text{Cr}(\text{CO})_4$ or *trans*- $[\text{P}(\text{OMe})_3]_2\text{Cr}(\text{CO})_4$, respectively, either by photolysis or by thermolysis. Photochemical displacement reaction with (diphenylphosphino)ethane furnished $[2-(\text{Me}_2\text{NCH}_2)\text{C}_6\text{H}_4]\text{HSi}=\text{Cr}[\text{Ph}_2\text{P}(\text{CH}_2)_2\text{PPh}_2](\text{CO})_3$ by subsequent displacement of two carbonyls of the metal moiety. Exchange reactions of the complex $[2-(\text{Me}_2\text{NCH}_2)\text{C}_6\text{H}_4]\text{HSi}=\text{Cr}(\text{CO})_5$ with Ph_3CX ($\text{X} = \text{Cl}, \text{BF}_4, \text{OSO}_2\text{CF}_3$) or $\text{CH}_3\text{COX}'$ ($\text{X}' = \text{Cl}, \text{Br}$) provide a direct entry to a series of functionalized complexes $[2-(\text{Me}_2\text{NCH}_2)\text{C}_6\text{H}_4]\text{XSi}=\text{Cr}(\text{CO})_5$. The liberated silylenes from complexes $\text{ArHSi}(\text{B})=\text{Fe}(\text{CO})_4$ ($\text{Ar} = \text{Ph}, 1\text{-Np}$) ($\text{B} = \text{DMI}$) can be trapped in the presence of *tert*-butyl alcohol or methanol to give di-*tert*-butoxysilanes or trimethoxysilanes, respectively.

Introduction

The chemistry of transition metal-silylene complexes gained interest when it was realized that they could participate in the elaboration of polysilanes^{1,2} or more generally organosilyl polymeric materials, whose the original structural properties are under active research.³ Base stabilization of transition metal carbene-like^{4,5} species ($\text{M}' = \text{Ge}, \text{Sn}$) is a classical method,^{6,7} which was

extended in 1987 by Zybilla⁸ and Tilley,⁹ who described the preparation of transition metal-silylene complexes stabilized with donor molecules coordinated to the unsaturated silicon atom. The coupling reaction of silicon(IV) dihalides with metal dianions afforded a series of organosilane diyl-transition metal complexes with the general formula $\text{R}_2\text{Si}(\text{B})=\text{M}(\text{CO})_n$. The chemistry of these silylene complexes was limited to ligand substitution reactions and some trapping experiments of the intermediary delivered silylenes.¹⁰

[®] Abstract published in *Advance ACS Abstracts*, February 15, 1995.

(1) (a) Aitken, C.; Harrod, J. F.; Samuel, E. *J. Am. Chem. Soc.* **1986**, *108*, 4059. (b) Aitken, C.; Harrod, J. F.; Samuel, E. *Can. J. Chem.* **1986**, *64*, 1677. (c) Harrod, J. F.; Yun, S. S. *Organometallics* **1987**, *6*, 1381. (d) Woo, H.-G.; Tilley, T. D. *J. Am. Chem. Soc.* **1989**, *111*, 8043. (e) Woo, H.-G.; Tilley, T. D. *J. Am. Chem. Soc.* **1989**, *111*, 3757. (f) Corey, J. Y.; Chang, L. S.; Corey, E. R. *Organometallics* **1987**, *6*, 1596. (g) Chang, L. S.; Corey, J. Y. *Organometallics* **1989**, *8*, 1885. (h) Sakakura, T.; Lautenschlager, H. J.; Nakajima, M.; Tanaka, M. *Chem. Lett.* **1991**, 913. (i) Aitken, C.; Barry, J.-P.; Gauvin, F.; Harrod, J. F.; Malek, A.; Rousseau, D. *Organometallics* **1989**, *8*, 1732. (j) Hengge, E.; Weinberger, M.; Jammegg, C. *J. Organomet. Chem.* **1991**, *410*, C1. (2) (a) Harrod, J. F.; Ziegler, T.; Tschinke, V. *Organometallics* **1990**, *9*, 897. (b) Yamashita, H.; Tanaka, M.; Goto, M. *Organometallics* **1992**, *11*, 3227. (c) Hengge, E.; Weinberger, M. *J. Organomet. Chem.* **1993**, *443*, 167. (d) Tilley, T. D. *Acc. Chem. Res.* **1993**, *26*, 22. (3) (a) Seyferth, D.; Lang, H.; Sobon, C. A.; Borm, J.; Tracy, H. J.; Bryson, N. *J. Inorg. Organomet. Polym.* **1992**, *1*, 59. (b) Corey, J. Y.; Zhu, X. M.; Bedard, T. C.; Lange, L. D. *Organometallics* **1991**, *10*, 924. (c) Dioumaev, V. K.; Harrod, J. F. *Organometallics* **1994**, *13*, 1548. (d) Corriu, R. J. P.; Enders, M.; Huille, S.; Moreau, J. J. E. *Chem. Mater.* **1994**, *6*, 15. (4) (a) Fischer, E. O.; Maasböl, A. *Angew. Chem., Int. Ed. Engl.* **1964**, *3*, 580. (b) Klabunde, U.; Fischer, E. O. *J. Am. Chem. Soc.* **1967**, *89*, 7141. (c) Fischer, E. O.; Beck, H. *J. Angew. Chem., Int. Ed. Engl.* **1970**, *9*, 72. (d) Fischer, E. O.; Maasböl, A. *Chem. Ber.* **1967**, *100*, 2245. (e) Aumann, R.; Fischer, E. O. *Chem. Ber.* **1968**, *101*, 954. (f) Lappert, M. F.; Pye, P. L. *J. Chem. Soc., Dalton Trans.* **1977**, 2172. (g) Kreissl, F. R.; Fischer, E. O.; Kreiter, C. G.; Weiss, K. *Angew. Chem., Int. Ed. Engl.* **1973**, *12*, 563. (h) Casey, C. P.; Burkhardt, T. J. *J. Am. Chem. Soc.* **1973**, *95*, 5833. (i) Dötz, K. H.; Fischer, H.; Hofmann, P.; Kreissl, F. R.; Schubert, U.; Weiss, K. *Transition Metal Carbene Complexes*; VCH: Weinheim, Germany, 1984; and references cited therein.

(5) (a) Aumann, R. In *Organometallics in Organic Synthesis*; de Meijere, A., tom Dieck, H., Eds.; Springer: Berlin, 1988; pp 69–83. (b) Parker, K. A.; Coburn, C. A. *J. Org. Chem.* **1991**, *56*, 1667. (c) Boger, D. L.; Jacobsen, I. C. *J. Org. Chem.* **1991**, *56*, 2209.

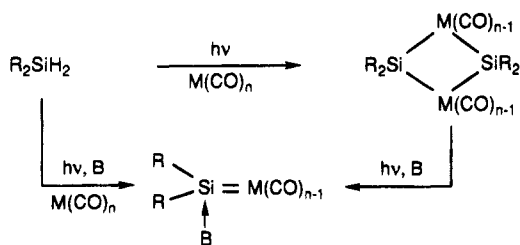
(6) (a) Jutzi, P.; Kanne, D.; Krüger, C. *Angew. Chem., Int. Ed. Engl.* **1986**, *25*, 164. (b) Jutzi, P.; Holtmann, U.; Bogge, H.; Müller, A. *J. Chem. Soc., Chem. Commun.* **1988**, 305. (c) Jutzi, P.; Möhrke, A. *Angew. Chem., Int. Ed. Engl.* **1989**, *28*, 762. (d) Jutzi, P. *Comments Inorg. Chem.* **1987**, *6*, 133. (e) Karsch, H. H.; Keller, U.; Gamper, S.; Müller, G. *Angew. Chem., Int. Ed. Engl.* **1990**, *29*, 295.

(7) (a) Petz, W. *Chem. Rev.* **1986**, *86*, 1019. (b) Jutzi, P.; Steiner, W. *Chem. Ber.* **1976**, *109*, 3473. (c) Jutzi, P.; Steiner, W.; König, E.; Huttner, G.; Frank, A.; Schubert, U. *Chem. Ber.* **1978**, *111*, 606. (d) Barrau, J.; Escudé, J.; Stagé, J. *Chem. Rev.* **1990**, *90*, 283. (e) Lappert, M. F.; Maskell, R. V. *J. Organomet. Chem.* **1984**, *264*, 217. (f) Marks, T. J.; Newman, A. R. *J. Am. Chem. Soc.* **1973**, *95*, 769. (g) Marks, T. J. *J. Am. Chem. Soc.* **1971**, *93*, 7090. (h) Cotton, J. D.; Davis, P. J.; Goldberg, D. E.; Lappert, M. F.; Thomas, K. M. *J. Chem. Soc., Chem. Commun.* **1974**, 89. (i) Neumann, W. P. *Chem. Rev.* **1991**, *91*, 311.

(8) (a) Zybilla, C.; Müller, G. *Angew. Chem., Int. Ed. Engl.* **1987**, *26*, 669. (b) Zybilla, C.; Wilkinson, D. L.; Leis, C.; Müller, G. *Angew. Chem., Int. Ed. Engl.* **1988**, *27*, 583. (c) Leis, C.; Zybilla, C.; Lachmann, J.; Müller, G. *Polyhedron* **1991**, *10*, 1163. (d) For a recent review, see: Zybilla, C.; Handwerker, H.; Friedrich, H. In *Advances in Organometallic Chemistry*; West, R., Stone, F. G. A., Eds.; Academic Press, Inc.: New York, 1994; Vol. 36, pp 229–281.

(9) (a) Straus, D. A.; Tilley, T. D.; Rheingold, A. L.; Geib, S. *J. Am. Chem. Soc.* **1987**, *109*, 5872. (b) Straus, D. A.; Grumbine, S. D.; Tilley, T. D. *J. Am. Chem. Soc.* **1990**, *112*, 7801. (c) Grumbine, S. D.; Chadha, R. K.; Tilley, T. D. *J. Am. Chem. Soc.* **1992**, *114*, 1518. (d) Tilley, T. D. In *The Silicon-Heteroatom Bond*; Patai, S., Rappoport, Z., Eds.; Wiley: New York, 1991; p 309.

Scheme 1



Another approach to organosilane-transition metal complexes was the photolysis of dihydrosilanes with metal carbonyls,¹¹ but a Lewis base was necessary to stabilize the organosilane-transition metal complex, either externally [with 1,3-dimethyl-2-imidazolidinone (DMI) or hexamethylphosphoric triamide (HMPA)] or intramolecularly coordinated with amino aryl groups directly attached to the silicon atom (Scheme 1).

In the present paper, we describe the preparation of 13 hydrosilane-transition metal complexes containing a functional SiH group at silicon obtained from the easily accessible trihydrosilanes RSiH_3 with $\text{M}(\text{CO})_n$, under photolytic conditions. The purpose of these studies is the formation of complexes that have a potent reactive group attached to the silicon atom. Moreover, since numerous techniques are available to investigate the bond order of the SiH functionality (^1H , ^{29}Si , or ^{13}C NMR, IR), we expect to have with this model a better understanding of the silicon-transition metal bond character.

Results and Discussion

(1) **Synthesis.** Addition of $\text{Fe}(\text{CO})_5$, $\text{RCpMn}(\text{CO})_3$ ($\text{R} = \text{H}, \text{CH}_3$), $\text{Cr}(\text{CO})_6$, or $\text{CpCo}(\text{CO})_2$ to the pentacoordinated primary silanes [2-[(dimethylamino)methyl]phenyl]silane (**1**), [8-[(dimethylamino)methyl]naphthyl]silane (**6**), or [8-[(dimethylamino)naphthyl]silane (**11**), in pentane under UV irradiation with a 450-W medium-pressure Hg lamp, affords transition metal-silane complexes **2–13** (Scheme 2).

(2) **Characterization.** Silanes and related stananes with intramolecular donor functions have been investigated extensively.^{12,13} Techniques used to characterize silicon-containing complexes are similar to

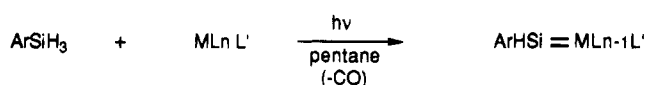
(10) Leis, C.; Wilkinson, D. L.; Handwerker, H.; Zybilla, C.; Müller, G. *Organometallics* **1992**, *11*, 514.

(11) (a) Corriu, R. J. P.; Lanneau, G. F.; Chauhan, B. P. S. *Organometallics* **1993**, *12*, 2001. (b) Corriu, R. J. P.; Lanneau, G. F.; Priou, C. *Angew. Chem., Int. Ed. Engl.* **1991**, *30*, 1130. (c) Chauhan, B. P. S.; Corriu, R. J. P.; Lanneau, G. F.; Priou, C.; Auner, N.; Handwerker, H.; Herdtweck, E. *Organometallics* **1995**, *14*, 1657.

(12) (a) Arya, P.; Boyer, J.; Corriu, R. J. P.; Lanneau, G. F.; Perrot, M. *J. Organomet. Chem.* **1988**, *346*, C11. (b) Arya, P.; Boyer, J.; Carré, F.; Corriu, R. J. P.; Lanneau, G. F.; Perrot, M.; Priou, C. *Angew. Chem., Int. Ed. Engl.* **1989**, *28*, 1016. (c) Corriu, R. J. P.; Lanneau, G. F.; Mehta, V. D. *J. Organomet. Chem.* **1991**, *419*, 9. (d) Brelrière, C.; Carré, F.; Corriu, R. J. P.; Poirier, M.; Royo, G.; Zwecker, J. *Organometallics* **1989**, *8*, 1831. (e) For a general review, see: Corriu, R. J. P.; Young, C. In *Hypervalent Silicon Compounds*; Patai, S.; Rappoport, Z., Eds.; Wiley: New York, 1989; p 1241. (f) Corriu, R. J. P. *Pure Appl. Chem.* **1988**, *60*, 99.

(13) (a) Van Koten, G.; Jastrzebski, J. T. B. H.; Noltes, J. G.; Spek, A. L.; Schoone, J. C. *J. Organomet. Chem.* **1978**, *148*, 233. (b) Van Koten, G.; Schaap, C. A.; Noltes, J. G. *J. Organomet. Chem.* **1975**, *99*, 157. (c) Van Koten, G.; Noltes, J. G. *J. Am. Chem. Soc.* **1976**, *98*, 5393. (d) Jastrzebski, J. T. B. H.; Van der Schaaf, P. A.; Boersma, J.; Van Koten, G.; Zoutberg, M. C.; Heijdenrijk, D. *Organometallics* **1989**, *8*, 1373. (e) Jastrzebski, J. T. B. H.; Van der Schaaf, P. A.; Boersma, J.; Van Koten, G.; de Ridder, D. J. A.; Heijdenrijk, D. *Organometallics* **1992**, *11*, 1521.

Scheme 2



2 $\text{M}=\text{Fe}$, $\text{L}=\text{CO}$, $n=4$, $\text{L}'=\text{CO}$

3a $\text{M}=\text{Mn}$, $\text{L}=\text{CO}$, $n=3$, $\text{L}'=\text{Cp}$

3b $\text{M}=\text{Mn}$, $\text{L}=\text{CO}$, $n=3$, $\text{L}'=\text{MeCp}$

4 $\text{M}=\text{Cr}$, $\text{L}=\text{CO}$, $n=5$, $\text{L}'=\text{CO}$

5 $\text{M}=\text{Co}$, $\text{L}=\text{CO}$, $n=2$, $\text{L}'=\text{Cp}$,

7 $\text{M}=\text{Fe}$, $\text{L}=\text{CO}$, $n=4$, $\text{L}'=\text{CO}$

8a $\text{M}=\text{Mn}$, $\text{L}=\text{CO}$, $n=3$, $\text{L}'=\text{Cp}$,

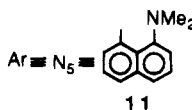
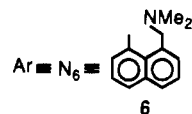
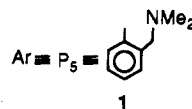
8b $\text{M}=\text{Mn}$, $\text{L}=\text{CO}$, $n=3$, $\text{L}'=\text{MeCp}$,

9 $\text{M}=\text{Cr}$, $\text{L}=\text{CO}$, $n=5$, $\text{L}'=\text{CO}$

10 $\text{M}=\text{Co}$, $\text{L}=\text{CO}$, $n=2$, $\text{L}'=\text{Cp}$

12 $\text{M}=\text{Mn}$, $\text{L}=\text{CO}$, $n=3$, $\text{L}'=\text{MeCp}$

13 $\text{M}=\text{Cr}$, $\text{L}=\text{CO}$, $n=5$, $\text{L}'=\text{CO}$



those used for their carbon analogues. In the present study, all the complexes have been characterized unambiguously by ^{29}Si , ^{13}C , and ^1H NMR, IR, and mass spectroscopy. However, our repeated efforts to study these complexes in solid state by X-ray crystallography have been unsuccessful.

(a) **^{29}Si -NMR Spectroscopy.** ^{29}Si -NMR chemical shifts of base-stabilized silane-transition metal complexes having at least one aromatic group on the silicon fall in the characteristic region of 80–150 ppm, which allows a clear distinction of silylene complexes from various silyl-metal σ -bonded compounds and also from dimeric moieties, which are typically observed at rather lower field, below 150 ppm. As would be expected by comparison with carbene complexes, ^{29}Si -NMR chemical shifts are 100 ppm upfield due to the rigid coordination of the donor group to the Si atom. The same phenomenon was observed by Tilley *et al.*¹⁴ for the cationic complex $[\text{Cp}^*(\text{PMe}_2)_2\text{Ru}=\text{SiR}_2]^+\text{BPh}_4^-$. This base-free silylene complex ($\text{R} = (S)\text{-}p\text{-tolyl}$), which gives a broad signal at +250.6 ppm in ^{29}Si NMR, readily coordinates with acetonitrile to give the corresponding base-stabilized complex at +53.3 ppm. Cobalt-silane-transition metal complex **5** (+95 ppm) displays only one signal slightly upfield than other silane-transition metal complexes having the same coordinating ligand (P_5), followed by iron and chromium silane-transition metal complexes **2** (+105 ppm) and **4** (+111 ppm), respectively. Manganese complexes **3a** and **3b** display more downfield shifts at +131 and +132 ppm, respectively. The same trends are observed by changing the coordinating ligand at silicon (N_6 , N_5 system) (Table 1).

Variable-temperature ^{29}Si -NMR studies of complexes **2–13** were carried out in toluene. ^{29}Si resonances are shifted slightly downfield with increasing temperature; for instance, **4** gives a signal (DEPT technique) at +108.4 ppm (233 K), which shifts to +112.6 ppm at 333 K.

(b) **Si-H Coupling Constants.** $^1J(\text{SiH})$ coupling constants for complexes **2–13** were measured by the

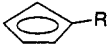
(14) Zhang, C.; Grumbine, S. D.; Tilley, T. D. *Polyhedron* **1991**, *10*, 1173.

Table 1. ^{29}Si NMR Chemical Shifts and Coupling Constants (Si–H) of Intramolecular Base-Stabilized Silanediyl–Transition Metal Complexes

products	compd	Ar≡P ₅	compd	Ar≡N ₆	compd	Ar≡N ₅
ArHSi=Fe(CO) ₄	2	+105 ^a ¹ J(SiH) = 180 ^b	7	+94 ¹ J(SiH) = 191		
ArHSi=MnCp(CO) ₂	3a	+131 ¹ J(SiH) = 157	8a	+120 ¹ J(SiH) = 165		
ArHSi=MnMeCp(CO) ₂	3b	+132 ¹ J(SiH) = 149	8b	+124 ¹ J(SiH) = 166	12	+142 ¹ J(SiH) = 164
ArHSi=Cr(CO) ₅	4	+111 ¹ J(SiH) = 162	9	+102 ¹ J(SiH) = 165	13	+120 ¹ J(SiH) = 165
ArHSi=CoCp(CO)	5	+95 ¹ J(SiH) = 162	10	+86 ¹ J(SiH) = 165		

^a Chemical shifts in ppm. ^b Coupling constants in hertz.

Table 2. ^{13}C -NMR Chemical Shifts of Silanediyl–Transition Metal Complexes 2–12

product	NMe ₂	NCH ₂	CO		aromatics
2	47.12 48.16	67.86	214.17 215.05		128.15, 128.96, 129.13 131.45, 133.24
3a	46.05 47.50	68.77	232.60 233.70	80.16	123.70, 129.25, 134.30 138.02, 139.80, 145.43
3b	46.28 47.62	68.91	233.11 233.54	14.17, ^a 79.04, 79.12, 80, 64, 81.03, 93.03 ^b	123.96, 129.64, 134.27 137.87, 140.24, 145.59
4	45.28 48.43	69.59	221.72 225.51		123.63, 129.93, 134.17 140.19, 142.28
5	46.17	66.72	207.37	80.58	123.65, 129.26, 134.51 140.81, 143.81
7	44.77 50.91	68.96	217.40		126.07, 127.60, 131.07 131.50, 133.85, 138.62
8a	45.01 50.08	68.61	232.52 234.31	80.21	125.50, 127.12, 131.06 131.61, 133.92, 138.91
8b	45.36 50.24	68.26	232.67 234.49	14.86, ^a 79.74, 80.56, 81.64, 82.40, 98.23 ^b	128.32, 130.13, 133.72 137.50, 140.99
9	45.03 50.01	69.33	233.01 226.09		125.74, 126.67, 130.75 131.03, 134.23, 136.75
10	45.17 49.21	66.97	207.73	80.99	125.72, 126.78, 130.18 131.06, 134.56, 139.02
12	50.18 53.86		232.87 234.01	15.16, ^a 80.98, 82.69, 82.93, 83.45, 98.90 ^b	127.51, 129.97, 132.04 142.78, 150.61

^a C*CH₃. ^b *CCH₃.

DEPTC technique. All complexes display one doublet, indicating the presence of only one Si–H bond. ¹J(SiH) values usually depend on the Fermi contact term and hence on the s-character of the Si–H bond.¹⁵ An increase or decrease in the s-character of the Si–H bond causes an increase or decrease in the coupling constant, respectively. Comparatively lower values of the ¹J(SiH) coupling constant in complexes **2–13** (Table 1) are indicative of a decrease in the s-character of the Si–H bond, implying very low effective electronegative values of the MLnL' moieties attached to silicon, according to Bent's rule.¹⁵

(c) **¹H-NMR and ¹³C-NMR Spectroscopic Data.** ¹H-NMR and ¹³C-NMR spectra provide definite evidence about the rigid coordination of the dimethylamino unit to the silicon atom¹² and also about the arrangement of CO groups around the metal.

For example, the ¹H-NMR spectrum of complex **4**, in benzene or toluene, displays two signals (1.85, 1.95 ppm) for methyl protons on nitrogen and the AB system [(2.69, 3.26 ppm, ²J(HH) = 13.80 Hz] for NCH₂ protons. Nitrogen inversion is hindered because of coordination to silicon, implying that the two methyl groups on nitrogen and methylene protons of the NCH₂ group are

in a disymmetric environment (diastereotopic). In the case of rapid nitrogen inversion, plus rapid C–N bond rotation, the two methyl groups on nitrogen as well as the methylene protons (NCH₂) would become equivalent. We must emphasize the observed phenomenon of rigid coordination prevails up to 105 °C. No coalescence was observed in variable-temperature ¹H-NMR experiments, neither for the NMe₂ group nor for the NCH₂ AB system ($\Delta G^\ddagger > 95 \text{ kJ mol}^{-1}$).¹⁶ Inequivalence of the two methyls of the NMe₂ groups is observed, similarly, in the ¹H NMR spectra of **3a**, **5**, **8b**, **9**, and **10**.

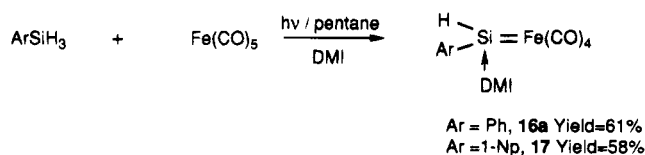
Rigid coordination of the NMe₂ unit to the Si atom is equally apparent in ¹³C-NMR spectra of manganese-, cobalt-, and iron-silanediyl complexes (Table 2). As an example, the ¹³C-NMR spectrum of complex **4** displays two methyl signals (45.28, 48.43 ppm), which are diastereotopic because of rigid coordination of the NMe₂ group to the Si atom.

The number of carbonyl carbons signals in ¹³C-NMR spectra of transition metal carbonyl complexes depends on the local symmetry of M(CO)_n.⁴¹ As expected, in the case of the chromium complexes, **4**, **9**, and **13**, two sets of signals (for one axial carbonyl and four equatorial carbonyls) were observed. In the case of complex **2**, two

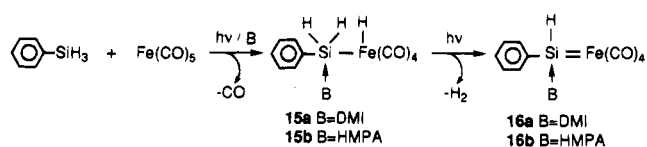
(15) (a) Bent, H. A. *Chem. Rev.* **1961**, *61*, 275. (b) Aylett, B. J. *J. Organomet. Chem. Lib.* **1980**, *9*, 327. (c) Aylett, B. J. *Adv. Inorg. Chem. Radiochem.* **1982**, *25*, 1. (d) Williams, E. A. In *Annual Reports on NMR Spectroscopy*; Webb, G. A., Ed.; Academic Press: London, 1983; pp 235–289.

(16) (a) Probst, R.; Leis, C.; Gamper, S.; Herdtweck, E.; Zybille, C.; Auner, N. *Angew. Chem., Int. Ed. Engl.* **1991**, *30*, 1132. (b) Handwerker, H.; Leis, C.; Probst, R.; Bissinger, P.; Grohmann, A.; Kiprof, P.; Herdtweck, E.; Blümel, J.; Auner, N.; Zybille, C. *Organometallics* **1993**, *12*, 2162.

Scheme 3



Scheme 4



signals at 214.17 (equatorial carbonyls) and 215 ppm (axial carbonyl) for carbonyl carbons were differentiated. In contrast to complex **2**, complex **7** gives only one signal (217.4 ppm) for carbonyl carbons, indicating rapid exchange on the NMR time scale between axial and equatorial carbonyls.

As expected, manganese complexes **3a**, **3b**, **8a**, **8b**, and **12** display two signals for two stereochemically different carbonyl carbons in ^{13}C NMR. We have carried out the variable-temperature ^{13}C -NMR study of complex **3b**. The two signals (233.11, 233.54 ppm) for carbonyl carbons, observed at room temperature, collapse to only one signal (233.08 ppm) at 90 °C, indicating fluxional behavior of the carbonyls at higher temperature. Such a result is noticeable because, as mentioned before and contrary to the structural behavior of the carbonyls, no change was observed (*vide infra*) in the ^{13}C -NMR spectrum of **3b** for the diastereotopic NMe_2 signals. Coordination of nitrogen to silicon is stronger enough to be maintained at high temperature.

(3) Synthesis of Intermolecular Base-Stabilized Silanediyl-Iron Tetracarbonyl Complexes. Primary silane PhSiH_3 was irradiated with 1 equiv of $\text{Fe}(\text{CO})_5$ in the presence of DMI in pentane. Separation of a black-red sticky solid started taking place after 10 min of irradiation. ^{29}Si NMR (toluene/ C_6D_6) of this solid showed the formation of **15a** (see later) and **16a**. IR analysis of the pentane solution indicated complete consumption of starting silane after 5 h. Washing of the precipitate with pentane furnished DMI-stabilized (phenylsilanediyl)iron(0) tetracarbonyl complex **16a** in good yield. DMI-stabilized (naphthylsilanediyl)iron(0) tetracarbonyl complex **17a** was prepared in the same manner (Scheme 3).

^{29}Si -NMR spectra (DEPTC, toluene/ C_6D_6) show only doublets for the monomeric hydridosilanediyl-iron(0) complexes [$^1J(\text{SiH}) = 199$ Hz for **16a** and $^1J(\text{SiH}) = 218$ Hz for **17**]. ^{29}Si chemical shifts of complexes **16a** (+83.52 ppm) and **17** (+81.51 ppm) fall in the characteristic region of intermolecular base-stabilized silanediyl complexes.¹⁰ ^{29}Si -NMR chemical shifts of DMI-stabilized complexes **16a** and **17**, measured at different temperatures move linearly downfield with increasing temperature, but $\Delta\delta$ is even less significant than in the case of intramolecular base-stabilized complexes, for example, δ value shifts in case of **16a** from +83.19 ppm at 233 K to +84.53 ppm at 313 K.

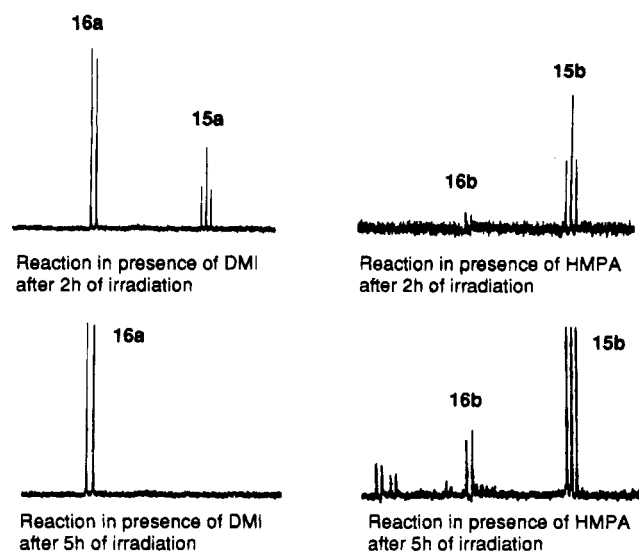


Figure 1.

(4) Mechanism of Formation of Silanediyl-Transition Metal Complexes. The Lewis base-induced insertion reaction of photochemically generated 16-e^- transition metal species into the Si-H bond of primary silanes represents an easy access to intramolecular or intermolecular base-stabilized hydrosilanediyl-metal complexes. NMR study of reaction mixtures indicates that formation of silanediyl complexes involves two steps: (i) insertion of 16-e^- metal species into the Si-H bond,¹⁷ i.e., formation of a silyl metal hydride intermediate, and (ii) H_2 elimination from the silyl metal hydride intermediate.

For instance, irradiation of phenylsilane with $\text{Fe}(\text{CO})_5$ in the presence of DMI provides strong evidence for the stepwise formation of **16a** (phenylsilanediyl)iron(0) tetracarbonyl-1,3-dimethyl-2-imidazolidinone. After 2 h of UV irradiation, the ^{29}Si -NMR spectrum of the mixture displays one triplet at -2.53 ppm [$^1J(\text{SiH}) = 176$ Hz, DEPTC] corresponding to **15a** and one doublet at +83.52 ppm [$^1J(\text{SiH}) = 199$ Hz, DEPTC] for **16a** (Scheme 4).

Hydrogen elimination from the silyl metal hydride intermediate **15a** is favored by strong coordination of DMI to the Si atom. In similar conditions, photoirradiation of PhSiH_3 with $\text{Fe}(\text{CO})_5$ in the presence of HMPA for 2 h furnishes, exclusively, silyl metal hydride intermediate **15b** [^{29}Si NMR +6.43 ppm, $^1J(\text{SiH}) = 176$ Hz, DEPTC]. Prolonged irradiation conditions lead to the mixture of **15b** and (phenylsilanediyl)iron(0) tetracarbonyl-hexamethylphosphoric triamide complex **16b** [^{29}Si NMR +72.01 ppm, $^1J(\text{SiH}) = 220.6$ Hz, $^3J(\text{SiP}) = +20.86$ Hz] (Figure 1).

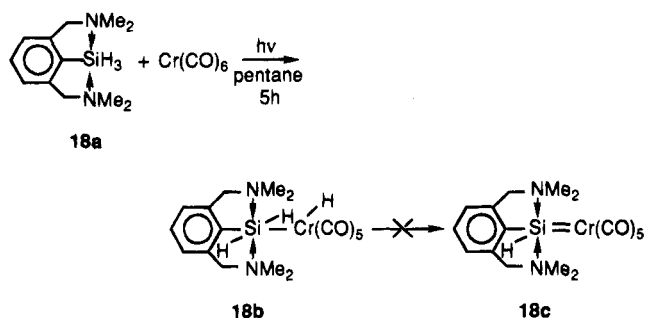
Weak coordination of HMPA to the Si atom leads to comparatively less basic Si-H bonds in intermediate **15b**. Hydrogen elimination from this intermediate is not favored due to less basic Si-H bonds. Small doublets observed downfield could be attributed to dimers, but no further experiment was performed in order to identify these byproducts.

In the case of activated rigid pentacoordinated silanes, we were not able to observe intermediate formation of

(17) (a) Jetz, W.; Graham, W. A. G. *Inorg. Chem.* **1971**, *10*, 4. (b) Jetz, W.; Graham, W. A. G. *Inorg. Chem.* **1971**, *10*, 1647. (c) Colomer, E.; Corriu, R. J. P.; Vioux, A. *Inorg. Chem.* **1979**, *18*, 695. (d) Colomer, E.; Corriu, R. J. P. *Top. Curr. Chem.* **1981**, *96*, 79. (e) Schubert, U. *Trans. Met. Chem.* **1991**, *16*, 136, and references cited therein.

(18) (a) van Koten, G. *Pure Appl. Chem.* **1989**, *61*, 1681; *Ibid.* **1990**, *62*, 1155. (b) Chuit, C.; Corriu, R. J. P.; Mehdi, A.; Reyé, C. *Angew. Chem., Int. Ed. Engl.* **1993**, *9*, 1311. (c) Carré, F.; Chuit, C.; Corriu, R. J. P.; Mehdi, A.; Reyé, C. *Angew. Chem., Int. Ed. Engl.* **1994**, *10*, 1097.

Scheme 5



a silyl–metal hydride complex, because the efficient activation of the NMe₂ unit to the silicon atom favors a hydrogen elimination step, giving a stable silylene–metal complex. In view of recent results¹⁸ obtained with less efficient interconverting intramolecular coordination of two NMe₂ groups at the Si and Sn atoms to stabilize cationic intermediates, we chose [[2,6-bis(dimethylamino)methyl]phenyl]silane (**18a**) to stabilize the silyl–metal hydride intermediate. As expected, photolysis of silane **18a** with Cr(CO)₆ furnished the desired intermediate **18b** in good yield, after 5 h of irradiation (Scheme 5).

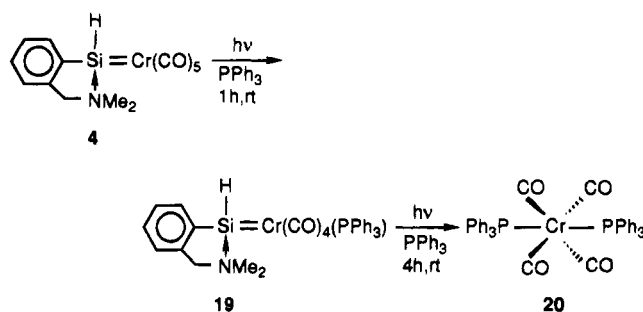
The stability of product **18b** can be accounted for by the less acidic Cr–H bond and comparatively less basic Si–H bonds because of weak coordination of the NMe₂ group to the silicon atom. Both factors do not favor elimination of hydrogen from intermediate **18b** to give the silylene–metal complex.

The above experiments suggest that selective hydrogen elimination from the silyl–metal hydride intermediate depends upon a combination of two factors: (a) acidity of the metal hydride bond; (b) basicity of the Si–H bond.

Reactivity of Base-Stabilized Silylene Complexes. “Base-free” silylene complexes have been considered as reactive intermediates in a variety of silylene transfer reactions.¹⁹ In many cases, transient silylene complexes have also been proposed as catalytically active species, for instance, in silylene transfer reactions to olefins and acetylenes.²⁰ Since relatively few reports⁸ are known concerning the reactivity of base-stabilized silanediyl–transition metal complexes, and since we have recently demonstrated the base-stabilized silanediyl–transition metal complexes as potential source of silylenes,¹¹ we have considered the reactivity of functional hydrosilanediyl–transition metal complexes for [[2-[(dimethylamino)methyl]phenyl]silanediyl]chromium(0) pentacarbonyl (**4**).

(5) Carbonyl Displacement Reactions. (1) Reaction with Triphenyl Phosphine. A toluene solution of [[2-[(dimethylamino)methyl]phenyl]silanediyl]chromium(0) pentacarbonyl (**4**) was photolyzed in the presence of 2 equiv of triphenylphosphine at room tempera-

Scheme 6



Scheme 7



ture. After 1 h of irradiation, a mixture consisting of complex [[2-[(dimethylamino)methyl]phenyl]silanediyl]-(triphenylphosphine)chromium(0) tetracarbonyl (**19**; +57 ppm) and complex *trans*-bis(triphenylphosphine)chromium(0) tetracarbonyl (**20**; +75 ppm) was observed in ³¹P NMR (Scheme 6).

Further photolysis of this mixture for 4 h allowed complete conversion to complex **20** (45% yield). This experiment indicates that the formation of complex **20** takes place by stepwise displacement of CO and the silylene unit. We were not able to identify the organosilicon part. No signal was observed in ²⁹Si NMR, using different programs (INVGATE, DEPTC, INEPT). Such behavior was already noted²¹ for aminoaryl silylenes, prepared by halodemetalation of pentacoordinated difluorosilanes. Hydrolysis of the reaction mixture gave siloxanes.

Thermolysis of complex **4** with triphenylphosphine furnished the same results. Refluxing complex **4** with 2 equiv of triphenylphosphine in toluene leads to the formation of complex **20** after 7 h, in 38% yield.

(b) Reaction with DPPE. One equivalent of 1,2-bis(diphenylphosphino)ethane (DPPE) was added to the toluene solution of freshly prepared complex **4** in a photochemical reactor. This mixture was irradiated for 1 h at room temperature (Scheme 7). After 1 h, the mixture was analyzed by ²⁹Si NMR, which established the formation of complex [[2-[(dimethylamino)methyl]phenyl]silanediyl][1,2-bis(diphenylphosphino)ethane]chromium(0) tetracarbonyl (**21**; +118.39 ppm (d, ²J(SiP) = 26.15 Hz, INVGATE) (d of d, ¹J(SiH) = 154.85 Hz, DEPTC)) and complex [[2-[(dimethylamino)methyl]phenyl]silanediyl][1,2-bis(diphenylphosphino)ethane]chromium(0) tricarbonyl (**22**; +123.93 ppm (t, ²J(SiP) = 20.6 Hz, INVGATE) (d of t, ¹J(SiH) = 144.73 Hz, DEPTC)) along with the remaining complex **4**. When this mixture was further photolyzed for 5 h at room temperature, total consumption of complex **4** and complex **21** took place to furnish complex **22** in 80% yield (Figure 2). In contrast to triphenylphosphine, complexation of the second phosphorus of the DPPE ligand dissociates the second carbonyl in place of the silylene unit. In the case of complex **21** (¹J(²⁹SiH) = 154.85 Hz), replacement of one carbonyl of complex **4** (¹J(SiH) = 162

(19) (a) Curtis, M. D.; Epstein, P. S. *Adv. Organomet. Chem.* **1981**, *19*, 213. (b) Yamamoto, K.; Okinoshima, H.; Kumada, M. *J. Organomet. Chem.* **1971**, *27*, C31. (c) Ojima, I.; Inaba, S.-I.; Kogure, T.; Nagai, Y. *J. Organomet. Chem.* **1973**, *55*, C7. (d) Kumada, M. *J. Organomet. Chem.* **1975**, *100*, 127.

(20) (a) Seyferth, D.; Shannon, M. L.; Vick, S. C.; Lim, T. F. O. *Organometallics* **1985**, *4*, 57. (b) Okinoshima, H.; Yamamoto, K.; Kumada, M. *J. Am. Chem. Soc.* **1972**, *94*, 9263. (c) Sakurai, H.; Kamiyama, Y.; Nakadaira, Y. *J. Am. Chem. Soc.* **1977**, *99*, 3879. (d) Pannell, K. H.; Cervantes, J.; Hernandez, C.; Cassias, J.; Vincenti, S. *Organometallics* **1985**, *5*, 1056.

(21) Corriu, R. J. P.; Lanneau, G. F.; Priou, C.; Soulaïrol, F.; Auner, N.; Probst, R.; Conlin, R.; Tan, C. *J. Organomet. Chem.* **1994**, *466*, 55.

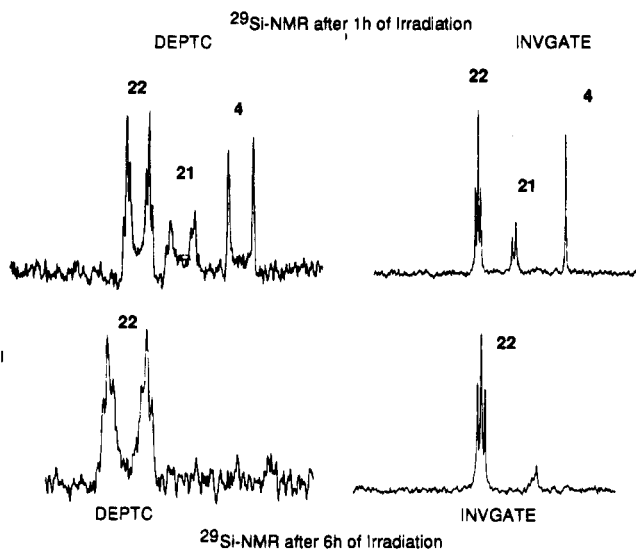
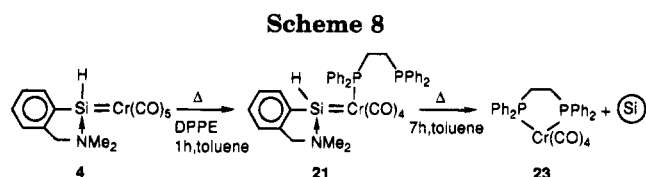


Figure 2.



Hz) by one phosphorus of the DPPE ligand decreases the Si-H coupling constant by 7.15 Hz. A downfield shift of 7.4 ppm for complex **21** (+118.39 ppm) in comparison to complex **4** (+111 ppm) in ^{29}Si NMR should also be noted. The same trend is observed for complex **22** (+123.93 ppm, $^1J(\text{SiH}) = 144.73$ Hz), when two carbonyls of complex **4** are replaced by a DPPE ligand, with, respectively, a further decrease in Si-H coupling constant of 10.12 Hz and downfield ^{29}Si chemical shift variation of 5.6 ppm (Figure 2).

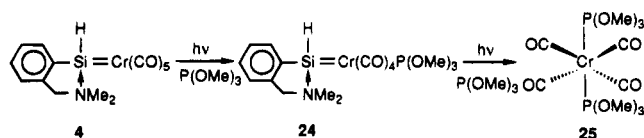
(b2) Thermolysis with DPPE. Freshly prepared complex **4** was dissolved in toluene, and 1 equiv of DPPE was added to this solution. The resulting mixture was refluxed for 1 h (Scheme 8). Formation of complex **21** and complex [1,2-bis(diphenylphosphino)ethanechromium(0) tetracarbonyl]**23** (**21:23**, about 1:1 ratio) was confirmed by ^{31}P NMR (**21:23**, about 1:1 ratio). As mentioned above, silylene or oligomeric silanes could not be identified by ^{29}Si -NMR techniques currently available. A total of 50% of **4** was consumed after 7 h of heating to produce complex **21** and complex **23** in a 1:3 ratio. The reaction was not complete, even after prolonged heating of the mixture.

(c) Reaction with Trimethyl Phosphite. Complex **4** was dissolved in 300 mL of toluene in a 500-mL quartz reaction vessel. Two equivalents of trimethyl phosphite were added to this solution, and the mixture was photolyzed for 1 h. Analysis of the crude mixture by spectroscopic methods revealed the formation of the complexes [[2-[(dimethylamino)methyl]phenyl]silylanyl]-(trimethylphosphite)chromium(0) tetracarbonyl (**24**) and 23 *trans*-bis(trimethylphosphite)chromium(0) tetracarbonyl (**25**; Scheme 9). Thermolysis of complex **4** furnished the same products after 7 h of refluxing.

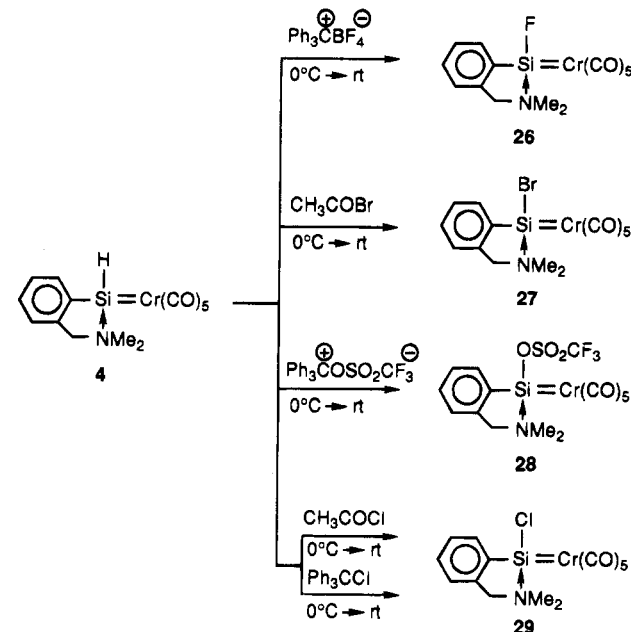
(22) (a) Grim, S. O.; Briggs, W. L.; Barth, R. C.; Tolman, C. A.; Jesson, J. P. *Inorg. Chem.* **1974**, *13*, 1095. (b) Carty, A. J.; Harris, R. K. *J. Chem. Soc., Chem. Commun.* **1967**, 234.

(23) (a) Bertrand, R. J.; Ogilvie, F. B.; Verkade, J. G. *J. Am. Chem. Soc.* **1970**, *92*, 1908. (b) Ogilvie, F. B.; Jenkins, J. M.; Verkade, J. G. *J. Am. Chem. Soc.* **1970**, *92*, 1916.

Scheme 9



Scheme 10



(d) Reaction with 2,3-Dimethylbutadiene. Complex **4** was photolyzed in the presence of a 10-fold excess of 2,3-dimethylbutadiene for 5 h at room temperature. ^{29}Si -NMR analysis of the crude mixture indicated complete consumption of **4**, but no new signal for a compound corresponding to the trapping product or compounds with the Si-H bond (DEPTC technique) were observed.

(6) Reactions of Si-H Bond. Tetracoordinated hydrosilanes are reactive species, and many substitutions and exchange processes have been developed with these starting materials.²⁴ Some experiments have been performed in order to extend such reactions to unsaturated base-stabilized hydrosilanydiyl-transition metal complexes.

(a) Reaction with Triphenylcarbonium Tetrafluoroborate. Addition of 1 equiv of triphenylcarbonium tetrafluoroborate to the freshly prepared complex **4** at 0 °C furnished complex [[2-[(dimethylamino)methyl]phenyl]fluorosilylanyl]chromium(0) pentacarbonyl (**26**) in 93% yield (Scheme 10).

(b) Reaction with Acetyl Bromide. One equivalent of acetyl bromide was added dropwise to the 50-mL toluene solution of complex **4** at 0 °C. Evaporation of solvent after 4 h furnished complex [[2-[(dimethylamino)methyl]phenyl]bromosilylanyl]chromium(0) pentacarbonyl (**27**) in 80% yield (Scheme 10).

(24) (a) Corey, J. Y.; West, R. *J. Am. Chem. Soc.* **1963**, *85*, 2430. (b) Sommer, L. H.; Bauman, D. L. *J. Am. Chem. Soc.* **1969**, *91*, 7076. (c) Corriu, R. J. P.; Henner, M. *J. Organomet. Chem.* **1974**, *74*, 1. (d) Corey, J. Y. *J. Am. Chem. Soc.* **1975**, *97*, 3237. (e) Schubert, U.; Scholz, G.; Müller, J.; Ackermann, K.; Wörle, B.; Stansfield, R. F. D. *J. Organomet. Chem.* **1986**, *306*, 303. (f) Corriu, R. J. P.; Lanneau, G. F.; Perrot, M. *Tetrahedron Lett.* **1988**, *29*, 1271. (g) For a recent review, see: Chuit, C.; Corriu, R. J. P.; Reye, C.; Young, J. C. *Chem. Rev.* **1993**, *93*, 1371.

Table 3. Comparison of ^{29}Si -NMR and ^{13}C -NMR Signals of Complexes 26–29

	26	27	28	29
^{29}Si NMR ^a (INVGATE)	+117.20 (d) $^1J(\text{SiF}) = 398 \text{ Hz}$	+119.38	+123.46	+122.97
^{13}C NMR ^a	45.70	46.33	45.12	46.22
NMe ₂	45.99		45.71	47.07
NCH ₂	68.38	68.33	68.57	68.17
CO	219.90 (eq) 224.52 (ax)	220.94 (eq) 224.48 (ax)	219.07 (eq) 222.33 (ax)	219.50 (eq) 223.30 (ax)
aromatics	124.26, 127.71 129.09, 131.51 134.48, 139.89	124.92, 130.89 131.90, 140.13 144.33	122.89, 130.53 132.29, 135.53 138.86, 140.53	124.45, 129.26 131.30, 133.40 139.13, 142.81

^a Chemical shifts in ppm.

(c) **Reaction with (Triphenylmethyl)trifluoromethanesulfonate.** Freshly prepared (triphenylmethyl)trifluoromethanesulfonate²⁵ (5 mL, CH_2Cl_2) solution was added dropwise to the toluene solution of **4** at 0 °C. Removal of solvents after 4 h afforded Ph_3CH and complex $[[2-[(\text{dimethylamino})\text{methyl}]\text{phenyl}]\text{trifluoromethanesulfonatesilanediy}]$ chromium(0) pentacarbonyl (**28**; Scheme 10).

(d) **Reaction with Chlorotriphenylmethane.** Chlorotriphenylmethane solution was added dropwise to the toluene solution of complex **4** at 0 °C. This mixture was stirred at room temperature for 24 h. Evaporation of solvent under reduced pressure furnished complex $[[2-[(\text{dimethylamino})\text{methyl}]\text{phenyl}]\text{chlorosilanediy}]$ chromium(0) pentacarbonyl (**29**) in 65% yield (Scheme 10).

(e) **Reaction with Acetyl Chloride.** The same procedure as for acetyl bromide reaction was applied with acetyl chloride to isolate complex **29** in 83% yield (Scheme 10).

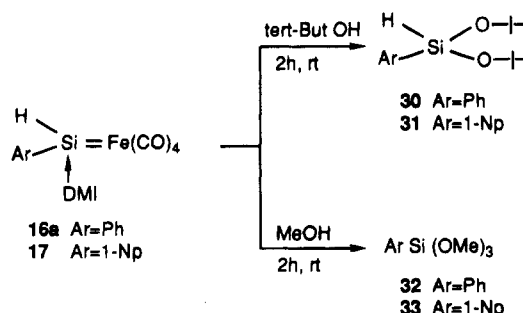
(f) **Reaction with *tert*-Butyl Alcohol.** **4** was dissolved in toluene, and a 10-fold excess of *tert*-butyl alcohol was added to this solution. The mixture was stirred at room temperature for 24 h. Evaporation of solvent and an excess *tert*-butyl alcohol furnished a yellow sticky solid which gave only one signal in ^{29}Si NMR (INVGATE) at -75.95 ppm . No signal for SiH was observed in ^{29}Si NMR by the DEPTC technique. We were not able to identify the product.

(g) **Reaction of Complexes 16a and 17 with Alcohols.** Reaction of (phenylsilanediy)iron(0) tetracarbonyl-1,3-dimethyl-2-imidazolidinone (**16a**) and (1-naphthylsilanediy)iron(0) tetracarbonyl-1,3-dimethyl-2-imidazolidinone (**17**) with *tert*-butyl alcohol or methanol in excess at room temperature for 24 h caused the cleavage of Si–Fe bonds to give quantitatively aryl-*tert*-butoxysilanes **30** (Ar = Ph) and **31** (Ar = 1-Np) and aryltrimethoxysilanes **32** (Ar = Ph) and **33** (Ar = 1-Np) (Scheme 11).

Conclusion

The dehydrogenative coupling reaction of primary organosilanes with transition metal carbonyls under photochemical conditions allows one to obtain Lewis base-stabilized silanediy–transition metal complexes with Si–H bond functionality, but strong nucleophiles are necessary to avoid further reactions. The formation of silanediy–transition metal complexes takes place in two steps: (1) insertion of the initially formed 16-e[−] metal moiety into the Si–H bond, giving a σ -bonded silyl metal hydride intermediate, and (2) elimination of

Scheme 11



hydrogen from this intermediate, with formation of a *base-stabilized* silanediy–transition metal complex. Such a mechanism supports the concept of silylene participation² in metal-catalyzed polymerization reactions of primary silanes.

Displacement of two carbonyls by DPPE provides a new entry to silanediy complexes suitable for model studies, and we expect a wide variety of applications in catalysis. Silanediy complexes with functionality X (X = F, Cl, Br, OSO_2CF_3) have also been synthesized in one-step reactions, allowing us to study the nature of silicon metal bonding on simple molecules.

Experimental Section

All reactions, unless otherwise mentioned, were carried out under an atmosphere of dry argon. Air-sensitive products and reagents were handled by standard Schlenk techniques. All solvents were dried and distilled from purple solutions of sodium/benzophenone or P_2O_5 , and glassware was dried in an oven at 110–120 °C prior to use. Commercially available chemicals were used as such without any further purification, except $\text{Fe}(\text{CO})_5$ and $\text{CH}_3\text{CpMn}(\text{CO})_3$, which were distilled before use. The synthesis of starting silanes has already been described in literature.¹²

^{29}Si , ^{13}C , ^1H , and ^{31}P -NMR spectra were recorded on Bruker WP 200 SY or AC 250 spectrometer. ^1H and ^{13}C chemical shifts were measured against Me_4Si using solvent resonances as standard locks. ^{29}Si chemical shifts were referenced to external Me_4Si in same solvent. IR spectra were recorded on Perkin-Elmer 1600 FT as KBr pellets, Nujol suspensions, or solutions in CaF_2 cells. The mass spectra were obtained on a JEOL JMS D100 apparatus by EI ionization at 30 or 70 eV. Elemental analyses were carried out by the Service Central de Microanalyse du CNRS or ENSC Montpellier. All photochemical reactions were performed in a quartz reaction vessel equipped with a water-cooled quartz finger, under a steady flow of argon. A 450-W Hanovia medium-pressure mercury lamp was placed inside the quartz finger.

[2-(Me₂NCH₂)C₆H₄]SiH=Fe(CO)₄. **[[2-(Dimethylamino)methyl]phenyl]silanediy]iron(0) tetracarbonyl (2).** A 350-mL pentane solution of $[[2-[(\text{dimethylamino})\text{methyl}]\text{phenyl}]\text{tri}(\text{hydro})\text{silane}$ (**1**; 3.30 g, 0.02 mol) was transferred under

(25) Straus, D. A.; Zhang, C.; Tilley, T. D. *J. Organomet. Chem.* **1989**, *369*, C13.

argon into a 500-mL quartz reaction vessel containing 2.63 mL (0.02 mol) of $\text{Fe}(\text{CO})_5$. This mixture was irradiated at room temperature for 5 h. A dark red thick oil started precipitating after 15 min. Reaction progress was monitored by IR. After complete disappearance of silane 1, pentane solution was removed with a cannula, and the dark red oil, [[2-(dimethylamino)methyl]phenyl]silanediyliron(0) tetracarbonyl (2), was washed with pentane and analyzed. Yield: 81%. Anal. Calcd for $\text{C}_{13}\text{H}_{13}\text{NO}_4\text{SiFe}$: C, 47.14; H, 3.92; N, 4.23. Found: C, 47.18; H, 3.86; N, 4.24. ^{29}Si NMR (toluene/ C_6D_6): δ 47.12 (NCH_3), 48.16 (NCH_3), $^1J(^{29}\text{Si}^1\text{H}) = 180$ Hz. ^{13}C NMR (C_6D_6): δ 47.12 (NCH_3), 48.16 (NCH_3), 67.86 (NCH_2), 124.00, 124.08, 131.45, 131.66 (C_6H_4), 214.17, 215.05 (CO). MS [EI, 70 eV; m/e (relative intensity %): 331 (M^+ , 0.8), 135 (32), 118 (10), 91 (35), 57 (100). IR (toluene, cm^{-1}): $\nu(\text{CO}, \text{SiH})$ 2040 (s), 1964 (s), 1924 (br).

The same procedure and stoichiometric quantities of reactants were used for the preparation of complexes 3–5.

[2-(Me_2NCH_2) C_6H_4] $\text{SiH}=\text{MnCp}(\text{CO})_2$. [[2-(Dimethylamino)methyl]phenyl]silanediyl(η^5 -cyclopentadienyl)manganese dicarbonyl (3a). mp: 136 °C (dec). Yield: 76%. Anal. Calcd for $\text{C}_{16}\text{H}_{16}\text{NO}_2\text{SiMn}$: C, 56.63; H, 5.30; N, 4.12. Found: C, 56.72; H, 5.39; N, 4.18. ^{29}Si NMR (toluene/ C_6D_6): δ +130.89 (INV-GATE), $^1J(^{29}\text{Si}^1\text{H}) = 156.8$ Hz (DEPTC). ^{13}C NMR (C_6D_6): δ 46.05 (NCH_3), 47.50 (NCH_3), 68.77 (NCH_2), 80.16 (C_5H_5), 123.7–145.4 (aromatics), 232.6, 233.7 (CO). ^1H NMR (C_6D_6): δ 1.79 (s, 3H, NCH_3), 2.11 (s, 3H, NCH_3), 3.91 [dd, (br), 2H, AB system, $^2J(^1\text{H}^1\text{H}) = 14.8$ Hz, NCH_2], 4.47 (s, 5H, Cp), 6.18 (s, 1H, SiH), 6.84, 7.09, 7.79 (4H, aromatics). MS [EI, 70 eV; m/e (relative intensity %): 339 (M^+ , 30), 283 (–2CO, 90), 162 (100), 135 (8), 119 (30), 91 (20). IR (C_6D_6 , cm^{-1}): $\nu(\text{CO}, \text{SiH})$ 1974, 1910, 1837.

[2-(Me_2NCH_2) C_6H_4] $\text{SiH}=\text{MnMeCp}(\text{CO})_2$. [[2-(Dimethylamino)methyl]phenyl]silanediyl(η^5 -methylcyclopentadienyl)manganese dicarbonyl (3b). Yield: 63%. Anal. Calcd for $\text{C}_{17}\text{H}_{20}\text{NO}_2\text{SiMn}$: C, 57.79; H, 5.66; N, 3.96. Found: C, 57.82; H, 5.965; N, 3.98. ^{29}Si NMR (toluene/ C_6D_6): δ +131 (INV-GATE), $^1J(^{29}\text{Si}^1\text{H}) = 149$ Hz (DEPTC). ^{13}C NMR (22 °C, C_6D_6): δ 14.87 (Cp^*CH_3), 46.28 (CH_3), 47.62 (NCH_3), 68.91 (NCH_2), 79.04, 79.12, 80.64, 81.03 (C_6H_4), 93.03 ($^*\text{CCH}_3$), 123.96, 134.27, 140.24, 145.59 (aromatics), 233.11, 233.54 (CO). ^{13}C NMR (90 °C, toluene- d_8): no change, except that the two carbonyls give one broad signal at δ 233.08 ppm. MS [EI, 70 eV; m/e (relative intensity %): 353 (M^+ , 19), 297 (–2CO, 100), 218 (2), 162 (87), 134 (18), 91 (85), 79 (58). IR (toluene, cm^{-1}): $\nu(\text{CO}, \text{SiH})$ 1971, 1904, 1838.

[2-(Me_2NCH_2) C_6H_4] $\text{SiH}=\text{Cr}(\text{CO})_5$. [[2-(Dimethylamino)methyl]phenyl]silanediylchromium(0) pentacarbonyl (4). Yield: 87%. Yellow solid, mp: 163–164 °C. Anal. Calcd for $\text{C}_{14}\text{H}_{13}\text{NO}_5\text{SiCr}$: C, 47.32; H, 3.66; N, 3.94. Found: C, 47.53; H, 3.96; N, 4.02. ^{29}Si NMR (C_6D_6): δ +110.94 (INV-GATE), $^1J(^{29}\text{Si}^1\text{H}) = 162.35$ Hz (DEPTC). ^{13}C NMR (C_6D_6): δ 45.28 (NCH_3), 48.43 (NCH_3), 69.59 (NCH_2), 123.63, 129.97, 134.17, 140.19, 142.28 (aromatics), 221.72, 225.51 (CO). ^1H NMR (C_6D_6): δ 1.85 (s, 3H, NCH_3), 1.95 (s, 3H, NCH_3), 2.65–2.73, 3.22–3.30 [dd, 2H, AB system, $^2J(^1\text{H}^1\text{H}) = 13.80$ Hz, NCH_2], 5.68 (s, 1H, SiH), 6.7–7.08 (aromatics). MS [EI, 30 eV; m/e (relative intensity %): 355 (M^+ , 48), 327 (–CO, 24), 299 (–2CO, 4), 271 (–3CO, 49), 243 (–4CO, 64), 216 (–5CO, 100), 162 (98), 135 (08), 119 (22), 91 (33), 52 (86). IR (toluene, cm^{-1}): $\nu(\text{CO}, \text{SiH})$ 1914 (br), 1978, 2042.

[2-(Me_2NCH_2) C_6H_4] $\text{HSi}=\text{CoCp}(\text{CO})$. [[2-(Dimethylamino)methyl]phenyl]silanediyl(η^5 -cyclopentadienyl)cobalt carbonyl (5). Yield: 71%. Anal. Calcd for $\text{C}_{15}\text{H}_{15}\text{NO}_3\text{SiCo}$: C, 57.14; H, 5.71; N, 4.44. Found: C, 57.21; H, 5.68; N, 4.49. ^{29}Si NMR (C_6D_6): δ +95 (INV-GATE), $^1J(^{29}\text{Si}^1\text{H}) = 162$ Hz (DEPTC). ^{13}C NMR (C_6D_6): δ 46.17 (NCH_3), 66.72 (NCH_2), 80.59 (Cp), 123.65, 134.51, 140.23, 143.81 (aromatics), 207.37 (CO). ^1H NMR (C_6D_6): δ 1.91 (s, 3H, NCH_3), 2.02 (s, 3H, NCH_3), 2.91–2.96, 3.35–3.40 [dd, 2H, AB system, $^2J(^1\text{H}^1\text{H}) = 12.40$ Hz, NCH_2], 4.89 (s, 5H, Cp), 5.75 (s, 1H, SiH), 6.74–6.76 (d, 1H, aromatic), 7.15 (m, 2H, aromatic), 7.80–7.72 (d,

1H, aromatic). MS [EI, 70 eV; m/e (relative intensity %): 315 (M^+ , 90), 285 (–CO, 100), 270 (20), 242 (25), 162 (85), 135 (28), 119 (53), 105 (16), 91 (38). IR (C_6D_6 , cm^{-1}): $\nu(\text{CO}, \text{SiH})$ 2053, 1957.

[8-(Me_2NCH_2) C_{10}H_6] $\text{HSi}=\text{Fe}(\text{CO})_4$. [[8-(Dimethylamino)methyl]naphthyl]-1-silanediyliron(0) tetracarbonyl (7). [8-(Dimethylamino)methyl]naphthyl]-1-trihydrosilane (6; 4.30 g, 0.02 mol) was diluted in 350 mL of pentane in a 500-mL photochemical reactor under argon. $\text{Fe}(\text{CO})_5$ (2.63 mL, 0.02 mol) was injected into this solution with a syringe. This yellow mixture was irradiated at room temperature under a steady flow of argon for 6 h. Reaction progress was monitored by IR. After 10 min of irradiation, a red-black solid starts separating from the solution. After complete consumption of silane 6, pentane solution was taken out with a cannula and the remaining solid was washed three times with pentane and identified as [[8-(dimethylamino)methyl]naphthyl]-1-silanediyliron(0) tetracarbonyl (7). Yield: 68%; mp: 132–133 °C (dec). Anal. Calcd for $\text{C}_{17}\text{H}_{15}\text{NO}_4\text{SiFe}$: C, 53.34; H, 3.93; N, 3.67. Found: C, 53.33; H, 3.90; N, 3.72. ^{29}Si NMR (toluene/ C_6D_6): δ +95.53 (INV-GATE), $^1J(^{29}\text{Si}^1\text{H}) = 191.39$ Hz (DEPTC). ^{13}C NMR (C_6D_6): δ 44.77 (NCH_3), 50.91 (NCH_3), 68.96 (NCH_2), 126.07, 127.60, 131.07, 131.50, 133.85, 138.62 (aromatics), 217.40 (CO), MS [EI, 30 eV; m/e (relative intensity %): 381 (M^+ , 11), 353 (–CO, 21), 297 (–3CO, 42), 269 (–4CO, 75), 224 (30), 212 (35), 185 (25), 169 (18), 141 (40), 58 (100). IR (C_6D_6 , cm^{-1}): $\nu(\text{CO}, \text{SiH})$ 2023, 1994, 1995, 1905.

The same method and stoichiometric quantities as above were used for the synthesis of complexes 8a–10.

[8-(Me_2NCH_2) C_{10}H_6] $\text{HSi}=\text{MnCp}(\text{CO})_2$. [[8-(Dimethylamino)methyl]naphthyl]-1-silanediyl(η^5 -cyclopentadienyl)manganese dicarbonyl (8a). Yield: 63%. mp: 210–211 °C (dec). Anal. Calcd for $\text{C}_{20}\text{H}_{22}\text{NO}_2\text{SiMn}$: C, 61.69; H, 5.14; N, 3.59. Found: C, 61.58; H, 5.19; N, 3.64. ^{29}Si NMR (C_6D_6): δ +119.82 (INV-GATE), $^1J(^{29}\text{Si}^1\text{H}) = 165.46$ Hz (DEPTC). ^{13}C NMR (C_6D_6): δ 45.01 (NCH_3), 50.08 (NCH_3), 68.61 (NCH_2), 80.21 (Cp), 125.50, 127.12, 131.06, 131.61, 133.92, 138.91 (aromatics), 232.52, 234.31 (CO). ^1H NMR (C_6D_6): δ 1.75 (s, 3H, NCH_3), 2.25 (s, 3H, NCH_3), 3.19–3.29, 3.90–4.00 [dd, 2H, AB system, $^2J(^1\text{H}^1\text{H}) = 13.01$ Hz, NCH_2], 4.29 (s, 5H, Cp), 6.25 (s, 1H, SiH), 6.71 (d, 1H, aromatic), 7.39 (t, 1H, aromatic), 7.61 (t, 2H, aromatics), 8.18 (d, 1H, aromatic). MS [EI, 30 eV; m/e (relative intensity %): 389 (M^+ , 40), 333 (–2CO, 100), 212 (69), 169 (90), 141 (20), 58 (18). IR (C_6D_6 , cm^{-1}): $\nu(\text{CO}, \text{SiH})$ 1974, 1903, 1838.

[8-(Me_2NCH_2) C_{10}H_6] $\text{HSi}=\text{MnMeCp}(\text{CO})_2$. [[8-(Dimethylamino)methyl]naphthyl]-1-silanediyl(η^5 -methylcyclopentadienyl)manganese dicarbonyl (8b). mp: 215–216 °C (dec). Yield: 68%. ^{29}Si NMR (C_6D_6): δ +124.49 (INV-GATE), $^1J(^{29}\text{Si}^1\text{H}) = 165.96$ Hz (DEPTC). ^{13}C NMR (toluene- d_8): δ 14.86 (Cp^*CH_3), 45.36 (NCH_3), 50.24 (NCH_3), 68.26 (NCH_2), 79.74, 80.56, 81.64, 82.40 (Cp), 98.23 ($^*\text{CCH}_3$), 128.52, 130.13, 133.08, 133.72, 137.50, 140.99 (aromatics), 232.67, 234.49 (CO). MS [EI, 30 eV; m/e (relative intensity %): 403 (M^+ , 21), 347 (–2CO, 100), 212 (52), 169 (60), 141 (10), 134 (8). IR (C_6D_6 , cm^{-1}): 1970, 1901, 1833.

[8-(Me_2NCH_2) C_{10}H_6] $\text{HSi}=\text{Cr}(\text{CO})_5$. [[8-(Dimethylamino)methyl]naphthyl]-1-silanediylchromium(0) pentacarbonyl (9). mp: 171–172 °C (dec). Yield: 73%. Anal. Calcd for $\text{C}_{18}\text{H}_{15}\text{NO}_5\text{SiCr}$: C, 53.33; H, 3.70; N, 3.45. Found: C, 53.38; H, 3.74; N, 3.39. ^{29}Si NMR (C_6D_6): δ +102.14 (INV-GATE), $^1J(^{29}\text{Si}^1\text{H}) = 165.33$ Hz (DEPTC). ^{13}C NMR (C_6D_6): δ 45.03 (NCH_3), 50.01 (NCH_3), 69.33 (NCH_2), 125.74, 126.67, 130.75, 131.03, 134.23, 136.75 (aromatics), 222.02, 226.09 (CO). ^1H NMR (C_6D_6): δ 1.79 (s, 3H, NCH_3), 1.96 (s, 3H, NCH_3), 3.15–3.21, 3.73–3.67 [dd, 2H, $^2J(^1\text{H}^1\text{H}) = 15.01$ Hz, NCH_2], 5.95 (s, 1H, SiH), 6.54 (d, 1H, aromatic), 7.07 (t, 1H, aromatic), 7.29 (t, 1H, aromatic), 7.51 (t, 2H, aromatic), 8.25 (d, 1H, aromatic). MS [EI, 70 eV; m/e (relative intensity %): 405 (M^+ , 10), 377 (–CO, 8), 321 (–3CO, 10), 293 (4CO, 12), 265 (–5CO, 100), 212 (6), 185 (7), 169 (18), 52 (50). IR (C_6D_6 , cm^{-1}): $\nu(\text{CO}, \text{SiH})$ 2032, 1982, 1911.

[8-(Me₂NCH₂)C₁₀H₆]HSi=CoCp(CO). [[8-(Dimethylamino)methyl]naphthyl]-1-silanediy[(η⁵-cyclopentadienyl)manganese carbonyl (10). Yield: 65%. Anal. Calcd for C₁₉H₂₀NOSiCo: C, 62.46; H, 5.47; N, 3.83. Found: C, 62.53; H, 5.52; N, 3.81. ²⁹Si NMR (C₆D₆): δ +85.99 (INVGATE), ¹J(²⁹Si¹H) = 164.79 Hz (DEPTC). ¹³C NMR (C₆D₆): δ 45.17 (NCH₃), 49.21 (NCH₃), 66.97 (NCH₂), 80.99 (Cp), 125.72, 126.78, 130.18, 131.06, 134.56, 139.02 (aromatics), 207.73 (CO). ¹H NMR (C₆D₆): δ 1.92 (s, 3H, NCH₃), 2.10 (s, 3H, NCH₃), 3.35–3.42, 3.89–3.92 [dd, 2H, AB system, ²J(¹H¹H) = 13.99 Hz, NCH₂], 4.90 (s, 5H, Cp), 5.98 (s, 1H, SiH), 6.70 (d, 1H, aromatic), 7.15 (m, 1H, aromatic), 7.38 (t, 1H, aromatic), 7.58 (t, 2H, aromatics), 8.41 (d, 1H, aromatic). IR (toluene, cm⁻¹): ν(CO, SiH) 2022, 1961.

[8-(Me₂N)C₁₀H₆]HSi=MnMeCp(CO)₂. [[8-[(Dimethylamino)naphthyl]-1-silanediy[(η⁵-methylcyclopentadienyl)manganese Dicarboxyl (12). [8-[(Dimethylamino)naphthyl]trihydrosilane (11; 4.04 g, 20 mmol) was dissolved in 350 mL of pentane and transferred to a photochemical reactor. Methylcyclopentadienylmanganese tricarbonyl (3.15 mL, 20 mmol) was added to that solution, and the mixture was irradiated at room temperature for 6 h. After completion of reaction, pentane was taken out with a cannula and the remaining solid was washed three times with pentane and analyzed. Yield: 60%. Anal. Calcd for C₂₀H₂₀NO₂SiMn: C, 61.69; H, 5.14; N, 3.59. Found: C, 61.72; H, 5.21; N, 3.41. ²⁹Si NMR (C₆D₆): δ +141.85 (INVGATE), ¹J(²⁹SiH) = 163.97 Hz (DEPTC). ¹³C NMR (C₆D₆): δ 15.16 (Cp*CH₃), 50.18 (NCH₃), 53.86 (NCH₃), 80.98, 82.69, 82.93, 83.45 (Cp), 98.90 (*CCH₃), 127.51, 129.97, 132.04, 142.78, 150.61 (aromatics), 232.87, 234.01 (CO). MS [EI, 30 eV; *m/e* (relative intensity %): 389 (M⁺, 20), 333 (-2CO, 100), 317 (10), 198 (81), 184 (28), 170 (10), 134 (30), 91 (5), 55 (18). IR (toluene, cm⁻¹): ν(CO, SiH) 1972, 1907, 1840.

[8-(Me₂N)C₁₀H₆]HSi=Cr(CO)₅. [[8-[(Dimethylamino)naphthyl]-1-silanediy]chromium(0) Pentacarbonyl (13). The same stoichiometric quantities and procedure as above were followed. Yield: 51%. Anal. Calcd for C₁₇H₁₃NO₅SiCr: C, 52.17; H, 3.32; N, 3.59. Found: C, 52.32; H, 3.45; N, 3.41. ²⁹Si NMR (toluene-*d*₆): δ +120.41 (INVGATE), ¹J(²⁹Si¹H) = 164.91 Hz (DEPTC). MS [EI, 30 eV; *m/e* (relative intensity %): 391 (M⁺, 10), 365 (-CO, 8), 307 (-3CO, 11), 279 (-4CO, 20), 252 (-5CO, 100), 199 (24), 185 (38), 171 (32), 154 (5), 52 (50). IR (C₆D₆, cm⁻¹): ν(CO, SiH) 1979, 1932, 1897.

(C₆H₅)₃(H)DMiSi=Fe(CO)₄. (Phenylsilanediy)iron(0) Tetracarbonyl-1,3-Dimethyl-2-imidazolidinone (16a). A solution of phenylsilane (2.6 g, 20 mmol) and 1,3-dimethyl-2-imidazolidinone (2.28 g, 20 mmol) in 350 mL of pentane was transferred into a 500-mL quartz reaction vessel. Iron pentacarbonyl (2.62 mL, 20 mmol) was added to this solution, and the mixture was irradiated at room temperature. Separation of a black-red sticky solid started taking place after 10 min of irradiation; complete disappearance of starting silane was observed after 5 h in IR spectrum. Pentane solution was taken out from the reactor, and the remaining solid **16a** was washed with pentane and analyzed. Yield: 61%. Anal. Calcd for C₁₅H₁₆N₂O₅SiFe: C, 46.39; H, 4.12; N, 7.21. Found: C, 46.40; H, 4.08; N, 7.16. ²⁹Si NMR (toluene/C₆D₆): δ +83.52 (INVGATE), ¹J(²⁹Si¹H) = 199 Hz (DEPTC). ¹³C NMR (C₆D₆): δ 29.87 (NCH₃), 46.97 (NCH₂), 127–142 (aromatics), 159.28 (>CO), 215.62, 216.34 (CO). IR (toluene, cm⁻¹): ν(CO, SiH) 2032, 1998, 1904, 1889 ν(>CO), 1708.

(1-C₁₀H₇)(H)DMiSi=Fe(CO)₄. (1-Naphthylsilanediy)iron(0) Tetracarbonyl-1,3-Dimethyl-2-imidazolidinone (17). The same procedure and molar quantities of 1-naphthylsilane and other reactants as for the preparation of complex **16a** were used to prepare complex **17**. Yield: 58%. Anal. Calcd for C₁₉H₁₈N₂O₅SiFe: C, 52.05; H, 4.10; N, 6.39. Found: C, 52.13; H, 4.12; N, 6.42. ²⁹Si NMR (toluene/C₆D₆): δ +81.51 (INVGATE), ¹J(²⁹Si¹H) = 218.61 Hz (DEPTC). MS [EI, 70 eV; *m/e* (relative intensity %): 439 (M⁺, 10), 411 (-CO,

0.5), 359 (0.5), 331 (0.4), 290 (0.8), 239 (0.8), 114 (100). IR (toluene, cm⁻¹): ν(CO, SiH) 2025, 1997, 1890, ν(>CO), 1711.

[2,6-(Me₂NCH₂)₂C₆H₃]H₂Si-CrH(CO)₅. Hydrido[[2,6-bis[(dimethylamino)methyl]phenyl]dihydrosilyl]pentacarbonyl Chromium (18b). In a 500-mL photochemical reactor, [2,6-bis(dimethylamino)methyl]phenylsilane^{18c} (**18a**; 2.22 g, 10 mmol) was diluted in 350 mL of pentane. Chromium hexacarbonyl (2.20 g, 10 mmol) was added to this solution, and precipitation started after 10 min of irradiation. After the disappearance of silane **18a**, pentane solution was taken out from the reaction vessel; the remaining solid was washed two times with pentane and identified as complex **18b**. Yield: 48%. Anal. Calcd for C₁₇H₂₂N₂O₅SiCr: C, 49.27; H, 5.31; N, 6.76. Found: C, 49.31; H, 5.38; N, 6.58. ²⁹Si NMR (CDCl₃): δ -44.89 (INVGATE), ¹J(²⁹Si¹H) = 265.98 Hz (DEPTC). ¹³C NMR (CDCl₃): δ 48.51 (NCH₃), 65.92 (NCH₂), 125.17, 135.34, 142.94 (aromatics), 216.95, 221.30, 224.45, 226.95 (CO). ¹H NMR (CDCl₃): δ 2.18 (s (br), 12 H, NCH₃), 3.50 (s (br), 4 H, NCH₂), 5.30 (s, 2H, SiH₂), 7.02–7.41 (d (br), 3H, aromatics), -5.48 [s (br), 1H, CrH)], MS [EI, 70 eV; *m/e* (relative intensity %): 412 (M⁺, 6), 356 (-2CO, 10), 300 (-4CO, 25), 272 (-5CO, 100), 229 (30), 176 (28), 149 (18), 133 (8), 105 (25), 58 (85).

(1a) Photolysis of 4 with Triphenylphosphine. Complex **4** (3.55 g, 10 mmol) was dissolved in 300 mL of toluene in a 500-mL photochemical reactor. Triphenylphosphine (5.24 g, 20 mmol, diluted in 20 mL of toluene) was added to this solution, and the resulting mixture was photolyzed for 1 h. ³¹P-NMR analysis of the mixture revealed the formation of complex [[2-[(dimethylamino)methyl]phenyl]silanediy](triphenylphosphine)chromium(0) tetracarbonyl (**19**; +57 ppm) and complex **20** (+75 ppm) along with remaining triphenyl phosphine. Further irradiation of this mixture for 4 h furnished complex **20** in 45% yield, after crystallization in pentane/toluene (30:70). No signal was observed by ²⁹Si-NMR spectroscopy. Characteristics of *trans*-[(C₆H₅)₃P]₂Cr(CO)₄, *trans*-bis(triphenylphosphine)chromium(0) tetracarbonyl (**20**). Anal. Calcd for C₄₀H₃₀CrO₄P₂: C, 69.77; H, 4.39; P, 9.0. Found: C, 69.79; H, 4.37; P, 8.91. ³¹P NMR (CDCl₃): δ +75.09. IR (CDCl₃, cm⁻¹): ν(CO) 1957. ¹H NMR (CDCl₃): δ 6.98 (m, 18H, aromatics), 7.81 (m, 12H, aromatics).

(1b) Thermolysis of 4 with Triphenylphosphine. Triphenylphosphine (1.04 g, 4 mmol) was added to 65-mL toluene solution of complex **4** (0.71 g, 2 mmol), and this mixture was refluxed for 1 h. ³¹P-NMR analysis of the crude mixture revealed the formation of complexes **19** and **20**. Further heating of the mixture for additional 6 h furnished complex **20**, yield 38%, after purification.

(2a) Photolysis of 4 with DPPE. In a 500-mL photochemical reactor, complex **4** (2 g, 5.6 mmol) was dissolved in 300 mL of toluene followed by addition of DPPE (2.22 g, 5.6 mmol), diluted in 50 mL of toluene. This mixture was irradiated at room temperature for 1 h. After 15 min of irradiation, the yellow solution turned reddish-orange. ²⁹Si-NMR analysis of the crude mixture established the formation of complex [[2-[(dimethylamino)methyl]phenyl]silanediy][1,2-bis(diphenylphosphino)ethane]chromium(0) tetracarbonyl (**21**), δ +118.39 [(d, ²J(²⁹Si³¹P) = 26.15 Hz (INVGATE), (d of d, ¹J(²⁹Si¹H) = 154.85 Hz (DEPTC))] and complex **22**, +123.93 [(t, ²J(²⁹Si³¹P) = 20.06 Hz (INVGATE), (d of t, ¹J(²⁹Si¹H) = 144.73 Hz (DEPTC)], along with remaining complex **4**. This mixture was further irradiated for 5 h. Solvent was evaporated under vacuum, and the resulting solid was washed two times with pentane. This solid was identified as complex **22**. Characteristics of [2-(Me₂NCH₂)C₆H₄]HSi=Cr[Ph₂P(CH₂)₂PPh₂](CO)₃. [[2-[(Dimethylamino)methyl]phenyl]silanediy][1,2-bis(diphenylphosphino)ethane]chromium(0) tricarbonyl (**22**). Yield: 80%. Anal. Calcd for C₃₈H₃₇NO₃P₂SiCr: C, 65.42; H, 5.30; N, 2.00. Found: C, 65.38; H, 5.36; N, 2.10. ²⁹Si NMR (C₆D₆, 22 °C): δ +123.93 [(t, ²J(²⁹Si³¹P) = 20.06 Hz, INVGATE) (d of t, ¹J(²⁹Si¹H) = 144.73, DEPTC)]. ¹³C NMR (C₆D₆): δ 29.79 (br, PCH₂), 46.39 (NCH₃), 45.12 (NCH₃), 69.79 (NCH₂), 125.08–

145.95 (aromatics), 221.22, 229.98 (CO). ^1H NMR (C_6D_6): δ 2.21 (br) (10 H, NCH_3 , PCH_2), 2.79–2.86, 3.62–3.55 [dd, 2H, AB system, $^2J(^1\text{H}^1\text{H}) = 17.51$ Hz, NCH_2], 6.28 (br, 1H, SiH), 6.71–7.42, 7.51–7.97 (m, 24H, aromatics). IR (C_6D_6 , cm^{-1}): $\nu(\text{CO}, \text{SiH})$ 2008, 1890, 1850.

(2b) Thermolysis of 4 with DPPE. Complex 4 (0.71 g, 2 mmol) was dissolved in 50 mL of toluene followed by addition of DPPE (0.796 g, 2 mmol, dissolved in 10 mL of toluene) in a 200-mL Schlenk tube. This mixture was refluxed for 1 h. ^{31}P -NMR analysis of the crude mixture established the formation of complex 21 [$\delta +50.52$ (d, P coordinated), $^3J(^{31}\text{P}^{31}\text{P}) = 35.56$ Hz, -11.60 (d, P uncoordinated)] and [1,2-bis(diphenylphosphino)ethane]chromium(0) tetracarbonyl (23 ($\delta +80.16$)) in 1:1 ratio along with remaining starting 4 and DPPE. Further heating of the mixture for 7 h consumed 50% of the complex 4 giving complexes 21 and 23 in 1:3 ratio. Yields and ratios are estimated from ^{31}P - and ^{29}Si -NMR signals. Complex 23 can be crystallized from the mixture with $\text{CHCl}_3/\text{toluene}$ (30:70) at -20 °C.

[$\text{Ph}_2\text{P}(\text{CH}_2)_2\text{PPh}_2$] $\text{Cr}(\text{CO})_4$. [1,2-Bis(diphenylphosphino)ethane]chromium(0) tetracarbonyl (23). ^1H NMR (C_6D_6): δ 2.15 (d, 4H, PCH_2), 6.91–7.02, 7.41–7.58 (m, 20H, aromatics). ^{31}P NMR (C_6D_6): δ 80.11. MS [EI, 30 eV; m/e (relative intensity %): 506 (M^+ , -2CO , 10), 450 (-4CO , 21), 398 (38), 370 (25), 289 (50), 275 (30), 262 (46), 18 (100), 152 (18), 107 (28), 51 (16)]. IR (C_6D_6 , cm^{-1}): $\nu(\text{CO})$ 2009, 1916, 1902, 1884.

(3) Photolysis of 4 with Trimethyl Phosphite. Trimethyl phosphite (1.18 mL, 10 mmol) in 8 mL of toluene was added to the 300-mL toluene solution of complex 4 (1.77 g, 5 mmol) in a photochemical reactor. ^{31}P NMR analysis of the mixture after 1 h of irradiation revealed the presence of [[2-[(dimethylaminomethyl)phenyl]silanediyl]trimethylphosphite]chromium(0) tetracarbonyl (24) ($\delta +194.23$) and complex *trans*-bis(trimethylphosphite)chromium(0) tetracarbonyl (+25) ($\delta +180.21$) along with some residual trimethyl phosphite. Further irradiation of the mixture for 6 h furnished only complex 25 (38% yield). No signal was observed in ^{29}Si NMR.

Thermolysis of 4 with Trimethyl Phosphite. The same results were obtained when complex 4 (0.71 g, 2 mmol) was refluxed with trimethyl phosphite (0.47 mL, 4 mmol) in a 150-mL Schlenk flask for 7 h. 25 was isolated in 31% yield, after successive extractions with pentane. Characteristics of *trans*-[(CH_3O) $_3\text{P}$] $\text{Cr}(\text{CO})_4$. *trans*-bis(trimethylphosphite)chromium(0) tetracarbonyl (25). ^1H NMR (C_6D_6): δ 3.41 (d, 18H, $^3J(^{13}\text{P}^1\text{H}) = 11.31$ Hz, OCH_3). ^{31}P NMR (CDCl_3): $\delta +180.02$. MS [EI, 30 eV; m/e (relative intensity %): 412 (M^+ , 20), 356 (-2CO , 10), 328 (-3CO , 12), 300 (-4CO , 100), 269 (22), 239 (8), 207 (12), 176 (32)].

[2-(Me_2NCH_2) C_6H_4] $\text{FSi}=\text{Cr}(\text{CO})_5$. [[2-[(Dimethylamino)methyl]phenyl]fluorosilanediyl]chromium(0) Pentacarbonyl (26). 4 (1.06 g, 3 mmol) was dissolved in 60 mL of toluene and kept at 0 °C. Triphenylcarbonium tetrafluoroborate (1 g, 3 mmol, dissolved in 5 mL of CH_2Cl_2) was added dropwise to this solution. The mixture was stirred at room temperature for 2 h. Evaporation of solvents furnished a white-yellow solid which was washed several times with pentane in order to separate triphenylmethane from the product. [[2-[(Dimethylamino)methyl]phenyl]fluorosilanediyl]chromium(0)pentacarbonyl (26) was isolated in 93% yield. Anal. Calcd for $\text{C}_{14}\text{H}_{12}\text{NO}_5\text{FSiCr}$: C, 45.04; H, 3.21; N, 3.75. Found: C, 45.16; H, 3.31; N, 3.81. ^{29}Si NMR (CDCl_3 , 22 °C): $\delta +117.20$ (INVGATE, d, $^1J(^{29}\text{Si}^{19}\text{F}) = 398.51$ Hz). ^{13}C NMR (CDCl_3): δ 45.70 (NCH_3), 45.99 (NCH_3), 68.38 (NCH_2), 124.26, 127.71, 129.09, 131.51, 134.48, 139.87 (aromatics), 219.96 (CO, eq), 224.52 (CO, ax). ^1H NMR (CDCl_3): δ 2.75 (s, 3H, NCH_3), 3.12 (s, 3H, NCH_3), 3.93–3.98, 4.67–4.72 [dd, 2H, AB system, $^2J(^1\text{H}^1\text{H}) = 12.51$ Hz, NCH_2], 7.20 (m, 2H, aromatics), 7.43 (d, H, aromatic), 7.99 (d, H, aromatic). ^{19}F NMR (CDCl_3): $\delta -117.33$. MS [EI, 70 eV; m/e (relative intensity %): 373 (M^+ , 11), 355 (20), 345 (5), 327 (22), 317 (8), 271 (8), 243 (10), 215

(40), 162 (18), 135 (6), 108 (40), 52 (100). IR (toluene, cm^{-1}): $\nu(\text{CO})$ 2051, 1983, 1915.

[2-(Me_2NCH_2) C_6H_4] $\text{BrSi}=\text{Cr}(\text{CO})_5$. [[2-[(Dimethylamino)methyl]phenyl]bromosilanediyl]chromium(0) Pentacarbonyl (27). Acetyl bromide (0.14 mL, 2 mmol) was added to the 50-mL toluene solution of complex 4 (0.71 g, 2 mmol) at 0 °C. After 4 h, evaporation of solvent furnished the complex [[2-[(dimethylamino)methyl]phenyl]bromosilanediyl]chromium(0) pentacarbonyl (27) in 80% yield. Anal. Calcd for $\text{C}_{14}\text{H}_{12}\text{NO}_5\text{BrSiCr}$: C, 38.70; H, 2.76; N, 3.22. Found: C, 38.82; H, 2.81; N, 3.18. ^{29}Si NMR (C_6D_6): $\delta +119.38$ (INV-GATE). ^{13}C NMR (C_6D_6 , 22 °C): δ 46.33 (NCH_3), 68.33 (NCH_2), 124.92, 130.89, 131.90, 140.13, 144.33 (aromatics), 220.94 (CO, eq), 224.48 (CO, ax). ^1H NMR (C_6D_6): δ 1.89 (s, 3H, NCH_3), 2.17 (s, 3H, NCH_3), 2.47–2.53, 3.89–3.94 [dd, 2H, AB system, $^2J(^1\text{H}^1\text{H}) = 13.99$ Hz, NCH_2], 6.65 (m, 1H, aromatic), 7.01 (m, 2H, aromatics), 7.98 (m, 1H, aromatic). MS [EI, 30 eV; m/e (relative intensity %): 434 (M^+ , 12), 406 ($-\text{CO}$, 18), 378 (-2CO , 8), 350 (-3CO , 14), 322 (-4CO , 23), 294 (-5CO , 71), 242 (9), 215 (14), 162 (100), 135 (34), 119 (70), 91 (32)]. IR (C_6D_6 , cm^{-1}): $\nu(\text{CO})$ 2051, 1970, 1919.

[2-(Me_2NCH_2) C_6H_4] $\text{OSO}_2\text{CF}_3\text{Si}=\text{Cr}(\text{CO})_5$. [[2-[(Dimethylamino)methyl]phenyl]trifluoromethanesulfonylsilanediyl]chromium(0) Pentacarbonyl (28). Freshly prepared (triphenylmethyl)trifluoromethanesulfonate (0.39 g, 1 mmol) was dissolved in 5 mL of CH_2Cl_2 and added dropwise to the toluene solution of 4 (0.35 g, 1 mmol) at 0 °C. The mixture was stirred for 4 h while the temperature was raised to room temperature. Removal of solvent under reduced pressure afforded [[2-[(dimethylamino)methyl]phenyl]trifluoromethanesulfonylsilanediyl]chromium(0) pentacarbonyl (28) in 82% yield. Anal. Calcd for $\text{C}_{15}\text{H}_{12}\text{NO}_6\text{SF}_3\text{SiCr}$: C, 35.78; H, 2.38; N, 2.78. Found: C, 35.81; H, 2.39; N, 2.89. ^{29}Si NMR (C_6D_6 , 22 °C): $\delta +123.54$ (INV-GATE). ^{13}C NMR (C_6D_6): δ 45.12 (NCH_3), 45.71 (NCH_3), 68.57 (NCH_2), 122.89, 130.53, 132.29, 135.53, 138.86, 1450.53 (aromatics, CF), 219.07 (CO, eq), 222.33 (CO, ax). ^1H NMR (C_6D_6): δ 1.69 (s, 3H, NCH_3), 2.07 (s, 3H, NCH_3), 2.59–2.65, 4.05–4.11 [dd, 2H, AB system, $^2J(^1\text{H}^1\text{H}) = 14.52$ Hz, NCH_2], 6.61 (m, 1H, aromatic), 7.35 (m, 2H, aromatics), 8.04 (m, 1H, aromatic). ^{19}F NMR (C_6D_6): $\delta -78.34$. MS [EI, 70 eV; m/e (relative intensity %): 503 (M^+ , 08), 484 (18), 408 (64), 389 (12), 361 (38), 318 (10), 242 (40), 162 (100), 104 (15), 58 (80)]. IR (C_6D_6 , cm^{-1}): $\nu(\text{CO})$ 2057, 1980, 1930; $\nu(\text{SO}_3)$ 1385.

[2-(Me_2NCH_2) C_6H_4] $\text{ClSi}=\text{Cr}(\text{CO})_5$. [[2-[(Dimethylamino)methyl]phenyl]chlorosilanediyl]chromium(0) Pentacarbonyl (29). Synthesis from Chlorotriphenylmethane. 4 (0.71 g, 2 mmol) was dissolved in 60 mL of toluene and kept at 0 °C. Chlorotriphenylmethane (0.55 g, 2 mmol) dissolved in 3 mL of CH_2Cl_2 was added dropwise, and the mixture stirred at room temperature for 24 h. Evaporation of solvent furnished [[2-[(dimethylamino)methyl]phenyl]chlorosilanediyl]chromium(0) pentacarbonyl (27) in 65% yield. Complex 2 was washed several times with pentane in order to remove triphenylmethane.

Synthesis from Acetyl Chloride. Acetyl chloride (0.70 mL, 0.01 mol) was added dropwise to the toluene solution of complex 4 (3.55 g, 0.01 mol) at 0 °C. The mixture was allowed to come to room temperature and stirred for 12 h. Evaporation of solvent in vacuo furnished [[2-[(dimethylamino)methyl]phenyl]chlorosilanediyl]chromium(0) pentacarbonyl (29) in 83% yield. Anal. Calcd for $\text{C}_{14}\text{H}_{12}\text{NO}_5\text{ClSiCr}$: C, 43.18; H, 3.08; N, 3.59. Found: C, 43.31; H, 3.13; N, 3.62. ^{29}Si NMR (CDCl_3 , 22 °C): $\delta +122.97$ (INV-GATE). ^{13}C NMR (CDCl_3): δ 46.22 (NCH_3), 47.07 (NCH_3), 68.17 (NCH_2), 124.45, 129.96, 131.30, 139.13, 142.81 (aromatics), 219.50 (CO, eq), 223.30 (CO, ax). ^1H NMR (toluene- d_8 , 22 °C): δ 2.16 (s, 3H, NCH_3), 2.42 (s, 3H, NCH_3), 2.82–2.88, 4.09–4.14 [dd, 2H, AB system, $^2J(^1\text{H}^1\text{H}) = 13.83$ Hz, NCH_2], 6.89 (m, 1H, aromatic), 7.30 (m, 2H, aromatics), 8.16 (m, 1H, aromatic). MS [EI, 70 eV; m/e (relative intensity %): 389 (M^+ , 12), 360 ($-\text{CO}$, 7), 333 (-2CO , 6), 305 (-3CO , 12), 277 (-4CO , 18), 249 (-5CO , 82), 196 (3),

162 (100), 135 (10), 119 (28), 105 (8), 52 (24). IR (CDCl₃, cm⁻¹): $\nu(\text{CO})$ 2051, 1979, 1923.

Reaction of 16a with *tert*-Butyl Alcohol. (Phenylsilyl)iron(0) tetracarbonyl-1,3-dimethyl-2-imidazolidinone (**16a**; 3.88 g, 10 mmol) was dissolved in 100 mL of toluene in a 200-mL Schlenk flask. A 10-fold excess of *tert*-butyl alcohol (7.4 g, 0.1 mol) was added dropwise to this solution, and the mixture was stirred at room temperature. After 2 h, the solvent and excess of *tert*-butyl alcohol were evaporated and the resulting mixture was chromatographed on a Florisil column (33 cm \times 2 cm). Di-*tert*-butoxyphenylsilane (**30**) was obtained as the first fraction with pentane in 68% yield. ²⁹Si NMR (CDCl₃): δ -46.99 (INVGATE), ¹J(²⁹Si¹H) = 238.25 Hz (DEPTC). ¹³C NMR (CDCl₃): δ 32.23 (CH₃), 74.11 (*CCH₃), 128.12, 130.23, 134.35 (aromatics). ¹H NMR (CDCl₃): δ 1.30 (s, 18H, CH₃), 5.13 (s, 1H, SiH), 7.21–7.43, 7.61–7.90 (m, 5H, aromatics). IR (CDCl₃, cm⁻¹): $\nu(\text{SiH})$ = 2171.

Reaction of 16a with Methanol. Methanol (4.05 mL, 0.1 mol) was added dropwise in a 110-mL toluene solution of complex **16a** (3.88 g, 10 mmol) at room temperature. This mixture was stirred for 2 h. Evaporation of solvent and excess methanol furnished a sticky slurry which was chromatographed on a Florisil column (33 cm \times 2 cm). Phenyltri-

methoxysilane **31** was isolated as the first fraction with pentane in 73% yield and compared with authentic sample.

Reaction of 4 with 2,3-Dimethylbutadiene. Freshly prepared complex **4** (3.55 g, 0.01 mol) was dissolved in 350 mL of toluene in a 500-mL photochemical reactor. A 10-fold excess of 2,3-dimethylbutadiene (11.4 mL, 0.1 mol) was added to this solution, and the mixture was irradiated for 5 h at room temperature. Evaporation of volatiles under reduced pressure furnished a red-yellow mixture. Analysis of the crude mixture by ²⁹Si NMR established complete consumption of starting complex **4**, but no new signal for compound corresponding to trapping product or having Si–H bonds (DEPTC technique) was observed.

Reaction of 4 with *tert*-Butyl Alcohol. *tert*-Butyl alcohol (7.4 g, 0.1 mol) was added to a 150-mL toluene solution of complex **4** (3.55 g, 10 mmol) in a 250-mL Schlenk flask. This mixture was stirred at room temperature for 24 h. Evaporation of solvent and excess *tert*-butyl alcohol furnished an orange-yellow sticky solid. ²⁹Si-NMR analysis of the crude product established the complete disappearance of starting complex **4**. A new signal at -79.95 ppm (no Si–H bond by DEPTC) was observed.

OM940938Z

Lewis Base Stabilized Transition Metal Complexes of Divalent Silicon Species

Bhanu P. S. Chauhan, Robert J. P. Corriu,* Gérard F. Lanneau,* and Christian Priou

Laboratoire des Précurseurs Organométalliques de Matériaux, UMR 044, Université Montpellier II, Case 007, Place Eugène Bataillon, 34095 Montpellier Cedex 05, France

Norbert Auner, Hermann Handwerker, and Eberhardt Herdtweck

Anorganisch-Chemisches Institut, Technische Universität München, Lichtenbergstrasse 4, 85748 Garching, Germany

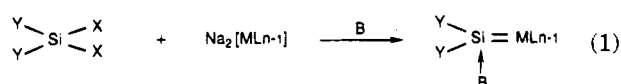
Received November 10, 1994[®]

A direct photochemical synthesis of silanediyl–iron tetracarbonyl complexes $\text{Ph}_2\text{Si}(\text{B})=\text{Fe}(\text{CO})_4$ [B = 1,3-dimethylimidazolidinone (DMI) or hexamethylphosphoric triamide (HMPA)] is described. The Lewis base character of DMI is strong enough to quantitatively convert the dimeric $[\text{Fe}_2(\text{CO})_8(\text{SiPh}_2)_2]$ to more stable $\text{Ph}_2\text{Si}(\text{DMI})=\text{Fe}(\text{CO})_4$. A series of organosilanediyl–transition metal complexes, of general formula $\text{ArAr}'\text{Si}=\text{MLn}$ [Ar = Ph, Ar' = [2-(Me₂NCH₂)C₆H₄], [8-(Me₂NCH₂)C₁₀H₆], [8-(Me₂N)C₁₀H₆]; Ar, Ar' = [2-(Me₂NCH₂)C₆H₄]; Ar = 1-Np, Ar' = [8-(Me₂NCH₂)C₁₀H₆]; or Ar = Me, Ar' = [2-(Me₂NCH₂)C₆H₄]] is directly obtained in the photochemical reaction of $\text{ArAr}'\text{SiH}_2$ with $\text{Fe}(\text{CO})_5$, $\text{Cr}(\text{CO})_6$, $\text{Mo}(\text{CO})_6$, and $\text{RCpMn}(\text{CO})_3$ (R = Me, H). Single-crystal X-ray structure analysis of the complex [2-(Me₂NCH₂)C₆H₄]₂Si=C₆H₅Fe(CO)₄ (**5a**) reveals a N→Si bond length of 1.962(2) Å and Si–Fe bond distance of 2.259(1) Å. The sum of bond angles at silicon, excluding the N-atom, is to 346.7°. Crystal data: C₁₉H₁₇FeNO₄Si, triclinic, space group *P*1 (No. 2), *a* = 8.284(2), *b* = 8.404(2), *c* = 13.497(3) Å; α = 97.02(1)°, β = 93.68(1)°, γ = 91.25(1)°, *V* = 930.3 Å³, *Z* = 2, *R* = 0.027, *R*_w = 0.030 based on 3171 reflections with (*I* > 0.00, all data). Strong intramolecular donor stabilization with the 8-[(dimethylamino)methyl]naphthyl ligand directly bonded to the silicon atom prevents further reactions, but typical experiments have been performed with less coordinated 8-[(dimethylamino)methyl]phenyl derivatives. Silanediyl–iron tetracarbonyl complexes react with acetylenes, dienes, and alcohols under UV irradiation, and trapping products of silylenes are isolated in good yields. A comparative study of different coordinating ligands has been carried out.

Introduction

The hypothetical participation of silanediyl–transition metal complexes¹ in the chemical transformations of organosilicon compounds is a subject under active research.² Although complexes of germanium(II) and tin(II) with group 5 and group 6 metal carbonyls are readily accessible, either from carbene-like species³ or from dihalides $\text{Y}_2\text{M}'\text{X}_2$,⁴ through dehalogenation with transition metal dianionic species, the dehalogenation method has only recently been applied to the synthesis of organosilanediyl–transition metal complexes.⁵ The reactions were performed in coordinating solvents, and products were isolated as monomeric stable species,

containing a solvent molecule coordinated to the unsaturated silicon (eq 1).

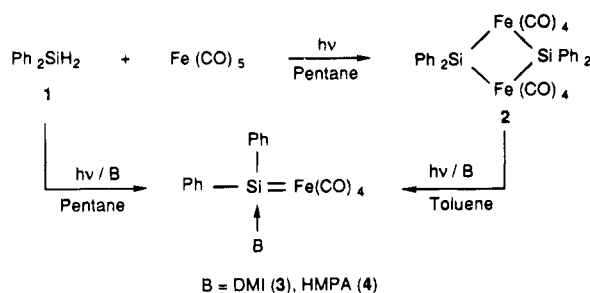


Transition metal compounds with σ-bonded silicon species are accessible by insertion of the Si–H bond

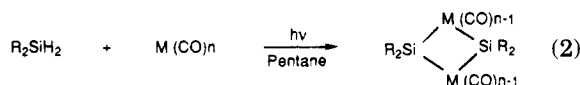
[®] Abstract published in *Advance ACS Abstracts*, March 1, 1995.
 (1) For recent reviews, see: (a) Tilley, T. D. In *The Silicon Heteroatom Bond*; Patai, S., Rappoport, Z., Eds.; Wiley: New York, 1991; pp 245–309. (b) Zybilla, C. *Top. Curr. Chem.* **1991**, *160*, 1. (c) Lickiss, P. D. *Chem. Soc. Rev.* **1992**, *21*, 271. (d) Tilley, T. D. *Acc. Chem. Res.* **1993**, *26*, 22. (e) Zybilla, C.; Handwerker, H.; Friedrich, H. *Adv. Organomet. Chem.* **1994**, *36*, 229.
 (2) (a) Aitken, C. T.; Harrod, J. F.; Samuel, E. *J. Am. Chem. Soc.* **1986**, *108*, 4059. (b) Aitken, C. T.; Harrod, J. F.; Gill, U. S. *Can. J. Chem.* **1987**, *65*, 1804. (c) Hayashi, T.; Yamashita, H.; Tanaka, M.; Goto, M. *Organometallics* **1992**, *11*, 3227. (d) Campbell, W. H.; Hilty, T. K.; Yurga, L. *Organometallics* **1989**, *8*, 2615. (e) Xin, S.; Aitken, C. T.; Harrod, J. F.; Mu, Y.; Samuel, E. *Can. J. Chem.* **1990**, *68*, 471. (f) Corey, J. Y.; Zhu X.; Bedard, T. C.; Lange, L. D. *Organometallics* **1991**, *10*, 924. (g) Mu, Y.; Aitken, C. T.; Cote, B.; Harrod, J. F.; Samuel, E. *Can. J. Chem.* **1991**, *69*, 264. (h) Banovetz, J. P.; Stein, K. M.; Waymouth, R. M. *Organometallics* **1991**, *10*, 3430. (i) Heyn, R. H.; Tilley, T. D. *J. Am. Chem. Soc.* **1992**, *114*, 1917.

(3) (a) Jutzli, P.; Steiner, W. *Chem. Ber.* **1976**, *109*, 3473. (b) Jutzli, P.; Steiner, W. König, E.; Huttner, G.; Frank, A.; Schubert, U. *Chem. Ber.* **1978**, *111*, 606. (c) Petz, W. *Chem. Rev.* **1986**, *86*, 1019. (d) Barrau, J.; Escudie, J.; Satgé, J. *Chem. Rev.* **1990**, *90*, 283. (e) Lappert, M. F.; Rowe, R. S. *Coord. Chem. Rev.* **1990**, *100*, 267. (f) Neumann, W. P. *Chem. Rev.* **1991**, *91*, 311. (g) Tokitoh, N.; Manmaru, K.; Okazaki, R. *Organometallics* **1994**, *13*, 167. (h) Lappert, M. F.; Maskell, R. V. *J. Organomet. Chem.* **1984**, *264*, 217. (i) Veith, M.; Becker, S.; Huch, V. *Angew. Chem., Int. Ed. Engl.* **1990**, *29*, 216. (j) Ellis, E. L.; Hitchcock, P. B.; Holmes, S. A.; Lappert, M. F.; Slade, M. J. *J. Organomet. Chem.* **1993**, *444*, 95.
 (4) (a) Marks, T. J. *J. Am. Chem. Soc.* **1971**, *93*, 7090. (b) Marks, T. J.; Newman, A. R. *J. Am. Chem. Soc.* **1973**, *95*, 769. (c) Jastrzebski, J. T. B. H.; Van Der Schaaf, P. A.; Boersma, J.; Van Koten, G.; Heijdenrijk, D.; Goubitz, K.; De Ridder, D. J. A. *J. Organomet. Chem.* **1989**, *367*, 55. (d) Lee, K.; Arif, A. M.; Gladysz, J. A. *Organometallics* **1991**, *10*, 751. (e) Cotton, J. D.; Davis, P. J.; Goldberg, D. E.; Lappert, M. F.; Thomas, K. M. *J. Chem. Soc., Chem. Commun.* **1974**, 893. (f) Huttner, G.; Weber, U.; Sigwarth, B.; Scheidsteger, O.; Lang, H.; Zsolnai, L. *J. Organomet. Chem.* **1985**, *282*, 331.
 (5) (a) Zybilla, C.; Müller, G. *Angew. Chem., Int. Ed. Engl.* **1987**, *26*, 669. (b) Zybilla, C.; Wilkinson, D. L.; Leis, C.; Müller, G. *Angew. Chem., Int. Ed. Engl.* **1988**, *27*, 583. (c) Leis, C.; Zybilla, C.; Lachmann, J.; Müller, G. *Polyhedron* **1991**, *10*, 1163. (d) Leis, C.; Wilkinson, D. L.; Handwerker, H.; Zybilla, C.; Müller, G. *Organometallics* **1992**, *11*, 514.

Scheme 1



under photochemical conditions.⁶ Irradiation of dihydrosilanes allowed the synthesis of dimers⁷ (eq 2).

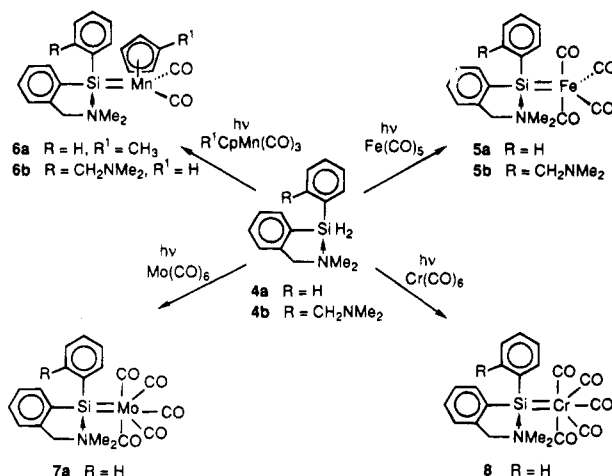


More recently, rearrangements giving Lewis base-stabilized monomeric silylene-transition metal species have been reported.⁸ The purpose of the present paper is to describe the direct photochemical preparation of new organosilanediyl-transition metal complexes, stabilized by either intermolecular coordination of Lewis bases, obtained with 1,3-dimethyl-2-imidazolidinone (DMI) and hexamethylphosphoric triamide (HMPA), as nucleophiles or intramolecular association with aminoaryl groups attached to the silicon atom. Furthermore, some representative examples in which silanediyl-transition metal complexes act as silylene sources are also reported.

Results

Synthesis of DMI-Stabilized Silanediyliron(0) Tetracarbonyl Complexes. Dihydrosilanes have been shown to react with iron pentacarbonyl to give iron carbonyl complexes containing bridging silyl ligands. UV irradiation of diphenylsilane **1** with equimolar amounts of $Fe(CO)_5$ in pentane gave the yellow-orange dimer⁷ **2**. In the presence of DMI, dimer **2** furnished the yellow base-stabilized monomer **3** (Scheme 1).

If the photochemical dehydrogenative coupling reaction of diphenylsilane is performed in the presence of DMI, **3** is obtained directly in 93% yield. Analytical data for **3** are consistent with the proposed structure. The ¹H NMR spectrum exhibits a broad singlet for the methyl groups (δ 4.18) and a singlet (δ 6.18) for the

Scheme 2. Photolysis of Silanes **4a** and **4b** with Transition Metal Carbonyls

methylene groups, which are shifted downfield, compared to free DMI (δ 2.70 and 3.25, respectively). The ²⁹Si NMR spectrum of the crude mixture, after washing with pentane and dissolving the oil in toluene, exhibits only a singlet at +91.3 ppm, emphasizing the selectivity of the reaction. The signal is shifted upfield compared to that of dimer **2** (+111 ppm). When silane **1** was irradiated with $Fe(CO)_5$ in the presence of HMPA in equimolar amounts, complex **4** was isolated in 43% yield after crystallization. The ²⁹Si NMR spectrum displays a doublet at +79.52 ppm ($^2J(^{31}P^{29}Si) = 23.86$ Hz), which is in good agreement with the literature values⁹ reported for HMPA-stabilized silanediyl-transition metal complexes synthesized by other methods.

Synthesis of Aminoaryl Silanediyl-Transition Metal Complexes. The photochemical reaction of 16- e^- metal species (generated from various transition metal carbonyls) with dihydroarylsilanes in the presence of internal donors provides a quite general route for the preparation of silanediyl-transition metal complexes in good yield (Scheme 2).

Addition of $Fe(CO)_5$, $R^1CpMn(CO)_3$, $Cr(CO)_6$, or $Mo(CO)_6$ to pentacoordinated [2-[(dimethylamino)methyl]phenyl]phenyldihydrosilane (**4a**) or bis[2-[(dimethylamino)methyl]phenyl]dihydrosilane (**4b**) in pentane under UV irradiation afforded the respective silanediylmetal complexes. The silanediyl-transition metal complexes were characterized unambiguously by ¹H, ²⁹Si, ¹³C, IR, and mass spectrometry. In some cases, the ¹H NMR spectroscopic data were not reliable, and only broad signals were detected at various temperatures, although they appeared in the expected regions (see Experimental Section). However, even in these cases, ¹³C NMR data could be recorded without such problems.

X-ray Structure of [2-[(Dimethylamino)methyl]phenyl]phenylsilanediyliron(0) Tetracarbonyl (5a). In order to elucidate the degree of coordination of donor ligand to silicon atom and to gain insight as to the way the silylene unit is bonded to the metal center, an X-ray structural analysis of complex **5a** was carried out. Crystals were grown in $CHCl_3$ /pentane (80/20) solution at $-20^\circ C$. The silanediyl ligand is coordinated to the $Fe(CO)_4$ fragment with a bond distance of Si-Fe of

(6) (a) Aylett, B. J. *J. Organomet. Chem. Lib.* **1980**, *9*, 327. (b) Jetz, W.; Graham, W. A. G. *Inorg. Chem.* **1971**, *10*, 1647. (c) Jetz, W.; Graham, W. A. G. *Inorg. Chem.* **1971**, *10*, 4. (d) Colomer, E.; Corriu, R. J. P. *Top. Curr. Chem.* **1981**, *96*, 79. (e) Colomer, E.; Corriu, R.; Vioux, A. *J. Chem. Soc., Chem. Commun.* **1976**, 175. (f) Schubert, U. *Trans. Met. Chem.* **1991**, *16*, 136. (g) Schubert, U.; Müller, C. *J. Organomet. Chem.* **1988**, *340*, 101. (h) Schubert, U.; Müller, C. *J. Organomet. Chem.* **1989**, *373*, 165.

(7) (a) Corriu, R. J. P.; Moreau, J. J. E. *J. Chem. Soc., Chem. Commun.* **1980**, 278. Carré, F. H.; Moreau, J. J. E. *Inorg. Chem.* **1982**, *8*, 3099.

(8) (a) Schmid, G.; Welz, E. *Angew. Chem., Int. Ed. Engl.* **1977**, *16*, 785. (b) Ueno, K.; Tobita, H.; Shimoi, M.; Ogino, H. *J. Am. Chem. Soc.* **1988**, *110*, 4092. (c) Horng, K. M.; Wang, S. L.; Liu, C. S. *Organometallics* **1991**, *10*, 631. (d) Takeuchi, T.; Tobita, H.; Ogino, H. *Organometallics* **1991**, *10*, 835. (e) Koe, J. R.; Tobita, H.; Ogino, H. *Organometallics* **1992**, *11*, 2479. (f) Woo, L. K.; Smith, D. A.; Young, V. G., Jr. *Organometallics* **1991**, *10*, 3977. (g) Pannell, K. H.; Rozell, J. M., Jr.; Hernandez, C. *J. Am. Chem. Soc.* **1989**, *111*, 4482. (h) Pannell, K. H.; Wang, L. J.; Rozell, J. M. *Organometallics*, **1989**, *8*, 550. (i) Malisch, W. *Chem. Ber.* **1974**, *107*, 3835. (j) Thum, G.; Malisch, W. *J. Organomet. Chem.* **1984**, *264*, C5. (k) Pi, Z.; Simons, R.; Tessier, C. Proceedings of the XXVII ACS Organosilicon Symposium, Troy, NY, March 1994.

(9) (a) Zybilla, C.; Wilkinson, D. L.; Leis, C.; Müller, G. *Angew. Chem., Int. Ed. Engl.* **1989**, *28*, 203. (b) Zybilla, C.; Müller, G. *Organometallics* **1988**, *7*, 514.

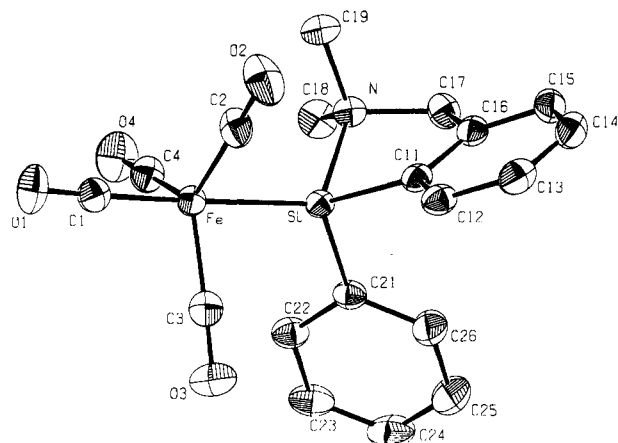


Figure 1. PLATON drawing (50% probability) of the molecular structure of **5a** in the solid state. Hydrogens have been omitted for clarity.

Table 1. Selected Bond Distances (Å) and Angles (deg) for **5a**

Bond Distances			
Fe-Si	2.259(1)	Si-N	1.962(2)
Fe-C1	1.786(3)	Si-C11	1.878(3)
Fe-C2	1.774(3)	Si-C21	1.891(3)
Fe-C3	1.779(3)	O1-C1	1.145(3)
Fe-C4	1.773(3)	O2-C2	1.150(3)
		O3-C3	1.149(3)
		O4-C4	1.152(3)
		N-C17	1.508(3)
		N-C18	1.498(3)
		N-C19	1.498(3)
Bond Angles			
Si-Fe-C1	175.2(1)	Si-N-C17	104.5(2)
Si-Fe-C2	84.6(1)	Si-N-C18	115.3(2)
Si-Fe-C3	85.3(1)	Si-N-C19	110.0(2)
Si-Fe-C4	90.4(1)	C17-N-C18	109.7(2)
C1-Fe-C2	91.0(1)	C17-N-C19	108.6(2)
C1-Fe-C3	95.3(1)	C18-N-C19	108.5(2)
C1-Fe-C4	93.6(1)	Fe-C1-O1	177.9(3)
C2-Fe-C3	120.4(1)	Fe-C2-O2	178.0(3)
C2-Fe-C4	123.6(1)	Fe-C3-O3	178.6(3)
C3-Fe-C4	115.1(1)	Fe-C4-O4	178.4(3)
Fe-Si-N	117.0(1)	Si-C11-C12	129.5(2)
Fe-Si-C11	122.6(1)	Si-C11-C16	111.4(2)
Fe-Si-C21	119.2(1)	N-C17-C16	107.3(2)
N-Si-C11	86.8(2)	Si-C21-C22	120.3(3)
N-Si-C21	100.0(2)	Si-C21-C26	122.5(2)
C11-Si-C21	104.8(1)		

2.259(1) Å. The N-Si bond distance of 1.962(2) Å is intermediate between the values of Si-N σ -bonds, which have been measured in the range 1.70–1.76 Å, and the sum of the van der Waals radii, which is 3.2 Å. A striking feature of the structure is the sum of the bond angles of the silanediyl unit, excluding the N-atom, giving 346.7°, which emphasizes the tendency of the whole system to pyramidalize around silicon. (Figure 1). A complete list of bond distances and angles of **5a** is given in Table 1.

A comparison can be made with the already known¹⁰ structural parameters of **8**. In agreement with the present data, a Si-Cr bond distance of 2.409(1) Å and a N-Si bond distance of 1.991(2) Å were found. The sum of bond angles of the three covalently bonded substituents at silicon in **8** amounts to 347.8°.

Dynamic Behavior of the Silanediyl-Transition Metal Complexes. An investigation of the molecular dynamics of compounds **5–8** provides insight into the

mechanism of intramolecular Lewis base coordination. For instance, the ¹H NMR spectrum of **5a** shows rigid coordination of the NMe₂ unit to silicon at 22°C in toluene, which leads to diastereotopic methyl groups at nitrogen and an AB system for the benzylic phenyl CH₂N protons. Temperature-dependent NMR spectra provide further information about rigid N → Si coordination. The Gibbs free energy for the dissociation of the donor group is relatively high ($\Delta G^\ddagger > 95$ kJ mol⁻¹), because no coalescence was observed up to 105 °C either for diastereotopic NMe₂ groups or for the benzylic protons (AB system). In contrast to the **5a**, the variable-temperature NMR spectrum of **8** showed¹⁰ coalescence for both methyl signals of the diastereotopic NMe₂ group and the AB system of CH₂N protons at 95 °C (ΔG^\ddagger 80.5 kJ mol⁻¹).

The ¹³C NMR spectra of **5–8** provide further information about the structure of the molecules. **5a** and **7a** show only one signal for the carbonyl carbons (CO), indicating rapid exchange at the NMR time scale between axial and equatorial carbonyl groups at room temperature. **6a** displays two different signals for the carbonyls at 238 and 235 ppm, respectively. Complexes **5a**, **6a**, **7a**, and **8** show two diastereotopic methyl signals for the NMe₂ group coordinated to the Si atom. No change is observed with increasing temperature.

When the phenyl group is ortho-substituted by another CH₂NMe₂ coordinating group (**5b** and **6b**), ¹³C NMR spectra indicate dramatic changes in the mode of coordination of the NMe₂ groups to the Si atom. In both cases, the NMe₂ groups give only one signal showing equivalence of the methyl groups at nitrogen. This phenomenon of equivalence takes place because both NMe₂ donor groups displace each other rapidly, thus permitting inversion at nitrogen and rotation around the C-N bonds.¹⁰ The carbonyl carbons in **5b** again give only one signal in ¹³C NMR, because of rapid exchange on the NMR time scale between axial and equatorial carbonyls. However, in the case of **6b**, the cyclopentadienyl carbons give only one signal, but two different signals are observed for the diastereotopic carbonyl carbons at 234.7 and 235 ppm, respectively.

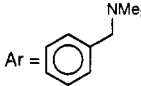
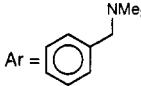
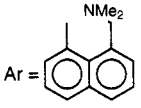
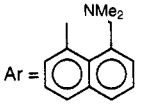
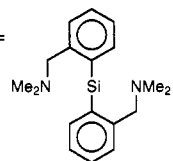
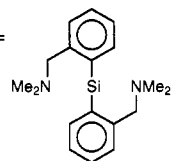
²⁹Si NMR measurements provide very powerful spectroscopic evidence for M=Si interaction in complexes **5–8**. **5a** gives one signal at +118 ppm, which lies in the characteristic range of 80–150 ppm for silanediyl-transition metal complexes having at least one phenyl group bonded to Si atom (see Table 2). Chemical shifts for complexes **5b** (+115 ppm), **7** (+111 ppm), and **8** (+122 ppm) also fall in the same region. Manganese complexes **6a** and **6b** display more downfield chemical shifts at +145 and +147 ppm, respectively, at room temperature. ²⁹Si NMR chemical shifts of silanediyl-transition metal complexes are not much influenced by introducing second donor groups at the silicon atom, as indicated by the chemical shifts of **5b** (+115 ppm) and **6b** (+147 ppm).

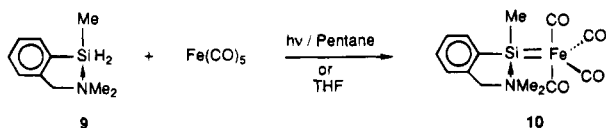
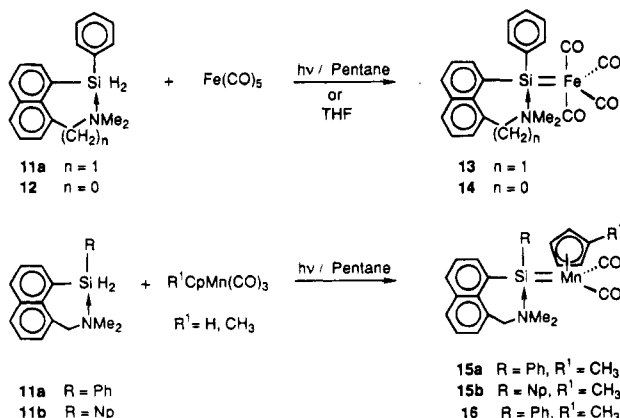
The effect of the noncoordinating ligand to silicon has been checked by replacing the phenyl by a methyl group. Addition of iron pentacarbonyl to a THF solution of [2-[(dimethylamino)methyl]phenyl]methyl-dihydro-silane (**9**) affords complex **10** in 2 h. In pentane, irradiation of the crude mixture is necessary to initiate the reaction (see Experimental Section) (Scheme 3).

Complex **10** displays spectroscopic characteristics similar to those for complexes **5–8**. The presence of two

(10) (a) Probst, R.; Leis, C.; Gamper, S.; Herdtweck, E.; Zybilla, C.; Auner, N. *Angew. Chem., Int. Ed. Engl.* **1991**, *30*, 1132. Handwerker, H.; Leis, C.; Probst, R.; Bissinger, P.; Grohmann, A.; Kiprof, P.; Herdtweck, E.; Blümel, J.; Auner, N.; Zybilla, C. *Organometallics* **1993**, *12*, 2162.

Table 2. ^{29}Si NMR and ^{13}C NMR (CO) Chemical Shifts of Silanediyl Transition Metal Complexes ^{29}Si NMR and ^{13}C NMR (CO) Chemical Shifts of Silanediyl Transition Metal Complexes

NMR (δ /ppm, CDCl_3) system	products	^{29}Si	^{13}C (CO)
 Ar = 	ArPhSi=Fe(CO) $_4$ (5a)	+118.1	216.1
	ArMeSi=Fe(CO) $_4$ (10)	+123.6	214.2
	ArPhSi=MnMeCp(CO) $_2$ (6a)	+145.2	234.7, 235.0
	ArPhSi=Cr(CO) $_5$ (8a)	+122, (121.2) ^a	221.3, 224.8
	ArPhSi=Mo(CO) $_5$ (7a)	+111.2	210.4, 212.5
 Ar = 	ArPhSi=Fe(CO) $_4$ (13)	+101.1	207
	ArPhSi=MnCp(CO) $_2$ (16)	+125.2	234.1, 236.3
	ArPhSi=MnMeCp(CO) $_2$ (15a)	+124.3	234.2, 237.4
	ArNpSi=MnMeCp(CO) $_2$ (15b)	+127.1	235.0, 237.4
	NMe $_2$ ArPhSi=Fe(CO) $_4$ (14)	+125.7	215.0
 BisArSi = 	bisArSi=Fe(CO) $_4$ (5b)	+115.0	216.6
	bisArSi=MnCp(CO) $_2$ (6b)	+147.4	234.6, 235.5
	bisArSi=Cr(CO) $_5$	+125.0 ^a	212.8, 227.2

^a See ref 10.**Scheme 3****Scheme 4**

signals for nonequivalent methyl groups at NMe $_2$ in ^{13}C NMR again indicates rigid coordination of the donor NMe $_2$ group to Si atom. Rapid exchange between equatorial and axial carbonyls takes place, giving rise to only one signal in the carbonyl region (214 ppm).

In order to explore the general approach of the reaction, we replaced the aminophenyl group with an aminonaphthyl group, possessing the coordinating system of the five-membered ring **14** (as in case of **5**–**10**) or the six-membered ring system **13**, **15a**–**16**, having the same coordinating NMe $_2$ groups. Amino(methyl-ene)naphthylsilanediyl-transition metal complexes **13**–**16** were synthesized either by addition of THF solutions of metal carbonyls Fe(CO) $_5$, R 1 CpMn(CO) $_3$ to silanes **11a**, **11b**, and **12** or by UV irradiation of pentane solutions of silanes with the respective metal carbonyls (Scheme 4).

The six-membered ring system used in **13** has already shown to be the more effective ligand for coordinating

to silicon species, either in hypervalent species, in which case increased activation of the Si–X bond is observed,¹¹ or in low-coordinating silicon species, since even the stabilized silanethione could be isolated as the monomeric base-stabilized species.^{12a–c}

The ^{13}C NMR spectra of complexes **13**, **14**, **15a**, **15b**, and **16** give two signals for the methyl of the diastereotopic NMe $_2$ group, indicating strong coordination of the amino donor group to the Si atom, as in the case of complexes **5**–**8**. For complexes **13** and **14** only one signal for the carbonyl carbon is observed at 217 and 215 ppm, respectively. Complexes **15a**–**16** permit distinction between carbonyls giving two signals in the range 235–237 ppm. The ^{29}Si NMR chemical shifts in manganese silanediyl complexes **15a**–**16** fall in the region +125 ppm, more downfield than for the corresponding iron silanediyl complex **13** (+101 ppm). The five-membered ring system **14** presents a fused geometry, with the NMe $_2$ group held in proximity to silicon. The strongly coordinated [8-[(dimethylamino)naphthyl]-1-phenyldihydrosilane **12** is less reactive;¹³ nevertheless under photolytic conditions iron tetracarbonyl complex **14** has been isolated and characterized (Table 2).

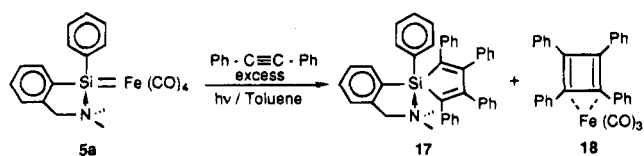
Reactivity of Silanediyl-Transition Metal Complexes as Silylene Sources. Silanediyl-transition metal complexes can be considered as reactive intermediates in a variety of silylene transfer reactions, for instance, in dehydrogenative coupling of silanes giving

(11) (a) Corriu, R. J. P.; Lanneau, G. F.; Perrot, M. *Tetrahedron Lett.* **1988**, *29*, 1271. (b) Corriu, R. J. P.; Lanneau, G. F.; Perrot-Petta, M.; Mehta, V. D. *Tetrahedron Lett.* **1990**, *31*, 2585. (c) Corriu, R. J. P.; Lanneau, G. F.; Mehta, V. D. *Heteroat. Chem.* **1991**, *2*, 461. (d) Corriu, R. J. P.; Lanneau, G. F.; Perrot-Petta, M. *Synthesis* **1991**, 954.

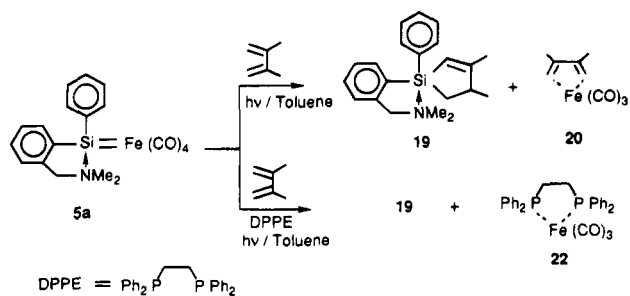
(12) (a) Priou C. Ph.D. Thesis, Université Montpellier II, Montpellier, France, 1990. (b) Arya, P.; Boyer, J.; Carré, F.; Corriu, R. J. P.; Lanneau, G. F.; Perrot, M.; Priou, C. *Angew. Chem., Int. Ed. Engl.* **1989**, *28*, 1016. (c) Corriu, R. J. P.; Lanneau, G. F.; Priou, C. *Angew. Chem., Int. Ed. Engl.* **1991**, *30*, 1130. (d) Corriu, R. J. P.; Moreau, J. J. E. *J. Chem. Soc., Chem. Commun.* **1973**, 38. (e) Corriu, R. J. P.; Moreau, J. J. E. *J. Organomet. Chem.* **1976**, *114*, 135.

(13) (a) Arya, P.; Boyer, J.; Corriu, R. J. P.; Lanneau, G. F.; Perrot, M. *J. Organomet. Chem.* **1988**, *346*, C11. (b) Corriu, R. J. P.; Lanneau, G. F.; Mehta, V. D. *J. Organomet. Chem.* **1991**, *419*, 9.

Scheme 5



Scheme 6

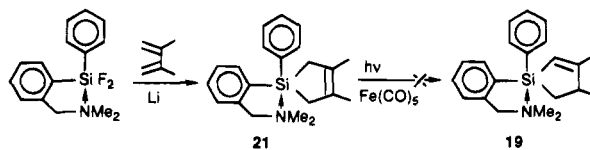


disilanes with late transition metal catalysts.¹⁴ In the case of the oligomerization reaction of chain polysilanes¹⁵ or in silylene transfer reactions with olefins and acetylenes, silanediyl metal complexes have also been proposed as reactive intermediates.¹⁶ Trapping experiments of silanediyl-transition metal complexes could provide strong evidence for such type of mechanism.

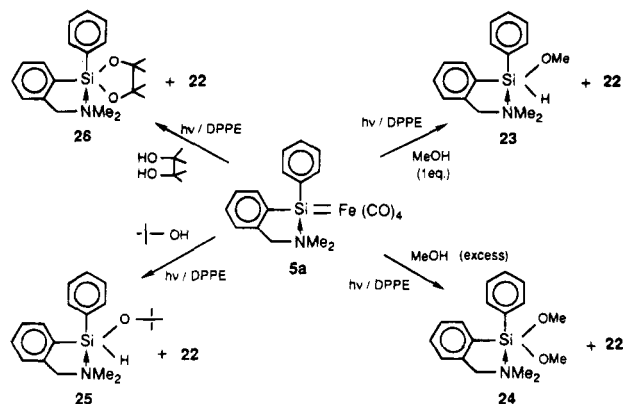
(1) Reaction with Diphenylacetylene. For trapping experiments, [2-[(dimethylamino)methyl]phenyl]phenylsilyliron(0) tetracarbonyl (**5a**) was chosen as the title complex. A toluene solution of complex **5a**, containing 10 equiv of diphenylacetylene was photolyzed for 5 h at room temperature. Formation of the silole [2-[(dimethylamino)methyl]phenyl]phenyl-1,2,3,4-tetraphenylsilacyclopent-2,4-diene (**17**) clearly demonstrates decomposition of the silanediyl complex **5a** into silylene. Besides the trapping product of silylene **17** and the metal complex **18**, traces of $\text{Fe}_3(\text{CO})_{12}$ were also observed (Scheme 5).

(2) Reaction with 2,3-Dimethylbutadiene. Photoirradiation of a toluene solution of complex **5a** in the presence of excess 2,3-dimethylbutadiene for 5 h afforded **19** and **20** in quantitative yield. The same trapping product **19** was obtained when the reaction was carried out in the presence of 1,2-bis(diphenylphosphino)ethane (DPPE), along with the formation of 1,2-bis(diphenylphosphino)ethaneiron(0) tricarbonyl complex (**22**; Scheme 6). [2-[(dimethylamino)methyl]phenyl]phenyl-3,4-dimethylsilacyclopent-2-ene (**19**) could be the isomerization product of the direct trapping compound [2-[(dimethylamino)methyl]phenyl]phenyl-3,4-dimethylsilacyclopent-3-ene (**21**).

Scheme 7



Scheme 8



However, irradiation of authentic¹⁷ **21** in the presence of $\text{Fe}(\text{CO})_5$ in pentane did not isomerize the species (Scheme 7).

(3) Reactions with Alcohols. Silanediyl-transition metal complexes also react with alcohols in the presence of DPPE under UV irradiation to afford alkoxy-silanes and iron complex **22**. Remarkably, silanediyl-iron carbonyl complex does not react with alcohols without irradiation. [2-[(Dimethylamino)methyl]phenyl]phenyl methoxysilane (**23**) was obtained from complex **5a** in the presence of 1 equiv of methanol. Excess of methanol afforded [2-[(dimethylamino)methyl]phenyl]phenyl dimethoxysilane (**24**). Irradiation of complex **5a** with *tert*-butyl alcohol or pinacol in the presence of DPPE produced the expected trapping products **25** and **26**, respectively, along with DPPE-iron(0) tricarbonyl complex **22** (Scheme 8).

Reactivity of [8-[(Dimethylamino)methyl]naphthyl]phenylsilyliron(0) Tetracarbonyl (13**).** The silanediyl complex **13** was submitted to trapping experiments under the same experimental conditions as for **5a**. Complex **13** is unexpectedly unreactive toward alcohols and unsaturated hydrocarbons. Iron carbonyls are known to be highly associative with sulfur. No reaction occurred when **13** was mixed with previously described silanethione^{12c} or elemental sulfur.

Irradiation of **13** in the presence of DPPE in THF for 5 h afforded 15% of complex **22**. Trapping experiments with methanol and dimethylbutadiene failed to isolate the expected dimethoxysilane or silacyclopentene. Some new signals (five) were observed in the ²⁹Si NMR spectra of the crude reaction mixtures, but only trimeric siloxane could be identified as one of the decomposition products. Trimeric siloxane **27** was obtained quantitatively after oxidation of **13** in THF under photolytic conditions or by just stirring the mixture at 25 °C in air for 5 h (Scheme 9).

Reactivity of DMI-Stabilized Diphenylsilyliron(0) Tetracarbonyl (3**).** The photochemical degradation of **3** in the presence of typical trapping agents afforded

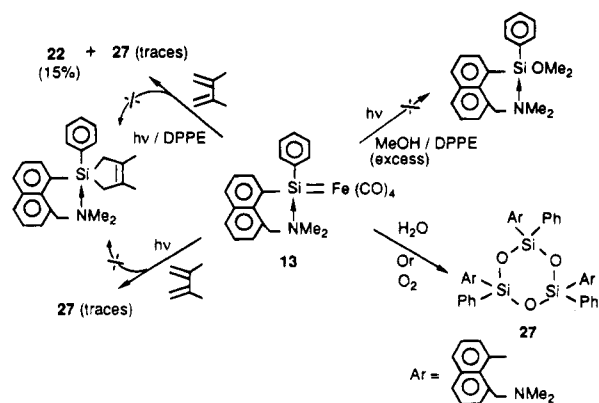
(14) (a) Aitken, C. T.; Harrod, J. F.; Samuel, E. *Can. J. Chem.* **1986**, *64*, 1677. (b) Harrod, J. F.; Yun, S. S. *Organometallics* **1987**, *6*, 1381. (c) Chang, L. S.; Corey, J. Y. *Organometallics* **1989**, *8*, 1885.

(15) (a) Brown-Wensley, K. A. *Organometallics* **1987**, *6*, 1590. (b) Zarate, E. A.; Tessier-Youngs, C. A.; Youngs, W. J. *J. Am. Chem. Soc.* **1988**, *110*, 4068. (c) Nakeno, T.; Nakamura, H.; Nagai, Y. *Chem. Lett.* **1989**, 83. (d) Aitken, C. T.; Barry, J. P.; Gauvin, F.; Harrod, J. F.; Malek, A.; Rousseau, D. *Organometallics* **1989**, *8*, 1732. (e) Jutzi, P.; Möhrke, A. *Angew. Chem., Int. Ed. Engl.* **1990**, *29*, 893. (f) McDonald, R.; Cowie, M. *Organometallics* **1990**, *9*, 2468. (g) Wang, W. D.; Eisenberg, R. *J. Am. Chem. Soc.* **1990**, *112*, 1833. (h) Lee, K.; Arif, A.; Gladysz, J. A. *Chem. Ber.* **1991**, *124*, 309.

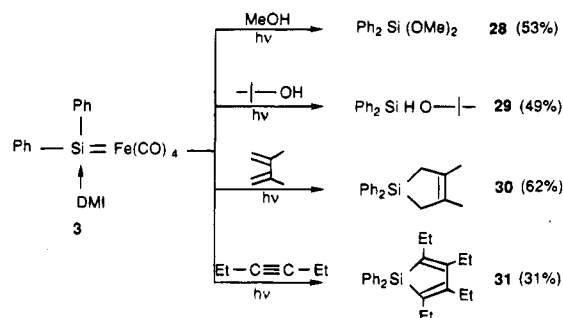
(16) (a) See: Gaspar P. P. *Silylenes*. In *Reactive Intermediates*; Moss, R., Jones, M., Eds.; Wiley: New York, 1985; p 333, and references cited therein. (b) Raabe G.; Michl, J. In *The Chemistry of Organic Silicon Compounds*; Patai, S., Rappoport, Z., Eds.; Wiley: New York, 1989; Chapter 17, p 1015.

(17) Corriu, R.; Lanneau, G.; Priou, C.; Soulaire, F.; Auner, N.; Probst, R.; Conlin, R.; Tan, C. *J. Organomet. Chem.* **1994**, *466*, 55.

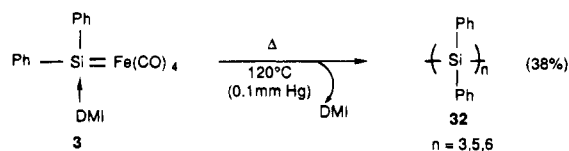
Scheme 9



Scheme 10



Scheme 11



products **28**–**31**, whose spectroscopic properties were compared with those of authentic samples.^{12d,e} **29** is the expected trapping product of the free silylene with *tert*-butyl alcohol, but **28** could be the direct product of methanolysis of complex **3** or could result from the consecutive methanolysis of Ph_2SiHOMe in the presence of excess methanol. Irradiation of **3** with an excess of 2,3-dimethylbutadiene afforded the expected trapping product 3,4-dimethyl-1,1-diphenylsilacyclopent-3-ene (**30**; 62% yield) and (2,3-dimethylbutadiene)iron tricarbonyl **20** (67%). Similarly the silole **31** (37%) was isolated in the photochemical reaction of **3** with an excess of 3-hexyne (Scheme 10).

Thermolysis of 3. Pyrolysis of **3** under vacuum at 120 °C led to the formation of the linear and cyclic trimer–pentamer of diphenylsilane. The mixture was analyzed by GPC after chromatography on Florisil (see Experimental Section). Two peaks were observed with average molecular weights of 532 and 1247, respectively. ¹H NMR spectroscopy showed the presence of only aromatic protons. No Si–O or Si–H vibration was detected in the IR spectrum (Scheme 11).

Discussion

The photolysis of dihydrosilanes with transition metal carbonyls in the presence of Lewis bases represents a new method for the preparation of base-stabilized silylene complexes. The formation of silanediyl com-

Scheme 12

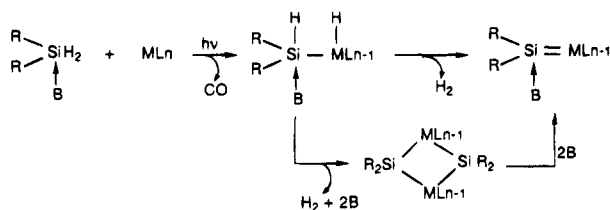
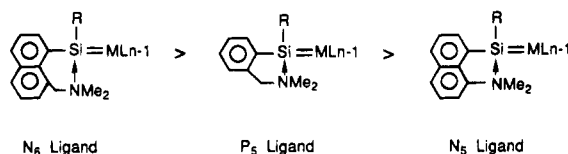


Chart 1



plexes may involve prior formation of a dimer which rearranges in the presence of base as shown by Ph_2SiH_2 with $\text{Fe}(\text{CO})_5$ adding 1,3-dimethyl-2-imidazolidinone. Another possibility is the direct intramolecular elimination of hydrogen gas, giving the products (Scheme 12).

Generally, yields of silanediyl complexes are in the order of 80–90%. Typically, reaction conditions need irradiation of the crude mixture for 5–8 h in pentane at room temperature. The silanediyl complex is not soluble in hydrocarbon, giving a solid or an oil, which deposits along the walls of the reactor. The excess of metal carbonyl and byproducts can easily be removed. Qualitatively, the reaction is strongly accelerated by changing the solvent from pentane to THF. For example, with **12a**, irradiation is not necessary to initiate the reaction, but with the less reactive **4a**, the reaction performed in THF without UV irradiation is slow and gives essentially byproducts.

In fact, two factors seem to be important to observe decomposition of the σ -bonded transition metal species: (i) the acidity of the M–H bond and (ii) the basicity of the Si–H bond. As expected, we observe a relative order of reactivity of $\text{Fe} > \text{Cr} > \text{Mn}$.

The effect of the intramolecular coordination with aminoaryl groups upon the lability of the $\text{Si}^{\delta+}\text{--H}^{\delta-}$ bond parallels the ability of these systems to form silanediyl¹⁸ complexes. The dihydrosilanes with an intramolecular six-membered-ring coordinating ligand are known to be more reactive than the compounds with five-membered-ring ligands (Chart 1).

For example, they react with acyl chlorides,^{11a} heterocumulenes,^{11b,d} keto groups,²³ and alcohols.²⁰ The same ligand is more efficient at stabilizing low-coordinated silicon species, silanethiones, silaimines, and silaphos-

(18) Corriu, R. J. P.; Lanneau, G. F.; Chauhan, B. P. S. *Organometallics* **1993**, *12*, 2001.

(19) Straus, D. A.; Grumbine, S. D.; Tilly, T. D. *J. Am. Chem. Soc.* **1990**, *112*, 7801.

(20) (a) Corriu, R. J. P.; Lanneau, G. F.; Perrot, M. *Tetrahedron Lett.* **1987**, *28*, 3941. (b) Boyer, J.; Brelrière, C.; Carré, F.; Corriu, R. J. P.; Kpton, A.; Poirier, M.; Royo, G.; Young, J. C. *J. Chem. Soc., Dalton Trans.* **1989**, *43*. (c) Boyer, J.; Brelrière, C.; Corriu, R. J. P.; Kpton, A.; Poirier, M.; Royo, G. *J. Organomet. Chem.* **1986**, *311*, C39. (d) Corriu, R. J. P.; Kpton, A.; Poirier, M.; Royo, G.; Corey, J. Y. *J. Organomet. Chem.* **1986**, *277*, C25.

(21) (a) Ishikawa, M.; Ohi, F.; Kumada, M. *J. Organomet. Chem.* **1975**, *186*, C23. (b) Okinoshima, H.; Yamamoto, K.; Kumada, M. *J. Am. Chem. Soc.* **1972**, *94*, 9263. (c) Ishikawa, M. *Organomet. Syn.* **1988**, *4*, 527. (d) For a recent review on siloles, see: Dubac, C.; Laporterie, A.; Manuel, G. *Chem. Rev.* **1990**, *90*, 215.

(22) Ittel, S. D.; Tolman, C. A.; Krusic, P. J.; English, A. D.; Jesson, J. P. *Inorg. Chem.* **1978**, *17*, 3432.

phenes.¹³ The stability of the system is also emphasized when the reactivity of the silanediyl complexes is considered. The N₆ model is strongly coordinated to the metal, preventing any approach of a nucleophile. More drastic conditions allow decomposition of the complex. With the less coordinating P₅ group, reactions are possible, but photochemical activation is necessary. The silylene, which is the expected decomposition product, can be trapped, either with alcohols or dienes, but any attempt to characterize the base-stabilized silylene was unsuccessful.

Conclusion

We have developed a new approach to Lewis base-stabilized silanediyl-transition metal complexes, based on the photochemical reaction of 16-e⁻ transition metal carbonyl species with dihydrosilanes in the presence of either external or internal donor molecules. Trapping experiments with acetylenes, dienes, and alcohols emphasize the efficiency of the silanediyl-transition metal complexes as silylene sources. The reactivity of these complexes is inversely proportional to their stability: the more coordinated the Lewis base adducts, the less reactive they are.

Experimental Section

All manipulations were carried out under an atmosphere of dry argon. Air-sensitive reagents and products were handled by standard Schlenk techniques. All solvents were dried and distilled from purple solutions of sodium/benzophenone or P₂O₅. Commercially available chemicals were used as such without any further purification. The synthesis of starting dihydrosilanes has been described²⁰ in the literature. ²⁹Si, ¹³C, ¹H, and ³¹P NMR spectra were recorded on a Bruker WP200 SY or AC 250 spectrometer. ¹H and ¹³C chemical shifts were measured against Me₄Si using solvent resonances as standard locks. ²⁹Si chemical shifts were referenced to external Me₄Si in the same solvent. IR spectra were recorded on a Perkin-Elmer 1600 FT instrument as KBr pellets, Nujol suspensions, or solutions in CaF₂ cells. The mass spectra were obtained on a JEOL JMS D100 apparatus by EI ionization at 70 or 30 eV. Elemental analyses were carried out by the Service Central de Microanalyse du CNRS or ENSC Montpellier. All photochemical reactions were performed at room temperature by use of an immersed Hanovia 450-W medium-pressure mercury lamp in a quartz reaction vessel under argon.

(C₆H₅)₂(DMI)Si=Fe(CO)₄. (Diphenylsilanediyl)iron(0) Tetracarbonyl-1,3-dimethyl-2-imidazolidinone (3). A solution of diphenylsilane 1 (3.69 g, 20 mmol) and 1,3-dimethyl-2-imidazolidinone (2.28 g, 20 mmol) in 350 mL of pentane was transferred into a 500-mL quartz reaction vessel. Iron pentacarbonyl (2.62 mL, 20 mmol) was added to this solution, and the mixture was irradiated at room temperature. Separation of a black-red sticky solid started taking place after 20 min of irradiation. Complete disappearance of ν(SiH), in the IR spectrum, was observed after 5 h. Pentane solution was removed from the reaction vessel, and the remaining solid 3 was washed with pentane and analyzed. Yield: 93%.

Synthesis of 3 from μ-(Diphenylsilanediyl)iron Tetracarbonyl (2). Freshly prepared μ-(diphenylsilanediyl)iron tetracarbonyl complex⁷ (2; 0.35 g, 5 mmol) was dissolved in 350 mL of toluene, and 1,3-dimethyl-2-imidazolidinone (1.14 g, 10 mmol) was injected dropwise to this solution. The

resulting mixture was irradiated for 1 h. Evaporation of solvent furnished complex 3 in 90% yield. Anal. Calcd for C₂₁H₂₀N₂O₅SiFe: C, 54.31; H, 4.31; N, 6.03. Found: C, 54.48; H, 4.49; N, 6.12. ¹H NMR (CDCl₃): δ 4.18 (br s, 6H, 2NCH₃), 6.18 (s, 4H, 2NCH₂), 7.01–7.98 (m, 10H, ArH) [uncoordinated DMI: ¹H NMR (CDCl₃) δ 2.70 (s, 6H, 2NCH₃), 3.25 (s, 4H, 2NCH₂)]. ¹³C NMR (CDCl₃): δ 28.63 (NCH₃), 48.12 (NCH₂) 125.35–143.44 (aromatics), 161.6 (>C=O), 217.6 (CO), MS [EI, 70 eV; *m/e* (relative intensity %): 437 (M⁺ - CO, 100), 396 (0.6), 361 (18), 317 (10) 182 (15), 154 (10), 114 (60). ²⁹Si NMR (toluene/C₆D₆): δ +91.30. IR (CDCl₃, cm⁻¹): ν(>C=O, CO), 1688 (>C=O), 2019, 1995 (CO).

(C₆H₅)₂HMPASi=Fe(CO)₄. (Diphenylsilanediyl)iron(0) Tetracarbonyl Hexamethylphosphorictriamide (4). The preparation of 4 was done analogously to the synthesis of complex 3. Complex 4 was crystallized from CHCl₃/C₇H₈ (40/60) mixture at -15 °C. mp: 121–122 °C. Yield: 43% Anal. Calcd for C₂₂H₂₈N₃O₅PSiFe: C, 49.90; H, 5.29. Found: C, 49.98; H, 5.39. ¹H NMR (CDCl₃): δ 2.52 (d, CH₃, 18H), 7.33, 7.69 (m, aromatics, 10H). ¹³C NMR (CDCl₃): δ 37.22 (NCH₃), 127.72, 128.18, 129.17, 130.83, 135.05, 143.56 (aromatics), 217.62 (CO). ²⁹Si NMR (CDCl₃): δ +79.52 [d, ²J(³¹P²⁹Si) = 23.86 Hz]. ³¹P-NMR (CDCl₃): δ +25. IR (CDCl₃, cm⁻¹): ν(CO), 2017, 1932, 1885. MS [EI, 30 eV; *m/e* (relative intensity %): 529 (M⁺, 15), 501 (-CO, 10) 473 (14), 445 (35), 417 (50), 360 (20), 322 (40), 314 (10), 266 (40), 236 (100), 182 (80), 135 (90), 119 (20), 92 (70), 56 (45).

[2-(Me₂NCH₂)C₆H₄]C₆H₅Si=Fe(CO)₄. [2-[(Dimethylamino)methyl]phenyl]phenylsilanediyliron(0) Tetracarbonyl (5a). In a 500-mL quartz reaction vessel, [2-[(dimethylamino)methyl]phenyl]phenyldihydrosilane (4a; 2.41 g, 10 mmol) was dissolved in 350 mL of pentane. To this colorless solution was added iron pentacarbonyl (1.31 mL, 10 mmol) by a syringe. This mixture was irradiated at room temperature for 5–6 h. A red solid started precipitating after 15 min. The progress of the reaction was monitored by IR. After complete disappearance of silane 4a, pentane was removed with a cannula and solid 5a was washed three times with pentane and isolated as a powder. mp: 130 °C dec. Yield: 3.25 g (80%). Anal. Calcd for C₁₉H₁₇NSiFeO₄: C, 56.0; H, 4.2; N, 3.4; Si, 6.7. Found: C, 56.03; H, 4.32; N, 3.54; Si, 6.61. ²⁹Si NMR (CDCl₃, 22 °C): δ +118. ¹H NMR (CDCl₃): δ 1.89 (s, 3H, NCH₃), 2.18 (s, 3H, NCH₃), 2.65, 2.73, 3.39, 3.47 [dd, 2H, AB system, ²J(¹H¹H) = 14.3 Hz, NCH₂], 6.65, 6.86, 7.11, 7.48, 7.82 (9H, aromatics). ¹³C NMR (CDCl₃): δ 47.73 (NCH₃), 49.57 (NCH₃), 68.60 (NCH₂), 123.73, 130.56, 136.52, 138.40, 139.34 (aromatics), 215.62 (CO). IR (CDCl₃, cm⁻¹): ν(CO) 1985, 1953, 1914, 1893. MS [EI, 70 eV; *m/e* (relative intensity %): 407 (M⁺, 15), 779 (24), 323 (65), 295 (100), 238 (26), 134 (26), 91 (28).

[2-(Me₂NCH₂)C₆H₄]₂Si=Fe(CO)₄. Bis[2-[(dimethylamino)methyl]phenyl]silanediyliron(0) Tetracarbonyl (5b). Bis[2-[(dimethylamino)methyl]phenyl]dihydrosilane (4b; 2.98 g, 10 mmol) was diluted in 350 mL of pentane in a 500-mL quartz reaction vessel. Iron pentacarbonyl (1.31 mL, 10 mmol) was added with a syringe. The yellow mixture was subjected to irradiation for 5 h at room temperature. A red-brown solid started precipitating after 15 min of irradiation. After complete disappearance of silane (monitored by IR), the pentane solution was removed from the vessel with a cannula and the remaining solid was washed two times with pentane. This solid was further purified by crystallization in a chloroform/toluene (80/20) mixture. Yield: 65%. Anal. Calcd for C₂₂H₂₄N₂O₄SiFe: C, 56.89; H, 5.17; N, 6.03. Found: C, 56.80; H, 5.20; N, 6.09. ²⁹Si NMR (CDCl₃): δ +115. ¹³C NMR (CDCl₃): δ 45.90 (NCH₃), 64.28 (NCH₂), 126.47, 127.90, 130.26, 131.17, 136.22, 145.12, (C₆H₄), 216.61 (CO). IR (CDCl₃, cm⁻¹): ν(CO) 1998 (br), 1889. MS [EI, 70 eV; *m/e* (relative intensity %): 408 (-2CO, 21), 380 (25), 352 (38), 309 (27), 296 (10), 238 (8), 135(40), 91 (100), 55 (40).

[2-(Me₂NCH₂)C₆H₄]C₆H₅Si=MnMeCp(CO)₂. [2-[(Dimethylamino)methyl]phenyl]phenylsilanediyl(η⁵-methyl-

(23) (a) Carré, F. H.; Corriu, R. J. P.; Lanneau, G. F.; Yu, Z. *Organometallics* **1991**, *10*, 1236. (b) Corriu, R. J. P.; Royo, G.; de Saxcé, A. *J. Chem. Soc., Chem. Commun.* **1980**, 892. (c) Arya, P.; Corriu, R. J. P.; Gupta, K.; Lanneau, G. F.; Yu, Z. *J. Organomet. Chem.* **1990**, *399*, 11. (d) Corriu, R. J. P.; Lanneau, G. F.; Yu, Z. *Tetrahedron* **1993**, *49*, 9019.

cyclopentadienyl)manganese Dicarboxyl (6a). mp: 133–134 °C. Yield: 63%. Anal. Calcd for $C_{23}H_{24}NSiMnO_2$: C, 64.33; H, 5.59; N, 3.26. Found: C, 64.38; H, 5.61; N, 3.29. ^{29}Si NMR ($CDCl_3$, 22 °C): δ +145. ^{13}C -NMR ($CDCl_3$): δ 22.9 (Cp-CH₃), 46.1 (NCH₃), 50.06 (NCH₃), 68.0 (NCH₂), 82.7, 83.1 (Cp), 98.7 (C-CH₃), 123.61, 130.23, 136.82, 138.50, 139.28 (aromatics), 235.0, 237.7 (CO). IR ($CDCl_3$, cm^{-1}): $\nu(CO)$ 1896, 1821. MS [EI, 70 eV; m/e (relative intensity %): 429 (M^+ , 10), 373 (18), 238 (6), 218 (24), 162 (27), 134 (100), 91 (12), 52 (44).

[2-(Me₂NCH₂)C₆H₄]₂Si=MnCp(CO)₂. Bis[2-[(dimethylamino)methyl]phenylsilanediyl(η^5 -cyclopentadienyl)-manganese Dicarboxyl (6b). The same procedure and stoichiometric quantities of reactants as in case of complex **6a** were used. The precipitated brown solid was washed with pentane and analyzed. mp: 139–141 °C dec. Yield: 68%. Anal. Calcd for $C_{25}H_{29}N_2O_2SiMn$: C, 63.55; H, 6.14; N, 5.93. Found: C, 63.25; H, 6.04; N, 5.98. ^{29}Si NMR ($CDCl_3$): δ +147. ^{13}C NMR ($CDCl_3$): δ 47.85 (NCH₃), 67.42 (NCH₂), 83.44 (C₅H₅), 127.64, 129.36, 132.76, 133.68, 136.63, 144.86 (aromatics), 234.67, 235.49 (CO). IR ($CDCl_3$, cm^{-1}): $\nu(CO)$ 1893, 1821. MS [EI, 70 eV; m/e (relative intensity %): 445 (–CO, 20), 416 (35), 402 (28), 354 (20), 296 (10), 238 (10), 135 (42), 91(80), 55 (100).

[2-(Me₂NCH₂)C₆H₄]₂C₆H₅Si=Mo(CO)₅. [2-(Dimethylamino)methyl]phenyl]phenylsilanediylmolybdenum(0) Pentacarbonyl (7a). Yellow sticky solid. Yield: 48%. Anal. Calcd for $C_{26}H_{17}NSiMoO_5$: C, 50.52; H, 3.57; N, 2.94. Found: C, 50.61; H, 3.59; N, 2.98. 1H NMR ($CDCl_3$): unresolved material. ^{29}Si NMR ($CDCl_3$): δ +111. ^{13}C NMR ($CDCl_3$, 22 °C): δ 47.4 (NCH₃), 50.1 (NCH₃), 68.1 (NCH₂), 123.63, 130.52, 136.51, 138.42, 139.34 (aromatics), 210.4, 212.56 (CO). IR ($CDCl_3$, cm^{-1}): $\nu(CO)$ 2055 (fine), 1926 (very large).

[2-(Me₂NCH₂)C₆H₄]₂C₆H₅Si=Cr(CO)₅. [2-(Dimethylamino)methyl]phenyl]phenylsilanediylchromium(0) Pentacarbonyl (8). The same procedure as above and stoichiometric quantities of reactants were used. The resulting yellow solid was washed three times with pentane and analyzed. mp: 171–172 °C (lit.¹⁰ mp 171 °C). Yield: 68%. Anal. Calcd for $C_{26}H_{17}NSiCrO_5$: C, 55.68; H, 3.97; N, 3.25. Found: C, 55.56; H, 3.61; N, 3.21. ^{29}Si NMR ($CDCl_3$, 22 °C): δ +122. 1H NMR ($CDCl_3$, 22 °C): δ 1.86 (s, 3H, NCH₃), 2.12 (s, 3H, NCH₃), 2.63, 2.71, 3.32, 3.40 [dd, 2H, AB system, $^2J(^1H^1H) = 14.01$ Hz, NCH₂], 6.06, 6.93, 7.08, 7.51, 7.92 (9H, aromatics). ^{13}C NMR ($CDCl_3$, 22 °C): δ 47.29 (NCH₃), 48.63 (NCH₃), 68.17 (NCH₂), 123.81, 128.83, 129.74, 134.60, 139.08, 142.81 (aromatics), 221.33, 224.85 (CO). IR ($CDCl_3$, cm^{-1}): $\nu(CO)$, 2055 (fine), 1926 (very large). MS [EI, 70 eV; m/e (relative intensity %): 431 (M^+ , 8), 403 (10), 347 (22), 319 (15), 291 (100), 238 (15), 134 (30), 91 (25).

[2-[(Me₂NCH₂)C₆H₄]₂CH₃Si=Fe(CO)₄. [2-[(Dimethylamino)methyl]phenyl]methylsilanediyliron(0) Tetracarbonyl (10). [2-[(Dimethylamino)methyl]phenyl]methylsilanediyliron(0) Tetracarbonyl (9; 0.35 g, 2 mmol) was dissolved in 15 mL of THF, and iron pentacarbonyl (0.26 mL, 2 mmol) diluted in 5 mL of THF was added dropwise to this solution. This mixture was stirred for a further 2 h at room temperature. Removal of solvent under vacuum furnished a red-brown solid which was washed with pentane and analyzed. Yield: 72%. Anal. Calcd for $C_{14}H_{15}NSiFeO_4$: C, 48.69; H, 4.34; N, 4.05. Found: C, 48.70; H, 4.35; N, 4.01. ^{29}Si NMR ($CDCl_3$, 22 °C): δ +123.6. ^{13}C NMR ($CDCl_3$): δ 5.0 (SiCH₃), 46.1 (NCH₃), 48.2 (NCH₃), 66.8 (NCH₂), 121–135 (aromatics), 214.5 (CO). IR ($CDCl_3$, cm^{-1}): $\nu(CO)$ 2040, 1945, 1905, 1890.

[8-(Me₂NCH₂)C₁₀H₆]-1-C₆H₅Si=Fe(CO)₄. [8-[(Dimethylamino)methyl]naphthyl]-1-phenylsilanediyliron(0) Tetracarbonyl (13). (1) **Synthesis in THF.** [8-[(Dimethylamino)methyl]naphthyl]-1-phenylsilanediyliron(0) Tetracarbonyl (11a; 0.52 g, 1.8 mmol) was diluted in 15 mL of THF at room temperature. Iron

pentacarbonyl (0.35 g, 1.8 mmol) diluted in 5 mL of THF was added dropwise to the stirred solution of silane. The mixture turned brown-red. After 1 h of stirring, THF was evaporated and the resulting solid was washed three times with pentane and crystallized in acetone. Yield: 75%.

(2) **Synthesis by Photoirradiation.** In a 500-mL photochemical reactor, [8-[(dimethylamino)methyl]naphthyl]-1-phenylsilanediyliron(0) Tetracarbonyl (12a; 3.0 g, 10.3 mmol) was dissolved in 350 mL of pentane. Iron pentacarbonyl (2.01 g, 10.3 mmol) was added with a syringe. This yellow mixture was irradiated at room temperature for 5 h under a constant flow of argon. The progress of the reaction was monitored by IR. After 15 min of irradiation, a brown-red solid started precipitating. After complete disappearance of the silane, the pentane solution was removed and the solid was washed with pentane and crystallized from acetone. Yield: 61%. The same procedure and molar quantities were used for the synthesis of complexes **14–16**. mp: 140–141 °C. Anal. Calcd for $C_{23}H_{19}NSiFeO_4$: C, 60.4; H, 4.2; N, 3.1; Si, 6.1. Found: C, 59.97; H, 4.60; N, 3.25; Si, 5.97. ^{29}Si NMR ($CDCl_3$): δ +101. ^{13}C NMR ($CDCl_3$): δ 50.39 (NCH₃), 51.40 (NCH₃), 68.30 (NCH₂), 125.1–139.6 (aromatics), 217 (CO). IR (CCl_4 , cm^{-1}): $\nu(CO)$ 1978, 1951, 1911, 1896. MS [EI, 70 eV; m/e (relative intensity %): 457 (M^+ , 5), 429 (9), 373 (20), 345 (30), 302 (12), 278 (8), 244 (14), 215 (18), 185 (43), 167 (20), 141 (80), 55 (100).

[8-(Me₂N)C₁₀H₆]-1-C₆H₅Si=Fe(CO)₄. [8-[(Dimethylamino)naphthyl]-1-phenylsilanediyliron(0) Tetracarbonyl (14). Yield: 56%. Anal. Calcd for $C_{22}H_{17}NSiFeO_4$: C, 59.59; H, 3.83; N, 3.16; Si, 6.32. Found: C, 59.61; H, 3.86; N, 3.14; Si, 6.30. ^{29}Si NMR ($CDCl_3$): δ +126. ^{13}C NMR ($CDCl_3$, 22 °C): δ 46.9 (NCH₃), 48.2 (NCH₃), 122.1–138.2 (aromatics), 215.0 (CO). IR ($CDCl_3$, cm^{-1}): $\nu(CO)$ 1977, 1954, 1914, 1894. MS [EI, 70 eV; m/e (relative intensity %): 443 (M^+ , 9), 415 (12), 359 (6), 331 (8), 276 (29), 26 (30), 200 (48), 185 (43), 168 (22), 84 (100), 53 (57).

[8-(Me₂NCH₂)C₁₀H₆]-1-C₆H₅Si=MnMeCp(CO)₂. [8-[(Dimethylamino)methyl]naphthyl]-1-phenylsilanediyl(η^5 -methylcyclopentadienyl)manganese Dicarboxyl (15a). mp: 230–231 °C. Yield: 45%. Anal. Calcd for $C_{27}H_{26}NSiMnO_2$: C, 67.64; H, 5.43; N, 2.92; Si, 5.84. Found: C, 67.50; H, 5.52; N, 3.09; Si, 5.15. ^{29}Si NMR ($CDCl_3$): δ +124. ^{13}C NMR ($CDCl_3$): δ 14.6 (Cp*CH₃), 45.0 (NCH₃), 48.0 (NCH₃), 65.9 (NCH₂), 85.5, 82.8 (C₅H₅), 103.1 (C*CH₃), 121.6–136.2 (aromatics), 234.1, 237.0 (CO). IR ($CDCl_3$, cm^{-1}): $\nu(CO)$ 1897, 1822. MS [EI, 70 eV; m/e (relative intensity %): 479 (M^+ , 18), 423 (81), 288 (21), 245 (62), 215 (30), 184 (31), 134 (100), 79 (62), 55 (81).

[8-(Me₂NCH₂)C₁₀H₆]-1-C₁₀H₇Si=MnMeCp(CO)₂. [8-[(Dimethylamino)methyl]naphthyl]-1-naphthylsilanediyl(η^5 -methylcyclopentadienyl)manganese Dicarboxyl (15b). mp (powder): 249–250 °C. Yield: 40%. Anal. Calcd for $C_{22}H_{28}N_3O_5PSiFe$: C, 49.90; H, 5.29; N, 7.93. Found: C, 49.98; H, 5.39; N, 8.01. The 1H NMR ($CDCl_3$) spectrum of the brown solution gives only broad signals in the expected region, even changing the probe temperature (two peaks at about 2–3 ppm). ^{29}Si NMR ($CDCl_3$): δ +127. ^{13}C NMR ($CDCl_3$): δ 15.0 (CpCH₃), 45.01 (NCH₃), 47.5 (NCH₃), 67.5 (NCH₂), 81.9, 83.1 (C₅H₅), 99.7 (C*CH₃), 125.3–141.7 (aromatics) 235, 237.4 (CO). IR ($CDCl_3$, cm^{-1}): $\nu(CO)$ 1892, 1818. MS [EI, 70 eV; m/e (relative intensity %): 529 (M^+ , 6), 473 (37), 338 (19), 295 (18), 265 (10), 185 (42), 141 (100), 115 (32), 55 (97).

[8-(Me₂NCH₂)C₁₀H₆]-1-C₆H₅Si=MnCp(CO)₂. [8-[(Dimethylamino)methyl]naphthyl]-1-phenylsilanediyl(η^5 -cyclopentadienyl)manganese dicarbonyl (16). mp (powder): 226–227 °C. Yield 62%. Anal. Calcd for $C_{26}H_{23}NSiMnO_2$: C, 67.24; H, 4.95; N, 3.01. Found: C, 67.18; H, 4.83; N, 3.08. 1H NMR ($CDCl_3$): unresolved material. ^{29}Si NMR ($CDCl_3$): δ +125.2. ^{13}C NMR ($CDCl_3$): δ 48.1 (NCH₃), 49.4 (NCH₃), 65.9 (NCH₂), 81.19 (C₅H₅), 124.62–142.46 (aromatics), 234.13, 236.34 (CO). IR ($CDCl_3$, cm^{-1}): $\nu(CO)$ 1888, 1821. MS [EI, 70 eV; m/e (relative intensity %): 464 (M^+ , 11), 408 (20), 288 (15), 245 (28), 215 (18), 184 (26), 141 (45), 79 (53), 55 (100).

Photolysis of Complex 5a with Diphenylacetylene. The freshly prepared complex **5a** (4.01g, 0.01mol) was diluted in 350 mL of toluene followed by addition of diphenylacetylene (8.90 g, 0.05 mol, diluted in 50 mL of toluene) and irradiated at 22 °C. The reaction progress was monitored by IR and TLC. The total irradiation time was 6 h. The solvent was stripped off and the crude mixture was chromatographed on a Florisil column (33 × 2 cm). Elution with pentane furnished unreacted diphenylacetylene as the first fraction. A yellowish sticky solid [2-[(dimethylamino)methyl]phenyl]phenylsilacyclopent-2,4-diene²¹ **17** was obtained as the second fraction with pentane/ether (80/20). Further washing of the column with ether gave tetraphenylcyclobutadieneiron tricarbonyl complex **18**.

[2-[(Dimethylamino)methyl]phenyl]phenylsilacyclopent-2,4 diene (17). Anal. Calcd for C₄₃H₃₇NSi: C, 86.72; H, 6.21; N, 2.35. Found: C, 86.05; H, 6.32; N, 2.56. ²⁹Si NMR (CDCl₃): δ -14.85. ¹³C NMR (CDCl₃): δ 44.01 (NCH₃), 64.83 (NCH₂), 125.2–135.8 (aromatics, C=C). ¹H NMR (CDCl₃): δ 1.52 (s, 6H, NCH₃), 2.61 (s, 2H, NCH₂) 6.8–7.92 (m, 29H, aromatics). MS [EI, 70 eV; *m/e* (relative intensity %): 580 (M⁺ -CH₃, 8), 551 (9), 538 (6), 505 (12), 461 (3), 289 (5), 256 (25), 240 (18), 211 (21), 191 (8), 178 (8), 165 (21), 134 (17), 105 (23), 91 (35), 77 (16), 58 (100).

Photolysis of Complex 5a in the Presence of 2,3-Dimethylbutadiene. A 10-fold excess of 2,3-dimethylbutadiene (8.25 g, 0.1 mol) was injected into a 350-mL toluene solution of freshly prepared complex **5a** (4.01 g, 0.01 mol). This mixture was irradiated at room temperature for 6 h. Toluene was evaporated and resulting mixture was chromatographed on a Florisil column (33 × 2 cm). [2-[(Dimethylamino)methyl]phenyl]phenyl-3,4-dimethylsilacyclopent-2-ene (**19**) was isolated in pentane/ether (90/10) as the first fraction. The second fraction contained 2,3-dimethylbutadieneiron tetracarbonyl complex **20**. Fe₃(CO)₁₂ was also isolated in trace amounts as the third fraction in ether.

19. Yield: 42%. Anal. Calcd for C₂₁H₂₇SiN: C, 78.50; H, 8.41; N, 4.36. Found: C, 78.61; H, 8.30; N, 4.12. ²⁹Si NMR (CDCl₃): δ +3.15. ¹H NMR (CDCl₃): δ 1.21 (d, 3H, CCH₃), 1.79 (s, 9H, C=CCH₃, NCH₃), 1.90 (s, 2H, SiCH₂), 2.70 (br, 1H, CH), 3.36 (s, 2H, NCH₂), 5.8 (s, 1H, C=CH), 7.12–7.80 (m, 9H, aromatics). ¹³C NMR (CDCl₃): δ 20.22 (CH₃), 20.80 (CH₃), 23.45 (SiCH₂), 42.21 (CH), 45.36 (NCH₃), 65.12 (NCH₂), 124.52–146.12 (aromatics, C=C). MS [EI, 70 eV; *m/e* (relative intensity %): 321 (M⁺, 24) 306 (-CH₃, 100), 278 (15), 239 (60), 228 (55), 207 (10), 195 (20).

20. Anal. Calcd for C₉H₁₀FeO₃: C, 48.64; H, 4.54. Found: C, 48.69; H, 4.83. IR (CDCl₃, cm⁻¹): ν(CO) 2043, 1970. MS [EI, 70 eV; *m/e* (relative intensity %): 222 (M⁺, 8), 194 (-CO, 30), 166 (-2CO, 40), 138 (-3CO, 100), 122 (40), 110 (18), 96 (24, 84 (15), 67 (12), 56 (62).

Photolysis of Complex 5a in the Presence of 2,3-Dimethylbutadiene and DPPE. A freshly prepared toluene (300 mL) solution of complex **5a** (4.01 g, 0.01 mol) was treated with 2,3-dimethylbutadiene (4.12 g, 0.05 mol) and transferred to a photochemical reactor. 1,2-Bis(diphenylphosphino)ethane (3.98 g, 0.01 mol) diluted in 50 mL of toluene was then added to this solution, and the mixture was irradiated for 5 h at room temperature. Analysis of the crude product established the formation of **19** and bis(diphenylphosphino)ethaneiron tricarbonyl **22** (by comparison with the authentic product,²² after crystallization) along with trace amounts of complex **20** by ²⁹Si NMR, ³¹P NMR, and mass spectra.

22. mp: 136 °C (dec). Yield: 58%. Anal. Calcd for C₂₉H₂₄P₂FeO₃: C, 64.70; H, 4.46. Found: C, 64.23; H, 4.52. IR (CDCl₃, cm⁻¹): ν(CO) 1980, 1911, 1892. ³¹P NMR (CDCl₃): δ +96.34. MS [EI, 70 eV; *m/e* (relative intensity %): 538 (M⁺, 7), 510 (-CO, 20), 482 (-2CO, 24), 454 (-3CO, 100), 425 (60), 397 (22), 289 (28), 275 (18), 262 (22), 183 (82).

Photolysis of Complex 5a with Alcohols in the Presence of DPPE. To a 300-mL toluene solution of complex **5a** (4.07 g, 0.01 mol), methanol (0.40 mL, 0.01 mol) was injected followed by addition of DPPE (3.98 g, 0.01 mol) diluted in 50

Table 3. Summary of Crystal Data and Details of Intensity Collection for 5a

Crystal Data	
formula	C ₁₉ H ₁₇ FeO ₄ Si
fw	407.3
cryst syst	triclinic
space group	P1 (No. 2)
<i>a</i> , Å	8.284(2)
<i>b</i> , Å	8.404(2)
<i>c</i> , Å	13.497(3)
α, deg	97.02(1)
β, deg	93.68(1)
γ, deg	91.25(1)
cell vol, Å ³	930.3
<i>Z</i> ; <i>d</i> _{calcd} , g cm ⁻³	2; 1.598
<i>F</i> (000)	968
cryst size, mm	0.75 × 0.48 × 0.20
cryst color and habit	colorless plates
Data Collection and Data Reduction	
diffractometer	Enraf-Nonius CAD4
radiation	Mo Kα (λ = 0.710 73 Å)
temp, K	193 ± 3
scan type	ω-scan
scan range, deg	0.75 + 0.30 tan θ
scan time, s	variable; max 60
2θ limits, deg; octants	4.0–50.0; ± <i>h</i> , + <i>k</i> , ± <i>l</i>
reflections collected	3488
no. of refls for ψ-scans	9
<i>m</i> (Mo Kα), cm ⁻¹	8.9
min/max transm factor	0.988/1.000
cryst decay, %	no
Solution and Refinement	
no. of independent data	3171
no. of observed data	3171 (<i>I</i> > 0.00)
no. of refined params	303
<i>R</i> _{merge}	0.009 (<i>F</i> _o)
<i>R</i> ^{<i>a</i>,<i>b</i>} indexes (all data)	<i>R</i> = 0.027, <i>R</i> _w = 0.030
GOF, ^c p	0.6377, 0.00
max/min peak final diff map, e Å ⁻³	0.55/-0.29
max shift/err	<0.001

$$^a R = \sum ||F_o| - |F_c|| / \sum |F_o|. \quad ^b R_w = [\sum w(|F_o| - |F_c|)^2 / \sum w|F_o|^2]^{1/2}. \quad ^c \text{GOF} = [\sum w(|F_o| - |F_c|)^2 / (\text{NO} - \text{NV})]^{1/2}.$$

mL of toluene). This mixture was photolyzed in a 500-mL reactor at room temperature. Removal of solvent furnished a very sticky solid which was chromatographed on a Florisil column. [2-[(Dimethylamino)methyl]phenyl]phenylmethoxysilane (**23**) was obtained as the first fraction by eluting the column with pentane/ether (90/10) in 61% yield. Complex **22** was obtained as the second fraction with pentane/ether (50/50) mixture in 56% yield.

The same molar quantities of complex **5a** and the procedure given above were followed for other trapping experiments with alcohols to obtain product **24** from methanol (0.80 mL, 0.02 mol), product **25** from *tert*-butyl alcohol (1.48 g, 0.02 mol), and product **26** from 2,3-dimethyl 2,3-butanediol (1.18 g, 0.01 mol). Products **23**, **24**, **25**, and **26** were analyzed by ²⁹Si NMR and ¹H NMR and compared with authentic samples.²³ Yields of the products **24**, **25**, and **26** were 57%, 68%, and 79%, respectively. In all the cases, complex **22** was isolated in 55–60% yield.

Photolysis of Complex 3 in the Presence of 2,3-Dimethylbutadiene. Freshly prepared complex **3** (4.64 g, 0.01 mol) was dissolved in 350 mL of toluene, and the solution was transferred to a 500-mL quartz vessel. 2,3-Dimethylbutadiene (11.4 mL, 0.1 mol) was added to this solution. This mixture was irradiated at 22 °C for 5 h. Toluene was evaporated under vacuum, and the black-red product was chromatographed on Florisil (33 × 2 cm) column. Product **30** was isolated in pentane/ether (80/20) as the first fraction in 62% yield. Elution with pentane/ether (50/50) furnished 2,3-dimethylbutadiene iron tetracarbonyl²⁴ (**20**) in 67% yield.

Table 4. Fractional Atomic Coordinates and Equivalent Isotropic Displacement Coefficients for Non-Hydrogen Atoms in 5a

atom	x	y	z	B_{eq}^a (Å ²)
Fe	0.51052(3)	0.28717(4)	0.13495(2)	1.831(5)
Si	0.31787(7)	0.26963(6)	0.24451(4)	1.66(1)
O1	0.7823(2)	0.3005(2)	0.0072(1)	3.60(4)
O2	0.7002(2)	0.0893(2)	0.2602(1)	4.27(4)
O3	0.5006(2)	0.6344(2)	0.1906(1)	3.56(4)
O4	0.2840(2)	0.1581(3)	-0.0321(1)	4.00(4)
N	0.1865(2)	0.0701(2)	0.2299(1)	1.95(3)
C1	0.6749(3)	0.2977(3)	0.0565(2)	2.39(4)
C2	0.6231(3)	0.1660(3)	0.2115(2)	2.76(5)
C3	0.5037(3)	0.4979(3)	0.1699(2)	2.37(4)
C4	0.3715(3)	0.2086(3)	0.0346(2)	2.58(4)
C11	0.3663(3)	0.2343(2)	0.3777(2)	1.96(4)
C12	0.4915(3)	0.2997(3)	0.4453(2)	2.38(4)
C13	0.5002(3)	0.2620(3)	0.5432(2)	2.83(5)
C14	0.3877(3)	0.1574(3)	0.5726(2)	2.85(5)
C15	0.2644(3)	0.0878(3)	0.5061(2)	2.63(4)
C16	0.2538(3)	0.1282(3)	0.4088(2)	2.12(4)
C17	0.1212(3)	0.0648(3)	0.3313(2)	2.39(4)
C18	0.0493(3)	0.0586(3)	0.1513(2)	2.65(4)
C19	0.2916(3)	-0.0711(3)	0.2083(2)	2.47(4)
C21	0.1523(3)	0.4213(2)	0.2513(2)	2.05(4)
C22	0.0907(3)	0.4805(3)	0.1644(2)	2.39(4)
C23	-0.0332(3)	0.5906(3)	0.1679(2)	2.85(5)
C24	-0.0947(3)	0.6451(3)	0.2566(2)	3.29(5)
C25	-0.0335(3)	0.5911(3)	0.3442(2)	3.85(6)
C26	0.0890(3)	0.4806(3)	0.3408(2)	3.11(5)

^a Anisotropically refined atoms are given in the form of the isotropic equivalent displacement parameter: $B_{eq} = (a^2\beta_{11} + b^2\beta_{22} + c^2\beta_{33})$.

30. Anal. Calcd for C₁₈H₂₀Si: C, 81.81; H, 7.57; Si, 10.60. Found: C, 81.84; H, 7.62; Si, 10.54. ²⁹Si NMR (CDCl₃): δ +02. ¹H NMR (CDCl₃): δ 1.58 (s, 6H, CH₃), 1.70 (s, 4H, CH₂) 7.18–7.20, 7.20–8.00 (m, 10H, aromatics). ¹³C NMR (CDCl₃): δ 20.08 (CH₃), 24.64 (CH₂), 128.64, 131.16, 134.44, 134.83 136.63 (aromatics, C=C). MS [EI, 70 eV; *m/e* (relative intensity %): 264 (M⁺, 92), 249 (8), 222 (18), 207 (10), 186(100), 182 (60), 171 (20), 155 (10), 145 (15), 105 (60), 77 (60).

Photolysis of Complex 3 in the Presence of Hex-3-yne. The same procedure and molar quantities of reactants were used. **31** was obtained as the first fraction with ether/pentane (30/70) in 37% yield. Traces of Fe₃(CO)₁₂ were also identified by IR spectroscopy.

24. Anal. Calcd for C₂₄H₃₀Si: C, 83.23; H, 8.67; Si, 8.09. Found: C, 83.18; H, 8.58; Si, 8.23. ²⁹Si NMR (CDCl₃): δ

-19.06. ¹H NMR (CDCl₃): δ 1.15 (t, 12H, CH₃), 2.58 (q, 8H, CH₂), 7.21–7.46 (m, 6H, aromatics), 7.61–7.82 (m, 4H, aromatics). ¹³C NMR (CDCl₃): δ 14.95 (CH₃), 20.12 (CH₂), 128.63, 130.82, 134.78, 145.48 (aromatics), MS [EI, 70 eV; *m/e* (relative intensity %): 346 (M⁺, 20), 319 (78), 278 (40), 264 (20), 235 (58), 221 (45), 207 (25), 182 (10092), 105 (90), 77 (42), 57 (43).

X-ray Data Collection, Structure Solution, and Refinement for [2-[(Dimethylamino)methyl]phenyl]phenylsilanediyliron(0) Tetracarbonyl (5a). Single crystals suitable for single-crystal X-ray structure analysis were grown from CHCl₃/*n*-pentane. A colorless plate-shaped crystal (ca. 0.75 × 0.48 × 0.20 mm) coated in silicon grease was mounted in a glass capillary. Data collection was performed on an Enraf-Nonius CAD4 four-circle diffractometer with graphite-monochromated Mo Kα radiation (λ = 0.710 73 Å) at low temperature (193 ± 3 K). Intensity data for 3488 reflections in the range 2.0° ≤ θ ≤ 25.0° (±*h*,*k*,±*l*) were collected by ω-scan; the maximum scan time amount, *t*_{max}, was 60 s. The intensity data were corrected for Lorentz and polarization effects and for absorption. After merging, all 3171 unique reflections (*I* > 0.0) were used in the refinement. The structure has been solved by direct methods and subsequent full-matrix least-squares refinement cycles and difference Fourier syntheses. All atoms are refined with anisotropic displacement parameters. Hydrogen atoms could be located and were freely refined. Refinement minimized the function Σω(|*F*_o| - |*F*_c|)², where ω = 1/σ² and converged yielding *R*w = 0.030. Residual electron density maxima and minima were 0.55 and -0.29 e Å⁻³. Crystal data and details of data collection are given in Table 3. Atomic coordinates are listed in Table 4. All calculations were performed on a MicroVAX 3100 computer using standard programs.²⁵

Acknowledgment. Helpful corrections of the English by Dr. W. Douglas were greatly appreciated.

Supplementary Material Available: A description of the X-ray single crystal structure determination, including tables of crystal data, data collection, and solution and refinement parameters, atomic coordinates, bond distances and angles, and the thermal parameters (12 pages). Ordering information is given on any current masthead page.

OM940854Q

(25) Scherer, W.; Kiprof, P.; Herdtweck, E.; Schmidt, R. E.; Birkhahn, M.; Massa, W. *STRUX-IV; A Program System to Handle X-ray Data*; TU München und University Marburg, Marburg, Germany, 1985/1987/1994 (includes the programs Multan 11/82, Ortep II, Platon, Schakal, and SDP).

(24) (a) Behrens, H.; Moll, M.; Popp, W.; Seibold, H. J.; Sepp, E.; Wurstl, P. *J. Organomet. Chem.* **1980**, *192*, 389. (b) Busch, M. A.; Clark, R. *Inorg. Chem.* **1975**, *94*, 219.

Synthesis and Reactivity of (η^3 -pentadienyl)Ir(PET₃)₂ and (η^3 -2,4-dimethylpentadienyl)Ir(PET₃)₂¹

John R. Bleeker* and Scott T. Luaders

Department of Chemistry, Washington University, St. Louis, Missouri 63130

Received November 7, 1994[®]

Treatment of [ClIr(PET₃)₂]₂ with potassium pentadienide or potassium 2,4-dimethylpentadienide produces (η^3 -pentadienyl)Ir(PET₃)₂ (**1**) or (η^3 -2,4-dimethylpentadienyl)Ir(PET₃)₂ (**2**) in high yield. In solution, compound **1** exists as a 70:30 equilibrium mixture of *anti*-pentadienyl (**1a**) and *syn*-pentadienyl (**1s**) isomers, while compound **2** exists exclusively in the *anti* form. Both **1a** and **2** undergo a low-energy fluxional process that exchanges the ends of the *anti*- η^3 -pentadienyl ligand via an 18e⁻ η^5 -pentadienyl intermediate. Treatment of **1** and **2** with Lewis bases, L, leads to the formation of known (pentadienyl)Ir(PET₃)₂L complexes. In particular, addition of 1 equiv of PET₃ to **1** and **2** produces ((1,4,5- η -pentadienyl)Ir(PET₃)₃ and *mer*-CH=C(Me)CH=C(Me)CH₂Ir(PET₃)₃(H), respectively, while addition of CO produces ((1,4,5- η -pentadienyl)Ir(PET₃)₂(CO))/((1-3- η -pentadienyl)Ir(PET₃)₂(CO) and ((1,4,5- η)-2,4-dimethylpentadienyl)Ir(PET₃)₂(CO), respectively. Compounds **1** and **2** also react with Lewis acids. Hence, treatment with triflic acid produces (η^5 -pentadienyl)Ir(PET₃)₂(H)⁺O₃SCF₃⁻ (**3**) and (η^5 -2,4-dimethylpentadienyl)Ir(PET₃)₂(H)⁺O₃SCF₃⁻ (**4**), respectively, while treatment with methyl triflate generates (η^5 -pentadienyl)Ir(PET₃)₂(CH₃)⁺O₃SCF₃⁻ (**5**) and (η^5 -2,4-dimethylpentadienyl)Ir(PET₃)₂(CH₃)⁺O₃SCF₃⁻ (**6**), respectively. Compounds **3–6** adopt unsymmetrical structures in which one phosphine resides under a pentadienyl edge while the other phosphine is situated under the pentadienyl mouth. Compound **3** undergoes a fluxional process in solution that involves rotation of the η^5 -pentadienyl ligand with respect to the Ir(PET₃)₂(H) fragment. Under this process, the two phosphines exchange positions and the two ends of the pentadienyl ligand become equivalent. Compounds **3–6** react with bis(triphenylphosphine)nitrogen(1+) chloride (PPN⁺Cl⁻), a source of Cl⁻, to produce (*syn*- η^3 -pentadienyl)Ir(PET₃)₂(H)(Cl) (**7**), (*syn*- η^3 -2,4-dimethylpentadienyl)Ir(PET₃)₂(H)(Cl) (**8**), (*syn*- η^3 -pentadienyl)Ir(PET₃)₂(CH₃)(Cl) (**9**), and (*syn*- η^3 -2,4-dimethylpentadienyl)Ir(PET₃)₂(CH₃)(Cl) (**10**), respectively. In these compounds, the phosphine ligands are situated *trans* to the pentadienyl ligands.

Introduction

During the past decade, there has been increasing interest in the chemistry of transition-metal complexes containing the acyclic pentadienyl ligand.² In part, this interest has been spurred by the pentadienyl ligand's ability to adopt a variety of bonding modes (including η^5 , η^3 , and η^1 modes) and expectations that interconversions between these bonding modes will lead to interesting chemistry. We now report the synthesis of a pair of (pentadienyl)iridium bis(phosphine) complexes whose solution-phase dynamic behavior and reaction chemistry illustrate the key role of facile pentadienyl ligand isomerizations.

Results and Discussion

A. Synthesis and Dynamic Behavior of (η^3 -pentadienyl)Ir(PET₃)₂ (1**) and (η^3 -2,4-dimethylpentadienyl)Ir(PET₃)₂ (**2**).** Treatment of [ClIr(PET₃)₂]₂³ with 2 equiv of potassium pentadienide⁴ or potassium 2,4-dimethylpentadienide⁴ leads to the production of

16e⁻ (η^3 -pentadienyl)Ir(PET₃)₂ (**1**) or (η^3 -2,4-dimethylpentadienyl)Ir(PET₃)₂ (**2**)⁵ in essentially quantitative yield (see Scheme 1). At room temperature, **1** exists as a 70:30 equilibrium mixture of *anti* (**1a**) and *syn* (**1s**) isomers, while **2** exists exclusively in the *anti* form. The *anti* and *syn* isomers can be readily distinguished by the chemical shift of the H3 proton; H3 for the *anti* isomer is less shielded by the metal center and appears substantially downfield from H3 for the *syn* isomer.⁶

In solution, both **1** and **2** exhibit dynamic behavior. The ¹H NMR spectrum of **2** at room temperature consists of just four pentadienyl signals (H1_{outer}/H5_{outer}, H1_{inner}/H5_{inner}, H3, and the pentadienyl methyl groups) due to a rapid "end-to-end" fluxional process that exchanges the two sides of the pentadienyl ligand via

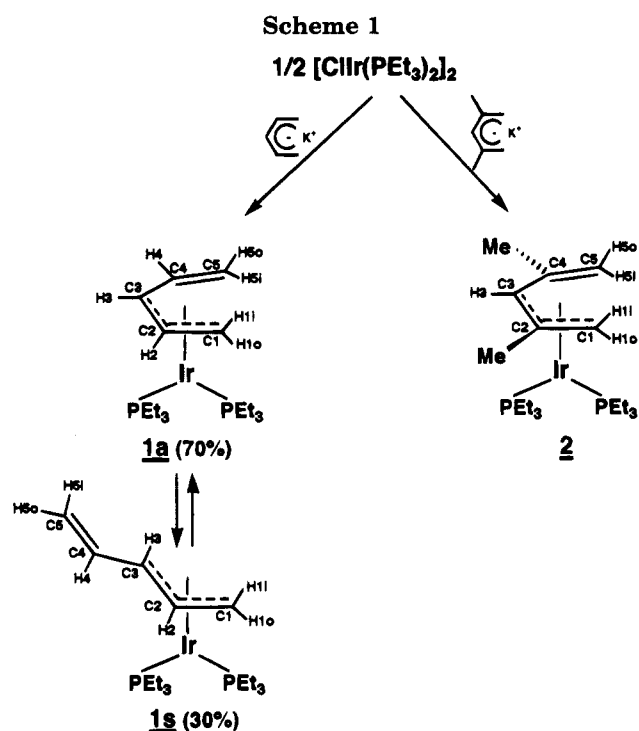
(3) (a) This species was synthesized by reacting [(cyclooctene)₂IrCl]₂^{3b} with 4 equiv of PET₃. (b) Herde, J. L.; Lambert, J. C.; Senoff, C. V. In *Inorganic Syntheses*; Parrshall, G. W., Ed.; McGraw-Hill: New York, 1974; Vol. 15, pp 18–20.

(4) Yasuda, H.; Ohnuma, Y.; Yamauchi, M.; Tani, H.; Nakamura, A. *Bull. Chem. Soc. Jpn.* **1979**, *52*, 2036.

(5) Earlier, we reported the synthesis of the analogous rhodium compound. See: Bleeker, J. R.; Donaldson, A. J. *Organometallics* **1986**, *5*, 2401.

(6) It is typical for "outer" allyl protons (such as H3 in **1a**) to resonate downfield from "inner" allyl protons (such as H3 in **1s**). This effect is usually attributed to the inner protons' closer proximity to the metal center: Collman, J. P.; Hegedus, L. S.; Norton, J. R.; Finke, R. G. *Principles and Applications of Organotransition Metal Chemistry*; University Science Books: Mill Valley, CA, 1987; pp 175–180.

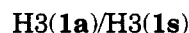
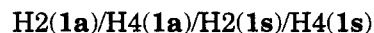
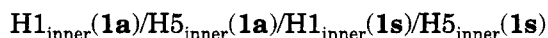
[®] Abstract published in *Advance ACS Abstracts*, February 15, 1995.
(1) Pentadienyl–Metal–Phosphine Chemistry. 28. Part 27: Bleeker, J. R.; Luaders, S. T.; Robinson, K. D. *Organometallics* **1994**, *13*, 1592.
(2) For leading reviews, see: (a) Ernst, R. D. *Chem. Rev.* **1988**, *88*, 1251. (b) Yasuda, H.; Nakamura, A. *J. Organomet. Chem.* **1985**, *285*, 15. (c) Powell, P. *Adv. Organomet. Chem.* **1986**, *26*, 125.



an η^5 -pentadienyl intermediate⁷ (see Scheme 2).⁸ Similarly, in the $^{13}\text{C}\{^1\text{H}\}$ NMR spectrum, only four pentadienyl signals are observed at room temperature: C1/C5, C2/C4, C3, and the pentadienyl methyl groups. The signals due to C1/C5 and C2/C4 are quite broad but sharpen upon heating to 50 °C. However, as the sample is cooled and the fluxional process is slowed, the ^1H NMR signals due to H1_{outer}/H5_{outer}, H1_{inner}/H5_{inner}, and the pentadienyl methyl groups begin to "decoalesce", ultimately disappearing into the base line at -60 °C. Temperatures cold enough to observe reemergence of separate signals due to H1_{outer}, H5_{outer}, H1_{inner}, H5_{inner}, and the pentadienyl methyl groups could not be achieved. In the $^{13}\text{C}\{^1\text{H}\}$ NMR spectrum, a similar decoalescence is observed upon cooling, and separate peaks due to C1, C5, C2, and C4 do reemerge at -80 °C. From this behavior, the free energy of activation, ΔG^\ddagger , for the end-to-end fluxional process in **2** is calculated to be 9.5 ± 0.5 kcal/mol. It should be noted that H3 and C3 are not affected by this process and hence their signals remain sharp over the entire temperature regime studied. Likewise, the phosphine ligands do not exchange under this process; one (P1 in Scheme 2) remains under the pentadienyl edges while the other (P2) remains under the open pentadienyl mouth. Hence, separate ^{31}P , ^1H , and ^{13}C NMR signals are observed for the two PEt_3 groups at all temperatures.

The NMR spectra for **1** are somewhat more complicated because of the presence of both *anti* (**1a**) and *syn*

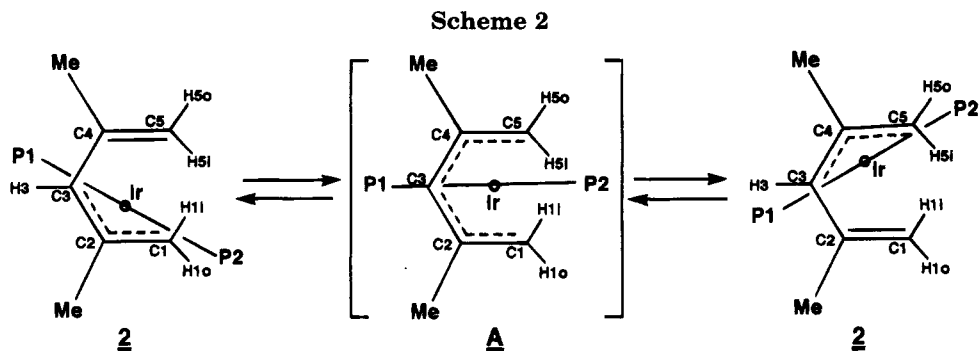
(**1s**) isomers. At room temperature, **1a** and **1s** are interconverting, probably via the mechanism outlined in Scheme 3, which involves sickle-shaped pentadienyl intermediates.⁹ This interconversion, together with a rapid end-to-end fluxional process in the *anti* isomer (cf. Scheme 2), causes the following signals to coalesce:



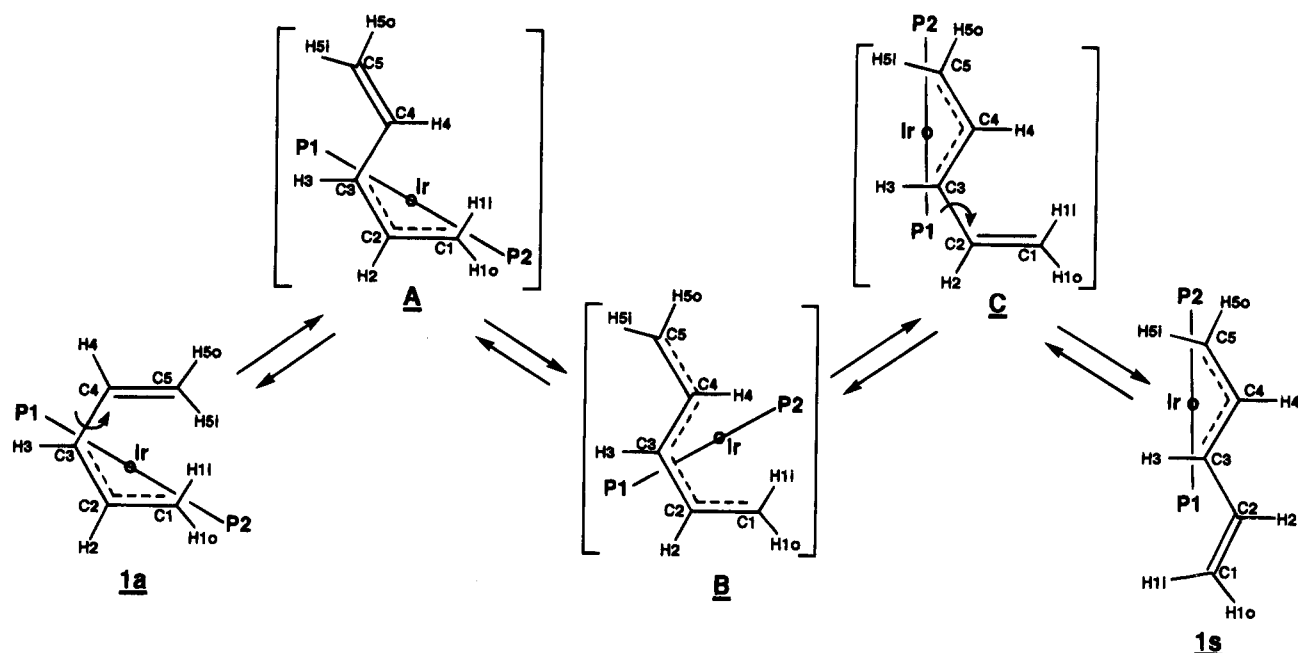
Therefore, at room temperature, the ^1H NMR spectrum of **1** consists of just four broad signals in the pentadienyl region. As the sample is cooled to -30 °C, the *anti* \rightleftharpoons *syn* interconversion slows down, causing the signals due to **1s** to decoalesce from those due to **1a**. Since **1s** does not undergo end-to-end exchange at this temperature, seven separate signals are observed for its seven inequivalent protons. However, at -30 °C, **1a** continues to undergo rapid end-to-end exchange and, therefore, only four ^1H NMR signals (H1_{outer}/H5_{outer}, H1_{inner}/H5_{inner}, H2/H4, and H3) are observed for it in the pentadienyl region. As the sample is cooled from -30 to -80 °C, the signals due to **1a** broaden somewhat but never fully decoalesce. On the basis of this behavior, ΔG^\ddagger for the end-to-end fluxional process in **1a** is calculated to be less than 7.5 kcal/mol.

The interconversion of *anti* and *syn* isomers can also be conveniently monitored in the $^{31}\text{P}\{^1\text{H}\}$ NMR spectrum. Each isomer exhibits two peaks in the $^{31}\text{P}\{^1\text{H}\}$ NMR spectrum due to the two inequivalent phosphine ligands: the edge phosphines (P1 in Scheme 3) and the mouth phosphines (P2). At room temperature, all four signals are observable, although each of the *anti* signals is beginning to coalesce with one of the *syn* signals. As the temperature is raised to 50 °C, coalescence progresses until only two signals are observed—one for the edge phosphines of **1a** and **1s** and one for the mouth phosphines of the two isomers. Cooling the sample below room temperature causes the signals to decoalesce; at -80 °C, the stopped-exchange spectrum of four very sharp peaks is observed.

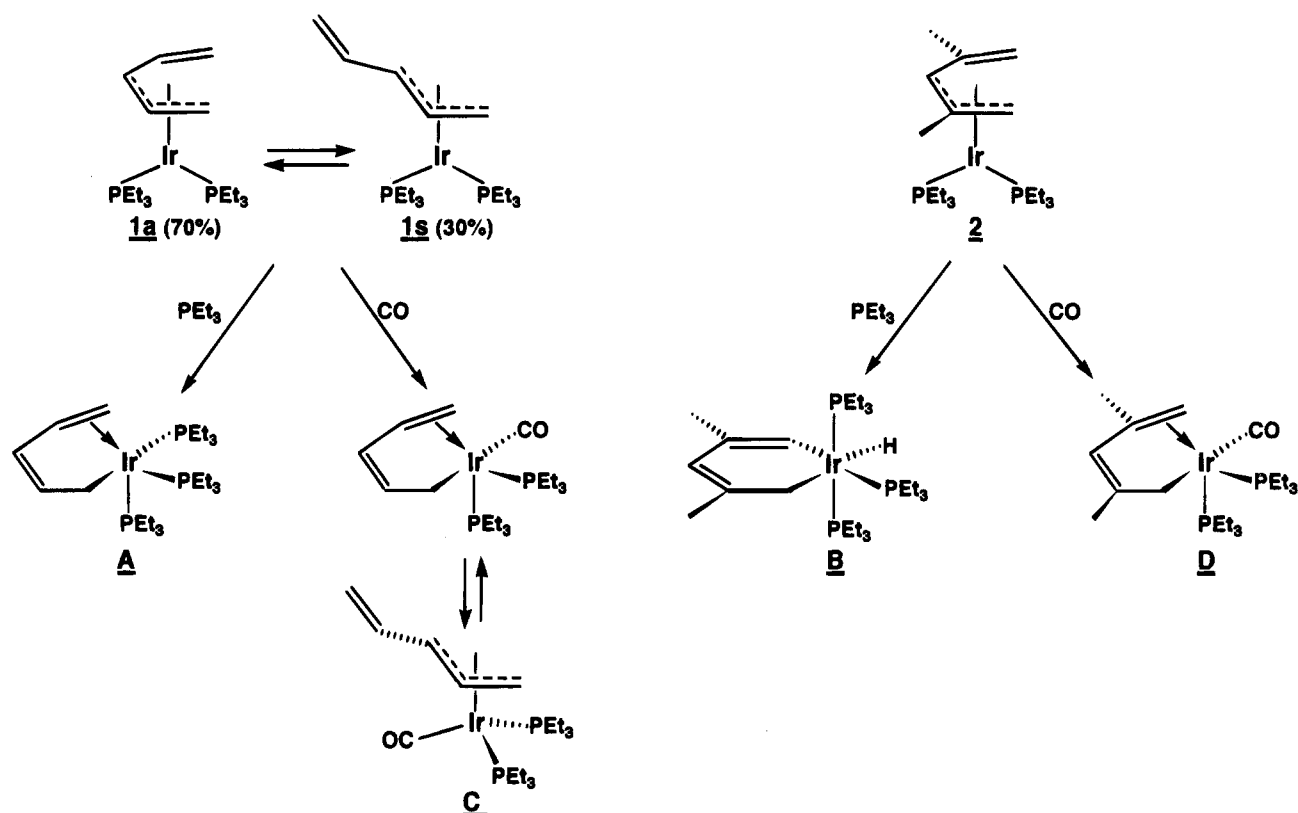
B. Reactions of Compounds 1 and 2 with Lewis Bases. Not surprisingly, $16e^-$ compounds **1** and **2** react readily with $2e^-$ donor reagents, such as PEt_3 and carbon monoxide, to produce $18e^-$ species. As shown in Scheme 4, addition of PEt_3 to **1** yields ((1,4,5- η)-pentadienyl)Ir(PEt_3)₃ (**A**) instantaneously at room temperature. Addition of PEt_3 to **2** is a slower reaction but ultimately yields the iridacycle *mer*- $\text{CH}=\text{C}(\text{Me})\text{CH}=\text{C}$ -



Scheme 3



Scheme 4



(Me)₂CH₂Ir(PEt₃)₃(H) (**B**) via a C–H bond activation process. Similarly, treatment of **1** with CO leads to an equilibrium mixture of ((1,4,5-η)-pentadienyl)Ir(PEt₃)₂(CO) and ((1-3-η)-pentadienyl)Ir(PEt₃)₂(CO) (**C**), while treatment of **2** with CO produces exclusively ((1,4,5-η)-2,4-dimethylpentadienyl)Ir(PEt₃)₂(CO) (**D**). All of these

(7) A similar fluxional process operates in the analogous rhodium system⁵ and in a series of isoelectronic (η³-cycloheptadienyl)PdL₂⁺ complexes (Mann, B. E.; Maitlis, P. M. *J. Chem. Soc., Chem. Commun.* **1976**, 1058).

(8) In Scheme 2, compound **2** and the proposed η⁵-pentadienyl intermediate (**A**) are drawn in projection to show the orientation of the pentadienyl ligand with respect to the Ir(PEt₃)₂ fragment.

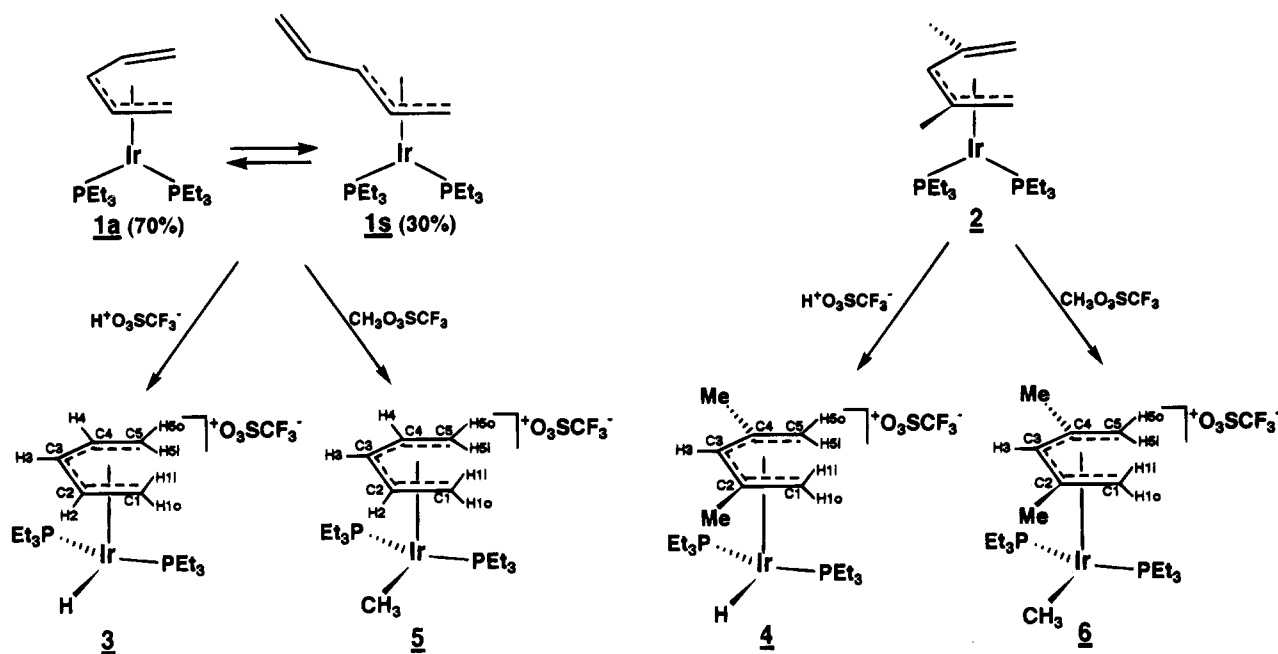
species have previously been isolated from the reactions of ClIr(PEt₃)₃ or ClIr(PEt₃)₂(CO) with potassium pentadienide or potassium 2,4-dimethylpentadienide.¹⁰

C. Reactions of Compounds 1 and 2 with Lewis Acids. Compounds **1** and **2** also react cleanly with electrophiles. As shown in Scheme 5, treatment of **1** and **2** with 1 equiv of triflic acid leads to electrophilic

(9) This "haptotropic rearrangement" has been examined theoretically for the isoelectronic (but hypothetical) species (η³-pentadienyl)Pt(PH₃)₂⁺: Silvestre, J.; Albright, T. A. *J. Am. Chem. Soc.* **1985**, *107*, 6829.

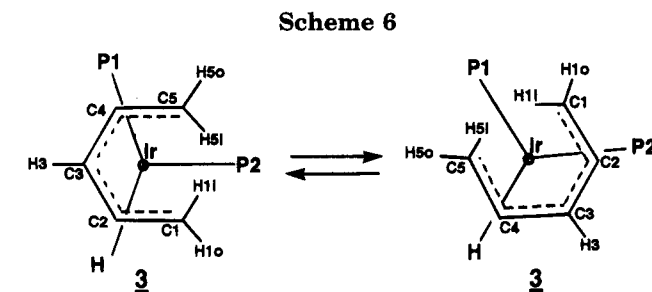
(10) (a) Bleeke, J. R.; Peng, W.-J. *Organometallics* **1987**, *6*, 1576. (b) Bleeke, J. R.; Boorsma, D.; Chiang, M. Y.; Clayton, T. W. Jr.; Haile, T.; Beatty, A. M.; Xie, Y.-F. *Organometallics* **1991**, *10*, 2391.

Scheme 5



attack at the electron-rich iridium center and isomerization of the pentadienyl ligand to the η^5 bonding mode, yielding the $18e^-$ cationic complexes (η^5 -pentadienyl)Ir(PEt₃)₂(H)⁺O₃SCF₃⁻ (**3**) and (η^5 -2,4-dimethylpentadienyl)Ir(PEt₃)₂(H)⁺O₃SCF₃⁻ (**4**), respectively.¹¹ Similarly, compounds **1** and **2** react cleanly with methyl triflate to produce compounds **5** and **6**, the methyl analogues of **3** and **4**. All of these compounds possess the unsymmetrical structure shown in Scheme 5, in which one of the PEt₃ ligands resides in the unique site under the open pentadienyl mouth, while the hydride or methyl ligand and the other PEt₃ group occupy the remaining sites under the pentadienyl edges. This ligand orientation is apparent from the ³¹P{¹H} NMR spectra of **3**–**6**, wherein the two phosphines give rise to separate signals. The unsymmetrical structure is also reflected in the ¹H and ¹³C{¹H} NMR spectra, where distinct signals are observed for the phosphine ligands and for each of the pentadienyl hydrogen and carbon atoms, although the signals for **3** are broad (*vide infra*). The hydride ligands in **3** and **4** resonate in the characteristic upfield region of the ¹H NMR spectrum (δ –16.5 for **3** and δ –17.3 for **4**) and in each case appear as a pseudotriplet due to coupling to the ³¹P centers of the phosphine ligands. Similarly, the methyl ligands in **5** and **6** give rise to characteristic upfield pseudotriplets at δ 0.5 and 0.2 in the ¹H NMR spectra.

As mentioned above, the ¹H NMR spectrum of **3** at room temperature exhibits broad signals in both the phosphine and pentadienyl regions; only the H3 peak is a sharp triplet. Likewise in the ¹³C{¹H} NMR spectrum, only the C3 signal is sharp. We believe that this broadening is caused by a fluxional process that involves rotation of the η^5 -pentadienyl ligand with respect to the Ir(PEt₃)₂(H) fragment (see Scheme 6).¹² Under this process, the two phosphines exchange positions and the two ends of the pentadienyl ligand become



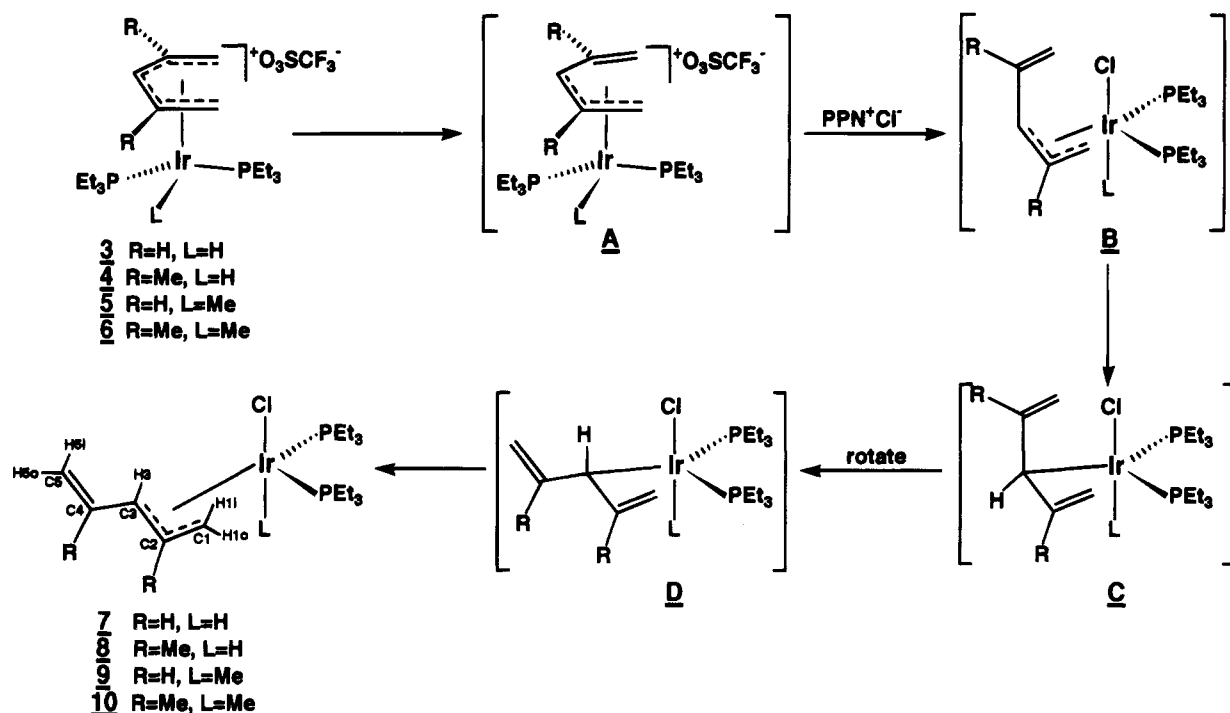
equivalent. Of course, H3 and C3 are unaffected by this process. When the sample is heated to 50 °C in *d*₆-acetone, additional line broadening occurs, although full coalescence of the exchanging signals is not achieved before the sample decomposes. Cooling the sample to –20 °C halts the fluxional process, and sharp stopped-exchange spectra are obtained. On the basis of this variable-temperature NMR behavior, ΔG^\ddagger for pentadienyl ligand rotation in **3** must exceed 16 kcal/mol. Unlike **3**, compounds **4**–**6** show no NMR signal broadening at room temperature.

D. Nucleophilic Addition of Cl⁻ to Cationic Compounds **3–**6**.** Cationic compounds **3**–**6** all undergo clean nucleophilic addition at iridium when treated with Cl⁻ (from bis(triphenylphosphine)nitrogen(1+) chloride) to produce (*syn*- η^3 -pentadienyl)Ir(PEt₃)₂(H)(Cl) (**7**), (*syn*- η^3 -2,4-dimethylpentadienyl)Ir(PEt₃)₂(H)(Cl) (**8**), (*syn*- η^3 -pentadienyl)Ir(PEt₃)₂(CH₃)(Cl) (**9**), and (*syn*- η^3 -2,4-dimethylpentadienyl)Ir(PEt₃)₂(CH₃)(Cl) (**10**), respectively (see Scheme 7). The *syn* geometry of the pentadienyl ligands in compounds **7**–**10** has been confirmed by carrying out NOESY (2D NOE) experiments. In each case, correlations are observed between H1_{inner} and H3, requiring a ligand geometry in which

(11) Similar metal-centered protonations are observed in the analogous rhodium system but are followed by rapid migration of the hydride ligand to the pentadienyl ligand: Bleeke, J. R.; Donaldson, A. J. *Organometallics* **1988**, *7*, 1588.

(12) Similar fluxional processes have been observed in other (η^5 -pentadienyl)metal complexes. See, for example: (a) Bleeke, J. R.; Stanley, G. G.; Kotyk, J. J. *Organometallics* **1986**, *5*, 1642. (b) Bleeke, J. R.; Moore, D. A. *Inorg. Chem.* **1986**, *25*, 3522. (c) Bleeke, J. R.; Hays, M. K.; Wittenbrink, R. J. *Organometallics* **1988**, *7*, 1417. (d) Bleeke, J. R.; Rauscher, D. J. *Organometallics* **1988**, *7*, 2328. (e) Newbound, T. D.; Stahl, L.; Ziegler, M. L.; Ernst, R. D. *Organometallics* **1990**, *9*, 2962. (f) Lin, W.-J.; Lee, G.-H.; Peng, S.-M.; Liu, R.-S. *Organometallics* **1991**, *10*, 2519.

Scheme 7



these protons reside in close proximity. The orientation of the phosphine ligands *trans* to the pentadienyl ligands in 7–10 has been unequivocally established by the observation of substantial C–P coupling (~ 30 Hz) on pentadienyl carbons C1 and C3 in the $^{13}\text{C}\{^1\text{H}\}$ NMR spectra.

As outlined in Scheme 7, these nucleophilic addition reactions probably proceed through the intermediacy of $16e^-$ (*anti*- η^3 -pentadienyl)Ir(PET₃)₂(L)⁺ (L = H, CH₃) species (A), which are attacked by Cl⁻. The resulting *anti* isomers of compounds 7–10 (B; Scheme 7) then rearrange to the *syn* isomers via C3-bound η^1 -pentadienyl intermediates (C and D; Scheme 7).¹³ In fact, when these reactions are monitored by NMR, the *anti* isomers (B) can be observed as intermediates, but these species cleanly convert to the thermodynamically preferred *syn* isomers over the course of several hours (compounds 9 and 10) or days (compounds 7 and 8).

Summary

(pentadienyl)Ir(PET₃)₂ (1) and (2,4-dimethylpentadienyl)Ir(PET₃)₂ (2) adopt $16e^-$ ground-state structures in which the pentadienyl ligands are coordinated to iridium in an η^3 fashion. However, low-energy fluxional processes involving $18e^-$ (η^5 -pentadienyl)Ir(PET₃)₂ intermediates occur in solution. Because compounds 1 and 2 are formally unsaturated ($16e^-$), they react readily with Lewis bases such as PET₃ and CO. However, they also possess electron-rich metal centers and are reactive toward Lewis acids such as triflic acid and methyl triflate. The cationic products of these Lewis acid reactions undergo nucleophilic attack at iridium by Cl⁻. Pentadienyl ligand interconversions play two key roles in this chemistry: (a) generating reactive sites at the metal center and (b) stabilizing intermediates and products.

(13) Similar $\eta^3 \rightleftharpoons \eta^1 \rightleftharpoons \eta^3$ interconversions are common in allyl-metal chemistry.⁶

Experimental Section

General Procedures. All manipulations were carried out under an atmosphere of purified nitrogen in a Vacuum Atmospheres drybox or by standard Schlenk techniques. Solvents were stored under nitrogen after being distilled from appropriate drying agents. [(cyclooctene)₂IrCl]₂,^{3b} potassium pentadienide–tetrahydrofuran,⁴ and potassium 2,4-dimethylpentadienide–tetrahydrofuran⁴ were synthesized using the literature methods. Triethylphosphine (Strem), carbon monoxide (Air Products), triflic acid (Aldrich), methyl triflate (Aldrich), and bis(triphenylphosphine)nitrogen(1+) chloride (PPN⁺Cl⁻; Aldrich) were used as received.

NMR experiments were generally performed on a Varian XL-300 spectrometer (¹H, 300 MHz; ¹³C, 75 MHz; ³¹P, 121 MHz). ¹H and ¹³C spectra were referenced to tetramethylsilane, while ³¹P spectra were referenced to external H₃PO₄. In most cases, ¹H assignments were made on the basis of COSY (¹H–¹H correlation spectroscopy) experiments, while ¹³C assignments were made using HMQC (¹³C–¹H heteronuclear correlation spectroscopy) data. High-resolution MS data were obtained on a VG ZAB-SE mass spectrometer. Microanalysis were performed by Galbraith Laboratories, Inc., Knoxville, TN.

Synthesis of (η^3 -pentadienyl)Ir(PET₃)₂ (1). Under nitrogen, [(cyclooctene)₂IrCl]₂ (0.50 g, 5.6×10^{-4} mol) was dissolved in 50 mL of tetrahydrofuran (THF). To this solution was added 4 equiv of triethylphosphine (0.26 g, 2.2×10^{-3} mol), generating an orange solution of [(PET₃)₂IrCl]₂. After removal of the volatiles (THF and cyclooctene) under vacuum, the residue was redissolved in 50 mL of THF. Potassium pentadienide–tetrahydrofuran (0.20 g, 1.1×10^{-3} mol) in 50 mL of THF was then added, causing the solution to turn dark red. After removal of the solvent under vacuum, the dark red residue was extracted with pentane and filtered through Celite. Removal of the pentane under vacuum yielded 0.46 g (83%) of compound 1 as a red oil. In solution, 1 existed as a 70:30 mixture of *anti* (1a) and *syn* (1s) isomers. HRMS: exact mass calcd for C₁₇H₃₇¹⁹³IrP₂ 496.200, found 496.202.

Room-Temperature NMR Data for Equilibrating Isomers 1a and 1s. Please refer to Scheme 1 for NMR atom

labels. ^1H NMR (C_6D_6 , 22 °C): δ 4.92 (br m, 2, H₂/H₄), 4.63 (br m, 1, H₃), 3.86 (br m, 2, H₁_{outer}/H₅_{outer}), 3.44 (br m, 2, H₁_{inner}/H₅_{inner}), 1.84–1.55 (br m, 12, PEt_3 CH₂'s), 1.08–0.72 (br m, 18, PEt_3 CH₃'s). $^{13}\text{C}\{^1\text{H}\}$ NMR (C_6D_6 , 22 °C): δ 114.0 (br m, C₂/C₄), 71.6 (br m, C₁/C₅), 64.9 (d, $J_{\text{C-P}}$ = 20.3 Hz, C₃), 23.2–20.0 (br m, PEt_3 CH₂'s), 9.0 (br s, PEt_3 CH₃'s). $^{31}\text{P}\{^1\text{H}\}$ NMR (C_6D_6 , 22 °C): δ 11.7, 10.9 (br humps, 1, PEt_3), 8.5, 7.6 (br humps, 1, PEt_3).

Low-Temperature NMR Data for Isomer 1a (70%). ^1H NMR ($\text{C}_6\text{D}_5\text{CD}_3$, -80 °C): δ 4.91 (m, 2, H₂/H₄), 4.58 (m, 1, H₃), 3.83 (m, 2, H₁_{outer}/H₅_{outer}), 3.42 (br m, 2, H₁_{inner}/H₅_{inner}), 1.81–1.45 (m, 12, PEt_3 CH₂'s), 1.05–0.65 (m, 18, PEt_3 CH₃'s). $^{31}\text{P}\{^1\text{H}\}$ NMR ($\text{C}_6\text{D}_5\text{CD}_3$, -80 °C): δ 11.5 (s, 1, PEt_3), 7.2 (s, 1, PEt_3).

Low-Temperature NMR Data for Isomer 1s (30%). ^1H NMR ($\text{C}_6\text{D}_5\text{CD}_3$, -80 °C): δ 6.39 (m, 1, H₄), 5.17 (m, 1, H₅), 4.98 (m, 1, H₅), 4.42 (m, 1, H₂), 3.32 (m, 1, H₃), 3.17 (m, 1, H₁_{outer}), 2.14 (m, 1, H₁_{inner}), 1.81–1.45 (m, 12, PEt_3 CH₂'s), 1.05–0.65 (m, 18, PEt_3 CH₃'s). $^{31}\text{P}\{^1\text{H}\}$ NMR ($\text{C}_6\text{D}_5\text{CD}_3$, -80 °C): δ 10.7 (s, 1, PEt_3), 8.3 (s, 1, PEt_3).

Synthesis of (η^3 -2,4-dimethylpentadienyl)Ir(PEt_3)₂ (2). A procedure identical with that described above for 1 was employed, except that potassium 2,4-dimethylpentadienide-tetrahydrofuran (0.23 g, 1.1×10^{-3} mol) was used in place of potassium pentadienide. The yield of 2 as an orange oil was 0.50 g (85%). HRMS: exact mass calcd for $\text{C}_{19}\text{H}_{41}^{193}\text{IrP}_2$ 524.232, found 524.230. Please refer to Scheme 1 for NMR atom labels. ^1H NMR (C_6D_6 , 20 °C): δ 4.16 (s, 1, H₃), 3.76 (s, 2, H₁_{outer}/H₅_{outer}), 3.67 (s, 2, H₁_{inner}/H₅_{inner}), 1.85 (s, 6, pentadienyl CH₂'s), 1.77–1.56 (m, 12, PEt_3 CH₂'s), 1.00–0.87 (m, 18, PEt_3 CH₃'s). $^{13}\text{C}\{^1\text{H}\}$ NMR (C_6D_6 , 20 °C): δ 125.3 (s, C₂/C₄), 76.6 (s, C₁/C₅), 68.5 (dd, $J_{\text{C-P}}$ = 26.0 Hz, 3.5 Hz, C₃), 26.8 (s, pentadienyl CH₂'s), 22.2 (d, $J_{\text{C-P}}$ = 29.0 Hz, PEt_3 CH₂), 20.6 (d, $J_{\text{C-P}}$ = 27.7 Hz, PEt_3 CH₂), 9.0 (s, PEt_3 CH₃), 8.9 (s, PEt_3 CH₃). $^{13}\text{C}\{^1\text{H}\}$ NMR ($\text{C}_6\text{D}_5\text{CD}_3$, -80 °C, selected peaks): δ 149 (br s, C₄), 106 (br s, C₅), 101 (br s, C₂), 68.5 (dd, $J_{\text{C-P}}$ = 26.0 Hz, 3.5 Hz, C₃), 46 (br s, C₁). $^{31}\text{P}\{^1\text{H}\}$ NMR (C_6D_6 , 20 °C): δ 11.6 (s, 1, PEt_3), 8.5 (s, 1, PEt_3).

Reaction of Compound 1 with PEt_3 . Compound 1 (0.20 g, 4.0×10^{-4} mol) was dissolved in 1 mL of *d*₆-benzene in an NMR tube, and PEt_3 (0.05 g, 4.0×10^{-4} mol) was added, causing the solution color to change rapidly from dark red to yellow. NMR spectroscopy showed quantitative conversion to ((1,4,5- η)-pentadienyl)Ir(PEt_3)₃, which we reported previously.¹⁰

Reaction of Compound 2 with PEt_3 . Compound 2 (0.20 g, 3.8×10^{-4} mol) was dissolved in 1 mL of *d*₆-benzene in an NMR tube, and PEt_3 (0.05 g, 3.8×10^{-4} mol) was added. NMR monitoring showed a slow conversion to *mer*- $\text{CH}=\text{C}(\text{Me})-\text{CH}=\text{C}(\text{Me})\text{CH}_2\text{Ir}(\text{PEt}_3)_3(\text{H})$, which we reported earlier.¹⁰ After 20 h, the reaction was 90% complete.

Reaction of Compound 1 with CO. Carbon monoxide was bubbled into a stirred solution of compound 1 (0.20 g, 4.0×10^{-4} mol) in 50 mL of tetrahydrofuran. Within several minutes, the solution color changed from dark red to yellow-orange. After removal of the volatiles under vacuum, the solid residue was extracted with pentane and filtered through Celite. Removal of the pentane under vacuum yielded 0.15 g (72%) of the previously reported equilibrium mixture of ((1,4,5- η)-pentadienyl)Ir(PEt_3)₂CO and ((1-3- η)-pentadienyl)Ir(PEt_3)₂(CO).¹⁰

Reaction of Compound 2 with CO. Carbon monoxide was bubbled into a stirred solution of compound 2 (0.20 g, 3.8×10^{-4} mol) in 50 mL of tetrahydrofuran. Within several minutes, the solution color changed from orange to light yellow. A workup procedure similar to that described above (Reaction of Compound 1 with CO) yielded 0.18 g (86%) of ((1,4,5- η)-2,4-dimethylpentadienyl)Ir(PEt_3)₂(CO), which we reported earlier.¹⁰

Synthesis of (η^5 -pentadienyl)Ir(PEt_3)₂(H)⁺O₃SCF₃⁻ (3). Compound 1 (0.20 g, 4.0×10^{-4} mol) was dissolved in 20 mL of diethyl ether, and the solution was cooled to -30 °C. Cold

(-30 °C) triflic acid (0.06 g, 4.0×10^{-4} mol) was added, and the solution was stirred briefly. Addition of 20 mL of pentane caused 3 to precipitate out of the solution as a white solid. After removal of the solvent by decantation, the solid was washed with diethyl ether and pentane and dried under vacuum. Yield: 0.16 g (62%). Anal. Calcd for $\text{C}_{18}\text{H}_{38}\text{F}_3\text{IrO}_3\text{P}_2\text{S}$: C, 33.48; H, 5.94. Found: C, 33.18; H, 5.86. Please refer to Scheme 5 for NMR atom labels. ^1H NMR ($(\text{CD}_3)_2\text{CO}$, 0 °C): δ 6.16 (m, 1, H₃), 6.03 (br m, 1, H₂), 5.76 (br m, 1, H₄), 4.30 (m, 1, H₅_{outer}), 3.20 (m, 1, H₁_{outer}), 1.99 (m, 1, H₅_{inner}), 0.95 (m, 1, H₁_{inner}), 2.45–1.75 (m, 12, PEt_3 CH₂'s), 1.38–0.78 (m, 18, PEt_3 CH₃'s), -16.50 (t, $J_{\text{H-P}}$ = 20.0 Hz, 1, Ir-H). $^{13}\text{C}\{^1\text{H}\}$ NMR ($(\text{CD}_3)_2\text{CO}$, 0 °C): δ 103.7 (s, C₄), 100.7 (s, C₂), 91.1 (d, $J_{\text{C-P}}$ = 9.1 Hz, C₃), 58.9 (s, C₅), 43.1 (d, $J_{\text{C-P}}$ = 25.5 Hz, C₁), 22.6 (d, $J_{\text{C-P}}$ = 36.5 Hz, PEt_3 CH₂'s), 21.6 (d, $J_{\text{C-P}}$ = 34.6 Hz, PEt_3 CH₂'s), 8.4 (s, PEt_3 CH₃'s), 8.1 (s, PEt_3 CH₃'s). $^{31}\text{P}\{^1\text{H}\}$ NMR ($(\text{CD}_3)_2\text{CO}$, 0 °C): δ 4.9 (br s, 1, PEt_3), -6.4 (br s, 1, PEt_3).

Synthesis of (η^5 -2,4-dimethylpentadienyl)Ir(PEt_3)₂(H)⁺O₃SCF₃⁻ (4). Compound 2 (0.50 g, 9.6×10^{-4} mol) was dissolved in 20 mL of diethyl ether and cooled to -30 °C. Cold (-30 °C) triflic acid (0.14 g, 9.6×10^{-4} mol) was added to the solution, and upon swirling, compound 4 began to precipitate out as a white solid. To complete the precipitation, the solution was stored at -30 °C for ~20 h. After removal of the solvent by decantation, the solid was washed with diethyl ether and pentane and dried under vacuum. Yield: 0.48 g (74%). Anal. Calcd for $\text{C}_{20}\text{H}_{42}\text{F}_3\text{IrO}_3\text{P}_2\text{S}$: C, 35.65; H, 6.30. Found: C, 34.28; H, 6.31. Please refer to Scheme 5 for NMR atom labels. ^1H NMR ($(\text{CD}_3)_2\text{CO}$, 20 °C): δ 6.22 (s, 1, H₃), 4.02 (s, 1, H₅_{outer}), 3.33 (s, 1, H₁_{outer}), 2.61 (s, 3, pentadienyl CH₂), 2.56 (s, 3, pentadienyl CH₂), 2.20 (m, 6, PEt_3 CH₂'s), 1.98 (s, 1, H₅_{inner}), 1.89 (m, 6, PEt_3 CH₂'s), 1.06 (m, 18, PEt_3 CH₃'s), 0.88 (s, 1, H₁_{inner}), -17.28 (t, $J_{\text{H-P}}$ = 21.4 Hz, 1, Ir-H).

$^{13}\text{C}\{^1\text{H}\}$ NMR ($(\text{CD}_3)_2\text{CO}$, 20 °C): δ 121.8 (s, C₄ or C₂), 117.5 (s, C₂ or C₄), 91.2 (d, $J_{\text{C-P}}$ = 10.1 Hz, C₃), 56.4 (s, C₅), 46.5 (d, $J_{\text{C-P}}$ = 28.4 Hz, C₁), 27.6 (s, pentadienyl CH₂), 26.0 (s, pentadienyl CH₂), 22.3 (d, $J_{\text{C-P}}$ = 31.4 Hz, PEt_3 CH₂'s), 21.8 (d, $J_{\text{C-P}}$ = 26.9 Hz, PEt_3 CH₂'s), 9.1 (s, PEt_3 CH₃'s), 8.1 (s, PEt_3 CH₃'s). $^{31}\text{P}\{^1\text{H}\}$ NMR ($(\text{CD}_3)_2\text{CO}$, 20 °C): δ 4.7 (d, $J_{\text{P-P}}$ = 10.5 Hz, 1, PEt_3), -4.7 (d, $J_{\text{P-P}}$ = 10.5 Hz, 1, PEt_3).

Synthesis of (η^5 -pentadienyl)Ir(PEt_3)₂(CH₃)⁺O₃SCF₃⁻ (5). Compound 1 (0.20 g, 4.0×10^{-4} mol) was dissolved in 20 mL of diethyl ether, and the solution was cooled to -30 °C. Cold (-30 °C) methyl triflate (0.07 g, 4.0×10^{-4} mol) was added. The solution was swirled for several minutes and then stored at -30 °C overnight, causing 5 to precipitate out of the solution as an orange-yellow solid. After removal of the solvent by decantation, the solid was washed with diethyl ether and pentane and dried under vacuum. Yield: 0.18 g (68%). Anal. Calcd for $\text{C}_{19}\text{H}_{40}\text{F}_3\text{IrO}_3\text{P}_2\text{S}$: C, 34.58; H, 6.12. Found: C, 34.22; H, 6.00. Please refer to Scheme 5 for NMR atom labels. ^1H NMR ($(\text{CD}_3)_2\text{CO}$, 22 °C): δ 6.48 (m, 1, H₃), 5.57 (m, 1, H₄), 5.25 (m, 1, H₂), 3.98 (m, 1, H₅_{outer}), 3.01 (m, 1, H₁_{outer}), 2.11 (m, 1, H₅_{inner}), 1.54 (m, 1, H₁_{inner}), 2.48–1.78 (m, 12, PEt_3 CH₂'s), 1.28–1.01 (m, 18, PEt_3 CH₃'s), 0.49 (t, $J_{\text{H-P}}$ = 5.5 Hz, 3, Ir-CH₃). $^{13}\text{C}\{^1\text{H}\}$ NMR ($(\text{CD}_3)_2\text{CO}$, 22 °C): δ 110.9 (s, C₄), 101.5 (s, C₂), 91.5 (d, $J_{\text{C-P}}$ = 10.7 Hz, C₃), 59.1 (s, C₅), 47.6 (d, $J_{\text{C-P}}$ = 31.9 Hz, C₁), 21.6 (d, $J_{\text{C-P}}$ = 35.5 Hz, PEt_3 CH₂'s), 18.7 (d, $J_{\text{C-P}}$ = 31.4 Hz, PEt_3 CH₂'s), 8.5 (s, PEt_3 CH₃'s), -26.7 (br s, Ir-CH₃). $^{31}\text{P}\{^1\text{H}\}$ NMR ($(\text{CD}_3)_2\text{CO}$, 22 °C): δ -9.9 (d, $J_{\text{P-P}}$ = 8.5 Hz, 1, PEt_3), -23.1 (d, $J_{\text{P-P}}$ = 8.5 Hz, 1, PEt_3).

Synthesis of (η^5 -2,4-dimethylpentadienyl)Ir(PEt_3)₂(CH₃)⁺O₃SCF₃⁻ (6). Compound 2 (0.60 g, 1.1×10^{-3} mol) was dissolved in 20 mL of diethyl ether, and the solution was cooled to -30 °C. Cold (-30 °C) methyl triflate (0.19 g, 1.1×10^{-3} mol) was added, and when the mixture was stirred for several minutes, compound 6 began to precipitate as a light brown solid. To complete the precipitation, the solution was stored at -30 °C for ~20 h. After removal of the solvent by decantation, the solid was washed with diethyl ether and pentane and dried under vacuum. Yield: 0.53 g (67%). Anal. Calcd for $\text{C}_{21}\text{H}_{44}\text{F}_3\text{IrO}_3\text{P}_2\text{S}$: C, 36.67; H, 6.46. Found: C, 36.36; H, 6.38. Please refer to Scheme 5 for NMR atom labels. ^1H

NMR ((CD₃)₂CO, 20 °C): δ 6.27 (m, 1, H₃), 3.83 (m, 1, H₅_{outer}), 2.63 (m, 1, H₁_{outer}), 2.44 (s, 3, pentadienyl CH₃), 2.31 (m, 4, PEt₃ CH₂'s), 2.14 (m, 4, PEt₃ CH₂'s), 2.07 (m, 1, H₅_{inner}), 1.93 (s, 3, pentadienyl CH₃), 1.66 (m, 4, PEt₃ CH₂'s), 1.05 (m, 18, PEt₃ CH₃'s), 1.01 (m, 1, H₁_{inner}), 0.20 (t, J_{H-P} = 5.4 Hz, 3, Ir-CH₃). ¹³C{¹H} NMR ((CD₃)₂CO, 20 °C): δ 122.1 (s, C₄ or C₂), 121.3 (s, C₂ or C₄), 92.3 (d, J_{C-P} = 11.4 Hz, C₃), 57.0 (s, C₅), 48.3 (d, J_{C-P} = 34.9 Hz, C₁), 25.0 (s, pentadienyl CH₃), 22.1 (s, pentadienyl CH₃), 21.0 (d, J_{C-P} = 35.6 Hz, PEt₃ CH₂), 18.7 (d, J_{C-P} = 30.3 Hz, PEt₃ CH₂), 9.3 (s, PEt₃ CH₃), 8.5 (s, PEt₃ CH₃), -18.5 (s, Ir-CH₃). ³¹P{¹H} NMR ((CD₃)₂CO, 20 °C): δ -9.6 (d, J_{P-P} = 6.6 Hz, 1, PEt₃), -21.8 (d, J_{P-P} = 6.6 Hz, 1, PEt₃).

Synthesis of (*syn*- η^3 -pentadienyl)Ir(PEt₃)₂(H)(Cl) (7). Compound **3** (0.20 g, 3.1 \times 10⁻⁴ mol) was dissolved in 5 mL of tetrahydrofuran, and solid bis(triphenylphosphine)nitrogen-(1+) chloride (PPN⁺Cl⁻; 0.18 g, 3.1 \times 10⁻⁴ mol) was added. After the solution was swirled for several minutes, 30 mL of pentane was added, causing PPN⁺O₃SCF₃⁻ to precipitate out. The solution was then filtered and evaporated to dryness. The resulting solid was dissolved in tetrahydrofuran and the solution stirred for several days in order to convert the product entirely to the *syn* isomer. Removal of the THF under vacuum yielded compound **7** (0.12 g, 73%) as a light yellow powder. Anal. Calcd for C₁₇H₃₆ClIrP₂: C, 38.37; H, 7.21. Found: C, 38.01; H, 7.15. Please refer to Scheme 7 for NMR atom labels. ¹H NMR (C₆D₆, 22 °C): δ 5.93 (m, 1, H₄), 5.23 (d, J_{H-H} = 17.4 Hz, 1, H₅), 5.02 (m, 1, H₂), 4.94 (d, J_{H-H} = 9.9 Hz, 1, H₅), 3.90 (m, 1, H₃), 2.97 (m, 1, H₁_{outer}), 2.70 (m, 1, H₁_{inner}), 1.92-1.48 (m, 12, PEt₃ CH₂'s), 0.98-0.71 (m, 18, PEt₃ CH₃'s), -25.42 (t, J_{H-P} = 15.0 Hz, 1, Ir-H). ¹³C{¹H} NMR (C₆D₆, 22 °C): δ 143.7 (s, C₄), 110.5 (s, C₅), 94.7 (s, C₂), 68.6 (d, J_{C-P} = 28.8 Hz, C₃), 46.4 (d, J_{C-P} = 28.8 Hz, C₁), 21.0 (d, J_{C-P} = 31.2 Hz, PEt₃ CH₂'s), 17.9 (d, J_{C-P} = 31.2 Hz, PEt₃ CH₂'s), 8.1 (s, PEt₃ CH₃'s), 8.0 (s, PEt₃ CH₃'s). ³¹P{¹H} NMR (C₆D₆, 22 °C): δ -7.3 (s, 1, PEt₃), -16.4 (s, 1, PEt₃).

Synthesis of (*syn*- η^3 -2,4-dimethylpentadienyl)Ir(PEt₃)₂(H)(Cl) (8). Compound **4** (0.20 g, 3.0 \times 10⁻⁴ mol) was dissolved in 5 mL of tetrahydrofuran, and solid PPN⁺Cl⁻ (0.17 g, 3.0 \times 10⁻⁴ mol) was added. After the solution was swirled for several minutes, 30 mL of pentane was added, causing PPN⁺O₃SCF₃⁻ to precipitate out. The solution was then filtered and evaporated to dryness. The resulting solid was redissolved in tetrahydrofuran and the solution stirred for several days to convert the product entirely to the *syn* isomer. Removal of the THF under vacuum yielded compound **8** (0.13 g, 77%) as a light yellow powder. Anal. Calcd for C₁₉H₄₂ClIrP₂: C, 40.73; H, 7.57. Found: C, 40.69; H, 7.50. Please refer to Scheme 7 for NMR atom labels. ¹H NMR (C₆D₆, 22 °C): δ 5.11 (s, 1, H₅), 5.07 (s, 1, H₅), 3.85 (d, J_{H-P} = 8.2 Hz, 1, H₃), 3.34 (m, 1, H₁_{outer}), 2.94 (m, 1, H₁_{inner}), 2.45 (s, 3, pentadienyl CH₃), 1.99 (s, 3, pentadienyl CH₃), 1.90-1.50 (m, 12, PEt₃ CH₂'s), 1.07-0.79 (m, 18, PEt₃ CH₃'s), -25.84 (t, J_{H-P} = 16.0 Hz, 1, Ir-H). ¹³C{¹H} NMR (C₆D₆, 22 °C): 112.6 (s, C₅), 70.4 (d, J_{C-P} = 29.9 Hz, C₃), 52.2 (d, J_{C-P} = 29.9 Hz, C₁), 25.6 (s, pentadienyl CH₃), 24.3 (s, pentadienyl CH₃), 21.0 (d, J_{C-P} = 30.7 Hz, PEt₃ CH₂'s), 18.8 (d, J_{C-P} = 30.7 Hz, PEt₃ CH₂'s), 8.6 (s, PEt₃ CH₃'s), 8.0 (s, PEt₃ CH₃'s). Note: Carbons C₂ and C₄ were not observed. ³¹P{¹H} NMR (C₆D₆, 22 °C): δ -8.5 (d, J_{P-P} = 3.0 Hz, 1, PEt₃), -15.6 (d, J_{P-P} = 3.0 Hz, 1, PEt₃).

Synthesis of (*syn*- η^3 -pentadienyl)Ir(PEt₃)₂(CH₃)(Cl) (9). Compound **5** (0.20 g, 3.0 \times 10⁻⁴ mol) was dissolved in 5 mL of tetrahydrofuran, and solid PPN⁺Cl⁻ (0.17 g, 3.0 \times 10⁻⁴ mol) was added. After the solution was swirled for several minutes, 30 mL of pentane was added, causing PPN⁺O₃SCF₃⁻ to precipitate out. The solution was then filtered and evaporated to dryness. After redissolving in tetrahydrofuran and stirring for several hours, the pure *syn* isomer of **9** (0.13 g, 80%) was obtained as a light yellow powder. Anal. Calcd for C₁₈H₄₀ClIrP₂: C, 39.58; H, 7.40. Found: C, 39.21; H, 7.23. Please refer to Scheme 7 for NMR atom labels. ¹H NMR (C₆D₆, 22 °C): δ 6.16 (m, 1, H₄), 5.36 (dd, J_{H-H} = 17.0, 2.5 Hz, 1, H₅),

5.11 (dd, J_{H-H} = 9.3 Hz, 2.5 Hz, 1, H₅), 4.65 (m, 1, H₃), 3.94 (m, 1, H₂), 3.21 (m, 1, H₁_{outer}), 3.14 (m, 1, H₁_{inner}), 1.95 (m, 6, PEt₃ CH₂'s), 1.82 (m, 6, PEt₃ CH₂'s), 1.05-0.80 (m, 18, PEt₃ CH₃'s), -0.08 (t, J_{H-P} = 4.8 Hz, 3, Ir-CH₃). ¹³C{¹H} NMR (C₆D₆, 22 °C): 141.5 (s, C₄), 110.9 (s, C₅), 110.1 (s, C₂), 73.8 (d, J_{C-P} = 30.2 Hz, C₃), 46.7 (d, J_{C-P} = 30.2 Hz, C₁), 18.1 (d, J_{C-P} = 29.6 Hz, PEt₃ CH₂'s), 15.9 (d, J_{C-P} = 29.6 Hz, PEt₃ CH₂'s), 8.6 (s, PEt₃ CH₃'s), -34.7 (t, J_{C-P} = 6.4 Hz, Ir-CH₃). ³¹P{¹H} NMR (C₆D₆, 22 °C): δ -20.2 (br s, 1, PEt₃), -29.6 (br s, 1, PEt₃).

Synthesis of (*syn*- η^3 -2,4-dimethylpentadienyl)Ir(PEt₃)₂(CH₃)(Cl) (10). Compound **6** (0.20 g, 2.9 \times 10⁻⁴ mol) was dissolved in 5 mL of tetrahydrofuran, and solid PPN⁺Cl⁻ (0.17 g, 2.9 \times 10⁻⁴ mol) was added. After the solution was swirled for several minutes, 30 mL of pentane was added, causing PPN⁺O₃SCF₃⁻ to precipitate out. The solution was then filtered and evaporated to dryness. After redissolving in tetrahydrofuran and stirring for several hours, the pure *syn* isomer of **10** (0.14 g, 84%) was obtained as a light yellow powder. Anal. Calcd for C₂₀H₄₄ClIrP₂: C, 41.83; H, 7.74. Found: C, 41.57; H, 7.54. Please refer to Scheme 7 for NMR atom labels. ¹H NMR (C₆D₆, 22 °C): δ 5.11 (s, 1, H₅), 5.06 (s, 1, H₅), 4.43 (d, J_{H-P} = 7.6 Hz, 1, H₃), 3.21 (d, J_{H-P} = 7.6 Hz, 1, H₁_{inner}), 3.00 (br s, 1, H₁_{outer}), 1.98 (s, 3, pentadienyl CH₃), 1.84 (s, 3, pentadienyl CH₃), 2.10-1.70 (m, 12, PEt₃ CH₂'s), 1.08-0.70 (m, 18, PEt₃ CH₃'s), 0.04 (t, J_{H-P} = 5.4 Hz, 3, Ir-CH₃). ¹³C{¹H} NMR (C₆D₆, 22 °C): 112.1 (s, C₅), 72.1 (d, J_{C-P} = 31.7 Hz, C₃), 47.6 (d, J_{C-P} = 31.7 Hz, C₁), 26.5 (s, pentadienyl CH₃), 19.0 (s, pentadienyl CH₃), 18.0 (d, J_{C-P} = 29.4 Hz, PEt₃ CH₂'s), 16.8 (d, J_{C-P} = 28.1 Hz, PEt₃ CH₂'s), 9.0 (s, PEt₃ CH₃'s), 8.5 (s, PEt₃ CH₃'s), -32.0 (br s, Ir-CH₃). Note: Carbons C₂ and C₄ were not observed. ³¹P{¹H} NMR (C₆D₆, 22 °C): δ -21.1 (d, J_{P-P} = 5.7 Hz, 1, PEt₃), -30.4 (d, J_{P-P} = 5.7 Hz, 1, PEt₃).

Solution Dynamics of Compounds 1-3. Exchange rate constants, k_c , at the coalescence temperature were calculated using the formula

$$k_c = \pi(\Delta\nu)/2^{1/2}$$

where $\Delta\nu$ is the difference in frequencies between the two exchanging sites in the stopped-exchange limit.¹⁴ These exchange rate constants were then used to determine the free energy of activation, ΔG^\ddagger at the coalescence temperature, T_c , from the Eyring equation

$$k_c = (k'/h)T_c e^{-\Delta G^\ddagger/RT_c}$$

where k' = Boltzmann's constant, h = Planck's constant, and R = ideal gas constant.¹⁵

Acknowledgment. We thank the National Science Foundation (Grants CHE-9003159 and CHE-9303516) and the donors of the Petroleum Research Fund, administered by the American Chemical Society, for support of this research. A loan of IrCl₃·3H₂O from Johnson-Matthey Alfa/Aesar is gratefully acknowledged. Washington University's High Resolution NMR Service Facility was funded in part by National Institutes of Health Biomedical Support Instrument Grant 1 S10 RR02004 and by a gift from Monsanto Co.

OM940845H

(14) Pople, J. A.; Schneider, W. G.; Bernstein, H. J. *High Resolution Nuclear Magnetic Resonance*; McGraw-Hill: New York, 1959; p 223.

(15) Lowry, T. H.; Richardson, K. S. *Mechanism and Theory in Organic Chemistry*; Harper and Row: New York, 1976; p 194.

Phosphapentadienyl–Iridium–Phosphine Chemistry.¹ Synthesis, Structure, and Spectroscopy of Phosphapentadienyl-Bridged Iridium Dimers

John R. Bleeker,* Alicia M. Rohde, and Kerry D. Robinson

Department of Chemistry, Washington University, St. Louis, Missouri 63130-4899

Received December 7, 1994[®]

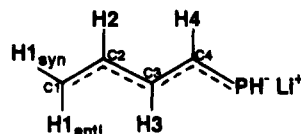
The reactions of new lithium phosphapentadienide reagents with $\text{ClIr}(\text{PR}_3)_3$ have been investigated. Treatment of $\text{ClIr}(\text{PET}_3)_3$ with lithium phosphapentadienide produced the phosphapentadienyl-bridged dimer $[(\mu\text{-}\eta^1\text{-phosphapentadienyl})\text{Ir}(\text{PET}_3)_2]_2$ (**1**) as a 1.4:1 mixture of *trans* (**1a**) and *cis* (**1b**) isomers. The analogous reaction involving $\text{ClIr}(\text{PET}_2\text{Ph})_3$ produced $[(\mu\text{-}\eta^1\text{-phosphapentadienyl})\text{Ir}(\text{PET}_2\text{Ph})_2]_2$ (**2**). Again, a 1.4:1 mixture of *trans* (**2a**) and *cis* (**2b**) isomers was obtained. The mechanism of *trans* \rightarrow *cis* isomer conversion was probed by means of a "crossover" experiment: pure samples of *trans* isomers **1a** and **2a** were combined and their conversion to the equilibrium mixture of *trans* and *cis* isomers was monitored. The absence of "mixed-dimer" products (i.e., those containing both $\text{Ir}(\text{PET}_3)_2$ and $\text{Ir}(\text{PET}_2\text{Ph})_2$ moieties) in these reactions ruled out a *trans* \rightarrow *cis* isomerization mechanism involving monomeric $(\text{phosphapentadienyl})\text{Ir}(\text{PR}_3)_2$ units and supported a mechanism involving dissociation of one iridium–phosphido bond, inversion at the resulting terminal phosphido center, and re-formation of the iridium–phosphido bond. Treatment of $\text{ClIr}(\text{PET}_3)_3$ with lithium 2,4-dimethylphosphapentadienide generated $[(\mu\text{-}\eta^1\text{-2,4-dimethylphosphapentadienyl})\text{Ir}(\text{PET}_3)_2]_2$ (**3**). Again, an equilibrium mixture of *trans* (**3a**) and *cis* (**3b**) isomers was obtained, but the presence of the bulky dimethylphosphapentadienyl ligand led to a higher fraction of *trans* isomer (**3a**:**3b** = 8:1). The structure of **3a** was confirmed by X-ray crystallography (triclinic, $P\bar{1}$, $a = 11.756(4)$ Å, $b = 12.011(3)$ Å, $c = 17.716(7)$ Å, $\alpha = 93.50(3)^\circ$, $\beta = 92.89(3)^\circ$, $\gamma = 108.67(3)^\circ$, $V = 2359.0(15)$ Å³, $Z = 2$, $R = 0.0277$, $R_w = 0.0345$).

During the past 15 years, the chemistry of pentadienyl–metal complexes has been extensively investigated.² The pentadienyl ligands in these complexes adopt a wide variety of bonding modes, and facile interconversion between these modes leads to interesting dynamic behavior and reactivity. In contrast, relatively little is known about heteropentadienyl ligands, i.e., analogues of pentadienyl in which one of the terminal CH_2 groups has been replaced with a heteroatom. In order to learn more about heteropentadienyl ligands and their bonding preferences we have begun to investigate a series of heteropentadienyl–iridium–phosphine complexes. Our general synthetic approach involves treating halo–iridium–phosphine precursors with anionic heteropentadienide reagents. Previously, we reported our findings in the oxapentadienyl,³ thiapentadienyl,⁴ and azapentadienyl⁵ ligand systems. We now describe the preparation of anionic phosphapentadienide reagents⁶ and the use of these novel reagents in the synthesis of phosphapentadienyl–iridium–phosphine complexes.⁷

Results and Discussion

A. Synthesis of Lithium Phosphapentadienide and Its Reactions with $\text{ClIr}(\text{PR}_3)_3$ Complexes.

Lithium phosphapentadienide was prepared in high yield by treating butadienylphosphine⁸ with *n*-butyllithium in diethyl ether/tetrahydrofuran (THF) at -98°C , followed by warming to room temperature. The ¹³C- $\{^1\text{H}\}$ NMR spectrum of this orange, THF-soluble species showed four downfield peaks at δ 154.0 (C4), 142.0 (C2), 122.0 (C3), and 95.6 (C1), with labeling as follows:



The C4 peak was split into a doublet ($J = 40$ Hz) due to carbon–phosphorus coupling. Similarly, the ¹H NMR spectrum included five downfield signals at δ 6.90 (H4), 6.09 (H2), 5.89 (H3), 4.12 (H1_{anti}), and 3.87 (H1_{syn}). The phosphido proton appeared at δ 1.88 and was split into a doublet of doublets as a result of large coupling ($J = 160$ Hz) to phosphorus and small coupling ($J = 12.5$ Hz)

[®] Abstract published in *Advance ACS Abstracts*, March 15, 1995.
(1) Pentadienyl–Metal–Phosphine Chemistry. 29. For the previous paper in this series, see: Bleeker, J. R.; Luaders, S. T. *Organometallics*, in press.

(2) For leading reviews, see: (a) Ernst, R. D. *Chem. Rev.* **1988**, *88*, 1251. (b) Yasuda, H.; Nakamura, A. *J. Organomet. Chem.* **1985**, *285*, 15. (c) Powell, P. *Adv. Organomet. Chem.* **1986**, *26*, 125.

(3) (a) Bleeker, J. R.; Haile, T.; Chiang, M. Y. *Organometallics* **1991**, *10*, 19. (b) Bleeker, J. R.; Haile, T.; New, P. R.; Chiang, M. Y. *Organometallics* **1993**, *12*, 517.

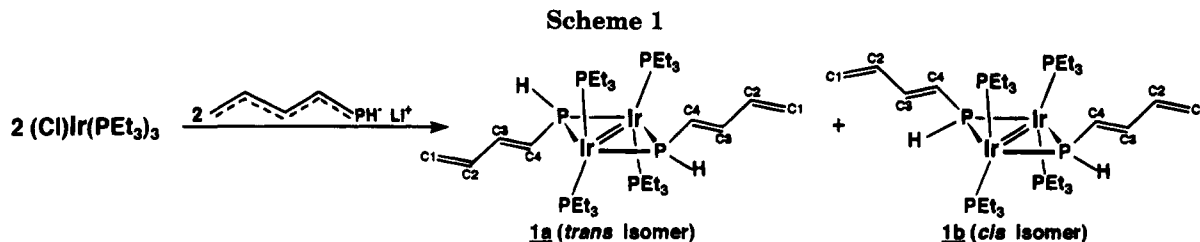
(4) Bleeker, J. R.; Ortwerth, M. F.; Chiang, M. Y. *Organometallics* **1992**, *11*, 2740.

(5) Bleeker, J. R.; Luaders, S. T.; Robinson, K. D. *Organometallics* **1994**, *13*, 1592.

(6) Recently, the first anionic phosphapentadienyl reagent was reported: Niecke, E.; Nieger, M.; Wenderoth, P. *J. Am. Chem. Soc.* **1993**, *115*, 6989.

(7) A communication describing portions of this work has appeared: Bleeker, J. R.; Rohde, A. M.; Robinson, K. D. *Organometallics* **1994**, *13*, 401.

(8) Cabioch, J. L.; Denis, J. M. *J. Organomet. Chem.* **1989**, *377*, 227.



to H4. Finally, the $^{31}\text{P}\{^1\text{H}\}$ NMR spectrum showed a peak at $\delta -107.1$ (with respect to an external H_3PO_4 standard). In the absence of decoupling, this signal split into a doublet-of-doublets-of-doublets pattern, as a result of large one-bond coupling to the phosphido proton ($J = 160$ Hz) and smaller couplings ($J = 26$ and 5 Hz) to other hydrogens in the phosphapentadienide chain.

Reaction of lithium phosphapentadienide with $\text{ClIr}(\text{PEt}_3)_3$ in tetrahydrofuran at 0°C , followed by warming to room temperature, produced the deep red phosphapentadienyl-bridged dimer $[(\mu-\eta^1\text{-phosphapentadienyl})\text{Ir}(\text{PEt}_3)_2]_2$ (**1**) in good yield (see Scheme 1). The $^{31}\text{P}\{^1\text{H}\}$ NMR spectrum of **1** clearly showed the presence of two solution phase isomers in a 1.4:1 ratio. The major isomer (*trans*, **1a**) exhibited a quintet ($J_{\text{P-P}} = 19$ Hz) at $\delta 68.0$ (intensity 1) for the two bridging phosphido groups and a triplet ($J_{\text{P-P}} = 19$ Hz) at $\delta -4.1$ (intensity 2) for the four equivalent PEt_3 ligands. The minor isomer (*cis*, **1b**) gave rise to three equal-intensity multiplets at $\delta 66.4$ (phosphido's), 1.0 (PEt_3 's), and -10.0 (PEt_3 's). The downfield ^{31}P NMR chemical shifts of the bridging phosphido ligands ($\delta 68.0$ in **1a** and $\delta 66.4$ in **1b**) are typical for compounds containing a strong metal-metal interaction,¹⁰ while the small P-P coupling constants (19 Hz in **1a**) are consistent with a tetrahedral geometry about each iridium center.¹¹ The ^{13}C and ^1H NMR signals of the phosphapentadienyl ligands in **1a** and **1b** were very similar to those of the anionic phosphapentadienide reagent. The only major difference was the position of the ^1H NMR signal for the phosphido hydrogens, which were shifted dramatically downfield (to $\delta 8.83$ in **1a** and $\delta 8.58$ in **1b**) and appeared as a complex multiplet due to their participation in an AA'XX' spin system.

The X-ray crystal structure of **1a**, which we reported earlier,⁷ showed the expected tetrahedral coordination geometry about each iridium center. Furthermore, the plane made by the two iridium centers and the two phosphido phosphorus atoms was oriented almost perpendicular to the plane containing the two iridium centers and the four PEt_3 phosphorus atoms; the dihedral angle was 94.6° . The Ir-Ir distance was $2.576(1)$ Å, consistent with the presence of a double bond as required for each metal to achieve an $18e^-$ count. The phosphapentadienyl ligand was essentially W-shaped with torsional angles of 179.2 and -175.5° for C1-C2-C3-C4 and C2-C3-C4-P1, respectively. The carbon-carbon bond lengths showed the expected pattern of alternation.

(9) Produced *in situ* by reacting $[(\text{cyclooctene})_2\text{IrCl}]_2$ with 6 equiv of PEt_3 in tetrahydrofuran.

(10) See, for example: (a) Garrou, P. E. *Chem. Rev.* **1981**, *81*, 229. (b) Carty, A. J. *Adv. Chem. Ser.* **1982**, No. 196, 163.

(11) See, for example: (a) Kreter, P. E.; Meek, D. W. *Inorg. Chem.* **1983**, *22*, 319. (b) Jones, R. A.; Norman, N. C.; Seeberger, M. H.; Atwood, J. L.; Hunter, W. E. *Organometallics* **1983**, *2*, 1629. (c) Burkhardt, E. W.; Mercer, W. C.; Geoffroy, G. L. *Inorg. Chem.* **1984**, *23*, 1779.

While phosphido-bridged iridium dimers of this general structure are known,^{11a,12} all contain dialkyl- or diarylphosphido groups. To our knowledge, this is the first example of a *primary* phosphido-iridium dimer and the first iridium system to exhibit *cis/trans* isomers. Perhaps the closest known analogue of **1** is $[(\mu\text{-P(H)(t-but)})\text{Rh}(\text{PMe}_2)_2]_2$, reported by Jones et al.^{11b} However, this complex possesses two substituents on the bridging phosphido group which are very different in size and, as a result, it exists only as the less sterically-encumbered *trans* isomer.

When a pure crystalline sample of *trans* isomer **1a** was redissolved in benzene, it slowly (over a period of several days) isomerized back to the equilibrium mixture of *cis* and *trans* isomers. Two plausible mechanisms can be envisaged for the isomerization in nonpolar solvents.¹³ The simplest is the dissociation of one iridium-phosphido bond, inversion at the resulting terminal phosphido phosphorus center, and re-formation of the iridium-phosphido bond (see Scheme 2).¹⁴ While phosphorus inversion barriers are generally quite high, Gladysz¹⁵ has recently shown that the ΔG^\ddagger for phosphorus inversion in terminal primary metal-phosphido complexes is remarkably low—in the range of 11–15 kcal/mol. A second possible mechanism involves reversible dissociation of dimers into monomeric (phosphapentadienyl)Ir(PEt₃)₂ complexes.¹⁶

In order to distinguish between these two mechanistic alternatives, we synthesized the diethylphenylphosphine analogue of **1**, $[(\mu-\eta^1\text{-phosphapentadienyl})\text{Ir}(\text{PEt}_2\text{-Ph})_2]_2$, **2**. Like **1**, compound **2** crystallized from toluene as the *trans* isomer but slowly converted in benzene solution to a 1.4:1 equilibrium mixture of *trans* (**2a**) and *cis* (**2b**) isomers. When crystalline samples of pure *trans* isomers **1a** and **2a** were dissolved together in benzene at room temperature, we observed the gradual formation of the *cis* isomers **1b** and **2b**.¹⁷ However, no additional peaks due to the "mixed" dimer, $(\text{PEt}_3)_2\text{Ir}(\mu-\eta^1\text{-phosphapentadienyl})_2\text{Ir}(\text{PEt}_2\text{Ph})_2$, were detected in either the phosphido or phosphine region of the ^{31}P

(12) (a) Mason, R.; Sotofte, I.; Robinson, S. D.; Uttley, M. R. *J. Organomet. Chem.* **1972**, *46*, C61. (b) Bellon, P. L.; Benedicenti, C.; Caglio, G.; Manassero, M. *J. Chem. Soc., Chem. Commun.* **1973**, 946. (c) Arif, A. M.; Heaton, D. E.; Jones, R. A.; Kidd, K. B.; Wright, T. C.; Whittlesey, B. R.; Atwood, J. L.; Hunter, W. E.; Zhang, H. *Inorg. Chem.* **1987**, *26*, 4065.

(13) In polar solvents, a third mechanism involving deprotonation/inversion/reprotonation of the bridging phosphido ligands may also be possible. See: Brown, M. P.; Buckett, J.; Harding, M. M.; Lynden-Bell, R. M.; Mays, M. J.; Woulfe, K. W. *J. Chem. Soc., Dalton Trans.* **1991**, 3097.

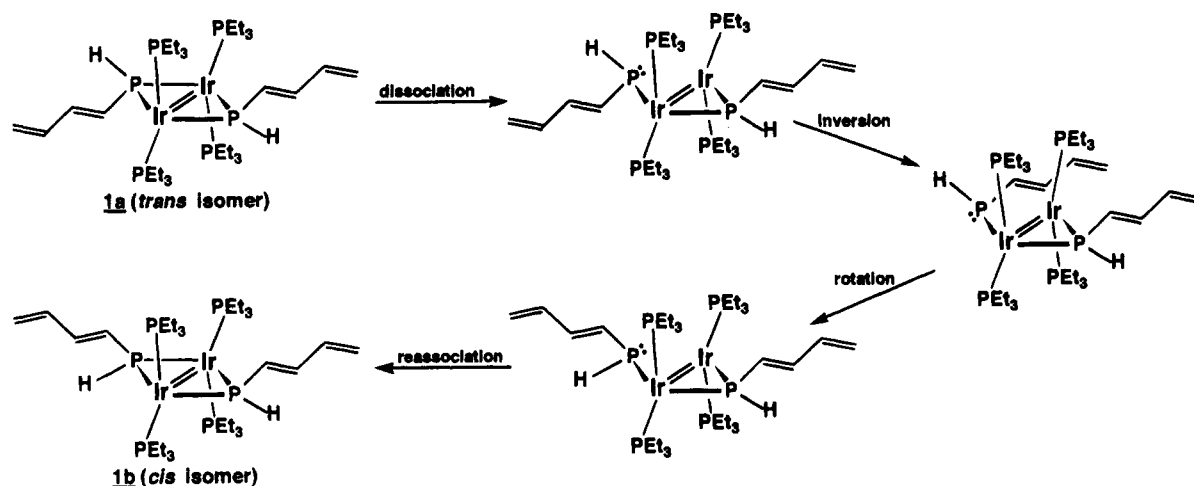
(14) A slight variation on this mechanism would involve simultaneous dissociation of two iridium-phosphido bonds, leaving each phosphapentadienyl ligand coordinated to a single iridium center. The dimer would remain intact, held together by metal-metal bonds.

(15) Zwick, B. D.; Dewey, M. A.; Knight, D. A.; Buhro, W. E.; Arif, A. M.; Gladysz, J. A. *Organometallics* **1992**, *11*, 2673.

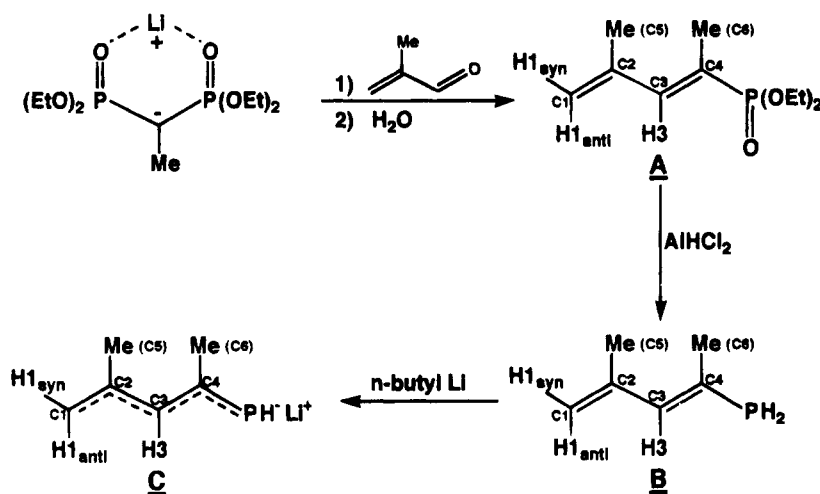
(16) An analogous mechanism has been postulated for the isomerization of a related rhodium dimer containing $\mu\text{-PMePh}$ ligands.^{11c}

(17) The reaction was carried out in the dark to eliminate the slow photoassisted decomposition of **1** and **2**.

Scheme 2



Scheme 3



NMR spectrum. This result rules out reversible dissociation of dimers into monomeric complexes *under these rather mild conditions* and supports the intramolecular process involving inversion at the phosphido phosphorus center (cf., Scheme 2).

B. Synthesis of Lithium 2,4-Dimethylphosphapentadienide and Its Reaction with $\text{ClIr}(\text{PEt}_3)_3$. Methylation of pentadienide or heteropentadienide reagents often has a dramatic effect on the chemistry of these species.¹⁸ In order to assess this effect in the phosphapentadienyl system, we set out to synthesize lithium 2,4-dimethylphosphapentadienide. Since the precursor phosphine, (dimethylbutadienyl)phosphine, had not previously been reported, we first developed a synthesis for this precursor, as shown in Scheme 3. The diethyl (dimethylbutadienyl)phosphonate (**A**, Scheme 3) was produced using the general procedure developed by Teulade and Savignac¹⁹ for the synthesis of vinylphosphonates. This species was then reduced to (dimethylbutadienyl)phosphine (**B**) with dichloroalane in tetraglyme and immediately collected at -196°C , following the procedure developed by Denis et al.⁸ Finally, treatment of this precursor phosphine with *n*-butyl-

lithium at -98°C , followed by warming to room temperature, yielded the desired lithium 2,4-dimethylphosphapentadienide (**C**) as an orange solid.

The $^{13}\text{C}\{^1\text{H}\}$ NMR spectrum of lithium 2,4-dimethylphosphapentadienide, like that of its unmethylated analogue, exhibited four downfield resonances between δ 160 and 100 for the carbon atoms in the phosphapentadienyl chain (C1, C2, C3, and C4). The peaks due to carbons C4 and C3 were split into doublets ($J = 44$ Hz and $J = 16$ Hz, respectively) as a result of carbon-phosphorus coupling. In addition, two methyl resonances (C5 and C6) appeared in the upfield region of the spectrum. The ^1H NMR spectrum showed the expected downfield signals for H3 and the H1's at δ 5.73 and 4.16, respectively. The methyl peaks appeared at δ 1.97 and 1.65, while the phosphido proton resonated at δ 2.06 and was split into a well-separated doublet ($J = 160$ Hz) due to phosphorus coupling. In the $^{31}\text{P}\{^1\text{H}\}$ NMR spectrum, the phosphido phosphorus appeared as a singlet at δ -75.0 . When coupled to protons, the signal split into a broad doublet with the expected P-H coupling of 160 Hz.

Treatment of $\text{ClIr}(\text{PEt}_3)_3$ ⁹ with lithium 2,4-dimethylphosphapentadienide led to the production of $[(\mu\text{-}\eta^1\text{-}2,4\text{-dimethylphosphapentadienyl})\text{Ir}(\text{PEt}_3)_2]_2$ (**3**), the 2,4-dimethylphosphapentadienyl analogue of **1**. The $^{31}\text{P}\{^1\text{H}\}$ NMR spectrum of the product showed an equilibrium

(18) See, for example: (a) Bleeke, J. R.; Boorsma, D.; Chiang, M. Y.; Clayton, T. W., Jr.; Haile, T.; Beatty, A. M.; Xie, Y.-F. *Organometallics* **1991**, *10*, 2391. (b) Reference 3b.

(19) Teulade, M.-P.; Savignac, P.; Aboujaoude, E. E.; Lietge, S.; Collignon, N. *J. Organomet. Chem.* **1986**, *304*, 283.

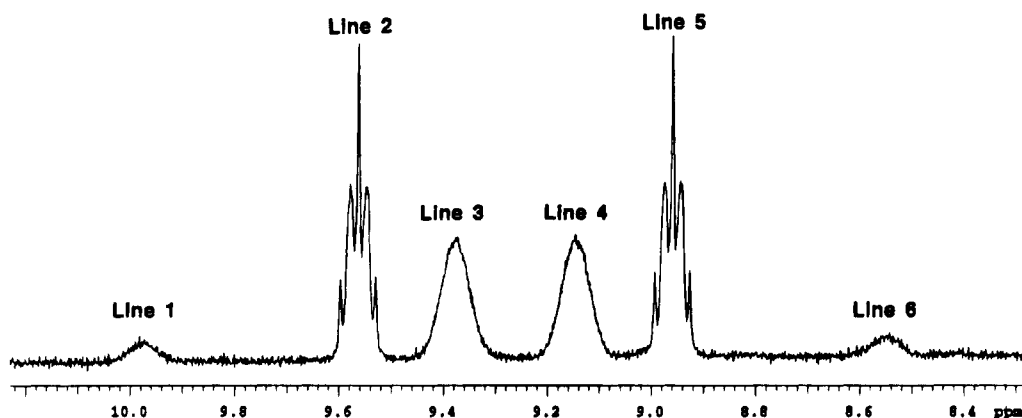


Figure 1. ^1H NMR signal (at 500 MHz) for the phosphido (P-H) protons in $[(\mu\text{-}\eta^1\text{-}2,4\text{-dimethylphosphapentadienyl})\text{Ir}(\text{PEt}_3)_2]_2$ (**3a**). The complex signal, which consists of six "lines" labeled 1–6 above, arises from the fact that the phosphido protons are part of an AA'XX' spin system, where A and A' are the phosphido protons and X and X' are the phosphido phosphorus atoms.

mixture of *trans* (**3a**) and *cis* (**3b**) isomers, but the presence of the bulky dimethylphosphapentadienyl ligand led to a higher fraction of *trans* isomer (**3a**:**3b** = 8:1). The *trans* isomer gave rise to a downfield quintet ($J_{\text{P-P}} = 20$ Hz) of intensity 1 (phosphido groups) and an upfield triplet ($J_{\text{P-P}} = 20$ Hz) of intensity 2 (PEt_3 's), while the *cis* isomer gave rise to three equal-intensity signals, one in the downfield (phosphido) region and two in the upfield (PEt_3) region. The ^{13}C and ^1H NMR spectra of **3** closely resembled those of the lithium 2,4-dimethylphosphapentadienide reagent, with one exception: the phosphido protons were shifted downfield (to δ 9.31 for **3a**) and appeared as a complex multiplet due to their participation in an AA'XX' spin system, where A and A' are the phosphido protons and X and X' are the phosphido phosphorus atoms.²⁰ The phosphido proton signal for **3a** (at 500 MHz) is reproduced in Figure 1. It consists of six "lines", a pair of quintets at δ 9.56 and 8.96, and a broad quartet with peaks at δ 9.97, 9.37, 9.14, and 8.54. Normally, the AA' pattern of an AA'XX' spin system consists of ten lines,²¹ but ours reduces to six because $J_{\text{A-A'}}$ (the coupling between the two phosphido protons) is vanishingly small.

From the positions of the six lines, arbitrarily labeled 1 → 6 in Figure 1, the values of $J_{\text{X-X'}}$, $J_{\text{A-X}}$, and $J_{\text{A-X'}}$ can be easily calculated. The separation between lines 1 and 3 yields a value of 300 Hz for $J_{\text{X-X'}}$ (the coupling between the two phosphido phosphorus atoms).²² Similarly, the separation between lines 2 and 5 yields a value of 300 Hz for $J_{\text{A-X}} + J_{\text{A-X'}}$. Finally, the separation between lines 1 and 4, together with the previously calculated value of $J_{\text{X-X'}}$, allows calculation of a value of 287 Hz for $J_{\text{A-X}} - J_{\text{A-X'}}$. Hence, $^1J_{\text{A-X}}$ (the coupling between a phosphido proton and the phosphido phosphorus to which it is directly bonded) is 293.5 Hz, while $^3J_{\text{A-X'}}$ (the coupling between a phosphido proton and the other phosphido phosphorus) is only 6.5 Hz. The quintet fine structure in lines 2 and 5 ($J = 8$ Hz) arises from coupling between the phosphido protons and the P centers on the four equivalent PEt_3 ligands.

Crystals of compounds **3a** were grown from a saturated toluene solution of **3a,b** at -40 °C, and its solid state structure was determined by a single crystal X-ray diffraction study. The compound crystallized with two independent molecules in the unit cell. Each molecule resided on a crystallographically-imposed inversion center, making the two $\text{Ir}(\text{PEt}_3)_2$ fragments and the two bridging 2,4-dimethylphosphapentadienyl ligands crystallographically equivalent. The ORTEP drawing of one of the independent molecules is presented in Figure 2, while important bond distances and angles are reported in the caption. A listing of atomic coordinates is given in Table 1.

As expected, the coordination geometry about iridium was approximately tetrahedral. In fact, the average of the six P–Ir–P angles was 109.6°. However, the presence of the methyl groups (particularly C6) on the phosphapentadienyl chain caused some tilting of the iridium–phosphine plane ($\text{Ir1/Ir1a/P2/P3/P2a/P3a}$) in order to minimize unfavorable steric contacts. This tilting was clearly seen in the individual P–Ir–P angles; P1–Ir1–P2 was expanded to 121.9(1)°, while P1–Ir1–P3 was contracted to 102.8(1)°. The dihedral angle between the iridium–phosphine plane ($\text{Ir1/Ir1a/P2/P3/P2a/P3a}$) and the iridium–phosphido plane (Ir1/Ir1a/P1/P1a) was 104.8°. (The analogous dihedral angle for compound **1a** was 94.6°.) The Ir1–Ir1a distance of 2.587(1) Å was typical for an iridium–iridium double bond. The bond distances along the phosphapentadienyl chain were normal except for C1–C2 and C2–C5, which were equal within experimental error (1.429(10) and 1.418(13) Å) and intermediate between typical signal and double bonds. This strongly suggested the presence of a 2-fold disorder, wherein methylene group C1 and methyl group C5 shared the two terminal positions. As a result of steric contacts between the methyl substituents, the central angle in the 2,4-dimethylphosphapentadienyl ligand (C2–C3–C4) expanded to 131.2(7)°. (The analogous angle in **1a** was 123.5(8)°.) In addition, angles C5–C2–C3 and C3–C4–C5 were expanded to 124.7(6) and 125.6(6)°, respectively.

In summary, we have synthesized new anionic phosphapentadienide reagents and have demonstrated that these reagents can be used to produce phosphapentadienyl–metal complexes via simple nucleophilic dis-

(20) The only other phosphido-bridged dimer for which this type of ^1H NMR pattern has been reported is $\text{Mn}_2(\mu\text{-PPhH})_2(\text{CO})_6$; see ref 13.

(21) Pople, J. A.; Schneider, W. G.; Bernstein, H. J. *High Resolution Nuclear Magnetic Resonance*; McGraw-Hill: New York 1959; p 141.

(22) This P–P coupling is unusually large for phosphorus atoms in a tetrahedral geometry and must result, at least in part, from the fact that the two phosphido P centers are part of a four-membered ring.

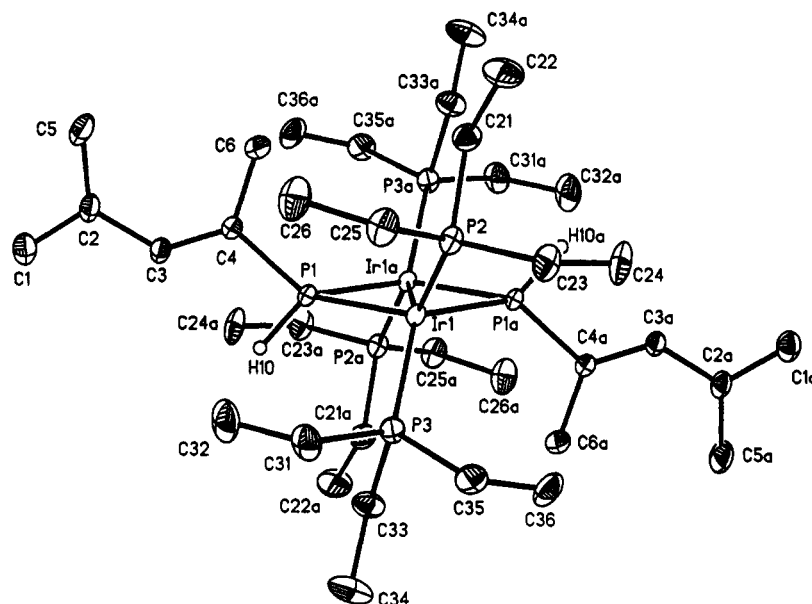


Figure 2. ORTEP drawing of $[(\mu\text{-}\eta^1\text{-}2,4\text{-dimethylphosphapentadienyl})\text{Ir}(\text{PEt}_3)_2]_2$ (**3a**). This compound crystallized with two independent molecules in the unit cell. Molecule 1, along with its distances and angles, is shown here. Selected bond distances (Å): Ir1–Ir1a, 2.587(1); Ir1–P, 2.294(2); Ir1–P1a, 2.295(2); Ir1–P2, 2.254(2); Ir1–P3, 2.261(2); C1–C2, 1.429(10); C2–C3, 1.459(9); C2–C5, 1.418(13); C3–C4, 1.351(8); C4–C6, 1.513(9); C4–P1, 1.831(6). Selected bond angles (deg): P1–Ir1–P1a, 111.3(1); P1–Ir1–P2, 121.9(1); P1–Ir1–P3, 102.8(1); P1a–Ir1–P2, 102.2(1); P1a–Ir1–P3, 122.4(1); P2–Ir1–P3, 96.8(1); Ir1–P1–Ir1a, 68.7(1); C1–C2–C3, 116.0(7); C1–C2–C5, 119.3(6); C5–C2–C3, 124.7(6); C2–C3–C4, 131.2(7); C3–C4–P1, 119.9(5); C3–C4–C6, 125.6(6); C6–C4–P1, 114.5(4); C4–P1–Ir1, 129.3(2); C4–P1–Ir1a, 128.0(2).

Table 1. Atomic Coordinates ($\times 10^4$) with Estimated Standard Deviations for Non-Hydrogen Atoms in $[(\mu\text{-}\eta^1\text{-}2,4\text{-Dimethylphosphapentadienyl})\text{Ir}(\text{PEt}_3)_2]_2$ (**3a**)^a

	x	y	z
Ir1	397(1)	9132(1)	114(1)
P1	1572(1)	11079(1)	235(1)
P2	770(2)	7805(1)	-708(1)
P3	947(2)	8446(2)	1186(1)
C1	5821(7)	14142(7)	475(5)
C2	5039(6)	13319(6)	-94(4)
C3	3891(6)	12585(5)	149(4)
C4	2914(5)	11821(5)	-250(3)
C5	5416(8)	13259(9)	-839(6)
C6	2801(7)	11507(7)	-1097(4)
C21	554(7)	8141(7)	-1680(4)
C22	605(10)	7256(9)	-2334(5)
C23	-131(7)	6215(6)	-741(5)
C24	-1476(7)	5921(7)	-899(6)
C25	2260(7)	7607(7)	-697(5)
C26	3333(8)	8728(8)	-745(6)
C31	2525(7)	8526(8)	1406(5)
C32	3460(8)	9758(9)	1443(6)
C33	676(8)	9266(7)	2032(4)
C34	979(11)	8921(9)	2816(5)
C35	238(8)	6875(6)	1364(5)
C36	-1124(8)	6474(7)	1330(5)

^a This compound crystallized with two independent molecules in the unit cell. Coordinates for the unique portion of molecule 1 are given here.

placement reactions. In the iridium–phosphine system described herein, the phosphapentadienyl ligand bonds preferentially in a bridging phosphido ($\mu\text{-}\eta^1$) mode. Other metal–ligand systems are now under investigation in order to learn more about phosphapentadienyl bonding preferences.

Experimental Section

General Procedures. All manipulations were carried out under an inert atmosphere (N_2) using either drybox or Schlenk techniques. Solvents were stored under nitrogen after being distilled from the appropriate drying agents. Diethyl eth-

ylphosphonate (Pfaltz and Bauer) was distilled before use. The following reagents were used without further purification: $\text{IrCl}_3 \cdot 3\text{H}_2\text{O}$ (Johnson Matthey), cyclooctene (Aldrich), 2-propanol (EM Science), triethylphosphine (Strem), diethylphenylphosphine (Strem), triethyl phosphite (Aldrich), 1,4-dichloro-*trans*-2-butene (Aldrich), potassium hydroxide (Aldrich), anhydrous ethanol (Midwestern Grain), lithium aluminum hydride (Aldrich), aluminum chloride (Aldrich), *n*-butyllithium (Aldrich), lithium diisopropylamide (Aldrich), diethyl chlorophosphate (Aldrich), methacrolein (Aldrich). $[(\text{Cyclooctene})_2\text{Ir}(\text{Cl})_2]^{23}$ and butadienylphosphine⁸ were prepared by the literature methods.

Nuclear magnetic resonance experiments were performed on Varian XL-300 MHz and VXR-500 MHz spectrometers. The ^1H and ^{13}C NMR spectra were referenced to tetramethylsilane, while ^{31}P spectra were referenced to external H_3PO_4 . Some ^1H peak assignments were determined using COSY (homonuclear shift-correlated spectroscopy) experiments. Some ^{13}C peak assignments were determined using APT (attached proton test), off-resonance ^{13}C (off-resonance ^1H -decoupled ^{13}C NMR spectroscopy), and/or HMQC (^1H detected multiple quantum coherence) experiments. One gram sealed ampules of deuterated NMR solvents were used without further purification (Cambridge Isotope Laboratories). In the NMR spectra reported below, carbon atoms were numbered starting at the end of the chain *opposite from phosphorus*.

Microanalyses were performed by Galbraith Laboratories, Inc., Knoxville, TN.

Synthesis of Lithium Phosphapentadiene. Under nitrogen, butadienylphosphine (2.0 g, 0.023 mol) was mixed with 50 mL of diethyl ether and 10 mL of tetrahydrofuran (THF) and cooled to $-98\text{ }^\circ\text{C}$ in a methanol/ $\text{N}_2(l)$ bath. *n*-Butyllithium (14.4 mL of a 1.6 M solution in hexanes, 0.023 mol) was diluted with ~ 10 mL of diethyl ether and added dropwise over a period of 30 min. A yellow/orange color formed immediately in the solution. After slowly warming to room temperature, the solution was stirred for 8 h and filtered through Celite. The solvent was then removed under vacuum,

(23) Herde, J. L.; Lambert, J. C.; Senoff, C. V. In *Inorganic Syntheses*; Parrshall, G. W., Ed.; McGraw-Hill: New York, 1974; Vol. 15, pp 18–20.

yielding lithium phosphapentadienide as a gummy orange solid (crude yield: 2.0 g, 95%). A free-flowing orange powder was obtained by washing the crude product with three 200 mL aliquots of diethyl ether. This powder was extremely air-sensitive, burning upon exposure to the atmosphere.

$^1\text{H NMR}$ (d_8 -THF, 25 °C): δ 6.90 (m, H4), 6.09 (m, H2), 5.89 (m, H3), 4.12 (d, $J_{\text{H-H}} = 16.1$ Hz, H1_{anti}), 3.87 (d, $J_{\text{H-H}} = 9.6$ Hz, H1_{syn}), 1.88 (dd, $J_{\text{H-P}} = 160$ Hz, $J_{\text{H-H}} = 12.5$ Hz, P-H).

$^{13}\text{C}\{^1\text{H}\}$ NMR (d_8 -THF, 25 °C): δ 154.0 (d, $J_{\text{C-P}} = 40$ Hz, C4), 142.0 (s, C2), 122.0 (br s, C3), 95.6 (s, C1).

$^{31}\text{P}\{^1\text{H}\}$ NMR (d_8 -THF, 25 °C): δ -107.2 (s).

^{31}P NMR (d_8 -THF, 25 °C): δ -107.2 (ddd, $J_{\text{P-H}} = 160$ Hz, 26 Hz, 5 Hz).

Synthesis of $[(\mu\text{-}\eta^1\text{-Phosphapentadienyl})\text{Ir}(\text{PEt}_3)_2]$ (1). Under nitrogen, triethylphosphine (0.16 g, 1.3 mmol) was added dropwise to a stirred solution of $[(\text{cyclooctene})_2\text{Ir}(\text{Cl})_2]$ (0.20 g, 0.22 mmol) in 10 mL of tetrahydrofuran (THF). The volatiles were removed under vacuum, and the resulting residue was redissolved in 50 mL of THF and cooled to 0 °C. Lithium phosphapentadienide (0.041 g, 0.45 mmol) in 20 mL of THF was added dropwise, causing the solution to turn a deep red color. After the mixture was stirred overnight, it was heated gently (at ~ 50 °C) for 4 h. The volatiles were then removed under vacuum, and the residue was extracted with toluene. The resulting red solution was filtered and evaporated to dryness, yielding 0.15 g (67%) of **1** as a 1.4:1 ratio of *trans* to *cis* isomers (**1a**:**1b**). When this product was redissolved in a minimal quantity of toluene and the solution cooled to -40 °C, **1a** crystallized as red plates. Compound **1a** was air- and light-stable for up to 1 week in crystalline form, but solutions of **1** in toluene and benzene were air- and light-sensitive. Anal. Calcd for $\text{C}_{32}\text{H}_{72}\text{Ir}_2\text{P}_6$: C, 37.41; H, 7.08. Found: C, 36.93; H, 6.64.

Trans Isomer 1a. $^1\text{H NMR}$ (C_6D_6 , 25 °C): δ 8.83 (AA'XX' multiplet, $^1J_{\text{H-P}} \approx 300$ Hz, $^2J_{\text{P-P}} \approx 300$ Hz, $^3J_{\text{H-P}} = 6.9$ Hz, 1, P-H), 6.82 (br m, 1, H3), 6.70 (br m, 1, H4), 6.55 (br m, 1, H2), 5.21 (d, $J_{\text{H-H}} = 16.5$ Hz, 1, H1_{anti}), 4.94 (d, $J_{\text{H-H}} = 9.6$ Hz, 1, H1_{syn}), 1.35 (br m, 12, PEt_3 CH_2 's), 0.98 (br m, 18, PEt_3 CH_3 's).

$^{13}\text{C}\{^1\text{H}\}$ NMR (C_6D_6 , 25 °C): δ 145.4 (C4), 138.7 (C2), 129.5 (C3), 115.2 (C1), 24.3 (PEt_3 CH_2 's), 9.0 (PEt_3 CH_3 's).

$^{31}\text{P}\{^1\text{H}\}$ NMR (C_6D_6 , 25 °C): δ 68.0 (quintet, $J_{\text{P-P}} = 19.0$ Hz, 1, phosphido P), -4.1 (triplet, $J_{\text{P-P}} = 19.0$ Hz, 2, PEt_3 's).

Cis Isomer 1b (Peak Positions Obtained from a Mixture of 1a and 1b). $^1\text{H NMR}$ (C_6D_6 , 25 °C): δ 8.58 (AA'XX' multiplet, $^1J_{\text{H-P}} \approx 300$ Hz, $^2J_{\text{P-P}} \approx 300$ Hz, $^3J_{\text{H-P}} \approx 6.9$ Hz, 1, P-H), 7.14-6.48 (m's, 3, H4, H3, H2), 5.17 (d, $J_{\text{H-H}} = 17.0$ Hz, H1_{anti}), 4.96 (d, $J_{\text{H-H}} = 9.0$ Hz, H1_{syn}), 1.35 (br m, 12, PEt_3 CH_2 's), 0.98 (br m, 18, PEt_3 CH_3 's).

$^{13}\text{C}\{^1\text{H}\}$ NMR (C_6D_6 , 25 °C): δ 146.7 (C4), 138.7 (C2), 129.8 (C3), 115.0 (C1), 25.1 (PEt_3 CH_2 's), 23.2 (PEt_3 CH_2 's), 9.3 (PEt_3 CH_3 's), 8.7 (PEt_3 CH_3 's).

$^{31}\text{P}\{^1\text{H}\}$ NMR (C_6D_6 , 25 °C): δ 66.4 (br m, 1, phosphido P), 1.0 (br m, 1, PEt_3), -10.0 (br m, 1, PEt_3).

Synthesis of $[(\mu\text{-}\eta^1\text{-Phosphapentadienyl})\text{Ir}(\text{PEt}_2\text{Ph})_2]$ (2). Compound **2** was synthesized and isolated in a manner directly analogous to the synthesis of compound **1**, using diethylphenylphosphine in place of triethylphosphine. Yield: 60%.

Trans Isomer 2a. $^1\text{H NMR}$ (C_6D_6 , 25 °C): δ 9.03 (AA'XX' multiplet, $^1J_{\text{H-P}} \approx 300$ Hz, $^2J_{\text{P-P}} \approx 300$ Hz, $^3J_{\text{H-P}} \approx 6.9$, 1, P-H), 7.67-7.00 (m's, 10, PEt_2Ph Ph's), ~ 6.95 (br m, partially obscured by PEt_2Ph Ph's, 1, H3), 6.70 (br m, 1, H4), 6.58 (m, 1, H2), 5.31 (d, $J_{\text{H-H}} = 14.1$ Hz, 1, H1_{anti}), 5.08 (d, $J_{\text{H-H}} = 9.6$ Hz, 1, H1_{syn}), 1.85-1.18 (m's, 8, PEt_2Ph CH_2 's), 0.85 (br m, 6, PEt_2Ph CH_3 's), 0.67 (br m, 6, PEt_2Ph CH_3 's).

$^{31}\text{P}\{^1\text{H}\}$ NMR (C_6D_6 , 25 °C): δ 71.1 (quintet, $J_{\text{P-P}} = 18.5$ Hz, 1, phosphido P), -2.1 (triplet, $J_{\text{P-P}} = 18.5$ Hz, 2, PEt_2Ph 's).

Cis Isomer 2b. $^{31}\text{P}\{^1\text{H}\}$ NMR (C_6D_6 , 25 °C): δ 71.1 (br m, 1, phosphido P), 5.3 (br m, 1, PEt_2Ph), -10.1 (br m, 1, PEt_2Ph).

Synthesis of Diethyl (Dimethylbutadienyl)phosphonate $[\text{CH}_2=\text{C}(\text{Me})\text{CH}=\text{C}(\text{Me})\text{P}(\text{O})(\text{OEt})_2]$. A slurry of lithium diisopropylamide (LDA) (11.0 g, 0.103 mol) in 70 mL of THF and 70 mL of pentane was cooled to -78 °C. Diethyl ethylphosphonate (8.14 g, 0.049 mol) in 15 mL of THF was added via addition funnel. Stirring was maintained for 5 min, as the reaction temperature was allowed to return to -78 °C. Diethyl chlorophosphate (8.89 g, 0.052 mol) in 20 mL of THF was added by cannulation. The reaction mixture was allowed to stir for 15 min at -78 °C, and then the dry ice/acetone bath was replaced with a -23 °C bath ($\text{CCl}_4/\text{dry ice}$) to complete the reaction (stirred ~ 30 min at -23 °C). Methacrolein (3.85 g, 0.055 mol) in 10 mL of THF was added to the reaction mixture via cannula. The -23 °C bath was then removed, and the reaction was allowed to stir for 2 h. Water (35 mL) was then added to the reaction mixture, and the solution was transferred to a separatory funnel. The solution was extracted with Et_2O (3 \times 50 mL), and the organic layer was dried over Na_2SO_4 . Diethyl ether was removed by vacuum aspiration, leaving diethyl (dimethylbutadienyl)phosphonate behind as a yellow liquid. This phosphonate product was further purified by distillation under vacuum. Yield: 7.06 g (66%) of spectroscopically pure light yellow liquid.

$^1\text{H NMR}$ (C_6D_6 , 22 °C): δ 7.25 (d, $J_{\text{H-P}} = 25$ Hz, 1, H3), 4.95 (s, 1, H1), 4.89 (s, 1, H1), 3.95 (m, 4, OEt CH_2 's), 1.97 (d, $J_{\text{H-P}} = 15$ Hz, 3, H6's), 1.62 (s, 3, H5's), 1.06 (t, $J_{\text{H-H}} = 7$ Hz, 6, OEt CH_3 's).

$^{31}\text{P}\{^1\text{H}\}$ NMR (C_6D_6 , 22 °C): δ 22.5 (s).

Synthesis of (Dimethylbutadienyl)phosphine $[\text{CH}_2=\text{C}(\text{Me})\text{CH}=\text{C}(\text{Me})\text{PH}_2]$. Dichloroalane was prepared *in situ* by the addition of AlCl_3 (21.3 g, 0.16 mol) to lithium aluminum hydride (LAH) (2.02 g, 0.053 mol) in 250 mL of tetraglyme at -20 °C. This slurry was allowed to stir for 30 min as it warmed to room temperature. The dichloroalane solution was then placed under dynamic vacuum, connected to a trap cooled with liquid nitrogen (-178 °C). Diethyl (dimethylbutadienyl)phosphonate (5.46 g, 0.025 mol) was added slowly (~ 30 min) to the AlHCl_2 solution, and (dimethylbutadienyl)phosphine was isolated in the cold trap as it was formed (~ 8 h). This phosphine product was further purified by trap-to-trap distillation in a tube equipped with an airtight stopcock and quickly transferred to a -40 °C freezer. Yield: 2.3 g (81%) of spectroscopically pure colorless liquid.

$^1\text{H NMR}$ (C_6D_6 , 25 °C): δ 6.33 (d, $J_{\text{H-P}} = 17$ Hz, 1, H3), 4.93 (s, 1, H1), 4.76 (s, 1, H1), 3.44 (d, $J_{\text{H-P}} = 194$ Hz, 2, P-H's), 1.88 (d, $J_{\text{H-P}} = 6$ Hz, 3, H6's), 1.62 (s, 3, H5's).

$^{31}\text{P}\{^1\text{H}\}$ NMR (C_6D_6 , 25 °C): δ -105.9 (s).

Synthesis of Lithium 2,4-Dimethylphosphapentadienide. Lithium 2,4-dimethylphosphapentadienide was synthesized in a manner directly analogous to the synthesis of lithium phosphapentadienide. Yield: 92%.

$^1\text{H NMR}$ (d_8 -THF, 25 °C): δ 5.73 (d, $J_{\text{H-P}} = 7.5$ Hz, 1, H3), 4.16 (s, 2, H1's), 2.06 (d, $J_{\text{H-P}} = 160$ Hz, P-H), 1.97 (d, $J_{\text{H-P}} = 9.8$ Hz, 3, H6's), 1.65 (s, 3, H5's).

$^{13}\text{C}\{^1\text{H}\}$ NMR (d_8 -THF, 25 °C): δ 159.8 (d, $J_{\text{C-P}} = 44$ Hz, C4), 143.6 (s, C2), 117.2 (d, $J_{\text{C-P}} = 16$ Hz, C3), 103.2 (s, C1), 26.4-25.8 (C5, C6).

$^{31}\text{P}\{^1\text{H}\}$ NMR (d_8 -THF, 25 °C): δ -75.0 (s).

^{31}P NMR (d_8 -THF, 25 °C): δ -75.0 (d, $^1J_{\text{P-H}} = 160$ Hz).

Synthesis of $[(\mu\text{-}\eta^1\text{-2,4-Dimethylphosphapentadienyl})\text{Ir}(\text{PEt}_3)_2]$ (3). Compound **3** was synthesized in a manner directly analogous to Compound **1**. The equilibrium ratio of the *trans*:*cis* isomers was 8:1. Yield: 40% crystalline **3a**. Anal. Calcd for $\text{C}_{36}\text{H}_{80}\text{Ir}_2\text{P}_6$: C, 39.91; H, 7.46. Found: C, 39.39; H, 7.51.

Trans Isomer 3a. $^1\text{H NMR}$ (C_6D_6 , 25 °C): δ 9.31 (AA'XX' multiplet, $^1J_{\text{H-P}} = 293.5$ Hz, $^2J_{\text{P-P}} = 300$ Hz, $^3J_{\text{H-P}} = 6.5$ Hz, 1, P-H), 6.39 (inverted t, $J = 18.6$ Hz, 1, H3), 5.07 (s, 1, H1), 5.03 (s, 1, H1), 2.46 (inverted t, $J = 10.5$ Hz, 3, H6's), 2.00 (s, 3, H5's), 1.41 (br m, 12, PEt_3 CH_2 's), 1.00 (br m, 18, PEt_3 CH_3 's).

$^{13}\text{C}\{^1\text{H}\}$ NMR (C_6D_6 , 25 °C): δ 145.1 (br s, C4 or C2), 143.1 (virtual triplet, $J_{\text{C-P}} = 15$ Hz, C2 or C4), 135.2 (virtual triplet,

$J_{C-P} = 21$ Hz, C3), 113.8 (C1), 24.1 (C5), 24.0 (PEt₃ CH₂'s), 20.8 (virtual triplet, $J_{C-P} = 15$ Hz, C6), 9.0 (PEt₃ CH₃'s).

³¹P{¹H} NMR (C₆D₆, 25 °C): δ 109.2 (quintet, $J_{P-P} = 20.0$ Hz, 1, phosphido P), -6.0 (triplet, $J_{P-P} = 20.0$ Hz, 2, PEt₃'s).

Cis Isomer 3b (from a Mixture of 3a and 3b). ³¹P{¹H} NMR (C₆D₆, 25 °C): δ 99.8 (m, 1, phosphido P), -0.5 (m, 1, PEt₃), -16.5 (m, 1, PEt₃).

Single Crystal X-ray Diffraction Study. A single crystal of **3a** (C₃₆H₈₀Ir₂P₆, red prism, 0.58 mm × 0.36 mm × 0.44 mm) was sealed in a glass capillary under inert atmosphere. Data were collected at 295 K on a Siemens R3m/V diffractometer using graphite monochromated Mo K α radiation ($\lambda = 0.71073$ Å). All data reduction and refinement were done using the Siemens SHELXTL PLUS package on a Micro VAX II computer.²⁴ Crystal data and details of data collection and structure analysis are summarized as follows: triclinic, $P\bar{1}$, $a = 11.756(4)$ Å, $b = 12.011(3)$ Å, $c = 17.716(7)$ Å, $\alpha = 93.50(3)^\circ$, $\beta = 92.89(3)^\circ$, $\gamma = 108.67(3)^\circ$, $V = 2359.0(15)$ Å³, $Z = 2$, $d_{\text{calcd}} = 1.511$ g/cm³, $\mu = 58.60$ cm⁻¹, θ - 2θ scanning technique, $+h, \pm k, \pm l$ collected, 9422 reflections with $3^\circ < 2\theta < 50^\circ$, 8291 independent reflections, 5876 reflections with $I > 3\sigma(I)$ used in refinement, semi-empirical absorption correction (min/max transmission factors = 0.4421/0.8876), $R = 0.0277$, $R_w = 0.0345$, goodness-of-fit = 0.95.

The positions of the iridium atoms were determined by direct methods. Remaining non-hydrogen atoms were found by successive full matrix least-squares refinement and difference Fourier map calculations. The iridium atoms, phosphorus

atoms, and carbon atoms were refined anisotropically. The phosphido hydrogens were located and refined isotropically. Hydrogen atoms for the terminal methylene and methyl groups of the phosphapentadienyl ligands were not included in the structure solution due to ambiguity in assigning these groups (*vide supra*). The remaining hydrogen atoms on the phosphapentadienyl ligands and phosphine ligands were placed at idealized positions and assumed the riding model. A common isotropic U value was refined.

Acknowledgment. We thank the National Science Foundation (Grants CHE-9003159 and CHE-9303516) and the donors of the Petroleum Research Fund, administered by the American Chemical Society, for support of this research. A loan of IrCl₃·3H₂O from Johnson-Matthey Alfa/Aesar is gratefully acknowledged. Washington University's X-ray Crystallography Facility was funded by the National Science Foundation's Chemical Instrumentation Program (Grant CHE-8811456). The High Resolution NMR Service Facility was funded in part by National Institutes of Health Biomedical Support Instrument Grant 1 S10 RR02004 and by a gift from Monsanto Co.

Supplementary Material Available: Tables containing a structure determination summary, final atomic coordinates, thermal parameters, bond lengths, and bond angles, and ORTEP drawings for the two crystallographically independent molecules of compound **3a** (11 pages). Ordering information is given on any current masthead page.

OM940934U

(24) Atomic scattering factors were obtained from the following: *International Tables for X-Ray Crystallography*; Kynoch Press: Birmingham, England, 1974; Vol. IV.

Chains and Stars in Organoplatinum Oligomers

Sudhir Achar and Richard J. Puddephatt*

Department of Chemistry, University of Western Ontario, London, Canada N6A 5B7

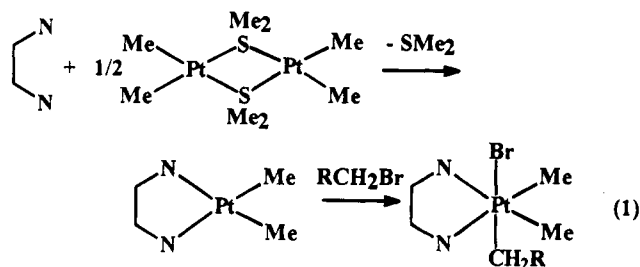
Received December 6, 1994[®]

A method for synthesis of new oligomers and a polymer containing organoplatinum centers is reported. Reaction of [PtMe₂(bu₂bipy)], **1b**, bu₂bipy = 4,4'-di-*tert*-butyl-2,2'-bipyridine, with 4-(bromomethyl)-4'-methyl-2,2'-bipyridine, **A**, gave the complex [PtBrMe₂(bu₂bipy)-(CH₂C₅H₃NC₅H₃NMe)], **2**, by oxidative addition of the C-Br bond to platinum(II). Reaction of **2** with [Pt₂Me₄(μ-SMe₂)₂], **B**, gave the Pt^{IV}Pt^{II} complex [PtBrMe₂(bu₂bipy)(μ-CH₂C₅H₃NC₅H₃NMe)PtMe₂], **3**, by displacement of the Me₂S ligands from **B** by the free bipyridine group of **2** to regenerate a reactive dimethylplatinum(II) center. Repetition of this cycle of reactions gave [PtBrMe₂(bu₂bipy){(μ-CH₂C₅H₃NC₅H₃NMe)PtBrMe₂}_n(CH₂C₅H₃NC₅H₃NMe)] (**4**, *n* = 1; **6**, *n* = 2) and [PtBrMe₂(bu₂bipy){(μ-CH₂C₅H₃NC₅H₃NMe)PtBrMe₂}_n(μ-CH₂C₅H₃NC₅H₃NMe)PtMe₂] (**5**, *n* = 1; **7**, *n* = 2). Reaction of **A** with **B** gave the insoluble polymer [{PtBrMe₂(μ-CH₂C₅H₃NC₅H₃NMe)]_n. Star-shaped oligomers containing platinum(IV) centers were obtained by reaction of 1,2,4,5-(BrCH₂)₄C₆H₂ with the complexes **1**, **3**, or **5** to give 1,2,4,5-[PtBrMe₂(bu₂bipy){(μ-CH₂C₅H₃NC₅H₃NMe)PtBrMe₂]_nCH₂]₄-C₆H₂ (*n* = 0, **10b**; *n* = 1, **11**; and *n* = 2, **12**, respectively).

Introduction

There is considerable current interest in the design and synthesis of oligomers and polymers having novel linear or branched structural features, which in the future may prove useful in "nanostructures", supermolecules, and new types of polymers.¹ The development of new strategies for synthesis of organic, organometallic, and inorganic compounds with branched structures of either "star" or "dendrimer" architecture has been a prominent feature in the explosive growth of this field.¹ It is a particular challenge in inorganic and organometallic chemistry where techniques for stepwise growth of oligomeric structures are still relatively undeveloped. There are a number of potential applications, for example as light harvesting antennae.¹ The project described below addresses the problem of how oligomeric organometallic compounds with "star" structures can be synthesized.

Complexes of the type [PtMe₂(NN)], **1**, in which NN represents a diimine ligand such as 2,2'-bipyridine, are very reactive in oxidative addition of alkyl halides, and this reaction has been used to synthesize many functionally substituted organoplatinum(IV) complexes.¹ For example, introduction of vinyl groups is easy and can give useful monomers for free radical initiated polymerization, yielding organoplatinum(IV) polymers, while use of bifunctional alkyl halides can give hydrocarbyl-bridged binuclear organoplatinum(IV) complexes.² The diimine complexes **1** are themselves easily prepared by displacement of Me₂S ligands from [Pt₂Me₄(μ-SMe₂)₂].² The sequence of reactions leading to functionally substituted organoplatinum(IV) complexes is shown in eq 1, R = functional substituent. If the group R contained



a diimine group, it follows that a second dimethylplatinum(II) group could be introduced and that repetition of the sequence could give organoplatinum oligomers. An adaptation of this method has recently been used to synthesize several oligomeric organoplatinum dendrimers, containing up to 28 platinum atoms.³ This article shows how oligomeric organoplatinum(IV) complexes in the form of chains or stars can be synthesized by using the basic reactions of eq 1 with the alkyl halide being 4-(bromomethyl)-4'-methyl-2,2'-bipyridine.

Results and Discussion

Synthesis of Chain Oligomers. The synthesis of the chain oligomers is outlined in Scheme 1. The platinum(II) complex [PtMe₂(bu₂bipy)], **1b**, bu₂bipy = 4,4'-di-*tert*-butyl-2,2'-bipyridine, was chosen as the plat-

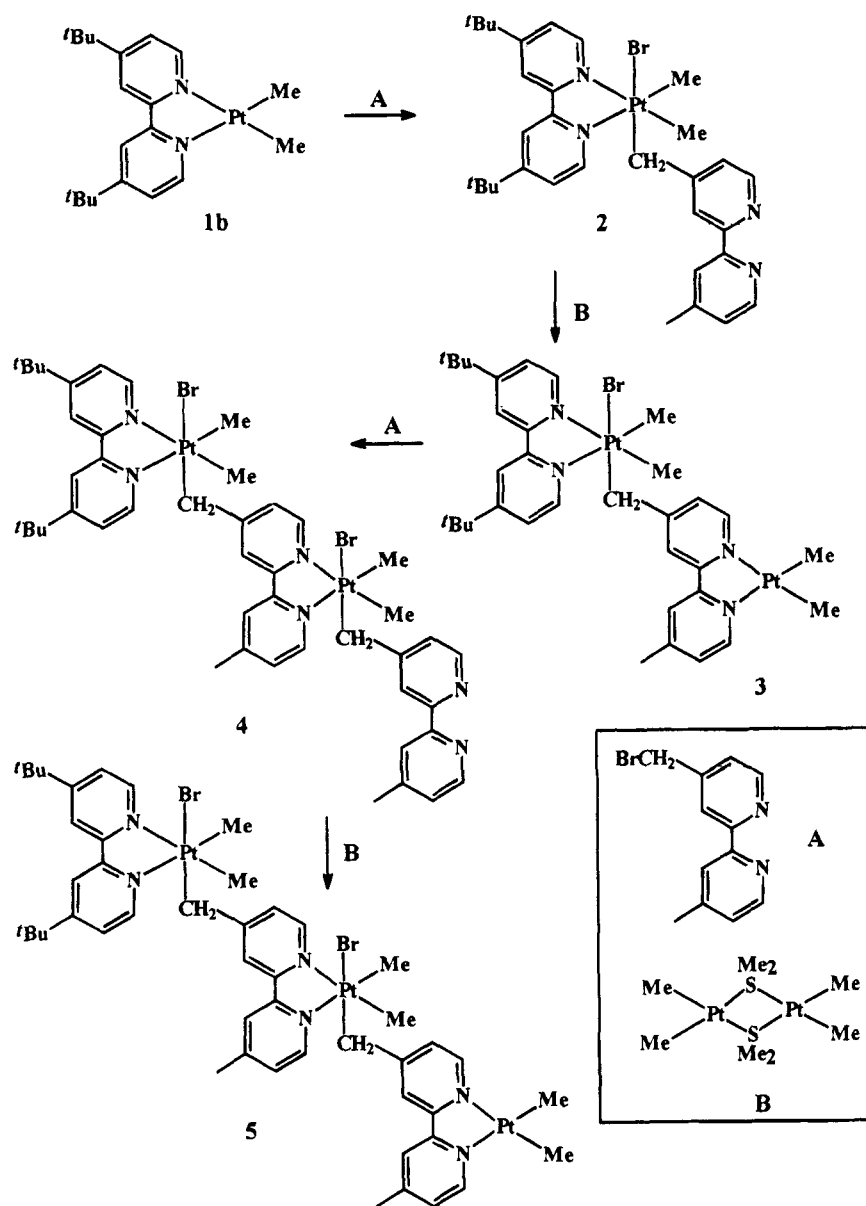
(2) (a) Jawad, J. K.; Puddephatt, R. J. *Organomet. Chem.* **1976**, *117*, 297. (b) Jawad, J. K.; Puddephatt, R. J. *J. Chem. Soc., Dalton. Trans.* **1977**, 1466. (c) Ferguson, G.; Parvez, M.; Monaghan, P. K.; Puddephatt, R. J. *J. Chem. Soc., Chem. Commun.* **1983**, 267. (d) Monaghan, P. K.; Puddephatt, R. J. *Organometallics* **1984**, *3*, 444. (e) Monaghan, P. K.; Puddephatt, R. J. *Organometallics* **1985**, *4*, 1406. (f) Scott, J. D.; Puddephatt, R. J. *Organometallics* **1986**, *5*, 1538. (g) Crespo, M.; Puddephatt, R. J. *Organometallics* **1987**, *6*, 2548. (h) Monaghan, P. K.; Puddephatt, R. J. *J. Chem. Soc., Dalton. Trans.* **1988**, 595. (i) Aye, K. T.; Canty, A. J.; Crespo, M.; Puddephatt, R. J.; Scott, J. D.; Watson, A. A. *Organometallics* **1989**, *8*, 1518. (j) Scott, J. D.; Puddephatt, R. J. *Organometallics* **1993**, *2*, 1643. (k) Achar, S.; Scott, J. D.; Puddephatt, R. J. *Organometallics* **1992**, *11*, 2325. (l) Achar, S.; Scott, J. D.; Vittal, J. J.; Puddephatt, R. J. *Organometallics* **1993**, *12*, 4592.

(3) (a) Achar, S.; Puddephatt, R. J. *Angew. Chem., Int. Ed. Engl.* **1994**, *33*, 847. (b) Achar, S.; Puddephatt, R. J. *J. Chem. Soc., Chem. Commun.* **1994**, 1895.

[®] Abstract published in *Advance ACS Abstracts*, March 1, 1995.

(1) (a) Mekelburger, H.-B.; Jaworek, W.; Vogtle, F. *Angew. Chem., Int. Ed. Engl.* **1992**, *31*, 1571. (b) Webber, S. E. *Chem. Rev.* **1990**, *90*, 1469. (c) Juris, A.; Balzani, V.; Campagna, S.; Denti, G.; Serroni, S.; Frei, G.; Gudel, H. U. *Inorg. Chem.* **1994**, *33*, 1491. (d) Seebach, D.; Lapierre, J. M.; Greiveldinger, G.; Skobridis, K. *Helv. Chim. Acta* **1994**, *77*, 1673.

Scheme 1



inimum(II) substrate since the bu_2bipy ligand gives complexes with higher solubility than the corresponding complexes of 2,2'-bipyridine. Complex **1b** is orange red in color due to the presence of a platinum(II)-diimine(π^*) metal to ligand charge transfer (MLCT) band in the visible region,⁴ and the platinum(IV) products of oxidative addition are colorless or pale yellow since the MLCT band is shifted to higher energy. Hence reactions are easily monitored by visible spectroscopy or simply by observing the bleaching of color as the platinum(II) complex is consumed.

The $\text{CH}_2\text{-Br}$ group of the reagent 4-(bromomethyl)-4'-methyl-2,2'-bipyridine, **A**, added rapidly to **1b** to give the pale yellow platinum(IV) complex **2**. The stereochemistry of the product **2** was established from the ^1H NMR spectrum. There was a single MePt resonance, a single *t*-Bu resonance and a single CH_2Pt resonance. Hence there must be a mirror plane and the product must be formed by *trans* oxidative addition. Close inspection showed the presence of two very low intensity

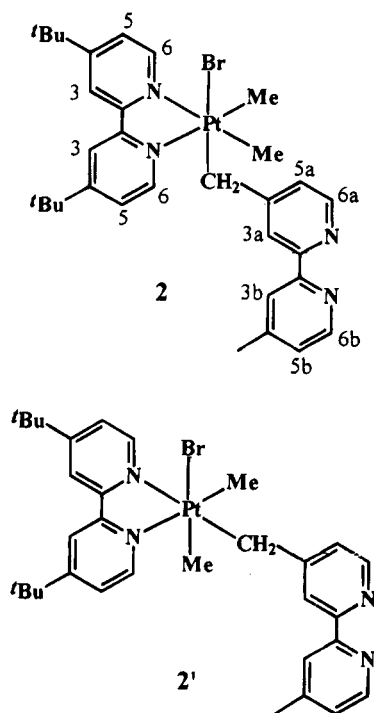
MePt resonances, assigned to a trace amount (*ca* 3%) of the product of *cis* oxidative addition, **2'**. No other resonances of the minor product were resolved, but all resonances of the major isomer were easily identified and assigned (see the Experimental Section). The protons H^{3a} , H^{5a} , and H^{6a} (see structure **2** in Chart 1) appear in the unusual chemical shift range $\delta = 6.5\text{--}7.1$ whereas H^{3b} , H^{5b} , and H^{6b} have more typical aromatic proton chemical shifts in the range $\delta = 7.9\text{--}8.4$. The assignment of the H^{3a} and H^{5a} resonances is confirmed by the observation of satellites due to coupling to ^{195}Pt , with $^4J(\text{PtH}) = 11$ and 12 Hz, respectively. The pattern of aromatic chemical shifts is attributed to the complex having a preferred conformation with the pyridyl group containing $\text{H}^{3a}\text{--H}^{6a}$ lying under the bu_2bipy ligand where the ring current effect can lead to shielding of the aromatic protons. A similar effect has been observed for some related benzylplatinum(IV) complexes.^{2,5}

The complex $[\text{Pt}_2\text{Me}_4(\mu\text{-SMe}_2)_2]$, **B**, is a convenient

(4) Chaudhury, N.; Puddephatt, R. J. *J. Organomet. Chem.* **1975**, *84*, 105.

(5) Byers, P. K.; Canty, A. J. *J. Chem. Soc., Chem. Commun.* **1988**, 639.

Chart 1



source of $\text{Me}_2\text{Pt}^{\text{II}}$ units by displacement of the SMe_2 ligands.² Thus the free bipyridine substituent in **2** can act as a ligand to displace Me_2S from **B** to give the mixed oxidation state $\text{Pt}^{\text{IV}}\text{Pt}^{\text{II}}$ complex **3**. Since a new bipyridine platinum(II) center is formed in this reaction, a color change from very pale yellow to red-orange is observed, due to a MLCT band in the visible region [platinum(II) $5d-\pi^*$ (diimine)].⁴ Many features of the ^1H NMR spectrum of **3** are similar to those in complex **2**, with the spectrum of **3** having two extra singlet resonances due to the new $\text{Me}_2\text{Pt}^{\text{II}}$ group, each having satellites due to coupling to ^{195}Pt with $^2J(\text{PtH}) = 83$ Hz.² Again, all resonances were sharp and well-resolved and full assignments are given in the Experimental Section. The FAB mass spectrum of **3** displays peaks due to $[\text{M} + 2]$ and $[\text{M} - (\text{Br} + 2\text{Me})]$.

The synthesis of complex **3** represents the end of the first growth cycle in which a dimethylplatinum(II) center undergoes oxidative addition, followed by generation of a new dimethylplatinum(II) center which is then able to participate in the next cycle (Scheme 1). The reaction between **3** and **A** gave the $\text{Pt}^{\text{IV}}\text{Pt}^{\text{IV}}$ complex **4**, which was easily isolated as a pale yellow solid. Unlike **2** and **3**, complex **4** cannot contain a plane of symmetry and so the ^1H NMR spectrum is considerably more complex. The spectrum contained two singlets due to the *t*-Bu groups at $\delta = 1.29$ and 1.41 , four MePt^{IV} resonances at $\delta = 1.20, 1.23, 1.53,$ and 1.57 each with satellites due to coupling to ^{195}Pt with $^2J(\text{PtH}) = 69-70$ Hz and two singlets due to the MeC groups at $\delta = 2.21$ and 2.38 . The CH_2Pt groups each gave an "AB" pattern, with overlapping peaks in the region $\delta = 2.45-3.00$; nonequivalence of the $\text{CH}^a\text{H}^b\text{Pt}$ protons is expected as a result of the lower symmetry of **4**. The aromatic protons of the bipyridine groups appeared at $\delta = 6.0-8.8$; 18 resonances are expected, but only 12 were resolved as separate peaks so full assignment was not attempted. The mass spectrum of **4** failed to show a molecular ion peak at $m/z = 1242$, but the highest mass

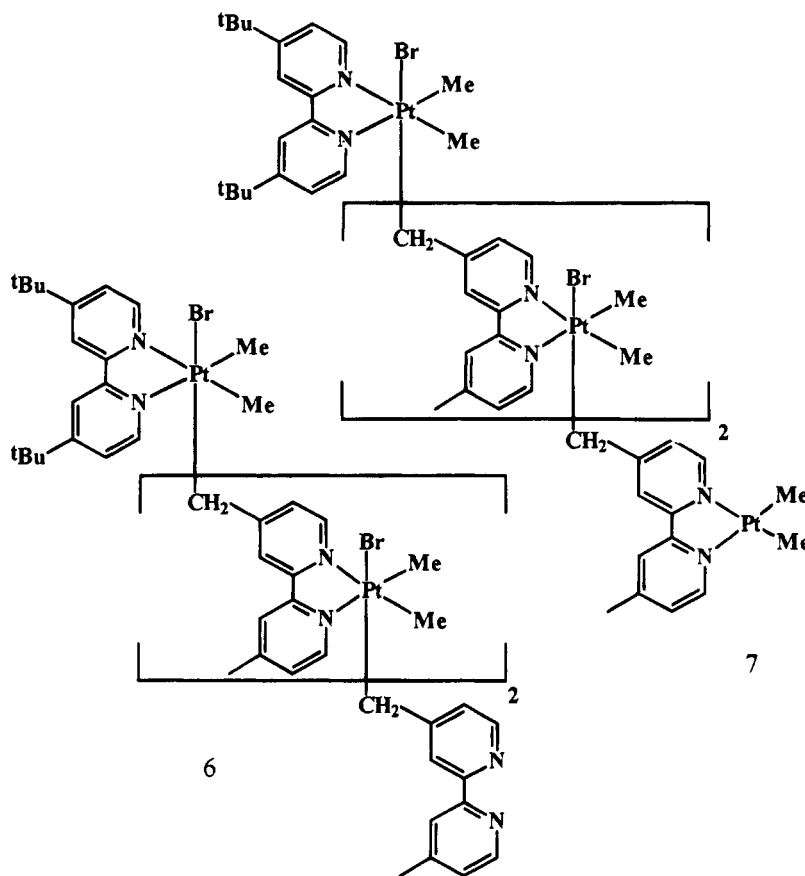
observed was at $m/z = 1212$ due to loss of two methyl groups.

Complex **4**, dissolved in benzene, reacted with **B** to give the red complex **5**, thus completing the second growth cycle. Complex **5** is a trinuclear $\text{Pt}^{\text{IV}}_2\text{Pt}^{\text{II}}$ complex. The ^1H NMR spectrum was similar to that of **4** but with two additional resonances due to the $\text{Me}_2\text{Pt}^{\text{II}}$ group at $\delta = 0.70$ and 0.82 , each with $^2J(\text{PtH}) = 82$ Hz.

In principle, the growth cycles should be capable of repetition to grow continually larger organoplatinum oligomers, but problems arise as the molecules grow in size. First, there is a general decrease in solubility with chain length, following the sequence $1 > 2 > 3 > 4 > 5$. All have reasonable solubility in dichloromethane, but those containing Pt^{II} centers react slowly with this solvent by oxidative addition of a C-Cl bond to the platinum(II) center,² and so this solvent cannot be used for synthetic reactions. Complexes **1**, **2**, and **3** are soluble in acetone but **4** and **5** are not. Complex **4** is soluble in benzene and **5** is soluble in acetone/benzene mixture though not in either solvent alone. Characterization by ^1H NMR and by FAB MS becomes more difficult as the molecular size increases further. We have completed one further growth cycle to give complexes **6** and **7** (Chart 2), but characterization of these complexes is less secure than for the complexes **1-5**. For example, in the ^1H NMR spectrum of **6**, the three MeC resonances were resolved but the MePt^{IV} groups overlapped and were not clearly resolved. There was no MePt^{II} resonance and the complex was pale yellow, thus proving that the oxidative addition reaction occurred quantitatively. Complex **7** was sparingly soluble in all common organic solvents and was clearly unsuitable as a precursor to further growth cycles.

Synthesis of an Organoplatinum Polymer. Reaction of the dimethylplatinum(II) complex **B** with reagent **A** occurred to give a red solution, which then became purple in color and finally became paler as a yellow powder precipitated from solution. This solid analyzed as $[\{\text{PtMe}_2\text{Br}(\text{CH}_2\text{C}_5\text{H}_3\text{NC}_5\text{H}_3\text{NMe})\}_n]$, **8**. These results are interpreted in terms of the reactions shown in Scheme 2. The first step involves displacement of SMe_2 from **B** by the bipyridyl group of **A**. This yields a dimethylplatinum(II) complex with an appended CH_2Br group, **9**. The geometry does not allow intramolecular oxidative addition to occur so intermolecular oxidative addition occurs instead. The dimethylplatinum(II) groups which give rise to the intense colors are then consumed, and the polymeric platinum(IV) product eventually precipitates. Monitoring by ^1H NMR at low temperature did not indicate any buildup of a long-lived intermediate. Hence it is deduced that the intermediate dimethylplatinum(II) complexes undergo oxidative addition at a rate competitive with their formation. The polymer was insoluble in acetone, benzene, and chlorinated solvents but did dissolve in dimethyl sulfoxide. A ^1H NMR spectrum of the polymer in $\text{dms-}d_6$ contained broad peaks characteristic of organoplatinum polymers. There were resonances in the aromatic and aliphatic regions having the expected intensities, but individual resonances were not resolved. There were no signals in the region $\delta = 4-5$ implying that all the bromomethyl groups had undergone the oxidative addition reaction. Because of the low solubility, the molecular weight of the polymer could not

Chart 2



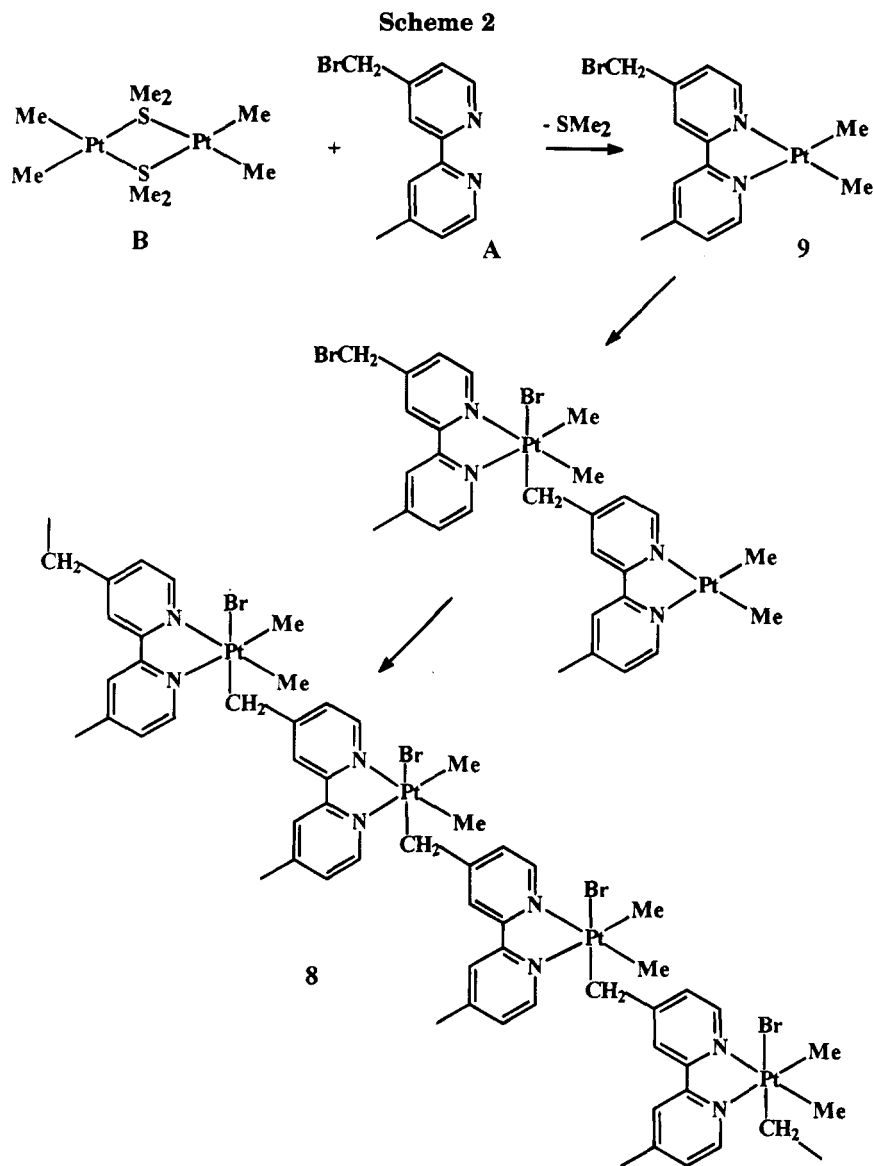
be determined. Scheme 2 shows the first proposed intermediate, a possible next step, and the final polymer in idealized form.

Synthesis of Star-Shaped Platinum(IV) Complexes. In the synthesis of dendrimeric organoplatinum(IV) complexes, it was found that the solubility of the products increased with increasing branching.³ Therefore, an attempt to synthesize more soluble oligomers by introducing branching was made. The results are shown in Scheme 3. The key reagent for this work is 1,2,4,5-tetrakis(bromomethyl)benzene, **C**, which can react with four organoplatinum(II) centers by oxidative addition of the C–Br bonds. Reagent **C** reacted with [PtMe₂(bipy)], bipy = 2,2'-bipyridine, to give the product [1,2,4,5-{PtBrMe₂(bipy)CH₂}₄C₆H₂], **10a**, which was very sparingly soluble. Fortunately, the corresponding product, **10b**, from [PtMe₂(bu₂bipy)] was soluble and was readily characterized by NMR. The ¹H NMR spectrum contained two MePt^{IV} resonances at $\delta = 0.77$ and 0.88 , each with ²J(PtH) = 68 Hz, and the CH₂Pt group gave rise to an "AB" spectrum with $\delta = 2.15$ [²J(PtH) = 91 Hz, ²J(HH) = 8 Hz] and *ca.* 1.5 [partly obscured by a *t*-Bu resonance. The nonequivalence of the Me₂Pt and CH₂Pt protons is expected since no plane of symmetry bisecting these groups is possible in **10**. The ¹⁹⁵Pt NMR spectrum of **10b** contained a sharp singlet at $\delta = -870$, thus proving the equivalence of the four platinum atoms. Molecular mechanics calculations, as well as simple steric considerations, suggest a conformation with *ortho* CH₂Pt substituents mutually *anti* with respect to the C₆H₂ ring as shown in Scheme 3.

In a similar way, reaction of **3** or **5** with **C** gave the star-shaped oligomers **11** and **12**, containing eight and

twelve platinum atoms, respectively, as shown in Scheme 3. The ¹H NMR spectra of these complexes contained only broad, poorly resolved resonances, but the integration of the spectra, together with the analytical data, supported the proposed formulations. For example, the spectrum of **11** gave envelopes of peaks at $\delta = 0.6$ – 1.8 (120 H, MePt + *t*-Bu), 2.1–3.2 (28H, CH₂Pt + MeC) and 6.0–8.8 (50H, aromatic protons). The ¹⁹⁵Pt NMR spectrum contained two resonances of equal intensity, a sharp resonance at $\delta = -911$ [with three partly resolved components at $\delta = -908, -911, -913$] and a broad resonance at $\delta = -855$. We suggest that the conformation of the C₆H₂(CH₂Pt)₄ unit is rigidly fixed but that more than one conformation of the outer shell of organoplatinum(IV) groups is possible, leading to non-equivalence. Because of steric hindrance to rotation about the C₆H₂–CH₂ and CH₂–Pt bonds, these less symmetrical conformations are essentially frozen on the NMR time scale and lead to broad resonances in both the ¹H and ¹⁹⁵Pt NMR spectra. Complex **12** contains a total of 516 atoms and has a calculated molecular weight of 6330. It is considerably more soluble than the linear precursor **5**, presumably as a result of the increased branching.

In order to obtain information about the size of the oligomers, GPC analysis of the platinum complexes **5**, **10b**, **11**, and **12** was carried out using THF solvent and polystyrene standards. The absolute molecular weights cannot be expected to be correct since the standards are linear and organic while the complexes have heavy metal content and, for **10b**–**12**, are not linear. Nevertheless, there is a correlation of the apparent molecular weight determined by GPC and the expected molecular weight, although it is not a linear relationship as shown



in Figure 1. The data are fully consistent with the proposed formulations.

Differential scanning calorimetric (DSC) and thermogravimetric analysis (TGA) were carried out on the linear organoplatinum complexes 2–7 and on the polymer 8. DSC thermograms revealed that only the complexes 2 and 3 exhibited melting endotherms prior to decomposition. TGA studies on the above complexes (Table 1) indicated that all of them decomposed over a wide temperature range, in most cases leaving a residue of metallic platinum, confirmed by XPS and EDX analysis on the residue.

Conclusions

A successful strategy for the step by step synthesis of linear, oligomeric organoplatinum complexes has been developed on the basis of oxidative addition reactions. The reactions occur in very high yield, but the ability to grow large oligomers is limited since the solubility decreases with chain length. An extension of the synthetic method gave the first examples of star-shaped multinuclear organoplatinum complexes. There are few examples of star type oligomers or polymers,^{1,6} and most are organic in nature. An organometallic example is

found in the reaction of $\text{Na}[\text{Co}(\text{CO})_4]$ with 1,2,4,5-tetrakis(bromomethyl)benzene to yield 1,2,4,5-tetrakis-((σ -methylene)tetracarbonyl)cobalt)benzene, which possesses four cobalt centers.⁷ This is closely related to the method used in the present work, but combination of the star-forming reaction with the method of growing linear oligomers has made it possible to form higher molecular weight oligomers based on organoplatinum compounds. The synthesis of unusual mixed oxidation state complexes⁸ as well as a new type of organometallic polymer⁹ is established in this work.

Experimental Section

The ^1H NMR spectra were recorded by using Varian Gemini 200 or XL-300 spectrometers, and ^{195}Pt spectra (on the more soluble complexes only), by using the XL-300 spectrometer. Chemical shifts are reported with respect to TMS or $\text{K}_2[\text{PtCl}_4]$. Mass spectra were recorded by using a Finnigan MAT 8320

(6) Jerome, R.; Henriouille-Granville, M.; Boutevin, B.; Robin, J. J. *Prog. Polym. Sci.* **1991**, *16*, 837.

(7) Ullah, S. S.; Azam, K. A.; Hashem, M. A.; Ahmed, I.; Karim, M. M.; Khan, S. M. A. *Indian J. Chem.* **1987**, *26A*, 831.

(8) Anderson, G. K. *Adv. Organomet. Chem.* **1993**, *35*, 1.

(9) (a) Pittman, C. U., Jr. *New Monomers and Polymers*; Plenum Press: New York, 1984. (b) Tomalia, D. A.; Naylor, A. M.; Goddard, W. A., III. *Angew. Chem., Int. Ed. Engl.* **1990**, *29*, 138.

Scheme 3

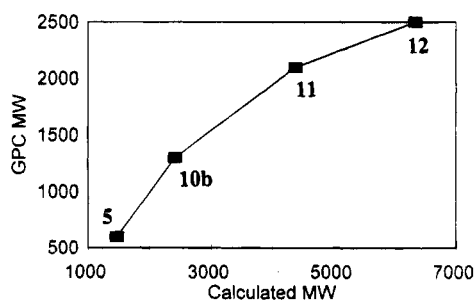
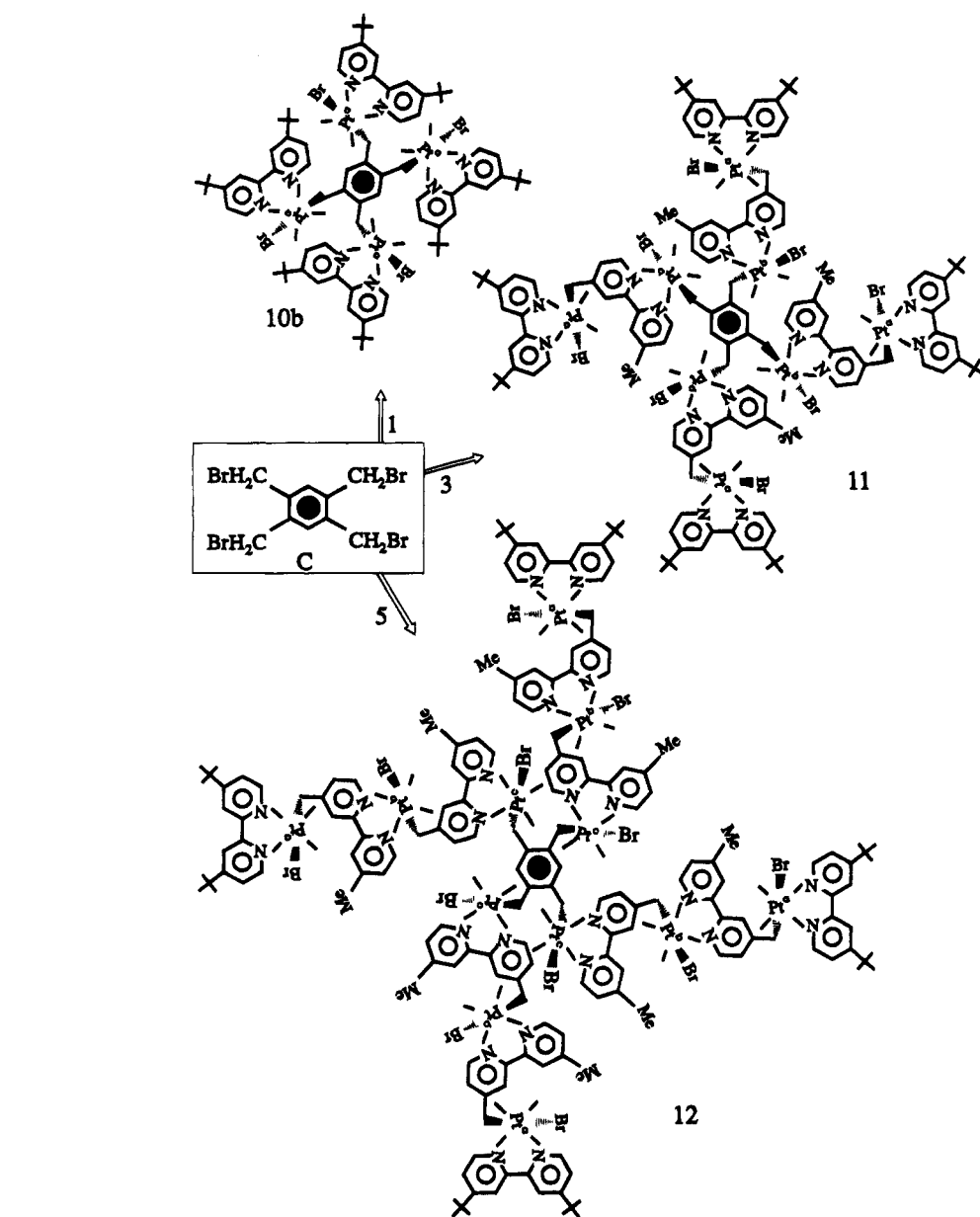


Figure 1. Graph of the calculated molecular weight of some platinum oligomers *versus* the apparent molecular weights determined by GPC using linear polystyrene standards.

mass spectrometer. Differential scanning calorimetry and thermogravimetric analysis were carried out employing Perkin-Elmer DSC7 and TGA7 instruments respectively. The heating rate was 20 °C/min, and a sample mass of 3–8 mg was used. Nitrogen was used as the purge gas. Gel permeation chromatography was performed on a Waters 600 GPC with Waters 410 differential refractometer as the detector. Millennium software was used to analyze the results. Two

Table 1. DSC and TGA Data for the Organoplatinum Compounds

complex	DSC, melting onset	TGA, decompos range and residue ^a (°C)
2	189 °C	168–840, 25 (26.7)
3	194 °C	120–940, 45 (39.7)
4	does not melt	134–940, 37 (31.4)
5	does not melt	30–940, 53 (39.8)
6	does not melt	220–940, 40 (33.7)
8	does not melt	119–940, 40.3 (39.9)

^a Residue observed at the maximum temperature; the value if the residue were metallic platinum is enclosed in parentheses.

ultrastayragel columns were used in series (10³ and 10² Å), and THF was used as the solvent. The system was calibrated with linear polystyrene standards. The complexes [Pt₂Me₄(μ-SMe₂)₂]² and [PtMe₂(bu₂bipy)]² and the diimine 4-(bromomethyl)-4'-methyl-2,2'-bipyridine¹⁰ were prepared by literature methods.

Complex 2. To a stirring red solution of [PtMe₂(bu₂bipy)], **1b**, (0.10 g) in acetone (10 mL) was added 4-(bromomethyl)-

(10) Gould, S.; Strouse, G. F.; Meyer, T. J.; Sullivan, B. P. *Inorg. Chem.* **1991**, *30*, 2942.

4'-methyl-2,2'-bipyridine (0.06 g) in acetone (5 mL). The color of the solution turned immediately to yellow. The solution was concentrated under vacuum, and the product was precipitated with pentane as a pale yellow solid. Yield: 88%. Anal. Calcd for $C_{32}H_{41}BrN_4Pt$: C, 50.8; H, 5.5; N, 7.4. Found: C, 50.8; H, 5.5; N, 7.3. Mass spectrum: $m/z = 757$ (12%) $[M]^+$, 676 (100%) $[M - Br]^+$, 646 (80%) $[M - (Br + 2Me)]^+$. 1H NMR in CD_2Cl_2 (300 MHz): $\delta = 1.28$ [s, 18H, *t*-Bu]; 1.48 [s, 6H, $^2J(PtH) = 69$ Hz, Me_2Pt]; 2.35 [s, 3H, MeC]; 2.81 [s, 2H, $^2J(PtH) = 97$ Hz, CH_2Pt]; 7.44 [dd, 2H, $^3J(H^6H^5) = 6$ Hz, $^4J(H^3H^5) = 2$ Hz, H^5 of bu_2bipy]; 7.88 [d, 2H, $^4J(H^6H^3) = 2$ Hz, H^3 of bu_2bipy]; 8.54 [d, 2H, $^3J(PtH) = 12$ Hz, $^3J(H^6H^5) = 6$ Hz, H^6 of bu_2bipy]; 6.54 [dd, 1H, $^4J(H^3H^5) = 2$ Hz, $^4J(PtH) = 11$ Hz, $^3J(H^6H^5) = 5.5$ Hz, H^{5a} of $CH_2bipyMe$]; 7.01 [m, 1H, $^4J(PtH) = 11$ Hz, H^{3a} of $CH_2bipyMe$]; 7.06 [m, 1H, $^3J(H^6H^5) = 5.5$ Hz, H^{6a} of $CH_2bipyMe$]; 7.92 [dd, 1H, $^3J(H^6H^5) = 5$ Hz, H^{5b} of $CH_2bipyMe$]; 7.98 [s, 1H, H^{3b} of $CH_2bipyMe$]; 8.37 [dd, 1H, $^3J(H^6H^5) = 5$ Hz, H^{6b} of $CH_2bipyMe$]; $\delta(Pt) = -940$. In addition, resonances of much lower intensity (*ca.* 3%), corresponding to the *cis* isomer were detected in the 1H NMR at $\delta = 1.19$ and 1.39 [s, 3H each, $^2J(PtH) = 69$ Hz, MePt], 2.78 [s, 2H, CH_2Pt].

Complex 3. To a solution of complex 2 (0.07 g) in benzene (10 mL) was added a solution of $[Pt_2Me_4(\mu-SMe_2)_2]$ (0.03 g) in ether (10 mL). An instant change in color to red was observed. The mixture was cooled to 0 °C for 1 day, during which time the product precipitated as a red solid which was separated and washed with ether. Yield: 80%. Anal. Calcd for $C_{34}H_{47}BrN_4Pt_2$: C, 41.6; H, 4.8; N, 5.7. Found: C, 41.3; H, 4.8; N, 5.5. Mass spectrum: $m/z = 984$ (30%) $[M + 2]^+$, 871 (28%) $[M - (Br + 2Me)]^+$. 1H NMR in CD_2Cl_2 (200 MHz): $\delta = 0.75$ [s, 3H, $^2J(PtH) = 85$ Hz, MePt^{II}]; 0.80 [s, 3H, $^2J(PtH) = 83$ Hz, MePt^{II}]; 1.35 [s, 18H, *t*-Bu]; 1.51 [s, 6H, $^2J(PtH) = 69$ Hz, Me_2Pt]; 2.32 [s, 3H, MeC]; 2.82 [s, 2H, $^2J(PtH) = 100$ Hz, CH_2Pt]; 7.52 [dd, 2H, H^5 of bu_2bipy]; 7.98 [d, 2H, H^3 of bu_2bipy]; 8.56 [d, 2H, H^6 of bu_2bipy]; 6.25 [m, 1H, H^{5a} of $CH_2bipyMe$]; 7.04 [s, 1H, H^{3a} of $CH_2bipyMe$]; 7.26 [d, 1H, H^{6a} of $CH_2bipyMe$]; 7.4 [s, 1H, H^{5b} of $CH_2bipyMe$]; 8.25 [d, 1H, H^{6b} of $CH_2bipyMe$]; 8.92 [d, 1H, H^{6b} of $CH_2bipyMe$].

Complex 4. This was synthesized by reaction of complex 3 and $BrCH_2bipyMe$ by a similar procedure employed to synthesize the complex 2. Yield: 75%. Anal. Calcd for $C_{46}H_{58}Br_2N_6Pt_2$: C, 44.5; H, 4.4; N, 6.8. Found: C, 43.6; H, 4.6; N, 6.5. Mass spectrum: $m/z = 1212$ (5%) $[M - 2Me + 1]^+$, 1166 (50%) $[M - 5Me]^+$. 1H NMR in CD_2Cl_2 (300 MHz): $\delta = 1.29$ and 1.41 [b, 9H each, *t*-Bu]; 1.20 and 1.23 [s, 3H each, Me_2Pt^b]; 1.53 and 1.57 [s, 3H each, $^2J(PtH) = 69$ Hz, Me_2Pt^a]; 2.21 and 2.38 [s, 3H each, Me of $CH_2bipyMe$]; 2.45–3.1 [unresolved, 4H, $2CH_2Pt$]; 6.0–8.8 [m, 18H, aromatic region].

Complex 5. To a solution of complex 4 (0.09 g) in benzene (12 mL) was added a solution of $[Pt_2Me_4(\mu-SMe_2)_2]$ (0.025 g) in benzene (5 mL). The solution turned red, and the product precipitated slowly. The red precipitate was separated from the solvent and washed with ether. Yield: 86%. Anal. Calcd for $C_{48}H_{64}Br_2N_6Pt_3$: C, 39.2; H, 4.4; N, 5.7. Found: C, 39.5; H, 4.5; N, 5.5. Mass spectrum: $m/z = 1340$ (40%) $[M - (2t-Bu + Me)]^+$, 1155 (100%) $[M - (Pt + 8Me)]^+$, 1126 (80%) $[M - (Pt + 10Me) + 1]$. Gel permeation chromatography: Apparent molecular weight = 600. 1H NMR in CD_2Cl_2 (300 MHz): $\delta = 0.70$ and 0.82 [s, 3H each, $^2J(PtH) = 82$ Hz, MePt^{II}]; 1.07 and 1.44 [s, 9H each, *t*-Bu], 1.21 and 1.23 [s, 3H each, MePt^b]; 1.54 and 1.56 [s, 3H each, $^2J(PtH) = 68$ Hz, MePt^a]; 2.30 and 2.40 [s, 3H each, Me of $CH_2bipyMe$]; 2.45–3.25 [m, 4H, $2CH_2Pt$]; 6.1–9.0 [m, 18H, aromatic region].

Complex 6. To a stirred suspension of complex 5 (0.075 g) in a 1:1 mixture of acetone:benzene (25 mL) was added the diimine $BrCH_2bipyMe$ (0.015 g) in acetone (2 mL). The suspended solid dissolved to give a pale yellow solution. After 2 h, the solvent was removed and the product was washed with ether and dried. Yield: 82%. Anal. Calcd for $C_{60}H_{75}Br_2N_6Pt_3$: C, 41.5; H, 4.3; N, 6.4. Found: C, 38.7; H, 4.2; N, 6.3. Mass spectrum: $m/z = 1653$ (100%) $[M - Br]^+$, 1558 (55%) $[M - (2Br + Me)]^+$, 1482 (55%) $[M - (2Br + 6Me)]^+$. 1H NMR in benzene- d_6 (200 MHz): $\delta = 1.0$ –1.8 [m, 36H, MePt and *t*-Bu]; 2.21, 2.34, and 2.40 [s, 3H each, Me of $CH_2bipyMe$]; 2.4–3.1 [m, 6H, CH_2Pt]; 5.5–9.0 [m, 24H, aromatic region].

Polymer 8. To a solution of $[Pt_2Me_4(\mu-SMe_2)_2]$ (0.075 g) in benzene (8 mL) was added a solution of 4-(bromomethyl)-4'-methyl-2,2'-bipyridine (0.07 g) in benzene (5 mL). The solution turned red instantly, followed by a change to purple and finally pale yellow. The pale yellow precipitate which formed was separated and washed with ether. Yield: 71%. Anal. Calcd for $(C_{14}H_{17}BrN_2Pt)_n$: C, 34.4; H, 3.5; N, 5.7. Found: C, 33.9; H, 3.6; N, 5.3. 1H NMR in $dmsO-d_6$ (200 MHz): $\delta = 0.8$ –1.8 [unresolved, 6H, MePt]; 2.0–3.0 [broad, partially hidden under the solvent peak, 5H, Me of $CH_2bipyMe$ and CH_2Pt]; 6.8–9.0 [broad, 6H, aromatic region].

Complex 10a. To a stirring solution of $[PtMe_2(bipy)]$, 1a (0.15 g), in acetone (10 mL) was added a solution of 1,2,4,5-tetrakis(bromomethyl)benzene (0.045 g) in acetone (5 mL). The solution color changed from orange red to yellow. After the solution was stirred for an additional 4 h, the solvent volume was reduced and the precipitate was separated and washed with ether. Yield: 80%. Anal. Calcd for $C_{58}H_{66}Br_4N_8Pt_4$: C, 35.3; H, 3.4; N, 5.7. Found: C, 35.0; H, 3.0; N, 6.0. FAB mass spectrum: m/z (%) = 1894 (10%) $[M - Br]^+$; calcd $[M - Br] = 1895$.

Similarly 10b and 11 were prepared.

Complex 10b. Anal. Calcd for $C_{90}H_{130}Br_4N_8Pt_4$: C, 44.6; H, 5.4; N, 4.6. Found: C, 43.8; H, 5.7; N, 4.3. 1H NMR in CD_2Cl_2 (300 MHz): $\delta = 0.65$ [s, 12H, $^2J(PtH) = 68$ Hz, Me_2Pt]; 0.88 [s, 12H, $^2J(PtH) = 68$ Hz, Me_2Pt]; 1.45 [s, 72H, *t*-Bu]; 2.1 [m, 4H, $^2J(PtH) = 91$ Hz, CH_2Pt]; 7.52 [d, 8H, H^5 of bu_2bipy]; 8.20 [s, 8H, H^3 of bu_2bipy]; 8.26 [d, 8H, H^6 of bu_2bipy]; 4.9 [m, C_6H_2]; $\delta(Pt) = -870$.

Complex 11. Anal. Calcd for $C_{146}H_{198}Br_8N_{16}Pt_8$: C, 40.1; H, 4.6; N, 5.1. Found: C, 39.1; H, 4.5; N, 4.9. 1H NMR in CD_2Cl_2 (300 MHz): $\delta = 0.6$ –1.8 [br, 120H, Me_2Pt and *t*-Bu]; 2.1–3.2 [br, 28H, CH_2Pt and MeC]; 6.0–8.8 [br, 50H, aromatic region]; $\delta(Pt) = -855$ [br, 4Pt]; -908, -911, -913 [s, 4Pt].

Complex 12. To a stirred suspension of 5 (0.150 g) in a 1:1 mixture of acetone:benzene (100 mL) was added a solution of 1,2,4,5-tetrakis(bromomethyl)benzene (0.008 g) in acetone (2 mL). The suspended red solid dissolved to give a pale yellow solution. After 1 day, the solvent was removed and the product was washed with ether and dried. Yield: 95%. Anal. Calcd for $C_{202}H_{266}Br_{12}N_{24}Pt_{12}$: C, 38.3; H, 4.2; N, 5.3. Found: C, 38.2; H, 4.2; N, 5.2. Gel permeation chromatography: Apparent molecular weight = 2500. 1H NMR in $dmsO-d_6$ (200 MHz): $\delta = 0.8$ –1.2 [br, 144H, MePt and *t*-Bu]; 2.1–3.0 [br, 48H, MeC and CH_2Pt]; 6.3–8.9 [br, 74H, aromatic region]; $\delta(Pt) = -871$ [br, 4Pt]; -895 [br, 4Pt]; -906 [s, 4Pt].

OM940925L

Conformations of (η^3 -Cyclohexenyl)palladium Systems. A Molecular Mechanics (MM2) Study

Björn Åkermark* and Johan D. Oslob

Department of Chemistry, Organic Chemistry, Royal Institute of Technology,
S-100 44 Stockholm, Sweden

Per-Ola Norrby*

Department of Medicinal Chemistry, Royal Danish School of Pharmacy, Universitetsparken 2,
DK-2100 Copenhagen, Denmark

Received November 29, 1994[Ⓢ]

The primary products from palladium(II)-assisted nucleophilic addition to 1,4-cyclohexadienes ((η^3 -cyclohexenyl)palladium complexes) have been investigated by molecular mechanics (MM2). The observed coupling constants can best be explained by a rapid equilibrium between chair- and boatlike conformations. Methods to estimate the relative amounts of the boat and chair conformations of the complexes are presented.

Palladium allyl complexes have been found to be very versatile and important reagents in organic synthesis.¹ Several palladium-catalyzed conversions of unsaturated substrates proceed *via* η^3 -allyl complexes. Included in the range of reactions available are functionalizations of cyclohexenes, 1,3-cyclohexadienes, and 1,4-cyclohexadienes, as well as acyclic 1,4- to 1,7-dienes.² In the palladium-catalyzed nucleophilic displacement of allylic acetates, another facile reaction with (η^3 -allyl)palladium intermediates, optically active products can be obtained by introduction of chiral ligands.^{3,4}

In most cases, (η^3 -allyl)palladium complexes will react with nucleophiles to form allylic products. We have previously studied ways to control the configuration of the product double bond and the regioselectivity of the nucleophilic attack.⁵ Complications arise from the fast dynamic equilibria in the η^3 -allyl moiety,⁶ the rates of which, depending on reaction conditions, are often comparable to the rate of nucleophilic attack.⁷

The selectivities in these reactions are determined by the energies and reactivities of the different isomers of the intermediate η^3 -allyl. In order to rationalize some of these effects, we have recently created a molecular mechanics (MM2) force field for the (η^3 -allyl)palladium moiety.⁸ The conformational preferences of the η^3 -allyl intermediates are especially important for rationalization and prediction of enantioselectivity in the reaction.

In order to elucidate these effects, it is advantageous to study systems where the above-mentioned complications arising from the fast isomerizations in the system (e.g., the η^3 - η^1 - η^3 isomerization) are absent. This is true in, for example, the η^3 -cyclohexenyl moiety, where the position of the side groups are locked by the ring. We have recently observed enantioselectivity in the palladium-catalyzed nucleophilic substitution of unsubstituted cyclohexenyl acetate in the presence of a chiral ligand.^{4,7} The enantioselectivity here clearly arises from a *conformationally induced reactivity difference* between the allyl termini in the (η^3 -cyclohexenyl)palladium complex.⁴ It is therefore very important to us to be able to correctly describe the conformations of the (η^3 -cyclohexenyl)palladium complexes. It has also been reported that the conformation of (η^3 -cyclohexenyl)palladium complexes governs the mode of attack by acetate.⁹

(η^3 -Cyclohexenyl)palladium complexes (e.g. 1) are intermediates in a palladium-assisted functionalization of 1,4-cyclohexadienes which we reported earlier (Scheme 1).^{2c,10} In the course of this investigation,^{2c,10} a large number of (η^3 -cyclohexenyl)palladium complexes were isolated and characterized. The conformation of these complexes was unclear but was assigned as overall "pseudochair" or "pseudoboat" from the vicinal couplings between allyl and ring methylene protons. However, in most cases the supposed diaxial couplings between ring methylene protons (H⁵ to H⁴ and H⁶) were suspiciously low. The numbering of the protons in the cyclohexenyl system is shown in the figure in the lower right corner of Chart 1. For example, in the prototypical compound 1, the couplings $J_{41,52}$ and $J_{42,52}$ were 7.8 and 5.7 Hz, respectively (Table 1). These values are in reasonable agreement with a previously observed palladium cyclohexenyl species in a chair conformation,⁹

[Ⓢ] Abstract published in *Advance ACS Abstracts*, March 1, 1995.

(1) Trost, B. M.; Verhoeven, T. R. In *Comprehensive Organometallic Chemistry*; Wilkinson, G., Ed.; Pergamon: Oxford, U.K., 1982; Vol. 8, pp 802–853.

(2) (a) Bäckvall, J.-E. *Acc. Chem. Res.* **1983**, *16*, 335–342. (b) Larock, R. C.; Takagi, K. *J. Org. Chem.* **1984**, *49*, 2701–2705. (c) Hall, S. S.; Åkermark, B. *Organometallics* **1984**, *3*, 1745–1748.

(3) (a) Godleski, S. A. In *Comprehensive Organic Synthesis*; Trost, B. M., Fleming, I., Eds.; Pergamon: Oxford, U.K., 1991; Vol. 4, Chapter 3.3, pp 585–661. (b) Harrington, J. P. *Transition Metals in Total Synthesis*; Wiley: New York, 1990.

(4) Peña-Cabrera, E.; Norrby, P.-O.; Sjögren, M.; Vitagliano, A.; deFelice, V.; Oslob, J.; Åkermark, B.; Helquist, P., manuscript in preparation.

(5) Sjögren, M.; Hansson, S.; Norrby, P.-O.; Åkermark, B.; Cucciolito, M. E.; Vitagliano, A. *Organometallics* **1992**, *11*, 3954–3964.

(6) Hansson, S.; Norrby, P.-O.; Sjögren, M. P. T.; Åkermark, B.; Cucciolito, M. E.; Giordano, F.; Vitagliano, A. *Organometallics* **1993**, *12*, 4940–4948 and references cited therein.

(7) Sjögren, M. Ph.D. Thesis, The Royal Institute of Technology, Stockholm, Sweden, 1993.

(8) (a) Norrby, P.-O.; Åkermark, B.; Haefner, F.; Hansson, S.; Blomberg, M. *J. Am. Chem. Soc.* **1993**, *115*, 4859–4867. (b) Norrby, P.-O. Ph.D. Thesis, The Royal Institute of Technology, Stockholm, Sweden, 1992.

(9) Grennberg, H.; Langer, V.; Bäckvall, J.-E. *J. Chem. Soc., Chem. Commun.* **1991**, 1190–1192.

(10) (a) Söderberg, B. C.; Åkermark, B.; Hall, S. S. *J. Org. Chem.* **1988**, *53*, 2925–2937. (b) Söderberg, B. C. Ph.D. Thesis, Royal Institute of Technology, Stockholm, Sweden, 1987.

Table 1. Calculated Percentages of the Boat Conformation, Together with Observed and Calculated Coupling Constants

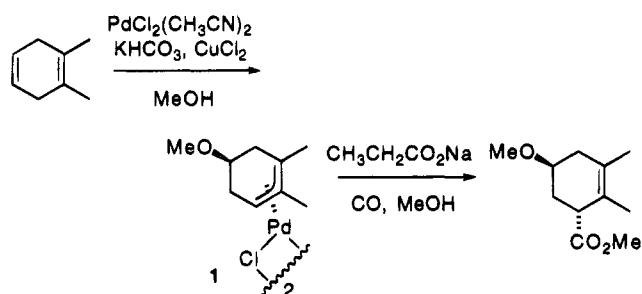
compd		calcd												obsd ⁱ
		eq 1 ^a						eq 2 ^b						
		method				method								
		1 ^c	2 ^d	3 ^e	4 ^{f,g}	1 ^c	2 ^d	3 ^e	4 ^{f,h}					
1	% boat	100.0	0.0	65.7	50.0	47.5	45.1	100.0	0.0	65.7	31.9	44.7	45.6	
	$J_{41,52}$	3.1	11.9	6.1	7.5	7.5	7.6	2.8	9.9	5.3	7.7	7.5	7.5	7.6
	$J_{42,52}$	5.6	6.6	5.9	6.1	5.9	5.7	3.2	6.7	4.4	5.6	5.9	5.9	5.8
	$J_{52,61}$	3.3	12.0	6.3	7.6	7.7	7.7	3.1	10.1	5.5	7.8	7.7	7.7	7.6
	$J_{52,62}$	5.5	6.3	5.8	5.9	5.7	5.5	3.2	6.4	4.3	5.4	5.7	5.8	5.8
	rms			0.99	0.15	0.08	0.15			1.88	0.26	0.08	0.08	
2	% boat	100.0	0.0	21.5	62.3	69.9	57.8	100.0	0.0	21.5	34.9	78.9	47.0	
	$J_{42,52}$	4.8	6.6	6.2	5.5	6.0	5.1	2.4	5.6	4.9	4.5	6.0	4.9	6
	$J_{52,61}$	2.3	12.4	10.2	6.1	6.0	6.2	1.4	9.4	7.7	6.6	6.0	6.4	6
	rms			3.00	0.34	0.00	0.62			1.41	1.15	0.00	0.84	
3	% boat	100.0	0.0	99.4	89.9	89.8	92.4	100.0	0.0	99.4	94.1	89.2	89.1	
	$J_{42,51}$	12.7	2.2	12.7	11.7	11.7	12.0	12.1	1.1	12.0	11.4	11.7	10.9	11.7
	$J_{42,52}$	4.9	7.9	4.9	5.2	5.2	5.1	4.1	7.1	4.1	4.3	5.2	4.4	5.2
	$J_{51,62}$	12.8	2.2	12.7	11.7	11.7	12.0	12.1	1.2	12.0	11.5	11.7	10.9	11.7
	$J_{52,62}$	4.9	8.0	4.9	5.2	5.2	5.1	4.1	7.0	4.1	4.3	5.2	4.4	5.2
	rms			0.74	0.02	0.00	0.19			0.80	0.68	0.01	0.79	
4	% boat	100.0	0.0	49.6	58.3	52.8	53.5	100.0	0.0	49.6	42.2	56.1	55.5	
	$J_{42,51}$	3.0	12.0	7.6	6.8	6.8	6.8	2.8	10.1	6.5	7.0	6.8	6.8	6.8
	$J_{42,52}$	5.7	6.4	6.1	6.0	5.6	5.6	3.4	6.5	5.0	5.2	5.6	5.6	5.6
	$J_{42,52}$	3.0	12.0	7.5	6.8	6.8	6.8	2.8	10.0	6.4	7.0	6.8	6.8	6.8
	$J_{52,62}$	5.7	6.5	6.1	6.0	5.6	5.7	3.4	6.5	5.0	5.2	5.6	5.6	5.6
	rms			0.63	0.30	0.01	0.04			0.51	0.30	0.01	0.02	
5	% boat	100.0	0.0	97.5	65.3	71.4	68.6	100.0	0.0	97.5	79.9	83.8	69.6	
	$J_{41,51}$	5.7	7.1	5.8	6.2	5.4	5.8	5.9	4.7	5.9	5.7	5.4	6.3	5.4
	$J_{42,51}$	12.4	2.3	12.2	8.9	8.8	8.8	10.5	1.8	10.3	8.8	8.8	8.7	8.8
	$J_{51,61}$	5.7	7.1	5.8	6.2	5.4	5.8	5.9	4.7	5.9	5.7	5.4	6.3	5.4
	$J_{51,62}$	12.4	2.3	12.2	8.9	8.8	8.8	10.5	1.9	10.3	8.8	8.8	8.7	8.8
	rms			2.40	0.58	0.00	0.26			1.10	0.18	0.00	0.66	
6	% boat	100.0	0.0	66.9	33.0	25.9	27.5	100.0	0.0	66.9	11.8	13.8	27.0	
	$J_{42,52}$	4.9	6.6	5.4	6.0	5.6	5.7	2.5	5.5	3.5	5.1	5.2	5.5	5.7
	$J_{52,61}$	3.0	12.0	6.0	9.0	9.1	9.1	2.8	9.9	5.2	9.1	9.1	8.8	9.1
	$J_{52,62}$	5.7	6.5	6.0	6.3	5.8	5.9	3.4	6.6	4.5	6.2	6.3	6.6	5.7
	rms			1.83	0.37	0.08	0.11			1.10	0.46	0.46	0.66	
7	% boat	100.0	0.0	48.6	26.6	26.5	26.6	100.0	0.0	48.6	19.9	25.4	27.0	
	$J_{42,52}$	5.7	5.7	5.7	5.7	4.1	5.3	4.7	3.2	3.9	3.5	4.2	4.4	4.1
	$J_{52,61}$	2.7	12.2	7.6	9.7	9.7	9.7	1.6	11.6	6.7	9.6	9.7	9.7	9.7
	$J_{52,62}$	6.2	6.0	6.1	6.1	6.1	6.1	5.3	5.3	5.3	5.3	6.0	6.1	6.1
	rms			1.51	0.91	0.01	0.68			1.77	0.59	0.11	0.16	
8	% boat	100.0	0.0	54.9	42.1	36.1	36.4	100.0	0.0	54.9	20.3	29.6	36.1	
	$J_{42,52}$	4.8	6.5	5.6	5.8	5.5	5.5	2.5	5.6	3.9	5.0	5.2	5.3	5.5
	$J_{52,61}$	3.4	12.0	7.3	8.4	8.5	8.5	3.2	10.1	6.3	8.7	8.5	8.4	8.5
	$J_{52,62}$	5.4	6.2	5.8	5.9	5.5	5.5	3.1	6.3	4.6	5.7	5.8	6.0	5.5
	rms			0.72	0.29	0.01	0.02			1.66	0.32	0.27	0.30	
9	% boat	100.0	0.0	61.3	38.8	36.7	33.9	100.0	0.0	61.3	19.5	22.3	33.2	
	$J_{41,52}$	3.0	12.0	6.4	8.5	8.5	8.5	2.7	10.0	5.5	8.5	8.5	8.3	8.3
	$J_{42,52}$	5.7	6.6	6.1	6.2	6.1	5.9	3.4	6.6	4.6	6.0	6.1	6.4	5.9
	$J_{52,61}$	3.3	11.9	6.7	8.6	8.6	8.6	3.1	9.9	5.7	8.6	8.6	8.5	8.8
	$J_{52,62}$	5.5	6.4	5.9	6.1	5.9	5.7	3.2	6.5	4.5	5.9	5.9	6.2	6.1
	rms			1.42	0.22	0.19	0.24			2.31	0.20	0.19	0.29	
10	% boat	100.0	0.0	31.8	41.6	35.7	36.7	100.0	0	31.8	23.9	20.2	37.5	
	$J_{41,52}$	2.9	11.9	9.0	8.1	8.2	8.2	2.7	9.9	7.8	8.2	8.2	8.0	8.2
	$J_{42,52}$	5.9	6.6	6.4	6.3	5.9	6.0	3.6	6.7	5.7	6.0	5.8	6.3	5.9
	$J_{52,61}$	3.0	11.8	9.0	8.2	8.2	8.2	2.8	9.8	7.6	8.1	8.2	8.0	8.2
	$J_{52,62}$	5.7	6.8	6.4	6.3	5.9	6.0	3.3	6.9	5.8	6.1	6.0	6.4	5.9
	rms			0.69	0.30	0.19	0.24			0.44	0.09	0.19	0.29	
11	% boat	100.0	0.0	68.5	36.9	18.0	31.2	100.0	0.0	68.5	18.6	9.8	34.2	
	$J_{42,52}$	4.8	6.5	5.4	5.9	4.9	5.6	2.4	5.5	3.4	4.9	4.3	5.2	3.8
	$J_{52,61}$	3.3	12.0	6.0	8.8	9.1	8.9	3.1	10.0	5.3	8.7	9.2	8.4	9.2
	$J_{52,62}$	5.5	6.3	5.8	6.0	4.8	5.7	3.2	6.4	4.2	5.8	5.3	6.1	5.8
	rms			2.05	1.25	0.84	1.06			2.46	0.69	0.42	0.95	
12	% boat	100.0	0.0	49.9	17.4	16.8	17.2	100.0	0.0	49.9	11.0	17.6	17.9	
	$J_{42,52}$	5.5	5.9	5.7	5.8	4.2	5.4	4.6	3.3	4.0	3.5	4.3	4.4	4.2
	$J_{52,61}$	2.9	12.3	7.6	10.6	10.7	10.7	1.8	11.7	6.8	10.6	10.7	10.7	10.7
	$J_{52,62}$	6.1	5.8	5.9	5.8	5.8	5.8	5.1	5.1	5.1	5.1	5.9	5.9	6
	rms			2.00	0.93	0.09	0.70			2.34	0.66	0.10	0.10	

Table 1 (Continued)

compd	calcd														obsd ⁱ
	eq 1 ^a							eq 2 ^b							
	method				method				method				method		
		1 ^c	2 ^d	3 ^e	4 ^{f,g}	1 ^c	2 ^d	3 ^e	4 ^{f,h}	1 ^c	2 ^d	3 ^e	4 ^{f,h}		
13	% boat	100.0	0.0	84.6	54.4	50.9	49.5	100.0	0.0	84.6	36.8	52.3	50.5		
	$J_{41,52}$	3.1	12.0	4.5	7.2	7.2	7.2	2.9	10.0	4.0	7.4	7.2	7.2	7.2	
	$J_{42,52}$	5.5	6.5	5.7	6.0	5.7	5.6	3.2	6.5	3.7	5.3	5.7	5.7	5.7	
	$J_{52,61}$	3.2	12.0	4.5	7.2	7.2	7.2	3.0	10.0	4.1	7.4	7.2	7.2	7.2	
	$J_{52,62}$	5.5	6.5	5.6	5.9	5.7	5.6	3.2	6.5	3.7	5.3	5.7	5.6	5.7	
	rms			1.91	0.18	0.01	0.08			2.64	0.30	0.02	0.04		
14	% boat	100.0	0.0	41.2	53.1	51.8	48.2	100.0	0.0	41.2	35.1	54.0	48.6		
	$J_{41,52}$	3.0	12.0	8.3	7.2	7.2	7.3	2.8	10.1	7.1	7.5	7.2	7.3	7.3	
	$J_{42,52}$	5.7	6.5	6.1	6.0	6.0	5.7	3.3	6.6	5.2	5.4	5.9	5.8	5.9	
	$J_{52,61}$	3.2	12.0	8.4	7.3	7.4	7.4	3.0	10.0	7.1	7.6	7.4	7.4	7.3	
	$J_{52,62}$	5.5	6.4	6.0	5.9	5.8	5.6	3.2	6.5	5.1	5.3	5.8	5.7	5.9	
	rms			0.75	0.09	0.06	0.20			0.52	0.39	0.05	0.12		
15	% boat	100.0	0.0	64.0	52.7	49.0	47.7	100.0	0.0	64.0	35.1	47.8	48.6		
	$J_{41,52}$	3.1	11.9	6.3	7.3	7.3	7.3	2.8	10.0	5.4	7.5	7.3	7.3	7.3	
	$J_{42,52}$	5.6	6.6	6.0	6.1	5.8	5.7	3.3	6.6	4.5	5.5	5.8	5.8	5.8	
	$J_{52,61}$	3.1	11.9	6.3	7.3	7.3	7.3	2.8	10.0	5.4	7.5	7.3	7.3	7.3	
	$J_{52,62}$	5.6	6.5	6.0	6.1	5.8	5.7	3.3	6.6	4.5	5.5	5.8	5.8	5.8	
	rms			0.74	0.19	0.00	0.07			1.62	0.26	0.01	0.02		
16	% boat	100.0	0.0	44.0	33.7	28.4	27.8	100.0	0.0	44.0	11.0	18.0	27.0		
	$J_{41,52}$	4.9	6.5	5.8	6.0	5.7	5.7	2.5	5.5	4.2	5.1	5.3	5.5	5.7	
	$J_{52,61}$	3.4	12.0	8.2	9.1	9.2	9.2	3.3	10.0	7.0	9.3	9.1	9.0	9.2	
	$J_{52,62}$	5.3	6.4	5.9	6.0	5.7	5.7	3.0	6.5	4.9	6.1	6.2	6.3	5.7	
	rms			0.57	0.24	0.01	0.03			1.59	0.40	0.38	0.41		

^a Reference 12. ^b Reference 14. ^c Boltzmann weighted average; eq 3. ^d Adjusted for best fit to observed couplings; eqs 4 and 5. ^e As in method 2, allowing for a variable systematic error in the Karplus equation. ^f As in method 2, but adjusting each coupling by a fixed value. ^g Couplings adjusted by 0.4 Hz. ^h Couplings adjusted by -0.8 Hz. ⁱ Reference 10.

Scheme 1



but a (cyclohexenyl)molybdenum complex in a chair conformation has been shown to have a diaxial coupling of 11.4 Hz,¹¹ in good agreement with a value calculated from the published X-ray structure using a modification of the Karplus equation.¹² Also, the compound **3**, which is believed to prefer a boat conformation, has a diaxial coupling of 11.7 Hz.^{2c,10}

It can be assumed that the observed coupling constants result from a fast equilibrium between boat and chair conformations in solution. According to preliminary MM2 calculations using the previously developed parameter set,⁸ both conformations are minima on the energy hypersurface for the compounds in Chart 1. In view of the above, we decided to reinvestigate the previously determined NMR coupling constants using a combination of molecular mechanics and Karplus type equations. The goal of this investigation is twofold: first, to elucidate the conformational preferences of (η^3 -cyclohexenyl)palladium complexes, and second, to evalu-

ate the accuracy of the molecular mechanics method for relative energies of different conformations of (η^3 -allyl)-palladium complexes. The second goal is especially important to us, since we are using this force field in the development of new chiral ligands for palladium-catalyzed reactions.^{4,7}

MM2 Calculations

We have recently shown, for a related system, that coupling constants calculated from molecular mechanics structures can be used to both verify structural assignments and determine the position of a fast equilibrium.¹³ The molecular mechanics calculations on our η^3 -cyclohexenyl complexes were performed using a recently developed force field which has been parameterized for very similar systems.⁸ For most of these simple structures, all minima on the energy hypersurface could easily be located by hand, but in a few cases (e.g., **8**) dihedral driver calculations were used to verify that all relevant conformations were found. For all conformations generated, vicinal couplings in the saturated part of the cyclohexenyl ring were calculated by two different Karplus-type methods: the simple relationship in eq 1¹² and the more complex are given by eq 2.¹⁴

$${}^3J = 7 - \cos \theta + 5 \cos 2\theta \quad (1)$$

$${}^3J = 13.7 \cos^2 \theta - 0.73 \cos \theta + \sum \Delta\chi_i \{0.56 - 2.47 \cos^2 \theta (\xi_i \theta + 16.9^\circ |\Delta\chi_i|)\} \quad (2)$$

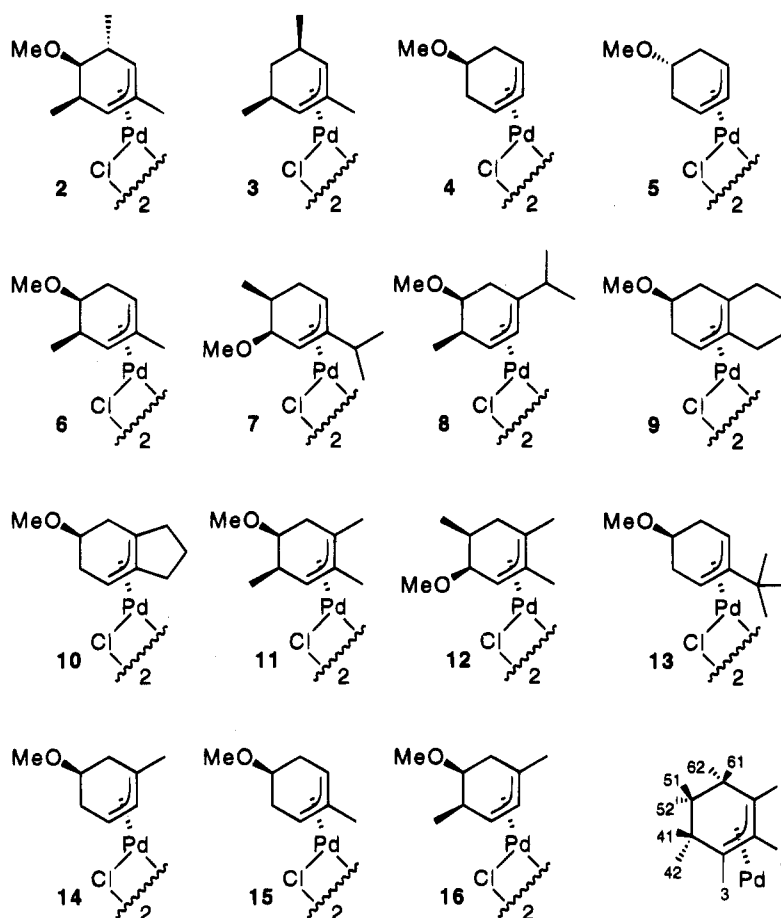
Here θ is a H-C-C-H dihedral angle, $\Delta\chi_i$ is the

(11) Faller, J. W.; Murray, H. H.; White, D. L.; Chao, K. H. *Organometallics* **1983**, *2*, 400-409.

(12) Bothner-By, A. A. *Adv. Magn. Reson.* **1965**, *1*, 195. The modified Karplus equation is shown in eq 1.

(13) Martin, J. T.; Norrby, P.-O.; Åkermark, B. *J. Org. Chem.* **1993**, *58*, 1400-1406.

(14) Haasnoot, C. A. G.; de Leeuw, F. A. A. M.; Altona, C. *Tetrahedron* **1980**, *36*, 2783-2792.

Chart 1. Complexes Investigated in This Work^a

^a The numbering of substituents in the cyclohexenyl moiety is given at the lower right. Protons trans to palladium have the second index "1"; protons cis to palladium have "2" in methylenes. When a carbon has only one proton bound to it, the second index is left out (e.g., H-5 in all structures except 3).

difference in electronegativity between hydrogen and one substituent on the ethane fragment under study, and ξ_i is a positional "sign" (+1 or -1) for one substituent.¹⁴

Under the assumption of fast conformational equilibrium, time-averaged coupling constants can now be calculated by taking a population-weighted average over all conformations (eq 3, where p_i is the population of, and J_i a coupling in, conformer i).

$$J_{\text{calc}} = \frac{\sum J_i p_i}{\sum p_i} \quad (3)$$

A few considerations must be made when calculating the Boltzmann populations (p_i) in eq 3. The Boltzmann factors should be calculated from free energies, whereas most molecular mechanics packages calculate a steric energy, which is similar but not identical with enthalpy. The simplest procedure is to just ignore the difference and calculate the populations directly from the steric energies. This will be designated as method 1 in this work. When the conformations are structurally similar, this may be a valid procedure. Even in the absence of normal mode analysis, a qualitative estimate of the difference in relative free energies between conformers can be obtained by driving some key torsional angles and comparing the curvature of the potential wells. A shallow well should lead to a higher entropy term and thus a higher population in one specific conformer.

Alternatively, errors in the calculated energies can be compensated for by treating the relative populations of the two major conformations (boat and chair) as variables and fitting the calculated coupling constants to the observed values by least-squares methods (eqs 4 and 5, where x is the fraction in the boat conformation and $e(x)$ is the error in x).¹³

$$J_{\text{calc}} = xJ_{\text{boat}} + (1-x)J_{\text{chair}} \quad (4)$$

$$x = \frac{\sum (J_{\text{boat}} - J_{\text{chair}})(J_{\text{obs}} - J_{\text{chair}})}{\sum (J_{\text{boat}} - J_{\text{chair}})^2} \quad (5)$$

$$e(J)_{\text{tot}} \approx (J_{\text{boat}} - J_{\text{chair}})[e(x)] \quad (6)$$

The J_{boat} and J_{chair} values are calculated using method 1. We still assume that energy error differences are negligible within one class of conformations. The accuracy of the relative populations thus obtained can be estimated from eq 6, where $e(J)_{\text{tot}}$ is a total coupling constant error, both experimental errors in the observed value and all errors in the coupling constant calculation. We assume this value to be 1–2 Hz, mainly due to the inaccuracy of the Karplus equations. As an ideal example, if two conformers are calculated to exist in a 50/50 equilibrium at ambient temperature and the maximum calculated coupling constant difference between the two conformers is 10 Hz, the error in the free

energy difference between the conformers can be expected to be 1–2 kJ/mol.

In some cases, usually due to linearly dependent systems and/or inaccuracies in the Karplus equation, meaningless values for the population (e.g., negative) can result. It is good practice to check the populations against those obtained from method 1 and, if possible, identify the sources of any differences. Very often, the populations simply display a small shift toward conformers with a more shallow minimum, that is, entropically favored conformers.

As an additional refinement, it is possible to compensate for small systematic errors in the Karplus equation. This is especially useful in a system like this, where a group with unknown properties (the allyl) is connected to the ethane fragment under study. This is most easily done by allowing a nonzero intercept in the linear regression, corresponding to a constant adjustment to the Karplus equation (method 3). A more ambitious project would be to try to determine the correct electronegativity of the allyl group from the available data, but no such attempt was made in the current work. Already addition of a nonzero intercept has to be considered an overinterpretation of the available data. Great care should be used when analyzing the results of this regression. For some of our compounds, we actually fit a line to two data points only. However, it was noted that in many cases the intercepts were very similar between different sets of data, possibly corresponding to a real systematic error in the application of the Karplus equations to these systems. As an additional way of determining relative populations (method 4), we therefore applied one fixed correction, corresponding to the median of the corrections determined by method 3, to all coupling constants before performing the least-squares fit (eq 5).

The arguments presented here depend on the validity of the Karplus equations.¹⁵ Although the general form of the equation is well-established, there is considerable variation in the literature on the values of the coefficients in the equation. It is certainly well-known that there are substituent effects on the coefficients¹⁶ and that electronegative substituents on the HC–CH fragment cause a slight decrease in the observed coupling,^{16a,17} thus giving somewhat lower maximum possible values for J . Our system is, in essence, three steps removed from the original Karplus ethane fragment,¹⁵ that is, it contains a six-membered ring, a methoxy group, and a η^3 -allyl system. Equation 1 takes the first of these points into account,¹² whereas equation 2 also accounts for the influence of the methoxy group.¹⁴ The good agreement in this paper (see below) suggests that, at least for protons on C⁴, C⁵, and C⁶, the coefficients are quite reasonable and that the couplings are not drastically affected by the presence of a η^3 -allyl group at the other end of the ring. The median correction (not considering differences in conformation) obtained from method 3 is less than 1 Hz for both Karplus-type equations. We have also seen a fairly large experimental value for J (11.7 Hz in **3**, Table 1), again suggesting

no large decreases in the Karplus coefficients due to the allyl group.

Calculations were done for all dimeric complexes (1–16). In some cases (compounds 7–9) dihedral driver calculations were performed in order to find all possible minimum energy conformations with respect to rotation of side groups. For computational efficiency, calculations were not performed on the true dimers but on complexes consisting of one palladium–cyclohexenyl moiety connected to another palladium atom via two chloride bridges. The results from these calculations are shown in Table 1, together with the observed couplings.¹⁰ A few calculations of the full dimers verify that the structures and relative energies of conformations in one ring are unaffected by the presence of a second ring.

Results and Discussion

The results in Table 1 nicely illustrate the advantage of utilizing the observed coupling constants in the calculation of relative populations according to eq 4 (method 2) instead of the more common reliance upon calculated energies (eq 3, method 1). In all cases, the expected error in populations estimated from eq 6 is low, due to the presence of at least one coupling constant with a large range of attainable values (a diaxial coupling in equilibrium with a diequatorial coupling).

A comparison of the two Karplus-type equations (eqs 1 and 2) shows surprisingly little difference. For the fitted methods (methods 2–4), this is in part due to the fitting, since a systematic error in the coupling constant calculation to some extent can be compensated by a shift in the predicted populations. However, this probably is not the only reason for the almost negligible difference between the simple eq 1 and the more recent eq 2. The explanation may be found in the way the two equations treat the electronegativity of the two substituents. It seems for eq 1 that the error from ignoring the large electronegativity of the methoxy group is to some extent cancelled by ignoring also the opposite effect of the allyl group, whereas eq 2 includes the large effect from the methoxy but not the small effect from the allyl. If, for each conformation, the two groups would affect the coupling in opposite directions, with the absolute effect of the allyl being about half that of the methoxy, both equations should give approximately the same error, but with opposite signs. The true magnitude of this effect can be estimated from the application of method 3. It should be stressed again that, for each case taken alone, method 3 is very prone to give spurious, false results. For this reason, we use the median instead of the mean as an estimator of the underlying systematic error in the Karplus-type equation. This estimated error is actually larger for the more elaborate eq 2, indicating a significant electronegative contribution to the coupling constants from the allyl group. It should be noted that when this correction is applied to the individual couplings before populations are calculated (method 4), the two Karplus-type equations yield almost identical calculated populations. The two main outliers are compounds **3** and **5**, as should be expected from the structural difference between these two compounds and the rest of the data set. Compound **3** lacks a methoxy group, and therefore the cancellation of errors in eq 1 no longer occurs, whereas the corrected eq 2 (method

(15) Karplus, M. *J. Chem. Phys.* **1959**, *30*, 11–15.

(16) (a) Karplus, M. *J. Am. Chem. Soc.* **1963**, *85*, 2870–2871. (b) Abraham, R. J.; Pachler, K. G. R. *Mol. Phys.* **1963–64**, *7*, 165–182.

(c) Abraham, R. J.; Thomas, W. A. *Chem. Commun.* **1965**, 431–433.

(17) Williamson, K. L. *J. Am. Chem. Soc.* **1963**, *85*, 516–519.

4) should still give accurate results. In compound **5**, the only compound in the series where the methoxy group is *cis* to the palladium, the dihedral relationship between the methoxy group and the observed protons has changed. The systematic difference between eqs 1 and 2 cannot, therefore, be expected to be the same for compounds **3** and **5** as for the other compounds in the investigation.

The results of the MM2 calculations allow us to come to some very useful conclusions. Because the geometry and energy calculations indicating an equilibrium significantly improve the agreement between the observed couplings and the model, we can say that the η^3 -cyclohexenyl ring in our palladium system is probably undergoing rapid conformational change between chair and boat conformations. Furthermore, these calculations also show that the $J_{52,42}$ coupling constant should be essentially unaffected by the conformation of the ring. Rather, it is $J_{52,41}$ that provides a clue to the equilibrium between chair and boat.

In our earlier work, we assigned the chair and boat conformations on the basis of the axial,axial vicinal couplings and on the values of the H-3,H-41 and H-3,H-42 (or H-1,H-6) couplings.^{2c,10} In this paper, we have shown that the axial,axial couplings are better described by invoking fluxionality. The $J_{3,41}$ values for boat conformations were ~ 6 Hz, while $J_{3,42}$ values were usually ~ 0 Hz, the latter corresponding to a dihedral angle of $\sim 90^\circ$. This assignment is certainly reasonable, and this coupling pattern was seen for **3** in this paper and for several compounds with endo substituents on C-5 that should force the ring into a boat conformation.^{2c,10} In a chair conformation, the dihedral angles H-3-C-3-C-4-H-41 and H-3-C-3-C-4-H-42 would be quite similar and so the assumption was made

that the coupling constants would be similar. This assumption is not nearly so reasonable, since the presence of the π -bond to the palladium from C-3 might be expected to affect the angular dependence of the coupling constant on the underside of the ring in quite a different way than on the top side of the ring. In addition, 3J allylic couplings in conventional organic systems are not known to be especially reliable indicators of bond angles.¹⁸ We feel, therefore, that the use of H^5 couplings is a better indicator of conformation and that the $J_{3,4}$ couplings are useful only when one coupling is ~ 0 Hz to indicate a system with the equilibrium very heavily in favor of the boat conformation.

Computational Details

All MM2 calculations were carried out using the MacMimic/MM2(91) package¹⁹ on a Macintosh Quadra, with added parameters for the (η^3 -allyl)palladium moiety.⁸ Coupling constants according to eq 1 were calculated with a home-developed macro in Microsoft Excel, whereas MacroModel²⁰ was used to calculate couplings according to eq 2. In this implementation, the electronegativity of the η^3 -allyl moiety is ignored.

Acknowledgment. Support from the Trygger Foundation and the Danish Medical Research Council is gratefully acknowledged. J.D.O. thanks the Royal Institute of Technology for a research scholarship.

OM940910N

(18) Garbisch, E. W., Jr. *J. Am. Chem. Soc.* **1964**, *86*, 5561–5564.

(19) MacMimic/MM2(91); InStar Software AB, IDEON Research Park, S-223 70 Lund, Sweden.

(20) MacroModel V4.0: Mohamadi, F.; Richards, N. G. J.; Guida, W. C.; Liskamp, R.; Caufield, C.; Chang, G.; Hendrickson, T.; Still, W. C. *J. Comput. Chem.* **1990**, *11*, 440.

Exploring Stereoselectivity through the Quantitative Analysis of Ligand Effects. Osmylation of Chiral (Acetoxyallyl)silanes

Beth A. Lorschach, Alfred Prock,* and Warren P. Giering*

Department of Chemistry, Metcalf Science and Engineering Center, Boston University,
Boston, Massachusetts 02215

Received October 13, 1994[®]

The diastereoselectivity of the catalytic osmylation of chiral (acetoxyallyl)silanes of the type $(R_3Si)(OAc)CHCH=CH_2$ is described by the equation $\log(\text{anti/syn}) = -(0.070 \pm 0.012)\chi - (0.002 \pm 0.002)\theta + (0.18 \pm 0.06)E_{ar} + 1.55 \pm 0.41$, with $n = 14$ and $r^2 = 0.74$. The analysis shows that the preference for the anti isomer increases as the electron donor capacity of the silyl groups and the number of pendent phenyl groups increases. Importantly, predicated on this method of analysis we find that the steric effect of the silyl group is at best small and that it is not statistically significant.

Introduction

The stereochemistry of the dihydroxylation of alkenes by osmium tetroxide (osmylation) has been the subject of study for over a decade.¹ A number of models have been offered to account for, to predict, and to understand the stereochemistry of this reaction. All of these models rest, to varying degrees, on steric arguments. Since the stereoselectivity of osmylation is greater for (*Z*)-alkenes than for (*E*)-alkenes, Kishi² suggested that the reaction occurred via the least congested ground state conformation of the alkene. In this transition state (**1a**), the OsO_4 approaches the alkene from the face opposite to the preexisting allylic hydroxy or alkoxy group and the allylic C-H bond eclipses the vinyl group. Predicated on the observation that the osmylation of (*E*)- α,β -unsaturated esters gave a single dihydroxyacetone, Stork³ envisioned the reaction as occurring via the transition state shown (**1b**) in Figure 1.

In this transition state, the hydroxy group is in the inside position, the small hydrogen is in the outside position, and the ethyl group is essentially antiperiplanar to the approaching OsO_4 . The positioning of the hydroxy group rather than the hydrogen group in what appears to be the more sterically demanding inside position suggested that the presence of the electronegative group in this position activates (or at least does not deactivate) the double bond. The largest group, ethyl, was positioned anti to the attacking osmium group. The osmylation of the *Z* isomer was suggested to occur via a transition state with a different structure. If the *Z*-isomer reacted via the analogous transition state (**1d**), then the carboxy group and the hydroxy group would clash, thereby sterically destabilizing the transition state. It was therefore proposed that the *Z*-isomer reacts via transition state **1c**, where the

smallest group, hydrogen, occupies the inside position and the hydroxy group takes up residence in the outside position. The stereoselectivity of the osmylation of the *Z*-isomer was found to be consistent with this model although the stereoselectivity is smaller than that observed for the *E*-isomer. Houk followed up on these ideas in his experimental and computational study of the cycloaddition of nitrile oxides to chiral allyl ethers,^{4a} allyl alcohols,^{4a} and chiral alkenes.^{4b} It was found that the ether groups preferred the inside position (inside alkoxy effect). It was suggested that the alkoxy group in this position minimized the electron-withdrawing interaction between the CO σ^* orbital and the π orbital. Although the CO σ^*/π interaction could also be minimized with the alkoxy group in the outside position, Houk suggested that there is repulsion (steric and/or dipolar) between the outside alkoxy oxygen and the oxygen of the nitrile oxide (and presumably the oxygens of the OsO_4 group in the osmylation reaction). Houk's model allows the electron-rich C-R bond to hyperconjugate with the double bond, thereby enhancing reactivity of the double bond toward electrophilic addition. Houk extended these studies to alkenes where the alkoxy group was replaced by an alkyl group. It was assumed that the alkyl groups exert only steric influence over the reaction. The stereochemical outcome of the osmylation of these alkenes was the same as that observed for the allyl ethers. Again the transition state for the reaction of these chiral alkenes was envisioned as involving a staggered conformation such as that shown in **1e** with the largest alkyl group anti to the approaching osmium group and the medium-sized group in the inside position. Houk's model leads to the expectation that the *E*-alkenes would exhibit the greatest stereoselectivity, which is contrary to Kishi's results.

Panek and Cirillo⁵ systematically but qualitatively examined the diastereoselectivity of the catalytic (trimethylamine oxide (TMAO) as the oxidant) osmylation

[®] Abstract published in *Advance ACS Abstracts*, February 15, 1995.

(1) (a) Schroder, M. *Chem. Rev.* **1980**, *80*, 187. (b) Johnson, R. A.; Sharpless, K. B. *Catalytic Asymmetric Dihydroxylation*. In *Catalytic Asymmetric Synthesis*; Ojima, I., Ed.; VCH: Weinheim, Germany, 1993; p 227.

(2) (a) Christ, W. J.; Cha, J. K.; Kishi, Y. *Tetrahedron Lett.* **1983**, *24*, 3947. (b) Christ, W. J.; Cha, J. K.; Kishi, Y. *Tetrahedron* **1984**, *40*, 2247.

(3) Stork, G.; Kahn, M. *Tetrahedron Lett.* **1983**, *24*, 3951.

(4) (a) Houk, K. N.; Moses, S. R.; Wu, Y. D.; Rondan, N. G.; Jager, V.; Schohe, R.; Fronczek, F. *J. Am. Chem. Soc.* **1984**, *106*, 3880. (b) Houk, K. N.; Duh, H. Y.; Wu, Y. D.; Moses, S. R. *J. Am. Chem. Soc.* **1986**, *108*, 2754.

(5) Panek, J. S.; Cirillo, P. F. *J. Am. Chem. Soc.* **1990**, *112*, 4873.

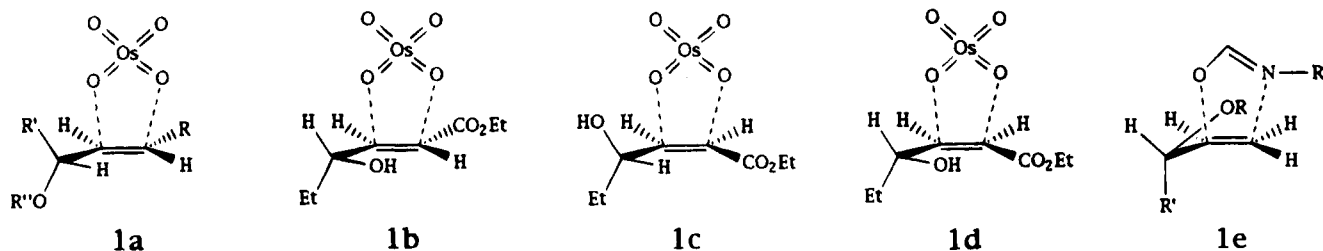
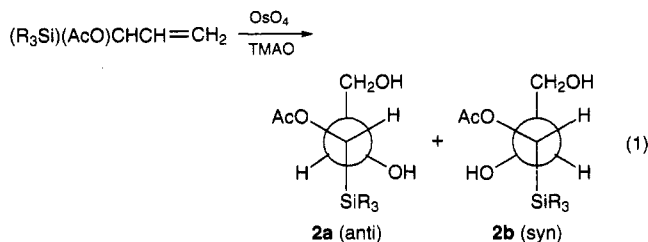


Figure 1. Possible transition states for the osmylation and addition of nitrile oxides to *Z*- and *E*-alkenes as proposed by Kishi,² Stork,³ and Houk.⁴

of five chiral (acetoxyallyl)silanes as a function of the size of the silyl group (eq 1). They observed for five allyl



silanes that the ratio of the anti (**2a**) and syn (**2b**) diastereomers increased from 6.5:1 for $\text{SiR}_3 = \text{SiMe}_3$ to 11.5:1 for $\text{SiR}_3 = \text{SiPh}_2\text{Me}$. This is a trend that appears to reflect the changes in the size of the silyl groups. These results were interpreted in terms of the Houk model.⁴

On the basis of their studies of substituted (*Z*)- and (*E*)-pentenes that bear silyl and sulfonyl groups, Vedejs et al.⁶ forcibly argued that electronic effects (hyperconjugation) are not important and that there are different transition states for the osmylation of the *Z*- and *E*-isomers. Vedejs suggested that the dominant factor controlling the transition state geometries is the placement of the allylic hydrogen in the most sterically demanding position. Thus, the exclusive product obtained when a chiral (*Z*)-silylpentene was osmylated could be envisioned as arising via transition state **3c**. Sterically, **3c** seems quite reasonable with the large silyl group antiperiplanar to the attacking osmium group, the small hydrogen in the inside position, and the methyl in the outside position. (It should be noted, however, that Houk proposed that in the cycloaddition of nitrile oxides to alkenes the outside position was more sterically congested because of interaction between the outside group and the oxygen of the attacking electrophile.^{4b}) The other diastereomer is not formed because of severe steric interactions between the methyl groups (**3a** or **3b**).

In contrast, Vedejs found that the *E*-isomer gives two diastereomers. He pointed out that if the osmylation of the *E*-isomer proceeded via a transition state analogous to **3c**, then transition state **4c** would be preferred on the basis of electronic (hyperconjugation) and steric factors. The major product from the *E*-isomer, however, arises from osmylation of the other face of the alkene and could occur via either transition state **4a** or **4b**. Since it made little sense that **4a** should be more stable than **4c**, Vedejs proposed that the nature of the transition state for the *E*-isomer was controlled by steric interactions between the incoming osmium and the

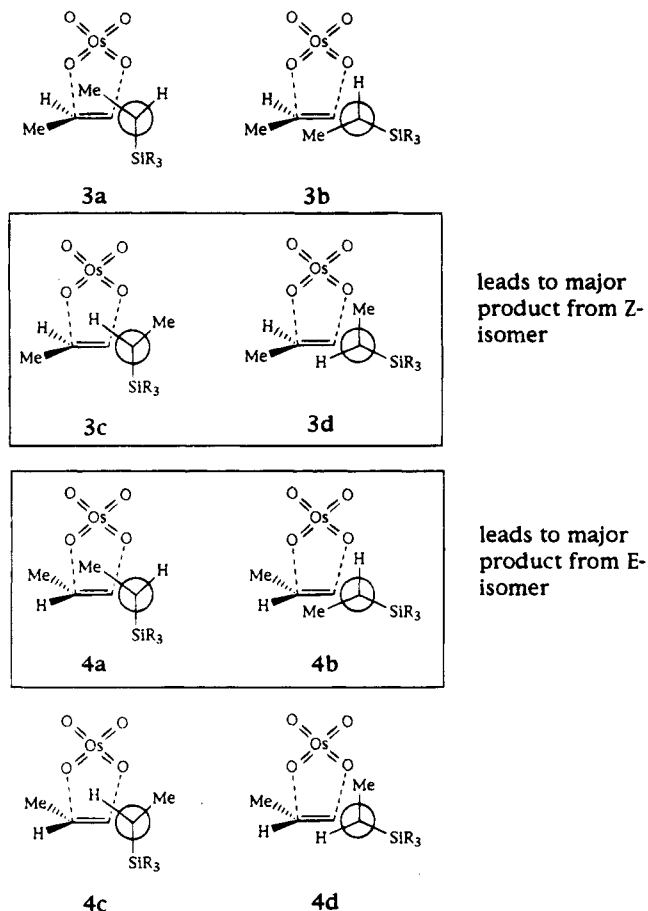


Figure 2. Various transition states discussed by Vedejs⁶ for the osmylation of *Z*- and *E*-alkenes.

stereogenic center. Thus, structure **3b** with the small hydrogen atom directed toward the incoming osmium seemed like a reasonable candidate for the transition state of this reaction.

Evans,⁷ in his study of the osmylation of 1,1-disubstituted alkenes, found evidence supporting either the Houk or Vedejs model but not the Kishi model.

Thus, the debate over the importance of electronic factors (hyperconjugation and inside alkoxy effect) as well as steric factors (congestion in the alkene, repulsive interactions between the alkene and approaching OsO_4) remains lively and we are left with a variety of transition state models for a reaction whose mechanism is only now becoming unraveled.⁸ Despite this plethora of experimental and theoretical work, there has been no systematic attempt to separate and quantitatively

(7) Evans, D. A.; Kaldor, S. W. *J. Org. Chem.* **1990**, *55*, 1698.

(6) (a) Vedejs, E.; McClure, C. K. *J. Am. Chem. Soc.* **1986**, *108*, 1094.
(b) Vedejs, E.; Dent, W. H., III *J. Am. Chem. Soc.* **1989**, *111*, 6861.

(8) (a) Henderson, I.; Sharpless, K. B.; Wong, C. H. *J. Am. Chem. Soc.* **1994**, *116*, 558. (b) Kolb, C. H.; Andersson, P. G.; Sharpless, K. B. *J. Am. Chem. Soc.* **1994**, *116*, 1278, and references therein.

assess the electronic and steric factors that influence the stereoselectivity of the osmylation of chiral alkenes. We have taken the opportunity to follow up and greatly expand on Panek and Cirillo's study⁵ of the stereoselectivity of the osmylation of chiral (acetoxiallyl)silanes. It was our expectation that we would be able to analyze the stereoselectivity in terms of the concepts embedded in the quantitative analysis of ligand effects (QALE). Recently, we reported that the stereoselectivity of the addition of hydride to the cationic carbene complexes $\eta\text{-Cp}(\text{CO})(\text{PR}_3)\text{Fe}[\text{C}(\text{OMe})\text{Me}]^+$ is correlated with the stereoelectronic parameters of the phosphine ligands.⁹ Herein, we report the results of our study of the osmylation of 14 chiral (acetoxiallyl)silanes. The results appear to indicate that the stereoselectivity of these osmylation reactions is influenced by the electronic properties of the silyl groups and to a much smaller extent, if at all, by the size of silyl groups.

Experimental Section

FT NMR spectra were measured on JEOL GSX-270 and Varian 400 MHz NMR spectrometers. IR spectra were measured on a Perkin-Elmer FT-IR spectrometer. All chlorosilanes were purchased from Huls America Co., except for (*p*-methoxyphenyl)dimethylchlorosilane, butyldiphenylchlorosilane, ethyldiphenylchlorosilane, and diethylmethylchlorosilane, which were synthesized in our laboratory by addition of the appropriate Grignard reagent to R_2SiCl_2 . All the chlorosilanes were distilled from quinoline prior to use. All solvents were purchased from commercial sources and distilled prior to use by standard methods. All reactions were performed under a nitrogen atmosphere, except for the osmylation reactions. The chiral (acetoxiallyl)silanes $(\text{R}_3\text{Si})(\text{AcO})\text{CHCH}=\text{CH}_2$ were prepared by acetylation of $(\text{R}_3\text{Si})(\text{HO})\text{CHCH}=\text{CH}_2$, which in turn was prepared by the silyl Wittig rearrangement of $(\text{R}_3\text{SiO})\text{CH}_2\text{CH}=\text{CH}_2$ as described by Panek and Cirillo.^{5,10} We found that the silyl Wittig rearrangement gave mixtures of $(\text{R}_3\text{Si})(\text{HO})\text{CHCH}=\text{CH}_2$ and $(\text{R}_3\text{SiO})\text{CH}_2\text{CH}=\text{CH}_2$ for the larger silyl groups. The materials were readily separated on silica gel using petroleum ether and then 5% ethyl acetate/petroleum ether. We were unable to synthesize $(\text{R}_3\text{Si})(\text{HO})\text{CHCH}=\text{CH}_2$ with silyl groups with $\theta > 143^\circ$. All compounds and their precursors were characterized by ^1H and ^{13}C NMR spectroscopy and IR spectroscopy. These values, which are displayed in the supplemental material, agree with available literature values.^{5,10}

The osmylation reactions were performed according to the protocol of Panek and Cirillo⁵ using TMAO as the oxidant and a catalytic amount of OsO_4 at 22°C in 8:1 acetone/water. The estimated crude yields of the diols ranged from 40% to 80%, which are comparable to those reported by Panek and Cirillo.⁵ Since the yields of the diols were modest, we were concerned that the diols might be unstable and therefore that the anti/syn ratios might not reflect the rates of formation of the diastereomers. The observation that the diols are stable under the reaction conditions employed and that samples of the diols are stable as the neat liquid or in chloroform-*d* at room temperature for several days suggests that the diols are not decomposing over the time frame of the experiments.

The ratio of the anti and syn isomers, **2a** and **2b**, respectively, were obtained from the NMR spectra of the crude product by cutting out and weighing the peaks for C(1) hydrogens of the allyl groups. The anti/syn ratios listed in Table 1 are the average of at least three separate experiments.

Table 1. Stereoelectronic Parameters for the Silyl Groups and the Ratio of the Anti and Syn Diastereomers That Result from the Catalytic Osmylation of $(\text{R}_3\text{Si})(\text{AcO})\text{CHCH}=\text{CH}_2$.

entry	SiR_3^a	χ^b	θ^c	E_{ar}^d	(anti/syn) ^{e,f}	log(anti/syn)
1	SiMe_3	8.55	118	0.00	5.35 (6.5)	0.728
2	$\text{SiMe}_2(p\text{-MeOPh})$	9.2	122	1.00	6.87	0.837
3	$\text{SiMe}_2(p\text{-MePh})$	9.5	122	1.00	6.91	0.839
4	SiMe_2Ph	10.6	122	1.00	5.41 (7.0)	0.733
5	SiMe_2Et	7.8	123	0.00	5.98	0.777
6	SiMeEt_2	7.05	127	0.00	5.91	0.772
7	SiEt_3	6.3	132	0.00	6.93 (7.5)	0.841
8	SiMe_2Cy	6.2	135	0.00	6.96	0.843
9	SiBu_3	5.25	136	0.00	6.43	0.869
10	SiMePh_2	12.1	136	2.00	5.48 (11.5)	0.740
11	$\text{SiMe}_2\text{-}t\text{-Bu}$	5.7	139	0.00	8.8 (11.3)	0.946
12	SiEtPh_2	11.3	141	2.00	7.09	0.851
13	SiBuPh_2	11.1	142	2.00	7.57	0.879
14	$\text{Si}(i\text{-Bu})_3$	5.7	143	0.00	6.85	0.836

^a The stereoelectronic parameters for phosphines were used for the isostructural silyl groups. ^b χ values (cm^{-1}) are taken from ref 11. ^c θ (deg) are taken from ref 12. ^d E_{ar} (dimensionless) are taken from ref 13. ^e Ratios were determined by cutting and weighing the peaks assigned to the protons on the C₁ stereocenter to which the silyl and acetyl groups are attached. ^f Values in parentheses were reported in ref 5.

The ratios differ by less than 5% from the average of the three values. The stereoelectronic parameters of the silyl groups are also presented in Table 1.

We repeated the measurements of the five anti/syn ratios reported by Panek and Cirillo⁵. Our values are consistently smaller than the literature data (given in parentheses in Table 1) but vary over about the same range. The largest deviations occur for the $\text{Si}(t\text{-Bu})\text{Me}_2$ and SiMePh_2 derivatives. We have used our values in the ensuing analysis.

Results and Discussion

For a number of years we and others (most notably Poë) have been investigating the manner in which systematic variations of the stereoelectronic properties of phosphines affect the chemical and spectroscopic properties of the phosphines and their organometallic and inorganic derivatives.¹⁴ The appropriate properties of these derivatives are related to the three stereoelectronic parameters χ , θ , and E_{ar} via eq 2.¹³

$$\text{property} = a(\chi) + b(\theta - \theta_{\text{st}})\lambda + c(E_{\text{ar}}) + d \quad (2)$$

In eq 2, χ is an electronic parameter and E_{ar} is the aryl effect parameter, which is only dependent on the number of phenyl groups attached to the phosphorus(III) compound. θ is Tolman's cone angle, and λ is a switching function that turns on the steric term after θ exceeds the steric threshold, θ_{st} . We have found that these phosphine stereoelectronic parameters are transferrable to alkyl groups, thioethers, arsines, and nitriles. To date, we have successfully correlated, via eq 2, over

(12) (a) Tolman, C. A. *Chem. Rev.* **1977**, *77*, 313. (b) First, have not used Brown's steric parameter, E_{T} , since there is no evidence for a steric effect, and therefore, this set of data does not provide a good test of the validity of E_{T} . Second, as Brown pointed out, these E_{T} values are system dependent. Brown, T. L.; Lee, K. J. *Coord. Chem. Rev.* **1993**, *128*, 89.

(13) Wilson, M. R.; Woska, D. C.; Prock, A.; Giering, W. P. *Organometallics* **1993**, *12*, 1742.

(9) Lorsbach, B. A.; Bennett, D. M.; Prock, A.; Giering, W. P. *Organometallics*, in press.

(10) Danheiser, R. L.; Fink, D. M.; Okano, K.; Tsai, Y. M.; Szczepanski, S. W. *J. Org. Chem.* **1985**, *50*, 5393.

(11) Bartik, T.; Himmler, T.; Schulte, H.-G.; Seevogel, K. *J. Organomet. Chem.* **1984**, *272*, 29.

Table 2. Compilation of Analyses of Kinetic and Thermodynamic Data for Reactions of Organosilanes^a

entry	reaction	n	a	b	c	d	θ_{st}	r ²
1	rate of dissociation of HSiR ₃ from (CO) ₅ Cr(HSiR ₃) ¹⁷	7	-0.069	0.118	0.80	0.77	136	0.966
2	rate of hydride abstraction by (Ph)(p-MeOPh)CH ⁺ from HSiR ₃ ^{13,18}	19	±0.028 -0.43	±0.028 -0.066	±0.12 1.05	±0.19 13.6	<103	0.961
3	rate of reaction between R ₃ SiH and O ₃ ¹⁹	19	±0.03 -0.117 ±0.007	±0.008 0.002 ±0.002	±0.12 +0.013 ±0.030	±1.3 2.82 ±0.33	>174	0.986
4	rate of reaction between R ₃ SiH and Br ₂ ²⁰	8	-0.117 ±0.008	0.043 ±0.001		3.74 ±0.05	133	0.998
5	rate of reaction between R ₃ SiH and KOH ²¹	9	0.15 ±0.06	-0.057 ±0.006		5.4 ±1.3	<123	0.996
6	rate of reaction between R ₃ SiH and HCl in 95%EtOH/H ₂ O ²²	11	0.13	-0.028	-0.37	2.8	<120	0.979
7	heat of reaction for the reaction between η-CpMn(CO) ₂ (heptane) and HSiR ₃ ²³	7	±0.02 -0.18	±0.005 -0.226	±0.08	±0.8 18.9	133	0.997
8	rate of addition of (p-MeOPh)(Ph)CH ⁺ to allylsilanes ^{14n,24}	8	±0.02 -0.26	±0.008 -0.026	0.15	±0.2 7.5	<118	0.934
9	ratio of diastereomers resulting from the benzannulation reaction between chromium alkenyl carbene complexes and chiral siloxyalkynes ²⁵	6	±0.20 -0.065	±0.025 0.0005	±0.64 -0.006	±4.5 1.38	>160	0.970
			±0.012	±0.003	±0.12	±0.42		

^a Analyses are based on eq 2: property = $a(\chi) + b(\theta - \theta_{st})\lambda + c(E_{ar}) + d$. Standard errors are written below the appropriate coefficients.

100 sets of data for various properties of organic, main group, and transition metal compounds.¹⁵

Since silyl groups are isostructural to the analogous phosphines, and since silicon is adjacent to phosphorus in the periodic table, it seemed reasonable that the stereoelectronic properties of silicon would be proportional to those of phosphorus. As a test of the validity of transferring the phosphorus(III) stereoelectronic parameters to silicon we analyzed (via eq 2) the appropriate kinetic data for reactions of organosilanes, some of which are collected in a paper by Cartledge.¹⁶ In contrast to our earlier analyses of data for organosilanes,^{13,14n} we restricted these analyses to data for silyl groups of the type SiX₃ where X = H, alkyl, and phenyl. The results of these analyses are presented in Table 2. We note in entry 8 (Table 2) that r² is large, but the

standard errors are also large enough to make the coefficients statistically indistinguishable from zero. This arises because of high correlation among the parameters of the set of silyl groups used in the study. The large value of r² suggests that with a better set of silyl groups a better fit could be obtained. Thus, in conclusion, we are of the opinion that the transference of the phosphorus(III) stereoelectronic parameters to silicon is valid.

Particularly relevant is our analysis (entry 9, Table 2) of the diastereoselectivity of the benzannulation reaction involving chiral siloxyalkynes as reported by Wulff²⁵ and as shown in the Scheme 1. Our analysis shows a good correlation between the stereochemical parameters and the stereoselectivity of the reaction.

We therefore analyzed log (anti/syn)²⁶ (Table 1) according to equation 2 and obtained eq 3. Below eq 3

(14) (a) Golovin, M. N.; Rahman, Md. M.; Belmonte, J. E.; Giering, W. P. *Organometallics* **1985**, *4*, 1981. (b) Dahlinger, K.; Falcone, F.; Poë, A. *J. Inorg. Chem.* **1986**, *25*, 2654. (c) Rahman, Md. M.; Liu, H.-Y.; Prock, A.; Giering, W. P. *Organometallics*, **1987**, *6*, 650-8. (d) Poë, A. *J. Pure Appl. Chem.* **1988**, *60*, 1209. (e) Golovin, N. G.; Meirowitz, R. E.; Rahman, Md. M.; Liu, H.; Prock, A.; Giering, W. P. *Organometallics* **1987**, *6*, 2285. (f) Lezhan, C.; Poë, A. *J. Inorg. Chem.* **1989**, *28*, 3641. (g) Rahman, Md. M.; Liu, H.-Y.; Eriks, K.; Prock, A.; Giering, W. P. *Organometallics* **1989**, *8*, 1-7. (h) Eriks, K.; Liu, H.-Y.; Koh, L.; Prock, A.; Giering, W. P. *Acta Crystallogr.* **1989**, *C45*, 1683. (i) Liu, H.; Fertal, D.; Tracey, A. A.; Eriks, K.; Prock, A.; Giering, W. P. *Organometallics* **1989**, *8*, 1454-8. (j) Eriks, E.; Liu, H.-Y.; Prock, A.; Giering, W. P. *Inorg. Chem.* **1989**, *28*, 1759-63. (k) Brodie, N. M.; Chen, L.; Poë, A. *Int. J. Chem. Kinet.* **1988**, *27*, 188. (l) Tracey, A. A.; Eriks, K.; Prock, A.; Giering, W. P. *Organometallics* **1990**, *9*, 1399. (m) Liu, H.-Y.; Eriks, E.; Prock, A.; Giering, W. P. *Organometallics* **1990**, *9*, 1758. (n) Panek, J.; Prock, A.; Eriks, K.; Giering, W. P. *Organometallics* **1990**, *9*, 2175. (o) Liu, H.-Y.; Eriks, E.; Prock, A.; Giering, W. P. *Acta Crystallogr.* **1990**, *C46*, 51. (p) Prock, A.; Giering, W. P.; Greene, J. E.; Meirowitz, R. E.; Hoffman, S. L.; Woska, D. C.; Wilson, M. Chang, R.; Chen, J.; Magnuson, R. H.; Eriks, K. *Organometallics* **1991**, *10*, 3479-85. (q) Woska, D. C.; Wilson, M. R.; Eriks, K.; Prock, A.; Giering, W. P. *Organometallics* **1992**, *11*, 3343. (r) Liu, H.; Eriks, K.; Prock, A.; Giering, W. P. *Acta Crystallogr.* **1992**, *C48*, 433. (s) Woska, D. C.; Bartholomew, J.; Greene, J. E.; Eriks, K.; Prock, A.; Giering, W. P. *Organometallics* **1993**, *12*, 304. (t) Fernandez, A. L.; Prock, A.; Giering, W. P. *Organometallics* **1994**, *13*, 2767.

(15) Bartholomew, J.; Bennett, D. M.; Chakar, F.; Fernandez, A. L.; Giering, W. P.; Lorschach, B. A.; Prock, A.; Wilson, M. R., unpublished results. Compilation of analyses is available upon request.

(16) Cartledge, F. K. *Organometallics* **1983**, *2*, 425.

(17) Zhang, S.; Dobson, G. R.; Brown, T. L. *J. Am. Chem. Soc.* **1991**, *113*, 6908.

(18) Mayr, H.; Basso, N.; Hagen, G. *J. Am. Chem. Soc.* **1992**, *114*, 3060.

(19) Spialter, L.; Pazdernik, L.; Bernstein, S.; Swansigerwa, W. A.; Buell, G. R.; Freeburger, M. E. *J. Am. Chem. Soc.* **1971**, *93*, 5682. Data were used as reported in ref 15.

(20) Hetflejes, J.; Mares, F.; Chvalovsky, V. *Collect. Czech. Chem. Commun.* **1972**, *37*, 1713. Data were used as reported in ref 15.

(21) Barie, W. P., Jr. Ph.D. Thesis, Pennsylvania State University, University Park, PA, 1954. Data were used as reported in ref 15.

(22) Steward, O. W.; Pierce, O. R. *J. Am. Chem. Soc.* **1961**, *83*, 4932.

(23) Hester, D. M.; Sun, J.; Harper, A. W.; Yang, G. K. *J. Am. Chem. Soc.* **1992**, *114*, 5234.

(24) Mayr, H.; Hagen, G. *J. Chem. Soc., Chem. Commun.* **1989**, 91.

(25) Hsung, R. P.; Wulff, W. D.; Rheingold, A. L. *J. Am. Chem. Soc.* **1994**, *116*, 6449.

(26) The modest yields of the diol products indicate that there might be selective loss of one of the diastereomers, thereby distorting our analysis. There are two pieces of information that suggest that this is not the case. First, we obtain a high-quality correlation between the stereoselectivities and the stereoelectronic parameters; if the observed stereoselectivity were dependent on the loss of the syn and anti isomers then the product yields would also correlate with the parameters. However, there is no correlation between product yields and the stereoelectronic parameters of the silyl groups. For example, the biggest variation in product yield was observed for the SiMe₂Cy (75%) and Si(*i*-Bu)₂ (40%) groups, which are quite similar in their stereoelectronic properties. Second, we have found no evidence that the diols are unstable under the reaction conditions.

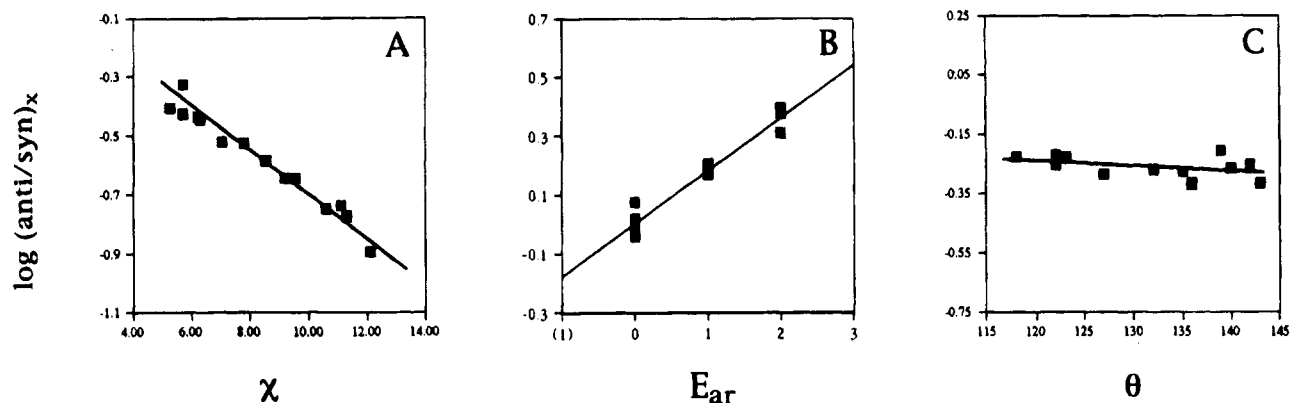
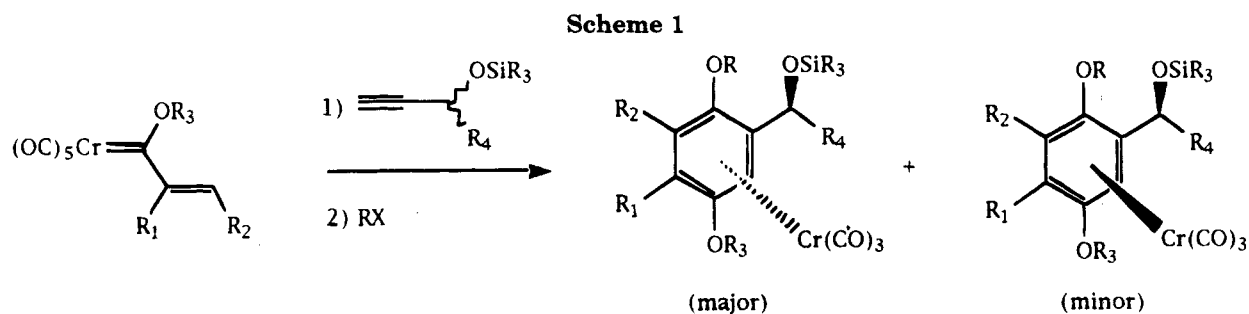


Figure 3. Stereoelectronic profiles for $\log(\text{anti/syn})$ of the diastereomers resulting from the osmylation of (acetoxiallyl)silanes (reaction 1): (A) electronic profile, $x = \chi$; (B) electronic profile, $x = E_{\text{ar}}$; (C) steric profile, $x = \theta$.



we give the standard errors, percent contribution of each variable based on the product of the range of variable times its coefficient divided by the sum of these terms for all three variables.

$$\log(\text{anti/syn}) = -(0.070)\chi - (0.0020)\theta + (0.18)E_{\text{ar}} + 1.55 \quad (3)$$

$$\pm 0.012 \quad \pm 0.002 \quad \pm 0.06 \quad \pm 0.41$$

$$n = 14; \quad r^2 = 0.74; \quad \chi (58\%); \quad \theta (8\%); \quad E_{\text{ar}} (34\%)$$

Based on an examination of the standard errors and 95% confidence limits, we find that the coefficients of χ and E_{ar} are statistically significant while the coefficient of θ is indistinguishable from zero.²⁷ Summarizing, we find from the analysis that (a) the anti/syn ratio might decrease as the size of the silyl group increases (larger θ) but this effect is small and not statistically significant, (b) the anti/syn ratio increases as the silyl groups become better electron donors (less positive χ), and (c) the anti/syn ratio increases as the number of aryl groups increases on the silyl group (larger E_{ar}).

We display in Figure 3 the steric and electronic profiles for the stereoselectivity of reaction 1. Each

profile shows the response of $\log(\text{anti/syn})$ to changes in a single parameter. Each profile also shows all the error involved in the analyses. A direct comparison of the importance of each parameter is readily seen since the scale on the Y axis is the same for each profile. The three stereoelectronic components of $\log(\text{anti/syn})$ were calculated by subtracting the appropriate terms from the experimental values of $\log(\text{anti/syn})$. Thus, each graph includes all the experimental error. For example, eq 4 shows how we calculated the data for the steric profile shown in Figure 3C.

$$\log(\text{anti/syn})_{\text{st}} = \log(\text{anti/syn})_{\text{exp}} + (0.070)\chi - (0.18)E_{\text{ar}} - 1.55 \quad (4)$$

The most important result is that the stereoselectivity for reaction 1 is weakly, if at all, determined by steric factors. It is understandable that, in their initial study on the stereoselectivity of reaction 2, Panek and Cirillo⁵ linked increasing size with increasing anti/syn ratio. For the trialkylsilyl groups employed in their study, χ and θ are closely correlated, i.e., as the electron donor capacity of the groups increases (which increases the anti/syn ratio according to eq 3), the size of the group increases. Likewise, for the phenylsilyl groups, θ and E_{ar} are closely correlated, i.e., as the number of pendent phenyl groups increases (which also increases the anti/syn ratio), the size of the silyl groups increase.

Unfortunately our results do not allow us to support one of the aforementioned models of the origins of stereoselectivity since each of these models rests, at least in part, on steric arguments and our results indicate that silyl steric effects are not controlling the stereochemistry of reaction 1.

The interpretation of eq 3 at the molecular level is problematic. The absence of a steric effect can be interpreted in two ways. Since the anti/syn ratio is a

(27) r^2 is best interpreted as a measure of the shape of the distribution of data, i.e., whether it is wide or narrow. A large value of r^2 is often, but not invariably, associated with a good fit. Similarly, a small value of r^2 can be associated with a good statistical model. These points are discussed in: Achen, C. H. *Interpreting and Using Regression*; Series No. 29; Sage Publications: London, 1982. (We thank a reviewer for bringing this monograph to our attention.) To answer the question whether a coefficient is statistically significant, the 95% confidence limits (2.23 times the standard errors for the present 10 degrees of freedom) are recognized as superior statistics. The standard deviation (or its square) is also used as a measure of goodness of fit; we show this information visually by means of the three profiles given in Figure 3. We conclude the fit of our data to the model is quite good. It must be noted that the error is not distributed among the three graphs, but by construction, the full error is present in each graph.

ratio of the rate constants for the formation of the anti and syn isomers the absence of steric effects might result because (1) there are no steric effects in either the anti or syn transition states or (2) there are significant but compensatory steric effects in both transition states. We cannot distinguish between these two models with the information in hand. The correlation of increasing anti/syn ratio with increasing electron donor capacity might reflect enhanced hyperconjugation in the anti transition state or an anti transition state with greater development of charge on the allyl group. Again we cannot distinguish between these interpretations. The aryl effect remains enigmatic. It is not obvious why increasing the number of phenyl groups would increase the anti/syn ratio.

It is noteworthy that the stereoselectivity of reactions can respond in different ways to variations in the χ and E_{ar} properties of the ligands. Thus, increasing both the electron donor capacity and the number of pendent phenyl groups on silicon increases the stereoselectivity of reaction 1. In contrast, for the addition of hydride to the cationic carbene complexes, $\eta\text{-Cp}(\text{CO})(\text{PR}_3)\text{Fe}[\text{C}(\text{OMe})\text{Me}]^+$, the preference for the anti isomer is enhanced by increasing electron donor capacity of the phosphine but decreased by increasing number of pendent phenyl groups on the phosphine and is independent of size until 145° , after which the anti/syn ratio rises dramatically.⁹ In the benzannulation reaction shown the scheme, the preference for the major isomer grows by increasing the electron donor capacity of the silyl group but is independent of both aryl and steric effects.

Conclusions

There are four important points to be gleaned from this work on stereoselectivity: (1) There can be little doubt that the reactivities of organosilanes are correlated via eq 2 with the stereoelectronic parameters χ , θ , and E_{ar} , which were transferred to the silyl groups from the isostructural phosphines. (2) The high quality of the fit of the stereoselectivity of reaction 1 and the benzannulation reaction (scheme) to eq 2 indicates that even small differences in free energies of activation can be analyzed in terms of these stereoelectronic parameters. (3) The results of the analysis of the stereoselectivity clearly show that the size of silyl group is not controlling the stereoselectivity of reaction 1 or benzannulation reaction. (4) The electronic effects of χ and E_{ar} can work in concert or opposition, depending on the system. Finally, our report illustrates that the factors controlling stereoselectivity can be rationally, systematically, and quantitatively probed.

Acknowledgment. We gratefully acknowledge John Houlihan (Senior Research Consultant for Statistics, Boston University) for his advice concerning these statistical analyses. We thank Professors James Panek, John Snyder (Boston University), and Dr. Pierre Cirillo (Boston University) for their many helpful discussions.

Supplementary Material Available: Spectroscopic data for the (acetoxyallyl)silanes and their precursors (10 pages). Ordering information is given on any current masthead page.

OM940789K

Isomers of $\text{SnPh}_2(\text{B}_5\text{H}_8)_2$: Synthesis and Characterization of μ, μ' - $\text{SnPh}_2(\text{B}_5\text{H}_8)_2$, $\mu, 2'$ - $\text{SnPh}_2(\text{B}_5\text{H}_8)_2$, and $\mu, 1'$ - $\text{SnPh}_2(\text{B}_5\text{H}_8)_2$

Hong Fang, Dong Zhao, Nigam P. Rath, Lee Brammer, and Lawrence Barton*

Department of Chemistry, University of Missouri—St. Louis, St. Louis, Missouri 63121

Received November 16, 1994[®]

The reaction between $\text{K}[\text{B}_5\text{H}_8]$ and SnCl_2Ph_2 in a 2:1 molar ratio affords either μ, μ' - $\text{SnPh}_2(\text{B}_5\text{H}_8)_2$ (**1**), $\mu, 2'$ - $\text{SnPh}_2(\text{B}_5\text{H}_8)_2$ (**2**), or $\mu, 1'$ - $\text{SnPh}_2(\text{B}_5\text{H}_8)_2$ (**3**) depending on the choice of solvent and conditions. **1** is formed if the reaction is carried out in the noncoordinating solvent CH_2Cl_2 at -35°C , whereas if the coordinating solvents Et_2O or THF are used, the products are **2** and **3**, respectively. **2** is also formed when **1** is treated with Et_2O , and **3** is formed when **1** is treated with THF. The species are characterized by ^1H , ^{11}B , ^{13}C , and ^{119}Sn NMR spectra. The crystal structures of all three isomers are reported. **1** crystallizes in the orthorhombic space group $Pna2_1$, with $a = 7.708(4) \text{ \AA}$, $b = 15.836(6) \text{ \AA}$, $c = 15.814(5) \text{ \AA}$, and $Z = 4$, **2** crystallizes in the monoclinic space group $C2/c$, with $a = 38.506(14) \text{ \AA}$, $b = 11.379(2) \text{ \AA}$, $c = 19.096(6) \text{ \AA}$, $\beta = 106.12(2)^\circ$, and $Z = 16$, and **3** crystallizes in the monoclinic space group $P2_1/c$, with $a = 9.662(2) \text{ \AA}$, $b = 9.868(2) \text{ \AA}$, $c = 21.009(4) \text{ \AA}$, $\beta = 92.07(2)^\circ$, and $Z = 4$. **3** is also prepared in the reaction between $\text{K}[\text{B}_5\text{H}_8]$ and $1-(\text{SnClPh}_2)\text{B}_5\text{H}_8$. If the reaction between $\text{K}[\text{B}_5\text{H}_8]$ and SnCl_2Ph_2 , in a 2:1 mole ratio, is carried out in THF, two isomers of **3** appear to be formed. **1–3** are the first structurally characterized examples of pentaboranyl(9) cages linked by a single heteroatom, and they differ only in the mode of attachment of the two B_5H_8 cages to the tin atom. In all three species, the Sn atom has approximately tetrahedral coordination with one cage bonding the tin atom through a three-center bond to two adjacent basal borons and the other cage bonding a similar bridging position in **1**, bonding to a basal boron atom of the second cage in **2** and bonding to the apical boron atom in **3**.

Introduction

Examples of borane clusters linked by single heteroatoms are quite rare. The large cage systems $[\text{Cu}(\text{B}_{10}\text{H}_9\text{N}_2)_2]^-$,¹ $[\text{Pd}(\text{B}_{10}\text{H}_{12})_2]^{2-}$,^{2a} $[\text{Pt}(\text{B}_{10}\text{H}_{12})_2]^{2-}$,^{2b} $[\text{Au}(\text{B}_{10}\text{H}_{13})_2]^{2-}$,³ $[\text{Au}(\text{B}_{10}\text{H}_{12})_2]^-$,³ $[\text{Zn}(\text{B}_{10}\text{H}_{12})_2]^{2-}$,^{4a} and $(\text{B}_{10}\text{H}_{13})_2\text{O}^{4b}$ have all been characterized by crystal structure determinations. Three systems based on hexaborane(10) are known. They include $\text{Mg}(\text{B}_6\text{H}_9)_2(\text{THF})_2$ ^{5a} and $\text{Pt}(\text{B}_6\text{H}_{10})_2\text{Cl}_2$,⁶ for which structures are also available, and $\text{Cd}(\text{B}_6\text{H}_9)_2$ ^{5a} which was identified spectroscopically. There are two reports for pentaboranyl(9) cages, one involving $\text{Hg}(\text{II})$ ⁷ and the other involving Si and Ge.⁸ In both cases, the species were characterized by low-field NMR spectroscopy. We recently described the characterization of a series of tris-(organyl)stannyl-substituted *nido*-penta- and hexabo-

ranes(9).⁹ We now report that selection of solvent and conditions allows individual isolation of three of the six possible linkage isomers of $\text{SnPh}_2(\text{B}_5\text{H}_8)_2$, and we also describe the crystal and molecular structures of μ, μ' - $\text{SnPh}_2(\text{B}_5\text{H}_8)_2$ (**1**), $\mu, 2'$ - $\text{SnPh}_2(\text{B}_5\text{H}_8)_2$ (**2**), and $\mu, 1'$ - $\text{SnPh}_2(\text{B}_5\text{H}_8)_2$ (**3**). A preliminary report of some of this work has appeared.¹⁰

Experimental Section

Materials. B_5H_9 was obtained from laboratory stock and distilled on the vacuum line before use. SnClPh_3 was obtained from Aldrich and used without further purification and SnCl_2Ph_2 was prepared as reported in the literature.¹¹ KH, obtained as a 20–25% mineral oil suspension from Alfa, was washed repeatedly before use with anhydrous pentane on the vacuum line until it was a free-flowing white powder. The activity of the powder, in reactions with methanol, was 85–95%. $1-(\text{SnClPh}_2)\text{B}_5\text{H}_8$ was prepared as described previously.^{9b} THF and diethyl ether were dried over LiAlH_4 , distilled from Na/benzophenone ketyl, and stored over it. CH_2Cl_2 was dried and distilled over P_2O_5 . Me_2O was stirred over LiAlH_4 at -78°C for several days and distilled on the vacuum line into a storage vessel. Pentane was dried over CaH_2 , distilled from Na/benzophenone, and stored over it. All solvents were reagent grade and were dried and distilled prior to use and stored in Pyrex vessels with Teflon stopcocks.

(9) (a) Barton, L.; Srivastava, D. K. *J. Chem. Soc., Dalton Trans.* **1992**, 1327. (b) Srivastava, D. K.; Rath, N. P.; Barton, L. *Organometallics* **1992**, *11*, 2263. (c) Srivastava, D. K.; Barton, L. *Organometallics* **1993**, *12*, 2864.

(10) Fang, H.; Zhao, D.; Brammer, L.; Barton, L. *J. Chem. Soc., Chem. Commun.* **1994**, 1531.

(11) Gilman, H.; Gist, L. A. *J. Org. Chem.* **1957**, *22*, 368.

[®] Abstract published in *Advance ACS Abstracts*, March 15, 1995.

(1) Ng, L.-L.; Ng, B. K.; Shelly, K.; Knobler, C. B.; Hawthorne, M. F. *Inorg. Chem.* **1991**, *30*, 4278.

(2) (a) Macgregor, S. A.; Scanlan, J. A.; Yellowless, L. J.; Welch, A. J. *Acta Crystallogr.* **1991**, *C47*, 513. (b) Macgregor, S. A.; Yellowless, L. J.; Welch, A. J. *Acta Crystallogr.* **1990**, *C46*, 1399.

(3) Wynd, A. J.; Welch, A. J. *J. Chem. Soc., Chem. Commun.* **1987**, 1174.

(4) (a) Greenwood, N. N.; McGinety, J. A.; Owen, J. D. *J. Chem. Soc. A* **1971**, 809. (b) Greenwood, N. N.; McDonald, W. S.; Spalding, T. R. *J. Chem. Soc., Dalton Trans.* **1980**, 1251.

(5) (a) Denton, D. L.; Clayton, W. R.; Mangion, M.; Shore, S. G.; Meyers, E. A. *Inorg. Chem.* **1976**, *15*, 541. (b) Rimmel, R. J.; Denton, D. L.; Leach, J. B.; Toft, M. A.; Shore, S. G. *Inorg. Chem.* **1981**, *20*, 1270.

(6) Brennan, J. P.; Schaeffer, R.; Davison, A.; Wreford, S. S. *J. Chem. Soc., Chem. Commun.* **1973**, 354.

(7) Hosmane, N. S.; Grimes, R. N. *Inorg. Chem.* **1979**, *18*, 2886.

(8) Gaines, D. F.; Ulman, J. *Inorg. Chem.* **1974**, *13*, 2792.

Table 1. NMR Data for Bis(pentaboranyl)diphenylstannanes

compd	$^{11}\text{B}^a$	$^1\text{H}^b$	$^1\text{H}\{^{11}\text{B}\}^b$	$^{13}\text{C}\{^1\text{H}\}^c$
μ, μ' - $\text{SnPh}_2(\text{B}_5\text{H}_8)_2^d$	-7.4 [d, 4B, B(4,5), B(4',5'), $^1J(^{11}\text{B}-^1\text{H}) = 155$ Hz] -10.8 [d, 4B, B(2,3), B(2',3'), $^1J(^{11}\text{B}-^1\text{H}) = 155$ Hz] -45.8 [d, 2B, B(1), B(1'), $^1J(^{11}\text{B}-^1\text{H}) = 176$ Hz]	-2.72 [s, br, 4H, $\text{H}_\mu(3,4)$, $\text{H}_\mu(2,5)$, $\text{H}_\mu(3',4')$, $\text{H}_\mu(2',5')$] -1.98 [s, br, 2H, $\text{H}_\mu(4,5)$, $\text{H}_\mu(4',5')$] 0.90 [q, br, 2H, H(1), H(1'), $J(^{11}\text{B}-^1\text{H}) = 180$ Hz] 1.5-3.7 [m, br, 8H, (H _i (2-5), H _i (2'-5'), J_{unres}) 7.34 [m, 6H, <i>p</i> -, <i>m</i> -C ₆ H ₅] 7.45 [m, 4H, <i>o</i> -C ₆ H ₅]	0.90 [s, 2H, H(1), H(1')] 2.67 [s, 4H, H _i (4,5), H _i (4',5')] 2.75 [s, 4H, H _i (2,3), H _i (2',3')]	144.7 [s, <i>i</i> -C ₆ H ₅] 135.0 [s, <i>o</i> -C ₆ H ₅ , $^2J(^{119}\text{Sn}-^{13}\text{C}) = 44$ Hz] 129.8 [s, <i>p</i> -C ₆ H ₅ , $^4J(^{119}\text{Sn}-^{13}\text{C}) = 14$ Hz] 129.2 [s, <i>m</i> -C ₆ H ₅ , $^3J(^{119}\text{Sn}-^{13}\text{C}) = 63$ Hz]
$\mu, 2'$ - $\text{SnPh}_2(\text{B}_5\text{H}_8)_2^d$	-2.6 [d, 1B, B(4'), $J(^{11}\text{B}-^1\text{H}) = 164$ Hz] -6.8 [d, 2B, B(3',5'), $^1J(^{11}\text{B}-^1\text{H}) = 155$ Hz] -8.2 [d, 2B, B(4,5), $^1J(^{11}\text{B}-^1\text{H}) = 164$ Hz] -10.8 [d, 2B, B(2,3), J_{unres}] -10.5 [s, 1B, B(2')] -48.0 [d, 2B, B(1), B(1'), $^1J(^{11}\text{B}-^1\text{H}) = 177$ Hz]	-2.75 [s, br, 2H, $\text{H}_\mu(3,4)$, $\text{H}_\mu(2,5)$] -2.0 [s, br, 3H, $\text{H}_\mu(4,5)$, $\text{H}_\mu(2',3')$, $\text{H}_\mu(2',5')$] -1.70 [s, br, 2H, $\text{H}_\mu(3',4')$, $\text{H}_\mu(4',5')$] 0.85 [q, br, 1H, H(1), $J(^{11}\text{B}-^1\text{H}) = 176$ Hz] 0.65 [q, br, 1H, H(1), or H(1'), $J(^{11}\text{B}-^1\text{H}) = 176$ Hz] 1.5-3.8 [m, br, 7H, H _i (2-5), H _i (3'-5'), J_{unres}] 7.30 [m, 6H, <i>p</i> -, <i>m</i> -C ₆ H ₅] 7.48 [m, 4H, <i>o</i> -C ₆ H ₅]	-2.25 [s, 1H, $\text{H}_\mu(4,5)$] -2.00 [s, 2H, $\text{H}_\mu(2',3')$, $\text{H}_\mu(2',5')$] 0.85 [s, 1H, H(1) or H(1')] 0.65 [s, 1H, H(1) or H(1')] 2.37 [s, 2H, H _i (4,5)] 2.52 [s, 2H, H _i (2,3)] 2.73 [s, 2H, H _i (3',5')] 2.80 [s, 1H, H _i (4')]	139 [s, br, <i>i</i> -C ₆ H ₅] 135.8 [s, <i>o</i> -C ₆ H ₅ , $^2J(^{119}\text{Sn}-^{13}\text{C}) = 42$ Hz] 128.8 [s, <i>p</i> -C ₆ H ₅ , $^4J(^{119}\text{Sn}-^{13}\text{C}) = 12$ Hz] 128.5 [s, <i>m</i> -C ₆ H ₅ , $^3J(^{119}\text{Sn}-^{13}\text{C}) = 54$ Hz]
$\mu, 1'$ - $\text{SnPh}_2(\text{B}_5\text{H}_8)_2^d$	-10.1 [d, br, with a shoulder 8B, B(2-5), B(2'-5'), $^1J(^{11}\text{B}-^1\text{H}) = 156$ Hz] -48.2 [d, 1B, B(1), $^1J(^{11}\text{B}-^1\text{H}) = 171$ Hz] -51.6 [s, 1B, B(1'), $^1J(^{11}\text{B}-^{119}\text{Sn}) = 1174$ Hz]	-2.75 [s, br, 2H, $\text{H}_\mu(3,4)$, $\text{H}_\mu(2,5)$] -2.15 [s, br, with a shoulder, 5H, $\text{H}_\mu(2',3')$, $\text{H}_\mu(3',4')$, $\text{H}_\mu(4',5')$, $\text{H}_\mu(2',5')$, shoulder $\text{H}_\mu(4,5)$] 0.60 [q, br, 1H, H(1), $J(^{11}\text{B}-^1\text{H}) = 175$ Hz] 1.4-3.5 [m, br, 8H, basal H _i] 7.31 [m, 6H, <i>p</i> -, <i>m</i> -C ₆ H ₅] 7.46 [m, 4H, <i>o</i> -C ₆ H ₅]	-2.35 [s, 1H, $\text{H}_\mu(4,5)$] -2.08 [s, 4H, $\text{H}_\mu(2'-5')$] 0.60 [s, 1H, H(1)] +2.34 [s, 2H, H _i (4,5)] 2.49 [s, 2H, H _i (2,3)] 2.58 [s, 4H, basal H _i]	141.4 [q, <i>i</i> -C ₆ H ₆ , $^2J(^{13}\text{C}-^{11}\text{B}) = 10.2$ Hz] 136.1 [s, <i>o</i> -C ₆ H ₅ , $^2J(^{119}\text{Sn}-^{13}\text{C}) = 44$ Hz] 128.6 [s, <i>p</i> -C ₆ H ₅ , $^4J(^{119}\text{Sn}-^{13}\text{C}) = 13$ Hz] 128.3 [s, <i>m</i> -C ₆ H ₅ , $^3J(^{119}\text{Sn}-^{13}\text{C}) = 58$ Hz]

^a Spectra observed at 96.3 MHz. ^b Spectra observed at 500 MHz. ^c Spectra observed at 76.6 MHz. ^d In CDCl₃ at 25 °C. ^e ^{11}B spectra observed in (C₂H₅)₂O; ¹H spectra observed in CDCl₃.

Table 2. Summary of Crystallographic Data for 1–3

	1	2	3
empirical formula	C ₁₂ H ₂₆ B ₁₀ Sn	C ₁₂ H ₂₆ B ₁₀ Sn	C ₁₂ H ₂₆ B ₁₀ Sn
fw	397.1	397.1	397.1
cryst color and habit	colorless needles	colorless rectangles	colorless cubes
cryst size, mm	0.3 × 0.2 × 0.2	0.35 × 0.30 × 0.20	0.45 × 0.40 × 0.30
cryst syst	orthorhombic	monoclinic	monoclinic
space group	<i>Pna</i> 2 ₁	<i>C</i> 2/ <i>c</i>	<i>P</i> 2 ₁ / <i>c</i>
unit cell dimens			
<i>a</i> , Å	7.708(4)	38.506(14)	9.622(2)
<i>b</i> , Å	15.836(6)	11.379(2)	9.868(2)
<i>c</i> , Å	15.814(5)	19.096(6)	21.009(4)
β, deg	90	106.12(2)	92.07(2)
<i>V</i> , Å ³	1930.3(14)	8038(4)	1993.6(7)
<i>Z</i> , molecules/cell	4	16	4
<i>D</i> _{calcd} , Mg m ⁻³	1.366	1.313	1.323
wavelength, Å	0.71073	0.71073	0.71073
scan type	<i>ω</i> -2θ	<i>ω</i> -2θ	<i>ω</i> -2θ
scan sp in <i>ω</i> (min, max), deg min ⁻¹	3.97–29.30	4.99–29.30	3.50–29.30
2θ range, deg	3.0–65.0	3.0–55.0	3.0–55.0
<i>T</i> , K	125(5)	125(5)	184(5)
abs coeff, mm ⁻¹	1.312	1.260	1.270
abs structure	0.03(10) ^a	N/A	N/A
no. of rflns collected	3618	9903	5162
no. of ind rflns	3618	9291 (<i>R</i> _{int} = 1.58%)	4609 (<i>R</i> _{int} = 2.38%)
no. of obsvd rflns	2062 (<i>F</i> > 4.0σ(<i>F</i>))	6442 (<i>F</i> > 4.0σ(<i>F</i>))	3813 (<i>F</i> > 4.0σ(<i>F</i>))
function minimized	Σ <i>w</i> (<i>F</i> _o ² - <i>F</i> _c ²)	Σ <i>w</i> (<i>F</i> _o - <i>F</i> _c)	Σ <i>w</i> (<i>F</i> _o - <i>F</i> _c)
final <i>R</i> (<i>F</i>), %	7.90	3.72	2.56
final <i>wR</i> (<i>F</i>) %	15.63 <i>R</i> (<i>F</i> ²)	3.12	2.57
goodness of fit, <i>S</i> (<i>F</i>)	1.046 <i>S</i> (<i>F</i> ²)	1.15	1.41

^a Flack parameter (SHELXL-93).

Apparatus. Standard high-vacuum line and drybox techniques were employed in this work.¹² NMR spectra were obtained on a Varian XL-300 spectrometer operating at 300.1, 96.3, 76.6, and 111.7 MHz to observe ¹H, ¹¹B, ¹³C, and ¹¹⁹Sn resonances, respectively. ¹H and ¹H{¹¹B} spectra were also recorded on a 500 MHz Bruker ARX-500 NMR spectrometer. Assignments were confirmed by selective decoupling experiments and heteronuclear 2D ¹¹B–¹H correlation spectra also run on the Bruker 500 MHz spectrometer. ¹¹B chemical shifts are reported in ppm, positive signs denoting a shift at a lower field with respect to Et₂O·BF₃ reference (0.0 ppm). ¹H and ¹³C chemical shifts were measured relative to SiMe₄ and CDCl₃, respectively. ¹¹⁹Sn chemical shifts were obtained with respect to SnMe₄ (0.0 ppm) as an external reference. Mass spectra were run as solids at 70 eV on a Varian/Mat 311A spectrometer equipped with a Technivent data system. IR spectra were run as KBr pellets on a Perkin-Elmer 1604 FT-IR spectrometer. Elemental analyses were performed by Atlantic Microlabs Inc.

Preparation of μ,μ'-SnPh₂(B₅H₈)₂ (1). KH (150 mg, 3.75 mmol) was placed in a 50 mL two-neck flask with one neck fitted with an extractor and the other neck stoppered. After evacuation, 0.4 mL of B₅H₉ (4 mmol) and 10 mL of Me₂O were condensed in at -198 °C. The mixture was warmed to -78 °C and stirred for 2 h. H₂ was pumped away at -196 °C, and the solvent was removed by evacuation overnight at -78 °C to afford solvent-free K[B₅H₈]. CH₂Cl₂, 10 mL, was condensed onto the K[B₅H₈], and under positive N₂ flow, a side-arm tip tube containing SnCl₂Ph₂ (510 mg, 1.5 mmol) was attached to the second neck of the reaction flask. After evacuation, the solution was stirred, the SnCl₂Ph₂ was added at -78 °C, and the resulting mixture stirred at -35 °C for 4 h. The reaction mixture was allowed to stir at -78 °C overnight and then warmed slowly over a period of 1 h to room temperature, stirred for an additional 1 h, and filtered at room temperature to remove KCl and unreacted K[B₅H₈]. The resultant clear filtrate was reduced to 2 mL under vacuum. Addition of 10 mL of pentane resulted in a trace of precipitate; so the solvent was removed and the residue dried under vacuum for 1 h at 25 °C to afford a waxy-white solid in 60% yield. The crude

Table 3. Atomic Coordinates (×10⁴) and Equivalent Isotropic Displacement Parameters (Å² × 10³) for 1

	<i>x</i>	<i>y</i>	<i>z</i>	<i>U</i> (eq) ^a
Sn	4652(1)	5126(1)	5000	23(1)
B(11)	2222(24)	3254(9)	4121(12)	35(4)
B(12)	3863(23)	3951(11)	4052(11)	36(4)
B(13)	2398(21)	3992(9)	4881(13)	34(5)
B(14)	558(22)	3963(13)	4161(14)	49(5)
B(15)	2097(20)	3882(11)	3304(13)	39(4)
B(21)	6498(29)	6822(12)	3579(13)	52(5)
B(22)	6742(24)	6218(11)	4460(11)	40(4)
B(23)	4949(20)	6100(11)	3748(11)	35(4)
B(24)	6432(24)	6015(12)	2896(11)	43(4)
B(25)	8151(29)	6085(16)	3632(12)	59(6)
C(11)	3111(16)	5940(9)	5796(10)	33(3)
C(12)	1732(16)	6411(8)	5484(9)	31(3)
C(13)	813(18)	6949(9)	6020(10)	36(3)
C(14)	1247(17)	7007(8)	6857(10)	32(3)
C(15)	2672(19)	6529(9)	7173(9)	34(3)
C(16)	3551(15)	6004(7)	6644(9)	24(3)
C(21)	6537(16)	4454(8)	5735(7)	25(3)
C(22)	6493(17)	3605(8)	5818(9)	27(3)
C(23)	7710(19)	3173(10)	6309(10)	36(3)
C(24)	9036(18)	3610(10)	6691(8)	34(3)
C(25)	9106(19)	4463(10)	6617(9)	38(3)
C(26)	7848(19)	4905(9)	6140(9)	37(3)

^a *U*(eq) is defined as one-third of the trace of the orthogonalized *U*_{ij} tensor.

product may be purified by recrystallization from hexane to afford white crystalline needles. Crystals suitable for X-ray diffraction are obtained by slow evaporation of hexane solutions. **1** melts with decomposition at about 98 °C and is very soluble in THF, CH₂Cl₂, and CHCl₃ and sparingly soluble in C₅H₁₂, C₆H₁₄, and Et₂O. Attempts to obtain satisfactory elemental analysis were unsuccessful, probably due to the high sensitivity to air and moisture. Anal. Calcd for C₁₂H₂₆B₁₀Sn: C, 36.31; H, 6.62. Found (1): C, 35.20; H, 6.14. Found (2): C, 35.11; H, 6.18. However mass spectral data were supportive of the formulation. The data for the (M - B₅H₈)⁺ ion [¹¹B₅¹²⁴Sn¹²C₆¹H₂₄]⁺ were selected since the molecular ion [¹¹B₁₀¹²⁴Sn¹²C₁₂¹H₃₁]⁺, although quite visible with a cutoff at *m/z* 405, was weak. The observed *m/z* values for the (M - B₅H₈)⁺ ion (relative intensity) were 327 (1.06), 328 (2.36), 329 (3.18), 330

Table 4. Atomic Coordinates ($\times 10^4$) and Equivalent Displacement Coefficients ($\text{\AA}^2 \times 10^3$) for 2

	x	y	z	$U(\text{eq})^a$
Sn(1)	3436(1)	8038(1)	668(1)	15(1)
B(11)	2886(2)	10298(5)	1344(3)	23(2)
B(12)	2908(1)	9327(5)	685(3)	25(2)
B(13)	3269(1)	9515(5)	1486(3)	21(2)
B(14)	3253(2)	11092(5)	1348(4)	33(2)
B(15)	2886(2)	10903(5)	539(3)	31(2)
B(21)	4144(1)	9899(4)	692(3)	19(2)
B(22)	4012(1)	8608(4)	984(3)	17(2)
B(23)	4247(1)	9743(5)	1599(3)	24(2)
B(24)	4590(2)	9804(5)	1130(3)	29(2)
B(25)	4357(2)	8687(5)	511(3)	28(2)
C(11)	3295(1)	6456(4)	1127(2)	18(1)
C(12)	3559(1)	5652(4)	1457(3)	23(1)
C(13)	3471(2)	4638(4)	1777(3)	31(2)
C(14)	3115(2)	4423(4)	1760(3)	35(2)
C(15)	2848(2)	5212(5)	1432(3)	33(2)
C(16)	2936(1)	6229(4)	1115(3)	23(2)
C(21)	3233(1)	7965(4)	-499(2)	18(1)
C(22)	3004(1)	7071(4)	-836(2)	20(1)
C(23)	2851(1)	7058(4)	-1588(3)	28(2)
C(24)	2926(1)	7966(4)	-2003(3)	25(2)
C(25)	3154(1)	8873(4)	-1677(3)	24(2)
C(26)	3308(1)	8871(4)	-929(3)	23(2)
Sn(2)	914(1)	618(1)	715(1)	16(1)
B(31)	437(1)	2911(5)	1549(3)	23(2)
B(32)	423(1)	1962(5)	855(3)	19(1)
B(33)	802(2)	2036(5)	1639(3)	21(2)
B(34)	822(2)	3614(5)	1551(3)	27(2)
B(35)	435(2)	3546(5)	754(3)	25(2)
B(41)	1641(1)	2458(5)	880(3)	24(2)
B(42)	1501(1)	1091(4)	1013(3)	20(2)
B(43)	1788(1)	1937(5)	1741(3)	27(2)
B(44)	2087(1)	2222(5)	1189(3)	27(2)
B(45)	1804(2)	1376(5)	458(3)	27(2)
C(31)	760(1)	-1014(3)	1091(2)	17(1)
C(32)	1018(1)	-1850(4)	1425(2)	20(1)
C(33)	911(1)	-2927(4)	1653(3)	23(2)
C(34)	549(1)	-3163(4)	1558(2)	26(2)
C(35)	292(1)	-2343(4)	1227(3)	23(2)
C(36)	394(1)	-1280(4)	993(3)	21(1)
C(41)	715(1)	633(4)	-454(2)	18(1)
C(42)	514(1)	-321(4)	-823(3)	22(1)
C(43)	395(1)	-333(5)	-1578(3)	31(2)
C(44)	476(1)	594(5)	-1978(3)	34(2)
C(45)	669(1)	1536(5)	-1623(3)	34(2)
C(46)	796(1)	1562(4)	-862(3)	27(2)

^a Equivalent isotropic U defined as one-third of the trace of the orthogonalized U_{ij} tensor.

(6.15), 331 (24.05), 332 (46.68), 333 (72.51), 334 (87.22), 335 (100), 336 (92.70), 337 (68.45), 338 (19.12), 339 (14.95), 340 (13.11), 341 (10.63), and 342 (1.33). The calculated¹³ m/z data were 327 (2.80), 328 (3.75), 329 (5.25), 330 (6.69), 331 (21.54), 332 (49.77), 333 (77.13), 334 (93.80), 335 (100), 336 (92.19), 337 (79.00), 338 (20.02), 339 (15.43), 340 (13.69), 341 (11.89), and 342 (2.32). The IR spectrum showed the following absorbances (cm^{-1}): 3061 (w), 2969 (w), 2592 (s, br), 1831 (w, br), 1478 (m), 1428 (m), 1261 (s), 1085 (s, br), 1067 (s), 1020 (s), 997 (m), 933 (m), 884 (m), 802 (s), 727 (s), 695 (s), 6107 (m), 444 (m).

Preparation of μ_2 - $\text{SnPh}_2(\text{B}_5\text{H}_8)_2$ (2). A two-neck reaction vessel attached to an extractor was charged with 170 mg of KH (4.25 mmol) in the drybox. After evacuation of the vessel on the vacuum line, 0.5 mL of B_5H_9 (4.8 mmol) and 15 mL of Et_2O was condensed in at -196°C . Deprotonation, under continued stirring, was carried out at -78°C overnight. The H_2 was pumped away at -196°C , and under positive nitrogen flow, the vessel was sealed with a tipper tube

Table 5. Atomic Coordinates ($\times 10^4$) and Equivalent Isotropic Displacement Coefficients ($\text{\AA}^2 \times 10^3$) for 3

	x	y	z	$U(\text{eq})^a$
Sn	3500(1)	5756(1)	1427(1)	25(1)
B(11)	1881(3)	8018(3)	137(1)	33(1)
B(12)	2140(3)	7695(3)	920(1)	33(1)
B(13)	2905(3)	6687(3)	342(1)	32(1)
B(14)	1249(3)	6501(3)	-76(2)	39(1)
B(15)	467(3)	7535(4)	521(2)	43(1)
B(21)	5500(3)	6705(3)	1697(1)	31(1)
B(22)	5803(3)	8168(3)	2097(2)	40(1)
B(23)	6396(4)	7909(4)	1312(2)	46(1)
B(24)	7175(3)	6331(4)	1567(2)	47(1)
B(25)	6560(3)	6600(4)	2353(2)	42(1)
C(11)	2056(2)	5699(3)	2189(1)	29(1)
C(12)	1006(3)	4727(3)	2217(1)	37(1)
C(13)	142(3)	4675(3)	2731(2)	47(1)
C(14)	303(3)	5580(4)	3223(2)	52(1)
C(15)	1332(3)	6550(3)	3203(2)	48(1)
C(16)	2203(3)	6607(3)	2690(1)	38(1)
C(21)	3666(3)	3712(3)	1091(1)	29(1)
C(22)	2550(3)	2986(3)	824(1)	37(1)
C(23)	2698(3)	1658(3)	629(1)	39(1)
C(24)	3984(3)	1025(3)	698(1)	38(1)
C(25)	5100(3)	1717(3)	962(1)	38(1)
C(26)	4943(3)	3053(3)	1157(1)	32(1)

^a Equivalent isotropic U defined as one-third of the trace of the orthogonalized U_{ij} tensor.

containing SnCl_2Ph_2 (645 mg, 1.9 mmol). SnCl_2Ph_2 was added to the borane anion, the mixture was allowed to warm to -78°C , and the resulting suspension was stirred at -78°C overnight. The reaction mixture became very viscous; so an additional 10 mL of Et_2O was added and the mixture stirred at -78°C for 3 h, then at -35°C for 4 h, and at ambient temperature for 15 min. The contents of the flask were filtered at -78°C to remove KCl and excess $\text{K}[\text{B}_5\text{H}_8]$ and the colorless filtrate was evaporated to dryness, resulting in 480 mg, or a 65% yield, of waxlike white solid product which on recrystallization from hexane gave colorless crystals. Crystals suitable for X-ray analysis were grown by slow evaporation from hexane. **2** melts at 74 – 76°C and has solubility properties similar to those of **1**. NMR spectra are given in Table 1. **2** is most easily identified by its ^{119}Sn NMR spectrum, which gives a broad 1:1:1:1 quartet at $\delta = -138.5$ ppm ($^1J(^{119}\text{Sn}-^{11}\text{B}) = 900$ Hz). Mass spectral data, observed for the $(\text{M} - \text{B}_5\text{H}_8)^+$ ion, [$^{11}\text{B}_5^{124}\text{Sn}^{12}\text{C}_6^{1}\text{H}_{24}$] $^+$, were m/z (relative intensity) 327 (6.04), 328 (0.00), 329 (8.82), 330 (8.43), 331 (22.40), 332 (48.77), 333 (81.94), 334 (95.53), 335 (100), 336 (96.35), 337 (74.73), 338 (22.61), 339 (17.59), 340 (15.59), 341 (17.59), and 342 (5.67). The calculated m/z data are the same as for **1**. The IR spectrum showed the following absorbances (cm^{-1}): 3058 (w), 2966 (w), 2589 (s, br), 1815 (w, br), 1479 (w), 1429 (m), 1262 (s), 1085 (s, br), 1073 (s), 1020 (s), 997 (m), 943 (w), 917 (w), 884 (m), 802 (s), 728.2 (s), 696 (s), 658 (w), 614 (m).

Preparation of μ_1 - $\text{SnPh}_2(\text{B}_5\text{H}_8)_2$ (3). 1 - $(\text{SnPh}_2\text{Cl})\text{B}_5\text{H}_8$ (2 mmol) in 20 mL of CH_2Cl_2 , was allowed to react with $\text{K}[\text{B}_5\text{H}_8]$ (2.5 mmol solid, from the reaction of 100 mg of KH with 3 mmol of B_5H_9 in 10 mL of Me_2O), stirring overnight at -78°C . The mixture was warmed to -35°C and stirred at that temperature for 3 h and then at ambient temperature for an additional 0.5 h. A white turbid solution was obtained. The contents of the flask were filtered slowly at -78°C in a vacuum extractor to remove KCl, and unreacted $\text{K}[\text{B}_5\text{H}_8]$, and after reduction of the volume of the colorless filtrate, 10 mL of C_5H_{12} was added. A precipitate was not obtained so the solvent was removed under vacuum. Recrystallization from hexane afforded colorless cubic crystals in 53% yield. The initial solid residue turns from off-white to pale yellow on drying. Slow evaporation from hexane affords crystals suitable for X-ray analysis. **3** has solubility properties similar to those of **1**, and it melts at 86 – 88°C . NMR spectral data are given in Table 1. **3** is easily recognized by its ^{119}Sn NMR spectrum which gives a broad 1:1:1:1 quartet at $\delta = -80.1$ ppm ($^1J(^{119}\text{Sn}-^{11}\text{B})$

(13) Program for the calculation of isotopic distributions from molecular formula: Stolz, W.; Korzenioski, R. W. In *Introduction to Organic Spectroscopy*; Lambert, J. B., Shurvell, H. F., Lightner, D. A., Cooks, R. G., Eds.; Macmillan: New York 1987, pp 401–406.

Table 6. Selected Bond Lengths and Bond Angles for $\mu_2\text{-SnPh}_2(\text{B}_5\text{H}_8)_2$ (1)

Bond Distances (Å)			
Sn-C(21)	2.143(11)	B(12)-B(15)	1.81(2)
Sn-C(11)	2.16(2)	B(13)-B(14)	1.82(3)
Sn-B(12)	2.47(2)	B(14)-B(15)	1.81(3)
Sn-B(13)	2.51(2)	B(21)-B(23)	1.67(2)
Sn-B(22)	2.51(2)	B(21)-B(24)	1.67(3)
Sn-B(23)	2.52(2)	B(21)-B(22)	1.70(3)
B(11)-B(15)	1.63(3)	B(21)-B(25)	1.73(3)
B(11)-B(13)	1.68(2)	B(22)-B(25)	1.72(3)
B(11)-B(12)	1.68(2)	B(22)-B(23)	1.79(2)
B(11)-B(14)	1.71(2)	B(23)-B(24)	1.77(3)
B(12)-B(13)	1.73(3)	B(24)-B(25)	1.77(3)
Bond Angles (deg)			
C(21)-Sn-C(11)	110.7(5)	B(11)-B(14)-B(13)	56.9(10)
C(21)-Sn-B(12)	97.0(5)	B(15)-B(14)-B(13)	87.7(11)
C(11)-Sn-B(12)	132.0(6)	B(11)-B(15)-B(14)	59.2(11)
C(21)-Sn-B(13)	98.9(5)	B(11)-B(15)-B(12)	58.3(10)
C(11)-Sn-B(13)	95.2(5)	B(14)-B(15)-B(12)	89.9(12)
B(12)-Sn-B(13)	40.7(6)	B(23)-B(21)-B(24)	63.9(11)
C(21)-Sn-B(22)	95.2(6)	B(23)-B(21)-B(22)	64.2(10)
C(11)-Sn-B(22)	98.0(6)	B(24)-B(21)-B(22)	95.9(13)
B(12)-Sn-B(22)	118.1(6)	B(23)-B(21)-B(25)	93.3(13)
B(13)-Sn-B(22)	155.8(6)	B(24)-B(21)-B(25)	62.5(12)
C(21)-Sn-B(23)	131.9(5)	B(22)-B(21)-B(25)	60.0(11)
C(11)-Sn-B(23)	98.2(5)	B(21)-B(22)-B(25)	60.9(12)
B(12)-Sn-B(23)	90.4(6)	B(21)-B(22)-B(23)	57.2(11)
B(13)-Sn-B(23)	116.3(6)	B(25)-B(22)-B(23)	89.7(12)
B(22)-Sn-B(23)	41.7(5)	B(21)-B(22)-Sn	126.5(12)
B(15)-B(11)-B(13)	98.4(11)	B(25)-B(22)-Sn	125.5(12)
B(15)-B(11)-B(12)	66.0(10)	B(23)-B(22)-Sn	69.3(7)
B(13)-B(11)-B(12)	61.9(10)	B(21)-B(23)-B(24)	58.1(10)
B(15)-B(11)-B(14)	65.4(11)	B(21)-B(23)-B(22)	58.6(10)
B(13)-B(11)-B(14)	64.9(10)	B(24)-B(23)-B(22)	89.3(10)
B(12)-B(11)-B(14)	97.7(11)	B(21)-B(23)-Sn	127.4(11)
B(11)-B(12)-B(13)	59.0(10)	B(24)-B(23)-Sn	127.5(10)
B(11)-B(12)-B(15)	55.7(10)	B(22)-B(23)-Sn	68.9(7)
B(13)-B(12)-B(15)	90.4(12)	B(21)-B(24)-B(25)	60.3(13)
B(11)-B(12)-Sn	129.9(12)	B(21)-B(24)-B(23)	58.1(11)
B(13)-B(12)-Sn	70.9(8)	B(25)-B(24)-B(23)	88.8(11)
B(15)-B(12)-Sn	129.0(10)	B(22)-B(25)-B(21)	59.1(11)
B(11)-B(13)-B(12)	59.1(10)	B(22)-B(25)-B(24)	92.0(13)
B(11)-B(13)-B(14)	58.2(11)	B(21)-B(25)-B(24)	57.2(12)
B(12)-B(13)-B(14)	92.0(13)	C(16)-C(11)-C(12)	119.3(14)
B(11)-B(13)-Sn	127.5(11)	C(16)-C(11)-Sn	118.3(9)
B(12)-B(13)-Sn	68.4(8)	C(12)-C(11)-Sn	122.4(19)
B(14)-B(13)-Sn	127.3(11)	C(22)-C(21)-Sn	122.0(10)
B(11)-B(14)-B(15)	55.4(10)	C(26)-C(21)-Sn	119.2(10)

= 1174 Hz). A very weak quartet is also seen under this one at $\delta = -75.8$ ppm. Mass spectral data, observed for the $(M - B_5H_8)^+$ ion, [$^{11}B_5^{124}Sn^{12}C_6^{1}H_{24}^{1+}$], were m/z (relative intensity) 327 (2.60), 328 (4.06), 329 (4.44), 330 (7.20), 331 (23.32), 332 (50.05), 333 (68.78), 334 (88.42), 335 (100), 336 (92.42), 337 (61.53), 338 (22.02), 339 (15.42), 340 (15.69), 341 (15.25), and 342 (2.65). The calculated m/z data are given above. The IR spectrum showed the following absorbancies (cm^{-1}): 3066 (w), 2983 (w), 2596 (s, br), 1844 (w), 1603 (w), 1479 (w), 1442 (s), 1429 (s), 1369 (s), 1351 (s), 1310 (m), 1261 (m), 1090 (m, br), 1070 (m), 1026 (m), 942 (w), 884 (w), 802 (s), 731.6 (m), 698 (s), 668 (w).

Rearrangement of 1 in CDCl_3 . If an NMR tube containing a sample of **1** was stored in CDCl_3 at ambient temperature and the NMR spectra were observed periodically, changes were noted in the ^{11}B , 1H , and ^{119}Sn spectra. The spectra were quite complex, indicative of mixtures, and only the ^{119}Sn spectra were easily interpreted. After 1 month at 25 °C the resonance at $\delta = -40.1$ ppm had diminished in intensity and a 1:1:1 quartet had grown in at $\delta = -138.5$ ppm, indicative of the presence of isomer **2**. After 4 months at 25 °C, the original signal was much smaller and a second 1:1:1 quartet had appeared at $\delta = -80.1$ ppm, indicative of the presence of isomer **3**. Changes are also observed in the 1H and ^{11}B NMR spectra which are also interpreted in terms of the slow rearrangement of **1** to **2** and then to **3**.

Table 7. Selected Bond Lengths and Bond Angles for $\mu_2\text{-SnPh}_2(\text{B}_5\text{H}_8)_2$ (2)

Bond Distances (Å)			
Sn(1)-B(12)	2.513(6)	B(15)-H(145)	1.239(56)
Sn(1)-B(13)	2.495(6)	B(15)-H(15)	1.122(50)
Sn(1)-B(22)	2.230(5)	B(21)-B(22)	1.697(7)
Sn(1)-C(11)	2.137(5)	B(21)-B(23)	1.674(7)
Sn(1)-C(21)	2.148(4)	B(21)-B(24)	1.693(7)
B(11)-B(12)	1.695(8)	B(21)-B(25)	1.689(8)
B(11)-B(13)	1.682(8)	B(21)-H(21)	1.050(51)
B(11)-B(14)	1.676(9)	B(22)-B(23)	1.810(7)
B(11)-B(15)	1.686(9)	B(22)-B(25)	1.802(9)
B(11)-H(11)	1.095(62)	B(22)-H(223)	1.252(51)
B(12)-B(13)	1.771(7)	B(22)-H(225)	1.263(57)
B(12)-B(15)	1.814(8)	B(23)-B(24)	1.791(9)
B(12)-H(12)	1.083(52)	B(23)-H(223)	1.277(55)
B(12)-H(125)	1.235(58)	B(23)-H(23)	1.086(58)
B(13)-B(14)	1.812(8)	B(23)-H(234)	1.191(57)
B(13)-H(13)	1.137(50)	B(24)-B(25)	1.797(8)
B(13)-H(134)	1.221(60)	B(24)-H(234)	1.323(60)
B(14)-B(15)	1.793(8)	B(24)-H(24)	1.091(56)
B(14)-H(134)	1.150(59)	B(24)-H(245)	1.285(56)
B(14)-H(14)	1.092(50)	B(25)-H(225)	1.366(58)
B(14)-H(145)	1.306(55)	B(25)-H(245)	1.224(48)
B(15)-H(125)	1.344(57)	B(25)-H(25)	1.130(56)
Bond Angles(deg)			
B(12)-Sn(1)-B(13)	41.4(2)	B(25)-B(21)-H(21)	133.7(31)
B(12)-Sn(1)-B(22)	125.1(2)	Sn(1)-B(22)-B(21)	121.9(3)
B(13)-Sn(1)-B(22)	92.5(2)	Sn(1)-B(22)-B(23)	131.5(3)
B(12)-Sn(1)-C(11)	100.9(2)	Sn(1)-B(22)-B(25)	134.0(3)
B(13)-Sn(1)-C(11)	99.9(2)	Sn(1)-B(22)-H(223)	113.0(28)
B(22)-Sn(1)-C(11)	118.7(2)	Sn(1)-B(22)-H(225)	114.0(24)
B(12)-Sn(1)-C(21)	88.5(2)	H(223)-B(22)-H(225)	96.7(34)
B(13)-Sn(1)-C(21)	126.4(2)	B(21)-B(23)-H(23)	133.6(27)
B(22)-Sn(1)-C(21)	109.8(2)	B(21)-B(23)-H(23)	133.2(28)
C(11)-Sn(1)-C(21)	109.4(2)	B(24)-B(23)-H(23)	135.9(28)
B(12)-B(11)-H(11)	127.7(27)	H(223)-B(23)-H(23)	106.2(41)
B(13)-B(11)-H(11)	128.2(27)	H(223)-B(23)-H(234)	94.1(36)
B(14)-B(11)-H(11)	134.2(27)	H(23)-B(23)-H(234)	109.2(37)
B(15)-B(11)-H(11)	133.6(26)	B(21)-B(24)-H(24)	130.8(28)
Sn(1)-B(12)-B(11)	126.7(3)	B(23)-B(24)-H(24)	133.2(31)
Sn(1)-B(12)-B(13)	68.8(3)	B(25)-B(24)-H(24)	135.6(30)
Sn(1)-B(12)-B(15)	125.3(4)	H(234)-B(24)-H(24)	113.6(36)
Sn(1)-B(12)-H(12)	92.8(29)	H(234)-B(24)-H(245)	95.6(35)
B(11)-B(12)-H(12)	129.3(32)	H(24)-B(24)-H(245)	112.4(41)
B(13)-B(12)-H(12)	140.6(26)	H(225)-B(25)-H(245)	96.2(34)
B(15)-B(12)-H(12)	127.5(26)	B(21)-B(25)-H(25)	132.1(25)
Sn(1)-B(12)-H(125)	89.5(27)	B(22)-B(25)-H(25)	128.0(28)
H(12)-B(12)-H(125)	107.4(37)	B(24)-B(25)-H(25)	140.8(28)
Sn(1)-B(13)-B(11)	128.5(3)	H(225)-B(25)-H(25)	103.9(36)
Sn(1)-B(13)-B(12)	69.8(3)	H(245)-B(25)-H(25)	113.3(39)
Sn(1)-B(13)-B(14)	125.5(4)	Sn(1)-C(11)-C(12)	120.5(3)
Sn(1)-B(13)-H(13)	95.6(30)	Sn(1)-C(11)-C(16)	120.7(3)
B(11)-B(13)-H(13)	126.6(33)	Sn(1)-C(11)-C(22)	120.8(3)
B(12)-B(13)-H(13)	143.7(28)	Sn(1)-C(21)-C(26)	120.5(3)
B(14)-B(13)-H(13)	123.6(27)	B(12)-H(125)-B(15)	89.3(37)
Sn(1)-B(13)-H(134)	96.0(29)	B(13)-H(134)-B(14)	99.6(48)
H(13)-B(13)-H(134)	110.7(37)	B(14)-H(145)-B(15)	89.6(39)
B(11)-B(14)-H(14)	131.0(33)	B(22)-H(223)-B(23)	91.4(37)
B(13)-B(14)-H(14)	131.4(27)	B(22)-H(225)-B(25)	86.4(31)
B(15)-B(14)-H(14)	137.9(28)	B(23)-H(234)-B(24)	90.7(33)
H(134)-B(14)-H(14)	113.0(38)	B(24)-H(245)-B(25)	91.4(35)
H(134)-B(14)-H(145)	90.5(37)	B(32)-Sn(2)-B(33)	41.5(2)
H(14)-B(14)-H(145)	115.4(38)	B(32)-Sn(2)-B(42)	124.4(2)
H(125)-B(15)-H(145)	89.2(35)	B(33)-Sn(2)-B(42)	91.4(2)
B(11)-B(15)-H(15)	135.4(31)	B(32)-Sn(2)-C(31)	101.9(2)
B(12)-B(15)-H(15)	132.2(27)	B(33)-Sn(2)-C(31)	101.8(2)
B(14)-B(15)-H(15)	138.0(27)	B(42)-Sn(2)-C(31)	118.7(2)
H(125)-B(15)-H(15)	109.6(35)	B(32)-Sn(2)-C(41)	92.6(2)
H(145)-B(15)-H(15)	110.3(38)	B(33)-Sn(2)-C(41)	130.0(2)
B(22)-B(21)-H(21)	131.7(30)	B(42)-Sn(2)-C(41)	107.8(2)
B(23)-B(21)-H(21)	128.4(31)	C(31)-Sn(2)-C(41)	107.7(2)
B(24)-B(21)-H(21)	130.4(30)		

Rearrangement of 1 in Et_2O . A 200 mg sample of **1** was dissolved in 15 mL of Et_2O at -78 °C and stirred for 2 days at -78 °C and then at ambient temperature for 1.5 h. The solution was filtered, and the colorless filtrate was evacuated until dry solid residue remained. NMR spectra of the resulting

Table 8. Selected Bond Lengths and Bond Angles for μ, μ' - $\text{SnPh}_2(\text{B}_5\text{H}_8)_2$ (3)

Bond Distances (Å)			
Sn-B(12)	2.532 (3)	B(15)-H(15)	1.115(29)
Sn-B(13)	2.504 (3)	B(15)-H(145)	1.274(31)
Sn-B(21)	2.197 (3)	B(21)-B(22)	1.691(4)
Sn-C(11)	2.157 (2)	B(21)-B(23)	1.691(5)
Sn-C(21)	2.145 (2)	B(21)-B(24)	1.685(4)
B(11)-B(12)	1.685 (4)	B(21)-B(25)	1.689(4)
B(11)-B(13)	1.689 (4)	B(22)-B(23)	1.783 (5)
B(11)-B(14)	1.671 (4)	B(22)-B(25)	1.785 (5)
B(11)-B(15)	1.676 (5)	B(22)-H(22)	1.048 (30)
B(11)-H(11)	1.043 (31)	B(22)-H(223)	1.275 (31)
B(12)-B(13)	1.752 (4)	B(22)-H(225)	1.338 (29)
B(12)-B(15)	1.795 (4)	B(23)-B(24)	1.802 (5)
B(12)-H(12)	1.100 (29)	B(23)-H(234)	1.259 (30)
B(12)-H(125)	1.298 (30)	B(23)-H(223)	1.216 (30)
B(13)-B(14)	1.801 (4)	B(23)-H(23)	1.074 (31)
B(13)-H(13)	1.015 (30)	B(24)-B(25)	1.794 (5)
B(13)-H(134)	1.249 (30)	B(24)-H(234)	1.404 (30)
B(14)-B(15)	1.803 (5)	B(24)-H(24)	1.042 (30)
B(14)-H(134)	1.221 (30)	B(24)-H(245)	1.285 (30)
B(14)-H(14)	1.039 (30)	B(25)-H(25)	1.033 (31)
B(14)-H(145)	1.288 (30)	B(25)-H(225)	1.253 (30)
B(15)-H(125)	1.265 (29)	B(25)-H(245)	1.235 (30)

Bond Angles (deg)			
B(12)-Sn-B(13)	40.7(1)	H(125)-B(15)-H(145)	89.9(19)
B(12)-Sn-B(21)	102.8(1)	H(15)-B(15)-H(145)	109.7(20)
B(13)-Sn-B(21)	104.4(1)	Sn-B(21)-B(22)	128.8(2)
B(12)-Sn-C(11)	89.7(1)	Sn-B(21)-B(23)	129.3(2)
B(13)-Sn-C(11)	123.5(1)	Sn-B(21)-B(24)	134.4(2)
B(21)-Sn-C(11)	113.6(1)	Sn-B(21)-B(25)	133.0(2)
B(12)-Sn-C(21)	128.0(1)	B(21)-B(22)-H(22)	131.4(17)
B(13)-Sn-C(21)	93.6(1)	B(23)-B(22)-H(22)	130.5(16)
B(21)-Sn-C(21)	114.3(1)	B(25)-B(22)-H(22)	137.8(17)
C(11)-Sn-C(21)	106.1(1)	H(22)-B(22)-H(223)	110.1(22)
B(11)-B(11)-H(11)	133.1(16)	H(22)-B(22)-H(225)	113.9(21)
B(13)-B(11)-H(11)	130.0(17)	H(223)-B(22)-H(225)	92.2(19)
B(14)-B(11)-H(11)	129.3(17)	H(234)-B(23)-H(223)	88.6(19)
B(15)-B(11)-H(11)	132.4(17)	B(21)-B(23)-H(23)	130.8(16)
Sn-B(12)-B(13)	127.5(2)	B(22)-B(23)-H(23)	135.5(16)
Sn-B(12)-B(15)	68.8(1)	B(24)-B(23)-H(23)	134.0(17)
Sn-B(12)-B(15)	124.8(2)	H(234)-B(23)-H(23)	106.2(21)
Sn-B(12)-H(12)	91.1(15)	H(223)-B(23)-H(23)	112.8(22)
B(11)-B(12)-H(12)	129.1(16)	B(21)-B(24)-H(24)	128.7(17)
B(13)-B(12)-H(12)	137.3(15)	B(23)-B(24)-H(24)	135.4(17)
B(15)-B(12)-H(12)	130.0(15)	B(25)-B(24)-H(24)	133.0(17)
Sn-B(12)-H(125)	91.5(13)	H(234)-B(24)-H(24)	113.4(21)
H(12)-B(12)-H(125)	110.6(20)	B(234)-B(24)-H(245)	95.7(18)
Sn-B(13)-B(11)	129.0(2)	H(24)-B(24)-H(245)	111.2(21)
Sn-B(13)-B(12)	70.5(1)	B(21)-B(25)-H(25)	134.4(17)
Sn-B(13)-B(14)	125.1(2)	B(22)-B(25)-H(25)	135.0(17)
Sn-B(13)-H(13)	92.3(16)	B(24)-B(25)-H(25)	135.0(17)
B(11)-B(13)-H(13)	128.0(17)	H(25)-B(25)-H(225)	106.9(22)
B(12)-B(13)-H(13)	139.8(17)	H(25)-B(25)-H(245)	107.4(22)
B(14)-B(13)-H(13)	127.7(16)	H(225)-B(25)-H(245)	91.3(20)
Sn-B(13)-H(134)	92.8(14)	Sn-C(11)-C(12)	122.4(2)
H(13)-B(13)-H(134)	110.8(22)	Sn-C(11)-C(16)	119.8(2)
B(11)-B(14)-H(14)	131.8(16)	Sn-C(21)-C(22)	123.4(2)
B(13)-B(14)-H(14)	135.4(16)	Sn-C(21)-C(26)	118.8(2)
B(15)-B(14)-H(14)	134.5(16)	B(13)-H(134)-B(14)	93.6(19)
H(134)-B(14)-H(14)	113.4(21)	B(12)-H(125)-B(15)	88.9(19)
H(134)-B(14)-H(145)	90.9(20)	B(23)-H(234)-B(24)	85.0(18)
H(14)-B(14)-H(145)	110.4(21)	B(14)-H(145)-B(15)	89.5(19)
B(11)-B(15)-H(15)	130.1(15)	B(22)-H(223)-B(23)	91.4(21)
B(12)-B(15)-H(15)	137.1(15)	B(22)-H(225)-B(25)	87.0(18)
B(14)-B(15)-H(15)	132.5(15)	B(24)-H(245)-B(25)	90.7(19)
H(125)-B(15)-H(15)	114.2(20)		

sample in CDCl_3 were identical to those observed for **2** prepared as described above and are listed in Table 1.

Rearrangement of 1 in THF. An NMR sample of **1** in THF was made up at -78°C and stored overnight. The resulting NMR spectrum indicated a mixture of **1** and **2**. After 2 days the spectrum had not changed. When the sample was allowed to warm to room temperature and remain there for 1 h, the ^1H and ^{11}B NMR spectra indicated the presence of only the isomer **3** and some decomposition product, most easily

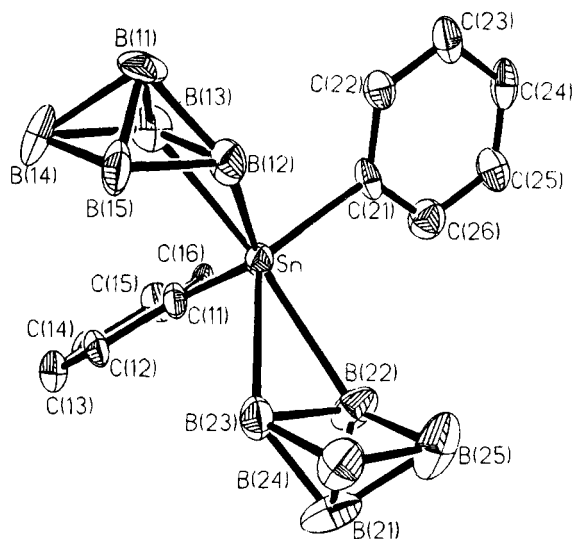


Figure 1. Projection view of μ, μ' - $\text{SnPh}_2(\text{B}_5\text{H}_8)_2$ (**1**). The thermal ellipsoids are at the 50% probability level.

observed as a broad single ^{119}Sn resonance at $\delta = -204$ ppm. The ^{119}Sn spectrum exhibited a quartet at $\delta = -75.8$ ppm, suggesting that this is the minor component observed above in the preparation of **3**. All other spectral data for the product mixture indicated that the major product of the reaction of **1** with THF at ambient temperature was **3**.

Reaction of $[\text{B}_5\text{H}_8]^-$ with SnCl_2Ph_2 in a 2:1 Mole Ratio in THF. Using the same procedure as described for the preparation of **1**, except that the reaction is carried out in THF, 263 mg (37% yield) of a viscous orange residue is obtained when 610 mg of SnCl_2Ph_2 (1.8 mmol) is added to $\text{K}[\text{B}_5\text{H}_8]$ prepared from 0.55 mL of B_5H_9 (5.3 mmol) and 190 mg of KH (4.75 mmol) in 20 mL of THF. NMR spectra were identical to those for **3** except that the ^{119}Sn spectrum exhibited two 1:1:1:1 quartets in approximately equal amounts at $\delta = -80.1$ and -75.8 ppm, suggesting that perhaps two isomers are present.

X-ray Structure Determinations. Colorless crystals of **1**, were obtained by slow evaporation of hexane solutions in the refrigerator at -20°C , and **2** and **3** crystals were grown similarly in the drybox at ambient temperature. Crystals of appropriate dimensions were mounted on glass fibers in random orientations. Preliminary examination and data collection were performed using a Siemens R3m/V automated single crystal X-ray diffractometer using graphite-monochromated Mo K α radiation ($\lambda = 0.71073$ Å) at 125(5) K for **1** and 2 and 184(5) K for **3**. Auto-indexing of 10 centered reflections from the rotation photograph indicated an orthorhombic lattice for **1** and a monoclinic lattice for **2** and **3**. Axial photographs were taken to confirm the Laue symmetry and cell lengths. Final cell constants and orientation matrices for data collection were calculated by least squares refinement of the setting angles for 20 reflections ($15^\circ < 2\theta < 30^\circ$). Intensity data were collected using ω - 2θ scans with variable scan speeds. Three representative reflections measured every 50 reflections showed <5% variation during data collection. Crystal data and intensity data collection parameters are listed in Table 2.

Data reduction, structure solution, and refinement were carried out using the SHELXTL-PLUS (VMS) software package.^{14a} Least-squares refinement for **1** was achieved using SHELXL-93.^{14b} Empirical absorption corrections were applied to the data using Ψ -scan curves. The structures were solved by the Patterson method and refined successfully in the space groups $Pna2_1$, $C2/c$, and $P2_1/c$, respectively for **1**-**3**. Full matrix least-squares refinement was carried out by minimizing $\sum w(F_o^2 - F_c^2)^2$ for **1** and $\sum w(F_o - F_c)^2$ for **2** and **3**. The non-

(14) (a) Sheldrick, G. M. Siemens Analytical X-Ray Division, Madison, WI, 1991. (b) Sheldrick, G. M. Siemens Analytical X-Ray Division, Madison, WI, 1993.

hydrogen atoms were refined anisotropically to convergence. The positional parameters of all hydrogen atoms except the bridging hydrogens of **1** were refined using a riding model.^{14b} Fixed isotopic temperature factors were used for all hydrogen atoms. Final residual values: (**1**) $R(F) = 7.90$ for reflections $I > 2\sigma(I)$, $wR(F^2) = 15.63\%$ for reflections $(F^2) > -3\sigma(F^2)$, $s = 1.026$; (**2**) $R(F) = 3.72$, $wR(F) = 3.12\%$, $s = 1.15$ for reflections $F > 4\sigma(F)$; (**3**) $R(F) = 2.56$, $wR(F) = 2.57\%$, $s = 1.41$ for reflections $F > 4\sigma(F)$. Structure refinement parameters are listed in Table 2. The atomic coordinates for the non-hydrogen atoms for **1–3** are listed in Tables 3–5 and selected bond distances and angles are given in Tables 6–8, respectively. Projection views of the molecule with non-hydrogen atoms represented by 50% probability ellipsoids for **1–3** are presented in Figures 1–3.

Results

Scheme 1 illustrates the reactions in which the species **1–3** are prepared, and it also illustrates the processes in which **1** is converted to **2** and **3**.

μ, μ' -SnPh₂(B₅H₈)₂ (1). Two B₅H₈ cages may be coupled to a SnPh₂ moiety by treatment of K[B₅H₈] with SnCl₂Ph₂ in a 2:1 molar ratio in CH₂Cl₂ to afford μ, μ' -SnPh₂(B₅H₈)₂ **1**. The ¹¹⁹Sn NMR spectrum gives a single broad resonance at $\delta = -40.1$ ppm, fwhm = 187 Hz, and it is useful to compare this with the analogous data for 2,3- μ -(SnPh₃)B₅H₈ which are -98.3 ppm and 108 Hz, respectively.^{9b} It is well-known that broad resonances, rather than resolved septets, are normally observed for bridging protons in boranes.¹⁵ Furthermore we observed single broad resonances for the tin atom in an analogous environment both for 2,3- μ -(SnPh₃)B₅H₈^{9b} and 2,3- μ -(SnPh₃)B₆H₉.^{9c} The ¹H spectrum gives two resonances in a 1:2 area ratio in the upfield region where bridging H atoms are normally observed, suggesting that the two cages are equivalent and each contains three bridging H atoms. The apical H atoms appear as a single 1:1:1:1 quartet [$J(^{11}\text{B}-^1\text{H}) = 176$ Hz], which on ¹¹B decoupling gives a sharp singlet, again suggesting that the two H atoms are equivalent. The basal H atoms are observed as two broad partially collapsed overlapping quartets which decouple to sharp singlets with area ratio 2:2. The ¹¹B spectrum gives the expected three doublets in a 2:2:1 area ratio which on ¹H decoupling collapse to singlets, as is typical for *nido*-pyramidal boranes. Selective ¹H-¹¹B decoupling experiments and ¹H{¹¹B}-¹¹B{¹H} correlated two-dimensional NMR measurements indicate that the higher field resonance of the two basal borons is due to the B(2,3) pair bonded to the tin atom.¹⁸ In previously reported work, the low-field resonances in 2,3- μ -bridged-substituted *nido*-pentaboranes were assigned to the boron atoms bonded to the substituent,¹⁶ but we believe this to be wrong in the case of all previous work.^{10,17,9b} Mass spectral ion cluster calculations for

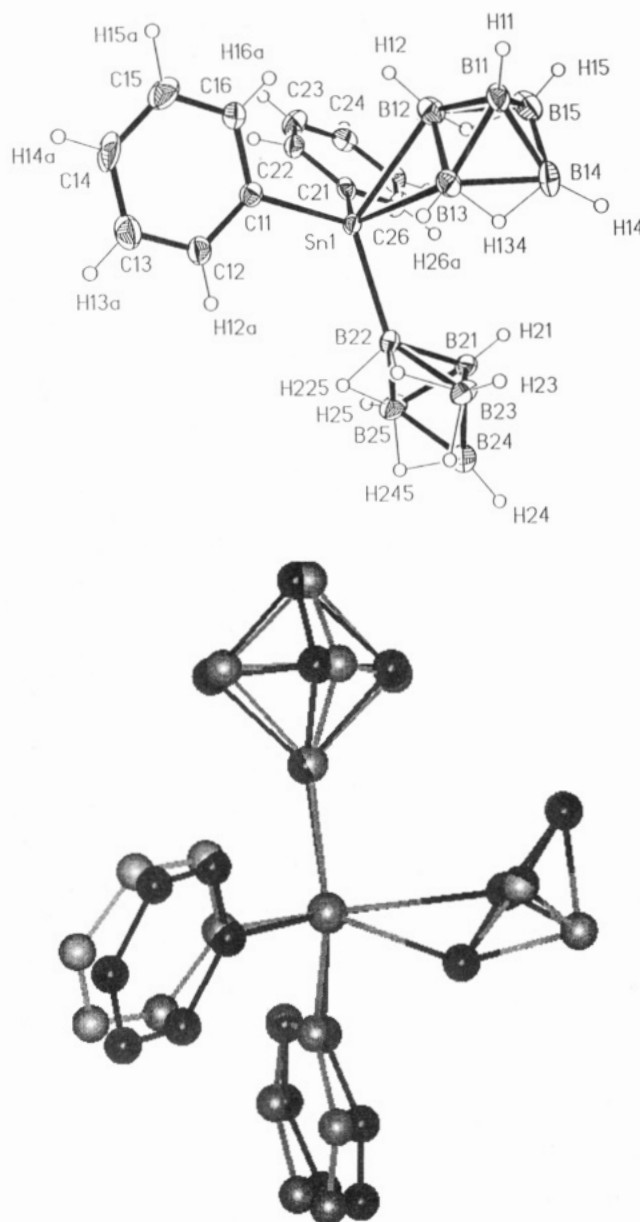


Figure 2. (a) Projection view of one of the two unique molecules in the unit cell of μ, μ' -SnPh₂(B₅H₈)₂ (**2**). The thermal ellipsoids are at the 50% probability level. (b) Superimposition of the two unique molecules in the unit cell of **2**.

the $[P - B_5H_8]^+$ envelope match the observed data very well when the isotopic abundances of Sn and B are used in a standard calculation.¹³ Also, the fragmentation mode is that expected for a system with the Sn substituent in a bridging position, since mass spectra of the series of stannylborane species we described earlier⁹ indicate that loss of the Ph group is not favored in bridging species.

$\mu, 2'$ -SnPh₂(B₅H₈)₂ (2). If **1** is stored in CDCl₃ at 25 °C for several weeks, changes are observed in the NMR spectra which are interpreted to indicate the presence of isomer **2** such that the ratio of isomers **1** and **2**, after a period of about 1 month, is approximately 2:1.¹⁹ A more vivid observation of this rearrangement is observed if **1** is treated with Et₂O. This, followed by

(15) (a) Schaeffer, R. *Prog. Boron Chem.* **1964**, *1*, 441. (b) Eaton, G. R.; Lipscomb, W. N. *NMR Studies of Boron Hydrides and Related Compounds* Benjamin: New York, 1969. (c) Shore, S. G. In *Boron Hydride Chemistry*; Muettterties, E. L., Ed.; Academic Press: New York, 1975; Chapter 3. (d) Todd, L. J.; Siedle, A. R. *Prog. NMR Spectrosc.* **1979**, *13*, 87.

(16) (a) Gaines, D. F.; Iorns, T. V. *J. Am. Chem. Soc.* **1967**, *89*, 4249. (b) Gaines, D. F.; Iorns, T. V. *J. Am. Chem. Soc.* **1968**, *90*, 6617. (c) Leach, J. B.; Oates, G.; Tang, S.; Onak, T. *J. Chem. Soc., Dalton Trans.* **1975**, 1018. (d) Greenwood, N. N.; Staves, J. *J. Chem. Soc., Dalton Trans.* **1977**, 1786.

(17) Rush, P. K.; Barton, L. *Polyhedron* **1985**, *4*, 1741.

(18) Fang, H.; Bould, J.; Wilking, J. B.; Barton, L. To be submitted.

(19) Srivastava, D. K.; Fang, H.; Rath, N. P.; Barton, L. *Spec. Publ.-R. Soc. Chem.* **1994**, No. 143, 310.

Scheme 1

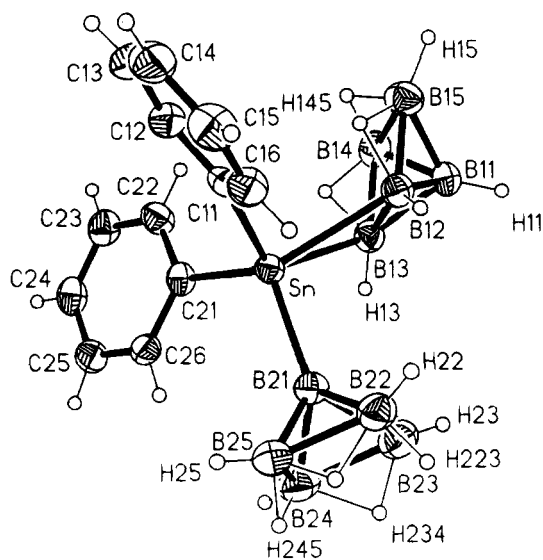
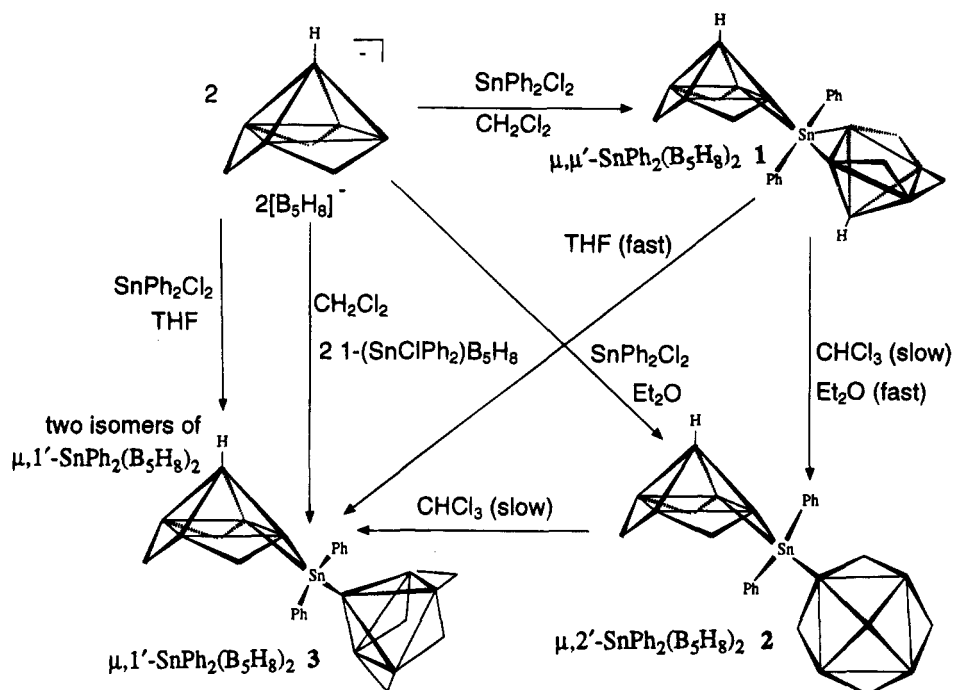


Figure 3. Projection view of $\mu, 1'-\text{SnPh}_2(\text{B}_5\text{H}_8)_2$ (**3**). The thermal ellipsoids are at the 50% probability level.

workup, results in the isolation of a material whose NMR spectral data were identical to those observed for **2** prepared as described below and listed in Table 1.

2 is best prepared if the reaction between $\text{K}[\text{B}_5\text{H}_8]$ and SnCl_2Ph_2 in a 2:1 mole ratio is allowed to proceed in Et_2O . NMR spectra and a crystal structure determination confirm the identity of **2**. The 96.25 MHz ^{11}B NMR spectrum, observed in CDCl_3 at ambient temperature, is given in Figure 4b and the $^{11}\text{B}\{^1\text{H}\}$ spectrum is given in Figure 4a. The basal boron resonances are easily interpreted in terms of the $\mu, 2'$ -structure. The resulting $^{11}\text{B}\{^1\text{H}\}$ spectrum shows a 1:2:2:3 pattern which arises from overlap of the 1:2:1 pattern from the cage bonded to the tin at the 2-position and a 2:2 pattern arising from the cage bonded to tin through a B–Sn–B bridge bond. The apical borons are seen as a single doublet of area 2, which on proton decoupling affords a

singlet. This observation was surprising since, on the basis of the ^1H spectrum described below, we expected to observe two resonances for apical boron atoms on the two cages. The Sn atom bonds to each cage in a different manner, rendering the two cages nonequivalent, and this should be reflected in the NMR spectra. However, if the ^{11}B spectrum is recorded at -75°C , two distinct apical boron resonances are just discerned, as seen in the inset in Figure 4a,b. The two different apical protons are clearly observed in the ^1H spectrum as two distinct overlapping 1:1:1:1 quartets, as seen in Figure 4d. On ^{11}B decoupling, these collapse to sharp singlets, as seen in the 500 MHz spectrum shown as Figure 4c.

$\mu, 1'-\text{SnPh}_2(\text{B}_5\text{H}_8)_2$ (**3**). If the ^{119}Sn NMR spectrum of the solution of **1** in CDCl_3 is observed after standing for 4 months, a second 1:1:1:1 quartet at -80.1 ppm, [$(^{11}\text{B}-^{119}\text{Sn}) = 1174$ Hz, fwhm = 200 Hz] assigned to a third isomer, $\mu, 1'-(\text{SnPh}_2)(\text{B}_5\text{H}_8)_2$, **3**, is observed such that the three isomers, **1**–**3** are present in approximately a 1:2:1 ratio. Traces of a second quartet under the major one, assigned to a second isomer and discussed later, are just visible at $\delta = -75.8$ ppm. The rearrangement of **1** is rapid in THF, affording **3**, and some decomposition product. The ^{119}Sn spectrum exhibits a quartet at $\delta = -75.8$ ppm. **3** is best prepared from the reaction between $1-(\text{SnClPh}_2)\text{B}_5\text{H}_8$ and $\text{K}[\text{B}_5\text{H}_8]$ in CH_2Cl_2 . The ^{119}Sn NMR spectrum of **3** exhibits the expected quartet arising from coupling to the directly bonded ^{11}B atom ($I = 3/2$), at $\delta = -80.1$ ppm, with small amounts of a second quartet at $\delta = -75.8$ ppm, under the major one. The ^{11}B NMR spectrum, shown in Figure 5b, exhibits two resonances in the high-field region where the apical B atom resonance is normally observed in B_5H_9 . These are a doublet at $\delta = -48.2$ ppm, which collapses to a singlet on proton decoupling (see Figure 5a), and a singlet at $\delta = -51.6$ ppm which is unaffected by decoupling. ^{119}Sn satellites are just discernible for the peak at -51.6 ppm with $J(^{11}\text{B}-^{119}\text{Sn}) = 1174$ Hz. The latter is assigned to the apical B atom on the B_5H_8 cage which is directly bonded to Sn, and the former is

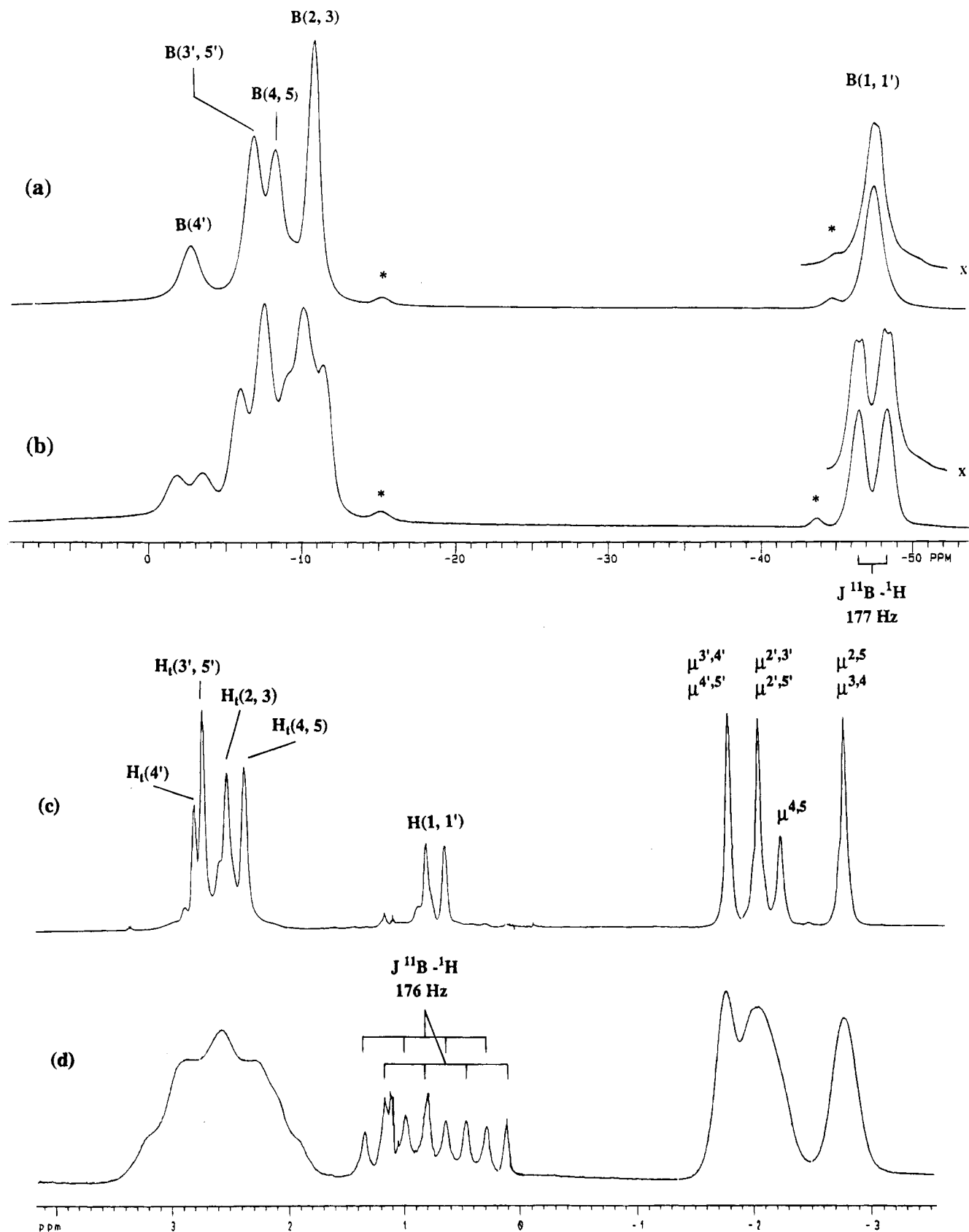


Figure 4. (a) 96.25 MHz $^{11}\text{B}\{^1\text{H}\}$ NMR spectrum of **2** at 25 °C with the B(1) resonance (x) observed at -75 °C inset. (b) 96.25 MHz ^{11}B NMR spectrum of **2** at 25 °C with the B(1) resonance (x) observed at -75 °C inset. (c) 500 MHz $^1\text{H}\{^{11}\text{B}\}$ NMR spectrum of **2**. (d) 500 MHz ^1H NMR spectrum of **2**. * impurity.

assigned to the apical boron on the other B_5H_8 cage, which still bears a terminal H atom. The basal region of the ^{11}B spectrum is clearly overlapped; so the individual boron resonances are difficult to discern.

Discussion

Formation of **1** as the sole product when the reaction between $\text{K}[\text{B}_5\text{H}_8]$ and SnCl_2Ph_2 is carried out in CH_2 -

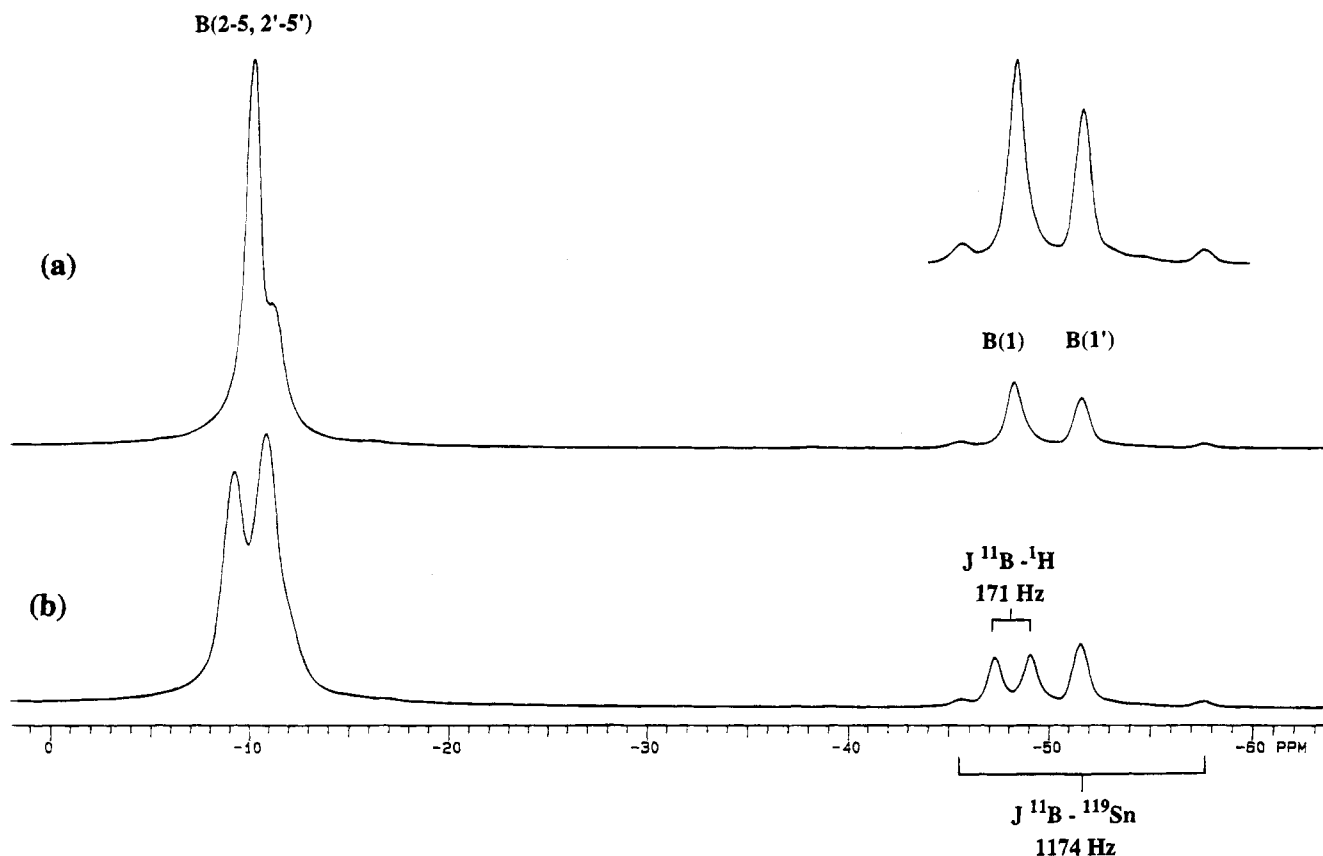


Figure 5. (a) 96.25 MHz $^{11}\text{B}\{^1\text{H}\}$ NMR spectrum of **3**. (b) 96.25 MHz ^{11}B NMR spectrum of **3**.

Cl_2 clearly is a consequence of the low basicity of the solvent. In the presence of stronger Lewis bases, 2,3- μ -substituted pentaboranes isomerize to the 2- and then the 1-isomer.^{20,21} Thus the use of a noncoordinating solvent precludes rapid isomerization of **1** to **2** and then **3**, but very slow rearrangement does take place even in the absence of base, as evidenced by the formation of **2** and then **3** from **1** in CDCl_3 over several months.¹⁹ In the presence of the moderately basic solvent Et_2O , the rearrangement of **1** to **2** is rapid. Similarly, if the reaction for the preparation of **1** is carried out in Et_2O , **2** is formed in good yield. Treatment of **1** with the stronger base, THF, allows formation of **3** in good yield. It is interesting to note that in the presence of a moderately strong base such as Et_2O , rearrangement of **1** to **3** does not occur. Although **3** appears to be the thermodynamically most stable product, it is the most reactive and thus we suspect that further reaction with Et_2O leads to degradation rather than isomerization. The alternative preparation of **3** from 1-(SnClPh_2) B_5H_8 and $[\text{B}_5\text{H}_8]^-$ in CH_2Cl_2 , is similarly analogous to our original preparation of 2,3- μ -(SnPh_3) B_5H_8 .^{9b} The electrophile $[\text{1}-(\text{SnPh}_2)\text{B}_5\text{H}_8]^+$ inserts into the vacant bridging site in $[\text{B}_5\text{H}_8]^-$, and in CH_2Cl_2 rapid rearrangement does not occur.

The formation of two isomers in THF is not completely understood, but two isomers of **3** can exist. Figure 6 illustrates this point. The two isomers differ only in

the way the open face of the B_5 cage, which is bonded to the Sn via a bridging site, is directed. The open face may point toward or away from the other B_5 cage. As indicated below, it appears that the latter, which is observed in the crystal structure determination, may be favored for steric reasons. Interestingly, different isomers are formed depending on the conditions used. The two isomers are distinguished by their ^{119}Sn NMR spectra. The product of the reaction between SnPh_2Cl_2 and $[\text{K}[\text{B}_5\text{H}_8]^-]$, in a 1:2 mole ratio in THF, gives equal amounts of species with ^{119}Sn quartets at $\delta = -75.8$ and -80.1 ppm. The product of the slow rearrangement of **1**, and **2**, in CHCl_3 , gives only a major quartet at $\delta = -80.1$ ppm; however, if **3** is obtained by treatment of **1** with THF, the species shows a ^{119}Sn resonance at $\delta = -75.8$ ppm. One might expect that the isomer formed in the slow rearrangement would be the thermodynamically more stable isomer although this point is not clear. The formation of **1**–**3** represents an interesting series of reactions whose extent is controlled by the nature of the solvent.

The structure of **1**, as illustrated in Figure 1, consists of two B_5H_8 cages linked by a SnPh_2 group such that the Sn atom replaces a bridging proton in each cage, and thus the cages share a bridging Sn atom. The Sn lies at the center of a distorted tetrahedron which comprises the two phenyl groups and the two B_5H_8 cages. The largest of the angles around Sn is that involving cage(1)–Sn–cage(2), measured at the centroids (X) of the bridged B–B bonds (121.6°), and the smallest angles are those between the centroids and the *ipso*-C atom which is away from the open face of the cage. These angles, 98.5 and 98.9° for X–Sn–C(21) and X'–Sn–C(11), respectively, suggest that the open face

(20) (a) Gaines, D. F. In *Boron Chemistry 4, Plenary Lectures at the 4th International Meeting on Boron Chemistry* (Salt Lake City, 1979); Parry, R. W.; Kodama, G. J., Eds.; Pergamon Press: Oxford, U.K., 1980; pp 73–79. (b) Gaines, D. F.; Walsh, J. L. *Inorg. Chem.* **1978**, *17*, 806. (c) Heppert, J. A.; Gaines, D. F. *Inorg. Chem.* **1983**, *22*, 3155. (d) Gaines, D. F.; Coons, D. E. *J. Am. Chem. Soc.* **1985**, *107*, 3266.

(21) Gaines, D. F.; Iorns, T. V. *Inorg. Chem.* **1971**, *10*, 1094.

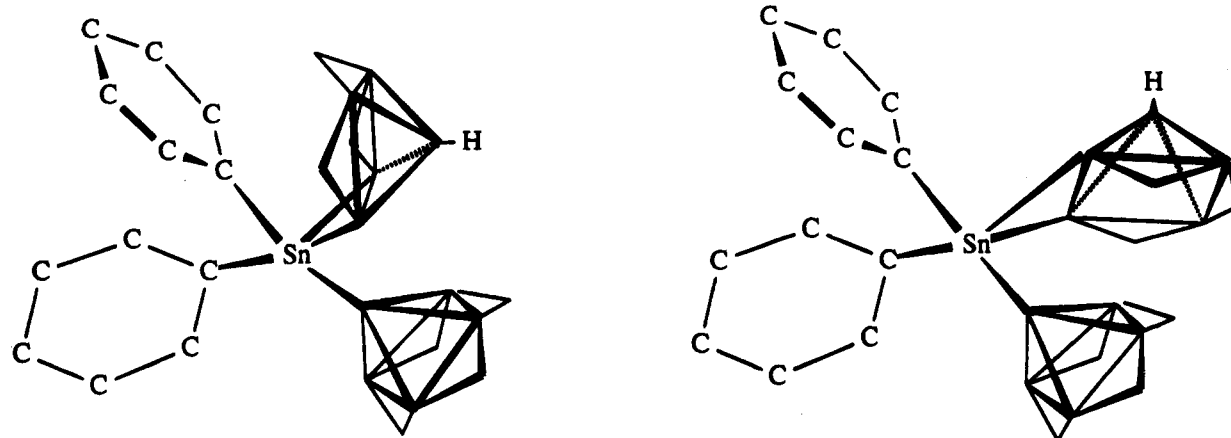


Figure 6. Two possible isomers of **3**.

of the cage is the more sterically hindered side. The two interplanar angles between the B(2)–B(3)–Sn and the basal B(2)–B(3)–B(4)–B(5) planes of the cage are smaller than those in all the other known 2,3-substituted pentaboranes(9) including **2** and **3**. This interplanar angle for the two cages averages 49.7° , compared to those for species with B,²² Be,²³ Si,²⁴ Sn,^{9b} Cu,²⁵ and Au²⁶ atoms bridging a single cage for which the reported angles are 52, 56.18, 51.7, 53, 52, and 54.7° , respectively. The angles in **1** are low presumably due to steric hindrance. The open faces of the B₅ cages do not point away from each other but are twisted so that the B(2)–B(3)–Sn planes in the two cages are at 117.5° to each other.

The structure of **2** is illustrated in Figure 2 and it consists of a SnPh₂ group coupled to one B₅H₈ cage at the basal boron B(22) and to the other cage by bridging the basal boron atoms B(12)–Sn–B(13). The unit cell contains two independent molecules which differ in their relative orientation of the B₅ cages, as indicated in Figure 2b. The Sn atom is located at the center of a distorted tetrahedron defined by the two attached C atoms of the phenyl groups, position B(2) in the terminally bonded cage, and the centroid (Y) of the B–B bond which is coordinated to Sn. The angles around the tin atom provide useful information about steric crowding. Of the six angles, four are close to the tetrahedral angle, but the other two reflect the steric hindrance of the open face of the B₅H₈ cage. The angles C(11)–Sn(1)–B(22) and C(31)–Sn(2)–B(42) are both 118.7° in the two molecules whereas the angles C(11)–Sn(1)–Y and C(31)–Sn(2)–Y are 101.1 and 102.7° , respectively. Where the phenyl group is closest to the open face of the B₅ cage containing the bridging H atoms, the angle is ca. 10° larger, reflecting the steric crowding caused by the bridging H atoms, and where the closed side of the cage points toward a phenyl group, the angle is ca. 10° smaller. The Sn atom lies well below the basal plane of the cage which it occupies a bridging position; the average angle between the basal boron plane and the BSnb plane in the two molecules is 52.9° , compa-

table to the value of 53° observed for the corresponding angle in 2,3- μ -(SnPh₃)B₅H₈.^{9b} The average boron–tin σ -bond distance is $2.233(5)$ Å, a little longer than that in **3** which is $2.197(3)$ Å. This would be expected since there is more steric crowding involving both bridge and terminal H atoms in the former which involves a basal boron than in the latter which involves an apical boron.

The structure of **3** is shown in Figure 3. The B₅ cage which is bonded to the Sn via a bridging site has its open face pointing away from the other B₅ cage. Presumably, this position is favored for steric reasons over the alternative structure in which the open face of the cage points toward the second B₅ cage. In the latter, the bridging H atoms would be much closer to the bridge-bonded cage and this configuration would be more sterically hindered than that with the hydrogen atoms pointing away from the σ -bonded cage. This is reflected somewhat in the structural data. The smallest of the "tetrahedral" angles, 104.5° , is B(21)–Sn–Z, where Z is the midpoint of the B(13)–B(12) bond. We would expect this angle to be large in the other isomer. The largest angles are those between the apical B atom attached to the tin and the *ipso*-carbon atoms of the phenyl groups: 114.3 and 113.6° . Presumably, there is more crowding between the phenyl hydrogens and the apically bonded cage than with the bridged bonded cage. The B–Sn distances in the bridging moiety, $2.504(3)$ and $2.532(3)$ Å are on average longer than the corresponding distances in 2,3- μ -(SnPh₃)B₅H₈, which are $2.467(4)$ and $2.512(5)$ Å. The angle between the planes Sn–B(12)–B(13) and B(12)–15) is 52.7° , again comparable to that for **2** and related systems.

There are six possible linkage isomers of SnPh₂–(B₅H₈)₂, and they are illustrated in Figure 7. That we were able to obtain only three in this study warrants some comment. The thermodynamic stabilities of **1**–**3** decrease in the order $\mu, 1' > \mu, 2' > \mu, \mu'$, and we have commented on this for the species 1-(SnPh₃)-, 2-(SnPh₃)-, and 2,3- μ -(SnPh₃)B₅H₈, previously.^{9b} The decreased stability is reflected in the B–Sn σ -bond lengths.²⁷ From the X-ray data, the B–Sn distance in **2** is longer than that in **3** by $0.033(5)$ Å. Gaines and co-workers showed that in the case of 2,3- μ -MR₃B₅H₈ species, when M = Si, Ge, an equilibrium exists in the presence of base such that the 2- and 1- isomers are present in an approximately 1:4 ratio.²¹ For MR₃ =

(22) Edverson, G. M.; Gaines, D. F.; Harris, H. A.; Campana, C. F. *Organometallics* **1990**, *9*, 401.

(23) Gaines, D. F.; Coleson, K. M.; Calabrese, J. C. *Inorg. Chem.* **1981**, *20*, 2185.

(24) Calabrese, J. C.; Dahl, L. F. *J. Am. Chem. Soc.* **1971**, *93*, 6042.

(25) Greenwood, N. N.; Howard, J. A.; McDonald, W. S. *J. Chem. Soc., Dalton Trans.* **1977**, 37.

(26) Alcock, N. W.; Parkhill, L.; Wallbridge, M. G. H. *Acta Crystallogr.* **1985**, *C41*, 716.

(27) Wieser, J. D.; Moody, D. C.; Huffmann, J. C.; Hildebrandt, R. C.; Schaeffer, R. L. *J. Am. Chem. Soc.* **1975**, *97*, 1074.

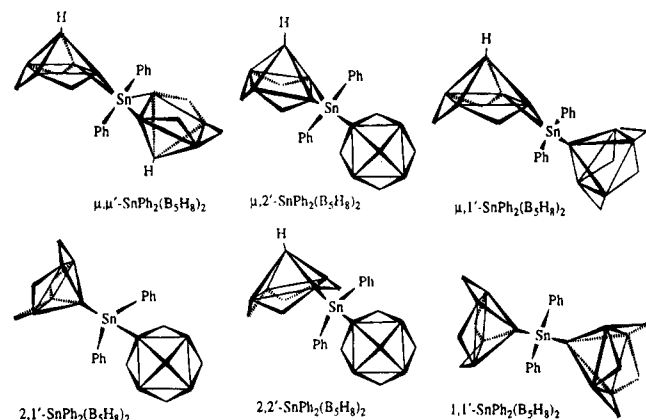


Figure 7. Six possible linkage isomers of $\text{SnPh}_2(\text{B}_5\text{H}_8)_2$.

Table 9. Comparison of ^{119}Sn NMR Data for Tin-Substituted Pentaboranes(9)

species	δ in ppm (form)	$J(^{119}\text{Sn}-^{11}\text{B})$, Hz	fwhm (Hz)
μ, μ' - $\text{SnPh}_2(\text{B}_5\text{H}_8)_2$, 1	-40.1 (singlet)	NA	187
$\mu, 2'$ - $\text{SnPh}_2(\text{B}_5\text{H}_8)_2$, 2	-138.5 (quartet)	900	244
$\mu, 1'$ - $\text{SnPh}_2(\text{B}_5\text{H}_8)_2$, 3	-80.1 (quartet)	1174	200
2,3-(SnPh_3) B_5H_8	-98.3 (singlet)	NA	108
1-(SnPh_3) B_5H_8	-89.2 (quartet)	1117	128
2-(SnPh_3) B_5H_8	-87.5 (quartet)	1061	<i>a</i>
1-(SnClPh_2) B_5H_8	72.1 (quartet)	1272	172

^a Difficult to measure accurately; see ref 9b.

SnPh_3 in a previous study, we observed complete conversion to the 1-isomer in the presence of THF and concluded that steric factors predominate in this system.^{9b} For the series 1–3, the thermal stability with respect to degradation to noncage products and the stability to air and water decreased in the sequence $\mu, \mu' > \mu, 2' > \mu, 1'$. Thus subsequent rearrangement of **3** competes with decomposition and this may account for our inability to prepare the other three isomers.

Our observation of direct ^{11}B – ^{119}Sn coupling in these pyramidal boranes is novel; the only previous such observations were those we reported for the series 2,3- μ -(SnPh_3) B_5H_8 , 1-(SnPh_3) B_5H_8 , 2-(SnPh_3) B_5H_8 , and 1-(SnClPh_2) B_5H_8 .^{9a,b} It is informative to compare these data. Table 9 lists the data for 1–3 and those previously described. The fwhm data for the last three species have not been previously reported. The trends for the two sets of compounds are consistent in that the fwhm data increase in the series 1 < 3 < 2 and in the series 2,3- μ -(SnPh_3) B_5H_8 < 1-(SnPh_3) B_5H_8 < 2-(SnPh_3) B_5H_8 ; the fwhm value for 2-(SnPh_3) B_5H_8 cannot be estimated with any confidence, so this latter trend is an assumption. The data for the former series are higher than those for the latter, reflecting additional coupling to a second bridging cage. Also the observation that the ^{11}B – ^{119}Sn coupling constant values increase

in the series 2-(SnPh_3) B_5H_8 < 1-(SnPh_3) B_5H_8 reflects the s-electron density in the respective substitution positions.²⁸ The same trend is seen in the ^{119}Sn – ^{11}B coupling constants for **2** and **3** which are larger for the apical boron in **3**, which can be considered to be sp hybridized, and smaller for the basal boron in **2** for which the orbitals contain more p-character.

1–3 represent the first examples of structurally characterized pentaborane cages linked by a single heteroatom group, although examples involving hexaborane cages linked by Mg^{5a} and Pt^{5b} are known and a Cd system was identified spectroscopically. The Cd species is analogous to the known species $\text{Hg}(\text{B}_5\text{H}_8)_2$ ⁷ and to the recently described $\text{Cd}(\text{B}_5\text{H}_8)_2$.²⁹ Structures of 2-substituted *nido*- B_5H_9 cages are rare; the only other examples are *trans*-(PMe_3)₂ $\text{Br}_2(\text{CO})\text{IrB}_5\text{H}_8$,^{30a} [μ -(Ph_2P) $\text{B}_5\text{H}_7\text{FeCp}(\text{CO})_2$],^{30b} and 2,3- $\text{Me}_2\text{B}_5\text{H}_7$, determined many years ago.^{30c} There are only two other fully characterized systems with a heteroatom in the 1-position of *nido*- B_5H_9 . They are 1-(SnPh_2Cl) B_5H_8 ^{9b} and the halogeno systems 1-Br-2,3- μ -(SiMe_3) B_5H_7 ²⁴ and 1- IB_5H_8 .³¹ We are continuing these studies and extending them to other species in which pentaborane(9) cages are bridged by heteroatoms.

Acknowledgment. We acknowledge support of Mallinckrodt Specialty Chemicals Co. for a Fellowship to H.F. and the National Science Foundation for a grant for the NMR spectrometer. L. Barton thanks the NSF, the Missouri Research Board and the UM–St. Louis Research Incentive Award Fund for research grants, and L. Brammer thanks the Missouri Research Board for support.

Supplementary Material Available: For 1–3 tables of mass spectral data, bond lengths and angles, anisotropic displacement coefficients, and H-atom coordinates and isotropic displacement coefficients and charts showing graphical representations of mass spectral data (23 pages). Ordering information is given on any current masthead page.

OM9408728

(28) Nöth, H.; Wrackmeyer, B. *Nuclear Magnetic Resonance Spectroscopy of Boron Compounds*; Diehl, P., Fluck, E., Kosfeld, R., Eds.; NMR, Basic Principles and Progress; Springer-Verlag: Berlin, 1978; Vol. 14, Chapter 8.

(29) Fang, H.; Bould, J.; Barton, L. *Abstracts of Papers*, 29th Regional Meeting of the American Chemical Society, Kansas City, MO, Nov 1994; American Chemical Society: Washington, DC, 1994; INORG 124.

(30) (a) Churchill, M. R.; Hackbarth, J. J.; Davison, A.; Traficante, D. D.; Wreford, S. S. *J. Am. Chem. Soc.* **1974**, *96*, 4041. (b) Goudreau, B. H.; Ostrander, R. L.; Spencer, J. T. *Inorg. Chem.* **1991**, *30*, 2066. (c) Friedman, L. B.; Lipscomb, W. N. *Inorg. Chem.* **1966**, *5*, 1752.

(31) Hall, L. H.; Block, S.; Perloff, A. *Acta Crystallogr.* **1965**, *19*, 658.

Promoter Effect of Chloride Ions on the Ruthenium-Catalyzed Hydroesterification of Ethylene with Methyl Formate. Design and Evaluation of New Poly- and Mononuclear Catalyst Precursors

Noël Lugan and Guy Lavigne*

Laboratoire de Chimie de Coordination du CNRS (UPR 8241), 205 route de Narbonne, 31077 Toulouse Cedex, France

Jean Marc Soulié, Sylvie Fabre, and Philippe Kalck*

Ecole Nationale Supérieure de Chimie de Toulouse, Institut National Polytechnique, 118, route de Narbonne, 31077 Toulouse Cedex, France

Jean Yves Saillard and Jean François Halet

Laboratoire de Chimie du Solide et Inorganique Moléculaire, Université de Rennes I, Avenue du Général Leclerc, 35042 Rennes Cedex, France

Received November 22, 1994[®]

The catalytic hydroesterification of ethylene with methyl formate to produce methyl propionate is shown to take place in the presence of trinuclear ruthenium carbonyl complexes modified by anionic nucleophiles such as amido (anilinopyridyl), alkoxy (pyridonate), or halide ligands, regarded as potential promoters. The best results (100% conversion, 99% selectivity) are obtained with the mixture $\text{Ru}_3(\text{CO})_{12} + [\text{PPN}]\text{Cl}$ (1/1) under the following experimental conditions: $[\text{HCOOMe}]/[\text{cat.}] = 345$, DMF solvent, $P(\text{C}_2\text{H}_4) = 20$ atm (at 25 °C), $T = 160$ °C, time = 12 h. The complex $[\text{PPN}][\text{Ru}_3(\mu_3\text{-Cl})(\text{CO})_9]$ (**3**) resulting from the addition of $[\text{PPN}]\text{-Cl}$ to $\text{Ru}_3(\text{CO})_{12}$ reacts cleanly with an excess of $[\text{PPN}]\text{Cl}$ in refluxing THF under a stream of inert gas to produce the unique dianionic species $[\text{PPN}]_2[\text{Ru}_4(\mu\text{-Cl})_2(\text{CO})_{11}]$ (**4**) (70% yield). The X-ray structure analysis of **4** is reported (triclinic $P\bar{1}$, No. 2, $a = 18.209(2)$ Å, $b = 18.877(3)$ Å, $c = 13.895(2)$ Å, $\alpha = 110.70(1)^\circ$, $\beta = 108.43(1)^\circ$, $\gamma = 87.43(1)^\circ$, $V = 4226(1)$ Å³, $Z = 2$, $R = 0.053$, $R_w = 0.069$). The dianionic tetranuclear unit of **4** consists of a basic triangular metal framework "Ru₃(CO)₉" one face of which is supported by a spiked "Ru(CO)₂Cl₂" fragment involving a 16e metal center exhibiting a square pyramidal geometry. Extended Hückel MO calculations indicate a large HOMO/LUMO gap (1.45 eV). Facile loss of Cl⁻ from the above dianion is induced by capture of CO, leading to the known butterfly complex $[\text{PPN}][\text{Ru}_4(\mu\text{-Cl})(\text{CO})_{13}]$ (**5**). Complex **4** also reacts with O₂ at 25 °C to provide the new oxo derivative $[\text{PPN}]_2[\text{Ru}_4(\mu_4\text{-O})(\mu\text{-Cl})_4(\text{CO})_{10}]$ (**6**). The structure of **6** has been determined by X-ray diffraction (triclinic $P1$, No. 2, $a = 13.226(5)$ Å, $b = 25.533(2)$ Å, $c = 12.771(3)$ Å, $\alpha = 92.39(1)^\circ$, $\beta = 114.77(3)^\circ$, $\gamma = 85.92(2)^\circ$, $V = 3906(2)$ Å³, $Z = 2$, $R = 0.038$, $R_w = 0.045$). Its dianionic unit consists of a distorted quadratic antiprism based on two rectangular faces Ru(μ-Cl)₂Ru and containing an encapsulated oxygen atom linked to the four ruthenium centers. The anionic complexes **4–6** also act as catalyst precursors for the hydroesterification reaction. Analysis of the solutions recovered at the end of all catalytic runs indicate the presence of $[\text{PPN}]_2[\text{Ru}_6(\text{C})(\text{CO})_{16}]$ as the principal metal-containing derivative. The probable mononuclear nature of the active species is suggested. A detailed investigation of the catalytic system based on $[\text{PPN}][\text{Ru}(\text{CO})_3\text{Cl}_3]$ (**7**) (prepared here in 81% yield by a new one-pot procedure) is reported. The results show that catalysis in the presence of the latter complex takes place readily without an induction period. Furthermore, a comparative evaluation of the four salts **7**, $[\text{PPN}][\text{Ru}(\text{CO})_3\text{I}_3]$ (**8**), $[\text{PPN}][\text{Ru}(\text{CO})_3\text{Cl}_2\text{I}]$ (**9**), and $[\text{PPN}][\text{Ru}(\text{CO})_3\text{ClI}_2]$ (**10**) as catalyst precursors reveals that chloride is a better promoter than iodide under the experimental conditions defined above, using DMF (or related amides) as solvent. Catalysis in the presence of **7** (and 3 equiv of NEt₃ as cocatalyst) is complete within 2 h (100% conversion and 99% selectivity; overall turnover frequency = 170 h⁻¹, corresponding to an initial activity of the order of 700 h⁻¹). Complex **7** is seen to react readily with DMF at 160 °C within 30 min to produce the new complex $[\text{PPN}][\text{Ru}(\text{CO})_2\text{Cl}_3(\eta^1\text{-DMF})]$ (**11**), isolated in 60% yield. The X-ray structure of **11** is reported (monoclinic $P2_1/c$, $a = 9.000(2)$ Å, $b = 21.176(2)$ Å, $c = 21.080(1)$ Å, $\beta = 93.89(8)^\circ$, $V = 4008.3(9)$ Å³, $Z = 4$, $R = 0.028$, $R_w = 0.030$). The three chloride ligands adopt a meridional arrangement, whereas the DMF ligand, bound via its oxygen atom, occupies one of the two apical sites.

Introduction

Methyl formate is a valuable feedstock in organic synthesis,^{1,2} and its "direct" addition to olefins for the

production of esters is of potential industrial importance.³ The homogeneous catalytic hydroesterification of ethylene with methyl formate was originally discov-

(1) (a) Röper, M. *Erdöl Kohle, Erdgas, Petrochem.* **1984**, *37*, 506 and references therein. (b) Lee, J. S.; Kim, J. C.; Kim, Y. G. *Appl. Catal.* **1990**, *57*, 1 and references therein.

[®] Abstract published in *Advance ACS Abstracts*, March 15, 1995.

Table 1. Performances of the Principal Ru-Based Catalytic Systems for the Hydroesterification of Ethylene with Methyl Formate (Selected Results)

author	precursor	solvent	conditions	activity (h ⁻¹)	ref
Sneeden et al.	RuCl ₂ (PPh ₃) ₃	methyl formate	190 °C 20 atm 18 h	16	4
Ueda et al.	RuH ₂ (PPh ₃) ₄	THF	90 °C 40 atm 23 h	<i>a</i>	7
Keim et al.	Ru ₃ (CO) ₁₂	toluene	230 °C 90 atm 20 h	230	8
Keim et al.	[Ru ₃ (CO) ₁₀ Cl] ⁻	toluene	230 °C 90 atm 20 h	50	8
Petit et al.	RuCl ₃ /2 [Et ₄ N]I	DMF	190 °C 55 atm 1 h	1450 ^b	11

^a Data not available; the reported [product]/[formate] ratio was 5.4.

^b Typical value taken from the patent;^{11b} such a value, measured at 65% conversion, is not directly comparable with Keim's results.⁸

ered by Sneeden and co-workers in 1983, using RuCl₂(PPh₃)₃ at 190 °C (Table 1).⁴ A Pd-based process at room temperature was then patented by Alper and co-workers.^{5,6} More recently, a number of modified Ru-based catalytic systems were also developed by several authors.⁷⁻¹¹ In particular, Keim and Becker⁸ reported that Ru₃(CO)₁₂ functions as a catalyst precursor notably superior to the chloride-containing complex [PPN][Ru₃(μ-Cl)(CO)₁₀]. Finally, a highly efficient catalytic procedure based on RuCl₃·*n*H₂O/[Et₄N]I was patented by the late Professor Petit and his co-workers.¹¹

An apparent negative influence of the chloride ion was noted by Keim,⁸ at a working temperature of 230 °C. This was in sharp contrast to the booster effect of iodide in the patented process at 190 °C.¹¹

(2) For additional leading references on formate-based organic reactions other than those discussed in this paper, see also: (a) Keister, J. B.; Gentile, R. *J. Organomet. Chem.* **1981**, *222*, 143. (b) Pruett, R. L.; Kacmarcik, R. T. *Organometallics* **1982**, *1*, 1693. (c) Thorn, D. L. *Organometallics* **1982**, *1*, 197. (d) Milstein, D. *J. Am. Chem. Soc.* **1986**, *108*, 3525. (e) Zahalka, H. A.; Alper, H.; Sasson, Y. *Organometallics* **1986**, *5*, 2497. (f) Vanhoye, D.; Melloul, S.; Castanet, Y.; Mortreux, A.; Petit, F. *Angew. Chem., Int. Ed. Engl.* **1988**, *27*, 683. (g) Bianchini, C.; Peruzzini, M.; Vizza, F.; Zanobini, F. *J. Organomet. Chem.* **1988**, *348*, C9. (h) Jenner, G.; Nahmed, E. M.; Leismann, H. *J. Organomet. Chem.* **1990**, *387*, 315. (i) Mathé, F.; Castanet, Y.; Mortreux, A.; Petit, F. *Tetrahedron Lett.* **1991**, *32*, 3989. (j) Jou, D.-C.; Cheng, C.-H. *J. Chinese Chem. Soc.* **1991**, *38*, 235. (k) Jenner, G.; Ben Taleb, A. *J. Mol. Catal.* **1992**, *77*, 247. (l) Jenner, G.; Ben Taleb, A. *J. Mol. Catal.* **1994**, *91*, 31. (m) Jenner, G. *J. Organomet. Chem.* **1994**, *469*, 99. (n) Grévin, J.; Kalck, P. *J. Organomet. Chem.* **1994**, *476*, C23.

(3) (a) Methyl methacrylate, directly obtained by a cross-coupling reaction between methyl propionate and methanol,^{3b,c} is used in the manufacture of poly(methyl methacrylate) (Plexiglas, or Altuglas). (b) Ueda, W.; Kurokawa, H.; Moro-Oka, Y.; Ikawa, T. *Chem. Lett.* **1985**, 819. (c) BASF Ger. Offen **1978**, *2*, 615, 887.

(4) Isnard, P.; Denise, B.; Sneeden, R. P. A.; Cognion, J. M.; Durual, P. *J. Organomet. Chem.* **1983**, *256*, 135.

(5) Alper, H.; Smith, D. J. U.S. Patent 4,665,213 to British Petroleum, 1987.

(6) (a) Mlekuz, M.; Joó, F.; Alper, H. *Organometallics* **1987**, *6*, 1591.

(b) Lin, I. J. B.; Alper, H. *J. Chem. Soc., Chem. Commun.* **1989**, 248. (7) Ueda, W.; Yokoyama, T.; Morikawa, Y.; Moro-oka, Y.; Ikawa, T. *J. Mol. Catal.* **1988**, *44*, 197.

(8) Keim, W.; Becker, J. *J. Mol. Catal.* **1989**, *54*, 95.

(9) Kondo, T.; Yoshii, S.; Tsuji, Y.; Watanabe, Y. *J. Mol. Catal.* **1989**, *50*, 31.

(10) For related coupling reactions between alkyl formates (other than methyl formate) and alkenes other than ethylene, see: Nahmed, M.; Jenner, G. *J. Mol. Catal.* **1990**, *59*, L15.

(11) (a) Legrand, C. Thèse de l'Université des Sciences et Techniques de Lille Flandres-Artois, July 8, 1991. (b) Legrand, C.; Castanet, Y.; Mortreux, A.; Petit, F. *Eur. Pat. Appl.* **1991**, 449 693 A (to Atochem). (c) Legrand, C.; Castanet, Y.; Mortreux, A.; Petit, F. *J. Chem. Soc., Chem. Commun.* **1994**, 1173.

With the aim to rationalize these discrepancies, we set out to evaluate the relative efficiency of a range of anionic nucleophiles as promoters for the hydroesterification reaction using Ru₃(CO)₁₂ as a catalyst precursor. The coordinating anions selected for this study included halides,^{12,13} as well as specific alkoxide, amide, and thiolate groups which were prone to function as hemilabile ligands.^{14,15} Indeed, in light of earlier findings, it might be anticipated that a stepwise introduction of ethylene and methyl formate in the coordination sphere of the cluster would be facilitated by bridge-opening reactions of the type encountered in the equilibria involving either [PPN][Ru₃(Cl)(CO)_{12-n}] (*n* = 1-3)^{12,13} or [PPN][Ru₃(μ-(C₆H₅)N(C₅H₄N))(CO)_{12-n}] (*n* = 2, 3) (Scheme 1).^{14,15} Kinetic data on such bridge-opening processes have now been obtained by Basolo and co-workers.¹⁶

We were obviously prepared to consider the alternate possibility that the above polymetallic species might act as sources of active mononuclear fragments generated *in situ* under catalytic conditions.

In a preliminary screening, triruthenium carbonyl complexes incorporating the above mentioned ancillary ligands were tested as catalyst precursors. Analysis of the results led us to a thorough investigation of the ruthenium/chloride system, found to be the most active in amide solvents under the specific conditions defined below. An unexpected outgrowth of this work was the discovery of new dianionic polymetallic ruthenium carbonyl halide complexes resulting from the incorporation of more than one chloride ligand into Ru₃(CO)₁₂. The unprecedented odd structures of these compounds are rationalized in terms of EHMO calculations. The observation that such polymetallic species are transformed under catalytic conditions led us to evaluate mononuclear complexes as alternate catalyst precursors. In particular, [PPN][Ru(CO)₃Cl₃] was found to be highly efficient, achieving the hydroesterification of ethylene under milder conditions than with other Ru-based catalytic systems. The latter complex reacts with the dimethylformamide solvent under catalytic conditions to give the new species [PPN][Ru(CO)₂Cl₃(η¹-OCHN-

(12) For fundamental reactions of anion-promoted ruthenium carbonyl species, see: (a) Lavigne, G.; Kaesz, H. D. *J. Am. Chem. Soc.* **1984**, *106*, 4647. (b) Zuffa, J. L.; Blohm, M. L.; Gladfelter, W. L. *J. Am. Chem. Soc.* **1986**, *108*, 552. (c) Zuffa, J. L.; Gladfelter, W. L. *J. Am. Chem. Soc.* **1986**, *108*, 4669. (d) Han, S.-H.; Geoffroy, G. L.; Dombek, B. D.; Rheingold, A. L. *Inorg. Chem.* **1988**, *27*, 4355. (e) Han, S.-H.; Song, J. S.; Macklin, P. D.; Nguyen, S. T.; Geoffroy, G. L. *Organometallics* **1989**, *8*, 2127. (f) Chin-Choy, T.; Harrison, W. T. A.; Stucky, G. D.; Keder, N.; Ford, P. C. *Inorg. Chem.* **1989**, *28*, 2028. (g) Rivomanana, S.; Lavigne, G.; Lugan, N.; Bonnet, J.-J.; Yanez, R.; Mathieu, R. *J. Am. Chem. Soc.* **1989**, *111*, 8959. (h) Rivomanana, S.; Lavigne, G.; Lugan, N.; Bonnet, J.-J. *Organometallics* **1991**, *10*, 2285. (i) Ramage, D. L.; Geoffroy, G. L.; Rheingold, A. L.; Haggerty, B. S. *Organometallics* **1992**, *11*, 1242. (j) Lillis, J.; Rokicki, A.; Chin, T.; Ford, P. C. *Inorg. Chem.* **1993**, *32*, 5040.

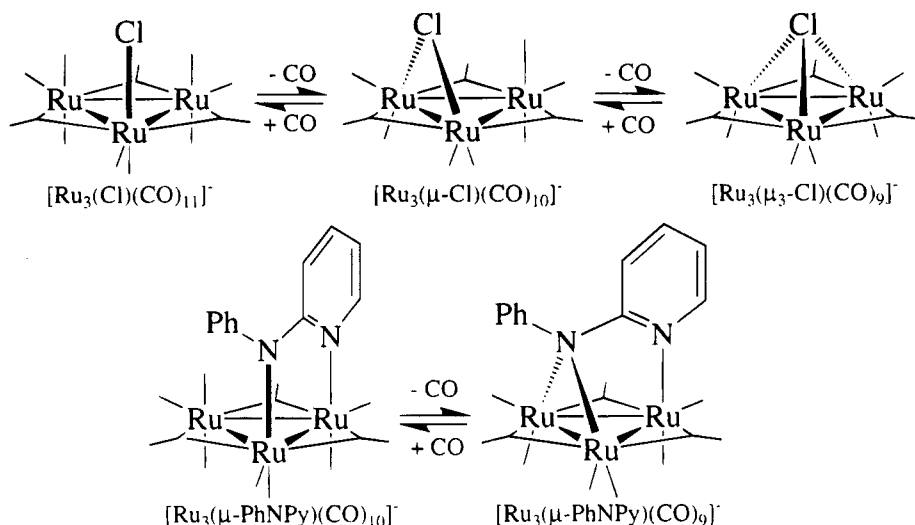
(13) For recent reviews, see: (a) Lavigne, G. In *The Chemistry of Metal Clusters*; Shriver, D., Adams, R. D., Kaesz, H. D., Eds.; VCH: New York, 1990; Chapter 5, pp 201-303 (see also references therein). (b) Lavigne, G.; Lugan, N.; Rivomanana, S.; Mulla, F.; Soulié, J. M.; Kalck, P. *J. Cluster Sci.* **1993**, *4*, 49.

(14) Lugan, N.; Laurent, F.; Lavigne, G.; Newcomb, T. P.; Liimatta, E. W.; Bonnet, J.-J. *J. Am. Chem. Soc.* **1990**, *112*, 8607.

(15) (a) Lugan, N.; Laurent, F.; Lavigne, G.; Newcomb, T. P.; Liimatta, E. W.; Bonnet, J.-J. *Organometallics* **1992**, *11*, 1351. (b) Nombel, P.; Lugan, N.; Mulla, F.; Lavigne, G. *Organometallics* **1994**, *13*, 4673.

(16) (a) Shen, J.-K.; Basolo, F. *Organometallics* **1993**, *12*, 2942. (b) Basolo, F. Personal communication.

Scheme 1

Table 2. Preliminary Screening of Various Catalyst Precursors^a

entry	catalyst precursor	solvent	conv (%)	selec (%)
1	$\text{Ru}_3(\mu\text{-H})(\mu\text{-PhNPy})(\text{CO})_9$	THF	0	0
2	$[\text{PPN}][\text{Ru}_3(\mu\text{-PhNPy})(\text{CO})_9]$	THF	28	77
3	$[\text{PPN}][\text{Ru}_3(\mu\text{-PhNPy})(\text{CO})_9]$	DMF	33	96
4	$[\text{PPN}][\text{Ru}_3(\mu\text{-OPy})(\text{CO})_{10}]$	THF	40	78
5	$[\text{PPN}][\text{Ru}_3(\mu\text{-OPy})(\text{CO})_{10}]$	DMF	58	88
6	$[\text{PPN}][\text{Ru}_3(\mu\text{-SPy})(\text{CO})_9]$	THF	0	0
7	$[\text{PPN}][\text{Ru}_3(\mu\text{-Cl})(\text{CO})_{10}]$	THF	2	93
8	$[\text{PPN}][\text{Ru}_3(\mu\text{-Cl})(\text{CO})_{10}]$	DMF	100	99

^a Experimental conditions: Catalyst precursor (0.235 mmol), HCO_2CH_3 (5 mL), $[\text{formate}]/[\text{cat.}] = 345$, solvent (15 mL), $P(\text{C}_2\text{H}_4) = 20$ atm, $T = 160$ °C, reaction time = 12 h.

$(\text{CH}_3)_2$]. A preliminary account of part of this work has been published.¹⁷

Results

A. Design and Evaluation of Polynuclear Catalyst Precursors. Preliminary screening of various promoters. Preliminary catalytic runs were first carried out in THF solution under the typical experimental conditions defined in Table 2 (entries 1, 2, 4, 6, 7). The catalyst precursors were preformed triruthenium carbonyl complexes incorporating various ancillary ligands regarded as potential promoters. Though the neutral hydrido species $\text{Ru}_3(\mu\text{-H})\{\mu\text{-}(\text{C}_6\text{H}_5)\text{N}(\text{C}_5\text{H}_4\text{N})\}(\text{CO})_9$ involving an anilinyridyl group as a ligand was totally inefficient (entry 1), the corresponding deprotonated anionic species $[\text{PPN}][\text{Ru}_3\{\mu\text{-}(\text{C}_6\text{H}_5)\text{N}(\text{C}_5\text{H}_4\text{N})\}(\text{CO})_9]$ was found to exhibit a moderate activity. Even better results were obtained with the complex $[\text{PPN}][\text{Ru}_3\{\mu\text{-O}(\text{C}_5\text{H}_4\text{N})\}(\text{CO})_{10}]$ bearing an alkoxyridyl group as the ancillary ligand. Noticeably, no activity was observed in the presence of $[\text{PPN}][\text{Ru}_3\{\mu\text{-S}(\text{C}_5\text{H}_4\text{N})\}(\text{CO})_9]$.

It is noteworthy that the chloride complex $[\text{PPN}][\text{Ru}_3(\mu\text{-Cl})(\text{CO})_{10}]$ generated *in situ* from $\text{Ru}_3(\text{CO})_{12}$ and $[\text{PPN}]\text{Cl}$ had no promoter effect in THF solvent (entry 7).

A recurrent observation was that, regardless of the nature of the anionic promoter, the red solutions recovered at the end of catalytic runs were all roughly

Table 3. Efficiency of Various Salts as Promoters for the Hydroesterification Reaction Based on $\text{Ru}_3(\text{CO})_{12}$ as a Catalyst Precursor in DMF Solvent^a

entry	promoter	conversion (%)	selec (%)	turnover
1	none	30	96	101
2	KI	56	91	182
3	$[\text{PPN}]\text{I}$	66	97	264
4	$[\text{NBu}_4]\text{F}$	74	87	223
5	NaCl	59	98	203
6	$[\text{PPN}]\text{Cl}$	100	99	339

^a Experimental conditions: $\text{Ru}_3(\text{CO})_{12}$ (0.235 mmol), promoter (0.235 mmol), HCO_2CH_3 (5 mL) ($[\text{formate}]/[\text{cat.}] = 345$), DMF (15 mL), $P(\text{C}_2\text{H}_4) = 20$ atm, $T = 160$ °C, reaction time = 12 h.

exhibiting the same infrared spectrum in the $\nu(\text{CO})$ region. The corresponding species was subsequently identified as $[\text{PPN}]_2[\text{Ru}_6\text{C}(\text{CO})_{16}]$ (*vide infra*).

In the pioneering work of Sneed and co-workers on the hydroesterification of ethylene (originally using methyl formate as solvent),⁴ it was noted that the presence of amide solvents such as *N*-methylpyrrolidone (NMP) or dimethylformamide (DMF) accelerates the decomposition of methyl formate, with production of CO. Using $\text{RuCl}_3 \cdot n\text{H}_2\text{O}$ in NMP/toluene mixtures, these authors observed for the first time good selectivities in methyl propionate. More recently, DMF proved to be essential as solvent for the mixture $\text{RuCl}_3 \cdot n\text{H}_2\text{O} + 2\text{-}[\text{NEt}_4]\text{I}$ used by Petit and co-workers in their patented hydroesterification process.¹¹

Under our experimental conditions, the activity of most doped catalyst precursors was also dramatically enhanced by the use of DMF (Table 2, entries 3, 5, 8). Surprisingly, the complex $[\text{PPN}][\text{Ru}_3(\mu\text{-Cl})(\text{CO})_{10}]$ which had been found inefficient in THF, became highly active in DMF, achieving 100% conversion and 99% selectivity!

This led us to evaluate the relative efficiency of various halide salts as promoters for the hydroesterification reaction in DMF solvent. Experiments reported in Table 3 revealed that (i) onium salts are better promoters than alkaline salts, and (ii) the chloride ion is superior to other halides. Considering these results, we set out to examine in detail the system based on $\text{Ru}_3(\text{CO})_{12}$ as a catalyst precursor and $[\text{PPN}]\text{Cl}$ as a promoter, using DMF as solvent.

As shown in Table 4, the optimum temperature for the $\text{Ru}_3(\text{CO})_{12}/[\text{PPN}]\text{Cl}$ system was found to be 160 °C.

(17) Lavigne, G.; Lugan, N.; Kalck, P.; Soulié, J. M.; Lerouge, O.; Saillard, J.-Y.; Halet, J.-F. *J. Am. Chem. Soc.* **1992**, *114*, 10669.

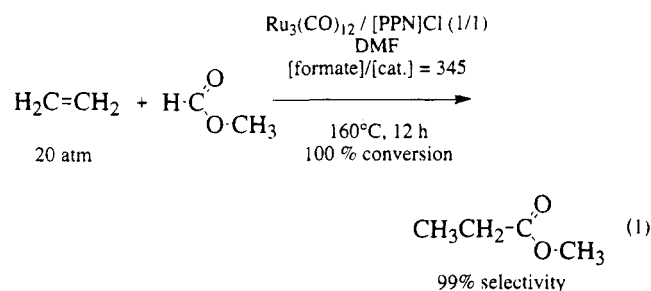
Table 4. Temperature Optimization for the System Using $\text{Ru}_3(\text{CO})_{12}$ + [PPN]Cl as Catalyst Precursor in DMF Solvent^a

entry	T (°C)	conv (%)	selec (%)	turnover
1	130	5	95	17
2	150	74	98	255
3	160	100	99	339
4	170	100	35	122
5	180	100	28	99

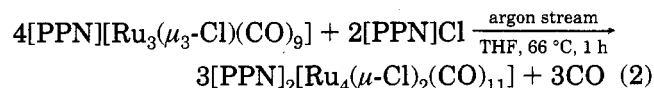
^a Experimental conditions: $\text{Ru}_3(\text{CO})_{12}$ (0.235 mmol), [PPN]Cl (0.235 mmol), HCO_2CH_3 (5 mL) ([formate]/[cat.] = 345), DMF (15 mL), $P(\text{C}_2\text{H}_5)_4$ = 20 atm, reaction time = 12 h.

Loss of selectivity in methyl propionate, with concomitant formation of methanol and CO, was observed as the temperature was raised above 180 °C.

In summary, at the end of the above preliminary study, the optimum conditions were those summarized below in eq 1. Noticeably, no attempts were made to optimize the reaction time of these preliminary experiments which were all carried out overnight.



Reaction of [PPN][$\text{Ru}_3(\mu_3\text{-Cl})(\text{CO})_9$] with an excess of halide ions. Formation of [PPN]₂[$\text{Ru}_4(\mu\text{-Cl})_2(\text{CO})_{11}$]. During the course of preliminary experiments aimed at evaluating the optimum Ru/halide ratio, we noted that when THF solutions of [PPN][$\text{Ru}_3(\mu_3\text{-Cl})(\text{CO})_9$] (**3**) were refluxed under an argon stream in the presence of an excess of [PPN]Cl, a characteristic blood red crystalline precipitate was progressively appearing over a period of 1 h. This new air sensitive complex was recovered in 70% yield after recrystallization from dichloromethane/hexane solutions. It was subsequently formulated as [PPN]₂[$\text{Ru}_4(\mu\text{-Cl})_2(\text{CO})_{11}$] (**4**) on the basis of an X-ray structure analysis (*vide infra*). The overall stoichiometry of the reaction corresponds to eq 2.



The structure of the dianionic cluster unit is represented here in a simplified structural drawing, whereas an ORTEP diagram is also provided in Figure 1.

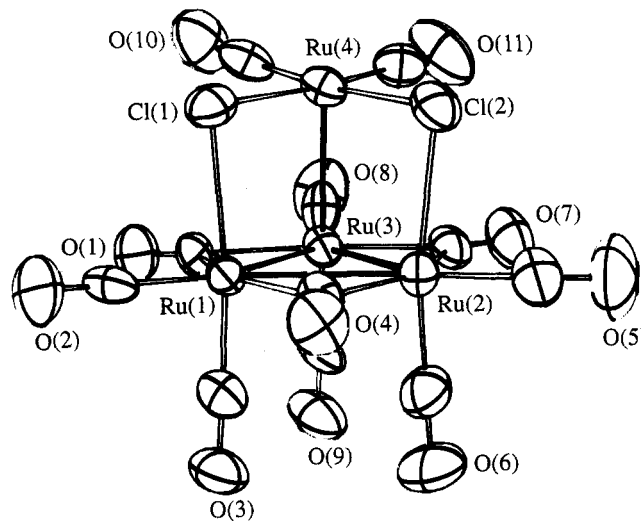
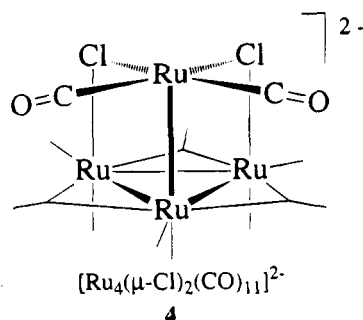


Figure 1. Perspective view of the dianionic unit of complex **4**. For clarity purposes, the labels of carbonyl groups are shown only at oxygen atoms.

This exotic architecture provides the image of a mononuclear unsaturated complex $[\text{Ru}(\text{CO})_2\text{Cl}_2]^{2-}$ that would be anchored onto the surface of a basic triangular cluster unit " $\text{Ru}_3(\text{CO})_9$ ". Indeed, the ruthenium center Ru(4) and its two neighboring halide atoms are respectively "spiked" on the three axial coordination sites of the basic trimetallic unit. Furthermore, the mean plane of the " $\text{Ru}(\text{CO})_2\text{Cl}_2$ " unit is roughly parallel to the plane of the triangular support (the dihedral angle is $4.8(1)^\circ$). The most striking feature is indeed the occurrence of a square pyramidal geometry about the 16e metal center Ru(4) (regarding Ru(3) as the "apical" atom). In the rare cases of mononuclear complexes where such a geometry is found,¹⁸⁻²⁰ the vacant octahedral site is generally protected by an agostic interaction.²¹ For example, in $\text{RuCl}_2(\text{PPh}_3)_3$, one of the phenyl groups of a triphenylphosphine ligand interacts directly with the metal through one of its H atoms ($\text{Ru} \cdots \text{H} = 2.59 \text{ \AA}$).¹⁹ In complex **4**, the shortest intermolecular contact involves Ru(4) and an H atom which belongs to one of the phenyl rings of a PPN cation ($\text{Ru}(4) \cdots \text{H}(53) = 2.919(9) \text{ \AA}$). The latter value is unusually short for a simple van der Waals contact. Furthermore, the exact geometrical location of H(53) on the "vacant" octahedral coordination site tends to indicate the occurrence a weak interaction which may be assimilated to an agostic interaction and is apparently sufficient to stabilize the coordinative unsaturation.

Extended Hückel molecular orbital calculations^{22,23} were carried out on **4**, with an idealized averaged structure of C_s symmetry (see Experimental Section). Its MO diagram (Figure 2) is based on the interaction between the respective fragments $\text{Ru}_3(\text{CO})_9$ (left) and $[\text{Ru}(\text{CO})_2\text{Cl}_2]^{2-}$ (right).

(18) El-Idrissi Rachidi, I.; Eisenstein, O.; Jean, Y. *New J. Chem.* **1990**, *14*, 671 and references therein.

(19) La Placa, S. J.; Ibers, J. A. *Inorg. Chem.* **1965**, *4*, 778.

(20) Cabeza, J. A.; Riera, V.; Villa-Garcia, M.; Ouahab, L.; Triki, S. *J. Organomet. Chem.* **1992**, *441*, 323.

(21) (a) Brookhart, M.; Green, M. L. H. *J. Organomet. Chem.* **1983**, *250*, 395. (b) Brookhart, M.; Green, M. L. H.; Wong, L.-L. *Prog. Inorg. Chem.* **1988**, *36*, 1.

(22) (a) Hoffmann, R. *J. Chem. Phys.* **1963**, *39*, 1397. (b) Hoffmann, R.; Lipscomb, W. N. *J. Chem. Phys.* **1962**, *36*, 2179.

(23) Ammeter, J. H.; Bürgi, H.-B.; Thibeault, J. C.; Hoffmann, R. *J. Am. Chem. Soc.* **1978**, *100*, 3686.

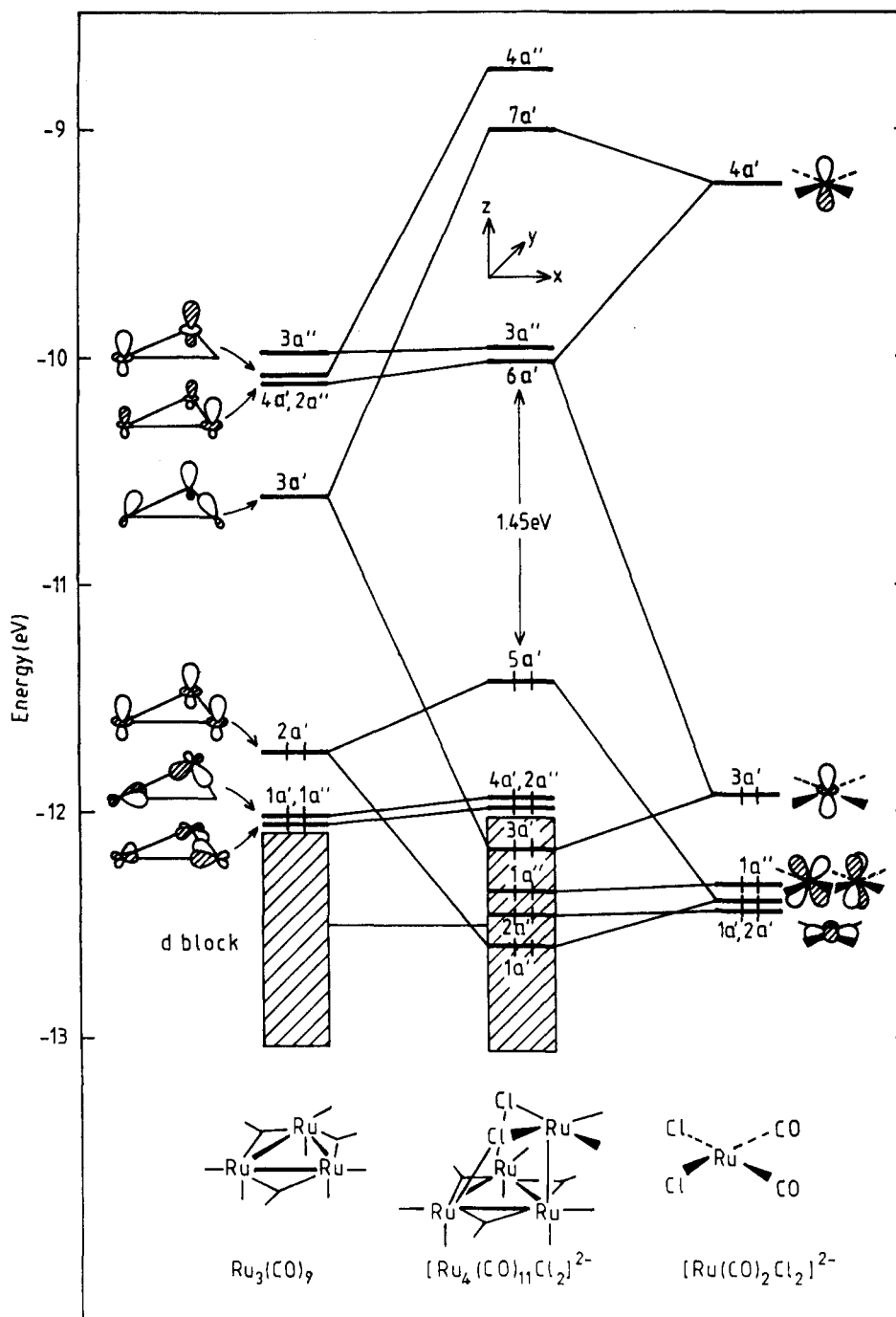


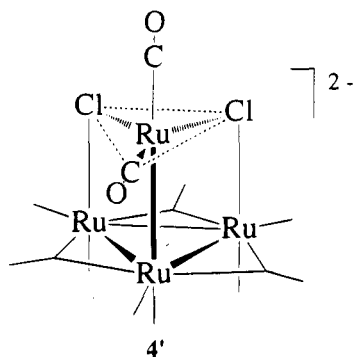
Figure 2. Interaction MO diagram for compound **4**, assuming an idealized structure of C_s symmetry.

The $[\text{Ru}(\text{CO})_2\text{Cl}_2]^{2-}$ moiety exhibits the usual electronic structure of stable 16-electron square planar species, with a large HOMO/LUMO gap separating the four nonbonding occupied d-type orbitals from the z-type LUMO. The electron deficiency of the 42-electron " $\text{Ru}_3(\text{CO})_9$ " fragment is illustrated by the presence of three empty acceptor orbitals lying in the -11 to -10 eV energy range ($3a'$, $4a'$, and $2a''$). The main bonding interactions between the two fragments involve the three acceptor orbitals of " $\text{Ru}_3(\text{CO})_9$ " on one side and the z^2 -type HOMO ($3a'$) and chlorine-localized occupied orbitals of $[\text{Ru}(\text{CO})_2\text{Cl}_2]^{2-}$ on the other side. These latter low-lying levels are not shown in Figure 2. The computed overlap population is 0.644, and the total charge transfer from $[\text{Ru}(\text{CO})_2\text{Cl}_2]^{2-}$ to $\text{Ru}_3(\text{CO})_9$ is 0.9 electron, of which *ca.* 0.32 come from Ru(4). There is

almost no π -electron transfer between the fragments. The main bonding interaction between Ru(4) and the $\text{Ru}_3(\text{CO})_9$ moiety occurs between the z^2 -type $3a'$ HOMO of $[\text{Ru}(\text{CO})_2\text{Cl}_2]^{2-}$ and the $3a'$ LUMO of $\text{Ru}_3(\text{CO})_9$. The HOMO ($5a'$)/LUMO ($6a'$) gap of **4** is rather large (1.45 eV), indicating a good thermodynamical stability. The HOMO, which is mainly localized on the triangular $\text{Ru}_3(\text{CO})_9$ entity (90%) is the out-of-phase component resulting from the 4-electron–two-orbital destabilizing interaction of the metallic $2a'$ MO of $\text{Ru}_3(\text{CO})_9$ with the $1a'$ (xz) MO of $[\text{Ru}(\text{CO})_2\text{Cl}_2]^{2-}$. The LUMO is the nonbonding combination deriving from the interaction of the metallic $4a'$ level of $\text{Ru}_3(\text{CO})_9$ on one side, with the upper $4a'$ (z) and the lower $3a'$ (z^2) orbitals of $[\text{Ru}(\text{CO})_2\text{Cl}_2]^{2-}$ on the other side. The participation of $\text{Ru}(\text{CO})_2\text{Cl}_2$ in this LUMO is fairly large (44%, of which 26% is coming

from Ru(4)). The overlap populations computed between the metal atoms are 0.133, 0.141, and 0.146 for the Ru(1)–Ru(2), Ru(1,2)–Ru(3), and Ru(3)–Ru(4) contacts, respectively. They reflect the differences observed in the metal–metal distances. The Ru(1,2)–Cl overlap populations are rather important and comparable to that found for Ru(4)–Cl (0.278 *vs* 0.337, respectively).

Thus, this orbital analysis supports our view of compound **4** as a saturated 48e triruthenium system bearing a mononuclear 16e square pyramidal metal fragment on one face. Although unprecedented in cluster chemistry, the square pyramidal arrangement around Ru(4) is not uncommon for 16e mononuclear species. Theoretical calculations by El Idrissi *et al.*¹⁸ have shown that such a geometry is favored for d⁶ ML₅ species having strong σ -donor ligands *trans* to the vacant octahedral site. This is obviously the case here, where a strong σ -type interaction exists between Ru(4) and Ru(1) (*vide supra*). The same authors have shown that the alternative trigonal bipyramidal structure is Jahn–Teller unstable.¹⁸ Our calculations on the tentative alternate theoretical model **4'** exhibiting such a



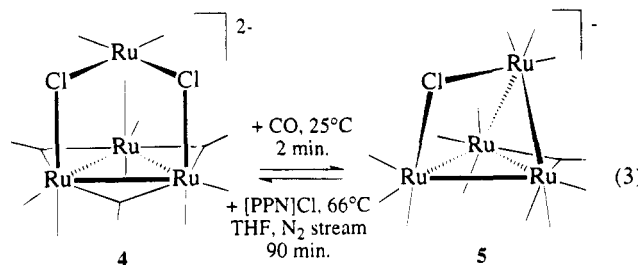
geometry indicate that the trigonal bipyramidal structure exhibits a triplet ground state and requires two electrons more to achieve a closed shell configuration, with a HOMO/LUMO gap of 1.03 eV. Thus, **4'** is less stable than **4** by almost 2 eV, with a very small Ru(3)–Ru(4) overlap population (0.036).

Calculations aimed at evaluating the acceptor capabilities of **4** were also performed: hypothetical introduction of a hydride ligand on the vacant coordination site of Ru(4), at a distance of 2.0 Å from the metal, resulted in a Ru(4)–H overlap population of 0.293. When the same calculations were made after replacement of the "Ru₃(CO)₉" unit by strong σ -donors such as CH₃⁻ or PH₃, the corresponding overlap populations became 0.346 and 0.366, respectively. These results suggest that the metal atom Ru(4) in **4** is a strong electrophilic center, although probably weaker than a 16-electron Ru^{II}L₅ mononuclear species.

An energy gap of 0.51 eV separates the 5a' HOMO of **4** from its next occupied 4a' neighbor orbital. Since the former is slightly Ru₃(CO)₉–Ru(CO)₂Cl₂ antibonding, its depopulation should lead to some shortening of the Ru(3)–Ru(4) distance. Unfortunately, this cannot be verified experimentally since the compound does not give a simple oxidized product.

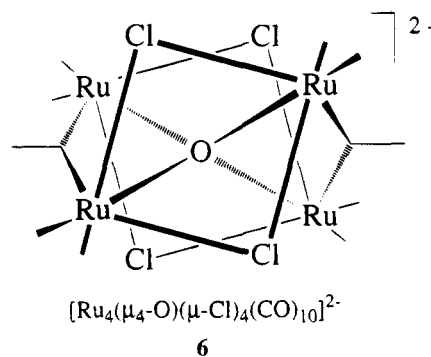
As expected due to its unsaturation, the compound was found to be highly reactive. However, to date, we have been unable to intercept any adduct resulting from simple capture of the vacant coordination site by an incoming nucleophile. In fact, addition of donor ligands

triggers further rearrangements of this rather unstable polymetallic architecture. Typically, reaction with CO takes place almost instantaneously at 25 °C and induces concomitant loss of one halide to give the known thermodynamically stable butterfly compound [PPN]₂[Ru₄(μ -Cl)(CO)₁₃] (**5**) (eq 3).²⁴



The reverse reaction takes place quantitatively in refluxing THF over a period of 90 min.

Oxygenation of [PPN]₂[Ru₄(μ -Cl)₂(CO)₁₁] and formation of [PPN]₂[Ru₄(μ_4 -O)(μ -Cl)₄(CO)₁₀]. Solutions of complex **4** rapidly turn yellow upon adventitious exposure to air, leading to a new compound obtained as bright yellow crystals. The new complex was formulated as [PPN]₂[Ru₄(μ_4 -O)(μ -Cl)₄(CO)₁₀] (**6**) on the basis of an X-ray structure analysis.



Complex **6** is a new member of the family of polymetallic oxo compounds.²⁵ The structure of its dianionic molecular unit is represented in both the simplified drawing shown here and a perspective view displayed in Figure 3.

The molecule appears as a cage built around a central oxygen atom exhibiting a distorted tetrahedral (sp³) geometry. The cage defined by Ru and Cl atoms is a slightly distorted quadratic antiprism (noncrystallographic D₂ symmetry) based on two rectangular faces Ru(μ -Cl)₂Ru. The unique oxygen is linked to four equivalent ruthenium centers. Each metal atom is surrounded by six ligands, namely, the central oxygen atom, three carbonyl groups (one bridging, two terminal), and two chloride atoms. The latter chloride ligands are in asymmetric bridging positions between two metal centers, in such a way that the coordination sphere of each metal center involves both a short (average value,

(24) Steinmetz, G. R.; Harley, A. D.; Geoffroy, G. L. *Inorg. Chem.* **1980**, *19*, 2985.

(25) (a) For a review on polymetallic oxo compounds, see: Bottomley, F.; Sutin, L. *Adv. Organomet. Chem.* **1988**, *28*, 339 and references therein. (b) Schleid, T.; Meyer, G. *J. Less-Common Met.* **1987**, *127*, 161. (c) Cotton, F. A.; Hong, B.; Shang, M. *Inorg. Chem.* **1993**, *32*, 4876. (d) Schauer, C. K.; Shriver, D. F. *Angew. Chem., Int. Ed. Engl.* **1987**, *26*, 255. (e) Schauer, C. K.; Voss, E. J.; Sabat, M.; Shriver, D. F. *J. Am. Chem. Soc.* **1989**, *111*, 7662.

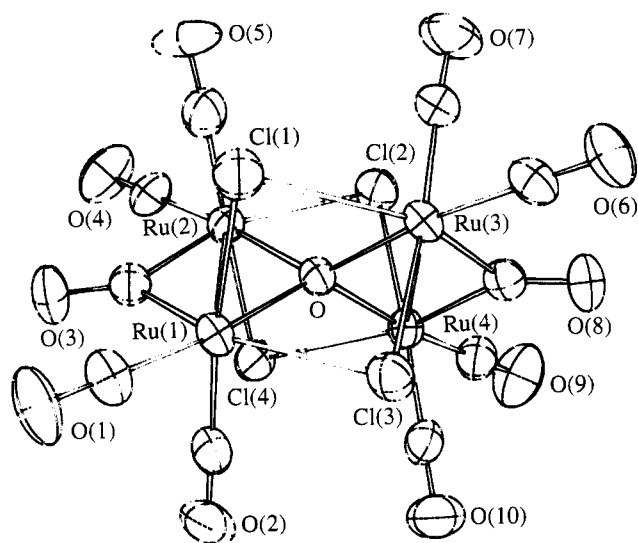


Figure 3. Perspective view of the dianionic unit of complex **6**. For clarity purposes, the labels of carbonyl groups are shown only at oxygen atoms.

2.461 Å) and a long (average value, 2.716 Å) Ru–Cl interaction. The chlorine atom which is the less strongly bound to the ruthenium center is the ligand which is the furthest away from the ideal octahedral site. Such a distortion can be attributed to steric repulsions between the chloride atoms within the double bridge, as suggested by the occurrence of rather short nonbonding contacts (Cl(1)··Cl(3) = 3.35 Å; Cl(2)··Cl(4) = 3.32 Å). In summary, the four metal atoms constitute a tetrahedron, the edges of which can be divided in three groups of two. The largest Ru–Ru separations (*ca.* 3.8 Å) correspond to the unbridged edges of the tetrahedron. The intermediate separations (*ca.* 3.2 Å) correspond to the Cl-bridged edges, whereas the CO-bridged ones are slightly shorter (*ca.* 3.1 Å).

The molecule can be described as an ensemble of four hexacoordinated ruthenium centers linked together through a unique oxo ligand. This simple picture is supported by EHMO calculations based on the experimental molecular structure. The large value of the calculated HOMO/LUMO gap (2.13 eV) is much more characteristic of a mononuclear ruthenium species rather than a compound presenting significant metal–metal interactions. Over the range –11.8 to –12.8 eV, the 14 highest occupied levels constitute a group being well isolated on the energy scale. This block is made from the 4×3 “ t_{2g} ” levels of the four independent metal centers mixed with two bonding MOs deriving from the two bridging carbonyls. The other occupied levels, predominantly ligands in character, lie below –14 eV.

The fact that the corresponding overlap populations between the metals are all slightly negative (average value = –0.023) indicates weak repulsive interactions and, hence, absence of Ru–Ru bonding. The strongest repulsions correspond to the shortest, CO-bridged Ru··Ru separations (–0.039 and –0.036 for Ru(1)··Ru(2) and Ru(3)··Ru(4), respectively). Repulsive interactions are also present between the chlorine atoms which are bridging the same metal–metal vector, as expected from the molecular structure (see above). The corresponding overlap populations are –0.010 and –0.011 for Cl(1)··Cl(3) and Cl(2)··Cl(4), respectively. The Ru–O and Ru–Cl (short bond) overlap populations

Table 5. Performances of Various Mono- and Dianionic Polymetallic Ruthenium Carbonyl Halide Complexes Used as Catalyst Precursors^a

entry	catalyst precursor	[substr]/ [cat.]	conv (%)	selec (%)	turnover
1	Ru ₃ (CO) ₁₂ + [PPN]Cl	345	100	99	339
2	[PPN][Ru ₄ (μ-Cl)(CO) ₁₃]	345	100	99	339
3	[PPN] ₂ [Ru ₄ (μ-Cl) ₂ (CO) ₁₁]	405	95	98	381
4	[PPN] ₂ [Ru ₄ (μ-Cl) ₄ (μ ₄ -O)(CO) ₁₀]	405	88	97	345
5	[PPN] ₂ [Ru ₆ C(CO) ₁₆]	901	53	44	207

^a Experimental conditions: HCO₂CH₃ (5 mL), DMF (15 mL), P(C₂H₅)₃ = 20 atm, T = 160 °C, reaction time = 12 h.

exhibit values of 0.234 and 0.308, respectively, thereby indicating substantial metal–ligand bonding, whereas the corresponding average value of 0.157 for the long Ru–Cl bonds indicates significantly weaker interactions. This suggests that a partial decoordination of one or several chlorine ligands should be possible in solution at reasonable temperatures, generating reactive coordination sites on one or several atoms.

Evaluation of the New Complexes as Catalyst Precursors. Identification of the Principal Metal-Containing Species at the End of Catalytic Runs. Following the isolation and characterization of the above dianionic species, we attempted to evaluate their efficiency as catalyst precursors (Table 5). It appeared that the performances obtained with [PPN]₂[Ru₄(μ-Cl)₂(CO)₁₁] (**4**), [PPN][Ru₄(μ-Cl)(CO)₁₃] (**5**), or [PPN]₂[Ru₄(μ₄-O)(μ-Cl)₄(CO)₁₀] (**6**) matched those obtained with Ru₃(CO)₁₂ + [PPN]Cl. The fact that complexes exhibiting rather different structures had roughly the same efficiencies was interpreted as a strong indication that they were just acting as the precursors to the same active species. Furthermore, it appeared that the solutions recovered at the end of all catalytic runs exhibited the same infrared pattern in the ν(CO) region, regardless of the nature of the anionic precursor. The species responsible for the observed infrared pattern was isolated from the solution, crystallized, and unambiguously identified as the known dianionic carbido complex [PPN]₂[Ru₆C(CO)₁₆].²⁶ However, only moderate performances (Table 5, entry 5) were recorded when the complex was used as a catalyst precursor, thereby indicating that it was not the active species, but an end product resulting from its decomposition.

Interestingly, [PPN]₂[Ru₆C(CO)₁₆] had been also isolated earlier by Dombek as a residual product in a related catalytic system, namely, the ruthenium-catalyzed syngas conversion to ethylene glycol, using KI as a promoter.²⁷ With this in mind, we reasoned that the two catalytic systems might possibly involve the same active species at the intermediate stage. In the glycol synthesis, the active species generated *in situ* upon reaction of Ru₃(CO)₁₂ with KI under hydrogen pressure had been proposed to be a mixture of [Ru₃(μ-H)(CO)₁₁][–] and [Ru(CO)₃I₃][–].²⁷ Though molecular hydrogen was not involved in our system, hydrido com-

(26) (a) This carbido complex had been originally obtained upon reaction of Ru₃(CO)₁₂ with ethylene in the presence of a base.^{26b,c} (b) Bradley, J. S.; Ansell, G. B.; Hill, E. W. *J. Organomet. Chem.* **1980**, *184*, C33–C35. (c) Johnson, B. F. G.; Lewis, J.; Sankey, S. W.; Wong, K.; McPartlin, M.; Nelson, W. J. H. *J. Organomet. Chem.* **1980**, *191*, C3–C7.

(27) (a) Dombek, B. D. *J. Am. Chem. Soc.* **1981**, *103*, 6508. (b) Dombek, B. D. *J. Organomet. Chem.* **1983**, *250*, 467. (c) Dombek, B. D. *Organometallics* **1985**, *4*, 1707. (d) Dombek, B. D. *J. Organomet. Chem.* **1989**, *372*, 151 and references therein.

Table 6. Evidence for the Efficiency of [PPN][Ru(CO)₃Cl₃]^a

entry	catalyst precursor	time (h)	conv (%)	selec (%)	TOF (h ⁻¹)
1	[HRu ₃ (CO) ₁₁] ⁻	12	100	25	8
2	[Ru(CO) ₃ Cl ₃] ⁻ + 2 [HRu ₃ (CO) ₁₁] ⁻	3	72	98	83
3	[Ru(CO) ₃ Cl ₃] ⁻	3	80	95	89

^a Experimental conditions: entry 1, [PPN][HRu₃(CO)₁₁] (0.235 mmol); entry 2, [PPN][Ru(CO)₃Cl₃] (0.235 mmol), [PPN][HRu₃(CO)₁₁] (0.470 mmol); entry 3, [PPN][Ru(CO)₃Cl₃] (0.235 mmol); HCO₂CH₃ (5 mL), DMF (15 mL), P(C₂H₄) = 20 atm, T = 160 °C.

plexes might have been generated *in situ* from ethylene or methyl formate under catalytic conditions. Thus, the activity of the mixture [Ru₃(μ-H)(CO)₁₁]⁻ + [Ru(CO)₃X₃]⁻ was evaluated in the formate/ethylene reaction, keeping in mind that such a mixture had been also found active in a conventional hydroalkoxycarbonylation process using CO + MeOH.²⁸ Whereas the results were still found totally negative when X was the iodide ligand, the use of the chloride-containing salt resulted in a spectacular rate enhancement and completion of the reaction within 3 h (Table 6, entry 2). Finally, the salt [PPN][Ru(CO)₃Cl₃] alone (entry 3) was found as active as the mixture [PPN][Ru(CO)₃Cl₃] + 2[PPN][Ru₃(μ-H)(CO)₁₁], which ruled out a participation of the latter salt in the present case.

The advantage of using [PPN][Ru(CO)₃Cl₃] instead of the Ru₃(CO)₁₂/[PPN]Cl mixture is illustrated by the diagram showing the respective evolution of the internal pressure as a function of time for the two systems (Figure 4): whereas the reaction initiated with the mixture Ru₃(CO)₁₂/[PPN]Cl starts only after an induction period of ca. 3 h, catalytic reaction takes place rapidly in the presence of [PPN][Ru(CO)₃Cl₃]. Thus, the mononuclear complex appears to be much closer to the active species than the former cluster. One may reasonably suggest that the induction period required to activate the cluster corresponds to the generation of active fragments of lower nuclearity. Even though slightly lower conversion rates and selectivities were obtained from the initial catalytic runs where the mononuclear complex was used as a precursor, we next found that the addition of an excess of [PPN]Cl (1 equiv) to the mononuclear complex [PPN][Ru(CO)₃Cl₃] allows us to match the performances obtained with the cluster, namely, 97% conversion and 98% selectivity, within a much shorter reaction time (*vide infra*). In view of further developments of a catalytic system based on the mononuclear precursor, it was first necessary to improve the yield of its preparation.

B. Design and Evaluation of Mononuclear Catalyst Precursors. "One Pot" Synthesis of [PPN][Ru(CO)₃Cl₃]. The complex [PPN][Ru(CO)₃Cl₃] can be readily obtained by treatment of the dimer [Ru(CO)₃Cl₂]₂ with [PPN]Cl in parallel with the procedure reported for iodide salts.²⁹ However, the published multistep procedure for the preparation of the antecedent bimetallic species [Ru(CO)₃Cl₂]₂ is not convenient for extensive use since it necessitates, first, the preparation of Ru₃(CO)₁₂ from the commercial ruthenium trichloride RuCl₃·3H₂O,³⁰ and then the reintroduction

of chloride ions *via* reaction with HCCl₃ in a reactor.³¹ The corresponding overall yield of [PPN][Ru(CO)₃Cl₃] never exceeds 28%, due to cumulated losses along the four individual steps.

While routinely preparing samples of Ru₃(CO)₁₂ *via* the method reported by Mantovani and Cenini,³⁰ namely, the two-step reduction of RuCl₃·nH₂O by CO and zinc, we were intrigued by slight variations in the color of the intermediate yellow solution obtained at the end of the first reduction step. Such variations occurred when the solution was kept overnight under CO at room temperature. We realized that the exact composition of this mixture (referred to as "lemon-yellow solution" in the published procedure³⁰) had never been determined before. A careful monitoring by infrared spectroscopy allowed us to identify the principal species present in this mixture (Scheme 2). Typically, when RuCl₃·nH₂O was refluxed in ethoxyethanol under a fast stream of carbon monoxide, a color change from dark brown to blood red was observed after 20 min. At that stage, the IR spectrum exhibited two bands of equal intensity at 2060 and 1990 cm⁻¹ that could be attributed to the polymeric complex [Ru(CO)₂Cl₂]_n (though it has been suggested that the latter species might be trimeric, its structure has in fact never been established).³² While the red color progressively turned yellow under prolonged reaction with CO, an additional band appeared at 2125 cm⁻¹, whereas the 2060 cm⁻¹ band was simultaneously enlarged and slightly shifted down to 2056 cm⁻¹. Such a spectral change was ascribed to the progressive formation of the dimeric complex [Ru(CO)₃Cl₂]₂ (2125 (s), 2050 (vs) cm⁻¹) at the expense of the polymeric species.³³ The complete transformation of the polymeric species into the colorless dimer was achieved upon prolonged treatment with CO for ca. 7 h at room temperature. Alternately, such a transformation could be more readily achieved under CO pressure (10 atm, 80 °C, 1 h). The dimeric compound [Ru(CO)₃Cl₂]₂ was recovered by evaporation of the solvent and then dissolved in THF. Further addition of [PPN]Cl allowed precipitation of the salt [PPN][Ru(CO)₃Cl₃]. After recrystallization from methanol, the overall yield of [PPN][Ru(CO)₃Cl₃] relative to the starting material RuCl₃·nH₂O was 81% (Scheme 2).

An X-ray structure analysis of the crystals confirmed that the compound is obtained as the *fac*-isomer, as established earlier from a structural analysis of the salt [H₅O₂][Ru(CO)₃Cl₃]·SbCl₅.³⁴

Synthesis of [PPN][Ru(CO)₃X_nX'_{3-n}] (X = Cl, X' = I, n = 1, 2). Whereas [PPN][Ru(CO)₃Br₃] was prepared by adaptation of the procedure published for [PPN][Ru(CO)₃I₃],²⁹ we needed samples of mixed chloride/iodide salts in order to evaluate the respective efficiency of these halide ions as promoters (*vide infra*). The salt [PPN][Ru(CO)₃Cl₂I] was prepared by simple reaction of the chloride dimer [Ru(CO)₃Cl₂]₂ with [PPN]I, whereas [PPN][Ru(CO)₃ClI₂] was obtained by reacting [Ru(CO)₃I₂]₂ with [PPN]Cl.

(31) Mantovani, A.; Cenini, S. *Inorg. Synth.* **1976**, *16*, 51 and references therein.

(32) Seddon, E. A.; Seddon, K. R. in *The Chemistry of Ruthenium*; Clark, R. J. H., Ed.; Elsevier: Amsterdam, Oxford, New York, Tokyo, 1984 (see also references therein).

(33) For a recent preparative procedure of the dimer, see: (a) Roberto, D.; Psaro, R.; Ugo, R. *Organometallics* **1993**, *12*, 2292. (b) Roberto, D.; Psaro, R.; Ugo, R. *J. Organomet. Chem.* **1993**, *451*, 123.

(34) Teulon, P.; Roziere, J. Z. *Anorg. Allg. Chem.* **1981**, *483*, 219.

(28) Hidai, M.; Koyasu, Y.; Chikanari, K.; Uchida, Y. *J. Mol. Catal.* **1987**, *40*, 243.

(29) For the synthesis of various salts of [Ru(CO)₃X₃]⁻ (X = I,^{29a} Cl^{29b}) see: (a) Zoeller, J. R. *Inorg. Chem.* **1966**, *25*, 3933. (b) Cleare, M. J.; Griffith, W. P. *Chem. Soc. A* **1969**, 372.

(30) Mantovani, A.; Cenini, S. *Inorg. Synth.* **1972**, *16*, 47.

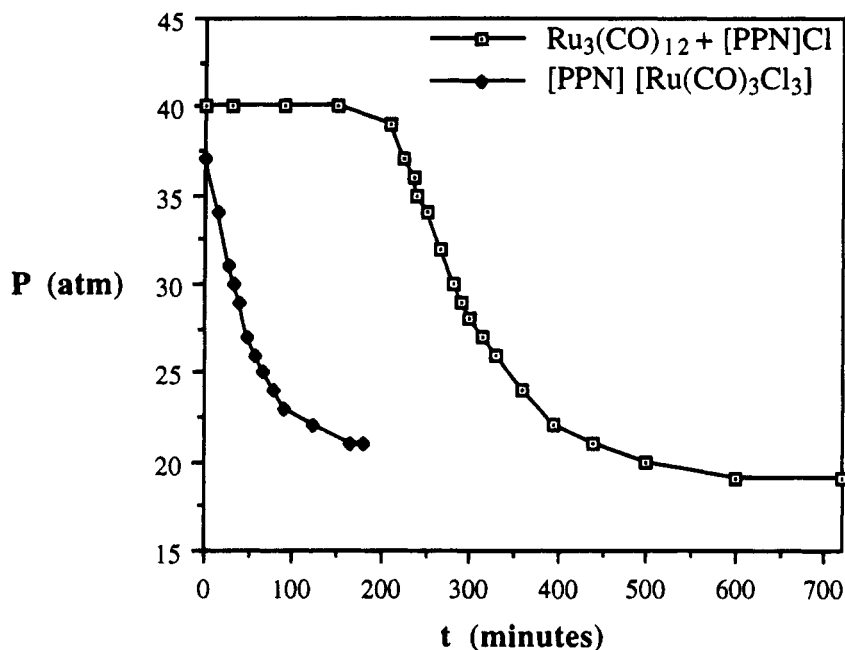
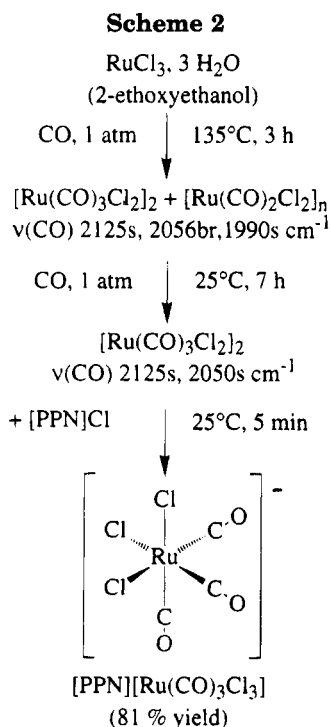


Figure 4. Comparative study of the relative efficiency of polynuclear and mononuclear ruthenium carbonyl chloride complexes as catalyst precursors under the experimental conditions defined in Table 6. The plots represent the evolution of the internal pressure within the reactor as a function of time.



Optimization of the Catalytic System Based on [PPN][Ru(CO)₃Cl₃]. Influence of the Temperature. The results of catalytic runs performed at various temperatures are reported in Table 7, whereas the corresponding graph tracing the evolution of the internal pressure as a function of time is displayed in Figure 5. The optimum activity was obtained at 180 °C. Interestingly, the plot corresponding to the catalytic run performed at 200 °C clearly showed a fast decrease of the ethylene pressure in the initial stage, followed after 10 min by a sudden pressure increase consistent with a decomposition of methyl formate into methanol and CO. It is noteworthy that, even though all the required substrates (MeOH + CO) necessary for a conventional

Table 7. Temperature Optimization for the System Using [PPN][Ru(CO)₃Cl₃] as Catalyst Precursor in DMF Solvent^a

entry	T (°C)	time (h)	conv (%)	selec (%)	turnover
1	120	12	57	96	16
2	140	6	74	96	41
3	160	3	80	95	89
4	180	2	100	97	170
5	200	2	100	38	74

^a Experimental conditions: [PPN][Ru(CO)₃Cl₃] (0.235 mmol), HCO₂CH₃ (5 mL), [formate]/[cat.] = 345, DMF (15 mL), P(C₂H₄) = 20 atm.

alkoxycarbonylation reaction were produced through the latter experiment at 200 °C, such a reaction did not occur. We also noted a critical influence of the temperature on the composition of the solutions recovered at the end of catalytic runs. Typically, whereas a yellow solution (IR ν(CO) 2003 (s), 1918 (vs)) was recovered when the working temperature was maintained at 160 °C or below, the red carbido complex [PPN]₂[Ru₆C(CO)₁₆] was systematically present at the end of all catalytic runs carried out above 180 °C. Since these changes might indicate a faster deactivation of the working catalyst at high temperatures, the working temperature was maintained at 160 °C in all further experiments. To date, attempts to isolate the yellow species detectable by IR have been unsuccessful.

Influence of the Solvent. Up to 10 different solvents were examined (Table 8, and selected results in Figure 6). DMF, DMA, and NMP gave the best results, whereas *N*-methylacetamide (NMA) was found to be inefficient. Apparently, catalysis takes place only when the nitrogen atom of the amide function is disubstituted.

Relative Efficiency of [PPN][Ru(CO)₃Cl₃], [PPN][Ru(CO)₃Br₃], [PPN][Ru(CO)₃I₃], and RuCl₃·*n*H₂O + 2[Et₄N]I. The results of a comparative study of these salts under our standard experimental conditions are displayed in Table 9. It appears that (i) the order of reactivity of halide ions for the species [PPN][Ru(CO)₃X₃] is Cl > Br > I, and (ii) the mixture RuCl₃·*n*H₂O

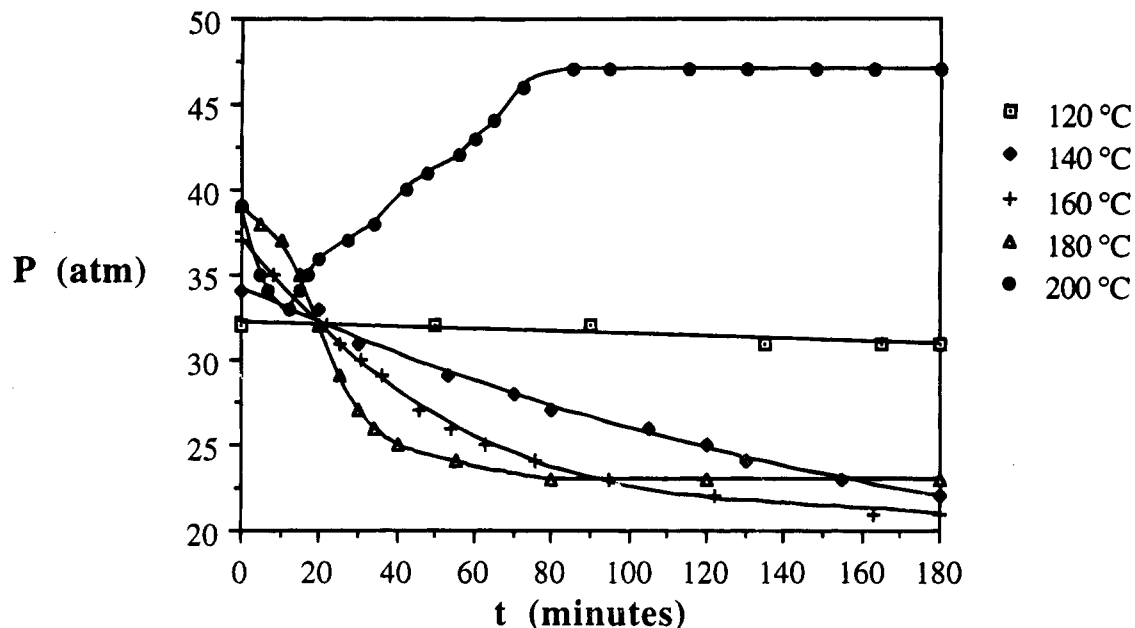


Figure 5. Temperature optimization for the catalytic system based on $[\text{PPN}][\text{Ru}(\text{CO})_3\text{Cl}_3]$. The plots represent the evolution of the internal pressure within the reactor as a function of time for different temperatures under the experimental conditions defined in Table 7.

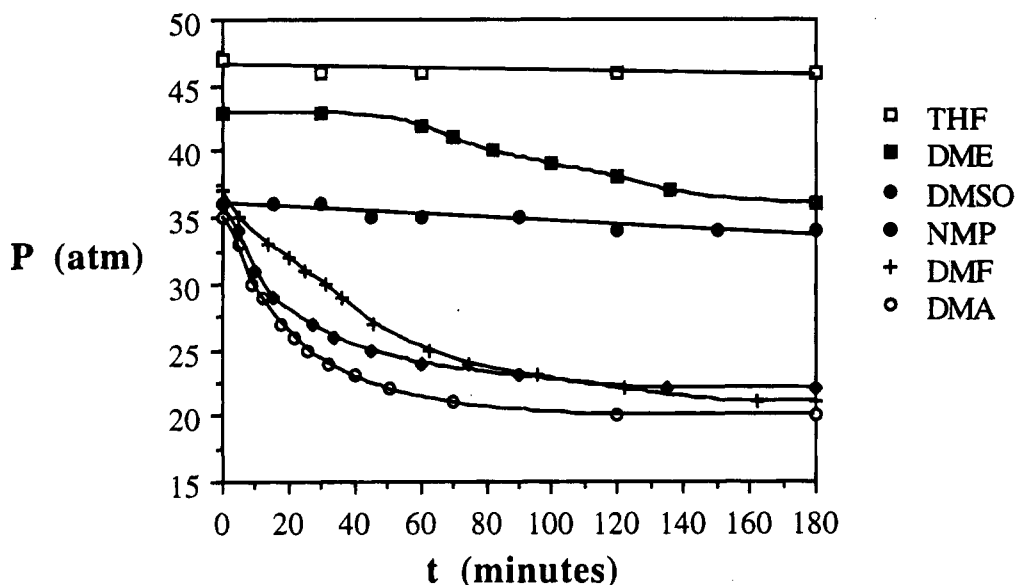


Figure 6. Influence of the solvent on the efficiency of the catalytic system based on $[\text{PPN}][\text{Ru}(\text{CO})_3\text{Cl}_3]$. The plots represent the evolution of the internal pressure within the reactor as a function of time under the experimental conditions defined in Table 8.

+ $2[\text{Et}_4\text{N}]\text{I}$ is still only moderately active and rather unselective under the mild conditions of our experiment.

Influence of Additional Promoters. As noted above, whereas all experiments using the clusters derived from mixtures of $\text{Ru}_3(\text{CO})_{12}$ + $[\text{PPN}]\text{Cl}$ as catalysts precursors led to 100% conversion, the maximum conversion rate obtained with $[\text{PPN}][\text{Ru}(\text{CO})_3\text{Cl}_3]$ did not exceed 80%. However, it was subsequently found that addition of 1 equiv of $[\text{PPN}]\text{Cl}$ allows us to achieve 100% conversion within 2 h (Table 10).

Triethylamine is commonly used as a cocatalyst in catalytic systems involving halide promoters. Petit and co-workers had already noted its positive influence on the activity of their system based on $\text{RuCl}_3 \cdot n\text{H}_2\text{O}$ + $2[\text{Et}_4\text{N}]\text{I}$. We just noted exactly the same effect on our system, namely, a prolongation of the linear phase of

Table 8. Influence of the Nature of the Solvent on the Activity of $[\text{PPN}][\text{Ru}(\text{CO})_3\text{Cl}_3]^a$

entry	solvent	time (h)	conv (%)	selec (%)	TOF (h^{-1})
1	THF	5	24	59	11
2	CH_3CN	3	7	96	8
3	TMEDA	3	32	9	4
4	HMPA	4	75	0	0
5	DME	5	49	97	34
6	DMSO	4	46	70	32
7	DMF	3	80	95	89
8	NMP	3	77	94	85
9	DMA	3	78	95	88
10	NMA	3	0	0	0

^a Experimental conditions: $[\text{PPN}][\text{Ru}(\text{CO})_3\text{Cl}_3]$ (0.235 mmol), HCO_2CH_3 (5 mL), solvent (15 mL), $P(\text{C}_2\text{H}_4) = 20$ atm, $T = 160$ °C.

the catalysis being optimum for a ratio $[\text{NEt}_3]/[\text{cat.}] = 3$ (see Table 11).

Table 9. Effect of the Nature of the Halide on the Efficiency of [PPN]Ru(CO)₃X₃; Comparison with the System Based on RuCl₃·3H₂O + 2[Et₄N]I^a

entry	catalyst precursor	time (h)	conv (%)	selec (%)	TOF (h ⁻¹)
1	[PPN]Ru(CO) ₃ Cl ₃	3	80	95	89
2	[PPN]Ru(CO) ₃ Br ₃	3	11	89	13
3	[PPN]Ru(CO) ₃ I ₃	4	2	82	2
4	RuCl ₃ ·3H ₂ O + 2[Et ₄ N]I	3	28	41	14

^a Experimental conditions: catalyst precursor (0.235 mmol), HCO₂CH₃ (5 mL), DMF (15 mL), P(C₂H₄) = 20 atm, T = 160 °C.

Table 10. Modulation of the Activity of [PPN][Ru(CO)₃Cl₃] by Addition of [PPN]Cl^a

entry	catalyst precursor	time (h)	conv (%)	selec (%)	TOF (h ⁻¹)
1	[PPN][Ru(CO) ₃ Cl ₃]	3	80	95	89
2	[PPN][Ru(CO) ₃ Cl ₃] + [PPN]Cl	3	97	98	112

^a Experimental conditions: [PPN][Ru(CO)₃Cl₃] (0.235 mmol), HCO₂CH₃ (5 mL), DMF (15 mL), P(C₂H₄) = 20 atm, T = 160 °C.

Table 11. Modulation of the Activity of [PPN][Ru(CO)₃Cl₃] by Addition of Variable Amounts of Triethylamine^a

entry	[NEt ₃]/[cat.]	time (h)	conv (%)	selec (%)	TOF (h ⁻¹)
1	458	4	0	0	0
2	50	2	41	35	25
3	25	2	59	57	60
4	10	2	61	82	88
5	6	2	86	98	146
6	3	2	100	98	170
7	2	2	82	95	136
8	0	3	80	95	89

^a Experimental conditions: [PPN][Ru(CO)₃Cl₃] (0.235 mmol), HCO₂CH₃ (5 mL), DMF (15 mL, except in run 1 where pure triethylamine was used as a solvent) P(C₂H₄) = 20 atm, T = 160 °C.

Table 12. Comparative Evaluation of the Salts [PPN][Ru(CO)₃I_nCl_{3-n}] (n = 0, 1, 2, 3) as Catalyst Precursors^a

entry	catalyst precursor	time (h)	conv (%)	selec (%)	TOF (h ⁻¹)
1	[PPN][Ru(CO) ₃ I ₃]	5	2	82	2
2	[PPN][Ru(CO) ₃ ClI ₂]	5	84	98	58
3	[PPN][Ru(CO) ₃ Cl ₂ I]	4	100	97	86
4	[PPN][Ru(CO) ₃ Cl ₃]	2	100	98	170

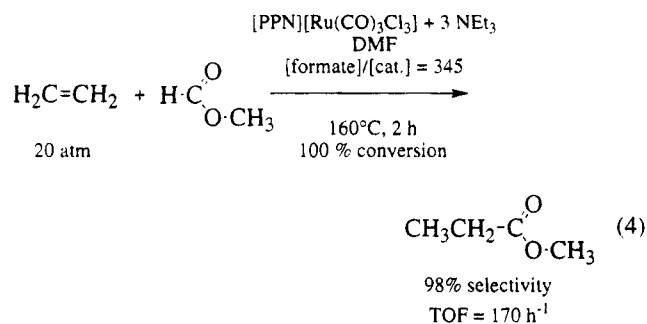
^a Experimental conditions: [PPN][Ru(CO)₃I_nCl_{3-n}] (n = 0, 1, 2, 3) (0.235 mmol), NEt₃ (0.705 mmol), HCO₂CH₃ (5 mL), DMF (15 mL), P(C₂H₄) = 20 atm, T = 160 °C.

Relative Efficiency of Mixed-Halide Complexes [PPN][Ru(CO)₃Cl_nI_{3-n}]. In order to ascertain our observation that the chloride ion is superior to the iodide, we were led to analyze the effect of a progressive substitution of the three iodide atoms of the complex [PPN][Ru(CO)₃I₃] by chloride atoms. The results shown respectively in Table 12 and Figure 7 provided further evidence that the chloride is by far the best promoter under mild experimental conditions.

The optimum performances of the catalytic system for a standard ethylene pressure of 20 atm are summarized in eq 4.

Poisonous Effect of CO. A very significant poisonous effect of CO was noted. Indeed, under the optimum experimental conditions defined in eq 4, a partial pressure of 3 atm of CO was found to inhibit almost completely the catalysis, leading to only 8% conversion and 80% selectivity. A similar poisonous effect was noted upon addition of 1 equiv of triphenylphosphine (43% conversion, 28% selectivity).

Attempted Alkoxy carbonylation Reaction. Finally, it was of interest to determine whether the



synthesis of methyl propionate could be alternately achieved *via* a conventional alkoxy carbonylation process starting from methanol + CO in the presence of our catalyst precursor. In a typical experiment using 0.235 mmol of [PPN][Ru(CO)₃Cl₃], 0.042 mol of methanol, 18 mL of DMF, 10 atm of C₂H₄, and 10 atm of CO, the rate of methanol conversion into methyl propionate was found to be only 69% after 6 h, thus corresponding to a turnover frequency of 27 h⁻¹, much lower than that obtained with methyl formate as a substrate.

Furthermore, an additional experiment where the reactor was loaded with nitrogen (7 atm) instead of ethylene (otherwise using the standard conditions of eq 4) revealed that the decomposition of methyl formate into MeOH + CO was limited to 7% after 2 h at 160 °C.

Evidence for the Implication of DMF in the Formation of the Active Species. When DMF solutions of the complex [PPN][Ru(CO)₃Cl₃] were heated in the absence of substrate at the temperature of the catalytic reaction, namely, 160 °C, infrared monitoring indicated the progressive formation of a new complex exhibiting two ν(CO) bands appearing at lower frequencies (2045 (s), 1975 (s) cm⁻¹) than those of the starting complex (2108 (s), 2031 (vs) cm⁻¹). The reaction was generally complete within 0.5 h, and the new compound was isolated as bright yellow crystals. An IR spectrum taken after redissolution of these crystals in dichloromethane revealed a third band at 1645 cm⁻¹ that had been previously masked in DMF solution by the characteristic ν(C=O) band of the solvent. The formulation of the complex as [PPN][Ru(CO)₂Cl₃(η¹-OCHN(CH₃)₂)] (11), consistent with analytical results, was ascertained by an X-ray structure determination.

A perspective view of the anionic unit of [PPN][Ru(CO)₂Cl₃(η¹-OCHN(CH₃)₂)] (11) is displayed in Figure 8. The complex results from the replacement of a CO ligand of [PPN][Ru(CO)₃Cl₃] by a DMF molecule coordinated through the oxygen atom. However, whereas the starting compound [PPN][Ru(CO)₃Cl₃] was isolated as the *fac*-isomer (*vide supra*), the three halides of the DMF-substituted derivative adopt a *mer*-arrangement of chloride atoms. One of the two axial sites is occupied by the oxygen atom of the coordinated DMF. Though the overall geometry is indeed octahedral, the complex may be alternately regarded as an unsaturated square pyramidal fragment "Ru(CO)₂Cl₃" being stabilized by a solvent molecule.

In a series of new experiments, we are now currently observing that the catalytic activity of [PPN][Ru(CO)₂Cl₃(η¹-OCHN(CH₃)₂)] slightly exceeds that found for [PPN][Ru(CO)₃Cl₃], due to a shortening of the initial induction period.

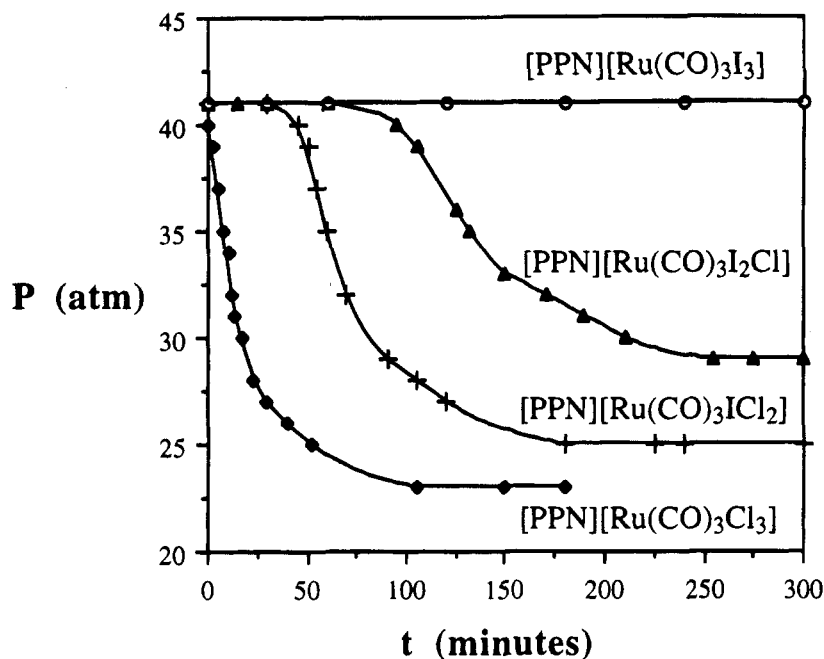


Figure 7. Influence of the I/Cl ratio on the efficiency of $[\text{PPN}][\text{Ru}(\text{CO})_3\text{I}_n\text{Cl}_{3-n}]$ as catalyst precursor under the experimental conditions defined in Table 9.

Discussion

Polymetallic Ruthenium Carbonyl Halide Complexes: Labile Combinations of Electron Deficient Skeletons and Electron Rich Anions. The associative mechanism by which the first chloride ion is incorporated into the coordination sphere of $\text{Ru}_3(\text{CO})_{12}$ has been well established from previous studies.¹² Let us just remind the reader here that the chloride-containing anions corresponding to the stepwise loss of CO from the initial adduct are $[\text{PPN}][\text{Ru}_3(\text{Cl})(\text{CO})_{11}]$ (**1**), $[\text{PPN}][\text{Ru}_3(\mu\text{-Cl})(\text{CO})_{10}]$ (**2**), and $[\text{PPN}][\text{Ru}_3(\mu_3\text{-Cl})(\text{CO})_9]$ (**3**) (Scheme 1). The less CO rich derivative **3** is formed quantitatively in refluxing THF but is stable only in the absolute absence of CO.^{12g,h} Otherwise, it rapidly rearranges to the well known butterfly complex $[\text{PPN}][\text{Ru}_4(\mu\text{-Cl})(\text{CO})_{13}]$ (**5**).²⁴

The present work reveals that incorporation of a second chloride ligand can be easily achieved under thermal activation to produce a dianionic species. Such a reaction may readily take place under the conditions of many catalytic systems where $\text{Ru}_3(\text{CO})_{12}$ is used in the presence of an excess of halide promoter. Though simple CO displacement by a chloride ligand from **3** would be expected to give a trinuclear substituted derivative of rough formula " $[\text{PPN}]_2[\text{Ru}_3(\text{Cl})_2(\text{CO})_8]$ ", such an intermediate is not seen, whereas the tetranuclear cluster $[\text{PPN}]_2[\text{Ru}_4(\mu\text{-Cl})_2(\text{CO})_{11}]$ (**4**) is isolated quantitatively in the presence of an excess of chloride (at least $1/2$ equiv).

For metal carbonyl complexes, aggregation *via* metal-metal bond formation is generally the only way to release the unsaturation created by thermally induced loss of CO. Here, capture of an additional chloride ligand may be regarded as a *spare means for the cluster to protect vacant coordination sites on electron-deficient metal centers*. The occurrence of a concomitant reorganization of the trimetal framework into a tetranuclear one reflects the important lability of ruthenium/carbonyl/halide aggregates. An intermolecular transfer of

metal/chloride/CO fragments is obviously required in such a transformation. It may be facilitated by transient formation of halide bridges between neighboring cluster units. A relevant type of "ligand-induced aggregation" was previously observed in the dimerization of the related anionic trinuclear species $[\text{PPN}][\text{Ru}_3(\text{CN})(\text{CO})_{11}]$ to the dianionic hexanuclear species $[\text{PPN}]_2[\text{Ru}_6(\mu\text{-CN})_2(\text{CO})_{20}]$, a coupling reaction assisted by the coordinated cyanide ligand.³⁵

A general observation is that the interaction of **4** with donor substrates does not give simple isolable adducts. Occupation of the apical coordination site of the unsaturated Ru center apparently triggers a complete reorganization of the polymetallic architecture. For example, addition of CO induces immediate loss of a halide ion and concomitant formation of a metal-metal bond to yield the butterfly complex **5**. Even more complicated is the reaction with oxygen, which involves disruption of metal-metal bonds, intermolecular scavenging of halide ions, and encapsulation of a single oxygen atom to give $[\text{PPN}]_2[\text{Ru}_4(\mu_4\text{-O})(\mu\text{-Cl})_4(\text{CO})_{10}]$ (**6**).

Thus, in account of the high lability of the above aggregates, it seems reasonable to ascribe their efficiency as catalyst precursors to the facile generation of active mononuclear ruthenium carbonyl halide fragments under catalytic conditions. The principal arguments consistent with such a view are the following: (i) catalysis in the presence of all the anionic ruthenium carbonyl chloride clusters considered here takes place only after an induction period (see an example in Figure 4); (ii) comparable conversion rates and selectivities are obtained, regardless of the different polymetallic architectures of these compounds, which means that there is no structure/activity relationship; (iii) all these compounds are transformed under catalytic conditions, and the principal dianionic species $[\text{PPN}]_2[\text{Ru}_6(\mu_6\text{-C})(\text{CO})_{16}]$ recovered at the end of the catalytic runs is only

(35) Lavigne, G.; Lukan, N.; Bonnet, J.-J. *J. Chem. Soc., Chem. Commun.* **1987**, 957.

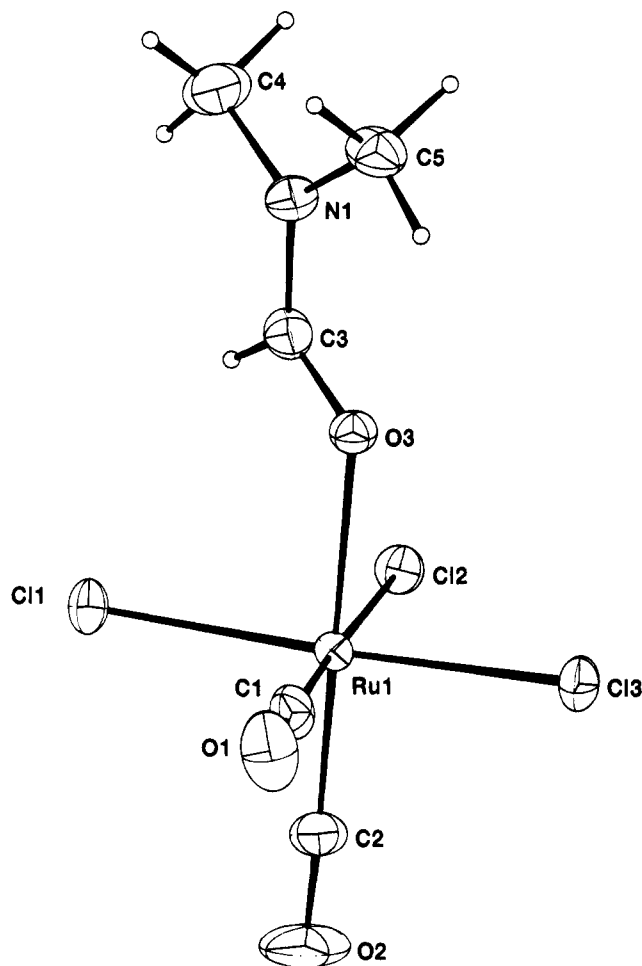


Figure 8. Perspective view of the anionic unit of complex 11.

moderately active and rather unselective in the production of methyl propionate.

[PPN][Ru(CO)₃Cl₃] as an Alternate Catalyst Precursor. According to Dombek,²⁷ the reaction of Ru₃(CO)₁₂ with iodide salts in the presence of CO/H₂ mixtures generates the two anionic complexes [Ru₃(μ-H)(CO)₁₁]⁻ and [Ru(CO)₃I₃]⁻, acting in concert to promote syngas conversion to ethylene glycol *via* intermolecular hydride transfer. These complexes were also taken into account in relevant Ru-based syngas reactions in molten salts developed by Knifton and co-workers.³⁶ Furthermore, the same mixture of anionic species was used by Hidai in the alkoxy-carbonylation of ethylene with MeOH + CO.²⁸ In that case, it was suggested that consecutive insertion of ethylene and CO into the Ru-H bond of the hydrido anion would give a propionyl intermediate, whereas a bimolecular reaction would then lead to propionyl iodide, subsequently converted into methyl propionate *via* reaction with methanol.²⁸

There are significant differences between our system using methyl formate as a substrate and the one proposed by Hidai for the alkoxy-carbonylation reaction using MeOH + CO. In particular, (i) we use exclusively the chloride-containing salt [PPN][Ru(CO)₃Cl₃] as a catalyst precursor, since the corresponding iodide de-

rivative proved to be inactive under our milder reaction conditions; (ii) the addition of [Ru₃(μ-H)(CO)₁₁]⁻ has no detectable influence on the activity of our catalytic system; (iii) the promoter effect of Cl⁻ is observed only in the amide type solvents, whereas the former iodide-promoted alkoxy-carbonylation reaction was performed in neat methanol; finally, (iv) the activity of our catalyst is quenched by small amounts of CO (3 atm), whereas a significant CO pressure is obviously required in a conventional alkoxy-carbonylation process starting from methanol.

Our observation of a significant poisoning effect of CO tends to indicate that the mechanism by which methyl formate is activated *in situ* in the present case is not a simple decomposition of methyl formate to methanol and free CO followed by a conventional hydroalkoxy-carbonylation process.

One may wonder whether the catalytic system presented here and the above mentioned patented process^{11b} involve the same active species. We have presently no answer to such a question. A puzzling point is that, even though both chloride and iodide ions are claimed to be necessary in the catalytic system based on RuCl₃·nH₂O + 2[NEt₄]I,^{11b} we find that the chloride-containing salt [PPN][Ru(CO)₃Cl₃] alone is active in our system and that the presence of iodide is detrimental (Figure 7). Though the turnover rates obtained with our chloride-based system do not match those reported in the patented process, it is noteworthy that (i) the respective values are not directly comparable³⁷ and (ii) those reported here were recorded under mild experimental conditions at which the former process is still only moderately active and rather unselective. Whereas the present chloride-based system appears to reach its optimum efficiency at milder conditions than recorded for other promoters, a major limiting factor is the temperature, which should not exceed 180 °C, above which the active species seems to be decomposed. This result is fully consistent with Keim's earlier observation that the halide-containing anion [Ru₃(μ-Cl)(CO)₁₀]⁻ is a much less efficient catalyst precursor than Ru₃(CO)₁₂ at 230 °C.⁸

Key Role of the Solvent. There is an apparent synergism in the combined effects of halide ions and amide solvents on the ruthenium-catalyzed ethylene/formate reaction. It has been suggested that partial decomposition of DMF under catalytic conditions might play a role in the formation of the active species.¹¹ Recently, des Abbayes and co-workers reported that amines (that might be possibly obtained in small amounts *via* partial decomposition of DMF) catalyze the decomposition of methyl formate to methanol and CO, even in the absence of metal.³⁸ To date, the only experimental evidence we have is that DMF is involved as a ligand at the intermediate stage. We are currently attempting to determine whether it either acts as a weakly coordinated ligand stabilizing a reactive five-coordinate intermediate or undergoes subsequent metal-assisted decomposition, with possible relevance to the

(37) The best TOF value of 1450 h⁻¹ reported in the patent^{11b} was measured at 65% conversion, whereas the recently published^{11c} value of 2300 h⁻¹ was measured at 25% conversion. In the present case, an attempt to estimate the turnover frequency of our system from the linear part of the pressure plot in the best catalytic run (Figure 7) led to an approximate value of 700 h⁻¹.

(38) Ramirez Vega, F.; Clement, J.-C.; Des Abbayes, H. *Tetrahedron Lett.* **1993**, *34*, 8117.

(36) Knifton, J. F. In *Aspects of Homogeneous Catalysis*; Ugo, R., Ed.; Reidel: Dordrecht, The Netherlands, 1988; Vol. 6, p 1 (see also references therein).

Table 13. Crystal and Intensity Data for the Complexes [PPN]₂[Ru₄(μ-Cl)₂(CO)₁₁] (4), [PPN]₂[Ru₄(μ₄-O)(μ-Cl)₄(CO)₁₀] (6), and [PPN][Ru(CO)₂Cl₃(η¹-OCHN(CH₃)₂)] (11)

compd	4	6	11
formula	C ₈₃ H ₆₀ N ₂ O ₁₁ P ₄ Cl ₂ Ru ₄ (+ 1.5CH ₂ Cl ₂)	C ₈₂ H ₆₀ N ₂ O ₁₁ P ₄ Cl ₄ Ru ₄	C ₄₁ H ₃₇ N ₂ O ₅ P ₂ Cl ₃ Ru
F _w	1860.5	1919.4	875.1
a, Å	18.209(2)	13.226(5)	9.000(2)
b, Å	18.877(3)	25.533(2)	21.176(2)
c, Å	13.895(2)	12.771(3)	21.080(1)
α, deg	110.70(1)	92.39(1)	90.00
β, deg	108.43(1)	114.77(3)	93.89(8)
γ, deg	87.43(1)	85.92(2)	90.00
V, Å ³	4226(1)	3906(2)	4008.3(9)
Z	2	2	4
space group	triclinic P $\bar{1}$ (No. 2)	triclinic P $\bar{1}$ (No. 2)	P2 ₁ /c (No. 14)
T, °C	23	23	-140
radiation, wavelength, Å	Mo Kα, λ(Mo Kα ₁) = 0.7093 Å (monochromator)		
linear abs coeff, cm ⁻¹	9.46	10.2	7.0
cryst shape	prismatic; 6 faces	prismatic; 6 faces	prismatic
boundary faces	{100}, {011}, {0,1,-1}	{010}, {011}, {1,-2,0}	
dist from faces to origin, cm	0.01, 0.011, 0.009	0.011, 0.018, 0.025	
min and max transm	0.812, 0.874	0.674, 0.828	0.92, 1.23
receiving aperture, mm	4.0 × 4.0	4.0 × 4.0	4.0 × 4.0
takeoff angle, deg	3.0	2.5	2.5
scan mode	ω-2θ	ω-2θ	ω-2θ
scan range, deg	0.85 + 0.345 tan θ	0.7 + 0.345 tan θ	0.8 + 0.345 tan θ
scan speed, deg min ⁻¹	4.1	4.1	variable (4.1-16.5)
background	moving position	fixed position at both ends	moving position
θ limit, deg	1.0-23.5	1.0-23.0	1.0-25.0
no. of data colld	12934	11249	5512
no. of unique data used	5493 (F _o ² > 4σ(F _o ²))	7753 (F _o ² > 4σ(F _o ²))	5219 (F _o ² > 3σ(F _o ²))
final no. of variables	523	460	470
R (on F _o) ^a	0.053	0.038	0.028
R _w (on F _o) ^a	0.069	0.045	0.030
w = 1/(σ(F _o) ² + p ² F _o ²)	p = 0.03	p = 0.013 (refined value)	no weight
S, Å ²	1.86	1.96	2.13

^a R = Σ||F_o| - |F_c||/Σ|F_o|; R_w = [Σw(|F_o| - |F_c||)²/(Σw|F_o|²)]^{1/2}. ^b Error in an observation of unit weight.

formation of the active species. To date, very little is known about the above mentioned yellow species which is seen by IR spectroscopy during the course of the catalysis. Attempts to isolate and characterize the latter complex are underway.

Concluding Remarks

In summary, the present contribution shows that, regardless of their nuclearity, various ruthenium carbonyl chloride complexes are susceptible to generating an active species achieving the catalytic hydroesterification of ethylene with methyl formate in amide solvents.

Due to the important lability of their ruthenium/chloride framework, the odd aggregates investigated in the first part of this work are susceptible to producing unsaturated fragments of lower nuclearity. This is probably the clue to their efficiency as catalyst precursors.

With the mononuclear complex [PPN][Ru(CO)₃Cl₃], or its DMF-substituted derivative [PPN][Ru(CO)₂Cl₃(η¹-OCHN(CH₃)₂)], we are much closer to the active species. These complexes, which were found to be much more active than the iodide derivative [PPN][Ru(CO)₃I₃], can be used in amide solvents without additives. They are of particular interest on account of their availability in high yield from commercial RuCl₃·nH₂O and their ability to catalyze the hydroesterification reaction under rather mild conditions. It is hoped that, due to their simplicity, these complexes will be amenable to a detailed mechanistic study of the catalytic system. To date, there is a growing number of new catalytic processes where methyl formate is involved as a substrate and still no firm evidence for the mechanism of its metal-mediated activation.^{1,2} Though direct C-H activation has been

observed in few instances,^{2d,g} the alternate possibility of a C-O cleavage within the ester function should be also considered as a working hypothesis, especially in light of the observation that aldehydes cannot be added to ethylene under the experimental conditions defined above.

Experimental Section

All synthetic manipulations were carried out under nitrogen atmosphere, using standard Schlenk techniques. Tetrahydrofuran was distilled under argon from sodium benzophenone ketyl just before use. Dichloromethane was distilled over P₂O₅. Bis(triphenylphosphoranylidene)ammonium chloride, [PPN]Cl, was obtained from Aldrich. RuCl₃·nH₂O (n = 3) was purchased from Johnson Matthey. The following starting materials were prepared according to published procedures: Ru₃(CO)₁₂,³⁰ [PPN][Ru₃(Cl)(CO)₁₁] (1),^{12b} [PPN][Ru₃(μ-Cl)(CO)₁₀] (2),^{12b} [PPN][Ru₃(μ₃-Cl)(CO)₉] (3),^{12b} [PPN][Ru₄(μ-Cl)(CO)₁₃] (5),²⁴ [PPN][Ru₃{μ-η²-O(C₅H₄N)}(CO)₁₀],¹⁵ [PPN][Ru₃{μ₃-η²-S(C₅H₄N)}(CO)₉],¹⁵ [PPN][Ru₃{μ₃-η²-N(C₆H₅)(C₅H₄N)}(CO)₉],¹⁵ [PPN][Ru₃(μ-H)(CO)₁₁],³⁹ and [Ru(CO)₃I₂].²⁹

Infrared spectra were recorded on a Perkin-Elmer 225 spectrophotometer with 0.1 mm cells equipped with CaF₂ windows. These spectra were calibrated against water vapor absorptions.

Preparation of the Complexes. Preparation of [PPN]₂[Ru₄(μ-Cl)₂(CO)₁₁] (4). The complex [PPN][Ru₃(μ₃-Cl)(CO)₉] (3) was prepared *in situ*^{12b} from Ru₃(CO)₁₂ (300 mg, 0.469 mmol) and [PPN]Cl (270 mg, 0.469 mmol) in 30 mL of freshly distilled THF. A continuous stream of argon was bubbled through the solution. Solid [PPN]Cl (135 mg, 0.235 mmol) was added, and the suspension was heated under reflux. Infrared monitoring indicated the formation of a new compound 4. The new IR bands were rapidly maximized and finally disappeared

(39) Lavigne, G.; Lugan, N.; Bonnet, J.-J. *Inorg. Chem.* **1987**, *26*, 2345.

Table 14. Fractional Atomic Coordinates and Isotropic or Equivalent Temperature Factors ($\text{\AA}^2 \times 100$) with Esd's in Parentheses for Compound 4

atom	<i>x/a</i>	<i>y/b</i>	<i>z/c</i>	<i>U</i> _{eq} / <i>U</i> _{iso}	atom	<i>x/a</i>	<i>y/b</i>	<i>z/c</i>	<i>U</i> _{eq} / <i>U</i> _{iso}
Ru(1)	0.68072(7)	0.70556(6)	0.02806(9)	3.74(7)	C(46)	0.6469(5)	-0.0261(5)	0.5407(6)	5.1(4)
Ru(2)	0.76129(7)	0.84317(6)	0.1960(1)	4.32(8)	C(51)	0.6069(4)	0.0395(4)	0.8038(7)	3.1(3)
Ru(3)	0.82989(7)	0.75244(6)	0.0439(1)	4.09(7)	C(52)	0.6149(4)	-0.0201(4)	0.8429(7)	3.7(3)
Ru(4)	0.73626(7)	0.83847(7)	-0.0639(1)	4.82(8)	C(53)	0.5552(4)	-0.0412(4)	0.8725(7)	4.8(4)
Cl(1)	0.7060(2)	0.9288(2)	0.0894(3)	5.9(3)	C(54)	0.4876(4)	-0.0027(4)	0.8631(7)	5.3(4)
Cl(2)	0.6142(2)	0.7707(2)	-0.1046(3)	5.4(2)	C(55)	0.4796(4)	0.0568(4)	0.8240(7)	6.1(4)
C(1)	0.7585(8)	0.6553(8)	-0.065(1)	4.8(9)	C(56)	0.5393(4)	0.0780(4)	0.7944(7)	5.4(4)
O(1)	0.7572(6)	0.5998(6)	-0.1364(9)	6.3(8)	C(61)	0.7720(5)	0.0815(5)	0.8620(6)	3.9(3)
C(2)	0.5900(9)	0.6403(9)	-0.041(1)	6(1)	C(62)	0.8392(5)	0.0781(5)	0.8330(6)	5.5(4)
O(2)	0.5338(7)	0.6034(7)	-0.078(1)	9(1)	C(63)	0.9119(5)	0.0941(5)	0.9129(6)	6.4(5)
C(3)	0.7209(9)	0.6473(9)	0.114(1)	6(1)	C(64)	0.9175(5)	0.1135(5)	1.0217(6)	6.9(5)
O(3)	0.7423(7)	0.6120(6)	0.1673(9)	8.1(9)	C(65)	0.8504(5)	0.1169(5)	1.0507(6)	7.6(5)
C(4)	0.6509(9)	0.7868(7)	0.157(1)	4.5(9)	C(66)	0.7776(5)	0.1009(5)	0.9709(6)	5.2(4)
O(4)	0.6006(6)	0.7929(6)	0.1927(9)	7.2(8)	C(71)	0.8155(6)	0.3889(4)	0.2389(8)	4.2(4)
C(5)	0.770(1)	0.934(1)	0.313(1)	7(1)	C(72)	0.8241(6)	0.4593(4)	0.2302(8)	6.4(5)
O(5)	0.7744(9)	0.9903(8)	0.382(1)	11(1)	C(73)	0.8643(6)	0.4668(4)	0.1635(8)	8.4(6)
C(6)	0.808(1)	0.7947(9)	0.292(1)	6(1)	C(74)	0.8958(6)	0.4039(4)	0.1054(8)	8.2(5)
O(6)	0.8362(8)	0.7661(8)	0.353(1)	11(1)	C(75)	0.8872(6)	0.3335(4)	0.1140(8)	8.0(5)
C(7)	0.8696(9)	0.8563(8)	0.173(1)	5(1)	C(76)	0.8470(6)	0.3261(4)	0.1807(8)	6.2(4)
O(7)	0.9231(7)	0.9002(6)	0.214(1)	7.6(9)	C(81)	0.8340(6)	0.3790(6)	0.447(1)	5.3(4)
C(8)	0.9043(9)	0.7438(8)	-0.025(1)	5(1)	C(82)	0.8076(6)	0.3632(6)	0.521(1)	9.6(6)
O(8)	0.9523(7)	0.7369(8)	-0.064(1)	10(1)	C(83)	0.8600(6)	0.3661(6)	0.621(1)	13.2(8)
C(9)	0.8830(9)	0.6955(8)	0.121(2)	7(1)	C(84)	0.9387(6)	0.3848(6)	0.646(1)	13.8(9)
O(9)	0.9149(6)	0.6581(7)	0.167(1)	9.2(9)	C(85)	0.9651(6)	0.4006(6)	0.571(1)	11.9(8)
C(10)	0.8259(9)	0.8928(9)	-0.040(1)	6(1)	C(86)	0.9128(6)	0.3977(6)	0.471(1)	7.7(5)
O(10)	0.8818(7)	0.9241(7)	-0.027(1)	11(1)	C(91)	0.7087(6)	0.2915(5)	0.2557(8)	4.7(4)
C(11)	0.750(1)	0.7746(9)	-0.189(2)	7(1)	C(92)	0.6359(6)	0.2892(5)	0.1807(8)	6.3(4)
O(11)	0.7573(8)	0.7368(7)	-0.269(1)	11(1)	C(93)	0.5942(6)	0.2196(5)	0.1137(8)	8.8(6)
P(1)	0.6778(2)	0.1985(2)	0.6929(3)	3.6(2)	C(94)	0.6254(6)	0.1523(5)	0.1218(8)	9.3(6)
N(1)	0.6508(6)	0.1320(6)	0.7192(9)	4.9(7)	C(95)	0.6982(6)	0.1546(5)	0.1968(8)	9.0(6)
P(2)	0.6801(2)	0.0628(2)	0.7568(3)	3.5(2)	C(96)	0.7399(6)	0.2242(5)	0.2638(8)	7.9(5)
P(3)	0.7641(2)	0.3808(2)	0.3253(3)	4.0(2)	C(101)	0.7821(5)	0.5800(5)	0.5109(6)	3.8(3)
N(2)	0.7062(6)	0.4442(6)	0.3440(9)	4.3(7)	C(102)	0.8087(5)	0.6329(5)	0.4780(6)	5.9(4)
P(4)	0.6942(2)	0.5216(2)	0.4257(3)	3.5(2)	C(103)	0.8787(5)	0.6763(5)	0.5418(6)	7.3(5)
C(13)	0.7753(6)	0.1974(5)	0.6893(6)	3.8(3)	C(104)	0.9221(5)	0.6668(5)	0.6384(6)	6.8(5)
C(14)	0.8348(6)	0.2448(5)	0.7773(6)	5.7(4)	C(105)	0.8955(5)	0.6139(5)	0.6712(6)	6.7(5)
C(15)	0.9114(6)	0.2396(5)	0.7768(6)	7.8(5)	C(106)	0.8255(5)	0.5705(5)	0.6075(6)	5.1(4)
C(16)	0.9284(6)	0.1869(5)	0.6884(6)	8.7(6)	C(111)	0.6341(6)	0.5716(5)	0.3475(6)	3.6(3)
C(17)	0.8689(6)	0.1395(5)	0.6004(6)	8.4(6)	C(112)	0.6138(6)	0.6445(5)	0.3968(6)	6.9(5)
C(18)	0.7924(6)	0.1447(5)	0.6009(6)	6.2(4)	C(113)	0.5648(6)	0.6817(5)	0.3335(6)	7.4(5)
C(21)	0.6157(5)	0.1957(5)	0.5641(7)	3.7(3)	C(114)	0.5361(6)	0.6460(5)	0.2208(6)	7.7(5)
C(22)	0.5394(5)	0.1653(5)	0.5292(7)	5.0(4)	C(115)	0.5563(6)	0.5731(5)	0.1715(6)	7.0(5)
C(23)	0.4874(5)	0.1661(5)	0.4313(7)	6.9(5)	C(116)	0.6054(6)	0.5359(5)	0.2348(6)	5.8(4)
C(24)	0.5118(5)	0.1973(5)	0.3683(7)	6.6(5)	C(121)	0.6463(5)	0.5071(4)	0.5122(8)	4.1(3)
C(25)	0.5882(5)	0.2277(5)	0.4032(7)	6.9(5)	C(122)	0.6447(5)	0.5667(4)	0.6058(8)	7.1(5)
C(26)	0.6401(5)	0.2269(5)	0.5011(7)	5.6(4)	C(123)	0.6030(5)	0.5565(4)	0.6694(8)	8.2(5)
C(31)	0.6716(5)	0.2885(5)	0.7927(6)	3.7(3)	C(124)	0.5630(5)	0.4867(4)	0.6393(8)	7.8(5)
C(32)	0.6773(5)	0.3561(5)	0.7752(6)	4.9(4)	C(125)	0.5646(5)	0.4271(4)	0.5456(8)	7.5(5)
C(33)	0.6762(5)	0.4255(5)	0.8557(6)	7.1(5)	C(126)	0.6062(5)	0.4372(4)	0.4821(8)	5.3(4)
C(34)	0.6694(5)	0.4274(5)	0.9538(6)	7.2(5)	C(101)	0.985(3)	0.071(1)	0.338(3)	19(3)
C(35)	0.6637(5)	0.3597(5)	0.9712(6)	6.8(5)	Cl(3)	0.9522(6)	0.1601(6)	0.3756(9)	23(1)
C(36)	0.6648(5)	0.2903(5)	0.8907(6)	5.8(4)	Cl(4)a	1.074(2)	0.065(2)	0.389(3)	17(2)
C(41)	0.6876(5)	-0.0200(5)	0.6472(6)	3.6(3)	Cl(4)b	1.051(2)	0.095(2)	0.295(2)	18(3)
C(42)	0.7307(5)	-0.0792(5)	0.6672(6)	4.9(4)	Cl(4)c	1.034(2)	0.065(2)	0.470(2)	20(3)
C(43)	0.7330(5)	-0.1446(5)	0.5807(6)	6.5(5)	Cl(5)	-0.018(2)	0.482(2)	-0.043(2)	18(3)
C(44)	0.6922(5)	-0.1506(5)	0.4742(6)	6.9(5)	C(201)	0.084(3)	0.475(2)	0.072(4)	25(5)
C(45)	0.6492(5)	-0.0914(5)	0.4542(6)	6.7(5)	Cl(6)	0.123(2)	0.548(2)	0.140(3)	25(4)

as the compound crystallized from the THF solution, even at reflux temperature (66 °C). After 90 min, the solution was allowed to cool and 10 mL of hexane was added. The blood red complex **4** was isolated by filtration (460 mg, 70% yield). Suitable crystals for the X-ray diffraction analysis were grown from dichloromethane/hexane mixtures. Dichloromethane molecules were subsequently found to be trapped in the lattice of these crystals (*vide infra*).

Noticeably, treatment of solutions of complex **4** with CO (1 atm, 2 min) results in the precipitation of 1 equiv of [PPN]Cl and concomitant formation of the known butterfly complex [PPN][Ru₄(μ-Cl)(CO)₁₃] (**5**). The reverse reaction takes place in refluxing THF within 90 min under a stream of inert gas.

4. Anal. Calcd for C₈₄H₆₂N₂Cl₄O₁₁P₄Ru₄ (%): (taking into account 1 mol of dichloromethane per mol of complex): C, 51.86; H, 3.21; N, 1.44. Found: C, 51.70; H, 3.09; N, 1.31. IR

(ν(CO), CH₂Cl₂): 2015 (m), 1971 (vs), 1960 (sh), 1919 (m), 1895 (vs) 1770 (s) cm⁻¹. ¹H NMR (acetone-*d*₆): δ 7.64–7.90 (m, phenyls, PPN⁺), 5.75 (dichloromethane solvate).

Preparation of [PPN]₂[Ru₄(μ₄-O)(μ-Cl)₄(CO)₁₀] (6**).** The starting complex **4** was prepared as indicated above, from 300 mg of Ru₃(CO)₁₂. The crystallized product was dissolved in 30 mL of freshly distilled dichloromethane, and the solution was stirred in a beaker for 1 h at room temperature in air. The initial blood red color progressively turned yellow. After evaporation of the solvent, the solid residue was recrystallized from acetone/ethanol, providing bright yellow crystals of **6** suitable for X-ray diffraction (150 mg, 22% yield calculated from Ru₃(CO)₁₂).

6. Anal. Calcd for C₈₂H₆₀N₂Cl₄O₁₁P₄Ru₄ (%): C, 51.31; H, 3.16; N, 1.46. Found: C, 50.60; H, 3.04; N, 1.31. IR (ν(CO), CH₂Cl₂): 2011 (vs), 1938 (vs), 1710 (m, br) cm⁻¹.

Table 15. Selected Interatomic Distances (Å) for 4, with Esd's in Parentheses

Ru-Ru			
Ru(1)-Ru(3)	2.812(2)	Ru(2)-Ru(3)	2.806(2)
	Ru(1)-Ru(2)	2.870(1)	
	Ru(3)-Ru(4)	2.766(2)	
Ru(1)-Ru(4)	3.502(2)	Ru(2)-Ru(4)	3.463(2)
Ru-Cl			
Ru(1)-Cl(1)	2.536(4)	Ru(2)-Cl(2)	2.534(4)
Ru(4)-Cl(1)	2.417(4)	Ru(4)-Cl(2)	2.416(4)
Ru-C (Bridging Carbonyl Groups)			
Ru(1)-C(1)	2.18(2)	Ru(2)-C(7)	2.13(2)
Ru(3)-C(1)	2.08(1)	Ru(3)-C(7)	2.10(1)
Ru(1)-C(4)	2.12(1)	Ru(2)-C(4)	2.14(1)
Ru-C (Terminal Carbonyl Groups)			
Ru(1)-C(2)	1.87(1)	Ru(2)-C(5)	1.87(1)
Ru(1)-C(3)	1.86(2)	Ru(2)-C(6)	1.84(2)
	Ru(3)-C(8)	1.87(2)	
	Ru(3)-C(9)	1.81(2)	
Ru(4)-C(10)	1.82(2)	Ru(4)-C(11)	1.84(2)
C-O (Bridging Carbonyl Groups)			
C(1)-O(1)	1.15(2)	C(7)-O(7)	1.16(2)
	C(4)-O(4)	1.15(2)	
C-O (Terminal Carbonyl Groups)			
C(2)-O(2)	1.13(2)	C(5)-O(5)	1.14(2)
C(3)-O(3)	1.14(2)	C(6)-O(6)	1.14(2)
	C(8)-O(8)	1.15(2)	
	C(9)-O(9)	1.13(2)	
C(10)-O(10)	1.14(2)	C(11)-O(11)	1.13(2)
Shortest Intermolecular Contact			
	Ru(4)···H(53)	2.919(9)	

Table 16. Selected Bond Angles (deg) for 4, with Esd's in Parentheses

Ru-Ru-Ru			
Ru(2)-Ru(1)-Ru(3)	59.18(4)	Ru(1)-Ru(2)-Ru(3)	59.39(4)
Ru(1)-Ru(3)-Ru(2)	61.43(4)		
Ru(1)-Ru(3)-Ru(4)	77.77(5)	Ru(2)-Ru(3)-Ru(4)	76.85(5)
Ru-Ru-Cl			
Ru(2)-Ru(1)-Cl(1)	94.07(8)	Ru(1)-Ru(2)-Cl(2)	95.60(8)
Ru(3)-Ru(1)-Cl(1)	92.9(1)	Ru(3)-Ru(2)-Cl(2)	94.1(1)
Ru(3)-Ru(4)-Cl(1)	96.7(1)	Ru(3)-Ru(4)-Cl(2)	97.9(1)
Ru-Ru-CO			
Ru(2)-Ru(1)-C(2)	148.3(5)	Ru(1)-Ru(2)-C(5)	154.3(6)
Ru(2)-Ru(1)-C(3)	92.9(4)	Ru(1)-Ru(2)-C(6)	93.3(4)
Ru(3)-Ru(1)-C(2)	152.3(5)	Ru(3)-Ru(2)-C(5)	146.0(6)
Ru(3)-Ru(1)-C(3)	92.1(5)	Ru(3)-Ru(2)-C(6)	91.3(5)
Ru(1)-Ru(3)-C(8)	147.0(4)	Ru(2)-Ru(3)-C(8)	148.6(4)
Ru(1)-Ru(3)-C(9)	96.5(6)	Ru(2)-Ru(3)-C(9)	98.1(6)
Ru(3)-Ru(4)-C(10)	88.6(6)	Ru(3)-Ru(4)-C(11)	87.0(6)
Ru(4)-Ru(3)-C(8)	94.8(5)	Ru(4)-Ru(3)-C(9)	173.7(6)
Cl-Ru-CO			
Cl(1)-Ru(4)-C(10)	91.7(6)	Cl(2)-Ru(4)-C(11)	94.5(5)
Cl(2)-Ru(4)-C(10)	173.4(6)	Cl(1)-Ru(4)-C(11)	176.1(6)
Cl-Ru-Cl			
Cl(1)-Ru(4)-Cl(2)	86.0(1)		

Preparation of [PPN][Ru(CO)₃Cl₃] (7) (One-Pot Procedure). The reaction was carried out in a 100 mL round bottom flask connected to a reflux condenser and equipped with a lateral gas inlet and a magnetic stir bar. RuCl₃·nH₂O (1 g, 3.82 mmol) was dissolved in 20 mL of 2-ethoxyethanol. A fast stream of CO gas was bubbled through the solution which was vigorously stirred and heated under reflux. The initial brown-black color turned gold yellow over a period of 3 h. The solution was then allowed to cool down to 25 °C under CO atmosphere. At that stage, infrared monitoring in the ν(CO) region indicated the presence of three bands at 2125 (s), 2056 (s, br), and 1990 (s) cm⁻¹. The solution was maintained under CO for 7 h more, during which it became almost colorless, and finally exhibited a ν(CO) pattern characteristic of the dimer [Ru(CO)₃Cl₂]₂, namely, 2125 (s) and 2050 (vs) cm⁻¹. The solvent was evaporated under reduced pressure at 40–50 °C

and the resulting oil was recovered with 100 mL of THF. A stoichiometric amount of [PPN]Cl (2.19 g, 3.82 mmol) was dissolved separately in the minimum amount of dichloromethane (3 mL) and added to the THF solution of the dimer. Infrared monitoring indicated an instantaneous reaction. After 5 min, the solvent was evaporated under reduced pressure and the resulting product was recrystallized in 5 mL of methanol at -25 °C. Colorless crystals of [PPN][Ru(CO)₃Cl₃] were recovered by filtration (2.55 g, 81% yield).

7. Anal. Calcd for C₃₉H₃₀NCl₃O₃P₂Ru (%): C, 56.43; H, 3.64; N, 1.69. Found: C, 55.92; H, 3.62; N, 1.88. IR (ν(CO), THF): 2108 (s), 2031 (vs) cm⁻¹.

Preparation of [PPN][Ru(CO)₃I₃] (8) from the Dimeric Species [Ru(CO)₃I₂]₂. Crystals of [Ru(CO)₃I₂]₂²⁹ (300 mg, 0.34 mmol) were dissolved in 20 mL of THF. Addition of a solution of [PPN]I (454 mg, 0.68 mmol) in dichloromethane (2 mL) resulted in a change in IR ν(CO) bands, indicating the formation of the anion. After evaporation of THF, the salt [PPN][Ru(CO)₃I₃] was recrystallized in the minimum amount of methanol at -25 °C and 620 mg of orange crystals were isolated (82% yield).

8. Anal. Calcd for C₃₉H₃₀NI₃O₃P₂Ru (%): C, 42.41; H, 2.74; N, 1.27. Found: C, 42.35; H, 2.49; N, 1.09. IR (ν(CO), THF): 2092 (s), 2025 (vs) cm⁻¹.

Preparation of [PPN][Ru(CO)₃Cl₂I] (9). The addition of 2 mL of a dichloromethane solution containing the salt [PPN]I (508 mg, 0.76 mmol) to a portion of the ethoxyethanol solution of the dimer [Ru(CO)₃Cl₂]₂ synthesized as above (2 mL = 0.38 mmol) resulted in the immediate evolution of a lemon yellow color. After evaporation of the ethoxyethanol, the resulting oil was dissolved in the minimum amount of methanol and crystallized at -25 °C, leading to 510 mg of the salt [PPN][Ru(CO)₃Cl₂I] (73% yield).

9. Anal. Calcd for C₃₉H₃₀NI₂O₃P₂Ru (%): C, 50.83; H, 3.28; N, 1.52. Found: C, 50.06; H, 3.48; N, 1.40. IR (ν(CO), THF): 2104 (s), 2028 (vs) cm⁻¹.

Preparation of [PPN][Ru(CO)₃ClI₂] (10). The complex was prepared by addition of a dichloromethane solution (2 mL) of [PPN]Cl (327 mg, 0.57 mmol) to a THF solution (20 mL) of the dimer [Ru(CO)₃I₂]₂ (250 mg, 0.28 mmol). The color of the solution remained orange. After evaporation of the solvent, the solid residue was recovered with the minimum amount of methanol and crystallized at -25 °C, leading to 395 mg of the salt [PPN][Ru(CO)₃ClI₂] (68% yield).

10. Anal. Calcd for C₃₉H₃₀NI₂O₃P₂Ru (%): C, 46.21; H, 2.99; N, 1.38. Found: C, 46.20; H, 3.38; N, 1.16. IR (ν(CO), THF): 2096 (s), 2025 (vs) cm⁻¹.

Preparation of [PPN][Ru(CO)₂Cl₃(η⁻¹-OCHN(CH₃)₂)] (11). The complex [PPN][Ru(CO)₃Cl₃] (195 mg, 0.235 mmol) was dissolved in 15 mL of dimethylformamide and heated under reflux at 160 °C. After 30 min, the initial light yellow color of the solution appeared much more intense, whereas infrared monitoring indicated spectroscopically quantitative transformation of the initial salt into a new species. After evaporation of the solvent, the resulting oil was recrystallized from acetone/heptane mixtures, leading to yellow crystals which were subsequently characterized as [PPN][Ru(CO)₂Cl₃(η⁻¹-OCHN(CH₃)₂)] (118 mg, 57% yield).

11. Anal. Calcd for C₄₁H₃₇N₂Cl₃O₃P₂Ru (%): C, 56.27; H, 4.26; N, 3.20. Found: C, 56.23; H, 4.20; N, 3.05. IR (ν(CO), CH₂Cl₂): 2045 (s), 1975 (s), 1645 (ms) cm⁻¹.

X-ray Structure Analyses. General Procedure. Table 13 summarizes crystal and intensity data for compounds 4, 6, and 11. Intensity data were respectively collected at 23 °C for 4 and 6, and at -140 °C for 11, on an Enraf-Nonius CAD4 diffractometer. The cell constants were obtained by least-squares refinement of the setting angles of 25 reflections in the range 26 < 2θ(Mo Kα₁) < 30°. Data reductions for 4 and 6 were carried out using the MOLEN crystallographic

Table 17. Fractional Atomic Coordinates and Isotropic or Equivalent Temperature Factors ($\text{Å}^2 \times 100$) with Esd's in Parentheses for Compound 6

atom	<i>x/a</i>	<i>y/b</i>	<i>z/c</i>	$U_{\text{eq}}/U_{\text{iso}}$	atom	<i>x/a</i>	<i>y/b</i>	<i>z/c</i>	$U_{\text{eq}}/U_{\text{iso}}$
Ru(1)	0.22911(4)	0.23840(2)	-0.00729(4)	3.77(3)	C(42)	0.6924(4)	-0.0516(2)	0.2258(3)	5.0(2)
Ru(2)	0.08744(4)	0.32289(2)	0.05636(4)	3.67(3)	C(43)	0.7456(4)	-0.1015(2)	0.2353(3)	6.3(2)
Ru(3)	0.05615(4)	0.17343(2)	0.05168(4)	3.58(3)	C(44)	0.7722(4)	-0.1310(2)	0.3338(3)	6.6(2)
Ru(4)	0.17382(4)	0.24205(2)	0.26487(4)	3.59(3)	C(45)	0.7455(4)	-0.1106(2)	0.4228(3)	6.7(2)
O	0.1356(3)	0.2436(2)	0.0896(3)	3.3(2)	C(46)	0.6922(4)	-0.0606(2)	0.4133(3)	5.0(2)
Cl(1)	0.0528(1)	0.20917(7)	-0.1571(1)	4.8(1)	C(51)	0.4554(3)	0.0233(2)	0.2658(3)	3.5(2)
Cl(2)	-0.0014(1)	0.29808(7)	0.2003(1)	5.2(1)	C(52)	0.4035(3)	-0.0115(2)	0.1745(3)	5.3(2)
Cl(3)	0.2387(1)	0.13934(6)	0.0644(1)	4.7(1)	C(53)	0.2905(3)	-0.0188(2)	0.1365(3)	6.4(2)
Cl(4)	0.2505(1)	0.33195(6)	0.2420(1)	4.2(1)	C(54)	0.2295(3)	0.0086(2)	0.1898(3)	5.3(2)
C(1)	0.2979(6)	0.2356(3)	-0.1091(6)	5.1(5)	C(55)	0.2814(3)	0.0434(2)	0.2812(3)	4.8(2)
O(1)	0.3406(5)	0.2351(2)	-0.1690(5)	9.0(4)	C(56)	0.3944(3)	0.0507(2)	0.3192(3)	4.1(2)
C(2)	0.3643(6)	0.2521(3)	0.1108(6)	4.8(5)	C(61)	0.6134(3)	0.0698(2)	0.2016(4)	3.3(2)
O(2)	0.4520(4)	0.2594(2)	0.1811(4)	6.6(4)	C(62)	0.5212(3)	0.0950(2)	0.1148(4)	4.8(2)
C(3)	0.1881(5)	0.3170(3)	-0.0280(5)	3.7(4)	C(63)	0.5353(3)	0.1257(2)	0.0349(4)	6.1(2)
O(3)	0.2182(4)	0.3498(2)	-0.0694(4)	6.7(4)	C(64)	0.6415(3)	0.1312(2)	0.0418(4)	5.8(2)
C(4)	0.0589(6)	0.3947(3)	0.0377(6)	5.1(5)	C(65)	0.7337(3)	0.1060(2)	0.1286(4)	5.0(2)
O(4)	0.0388(5)	0.4387(2)	0.0227(5)	8.0(4)	C(66)	0.7196(3)	0.0753(2)	0.2085(4)	4.0(2)
C(5)	-0.0373(7)	0.3161(3)	-0.0807(7)	5.6(5)	C(71)	0.5332(3)	0.3734(2)	0.6137(4)	3.7(2)
O(5)	-0.1170(5)	0.3173(2)	-0.1643(5)	7.4(4)	C(72)	0.4779(3)	0.3346(2)	0.5341(4)	4.7(2)
C(6)	-0.0003(5)	0.1077(3)	0.0313(6)	4.7(5)	C(73)	0.5272(3)	0.3087(2)	0.4674(4)	5.9(2)
O(6)	-0.0363(4)	0.0675(2)	0.0247(4)	6.6(4)	C(74)	0.6319(3)	0.3216(2)	0.4801(4)	6.3(2)
C(7)	-0.0866(6)	0.1992(3)	0.0235(6)	4.8(5)	C(75)	0.6873(3)	0.3604(2)	0.5596(4)	6.6(2)
O(7)	-0.1778(4)	0.2110(2)	0.0044(5)	7.8(4)	C(76)	0.6379(3)	0.3863(2)	0.6264(4)	5.5(2)
C(8)	0.0971(5)	0.1733(3)	0.2239(5)	4.1(4)	C(81)	0.5302(3)	0.3672(2)	0.8356(4)	4.0(2)
O(8)	0.0813(4)	0.1422(2)	0.2813(4)	5.7(3)	C(82)	0.6406(3)	0.3473(2)	0.8823(4)	5.8(2)
C(9)	0.1916(6)	0.2442(3)	0.4164(6)	5.1(5)	C(83)	0.6847(3)	0.3215(2)	0.9878(4)	7.7(3)
O(9)	0.2023(5)	0.2451(2)	0.5107(4)	8.8(4)	C(84)	0.6184(3)	0.3157(2)	1.0465(4)	8.6(3)
C(10)	0.3094(6)	0.2040(3)	0.3157(6)	4.5(5)	C(85)	0.5080(3)	0.3356(2)	0.9998(4)	8.5(3)
O(10)	0.3946(4)	0.1819(2)	0.3519(4)	6.2(4)	C(86)	0.4639(3)	0.3614(2)	0.8944(4)	5.9(2)
P(1)	0.7323(1)	0.10010(6)	0.5159(1)	3.4(1)	C(91)	0.5162(4)	0.4680(2)	0.7381(3)	3.6(2)
N(1)	0.6462(4)	0.0606(2)	0.4337(4)	3.7(3)	C(92)	0.4942(4)	0.5018(2)	0.6471(3)	4.9(2)
P(2)	0.5996(1)	0.03324(6)	0.3112(1)	3.28(9)	C(93)	0.5186(4)	0.5544(2)	0.6697(3)	6.1(2)
P(3)	0.4725(1)	0.40216(7)	0.7047(1)	3.5(1)	C(94)	0.5649(4)	0.5733(2)	0.7833(3)	7.3(2)
N(2)	0.3428(4)	0.3974(2)	0.6454(4)	4.4(3)	C(95)	0.5869(4)	0.5396(2)	0.8744(3)	7.3(2)
P(4)	0.2285(1)	0.43049(7)	0.6047(1)	3.8(1)	C(96)	0.5625(4)	0.4869(2)	0.8518(3)	5.9(2)
C(11)	0.7744(3)	0.1466(2)	0.4426(3)	3.5(2)	C(101)	0.1955(3)	0.4668(1)	0.4766(4)	4.2(2)
C(12)	0.6923(3)	0.1798(2)	0.3631(3)	4.4(2)	C(102)	0.2337(3)	0.4456(1)	0.3963(4)	5.3(2)
C(13)	0.7205(3)	0.2146(2)	0.3001(3)	5.4(2)	C(103)	0.2076(3)	0.4719(1)	0.2938(4)	6.0(2)
C(14)	0.8308(3)	0.2162(2)	0.3166(3)	6.1(2)	C(104)	0.1434(3)	0.5194(1)	0.2717(4)	6.6(2)
C(15)	0.9130(3)	0.1830(2)	0.3962(3)	5.7(2)	C(105)	0.1052(3)	0.5405(1)	0.3521(4)	6.5(2)
C(16)	0.8848(3)	0.1482(2)	0.4591(3)	4.6(2)	C(106)	0.1313(3)	0.5142(1)	0.4546(4)	5.5(2)
C(21)	0.8571(3)	0.0665(1)	0.6147(3)	3.4(2)	C(111)	0.2216(4)	0.4770(2)	0.7115(4)	4.1(2)
C(22)	0.9237(3)	0.0904(1)	0.7190(3)	4.9(2)	C(112)	0.2663(4)	0.5257(2)	0.7223(4)	5.9(2)
C(23)	1.0198(3)	0.0636(1)	0.7965(3)	5.5(2)	C(113)	0.2588(4)	0.5626(2)	0.8032(4)	6.9(2)
C(24)	1.0494(3)	0.0128(1)	0.7697(3)	5.9(2)	C(124)	-0.0395(3)	0.3139(2)	0.5335(3)	5.9(2)
C(25)	0.9829(3)	-0.0111(1)	0.6654(3)	6.7(2)	C(125)	-0.0544(3)	0.3509(2)	0.4503(3)	6.1(2)
C(26)	0.8867(3)	0.0157(1)	0.5879(3)	5.5(2)	C(126)	0.0269(3)	0.3862(2)	0.4699(3)	4.9(2)
C(31)	0.6729(4)	0.1377(1)	0.5988(4)	3.5(2)	C(114)	0.2068(4)	0.5508(2)	0.8732(4)	7.3(2)
C(32)	0.5941(4)	0.1160(1)	0.6265(4)	5.2(2)	C(115)	0.1621(4)	0.5021(2)	0.8624(4)	8.2(3)
C(33)	0.5483(4)	0.1449(1)	0.6931(4)	7.1(2)	C(116)	0.1696(4)	0.4652(2)	0.7816(4)	6.4(2)
C(34)	0.5813(4)	0.1954(1)	0.7320(4)	7.2(2)	C(121)	0.1232(3)	0.3845(2)	0.5727(3)	3.6(2)
C(35)	0.6601(4)	0.2170(1)	0.7043(4)	6.6(2)	C(122)	0.1381(3)	0.3475(2)	0.6559(3)	5.4(2)
C(36)	0.7059(4)	0.1882(1)	0.6377(4)	5.0(2)	C(123)	0.0568(3)	0.3122(2)	0.6363(3)	6.0(2)
C(41)	0.6656(4)	-0.0311(2)	0.3149(3)	3.4(2)	C(42)	0.6924(4)	-0.0516(2)	0.2258(3)	5.0(2)

computing package.⁴⁰ The intensities measured for these two compounds were corrected for absorption by using a numerical method based on Gaussian integration.⁴¹ Data reduction and treatment for compound **11** were carried out with the CRYSTALS package.⁴² In that case, empirical absorption corrections were applied by using the program DIFABS.⁴³

All three structures were solved by using the SHELXS-86 package.^{44a} The structures of **4** and **6** were refined by using the SHELX-76 package,^{44b} whereas the structure of **11** was refined by using the CRYSTALS package.⁴² In all three cases,

(40) *MOLen, Package for Crystal Structure Analysis*. Enraf Nonius: Delft, The Netherlands, 1990.

(41) Coppens, P.; Leiserowitz, L.; Rabinovitch, D. *Acta Crystallogr.* **1965**, *18*, 1035.

(42) Watkin, D. J.; Carruthers, J. R.; Betteridge, P. W. *CRYSTALS User Guide*, Chemical Crystallography Laboratory; University of Oxford: Oxford, England, 1985.

(43) Walker, N.; Stuart, D. *Acta Crystallogr.* **1983**, *39*, 158.

direct methods allowed us to locate at least the heavier atoms. All remaining non-hydrogen atoms were located by the usual combination of full matrix least-squares refinement and difference electron density syntheses.

Atomic scattering factors were taken from the usual tabulations.⁴⁵ All non-hydrogen atoms of the anionic units were allowed to vibrate anisotropically. Due to the high number of variable parameters for **4** and **6**, all phenyl rings of the corresponding PPN cations were treated as rigid groups with idealized geometry (C-C = 1.495 Å; C-H = 0.97 Å).

(44) (a) Sheldrick, G. M. *SHELXS-86 Program for Crystal Structure Solution*; University of Göttingen, Federal Republic of Germany, 1986. (b) Sheldrick, G. M. *SHELX-76 Program for Crystal Structure Determination*; University of Cambridge: Cambridge, England, 1976.

(45) (a) Cromer, D. T.; Waber, J. T. *International Tables for X-ray Crystallography*; Kynoch Press: Birmingham, England, 1974; Vol. 4, Table 2.2B. (b) Cromer, D. T.; Waber, J. T. *International Tables for X-ray Crystallography*; Kynoch Press: Birmingham, England, 1974; Vol. 4, Table 2.3.1.

Table 18. Selected Interatomic Distances (Å) for 6, with Esd's in Parentheses

Ru-Ru			
Ru(1)-Ru(2)	3.063(1)	Ru(3)-Ru(4)	3.057(1)
Ru(1)··Ru(3)	3.262(1)	Ru(3)··Ru(4)	3.199(1)
Ru-O			
Ru(1)-O	2.080(5)	Ru(3)-O	2.078(4)
Ru(2)-O	2.084(4)	Ru(4)-O	2.079(4)
Ru-Cl (Short Bonds)			
Ru(1)-Cl(1)	2.459(2)	Ru(3)-Cl(3)	2.449(2)
Ru(2)-Cl(4)	2.463(2)	Ru(4)-Cl(2)	2.474(2)
Ru-Cl (Long Bonds)			
Ru(1)-Cl(3)	2.702(2)	Ru(3)-Cl(1)	2.836(2)
Ru(2)-Cl(2)	2.678(2)	Ru(4)-Cl(4)	2.649(2)
Ru-C (Terminal Carbonyl Groups)			
Ru(1)-C(1)	1.870(9)	Ru(3)-C(6)	1.850(7)
Ru(1)-C(2)	1.838(6)	Ru(3)-C(7)	1.844(8)
Ru(2)-C(4)	1.850(8)	Ru(4)-C(9)	1.848(8)
Ru(2)-C(5)	1.848(7)	Ru(4)-C(10)	1.846(7)
Ru-C (Bridging Carbonyl Groups)			
Ru(1)-C(3)	2.039(6)	Ru(3)-C(8)	2.033(7)
Ru(2)-C(3)	2.029(8)	Ru(4)-C(8)	2.030(6)
C-O (Terminal Carbonyl Groups)			
C(1)-O(1)	1.12(1)	C(6)-O(6)	1.147(9)
C(2)-O(2)	1.153(8)	C(7)-O(7)	1.15(1)
C(4)-O(4)	1.143(9)	C(9)-O(9)	1.15(1)
C(5)-O(5)	1.143(8)	C(10)-O(10)	1.140(9)
C-O (Bridging Carbonyl Groups)			
C(3)-O(3)	1.184(9)	C(8)-O(8)	1.188(9)

Specific Details for the Structure Solution of Compound 4. (a) Evidence for the Occurrence of a Square Pyramidal Geometry about the Metal Center Ru(4). After localization and refinement of the two bis(triphenylphosphine)iminium cations and of the dianionic unit $[\text{Ru}_4(\mu\text{-Cl})_2(\text{CO})_{11}]^-$, the environment of the atom Ru(4) appeared to be of square pyramidal type. The highest residual peaks in the Fourier map, all located far away from the metal center Ru(4), were consistent with the presence of dichloromethane solvent molecules (see below the treatment of the disorder problem). Though no residual peaks appeared around the metal center Ru(4), attempts to introduce an additional CO group in an idealized position on its vacant octahedral site (in *trans* position relative to Ru(3)) were made with the aim of ascertaining the observed geometry. The refinement of the corresponding "phantom" C and O atoms did not converge. Furthermore, it appeared that the idealized position of the oxygen would come in unacceptable short contact with H(53), a hydrogen atom belonging to one of the two PPN cations. This drew our attention to the fact that the latter H atom was in fact "filling" the vacant octahedral site of the Ru(4) center. The intermolecular $\text{Ru} \cdots \text{H}$ contact $\text{Ru}(4) \cdots \text{H}(53) = 2.92 \text{ \AA}$ reflects the existence of a weak interaction, which may account for the stabilization of the unsaturated complex. The occurrence of such a short intermolecular distance also ruled out the presence of any other ligand between Ru(4) and H(53). At that stage of the refinement, the intermediate *R* value before introducing the solvent molecules in the model was *R* = 0.08.

(b) Location and Refinement of Disordered Dichloromethane Solvent Molecules in the Lattice. A total intensity loss of 9.6% was observed during data collection and corrected by using the program LINDECAY in the MOLEN package. Such a decrease might be ascribed to the loss of dichloromethane molecules from the lattice, thus rendering the determination of the exact occupancy factor of these molecules problematic. The approximate estimated value (from analysis and NMR data) was between 1 and 1.5 molecules of dichloromethane per molecule of complex 4. Solvent molecules were detected in two different "holes" in the lattice, far away from the atom Ru(4).

First Dichloromethane Molecule. The difference Fourier map provided clear evidence that the molecule was

Table 19. Selected Bond Angles (deg) for 6, with Esd's in Parentheses

Ru-O-Ru			
Ru(1)-O-Ru(2)	94.7(2)	Ru(3)-O-Ru(4)	94.7(2)
Ru(1)-O-Ru(3)	103.3(2)	Ru(2)-O-Ru(4)	100.4(2)
Ru(1)-O-Ru(4)	134.6(2)	Ru(2)-O-Ru(3)	136.2(2)
Ru-Ru-Cl			
Ru(2)-Ru(1)-Cl(1)	86.69(5)	Ru(4)-Ru(3)-Cl(3)	89.19(4)
Ru(1)-Ru(2)-Cl(4)	86.90(5)	Ru(3)-Ru(4)-Cl(2)	86.99(4)
Ru(2)-Ru(1)-Cl(3)	118.24(5)	Ru(4)-Ru(3)-Cl(1)	115.66(4)
Ru(1)-Ru(2)-Cl(2)	118.64(4)	Ru(3)-Ru(4)-Cl(4)	119.44(4)
Ru-Cl-Ru			
Ru(1)-Cl(1)-Ru(3)	75.68(5)	Ru(1)-Cl(3)-Ru(3)	78.41(5)
Ru(2)-Cl(4)-Ru(4)	77.37(5)	Ru(2)-Cl(2)-Ru(4)	76.65(6)
Cl-Ru-Cl			
Cl(1)-Ru(1)-Cl(3)	80.68(5)	Cl(1)-Ru(3)-Cl(3)	78.16(6)
Cl(2)-Ru(2)-Cl(4)	80.27(6)	Cl(2)-Ru(4)-Cl(4)	80.66(6)
Ru-Ru-CO			
Ru(2)-Ru(1)-C(1)	134.0(2)	Ru(4)-Ru(3)-C(6)	133.0(2)
Ru(1)-Ru(2)-C(4)	135.9(3)	Ru(3)-Ru(4)-C(9)	136.4(2)
Ru(2)-Ru(1)-C(2)	97.3(2)	Ru(4)-Ru(3)-C(7)	96.0(2)
Ru(1)-Ru(2)-C(5)	94.2(3)	Ru(3)-Ru(4)-C(10)	95.8(2)
Cl-Ru-CO (Terminal CO Ligands)			
Cl(1)-Ru(1)-C(1)	92.5(2)	Cl(3)-Ru(3)-C(6)	93.9(2)
Cl(4)-Ru(2)-C(4)	93.4(2)	Cl(2)-Ru(4)-C(9)	92.5(2)
Cl(1)-Ru(1)-C(2)	173.1(2)	Cl(3)-Ru(3)-C(7)	173.2(2)
Cl(4)-Ru(2)-C(5)	178.4(3)	Cl(2)-Ru(4)-C(10)	176.4(2)
Cl(3)-Ru(1)-C(2)	92.5(2)	Cl(1)-Ru(3)-C(7)	95.6(2)
Cl(2)-Ru(2)-C(5)	98.2(3)	Cl(4)-Ru(4)-C(10)	95.9(2)
Cl(2)-Ru(2)-C(4)	104.8(3)	Cl(4)-Ru(4)-C(9)	103.4(2)
Cl(3)-Ru(1)-C(2)	106.9(2)	Cl(1)-Ru(3)-C(6)	110.8(2)
Cl-Ru-CO (Bridging CO Ligands)			
Cl(1)-Ru(1)-C(3)	96.6(1)	Cl(3)-Ru(3)-C(8)	96.3(2)
Cl(4)-Ru(2)-C(3)	90.5(1)	Cl(2)-Ru(4)-C(8)	94.9(2)
Cl(3)-Ru(1)-C(3)	159.2(2)	Cl(1)-Ru(3)-C(8)	156.7(2)
Cl(2)-Ru(2)-C(3)	158.9(2)	Cl(4)-Ru(4)-C(8)	160.6(2)
C-Ru-C			
C(1)-Ru(1)-C(2)	88.7(3)	C(6)-Ru(3)-C(7)	85.7(3)
C(4)-Ru(2)-C(5)	86.6(3)	C(9)-Ru(4)-C(10)	87.1(3)
C(1)-Ru(1)-C(3)	93.7(3)	C(6)-Ru(3)-C(8)	92.0(3)
C(2)-Ru(1)-C(3)	90.1(2)	C(7)-Ru(3)-C(8)	90.4(3)
C(4)-Ru(2)-C(3)	94.6(3)	C(9)-Ru(4)-C(8)	95.6(3)
C(5)-Ru(2)-C(3)	91.1(3)	C(10)-Ru(4)-C(8)	88.7(3)

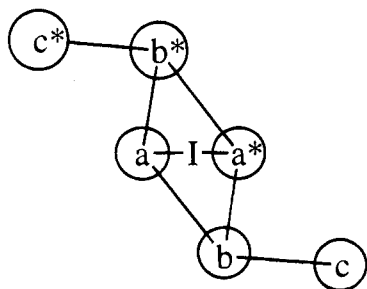
disordered. Indeed, the carbon atom labeled as C(101) (occupancy factor = 1) was surrounded by four peaks which appeared to be chloride atoms. The highest one, subsequently labeled as Cl(3), could be correctly refined with an occupancy factor of 1.0. The three additional peaks, of lower intensity, were consistent with a statistical distribution of the second halide atom over these three sites, referred to as Cl(4a), Cl(4b), and Cl(4c). The respective occupancy factors were determined as follows: in a first step, the refined isotropic *B* value found for Cl(3) was ascribed to Cl(4a), Cl(4b), and Cl(4c) and fixed. These atoms were then subsequently refined with variable occupancy factors which converged to roughly equal values (within experimental error). In a second step, the three occupancy factors were set exactly at 0.33, whereas the isotropic *B*'s were refined. In the final stage, all five atoms of this disordered molecule were refined with anisotropic thermal parameters.

Second Dichloromethane Molecule. A second disordered molecule was located in the lattice. The lower intensities of the corresponding residual peaks indicated partial occupancy of these sites. Chart 1 provides a projection of the distribution of the corresponding electron density residues **a**, **b**, and **c**, appearing close to the inversion center noted I on the drawing (*x* = 0, *y* = 0.5, *z* = 0). The peaks **a***, **b***, and **c*** are respectively related to **a**, **b**, and **c**, through the inversion center I. The six peaks are roughly coplanar.

In account of the interatomic distances and angles between these peaks, it appeared that the three atoms of the dichloromethane molecule Cl-C-Cl could be respectively entered

Table 20. Fractional Atomic Coordinates and Equivalent Temperature Factors (\AA^2) for Compound 11

atom	<i>x/a</i>	<i>y/b</i>	<i>z/c</i>	<i>U</i> (eq)
Ru(1)	0.51325(3)	0.01423(1)	0.75788(1)	0.0235
Cl(1)	0.65192(9)	0.11061(4)	0.76302(4)	0.0276
Cl(2)	0.44385(9)	0.03332(4)	0.64607(4)	0.0328
Cl(3)	0.3860(1)	0.08412(4)	0.75082(5)	0.0394
O(1)	0.5930(4)	-0.0162(4)	0.8946(1)	0.0526
O(2)	0.2435(4)	0.0833(2)	0.7899(2)	0.0638
O(3)	0.7101(2)	-0.0335(1)	0.7303(1)	0.0303
N(1)	0.9182(3)	-0.0317(1)	0.6751(1)	0.0378
C(1)	0.5642(4)	-0.0040(2)	0.8426(2)	0.0358
C(2)	0.3457(4)	0.0558(2)	0.7785(2)	0.0410
C(3)	0.7939(4)	-0.0065(2)	0.6936(2)	0.0352
C(4)	0.9614(4)	-0.0947(2)	0.6955(2)	0.044
C(5)	1.0099(5)	0.0010(2)	0.6316(2)	0.0559
P(1)	1.10208(8)	0.026638(4)	1.02159(3)	0.0194
P(2)	0.94261(8)	0.16712(4)	0.94444(3)	0.0175
N(2)	1.0596(3)	0.1987(1)	0.9943(1)	0.0215
C(10)	1.2214(3)	0.3089(2)	0.9713(1)	0.0241
C(11)	1.2428(4)	0.3738(2)	0.9771(2)	0.0365
C(12)	1.3371(4)	0.4044(2)	0.9381(2)	0.0421
C(13)	1.4095(4)	0.3709(3)	0.8935(2)	0.0436
C(14)	1.3902(4)	0.3072(2)	0.8882(2)	0.0398
C(15)	1.2959(4)	0.2754(2)	0.9269(2)	0.0322
C(20)	1.2033(3)	0.2531(2)	1.0969(1)	0.0226
C(21)	1.2919(4)	0.3002(2)	1.1252(2)	0.0336
C(22)	1.3788(4)	0.2872(2)	1.1807(2)	0.0368
C(23)	1.3782(4)	0.2281(2)	1.2067(2)	0.0364
C(24)	1.2885(4)	0.1810(2)	1.1796(2)	0.0322
C(25)	1.2002(4)	0.1936(2)	1.1245(1)	0.0264
C(30)	0.9457(3)	0.3172(1)	1.0326(1)	0.0238
C(31)	0.8809(4)	0.3506(2)	0.9810(2)	0.0306
C(32)	0.7519(4)	0.3849(2)	0.9868(2)	0.0416
C(33)	0.6862(4)	0.3854(2)	1.0438(2)	0.0435
C(34)	0.7490(4)	0.3528(2)	1.0955(2)	0.0395
C(35)	0.8795(4)	0.3190(2)	1.0905(2)	0.0323
C(40)	0.7626(3)	0.1593(1)	0.9756(1)	0.0218
C(41)	0.6412(3)	0.1377(2)	0.9368(1)	0.0270
C(42)	0.5049(4)	0.1293(2)	0.9620(2)	0.0343
C(43)	0.4885(4)	0.1431(2)	1.0252(2)	0.0354
C(44)	0.6068(4)	0.1650(2)	1.0639(2)	0.0341
C(45)	0.7445(4)	0.1729(2)	1.0393(1)	0.0275
C(50)	1.0103(3)	0.0894(1)	0.9273(1)	0.0202
C(51)	1.1270(3)	0.0628(2)	0.9655(1)	0.0245
C(52)	1.1805(4)	0.0036(2)	0.9505(2)	0.0312
C(53)	1.1181(4)	-0.0288(2)	0.8988(2)	0.0362
C(54)	0.9994(4)	-0.0036(2)	0.8627(2)	0.0351
C(55)	0.9456(4)	0.0557(2)	0.8763(1)	0.0280
C(60)	0.9152(3)	0.2070(1)	0.8693(1)	0.0191
C(61)	1.0179(3)	0.1984(2)	0.8237(1)	0.0274
C(62)	0.9995(4)	0.2298(2)	0.7663(2)	0.0343
C(63)	0.8794(4)	0.2695(2)	0.7541(2)	0.0341
C(64)	0.7781(4)	0.2786(2)	0.7993(2)	0.0328
C(65)	0.7956(3)	0.2476(1)	0.8570(2)	0.0263

Chart 1

on the sites **a**–**b**–**c**. The short distance **a**–**a*** = 1.13 Å ruled out the possibility of simultaneous occupation of the sites **a**–**b**–**c** and **a***–**b***–**c***. A maximum occupancy factor of 0.5 could thus be expected. However, the observation of an abnormal high value for the residue **b** led us to suspect that the disorder was more intricate than expected and also involved another alternate orientation in which the atoms Cl–C–Cl would roughly correspond with the residues **b**–**a**–**b***

Table 21. Selected Interatomic Distances (\AA) for 11, with Esd's in Parentheses

Ru-Cl			
Ru(1)–Cl(1)	2.3905(8)	Ru(1)–Cl(2)	2.4309(8)
Ru(1)–Cl(3)	2.3762(9)		
Ru-O			
Ru(1)–O(3)	2.154(2)		
Ru-C and C-O			
Ru(1)–C(1)	1.855(4)	C(1)–O(1)	1.138(4)
Ru(1)–C(2)	1.824(4)	C(2)–O(2)	1.130(4)
DMF Ligand			
O(3)–C(3)	1.254(4)	N(1)–C(3)	1.323(4)
N(1)–C(4)	1.452(5)	N(1)–C(5)	1.449(5)
[PPN] ⁺ Cation			
P(1)–C(10)	1.800(3)	P(1)–C(20)	1.798(3)
P(1)–C(30)	1.799(3)	P(1)–N(2)	1.581(3)
P(2)–C(40)	1.796(3)	P(2)–C(50)	1.800(3)
P(2)–C(60)	1.798(3)	P(2)–N(2)	1.584(2)
C(10)–C(11)	1.393(5)	C(11)–C(12)	1.382(5)
C(12)–C(13)	1.376(7)	C(13)–C(14)	1.363(7)
C(14)–C(15)	1.390(5)	C(10)–C(15)	1.383(5)
C(20)–C(21)	1.386(4)	C(21)–C(22)	1.390(5)
C(22)–C(23)	1.366(6)	C(23)–C(24)	1.382(6)
C(24)–C(25)	1.388(4)	C(20)–C(25)	1.390(4)
C(30)–C(31)	1.393(4)	C(31)–C(32)	1.382(5)
C(32)–C(33)	1.373(6)	C(33)–C(34)	1.379(6)
C(34)–C(35)	1.386(5)	C(30)–C(35)	1.394(4)
C(40)–C(41)	1.396(4)	C(41)–C(42)	1.381(4)
C(42)–C(43)	1.382(5)	C(43)–C(44)	1.376(5)
C(44)–C(45)	1.387(4)	C(40)–C(45)	1.393(4)
C(50)–C(51)	1.398(4)	C(51)–C(52)	1.387(5)
C(52)–C(53)	1.375(5)	C(53)–C(54)	1.377(5)
C(54)–C(55)	1.383(5)	C(50)–C(55)	1.384(4)
C(60)–C(61)	1.390(4)	C(61)–C(62)	1.380(4)
C(62)–C(63)	1.380(5)	C(63)–C(64)	1.377(5)
C(64)–C(65)	1.381(5)	C(60)–C(65)	1.389(4)

or **b**–**a***–**b***. Thus, whereas the site **c** is only occupied by a chloride atom (labeled Cl(6) in the listing of atomic coordinates), sites **a** and **b** are each alternately occupied by C and Cl atoms. Such a disorder was treated empirically as follows: two atoms labeled as Cl(5) and C(201) were respectively entered on the sites **a** and **b** with imposed *B* parameters of 15 \AA^2 (average *B* value obtained from the first disordered molecule). The *f* table of carbon was used for both atoms, and the occupancy factor was set as a variable to allow the system to adjust the accurate number of electrons on each site. In the following cycles, the refined occupancy factors (Cl(5), *K* = 1.37(3); C(201), *K* = 0.98(3)) were blocked, whereas the *B* values were refined. The occupancy factor of Cl(6) (*K* = 0.35(3)) on site **c** was determined by the same procedure. In that case, the *f* table of Cl was indeed used. In the final cycles, anisotropic thermal parameters were used for all non-hydrogen atoms of the disordered molecule.

After refinement of these solvent molecules, the highest residue in the final Fourier difference map was found close to the carbons atoms C(94) and C(95) of one of the phenyl rings. The relatively high value of the final *R* = 0.053, is obviously due to the large number of rigid groups in the structure (12 phenyl rings in the cations).

Final atomic coordinates and $100U_{\text{eq}}$ (or $100U_{\text{iso}}$) for **4** are given in Table 14. Selected interatomic distances and interatomic bond angles of interest are given in Tables 15 and 16, respectively.

Final atomic coordinates and $100U_{\text{eq}}$ (or $100U_{\text{iso}}$) for **6** are given in Table 17. Selected interatomic distances and interatomic bond angles of interest are given in Tables 18 and 19, respectively.

Final atomic coordinates and $100U_{\text{eq}}$ (or $100U_{\text{iso}}$) for **11** are given in Table 20. Selected interatomic distances and interatomic bond angles of interest are given in Tables 21 and 22, respectively.

Table 22. Selected Bond Angles (deg) for 11, with Esd's in Parentheses

Ru Environment			
Cl(1)–Ru(1)–Cl(2)	90.04(3)	Cl(1)–Ru(1)–Cl(3)	177.13(3)
Cl(1)–Ru(1)–C(1)	92.3(1)	Cl(1)–Ru(1)–C(2)	90.9(1)
Cl(1)–Ru(1)–O(3)	88.65(6)	Cl(2)–Ru(1)–Cl(3)	89.67(3)
Cl(2)–Ru(1)–C(1)	177.5(1)	Cl(2)–Ru(1)–C(2)	89.3(1)
Cl(2)–Ru(1)–O(3)	88.77(6)	Cl(3)–Ru(1)–C(1)	87.9(1)
Cl(3)–Ru(1)–C(2)	92.0(1)	Cl(3)–Ru(1)–O(3)	88.49(6)
C(1)–Ru(1)–C(2)	91.4(2)	C(1)–Ru(1)–O(3)	90.5(1)
C(2)–Ru(1)–O(3)	178.1(1)		
Ru-C-O			
Ru(1)–C(1)–O(1)	178.4(3)	Ru(1)–C(2)–O(2)	177.4(4)
Ru-O-C			
Ru(1)–O(3)–C(3)	119.5(2)		
DMF Ligand			
O(3)–C(3)–N(1)	123.6(3)	C(3)–N(1)–C(4)	120.8(3)
C(3)–N(1)–C(5)	121.5(3)	C(4)–N(1)–C(5)	117.6(3)
[PPN] Cation			
P(1)–N(2)–P(2)	139.2(2)		
N(2)–P(1)–C(10)	112.2(1)	N(2)–P(1)–C(20)	105.9(1)
N(2)–P(1)–C(30)	114.7(1)	N(2)–P(2)–C(40)	111.8(1)
N(2)–P(2)–C(50)	107.5(1)	N(2)–P(2)–C(60)	115.6(1)
C(10)–P(1)–C(20)	108.1(1)	C(10)–P(1)–C(30)	106.3(1)
C(20)–P(1)–C(30)	109.5(1)	C(40)–P(2)–C(50)	108.4(1)
C(40)–P(2)–C(60)	107.0(1)	C(50)–P(2)–C(60)	106.3(1)

Tables of anisotropic thermal parameters and hydrogen coordinates for **4**, **6** and **11** are available as supplementary material.

Extended Hückel MO Calculations. All calculations were carried out within the extended Hückel method,²² using the modified Wolfsberg–Helmholz formula.²³ Standard atomic parameters were taken for H, C, O, P, and Cl. The exponent (ζ) and the valence shell ionization potential (H_{ii} in eV) for Ru were respectively 2.078, –8.60 for 5s and 2.043, –5.10 for 5p. The H_{ii} value for 4d was set equal to –12.20. A linear combination of two Slater-type orbitals ($\zeta_1 = 5.378$, $c_1 = 0.5340$; $\zeta_2 = 2.203$, $c_2 = 0.6365$) was used to represent the atomic 4d orbitals. The model used for the calculations was based on the idealized C_s structure of **4**. The following distances (Å) were used in **4** and **4'**: Ru–Ru = 2.815; Ru–C(O) = 1.85; Ru–(4)–Cl = 2.42; C–O = 1.14. The Ru–CH₃ and Ru–PH₃ distances in [RuCl₂(CO)₂(CH₃)]³⁻ and [RuCl₂(CO)₂(PH₃)]²⁻ models were respectively set equal to 2.0 and 2.25 Å. Due to the lack of symmetry in **6**, the corresponding calculations were performed on the experimental molecular structure. All the averaged idealized structures which were tested presented too large steric repulsions between ligands.

Catalytic Runs. Catalytic runs were carried out in a 100 mL stainless steel autoclave equipped with a manometer, gas and liquid inlets, and a magnetic stirrer. The general experimental procedure was as follows: the catalyst precursor was

entered as a solid into the reactor which was then rapidly closed and degased under reduced pressure. The solvent (THF or amide type solvents) and the substrate (methyl formate) were mixed together in a Schlenk tube and introduced next into the reactor. Finally, the appropriate pressure of ethylene (20 bar, representing an excess relative to the formate concentration) was supplied at room temperature. The catalytic runs were started by immersion of the reactor into a thermostated oil bath. The working temperature, measured with an internal thermocouple, was reached within 20 min. The time counter was started when the working temperature was reached. Samples were analyzed by gas chromatography on an INTERSMAT IGC 120 DFB equipped with a 1/8 in. × 3 m column filled with 10% Carbowax 20 M on Chromosorb W 80–100 mesh. Decane was used as the internal standard. In our hands, the ruthenium-catalyzed hydroesterification of ethylene with methyl formate appeared as a clean reaction, since the only adventitious byproducts were found to be methanol, CO, and traces (always less than 2%) of diethyl ketone. Thus, standard plots were made from pure samples of methyl propionate, methanol, and diethyl ketone. In the present work, conversion rate, selectivity, turnover, and turnover frequency are respectively defined as follows:

Conversion (%) = ratio between the number of moles of methyl formate consumed, N_c , and the initial number of moles of methyl formate, N_i .

Selectivity (%) = ratio between the number of moles of methyl propionate produced, N_p , and the total number of moles of products formed throughout the reaction (methyl propionate + methanol + diethyl ketone).

Turnover number (TN) = number of moles of methyl propionate produced per mole of catalyst.

Turnover frequency (TOF) = turnover per time unit (h^{-1}).

Acknowledgment. We acknowledge the generous financial support of this work by the CNRS and the “Region Midi-Pyrénées”. We wish to thank Herbert D. Kaesz for helpful discussions and Bruno Donnadiu for his technical assistance in the utilization of the CRYSTALS package now available in our laboratory. We also thank the “Ministère de l'Enseignement Supérieur et de la Recherche” for a fellowship to Jean Marc Soulié, and the Ecole Nationale de Chimie for a fellowship to Sylvie Fabre.

Supplementary Material Available: Tables of anisotropic thermal parameters and hydrogen coordinates for the three structures (8 pages). Ordering information is given on any masthead page.

OM940891H

Reactivity of the Diruthenium(I) Diphosphine- and Acetate-Bridged Species

$[\text{Ru}_2(\text{CO})_4(\mu\text{-O}_2\text{CMe})(\mu\text{-DPPM})_2][\text{BF}_4]$

Kom-Bei Shiu,* Wei-Ning Guo, and Tsung-Jung Chan

Department of Chemistry, National Cheng Kung University, Tainan, Taiwan 701, Republic of China

Ju-Chun Wang and Lin-Shu Liou

Department of Chemistry, Soochow University, Taipei, Taiwan 111, Republic of China

Shie-Ming Peng and Ming-Chu Cheng

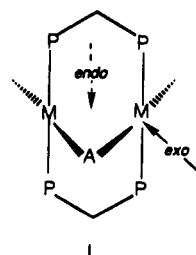
Department of Chemistry, National Taiwan University, Taipei, Taiwan 106, Republic of China

Received September 6, 1994[®]

Reactions of the cationic singly bridged A-frame complex $[\text{Ru}_2(\text{CO})_4(\mu\text{-O}_2\text{CMe})(\mu\text{-DPPM})_2]^+$ (**2**) with I^- , N_3^- , and Pz'^- , via $\text{HPz}'/\text{Et}_3\text{N}$ ($\text{HPz}' = 3,5\text{-dimethylpyrazole}$), in MeOH yield two types of neutral dibridged A-frame products, $[\text{Ru}_2(\text{CO})_2(\mu\text{-CO})(\mu\text{-X})\text{X}(\mu\text{-DPPM})_2]$ ($\text{X} = \text{I}$ (**3**), N_3 (**4**)) and $[\text{Ru}_2(\text{CO})_3(\mu\text{-Pz}')\text{H}(\mu\text{-DPPM})_2]$ (**10**). Complexes **3**, **4**, and **10** have been characterized by spectroscopic data and X-ray crystallography: **3**· Et_2O , $a = 12.779(4)$ Å, $b = 27.447(11)$ Å, $c = 15.487(4)$ Å, $\beta = 95.676(23)^\circ$, $V = 5405(3)$ Å³, monoclinic, $P2_1/c$; $Z = 4$, refined to $R = 0.041$, $R_w = 0.034$, and $\text{GOF} = 1.33$; **4**· CH_2Cl_2 , $a = 19.764(2)$ Å, $b = 14.647(2)$ Å, $c = 20.033(2)$ Å, $\beta = 97.532(8)^\circ$, $V = 5749(1)$ Å³, monoclinic, $P2_1/c$; $Z = 4$, refined to $R = 0.058$, $R_w = 0.086$, and $\text{GOF} = 1.16$; **10**· CH_2Cl_2 , $a = 13.046(2)$ Å, $b = 15.179(3)$ Å, $c = 28.226(5)$ Å, $\beta = 95.93(1)^\circ$, $V = 5559(1)$ Å³, monoclinic, $P2_1/c$, $Z = 4$, refined to $R = 0.074$, $R_w = 0.081$, and $\text{GOF} = 1.70$. The Ru–Ru distance is $3.0147(15)$ Å in **3**, $3.020(1)$ Å in **4**, and $2.891(3)$ Å in **10**. Complex **3** reacts with PMe_3 and $\text{P}(\text{OMe})_3$ to give $[\text{Ru}_2(\text{CO})_3\text{I}_2(\text{PMe}_3)(\mu\text{-DPPM})_2]$ (**8**) and $[\text{Ru}_2(\text{CO})_3\text{I}_2\{\text{P}(\text{OMe})_3\}(\mu\text{-DPPM})_2]$ (**9**), respectively, whereas no reaction between **4** and these phosphine ligands was observed even under forcing conditions. This difference in reactivity, accompanied with the spectral evidences of **8** and **9**, reflects apparently the greater importance of a facile switch from a bridging to terminal group relative to the cleavage of the dative Ru–Ru bond in the double-bridged A-frame complexes such as **3** and **4** to form isolable adducts such as **8** and **9**.

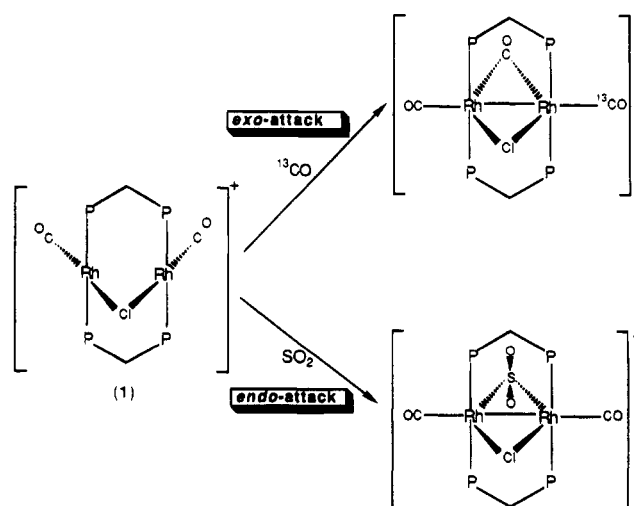
Introduction

Binuclear complexes of two bridging bis(diphenylphosphino)methane (DPPM) ligands with a singly bridged A-frame geometry (**1**) have recently attracted a significant amount of interest because of their rich chemistry and potential as catalysts, catalyst precursors, or model compounds to study the metal–metal cooperativity effects in binding and activation of substrates.^{1–4} One



important focus of many of these studies has centered on the binding of small molecules, either at *endo* (i.e. bridging) or *exo* (i.e. terminal) sites of the complexes.

Scheme 1



In this regard, rarely encountered cationic complexes such as $[\text{Rh}_2(\mu\text{-Cl})(\text{CO})_2(\mu\text{-DPPM})_2]^+$ (**1**) are more interesting than the numerous neutral species, for **1** displays

[®] Abstract published in *Advance ACS Abstracts*, March 15, 1995.

(1) Puddephatt, R. J. *Chem. Soc. Rev.* **1983**, 12, 99.

(2) Balch, A. L. In *Homogeneous Catalysis with Metal Phosphine Complexes*; Pignolet, L. H., Ed.; Plenum: New York, 1983; pp 167–213.
(3) Chaudret, B.; Delavaux, B.; Poilblanc, R. *Coord. Chem. Rev.* **1988**, 86, 191.

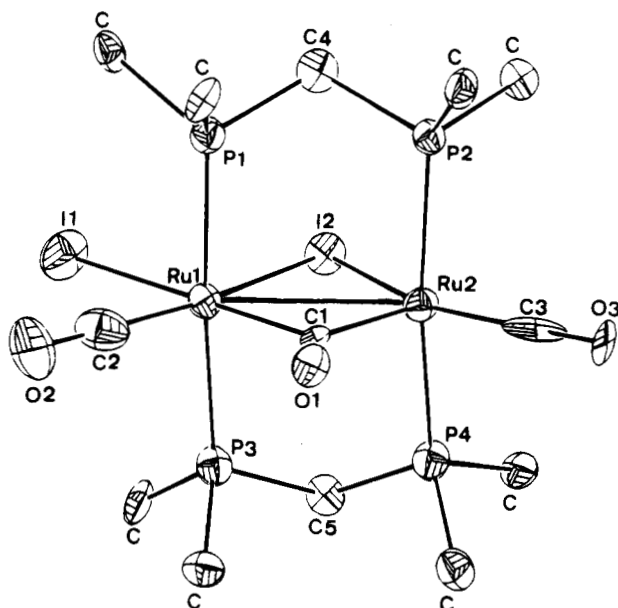


Figure 1. Perspective drawing with 30% probability ellipsoids and numbering scheme (only the *ipso* carbon atom of each phenyl group has been retained for clarity) for **3**.

substrate-dependent reactivity; SO₂ enters the symmetry-allowed⁵ *endo* pocket, whereas ¹³CO chooses the *exo* addition to produce doubly bridged A-frame complexes (Scheme 1).⁶

In this paper, we present the following new information: (1) reactions of the cationic singly bridged A-frame complex [Ru₂(CO)₄(μ-O₂CMe)(μ-DPPM)₂]⁺ (**2**)⁷ with different halide and pseudohalide anions, yielding two types of neutral doubly bridged A-frame products with the entering groups at both sites, (2) reactivity of two dimeric products with a Ru–Ru distance longer than 3.0 Å toward PR₃ (R = Me, OMe, Ph) and (3) the X-ray structures of three reaction products obtained from **2**.

Results and Discussion

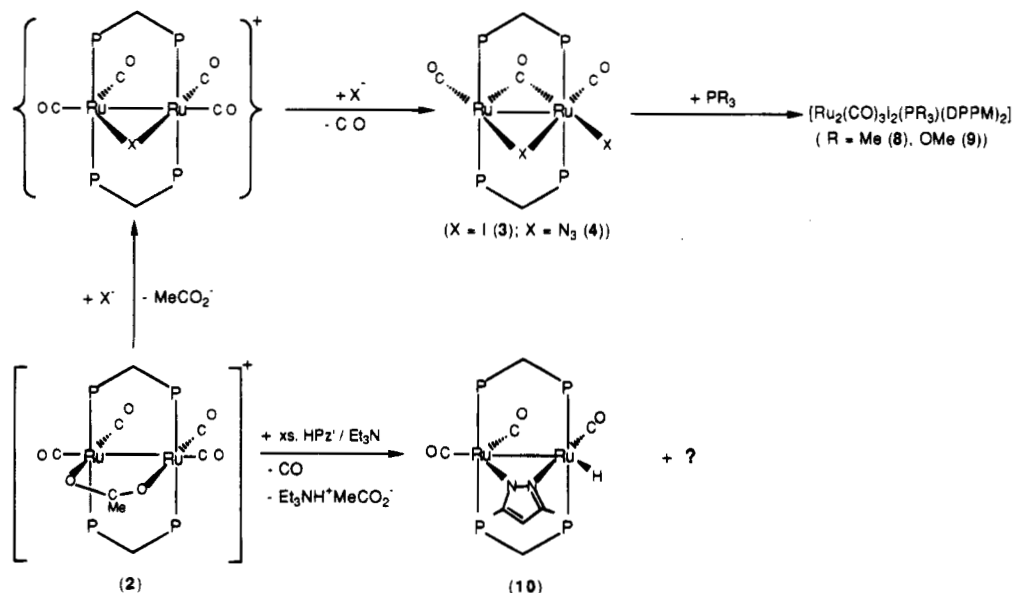
The cation–anion annihilation reaction between **2** and iodide did not occur at ambient temperature. However,

Table 1. Selected Bond Lengths (Å) and Angles (deg) for **3**, **4**, and **10**

(a) Compound 3			
Ru(1)–Ru(2)	3.0147(15)	Ru(1)–I(1)	2.7674(15)
Ru(1)–I(2)	2.8252(15)	Ru(2)–I(2)	2.7556(15)
Ru(1)–C(1)	2.179(10)	Ru(1)–C(2)	1.847(12)
Ru(2)–C(1)	2.014(10)	Ru(2)–C(3)	1.879(12)
Ru(1)–P(1)	2.408(3)	Ru(1)–P(3)	2.426(3)
Ru(2)–P(2)	2.344(3)	Ru(2)–P(4)	2.328(3)
C(1)–O(1)	1.069(12)	C(2)–O(2)	1.141(14)
C(3)–O(3)	1.056(14)		
Ru(1)–I(2)–Ru(2)	65.38(3)	C(3)–Ru(2)–I(2)	155.2(4)
		Ru(1)–C(1)–Ru(2)	91.9(4)
(b) Compound 4			
Ru(1)–Ru(2)	3.020(1)	Ru(1)–P(1)	2.342(2)
Ru(1)–P(3)	2.344(2)	Ru(1)–N(1)	2.167(8)
Ru(1)–C(1)	1.855(11)	Ru(1)–C(2)	1.981(9)
Ru(2)–P(2)	2.388(3)	Ru(2)–P(4)	2.380(3)
Ru(2)–N(1)	2.181(7)	Ru(2)–N(4)	2.166(9)
Ru(2)–C(2)	2.071(9)	Ru(2)–C(3)	1.844(10)
N(1)–N(2)	1.178(13)	N(2)–N(3)	1.109(18)
N(4)–N(5)	1.202(13)	N(5)–N(6)	1.136(15)
C(1)–O(1)	1.147(14)	C(2)–O(2)	1.192(11)
C(3)–O(3)	1.133(13)		
Ru(1)–C(2)–Ru(2)	96.4(4)	C(1)–Ru(1)–N(1)	173.0(4)
N(1)–N(2)–N(3)	177.9(14)	Ru(1)–N(1)–Ru(2)	88.0(3)
		N(4)–N(5)–N(6)	175.1(11)
(c) Compound 10			
Ru(1)–Ru(2)	2.891(3)	Ru(1)–P(1)	2.526(7)
Ru(1)–P(3)	2.536(7)	Ru(1)–N(1)	2.260(18)
Ru(1)–C(1)	1.788(27)	Ru(1)–C(2)	1.742(25)
Ru(2)–P(2)	2.512(7)	Ru(2)–P(4)	2.541(7)
Ru(2)–N(2)	1.993(17)	Ru(2)–C(3)	1.673(23)
N(1)–N(2)	1.346(24)	N(1)–C(7)	1.235(28)
N(2)–C(9)	1.354(29)	C(7)–C(8)	1.470(34)
C(9)–C(8)	1.277(30)	C(6)–C(7)	1.398(30)
C(9)–C(10)	1.485(30)	C(1)–O(1)	1.221(32)
C(2)–O(2)	1.119(32)	C(3)–O(3)	1.058(27)
Ru(1)–N(1)–N(2)	114.9(2)	N(1)–N(2)–Ru(2)	107.1(13)
Ru(1)–C(2)–O(2)	151.4(22)	C(1)–Ru(1)–N(1)	134.8(9)
C(2)–Ru(1)–C(1)	100.2(12)	C(3)–Ru(2)–N(2)	168.6(9)

when the mixture of the two ions was heated under reflux, an orange-red precipitate of **3** gradually formed. Two iodide ions were needed for a complete conversion of every cation **2** into [Ru₂(CO)₂(μ-CO)(μ-I)(μ-DPPM)₂] (**3**). The single-crystal X-ray diffraction structure of this

Scheme 2



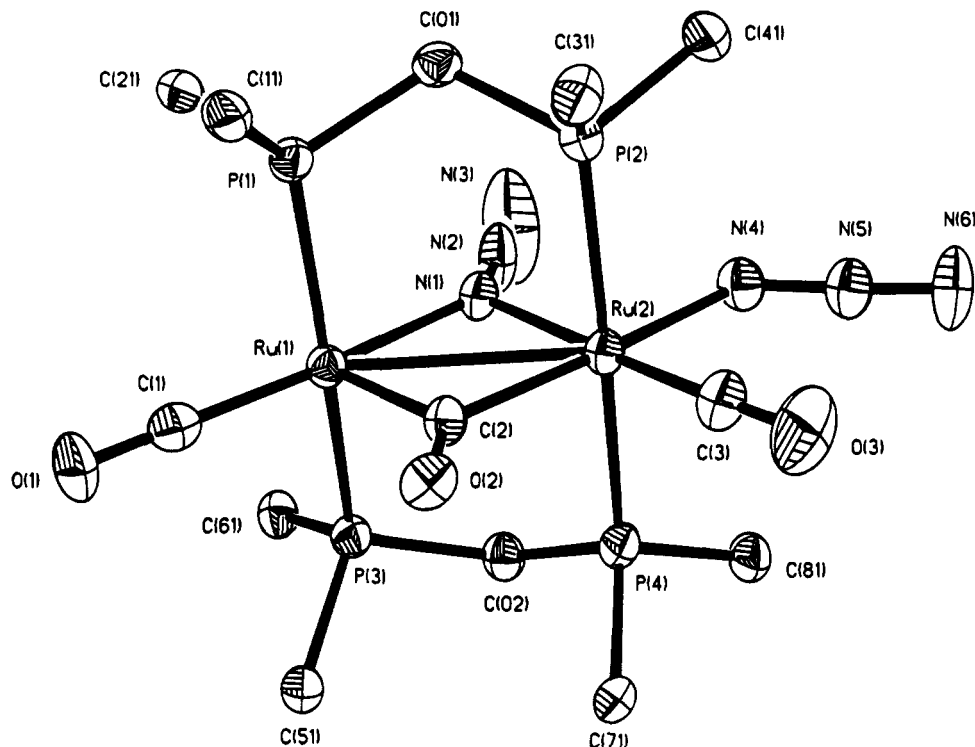


Figure 2. Perspective drawing with 30% probability ellipsoids and numbering scheme (only the *ipso* carbon atom of each phenyl group has been retained for clarity) for **4**.

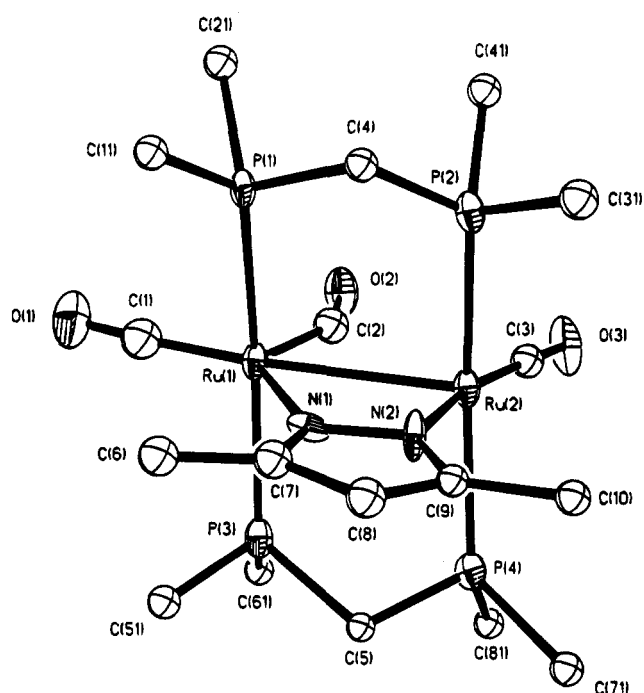


Figure 3. Perspective drawing with 30% probability ellipsoids and numbering scheme (only the *ipso* carbon atom of each phenyl group has been retained for clarity) for **10**.

product then revealed that it is a doubly bridged A-frame complex with an unsymmetrical disposition of two iodide groups (Figure 1). Presumably, **2** reacts with one iodide anion to give $[\text{Ru}_2(\text{CO})_4(\mu\text{-I})(\mu\text{-DPPM})_2]^+$ (**5**), having a structure similar to that of $[\text{Ru}_2(\text{CO})_4(\mu\text{-I})_2(\mu\text{-DPPM})_2]^+$ (**6**),⁸ and then reacts with another iodide anion to yield one CO and **3** (Scheme 2). It is also possible that **3** can be prepared from reaction of the related complex $[\text{Ru}_2(\text{CO})_4(\mu\text{-I})_2(\mu\text{-DPPM})]$ (**7**)⁹ with DPPM. From Table 1, it is clear that the bridging iodide and carbonyl ligands are also unsymmetrically placed ($\text{Ru}(1)\text{-I}(2) = 2.8252(15) \text{ \AA}$; $\text{Ru}(2)\text{-I}(2) = 2.7556(15) \text{ \AA}$; $\text{Ru}(1)\text{-C}(1) = 2.179(10) \text{ \AA}$; $\text{Ru}(2)\text{-C}(1) = 2.014(10) \text{ \AA}$). Such a feature was observed previously in **1**.⁶ Since either terminal iodide or carbonyl ligands are connected with Ru at a short distance of $2.7674(15) \text{ \AA}$ for $\text{Ru}(1)\text{-I}$, $1.847(12) \text{ \AA}$ for $\text{Ru}(1)\text{-C}(2)$, and $1.879(12) \text{ \AA}$ for $\text{Ru}(2)\text{-C}(3)$, it is quite obvious that **3** has the two weak bridges $\text{Ru}(1)\text{-C}(1)$ and $\text{Ru}(1)\text{-I}(2)$. Two ruthenium atoms in **3** are separated by a distance of $3.0147(15) \text{ \AA}$ with one trigonal-bipyramidal and one octahedral Ru center. This value is much larger than that of $2.821(1) \text{ \AA}$ in **6** or that of $2.7074(6) \text{ \AA}$ in **7**. The multiplicity of phosphorus signals observed in a $^{31}\text{P}\{^1\text{H}\}$ NMR spectrum reflects that **3** is diamagnetic. Conventional electron counting would predict a single Ru-Ru bond for this 34-electron species, and the long $\text{Ru}(1)\text{-Ru}(2)$ bond may be classified as a dative bond, donating an electron pair from the 18-electron $\text{Ru}(1)$ center to the 16-electron $\text{Ru}(2)$ center.¹⁰ Apparently **3** has also a weak Ru-Ru bond, despite the two weak bridges. Reactivity of this complex toward Lewis bases such as phosphine ligands PR_3 was hence studied. Complex **3** reacts as expected with PR_3 to produce the adducts $[\text{Ru}_2(\text{CO})_3\text{I}_2(\text{PR}_3)(\mu\text{-DPPM})_2]$ ($\text{R} = \text{Me}$ (**8**), OMe (**9**)). Each

(6) (a) Cowie, M.; Mague, J. T.; Sanger, A. R. *J. Am. Chem. Soc.* **1973**, *100*, 3628. (b) Mague, J. T.; Sanger, A. R. *Inorg. Chem.* **1979**, *18*, 1224. (c) Sanger, A. R. *J. Chem. Soc., Dalton Trans.* **1981**, 221. (7) Sherlock, S. J.; Cowie, M.; Singleton, E.; Steyn, M. M. d. V. *Organometallics* **1988**, *7*, 1663.

(8) Johnson, K. A.; Gladfelter, W. L. *Organometallics* **1990**, *9*, 2101.

(9) Colombie, A.; Lavigne, G.; Bonnet, J.-J. *J. Chem. Soc., Dalton Trans.* **1986**, 899.

(4) Parshall, G. W.; Ittel, S. D. *Homogeneous Catalysis: The Applications and Chemistry of Catalysis by Soluble Transition Metal Complexes*, 2nd ed.; Wiley: New York, 1992.

(5) Hoffman, D. M.; Hoffmann, R. *Inorg. Chem.* **1981**, *20*, 3543.

Table 2. Fractional Atomic Coordinates and B_{eq} Values^a for 3

	x	y	z	B _{eq}		x	y	z	B _{eq}
Ru(1)	0.18664(7)	0.85946(3)	0.25731(6)	1.89(4)	C(22B)	0.4381(10)	0.8921(4)	-0.0668(9)	4.2(7)
Ru(2)	0.32567(8)	0.91693(3)	0.14830(6)	1.94(4)	C(23B)	0.5176(10)	0.8811(5)	-0.1171(9)	4.9(8)
I(1)	0.17294(8)	0.77178(3)	0.34373(6)	4.08(4)	C(24B)	0.5353(10)	0.8346(5)	-0.1432(9)	4.8(8)
I(2)	0.38749(7)	0.82811(3)	0.21896(5)	2.78(4)	C(25B)	0.4707(10)	0.7983(5)	-0.1168(9)	4.5(7)
P(1)	0.10642(23)	0.82323(11)	0.12539(19)	2.06(14)	C(26B)	0.3912(9)	0.8095(4)	-0.0668(8)	3.5(6)
P(2)	0.26658(23)	0.87344(11)	0.02256(19)	1.91(13)	C(31A)	0.2108(9)	0.9583(4)	0.4179(7)	2.5(5)
P(3)	0.27135(24)	0.90176(11)	0.38283(19)	2.23(14)	C(32A)	0.1160(9)	0.9743(4)	0.3835(8)	3.1(6)
P(4)	0.41647(24)	0.95549(12)	0.26690(19)	2.30(14)	C(33A)	0.0704(11)	1.0177(5)	0.4131(9)	5.5(8)
C(1)	0.1826(8)	0.9287(4)	0.1883(6)	1.6(5)	C(34A)	0.1272(14)	1.0433(5)	0.4764(10)	7.0(10)
O(1)	0.1253(5)	0.95718(24)	0.1817(4)	2.1(3)	C(35A)	0.2257(12)	1.0292(6)	0.5093(10)	6.3(9)
C(2)	0.0550(9)	0.8698(4)	0.2935(8)	3.4(6)	C(36A)	0.2654(11)	0.9860(5)	0.4805(9)	5.0(8)
O(2)	-0.0246(6)	0.8740(3)	0.3202(6)	5.0(5)	C(31B)	0.3001(9)	0.8692(4)	0.4846(7)	2.7(6)
C(3)	0.3404(9)	0.9737(4)	0.0828(7)	3.0(6)	C(32B)	0.2584(10)	0.8799(5)	0.5605(8)	4.3(7)
O(3)	0.3536(7)	1.0048(3)	0.0452(5)	3.7(4)	C(33B)	0.2874(11)	0.8550(6)	0.6357(8)	6.2(10)
C(4)	0.2006(9)	0.8160(4)	0.0432(7)	2.4(5)	C(34B)	0.3559(11)	0.8172(5)	0.6364(8)	5.0(7)
C(5)	0.4056(8)	0.9231(4)	0.3693(7)	2.0(5)	C(35B)	0.3972(11)	0.8049(4)	0.5645(9)	4.6(7)
C(11A)	-0.0053(8)	0.8519(4)	0.0625(7)	1.9(5)	C(36B)	0.3719(10)	0.8304(5)	0.4872(8)	4.1(7)
C(12A)	-0.0423(9)	0.8332(4)	-0.0177(7)	2.8(5)	C(41A)	0.3855(9)	1.0180(4)	0.2954(7)	2.6(6)
C(13A)	-0.1279(10)	0.8531(5)	-0.0661(7)	3.9(7)	C(42A)	0.2989(9)	1.0412(4)	0.2569(9)	2.8(6)
C(14A)	-0.1790(10)	0.8927(5)	-0.0325(8)	4.1(7)	C(43A)	0.2743(9)	1.0880(4)	0.2800(8)	3.6(6)
C(15A)	-0.1465(9)	0.9106(4)	0.0458(8)	3.2(6)	C(44A)	0.3402(11)	1.1122(4)	0.3402(8)	4.0(7)
C(16A)	-0.0602(8)	0.8907(5)	0.0938(7)	2.8(6)	C(45A)	0.4263(10)	1.0913(4)	0.3810(9)	4.2(7)
C(11B)	0.0470(9)	0.7624(4)	0.1300(7)	2.1(5)	C(46A)	0.4502(9)	1.0433(4)	0.3594(8)	3.5(6)
C(12B)	0.0738(9)	0.7236(4)	0.0805(8)	3.2(6)	C(41B)	0.5570(8)	0.9585(4)	0.2598(7)	2.4(5)
C(13B)	0.0189(11)	0.6814(5)	0.07777(8)	4.3(7)	C(42B)	0.6034(10)	0.9988(5)	0.2255(10)	4.9(8)
C(14B)	-0.0637(10)	0.6752(5)	0.1298(9)	4.7(8)	C(43B)	0.7084(12)	1.0005(6)	0.2167(11)	6.6(9)
C(15B)	-0.0888(10)	0.735(5)	0.1811(9)	4.4(7)	C(44B)	0.7715(10)	0.9630(5)	0.2420(9)	4.9(8)
C(16B)	-0.0350(9)	0.7568(5)	0.1803(8)	3.4(6)	C(45B)	0.7300(10)	0.9220(5)	0.2725(10)	5.2(8)
C(21A)	0.1750(8)	0.9023(4)	-0.0590(7)	2.0(5)	C(46B)	0.6245(9)	0.9205(4)	0.2825(8)	3.6(7)
C(22A)	0.1535(9)	0.8803(4)	-0.1421(7)	2.9(6)	C(51)	0.2983(19)	0.3132(8)	0.0519(14)	13.8(18)
C(23A)	0.0801(9)	0.9013(5)	-0.2019(8)	3.5(6)	C(52)	0.234(3)	0.2761(10)	0.095(4)	39.0(53)
C(24A)	0.0268(9)	0.9421(4)	-0.1817(7)	2.9(6)	O(53)	0.3175(12)	0.2627(6)	-0.0327(13)	18.2(15)
C(25A)	0.0486(9)	0.9639(4)	-0.1023(7)	2.8(6)	C(54)	0.3235(18)	0.2120(10)	-0.0974(22)	21.0(27)
C(26A)	0.1229(8)	0.9440(4)	-0.0408(7)	2.3(5)	C(55)	0.3224(24)	0.2187(10)	-0.217(4)	46.3(64)
C(21B)	0.3742(8)	0.8562(4)	-0.0396(7)	2.2(5)					

$$^a B_{eq} = \frac{8}{3}\pi^2(U_{11}(aa)^2 + U_{22}(bb)^2 + U_{33}(cc)^2 + 2U_{12}aa*bb(\cos \gamma) + 2U_{13}aa*cc(\cos \beta) + 2U_{23}bb*cc(\cos \alpha)).$$

adduct displays three carbonyl stretching bands in CH₂-Cl₂ with one band at the lowest frequency of 1742 cm⁻¹ for **8** and 1826 cm⁻¹ for **9**, indicating that **8** and **9** may retain the carbonyl bridge or semibrige,¹¹ but whether the iodide bridge or the Ru-Ru bond is cleaved in these adducts should be the subject of a further structural analysis. Since there is an open terminal site around Ru(2), it appears probable that an initial terminal attack of PR₃ will occur, leading to the formation of the adducts with cleavage of either the Ru-Ru dative bond¹⁰ or the weak iodide bridge. The fact that **2** fails to react with PPh₃ is probably due to the steric nature of this phosphine ligand.

Reaction of **1** with azide follows similarly to give [Ru₂(CO)₂(μ-CO)(μ-N₃)(N₃(μ-DPPM))₂] (**4**). The bridging azide group adopts an end-on coordination mode with ∠N(1)-N(2)-N(3) = 177.9(14)° (Figure 2), though it is able to bridge the metals in an end-to-end mode.¹² To the best of our knowledge, **4** is the first dinuclear carbonyl

complex containing both the terminal and bridging azides. Complex **4** has also a long dative Ru-Ru bond of 3.020(1) Å, but it has only one apparently weak Ru(2)-C(2) bridge (Ru(2)-C(2) = 2.071(9) Å; Ru(1)-C(2) = 1.981(9) Å; Ru(1)-C(1) = 1.855(11) Å; Ru(2)-C(3) = 1.844(10) Å; Ru(1)-N(1) = 2.167(8) Å; Ru(2)-N(1) = 2.181(7) Å; Ru(2)-N(4) = 2.166(9) Å). By comparison of the Ru-C bridging bond distances in **4** with those in **3**, it is evident that the "weak" Ru(2)-C(2) bond in **4** is significantly shorter than the "weak" Ru(1)-C(1) bond in **3**. Thus, from the fact that **4** does not react at all with PMe₃, P(OMe)₃, or PPh₃ under the forcing conditions, even though **4** has a more open terminal site around one Ru center to potentially accept an incoming nucleophile than does **3** (∠C(1)-Ru(1)-N(1) = 173.0(4)° in **4** versus ∠C(3)-Ru(2)-I(2) = 155.2(4)° in **3**), a successful adduct formation of the doubly bridged A-frame complexes such as **3** and **4** with the added molecules appears to involve a switch from a bridging to a terminal group rather than the cleavage of the long dative Ru-Ru bond after an initial terminal attachment of the molecules at the open site. If such a switch would be blocked either thermodynamically or kinetically, no isolable adduct would form. In this regard, the facile conversion from a bridging to a terminal iodide in **3** helps formation of **8** and **9**, but the stubborn carbonyl and azide bridges in **4** inhibit any PR₃-adduct formation.

(12) (a) Vicente, R.; Escuer, A.; Ribas, J.; Solans, X. *Inorg. Chem.* **1992**, *31*, 1726. (b) Escuer, A.; Vicente, R.; Ribas, J.; Fallas, M. S. E.; Solans, X.; Font-Bardia, M. *Inorg. Chem.* **1993**, *32*, 3727. (c) Cortes, R.; Pizzaro, J. L.; Lezama, L.; Arriortua, M. I.; Rojo, T. *Inorg. Chem.* **1994**, *33*, 2697.

(10) (a) Langebach, H.-J.; Vahrenkamp, H. *Chem. Ber.* **1979**, *112*, 3390, 3773. (b) Breen, M. J.; Duttera, M. R.; Geoffroy, G. L.; Novotnak, G. C.; Roberts, D. A.; Shulman, P. M.; Steinmetz, G. R. *Organometallics* **1981**, *1*, 1008. (c) Roberts, D. A.; Steinmetz, G. R.; Breen, M. J.; Shulman, P. M.; Morrison, E. D.; Duttera, M. R.; DeBrosse, C. W.; Whittle, R. R.; Geoffroy, G. L. *Organometallics* **1983**, *2*, 846. (d) Mercer, W. C.; Whittle, R. R.; Burkhardt, E. W.; Geoffroy, G. L. *Organometallics* **1985**, *4*, 68. (e) Shyu, S.-G.; Wojcicki, A. *Organometallics* **1985**, *4*, 1457. (f) Powell, J.; Coutoure, C.; Gregg, M. R. *J. Chem. Soc., Chem. Commun.* **1988**, 1208. (g) Baker, R. T.; Calabrese, J. C.; Krusic, P. J.; Therien, M. J.; Troglor, W. C. *J. Am. Chem. Soc.* **1988**, *110*, 8392. (h) Jenkins, H. A.; Loeb, S. J.; Stephan, D. W. *Inorg. Chem.* **1989**, *28*, 1998. (i) Powell, J.; Sawyer, J. F.; Stainer, M. V. R. *Inorg. Chem.* **1989**, *28*, 4461. (j) Shyu, S.-G.; Hsu, J.-Y.; Lin, P.-J.; Wu, W.-J.; Peng, S.-M.; Lee, G.-H.; Wen, Y.-S. *Organometallics* **1994**, *13*, 1699. (11) Horwitz, C. P.; Schriver, D. F. *Adv. Organomet. Chem.* **1984**, *23*, 219.

Table 3. Atomic Coordinates ($\times 10^4$) and Equivalent Isotropic Displacement Coefficients^a ($\text{\AA}^2 \times 10^3$) for 4

	x	y	z	U(eq)		x	y	z	U(eq)
Ru(1)	4576(1)	532(1)	2433(1)	35(1)	C(36)	6376	-405	4256	58(4)
Ru(2)	5680(1)	-887(1)	2401(1)	37(1)	C(31)	6721	159	3852	50(3)
P(1)	5352(1)	1602(2)	2954(1)	38(1)	C(42)	7536(5)	763(5)	2211(6)	144(10)
P(2)	6486(1)	186(2)	2935(1)	41(1)	C(43)	8149	623	1950	184(14)
P(3)	3803(1)	-311(2)	1687(1)	38(1)	C(44)	8528	-167	2114	142(11)
P(4)	4863(1)	-1867(2)	1786(1)	41(1)	C(45)	8296	-818	2539	139(10)
O(1)	3489(4)	1108(5)	3261(4)	70(3)	C(46)	7683	-678	2799	115(8)
O(2)	4786(4)	-816(4)	3505(3)	50(2)	C(41)	7303	112	2636	56(4)
O(3)	6234(5)	-2386(6)	3316(5)	97(4)	C(52)	2533(4)	-1203(5)	1538(3)	72(5)
N(1)	5302(4)	236(5)	1740(4)	42(3)	C(53)	1997	-1667	1778	80(5)
N(2)	5444(5)	463(6)	1212(5)	67(4)	C(54)	2014	-1824	2466	83(6)
N(3)	5559(9)	693(11)	711(7)	164(9)	C(55)	2567	-1518	2915	74(5)
N(4)	6365(4)	-1157(6)	1665(4)	49(3)	C(56)	3103	-1055	2675	57(4)
N(5)	6767(5)	-1776(6)	1677(4)	55(3)	C(51)	3085	-897	1987	47(3)
N(6)	7160(6)	-2334(7)	1649(5)	89(5)	C(62)	3086(4)	1194(5)	1185(3)	77(5)
C(01)	6225(5)	1368(6)	2769(5)	43(3)	C(63)	2775	1780	688	101(6)
C(02)	4226(5)	-1211(7)	1240(4)	45(3)	C(64)	2768	1560	10	89(6)
C(1)	3909(5)	890(7)	2949(5)	47(3)	C(65)	3073	754	-172	78(5)
C(2)	4947(5)	-509(6)	2997(4)	36(3)	C(66)	3384	268	325	62(4)
C(3)	6011(6)	-1810(7)	2979(5)	54(4)	C(61)	3390	388	1003	46(3)
C(12)	5115(3)	1238(4)	4263(3)	56(4)	C(72)	3784(4)	-3079(5)	1827(3)	75(5)
C(13)	5224	1335	4961	70(5)	C(73)	3368	-3672	2137	94(7)
C(14)	5683	1989	5255	80(5)	C(74)	3506	-3840	2826	91(7)
C(15)	6033	2545	4851	83(5)	C(75)	4060	-3415	3207	81(6)
C(16)	5924	2448	4152	67(4)	C(76)	4475	-2822	2897	64(4)
C(11)	5465	1794	3858	45(3)	C(71)	4337	-2654	2207	50(4)
C(22)	5155(4)	2834(5)	1895(3)	73(5)	C(82)	5411(4)	-3486(5)	1393(4)	77(5)
C(23)	4916	3641	1578	99(7)	C(83)	5718	-4054	961	100(7)
C(24)	4651	4330	1948	104(7)	C(84)	5829	-3738	328	120(8)
C(25)	4624	4212	2635	98(7)	C(85)	5632	-2855	126	100(7)
C(26)	4863	3404	2952	72(5)	C(86)	5325	-2287	558	73(5)
C(21)	5128	2715	2582	49(4)	C(81)	5215	-2603	1192	51(4)
C(32)	7250(4)	718(5)	4145(3)	68(5)	Cl(1)	7275(6)	2396(9)	95(11)	510(14)
C(33)	7434	712	4841	89(6)	Cl(2)	6267	3542	157	335(8)
C(34)	7089	149	5245	81(5)	C(91)	6740	2722	690	313(22)
C(35)	6560	-410	4953	76(5)					

^a Equivalent isotropic U , defined as one-third of the trace of the orthogonalized U_{ij} tensor.

In order to get some other information about the paucity of reactivity of **4** toward PR_3 , a parallel reaction of **2** with another pseudohalide, Pz'^- , obtained *in situ* from deprotonation of HPz' with Et_3N , was also carried out. Unfortunately, this experiment did not give us any directly related information but did result in something unexpected. The reaction was found to be complicated with at least two different products, as indicated by two triplet signals at -10.31 and -10.55 ppm in a ^1H NMR spectrum of the reaction mixture dissolved in CD_2Cl_2 . Unlike **4**, one product **10**, separated cleanly from the mixture, does not contain two but one pseudohalide (i.e. Pz'^-) and one hydride. The crystal structure of $[\text{Ru}_2(\text{CO})_3(\mu\text{-Pz}')(\text{H})(\mu\text{-DPPM})_2]$ (**10**) was determined (Figure 3) to have structural features similar to those of **3** and **4**, except for a much shorter Ru-Ru distance of 2.891-(3) Å and two more unsymmetrical bridging ligands (Ru(1)-N(1) = 2.260(18) Å; Ru(2)-N(2) = 1.993(17) Å; Ru(1)-C(2) = 1.742(25) Å; Ru(2)-C(2) = 2.612(27) Å). Carbonyl C(2)O(2) can even be classified as a semibridging carbonyl with an asymmetry parameter, Ω ,¹¹ of 2.15 and appears to form a stronger bonding with Ru(1) than with Ru(2). Although the terminal hydride position in **10** could not be located from the last difference Fourier map, its position can be inferred to be connected to Ru(2), since the vacancy around this atom is larger than that around Ru(1). The hydride location is probably included in one mirror plane of **10** and is *cis* to the Pz' nitrogen atom N(2), the carbonyl C(3)O(3), and two equivalent phosphorus atoms P(2) and P(4) while being *trans* to C(2)O(2), as is supported by the presence of a triplet signal at -10.31 ppm ($^2J_{\text{P,H}} = 19$ Hz) in the ^1H

NMR spectrum.¹³ The relatively long distance of 2.612-(27) Å between Ru(2) and C(2) compared to that of 1.742(25) between C(2) and Ru(1) is compatible with the high *trans* influence of the hydride ligand in **10**.¹⁴ Alternatively speaking, carbonyl C(2)O(2) in a semibridging structure with $\angle\text{Ru}(1)\text{-C}(2)\text{-O}(2) = 151.4(22)^\circ$ in **10** rather than a symmetrical or nearly symmetrical bridging structure like that found in **3** or **4** may act as a better π -acceptor with the π^* orbital of CO tipped toward Ru(2) to dissipate effectively the accumulated charge density on this atom,¹⁵ when a superior σ -donor (i.e. hydride) is at this atom and is *trans* to C(2)O(2) (Scheme 2).

Conclusions

The cationic single-bridged A-frame complex **2** is a convenient starting material to form different types of double-bridged A-frame products **3**, **4**, and **10**. The specific type of product appears to be dependent on the substrate used. The different reactivities of **3** and **4** toward phosphine ligands and the spectral evidence of the resulting phosphine adducts **8** and **9** reflect apparently the greater importance of a facile switch from a bridging to a terminal group relative to the cleavage of the dative Ru-Ru bond in a double-bridged A-frame

(13) Schreiner, S.; Gallaher, T. N.; Parsons, H. F. *Inorg. Chem.* **1994**, *33*, 3021.

(14) Douglas, B. E.; McDaniel, D. H.; Alexander, J. J. *Concepts and Models of Inorganic Chemistry*, 3rd ed.; Wiley: New York, 1994; p 525.

(15) Cotton, F. A. *Prog. Inorg. Chem.* **1976**, *21*, 1.

Table 4. Atomic Coordinates ($\times 10^4$) and Equivalent Isotropic Displacement Coefficients^a ($\text{\AA}^2 \times 10^3$) for 10

	x	y	z	U(eq)		x	y	z	U(eq)
Ru(1)	1551(2)	1651(1)	1682(1)	29(1)	C(32)	572(12)	5425(10)	1424(4)	51(8)
Ru(2)	1178(2)	2737(1)	840(1)	30(1)	C(33)	689	6267	1238	60(8)
Cl(1)	4591(9)	7683(8)	1221(3)	134(5)	C(34)	302	6455	770	65(9)
Cl(2)	5615(8)	6433(7)	1792(3)	126(5)	C(35)	-203	5801	487	51(8)
P(1)	451(5)	2537(4)	2193(2)	28(2)	C(36)	-319	4959	673	33(6)
P(2)	-12(6)	3601(4)	1310(2)	34(3)	C(31)	68	4771	1141	40(7)
P(3)	2926(6)	943(4)	1234(2)	35(3)	C(42)	-1876(14)	2730(10)	1162(5)	65(8)
P(4)	2617(5)	2129(4)	393(2)	32(2)	C(43)	-2933	2599	1166	94(11)
N(1)	2552(13)	2855(12)	1628(6)	31(7)	C(44)	-3530	3229	1371	88(10)
N(2)	2318(5)	3348(11)	1235(6)	35(7)	C(45)	-3069	3990	1572	74(9)
C(4)	260(18)	3643(13)	1921(7)	30(6)	C(46)	-2011	4121	1568	48(7)
C(5)	3566(16)	1684(14)	781(6)	25(6)	C(41)	-1415	3491	1363	34(6)
C(6)	3622(18)	2891(15)	2294(8)	40(7)	C(52)	4854(14)	1114(9)	1589(5)	49(8)
C(7)	3256(19)	3266(16)	1856(8)	37(6)	C(53)	5704	821	1889	60(9)
C(8)	3530(19)	4058(15)	1597(8)	38(7)	C(54)	5629	60	2160	70(9)
C(9)	2931(18)	4063(15)	1210(7)	26(6)	C(55)	4705	-409	2131	71(9)
C(10)	2834(18)	4745(14)	831(7)	30(6)	C(56)	3855	-116	1831	66(9)
C(01)	5705(26)	7387(23)	1450(11)	116(13)	C(51)	3930	645	1561	35(7)
O(1)	1403(17)	139(12)	2358(6)	77(9)	C(62)	3433(10)	-430(10)	617(5)	45(7)
O(2)	-169(15)	942(11)	1156(5)	57(8)	C(63)	3216	-1249	406	56(8)
O(3)	-307(13)	2163(11)	157(5)	63(7)	C(64)	2339	-1712	503	69(9)
C(1)	1515(22)	769(18)	2100(9)	54(8)	C(65)	1678	-1357	812	78(10)
C(2)	529(21)	1349(17)	1267(9)	43(8)	C(66)	1895	-539	1023	49(8)
C(3)	267(19)	2370(16)	426(8)	37(7)	C(61)	2773	-75	926	31(6)
C(12)	1309(13)	2181(8)	3027(5)	57(8)	C(72)	4507(12)	3114(10)	99(5)	57(8)
C(13)	1649	2339	3505	52(7)	C(73)	4948	3762	-166	72(9)
C(14)	1566	3181	3695	76(10)	C(74)	4326	4266	-494	70(9)
C(15)	1143	3865	3408	71(9)	C(75)	3265	4123	-557	51(8)
C(16)	803	3708	2931	40(7)	C(76)	2824	3475	-292	43(7)
C(11)	886	2866	2741	31(6)	C(71)	3445	2971	36	33(7)
C(22)	-1556(13)	2726(8)	2649(5)	62(8)	C(82)	3322(10)	1119(10)	-379(5)	37(7)
C(23)	-2421	2372	2832	77(9)	C(83)	3191	406	-692	75(10)
C(24)	-2641	1477	2779	62(8)	C(84)	2340	-148	-682	59(8)
C(25)	-1996	934	2543	47(7)	C(85)	1619	12	-359	51(8)
C(26)	-1132	1287	2360	40(7)	C(86)	1750	725	-47	44(7)
C(21)	-912	2183	2413	36(6)	C(81)	2602	1279	-57	32(6)

^a Equivalent isotropic U , defined as one-third of the trace of the orthogonalized U_{ij} tensor.

complexes to form isolable adducts. Further studies on the synthetic uses of **2–4**, the hydride source, and isolation of the second hydride compound are currently in progress in our laboratory.

Experimental Section

General Comments. All solvents were dried and purified by standard methods (ethers, paraffins, and arenes from potassium with benzophenone as indicator; halocarbons and acetonitrile from CaH₂ and alcohols from the corresponding alkoxide) and were freshly distilled under nitrogen immediately before use. All reactions and manipulations were carried out in standard Schlenkware, connected to a switchable double manifold providing vacuum and nitrogen. Reagents were used as supplied by Aldrich. ¹H and ³¹P NMR spectra were measured on a Bruker AMC-400 or a Varian Unity Plus-400 (¹H, 400 MHz; ³¹P, 162 MHz) NMR spectrometer. ¹H chemical shifts (δ in ppm, J in Hz) are defined as positive downfield relative to internal MeSi₄ (TMS) or the deuterated solvent, while ³¹P chemical shifts are defined as positive downfield relative to external 85% H₃PO₄. The IR spectra, calibrated with polystyrene, were recorded on a Hitachi Model 270–30 instrument. The following abbreviations are used: s, strong; m, medium; w, weak. Microanalyses were carried out by the staff of the Microanalytical Service of the Department of Chemistry, National Cheng Kung University.

Synthesis of [Ru₂(CO)₂(μ -CO)(μ -I)(μ -DPPM)₂] (3**).** A suspension of [Ru₂(CO)₄(μ -O₂CMe)(μ -DPPM)₂][BF₄] (**2**;⁷ 157 mg, 0.128 mmol) and NaI (48 mg, 0.32 mmol) in MeOH (25 mL) was heated under reflux for 5 h, giving an orange-red precipitate, which was collected by filtration. Recrystallization from CH₂Cl₂/MeOH gave the pure product **3** (131 mg, 78%). Anal. Calcd for C₅₃H₄₄I₂O₂P₄Ru₂: C, 48.64; H, 3.58. Found: C, 48.45; H,

3.56. ³¹P{¹H} NMR (25 °C, acetone-*d*₆/CH₂Cl₂ (1/1), 162 MHz): δ 14.79 (m, 2 P), 28.15 (m, 2 P). IR (CH₂Cl₂): ν_{CO} 1982 m, 1912 s, 1712 m cm⁻¹.

Synthesis of [Ru₂(CO)₂(μ -CO)(μ -N₃)(N₃)(μ -DPPM)₂] (4**).** The orange-yellow compound **4** was prepared in a yield of 70% by a procedure similar to that for **3**. Anal. Calcd for C₅₃H₄₄N₆O₃P₄Ru₂: C, 55.88; H, 3.90; N, 7.37. Found: C, 55.70; H, 4.10; N, 7.48. ³¹P{¹H} NMR (25 °C, CDCl₃, 162 MHz): δ 20.15–23.16 (m, 4 P). IR (CH₂Cl₂): ν_{CO} 1960 m, 1914 s, 1696 m cm⁻¹.

Synthesis of [Ru₂(CO)₃I₂(PR₃)(μ -DPPM)₂] (R = Me (8**), OMe (**9**)).** To an orange-red suspension of **2** (153 mg, 0.117 mmol) in THF (25 mL) was added PMe₃ (0.5 mL, 1.0 M in THF). The mixture was stirred for 10 min at ambient temperature, and some orange-yellow precipitate formed. This mixture was then heated under reflux for 3 h to give a complete conversion. The precipitate formed was collected by filtration, washed three times with 15 mL of Et₂O, and vacuum-dried. Recrystallization from CH₂Cl₂/MeOH gave the pure product **8** (81 mg, 50%). Anal. Calcd for C₅₆H₅₃I₂O₃P₅Ru₂: C, 48.57; H, 3.86. Found: C, 48.35; H, 3.86. ³¹P{¹H} NMR (25 °C, acetone-*d*₆, 162 MHz): δ -15.80 (m, 1 P), 22.06 (m, 2 P), 30.28 (m, 2 P). IR (CH₂Cl₂): ν_{CO} 1946 sh, 1926 s, 1742 m cm⁻¹. Compound **9** was obtained similarly in a yield of 48%. Anal. Calcd for C₅₆H₅₃I₂O₆P₅Ru₂Et₂O: C, 47.82; H, 4.21. Found: C, 47.60; H, 4.04. ³¹P{¹H} NMR (25 °C, acetone-*d*₆, 162 MHz): δ -28.33 (m, 2 P), 38.12 (m, 2 P), 96.70 (m, 1 P). IR (CH₂Cl₂): ν_{CO} 1984 m, 1908 s, 1826 m cm⁻¹. The presence of diethyl ether solvate was confirmed by ¹H NMR spectroscopy.

Synthesis of [Ru₂(CO)₃(μ -Pz')H(μ -DPPM)₂] (10**).** A suspension of **2** (200 mg, 0.163 mmol), HPz' (20 mg, 0.208 mmol), and Et₃N (0.5 mL) in MeOH (15 mL) was heated under reflux for 36 h, giving a yellow precipitate, which was collected by

Table 5. Crystal Data for 3, 4, and 10

compd	3	4	10
formula	C ₅₇ H ₅₄ I ₂ O ₄ P ₄ Ru ₂	C ₅₄ H ₄₆ Cl ₂ N ₆ O ₃ P ₄ Ru ₂	C ₅₉ H ₅₄ Cl ₂ N ₂ O ₃ P ₄ Ru ₂
fw	1385.88	1223.89	1235.91
diffractometer used	Nonius CAD4	Siemens P4	Siemens P4
space group	monoclinic, <i>P</i> ₂ ₁ / <i>c</i>	monoclinic, <i>P</i> ₂ ₁ / <i>n</i>	monoclinic, <i>P</i> ₂ ₁ / <i>c</i>
<i>a</i> , Å	12.779(4)	19.764(2)	13.046(2)
<i>b</i> , Å	27.447(11)	14.647(2)	15.179(3)
<i>c</i> , Å	15.487(4)	20.033(2)	28.226(5)
β , deg	95.676(23)	97.532(8)	95.93(1)
<i>V</i> , Å ³	5405(3)	5749(1)	5559(1)
<i>Z</i>	4	4	4
<i>D</i> _{calcd} , g cm ⁻³	1.699	1.414	1.468
λ (Mo K α), Å	0.709 30	0.710 73	0.710 73
<i>F</i> (000)	2713	2519	2480
unit cell detn: no. 2 θ range, deg	24, 18–31	25, 10–13	25, 10–13
scan type	θ –2 θ	θ – ω	θ – ω
2 θ range, deg	2–45	4–50	4–45
<i>h</i> , <i>k</i> , <i>l</i> range	±13, 29, 16	24, 18, ±24	15, 17, ±31
μ (Mo K α), cm ⁻¹	18.3	7.75	8.0
cryst size, mm	0.10 × 0.10 × 0.30	0.4 × 0.4 × 0.5	0.1 × 0.2 × 0.4
transmissn factor	0.859–1.000	0.421–0.491	0.865–0.939
temp, K	298	298	298
no. of measd rflns	7069	10968	8061
no. of unique rflns	7069	10197	7320
no. of obsd rflns (<i>N</i> _o)	3830 (>2 σ)	6067 (>4 σ)	2608 (>6 σ)
<i>R</i> , ^a <i>R</i> _w ^a	0.041, 0.034	0.058, 0.086	0.074, 0.081
GOF ^a	1.33	1.16	1.70
refinement program	NRCVAX	SHELXTL–PLUS	SHELXTL–PLUS
no. of ref params (<i>N</i> _p)	623	536	258
weighting scheme	$[\sigma^2(F_o)]^{-1}$	$[\sigma^2(F_o) + 0.003F_o^2]^{-1}$	$[\sigma^2(F_o) + 0.005F_o^2]^{-1}$
<i>g</i> (2nd ext coeff) × 10 ⁴	0.314(11)	0	0
(Δ / σ) _{max}	0.074	0.001	0.001
(ΔQ) _{max} , (ΔQ) _{min} , e Å ⁻³	–3.6, 3.5	–0.7, 1.3	–1.3, 0.9
solvent	Et ₂ O	CH ₂ Cl ₂	CH ₂ Cl ₂

$$^a R = [\sum(|F_o| - |F_c|)/\sum|F_o|], R_w = [\sum w(|F_o| - |F_c|)^2/\sum w|F_o|^2]^{1/2}, GOF = [\sum w(|F_o| - |F_c|)^2/(N_o - N_p)]^{1/2}.$$

filtration. Recrystallization from CH₂Cl₂/Et₂O gave the pure product **4** (90 mg, 48%). Anal. Calcd for C₅₈H₅₂N₂O₃P₄Ru₂: C, 60.52; H, 4.55; N, 2.43. Found: C, 60.45; H, 4.56; N, 2.37. ³¹P{¹H} NMR (25 °C, CD₂Cl₂, 162 MHz): δ 19.54 (m, 2 P), 33.45 (m, 2 P). IR (CH₂Cl₂): ν_{CO} 1924 s, 1876 s, 1810 m cm⁻¹.

Single-Crystal X-ray Diffraction Studies of 3, 4, and 10. Suitable single crystals were grown from CH₂Cl₂/hexane or CH₂Cl₂/Et₂O at ambient temperature and chosen for the single-crystal structure determination. Atomic coordinates and equivalent isotropic displacement coefficients for **3**, **4**, and **10** are listed in Tables 2–4, respectively. The X-ray diffraction data were measured on a four-circle diffractometer. Intensities of 3 standard reflections were monitored every 1 h or every 500 reflections throughout the data measurement. The variation was less than 2% for **3**, 5% for **4**, and 12% for **10**. For **3**, the structure was solved by the heavy-atom method and refined by a full-matrix least-squares procedure using NRCVAX.¹⁶ For **4** and **10**, the structure was solved by direct methods and refined by a full-matrix least-squares procedure using SHELXTL-PLUS.¹⁷ Two chlorine atoms and one carbon

atom of the CH₂Cl₂ solvate in **4** were located from difference Fourier maps, and this solvent molecule was refined as a rigid group using the SHELXTL command DFIX 6. Hydrogen positions, except those of Pz⁻ and H⁻ of **10**, were either located from the difference maps or calculated at idealized locations. The other essential details of the single-crystal data measurements and refinements are given in Table 5.

Acknowledgment is made to the National Science Council of the Republic of China for financial support of this research (Contract No. NSC84-2113-M006-010).

Supplementary Material Available: Tables of all bond lengths and angles, anisotropic displacement coefficients, and hydrogen coordinates for **3**, **4**, and **10** (14 pages). Ordering information is given on any current masthead page.

OM9407013

(16) Gabe, E. J.; Le Page, Y.; Charland, J.-P.; Lee, F. L.; White, P. S. *J. Appl. Crystallogr.* **1989**, *22*, 384.

(17) Siemens Analytical X-ray Instruments Inc., Karlsruhe, Germany, 1991.

Coordination of Polythiaether Macrocycles to Metal Cluster Complexes. 2. Coordination of Polythiaether Macrocycles to Hexaruthenium Carbido Carbonyl Clusters

Richard D. Adams,* Stephen B. Falloon, Kenneth T. McBride, and John H. Yamamoto

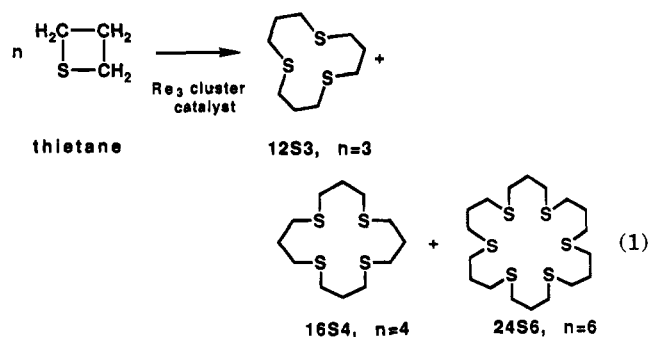
Department of Chemistry and Biochemistry, University of South Carolina, Columbia, South Carolina 29208

Received November 28, 1994[®]

The synthesis and structural characterizations of $\text{Ru}_6(\mu_6\text{-C})$ cluster complexes containing the polythiaether macrocycle ligands 1,5,9-trithiacyclododecane (12S3), 1,5,9,13-tetrathiacyclohexadecane (16S4), and 1,4,7-trithiacyclononane (9S3) are reported. The reactions of $\text{Ru}_6(\text{CO})_{17}(\mu_6\text{-C})$, **1**, with 12S3 and 16S4 in refluxing octane solvent have yielded the new cluster complexes $\text{Ru}_6(\text{CO})_{13}(\mu\text{-}\eta^3\text{-12S3})(\mu_6\text{-C})$, **2**, in 78% yield, and $\text{Ru}_6(\text{CO})_{15}(\mu\text{-}\eta^2\text{-16S4})(\mu_6\text{-C})$, **3**, in 58% yield, respectively. The reaction of **1** with 9S3 in refluxing hexane solvent has yielded the new cluster complex $\text{Ru}_6(\text{CO})_{14}(\eta^3\text{-9S3})(\mu_6\text{-C})$, **4**, in 93% yield. All three products were characterized by a combination of IR, ^1H NMR, and single crystal X-ray diffraction analyses. All three compounds contain octahedral Ru_6 clusters with a carbido ligand in the center. In compound **2** the three sulfur atoms of the 12S3 ligand are coordinated to one ruthenium atom but one of the sulfur atoms simultaneously serves as a bridge to an adjacent ruthenium atom. In compound **3** only two of the four sulfur atoms of the 16S4 ligand are coordinated to the cluster and they are coordinated to two adjacent ruthenium atoms. In compound **4** the three sulfur atoms of the 9S3 ligand are coordinated to one ruthenium atom only. When heated to 105 °C for 18 h, compound **4** was converted to the new compound $\text{Ru}_6(\text{CO})_{14}(\mu_3\text{-}\eta^3\text{-SCH}_2\text{CH}_2\text{SCH}_2\text{CH}_2\text{S})(\mu_5\text{-C})$, **5**, in 68% yield. The evolution of ethylene was observed by ^1H NMR spectroscopy. Compound **5** was obtained in one step from the reaction of **1** with 9S3 in refluxing octane solvent in 36% yield. Compound **5** was characterized crystallographically and was shown to consist of a "spiked" square pyramidal cluster of six metal atoms with the carbido ligand in the center of the base of the square pyramid. The spike is bonded to one of the metal atoms in the base of the square pyramid. The 9S3 ligand was converted into a triply bridging 3-thiapentane-1,5-dithiolato ligand. All three sulfur atoms form bridges between the ruthenium spike and the Ru_5 square pyramid. Crystal data: for **2**· C_6H_6 , space group = $P\bar{1}$, $a = 16.755(2)$ Å, $b = 11.647(2)$ Å, $c = 11.355(2)$ Å, $\alpha = 61.30(1)^\circ$, $\beta = 89.78(1)^\circ$, $\gamma = 101.76(2)^\circ$, $Z = 2$, 2648 reflections, $R = 0.032$; for **3**: space group = $Pnma$, $a = 23.373(3)$ Å, $b = 17.643(2)$ Å, $c = 9.453(2)$ Å, $Z = 4$, 1854 reflections, $R = 0.030$; for **4**· C_6H_6 , space group = $P2_1/a$, $a = 13.366(2)$ Å, $b = 20.746(6)$ Å, $c = 13.059(3)$ Å, $\beta = 90.75(1)^\circ$, $Z = 4$, 3345 reflections, $R = 0.025$; for **5**· CH_2Cl_2 , space group = $P2_1/c$, $a = 13.669(2)$ Å, $b = 15.610(3)$ Å, $c = 15.476(2)$ Å, $\beta = 92.46(1)^\circ$, $Z = 4$, 4526 reflections, $R = 0.033$.

Introduction

We have recently developed new procedures for the preparation of polythiaether macrocycles that involve the catalytic cyclooligomerization of thietanes, eq (1).^{1,2} Polythiaether macrocycles have recently attracted attention because of their ability to serve as ligands for the transition elements.³ To date, however, there have been very few reports on metal carbonyl cluster com-



plexes that contain polythiaether macrocycles as ligands.^{4,5} We have recently shown that the trithia macrocycle 12S3 can be attached to the pentaruthenium carbido carbonyl cluster complex $\text{Ru}_5(\text{CO})_{15}(\mu_5\text{-C})$ in a

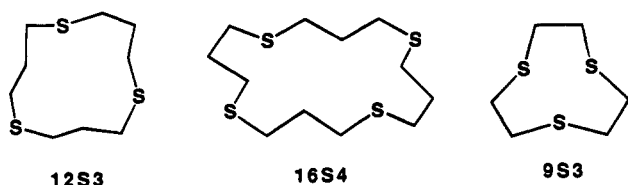
[®] Abstract published in *Advance ACS Abstracts*, March 15, 1995.
 (1) (a) Adams, R. D.; Falloon, S. B. *J. Am. Chem. Soc.* **1994**, *116*, 10540. (b) Adams, R. D.; Cortopassi, J. E.; Falloon, S. B. *J. Organomet. Chem.* **1993**, *463*, C5.

(2) Adams, R. D.; Falloon, S. B. *Organometallics* **1995**, *14*, 1748.

(3) (a) Cooper, S. R., Ed. *Crown Compounds: Toward Future Applications*; VCH Publishers: New York, 1992. (b) Cooper, S. R.; Rawle, S. C. *Struct. Bonding* **1990**, *72*, 1. (c) Blake, A. J.; Schröder, M. *Adv. Inorg. Chem.* **1990**, *35*, 1. (d) Cooper, S. R. *Acc. Chem. Res.* **1988**, *21*, 141.

sequence of decarbonylation steps that leads ultimately to a tridentate coordination in which one of the sulfur atoms also serves as a bridge between two metal atoms.⁵

In this report, the results of our studies of the complexation of three different polythiaether macrocycles **1**, **5**, 9-trithiacyclododecane (12S3), 1,5,9,13-tetra-



thiacyclohexadecane (16S4), and 1,4,7-trithiacyclononane (9S3) to the hexaruthenium carbido cluster $\text{Ru}_6(\text{CO})_{17}(\mu_6\text{-C})$, **1**, are described. These studies further demonstrate that the thiaether ligands are able to change their conformations in order to serve as more effective ligands. We have also found additional evidence that those ligands that contain C_2H_4 groupings between pairs of sulfur atoms are subject to degradation through the elimination of C_2H_4 under mild conditions. The 9S3 complex $\text{Ru}_6(\text{CO})_{14}(\eta^3\text{-9S3})(\mu_6\text{-C})$, **4**, was found to undergo elimination of ethylene to yield a new hexanuclear complex $\text{Ru}_6(\text{CO})_{14}(\mu_3\text{-}\eta^3\text{-SCH}_2\text{CH}_2\text{SCH}_2\text{CH}_2\text{S})(\mu_5\text{-C})$, **5**, containing a 3-thiapentane-1,5-dithiolato ligand when heated to 105 °C.

Experimental Section

General Data. Reagent grade solvents were stored over 4Å molecular sieves. All reactions were performed under a nitrogen atmosphere. Infrared spectra were recorded on a Nicolet 5DXB FTIR spectrophotometer. ^1H NMR spectra were recorded on a Bruker AM-500 FT-NMR spectrometer. $\text{Ru}_6(\text{CO})_{17}(\mu_6\text{-C})$, **1**, was prepared by the previously reported procedure.⁶ 1,5,9-Trithiacyclododecane, 12S3, was prepared by the catalytic cyclooligomerization of thietane.^{1a} 1,5,9,13-Tetrathiahexadecane, 16S4, and 1,4,7-trithiacyclononane, 9S3, were purchased from Aldrich Chemical Co. and were used without further purification. Elemental analyses were performed by Oneida Research Services, Whitesboro, NY.

Preparation of $\text{Ru}_6(\text{CO})_{13}(\mu\text{-}\eta^3\text{-12S3})(\mu_6\text{-C})$, **2.** A 20.0-mg amount of **1** (0.0183 mmol) and a 5.3-mg amount of 12S3 (0.024 mmol) were dissolved in 30 mL of octane. The solution was brought to reflux and maintained for 4 h in the presence of a slow purge with nitrogen. After cooling of the solution to room temperature, a brown precipitate formed. The solid was washed with 3 × 10 mL portions of hexanes and dissolved with 30 mL of CH_2Cl_2 , and the mixture was filtered under nitrogen. The solvent was removed under vacuum. This yielded 17.2-mg of $\text{Ru}_6(\text{CO})_{13}(\mu\text{-}\eta^3\text{-12S3})(\mu_6\text{-C})$, **2**, in 78% yield. Analytical samples were obtained by recrystallization from CH_2Cl_2 /benzene (2/1) solutions by slow evaporation of solvent at 25 °C. Analytical and spectral data for **2** are as follows. IR (ν_{CO} , cm^{-1} , in CH_2Cl_2): 2078 (m), 2039 (vs), 2024 (vs), 1999 (m, sh), 1975 (w, sh), 1836 (w). ^1H NMR (δ in CDCl_3): 3.1 (m, 4H), 2.85 (dd, 4H), 2.57 (dd, 4H), 2.2 (m, 4H), 1.84 (q, 2H). Anal. Calc (found) for C_6H_6 : C, 27.15 (26.38); H, 1.88 (1.72).

Preparation of $\text{Ru}_6(\text{CO})_{15}(\mu\text{-}\eta^2\text{-16S4})(\mu_6\text{-C})$, **3.** A 20.0-mg amount of **1** (0.0183 mmol) and 6.5 mg of 16S4 (0.022 mmol) were dissolved in 30 mL of octane. The solution was brought to reflux and maintained for 2 h in the presence of a

slow purge with nitrogen. After cooling of the solution to room temperature, a brown precipitate formed. The solid was washed with 3 × 10 mL portions of hexane and then dissolved with 30 mL of CH_2Cl_2 , and the mixture was filtered under nitrogen. The solvent was then removed under vacuum to yield 6.8-mg of $\text{Ru}_6(\text{CO})_{15}(\mu\text{-}\eta^2\text{-16S4})(\mu_6\text{-C})$, **3**, in 58% yield. Analytical samples were obtained by recrystallization by slow evaporation of solvent from a CH_2Cl_2 /hexane (2/1) solution at -20 °C. Spectral data for **3** are as follows. IR (ν_{CO} , cm^{-1} , CH_2Cl_2): 2073 (m), 2033 (s), 2018 (vs), 2003 (m, sh), 1969 (w), 1825 (w). ^1H NMR (δ in CDCl_3): 2.47–2.77 (m, 8H), 3.34–3.48 (m, 16H). Anal. Calc (found) for **3**: C, 25.19 (25.45); H, 1.81 (1.81).

Preparation of $\text{Ru}_6(\text{CO})_{14}(\eta^3\text{-9S3})(\mu_6\text{-C})$, **4.** A 20.0-mg amount of **1** (0.0183 mmol) and 3.9 mg of 9S3 (0.022 mmol) were dissolved in 30 mL of hexane, and then the solution was heated to reflux with a nitrogen purge for 4 h. The solvent was then removed under vacuum, and the crude product dissolved in a minimal amount of CH_2Cl_2 and separated by column chromatography on silica gel (12 mm × 200 mm). Elution with hexane yielded 4.4 mg of unreacted $\text{Ru}_6(\text{CO})_{17}(\mu_6\text{-C})$, and elution with CH_2Cl_2 yielded 15.9 mg of $\text{Ru}_6(\text{CO})_{14}(\eta^3\text{-9S3})(\mu_6\text{-C})$, **4**, in 93% yield (based on **1** consumed). Analytical and spectral data for **4** are as follows. IR (ν_{CO} , cm^{-1} , in CH_2Cl_2): 2066 (m), 2017 (vs), 1975 (w, br), 1800 (w, br). ^1H NMR (δ in CD_2Cl_2): 2.78 (m, 6H, $^2J_{\text{H-H}} = -13.9$ Hz, $^3J_{\text{H-H}} = 7.0$ Hz, $^3J_{\text{H-H}} = 6.7$ Hz), 2.33 (m, 6H, $^2J_{\text{H-H}} = -13.9$ Hz, $^3J_{\text{H-H}} = 7.0$ Hz, $^3J_{\text{H-H}} = 6.7$ Hz). Anal. Calc (found) for **4** (crystals obtained from CH_2Cl_2): C, 21.18 (20.38); H, 1.02 (1.05).

Preparation of $\text{Ru}_6(\text{CO})_{14}(\mu_3\text{-}\eta^3\text{-SCH}_2\text{CH}_2\text{SCH}_2\text{CH}_2\text{S})(\mu_5\text{-C})$, **5.** A 20.0-mg amount of **1** (0.0183 mmol) and 3.9 mg of 9S3 (0.022 mmol) were dissolved in 30 mL of octane, and then the solution was heated to reflux with a nitrogen purge for 2 h. The solvent was then removed under vacuum, and the crude product was dissolved in a minimal amount of CH_2Cl_2 and separated by column chromatography on silica gel (12 mm × 200 mm). Elution with hexane yielded 1.2 mg of unreacted $\text{Ru}_6(\text{CO})_{17}(\mu_6\text{-C})$, and elution with CH_2Cl_2 yielded 7.3 mg of $\text{Ru}_6(\text{CO})_{14}(\mu_3\text{-}\eta^3\text{-SCH}_2\text{CH}_2\text{SCH}_2\text{CH}_2\text{S})(\mu_5\text{-C})$, **5**, in 36% yield. Analytical and spectral data for **5** are as follows. IR (ν_{CO} , cm^{-1} , in CH_2Cl_2): 2085 (s), 2056 (vs), 2035 (m), 2022 (vs), 2003 (m, sh), 1975 (w, br). ^1H NMR (δ in CD_2Cl_2): 4.26 (dd, $J = 7.5$ Hz, 13.0 Hz, 1H), 3.91 (dd, $J_{\text{H-H}} = 7.9$ Hz, $J_{\text{H-H}} = 13.3$ Hz, 1H), 3.65 (dd, $J_{\text{H-H}} = 5.5$ Hz, 10.6 Hz, 1H), 3.3–3.42 (m, 2H), 3.2 (ddd, $J_{\text{H-H}} = 7.9$ Hz, $J_{\text{H-H}} = 11.0$ Hz, 11.0 Hz, 1H), 2.9 (ddd, $J_{\text{H-H}} = 8.3$ Hz, 11.0 Hz, 11.0 Hz, 1H), 2.5 (ddd, $J_{\text{H-H}} = 6.6$ Hz, 10.8 Hz, 13.2 Hz, 1H). Anal. Calc (found) for **5-CH}_2\text{Cl}_2: C, 19.25 (20.23); H, 0.81 (0.42).**

Conversion of **4 to **5**.** An NMR tube was charged with a 4.5 mg sample of **4** in toluene- d_6 under a nitrogen atmosphere and placed in an oil bath at 105 °C for 18 h. An NMR spectrum recorded after this period showed the formation of ethylene as a sharp singlet at 5.25 ppm. The solvent was then removed, and 3.0 mg of **5** (68% yield) was isolated from the sample by TLC.

Reaction of $\text{Ru}_6(\text{CO})_{13}(\mu\text{-}\eta^3\text{-12S3})(\mu_6\text{-C})$, **2, with CO.** A 25.0-mg amount of **2** was dissolved in 40 mL of THF, and the solution was heated to reflux under a slow purge of CO for 5 h. The solvent was then removed under vacuum and the crude product separated by TLC using a CH_2Cl_2 /hexane (1:1) eluant. This yielded 10.0 mg of **1** (45% yield).

Crystallographic Analysis. Crystals of **2** suitable for diffraction analysis were grown by slow evaporation of solvent from a solution in a CH_2Cl_2 /benzene (2/1) solvent mixture at 25 °C. Crystals of **3** and **5** suitable for diffraction analysis were grown by slow evaporation of solvent from a solution in a CH_2Cl_2 /hexane (2/1) solvent mixture at -20 °C. Crystals of **4** suitable for diffraction analysis were grown by slow evaporation of solvent from a solution in a CH_2Cl_2 /benzene (2/1) solvent mixture at 25 °C. All crystals used for the diffraction measurements were mounted in thin-walled glass capillaries. Diffraction measurements were made on a Rigaku AFC6S fully automated four-circle diffractometer using graphite-monochro-

(4) Edwards, A. J.; Johnson, B. F. G.; Khan, F. K.; Lewis, J.; Raithby, P. R. *J. Organomet. Chem.* **1992**, 426, C44.

(5) Adams, R. D.; Falloon, S. B.; McBride, K. T. *Organometallics* **1994**, 13, 4870.

(6) Nicholls, J. N.; Vargas, M. D. *Inorg. Synth.* **1983**, 26, 281.

Table 1. Crystallographic Data for Compounds 2–5

	compound			
	2	3	4	5
empirical formula	Ru ₆ S ₃ O ₁₃ C ₂₃ H ₁₈ ·C ₆ H ₆	Ru ₆ S ₄ O ₁₅ C ₂₈ H ₂₄	Ru ₆ S ₃ O ₁₄ C ₂₁ H ₁₂ ·C ₆ H ₆	Ru ₆ S ₃ O ₁₄ C ₁₉ H ₁₀ ·CH ₂ Cl ₂
fw	1283.10	1335.15	1269.03	1247.80
cryst system	triclinic	orthorhombic	monoclinic	monoclinic
lattice params				
<i>a</i> (Å)	16.755(2)	23.373(3)	13.366(2)	13.669(2)
<i>b</i> (Å)	11.647(2)	17.643(2)	20.746(6)	15.610(3)
<i>c</i> (Å)	11.355(2)	9.453(2)	13.059(3)	15.476(2)
α (deg)	61.30(1)	90.0	90.0	90.0
β (deg)	89.78(1)	90.0	90.75(1)	92.46(1)
γ (deg)	101.76(2)	90.0	90.0	90.0
<i>V</i> (Å ³)	1889.5(6)	3898.2(8)	3621(1)	3299.1(8)
space group	<i>P</i> $\bar{1}$ (No. 2)	<i>Pnma</i> (No. 62)	<i>P2</i> ₁ / <i>a</i> (No. 14)	<i>P2</i> ₁ / <i>c</i> (No. 14)
<i>Z</i> value	2	4	4	4
<i>D</i> _{calc} (g/cm ³)	2.26	2.28	2.33	2.51
μ (Mo K α) (cm ⁻¹)	25.63	25.45	26.23	30.90
temp (°C)	20	20	20	20
2 θ _{max} (deg)	41	46	44	48
no. obs <i>I</i> > 3 σ (<i>I</i>)	2648	1854	3345	4526
no. variables	430	256	452	402
residuals: ^a <i>R</i> ; <i>R</i> _w	0.032; 0.028	0.030; 0.030	0.025; 0.025	0.033; 0.042
GOF	1.56	1.49	1.41	2.52
max shift final cycle	0.01	0.04	0.02	0.15
largest peak in final diff map (e/Å ³)	0.85	0.43	0.48	1.24
abs corr, max/min	empirical, 1.0/0.83	empirical, 1.0/0.79	empirical, 1.0/0.66	empirical, 1.0/0.66

$$^a R = \sum_{hk} (|F_o| - |F_c|) / \sum_{hk} |F_o|, R_w = [\sum_{hk} w(|F_o| - |F_c|)^2 / \sum_{hk} w F_o^2]^{1/2}, w = 1/\sigma^2(F_o). \text{ GOF} = [\sum_{hk} (|F_o| - |F_c|/\sigma(F_o))^2 / (n_{\text{data}} - n_{\text{vari}})].$$

mated Mo K α radiation. The unit cells of the crystals were determined and refined from 15 randomly selected reflections obtained by using the AFC6 automatic search, center, index, and least-squares routines. Crystal data, data collection parameters, and results of the analyses are listed in Table 1. All data processing was performed on a Digital Equipment Corp. VAXstation 3520 computer by using the TEXSAN motif structure solving program library obtained from the Molecular Structure Corp., The Woodlands, TX. Neutral atom scattering factors were calculated by the standard procedures.^{7a} Anomalous dispersion corrections were applied to all non-hydrogen atoms.^{7b} Lorentz/polarization (*Lp*) and absorption corrections (empirical based on ψ -scans) were applied to the data for each structure. Full matrix least-squares refinements minimized the function $\sum_{hk} w(|F_o| - |F_c|)^2$, where $w = 1/\sigma^2(F)$, $\sigma(F) = \sigma(F_o^2)/2F_o$, and $\sigma(F_o^2) = [\sigma(I_{\text{raw}})^2 + (0.02I_{\text{net}})^2]^{1/2}/Lp$.

Compound **2** crystallized in the triclinic crystal system. The space group *P* $\bar{1}$ was assumed and confirmed by the successful solution and refinement of the structure. The structure was solved by a combination of direct methods (MITHRIL) and difference Fourier syntheses. All non-hydrogen atoms were refined with anisotropic thermal parameters. The positions of the hydrogen atoms on the 12S3 ligand were calculated by assuming idealized tetrahedral geometries at the carbon atoms with C–H distances of 0.95 Å. The scattering contributions of the hydrogen atoms were included in the structure factor calculations, but their positions were not refined. In the final stages of the analysis two formula equivalents of benzene that had cocrystallized from the crystallization solvent were located in the lattice. There were both centered about centers of symmetry. They were added to the analysis and satisfactorily refined with isotropic thermal parameters for the carbon atoms.

Compound **3** crystallized in the orthorhombic crystal system. The patterns of systematic absences observed during the collection of the intensity data were consistent with either of the space groups *Pnma* or *Pna2*₁. The centrosymmetric space group *Pnma* was selected and confirmed by the successful solution and refinement of the structure. The structure was solved by a combination of direct methods (MITHRIL) and

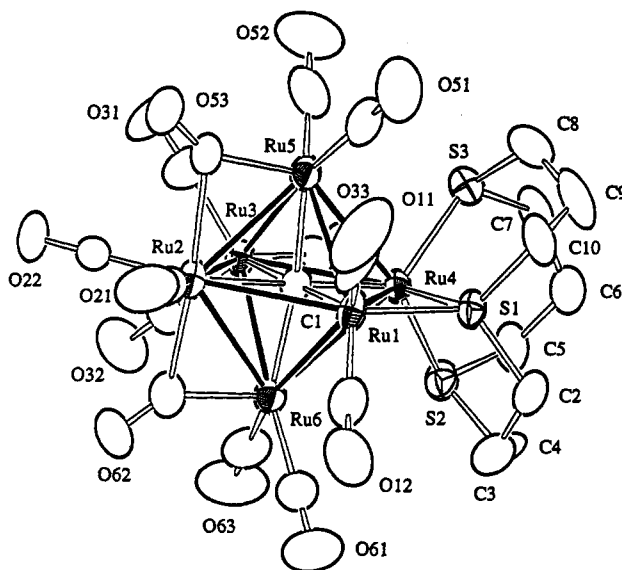


Figure 1. ORTEP diagram of Ru₆(CO)₁₃(μ - η^3 -12S3)(μ_6 -C)₂, showing 40% probability thermal ellipsoids.

difference Fourier syntheses. All non-hydrogen atoms were refined with anisotropic thermal parameters. The positions of the hydrogen atoms on the 16S4 ligand were calculated by assuming idealized tetrahedral geometries at the carbon atoms with C–H distances of 0.95 Å. The scattering contributions of the hydrogen atoms were included in the structure factor calculations, but their positions were not refined.

Compounds **4** and **5** both crystallized in the monoclinic crystal system. The space groups *P2*₁/*a* and *P2*₁/*c*, respectively, were identified uniquely on the basis of the patterns of systematic absences observed during the collection of the intensity data. Both structures were solved by a combination of direct methods (MITHRIL) and difference Fourier syntheses. All non-hydrogen atoms were refined with anisotropic thermal parameters. The positions of the hydrogen atoms on the 9S3 ligand were calculated by assuming idealized tetrahedral geometries at the carbon atoms with C–H distances of 0.95 Å. The scattering contributions of the hydrogen atoms were included in the structure factor calculations, but their positions

(7) (a) *International Tables for X-ray Crystallography*; Kynoch Press: Birmingham, England, 1975; Vol. IV, Table 2.2B, pp 99–101. (b) *Ibid.*, Table 2.3.1, pp 149–150.

Table 2. Positional Parameters and $B(\text{eq})$ Values for **2 (\AA^2)**

atom	<i>x</i>	<i>y</i>	<i>z</i>	<i>B</i> (eq)
Ru(1)	0.37109(6)	0.0426(1)	0.1604(1)	3.65(8)
Ru(2)	0.29892(6)	-0.1001(1)	0.4454(1)	3.55(7)
Ru(3)	0.14721(5)	-0.0221(1)	0.35095(9)	3.12(7)
Ru(4)	0.22738(6)	0.1216(1)	0.07375(9)	2.86(7)
Ru(5)	0.30070(6)	0.1750(1)	0.2811(1)	3.80(8)
Ru(6)	0.22371(6)	-0.1735(1)	0.2605(1)	3.40(7)
S(1)	0.3443(2)	0.1806(3)	-0.0520(3)	3.6(2)
S(2)	0.1404(2)	0.0401(3)	-0.0457(3)	4.1(2)
S(3)	0.2007(2)	0.3369(3)	-0.0172(3)	3.9(2)
O(11)	0.5415(6)	0.166(2)	0.189(1)	12(1)
O(12)	0.4481(6)	-0.155(1)	0.127(1)	8(1)
O(21)	0.4616(6)	-0.157(1)	0.540(1)	8(1)
O(22)	0.2179(6)	-0.226(1)	0.7299(9)	7.1(8)
O(31)	0.1018(6)	0.071(1)	0.544(1)	8(1)
O(32)	0.0185(6)	-0.283(1)	0.514(1)	9(1)
O(33)	0.0298(5)	0.1081(9)	0.1549(9)	5.6(8)
O(51)	0.4533(7)	0.402(1)	0.162(1)	10(1)
O(52)	0.2123(9)	0.362(1)	0.310(2)	11(1)
O(53)	0.3524(6)	0.1018(9)	0.5555(8)	6.8(8)
O(61)	0.2803(8)	-0.330(1)	0.141(1)	10(1)
O(62)	0.2482(6)	-0.400(1)	0.5248(9)	6.2(8)
O(63)	0.0571(6)	-0.341(1)	0.279(1)	9(1)
C(1)	0.2580(7)	0.010(1)	0.256(1)	3.3(8)
C(2)	0.3463(8)	0.133(1)	-0.182(1)	5(1)
C(3)	0.288(1)	0.006(1)	-0.144(1)	6(1)
C(4)	0.198(1)	0.017(1)	-0.167(1)	6(1)
C(5)	0.0884(7)	0.162(1)	-0.163(1)	5(1)
C(6)	0.1355(7)	0.307(1)	-0.238(1)	5(1)
C(7)	0.1360(7)	0.378(1)	-0.155(1)	5(1)
C(8)	0.2935(8)	0.468(1)	-0.107(1)	6(1)
C(9)	0.3510(8)	0.452(1)	-0.198(1)	7(1)
C(10)	0.4012(7)	0.356(1)	-0.141(1)	5(1)
C(11)	0.4761(9)	0.119(2)	0.179(1)	7(1)
C(12)	0.4164(8)	-0.083(2)	0.142(1)	6(1)
C(21)	0.3993(9)	-0.134(1)	0.500(1)	5(1)
C(22)	0.2484(7)	-0.179(1)	0.622(1)	4(1)
C(31)	0.1187(8)	0.040(1)	0.470(1)	6(1)
C(32)	0.0678(8)	-0.185(1)	0.451(1)	5(1)
C(33)	0.0837(8)	0.068(1)	0.210(1)	5(1)
C(51)	0.395(1)	0.317(2)	0.205(1)	7(1)
C(52)	0.246(1)	0.286(2)	0.296(2)	7(1)
C(53)	0.3303(7)	0.090(1)	0.465(1)	4(1)
C(61)	0.2621(9)	-0.268(1)	0.185(1)	6(1)
C(62)	0.2526(7)	-0.288(1)	0.445(1)	4(1)
C(63)	0.1217(9)	-0.275(1)	0.273(1)	6(1)
C(71)	0.959(1)	0.542(2)	0.887(2)	8.9(5)
C(72)	0.932(1)	0.418(2)	1.000(2)	7.7(4)
C(73)	0.971(1)	0.379(2)	1.109(2)	8.5(4)
C(81)	0.459(1)	0.596(2)	0.458(2)	7.5(4)
C(82)	0.4290(9)	0.486(2)	0.447(1)	6.4(3)
C(83)	0.472(1)	0.390(2)	0.490(2)	7.1(4)

Table 3. Intramolecular Distances for **2^a**

Ru(1)–Ru(2)	2.947(2)	Ru(4)–S(3)	2.352(3)
Ru(1)–Ru(4)	2.768(2)	Ru(4)–C(1)	1.98(1)
Ru(1)–Ru(5)	2.900(2)	Ru(5)–C(1)	2.06(1)
Ru(1)–Ru(6)	2.902(2)	Ru(6)–C(1)	2.08(1)
Ru(1)–S(1)	2.276(3)	S(1)–C(2)	1.81(1)
Ru(1)–C(1)	2.05(1)	S(1)–C(10)	1.82(1)
Ru(2)–Ru(3)	2.909(2)	S(2)–C(4)	1.83(1)
Ru(2)–Ru(5)	2.823(2)	S(2)–C(5)	1.81(1)
Ru(2)–Ru(6)	2.834(1)	S(3)–C(7)	1.83(1)
Ru(2)–C(1)	2.11(1)	S(3)–C(8)	1.82(1)
Ru(3)–Ru(4)	2.916(1)	O–C(av)	1.15(2)
Ru(3)–Ru(5)	2.888(1)	C(2)–C(3)	1.45(2)
Ru(3)–Ru(6)	2.907(2)	C(3)–C(4)	1.56(2)
Ru(3)–C(1)	2.01(1)	C(5)–C(6)	1.50(2)
Ru(4)–Ru(5)	2.926(1)	C(6)–C(7)	1.53(2)
Ru(4)–Ru(6)	3.037(2)	C(8)–C(9)	1.51(2)
Ru(4)–S(1)	2.199(3)	C(9)–C(10)	1.44(2)
Ru(4)–S(2)	2.357(3)		

^a Distances are in angstroms. Estimated standard deviations in the least significant figure are given in parentheses.

were not refined. In the final stages of the analysis of compound **4** one formula equivalent of benzene that had cocrystallized from the crystallization solvent was located in

Table 4. Intramolecular Bond Angles for **2^a**

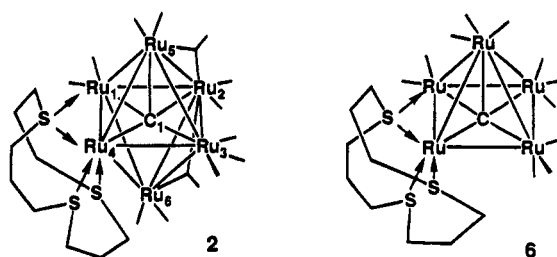
Ru(2)–Ru(1)–Ru(4)	91.40(4)	Ru(1)–Ru(5)–Ru(3)	89.28(5)
Ru(2)–Ru(1)–Ru(5)	57.72	Ru(1)–Ru(5)–Ru(4)	56.75(4)
Ru(2)–Ru(1)–Ru(6)	57.96	Ru(2)–Ru(5)–Ru(3)	61.24(4)
Ru(2)–Ru(1)–S(1)	141.66(9)	Ru(2)–Ru(5)–Ru(4)	90.78(5)
Ru(4)–Ru(1)–Ru(5)	62.09(4)	Ru(3)–Ru(5)–Ru(4)	60.21(4)
Ru(4)–Ru(1)–Ru(6)	64.72(3)	Ru(1)–Ru(6)–Ru(2)	61.82(4)
Ru(4)–Ru(1)–S(1)	50.55(8)	Ru(1)–Ru(6)–Ru(3)	88.87(5)
Ru(5)–Ru(1)–Ru(6)	90.48(4)	Ru(1)–Ru(6)–Ru(4)	55.52(3)
Ru(5)–Ru(1)–S(1)	94.3(1)	Ru(1)–Ru(6)–C(1)	45.1(3)
Ru(6)–Ru(1)–S(1)	101.24(8)	Ru(1)–Ru(6)–C(61)	94.6(4)
Ru(1)–Ru(2)–Ru(3)	87.97(3)	Ru(1)–Ru(6)–C(62)	98.3(3)
Ru(1)–Ru(2)–Ru(5)	60.30(4)	Ru(1)–Ru(6)–C(63)	162.2(4)
Ru(1)–Ru(2)–Ru(6)	60.22(4)	Ru(2)–Ru(6)–Ru(3)	60.87(4)
Ru(3)–Ru(2)–Ru(5)	60.50(4)	Ru(2)–Ru(6)–Ru(4)	88.32(5)
Ru(3)–Ru(2)–Ru(6)	60.81(4)	Ru(3)–Ru(6)–Ru(4)	58.71(4)
Ru(5)–Ru(2)–Ru(6)	93.48(4)	Ru(1)–S(1)–Ru(4)	76.41(9)
Ru(2)–Ru(3)–Ru(4)	89.26(4)	Ru(1)–S(1)–C(2)	120.6(4)
Ru(2)–Ru(3)–Ru(5)	58.27(4)	Ru(1)–S(1)–C(10)	118.9(5)
Ru(2)–Ru(3)–Ru(6)	58.32(4)	Ru(4)–S(1)–C(2)	118.3(4)
Ru(4)–Ru(3)–Ru(5)	60.53(4)	Ru(4)–S(1)–C(10)	120.2(5)
Ru(4)–Ru(3)–Ru(6)	62.86(4)	C(2)–S(1)–C(10)	102.4(6)
Ru(5)–Ru(3)–Ru(6)	90.60(4)	Ru(4)–S(2)–C(4)	112.1(5)
Ru(1)–Ru(4)–Ru(3)	91.32(4)	Ru(4)–S(2)–C(5)	113.2(5)
Ru(1)–Ru(4)–Ru(5)	61.16(4)	C(4)–S(2)–C(5)	98.4(6)
Ru(1)–Ru(4)–Ru(6)	59.77(4)	Ru(4)–S(3)–C(7)	114.6(5)
Ru(1)–Ru(4)–S(1)	53.04(8)	Ru(4)–S(3)–C(8)	111.1(5)
Ru(1)–Ru(4)–S(2)	124.0(1)	C(7)–S(3)–C(8)	99.7(6)
Ru(1)–Ru(4)–S(3)	128.88(9)	S(1)–C(2)–C(3)	112(1)
Ru(3)–Ru(4)–Ru(5)	59.26(4)	C(2)–C(3)–C(4)	115(1)
Ru(3)–Ru(4)–Ru(6)	58.43(4)	S(2)–C(4)–C(3)	117(1)
Ru(3)–Ru(4)–S(1)	144.21(8)	S(2)–C(5)–C(6)	117.3(9)
Ru(3)–Ru(4)–S(2)	105.50(7)	C(5)–C(6)–C(7)	113(1)
Ru(3)–Ru(4)–S(3)	104.3(1)	S(3)–C(7)–C(6)	118(1)
Ru(5)–Ru(4)–Ru(6)	87.38(4)	S(3)–C(8)–C(9)	119(1)
Ru(5)–Ru(4)–S(1)	95.2(1)	C(8)–C(9)–C(10)	120(1)
Ru(5)–Ru(4)–S(2)	164.74(7)	S(1)–C(10)–C(9)	114.7(9)
Ru(5)–Ru(4)–S(3)	85.6(1)	Ru(2)–C(53)–Ru(5)	83.1(6)
Ru(6)–Ru(4)–S(1)	99.1(1)	Ru(2)–C(53)–O(53)	129.1(9)
Ru(6)–Ru(4)–S(2)	84.37(8)	Ru(5)–C(53)–O(53)	148(1)
Ru(6)–Ru(4)–S(3)	162.4(1)	Ru(2)–C(62)–Ru(6)	85.7(5)
S(1)–Ru(4)–S(2)	98.7(1)	Ru(2)–C(62)–O(62)	133(1)
S(1)–Ru(4)–S(3)	97.6(1)	Ru(6)–C(62)–O(62)	141(1)
S(2)–Ru(4)–S(3)	98.5(1)	Ru–C–O(av)	176(1)
Ru(1)–Ru(5)–Ru(2)	61.98(4)		

^a Angles are in degrees. Estimated standard deviations in the least significant figure are given in parentheses.

a general position in the lattice. It was added to the analysis and satisfactorily refined with anisotropic thermal parameters for the carbon atoms. In the final stages of the analysis of compound **5** one formula equivalent of CH_2Cl_2 that had cocrystallized from the crystallization solvent was located in a general position in the lattice. It was added to the analysis and satisfactorily refined with anisotropic thermal parameters for the chlorine atoms and an isotropic thermal parameter for the carbon atom.

Results and Discussion

The reaction of $12\text{S}3$ with $\text{Ru}_6(\text{CO})_{17}(\mu_6\text{-C})$, **1**, in octane solvent at reflux produced only one compound $\text{Ru}_6(\text{CO})_{13}(\mu\text{-}\eta^3\text{-}12\text{S}3)(\mu_6\text{-C})$, **2**, in 78% yield. Compound



2 was characterized by a combination of IR, ^1H NMR,

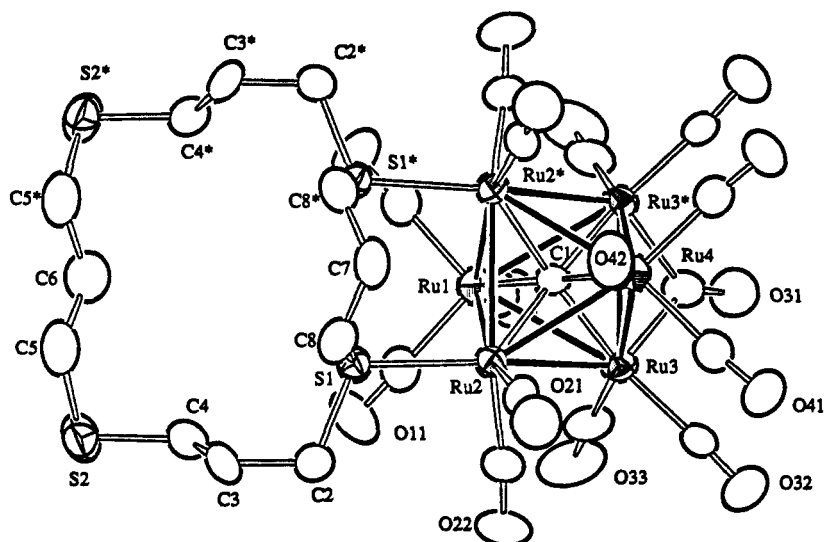


Figure 2. ORTEP diagram of $\text{Ru}_6(\text{CO})_{15}(\mu\text{-}\eta^2\text{-16S4})(\mu_6\text{-C})$, **3**, showing 40% probability thermal ellipsoids.

and single crystal X-ray diffraction analysis. An ORTEP drawing of the molecular structure of **2** is shown in Figure 1. Final atomic positional parameters are listed in Table 2. Selected interatomic distances and angles are listed in Tables 3 and 4, respectively. The molecule contains an octahedral Ru_6 cluster with a carbido ligand inside the cluster. This is structurally analogous to that of the parent complex **1**.⁸ The 12S3 ligand exhibits a $\mu\text{-}\eta^3$ tridentate coordination. All three sulfur atoms are coordinated to one ruthenium atom Ru(4), but one of the sulfur atoms S(1) also uses its second lone pair of electrons to coordinate to one of the neighboring ruthenium atoms Ru(1) and forms a bridging interaction. A similarly coordinated 12S3 ligand was found in the complex $\text{Ru}_5(\text{CO})_{11}(\mu\text{-}\eta^3\text{-12S3})(\mu_5\text{-C})$, **6**, that was recently obtained by us from the reaction of $\text{Ru}_5(\text{CO})_{15}(\mu_5\text{-C})$ with 12S3⁵ and the compound $\text{Ru}_6(\text{CO})_{15}(\mu_4\text{-}\eta^2\text{-CO})(\mu\text{-}\eta^3\text{-12S3})$, **7**, that was obtained from the reaction of 12S3 with $\text{Ru}_3(\text{CO})_{12}$.⁴

The metal-metal bond distances in **2** are similar to those found in **1**, but as found in **6**, the macrocycle does produce significant effects on these distances. For example, the sulfur-bridged metal-metal bond, Ru(1)-Ru(4), is the shortest in the molecule, 2.768(2) Å, while the other metal-metal bonds to Ru(4), Ru(3)-Ru(4) = 2.916(1) Å, Ru(4)-Ru(5) = 2.926(1) Å, and Ru(4)-Ru(6) = 3.037(2) Å, are the longest in the molecule. There are two metal-metal bonds that contain bridging carbonyl ligands, Ru(2)-Ru(5) and Ru(2)-Ru(6), and these bonds also have relatively short lengths, 2.823(2) and 2.834(1) Å, respectively. The carbido ligand does not lie in the exact center of the Ru_6 octahedron but is shifted closer to the metal atom coordinated to the 12S3 ligand (e.g. Ru(4)-C(1) = 1.98(1), Ru(2)-C(1) = 2.11(1) Å). A similar shift of the carbido ligand was observed in **6**. In **2**, **6**, and **7** the 12S3 ligand adopts a conformation in which the three sulfur atoms point toward the inside of the ring to facilitate coordination to the metal atoms. However, this is quite unlike the free molecule and many mononuclear metal complexes where the lone pairs on the sulfur atoms do not point to the inside of

Table 5. Positional Parameters and $B(\text{eq})$ Values (\AA^2) for **3**

atom	x	y	z	$B(\text{eq})$
Ru(1)	0.97861(4)	1/4	0.37176(9)	3.19(5)
Ru(2)	1.04277(3)	0.16581(4)	0.15828(8)	2.92(3)
Ru(3)	0.91790(3)	0.16984(3)	0.15570(8)	3.14(3)
Ru(4)	0.98500(4)	1/4	-0.0598(1)	3.02(5)
S(1)	1.13074(9)	0.1600(1)	0.2865(2)	3.4(1)
S(2)	1.2316(1)	0.0935(2)	0.7285(3)	5.5(1)
O(11)	0.8713(4)	1/4	0.555(1)	6.6(6)
O(12)	1.0335(3)	0.3778(4)	0.5394(7)	6.3(4)
O(21)	1.0964(3)	0.0960(4)	-0.0994(7)	6.4(4)
O(22)	1.0032(3)	0.0074(4)	0.228(1)	7.9(5)
O(31)	0.8042(4)	1/4	0.157(1)	6.0(5)
O(32)	0.8586(3)	0.0491(4)	-0.0163(7)	6.4(4)
O(33)	0.8703(4)	0.0854(4)	0.4026(8)	9.4(5)
O(41)	0.9264(3)	0.3681(4)	-0.2419(7)	5.7(4)
O(42)	1.0853(4)	1/4	-0.261(1)	5.9(5)
C(1)	0.9829(5)	1/4	0.157(1)	2.9(5)
C(2)	1.1486(3)	0.0644(5)	0.342(1)	4.2(4)
C(3)	1.1964(3)	0.0632(5)	0.4524(9)	4.1(4)
C(4)	1.1775(4)	0.0918(5)	0.5951(9)	4.1(4)
C(5)	1.2695(4)	0.1770(6)	0.685(1)	5.8(6)
C(6)	1.2377(6)	1/4	0.699(1)	5.9(9)
C(7)	1.1888(5)	1/4	0.088(1)	4.2(7)
C(8)	1.1914(3)	0.1761(5)	0.170(1)	4.4(4)
C(11)	0.9109(6)	1/4	0.488(1)	4.4(7)
C(12)	1.0146(4)	0.3312(5)	0.4703(9)	4.2(4)
C(21)	1.0761(4)	0.1258(5)	-0.006(1)	4.2(5)
C(22)	1.0138(4)	0.0684(5)	0.203(1)	5.0(5)
C(31)	0.8542(5)	1/4	0.157(1)	3.9(6)
C(32)	0.8812(4)	0.0969(5)	0.045(1)	3.9(4)
C(33)	0.8891(4)	0.1197(5)	0.309(1)	5.2(6)
C(41)	0.9471(4)	0.3261(5)	-0.164(1)	4.0(4)
C(42)	1.0490(5)	1/4	-0.183(1)	4.5(7)

the ring.⁹ In **2** the 12S3 ligand serves as an 8 electron donor and the cluster attains the expected 86 electron configuration.

When exposed to a CO atmosphere in a THF solution for 5 h at 67 °C, compound **2** was converted back to **1** in 45% yield by loss of the 12S3 ligand. Thus, the 12S3 substitution of **1** is not fully reversible, but the 12S3 ligand can be displaced to a significant degree by CO under these mild conditions.

The compound $\text{Ru}_6(\text{CO})_{15}(\mu\text{-}\eta^2\text{-16S4})(\mu_6\text{-C})$, **3**, was obtained in 58% yield from the reaction of 16S4 with octane solvent at reflux. Compound **3** was also characterized by a single crystal X-ray diffraction analysis.

(8) (a) Braga, D.; Grepioni, F.; Dyson, P. J.; Johnson, B. F. G.; Frediani, P.; Bianchi, M.; Piacenti, F. *J. Chem. Soc., Dalton Trans.* **1992**, 2562. (b) Sirigu, A.; Bianchi, M.; Benedetti, E. *Chem Commun.* **1989**, 596.

(9) (a) Rawle, S. C.; Admans, G. A.; Cooper, S. R. *J. Chem. Soc., Dalton Trans.* **1988**, 93.

Table 6. Intramolecular Distances for 3^a

Ru(1)–Ru(2)	2.920(1)	Ru(3)–C(32)	1.867(9)
Ru(1)–Ru(3)	2.861(1)	Ru(3)–C(3)	1.83(1)
Ru(1)–C(1)	2.03(1)	Ru(4)–C(1)	2.05(1)
Ru(1)–C(11)	1.93(1)	Ru(4)–C(41)	1.89(1)
Ru(1)–C(12)	1.90(1)	Ru(4)–C(42)	1.90(1)
Ru(2)–Ru(2*)	2.971(1)	S(1)–C(2)	1.814(8)
Ru(2)–Ru(3)	2.9197(9)	S(1)–C(8)	1.819(8)
Ru(2)–Ru(4)	2.878(1)	S(2)–C(4)	1.786(9)
Ru(2)–S(1)	2.389(2)	S(2)–C(5)	1.77(1)
Ru(2)–C(1)	2.041(8)	C(2)–C(3)	1.53(1)
Ru(2)–C(21)	1.874(9)	C(3)–C(4)	1.51(1)
Ru(2)–C(22)	1.90(1)	C(5)–C(6)	1.49(1)
Ru(3)–Ru(3*)	2.829(1)	C(7)–C(8)	1.52(1)
Ru(3)–Ru(4)	2.934(1)	S(1)–S(1*)	3.18(4)
Ru(3)–C(1)	2.076(8)	O–C(av)	1.14(1)
Ru(3)–C(31)	2.05(1)		

^a Distances are in angstroms. Estimated standard deviations in the least significant figure are given in parentheses.

Table 7. Intramolecular Bond Angles for 3^a

Ru(2)–Ru(1)–Ru(2*)	61.14(3)	Ru(2)–Ru(3)–Ru(4)	58.88(3)
Ru(2)–Ru(1)–Ru(3)	60.66(2)	Ru(2)–Ru(3)–C(31)	137.9(2)
Ru(2)–Ru(1)–Ru(3*)	90.73(3)	Ru(2)–Ru(3)–C(32)	116.6(3)
Ru(2)–Ru(1)–C(11)	144.7(2)	Ru(2)–Ru(3)–C(33)	110.5(3)
Ru(2)–Ru(1)–C(12*)	119.5(3)	Ru(3)–Ru(3*)–Ru(4)	61.18(2)
Ru(2)–Ru(1)–C(12)	74.2(2)	Ru(3)–Ru(3*)–C(31)	46.5(2)
Ru(3)–Ru(1)–Ru(3*)	59.25(3)	Ru(3)–Ru(3*)–C(32)	133.6(2)
Ru(3)–Ru(1)–C(11)	90.1(3)	Ru(3)–Ru(3*)–C(33)	118.9(3)
Ru(3)–Ru(1)–C(12*)	160.1(3)	Ru(4)–Ru(3)–C(31)	93.3(3)
Ru(3)–Ru(1)–C(12)	101.3(3)	Ru(4)–Ru(3)–C(32)	100.9(3)
C(11)–Ru(1)–C(12*)	94.8(4)	Ru(4)–Ru(3)–C(33)	168.9(3)
C(12)–Ru(1)–C(12*)	97.5(5)	C(31)–Ru(3)–C(32)	98.3(4)
Ru(1)–Ru(2)–Ru(2*)	59.43(2)	C(31)–Ru(3)–C(33)	93.6(4)
Ru(1)–Ru(2)–Ru(3)	58.67(3)	C(32)–Ru(3)–C(33)	86.7(4)
Ru(1)–Ru(2)–Ru(4)	89.52(3)	Ru(2)–Ru(4)–Ru(2*)	62.15(3)
Ru(1)–Ru(2)–S(1)	96.49(6)	Ru(2)–Ru(4)–Ru(3)	60.30(2)
Ru(1)–Ru(2)–C(21)	167.7(3)	Ru(2)–Ru(4)–Ru(3*)	90.13(3)
Ru(1)–Ru(2)–C(22)	97.0(3)	Ru(2)–Ru(4)–C(41)	164.1(3)
Ru(2*)–Ru(2)–Ru(3)	88.61(2)	Ru(2)–Ru(4)–C(41)	103.1(3)
Ru(2*)–Ru(2)–Ru(4)	58.92(2)	Ru(2)–Ru(4)–C(42)	94.0(3)
Ru(2*)–Ru(2)–S(1)	92.46(5)	Ru(3*)–Ru(4)–Ru(3)	57.63(3)
Ru(2*)–Ru(2)–C(21)	112.2(3)	Ru(3*)–Ru(4)–C(41)	117.1(3)
Ru(2*)–Ru(2)–C(22)	155.0(3)	Ru(3)–Ru(4)–C(41)	76.6(3)
Ru(3)–Ru(2)–Ru(4)	60.81(3)	Ru(3*)–Ru(4)–C(42)	148.0(2)
Ru(3)–Ru(2)–S(1)	149.95(6)	C(41*)–Ru(4)–C(41)	90.9(5)
Ru(3)–Ru(2)–C(21)	114.7(3)	C(41)–Ru(4)–C(42)	92.9(4)
Ru(3)–Ru(2)–C(22)	70.5(3)	Ru(2)–S(1)–C(2)	112.6(3)
Ru(4)–Ru(2)–S(1)	142.15(6)	Ru(2)–S(1)–C(8)	110.9(3)
Ru(4)–Ru(2)–C(21)	78.3(3)	C(2)–S(1)–C(8)	98.1(4)
Ru(4)–Ru(2)–C(22)	117.5(3)	C(4)–S(2)–C(5)	101.9(4)
S(1)–Ru(2)–C(21)	92.7(3)	S(1)–C(2)–C(3)	112.2(6)
S(1)–Ru(2)–C(22)	98.9(3)	C(2)–C(3)–C(4)	113.1(7)
C(21)–Ru(2)–C(22)	89.6(4)	S(2)–C(4)–C(3)	115.5(6)
Ru(1)–Ru(3)–Ru(2)	60.68(3)	S(2)–C(5)–C(6)	116.7(7)
Ru(1)–Ru(3)–Ru(3*)	60.37(2)	C(5)–C(6)–C(5*)	119(1)
Ru(1)–Ru(3)–Ru(4)	89.56(3)	C(8)–C(7)–C(8*)	119(1)
Ru(1)–Ru(3)–C(31)	90.9(3)	S(1)–C(8)–C(7)	114.3(7)
Ru(1)–Ru(3)–C(32)	165.6(2)	Ru–C–O(av)	175.0(8)
Ru(1)–Ru(3)–C(33)	81.7(3)	Ru(3)–C(31)–Ru(3)	87.1(5)
Ru(2)–Ru(3)–Ru(3*)	91.39(2)	Ru(3)–C(31)–O(31)	136.5(2)

^a Angles are in degrees. Estimated standard deviations in the least significant figure are given in parentheses.

An ORTEP drawing of the molecular structure of **3** is shown in Figure 2. Final atomic positional parameters are listed in Table 5. Selected interatomic distances and angles are listed in Tables 6 and 7, respectively. The molecule lies on a crystallographic reflection plane and thus contains a rigorously imposed reflection symmetry. The atoms Ru(1), C(1), and Ru(4) and the carbonyl ligands C(12)–O(12), C(31)–O(31), and C(42)–O(42) lie on the symmetry plane. This molecule also contains an octahedral Ru₆C cluster; however, unlike **2** the 16S4 ligand in **3** is only partially coordinated. Two of the sulfur atoms, S(1) and S(1*), are coordinated to adjacent

Table 8. Positional Parameters and B(eq) Values (Å²) for 4

atom	x	y	z	B(eq)
Ru(1)	0.44354(4)	0.03082(3)	0.23765(4)	2.97(3)
Ru(2)	0.39331(4)	0.16749(3)	0.20264(4)	3.34(3)
Ru(3)	0.19324(4)	0.14725(3)	0.26118(4)	2.95(3)
Ru(4)	0.22377(4)	0.00979(3)	0.26676(4)	2.57(2)
Ru(5)	0.30220(4)	0.06848(3)	0.08465(4)	3.04(3)
Ru(6)	0.34943(4)	0.10164(3)	0.39195(4)	2.93(3)
S(1)	0.1377(1)	−0.02854(9)	0.4091(1)	3.32(8)
S(2)	0.0784(1)	−0.0096(1)	0.1748(1)	3.9(1)
S(3)	0.2645(1)	−0.09710(9)	0.2375(2)	4.4(1)
O(11)	0.4992(5)	−0.0967(3)	0.3318(4)	6.2(3)
O(12)	0.6644(4)	0.0384(3)	0.1906(4)	6.3(3)
O(14)	0.4248(4)	−0.0499(3)	0.0423(4)	4.4(3)
O(21)	0.4412(5)	0.2811(4)	0.3387(6)	10.6(5)
O(22)	0.3098(6)	0.2588(3)	0.0421(6)	9.1(5)
O(23)	0.5975(4)	0.1724(3)	0.1028(5)	7.0(4)
O(31)	0.0408(4)	0.1089(3)	0.4184(4)	6.0(3)
O(32)	0.1885(5)	0.2870(3)	0.3317(5)	7.8(4)
O(33)	0.0449(4)	0.1648(3)	0.0844(4)	6.5(3)
O(51)	0.3936(4)	0.1294(3)	−0.1028(4)	7.0(4)
O(52)	0.1547(4)	0.0023(3)	−0.0577(4)	6.9(4)
O(61)	0.3507(5)	0.2205(3)	0.5244(5)	7.4(4)
O(62)	0.5672(4)	0.0763(3)	0.4472(4)	6.8(3)
O(63)	0.2784(4)	0.0323(3)	0.5811(4)	5.7(3)
C(1)	0.3097(4)	0.0839(3)	0.2401(4)	2.4(3)
C(2)	0.0123(5)	−0.0513(4)	0.3641(5)	4.0(4)
C(3)	−0.0204(5)	−0.0164(4)	0.2688(5)	4.4(4)
C(4)	0.0818(7)	−0.0942(4)	0.1310(6)	5.7(5)
C(5)	0.1866(7)	−0.1203(4)	0.1286(7)	6.3(5)
C(6)	0.2075(6)	−0.1461(4)	0.3396(7)	5.5(5)
C(7)	0.1928(6)	−0.1076(4)	0.4347(6)	4.7(4)
C(11)	0.4754(5)	−0.0487(4)	0.2967(5)	3.6(4)
C(12)	0.5819(6)	0.0375(4)	0.2059(5)	4.0(4)
C(14)	0.4031(4)	−0.0053(4)	0.0903(5)	3.1(3)
C(21)	0.4231(6)	0.2368(5)	0.2897(7)	6.3(5)
C(22)	0.3390(6)	0.2235(4)	0.1002(7)	5.6(5)
C(23)	0.5231(6)	0.1670(3)	0.1432(6)	4.3(4)
C(31)	0.0995(5)	0.1213(4)	0.3578(6)	4.1(4)
C(32)	0.1914(6)	0.2356(4)	0.3019(6)	4.8(4)
C(33)	0.1040(6)	0.1572(3)	0.1472(6)	4.0(4)
C(51)	0.3587(5)	0.1075(4)	−0.0319(6)	4.4(4)
C(52)	0.2106(6)	0.0253(4)	−0.0024(5)	4.7(4)
C(61)	0.3513(5)	0.1756(4)	0.4723(6)	4.4(4)
C(62)	0.4894(6)	0.0786(4)	0.4099(5)	4.6(4)
C(63)	0.3037(5)	0.0562(4)	0.5057(6)	3.8(4)
C(71)	0.6429(8)	0.3113(6)	−0.3433(8)	7.0(6)
C(72)	0.5631(8)	0.2700(6)	−0.3456(8)	7.2(7)
C(73)	0.5322(7)	0.2426(4)	−0.257(1)	6.9(6)
C(74)	0.579(1)	0.2573(6)	−0.1669(9)	8.4(8)
C(75)	0.6578(9)	0.2990(7)	−0.166(1)	8.4(8)
C(76)	0.6890(7)	0.3259(5)	−0.254(1)	7.7(7)

metal atoms, Ru(2) and Ru(2*), Ru(2)–S(1) = 2.389(2) Å. The other two sulfur atoms S(2) and S(2*) are uncoordinated. There is no shortening of the 16S4 bridged metal–metal bond in this molecule. In fact, in this case this is the longest metal–metal bond in the molecule, Ru(2)–Ru(2*) = 2.971(1) Å. The 16S4 ligand has changed its conformation from that observed in the free molecule.¹⁰ In the free molecule two nonadjacent sulfur atoms lie in exo-positions at the corners of a rectangular molecule. The other two are endo and lie along the edges of the rectangle; see the diagram in the Introduction. In **3** two adjacent sulfur atoms have endo-configurations and are coordinated to the two ruthenium atoms of the cluster while the two uncoordinated sulfur atoms have exo-configurations. This appears to be a newly observed conformation of this ligand and is undoubtedly a consequence of directing influences from its coordination to the cluster. Note, the distance between the two coordinated sulfur atoms is 3.176(4) Å

(10) Blake, A. J.; Gould, R. O.; Halcrow, M. A.; Schröder, M. *Acta Crystallogr.* **1993**, *B49*, 773.

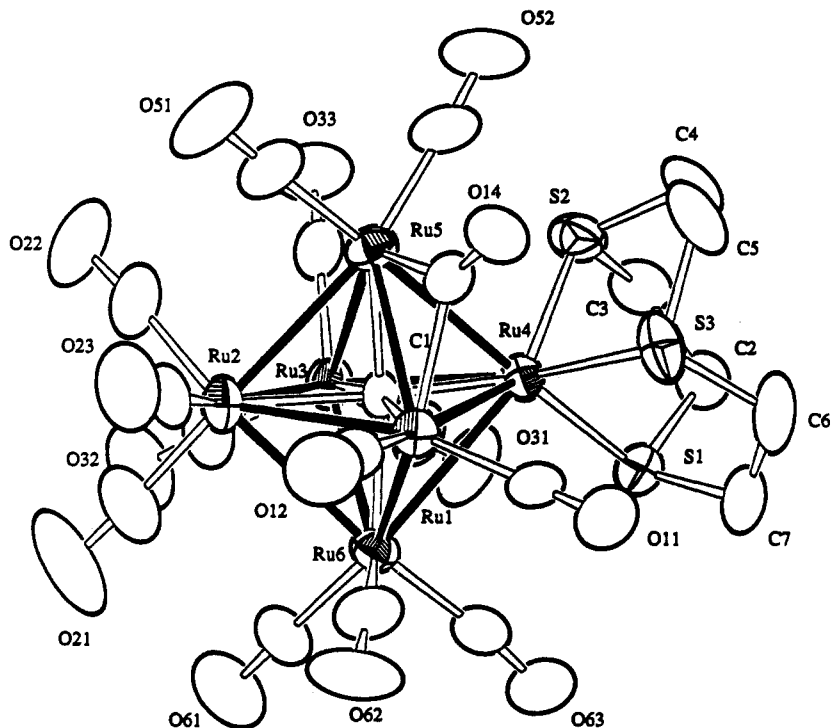


Figure 3. ORTEP diagram of $\text{Ru}_6(\text{CO})_{14}(\eta^3\text{-9S3})(\mu_6\text{-C})$, **4**, showing 40% probability thermal ellipsoids.

Table 9. Intramolecular Distances for **4^c**

Ru(1)–Ru(2)	2.948(1)	Ru(4)–S(2)	2.306(2)
Ru(1)–Ru(4)	2.9988(8)	Ru(4)–S(3)	2.316(2)
Ru(1)–Ru(5)	2.8413(8)	Ru(4)–C(1)	1.954(6)
Ru(1)–Ru(6)	2.8049(9)	Ru(4)–C(1)	2.056(6)
Ru(1)–C(1)	2.101(6)	Ru(6)–C(1)	2.079(6)
Ru(2)–Ru(3)	2.8221(8)	S(1)–C(2)	1.830(7)
Ru(2)–Ru(5)	2.8331(9)	S(1)–C(7)	1.826(7)
Ru(2)–Ru(6)	2.8913(9)	S(2)–C(3)	1.821(7)
Ru(2)–C(1)	2.123(6)	S(2)–C(4)	1.846(8)
Ru(3)–Ru(4)	2.882(1)	S(3)–C(5)	1.817(9)
Ru(3)–Ru(5)	3.1926(9)	S(3)–C(6)	1.848(8)
Ru(3)–Ru(6)	2.8419(8)	O–C(av)	1.140(8)
Ru(3)–C(1)	2.059(6)	C(2)–C(3)	1.50(1)
Ru(4)–Ru(5)	2.8814(9)	C(4)–C(5)	1.50(1)
Ru(4)–Ru(6)	3.0088(8)	C(6)–C(7)	1.49(1)
Ru(4)–S(1)	2.338(2)		

^c Distances are in angstroms. Estimated standard deviations in the least significant figure are given in parentheses.

and the distance between the two ruthenium atoms is 2.971(1) Å. Interestingly, although it is the endo sulfurs S(1) and S(1*) that are metal coordinated, the coordination involves the lone pairs of electrons that point away from the interior of the ring. Coordination to the two interior lone pairs would probably generate severe steric interactions between some of the carbonyl ligands and the remainder of the 16S4 ring. Studies have shown that when the 16S4 ligand is coordinated to a single metal atom, the metal generally lies inside the ring and all four of the sulfur atoms adopt endo-configurations.^{1b,11–14} The carbido carbon lies almost exactly in the center of the Ru_6 cluster in this molecule. There is one bridging carbonyl ligand C(31)–O(31), and

Table 10. Intramolecular Bond Angles for **4^c**

Ru(2)–Ru(1)–Ru(4)	86.45(2)	Ru(6)–Ru(4)–S(3)	124.41(5)
Ru(2)–Ru(1)–Ru(5)	58.56(2)	S(1)–Ru(4)–S(2)	86.28(6)
Ru(2)–Ru(1)–Ru(6)	60.28(2)	S(1)–Ru(4)–S(3)	85.68(7)
Ru(4)–Ru(1)–Ru(5)	59.05(2)	S(2)–Ru(4)–S(3)	86.88(7)
Ru(4)–Ru(1)–Ru(6)	62.35(2)	Ru(1)–Ru(5)–Ru(2)	62.60(2)
Ru(5)–Ru(1)–Ru(6)	93.49(3)	Ru(1)–Ru(5)–Ru(3)	86.47(2)
Ru(1)–Ru(2)–Ru(3)	91.70(2)	Ru(1)–Ru(5)–Ru(4)	63.20(2)
Ru(1)–Ru(2)–Ru(5)	58.84(2)	Ru(2)–Ru(5)–Ru(3)	55.47(2)
Ru(1)–Ru(2)–Ru(6)	57.41(2)	Ru(2)–Ru(5)–Ru(4)	90.91(3)
Ru(3)–Ru(2)–Ru(5)	68.74(2)	Ru(3)–Ru(5)–Ru(4)	56.36(2)
Ru(3)–Ru(2)–Ru(6)	59.64(2)	Ru(1)–Ru(6)–Ru(2)	62.31(3)
Ru(5)–Ru(2)–Ru(6)	91.83(3)	Ru(1)–Ru(6)–Ru(3)	94.33(3)
Ru(1)–Ru(3)–Ru(4)	91.13(2)	Ru(1)–Ru(6)–Ru(4)	61.99(2)
Ru(2)–Ru(3)–Ru(5)	55.79(2)	Ru(2)–Ru(6)–Ru(3)	58.97(2)
Ru(2)–Ru(3)–Ru(6)	61.39(2)	Ru(2)–Ru(6)–Ru(4)	87.29(3)
Ru(4)–Ru(3)–Ru(5)	56.36(2)	Ru(3)–Ru(6)–Ru(4)	58.93(2)
Ru(4)–Ru(3)–Ru(6)	63.43(2)	Ru(4)–S(1)–C(2)	106.9(2)
Ru(5)–Ru(3)–Ru(6)	85.70(2)	Ru(4)–S(1)–C(7)	104.4(3)
Ru(1)–Ru(4)–Ru(3)	89.51(2)	C(2)–S(1)–C(7)	101.1(3)
Ru(1)–Ru(4)–Ru(5)	57.75(2)	Ru(4)–S(2)–C(3)	106.0(2)
Ru(1)–Ru(4)–Ru(6)	55.66(2)	Ru(4)–S(2)–C(4)	107.7(3)
Ru(1)–Ru(4)–S(1)	130.02(5)	C(3)–S(2)–C(4)	99.0(4)
Ru(1)–Ru(4)–S(2)	141.20(5)	Ru(4)–S(3)–C(5)	104.4(3)
Ru(1)–Ru(4)–S(3)	83.43(5)	Ru(4)–S(3)–C(6)	107.9(3)
Ru(3)–Ru(4)–Ru(5)	67.28(2)	C(5)–S(3)–C(6)	100.5(4)
Ru(3)–Ru(4)–Ru(6)	57.64(2)	S(1)–C(2)–C(3)	113.5(5)
Ru(3)–Ru(4)–S(1)	106.60(5)	S(2)–C(3)–C(2)	113.0(5)
Ru(3)–Ru(4)–S(2)	92.36(6)	S(2)–C(4)–C(5)	112.0(5)
Ru(3)–Ru(4)–S(3)	167.63(6)	S(3)–C(5)–C(4)	114.4(6)
Ru(5)–Ru(4)–Ru(6)	88.53(3)	S(3)–C(6)–C(7)	111.5(5)
Ru(5)–Ru(4)–S(1)	171.11(5)	S(1)–C(7)–C(6)	112.7(5)
Ru(5)–Ru(4)–S(2)	87.53(5)	Ru–C–O(av)	176.5(8)
Ru(5)–Ru(4)–S(3)	100.35(5)	Ru(1)–C(14)–Ru(5)	85.9(3)
Ru(6)–Ru(4)–S(1)	93.45(5)	Ru(1)–C(14)–O(14)	135.2(5)
Ru(6)–Ru(4)–S(2)	148.64(6)	Ru(5)–C(14)–O(14)	138.6(5)

^c Angles are in degrees. Estimated standard deviations in the least significant figure are given in parentheses.

(11) Pett, V. B.; Diaddario, Jr. L. L.; Dockal, E. R.; Corfield, P. W.; Ceccarelli, C.; Glick, M. D.; Ochrymowycz, L. A.; Rorabacher, D. B. *Inorg. Chem.* **1983**, *22*, 3661.

(12) Jones, T. E.; Sokol, L. S. W. L.; Rorabacher, D. B.; Glick, M. D. *J. Chem. Soc., Chem. Commun.* **1979**, 140.

(13) Cragel, J., Jr.; Pett, V. B.; Glick, M. D.; DeSimone, R. E. *Inorg. Chem.* **1978**, *17*, 2885.

(14) DeSimone, R. E.; Glick, M. D. *Inorg. Chem.* **1978**, *17*, 3574.

the associated metal–metal bond Ru(3)–Ru(3*) is the shortest in the cluster, 2.829(1) Å.

The reaction of 9S3 with **1** in hexane solvent at reflux produced the compound $\text{Ru}_6(\text{CO})_{14}(\eta^3\text{-9S3})(\mu_6\text{-C})$, **4**, in 93% yield. Compound **4** was also characterized by a single crystal X-ray diffraction analysis, and an ORTEP

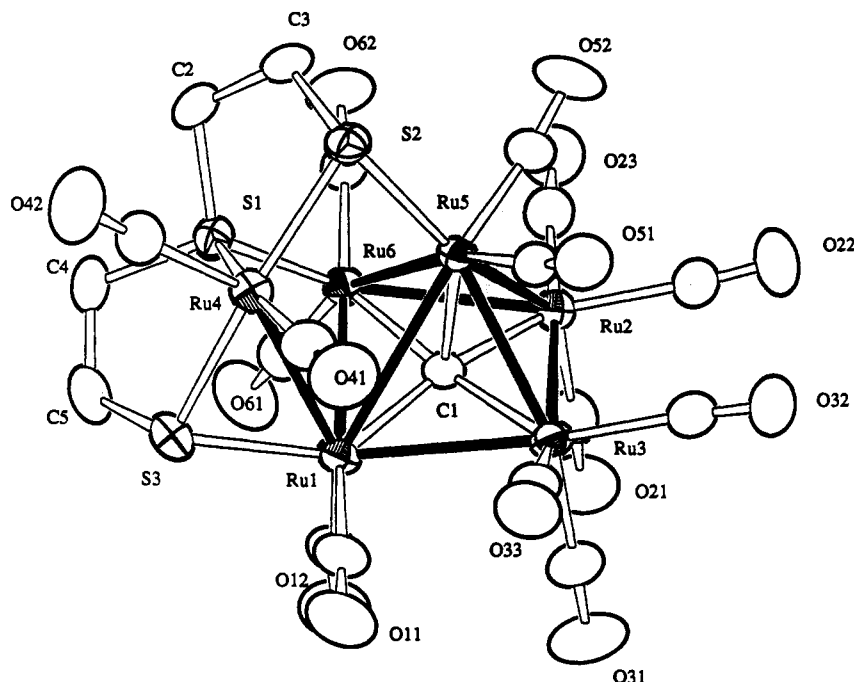
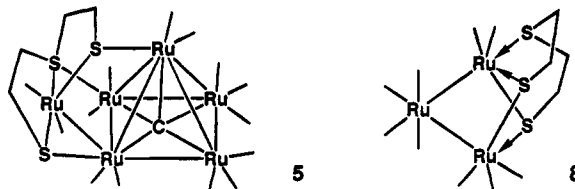


Figure 4. ORTEP diagram of $\text{Ru}_6(\text{CO})_{14}(\mu_3\text{-}\eta^3\text{-SCH}_2\text{CH}_2\text{SCH}_2\text{CH}_2\text{S})(\mu_5\text{-C})$, **5**, showing 40% probability thermal ellipsoids.

drawing of its molecular structure is shown in Figure 3. Final atomic positional parameters are listed in Table 8. Selected interatomic distances and angles are listed in Tables 9 and 10, respectively. This molecule also contains an octahedral Ru_6 cluster with a carbido ligand inside the cluster. The 9S3 ligand exhibits a η^3 -tridentate coordination with all three sulfur atoms coordinated to one ruthenium atom, Ru(4). In this regard the molecule is very similar to **2**, but unlike **2** where one of the sulfur atoms uses its second lone pair of electrons to coordinate to one of the neighboring ruthenium atoms, in **4** this interaction has not developed. In this case the 9S3 ligand is simply a six-electron donor. As a result, the cluster contains one more carbonyl ligand than **2** to make up for the lack of donation due to the absence of the bridging interaction. One of the metal-metal bonds is unusually long, Ru(3)-Ru(5) = 3.1926(9) Å. There seems to be no simple explanation for this in terms of steric or electronic effects. The shortest metal-metal bond is Ru(1)-Ru(6) at 2.8049(9) Å, and there seems to be no simple explanation for this either. As in **2**, the carbido ligand is displaced from the center of the Ru_6 octahedron toward the metal atom containing the 9S3 ligand, Ru(4)-C(1) = 1.954(6) Å vs Ru(2)-C(1) = 2.123(6) Å. The molecule contains one bridging carbonyl ligand C(14)-O(14). All the others are normal terminal ligands. The ^1H NMR spectrum of **4** has the form of a $\text{AA}'\text{BB}'$ spectrum with multiplets at 2.78 (6H) and 2.33 (6H) ppm and three coupling constants, $^2J_{\text{H-H}} = -13.9$ Hz, $^3J_{\text{H-H}} = 7.0$ Hz, $^3J_{\text{H-H}} = 6.7$ Hz, that were fitted by computer simulation. Since the molecule has no symmetry in the solid state, this indicates that, in solution, it is probably undergoing dynamical rearrangements that lead to an averaging of the three ethylene groups in the 9S3 ligand.

It seemed likely that the 9S3 analogue of **2** could be prepared by a simple decarbonylation of **4**. In an attempt to prepare such a species, a solution of **1** and 9S3 in octane solvent was heated to reflux for 2 h. From

this reaction the new compound $\text{Ru}_6(\text{CO})_{14}(\mu_3\text{-}\eta^3\text{-SCH}_2\text{CH}_2\text{SCH}_2\text{CH}_2\text{S})(\mu_5\text{-C})$, **5**, was isolated in 36% yield.



Compound **5** was characterized by a single crystal X-ray diffraction analysis, and an ORTEP drawing of its molecular structure is shown in Figure 4. Final atomic positional parameters are listed in Table 11. Selected interatomic distances and angles are listed in Tables 12 and 13, respectively. As can be seen, compound **5** is not the 9S3 analogue of **2**. It does not even contain an octahedral Ru_6 carbido cluster. In fact, it does not even contain a 9S3 ligand. The molecule does contain a "spiked" square pyramidal cluster of six ruthenium atoms and one carbido ligand. The carbido ligand lies in the center of the square base as is typical of M_5C clusters. The sixth metal atom Ru(4) is linked to one of the metal atoms in the square base, Ru(1), by a single metal-metal bond and bridging interactions to a 3-thiapentane-1,5-dithiolato ligand. The latter was evidently formed from the 9S3 ligand by the elimination of ethylene. Indeed, the formation of ethylene was confirmed by ^1H NMR spectroscopy after heating a sample of **4** in an NMR tube in toluene- d_8 solvent at 105 °C. From this reaction, **5** was obtained in an even better yield, 68%. The elimination of ethylene from ethanedithiolato ligands¹⁵ and ethylene-linked thioethers¹⁶ has been observed previously. A 3-thiapentane-1,5-dithiolato ligand was found in the complex $\text{Ru}_3(\text{CO})_9(\mu_3\text{-}\eta^3\text{-SCH}_2\text{CH}_2\text{SCH}_2\text{CH}_2\text{S})$, **8**, which was formed by the

(15) McKenna, M.; Wright, L. L.; Miller, D. J.; Tanner, L.; Haltiwanger, R. C.; Rakowski DuBois, M. *J. Am. Chem. Soc.* **1983**, *105*, 5329.

(16) Adams, R. D.; Yamamoto, J. H. *Inorg. Chim. Acta*, in press.

Table 11. Positional Parameters and $B(\text{eq})$ Values (\AA^2) for **5**

atom	x	y	z	$B(\text{eq})$
Ru(1)	0.32525(4)	0.07359(3)	0.79432(3)	2.81(2)
Ru(2)	0.27874(4)	0.03792(4)	0.54117(3)	3.17(2)
Ru(3)	0.21117(4)	0.15851(3)	0.66156(4)	3.16(2)
Ru(4)	0.19741(4)	-0.06293(3)	0.86282(3)	3.00(2)
Ru(5)	0.15779(4)	-0.01336(3)	0.67653(3)	2.58(2)
Ru(6)	0.35234(4)	-0.07036(3)	0.67613(3)	2.58(2)
Cl(1)	0.7075(3)	0.0516(3)	0.8443(3)	12.8(3)
Cl(2)	0.8588(3)	-0.0736(2)	0.8665(5)	15.8(3)
S(1)	0.3104(1)	-0.1459(1)	0.7951(1)	2.90(7)
S(2)	0.0905(1)	-0.1264(1)	0.7571(1)	3.22(7)
S(3)	0.3451(1)	-0.0035(1)	0.9254(1)	3.77(8)
O(11)	0.2782(5)	0.2199(4)	0.9153(4)	7.3(4)
O(12)	0.5198(4)	0.1535(4)	0.7629(5)	7.3(4)
O(21)	0.4513(5)	0.1508(4)	0.5066(4)	7.1(4)
O(22)	0.1410(6)	0.1050(4)	0.3947(4)	7.7(4)
O(23)	0.3362(5)	-0.1032(4)	0.4174(4)	7.0(4)
O(31)	0.3569(4)	0.3018(4)	0.6486(5)	7.8(4)
O(32)	0.0699(5)	0.2375(4)	0.5263(4)	6.8(3)
O(33)	0.0885(4)	0.2373(4)	0.8014(4)	6.0(3)
O(41)	0.0516(5)	0.0720(4)	0.9179(5)	6.7(4)
O(42)	0.1449(5)	-0.1816(4)	1.0075(4)	7.2(4)
O(51)	-0.0373(4)	0.0803(3)	0.6883(4)	5.4(3)
O(52)	0.0890(5)	-0.1054(4)	0.5146(4)	7.3(4)
O(61)	0.5749(4)	-0.0651(4)	0.6887(4)	6.4(3)
O(62)	0.3517(5)	-0.2328(4)	0.5676(4)	6.0(3)
C(1)	0.2895(4)	0.0471(4)	0.6713(4)	2.8(3)
C(2)	0.2472(5)	-0.2462(4)	0.7764(5)	3.7(3)
C(3)	0.1496(5)	-0.2283(4)	0.7287(5)	3.9(3)
C(4)	0.4029(5)	-0.1712(5)	0.8770(4)	4.0(3)
C(5)	0.4393(6)	-0.0883(5)	0.9171(5)	4.8(4)
C(11)	0.2915(5)	0.1647(5)	0.8703(5)	4.3(4)
C(12)	0.4469(6)	0.1206(5)	0.7762(5)	4.3(4)
C(21)	0.3842(6)	0.1077(5)	0.5169(5)	4.4(4)
C(22)	0.1904(7)	0.0830(5)	0.4504(5)	5.0(4)
C(23)	0.3152(6)	-0.0530(5)	0.4670(5)	4.7(4)
C(31)	0.3020(5)	0.2488(5)	0.6527(5)	4.4(4)
C(32)	0.1213(6)	0.2059(5)	0.5743(6)	4.7(4)
C(33)	0.1346(5)	0.2080(5)	0.7510(5)	4.3(4)
C(41)	0.1065(6)	0.0224(5)	0.8991(5)	4.6(4)
C(42)	0.1673(5)	-0.1383(5)	0.9536(5)	4.2(4)
C(51)	0.0377(5)	0.0488(4)	0.6861(4)	3.5(3)
C(52)	0.1223(6)	-0.0659(5)	0.5710(5)	4.0(3)
C(61)	0.4909(6)	-0.0665(5)	0.6848(5)	3.9(3)
C(62)	0.3512(5)	-0.1689(5)	0.6066(4)	3.7(3)
C(99)	0.793(2)	-0.013(1)	0.808(1)	16.9(7)

reaction of **9S3** with $\text{Ru}_3(\text{CO})_{12}$ in THF solvent.¹⁷ All three sulfur atoms of the 3-thiapentane-1,5-dithiolato ligand are coordinated, and each serves as a bridge between the Ru_5 cluster and the Ru(4) spike. The thioether sulfur S(1) bridges the nonbonded pair Ru(4) and Ru(6). The thiolato sulfur S(2) bridges the nonbonded pair Ru(4) and Ru(5), and the thiolato sulfur S(3) bridges the bonded pair Ru(1) and Ru(4). The thiapentanedithiolato ligand serves as a 10 electron donor in this molecule. Overall the complex contains a total of 90 valence electrons which is in accord with the polyhedral skeletal electron pair theory and the effective atomic number rule.¹⁸

Interestingly, the loss of ethylene from complex **4** is more facile than loss of CO which should have produced a stable species analogous to **2**. In contrast, the reaction of **1** with **12S3** proceeds to **2** because the formation of a

Table 12. Intramolecular Distances for **5^a**

Ru(1)-Ru(3)	2.8521(8)	Ru(4)-S(2)	2.364(2)
Ru(1)-Ru(4)	2.9800(9)	Ru(4)-S(3)	2.390(2)
Ru(1)-Ru(5)	3.1699(8)	Ru(4)-C(41)	1.917(9)
Ru(1)-Ru(6)	2.9309(8)	Ru(4)-C(42)	1.882(8)
Ru(1)-S(3)	2.366(2)	Ru(5)-Ru(6)	2.8044(8)
Ru(1)-C(1)	1.992(7)	Ru(5)-S(2)	2.369(2)
Ru(1)-C(11)	1.906(8)	Ru(5)-C(1)	2.044(6)
Ru(1)-C(12)	1.850(8)	Ru(5)-C(51)	1.914(8)
Ru(2)-Ru(3)	2.8310(9)	Ru(5)-C(52)	1.872(8)
Ru(2)-Ru(5)	2.8390(9)	Ru(6)-S(1)	2.281(2)
Ru(2)-Ru(6)	2.8374(8)	Ru(6)-C(1)	2.022(6)
Ru(2)-C(1)	2.013(7)	Ru(6)-C(61)	1.892(8)
Ru(2)-C(21)	1.854(9)	Ru(6)-C(62)	1.870(8)
Ru(2)-C(22)	1.934(9)	S(1)-C(2)	1.820(7)
Ru(2)-C(23)	1.899(9)	S(1)-C(4)	1.811(7)
Ru(3)-Ru(5)	2.7925(9)	S(2)-C(3)	1.858(7)
Ru(3)-C(1)	2.048(6)	S(3)-C(5)	1.881(8)
Ru(3)-C(31)	1.893(8)	C(2)-C(3)	1.55(1)
Ru(3)-C(32)	1.926(9)	C(4)-C(5)	1.52(1)
Ru(3)-C(33)	1.92(1)	O-C(av)	1.130(8)
Ru(4)-S(1)	2.303(2)		

^a Distances are in angstroms. Estimated standard deviations in the least significant figure are given in parentheses.

Table 13. Intramolecular Bond Angles for **5^a**

Ru(3)-Ru(1)-Ru(4)	106.12(2)	Ru(2)-Ru(5)-S(2)	148.16(5)
Ru(3)-Ru(1)-Ru(5)	106.12(2)	Ru(3)-Ru(5)-Ru(6)	93.06(2)
Ru(3)-Ru(1)-Ru(6)	89.23(2)	Ru(3)-Ru(5)-S(2)	150.26(5)
Ru(3)-Ru(1)-S(3)	153.36(5)	Ru(6)-Ru(5)-S(2)	98.85(5)
Ru(4)-Ru(1)-Ru(5)	58.55(2)	Ru(1)-Ru(6)-Ru(2)	87.27(2)
Ru(4)-Ru(1)-Ru(6)	76.43(2)	Ru(1)-Ru(6)-Ru(5)	67.06(2)
Ru(4)-Ru(1)-S(3)	51.55(5)	Ru(1)-Ru(6)-S(1)	81.37(5)
Ru(5)-Ru(1)-Ru(6)	54.56(2)	Ru(2)-Ru(6)-Ru(5)	60.42(2)
Ru(5)-Ru(1)-S(3)	109.20(5)	Ru(2)-Ru(6)-S(1)	144.01(5)
Ru(6)-Ru(1)-S(3)	97.56(5)	Ru(5)-Ru(6)-S(1)	83.76(5)
Ru(3)-Ru(2)-Ru(5)	59.01(2)	Ru(4)-S(1)-Ru(6)	105.83(7)
Ru(3)-Ru(2)-Ru(6)	91.55(2)	Ru(4)-S(1)-C(2)	104.1(3)
Ru(5)-Ru(2)-Ru(6)	59.21(2)	Ru(4)-S(1)-C(4)	106.0(3)
Ru(1)-Ru(3)-Ru(2)	88.93(2)	Ru(6)-S(1)-C(2)	117.1(2)
Ru(1)-Ru(3)-Ru(5)	68.32(2)	Ru(6)-S(1)-C(4)	119.3(3)
Ru(2)-Ru(3)-Ru(5)	60.64(2)	C(2)-S(1)-C(4)	103.0(3)
Ru(1)-Ru(4)-S(1)	79.95(5)	Ru(4)-S(2)-Ru(5)	79.04(6)
Ru(1)-Ru(4)-S(2)	114.06(5)	Ru(4)-S(2)-C(3)	105.9(2)
Ru(1)-Ru(4)-S(3)	50.83(5)	Ru(5)-S(2)-C(3)	109.2(3)
S(1)-Ru(4)-S(2)	81.68(6)	Ru(1)-S(3)-Ru(4)	77.61(6)
S(1)-Ru(4)-S(3)	80.24(7)	Ru(1)-S(3)-C(5)	110.8(3)
S(2)-Ru(4)-S(3)	158.35(7)	Ru(4)-S(3)-C(5)	106.2(3)
Ru(1)-Ru(5)-Ru(2)	82.79(2)	S(1)-C(2)-C(3)	107.8(5)
Ru(1)-Ru(5)-Ru(3)	56.73(2)	S(2)-C(3)-C(2)	114.5(5)
Ru(1)-Ru(5)-Ru(6)	58.38(2)	S(1)-C(4)-C(5)	107.7(5)
Ru(1)-Ru(5)-S(2)	107.67(5)	S(3)-C(5)-C(4)	114.2(5)
Ru(2)-Ru(5)-Ru(3)	60.35(2)	Ru-C-O(av)	175.9(7)
Ru(2)-Ru(5)-Ru(6)	60.36(2)		

^a Angles are in degrees. Estimated standard deviations in the least significant figure are given in parentheses.

4-heptane-1,7-dithiolato ligand would require the loss of a trimethylene group which is a much less stable fragment than ethylene.

Acknowledgment. This research was supported by the Office of Basic Energy Sciences of the U.S. Department of Energy.

Supplementary Material Available: Tables of hydrogen positional and thermal parameters and anisotropic thermal parameters (12 pages). Ordering information is given on any current masthead page.

OM940903Z

(17) Rossi, S.; Kallinen, K.; Pursianinen, J.; Pakkanen, T. T.; Pakkanen, T. A. *J. Organomet. Chem.* **1992**, *440*, 367.

(18) Mingos, D. M. P.; May, A. S. In *The Chemistry of Metal Cluster Complexes*; Shriver, D. F., Kaesz, H. D., Adams, R. D., Eds.; VCH Publishers: New York, 1990; Chapter 2.

Catalytic Cyclooligomerization of Thietane by Dirhenium Carbonyl Complexes

Richard D. Adams* and Stephen B. Falloon

Department of Chemistry and Biochemistry, University of South Carolina,
Columbia, South Carolina 29208

Received January 23, 1995[®]

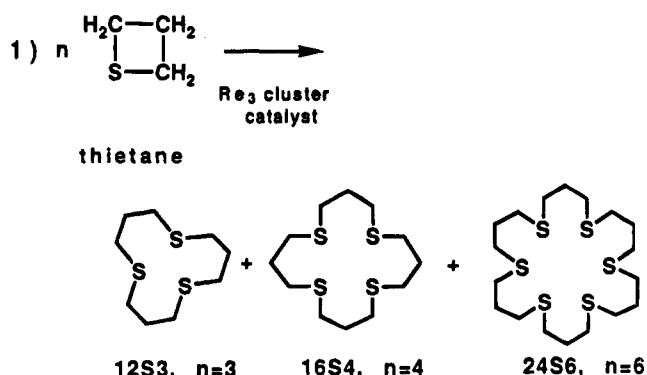
The reactions of $\text{Re}_2(\text{CO})_9(\text{NCMe})$, **1**, with thietane and 1,5,9-trithiacyclododecane, **12S3**, have yielded the compounds $\text{Re}_2(\text{CO})_9(\text{SCH}_2\text{CH}_2\text{CH}_2)$, **2**, $\text{Re}_2(\text{CO})_9(\text{SCH}_2\text{CH}_2\text{CH}_2\text{SCH}_2\text{CH}_2\text{CH}_2\text{SCH}_2\text{CH}_2\text{CH}_2)$, **3**, and $[\text{Re}_2(\text{CO})_9]_2(\text{SCH}_2\text{CH}_2\text{CH}_2\text{SCH}_2\text{CH}_2\text{CH}_2\text{SCH}_2\text{CH}_2\text{CH}_2)$, **4**, respectively. The molecular structures of **3** and **4** were established by single-crystal X-ray diffraction analyses. The structure of **3** is analogous to that of $\text{Re}_2(\text{CO})_{10}$ but has a **12S3** ligand coordinated to one of the rhenium atoms in an equatorial coordination site. Compound **4** is similar to **3**, but has two $\text{Re}_2(\text{CO})_9$ units attached to two adjacent thioether sulfur atoms on a single molecule of **12S3**. The reaction of **2** with thietane was found to yield **3** together with large amounts of the free molecule **12S3** by a cyclotrimerization process that is catalytic in **2**. Small amounts of 1,5,9,13,17,21-hexathiacyclotetracosane, **24S6**, are formed in this catalytic reaction in the early stages, but its yield increases substantially in the later stages of the reaction. A kinetic study showed that the catalytic formation of **12S3** is first order in the concentration of **2**, which is consistent with the catalysis being produced by **2** and not by mononuclear metal fragments. The PMe_2Ph derivative of **2**, $\text{Re}_2(\text{CO})_8(\text{PMe}_2\text{Ph})(\text{SCH}_2\text{CH}_2\text{CH}_2)$, **5**, was also prepared. It also catalyzes the cyclooligomerization of thietane to **12S3** and **24S6**, but the rate is lower and the selectivity for **12S3** is substantially lower than that of **2**. Crystal data for **3**: space group = $P2_1/c$, $a = 14.545(4)$ Å, $b = 13.425(4)$ Å, $c = 14.682(3)$ Å, $\beta = 118.24(1)^\circ$, $Z = 4$, 3148 reflections, $R = 0.035$. For **4**: $^{1/2}\text{C}_6\text{H}_{14}$: space group = $P2_1/n$, $a = 16.215(3)$ Å, $b = 9.836(4)$ Å, $c = 27.171(8)$ Å, $\beta = 99.71(2)^\circ$, $Z = 4$, 3742 reflections, $R = 0.036$.

Introduction

The cleavage of carbon-sulfur bonds in sulfur-containing heterocycles is an integral step in the important process of hydrodesulfurization of these molecules for the purification of fossil fuels.¹⁻³ In recent studies we have demonstrated the controlled opening of the saturated four-membered sulfur-containing heterocycles known as thietanes by nucleophiles when the thietane is coordinated as a bridging ligand in metal cluster complexes.^{4,5} We have found that thietanes, themselves, are also capable of producing ring-opening

additions upon coordinated thietanes, and in these cases ring-opening oligomerization processes ensue.^{6,7} Using

the trirhenium complex $\text{Re}_3(\text{CO})_{10}(\mu\text{-SCH}_2\text{CH}_2\text{CH}_2)(\mu\text{-H})_3$ we have recently developed the first example of a process that leads to the production of polythioether macrocycles catalytically, eq 1; **12S3** = 1,5,9-trithiacyclododecane, **16S4** = 1,5,9,13-tetrathiacyclohexadecane, and **24S6** = 1,5,9,13,17,21-hexathiacyclotetracosane.^{7a} Polythioether macrocycles have recently attracted considerable interest for their potential to serve as ligands for the transition metals.⁸



In this report our studies of the coordination of thietane and **12S3** to the dirhenium grouping Re_2 -

(5) Adams, R. D.; Cortopassi, J. E.; Falloon, S. B. *Organometallics* 1992, 11, 3794.

[®] Abstract published in *Advance ACS Abstracts*, March 15, 1995.

(1) (a) Angelici, R. J. *Acc. Chem. Res.* 1988, 21, 387. (b) Friend, C. M.; Roberts, J. T. *Acc. Chem. Res.* 1988, 21, 394. (c) Markel, E. J.; Schrader, G. L.; Sauer, N. N.; Angelici, R. J. *J. Catal.* 1989, 116, 11. (d) Prins, R.; De Beer, V. H. H.; Somorjai, G. A. *Catal. Rev. Sci. Eng.* 1989, 31, 1. (e) Sauer, N. N.; Markel, E. J.; Schrader, G. L.; Angelici, R. J. *J. Catal.* 1989, 117, 295. (f) Kwart, H.; Schuit, G. C. A.; Gates, B. C. *J. Catal.* 1980, 61, 128. (g) Curtis, M. D.; Penner-Hahn, J. E.; Schwank, J.; Beralt, O.; McCabe, D. J.; Thompson, L.; Waldo, G. *Polyhedron* 1988, 7, 2411. (h) Ogilvy, A. E.; Draganjac, M.; Rauchfuss, T. B.; Wilson, S. R. *Organometallics* 1988, 7, 1171. (i) Kaesz, H. D.; King, R. B.; Manuel, T. A.; Nichols, L. D.; Stone, F. G. A. *J. Am. Chem. Soc.* 1960, 82, 4749. (j) Luo, L.; Ogilvy, A. E.; Rauchfuss, T. B.; Rheingold, A. L.; Wilson, S. R. *Organometallics* 1991, 10, 1002 and references therein.

(2) (a) Roberts, J. T.; Friend, C. M. *J. Am. Chem. Soc.* 1987, 109, 7899. (b) Roberts, J. T.; Friend, C. M. *J. Am. Chem. Soc.* 1987, 109, 3872.

(3) Calhorda, M. J.; Hoffmann, R.; Friend, C. M. *J. Am. Chem. Soc.* 1988, 110, 749.

(4) (a) Adams, R. D. *J. Cluster. Sci.* 1992, 3, 263. (b) Adams, R. D.; Pompeo, M. P. *Organometallics* 1992, 11, 1460. (c) Adams, R. D.; Belinski, J. A.; Pompeo, M. P. *Organometallics* 1991, 10, 2539. (d) Adams, R. D.; Belinski, J. A.; Pompeo, M. P. *Organometallics* 1992, 11, 3129.

(CO)₉ are described. We have found that the complex $\text{Re}_2(\text{CO})_9(\text{SCH}_2\text{CH}_2\text{CH}_2)$ is also capable of producing 12S3 and 24S6 catalytically. Interestingly, the selectivity for 12S3 formation is much higher than that found with the trirhenium complex $\text{Re}_3(\text{CO})_{10}[\mu\text{-SCH}_2\text{CH}_2\text{CH}_2](\mu\text{-H})_3$. Unlike the trirhenium complex in which the thietane molecule is a bridging ligand, the thietane and polythioether macrocycles in these $\text{Re}_2(\text{CO})_9$ complexes are coordinated to one metal atom only.

Experimental Section

General Data. Unless otherwise indicated, all reactions were performed under a nitrogen atmosphere. Reagent grade solvents were stored over 4-Å molecular sieves. $\text{Re}_2(\text{CO})_9(\text{NCMe})$,⁹ $\text{Re}_2(\text{CO})_9(\text{NCMe})_2$,⁹ and $\text{Re}_2(\text{CO})_9(\text{PMe}_2\text{Ph})$ ⁹ were prepared according to the published procedures. $\text{Re}_2(\text{CO})_{10}$ was purchased from Strem Chemicals Inc. and was used without further purification. Trimethylamine *N*-oxide dihydrate (Aldrich) was dehydrated by using a Dean–Stark apparatus with benzene as the solvent prior to use. 1,5,9-Trithiacyclododecane, 12S3, was prepared as described in our previous report.^{7a} Thietane was purchased from Aldrich and was purified by vacuum distillation before use. All other reagents were purchased from Aldrich and were used as received. Infrared spectra were recorded on a Nicolet 5DXB FTIR spectrophotometer. ¹H NMR spectra were obtained on Bruker AM-300 or AM-500 spectrometers operating at 300 or 500 MHz, respectively. ¹³C NMR spectra were obtained on a Bruker AM-500 spectrometer operating at 125.76 MHz. Separations were performed by TLC in air on Analtech 0.25-mm silica gel 60-Å F₂₅₄ plates. Elemental analyses were performed by Oneida Research Services, Whitesboro, NY.

Preparation of $\text{Re}_2(\text{CO})_9(\text{SCH}_2\text{CH}_2\text{CH}_2)$, **2.** A 52.0-mg amount of $\text{Re}_2(\text{CO})_9(\text{NCMe})$, **1**, (0.078 mmol) was dissolved in 30 mL of acetone in a 50-mL three-neck round bottom flask equipped with a stir bar, a reflux condenser, and a nitrogen inlet. A 25-μL amount of thietane (0.34 mmol) was added, and the resulting solution was stirred at reflux for 2 h. The volatiles were removed *in vacuo*, and the products were separated by TLC using a hexane/methylene chloride 2/1 solvent mixture to yield 21.0 mg of $\text{Re}_2(\text{CO})_9(\text{SCH}_2\text{CH}_2\text{CH}_2)$, **2**, 67% yield, and 22.2 mg of unreacted **1**. IR ν_{CO} for **2** (cm⁻¹ in hexane): 2104 (m), 2043 (s), 2017 (m), 1997 (vs), 1991 (vs), 1978 (w), 1970 (s), 1957 (w), 1935 (s). ¹H NMR spectra for **2** (δ in CDCl₃): 3.66 (t, 4H, *J*_{H-H} = 7.7 Hz), 2.88 (quintet, 2H, *J*_{H-H} = 7.7 Hz). The mass spectrum of **2** showed the parent ion at *m/e* = 698. Ions at 670, 586, 558, 530, and 502 are attributed to the loss of 1, 4, 5, 6, and 7 CO ligands from the parent ion, respectively. Additional ions at 628, 600, and 572 are attributed to M⁺ - 3 CH₂ groups and 1-3 CO ligands. The loss of three CH₂ groups is indicative of fragmentation of the thietane ligand.

Preparation of $\text{Re}_2(\text{CO})_9(\text{SCH}_2\text{CH}_2\text{CH}_2\text{SCH}_2\text{CH}_2\text{CH}_2\text{SCH}_2\text{CH}_2\text{CH}_2)$, **3, and $[\text{Re}_2(\text{CO})_9]_2(\text{SCH}_2\text{CH}_2\text{CH}_2\text{SCH}_2\text{CH}_2\text{CH}_2\text{SCH}_2\text{CH}_2\text{CH}_2)$, **4**.** A 78.0-mg amount of **1** (0.12 mmol) was dissolved in 30 mL of acetone in a 50-mL three-neck round bottom flask equipped with a stir bar, a reflux

condenser, and a nitrogen inlet. A 26.0-mg amount of 12S3 (0.12 mmol) was added, and the resulting solution was stirred at reflux for 3 h. The volatiles were removed *in vacuo*, and the products were separated by TLC using a hexane/methylene chloride 3/1 solvent mixture to yield 69.5 mg of $\text{Re}_2(\text{CO})_9(\text{SCH}_2\text{CH}_2\text{CH}_2\text{SCH}_2\text{CH}_2\text{CH}_2\text{SCH}_2\text{CH}_2\text{CH}_2)$, **3**, 70% yield, and 14.4 mg of $[\text{Re}_2(\text{CO})_9]_2(\text{SCH}_2\text{CH}_2\text{CH}_2\text{SCH}_2\text{CH}_2\text{CH}_2\text{SCH}_2\text{CH}_2\text{CH}_2)$, **4**, 9% yield. IR ν_{CO} for **3** (cm⁻¹ in hexane): 2102 (m), 2039 (s), 2014 (m), 1988 (vs), 1977 (w), 1966 (s), 1951 (w), 1933 (s). ¹H NMR spectra for **3** (δ in CDCl₃): 3.01 (t, 4H, *J*_{H-H} = 7.2 Hz), 2.73 (t, 4H, *J*_{H-H} = 6.3 Hz), 2.59 (t, 4H, *J*_{H-H} = 6.2 Hz), 2.00 (quintet, 4H, *J*_{H-H} = 7.0 Hz), 1.80 (quintet, 2H, *J*_{H-H} = 6.3 Hz). Anal. Calcd for **3**: C, 25.54; H, 2.14. Found: C, 25.36; H, 1.69. IR ν_{CO} for **4** (cm⁻¹ in CH₂Cl₂): 2102 (m), 2040 (s), 1989 (vs), 1962 (s), 1926 (s). ¹H NMR spectra for **4** (δ in CDCl₃): 3.13 (t, br, 4H), 2.89 (t, br, 4H), 2.65 (t, br, 4H), 2.12 (quintet, br, 2H), 1.94 (quintet, br, 4H). Anal. Calcd for **4**: C, 22.04; H, 1.23. Found: C, 22.28; H, 1.27.

Preparation of ¹³CO-Enriched $\text{Re}_2(\text{CO})_{10}$. A 152-mg amount of $\text{Re}_2(\text{CO})_9(\text{MeCN})_2$ (0.22 mmol) and 7 mL of octane were placed in a Parr high-pressure reaction unit. The reactor was cooled in liquid nitrogen, and three freeze-pump-thaw cycles were performed. The reaction unit was then placed under vacuum, and ¹³CO was introduced to the reaction unit to a pressure of 1 atm at 25 °C. The unit was then sealed and placed in an oil bath at 150 °C for 24 h. After cooling, the volatiles were removed *in vacuo*, and the product was separated by TLC using hexane solvent to yield 134 mg of ¹³C-enriched $\text{Re}_2(\text{CO})_{10}$ (**5**). A mass spectrum of the product showed that the $\text{Re}_2(\text{CO})_{10}$ was enriched with ¹³CO to approximately 40%. As expected, the ¹³C NMR spectrum in CDCl₃ showed two broad CO resonances at 191.00 (8CO) and 181.78 (2CO) ppm. This sample was used in the preparation of the substituted derivatives listed below.

Preparation of ¹³CO-Enriched **2.** A 55.6-mg amount of **1** (40% enriched with ¹³CO) was converted to **2** (40% enriched with ¹³CO) in 63% yield by the procedure described above. The ¹³C NMR spectrum of this sample showed the following resonances in CDCl₃ (ppm): at 25 °C, 199.87, 194.4 (br), 191.97, 187.77, 185.3 (br); at -80 °C (in CDCl₃), 201.02 (2CO), 195.52 (4CO), 193.57 (1CO), 188.9 (1CO), 185.66 (1CO).

Preparation of ¹³CO-Enriched **3.** A 102-mg amount of **1** (40% enriched with ¹³CO) was converted to **3** (40% enriched with ¹³CO) in 70% yield by the procedure described above. A 20.5-mg amount of **4** (40% enriched with ¹³CO) in 9% yield was also obtained. ¹³C NMR for **3** (in CDCl₃, δ in ppm): 201.35, 195.17 (br), 191.47, 188.08, 184.42 (br); at -80 °C, 202.22 (2CO), 196.35 (4CO), 193.07 (1CO), 189.12 (1CO), 185.99 (1CO). ¹³C NMR for **4** (at 25 °C in CDCl₃, δ in ppm): 201.24, 195.1 (br), 191.20, 187.79, 184.6 (br).

Catalytic Cyclooligomerizations. All catalytic reactions were performed under nitrogen in 25-mL three-neck round bottom flasks equipped with a stir bar, a reflux condenser, and a nitrogen inlet, using preweighed amounts of recrystallized catalyst and thietane without solvent at the reflux temperature of the thietane by heating in an oil bath. Unless indicated otherwise, the reaction apparatus was routinely wrapped completely in aluminum foil to minimize possible effects of light on the reaction. Results of the experiments are listed in Table 1.

A typical treatment is as follows: a 6.0-mL amount of thietane (81 mmol) and a 15.0-mg amount of **2** was added to the 25-mL three-neck round bottom flask. The reaction mixture was heated to reflux and was stirred under nitrogen at this temperature for 24 h. After cooling, the excess thietane was removed *in vacuo*. The resulting residue weighed 829 mg. A ¹H NMR spectrum was taken of a portion of the residue. The spectrum showed two products only: 1,5,9-trithiacyclododecane,¹⁰ $\text{SCH}_2\text{CH}_2\text{CH}_2\text{SCH}_2\text{CH}_2\text{CH}_2\text{SCH}_2\text{CH}_2\text{CH}_2$, 12S3 [¹H NMR (δ in CDCl₃): 2.67 (t, 12H, *J*_{H-H} = 6.7 Hz),

(6) Adams R. D.; Pompeo, M. P. *J. Am. Chem. Soc.* **1991**, *113*, 1619.

(7) (a) Adams, R. D.; Falloon, S. B. *J. Am. Chem. Soc.* **1994**, *116*, 10540. (b) Adams, R. D.; Cortopassi, J. E.; Falloon, S. B. *J. Organomet. Chem.* **1993**, *463*, C5.

(8) (a) Cooper, S. R. In *Crown Compounds: Toward Future Applications*; Cooper, S. R., Ed.; VCH Publishers: New York, 1992; Chapter 15. (b) Cooper, S. R.; Rawley, S. C. *Struct. Bonding* **1990**, *72*, 1. (c) Blake, A. J.; Schröder, M. *Adv. Inorg. Chem.* **1990**, *35*, 1. (d) Cooper, S. R. *Acc. Chem. Res.* **1988**, *21*, 141.

(9) Koelle, U. *J. Organomet. Chem.* **1978**, *155*, 53

Table 1. Results of the Catalytic Cyclooligomerization of Thietane by Dirhenium Complexes

catalyst ^a	catalyst amt (mg)	reagent amt (mL)	products	ratio ^b	reactn time (h)	product amt (mg)	TOF for 12S3 ^c
Re ₂ (CO) ₁₀	20.0	4.0	12S3/24S6	3.5/1	24	55	0.3
1	17.0	4.0	12S3/24S6	3.6/1	24	527	3.0
2	15.0	6.0	12S3/24S6	5.7/1	24	829	6.1
2	15.0	6.0	12S3/24S6	1.3/1	72	2070	3.8
2 ^d	16.8	6.0	12S3/24S6	1.6/1	24	849	4.0
3	12.0	6.0	12S3/24S6	5.6/1	24	530	6.0
5 ^e	8.0	4.0	12S3/24S6	1.8/1	24	153	1.9

^a All reactions were performed at the boiling point of thietane, 94 °C. ^b Product ratios were determined by NMR. ^c TOF = moles of 12S3/moles of catalyst·hour. ^d Performed in the presence of light, see Experimental Section. ^e Mixture of isomers, see Experimental Section.

1.87 (q, 6H, $J_{H-H} = 6.7$ Hz) and 1,5,9,13,17,21-hexathiacyclotetacosane, 24S6¹¹ [¹H NMR (δ in CDCl₃): 2.60 (t, 24H, $J_{H-H} = 7.2$ Hz), 1.84 (q, 12H, $J_{H-H} = 7.2$ Hz)], which were present in a 5.7/1 ratio based on the NMR integration. The products were separated by TLC using a hexane/chloroform/ethyl acetate 2/1/1 solvent mixture as the eluent to give two bands. The first band contained the macrocycle 12S3,¹⁰ and the second band contained the macrocycle 24S6.¹¹ In general, the nonvolatile residues are completely soluble in methylene chloride, which indicates the near absence of polymer formation. The results of these tests are listed in Table 1.

Catalytic Cyclooligomerization of Thietane by 2: Long-Term Test. Under a nitrogen atmosphere was added 6.0 mL (54.0 mmol) of thietane to a 25-mL three-neck round bottom flask equipped with a stir bar, a reflux condenser, a nitrogen inlet, and 15.0 mg (0.022 mmol) of **2**. The thietane itself served as the solvent in this reaction. The solution was heated to reflux and was stirred under nitrogen at this temperature for 72 h. After cooling, the unreacted thietane was removed *in vacuo*. The resulting residue weighed 2.07 g. A ¹H NMR spectrum was taken of a portion of the residue. The spectrum showed the presence of only two products, 12S3 and 24S6, in a 1.3/1 ratio based on the NMR integration.

Catalytic Cyclooligomerization by 2 in the Presence of Light. A 6.0-mL amount of thietane (81 mmol) was added to a 25-mL three-neck round bottom flask equipped with a stir bar, a reflux condenser, a nitrogen inlet, and 16.8 mg (0.024 mmol) of **2**. The reaction mixture was heated to reflux and was stirred under nitrogen at this temperature for 24 h with a 100-W lamp placed 6 in. from the reaction flask. After cooling, the excess thietane was removed *in vacuo*. The resulting residue weighed 849 mg. A ¹H NMR spectrum was taken of a portion of the residue and showed that it consisted entirely of 12S3 and 24S6 in a 1.55/1 ratio.

Catalytic Cyclooligomerization of Thietane by 1. A 4.0-mL amount of thietane (54.0 mmol) was added to a 25-mL three-neck round bottom flask equipped with a stir bar, a reflux condenser, a nitrogen inlet and 17.0 mg (0.026 mmol) of **1**. The solution was heated to reflux and was stirred under nitrogen at this temperature for 24 h. After cooling, the excess thietane was removed *in vacuo*. The resulting residue weighed 527 mg. An NMR spectrum taken of a portion of the residue showed only two products, 12S3 and 24S6, which were in a 3.6/1 ratio based on integration.

Analysis of the Metal-Containing Species after Catalysis by Using ¹³CO-Enriched 2 as the Catalyst. A 2.5-mL amount of thietane (34.0 mmol) was added to a 25-mL 3-neck round bottom flask equipped with a stir bar, a reflux condenser, a nitrogen inlet, and 20.0 mg (0.029 mmol) of ¹³CO-enriched **2**. The reaction was heated to reflux and was stirred under nitrogen at this temperature for 1 h. After cooling, the excess thietane was removed *in vacuo*. The entire residue was dissolved in CDCl₃, and a ¹³C NMR spectrum was recorded. It showed the presence of only two metal-containing products, compounds **2** and **3** in a 2/1 ratio. There were no

detectable amounts of any other metal carbonyl complexes present in these solutions as measured by ¹³C NMR spectroscopy in the CO region. A 47-mg amount of 12S3 was formed in this reaction.

Analysis of the Metal-Containing Species after Catalysis by Using ¹³CO Enriched 3 as the Catalyst. A 5.0-mL amount of thietane (68.0 mmol) was added to a 25-mL three-neck round bottom flask equipped with a stir bar, a reflux condenser, a nitrogen inlet, and 31.0 mg (0.037 mmol) of **3**. The reaction mixture was heated to reflux and was stirred under nitrogen at this temperature for 1 h. After cooling, the excess thietane was removed *in vacuo*. The residue was dissolved in CDCl₃, and a ¹³C NMR spectrum was recorded. It showed the presence of only two metal-containing products, compounds **2** and **3** in a 1/1 ratio. In reactions that were allowed to proceed for 6 h, the ratio of **2/3** was 2/1, the same as found when **2** was used as the catalyst. No detectable amounts of any other metal-carbonyl complexes were found in these solutions as determined by ¹³C NMR spectroscopy in the CO region. After 1 h of catalysis, 27 mg of 12S3 was isolated from this residue.

Analysis of the Metal-Containing Species after Catalysis by Using ¹³CO-Enriched 1 as the Catalyst. A 4.0-mL amount of thietane (54.0 mmol) was added to a 25-mL three-neck round bottom flask equipped with a stir bar, a reflux condenser, a nitrogen inlet, and 20.0 mg (0.037 mmol) of Re₂(¹³CO)₉(NCMe). The reaction mixture was heated to reflux and was stirred under nitrogen at this temperature for 1 h. After cooling, the excess thietane was removed *in vacuo*. The residue was dissolved in CDCl₃, and a ¹³C NMR spectrum was recorded. It showed the presence of only two metal-containing products, compounds **2** and **3** in a 2/1 ratio. A 52-mg amount of 12S3 was subsequently isolated from this residue. There were no detectable amounts of any other metal-carbonyl complexes present in these solutions as determined by ¹³C NMR spectroscopy in the CO region.

Study of the Dependence of the Rate of Catalysis on the Concentration of 2. In a typical procedure a 4.0-mL amount of thietane (54 mmol) was added to a 25-mL three-neck round bottom flask equipped with a stir bar, a reflux condenser, and a nitrogen inlet. An appropriate amount of the catalyst **2** was added under nitrogen. All measurements were made at 93.0 ± 0.1 °C for a period of 1 h and were repeated in duplicate. At the end of 1 h, the excess thietane was removed *in vacuo*, and the amount of product was then determined by weighing the resulting residue and subtracting the preweighed weight of the catalyst. NMR spectra of the residues showed the presence of only one product, 12S3, and the remaining catalyst.

Preparation of Re₂(CO)₉(SCH₂CH₂CH₂)(PMe₂Ph), 5. A 55.0-mg amount of Re₂(CO)₉(PMe₂Ph) (0.072 mmol) was dissolved in 30 mL of acetone in a 50-mL three-neck round bottom flask equipped with a stir bar, a reflux condenser, and a nitrogen inlet. A 20- μ L amount of thietane (0.27 mmol) and a 3.0-mg amount (0.041 mmol) of Me₃NO was added, and the resulting solution was stirred at reflux for 12 h. The volatiles were removed *in vacuo*, and the products were separated by TLC using a hexane/acetone 3/1 solvent mixture to yield 20.1 mg of Re₂(CO)₉(SCH₂CH₂CH₂)(PMe₂Ph), **5**, 35% yield. IR ν_{CO}

(10) Rawle, S. C.; Admans, G. A.; Cooper, S. R. *J. Chem. Soc., Dalton Trans.* 1988, 93.

(11) Ochrymowycz, L. A.; Mak, C.-P.; Michna, J. D. *J. Org. Chem.* 1974, 14, 2079.

Table 2. Crystallographic Data for Compounds 3 and 4

	3	4
formula	Re ₂ S ₃ O ₉ C ₁₈ H ₁₈	Re ₄ S ₃ O ₁₈ C ₂₇ H ₁₈ ^{1/2} C ₆ H ₁₄
formula wt	846.93	1471.44
cryst syst	monoclinic	monoclinic
lattice param		
<i>a</i> (Å)	14.545(4)	16.215(3)
<i>b</i> (Å)	13.425(4)	9.836(4)
<i>c</i> (Å)	14.682(3)	27.171(8)
α (deg)	90.0	90.0
β (deg)	118.24(1)	99.71(2)
γ (deg)	90.0	90.0
<i>V</i> (Å ³)	2526(1)	4271(2)
space group	<i>P</i> ₂ / <i>C</i> , No. 14	<i>P</i> ₂ / <i>n</i> , No. 14
<i>Z</i>	4	4
<i>D</i> _{calc} (g/cm ³)	2.23	2.36
μ(Mo Kα) (cm ⁻¹)	98.7	115.2
temp (°C)	20	20
2θ _{max} (deg)	48.0	45.0
no. of obs used (<i>I</i> > 3σ(<i>I</i>))	3148	3742
no. of variables	290	470
residuals: <i>R</i> , <i>R</i> _w ^a	0.035, 0.033	0.036, 0.037
goodness of fit indicator	2.28	1.81
max shift in final cycle	0.02	0.01
largest peak in final diff map (e Å ⁻³)	1.68	1.11
abs cor	empirical	empirical

^a $R = \sum_{hkl} (|F_{obs}| - |F_{calc}|) / \sum_{hkl} |F_{obs}|$; $R_w = [\sum_{hkl} w(|F_{obs}| - |F_{calc}|)^2] / \sum_{hkl} w |F_{obs}|^2$; $w = 1/\sigma^2(F_{obs})$; $GOF = [\sum_{hkl} (|F_{obs}| - |F_{calc}|) / \sigma(F_{obs})] / (n_{data} - n_{vari})$.

for **5** (cm⁻¹ in CH₂Cl₂): 2068 (w), 2011 (m), 1965 (vs), 1940 (m), 1906 (m). ¹H NMR spectra for **5** (δ in CDCl₃) indicate that this compound exists in solution as a mixture of two isomers which could not be separated by TLC: major isomer, 7.46 (m, 5H), 3.59 (t, 4H, *J*_{H-H} = 7.7 Hz), 2.77 (quintet, 2H, *J*_{H-H} = 7.7 Hz), 2.14 (d, 6H, *J*_{P-H} = 8.6 Hz); minor isomer, 7.46 (m, 5H), 3.57 (t, 4H, *J*_{H-H} = 7.7 Hz), 2.77 (quintet, 2H, *J*_{H-H} = 7.7 Hz), 1.99 (d, 6H, *J*_{P-H} = 8.4 Hz). The mass spectrum of **5** showed the parent ion at *m/e* = 808 and ions corresponding to the loss of the thietane ligand and each of 7 CO ligands.

Catalytic Cyclooligomerization of Thietane by 5. A 4.0-mL amount of thietane (54.0 mmol) was added to a 25-mL three-neck round bottom flask equipped with a stir bar, reflux condenser, a nitrogen inlet, and an 8.0-mg amount (0.010 mmol) of **5**. The solution was heated to reflux and was stirred under nitrogen at this temperature for 24 h. After cooling, the excess thietane was removed *in vacuo*. The resulting residue weighed 153 mg. A ¹H NMR spectrum taken of a portion of the residue showed the presence of only two products, 12S3 and 24S6 in a 1.78/1 ratio.

Crystallographic Analyses. Colorless crystals of **3** and **4** suitable for X-ray diffraction analysis were grown from solution in a 2/1 CH₂Cl₂/hexane solvent mixture by slow evaporation of solvent at 25 °C. The crystals used in intensity measurements were mounted in thin-walled glass capillaries. Diffraction measurements were made on a Rigaku AFC6S fully automated four-circle diffractometer using graphite-monochromated Mo Kα radiation. The unit cells were determined and refined from 15 randomly selected reflections obtained by using the AFC6S automatic search, center, index, and least-squares routines. Crystal data, data collection parameters, and results of these analyses are listed in Table 2. All data processing was performed on a Digital Equipment Corp. VAXstation 3520 computer by using the TEXSAN structure-solving program library obtained from the Molecular Structure Corp., The Woodlands, TX. Neutral atom scattering factors were calculated by the standard procedures.^{12a} Anomalous dispersion corrections were applied to all non-hydrogen atoms.^{12b} Lorentz-polarization (Lp) and absorption corrections were applied in each analysis. Full matrix least-squares refinements minimized the function $\sum_{hkl} w(|F_o| - |F_c|)^2$, where $w = 1/\sigma(F)^2$, $\sigma(F) = \sigma(F_o^2)/2F_o$, and $\sigma(F_c^2) = [\sigma(I_{raw})^2 + (0.02I_{net})^2]^{1/2}/Lp$.

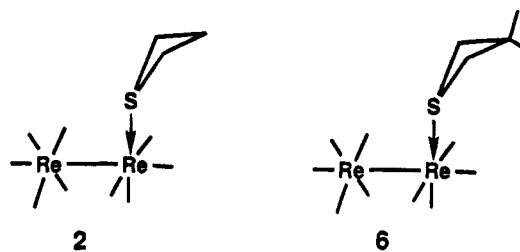
For each analysis the positions of all hydrogen atoms on the ligands were calculated by assuming idealized geometries and C-H = 0.95 Å. Their contributions were added to the structure factor calculations, but their positions were not refined.

Compound **3** crystallized in the monoclinic crystal system. The space group *P*₂/*c* was established on the basis of the patterns of systematic absences observed during the collection of data. The structure was solved by a combination of direct methods (MITHRIL) and difference Fourier syntheses. All non-hydrogen atoms were refined with anisotropic thermal parameters.

Compound **4** crystallized in the monoclinic crystal system. The space group *P*₂/*n* was established on the basis of the patterns of systematic absences observed during the collection of data. The structure was solved by a combination of direct methods (MITHRIL) and difference Fourier syntheses. All non-hydrogen atoms were refined with anisotropic thermal parameters. In the final stages of the analysis a molecule of hexane was located in the lattice positioned about a center of symmetry. The carbon atoms were refined partially on their positional parameters using an isotropic thermal parameter and were subsequently fixed for the final cycles of refinement when they failed to converge.

Results

The compound Re₂(CO)₉(SCH₂CH₂CH₂), **2**, has been obtained in 67% yield from the reaction of **1** with thietane. Compound **2** is spectroscopically similar to the related compound Re₂(CO)₉(SCH₂CMe₂CH₂), **6**, which we have prepared and structurally characterized previously.¹³ Compound **6** contains a 3,3-dimethylthietane ligand terminally coordinated in an equatorial site on one of the two metal atoms. Compound **2** is believed to be structurally similar to **6**.



The ¹³C NMR spectrum of **2** in the CO region was also obtained. The spectrum at 25 °C in CDCl₃ exhibits five resonances: 199.87, 194.4 (br), 191.97, 187.77, and 185.3 (br). Two of these are very broad. This broadening appears to be due to partial coupling to the neighboring rhenium nuclei due to incomplete quadrupolar relaxation effects.¹⁴ At -80 °C the quadrupole relaxation has removed nearly all of the coupling, and five relatively sharp resonances with relative intensities based on the proposed structure are observed: 201.02 (2C), 195.52 (4C), 193.57 (1C), 188.9 (1C), and 185.66 (1C). This spectrum is consistent with the proposed structure **2** assuming that conformational rotations about the Re-Re bond are rapid on the NMR time scale and thus

(12) (a) *International Tables for X-ray Crystallography*; Kynoch Press: Birmingham, England, 1975; Vol. IV, Table 2.2B, pp 99-101; (b) Table 2.3.1, pp 149-150.

(13) Adams, R. D.; Belinski, J. A.; Schierlmann, J. *J. Am. Chem. Soc.* **1991**, *113*, 9004.

(14) Todd, L. J.; Wilkinson, J. R. *J. Organomet. Chem.* **1974**, *80*, C31.

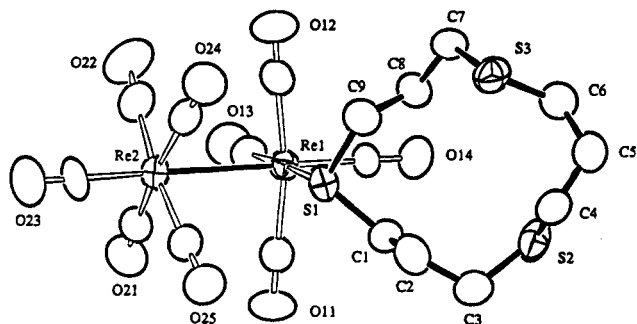


Figure 1. An ORTEP diagram of $\text{Re}_2(\text{CO})_9(\text{SCH}_2\text{CH}_2\text{CH}_2\text{SCH}_2\text{CH}_2\text{CH}_2)$ (**3**) showing 50% probability thermal ellipsoids. Selected interatomic distances (Å) and angles ($^\circ$) are as follows: $\text{Re}(1)\text{--Re}(2) = 3.0554(8)$, $\text{Re}(1)\text{--S}(1) = 2.498(3)$, $\text{S}(1)\text{--C}(1) = 1.81(1)$, $\text{S}(1)\text{--C}(9) = 1.82(1)$, $\text{S}(2)\text{--C}(3) = 1.77(1)$, $\text{S}(2)\text{--C}(4) = 1.80(1)$, $\text{S}(3)\text{--C}(6) = 1.81(1)$, $\text{S}(3)\text{--C}(7) = 1.80(1)$, $\text{Re}(2)\text{--Re}(1)\text{--S}(1) = 87.96(6)$, $\text{C}(1)\text{--S}(1)\text{--C}(9) = 100.9(5)$.

Table 3. Positional Parameters and $B(\text{eq})$ for **3**

atom	x	y	z	$B(\text{eq})$
Re(1)	0.35418(4)	0.01513(3)	0.67006(3)	3.07(2)
Re(2)	0.20329(4)	0.16344(3)	0.68637(3)	3.90(2)
S(1)	0.4976(2)	0.1364(2)	0.7684(2)	3.6(1)
S(2)	0.8523(3)	0.0196(2)	0.9155(3)	5.2(1)
S(3)	0.7735(3)	0.2256(2)	0.6850(2)	4.9(1)
O(11)	0.3855(7)	-0.0632(5)	0.8841(6)	6.0(4)
O(12)	0.2972(7)	0.1156(6)	0.4590(6)	6.3(4)
O(13)	0.1699(7)	-0.1256(6)	0.5519(6)	6.1(4)
O(14)	0.5110(6)	-0.1274(5)	0.6559(6)	5.1(3)
O(21)	0.1135(7)	-0.0207(6)	0.7483(7)	6.4(4)
O(22)	0.0563(8)	0.1134(8)	0.4553(7)	8.9(5)
O(23)	0.0581(9)	0.3169(7)	0.7077(8)	8.7(6)
O(24)	0.3128(7)	0.3179(6)	0.6118(6)	6.3(4)
O(25)	0.3758(8)	0.1825(6)	0.9159(6)	6.4(4)
C(1)	0.6083(9)	0.0665(7)	0.8615(7)	4.0(4)
C(2)	0.699(1)	0.1275(9)	0.9316(8)	5.3(5)
C(3)	0.799(1)	0.066(1)	0.9931(8)	5.5(5)
C(4)	0.921(1)	0.1290(8)	0.9091(8)	4.6(5)
C(5)	0.947(1)	0.122(1)	0.823(1)	5.9(6)
C(6)	0.854(1)	0.115(1)	0.7159(9)	5.9(6)
C(7)	0.6510(9)	0.1741(8)	0.5907(7)	4.4(5)
C(8)	0.5899(9)	0.1187(7)	0.6347(8)	4.1(4)
C(9)	0.5505(9)	0.1883(7)	0.6884(8)	4.1(4)
C(11)	0.3741(9)	-0.0352(7)	0.8059(8)	3.9(4)
C(12)	0.317(1)	0.0806(7)	0.5365(9)	4.1(5)
C(13)	0.2371(9)	-0.0741(8)	0.5970(8)	4.0(4)
C(14)	0.4516(8)	-0.0744(7)	0.6607(7)	3.4(4)
C(21)	0.145(1)	0.049(1)	0.7252(9)	5.0(6)
C(22)	0.107(1)	0.132(1)	0.539(1)	5.8(6)
C(23)	0.112(1)	0.259(1)	0.701(1)	5.7(6)
C(24)	0.271(1)	0.2606(8)	0.6399(8)	4.5(5)
C(25)	0.312(1)	0.1782(8)	0.8314(9)	4.5(5)

average the four equatorially positioned CO groups on the $\text{Re}(\text{CO})_5$ grouping.

Two products, $\text{Re}_2(\text{CO})_9(\text{SCH}_2\text{CH}_2\text{CH}_2\text{SCH}_2\text{CH}_2\text{CH}_2\text{SCH}_2\text{CH}_2\text{CH}_2)$ **3**, 70% yield, and $[\text{Re}_2(\text{CO})_9]_2\text{-(SCH}_2\text{CH}_2\text{CH}_2\text{SCH}_2\text{CH}_2\text{CH}_2\text{SCH}_2\text{CH}_2\text{CH}_2)$, **4**, 9% yield, were obtained when equimolar amounts of **1** and 12S3 were allowed to react in an acetone solution at reflux. Both of these products were characterized by combination of IR, ^1H NMR, ^{13}C NMR, and single-crystal X-ray diffraction analyses. An ORTEP diagram of the molecular structure of **3** is shown in Figure 1. Final atomic positional parameters are listed in Table 3. The molecule is structurally similar to compound **6**, with a 12S3 ligand coordinated through one of its sulfur atoms

to one of the rhenium atoms in an equatorial site. The equatorially positioned ligands on the two metal atoms adopted a staggered rotation conformation similar to that found in $\text{Re}_2(\text{CO})_{10}$ ¹⁵ and **6**.¹³ The Re- Re distance in **3**, 3.0554(8) Å, is similar to that found in $\text{Re}_2(\text{CO})_{10}$, 3.041(1) Å,¹⁵ and in **6**, 3.0422(8) Å.⁹ The 12S3 ligand exhibits the same conformation as that found for the free molecule in the solid state and in a number of its coordination complexes.¹⁶ The coordinated sulfur atom is pyramidal, so all of the hydrogen atoms on the ligand are inequivalent according to the solid state structure, but the ^1H NMR spectrum of the complex in solution at 25 $^\circ\text{C}$ is very simple [3.01 (t, 4H, $J_{\text{H-H}} = 7.2$ Hz), 2.73 (t, 4H, $J_{\text{H-H}} = 6.3$ Hz), 2.59 (t, 4H, $J_{\text{H-H}} = 6.2$ Hz), 2.00 (quintet, 4H, $J_{\text{H-H}} = 7.0$ Hz), 1.80 (quintet, 2H, $J_{\text{H-H}} = 6.3$ Hz)] and consistent with a C_{2v} symmetry. This can be explained by a combination of rapid conformational rearrangements in the ring and inversions in configuration at the coordinated sulfur atom.¹⁷ The ^{13}C NMR spectrum of **3** in the CO region at 25 $^\circ\text{C}$ is similar to that of **2**: [201.35, 195.17 (br), 191.47, 188.08, and 184.42 (br)] in which two of the resonances are broadened due to incomplete quadrupole relaxation of the coupling to the rhenium nuclei.¹⁴ At -80 $^\circ\text{C}$ sharp resonances were observed for all of the resonances: 202.22 (2CO), 196.35 (4CO), 193.07 (1CO), 189.12 (1CO), 185.99 (1CO).

An ORTEP diagram of the molecular structure of **4** is shown in Figure 2. Final atomic positional parameters are listed in Table 4. This molecule is very similar to that of **3** except that it has two $\text{Re}_2(\text{CO})_9$ groups coordinated to one 12S3 ring. The $\text{Re}_2(\text{CO})_9$ groups are coordinated to different sulfur atoms. The Re- Re distances, $\text{Re}(1)\text{--Re}(2) = 3.049(1)$ and $\text{Re}(3)\text{--Re}(4) = 3.052(1)$, are quite similar to those found in **3**, **6**, and $\text{Re}_2(\text{CO})_{10}$. The conformation of the 12S3 ligand is again the same as that found in the free molecule **3** and other related 12S3 complexes. The ability of 12S3 to coordinate more than one sulfur atom to separate metal units has been observed previously. Indeed, in the complex $[\text{Ag}(12\text{S3})](\text{CF}_3\text{SO}_3)\text{NMe}$, each sulfur atom of the 12S3 ligand is coordinated to a silver atom in the solid state.^{16c} In the solid state structure the two metal-coordinated sulfur atoms are conformationally different and thus inequivalent; however, the ^1H NMR spectrum of **4** at 25 $^\circ\text{C}$ indicates that the structure has an overall C_{2v} symmetry, [$\delta = 3.13$ (t, br, 4H), 2.89 (t, br, 4H), 2.65 (t, br, 4H), 2.12 (quintet, br, 2H), 1.94 (quintet, br, 4H) ppm], indicating that conformational averaging and inversions of configuration at the pyramidally coordinated sulfur atoms are rapid on the NMR time scale. The ^{13}C NMR for **4** in the CO region can be interpreted in terms of two equivalent $\text{Re}_2(\text{CO})_9$ groups although the CO ligands within a given $\text{Re}_2(\text{CO})_9$ group are not averaged: 201.24 (2CO), 195.1 (br) (4CO), 191.20 (1CO), 187.79 (1CO), 184.6 (br) (1CO) ppm. Broadening in some of the resonances is believed to be due to incom-

(15) Churchill, M. R.; Amoh, K. N.; Wasserman, H. *J. Inorg. Chem.* **1981**, *20*, 1609.

(16) (a) Rawle, S. C.; Admans, G. A.; Cooper, S. R. *J. Chem. Soc., Dalton Trans.* **1988**, 93. (b) Edwards, A. J.; Johnson, B. F. G.; Khan, F. K.; Lewis, J.; Raithby, P. R. *J. Organomet. Chem.* **1992**, *426*, C44. (c) Blower, P. J.; Clarkson, J. A.; Rawle, S. C.; Hartman, J. R.; Wolf, R. E.; Yagbasan, R.; Bott, S. G.; Cooper, S. R. *J. Chem. Soc., Dalton Trans.* **1989**, *28*, 4040.

(17) (a) Abel, E. W.; Bharagara, S. K. Orrell, K. G. *Prog. Inorg. Chem.* **1984**, *32*, 1. (b) Wu, H.; Lucas, C. R. *Inorg. Chem.* **1992**, *31*, 2354.

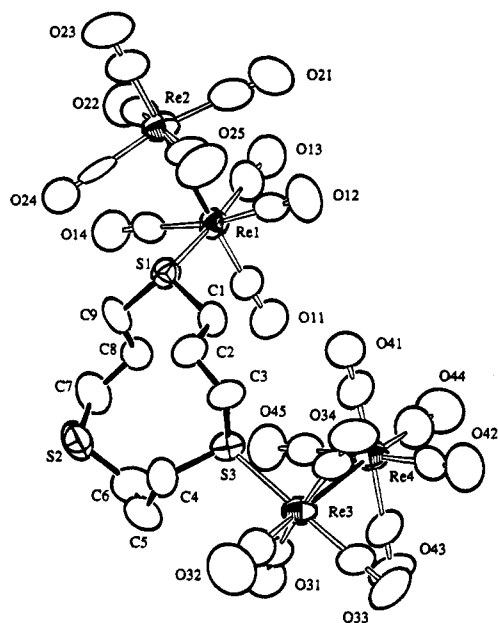


Figure 2. An ORTEP diagram of $[\text{Re}_2(\text{CO})_9]_2(\text{SCH}_2\text{CH}_2\text{CH}_2\text{SCH}_2\text{CH}_2\text{CH}_2\text{SCH}_2\text{CH}_2\text{CH}_2\text{SCH}_2\text{CH}_2\text{CH}_2)$, (**4**) showing 50% probability thermal ellipsoids. Selected interatomic distances (Å) and angles ($^\circ$) are as follows: $\text{Re}(1)\text{--Re}(2) = 3.049(1)$, $\text{Re}(3)\text{--Re}(4) = 3.052(1)$, $\text{Re}(1)\text{--S}(1) = 2.499(4)$, $\text{Re}(3)\text{--S}(3) = 2.501(4)$, $\text{S}(1)\text{--C}(1) = 1.80(1)$, $\text{S}(1)\text{--C}(9) = 1.82(1)$, $\text{S}(2)\text{--C}(6) = 1.81(2)$, $\text{S}(2)\text{--C}(7) = 1.77(2)$, $\text{S}(3)\text{--C}(3) = 1.83(2)$, $\text{S}(3)\text{--C}(4) = 1.86(2)$, $\text{Re}(2)\text{--Re}(1)\text{--S}(1) = 88.1(1)$, $\text{Re}(4)\text{--Re}(3)\text{--S}(3) = 90.1(1)$, $\text{C}(1)\text{--S}(1)\text{--C}(9) = 102.0(8)$, $\text{C}(3)\text{--S}(3)\text{--C}(4) = 99.7(9)$.

plete quadrupole relaxation of the coupling to the rhenium nuclei.¹⁴

Catalytic Cyclooligomerization of Thietane. We have shown previously that thietane can be cyclooligomerized catalytically by the trirhenium complex

$\text{Re}_3(\text{CO})_{10}(\mu\text{--SCH}_2\text{CH}_2\text{CH}_2)(\mu\text{--H})_3$, **7**,^{7a} In those reactions the cyclooligomers **12S3** and **24S6** were the two principal products and the amount of **24S6** was substantially greater than that of the **12S3**. Accordingly, we have also investigated the ability of $\text{Re}_2(\text{CO})_{10}$ and compounds **1**, **2**, **3**, and **5** to produce cyclooligomerization of thietane. As in the previous studies, these reactions were performed in pure thietane solutions at the reflux temperature of thietane (94 $^\circ\text{C}$). All of these compounds produce cyclooligomerization of thietane catalytically to yield **12S3** and **24S6**, see Table 1. No other cyclooligomers were formed. The catalytic activity of $\text{Re}_2(\text{CO})_{10}$ is much less than that of **1**, **2**, **3**, or **5**. Compounds **2** and **3** are the most active and have virtually the same activity and selectivity for **12S3** formation. In fact, **2** is only slightly less active than **7**.^{7a} A major difference between **2** and **7** is in the relative amounts of the **12S3** and **24S6** that are formed. With **2**, **12S3** was by far the major product after a 24-h period, whereas with **7**, **24S6** was by far the major product. The **12S3/24S6** ratios were 5.7/1 and 1/3.5 for **2** and **7**,^{7a} respectively. With **2** it was observed that the relative amount of **24S6** increases as the reaction progresses, but even after 72 h, the amount of **12S3** was still greater than that of **24S6**, see Table 1. The activity of **1** was similar to that of **2**, but the amount of **24S6** was significantly higher than that obtained from **2** in the first 24 h. The activity of $\text{Re}_2(\text{CO})_{10}$ is only about $1/20$ that of **2**. We have also

Table 4. Positional Parameters and $B(\text{eq})$ for **4**

atom	x	y	z	$B(\text{eq})$
Re(1)	0.13252(4)	0.15792(6)	0.38266(2)	4.05(3)
Re(2)	0.26621(4)	0.17362(8)	0.31626(3)	4.94(4)
Re(3)	-0.35134(4)	-0.14972(7)	0.35174(3)	4.45(3)
Re(4)	-0.30629(4)	0.11810(7)	0.40645(3)	4.64(3)
S(1)	0.0766(2)	-0.0489(4)	0.3350(2)	4.1(2)
S(2)	-0.0050(3)	-0.4588(4)	0.4198(2)	6.5(3)
S(3)	-0.1997(3)	-0.1949(4)	0.3511(2)	4.4(2)
O(11)	-0.0007(9)	0.152(1)	0.4492(5)	7.7(8)
O(12)	0.0259(9)	0.343(1)	0.3019(5)	8.5(8)
O(13)	0.2116(8)	0.410(1)	0.4370(5)	7.9(8)
O(14)	0.2634(8)	-0.030(1)	0.4476(4)	6.8(7)
O(21)	0.233(1)	0.486(2)	0.3186(7)	10(1)
O(22)	0.3969(8)	0.191(1)	0.4144(5)	7.6(7)
O(23)	0.396(1)	0.183(2)	0.2480(5)	8.8(9)
O(24)	0.2727(8)	-0.144(1)	0.3259(6)	7.5(8)
O(25)	0.1146(8)	0.145(2)	0.2298(5)	9.0(9)
O(31)	-0.330(1)	-0.268(1)	0.4608(5)	8.3(9)
O(32)	-0.405(1)	-0.416(1)	0.2956(6)	11(1)
O(33)	-0.5355(7)	-0.086(1)	0.3556(6)	9.1(9)
O(34)	-0.3703(8)	0.029(2)	0.2566(5)	8.5(8)
O(41)	-0.1978(9)	0.192(1)	0.3275(5)	7.3(8)
O(42)	-0.457(1)	0.252(1)	0.3362(6)	9(1)
O(43)	-0.4309(8)	0.011(2)	0.4744(6)	8.5(9)
O(44)	-0.264(1)	0.369(1)	0.4731(6)	9(1)
O(45)	-0.1579(8)	-0.052(1)	0.4657(4)	7.2(7)
C(1)	-0.036(1)	-0.035(1)	0.3239(6)	4.5(8)
C(2)	-0.078(1)	-0.150(2)	0.2931(5)	4.8(8)
C(3)	-0.173(1)	-0.148(2)	0.2907(5)	4.6(8)
C(4)	-0.181(1)	-0.381(2)	0.3498(8)	7(1)
C(5)	-0.176(1)	-0.451(2)	0.400(1)	8(1)
C(6)	-0.104(1)	-0.406(2)	0.4366(7)	7(1)
C(7)	0.064(1)	-0.332(2)	0.4494(6)	6(1)
C(8)	0.058(1)	-0.192(1)	0.4241(6)	4.5(8)
C(9)	0.093(1)	-0.198(1)	0.3749(6)	5.0(8)
C(11)	0.050(1)	0.152(2)	0.4236(7)	6(1)
C(12)	0.065(1)	0.275(2)	0.3307(7)	5(1)
C(13)	0.183(1)	0.316(2)	0.4163(7)	6(1)
C(14)	0.217(1)	0.040(2)	0.4243(6)	4.7(9)
C(21)	0.245(1)	0.372(2)	0.3177(8)	7(1)
C(22)	0.350(1)	0.189(2)	0.3791(7)	5(1)
C(23)	0.349(1)	0.180(2)	0.2749(8)	7(1)
C(24)	0.271(1)	-0.027(2)	0.3230(6)	5(1)
C(25)	0.170(1)	0.156(2)	0.2609(7)	6(1)
C(31)	-0.336(1)	-0.229(2)	0.4212(8)	6(1)
C(32)	-0.385(1)	-0.318(2)	0.3169(7)	7(1)
C(33)	-0.467(1)	-0.111(2)	0.3545(7)	5(1)
C(34)	-0.363(1)	-0.040(2)	0.2920(7)	6(1)
C(41)	-0.240(1)	0.165(2)	0.3567(7)	6(1)
C(42)	-0.402(1)	0.203(2)	0.3621(8)	6(1)
C(43)	-0.385(1)	0.051(2)	0.4500(7)	6(1)
C(44)	-0.280(1)	0.274(2)	0.4475(7)	7(1)
C(45)	-0.210(1)	0.011(2)	0.4445(6)	4.6(9)
C(51)	0.0291	0.0448	0.0171	20.8
C(52)	0.0764	0.0849	0.0626	15.6
C(53)	0.0418	0.0194	0.1058	14.5

prepared a phosphine derivative of **2**, $\text{Re}_2(\text{CO})_8(\text{PMe}_2\text{Ph})(\text{SCH}_2\text{CH}_2\text{CH}_2)$, **5**, and tested it for its ability to produce cyclooligomerizations of thietane. The activity of **5** is lower than that of **2** or **3**, and its selectivity for **12S3** is also lower, but it is significantly more active than $\text{Re}_2(\text{CO})_{10}$.

To obtain more information about the mechanism a kinetic study of the rate of formation of **12S3** as a function of the concentration of **2** was performed. A plot of these results is shown in Figure 3. As can be seen, the plot is linear in the concentration of **2**. This indicates that the catalysis is being produced by **2** and not by mononuclear fragments derived from **2**.¹⁸

(18) Laine, R. M. *J. Mol. Catal.* **1982**, *14*, 137. (b) Hilal, H. S.; Jondi, W.; Khalaf, S.; Abu-Halawa, R. *J. Organomet. Chem.* **1993**, *452*, 161. (c) Hilal, H. S.; Khalaf, S.; Jondi, W. *J. Organomet. Chem.* **1993**, *452*, 167.

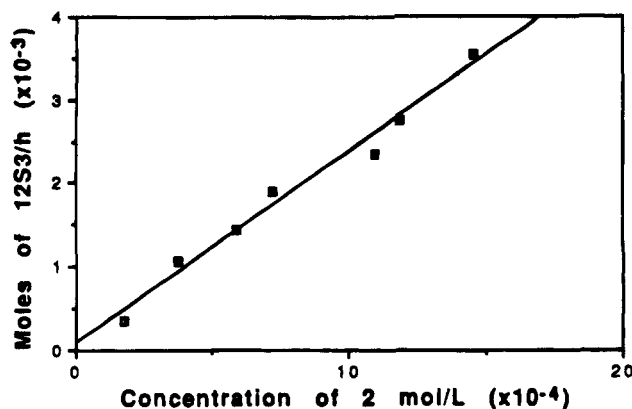
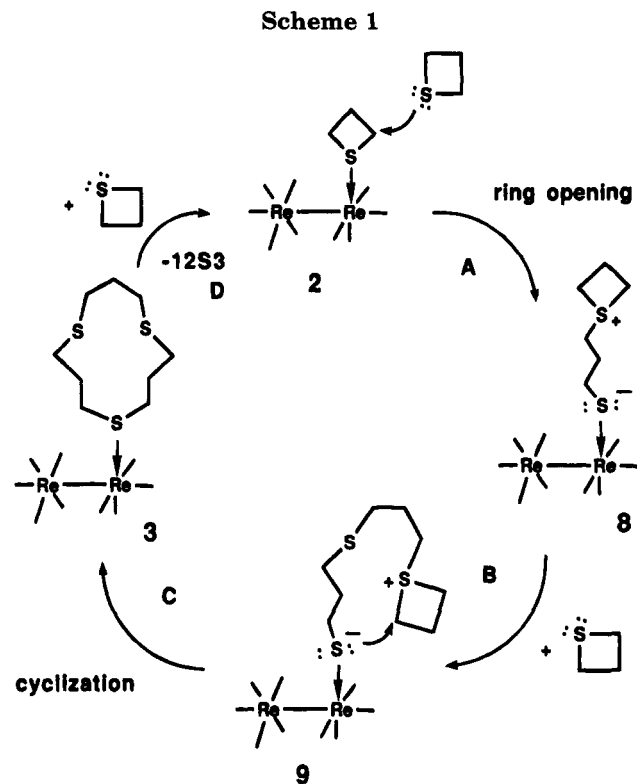


Figure 3. A plot of the rate of formation of 12S3 as a function of the concentration of **2**. Rates were determined after the first 1 h of reaction time.

Catalytically active solutions obtained from **2** were examined by ^{13}C NMR spectroscopy. For this purpose compound **2** was prepared in a form enriched to 40% with ^{13}C in the CO ligands. Catalysis was performed for a period of 1 h, and after removal of all volatile components a ^{13}C NMR spectrum was recorded of the entire residue. It showed the presence of only two metal-containing products, compounds **2** and **3** in a 2/1 ratio. A 47-mg amount of 12S3 was also obtained in this reaction. In a similar manner the catalysis produced by **3** was also examined by ^{13}C NMR spectroscopy using a sample of **3** enriched by 40% with ^{13}C . After 1 h an NMR spectrum of the residue showed the presence of only the two complexes **2** and **3** in a 1/1 ratio. After 6 h this ratio had changed to 2/1. Similarly, a test of the catalysis of **1** was performed using ^{13}C -enriched **1**. At the end of the catalysis, a ^{13}C NMR spectrum of the residue showed the presence of only two metal-containing products, compounds **2** and **3**, in a 2/1 ratio.

A proposed mechanism for the catalytic cyclotrimerization of thietane by **2** and **3** is shown in Scheme 1. It is proposed that the coordination of the thietane molecule to one of the rhenium atoms in **2** activates it toward nucleophilic addition of an uncoordinated thietane molecule at one of the methylene groups bonded to the coordinated sulfur atom. The activation occurs by the removal of some of the electron density from the sulfur atom by the metal atom. This should lead to the formation of a partial positive charge at the sulfur atom and to a lesser extent at the neighboring carbon atoms. This is apparently sufficient to promote a nucleophilic addition at the neighboring α -carbon atoms of the coordinated thietane, by the sulfur atom of an uncoordinated thietane molecule, resulting in the cleavage of the carbon-sulfur bond and opening the four-membered ring, step A.^{4b} This will lead to a zwitterionic intermediate, such as **8**, containing a negatively charged terminally coordinated thiolate grouping and a positively charged thietanium group linked to the thiolate sulfur atom via a trimethylene tether. Similar ring-opening reactions have been observed for thietane ligands in bridging coordination modes.⁴⁻⁷ The dangling thietanium group should be sufficiently reactive to react with uncoordinated thietane molecules spontaneously by ring-opening additions, step B. The cationic ring-opening polymerization of thietanes via thietanium intermediates is well-known.¹⁹ Polymerization



could ensue, but instead a ring-opening cyclization occurs after the addition of a second molecule of thietane by an attack of the coordinated thiolato sulfur atom at one of the α -carbon atoms of the thietanium ring, step C, which leads to the 12S3 complex **3**.

The tendency toward cyclization in these complexes may be enhanced by the zwitterionic nature of the intermediate **9**, which should tend to keep the head and tail of the growing chain proximate to one another. Catalyst **2** can be regenerated from **3** simply by the substitution of the 12S3 ligand by thietane, step D in the scheme. This step should be enhanced in the solvent-free thietane solutions used in these studies. A mechanism similar to this has been proposed for the Lewis acid catalyzed cyclooligmerization of oxetane by BF_3 .²⁰ The observed catalysis by **3** is also explained by the proposed catalytic cycle since **3** is a species in the cycle. Indeed, the catalytic activity of **3** is not significantly different from that of **2**. This can be seen in the turnover frequencies (TOF) for the formation of 12S3 by **2** and **3** as shown in Table 1. The catalysis by **1** can be explained by a similar mechanism by adding as a first step the substitution of its NCMe ligand by thietane. The presence of **2** and **3** in the catalyst solutions of **1** was confirmed by ^{13}C NMR spectroscopy. Interestingly, all the resonances detected by ^{13}C NMR spectroscopy in the CO region of these catalytic reactions can be explained, indicating that the catalysis is very clean, at least in the early stages. The catalysis by $\text{Re}_2(\text{CO})_{10}$ can also be explained by this cycle, but this would require the displacement of a less labile CO ligand from the $\text{Re}_2(\text{CO})_{10}$ by the thietane. This should be much slower than the NCMe displacement in **1**; thus $\text{Re}_2(\text{CO})_{10}$ should be a poorer catalyst, as observed.

(19) (a) Goethals, E. J. *Makromol. Chem., Macromol. Symp.* **1991**, 42/43, 51. (b) Goethals, E. J.; Drijvers, W.; van Ooteghem, D.; Buyle, A. M. *J. Macromol. Sci., Chem.* **1973**, A7, 1375. (c) Goethals, E. J.; Florquin, S. M. *Makromol. Chem.* **1981**, 182, 3371.

(20) Dale, J.; Fredriksen, S. B. *Acta Chem. Scand.* **1991**, 45, 82.

The catalysis by **5** can be explained by a mechanism similar to that for **2**. However, since phosphines are better donors than CO, the replacement of a CO ligand by the PMe_2Ph ligand in **5** will result in more electron density at the metal atoms. Accordingly, there should be less removal of electron density from the sulfur atom of the coordinated thietane ligand in **5** than in **2**. Thus, ring-opening addition in the catalytic cycle for **5** may be slower than for **2**, and the overall catalytic activity is lower, as observed.

The formation of **24S6** could be explained by a mechanism similar to that shown in Scheme 1 for **12S3** by allowing the addition of 4 equiv of thietane to the intermediate **8** prior to the cyclization step C. It is not yet clear to us why the formation of **24S6** is increased relative to that of **12S3** with longer reaction periods. We have shown that **12S3** is not converted to **24S6** in the presence of **2** in heptane solvent at 93 °C, which seems to rule out the possibility that the **12S3** is being converted to the **24S6** under the reaction conditions.

We have observed previously that visible light can promote the opening of thietane ligands in dirhenium complexes.¹³ Accordingly, we investigated the effects of visible light on this catalysis. We have found that the formation of **24S6** is substantially increased at the expense of **12S3** formation in the presence of visible light. This indicates that there are factors that can promote the formation of **24S6**. Other mechanisms may also be involved. It is possible that thietane could react with the **12S3** ligand in **3** in a ring-opening process that could lead to the transformation of some of the **12S3** into **24S6**. Alternatively, it is possible that **12S3** could

react with **2** by opening the coordinated thietane ligand leading to the formation of a thiolato ligand containing a **12S3** grouping linked to the Re_2 group by a $\text{SCH}_2\text{-CH}_2\text{CH}_2$ chain at a sulfonium center. An opening of the **12S3** grouping at this sulfonium center by thietane could lead to enlargement of the **12S3** ring. These processes would be less important in the early stages of the catalysis when there is little **12S3** present in the solutions. Further studies of the formation of **24S6** are in progress.

The fundamental difference between the catalytic activity of the dirhenium complexes reported here and that of **7^{7a}** is that, with **7**, the thietane ligand is coordinated in a bridging mode, whereas for the dirhenium complexes it appears that only terminal coordination is involved. It thus appears that the ability of heavy metals to activate thietanes toward ring-opening reactions through coordination has a wider scope than we originally suspected. We suspect that a wider range of metal-promoted organic reactions of thietanes can be anticipated as well.

Acknowledgment. These studies were supported by the Office of Basic Energy Sciences of the U.S. Department of Energy.

Supplementary Material Available: Tables of interatomic distances and angles and anisotropic thermal parameters (14 pages). Ordering information is given on any current masthead page.

OM950048Z

α -Sulfonyl Carbanion-Transition-Metal Bonds. Alkali-Metal α -Sulfonyl Carbanions and Their Reactivity with Metal Complexes

Pier Giorgio Cozzi and Carlo Floriani*

Institut de Chimie Minérale et Analytique, BCH, Université de Lausanne, CH-1015 Lausanne, Switzerland

Angiola Chiesi-Villa and Corrado Rizzoli

Dipartimento di Chimica, Università di Parma, I-43100 Parma, Italy

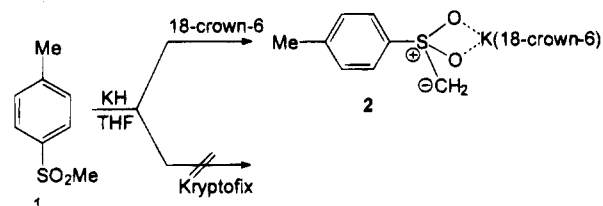
Received December 9, 1994[®]

Deprotonation of *p*-MeC₆H₄SO₂Me (**1**) with KH in THF in the presence of 18-crown-6 led to the isolation of the ion contact pair [*p*-MeC₆H₄S(CH₂)O₂- - K(18-crown-6)] (**2**). The α -sulfonyl carbanion has been involved in the derivatization of both early- and late-transition-metal complexes. When the deprotonation of **1** *in situ* was followed by a reaction with Cp₂-TiCl₂ (Cp = η^5 -C₅H₅), we obtained a Ti-C-bonded α -sulfonyl complex, [Cp₂Ti(Cl)(CH₂SO₂C₆H₄Me-*p*)] (**4**), while the reaction of **2** with Cp₂ZrCl₂ led to a 1:1 mixture of Zr-C- and Zr-O-bonded α -sulfonyl complexes, [Cp₂Zr(Cl)(CH₂SO₂C₆H₄Me-*p*)] (**5a**) and [Cp₂Zr(Cl)(O₂S(CH₂)C₆H₄Me-*p*)] (**5b**). The reaction of the α -sulfonyl carbanion derived from **1** with [*cis*-Pd(PPh₃)₂Cl₂] gave a Pd-C-bonded α -sulfonyl complex occurring with the isomerization of the metal center, [*trans*-(PPh₃)₂(Cl)Pd-CH₂SO₂(*p*-MeC₆H₄)] (**7**). Crystallographic details: **2** is monoclinic, space group *P*2₁/*c*, with *a* = 8.635(2) Å, *b* = 14.879(3) Å, *c* = 19.589(3) Å, $\alpha = \gamma = 90^\circ$, $\beta = 96.30(2)^\circ$, *Z* = 4, and *R* = 0.057; **4** is monoclinic, space group *C*2/*c*, with *a* = 22.318(3) Å, *b* = 9.727(2) Å, *c* = 16.267(3) Å, $\alpha = \gamma = 90^\circ$, $\beta = 100.08(2)^\circ$, *Z* = 8, and *R* = 0.047.

The importance of sulfones in organic synthesis stems from their easy conversion into the corresponding α -sulfonyl carbanions, which are employed in a variety of C-C bond formation reactions. The sulfone group has proved to be enormously valuable in some of the most demanding and difficult total syntheses carried out in recent years.¹ A number of X-ray structural determinations of α -sulfonyl carbanions were reported by the Boche² and Gais³ groups. Such studies were principally devoted to illustrating the configurational and structural characteristics of lithium α -sulfonyl carbanions. Other significant crystal structure determinations have been carried out on organometallic titanium alkoxide⁴ and potassium derivatives⁵ of α -sulfonyl carbanions. As an extension of our study into the fundamental aspects of α -carbanions and enolates,⁶ we report here our preliminary investigation into this closely related field.

Deprotonation of methyl *p*-tolyl sulfone (**1**) was carried out with KH in THF, and the suspension was then treated with either 18-crown-6 or 2,2,2-Kryptofix. The potassium ion pair **2**, fully characterized including the

X-ray analysis reported in Figure 1, is an extremely air-sensitive compound. In Table 1, we report significant bond distances and angles for this complex.



(1)

The CH₂SO₂C₆H₄Me anion interacts with the potassium atom of the K(18-crown-6) cation through the O7 and O8 oxygen atoms as an asymmetric chelating ligand (Figure 1). The plane through K, O7, and O8 is tilted with respect to the oxygen mean plane by 71.6(1)°. The cation has a typical geometry with the potassium atom protruding by 0.803(1) Å from the mean least-squares plane running through the six oxygen atoms. The distortions of the oxygen atoms from the mean plane range from -0.258(4) to 0.232(4) Å. The sulfur atom lies on the plane of the aromatic ring, which is ap-

* To whom correspondence should be addressed.
[®] Abstract published in *Advance ACS Abstracts*, March 15, 1995.
 (1) Simpkins, N. J. In *Sulphones in Organic Synthesis*; Pergamon: Oxford, U.K., 1993.
 (2) Hollstein, W.; Harms, K.; Marsch, M.; Boche, G. *Angew. Chem., Int. Ed. Engl.* **1988**, *27*, 846. Boche, G. *Angew. Chem., Int. Ed. Engl.* **1989**, *28*, 277.
 (3) Gais, H.-J.; Hellman, G.; Gunther, H.; Lopez, F.; Lindner, H. J.; Braun, S. *Angew. Chem., Int. Ed. Engl.* **1989**, *28*, 1025. Gais, H. J.; Hellman, G.; Lindner, H. *Angew. Chem., Int. Ed. Engl.* **1990**, *29*, 100.
 (4) Gais, H.-J.; Vollhardt, J.; Lindner, H.; Paulus, M. *Angew. Chem., Int. Ed. Engl.* **1988**, *27*, 1450.
 (5) Gais, H.-J.; Vollhardt, J.; Kruger, C. *Angew. Chem., Int. Ed. Engl.* **1988**, *27*, 1092.

(6) (a) Veya, P.; Floriani, C.; Chiesi-Villa, A.; Guastini, C. *Organometallics* **1991**, *10*, 1652, 2991. (b) Veya, P.; Floriani, C.; Chiesi-Villa, A.; Guastini, C. *J. Chem. Soc., Chem. Commun.* **1991**, 116. *Organometallics* **1993**, *12*, 253. (c) Veya, P.; Floriani, C.; Chiesi-Villa, A.; Guastini, C.; Dedieu, A.; Ingold, F.; Braunstein, P. *Organometallics* **1993**, *12*, 4359. (d) Veya, P.; Floriani, C.; Chiesi-Villa, A.; Rizzoli, C. *Organometallics* **1993**, *12*, 4646. (e) Veya, P.; Floriani, C.; Chiesi-Villa, A.; Rizzoli, C. *Organometallics* **1993**, *12*, 4892. (f) Veya, P.; Floriani, C.; Chiesi-Villa, A.; Guastini, C. *Organometallics* **1994**, *13*, 208. (g) Veya, P.; Floriani, C.; Chiesi-Villa, A.; Rizzoli, C. *Organometallics* **1994**, *13*, 441. (h) Cozzi, P. G.; Veya, P.; Floriani, C.; Chiesi-Villa, A.; Rizzoli, C. *Organometallics* **1994**, *13*, 1528.

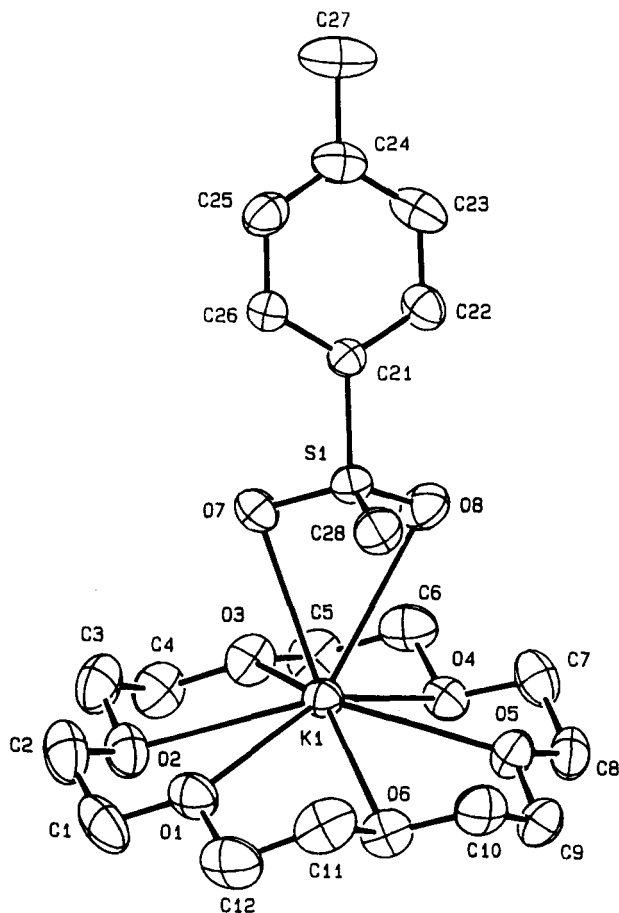


Figure 1. ORTEP drawing for complex **2** (30% probability ellipsoids).

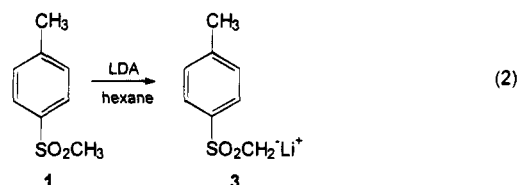
Table 1. Relevant Bond Distances (Å) and Angles (deg) for Complex **2**

K1-O1	2.888(5)	K1-O7	2.879(4)
K1-O2	3.020(4)	K1-O8	3.094(4)
K1-O3	2.861(5)	S1-O7	1.456(4)
K1-O4	2.975(4)	S1-O8	1.459(5)
K1-O5	2.807(3)	S1-C21	1.810(4)
K1-O6	2.894(5)	S1-C28	1.621(6)
O7-K1-O8	48.6(1)	O7-S1-C21	102.8(2)
C21-S1-C28	115.7(3)	O7-S1-O8	115.4(2)
O8-S1-C28	109.8(3)	K1-O7-S1	88.8(2)
O8-S1-C21	103.4(2)	K1-O8-S1	80.6(2)
O7-S1-C28	109.6(3)		

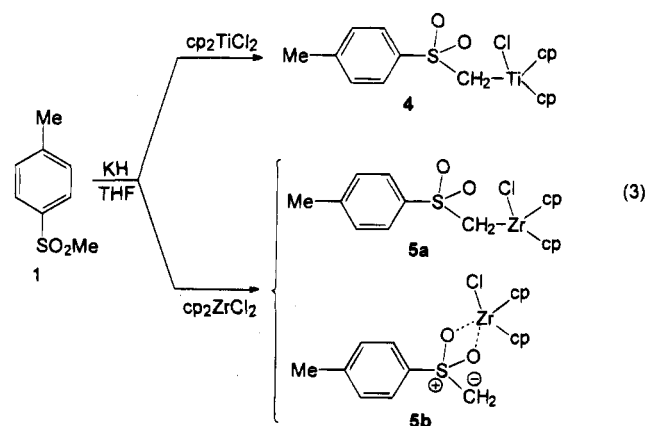
proximately coplanar with the K, O7, and O8 plane (dihedral angle of 11.3(1)°). The S-C_{ipso} bond distance corresponds well to a single bond, while the S-C28 and S-O distances are consistent with some degree of double-bond character. There is one feature which deserves particular attention, *i.e.* the orientation of the O7, O8, C28 group of atoms which is roughly parallel to the 18-crown-6 oxygen plane (dihedral angle of 15.7-(1)°), causing the C28 atom to approach the potassium at a distance of 3.403(6) Å, indicative of a weak bonding interaction between the two atoms. We assume that the negative charge is delocalized over all three of the atoms without significantly affecting the values of the bond distances. Accordingly, the small influence of the charge distribution on the S-O distances is further demonstrated by comparing these distances with those of complex **4** (see below), where an expected shortening is not observed, in spite of the charge localization on the carbon atom. The attempt to prepare a naked form of the α -sulfonyl carbanion by carrying out the depro-

tonation (eq 1) in the presence of Kryptofix gave only uncharacterized decomposition products. This may be due to the very high reactivity of the naked species.

For studying the complexation of α -sulfonyl carbanions with transition metals, we prepared the lithium α -sulfonyl carbanion **3**, using the recently described LDA-hexane methodology (eq 2).⁷



We studied the reactivity of lithium and potassium derivatives of methyl *p*-tolyl sulfone with early and late transition metals in order to discover a general approach to organometallic α -sulfonyl carbanion derivatives. However, since the use of the lithium derivative **3** proved troublesome in the isolation and purification of the metal complexes, the potassium complex **2** has been used instead, and to good effect, in the synthesis of transition-metal α -sulfonyl carbanion complexes. Despite the fact that Cp₂MCl₂ (M = Ti, Zr, Cp = η^5 -C₅H₅) reacts with the ion-pair forms of α -sulfonyl anions to give only decomposition products,^{8g} the corresponding reactions with the α -sulfonyl carbanion generated *in situ* give characterizable products (eq 3).



Complex **4** has been fully characterized, including an X-ray crystal analysis. A picture of **4** is shown in Figure 2. A chlorine atom and the C17 carbon atom of the α -sulfonyl anion are coordinated to titanium in the equatorial plane of the Cp₂Ti unit. The Ti-C bond distance is remarkably longer than the values generally observed for organotitanium derivatives of Ti(IV).⁸ The S1-C17 bond distance (1.743(5) Å) is also much longer than the corresponding one in complex **2** (1.621(6) Å), while the sulfur-oxygen distances are not significantly different from those observed in complex **2**. The aromatic ring is nearly perpendicular to the equatorial plane, with the dihedral angle between the Ti, C11, C17, and the C11, ..., C16 planes being 96.4(1)°. The sulfur atom is significantly displaced from the ring plane by 0.085(1) Å. The C17-S1-C11-C16 torsion angle is

(7) Kim, Y.-J.; Bernstein, P.; Galiano Roth, A. S.; Romesberg, F. E.; Willard, P. G.; Fuller, D. J.; Harrison, A. T.; Collum, D. B. *J. Org. Chem.* **1991**, *56*, 4435.

(8) Solari, E.; Floriani, C.; Chiesi-Villa, A.; Rizzoli, C. *J. Chem. Soc., Dalton Trans.* **1992**, 367 and references therein.

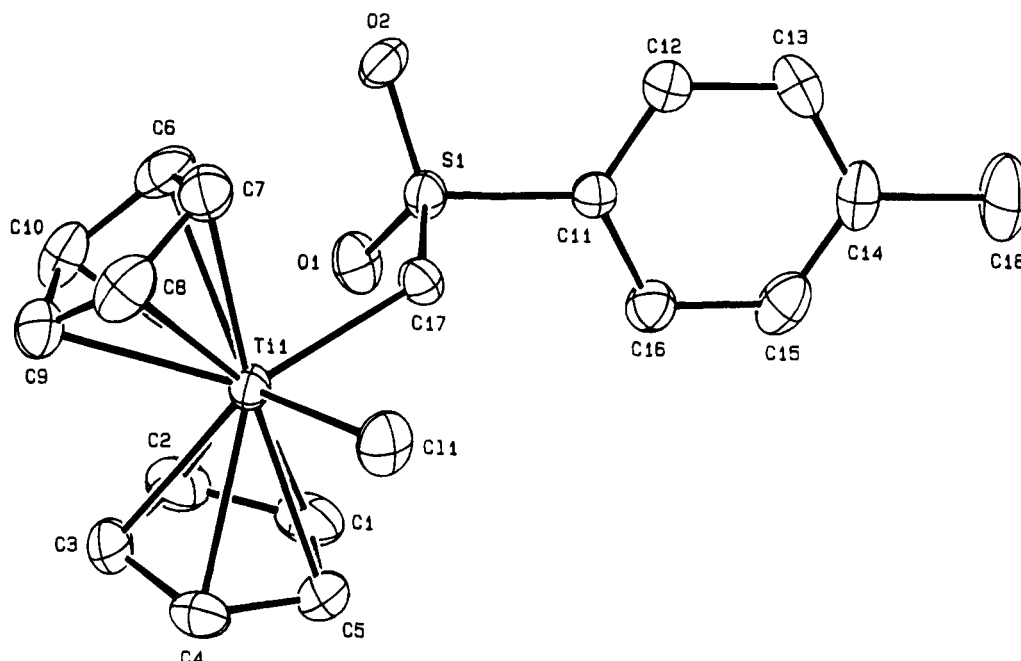


Figure 2. ORTEP drawing for complex **4** (30% probability ellipsoids).

Table 2. Relevant Bond Distances (Å) and Angles (deg) for Complex **4**^a

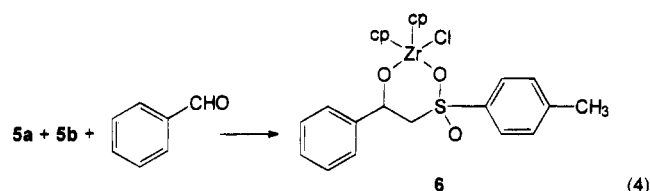
Ti1–Cp1	2.068(7)	S1–O1	1.447(4)
Ti1–Cp2	2.059(6)	S1–O2	1.448(4)
Ti1–Cl1	2.347(2)	S1–C11	1.771(4)
Ti1–C17	2.244(5)	S1–C17	1.743(5)
Cp2–Ti1–C17	106.7(2)	O2–S1–C17	109.5(2)
Cp1–Ti1–C17	106.4(2)	O1–S1–C17	111.3(2)
Cp1–Ti1–Cp2	131.4(3)	O1–S1–C11	106.8(2)
Cl1–Ti1–C17	87.0(1)	O1–S1–O2	115.8(2)
Cl1–Ti1–Cp2	108.1(2)	O2–S1–C11	108.1(2)
Cl1–Ti1–Cp1	108.2(2)	C11–S1–C17	104.7(2)
Ti1–C17–S1	126.7(3)		

^a Cp1 and Cp2 refer to the centroids of the cyclopentadienyl rings C1–C5 and C6–C10, respectively.

76.4(4)°. The geometries of the α -sulfonyl carbanion in complexes **2** and **4** are very similar except for a rotation of about 20° of the aromatic ring around the C–S bond as shown by the following torsion angles: complex **2**, C26–C21–S1–O7 = 37.8(4)°, C22–C21–S1–O8 = –22.6(5)°; complex **4**, C12–C11–S1–O2 = 15.4(5)°, C16–C11–S1–O1 = –41.7(5)°. The presence of a Ti–C bond in **4**, and likewise in related compounds,⁴ makes such complexes particularly useful for reactivity studies. In addition, complex **4** contains a Ti–Cl group available for further functionalization.

The α -sulfonyl carbanion has bonding sites for both carbophilic and oxophilic metals. Therefore, when we shifted our attention onto zirconium, which is much more oxophilic than titanium, we found that the use of Cp₂ZrCl₂, as shown in eq 3, led to a 1:1 mixture of metal–C-bonded (**5a**) and metal–O-bonded (**5b**) sulfonyl carbanions. The NMR spectrum of one of the two complexes is quite close to that of **4**, while the spectrum of the other one, which we believe to be the O-bonded form, is remarkably different. The presence of two Cp resonances is in agreement with the presence of a bidentate form of the α -sulfonyl fragment in **5b** and accounts for the fact that we did not observe interconversion between the two forms. This latter observation also rules out a possible C,O bidentate bonding mode.

Complexes **5** have been found to be fairly unreactive, although they both react slowly over a period of several days with a typical electrophile, namely benzaldehyde, to afford the same expected product, **6**, contaminated with small impurities derived from deoxygenation pathways^{6g} (eq 4).

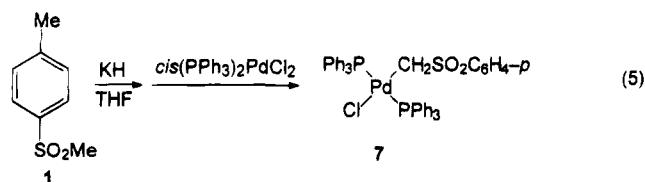


Complex **6** could only be isolated as an oil and was therefore only characterized by ¹H NMR spectroscopy. Attempts to isolate the organometallic product in a cationic form^{6e,9} afforded only secondary products of decomposition.

We have further shown that late transition metals are amenable to this sort of chemistry.^{6d,6g} α -Sulfonyl potassium carbanions react with [*cis*-(PPh₃)₂PdCl₂] to give the Pd–C-bonded product [*trans*-(PPh₃)₂(Cl)Pd(CH₂–SOAr)], where Ar = C₆H₅ or *p*-MeC₆H₄. The reaction of [*cis*-(PPh₃)₂PdCl₂] with the α -sulfonyl anion from **1** parallels the reaction we reported with α -sulfonyl derivatives, including the isomerization of the metal center, thus leading to **7**.^{6g} It is noteworthy that in these reactions no reduction of the palladium center was observed, despite the reducing nature of such carbanions.

Complex **7** is stable and can be handled in air, but we have experienced some difficulties in completely eliminating the potassium chloride byproduct of this reaction. This is probably the result of the strong coordinative interaction of the potassium ion with the oxygens of the sulfone moiety. The NMR data, quite close to those of the analogous α -sulfonyl derivatives,^{6g}

(9) Berno, P.; Floriani, C.; Chiesi-Villa, A.; Guastini, C. *Organometallics* **1990**, *9*, 1995.



for which the X-ray analysis is available, allows a confident attribution of the structure for 7.

The reactivity of Pd α -sulfonyl carbanions and the use of the titanium complex as a starting material in organometallic chemistry is under investigation.

Experimental Section

All operations were carried out under an atmosphere of purified nitrogen. All solvents were purified by standard methods and freshly distilled prior to use. NMR spectra were recorded on a 200-AC Bruker instrument. Methyl *p*-tolyl sulfone (1) was prepared according to the literature.¹⁰

Preparation of 2. To a solution of 1 (2.02 g, 11.87 mmol) in THF (220 mL) was added KH (0.477 g, 11.92 mmol). The resulting mixture was stirred at room temperature overnight, and then 18-crown-6 (3.15 g, 11.92 mmol) was added. After a few minutes, a yellow mixture was obtained; the mixture was filtered, and the THF was removed. Diethyl ether was added (60 mL), and the resulting yellow-green product was collected via filtration (2.6 g, 46%). The very sensitive product was purified by extraction with Et₂O. ¹H NMR (δ): 8.38 (d, 2 H, $J = 8$ Hz, AA'BB' system, Ar); 7.12 (d, 2 H, $J = 8$ Hz, AA'BB' system, Ar); 3.32 (s, 24 H, 18-crown-6); 2.31 (s, 2 H, CH₂); 2.04 (s, 3 H, CH₃). ¹³C NMR (δ): 129.02, 126.21 (Ar); 70.96 (18-crown-6); 38.92 (CH₂); 21.78 (Me). Anal. Calcd for C₂₀H₃₃KO₈S: C, 50.78; H, 6.98. Found: C, 50.76; H, 7.48.

Preparation of 3. To a solution of diisopropylamine (16.2 g, 160 mmol) in *n*-hexane (80 mL) was added a solution of butyllithium in hexane (100 mL, 1.6 M, 160 mmol) in a dropwise manner with stirring at room temperature. The pale yellow solution was stirred for 1 h, and then a solution of 1 (27.2 g, 160 mmol) in toluene (80 mL) was added dropwise by cannula. The lithium derivative immediately started to precipitate. The resulting suspension was filtered, and the solvent was removed at low pressure overnight. The residual white powder was stored in sealed ampules (26 g, 92%). ¹H NMR (pyridine-*d*₅; δ): 8.22 (d, 2 H, $J = 8$ Hz); 7.11 (d, 2 H, $J = 8$ Hz); 2.41 (s, 2 H); 2.17 (s, 3 H). Anal. Calcd for C₇H₉LiO₂S: C, 54.56; H, 5.11. Found: C, 54.01; H, 5.68.

Preparation of 4. To a solution of 1 (1.3 g, 7.64 mmol) in THF (200 mL) was added KH (0.316 g, 7.9 mmol), and the mixture was stirred overnight at room temperature. The resulting white slurry was cooled to 0 °C with an ice bath, and Cp₂TiCl₂ (1.96 g, 7.89 mmol) was added. The red mixture was stirred at 0 °C for 6 h and then warmed to room temperature. The red mixture was stirred for a 1 day further at room temperature, and the KCl was filtered off. The resulting orange-red solution was concentrated to about 15 mL, and then Et₂O (5 mL) was added in a dropwise manner. After a few hours the solid product was collected via filtration (35%). Another crop of the product was obtained after allowing the remaining filtrate to stand for a few days at -20 °C (56% total yield). ¹H NMR (200 MHz, CD₂Cl₂; δ): 7.73 (d, 2 H, $J = 8.3$ Hz, AA'BB' system, Ar); 7.3 (d, 2 H, $J = 8.3$ Hz, AA'BB' system, Ar); 6.69 (s, 10 H, Cp); 3.14 (s, 2 H, CH₂); 2.41 (s, 3 H, Me). ¹³C NMR (CD₂Cl₂; δ): 144.25, 143.25, 130.27, 126.78 (Ar); 119.24 (Cp); 66.36 (CH₂); 21.93 (Me). Anal. Calcd for C₁₈H₁₉O₂ClSTi: C, 56.19; H, 4.96. Found: C, 56.07; H, 5.00.

Preparation of 5. To a solution of 1 (1.08 g, 6.375 mmol) in THF (150 mL) was added KH (0.255 g, 6.375 mmol), and the mixture was stirred at room temperature overnight. The

Table 3. Experimental Data for the X-ray Diffraction Studies for Complexes 2 and 4

	2	4
formula	C ₂₀ H ₃₃ KO ₈ S	C ₁₈ H ₁₉ ClO ₂ STi
M_r	472.6	382.8
cryst syst	monoclinic	monoclinic
space group	$P2_1/c$	$C2/c$
cell params at 298 K ^a		
a , Å	8.635(2)	22.318(3)
b , Å	14.879(3)	9.727(2)
c , Å	19.589(3)	16.267(3)
β , deg	96.30(2)	100.08(2)
V , Å ³	2501.6(9)	3476.9(11)
Z	4	8
d_{calcd} , g cm ⁻³	1.255	1.462
cryst dims, mm	0.15 × 0.35 × 0.45	0.18 × 0.21 × 0.68
linear abs coeff, cm ⁻¹	29.76	68.04
diffractometer	Siemens AED	Siemens AED
diffractometer geometry	equatorial	equatorial
scan type	$\theta/2\theta$	$\theta/2\theta$
scan speed, deg min ⁻¹	3–12	3–12
scan width, deg	b	b
radiation	c	c
data colln range of 2θ range, deg	6–140	6–140
no. of rflns measd	$\pm h, k, l$	$\pm h, k, l$
unique total data	4732	3296
criterion for observn	$I > 2\sigma(I)$	$I > 2\sigma(I)$
no. of unique obsd data (NO)	2419	2008
no. of params refined (NV)	271	208
overdetermn ratio (NO/NV)	8.9	9.7
transmiss factors	0.498–1.000	0.712–1.000
$R = \sum \Delta F /\sum F_o $	0.057	0.047
$R_w = [\sum w^{1/2} \Delta F /\sum w^{1/2} F_o]$	0.071	0.057
$GOF = [\sum w \Delta F ^2/(\text{NO} - \text{NV})]^{1/2}$	1.008	0.996
largest shift/esd, final cycle	0.002	0.001
largest peak, e Å ⁻³	0.25	0.41

^a Unit cell parameters were obtained by a least-squares analysis of the setting angles of 25 carefully centered reflections chosen from diverse regions of reciprocal space. ^b $(\theta - 0.6) - (\theta + (0.6 + \Delta\theta))$; $\Delta\theta = [(\lambda\alpha_2 - \lambda\alpha_1)/\lambda](\tan \theta)$. ^c Graphite-monochromated Cu K α ($\lambda = 1.54178$ Å).

resulting white slurry was cooled to 0 °C, and Cp₂ZrCl₂ (1.8 g, 6.375 mmol) was added. The yellow mixture was stirred at 0 °C for 5 h and then warmed to room temperature. The mixture was stirred at room temperature for 1 day more, and then the KCl was removed by filtration. The THF was removed, and ether was then added. The resulting white powder was filtered and collected (72%). The NMR spectra in several different solvents showed an equimolar mixture of two organometallic products. The positions of the signals of the two species are, however, solvent dependent. In THF, a 0.2 M solution of the two species showed no transformation of one species into another after 3 days of stirring at room temperature and then heating. ¹H NMR (CD₂Cl₂; δ): 7.74 (d, 2 H, $J = 8.26$ Hz, AA'BB' system, Ar); 7.66 (d, 2 H, $J = 8.26$ Hz, AA'BB' system, Ar); 7.30 (d, 4 H, $J = 8.26$ Hz, AA'BB' system, Ar); 6.61 (s, 10 H, Cp); 6.48 (s, 5 H, Cp); 6.37 (s, 5 H, Cp); 2.75 (s, 2 H, CH₂); 2.40 (s, 5 H, CH₂ and Me); 2.29 (s, 3 H, Me). Anal. Calcd for C₁₈H₁₉ClO₂SZrEt₂O: C, 52.8; H, 5.8. Found: C, 52.57; H, 5.04.

Reaction of 5 with Benzaldehyde: Preparation of 6.

In an NMR tube, complex 5 (0.064 g, 0.128 mmol) was suspended in C₆D₆ and then benzaldehyde (0.013 mL, 0.128 mmol) was added. The NMR tube was then frozen, sealed, and warmed to room temperature; the contents were then allowed to react for 2 days. NMR spectra were then run on the resulting orange solution. ¹H NMR (C₆D₆; δ): 7.76 (d, 2 H, $J = 8.0$ Hz, AA'BB' system, Ar); 7.28–7.00 (m, 5 H, Ar); 6.66 (d, 2 H, $J = 8.0$ Hz, AA'BB' system, Ar); 6.31 (s, 5 H, Cp); 6.03–6.00 (m, 5 H, Cp); 5.97 (dd, 1 H, $J = 3.8$ Hz, CHOZrCp₂); 3.20 (dd, 1 H, $J = 8.16$ Hz, CH₂SO₂Ar); 3.00 (dd, 1 H, $J = 3.16$ Hz, CH₂SO₂Ar); 1.88 (s, 3 H, CH₃Ar).

Preparation of 7. To a solution of 1 (0.364 g, 2.14 mmol) in THF (80 mL) was added KH (0.085 g, 2.14 mmol), and the mixture was stirred at room temperature overnight. [*cis*-

(10) *Organic Synthesis*; Wiley: New York, 1963; Collect. Vol. IV, p 674.

Table 4. Fractional Atomic Coordinates ($\times 10^4$) for Complex 2

atom	<i>x/a</i>	<i>y/b</i>	<i>z/c</i>
K1	4685.1(12)	7599.8(7)	3143.7(5)
S1	2387.0(14)	7627.4(8)	1747.0(6)
O1	6950(5)	9035(3)	3220(2)
O2	4538(6)	9223(2)	4060(2)
O3	2323(5)	7833(3)	4045(2)
O4	3297(4)	6043(2)	3810(2)
O5	5826(4)	5845(2)	3033(2)
O6	7923(5)	7272(3)	2971(2)
O7	2347(4)	8420(2)	2181(2)
O8	2163(4)	6771(3)	2085(2)
C1	6881(11)	9758(5)	3685(4)
C2	5193(12)	9979(4)	3764(4)
C3	2935(10)	9351(5)	4137(4)
C4	2342(8)	8588(5)	4495(3)
C5	1649(7)	7048(5)	4317(3)
C6	1734(7)	6293(5)	3835(3)
C7	3481(8)	5304(4)	3374(3)
C8	5129(8)	5102(4)	3363(3)
C9	7443(7)	5710(4)	2962(3)
C10	7980(7)	6482(5)	2564(3)
C11	8473(8)	8043(6)	2627(4)
C12	8538(8)	8804(5)	3130(4)
C21	634(5)	7747(3)	1157(2)
C22	-226(7)	6997(4)	943(3)
C23	-1574(8)	7097(5)	495(3)
C24	-2083(6)	7923(5)	250(3)
C25	-1174(7)	8658(4)	460(3)
C26	168(6)	8583(3)	915(2)
C27	-3550(8)	8007(7)	-249(3)
C28	4007(6)	7608(4)	1400(3)

Table 5. Fractional Atomic Coordinates ($\times 10^4$) for Complex 4

atom	<i>x/a</i>	<i>y/b</i>	<i>z/c</i>
Ti1	3540.0(3)	580.6(9)	1777.7(5)
Cl1	4400.7(6)	1141.7(17)	1198.7(9)
S1	3818.4(4)	-2470.5(12)	3005.5(7)
O1	3479(2)	-1853(4)	3591(2)
O2	3511(1)	-3562(4)	2491(2)
C1	3734(3)	1172(7)	3236(4)
C2	3107(3)	1232(7)	2944(4)
C3	3004(2)	2318(7)	2368(4)
C4	3560(3)	2891(6)	2280(4)
C5	4009(2)	2155(7)	2829(4)
C6	2909(3)	-1258(7)	1175(4)
C7	3261(3)	-850(7)	585(4)
C8	3083(3)	481(7)	336(4)
C9	2643(2)	894(6)	790(4)
C10	2535(2)	-190(8)	1303(4)
C11	4492(2)	-3158(5)	3601(3)
C12	4712(2)	-4402(6)	3385(3)
C13	5252(2)	-4913(7)	3829(4)
C14	5577(2)	-4170(7)	4481(4)
C15	5347(2)	-2941(7)	4703(4)
C16	4806(2)	-2403(6)	4268(3)
C17	4070(2)	-1231(5)	2371(3)
C18	6183(3)	-4699(9)	4938(5)

(PPh₃)PdCl₂] (1.50 g, 2.14 mmol) was added at room temperature, and the mixture was stirred for 2 days. The THF was removed, and CH₂Cl₂ (120 mL) was added. Small quantities of a yellow solid were eliminated by filtration. CH₂Cl₂ was removed, and Et₂O was added. The resulting yellow solid was isolated by filtration and dried under vacuum (1.1 g, 70%). We were unable to make the product free of KCl. ¹H NMR (C₆D₆; δ): 8.05–7.98 (m, 12 H, Ar); 7.14–7.11 (m, 18 H, Ar); 6.83 (d, 2 H, *J* = 8.77 Hz, AA'BB' system, tolyl); 6.68 (d, 2 H, *J* = 8.77 Hz, AA'BB' system, tolyl); 2.65 (t, 2 H, *J* = 7.68 Hz,

CH₂); 1.87 (s, 3 H, Me). ¹³C NMR (C₆D₆; δ): 144.11, 141.2 (tol); 136.58–127.21 (Ar); 21.45 (Me); 1.68 (CH₂). ³¹P NMR (C₆D₆; δ): 28.77 (PPh₃).

Crystallography. The crystals selected for study were mounted in glass capillaries and sealed under nitrogen. The reduced cells were obtained with use of TRACER.¹¹ Crystal data and details associated with data collection are given in Table 3. Data were collected at room temperature (295 K) on a single-crystal diffractometer. For intensities and background, individual reflection profiles were analyzed.¹² The structure amplitudes were obtained after the usual Lorentz and polarization corrections,¹³ and the absolute scale was established by the Wilson method.¹⁴ Data for both complexes were corrected for absorption using the program ABSORB.¹⁵ The function minimized during the full-matrix least-squares refinement was $\Delta w|\Delta F|^2$. Weights were applied according to the scheme $w = k/[\sigma^2(F_o) + |g|F_o^2]$. Anomalous scattering corrections were included in all structure factor calculations.^{16b} Scattering factors for neutral atoms were taken from ref 16a for non-hydrogen atoms and from ref 17 for H. Among the low-angle reflections no correction for secondary extinction was deemed necessary.

Solution and refinement were based on the observed reflections. The structures were solved by using SHELX86¹⁸ for complex 2 and by the heavy-atom method starting from a three-dimensional Patterson map for complex 4. Refinement was first done isotropically and then anisotropically for non-H atoms. Both structures were refined straightforwardly. All the hydrogen atoms were located from difference Fourier maps and introduced in the subsequent refinements as fixed-atom contributions with isotropic *U*'s fixed at 0.08 and 0.10 Å² for 2 and 4, respectively.

The final difference maps showed no unusual feature, with no significant peak above the general background. Final atomic coordinates are listed in Tables 4 and 5 for non-H atoms and in Tables S1 and S2 for hydrogens. Thermal parameters are given in Tables S3 and S4 and bond distances and angles in Tables S5 and S6.¹⁹

Acknowledgment. We thank the Fonds National Suisse de la Recherche Scientifique (Grant No. 20–40268.94) for financial support.

Supplementary Material Available: Listings of anisotropic thermal parameters, atomic coordinates for hydrogen atoms, and all bond lengths and angles (Tables S1–S6) for complexes 2 and 4 (6 pages). Ordering information is given on any current masthead page.

OM940939R

(11) Lawton, S. L.; Jacobson, R. A. "TRACER", a Cell Reduction Program; Ames Laboratory, Iowa State University of Science and Technology: Ames, IA, 1965.

(12) Lehmann, M. S.; Larsen, F. K. *Acta Crystallogr., Sect. A: Cryst. Phys., Diff., Theor. Gen. Crystallogr.* **1974**, *A30*, 580.

(13) Data reduction, structure solution, and refinement were carried out on a Gould 32/77 computer using: Sheldrick, G. "SHELX-76: System of Crystallographic Computer Programs"; University of Cambridge: Cambridge, England, 1976.

(14) Wilson, A. J. C. *Nature* **1942**, *150*, 151.

(15) Uguzzoli, F. ABSORB, a program for F_o Absorption Correction. In *Comput. Chem.* **1987**, *11*, 109.

(16) (a) *International Tables for X-ray Crystallography*; Kynoch Press: Birmingham, England, 1974; Vol. IV, p 99. (b) *Ibid.*, p 149.

(17) Stewart, R. F.; Davidson, E. R.; Simpson, W. T. *J. Chem. Phys.* **1965**, *42*, 3175.

(18) Sheldrick, G. "SHELX-86: a FORTRAN-77 Program for the Solution of Crystal Structure from Diffraction Data"; University of Cambridge: Cambridge, England, 1986.

(19) See the paragraph at the end of paper regarding supplementary material.

Reactions of $M(C_5H_4R)Cl_4$ Complexes ($R = H, CH_3$) with Pentadienyl Anions: Pathway Variations for Niobium vs Tantalum

Atta M. Arif,¹ Richard D. Ernst,^{*1} Enrique Meléndez,¹
Arnold L. Rheingold,^{*2} and Thomas E. Waldman¹

Departments of Chemistry, University of Utah, Salt Lake City, Utah 84112, and
University of Delaware, Newark, Delaware 19716

Received November 15, 1994[®]

The reactions of $Nb(C_5H_5)Cl_4$ or $Nb(CH_3C_5H_4)Cl_4$ compounds with 4 equiv of various pentadienyl anions lead initially to $Nb(RC_5H_4)(\eta^5-Pdl)(\eta^3-Pdl)$ complexes, for $Pdl = C_5H_7$ or $2,4-C_7H_{11}$ ($C_7H_{11} =$ dimethylpentadienyl). For the $2,4-C_7H_{11}$ complexes, subsequent intramolecular coupling between the two Pdl ligands occurs on standing at room temperature, leading to $Nb(RC_5H_4)(\eta^8-2,4,7,9-tetramethyl-1,3,7,9-decatetraene)$ complexes. These contain one η^4 -cis-diene and one η^4 -trans-diene coordinated to the metal center. This has been confirmed crystallographically for the $R = H$ complex, which crystallizes in the orthorhombic space group $Pcc2$ with $a = 14.061(3)$ Å, $b = 14.273(3)$ Å, $c = 8.045(1)$ Å, and $Z = 4$. For related tantalum reactions, a different course is followed, leading to isolation of $Ta(C_5H_5)_2(\eta^3-Pdl)$ complexes ($Pdl = 2,3-C_7H_{11}; 2,4-C_7H_{11}; 1,5-(Me_3Si)_2C_5H_5$), apparently via disproportionation. A structural study on the $2,3-C_7H_{11}$ complex revealed that its mode of coordination involved localized Ta–C and Ta–olefinic interactions, through the 1, 4, and 5 positions of the open dienyl ligand. The compound crystallizes in the monoclinic space group $P2_1/c$ with $a = 7.887(2)$ Å, $b = 14.433(3)$ Å, $c = 12.645(3)$ Å, and $\beta = 97.93(2)^\circ$ for $Z = 4$. However, for the $1,5-(Me_3Si)_2C_5H_5$ complex, the more usual allylic mode of coordination is observed. This compound crystallizes in the monoclinic space group $P2_1/n$, with $a = 7.422(1)$ Å, $b = 23.934(5)$ Å, $c = 13.059(2)$ Å, and $\beta = 97.52(1)^\circ$ for $Z = 4$.

In order to allow for more direct comparisons to be made between cyclopentadienyl and pentadienyl ligands, we have devoted a fair degree of our efforts to the preparations and studies of compounds simultaneously containing ligands of both types ("half-open metallocenes").³ In such species, differences that might otherwise exist between related cyclopentadienyl and pentadienyl compounds with regard to their symmetries, steric environments, or spin configurations are eliminated. As a result, more direct comparisons can be made between the two types of ligands, whether in regards to their physical natures, or chemical reactions. Herein we report our efforts to prepare such complexes of niobium and tantalum, from reactions of $M(C_5H_4R)Cl_4$ complexes with four equiv of pentadienyl anions. These reactions have been found to proceed along much differing paths for the two metals, in neither case leading to a half-open metallocene. As will be seen in the case of niobium, reduction of the Nb(V) starting materials to isolable mono(cyclopentadienyl)Nb(III) species occurs, followed by slower intramolecular coupling reactions between pentadienyl ligands. In contrast, for

tantalum bis(cyclopentadienyl)Ta(III) species are isolated, presumably through a combination of reduction and disproportionation. In these tantalum complexes η^3 -Pdl coordination is present for a single ligand, although this has been found to occur in most cases through localized alkyl/ene bonding, involving the 1, 4, and 5 positions, rather than through the usual allylic bonding mode.

Experimental Section

The compounds described herein are mostly air-sensitive. They were therefore prepared, handled, and stored under nitrogen or in a glovebox, while solutions were manipulated under nitrogen. Hydrocarbon and ethereal solvents were predried and distilled under nitrogen from Na/benzophenone prior to use. Magnetic and spectroscopic data were obtained as previously described.⁴ The starting dienes,⁵ dienyl anions,⁶ and metal complexes⁷ were either purchased or prepared by standard methods. The ¹³C NMR spectra were not integrated, but numbers of carbon atoms are provided in accord with their assignments.

(Cyclopentadienyl)(η^5 -2,4-dimethylpentadienyl)(η^3 -2,4-dimethylpentadienyl)niobium, $Nb(C_5H_5)(\eta^5-2,4-C_7H_{11})(\eta^3-2,4-C_7H_{11})$, **2a**. To a THF solution (40 mL) of $Nb(C_5H_5)_2$

(4) Newbound, T. D.; Stahl, L.; Ziegler, M. L.; Ernst, R. D. *Organometallics* **1990**, *9*, 2962.

(5) Jitkow, O. N.; Bogert, M. T. *J. Am. Chem. Soc.* **1941**, *63*, 1979.

(6) (a) Wilson, D. R.; Stahl, L.; Ernst, R. D. In *Organometallic Synthesis*; King, R. B., Eisch, J. J., Eds.; Academic Press: New York, 1986; Vol. 3, p 136. (b) Yasuda, H.; Nishi, T.; Lee, K.; Nakamura, A. *Organometallics* **1983**, *2*, 21.

(7) Brunner, M. J.; DeCian, A.; Green, M. L. H.; Moreau, J. J. E.; Sigantoria, N. *J. Chem. Soc., Dalton Trans.* **1980**, 2155.

[®] Abstract published in *Advance ACS Abstracts*, March 1, 1995.

(1) University of Utah.

(2) University of Delaware.

(3) (a) Freeman, J. W.; Hallinan, N. C.; Arif, A. M.; Gedridge, R. W.; Ernst, R. D.; Basolo, F. *J. Am. Chem. Soc.* **1991**, *113*, 6509. (b) Elschenbroich, Ch.; Bilger, E.; Ernst, R. D.; Wilson, D. R.; Kralik, M. S. *Organometallics* **1985**, *4*, 2068. (c) Ernst, R. D.; Ma, H.; Sergeson, G.; Zahn, T.; Ziegler, M. L. *Ibid.* **1987**, *6*, 848. (d) Gleiter, R.; Hyla-Kryspin, I.; Ziegler, M. L.; Sergeson, G.; Green, J. C.; Stahl, L.; Ernst, R. D. *Ibid.* **1989**, *8*, 298. (e) Gedridge, R. W.; Hutchinson, J. P.; Rheingold, A. L.; Ernst, R. D. *Ibid.* **1993**, *12*, 1553. (f) Trakarnpruk, W.; Arif, A. M.; Ernst, R. D. *Ibid.* **1994**, *13*, 2423.

$\text{Cl}_4\text{-THF}$ (1.0 g, 2.7 mmol) under nitrogen at -78°C was added potassium 2,4-dimethylpentadienide (1.4 g, 11 mmol) in 40 mL of THF dropwise. The mixture was stirred for 4 h at -78°C , and the solvent was removed in vacuo at -5°C . The crude product was extracted in cold pentane and filtered on a cold frit. The solution was concentrated to about 15 mL and cooled to -78°C for 2 days, yielding a bright-orange crystalline product. Warming this compound to room temperature for a period of 1 day leads to an isomerization to (cyclopentadienyl)- $(\eta^8\text{-}2,4,7,9\text{-tetramethyl-}1,3,7,9\text{-decatetraene})\text{niobium}$. The yield is 55–60% (0.52–0.56 g) depending on the reaction conditions.

Infrared data (Nujol mull): 3080 (w), 1606 (ms), 1513 (m), 1310 (m), 1250 (w), 1212 (w), 1161 (w), 1121 (w), 980 (w), 970 (w), 885 (ms), 865 (s), 820 (m), 804 (s).

^1H NMR (toluene- d_6 , -72°C): δ 5.11 (s, 1H), 4.66 (s, 1H), 4.44 (s, 5H), 2.91 (s, 1H), 2.70 (s, 1H), 2.35 (s, 1H), 1.82 (s, 3H), 1.71 (s, 3H), 1.65 (s, 3H), 1.60 (s, 1H), 1.55 (d, 1H, $J = 3$ Hz), 1.42 (s, 1H), 1.29 (s, 3H), 0.92 (s, 1H), -0.06 (d, 1H, $J = 3$ Hz).

^{13}C NMR (toluene- d_6 , -72°C): δ 144.8 (s, 1C), 137.6 (s, 1C), 114.14 (t, 1C, $J = 154$ Hz), 114.07 (s, 1C), 109.1 (d, 1C, $J = 159$ Hz), 96.0 (d, 5C, $J = 174$ Hz), 83.3 (d, 1C, $J = 147$ Hz), 75.2 (s, 1C), 46.6 (t, 1C, $J = 152$ Hz), 45.8 (t, 1C, $J = 149$ Hz), 41.8 (t, 1C, $J = 148$ Hz), 24.8 (q, 1C, $J = 126$ Hz), 23.9 (q, 1C, $J = 126$ Hz), 22.6 (q, 1C, $J = 127$ Hz), 19.7 (q, 1C, $J = 124$ Hz).

MS (EI) [m/z (relative intensity)]: 55 (32), 67 (11), 79 (11), 81 (43), 83 (28), 95 (32), 96 (58), 97 (51), 107 (12), 111 (13), 179 (11), 235 (29), 249 (100), 250 (27), 291 (27), 348 (7).

(Cyclopentadienyl)($\eta^5\text{-pentadienyl}$)($\eta^3\text{-pentadienyl}$)-niobium, $\text{Nb}(\text{C}_5\text{H}_5)(\eta^5\text{-C}_5\text{H}_7)(\eta^3\text{-C}_5\text{H}_7)$, **1a.** This air sensitive light-brown compound is isolated in an analogous manner as described for $\text{Nb}(\text{C}_5\text{H}_5)(\eta^5\text{-}2,4\text{-C}_7\text{H}_{11})(\eta^3\text{-}2,4\text{-C}_7\text{H}_{11})$, substituting potassium pentadienide for potassium 2,4-dimethylpentadienide. Crystallization is carried out from a toluene/pentane mixture. The yield is about 55% (0.42 g) based on $\text{Nb}(\text{C}_5\text{H}_5)\text{-Cl}_4\text{-THF}$.

Infrared data (Nujol mull): 3160 (w), 1636 (w), 1612 (m), 1307 (m), 1261 (s), 1195 (w), 1167 (m), 967 (s), 860 (m), 805 (s).

^1H NMR (benzene- d_6 , 18°C): δ 5.83 (dt, 1H, $J = 16.7, 10$ Hz), 5.48 (app t, 1H, $J = J' = \text{ca. } 7$ Hz), 4.87 (d of d, 1H, $J = 16.7, 1.8$ Hz), 4.71 (d of d, 1H, $J = 1.8, 10$ Hz), 4.48 (s, 5H), 4.05 (dt, 1H, $J = 8.6, 13.0$ Hz), 2.76 (t, 1H, $J = 5.2$ Hz), 2.62 (d, 1H, $J = 8.7$ Hz), 2.52 (m, 1H), 2.09 (overlapping resonances, 2H), 1.82 (d of d, 1H, $J = 2.3, 6.5$ Hz), 1.72 (br dd, 1H, $J = 2, 10$ Hz), 1.49 (d of d, 1H, $J = 3, 8.7$ Hz), 0.73 (d of d, 1H, $J = 3, 12.7$ Hz).

^{13}C NMR (benzene- d_6 , 18°C): δ 141.3 (d, 1C, $J = 143$ Hz), 104.7 (t, 1C, $J = 156$ Hz), 100.9 (d, 1C, $J = 156$ Hz), 94.5 (d, 5C, $J = 175$ Hz), 93.1 (d, 1C, $J = 153$ Hz), 78.8 (d, 1C, $J = 154$ Hz), 69.6 (d, 1C, $J = 162$ Hz), 51.7 (t, 1C, $J = 160$ Hz), 32.0 (t, 1C, $J = 153$ Hz). One CH and one CH_2 resonance could not be assigned with certainty due to the apparent presence of a second isomeric compound.

MS (EI) [m/z (relative intensity)]: 57 (17), 59 (33), 81 (11), 83 (14), 95 (12), 109 (10), 125 (14), 175 (15), 177 (26), 179 (29), 221 (22), 232 (13), 233 (37), 234 (17), 235 (100), 287 (17), 288 (11), 289 (29), 290 (12), 291 (38).

Anal. Calcd for $\text{C}_{15}\text{H}_{19}\text{Nb}$: C, 61.65; H, 6.55. Found: C, 62.28; H, 6.72.

(Methylcyclopentadienyl)($\eta^5\text{-}2,4\text{-dimethylpentadienyl}$)-($\eta^3\text{-}2,4\text{-dimethylpentadienyl}$)niobium, $\text{Nb}(\text{CH}_3\text{C}_5\text{H}_4)(\eta^5\text{-}2,4\text{-C}_7\text{H}_{11})(\eta^3\text{-}2,4\text{-C}_7\text{H}_{11})$, **3a.** A solution of 1.0 g of $\text{Nb}(\text{CH}_3\text{C}_5\text{H}_4)\text{-Cl}_4\text{-THF}$ (2.6 mmol) in 50 mL of THF was treated with 1.4 g of potassium 2,4-dimethylpentadienide (10 mmol) at -78°C . The resulting brown solution was stirred for 5 h at -78°C and the solvent was removed in vacuo at -5°C . The crude product was extracted in cold hexane and filtered on a coarse frit. Cooling of the light-orange hexane solution

to -78°C yielded an orange air-sensitive crystalline compound. This compound may be isolated in 62% yield (0.58 g), and it readily isomerizes to the corresponding niobium-decatetraene compound when the solution is warmed to room temperature.

Infrared data (Nujol mull): 3075 (w), 1604 (m), 1516 (w), 1496 (mw), 1309 (m), 1247 (w), 1211 (w), 977 (w), 933 (w), 883 (s), 864 (s), 798 (s).

^1H NMR (toluene- d_8 , -72°C): δ 5.04 (s, 1H), 4.57 (s, 1H), 4.52 (s, 1H), 4.19 (s, 1H), 3.95 (s, 1H), 3.77 (s, 1H), 2.85 (s, 1H), 2.68 (s, 1H), 2.25 (s, 1H), 1.83 (s, 3H), 1.76 (s, 3H), 1.68 (s, 3H), 1.58 (s, 3H), 1.47 (d, 1H, $J = 3$ Hz), 1.35 (s, 1H), 1.33 (s, 1H), 1.24 (s, 3H), 0.92 (s, 1H), -0.02 (s, 1H).

^{13}C NMR (toluene- d_8 , -72°C): δ 144.8 (s, 1C), 138.3 (s, 1C), 114.1 (s, 1C), 114.0 (t, 1C, $J = 155$ Hz), 110.4 (d, 1C, $J = 156$ Hz), 97.0 (d, 2C, $J = 177$ Hz), 94.8 (d, 1C, $J = 173$ Hz), 94.6 (s, 1C), 94.1 (d, 1C, $J = 177$ Hz), 83.2 (d, 1C, $J = 157$ Hz), 76.1 (s, 1C), 50.0 (t, 1C, $J = 151$ Hz), 47.9 (t, 1C, $J = 149$ Hz), 42.6 (t, 1C, $J = 151$ Hz), 25.0 (q, 1C, $J = 126$ Hz), 23.9 (q, 1C, $J = 124$ Hz), 22.5 (q, 1C, $J = 129$ Hz), 19.9 (q, 1C, $J = 124$ Hz), 16.0 (q, 1C, $J = 128$ Hz).

MS (EI) [m/z (relative intensity)]: 95 (10), 250 (29), 261 (13), 263 (61), 264 (64), 265 (10), 278 (100), 279 (10), 302 (12), 304 (10), 305 (11), 314 (10), 318 (12), 360 (24), 362 (73), 363 (11).

(Cyclopentadienyl)($\eta^8\text{-}2,4,7,9\text{-tetramethyl-}1,3,7,9\text{-decatetraene}$)niobium, $\text{Nb}(\text{C}_5\text{H}_5)(\eta^8\text{-}2,4,7,9\text{-C}_{14}\text{H}_{22})$, **2b.** To a magnetically stirred solution of 1.0 g (2.7 mmol) of $\text{Nb}(\text{C}_5\text{H}_5)\text{-Cl}_4\text{-THF}$ in 50 mL of THF under nitrogen at -78°C was added 1.4 g (11 mmol) of potassium 2,4-dimethylpentadienide in 50 mL of THF dropwise. The solution was allowed to stir at -78°C for 2 h, thereby developing a red-brown color. The reaction mixture was then stirred for 6 h at room temperature. The solvent was removed in vacuo and the crude solid extracted with several portions of hexane and filtered on a coarse frit. The brown-red solution was concentrated under reduced pressure. On cooling to -78°C for several days a red-orange crystalline product was obtained (0.56 g, 60% yield).

Melting point (nitrogen-filled, sealed capillary): 153–155 $^\circ\text{C}$.

Infrared data (Nujol mull): 3160 (w), 1519 (m), 1501 (ms), 1312 (m), 1273 (w), 1230 (w), 1160 (m), 1103 (m), 972 (mw), 917 (m), 890 (s), 823 (m), 800 (s).

^1H NMR (benzene- d_6 , ambient): δ 4.69 (s, 5H), 3.38 (s, 1H), 2.76–2.90 (multiplets, 3H), 1.88 (m, 1H), 1.85 (s, 3H), 1.83 (s, 3H), 1.70 (b, 1H), 1.57 (s, 3H), 1.36–1.39 (multiplets, 2H), 1.28 (s, 3H), 1.19 (d, 1H, $J = 5$ Hz), 0.36 (d, 1H, $J = 5$ Hz).

^{13}C NMR benzene- d_6 , ambient): 138.4 (s, 1C), 124.5 (s, 1C), 115.0 (s, 1C), 107.8 (d, 1C, $J = 149$ Hz), 100.4 (d, 5C, $J = 172$ Hz), 98.6 (d, 1C, $J = 149$ Hz), 78.9 (s, 1C), 57.8 (t, 1C, $J = 124$ Hz), 48.0 (t, 1C, $J = 154$ Hz), 39.5 (t, 1C, $J = 149$ Hz), 37.1 (t, 1C, $J = 130$ Hz), 26.4 (q, 1C, $J = 126$ Hz), 25.2 (q, 1C, $J = 125$ Hz), 22.6 (q, 1C, $J = 120$ Hz), 22.3 (q, 1C, $J = 127$ Hz).

MS (EI) [m/z (relative intensity)]: 55 (22), 67 (79), 79 (11), 81 (11), 91 (11), 93 (22), 95 (100), 96 (12), 105 (13), 107 (24), 108 (10), 109 (12), 119 (21), 121 (19), 133 (14), 147 (11), 175 (69), 249 (14), 250 (19), 264 (22), 348 (16).

Anal. Calcd for $\text{C}_{19}\text{H}_{27}\text{Nb}$: C, 65.50; H, 7.81. Found: C, 65.35; H, 7.61.

(Methylcyclopentadienyl)($\eta^8\text{-}2,4,7,9\text{-tetramethyl-}1,3,7,9\text{-decatetraene}$)niobium, $\text{Nb}(\text{CH}_3\text{C}_5\text{H}_4)(\eta^8\text{-}2,4,7,9\text{-C}_{14}\text{H}_{22})$, **3b.** A bright red solution of 1.0 g (2.6 mmol) of $\text{Nb}(\text{CH}_3\text{C}_5\text{H}_4)\text{-Cl}_4\text{-THF}$ in 50 mL of THF was cooled under nitrogen to -78°C , and 1.4 g (10 mmol) of the potassium salt of the 2,4-dimethylpentadienide anion dissolved in THF was added in a dropwise manner. The reaction mixture was stirred for 2 h at -78°C and allowed to warm to room temperature, resulting in a brown-red solution. After 6 h, the solvent was removed in vacuo, and the crude product was extracted with several portions of hexane and filtered on a coarse frit. The orange-brown solution was reduced in volume to about 15 mL and cooled to -78°C , yielding a dark-red, air-sensitive crystalline product (0.54 g, 58% yield). The compound is very soluble in hexane and can be recrystallized from pentane.

Table 1. Crystallographic Data for $Nb(C_5H_5)[\eta^8-2,4,7,9-(CH_3)_4-1,3,7,9-C_{10}H_{10}]$ (A), $Ta(C_5H_5)_2(\eta^3-2,3-C_7H_{11})$ (B), and $Ta(C_5H_5)_2[\eta^3-1,5-(Me_3Si)_2C_5H_5]$ (C)

	A	B	C
formula	$C_{19}H_{27}Nb$	$C_{17}H_{21}Ta$	$C_{21}H_{33}Si_2Ta$
fw	348.3	406.3	522.6
cryst system	orthorhombic	monoclinic	monoclinic
space group	$Pcc2$	$P2_1/c$	$P2_1/n$
<i>a</i> , Å	14.061(3)	7.887(2)	7.422(1)
<i>b</i> , Å	14.273(3)	14.433(3)	23.934(5)
<i>c</i> , Å	8.045(1)	12.645(3)	13.059(2)
β , deg	90	97.93(2)	97.52(1)
<i>V</i> , Å ³	1614	1426	2300
<i>Z</i>	4	4	4
cryst dimens, mm	0.20 × 0.20 × 0.64	0.31 × 0.25 × 0.22	0.03 × 0.28 × 0.52
cryst color	red	yellow	purple
<i>D</i> (calc), g cm ⁻³	1.43	1.89	1.54
μ (Mo K α), cm ⁻¹	7.07	76.02	51.34
temp, K	298	293	298
<i>T</i> (max)/ <i>T</i> (min)	1.061	2.370	2.729
diffractometer	Siemens P4	Nicolet P $\bar{1}$	Nicolet R3m
monochromator	graphite	graphite	graphite
λ (Mo K α)	0.710 73	0.710 73	0.710 73
2 θ scan range	4–55	2–51	4–46
data collected (<i>h,k,l</i>)	+17,+17,+10	+9,+17, \pm 15	\pm 9,+27,+15
reflins colcd	2221	2997	3502
indpt reflns	2047	2613	3205
indpt obsd reflns	1621 (3 σ)	2034 (3 σ)	2065 (5 σ)
<i>R</i> (<i>F</i>), %	7.3	3.4	3.4
<i>R</i> (<i>wF</i>), %	8.8	3.8	3.5
$\Delta\sigma$ (max)	0.03	0.001	0.02
$\Delta(\rho)$, e Å ⁻³	2.89	1.42	0.73
<i>N</i> _o / <i>N</i> _v	12.1	12.5	9.5

Melting point (nitrogen-filled, sealed capillary): 148–9 °C.

Infrared data (Nujol mull): 3170 (w), 1516 (mw), 1501 (mw), 1312 (m), 1272 (m), 1261 (m), 1240 (w), 1232 (m), 1166 (w), 962 (w), 917 (s), 891 (s), 852 (s), 795 (s).

¹H NMR (benzene-*d*₆, ambient): δ 4.79 (q, 1H, *J* = 2 Hz), 4.55 (q, 1H, *J* = 2 Hz), 4.29 (q, 1H, *J* = 2 Hz), 4.13 (q, 1H, *J* = 2 Hz), 3.40 (s, 1H), 2.76–2.90 (multiplets, 3H), 1.89 (s, 3H), 1.86 (s, 3H), 1.81 (s, 3H), 1.68 (br, 2H), 1.58 (s, 3H), 1.33–1.36 (multiplets, 2H), 1.32 (s, 3H), 1.07 (d, 1H, *J* = 5 Hz), 0.51 (d, 1H, *J* = 5 Hz).

¹³C NMR (benzene-*d*₆, ambient): δ 139.1 (s, 1C), 125.1 (s, 1C), 114.7 (s, 1C), 108.1 (d, 1C, *J* = 146 Hz), 104.1 (d, 1C, *J* = 176 Hz), 99.8 (d, 1C, *J* = 174 Hz), 99.0 (d, 1C, *J* = 181 Hz), 98.4 (s, 1C), 98.37 (d, 1C, *J* = 177 Hz), 98.3 (d, 1C, *J* = 157 Hz), 78.9 (s, 1C), 57.9 (t, 1C, *J* = 124 Hz), 51.9 (t, 1C, *J* = 149 Hz), 41.0 (t, 1C, *J* = 147 Hz), 37.1 (t, 1C, *J* = 126 Hz), 26.4 (q, 1C, *J* = 127 Hz), 25.0 (q, 1C, *J* = 130 Hz), 22.6 (q, 1C, *J* = 125 Hz), 22.3 (q, 1C, *J* = 125 Hz), 15.3 (q, 1C, *J* = 126 Hz).

MS (EI) [*m/z* (relative intensity)]: 95 (14), 250 (16), 262 (13), 263 (58), 264 (60), 278 (100), 302 (10), 360 (12), 362 (72).

Anal. Calcd for $C_{20}H_{29}Nb$: C, 66.29; H, 8.06. Found: C, 66.04; H, 7.91.

Ta(C₅H₅)₂($\eta^3-2,4-C_7H_{11}$), 5. To a yellow solution of 1.0 g (2.6 mmol) of Ta(C₅H₅)Cl₄ in 40 mL of THF under nitrogen at –78 °C was added dropwise 1.4 g (10 mmol) of the potassium salt of the 2,4-dimethylpentadienyl anion dissolved in 65 mL of THF. The resulting green solution was allowed to warm to room temperature. The solution was stirred an additional 6 h, and the solvent was removed in vacuo. The crude product was extracted with several portions of hexane and filtered on a coarse frit. The green solution was concentrated to 15 mL and cooled to –78 °C, yielding a light-brown air-sensitive crystalline compound, mp 91–93 °C. The yield was 30% (0.16 g) based on Ta(C₅H₅)Cl₄.

Infrared data (Nujol mull): 3111 (m), 3000 (w), 1633 (m), 1308 (m), 1280 (mw), 1268 (w), 1171 (m), 1124 (m), 972 (m), 930 (w), 917 (w), 904 (m), 840 (m), 829 (m), 813 (s).

¹H NMR (benzene-*d*₆, ambient): δ 6.31 (s, 1H), 4.65 (s, 10H), 1.88 (s, 6H), 1.81 (d, 2H, *J* = 9 Hz), 1.22 (d, 2H, *J* = 9 Hz).

¹H NMR (toluene-*d*₈, –78 °C): δ 6.44 (s, 1H), 4.72 (s, 5H), 4.25 (s, 5H), 2.79 (d, 1H, *J* = 10 Hz), 2.06 (s, 3H), 1.88 (s, 3H), 1.33 (d, 1H, *J* = 10 Hz), 1.08 (s, 1H), 0.77 (s, 1H). ΔG^\ddagger

(coalescence of Cp's, *T*_c = 220 K): 10.2 ± 0.2 kcal/mol. ΔG^\ddagger (coalescence of CH₃'s, *T*_c = 211 K): 10.2 ± 0.2 kcal/mol.

¹³C NMR (benzene-*d*₆, ambient): δ 135.9 (d, 1C, *J* = 154 Hz), 98.0 (d, 10C, *J* = 176 Hz), 28.5 (q, 2C, *J* = 123 Hz), 21.2 (t, 2C, *J* = 136 Hz). The expected quaternary carbon resonance was not visible.

MS (EI) [*m/z* (relative intensity)]: 95 (10), 311 (11), 312 (100), 326 (12), 341 (10), 406 (54).

Anal. Calcd for $C_{17}H_{21}Ta$: C, 50.25; H, 5.21. Found: C, 49.86; H, 5.24.

Ta(C₅H₅)₂($\eta^3-2,3-C_7H_{11}$), 4. To 0.80 g (2.1 mmol) of Ta(C₅H₅)Cl₄ in 50 mL of THF under nitrogen at –78 °C was added 1.1 g (8.3 mmol) of potassium 2,3-dimethylpentadienide in 50 mL of THF. The reaction mixture was allowed to warm slowly to room temperature and was then stirred for 8 h more. The solvent was removed under reduced pressure and the residue extracted with hexane. The extracts were filtered on a coarse frit, and the resulting yellow-green solution was concentrated to 15 mL. On cooling of this solution to –78 °C for several days, an oily brown solid precipitated. After removal of the supernatant liquid, the oily residue was left under vacuum for about 10–14 days, affording a yellow crystalline product in 20% yield (0.09 g). Pairs of C₅H₅ and CH₃ resonances could be observed at (4.75, 4.39) and (1.76, 1.65) ppm, respectively. Other assignments are uncertain, due to the apparent presence of a second isomer in solution.

Infrared data (Nujol mull): 3090 (w), 1607 (m), 1305 (m), 1262 (mw), 1170 (w), 1155 (mw), 1098 (m), 971 (w), 937 (w), 893 (m), 845 (w), 810 (s).

Anal. Calcd for $C_{17}H_{21}Ta$: C, 50.25; H, 5.21. Found: C, 50.33; H, 5.68.

Ta(C₅H₅)₂($\eta^3-1,5-(SiMe_3)_2C_5H_5$), 6. To a magnetically stirred solution of 0.50 g (1.3 mmol) of (C₅H₅)₂TaCl₄ in 20 mL of THF under nitrogen at –78 °C was added 1.3 g (5.2 mmol) of potassium 1,5-bis(trimethylsilyl)pentadienide dissolved in 35 mL of THF. The mixture was stirred at –78 °C for 1 h, then warmed to room temperature, and allowed to stir an additional 4 h. The solvent was removed in vacuo and the crude product extracted with pentane and filtered on a coarse frit. Cooling of this dark-brown solution to –78 °C for several days afforded a dark-purple crystalline product (mp 150–151 °C) in 30% yield (0.10 g).

Table 2. Positional ($\times 10^4$) and Isotropic Thermal Parameters ($\text{\AA}^2 \times 10^3$) for $\text{Nb}(\text{C}_5\text{H}_5)[\eta^8\text{-2,4,7,9-(CH}_3)_4\text{-1,3,7,9-C}_{10}\text{H}_{10}]$

atom	x	y	z	U^a
Nb	2442.9(7)	2749.2(7)	5000	28.6(4)*
C(1)	2803(14)	1654(14)	7111(27)	51(4)
C(2)	1811(15)	1930(12)	7402(26)	52(4)
C(3)	1801(14)	2928(14)	7729(24)	52(4)
C(4)	2760(14)	3158(14)	7843(28)	51(4)
C(5)	3338(13)	2471(11)	7388(23)	37(3)
C(6)	939(10)	3381(10)	4631(26)	52(6)*
C(7)	1248(11)	3339(12)	2784(28)	52(6)*
C(8)	1528(10)	2509(8)	2267(18)	26(2)
C(9)	1648(13)	1633(10)	3328(26)	48(5)*
C(10)	2240(12)	903(13)	2536(22)	45(5)*
C(11)	3206(12)	1265(11)	1896(19)	44(5)*
C(12)	3686(11)	1832(10)	3179(19)	39(4)*
C(13)	3646(11)	2784(9)	2975(22)	35(3)
C(14)	3814(10)	3519(10)	4228(22)	39(3)
C(15)	3088(9)	4204(8)	4168(14)	28(3)*
C(16)	1226(12)	4174(11)	1848(26)	59(6)*
C(17)	669(12)	1198(14)	4068(23)	60(6)*
C(18)	4392(14)	1315(15)	4338(41)	101(11)*
C(19)	4734(9)	3589(9)	5164(21)	39(3)

* Asterisk indicates equivalent isotropic U defined as one-third of the trace of the orthogonalized U_{ij} tensor.

Infrared data (Nujol mull): 3188 (w), 1572 (ms), 1311 (m), 1259 (m), 1247 (s), 1220 (w), 1160 (m), 1113 (w), 1019 (mw), 998 (mw), 864 (s), 839 (s), 834 (s), 810 (w).

^1H NMR (benzene- d_6 , ambient): δ 6.67 (d of d, 1H, $J = 7$, 18 Hz), 5.45 (d, 1H, $J = 18$ Hz), 4.51 (s, 5H), 4.18 (s, 5H), 2.16 (dd, 1H, $J = 13$, 16 Hz), 2.04 (dd, 1H, $J = 7$, 13 Hz), 0.28 (s, 9H), 0.25 (s, 9H), -0.29 (d, 1H, $J = 16$ Hz).

^{13}C NMR (benzene- d_6 , ambient): δ 154.3 (d, 1C, $J = 150$ Hz), 113.2 (d, 1C, $J = 137$ Hz), 91.4 (d, 5C, $J = 175$ Hz), 85.5 (d, 5C, $J = 174$ Hz), 68.2 (d, 1C, $J = 158$ Hz), 56.2 (d, 1C, $J = 149$ Hz), 37.3 (d, 1C, $J = 127$ Hz), 1.89 (q, 3C, $J = 118$ Hz), 0.13 (q, 3C, $J = 118$ Hz).

MS (EI) [m/z (relative intensity)]: 312 (100), 448 (10), 522 (48).

Anal. Calcd for $\text{C}_{21}\text{H}_{33}\text{Si}_2\text{Ta}$: C, 45.37; H, 5.98. Found: C, 44.92; H, 5.38.

X-ray Crystallography for $\text{Nb}(\text{C}_5\text{H}_5)(\eta^8\text{-2,4,7,9-C}_{14}\text{H}_{22})$ (2b). Crystal, data collection, and refinement parameters are given in Table 1. Suitable crystals were selected and mounted with epoxy cement to glass fibers. The unit-cell parameters were obtained by the least-squares refinement of the angular settings of 24 reflections ($20^\circ \leq 2\theta \leq 24^\circ$). All of the examined crystal specimens showed approximately 5% of the diffracted radiation from a satellite or twin. About 100 data were rejected due to background contributions from the secondary diffraction source, as judged from their poor fit to a learned peak profile.

The systematic absences in the diffraction data are consistent for space groups $Pcc2$ and $Pccm$. Departures of the molecule from mirror plane symmetry suggested the noncentrosymmetric alternative. The centrosymmetric option was also explored but was abandoned because of chemically unreasonable results during refinement.

The structure was solved using direct methods, completed by subsequent difference Fourier syntheses, and refined by full-matrix least-squares procedures. The niobium atom, C(6), C(7), and C(9)–C(18) were refined with anisotropic displacement coefficients. All other remaining non-hydrogen atoms were refined isotropically. Hydrogen atoms were treated as idealized contributions. The largest remaining peak in the difference map (2.89 e \AA^{-3}) is a noise peak associated with the niobium atom at a distance of 0.82 \AA , perhaps due to less than adequate correction for absorption, despite a low 1.06 transmission ratio.

All software and sources of the scattering factors are contained in the SHELXTL (5.1 Data General Eclipse 32K

Table 3. Pertinent Bonding Parameters for $\text{Nb}(\text{C}_5\text{H}_5)[\eta^8\text{-2,4,7,9-(CH}_3)_4\text{-1,3,7,9-C}_{10}\text{H}_{10}]$

Bond Distances (\AA)			
Nb–C(1)	2.363(20)	C(3)–C(4)	1.391(29)
Nb–C(2)	2.427(20)	C(4)–C(5)	1.324(26)
Nb–C(3)	2.387(20)	C(6)–C(7)	1.549(31)
Nb–C(4)	2.402(22)	C(7)–C(8)	1.315(21)
Nb–C(5)	2.331(18)	C(7)–C(16)	1.411(26)
Nb–C(6)	2.317(14)	C(8)–C(9)	1.524(21)
Nb–C(7)	2.590(20)	C(9)–C(10)	1.477(25)
Nb–C(8)	2.570(15)	C(9)–C(17)	1.623(25)
Nb–C(9)	2.366(18)	C(10)–C(11)	1.541(24)
Nb–C(12)	2.630(15)	C(11)–C(12)	1.476(22)
Nb–C(13)	2.349(16)	C(12)–C(13)	1.369(20)
Nb–C(14)	2.304(15)	C(12)–C(18)	1.548(30)
Nb–C(15)	2.363(12)	C(13)–C(14)	1.474(22)
C(1)–C(2)	1.469(28)	C(14)–C(15)	1.414(19)
C(1)–C(5)	1.405(25)	C(14)–C(19)	1.501(21)
C(2)–C(3)	1.449(26)		
Bond Angles (deg)			
C(2)–C(1)–C(15)	105.0(16)	C(10)–C(9)–C(17)	111.5(13)
C(1)–C(2)–C(13)	107.6(16)	C(9)–C(10)–C(11)	113.9(15)
C(2)–C(3)–C(14)	103.5(17)	C(10)–C(11)–C(12)	110.7(13)
C(3)–C(4)–C(5)	113.7(18)	C(11)–C(12)–C(13)	116.2(14)
C(4)–C(5)–C(1)	109.3(17)	C(11)–C(12)–C(18)	116.9(15)
C(6)–C(7)–C(8)	115.0(16)	C(13)–C(12)–C(18)	124.9(15)
C(6)–C(7)–C(16)	118.2(16)	C(12)–C(13)–C(14)	128.2(15)
C(8)–C(7)–C(16)	126.8(20)	C(13)–C(14)–C(15)	110.7(13)
C(7)–C(8)–C(9)	126.5(16)	C(13)–C(14)–C(19)	121.9(13)
C(8)–C(9)–C(10)	113.6(16)	C(15)–C(14)–C(19)	126.4(13)
C(8)–C(9)–C(17)	115.2(14)		

version) program libraries. Positional parameters are collected in Table 2, and selected bond distances and angles are listed in Table 3.

X-ray Crystallography for $\text{Ta}(\text{C}_5\text{H}_5)_2[\eta^8\text{-1,5-(Me}_3\text{Si)}_2\text{C}_5\text{H}_5]$ (6). A crystal suitable for X-ray structural determination was mounted on a glass fiber with epoxy cement. Crystal, data collection, and refinement parameters are collected in Table 1. The unit-cell parameters were obtained from the least squares fit of 25 reflections ($20^\circ \leq 2\theta \leq 25^\circ$). The systematic absences in the diffraction data uniquely established the space group as $P2_1/n$. A semi-empirical correction factor for absorption was applied (216 ψ -scans, $T_{\text{max}}/T_{\text{min}} = 2.729$).

The structure was solved by direct methods which located the Ta atom. The remaining non-hydrogen atoms were located through subsequent difference Fourier syntheses. All hydrogen atoms were included as idealized isotropic contributions ($d_{\text{CH}} = 0.960 \text{ \AA}$, $U = 1.2U$ for attached C). All non-hydrogen atoms were refined with anisotropic thermal parameters. Positional parameters are collected in Table 4, and selected bond distances and angles are listed in Table 5. All software and the sources of the scattering factors are contained in the SHELXTL (5.1) program library.⁸

X-ray Crystallography for $\text{Ta}(\text{C}_5\text{H}_5)_2(2,3\text{-C}_7\text{H}_{11})$ (4). A single crystal of the compound was mounted in a glass capillary under nitrogen, and transferred to a Nicolet-Siemens $P1$ autodiffractometer. Unit cell parameters were determined through standard software routines and along with the diffraction data indicated monoclinic Laue symmetry, with extinctions uniquely characteristic of space group $P2_1/c$, with $a = 7.887(2) \text{ \AA}$, $b = 14.433(3) \text{ \AA}$, $c = 12.645(3) \text{ \AA}$, $\beta = 97.93(2)^\circ$, and $V = 1425.6 \text{ \AA}^3$ for $Z = 4$. ψ -scan data were used to apply an absorption correction (relative transmission range 0.4195–0.9944).

The tantalum atom position was determined by direct methods, after which the carbon atoms were located from difference Fourier maps. Refinements utilized an "ignorance" factor of 0.05 in the weighing scheme. Once convergence was near, the hydrogen atom locations could also be found from a difference Fourier map, and these atoms were then included as fixed contributions. Positional and thermal parameters are

(8) Sheldrick, G. Siemens XRD, Madison, WI.

Table 4. Positional ($\times 10^3$) and Isotropic Thermal Parameters ($\text{\AA}^2 \times 10^3$) for $Ta(C_5H_5)_2(2,3-C_7H_{11})$

atom	x	y	z	B
Ta	58.97(4)	169.75(2)	300.20(3)	2.553(6)
C(1)	179(1)	87.3(7)	447.5(7)	3.6(2)
C(2)	149(1)	28.1(6)	355.7(7)	2.7(2)
C(3)	282(1)	-2.9(6)	289.3(7)	2.8(2)
C(4)	246(1)	18.1(7)	186.0(8)	3.4(2)
C(5)	88(1)	77.6(8)	155.9(8)	3.7(2)
C(6)	431(1)	-58.2(7)	342.0(9)	4.2(2)
C(7)	350(2)	-10(1)	99.1(9)	5.6(3)
C(8)	359(1)	218.4(8)	321(9)	4.8(3)
C(9)	293(1)	233.6(7)	213.3(9)	4.6(2)
C(10)	165(2)	300.2(8)	208(1)	6.0(3)
C(11)	151(2)	329.0(8)	313(1)	6.4(3)
C(12)	270(2)	277.8(8)	384(1)	5.3(3)
C(13)	-200(1)	254.6(9)	289(1)	7.5(4)
C(14)	-171(2)	223(1)	393(1)	6.8(4)
C(15)	-188(1)	128(1)	390(1)	6.3(3)
C(16)	-219(1)	98.2(9)	287(1)	7.0(4)
C(17)	-228(1)	177(1)	219(1)	6.8(4)

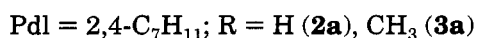
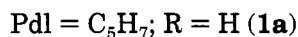
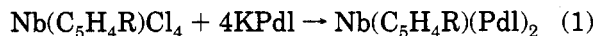
Table 5. Pertinent Bonding Parameters for $Ta(C_5H_5)_2(2,3-C_7H_{11})$

Bond Distances (\AA)			
Ta-C(1)	2.302(4)	C(3)-C(4)	1.333(6)
Ta-C(2)	2.245(4)	C(3)-C(6)	1.497(6)
Ta-C(5)	2.296(5)	C(4)-C(5)	1.517(6)
Ta-C(8)	2.450(4)	C(4)-C(7)	1.512(6)
Ta-C(9)	2.454(4)	C(8)-C(9)	1.402(8)
Ta-C(10)	2.421(5)	C(8)-C(12)	1.427(7)
Ta-C(11)	2.410(5)	C(9)-C(10)	1.389(8)
Ta-C(12)	2.414(5)	C(10)-C(11)	1.408(9)
Ta-C(13)	2.370(5)	C(11)-C(12)	1.408(9)
Ta-C(14)	2.415(6)	C(13)-C(14)	1.38(1)
Ta-C(15)	2.457(5)	C(13)-C(17)	1.42(1)
Ta-C(16)	2.409(5)	C(14)-C(15)	1.367(9)
Ta-C(17)	2.358(5)	C(15)-C(16)	1.36(1)
C(1)-C(2)	1.434(6)	C(16)-C(17)	1.42(1)
C(2)-C(3)	1.499(5)		
Bond Angles (deg)			
C(1)-C(2)-C(3)	125.7(4)	C(9)-C(10)-C(11)	108.1(6)
C(2)-C(3)-C(4)	114.3(4)	C(10)-C(11)-C(12)	108.3(5)
C(2)-C(3)-C(6)	118.3(4)	C(8)-C(12)-C(11)	107.2(5)
C(4)-C(3)-C(6)	127.2(4)	C(14)-C(13)-C(17)	108.7(6)
C(3)-C(4)-C(5)	115.5(4)	C(13)-C(14)-C(15)	107.7(7)
C(3)-C(4)-C(7)	126.0(4)	C(14)-C(15)-C(16)	110.3(7)
C(5)-C(4)-C(7)	118.5(4)	C(15)-C(16)-C(17)	108.0(6)
C(9)-C(8)-C(12)	107.5(5)	C(13)-C(17)-C(16)	105.2(6)
C(8)-C(9)-C(10)	108.9(5)		

included in Table 6, while selected bond distances and angles are given in Table 7.

Results and Discussion

The reactions of $Nb(C_5H_4R)Cl_4$ ($R = H, CH_3$) complexes with four equiv of either KC_5H_7 or $K(2,4-C_7H_{11})$ ($C_7H_{11} = \text{dimethylpentadienyl}$) led, at least initially, to apparent Nb(III) complexes (eq 1). That reduction of



the Nb(V) center would occur could be expected, on the basis of the fact that pentadienyl ligands greatly favor metals in low oxidation states,⁹ even bringing about spontaneous reduction of Zr(IV) or Hf(IV) to their divalent states.¹⁰ The isolated compounds are air-

Table 6. Positional ($\times 10^4$) and Isotropic Thermal Parameters ($\text{\AA}^2 \times 10^3$) for $Ta(C_5H_5)_2[1,5-(Me_3Si)_2C_5H_5]$

atom	x	y	z	U
Ta	1394.2(5)	1971.6(2)	127.5(3)	39.7(1)
Si(1)	-1244(4)	879(2)	1459(2)	60(1)
Si(2)	-2102(5)	4065(2)	714(3)	69(1)
C(1)	-982(13)	1419(4)	474(8)	49(4)
C(2)	-1533(11)	1995(5)	535(7)	48(4)
C(3)	-1410(12)	2389(4)	-277(7)	44(3)
C(4)	-1660(12)	2999(4)	-169(7)	47(3)
C(5)	-2056(14)	3294(4)	638(8)	49(4)
C(6)	-3348(18)	443(5)	1051(11)	95(6)
C(7)	-1484(20)	1194(6)	2752(8)	88(6)
C(8)	734(18)	393(6)	1564(10)	90(6)
C(9)	-1582(20)	4370(6)	-533(9)	91(6)
C(10)	-328(21)	4393(6)	1794(9)	105(7)
C(11)	-4351(20)	4329(6)	980(11)	113(8)
C(12)	741(16)	1609(6)	-1594(8)	87(6)
C(13)	1995(23)	1226(6)	-1020(10)	88(7)
C(14)	3572(18)	1531(7)	-822(9)	87(6)
C(15)	3304(22)	2045(7)	-1226(10)	97(7)
C(16)	1590(20)	2105(6)	-1667(9)	80(6)
C(17)	1564(16)	2411(8)	1740(9)	98(7)
C(18)	2537(33)	1928(10)	1916(12)	145(11)
C(19)	3966(26)	1970(8)	1407(14)	127(9)
C(20)	3957(19)	2455(9)	957(10)	94(7)
C(21)	2483(23)	2750(6)	1102(12)	91(7)

Table 7. Selected Bond Distances and Angles for $Ta(C_5H_5)_2[1,5-(Me_3Si)_2C_5H_5]$

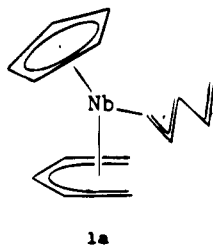
Bond Distances (\AA)			
Ta-C(1)	2.297(10)	Si(1)-C(1)	1.852(11)
Ta-C(2)	2.304(9)	Si(1)-C(6)	1.896(13)
Ta-C(3)	2.306(9)	Si(1)-C(7)	1.879(12)
Ta-C(12)	2.399(11)	Si(1)-C(8)	1.863(14)
Ta-C(13)	2.409(14)	Si(2)-C(5)	1.849(11)
Ta-C(14)	2.405(14)	Si(2)-C(9)	1.870(13)
Ta-C(15)	2.412(15)	Si(2)-C(10)	1.880(13)
Ta-C(16)	2.389(12)	Si(2)-C(11)	1.860(16)
Ta-C(17)	2.342(14)	C(12)-C(13)	1.444(19)
Ta-C(18)	2.381(16)	C(12)-C(16)	1.354(21)
Ta-C(19)	2.367(18)	C(13)-C(14)	1.376(21)
Ta-C(20)	2.365(16)	C(14)-C(15)	1.342(23)
Ta-C(21)	2.339(14)	C(15)-C(16)	1.333(20)
C(1)-C(2)	1.443(15)	C(17)-C(18)	1.367(29)
C(2)-C(3)	1.431(14)	C(17)-C(21)	1.402(22)
C(3)-C(4)	1.483(14)	C(18)-C(19)	1.328(31)
C(4)-C(5)	1.332(14)	C(19)-C(20)	1.299(28)
		C(20)-C(21)	1.335(23)
Bond Angles (deg)			
C(1)-C(2)-C(3)	122.9(9)	C(19)-C(20)-C(21)	111.3(16)
C(2)-C(3)-C(4)	123.9(9)	C(17)-C(21)-C(20)	104.5(14)
C(3)-C(4)-C(5)	129.8(9)	C(1)-Si(1)-C(6)	110.3(5)
Si(1)-C(1)-C(2)	125.0(8)	C(1)-Si(1)-C(7)	112.0(6)
Si(2)-C(5)-C(4)	125.3(8)	C(1)-Si(1)-C(8)	109.5(6)
C(13)-C(12)-C(16)	108.6(11)	C(6)-Si(1)-C(7)	107.5(7)
C(12)-C(13)-C(14)	103.6(12)	C(6)-Si(1)-C(8)	106.8(6)
C(13)-C(14)-C(15)	109.5(13)	C(7)-Si(1)-C(8)	110.5(6)
C(14)-C(15)-C(16)	110.7(14)	C(5)-Si(2)-C(9)	109.6(6)
C(12)-C(16)-C(15)	107.5(13)	C(5)-Si(2)-C(10)	108.3(5)
C(18)-C(17)-C(21)	107.6(14)	C(5)-Si(2)-C(11)	111.9(6)
C(17)-C(18)-C(19)	106.9(18)	C(9)-Si(2)-C(10)	109.6(6)
C(18)-C(19)-C(20)	109.7(18)	C(9)-Si(2)-C(11)	108.8(7)
		C(10)-Si(2)-C(11)	108.6(7)

sensitive and have been characterized through normal analytical and spectroscopic methods.

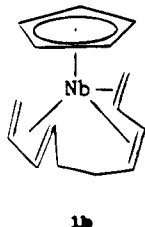
Given that one could not expect η^5 coordination for both PdI ligands (which would lead to a 20 electron count), two general bonding modes seemed plausible for the above complexes. First, an 18 electron count could result if one PdI ligand were bound in η^5 fashion, the other η^3 , as in **1a**. Second, an intramolecular coupling between the two PdI ligands could take place, converting them (at least initially) to a 2,4,7,9-tetramethyl-1,3,7,9-decatetraene, which could bind in η^8 fashion to the niobium center, again leading to an 18 electron complex,

(9) Ernst, R. D. *Chem. Rev.* **1988**, *88*, 1255.

(10) Waldman, T. E.; Stahl, L.; Wilson, D. R.; Arif, A. M.; Hutchinsson, J. P.; Ernst, R. D. *Organometallics* **1993**, *12*, 1543.



such as **1b**. These two possibilities should be readily



distinguishable through both IR and NMR spectroscopy. Indeed, all three complexes displayed a C–C stretching vibrational mode just over 1600 cm^{-1} , indicative of a free olefinic bond and, hence, a η^3 -Pd ligand. This formulation was further supported by the ^1H and ^{13}C NMR spectra. Thus, in the ^1H NMR spectra of **2a** and **3a**, one finds two downfield resonances which may be attributed to a terminal vinyl group, while three such resonances may be found for **1a**. In the ^{13}C NMR spectra for each of these complexes, three of the CH_2 resonances are found between 32 and 55 ppm, consistent with their being bound to the metal center, while a fourth one is located between 104–115 ppm, consistent again with a free olefinic bond. Additionally, the $J(^{13}\text{C}-\text{H})$ values for all of these types of CH_2 groups fall in the range 148–160 Hz, consistent with sp^2 hybridization, whereas a coupling reaction would lead to formal sp^3 hybridization and significantly smaller coupling constants. While these data leave no doubt that the complexes contain both η^5 - and η^3 -bound Pd ligands, unfortunately they do not unequivocally establish the skeletal frameworks of all the ligands. For **2a** and **3a**, the presence of methyl groups on the 2 and 4 positions prevents assessment of *cis* vs *trans* dispositions about the C(2)–C(3) and C(3)–C(4) bonds whereas it should in principle be possible to make such a determination for **1a**. Unfortunately, a high degree of spectral complexity, due primarily to the overlap of resonances and the presence of a minor second isomer, prevented a full assignment of the peaks. However, the presence of a simple triplet at 5.48 ppm with a proton–proton coupling constant of ca. 7 Hz¹¹ suggests the presence of a U conformation for the η^5 - C_5H_7 ligand, as is generally expected,¹² although η^5 -S structures may also exhibit such features due to the nonplanarity of their dienylic skeletons.^{3a} Thus, while very unlikely, the η^5 -S coordination mode may not be entirely eliminated from consideration. For the η^3 -bound ligand, a W conformation is expected, although an S or U conformation would represent only a minor perturbation of the allylic

(11) That this peak does not arise from the η^3 - C_5H_7 ligand may be ascertained from the fact that the CH (free olefinic) resonance for the η^3 ligand can be assigned as the peak at δ 5.83. Besides its 10 and 16.7 Hz couplings to C(5), there is an additional coupling with C(3) of 10 Hz. That is not seen in the peak at δ 5.48. The splitting patterns of the olefinic resonances also eliminate the possibility of η^3 coordination through the 1, 2, and 5 positions.

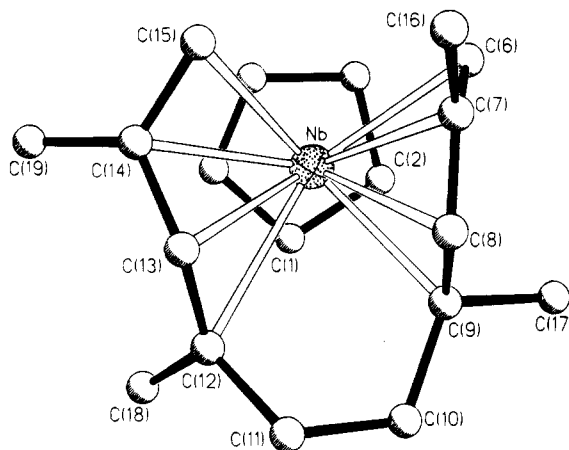
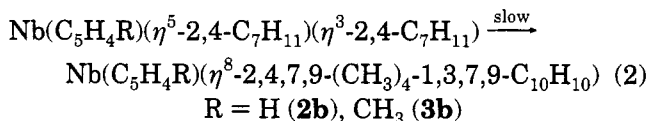


Figure 1. Perspective view and numbering scheme for $\text{Nb}(\text{C}_5\text{H}_5)[\eta^8\text{-}2,4,7,9\text{-}(\text{CH}_3)_4\text{-}1,3,7,9\text{-}\text{C}_{10}\text{H}_{10}]$.

coordination. For **2a** and **3a**, one can also presume η^5 -U coordination. Although the free 2,4- C_7H_{11} anion exhibits some preference for the U conformation,¹⁴ it seems unlikely that the η^3 -bound 2,4- C_7H_{11} ligand exists in the U conformation, as one would expect facile interconversion of each ligand between the η^5 and η^3 modes, thereby rendering them equivalent in their NMR spectra.

The 2,4- C_7H_{11} complexes (**2a** and **3a**) undergo a slow transformation on standing at room temperature, eq 2.



Telling spectroscopic features for the new products include a lack of a free olefinic C–C stretch over 1600 cm^{-1} , and two $J(^{13}\text{C}-\text{H})$ coupling constants falling in the range 124–130 Hz, signifying formal sp^3 hybridization, while the other two $J(^{13}\text{C}-\text{H})$ coupling constants (147–154 Hz) were still characteristic of sp^2 hybridization. These data clearly demonstrate that an intramolecular coupling has occurred between the two ligands, converting them to a 2,4,7,9-tetramethyl-1,3,7,9-decatetraene ligand. With η^8 coordination, the complex achieves the 18 electron configuration.

The structure of complex **2b** is shown in Figure 1, while pertinent positional and bonding parameters are provided in Tables 2 and 3. As suggested by the ^{13}C NMR spectra, the two dienylic fragments have coupled to yield an η^8 -1,3,7,9-decatetraene complex which as a result possesses the 18 electron configuration. Such intramolecular couplings have been previously observed in other systems,¹⁵ although intermolecular coupling is

(12) The alternative η^5 -S (sickle) mode may be found in some d^4 18 electron complexes.^{3a,10,13}

(13) (a) Lee, G. H.; Peng, S.-M.; Lee, T.-W.; Liu, R.-S. *Organometallics* **1986**, *5*, 2378. (b) Green, M.; Nagle, K. R.; Woolhouse, C. M.; Williams, D. J. *J. Chem. Soc., Chem. Commun.* **1987**, 1793. (c) Sivacek, T. M.; Katz, T. J.; Chiang, M. Y.; Yang, X.-Q. *Organometallics* **1989**, *8*, 1620. (d) Herrmann, W. A.; Fischer, R. A.; Herdtweck, E. *Ibid.* **1989**, *8*, 2821. (e) Bovino, S. C.; Coates, G. W.; Banovetz, J. P.; Waymouth, R. M.; Straus, D. A.; Ziller, J. W. *Inorg. Chim. Acta* **1993**, *203*, 179.

(14) (a) Schlosser, M.; Rauchschalbe, G. *J. Am. Chem. Soc.* **1978**, *100*, 3258. (b) Yasuda, H.; Yamauchi, M.; Nakamura, A.; Sei, T.; Kai, Y.; Yasuoka, N.; Kasai, N. *Bull. Chem. Soc. Jpn.* **1980**, *53*, 1089. (c) Yasuda, H.; Ohnuma, Y.; Nakamura, A.; Kai, Y.; Yasuoka, N.; Kasai, N. *Ibid.* **1980**, *53*, 1101.

(15) (a) Bleeke, J. R.; Kotyk, J. *J. Organometallics* **1983**, *2*, 1263. (b) Bleeke, J. R.; Hays, M. K.; Wittenbrink, R. *J. Ibid.* **1988**, *7*, 1417.

more common.¹⁶ Interestingly, the two isolated η^4 -diene units are bound in entirely different forms, one as a *trans*-diene, the other as a *cis*-diene (perhaps better described as an enediyl; *vide infra*). This provided the first crystallographically established example of such mixed coordination, although another example had been spectroscopically identified around the same time.¹⁷ The bonding of the *cis*-diene fragment to the metal center can be seen to involve enediyl coordination

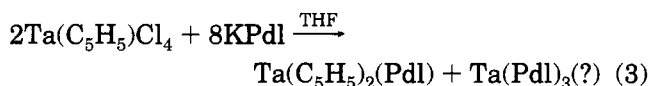


as revealed by the long-short-long pattern of C-C bond distances in the C(6-9) fragment (1.549(31), 1.315(21), 1.524(21) Å). The corresponding metal-carbon bond lengths follow the usual short-long-long-short trend for such a situation (2.317(14), 2.590(20), 2.570(15), 2.366(18) Å). As is often observed in metal-pentadienyl structures, the presence of a methyl substituent on an internal diene (or dienyl) carbon atom leads to a contraction of the C-C-C bond angle about that atom, i.e., 115.0(16)° around C(7) vs 126.5(16)° around C(8).¹⁸ The methyl (C(16), C(17)) and methylene (C(10)) substituents experience fairly normal distortions out of the idealized diene plane, by 0.125, -1.295, and 0.360 Å, respectively, corresponding to tilts of 5.1, -52.9, and 14.1°, negative values indicating tilts away from the metal center. The bonding in the η^4 -*trans*-diene portion (C(12)-C(15)) is much different but typical of the type normally seen in the other (relatively few) complexes having this bonding mode.¹⁹ Thus, the short-long-short pattern of C-C distances (1.369(20), 1.474(22), 1.414(19) Å) is consistent with a neutral diene fragment, and the M-C bond lengths follow a long-short-short-long pattern (2.630(15), 2.349(16), 2.304(15), 2.363(12) Å). The significant difference between the Nb-C(12) and Nb-C(15) bond lengths is likely a result of strain imposed on the diene coordination by the C(10)-C(11) bridge. Such strain may also be indicated by the differences between the C(12)-C(13)-C(14) and C(13)-C(14)-C(15) bond angles, 128.2(15) vs 110.7(13)°, respectively—a difference far larger than could be expected based on the presence of a methyl

substituent on C(14). That the distortion is much more noticeable for the diene rather than enediyl fragment suggests the former is not bound as strongly to the metal as the latter, as could be expected. In accord with previous observations, then, the η^4 -*trans*-coordination mode seems to necessitate a diene rather than an enediyl contribution. Some reasons for this have been provided previously.¹⁹

The *trans*-diene fragment is decidedly nonplanar, having a C(12)-C(13)-C(14)-C(15) torsion angle of -132.9°. This renders the relative substituent tilts less meaningful; nevertheless, the tilts of C(11), C(18), and C(19) from the C(12-14) plane are 16.5, -28.2, and -45.9°, respectively, while the tilt of C(19) from the C(13-15) plane is 9.1°. For purposes of comparison, the Nb-C(C₅H₅) bond lengths average 2.382(9) Å.

In contrast to the reactions for Nb(C₅H₅)Cl₄, those of Ta(C₅H₅)Cl₄ with four equiv of various pentadienyl anions lead to *bis*(cyclopentadienyl) complexes, as in eq 3. No additional products, such as the expected Ta(PdI)₃

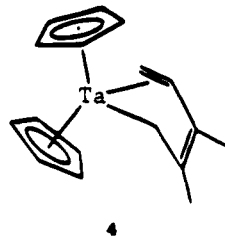


PdI = 2,3-C₇H₁₁ (**4**); 2,4-C₇H₁₁ (**5**);

1,5-(Me₃Si)₂C₅H₅ (**6**)

compound could be isolated from solution readily, as anything else in solution appeared to be very soluble and most likely an oil. It might be expected, however, that such a species would bear some similarity to the mono(cyclopentadienyl) complexes of niobium (*vide supra*), which initially possessed combinations of η^3 - and η^5 -bound pentadienyl ligands, which underwent coupling on standing.

The Ta(C₅H₅)₂(PdI) complexes were characterized analytically and through IR and NMR spectroscopic data. For such complexes to achieve the 18 electron configuration, one would expect to find η^3 -PdI coordination, presumably involving an allylic fragment, leaving a free olefinic bond. Indeed, IR bands were observed around 1600 cm⁻¹ for these compounds (see Experimental Section). However, for either **4** or **5**, one would therefore expect to have two or three²⁰ vinylic hydrogen atoms present, whereas their ¹H NMR spectra revealed zero or one such resonances, respectively. A mode of η^3 coordination in accord with these data, and established from an X-ray diffraction study for **4** (*vide infra*), is that shown as follows:



In such a situation, one has a localized Ta-C single bond on one end of the ligand, olefinic coordination to the tantalum center from the other end, and a free olefin in between. This provided the first example of such η^3 -

(20) The unsymmetric η^3 -2,3-C₇H₁₁ ligand could exist in two forms, one having two vinylic hydrogen atoms, the other three. The η^3 -2,4-C₇H₁₁ ligand would have two vinylic hydrogen atoms.

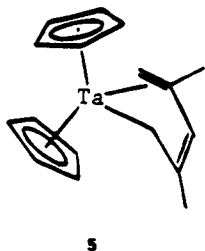
(16) (a) Jotham, R. W.; Kettle, S. F. A.; Moll, D. B.; Stamper, P. J. *Organomet. Chem.* **1976**, *118*, 59. (b) Sapienza, R. S.; Riley, P. E.; Davis, R. E.; Pettit, R. *Ibid.* **1976**, *121*, C35. (c) Connelly, N. G.; Kelly, R. L.; Kitchen, M. C.; Mills, R. M.; Stensfield, R. F. D.; Shiteley, M. W.; Whiting, S. M.; Woodward, P. J. *J. Chem. Soc., Dalton Trans.* **1981**, 1317. (d) Geiger, W. E.; Gennett, T.; Lane, G. A.; Salzer, A.; Rheingold, A. L. *Organometallics* **1986**, *5*, 352. (e) Noda, I.; Yasuda, H.; Nakamura, A. *Ibid.* **1983**, *2*, 1207. (f) Connelly, N. G.; Freeman, M. J.; Orpen, A. G.; Sheridan, J. B.; Symonds, A. N. D.; Whiteley, M. W. *J. Chem. Soc., Dalton Trans.* **1985**, 1027. (g) Wilson, D. R.; Ernst, R. D.; Kralik, M. S. *Organometallics* **1984**, *3*, 1442. (h) Ernst, R. D.; Ma, H.; Sergeson, G.; Zahn, T.; Ziegler, M. L. *Ibid.* **1987**, *6*, 848. (i) Ma, H.; Weber, P.; Ziegler, M. L.; Ernst, R. D. *Ibid.* **1986**, *5*, 2009. (j) Newbound, T. D.; Arif, A. M.; Wilson, D. R.; Rheingold, A. L.; Ernst, R. D. *J. Organometallic Chem.* **1992**, *435*, 73.

(17) (a) Okamoto, T.; Yasuda, H.; Nakamura, A.; Kai, Y.; Kanehisa, N.; Kasai, N. *J. Am. Chem. Soc.* **1988**, *110*, 5008. (b) Melendez, E.; Arif, A. M.; Rheingold, A. L.; Ernst, R. D. *Ibid.* **1988**, *110*, 8703.

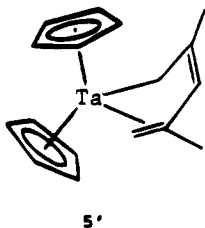
(18) Ernst, R. D. *Struct. Bond. (Berlin)* **1984**, *57*, 1.

(19) (a) Erker, G.; Krüger, C.; Müller, G. *Adv. Organomet. Chem.* **1985**, *24*, 1. (b) Yasuda, H.; Nakamura, A. *Angew. Chem., Int. Ed. Engl.* **1987**, *26*, 723. (c) Hunter, A. D.; Legzdins, P.; Nurse, C. R.; Einstein, F. W. B.; Willis, A. C. *J. Am. Chem. Soc.* **1985**, *107*, 1791. (d) Benyunes, S. A.; Green, M.; Grimshire, M. J. *Organometallics* **1989**, *8*, 2268. (e) Fagan, P. J.; Mahoney, W. S.; Calabrese, J. C.; Williams, I. D. *Ibid.* **1990**, *9*, 1843. (f) Benyunes, S. A.; Day, J. P.; Green, M.; Al-Saadoon, A. W.; Waring, T. L. *Angew. Chem., Int. Ed. Engl.* **1990**, *29*, 1416. (g) Ernst, R. D.; Melendez, E.; Stahl, L.; Ziegler, M. L. *Organometallics* **1991**, *10*, 3635.

pentadienyl coordination, and these compounds are then essentially $\text{Ta}(\text{C}_5\text{H}_5)_2(\text{olefin})(\text{alkyl})$ variants.²¹ Subsequently, this coordination mode has also been found for several (pentadienyl)iridium phosphine complexes.²² However, for **5**, the room-temperature ^1H NMR spectrum indicated, in addition to equivalent C_5H_5 ligands, apparent mirror plane symmetry for the 2,4- C_7H_{11} ligand such that one end of the ligand was equivalent to the other, i.e., a 1:6:2:2 pattern. Not surprisingly, the apparent higher symmetry was simply the result of a fluxional process, and at low temperatures a lower symmetry pattern was revealed, in which the two C_5H_5 ligands became inequivalent, as did the two ends of the 2,4- C_7H_{11} ligand. From the coalescence temperatures and spectral shifts, a value of $\Delta G^\ddagger = 10.2 \pm 0.2$ kcal/mol can be obtained for the fluxional process.²³ In this case the allyl-ene coordination for the 2,4- C_7H_{11} ligand can be represented similarly as



Regarding the mechanism by which site exchange occurs, the easiest pathway might appear to be a simple rocking of the ligand in such a way as to reverse the interactions each side experiences, as in **5'**, although it is also possible that an 18 electron intermediate having η^5 -2,4- C_7H_{11} coordination could be involved, should η^5 - η^3 slippage of a C_5H_5 ligand occur.²⁴



One way in which it might be possible to destabilize the localized η^3 coordination mode in favor of the usual η^3 allylic mode would be to place bulky substituents on the two terminal carbon centers, both of which interact with the metal in the former mode but only one of which interacts in the latter. Indeed, the ^1H NMR spectrum of **6** contained two resonances in the vinylic region; however, this would be expected for either coordination mode. Some information could be gleaned from the proton-proton coupling constants between the hydrogen atoms on carbon atom positions 2, 3, and 4. The H(2)-

(21) Guggenberger, L. J.; Schrock, R. R. *J. Am. Chem. Soc.* **1975**, *97*, 6577.

(22) Bleeke, J. R.; Boorsma, D.; Chiang, M. Y.; Clayton, T. W., Jr.; Haile, T.; Beatty, A. M.; Xie, Y.-F. *Organometallics* **1991**, *10*, 2391.

(23) (a) For the two C_5H_5 resonances, $\delta\nu = 141$ Hz and $T_c = 220$ K, while, for the two CH_3 resonances, $\delta\nu = 54$ Hz and $T_c = 211$ K. (b) Gunther, H. In *NMR Spectroscopy*; Wiley: New York, 1980, p 243. (c) Kessler, H. *Angew. Chem.* **1970**, *9*, 219.

(24) Interestingly, the transition from a η^3 - to η^5 -bound ligand could occur by coordination to either side of the free C(2,3) olefinic bond. In one case this would lead to η^5 -S (sickle) coordination; in the other this would lead to η^5 -U coordination. Possibly, then, conversions between η^5 -S and η^5 -U bonding modes in other systems might utilize the η^3 -C(1,4,5) bonding mode as an intermediate.

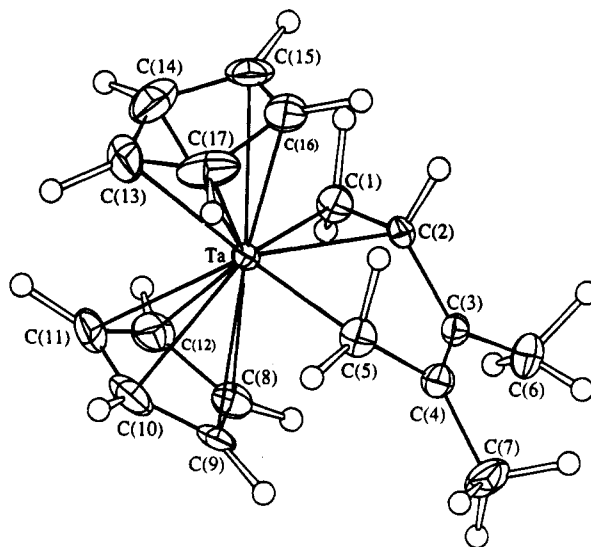


Figure 2. Solid state structure of $\text{Ta}(\text{C}_5\text{H}_5)_2(\eta^3\text{-}2,3\text{-C}_7\text{H}_{11})$.

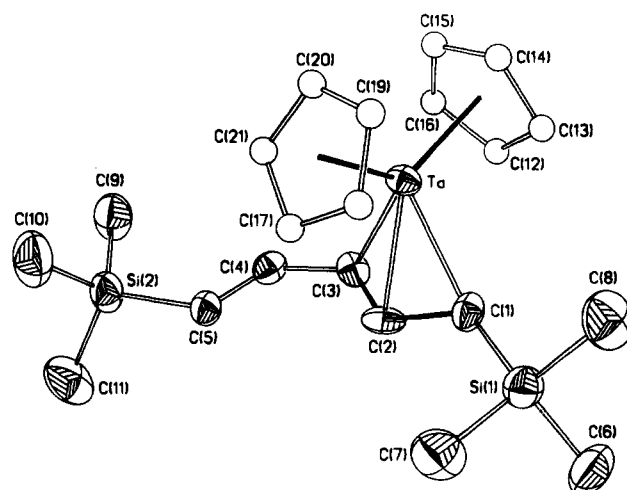
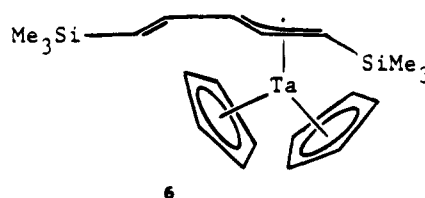


Figure 3. Solid state structure of $\text{Ta}(\text{C}_5\text{H}_5)_2[\eta^3\text{-}1,5\text{-(Me}_3\text{Si)}_2\text{C}_5\text{H}_5]$.

H(3), H(3)-H(4), and H(4)-H(5) couplings were found to be 13, 7, and 18 Hz, respectively, demonstrating that the diene group was present in a S (sickle) conformation. Given that the resonance for the 5-position clearly indicates an olefinic site (5.45 ppm), while the resonance for the 4-position (6.67 ppm) has J values of 7 and 18 Hz, these data are consistent with the usual allyl mode found by the X-ray diffraction study (vide infra).

The structures of **4** and **6** are presented in Figures 2 and 3, and pertinent bonding parameters are given in Tables 4-7. One can note that, for the former complex, the η^3 -dienyl coordination occurs through the 1, 2, and 5 positions of the ligand, rather than through the 1, 2, and 3 positions shown as follows



which would characterize an allyl complex and is actually observed for the latter complex (Figure 3). Apparently, the presence of Me_3Si substituents on the

1 and 5 positions destabilizes the 1, 2, 5 bonding mode, leading to adoption of the 1, 2, 3 (allylic) mode.

The $Ta(C_5H_5)_2$ fragments themselves are not too different, as average²⁵ Ta–C bond distances of 2.416(2) and 2.381(5) Å and ring–ring dihedral angles of 130.4 and 131.5° are observed for the respective complexes. Actually, in each case one of the C_5H_5 ligand planes makes a closer approach to the Ta center, by 2.114 vs 2.086 and 2.101 vs 2.061 Å, respectively.²⁰ (As it is clear from some of the Cp C–C bond lengths that there is significant librational disorder, it should be more appropriate to compare these Ta–ligand plane separations.)

The differing coordination modes for the two complexes are revealed and reflected by the carbon–carbon lengths. Thus, for **4**, the C–C bond lengths from C(1) to C(5) are 1.434(6), 1.499(5), 1.333(6), and 1.517(6) Å, while those for **6** are 1.443(15), 1.431(14), 1.483(14), and 1.332(14) Å, consistent with their respective bonding schemes (*vide supra*). Interestingly, all of the Ta–allyl bonds in **6** are of similar length, 2.300 Å, as are two of the three Ta–C bonds to the 2,3- C_7H_{11} ligand. Only the Ta–C(2) bond for **4** is significantly different, at 2.245–(4) Å. The fact that one bond in **4** is shorter than those in **6** might reflect an enhanced bonding interaction for **4**, wherein all three of its attached carbon atoms lie in the same plane as the metal center, where the appropriate metal orbitals for bonding are located. However, it is interesting that the Ta– C_5H_5 bonds in **6** are slightly shorter than those in **4**; *vide supra*. Of course, the fact that the three metal-bound dienyl carbon atoms in **4** are not contiguous could lead to greater steric demands.

One can also note some significant distortions which occur in the dienyl ligands as a result of their coordination. Thus, the C(1)–C(2)–C(3)–C(4) and C(2)–C(3)–C(4)–C(5) torsion angles in **4** are –123.3 and 6.0°, respectively. The large angle about the C(2)–C(3) bond clearly indicates that the two localized olefinic bonds in **4** are not appreciably conjugated, as can also be noted from Figure 1. The corresponding torsion angles around the C(1)–C(2), C(2)–C(3), C(3)–C(4), and C(4)–C(5) bonds in **6** are –175.9, –169.0, –1.2, and 173.4°, indicating only relatively small incremental deviations from planarity, despite the large size of the Me_3Si substituents. Finally, while the C(1)–C(2)–C(3) and C(2)–C(3)–C(4) bond angles in **6** are quite normal (Table 7; however, some expansion about C(4) is observed, apparently due to steric interactions for the $Me_3Si(2)$ group), those for **4** are significantly different, being 125.7(4), 114.3(4), and 115.5(4)° around C(2), C(3), and C(4), respectively. While one generally sees some

contraction of the C–C–C angles upon methylation of the central atom, the angles still generally exceed 120°, the most notable exceptions involving η^5 -sickle coordination



for which small angles work to keep the two ends of the dienyl ligand in relatively reasonable proximity. The situation for C(3) and C(4) in **4** seems similar, and it can readily be seen in Figure 1 that small angles about C(3) and C(4) would allow for the metal-bound olefin (C(1), C(2)) and alkyl (C(5)) units to remain fairly close, thereby leading to simultaneously effective bonding to the metal center for each unit.

For metal centers like niobium and tantalum, which often display similar chemistry, it is surprising that the reaction courses reported herein should differ so greatly and be essentially unchanged even with quite significant variations in pentadienyl ligand substituents. As to the cause for such a difference, at this point, one can only speculate. Should the initial reduction steps for the tantalum reactions proceed via intermolecular pentadienyl–pentadienyl coupling,²⁶ this might allow for a more facile exchange of ligands, thus bringing about the observed disproportionation. Possibly the utilization of a bulkier complex such as $Ta(C_5Me_5)Cl_4$ in these reactions might allow for the isolation of key intermediates in these processes. It is notable for the tantalum reactions, however, that variations in the pentadienyl substituents can be used to favor either the normal allylic η^3 coordination mode or the localized η^3 σ -alkyl/ π -olefin mode. This is reminiscent of η^5 -bound pentadienyl ligands, for which at least two bonding modes (η^5-U and η^5-S) have been observed. Finally, the uncoupled niobium and tantalum pentadienyl complexes are uncommon examples of metal pentadienyl compounds in “higher” oxidation states; this situation is most likely responsible for the intramolecular coupling observed for the $Nb(C_5H_5)(Pd)_2$ species.

Acknowledgment. R.D.E. is grateful to the National Science Foundation for generous support of this research.

Supplementary Material Available: Tables of anisotropic thermal parameters, hydrogen atom parameters, and least-squares planes (7 pages). Ordering information is given on any current masthead page.

OM940863Z

(26) This might be brought about by the greater reluctance of the tantalum complexes to undergo formal reduction.

(25) The esd's accompanying average values are derived from the esd's of the individual values being averaged and, therefore, reflect the uncertainty in the average, but not the distribution, of the individual values.

Homogeneous Multimetallic Catalysts. 11.¹ Carbonylation of Aryl Iodides with HSiEt₃ Catalyzed by Pd-Co Bimetallic Systems

Yoshihiko Misumi, Youichi Ishii, and Masanobu Hidai*

Department of Chemistry and Biotechnology, Faculty of Engineering, The University of Tokyo,
Hongo, Bunkyo-ku, Tokyo 113, Japan

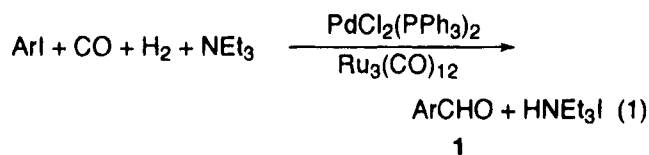
Received November 28, 1994[®]

The PdCl₂(PPh₃)₂-Ru₃(CO)₁₂ or PdCl₂(PPh₃)₂-Co₂(CO)₈ bimetallic catalyst has been found to be effective for carbonylation of aryl iodides and HSiEt₃ to give benzyl silyl ether as the major product, although neither PdCl₂(PPh₃)₂, Ru₃(CO)₁₂, nor Co₂(CO)₈ alone had any appreciable catalytic activity. Addition of NEt₃ to the Pd-Co mixed-metal-catalyzed carbonylation reaction remarkably changed the selectivity of the products, and 1,2-diaryl-1,2-disiloxyethane was obtained as the major product. Studies on the hydrosilylation of 4-TolCHO with HSiEt₃ under CO revealed that the formation of benzyl silyl ether in the former reaction may proceed through the formylation of aryl iodide followed by hydrosilylation of the resulting aldehyde. In contrast, the aldehyde was not included as an intermediate in the formation of 1,2-diaryl-1,2-disiloxyethane in the latter reaction. An aroylcobalt complex ArCOC_o(CO)₃(PPh₃) was suggested as an intermediate for the 1,2-diaryl-1,2-disiloxyethane production based on the following observations: (1) the aroylcobalt complex ArCOC_o(CO)₃(PPh₃) can be produced from aryl iodide, [Co(CO)₄]⁻, and PPh₃ with a Pd(0) catalyst; (2) hydrosilylation of the aroylcobalt complex ArCOC_o(CO)₃(PPh₃) under 50 atm of CO pressure produced 1,2-diaryl-1,2-disiloxyethane as the major product. The detailed mechanisms are proposed for the catalytic carbonylations of aryl iodides with HSiEt₃ by using the bimetallic catalysts.

Introduction

Homogeneous bimetallic or multimetallic catalysis has recently attracted much attention for its unique or enhanced catalytic activity and selectivity.² In spite of a considerable number of bimetallic catalyst systems having been developed and used in a variety of synthetic reactions, the reaction mechanism or the origin of the synergism has been elucidated in only limited examples. We have continuously focused our attention on bimetallic catalysts with the intention of developing novel and effective catalytic systems and already reported several bimetallic catalysts including the Co₂(CO)₈-RuCl₃ system for homologation of methanol,³ the Co₂(CO)₈-Ru₃(CO)₁₂ system for hydroformylation of olefins,⁴ and the PdCl₂(PPh₃)₂-Ru₃(CO)₁₂ system for formylation of aryl iodides and vinyl iodides (eq 1).¹

In these carbonylation reactions with CO/H₂, the bimetallic catalysts exhibited much higher activity than the corresponding single-metal catalysts. We proposed that the synergistic effects can be explained by the dinuclear reductive elimination reactions between acylcobalt or acylpalladium intermediates and hydridoru-



thenium species to give the corresponding aldehydes.^{1,3-5} Very recently, a related bimetallic mechanism was proposed for the remarkable rate enhancement in the hydroformylation of 1-alkenes catalyzed by a dinuclear rhodium complex.⁶

On the other hand, catalytic carbonylation with CO/HSiR₃ instead of CO/H₂ has been noted as a useful tool for organic syntheses.⁷ Considering the formal similarity in the reactivities toward organometallic compounds between dihydrogen and hydrosilanes,⁸ we have embarked on the investigation into catalytic carbonylation of aryl iodides (ArI) with CO/HSiEt₃ by using bimetallic catalyst systems. This has led us to the finding that Pd-Co and Pd-Ru mixed-metal catalysts were specifically effective for formation of ArCHO (1), ArCH₂OSiEt₃ (2), and (ArCHOSiEt₃)₂ (3) (1-3a; Ar = 4-Tol; 1-3b,

[®] Abstract published in *Advance ACS Abstracts*, March 15, 1995.

(1) Part 10: Misumi, Y.; Ishii, Y.; Hidai, M. *J. Mol. Catal.* **1993**, *78*, 1.

(2) (a) Braunstein, P.; Rose, J. In *Stereochemistry of Organometallic and Inorganic Compounds*; Bernal, I., Ed.; Elsevier: Amsterdam, 1989; Vol. 3, pp 3-138. (b) Roberts, D. A.; Geoffroy, G. L. In *Comprehensive Organometallic Chemistry*; Wilkinson, G., Stone, F. G. A., Abel, E. W., Eds.; Pergamon: Oxford, U.K., 1982; Vol. 6, pp 763-877.

(3) Hidai, M.; Orisaku, M.; Ue, M.; Koyasu, Y.; Kodama, T.; Uchida, Y. *Organometallics* **1983**, *2*, 292.

(4) (a) Hidai, M.; Fukuoka, A.; Koyasu, Y.; Uchida, Y. *J. Mol. Catal.* **1986**, *35*, 29. (b) Hidai, M.; Matsuzaka, H. *Polyhedron* **1988**, *7*, 2369. (c) Ishii, Y.; Sato, M.; Matsuzaka, H.; Hidai, M. *J. Mol. Catal.* **1989**, *54*, L13.

(5) Koyasu, Y.; Fukuoka, A.; Uchida, Y.; Hidai, M. *Chem. Lett.* **1985**, 1083.

(6) Broussard, M. E.; Juma, B.; Train, S. G.; Peng, W.-J.; Laneman, S. A.; Stanley, G. G. *Science* **1993**, *260*, 1784.

(7) (a) Murai, S.; Sonoda, N. *Angew. Chem., Int. Ed. Engl.* **1979**, *18*, 837. (b) Matsuda, I.; Ogiso, A.; Sato, S.; Izumi, Y. *J. Am. Chem. Soc.* **1989**, *111*, 2332. (c) Ojima, I.; Ingallina, P.; Donovan, R. J.; Clos, N. *Organometallics* **1991**, *10*, 38. (d) Doyle, M. P.; Shanklin, M. S. *Organometallics* **1994**, *13*, 1081. (e) Zhou, J.-Q.; Alper, H. *Organometallics* **1994**, *13*, 1586. (f) Ojima, I.; Tsai, C.-Y. *J. Am. Chem. Soc.* **1994**, *116*, 3643.

(8) Tilley, T. D. In *The Chemistry of Organic Silicon Compounds*; Patai, S., Rappoport, Z., Eds.; John Wiley & Sons: Chichester, U.K., 1989; pp 1417-1419.

Table 1. Carbonylation of 4-TolI Catalyzed by Palladium and/or Various Metal Carbonyls^a

entry	cat.	amt of NEt ₃ (mmol)	conv ^b (%)	yield (%) ^b			
				1a	2a	3a	Et ₃ SiI ^c
1	PdCl ₂ (PPh ₃) ₂		10	3	0	2	9
2	PdCl ₂ (PPh ₃) ₂	3	4	2	0	0	2
3	Ru ₃ (CO) ₁₂		5	0	1	0	
4	Ru ₃ (CO) ₁₂	3	0	0	0	0	
5	Co ₂ (CO) ₈		4	0	0	0	
6	Co ₂ (CO) ₈	3	5	0	0	0	
7	PdCl ₂ (PPh ₃) ₂ -Ru ₃ (CO) ₁₂		79	10	40	4	
8	PdCl ₂ (PPh ₃) ₂ -Ru ₃ (CO) ₁₂	3	64	17	10	3	
9	PdCl ₂ (PPh ₃) ₂ -Co ₂ (CO) ₈		85	0	76	0	80
10	PdCl ₂ (PPh ₃) ₂ -Co ₂ (CO) ₈	3	70	2	6	57	30

^a Reaction conditions: 4-TolI (2.5 mmol), HSiEt₃ (7.5 mmol), metal complex (0.05 mmol as metal atom), C₆H₆ (5 mL), CO (50 atm), 80 °C, 3 h. ^b Determined by GLC analysis. ^c Determined as Et₃SiOEt.

Ar = Ph; **1-3c**, Ar = 4-MeOC₆H₄; **1-3d**, Ar = 4-FC₆H₄. In this paper we wish to describe the scope of these reactions and elucidate the bimetallic mechanisms.

Results and Discussion

Catalytic Carbonylation of Aryl Iodides with CO/HSiEt₃. Table 1 shows the results of the carbonylation reaction of 4-TolI with CO/HSiEt₃ catalyzed by PdCl₂(PPh₃)₂ and/or some metal carbonyl complexes at 80 °C. None of the complexes showed any more than a marginal catalytic activity for this reaction by itself. Thus, when PdCl₂(PPh₃)₂ was employed as the catalyst, the total yield of the carbonylation products was only 5% (entry 1). No more than 1% of the carbonylation products were detected in the reactions using Cr(CO)₆, Mo(CO)₆, W(CO)₆, Mn₂(CO)₁₀, Fe(CO)₅, Ru₃(CO)₁₂, and Co₂(CO)₈. The catalytic activities of mixed-metal catalysts PdCl₂(PPh₃)₂-Cr(CO)₆, -Mo(CO)₆, -W(CO)₆, -Mn₂(CO)₁₀, and -Fe(CO)₅ were also poor and almost equal to or less than that of PdCl₂(PPh₃)₂. In sharp contrast, when Ru₃(CO)₁₂ or Co₂(CO)₈ was used in combination with PdCl₂(PPh₃)₂, 4-TolI was effectively carbonylated to give 4-TolCHO (**1a**), 4-methylbenzyl triethylsilyl ether (**2a**), and 1,2-bis(4-tolyl)-1,2-bis(triethylsiloxy)ethane (**3a**), where **2a** was the major product (entries 7 and 9). These results clearly show that the synergistic effect between palladium and ruthenium or cobalt enabled the carbonylation reaction of 4-TolI with CO/HSiEt₃.

These reactions with CO/HSiEt₃ do not require the addition of a base, which is indispensable for the formylation reaction of ArI with CO/H₂ in order to quench the HI formed, and the formation of Et₃SiI was observed in this case. Interestingly, the addition of NEt₃ to the Pd-Co bimetallic system dramatically changed the distribution of the carbonylation products, where **3a** became the major product (57% yield at 70% conversion, entry 10). A similar change was not observed in the Pd-Ru-catalyzed reaction (entry 8). The diastereomer ratio of **3a** was almost 1:1 in every case. It should be pointed out that dimeric 1,2-diol derivatives were first obtained from the catalytic carbonylation of aryl iodides with CO/hydrosilane by using the Pd-Co bimetallic system in the presence of NEt₃.

The Et₃SiI formed in the Pd-Co-catalyzed reaction was determined by GLC analysis after being converted into Et₃SiOEt by treatment with NEt₃/EtOH. It was found that the yield of Et₃SiI was almost equal to that

Table 2. Carbonylation of ArI Catalyzed by PdCl₂(PPh₃)₂ and/or Co₂(CO)₈^a

entry	Ar	cat.	amt of NEt ₃ (mmol)	conv ^b (%)	yield (%) ^b		
					1	2	3
1	4-Tol	Pd		10	3	0	2
2		Co		4	0	0	0
3		Pd-Co		85	0	76	0
4		Pd-Co	3	70	2	6	57
5	Ph	Pd		25	0	0	0
6		Co		3	3	0	0
7		Pd-Co		62	1	61	0
8		Pd-Co	3	67	0	4	52
9	4-CH ₃ OC ₆ H ₄	Pd		13	3	0	0
10		Co		4	0	3	0
11		Pd-Co		83	0	81	0
12		Pd-Co	3	80	0	2	57
13	4-FC ₆ H ₄	Pd		10	7	0	0
14		Co		6	5	0	0
15		Pd-Co		54	1	38	0
16		Pd-Co	3	54	3	0	28

^a Reaction conditions are the same as shown in Table 1 except ArI (2.5 mmol) was used instead of 4-TolI. ^b Determined by GLC analysis.

of **2a** in the reaction without NEt₃, while in the presence of NEt₃ it was about half that of **3a**. On the basis of these observations, the carbonylation reactions are considered to follow eq 2 or 3, depending upon the absence or the presence of NEt₃, respectively.

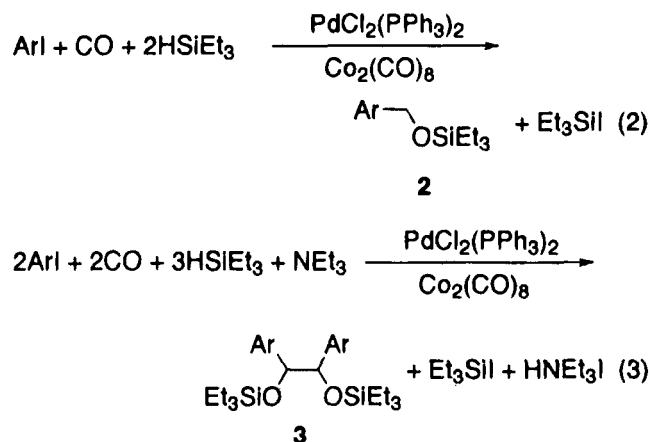


Table 2 summarizes the results of carbonylation reactions of some ArI with CO/HSiEt₃ by using PdCl₂(PPh₃)₂ and/or Co₂(CO)₈ catalysts. Similarly to the reaction of 4-TolI with CO/HSiEt₃, benzyl silyl ether (**2**) or 1,2-diaryl-1,2-disiloxyethane (**3**) was selectively obtained from the carbonylation of ArI, although the reaction rate exhibited a dependency on the Ar group of the substrate.

The carbonylation reaction of ArI with CO/HSiEt₃ by the Pd-Co mixed catalyst is especially interesting in the point that a specific combination of two catalytically ineffective complexes displays a remarkable synergistic effect, and the distribution of the products is completely changed upon the addition of NEt₃. We have therefore investigated the reaction mechanism of this Pd-Co-catalyzed reaction to elucidate the origin of the synergism.

Reaction of Tolualdehyde with Triethylsilane under CO Pressure. Two possible reaction mechanisms may be considered for the above mentioned carbonylation of aryl iodide with CO/HSiEt₃. One includes the formylation of aryl iodide to form the

Table 3. Reaction of 4-TolCHO with HSiEt₃ Catalyzed by Palladium and/or Cobalt under Various Conditions^a

entry	cat.	CO pressure (atm)	amt of NEt ₃ (mmol)	amt of 4-TolI (mmol)	conv ^b (%)	yield (%) ^b	
						2a	3a
1	Pd				2	0	0
2				0.1	98	71	4
3		50			5	0	1
4		50		0.1	30	9	20
5		50	3		5	0	0
6		50	3	0.1	1	0	0
7	Co				100	100	0
8				0.1	100	99	1
9		50			100	21	14
10		50		0.1	100	29	16
11		50	3		5	0	0
12		50	3	0.1	4	0	0
13	Pd-Co	50			7	1	0
14		50		0.1	100	96	3
15 ^c		50			100	88	5
16		50	3		6	0	0
17		50	3	0.1	5	0	0

^a Reaction conditions: 4-TolCHO (2.5 mmol), HSiEt₃ (7.5 mmol), metal complex (0.05 mmol as metal atom), C₆H₆ (5 mL), 80 °C, 3 h. ^b Determined by GLC analysis. ^c Me₃SiI (0.1 mmol).

corresponding aldehyde as the intermediate and the following hydrosilylation or silylation to give the silyl ethers **2** or **3**. In the other mechanism, silyl ethers are directly formed from aryl iodide on organometallic species, not via the free aldehyde. In fact, the hydrosilylation of **1** to give **2** is well-known to be catalyzed by a variety of metal complexes,⁹ while NiCl₂-Et₂S¹⁰ and Co₂(CO)₈¹¹ are effective for the silylation of **1** to form **3**, although the latter reactions require much higher temperatures (120–140 °C) than the present bimetallic carbonylation (80 °C). Therefore, we have examined the reaction of **1a** with HSiEt₃ under the catalytic carbonylation conditions in order to obtain information about the reaction mechanism.

The results are summarized in Table 3. When CO was not pressurized, PdCl₂(PPh₃)₂ was an effective hydrosilylation catalyst for **1a** in the presence of a catalytic amount of 4-TolI (entry 2). However, under CO pressure (50 atm), the activity of palladium was strongly suppressed. Only when the reaction was conducted in the presence of 4-TolI without NEt₃ were **2a** and **3a** obtained in low yields without selectivity (entry 4). As is well-known, Co₂(CO)₈ showed a very high activity for the hydrosilylation of **1a** to give **2a** when CO was not pressurized (entries 7 and 8). Again under CO pressure, the selectivity of the cobalt catalyst was lost (entries 9 and 10). Surprisingly, when the palladium and cobalt catalysts were used together in the presence of tolyl iodide without NEt₃, the hydrosilylation of the aldehyde proceeded smoothly to give **2a** (entry 14). An addition of a catalytic amount of Me₃SiI instead of tolyl iodide was also effective (entry 15). It is of great interest that the use of the mixed-metal catalyst cancels the negative effect of the CO pressure toward the catalysis. A cooperative effect of the two metal species obviously seems to play a critical role in the selective formation of **2a** under CO pressure. As is

seen in entries 14 and 15, this Pd-Co-catalyzed hydrosilylation requires aryl or silyl iodide as a cocatalyst. Because ArI can be easily converted into carbonylation products and Et₃SiI by the reaction of eq 2, the latter might act as the true cocatalyst. However, we must await further investigations to elucidate the role of the iodide cocatalyst and the detailed mechanism of the bimetallic catalysis. On the basis of these observations, it may be concluded that aldehyde **1** is a highly probable intermediate for the catalytic carbonylation of ArI to form **2** (eq 2).

It should also be mentioned that the Pd-Co mixed system was not effective for the hydrosilylation of **1a** in the presence of NEt₃. In this case, the conversion of **1a** was very low regardless of the addition of tolyl iodide and neither **2a** nor **3a** was obtained (entries 16 and 17). This fact clearly indicates that **1** cannot be the intermediate for the carbonylation of ArI to form **3** (eq 3).

Mechanism for the Catalytic Formation of 2 from Aryl Iodides and CO/HSiEt₃. As described above, we suppose that the carbonylation in the absence of NEt₃ (eq 2) proceeds via the aldehyde intermediate. Scheme 1 depicts the proposed total mechanism for this reaction.

ArI is first taken into the catalytic cycle by the oxidative addition to a Pd(0) species, and the following CO insertion leads to the formation of an aroylpalladium complex ArCOPdI(PPh₃)₂.¹² On the other hand, the reaction of Co₂(CO)₈ with HSiEt₃ is supposed to give a hydrosilylcobalt complex H(SiEt₃)Co(CO)₃ as the primary product.¹³ Since neither single-metal catalyst, PdCl₂(PPh₃)₂ nor Co₂(CO)₈, is effective for the carbonylation of ArI with CO/HSiEt₃, the bimetallic reaction between the aroylpalladium and hydridocobalt complexes should be included in the catalysis. As is referred to in the Introduction, we have previously found that the reaction of an aroylpalladium complex with certain hydridometal species yields the corresponding aldehyde, which constitutes the key step in the bimetallic formylation of ArI with CO/H₂.¹ In the present carbonylation with CO/HSiEt₃, a similar dinuclear reductive elimination between the aroylpalladium complex and a hydridocobalt species such as H(SiEt₃)Co(CO)₃ is assumed to produce the aldehyde ArCHO. An equimolar amount of Et₃SiI should also be formed at this stage, and the Pd(0) and Co(0) species are regenerated. Further reaction of the aldehyde and HSiEt₃ by the Pd-Co mixed-metal catalyst selectively produces **2** under the catalytic conditions. It is noteworthy that both the formylation of ArI giving ArCHO and the hydrosilylation of ArCHO forming **2** are catalyzed by the Pd-Co bimetallic catalyst.

When NEt₃ is added to the reaction system, H(SiEt₃)Co(CO)₃ is converted into the carbonylcobaltate anion [Co(CO)₄]⁻.¹³ This prevents the aroylpalladium complex from undergoing the dinuclear reductive elimination with the hydridocobalt; therefore the aldehyde formation is suppressed in the presence of NEt₃. The results shown in Tables 1 and 2 are in agreement with these discussions and the formation of **3** should be attributed to a completely different mechanism.

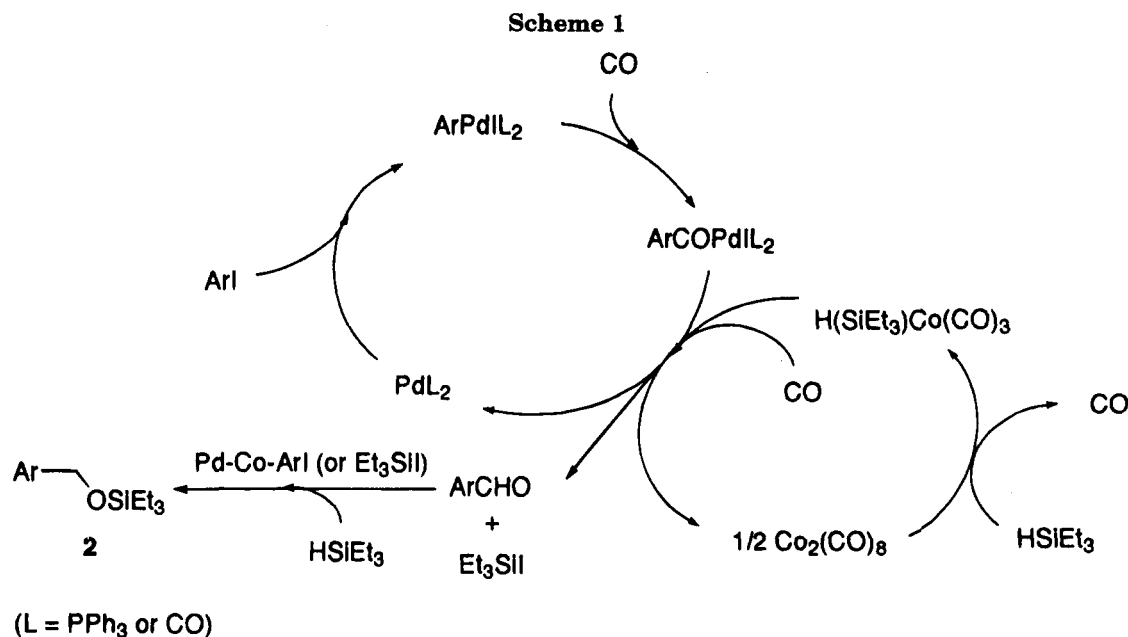
(9) Ojima, I. In *The Chemistry of Organic Silicon Compounds*; Patai, S., Rappoport, Z., Eds.; John Wiley & Sons: Chichester, U.K., 1989; pp 1499–1501.

(10) Frainnet, E.; Bourhis, R.; Simonin, F.; Moulines, F. *J. Organomet. Chem.* **1976**, *105*, 17.

(11) Murai, S. Private communication.

(12) Kudo, K.; Hidai, M.; Uchida, Y. *J. Organomet. Chem.* **1971**, *33*, 393.

(13) Sisak, A.; Ungváry, F.; Markó, L. *Organometallics* **1986**, *5*, 1019.



Hydrosilylation of Arylcobalt Complexes under CO Pressure. Very recently, we have reported that a Pd(0) complex catalyzes the formation of arylcobalt complexes $\text{ArCOC}(\text{CO})_3(\text{PPh}_3)$ from ArI , $[\text{Co}(\text{CO})_4]^-$, and PPh_3 .¹⁴ Because $[\text{Co}(\text{CO})_4]^-$ is generated from $\text{Co}_2(\text{CO})_8$ ¹³ or $\text{Co}_2(\text{CO})_6(\text{PPh}_3)_2$ and a hydrosilane/CO under basic conditions (vide infra), it is reasonable to assume that $\text{ArCOC}(\text{CO})_3(\text{PPh}_3)$ is formed during the bimetallic carbonylation in the presence of NEt_3 (eq 3). Therefore, we have examined the hydrosilylation of the arylcobalt complexes under the catalytic carbonylation conditions.

Some studies were already reported on the reactions of acylmetal complexes with hydrosilanes.¹⁵ Cutler et al. reported that $\text{MeCOC}(\text{CO})_3(\text{PPh}_3)$ reacts with HSiEt_3 smoothly to give EtOSiEt_3 and $\text{Et}_3\text{SiCo}(\text{CO})_3(\text{PPh}_3)$ under a nitrogen atmosphere at room temperature, while the addition of CO or RCHO completely inhibits this reaction.¹⁶ They also reported similar reactions of acylmanganese complexes.¹⁷ However, reactivities of acyl complexes toward HSiR_3 under CO pressure have not been investigated so far, and furthermore the coupling of an acyl ligand leading to the formation of 1,2-disiloxyethanes has never been observed.

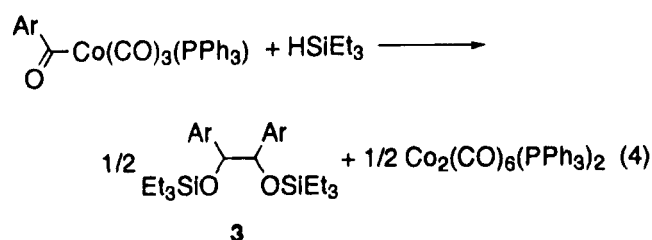
The results of reactions between some arylcobalt complexes and HSiEt_3 are tabulated in Table 4. The arylcobalt complex 4-TolCOC $(\text{CO})_3(\text{PPh}_3)$ reacted with 3 equiv of HSiEt_3 at room temperature under a nitrogen atmosphere to give a mixture of **2a** (44%) and **3a** (18%) (entry 1). The result was different from that of the reaction between $\text{MeCOC}(\text{CO})_3(\text{PPh}_3)$ and HSiEt_3 in that an appreciable amount of **3a** was obtained, although **2a** was still the major product. Under an atmospheric pressure of CO, **1a** was formed in addition to **2a** and **3a**, but the reaction was not selective. In contrast, the reaction under 50 atm of CO did not proceed at room temperature. When the reaction was performed at 80 °C under 50 atm of CO, a dimeric silyl

Table 4. Reactions of $\text{ArCOC}(\text{CO})_{4-n}(\text{PPh}_3)_n$ and HSiEt_3^a

entry	Ar	n	amt of $\text{Co}_2(\text{CO})_8$ (mmol)	amt of NEt_3 (mmol)	CO pressure (atm)	yield (%) ^b		
						1	2	3
1 ^c	4-Tol	1			0	1	44	18
2 ^c		1			1	41	31	21
3		1			50	1	20	68
4		1		3	50	0	1	67
5		1	0.025		50	6	11	71
6		1	0.025	3	50	4	3	76
7 ^d		0		3	50	41	10	2
8	Ph	1		3	50	15	3	60
9	4-MeOC ₆ H ₄	1		3	50	11	9	36
10	4-FC ₆ H ₄	1		3	50	15	4	46

^a Reaction conditions: $\text{ArCOC}(\text{CO})_{4-n}(\text{PPh}_3)_n$ (0.5 mmol), HSiEt_3 (1.5 mmol), C_6H_6 (5 mL, except for entry 7), 80 °C (except for entries 1 and 2), 3 h. ^b Determined by GLC analysis. ^c At room temperature. ^d C_6H_6 (3 mL), hexane (2 mL).

ether **3a** was obtained as the major product (entry 3, eq 4). Addition of NEt_3 further suppressed the formation



of **2a** and the selectivity of **3a** became quite high (entry 4). Use of a catalytic amount of $\text{Co}_2(\text{CO})_8$ was also found effective for inhibiting the formation of **2a** (entries 5 and 6). Similarly, other arylcobalt complexes reacted with HSiEt_3 to form **3** as the major products (entries 8–10). In contrast, the hydrosilylation of 4-TolCOC $(\text{CO})_4$ did not give **3a** selectively (entry 7). From these results, it is clear that $\text{ArCOC}(\text{CO})_3(\text{PPh}_3)$ is a highly probable intermediate for the catalytic formation of **3** in the carbonylation of ArI with CO/ HSiEt_3 in the presence of NEt_3 .

Extensive studies have been done concerning catalyzed¹⁸ and uncatalyzed¹⁷ reactions of acyl complexes with hydrosilanes to give siloxyalkyl complexes. Treatment of silyl complexes with aromatic aldehydes also

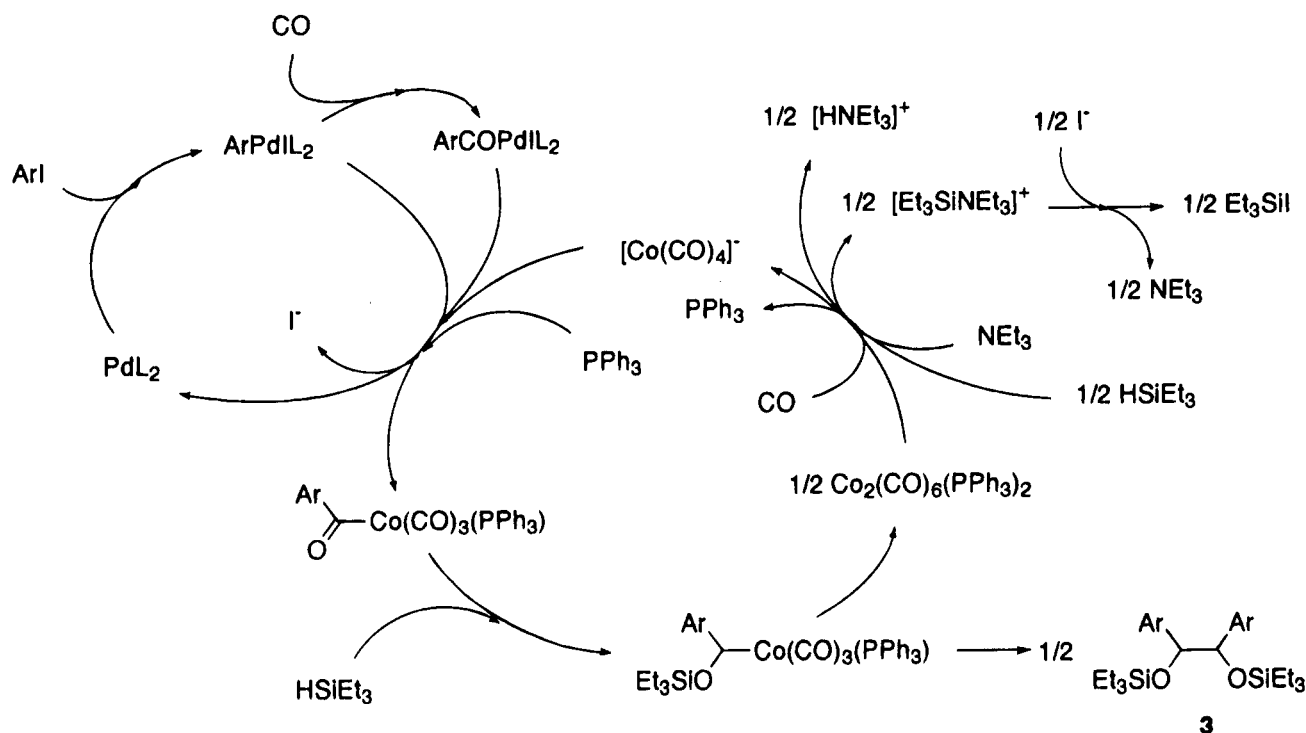
(14) Misumi, Y.; Ishii, Y.; Hidai, M. *Chem. Lett.* **1994**, 695.

(15) (a) Wegmen, R. W. *Organometallics* **1986**, *5*, 707. (b) Kovács, I.; Sisak, A.; Ungváry, F.; Markó, M. *Organometallics* **1988**, *7*, 1025.

(16) Gregg, B. T.; Cutler, A. R. *Organometallics* **1992**, *11*, 4276.

(17) Gregg, B. T.; Hanna, P. K.; Crawford, E. J.; Cutler, A. R. *J. Am. Chem. Soc.* **1991**, *113*, 384.

Scheme 2



(L = PPh₃ or CO)

forms siloxyalkyl complexes such as Mn(CO)₅-(CHPhOSiEt₃), which in turn undergo thermolysis to give 1,2-disiloxyethanes via the homolytic fission of the metal–siloxyalkyl bond followed by radical coupling.¹⁹ Therefore, it may be considered that the reaction of eq 4 proceeds through the formation of the siloxybenzylcobalt complex ArCH(OSiEt₃)Co(CO)₃(PPh₃), the subsequent homolytic fission of the Co–C bond to liberate the siloxybenzyl radical (OSiEt₃)ArCH•, and the coupling of the radical to form **3**. Obviously, the aryl group favors this process by stabilizing the siloxyalkyl radical.

Mechanism for the Catalytic Formation of **3**.

The reaction mechanism for the catalytic formation of **3** is proposed in Scheme 2.

In this mechanism, ArI first reacts with a Pd(0) species through oxidative addition, and the aryl or aroyl group is then transferred from the palladium to the cobalt center by the reaction of ArPdIL₂ or ArCOPdIL₂ (L = PPh₃ or CO) with [Co(CO)₄][−] to give the aroyl complex ArCOC(CO)₃(PPh₃). The anion [Co(CO)₄][−] may be formed by the reaction of Co₂(CO)₈ or Co₂(CO)₆(PPh₃)₂ with HSiEt₃ and NEt₃. It was actually confirmed by the IR spectrum that the reaction of Co₂(CO)₆(PPh₃)₂ with HSiEt₃ and NEt₃ under CO pressure forms [Co(CO)₄][−]. It was also confirmed that anion complex [Co(CO)₃(PPh₃)][−] reacts with 1 atm of CO to form [Co(CO)₄][−]. Hydrosilylation of the aroyl complex gives the siloxybenzyl complex ArCH(OSiEt₃)Co(CO)₃(PPh₃), which leads to the formation of **3** via the coupling of the siloxybenzyl radical formed by the homolytic cleavage of the Co–C bond, concurrent with regeneration of

Co₂(CO)₆(PPh₃)₂. Et₃SiI may be formed from [Et₃SiNEt₃]⁺ and I[−]. This mechanism is in full agreement with the stoichiometry shown in eq 3.

Finally, it should be emphasized that this provides a rare example in which the organic group transfer from one metal center to another has been revealed to function as a key step in the actual homogeneous catalytic reaction. The bimetallic systems seem to have the potential to enable the unique reactions which are inaccessible through single-metal catalysts.

Conclusions

By using a new bimetallic catalyst composed of PdCl₂-(PPh₃)₂ and Co₂(CO)₈, we have developed the novel carbonylation reaction of ArI with CO/HSiEt₃. The reaction products were strongly affected by the addition of NEt₃. In the reaction without NEt₃, we proposed the reaction mechanism including the dinuclear reductive elimination between an aroylpalladium complex and a hydridocobalt species to give aldehyde **1** as an initial product, which is further transformed to **2** by the bimetallic catalyst. In contrast, in the reaction with NEt₃, the aryl or aroyl group transfer from the palladium center to the cobalt has been shown to be an important step, which leads to the formation of **3**. These mechanistic studies, we believe, not only demonstrate new possibilities of bimetallic catalysis but also provide a guiding principle in designing bimetallic catalysts.

Experimental Section

General Procedure. All catalytic reactions including carbonylation of aryl iodides and hydrosilylation of aldehydes were performed in a 50 mL stainless-steel autoclave. Reactions of aroylcobalt complexes and hydrosilanes under 50 atm of CO were also performed by using the same autoclave, while

(18) (a) Hanna, P. K.; Gregg, B. T.; Cutler, A. R. *Organometallics* **1991**, *10*, 31. (b) Crawford, E. J.; Hanna, P. K.; Cutler, A. R. *J. Am. Chem. Soc.* **1989**, *111*, 6891. (c) Akita, M.; Mitani, O.; Moro-oka, Y. *J. Chem. Soc., Chem. Commun.* **1989**, 527.

(19) Gladysz, J. A. *Acc. Chem. Res.* **1984**, *17*, 326.

those under 1 atm of N_2 or CO were carried out in a 20 mL Schlenk tube. Benzene was freshly distilled from sodium benzophenone prior to use. Reagents including NEt_3 , PhI , $EtOH$, $HSiEt_3$, and 4-TolCHO were also dried and distilled prior to use. Complexes $PdCl_2(PPh_3)_2$,²⁰ $ArCOC(CO)_3(PPh_3)$,¹⁴ $Co_2(CO)_8(PPh_3)_2$,²¹ and $Na[Co(CO)_3(PPh_3)]$ ²¹ were prepared according to the literature method. Other organic reagents and metal carbonyls were used as received.

Quantitative GLC analyses were carried out on a Shimadzu GC-14A instrument equipped with a flame ionization detector and a 25 m \times 0.25 mm fused-silica capillary column CBP 1 or CBP 10. 1H and ^{13}C NMR spectra were measured on a JEOL GMN-270 spectrometer. MS and HRMS were recorded on a JEOL JMS-AX505H mass spectrometer. IR spectra were recorded with a Shimadzu FTIR-8100M spectrometer by using a NaCl cell. Elemental analysis was performed with a Perkin-Elmer 2400II CHN Analyzer.

Catalytic Carbonylation of Aryl Iodides with $HSiEt_3$. In a typical run, 4-TolI (0.545 g, 2.5 mmol), $HSiEt_3$ (0.872 g, 7.5 mmol), $PdCl_2(PPh_3)_2$ (0.035 g, 0.05 mmol), $Co_2(CO)_8$ (0.0086 g, 0.025 mmol), and benzene (5 mL) as a solvent were charged in an autoclave under nitrogen. The autoclave was pressurized to 50 atm with CO at room temperature, and heated to 80 °C in an oil bath. The reaction was allowed to proceed at this temperature for 3 h with magnetic stirring. After the reaction, the autoclave was rapidly cooled to room temperature, and the pressure was slowly released. Then NEt_3 (3 mmol) and $EtOH$ (3 mmol) were added with stirring under nitrogen to quench Et_3SiI formed during the carbonylation. Tetradecane (ca. 0.5 g) was added to the reaction mixture as an internal standard, and the liquid phase was analyzed by GLC, which showed that the conversion of 4-TolI and the yields of **2a** and Et_3SiI were 85%, 76%, and 80%, respectively. A similar reaction in the presence of NEt_3 (0.303 g, 3 mmol) afforded a mixture of **1a** (2%), **2a** (6%), **3a** (57%), and Et_3SiI (30%) at 70% conversion of 4-TolI. Compounds **2a-d** and **3a-d** were fully identified by 1H NMR¹⁰ and MS or HRMS after purification by silica-gel column chromatography and bulb-to-bulb distillation. The spectral data for newly synthesized compounds **2d** and **3d** are as follows.

4-FC₆H₄CH₂OSiEt₃ (2d). Colorless oil. 1H NMR ($CDCl_3$): δ 0.64 (q, $J = 7.8$ Hz, 6 H), 0.97 (t, $J = 7.8$ Hz, 9 H), 4.69 (s, 2 H), 7.01 (pseudo-t, $J = 8.8$ Hz, 2 H), 7.29 (dd, $J = 8.3$ and 5.6 Hz, 2 H). ^{13}C NMR ($CDCl_3$): δ 4.5, 6.7, 64.1, 115.0 (d, $^2J_{FC} = 22$ Hz), 127.8 (d, $^3J_{FC} = 7$ Hz), 137.0 (d, $^4J_{FC} = 4$ Hz), 161.9 (d, $^1J_{FC} = 244$ Hz). HRMS calcd for $C_{13}H_{21}OFSi$: 240.1346. Found: 240.1352.

(4-FC₆H₄CHOSiEt₃)₂ (3d). Colorless oil (mixture of diastereomers). 1H NMR ($CDCl_3$): δ 0.20–0.30, 0.45–0.54 (m, 12 H each), 0.68 (t, $J = 7.8$ Hz, 18 H) 0.87 (t, $J = 7.8$ Hz, 18 H), 4.45, 4.71 (s, 2 H each), 6.77–6.99 (m, 12 H), 7.25 (dd, $J = 8.6$ and 5.6 Hz, 4 H). ^{13}C NMR ($CDCl_3$): δ 4.5, 4.8, 6.5, 6.7, 78.2, 79.1, 113.7 (d, $^2J_{FC} = 22$ Hz), 114.2 (d, $^2J_{FC} = 21$ Hz), 128.91 (d, $^3J_{FC} = 7$ Hz), 128.96 (d, $^3J_{FC} = 9$ Hz), 136.6 (d, $^4J_{FC} = 2$ Hz), 138.7 (d, $^4J_{FC} = 4$ Hz), 162.0 (d, $^1J_{FC} = 246$ Hz), 162.2 (d, $^1J_{FC} = 245$ Hz). Anal. Calcd for $C_{26}H_{40}O_2F_2Si_2$: C, 65.23; H, 8.42. Found: C, 65.14; H, 8.59.

(20) Trost, B. M.; Verhoeven, T. R. In *Comprehensive Organometallic Chemistry*; Wilkinson, G., Stone, F. G. A., Abel, E. W., Eds.; Pergamon: Oxford, U.K., 1982; Vol. 8, p 801.

(21) Tso, C. C.; Cutler, A. R. *Polyhedron* **1993**, *12*, 149.

Hydrosilylation of 4-TolCHO under CO Pressure. In a typical run, 4-TolCHO (0.300 g, 2.5 mmol), $HSiEt_3$ (0.872 g, 7.5 mmol), $PdCl_2(PPh_3)_2$ (0.035 g, 0.05 mmol), $Co_2(CO)_8$ (0.0086 g, 0.025 mmol), and benzene (5 mL) as a solvent were charged in an autoclave under nitrogen. The autoclave was immediately pressurized to 50 atm with CO at room temperature and heated to 80 °C in an oil bath. The reaction was allowed to proceed at this temperature for 3 h with magnetic stirring. After the reaction, the autoclave was rapidly cooled to room temperature, and the pressure was slowly released. Tetradecane (ca. 0.5 g) was added to the reaction mixture as an internal standard. The liquid phase was analyzed by GLC, which indicated that all the 4-TolCHO was consumed, and **2a** and **3a** were formed in 96% and 3% yields, respectively.

Hydrosilylation of $ArCOC(CO)_3(PPh_3)$. For entry 1 or 2 in Table 4, $HSiEt_3$ (0.174 g, 1.5 mmol) was added to a benzene solution (5 mL) of 4-TolCOC(CO)₃(PPh₃) (0.262 g, 0.5 mmol) and tetradecane (ca. 0.05 g) as an internal standard, and the resulting mixture was stirred under N_2 or CO, respectively. After 3 h, the liquid phase was analyzed by GLC.

For entries 3–6 and 8–10, $ArCOC(CO)_3(PPh_3)$ (0.262 g, 0.5 mmol), $HSiEt_3$ (0.174 g, 1.5 mmol), and benzene (5 mL) were charged in an autoclave under nitrogen. For entries 5 and 6, $Co_2(CO)_8$ (0.086 g, 0.025 mmol) was charged in addition. For entry 7, 4-TolCOC(CO)₄ in hexane (2 mL) prepared from 4-TolCOCl (0.078 g, 0.5 mmol) and $K[Co(CO)_4]$ (0.5 mmol) in THF (1 mL) and ether (4 mL)²² was charged in an autoclave under nitrogen, and benzene (3 mL), $HSiEt_3$ (0.174 g, 1.5 mmol), and NEt_3 (0.303 g, 3 mmol) were added. The autoclave was pressurized to 50 atm with CO at room temperature, and heated to 80 °C in an oil bath with stirring. After 3 h, the autoclave was cooled and the pressure was released. Then tetradecane (ca. 0.05 g) was added as an internal standard, and the liquid phase was analyzed by GLC. In the case of entry 5 in Table 4, the formation of $Co_2(CO)_6(PPh_3)_2$ (0.101 g, 50%) was confirmed by the IR spectrum (1958 cm^{-1} , $CHCl_3$).²³

Conversion of $Co_2(CO)_6(PPh_3)_2$ into $[Co(CO)_4]^-$. $Co_2(CO)_6(PPh_3)_2$ (0.020 g, 0.025 mmol), $HSiEt_3$ (0.029 g, 0.25 mmol), NEt_3 (0.303 g, 3 mmol), and THF (5 mL) as a solvent were charged in an autoclave under nitrogen. The autoclave was immediately pressurized to 50 atm with CO at room temperature and heated to 80 °C in an oil bath. The reaction was allowed to proceed at this temperature for 3 h with magnetic stirring. After the reaction, the autoclave was rapidly cooled to room temperature, and the pressure was slowly released. The IR spectrum of the resulting mixture showed an absorption at 1887 cm^{-1} which is assignable to $[Co(CO)_4]^-$.

A THF solution of $Na[Co(CO)_3(PPh_3)]$ (0.05 mol dm^{-3}) was allowed to react with 1 atm of CO. In the IR spectrum of the resulting solution, absorptions at 1931, 1856, and 1811 cm^{-1} due to $[Co(CO)_3(PPh_3)]^-$ remarkably decreased and a strong absorption at 1888 cm^{-1} assignable to $[Co(CO)_4]^-$ was observed.

Supplementary Material Available: 1H and ^{13}C NMR spectra for **2d** and **3d** (4 pages). Ordering information is given on any current masthead page.

OM9409074

(22) Heck, R. F.; Breslow, D. *J. Am. Chem. Soc.* **1962**, *84*, 2499.

(23) Manning, A. R. *J. Chem. Soc. A* **1968**, 1135.

Mixed-Valence Biferroceniums: Pronounced Effects of Cation–Anion Interactions on the Intramolecular Electron-Transfer Rate

Teng-Yuan Dong,^{*,1} Chun-Hsun Huang,¹ Chung-Kay Chang,¹
Hsing-Ching Hsieh,¹ Shie-Ming Peng,² and Gene-Hsiang Lee²

Department of Chemistry, National Sun Yat-sen University, Kaohsiung, Taiwan, ROC, and
Department of Chemistry, National Taiwan University, Taipei, Taiwan, ROC

Received November 14, 1994[®]

Relatively minor perturbations caused by the cation–anion interactions in 1',2',3',1''',2''',3'''-hexaethylbiferrocenium triiodide (**1**) and 1',2',4',1''',2''',4'''-hexaethylbiferrocenium triiodide (**2**) have pronounced effects on the electronic structure and the rate of intramolecular electron transfer. The X-ray structure of **1** has been determined at 298 K: $P2_1/c$, $a = 9.433(3)$ Å, $b = 18.597(3)$ Å, $c = 10.425(3)$ Å. $\beta = 110.24(2)^\circ$, $Z = 2$, $D_{\text{calcd}} = 1.779$ g cm⁻³, $R_F = 0.037$, and $R_{wF} = 0.035$. The isomeric **2** crystallizes in the monoclinic space group $P2_1/n$ with two molecules in a unit cell with dimensions $a = 12.214(9)$ Å, $b = 11.516(10)$ Å, $c = 12.222(7)$ Å. $\beta = 103.36(5)^\circ$; $R_F = 0.055$, and $R_{wF} = 0.055$. The neutral compound 1',2',3',1''',2''',3'''-hexaethylbiferrocene crystallizes in the triclinic space group $P\bar{1}$ with one molecule in a unit cell with dimensions $a = 7.999(1)$ Å, $b = 8.981(3)$ Å, $c = 11.222(2)$ Å. $\alpha = 112.08(2)^\circ$, $\beta = 76.47(1)^\circ$, $\gamma = 113.80(2)^\circ$; $R_F = 0.027$, and $R_{wF} = 0.032$. The variable-temperature ⁵⁷Fe Mössbauer data indicate that **1** is delocalized on the Mössbauer time scale in the solid state above 170 K. However, the electron-transfer rate in **2** is localized on the Mössbauer time scale at 300 K (electron-transfer rate $< \sim 10^7$ s⁻¹). We suggest that the difference in rates of electron transfer in **1** and **2** is a result of difference in the cation–anion interactions. A comparison of electron-transfer rates in solid state and solution state is also presented.

Introduction

We undertook the present work in the hope that comparison of molecular structures would improve our understanding of the factors that control the rate of intramolecular electron transfer in the solid state for a series of mixed-valence biferrocenium salts. In the solid state, the rate of electron transfer for a given mixed-valence cation is influenced by various structural factors and lattice dynamics,^{3–7} including the electronic and vibronic coupling between two metal ions,^{8–11} the nature of the counterion,^{12–14} and cation–anion interactions.¹⁵ The work to be reported is a refinement and extension

of our earlier preliminary results^{16,17} on the rates of intramolecular electron transfer in a series of alkyl-substituted biferrocenium salts. To further confirm the correlation of structure and rate of electron transfer, we prepared two new mixed-valence polyethylbiferrocenium triiodides (Chart 1; **1** and **2**).

In our original publication,^{11,18} a significant influence on the electron-transfer rate in mixed-valence biferrocenium salt **3** was observed when the cyclopentadienyl (Cp) rings in the ferrocenyl moieties were linked by an interannular trimethylene bridge. We proposed that such a structural modification would lead to increased metal–ligand interactions as the rings tilt. A recent interesting finding is that there is a correlation between the tilt angle and the rate of electron transfer in the series of biferrocenium salts **5–8** and **16**.^{16,17} We proposed a model to explain the difference in the rates of electron transfer of these mixed-valence cations. We suggested that this is a result of difference in the degree of tilting of the Cp rings from a parallel geometry. However, our present physical measurements for **1** and **2** have stimulated us to extend this model to consider characteristics of the cation–anion interactions. Consideration is taken of how the triiodide counterion can interact with the cation to influence the electronic coupling between the Fe centers. In so doing, our new

[®] Abstract published in *Advance ACS Abstracts*, March 1, 1995.

(1) National Sun Yat-sen University.

(2) National Taiwan University.

(3) Cohn, M. J.; Dong, T.-Y.; Hendrickson, D. N.; Geib, S. J.; Rheingold, A. L. *J. Chem. Soc., Chem. Commun.* **1985**, 1095.

(4) Dong, T.-Y.; Hendrickson, D. N.; Iwai, K.; Cohn, M. J.; Rheingold, A. L.; Sano, H.; Motoyama, S. *J. Am. Chem. Soc.* **1985**, *107*, 7996.

(5) Iijima, S.; Saida, R.; Motoyama, I.; Sano, H. *Bull. Chem. Soc. Jpn.* **1981**, *54*, 1375.

(6) Nakashima, S.; Katada, M.; Motoyama, I.; Sano, H. *Bull. Chem. Soc. Jpn.* **1987**, *60*, 2253.

(7) Kai, M.; Katada, M.; Sano, H. *Chem. Lett.* **1988**, 1523.

(8) Dong, T.-Y.; Lee, T. Y.; Lee, S. H.; Lee, G. H.; Peng, S. M. *Organometallics* **1994**, *13*, 2337.

(9) Dong, T.-Y.; Ke, T. J.; Peng, S. M.; Yeh, S. K. *Inorg. Chem.* **1989**, *28*, 2103.

(10) Dong, T.-Y.; Hwang, M. Y.; Wen, Y. S. *J. Organomet. Chem.* **1990**, *391*, 377.

(11) Dong, T.-Y.; Lee, T. Y.; Lin, H. M. *J. Organomet. Chem.* **1992**, *427*, 101.

(12) Dong, T.-Y.; Schei, C. C.; Hsu, T. L.; Lee, S. L.; Li, S. J. *Inorg. Chem.* **1991**, *30*, 2457.

(13) Webb, R. J.; Geib, S. J.; Staley, D. L.; Rheingold, A. L.; Hendrickson, D. N. *J. Am. Chem. Soc.* **1990**, *112*, 5031.

(14) Dong, T.-Y.; Kambara, T.; Hendrickson, D. N. *J. Am. Chem. Soc.* **1986**, *108*, 5857.

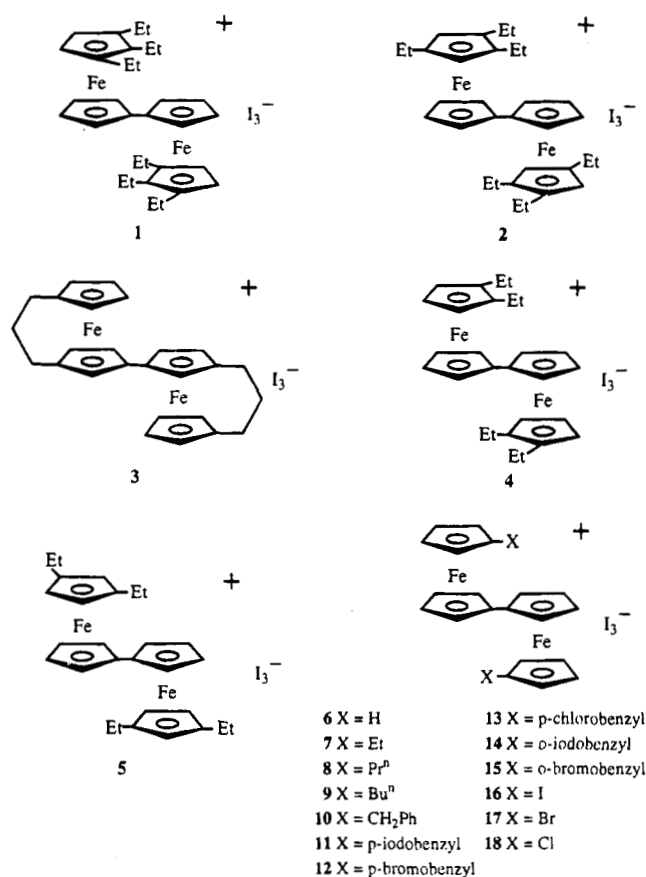
(15) Kambara, T.; Hendrickson, D. N.; Dong, T.-Y.; Cohn, M. J. *J. Chem. Phys.* **1987**, *86*, 2362.

(16) Dong, T.-Y.; Chang, C. K.; Huang, C. H.; Wen, Y. S.; Lee, S. L.; Chen, J. A.; Yeh, W. Y.; Yeh, A. *J. Chem. Soc., Chem. Commun.* **1992**, 526.

(17) Dong, T.-Y.; Huang, C. H.; Chang, C. K.; Wen, Y. S.; Lee, S. L.; Chen, J. A.; Yeh, W. Y.; Yeh, A. *J. Am. Chem. Soc.* **1993**, *115*, 6357.

(18) Dong, T.-Y.; Chou, C. Y. *J. Chem. Soc., Chem. Commun.* **1990**, 1332.

Chart 1



model allows for a more realistic description of the mixed-valence biferrocenium salts 1–18. Our explanation is general and is applicable to other mixed-valence systems. Before the new model is described, the physical properties of 1 and 2 will be presented.

Experimental Section

General Information. The starting materials 1',2'-diethyl-1-bromoferrocene and 1',3'-diethyl-1-bromoferrocene were prepared according to our previous literature procedure.¹⁷ All solvents were dried and distilled under a nitrogen atmosphere. All procedures involving air-sensitive materials were performed under the strict exclusion of air. Chromatography was carried out on neutral alumina (activity II) or silica gel (70–230 mesh).

Acetylation of 1',2'-Diethyl-1-bromoferrocene. The acetylating reagent was prepared according to the Friedel–Crafts synthesis by mixing 0.66 mL (9.7 mmol) of acetyl chloride and excess AlCl₃ in dry CH₂Cl₂ (100 mL) at 0 °C under N₂. The excess of AlCl₃ was filtered off with glass wool.

The acetylating reagent was added by means of a dropping funnel over a period of ~1 h to a solution of 1',2'-diethyl-1-bromoferrocene (2.59 g, 8.1 mmol) in dry CH₂Cl₂ (100 mL) at 0 °C. The mixture was stirred for 4 h at 0 °C and then 1 h at room temperature. The reaction mixture was then poured into an ice–water mixture. The resulting mixture was separated after the reduction of ferrocenium cation with aqueous Na₂S₂O₃. The organic layer was washed with saturated aqueous NaHCO₃ and with water, and then it was dried over MgSO₄. The solvent was removed, and the red oily residue was chromatographed on Al₂O₃. The first band eluted with *n*-hexane–CH₂Cl₂ (7:3) was the starting material. The second band was a mixture of 19 and 20. This mixture could be separated by rechromatographing on silica gel using *n*-hexane–ethyl acetate

(15:1) as the eluent. The first and third bands were 19 (40%) and 20 (15%). The second band was uncharacterized. The physical properties of 19 are as follows. ¹H NMR (CDCl₃, ppm): 1.20 (t, 6H, CH₃), 2.49 (s, 3H, COCH₃), 2.59 (q, 4H, CH₂), 3.96 (t, 2H, Cp), 4.21 (m, 3H, Cp), 4.45 (t, 1H, Cp). Mass spectrum: M⁺ at *m/z* 362.

Reduction of 19. The reduction reaction was carried out by carefully adding, with stirring, small portions of AlCl₃ to a mixture of the ferrocene compound and LiAlH₄ in dry ether. After 30 min, the solution became yellow, an excess of H₂O was added to it, and the ether layer was separated. The ether layer was washed with H₂O and dried over MgSO₄. After the evaporation of the solvent, the crude product was chromatographed on Al₂O₃, eluting with hexane. The first band was the desired compound (21). The yields were ~85%. The physical properties of 21 are as follows. ¹H NMR (CDCl₃, ppm): 1.12 (td, 9H, CH₃), 2.33 (m, 6H, CH₂), 3.85 (t, 2H, Cp), 3.94 (d, 2H, Cp), 4.04 (t, 2H, Cp); mass spectrum: M⁺ at *m/z* 348.

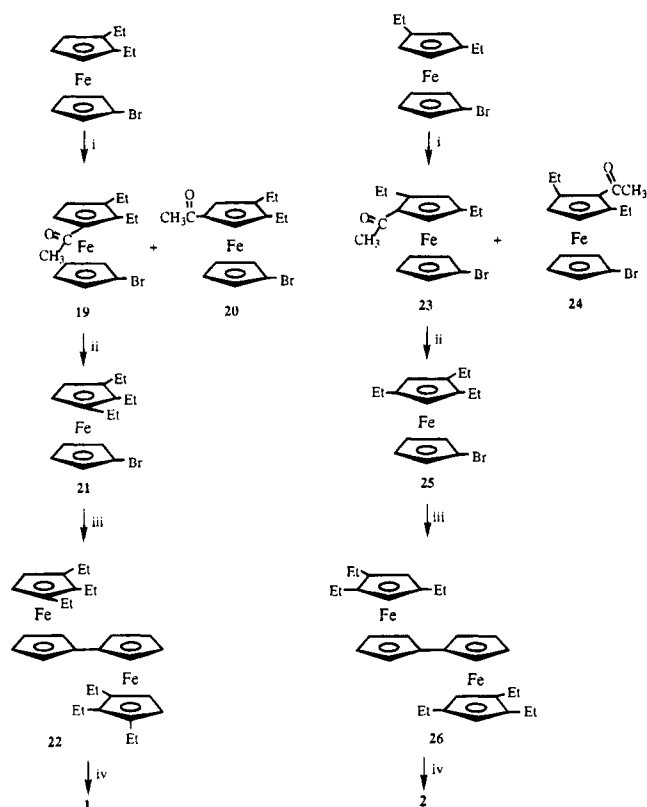
Acetylation of 1',3'-Diethyl-1-bromoferrocene. The Friedel–Crafts reaction of 1',3'-diethyl-1-bromoferrocene was carried out according to the same procedure as the acetylation of 1',2'-diethyl-1-bromoferrocene. The red oily residue was chromatographed on Al₂O₃. The first band eluted with *n*-hexane–CH₂Cl₂ (7:3) was the recovered starting material. The second band was a mixture of 23 and 24. Similarly, this mixture could be separated into three bands by rechromatographing on silica gel using *n*-hexane–ethyl acetate (15:1) as the eluent. The first and third bands were 23 (35%) and 24 (9%), respectively. The second band was uncharacterized. The physical properties of 23 are as follows. ¹H NMR (CDCl₃, ppm): 1.17 (t, 6H, CH₃), 2.37 (s, 3H, COCH₃), 2.61 (m, 4H, CH₂), 3.99 (t, 2H, Cp), 4.03 (t, 2H, Cp), 4.19 (t, 1H, Cp), 4.48 (t, 1H, Cp). Mass spectrum: M⁺ at *m/z* 362.

Reduction of 23. Reduction of 23 with LiAlH₄–AlCl₃ in dry ether was carried out in a manner similar to the reduction of 19. ¹H NMR (CDCl₃, ppm) of 25: 1.27 (t, 9H, CH₃), 2.31 (m, 6H, CH₂), 3.88 (dd, 2H, Cp), 3.94 (d, 2H, Cp), 4.08 (dd, 2H, Cp); mass spectrum: M⁺ at *m/z* 348.

Ullmann Reaction of 21 and 25. Compounds 22 and 26 were prepared by the Ullmann coupling procedure as shown in Scheme 1. A mixture of the corresponding bromoferrocene (1 g) and activated copper (5 g) was heated under N₂ at 110–120 °C for 24 h. After cooling to room temperature, the reaction mixture was repeatedly extracted with CH₂Cl₂ until the CH₂Cl₂ extracts appeared colorless. The extracts were evaporated and chromatographed on neutral Al₂O₃. The first band eluted with hexane yielded starting material. Continued elution with hexane afforded the desired compound. Compounds 22 and 26 were recrystallized from hexane. The yields were ~70%. The physical properties of 22 are as follows: ¹H NMR (CDCl₃, ppm): 1.00 (t, 18H, CH₃), 2.03 (q, 12H, CH₂), 3.74 (s, 4H, Cp), 3.98 (d, 4H, Cp), 4.04 (d, 4H, Cp). mp: 51.5–52.3 °C. Mass spectrum: M⁺ at *m/z* 538. The physical properties of 26 are as follows: ¹H NMR (CDCl₃, ppm): 1.02 (t, 18H, CH₃), 2.08 (q, 12H, CH₂), 3.69 (s, 4H, Cp), 3.93 (d, 4H, Cp), 4.01 (d, 4H, Cp). mp: 40.8–41.5 °C. Mass spectrum: M⁺ at *m/z* 538.

Mixed-Valence Compounds 1 and 2. Crystalline samples of 1 and 2 were prepared by adding a benzene–hexane (1:1) solution containing a stoichiometric amount of iodine to a benzene–hexane (1:1) solution of the corresponding biferrocene at 0 °C. The resulting dark crystals were filtered and washed repeatedly with cold hexane. A more crystalline sample can be prepared by slowly diffusing hexane into a CH₂Cl₂ solution containing the corresponding biferrocenium triiodide salt. Anal. Calcd for 1 (C₃₂H₄₂Fe₂I₃): C, 41.82; H, 4.61. Found: C, 41.47; H, 4.64. Anal. Calcd for 2 (C₃₂H₄₂Fe₂I₃): C, 41.82; H, 4.61. Found: C, 41.55; H, 4.50.

Physical Methods. ⁵⁷Fe Mössbauer measurements were made on a constant-velocity instrument which has been

Scheme 1^a

^a Reagents and conditions: (i) $\text{AcCl}-\text{AlCl}_3$; (ii) $\text{AlCl}_3-\text{LiAlH}_4$; (iii) activated Cu; (iv) I_2 .

previously described.¹⁹ Velocity calibrations were made using a 99.99% pure 10 μm iron foil. Typical line widths for all three pairs of iron lines fell in the range 0.24–0.27 mm s^{-1} . Isomer shifts are reported relative to iron foil at 300 K but are uncorrected for temperature-dependent, second-order Doppler effects. It should be noted that the isomer shifts illustrated in the figures are plotted as experimentally obtained. Tabulated data is provided.

¹H NMR spectra were run on a Bruker AMX500 spectrometer. Mass spectra were obtained with a VG250–70S system. The near-IR spectra were recorded from 2600 to 900 nm in CH_2Cl_2 by using 1.0 cm quartz cells with a Hitachi U-3501 spectrophotometer. The IR spectra were obtained with a Bio-Rad spc3200 spectroscope.

Electrochemical measurements were carried out with a BAS 100B system. Cyclic voltammetry was performed with a stationary glassy carbon working electrode, which was cleaned after each run. These experiments were carried out with 1×10^{-3} M solutions of ferrocene in dry $\text{CH}_2\text{Cl}_2-\text{CH}_3\text{CN}$ (1:1) containing 0.1 M of $(n\text{-C}_4\text{H}_9)_4\text{NPF}_6$ as supporting electrolyte. The potentials quoted in this work are relative to a Ag/AgCl electrode at 25 °C. Under these conditions, ferrocene shows a reversible one-electron oxidation wave ($E_{1/2} = 0.37$ V).

Crystal Structure Determinations. The crystals of **1**, **2**, and **22** were mounted, and data were collected on an Enraf-Nonius CAD4 diffractometer at 298 K. Absorption corrections based on ψ -scans for **1**, **2**, and **22** were applied. The structures were solved by the heavy atom method. Positional and anisotropic thermal parameters for non-hydrogen atoms were refined by the full-matrix least-squares method. H atoms were introduced in calculated positions and refined isotropically. Further details are given in Table 1. Atomic positional parameters for **1** are listed in Table 2, and Table 3 contains

(19) Dong, T.-Y.; Schei, C. C.; Hwang, M. Y.; Lee, T. Y.; Yeh, S. K.; Wen, Y. S. *Organometallics* **1992**, *11*, 573.

Table 1. Experimental and Crystal Data for the X-ray Structures

	1	2	22
formula	$\text{C}_{32}\text{H}_{42}\text{Fe}_2\text{I}_3$	$\text{C}_{32}\text{H}_{42}\text{Fe}_2\text{I}_3$	$\text{C}_{32}\text{H}_{42}\text{Fe}_2$
MW	919.08	919.08	538.38
cryst syst	monoclinic	monoclinic	triclinic
space group	$P2_1/c$	$P2_1/n$	$P\bar{1}$
<i>a</i> , Å	9.433(3)	12.214(9)	7.999(1)
<i>b</i> , Å	18.597(3)	11.516(10)	8.981(3)
<i>c</i> , Å	10.425(3)	12.222(7)	11.222(2)
α , deg			112.08(2)
β , deg	110.24(2)	103.36(5)	76.47(1)
γ , deg			113.80(2)
<i>V</i> , Å ³	1715.9(8)	1672.5(2)	680.4(3)
<i>Z</i>	2	2	1
<i>D</i> _{calcd} , g cm ⁻³	1.779	1.825	1.314
μ , mm ⁻¹	3.54	3.63	1.08
λ , Å	0.709 30	0.709 30	0.709 30
2 θ limits, deg	44.9	44.8	44.8
max, min trans coeff	0.998, 0.895	1.0, 0.716	0.998, 0.852
<i>R</i> _F	0.037	0.055	0.027
<i>R</i> _{wF}	0.035	0.055	0.032

Table 2. Atom Coordinates and Thermal Parameters (Å²) for **1**

	<i>x</i>	<i>y</i>	<i>z</i>	<i>B</i> _{iso} ^a
I1	0.97503(8)	0.88661(4)	0.18346(7)	7.18(4)
I2	1.0	1.0	0.0	5.16(4)
Fe	0.5613(1)	0.03029(6)	0.2862(1)	3.79(6)
C1	0.5123(8)	-0.0196(4)	0.4448(7)	3.2(4)
C2	0.396(1)	-0.0336(5)	0.3178(8)	6.1(5)
C3	0.457(2)	-0.0670(5)	0.234(1)	11(1)
C4	0.611(2)	-0.0773(4)	0.300(1)	10.0(9)
C5	0.651(1)	-0.0451(5)	0.435(1)	6.6(6)
C6	0.7298(8)	0.1029(4)	0.2889(7)	3.6(4)
C7	0.6185(8)	0.1390(3)	0.3301(7)	3.2(4)
C8	0.4746(8)	0.1312(4)	0.2206(7)	3.5(4)
C9	0.5012(9)	0.0921(4)	0.1135(7)	3.9(4)
C10	0.6572(9)	0.0745(4)	0.1568(7)	4.0(4)
C11	0.898(1)	0.0978(5)	0.3679(9)	5.8(5)
C12	0.986(1)	0.1555(6)	0.327(1)	8.0(7)
C13	0.6461(9)	0.1760(4)	0.4636(8)	4.7(5)
C14	0.683(1)	0.2550(5)	0.460(1)	8.4(7)
C15	0.3275(9)	0.1617(5)	0.216(1)	6.0(5)
C16	0.294(1)	0.2346(5)	0.143(1)	9.7(8)

^a *B*_{iso} is the mean of the principal axes of the thermal ellipsoid.

selected bond lengths and angles. Final atomic coordinates for **2** are given in Table 4, with selected bond lengths and angles in Table 3. Final positional and thermal parameters and selected bond lengths and angles for **22** are given in Tables 5 and 3, respectively. Complete tables of interatomic distances and angles and of thermal parameters for these compounds are supplied as supplementary materials.

1',2',3',1''',2''',3''''-Hexaethylbiferrocenium Triiodide (1). A dark needlelike crystal measuring 0.10 × 0.13 × 0.50 mm, grown by layering hexane on a CH_2Cl_2 solution of **1**, was attached to a quartz fiber with hydrocarbon grease. Cell dimensions were obtained from 25 reflections with $2\theta < 27.80^\circ$. The $\theta-2\theta$ scan technique was used to record the intensities for all reflections for which $1^\circ < 2\theta < 44.9^\circ$. Of the 2232 unique reflections, there were 1620 reflections with $F_o > 2.0\sigma(F_o^2)$, where $\sigma(F_o^2)$ values were estimated from counting statistics. These data were used in the final refinement of structural parameters.

1',2',4',1''',2''',4''''-Hexaethylbiferrocenium Triiodide (2). A dark crystal (0.10 × 0.30 × 0.50 mm) was obtained by following the same procedure as described for **1**. Data were collected to a 2θ value of 44.8° . The unit cell dimensions were obtained from 25 reflections with $19.80^\circ < 2\theta < 23.18^\circ$. Of the 2174 unique reflections, there were 1573 reflections with $F_o > 2.0\sigma(F_o^2)$. These data were used in the final refinement of structural parameters.

1',2',3',1''',2''',3''''-Hexaethylbiferrocene (22). An orange

Table 3. Selected Bond Distances (Å) and Bond Angles (deg)

	1	2	22
Bond Distances			
I1-I2	2.9106(9)	2.904(2)	
Fe-C1	2.082(7)	2.09(1)	2.069(3)
Fe-C2	2.075(8)	2.07(1)	2.037(3)
Fe-C3	2.04(1)	2.06(1)	2.024(3)
Fe-C4	2.049(8)	2.03(1)	2.044(3)
Fe-C5	2.046(8)	2.05(1)	2.051(3)
Fe-C6	2.079(7)	2.04(1)	2.051(3)
Fe-C7	2.101(7)	2.05(1)	2.045(3)
Fe-C8	2.067(7)	2.05(2)	2.046(3)
Fe-C9	2.044(7)	2.15(2)	2.032(3)
Fe-C10	2.040(7)	2.06(1)	2.033(3)
C1-C1 ^a	1.45(1)	1.44(2)	1.457(6)
C1-C2	1.42(1)	1.43(2)	1.420(4)
C1-C5	1.42(1)	1.43(2)	1.427(4)
C2-C3	1.35(2)	1.44(2)	1.423(5)
C3-C4	1.39(2)	1.38(2)	1.395(7)
C4-C5	1.46(2)	1.40(2)	1.415(5)
C6-C7	1.43(1)	1.48(2)	1.428(4)
C6-C10	1.41(1)	1.42(2)	1.422(4)
C7-C8	1.45(1)	1.38(3)	1.429(4)
C8-C9	1.42(1)	1.34(3)	1.422(5)
C9-C10	1.42(1)	1.50(2)	1.409(5)
Bond Angles			
I2-I1-I2 ^b	180.0	180.0	
C2-C1-C5	107.8(7)	107(1)	106.9(3)
C1-C2-C3	108.9(1)	108(1)	108.9(3)
C2-C3-C4	110(1)	108(1)	108.9(3)
C3-C4-C5	107.3(8)	110(1)	107.7(3)
C1-C5-C4	105.7(9)	108(1)	108.7(3)
C7-C6-C10	108.0(6)	103(1)	107.2(3)
C6-C7-C8	107.5(6)	105(1)	108.6(3)
C7-C8-C9	107.3(6)	119(2)	106.9(3)
C8-C9-C10	108.2(6)	100(2)	108.9(3)
C6-C10-C9	108.8(6)	113(1)	108.4(3)

^a Symmetry equivalents: 1 - x, -y, 1 - z for **1**; 1 - x, -y, 1 - z for **2**; -x, -y, -z for **22**. ^b Symmetry equivalents: 2 - x, 2 - y, -z for **1**; 2 - x, -y, -z for **2**.

Table 4. Atom Coordinates and Thermal Parameters (Å²) for 2

	x	y	z	B _{iso} ^a
I1	0.8969(1)	0.1202(1)	0.15946(9)	7.70(7)
I2	1.0	0.0	0.0	5.48(7)
Fe	0.6742(2)	0.1087(2)	0.4728(2)	5.7(1)
C1	0.5151(9)	0.035(1)	0.4565(9)	4.6(7)
C2	0.507(1)	0.158(1)	0.446(1)	6.2(8)
C3	0.553(1)	0.192(1)	0.353(1)	6.6(8)
C4	0.590(1)	0.092(1)	0.310(1)	6.4(8)
C5	0.5677(9)	-0.005(1)	0.370(1)	4.9(7)
C6	0.820(1)	0.024(1)	0.543(1)	6.4(8)
C7	0.776(1)	0.087(2)	0.630(1)	8(1)
C8	0.776(1)	0.202(2)	0.599(2)	13(1)
C9	0.811(1)	0.231(2)	0.507(2)	11.9(1)
C10	0.842(1)	0.114(1)	0.472(1)	7.2(9)
C11	0.842(1)	-0.01(2)	0.532(1)	9(1)
C12	0.861(1)	-0.137(1)	0.415(2)	10(1)
C13	0.747(2)	0.034(2)	0.725(2)	14(1)
C14	0.696(2)	0.130(2)	0.799(1)	14(2)
C15	0.814(2)	0.340(2)	0.416(2)	8(2)
C15'	0.827(4)	0.347(3)	0.512(4)	11(3)
C16	0.898(2)	0.385(2)	0.448(2)	18(2)

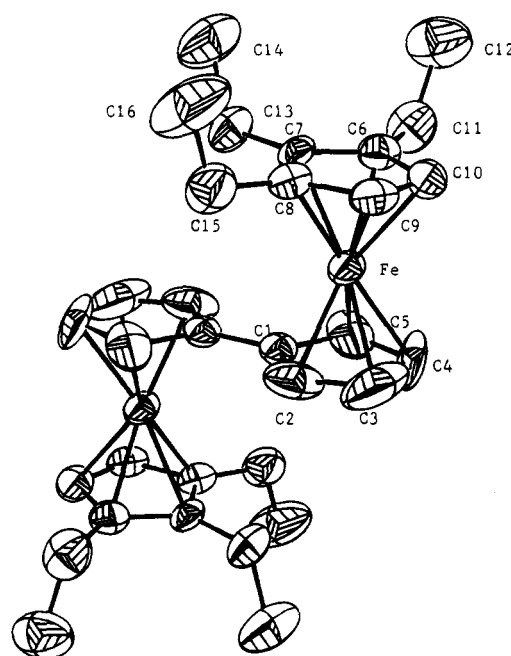
^a B_{iso} is the mean of the principal axes of the thermal ellipsoid.

crystal (0.19 × 0.44 × 0.50 mm), which was grown by slow evaporation from a hexane solution, was used for data collection at 298 K. Cell dimensions were obtained from 20 reflections with 14.70° < 2θ < 32.25°. Data were collected to a 2θ value of 44.8°. The unit cell dimensions were obtained from 25 reflections with 19.80° < 2θ < 23.18°. Of the 1773 unique reflections, there were 1475 reflections with F_o > 2.5 σ (F_o²).

Table 5. Atom Coordinates and Thermal Parameters (Å²) for 22

	x	y	z	B _{iso} ^a
Fe	0.05782(6)	0.11599(5)	0.23969(4)	3.01(2)
C1	-0.0302(4)	-0.0263(4)	0.0578(3)	3.0(1)
C2	0.0498(5)	-0.1109(4)	0.1002(3)	3.9(2)
C3	-0.0529(6)	-0.1383(4)	0.2167(3)	5.1(2)
C4	-0.1932(5)	-0.0715(5)	0.2477(3)	5.3(2)
C5	-0.1801(4)	-0.0011(4)	0.1508(3)	4.1(2)
C6	0.2071(4)	0.3643(4)	0.2433(3)	3.2(2)
C7	0.3247(4)	0.2794(4)	0.2426(3)	3.0(2)
C8	0.2691(4)	0.2225(4)	0.3534(3)	3.4(2)
C9	0.1171(5)	0.2732(4)	0.4216(3)	4.1(2)
C10	0.0785(4)	0.3586(4)	0.3545(3)	3.9(2)
C11	0.2159(5)	0.4489(4)	0.1487(3)	4.5(2)
C12	0.3041(6)	0.6401(5)	0.1969(4)	6.3(3)
C13	0.4823(4)	0.2583(4)	0.1427(3)	4.1(2)
C14	0.6601(5)	0.4106(5)	0.1718(3)	5.2(2)
C15	0.3559(5)	0.1307(4)	0.3932(3)	4.9(2)
C16	0.5128(5)	0.2498(5)	0.4752(4)	5.8(2)

^a B_{iso} is the mean of the principal axes of the thermal ellipsoid.

**Figure 1.** ORTEP drawing of the mixed-valence cation in **1**.

Results and Discussion

Structural Studies. X-ray crystallographic studies were undertaken to help us to elucidate the structures and geometric influences on the rate of intramolecular electron transfer. Figures 1–3 display the ORTEP views of the three molecules. They adopt the usual trans conformation as found for most biferrocenium cations and biferrocenes. Only a few cis conformation biferrocenes are known,²⁰ and in all cases, the molecule is held in a cis conformation by a bridge between the 2,2'' positions of the fulvalenide ligand. The fulvalenide ligand in **1**, **2**, and **22** is planar with a crystallographically imposed 0°.

For **1** and **2**, the average distances from the iron atom to the two Cp rings are 1.672(5) and 1.676(9) Å, respectively. Furthermore, there is no significant difference between Fe–Cp distance and Fe–fulvalenide distance. In the case of **1**, the average Fe–Cp distance

(20) Zhang, W.; Wilson, S. R.; Hendrickson, D. N. *Inorg. Chem.* **1989**, *28*, 4160, and references therein.

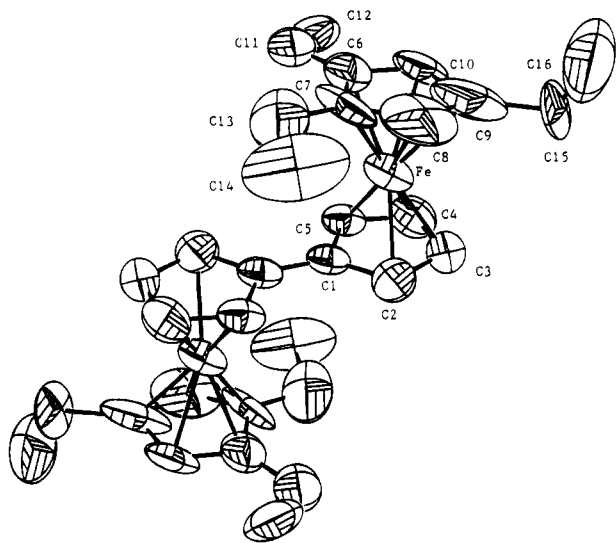


Figure 2. ORTEP drawing of the mixed-valence cation in **2**.

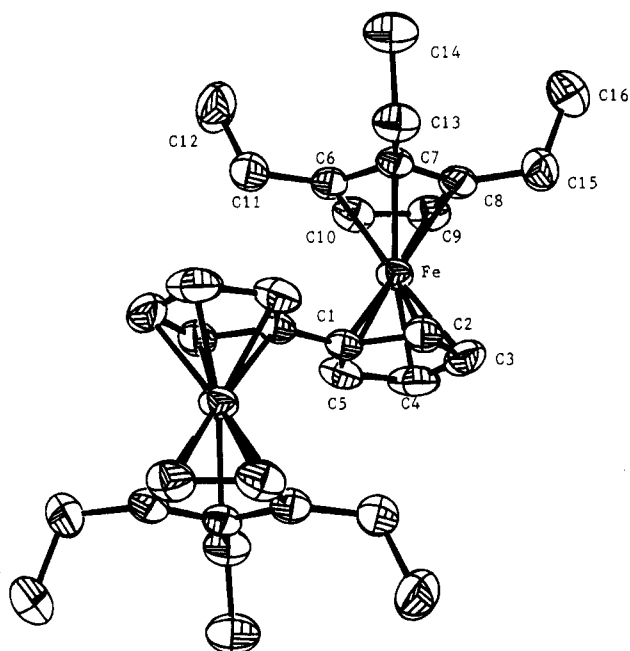


Figure 3. ORTEP drawing of **22**.

(1.672(5) Å) is larger than that for the neutral **22** (1.648(2) Å). Inspection of the Fe–Cp distances in **1** and **2** shows that both distances lie midway between the value of 1.65 Å found²¹ for ferrocene and the value of 1.70 Å found²² for the ferrocenium ion. Mean bond distances from the Fe atom to the rings carbon atoms in **1**, **2**, and **22** are 2.062(8), 2.06(1), and 2.043(3) Å, respectively. Furthermore, the average Fe–C distance in **1** is marginally larger than that in the corresponding neutral biferrocene **22**. The average Fe–C distances in **1** and **2** are very similar, and the values also lie midway between the 2.045 Å observed²¹ for ferrocene and 2.075 Å observed²² for ferrocenium cations. Such an increase in Fe–C and Fe–Cp distances has been observed¹⁹ when ferrocenes are oxidized to the corresponding ferrocenium cations.

The average C–C bond distances in the Cp rings for **1**, **2**, and **22** are 1.42(1), 1.42(1), and 1.419(5) Å, respectively. These values agree well with that in ferrocene (1.42 Å).²¹ The respective dihedral angles between the two least-squares planes of the Cp rings for a given ferrocenyl moiety in **1**, **2**, and **22** are 3.9(4)°, 4.4(7)°, and 1.6(2)°.

The triiodides anions in **1** and **2** are also at the inversion center, showing a symmetric structure. The corresponding I–I bond distances in **1** and **2** are 2.9106(9) and 2.904(2) Å, which are in accord with the accepted value of 2.92 Å reported²³ for the free triiodide ion.

An interesting finding is that the three ethyl substituents on the Cp ring are situated differently. In **1**, the three ethyl substituents are perpendicular to the fulvalenide ligand and this is in contrast to **2**, in which the ethyl substituents stand parallel to the fulvalenide ligand. In both compounds, a three-dimensional hydrogen bonding is clearly found between the Cp hydrogen atoms and the iodine atoms (~3.6 to ~4.1 Å). There is also a hydrogen bond network between ethyl groups and triiodide anions. Consequently, the packing arrangements of the cations and anions in **1** and **2** are different (Figures 4 and 5). In the case of **2**, the packing arrangement can be described as steplike columns. It appears that the parallel ethyl groups on the Cp ring in **2** lead to further slippage of the cations from the steplike stacks seen in **6–10**.^{4,24,25} However, the packing arrangement in **1** cannot be described as layer or column structures found in the series of mixed-valence biferrocenium salts **5–10**, **12**, **14**, and **16**. In both compounds, there is no Cp–Cp overlap between neighboring cations in the solid-state structure. In the case of **8**, the Cp–Cp interplanar distance is ~3.5 Å and an intermolecular π – π interaction is expected between neighboring cations.

The positioning of the triiodide anion relative to the mixed-valence cation in **2** apparently is also unusual. The triiodide moiety in **2** is parallel to the fulvalenide ligand, rather than perpendicular to the fulvalenide ligand as found in **5–9**.^{4,24,25} This type of arrangement is also observed^{19,26} in **10** and **12**. The change of the relative positions of the ethyl substituents from 1',2',4',1''',2''',4''' in **2** to 1',2',3',1''',2''',3''' in **1** leads a dramatic difference in packing arrangement. As shown in Figure 4, **1** is the first mixed-valence biferrocenium salt that contains both parallel and perpendicular fulvalenide–triiodide arrangements.

In our previous papers,^{16,17} we suggested that the degree of tilting of the Cp rings from the parallel geometry plays an important role in determining the rates of electron transfer in the series of mixed-valence biferrocenium salts. However, the deviations of the Cp rings from parallel position were found not to correlate well with the critical temperature for electronic delocalization–localization in the case of mixed-valence biferrocenium salts **1** and **2**. Hence, we suggest that the interactions between cations and anions in **1** and **2**

(23) Runsink, J.; Swen-Walstra, S.; Mighelsen, T. *Acta Crystallogr., Sect. B* **1972**, *28*, 1331.

(24) Konno, M.; Sano, H. *Bull. Chem. Soc. Jpn.* **1988**, *61*, 1455.

(25) Konno, M.; Hyodo, S.; Iijima, S. *Bull. Chem. Soc. Jpn.* **1982**, *55*, 2327.

(26) Webb, R. J.; Dong, T.-Y.; Pierpont, C. G.; Boone, S. R.; Chadha, R. K.; Hendrickson, D. N. *J. Am. Chem. Soc.* **1991**, *113*, 4806.

(21) Seiler, P.; Dunitz, J. D. *Acta Crystallogr., Sect. B* **1979**, *35*, 1068.
(22) Mammano, N. J.; Zalkin, A.; Landers, A.; Rheingold, A. L. *Inorg. Chem.* **1977**, *16*, 297.

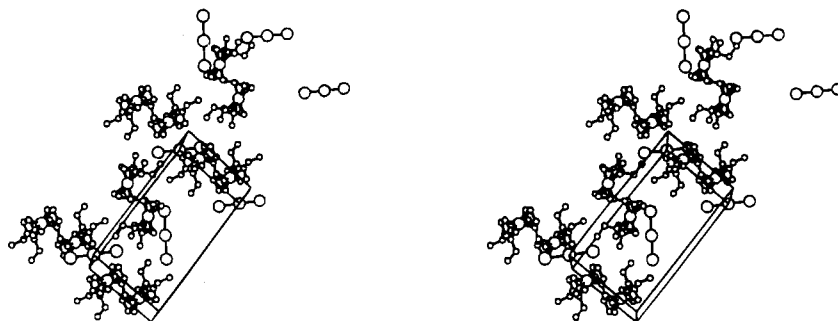


Figure 4. Packing arrangement of 1.

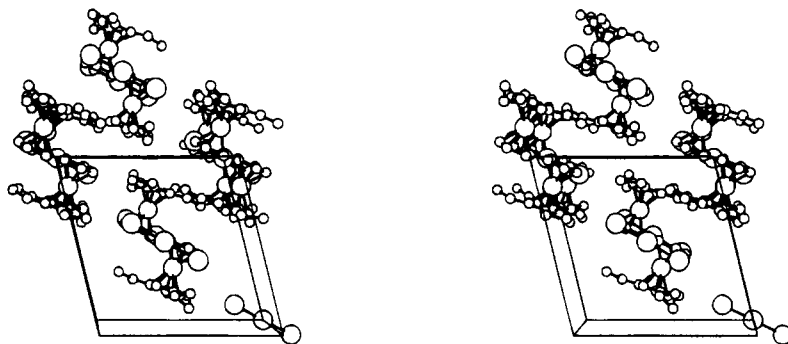


Figure 5. Packing arrangement of 2.

Table 6. Electrochemical Data for Various Biferrocenes

compound	$E_{1/2}^a$ (V)	$\Delta E_{1/2}^b$ (V)	ΔmV^c	I_c/I_a^d	$10^{-5} \times K_{com}$
ferrocene	0.37		70	1.02	
biferrocene	0.28	0.31	70	1.01	1.80
	0.59		75	1.01	
1',1'''-diethylbiferrocene	0.20	0.36	68	1.01	12.6
	0.56		70	1.02	
1',2',1''',2'''-tetraethylbiferrocene	0.16	0.37	70	1.13	18.7
	0.53		71	1.01	
1',3',1''',3'''-tetraethylbiferrocene	0.15	0.37	67	0.97	18.7
	0.52		65	1.02	
22	0.17	0.38	70	1.27	27.6
	0.55		70	1.02	
26	0.15	0.38	74	1.00	27.6
	0.53		63	1.07	

^a All half-wave potentials are referred to the AgCl/Ag electrode. ^b Peak separation between two waves. ^c Peak-to-peak separation between the resolved reduction and oxidation wave maxima. ^d Peak-current ratio between cathode and anode.

can also have a pronounced impact on the rate of intramolecular electron transfer. In other words, the positioning of the triiodide anion relative to the mixed-valence cation plays an important role in determining the rate of electron transfer. We suggest that the hydrogen bond networks between the alkyl substituent and the triiodide anion in the series of mixed-valence biferrocenium salts play a crucial role in controlling the magnitude of cation-anion interactions and the degree of tilting of the Cp rings from parallel geometry. A detailed discussion of the effects of structural characteristics on the rate of intramolecular electron transfer in mixed-valence biferrocenium salt will be presented in the later section.

Electrochemical Results. Electrochemical data for **22** and **26**, as well as those for some other relevant compounds, are shown in Table 6. As shown in Figure 6, the neutral compounds **22** and **26** undergo two successive reversible one-electron oxidations to yield the mono and then the dication. Electrochemical revers-

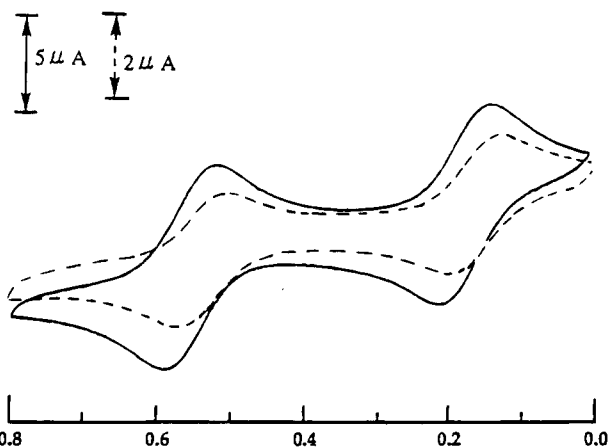


Figure 6. Cyclic voltammograms of **22** (—) and **26** (---); $\nu = 100 \text{ mV s}^{-1}$.

ibility was demonstrated by the peak-to-peak separation between the resolved reduction and oxidation wave maxima.

The effect of ethyl substituents on the stability of the Fe(III) state is illustrated by the shift of half-wave potentials. In a general way, electron-donating groups stabilize the ferrocenium cation, lowering the half-wave potential, and electron-withdrawing groups have the opposite effect. The comparison of the half-wave potentials of ethyl biferrocene with that of biferrocene indicates that the ethyl group clearly acts as a net electron donor. However, it is clear that the electronic effect of the ethyl substituent on half-wave potential is not additive. Hence, an extra ethyl substituent on the Cp ring of **22** and **26** does not lower the half-wave potentials in comparison with 1',2',1''',2'''-tetraethylbiferrocene or 1',3',1''',3'''-tetraethylbiferrocene.

It has been shown that the magnitude of the peak-to-peak separation ($\Delta E_{1/2}$) gives an indication of the interaction through the fulvalenide bridge between the

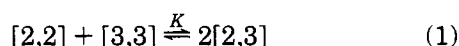
Table 7. Absorption Maximum of IT Band and Activation Parameters

compd	ν_{\max}^a	ϵ_{\max}^b	$\Delta\nu_{1/2(\text{obsd})}^a$	$\Delta\nu_{1/2(\text{calcd})}^a$	α^2	H_{ab}	$10^{-12} \times K_{\text{et}}$
6	4878	958	3384	3357	0.0108	508	1.55
7	5035	1104	2892	3410	0.0103	512	1.29
4	5000	1089	2602	3398	0.0092	480	1.19
5	5120	1163	2483	3439	0.0092	491	1.06
1	5074	1173	2397	3424	0.0090	482	1.09
2	5074	1197	2282	3424	0.0088	475	1.06

^a In cm^{-1} . ^b In $\text{M}^{-1} \text{cm}^{-1}$.

two Fe sites.²⁷ A comparison of the magnitude of $\Delta E_{1/2}$ for various ethyl-substituted biferrocenes indicates that the magnitude of interaction between the two Fe sites in these compounds is similar. However, a comparison of the $\Delta E_{1/2}$ values for ethyl-substituted biferrocenes with that for biferrocene indicates that the interaction between the two Fe sites in ethyl-substituted biferrocene is larger than that in biferrocene.

Coulometry experiments show that each of the two waves is a one-electron-transfer process. In eq 1, the



abbreviation [3,3] denotes the dioxidized cation, [2,3] the monooxidized cation, and [2,2] the neutral compound. Comproportionation equilibrium constants K for various biferrocenes are shown in Table 6. In the studies of electron-transfer rate in the solution state, quantitative calculations based on the concentration of [2,3] have been corrected for this equilibrium.

Electron Transfer in the Solution State. Mixed-valence compounds **1**, **2**, and **4–7** exhibit an IT band at $\sim 5000 \text{ cm}^{-1}$ in the near-IR absorption spectrum. An intervalence transition (IT band) has been defined as metal-to-metal charge transfer. A description of the width of the IT band, the extent of electron delocalization, and the electron-transfer properties of mixed-valence dimers has been given by Hush.²⁸ This work is based on Hush's electron-transfer model. Hush derived an expression for the bandwidth (in cm^{-1}) at half-maximum of the IT band of a localized, homo-nuclear mixed-valence dimer at 300 K as

$$\Delta\nu_{1/2} = [2310\nu_{\max}]^{1/2} \quad (2)$$

where ν_{\max} is the frequency (in cm^{-1}) of the absorption maximum. The absorption maximum of IT bands in the series of mixed-valence biferrocenium and activation parameters calculated were collected in Table 7. An interesting finding is that the IT bands of ethyl-substituted biferrocenium cations are all sharper than what is expected on the basis of eq 2. An agreement, to about $\sim 10\%$, between $\Delta\nu_{1/2(\text{calcd})}$ and $\Delta\nu_{1/2(\text{obsd})}$ is usually taken as an indication that the Hush model is a satisfactory description of a localized mixed-valence system. In the case of **6**, a good agreement is observed. For localized dimers, the IT bands tend to be very broad and symmetrical, whereas the delocalized dimers have narrower profiles that are asymmetric broader on the blue side than on the red side.²⁸ For example, the IT band in the delocalized Creutz–Taube ion is ~ 6 times

sharper than that predicted by eq 2.²⁹ The Hush model is derived for the high-temperature limit, the criterion for that limit being $2RT > h\nu$, where $h\nu$ is the energy associated with a metal–ligand vibrational transition. It is possible that we are not at the high-temperature limit for either a Fe(II)–Cp or a Fe(III)–Cp vibration in ethyl-substituted biferrocenium cation. Owing to the ethyl substituent, the Fe–Cp vibrational energy in **1**, **2**, **4**, **5**, and **7** is higher than that in **6**. Possibly as a consequence of this fact, Hush's correlation of band energy with bandwidth (at room temperature, eq 2) fails.

The extent of electron delocalization for a given mixed-valence biferrocenium cation can be calculated from eq 3. The average value (5.1 Å) of Fe–Fe distances

$$\alpha^2 = \{4.24 \times 10^{-4} \epsilon_{\max}(\Delta\nu_{1/2})\} / \{\nu_{\max} d^2\} \quad (3)$$

in a series of dialkyl mixed-valence biferrocenium cation is used as donor–acceptor distance.^{4,24,30} In this man-

$$H_{\text{ab}} = \nu_{\max} \alpha \quad (4)$$

$$K_{\text{et}} = \nu_{\text{et}} \exp(-\nu_{\max}/4K_{\text{B}}T) \quad (5)$$

$$\nu_{\text{et}} = (2\pi/\hbar)H_{\text{ab}}^2(\pi/K_{\text{B}}T\nu_{\max})^{1/2}$$

ner, the values of α^2 for the series of biferrocenium cations were obtained and collected in Table 7. As shown in Table 7, it can be concluded that these biferrocenium cations are examples of class II mixed-valence compounds.^{31,32}

The magnitude of the electronic coupling can be estimated by using eq 4. Finally, the rate constant (K_{et}) of intramolecular electron transfer can be calculated from eq 5, where ν_{et} is the hopping frequency. From the rate constants illustrated in Table 7, the electron-transfer rates in the series of ethyl-substituted biferrocenium cations are quite similar. This similarity in rate clearly indicates that the extra ethyl substituent in **1**, **2**, **4**, and **5** does not play an important role in determining the rate of electron transfer in solution state. This is in agreement with the electrochemical measurement.

⁵⁷Fe Mössbauer Characteristics. The dependence of sample history in Mössbauer spectra has been noted for a few mixed-valence biferrocenium salts.⁴ To examine this phenomenon more thoroughly, we prepared samples of **1** and **2** by two different methods as described in the Experimental Section. In our case, the samples prepared by two different methods gave essentially identical variable-temperature ⁵⁷Fe Mössbauer spectra. Some of these spectra for mixed-valence **1** are illustrated in Figure 7 and fitting parameters are collected in Table 8. The examination of these spectra shows that in the 77–170 K region **1** is converting from valence trapped to valence detrapped and this process is completed by 170 K. The features in the low-temperature Mössbauer spectrum are two doublets, one for an Fe(III) site and the other for an Fe(II) site. Both

(29) Creutz, C.; Taube, H. *J. Am. Chem. Soc.* **1973**, *95*, 1086.

(30) Webb, R. J.; Rheingold, A. L.; Geib, S. J.; Staley, D. L.; Hendrickson, D. N. *Angew. Chem., Int. Ed. Engl.* **1989**, *28*, 1388.

(31) Brown, D. B., Ed. *Mixed-Valence Compounds, Theory and Applications in Chemistry, Physics, Geology and Biology*; Reidel Publishing Co.: Boston, MA, 1980.

(32) Day, P. *Int. Rev. Phys. Chem.* **1981**, *1*, 149.

(27) Morrison, W. H. Jr.; Krogsrud, S.; Hendrickson, D. N. *Inorg. Chem.* **1973**, *12*, 1998.

(28) Hush, N. S. *Prog. Inorg. Chem.* **1967**, *8*, 391.

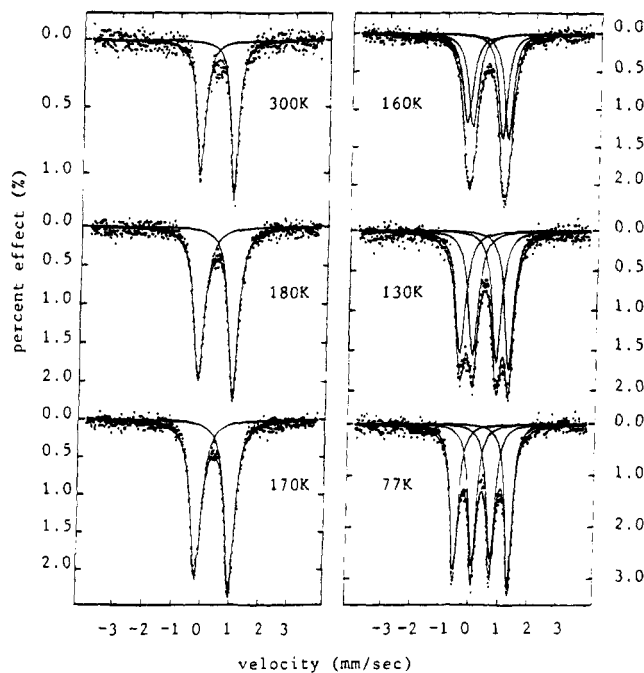


Figure 7. Variable-temperature ^{57}Fe Mössbauer spectra of **1**.

Table 8. ^{57}Fe Mössbauer Least-Squares-Fitting Parameters

compd	T (K)	ΔE_Q^a	δ^b	Γ^c
1	300	1.179	0.441	0.352, 0.297
	180	1.196	0.492	0.442, 0.389
	170	1.179	0.493	0.448, 0.400
	160	1.401	0.506	0.398, 0.351
		1.012	0.500	0.417, 0.349
	130	1.658	0.513	0.400, 0.378
2	300	0.813	0.507	0.406, 0.359
		1.868	0.509	0.339, 0.323
	77	0.627	0.510	0.314, 0.287
		2.039	0.406	0.286, 0.290
		0.522	0.412	0.432, 0.395
		2.031	0.405	0.283, 0.286
	0.521	0.411	0.429, 0.392	

^a Quadrupole splitting (in mm s^{-1}). ^b Isomer shift referred to iron foil (in mm s^{-1}). ^c Full width at half-height taken from the least-squares-fitting program. The width for the line at more positive velocity is listed first for the doublet.

doublets have the same area. This pattern of two doublets is what is expected for a mixed-valence biferrocenium cation that is valence trapped on the Mössbauer time scale ($\sim 10^7 \text{ s}^{-1}$). At temperatures above 170 K, the spectrum of this sample shows a single quadrupole-split doublet which is characteristic of a valence-detraped cation in which the electron-transfer rate exceeds $\sim 10^7 \text{ s}^{-1}$. At 170 K, the valence-detraped doublet has $\Delta E_Q = 1.179 \text{ mm s}^{-1}$. There is one interesting aspects of the temperature dependence of the Mössbauer spectra shown in Figure 7. The two valence-trapped doublets at low-temperature Mössbauer spectrum just move together as the temperature is increased. There is very little line broadening evident in the averaging process. Absence of line broadening in variable-temperature Mössbauer spectra has been noted^{3,4,33} for a few mixed-valence biferrocenium salts. A description of this averaging process will be given in a later section.

(33) Dong, T.-Y.; Cohn, M. J.; Hendrickson, D. N.; Pierpont, C. G. *J. Am. Chem. Soc.* **1985**, *107*, 4777.

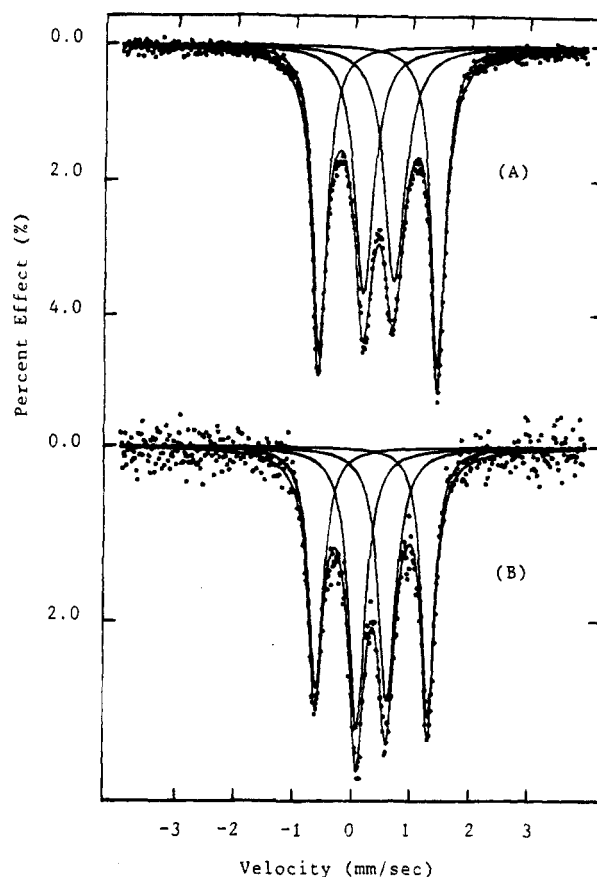


Figure 8. ^{57}Fe Mössbauer spectra of **2** at 300 (A) and 77 K (B).

^{57}Fe Mössbauer spectra were collected at 77 and 300 K for **2**. As shown in Figure 8, this mixed-valence compound shows two doublets in the 300 K Mössbauer spectrum (Fe(II) site, $\Delta E_Q = 2.039 \text{ mm s}^{-1}$; Fe(III) site, $\Delta E_Q = 0.522 \text{ mm s}^{-1}$). This pattern is expected for a mixed-valence cation that is valence trapped on the time scale of the Mössbauer technique (electron-transfer rate $< \sim 10^7 \text{ s}^{-1}$).

The Mössbauer results indicate that the change of the relative positions of the ethyl substituents from 1',2',3',1''',2''',3''' in **1** to 1',2',4',1''',2''',4''' in **2** leads to a reduction in the intramolecular electron-transfer rate. We believe that this difference in rate is not only due to a difference in electronic and steric effects of the ethyl substituents. First, it is clear that the electronic effect of the ethyl substituent is not additive by comparing the transition temperatures of **1**, **2**, **4**,^{16,17} **5**, **6**,^{3,4} and **7**: 170, >300, 195, 125, >300, and 275 K, respectively. In the comparison of the transition temperature of **1** or **2** with **5**, an extra ethyl substituent on the Cp ring of **1** or **2** does not increase the rate of electron transfer. Instead, the rates of electron transfer in **1** and **2** are decreased. Similarly, the electron-transfer rate in **1** is also slower than that in **5**. However, an extra ethyl substituent on the Cp ring of **4** and **5** does increase the rate of electron transfer, as shown by a comparison of the transition temperature of **4** and **5** with **7**. Further evidence can be gleaned from the electrochemical data of neutral ethylbiferrocenes. These compounds show two one-electron oxidation waves (Table 6). It has been shown that the peak-to-peak separation ($\Delta E_{1/2}$) can gauge the interaction between two Fe sites. As shown in Table 6, the magnitudes of the electronic interactions

between the two Fe atoms in ethylbiferrocenes are nearly equivalent.

Second, it is possible that the relative position of ethyl substituents on a given Cp ring plays an interesting role in controlling the rate of electron transfer in the solid state. The rate of electron transfer will be increased if two ethyl substituents are relative in meta position. The Mössbauer results indicate that the electron-transfer rate in 1',3',1''',3''''-tetraethylbiferrocenium triiodide (**5**) is faster than that in 1',2',1''',2''''-tetraethylbiferrocenium triiodide (**4**).^{16,17} Similarly, in **2** there are two pairs of ethyl substituents in the meta position. Consequently, the rate of electron transfer in **2** is faster than that in **1**.

We suggest that the difference in rates of electron transfer in the series of ethylbiferrocenium cations is a result of structural difference in the solid state. We believe that the magnitude of cation-anion interaction and the Cp ring tilting in the ferrocenyl moiety play a crucial role in intramolecular electron transfer in the biferrocenium system. The ethyl substituents on the Cp ring modify the local structure of the biferrocenium cation and lead to a difference of electron-transfer rate. More detailed discussion will be presented in a later section.

IR Spectroscopy. IR spectroscopy has proven to be useful to tell whether a given mixed-valence biferrocenium cation is delocalized or not.^{4,33} When Fe(II) metallocene is oxidized to Fe(III) metallocene, there is a dramatic change in the IR spectrum. It has been shown that the perpendicular C-H bending band is the best diagnosis of the oxidation state. This band is seen at 815 cm⁻¹ for ferrocene and at 851 cm⁻¹ for ferrocenium triiodide. Mixed-valence biferrocenium cations that have a nonegligible potential energy barrier for electron transfer should exhibit one C-H bending mode for the Fe(II) moiety and one for the Fe(III) moiety.

Infrared spectra were run for KBr pellets of **1** and **2**. In **1**, for the perpendicular C-H bending region there are relatively strong bands at 820 and 834 cm⁻¹. Similarly, there are C-H bending bands at 818 and 839 cm⁻¹ for **2**. It is clear that, on the IR time scale, the mixed-valence cations **1** and **2** have both Fe(II) and Fe(III) moieties. In other words, the electron-transfer rates in the cations of **1** and **2** are less than ~10¹² s⁻¹ at 300 K.

Factors in Controlling the Rate of Electron Transfer in the Solid State. The goal of this section is to present an explanation for the differences of electron-transfer rates in the series of mixed-valence biferrocenium cations.

In the last few years there has been considerable progress made in understanding what factors control the rate of intramolecular electron transfer in the solid state for mixed-valence biferrocenium salts.^{4,13-19,34-37} Three different types of temperature dependencies have been observed in a series of various disubstituted biferrocenium triiodide compounds. There are those that are valence trapped at all temperatures, those that

are valence detrapped at all temperatures, and those that are valence trapped at low temperature to valence detrapped at some higher temperatures with no discernible line broadening in the averaging process. If intramolecular electron transfer for a biferrocenium cation were slow on the Mössbauer time scale (rate <~10⁷ s⁻¹) at low temperature and then increased with increasing temperature, the rate should go through the range where coalescence effects would be seen. The line widths of Fe(II) and Fe(III) doublets would be expected to broaden as the electron-transfer rate goes through the ⁵⁷Fe Mössbauer window (~10⁷ s⁻¹). This is not seen for mixed-valence compounds **1** and **2**. Hendrickson suggested^{4,13,15} that what is affecting the Mössbauer spectrum and imparting a temperature dependence is the onset of lattice dynamics (a second-order phase transition). As the temperature of a compound is increased, the thermal energy could achieve the value necessary to trigger off a cooperative change in the crystal lattice. In Hendrickson's theoretical model,¹⁵ the factors that are potentially important in controlling the rate of intramolecular electron transfer in a mixed-valence biferrocenium cation include the effective barrier for charge oscillation in the anion and the intermolecular cation-cation and cation-anion interactions. It is possible that the onset of vibrational motion involving the I₃⁻ counterion controls the rate of electron transfer in mixed-valence biferrocenium triiodide salts. When the I₃⁻ counterion is thermally activated, it interconverts between two configurations, I_a⁻-I_b-I_c and I_a-I_b-I_c⁻. In each of these limiting forms the two iodine-iodine bond lengths are not equal. The oscillatory charge motion associated with it controls whether charge can be pulled back and forth in the mixed-valence cation.

In our previous paper,¹⁷ we found that the deviations of the Cp rings from the parallel position correlate quite well with the Mössbauer critical temperature for electronic delocalization-localization in mixed-valence biferrocenium salts. The Cp tilt angles in each ferrocenyl moiety for **6**, **7**, **5**, and **16** are 0.3, 4.8, 5.9 and 15.6°, respectively. The transition temperatures from localized to delocalized states on the Mössbauer time scale for **6**, **7**, **5**, and **16** are 365, 275, 125, and <4.2 K, respectively. In our previous paper,¹⁷ we also found that the HOMO-LUMO gap in biferrocenium cation decreases as the tilt angle increase. Bending back the Cp rings leads to a larger extent of metal-ligand interactions. We found that the metal nonbonding orbitals (d_{x²-y²}, d_{xy}) start to interact with ligand π orbitals. Here, the question is to have a reasonable explanation for the difference of electron-transfer rates in new mixed-valence compounds **1** and **2**. The tilt angles of the two Cp rings in the ferrocenyl moiety for **1** and **2** are 3.9° and 4.4°, respectively. The respective Mössbauer localized-delocalized transition temperatures for **1** and **2** are 170 and >300 K. Thus, it cannot fit into the correlation of tilt angle with electron-transfer rate. We believe that the cation-anion interaction in **1** and **2** plays a predominant role in determining the electron-transfer rate. We suggest that the deviation of the correlation results from the difference of packing arrangements for triiodide anions. As discussed in the X-ray section, one of the triiodide anions in **1** is perpendicular to the fulvalenide ligand, not parallel to the fulvalenide ligand

(34) Dong, T.-Y.; Hendrickson, D. N.; Pierpont, C. G.; Moore, M. F. *J. Am. Chem. Soc.* **1986**, *108*, 963.

(35) Moore, M. F.; Wilson, S. R.; Cohn, M. J.; Dong, T.-Y.; Mueller-Westerhoff, U. T.; Hendrickson, D. N. *Inorg. Chem.* **1985**, *24*, 4559.

(36) Dong, T.-Y.; Kambara, T.; Hendrickson, D. N. *J. Am. Chem. Soc.* **1986**, *108*, 4423.

(37) Sorai, M.; Nishimori, A.; Hendrickson, D. N.; Dong, T.-Y.; Cohn, M. J. *J. Am. Chem. Soc.* **1987**, *109*, 4266.

as found in **2**. In other words, the charge oscillation of the I_3^- anion in **1** is parallel to the electron-transfer pathway and this leads to a stronger ability to pull the charge back and forth in the mixed-valence cation. Furthermore, the impact of relative cation–anion position on the electron-transfer rate can be also applied to the case of **12** and **14** reported in our previous paper.¹⁹ The I_3^- moiety in **12** is parallel to the fulvalenide ligand rather than perpendicular to the fulvalenide ligand as found in **14**. Thus, **14** has a faster electron-transfer rate than **12**. The critical transition temperatures of **12** and **14** in variable-temperature Mössbauer studies are 200 and <77 K, respectively.

Comparison of Electron-Transfer Rate in Solid and Solution States. Mössbauer spectra indicating the presence of localized electronic structure at 300 K have been observed for **2** in the solid state. In the studies of variable-temperature Mössbauer technique, **1** converts from valence trapped to valence detrapped and this process is completed by 170 K. The energy and the line shape of the IT band clearly indicate that the intramolecular electron-transfer rates in **1** and **2** in solution are greater than in the solid state. In the solid state, the rate of electron transfer for a given mixed-valence cation is influenced by various structural factors

and lattice dynamics, including the electronic and vibronic couplings between two metal ions, the nature of the counterion, and cation–anion interactions. In general, the electron-transfer rate for a given mixed-valence biferrocenium cation in the solution state is greater than that in the solid state. In the solid state, we have demonstrated that relatively minor perturbations caused by interactions between neighboring cations and anions have pronounced effects on electron transfer. In solution, the manner in which the mixed-valence cation is solvated also influences the rate of intramolecular electron transfer. If ion pairing is present, the anion must move rapidly so as not to limit the rate of intramolecular electron transfer.

Acknowledgment. Our work was generously supported by the National Science Council (NSC84-2113-M-110-015) and National Sun Yat-sen University. We gratefully acknowledge this support.

Supplementary Material Available: Complete tables of positional parameters, bond lengths and angles, and thermal parameters for **1**, **2**, and **22** (23 pages). Ordering information is given on any current masthead page.

OM940860M

An Unprecedented Bending of a Bridging Diynyl Ligand in an Unsymmetrical Binuclear Rhodium(I) Complex

Helmut Werner,* Olaf Gevert, Paul Steinert, and Justin Wolf

Institut für Anorganische Chemie der Universität Würzburg, Am Hubland,
D-97074 Würzburg, Germany

Received November 8, 1994[®]

The reaction of $[\text{Rh}(\eta^2\text{-O}_2\text{CCH}_3)(\text{PiPr}_3)_2]$ (**2**) with 2 equiv of phenylbutadiyne leads, in the presence of Na_2CO_3 , to the formation of the five-coordinate bis(diynyl)hydridorhodium(III) complex $[\text{RhH}(\text{C}\equiv\text{CC}\equiv\text{CPh})_2(\text{PiPr}_3)_2]$ (**3**). While **3** reacts with pyridine to give the stable octahedral compound $[\text{RhH}(\text{C}\equiv\text{CC}\equiv\text{CPh})_2(\text{py})(\text{PiPr}_3)_2]$ (**4**), on treatment with carbon monoxide the square-planar complex *trans*- $[\text{Rh}(\text{C}\equiv\text{CC}\equiv\text{CPh})(\text{CO})(\text{PiPr}_3)_2]$ (**6**) is formed via the spectroscopically characterized 1:1 adduct **5** as a labile intermediate. Compound **6**, which has also been prepared from $[\text{Rh}(\eta^3\text{-CH}_2\text{C}_6\text{H}_5)(\text{PiPr}_3)_2]$ (**7**), CO, and phenylbutadiyne, reacts with $[\text{RhCl}(\text{PiPr}_3)_2]_n$ (**1**) to yield the binuclear complex $[\text{Rh}(\text{CO})(\text{PiPr}_3)_2(\eta^1, \eta^2\text{-C}\equiv\text{CC}\equiv\text{CPh})\text{-RhCl}(\text{PiPr}_3)_2]$ (**8**). The X-ray structural analysis of **8** (triclinic space group $P\bar{1}$ (No. 2) with $a = 12.460(2)$ Å, $b = 13.954(2)$ Å, $c = 16.431(2)$ Å, $\alpha = 97.98(1)^\circ$, $\beta = 91.47(1)^\circ$, $\gamma = 109.61(1)^\circ$, $V = 2657(1)$ Å³, and $Z = 2$) reveals a square-planar coordination around each of the metal centers which are bridged by a strongly bent diynyl ligand. The reaction of **1** with phenylbutadiyne leads, via the isomeric diyne and diynyl hydrido species **9** and **10** as intermediates, to the alkynyl-substituted vinylidenerhodium(I) complex *trans*- $[\text{RhCl}(\text{=C}=\text{CHC}\equiv\text{CPh})(\text{PiPr}_3)_2]$ (**11**). In the presence of pyridine the diynyl(hydrido)rhodium derivative $[\text{RhH}(\text{C}\equiv\text{CC}\equiv\text{CPh})\text{Cl}(\text{py})(\text{PiPr}_3)_2]$ (**12**) is obtained.

Introduction

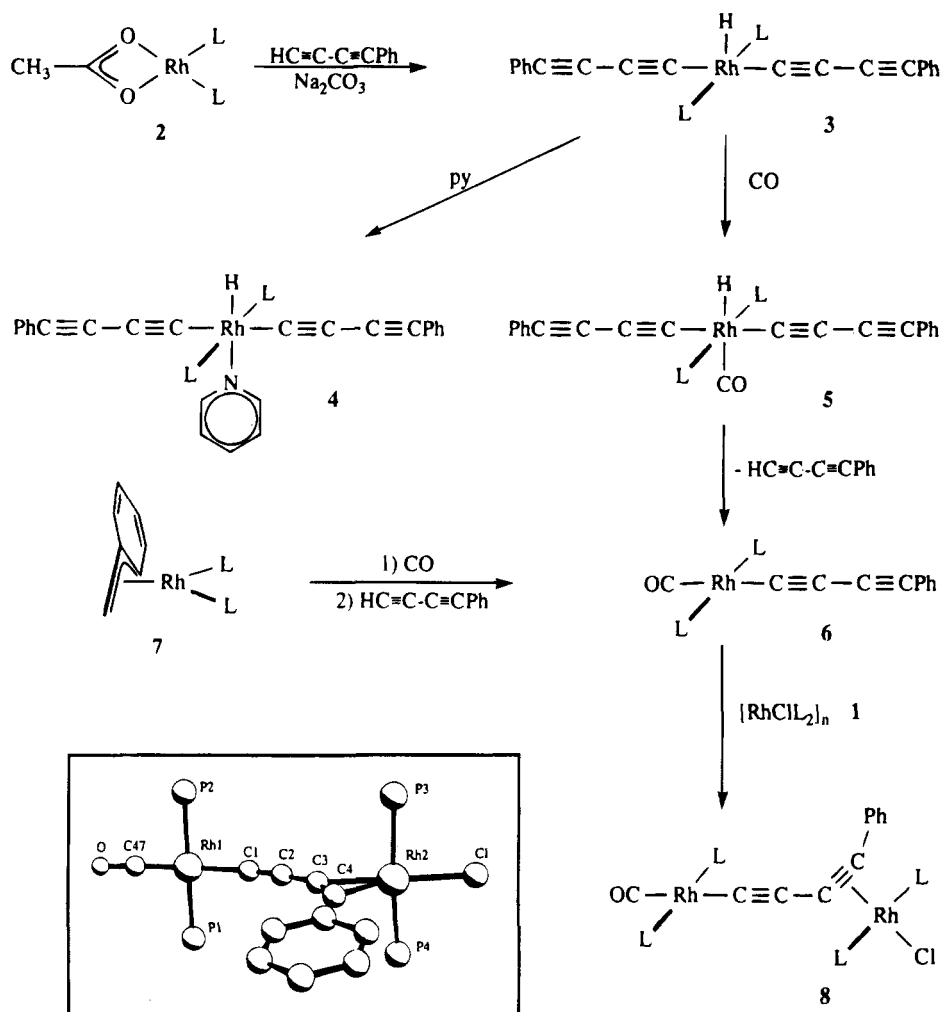
We have recently shown that the displacement of the chloro ligand in $[\text{RhCl}(\text{PiPr}_3)_2]_n$ (**1**) by acetate alters the course of the reaction of the corresponding rhodium(I) complex $[\text{Rh}(\eta^2\text{-O}_2\text{CCH}_3)(\text{PiPr}_3)_2]$ (**2**) with phenylacetylene quite significantly. While compound **1** reacts with $\text{HC}\equiv\text{CPh}$ to give the square-planar vinylidene complex *trans*- $[\text{RhCl}(\text{=C}=\text{CHPh})(\text{PiPr}_3)_2]$,¹ the octahedral alkynyl(hydrido)rhodium(III) species $[\text{RhH}(\text{C}\equiv\text{CPh})(\eta^2\text{-O}_2\text{CCH}_3)(\text{PiPr}_3)_2]$ is initially formed on treatment of **2** with the same 1-alkyne.² In the presence of base, this further reacts with a second molecule of $\text{HC}\equiv\text{CPh}$ to give *trans*- $[\text{Rh}(\text{C}\equiv\text{CPh})(\text{=C}=\text{CHPh})(\text{PiPr}_3)_2]$.² Following the observation that $\text{HC}\equiv\text{CC}\equiv\text{CH}$ as the most simple diyne behaves similarly as $\text{HC}\equiv\text{CH}$ and $\text{HC}\equiv\text{CPh}$ toward the chloro compound **1**,³ we were interested to find out whether butadiyne or derivatives thereof would react with the acetato derivative **2** to afford preferentially either an alkynyl-substituted vinylidenerhodium(I) or a diynyl(hydrido)rhodium(III) complex. During these investigations on the reactivity of compounds **1** and **2** toward $\text{HC}\equiv\text{CC}\equiv\text{CPh}$ a four-coordinate carbonyl(diynyl)rhodium(I) complex has been prepared which on subsequent treatment with **1** yields an unsymmetrical binuclear product containing a strongly bent σ, π -bonded diynyl ligand in a bridging position.

Results and Discussion

Reaction of the Acetato Complex 2 with $\text{HC}\equiv\text{CC}\equiv\text{CPh}$. In contrast to 1,4- $\text{C}_6\text{H}_4(\text{C}\equiv\text{CH})_2$ which has already been used by us⁴ as well as by Marder et al.⁵ to prepare bi- and polynuclear diynylrhodium complexes, the more simple butadiyne $\text{HC}\equiv\text{CC}\equiv\text{CH}$ is difficult to handle due to its high tendency for polymerization and its explosive behavior in the presence of air. Although we have previously used butadiyne,³ we decided for good reasons to employ the phenyl derivative for our studies with the acetato compound **2**. Phenylbutadiyne is obtained from the alkynol $\text{PhC}\equiv\text{CC}\equiv\text{CMe}_2\text{OH}$ on heating with a catalytic amount of solid KOH to 70 °C and, after distillation into a cold trap (-190 °C), is used as a diluted solution in pentane.⁶ This solution reacts with a mixture of **2** and Na_2CO_3 which is suspended in diethyl ether almost instantaneously to give the bis(diynyl) hydrido complex **3** in ca. 60% yield. The orange-brown microcrystalline solid is soluble in most common organic solvents, excluding pentane and hexane, and in the solid form only slightly air-sensitive. The structural proposal shown in Scheme 1 is mainly supported by the ³¹P NMR spectrum which displays only one doublet for the two equivalent phosphine ligands and by the chemical shift of the hydride signal in the ¹H NMR spectrum (δ -28.75) which is similar to that of the crystallographically characterized bis(alkynyl)hydridorhodium(III) derivative $[\text{RhH}(\text{C}\equiv\text{CCiPr}_2\text{OH})_2(\text{PiPr}_3)_2]$.⁷ With regard to the course of the reaction of **2** with $\text{HC}\equiv\text{CC}\equiv\text{CPh}$ and Na_2CO_3 , in

[®] Abstract published in *Advance ACS Abstracts*, March 15, 1995.
(1) (a) Garcia Alonso, F. J.; Höhn, A.; Wolf, J.; Otto, H.; Werner, H. *Angew. Chem.* **1985**, *97*, 401-402; *Angew. Chem., Int. Ed. Engl.* **1985**, *24*, 406-407. (b) Werner, H.; Garcia, Alonso, F. J.; Otto, H.; Wolf, J. *Z. Naturforsch.* **1988**, *43B*, 722-726.
(2) Schäfer, M.; Wolf, J.; Werner, H. *J. Organomet. Chem.* **1995**, *485*, 85-100.
(3) Rappert, T.; Nürnberg, O.; Werner, H. *Organometallics* **1993**, *12*, 1359-1364.

(4) (a) Werner, H.; Rappert, T.; Wolf, J. *Isr. J. Chem.* **1990**, *30*, 377-384. (b) Rappert, T. Dissertation, Universität Würzburg, 1992.
(5) Fyfe, H. B.; Mlekuz, M.; Zargarian, D.; Taylor, N. J.; Marder, T. B. *J. Chem. Soc., Chem. Commun.* **1991**, 188-189.
(6) Brandsma, L. *Preparative Acetylenic Chemistry*; Elsevier: Amsterdam, 1988; pp 212-214 and 290.

Scheme 1^a

^a L = $\text{P}i\text{Pr}_3$.

agreement with previous findings,^{1,2,7,8} we note that the thermodynamic stability of the $[\text{L}_n\text{RhH}(\text{C}\equiv\text{CR})]$ and $[\text{L}_n\text{Rh}(\text{C}\equiv\text{CHR})]$ isomers significantly depends both on the substituent R of the alkyne (or diyne) and the remaining ligands L with the possible trend that complexes $\text{RhH}(\text{C}\equiv\text{CR})_2$ less easily rearrange to rhodium vinylidenes than $\text{RhH}(\text{C}\equiv\text{CR})$ species.

Although compound **3** slowly decomposes in solution, it readily reacts with pyridine and carbon monoxide in pentane at -20°C to give the corresponding 1:1 adducts **4** and **5**, respectively. While the pyridine complex **4** is remarkably stable and only moderately soluble in benzene, the carbonyl compound **5** is rather labile and on warming in pentane to room temperature eliminates phenylbutadiyne to yield the square-planar diynylrhodium(I) complex **6**. The most characteristic features for the octahedral intermediate **5** are the doublet in the ^{31}P NMR spectrum at δ 56.87 and the resonance for the Rh-H proton in the ^1H NMR spectrum at δ -8.72 which is shifted by 20 ppm to lower field compared with **3**.

The rhodium(I) compound **6** which is a light-yellow solid resembles in most of its properties the analogous alkynyl(carbonyl)metal derivatives *trans*- $[\text{Rh}(\text{C}\equiv\text{CR})-$

$(\text{CO})(\text{P}i\text{Pr}_3)_2]$ (R = Me, Ph).⁸ It can also be prepared in more than 80% yield if a solution of the π -benzyl complex **7**⁹ in pentane at -20°C is first treated with carbon monoxide and then, upon cooling to -78°C , with 1 equiv of phenylbutadiyne. Since after CO is passed through the solution of **7** a rapid change of color from red to light-yellow occurs, we assume that initially a σ -benzyl species $[\text{Rh}(\text{CH}_2\text{C}_6\text{H}_5)(\text{CO})(\text{P}i\text{Pr}_3)_2]$ is formed⁹ which reacts with $\text{HC}\equiv\text{CC}\equiv\text{CPh}$ by protolytic cleavage of the Rh- $\text{CH}_2\text{C}_6\text{H}_5$ bond to give the final product. The diynyl complex **6** has been characterized by elemental analysis and IR as well as NMR spectroscopy. While the ^{31}P NMR spectrum shows the expected single resonance (doublet with a larger Rh-P coupling than found for **3** and **5**), the ^{13}C NMR spectrum displays four signals for the carbon atoms of the Rh-C \equiv CC \equiv C chain at δ 126.33, 102.22, 79.15, and 71.95 which due to the decreasing P-C coupling constant along this sequence are supposedly assigned to C1-C4. Since in the ^1H NMR spectrum of **6** only one doublet of virtual triplets¹⁰ for the PCHCH_3 protons appears, there is no doubt that the phosphine ligands are in *trans* disposition.

In order to find out whether in contrast to *trans*- $[\text{RhCl}(\text{C}\equiv\text{C}(\text{R})\text{C}\equiv\text{CSiMe}_3)(\text{P}i\text{Pr}_3)_2]$ (R = H, SiMe_3)³ the

(7) Wiedemann, R.; Mahr, N.; Steinert, P.; Werner, H. Unpublished results. See: Wiedemann, R. Diploma Thesis, Universität Würzburg, 1991.

(8) Schäfer, M. Dissertation, Universität Würzburg, 1994.

(9) Werner, H.; Schäfer, M.; Nürnberg, O.; Wolf, J. *Chem. Ber.* **1994**, *127*, 27-38.

(10) Harris, R. K. *Canad. J. Chem.* **1964**, *42*, 2275-2281.

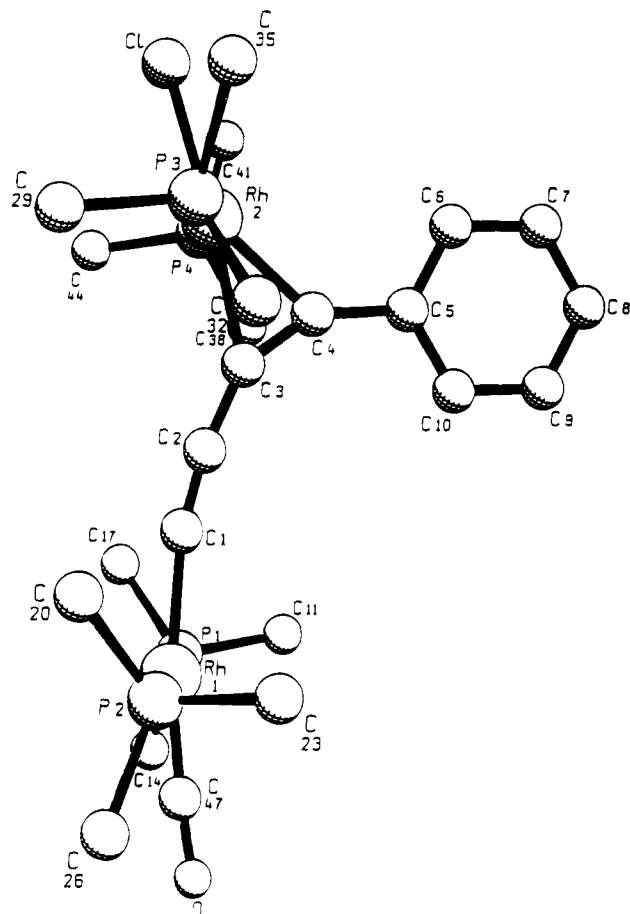


Figure 1. Molecular structure of **8** viewed perpendicular to the Rh–P axes. (The CH₃ carbon atoms of the isopropyl groups are omitted for clarity.)

outer C≡C bond in **6** can be used for π -coordination, the carbonyl diyne complex was treated with **1**. Both compounds react with each other in diethyl ether at 0 °C to give a yellow microcrystalline solid in nearly quantitative yield. The ¹H, ¹³C, and ³¹P NMR spectra of product **8** (Scheme 1) confirm that two different [Rh-(*PiPr*₃)₂] units are present which together with the data of the elemental analysis indicate that an unsymmetrical binuclear rhodium complex is formed. This has been substantiated by an X-ray crystal structure analysis. The SCHAKAL drawing in Figure 1 reveals that the butadiynyl ligand is σ -bonded to a [Rh(CO)(*PiPr*₃)₂] and π -bonded to a [RhCl(*PiPr*₃)₂] fragment, both of which contain *trans*-disposed phosphine ligands. The most remarkable feature, however, is the crescent-shaped structure of the Rh–C≡CC≡C–C(Ph) chain which leads to an angle between the Rh–C1 and C4–C5 axes of about 95°. Whereas the deviation of the bond angles Rh–C1–C2 (167.9(3)°) and C1–C2–C3 (171.9(4)°) from the 180° value is only modest, the rehybridization of the carbon atoms C3 and C4 results in a bending of the C2–C3–C4 and C3–C4–C5 axes (149.5(4) and 147.5(4)°, respectively) which is similar to that found in the chelate nickel complex [Ni(η^2 -HC≡CC≡CH)(*iPr*₂PCH₂CH₂CH₂PiPr₂)] (146.2(6)°).¹¹ For other substituted

Table 1. Selected Bond Distances and Angles with Esd's for Compound **8**

Bond Distances (Å)			
Rh1–P1	2.316(1)	Rh2–Cl	2.369(1)
Rh1–P2	2.314(1)	Rh2–C3	2.154(4)
Rh1–C1	2.061(4)	Rh2–C4	2.041(4)
Rh1–C47	1.884(5)	C1–C2	1.213(5)
C47–O	1.133(5)	C2–C3	1.393(6)
Rh2–P3	2.350(1)	C3–C4	1.271(5)
Rh2–P4	2.354(1)	C4–C5	1.440(5)
Bond Angles (deg)			
P1–Rh1–P2	178.22(4)	P3–Rh2–Cl	88.35(4)
P1–Rh1–C1	90.1(1)	P3–Rh2–C3	91.3(1)
P1–Rh1–C47	90.4(1)	P3–Rh2–C4	95.2(1)
P2–Rh1–C1	90.3(1)	P4–Rh2–C1	87.49(4)
P2–Rh1–C47	89.5(1)	P4–Rh2–C3	92.0(1)
Rh1–C47–O	176.0(5)	P4–Rh2–C4	93.3(1)
Rh1–C1–C2	167.9(3)	Cl–Rh2–C3	175.2(1)
C1–Rh1–C47	171.4(2)	Cl–Rh2–C4	149.6(1)
C1–C2–C3	171.9(4)	Rh2–C3–C2	142.9(3)
C2–C3–C4	149.5(4)	Rh2–C3–C4	67.6(2)
C3–C4–C5	147.5(4)	Rh2–C4–C3	77.3(2)
C4–C5–C6	121.7(4)	Rh2–C4–C5	134.9(3)
C4–C5–C10	119.4(4)	C3–Rh2–C4	35.2(1)
P3–Rh2–P4	169.51(4)		

butadiyne metal compounds a smaller bending of the C–C–C angle (156(2) and 158.5(5)°) has been observed.^{3,12}

The rhodium, the four carbon atoms of the diyne chain, and the *ipso*-carbon atom of the phenyl group lie exactly in the same plane which is almost perpendicular to the planes containing the metal centers, the phosphorus atoms, and the Cl or CO ligands. The dihedral angle between [Rh1, P1, P2, C1, C47] and [C1, C2, C3, C4, C5] is 82.0(2)° and that between [Rh2, P3, P4, C1] and [C1, C2, C3, C4, C5] is 85.4(2)°. The two rhodium-containing planes [Rh1, P1, P2, C1, C47] and [Rh2, P3, P4, C1] are slightly tilted with respect to each other which could be due to some steric hindrance between the phenyl group and the trisopropylphosphine ligands. Although the coordination around Rh2 can be described as square-planar, the Rh2–C3 and Rh2–C4 distances differ significantly (2.154(4) and 2.041(4) Å) which is in marked contrast to the above-mentioned nickel complex¹¹ but very similar to the situation found in the mononuclear diynerhodium(I) compound *trans*-[RhCl(η^2 -Me₃SiC≡CC≡CSiMe₃)(*PiPr*₃)₂].³ The C3–C4 bond (see Table 1) is elongated by ca. 0.06 Å compared to C1–C2 and by ca. 0.08 Å compared with that in free butadiyne.¹³

The bond length Rh–C1 of 2.061(4) Å is slightly longer than that found for the Rh–C(sp) single bond in the five-coordinated alkynyl complex [Rh(C≡CCH₂OMe)(HgPh)Cl(*PiPr*₃)₂] (1.986(5) Å)¹⁴ and in the six-coordinate bis(alkynyl)hydridorhodium(III) derivative [RhH(C≡CSiMe₃)₂(py)(*PiPr*₃)₂] (2.032(6) and 2.020(6) Å, respectively).¹⁵ The distance Rh–C1 is, however, almost identical to the Ru–C distances of the ruthenium compounds [Ru(C≡CC≡CR)₂(CO)₂(PEt₃)₂] (R = H, SiMe₃) where two diyne units are linked to the metal center.¹⁶

(12) Cash, G. G.; Pettersen, R. C. *J. Chem. Soc., Dalton Trans.* **1979**, 1630–1633.

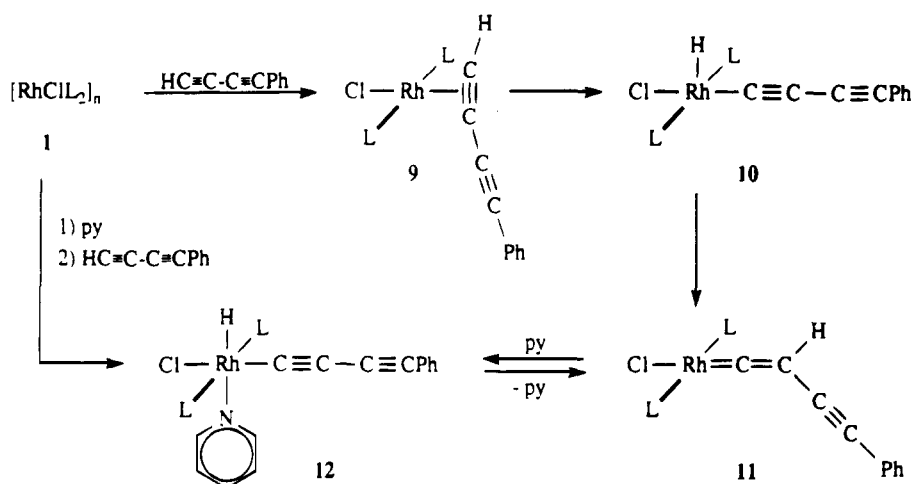
(13) Pauling, L.; Springall, H. D.; Palmer, K. J. *J. Am. Chem. Soc.* **1939**, *61*, 927–937.

(14) Baum, M.; Mahr, N.; Werner, H. *Chem. Ber.* **1994**, *127*, 1877–1886.

(15) Werner, H.; Baum, M.; Schneider, D.; Windmüller, B. *Organometallics* **1994**, *13*, 1089–1097.

(16) Sun, Y.; Taylor, N. J.; Carty, A. J. *Organometallics* **1992**, *11*, 4293–4300.

(11) Bonrath, W.; Pörschke, K. R.; Wilke, G.; Angermund, K.; Krüger, C. *Angew. Chem.* **1988**, *100*, 853–855; *Angew. Chem., Int. Ed. Engl.* **1988**, *27*, 833–835.

Scheme 2^a

^a L = $\text{P}(\text{iPr})_3$.

The Rh–Cl, Rh–CO, and Rh–P bond lengths in **8** correspond to what could be expected for square-planar complexes of rhodium(I).^{1,3,17} and deserve no further comments.

Reaction of the Chloro Complex 1 with $\text{HC}\equiv\text{CC}\equiv\text{CPh}$. Since compound **1** is monomeric in solution¹⁸ and therefore contains a coordinatively unsaturated metal center, it is not surprising that it readily reacts both with alkynes¹⁹ as well as diynes. If a solution of **1** in pentane is treated at -20°C with $\text{HC}\equiv\text{CC}\equiv\text{CPh}$, after a few minutes a light-yellow precipitate is formed which has to be quickly separated from the remaining solution. The ³¹P NMR spectrum of the new compound (if measured in CDCl_3 at -20°C) displays two doublets of unequal intensity and with different rhodium–phosphorus coupling constants. The more intense signal at δ 34.36 with $J(\text{RhP}) = 112$ Hz resembles both in the chemical shift and in the size of Rh–P coupling the resonance observed in the ³¹P NMR spectrum of *trans*- $[\text{RhCl}(\eta^2\text{-Me}_3\text{SiC}\equiv\text{CC}\equiv\text{CSiMe}_3)(\text{P}(\text{iPr})_3)_2]$,³ and thus we assume that it belongs to the initially formed π -alkyne complex **9** (Scheme 2). The less intense signal appears (in CDCl_3) at δ 49.85, and since it shows a Rh–P coupling (96 Hz) which is almost identical to that of $[(\text{P}(\text{iPr})_3)_2\text{Cl}(\text{H})\text{Rh}(\text{C}\equiv\text{CC}\equiv\text{C})\text{Rh}(\text{H})\text{Cl}(\text{P}(\text{iPr})_3)_2]$,³ we attribute this doublet to the five-coordinate diynyl(hydrido)rhodium(III) derivative **10**. The ¹H NMR spectrum of the yellow precipitate supports this proposal because it displays in the high-field region at δ -27.50 a doublet of triplets [$J(\text{RhH}) = 42.1$, $J(\text{PH}) = 12.3$ Hz] which again is very similar to that of the above mentioned $\text{HRh}(\text{C}\equiv\text{CC}\equiv\text{C})\text{RhH}$ species.³

Stirring a solution of the mixture of **9** and **10** in diethyl ether for 2 h at room temperature leads to a change of color from yellow to green, and after the solvent has been removed dark-green crystals are isolated in about 80% yield. Compound **11** which is

soluble in most common organic solvents has been characterized by elemental analysis and IR as well as NMR spectroscopy. The most typical feature besides the doublet in the ³¹P NMR spectrum at δ 42.92 ($J(\text{RhP}) = 133.7$ Hz) and the C=CH proton signal in the ¹H NMR spectrum at δ 1.03 are the low-field resonances at δ 293.76 and 91.46 (both doublets of triplets due to Rh–C and P–C coupling) in the ¹³C NMR spectrum which are characteristic of compounds of the general type *trans*- $[\text{RhCl}(\text{C}=\text{CRR}')(\text{P}(\text{iPr})_3)_2]$.^{1,3,4,14,15}

The octahedral pyridine adduct **12** (Scheme 2) is most conveniently prepared on stepwise reaction of **1** with pyridine and phenylbutadiyne at -20°C . However, if in analogy to previous work^{3,20} the mixture of **9** and **10** is treated with pyridine in diethyl ether at 0°C , besides **12** the vinylidene complex **11** is equally formed. Although **11** slowly reacts with pyridine to give **12**, only in the presence of a larger excess of NC_5H_5 the equilibrium can be completely shifted to the side of the rhodium(III) species. Therefore, the synthetic route to **12** using **1** as the starting material is preferred. Compound **12** is a white crystalline solid which can be briefly handled in air but even if stored under argon slowly decompose to give dark oily, possibly polymeric products.

Experimental Section

All reactions were carried out under an atmosphere of argon by Schlenk tube techniques. The starting materials $[\text{RhCl}(\text{P}(\text{iPr})_3)_2]_n$ (**1**),²¹ $[\text{Rh}(\eta^2\text{-O}_2\text{CCH}_3)(\text{P}(\text{iPr})_3)_2]$ (**2**),⁹ $[\text{Rh}(\eta^3\text{-CH}_2\text{C}_6\text{H}_5)(\text{P}(\text{iPr})_3)_2]$ (**7**),⁹ and $\text{HC}\equiv\text{CC}\equiv\text{CPh}$ ^{6,22} were prepared as described in the literature. NMR spectra were recorded at room temperature on Bruker AC 200 and Bruker AMX 400 instruments, and IR spectra, on a Perkin-Elmer 1420 infrared spectrophotometer. Melting points were measured by DTA.

Preparation of $[\text{RhH}(\text{C}\equiv\text{CC}\equiv\text{CPh})_2(\text{P}(\text{iPr})_3)_2]$ (3**).** Diethyl ether (15 mL) was poured on a mixture of **2** (237 mg, 0.49 mmol) and excess Na_2CO_3 (ca. 500 mg), and upon cooling of the mixture to 0°C , a solution of phenylbutadiyne (124 mg, 0.98 mmol) in 10 mL of pentane was added. After the mixture was stirred for 5 min, the solution was separated and stored

(17) (a) Nürnberg, O.; Werner, H. *J. Organomet. Chem.* **1993**, *460*, 163–175. (b) Wiedemann, R.; Steinert, P.; Schäfer, M.; Werner, H. *J. Am. Chem. Soc.* **1993**, *115*, 9864–9865. (c) Werner, H.; Rappert, T.; Wiedemann, R.; Wolf, J.; Mahr, N. *Organometallics* **1994**, *13*, 2721–2727.

(18) Schneider, D.; Werner, H. *Angew. Chem.* **1991**, *103*, 710–712; *Angew. Chem., Int. Ed. Engl.* **1991**, *30*, 700–702.

(19) Short reviews: (a) Werner, H. *Nachr. Chem. Tech. Lab.* **1992**, *40*, 435–444. (b) Werner, H. *J. Organomet. Chem.* **1994**, *475*, 45–55.

(20) Rappert, T.; Nürnberg, O.; Mahr, N.; Wolf, J.; Werner, H. *Organometallics* **1992**, *11*, 4156–4164.

(21) Werner, H.; Wolf, J.; Höhn, A. *J. Organomet. Chem.* **1985**, *287*, 395–407.

(22) Gevert, O. Diploma Thesis, Universität Würzburg, 1994.

in a cooled Schlenk tube at 0 °C. The orange-brown precipitate was extracted twice with 5 mL of diethyl ether each, and the extracts were combined with the reaction solution. After the solvent was removed in vacuo, the yellow residue was repeatedly washed with small portions of acetone (−20 °C) and dried in vacuo: yield 203 mg (61%); mp 64 °C dec; IR (KBr) $\nu(\text{C}\equiv\text{C})$ 2140, 2010 cm^{-1} ; ^1H NMR (CDCl_3 , 200 MHz) δ 7.35 (m, C_6H_5), 2.92 (m, PCHCH_3), 1.37 [dvt, $N = 13.8$, $J(\text{HH}) = 6.5$ Hz, PCHCH_3], −28.75 [dt, $J(\text{RhH}) = 52.2$, $J(\text{PH}) = 11.7$ Hz, RhH]; ^{31}P NMR (C_6D_6 , 81.0 MHz) δ 53.77 [d, $J(\text{RhP}) = 97.4$]. Anal. Calcd for $\text{C}_{38}\text{H}_{53}\text{P}_2\text{Rh}$: C, 67.73; H, 7.93. Found: C, 67.54; H, 7.98.

Preparation of $[\text{RhH}(\text{C}\equiv\text{CC}\equiv\text{CPh})_2(\text{py})(\text{PiPr}_3)_2]$ (4). A suspension of **3** (120 mg, 0.18 mmol) in 5 mL of pentane was treated at −20 °C with excess pyridine (0.1 mL) and under continuous stirring slowly warmed to room temperature (ca. 5–8 min). A white precipitate was formed, which was filtered off, washed three times with 2 mL of pentane each (0 °C), and dried in vacuo: yield 130 mg (96%); mp 117 °C dec; IR (KBr) $\nu(\text{C}\equiv\text{C})$ 2140, 2010 cm^{-1} ; ^1H NMR (C_6D_6 , 200 MHz) δ 8.50–6.80 (m, C_6H_5 and NC_5H_5), 2.84 (m, PCHCH_3), 1.17 [dvt, $N = 14.5$, $J(\text{HH}) = 7.3$ Hz, PCHCH_3], −17.51 [dt, $J(\text{RhH}) = 17.4$, $J(\text{PH}) = 13.1$ Hz, RhH]; ^{31}P NMR (C_6D_6 , 81.0 MHz) δ 42.16 [d, $J(\text{RhP}) = 94.5$ Hz]. Anal. Calcd for $\text{C}_{43}\text{H}_{55}\text{NP}_2\text{Rh}$: C, 68.52; H, 7.75; N, 1.86. Found: C, 68.56; H, 7.59; N, 1.99.

Intermediate Formation of $[\text{RhH}(\text{C}\equiv\text{CC}\equiv\text{CPh})_2(\text{CO})(\text{PiPr}_3)_2]$ (5). A slow stream of CO was passed for 2 min through a suspension of **3** (50 mg, 0.07 mmol) in 5 mL of pentane at −20 °C. After the reaction mixture was stirred for 5 min at the same temperature, the solvent was removed in vacuo. The ^1H and ^{31}P NMR spectra of the yellow-brown residue, measured at −20 °C, reveal the presence of at least two compounds of which **5** is the main component: ^1H NMR (C_6D_6 , 200 MHz) δ 7.25 (m, C_6H_5), 2.75 (m, PCHCH_3), 1.23 [dvt, $N = 14.5$, $J(\text{HH}) = 7.3$ Hz, PCHCH_3], −8.72 [dt, $J(\text{RhH}) = 8.7$, $J(\text{PH}) = 9.4$ Hz, RhH]; ^{31}P NMR (C_6D_6 , 81.0 MHz) δ 56.87 [d, $J(\text{RhP}) = 87.5$ Hz].

Preparation of $trans$ - $[\text{Rh}(\text{C}\equiv\text{CC}\equiv\text{CPh})(\text{CO})(\text{PiPr}_3)_2]$ (6). Method a. The yellow-brown solid, obtained from **3** and CO at −20 °C as described above, was dissolved in 3 mL of toluene at room temperature. The solution was stirred for 3 min, the solvent was removed, and the residue was recrystallized from 2 mL of acetone (25 to −78 °C). A bright-yellow solid was obtained, yield ca. 90%.

Method b. A slow stream of CO was passed for 2 min through a solution of **7** (80 mg, 0.16 mmol) in 5 mL of pentane at −20 °C which was accompanied by a change of color from red to light-yellow. After the solution was stirred for 10 min at −20 °C under a CO atmosphere, it was cooled to −78 °C and then a solution of phenylbutadiyne (20 mg, 0.16 mmol) in 2 mL of pentane was added dropwise. The reaction mixture was stirred for 10 min at −78 °C, the volatile components were removed in vacuo, and the residue was worked up as described in method a: yield 75 mg (89%); mp 158 °C dec; IR (KBr) $\nu(\text{C}\equiv\text{C})$ 2150, $\nu(\text{C}=\text{O})$ 1935 cm^{-1} ; ^1H NMR (C_6D_6 , 200 MHz) δ 7.10 (m, C_6H_5), 2.45 (m, PCHCH_3), 1.27 [dvt, $N = 13.9$, $J(\text{HH}) = 6.9$ Hz, PCHCH_3]; ^{13}C NMR (C_6D_6 , 100.6 MHz) δ 196.03 [dt, $J(\text{RhC}) = 58.9$, $J(\text{PC}) = 13.8$ Hz, CO], 132.45, 128.27, 127.24 (all s, C_6H_5), 106.33 (s, *ipso*-C of C_6H_5), 126.33 [dt, $J(\text{RhC}) = 43.4$, $J(\text{PC}) = 21.6$ Hz], 102.22 [dt, $J(\text{RhC}) = 12.7$, $J(\text{PC}) = 3.2$ Hz], 79.15 (m), 71.95 [t, br, $J(\text{PC}) = 2.1$ Hz] (these four signals are assigned to the carbon atoms of the C_4 chain), 26.32 [vt, $N = 23.3$ Hz, PCHCH_3], 20.42 (s, PCHCH_3); ^{31}P NMR (C_6D_6 , 81.0 MHz) δ 54.21 [d, $J(\text{RhP}) = 125$ Hz]. Anal. Calcd for $\text{C}_{29}\text{H}_{47}\text{OP}_2\text{Rh}$: C, 60.42; H, 8.22. Found: C, 59.98; H, 8.03.

Preparation of $trans$ - $[\text{Rh}(\text{CO})(\text{PiPr}_3)_2(\eta^1, \eta^2\text{-C}\equiv\text{CC}\equiv\text{CPh})\text{RhCl}(\text{PiPr}_3)_2]$ (8). A solution of **6** (102 mg, 0.18 mmol) in 5 mL of diethyl ether was treated at 0 °C with a solution of **1** (83 mg, 0.18 mmol for $n = 1$) in 5 mL of diethyl ether. With continuous stirring, the solution was slowly warmed to room temperature (ca. 20 min), the solvent was then removed, and the residue was dissolved in 3 mL of acetone. After the

solution was stored at −78 °C, a yellow microcrystalline precipitate was formed which was filtered off, repeatedly washed with small portions of acetone (0 °C), and dried: yield 157 mg (85%); mp 117 °C dec; IR (KBr) $\nu(\eta^1\text{-C}\equiv\text{C})$ 1995, $\nu(\text{C}=\text{O})$ 1930, $\nu(\eta^2\text{-C}\equiv\text{C})$ 1800 cm^{-1} ; ^1H NMR (C_6D_6 , 400 MHz) δ 8.20 (m, *ortho*-H of C_6H_5), 7.36 (m, *meta*-H of C_6H_5), 7.14 (m, *para*-H of C_6H_5), 2.72, 2.61 (both m, PCHCH_3), 1.57 [dvt, $N = 13.5$, $J(\text{HH}) = 6.9$ Hz, PCHCH_3], 1.47 [dvt, $N = 13.9$, $J(\text{HH}) = 7.1$ Hz, PCHCH_3], 1.38 [dvt, $N = 12.9$, $J(\text{HH}) = 6.3$ Hz, PCHCH_3]; ^{13}C NMR (C_6D_6 , 100.6 MHz) δ 196.55 [dt, $J(\text{RhC}) = 58.4$, $J(\text{PC}) = 14.6$ Hz, CO], 131.62 (s, *ipso*-C of C_6H_5), 130.58, 127.82, 126.02 (all s, C_6H_5), 139.32 [dt, $J(\text{RhC}) = 44.3$, $J(\text{PC}) = 21.1$ Hz], 106.29, 82.28, 65.51 (all m), (these four signals are assigned to the carbon atoms of the C_4 chain), 26.52 [vt, $N = 21.3$ Hz, PCHCH_3], 23.38 [vt, $N = 17.0$ Hz, PCHCH_3], 21.32, 20.73, 20.09 (all s, PCHCH_3); ^{31}P NMR (C_6D_6 , 162.0 MHz) δ 55.10 [d, $J(\text{RhP}) = 126.4$ Hz], 33.76 [d, $J(\text{RhP}) = 119.2$ Hz]. Anal. Calcd for $\text{C}_{47}\text{H}_{89}\text{ClOP}_4\text{Rh}_2$: C, 54.52; H, 8.66. Found: C, 54.66; H, 8.43.

Preparation of $trans$ - $[\text{RhCl}(\text{C}\equiv\text{CHC}\equiv\text{CPh})(\text{PiPr}_3)_2]$ (11). A solution of **1** (293 mg, 0.64 mmol for $n = 1$) in 10 mL of pentane was treated dropwise at −20 °C with a solution of phenylbutadiyne (80 mg, 0.64 mmol) in 8 mL of pentane. After the solution was stirred for 3–5 min, a light-yellow solid precipitated which was separated from the mother liquor and dried in vacuo. The solid was dissolved in 5 mL of diethyl ether, and the solution was stirred for 2 h at room temperature. The volatile components were removed in vacuo, and the residue was dissolved in 2 mL of acetone. After the solution was stored for 16 h at −78 °C, a dark-green precipitate was formed which was filtered off, repeatedly washed with acetone (0 °C), and dried: yield 301 mg (80%); mp 73 °C dec; IR (KBr) $\nu(\text{C}\equiv\text{C})$ 2170, $\nu(\text{C}=\text{C})$ 1605 cm^{-1} ; ^1H NMR (CDCl_3 , 200 MHz) δ 7.26 (m, C_6H_5), 2.87 (m, PCHCH_3), 1.40 [dvt, $N = 13.7$, $J(\text{HH}) = 7.1$ Hz, PCHCH_3], 1.03 [dt, $J(\text{RhH}) = 0.7$, $J(\text{PH}) = 3.1$ Hz, $\text{Rh}=\text{C}=\text{CH}$]; ^{13}C NMR (CDCl_3 , 50.3 MHz) δ 298.76 [dt, $J(\text{RhC}) = 62.3$, $J(\text{PC}) = 16.5$ Hz, $\text{Rh}=\text{C}$], 130.90, 129.85, 127.61 (all s, C_6H_5), 125.37 (s, *ipso*-C of C_6H_5), 100.24 (s, $\text{C}\equiv\text{CPh}$), 91.46 [dt, $J(\text{RhC}) = 17.8$, $J(\text{PC}) = 6.0$ Hz, $\text{Rh}=\text{C}=\text{C}$], 67.10 [t, br, $J(\text{PC}) = 3.5$ Hz, $\text{C}\equiv\text{CPh}$], 24.00 [vt, $N = 20.3$ Hz, PCHCH_3], 20.74 (s, PCHCH_3); ^{31}P NMR (CDCl_3 , 81.0 MHz) δ 42.92 [d, $J(\text{RhP}) = 133.7$ Hz]. Anal. Calcd for $\text{C}_{28}\text{H}_{48}\text{ClP}_2\text{Rh}$: C, 57.49; H, 8.27. Found: C, 57.20; H, 8.21.

Preparation of $[\text{RhH}(\text{C}\equiv\text{CC}\equiv\text{CPh})\text{Cl}(\text{py})(\text{PiPr}_3)_2]$ (12). A solution of **1** (163 mg, 0.40 mmol for $n = 1$) in 15 mL of diethyl ether was treated first with pyridine (0.1 mL, 1.2 mmol) and then at −20 °C with a solution of phenylbutadiyne (50 mg, 0.40 mmol) in 5 mL of pentane. An almost immediate change of color from red to light-yellow occurred. After the reaction mixture was stirred for 15 min at 0 °C, the volatile components were removed and the yellow-green residue was repeatedly washed with small portions of acetone (0 °C) and dried in vacuo: yield 155 mg (58%); mp 78 °C dec; IR (KBr) $\nu(\text{C}\equiv\text{C})$ 2165, 2050 cm^{-1} ; ^1H NMR (C_6D_6 , 200 MHz) δ 9.77 (m, *ortho*-H of NC_5H_5), 7.44–6.64 (m, C_6H_5 and NC_5H_5), 2.93 (m, PCHCH_3), 1.54 [dvt, $N = 13.9$, $J(\text{HH}) = 7.3$ Hz, PCHCH_3], 1.33 [dvt, $N = 13.1$, $J(\text{HH}) = 6.2$ Hz, PCHCH_3], −17.03 [dt, $J(\text{RhH}) = 13.1$, $J(\text{PH}) = 13.1$ Hz, RhH]; ^{31}P NMR (C_6D_6 , 81.0 MHz) δ 38.38 [d, $J(\text{RhP}) = 97.4$ Hz]. Anal. Calcd for $\text{C}_{33}\text{H}_{53}\text{ClNP}_2\text{Rh}$: C, 59.68; H, 8.04; N, 2.11. Found: C, 59.56; H, 8.35; N, 2.07.

X-ray Structural Analysis of 8. Single crystals were grown from diethyl ether at −20 °C. Crystal data (from 23 reflections, $10^\circ < \theta < 12^\circ$): triclinic, space group $P\bar{1}$ (No. 2), $a = 12.460(2)$ Å, $b = 13.954(2)$ Å, $c = 16.431(2)$ Å, $\alpha = 97.98(1)^\circ$, $\beta = 91.47(1)^\circ$, $\gamma = 109.61(1)^\circ$, $V = 2657(1)$ Å³, $Z = 2$, $D_{\text{calcd}} = 1.284$ g cm^{−3}, $\mu(\text{Mo K}\alpha) = 8.0$ cm^{−1}. Crystal size: $0.13 \times 0.23 \times 0.40$ mm. Solution details: Enraf-Nonius CAD4 diffractometer, Mo K α radiation (0.709 30 Å), graphite monochromator, zirconium filter (factor 16.4), $T = 293$ K, ω/θ -scan, maximum $2\theta = 42^\circ$, 6064 reflections measured, 5388 independent, 4867

regarded as being observed [$F_o > 3\sigma(F_o)$]; intensity data corrected for Lorentz and polarization effects, empirical absorption correction (ψ -scan method) applied, minimum transmission 95.82%; structure solved by direct methods (SHELXS-86); atomic coordinates and anisotropic thermal parameters refined by full-matrix least squares (Enraf-Nonius SDP);²³ positions of the hydrogen atoms calculated according to ideal geometry and used only in structure factor calculation; $R = 0.035$, $R_w = 0.035$; reflection/parameter ratio 9.81; residual electron density $\pm 1.53/-0.52$ e \AA^{-3} .

(23) Frenz, B. A. The Enraf-Nonius CAD 4 SDP—a real time system for concurrent X-ray data collection and structure determination. In *Computing in Crystallography*; Delft University Press: Delft, Holland, 1978; pp 64–71.

Acknowledgment. We thank the Volkswagen Stiftung and the Fonds der Chemischen Industrie for financial support. We also gratefully acknowledge support by Mrs. U. Neumann, Mrs. R. Schedl, and Mr. C. P. Kneis (elemental analysis and DTA), Mrs. M. L. Schäfer, Dr. W. Buchner, and Mr. B. Stempfle (NMR measurements) and Degussa AG (chemicals).

Supplementary Material Available: Tables of data collection parameters, bond lengths and angles, positional and thermal parameters, and least-squares planes for **8** (15 pages). Ordering information is given on any current masthead page.

OM9408472

Effect of Charge on Structure: Stepwise Protonation of $[\text{EFe}_3(\text{CO})_9]^{2-}$ (E = Se, Te) and Isolation of the Novel Mixed-Metal Cluster $[\text{TeFe}_3(\text{CO})_9(\mu\text{-CuCl})]^{2-}$

Robert E. Bachman, Kenton H. Whitmire,* and Jaap van Hal

Department of Chemistry, Rice University, P.O. Box 1892, Houston, Texas 77251

Received June 1, 1994[⊗]

The clusters $[\text{EFe}_3(\text{CO})_9]^{2-}$ (E = Se, Te) were protonated stepwise with triflic acid to produce both the monohydride clusters $[\text{HFe}_3(\text{CO})_9]^-$ and the dihydride clusters $\text{H}_2\text{EFe}_3(\text{CO})_9$. The effect of the presence of the hydrides as well as that of the overall cluster charge on the structure was probed both spectroscopically and crystallographically. The ^{13}C NMR shifts and the IR stretching frequencies of the carbonyl ligands was found to be correlated with the cluster charge in a linear fashion. $[\text{PPN}][\text{HSeFe}_3(\text{CO})_9]$ crystallizes in the monoclinic space group $P2_1/c$ (No. 14) with $a = 9.359(2)$ Å, $b = 29.648(6)$ Å, $c = 16.057(3)$ Å, $\beta = 101.23(3)^\circ$ and $V = 4370.1(15)$ Å³. The isostructural telluride $[\text{PPN}][\text{HTeFe}_3(\text{CO})_9]$ also crystallizes in the monoclinic space group $P2_1/n$ (No. 14) with $a = 8.925(2)$ Å, $b = 13.985(3)$ Å, $c = 35.798(7)$ Å, $\beta = 97.13(3)^\circ$, and $V = 4433.6(16)$ Å³. $\text{H}_2\text{SeFe}_3(\text{CO})_9$ crystallizes in the monoclinic space group $P2_1/n$ with $a = 8.862(2)$ Å, $b = 11.503(2)$ Å, $c = 14.936(3)$ Å, $\beta = 103.28(3)^\circ$, and $V = 1481.9(5)$ Å³. The tellurium analog $\text{H}_2\text{TeFe}_3(\text{CO})_9$ crystallizes in the centrosymmetric triclinic space group $P\bar{1}$ (No. 2) with $a = 7.8814(4)$ Å, $b = 8.9414(7)$ Å, $c = 11.8243(4)$ Å, $\alpha = 82.318(5)^\circ$, $\beta = 77.664(4)^\circ$, $\gamma = 69.303(4)^\circ$, and $V = 759.95(8)$ Å³. The reaction of $[\text{TeFe}_3(\text{CO})_9]^{2-}$ with either CuCl or Et_3PCuCl produced the unusual cluster $[\text{TeFe}_3(\text{CO})_9(\mu\text{-CuCl})]^{2-}$. A crystallographic study of the $[\text{PPN}]^+$ salt confirmed the presence of the chloride ligand. $[\text{PPN}]_2[\text{TeFe}_3(\text{CO})_9(\mu\text{-CuCl})]$, which crystallizes in the orthorhombic space group $Pbca$ (No. 61) with $a = 24.274(5)$ Å, $b = 21.634(4)$ Å, $c = 30.363(6)$ Å, and $V = 15944.9(54)$ Å³, is therefore the first example of a mixed iron-copper cluster which retains a halide ligand bound to copper.

Introduction

Transition metal clusters have been studied for some time as potential catalysts and catalyst precursors.¹ Since many catalytic processes involve the transfer of hydrogen, clusters containing hydride ligands are of particular interest. For example, $[\text{HRu}_3(\text{CO})_{11}]^-$ has been shown to be an active catalyst for hydroformylation but it unfortunately suffers from a short catalyst lifetime.² The problem of rapid catalyst degradation is common for cluster-based systems, but the incorporation of main-group hetero-atoms appears to increase the stability of the cluster framework.³ Therefore, clusters which contain both hydride ligands and main-group fragments are attractive targets as potential catalysts which will be better able to resist degradation.

A common method for the production of main-group-transition-metal clusters which contain one or more hydride ligands is by the protonation of anionic clusters. However, in several cases, changing the method used to protonate these heteroatomic clusters drastically changes the product which is isolated. An example of this phenomenon is the cluster $[\text{Sb}\{\text{Fe}(\text{CO})_4\}_4]^{3-}$.⁴ When

this cluster is protonated with 1 equiv of triflic acid, the major product is $[\text{HSbFe}_4(\text{CO})_{13}]^{2-}$, in which a protonation induced metal-metal bond-forming reaction has occurred. This monohydride can be protonated again with a second 1 equiv of triflic acid to yield $[\text{H}_2\text{SbFe}_4(\text{CO})_{13}]^-$. However, if 2 equiv of triflic acid are added directly to $[\text{SbFe}_4(\text{CO})_{16}]^{3-}$, the major product is $[\text{Sb}_2\text{Fe}_5(\text{CO})_{17}]^{2-}$,⁴ presumably arising from direct oxidation of the starting cluster. The possibility of differing outcomes dependent on the reaction conditions employed prompted the careful investigation of the protonation of $[\text{PPN}]_2[\text{TeFe}_3(\text{CO})_9]$ (**Ia**) and $[\text{PPN}]_2[\text{SeFe}_3(\text{CO})_9]$ (**Ib**). The protonation of **I** was found to proceed stepwise. While the first protonation is clean in both cases yielding a monohydrido cluster with a bridging hydride, the second protonation was more delicate and extreme care was needed to prevent oxidation to $\text{E}_2\text{Fe}_3(\text{CO})_9$ instead of protonation. Since Cu^+ is isolobal with H^+ , the oxidation of **Ia** with Cu(I) reagents was also investigated. The surprising outcome of this work was the preparation and structural characterization of a mixed-metal cluster which incorporates an intact CuCl fragment.

Experimental Procedures

General Considerations. All manipulations were performed with oven-dried Schlenkware using standard tech-

[⊗] Abstract published in *Advance ACS Abstracts*, March 15, 1995.
(1) Gates, B. C., Ed. *Metal Clusters in Catalysis*; Elsevier: Amsterdam, 1986.

(2) Süß-Fink, G.; Herrmann, G. *J. Chem. Soc., Chem. Commun.* **1985**, 735.

(3) (a) Churchill, M. R.; Fettinger, J. C.; Whitmire, K. H. *J. Organomet. Chem.* **1985**, *284*, 13. (b) Whitmire, K. H. *J. Coord. Chem.* **1988**, *17*, 95. (c) Herrmann, W. A. *Angew. Chem., Int. Ed. Engl.* **1986**, *25*, 56. (d) Compton, N. A.; Errington, R. J.; Norman, N. C. *Adv. Organomet. Chem.* **1990**, *31*, 91. (e) Mathur, P.; Chakrabarty, D.; Mavunkal, I. *J. Cluster Sci.* **1993**, *4*, 351.

(4) (a) Luo, S.; Whitmire, K. H. *Inorg. Chem.* **1989**, *28*, 1424. (b) Whitmire, K. H.; Leigh, J. S.; Luo, S.; Shieh, M.; Fabiano, M. D. *New J. Chem.* **1988**, *12*, 397.

niques on a Schlenk line or in a Vacuum Atmospheres drybox.⁵ Solvents were distilled from the appropriate drying agent under nitrogen prior to use: THF and ether (Na/Ph₂CO); hexanes (LiAlH₄); dichloromethane and acetonitrile (CaH₂). The trifluoromethanesulfonic acid (triflic acid) was carefully distilled under vacuum before use, and the CuCl (Aldrich) was dried in vacuo overnight before use to ensure dryness. Bis-(triphenylphosphine)ammonium chloride, [PPN]Cl,⁶ [PPN]₂[TeFe₃(CO)₉] (**Ia**)⁷, and [PPN]₂[SeFe₃(CO)₉] (**Ib**)⁷ were prepared according to literature methods.

Solution IR spectra were recorded in 0.1 mm path length CaF₂ cells on a Perkin-Elmer Model 1640 FTIR spectrophotometer. ¹H and ¹³C spectra were obtained on a Bruker AF 300 spectrometer in the solvent noted. Electron impact mass spectra were obtained on a Finnigan 3300 spectrometer, and fast atom bombardment mass spectra were obtained on either a Finnigan MAT 95 (FAB) or a Fisons/VG Analytical Autospec 3000 (EI) spectrometer. Elemental analyses were performed on a Carlo Erba Instruments NA 1500 series 2 analyzer.

Preparation of [PPN][HTeFe₃(CO)₉] (IIa). A stock solution of 0.5 mL of trifluoromethanesulfonic acid (triflic acid) diluted to a total volume of 55 mL with acetonitrile (to yield a final concentration of 0.1 mmol/mL) was prepared. A 500 mg (0.31 mmol) amount of **Ia** was dissolved in 35 mL of CH₂Cl₂, and the resulting red solution was cooled to -78 °C in a dry ice/acetone bath. A 1 equiv amount (3.1 mL) of the dilute acid solution was then added dropwise. After 5 min the reaction was complete by IR. The solvent was removed *in vacuo* to yield an oily solid. The solids were extracted into 40 mL of ether, and the resulting solution was filtered through Celite to remove [PPN][O₃SCF₃], which is formed as a byproduct of the reaction, along with a small amount of other insoluble material. The solution was concentrated to approximately 10 mL and held at -20 °C for several days to yield 313 mg of dark red crystalline product (93%). IR (Et₂O, cm⁻¹): 2043 w, 2000 s, 1975 vs, 1958 m, 1940 sh, 1909 w. ¹H NMR (CD₃CN, ppm): 7.6–7.4 m, -22.02 s. ¹³C NMR (CD₃CN, ppm): 215.8 (CO), 134.5, 131.6 d (*J*_{P-C} = 208 Hz), 128.9, 127.4. Anal. Calcd for C₄₅H₃₁Fe₃NO₉P₂Te: C, 49.7; H, 2.87; N, 1.29. Found: C, 48.9 (49.8); H, 2.76 (2.72); N, 1.44 (1.11). Negative ion FAB-MS in nitrobenzyl alcohol (NBA): calcd for [HTeFe₃(CO)₉]⁻, *m/z* 548.7; obsd, *m/z* 548.4.

Preparation of H₂TeFe₃(CO)₉ (IIIa). **Ia**, 500 mg (0.31 mmol), was dissolved in 35 mL of CH₂Cl₂. The solution was cooled to -78 °C in a dry ice/acetone bath, and 6.2 mL of the triflic acid solution prepared above was added dropwise. As the addition neared completion, the reaction was monitored closely by IR. Addition of more than 2 equiv of acid led to the formation of Fe₃(CO)₉Te₂ as an impurity which is very difficult to remove. After the addition was complete the solvent was removed *in vacuo* and the residues were extracted with 30 mL of ether. After filtering of the solution through Celite to remove the solid salts formed in the reaction, the solvent was concentrated under reduced pressure to approximately 10 mL. Deep red/black crystals formed on standing at -20 °C. A 165 mg amount (97% yield) of crystalline product was obtained. IR (Et₂O, cm⁻¹): 2098 w, 2060 vs, 2038 vs, 2000 m. ¹H NMR (CD₃CN, ppm): -23.49. ¹³C NMR (CD₃CN, ppm): 208.0. MS (EI) (*m/z*): 550 (M⁺), 522 (M⁺ - CO), 494 (M⁺ - 2CO), 438 (M⁺ - 4CO), 410 (M⁺ - 5CO), 382 (M⁺ - 6CO), 354 (M⁺ - 7CO), 326 (M⁺ - 8CO), 298 (TeFe₃⁺), 242 (TeFe₂⁺). Anal. Calcd for C₉H₂Fe₃O₉Te: C, 19.7; H, 0.37. Found: C, 18.8; H, 0.75. Upon investigation of the low C analysis it was discovered that H₂TeFe₃(CO)₉ is unstable in the solid state as well as in solution, converting to Te₂Fe₃(CO)₉. An analysis of CO content for a freshly prepared sample gave 0.015 mol of CO/g of sample as compared to a theoretical value of 0.016 mol/g.

Preparation of [PPN]₂[TeFe₃(CO)₉(μ-CuCl)] (IV). A solution of 100 mg (0.06 mmol) of **Ia** in 5 mL of CH₂Cl₂ was prepared. Approximately 10 mg (0.10 mmol) of solid anhydrous CuCl was then added, and the mixture was allowed to stand for approximately 8 h. During this time the solution changed from deep red to magenta in color. The reaction mixture was then carefully layered with ether and allowed to stand for 1 week. Long deep red rectangular prism-shaped crystals of **IV** were isolated by filtration along with colorless needles of [PPN][CuCl₂] (identified by X-ray crystallography). The crystals were washed with minimal methanol to remove the [PPN][CuCl₂], and the product was then dried *in vacuo*. Yield: 80.4 mg (76%). IR (CH₂Cl₂, cm⁻¹): 2007 w, 1943 vs, 1917 msh, 1880 w, 1864, w. ¹H NMR (CD₃CN, ppm): 7.6–7.4 m. ¹³C NMR (CD₃CN, ppm): 221.5 (CO), 135.2, 132.3 d (*J*_{P-C} = 208 Hz), 129.4, 128.0. Analyses are complicated by the observation that crystals of the adduct always form concomitantly with crystals of [PPN]₂[TeFe₃(CO)₉] and [PPN]-[CuCl₂]. Duplicate analyses were obtained. Calcd for C₈₁H₆₀-ClCuFe₃N₂O₉P₄Te: C, 56.4; H, 3.51; N, 1.62. Found: C, 55.8; (55.4); H, 3.87 (3.48); N, 1.75 (1.69). Negative ion FAB-MS in NBA: calcd for [HTeFe₃(CO)₉(CuCl)]⁻, *m/z* 1184.7; observed, *m/z* 1184.4.

Preparation of [PPN][HSeFe₃(CO)₉] (IIb). A stock solution was prepared from 0.5 mL of triflic acid diluted to a total volume of 55 mL with acetonitrile (final concentration was 0.1 mmol/mL). A 500 mg (0.32 mmol) amount of **Ib** was dissolved in 35 mL of CH₂Cl₂. After cooling of the resulting red solution to -78 °C in a dry ice/acetone bath, 3.2 mL of the acid solution was added dropwise. After 5 min the reaction was complete as determined by IR spectroscopy. The solvent was removed *in vacuo* to yield an oily solid which was extracted into 40 mL of ether. The resulting solution was filtered through Celite to remove the [PPN][O₃SCF₃] formed as a byproduct along with a small amount of dark insoluble material. The solution was concentrated to approximately 10 mL and held at -20 °C for several days to yield 302 mg of dark red crystalline product (94% based on Se). IR (Et₂O, cm⁻¹): 2055 w, 2049 w, 2035 w, 2005 s, 1978 vs, 1961 m, 1910 w. ¹H NMR (CD₃CN, ppm): 7.6–7.4 m, -22.72 s. ¹³C NMR (CD₃CN, ppm): 215.2 (CO), 134.5, 131.6 d (*J*_{P-C} = 207 Hz), 128.8, 127.4. Anal. Calcd for C₄₅H₃₁Fe₃NO₉P₂Se: C, 52.1; H, 3.01; N, 1.35. Found: C, 51.91 (51.85); H, 3.17 (3.19); N, 1.33 (1.29). Negative ion FAB-MS in NBA: calcd for [HSeFe₃(CO)₉]⁻, *m/z* 500.7; observed, *m/z* 500.5.

Preparation of H₂SeFe₃(CO)₉ (IIIb). **Ib**, 500 mg (0.32 mmol), was dissolved in 35 mL of CH₂Cl₂. The solution was cooled to -78 °C in a dry ice/acetone bath, and 6.4 mL of the triflic acid solution prepared above was added dropwise. During the addition of the second 1 equiv of acid, Fe₃(CO)₉Se₂ formed in competition with the desired product. It was not possible to isolate a pure sample of **IIIb** as it formed an intractable mixture with the diselenide cluster which is present in significant quantities. Chromatography over fluorisil led to decomposition of **IIIb** and isolation of pure Fe₃(CO)₉Se₂. Attempts to separate the two compounds by sublimation also failed. When a hexane solution containing a mixture of the two compounds was cooled to -20 °C crystals of both materials were isolated. IR (hexane, cm⁻¹) of mixture (bands assigned to Fe₃(CO)₉Se₂ are italic): 2103 m, 2066 s, 2046 vs, 2037 s, 2032 sh, 2010 s, 2000 m, 1989 w, 1984 w, 1959 w. ¹H NMR (CD₃CN, ppm): -24.13. ¹³C NMR (CD₃CN, ppm): 207.6. MS (EI) (*m/z*): peaks due to H₂SeFe₃(CO)₉, 501 (M⁺), 473 (M⁺ - CO), 445 (M⁺ - 2CO), 417 (M⁺ - 3CO), 389 (M⁺ - 4CO), 361 (M⁺ - 5CO), 333 (M⁺ - 6CO), 305 (M⁺ - 7CO), 277 (M⁺ - 8CO), 249 (H₂SeFe₃⁺), 247 (SeFe₃⁺), 191 (SeFe₂⁺); peaks due to Fe₃(CO)₉Se₂, 550 (M⁺ - CO), 522 (M⁺ - 2CO), 354 (M⁺ - 8CO), 270 (Se₂Fe₂⁺), 247 (SeFe₃⁺), 191 (SeFe₂⁺). No elemental analysis was performed because of the difficulty in separating the two compounds.

(5) Shriver, D. F.; Drezdson, M. A. *The Manipulation of Air Sensitive Compounds*; Wiley: New York, 1986.

(6) Ruff, J. K.; Schlientz, W. S. *Inorg. Synth.* **1975**, *15*, 84.

(7) Bachman, R. E.; Whitmire, K. H. *Inorg. Chem.*, in press.

Table 1. Crystal Data and Structure Refinement Parameters for IIa, IIIa, IV, IIb, and IIIb

	IIa	IIIa	IV	IIb	IIIb
empirical formula	C ₄₅ H ₃₁ Fe ₃ NO ₉ P ₂ Te	C ₉ H ₂ Fe ₃ O ₉ Te	C ₈₁ H ₆₀ ClCuFe ₃ N ₂ O ₉ P ₄ Te	C ₄₅ H ₃₁ Fe ₃ NO ₉ P ₂ Se	C ₉ H ₂ Fe ₃ O ₉ Se
fw	1086.80	549.26	1723.33	1038.16	500.62
temp	223(2) K	223(2) K	223(2) K	223(2) K	223(2) K
wavelength	0.710 69 Å	0.710 69 Å	0.710 69 Å	0.710 69 Å	0.710 69 Å
cryst system	monoclinic	triclinic	orthorhombic	monoclinic	monoclinic
space group	<i>P2₁/n</i> (No. 14)	<i>P</i> $\bar{1}$ (No. 2)	<i>Pbca</i> (No. 61)	<i>P2₁/c</i> (No. 14)	<i>P2₁/n</i>
unit cell dimens					
<i>a</i> (Å)	8.925(2)	7.8814(4)	24.274(5)	9.359(2)	8.862(2)
<i>b</i> (Å)	13.985(3)	8.9414(7)	21.634(4)	29.648(6)	11.503(2)
<i>c</i> (Å)	35.798(7)	11.8243(4)	30.363(6)	16.057(3)	14.936(3)
α (deg)		82.318(5)			
β (deg)	97.13(3)	77.664(4)		101.23(3)	103.28(3)
γ (deg)		69.303(4)			
<i>V</i>	4433.6(16) Å ³	759.95(8) Å ³	15944.9(54) Å ³	4370.1(15) Å ³	1481.9(5) Å ³
<i>Z</i>	4	2	8	4	4
<i>D</i> (calcd)	1.628 g/cm ³	2.400 g/cm ³	1.436 g/cm ³	1.578 g/cm ³	2.244 g/cm ³
abs coeff	1.741 mm ⁻¹	4.744 mm ⁻¹	1.326 mm ⁻¹	1.945 mm ⁻¹	5.392 mm ⁻¹
<i>F</i> (000)	2160	516	6944	2088	960
θ range for data collcn	2.25–24.98°	2.44–27.50°	2.04–24.98°	2.22–20.00°	2.26–27.49°
index ranges	–10 ≤ <i>h</i> ≤ 10, –16 ≤ <i>k</i> ≤ 0, –38 ≤ <i>l</i> ≤ 10	0 ≤ <i>h</i> ≤ 9, –10 ≤ <i>k</i> ≤ 11, –15 ≤ <i>l</i> ≤ 15	0 ≤ <i>h</i> ≤ 26, 0 ≤ <i>k</i> ≤ 25, –36 ≤ <i>l</i> ≤ 0	0 ≤ <i>h</i> ≤ 8, 0 ≤ <i>k</i> ≤ 28, –15 ≤ <i>l</i> ≤ 15	0 ≤ <i>h</i> ≤ 10, 0 ≤ <i>k</i> ≤ 14, –19 ≤ <i>l</i> ≤ 18
reflns collcd	6418	3683	11 242	4250	3145
independent reflctns	6289 [<i>R</i> (int) = 0.0252]	3432 [<i>R</i> (int) = 0.0118]	11 242	3924 [<i>R</i> (int) = 0.0171]	2932 [<i>R</i> (int) = 0.0159]
data/restraints/params	6243/0/554	3432/0/208	11229/44/920	3861/0/554	2930/0/208
goodness-of-fit on <i>F</i> ²	1.087	1.091	1.072	1.196	1.003
final <i>R</i> indices [<i>I</i> > 2σ(<i>I</i>)]	<i>R</i> ₁ = 0.0306, <i>wR</i> ₂ = 0.0660	<i>R</i> ₁ = 0.0381, <i>wR</i> ₂ = 0.1110	<i>R</i> ₁ = 0.0841, <i>wR</i> ₂ = 0.2308	<i>R</i> ₁ = 0.0507, <i>wR</i> ₂ = 0.1348	<i>R</i> ₁ = 0.0226, <i>wR</i> ₂ = 0.0491
<i>R</i> indices (all data)	<i>R</i> ₁ = 0.0580, <i>wR</i> ₂ = 0.0947	<i>R</i> ₁ = 0.0415, <i>wR</i> ₂ = 0.1139	<i>R</i> ₁ = 0.1944, <i>wR</i> ₂ = 0.3105	<i>R</i> ₁ = 0.0947, <i>wR</i> ₂ = 0.2721	<i>R</i> ₁ = 0.0359, <i>wR</i> ₂ = 0.0567
largest diff peak and hole	0.418 and –0.379 e Å ⁻³	1.338 and –1.190 e Å ⁻³	1.795 and –0.720 e Å ⁻³	0.437 and –0.463 e Å ⁻³	0.329 and –0.271 e Å ⁻³

X-ray Crystallography

General Considerations. All crystals were mounted with epoxy cement on the tip of a glass fiber. The data were collected using the TEXSAN automatic data collection series⁸ on a Rigaku AFC5S diffractometer using Mo K α radiation (λ = 0.710 69 Å). The crystallographic data collection parameters for each compound are summarized in the appropriate appendices. Unless otherwise noted, the data were collected at 223 K and were corrected for Lorentz and polarization effects and for absorption using ψ -scans. Crystal and instrument stability were checked by measuring three standard reflections every 150 observations. The analytical form of the scattering factors for the appropriate neutral atoms were corrected for both the real ($\Delta f'$) and imaginary ($\Delta f''$) components of anomalous dispersion.⁹ In all cases structure solution was carried out with the SHELXTL-PC package¹⁰ and the structure refinements were performed on *F*² with SHELXL-93.¹¹ The function minimized was $wR_2 = [\sum\{w(F_o^2 - F_c^2)^2\}/\sum\{wF_o^2\}]^{0.5}$, with $w = [\sum^2 F_o^2 + (aP)^2 + bP]^{-1}$ and $P = 0.33F_o^2 + 0.67F_c^2$. Additionally, a residual *R*₁ was calculated. This residual is included to make comparisons with refinements carried out on *F* more convenient. This scaling is necessary because, due to statistical factors, the residuals for refinement on *F*² are normally two to three times larger than those for the same refinement carried out on *F*. Table 1 contains a summary of the crystallographic and structure refinement parameters for all five structures.

Structure of IIa. A red regular prism approximately 0.4 × 0.3 × 0.5 mm in size was cut from a larger crystal and used for data collection. The unit cell was determined to be monoclinic from a least squares analysis of 25 reflections (6.75° ≤ 2θ ≤ 12.0°). The space group *P2₁/n* (No. 14) was chosen on the basis of systematic absences. All non-hydrogen atoms were refined anisotropically while the hydride ligand was located crystallographically and refined isotropically. The hydrogen atoms on the cation were included in calculated positions using

(8) *International Tables for X-ray Crystallography*; Kynoch: Birmingham, England, 1974; Vol. 4, pp 99–101 and 149–150.

(9) TEXSAN: Single Crystal Structure Analysis Software, v. 5.0.

(10) SHELXTL PC v. 4.2. Siemens Crystallographic Research Systems: Madison, WI, 1990.

Table 2. Atomic Coordinates (×10⁴) and Equivalent Displacement Parameters (Å² × 10³) for IIa

atom	<i>x</i>	<i>y</i>	<i>z</i>	<i>U</i> (eq) ^a
Te(1)	4497(1)	6421(1)	3788(1)	45(1)
Fe(1)	5074(1)	4813(1)	3545(1)	36(1)
Fe(2)	2244(1)	5583(1)	3460(1)	37(1)
Fe(3)	3530(1)	5033(1)	4124(1)	43(1)
O(11)	6381(4)	5044(3)	2840(1)	60(1)
O(12)	4421(4)	2768(2)	3565(1)	64(1)
O(13)	8016(4)	4727(3)	3996(1)	80(1)
O(21)	307(6)	3925(4)	3356(2)	120(2)
O(22)	142(4)	6775(3)	3808(1)	75(1)
O(23)	1457(5)	6352(3)	2706(1)	86(1)
O(31)	1640(5)	6007(4)	4614(1)	108(2)
O(32)	6027(5)	4581(3)	4700(1)	72(1)
O(33)	2032(6)	3185(3)	4137(1)	107(2)
C(11)	5855(5)	4974(3)	3116(2)	44(1)
C(12)	4682(5)	3574(4)	3563(1)	45(1)
C(13)	6843(6)	4764(4)	3823(1)	51(1)
C(21)	1066(6)	4571(4)	3408(2)	63(2)
C(22)	989(5)	6304(4)	3676(1)	50(1)
C(23)	1837(5)	6071(4)	3005(2)	50(1)
C(31)	2379(6)	5636(4)	4418(1)	61(2)
C(32)	5051(6)	4779(4)	4474(2)	52(1)
C(33)	2621(7)	3912(4)	4122(2)	66(2)

^a *U*(eq) is defined as one-third of the trace of the orthogonalized *U_{ij}* tensor.

a riding model. The refinement converged with final residuals of *R*₁ = 0.0306 and *wR*₂ = 0.0660 for 554 parameters and 4158 observed (*I* > 2σ(*I*)) reflections. Selected positional and displacement parameters are included in Table 2, and selected bond metrics may be found in Table 3.

Structure of IIIa. A black square plate 0.5 × 0.1 × 0.5 mm in size was chosen for data collection. The unit cell was determined by least squares refinement of 24 reflections (7.0° ≤ 2θ ≤ 15.5°), and the crystal system was shown to be triclinic. The more prevalent space group, *P* $\bar{1}$ (No. 2), was chosen on the basis of intensity statistics and shown to be correct by successful refinement of the structure. The hydrogen atoms were located in the difference map and refined isotropically, while the non-hydrogen atoms were refined anisotropically.

(11) Sheldrick, G. M. SHELXS-93, Göttingen, Germany, 1993.

Table 3. Bond Lengths (Å) and Angles (deg) for IIa

Lengths			
Te(1)-Fe(1)	2.4877(8)	Fe(1)-Fe(3)	2.6447(11)
Te(1)-Fe(3)	2.4918(9)	Fe(1)-Fe(2)	2.7276(10)
Te(1)-Fe(2)	2.4927(9)	Fe(2)-Fe(3)	2.6237(11)
Fe(1)-H(1)	1.65(4)	Fe(2)-H(1)	1.60(4)
Fe-C	1.757(6)-1.778(6)	C-O	1.130(6)-1.152(6)
Angles			
Fe(1)-Te(1)-Fe(3)	64.16(3)	H(1)-Fe(2)-Fe(1)	34(2)
Fe(1)-Te(1)-Fe(2)	66.41(2)	C(22)-Fe(2)-Fe(1)	144.0(2)
Fe(3)-Te(1)-Fe(2)	63.52(3)	C(21)-Fe(2)-Fe(1)	103.1(2)
H(1)-Fe(1)-C(13)	177(2)	C(23)-Fe(2)-Fe(1)	109.8(2)
H(1)-Fe(1)-C(12)	87(2)	Te(1)-Fe(2)-Fe(1)	56.70(3)
C(13)-Fe(1)-C(12)	96.3(2)	H(1)-Fe(2)-C(22)	177(2)
H(1)-Fe(1)-C(11)	85.0(14)	H(1)-Fe(2)-C(21)	85(2)
C(13)-Fe(1)-C(11)	94.1(2)	C(22)-Fe(2)-C(21)	95.9(2)
C(12)-Fe(1)-C(11)	104.8(2)	H(1)-Fe(2)-C(23)	86(2)
H(1)-Fe(1)-Te(1)	85.0(14)	C(22)-Fe(2)-C(23)	96.6(2)
C(13)-Fe(1)-Te(1)	92.8(2)	C(21)-Fe(2)-C(23)	99.3(2)
C(11)-Fe(1)-Fe(3)	163.8(2)	H(1)-Fe(2)-Te(1)	86(2)
Te(1)-Fe(1)-Fe(3)	57.99(2)	C(22)-Fe(2)-Te(1)	92.5(2)
H(1)-Fe(1)-Fe(2)	32.4(14)	Fe(3)-Fe(2)-Fe(1)	59.20(3)
C(13)-Fe(1)-Fe(2)	146.4(2)	C(32)-Fe(3)-C(33)	97.8(3)
C(12)-Fe(1)-Fe(2)	101.9(2)	C(32)-Fe(3)-C(31)	97.3(2)
C(11)-Fe(1)-Fe(2)	108.1(2)	C(33)-Fe(3)-C(31)	97.1(3)
Te(1)-Fe(1)-Fe(2)	56.88(2)	C(32)-Fe(3)-Te(1)	102.5(2)
Fe(3)-Fe(1)-Fe(2)	58.44(3)	C(33)-Fe(3)-Te(1)	151.2(2)
C(12)-Fe(1)-Te(1)	145.2(2)	C(31)-Fe(3)-Te(1)	100.2(2)
C(11)-Fe(1)-Te(1)	107.95(14)	C(32)-Fe(3)-Fe(2)	155.9(2)
H(1)-Fe(1)-Fe(3)	85.6(14)	C(33)-Fe(3)-Fe(2)	96.2(2)
C(13)-Fe(1)-Fe(3)	94.6(2)	C(31)-Fe(3)-Fe(2)	100.2(2)
C(12)-Fe(1)-Fe(3)	87.8(2)	Te(1)-Fe(3)-Fe(2)	58.26(2)
C(21)-Fe(2)-Te(1)	149.8(2)	C(32)-Fe(3)-Fe(1)	95.9(2)
C(23)-Fe(2)-Te(1)	108.4(2)	C(33)-Fe(3)-Fe(1)	100.3(2)
H(1)-Fe(2)-Fe(3)	87(2)	C(31)-Fe(3)-Fe(1)	156.5(2)
C(22)-Fe(2)-Fe(3)	90.0(2)	Te(1)-Fe(3)-Fe(1)	57.84(2)
C(21)-Fe(2)-Fe(3)	92.8(2)	Fe(2)-Fe(3)-Fe(1)	62.36(3)
C(23)-Fe(2)-Fe(3)	165.5(2)	Fe(2)-H(1)-Fe(1)	114(2)
Te(1)-Fe(2)-Fe(3)	58.22(3)	Fe-C-O	174.3(5)-178.3(5)

Table 4. Atomic Coordinates ($\times 10^4$) and Equivalent Displacement Parameters ($\text{Å}^2 \times 10^3$) for IIIa

atom	x	y	z	$U(\text{eq})^a$
Te(1)	730(1)	2114(1)	3941(1)	35(1)
Fe(1)	499(1)	2357(1)	1859(1)	32(1)
Fe(2)	1660(1)	4340(1)	2761(1)	29(1)
Fe(3)	3742(1)	1190(1)	2578(1)	34(1)
O(11)	-76(9)	-649(6)	1719(6)	86(2)
O(12)	-3383(6)	4317(7)	2036(7)	102(3)
O(13)	1801(10)	2936(9)	-601(5)	90(2)
O(21)	-1887(6)	6862(5)	3347(4)	59(1)
O(22)	3017(9)	6128(10)	747(7)	138(4)
O(23)	3423(7)	5018(8)	4469(5)	80(2)
O(31)	6291(7)	914(7)	4114(5)	77(2)
O(32)	3952(9)	-2145(6)	2893(9)	118(3)
O(33)	6301(11)	929(10)	369(7)	119(3)
C(11)	155(9)	511(7)	1775(5)	50(1)
C(12)	-1871(8)	3544(7)	1953(7)	58(2)
C(13)	1295(9)	2713(7)	354(5)	51(1)
C(21)	-528(7)	5876(6)	3131(4)	39(1)
C(22)	2491(9)	5454(9)	1529(6)	72(2)
C(23)	2720(7)	4786(6)	3809(5)	43(1)
C(31)	5303(8)	1004(7)	3530(6)	49(1)
C(32)	3860(9)	-860(8)	2777(9)	71(2)
C(33)	5309(11)	1026(10)	1222(7)	75(2)

^a $U(\text{eq})$ is defined as one-third of the trace of the orthogonalized U_{ij} tensor.

Final refinement on F^2 converged with $R_1 = 0.0381$ and $wR_2 = 0.1110$ for 208 parameters and 3145 observed reflections ($I > 2\sigma(I)$). The positional and displacement parameters are included in Table 4 and the bond metrics are listed in Table 5.

Structure of IV. A deep purple plate $0.3 \times 0.1 \times 0.4$ mm in size was chosen for data collection. The unit cell was determined by least squares refinement of 25 reflections (7.0°

Table 5. Bond Lengths (Å) and Angles (deg) for IIIa

Distances			
Te(1)-Fe(1)	2.4831(7)	Fe(1)-Fe(3)	2.6741(9)
Te(1)-Fe(3)	2.5001(7)	Fe(2)-H(2)	1.47(11)
Te(1)-Fe(2)	2.5089(7)	Fe(2)-H(1)	1.50(7)
Fe(1)-H(2)	1.69(11)	Fe(2)-Fe(3)	2.7229(9)
Fe(1)-Fe(2)	2.6809(9)	Fe(3)-H(1)	1.67(6)
Fe-C	1.780(6)-1.794(5)	C-O	1.117(8)-1.138(7)
Angles			
Fe(1)-Te(1)-Fe(3)	64.91(2)	H(2)-Fe(2)-Te(1)	90(5)
Fe(1)-Te(1)-Fe(2)	64.96(2)	H(1)-Fe(2)-Te(1)	87(3)
Fe(3)-Te(1)-Fe(2)	65.86(2)	C(23)-Fe(2)-Te(1)	97.3(2)
H(2)-Fe(1)-C(12)	86(4)	C(22)-Fe(2)-Te(1)	159.8(3)
H(2)-Fe(1)-C(13)	77(4)	C(21)-Fe(2)-Te(1)	95.7(2)
C(12)-Fe(1)-C(13)	99.6(3)	H(2)-Fe(2)-Fe(1)	34(5)
H(2)-Fe(1)-C(11)	175(4)	H(1)-Fe(2)-Fe(1)	85(3)
C(12)-Fe(1)-C(11)	95.0(3)	C(23)-Fe(2)-Fe(1)	151.8(2)
C(13)-Fe(1)-C(11)	97.9(3)	C(22)-Fe(2)-Fe(1)	104.6(3)
H(2)-Fe(1)-Te(1)	86(4)	C(21)-Fe(2)-Fe(1)	98.1(2)
C(13)-Fe(1)-Fe(2)	100.2(2)	Te(1)-Fe(2)-Fe(1)	57.05(2)
C(11)-Fe(1)-Fe(2)	154.7(2)	H(2)-Fe(2)-Fe(3)	85(5)
Te(1)-Fe(1)-Fe(2)	57.98(2)	H(1)-Fe(2)-Fe(3)	33(3)
Fe(3)-Fe(1)-Fe(2)	61.12(2)	Fe(1)-Fe(2)-Fe(3)	59.31(2)
C(12)-Fe(1)-Te(1)	99.3(3)	H(1)-Fe(3)-C(32)	177(2)
C(13)-Fe(1)-Te(1)	153.2(2)	H(1)-Fe(3)-C(31)	85(2)
C(11)-Fe(1)-Te(1)	99.2(2)	C(32)-Fe(3)-C(31)	95.6(3)
H(2)-Fe(1)-Fe(3)	83(4)	H(1)-Fe(3)-C(33)	86(2)
C(11)-Fe(1)-Fe(3)	98.7(2)	C(32)-Fe(3)-C(33)	96.8(4)
C(12)-Fe(1)-Fe(3)	154.9(3)	C(31)-Fe(3)-C(33)	99.1(4)
C(13)-Fe(1)-Fe(3)	99.2(2)	H(1)-Fe(3)-Te(1)	84(2)
Te(1)-Fe(1)-Fe(3)	57.85(2)	C(32)-Fe(3)-Te(1)	93.2(3)
H(2)-Fe(1)-Fe(2)	30(4)	C(31)-Fe(3)-Te(1)	100.3(2)
C(12)-Fe(1)-Fe(2)	99.2(2)	C(33)-Fe(3)-Te(1)	157.1(3)
C(23)-Fe(2)-Fe(3)	98.3(2)	H(1)-Fe(3)-Fe(1)	82(2)
C(22)-Fe(2)-Fe(3)	108.1(2)	C(32)-Fe(3)-Fe(1)	96.8(2)
C(21)-Fe(2)-Fe(3)	150.5(2)	C(31)-Fe(3)-Fe(1)	154.8(2)
Te(1)-Fe(2)-Fe(3)	56.92(2)	C(33)-Fe(3)-Fe(1)	101.0(3)
H(2)-Fe(2)-H(1)	97(5)	Te(1)-Fe(3)-Fe(1)	57.24(2)
H(2)-Fe(2)-C(23)	173(5)	H(1)-Fe(3)-Fe(2)	29(2)
H(1)-Fe(2)-C(23)	82(3)	C(32)-Fe(3)-Fe(2)	148.5(2)
H(2)-Fe(2)-C(22)	75(5)	C(31)-Fe(3)-Fe(2)	99.9(2)
H(1)-Fe(2)-C(22)	82(3)	C(33)-Fe(3)-Fe(2)	107.4(3)
C(23)-Fe(2)-C(22)	98.5(4)	Te(1)-Fe(3)-Fe(2)	57.23(2)
H(2)-Fe(2)-C(21)	85(5)	Fe(1)-Fe(3)-Fe(2)	59.56(2)
H(1)-Fe(2)-C(21)	177(3)	Fe(2)-H(1)-Fe(3)	118(4)
C(23)-Fe(2)-C(21)	95.6(2)	Fe(2)-H(2)-Fe(1)	116(7)
C(22)-Fe(2)-C(21)	95.3(3)	Fe-C-O	178.4(8)-179.9(7)

$\leq 2\theta \leq 11.50^\circ$), and the crystal system was shown to be orthorhombic. The space group, $Pbca$ (No. 61), was selected on the basis of systematic absences and intensity statistics. The non-hydrogen atoms were refined anisotropically. Hydrogen atoms were included in calculated positions using a riding model with a fixed common displacement parameter. Final refinement on F^2 converged with $R_1 = 0.0841$ and $wR_2 = 0.2994$ for 920 parameters and 5921 observed reflections ($I > 2\sigma(I)$). Selected positional and displacement parameters are listed in Table 6, and the important bond metrics are given in Table 7.

Structure of IIb. An irregular chunk approximately $0.15 \times 0.15 \times 0.5$ mm in size was mounted for data collection. The unit cell was determined to be monoclinic from least squares refinement of 25 reflections ($7.0^\circ \leq 2\theta \leq 15.0^\circ$). The space group was initially chosen as Pc (No. 9) on the basis of systematic absences and intensity statistics. Unsatisfactory behavior during refinement led to the selection of the related, and more common, centric space group $P2_1/c$ (No. 14). Successful refinement of the structure indicated that this was indeed the proper choice. The hydride ligand bound to the metal atoms was located in the difference map during the structure refinement. The non-hydrogen atoms were refined anisotropically, and the hydride was refined isotropically. The hydrogen atoms of the cation were included in calculated positions using a riding model. The refinement on F^2 converged with $R_1 = 0.0507$ and $wR_2 = 0.1348$ for 554 parameters

Table 6. Atomic Coordinates ($\times 10^4$) and Equivalent Isotropic Displacement Parameters ($\text{\AA}^2 \times 10^3$) for IV

atom	x	y	z	$U(\text{eq})^a$
Te(1)	1912(1)	269(1)	562(1)	50(1)
Cu(1)	1657(1)	-103(1)	1781(1)	56(1)
Fe(2)	2885(1)	212(1)	812(1)	41(1)
Fe(1)	2115(1)	-548(1)	1118(1)	41(1)
Fe(3)	2102(1)	688(1)	1311(1)	42(1)
Cl(1)	1218(2)	-374(2)	2365(1)	63(1)
O(11)	2761(4)	-972(5)	1870(3)	62(3)
O(12)	1063(5)	-1148(6)	1274(4)	83(4)
O(13)	2456(6)	-1546(6)	536(4)	87(4)
O(21)	3649(5)	6(5)	1535(4)	61(3)
O(22)	3334(5)	-581(6)	129(4)	73(3)
O(23)	3390(5)	1346(6)	473(4)	66(3)
O(31)	2717(5)	581(5)	2145(4)	63(3)
O(32)	2450(5)	1960(6)	1151(4)	68(3)
O(33)	985(6)	1120(7)	1473(5)	106(5)
C(11)	2512(6)	-785(7)	1587(5)	47(4)
C(12)	1471(7)	-831(9)	1222(5)	62(5)
C(13)	2331(7)	-1140(8)	761(5)	53(4)
C(21)	3349(6)	84(6)	1256(5)	38(3)
C(22)	3150(7)	-261(8)	403(6)	58(4)
C(23)	3190(6)	914(9)	605(5)	56(4)
C(31)	2472(7)	599(6)	1832(5)	47(4)
C(32)	2328(6)	1468(9)	1192(5)	55(4)
C(33)	1436(7)	910(9)	1436(6)	75(6)

^a $U(\text{eq})$ is defined as one-third of the trace of the orthogonalized U_{ij} tensor.

and 2899 observed reflections ($I > 2\sigma(I)$). Selected positional and displacement parameters are given in Table 8, and the noteworthy bond metrics are included in Table 9.

Structure of IIIb. A deep red irregular prism approximately $0.25 \times 0.20 \times 0.40$ mm in size was chosen for data collection. The unit cell was determined by least squares refinement of 25 reflections ($6.50^\circ \leq 2\theta \leq 12.25^\circ$), and the crystal system was shown to be monoclinic. The space group, $P2_1/n$ (No. 14), was chosen on the basis of systematic absences and intensity statistics. The hydride ligands were located in the difference map during refinement and included in the model. The non-hydrogen atoms were refined anisotropically while the hydride ligands were refined isotropically. Final refinement on F^2 converged with $R_1 = 0.0226$ and $wR_2 = 0.0530$ for 208 parameters and 2434 observed reflections ($I > 2\sigma(I)$). The positional and displacement parameters are included in Table 10, and the bond metrics are included in Table 11.

Results

Protonation of I with Triflic Acid. When compounds **I** are allowed to react with 1 equiv of triflic acid in CH_2Cl_2 at -78°C , the monoanions **II** can be isolated cleanly and essentially quantitatively as the $[\text{PPN}]^+$ salts along with $[\text{PPN}][\text{O}_3\text{SCF}_3]$ as a byproduct. The products, unlike the starting material or the byproduct, are completely soluble in both THF and ether. Extraction into ether, therefore, offers a convenient method for purification. When ethereal solutions of **II** are cooled to -20°C for several days, the clusters crystallize as irregular blocks in high yield. The ^1H NMR reveals hydride signals at approximately -22 ppm for both **IIa** and **IIb** (Table 12) indicative of a bridging environment. In both cases the CO ligands show only one resonance at 215.2 ppm in the ^{13}C NMR spectrum. The IR spectra, which are essentially identical for both **IIa** and **IIb**, show a shift of approximately $40\text{--}60\text{ cm}^{-1}$ relative to the dianionic starting materials. The lower overall molecular symmetry of the monoanions is also reflected in the IR spectra which contain several more bands than the spectra of the starting clusters.

Table 7. Selected Bond Lengths (\AA) and Angles (deg) for IV

Lengths			
Te(1)–Fe(2)	2.485(2)	Cu(1)–Fe(1)	2.492(3)
Te(1)–Fe(3)	2.492(2)	Fe(2)–Fe(3)	2.639(3)
Te(1)–Fe(1)	2.493(2)	Fe(2)–Fe(1)	2.656(3)
Cu(1)–Cl(1)	2.150(4)	Fe(1)–Fe(3)	2.738(3)
Cu(1)–C(12)	2.36(2)	Fe–C	1.71(2)–1.83(2)
Cu(1)–Fe(3)	2.478(3)	C–O	1.11(2)–1.22(2)
Cu(1)–C(33)	2.49(2)		
Angles			
Fe(2)–Te(1)–Fe(3)	64.06(7)	C(22)–Fe(2)–Te(1)	99.4(5)
Fe(2)–Te(1)–Fe(1)	64.49(7)	C(21)–Fe(2)–Te(1)	147.4(4)
Fe(3)–Te(1)–Fe(1)	66.61(7)	C(23)–Fe(2)–Te(1)	104.0(5)
Cl(1)–Cu(1)–C(12)	108.5(5)	C(22)–Fe(2)–Fe(3)	155.4(5)
Cl(1)–Cu(1)–Fe(3)	151.6(2)	C(21)–Fe(2)–Fe(3)	94.7(4)
C(12)–Cu(1)–Fe(3)	97.5(4)	C(23)–Fe(2)–Fe(3)	99.6(5)
Cl(1)–Cu(1)–C(33)	118.8(5)	Te(1)–Fe(2)–Fe(3)	58.10(7)
C(12)–Cu(1)–C(33)	104.1(7)	C(22)–Fe(2)–Fe(1)	98.5(5)
Fe(3)–Cu(1)–C(33)	40.7(4)	C(21)–Fe(2)–Fe(1)	94.9(4)
Cl(1)–Cu(1)–Fe(1)	141.4(2)	C(23)–Fe(2)–Fe(1)	158.8(5)
C(12)–Cu(1)–Fe(1)	41.1(4)	Te(1)–Fe(2)–Fe(1)	57.92(7)
Fe(3)–Cu(1)–Fe(1)	66.85(8)	Fe(3)–Fe(2)–Fe(1)	62.26(8)
C(33)–Cu(1)–Fe(1)	95.5(5)	C(33)–Fe(3)–C(32)	93.9(8)
C(11)–Fe(1)–Cu(1)	73.1(5)	C(23)–Fe(3)–C(31)	107.3(8)
C(12)–Fe(1)–Te(1)	101.4(6)	C(32)–Fe(3)–C(31)	97.0(7)
C(13)–Fe(1)–Te(1)	99.0(5)	C(33)–Fe(3)–Cu(1)	69.9(6)
C(11)–Fe(1)–Te(1)	147.8(5)	C(32)–Fe(3)–Cu(1)	153.0(5)
Cu(1)–Fe(1)–Te(1)	100.68(9)	C(31)–Fe(3)–Cu(1)	69.1(5)
C(12)–Fe(1)–Fe(2)	158.5(6)	C(33)–Fe(3)–Te(1)	97.3(7)
C(13)–Fe(1)–Fe(2)	91.5(5)	C(32)–Fe(3)–Te(1)	102.4(5)
C(11)–Fe(1)–Fe(2)	94.4(5)	C(31)–Fe(3)–Te(1)	147.4(4)
Cu(1)–Fe(1)–Fe(2)	110.97(10)	Cu(1)–Fe(3)–Te(1)	101.13(9)
Te(1)–Fe(1)–Fe(2)	57.59(7)	C(33)–Fe(3)–Fe(2)	155.2(7)
Cu(1)–Fe(1)–Fe(3)	56.32(8)	C(32)–Fe(3)–Fe(2)	91.9(5)
Te(1)–Fe(1)–Fe(3)	56.66(7)	C(31)–Fe(3)–Fe(2)	95.9(4)
Fe(2)–Fe(1)–Fe(3)	58.57(7)	Cu(1)–Fe(3)–Fe(2)	111.98(10)
C(12)–Fe(1)–Fe(3)	107.5(6)	Te(1)–Fe(3)–Fe(2)	57.84(7)
C(13)–Fe(1)–Fe(3)	147.9(5)	C(33)–Fe(3)–Fe(1)	109.2(7)
C(11)–Fe(1)–Fe(3)	96.7(5)	C(32)–Fe(3)–Fe(1)	149.9(5)
C(12)–Fe(1)–C(13)	97.2(8)	C(31)–Fe(3)–Fe(1)	94.4(4)
C(12)–Fe(1)–C(11)	104.0(7)	Cu(1)–Fe(3)–Fe(1)	56.82(8)
C(13)–Fe(1)–C(11)	96.9(7)	Te(1)–Fe(3)–Fe(1)	56.72(6)
C(12)–Fe(1)–Cu(1)	65.2(5)	Fe(2)–Fe(3)–Fe(1)	59.17(7)
C(13)–Fe(1)–Cu(1)	155.8(5)	O(12)–C(12)–Fe(1)	167(2)
C(22)–Fe(2)–C(21)	102.4(7)	O(33)–C(33)–Fe(3)	171(2)
C(22)–Fe(2)–C(23)	95.4(7)	Fe–C–O	167(2)–
C(21)–Fe(2)–C(23)	97.7(7)		179.2(1.2)

When a second 1 equiv of triflic acid is added to **IIa** in CH_2Cl_2 at -78°C , the neutral cluster **IIIa** is produced, again in nearly quantitative yield. Care must be taken during the addition of this second 1 equiv of acid not to pass the equivalence point. If excess triflic acid is added, the known cluster, $\text{Fe}_3(\text{CO})_9\text{Te}_2$, is also formed. These two neutral species are practically impossible to separate due to their similar solubilities. Chromatographic separation over silica gel or florisil is not possible because the **IIIa** decomposes when in contact with the chromatographic media. **IIIa** is soluble in hexane, ether, and most other organic solvents. The ^1H NMR displays a single signal at -23.48 ppm again consistent with a bridging configuration for the hydrides which in this case are equiv by symmetry. The carbonyls display a single resonance at 208.5 ppm in the ^{13}C NMR spectrum. As with **IIa**, the IR spectrum in the CO region contains a more complex band pattern than the highly symmetric starting material, **Ia**. Both of these facts indicate that the hydride ligands are bound to the iron atoms rather than the tellurium atom. The EI mass spectrum displays the parent ion at 550 mass units, with the proper isotopic distribution pattern, and a stepwise loss of CO to the bare metal core. **IIIa** is unstable even in the solid state, decomposing slowly to $\text{Te}_2\text{Fe}_3(\text{CO})_9$.

Table 8. Atomic Coordinates ($\times 10^4$) and Equivalent Isotropic Displacement Parameters ($\text{\AA}^2 \times 10^3$) for **IIb**

atom	x	y	z	$U(\text{eq})^a$
Se(1)	-232(2)	3868(1)	6541(1)	43(1)
Fe(1)	50(2)	4374(1)	7648(1)	37(1)
Fe(2)	851(2)	3526(1)	7814(1)	40(1)
Fe(3)	-1975(2)	3757(1)	7376(1)	36(1)
O(11)	2894(12)	4792(4)	7690(6)	67(3)
O(12)	-1652(12)	5155(4)	6909(7)	67(3)
O(13)	-84(10)	4514(3)	9435(6)	59(3)
O(21)	1352(12)	3524(4)	9672(7)	74(3)
O(22)	1100(16)	2566(4)	7440(8)	104(5)
O(23)	3845(15)	3723(5)	7685(9)	111(5)
O(31)	-3594(13)	2944(4)	6723(7)	79(4)
O(32)	-4078(13)	4387(4)	6460(7)	84(4)
O(33)	-2928(12)	3859(4)	9002(7)	73(3)
C(11)	1785(19)	4617(5)	7662(8)	48(4)
C(12)	-991(17)	4841(5)	7196(9)	46(4)
C(13)	-42(14)	4459(4)	8732(10)	41(4)
C(21)	1181(15)	3534(5)	8948(11)	51(4)
C(22)	983(17)	2945(6)	7581(10)	61(4)
C(23)	2641(19)	3649(5)	7738(10)	58(4)
C(31)	-2951(16)	3273(5)	6959(8)	44(4)
C(32)	-3235(17)	4143(5)	6829(9)	52(4)
C(33)	-2563(15)	3828(5)	8359(10)	48(4)

^a $U(\text{eq})$ is defined as one-third of the trace of the orthogonalized U_{ij} tensor.

Table 9. Bond Lengths (\AA) and Angles (deg) for **IIb**

Lengths			
Se(1)-Fe(1)	2.302(2)	Fe(2)-H(1)	1.75(12)
Se(1)-Fe(2)	2.329(2)	Fe(2)-Fe(3)	2.689(3)
Se(1)-Fe(3)	2.329(2)	Fe(3)-H(1)	1.62(12)
Fe(1)-Fe(3)	2.609(3)	Fe-C	1.74(2)-1.79(2)
Fe(1)-Fe(2)	2.621(3)	C-O	1.14(2)-1.17(2)
Angles			
Fe(1)-Se(1)-Fe(2)	68.93(8)	C(23)-Fe(2)-Fe(1)	93.0(5)
Fe(1)-Se(1)-Fe(3)	68.56(8)	C(22)-Fe(2)-Fe(1)	160.2(5)
Fe(2)-Se(1)-Fe(3)	70.52(8)	C(21)-Fe(2)-Fe(1)	94.5(5)
C(11)-Fe(1)-C(13)	98.5(6)	C(23)-Fe(2)-Fe(3)	147.0(5)
C(11)-Fe(1)-C(12)	96.7(7)	C(22)-Fe(2)-Fe(3)	107.3(5)
C(13)-Fe(1)-C(12)	99.4(6)	C(21)-Fe(2)-Fe(3)	103.2(5)
C(11)-Fe(1)-Se(1)	104.0(4)	Se(1)-Fe(2)-Fe(3)	54.74(7)
C(13)-Fe(1)-Se(1)	146.0(4)	Fe(1)-Fe(2)-Fe(3)	58.84(7)
C(12)-Fe(1)-Se(1)	102.9(5)	Fe(1)-Fe(3)-Fe(2)	59.28(7)
C(11)-Fe(1)-Fe(3)	157.1(5)	H(1)-Fe(3)-C(32)	175(4)
C(13)-Fe(1)-Fe(3)	95.3(4)	H(1)-Fe(3)-C(31)	84(4)
C(12)-Fe(1)-Fe(3)	99.1(5)	C(32)-Fe(3)-C(31)	95.3(6)
Se(1)-Fe(1)-Fe(3)	56.20(7)	H(1)-Fe(3)-C(33)	81(4)
C(11)-Fe(1)-Fe(2)	98.4(5)	C(32)-Fe(3)-C(33)	94.2(7)
C(13)-Fe(1)-Fe(2)	96.0(4)	C(31)-Fe(3)-C(33)	101.9(6)
C(12)-Fe(1)-Fe(2)	156.6(5)	H(1)-Fe(3)-Se(1)	90(4)
Se(1)-Fe(1)-Fe(2)	56.01(7)	C(32)-Fe(3)-Se(1)	95.6(5)
Fe(3)-Fe(1)-Fe(2)	61.88(7)	C(31)-Fe(3)-Se(1)	105.4(4)
Se(1)-Fe(2)-Fe(1)	55.07(7)	C(33)-Fe(3)-Se(1)	149.9(5)
H(1)-Fe(2)-Fe(3)	35(4)	H(1)-Fe(3)-Fe(1)	91(4)
H(1)-Fe(2)-C(23)	177(4)	C(32)-Fe(3)-Fe(1)	91.2(5)
H(1)-Fe(2)-C(22)	85(4)	C(31)-Fe(3)-Fe(1)	160.2(5)
C(23)-Fe(2)-C(22)	94.7(7)	C(33)-Fe(3)-Fe(1)	96.2(5)
H(1)-Fe(2)-C(21)	82(4)	Se(1)-Fe(3)-Fe(1)	55.24(7)
C(23)-Fe(2)-C(21)	95.2(7)	H(1)-Fe(3)-Fe(2)	39(4)
C(22)-Fe(2)-C(21)	102.9(7)	C(32)-Fe(3)-Fe(2)	145.9(5)
H(1)-Fe(2)-Se(1)	87(4)	C(31)-Fe(3)-Fe(2)	107.7(5)
C(23)-Fe(2)-Se(1)	96.1(5)	C(33)-Fe(3)-Fe(2)	104.9(4)
C(22)-Fe(2)-Se(1)	105.9(5)	Se(1)-Fe(3)-Fe(2)	54.74(7)
C(21)-Fe(2)-Se(1)	148.0(5)	Fe(3)-H(1)-Fe(2)	106(7)
H(1)-Fe(2)-Fe(1)	88(4)	Fe-C-O	176.6(12)-179(2)

In contrast to the reactivity seen with **IIa**, addition of a second 1 equiv of triflic acid to **IIb** does not cleanly produce **IIIb**. In this case a mixture of **IIIb** and the oxidation product, $\text{Se}_2\text{Fe}_3(\text{CO})_9$, is produced. The presence of the undesired product, $\text{Se}_2\text{Fe}_3(\text{CO})_9$, can be seen easily in both the IR and mass spectra. Both clusters are formed regardless of the temperature of reaction or

Table 10. Atomic Coordinates ($\times 10^4$) and Equivalent Isotropic Displacement Parameters ($\text{\AA}^2 \times 10^3$) for **IIIb**

atom	x	y	z	$U(\text{eq})^a$
Se(1)	2193(1)	1114(1)	4473(1)	27(1)
Fe(1)	1765(1)	1998(1)	3023(1)	25(1)
Fe(2)	-254(1)	1946(1)	4120(1)	24(1)
Fe(3)	2321(1)	3111(1)	4643(1)	24(1)
O(11)	5022(3)	1783(2)	2926(2)	62(1)
O(12)	716(3)	-157(2)	2034(2)	54(1)
O(13)	771(3)	3669(2)	1515(2)	56(1)
O(21)	-2281(3)	-14(2)	3357(1)	47(1)
O(22)	-926(3)	1779(2)	5939(1)	45(1)
O(23)	-2319(3)	3946(2)	3588(2)	51(1)
O(31)	5665(3)	3587(2)	5041(2)	55(1)
O(32)	2301(3)	3140(2)	6595(1)	49(1)
O(33)	967(3)	5420(2)	4193(2)	50(1)
C(11)	3761(4)	1857(3)	2952(2)	37(1)
C(12)	1130(3)	681(3)	2408(2)	35(1)
C(13)	1160(4)	3010(3)	2080(2)	34(1)
C(21)	-1507(3)	746(3)	3647(2)	32(1)
C(22)	-650(3)	1842(2)	5230(2)	31(1)
C(23)	-1528(3)	3167(3)	3796(2)	33(1)
C(31)	4366(4)	3413(3)	4876(2)	34(1)
C(32)	2276(3)	3127(2)	5827(2)	32(1)
C(33)	1496(3)	4531(3)	4388(2)	32(1)

^a $U(\text{eq})$ is defined as one-third of the trace of the orthogonalized U_{ij} tensor.

the rate of acid addition. Both components of the mixture are soluble in hexane, ether, and most other organic solvents. As with **IIIa**, chromatography results in the decomposition of the **IIIb** and only the isolation of $\text{Se}_2\text{Fe}_3(\text{CO})_9$. Attempts to separate the two materials by sublimation also failed. **IIIb** shows a single signal in the bridging hydride region of the ^1H NMR at -24.1 ppm similarly to the $\text{E} = \text{Te}$ case. The carbonyl carbons resonate at 207.6 ppm in the ^{13}C NMR spectrum. Crystals of **IIIb**, along with separate crystals of $\text{Se}_2\text{Fe}_3(\text{CO})_9$, can be grown from a hexane solution at -20 °C.

Structures of IIa,b. Both **IIa** and **IIb** crystallize in the monoclinic space group No. 14 (**IIa** in $P2_1/n$ and **IIb** in $P2_1/c$) with one anion and one cation in the asymmetric unit. In both cases there are no significant contacts between the cation and the anion. A diagram showing the molecular geometry and atom labeling for **IIa** is shown in Figure 1, while **IIb** is shown in Figure 2. For **IIa**, the $\text{Te}-\text{Fe}$ distances average $2.491(3)$ \AA ¹² with little overall variation ($2.4877(8)$ – $2.4927(9)$ \AA). In contrast, the $\text{Fe}-\text{Fe}$ distances ($2.6447(11)$, $2.6237(11)$, and $2.7276(10)$ \AA) show a much larger degree of variation. As expected, the longest of the three $\text{Fe}-\text{Fe}$ bonds is that bridged by the hydride ligand where $\text{Fe}-\text{H}$ distances of 1.65(4) and 1.60(4) \AA were found.

IIIb is isostructural with **IIa** but both $\text{Se}-\text{Fe}$ and $\text{Fe}-\text{Fe}$ distances are shorter than the corresponding distances in **IIa** as a result of the smaller size of selenium. The $\text{Se}-\text{Fe}$ distances average 2.320 \AA , but the bond between the selenium and the unique iron atom is significantly shorter at 2.302(2) \AA . The two unbridged $\text{Fe}-\text{Fe}$ bonds are 2.609(3) and 2.621(3) \AA , while the $\text{Fe}-\text{Fe}$ bond which is bridged by the hydride is slightly longer at 2.689(3) \AA . The hydride location for this compound was less well-determined as seen in the higher errors for the $\text{Fe}-\text{H}$ distances (1.75(12) and 1.62-

(12) Esd's of average values are calculated with the scatter formula:

$$\sigma = \left[\sum_{i=1}^{i=N} \{d_i - \bar{d}\}^2 / (N - 1) \right]^{1/2}$$

Table 11. Bond Lengths (Å) and Angles (deg) for IIIb

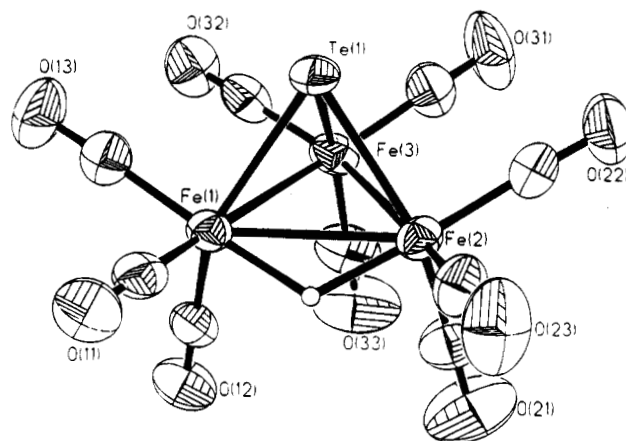
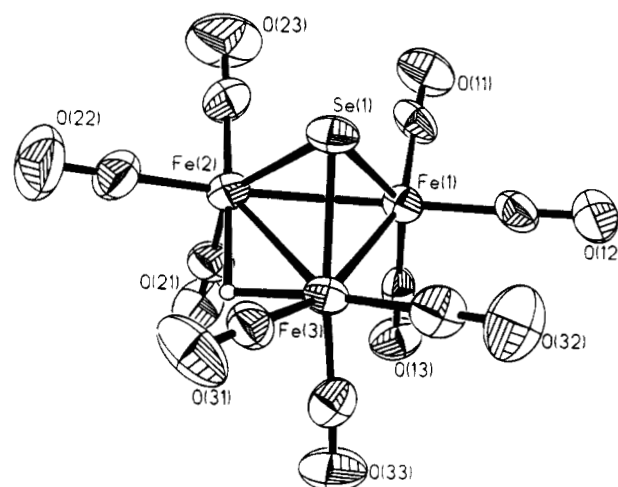
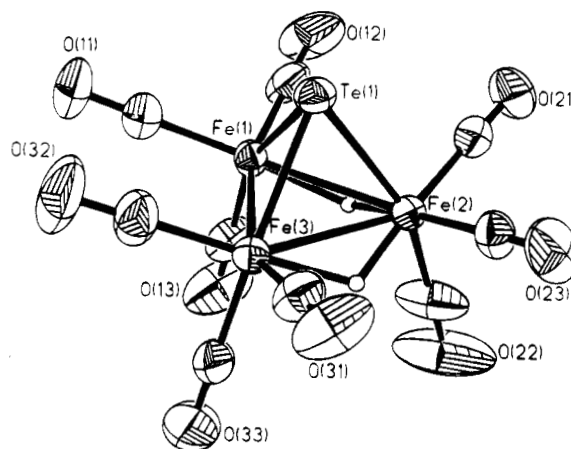
		Lengths	
Se(1)-Fe(3)	2.3106(6)	Fe(1)-Fe(2)	2.6897(9)
Se(1)-Fe(2)	2.3174(7)	Fe(2)-H(1)	1.64(3)
Se(1)-Fe(1)	2.3436(6)	Fe(2)-Fe(3)	2.6065(8)
Fe(1)-H(1)	1.55(3)	Fe(3)-H(2)	1.67(3)
Fe(1)-H(2)	1.62(3)	Fe-C	1.776(3)-1.811(3)
Fe(1)-Fe(3)	2.6813(7)	C-O	1.128(3)-1.144(3)
Angles			
Fe(3)-Se(1)-Fe(2)	68.56(2)	H(1)-Fe(2)-C(22)	173.4(11)
Fe(3)-Se(1)-Fe(1)	70.35(2)	H(1)-Fe(2)-C(23)	81.0(11)
Fe(2)-Se(1)-Fe(1)	70.49(3)	C(22)-Fe(2)-C(23)	93.29(13)
H(1)-Fe(1)-H(2)	89(2)	H(1)-Fe(2)-C(21)	90.0(11)
H(1)-Fe(1)-C(12)	88.5(11)	C(22)-Fe(2)-C(21)	94.45(12)
H(2)-Fe(1)-C(12)	175.5(11)	C(23)-Fe(2)-C(21)	101.55(14)
H(1)-Fe(1)-C(11)	176.2(11)	H(1)-Fe(2)-Se(1)	86.0(11)
H(2)-Fe(1)-C(11)	87.2(12)	C(22)-Fe(2)-Se(1)	97.72(10)
C(12)-Fe(1)-C(11)	95.19(13)	C(23)-Fe(2)-Se(1)	151.78(10)
H(1)-Fe(1)-C(13)	80.9(12)	C(21)-Fe(2)-Se(1)	103.39(10)
H(2)-Fe(1)-C(13)	77.7(11)	H(1)-Fe(2)-Fe(3)	81.7(11)
C(13)-Fe(1)-Fe(3)	110.81(9)	C(22)-Fe(2)-Fe(3)	95.85(10)
Se(1)-Fe(1)-Fe(3)	54.25(2)	C(23)-Fe(2)-Fe(3)	97.57(10)
H(1)-Fe(1)-Fe(2)	33.5(11)	C(21)-Fe(2)-Fe(3)	157.69(10)
H(2)-Fe(1)-Fe(2)	83.2(11)	Se(1)-Fe(2)-Fe(3)	55.60(2)
C(12)-Fe(1)-Fe(2)	96.84(9)	H(1)-Fe(2)-Fe(1)	31.4(11)
C(11)-Fe(1)-Fe(2)	146.32(10)	C(22)-Fe(2)-Fe(1)	150.67(10)
C(13)-Fe(1)-Fe(2)	111.64(10)	C(23)-Fe(2)-Fe(1)	106.48(9)
C(12)-Fe(1)-C(13)	98.21(13)	C(32)-Fe(3)-C(31)	93.28(13)
C(11)-Fe(1)-C(13)	97.53(14)	C(33)-Fe(3)-C(31)	102.00(13)
H(1)-Fe(1)-Se(1)	87.1(11)	H(2)-Fe(3)-Se(1)	89.2(11)
H(2)-Fe(1)-Se(1)	89.5(11)	C(32)-Fe(3)-Se(1)	96.19(9)
C(12)-Fe(1)-Se(1)	94.13(10)	C(33)-Fe(3)-Se(1)	150.95(9)
C(11)-Fe(1)-Se(1)	93.57(10)	C(31)-Fe(3)-Se(1)	103.64(10)
C(13)-Fe(1)-Se(1)	162.55(9)	H(2)-Fe(3)-Fe(2)	84.8(11)
H(1)-Fe(1)-Fe(3)	80.7(11)	C(32)-Fe(3)-Fe(2)	94.90(9)
H(2)-Fe(1)-Fe(3)	36.1(11)	C(33)-Fe(3)-Fe(2)	96.79(9)
C(12)-Fe(1)-Fe(3)	146.76(10)	C(31)-Fe(3)-Fe(2)	158.62(10)
C(11)-Fe(1)-Fe(3)	96.66(10)	Se(1)-Fe(3)-Fe(2)	55.85(2)
C(21)-Fe(2)-Fe(1)	102.32(9)	H(2)-Fe(3)-Fe(1)	34.7(11)
Se(1)-Fe(2)-Fe(1)	55.21(2)	C(32)-Fe(3)-Fe(1)	149.44(9)
Fe(3)-Fe(2)-Fe(1)	60.81(2)	C(33)-Fe(3)-Fe(1)	105.16(9)
H(2)-Fe(3)-C(32)	173.3(11)	C(31)-Fe(3)-Fe(1)	103.61(9)
H(2)-Fe(3)-C(33)	77.6(11)	Se(1)-Fe(3)-Fe(1)	55.404(14)
C(32)-Fe(3)-C(33)	95.77(13)	Fe(2)-Fe(3)-Fe(1)	61.13(3)
H(2)-Fe(3)-C(31)	89.3(11)	Fe(3)-H(2)-Fe(1)	109(2)
Se(1)-Fe(1)-Fe(2)	54.30(2)	Fe(1)-H(1)-Fe(2)	115(2)
Fe(3)-Fe(1)-Fe(2)	58.06(2)	Fe-C-O	177.4(3)-179.3(2)

Table 12. NMR Shifts (ppm) for the Hydride Ligands of I-III

compd	¹ H (hydride)	¹³ C (carbonyl)
Ia		223.7
IIa	-22.02	215.8
IIIa	-23.49	208.0
Ib		220.0
IIb	-22.72	215.2
IIIb	-24.13	207.6

(12) Å). The general structural features are, however, in agreement with those found for IIa.

Structures of IIIa,b. IIIa crystallizes in the triclinic space group $P\bar{1}$ (No. 2), while IIIb crystallizes in the monoclinic space group $P2_1/n$ (No. 14). Diagrams showing the molecular geometry and atom labeling scheme for IIIa and IIIb are shown in Figures 3 and 4, respectively. The Te-Fe distances in IIIa vary significantly from 2.4831(7) to 2.5089(7) Å, with an average value of 2.497 Å. The Fe-Fe distances also show a significant variation at 2.6741(9), 2.6809(9), and 2.7229(9) Å. The hydrides were located crystallographically, but the position of one of them has a high degree of uncertainty associated with it; this is reflected in the errors present in the Fe-H bond distances: 1.68(11), 1.47(11), 1.67(6), and 1.50(7) Å. Although the uncer-

**Figure 1.** Diagram of the anion of IIa showing the displacement ellipsoids (50% probability level) and the atomic labeling scheme.**Figure 2.** Diagram of the anion of IIb showing the displacement ellipsoids (50% probability level) and the atomic labeling scheme.**Figure 3.** Diagram of the molecule IIIa showing the displacement ellipsoids (50% probability level) and the atomic labeling scheme.

tainty of these positions is high, they are consistent with those seen for IIIb for which it was possible to locate the hydride ligands with a higher degree of certainty. As with the monoanions (IIa,b), IIIa and IIIb are isostructural with the largest structural differences being the shorter E-M and M-M bond lengths for the smaller selenide-containing compound. The Fe-

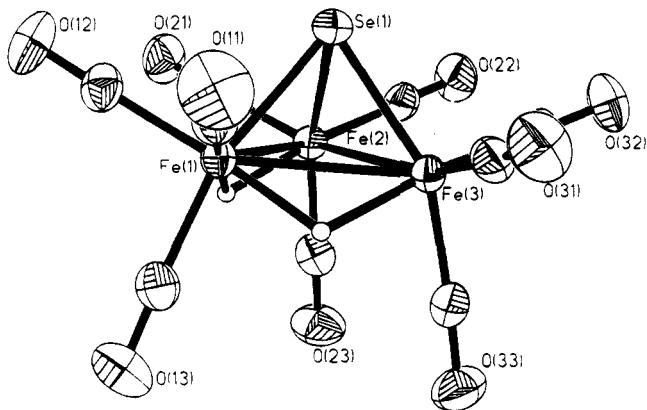


Figure 4. Diagram of the molecule **IIIb** showing the displacement ellipsoids (50% probability level) and the atomic labeling scheme.

Fe distances are 2.690(1) and 2.681(1) Å for the hydride-bridged bonds and 2.607(1) Å for the unbridged bond. The Se–Fe distances in **IIIb** are also grouped into two short, 2.311(1) and 2.317(1) Å, and one long distance, 2.344(1) Å. The Fe–H distances are 1.67(3), 1.62(3), 1.55(3), and 1.64(3) Å.

Reaction of Ia with CuCl. When **Ia** is placed in solution over solid CuCl, the copper salt slowly dissolves and the solution changes color from deep red to dark purple. The halide is not displaced from the copper center; rather, the intact CuCl forms a Lewis acid–base adduct with the cluster. If Et₃PCuCl is used instead of CuCl, the reaction rate is significantly accelerated but the outcome remains unchanged. The IR of the adduct in CH₂Cl₂ retains the simple pattern seen for the starting material but shifted approximately 20 cm⁻¹ higher in energy. If the solution is layered with ether, a mixture of **Ia**, **IV**, and colorless crystals of [PPN][CuCl₂] can be isolated. The [PPN][CuCl₂] can be removed by washing the mixture with methanol. If **Ia** is left standing over a large excess of CuCl for several days, the anionic cluster is oxidized to the known cluster Te₂Fe₃(CO)₉. The crystals used for the structural study were grown from the reaction of **Ia** with Et₃PCuCl.

Structure of IV. **IV** crystallizes in the orthorhombic space group *Pbca* (No. 60) with one cluster anion and two cations in the asymmetric unit. The presence of a chloride bound to the copper, rather than the expected triethylphosphine, was verified on the basis of the cation/anion ratio (2:1). Also, the closest contacts between the chloride and the phenyl rings of the cations are between 3.60 and 4.00 Å. These close contacts do not provide enough space in the lattice for the presence of the ethyl groups which would be associated with the the phosphorus atom. As can be seen in the diagram of the anion (Figure 5), the copper chloride unit bridges an iron–iron bond of the cluster. Additionally, the copper interacts with two of the CO ligands such that the CO's adopt a weakly semibridging geometry. The Cu–C distances are 2.359(3) and 2.488(18) Å, and the corresponding Fe–C–O angles are 166.5(1.6) and 170.6(1.6)°. The two unbridged Fe–Fe bonds are 2.639(3) and 2.656(3) Å, while the bridged bond is significantly longer at 2.738(3) Å. The Te–Fe distances are 2.485(2), 2.492(2), and 2.493(2) Å. The Cu–Cl distance is normal at 2.150(4) Å.

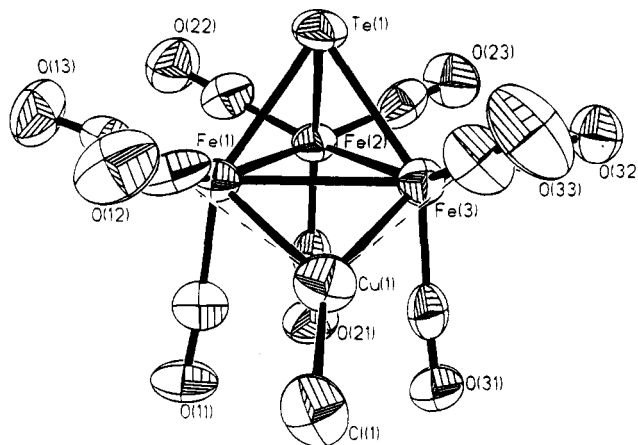


Figure 5. Diagram of the anion of **IV** showing the displacement ellipsoids (50% probability level) and the atomic labeling scheme.

Table 13. Comparison of the Average E–M and M–M Bond Distances (Å) in the [H₂EFe₃(CO)₉]^{(2-x)-} Clusters

cluster	E–M dists	M–M dists	cluster	E–M dists	M–M dists
[SFe ₃ (CO) ₉] ²⁻	2.190	2.584	Ia	2.49(2)	2.631(5)
Ib	2.322(4)	2.610(11)	IIa	2.491(3)	2.665
IIb	2.320	2.640	IIIa	2.497	2.693
IIIb	2.32(4)	2.66(4)			

Discussion

The cluster anions [EFe₃(CO)₉]²⁻ (E = Se, Te) are readily protonated to give mono- and dihydrido clusters, but the second protonations must be carried out very carefully as excess acid leads to oxidation and formation of E₂Fe₃(CO)₉. This situation is worse for E = Se than for E = Te, and in the former case the dihydride could not be isolated in pure form. A similar observation has been made in the case of E = S.¹³ The average E–M and M–M bonds for all six clusters along with the related [SFe₃(CO)₉]²⁻ cluster^{13a} are shown in Table 13. Structural reports of the hydrido sulfur compounds have not yet appeared. The average E–M distances remain relatively constant in both the selenium and tellurium series. For selenium this average value is approximately 2.32 Å, and the average tellurium–iron bond distance is 0.17 Å longer. While the average distance remains the same for all members of a given series, there is a striking difference in the variation of these bond lengths which can be seen within a given cluster in some cases. The Se–Fe bonds in **Ib** are fairly uniform ranging from 2.318(3) to 2.326(3) Å. In contrast, the Se–Fe bonds in **IIb** range from 2.302(2) to 2.329(2) Å and those in **IIIb** are clearly divided into one longer bond (2.3436(6) Å) and two shorter bonds (2.3174(7) and 2.3106(6) Å). The longer bond is to the iron atom bound to both hydride ligands. For **IIIa**, a similar pattern emerges but the difference in bond lengths is smaller (0.009–0.026 Å). It appears that the hydrogen atoms compete more effectively than the main-group atoms for the electron density on the iron atom. However, whether these variations have any effect on the chemistry of the molecules is not clear because of the large degree of variation in the Te–Fe bond lengths of **Ia** and **IIa**.

(13) (a) Fischer, K.; Deck, W.; Schwarz, M.; Vahrenkamp, H. *Chem. Ber.* **1985**, *118*, 4946. (b) Markó, L.; Takács, J.; Sándor, P.; Markó-Monostory, B. *Inorg. Chim. Acta* **1980**, *45*, L189. (c) Markó, L.; Takács, J. *Inorg. Synth.* **1989**, *26*, 243.

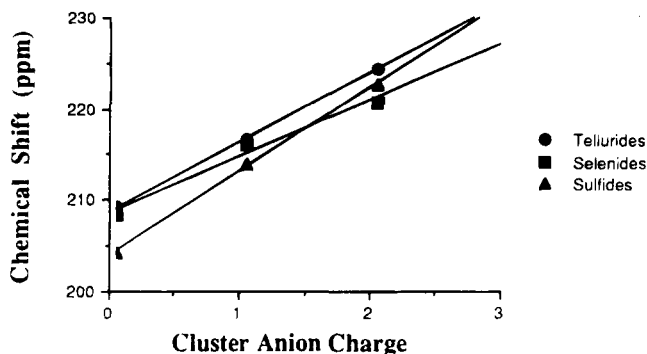


Figure 6. Correlation of the ^{13}C NMR shifts of the carbonyl ligands with cluster charge. The data for the sulfides is taken from ref 13b.

The protonations have a much larger effect on the iron–iron bond distances. With the addition of each hydrogen ligand the average Fe–Fe bond distance in the cluster lengthens by between 0.20 and 0.30 Å (Table 13), while the unbridged distances increase only slightly. This lengthening of the hydride-bridged metal–metal bonds is expected upon the creation of a three-center, two-electron bond from the addition of a proton to the system.

The removal of electron density from the cluster core upon protonation can also be seen spectroscopically. A roughly linear relationship exists between cluster charge and the averaged ^{13}C NMR chemical shifts for the carbonyl ligands (Figure 6). The shifts are consistent with each proton localizing charge away from the cluster framework. The observation of a single ^{13}C signal for each of these compounds indicates rapid equilibration of the CO environments common to cluster compounds of this type. The IR data show a similar stepwise shift of approximately 40–50 cm^{-1} higher in energy on the addition of each proton.

From the crystallographic and spectroscopic data, it is clear that the thermodynamically preferred location of the protons is on the iron–iron bonds. However, the initial site of electrophilic attack could be at Se or Te. In iron carbide and iron nitride clusters electrophiles have been shown to attack at the main-group atom.¹⁴ Compounds isoelectronic and isostructural to $[\text{HAs}\{\text{Fe}(\text{CO})_4\}_3]^{2-}$ would be the expected initial products. The protonations of **Ia,b** were examined by NMR spectroscopy at low temperature (220 K) in order to see if such intermediates could be detected. Even at this temperature, however, the only signals observed corresponded to the transition-metal hydride species. The most satisfactory interpretation of this observation is that the electrophilic attack takes place exclusively at the iron–iron bond rather than the chalcogen atom. However, the possibility of attack at the chalcogen atom followed by a very rapid migration of the hydride ligand cannot be ruled out.

The basicity of the metal–metal bonds in **Ia** can also be seen in the surprising result of the reaction between the cluster and either Et_3PCuCl or CuCl . Copper(I) salts are normally very good mild oxidants of clusters such as these. In cases where a Cu^+ fragment is incorporated in to the cluster it is frequently found

bridging a metal–metal bond similar to H^+ as expected by the isolobal analogy. However, in this case the cluster acting as a Lewis base binds an intact molecule of copper chloride through an iron–iron bond. When Et_3PCuCl is used in place of CuCl , the phosphine is displaced preferentially to the chloride. In all other instances reported to date the reaction of transition-metal carbonylates with L_nCuX (L = phosphine, X = halide) the halide is displaced preferentially to the neutral ligands.^{15–22} Even in a few cases where naked copper halides are employed, no halide incorporation occurs.

Since the crystals used for the structural determination were synthesized from Et_3PCuCl , it was of some concern that the chloride could be a phosphine in which the ethyl groups are extremely disordered. This possibility was ruled out in two ways. The cation/anion ratio in the unit cell is 2:1. If the neutral phosphine were present rather than the chloride, the cluster charge should only be negative one and correspondingly the cation/anion ratio should be 1:1. Additionally, the shortest intermolecular contacts present between the chloride and the phenyl rings of the cation are only 3.60–4.00 Å. Therefore, the cavity around the chloride position is too small to accommodate the alkyl groups of a trialkylphosphine. This was also confirmed by the synthesis of **IV** from CuCl in the absence of PEt_3 .

Structurally, the adduct with CuCl is similar to **IIa**. The Fe–Fe bond to which the copper is bound is the longest at 2.738(3) Å compared with 2.639(3) and 2.656(3) Å for the Fe–Fe bonds which are not bridged by copper. For comparison the hydride-bridged Fe–Fe bond in **IIa** is 2.7276(10) Å. The Cu–Fe distances (2.478(3) and 2.492(3) Å) fall in the middle of the range of values found for other copper iron clusters: $[\text{Et}_4\text{N}]_2\text{[Cu}_3\text{Fe}_3(\text{CO})_{12}]$ (2.421 Å),¹⁵ $[\text{Et}_4\text{N}]_3\text{[Cu}_5\text{Fe}_4(\text{CO})_{16}]$ (2.437 Å),¹⁵ $\text{Fe}_2(\text{CO})_7(\text{PPh}_2)(\text{CuPPh}_3)$ (2.495 Å),¹⁶ $[(\text{diphos})_2\text{Cu}]_2\text{[Cu}_6\text{Fe}_4(\text{CO})_{16}]$ (2.466 Å),¹⁷ $\{(\text{Ph}_3\text{P})_2\text{Cu}\}_2\text{Fe}(\text{CO})_4$ (2.510 Å),¹⁷ $[\text{PPN}][\text{Fe}_4(\text{CuPPh}_3)(\text{CO})_{13}]$ (2.556 Å),¹⁸ and $\text{Fe}_2(\text{CO})_8\{\text{CuP}^t\text{Bu}_3\}_2$ (2.565 Å).¹⁹

Another interesting feature of this mixed-metal structure is the interaction of two of the carbonyls of the cluster with the copper. These two carbonyls act in a semibridging fashion with C–Cu distances of 2.359(16) and 2.488(18) Å. This interaction can also be seen by its effect on the Fe–C–O angles. For the two bridging carbonyls these angles are 166.5(1.6) and 170.6(1.6)°, respectively. For comparison, the other carbonyls have an average Fe–C–O angle of 177°. It is also informative to consider this novel structure from a mechanistic perspective. When **Ia** is left standing over excess CuCl for several days, the primary outcome is oxidation to $\text{Te}_2\text{Fe}_3(\text{CO})_9$. In light of this reactivity, it is conceptually appealing to postulate that the formation of **IV** repre-

(15) Doyle, G.; Eriksen, K. A.; Van Engen, D. *J. Am. Chem. Soc.* **1986**, *108*, 445.

(16) Ferrer, M.; Reina, R.; Rossell, O.; Seco, M.; Solans, X. *J. Chem. Soc., Dalton Trans.* **1991**, 347.

(17) Doyle, G.; Eriksen, K. A.; Van Engen, D. *J. Am. Chem. Soc.* **1985**, *107*, 7914.

(18) Horwitz, C. P.; Holt, E. M.; Brock, C. P.; Shriver, D. F. *J. Am. Chem. Soc.* **1985**, *107*, 8136.

(19) Deng, H.; Knoepfel, D. W.; Shore, S. G. *Organometallics* **1992**, *11*, 3472.

(20) Doyle, G.; Heaton, B. T.; Occhiello, E. *Organometallics* **1985**, *4*, 1224.

(21) Deng, H.; Shore, S. G. *Organometallics* **1991**, *10*, 3486.

(22) Horwitz, C. P.; Shriver, D. F. *J. Am. Chem. Soc.* **1985**, *107*, 8147.

(14) (a) Bogda, P. L.; Woodcock, C.; Shriver, D. F. *Organometallics* **1987**, *6*, 1377. (b) Bradley, J. S. *Adv. Organomet. Chem.* **1983**, *22*, 1 and references contained therein.

sents the very first step in the oxidation mechanism. An important feature of this compound is that the coordination to the CuCl fragment is reversible. Addition of Et₂O causes regeneration of starting cluster which co-crystallizes with the product and [PPN][CuCl₂]. The cluster can thus be viewed as a complex ligand to CuCl as found in a range of L → CuCl complexes.

Conclusion

Protonation readily occurs sequentially at the iron centers in the dianions [EFe₃(CO)₉]²⁻ (E = Se, Te). Spectroscopic evidence indicates that there is a regular decrease in the overall electron density in the cluster cores of **I** and **II** upon protonation. Lengthening of the hydride-bridged Fe–Fe bonds, along with smaller increases in the unbridged bonds, is confirmed crystallographically. The dihydrido compounds **III** are susceptible to oxidation which, under appropriate circumstances, yields the well-known E₂Fe₃(CO)₉ clusters. The characterization of the Lewis acid–base adduct **IV**

shows an unusual variation in Cu(I) chemistry in that the carbonyl cluster functions as a ligand to the neutral CuCl moiety while, in all other known systems, displacement of the halide occurs preferentially. This indicates a very subtle mediation in the electronic capabilities by the main group element in E/M cluster compounds.

Acknowledgment. K.H.W. wishes to thank the National Science Foundation and the Robert A. Welch Foundation for financial support of this work. R.E.B. wishes to thank the NSF for a Predoctoral Fellowship. Dr. Terry Marriott, Finnigan MAT, and VG Analytical are acknowledged for help in obtaining the mass spectral analyses.

Supplementary Material Available: Complete tables of the bond metrics as well as the positional and anisotropic displacement parameters for **IIa,b**, **IIIa,b**, and **IV** (57 pages). Ordering information is given on any current masthead page.

OM9404994

Synthesis and Characterization of *fac*-Tris(trimethylphosphino)iridium(III) Silane Complexes[†]

Eugene A. Zarate,[‡] Vance O. Kennedy,[‡] Judith A. McCune,[§]
Richard S. Simons,[§] and Claire A. Tessier^{*,§}

Departments of Chemistry, The University of Akron, Akron, Ohio 44325-3601, and
Case Western Reserve University, 10900 Euclid Avenue, Cleveland, Ohio 44106-7078

Received April 27, 1994[®]

The synthesis and characterization of iridium(III) silyl complexes of the form IrHX(PMe₃)₃-SiRR'₂ (X = H or D; R = H, D, Cl, or Ph; R' = Ph or *t*-Bu) are described. The complexes are prepared by the oxidative addition of SiXRR'₂ to IrH(PMe₃)₄ with the loss of PMe₃. Three of the complexes have been characterized by single-crystal X-ray diffraction techniques: IrH₂(PMe₃)₃(SiHPh₂), triclinic, space group *P* $\bar{1}$, *a* = 9.793(2) Å, *b* = 16.385(2) Å, *c* = 16.807(4) Å, α = 88.32(2)°, β = 99.70(2)°, γ = 94.72(2)°, *V* = 2649.0(10) Å³, *Z* = 4; IrH₂(PMe₃)₃(SiCl(*t*-Bu)₂), orthorhombic, space group *Pbca*, *a* = 18.519(3) Å, *b* = 15.264(2) Å, *c* = 18.982(3) Å, *V* = 5635.6(15) Å³, *Z* = 8; and IrH₂(PMe₃)₃(SiPh₃), *C*2/*c*, *a* = 34.011(7) Å, *b* = 9.779(2) Å, *c* = 18.733(4) Å, β = 105.46(3)°, *V* = 5998(2) Å³, *Z* = 8. Refinement to convergence gave the conventional and weighted agreement factors *R* = 0.038 and *R*_w = 0.042, *R* = 0.037 and *R*_w = 0.040, and *R* = 0.061 and *R*_w = 0.075 for each structure, respectively.

Introduction

The oxidative addition of silyl hydrides to transition-metal centers is a step in catalytic cycles such as hydrosilylation,¹ dehydrogenative coupling of silanes,² alkyl redistribution reactions of silanes,³ and silylene transfer reactions⁴ by the late transition metals and is a major route for the formation of metal-silicon bonds.⁵ Iridium silyl complexes of general formula IrX(Y)(SiR₃)(PMe₃)₃ are of recent interest because they can be formed by the oxidative addition of a silyl chloride⁶ or can oxidatively add to carbon hydrogen bonds.⁷ As part of an ongoing study of the interaction of transition metals with silanes, we report the reactions of silanes,

most of which contain two reactive substituents, with IrH(PMe₃)₄ to form iridium-silyl complexes.

Experimental Section

All reactions were carried out under an argon atmosphere using standard Schlenk techniques⁸ with greaseless glassware. IrCl₃·3H₂O was purchased from Johnson Matthey. Trichlorosilane, triphenylchlorosilane, diphenyldichlorosilane, and di-*tert*-butyldichlorosilane were obtained from Hüls America and were degassed before using. Di-*tert*-butylchlorosilane was synthesized from trichlorosilane and *tert*-butyllithium (Aldrich).⁹ The dihydridosilanes di-*tert*-butylsilane and diphenylsilane or the corresponding deuterides were produced by treating the dichlorosilanes with a slight excess of either lithium aluminum hydride or lithium aluminum deuteride.^{9,10} The silyl hydrides were characterized by the Si-H stretches in their IR spectra, and the silyl deuterides were characterized by the absence of the Si-H stretch and the presence of an Si-D stretch at 1548 cm⁻¹ for Ph₂SiD₂ ($\bar{\nu}(\text{Si-H})/\bar{\nu}(\text{Si-D}) = 1.382$) and 1532 cm⁻¹ for (*t*-Bu)₂SiD₂ ($\bar{\nu}(\text{Si-H})/\bar{\nu}(\text{Si-D}) = 1.380$). (See Table 2.) All solvents were freshly distilled under nitrogen from sodium and benzophenone. The NMR samples were dissolved in deuterated solvents under inert atmosphere conditions. The ¹H, ¹³C, and ³¹P NMR spectra were recorded at 200 MHz. The ¹H spectra were referenced to the residual proton resonance of the solvent; the ¹³C spectra were referenced to the ¹³C resonance of the solvent; and the ³¹P spectra were referenced to external 85% H₃PO₄, such that shifts to higher frequencies relative to the reference are taken as positive. The ²⁹Si NMR spectra were obtained at 300 MHz using the DEPT pulse sequence¹¹ and were referenced to external TMS. The mass spectra were obtained from B.F. Goodrich using the field desorption (FD-MS) mode. Elemental

* To whom correspondence should be addressed.

[†] Presented in part at the XXIII Organosilicon Symposium, Midland, MI, April 20-21, 1990.

[‡] Case Western Reserve University.

[§] University of Akron.

[®] Abstract published in *Advance ACS Abstracts*, March 15, 1995.

(1) (a) Ojima, I. In *The Chemistry of Organic Silicon Compounds*; Patai, S., Rappoport, Z., Eds.; John Wiley and Sons: New York, 1989; Vol. 2, Chapter 25. (b) Koga, N.; Morokuma, K. *J. Am. Chem. Soc.* **1993**, *115*, 6883.

(2) (a) Tessier, C. A.; Kennedy, V. O.; Zarate, E. A. In *Inorganic and Organometallic Oligomers and Polymers*; Harrod, J. F., Laine, R. M., Eds.; Kluwer: Dordrecht, The Netherlands, 1991; pp 13-22 and references therein. (b) Tilley, T. D.; Woo, H.-G. *Ibid.*, pp 3-11. (c) Corey, J. In *Advances in Silicon Chemistry*; Larson, G., Ed.; JAI: Greenwich, CT, 1991; Vol. 1, p 327.

(3) Curtis, M. D.; Epstien, P. S. *Adv. Organomet. Chem.* **1981**, *19*, 213-255.

(4) (a) Okinoshima, H.; Yamamoto, K.; Kumada, M. *J. Am. Chem. Soc.* **1972**, *94*, 9263. (b) Sakurai, H.; Kamiyama, Y.; Nakadaira, Y. *J. Am. Chem. Soc.* **1977**, *99*, 3879. (c) Seyferth, D.; Shannon, M. L.; Vicks, S. C.; Lim, T. F. O. *Organometallics* **1985**, *4*, 57. (d) Pannell, K. H.; Cervantes, J.; Hernandez, C.; Cassias, J.; Vincenti, S. *Organometallics* **1986**, *5*, 1056.

(5) (a) Tilley, T. D. In *The Chemistry of Organic Silicon Compounds*; Patai, S.; Rappoport, Z., Eds.; John Wiley and Sons: New York, 1989; Vol. 2, Chapter 24. (b) Tilley, T. D. In *The Silicon-Heteroatom Bond*; Patai, S.; Rappoport, Z., Eds.; John Wiley and Sons: New York, 1991; Chapter 10.

(6) Zlota, A. A.; Frolow, F.; Milstein, D. *J. Chem. Soc., Chem. Commun.* **1989**, 1826.

(7) Aizenberg, M.; Milstein, D. *Angew. Chem., Int. Ed. Engl.* **1994**, *33*, 317.

(8) Shriver, D. F.; Drezdson, M. A. *The Manipulation of Air-Sensitive Compounds*, 2nd ed.; John Wiley and Sons: New York, 1986.

(9) Triplett, K.; Curtis, M. D. *J. Organomet. Chem.* **1976**, *107*, 23-32.

(10) Weidenbruch, M.; Peter, W. *Angew. Chem., Int. Ed. Engl.* **1975**, *14*, 642-643.

(11) Blinka, T. A.; Helmer, B. J.; West, R. *Adv. Organomet. Chem.* **1984**, *23*, 193.

Table 1. ¹H NMR Resonance Frequencies for Complexes 1–4^a

compd	δ(Ir–H)	δ(Si–H)	δ(cis-P(CH ₃) ₃) ^b	δ(trans-P(CH ₃) ₃) ^c	δ(C ₆ H ₅)	δ(C(CH ₃) ₃)
1	–12.12 (dd, 92.6 Hz, 17.6 Hz)	5.51 (q, 8.5 Hz)	1.19 (d, 7.1 Hz)	1.29 (d, 7.2 Hz)	8.29 (d, 7.9 Hz), 7.29 (t, 7.2 Hz), 7.12 (d, 7.4 Hz)	
1(D)	–12.10 (dt, 111.6 Hz, 19.5 Hz)		1.17 (d, 7.2 Hz)	1.28 (d, 7.4 Hz)	8.29 (d, 8.0 Hz), 7.29 (t, 7.2 Hz), 7.13 (d, 7.4 Hz)	
2	–13.06 (dd, 92.6 Hz, 16.4 Hz)	4.50 (q, 9.0 Hz)	1.37 (d, 6.9 Hz)	1.24 (d, 7.2 Hz)		1.53 (s)
2(D)	–13.03 (dt, 116.3 Hz, 21.1 Hz)		1.33 (d, 7.0 Hz)	1.25 (d, 7.3 Hz)		1.53 (s)
3	–13.16 (dd, 89.6 Hz, 16.2 Hz)		1.33 (d, 7.3 Hz)	1.15 (d, 7.7 Hz)		1.50 (s)
4	–12.16 (dd, 91.6 Hz, 18.7 Hz)		1.04 (d, 7.3 Hz)	1.32 (d, 7.6 Hz)	8.10 (d, 7.6 Hz), 7.28 (t, 7.2 Hz), 7.19 (d) ^d	

^a s = singlet, d = doublet, t = triplet, q = quartet, m = multiplet, dd = doublet of doublets, dt = doublet of triplets. All spectra were run in C₆D₆.

^b Signal for the protons bound to the two trimethylphosphine ligands *cis* to the silyl ligand. ^c Signal for the protons bound to the trimethylphosphine ligand *trans* to the silyl ligand. ^d Coupling constant unavailable due to interference from the solvent.

Table 2. IR Data for Complexes 1–4

compd	$\bar{\nu}$ (Ir–H) (cm ^{–1})	$\bar{\nu}$ (Si–H) (cm ^{–1})	$\bar{\nu}$ (Ir–D) or $\bar{\nu}$ (Si–D) (cm ^{–1})
1	2002 (s) 2042 (s)	2018 (s)	
1(D)	2000 (m) 2042 (m)		1439 (m)
2	2006 (s) 2172 (w, br)	1952 (s)	
2(D)	2005 (m) 2170 (w, br)		1420 (s)
3	2031 (s) 2105 (s)		
4	2055 (m) 2065 (m)		
SiH ₂ (Ph) ₂		2139 (vs)	
SiD ₂ (Ph) ₂			1548 (vs)
SiH ₂ (<i>t</i> -Bu) ₂		2114 (vs)	
SiD ₂ (<i>t</i> -Bu) ₂			1532 (s), 1545 (s) ^a
SiH(Ph) ₃		2110 (s)	
SiHCl(<i>t</i> -Bu) ₂		2136 (s)	

^a The peaks are nearly indistinguishable.

analyses were performed by either Schwarzkopf Microanalytical Laboratory or Oneida Research Services, Inc., with the aid of a combustion catalyst. Uncorrected melting points were recorded in capillaries sealed under argon unless otherwise stated.

Synthesis of the Iridium Complexes. The complex IrH(PMe₃)₄ was synthesized from IrCl(PMe₃)₄.¹² The complex IrCl(PMe₃)₄ was prepared¹³ from [Ir(C₆H₁₄)Cl]₂, which in turn was prepared¹⁴ from IrCl₃·3H₂O. The products 1–4 were moderately air-stable in the solid state, but were unstable as solutions in air. The ¹H NMR and infrared data for compounds 1–4 are given in Tables 1 and 2, respectively.

Synthesis of IrH₂(PMe₃)₃SiHPh₂, 1. To a stirred solution of IrH(PMe₃)₄ (0.41 g, 0.82 mmol) in toluene (12 mL) was added SiH₂Ph₂ (0.25 mL, 1.35 mmol), dropwise via syringe. A vigorous reaction immediately took place. The reaction was stirred at room temperature for 48 h, during which the original brown solution lightened to a yellow orange color. The solvent was removed under vacuum, and the resulting solid was washed with 2 mL of hexane. The yield was 87%. Colorless crystals suitable for X-ray analysis were obtained upon recrystallization from benzene. Anal. Calcd for IrP₃SiC₂₁H₄₀: C, 41.64; H, 6.66. Found: C, 41.79; H, 6.56. ¹³C[¹H] (C₆D₆): 137.4, 128.8, 127.8, 127.2 (s, SiPh); 27.5 (d of t, 26 Hz, 4 Hz, 1P(CH₃)₃); 23.8 (t of d, 16 Hz, 5 Hz, 2P(CH₃)₃). ³¹P[¹H]

(12) (a) Thorn, D. L.; Tulip, T. H. *Organometallics* **1982**, *1*, 1580–1586. (b) Analytical data for this compound: mp 190–192 °C. Anal. Calcd for IrP₃C₁₂H₃₇: C, 28.97; H, 7.50. Found: C, 28.83; H, 7.41.

(13) (a) Herskovitz, T. *Inorg. Synth.* **1982**, *21*, 99–103. (b) Analytical and other data for this compound: mp 185–187 °C. Anal. Calcd for IrP₃Cl₂H₃₆: C, 27.09; H, 6.82; P, 23.29; Cl, 6.66. Found: C, 27.92; H, 6.85; P, 21.28; Cl, 6.49. The compound initially formed by following the synthesis in ref 9a was thought to be a species of higher coordination than IrCl(PMe₃)₄. After the sample was subjected to vacuum (at about 0.1 Torr) for several hours (until the color changed to that of the desired product), IrCl(PMe₃)₄ was obtained.

(14) (a) Herde, J. L.; Lambert, J. C.; Senoff, C. V. *Inorg. Synth.* **1974**, *15*, 18–20. (b) Herde, J. L.; Senoff, C. V. *Inorg. Nucl. Chem. Lett.* **1971**, *7*, 1029–1031.

(C₆D₆): –60.9 (d, 21 Hz, 2P); –62.3 (t, 22 Hz, 1P). ²⁹Si (DEPT, C₆D₆): –0.323 (d of t, 128 Hz, 10 Hz).

Synthesis of IrHD(PMe₃)₃SiDPh₂, 1(D). To a stirred solution of IrH(PMe₃)₄ (0.33g, 0.67 mmol) in toluene (10 mL) was added SiD₂Ph₂ (0.13 mL, 0.70 mmol), dropwise via syringe. A vigorous reaction immediately took place, and the solution lightened to a yellow color. The reaction was stirred at room temperature for 5 days. The solution was then reduced to half its original volume under vacuum, causing the precipitation of the colorless crystals of 1(D). The solution was filtered, and the solid 1(D) was washed with 2 mL of hexane: mp (in air) 178–180 °C. Anal. Calcd for IrP₃SiC₂₁H₃₈D₂: C, 41.50; H, 6.96; P, 15.29. Found: C, 42.00; H, 6.64; P, 15.69 (where D = H for anal. calcd). ¹³C[¹H] (C₆D₆) d 137.4 (one obscured), 127.7, 127.2 (s, SiPh); 27.5 (pseudo d of t, 26 Hz, 4 Hz, 1P(CH₃)₃); 23.7 (pseudo t of d, 14 Hz, 4 Hz, 2P(CH₃)₃). ³¹P[¹H] (C₆H₆ with 15% C₆D₆): –60.4 (pseudo d, 21 Hz, 2P); –61.5 (pseudo t, 22 Hz, 1P).

Synthesis of IrH₂(PMe₃)₃SiH(*t*-Bu)₂, 2. To a stirred solution of IrH(PMe₃)₄ (0.51 g, 1.02 mmol) in toluene (12 mL) was added SiH₂(*t*-Bu)₂ (0.25 mL, 1.26 mmol), dropwise via syringe. After 48 h, half of the solvent was removed under vacuum and the flask immersed in a –78 °C bath for 24 h. The resulting colorless solid 2 was filtered from the solution and was washed with hexanes (2 mL). The yield was 71%. ¹³C[¹H] (C₆H₆): 34.0 (s, C(CH₃)₃); 29.5 (C(CH₃)₃); 27.5 (d of t, 26 Hz, 4 Hz, 1P(CH₃)₃); 23.8 (t of d, 16 Hz, 6 Hz, 2P(CH₃)₃). ²⁹Si (DEPT, C₆D₆): 23.7 (d of t, 126 Hz, 9 Hz).

Synthesis of IrHD(PMe₃)₃SiD(*t*-Bu)₂, 2(D). This complex was prepared from SiD₂(*t*-Bu)₂ (0.07 mL, 0.33 mmol) and IrH(PMe₃)₄ (0.16 g, 0.32 mmol) in toluene (5 mL) using the same procedure as for 2, except for a reaction time of 3 days. The yield was 44%; mp 163–164 °C. Anal. Calcd for IrP₃SiC₁₇H₄₆D₂: C, 35.96; H, 8.87; P, 16.37 (where D = H for anal. calcd). Found: C, 35.86; H, 8.25; P, 17.88. ¹³C[¹H] (C₆D₆): 33.4 (pseudo s that contains both C(CH₃)₃ and C(CH₃)₃); 27.2 (pseudo d, 24 Hz, 1P(CH₃)₃); 24.7 (pseudo d, 28 Hz, 2P(CH₃)₃). ³¹P[¹H] (C₆D₆): –62.0 (pseudo d (shows minor additional splittings), 18 Hz, 2P); –63.3 (pseudo d, 16 Hz, 1P). FD-MS: calcd *m/z* for (¹⁹³IrP₃SiC₁₇H₄₆D₂)(M⁺) 568, found 568; calcd *m/z* for (¹⁹¹IrP₃SiC₁₇H₄₆D₂)(M⁺) 566, found 566.

Synthesis of IrH₂(PMe₃)₃SiCl(*t*-Bu)₂, 3. The dropwise addition of SiHCl(*t*-Bu)₂ (0.09 mL, 0.45 mmol) to a stirred solution of IrH(PMe₃)₄ (0.22 g, 0.45 mmol) in toluene (2 mL) caused the precipitation of a fine colorless powder. After 3 days, the suspension was filtered and the solid 4 was dried under vacuum. Complex 4 was washed with cold hexanes (2 × 2 mL). The yield was 71%. Anal. Calcd for IrClP₃SiC₁₇H₄₇: C, 34.02; H, 7.89. Found: C, 33.74; H, 7.71. ¹³C[¹H] (C₆D₆): 51.5 (pseudo s, 3P(CH₃)₃); 44.7 (s, C(CH₃)₃); 39.2 (s, C(CH₃)₃). ³¹P[¹H] (CDCl₃): –61.4 (d, 16 Hz, 2P); –63.8 (t, 16 Hz, 1P).

Synthesis of IrH₂(PMe₃)₃SiPh₃, 4. To a stirred solution of IrH(PMe₃)₄ (0.10 g, 0.20 mmol) in toluene (1 mL) was added SiHPh₃ (0.05 g, 0.20 mmol). A vigorous reaction took place followed by the precipitation of colorless crystals. The mixture was filtered and allowed to sit overnight, causing a second crop of crystals to form. The total yield was 81%. The solvent was removed under vacuum, and the product 4 was recrystallized from toluene, yielding crystals which were

Table 3. Summary of Crystallographic Data for 1, 3, and 4

	1	3	4
formula	IrP ₃ SiC ₂₁ H ₄₀	IrClP ₃ SiC ₁₇ H ₄₇	IrP ₃ SiC ₂₇ H ₄₄
formula wt, amu	605.76	600.23	681.80
crystal syst	triclinic	orthorhombic	monoclinic
space group	P $\bar{1}$ (No. 2)	<i>Pbca</i> (No. 61)	<i>C2/c</i> (No. 15)
<i>a</i> , Å	9.793(2)	18.519(3)	34.011(7)
<i>b</i> , Å	16.385(2)	15.264(2)	9.779(2)
<i>c</i> , Å	16.807(4)	18.982(3)	18.733(4)
α , deg	88.32(2)	90	90
β , deg	99.70(2)	90	105.46(3)
γ , deg	94.72(2)	90	90
<i>V</i> , Å ³	2649.(1)	5636(2)	5998(2)
<i>Z</i>	4	8	8
ρ (calcd), g cm ⁻³	1.52	1.49	1.51
cryst dimens, mm ³	0.1 × 0.3 × 0.3	0.2 × 0.2 × 0.4	0.2 × 0.3 × 0.3
diffractometer	Syntex P2 ₁	Syntex P2 ₁	Syntex P2 ₁
radiation	Mo K α (0.710 73 Å)	Mo K α (0.710 73 Å)	Mo K α (0.710 73 Å)
temp, K	296	296	130
scan type	2 θ - θ	2 θ - θ	ω
2 θ scan limits, deg	3.0-50.0	3.0-50.0	3.5-50.0
linear abs coeff, cm ⁻¹	52.51	52.81	46.44
total no. of rflns scanned	103 17 (322 stds)	5446 (165 stds)	5580 (173 stds)
unique rflns	8901	4048	3950
final no. of variables	469	208	289
goodness of fit	1.1879	1.1164	0.98
<i>R</i> (<i>F</i>)	0.038 ($F_o^2 \geq 3\sigma(F_o^2)$)	0.037 ($F_o^2 \geq 3\sigma(F_o^2)$)	0.061 ($F_o \geq 4\sigma(F_o)$)
<i>R</i> _w (<i>F</i>)	0.042 ($F_o^2 \geq 3\sigma(F_o^2)$)	0.040 ($F_o^2 \geq 3\sigma(F_o^2)$)	0.075 ($F_o \geq 4\sigma(F_o)$)

suitable for X-ray analysis. Anal. Calcd for IrP₃SiC₂₇H₄₄: C, 47.56; H, 6.50. Found: C, 47.63; H, 6.32. ³¹P[¹H] (C₆D₆): -58.8 (pseudo s, 2P); -61.4 (pseudo t, 1P). ²⁹Si (DEPT, C₆D₆): 0.094 (d of t, 134 Hz, 8 Hz).

X-ray Structures for Compounds 1, 3, and 4. A colorless single crystal of each compound was chosen for examination by X-ray diffraction methods. The dimensions of the crystals were as follows: **1**, 0.1 × 0.3 × 0.3 mm³; **3**, 0.2 × 0.2 × 0.4 mm³; and **4**, 0.2 × 0.3 × 0.3 mm³. Each crystal was mounted on the end of a thin glass fiber in air. Diffraction measurements were performed on a Syntex P2₁ automated four-circle diffractometer at room temperature for **1** and **3** and at 130 K for **4**. Compound **1** is triclinic, and no systematic absences were observed, suggesting the space group *P* $\bar{1}$. Compound **3** is orthorhombic with systematic absences (*0kl*, *k* = 2*n* + 1; *h0l*, *l* = 2*n* + 1; *hkl*, *h* = 2*n* + 1) indicating the centrosymmetric space group *Pbca*. Compound **4** is monoclinic with systematic absences (*hkl*, *h* + *k* = 2*n* + 1; *h0l*, *l* = 2*n* + 1) indicating the space group *C2/c* with one molecule per asymmetric unit, or the space group *Cc* with two molecules per asymmetric unit. The structure refined satisfactorily in the space group *C2/c*. Data were corrected for Lorentz and polarization factors and reduced to [*F*_o] values. Details relevant to data collection and refinement appear in Table 3.

The analytical form of the scattering factors for neutral iridium, chlorine, phosphorus, silicon, and carbon was used throughout the analyses,^{15a} and the contributions of all non-hydrogen atoms were corrected for both real (*Df'*) and imaginary (*Df''*) components of anomalous dispersion.^{15b} Structures **1**, **3**, and **4** were solved by direct methods.¹⁶ The remaining atoms were located via a series of difference-Fourier syntheses, each being phased by an increasing number of atoms. The unit cells of **1**, **3**, and **4** contain two, one, and one molecules per asymmetric unit, respectively. For all three complexes, all hydrogen atoms, except those bound to iridium or silicon, whose approximate positions could be obtained from the

electron density maps were placed in idealized positions. The remaining hydrogen atoms were included by calculation (based upon C-H = 0.95 Å, tetrahedral or trigonal angles, and idealized thermal parameters with *B* = 1.0 Å² greater than those of the carbon atom to which they are attached).¹⁷ The hydrogen atoms bound to iridium or silicon were selected from among the highest maxima surrounding the metal and the silicon atoms in the final difference-Fourier syntheses, and their existence is consistent with the ¹H NMR and IR data as well as the coordination of the iridium and silicon atoms. In **4** the hydrogen atoms on iridium were not located. Numerical absorption corrections were performed for all the structures of **1** and **3** and were based on the indexed and measured faces of each crystal and the contents of each unit cell. An empirical absorption correction was performed on the structure of **4**. Refinement for **1** and **3** was based on *F*² and included reflections with *F*_o² ≥ 3(*F*_o²). Refinement for **4** was based on *F* and included reflections with *F*_o > 4(*F*_o). Full-matrix least-squares refinement of positional and anisotropic thermal parameters of **1** and **3** for all non-hydrogen atoms led to final convergence with *R* = 0.038, *R*_w = 0.042, and GOF = 1.19 for 469 variables and 8901 reflections for **1**; *R* = 0.037, *R*_w = 0.040, and GOF = 1.16 for 208 variables and 4272 reflections for **3**; and *R* = 0.061, *R*_w = 0.075, and GOF = 0.98 for 289 variables and 5288 reflections for **4**. Positional parameters for the structures of **1**, **3**, and **4** are provided in Tables 4, 5, and 6, respectively.

Results and Discussion

The reactions of several phenyl- or *tert*-butylsilanes with IrH(PMe₃)₄ proceed at room temperature and produce the complexes **1-4** in high yield (eq 1). In each case the net reaction involves the loss of a trimethylphosphine ligand from the iridium reagent and oxidative addition of a Si-H (or Si-D) bond to the iridium, leading to the formation of Ir-Si and Ir-H (or Ir-D) bonds. As expected, preferential oxidative addition of Si-H instead of Si-Cl to the iridium center occurred in the case of (*t*-Bu)₂SiHCl to give **3**. Interestingly, an

(15) (a) *International Tables for X-Ray Crystallography*; Kynoch Press: Birmingham, England, 1974; Vol. IV, pp 99-101. (b) *Ibid.*, pp 149-150.

(16) (a) Main, P.; Fiske, S. J.; Hulls, S. E.; Lessinger, L.; Germain, G.; Declercq, J. P.; Woolfson, M. M. *Multan 80, A system of computer programs for the automatic solution of crystal structures from X-ray diffraction data*; Universities of York and Louvain: York, England, and Louvain, Belgium, 1980. (b) Sheldrick, G. M. *SHELXTL, Crystallographic Computing System*, revision 5.1; Nicolet Instruments Division: Madison, WI, 1986.

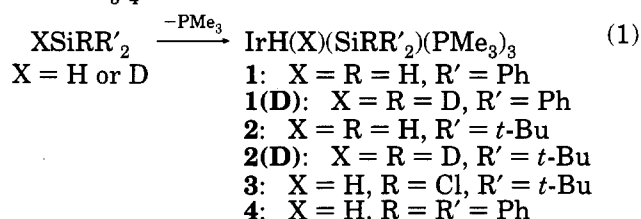
(17) (a) Churchill, M. R. *Inorg. Chem.* **1983**, *12*, 1213-1214. (b) Hamilton, W. C.; Ibers, J. A. *Hydrogen Bonding in Solids*; W. A. Benjamin: New York, 1968; pp 63-66.

Table 4. Positional Parameters for the Non-Hydrogen Atoms of IrH₂(PMe₃)₃(SiHPh₂) (1)

atom	<i>x/a</i>	<i>y/b</i>	<i>z/c</i>
Ir(1)	0.80250(4)	0.74430(2)	0.58140(2)
Ir(2)	0.82810(4)	0.74014(2)	0.09079(2)
P(1)	0.9740(3)	0.7981(2)	0.5117(1)
P(2)	0.7248(3)	0.8654(2)	0.6177(2)
P(3)	0.6289(3)	0.7052(2)	0.4755(2)
P(4)	0.8921(3)	0.7201(2)	-0.0321(2)
P(5)	0.7846(3)	0.6054(2)	0.1309(2)
P(6)	0.6043(3)	0.7760(2)	0.0456(2)
Si(1)	0.9021(3)	0.6172(2)	0.5978(1)
Si(2)	0.9326(3)	0.8758(2)	0.1021(2)
C(1)	1.0919(9)	0.6230(5)	0.6511(5)
C(2)	1.1299(10)	0.6606(6)	0.7262(6)
C(3)	1.2671(11)	0.6669(7)	0.7636(6)
C(4)	1.3683(11)	0.6363(7)	0.7300(7)
C(5)	1.3344(11)	0.5972(7)	0.6570(7)
C(6)	1.1958(9)	0.5903(6)	0.6188(5)
C(7)	0.8175(9)	0.5312(5)	0.6560(5)
C(8)	0.7204(11)	0.5409(6)	0.7047(6)
C(9)	0.6682(12)	0.4756(7)	0.7493(7)
C(10)	0.7125(12)	0.4001(7)	0.7438(6)
C(11)	0.8040(13)	0.3878(7)	0.6923(7)
C(12)	0.8567(11)	0.4517(6)	0.6499(6)
C(13)	1.1429(11)	0.8293(8)	0.5751(7)
C(14)	1.0359(11)	0.7314(7)	0.4408(6)
C(15)	0.9434(12)	0.8887(7)	0.4479(7)
C(16)	0.8566(12)	0.9335(7)	0.6793(7)
C(17)	0.5913(11)	0.8530(7)	0.6822(7)
C(18)	0.6447(14)	0.9383(7)	0.5427(7)
C(19)	0.6072(13)	0.5969(7)	0.4522(8)
C(20)	0.4546(12)	0.7217(9)	0.4893(7)
C(21)	0.6285(12)	0.7506(7)	0.3750(6)
C(22)	1.1156(9)	0.8877(5)	0.1631(5)
C(23)	1.1543(10)	0.8420(6)	0.2335(6)
C(24)	1.2847(13)	0.8548(7)	0.2787(7)
C(25)	1.3824(11)	0.9108(8)	0.2537(7)
C(26)	1.3493(12)	0.9533(7)	0.1833(7)
C(27)	1.2175(11)	0.9418(6)	0.1367(6)
C(28)	0.8458(9)	0.9553(6)	0.1511(5)
C(29)	0.7965(11)	0.9438(6)	0.2241(6)
C(30)	0.7426(11)	1.0025(7)	0.2616(6)
C(31)	0.7286(11)	1.0800(7)	0.2260(7)
C(32)	0.7762(13)	1.0938(7)	0.1550(7)
C(33)	0.8346(11)	1.0329(7)	0.1180(6)
C(34)	1.0773(14)	0.7183(10)	-0.0276(9)
C(35)	0.8290(15)	0.6264(9)	-0.0881(7)
C(36)	0.8549(15)	0.7975(8)	-0.1116(6)
C(37)	0.6318(14)	0.5403(7)	0.0848(8)
C(38)	0.7707(15)	0.5947(7)	0.2377(6)
C(39)	0.9201(14)	0.5362(7)	0.1257(8)
C(40)	0.4921(13)	0.7619(8)	0.1215(8)
C(41)	0.5776(13)	0.8821(8)	0.0089(8)
C(42)	0.4994(11)	0.7195(9)	-0.0380(7)

iridium reagent similar to the one in this study, IrCl(PMe₃)₃(C₈H₁₄), was found to oxidatively add to the Si-Cl bond of MeSiCl₃ at room temperature in 90% yield.⁶ The complexes 1-4 are moderately air-stable solids, but in solution they are air-sensitive. Recently the rhodium analog of 4 was reported.¹⁸

HIr(PMe₃)₄ +



The different possible isomers that could be formed

Table 5. Positional Parameters for the Non-Hydrogen Atoms of IrH₂(PMe₃)₃(SiCl(*t*-Bu)₂) (3)

atom	<i>x/a</i>	<i>y/b</i>	<i>z/c</i>
Ir(1)	0.94772(2)	0.21924(3)	0.58867(2)
Cl(1)	1.1408(2)	0.2299(2)	0.5286(2)
P(1)	0.8731(2)	0.3281(2)	0.6339(2)
P(2)	0.8731(2)	0.1089(2)	0.5817(2)
P(3)	0.9477(2)	0.2668(2)	0.4723(2)
Si(1)	1.0709(1)	0.2440(2)	0.6207(2)
C(1)	1.1059(6)	0.3569(8)	0.6552(7)
C(2)	1.0640(7)	0.3855(10)	0.7217(8)
C(3)	1.0963(8)	0.4237(8)	0.5979(8)
C(4)	1.1874(7)	0.3602(9)	0.6748(8)
C(5)	1.1110(7)	0.1500(9)	0.6786(7)
C(6)	1.0837(9)	0.0597(9)	0.6550(9)
C(7)	1.0890(9)	0.1607(10)	0.7568(7)
C(8)	1.1949(7)	0.1433(11)	0.6752(9)
C(9)	0.7762(6)	0.3237(9)	0.6099(7)
C(10)	0.8619(7)	0.3294(11)	0.7288(6)
C(11)	0.8899(7)	0.4452(9)	0.6147(9)
C(12)	0.9013(7)	0.0013(8)	0.5702(8)
C(13)	0.7894(7)	0.1049(10)	0.5160(9)
C(14)	0.8104(9)	0.0903(11)	0.6638(9)
C(15)	0.8613(7)	0.3009(10)	0.4341(7)
C(16)	1.0031(7)	0.3594(9)	0.4444(7)
C(17)	0.9788(8)	0.1836(10)	0.4099(7)

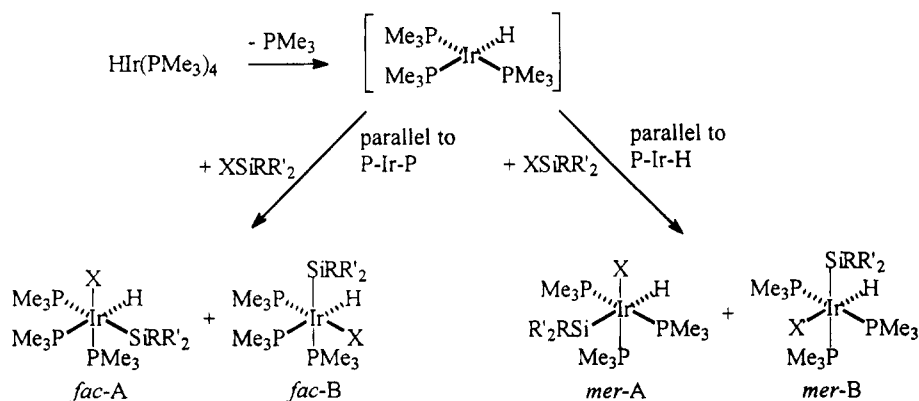
Table 6. Positional Parameters and Equivalent Isotropic Displacement Parameters (Å²) for the Non-Hydrogen Atoms of IrH₂(PMe₃)₃(SiPh₃) (4)

atom	<i>x/a</i>	<i>y/b</i>	<i>z/c</i>	<i>U</i> (eq) ^a
Ir(1)	0.3708(1)	0.3079(1)	0.0795(1)	0.026(1)
Si(1)	0.3587(1)	0.1861(4)	-0.0345(2)	0.028(1)
P(1)	0.3436(1)	0.4490(4)	0.1539(2)	0.035(1)
P(2)	0.3977(1)	0.1320(5)	0.1615(2)	0.037(1)
P(3)	0.4314(1)	0.4174(5)	0.0827(2)	0.038(1)
C(1)	0.3154(4)	0.2595(14)	-0.1107(8)	0.024(5)
C(2)	0.2894(5)	0.359(2)	-0.1004(10)	0.053(7)
C(3)	0.2557(5)	0.4026(18)	-0.1582(9)	0.047(6)
C(4)	0.2485(6)	0.3483(18)	-0.2279(10)	0.050(7)
C(5)	0.2746(5)	0.2474(18)	-0.2413(9)	0.043(6)
C(6)	0.3061(5)	0.2051(17)	-0.1843(8)	0.036(5)
C(7)	0.3402(5)	0.0002(17)	-0.0358(8)	0.040(6)
C(8)	0.3134(5)	-0.0332(16)	0.0072(9)	0.042(6)
C(9)	0.2962(6)	-0.1629(18)	0.0072(11)	0.052(7)
C(10)	0.3069(6)	-0.2645(19)	-0.0381(10)	0.055(7)
C(11)	0.3320(7)	-0.2325(17)	-0.0813(10)	0.055(8)
C(12)	0.3489(5)	-0.1046(17)	-0.0799(9)	0.045(6)
C(13)	0.4023(5)	0.1758(17)	-0.0807(8)	0.038(6)
C(14)	0.4084(5)	0.2734(15)	-0.1296(9)	0.039(6)
C(15)	0.4421(5)	0.2753(18)	-0.1561(9)	0.045(7)
C(16)	0.4709(5)	0.171(2)	-0.1384(11)	0.054(8)
C(17)	0.4659(5)	0.071(2)	-0.0902(10)	0.051(7)
C(18)	0.4329(5)	0.0712(19)	-0.0631(8)	0.043(6)
C(19)	0.3471(6)	0.417(2)	0.2517(9)	0.057(8)
C(20)	0.2880(5)	0.457(2)	0.1195(11)	0.059(7)
C(21)	0.3557(6)	0.6305(19)	0.1582(10)	0.049(7)
C(22)	0.4225(6)	-0.0130(19)	0.1305(11)	0.059(8)
C(23)	0.4376(6)	0.182(2)	0.2462(11)	0.071(7)
C(24)	0.3626(5)	0.0371(19)	0.2016(9)	0.049(7)
C(25)	0.4278(7)	0.547(2)	0.0132(11)	0.068(9)
C(26)	0.4756(5)	0.3209(19)	0.0750(10)	0.048(6)
C(27)	0.4562(5)	0.517(3)	0.1645(11)	0.071(9)

^a Equivalent isotropic *U*, defined as one-third of the trace of the orthogonalized *U*_{ij} tensor.

from the reaction of IrH(PMe₃)₄ and XSiRR'₂ (X = H or D) are shown in Scheme 1. Scheme 1 was formulated on the basis of accepted mechanisms¹⁹ of *cis* addition to the 16-electron square planar Ir(I) intermediate HIr(PMe₃)₃. Loss of a PMe₃ ligand from IrH(PMe₃)₄ would result in the formation of such an intermediate. The Si-H (or Si-D) bond of the silane could oxidatively

Scheme 1



add to the planar intermediate either parallel to the P–Ir–P axis or parallel to the P–Ir–H axis. Addition parallel to the P–Ir–P axis would give two *fac* isomers which are mirror images of each other and therefore indistinguishable by NMR spectroscopy. In both *fac* isomers the H and X substituents occupy *cis* positions. Addition parallel to the P–Ir–H axis would give two *mer* isomers which are not mirror images of each other. In only one of the two *mer* isomers (*mer-A*) are the H and X substituents found in *cis* positions.

The ^1H NMR spectra of 1–4 are listed in Table 1. All complexes show a similar pattern for the protons of the PMe_3 ligands with a resonance for two equivalent (or nearly equivalent in 1(D) and 2(D)) phosphine ligands and a separate resonance for the third phosphine, in the range 1.04–1.37 ppm with the appropriate integrations. Each ^1H NMR signal for the methylphosphines is split into a doublet, $^1J(\text{PH}) = 6.9\text{--}7.7$ Hz, by the phosphorus to which it is attached. The ^1H NMR signal of the phosphines is only consistent with the facial isomers. Two trimethylphosphine ligands situated in a *trans* orientation as in the meridional isomers would give rise to a pseudo triplet/doublet pattern.^{20,21} The silicon hydride resonances of complexes 1 and 2 are quartets with overlapping splittings from the phosphorus atoms, in the appropriate regions of the ^1H NMR spectra (4.50–5.51 ppm). The iridium hydride signals are observed as multiplets with a chemical shift range of –12.01 to –13.16 ppm.²² The iridium hydride resonances for the undeuterated 1–4 exhibit second-order behavior because they are chemically equivalent but magnetically inequivalent with respect to the phosphine ligands. The iridium hydride signal for each undeuterated compound is an apparent doublet of doublets, showing two very different couplings to phosphorus atoms ($^2J(\text{PH}) = 16\text{--}18$ and $90\text{--}92$ Hz). On the basis of similarities with the spectra of related iridium hydride complexes, the smaller $^2J(\text{PH})$ is assigned to coupling to *cis* phosphines and the larger to coupling to *trans* phosphines.^{6,7,19,23} The Ir–H signal of the complexes containing only one iridium hydride, 1(D) and 2(D), appears as the expected doublet of triplets showing two very different couplings

to phosphorus atoms ($^2J(\text{PH}_{\text{cis}}) = 20\text{--}23$ Hz and $^2J(\text{PH}_{\text{trans}}) = 100\text{--}116$ Hz) and unresolved deuterium splittings.

Other NMR spectra of 1–4 were obtained. The ^{31}P – $[\text{H}]$ NMR spectra of 1, 1(D), 2(D), and 3 all show the presence of two different types of phosphine ligands, one of which is split into a doublet by one phosphorus atom and the other of which is split into a triplet by two equivalent phosphorus atoms. Apparently in 1(D) and 2(D) two of the three inequivalent phosphines of the *fac* isomers are in almost identical environments. The DEPT ^{29}Si NMR spectra of compounds 1, 2, and 4 were obtained. The ^{29}Si signals are observed in the range 0–24 ppm, each as a doublet of doublets due to splitting from *trans* ($^2J(\text{PSi}_{\text{trans}}) = 126\text{--}128$ Hz) and *cis* ($^2J(\text{PSi}_{\text{cis}}) = 8\text{--}10$ Hz) phosphine ligands. No evidence for agostic Ir–H–Si interactions, in the form of a significant silicon–hydrogen coupling in the range of 20–136 Hz,²⁴ is observed. The solution ^{13}C – $[\text{H}]$ NMR spectra for the compounds 1–4 show the expected resonances and splitting patterns and are consistent with the other NMR results. There was no evidence for fluxional behavior or slow interconversions between species at room temperature.

The infrared stretching frequencies of the Ir–H and the Si–H bands for the solid state samples (Nujol mulls) of 1–4 are summarized in Table 2. Because the Ir–H and Si–H bands occur at similar regions of the IR spectrum,²⁵ assignments of the Si–H bands for complexes 1 and 2 have been positively made by synthesizing their deuterated analogs 1(D) and 2(D) and comparing their spectra. The band that disappears from the 2200–1950 cm^{-1} region of the spectrum of 1 and 2 on deuteration is assigned to the Si–H stretch. In each case a new band appears with approximately $(1/\sqrt{2})(\bar{\nu}(\text{Si–H}))$ of 1 and 2 in the spectrum of 1(D) and 2(D), respectively. This new band is thought to be the Si–D stretch, but it could also be the Ir–D stretch as at least one band is expected for each. The presence of unrelated signals in the region, however, does not allow for more precise assignments. On the basis of the deuteration studies, two Ir–H stretches are assigned

(20) Harris, R. K. *Can. J. Chem.* **1964**, *42*, 2275.

(21) For a recent example see: Aizenberg, M.; Milstein, D. *J. Chem. Soc., Chem. Commun.* **1994**, 411.

(22) Crabtree, R. H.; Felkin, H.; Fillebeen-Khan, T.; Morris, G. E. *J. Organomet. Chem.* **1979**, *163*, 183.

(23) (a) Harrod, J. F.; Yorke, W. J. *Inorg. Chem.* **1981**, *20*, 1156. (b) Yang, N. K.; Chung, D.-E.; Ko, J.; Kang, S. O. *Bull. Korean Chem. Soc.* **1992**, *13*, 627.

(24) (a) Schubert, U. *Adv. Organomet. Chem.* **1990**, *30*, 151. (b) Crabtree, R. H. *Angew. Chem., Int. Ed. Engl.* **1993**, *32*, 789. (c) Driess, M.; Reigys, M.; Pritzko, H. *Angew. Chem., Int. Ed. Engl.* **1992**, *31*, 1510.

(25) Nakamoto, K. *Infrared and Raman Spectra of Inorganic and Coordination Compounds*, 4th edition; John Wiley and Sons: New York, 1986; pp 323–4, 384–5.

Table 7. Selected Bonding Parameters for IrH₂(PMe₃)₃(SiHPh₂) (1)

Bond Lengths (Å)			
Ir(1)–Si(1)	2.361(3)	Si(1)–C(7)	1.905(9)
Ir(2)–Si(2)	2.369(3)	Si(2)–C(22)	1.907(9)
Si(1)–H(c)	1.184	Si(2)–C(28)	1.891(10)
Si(2)–H(f)	1.219	Ir(1)–P(1)	2.308(3)
Ir(1)–H(a)	1.218	Ir(1)–P(2)	2.316(3)
Ir(1)–H(b)	1.215	Ir(1)–P(3)	2.310(3)
Ir(2)–H(d)	1.119	Ir(2)–P(4)	2.297(3)
Ir(2)–H(e)	1.341	Ir(2)–P(5)	2.316(3)
Si(1)–C(1)	1.918(9)	Ir(2)–P(6)	2.313(3)
Bond Angles (deg)			
Ir(1)–Si(1)–C(1)	114.6(3)	P(5)–Ir(2)–Si(2)	156.3(1)
Ir(1)–Si(1)–C(7)	118.9(3)	P(6)–Ir(2)–Si(2)	96.0(1)
Ir(2)–Si(2)–C(22)	115.6(3)	P(1)–Ir(1)–P(2)	99.0(1)
Ir(2)–Si(2)–C(28)	119.0(3)	P(1)–Ir(1)–P(3)	100.6(1)
Ir(1)–Si(1)–H(c)	104.0	P(2)–Ir(1)–P(3)	100.7(1)
Ir(2)–Si(1)–H(f)	107.1	P(4)–Ir(2)–P(5)	100.0(1)
C(1)–Si(1)–H(c)	109.0	P(4)–Ir(2)–P(6)	98.6(1)
C(7)–Si(1)–H(c)	107.4	P(5)–Ir(2)–P(6)	100.7(1)
C(28)–Si(1)–H(f)	106.1	P(5)–Ir(2)–H(e)	77.0
C(1)–Si(1)–C(7)	102.5(4)	P(6)–Ir(2)–H(d)	152.5
C(22)–Si(2)–C(28)	100.6(4)	P(6)–Ir(2)–H(e)	98.4
Si(1)–Ir(1)–H(a)	81.9	P(1)–Ir(1)–H(a)	76.4
Si(1)–Ir(1)–H(b)	81.3	P(1)–Ir(1)–H(b)	162.3
Si(2)–Ir(2)–H(d)	57.6	P(2)–Ir(1)–H(a)	81.9
Si(2)–Ir(2)–H(e)	84.1	P(2)–Ir(1)–H(b)	83.4
H(a)–Ir(1)–H(b)	86.7	P(3)–Ir(1)–H(a)	176.3
H(d)–Ir(2)–H(e)	87.2	P(3)–Ir(1)–H(b)	96.1
P(1)–Ir(1)–Si(1)	91.2(1)	P(4)–Ir(2)–H(d)	77.5
P(2)–Ir(1)–Si(1)	158.3(1)	P(4)–Ir(2)–H(e)	163.0
P(3)–Ir(1)–Si(1)	96.1(1)	P(5)–Ir(2)–H(d)	106.8
P(4)–Ir(2)–Si(2)	93.9(1)		

for each complex 1–4. Two stretches are expected for the *fac* isomers according to symmetry. This result is consistent with the solid state X-ray crystallographic results for 1 and 3 (see below) and the above solution ¹H NMR results. For the deuterated compounds 1(D) and 2(D) two Ir–H stretches are observed whereas only one would be expected. We attribute this to solid state effects.

The observation of the formation of exclusively facial isomers can be best rationalized by invoking the accepted mechanisms of oxidative addition to Ir(I) centers shown in Scheme 1. Only preferential *cis* addition of R₃Si–H parallel to the P–Ir–P axis yields *cis* dihydride products in which the silicon is *trans* to a phosphine (*fac* isomers), as is implied spectroscopically for complexes 1–4 and is observed crystallographically for 1, 3, and 4 (see below). Either orientation of R₃SiH parallel to the P–Ir–P axis is sterically and electronically equivalent and produces *cis* dihydride products. Thereby apparent scrambling of the H and D positions in 1(D) and 3(D) observed in the infrared spectra can also be accounted for.

The X-ray crystal structures of 1, 3, and 4 have been determined. Selected distances and angles for the structures of 1, 3, and 4 are listed in Tables 7, 8 and 9, respectively. ORTEP drawings of 1, 3, and 4 are shown in Figures 1–3, respectively. Two independent molecules of 1 are present in the unit cell. Though the arrangement of the substituents around the silicon atoms in the two molecules of 1 is different (see below), the differences between the angles and distances are minor and therefore only one of the molecules is represented in Figure 1. The hydrogen atoms on iridium were located for 1 and 3 but not for 4. The crystal structure of 4 had to be determined at 130 K

Table 8. Selected Bonding Parameters for IrH₂(PMe₃)₃(SiCl(*t*-Bu)₂) (3)

Bond Lengths (Å)			
Ir(1)–Si(1)	2.291(3)	Ir(1)–H(b)	1.244
Cl(1)–Si(1)	2.187(4)	Ir(1)–P(1)	2.326(3)
Si(1)–C(1)	1.95(1)	Ir(1)–P(2)	2.329(3)
Si(1)–C(5)	1.96(1)	Ir(1)–P(3)	2.325(3)
Ir(1)–H(a)	1.365		
Bond Angles (deg)			
P(1)–Ir(1)–P(2)	97.4(1)	Ir(1)–Si(1)–Cl(1)	110.3(2)
P(1)–Ir(1)–P(3)	97.3(1)	Ir(1)–Si(1)–C(1)	122.8(4)
P(2)–Ir(1)–P(3)	99.9(1)	Ir(1)–Si(1)–C(5)	112.9(4)
P(1)–Ir(1)–Si(1)	111.1(1)	Cl(1)–Si(1)–C(1)	99.1(4)
P(2)–Ir(1)–Si(1)	141.8(1)	Cl(1)–Si(1)–C(5)	98.8(4)
P(3)–Ir(1)–Si(1)	101.1(1)	C(1)–Si(1)–C(5)	109.5(6)
P(1)–Ir(1)–H(a)	81.1	P(3)–Ir(1)–H(b)	96.9
P(1)–Ir(1)–H(b)	161.6	Si(1)–Ir(1)–H(a)	66.4
P(2)–Ir(1)–H(a)	85.9	Si(1)–Ir(1)–H(b)	62.6
P(2)–Ir(1)–H(b)	90.0	H(a)–Ir(1)–H(b)	84.1
P(3)–Ir(1)–H(a)	176.5		

Table 9. Selected Bonding Parameters for IrH₂(PMe₃)₃(SiPh₃) (4)

Bond Lengths (Å)			
Ir(1)–P(1)	2.323(5)	Si(1)–C(1)	1.90(2)
Ir(1)–P(2)	2.324(4)	Si(1)–C(7)	1.92(2)
Ir(1)–P(3)	2.306(5)	Si(1)–C(13)	1.91(2)
Ir(1)–Si(1)	2.382(4)		
Bond Angles (deg)			
Ir(1)–Si(1)–C(1)	113.5(5)	P(2)–Ir(1)–Si(1)	99.6(2)
Ir(1)–Si(1)–C(7)	117.6(5)	P(1)–Ir(1)–Si(1)	146.4(1)
Ir(1)–Si(1)–C(13)	117.6(5)	P(3)–Ir(1)–Si(1)	101.3(2)
C(1)–Si(1)–C(7)	99.3(6)	P(1)–Ir(1)–P(2)	101.1(2)
C(7)–Si(1)–C(13)	103.6(8)	P(1)–Ir(1)–P(3)	101.8(2)
C(1)–Si(1)–C(13)	102.7(7)	P(2)–Ir(1)–P(3)	97.8(2)

because at room temperature only a poor structure (*R* = 12.2%, carbon atoms left isotropic) could be obtained.

In the solid state, both 1 and 3 assume distorted octahedral arrangements in which a PMe₃ ligand and the silyl group occupy the axial positions, and the four equatorial positions are occupied by two iridium hydrides and two PMe₃ ligands such that each iridium hydride is roughly *trans* to a phosphine. Complex 4 assumes a similar structure, but the quality of the refinement did not permit the location of the iridium hydrides. The solid state geometries for complexes 1, 3, and 4 show a *facial* arrangement of the phosphine ligands.

Trends in the *cis*-P–Ir–P, *trans*-Si–Ir–P, and C–Si–C angles and Ir–Si and Si–C distances allow us to conclude that the steric bulk of the silyl fragments increases in the order SiPh₂H (1) < SiPh₃ (4) < Si(*t*-Bu)₂Cl (3). The long Si–Cl bond length of 2.184 Å in 3 is also consistent with the greater steric bulk of the Si(*t*-Bu)₂Cl fragment. Other Si–Cl bond lengths in iridium(III) complexes of less sterically hindered silanes range from 2.094 to 2.139 Å.²⁶ The Ir–Si distances of the two molecules of 1 (2.361(3) and 2.369(3) Å) and that of 4 (2.382(4) Å) are shorter than that of 3 (2.392(3) Å). These distances are also short when compared to other Ir(III)–Si distances of mononuclear unstrained complexes, which range from 2.390 to 2.416 Å^{26,27} with the exception of the 2.299 Å distance observed in the

(26) Hays, M. K.; Eisenberg, R. *Inorg. Chem.* **1991**, *30*, 2623.(27) (a) Fernández, M. J.; Eseruelas, M. A.; Oro, L. A.; *Organometallics* **1987**, *6*, 1751. (b) Rappoli, B. J.; Janik, T. S.; Churchill, M. R. Thompson, J. S.; Atwood, J. D. *Organometallics* **1988**, *7*, 1939. (c) Ricci, J. S.; Koetzle, T. F.; Fernandez, M.-J.; Maitlis, P. M.; Green, J. C. *J. Organomet. Chem.* **1986**, *299*, 383.

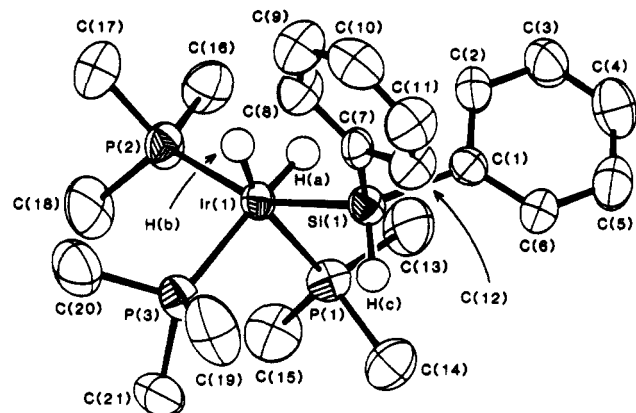


Figure 1. ORTEP labeling diagram for one molecule of $\text{IrH}_2(\text{PMe}_3)_3(\text{SiHPh}_2)$ (**1**). The thermal ellipsoids are drawn at the 50% probability level. The hydrogen atoms, except those bound to iridium and silicon, have been omitted for clarity.

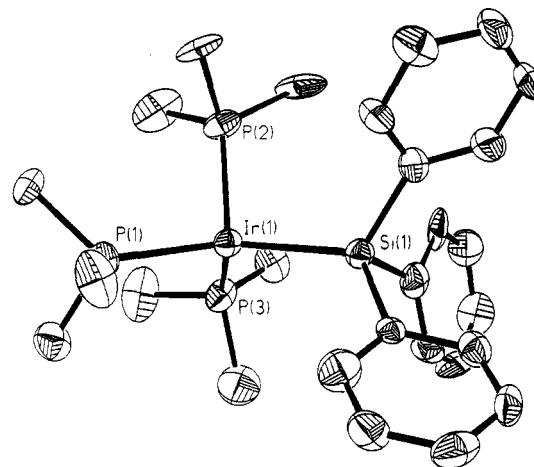


Figure 3. Thermal ellipsoid labeling diagram for $\text{IrH}_2(\text{PMe}_3)_3(\text{SiPh}_3)$ (**4**). The thermal ellipsoids are drawn at the 50% probability level. The hydrogen atoms on iridium were not found, and all other hydrogen atoms have been omitted for clarity.

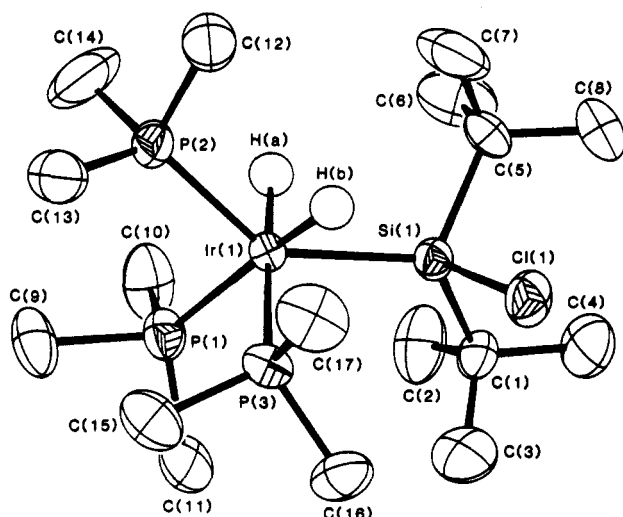


Figure 2. ORTEP labeling diagram for $\text{IrH}_2(\text{PMe}_3)_3(\text{SiCl}(t\text{-Bu})_2)$ (**3**). The thermal ellipsoids are drawn at the 50% probability level. The hydrogen atoms, except those bound to iridium, have been omitted for clarity.

complex $\text{Ir}(\text{PMe}_3)_3\text{Cl}_2(\text{SiMeCl}_2)$.⁶ The tendency toward shorter Ir(III)–Si bond lengths in complexes with three PMe_3 ligands may be due to the small steric requirements of the PMe_3 ligand relative to other phosphine ligands. In all three complexes the Ir–P(*trans*) (with respect to the silicon atom) distance is marginally longer than Ir–P(*cis*) distances. The range of Ir–P bond distances in **1**, **3**, and **4** are comparable to each other and to those of other Ir(III) complexes with three PMe_3 ligands.^{6,7,28}

The hydrides on iridium and silicon of **1** and **3** were located in the difference maps but were not refined. The lack of long Ir–Si bonds and the positions of the hydrides of **1** and **3** indicate that all hydrides are terminal, and no evidence was found for agostic Si–H or H–H bonding to iridium, in agreement with NMR spectral data. This is consistent with the observation that agostic Si–H interactions with iridium have been

only observed at low temperatures.²⁹ A computational study of the oxidative addition of SiH_4 to the related 14-electron complex $\text{RhCl}(\text{PH}_3)_2$ indicates that an agostic $\eta^2\text{-SiH}_4$ complex is a transition state but not an intermediate.³⁰

Crystallographic studies of mononuclear complexes of diphenylsilane are available when the metal is iridium (**1**), ruthenium,³¹ chromium,³² and manganese³³ (two examples). There exists a relationship between the C–Si–C angle of the diphenylsilane ligand and the extent of oxidative addition. In the former two complexes the C–Si–C angle is in the range $100.5\text{--}102.5^\circ$ and the Si–H has fully oxidatively added to the metal, whereas in the latter three complexes the angle increases to $105.9\text{--}107.0^\circ$ and the Si–H interacts in an agostic fashion.

A long-range goal of this research is to find ways to induce elimination of X–Y from an X–Ir–Si–Y moiety to give Ir=Si bonds or (Ir–Si)₂ rings. The success of an elimination process may depend on the relative arrangement of the X and Y substituents around the Ir–Si bond and/or whether steric interactions impede X and Y from attaining the correct arrangement. Views of both the molecules of **1** and the complexes **3** and **4** are shown in Figure 4. Each molecule has been drawn looking down the Si–Ir axis with the Si atom forward such that the phosphine is *trans* to the silicon and the two iridium hydrides are toward the bottom of the drawing. The two molecules of **1** have very different orientations of the phenyl groups; however, in both, the phenyl groups are staggered relative to the *cis*-phosphines. In the first molecule of **1** the hydrides are symmetrically disposed whereas in the second molecule a hydride on silicon H(f) is nearly opposite to the iridium hydride H(e) (dihedral angle = 169°). In **3** and **4** a *cis*-phosphine is eclipsed with a hydrocarbon substituent

(28) (a) Herskovitz, T.; Guggenberger, L. *J. Am. Chem. Soc.* **1976**, *98*, 1615. (b) Thorn, D. L.; Tulip, T. H. *J. Am. Chem. Soc.* **1981**, *103*, 5984. (c) Thorn, D. L.; Harlow, R. L. *J. Am. Chem. Soc.* **1989**, *111*, 2575. (d) Merola, J. S.; Lapido, F. T. *Inorg. Chem.* **1990**, *29*, 4172. (e) Baker, R. T.; Ovenall, D. W.; Calabrese, J. C.; Westcott, S. A.; Taylor, N. J.; Williams, I. D.; Marder, T. B. *J. Am. Chem. Soc.* **1990**, *112*, 9399.

(29) Luo, X.-L.; Crabtree, R. H. *J. Am. Chem. Soc.* **1989**, *111*, 2527.

(30) Koga, N.; Morokuma, K. *J. Am. Chem. Soc.* **1993**, *115*, 6883.

(31) Straus, D. A.; Zhang, C.; Quimbata, G. E.; Grumbine, S. D.; Heyn, R. H.; Tilley, T. D.; Rheingold, A. L.; Geib, S. J. *J. Am. Chem. Soc.* **1990**, *112*, 2673.

(32) Schubert, U.; Müller, J.; Alt, H. G. *Organometallics* **1987**, *6*, 469.

(33) Schubert, U.; Scholz, G.; Müller, J.; Ackermann, K.; Wörle, B.; Stansfield, R. F. D. *J. Organomet. Chem.* **1986**, *306*, 303.

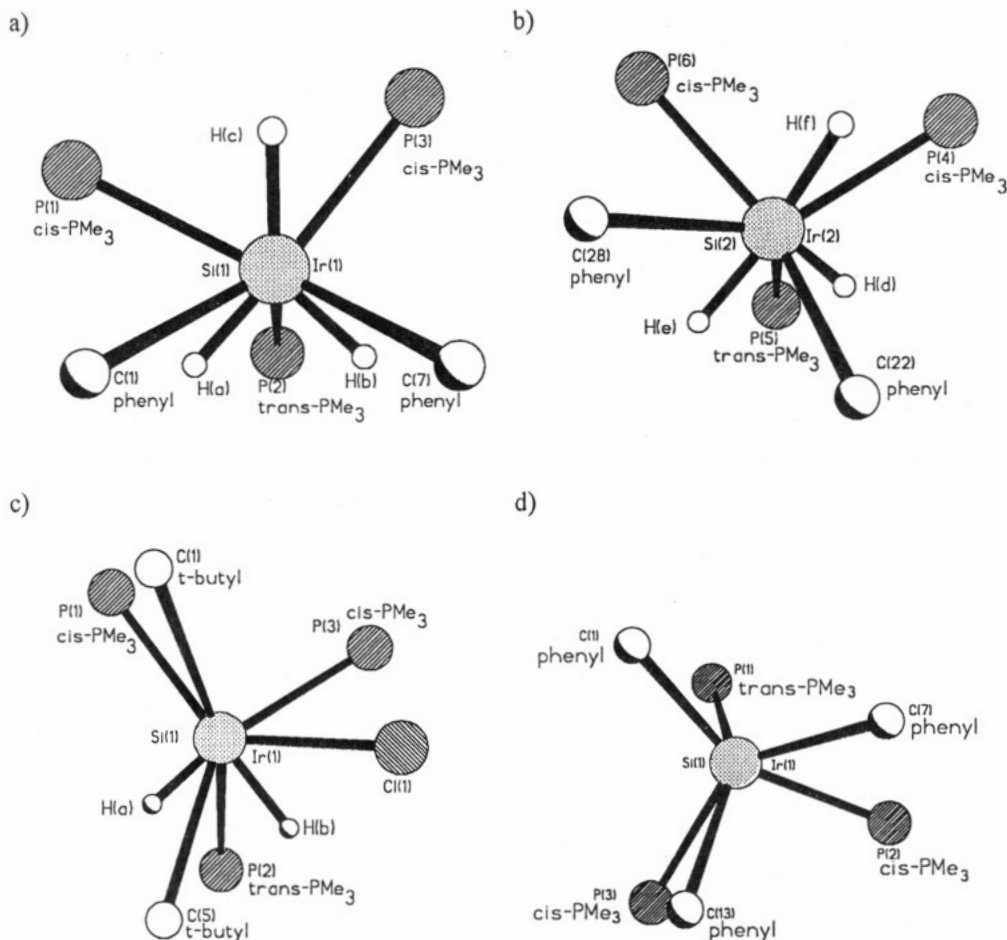


Figure 4. Projections of both molecules of **1** (a and b), **3** (c), and **4** (d) down the Ir–Si bond with the silicon atom in front.

on the silicon. Crystal-packing forces cannot be eliminated as a reason, though there are no close intermolecular contacts. In **3** the silyl chloride is on the same side of the Ir–Si bond as the iridium hydride H(b) (dihedral angle = 46°).

The spectroscopic and crystallographic results presented within this paper show that monomeric iridium–silyl complexes are formed by the reaction of a silane with an iridium(I) phosphine compound. Though spectral results indicate free rotation around the Ir–Si bond, crystallographic results of **3** and preliminary reaction studies indicate that steric hindrance may impede reactions of the di(*tert*-butyl)silyl complexes.³⁴ Further studies of **1–4** will be directed toward understanding the reaction chemistry of the hydride or chloride substituents on the silyl groups or the iridium center with the goal of forming Ir=Si bonds or (Ir–Si)₂ rings. Other reactions pathways are possible. Recently, thermolysis of Ir(PMe₃)₃(SiPh₃)(Me)H gave methane and an iridasilacyclobutane complex in which the *ortho* C–H on the phenyl ring had been activated.⁷ Loss of H₂ from **4** could give a similar complex. The reactions of silanes

which contain more than one reactive substituent with IrCl(PMe₃)₄ are also being investigated.

Acknowledgment. We thank Wiley Youngs and Peter Rinaldi for many useful discussions, James Howe (deceased) for library research, and a reviewer for ref 20. Acknowledgment is made to the donors of the Petroleum Research Fund, administered by the American Chemical Society, the Office of Naval Research, and the University of Akron Faculty Research Committee for support of this research. NMR facilities were supported by a State of Ohio Board of Regents Academic Challenge Grant and a grant from the National Science Foundation Chemical Instrumentation Program (CHE-8820644). We thank Robert Lattimer of B.F. Goodrich for FD-MS. V.O.K. would like to thank NASA–Lewis Research Center for a NASA Fellowship.

Supplementary Material Available: Complete data collection parameters, thermal parameters, and complete tables of bond lengths and angles for the structures of **1**, **3**, and **4** (15 pages). Ordering information is given on any current masthead page.

(34) Zarate, E. A.; Tessier, C. Unpublished results.

Rate and Mechanism of Oxidative Addition of Aryl Triflates to Zerovalent Palladium Complexes. Evidence for the Formation of Cationic (σ -Aryl)palladium Complexes

Aenny Jutand* and Adil Mosleh

Ecole Normale Supérieure, Département de Chimie, CNRS URA 1679, 24 Rue Lhomond, 75231 Paris Cedex 5, France

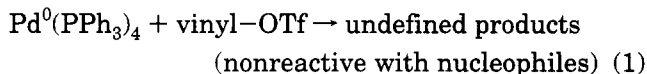
Received June 17, 1994[®]

The rate of oxidative addition of $\text{Pd}^0(\text{PPh}_3)_4$ to aryl triflates is monitored by amperometry and conductivity measurements in DMF. The kinetics follow a Hammett correlation, the oxidative addition being faster when the aryl group is substituted with an electron-withdrawing group. This reaction proceeds in the absence of deliberately added halides, to afford a unique, well-defined, stable arylpalladium complex that has been characterized for the first time, by conductivity measurements and mass and IR spectroscopies, as a cationic complex $\text{Ar-Pd}(\text{PPh}_3)_2^+$ with CF_3SO_3^- as the counteranion. The oxidative addition is faster in the presence of added chloride and affords neutral complexes *trans*- $\text{Ar-PdX}(\text{PPh}_3)_2$. The aryl triflates are found to be less reactive with $\text{Pd}^0(\text{PPh}_3)_4$ than aryl iodides but slightly more reactive than aryl bromides.

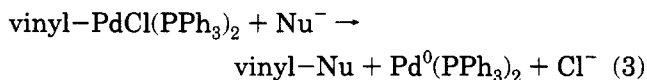
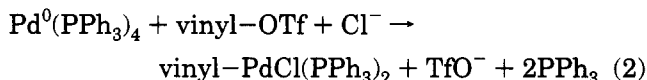
Introduction

The field of palladium-catalyzed coupling reactions involving aryl and vinyl triflates is extensive.¹⁻⁸ There is a general agreement on the fact that the first step of

the catalytic cycle is an oxidative addition of the aryl or vinyl triflate to a palladium(0) complex. However some palladium-catalyzed cross-coupling reactions of triflate derivatives are efficient only when performed in the presence of a large excess of chloride anion relative to the catalyst.¹⁻³ Extra chloride is always necessary in the case of coupling reactions involving vinyl triflates.^{1,2} In those cases, it was clearly established by Stille that the (σ -vinyl)palladium(II) complexes resulting from the oxidative addition were not stable:^{2b}



Performing the oxidative addition in the presence of chloride afforded a stable (σ -vinyl)palladium chloride complex, directly or via a hypothetical cationic complex $\text{vinyl-Pd}(\text{PPh}_3)_n^+, \text{TfO}^-$ ($n = 2$ or 3).^{2b}



By analogy, aryl triflates were declared also to react via similar pathways. It was supposed that the oxidative addition of aryl triflates the zerovalent palladium complexes afforded nonstable, possibly cationic complexes $\text{aryl-PdL}_n^+, \text{TfO}^-$ ($n = 2$ or 3 ?),⁵ whereas stable aryl-PdCIL_2 complexes would be produced in the presence of chloride.^{3a,7a} Only one isolation of a stable (σ -

(5) Aoki, S.; Fujimura, T.; Nakamura, E.; Kuwajima, I. *J. Am. Chem. Soc.* **1988**, *110*, 3296.

(6) Cabri, W.; Candiani, I.; Bedeshi, A.; Santi, R. *Tetrahedron Lett.* **1991**, *32*, 1753.

(7) (a) Farina, V.; Krishnan, B.; Marshall, D. R.; Roth, G. P. *J. Org. Chem.* **1993**, *58*, 5434. (b) Ciattini, P. G.; Morera, E.; Ortar, G. *Tetrahedron Lett.* **1994**, *35*, 2405.

(8) (a) Jutand, A.; Negri, S.; Mosleh, A. *J. Chem. Soc., Chem. Commun.* **1992**, 1729. (b) Jutand, A.; Mosleh, A. *Synlett* **1993**, 568.

* To whom all correspondence should be addressed.

[®] Abstract published in *Advance ACS Abstracts*, March 15, 1995.

(1) (a) Stille, J. K. *Pure Appl. Chem.* **1985**, *57*, 1771. (b) Stille, J. K. *Angew. Chem., Int. Ed. Engl.* **1986**, *25*, 508. (c) Scott, W. J.; McMurry, J. E. *Acc. Chem. Res.* **1988**, *21*, 47.

(2) (a) Scott, W. J.; Crisp, G. T.; Stille, J. K. *J. Am. Chem. Soc.* **1984**, *106*, 4630. (b) Scott, W. J.; Stille, J. K. *J. Am. Chem. Soc.* **1986**, *108*, 3033.

(3) (a) Echavarren, A. M.; Stille, J. K. *J. Am. Chem. Soc.* **1987**, *109*, 5478; **1988**, *110*, 1557. (b) Krolski, M. E.; Renaldo, A. F.; Rudisill, D. E.; Stille, J. K. *J. Org. Chem.* **1988**, *53*, 1170. (c) Martorell, G.; Garcia-Raso, A.; Saa, J. M. *Tetrahedron Lett.* **1990**, *31*, 2357. (d) Chen, Q.-Y.; He, Y.-B. *Chin. J. Chem.* **1990**, *451*. (e) Saa, J. M.; Martorell, G.; Garcia-Raso, A. *J. Org. Chem.* **1992**, *57*, 678. (f) Badone, D.; Cecchi, R.; Guzzi, U. *J. Org. Chem.* **1992**, *57*, 6321. (g) Saa, J. M.; Martorell, G. *J. Org. Chem.* **1993**, *58*, 1963. (h) Andersson, C. M.; Hallberg, A. *J. Org. Chem.* **1988**, *53*, 2112.

(4) (a) Cacchi, S.; Ciattini, P. G.; Morera, E.; Ortar, G. *Tetrahedron Lett.* **1986**, *27*, 3931. (b) Chen, Q.-Y.; He, Y.-B.; Yang, Z.-Y. *J. Chem. Soc., Chem. Commun.* **1986**, 1452. (c) Peterson, G. A.; Kung, F.-A.; McCallum, J. S.; Wulff, W. D. *Tetrahedron Lett.* **1987**, *28*, 1381. (d) Orsini, F.; Pelizzoni, F.; Vallarino, L. M. *J. Organomet. Chem.* **1989**, *367*, 375. (e) Arcadi, A.; Cacchi, S.; Marinelli, F. *Tetrahedron Lett.* **1989**, *30*, 2581. (f) Hirota, K.; Isobe, Y.; Maki, Y. *J. Chem. Soc., Perkin Trans. 1* **1989**, *12*, 2513. (g) Takagi, K.; Sakakibara, Y. *Chem. Lett.* **1989**, *11*, 1957. (h) Cabri, G. W.; De Bernardinis, S.; Francalanci, F.; Penco, S. *J. Org. Chem.* **1990**, *55*, 350. (i) Saa, J. M.; Dopico, M.; Martorell, G.; Garcia-Raso, A. *J. Org. Chem.* **1990**, *55*, 991. (j) Cabri, W.; Candini, I.; Bedeschi, A.; Santi, R. *J. Org. Chem.* **1990**, *55*, 3654. (k) Takayuki, O. E.; Miyaura, N.; Susuki, A. *Synlett* **1990**, 221. (l) Fu, J. M.; Snieckus, V. *Tetrahedron Lett.* **1990**, *31*, 1665. (m) Hatanaka, Y.; Hiyama, T. *Tetrahedron Lett.* **1990**, *31*, 2719. (n) Hatanaka, Y.; Hiyama, T. *J. Am. Chem. Soc.* **1990**, *112*, 7793. (o) Arcadi, A.; Burini, A.; Cacchi, S.; Delmastro, M.; Marinelli, F.; Pietroni, B. *Synlett* **1990**, 47. (p) Takayuki, O. E.; Miyaura, N.; Susuki, A. *Synlett* **1990**, 221. (q) Ozawa, F.; Kubo, A.; Hayashi, T. *J. Am. Chem. Soc.* **1991**, *113*, 1417. (r) Carfagna, C.; Musco, A.; Sallèse, G.; Santi, R.; Fiorani, T. *J. Org. Chem.* **1991**, *56*, 261. (s) Cabri, W.; Candiani, I.; De Bernardinis, S.; Francalanci, F.; Penco, S.; Santi, R. *J. Org. Chem.* **1991**, *56*, 5796. (t) Prince, P.; Gaudour, D. R. *Synlett* **1991**, 405. (u) Cabri, W.; Candiani, I.; Bedeshi, A.; Santi, R. *Synlett* **1992**, 871. (v) Cabri, W.; Candiani, I.; Bedeshi, A.; Penco, S. *J. Org. Chem.* **1992**, *57*, 1481. (w) Cabri, W.; Candiani, I.; Bedeshi, A.; Roberto, S. *J. Org. Chem.* **1992**, *57*, 3558. (x) Alami, M.; Ferri, F.; Linstrumelle, G. *Tetrahedron Lett.* **1993**, *34*, 6403. (y) Ozawa, F.; Kubo, A.; Matsumoto, Y.; Hayashi, T. *Organometallics* **1993**, *12*, 4188.

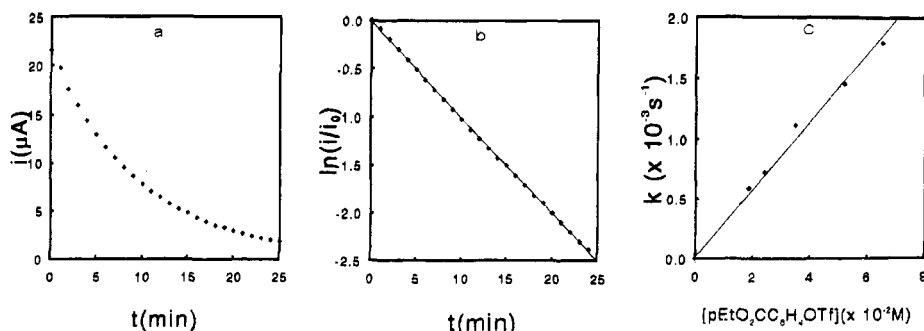
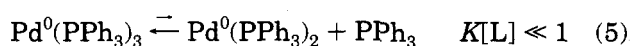
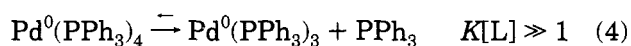


Figure 1. Kinetics of oxidative addition of $\text{Pd}^0(\text{PPh}_3)_4$ to $p\text{-EtO}_2\text{CC}_6\text{H}_4\text{OTf}$, in DMF at 20°C : (a) Variation of the oxidation plateau current i of $\text{Pd}^0(\text{PPh}_3)_4$, 2 mM, at $+0.18\text{ V}$, at a rotating gold disk electrode ($\phi = 2\text{ mm}$, $\omega = 105\text{ rad s}^{-1}$), in the presence of $p\text{-EtO}_2\text{CC}_6\text{H}_4\text{OTf}$, 65 mM, as a function of time; (b) variation of $\ln(i/i_0)$ as a function of time; (c) variation of the slope k of the straight line in (b), as a function of $p\text{-EtO}_2\text{CC}_6\text{H}_4\text{OTf}$ concentration.

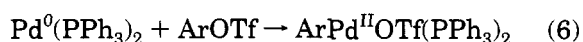
aryl)palladium complex has been reported in the particular case of $p\text{-ClC}_6\text{H}_4\text{PdOSO}_2\text{Rf}(\text{PPh}_3)_2$ ($\text{Rf} = \text{CF}_2\text{CF}_2\text{-OCF}_2\text{CF}_2\text{H}$).^{3d} It has also been reported recently that, in the absence of chloride, no clear-cut oxidative addition was detected under stoichiometric conditions in NMP.^{7a} But careful examination of published results, concerning palladium-catalyzed cross-coupling reactions of aryl triflates, shows that the reactivity of aryl triflates is more difficult to rationalize than that of vinyl triflates, since high yields of coupling products can be achieved in the absence of purposely added chloride.⁴⁻⁷ It seems that extra chloride is required in coupling reactions with organostannanes.^{3a-g} Recent papers demonstrate that addition of extra chloride can inhibit the palladium-catalyzed coupling reaction of aryl triflates^{5,6} even with organostannanes.⁷ The effect of chloride seems to be strongly dependent on the solvent^{3h,7} and on the ligand of the palladium.^{6,7} These results tend to suggest that the postulated role played by chloride in the oxidative addition is not so evident. The fact that cross-coupling reactions can be achieved in the absence of chloride suggests that the oxidative addition of $\text{Pd}^0(\text{PPh}_3)_4$ with aryl triflates should result in the formation of a well-defined product, able to react with nucleophiles. This prompted us to publish some results on the investigation of the mechanism of oxidative addition of aryl triflates to palladium(0) complexes.

Results and Discussion

Rate of the Oxidative Addition of $\text{Pd}^0(\text{PPh}_3)_4$ to Aryl Triflates. The oxidative addition of aryl triflates to $\text{Pd}^0(\text{PPh}_3)_4$ was investigated in DMF since this solvent is commonly used in cross-coupling reactions catalyzed by palladium(0) complexes. It is known that oxidative additions of aryl halides to $\text{Pd}^0(\text{PPh}_3)_4$ proceed via a low-ligated zerovalent palladium complex $\text{Pd}^0(\text{PPh}_3)_2$ formed after decomplexation of the ligand via reversible reactions:⁹⁻¹¹

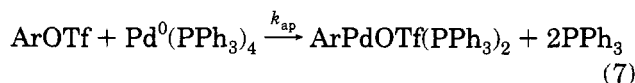


By analogy, it seems reasonable to suppose that oxidative addition to aryl triflates also proceeds via the low-ligated complex $\text{Pd}^0(\text{PPh}_3)_2$:



Since the equilibrium constant of reaction 5 is not

precisely known in DMF,¹⁰ only the apparent rate constant of the overall reaction 7 can be determined.



The complex $\text{Pd}^0(\text{PPh}_3)_4$, 2 mM in DMF containing $n\text{Bu}_4\text{-NBF}_4$ (0.3 M), was characterized by its oxidation peak at $E^{\text{p}} = +0.11\text{ V vs SCE}$. This oxidation peak disappeared in the presence of an aryl triflate demonstrating that the oxidative addition took place. Therefore the reactivity of the zerovalent palladium complex with aryl triflates could be monitored by amperometry. A kinetic investigation of this reaction was carried out using steady state cyclic voltammetry, performed at a rotating disk electrode, as the analytical technique.^{9,10} The electrode was polarized at a potential ($+0.18\text{ V vs SCE}$ in DMF) on the plateau of the oxidation wave of the zerovalent palladium complex, and the resulting current was recorded as a function of time, after addition of an excess of an aryl triflate, at 20°C . A typical curve is represented in Figure 1a. A plot of $\ln(i/i_0)$ as a function of time results in a straight line ($\ln(i/i_0) = -kt$, Figure 1b) demonstrating that the oxidative addition is first order in palladium(0). A plot of the slope k , as a function of the aryl triflate concentration, also resulted in a straight line (Figure 1c) showing that the oxidative addition is first order in the aryl triflate: $d[\text{Pd}^0]/dt = -k_{\text{ap}}[\text{Pd}^0][\text{ArOTf}]$, $k = k_{\text{ap}}[\text{ArOTf}]$. The value of the apparent rate constant of the oxidative addition could then be deduced from the slope of the straight line represented in Figure 1b.

The same experiments were performed with aryl triflates substituted in the para position by electron-withdrawing or donor groups Z. A plot of the variation of $\log(k_{\text{ap}}^{\text{Z}}/k_{\text{ap}}^{\text{H}})$ as a function of the σ Hammett constants showed that the oxidative addition follows a Hammett correlation with $\rho = +2.55$ (Figure 2). The positive value of ρ indicates that the oxidative addition of aryl triflates to $\text{Pd}^0(\text{PPh}_3)_4$ is faster when the aryl triflate is substituted by an electron-withdrawing group, in which case the site of the nucleophilic attack by $\text{Pd}^0(\text{PPh}_3)_4$ bears a more positive charge. The ρ value determined in the case of aryl triflates, $\rho = 2.55$ in DMF,

(9) (a) Fauvarque, J. F.; Pflüger, F.; Troupel, M. *J. Organomet. Chem.* **1981**, *208*, 419. (b) Amatore, C.; Pflüger, F. *Organometallics* **1990**, *9*, 2276.

(10) Amatore, C.; Jutand, A.; Khalil, F.; M'Barki, M.-A.; Mottier, L. *Organometallics* **1993**, *12*, 3168.

(11) (a) Mann, B. E.; Musco, A. *J. Chem. Soc., Dalton Trans* **1968**, 1530. (b) Kuran, W.; Musco, A. *Inorg. Chim. Acta* **1975**, *12*, 187.

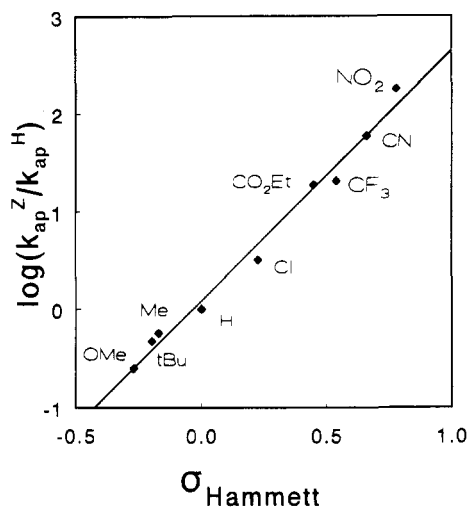


Figure 2. Hammett plot for the oxidative addition of $\text{Pd}^0(\text{PPh}_3)_4$, 2 mM, to para-substituted aryl triflates, $p\text{-Z-C}_6\text{H}_4\text{-OTf}$, in DMF at 20 °C. Regression line: $\log(k_{\text{ap}}^{\text{Z}}/k_{\text{ap}}^{\text{H}}) = 0.086 + 2.55 \sigma$. Correlation coefficient: 0.993.

can be compared with that already reported for para-substituted aryl iodides, $\rho = 2.0$ in THF^{9a} or $\rho = 2.3$ in toluene.^{9b} The slightly higher value of ρ found for aryl triflates shows that the aryl group of the transient intermediate, involved in the oxidative addition of aryl triflates to $\text{Pd}^0(\text{PPh}_3)_4$, develops a greater positive charge than that involved in the case of aryl iodides.

Investigation of the Oxidative Addition of Aryl Triflates to $\text{Pd}^0(\text{PPh}_3)_4$ by Conductivity Measurements. As shown above, electrochemical techniques allowed the investigation of the reactivity of $\text{Pd}^0(\text{PPh}_3)_4$ with aryl triflates by monitoring the disappearance of the palladium(0) complex. It was then necessary to employ other techniques in order to characterize the resulting product as well as its rate of formation. Since it is often postulated that oxidative addition of aryl triflates to $\text{Pd}^0(\text{PPh}_3)_4$ may afford cationic arylpalladium complexes,^{5,7a} we investigated the oxidative addition by conductivity measurements.^{12,13a} The selected aryl triflate was substituted by an electron-withdrawing group and used in large excess in order to get relatively fast oxidative addition at room temperature (see above), so as to prevent possible decomposition of the palladium(0) complex or of the resulting arylpalladium(II) complex.¹⁴

Starting from nonconducting solutions of $\text{Pd}^0(\text{PPh}_3)_4$, 2 mM in DMF at 20 °C (residual conductance $\Omega = 2 \mu\text{S}$), the addition of an aryl triflate (5 equiv of $p\text{-NO}_2\text{C}_6\text{H}_4\text{-OTf}$) resulted in an increase of the solution conductance as a function of time, up to a plateau ($\Omega_{\text{lim}} = 76 \mu\text{S}$). A typical evolution of the solution conductance as a function of time is represented in Figure 3a.

The formation of a plateau in the same time scale as that observed for the oxidative addition monitored by amperometry (see above) indicates the completion of the oxidative addition. These preliminary results demonstrate that the oxidative addition leads to ionic species,

(12) (a) Geary, W. J. *Coord. Chem. Rev.* **1971**, *7*, 81. (b) Denaro, A. R. In *Elementary Electrochemistry*; Butterworths: London, 1965.

(13) (a) Stang, P. J.; Kovalski, M. H.; Schiavelli, M. D.; Longford, D. J. *Am. Chem. Soc.* **1989**, *111*, 3347. (b) Lawrance, G. *Chem. Rev.* **1986**, *86*, 17.

(14) The stoichiometric reaction of $\text{Pd}^0(\text{PPh}_3)_4$ with PhOTf in NMP at room temperature was found to be very slow.^{7a}

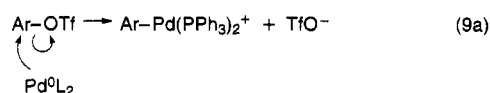
presumably the anion TfO^- and a cationic palladium complex, with a molar conductivity, $\Lambda_{\text{M}} = 41 \Omega^{-1} \text{cm}^2 \text{mol}^{-1}$, characteristic of a 1:1 ionic species in DMF.^{12a} The cationic palladium complex seems to be relatively stable as indicated by the length of the plateau (more than 25 min, since the experiment was voluntarily stopped after that time). Plotting the variation of the final conductance Ω_{lim} measured by the plateau magnitude as a function of $\text{Pd}^0(\text{PPh}_3)_4$ concentration (in the range from 10^{-4} to 3×10^{-3} M) results in a straight line (Figure 4a). This demonstrates that, in DMF, the ionic species which result from the oxidative addition are not involved in ion pairs but are completely dissociated.¹² Performing analogous experiments in THF in the same range of concentration afforded similar results except that the final conductance Ω_{lim} varies linearly as a function of the square root of the palladium concentration (Figure 4b). In THF, a less dissociating and co-ordinating solvent than DMF, the ionic species which result from the oxidative addition are partially ion paired. In toluene, a poorly co-ordinating and dissociating solvent, the resulting solutions were not conducting, showing that the arylpalladium complex is probably totally ion paired (see below).

Since we were able to monitor the formation of the ionic species as a function of time by conductance measurements, an investigation of the kinetics of the formation of the ionic species was possible. In the case of the reaction of $\text{Pd}^0(\text{PPh}_3)_4$ with $p\text{-NO}_2\text{C}_6\text{H}_4\text{OTf}$, in DMF, a plot of $\ln((\Omega_{\text{lin}} - \Omega)/\Omega_{\text{lim}})$ as a function of time resulted in a straight line, demonstrating that the formation of the cationic arylpalladium complex is a first-order process in palladium(0) (Figure 3b). From the slope, the apparent rate constant was found to be $k_{\text{ap}} = 0.35 \pm 0.02 \text{ M}^{-1} \text{ s}^{-1}$; this value is close to that found for the disappearance of $\text{Pd}^0(\text{PPh}_3)_4$ determined by amperometry ($k_{\text{ap}} = 0.32 \text{ M}^{-1} \text{ s}^{-1}$; see above). These results demonstrate that the rate of formation of the cationic product resulting from the oxidative addition is the same as that for the disappearance of $\text{Pd}^0(\text{PPh}_3)_4$. This means that the cationic arylpalladium complex is either formed in an elementary step (reaction 9a) or in several consecutive steps but, in the latter case, with intermediate complexes in very negligible concentration. If the formation of the cationic arylpalladium complex were to proceed via ionization of a neutral complex (reaction 9b), this latter complex would not accumulate in solution and the rate of ionization would be fast relative to that of the oxidative addition of $\text{Pd}^0(\text{PPh}_3)_4$ to the aryl triflate, the latter being the rate-determining step of the overall reaction (reaction 9b).

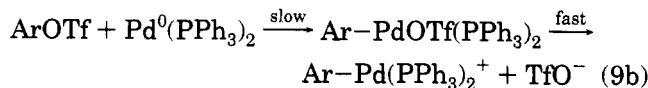
In DMF



via the following mechanisms:



or



the resulting cation being strongly solvated by DMF.

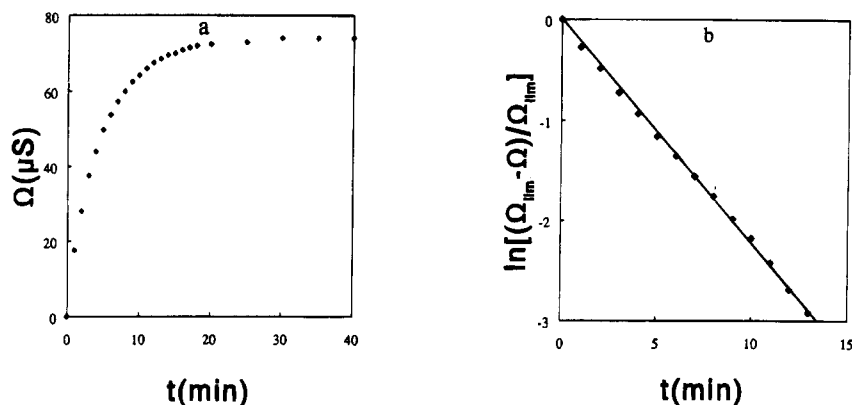


Figure 3. Kinetics of oxidative addition of $\text{Pd}^0(\text{PPh}_3)_4$ to $p\text{-NO}_2\text{C}_6\text{H}_4\text{OTf}$, in DMF at 20°C : (a) Variation of the conductance Ω of a solution of $\text{Pd}^0(\text{PPh}_3)_4$, 2 mM, in the presence of $p\text{-NO}_2\text{C}_6\text{H}_4\text{OTf}$, 10 mM, as a function of time; (b) variation of $\ln[(\Omega_{\text{lim}} - \Omega)/\Omega_{\text{lim}}]$ as a function of time. The final conductance is noted as Ω_{lim} .

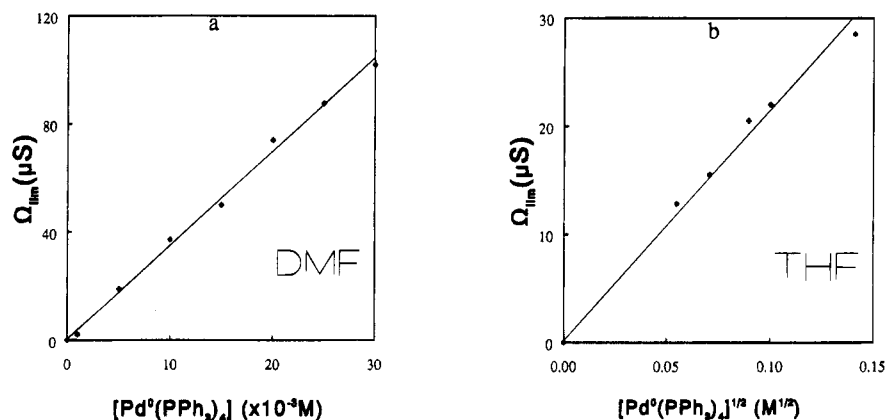
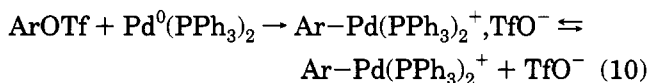


Figure 4. (a) Variation of the final conductance Ω_{lim} of a solution of $\text{Pd}^0(\text{PPh}_3)_4$, 2 mM, and $p\text{-NO}_2\text{C}_6\text{H}_4\text{OTf}$, 20 mM, as a function of the palladium concentration, in DMF. (b) Variation of the final conductance Ω_{lim} of a solution of $\text{Pd}^0(\text{PPh}_3)_4$, 2 mM, and $p\text{-NO}_2\text{C}_6\text{H}_4\text{OTf}$, 20 mM, as a function of the square root of the palladium concentration, in THF.

In THF



A complex has been isolated from the reaction of $p\text{-NO}_2\text{C}_6\text{H}_4\text{OTf}$ with $\text{Pd}^0(\text{PPh}_3)_4$. A solution of the isolated complex, 2 mM in DMF, exhibited a conductance of $63 \mu\text{S}$ (molar conductivity, $\Lambda_{\text{M}} = 35 \Omega^{-1} \text{cm}^2 \text{mol}^{-1}$), proving the 1:1 ionic character of the isolated complex.^{12a} Its IR spectrum exhibited two bands at 1265 and 637cm^{-1} characteristic of anionic CF_3SO_3^- .¹³ The ionic structure of the complex has also been confirmed by fast atom bombardment mass spectrometry. Its FAB mass spectrum exhibited a peak at m/e 752 that corresponds to the mass of the cation M^+ : $p\text{-NO}_2\text{C}_6\text{H}_4\text{Pd}(\text{PPh}_3)_2^+$. The pattern of the mass peak of the cation is exactly the same as the predicted and simulated one, according to the formula $\text{C}_{42}\text{H}_{34}\text{NO}_2\text{P}_2\text{-Pd}$, taking account of the palladium isotopes (Isomass). The mass spectrum also showed a peak at m/e 630 characteristic of $[\text{M} - \text{NO}_2\text{C}_6\text{H}_4]^+$ and one at m/e 430 characteristic of $[\text{M} - \text{PPh}_3]^+$ that confirm the presence of the $\text{NO}_2\text{C}_6\text{H}_4^-$ ligand on the palladium. Also was detected a mass peak at m/e 149 characteristic of the anion CF_3SO_3^- .

When the oxidative addition was performed in pure toluene, a nonpolar solvent, the resulting solution was not conducting at all (see above). The nonconductivity could be due to either the formation of a covalent

complex or of a totally ion-paired complex. An orange solid was isolated from toluene. Its IR spectrum exhibited the two bands at 637 and 1270cm^{-1} characteristic of anionic CF_3SO_3^- .¹³ The band at 1220cm^{-1} assigned to a covalent CF_3SO_3^- ^{13b} (which was present in the initial aryl triflate) was not observed in the resulting arylpalladium complex. These results demonstrate that the arylpalladium complex is not covalent in toluene but totally ion paired. This suggests that the oxidative addition proceeds via the mechanism described in eq 9a.

Another complex has been isolated from the $p\text{-ClC}_6\text{H}_4\text{OTf}$ with $\text{Pd}^0(\text{PPh}_3)_4$. A solution of this isolated complex, 2 mM in DMF, exhibited a conductance of $103 \mu\text{S}$ (molar conductivity, $\Lambda_{\text{M}} = 57 \Omega^{-1} \text{cm}^2 \text{mol}^{-1}$). Its IR spectrum exhibited the two bands at 1270 and 635cm^{-1} characteristic of anionic triflate. The ionic structure of the complex has also been confirmed by mass spectrometry. Its FAB mass spectrum as well as its ESI mass spectrum exhibited peaks at m/e 741 and 743 that correspond to the mass of the cation M^+ $p\text{-ClC}_6\text{H}_4\text{Pd}(\text{PPh}_3)_2^+$. The pattern of the mass peaks of the cation is exactly the same as the predicted one ($\text{C}_{42}\text{H}_{34}\text{ClPdP}_2$), taking account of the palladium and chloride isotopes.

A propos, this means that the palladium in the cationic complex is ligated by only two phosphine ligands and not three, as it has been demonstrated for cationic vinylplatinum complexes^{13a} (the third ligand could originate from $\text{Pd}^0(\text{PPh}_3)_4$). By analogy with

Table 1. ^{31}P NMR Shift of the (σ -Aryl)palladium Complexes Resulting from the Oxidative Addition of $\text{Pd}(\text{PPh}_3)_4$ with Aryl Triflates in the Absence or in the Presence of Halides^a

no.	complex	solvent	Ar-PdL ₂ OTf δ_1 (ppm) ^a	Ar-PdCIL ₂ δ_2 (ppm) ^a	Ar-PdBrL ₂ δ_3 (ppm) ^a
1	<i>p</i> -NO ₂ C ₆ H ₄ PdCl(PPh ₃) ₂ ^b	DMF		24.52	
2	Pd(PPh ₃) ₄ + <i>p</i> -NO ₂ C ₆ H ₄ OTf	DMF	22.01		
3	<i>p</i> -NO ₂ C ₆ H ₄ Pd(PPh ₃) ₂ OTf ^b	DMF	21.94		
4	Pd(PPh ₃) ₄ + <i>p</i> -NO ₂ C ₆ H ₄ OTf + LiCl (1 eq) ^c	DMF	none	24.48	
5	Pd(PPh ₃) ₄ + <i>p</i> -NO ₂ C ₆ H ₄ OTf + LiCl (5 eq) ^c	DMF	none	24.47	
6	Pd(PPh ₃) ₄ + LiCl (1 eq) + <i>p</i> -NO ₂ C ₆ H ₄ OTf ^d	DMF	none	24.41	
7	Pd(PPh ₃) ₄ + <i>p</i> -NO ₂ C ₆ H ₄ OTf + nBu ₄ NCl (1 eq) ^c	DMF	none	24.47	
8	Pd(PPh ₃) ₄ + <i>p</i> -NO ₂ C ₆ H ₄ OTf + ZnCl ₂ (1 eq) ^c	DMF	none	24.37	
9	<i>p</i> -NO ₂ C ₆ H ₄ Pd(PPh ₃) ₂ OTf ^b + ZnCl ₂ (1 eq)	DMF	none	24.38	
10	<i>p</i> -NO ₂ C ₆ H ₄ PdCl(PPh ₃) ₂ ^b	THF		24.10	
11	Pd(PPh ₃) ₄ + <i>p</i> -NO ₂ C ₆ H ₄ OTf	THF	22.02		
12	Pd(PPh ₃) ₄ + <i>p</i> -NO ₂ C ₆ H ₄ OTf + nBu ₄ NCl (1 eq) ^c	THF	none	23.99	
13	<i>p</i> -NO ₂ C ₆ H ₄ PdBr(PPh ₃) ₂ ^b	DMF			24.19
14	Pd(PPh ₃) ₄ + <i>p</i> -NO ₂ C ₆ H ₄ OTf + nBu ₄ NBr (0.35 eq) ^c	DMF	22.00		24.19
15	Pd(PPh ₃) ₄ + <i>p</i> -NO ₂ C ₆ H ₄ OTf + nBu ₄ NBr (1 eq) ^c	DMF	none		24.19
16	<i>p</i> -CF ₃ C ₆ H ₄ PdCl(PPh ₃) ₂ ^b	DMF		24.70	
17	Pd(PPh ₃) ₄ + <i>p</i> -CF ₃ C ₆ H ₄ OTf	DMF	22.02		
18	Pd(PPh ₃) ₄ + <i>p</i> -CF ₃ C ₆ H ₄ OTf + nBu ₄ NCl (1 eq) ^c	DMF	none	24.71	
19	<i>p</i> -CF ₃ C ₆ H ₄ PdCl(PPh ₃) ₂ ^b	TMF		24.38	
20	Pd(PPh ₃) ₄ + <i>p</i> -CF ₃ C ₆ H ₄ OTf	THF	22.20		
21	Pd(PPh ₃) ₄ + <i>p</i> -CF ₃ C ₆ H ₄ OTf + nBu ₄ NCl (1 eq) ^c	THF	none	24.21	
22	<i>p</i> -CH ₃ C ₆ H ₄ PdCl(PPh ₃) ₂ ^b	DMF		24.32	
23	Pd(PPh ₃) ₄ + <i>p</i> -CH ₃ C ₆ H ₄ OTf	DMF	20.87		
24	Pd(PPh ₃) ₄ + <i>p</i> -CH ₃ C ₆ H ₄ OTf + LiCl (1 eq) ^c	DMF	none	24.32	
25	<i>p</i> -ClC ₆ H ₄ Pd(PPh ₃) ₂ OTf ^b	DMF	23.20		

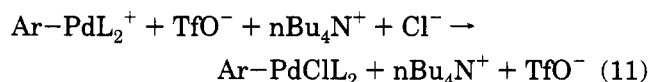
^a In every case the ratio ArOTf/Pd(0)L₄ was equal to 10 except entries 23 and 24 where it was equal to 65. δ values are relative to H₃PO₄ (external reference). ^b Isolated product. ^c The compounds were introduced into the NMR tube as follows: first PdL₄, second ArOTf. A ^{31}P NMR spectrum was then recorded in order to detect the signal of the corresponding (σ -aryl)palladium triflate. Halide salts were then added (the equivalents in parentheses were relative to PdL₄). ^d The chloride salt was added to the palladium(0) complex before the aryl triflate.

platinum complexes, it is often mentioned in the literature that cationic vinyl-^{2b} and arylpalladium^{5,7a} complexes might contain three phosphine ligands. We demonstrate here that cationic (σ -aryl)palladium complexes can be stable and isolated when ligated by only two triphenylphosphine ligands.

From these results it can be assumed that the reaction of aryl triflates to Pd⁰(PPh₃)₄ affords a cationic arylpalladium complex Ar-Pd(PPh₃)₂⁺ with CF₃SO₃⁻ as the counteranion, which is rather stable in solution. In DMF the complex is completely dissociated whereas in THF it is partially ion-paired. The cationic character of the arylpalladium complex is therefore clearly established for the first time.

Reaction of Halides with Cationic Arylpalladium Complexes Monitored by Conductimetry. After complete reaction of Pd⁰(PPh₃)₄ (2 mM) with *p*-NO₂C₆H₄OTf monitored by conductance measurement in DMF, the final conductance was found to be 76 μS and assigned to the conductance of a 2 mM solution of Ar-Pd(PPh₃)₂⁺ and TfO⁻. Addition of 1 equiv of chloride, introduced as nBu₄NCl, immediately resulted in a conductance of 133 μS , while the yellow solution simultaneously turned to pale yellow. The intrinsic conductance of a 2 mM solution of nBu₄NCl was found to be 131 μS . If no reaction occurred by addition of chloride, the conductance of the resulting solution would have been the sum of the two intrinsic conductances 76 + 131, that is, 207 μS . The fact that the conductance was found to be 133 rather than 207 μS after addition of chloride means that chloride has reacted with the cationic arylpalladium complex to form a neutral species responsible for the low conductance observed. Since the conductance of a 2 mM solution of nBu₄NOTf was

determined to be 121 μS , a value close to 133 μS , we can assume that



^{31}P NMR Investigation of the Oxidative Addition of Aryl Triflates to Pd⁰(PPh₃)₄ in the Absence or Presence of Halide. As for conductance measurements, we focused our study on very reactive aryl triflates substituted with electron-withdrawing groups (see above). In other cases, they were used in large excess in order to get a fast oxidative addition. Indeed, until now, any attempt to characterize the product resulting from the oxidative addition of Pd⁰(PPh₃)₄ with aryl triflates by ^{31}P NMR has been undertaken in stoichiometric conditions with poorly reactive aryl triflates, resulting in very slow reactions in NMP (1-methyl-2-pyrrolidinone) or THF.^{7a,14} On the other hand, the application of heat to accelerate the oxidative addition resulted in a decomposition of the palladium(0) complex in THF.^{7a}

The ^{31}P NMR spectrum of a solution of Pd⁰(PPh₃)₄ exhibited a broad signal ($\Delta = 480$ Hz) at 13.56 ppm vs H₃PO₄ in DMF (9.05 ppm in THF) characteristic of the species Pd⁰(PPh₃)₃, Pd⁰(PPh₃)₂, and PPh₃ in a fast equilibrium¹⁰ (eqs 4 and 5).

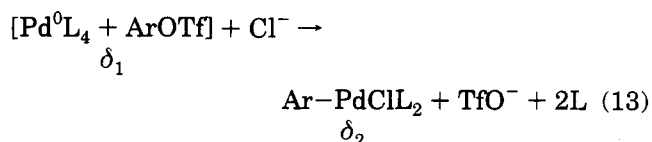
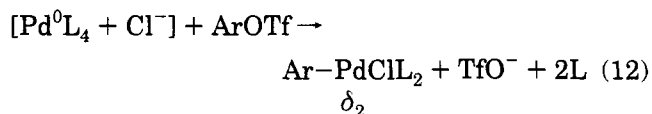
Addition of aryl triflates resulted in the disappearance of the broad signal and the appearance of two sharp signals. The signal at -5.47 ppm is characteristic of the free triphenylphosphine ligand. The release of triphenylphosphine proves that the oxidative addition occurred and that it afforded a single palladium complex, exhibiting a unique sharp singlet at δ_1 in THF or

DMF (Table 1: entries 2, 11, 17, 20, and 23). The observed unique singlet proves that the palladium complex resulting from the oxidative addition has only equivalent phosphine ligands, at most two ligands. The presence of three ligands on the palladium would result in a more complicated ^{31}P NMR spectrum, due to coupling between nonequivalent phosphorus atoms, as was observed in the case of vinylplatinum complexes.^{13a}

^{31}P NMR experiments were performed at relatively long time scales, about 20 min, indicating mixing time and ^{31}P NMR recording time. The presence of only one well-defined signal is indicative of the stability of the complex resulting from the oxidative addition.

It is mentioned in the literature that stable arylpalladium complexes could only be obtained when the oxidative addition of aryl triflates was performed in the presence of chloride.^{3a,7a} It has been established that the addition of chlorides to $\text{Pd}^0(\text{PPh}_3)_4$ results in the formation of palladium(0) complexes ligated by chloride anions *viz.* $\text{Pd}^0(\text{PPh}_3)_3\text{Cl}^-$.^{2b,15} Reaction of such a complex with an aryl triflate was supposed to afford the corresponding stable arylpalladium chloride complex.^{3a,7a} We found in agreement with published results^{3d,7a} that, when chloride anions were introduced into the NMR tube together with the palladium(0), before the addition of the aryl triflates (Table 1: entry 6), the ^{31}P NMR signal at δ_1 was not observed. However another signal was observed at δ_2 identical to the signal of an authentic sample of the corresponding *trans*-(σ -aryl)palladium chloride complex, $\text{Ar-PdCl}(\text{PPh}_3)_2$,¹⁶ observed independently (Table 1: entry 1).

However when at least 1 equiv of halide relative to the palladium(0) complex was introduced after complete reaction of palladium(0) with the aryl triflate (the end of the oxidative addition was systematically checked by the presence of the sharp signal at δ_1 , together with free phosphine), we observed, in all cases, that the signal at δ_1 completely disappeared and was replaced by a signal at δ_2 (or δ_3) characteristic of the corresponding arylpalladium chloride (or bromide) complex.¹⁶ A fast reaction occurred between the halide and the complex already formed *in situ* in the NMR tube to afford the (σ -aryl)palladium halide derivative, whatever the aryl triflate, the halide (chloride, bromide), the counterion (Li^+ , Zn^{2+} , nBu_4N^+), or the solvent. So, introduction of only 1 equiv of halide, either before or after the oxidative addition took place, resulted in the formation of the same chemical species.

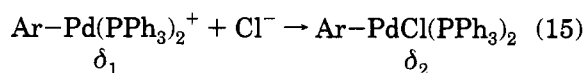
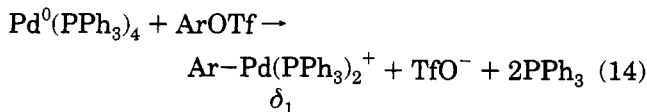


This means that the sharp signal observed at δ_1 characterizes a well-defined product that can be assigned as a stable (σ -aryl)palladium complex, highly

Table 2. Apparent Rate Constant of the Oxidative Addition of $\text{Pd}(\text{PPh}_3)_4$ to PhX (X = I, Br, OTf) Determined in DMF at 20 °C

k_{ap} ($\text{M}^{-1} \text{s}^{-1}$)	PhX		
	PhI ¹⁰	PhOTf	PhBr
	17	1.7×10^{-3}	10^{-3}

reactive toward halide. Since we have already characterized this complex as a cationic species, we are therefore inclined to conclude that the signal at δ_1 is indicative of the cationic complex $\text{Ar-Pd}(\text{PPh}_3)_2^+$.¹⁷



Rate of Oxidative Addition of $\text{Pd}^0(\text{PPh}_3)_4$ to Aryl Triflates in the Presence of Chloride Anions. In order to better characterize the role of chloride anions in the oxidative addition of $\text{Pd}^0(\text{PPh}_3)_4$ to aryl triflates, the apparent rate constant of this reaction was measured by amperometry in the presence of chloride. In the case of *p*- $\text{NO}_2\text{C}_6\text{H}_4\text{OTf}$, the following rate constants were determined at 20 °C: $k_{\text{ap}} = 0.32 \text{ M}^{-1} \text{ s}^{-1}$ (0 equiv of Cl^-); $0.36 \text{ M}^{-1} \text{ s}^{-1}$ (10 equiv of Cl^-); $0.59 \text{ M}^{-1} \text{ s}^{-1}$ (150 equiv of Cl^-). This results show that the presence of chloride anions slightly enhances the rate of the oxidative addition but that this effect becomes significant only when chloride are present in large excess.¹⁸ It can be noted that when chloride anions were found to be essential for cross-coupling reactions to proceed, they were always used in large amounts (in excess relative to the aryl triflate, which means from 30 to 200 equiv relative to the palladium catalyst).¹⁻³ However, in the case of less reactive aryl triflates such as PhOTf, the effect of chloride was found to be more important. Indeed, the corresponding apparent rate constants were respectively $k_{\text{ap}} = 1.7 \times 10^{-3} \text{ M}^{-1} \text{ s}^{-1}$ (0 equiv of Cl^-) and $33 \times 10^{-3} \text{ M}^{-1} \text{ s}^{-1}$ (150 equiv of Cl^-). The same observation was made for an aryl triflate of another series, the 1-naphthyl triflate: $k_{\text{ap}} = 7.5 \times 10^{-2} \text{ M}^{-1} \text{ s}^{-1}$ (0 equiv of Cl^-) and $43 \times 10^{-2} \text{ M}^{-1} \text{ s}^{-1}$ (150 equiv of Cl^-). These results confirm the accelerating effect of LiCl , observed during the oxidative addition of PhOTf with $\text{Pd}^0(\text{PPh}_3)_4$ in NMP.^{7a}

Comparison of the Rate of the Oxidative Addition of $\text{Pd}^0(\text{PPh}_3)_4$ to Aryl Triflates with that to Aryl Halides. Since aryl triflates are now more widely used than aryl halides in palladium-catalyzed cross-coupling reactions, it was interesting to compare the reactivity of $\text{Pd}^0(\text{PPh}_3)_4$ with aryl halides and triflates. The apparent rate constant of the oxidative addition was determined by amperometry as described above. From the results presented in the Table 2, the following order of reactivity was established: $\text{PhI} \gg \text{PhOTf} > \text{PhBr}$.

(17) Neutral arylpalladium complexes are generally square planar.¹⁶ By ^{31}P NMR spectroscopy performed on the cationic complex, the two ligands PPh_3 were found to be equivalent (only one signal). This implies that the two ligands have a *trans* configuration in the cationic complex. DMF is the fourth ligand which is in a *trans* position relative to the aryl group.

(18) A similar effect was found in the case of the oxidative addition of $\text{Pd}^0(\text{PPh}_3)_4$ to aryl iodides in the presence of chloride anions. See ref 15.

(15) Amatore, C.; Azzabi, M.; Jutand, A. *J. Am. Chem. Soc.* **1991**, *113*, 8375.

(16) Fitton, P.; Rick, E. A. *J. Organomet. Chem.* **1971**, *28*, 287.

This shows that aryl triflates are much less reactive than aryl iodides (by a factor 10^4) but slightly more reactive than aryl bromides in DMF.¹⁹

These results are consistent with those reported in literature concerning the comparative reactivity of aryl triflates and halides in $\text{Pd}^0(\text{PPh}_3)_4$ -catalyzed coupling reactions, performed in the absence of chlorides.^{4x} This tends to show that, for a given nucleophile, the oxidative addition of $\text{Pd}^0(\text{PPh}_3)_4$ to the aryl derivative is the rate-determining step of the overall catalytic reaction.

Conclusion

The reaction of $\text{Pd}^0(\text{PPh}_3)_4$ with aryl triflates is an oxidative addition which is faster when the aryl group is substituted by electron-withdrawing groups. This reaction proceeds in the absence of purposely added halides to afford well-defined arylpalladium complexes that have been characterized for the first time as cationic complexes, $\sigma\text{-Ar-Pd}(\text{PPh}_3)_2^+$. The relative stability of these cationic complexes can explain why some palladium-catalyzed cross-coupling reactions can be achieved in good yield in the absence of chloride. Addition of chloride either before or after the oxidative addition results in the formation of a neutral species, the *trans* complex: $\sigma\text{-Ar-PdCl}(\text{PPh}_3)_2$. If palladium-catalyzed reactions are inhibited by the presence of chloride, it certainly means that the reaction proceeds via a cationic arylpalladium complex⁵ as is sometimes postulated in Heck reactions. By contrast, some palladium-catalyzed cross-coupling reactions are only possible when performed in the presence of chloride.^{3a-g} In this case, it can be assumed that the oxidative addition is faster but does not afford a cationic complex. The overall reaction proceeds via the neutral complex ArPdClL_2 .²¹ In the case of poorly reactive nucleophiles such as organostannanes,^{3a-g,7a} we suppose that cationic complexes would not be stable enough (compared to neutral species ArPdClL_2) to allow nucleophilic attack,²¹ the latter being the rate-determining step.^{3d,7a} We cannot exclude the hypothesis that the oxidative addition performed in the presence of chloride would not afford directly the stable *trans*- ArPdClL_2 complex, but first a transient pentacoordinated complex $\text{ArPdCl}_2\text{L}_2^-$, which is supposed to be more reactive with nucleophiles

than the stable *trans* neutral complex, as recently reported by one of us.²²

Experimental Section

³¹P NMR spectra were recorded on a Bruker spectrometer (162 MHz) using H_3PO_4 as an external reference. ¹³C and ¹H NMR (63 and 250 MHz) spectra were recorded on a Bruker spectrometer. IR spectroscopy was performed on a Perkin-Elmer 599 spectrometer. FAB mass spectroscopy was performed on a Nermag R 10-10 spectrometer, and ESI mass spectroscopy, on a VGBIOQ (Altrincham) spectrometer.

Conductivity measurements were performed using a Tacussel CD 6NG conductimeter. The cell constant was determined to be 0.9.

Chemicals. DMF was distilled from calcium hydride under vacuum and kept under argon. LiCl , ZnCl_2 , and $n\text{Bu}_4\text{NCl}$ were commercial and dried under vacuum before use. Authentic samples of *p*- $\text{Z-C}_6\text{H}_4\text{PdCl}(\text{PPh}_3)_2$ ($\text{Z} = \text{NO}_2, \text{CN}, \text{CF}_3$),¹⁶ $\text{Pd}^0(\text{PPh}_3)_4$,²³ and para-substituted aryl triflates^{4f,24} were prepared according to described procedures.

³¹P NMR Investigations. A 23 mg amount of $\text{Pd}^0(\text{PPh}_3)_4$ was introduced into an NMR tube filled with argon and equipped with a septum. The tube was filled with 3 mL of DMF followed by the appropriate amount of aryl triflate (see Table 1). In some experiments, the chloride salt was introduced before the aryl triflate (see Table 1). At least 0.2 mL of acetone-*d*₆ was added to the solution.

Electrochemical Setup and Electrochemical Procedure for Steady State Voltammetry. Cyclic voltammetry was performed with a wave-form generator, PAR Model 175. The cyclic voltammograms were recorded with a Nicolet 3091 digital oscilloscope. Experiments were carried out in a three-electrode cell connected to a Schlenk line. The counter electrode was a platinum wire of ca. 1 cm² apparent surface area; the reference was a saturated calomel electrode (Tacussel) separated from the solution by a bridge (3 mL) filled with a 0.3 M $n\text{Bu}_4\text{NBF}_4$ solution in DMF. A 12 mL volume of DMF containing 0.3 M $n\text{Bu}_4\text{NBF}_4$ was poured into a cell. A 28 mg sample (2×10^{-3} M) of $\text{Pd}^0(\text{PPh}_3)_4$ was then introduced into the cell under argon. The kinetic measurements were performed by steady state voltammetry at a rotating disk electrode (gold disk, $\phi = 2$ mm, inserted into a Teflon holder, Tacussel EDI 65109) with a scan rate of 0.02 V s⁻¹ and an angular velocity of 105 rad s⁻¹ (Tacussel controvit).^{9,10} The RDE was polarized on the plateau of the oxidation wave of $\text{Pd}^0(\text{PPh}_3)_4$. The appropriate amount of the aryl triflate was then added to the cell and the oxidation current recorded as a function of time up to 100% conversion, in order to follow the kinetics of oxidative addition with ArOTf .

Synthesis of *p*- $\text{ClC}_6\text{H}_4\text{Pd}(\text{PPh}_3)_2^+\text{TfO}^-$. This compound was synthesized according to the procedure used for the synthesis of *p*- $\text{ClC}_6\text{H}_4\text{PdOSO}_2\text{Rf}(\text{PPh}_3)_2$ ($\text{Rf} = \text{CF}_2\text{CF}_2\text{OCF}_2\text{-CF}_2\text{H}$).^{3d} The synthesis was carried out in a Schlenk tube under argon. A mixture of 0.62 g (2.4 mmol) of *p*- $\text{ClC}_6\text{H}_4\text{OTf}$ and 1.61 g (1.4 mmol) of $\text{Pd}^0(\text{PPh}_3)_4$ in 8 mL of DMF and 8 mL of benzene had been heated at 80–90 °C for 30 h. Evaporation of the solvent under vacuum afforded a yellow solid which was washed with ethyl ether. The complex was dissolved in dichloromethane and precipitated in hexane. A 1.02 g amount of a pale yellow powder was collected. Yield: 82%.

³¹P NMR (162 MHz, DMF, acetone-*d*₆, H_3PO_4) (δ , ppm): 23.20. ¹H NMR (250 MHz, CDCl_3 , TMS) (δ , ppm): 7.41 (d, 2H, $J = 8$ Hz), 7.46 (d, 2H, $J = 8$ Hz), 7.62 (dd, 6H, $J = 7.5$ Hz, $J = 2$ Hz), 7.68 (dd, 6H, $J = 7.5$ Hz, $J = 2$ Hz), 7.78 (t, 6H, $J = 7.5$ Hz), 7.79 (t, 6H, $J = 7.5$ Hz), 7.91 (td, 6H, $J = 7.5$ Hz, $J = 2$ Hz). ¹³C NMR (63 MHz, CDCl_3 , TMS) (δ , ppm): 117.45

(19) In the seminal paper relative to the qualitative comparison of the rate of oxidative addition of $\text{Pd}^0(\text{PPh}_3)_4$ with aryl halides,¹⁶ Fitton reported that the order of reactivity in benzene was found to be $\text{ArI} > \text{ArBr} > \text{ArCl} > \text{ArF}$, i.e., with the Ar–X bond cleavage being the rate-determining step. In a classical $\text{S}_{\text{N}}\text{Ar}$ mechanism, the order of reactivity would be the reverse since the formation of the Meisenheimer complex, which is usually the rate-determining step, is faster when the halide has a high electronegativity, such as fluoride, but is a poor leaving group. Indeed an increase of the electronegativity of the halide favors the attack of the nucleophile that affords the Meisenheimer complex.²⁰ If the oxidative addition were to proceed via a Meisenheimer complex, it would not obey the classical $\text{S}_{\text{N}}\text{Ar}$ mechanism, but a mechanism where the second step, namely cleavage of the C–X bond in the Meisenheimer complex, would be the rate-determining step. Since TfO^- is a better leaving group than I^- , the oxidative addition should be faster with PhOTf than with PhI . Since the reverse was observed, it is highly improbable that the oxidative addition of $\text{Pd}^0(\text{PPh}_3)_4$ with aryl triflates proceeds through a Meisenheimer complex. It has also been shown recently that, in the case of aryl halides, the oxidative addition proceeds via a concerted mechanism.^{9b} This is why we are inclined to favor a concerted mechanism in the case of aryl triflates as mentioned in the text (eq 9a).

(20) March, J. *Advanced Organic Chemistry. Reactions, Mechanisms, and Structure*, 3rd ed.; Wiley Interscience: New York, 1985; pp 576–578.

(21) Osawa, F.; Kurihara, K.; Fujimori, M.; Hidaka, T.; Toshiyama, T.; Yamamoto, A. *Organometallics* 1989, 8, 180.

(22) Amatore, C.; Jutand, A.; Suarez, A. *J. Am. Chem. Soc.* 1993, 115, 9531.

(23) Rosevear, D. T.; Stone, F. G. H. *J. Chem. Soc. A* 1968, 164.

(24) Stang, P. J.; Hanack, M.; Subramanian, L. *Synthesis* 1982, 85.

(q, $J_{CF} = 90$ Hz, CF_3) 128.38 (s, C-Pd), 130.34 (d, CH-C-Pd), 130.62 (d, PPh₃), 130.71 (s, C-Cl), 130.82 (d, PPh₃), 134.02 (d, CH-C-Cl), 134.27 (d, PPh₃), 134.44 (d, PPh₃), 135.69 (d, PPh₃), 135.74 (d, PPh₃). IR (KBr) (cm^{-1}): $\nu_{C=C}$, 1550, 1480, 1435; $\nu_{S=O}$, 1270; ν_{S-O} , 635; ν_{Pd-P} , 540, 520, 510. FAB mass spectrum (3-nitrobenzylalcohol matrix) (I^+ , M^+ ; m/e): 743, 741. ESI mass spectrum (methanol) (m/e): M^+ , 743, 741; $[M + H - Cl]^+$, 707. Anal. Calcd for $C_{43}H_{34}ClF_3O_3P_2PdS \cdot 2CH_2Cl_2$: C, 50.92; H, 3.61. Found: C, 50.72, H, 3.45.

Synthesis of $p\text{-NO}_2\text{C}_6\text{H}_4\text{Pd}(\text{PPh}_3)_2^+, \text{TfO}^-$. The same procedure as above was used: 0.65 g (2.4 mmol) of $p\text{-NO}_2\text{C}_6\text{H}_4\text{-OTf}$ and 1.61 g (1.4 mmol) of $\text{Pd}^0(\text{PPh}_3)_4$ in 8 mL of DMF and 8 mL of benzene. A 0.99 g amount of orange powder was collected. Yield: 79%.

^{31}P NMR (162 MHz, DMF, acetone- d_6 , H_3PO_4) (δ , ppm): 21.94. ^1H NMR (250 MHz, CDCl_3 , TMS) (δ , ppm): 6.90 (d, 2H, $J = 8$ Hz), 7.12 (d, 2H, $J = 8$ Hz), 7.27–7.53 (m, 30 H). IR (KBr) (cm^{-1}): $\nu_{N=O}$, 1645; $\nu_{C=C}$, 1550, 1500, 1435; ν_{C-NO_2} , 1340;

$\nu_{N=O}$, 1280; $\nu_{S=O}$, 1265; ν_{C-N} , 860; ν_{C-S} , 695; ν_{S-O} , 637; ν_{Pd-P} , 520, 505, 495. FAB mass spectrum (3-nitrobenzylalcohol matrix) (m/e): I^+ , M^+ , 752; $[M - \text{NO}_2\text{C}_6\text{H}_4]^+$, 630; $[M - \text{PPh}_3]^+$, 490; $[M - (\text{NO}_2\text{C}_6\text{H}_4 + \text{PPh}_3)]^+$, 368; I^- , 149. Anal. Calcd for $C_{43}H_{34}F_3NO_5P_2PdS \cdot CH_2Cl_2$: C, 53.54; H, 3.68; N, 1.42. Found: C, 53.35; H, 3.70; N, 1.44.

Acknowledgment. This work has been supported in part by the Centre National de la Recherche Scientifique (CNRS, URA 1679, "Processus d'Activation Moléculaire") and the Ecole Normale Supérieure. We thank Mrs. Annick Dupont for the ESI data obtained in the Laboratoire de Spectroscopie de Masse Bio-Organique in Strasbourg, France. We thank Mr. Alan Brown for helpful comments on the English.

OM940476P

Rates and Mechanism of the Formation of Zerovalent Palladium Complexes from Mixtures of Pd(OAc)₂ and Tertiary Phosphines and Their Reactivity in Oxidative Additions

Christian Amatore,* Emmanuelle Carré, Anny Jutand,* and Mohamed Amine M'Barki†

Département de Chimie, Ecole Normale Supérieure, URA CNRS 1679, 24 Rue Lhomond, 75231 Paris Cédex 5, France

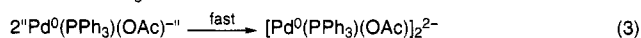
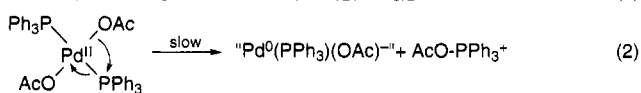
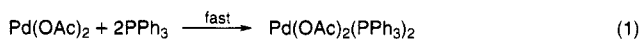
Received November 3, 1994[⊗]

Mixtures of Pd(OAc)₂ and tertiary phosphines spontaneously afford palladium(0) complexes. Kinetic investigations demonstrate that this reaction proceeds from the complex Pd(OAc)₂(PPh₃)₂ via an inner-sphere reduction which is the rate-determining step of the overall reaction. The phosphine is thus oxidized to the corresponding phosphine oxide. The formation of the palladium(0) complex is sensitive to electronic and steric factors. The more the triarylphosphine is substituted by electron-withdrawing groups, the faster the reaction. The palladium(0) complex thus formed reacts with phenyl iodide via an oxidative addition, and this reaction is faster when the phosphine is more electron-rich.

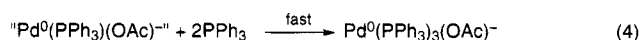
Introduction

We have reported in a previous paper¹ that catalytic systems commonly used in Heck^{2,3} reactions, consisting of Pd(OAc)₂(PPh₃)₂ or a mixture of Pd(OAc)₂ and *n*PPh₃ (*n* ≥ 2), spontaneously and quantitatively generate *in situ* a zerovalent palladium complex able to activate aryl iodides via an oxidative addition. Indeed, we demonstrated by means of analytical techniques such as ³¹P NMR spectroscopy and cyclic voltammetry that triphenylphosphine was able to reduce Pd(OAc)₂ into a zerovalent palladium complex, from the complex Pd-

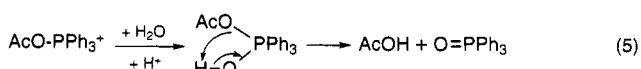
(OAc)₂(PPh₃)₂, triphenylphosphine being oxidized to triphenylphosphine oxide. Data at hand were consistent with the following tentative mechanism:¹



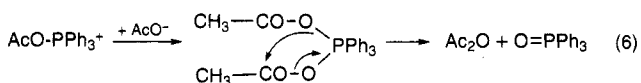
In the presence of excess phosphine:⁴



The formation of triphenylphosphine oxide could be interpreted as follows:



or



We wish to extend these preliminary results by reporting further kinetic data and investigating the effect of various tertiary phosphines. Also we report data on the reactivity of the resulting palladium(0) complexes in oxidative addition with phenyl iodide.

Results and Discussion

a. Kinetic Data on the Formation of Zerovalent Palladium from Pd(OAc)₂ + *n*PPh₃ (*n* > 2) in DMF.

As we have already reported,¹ mixtures of Pd(OAc)₂ and *n*PPh₃ (*n* ≥ 2) immediately afforded a bivalent palladium complex Pd(OAc)₂(PPh₃)₂, detected and characterized by its reduction peak in cyclic voltammetry at *E*_{Red}^P = -1.38 V vs SCE in DMF. This system led spontaneously but slowly to a palladium(0) complex

* To whom any correspondence should be addressed.
 † Present address: Université Ibn Tofail, Faculté des Sciences, BP 133, 14000 Kénitra, Morocco.
 ⊗ Abstract published in *Advance ACS Abstracts*, March 15, 1995.
 (1) Amatore, C.; Jutand, A.; M'Barki, M. A. *Organometallics* **1992**, *11*, 3009.
 (2) For reviews, see: (a) Heck, R. F. *Acc. Chem. Res.* **1979**, *12*, 146. (b) Tsuji, J. *Organic Syntheses via Palladium Compounds*; Springer Verlag: New York, 1980. (c) Kumada, M. *Pure Appl. Chem.* **1980**, *52*, 669. (d) Negishi, E. I. *Acc. Chem. Res.* **1982**, *15*, 340. (e) Heck, R. F. *Org. React.* **1982**, *27*, 345. (f) Heck, R. F. *Palladium Reagents in Organic Syntheses*; Academic Press: New York, 1985. (g) Stille, J. K. *Angew. Chem., Int. Ed. Engl.* **1986**, *25*, 508.
 (3) (a) Yamane, T.; Kikukawa, K.; Takagi, M.; Matsuda, T. *Tetrahedron* **1973**, *29*, 955. (b) Dieck, H. A.; Heck, R. F. *J. Am. Chem. Soc.* **1974**, *96*, 1133. (c) Dieck, H. A.; Heck, R. F. *J. Org. Chem.* **1975**, *40*, 1083. (d) Patel, B. A.; Heck, R. F. *J. Org. Chem.* **1978**, *43*, 3898. (e) Tsuji, J.; Yamakawa, T.; Kaito, M.; Mandai, T. *Tetrahedron Lett.* **1978**, 2075. (f) Ziegler, C. B.; Heck, R. F. *J. Org. Chem.* **1978**, *43*, 2941. (g) Patel, B. A.; Dickerson, J. E.; Heck, R. F. *J. Org. Chem.* **1978**, *43*, 5018. (h) Shimizu, I.; Yamada, T.; Tsuji, J. *Tetrahedron Lett.* **1980**, *21*, 3199. (i) Johnson, P. Y.; Wen, J. Q. *J. Org. Chem.* **1981**, *46*, 2767. (j) Kim, J.-I. I.; Patel, B. A.; Heck, R. F. *J. Org. Chem.* **1981**, *46*, 1067. (k) Hallberg, A.; Westerlund, C. *Chem. Lett.* **1982**, 1993. (l) Fiaud, J. C.; Aribi-Zouieche, L. *Tetrahedron Lett.* **1982**, *23*, 5279. (m) Mori, M.; Oda, I.; Ban, Y. *Tetrahedron Lett.* **1982**, *23*, 5315. (n) O'Connor, J. M.; Stallman, B. J.; Clark, W. G.; Shu, A. Y. L.; Spada, R. E.; Stevenson, T. M.; Dieck, H. A. *J. Org. Chem.* **1983**, *48*, 807. (o) Bäckvall, J. E.; Nordberg, R. E.; Vågberg, J. *Tetrahedron Lett.* **1983**, *24*, 411. (p) Cacchi, S.; Morera, E.; Ortari, G. *Tetrahedron Lett.* **1984**, *25*, 2271. (q) Mori, M.; Kanda, N.; Oda, I.; Ban, Y. *Tetrahedron* **1985**, *23*, 5465. (r) Karabelas, K.; Westerlund, C.; Hallberg, A. *J. Org. Chem.* **1985**, *50*, 3896. (s) Andersson, C. M.; Karabelas, K.; Hallberg, A. *J. Org. Chem.* **1985**, *50*, 3891. (t) Mori, M.; Kimura, M.; Uozumi, Y.; Ban, Y. *Tetrahedron Lett.* **1985**, *26*, 5947. (u) Andersson, C. M.; Hallberg, A. *J. Org. Chem.* **1987**, *52*, 3529. (v) Nilsson, K.; Hallberg, A. *Acta Chem. Scand. B* **1987**, *41*, 569. (w) Nilsson, K.; Hallberg, A. *Acta Chem. Scand.* **1990**, *44*, 288. (x) Andersson, C. M.; Larsson, J.; Hallberg, A. *J. Org. Chem.* **1990**, *52*, 5757.

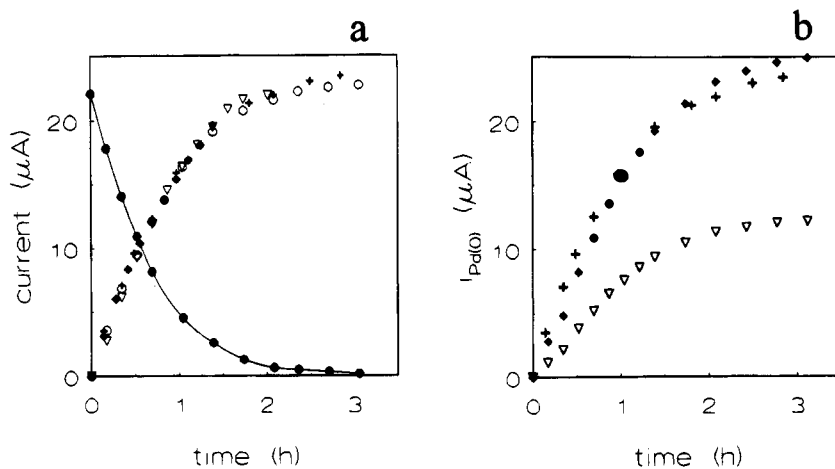


Figure 1. Variation of the plateau currents at a rotating gold disk electrode ($\phi = 2$ mm; $v = 0.02$ V s $^{-1}$; $\omega = 105$ rad s $^{-1}$) of the system Pd(OAc) $_2$ and PPh $_3$ as a function of time in DMF (nBu $_4$ NBF $_4$, 0.3 M) at 25 °C. (a) Variation of the reduction current at a potential of -1.30 V of the divalent palladium complex formed *in situ* from the mixture Pd(OAc) $_2$ (2 mM) and PPh $_3$ (20 mM) (●). Variation of the oxidation current at a potential of $+0.4$ V of the zerovalent palladium generated from the mixture Pd(OAc) $_2$ (2 mM) and PPh $_3$ (8 mM) (◆), PPh $_3$ (10 mM) (▽), and PPh $_3$ (20 mM) (+ and ○). (b) Variation of the oxidation current at a potential of $+0.4$ V of the zerovalent palladium generated from the mixture PPh $_3$ (20 mM) and Pd(OAc) $_2$ (2 mM) (+), Pd(OAc) $_2$ (1 mM) (▽), and Pd(OAc) $_2$ (1 mM) (◆) (same as ▽ but $2xi_{Pd(0)}$ is plotted to facilitate the comparison because of the concentration change).

detected by its oxidation peak in cyclic voltammetry at $E^{p_{Ox}} = +0.054$ V vs SCE in DMF. The palladium(0) oxidation peak current increased as a function of time at the expense of the reduction peak current of Pd(OAc) $_2$ (PPh $_3$) $_2$. Due to the instability of the palladium(0) complex generated from the mixture of Pd(OAc) $_2$ and 2PPh $_3$, kinetic investigations were achieved in the presence of excess triphenylphosphine ($n > 2$). In those cases a saturated stable complex, Pd 0 (PPh $_3$) $_3$ (OAc) $^-$, was obtained 4 and detected by its oxidation peak. Kinetic investigation of this system could be achieved using steady state voltammetry, performed at a rotating disk electrode. 1 The electrode was polarized at a potential of $+0.4$ V in DMF, on the plateau of the oxidation wave of the zerovalent palladium, and the resulting current was recorded as a function of time. The same technique was used to monitor the disappearance of the starting divalent complex Pd(OAc) $_2$ (PPh $_3$) $_2$, upon polarization on the plateau current of its reduction wave at -1.30 V in DMF.

From the curves presented in Figure 1a, we can observe that the rate of formation of the palladium(0) complex is not affected by the triphenylphosphine concentration, demonstrating that the formation of the palladium(0) complex is zero order in triphenylphosphine. The half life time $t_{1/2}$ for the generation of the palladium(0) complex was independent of the initial Pd(OAc) $_2$ concentration ([Pd(OAc) $_2$] = 2 mM, $t_{1/2} = 44$ min; [Pd(OAc) $_2$] = 1 mM, $t_{1/2} = 47$ min). This identity was even more striking when the variation of the palladium(0) concentration was plotted as a function of time (Figure 1b). Indeed when the data for [Pd(OAc) $_2$] = 1 mM (▽) were multiplied by a factor of 2 to account for the change of concentration, the resulting plot (◆) became exactly superimposable on that obtained for an initial concentration of [Pd(OAc) $_2$] = 2 mM (+). This

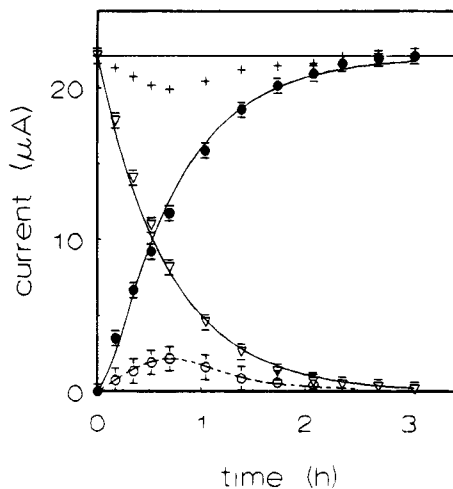


Figure 2. Variation of the plateau currents at a rotating gold disk electrode ($\phi = 2$ mm; $v = 0.02$ V s $^{-1}$; $\omega = 105$ rad s $^{-1}$) of the system Pd(OAc) $_2$ (2 mM) and PPh $_3$ (20 mM) as a function of time in DMF (nBu $_4$ NBF $_4$, 0.3 M) at 25 °C, variation of the reduction current at a potential of -1.30 V of the divalent palladium complex (▽), variation of the oxidation current at a potential of $+0.4$ V of the zerovalent palladium (●), sum of the experimental reduction and oxidation currents (+), and difference between the theoretical sum of the reduction and oxidation currents (22.07 μ A, horizontal solid lines) and the experimental one (○, dashed line). The solid lines are the theoretical predictions according to reactions 2 and 4 with $k_1 = 4.2 \times 10^{-4}$ s $^{-1}$ and $k_2' = 1.8 \times 10^{-3}$ s $^{-1}$.

demonstrates that the formation of the palladium(0) complex is first order in palladium(II) and thus that the palladium(0) complex is spontaneously produced from the bivalent complex Pd(OAc) $_2$ (PPh $_3$) $_2$ by an intramolecular reaction.

The sum of the oxidation current of the palladium(0) complex and the reduction current of Pd(OAc) $_2$ (PPh $_3$) $_2$ was not constant as a function of time (See Figure 2) evidencing the formation of an intermediate complex (dashed curve in Figure 2) prior the formation of the final complex Pd 0 (PPh $_3$) $_3$ (OAc) $^-$. The rate of disappear-

(4) Evidence for the ligation of the palladium(0) complex by an acetate anion and its consequences on the rate of oxidative addition will be published later: Amatore, C.; Carré, E.; Jutand, A.; M'Barki, M. A.; Meyer, G. Unpublished results (1994), manuscript in preparation.

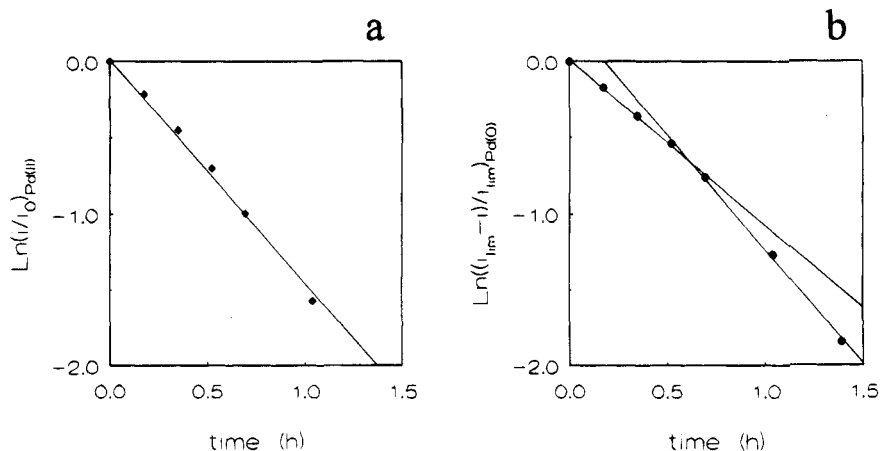
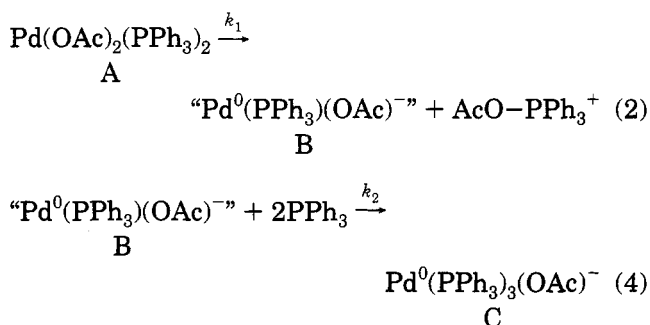


Figure 3. Kinetics of the disappearance of the palladium(II) complex and of the formation of the palladium(0) complex from the mixture $\text{Pd}(\text{OAc})_2$ (2 mM) and PPh_3 (20 mM) in DMF at 25 °C: (a) Variation of the reduction current of the palladium(II) complex, $\ln(i/i_0)$ as a function of time; (b) variation of the oxidation current of the palladium(0) complex, $\ln((i_{\text{lim}} - i)/i_{\text{lim}})$ as a function of time.

ance of the complex $\text{Pd}(\text{OAc})_2(\text{PPh}_3)_2$, represented by the plot of the variation of $\ln(i/i_0)_{\text{Pd(II)}}$ (i : reduction current at -1.3 V at t ; i_0 at $t = 0$) as a function of time (Figure 3a), follows a kinetic law first order in palladium(II) with a rate constant $k_1 = 4.1 \times 10^{-4} \text{ s}^{-1}$ at 25 °C. However, the rate of formation of the complex $\text{Pd}^0(\text{PPh}_3)_3(\text{OAc})^-$ does not follow a simple first order kinetic law, since the plot of the variation of $\ln((i_{\text{lim}} - i)/i_{\text{lim}})_{\text{Pd(0)}}$ (i , oxidation current at $+0.4$ V at t ; i_{lim} , limit of i at infinite time) as a function of time (Figure 3b) does not afford a straight line with zero intercept.

These data are indicative of the formation of an intermediate complex prior the formation of the final complex $\text{Pd}^0(\text{PPh}_3)_3(\text{OAc})^-$, according to the following mechanism:



The formation of the final product $\text{Pd}^0(\text{PPh}_3)_3(\text{OAc})^-$ (C) obeys the following kinetic law⁵ (see Experimental Section):

$$[\text{C}] = [\text{A}]_0 - [\text{A}]_0(k'_2 e^{-k_1 t} - k_1 e^{-k'_2 t}) / (k'_2 - k_1)$$

$$k'_2 = k_2 [\text{PPh}_3]^2$$

When long times are considered, this equation simplifies into

$$\ln([\text{A}]_0 - [\text{C}] / [\text{A}]_0) = \ln(k'_2 / (k'_2 - k_1)) - k_1 t = \ln((i_{\text{lim}} - i) / i_{\text{lim}})$$

From the slope of the straight line obtained at long

times (Figure 3b) we get $k_1 = 4.2 \times 10^{-4} \text{ s}^{-1}$, a value which is close to that of the rate constant found for the disappearance of $\text{Pd}(\text{OAc})_2(\text{PPh}_3)_2$, $4.1 \times 10^{-4} \text{ s}^{-1}$ (Figure 3a). From the intercept we can calculate $k'_2 = 1.8 \times 10^{-3} \text{ s}^{-1}$ and $k_2 = 4.5 \text{ M}^{-2} \text{ s}^{-1}$. The fact that $k'_2 > k_1$ further establishes our above claim that the intramolecular step 2 is the rate-determining step of the overall reaction 2 + 4.¹ Moreover such a larger value of k'_2 explains why most of the data in Figure 1a concerning the formation of the palladium(0) are almost superimposed when the phosphine concentration varies. Indeed, the result of varying the phosphine concentration amounts only in a slight shift of the data near the origin of time. Since k'_2 increases like $[\text{PPh}_3]^2$, this effect rapidly cancels at large phosphine concentration.

From the experimental values of k_1 and k'_2 , the values of the concentrations [B] and [C] may be determined at any time as well as the theoretical curves for the disappearance of the palladium(II) complex and for the formation of the palladium(0) complex. The theoretical curves, represented in solid lines in Figure 2, fit the experimental data. These results confirm that a palladium(0) complex is formed directly from $\text{Pd}(\text{OAc})_2(\text{PPh}_3)_2$ by an inner-sphere reduction and that this reaction 2 is the rate-determining step. The final palladium(0) complex $\text{Pd}^0(\text{PPh}_3)_3(\text{OAc})^-$ is then formed by a faster reaction 4 from the original palladium(0) complex obtained in reaction 2 with triphenylphosphine.

Influence of Water on the Rate of Formation of the Palladium(0) Complex from the Mixture $\text{Pd}(\text{OAc})_2 + 10\text{PPh}_3$ in DMF. Just after our former paper concerning triphenylphosphine,¹ Osawa and Hayashi have reported that the complex $\text{Pd}(\text{OAc})_2$ combined with 3 equiv of the ligand Binap afforded spontaneously and quantitatively a zerovalent palladium complex $\text{Pd}^0(\text{Binap})_2$ and Binap oxide.⁶ Their reaction was performed in the presence of known amounts of added water, the presence of which was found by these authors to be essential for the quantitative formation of the palladium(0) complex. Using solvents without water resulted in low conversion in palladium(0) complex, while the conversion and the rate of formation of the palladium(0) complex were enhanced by the presence

(5) Benson, S. W. *The Foundations of Chemical Kinetics*; McGraw-Hill Book Co. Inc.: New York, Toronto, London, 1960; p 33.

(6) Ozawa, F.; Kubo, A.; Hayashi, T. *Chem. Lett.* **1992**, 2177.

of an increasing amount of water. In our case, all reactions were performed in the absence of purposely added water but the amount of residual water in carefully distilled DMF had not been determined. However, we found that the presence of purposely added water (10 equiv) did not affect the rate of the formation of the palladium(0) complex ($k_1 = 3.9 \times 10^{-4} \text{ s}^{-1}$). It means that if residual water was involved in the mechanism of the formation of zerovalent palladium, this reaction would take place after the rate-determining step, *viz.* after the intramolecular reduction step 2.

After complete conversion of $\text{Pd}(\text{OAc})_2(\text{PPh}_3)_2$ to $\text{Pd}^0(\text{PPh}_3)_3(\text{OAc})^-$, a reduction peak was detected in cyclic voltammetry at -1.61 V in DMF. Addition of 1 equiv of acetic acid resulted in the same reduction peak with a double magnitude, demonstrating that acetic acid was formed in a quantitative yield during the conversion of $\text{Pd}(\text{OAc})_2(\text{PPh}_3)_2$ to $\text{Pd}^0(\text{PPh}_3)_3(\text{OAc})^-$. Since the resulting palladium(0) is ligated by one acetate,⁴ 1 equiv of acetic acid can only be produced by reaction 5. This implies that, in this experiment, the role of water (*viz.* the residual water in our experiments) is to convert an intermediate phosphonium salt into triphenylphosphine oxide (eq 5) as in the Mitsunobu reaction.⁷ Osawa and Hayashi's results⁶ could then be interpreted by considering that, at least under their conditions, the intramolecular step 2 is a reversible reaction that could be shifted to the formation of the palladium(0) complex by reaction of water with the postulated phosphonium salt, according to a reaction similar to reaction 5.

Influence of a Trialkylamine on the Rate of Formation of the Palladium(0) Complex from the Mixture $\text{Pd}(\text{OAc})_2 + 10\text{PPh}_3$, in DMF. Before we¹ and, later, Hayashi's group⁶ demonstrated that the triphenylphosphine was able to reduce the palladium acetate into a palladium(0) complex, it was very often suggested that a trialkylamine, which is always present and essential in order for the Heck reaction^{2,3} to proceed, was the reductant able to reduce the palladium acetate to palladium(0),⁸ especially when the Heck reactions were performed in the absence of any phosphine.⁹ Investigation by cyclic voltammetry of the $\text{Pd}(\text{OAc})_2$ salt, alone or in the presence of triethylamine (2 equiv), afforded badly resolved reduction peaks. In the oxidation range, no oxidation peaks could be detected except that of the triethylamine at $+0.89 \text{ V}$. However, in the absence of any authentic sample of the postulated palladium(0) complex formed in the case where the triethylamine could reduce the palladium acetate, it is hazardous at this stage to conclude whether triethylamine is able or not to reduce $\text{Pd}(\text{OAc})_2$ under our experimental conditions.¹⁰ It is why we have investigated the kinetics of the formation of the palladium(0) complex from the mixture $\text{Pd}(\text{OAc})_2 + 50 \text{ equiv of NEt}_3$

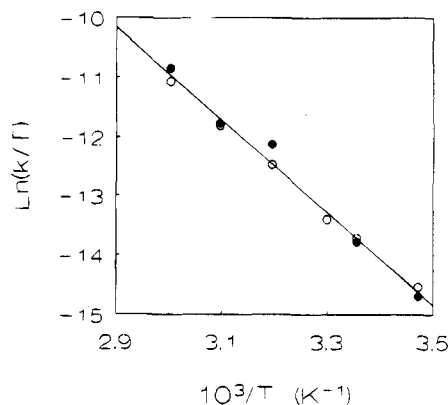


Figure 4. Arrhenius plot for the disappearance of the palladium(II) complex (O) and for the formation of the palladium(0) complex (●) from the mixture $\text{Pd}(\text{OAc})_2$ (2 mM) and PPh_3 (20 mM) in DMF (k , s^{-1}).

in the presence of 10 equiv of PPh_3 in order that a stable palladium(0) complex might be detected. A similar study as described above showed that, in the presence or in the absence of the amine, palladium(0) was formed with an identical rate constant of $k_1 = 4.0 \times 10^{-4} \text{ s}^{-1}$ at $25 \text{ }^\circ\text{C}$. So it is inferred that were triethylamine able to reduce the palladium acetate, this reaction would be much slower than the reduction by triphenylphosphine. When the reaction was performed in the presence of triethylamine, the reduction peak of acetic acid was of course not detected because of its reaction with the amine.

Influence of the Temperature on the Rate of Formation of the Palladium(0) Complex from the Mixture $\text{Pd}(\text{OAc})_2 + 10\text{PPh}_3$ in DMF. The rate constant of disappearance of $\text{Pd}(\text{OAc})_2(\text{PPh}_3)_2$ (calculated as in Figure 3a) and that of formation of the palladium(0) complex (calculated as in Figure 3b by considering the limiting straight line at long times) from the mixture $\text{Pd}(\text{OAc})_2$ (2 mM) and PPh_3 (10 equiv) were determined at various temperatures in the range $15\text{--}60 \text{ }^\circ\text{C}$, in DMF. The results showed that the rate of formation of the palladium(0) complex increases with the temperature (*e.g.* $t_{1/2} = 5620 \text{ s}$ at $15 \text{ }^\circ\text{C}$ and $t_{1/2} = 106 \text{ s}$ at $60 \text{ }^\circ\text{C}$). The rate of disappearance of the complex $\text{Pd}(\text{OAc})_2(\text{PPh}_3)_2$ also increases with the temperature. An Arrhenius plot for both reactions (disappearance of Pd(II) and formation of Pd(0)) afforded a common straight line (Figure 4) and allowed an evaluation of the activation parameters: $\Delta H^\ddagger = 65 \text{ kJ mol}^{-1}$ and $\Delta S^\ddagger = -94 \text{ J mol}^{-1} \text{ K}^{-1}$ for reaction 2.

The fact that either considering the rate of disappearance of the palladium(II) complex or that of the formation of the palladium(0) complex affords similar values of ΔH^\ddagger and ΔS^\ddagger further supports that the elemental reaction 2 that produces palladium(0) from $\text{Pd}(\text{OAc})_2(\text{PPh}_3)_2$ is the rate-determining step of the overall reaction. The negative value found for the entropy means that the palladium(II) complex of the transition state is more organized than the original complex $\text{Pd}(\text{OAc})_2(\text{PPh}_3)_2$. It is therefore reasonable to propose that the palladium(0) complex is produced by a sort of reductive elimination occurring in the inner sphere of the palladium(II) complex (reaction 2). All these results clarify and confirm the mechanism we have already proposed (reactions 1, 2, 4, and 5).¹

(7) Pautard-Cooper, A.; Slayton, A. E. *J. Org. Chem.* **1989**, *54*, 2485.

(8) Collman, J. P.; Hegedus, L. S.; Norton, J. R.; Finke, R. G. *Principles and Applications of Organotransition Metal Chemistry*, 2nd ed.; University Science Books: Mill Valley, CA, 1987; p 725.

(9) Ziegler, C. B., Jr.; Heck, R. F. *J. Org. Chem.* **1978**, *43*, 2941.

(10) Were the amine able to reduce the palladium acetate, it would result in the formation of palladium metal in the absence of any ligand able to stabilize the palladium(0). This metallic palladium could not be of course detected by cyclic voltammetry. It was reported that triethylamine partially reduces complexes such as $\text{PdCl}_2(\text{RCN})$ ($\text{R} = \text{Ph}$ or Me) into metallic palladium. See: McCrindle, R.; Ferguson, G.; Arsenault, G. J.; McAllees, A. J.; Stephenson, D. K. *J. Chem. Res. Synop.* **1984**, 360.

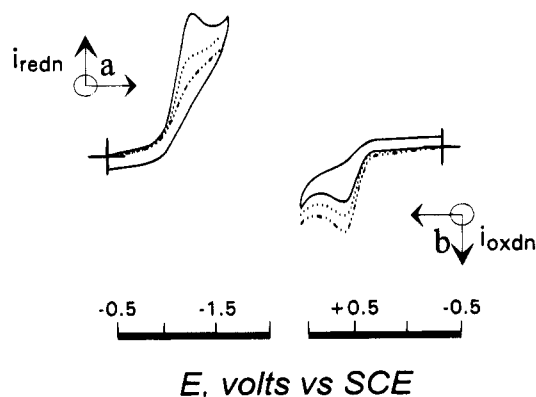
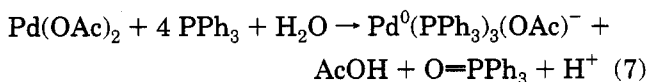


Figure 5. (a) Cyclic voltammetry of $\text{Pd}(\text{OAc})_2((p\text{-CF}_3\text{-C}_6\text{H}_4)_3\text{P})_2$ generated from $\text{Pd}(\text{OAc})_2$ (2 mM) and $(p\text{-CF}_3\text{-C}_6\text{H}_4)_3\text{P}$ (20 mM) in DMF ($n\text{Bu}_4\text{NBF}_4$, 0.3 M) at a stationary gold disk electrode ($\phi = 0.5$ mm) with a scan rate of 0.2 V s^{-1} . The cathodic scan, from -0.4 to -1.7 V, has been performed as a function of time: (—) 6, (···) 12, (-··-) 19 mn. Only forward scans are shown for 12 and 19 mn for simplification. (b) Cyclic voltammetry of the palladium(0) complex generated *in situ* from $\text{Pd}(\text{OAc})_2$ (2 mM) and $(p\text{-CF}_3\text{-C}_6\text{H}_4)_3\text{P}$ (20 mM), in DMF (0.3 M $n\text{Bu}_4\text{NBF}_4$) at the same electrode, with a scan rate of 0.2 V s^{-1} . The anodic scan, from -0.6 to $+1$ V, has been performed as a function of time: (—) 9, (···) 13, (-··-) 21 mn.

In the presence of at least four phosphine ligands, a stable complex could be accumulated:



b. Kinetic Data on the Formation of Zerovalent Palladium from $\text{Pd}(\text{OAc})_2$ and a Series of Tertiary Phosphines in DMF. The formation of palladium(0) complexes from mixtures of $\text{Pd}(\text{OAc})_2$ and tertiary phosphines¹¹ was first investigated by considering triarylphosphines para-substituted by electron-withdrawing or -donating groups Z: $(p\text{Z-C}_6\text{H}_4)_3\text{P}$. The reaction was investigated with mixtures of $\text{Pd}(\text{OAc})_2$ and 10 equiv of the triarylphosphines in order to obtain a stable palladium(0) complex (reaction 6).

The behavior of these systems was similar to that previously observed for triphenylphosphine. Indeed, whatever the triarylphosphine, the mixture of $\text{Pd}(\text{OAc})_2$ and 10 equiv of $(p\text{Z-C}_6\text{H}_4)_3\text{P}$ in DMF, immediately afforded a bivalent palladium complex $\text{Pd}(\text{OAc})_2((p\text{Z-C}_6\text{H}_4)_3\text{P})_2$ detected by its reduction peak (see Figure 5a and Table 1). As expected, the resulting complexes were more easily reduced when the triarylphosphines were substituted by an electron-withdrawing group (see Table 1). The resulting palladium(II) complexes were not stable and led spontaneously to species detected by their oxidation peak (see Figure 5b and Table 1). Their oxidation peak current increased with time concomitantly with a decrease of the reduction peak current of the divalent palladium complexes $\text{Pd}(\text{OAc})_2((p\text{Z-C}_6\text{H}_4)_3\text{P})_2$ (Figure 5a,b). After addition of iodobenzene, the oxidation peaks were no more observed, evidencing that the species that was formed from spontaneous evolution of the complex $\text{Pd}(\text{OAc})_2((p\text{Z-C}_6\text{H}_4)_3\text{P})_2$ was a zerovalent palladium complex able to react with iodobenzene by

(11) The influence of various phosphines on the Heck reaction has been investigated. See ref 9.

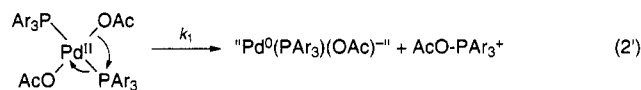
Table 1. Reduction and Oxidation Peak Potentials of the $\text{Pd}(\text{OAc})_2((p\text{Z-C}_6\text{H}_4)_3\text{P})_2$ and $\text{Pd}^0((p\text{Z-C}_6\text{H}_4)_3\text{P})_3(\text{OAc})^-$ Complexes

Z	σ Hammett	$\text{Pd}(\text{OAc})_2((p\text{Z-C}_6\text{H}_4)_3\text{P})_2$ $E_{\text{Red.}}^{\text{p}}, \text{V vs SCE}^a$	$\text{Pd}^0((p\text{Z-C}_6\text{H}_4)_3\text{P})_3(\text{OAc})^-$ $E_{\text{Ox.}}^{\text{p}}, \text{V vs SCE}^a$
CF_3	+0.54	-1.20 ₅	+0.54 ₅
Cl	+0.227	n.d.	+0.25 ₅
F	+0.062	-1.33 ₅	+0.20 ₅
H	0	-1.39 ₅	+0.05 ₅
CH_3	-0.170	-1.42 ₅	-0.03 ₅
CH_3O	-0.268	-1.50 ₅	-0.10 ₅

^a Determined at 0.2 V s^{-1} at a stationary gold disk electrode ($\phi = 0.5$ mm) in DMF containing $n\text{Bu}_4\text{NBF}_4$ (0.3 M), at 25°C .

an oxidative addition. As expected, the resulting zerovalent complexes $\text{Pd}^0((p\text{Z-C}_6\text{H}_4)_3\text{P})_3(\text{OAc})^-$ were more easily oxidized when the triarylphosphines were substituted by an electron donor group (Table 1). A kinetic study similar to that mentioned above for triphenylphosphine allowed the determination of the rate constant of the formation of the palladium(0) complex, k_1^Z . We observed that the rate of this reaction was faster when the triarylphosphine was substituted by an electron-withdrawing group. In order to obtain reasonable reaction times in the case of electron-donating substituents and to allow comparison between phosphines, all reactions were performed at 60°C . A plot of the variation of $\log(k_1^Z/k_1^{\text{H}})$ as a function of the σ Hammett constants showed that the rates of formation of palladium(0) complexes from $\text{Pd}(\text{OAc})_2((p\text{Z-C}_6\text{H}_4)_3\text{P})_2$ follow a Hammett correlation with a positive value of $\rho = +0.9$ (Figure 6a).

These results show that the formation of the palladium(0) complex according to reaction 2' is favored



when the electronic density on the phosphorous is low (electron-withdrawing group) *i.e.* when it is prompt to be attacked by the acetate leading to the reductive elimination-like step. However it should be mentioned that, at 25°C , the determination of ρ , made in the case of electron-withdrawing groups, led to $\rho = +2.4$ (Figure 6b). This shows that reaction 2' proceeds through a transition state, in which the stabilizing effects due to phosphine electronic properties become less effective at higher temperatures.

Results concerning other tertiary phosphines such as PPh_2Me , PMe_2Ph , and PBU_3 ¹² are more difficult to rationalize when compared with triphenylphosphine. In this series, we can observe from Figure 7a,b that no correlation is found between the rate of formation k_1 of the palladium(0) complex with either electronic factors (as evaluated from $\text{p}K$ values¹³) or steric ones (as evaluated from cone angles θ ¹⁴) when both parameters vary. However, when only electronic factors vary (such as in para-substituted triarylphosphines), a good correlation is obtained (Figure 6). This suggests that when both factors are varied, the rate constant is sensitive to

(12) (a) Mandai, T.; Matsumoto, T.; Tsuji, J. *Tetrahedron Lett.* **1993**, *34*, 2513. (b) Ono, K.; Fugami, K.; Tanaka, S.; Tamaru, Y. *Tetrahedron Lett.* **1994**, *35*, 4133.

(13) Zizelman, P. M.; Amatore, C.; Kochi, J. K. *J. Am. Chem. Soc.* **1984**, *106*, 3771.

(14) Tolman, C. A. *Chem. Rev.* **1977**, *77*, 313.

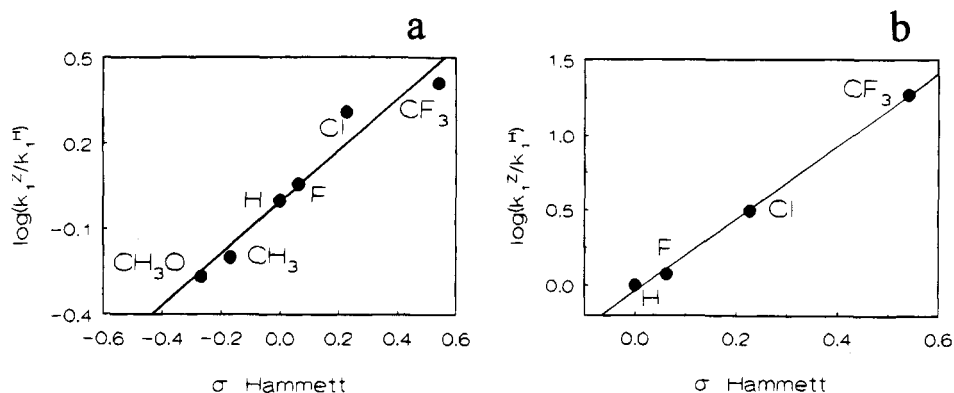


Figure 6. Hammett plot for the rate of the formation of the palladium(0) complex generated from the mixture $\text{Pd}(\text{OAc})_2$ (2 mM) and a series of *para*-substituted triarylphosphines (*p*- $\text{Z}-\text{C}_6\text{H}_4$) $_3\text{P}$ (20 mM) in DMF (k_1 , s^{-1}): (a) At 60 °C ($\rho = +0.9$; $r = 0.973$); (b) at 25 °C ($\rho = +2.4$; $r = 0.998$).

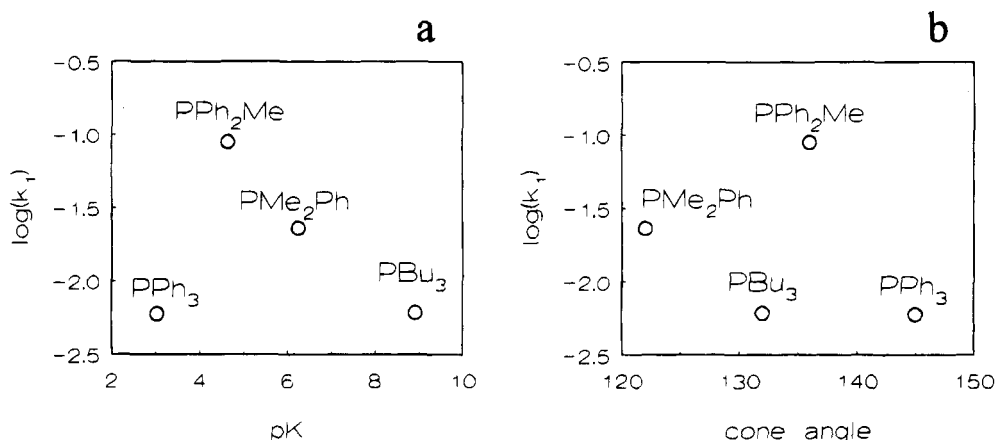


Figure 7. Variation of the rate of formation, k_1 (s^{-1}), of the palladium(0) complex from mixtures of $\text{Pd}(\text{OAc})_2$ (2 mM) and a series of tertiaryphosphines (20 mM) in DMF at 60 °C: (a) As a function of the $\text{p}K$ of the phosphine; (b) as a function of the cone angle of the phosphine.

both variations. However, a simple linear relationship of the kind¹³

$$\log k_1 = A + B\text{p}K + C\theta \quad (8)$$

does not hold any better. This is evidenced in Figure 7a,b by the nonlinear variations for the series PPh_3 , PPh_2Me , and PMe_2Ph . Indeed, in this series, θ and $\text{p}K$ values correlate linearly ($r = 0.99$):¹³

$$\theta = 167.3 - 7.1\text{p}K \quad (9)$$

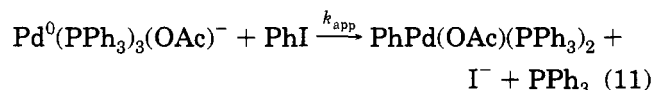
Were a two-parameter linear equation such as that in (9) to hold, owing to the fortuitous relationship in (9), one would obtain a linear correlation with either $\text{p}K$ or θ values for the series PPh_3 , PPh_2Me , and PMe_2Ph . Taking into account the fact that when θ is constant (Figure 6), a good correlation is observed with electronic factors, it appears that the absence of correlation observed in Figure 7a,b stems from the fact that cone angle parameter is involved through nonlinear contributions. In practice, an extremely good correlation ($r = 0.999$) is obtained by considering a quadratic involvement of the cone angle:

$$\log k_1 = 1.00 - 0.35\text{p}K - 8.7 \times 10^{-3}(\theta - 129)^2 \quad (10)$$

Such a quadratic dependence on cone angle suggests that two opposing effects are involved when the steric

parameters are modified. This may be rationalized by the following interpretation: when θ increases, steric constraint builds up in the $\text{Pd}(\text{OAc})_2(\text{PR}_3)_2$ complex thus favoring its reorganization to a nonplanar geometry. This would favor transition to the activated complex involved in reaction 2'. Conversely, when θ is too large, it is probable that intramolecular attack on the phosphine by the acetate is disfavored. Due to these antagonist effects, one should observe an optimum value of steric parameters. Equation 10 indicates that this optimum value is close to a cone angle of 129°.

c. Kinetic Data on the Oxidative Addition of Phenyl Iodide with Palladium(0) Complexes Generated from $\text{Pd}(\text{OAc})_2$ and Tertiary Phosphines, in DMF. Reactivity of the Palladium(0) Complex Generated from $\text{Pd}(\text{OAc})_2$ and 10 PPh_3 . The oxidation peak ($E^{\text{p}} = +0.054$ V vs SCE) of the complex $\text{Pd}^0(\text{PPh}_3)_3(\text{OAc})^-$, generated from the mixture of $\text{Pd}(\text{OAc})_2$, 2 mM in DMF, combined with 10 equiv of triphenylphosphine, disappeared in the presence of phenyl iodide, demonstrating that the oxidative addition in eq 11 took place, the final product of the reaction



being $\text{PhPd}(\text{OAc})(\text{PPh}_3)_2$.^{1,4} Therefore the reactivity of

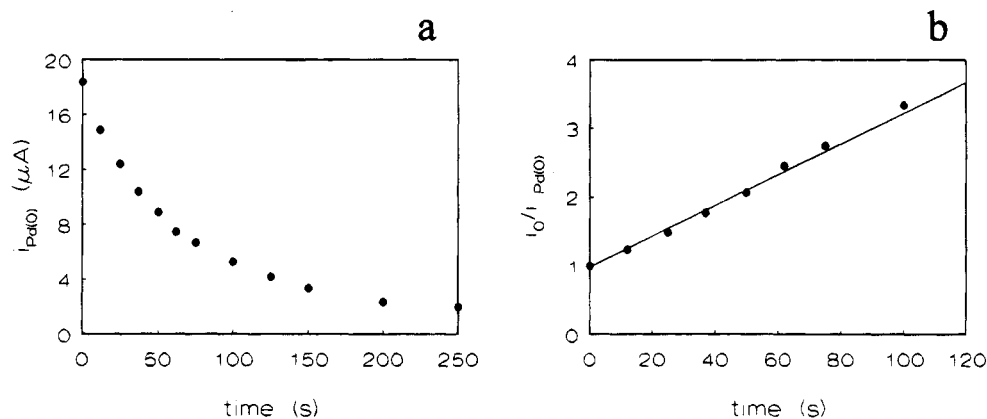


Figure 8. Oxidative addition of phenyl iodide (2 mM) with the palladium(0) complex quantitatively generated *in situ* from Pd(OAc)₂ (2 mM) and PPh₃ (20 mM), in DMF (nBu₄NBF₄, 0.3 M) at 25 °C: (a) Variation of the oxidation plateau current $i_{Pd(0)}$ at +0.2 V, at a rotating gold disk electrode ($\phi = 2$ mm; $v = 0.02$ Vs⁻¹; $\omega = 105$ rad s⁻¹) in the presence of phenyl iodide (2 mM) as a function of time; (b) variation of i_0/i as a function of time.

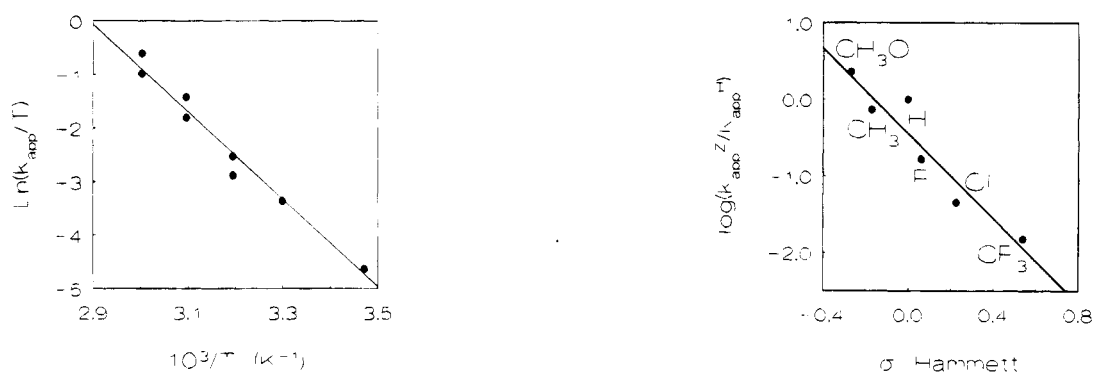


Figure 9. Arrhenius plot for the oxidative addition of phenyl iodide with the palladium(0) complex generated from Pd(OAc)₂ (2 mM) and PPh₃ (20 mM), in DMF (nBu₄NBF₄, 0.3 M) (k_{app} , M⁻¹ s⁻¹).

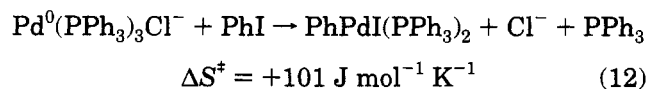
Figure 10. Hammett plot for the oxidative addition of phenyl iodide with the palladium(0) complex generated from mixtures of Pd(OAc)₂ (2 mM) and a series of para-substituted triarylphosphines (*p*-Z-C₆H₄)₃P (20 mM) in DMF (nBu₄NBF₄, 0.3 M) at 25 °C ($\rho = -2.8$; $r = 0.951$).

the zerovalent palladium complex with phenyl iodide could be monitored by amperometry. A kinetic investigation of this oxidative addition was carried out using steady state cyclic voltammetry, performed at a rotating disk electrode, as the analytical technique.^{1,15} After complete conversion of the palladium(II) complex to the palladium(0) complex, the electrode was polarized at a potential of +0.20 V on the plateau of the oxidation wave of the palladium(0) complex, and the resulting oxidation current was recorded as a function of time, after addition of 1 equiv of phenyl iodide. A typical curve is represented in Figure 8a.

A plot of the ratio i_0/i as a function of time results in a straight line ($i_0/i = -k_{app}cot + 1$; Figure 8b) demonstrating that the oxidative addition is first order in palladium(0) and in phenyl iodide. The value of the apparent rate constant of the oxidative addition could then be deduced from the slope of the straight line represented in Figure 8b and was found to be $k_{app} = 12$ M⁻¹ s⁻¹, at 25 °C.

The reactivity of phenyl iodide with the palladium(0) complex was investigated at various temperatures in the range 15–60 °C. An Arrhenius plot afforded a straight line (Figure 9) and allowed the determination of the activation parameters: $\Delta H^\ddagger = 60 \pm 7$ kJ mol⁻¹ and $\Delta S^\ddagger = -1 \pm 1$ J mol⁻¹ K⁻¹. These values have to be compared to that found for the oxidative addition of

PhI with Pd⁰(PPh₃)₄, in the presence of 50 equiv of PPh₃,^{15a} $\Delta H^\ddagger = 77$ kJ mol⁻¹ and $\Delta S^\ddagger = +14$ J mol⁻¹ K⁻¹, and to that of Pd⁰(PPh₃)₄, in the presence of 100 equiv of chloride anions,^{15b} $\Delta H^\ddagger = 95$ kJ mol⁻¹ and $\Delta S^\ddagger = +101$ J mol⁻¹ K⁻¹. The values of ΔH^\ddagger are comparable for the three systems. However the values of ΔS^\ddagger are very different. The high value $\Delta S^\ddagger = +101$ J mol⁻¹ K⁻¹ found in the case of the oxidative addition of Pd⁰(PPh₃)₄ in the presence of chloride anions was interpreted by the cleavage of two bonds (*viz.* Pd–Cl and Pd–PPh₃) from the complex Pd⁰(PPh₃)₃Cl⁻ during the oxidative addition (eq 12).^{15b} The small value of ΔS^\ddagger found in the



present paper seems to indicate that cleavage of only one bond occurred, despite the presence of an acetate anion ligated to the palladium(0) in Pd⁰(PPh₃)₃(OAc)⁻.⁴ A tentative explanation could be the formation of a transient pentacoordinated anionic *o*-arylpalladium complex in which the palladium(II) would remain li-

(15) (a) Fauvarque, J. F.; Pflüger, F.; Troupel, M. *J. Organomet. Chem.* **1981**, *208*, 419. (b) Amatore, C.; Azzabi, M.; Jutand, A. *J. Am. Chem. Soc.* **1991**, *113*, 8375.

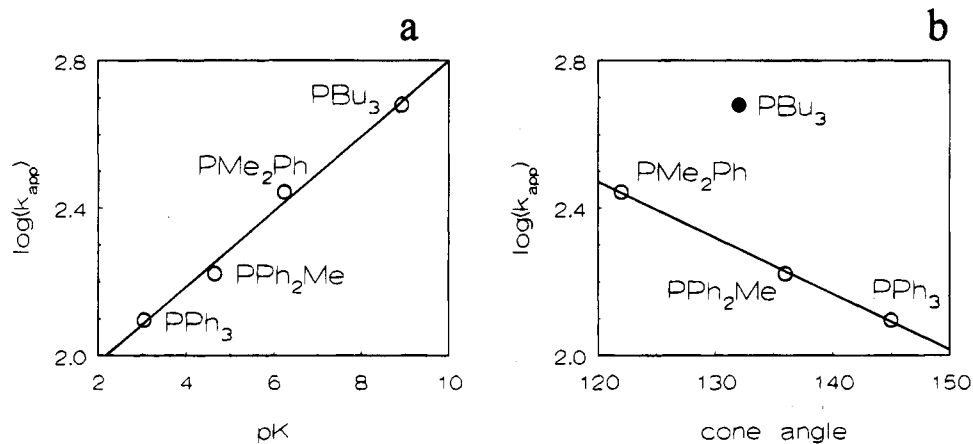
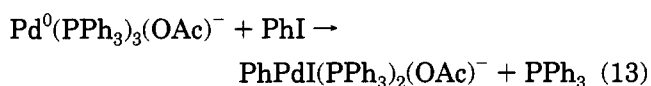
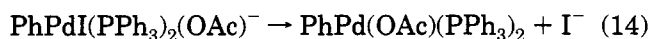


Figure 11. Variation of the rate of the oxidative addition, k_{app} ($M^{-1} s^{-1}$), of phenyl iodide with the palladium(0) complex generated from mixtures of $Pd(OAc)_2$ (2 mM) and a series of tertiary phosphines (20 mM) in DMF at 60 °C: (a) As a function of the pK of the phosphine (slope = +0.10; $r = 0.995$); (b) as a function of the cone angle of the phosphine (slope = -0.015; $r = 0.999$, except for PBu_3).

gated by an acetate anion.¹⁶



$$\Delta S^\ddagger = -1 \text{ J mol}^{-1} \text{ K}^{-1}$$



This hypothesis is indeed supported by the fact that the final product of the oxidation addition is not $PhPdI(PPh_3)_2$ but $PhPd(OAc)(PPh_3)_2$.^{1,4}

Reactivity of the Palladium(0) Complex Generated from $Pd(OAc)_2$ and $10PAr_3$. The same experiments were performed with triarylphosphines substituted in the para position by electron-withdrawing or -donating groups, Z. A plot of the variation of $\log(k_{app}^Z/k_{app}^H)$ as a function of the σ Hammett constants showed that the oxidative addition follows a Hammett correlation with $\rho = -2.8$ (Figure 10). As expected, the negative value of ρ indicates that the oxidative addition of phenyl iodide with $Pd^0((pZ-C_6H_4)_3P)_3(OAc)^-$ is faster when the aryl group of the triarylphosphine is substituted by an electron-donating group, in which case the nucleophilicity of the palladium(0) complex is enhanced.

Reactivity of the Palladium(0) Complex Generated from $Pd(OAc)_2$ and $10PR_3$. The apparent rate constant of the oxidative addition with phenyl iodide has been determined for different tertiary phosphines. The logarithm of the apparent rate constant varied linearly with the pK of the phosphine (Figure 11a). As expected, the oxidative addition of phenyl iodide with the palladium(0) complex is favored when the ligand is more basic. No correlation was found when considering the cone angle (Figure 11b). However, in the series PPh_3 , PPh_2Me , and PMe_2Ph , since θ and pK values correlate (see eq 9),¹³ a good correlation was found for the cone angle (Figure 11b); the higher the cone angle of the phosphine, the lower the reactivity of the palladium(0) complex.

(16) Anionic pentacoordinated arylpalladium complexes $ArPdI(PPh_3)_2Cl^-$ have been reported as intermediates in oxidative additions. See: Amatore, C.; Jutand, A.; Suarez, A. *J. Am. Chem. Soc.* **1993**, *115*, 9531.

Conclusion

Mixtures of $Pd(OAc)_2$ and tertiary phosphines afford spontaneously a palladium(0) complex and the corresponding phosphine oxide. The reaction proceeds via a reductive elimination performed on a palladium(II) complex, $Pd(OAc)_2(PR_3)_2$. This inner-sphere reduction is the rate-determining step of the overall reaction. The reaction seems to be general since it occurs with aromatic phosphines as well as with aliphatic phosphines. The rate of formation of the palladium(0) complex is higher when the triarylphosphine is substituted by an electron-withdrawing group. The resulting palladium(0) complex $Pd^0(PR_3)_3(OAc)^-$ undergoes oxidative addition with phenyl iodide. The rate of this reaction is higher when the triarylphosphine is substituted by an electron-donating group and when the phosphine is more basic.

We also observed that mixtures of triphenylphosphine with other bivalent palladium salts such as $Pd(O-COCF_3)_2$ and $Pd(Acac)_2$ ($Acac = acetylacetonate$) result in the formation of palladium(0) complexes and triphenylphosphine oxide.¹⁷ When the bivalent palladium does not contain an oxygenated ligand such as in the cationic complex $Pd(PPh_3)_2(BF_4)_2$, stable palladium(0) complexes are spontaneously formed, provided water and triphenylphosphine are present in solution.¹⁸ It seems that the spontaneous reduction of bivalent palladium complexes to zerovalent palladium by triphenylphosphine is a general reaction that occurs as soon as the divalent palladium is combined with an oxygenated ligand such as NO_3^- ,¹⁹ AcO^- ,^{1,4} $CF_3CO_2^-$,¹⁷ $Acac^-$,¹⁷ oxide,¹⁹ or OH^- .^{18,20}

Experimental Section

All the experiments were performed under argon.

Chemicals. DMF was distilled from calcium hydride. Iodobenzene and triethylamine were commercial and used after filtration on alumina. $Pd(OAc)_2$, $Pd(OCOCF_3)_2$, $Pd-$

(17) As observed in preliminary studies involving different bivalent palladium salts with oxygenated and nonoxygenated anions: Amatore, C.; Jutand, A.; M'Barki, M. A. Unpublished results (1994).

(18) Amatore, C.; Jutand, A.; Medeiros, M. J. Unpublished results (1994), manuscript in preparation.

(19) Malatesta, L.; Angoletta, M. *J. Chem. Soc.* **1957**, 1186.

(20) Grushin, V. V.; Alper, H. *Organometallics* **1993**, *12*, 1890.

(Acac)₂, and triphenylphosphine were commercial (Janssen). The other trialkyl- and arylphosphines were also from a commercial source (Strem Chemicals). Pd(PPh₃)₂(BF₄)₂ was synthesized according to a published procedure.²¹

Electrochemical Setup and Electrochemical Procedure for Cyclic Voltammetry. Cyclic voltammetry was performed with a homemade potentiostat²² and a wave-form generator, PAR Model 175. The cyclic voltammograms were recorded with a Nicolet 3091 digital oscilloscope. Experiments were carried out in a three-electrode cell connected to a Schlenk line. The cell was equipped with a double envelope in order to perform the reactions at different temperatures, using a Lauda M3 thermostat. The counter electrode was a platinum wire of ca. 1 cm² apparent surface area; the reference was a saturated calomel electrode (Tacussel) separated from the solution by a bridge (3 mL) filled with a 0.3 M nBu₄NBF₄ solution in DMF. A 12-mL volume of DMF containing 0.3 M nBu₄NBF₄, was poured into the cell. A 5.4-mg amount (2 × 10⁻³ M) of Pd(OAc)₂ was then added, followed by the suitable amount of the desired phosphine. The cyclic voltammetry was performed at a stationary disk electrode (a gold disk made from cross section of wire ($\phi = 0.5$ mm) sealed into glass) at a scan rate of 0.2 V s⁻¹.

The kinetic measurements were performed by steady state cyclic voltammetry at a rotating disk electrode (a gold disk ($\phi = 2$ mm) inserted into a Teflon holder, Tacussel EDI 65109) at a scan rate of 0.02 V s⁻¹ and an angular velocity of 105 rad s⁻¹ (Tacussel controvit). The RDE potential was set on the plateau of the reduction wave of the bivalent palladium complex, and the reduction current was monitored as a function of time up to 100% conversion. In another set of experiments, the RDE was polarized on the plateau of the oxidation wave of the zerovalent palladium complex, and the oxidation current was monitored as a function of time. When the limit of the oxidation current was reached, the suitable amount of iodobenzene was added to the cell and the oxidation current recorded to follow the kinetics of oxidative addition with PhI.^{1,15}

Derivation of Kinetic Laws Corresponding to the Mechanism Represented by Reactions 2 and 4.⁵ With the notations in eqs 2 and 4, one has

$$d[A]/dt = -k_1[A]$$

Straightforward integration affords

$$[A] = [A]_0 e^{-k_1 t}$$

and

$$d[B]/dt = k_1[A] - k'_2[B] = k_1[A]_0 e^{-k_1 t} - k'_2[B]$$

$$k'_2 = k_2[L]^2$$

$$d[B]/dt + k'_2[B] = k_1[A]_0 e^{-k_1 t}$$

$$[B] = (e^{-k_1 t} - e^{-k'_2 t})(k_1[A]_0)/(k'_2 - k_1)$$

The formation of the final product Pd⁰(PPh₃)₃(OAc)⁻ (C) obeys the following kinetic law:

$$d[C]/dt = k'_2[B] = k'_2(e^{-k_1 t} - e^{-k'_2 t})(k_1[A]_0)/(k'_2 - k_1)$$

From where it follows that

$$[C] = [A]_0 - [A]_0(k'_2 e^{-k_1 t} - k_1 e^{-k'_2 t})/(k'_2 - k_1)$$

Since at long times, $k'_2 e^{-k_1 t} > k_1 e^{-k'_2 t}$, we get

$$([A]_0 - [C])/[A]_0 \approx (k'_2 e^{-k_1 t})/(k'_2 - k_1)$$

That is

$$\ln(([A]_0 - [C]) / [A]_0) \approx \ln(k'_2 / (k'_2 - k_1)) - k_1 t \approx \ln((i_{lim} - i) / i_{lim})$$

Acknowledgment. This work has been supported in part by the Centre National de la Recherche Scientifique (CNRS, URA 1679, "Processus d'Activation Moléculaire") and the Ministère de l'Enseignement Supérieur et de la Recherche (Ecole Normale Supérieure, Département de Chimie).

OM940838T

(21) Bushnell, G. W.; Dixon, K. R. *Can. J. Chem.* **1972**, *50*, 3694.

(22) Amatore, C.; Lefrou, C.; Pflüger, F. *J. Electroanal. Chem.* **1989**, *270*, 43.

[N,N'-Bis(trimethylsilyl)benzamidinato]titanium and -zirconium Compounds. Synthesis and Application as Precursors for the Syndiospecific Polymerization of Styrene

Juan C. Flores, James C. W. Chien, and Marvin D. Rausch

Organometallics, 1995, 14 (4), 1827-1833 • DOI: 10.1021/om00004a040 • Publication Date (Web): 01 May 2002

Downloaded from <http://pubs.acs.org> on March 9, 2009

More About This Article

The permalink <http://dx.doi.org/10.1021/om00004a040> provides access to:

- Links to articles and content related to this article
- Copyright permission to reproduce figures and/or text from this article



[*N,N'*-Bis(trimethylsilyl)benzamidinato]titanium and -zirconium Compounds. Synthesis and Application as Precursors for the Syndiospecific Polymerization of Styrene

Juan C. Flores, James C. W. Chien, and Marvin D. Rausch*

Department of Chemistry and Department of Polymer Science & Engineering,
University of Massachusetts, Amherst, Massachusetts 01003

Received October 31, 1994[®]

Ti(O-*i*-Pr)₃Cl reacts with Li[C₆H₅C(NSiMe₃)₂]·Et₂O to give [η-C₆H₅C(NSiMe₃)₂]Ti(O-*i*-Pr)₃ (**1**) in quantitative yield. Mild thermolysis of **1** promotes the elimination of C₆H₅CN to form Ti(O-*i*-Pr)₃N(SiMe₃)₂ (**2**), which is also synthesized from the reaction of Ti(O-*i*-Pr)₃Cl and Li[N(SiMe₃)₂]·Et₂O. Treatment of the dimer {[η-C₆H₅C(NSiMe₃)₂]TiCl₃]₂ (**3**) with donor ligands produces the corresponding monomeric adducts [η-C₆H₅C(NSiMe₃)₂]TiCl₃·L (L = THF (**4**); PMe₃ (**5**)). Partial alkylation of the dimer **3** with 2 equiv of methyllithium gives {[η-C₆H₅C(NSiMe₃)₂]Ti(Me)Cl₂]₂ (**6**); however, treatment with 6 equiv leads to the formation of the bis(benzamidinate) compound [η-C₆H₅C(NSiMe₃)₂]₂TiMe₂ (**7**). Compound **7** is synthesized in better yield by the reaction between [η-C₆H₅C(NSiMe₃)₂]₂TiCl₂ (**8**) and methyllithium. The same reaction but with the zirconium dichloride analog [η-C₆H₅(NSiMe₃)₂]₂ZrCl₂ (**9**) also gives [η-C₆H₅C(NSiMe₃)₂]₂ZrMe₂ (**10**) in good yield. The catalytic systems **1**/methylaluminumoxane (MAO), **3**/MAO, **4**/MAO, and **5**/MAO are active for styrene polymerization, forming syndiotactic polymer in a highly stereospecific process. The systems **1**/MAO, **3**/MAO, **8**/MAO, and **9**/MAO show low activity as ethylene polymerization catalysts. The cationic systems **1**/triisobutylaluminum (TIBA)/Ph₃C⁺[B(C₆F₅)₄]⁻ (**11**) or **7,10/11** were not effective as olefin polymerization catalysts.

Introduction

There is remarkable worldwide research activity and interest in the development of new homogeneous Ziegler–Natta catalysts for the stereoregulated polymerization of α-olefins. Most of this research has been carried out with group 4 mono- and bis(η⁵-cyclopentadienyl) or -(indenyl) compounds, since Kaminsky, Ewen, Ishihara, and others have demonstrated that their use with MAO produces highly iso- or syndiotactic poly-α-olefins at very high reaction rates.^{1–5} Further studies have demonstrated that the so-called “cationic systems”,

such as [*rac*-Et(Ind)₂ZrMe]⁺ or (C₅Me₅)TiMe₂⁺, obtained from the reaction between *rac*-Et(Ind)₂ZrMe₂ or (C₅Me₅)TiMe₃ with Ph₃C⁺[B(C₆F₅)₄]⁻ (**11**), exhibit high activities in stereoselective propylene^{6,7} or styrene^{5,8} polymerizations.

The bidentate *N,N'*-bis(trimethylsilyl)benzamidinate ligand [η-RC(NSiMe₃)₂] (R = C₆H₅ or substituted phenyls),⁹ being a formal three-electron-donating group, has been regarded as a steric equivalent of η⁵-C₅H₅ and η⁵-C₅Me₅,¹⁰ and was recently reported as a promising alternative to the well-known cyclopentadienyl ligands.¹¹ A variety of [*N,N'*-bis(trimethylsilyl)benzamidinato]-metal compounds have been described in the literature,^{10–12} including several group 4 mono(benzamidinate) {[η-C₆H₅C(NSiMe₃)₂]MCl₃]₂ (M = Ti, Zr)¹³ and bis(benzamidinate) [η-C₆H₅C(NSiMe₃)₂]₂MCl₂ (M = Ti,

[®] Abstract published in *Advance ACS Abstracts*, March 15, 1995.

(1) (a) Sinn, H.; Kaminsky, W.; Vollmer, H.-J.; Wolcott, R. *Angew. Chem.* **1980**, *92*, 396. (b) Sinn, H.; Kaminsky, W. *Adv. Organomet. Chem.* **1980**, *18*, 99. (c) Kaminsky, W.; Kùlper, K.; Brintzinger, H. H.; Wild, F. R. W. *P. Angew. Chem., Int. Ed. Engl.* **1985**, *24*, 507. (d) Ewen, J. A. *J. Am. Chem. Soc.* **1984**, *106*, 6355. (e) Ewen, J. A. In *Catalytic Polymerization of Olefins*; Keii, T., Soga, K., Eds.; Elsevier: New York, 1986; p 271. (f) Rieger, B.; Chien, J. C. W. *Polym. Bull.* **1989**, *21*, 159. (g) Rieger, B.; Mu, X.; Mallin, D. T.; Rausch, M. D.; Chien, J. C. W. *Macromolecules* **1990**, *23*, 2559. (h) Llinás, G. H.; Day, R. O.; Rausch, M. D.; Chien, J. C. W. *Organometallics* **1993**, *12*, 1283. (i) Llinás, G. H.; Dong, S.-H.; Mallin, D. T.; Rausch, M. D.; Lin, Y.-G.; Winter, H. H.; Chien, J. C. W. *Macromolecules* **1992**, *25*, 1242. (j) Erker, G.; Aulbach, M.; Knickmeier, M.; Wingbermhùhle, D.; Krùger, C.; Nolte, M.; Werner, S. *J. Am. Chem. Soc.* **1993**, *115*, 4590.

(2) (a) Ewen, J. A.; Haspeslagh, L.; Atwood, J. L.; Zhang, H. *J. Am. Chem. Soc.* **1987**, *109*, 6544. (b) Ewen, J. A.; Jones, R. L.; Razavi, A. *J. Am. Chem. Soc.* **1988**, *110*, 6255. (c) Fierro, R.; Yu, Z.; Rausch, M. D.; Dong, S.-H.; Alvarez, D.; Chien, J. C. W. *J. Polym. Sci., Part A: Polym. Chem.* **1994**, *32*, 661.

(3) (a) Soga, K.; Yanagihara, H. *Makromol. Chem. Rapid Commun.* **1988**, *9*, 23. (b) Ishihara, N.; Seimiya, T.; Kuramoto, M.; Voi, M. *Macromolecules* **1986**, *19*, 2464. (c) Ishihara, N.; Kuramoto, M.; Voi, M. *Macromolecules* **1988**, *21*, 3356.

(4) Ready, T. E.; Chien, J. C. W.; Rausch, M. D. *Macromolecules* **1993**, *26*, 5822.

(5) Kucht, H.; Kucht, A.; Chien, J. C. W.; Rausch, M. D. *Appl. Organomet. Chem.*, in press.

(6) Chien, J. C. W.; Tsai, W.-M.; Rausch, M. D. *J. Am. Chem. Soc.* **1991**, *113*, 8570.

(7) (a) Jordan, R. F. *J. Chem. Educ.* **1988**, *65*, 285. (b) Bochmann, M.; Lancaster, S. J. *Organometallics* **1993**, *12*, 633. (c) Tsai, W.-M.; Rausch, M. D.; Chien, J. C. W. *Appl. Organomet. Chem.* **1993**, *7*, 71.

(8) Pellicchia, C.; Longo, P.; Proto, A.; Zambelli, A. *Makromol. Chem. Rapid Commun.* **1992**, *13*, 265.

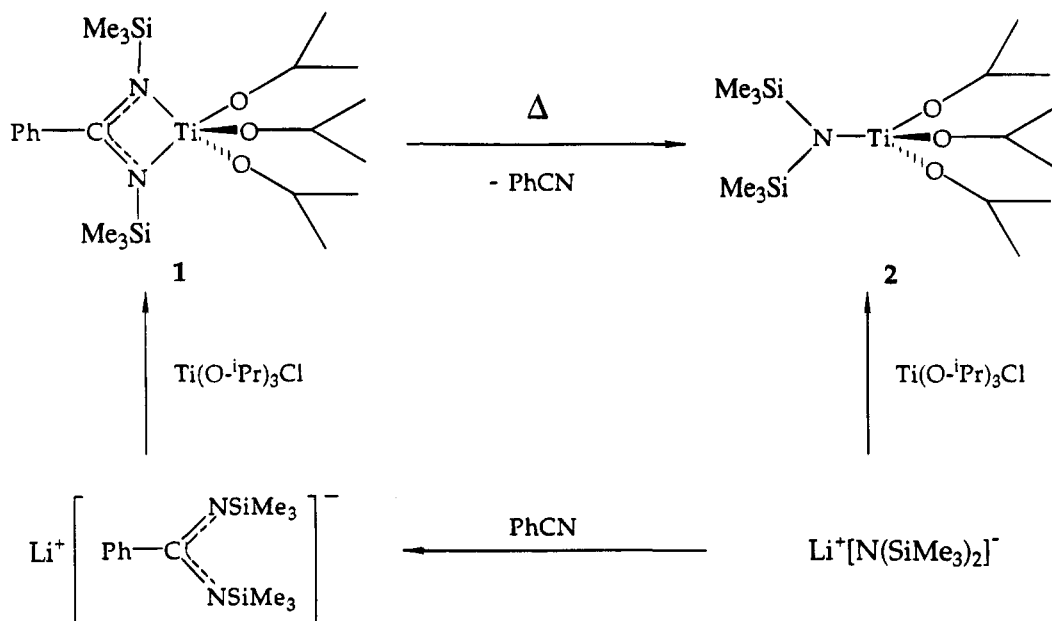
(9) Boeré, R. T.; Oakley, R. T.; Reed, R. W. *J. Organomet. Chem.* **1987**, *331*, 161.

(10) Wedler, M.; Knùsel, F.; Noltemeyer, M.; Edelmann, F. T. *J. Organomet. Chem.* **1990**, *388*, 21.

(11) Duchateau, R.; van Wee, C. T.; Meetsma, A.; Teuben, J. H. *J. Am. Chem. Soc.* **1993**, *115*, 4931.

(12) (a) Dehnicke, K.; Ergezinger, C.; Hartmann, E.; Zinn, A.; Hùsler, K. *J. Organomet. Chem.* **1988**, *352*, C1. (b) Buijink, J.-K.; Noltemeyer, M.; Edelmann, F. T. *Z. Naturforsch.* **1991**, *46B*, 1328. (c) Wedler, M.; Knùsel, F.; Edelmann, F. T.; Behrens, U. *Chem. Ber.* **1992**, *125*, 1313. (d) Wedler, M.; Recknagel, A.; Gilje, J. W.; Noltemeyer, M.; Edelmann, F. T. *J. Organomet. Chem.* **1992**, *426*, 295. (e) Kilimann, V.; Noltemeyer, M.; Edelmann, F. T. *J. Organomet. Chem.* **1993**, *443*, 35. (f) Edelmann, F. T.; Ziegler, W.; Behrens, U. *J. Organomet. Chem.* **1992**, *426*, 261.

Scheme 1



Zr)¹⁴ complexes. More recently, (η^5 -cyclopentadienyl)-benzamidinate compounds $\{(\eta^5\text{-C}_5\text{R}_5)[\eta\text{-C}_6\text{H}_5\text{C}(\text{NSiMe}_3)_2]\text{-MX}_2\}$ (R = H, Me; M = Ti, Zr, Hf; X = Cl, alkyl)¹⁵ have been found to be active for the polymerization of ethylene and propylene.

Since the geometric, steric, and electronic effects of the ligands attached to the metal center are of critical importance in determining the rate and stereospecificity of polymerization catalysis, it was of interest to determine the change produced when, instead of mono- or bis(cyclopentadienyl)metal compounds, mono- and bis(benzamidinate) group 4 compounds are the precursors in polymerizations using MAO or **11** as cocatalysts. Therefore, the purpose of the present study was to synthesize new *N,N'*-bis(trimethylsilyl)benzamidinate derivatives of titanium and zirconium and investigate their utility as catalysts in the polymerization of styrene, ethylene, and propylene.

Results and Discussion

Synthesis. $[\eta\text{-C}_6\text{H}_5\text{C}(\text{NSiMe}_3)_2]\text{Ti}(\text{O-}i\text{-Pr})_3$ (**1**) was prepared as an oil in quantitative yield by the reaction of $\text{Li}[\text{C}_6\text{H}_5\text{C}(\text{NSiMe}_3)_2]$ with $\text{Ti}(\text{O-}i\text{-Pr})_3\text{Cl}$ in ethyl ether at 0 °C. Compound **1** was obtained in analytical purity simply by filtration of LiCl and solvent removal. The product was found to be thermally unstable and could not be further purified. Thus, attempted fractional distillation of **1** at 10^{-3} mmHg resulted in decomposition, producing benzonitrile as the main product in the first fraction and pure $\text{Ti}(\text{O-}i\text{-Pr})_3\text{N}(\text{SiMe}_3)_2$ (**2**) in the second fraction. This behavior was also detected in solution by ¹H NMR (Scheme 1). A sample of **1** in CDCl₃ over the course of several days at 25 °C and monitored by ¹H NMR, showed the gradual formation of **2** (δ 0.20 (s, SiMe₃), 1.25 (d, $J = 6$ Hz, C(H)Me₂), 4.55 (hept, $J = 6$ Hz, C(H)Me₂)), together with the disappearance of the

corresponding signal for **1** (δ -0.11 (s, SiMe₃), 1.28 (d, $J = 6$ Hz, C(H)Me₂), 4.76 (hept, $J = 6$ Hz, C(H)Me₂)) and changes in the splitting pattern of the multiplet in the aromatic region. The amido compound **2** was also prepared in better yield (97%) by the direct reaction of $\text{Li}[\text{N}(\text{SiMe}_3)_2]$ with $\text{Ti}(\text{O-}i\text{-Pr})_3\text{Cl}$. The conversion of **1** to **2** can be visualized (Scheme 1) by means of a sigmatropic shift of one trimethylsilyl group¹⁶ to the other nitrogen atom along the NCN-benzamidinate framework, with the subsequent elimination of benzonitrile. Curiously, this pathway represents the reverse process of formation of the benzamidinate ligand, which involves the addition of $\text{Li}[\text{N}(\text{SiMe}_3)_2]$ to benzonitrile and migration of one SiMe₃ group to the nitrile nitrogen.⁹ The conversion of **1** to **2** is likely due to the steric relief produced in **2** compared to **1**.

The compound $[\eta\text{-}N,N'\text{-bis}(\text{trimethylsilyl})\text{benzamidinate}]\text{titanium trichloride}$ (**3**) is known to exist as a dimer, with chloro bridges connecting the two electron-deficient titanium atoms.¹³ We have found that this dimer is easily broken by using electron-donor solvents or ligands (Scheme 2). Thus, simple recrystallization of **3** from tetrahydrofuran (THF) afforded the monomer $[\eta\text{-C}_6\text{H}_5\text{C}(\text{NSiMe}_3)_2]\text{TiCl}_3 \cdot \text{THF}$ (**4**). As expected, elemental analysis and ¹H NMR revealed the coordination of just one molecule of THF per titanium atom. The THF molecule remained coordinated in solution, as observed by ¹H-NMR in CDCl₃ (δ 1.92 (m, THF), 3.96 (m, THF)), but was replaced by addition of 1 equiv of a stronger electron-donating ligand such as PMe₃. This latter reaction was carried out in THF and led to the formation of $[\eta\text{-C}_6\text{H}_5\text{C}(\text{NSiMe}_3)_2]\text{TiCl}_3 \cdot \text{PMe}_3$ (**5**) (Scheme 2). A ¹H-NMR spectrum of **5** in CDCl₃ showed the corresponding phosphine doublet at δ 1.44 ($J_{\text{P-H}} = 9$ Hz), whereas the ³¹P{¹H}-NMR spectrum exhibited a singlet at δ -13.9, confirming the coordination of phosphorus to titanium.

A typical alkylation reaction of **3** with 2 equiv of methylolithium produced $\{[\eta\text{-C}_6\text{H}_5\text{C}(\text{NSiMe}_3)_2]\text{Ti}(\text{Me})-$

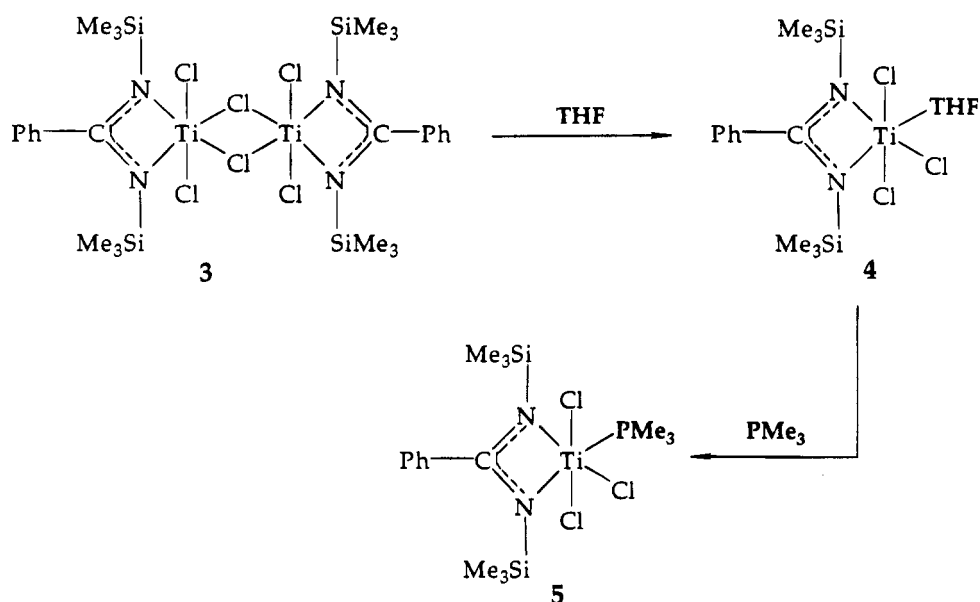
(13) Fenske, D.; Hartmann, E.; Dehnicke, K. *Z. Naturforsch.* **1988**, *43B*, 1611.

(14) Roesky, H. W.; Meller, B.; Noltemeyer, M.; Schmidt, H.-G.; Scholz, V.; Sheldrick, G. M. *Chem. Ber.* **1988**, *121*, 1403.

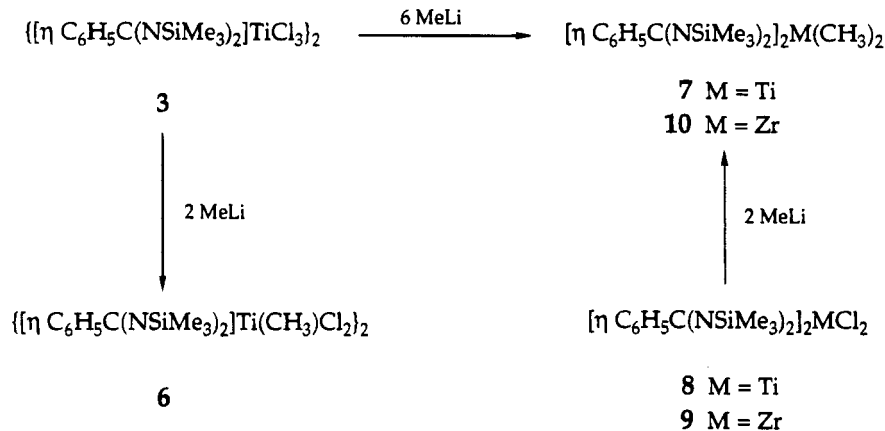
(15) Chernega, A. N.; Gómez, R.; Green, M. L. H. *J. Chem. Soc., Chem. Commun.* **1993**, 1415.

(16) (a) Abel, E. W.; Duster, M. O. *J. Organomet. Chem.* **1971**, *33*, 161. (b) Ashe, A. J. *J. Am. Chem. Soc.* **1970**, *92*, 1233.

Scheme 2



Scheme 3



Cl₂)₂ (6), which most likely exists as a dimer because of the stabilization resulting from the formation of chloro bridge bonds in this type of compound (*vide supra*). Compound 6 was characterized by ¹H-NMR spectrometry in benzene-*d*₆. A notable feature is the low-field chemical shift observed for the methyl group attached to titanium at δ 2.30.^{17c,d}

When the same reaction was carried out with 6 equiv of methyllithium, the unexpected bis(benzamidinato) compound [η -C₆H₅C(NSiMe₃)₂]₂TiMe₂ (7) was isolated in 24% yield based on Ti (Scheme 3). Six equivalents of LiCl were collected from this reaction, so it can be concluded that complete alkylation had occurred. One explanation for this result could involve formation of the corresponding trimethyltitanium compound [η -C₆H₅C(NSiMe₃)₂]₂TiMe₃. This coordinatively unsaturated intermediate might be unstable enough to react with another molecule of [η -C₆H₅C(NSiMe₃)₂]₂TiMe₃, resulting in the formation of 7 together with TiMe₄ (Scheme 4). The latter product would decompose under these conditions.^{17a} The free coordination position in the octahedral titanium environment of “[η -C₆H₅C(NSiMe₃)₂]-

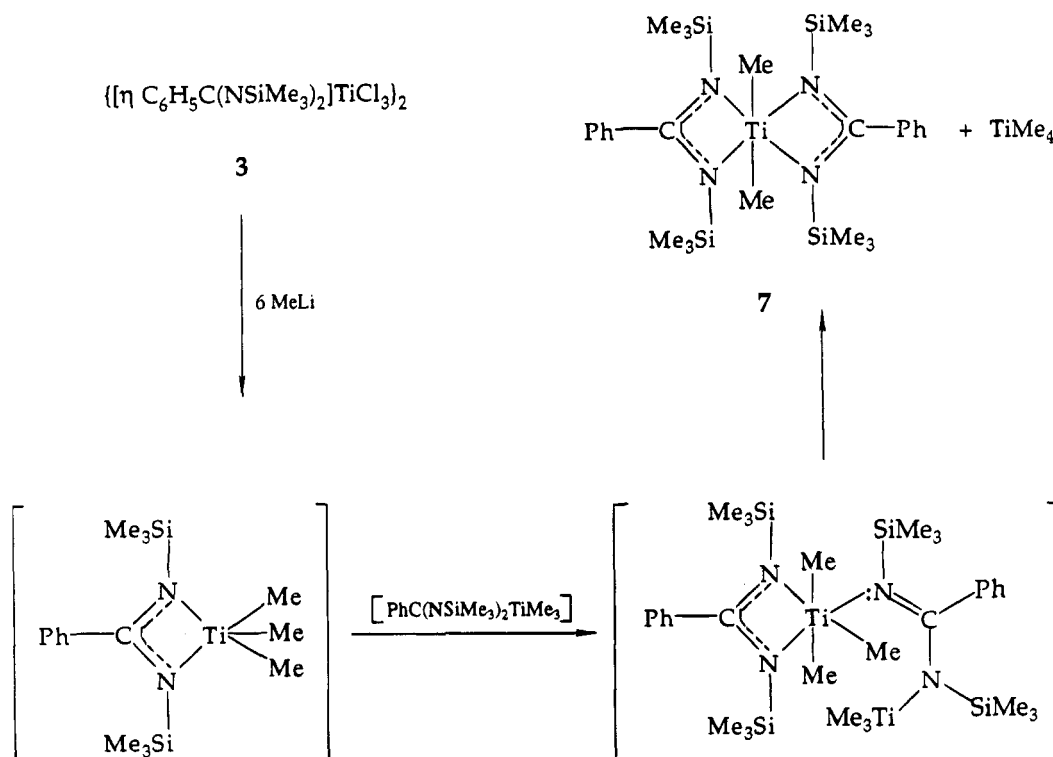
TiMe₃” probably plays an important role by providing a site for coordination of a nitrogen of the second benzamidinato molecule. A subsequent exchange of Ti-C and Ti-N bonds would complete the process. In another attempt to prepare a trimethyltitanium monobenzamidinato complex starting with the phosphine adduct 5, the desired product again could not be isolated. However, the dimethyltitanium bis(benzamidinato) product 7 was also not detected. In this case, the free coordination position was most likely occupied by the phosphine ligand.

Compound 7 was also synthesized in 99% yield by the direct reaction of methyllithium and [η -C₆H₅C(NSiMe₃)₂]₂TiCl₂ (8)¹⁴ and was found to be fairly stable compared to dimethyltitanocenes.^{17b,18} Also compared to the latter, the ¹H-NMR spectrum of 7 shows a singlet for the CH₃Ti protons shifted significantly to lower field (δ 1.94 in benzene-*d*₆). The zirconium analog [η -C₆H₅C(NSiMe₃)₂]₂ZrMe₂ (10) was likewise readily prepared in 98% yield by a reaction of the corresponding dichloride (9)¹⁴ and methyllithium. The ¹H-NMR spectrum of 10 exhibits a singlet at δ 0.44 for the CH₃Zr protons.

(17) (a) Wailes, P. C.; Coutts, R. S. P.; Weigold, H. *Organometallic Chemistry of Titanium, Zirconium and Hafnium*; Academic Press: New York, 1974; p 22. (b) *Ibid.*, p 89. (c) Samuel, E.; Ferner, R.; Bigorgne, M. *Inorg. Chem.* **1973**, *12*, 881. (d) Mena, M.; Royo, P.; Serrano, R. *Organometallics* **1989**, *8*, 476.

(18) (a) Gómez, R.; Cuenca, T.; Royo, P. Hovortreydt, E. *Organometallics* **1991**, *10*, 2516. (b) Demerseman, B.; Mahé, R.; Dixneuf, P. H. *J. Chem. Soc., Chem. Commun.* **1984**, 1394. (c) Bercaw, J. E.; Marvich, R. H.; Bell, L. G.; Brintzinger, H. H. *J. Am. Chem. Soc.* **1972**, *94*, 1219.

Scheme 4

Table 1. Styrene Polymerization Catalyzed by **3**/MAO^a

run	[cat.] (mM)	Al/Ti	T_p (°C)	yield of PS (mg)	$10^{-5}A^b$	SY ^c	T_m (°C)
1	0.050	4000	25	28	1.7	93	
2	0.025	4000	25	30	3.7	93	270
3	0.025	2000	25	36	4.4	94	272
4	0.025	2000	50	46	5.6	85	265

^a $V = 50$ mL of toluene + 5.0 mL of styrene; $t_p = 1.5$ h. ^b g of PS/(mol of Ti·mol of styrene·h). ^c Weight % of *s*-PS insoluble in refluxing 2-butanone.

Polymerization Catalysis. In this study, it was found that the mono[bis(trimethylsilyl)benzamidinato]titanium compounds **1**, **3**, **4**, and **5** when activated with methylaluminoxane (MAO) were active in the polymerization of styrene. In contrast, **8**/MAO was completely inactive in this regard. Table 1 summarizes some representative results for **3**/MAO. ¹³C-NMR spectra of the polystyrene (PS) fractions insoluble in refluxing 2-butanone showed them to be highly syndiotactic (Figure 1).^{3b,19} The yield (SY) of syndiotactic polystyrene (*s*-PS) (weight % of product remaining after 2-butanone extraction) was very high for this catalytic system, being a maximum in run 3 (94%).

The activity of this polymerization system was followed as a function of reaction time and began to decrease after *ca.* 2 h. This fact, together with the lack of reactivity for **8**/MAO suggests that the catalytic intermediate may become deactivated through the formation of a bis(benzamidinato)titanium species. Such a process would be similar to the observed alkylation of **3** with methyllithium as discussed above. The different polymerization behaviors of **3** and **8** toward styrene resemble the differences reported previously for CpTiCl₃ and Cp₂TiCl₂.^{3c} The activity of **3** [*i.e.*, 5.6×10^5 g of PS/(mol of Ti·mol of styrene·h)] was lower than that found for IndTiCl₃ or CpTiCl₃, but the syndiospeci-

ficity as measured by SY was similar to that for IndTiCl₃ and higher than that for CpTiCl₃.⁴

The trialkoxytitanium compound **1**, the THF adduct **4**, and the trimethylphosphine adduct **5** were also tested for styrene polymerization with MAO as the cocatalyst. The results obtained under the same conditions are summarized in Table 2. The order of reactivity was **3** > **1** > **4** > **5**. The thermal conversion of **1** to Ti(*O-i*-Pr)₃N(SiMe₃)₂ (**2**) under mild conditions may be responsible for its low activity, since **2**/MAO was found to be completely inactive. Compounds **4** and **5** behaved as expected; the coordination of electron-donating ligands to the metal center suppressed the activity. Even so, the syndiotactic yields of the *s*-PS were comparable to those observed for **3**/MAO.

Compounds **3** and **1** were supported on silica following the Soga procedure.²⁰ The titanium contents of these SiO₂-supported catalysts, as measured by atomic absorption spectrometry, were 7.1×10^{-2} and 4.4×10^{-2} mmol/g, respectively. After activation with TIBA,²⁰ both were found inactive for styrene polymerization.

In addition to these studies, an investigation on the activity of these (benzamidinato)metal compounds as ethylene polymerization catalysts was carried out. Using the conditions shown in Table 3, **3**/MAO, **1**/MAO, **8**/MAO, and **9**/MAO reacted very slowly with ethylene compared with the Cp₂ZrCl₂/MAO system.^{1a,b,21} The T_m values found for these polyethylenes suggest a large k_p/k_{tr} ratio, where K_p and k_{tr} are the rate constants for propagation and transfer, respectively.^{1h}

As was found with group 4 metallocenes, the zirconium compound **9** in this study was more active than the titanium analog **8** (runs 10 and 11). It is noteworthy that the bis(benzamidinato) compound **8** (run 10) was

(20) Soga, K.; Kaminaka, M. *Makromol. Chem.* **1993**, *194*, 1745.

(21) Chien, J. C. W.; Wang, B.-P. *J. Polym. Sci., Part A* **1990**, *28*, 15.

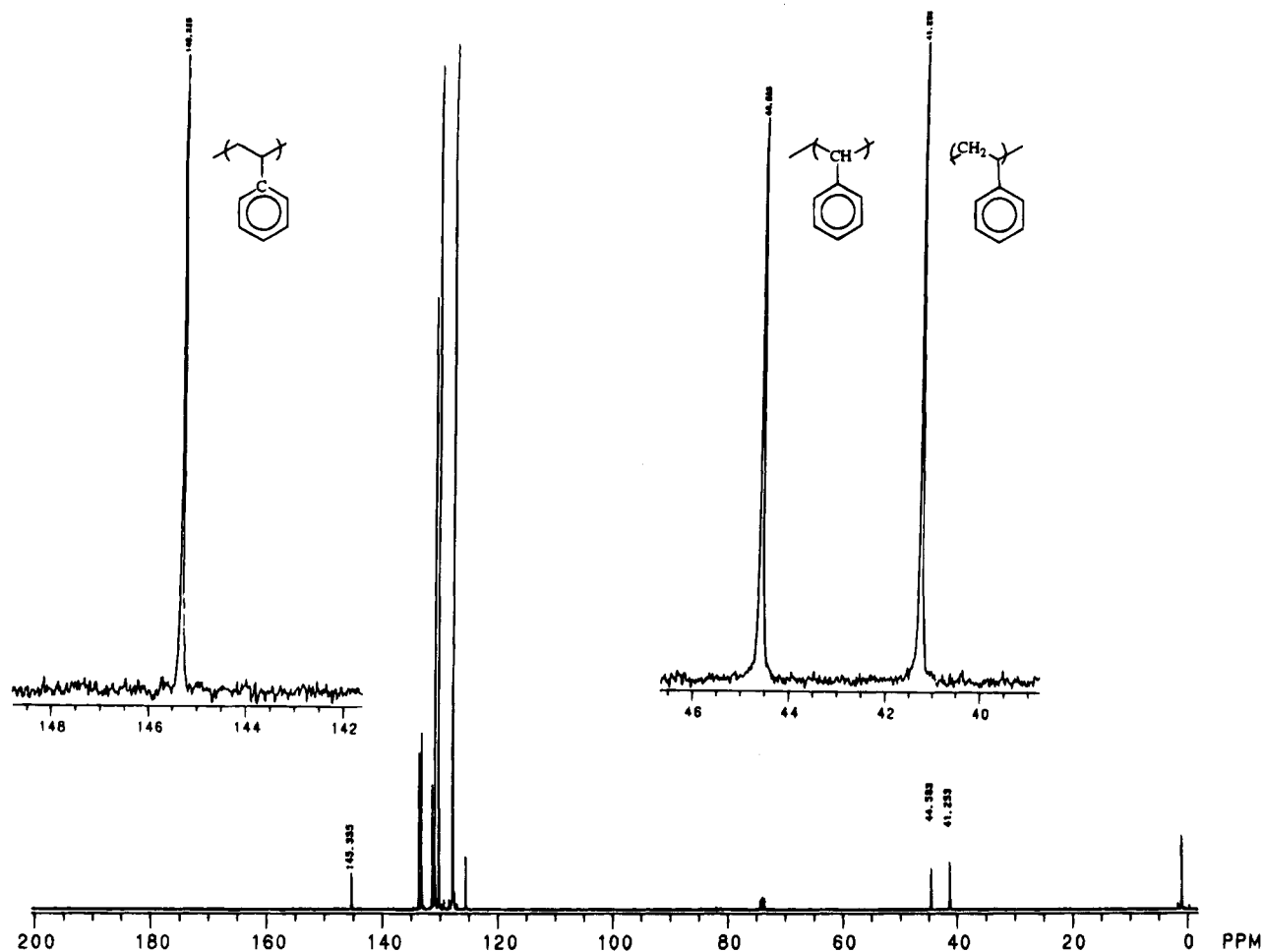


Figure 1. ^{13}C -NMR in 1,2,4-trichlorobenzene of polystyrene produced by **3**/MAO.

Table 2. Styrene Polymerization Catalyzed by **3**, **1**, **4**, and **5**/MAO^a

run	cat.	yield of PS (mg)	$10^{-5}A^b$	SY ^c	T_m (°C)
3	3	36	4.4	94	272
5	1	19	2.3	95	272
6*	4	30	1.8	93	273
7*	5	19	1.2	95	273

^a $V = 50$ mL of toluene + 5.0 mL of styrene (* $V = 100$ mL of toluene + 10 mL of styrene); $t_p = 25$ °C; [cat.] = 0.025 mM; Al/Ti = 2000. ^b g of PS/(mol of Ti·mol of styrene). ^c SY = weight % of *s*-PS insoluble in refluxing 2-butanone.

Table 3. Ethylene Polymerization Catalyzed by **3**, **1**, **8**, and **9**/MAO^a

run	cat.	yield of PE (mg)	$10^{-4}A^b$	T_m (°C)
8	3	42	5.5	137
9	1	13	1.7	136
10	8	12	1.6	137
11	9	32	4.2	137

^a $V = 50$ mL toluene; $T_p = 20$ °C; $P_{\text{ethylene}} = 10$ psig ($[\text{C}_2\text{H}_4] = 0.03076$ M); Al/Ti = 2000; [cat.] = 0.025 mM; $t_p = 2$ h. ^b g of PE/(mol of Ti or Zr)·(C₂H₄)_h.

inferior in activity to the corresponding mono(benzamidinate) compound **3** (run 8), and the latter was superior to the trialkoxide **1** (run 9) in ethylene polymerization. None of the catalytic systems included in Table 3 were active in propylene polymerization under similar conditions and 20 psig monomer pressure.

The system **3**/TIBA/Ph₃C⁺[B(C₆F₅)₄]⁻ was inactive for styrene polymerization. Also, the systems **7** or **10**/Ph₃C⁺[B(C₆F₅)₄]⁻ were inactive for ethylene or propyl-

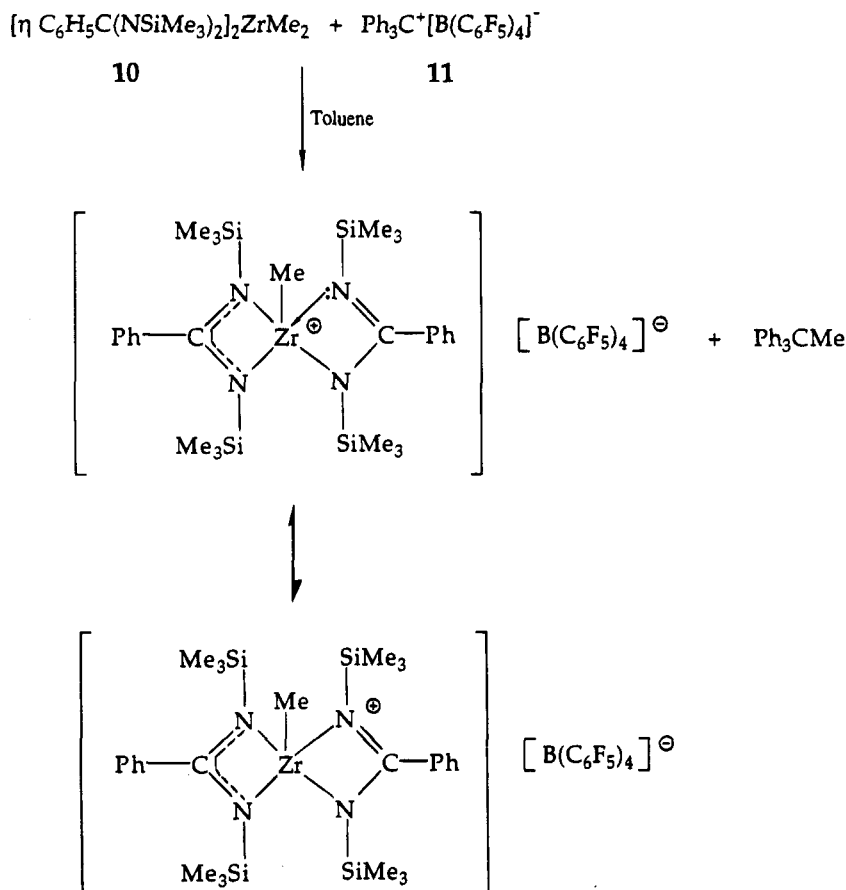
ene polymerizations. This unexpected behavior is in contrast with metallocene and half-sandwich alkylated group 4 compounds.⁵⁻⁸ A possible explanation could be that, after extraction of one alkyl group and formation of the cationic, electrophilic center, the latter is neutralized by a basic nitrogen attached to it, forming a σ -bond and transferring the positive charge from the metal onto nitrogen (Scheme 5). In fact, in a preparative scale reaction of **10** (0.39 g, 0.60 mol) with 1 equiv of Ph₃C⁺[B(C₆F₅)₄]⁻ (0.55 g, 0.60 mmol) in toluene, the color of the orange borate salt solution disappeared as soon as it was added to the colorless solution of **10**, and Ph₃CCH₃ was separated, as detected by ¹H NMR, from the reaction mixture in 94% yield. This reaction is currently under study in an attempt to characterize the resulting organometallic compound.

In conclusion, we have synthesized several new *N,N'*-bis(trimethylsilyl)benzamidinate complexes of titanium and zirconium and have investigated their reactivities and stabilities. We have found that these compounds are active in Ziegler-Natta polymerization reactions with styrene and ethylene, with MAO as a cocatalyst. They show a parallel behavior to mono- and bis-(cyclopentadienyl) group 4 metal compounds in terms of relative activity. Noteworthy is the high syndiospecificity achieved with mono(benzamidinato)titanium compounds in their catalytic reaction with styrene.

Experimental Section

All operations were performed under an argon atmosphere using Schlenk or glovebox techniques. Argon was deoxygen-

Scheme 5



ated with activated BTS catalyst and dried with molecular sieves and P_2O_5 . Solvents were purified as described elsewhere.²² Methylaluminoxane (MA) was purchased from Akzo, and other chemicals were from Aldrich. Styrene was distilled from CaH_2 and stored at -25°C under argon in darkness. $\text{Li}[\text{N}(\text{SiMe}_3)_2] \cdot \text{Et}_2\text{O}$, $\text{Li}[\text{C}_6\text{H}_5\text{C}(\text{NSiMe}_3)_2] \cdot \text{Et}_2\text{O}$, $\text{C}_6\text{H}_5\text{C}(\text{NSiMe}_3)_2\text{N}(\text{SiMe}_3)_2$,^{9,23} $[\eta\text{-C}_6\text{H}_5\text{C}(\text{NSiMe}_3)_2]_2\text{TiCl}_3$,¹³ $[\eta\text{-C}_6\text{H}_5\text{C}(\text{NSiMe}_3)_2]_2\text{MCl}_2$ ($\text{M} = \text{Ti}, \text{Zr}$),¹⁴ and $\text{Ph}_3\text{C}^+[\text{B}(\text{C}_6\text{F}_5)_4]^-$ ⁶ were synthesized according to published procedures. NMR spectra were recorded on IBM ESP 200 and IBM ESP 80 spectrometers. Chemical shifts (δ) are reported relative to external TMS (^1H) or H_3PO_4 (^{31}P). IR spectra were recorded on a Perkin-Elmer 1310 spectrophotometer. Elemental analyses were performed by the University of Massachusetts Microanalytical Laboratory.

Synthesis of $[\eta\text{-C}_6\text{H}_5\text{C}(\text{NSiMe}_3)_2]_2\text{Ti}[\text{OC}(\text{H})\text{Me}_2]_3$ (1). A solution of $\text{Li}[\text{PhC}(\text{NSiMe}_3)_2] \cdot \text{Et}_2\text{O}$ (7.14 g, 20.7 mmol) in 100 mL of ethyl ether was added dropwise to a solution of $\text{Ti}(\text{O}-i\text{-Pr})_3\text{Cl}$ (5.40 g, 20.7 mmol) in ethyl ether (50 mL) and out of light. After the addition was completed, stirring was continued for 1.5 h. Filtration of the LiCl precipitate and thorough evaporation of the solvent (all manipulations at 0°C and out of light) gave a clear, slightly pale-yellow oil. This oil, without further purification, was characterized as compound 1 spectroscopically and was analytically pure (10.10 g, 99.8%). The product was stored at -25°C and in darkness.

Anal. Calcd for $\text{C}_{22}\text{H}_{44}\text{N}_2\text{Si}_2\text{O}_3\text{Ti}$: C, 54.07; H, 9.08; N, 5.73. Found: C, 53.82; H, 8.82; N, 5.66. ^1H NMR (CDCl_3): δ -0.11 (s, 18 H, SiMe_3), 1.28 (d, $J = 6.0$ Hz, 18 H, $\text{OC}(\text{H})\text{Me}_2$), 4.76 (hept, $J = 6.0$ Hz, 3 H, $\text{OC}(\text{H})\text{Me}_2$), 7.10–7.40 (m, 5 H, Ph). IR (CH_2Cl_2): no $\nu_{\text{C}=\text{N}}$ band, $\nu_{\text{C}=\text{N}}$ 1500, $\nu_{(i\text{-Pr})}$ 1360 (d) and 1155, ν_{SiMe_3} 1235 and 835 cm^{-1} .

Synthesis of $\text{Ti}(\text{O}-i\text{-Pr})_3\text{N}(\text{SiMe}_3)_2$ (2). Method A. Reaction between $\text{Li}[\text{N}(\text{SiMe}_3)_2] \cdot \text{Et}_2\text{O}$ and $\text{Ti}(\text{O}-i\text{-Pr})_3\text{Cl}$. $\text{Li}[\text{N}(\text{SiMe}_3)_2] \cdot \text{Et}_2\text{O}$ (0.50 g, 2.1 mmol) and $\text{Ti}(\text{O}-i\text{-Pr})_3\text{Cl}$ (0.54 g, 2.1 mmol) were mixed in a Schlenk tube. Ethyl ether (20 mL) was then added at 0°C , and the reaction mixture was stirred for 2 h. Filtration of the precipitate and evaporation of the solvent gave **2** as a colorless oil (0.78 g, 97%).

Method B. Thermal Decomposition of $[\eta\text{-C}_6\text{H}_5\text{C}(\text{NSiMe}_3)_2]_2\text{Ti}(\text{O}-i\text{-Pr})_3$ (1). Fractional distillation of **1** (9.75 g, 19.9 mmol) was carried out in a distillation unit equipped with a 15 cm Vigreux column. The first fraction (bp $25\text{--}30^\circ\text{C}/10^{-3}$ mmHg) was characterized as predominantly benzonitrile by IR spectroscopy. A second fraction (bp $88\text{--}90^\circ\text{C}/10^{-3}$ mmHg) was identified as pure **2**, obtained as a colorless liquid (5.5 g, 73%).

Anal. Calcd for $\text{C}_{15}\text{H}_{39}\text{NO}_3\text{Si}_2\text{Ti}$: C, 46.73; H, 10.19; N, 3.63. Found: C, 46.85; H, 10.40; N, 3.63. ^1H NMR (CDCl_3): δ 0.20 (s, 18 H, SiMe_3), 1.25 (d, $J = 6$ Hz, 18 H, $\text{OC}(\text{H})\text{Me}_2$), 4.55 (hept, $J = 6$ Hz, 3 H, $\text{OC}(\text{H})\text{Me}_2$). IR (CH_2Cl_2): no $\nu_{\text{C}=\text{N}}$ band, $\nu_{(i\text{-Pr})}$ 1360 (d) and 1150, ν_{SiMe_3} 1230 and 840 cm^{-1} .

Synthesis of $[\eta\text{-C}_6\text{H}_5\text{C}(\text{NSiMe}_3)_2]_2\text{TiCl}_3 \cdot \text{THF}$ (4). $\{[\eta\text{-C}_6\text{H}_5\text{C}(\text{NSiMe}_3)_2]_2\text{TiCl}_3\}_2$ (0.53 g, 1.27 mmol based on Ti) was dissolved in THF (10 mL) at room temperature, and the solution was stirred for 1 h. The solvent was then thoroughly removed under reduced pressure, producing **4** as a red crystalline solid in quantitative yield (0.62 g, 100%).

Anal. Calcd for $\text{C}_{17}\text{H}_{31}\text{N}_2\text{OSi}_2\text{TiCl}_3$: C, 41.68; H, 6.38; N, 5.72. Found: C, 41.43; H, 6.21; N, 5.82. ^1H NMR (CDCl_3): δ 0.17 (s, 18 H, SiMe_3), 1.92 (m, 4 H, THF), 3.96 (m, 4 H, THF), 7.20–7.60 (m, 5 H, Ph).

Synthesis of $[\eta\text{-C}_6\text{H}_5\text{C}(\text{NSiMe}_3)_2]_2\text{TiCl}_3 \cdot \text{PMe}_3$ (5). A solution of $\{[\eta\text{-C}_6\text{H}_5\text{C}(\text{NSiMe}_3)_2]_2\text{TiCl}_3\}_2$ (2.30 g, 55.0 mmol based on Ti) in THF (30 mL) was treated with PMe_3 (0.58 mL, 55 mmol) at room temperature. The solution turned immediately from red to orange, but stirring was continued for an additional 2 h. Concentration and cooling of the solution

(22) Perrin, D. D.; Armarego, W. L. F. *Purification of Laboratory Chemicals*, 2nd ed.; Pergamon Press: Oxford, U.K., 1990.

(23) Sanger, A. R. *Inorg. Nucl. Chem. Lett.* **1973**, *9*, 351.

allowed the collection of a first fraction of orange-red crystals (1.53 g), identified as compound **5**. The filtrate afforded a second fraction (0.94 g), for a total yield of 2.47 g (91%).

Anal. Calcd for $C_{16}H_{32}N_2PSi_2TiCl_3$: C, 38.90; H, 6.53; N, 5.67. Found: C, 38.76; H, 6.52; N, 5.46. 1H NMR ($CDCl_3$): δ 0.11 (s, 18 H, $SiMe_3$), 1.44 (d, $^2J_{P-H} = 9.0$ Hz, 9 H, PMe_3), 7.10–7.50 (m, 5 H, Ph). $^{31}P\{^1H\}$ NMR: δ -13.9 (s, PMe_3).

Synthesis of $[\eta-C_6H_5C(NSiMe_3)_2]Ti(Me)Cl_2$ (6**).** To a solution of the dimer $\{[\eta-C_6H_5C(NSiMe_3)_2]TiCl_3\}_2$ (1.40 g, 1.67 mmol) in ethyl ether (30 mL) at $-20^\circ C$ was added methyllithium (2.40 mL, 3.35 mmol, 1.4 M ethyl ether solution) dropwise and very slowly. Once the addition was completed, the reaction mixture was stirred for 3 h at $-20^\circ C$. Lithium chloride was filtered, and the solution was concentrated under reduced pressure until ca. 10 mL remained. Cooling the solution overnight produced **6** as a thermally- and air-sensitive, yellow-orange solid (1.00 g, 78%). 1H NMR (C_6D_6): δ 0.13 (s, 18 H, $SiMe_3$), 2.30 (s, 3 H, TiMe), 6.70–7.20 (m, 5 H, Ph).

Synthesis of $[\eta-C_6H_5C(NSiMe_3)_2]TiMe_2$ (7**). Method A. Reaction between $\{[\eta-C_6H_5C(NSiMe_3)_2]TiCl_3\}_2$ and Six Equivalents of Methyllithium.** Methyllithium (8.10 mL, 11.3 mmol, 1.4 M ethyl ether solution) was added to a solution of $\{[\eta-C_6H_5C(NSiMe_3)_2]TiCl_3\}_2$ (1.58 g, 1.89 mmol) in 60 mL of either pentane or ethyl ether at $-10^\circ C$. After the reaction mixture had warmed to room temperature, stirring was continued for 2 h at $25^\circ C$. LiCl was filtered from the dark solution. Evaporation of the solvent under reduced pressure gave a crystalline solid mixed with a dark oil. Recrystallization from pentane afforded an orange crystalline solid which was characterized as **7** (0.54 g, 24% based on Ti).

Method B. Reaction between $[\eta-C_6H_5C(NSiMe_3)_2]_2TiCl_2$ and Two Equivalents of Methyllithium. Methyllithium (2.20 mL, 3.10 mmol, 1.4 M ethyl ether solution) was slowly added to a solution of $[\eta-C_6H_5C(NSiMe_3)_2]_2TiCl_2$ (1.00 g, 1.55 mmol) in ethyl ether (40 mL) at $-20^\circ C$. After the addition was completed, the reaction mixture was allowed to warm gradually to room temperature and stirred vigorously for 3 h. The byproduct, LiCl, was separated by filtration

through Celite, and the solvent was removed under vacuum. The orange residue was recrystallized from pentane, producing **7** as orange crystals in almost quantitative yield (0.93 g, 99%).

Anal. Calcd for $C_{28}H_{52}N_4Si_4Ti$: C, 55.59; H, 8.66; N, 9.26; Cl, 0.00. Found: C, 55.34; H, 8.58; N, 9.23; Cl, not detected. 1H NMR (C_6D_6): δ 0.14 (s, 36 H, $SiMe_3$), 1.94 (s, 6 H, TiMe), 7.00–7.40 (m, 10 H, Ph). 1H NMR ($CDCl_3$): δ -0.07 (s, 36 H, $SiMe_3$), 1.43 (s, 6 H, TiMe), 7.35–7.45 (m, 10 H, Ph).

Synthesis of $[\eta-C_6H_5C(NSiMe_3)_2]_2ZrMe_2$ (10**).** Methyllithium (3.20 mL, 4.44 mmol, 1.4 M ethyl ether solution) was added dropwise to a solution of $[\eta-C_6H_5C(NSiMe_3)_2]_2ZrCl_2$ (1.53 g, 2.22 mmol) in ethyl ether (40 mL) at $-10^\circ C$. Using the same procedure described above for **7**, **10** was obtained as a white crystalline precipitate (1.40 g, 98%).

Anal. Calcd for $C_{28}H_{52}N_4Si_4Zr$: C, 51.87; H, 8.08; N, 8.64. Found: C, 51.39; H, 8.04; N, 8.38. 1H NMR ($CDCl_3$): δ -0.08 (s, 36 H, $SiMe_3$), 0.44 (s, 6 H, ZrMe), 7.20–7.50 (m, 10 H, Ph).

Polymerization Studies. Polymerizations were carried out in toluene in 250 mL crown-capped glass pressure reactors equipped with magnetic stirring and thermostated to the desired temperature. For MAO-catalyzed polymerizations, toluene was added first (50 mL), followed by styrene (5.0 mL), MAO, and finally the appropriate benzamidinate precursor. The polymerization reactions were terminated by addition of acidified methanol. The polymer was washed with methanol and dried in vacuo to constant weight. The polymer obtained was extracted with refluxing 2-butanone for 12 h and the insoluble fraction again dried in vacuo to constant weight. DSC of polymers was performed on a Perkin-Elmer Thermal System IV.

Acknowledgment. J.C.F. is indebted to MEC (Spain) for a postdoctoral fellowship. We are also grateful to Dr. M. Malanga, Dow Chemical Co., for assistance in obtaining the ^{13}C -NMR polystyrene spectra.

OM9408223

Density Functional Study of Intermediates in the Nickel-Catalyzed Homo-Diels–Alder Reaction of Norbornadiene with Alkenes

M. M. Gugelchuk* and J. Wisner

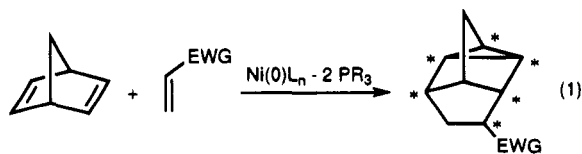
Department of Chemistry, University of Waterloo, Waterloo, Ontario, Canada N2L 3G1

Received November 28, 1994[®]

A theoretical study of proposed organonickel intermediates in the nickel-catalyzed homo-Diels–Alder reaction has been carried out employing density functional theory (DFT) methods to investigate the mechanism of this reaction. Predicted geometries and relative energies of various ground-state complexes important to the mechanistic pathway are discussed. The effects of the level of theory (local or nonlocal, gradient versus SCF corrections) and integration mesh size on relative energies, dipole moments, and Mulliken atomic charges were also investigated. Calculations using the local density approximation were insensitive to the mesh size. However, there are very large variations in the calculated total energies with nonlocal methods that were dependent on both the mesh size and whether the nonlocal corrections were applied in a gradient manner or self-consistently. Dipole moments and atomic charges were much less sensitive. All calculations gave approximately the same relative ordering of the energetics. Some intermediates have been shown to follow a more energetically feasible pathway than others and can be useful in rationalization of the experimentally observed stereo- and regioselectivity.

Introduction

The nickel-catalyzed homo-Diels–Alder reaction of norbornadienes (NBD) with electron-deficient olefins (shown in eq 1) has been reported to proceed with high degrees of stereo- and even enantioselectivity.^{1,2} In contrast to the uncatalyzed process,^{1c,3} the catalytic reaction affords the exo isomer predominantly and endo–exo isomerization of the products is negligible under the reaction conditions. This stereoselectivity is influenced by the steric nature of an added phosphorus ligand^{1b} and the steric bulk of the olefin substituent.^{1c,4a} A particularly attractive synthetic aspect of this chemistry is in the construction of polycyclic natural products with well-defined stereochemistry via cycloaddition–fragmentation sequences. Recently, the influence of norbornadiene substituents on regio- and stereoselectivity in the deltacyclane product has been examined with encouraging results.^{4b,c} Because of its synthetic potential, delineation of the factors responsible for the observed selectivity is quite desirable.



While formally a [2+2+2] cycloaddition, this reaction most likely occurs through a sequence of steps and a

series of intermediate organonickel complexes having discrete metal–carbon σ bonds. It is evident that a major gap exists in understanding the mechanistic details of this reaction. The organometallic intermediates have been postulated mainly on the basis of plausibility arguments or in relation to known stable molecules (cf. Figure 1).^{1,5} Early on, Schrauzer put forth the concept of a concerted, π -complex multicenter mechanism⁵ which involves a single intermediate (1) arising from the simultaneous coordination of NBD, the olefin, and the phosphorus ligand. This simple model was useful to rationalize the propensity for exo stereochemistry by assuming that tetrahedral coordination of NBD and the olefin takes place in the less-hindered configuration between the olefin substituent and phosphorus ligand. However, later investigations have largely discredited the idea of such a concerted pathway.^{1c,6,7}

On the basis of work with quadricyclane, Noyori proposed a stepwise mechanism^{1c} involving a nortricyclane complex (2) formed from 1 by an internal oxidative coupling process. This type of complex had been suggested earlier in the catalytic isomerization of quadri-

(4) (a) Lautens, M.; Edwards, L. G. *Tetrahedron Lett.* **1989**, *30*, 6813.

(b) Lautens, M.; Tam, W.; Edwards, L. G. *J. Chem. Soc., Perkin Trans. 1* **1994**, 2143. (c) Lautens, M.; Edwards, L. G. *J. Org. Chem.* **1991**, *56*, 3761.

(5) (a) Schrauzer, G. N. *Adv. Catal. Relat. Subj.* **1968**, *18*, 373. (b) Schrauzer, G. N. *Adv. Organomet. Chem.* **1964**, *2*, 1. (c) Schrauzer, G. N.; Glockner, P. *Chem. Ber.* **1964**, *97*, 2451. (d) Schrauzer, G. N.; Eichler, S. *Chem. Ber.* **1962**, *95*, 2764.

(6) Cassar, L.; Halpern, J. *J. Chem. Soc., Chem. Commun.* **1970**, 1082.

(7) (a) Pardigon, O.; Buono, G. *Tetrahedron: Asymmetry* **1993**, *4*, 1977. (b) Duan, I.-F.; Cheng, C.-H.; Shaw, J.-S.; Cheng, S.-S.; Liou, K. F. *J. Chem. Soc., Chem. Commun.* **1991**, 1347. (c) Brunner, H.; Prester, F. *J. Organomet. Chem.* **1991**, *414*, 401. (d) Lautens, M.; Lautens, J. C.; Smith, A. C. *J. Am. Chem. Soc.* **1990**, *112*, 5627. (e) Lautens, M.; Crudden, C. M. *Organometallics* **1989**, *8*, 2733. (f) Lyons, J. E.; Myers, H. K.; Schneider, A. *Ann. N.Y. Acad. Sci.* **1980**, *333*, 273. (g) Lyons, J. E.; Myers, H. K.; Schneider, A. *J. Chem. Soc., Chem. Commun.* **1978**, 636.

[®] Abstract published in *Advance ACS Abstracts*, March 15, 1995.

(1) (a) Yoshikawa, S.; Kiji, J.; Furukawa, J. *Bull. Chem. Soc. Jpn.* **1976**, *49*, 1093. (b) Yoshikawa, S.; Aoki, K.; Kiji, J.; Furukawa, J. *Bull. Chem. Soc. Jpn.* **1975**, *48*, 3239. (c) Noyori, R.; Umeda, I.; Kawauchi, H.; Takaya, H. *J. Am. Chem. Soc.* **1975**, *97*, 812.

(2) Brunner, H.; Muschiol, M.; Prester, F. *Angew. Chem., Int. Ed. Engl.* **1990**, *29*, 652.

(3) (a) Kobuke, Y.; Sugimoto, T.; Furukawa, J.; Fueno, T. *J. Am. Chem. Soc.* **1972**, *94*, 3633. (b) Cookson, R. C.; Dance, J.; Hudec, J. *J. Chem. Soc.* **1964**, 5416.

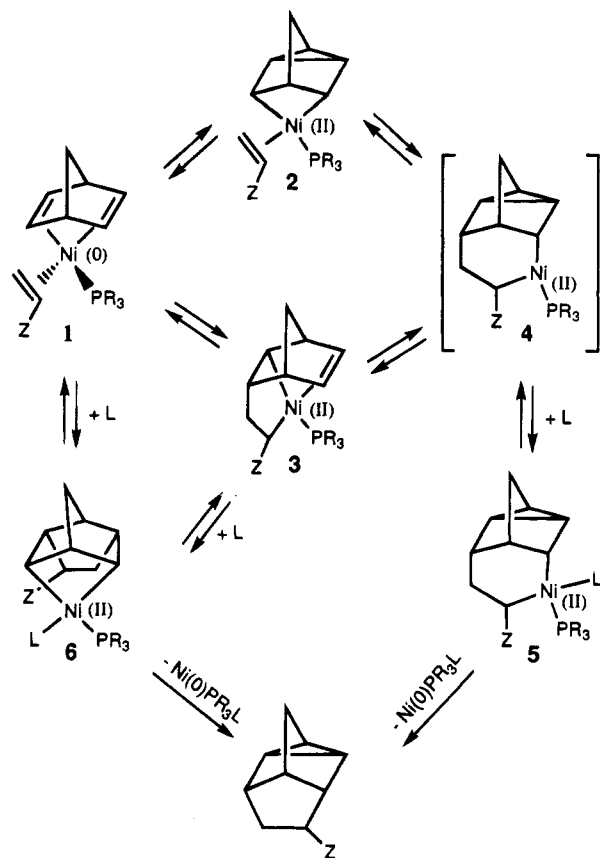


Figure 1. Possible stepwise mechanisms of nickel-catalyzed cycloaddition of olefins with NBD.

cyclane to norbornadiene by rhodium.⁶ Insertion of the coordinated olefin into the Ni–C σ bond of the metalocycle would give intermediate **4**. Associative reductive elimination (through complex **5**) would yield the cycloaddition product. Support for complexes **4** and **5** arises from related cobalt-catalyzed cycloadditions⁷ of ethylene to NBD which yields vinyltricyclanes presumably through β -elimination from these type of intermediates. The insertion of unsaturated molecules into the Ni–C σ bond of nickelacycles is well documented.⁸

Alternatively, oxidative coupling of one π bond of NBD with the coordinated olefin could produce a π -homoallylic nickel(II) intermediate (**3**) that undergoes electronic reorganization to give **4** or **5**. π -Homoallylic norbornadienyl palladium complexes have been isolated, and closure to the nortricyclenyl system has been demonstrated upon addition of a donor ligand such as pyridine or phosphines.⁹ Whether electronic reorganization occurs prior to or as a result of ligand association is unknown. A final possibility is that the complexed olefin could add to NBD in a concerted manner (or stepwise through **3**) to form complex **6**, which, via reductive elimination, would complete the three-membered ring. Some evidence for such a manifold can be found in the isolation of such complexes from homo-Diels–Alder addition of alkynes to NBD–rhodium complexes.¹⁰

(8) Campora, J.; Gutierrez, E.; Monge, A.; Palma, P.; Poveda, M. L.; Ruiz, C.; Carmona, E. *Organometallics* **1994**, *13*, 1728 and references therein.

(9) (a) Green, M.; Hancock, R. I. *J. Chem. Soc. A* **1967**, 2054. (b) Coulson, D. R. *J. Am. Chem. Soc.* **1969**, *91*, 200. (c) Forsellini, E.; Bombieri, G.; Crociani, B.; Boschi, T. *J. Chem. Soc., Chem. Commun.* **1970**, 1203. (d) Hines, L. F.; Stille, J. K. *J. Am. Chem. Soc.* **1972**, *94*, 485.

The direct involvement of bis(phosphine) nickel complexes has not been determined but may be plausible since the catalyst systems typically used contain Ni/P in a 1:2 ratio. Related to this issue, studies by Grubbs and co-workers¹¹ have shown that bis(phosphine) nickelacycles prefer a reductive elimination decomposition pathway whereas three-coordinate monophosphine nickelacycles predominantly undergo β -elimination. Also, chelated diphosphines are known to retard the rate of the homo-Diels–Alder reaction by effectively competing with NBD for binding to the metal.^{1b} Questions as to thermodynamic versus kinetic control at the individual steps have not been thoroughly investigated, but experimental studies suggest the formation of the delta-cyclane product is irreversible under the reaction conditions.

As a preliminary step toward modeling the regio- and stereochemistry of this reaction, we have undertaken a study of proposed organonickel intermediates employing density functional theory (DFT) methods.¹² A number of articles evaluating the use of DFT methods for organometallic calculations have already appeared in the literature.¹³ DFT has the advantage over traditional *ab initio* methods in that electron correlation is specifically treated and the computational demand is significantly less for large systems. In this paper we examine the predicted geometries and relative energies of the various ground-state complexes in order to gain some insight into the mechanistic pathway. The effects of the level of theory and integration mesh size on relative energies, dipole moments, and Mulliken atomic charges are also presented.

Computational Details

Local density calculations were performed with the program DMOL¹⁴ using the Hedin–Lundqvist/Janak–Moruzzi–Williams (JMW) parametrization¹⁵ of the correlation energy of the homogeneous electron gas. Double-numerical plus polarization (DNP) basis sets were used for all atoms. This basis set uses approximately two atomic orbitals for each occupied orbital in the free atom together with polarization functions and is comparable in quality to the standard Gaussian 6-31G** basis set. Geometry optimizations employed the BFGS quasi-Newton–Raphson minimizer in Cartesian space and have a maximum allowed gradient of 0.001. No symmetry constraints were imposed on the structures. The mesh size used for evaluation of the integrals in geometry optimizations was the “MEDIUM” mesh defined in the program. In most cases, the

(10) Evans, J. A.; Kemmitt, R. D. W.; Kimura, B. Y.; Russell, D. R. *J. Chem. Soc., Chem. Commun.* **1972**, 509.

(11) (a) Grubbs, R. H.; Miyashita, A. *J. Am. Chem. Soc.* **1978**, *100*, 7416. (b) Grubbs, R. H.; Miyashita, A.; Liu, M.-I. M.; Burk, P. L. *J. Am. Chem. Soc.* **1977**, *99*, 3863.

(12) (a) Anzelm, J.; Labanowski, J. K. *Density Functional Methods in Chemistry*; Springer-Verlag: New York, 1991. (b) Parr, R. G.; Yang, W. *Density-Functional Theory of Atoms and Molecules*; Oxford University Press: New York, 1989.

(13) (a) Norrby, P.-O.; Kolb, H. C.; Sharpless, K. B. *Organometallics* **1994**, *13*, 344. (b) Branchadell, V.; Deng, L.; Ziegler, T. *Organometallics* **1994**, *13*, 3115. (c) Woo, T. K.; Fan, L.; Ziegler, T. *Organometallics* **1994**, *13*, 2252. (d) Stanton, R. V.; Merz, K. M., Jr. *J. Chem. Phys.* **1994**, *100*, 434. (e) Sosa, C.; Anzelm, J.; Elkin, B. C.; Wimmer, E.; Dobbs, K. D.; Dixon, D. A. *J. Phys. Chem.* **1992**, *96*, 6630. (f) Fan, L.; Ziegler, T. *J. Chem. Phys.* **1991**, *94*, 6057. (g) Ziegler, T. *Chem. Rev.* **1991**, *91*, 651 and references therein.

(14) (a) DMOL, Version 3.2; Biosym Technologies, Inc.: San Diego, CA, 1993. (b) Delley, B. *J. Chem. Phys.* **1990**, *92*, 508.

(15) (a) Hedin, L.; Lundqvist, B. I. *J. Phys. C* **1971**, *4*, 2064. (b) Hedin, L.; Lundqvist, B. I.; Lundqvist, S. *Solid State Commun.* **1971**, *9*, 537. (c) Janak, J. F.; Moruzzi, V. L.; Williams, A. R. *Phys. Rev. B* **1975**, *12*, 1257.

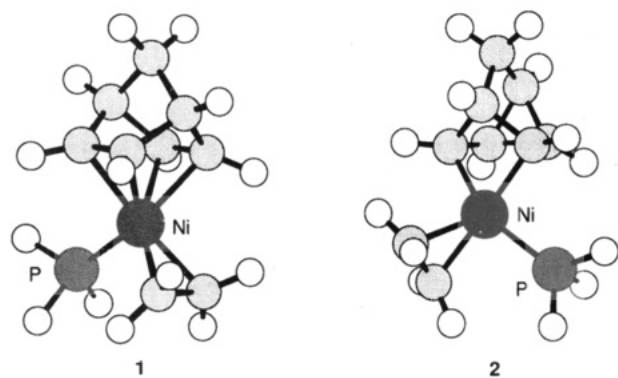


Figure 2. Optimized geometries for complexes 1 and 2.

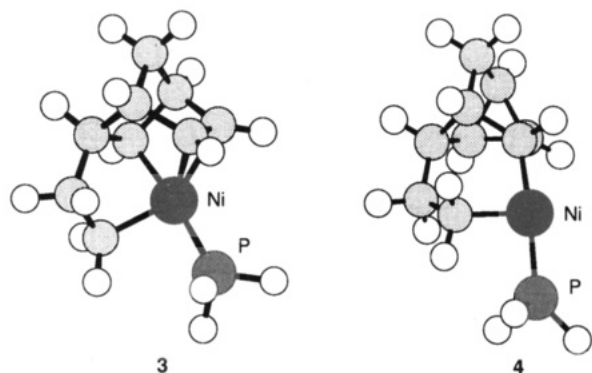


Figure 3. Optimized geometries for complexes 3 and 4.

"FINE" mesh was necessary to complete the optimizations. Nonlocal density corrections (gradient and self-consistent types) were calculated for the optimized geometries using the Becke (B88) functional for exchange¹⁶ and the Lee–Yang–Parr (LYP) functional for correlation¹⁷ with both the MEDIUM and FINE meshes. All other parameters were left at the default values contained in the DMOL program.

Results and Discussion

Geometries. The calculated structures of the complexes shown in Figure 1 can only be compared to similar metal complexes^{9c,10,18} due to a lack of structural data on the specific compounds. However, it is known that the combined sources of error in LDA-calculated structures typically give rise to a level of accuracy of 0.01–0.02 Å for main group bond lengths, 0.03 Å for metal–ligand distances, and 1–2° for bond angles.^{12b} In particular, carbon–carbon and metal–ligand distances are generally too short whereas carbon–hydrogen bond lengths are too long. Figures 2–4 show the LDA-optimized geometries of complexes 1–6, and selected geometric parameters are summarized in Tables 1 and 2. The numbering scheme is given in Table 2. Overall, the predicted structures are in good agreement with available experimental data.

Taking the midpoint of the C=C double bonds as the point of attachment to the Ni atom, the coordination sphere of complex 1 is tetrahedral as expected with four-coordinate Ni(0) complexes. There is some distortion due to the small bite angle (74°) of the chelating NBD. The independent Ni–C₇ bond lengths of the NBD ligand exhibit significant asymmetry in that the carbons syn to the phosphine are more loosely bound to the metal

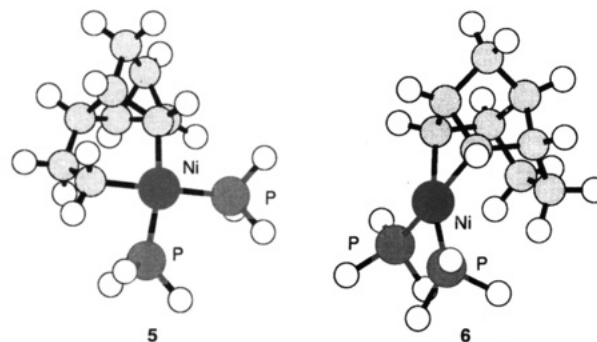


Figure 4. Optimized geometries for nickel bis(phosphine) complexes 5 and 6.

Table 1. Selected Bond Distances^a for Complexes 1–6

bond	1	2	3	4	5	6
Ni–C2	2.10	2.64	2.05	2.70	2.78	1.95
Ni–C3	2.06	1.97	2.04	1.87	1.95	2.88
Ni–C5	2.05	1.94	2.51	3.28	3.30	2.88
Ni–C6	2.09	2.60	1.95	3.46	3.48	1.95
Ni–C8	2.00	2.04	1.94	1.90	1.94	2.98
Ni–C9	2.01	1.98	2.53	2.86	2.89	2.96
C2–C3	1.39	1.52	1.39	1.51	1.51	1.54
C5–C6	1.39	1.51	1.52	1.52	1.52	1.55
C8–C9	1.40	1.39	1.53	1.51	1.52	1.54
C4–C5	1.53	1.52	1.55	1.54	1.53	1.54
C3–C4	1.53	1.53	1.54	1.52	1.53	1.54
C1–C2	1.53	1.52	1.52	1.53	1.52	1.53
C1–C6	1.54	1.53	1.54	1.50	1.51	1.53
C4–C7	1.53	1.53	1.53	1.53	1.53	1.51
C1–C7	1.54	1.50	1.53	1.51	1.51	1.52
Ni–P10	2.15	2.13	2.14	2.12	2.10	2.12
C3–C5	2.36	2.14	2.52	2.35	2.38	2.32
C2–C6	2.37	1.51	2.32	1.51	1.51	2.16
C8–C3	2.98	4.00	3.50	2.58	2.65	1.53
C8–C5	3.52	3.23	2.48	2.53	2.54	2.44
C9–C3	3.51	3.73	3.14	2.88	2.95	2.43
C9–C5	3.04	2.81	1.53	1.52	1.52	1.53
X1–Ni	1.96		1.92			
X2–Ni	1.95					
X3–Ni	1.88	1.88				
Ni–P11					2.12	2.12

^a X1 = centroid of C2–C3 double bond, X2 = centroid of C5–C6 double bond, and X3 = centroid of C8–C9 double bond. All values given in angstroms.

than the corresponding anti carbons ($\Delta \approx 0.035$ Å). This is reminiscent of the trans influence seen in square planar complexes. Approximate C_{2v} symmetry is observed for the NBD ligand. Strong back-donation from the metal is reflected in the lengthening of the C=C double bonds (1.39 Å) of the complex compared to free NBD (1.333 Å).¹⁹ The allylic C–C single-bond distances (1.53–1.54 Å) are slightly longer than those found in free NBD (1.522 Å). This is consistent with crystallographic data of known metal–NBD complexes and is thought to reflect a perturbation of the σ framework upon complexation.¹⁸ The coordinated ethylene is symmetrically bound and shows the normal C=C bond lengthening. In comparison to the NBD ligand, the Ni–C₇ distances of the ethylene ligand are much shorter (average $\Delta \approx 0.08$ Å).

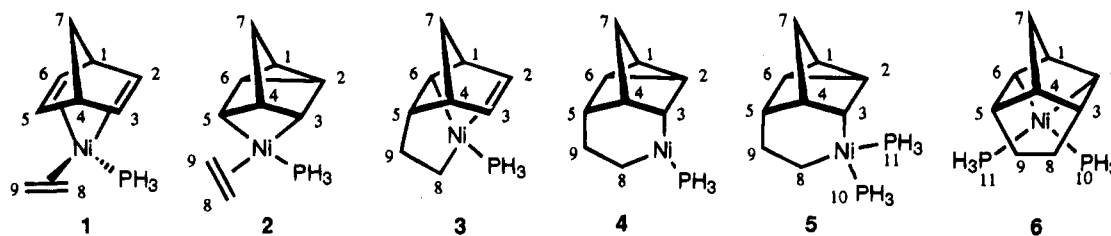
Complex 2 has a distorted square planar geometry about the nickel(II) center. The rigid bidentate nortricyclene ligand has a bite angle of 66°, otherwise the bond angles of the nickelacyclobutane moiety are close

(16) Becke, A. D. *J. Chem. Phys.* **1988**, *88*, 2547.

(17) Lee, C.; Yang, W.; Parr, R. G. *Phys. Rev. B* **1988**, *37*, 785.

(18) Eyring, M. W.; Radonovich, L. J. *Organometallics* **1985**, *4*, 1841.

(19) (a) Wilcox, C. F., Jr.; Winstein, S.; McMillan, W. G. *J. Am. Chem. Soc.* **1960**, *82*, 5450. (b) Yokozeki, A.; Kuchitsu, K. *Bull. Chem. Soc. Jpn.* **1971**, *44*, 2356.

Table 2. Selected Bond Angles^a for Complexes 1–6

angle	1	2	3	4	5	6	angle	1	2	3	4	5	6
C2–Ni–C3	39	35	40	32	31	30	Ni–C9–C8	69	67	50	38	38	76
C5–Ni–C6	39	35	37	26	26	30	C1–C2–C3	106	108	104	107	108	104
C8–Ni–C9	41	40	37	29	29	30	C1–C6–C5	106	108	107	107	106	104
C2–Ni–C6	69	34	71	25	25	67	C2–C3–C4	106	98	108	97	96	102
C3–Ni–C5	70	66	66	45	45	47	C4–C5–C6	106	98	98	97	96	102
C2–Ni–C5	83	60	82	47	46	65	C2–C1–C6	101	60	98	60	60	90
C3–Ni–C6	83	60	81	42	42	65	C3–C4–C5	101	89	109	100	102	98
C3–Ni–C8	94	172	123	86	86	30	C5–C9–C8	98	94	108	113	113	105
C5–Ni–C9	97	91	35	28	28	30	C3–C8–C9	100	69	64	85	86	104
C3–Ni–C9	119	142	86	72	72	49	C3–Ni–P10	133	92	104	175	169	97
C5–Ni–C8	121	108	66	50	50	49	C5–Ni–P10	132	153	141	131	125	100
Ni–C2–C3	69	48	70	42	42	111	C6–Ni–C8	160	113	80	74	74	78
Ni–C3–C2	72	97	71	106	107	39	C6–Ni–P10	96	120	174	134	131	163
Ni–C5–C6	72	97	51	84	84	40	C8–Ni–P10	101	91	94	90	84	87
Ni–C6–C5	69	48	92	70	71	110	C3–Ni–P11					92	142
Ni–C2–C1	95	121	94	145	145	94	C8–Ni–P11					171	117
Ni–C6–C1	95	122	97	102	104	94	P10–Ni–P11					98	98
Ni–C3–C4	94	93	101	126	123	101	C2–Ni–P10	96	93	116	145	148	98
Ni–C5–C4	95	94	83	67	68	102	C2–Ni–P11					77	163
Ni–C8–C9	70	72	93	113	113	74	C6–Ni–P11					98	96
X1–Ni–X2	74						X1–Ni–X3	124					
X1–Ni–P10	115		111				X2–Ni–X3	127					
X2–Ni–P10	114						X3–Ni–P10	101	104				
X3–Ni–C3	107	161					X3–Ni–C5	110	100				
X1–Ni–C6	75		75				X1–Ni–C8	108		138			

^a X1 = centroid of C2–C3 double bond, X2 = centroid of C5–C6 double bond, X3 = centroid of C8–C9 double bond. All angles given in degrees.

to 90°. A stronger trans influence for ethylene over phosphine is apparent with the Ni–C_σ bond trans to ethylene being longer by 0.03 Å than its counterpart cis to ethylene and is consistent with the known ordering of trans directors.²⁰ The individual Ni–C_π bond lengths vary widely ($\Delta = 0.06$ Å), which results in a slip distortion of the ethylene ligand such that the midpoint of the C=C bond lies well out of the plane defined by Ni and the other ligands. Also, the alkene conformation has a 20° twist from perpendicular with respect to the square plane, most likely to reduce steric interactions within the complex. There is a close contact (2.14 Å) between the C5 hydrogen of the norbornene and one of the C9 hydrogens in the optimized structure. All other features appear normal.

A distorted square planar geometry is also found about the Ni(II) center in the π -homoallylic complex **3**. There is clear departure from local C_s symmetry in the norbornenyl moiety, the most prominent being that the C2–C1–C6 bond angle (98°) is much more acute than the C3–C4–C5 angle (109°). Concerning the predicted Ni–C bond distances of the π -homoallylic system (1.95 and 2.04–2.05 Å), the Ni–C6 bond is significantly shorter and most likely a result of the trans influence in combination with the geometrical constraints of the ligand. It is clear that the C6 carbon retains substantial sp² character. The dihedral angle H1–C1–C6–H6 (6.6°) is comparable to that found in the NBD complex

(average 2.4°) but very different from that expected for sp³ character, as seen in the H4–C4–C5–H5 angle (61.4°). Due to the tridentate nature of the ligand, the nickelacyclopentane ring resulting from insertion of the ethylene fragment adopts an envelope conformation with the nickel atom being the out-of-plane atom. This gives rise to an eclipsed conformation about the C5–C9 bond.

Complexes **4** and **5** differ with respect to coordination number. Both complexes exhibit square planar geometry about the nickel(II) atom. The only significant differences were found in the Ni–C bond distances which are shorter in the 14-electron complex compared to the 16-electron complex. Most notable is the lengthening of the Ni–C3 single bond by 0.08 Å upon coordination of the second phosphine (cf. Table 1). In contrast to complex **3**, the larger six-ring metallocycles adopt a staggered conformation about the C5–C9 bond. However, this conformation produces very close contacts between the exo-C8 and the C4 bridgehead hydrogens (2.06–2.15 Å). The calculated structure of complex **6** has nearly perfect C_s symmetry. Coordination around the metal is slightly distorted from a square planar arrangement. Bond angles about the nickelacyclobutane moiety are identical to those in complex **2**.

Relative Energies. While the local density approximation has been quite successful in predicting molecular structures, nonlocal exchange/correlation corrections to the total energy are crucial for the quantitative prediction of reaction energetics. LDA

(20) Crabtree, R. H. *The Organometallic Chemistry of the Transition Metals*, 2nd ed.; John Wiley & Sons, Inc.: New York, 1994; p 6.

Table 3. Comparison of Relative Energies as Functions of Theory Level and Mesh Size^a

level/mesh	1 + PH ₃	2 + PH ₃	3 + PH ₃	4 + PH ₃	5	6
JMW/M	0.0	27.6	10.3	12.0	-23.0	-38.9
JMW/F	0.0	27.6	10.2	11.9	-23.2	-39.1
JMW-B88e/M	0.0	26.2	18.1	13.9	10.6	-4.0
JMW-B88e/F	0.0	26.0	18.1	13.8	10.4	-4.2
LYPe-B88e/M	0.0	-26.9	14.5	10.4	-0.1	-10.8
LYPe-B88e/F	0.0	26.6	16.0	13.3	2.2	-12.4
JMW-B88m/M	0.0	18.7	14.9			-28.8
JMW-B88m/F	0.0	13.0	9.3	-12.6	-72.0	-74.2
LYPm-B88m/M	0.0	23.3	16.0	5.7	-14.2	-22.6
LYPm-B88m/F	0.0	18.5	-15.0	1.8	-35.6	-41.1

^a JMW = Hedin-Lundqvist/Janak-Moruzzi-Williams local correlation. B88e = Becke nonlocal exchange gradient correction. B88m = Becke nonlocal exchange self-consistent correction. LYPe = Lee-Yang-Parr nonlocal correlation gradient correction. LYPm = Lee-Yang-Parr nonlocal correlation self-consistent correction. M = medium mesh. F = fine mesh. Relative energies are given in kcal/mol.

reaction energies are grossly overestimated, whereas nonlocal corrections provide reaction energies that approach the average error of Hartree-Fock methods (≈ 7 kcal/mol).^{12b} Since the magnitude of the exchange energy is significantly larger than that of the correlation energy, the usual practice is to treat corrections to the local exchange and correlation energies separately. These nonlocal corrections can be applied by a perturbative approach in which LDA densities are used to evaluate the gradient terms or by a self-consistent approach in which nonlocal densities are generated. The self-consistent method gives lower calculated total energies compared to the perturbative method, but the difference is reported to be less than 1 kcal/mol for small molecules.^{12c} Another variable to be considered is the effect of the integration mesh size on the total energy.

To gain a better understanding of how these factors influence the predicted reaction energies and the electronic structures (as reflected in the dipole moments and Mulliken charges), we carried out a systematic examination of the calculated single-point energies using the LDA-optimized geometries of complexes 1-6. Calculated total energies for each complex are provided in the supplementary material. The resulting relative energies are summarized in Table 3.

In general, local density and nonlocal perturbative energies are rather insensitive to the size of the integration mesh. The average energy difference due to mesh size was less than 1 kcal/mol. However, there were substantial differences in the nonlocal energies obtained by the self-consistent approach upon changing from a MEDIUM to a FINE mesh. Using the FINE integration mesh, the calculated energies were on the order of 30 and 50 kcal/mol lower for the 112- and 130-electron systems, respectively. The magnitude of this energy difference was greater as the number of electrons increased. Obviously, the greater numerical precision of the FINE mesh plays an important role in calculating the self-consistent nonlocal energies of these transition metal complexes. Of note, there is virtually no difference in the predicted total energies of the PH₃ molecule (18 electrons) with respect to mesh size (cf. Table 4). In two cases, SCF convergence with the B88 functional could not be achieved using the MEDIUM mesh even after several attempts with decreased charge and spin density mixing coefficients and performing charge smearing at the Fermi level.

Table 4. LYPm-B88m/F Mulliken Charges and Dipole Moments for Complexes 1-6

atom	1	2	3	4	5	6
C1	-0.397	-0.289	-0.359	-0.302	-0.316	-0.277
C2	-0.373	-0.270	-0.345	-0.281	-0.207	-0.491
C3	-0.310	-0.531	-0.345	-0.541	-0.560	-0.317
C4	-0.399	-0.304	-0.398	-0.332	-0.319	-0.350
C5	-0.330	-0.481	-0.270	-0.304	-0.298	-0.309
C6	-0.364	-0.279	-0.441	-0.294	-0.308	-0.499
C7	-0.642	-0.661	-0.617	-0.634	-0.622	-0.633
C8	-0.647	-0.594	-0.782	-0.714	-0.750	-0.604
C9	-0.625	-0.634	-0.606	-0.598	-0.594	-0.586
Ni	-0.039	-0.065	-0.051	-0.029	-0.210	-0.209
P10	-0.310	-0.218	-0.278	-0.291	-0.210	-0.250
P11					-0.235	-0.226
μ (D)	1.063	1.895	1.712	1.382	2.660	2.178

When we compared the energetic results based on the nonlocal method used at a given mesh size, the SCF nonlocal energies of the organonickel complexes were significantly lower (in the range of 30-180 kcal/mol) than those obtained by the perturbative approach. This is much larger than the 1 kcal/mol typically cited for small systems. For PH₃, the SCF nonlocal energies were also lower by 3-5 kcal/mol. In addition, with a FINE mesh these differences were much larger for the 130-electron complexes (172-184 kcal/mol) than the 112-electron species (27-32 kcal/mol). There was no apparent trend in the relative magnitude of the differences with a MEDIUM integration mesh. A closer look at possible explanations, particularly with regard to errors due to truncation in the numerical analysis and the implementation of the LYP functional in the DMOL program,²¹ is warranted. We also find the total calculated charge densities are about an order of magnitude less accurate for the nickel complexes compared to the simple phosphine. To illustrate, the MEDIUM mesh at the LYP-B88/SCF level generated 44 680 integration points for complex 1 and a model charge density of 111.999 771 electrons (error: 3×10^{-4}). The FINE mesh generated 88 350 integration points and a slightly more accurate charge density of 111.999 910 electrons (error: 9×10^{-5}). In the phosphine case, either mesh size gave an error in the calculated charge density of about 3×10^{-5} .

There were only modest changes in the Mulliken atomic charges and dipole moments of the complexes as a result of changing the theory level or mesh size. A summary of the calculated charges and dipole moments for all complexes at the LYPm-B88m/F level is given in Table 4. A complete tabulation of these properties as a function of level is given in the supplementary material. For each complex, the nonlocal SCF methods (FINE mesh) gave the lowest dipole moments. In a relative sense, the predicted charge densities at the nickel atom are consistent with conventional descriptions of metal-ligand bonding. Complex 1, with three strongly back-bonding π -alkene ligands, has only a slight excess of electron density at the metal, whereas the metal in complexes 2 and 3 (only one π -alkene ligand) is more electron-rich. The bis(phosphine) complexes 5 and 6 have much more electron-rich nickel environments.

All nonlocal calculations gave more or less the same qualitative energy orderings among the various species (summarized in Figure 5). In the SCF approach, the

(21) Release notes to this version of DMOL caution that the LYP functional has not been properly tested.

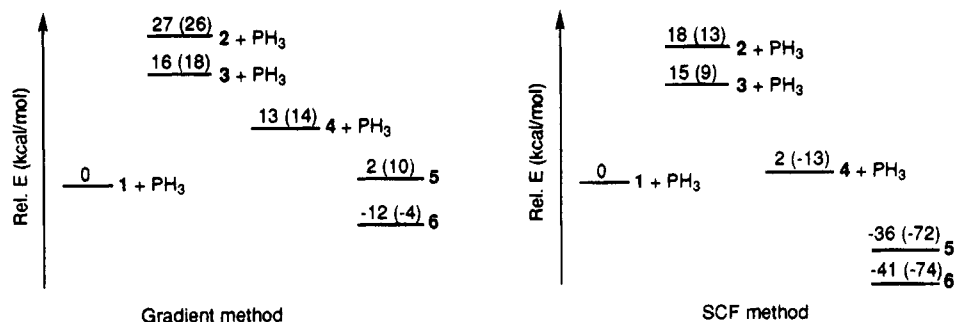


Figure 5. Summary of LYP-B88/F relative energies for all organonickel species. The corresponding JWM-B88/F energies are given in parentheses.

addition of nonlocal correlation corrections had a large influence on the relative energies compared to using nonlocal exchange corrections alone, but was of minor importance in the perturbative approach. The calculations indicate that commonly proposed intermediates **2** and **3** are formed endothermically from complex **1**. A more energetically favorable path would be the direct formation of **5** or **6**. The entropy change would be expected to be negative in all these transformations due to losses of rotational and/or translational degrees of freedom. It has been estimated that, for bimolecular complexations, the ΔS term is less than or equal to -36 cal/mol K.²² This would still suggest that the direct formation of **5** or **6** from **1** + phosphine is energetically accessible.

We are currently examining the influence of substituents on the stabilities of these intermediates, particularly in the case of **5** and **6**, as these would be the final intermediates before the irreversible reductive elimination step. Determination of substituent effects is necessary to provide further insight into the control of regiochemistry. Experimental studies have revealed a dominant electronic influence on the regiochemical outcome.⁴ With regard to stereoselectivity, it is obvious that, for steric reasons, the exo orientation of an olefin substituent would be more favorable in any of the complexes. Preliminary molecular mechanics calculations using a modified MM2 force field²³ have indicated that complexes **3**, **4**, and **5** give good quantitative

agreement with the observed exo stereoselectivity, but more detailed studies are needed to test their viability as predictive models for this chemistry.

Conclusions

We have presented the results of a DFT study on some possible intermediates in the nickel-catalyzed homo-Diels–Alder reaction. It would be preferable to compare the relevant transition-state energies, and we are currently carrying out this investigation. Reports on DFT transition-state calculations are relatively few at present, and more studies are needed to test the reliability of the method. Work is also in progress on determining the influence of substituents on the relative energies of these intermediates using a combined electronic structure/molecular mechanics approach and will be reported in due course.

Acknowledgment. We are grateful to the Natural Sciences and Engineering Research Council (NSERC) Canada for financial support. We also thank Professor Mark Lautens for helpful discussions.

Supplementary Material Available: Tables of calculated total energies, Mulliken charges, and dipole moments as functions of level of theory and mesh size for complexes **1**–**6** (4 pages). Ordering information is given on any current masthead page.

OM940900M

(22) Page, M. I. In *Enzyme Mechanisms*; Page, M. I., Williams, A., Eds.; The Royal Society of Chemistry: Burlington House, London, 1987; p 6.

(23) Gugelchuk, M. M.; Houk, K. N. *J. Am. Chem. Soc.* **1994**, *116*, 330.

Synthesis and X-ray Structure of Intramolecularly Coordinated Silyl Cations

Johannes Belzner,^{*,†} Dirk Schär,[†] Boris O. Kneisel,[‡] and Regine Herbst-Irmer[‡]

Institut für Organische Chemie der Georg-August-Universität Göttingen, Tammannstrasse 2, D-37077 Göttingen, Germany, and Institut für Anorganische Chemie der Georg-August-Universität Göttingen, Tammannstrasse 4, D-37077 Göttingen, Germany

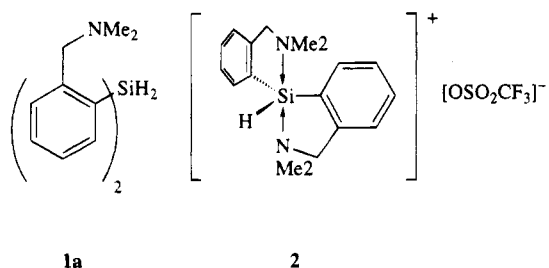
Received December 6, 1994[®]

Bis[2-((dimethylamino)methyl)phenyl]silyl triflate and [2-((dimethylamino)methyl)phenyl]phenylsilyl triflate were prepared by treatment of the corresponding dihydrosilanes with trimethylsilyl triflate in excellent yield. X-ray crystallography shows $[\text{Ar}_2\text{SiH}]^+[\text{OSO}_2\text{CF}_3]^-$ ($\text{Ar} = 2\text{-}(\text{Me}_2\text{NCH}_2)\text{C}_6\text{H}_4$; triclinic, $P\bar{1}$, $a = 8.421(2) \text{ \AA}$, $b = 9.892(3) \text{ \AA}$, $c = 13.183(4) \text{ \AA}$, $\alpha = 82.78(2)^\circ$, $\beta = 74.00(1)^\circ$, $\gamma = 75.84(2)^\circ$, $Z = 2$) to exist in the solid state as a separated ion pair with a pentacoordinated cationic silicon center, whereas $[\text{Ar}(\text{Ph})\text{SiH}]^+[\text{OSO}_2\text{CF}_3]^-$ (monoclinic, $P2_1/n$, $a = 8.923(2) \text{ \AA}$, $b = 9.957(2) \text{ \AA}$, $c = 20.132(3) \text{ \AA}$, $\beta = 98.74(1)^\circ$, $Z = 4$) forms a tight ion pair, in which the triflate anion occupies one axial position of the trigonal bipyramid around silicon.

While trivalent silyl cations are stable in the gas phase,¹ the electron-deficient silicon center almost inevitably undergoes coordinative interaction with either its counterion or with the solvent in the solid or in solution.² The formation of intermolecular complexes between silyl cations and Lewis bases in solution has been well investigated;³ furthermore, some solid-state structures of such intermolecularly coordinated silyl cations were determined.⁴ Recently, Corriu⁵ provided some evidence for the formation of an intramolecularly pentacoordinated silyl cation (siliconium ion) using the tridentate 2,6-bis((dimethylamino)methyl)phenyl substituent. In contrast, Willcott⁶ proved unambiguously that a quite similar compound exists in solution as an equilibrium mixture of two tetracoordinated structures. Very recently, Corriu⁷ published the first X-ray structure of an intramolecularly coordinated siliconium ion using the conformationally rigid 8-(dimethylamino)naphthalene substituent; herein we report the synthesis and the solid-state structure of two siliconium ions bearing the 2-((dimethylamino)methyl)phenyl substituent,

thus showing that, against first assumptions,^{5a} this substituent is highly suitable to stabilize a cationic silicon center via intramolecular coordination.

When bis[2-((dimethylamino)methyl)phenyl]silane (**1a**) was treated with trimethylsilyl triflate, bis[2-((dimethylamino)methyl)phenyl]silyl triflate (**2**)⁸ was isolated as a white solid in excellent yield; its solubility properties (insoluble in hexane, diethyl ether, and benzene, soluble in dichloromethane and chloroform) are in good agreement with an ionic structure.



The ¹H NMR spectrum provides evidence for a strong coordination of both NMe₂ groups to the silicon center: the methyl protons of the dimethylamino group as well as the benzylic protons are chemically inequivalent to each other and give rise to two singlets at δ 2.56 and 2.76 as well as a characteristic AB pattern at δ 4.27 and 4.33. Of further diagnostic value for the structural elucidation of **2** is the ²⁹Si–¹H coupling constant of 272 Hz, which is significantly increased compared to that found for covalent **1a** and does reflect the enhanced s character of the Si–H bond, as is expected for sp²-hybridized silicon.⁹ The SiH signal, whose ²⁹Si satellites allow the determination of the ²⁹Si–¹H coupling constant, is found at δ 4.60, thus showing an upfield shift of about 0.25 ppm in comparison to the starting silane **1a**. The same trend is observed in the ²⁹Si NMR spectrum: hydride abstraction from **1a** is accompanied

[†] Institut für Organische Chemie der Georg-August-Universität Göttingen.

[‡] Institut für Anorganische Chemie der Georg-August-Universität Göttingen.

[®] Abstract published in *Advance ACS Abstracts*, March 1, 1995.

(1) See e.g.: Schwarz, H. In *The Chemistry of Organic Silicon Compounds*; Patai, S., Rappoport, Z., Eds.; Wiley: Chichester, U.K., 1989; pp 446–450, and references cited therein.

(2) See e.g.: (a) Lambert, J. B.; Zhang, S.; Ciro, S. M. *Organometallics* **1994**, *13*, 2430–2443. (b) Prakash, G. K. S.; Keyaniyan, S.; Aniszfeld, R.; Heiliger, L.; Olah, G. A.; Stevens, R. C.; Choi, H.-K.; Bau, R. *J. Am. Chem. Soc.* **1987**, *109*, 5123–5126. (c) Reed, C. A.; Xie, Z.; Bau, R.; Benesi, A. *Science* **1993**, *262*, 402–404.

(3) See e.g.: Bassindale, A. R.; Stout, T. *Tetrahedron Lett.* **1985**, *26*, 3403–3406 and references cited therein.

(4) (a) Hensen, K.; Zengerly, T.; Pickel, P.; Klebe, G. *Angew. Chem.* **1983**, *95*, 739; *Angew. Chem., Int. Ed. Engl.* **1983**, *22*, 725. (b) Hensen, K.; Zengerly, T.; Müller, T.; Pickel, P. *Z. Anorg. Allg. Chem.* **1988**, *558*, 21–27.

(5) (a) Chuit, C.; Corriu, R. J. P.; Mehdi, A.; Reyé, C. *Angew. Chem.* **1993**, *105*, 1372–1375; *Angew. Chem., Int. Ed. Engl.* **1993**, *32*, 1311–1314. (b) Carré, F.; Chuit, C.; Corriu, R. J. P.; Mehdi, A.; Reyé, C. *Angew. Chem.* **1994**, *106*, 1152–1154; *Angew. Chem., Int. Ed. Engl.* **1994**, *33*, 1097.

(6) Benin, V. A.; Martin, J. C.; Willcott, M. R. *Tetrahedron Lett.* **1994**, *35*, 2133–2136.

(7) Brelière, C.; Carré, R.; Corriu, R.; Wong Chi Man, M. *J. Chem. Soc., Chem. Commun.* **1994**, 2333–2334.

(8) Alternatively, **2** may be prepared by reaction of cyclotrisilane (Ar_2Si)₃ with trimethylsilyl triflate.

(9) Jutzli, P.; Bunte, E.-A. *Angew. Chem.* **1992**, *104*, 1636–1638; *Angew. Chem., Int. Ed. Engl.* **1992**, *31*, 1605.

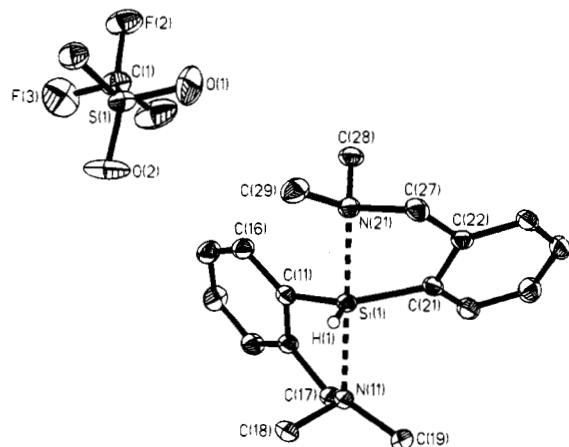


Figure 1. Crystal structure of **2**. Hydrogen atoms not bonded to silicon are omitted for clarity; displacement ellipsoids are at the 50% probability level.

Table 1. Selected Bond Lengths (Å) and Bond Angles (deg) in Triflate **2**

Si(1)–C(11)	1.874(2)	Si(1)–C(21)	1.882(2)	Si(1)–H(1)	1.34(2)
Si(1)–N(21)	2.072(2)	Si(1)–N(11)	2.052(2)		
C(11)–Si(1)–C(21)	119.8(1)	C(21)–Si(1)–H(1)	116.3(9)		
H(1)–Si(1)–C(11)	123.8(9)	N(11)–Si(1)–N(21)	171.2(1)		
H(1)–Si(1)–N(11)	86.8(9)	C(21)–Si(1)–N(11)	98.9(1)		
C(11)–Si(1)–N(11)	84.3(1)	H(1)–Si(1)–N(21)	84.5(9)		
C(21)–Si(1)–N(21)	83.7(1)	C(11)–Si(1)–N(21)	101.8(1)		

by an upfield shift of the ^{29}Si NMR resonance in **2** ($\delta(\mathbf{1a}) -45.0$; $\delta(\mathbf{2}) -51.6$). Thus, upon conversion of the dihydrosilane **1a** to the triflate **2**, NMR spectroscopic behavior is found which parallels the observations made for 8-(dimethylamino)naphthalene-substituted silanes⁷ but is in contrast with that reported for the 2,6-bis-((dimethylamino)methyl)phenyl-substituted system; in this case, the ^1H NMR signal of the SiH proton and the ^{29}Si NMR signal are shifted downfield upon going from the dihydrosilane to the corresponding siliconium ion.^{5a}

Colorless crystals of **2** suitable for X-ray analysis (Table 1) were obtained by crystallization from dichloromethane/diethyl ether (10:1). The X-ray structure (Figure 1) clearly proves the ionic structure of **2**. There exists no interaction between the silicon center and the triflate anion: the shortest silicon–oxygen distance is 4.165 Å, which is greater by far than the sum of the van der Waals radii of both elements (3.62 Å).¹⁰ The coordination geometry around silicon is that of a slightly distorted trigonal bipyramid, in which both dimethylamino groups occupy the axial positions. The Si–N distances are 2.052(2) and 2.072(2) Å, respectively, and resemble those found in the intermolecularly pentacoordinated imidazole complex **3** (2.034(3) and 2.005(3) Å).^{4b} These distances are significantly longer than a covalent Si–N bond distance (1.70–1.76 Å)¹¹ but smaller than the dative Si–N bond distance in neutral pentacoordinated silicon compounds bearing the 2-((dimethylamino)methyl)phenyl substituent (e.g. 2.291(2) Å in **1b**).¹² H(1), C(11), and C(21) form the equatorial plane; their bond angles to the central silicon atom sum up to

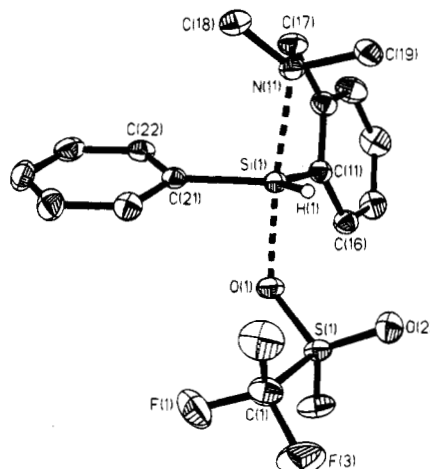
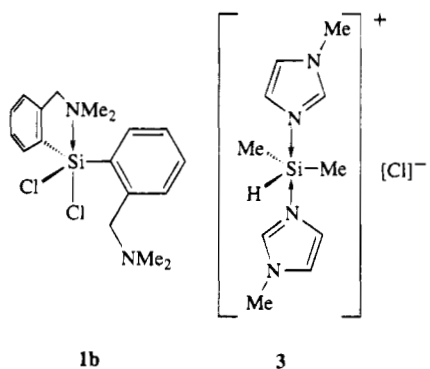


Figure 2. Crystal structure of **4**. Hydrogen atoms not bonded to silicon are omitted for clarity; displacement ellipsoids are at the 50% probability level.

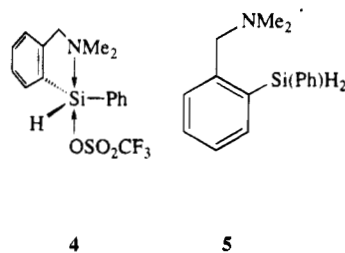
Table 2. Selected Bond Lengths (Å) and Bond Angles (deg) in Triflate **4**

Si(1)–C(11)	1.866(2)	Si(1)–C(21)	1.857(2)	Si(1)–H(1)	1.35(2)
Si(1)–O(1)	1.951(1)	Si(1)–N(11)	2.052(2)	Si(1)–O(1)	1.486(1)
S(1)–O(2)	1.421(2)	S(1)–O(3)	1.422(2)		
C(11)–Si(1)–C(21)	116.4(1)	C(21)–Si(1)–H(1)	116.0(8)		
H(1)–Si(1)–C(11)	127.6(8)	N(11)–Si(1)–O(1)	174.3(1)		
H(1)–Si(1)–O(1)	88.2(9)	C(21)–Si(1)–O(1)	89.4(1)		
C(11)–Si(1)–O(1)	93.5(1)	H(1)–Si(1)–N(11)	88.5(9)		
C(21)–Si(1)–N(11)	96.2(1)	C(11)–Si(1)–N(11)	84.9(1)		
Si(1)–C(11)–C(12)	113.7(1)	Si(1)–C(11)–C(16)	128.0(1)		
Si(1)–C(21)–C(22)	122.3(1)	Si(1)–C(21)–C(26)	120.2(1)		

360(2)°, thus manifesting the total flattening of the silicon center.



In an analogous manner, [2-((dimethylamino)methyl)phenyl]phenylsilyl triflate (**4**) was prepared from the corresponding dihydrosilane **5^{5a}** in 91% yield. Again, the



solubility properties as well as the increased ^{29}Si – ^1H coupling constant (290 Hz) argue for an ionic structure, which was eventually established for the solid state by single-crystal X-ray diffraction (Figure 2). The silicon center of **4** is pentacoordinated with Si(1), C(11), C(21),

(10) Bondi, A. *J. Phys. Chem.* **1964**, *68*, 441–451.

(11) Sheldrick, W. S. In *The Chemistry of Organic Silicon Compounds*; Patai, S., Rappoport, Z., Eds.; Wiley: Chichester, U.K., 1989; p 254.

(12) Probst, R.; Leis, C.; Gamper, S.; Herdtweck, E.; Zybille, L.; Auner, N. *Angew. Chem.* **1991**, *103*, 1155–1157; *Angew. Chem., Int. Ed. Engl.* **1991**, *30*, 1132–1134.

and H(1) forming the central plane of a trigonal bipyramid (sum of the bond angles $360(2)^\circ$). The twist angle between this plane and the phenyl substituent amounts to 18.2° , whereas the 2-((dimethylamino)methyl)phenyl substituent is located almost perpendicular to the central plane (twist angle 79.1°). Correspondingly, the dimethylamino group is brought into an apical position. In order to accomplish an optimal coordination of the lone pair at nitrogen to the silicon center, the bond angles around C(11) show, in contrast to the angles around C(21), appreciable deviation from 120° : the endocyclic angle Si(1)–C(11)–C(12) is reduced to $113.7(1)^\circ$, whereas the exocyclic angle Si(1)–C(11)–C(16) is widened up to $128.0(1)^\circ$. The resulting Si–N distance is $2.052(2)$ Å, which is similar to those found in **2**; however, the second axial position of the trigonal bipyramid is now occupied by the triflate anion. The Si–O distance of $1.951(1)$ Å is distinctly longer than typical covalent Si–O bond lengths, which range between 1.61 and 1.74 Å,¹³ and is elongated significantly even in comparison to the Si–O distance in protonated ${}^t\text{Bu}_3\text{SiOH}$ ($1.779(9)$ Å)¹⁴ as well as to the exceptionally long Si–O bond ($1.853(5)$ Å) found in a ruthenium-substituted silyl triflate.¹⁵ Thus, **4** may be described as a tight ion pair between an intramolecularly coordinated silyl cation and a triflate anion. However, there is also some covalent bonding interaction between Si(1) and O(1) in **4** present, which is reflected by the lengthening of the S(1)–O(1) ($1.486(1)$ Å) bond relative to the S(1)–O(2) and S(1)–O(3) bonds ($1.421(2)$ and $1.422(2)$ Å, respectively).

It is of interest to note that **4** does not form a tetracoordinated silyl cation, as is known for the reaction products of Me_3SiI with pyridine^{4a} or of Me_3SiCl with *N*-methylimidazole,^{4b} but prefers pentacoordination with inclusion of the triflate anion into its coordination sphere. Experiments which focus on to the synthesis of a tetrahedral silyl cation by substituting the triflate anion in **4** by a less nucleophilic counterion are under way.

Experimental Section

${}^1\text{H}$ NMR and ${}^{13}\text{C}$ NMR spectra were recorded on a Bruker AM 250 (${}^1\text{H}$ NMR, 250 MHz; ${}^{13}\text{C}$ NMR, 62.9 MHz). C_q , CH, CH_2 , and CH_3 were determined using the DEPT pulse sequence. ${}^{29}\text{Si}$ NMR spectra were recorded on a Bruker AMX 300 (59.6 MHz) using a refocused INEPT pulse sequence. Chemical shifts refer to δ_{TMS} 0.0. Mass spectra were recorded on a Varian MAT 311 A. Melting points are uncorrected. Elemental analyses were performed at Mikroanalytisches Labor der Georg-August-Universität Göttingen.

All manipulations were carried out under an inert argon atmosphere using carefully dried glassware. Ethereal solvents used were dried by refluxing over sodium and distilled immediately before use; dichloromethane was dried using molecular sieves (4 Å).

Bis[2-((dimethylamino)methyl)phenyl]silyl Triflate (2). To a stirred solution of 775 mg (2.6 mmol) of **1a**¹⁶ in 20 mL of

(13) Sheldrick, W. S. In *The Chemistry of Organic Silicon Compounds*; Patai, S., Rappoport, Z., Eds.; Wiley: Chichester, U.K., 1989; p 263.

(14) Xie, Z.; Bau, R.; Reed, C. A. *J. Chem. Soc., Chem. Commun.* **1994**, 2519–2520.

(15) Straus, D. A.; Zhang, C.; Quimbata, G. E.; Grumbine, S. D.; Heyn, R. H.; Tilley, D.; Rheingold, A. L.; Geib, S. J. *J. Am. Chem. Soc.* **1990**, *112*, 2673–2681.

(16) Auner, N.; Probst, R.; Hahn, F.; Herdtweck, E. *J. Organomet. Chem.* **1993**, *459*, 25–41.

Table 3. Summary of Crystal Data, Details of Intensity Collection, and Least-Squares Refinement Parameters for **2** and **4**

	2	4
empirical formula	$\text{C}_{19}\text{H}_{25}\text{N}_2\text{O}_3\text{F}_3\text{SiS}$	$\text{C}_{16}\text{H}_{18}\text{NO}_3\text{F}_3\text{SiS}$
M_r	446.56	389.46
cryst size (mm)	$0.7 \times 0.6 \times 0.6$	$0.9 \times 0.8 \times 0.8$
cryst syst	triclinic	monoclinic
space group	$P\bar{1}$	$P2_1/m$
a (Å)	8.421 (2)	8.923 (2)
b (Å)	9.892 (3)	9.957 (2)
c (Å)	13.183 (4)	20.132 (3)
α (deg)	82.78 (2)	90
β (deg)	74.00 (1)	98.74(1)
γ (deg)	75.84(2)	90
V (Å ³)	1021.5(5)	1767.9(6)
Z	2	4
D_{expt} (g cm ⁻³)	1.452	1.463
μ (mm ⁻¹)	0.268	0.296
$F(000)$	468	808
2θ range (deg)	$8 \leq 2\theta \leq 50$	$8 \leq 2\theta \leq 50$
range of hkl	$-9 \leq h \leq 10$ $-11 \leq k \leq 11$ $-24 \leq l \leq 15$	$-10 \leq h \leq 10$ $-11 \leq k \leq 11$ $-24 \leq l \leq 15$
no. of rflns coll	6274	6440
no. of indep rflns	3598	3114
$R(\text{int})$	0.0668	0.0674
no. of data	3598	3106
no. of params	270	232
S	1.035	1.063
g_1	0.0335	0.0389
g_2	0.6542	0.7821
$R1$ ($F > 4\sigma(F)$)	0.0404	0.0425
w $R2$ (all data)	0.1089	0.0933
largest diff peak (e Å ⁻³)	0.268	0.539
largest diff hole (e Å ⁻³)	-0.406	-0.322

ether was added dropwise at 0 °C 0.5 mL (2.6 mmol) of trimethylsilyl triflate. The resulting suspension was warmed to ambient temperature and stirred for another 30 min. Evaporation of the solvent left a white solid, which after being washed twice with 10 mL of hexane yielded 1.153 g (99%) of **2** (mp 144 °C). ${}^1\text{H}$ NMR (CDCl_3): δ 2.56 (s, 6 H, NCH_3), 2.76 (s, 6 H, NCH_3), 4.27, 4.33 (AB system, $J = 15$ Hz, 4 H, NCH_2), 4.60 (s (d, ${}^1J_{\text{Si-H}} = 272$ Hz), 1 H, SiH), 7.35–7.53 (m, 6 H, aromatic H), 7.75 (d, ${}^3J = 7$ Hz, 2 H, 6-H). ${}^{13}\text{C}$ NMR (CDCl_3): δ 45.0 (NCH_3), 47.1 (NCH_3), 64.5 (NCH_2), 120.8 (q, ${}^1J_{\text{C-F}} = 321$ Hz, CF_3), 127.0 (ar CH), 127.9 (ar C_q), 128.2 (ar CH), 131.9 (ar CH), 135.3 (ar CH), 144.3 (ar C_q). ${}^{29}\text{Si}$ NMR (CDCl_3): δ -51.6 (d, ${}^1J_{\text{Si-H}} = 272$ Hz). Anal. Calcd for $\text{C}_{19}\text{H}_{25}\text{F}_3\text{N}_2\text{O}_3\text{Si}$: C, 51.22; H, 5.43; N, 6.29. Found: C, 51.06; H, 5.60; N, 6.71.

[2-((Dimethylamino)methyl)phenyl]phenylsilane (5). To a stirred suspension of 1.00 g (26.4 mmol) of LiAlH_4 in 20 mL of ether was added at 0 °C a suspension of 4.39 g (14.1 mmol) of [2-((dimethylamino)methyl)phenyl]phenyldichlorosilane¹⁷ in 20 mL of ether. The mixture was stirred for 5 min at 0 °C, warmed to ambient temperature, and, after being stirred for another 60 min, hydrolyzed at -35 °C by subsequent addition of 1 mL of H_2O , 1 mL of 20% NaOH solution and 3 mL of H_2O . The white precipitate was filtered off and washed twice with 5 mL of ether, and the combined ethereal phases were evaporated. The remaining oil was redissolved in 15 mL of hexane and dried with MgSO_4 . Evaporation of the solvents yielded 3.41 g (100%) of analytically pure **5**. ${}^1\text{H}$ NMR (C_6D_6): δ 1.80 (s, 6 H, $\text{N}(\text{CH}_3)_2$), 3.20 (s, 2 H, NCH_2), 5.14 (s (d, ${}^1J_{\text{Si-H}} = 208$ Hz), 2 H, SiH_2), 6.93 (d, ${}^3J = 7$ Hz, 1 H, ar H), 7.03 (dd, ${}^3J = 7$ Hz, 1 H, ar H), 7.10–7.27 (m, 4 H, ar H), 7.62–7.69 (m, 3 H, ar H). ${}^{13}\text{C}$ NMR (C_6D_6): δ 43.5 (NCH_3), 63.8 (NCH_2), 127.0 (ar CH), 127.1 (ar CH), 128.0 (2 ar CH), 128.7 (ar CH), 129.8 (ar CH), 133.1 (ar C_q), 135.1 (2

(17) Handwerker, H.; Lies, C.; Probst, R.; Bissinger, P.; Grohmann, A.; Kipf, P.; Herdtweck, E.; Blümel, J.; Auner, N.; Zybll, C. *Organometallics* **1993**, *12*, 2162–2176.

Table 4. Atomic Coordinates ($\times 10^4$) and Equivalent Isotropic Displacement Parameters ($\text{\AA}^2 \times 10^3$) for **2**^a

	<i>x</i>	<i>y</i>	<i>z</i>	<i>U</i> (eq)
Si(1)	2578(1)	6965(1)	7354(1)	18(1)
C(11)	2693(3)	8575(2)	6445(2)	20(1)
C(12)	2973(3)	9658(2)	6919(2)	21(1)
C(13)	3024(3)	10957(2)	6394(2)	27(1)
C(14)	2798(3)	11185(2)	5382(2)	31(1)
C(15)	2591(3)	10121(2)	4884(2)	31(1)
C(16)	2542(3)	8821(2)	5408(2)	24(1)
C(17)	3266(3)	9331(2)	8008(2)	23(1)
N(11)	3884(2)	7798(2)	8130(1)	20(1)
C(18)	5705(3)	7432(2)	7557(2)	26(1)
C(19)	3767(3)	7293(2)	9254(2)	27(1)
C(21)	620(2)	6908(2)	8457(2)	21(1)
C(22)	4(3)	5729(2)	8418(2)	21(1)
C(23)	-1413(3)	5438(2)	9171(2)	27(1)
C(24)	-2246(3)	6330(3)	9962(2)	29(1)
C(25)	-1697(3)	7529(3)	9997(2)	30(1)
C(26)	-277(3)	7815(2)	9245(2)	25(1)
C(27)	953(3)	4849(2)	7508(2)	25(1)
N(21)	1527(2)	5838(2)	6591(1)	21(1)
C(28)	28(3)	6612(2)	6211(2)	26(1)
C(29)	2763(3)	5033(2)	5729(2)	29(1)
S(1)	3262(1)	6980(1)	2536(1)	28(1)
O(1)	1996(3)	6479(2)	3367(2)	56(1)
O(2)	4546(3)	7372(2)	2878(2)	55(1)
O(3)	3841(2)	6203(2)	1611(1)	32(1)
C(1)	2102(3)	8635(3)	2079(2)	36(1)
F(1)	1348(2)	9499(2)	2841(2)	63(1)
F(2)	900(2)	8463(2)	1656(1)	49(1)
F(3)	3125(2)	9287(2)	1326(2)	61(1)

^a *U* (eq) is defined as one-third of the trace of the orthogonalized U_{ij} tensor.

ar CH), 138.3 (ar C_q), 139.0 (ar CH), 146.4 (ar C_q). ²⁹Si NMR (C₆D₆): δ -43.3 (t, ¹*J*_{Si-H} = 208 Hz). MS (EI, 70 eV): *m/z* (relative intensity) 241 (28) [M⁺], 240 (33) [M⁺ - H], 226 (6) [M⁺ - Me], 195 (80) [M⁺ - NMe₂ - 2H], 181 (7) [M⁺ - CH₂-NMe₂ - 2H], 164 (100) [M⁺ - C₆H₅], 148 (64) [M⁺ - C₆H₅ - Me - H], 105 (56) [M⁺ - C₆H₄CH₂NMe - 2H], 58 (41) [CH₂-NMe₂⁺], 44 (12) [NMe₂⁺]. Anal. Calcd for C₁₅H₁₉NSi: C, 74.21; H, 7.97; N, 6.92. Found: C, 74.40; H, 7.89; N, 6.82.

[2-(Dimethylamino)methylphenyl]phenylsilyl Triflate (4). To a stirred solution of 938 mg (3.9 mmol) of **5** in 15 mL of ether was added dropwise at 0 °C 0.7 mL (3.9 mmol) of trimethylsilyl triflate. The solution was warmed to ambient temperature and stirred for another 45 min. Evaporation of the solvent left a white solid, which was washed three times with 10 mL of hexane, yielding 1.385 g (91%) of **4** (mp 102 °C). ¹H NMR (CDCl₃): δ 1.93 (s, 3 H, NCH₃), 2.48 (s, 3 H, NCH₃), 3.76, 3.81 (AB system, *J* = 15 Hz, 2 H, NCH₂), 5.22 (s (d, ¹*J*_{Si-H} = 290 Hz), 1 H, SiH), 7.20-7.54 (m, 8 H, ar H), 8.09 (d, ³*J* = 7 Hz, 1 H, 6-H). ¹³C NMR (CDCl₃): δ 46.1 (NCH₃), 46.6 (NCH₃), 63.3 (NCH₂), 119.3 (q, ¹*J*_{C-F} = 319 Hz, CF₃), 125.1 (ar CH), 128.4 (2 ar CH), 128.6 (ar CH), 129.5 (ar C_q), 130.1 (ar CH), 131.8 (ar CH), 132.5 (2 ar CH), 133.2 (ar C_q), 138.2 (ar CH), 143.4 (ar C_q). ²⁹Si NMR (CDCl₃): δ -56.2 (d, ¹*J*_{Si-H} = 294 Hz). Anal. Calcd for C₁₆H₁₈F₃NO₃SSi: C, 49.34; H, 4.66; N, 3.60. Found: C, 49.17; H, 4.85; N, 3.42.

X-ray Structure Determination for 2 and 4. Crystal data, data collection, and least-squares parameters are sum-

Table 5. Atomic Coordinates ($\times 10^4$) and Equivalent Isotropic Displacement Parameters ($\text{\AA}^2 \times 10^3$) for **4**^a

	<i>x</i>	<i>y</i>	<i>z</i>	<i>U</i> (eq)
Si(1)	3086(1)	5140(1)	1333(1)	18(1)
C(11)	4387(2)	5060(2)	2151(1)	20(1)
C(12)	4510(2)	3781(2)	2436(1)	25(1)
C(13)	5409(3)	3549(2)	3048(1)	34(1)
C(14)	6206(3)	4597(3)	3383(1)	37(1)
C(15)	6092(2)	5880(2)	3112(1)	31(1)
C(16)	5181(2)	6110(2)	2503(1)	24(1)
C(17)	3603(2)	2678(2)	2052(1)	27(1)
N(11)	3310(2)	3089(2)	1333(1)	22(1)
C(18)	1992(2)	2337(2)	973(1)	30(1)
C(19)	4660(2)	2743(2)	1018(1)	29(1)
C(21)	1023(2)	5161(2)	1380(1)	19(1)
C(22)	442(2)	4775(2)	1959(1)	24(1)
C(23)	-1086(2)	4818(2)	1985(1)	31(1)
C(24)	-2089(2)	5255(2)	1435(1)	34(1)
C(25)	-1544(2)	5637(2)	857(1)	31(1)
C(26)	-11(2)	5598(2)	830(1)	24(1)
S(1)	3974(1)	8090(1)	985(1)	22(1)
O(1)	3081(2)	7098(1)	1313(1)	23(1)
O(2)	5239(2)	7518(2)	736(1)	34(1)
O(3)	4182(2)	9303(2)	1360(1)	34(1)
C(1)	2649(2)	8535(2)	237(1)	30(1)
F(1)	1350(2)	8977(2)	393(1)	47(1)
F(2)	2358(2)	7489(2)	-168(1)	44(1)
F(3)	3244(2)	9492(2)	-96(1)	52(1)

^a *U* (eq) is defined as one-third of the trace of the orthogonalized U_{ij} tensor.

marized in Table 3. Data for **2** were collected on a STOE-Siemens-AED diffractometer and data for **4** on a STOE-Siemens-Huber four-circle diffractometer, both at -120 °C using graphite-monochromated Mo K α radiation (λ = 0.71073 Å). Both structures were solved by direct methods.¹⁸ All non-hydrogen atoms were refined anisotropically.¹⁹ A riding model starting from calculated positions was employed for all hydrogen atoms—except hydrogens bonded to silicon, which were refined freely using isotropic displacement parameters. The structures were refined against F^2 with the weighting scheme $w^{-1} = \sigma^2(F_o^2) + (g_1P)^2 + g_2P$, where $P = (F_o^2 + 2F_c^2)/3$. The *R* values are defined as $R1 = \sum ||F_o| - |F_c|| / \sum |F_o|$ and $wR2 = [\sum w(F_o^2 - F_c^2)^2 / \sum wF_o^4]^{1/2}$. Atomic coordinates for **2** and **4** are given in Tables 4 and 5, respectively.

Acknowledgment. This work was supported by the Deutsche Forschungsgemeinschaft, the Fonds der Chemischen Industrie, and the Graduiertenförderung des Landes Niedersachsen.

Supplementary Material Available: For **2** and **4**, tables of crystal data and structure refinement details, atomic coordinates, bond lengths and angles, anisotropic displacement parameters, and hydrogen atom coordinates (10 pages). Ordering information is given on any current masthead page.

OM9409276

(18) Sheldrick, G. M. *Acta Crystallogr.* **1990**, *A46*, 467.

(19) Sheldrick, G. M. SHELXL-93, Program for Crystal Structure Refinement; University of Göttingen, Göttingen, Germany, 1993.

A New Reaction of Coordinated Sulfoxides: Facile and Highly Diastereoselective Deprotonation of a Chiral, Cationic Rhenium DMSO Complex to an Ylide and Subsequent [1,2] Migration of Rhenium from Sulfur to Carbon

Oliver Meyer, Atta M. Arif, and J. A. Gladysz*

Department of Chemistry, University of Utah, Salt Lake City, Utah 84112

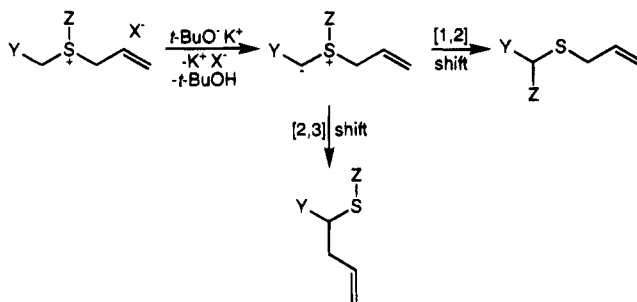
Received December 1, 1994[®]

Reaction of the chiral, cationic sulfur-ligated DMSO complex $[(\eta^5\text{-C}_5\text{H}_5)\text{Re}(\text{NO})(\text{PPh}_3)_2(\text{S}(\text{O})(\text{CH}_3)_2)]^+\text{BF}_4^-$ and $t\text{-BuO}^-\text{K}^+$ (CH_2Cl_2 , -80°C) gives the neutral alkyl complex $(\eta^5\text{-C}_5\text{H}_5)\text{Re}(\text{NO})(\text{PPh}_3)(\text{CH}_2\text{S}(\text{O})(\text{CH}_3))$ (**2**) in 96% yield as a 99:1 mixture of *SR,RS/SS,RR* Re,S configurational diastereomers. An intermediate ylide with a $\text{ReS}(\text{O})(\text{CH}_3)(\text{CH}_2^-)$ linkage is proposed. Subsequent [1,2] migration of rhenium from sulfur to carbon then gives **2**. In CDCl_3 at room temperature, **2** slowly equilibrates to a 4:96 *SR,RS/SS,RR* mixture. A mechanism involving epimerization at sulfur and the methyldene complex $[(\eta^5\text{-C}_5\text{H}_5)\text{Re}(\text{NO})(\text{PPh}_3)(=\text{CH}_2)]^+\text{X}^-$ (4^+X^-) is supported by (1) enhanced rates in the presence of catalytic amounts of HOTf, which presumably convert the $-\text{S}(\text{O})\text{CH}_3$ moieties to better leaving groups, HOSCH_3 , (2) reduced rates in the presence of pyridine, and (3) trapping of 4^+X^- with $\text{P}(p\text{-tol})_3$. The crystal structure of (*SS,RR*)-**2** is determined, and possible origins of the kinetic and thermodynamic selectivities are discussed.

Carbanions adjacent to sulfoxide groups are easily generated and see abundant use in synthetic organic chemistry.¹ Such carbanions are also chiral, and can often be prepared—in some cases as $\text{S}=\text{NR}$ derivatives—in nonracemic form. Accordingly, numerous applications in enantioselective syntheses have been developed.² Surprisingly, there do not appear to have been prior attempts to generate carbanions from metal-bound sulfoxides.³ In view of the growing number of chiral metal complexes available in enantiomerically pure form and the facile binding and detachment of sulfur donor ligands from many metal fragments,⁴ we thought that such species would have good prospects for applications in enantioselective syntheses.

In previous studies, we have shown that sulfide and sulfoxide ligands are easily coordinated to the chiral rhenium Lewis acid $[(\eta^5\text{-C}_5\text{H}_5)\text{Re}(\text{NO})(\text{PPh}_3)]^+$ (**I**).^{5–7} When diallyl sulfide complexes of **I** are treated with $t\text{-BuO}^-\text{K}^+$, sulfur ylides are generated that undergo rapid [2,3] sigmatropic rearrangements.⁷ A generic

Scheme 1. Representative Sulfur Ylide Rearrangements



version of this well-known reaction is sketched in Scheme 1. The resulting thiolate complexes contain new carbon stereocenters, and one configuration greatly dominates. Organic sulfides of high enantiomeric purities can subsequently be isolated. However, sulfur ylides sometimes undergo [1,2] sigmatropic rearrangements, an alternative also diagrammed in Scheme 1. In fact, the deprotonation of simple sulfoxide complexes of **I** leads to rapid [1,2] migrations of rhenium, as described in the new chemistry below.

Results

The sulfur-ligated DMSO complex $[(\eta^5\text{-C}_5\text{H}_5)\text{Re}(\text{NO})(\text{PPh}_3)_2(\text{S}(\text{O})(\text{CH}_3)_2)]^+\text{BF}_4^-$ (1^+BF_4^-)⁵ was dissolved in CH_2Cl_2 at -80°C and treated with 1.0 equiv of $t\text{-BuO}^-\text{K}^+$ in THF (Scheme 2). Workup gave an orange solid (**2**) in 96% yield, which was characterized by microanalysis and IR and NMR (^1H , ^{13}C , ^{31}P) spectroscopy (Experimental Section). Complex **2** exhibited spectroscopic features typical of neutral alkyl complexes

[®] Abstract published in *Advance ACS Abstracts*, March 15, 1995.

(1) Oae, S.; Uchida, Y. In *The Chemistry Of Sulphones and Sulphoxides*; Patai, S., Rappoport, Z., Stirling, C., Eds.; Wiley: New York, 1988; pp 583–664.

(2) (a) Walker, A. J. *Tetrahedron: Asymmetry* **1992**, *3*, 961. (b) Posner, G. H. In *The Chemistry Of Sulphones and Sulphoxides*; Patai, S., Rappoport, Z., Stirling, C., Eds.; Wiley: New York, 1988; pp 823–849. (c) Johnson, C. R. *Aldrichim. Acta* **1985**, *18*, 3.

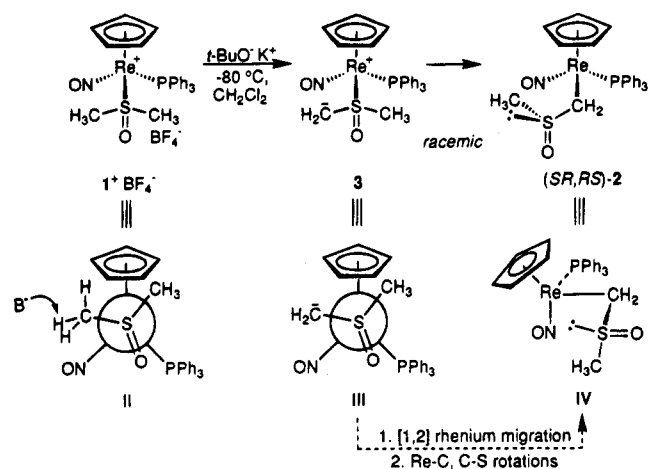
(3) Davies, J. A. *Adv. Inorg. Chem. Radiochem.* **1981**, *24*, 115.

(4) (a) Schenk, W. A.; Frisch, J.; Adam, W.; Prechtel, F. *Angew. Chem., Int. Ed. Engl.* **1994**, *33*, 1609. (b) Faller, J. W.; Ma, Y. *Organometallics* **1992**, *11*, 2726.

(5) Quirós Mendez, N.; Arif, A. M.; Gladysz, J. A. *Organometallics* **1991**, *10*, 2199.

(6) Boone, B. J.; Arif, A. M.; Gladysz, J. A. Manuscript in preparation.

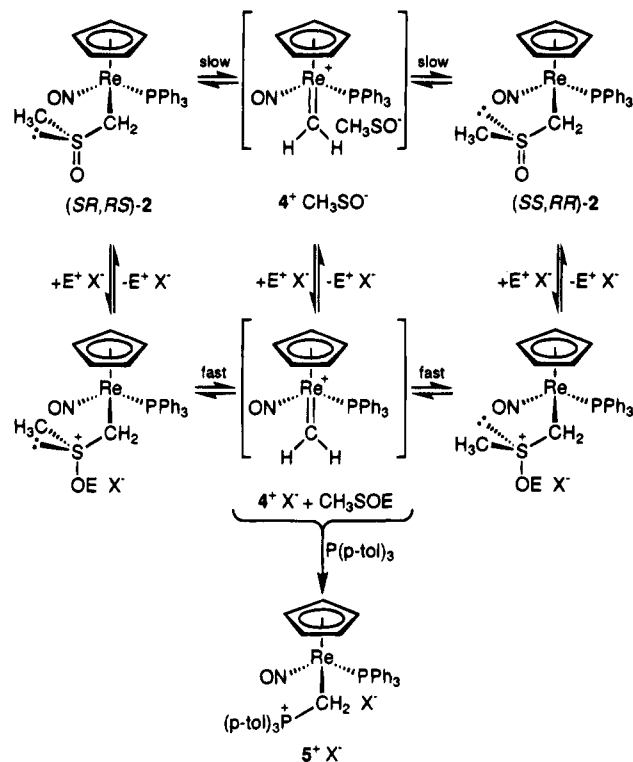
(7) (a) Cagle, P. C.; Arif, A. M.; Gladysz, J. A. *J. Am. Chem. Soc.* **1994**, *116*, 3655. (b) Cagle, P. C.; Weickhardt, K.; Meyer, O.; Arif, A. M.; Gladysz, J. A. Manuscript in preparation.

Scheme 2. Deprotonation and Rearrangement of DMSO Complex $1^+BF_4^-$ 

of the rhenium fragment I.⁸ These included an IR ν_{NO} value much lower than that of $1^+BF_4^-$ (1638 vs 1718 cm^{-1}), a phosphorus-coupled ReC ^{13}C NMR signal (15.3 ppm, d, $J_{CP} = 3.9$ Hz), and phosphorus-coupled ReCHH' 1H NMR signals (δ 3.70, 3.25; 2 dd). Hence, 2 was formulated as the alkyl or α -sulfinyl complex $(\eta^5-C_5H_5)Re(NO)(PPh_3)(CH_2S(O)CH_3)$. Free DMSO exhibits an IR ν_{SO} band at 1057 cm^{-1} , and 2 gave three absorptions in this region (1093 (m), 1015 (m), 998 (m sh)). A UV/visible spectrum showed, in addition to the intense band at ca. 234 nm characteristic of all adducts of I, a unique absorption at 306 nm (ϵ 2200 $M^{-1}\text{ cm}^{-1}$, CH_2Cl_2).

As illustrated in Scheme 2, $1^+BF_4^-$ and $t-BuO^-K^+$ likely first react to give the ylide or zwitterion 3 , derived from deprotonation of a methyl group. The formal positive charge can be placed on either sulfur, phosphorus, nitrogen, or rhenium. A [1,2] migration of rhenium from sulfur to carbon would then give 2 . No trace of the species that would result from a [1,2] migration of the remaining methyl group, sulfenate complex $(\eta^5-C_5H_5)Re(NO)(PPh_3)(S(O)CH_2CH_3)$, was detected. Hence, the electropositive rhenium fragment I has a much higher migratory aptitude than a methyl group.

In contrast to precursor $1^+BF_4^-$, 2 contains two stereocenters—one at rhenium and one at sulfur. Accordingly, two diastereomers are possible. Indeed, 2 was isolated as a 99:1 mixture of $SR,RS/SS,RR$ diastereomers,⁹ the configurations of which were assigned from a crystal structure below. Thus, the reaction is highly diastereoselective. Furthermore, the 99:1 ratio constitutes only a lower boundary to the actual diastereoselectivity. When a sample was kept in $CDCl_3$ at room temperature, slow epimerization occurred. After 7 days, a 4:96 $SR,RS/SS,RR$ mixture had formed, as assayed by ^{31}P NMR.¹⁰ This ratio did not change after an additional 14 days. Hence, (SR,RS) - 2 is less stable than

Scheme 3. Some Possible Mechanisms of Epimerization of 2 

(SS,RR) - 2 , and the kinetic and thermodynamic diastereomer ratios diverge dramatically.

We sought to probe the mechanism of epimerization. In extensive studies to date, only alkoxide and amido complexes of I have been observed to lose configuration at rhenium near room temperature.^{11,12} Thus, we suspected that the sulfur stereocenter of 2 was labile. Importantly, when a $CHCl_3$ solution of a 95:5 $SR,RS/SS,RR$ mixture was treated with HOTf (ca. 0.5 mol %; OTf = $OS(O)_2CF_3$), epimerization was catalyzed. After 0.25 and 6.25 h, 56:64 and 5:95 $SR,RS/SS,RR$ mixtures were present. Conversely, when a $CDCl_3$ solution of a 99:1 $SR,RS/SS,RR$ mixture was treated with pyridine (1.5 equiv), epimerization was slowed. After 7 and 21 days, 25:75 and 4:96 $SR,RS/SS,RR$ mixtures were present.

We envisioned, based upon the preceding data, the epimerization mechanism shown in Scheme 3, in which adventitious electrophiles assist the formal dissociation of a $-S(O)CH_3$ or $-OSCH_3$ moiety.¹³ This would generate the methylenidene complex $[(\eta^5-C_5H_5)Re(NO)(PPh_3)(=CH_2)]^+X^-$ (4^+X^-), which has been previously isolated¹⁴ and shown to readily alkylate phosphorus, nitrogen, and sulfur nucleophiles.¹⁴⁻¹⁶ Accordingly, when a $CDCl_3$

(8) Kiel, W. A.; Lin, G.-Y.; Bodner, G. S.; Gladysz, J. A. *J. Am. Chem. Soc.* **1983**, *105*, 4958 and references therein.

(9) (a) The configuration at rhenium is specified before that at sulfur, utilizing the priority sequence $\eta^5-C_5H_5 > PPh_3 > NO > CH_2S(O)CH_3$. See: Stanley, K.; Baird, M. C. *J. Am. Chem. Soc.* **1975**, *97*, 6598. Sloan, T. E. *Top. Stereochem.* **1981**, *12*, 1. Lecomte, C.; Dusausoy, Y.; Protas, J.; Tirouflet, J.; Dormand, J. *J. Organomet. Chem.* **1974**, *73*, 67. Isomer ratios are normalized to 100, and error limits on each integer are ± 2 ; e.g., 4:96 $\equiv (4 \pm 2):(96 \pm 2)$.

(10) Additional data: 1 day, 38:62; 3 days, 15:85; 4 days, 8:92.

(11) Saura-Llamas, I.; Gladysz, J. A. *J. Am. Chem. Soc.* **1992**, *114*, 2136.

(12) (a) Dewey, M. A.; Gladysz, J. A. *Organometallics* **1990**, *9*, 1351. (b) Richter-Addo, G. B.; Knight, A. D.; Dewey, M. A.; Arif, A. M.; Gladysz, J. A. *J. Am. Chem. Soc.* **1993**, *115*, 11863.

(13) Barrett, G. C.; Hogg, D. R. In *The Chemistry Of Sulphenic Acids and Their Derivatives*; Patai, S., Ed.; Wiley: New York, 1990; pp 14-15 and 371-373.

(14) (a) Tam, W.; Lin, G.-Y.; Wong, W.-K.; Kiel, W. A.; Wong, V. K.; Gladysz, J. A. *J. Am. Chem. Soc.* **1982**, *104*, 141. (b) Merrifield, J. H.; Lin, G.-Y.; Kiel, W. A.; Gladysz, J. A. *J. Am. Chem. Soc.* **1983**, *105*, 5811.

(15) McCormick, F. B.; Gleason, W. B.; Zhao, X.; Heah, P. C.; Gladysz, J. A. *Organometallics* **1986**, *5*, 1778.

(16) Crocco, G. L.; Lee, K. E.; Gladysz, J. A. *Organometallics* **1990**, *9*, 2819.

Table 1. Summary of Crystallographic Data for (SS,RR) - $(\eta^5\text{-C}_5\text{H}_5)\text{Re}(\text{NO})(\text{PPh}_3)(\text{CH}_2\text{S}(\text{O})\text{CH}_3)$ ((SS,RR) -2**)**

mol formula	$\text{C}_{25}\text{H}_{25}\text{NOPReS}$
mol wt	620.722
cryst syst	orthorhombic
space group	$Pna2_1$ (No. 33)
cell dimens (16 °C)	
a , Å	9.568(1)
b , Å	19.916(3)
c , Å	12.976(2)
V , Å ³	2472.60
Z	4
d_{calc} , g/cm ³	1.667
d_{obs} , g/cm ³ ($\text{Et}_2\text{O}/\text{CH}_2\text{I}_2$)	1.68
cryst dimens, mm	$0.43 \times 0.25 \times 0.25$
diffractometer	Syntex P1
radiation, Å	$\lambda(\text{Mo K}\alpha)$, 0.710 73
data colln method	θ - 2θ
scan speed, deg/min	3.0
no. of reflns measured	2567
range/indices (hkl)	0-11, 0-23, -14 to 0
scan range	$K_{\alpha 1} - 1.25$ to $K_{\alpha 2} + 1.25$
2θ limit, deg	3.00-50.00
std reflns check	1 X-ray h
total unique data	2513
no. of obsd data, $I > 3\sigma(I)$	1645
abs coeff, cm ⁻¹	51.458
min transm, %	92.40
max transm, %	99.99
no. of variables	279
goodness of fit	1.6276
$R = \sum F_o - F_c / \sum F_o $	0.0366
$R_w = \sum F_o - F_c w^{1/2} / \sum F_o w^{1/2}$	0.0585
$\Delta\sigma$ (max)	0.010
$\Delta\rho$ (max), e/Å ³	1.293 (ca. 0.850 Å from Re)

solution of **2** (99:1 $SR,RS/SS,RR$) was treated with the phosphine $\text{P}(p\text{-tol})_3$ (4 equiv), the phosphonium salt $[(\eta^5\text{-C}_5\text{H}_5)\text{Re}(\text{NO})(\text{PPh}_3)(\text{CH}_2\text{P}(p\text{-tol})_3)]^+\text{X}^-$ (5^+X^-) slowly formed. After 1 day, a 57:43 mixture of **2** (26:74 $SR,RS/SS,RR$) and 5^+X^- was present. After 7 days, conversion was >99% complete. The hexafluorophosphate salt 5^+PF_6^- has been previously characterized.¹⁶ Thus, the ammonium salt $\text{NH}_4^+\text{PF}_6^-$ was added to a preparative reaction. Workup gave 5^+PF_6^- in 43% yield. The ¹H and ³¹P NMR spectra matched those reported earlier.

In order to confirm the configurations given for **2** above, a crystal structure was sought. Thus, heptane vapor was allowed to slowly diffuse into a CH_2Cl_2 solution of the kinetic product (SR,RS)-**2**. Orange prisms formed, and X-ray data were collected as outlined in Table 1 and the Experimental Section. Refinement yielded the structures in Figure 1. A sulfur lone pair (LP) position was calculated. Atomic coordinates and selected bond lengths, bond angles, and torsion angles are summarized in Tables 2 and 3. Interestingly, these data showed that a crystal of the thermodynamic product (SS,RR)-**2** had been isolated. As a check, the crystal utilized was dissolved in CD_2Cl_2 . A ³¹P NMR spectrum confirmed the assignment (21.8 ppm).¹⁷

Some extensions of Scheme 2 were briefly explored. Complex **2** rapidly reacted with Br_2 and NBS. However, in no case was any bromodimethyl sulfoxide¹⁸ detected by IR or ¹H NMR. Reactions of other symmetrical sulfoxide complexes of **1** and $t\text{-BuO}^-\text{K}^+$ were examined.

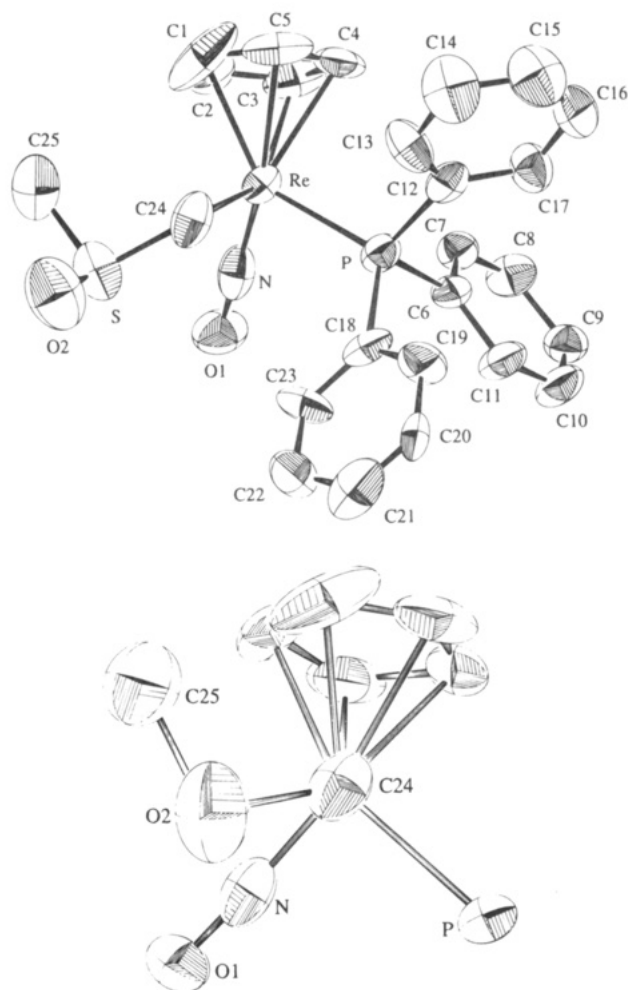


Figure 1. Structure of (SS,RR) - $(\eta^5\text{-C}_5\text{H}_5)\text{Re}(\text{NO})(\text{PPh}_3)(\text{CH}_2\text{S}(\text{O})\text{CH}_3)$ ((SS,RR) -**2**): (top) numbering diagram; (bottom) Newman-type projection with phenyl rings omitted and sulfur obscured by O2.

These appeared to give analogous rearrangement products but were not further studied since the ligating carbons were now also stereocenters, complicating analyses of the epimerizations. The dimethyl sulfide complex of **1**,⁵ which is likely less acidic than 1^+BF_4^- , did not give comparable chemistry. Finally, when 1^+BF_4^- and $t\text{-BuO}^-\text{K}^+$ were combined as in Scheme 2 but in the presence of CH_3I , only **2** (and unreacted 1^+BF_4^-) were detected.

Discussion

The preceding data establish a new base-promoted reaction of coordinated sulfoxides. With neutral metal complexes, there is abundant precedent for the generation of carbanions on coordinated ligands. However, analogous deprotonations of cationic metal complexes appear to have received much less attention.¹⁹ In many cases, the latter will give ylides or zwitterions—species that in our opinion have considerable potential for unusual rearrangements or synthetic applications. For

(17) This spectrum required several hours to acquire. A spectrum of a known $SR,RS/SS,RR$ mixture was subsequently recorded under identical conditions (23.4/21.8 ppm). The bulk sample of crystals was a 80:20 $SR,RS/SS,RR$ mixture. Thus, X-ray data were collected on the minor diastereomer present.

(18) Iriuchijima, S.; Tsuchihashi, G.-I. *Synthesis* **1970**, 588.

(19) Robertson, M. J.; White, C. J.; Angelici, R. J. *J. Am. Chem. Soc.* **1994**, *116*, 5190.

(20) See, for example: Wiegand, B. C.; Friend, C. M. *Chem. Rev.* **1992**, *92*, 491 and references therein.

Table 2. Atomic Coordinates and Equivalent Isotropic Thermal Parameters of Located Atoms of $(SS,RR)\text{-}2^a$

atom	x	y	z	B (\AA^2)
Re	0.99559(4)	0.96274(2)	0.993	3.370(9)
S	1.0028(4)	1.1190(2)	0.9032(4)	5.7(1)
P	1.1900(3)	0.9070(2)	0.9158(3)	3.44(6)
O1	1.177(1)	1.0363(5)	1.1346(8)	5.6(3)
O2	1.008(1)	1.1642(8)	0.810(2)	8.6(5)
N	1.105(1)	1.0075(5)	1.0697(9)	4.3(3)
C1	0.761(1)	0.960(1)	0.974(2)	8.6(5)
C2	0.787(1)	0.9532(8)	1.075(1)	5.1(4)
C3	0.860(1)	0.8942(8)	1.085(2)	6.0(4)
C4	0.874(1)	0.8629(6)	0.981(2)	4.6(3)
C5	0.808(1)	0.9069(9)	0.918(1)	5.9(3)
C6	1.296(1)	0.8638(6)	1.010(1)	3.6(3)
C7	1.238(1)	0.8380(6)	1.098(1)	3.4(3)
C8	1.311(1)	0.8037(7)	1.169(1)	4.2(3)
C9	1.453(1)	0.7905(7)	1.152(1)	3.8(3)
C10	1.514(1)	0.8161(9)	1.067(2)	4.8(4)
C11	1.437(1)	0.8530(6)	0.993(2)	4.3(3)
C12	1.138(1)	0.8396(7)	0.824(1)	3.7(3)
C13	1.059(2)	0.8592(7)	0.742(1)	4.7(3)
C14	1.008(2)	0.814(1)	0.669(2)	6.9(5)
C15	1.052(2)	0.747(1)	0.682(1)	6.7(4)
C16	1.132(2)	0.7260(7)	0.762(1)	6.0(4)
C17	1.179(2)	0.7736(7)	0.832(1)	4.6(3)
C18	1.322(1)	0.9557(7)	0.844(1)	4.2(3)
C19	1.389(1)	0.9280(7)	0.757(1)	4.8(3)
C20	1.494(1)	0.9634(6)	0.709(2)	4.7(4)
C21	1.526(2)	1.022(1)	0.739(2)	6.9(5)
C22	1.454(2)	1.0559(8)	0.825(2)	6.6(2)
C23	1.358(1)	1.0194(7)	0.874(1)	5.2(3)
C24	1.000(1)	1.0355(7)	0.858(2)	4.9(4)
C25	0.831(2)	1.130(1)	0.944(2)	9.5(7)

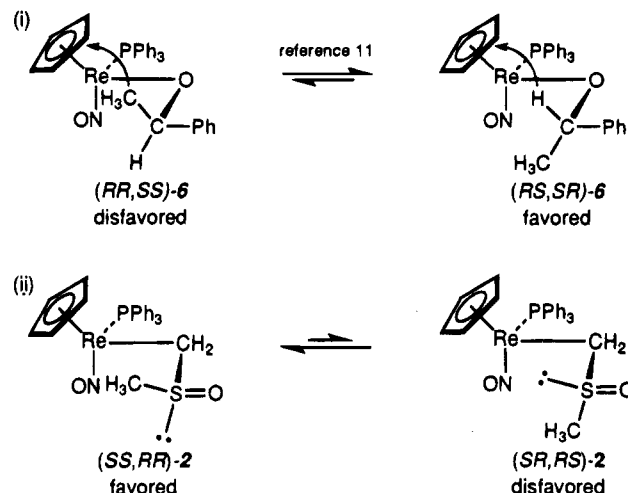
^a Anisotropically refined atoms are given in the form of the isotropic equivalent displacement parameter defined as $(4/3)[a^2B(1,1) + b^2B(2,2) + c^2B(3,3) + ab(\cos \gamma)B(1,2) + ac(\cos \beta)B(1,3) + bc(\cos \alpha)B(2,3)]$.

Table 3. Selected Bond Lengths (\AA), Bond Angles (deg), and Torsion Angles (deg) in $(SS,RR)\text{-}2$

Re-P	2.386(4)	Re-C5	2.32(2)
Re-N	1.70(2)	Re-C24	2.28(2)
Re-C1	2.26(2)	S-O2	1.51(3)
Re-C2	2.27(1)	S-C24	1.77(2)
Re-C3	2.23(2)	S-C25	1.74(3)
Re-C4	2.31(1)	N-O1	1.23(1)
P-Re-N	90.5(4)	C1-C2-C3	106(2)
P-Re-C24	87.5(4)	C2-C3-C4	108(2)
N-Re-C24	96.1(6)	C3-C4-C5	104(2)
Re-C24-S	110(1)	C4-C5-C1	109(2)
C24-S-O2	107(1)	C5-C1-C2	113(2)
C24-S-C25	102(9)	Re-N-O1	173(1)
O2-S-C25	101(1)		
N-Re-C24-S	-38.0(0.7)	P-Re-C24-S	-128.3(0.5)
Re-C24-S-O2	179.2(0.6)	Re-C24-S-C25	-75.0(1.0)
Re-C24-S-LP	53.0(0.7)		

example, new methods for activating sulfur donor ligands can potentially impact upon catalytic hydro-sulfurization technology.²⁰

There are several interesting stereochemical aspects of the above transformations. First, the highly diastereoselective formation of $(SR,RS)\text{-}2$ suggests that only one of the two diastereotopic methyl groups in DMSO complex 1^+BF_4^- is deprotonated. If it were possible to label one methyl group selectively, this could be tested. However, since 1^+BF_4^- is prepared from free DMSO,⁵ an enantiomerically pure $^*\text{CH}_3\text{S}(\text{O})\text{CH}_3$ species would be required. Regardless, the formation of $(SR,RS)\text{-}2$ is consistent with the transition state model **II** in Scheme 2. This model employs, as an arbitrary starting point, the Re-S conformation in crystalline 1^+BF_4^- .⁵ How-

Scheme 4. Models for Diastereomeric Equilibria in (i) $\text{OCH}(\text{CH}_3)\text{Ph}$ and (ii) $\text{CH}_2\text{S}(\text{O})\text{CH}_3$ Complexes of I^{24} 

ever, this in turn has the intuitively satisfying consequence that deprotonation must occur on the methyl group in the least hindered interstice—that between the small nitrosyl and medium-sized cyclopentadienyl ligands.^{16,21}

As noted above, attempts to trap the ylide **3** prior to rearrangement have to date been unsuccessful. However, we have previously generated a conceptually related species by deprotonation of the methylene group of phosphonium salt $[(\eta^5\text{-C}_5\text{H}_5)\text{Re}(\text{NO})(\text{PPh}_3)(\text{CH}_2\text{PPh}_3)]^+\text{PF}_6^-$.¹⁶ The resulting ylide could be observed by ³¹P NMR, and reaction with CH_3OTf gave a phosphonium salt with a new C_α stereocenter. Only one product diastereomer could be detected. If species such as **3** could be similarly intercepted, there would be attractive possibilities for enantioselective syntheses of free sulfoxides.

The 4:96 $(SR,RS)\text{-}2/(SS,RR)\text{-}2$ equilibrium ratio (CHCl_3 , 298 K) corresponds to a ΔG value of 1.9 kcal/mol. At present, we find it difficult to formulate a simple explanation for this stability difference. We have previously obtained equilibrium data for related adducts of **I** in which (1) the ligating atom bears only lone pairs or hydrogen atoms and (2) the atom β to rhenium bears three sterically distinct substituents (L, M, S).^{11,12,22} For example, the diastereomeric alkoxide complexes $(\eta^5\text{-C}_5\text{H}_5)\text{Re}(\text{NO})(\text{PPh}_3)(\text{OCH}(\text{CH}_3)\text{Ph})$ (**6**), illustrated in Scheme 4, equilibrate to (82–83):(18–17) $RS,SR/RR,SS$ mixtures in C_6D_6 at 65 °C.^{12,23,24} The direction of this equilibrium can be rationalized by a model in which antiperiplanar conformations or 180° torsion angles are maintained along the $\text{Ph}_3\text{P-Re-O-C-R}_L$ backbone—a linkage that contains the bulkiest rhenium (PPh_3) and carbon (R_L) substituents. This predicts that $(RR,SS)\text{-}6$ should experience a destabilizing interaction between

(21) (a) Davies, S. G.; Dordor-Hedgecock, I. M.; Sutton, K. H.; Whittaker, M. *J. Am. Chem. Soc.* **1987**, *109*, 5711. (b) Mackie, S. C.; Baird, M. C. *Organometallics* **1992**, *11*, 3712.

(22) Winter, C. H.; Arif, A. M.; Gladysz, J. A. *Organometallics* **1989**, *8*, 219.

(23) Dalton, D. M.; Fernández, J. M.; Emerson, K.; Larsen, R. D.; Arif, A. M.; Gladysz, J. A. *J. Am. Chem. Soc.* **1990**, *112*, 9198.

(24) For ease of comparison, eq 1 of Scheme 4 is illustrated as a carbon as opposed to rhenium epimerization.

the cyclopentadienyl ligand and the methyl alkoxide substituent (Scheme 4). However, the crystal structure of (*RS,SR*)-**6** shows that the conformation utilized in the model is approximate (P–Re–O–C and Re–O–C–C_{Ph} torsion angles = 158 and 149°).²³

There are several ambiguities in applying this model to (*SR,RS*)-**2** and (*SS,RR*)-**2**. First, there is not a large size difference between the three sulfur substituents (methyl, oxygen, lone pair). Second, there is a striking antiperiplanar relationship of the O=S and C–Re bonds in crystalline (*SS,RR*)-**2**, as reflected by the O=S–C–Re torsion angle (179.2(6)°) and the bottom view in Figure 1. This suggests a possible electronic control element. However, crystal structures of two other complexes with M–CH₂S(O)R linkages have been determined, and one shows a O=S–C–M angle of only 71°.²⁵ Third, the P–Re–C–S torsion angle (128.3(5)°) is the lowest observed to date in a compound fulfilling criterion (1) above. This places the *S*-methyl group in (*SS,RR*)-**2** further from the cyclopentadienyl ligand than the *C*-methyl group in (*RR,SS*)-**6**. Hence, we hesitate based upon the limited data available to ascribe the appreciable stability difference to a single feature.

Finally, there is abundant precedent for the epimerization mechanism in Scheme 3. First, the sulfonium salt [(η^5 -C₅H₅)Re(NO)(PPh₃)(CH₂S(CH₃)₂)]⁺PF₆[−] has previously been shown to be in facile equilibrium with methylenide complex **4**⁺PF₆[−] and free dimethyl sulfide.¹⁵ Second, organic sulfoxides can undergo heterolytic sulfur–carbon bond cleavage reactions in the presence of electrophiles.²⁶ These entail initial electrophile attack at the sulfoxide oxygen and are particularly facile when a stabilized carbocation is generated. Third, although species such as [−]OSCH₃ and HOSCH₃ are usually encountered only as reactive intermediates, they have been shown to serve as leaving groups and/or nucleophiles in a variety of transformations.¹³

The chemistry of ylides derived by the deprotonation of other adducts of **I** and neutral donor ligands is under active investigation. Additional reactions will be described in future reports from this laboratory.^{7b}

Experimental Section

General procedures and CH₂Cl₂ and toluene purifications were identical with those given in a recent paper.²⁷ The following were used as received: CDCl₃, CHCl₃, *t*-BuO[−]K⁺ (1.0 M in THF), HOTf, P(*p*-tol)₃, NH₄⁺PF₆[−].

(η^5 -C₅H₅)Re(NO)(PPh₃)(CH₂S(O)CH₃) (**2**). **A.** A Schlenk flask was charged with [(η^5 -C₅H₅)Re(NO)(PPh₃)(S(O)(CH₃)₂)]⁺BF₄[−] (1⁺BF₄[−]; 0.557 g, 0.786 mmol), CH₂Cl₂ (20 mL), and a stir bar, and cooled to −80 °C (CO₂/acetone). Then *t*-BuO[−]K⁺ (0.786 mL, 0.786 mmol, 1.0 M in THF) was added with stirring. The red solution turned orange. After 30 min, the solvent was removed via rotary evaporation, and the orange-red residue was dissolved in toluene (20 mL). The solution was filtered through a Celite pad (1 cm), which was washed with toluene

(60 mL) until the eluate was colorless. The solvent was removed via rotary evaporation to give **2** as an orange solid, which was dried under oil pump vacuum (0.467 g, 0.752 mmol, 96%; 99:1 *SR,RS/SS,RR*),⁹ mp 183 °C dec. Calcd for C₂₅H₂₅NO₂PrE: C, 48.37; H, 4.07. Found: C, 48.16; H, 4.13. IR (cm^{−1}, KBr): 1638 (vs) (ν_{NO}), 1434 (m), 1093 (m), 1015 (m), 998 (m sh). UV/vis (nm (ϵ , M^{−1} cm^{−1}), 1.1 × 10^{−4} M in CH₂Cl₂): 306 (2200).

B. A 5 mm NMR tube was charged with **2** (0.0149 g, 0.0240 mmol; 99:1 *SR,RS/SS,RR*) and CDCl₃ (0.5 mL) and capped with a septum. The isomerization to (*SS,RR*)-**2** was monitored by ³¹P NMR. Data: see text.

C. A 5 mm NMR tube was similarly charged with **2** (0.0129 g, 0.0208 mmol; 99:1 *SR,RS/SS,RR*), CDCl₃ (0.6 mL), and pyridine (0.0025 g, 0.0026 mL, 0.0320 mmol) and capped with a septum. Data: see text.

NMR for (*SR,RS*)-**2**: ¹H (δ , CDCl₃) 7.44–7.20 (m, 3C₆H₅), 5.10 (s, C₅H₅), 3.70 (dd, $J_{\text{HH}} = 11.5$ Hz, $J_{\text{HP}} = 9.6$ Hz, ReCH), 3.25 (dd, $J_{\text{HH}} = 11.5$ Hz, $J_{\text{HP}} = 2.4$ Hz, ReCH'), 2.59 (s, CH₃); ¹³C{¹H} (ppm, CDCl₃) 134.6 (d, $J_{\text{CP}} = 53.1$ Hz, *i*-Ph), 133.3 (d, $J_{\text{CP}} = 10.5$ Hz, *o*-Ph), 130.4 (d, $J_{\text{CP}} = 2.2$ Hz, *p*-Ph), 128.5 (d, $J_{\text{CP}} = 10.4$ Hz, *m*-Ph), 89.6 (s, C₅H₅), 41.2 (s, SCH₃), 15.3 (d, $J_{\text{CP}} = 3.9$ Hz, ReCHH'); ³¹P{¹H} (ppm, CDCl₃/CD₂Cl₂) 23.6/23.4 (s). NMR for (*SS,RR*)-**2**: ¹H (δ , CDCl₃) 7.44–7.20 (m, 3C₆H₅), 5.08 (s, C₅H₅), 3.48 (dd, $J_{\text{HH}} = 12.3$ Hz, $J_{\text{HP}} = 8.1$ Hz, ReCH), 3.27 (br d, $J_{\text{HH}} = 11.1$ Hz, ReCH'), 2.55 (s, CH₃); ¹³C{¹H} (ppm, CDCl₃) 135.1 (d, $J_{\text{CP}} = 53.4$ Hz, *i*-Ph), 133.3 (d, $J_{\text{CP}} = 10.3$ Hz, *o*-Ph), 130.4 (d, $J_{\text{CP}} = 2.2$ Hz, *p*-Ph), 128.7 (d, $J_{\text{CP}} = 10.5$ Hz, *m*-Ph), 90.1 (s, C₅H₅), 39.3 (s, SCH₃), 21.2 (d, $J_{\text{CP}} = 3.9$ Hz, ReCHH'); ³¹P{¹H} (ppm, CDCl₃/CD₂Cl₂) 22.0/21.8 (s).

[(η^5 -C₅H₅)Re(NO)(PPh₃)(CH₂P(*p*-tol)₃)]⁺X[−] (5⁺X[−]). **A.** A 5 mm NMR tube was charged with **2** (0.0149 g, 0.0240 mmol; 99:1 *SR,RS/SS,RR*), CDCl₃ (0.5 mL), and P(*p*-tol)₃ (0.0299 g, 0.0982 mmol) and capped with a septum. After ca. 0.5 h, a ³¹P NMR spectrum showed **2** (93:7 *SR,RS/SS,RR*; 23.6, 22.0 ppm) and P(*p*-tol)₃ (−7.0 ppm). After 7 days, the formation of 5⁺X[−] (41.6, d, $J_{\text{PP}} = 17.6$ Hz; 22.0, d, $J_{\text{PP}} = 17.7$ Hz) was complete.

B. A Schlenk flask was charged with **2** (0.107 g, 0.172 mmol; 99:1 *SR,RS/SS,RR*), CHCl₃ (30 mL), P(*p*-tol)₃ (0.263 g, 0.865 mmol), HOTf (5 μ L), and a stir bar. The mixture was stirred for 14 days. The solvent was removed via rotary evaporation and the dark brown residue dissolved in acetone (50 mL). Then NH₄⁺PF₆[−] (2.910 g, 17.8 mmol) was added with stirring. After 1 h, the solvent was removed and the residue dissolved in CH₂Cl₂ (20 mL). The dark brown solution was filtered through silica gel (10 cm), which was washed with CH₂Cl₂ (100 mL). The solvent was removed by rotary evaporation. The residue was washed with ether (20 mL) and pentane (60 mL) to give 5⁺PF₆[−] (0.076 g, 0.074 mmol, 43%)¹⁶ as a dark orange solid.

NMR: ¹H (δ , CDCl₃/CD₂Cl₂) 7.26–7.55/7.30–7.50 (m, 3C₆H₅), 4.68/4.71 (s, C₅H₅), 3.04/3.18 (ddd, $J_{\text{HH}} = 14.1/14.1$ Hz, $J_{\text{HP}} = 10.5/10.8$ Hz, $J_{\text{HP}} = 8.1/7.9$ Hz, ReCH), 2.87/2.53 (dd, $J_{\text{HH}} = 15.1/14.4$ Hz, $J_{\text{HP}} = 15.1/13.2$ Hz, ReCH'), 2.41/2.45 (s, CH₃); ³¹P{¹H} (ppm, CDCl₃, CD₂Cl₂) 40.9/40.3 (d, $J_{\text{PP}} = 18.3/18.3$ Hz, P(*p*-tol)₃), 21.6/20.8 (d, $J_{\text{PP}} = 18.2/18.2$ Hz, PPh₃).

Crystallography. An orange prism of (*SS,RR*)-**2** was grown over the course of 2 days by diffusion of heptane vapor into a CH₂Cl₂ solution of the opposite diastereomer, (*SR,RS*)-**2** (NMR data: see text). Data were collected as outlined in Table

(25) (a) Kneuper, H.-J.; Zimmermann, C.; Harms, K.; Boche, G. *Chem. Ber.* **1989**, *122*, 1043. (b) Veya, P.; Floriani, C.; Chiesi-Villa, A.; Rizzoli, C. *Organometallics* **1994**, *13*, 441. (c) See also: Stein, J.; Fackler, J. P., Jr.; Pappalardo, C.; Chen, H.-W. *J. Am. Chem. Soc.* **1981**, *103*, 2192.

(26) De Lucchi, O.; Miotti, U.; Modena, G. *Org. React.* **1991**, *40*, 157.

(27) Knight, D. A.; Dewey, M. A.; Stark, G. A.; Bennett, B. K.; Arif, A. M.; Gladysz, J. A. *Organometallics* **1993**, *12*, 4523.

(28) Frenz, B. A. The Enraf-Nonius CAD4 SDP - - A Real-time System for Concurrent X-ray Data Collection and Crystal Structure Determination. In *Computing and Crystallography*; Schenk, H., Olthof-Hazelkamp, R., van Koningsveld, H., Bassi, G. C., Eds.; Delft University Press: Delft, Holland, 1978; pp 64–71.

(29) Cromer, D. T.; Waber, J. T. In *International Tables for X-ray Crystallography*; Ibers, J. A., Hamilton, W. C., Eds.; Kynoch: Birmingham, England, 1974; Vol. IV, Tables 2.2B and 2.3.1, pp 72–98, 149–150.

1. Cell constants were obtained from 30 reflections with $10^\circ < 2\theta < 15^\circ$. The space group was determined from systematic absences ($0kl$ $k + l = 2n + 1$, $h0l$ $h = 2n + 1$) and subsequent least-squares refinement. Lorentz, polarization, and empirical absorption (ψ scans) corrections were applied. The structure was solved by standard heavy-atom techniques with the SDP/VAX package.²⁸ Non-hydrogen atoms were refined with anisotropic thermal parameters. Hydrogen atoms were calculated and added to the structure factor calculations but were not refined. Scattering factors, and $\Delta f'$ and $\Delta f''$ values, were taken from the literature.²⁹

Acknowledgment. We thank the NSF for support of this research and the Deutsche Forschungsgemeinschaft (DFG) for a fellowship (O.M.).

Supplementary Material Available: Anisotropic thermal parameters for (*SS,RR*)-**2** (1 page). Ordering information is given on any current masthead page.

OM940919P

Synthesis and Reaction Behavior of the Novel Mono(σ -alkynyl)titanocene Chloride $[(\eta^5\text{-C}_5\text{H}_2\text{SiMe}_3)_2\text{SiMe}_2]_2\text{Ti}(\text{Cl})(\text{CCSiMe}_3)$

H. Lang,* S. Blau, H. Pritzkow, and L. Zsolnai

Ruprecht-Karls-Universität Heidelberg, Anorganisch-Chemisches Institut, Im Neuenheimer Feld 270, D-69120 Heidelberg, Germany

Received November 28, 1994[®]

The reaction of $[(\eta^5\text{-C}_5\text{H}_2\text{SiMe}_3)_2\text{SiMe}_2]_2\text{TiCl}_2$ (**1**) with 1 equiv of LiCCSiMe_3 (**2**) yields the novel mono(σ -alkynyl)titanocene chloride $[(\eta^5\text{-C}_5\text{H}_2\text{SiMe}_3)_2\text{SiMe}_2]_2\text{Ti}(\text{Cl})(\text{CCSiMe}_3)$ (**3**). **3** can be used as an organometallic chelating ligand for the stabilization of monomeric $[\text{CuX}]$ entities $[\text{X} = \text{Cl}, \text{Br}, \text{O}_2\text{CMe}]$, yielding $\{[(\eta^5\text{-C}_5\text{H}_2\text{SiMe}_3)_2\text{SiMe}_2]_2\text{Ti}(\text{Cl})(\text{CCSiMe}_3)\}\text{CuX}$ [**5a**, $\text{X} = \text{Cl}$; **5b**, $\text{X} = \text{Br}$; **5c**, $\text{X} = \text{O}_2\text{CMe}$]. The X-ray structure analyses of **3** and **5a** are reported. Crystals of **3** are orthorhombic, space group $Pna2_1$, with $a = 20.22(2)$ Å, $b = 10.949(8)$ Å, $c = 29.53(3)$ Å, $V = 6537(9)$ Å³, and $Z = 8$; crystals of **5a** are triclinic, space group $P\bar{1}$ with $a = 11.195(3)$ Å, $b = 11.502(3)$ Å, $c = 14.788(4)$ Å, $\alpha = 96.27(2)^\circ$, $\beta = 110.62(2)^\circ$, $\gamma = 100.90(2)^\circ$, $V = 1717.7(8)$ Å³, and $Z = 2$.

Introduction

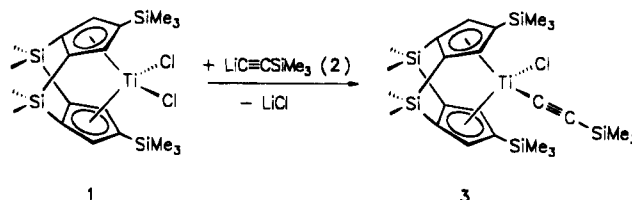
While mono(σ -alkynyl)zirconocene compounds are well studied,¹ the corresponding titanocene species are known to exchange ligands in solution to yield titanocene dichlorides and bis(alkynyl)titanocenes.² Recently, we have shown that the latter can successfully be used as organometallic chelating ligand (organometallic π -tweezers) for the stabilization of low-valent metal carbonyl building blocks $\text{M}(\text{CO})$ ($\text{M} = \text{Ni}, \text{Co}$)³ and various $\text{Fe}(\text{II})$,⁴ $\text{Cu}(\text{I})$,^{4,5} and $\text{Ag}(\text{I})$ ⁶ fragments, whereas titanocene dichlorides neither interact with $\text{Ni}(\text{CO})_4$ nor with $[\text{MX}]$ aggregates ($\text{M} = \text{Cu}, \text{Ag}$; $\text{X} =$ singly bonded ligand).

Here, we describe the synthesis of the first stable mono(σ -alkynyl)titanocene chloride $[(\eta^5\text{-C}_5\text{H}_2\text{SiMe}_3)_2\text{SiMe}_2]_2\text{Ti}(\text{Cl})(\text{C}\equiv\text{CSiMe}_3)$ (**3**) and its reaction with $[\text{CuX}]$ ($\text{X} = \text{Cl}, \text{Br}, \text{O}_2\text{CMe}$); the solid state structures of **3** and $\{[(\eta^5\text{-C}_5\text{H}_2\text{SiMe}_3)_2\text{SiMe}_2]_2\text{Ti}(\text{Cl})(\text{C}\equiv\text{CSiMe}_3)\}\text{CuCl}$ (**5a**) are discussed.

Results and Discussion

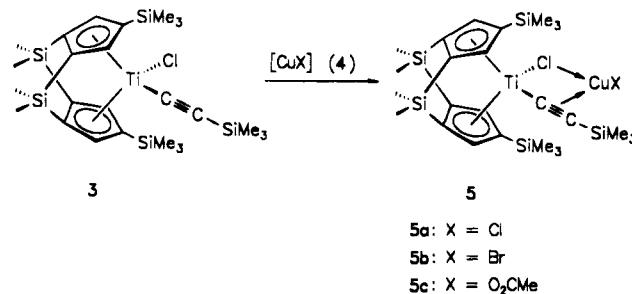
The doubly Me_2Si -bridged titanocene dichloride $[(\eta^5\text{-C}_5\text{H}_2\text{SiMe}_3)_2\text{SiMe}_2]_2\text{TiCl}_2$ (**1**)⁷ reacts at 25 °C in Et_2O with equimolar amounts of $\text{LiC}\equiv\text{CSiMe}_3$ (**2**) to form the mono(σ -(trimethylsilyl)ethynyl)titanocene chloride $[(\eta^5\text{-C}_5\text{H}_2\text{SiMe}_3)_2\text{SiMe}_2]_2\text{Ti}(\text{Cl})(\text{C}\equiv\text{CSiMe}_3)$ (**3**) in 97% yield.

$[(\eta^5\text{-C}_5\text{H}_2\text{SiMe}_3)_2\text{SiMe}_2]_2\text{Ti}(\text{Cl})(\text{C}\equiv\text{CSiMe}_3)$ (**3**) in 97% yield.



Extraction of the crude material with *n*-pentane and evaporation of the solvent affords an orange residue, which can be crystallized from *n*-pentane at -30 °C. Crystals of **3** are remarkably stable toward air for several months. As in the solid state, **3** is stable in solution; the formation of $[(\eta^5\text{-C}_5\text{H}_2\text{SiMe}_3)_2\text{SiMe}_2]_2\text{Ti}(\text{C}\equiv\text{CSiMe}_3)_2$ is not observed.

Addition of **3** to a suspension of the copper(I) compounds $[\text{CuX}]$ (**4a**, $\text{X} = \text{Cl}$; **4b**, $\text{X} = \text{Br}$; **4c**, $\text{X} = \text{O}_2\text{CMe}$), in a 1:1 molar ratio, leads to the formation of the complexes $\{[(\eta^5\text{-C}_5\text{H}_2\text{SiMe}_3)_2\text{SiMe}_2]_2\text{Ti}(\text{Cl})(\text{C}\equiv\text{CSiMe}_3)\}\text{CuX}$ [**5a**, $\text{X} = \text{Cl}$; **5b**, $\text{X} = \text{Br}$; **5c**, $\text{X} = \text{O}_2\text{CMe}$] in 85–90% yield. Compounds **5a–c** feature a monomeric CuX



unit, with the copper atom in an essentially trigonal-planar environment. Complexes **5a–c** are soluble in benzene, THF, and acetone and can be isolated as red crystalline solids by cooling their THF solutions to -30 °C. In the solid state **5** can be handled in air for short periods of time.

Compounds **5a–c** are monomeric as cryoscopic molecular weight determinations in benzene have shown.

[®] Abstract published in *Advance ACS Abstracts*, March 1, 1995.

(1) Erker, G.; Frömberg, W.; Benn, R.; Mynott, R.; Angermund, K.; Krüger, C. *Organometallics* **1989**, *8*, 911.

(2) Lang, H.; Seyferth, D. *Z. Naturforsch.* **1990**, *45b*, 212. For the synthesis of related $(\eta^5\text{-C}_5\text{H}_5)_2\text{Ti}(\text{C}\equiv\text{CSiMe}_3)_2$, see also: Wood, G. L.; Knobler, C. B.; Hawthorne, M. F. *Inorg. Chem.* **1989**, *28*, 382.

(3) Yasufuku, K.; Yamazaki, H. *Bull. Chem. Soc. Jpn.* **1972**, *45*, 2664. Lang, H.; Zsolnai, L. *J. Organomet. Chem.* **1991**, *406*, C5. Lang, H.; Imhof, W. *Chem. Ber.* **1992**, *125*, 1307. Lang, H.; Herres, M.; Zsolnai, L. *Bull. Chem. Soc. Jpn.* **1993**, *66*, 429. Lang, H.; Herres, M.; Imhof, W. *J. Organomet. Chem.* **1994**, *465*, 283.

(4) Lang, H.; Herres, M.; Zsolnai, L.; Fritz, M. *J. Organomet. Chem.* **1991**, *409*, C7. Herres, M.; Lang, H. *J. Organomet. Chem.*, in press.

(5) Lang, H.; Köhler, K.; Blau, S. *Coord. Chem. Rev.*, in press and literature cited therein.

(6) Lang, H.; Herres, M.; Zsolnai, L. *Organometallics* **1993**, *12*, 5008.

(7) Lang, H.; Blau, S.; Muth, A.; Weiss, K.; Neugebauer, U. *J. Organomet. Chem.*, in press.

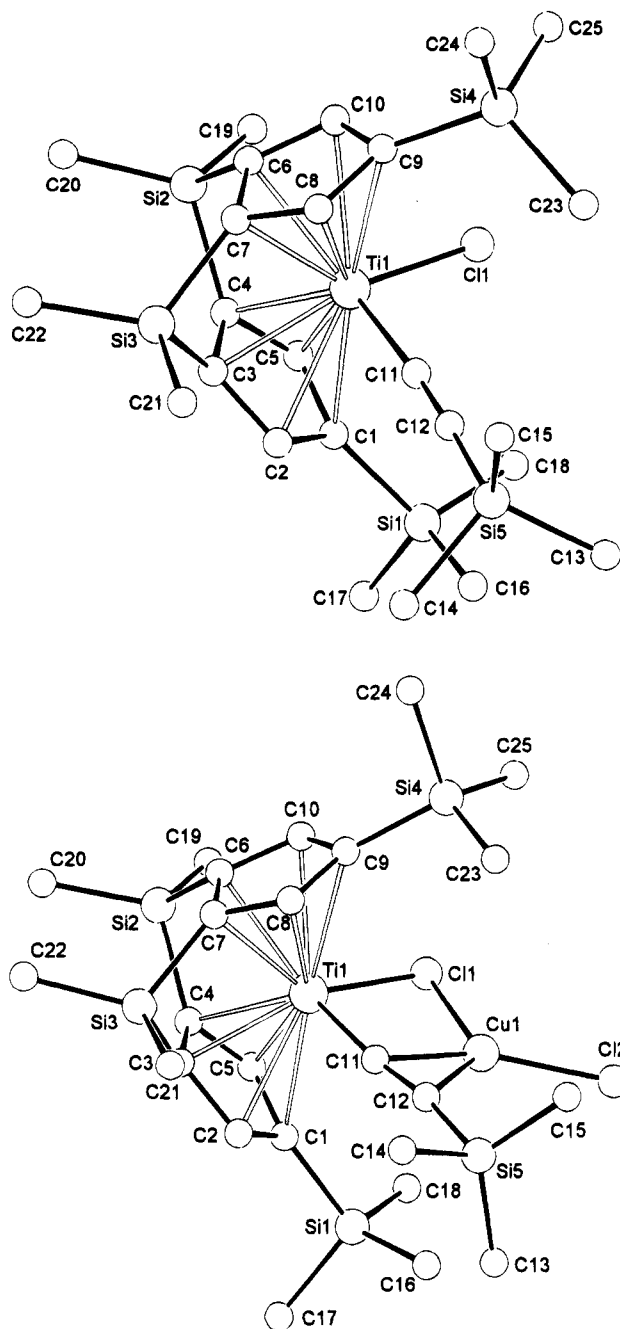


Figure 1. Molecular structures of **3** (top) and **5a** (bottom), showing the atomic numbering schemes.

The ^1H - and $^{13}\text{C}\{^1\text{H}\}$ -NMR spectra of **5a**–**5c** remain essentially unchanged in the temperature range 200–317 K, and the data are consistent with monomeric species in solution.

In order to establish the solid state structure of **3** and **5a**–**c**, an X-ray diffraction study was exemplarily carried out on single crystals of **3** and **5a** (Figure 1, Tables 1–4). The CuCl moiety in **5a** is cooperatively bonded to a chloro substituent (Cl(1)) as well as to a C \equiv C triple bond (C(11)–C(12)). The atoms Ti(1), Cu(1), C(11), C(12), Cl(1), Cl(2), and Si(5) form a plane (maximum atomic deviation 0.058 Å) (Table 3). The copper atom possesses a trigonal-planar environment, comprising the C₂ building block (C(11)–C(12)) and both chloro atoms (Cl(1), Cl(2)), and represents the first example in copper(I) chemistry for which the monomeric structure of the copper(I) moiety is brought about by one η^2 -coordinated Me₃SiC \equiv C ligand and one η^1 -bonded chloro group (Cl-

Table 1. Crystallographic Parameters for **3** and **5a**

	3	5a
formula	C ₅₀ H ₄₆ Cl ₂ Si ₁₀ Ti ₂	C ₂₅ H ₄₃ Cl ₂ CuSi ₅ Ti
fw	1134.76	666.38
cryst syst	orthorhombic	triclinic
space group	<i>Pna</i> 2 ₁ (No. 33)	<i>P</i> 1 (No. 2)
<i>a</i> , Å	20.22(2)	11.195(3)
<i>b</i> , Å	10.949(8)	11.502(3)
<i>c</i> , Å	29.53(3)	14.788(4)
α , deg		96.27(2)
β , deg		110.62(2)
γ , deg		100.90(2)
<i>V</i> , Å ³	6537(9)	1717.7(8)
ρ_{calc} , gcm ⁻³	1.153	1.288
<i>Z</i>	8	2
cryst size, mm ³	0.3 × 0.2 × 0.3	0.3 × 0.3 × 0.5
diff model	Siemens R3m/V	Siemens R3m/V
abs coeff, mm ⁻¹	0.539	1.195
radiation (λ , Å)	Mo K α (0.710 73)	Mo K α (0.710 73)
temp, K	200	295
scan mode	ω -scan	ω -scan
scan range, deg	1.20	1.20
scan speed, deg min ⁻¹	5.0–29.3	3.6–29.3
2 θ range, deg	4.0–48.1	3.0–50.0
index ranges	0 ≤ <i>h</i> ≤ 23 –12 ≤ <i>k</i> ≤ 0 0 ≤ <i>l</i> ≤ 33	0 ≤ <i>h</i> ≤ 13 –13 ≤ <i>k</i> ≤ 13 –17 ≤ <i>l</i> ≤ 16
no. of unique data	5261	6096
no. obsd [<i>I</i> ≥ 2 σ (<i>I</i>)]	3373	3830
<i>R</i> ₁ ^a	0.066	0.073
<i>wR</i> ₂ ^b	0.198	0.140

^a *R*₁ = $[\sum||F_o| - |F_c||/\sum|F_o|]$ only for observed reflections. ^b *wR*₂ = $[\sum|F_o^2 - F_c^2|^2/\sum|F_o^2|]$ ^{0.5} for all reflections.

Table 2. Selected Bond Lengths (Å) and Angles (deg) for **3** and **5a**

	3	5a
Bond lengths		
Cu(1)–C(11)		2.000(6)
Cu(1)–C(12)		2.104(6)
Cu(1)–Cl(2)		2.163(2)
Cu(1)–Cl(1)		2.344(2)
Cu(1)–Ti(1)		2.910(2)
Ti(1)–C(11)	2.10(2)	2.083(6)
Ti(1)–Cl(1)	2.320(4)	2.357(2)
C(11)–C(12)	1.20(2)	1.216(8)
Angles		
C(11)–Cu(1)–Cl(2)		153.5(2)
C(12)–Cu(1)–Cl(2)		119.2(2)
Cl(2)–Cu(1)–Cl(1)		108.84(8)
Cu(1)–C(11)–Ti(1)		90.9(2)
C(12)–C(11)–Ti(1)	176(1)	168.4(5)
C(11)–C(12)–Si(5)	174(1)	164.2(6)
C(11)–Ti(1)–Cl(1)	99.8(4)	94.9(2)

(1)). As a result of the dative Cl(1)–Cu(1) bonding the Ti(1)–Cl(1) bond is slightly lengthened from 2.320(4) Å in **3** to 2.357(2) Å in **5a**. The Cu(1)–Cl(1) interatomic distance of 2.344(2) Å in **5a** is significantly longer than the according Cu(1)–Cl(2) bond length of 2.163(2) Å due to different bonding types. These data are in agreement with Cu–Cl bond distances found in compounds of type $[(\eta^5\text{-C}_5\text{H}_4\text{SiMe}_3)_2\text{Ti}(\text{C}\equiv\text{CSiMe}_3)_2]\text{CuCl}$ [Cu–Cl: 2.182(3) Å]⁸ and $(\text{dppe})(\text{CO})_3\text{Mn}[(\eta^2\text{-C}\equiv\text{CPh})\text{CuCl}]$ [dppe = bis(diphenylphosphino)ethane] [Cu–Cl: 2.120(1) Å],^{9,10} containing terminal copper–chloride units, and $[(\eta^5\text{-C}_5\text{H}_5)(\text{CO})_2\text{Fe}(\eta^2\text{-C}\equiv\text{CPh})\text{CuCl}]_2$ [Cu–Cl: 2.267(5) Å],¹¹

(8) Lang, H.; Herres, M.; Köhler, K.; Blau, S.; Weinmann, S.; Weinmann, M.; Rheinwald, G.; Zsolnai, L. *J. Organomet. Chem.*, in press.

(9) Solans, X.; Solans, J.; Miravittles, C.; Miguel, D.; Riera, V.; Rubio-Gonzales, J. M. *Acta Crystallogr.* **1986**, *C42*, 975.

(10) Bruce, M. I.; Abu Salah, O. M.; Davies, R. E.; Raghavan, N. V. *J. Organomet. Chem.* **1974**, *64*, C48.

Table 3. Atomic Coordinates ($\times 10^4$) and Equivalent Isotropic Displacement Parameters ($\text{\AA}^2 \times 10^3$) for 3^a

atom	x	y	z	U_{eq}	atom	x	y	z	U_{eq}
Ti(1)	1773(1)	3347(2)	3145(1)	35(1)	C(16)	3684(8)	2717(16)	2348(6)	87(5)
Ti(2)	4188(1)	-402(2)	5101(1)	46(1)	C(17)	3896(14)	5628(27)	2344(11)	53(7)
Cl(1)	2497(2)	3347(3)	3754(1)	51(1)	C(17X)	3809(16)	5266(31)	2152(12)	63(9)
Cl(2)	4254(2)	-1698(4)	5722(2)	83(1)	C(18)	3977(7)	4280(17)	3173(7)	91(6)
Si(1)	3545(2)	4204(3)	2626(1)	50(1)	C(19)	1361(8)	6287(13)	3837(6)	78(5)
Si(2)	961(2)	5724(3)	3319(2)	54(1)	C(20)	288(7)	6763(12)	3153(8)	93(6)
Si(3)	685(2)	3769(4)	2396(1)	55(1)	C(21)	769(7)	2474(15)	2007(5)	73(4)
Si(4)	1230(2)	767(3)	3994(1)	44(1)	C(22)	26(8)	4817(17)	2186(6)	87(6)
Si(5)	2403(2)	-530(4)	2281(2)	68(1)	C(23)	1948(6)	-144(12)	3777(5)	56(4)
Si(6)	4557(8)	3830(19)	5817(9)	64(4)	C(24)	489(6)	-264(12)	4024(6)	62(4)
C(38)	3707(16)	4469(34)	5755(14)	106(12)	C(25)	1444(8)	1390(13)	4558(5)	66(4)
C(39)	5100(13)	4836(26)	5418(10)	67(7)	C(26)	3409(5)	304(12)	4582(4)	43(3)
C(40)	4812(21)	3808(43)	6358(13)	119(14)	C(27)	3243(5)	913(13)	4985(4)	48(3)
Si(6X)	4766(16)	3655(38)	5831(14)	120(12)	C(28)	3034(6)	84(13)	5328(5)	60(4)
C(38X)	3919(24)	4486(45)	5992(18)	87(14)	C(29)	3068(6)	-1099(13)	5127(5)	57(4)
C(39X)	5313(21)	4685(42)	5603(16)	77(12)	C(30)	3293(6)	-972(13)	4667(5)	56(4)
C(40X)	5019(34)	3209(64)	6410(21)	137(26)	C(31)	4675(6)	-139(12)	4390(5)	50(3)
Si(7)	4014(2)	905(4)	4155(1)	48(1)	C(32)	4561(6)	-1456(12)	4458(5)	56(4)
Si(8)	3748(2)	-2231(4)	4350(2)	70(1)	C(33)	5008(7)	-1784(15)	4802(6)	74(5)
Si(9)	6076(2)	-758(6)	5385(2)	103(2)	C(34)	5392(6)	-781(13)	4967(6)	64(4)
Si(10)	2738(2)	369(5)	5917(2)	79(2)	C(35)	5164(6)	223(13)	4684(5)	51(3)
C(1)	2627(5)	4474(10)	2693(4)	42(3)	C(36)	4441(7)	1274(13)	5399(4)	53(3)
C(2)	2122(6)	4036(11)	2405(5)	46(3)	C(37)	4558(7)	2282(15)	5555(5)	66(4)
C(3)	1515(6)	4500(11)	2520(4)	43(3)	C(41)	4230(7)	2516(12)	4270(4)	58(4)
C(4)	1618(6)	5290(11)	2894(5)	48(3)	C(42)	3833(7)	737(15)	3553(5)	65(4)
C(5)	2311(6)	5275(10)	2983(4)	44(3)	C(43)	3502(8)	-2492(17)	3766(6)	93(6)
C(6)	746(6)	4062(10)	3384(5)	44(3)	C(44)	3703(9)	-3690(15)	4645(8)	101(7)
C(7)	646(5)	3264(11)	2999(4)	43(3)	C(45X)	5846(24)	451(44)	5895(18)	130(16)
C(8)	803(5)	2068(10)	3156(4)	41(3)	C(46X)	6496(29)	-2392(53)	5198(20)	179(23)
C(9)	1006(6)	2087(11)	3617(4)	42(3)	C(47X)	6736(20)	265(42)	5131(16)	110(13)
C(10)	950(6)	3324(11)	3739(5)	46(3)	C(45)	6304(31)	902(56)	5546(26)	194(26)
C(11)	2070(6)	1728(13)	2823(5)	50(3)	C(46)	5900(18)	-1570(33)	5879(13)	94(11)
C(12)	2237(6)	840(13)	2614(5)	53(3)	C(47)	6800(28)	-916(64)	5161(21)	173(23)
C(13)	3261(19)	-1071(41)	2388(15)	103(13)	C(48)	2199(16)	1874(29)	5889(12)	70(9)
C(14)	2406(20)	45(37)	1658(13)	83(11)	C(49)	3434(17)	640(35)	6313(12)	58(10)
C(15)	1813(22)	-1708(42)	2381(16)	105(15)	C(50)	2213(16)	-859(31)	6125(11)	69(9)
C(13X)	2956(19)	-1572(35)	2571(13)	91(11)	C(48X)	1992(28)	1072(53)	5910(22)	174(23)
C(14X)	2716(23)	-222(44)	1751(15)	105(14)	C(49X)	3325(19)	1066(39)	6288(15)	76(13)
C(15X)	1558(15)	-1400(29)	2254(11)	61(8)	C(50X)	2509(26)	-1304(44)	6164(19)	129(18)

^a U_{eq} is defined as one-third of the trace of the orthogonalized U_{ij} tensor.

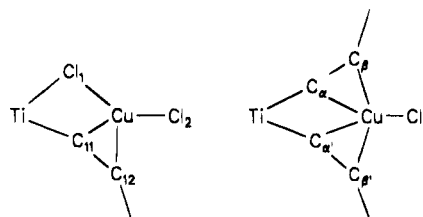


Figure 2. Schematic representation of $\{[(\eta^5\text{-C}_5\text{H}_2\text{-SiMe}_3)\text{SiMe}_2]_2\text{Ti}(\text{Cl})(\text{C}\equiv\text{CSiMe}_3)\text{CuCl}$ (**5a**, left) and $[(\eta^5\text{-C}_5\text{H}_4\text{SiMe}_3)_2\text{Ti}(\text{C}\equiv\text{CSiMe}_3)_2]\text{CuCl}^4$ (right).

$[(\eta^2\text{-Me}_3\text{SiC}\equiv\text{CSiMe}_3)\text{CuCl}]_2$ [Cu-Cl: 2.279(1), 2.281(1) \AA],¹² and $[(\eta^2\text{-tmtch})\text{CuCl}]_2$ (tmtch = 3,3,6,6-tetramethyl-1-thia-4-cycloheptyne, $\text{C}_{10}\text{H}_{16}\text{S}$) [Cu-Cl: 2.267(2), 2.283(2) \AA],¹³ dimeric compounds, which exhibit bridging copper-chloride entities.

As a result of the η^2 -coordination of the $\text{C}\equiv\text{C}$ triple bond to the copper atom the angle $\text{Cl}(1)\text{-Ti}(1)\text{-C}(11)$ in **3** decreases from 99.8° to $94.9(2)^\circ$ in **5a**. This leads to a deformation of the $\text{Ti-C}\equiv\text{C-Si}$ unit in **5a** [$\text{Ti-C}(11)\text{-C}(12) = 168.4(5)^\circ$, $\text{C}(11)\text{-C}(12)\text{-Si}(5) = 164.2(6)^\circ$], which is almost linear in **3** [$\text{Ti}(1)\text{-C}(11)\text{-C}(12) = 176(1)^\circ$, $\text{C}(11)\text{-C}(12)\text{-Si}(5) = 174(1)^\circ$]. Through this de-

formation different copper-carbon bond lengths [Cu(1)-C(11) = 2.000(6) \AA , Cu(1)-C(12) = 2.104(6) \AA] are observed (Figure 2). Similar bonding situations were found in compounds of the type $[(\eta^5\text{-C}_5\text{H}_4\text{SiMe}_3)_2\text{Ti}(\text{C}\equiv\text{CSiMe}_3)_2]\text{MX}$ (M = Cu, Ag; X = singly bonded inorganic or organic ligand) in which the bis(alkynyl)titanocene acts as "organometallic π tweezers" (Figure 2).³⁻⁶ The $\text{D}(1)\text{-Ti}(1)\text{-D}(2)$ angles [D(1), D(2) = centroids of the cyclopentadienyl ligands] are thereby not influenced (Table 3).

The η^2 -coordination of the $\text{C}\equiv\text{C}$ unit to a CuCl entity in **5a** is additionally confirmed by IR spectroscopy: The $\text{C}\equiv\text{C}$ -stretching vibration is shifted from 2023 cm^{-1} in **3** to 1905 cm^{-1} in **5a**, indicating a weaker $\text{C}\equiv\text{C}$ bond in **5a**.⁶ The same observation is made for **5b** (1905 cm^{-1}) and **5c** (1909 cm^{-1}), a phenomenon typical for π -bonding of alkynes to copper(I) moieties in which the alkyne ligand is acting as a 2-electron donor.⁵ The O_2CMe unit in **5c** is bidentate bonded to the copper atom as evidenced by the difference of the asymmetric (1561 cm^{-1}) and the symmetric (1421 cm^{-1}) O_2C stretching vibration.¹⁴

In the $^{13}\text{C}\{^1\text{H}\}$ -NMR spectra it is found that upon η^2 -coordination of the (trimethylsilyl)ethynyl ligand to the copper atom in **5a-c**, the resonance signals of the C_α

(11) Bruce, M. I.; Clark, R.; Howard, J.; Woodward, P. *J. Organomet. Chem.* **1972**, *42*, C107. Abu Salah, O. M.; Bruce, M. I. *J. Chem. Soc., Dalton Trans.* **1974**, 2302.

(12) Aleksandrov, G. G.; Gol'ding, I. R.; Sterlin, S. R.; Sladkov, A. M.; Struchkov, Yu. T.; Garbuzova, I. A.; Aleksanyan, V. T. *Izv. Akad. Nauk SSR, Ser. Khim.* **1980**, *12*, 2679 (Engl. Transl., 1858).

(13) Olbrich, F.; Schmidt, G.; Behrens, U.; Weiss, E. *J. Organomet. Chem.* **1991**, *418*, 421.

(14) Nakamoto, K. *Infrared and Raman Spectra of Inorganic and Coordination Compounds*, 3rd ed.; Wiley Interscience: New York, 1977.

Table 4. Atomic Coordinates ($\times 10^4$) and Equivalent Isotropic Displacement Parameters ($\text{\AA}^2 \times 10^3$) for **5a^a**

atom	x	y	z	U_{eq}
Cu(1)	3916(1)	1052(1)	2261(1)	60(1)
Ti(1)	2204(1)	2707(1)	1893(1)	41(1)
Cl(1)	1646(2)	603(1)	1338(1)	56(1)
Cl(2)	4554(2)	-610(2)	2294(2)	97(1)
Si(1)	2255(2)	1185(2)	4261(2)	60(1)
Si(2)	-469(2)	3444(2)	1084(1)	59(1)
Si(3)	2570(2)	5478(2)	2487(1)	59(1)
Si(4)	3390(2)	2188(2)	-410(1)	56(1)
Si(5)	7110(2)	2934(2)	3657(2)	66(1)
C(1)	1882(6)	2306(5)	3440(4)	45(2)
C(2)	2597(6)	3511(5)	3587(4)	48(2)
C(3)	1858(6)	4144(5)	2918(4)	47(2)
C(4)	609(6)	3304(6)	2341(4)	48(2)
C(5)	665(6)	2213(5)	2671(4)	47(2)
C(6)	987(6)	3656(6)	725(4)	49(2)
C(7)	2252(6)	4473(5)	1302(4)	49(2)
C(8)	3194(6)	4025(5)	1051(4)	49(2)
C(9)	2598(6)	2960(5)	332(4)	46(2)
C(10)	1248(6)	2752(6)	155(4)	49(2)
C(11)	4205(6)	2839(5)	2621(4)	46(2)
C(12)	5309(6)	2694(6)	2998(4)	52(2)
C(13A)	7306(49)	2432(82)	4762(42)	264(53)
C(14A)	7717(58)	4541(46)	3846(67)	363(73)
C(15A)	7696(58)	2232(73)	2868(54)	290(73)
C(13B)	7554(22)	3171(25)	4970(16)	118(10)
C(14B)	7897(24)	4244(25)	3375(20)	158(16)
C(15B)	7680(28)	1656(30)	3295(25)	171(17)
C(16)	3977(7)	1117(7)	4645(5)	85(2)
C(17)	1940(9)	1739(8)	5364(6)	96(3)
C(18)	1115(10)	-296(7)	3612(7)	120(4)
C(19)	-1659(7)	2020(7)	385(5)	86(3)
C(20)	-1340(8)	4660(7)	1047(6)	93(3)
C(21)	4357(7)	6034(6)	3204(6)	86(2)
C(22)	1762(8)	6748(6)	2375(6)	88(3)
C(23A)	5062(39)	2382(68)	275(37)	161(33)
C(24A)	3185(63)	3016(42)	-1490(31)	103(17)
C(25A)	2486(55)	613(27)	-907(45)	113(21)
C(23B)	4598(27)	1393(25)	305(15)	116(9)
C(24A)	4257(27)	3358(13)	-864(21)	105(9)
C(25B)	2079(18)	1147(22)	-1435(14)	105(7)

^a U_{eq} is defined as one-third of the trace of the ortho-gonalized U_{ij} tensor.

and C_β atoms in the Ti-C≡C-Si entity (at 163.7 and 133.1 ppm in **3**) are slightly shifted downfield (**5a**, 165.1, 134.3 ppm; **5b**, 167.2, 135.0 ppm; **5c**, 167.1, 134.1 ppm). This is in agreement with the observation generally made by changing from noncoordinated to η^2 -coordinated alkynes.^{5,15} This also results in a high-field shift of the proton signals of the (trimethylsilyl)ethynyl groups in the ¹H-NMR spectra of **5a-c**.

Experimental Section

General Comments. All reactions were carried out under an atmosphere of nitrogen using standard Schlenk techniques. Tetrahydrofuran (THF) and diethyl ether (Et₂O) were purified by distillation from sodium/benzophenone ketyl; *n*-pentane was purified by distillation from calcium hydride. Infrared spectra were obtained with a Perkin-Elmer 983G spectrometer. ¹H-NMR spectra were recorded on a Bruker AC 200 spectrometer operating at 200.132 MHz in the Fourier transform mode; ¹³C-NMR spectra were recorded at 50.323 MHz. Chemical shifts are reported in δ units (parts per million) downfield from tetramethylsilane with the solvent as the reference signal. FAB and EI mass spectra were recorded on a Finnigan 8230 mass spectrometer operating in the positive-ion mode. Melting points were determined with use of analytically pure samples, which were sealed in nitrogen-purged capillaries on a Gallen-

kamp MFB 595 010 M melting point apparatus. Microanalyses were performed by the Organisch-Chemisches Institut der Universität Heidelberg.

(A) Synthesis of **3.** [η^5 -C₅H₂SiMe₃]₂TiCl₂ (**1**)⁷ (1.0 g, 1.98 mmol) was added at 25 °C in one portion to a solution of LiCCSiMe₃ (**2**)¹⁶ (0.2 g, 1.98 mmol) in 100 mL of Et₂O. After the solution was stirred for 2 h the solvent was evaporated and the residue was extracted with 50 mL of *n*-pentane. Crystallization at -30 °C yielded **3** (1.1 g, 1.92 mmol; 97%) as an orange-colored solid.

Data for **3.** Mp: 142 °C. IR (KBr): 2023 (w) [$\nu_{C=C}$] cm⁻¹. ¹H-NMR: δ [CDCl₃] 0.10 (s, SiMe₃, 9H), 0.35 (s, SiMe₃, 18H), 0.48 (s, SiMe, 3H), 0.50 (s, SiMe, 3H), 0.71 (s, SiMe, 3H), 0.84 (s, SiMe, 3H), 6.71 (d, $J_{HH} = 1.4$ Hz, Cp, 2H), 7.38 (d, $J_{HH} = 1.4$ Hz, Cp, 2H). ¹³C{¹H}-NMR: δ [CDCl₃] -5.4 (s, SiMe), -4.5 (s, SiMe), 0.1 (s, SiMe₃, SiMe), 1.0 (s, SiMe), 1.9 (s, SiMe₃), 110.6 (s, Cp), 116.2 (s, Cp), 133.1 (s, CC-Si), 134.2 (s, Cp), 144.7 (s, Cp), 144.9 (s, Cp), 163.7 (s, CC-Ti). EI-MS [m/z (rel int)]: 566 (100), M⁺; 551 (31), M⁺ - Me; 493 (20), M⁺ - SiMe₃; 478 (23), M⁺ - SiMe₄; 459 (53), M⁺ - Cl - SiMe₃; 434 (29), M⁺ - Cl - C₂SiMe₃; 386 (24), M⁺ - Cl - 2SiMe₃. Anal. Calcd for C₂₅H₄₃ClSi₅Ti (567.38): C, 52.92; H, 7.64. Found: C, 52.67; H, 7.39.

(B) Synthesis of **5a-c.** To a solution of [η^5 -C₅H₂-SiMe₃]₂Ti(Cl)(C≡CSiMe₃) (**3**) (150 mg, 0.26 mmol) in THF (20 mL) the appropriate [CuX]_n (**4a**, 30 mg; **4b**, 43 mg; **4c**, 37 mg; 0.30 mmol) was added in one portion. The suspension was stirred in the dark for 2 h at 25 °C and afterward filtered through a pad of Celite (5.0 × 2.5 cm²; THF). On concentrating the filtrate and cooling it to -30 °C compound **5** (**5a**, 156 mg, 0.23 mmol, 90%; **5b**, 157 mg, 0.22 mmol, 85%; **5c**, 152 mg, 0.22 mmol, 85%) was obtained as a red crystalline solid.

Data for **5a.** Mp: 180 °C (dec). IR (KBr): 1905 (w) [$\nu_{C=C}$] cm⁻¹. ¹H-NMR: δ [CDCl₃] 0.26 (s, SiMe₃, 18H), 0.31 (s, SiMe₃, 9H), 0.49 (s, SiMe, 3H), 0.60 (s, SiMe, 3H), 0.78 (s, SiMe, 3H), 0.92 (s, SiMe, 3H), 6.43 (d, $J_{HH} = 1.2$ Hz, Cp, 2H), 6.97 (d, $J_{HH} = 1.2$ Hz, Cp, 2H). ¹³C{¹H}-NMR: δ [CDCl₃] -5.5 (s, SiMe), -4.5 (s, SiMe), -0.2 (s, SiMe₃), 0.9 (s, SiMe), 1.4 (s, SiMe), 111.3 (s, Cp), 115.2 (s, Cp), 134.3 (s, C≡C-Si), 135.0 (s, Cp), 140.1 (s, Cp), 141.6 (s, Cp, 2C), 165.1 (s, C≡C-Ti, 1C). FAB-MS [m/z (rel int)]: 666 (18), M⁺; 631 (100) M⁺ - Cl. Anal. Calcd for C₂₅H₄₃Cl₂CuSi₅Ti (666.38): C, 45.06; H, 6.50. Found: C, 45.20; H, 6.36.

Data for **5b.** Mp: 142 °C (dec). IR (KBr): 1905 (w) [$\nu_{C=C}$] cm⁻¹. ¹H-NMR: δ [CDCl₃] 0.28 (s, SiMe₃, 18H), 0.35 (s, SiMe₃, 9H), 0.52 (s, SiMe, 3H), 0.62 (s, SiMe, 3H), 0.81 (s, SiMe, 3H), 0.95 (s, SiMe, 3H), 6.46 (d, $J_{HH} = 1.2$ Hz, Cp, 2H), 7.01 (d, $J_{HH} = 1.2$ Hz, Cp, 2H). ¹³C{¹H}-NMR: δ (acetone-*d*₆) -5.4 (s, SiMe), -4.5 (s, SiMe), 0.0 (s, SiMe₃), 0.1 (s, SiMe₃), 1.5 (s, SiMe), 1.6 (s, SiMe), 112.9 (s, Cp), 116.8 (s, Cp), 135.0 (s, C≡C-Si), 135.3 (s, Cp), 141.2 (s, Cp), 142.6 (s, Cp), 167.2 (s, C≡C-Ti). EI-MS [m/z (rel int)]: 710 (1) M⁺; 566 (100), M⁺ - CuBr; 551 (10), M⁺ - CuBr - Me; 493 (24), M⁺ - CuBr - SiMe₃; 478 (28) M⁺ - CuBr - SiMe₄; 458 (40), M⁺ - CuBr - Cl - SiMe₃; 383 (35), M⁺ - CuBr - C₂Si₂Me₇. Anal. Calcd for C₂₅H₄₃BrClCuSi₅Ti (710.83): C, 42.24; H, 6.10. Found: C, 41.76; H, 5.86.

Data for **5c.** Mp: 203 °C. IR (KBr): 1909 (w) [$\nu_{C=C}$] cm⁻¹; 1561 (m), 1421 (m) [ν_{CO_2}] cm⁻¹. ¹H-NMR: δ (CDCl₃) 0.28 (s, SiMe₃, 18H), 0.31 (s, Me, 3H), 0.33 (s, SiMe₃, 9H), 0.51 (s, SiMe, 3H), 0.62 (s, SiMe, 3H), 0.80 (s, SiMe, 3H), 0.94 (s, SiMe, 3H), 6.45 (d, $J_{HH} = 0.9$ Hz, Cp, 2H), 6.99 (d, $J_{HH} = 0.9$ Hz, Cp, 2H). ¹³C{¹H}-NMR: δ (acetone-*d*₆) -5.4 (s, SiMe), -4.5 (s, SiMe), 0.0 (s, SiMe₃), 1.5 (s, SiMe₃), 1.5 (s, SiMe), 20.5 (s, Me), 112.6 (s, Cp), 116.5 (s, Cp), 134.1 (s, C≡C-Si), 135.0 (s, Cp), 141.0 (s, Cp), 142.6 (s, Cp), 167.1 (s, C≡C-Ti), 171.9 (s, O₂C). FAB-MS [m/z (rel int)]: 653 (42), M⁺ - Cl; 631 (100), M⁺ - O₂CMe. Anal. Calcd for C₂₇H₄₆ClCuO₂Si₅Ti (689.97): C, 47.00; H, 6.72. Found: C, 48.03; H, 6.70.

(15) Wrackmeyer, B.; Horchler, K. *Prog. NMR Spectrosc.* **1990**, *22*, 209.

(16) Lang, H.; Keller, H.; Imhof, W.; Martin, S. *Chem. Ber.* **1990**, *123*, 417 and literature cited therein.

X-ray Structure Determinations of 3 and 5a. The structures of compounds **3** and **5a** were determined from single crystal X-ray diffraction data, which were collected using a Siemens R3m/V (Nicolet Syntex) diffractometer. Crystallographic data for **3** and **5a** are given in Table 1.

The structures of **3** and **5a** were solved by direct methods (SHELXS 86¹⁷). An empirical absorption correction was applied. The structures were refined by the least-squares method based on F^2 with all measured reflections (SHELXL 93¹⁸).

Two of the trimethylsilyl groups (C(13)–C(15); C(23)–C(25)) in **5a** are disordered and were refined by two sets (site occupation factor 0.66/0.34, 0.68/0.32). The carbon atoms of the cyclopentadienyl rings (C(1)–C(10)) in **3** were refined

isotropically. All other heavy atoms were refined anisotropically. The hydrogen atoms were placed in calculated positions, and their temperature factors were refined isotropically.

Acknowledgment. We are grateful to the Deutsche Forschungsgemeinschaft, the Volkswagenstiftung, and the Fonds der Chemischen Industrie for financial support. We thank Prof. Dr. G. Huttner and Dr. Th. Seitz for many discussions and Th. Jannack for carrying out the MS measurements.

Supplementary Material Available: Tables of crystallographic parameters, hydrogen parameters, anisotropic thermal parameters, and bond distances and angles (17 pages). Ordering information is given on any current masthead page.

OM9409027

(17) SHELXS 86: Sheldrick, G. M. Program for Crystal Structure Determination, University of Göttingen, 1986.

(18) SHELXL 93: Sheldrick, G. M. Program for Crystal Structure Determination, University of Göttingen, 1993.

Tungsten–Carbon, Carbon–Carbon, and Carbon–Hydrogen Bond Activations in the Chemistry of 1,2-W₂R₂(OR')₄ (W≡W) Complexes. 4. Phosphine- and Amine-Promoted Ligand Migrations and α-CH Activations in the Formation of Alkylidynehydridoditungsten Compounds

Reed J. Blau, Malcolm H. Chisholm,* Bryan W. Eichhorn, John C. Huffman,
Keith S. Kramer, Emil B. Lobkovsky, and William E. Streib

*Department of Chemistry and Molecular Structure Center, Indiana University,
Bloomington, Indiana 47405*

Received September 26, 1994[®]

Lewis bases [PMe₃ or quinuclidine (Quin)] and 1,2-W₂(CH₂Ph)₂(O-*i*-Pr)₄ react in toluene and hexane at room temperature to give benzyldiyne hydrido compounds, W₂(μ-H)(μ-CPh)(O-*i*-Pr)₄L_x, where L = Quin, *x* = 2, and L = PMe₃, *x* = 3 and 2, by way of a double α-CH activation and elimination of toluene. Similarly, 1,2-W₂(*i*-Bu)₂(O-*i*-Pr)₄ and PMe₃ yields the alkylidyne hydride W₂(μ-H)(μ-C-*i*-Pr)(O-*i*-Pr)₄(PMe₃)₃ and isobutane. By contrast, addition of bisdimethylphosphinomethane (dmpm) yields adducts 1,2-W₂(CH₂R)₂(O-*i*-Pr)₄(dmpm), where R = Ph and *i*-Pr, that are relatively inert in solution at room temperature with respect to α-CH activation and formation of alkylidyne bridge complexes. The rate of formation of the benzyldiyne hydrido compounds has been studied in the presence of excess L. The formation of W₂(μ-H)(μ-CPh)(O-*i*-Pr)₄(Quin)₂ was approximately half-order in [Quin], while for PMe₃ there was an inverse dependence on [PMe₃]. These observations are attributed to differences in the relative equilibria involving the reversible uptake of L by 1,2-W₂(CH₂Ph)₂(O-*i*-Pr)₄ to give 1,2-W₂(CH₂Ph)₂(O-*i*-Pr)₄L₂ by way of a monoligated intermediate 1,2-W₂(CH₂Ph)₂(O-*i*-Pr)₄L. The kinetic isotope effects, *k*_{HH}/*k*_{DD} of 5.0(6) at 25 °C and 3.4(4) at 22 °C were observed for the liberation of toluene and toluene-*d*₈ for the reactions employing Quin and PMe₃, respectively, and the protio- and perdeuteriobenzyl-containing compounds. A discussion of the likely mechanism of formation of the hydrido alkylidyne bridged complexes is presented with emphasis on ligand induced benzyl/alkyl migration across the W≡W bond as reported in a previous paper for the reaction between 1,2-Mo₂(CH₂Ph)₂(O-*i*-Pr)₄ and PMe₃ to give (PMe₃)₃(PhCH₂)₂(*i*-PrO)Mo≡Mo(O-*i*-Pr)₃ (Chisholm, M. H.; et al. *Organometallics* 1992, 11, 4029). Support for elimination of toluene from one metal center is seen in the formation of the kinetic product (PMe₃)₃(*i*-PrO)W(μ-H)(μ-CPh)W(O-*i*-Pr)₃ which, by dissociation of PMe₃ and alkoxide migration, yields (PMe₃)₃(*i*-PrO)₂W(μ-H)(μ-CPh)W(O-*i*-Pr)₂(PMe₃). All the new compounds have been characterized by NMR studies, infrared spectroscopy, elemental analyses, and single crystal X-ray crystallography. The μ-alkylidyne hydrido complexes contain a central W₂⁸⁺ core with W–W distances typical of a W=W bond, ~2.5 Å, while the dmpm adducts contain W≡W bonds of distance ~2.3 Å. Crystal data: (i) For W₂(μ-H)(μ-CPh)(O-*i*-Pr)₄(PMe₃)₃ at –157 °C, *a* = 23.786(5) Å, *b* = 10.946(2) Å, *c* = 14.153(3) Å, *Z* = 4, *d*_{calcd} = 1.66 g/cm³ and space group P2₁2₁2₁. For W₂(μ-H)(μ-CPh)(O-*i*-Pr)₄(PMe₃)₂ at –143 °C, *a* = 11.441(4) Å, *b* = 13.223(6) Å, *c* = 21.892(8) Å, β = 94.21(2)°, *Z* = 4, *d*_{calcd} = 1.70 g/cm³, and space group P2₁/*c*. For W₂(μ-H)(μ-CPh)(O-*i*-Pr)₄(Quin)₂ at –152 °C, *a* = 17.942(6) Å, *b* = 9.976(3) Å, *c* = 19.788(8) Å, β = 94.82(2)°, *Z* = 4, *d*_{calcd} = 1.725 g/cm³, and space group P2₁/*c*. (ii) For W₂(μ-H)(μ-C-*i*-Pr)(O-*i*-Pr)₄(PMe₃)₃ at –170 °C, *a* = 19.122(4) Å, *b* = 20.749(3) Å, *c* = 19.817(3) Å, β = 114.45(1)°, *Z* = 8, *d*_{calcd} = 1.65 g/cm³, and space group P2₁/*a*. (iii) For W₂(*i*-Bu)₂(O-*i*-Pr)₄(dmpm) at –168 °C, *a* = 9.855(2) Å, *b* = 18.832(4) Å, *c* = 18.176(3) Å, β = 94.87(1)°, *Z* = 4, *d*_{calcd} = 1.69 g/cm³, and space group P2₁/*n*. (iv) For W₂(CH₂Ph)₂(O-*i*-Pr)₄(dmpm) at –172 °C, *a* = 15.020(2) Å, *b* = 29.207(4) Å, *c* = 17.774(2) Å, β = 111.63(1)°, *Z* = 8, *d*_{calcd} = 1.69 g/cm³, and space group P2₁/*n*.

Introduction

In preceding papers,^{1–3} we described the reactions of the 1,2-W₂(CH₂R)₂(O-*i*-Pr)₄ compounds with alkynes.

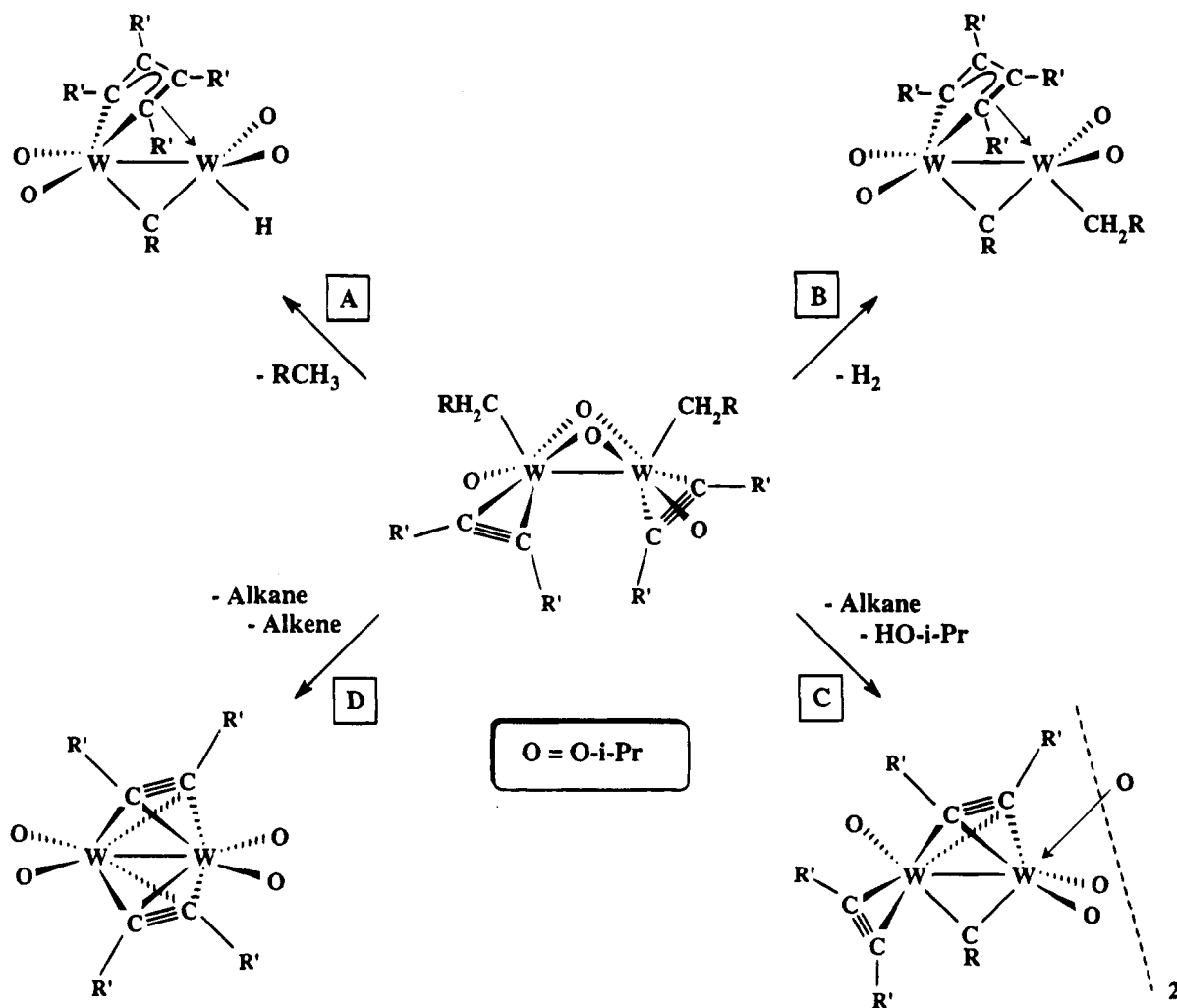
The reactions of the bis(alkyne) compounds of formula W₂(CH₂R)₂(MeCCMe)₂(O-*i*-Pr)₄, outlined in Scheme 1, include β-hydrogen elimination and three types of α-hydrogen abstraction. In reactions A and B of Scheme

[®] Abstract published in *Advance ACS Abstracts*, February 15, 1995.
(1) Chisholm, M. H.; Eichhorn, B. W.; Huffman, J. C. *Organometallics* 1989, 8, 80.

(2) Chisholm, M. H.; Eichhorn, B. W.; Folting, K.; Huffman, J. C. *Organometallics* 1989, 8, 49.

(3) Chisholm, M. H.; Eichhorn, B. W. *Organometallics* 1989, 8, 67.

Scheme 1



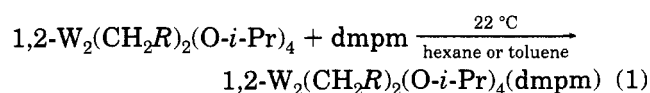
1, mechanistic studies indicated that a rate-determining coupling of alkyne ligands triggered a series of events that included a double α -hydrogen activation of one alkyl ligand. When the alkyl ligand contained β -hydrogens, the subsequent α -hydrogen abstraction pathway was altered, reaction C, and became competitive with β -hydrogen elimination¹ outlined in reaction D. In studies concerning the chemistry of $1,2\text{-Mo}_2(\text{CH}_2\text{Ph})_2(\text{O-}i\text{-Pr})_4$ and PMe_3 , we showed that metal-to-metal benzyl migrations were facile and reversible at room temperature.⁴ We have observed a similar but non-reversible 1,2-methyl shift in the reaction between $1,2\text{-W}_2\text{Me}_2(\text{O-}t\text{-Bu})_4(\text{py})_2$ and $\text{MeC}\equiv\text{CMe}$ to produce $1,1\text{-W}_2\text{Me}_2(\text{O-}t\text{-Bu})_4(\mu\text{-C}_2\text{Me}_2)(\text{py})$.²

In Pt and Pd binuclear metal-alkyl complexes, metal-to-metal alkyl migrations have been well documented,^{5,6} and in one instance, reversible methyl migrations were shown to be rapid on the NMR time scale even at -100°C .⁵ Such migrations are relevant to a variety of reactions of general interest, including reductive elimination of organic molecules from dinuclear metal cen-

ters.⁷ In this paper we describe our studies of the reactions between $1,2\text{-W}_2(\text{CH}_2R)_2(\text{O-}i\text{-Pr})_4$ compounds ($R = \text{Ph}, i\text{-Pr}$), Lewis bases PMe_3 , and quinuclidine which yield bridging alkyldiene hydrido complexes by way of elimination of $R\text{CH}_3$. By contrast we show that the addition of the bidentate ligand $\text{Me}_2\text{PCH}_2\text{PMe}_2(\text{dmpm})$ yields 1:1 adducts $1,2\text{-W}_2R_2(\text{O-}i\text{-Pr})_4(\text{dmpm})$ wherein the dmpm ligand spans the M-M unit. These compounds are relatively kinetically inert to the formation of alkyldiene hydrido compounds by way of α -CH activations.

Synthesis

Addition of the diphosphine $\text{Me}_2\text{PCH}_2\text{PMe}_2(\text{dmpm})$, well-known to bridge M-M bonded complexes,⁸ leads to the formation of $\text{W}_2(\text{CH}_2R)_2(\text{O-}i\text{-Pr})_4(\text{dmpm})$ according to eq 1, where $R = \text{Ph}$ and $i\text{-Pr}$. These compounds are



air-sensitive hydrocarbon-soluble species that are rela-

(7) (a) Norton, J. R. *Acc. Chem. Res.* **1979**, *12*, 139. (b) Bergman, R. G. *Acc. Chem. Res.* **1980**, *13*, 113. (c) Trinquier, G.; Hoffmann, R. *Organometallics* **1984**, *3*, 370.

(8) Cotton, F. A.; Walton, R. A. *Multiple Bonds Between Metal Atoms*, 2nd ed.; Oxford University Press: New York, 1993.

(4) (a) Chisholm, M. H.; Huffman, J. C.; Tatz, R. J., *J. Am. Chem. Soc.* **1984**, *106*, 5385. (b) Chisholm, M. H.; Foltz, K.; Huffman, J. C.; Kramer, K. S.; Tatz, R. J. *Organometallics* **1992**, *11*, 4029.

(5) Kellenberger, B.; Young, S. J.; Stille, J. K., *J. Am. Chem. Soc.* **1985**, *107*, 6105.

(6) (a) Ling, S. S. M.; Payne, N. C.; Puddephatt, R. J., *Organometallics* **1985**, *4*, 1546. (b) Arnold, D. P.; Bennett, M. A.; McLaughlin, G. M.; Robertson, G. B.; Whittaker, M. J. *J. Chem. Soc., Chem. Commun.* **1983**, 32.

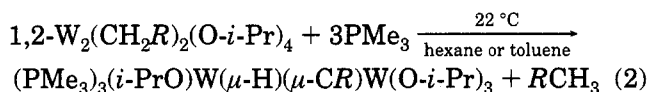
Table 1. Summary of Crystallographic Data^a

	I	II	III	IV	V	VI
empirical formula	W ₂ C ₂₈ H ₆₁ P ₃ O ₄	C ₂₅ H ₅₂ O ₄ P ₂ W ₂	C ₃₃ H ₆₀ N ₂ O ₄ W ₂	C ₂₅ H ₆₃ O ₄ P ₃ W ₂	W ₂ C ₃₁ H ₃₉ P ₂ O ₄	C ₂₅ H ₆₀ O ₄ P ₂ W ₂
color of crystal	dark red	red	reddish brown	black	black	dark red
crystal dimens (mm)	0.10 × 0.08 × 0.08	0.40 × 0.36 × 0.25	0.06 × 0.07 × 0.10	0.40 × 0.30 × 0.15	0.15 × 0.10 × 0.12	0.12 × 0.20 × 0.24
space group	P2 ₁ 2 ₁ 2 ₁	P2 ₁ /c	P2 ₁ /c	P2 ₁ /a	P2 ₁ /n	P2 ₁ /n
temp (°C)	-157	-143	-152	-170	-172	-168
cell dimens						
a (Å)	23.786(5)	11.441(4)	17.942(6)	19.122(4)	15.020(20)	9.855(2)
b (Å)	10.946(2)	13.223(6)	9.976(3)	20.749(3)	29.207(4)	18.832(4)
c (Å)	14.153(3)	21.892(8)	19.788(8)	19.817(3)	17.774(2)	18.176(3)
β (deg)		94.21(2)	94.82(2)	114.45(1)	111.63(1)	94.87(1)
Z (molecules/cell)	4	4	4	8	8	4
vol (Å ³)	3684.87	3302.93	3529.44	7157.91	7248.56	3361.29
d _{calc} (g/cm ³)	1.663	1.702	1.72	1.649	1.691	1.688
wavelength (Å)	0.710 69	0.710 69	0.710 69	0.716 09	0.710 69	0.710 69
mol wt	922.41	846.33	916.55	888.39	922.43	854.39
linear abs coeff (cm ⁻¹)	65.286	72.300	66.887	67.184	65.963	71.051
detector-to-sample dist (cm)	22.5	22.5	22.5	22.5	22.5	22.5
sample-to-source dist (cm)	23.5	23.5	23.5	23.5	23.5	23.5
av ω scan width at half-height	0.25	0.25	0.25	0.25	0.25	0.25
scan speed (deg/min)	4.0	8.0	4.0	8.0	8.0	8.0
scan width (deg + dispersion)	2.0	1.6	1.8	2.0	1.8	1.8
individ bkgrd (s)	6	4	8	4	3	4
aperture size (mm)	3.0 × 4.0	3.0 × 4.0	3.0 × 4.0	3.0 × 4.0	3.0 × 4.0	3.0 × 4.0
2θ range (deg)	6-45	6-45	6-45	6-45	6-45	6-45
total no. of reflns collected	2810	5727	5200	14 830	11 373	5699
no. of unique intensities	2744	4344	4625	9364	9494	4410
no. with F > 0.0		4054	4266	8565	8000	4185
no. with F > 2.33σ(F)				6423	5643	
no. with F > 3.0σ(F)	2318	3762	3811			3927
R(F)	0.0492	0.1069	0.0448	0.0658	0.0588	0.0390
R _w (F)	0.0477	0.1085	0.0415	0.0670	0.0595	0.0381
goodness of fit for last cycle	0.9782	2.573	0.978	1.522	1.175	1.226
max δ/σ for last cycle	0.05	0.05	0.05	0.006	0.38	0.08

^a I, W₂(μ-H)(μ-CPh)(O-*i*-Pr)₄(PMe₃)₃; II, W₂(μ-H)(μ-CPh)(O-*i*-Pr)₄(PMe₃)₂; III, W₂(μ-H)(μ-CPh)(O-*i*-Pr)₄(Quin)₂; IV, W₂(μ-H)(μ-C-*i*-Pr)(O-*i*-Pr)₄(PMe₃)₃; V, W₂(CH₂Ph)₂(O-*i*-Pr)₄(Me₂PCH₂PMe₂); VI, W₂(*i*-Bu)₂(O-*i*-Pr)₄(Me₂PCH₂PMe₂).

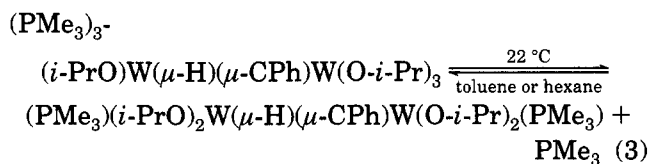
tively thermally persistent at room temperature. The compound where R = *i*-Pr decomposes over a period of 2 weeks at room temperature.

In contrast, addition of PMe₃ (≥3 equiv) leads to the facile formation of the μ-alkylidynehydridoditungsten complexes with liberation of alkane (1 equiv) according to eq 2. When only 2 or less equivalents of PMe₃ is



added, then reaction 2 occurs but some starting material, 1,2-W₂(CH₂R)₂(O-*i*-Pr)₄, remains.

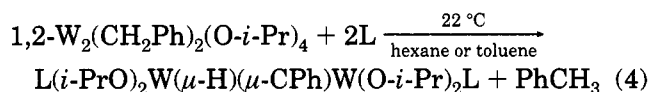
The product (PMe₃)₃(*i*-PrO)W(μ-H)(μ-CPh)W(O-*i*-Pr)₃ formed in eq 2 is apparently the kinetic product since with time in solution it reacts according to eq 3. Removal of the solvent and excess PMe₃ has allowed the isolation of pure (PMe₃)₂(*i*-PrO)₂W(μ-H)(μ-CPh)W(O-*i*-Pr)₂(PMe₃).



It is interesting to note that the equilibrium 3 involves the overall loss of PMe₃ and the migration of PMe₃ and OR ligands between the two tungsten atoms. The formal migration of PMe₃ may well involve dissociation followed by association at the other metal center. Equilibrium 3 has not been observed for the μ-*iso*-butylidyne complex (PMe₃)₃(*i*-PrO)W(μ-H)(μ-C-*i*-Pr)W-

(O-*i*-Pr)₃ under similar conditions, which implies that the PMe₃ ligands are more tightly bound.

Addition of quinuclidine, a bulky basic amine, to 1,2-W₂(CH₂Ph)₂(O-*i*-Pr)₄ proceeds to give only the symmetrically substituted μ-benzylidyne hydride complex according to eq 4, even when excess quinuclidine is present.



Solid-State and Molecular Structures. A summary of crystallographic data is given in Table 1 for the six compounds that have been structurally characterized in this study. Atomic coordinates are given in Tables 2-7.

(a) W₂(CH₂R)₂(O-*i*-Pr)₄(dmpm), where R = Ph and *i*-Pr. For R = Ph, in the space group P2₁/n, there are two crystallographically independent molecules in the unit cell that are chemically very similar. An ORTEP drawing of one of the molecules is given in Figure 1. The two molecules have been designated A and B, and a comparison of pertinent bond distances and angles is given in Tables 8 and 9, respectively.

For R = *i*-Pr, there is only one unique molecule in the unit cell and an ORTEP drawing of this showing the atom number scheme is given in Figure 2. Selected bond distances and angles are given in Table 10.

Both compounds are structurally very similar and contain W≡W bonds of distance 2.346-2.349 Å spanned by the bridging dmpm ligand. As is evident from the views in Figure 1, a twisting of the dmpm ligand allows for a staggered geometry about the W₂O₄C₂P₂ skeleton.

Table 2. Fraction Coordinates and Isotropic Thermal Parameters for $W_2(i-Bu)_2(O-i-Pr)_4(Me_2PCH_2PMe_2)$

Atom	10^4x	10^4y	10^4z	$10B_{iso}$
W(1)	2288.0(4)	1809.6(2)	6037.9(2)	9
W(1)	3155.9(4)	2848.1(2)	5537.0(2)	9
C(3)	1338(10)	3268(6)	4916(6)	16
C(4)	1510(11)	4048(6)	4668(6)	20
C(5)	2713(13)	4155(7)	4222(8)	33
C(6)	208(12)	4326(6)	4227(7)	25
C(7)	4139(9)	1182(5)	6125(6)	14
C(8)	4089(11)	486(6)	6573(6)	18
C(9)	5419(13)	87(6)	6622(9)	37
C(10)	2926(12)	5(6)	6279(7)	24
O(11)	3913(6)	2563(4)	4656(4)	14
C(12)	4265(10)	1953(5)	4267(5)	14
C(13)	3872(11)	2067(6)	3446(6)	19
C(14)	5785(11)	1808(6)	4432(6)	17
O(15)	4822(7)	3128(4)	6149(4)	15
C(16)	5625(10)	3739(6)	6030(6)	20
C(17)	6537(11)	3615(6)	5400(6)	24
C(18)	6464(11)	3903(5)	6741(6)	18
O(19)	655(7)	1982(3)	6571(4)	13
C(20)	-424(10)	1460(5)	6567(5)	14
C(21)	-1783(11)	1832(7)	6483(7)	26
C(22)	-268(12)	1003(6)	7260(6)	25
O(23)	1432(7)	1267(4)	5244(4)	15
C(24)	866(10)	1334(6)	4512(5)	15
C(25)	-623(11)	1549(6)	4510(6)	23
C(26)	1032(11)	650(6)	4106(6)	25
P(27)	2176(3)	3575(1)	6554(1)	13
C(28)	2781(12)	3175(6)	7438(6)	20
P(29)	3274(3)	2232(1)	7318(1)	12
C(30)	2692(11)	4508(6)	6707(6)	18
C(31)	335(11)	3645(6)	6598(6)	21
C(32)	5098(10)	2208(6)	7581(6)	16
C(33)	2612(11)	1826(6)	8126(6)	18

Table 3. Fractional Coordinates and Isotropic Thermal Parameters for $W_2(CH_2Ph)_2(O-i-Pr)_4(Me_2PCH_2PMe_2)$

atom	10^4x	10^4y	10^4x	$10B_{iso}$	atom	10^4x	10^4y	10^4x	$10B_{iso}$
W(1A)	7206(1)	87.4(4)	7867(1)	17	W(2B)	8067(1)	2359.3(4)	1961(1)	19
W(2A)	7863(1)	162.6(3)	6862(1)	16	P(3B)	8818(5)	3141(2)	2443(4)	29
P(3A)	8743(5)	-590(2)	7333(4)	23	C(4B)	7875(17)	3519(9)	2410(16)	31(5)
C(4A)	7840(18)	-1015(9)	7318(16)	33(5)	P(5B)	6798(5)	3205(3)	2460(4)	29
P(5A)	6745(5)	-741(2)	7362(3)	25	C(6B)	9381(20)	3439(10)	1814(17)	41(6)
C(6A)	9325(19)	-860(10)	6729(17)	38(6)	C(7B)	9753(18)	3206(10)	3460(16)	34(5)
C(7A)	9676(15)	-638(8)	8317(13)	20(4)	C(8B)	5870(21)	3302(11)	1483(19)	46(6)
C(8A)	5806(16)	-876(9)	6380(14)	26(5)	C(9B)	6397(21)	3572(11)	3107(18)	45(6)
C(9A)	6465(19)	-1171(10)	7987(16)	37(5)	C(10B)	9552(16)	2122(8)	2694(14)	22(4)
C(10A)	9306(15)	440(8)	7535(13)	20(4)	C(11B)	10147(14)	2129(7)	2197(12)	15(4)
C(11A)	9941(17)	371(9)	7054(15)	28(5)	C(12B)	11050(16)	2356(9)	2479(15)	30(5)
C(12A)	10835(17)	212(9)	7417(14)	27(5)	C(13B)	11657(20)	2362(11)	2035(18)	44(6)
C(13A)	11430(21)	119(11)	6969(19)	47(6)	C(14B)	11363(19)	2144(10)	1293(16)	35(5)
C(14A)	11124(21)	219(11)	6194(19)	46(6)	C(15B)	10485(18)	1908(9)	985(16)	32(5)
C(15A)	10239(21)	402(11)	5849(19)	45(6)	C(16B)	9889(15)	1908(8)	1444(14)	23(4)
C(16A)	9610(16)	501(8)	6240(14)	25(5)	C(17B)	5863(16)	2195(8)	2270(14)	22(4)
C(17A)	5699(14)	219(8)	7149(13)	18(4)	C(18B)	5354(14)	2289(8)	2841(13)	18(4)
C(18A)	5189(16)	162(9)	7729(14)	26(5)	C(19B)	5594(17)	2112(9)	3578(15)	31(5)
C(19A)	5240(15)	473(8)	8351(14)	21(4)	C(20B)	5185(19)	2223(10)	4128(17)	39(6)
C(20A)	4791(18)	412(10)	8860(16)	34(5)	C(21B)	4493(17)	2577(10)	3908(15)	31(5)
C(21A)	4280(17)	25(9)	8846(15)	30(5)	C(22B)	4241(19)	2760(10)	3151(17)	38(6)
C(22A)	4175(19)	-302(10)	8245(17)	37(6)	C(23B)	4647(16)	2633(9)	2609(15)	28(5)
C(23A)	4640(18)	-233(10)	7682(16)	34(5)	O(24B)	7775(10)	1776(5)	1442(9)	23(3)
O(24A)	7486(10)	729(5)	6334(9)	19(3)	C(25B)	7194(16)	1382(9)	1352(14)	23(4)
C(25A)	6875(18)	1116(10)	6285(16)	32(5)	C(26B)	6301(21)	1427(11)	596(18)	44(6)
C(26A)	5946(18)	1073(10)	5605(17)	36(5)	C(27B)	7760(20)	975(11)	1317(18)	40(6)
C(27A)	7391(19)	1543(10)	6216(17)	38(6)	O(28B)	7304(11)	2761(6)	1063(10)	26(3)
O(28A)	7140(10)	-243(5)	5961(9)	20(3)	C(29B)	7446(33)	2875(17)	314(29)	72(9)
C(29A)	7351(15)	-276(8)	5251(14)	21(4)	C(30B)	6956(36)	3177(19)	-176(32)	32(8)
C(30A)	7012(22)	-749(12)	4873(20)	52(7)	C(31B)	7293(42)	2365(23)	-166(38)	49(9)
C(31A)	6772(18)	132(10)	4649(16)	36(5)	O(32B)	8185(10)	2777(5)	3861(9)	22(3)
O(32A)	8052(10)	-277(5)	8772(9)	21(3)	C(33B)	7974(17)	2870(9)	4552(15)	28(5)
C(33A)	7831(17)	-403(9)	9474(15)	29(5)	C(34B)	8504(21)	3273(11)	4974(18)	45(6)
C(34A)	8490(22)	-763(12)	9903(20)	51(7)	C(35B)	8290(17)	2485(9)	5143(15)	30(5)
C(35A)	7858(29)	17(16)	9994(26)	82(9)	O(36B)	7619(9)	1821(5)	3479(8)	17(3)
O(36A)	7329(10)	676(5)	8363(9)	21(3)	C(37B)	8137(18)	1404(10)	3578(15)	31(5)
C(37A)	7860(14)	1079(8)	8435(12)	15(4)	C(38B)	9085(21)	1450(11)	4336(19)	45(6)
C(38A)	8790(15)	1079(8)	9198(13)	20(4)	C(39B)	7539(23)	1012(13)	3655(21)	54(7)
C(39A)	7247(19)	1473(10)	8477(17)	36(5)	C(40B)	6346(37)	2951(19)	-274(32)	36(9)
W(1B)	7391(1)	2391.7(4)	2957(1)	17	C(41B)	8125(104)	2688(55)	170(93)	159(11)

The staggered conformation is emphasized by the view looking down the M–M axis, as shown at the bottom of Figure 1. Each molecule has virtual C_2 symmetry, and the CH_2R ligands are in all cases cis to W–P bonds. This leads to two types of O-*i*-Pr groups, namely, those trans to W– CH_2R ligands and those trans to W–P bonds. The W–O bonds that are trans to W– CH_2R bonds are notably longer than those that are trans to the phosphine ligands, which implies a trans-influence order $RCH_2 > PR_3$.⁹ The local geometry about each tungsten atom is essentially square planar, and these structures are very similar to that reported previously for 1,2- $Mo_2(CH_2Ph)_2(O-i-Pr)_4(dmpm)$.^{4b}

(b) $(PMe_3)_3(i-PrO)W(\mu-H)(\mu-CR)W(O-i-Pr)_3$, where $R = Ph$ and *i*-Pr. These two ditungsten compounds are closely related. The bridging hydride was not crystallographically located for $R = Ph$, but for $R = i-Pr$, where there were two independent molecules in the unit cell, in one instance there was evidence for a hydride bridge.

An ORTEP view of the benzyldiene complex is shown in the top of Figure 3, and a related view of one of the isobutyldiene molecules is shown in the bottom. The W–W distance of ~ 2.50 Å is typical of a $(W=W)^{8+}$ core but one tungsten is in a pseudooctahedral geometry, being bound to one terminal OR and three PMe_3 ligands in addition to the bridging hydride and alkylidene groups. The other tungsten is five coordinate, being bonded to three terminal OR ligands and the bridging hydride and alkylidene. While we are inclined to place

Table 4. Fractional Coordinates and Isotropic Thermal Parameters for W₂(μ-H)(μ-C-*i*-Pr)(O-*i*-Pr)₄(PMe₃)₃

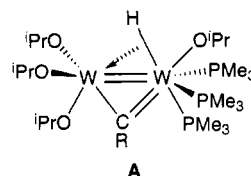
atom	10 ⁴ x	10 ⁴ y	10 ⁴ z	10B _{iso}
W(1)A	1475.3(5)	2385.9(4)	8876.0(5)	13
W(2)A	1641.2(5)	1240.1(4)	9309.3(5)	13
C(3)A	952(12)	1976(10)	9435(11)	15(4)
C(4)A	389(13)	1976(11)	9796(12)	22(4)
C(5)A	-129(14)	1380(12)	9572(13)	27(5)
C(6)A	800(14)	1992(13)	10658(14)	29(5)
P(7)A	473(3)	2134(3)	7615(3)	18
C(8)A	733(13)	1549(12)	7062(13)	23(4)
C(9)A	-431(13)	1792(12)	7555(13)	25(5)
C(10)A	156(15)	2820(13)	6979(14)	33(5)
P(11)A	750(3)	3378(3)	8953(3)	19
C(12)A	885(13)	3685(12)	9861(12)	22(4)
C(13)A	911(13)	4086(12)	8502(13)	26(5)
C(14)A	-299(13)	3379(12)	8546(13)	26(5)
P(15)A	2629(3)	2783(3)	9969(3)	18
C(16)A	2610(14)	2747(13)	10874(14)	29(5)
C(17)A	3561(14)	2405(13)	10183(13)	28(5)
C(18)A	2894(14)	3624(13)	9939(14)	28(5)
O(19)A	1890(8)	3002(7)	8307(8)	21(3)
C(20)A	2237(15)	2938(14)	7795(15)	34(5)
C(21)A	2413(16)	3583(14)	7575(15)	38(6)
C(22)A	2879(17)	2518(16)	8010(17)	45(6)
O(23)A	930(8)	735(8)	8554(8)	21(3)
C(24)A	922(13)	28(12)	8585(13)	23(5)
C(25)A	935(14)	-243(13)	7885(14)	29(5)
C(26)A	207(14)	-168(13)	8693(14)	29(5)
O(27)A	1660(8)	919(7)	10252(8)	17(3)
C(28)A	2092(13)	428(12)	10726(13)	25(5)
C(29)A	1541(17)	30(15)	10940(16)	43(6)
C(30)A	2741(16)	704(14)	11379(15)	38(6)
O(31)A	2712(8)	968(17)	9807(8)	19(3)
C(32)A	3247(12)	874(11)	9460(12)	19(4)
C(33)A	2938(15)	409(14)	8811(15)	36(6)
C(34)A	3986(14)	640(13)	10074(14)	32(5)
W(1)B	1495(1)	3317.5(5)	13810(1)	16
W(2)B	2179(1)	4333.6(5)	14406(1)	17
C(3)B	2600(14)	3481(13)	14163(14)	29(5)
C(4)B	3391(16)	3283(14)	14292(15)	38(6)
C(5)B	3908(15)	3096(14)	15075(15)	34(5)
C(6)B	3794(16)	3773(15)	13996(16)	40(6)
P(7)B	1536(4)	2828(3)	14984(4)	26
C(8)B	1063(15)	3242(14)	15491(14)	34(5)
C(9)B	2543(15)	2710(14)	15732(15)	37(6)
C(10)B	1052(15)	2045(14)	14869(15)	37(6)
P(11)B	1815(4)	2234(3)	13420(4)	26
C(12)B	2202(14)	2188(13)	12713(14)	32(5)
C(13)B	1020(17)	1696(16)	12997(17)	45(6)
C(14)B	2525(16)	1713(14)	14103(15)	39(6)
P(15)B	1111(4)	3755(3)	12526(3)	23
C(16)B	1873(15)	3955(14)	12235(14)	34(5)
C(17)B	566(15)	4498(14)	12282(15)	34(5)
C(18)B	472(15)	3262(13)	11771(14)	33(5)
O(19)B	387(9)	2930(8)	13393(9)	28(3)
C(20)B	-307(16)	3142(14)	13124(15)	37(6)
C(21)B	-882(16)	2645(15)	12648(16)	40(6)
C(22)B	-592(18)	3464(16)	13639(17)	49(7)
O(23)B	3220(10)	4443(9)	15114(10)	38(4)
C(24)B	3506(14)	4941(13)	15675(14)	29(5)
C(25)B	4251(17)	5186(16)	15672(17)	46(7)
C(26)B	3659(19)	4686(17)	16425(18)	53(7)
O(27)B	1964(10)	4619(9)	15256(10)	34(4)
C(28)B	1197(16)	4851(14)	15174(16)	39(6)
C(29)B	1317(17)	4984(16)	15977(17)	44(6)
C(30)B	973(18)	5435(17)	14700(18)	50(7)
O(31)B	2119(9)	4894(8)	13629(9)	29(3)
C(32)B	2405(15)	5544(14)	13740(15)	36(6)
C(33)B	3105(21)	5564(19)	13582(20)	62(8)
C(34)B	1810(19)	6001(18)	13267(19)	56(7)

the bridging hydride in the same plane as the W₂(μ-C) moiety, it is quite certain that the W-μ-C distances are different, with the shorter distance associated with the six-coordinate W atom that is bonded to three PMe₃

Table 5. Fractional Coordinates and Isotropic Thermal Parameters for W₂(μ-H)(μ-CPh)(O-*i*-Pr)₄(PMe₃)₃

atom	10 ⁴ x	10 ⁴ y	10 ⁴ z	10B _{iso}
W(1)	1579.1(3)	7461(1)	5382(1)	10
W(2)	543.3(3)	7716(1)	5001(1)	11
P(3)	1488(3)	5236(6)	5799(5)	17
C(4)	1191(9)	4211(19)	4918(19)	17(4)
C(5)	1054(11)	4906(25)	6809(20)	23(5)
C(6)	2137(10)	4430(22)	6115(17)	16(5)
P(7)	2471(2)	7158(6)	4457(4)	15
C(8)	3109(10)	7182(25)	5193(19)	29(6)
C(9)	2648(11)	8232(24)	3528(18)	23(5)
C(10)	2583(11)	5749(24)	3770(19)	23(5)
P(11)	1755(3)	9717(6)	5449(5)	19
C(12)	1584(10)	10649(21)	4441(17)	19(5)
C(13)	2486(12)	10217(28)	5735(22)	34(6)
C(14)	1381(11)	10507(25)	6411(20)	24(5)
O(15)	2112(6)	7530(22)	6541(10)	24
C(16)	2126(10)	7220(25)	7484(17)	23(5)
C(17)	2728(11)	7258(28)	7842(18)	31(6)
C(18)	1740(15)	7915(35)	8082(26)	54(8)
C(19)	1217(8)	7404(24)	4123(14)	13(4)
C(20)	1248(8)	7328(22)	3086(14)	12(4)
C(21)	1291(9)	6248(20)	2650(17)	9(4)
C(22)	1354(12)	6159(26)	1625(22)	27(6)
C(23)	1357(11)	7181(26)	1124(19)	30(6)
C(24)	1312(9)	8353(20)	1567(17)	8(4)
C(25)	1247(11)	8393(24)	2486(20)	23(5)
O(26)	404(6)	9417(14)	5149(12)	16
C(27)	-93(10)	10176(21)	4932(20)	23(5)
C(28)	-573(13)	9851(26)	5585(21)	32(6)
C(29)	67(11)	11465(23)	4925(22)	29(5)
O(30)	222(6)	6226(13)	5492(11)	13
C(31)	-373(10)	5972(24)	5626(19)	24(5)
C(32)	-529(14)	6430(29)	6556(13)	41(7)
C(33)	-443(14)	4626(30)	5531(25)	41(7)
O(34)	-17(5)	7707(14)	4006(10)	12
C(35)	-130(9)	7352(25)	3073(15)	18(4)
C(36)	-671(11)	7912(24)	2757(18)	27(5)
C(37)	-170(13)	5940(27)	3020(22)	33(6)

ligands. Similarly, the refinement of the bridging hydride μ-H(193) revealed an asymmetry with W(3)-H = 1.62 Å and W(4)-H = 2.00 Å, although clearly the location and refinement of this bridging hydride may be questionable. The point that is being made, however, is that there would seem to be evidence for an internal charge compensation within the (W=W)⁸⁺ moiety despite the presence of three terminal OR groups on one W atom and only one OR group on the other. In a formal or valence bond description one could write the W₂(μ-CR) group as a W-C double and single bond and the W-H bond as a donor as shown schematically in A.



The only other point of note is that the W-OR bond that is trans to the W=C bond of the μ-alkylidyne is extremely long for a terminal WOR group, namely, 2.07–2.10 Å, which presumably reflects the high trans influence of the W=C bond.⁹

Selected bond distances and angles are given in Tables 11 (R = Ph) and 12 (R = *i*-Pr).

W₂(μ-H)(μ-CPh)(O-*i*-Pr)₄L₂, where L = PMe₃ and Quinuclidine. An ORTEP drawing of the PMe₃ molecule is shown in the top of Figure 4, and a summary of pertinent bond distances and angles is given in Table

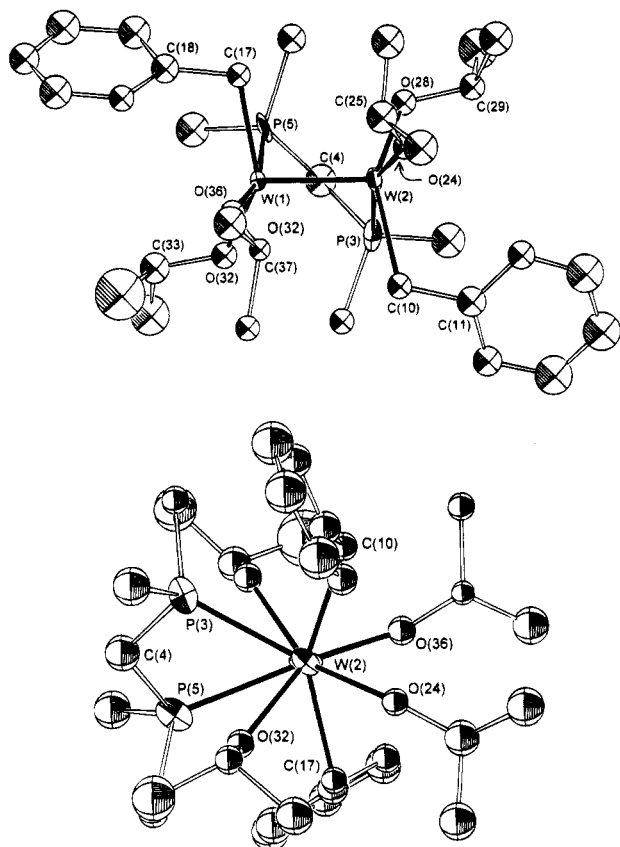


Figure 1. ORTEP drawing (50% probability ellipsoids) showing the molecular structure (molecule **A**) of $W_2(CH_2-Ph)_2(O-i-Pr)_4(dmpm)_2$ (top) and a view looking down the M–M axis (bottom).

Table 6. Fractional Coordinates and Isotropic Thermal Parameters for $W_2(\mu-H)(\mu-CPh)(O-i-Pr)_4(PMe_3)_2$

atom	10^4x	10^4y	10^4z	$10B_{iso}$
W(1)	3587(1)	2253(1)	1453(1)	13
W(2)	1582(1)	2950(1)	1427(1)	12
P(3)	62(8)	3538(6)	2158(4)	14
P(4)	5264(8)	1737(7)	2220(4)	17
O(5)	1534(20)	4398(17)	1262(12)	22
O(6)	4759(16)	3111(14)	1221(10)	0
O(7)	329(19)	2098(16)	1121(13)	24
O(8)	3663(22)	825(17)	1205(12)	24
C(9)	2664(28)	2559(25)	2811(15)	15(6)
C(10)	2668(33)	2608(31)	4124(18)	28(8)
C(11)	2606(27)	2635(25)	2135(15)	14(6)
C(12)	2304(33)	1666(30)	3135(18)	25(7)
C(13)	2306(32)	1675(29)	3770(18)	25(7)
C(14)	3020(31)	3483(28)	3163(17)	22(7)
C(15)	3036(35)	3421(32)	3805(19)	31(8)
C(16)	-1293(29)	3835(26)	1657(16)	19(6)
C(17)	-505(36)	2669(30)	2718(20)	33(8)
C(18)	452(33)	4669(33)	2583(18)	26(8)
C(19)	6580(34)	1411(31)	1831(19)	29(8)
C(20)	5054(45)	665(41)	2687(24)	48(11)
C(21)	5867(38)	2743(35)	2734(22)	36(9)
C(22)	2193(28)	5083(25)	908(16)	16(6)
C(23)	1789(30)	4976(27)	213(17)	20(7)
C(24)	1973(33)	6110(30)	1146(18)	26(7)
C(25)	4983(24)	3599(22)	661(13)	6(5)
C(26)	5601(27)	4614(24)	762(15)	13(6)
C(27)	5592(42)	2996(39)	233(24)	45(10)
C(28)	-43(31)	1576(28)	520(17)	23(7)
C(29)	-298(35)	2264(32)	72(20)	31(8)
C(30)	-1015(44)	1006(41)	662(25)	49(11)
C(31)	2955(30)	178(27)	893(17)	21(7)
C(32)	2126(34)	-252(30)	1296(19)	27(8)
C(33)	3736(38)	-624(34)	607(21)	35(9)

13. The hydride was not crystallographically located but can be viewed to occupy a site bridging the two

Table 7. Fractional Coordinates and Isotropic Thermal Parameters for $W_2(\mu-H)(\mu-CPh)(O-i-Pr)_4(Quin)_2$

atom	10^4x	10^4y	10^4z	$10B_{iso}$
W(1)	7712.6(3)	300(1)	8654.0(2)	12
W(2)	7244.9(3)	-1176(1)	7728.8(2)	12
O(3)	6927(4)	937(9)	9175(4)	19
C(4)	6150(7)	737(13)	9220(7)	21
C(5)	5930(8)	1389(15)	9861(6)	25
C(6)	5723(7)	1297(14)	8595(7)	23
O(7)	8679(4)	-210(8)	9094(4)	15
C(8)	8929(6)	-1447(12)	9368(7)	17
C(9)	8716(8)	-1612(14)	10089(7)	28
C(10)	9752(7)	-1628(14)	9312(7)	24
N(11)	8215(5)	2417(10)	8909(5)	15
C(12)	8404(6)	2480(13)	9660(6)	18
C(13)	8637(7)	3902(13)	9891(7)	20
C(14)	8798(7)	4716(14)	9275(6)	22
C(15)	9328(7)	3929(14)	8883(7)	21
C(16)	8911(7)	2678(13)	8561(6)	20
C(17)	8083(7)	4928(14)	8819(60)	21
C(18)	7684(7)	3546(11)	8708(6)	17
O(19)	8013(4)	-2276(9)	7396(4)	19
C(20)	8788(6)	-2580(13)	7557(6)	14
C(21)	8993(8)	-3775(16)	7161(7)	29
C(22)	9244(7)	-1345(15)	7400(7)	26
O(23)	6234(4)	-1885(9)	7817(4)	19
C(24)	5950(7)	-2623(13)	8340(6)	18
C(25)	6057(7)	-4088(14)	8213(7)	25
C(26)	5124(7)	-2267(15)	8358(8)	30
N(27)	6764(5)	-1205(10)	6581(5)	14
C(28)	6088(6)	-374(14)	6467(6)	19
C(29)	5667(7)	-666(15)	5777(7)	25
C(30)	6176(7)	-1477(13)	5345(6)	19
C(31)	6312(8)	-2835(14)	5659(7)	24
C(32)	6556(7)	-2638(13)	6424(7)	20
C(33)	6918(8)	-755(13)	5361(7)	21
C(34)	7311(8)	-779(15)	6087(7)	28
C(35)	7517(6)	733(13)	7676(6)	17
C(36)	7538(7)	1875(12)	7192(6)	15
C(37)	8191(7)	2103(12)	6833(6)	15
C(38)	8198(8)	3132(15)	6384(6)	24
C(39)	7598(9)	3973(14)	6255(7)	27
C(40)	6977(7)	3745(14)	6604(7)	21
C(41)	6934(7)	2737(13)	7057(6)	16

tungsten atoms so as to complete a trigonal-bipyramidal coordination environment at each metal atom with the $\mu-H$ and terminal PMe_3 groups in axial sites. The $\mu-CPh$ ligand occupies a common equatorial position and is symmetrically bonded to the two tungsten atoms. The W–W distance of 2.47 Å is again typical of one seen in $(W=W)^{8+}$ -containing compounds. The quality of the structural determination is poor for the reasons noted in the Experimental Section, but we offer the structural determination since it is consistent with the solution NMR data and structurally related to the quinuclidine derivative described below.

An ORTEP drawing of the quinuclidine molecule is shown in the bottom of Figure 4 and pertinent bond distances and angles are given in Table 14. The bridging hydride was not structurally located but is again assumed to complete a trigonal-bipyramidal geometry about each tungsten with the W–quinuclidine and $\mu-H$ groups being mutually trans. The $\mu-CPh$ ligand occupies a common equatorial site and the W–C distances 1.984(13) and 1.971(13) Å imply a symmetrical benzylidyne bridge. The W–W distance of 2.443(1) Å is again typical of a $(W=W)^{8+}$ -containing compound. The W–O distances span the range 1.92–1.97 Å and are suggestive of some RO p to W d bonding.

Solution NMR Characterization Data. (a) $W_2-(CH_2R)_2(O-i-Pr)_4(dmpm)$. The 1H NMR spectrum of the compound where $R = Ph$ recorded at 300 MHz at

Table 8. Bond Distances for W₂(CH₂Ph)₂(O-*i*-Pr)₄(Me₂PCH₂PMe₂)

	distances(Å)			distances(Å)	
	molecule A	molecule B		molecule A	molecule B
W(1)–W(2)	2.3476(13)	2.3456(14)	W(2)–O(24)	1.891(15)	1.901(16)
W(1)–W(2)	1.968(15)	1.957(15)	W(2)–O(28)	1.977(15)	1.968(16)
W(11)–O(36)	1.923(16)	1.869(15)	W(2)–C(10)	2.217(22)	2.227(23)
W(1)–C(17)	2.188(21)	2.236(22)	W(2)–P(3)	2.543(7)	2.552(7)
W(1)–P(5)	2.581(7)	2.577(7)			

Table 9. Bond Angles for W₂(CH₂Ph)₂(O-*i*-Pr)₄(Me₂PCH₂PMe₂)

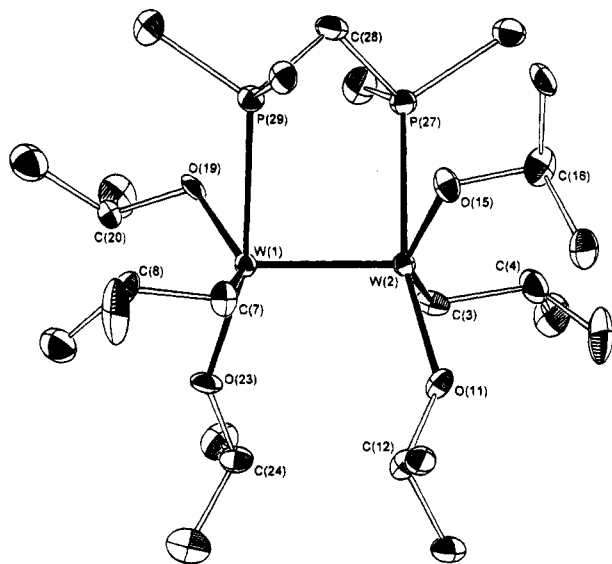
	angles (deg)	
	molecule A	molecule B
W(2)–W(1)–O(32)	110.3(4)	109.7(4)
W(2)–W(1)–O(36)	105.7(4)	106.7(4)
W(2)–W(1)–C(17)	100.3(6)	102.5(6)
W(2)–W(1)–P(5)	87.3(2)	88.2(2)
O(32)–W(1)–O(36)	100.9(6)	99.1(6)
O(32)–W(1)–C(17)	142.6(7)	142.0(7)
O(36)–W(1)–C(17)	90.7(7)	90.3(8)
O(36)–W(1)–P(5)	166.5(3)	151.2(10)
O(32)–W(1)–P(5)	77.5(5)	77.4(5)
C(17)–W(1)–P(5)	83.1(6)	84.0(6)
W(1)–W(2)–O(24)	109.1(4)	108.4(5)
W(1)–W(2)–O(28)	107.5(4)	108.7(5)
W(1)–W(2)–C(10)	103.3(6)	100.6(6)
W(1)–W(2)–P(3)	89.0(2)	88.4(2)
O(24)–W(2)–O(28)	98.7(6)	99.9(7)
O(24)–W(2)–C(10)	90.1(7)	90.5(8)
O(28)–W(2)–C(10)	142.8(7)	143.7(8)
O(24)–W(2)–P(3)	161.4(22)	162.7(25)
O(28)–W(2)–P(3)	79.1(4)	78.0(5)
C(10)–W(2)–P(3)	81.5(6)	88.4(2)
W(2)–O(24)–C(25)	142.5(14)	142.9(14)
W(2)–O(28)–C(29)	122.1(13)	120.5(17)
W(1)–O(32)–C(33)	123.0(13)	124.3(14)
W(2)–O(36)–C(37)	138.8(13)	144.3(14)
P(3)–C(4)–P(5)	112.0(15)	112.0(15)
W(2)–C(10)–C(11)	110.2(15)	109.7(14)
W(1)–C(17)–C(18)	105.3(14)	105.0(14)

Table 10. Bond Distances and Bond Angles for W₂(*i*-Bu)₂(O-*i*-Pr)₄(Me₂PCH₂PMe₂)

Bond Distances (Å)					
W(1)–W(2)	2.3490(7)	W(1)–O(23)	1.906(6)	W(2)–O(11)	1.900(6)
W(1)–P(29)	2.5706(27)	W(1)–C(7)	2.168(10)	W(2)–O(15)	1.975(7)
W(1)–O(19)	1.975(7)	W(2)–P(27)	2.5540(26)	W(2)–C(3)	2.183(10)
Bond Angles (deg)					
W(2)–W(1)–P(29)	88.37(6)	P(27)–W(2)–O(11)	163.87(22)		
W(2)–W(1)–O(19)	113.09(19)	P(27)–W(2)–O(15)	78.26(21)		
W(2)–W(1)–O(23)	107.78(21)	P(27)–W(2)–C(3)	80.56(27)		
W(2)–W(1)–C(7)	98.63(26)	O(11)–W(2)–O(15)	100.53(28)		
P(29)–W(1)–O(19)	76.48(19)	O(11)–W(2)–C(3)	91.8(3)		
P(29)–W(1)–O(23)	163.80(22)	O(15)–W(2)–C(3)	143.3(3)		
P(29)–W(1)–C(7)	81.46(28)	W(2)–P(27)–C(28)	107.5(4)		
O(19)–W(1)–O(23)	97.61(27)	W(1)–P(29)–C(28)	108.6(3)		
O(19)–W(1)–C(7)	140.3(3)	W(2)–O(11)–C(12)	141.7(6)		
O(23)–W(1)–C(7)	94.5(3)	W(2)–O(15)–C(16)	125.2(6)		
W(1)–W(2)–P(27)	89.60(6)	W(1)–O(19)–C(20)	121.0(6)		
W(1)–W(2)–O(11)	105.86(21)	W(1)–O(23)–C(24)	141.7(6)		
W(1)–W(2)–O(15)	108.43(19)	W(2)–C(3)–C(4)	112.8(7)		
W(1)–W(2)–C(3)	101.05(28)	W(1)–C(7)–C(8)	115.9(6)		

Table 11. Selected Bond Distances and Angles for W₂(μ-H)(μ-CPh)(O-*i*-Pr)₄(PMe₃)₃

Bond Distances (Å)					
W(1)–W(2)	2.5374(14)	W(1)–O(15)	2.074(14)	W(2)–O(34)	1.940(14)
W(1)–P(3)	2.515(7)	W(1)–C(19)	1.980(20)	W(2)–C(19)	2.056(19)
W(1)–P(7)	2.515(6)	W(2)–O(26)	1.903(15)	C(19)–C(20)	1.47(3)
W(1)–P(11)	2.506(7)	W(2)–O(30)	1.930(14)		
Bond Angles (deg)					
P(3)–W(1)–P(7)	93.85(22)	O(26)–W(2)–C(19)	111.4(9)		
P(3)–W(1)–P(11)	163.64(22)	O(30)–W(2)–O(34)	89.1(6)		
P(3)–W(1)–O(15)	84.4(7)	O(30)–W(2)–C(19)	112.7(9)		
P(3)–W(1)–C(19)	98.3(8)	O(34)–W(2)–C(19)	95.5(7)		
P(7)–W(1)–P(11)	90.50(22)	W(1)–O(15)–C(16)	140.6(15)		
P(7)–W(1)–O(15)	84.4(4)	W(2)–O(26)–C(27)	131.9(13)		
P(7)–W(1)–C(19)	84.0(6)	W(2)–O(30)–C(31)	126.4(14)		
P(11)–W(1)–O(15)	80.4(7)	W(2)–O(34)–C(35)	144.7(13)		
O(15)–W(1)–C(19)	97.9(8)	O(15)–C(16)–C(17)	109.9(19)		
O(15)–W(1)–C(19)	168.2(7)	W(1)–C(19)–W(2)	77.9(7)		
O(26)–W(2)–O(30)	135.9(7)	W(1)–C(19)–C(20)	151.3(15)		
O(26)–W(2)–O(34)	88.0(6)	W(2)–C(19)–C(20)	130.6(14)		

Figure 2. ORTEP drawing showing the molecular structure of W₂(*i*-Bu)₂(O-*i*-Pr)₄(dmpm).

22 °C in benzene-*d*₆ is entirely consistent with expectations based on the solid-state molecular structure that has a virtual C₂ axis of symmetry. Of particular note are the presence of two types of OR ligands with their characteristic septets for the methyne proton resonances of the O-*i*-Pr ligands and the benzylic methylene protons that are diastereotopic and, in addition, show coupling to ³¹P. The isopropyl methyl groups also appear as two

sets of diastereotopic groups for which the two sets of doublets partially overlap to give apparent triplets. At 22 °C there are two PMe₃ groups, which because of virtual coupling also appear as triplets, and this indicates that rotation about the W≡W bond is slow on ¹H NMR time scale; *i.e.*, the staggered conformation is maintained in solution. The ³¹P{¹H} spectrum shows a singlet at δ –1.04 flanked by tungsten satellites (¹⁸³W, *I* = 1/2, 14.4%). The satellite pattern is consistent for an AA'X spin system. The actual and simulated spectra are shown in Figure 5.

The ¹H spectrum for the complex where *R* = *i*-Pr at –20 °C is similar to that described above for *R* = Ph, but at room temperature there is some broadening of the OR methyne septets and the diastereotopic CH₂A_b protons of the isobutyl ligand. Presumably this molecule (*R* = *i*-Pr) is more dynamically labile. The ³¹P{¹H} NMR spectrum shows a pattern analogous to that found for *R* = Ph.

(b) (PMe₃)₃(*i*-PrO)W(μ-H)(μ-CR)W(O-*i*-Pr)₃. On the ¹H and ³¹P NMR time scale, the stereochemistry at

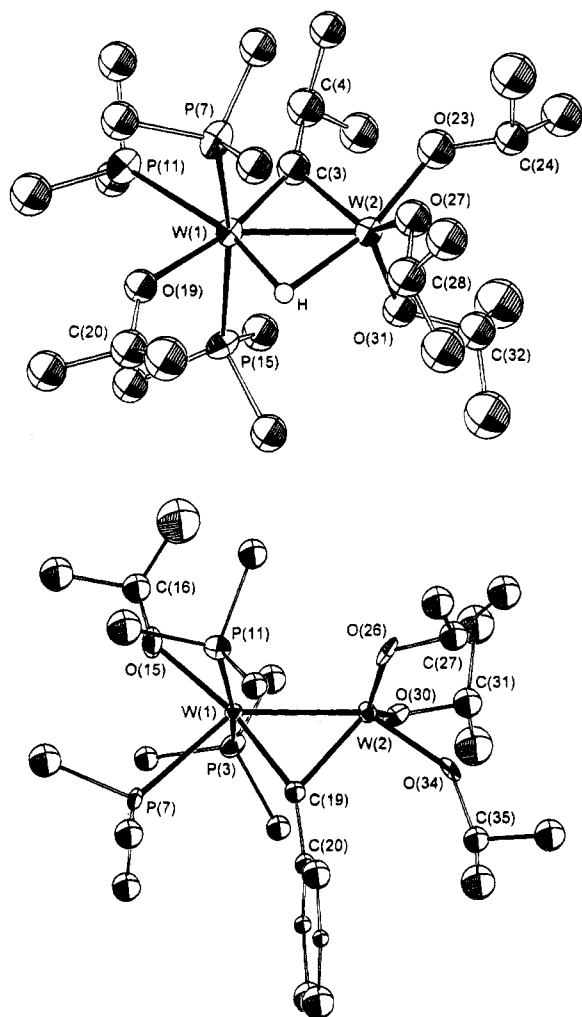


Figure 3. ORTEP drawing (50% probability ellipsoids) showing the molecular structure of $(\text{PMe}_3)_3(i\text{-PrO})\text{W}(\mu\text{-H})(\mu\text{-CPh})\text{W}(\text{O-}i\text{-Pr})_3$ (top) and an ORTEP drawing showing the molecular structure of $(\text{PMe}_3)_3(i\text{-PrO})\text{W}(\mu\text{-H})(\mu\text{-C-}i\text{-Pr})\text{W}(\text{O-}i\text{-Pr})_3$ (bottom).

the six-coordinate tungsten atoms ($R = \text{Ph}, i\text{-Pr}$) is rigid while that at the five-coordinate tungsten is labile; *i.e.*, the O-*i*-Pr ligands appear in the ratio 1:3 and there are two types of PMe_3 groups in the integral ratio 2:1. The NMR data are thus consistent with a facile turnstile rotation for the three terminal OR groups at the TBP tungsten atom. The hydride resonance appears at ~ 8.3 ($R = \text{Ph}$) as a doublet of triplets due to coupling to the adjacent WPMe_3 groups at the stereochemical rigid W atom. For $R = i\text{-Pr}$, the hydride signal is at ~ 4.0 and appears as a multiplet. In the latter compound ($R = i\text{-Pr}$), coupling to ^{183}W , $I = 1/2$, 14.5% natural abundance, was not clearly resolved but for $R = \text{Ph}$ two couplings were observed, $J_{^{183}\text{W}-\text{H}} \approx 108$ and 130 Hz, consistent with a hydride bridging two different W atoms. The μ -alkylidyne carbon appears at ~ 300 in the ^{13}C spectrum for $R = i\text{-Pr}$, but coupling to ^{183}W and ^{31}P was not detected.

(c) $\text{W}_2(\mu\text{-H})(\mu\text{-CPh})(\text{O-}i\text{-Pr})_4\text{L}_2$, where $\text{L} = \text{PMe}_3$ and Quinuclidine. By ^1H NMR spectroscopy, they show just one O-*i*-Pr ligand with diastereotopic methyl groups. The hydride appears at δ 5.29 as a 1:2:1 triplet ($\text{L} = \text{PMe}_3$) with $J_{^{183}\text{W}-\text{H}} = 148$ Hz. In the ^{31}P NMR spectrum, the PMe_3 groups give rise to a signal at $\delta \sim -25$ with $J_{^{183}\text{W}-^{31}\text{P}} \approx 220$ Hz. The alkylidyne carbon signal was not detected in this compound. However, for $\text{L} = \text{quinuclidine}$, $\delta \mu\text{-CPh}$ was observed at ~ 300 with $J_{^{183}\text{W}-^{13}\text{C}} \approx 147$ Hz. The hydride was seen at $\delta -0.8$ with $J_{^{183}\text{W}-\text{H}} = 168$ Hz. The relative intensity of the satellites indicated a symmetrical $\text{W}_2(\mu\text{-H})$ moiety. Again there was only one type of O-*i*-Pr ligand with diastereotopic methyl groups.

The ^1H , ^{13}C , and ^{31}P NMR data are summarized in Table 15. Collectively, the NMR data are entirely consistent (reconcilable) with the observed solid-state molecular structure.

Mechanistic Considerations and Studies of Kinetics. The addition of PMe_3 to $1,2\text{-W}_2(\text{CH}_2\text{Ph})_2(\text{O-}i\text{-Pr})_4$ at low temperatures (~ -50 °C) in toluene- d_8

Table 12. Selected Bond Distances and Angles (°) for $\text{W}_2(\mu\text{-H})(\mu\text{-C-}i\text{-Pr})(\text{O-}i\text{-Pr})_4(\text{PMe}_3)_3$

	distances (Å)		distances (Å)		
	molecule A	molecule B	molecule A	molecule B	
W(1)–W(2)	2.5030(13)	2.5043(14)	W(2)–O(23)	1.872(15)	
W(1)–P(7)	2.495(6)	2.509(6)	W(2)–O(27)	1.970(15)	
W(1)–P(11)	2.521(96)	2.533(7)	W(2)–O(31)	1.952(14)	
W(1)–P(15)	2.507(6)	2.508(6)	W(2)–C(3)	2.099(21)	
W(1)–O(19)	2.068(15)	2.090(16)	W(1)–H	1.6218(9)	
W(1)–C(3)	1.969(20)	1.961(25)	W(2)–H	1.9963(10)	
angles (deg)		angles (deg)			
	molecule A	molecule B	molecule A	molecule B	
W(2)–W(1)–P(7)	94.62(15)	95.38(16)	W(1)–W(2)–O(31)	113.9(4)	106.8(5)
W(2)–W(1)–P(11)	138.57(14)	138.24(16)	W(1)–W(2)–C(3)	49.7(6)	49.6(7)
W(2)–W(1)–P(15)	94.29(14)	92.86(16)	O(23)–W(2)–O(27)	107.0(6)	81.9(7)
W(2)–W(1)–O(19)	138.7(4)	139.1(5)	O(23)–W(2)–O(31)	120.3(6)	102.6(7)
W(2)–W(1)–C(3)	54.4(6)	53.9(8)	O(23)–W(2)–C(3)	102.6(7)	83.5(9)
P(7)–W(1)–P(11)	91.01(20)	90.30(21)	O(27)–W(2)–O(31)	79.6(6)	122.9(7)
P(7)–W(1)–P(15)	166.11(19)	166.04(22)	O(27)–W(2)–C(3)	84.2(7)	133.3(9)
P(7)–W(1)–O(19)	83.8(4)	81.3(5)	O(31)–W(2)–C(3)	136.9(7)	103.5(9)
P(7)–W(1)–C(3)	96.6(6)	97.1(7)	W(1)–O(19)–C(20)	136.5(15)	137.4(17)
P(11)–W(1)–P(15)	89.36(20)	91.04(21)	W(2)–O(23)–C(24)	122.8(13)	126.5(15)
P(11)–W(1)–O(19)	82.7(4)	82.6(5)	W(2)–O(27)–C(28)	131.0(13)	123.1(15)
P(11)–W(1)–C(3)	84.2(6)	84.4(8)	W(2)–O(31)–C(32)	126.4(12)	124.1(15)
P(15)–W(1)–O(19)	82.5(4)	85.1(5)	W(1)–C(3)–W(2)	75.9(7)	76.5(9)
P(15)–W(1)–C(3)	97.3(6)	96.8(7)	W(1)–C(3)–C(4)	152.8(17)	152.2(21)
O(19)–W(1)–C(3)	166.9(7)	166.9(9)	W(1)–C(3)–C(4)	131.2(16)	131.2(19)
W(1)–W(2)–O(23)	108.1(5)	128.8(6)	W(2)–W(1)–H	52.75(40)	
W(1)–W(2)–O(27)	126.6(4)	113.6(5)	W(1)–W(2)–H	40.29(3)	

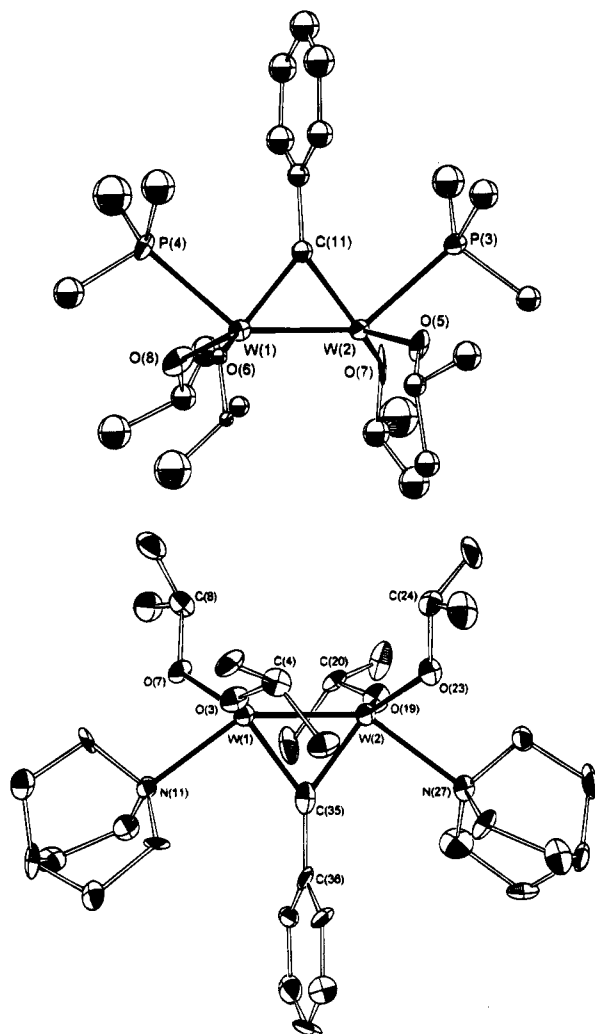


Figure 4. ORTEP drawing (50% probability ellipsoids) showing the molecular structure of $W_2(\mu\text{-CPh})(\mu\text{-H})(\text{O-}i\text{-Pr})_4(\text{PMe}_3)_2$ (top) and an ORTEP drawing showing the molecular structure of $W_2(\mu\text{-H})(\mu\text{-CPh})(\text{O-}i\text{-Pr})_4(\text{quin})_2$ (bottom).

Table 13. Selected Bond Distances and Angles for the $W_2(\mu\text{-H})(\mu\text{-CPh})(\text{O-}i\text{-Pr})_4(\text{PMe}_3)_2$ Molecule^a

Bond Distances (Å)			
W(1)–W(2)	2.4697(21)	W(2)–C(11)	1.92(3)
W(1)–C(11)	2.00(3)		
Bond Angles (deg)			
W(2)–O(5)–C(22)	135.1(20)	W(1)–C(11)–W(2)	78.1(12)
W(1)–O(6)–C(25)	133.8(17)	W(1)–C(11)–C(9)	138.0(24)
W(2)–O(7)–C(28)	136.9(21)	W(2)–C(11)–C(9)	143.4(24)
W(1)–O(8)–C(31)	136.1(22)		

^a Attempts to produce single crystals were unsuccessful, and the data reported here were obtained from a twinned crystal fragment. The structure was refined to $R_w(F) = 10.9\%$, and therefore, only a limited number of bond distances and angles are reported.

yields an adduct formulated as $1,2\text{-}W_2(\text{CH}_2\text{Ph})_2(\text{O-}i\text{-Pr})_4(\text{PMe}_3)_2$ —an analogue of the dimolybdenum complex previously described.^{4b} Upon warming the solution to $\sim -5^\circ\text{C}$, the compound $(\text{PMe}_3)_3(i\text{-PrO})W(\mu\text{-H})(\mu\text{-CPh})W(\text{O-}i\text{-Pr})_3$ is formed along with the evolution of toluene. We have followed the rate of formation of the hydrido-bridged alkylidyne complex in the presence of an excess of added $[\text{PMe}_3]$, under which conditions we observe an inverse dependence on the concentration $[\text{PMe}_3]$; *i.e.*, excess PMe_3 slows the rate of formation of the alkylidyne

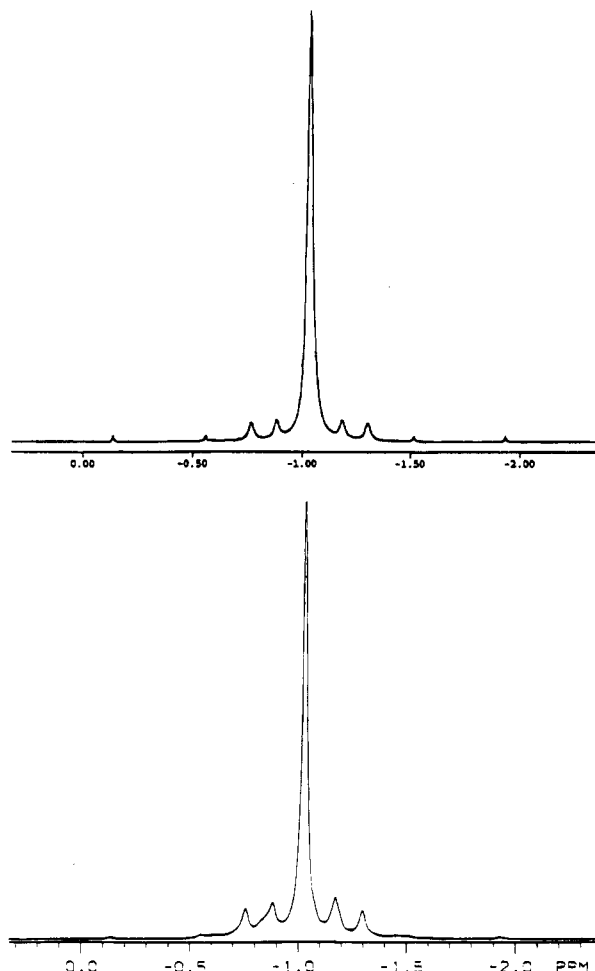


Figure 5. $^{31}\text{P}\{^1\text{H}\}$ NMR spectrum of $W_2(\text{CH}_2\text{Ph})_2(\text{O-}i\text{-Pr})_4(\text{dmpm})$ (bottom) and its spectral simulation (top). The central resonance is flanked by ^{183}W ($I = 1/2$, 14.4%) satellites giving rise to a $\text{AA}'\text{X}$ pattern where $^1J_{^{183}\text{W}-^{31}\text{P}} = 120\text{ Hz}$, $^2J_{^{183}\text{W}-^{31}\text{P}} = 3\text{ Hz}$, and $^2J_{^{31}\text{P}-^{31}\text{P}} = 92\text{ Hz}$.

Table 14. Selected Bond Distances and Angles for $W_2(\mu\text{-H})(\mu\text{-CPh})(\text{O-}i\text{-Pr})_4(\text{Quin})_2$

Bond Distances (Å)			
W(1)–W(2)	2.4425(10)	W(1)–C(35)	1.984(13)
W(1)–O(3)	1.923(8)	W(2)–O(19)	1.921(8)
W(1)–O(7)	1.941(7)	W(2)–O(23)	1.969(7)
W(1)–N(11)	2.335(10)	C(35)–C(36)	1.492(18)
W(2)–N(27)	2.361(10)		
W(2)–O(3)	1.971(13)		
Bond Angles (deg)			
W(2)–W(1)–O(3)	112.36(25)	W(1)–W(2)–C(35)	52.1(4)
W(2)–W(1)–O(7)	114.58(25)	W(1)–W(2)–O(23)	121.1(4)
W(2)–W(1)–N(11)	144.03(23)	W(1)–O(3)–C(4)	139.1(8)
W(2)–W(1)–C(35)	51.6(4)	W(1)–O(7)–C(8)	130.3(7)
O(3)–W(1)–O(7)	120.9(3)	W(2)–O(19)–C(20)	139.0(7)
O(3)–W(1)–N(11)	82.6(3)	W(2)–O(23)–C(24)	130.4(7)
W(1)–W(2)–O(19)	112.98(25)	W(1)–C(35)–W(2)	76.3(5)
W(1)–W(2)–O(23)	114.29(25)	W(1)–C(35)–C(36)	141.3(9)
W(1)–W(2)–N(27)	143.43(25)	W(2)–C(35)–C(36)	142.4(9)

dyne hydride complex. At very low concentrations of added $[\text{PMe}_3]$ ($\sim 4.0 \times 10^{-2}\text{ M}$) the formation of $W_2(\text{O-}i\text{-Pr})_4(\mu\text{-H})(\mu\text{-CPh})(\text{PMe}_3)_3$ is clearly seen to precede the formation of $W_2(\text{O-}i\text{-Pr})_4(\mu\text{-H})(\mu\text{-CPh})(\text{PMe}_3)_2$. It thus shows that the asymmetric trisphosphine complex is the kinetic product and the symmetrical bisphosphine complex the thermodynamic product in the absence of an excess of PMe_3 . Furthermore, in a separate study, the conversion of $W_2(\text{O-}i\text{-Pr})_4(\mu\text{-H})(\mu\text{-CPh})(\text{PMe}_3)_2$ to the asymmetric PMe_3 compound was shown to be first order in added $[\text{PMe}_3]$, whereas the reverse reaction was

Table 15. NMR Data^{a,b}

$W_2(\mu-H)(\mu-CPh)(O-i-Pr)_4(PMe_3)_3$		
1H NMR (benzene- <i>d</i> ₆ , 22 °C)	$^{13}C\{^1H\}$ NMR (benzene- <i>d</i> ₆ , 22 °C)	$^{31}P\{^1H\}$ NMR (toluene- <i>d</i> ₈ , 22 °C)
WH (8.28, dt, 1 H, $trans^2J_{ip-H} = 43.7$, $cis^2J_{ip-H} = 4.7$, $^1J_{isW-H} \approx 108, 130$); $\mu-CPh$, meta (7.27, t, 2 H, 7.6), ortho (6.82, d, 2 H, 7.8), para (6.76, t, 1 H, 7.4); $OCHMe_2$ (4.56, sept, 3 H, 6.0), (3.92, m, 1 H); PMe_3 , cis to H (1.59, t, 18 H, $J_{ip-H} = 3.3$); trans to H (1.06, d, 9 H, $J_{ip-H} = 6.5$); $OCHMe_2$ (1.32, d, 6 H, 6.0), (1.29, d, 18 H, 6.0)	+5 equiv of excess PMe_3 ($\delta = 16.4$ ppm); $\mu-CPh$, ipso (175.5, dt, $^3J_{ip-^{13}C} \approx 5$), ortho (125.9, d, $^4J_{ip-^{13}C} \approx 2$), meta (125.7), para (123.2); $OCHMe_2$ (75.6, rel intensity 3), (70.1, rel intensity 1); $OCHMe_2$ (28.7, rel intensity 1), (27.4, rel intensity 3); PMe_3 (20.6, d, $J_{ip-^{13}C} = 17.8$), (19.4, t, $J_{ip-^{13}C} = 12.1$)	PMe_3 , cis to H (-20.7, d, $^2J_{ip-^{31}P} = 8.5$, $^1J_{ip-^{31}P} = 280$); trans to H (-40.7, t, $^2J_{ip-^{31}P} = 8.5$, $^1J_{isW-^{31}P} = 188$)
$W_2(\mu-H)(\mu-CPh)(O-i-Pr)_4(PMe_3)_2$		
1H NMR (benzene- <i>d</i> ₆ , 22 °C)	$^{13}C\{^1H\}$ NMR (benzene- <i>d</i> ₆ , 22 °C)	$^{31}P\{^1H\}$ NMR (benzene- <i>d</i> ₆ , 22 °C)
$\mu-CPh$, meta (7.16, tt, 2, ~8), ortho (6.83, dm, 2, ~6.9), para (6.65, tt, 1, ~7.1); WH (5.29, t, 1, $^2J_{ip-H} = 65.5$, $^1J_{isW-H} = 148.5$, total satellite intensity 24%); $OCHMe_2$ (5.02, sept, 4, 6.0); $OCHMe_2$ (1.46, d, 12, 6.0), (1.41, d, 12, 6.0); PMe_3 (0.86, d, 18, $J_{ip-H} = 7.7$)	$\mu-CPh$, ipso (174.4, t, $^3J_{ip-^{31}P} = 7.0$), ortho (129.1), meta (126.1), para (123.8); $OCHMe_2$ (84.2, m); $OCHMe_2$ (28.2), (27.7); PMe_3 (12.9, d, $J_{ip-^{13}C} = 19.8$)	PMe_3 (-24.7, s, $^1J_{isW-^{31}P} = 221.5$ with $J_{ip-^{31}P} = 3.5$)
$W_2(\mu-H)(\mu-CPh)(O-i-Pr)_4(Quin)_2$		
1H NMR (benzene- <i>d</i> ₆ , 22 °C)	$^{13}C\{^1H\}$ NMR (benzene- <i>d</i> ₆ , 22 °C)	
$\mu-CPh$, meta (7.28, t, 2 H, 8.0), ortho (6.94, d, 2 H, 6.6), para (6.66, t, 1 H, 7.0), $OCHMe_2$ (5.27, sept, 4, H, 6.3); Quin (3.11, m, 12 H), 53, m-br, 12 H), (0.99, m-br, 1 H); $OCHMe_2$ (1.65, d, 12 H, 6.0), (1.43, d, 12 H, 6.0); WH, (-0.79, s, 1 H, $^1J_{isW-H} = 168$, total intensity 24%)	$\mu-CPh$ (300.4, $^1J_{isW-^{13}C} = 147$, total satellite intensity 24%); $\mu-CPh$, ipso (170.0), ortho, meta (131.7), (126.4), para (123.5); $OCHMe_2$ (82.8); Quin, α (48.8); Quin [β], and $OCHMe_2$ (28.3), (27.8), (26.3); Quin, γ (20.9)	
$W_2(CH_2Ph)_2(O-i-Pr)_4(PMe_3)_2$		
1H NMR (benzene- <i>d</i> ₆ , 22 °C)	^{13}C NMR	$^{31}P\{^1H\}$ NMR (toluene- <i>d</i> ₈ , -60 °C)
CH_2Ph , ortho (7.32, d, 4 H, 7.5), meta (7.15, t, 4 H, 7.5), para (6.91, t, 4 H, 7.5); $OCHMe_2$ (6.39, sept br, 2 H); CH_2Ph (4.21, t br, 2 H); $OCHMe_2$ (3.73, sept, 2 H, 5.7); CH_2Ph (2.54, t br, 2 H); $OCHMe_2$ (1.80, d, 6 H, 5.7), (1.67, d, 6 H, 5.7); PMe_3 (~1.4, s br, 9 H); $OCHMe_2$ (1.26, d, 6 H, 5.7), (1.12, d, 6 H, 5.7)	n/r	PMe_3 (-1.2, $^1J_{isW-^{31}P} = 130$, $^2J_{ip-^{31}P} = 16$, $^3J_{ip-^{31}P} = 6$)
$W_2(CH_2Ph)_2(O-i-Pr)_4(dmpm)$		
1H NMR (benzene- <i>d</i> ₆ , 22 °C)	$^{13}C\{^1H\}$ NMR (benzene- <i>d</i> ₆ , 22 °C)	$^{31}P\{^1H\}$ NMR (benzene- <i>d</i> ₆ , 22 °C, 146)
CH_2Ph , ortho (7.20, d, 4H, 7.2), meta (7.08, t, 4H, 7.5), para (6.84, t, 2H, 7.5); $OC(H)Me_2$ (5.76, br septet, 2H, 5.6); CH_2Ph (4.06, m, 2H); $OC(H)Me_2$ (3.83, septet, 2H, $J = 6.2$); CH_2Ph (2.85, m, 2H); $Me_2PCH_2PMe_2$ (2.20, t, 2H, $J_{ip-H} = 9.1$), (13.8, t, $J_{ip-^{13}C} = 11.3$); $Me_2PCH_2PMe_2$ (2.07, t, 6H, $J_{ip-H} = 4.4$); $OC(H)Me_2$ (1.68, d, 6H, 5.6), (1.66, d, 6H, 5.6), (1.07, d, 6H, 6.2), (1.05, d, 6H, 6.2); $Me_2PCH_2PMe_2$ (0.64, t, 6H, $J_{ip-^{31}P} = 2.9$)	CH_2Ph , ipso (148.6), ortho/meta (129.4), para (122.4); $OCHMe_2$ (82.1, 70.3); CH_2Ph (55.6); $Me_2PCH_2PMe_2$ (44.7, t, $J_{ip-^{13}C} = 26.5$); $OCHMe_2$ (27.1, 26.7, 26.5, 26.1); $Me_2PCH_2PMe_2$ (19.4, t, $J_{ip-^{13}C} = 9.4$)	$Me_2PCH_2PMe_2$ (s, -1.05, $^1J_{isW-^{31}P} = 120$, $^2J_{ip-^{31}P} = 3$), $^2J_{ip-^{31}P} = 92$)
$W_2(i-Bu)_2(O-i-Pr)_4(dmpm)$		
1H NMR (benzene- <i>d</i> ₆ , 300 MHz, -20 °C)	^{13}C NMR	$^{31}P\{^1H\}$ NMR (benzene- <i>d</i> ₆ , 146 MHz, 22 °C)
$OC(H)Me_2$ (5.62, septet, 2H, $J = 5.9$), (4.16, septet, 2H, $J = 6.2$); $CH_2C(H)Me_2$ (3.13, m, 2H); $Me_2PCH_2PMe_2$ (2.29, t, 2H, $J_{ip-H} = 9.3$); $Me_2PCH_2PMe_2$ (1.95, t, 6H, $J_{ip-H} = 4.4$), (0.95, br s, 6H); $OC(H)Me_2$ (1.70, d, 6H, 5.9), (1.56, d, 6H, 5.9), (1.28, d, 6H, 6.2), (1.23, d, 6H, 6.2); $CH_2C(H)Me_2$ (1.19, d, 6H, 6.5), (0.99, d, 6H, 6.5); $CH_2C(H)Me_2$ (observed by 1.56 doublet)	n/r	$Me_2PCH_2PMe_2$ (1.51, s, $^1J_{isW-^{31}P} \approx 100$, $^2J_{ip-^{31}P} \approx 3$, $^2J_{ip-^{31}P} \approx 90$)
$W_2(\mu-H)(\mu-CC(H)Me_2)(O-i-Pr)_4(PMe_3)_3$		
1H NMR (benzene- <i>d</i> ₆ , 22 °C)	^{13}C NMR	$^{31}P\{^1H\}$ NMR (benzene- <i>d</i> ₆ , 22 °C)
$OCHMe_2$ (6.38, sept, 1H, 6.6), (5.05, sept, 3H, 5.7); WH (3.96, m, 1H); $OCHMe_2$ (1.59, d, 6H, 6.6), (1.44, d, 18H, 5.7); PMe_3 (1.43, t, 18H, $J_{ip-H} = 4.2$), (1.38, d, 9H, $J_{ip-H} = 5.7$)	n/r	PMe_3 (-19.8, d, $^2J_{ip-^{31}P} = 5.4$, $^1J_{isW-^{31}P} = 275.5$), (-32.7, br s, $J_{isW-^{31}P} = 165.3$)

^a 1H NMR data are reported as follows: assignment (chemical shift in ppm, multiplicity, relative intensity, H-H coupling constant in hertz, heteronuclear coupling constants in hertz). $^{13}C\{^1H\}$ NMR data are reported as follows: assignment (chemical shift in ppm, heteronuclear coupling constants in hertz). ^{31}P NMR data are reported as follows: assignment (chemical shift in ppm, multiplicity, coupling constant). ^b s, singlet; d, doublet; t, triplet; q, quartet; sept, septet; m, multiplet; n/r, not recorded.

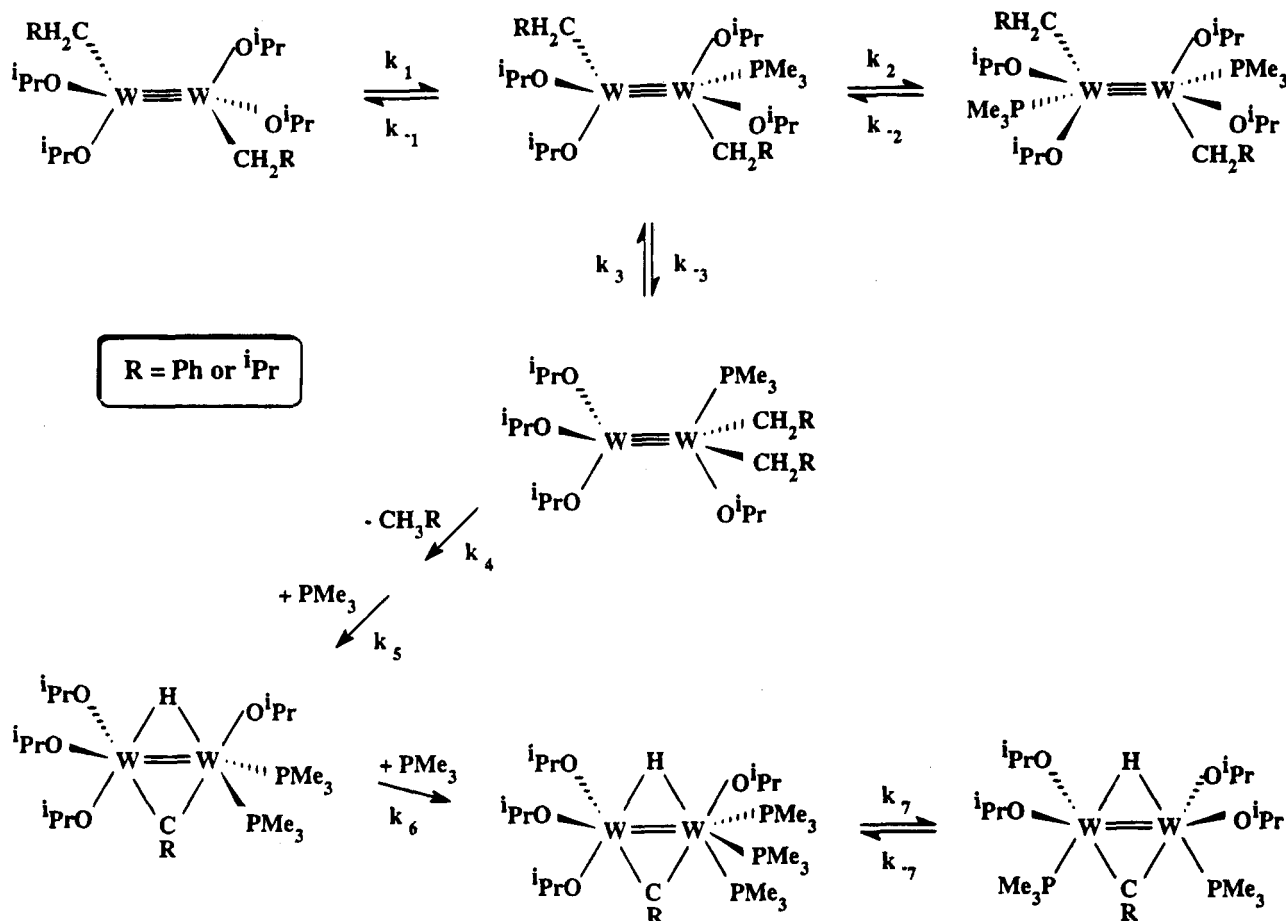
suppressed by added PMe_3 . This establishes the equilibrium 3.

In the case of the bulky quinuclidine ligand, the formation of the symmetrical $W_2(O-i-Pr)_4(\mu-H)(\mu-CPh)L_2$ ($L =$ quinuclidine) complex was much slower than that for when $L = PMe_3$ and the rate of formation of the hydrido benzylidyne complex was approximately half-order in added quinuclidine. No simple adducts

1,2- $W_2(CH_2Ph)_2(O-i-Pr)_4L_2$ are seen by 1H NMR for $L =$ quinuclidine.

We have also determined the kinetic isotope effect k_H/k_D by the comparisons of rates for CH_2Ph versus CD_2Ph . For $L = PMe_3$ at 25 °C in toluene-*d*₈, $k_H/k_D = 3.4(4)$, and for $L =$ quinuclidine at 22 °C $k_H/k_D = 5.0(6)$. Both of these findings imply that C-H/C-D bond breaking are important and may even be rate limiting. These

Scheme 2



isotope effects are comparable to other α -CH activation processes and cyclometalations at early transition metal centers.¹⁰

We propose that the overall reaction pathway for $L = PMe_3$ proceeds according to the reaction sequences depicted in Scheme 2. The reversible addition of PMe_3 to $1,2-W_2(CH_2Ph)_2(O-i-Pr)_4$ yields a kinetically unreactive $1,2-W_2(CH_2Ph)_2(O-i-Pr)_4L_2$ complex with respect to α -CH bond activation. This view is supported by the fact that the bridging bidentate phosphine adducts $1,2-W_2(CH_2R)_2(O-i-Pr)_4(dmpe)$ are notably less reactive toward α -CH activation. Moreover, in the presence of an excess of PMe_3 the rate of α -CH activation is suppressed.

The proposed α -CH activation pathway involves the 1,2-migration of $CH_2R/O-i-Pr$ ligands and the formation of $1,1-W_2(CH_2R)_2(O-i-Pr)_4L$. In the case of molybdenum, such a compound was isolated and structurally characterized.^{4b} The $1,1-W_2(CH_2R)_2(O-i-Pr)_4L$ compounds are now well suited for α -CH activation. The elimination of alkane by hydrogen atom transfer between adjacent alkyl groups is well documented in mononuclear chemistry and is known to be assisted by the addition of Lewis bases such as tertiary phosphines. Perhaps the classic or textbook example of such a reaction was discovered by Clark and Schrock and in their study of the reaction between $(Me_3CCH_2)_3WCCMe_3$ and $dmpe$ to give $(Me_3CCH_2)(Me_3CCH=)(Me_3CC)W(dmpe)$.¹¹ In part the role of base is to increase the coordination number of the metal, and this in turn

will both weaken the metal-carbon bond and force neighboring alkyl groups into closer proximity.

In Scheme 2, we do not wish to imply that we know whether or not a second equivalent of phosphine is required in the elimination of alkane. However, elimination of alkane will generate a coordinatively unsaturated metal center which would be expected to be labile to uptake of PMe_3 and further α -CH activation yielding the alkylidyne hydride complex $(PMe_3)_3(i-PrO)W(\mu-H)(\mu-CPh)W(O-i-Pr)_3$. Thus the kinetic product, with three terminal OR ligands on one end, has a memory of its parent reactive intermediate.

We speculate that quinuclidine plays a similar role in promoting the alkyl group migration and that a compound of formula $W_2(CH_2R)_2(O-i-Pr)_4L$ is a reactive intermediate. Since quinuclidine is much larger than PMe_3 , the asymmetric adduct may more readily be converted to the thermodynamic symmetric product $L(i-PrO)_2W(\mu-H)(\mu-CR)W(O-i-Pr)_2L$.

Concluding Remarks

In the ground state, the coordination chemistries of ethane-like M_2X_6 and $M_2X_4Y_2$ compounds of molybdenum and tungsten are very similar.¹² However, their reactivities are known to differ in two significant respects: 1. The conversion of a d^3-d^3 to a d^4-d^4 compound is more facile for molybdenum relative to

(10) Ryabov, A. D. *Chem. Rev.* **1990**, *90*, 403, and references therein.

(11) (a) Clark, D. N.; Schrock, R. R., *J. Am. Chem. Soc.* **1978**, *100*, 6774. (b) Churchill, M. R.; Youngs, W. J. *Inorg. Chem.* **1979**, *9*, 2454.
(12) Chisholm, M. H. *Acc. Chem. Res.* **1990**, *23*, 419.

Table 16. Pseudo-First-Order Rate Constants (k_{obs})

run	substrate	product	Lewis base (L)	[L] _{av} (M)	k_{obs} (s ⁻¹)
1	1,2-W ₂ (CD ₂ C ₆ D ₅) ₂ (O- <i>i</i> -Pr) ₄ ^a	W ₂ (μ-D)(μ-CC ₆ D ₅)(O- <i>i</i> -Pr) ₄ (quin) ₂	Quin	0.19	3.6(3) × 10 ⁻⁶
2	W ₂ (CH ₂ Ph) ₂ (O- <i>i</i> -Pr) ₄ ^a	W ₂ (μ-H)(μ-CPh)(O- <i>i</i> -Pr) ₄ (Quin) ₂	Quin	0.19	1.8(1) × 10 ⁻⁵
3				0.30	2.3(2) × 10 ⁻⁵
4				0.42	2.6(3) × 10 ⁻⁵
5	1,2-W ₂ (CD ₂ C ₆ D ₅) ₂ (O- <i>i</i> -Pr) ₄ (PMe ₃) ₂ ^b	W ₂ (μ-D)(μ-CC ₆ D ₅)(O- <i>i</i> -Pr) ₄ (PMe ₃) ₃	PMe ₃	0.24	7.2(3) × 10 ⁻⁵
6	1,2-W ₂ (CH ₂ Ph) ₂ (O- <i>i</i> -Pr) ₄ (PMe ₃) ₂ ^b	W ₂ (μ-H)(μ-CPh)(O- <i>i</i> -Pr) ₄ (PMe ₃) ₃	PMe ₃	0.24	2.3(1) × 10 ⁻⁴
7				0.48	1.5(1) × 10 ⁻⁴
8				0.72	1.4(1) × 10 ⁻⁴
9	W ₂ (μ-H)(μ-CPh)(O- <i>i</i> -Pr) ₄ (PMe ₃) ₂ ^c	W ₂ (μ-H)(μ-CPh)(O- <i>i</i> -Pr) ₄ (PMe ₃) ₃	PMe ₃	0.26	2.0(2) × 10 ⁻⁴
10				0.54	4.5(2) × 10 ⁻⁴

^a 25 °C and [W₂]_{total} = 0.038 M. ^b 22 °C and [W₂]_{total} = 0.038 M. ^c 22 °C and [W₂]_{total} = 0.047 M.

tungsten, and conversely, (2) oxidative addition occurs more readily for tungsten than molybdenum.¹³ The latter is easily understood in terms of (i) orbital energetics and (ii) metal–ligand bond strengths. For example, the M₂(μ-CO)(O-*t*-Bu)₆ compounds show $\nu(\text{CO}) = 1670$ (M=Mo) and 1598 cm⁻¹, (M=W) reflecting the ability of the W–W bond to backbond more readily to the π -acceptor C–O ligand relative to the Mo–Mo bond.¹⁴ Similarly, C–C double bonds form isolable adducts with W₂(OR)₆ compounds, but none are known for Mo₂(OR)₆ compounds.¹⁵

We suggest that the different chemistries that are observed in the reactions between 1,2-M₂(CH₂Ph)₂(O-*i*-Pr)₄ and PMe₃ reflect these general principles. For molybdenum, the binding of PMe₃ is weak and reversible and merely induces facile benzyl for alkoxide group migrations between the metal centers. For tungsten, the binding of PMe₃ is stronger, and although we do not see the 1,1-W₂(CH₂Ph)₂(O-*i*-Pr)₄L compound, α -CH activation at the W₂⁶⁺ center occurs such that a (W=W)⁸⁺ compound results. We propose that the CH₂R migration is intimately involved in the first α -CH activation step since the 1,2-W₂(CH₂R)₂(O-*i*-Pr)₄(dmpm) adducts are isolable and not prone to this reaction. Similarly, the presence of an excess of PMe₃ suppresses the α -CH activation because the bis(phosphine) adduct, 1,2-W₂(CH₂-Ph)₂(O-*i*-Pr)₄L₂, is favored. It should be recalled that the addition of PMe₃ to 1,2-Mo₂Br₂(CH₂SiMe₃)₄ also induced the elimination of Me₄Si (2 equiv) and formation of (PMe₃)₂(Br)(Me₃SiCH=)Mo≡Mo(=CHSiMe₃)(Br)-(PMe₃)₂.¹⁶

The actual mechanism of α -CH activation at the dinuclear center remains unclear in as much as we cannot distinguish between a direct C••H••C transfer or one that involves the intermediacy of an alkylidene–hydride prior to elimination of alkane. The formation of the resultant W₂(μ-H)(μ-CR)-containing compounds is not surprising because the rupture of one C–H bond is compensated for by the formation of the μ-CR and μ-H ligands, which in turn assist in M–M bonding by orbital mixing. We have previously observed, for example, that formation of μ-alkylidynes by α -CH activation of alkylidenes is favorable even when elimination of an alkoxide ligand as an alcohol is required.¹⁷

Experimental Section

General Procedures. Standard Schlenk procedures and Vacuum Atmospheres Co. Dri-Lab Systems were used for all syntheses and sample manipulations. Solvents were distilled under N₂ from Na/benzophenone and stored in solvent bottles over 4 Å molecular sieves.

The ¹H NMR spectra were recorded in dry and deoxygenated benzene-*d*₆ or toluene-*d*₈ using either a Varian XL-300 (300 MHz) or a Nicolet NT-360 (360 MHz) spectrometer. The data were calibrated against the residual protio impurities set at 7.15 (benzene-*d*₆) or 2.09 ppm (toluene-*d*₈). The ¹³C NMR spectra were recorded on a Varian XL-300 at 75 MHz. The data were calibrated against the central carbon resonances set at 128.0 (benzene-*d*₆) or 20.4 ppm (toluene-*d*₈). The ³¹P NMR spectra were recorded on a Nicolet NT-360 at 146.2 MHz using dry and deoxygenated benzene-*d*₆ or toluene-*d*₈ solvents. The spectra were calibrated against an external H₃PO₄ standard set at 0.0 ppm. The IR spectra were obtained from KBr pellets. The data were calibrated against the polystyrene absorbance at 1601 cm⁻¹.

Elemental analyses were performed by Alfred Bernhardt Mikroanalytisches Laboratorium, Elbach, Germany, Schwarzkopf Microanalytical Laboratory, Woodside, NY, and Oneida Research Services, Whitesboro, NY.

Chemicals. 1,2-W₂(CH₂Ph)₂(O-*i*-Pr)₄ and 1,2-W₂(*i*-Bu)₂(O-*i*-Pr)₄ were prepared according to previously described procedures.¹⁸ Trimethylphosphine was synthesized from P(OPh)₃ and CH₃MgBr and purified by distillation.¹⁹ Quinuclidine was purchased commercially.

Kinetics. Reaction rates were monitored by ¹H NMR spectroscopy using a Nicolet NT-360 NMR spectrometer equipped with an automated kinetics software package (KINET). Solutions of 1,2-W₂(CH₂Ph)₂(O-*i*-Pr)₄ and quinuclidine were prepared in a drybox by mixing the accurately preweighed solids [1,2-W₂(CH₂Ph)₂(O-*i*-Pr)₄ and Quin] in 5 mm Pyrex NMR tubes with glass extensions and charging the tubes with dry, deoxygenated benzene-*d*₆ (500 μL) using a microliter syringe. The solutions were then frozen at –198 °C, and the tubes were evacuated and sealed with a torch. The four experiments (see Table 16) were run simultaneously at room temperature (25 °C) and were monitored periodically over a 3–6 day period. The relative concentrations of 1,2-W₂(CH₂-Ph)₂(O-*i*-Pr)₄ and W₂(μ-H)(μ-CPh)(O-*i*-Pr)₄(Quin)₂ were determined by comparing the integrals of O-*i*-Pr methine septets of the respective compounds, assuming that the sum of the two remained constant. The initial ratio of [1,2-W₂(CH₂Ph)₂(O-*i*-Pr)₄]/[1,2-W₂(CH₂Ph)₂(O-*i*-Pr)₄]₀ or A/A₀ was normalized to 1.0 for run 4 (Table 16) and was rigorously 1.0 for runs 1–3. Solutions of W₂(μ-H)(μ-CPh)(O-*i*-Pr)₄(PMe₃)₂ + PMe₃ and 1,2-W₂(CH₂Ph)₂(O-*i*-Pr)₄ + PMe₃ were prepared by charging extended 5 mm Pyrex NMR tubes with accurately weighed W₂ substrate [1,2-W₂(CH₂Ph)₂(O-*i*-Pr)₄ or W₂(μ-H)(μ-CPh)(O-*i*-Pr)₄(PMe₃)₂] and dry, deoxygenated benzene-*d*₆ (500 mL) in a

(13) Chisholm, M. H. *Polyhedron* **1986**, *5*, 25.

(14) Blower, P. J.; Chisholm, M. H.; Clark, D. N.; Eichhorn, B. W. *Organometallics* **1986**, *5*, 2125.

(15) Chacon, S. T.; Chisholm, M. H.; Eisenstein, O.; Huffman, J. C. *J. Am. Chem. Soc.* **1992**, *114*, 8497.

(16) Ahmed, K. J.; Chisholm, M. H.; Rothwell, I. P.; Huffman, J. C. *J. Am. Chem. Soc.* **1982**, *104*, 6453.

(17) Chisholm, M. H.; Eichhorn, B. W.; Huffman, J. C. *Organometallics* **1987**, *6*, 2264.

(18) Chisholm, M. H.; Eichhorn, B. W.; Foltling, K.; Huffman, J. C.; Tatz, R. J. *Organometallics* **1986**, *5*, 1599.

(19) Luethens, M. L.; Sattelberger, A. P.; Murray, H. H.; Basil, J. D.; Fackler, J. P., Jr. *Inorg. Synth.* **1990**, *28*, 305.

drybox. The solutions were then frozen to -198°C , and the appropriate amount of PMe_3 was condensed into the NMR tubes using a calibrated vacuum manifold. The NMR tubes were then sealed with a torch and kept frozen until the experiments were run. The reactions were monitored in an NMR probe at 22°C using preset delays and acquisition times loaded into the KINET program. The probe temperatures were calibrated against an external MeOH standard. Each experiment took $\sim 3\text{--}8$ h. The disappearance of W_2 reagent [$1,2\text{-}W_2(\text{CH}_2\text{Ph})_2(\text{O-}i\text{-Pr})_4$ or $W_2(\mu\text{-H})(\mu\text{-CPh})(\text{O-}i\text{-Pr})_4(\text{PMe}_3)_2$] was followed by monitoring the absolute integral intensity decay of the $\text{O-}i\text{-Pr}$ methine septet of the respective compounds. The integral of the first data set was always normalized to 1.0.

Each experiment was monitored for not less than 2.5 half-lives. The rate constants were calculated by standard least-squares plots using a computer package written by Professor J. G. Gajewski. The reported errors are the least-squares standard deviations.

$W_2(\mu\text{-H})(\mu\text{-CC(H)Me}_2)(\text{O-}i\text{-Pr})_4(\text{PMe}_3)_3$. In a Schlenk flask, $W_2(i\text{-Bu})_2(\text{O-}i\text{-Pr})_4$ (0.500 g, 0.666 mmol) was dissolved in hexane (10 mL). PMe_3 (0.414 mL, 4.00 mmol) was then added to the stirring orange solution by microliter syringe. After 0.5 h the now purple reaction mixture was evaporated to dryness *in vacuo*. Hexane (2.5 mL) was added to dissolve the resulting purple powder. After 3 weeks of cooling at -20°C , large purple crystals were isolated by removing the supernatant liquid and drying *in vacuo* (yield 0.226 g, 38%). Anal. Calcd for $W_2O_4P_3C_{25}H_{63}$: C, 33.80; H, 7.15. Found: C, 33.60; H, 6.90.

$1,2\text{-}W_2(i\text{-Bu})_2(\text{O-}i\text{-Pr})_4(\text{dmpm})$. In a Schlenk flask, $W_2(i\text{-Bu})_2(\text{O-}i\text{-Pr})_4$ (0.260 g, 0.347 mmol) was dissolved in toluene (10 mL). dmpm (0.05 g, 0.367 mmol) was then added to the stirring orange solution by microliter syringe. An immediate color change to maroon occurred. After 15 min, the volume of toluene was reduced until the product began precipitating from the reaction mixture. The flask was warmed gently to redissolve the precipitate and then cooled to -20°C . Two crops of crystals were isolated (yield 0.244 g, 82%). IR data (KBr pellet) cm^{-1} : 1454 (w), 1373 (m), 1360 (m), 1323 (m), 1291 (w), 1277 (w), 1161 (s), 1119 (s), 1001 (s), 957 (s), 926 (s), 839 (m), 764 (w), 737 (w), 681 (w), 658 (w), 592 (s), 455 (w).

$1,2\text{-}W_2(\text{CH}_2\text{Ph})_2(\text{O-}i\text{-Pr})_4(\text{dmpm})$. In a Schlenk flask, $W_2(\text{CH}_2\text{Ph})_2(\text{O-}i\text{-Pr})_4$ (0.200 g, 0.254 mmol) was dissolved in toluene (15 mL). dmpm (40.5 mg, 0.298 mmol) was added to the red-orange solution. After 15 min of stirring, the resulting burgandy reaction mixture was reduced in volume and cooled to 0°C . After 2 days, crystals were isolated by removing the supernatant liquid and drying *in vacuo* (yield 0.190 g, 81%). Anal. Calcd for $W_2O_4P_2C_{31}H_{56}$: C, 40.37; H, 6.12. Found: C, 40.46; H, 6.24. IR data (KBr pellet) cm^{-1} : 2963 (s), 2920 (m), 2867 (w), 1593 (m), 1487 (m), 1448 (w), 1373 (m), 1369 (m), 1321 (m), 1277 (w), 1196 (w), 1163 (m), 1124 (s), 1107 (s), 1032 (w), 1001 (s), 952 (vs), 930 (m), 898 (w), 843 (m), 831 (m), 745 (m), 702 (m), 592 (m).

$W_2(\mu\text{-H})(\mu\text{-CPh})(\text{O-}i\text{-Pr})_4(\text{Quin})_2$. In a Schlenk reaction flask, $1,2\text{-}W_2(\text{CH}_2\text{Ph})_2(\text{O-}i\text{-Pr})_4$ (400 mg, 0.51 mmol) and quinuclidine (117 mg, 1.1 mmol) were dissolved in hexane (15 mL) at room temperature. The resulting red-brown solution was stirred at room temperature for 7 days, during which time it turned burgundy red. The reaction mixture was then filtered through a fine frit, concentrated to ~ 1 mL total volume, and cooled to -20°C . After 3 weeks at -20°C , small dark crystals were harvested by removing the supernatant liquid via cannula and drying *in vacuo* (crystalline yield 186 mg, 40%). Anal. Calcd for $W_2O_4C_{33}H_{60}N_2$: C, 43.25; H, 6.60; N, 3.06. Found: C, 43.48; H, 6.12; N, 2.88.

$W_2(\mu\text{-H})(\mu\text{-CPh})(\text{O-}i\text{-Pr})_4(\text{PMe}_3)_2$. In a Schlenk reaction vessel, $1,2\text{-}W_2(\text{CH}_2\text{Ph})_2(\text{O-}i\text{-Pr})_4$ (410 mg, 0.52 mmol) was dissolved in hexane (20 mL), frozen at -198°C , and the vessel evacuated. Using a calibrated vacuum manifold, PMe_3 (3.0 equiv, 1.6 mmol) was condensed into the flask and the resulting frozen mixture was then rapidly warmed to room

temperature. The red-brown solution was stirred at room temperature for 5 h, during which time it turned aqua blue-green. The reaction mixture was then warmed to $\sim 45^\circ\text{C}$ and stirred for an additional 4 days under vacuum. Approximately every 6 h, the volatile gases (PMe_3) were removed from the reaction flask under dynamic vacuum. The aqua blue-green solution slowly turned royal blue and then bright purple after 2 days at 45°C . After 4 days, the purple solution was evaporated to dryness, and the residue extracted into pentane (~ 2 mL) and cooled to -20°C . After 48 h, dark crystals were harvested by removing the supernatant liquid via cannula and drying *in vacuo* (total crystalline yield 160 mg, 36%). The best X-ray quality crystals were obtained from Et_2O recrystallizations. Anal. Calcd for $W_2O_4P_2C_{25}H_{52}$: C, 35.48, H, 6.19. Found: C, 33.13; H, 5.96. IR data (KBr pellet) cm^{-1} : 3045 (w), 2960 (vs), 2900 (s), 2850 (m), 1620 (w) br, 1580 (m), 1479 (m), 1460 (w), 1430 (w), 1415 (w), 1382 (s), 1369 (m), 1358 (s), 1315 (s), 1299 (m), 1280 (m), 1273 (m), 1160 (m), 1116 (vs), 974 (vs), 959 (vs), 842 (m), 761 (m), 738 (w), 730 (w), 700 (m), 601 (m), 578 (m).

$W_2(\mu\text{-H})(\mu\text{-CPh})(\text{O-}i\text{-Pr})_4(\text{PMe}_3)_3$. In a Schlenk reaction vessel, $1,2\text{-}W_2(\text{CH}_2\text{Ph})_2(\text{O-}i\text{-Pr})_4$ (154 mg, 0.19 mmol) was dissolved in pentane (8 mL) and frozen at -198°C . Using a calibrated vacuum manifold, PMe_3 (5.0 equiv) was condensed into the flask. The frozen mixture was warmed to room temperature and backfilled with N_2 . The solution was stirred for 12 h, during which time it turned from red-brown to aqua blue-green. After 12 h, the volume of solution was reduced to ~ 2 mL and cooled to -20°C . After 48 h, dark cubic crystals were isolated by removing the supernatant liquid via cannula and drying *in vacuo* (crystalline yield 67 mg, 37%).

The compound was spectroscopically pure as determined by ^{31}P NMR, ^1H NMR, and ^{13}C NMR, but repeated elemental analysis did not yield satisfactory analytical data. Anal. Calcd for $W_2O_4C_{28}H_{61}P_3$: C, 36.46; H, 6.67. Found: first analysis, C, 37.43; H, 6.41; second analysis, C, 35.76; H, 6.61. Both samples were handled in an inert atmosphere. IR data (KBr pellet) cm^{-1} : 3040 (vw), 2960 (s), 2902 (s), 2800 (vw), 1620 (m) br, 1579 (m), 1476 (w), 1423 (w), 1381 (m), 1370 (w), 1360 (m), 1321 (m), 1297 (w), 1288 (w), 1272 (m), 1151 (m), 1132 (s), 1111 (vs), 982 (vs), 948 (vs), 843 (m), 760 (m), 715 (w), 693 (m), 660 (w), 603 (m).

$1,2\text{-}W_2(\text{CH}_2\text{Ph})_2(\text{O-}i\text{-Pr})_4(\text{PMe}_3)_2$. In a Schlenk reaction vessel, $W_2(\text{CH}_2\text{Ph})_2(\text{O-}i\text{-Pr})_4$ (284 mg, 0.36 mmol) was dissolved in THF (12 mL), frozen at -198°C , and the vessel evacuated. Using a calibrated vacuum manifold, PMe_3 (3.0 equiv, 1.08 mmol) was condensed onto the frozen mixture. The flask was then placed in a -10°C EtOH/dry ice bath. The solution was stirred at -10°C for 30 min, during which time the color turned from red-brown to orange-yellow. The solution was then concentrated to ~ 1 mL and cooled to -20°C . After 48 h, brown crystals formed in the solution and were isolated by removing the supernatant liquid at -20°C and drying *in vacuo*. The crystalline material melted and decomposed before it could be removed from the reaction flask in the drybox. ^1H NMR analysis of the resulting oil revealed small quantities of $1,2\text{-}W_2(\text{CH}_2\text{Ph})_2(\text{O-}i\text{-Pr})_4(\text{PMe}_3)_2$ and $W_2(\mu\text{-H})(\mu\text{-CPh})(\text{O-}i\text{-Pr})_4(\text{PMe}_3)_3$ along with many other unidentified compounds.

Crystallographic Studies. General operating procedures and listings of programs have been given previously.²⁰

$W_2(\text{CH}_2\text{Ph})_2(\text{O-}i\text{-Pr})_4(\text{dmpm})$. A suitable crystal was located and transferred to the goniostat, using standard inert atmosphere handling techniques employed by the IUMSC, and cooled to -170°C for characterization and data collection.

A systematic search of a limited hemisphere of reciprocal space located a set of diffraction maxima with symmetry and systematic absences corresponding to the unique monoclinic space group $P2_1/n$. Subsequent solution and refinement of the structure confirmed this choice.

(20) Chisholm, M. H.; Foltling, K.; Huffman, J. C.; Kirkpatrick, C. C. *Inorg. Chem.* **1984**, *23*, 1021.

Data were collected in the usual manner by use of a continuous θ - 2θ scan with fixed backgrounds. Data were reduced to a unique set of intensities and associated σ 's in the usual manner. The structure was solved by a combination of direct methods (MULTAN78) and Fourier techniques. Two independent molecules are present in the asymmetric cell. There is a disorder involving one isopropyl group on the molecule designated as "B". A difference Fourier synthesis revealed the location of some, but not all, hydrogen atoms. All hydrogen atoms positions were therefore calculated using idealized geometries and $d(\text{C-H}) = 0.95 \text{ \AA}$. These calculated positions were fixed for the final cycles of refinement. No attempt was made to place the hydrogens on the disordered isopropyl group.

The crystal was poorly formed, and attempts to apply an absorption correction based on estimated Miller indexes for the "faces" did not significantly improve the data. Several of the carbon atoms converged to nonpositive values when allowed to go anisotropic, and little improvement was seen in the residuals. For this reason, only the metal and phosphorus atoms were allowed to vary anisotropically in the final cycles.

A final difference Fourier was featureless, with the largest peak being 0.74 e/\AA^3 , except at the metal positions, where peaks of 1.4 – 2.3 e/\AA^3 were located.

W₂(O-*i*-Pr)₄(μ -C-*i*-Pr)(μ -H)(PMe₃)₃. A fragment of irregular form was mounted using silicone grease, transferred to a goniostat, and cooled to $-170 \text{ }^\circ\text{C}$ for characterization and data collection. A systematic search of a limited hemisphere of reciprocal space revealed symmetry and systematic absences corresponding to the unique monoclinic group $P2_1/a$. No absorption correction was made.

The structure was solved by a usual combination of direct methods (MULTAN78) and Fourier techniques. The W and P atom positions were obtained from an initial E -map, and the remainder of the non-hydrogen atoms were found in subsequent iterations of least-squares refinement and difference Fourier calculations. After partial refinement of the non-hydrogen atoms, a difference Fourier revealed some but not all hydrogen atoms. There were numerous peaks within 2 \AA of the W atoms. One of these peaks looked like a hydrogen bridge between W(1)B and W(2)B atoms. It was put into the SDT file as H(B). All hydrogen atoms (except the hydride bridge) were introduced in fixed calculated positions. Attempts to refine oxygen and carbon atoms anisotropically were unsuccessful, with several atoms converting to nonpositive thermal parameters. In the final cycles of least-squares refinement, only W and P atoms were varied with anisotropic thermal parameters. A final difference Fourier had numerous tungsten residual peaks on the vicinity of the tungsten atoms.

W₂(*i*-Bu)₂(O-*i*-Pr)₄(dmpm). A crystal of suitable size was cleaved from a large piece of the sample in a nitrogen atmosphere glovebag. The crystal was mounted by use of silicone grease and was transferred to a goniostat, where it was cooled to $-168 \text{ }^\circ\text{C}$ for characterization and data collection. A systematic search of a limited hemisphere of reciprocal space revealed intensities with Laue symmetry and systematic absences consistent with space group $P2_1/n$, which was later confirmed by the successful solution of the structure. Following complete intensity data collection and correction for absorption, data processing gave a residual of 0.029 for the averaging of 1014 unique intensities which had been measured more than once. Four standards measured every 400 data showed no significant trends.

The structure was solved using a combination of direct methods (MULTAN78) and Fourier techniques. The tungsten positions were determined from an initial E -map, and the remaining non-hydrogen atoms were obtained from subsequent iterations of least-squares refinement and difference Fourier calculation. Hydrogens were included in calculated positions but were not refined. Hydrogen thermal parameters were fixed at one plus the isotropic thermal parameter of the atom to which they were bonded.

In the final cycles of refinement, the non-hydrogen atoms were varied with anisotropic thermal parameters to a final $R(F) = 0.039$. The largest peak in the final difference map was a tungsten residual of 1.7 e/\AA^3 .

W₂(μ -H)(μ -CPh)(O-*i*-Pr)₄(PMe₃)₃. A suitable crystal was located and transferred to the goniostat, using standard inert atmosphere handling techniques employed by the IUMSC, and cooled to $-157 \text{ }^\circ\text{C}$ for characterization and data collection. The sample used was cleaved from a larger crystal and approximated a cube although the faces were poorly formed.

A systematic search of a limited hemisphere of reciprocal space located a set of diffraction maxima with orthorhombic symmetry and systematic absences corresponding to $P2_12_12_1$.

Subsequent solution and refinement confirmed this choice. Data were collected in the usual manner by use of a continuous θ - 2θ scan technique. Data were reduced in the usual manner. The structure was solved by a combination of direct methods (MULTAN78) and Fourier techniques and refined by full-matrix least-squares analysis. Many of the hydrogen atom positions were visible in a difference Fourier phased on the non-hydrogen parameters. The positions of all hydrogens were calculated and placed in fixed idealized ($d(\text{C-H}) = 0.95 \text{ \AA}$) positions for the final cycles. The hydrogen atoms were assigned a thermal parameters of $1 + B_{\text{iso}}$ of the carbon atom to which they were bound. During the refinement, many of the anisotropic thermal parameters for the carbon atoms converged to nonpositive definite thermal parameters. When the data were corrected for absorption, several still refused to "behave". Since the number of observations was limited, it was decided to use isotropic parameters for the carbon atoms. In fact, the residual was essentially unchanged for the two refinements.

A final difference Fourier was essentially featureless, with the largest peak being 1.21 e/\AA^3 , located near the tungsten. There were four other peaks of intensity 1.0 – 1.2 within 1.1 \AA of the two tungsten atoms. Examination of the difference map failed to locate a peak (in the top 30) that could reasonably be assigned as a hydride.

W₂(μ -H)(μ -CPh)(O-*i*-Pr)₄(PMe₃)₂. It was very difficult to find a good single crystal, probably due to a twinning problem. The crystal selected was not single; it appeared to have a fragment of $\sim 25\%$. However, we decided to go on with the data collection in the usual manner. A relatively fast scan rate was used. At the conclusion of the structure determination, an attempt was made to identify the orientation of the fragment (or twin). It turned out that the fragment was approximately aligned with the main crystal, with $c(\text{frag})$ on $a(\text{main})$, $a(\text{frag})$ on $-c(\text{main})$, and an angle of $\sim 4^\circ$ between the b -axes. No attempts were made to remove the data from the fragment (twin).

The crystal was characterized in the usual manner, a systematic search of a limited hemisphere of reciprocal space yielded a set of reflections that exhibited monoclinic symmetry. A systematic extinction of $0k0$ for $k = 2n + 1$ was observed, while the extinctions in the $h01$ zone were ambiguous due to the presence of the fragment. It was decided to proceed in the monoclinic space group $P2_1/c$. A total of 5727 reflections measured yielded a set of 4344 unique reflections. The R for the averaging was 0.089 for 1045 reflections measured more than once. A total of 3762 reflections were considered observed by the criterion $F > 3.0\sigma(F)$ and were used for the solution and refinement of the structure.

The structure was solved by the usual combination of direct methods and Fourier techniques. All non-hydrogen atoms were readily located. Least-squares refinement using anisotropic thermal parameters on the W, P, and O atoms and isotropic thermal parameters on the C atoms lead to a final R of only 0.107 . The difference map at this point contained several peaks of $\sim 4 \text{ e/\AA}^3$, all in the general area of the molecule. Since we knew that the quality of the data was poor due to the presence of the fragment, refinement was stopped at this point. No hydrogen atoms were considered; no space-filling

plots were drawn. Though this study was unsatisfactory from a reliable crystallographic viewpoint, it did serve to unambiguously characterize the gross structural features of the molecule, which are seen to be related to the well-characterized compound described below.

$W_2(\mu-H)(\mu-CPh)(O-i-Pr)_4(Quin)_2$. A well-formed small crystal was selected using inert atmosphere handling techniques. The crystal was transferred to the goniostat, where it was cooled to -152 °C for characterization and data collection. A systematic search of a limited hemisphere of reciprocal space yielded a set of reflections that exhibited monoclinic symmetry and systematic extinctions of $0k0$ for $k = 2n + 1$ and $h01$ for $1 = 2n + 1$, identifying the space group as $P2_1/c$. Data collection was carried out in the usual manner. A total of 5200 reflections was collected. After processing and averaging of equivalent reflections, a unique set of 4625 reflections was obtained. The R for the averaging was 0.066 for 1232 reflections measured more than once. An absorption correction was carried out; the R for the averaging improved to 0.045.

The structure was solved by the usual combination of direct methods and heavy atom Fourier methods. All non-hydrogen atoms were readily located, and the hydrogen atoms were

located in a subsequent difference Fourier. The μ -hydrogen atom was visible in a difference Fourier and was included in the refinements. The structure was refined using full-matrix least-squares fit with anisotropic thermal parameters on all non-hydrogen atoms and isotropic thermal parameters on the hydrogen atoms. The final R was 0.045 for 3811 reflections considered observed by the criterion $F > 3.0\sigma(F)$.

The final difference Fourier was essentially featureless except for a few peaks of $1 e/\text{\AA}^3$ in the immediate vicinity of the W atoms.

Acknowledgment. We thank the National Science Foundation and the Wrubel Computing Center for support. B.W.E. was the 1986/87 Indiana University SOHIO Fellow.

Supplementary Material Available: Tables of anisotropic thermal parameters, complete listings of bond distances and bond angles (64 pages). See any current masthead page for ordering information.

OM940742Z

Five-Membered-Niobacycle Formation from an Allyl–Alkyne Coupling Reaction

Fabienne Biasotto, Michel Etienne,* and Françoise Dahan

Laboratoire de Chimie de Coordination du CNRS, UPR 8241, 205 route de Narbonne,
31 077 Toulouse Cedex, France

Received December 28, 1994[®]

Reaction of $\text{Tp}^*\text{NbCl}_2(\text{PhC}\equiv\text{CR})$ ($\text{R} = \text{CH}_3, \text{Ph}$) with 1 equiv of allyl Grignard gives moderate yield of five-membered niobacycles $\text{Tp}^*(\text{Cl})\text{Nb}[\text{C}(\text{Ph})\text{C}(\text{R})\text{CHCH}(\text{CH}_3)]$ resulting from an allyl–alkyne coupling reaction accompanied by a 1,3-hydrogen shift in the allyl moiety. Both the spectroscopic and X-ray crystal data indicate an η^4 -butadienyl formulation is appropriate for the new ligand.

Introduction

We have recently discovered rare cases of room-temperature stable *n*-alkyl- (ethyl and *n*-propyl) niobium alkyne complexes $\text{Tp}^*\text{Nb}(\text{Cl})(\text{CH}_2\text{CH}_2\text{R})(\text{PhC}\equiv\text{CR}')$ ($\text{R} = \text{H}, \text{CH}_3$; $\text{Tp}^* = \text{hydrotris}(3,5\text{-dimethylpyrazolyl})\text{-borate}$) where an α -agostic interaction is preferred over a more commonly observed β -agostic interaction.^{1–3} This is more likely due to the use of the bulky Tp^* ligand which prevents the sterically demanding bending of the alkyl group that would be necessary for the β -agostic interaction to occur.^{1,4} Upon heating, an intramolecular exchange of the niobium-bound alkyl group with the alkyne substituent is observed, the α -agostic interaction assisting the reaction.³ A benzyl complex, shown to be nonagostic, merely decomposes upon thermolysis.³ In order to understand more in depth the occurrence of such α -agostic interactions and rearrangements, we are studying the effects of substitution at C α . In this note, we report on the allyl–alkyne coupling reaction that results from allyl Grignard addition to the dichloro alkyne complexes $\text{Tp}^*\text{NbCl}_2(\text{PhC}\equiv\text{CR}')$. We present first spectroscopic and crystallographic data on the five-membered niobacycles which are formed, and then we briefly discuss a possible reaction pathway.

Results and Discussion

Synthesis and Spectroscopic Data. The treatment of a red-purple toluene solution of $\text{Tp}^*\text{NbCl}_2(\text{PhC}\equiv\text{CCH}_3)$ (**1a**)⁵ with 1 equiv of allylmagnesium chloride between -30 °C and room temperature leads to an orange-brown slurry shown by ¹H NMR to contain a single organoniobium complex apart from ill-defined signals due to unknown decomposition products. The orange crystalline compound is isolated in 25% yield after chromatographic workup and crystallization. It

has been characterized as the niobacycle $\text{Tp}^*(\text{Cl})\text{Nb}[\text{C}(\text{Ph})\text{C}(\text{CH}_3)\text{C}(\text{H})\text{CH}(\text{CH}_3)]$ (**2a**) on the basis of elemental analysis and ¹H and ¹³C NMR data. Starting from the diphenylacetylene complex $\text{Tp}^*\text{NbCl}_2(\text{PhC}\equiv\text{CPh})$ (**1b**), a similar compound $\text{Tp}^*(\text{Cl})\text{Nb}[\text{C}(\text{Ph})\text{C}(\text{Ph})\text{C}(\text{H})\text{CH}(\text{CH}_3)]$ (**2b**) has been obtained and fully identified by an X-ray crystallographic analysis. These events are summarized in Scheme 1.

Thus, compounds **2a,b** result from the coupling of the 4e-donor alkyne in **1a,b** with a rearranged allyl group. This rearrangement involves a 1,3-hydrogen shift.

In the ¹H and ¹³C NMR in benzene-*d*₆ of **2a,b** each set of the Tp^* hydrogens and carbons appears in a 1:1:1 ratio in accord with the lack of plane of symmetry in these niobacycles. For **2a**, the rearranged allyl group is identified by a doublet integrating for one proton at δ 5.49 attributed to H γ (we assign the α position to the phenyl attached carbon; see Scheme 1), coupled (³*J*_{HH} = 12.4 Hz) to a shielded *anti* proton H δ (δ 1.62). H δ shows additional coupling (³*J*_{HH} = 5.5 Hz) with a methyl group (δ 2.42) bound to the same C δ carbon. The C γ and C δ carbons give ¹³C NMR signals at δ 112.2 (d, ¹*J*_{CH} = 150 Hz) and δ 93.4 (d, ¹*J*_{CH} = 133 Hz), respectively. The latter coupling constant indicate substantial sp³ hybridization for C δ , which is furthermore slightly broadened by the niobium nucleus. The formerly phenylpropyne ligand is now identified by a niobium-broadened carbene-like resonance assigned to C α (δ 240.0) and by a second quaternary signal at δ 105.8 attributed to C β . Similar key spectral data have been obtained for **2b**.

Solid State Molecular Structure of 2b. An ORTEP drawing resulting from an X-ray diffraction analysis on a single crystal of **2b** is shown in Figure 1. Table 1 summarizes the crystallographic and solution and refinement data, and atomic coordinates are to be found in Table 2. Table 3 provides relevant bond lengths and angles. The overall geometry around the niobium center is that of a distorted octahedron if C(2) and C(3) are neglected in defining the metal coordination sphere, or a capped octahedron may be visualized when considering the interaction of the C(2)–C(3) bond with the niobium center. The almost planar four-carbon chain (torsional angle C(1)–C(2)–C(3)–C(4) = $-5.7(7)^\circ$) is η^4 -bound to the niobium center via a double bond with C(1)

[®] Abstract published in *Advance ACS Abstracts*, March 15, 1995.

(1) Brookhart, M.; Green, M. L. H.; Wong, L.-L. *Prog. Inorg. Chem.* **1988**, *36*, 1.

(2) Etienne, M. *Organometallics* **1994**, *13*, 410.

(3) Etienne, M.; Biasotto, F.; Mathieu, R. *J. Chem. Soc., Chem. Commun.* **1994**, 1661.

(4) A similar preference, also proposed to lie to steric grounds, has appeared in cationic hafnocene complexes: Guo, Z.; Swenson, D. C.; Jordan, R. F. *Organometallics* **1994**, *13*, 1424.

(5) Etienne, M.; White, P. S.; Templeton, J. L. *Organometallics* **1991**, *10*, 3801.

Scheme 1

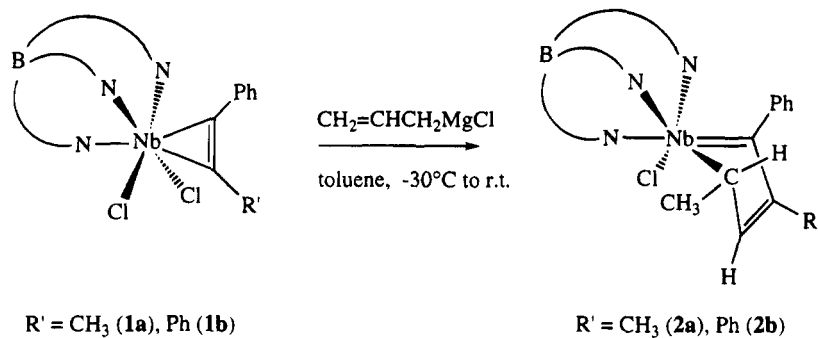


Table 1. Experimental Data for the X-ray Study of
Tp*(Cl)Nb[C(Ph)C(Ph)CHCH(CH₃)]·0.5C₆H₁₄ (2b)

formula	C ₃₅ H ₄₄ BN ₆ ClNb
f _w	687.94
cryst system	monoclinic
space group	P2 ₁ /n (No. 14)
a, Å	10.640(1)
b, Å	14.539(2)
c, Å	23.031(2)
β, deg	102.38(1)
V, Å ³	3480.0(8)
Z	4
F(000)	1436
ρ _{calcd} , g cm ⁻³	1.313
temp, K	293
radiation	graphite monochromated, λ(Mo Kα) = 0.710 73 Å
cryst size, mm	0.40 × 0.40 × 0.30
μ, mm ⁻¹	0.42
scan mode	ω-2θ
2θ max, deg	48
scan range, deg	0.80 + 0.35 tan θ
no. of rflns measd	5769 (0 ≤ h ≤ 12, 0 ≤ k ≤ 16, -26 ≤ l ≤ 26)
no of indep rflns	5455 (R _{av} = 0.025 on I)
final no. of variables	392
R ^a	0.033 [3747 rflns with F _o ² > 3σ(F _o ²)]
R _w ^b	0.034 (with unit weights)
goodness of fit	1.175

$$^a R = \frac{\sum ||F_o| - |F_c||}{\sum |F_o|}, \quad ^b R_w = \frac{[\sum w(|F_o| - |F_c|)^2 / \sum w |F_o|^2]^{1/2}}$$

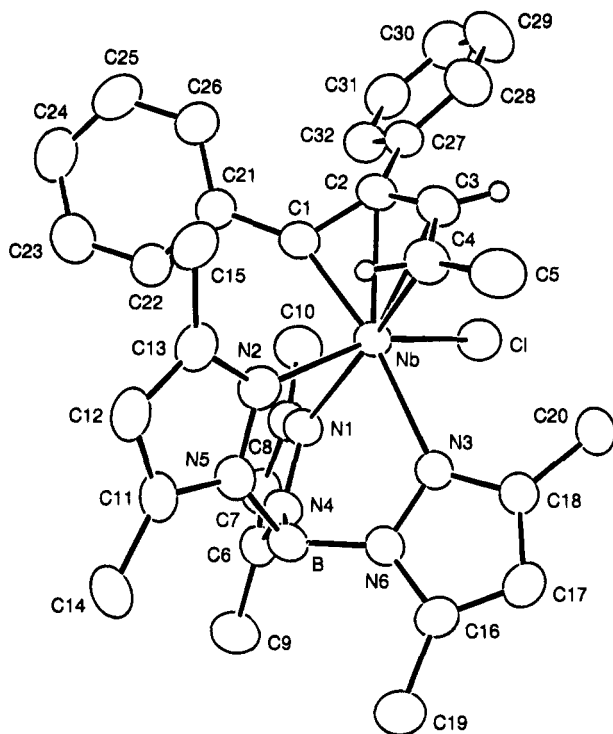


Figure 1. ORTEP plot of 2b.

[Nb-C(1) = 1.993(4) Å; Nb=C = 2.026 Å in Cp*Nb(=CHPh)(NR)(PMe₃)⁶], a single bond with C(4) [Nb-C(4) = 2.277(5) Å; Nb-C = 2.316(8) Å in Cp₂Nb(CH₂-CH₃)(C₂H₄)⁷], and with C(2) and C(3) unsymmetrically interacting with the metal center (Nb-C(2) = 2.334(4); Nb-C(3) = 2.370(5) Å). The five-membered niobacycle is folded about the C(1)-C(4) axis (109.4(2)°). There is appreciable electron delocalization over the four-carbon chain although C(1)-C(2) is slightly longer than C(3)-C(4) (1.439(7), 1.392(7) Å, respectively). C(2)-C(3) (1.418(6) Å) is, within 3σ, similar to the two other C-C bond lengths. All of these carbons are sp²-hybridized but, taking also into account the reduced ¹J_{CH} of 136 Hz, C(4) (Cδ) retains some sp³ character. The bonding at C(4) is reminiscent of that in diene- (butenediyl) niobium complexes.⁸

Structural Discussion. Both the spectroscopic data for 2a,b and the crystallographic data for 2b are characteristic of a now well-known family of η⁴-butadi-

enyl (η⁴-C₄R₅) group 6 metal complexes as exemplified by the work of Davidson,⁹ Green,¹⁰ Templeton,¹¹ and their co-workers. Somewhat related (η³-butadienyl)-niobium complexes have also been fully characterized.¹² The three resonance forms shown in Scheme 2 nicely account for all of the data. The carbene-like Cα, the single bond between Nb and Cδ, and sp³ character at Cδ are noteworthy.

However, the data also fit with a heteroatom-containing class of group 5 metal complexes as described more recently by Curtis and co-workers¹³ and by some of us.¹⁴ These complexes are oxa- or azametallacycles

(9) Carlton, L.; Davidson, J. L.; Ewing, P.; Manojlovic-Muir, L.; Muir, K. W. *J. Chem. Soc., Chem. Commun.* **1985**, 1474.

(10) (a) Conole, G. C.; Green, M.; McPartlin, M.; Reeve, C.; Woolhouse, C. M. *J. Chem. Soc., Chem. Commun.* **1988**, 1310. (b) Green, M.; Mahon, M. F.; Molloy, K. C.; Nation, C. B. M.; Woolhouse, C. M. *J. Chem. Soc., Chem. Commun.* **1991**, 1587.

(11) (a) Morrow, J. R.; Tonker, T. L.; Templeton, J. L. *J. Am. Chem. Soc.* **1985**, *107*, 5004. (b) Feng, S. G.; Gamble, A. S.; Templeton, J. L. *Organometallics* **1989**, *8*, 2024.

(12) (a) Herberich, G. E.; Hessner, B.; Mayer, H. *J. Organomet. Chem.* **1986**, *314*, 123. (b) Herberich, G. E.; Mayer, H. *Organometallics* **1990**, *9*, 2655.

(13) (a) Curtis, M. D.; Real, J. *J. Am. Chem. Soc.* **1986**, *108*, 4668. (b) Curtis, M. D.; Real, J.; Hirpo, W.; Butler, W. M. *Organometallics* **1990**, *9*, 66. (c) Hirpo, W.; Curtis, M. D. *Organometallics* **1994**, *13*, 2706.

(14) Etienne, M.; White, P. S.; Templeton, J. L. *Organometallics* **1993**, *12*, 4010.

(6) Cockcroft, J. K.; Gibson, V. C.; Howard, J. A. K.; Pool, A. D.; Siemeling, U.; Wilson, C. *J. Chem. Soc., Chem. Commun.* **1992**, 1668.

(7) Guggenberger, L. J.; Meakin, P.; Tebbe, F. N. *J. Am. Chem. Soc.* **1974**, *96*, 5420.

(8) Okamoto, T.; Yasuda, H.; Nakamura, A.; Kai, Y.; Kanehisa, N.; Kasai, N. *J. Am. Chem. Soc.* **1988**, *110*, 5008.

Scheme 2

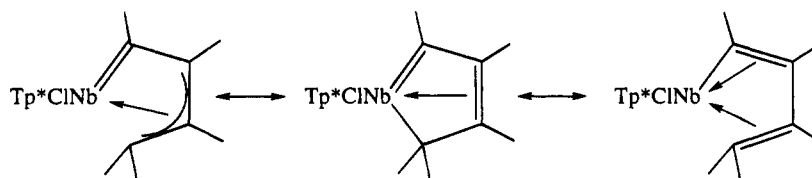


Table 2. Fractional Atomic Coordinates and Isotropic or Equivalent Isotropic Temperature Factors ($\text{\AA}^2 \times 100$) with Esd's in parentheses for 2b

atom ^b	x/a	y/b	z/c	$U_{\text{eq}}^a/U_{\text{iso}}$
Nb	0.58326(4)	0.55177(3)	0.80503(2)	4.06(2)*
C1	0.6192(1)	0.39218(8)	0.82883(5)	6.11(8)*
C(1)	0.4478(4)	0.5612(3)	0.7307(2)	4.6(3)*
C(2)	0.5306(4)	0.5001(3)	0.7068(2)	4.8(3)*
C(3)	0.6649(4)	0.5173(4)	0.7195(2)	5.5(3)*
C(4)	0.7272(4)	0.5932(4)	0.7495(2)	5.5(3)*
C(5)	0.8667(5)	0.6116(5)	0.7580(3)	9.4(5)*
N(1)	0.4481(3)	0.5574(3)	0.8680(1)	4.5(2)*
N(2)	0.5549(3)	0.7104(2)	0.8146(2)	4.7(2)*
N(3)	0.7336(3)	0.5812(2)	0.8932(2)	4.6(2)*
N(4)	0.4732(3)	0.6110(3)	0.9184(2)	4.6(2)*
N(5)	0.5528(3)	0.7463(3)	0.8701(2)	4.8(2)*
N(6)	0.7095(3)	0.6416(2)	0.9351(2)	4.3(2)*
B	0.5765(5)	0.6865(4)	0.9260(2)	4.7(3)*
C(6)	0.3905(4)	0.5889(3)	0.9536(2)	5.3(3)*
C(7)	0.3108(5)	0.5214(3)	0.9251(2)	5.9(3)*
C(8)	0.3474(4)	0.5038(3)	0.8722(2)	4.9(3)*
C(9)	0.3933(5)	0.6326(4)	1.0122(2)	7.6(4)*
C(10)	0.2894(5)	0.4360(4)	0.8249(2)	6.8(3)*
C(11)	0.5286(5)	0.8373(3)	0.8661(3)	5.9(3)*
C(12)	0.5139(5)	0.8611(3)	0.8078(3)	6.7(4)*
C(13)	0.5316(5)	0.7821(3)	0.7766(2)	5.7(3)*
C(14)	0.5155(6)	0.8964(4)	0.9176(3)	9.1(5)*
C(15)	0.5267(5)	0.7782(4)	0.7118(2)	7.6(4)*
C(16)	0.8137(4)	0.6496(3)	0.9803(2)	4.4(3)*
C(17)	0.9063(4)	0.5927(3)	0.9674(2)	4.9(3)*
C(18)	0.8538(4)	0.5507(3)	0.9138(2)	4.9(3)*
C(19)	0.8172(5)	0.7117(4)	1.0314(2)	6.3(3)*
C(20)	0.9167(5)	0.4803(4)	0.8823(2)	7.7(4)*
C(21)	0.3233(4)	0.5983(3)	0.7008(2)	4.6(3)*
C(22)	0.2494(4)	0.6470(3)	0.7332(2)	5.4(3)*
C(23)	0.1358(5)	0.6879(4)	0.7058(3)	6.8(4)*
C(24)	0.0905(5)	0.6792(4)	0.6455(3)	6.7(4)*
C(25)	0.1601(5)	0.6300(4)	0.6127(2)	6.3(3)*
C(26)	0.2765(5)	0.5902(3)	0.6400(2)	5.6(3)*
C(27)	0.4837(4)	0.4114(3)	0.6758(2)	4.9(3)*
C(28)	0.5596(6)	0.3644(4)	0.6434(2)	7.1(4)*
C(29)	0.5166(6)	0.2843(4)	0.6138(3)	8.6(5)*
C(30)	0.3984(6)	0.2508(4)	0.6149(3)	7.9(4)*
C(31)	0.3215(5)	0.2959(4)	0.6459(2)	6.8(4)*
C(32)	0.3634(5)	0.3752(3)	0.6760(2)	5.7(3)*
C(1s)	0.5321(8)	0.5448(4)	0.4985(3)	20.7(7)
C(2s)	0.7118(8)	0.6296(8)	0.5603(5)	21.8(5)
C(3s)	0.6707(5)	0.5417(9)	0.5275(9)	19.7(9)
C(4s)	0.5849(13)	0.5839(11)	0.5581(5)	17.6(8)

^a Asterisk indicates $U_{\text{eq}} = \frac{1}{3}[U_{11} + U_{22} + U_{33}]$. ^b C(3s) and C(4s) have an occupancy factor of 0.5.

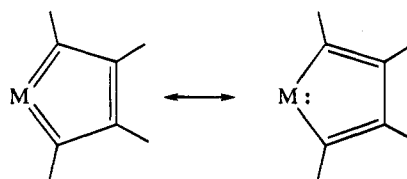
where -O- or -NR- groups replace the -CH(CH₃)- group at the δ position. Curtis has carefully analyzed this situation,¹³ and he has proposed a metallacyclopentatriene formulation akin to that found in some more symmetrical group 6^{13b,15} and group 5 metal complexes.¹⁶ In this case, two resonance forms may be drawn as in Scheme 3.¹³

As we mentioned just above, the oxa- and azametallacycles may be viewed through both the η^4 -butadienyl

Table 3. Selected Bond Lengths (\AA) and Angles (deg) for Complex $\text{Tp}^*(\text{Cl})\text{Nb}[\text{C}(\text{Ph})\text{C}(\text{Ph})\text{CHCH}(\text{CH}_3)]$ (2b)

Bond Lengths			
Nb-N(1)	2.252(4)	C(1)-C(2)	1.439(7)
Nb-N(2)	2.343(4)	C(1)-C(21)	1.459(6)
Nb-N(3)	2.339(4)	C(2)-C(3)	1.418(6)
Nb-Cl	2.396(1)	C(2)-C(27)	1.508(6)
Nb-C(1)	1.993(4)	C(3)-C(4)	1.392(7)
Nb-C(2)	2.334(4)	C(4)-C(5)	1.479(7)
Nb-C(3)	2.370(5)	C(3)-H(C3)	0.97(3)
Nb-C(4)	2.277(5)	C(4)-H(C4)	0.97(3)
Bond Angles			
C(1)-Nb-C(2)	37.8(2)	Nb-C(3)-C(4)	69.0(3)
C(1)-Nb-C(3)	68.1(2)	C(2)-C(3)-C(4)	126.4(5)
C(1)-Nb-C(4)	87.0(2)	C(2)-C(3)-H(C3)	118(2)
C(2)-Nb-C(3)	35.1(2)	C(4)-C(3)-H(C3)	114(2)
C(2)-Nb-C(4)	65.9(2)	Nb-C(3)-H(C3)	124(3)
C(3)-Nb-C(4)	34.8(2)	Nb-C(4)-C(3)	76.3(3)
Nb-C(1)-C(2)	84.0(2)	Nb-C(4)-C(5)	138.6(4)
Nb-C(2)-C(1)	58.1(2)	Nb-C(4)-H(C4)	83(3)
Nb-C(2)-C(3)	73.9(3)	C(3)-C(4)-C(5)	124.5(5)
C(1)-C(2)-C(3)	119.1(4)	C(3)-C(4)-H(C4)	119(2)
Nb-C(3)-C(2)	71.1(3)	C(5)-C(4)-H(C4)	109(2)

Scheme 3



and the metallacyclopentatriene formulations. Actually, we propose that these heteroatom-containing complexes are bridges between the two descriptions, but again the data for **2a,b** clearly point to the η^4 -butadienyl formulation (Scheme 2).

To our knowledge, **2a,b** are the first compounds of this kind in niobium chemistry. The niobium has 16 valence electrons and, formally, the oxidation state is +3 (d^2) or +5 (d^0) with the η^4 -butadienyl ligand giving 6 (monoanionic ligand) or 8 (trianionic ligand) electrons. η^3 -Butadienyl complexes in the bent niobocene series have been described by Herberich and co-workers:¹² the electron count for the metal is 18 with no interaction of the C β -C γ bond with the niobium center (Nb-C = 2.78 and 2.79 \AA in a typical example,^{12b} $(\text{Cp}_2\text{Nb}[\text{C}(\text{Et})\text{C}(\text{Et})\text{C}(\text{CO}_2\text{Me})\text{CH}(\text{CO}_2\text{Me})])$.

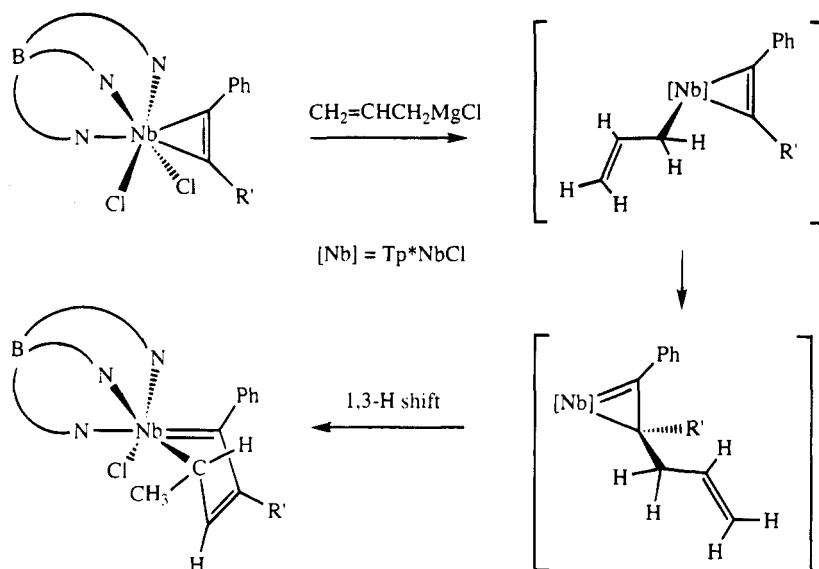
Mechanistic Consideration. Finally, we would like to briefly discuss a possible pathway for this "allyl-alkyne" coupling reaction. Recall first that (η^1 -allyl)-niobium complexes are known.¹⁷ Although it is well-known that allylic hydrogens are quite mobile via acid-base catalysis, rearrangement of an η^1 -allyl complex to

(15) (a) Hirpo, W.; Curtis, M. D. *J. Am. Chem. Soc.* **1988**, *110*, 5218. (b) Kerschner, J. L.; Fanwick, P. E.; Rothwell, I. P. *J. Am. Chem. Soc.* **1988**, *110*, 8235. (c) Kriley, C. E.; Kerschner, J. L.; Fanwick, P. E.; Rothwell, I. P. *Organometallics* **1993**, *12*, 2051.

(16) (a) Hessen, B.; Teuben, J. H. *J. Organomet. Chem.* **1989**, *367*, C18. (b) Hessen, B.; Meetsma, A.; Van Bolhuis, F.; Teuben, J. H. *Organometallics* **1990**, *9*, 1925.

(17) For a recent example, see: Chernega, A. N.; Green, M. L. H.; Suarez, A. G. *J. Chem. Soc., Dalton Trans.* **1993**, 3031.

Scheme 4



an η^1 -vinyl complex (rearrangement of an η^1 -prop-2-ene complex to an η^1 -prop-1-ene complex) prior to alkyne coupling is unlikely in this system since we have recently isolated¹⁸ the thermally stable (up to 353 K) complex $\text{Tp}^*\text{Nb}(\text{Cl})(\text{CPh}=\text{C}(\text{Et})_2)(\text{PhC}\equiv\text{CCH}_3)$, containing 4e-donor alkyne and η^1 -vinyl ligands. In niobocene complexes, coupling of η^1 -vinyls with 2e-donor alkynes is known,¹² whereas η^2 -vinyls couple to 4e-donor alkynes in group 6 metal complexes.¹⁹ The required 1,3-hydrogen shift could occur after allyl-alkyne coupling via C α attack at the coordinated alkyne carbon. In support of this proposal, we recently described a similar mechanism which accounts for alkyl group exchange between the alkyne and the niobium center.³ A possible sequence of events is depicted in Scheme 4. The driving force for the 1,3-shift in a putative allyl-substituted η^2 -vinyl intermediate would be the formation of a conjugated carbon chain.

Experimental Section

General Methods. All reactions and workup procedures were performed under an atmosphere of dried dinitrogen using conventional vacuum line and Schlenk tube techniques. Toluene was dried and distilled by refluxing over sodium-benzophenone under argon. *n*-Hexane was dried and distilled over CaH_2 under argon. These solvents were then stored over molecular sieves under a dinitrogen atmosphere. Column chromatography was performed on silica gel. Allylmagnesium chloride (2.0 M in tetrahydrofuran) was purchased. Benzene- d_6 was stored over molecular sieves. ^1H NMR data were acquired at 200 or 250 MHz, and ^{13}C NMR data at 50.3 or 62.9 MHz. Elemental analyses were performed in the Analytical Service of our laboratory.

Complexes $\text{Tp}^*\text{Nb}(\text{Cl})[\text{C}(\text{Ph})\text{C}(\text{R})\text{C}(\text{H})\text{CHCH}_3]$ (**2a,b**) are synthesized according to the same procedure described in detail for **2a** starting from the appropriate alkyne complex.⁵

$\text{Tp}^*\text{Nb}(\text{Cl})[\text{C}(\text{Ph})\text{C}(\text{CH}_3)\text{C}(\text{H})\text{CH}(\text{CH}_3)]$ (**2a**). A vigorously stirred toluene (50 mL) solution of $\text{Tp}^*\text{NbCl}_2(\text{PhC}\equiv\text{CCH}_3)$ (**1a**) (0.580 g, 1.0 mmol) cooled to -30°C is treated dropwise with allylmagnesium chloride (0.50 mL, 1.0 mmol). Slow warming to room temperature over 4 h gives an orange brown slurry. Concentration to ca. 25 mL, addition of hexane (10

mL), and filtration through Celite (subsequently rinsed with hexane three times) leads to an oil which is further purified by column chromatography. Elution with a 1:1 (v) toluene/hexane mixture gives an orange solution, from which, after evaporation to dryness and recrystallization from a toluene/hexane mixture at $+5^\circ\text{C}$, compound **2a** is obtained as orange microcrystals in 25% yield (0.150 g; 0.25 mmol). ^1H NMR: δ = 6.98–6.56 (m, 5H, C_6H_5), 5.76, 5.74, 5.21 (1H each, Tp^*CH), 5.49 (d, J = 12.4 Hz, 1H, CHCHCH_3), 2.42 (d, J = 5.5 Hz, 3H, CHCHCH_3), 2.80, 2.30, 2.22, 2.19, 2.18, 2.00, 1.17 (3H each, Tp^*CH_3 and β - CH_3), 1.62 (pseudosextet, J = 12.3, 5.5 Hz, 1H, CHCHCH_3). ^{13}C NMR (except phenyl resonances): δ = 240.0 (NbC), 152.7, 152.2, 152.0, 144.6, 144.5, 140.5 (Tp^*CCH_3), 112.2 (d, J_{CH} = 150 Hz, CHCHCH_3), 108.7, 108.3; 108.0 (Tp^*CH), 105.8 (NbCPhCCH $_3$), 93.4 (d, J_{CH} = 133 Hz, CHCHCH_3), 20.8, 19.0, 17.4, 16.9, 16.8, 13.7, 13.3, 13.1 (CHCHCH_3 , β - CH_3 and Tp^*CH_3). Anal. Calcd for $\text{C}_{27}\text{H}_{35}\text{BClN}_6$: C, 55.7; H, 6.00; N, 14.4. Found: C, 55.8; H, 5.9; N, 14.9.

2b. ^1H NMR: δ = 8.18 (d, J = 7 Hz, 2H, NbCPhC-*o*- C_6H_5), 7.36 (t, J = 7 Hz, 2H, NbCPhC-*m*- C_6H_5), 7.21 (t, J = 7 Hz, 1H, NbCPhC-*p*- C_6H_5), 6.81–6.45 (m, 5H, NbCC $_6\text{H}_5$), 5.86 (d, J = 12.5 Hz, 1H, CHCHCH_3), 5.75 (s, 2H, Tp^*CH), 5.24 (s, 1H, Tp^*CH), 2.64, 2.30, 2.21, 2.09, 2.01, 1.18 (s, 3H each, Tp^*CH_3), 2.37 (d, J = 5.5 Hz, 3H, CHCHCH_3), 1.75 (pseudosextet, J = 12.4, 5.8 Hz, 1H, CHCHCH_3). ^{13}C NMR (except phenyl resonances): δ = 235.7 (NbC), 114.2 (NbCPhCPh), 153.2, 152.0, 151.9, 146.2, 142.4, 140.9 (Tp^*CCH_3), 108.8, 108.5, 108.2 (Tp^*CH), 95.6 (d, J = 136 Hz, CHCHCH_3), 20.7 (d, J = 127 Hz, CHCHCH_3), 17.6, 17.1, 17.1, 13.6, 13.4, 13.0 (Tp^*CH_3). Anal. Calcd for $\text{C}_{32}\text{H}_{37}\text{BClN}_6\text{Nb}\cdot 0.5\text{C}_6\text{H}_{14}$: C, 61.1; H, 6.45; N, 12.2. Found: C, 61.7; H, 6.6; N, 11.8. One of these crystals was selected for the X-ray crystal study.

X-ray Diffraction Study. Data collection, crystal, and refinement parameters are collected in Table 1. Diffraction measurements were made on an Enraf-Nonius CAD4 diffractometer. The unit cell parameters were obtained from a least-squares fit of 25 reflections (with θ between 12.5 and 16°). Data were collected with the ω - 2θ scan technique and a variable scan rate with a maximum scan time of 60 s per reflection. The intensities of three standard reflections were monitored every 2 h. No significant variations were observed. Lorentz and polarization corrections and empirical absorption corrections²⁰ from ψ scans were applied using the MolEN package,²¹

(20) North, A. C. T.; Phillips, D. C.; Mathews, F. S. *Acta Crystallogr., Sect. A*, **1968**, *A21*, 351.

(21) Fair, C. K. *MolEN. Structure Solution Procedures*; Enraf-Nonius: Delft, Holland, 1990.

(18) Etienne, M. Unpublished result.

(19) Templeton, J. L. *Adv. Organomet. Chem.* **1989**, *29*, 1.

and the data were reduced to $|F_o|$ values. The structure was solved by Patterson methods using the program SHELXS86.²² Full-matrix least-squares refinement was made with the SHELX76 program.²³ All non-H atoms of the complex were refined anisotropically. A disordered half solvent molecule (*i.e.* hexane) was found and refined isotropically. Solvent H atoms were not calculated. All other H atoms were geometrically placed, except those bonded to C(3) and C(4) atoms which were isotropically refined. H isotropic thermal parameters were first refined and then kept fixed. The maximum shifts to esd ratio in the last full-matrix least-squares cycle were 0.129 for solvent and 0.004 for other parameters. The final difference Fourier map showed no peaks higher than $0.76 \text{ e } \text{\AA}^{-3}$ near the

(22) Sheldrick, G. M. *SHELXS86. Program for Crystal Structure Solution*; University of Gottingen: Gottingen, FRG, 1986.

(23) Sheldrick, G. M. *SHELX76. Program for Crystal Structure Determination*; University of Cambridge: Cambridge, U.K., 1976.

disordered C_6H_{14} , nor any deeper than $-0.57 \text{ e } \text{\AA}^{-3}$. Atomic scattering factors were taken from ref 24. Crystallographic plot was made with ORTEP.²⁵ All calculations were performed on a MicroVax 3400.

Supplementary Material Available: Crystal structure data for **2b**, including tables of hydrogen positional and thermal parameters, anisotropic thermal parameters, bond distances, bond angles, torsion angles, and least-squares plane equations (5 pages). Ordering information is given on any current masthead page.

OM940992F

(24) *International Tables for X-Ray Crystallography*; Kynoch Press: Birmingham, U.K., 1974; Vol. IV.

(25) Johnson, C. K. *ORTEP*. Report ORNL-3794; Oak Ridge National Laboratory: Oak Ridge, TN, 1965.

Alkyl, Alkylidene, and Alkylidyne Complexes of Rhenium

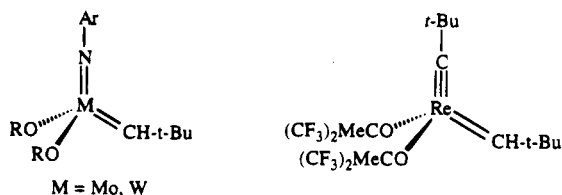
Anne M. LaPointe and Richard R. Schrock*

Room 6-331, Department of Chemistry, Massachusetts Institute of Technology,
Cambridge, Massachusetts 02139Received December 13, 1994[®]

The reaction of $\text{Re}(\text{C-}t\text{-Bu})(\text{CH-}t\text{-Bu})(\text{CH}_2\text{-}t\text{-Bu})_2$ with triflic acid, pentafluorophenol, $\text{HBF}_4\cdot\text{OEt}_2$, or $[\text{H}(\text{OEt}_2)_2]^+[\text{BAR}^{\text{F}}_4]^-$ ($\text{Ar}^{\text{F}} = 3,5\text{-C}_6\text{H}_3(\text{CF}_3)_2$) yields complexes of the general formula $\text{Re}(\text{C-}t\text{-Bu})(\text{CH}_2\text{-}t\text{-Bu})_3\text{X}$ ($\text{X} = \text{OTf}, \text{OC}_6\text{F}_5, \text{BF}_4, \text{BAR}^{\text{F}}_4$) in 60–80% yield. $\text{Re}(\text{C-}t\text{-Bu})(\text{CH}_2\text{-}t\text{-Bu})_3\text{X}$ reacts with coordinating ligands L ($\text{L} = \text{py}, \text{CH}_3\text{CN}, \text{CD}_3\text{OD}, \text{THF}$) to form neopentane and $\text{Re}(\text{C-}t\text{-Bu})(\text{CH-}t\text{-Bu})(\text{CH}_2\text{-}t\text{-Bu})(\text{L})_n\text{X}$ ($n = 1\text{--}3$). The reaction of $\text{Re}(\text{C-}t\text{-Bu})(\text{CH-}t\text{-Bu})(\text{CH}_2\text{-}t\text{-Bu})(\text{py})_2(\text{OTf})$ with NaC_5H_5 , NaL_{OEt} ($\text{L}_{\text{OEt}} = [\text{CpCo}(\text{PO}(\text{OEt})_2)_3]$, or NaHBpz_3 in THF yields $\text{Re}(\text{C-}t\text{-Bu})(\text{CH-}t\text{-Bu})(\text{CH}_2\text{-}t\text{-Bu})(\eta^5\text{-C}_5\text{H}_5)$, $\text{Re}(\text{C-}t\text{-Bu})(\text{CH-}t\text{-Bu})(\text{CH}_2\text{-}t\text{-Bu})(\text{L}_{\text{OEt}})$, or $\text{Re}(\text{C-}t\text{-Bu})(\text{CH-}t\text{-Bu})(\text{CH}_2\text{-}t\text{-Bu})(\text{HBpz}_3)$, respectively, while the reaction between $\text{Re}(\text{C-}t\text{-Bu})(\text{CH-}t\text{-Bu})(\text{CH}_2\text{-}t\text{-Bu})(\text{py})_2(\text{OTf})$ and 1,4,7-trithiacyclononane produces colorless $[\text{Re}(\text{C-}t\text{-Bu})(\text{CH-}t\text{-Bu})(\text{CH}_2\text{-}t\text{-Bu})(\eta^3\text{-S}_3\text{C}_6\text{H}_{12})]^+[\text{OTf}]^-$ in 96% yield. $\text{Re}(\text{C-}t\text{-Bu})(\text{CH-}t\text{-Bu})(\text{CH}_2\text{-}t\text{-Bu})(\text{L})$ ($\text{L} = \text{Cp}, \text{L}_{\text{OEt}}$) and $[\text{Re}(\text{C-}t\text{-Bu})(\text{CH-}t\text{-Bu})(\text{CH}_2\text{-}t\text{-Bu})(\eta^3\text{-S}_3\text{C}_6\text{H}_{12})]^+[\text{OTf}]^-$ react with triflic acid to form $\text{Re}(\text{C-}t\text{-Bu})(\text{CH-}t\text{-Bu})(\text{L})(\text{OTf})$ or $[\text{Re}(\text{C-}t\text{-Bu})(\text{CH-}t\text{-Bu})(\text{OTf})(\eta^3\text{-S}_3\text{C}_6\text{H}_{12})]^+[\text{OTf}]^-$, respectively. A similar reaction between $\text{Re}(\text{C-}t\text{-Bu})(\text{CH-}t\text{-Bu})(\text{CH}_2\text{-}t\text{-Bu})(\text{L}_{\text{OEt}})$ and $[\text{H}(\text{OEt}_2)_2]^+[\text{BAR}^{\text{F}}_4]^-$ in ether produces $[\text{Re}(\text{C-}t\text{-Bu})(\text{CH-}t\text{-Bu})(\text{OEt}_2)(\text{L}_{\text{OEt}})]^+[\text{BAR}^{\text{F}}_4]^-$. $\text{Re}(\text{C-}t\text{-Bu})(\text{CH-}t\text{-Bu})(\text{CH}_2\text{-}t\text{-Bu})(\text{py})_2(\text{OTf})$ reacts with $\text{H}_2\text{C}=\text{CHR}$ ($\text{R} = \text{OCH}_2\text{CH}_3, \text{C}_6\text{H}_5$) to yield neohexene and $\text{Re}(\text{C-}t\text{-Bu})(\text{CHR})(\text{CH}_2\text{-}t\text{-Bu})(\text{py})_2(\text{OTf})$ complexes. $\text{Re}(\text{C-}t\text{-Bu})(\text{CH-}t\text{-Bu})(\text{CH}_2\text{-}t\text{-Bu})(\text{py})_2(\text{OTf})$ reacts with ethylene to form the unstable methylidene complex, $\text{Re}(\text{C-}t\text{-Bu})(\text{CH}_2)(\text{CH}_2\text{-}t\text{-Bu})(\text{py})_2(\text{OTf})$, which can be trapped upon addition of bpy to yield red $\text{Re}(\text{C-}t\text{-Bu})(\text{CH}_2)(\text{CH}_2\text{-}t\text{-Bu})(\text{bpy})(\text{OTf})$. $\text{Re}(\text{C-}t\text{-Bu})(\text{CH-}t\text{-Bu})(\text{CH}_2\text{-}t\text{-Bu})(\text{py})_2(\text{OTf})$ reacts with excess ethylene to form colorless $\text{Re}(\text{C-}t\text{-Bu})[(\text{CH}_2)_3\text{-}t\text{-Bu}](\text{C}_2\text{H}_4)(\text{py})_2(\text{OTf})$ in 85% yield. $\text{Re}(\text{C-}t\text{-Bu})(\text{CH-}t\text{-Bu})(\text{CH}_2\text{-}t\text{-Bu})(\text{CH}_3\text{CN})(\text{OTf})$ metathesizes 100 equiv of *cis*-2-pentene in less than 5 min, but the catalyst is not long-lived.

Introduction

Rhenium is one of three metals (along with molybdenum and tungsten) that are active in classical olefin metathesis systems.¹ In the early 1980s, evidence began to accumulate in favor of the proposition that the metal is in its highest possible oxidation state in classical olefin metathesis systems involving these metals (if the alkylidene ligand is viewed as a dianion).² A variety of four-coordinate d^0 alkylidene complexes of molybdenum,^{3,4} tungsten,⁵ and rhenium^{6–8} were prepared and employed for the metathesis of acyclic and cyclic olefins. The most successful and best understood single-component olefin metathesis catalysts are the pseudotetrahedral species shown below.



The rates of metathesis of olefins by $\text{Re}(\text{C-}t\text{-Bu})(\text{CH-}t\text{-Bu})[\text{OCMe}(\text{CF}_3)_2]_2$ and its variations are estimated to

[®] Abstract published in *Advance ACS Abstracts*, March 15, 1995.
 (1) Ivin, K. J. *Olefin Metathesis*; Academic: New York, 1983.
 (2) Schrock, R. R. *J. Organomet. Chem.* **1986**, *300*, 249.
 (3) Schrock, R. R.; Murdzek, J. S.; Bazan, G. C.; Robbins, J.; DiMare, M.; O'Regan, M. *J. Am. Chem. Soc.* **1990**, *112*, 3875.
 (4) Schrock, R. R.; Crowe, W. E.; Bazan, G. C.; DiMare, M.; O'Regan, M. B.; Schofield, M. H. *Organometallics* **1991**, *10*, 1832.

be 2 orders of magnitude slower than the fastest Mo- or W-based systems.⁸ In some cases alkylidene complexes will metathesize olefins rapidly only in the presence of Lewis acids such as AlCl_3 .^{9–12} In these mixtures, it is presumed that cationic species are the most active species for olefin metathesis and that they may be present only in low concentrations. Such a presumption is consistent with recent observations that well-defined cationic early-¹³ and late-transition-metal¹⁴ catalysts are especially active for the polymerization of olefins. Therefore we felt that a cationic alkylidene complex of rhenium might metathesize olefins at a rate comparable to that of the most active four-coordinate neutral molybdenum or tungsten catalysts. Very recently a variety of cationic tungsten alkylidene com-

(5) Schrock, R. R.; DePue, R. T.; Feldman, J.; Yap, K. B.; Yang, D. C.; Davis, W. M.; Park, L. Y.; DiMare, M.; Schofield, M.; Anhaus, J.; Walborsky, E.; Evtitt, E.; Krüger, C.; Betz, P. *Organometallics* **1990**, *9*, 2262.

(6) Toreki, R.; Schrock, R. R. *J. Am. Chem. Soc.* **1990**, *112*, 2448.

(7) Toreki, R.; Schrock, R. R. *J. Am. Chem. Soc.* **1992**, *114*, 3367.

(8) Toreki, R.; Vaughan, G. A.; Schrock, R. R.; Davis, W. M. *J. Am. Chem. Soc.* **1993**, *115*, 127.

(9) Blosch, L. L.; Abboud, K.; Boncella, J. M. *J. Am. Chem. Soc.* **1991**, *113*, 7066.

(10) Flatt, B. T.; Grubbs, R. H.; Blanski, R. L.; Calabrese, J. C.; Feldman, J. *Organometallics* **1994**, *13*, 2728.

(11) Schofield, M. H.; Schrock, R. R.; Park, L. Y. *Organometallics* **1991**, *10*, 1844.

(12) Youinou, M. T.; Kress, J.; Fischer, J.; Aguero, A.; Osborn, J. A. *J. Am. Chem. Soc.* **1988**, *110*, 1488.

(13) Hlatky, G. G.; Turner, H. W.; Eckman, R. R. *J. Am. Chem. Soc.* **1989**, *111*, 2728.

(14) Brookhart, M.; Grant, B.; Volpe, A. F., Jr. *Organometallics* **1992**, *11*, 3920.

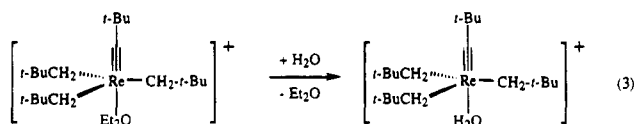
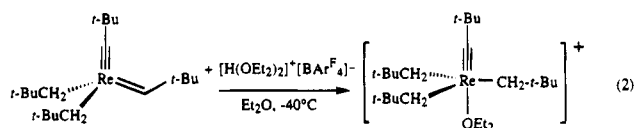
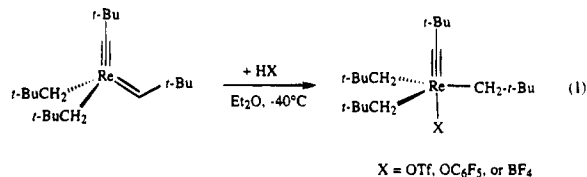
plexes were reported.^{9,15,16} However, these coordinatively saturated complexes do not metathesize olefins in the absence of a cocatalyst. The challenge then is to prepare cationic alkylidene complexes that are not coordinatively or sterically saturated, that do not interact strongly with the anion, and that do not decompose to alkylidyne complexes¹⁷ via loss of an α proton.

Although the primary goal of the research described here was to prepare cationic rhenium alkylidene complexes that were more active metathesis catalysts than $\text{Re}(\text{C-}t\text{-Bu})(\text{CH-}t\text{-Bu})[\text{OCMe}(\text{CF}_3)_2]_2$, another goal was to continue to search for rhenium alkylidene complexes that are stable to a range of functional groups, including alcohols and water. The alkylidene and alkylidyne ligands in the $\text{Re}(\text{C-}t\text{-Bu})(\text{CH-}t\text{-Bu})$ core are stable to water under some circumstances. For example, $[\text{Re}(\text{C-}t\text{-Bu})(\text{CH-}t\text{-Bu})\text{Cl}_2]_x$ can be dissolved in water and be recovered unchanged by removing the water *in vacuo*.⁷ Therefore we chose to focus on rhenium neopentylidene/neopentylidyne complexes that contain ligands that are not readily protonated, such as neopentyl, tris(pyrazolyl)borate (HBpz₃), 1,4,7-trithiacyclononane, $\eta^5\text{-C}_5\text{H}_5$, or $[\text{CpCo}(\text{PO}(\text{OEt})_2)_3]^+$ ("LOEt"),¹⁸ and counterions X that are relatively poor ligands, i.e., triflate,¹⁹ tetrafluoroborate, or $\text{B}[3,5\text{-(CF}_3)_2\text{C}_6\text{H}_3]_4$ ("BAR^F₄").¹⁴

Synthesis of $\text{Re}(\text{C-}t\text{-Bu})(\text{CH}_2\text{-}t\text{-Bu})_3\text{X}$. Our first goal was to prepare complexes of the type $[\text{Re}(\text{C-}t\text{-Bu})(\text{CH-}t\text{-Bu})(\text{CH}_2\text{-}t\text{-Bu})_n]_x^+$. The route we chose was to prepare complexes of the type $\text{Re}(\text{C-}t\text{-Bu})(\text{CH}_2\text{-}t\text{-Bu})_3\text{X}$ in which X was either a noncoordinating or weakly coordinating anion (triflate, $\text{BAR}^{\text{F}}_4^-$, or BF_4^-) and in which α -hydrogen abstraction reactions would be facile. The reaction of $\text{Re}(\text{C-}t\text{-Bu})(\text{CH-}t\text{-Bu})(\text{CH}_2\text{-}t\text{-Bu})_2$ with HX was investigated, since the reaction of $\text{Re}(\text{C-}t\text{-Bu})(\text{CH-}t\text{-Bu})(\text{CH}_2\text{-}t\text{-Bu})_2$ with HCl had been previously found to yield $\text{Re}(\text{C-}t\text{-Bu})(\text{CH}_2\text{-}t\text{-Bu})_3\text{Cl}$.^{20,21}

$\text{Re}(\text{C-}t\text{-Bu})(\text{CH-}t\text{-Bu})(\text{CH}_2\text{-}t\text{-Bu})_2$ reacts with a variety of acids as shown in equations 1 and 2. The products are highly crystalline yellow solids that are obtained in yields that range from 60–80%. Wilkinson and co-workers reported the synthesis of $\text{Re}(\text{CSiMe}_3)(\text{CH}_2\text{-SiMe}_3)_3\text{Cl}$ and found in an X-ray study that it was a trigonal bipyramid with the trimethylsilylmethyl ligands occupying the equatorial sites.²² When X = OC_6F_5 or OTf the structure is likely to be analogous to that of $\text{Re}(\text{CSiMe}_3)(\text{CH}_2\text{-SiMe}_3)_3\text{Cl}$. Since BF_4^- is known to coordinate through one of the fluorides in a variety of circumstances, we assume that it also coordinates to rhenium in this situation.

When the noncoordinating anion $\text{BAR}^{\text{F}}_4^-$ is employed, the resulting crystalline complex contains 1 equiv of ether, which we assume to be bound to the metal (eq 2). This ether is relatively labile and partially lost *in vacuo*. Therefore elemental analysis has not been correct or reproducible. A second problem is that if



traces of water are present in either $[\text{H}(\text{OEt}_2)_2]^+[\text{BAR}^{\text{F}}_4]^-$ or any solvent of recrystallization, highly crystalline $[\text{Re}(\text{C-}t\text{-Bu})(\text{CH}_2\text{-}t\text{-Bu})_3(\text{H}_2\text{O})]^+[\text{BAR}^{\text{F}}_4]^- (\text{Et}_2\text{O})$ crystallizes as yellow blocks. A similar situation has been observed by Brookhart and co-workers in cationic Rh chemistry.²³ It should be noted that $[\text{Re}(\text{C-}t\text{-Bu})(\text{CH}_2\text{-}t\text{-Bu})_3(\text{H}_2\text{O})]^+[\text{BAR}^{\text{F}}_4]^- (\text{Et}_2\text{O})$ is extremely crystalline and is isolated preferentially even if less than 1 equiv of water is present. The water is slowly lost *in vacuo*.

The water molecule in $[\text{Re}(\text{C-}t\text{-Bu})(\text{CH}_2\text{-}t\text{-Bu})_3(\text{H}_2\text{O})]^+[\text{BAR}^{\text{F}}_4]^- (\text{Et}_2\text{O})$ can be observed by IR ($\nu_{\text{O-H}} = 3640$, br) and ¹H NMR in CD_2Cl_2 (broad singlet at 7 ppm). In the ¹H NMR spectrum, resonances associated with the alkyl and alkylidyne groups are shifted from the resonances for $[\text{Re}(\text{C-}t\text{-Bu})(\text{CH}_2\text{-}t\text{-Bu})_3(\text{Et}_2\text{O})]^+[\text{BAR}^{\text{F}}_4]^-$, so water is not merely present in the crystal lattice. Addition of D_2O leads to H/D exchange on the NMR time scale at 25 °C, while addition of ether to a sample of $[\text{Re}(\text{C-}t\text{-Bu})(\text{CH}_2\text{-}t\text{-Bu})_3(\text{H}_2\text{O})]^+[\text{BAR}^{\text{F}}_4]^- (\text{Et}_2\text{O})$ results in only a single average ether resonance. We do not know whether the ether molecule is associated with the BAR^{F}_4 counterion, or whether it is weakly hydrogen bonded to the water ligand. Hydrogen bonding between pyridine and coordinated water has been observed by X-ray crystallography in $[\text{Re}(\text{C-}t\text{-Bu})(\text{CH-}t\text{-Bu})(\text{CH}_2\text{-}t\text{-Bu})(\text{py})_2(\text{H}_2\text{O}\cdot\text{py})]^+[\text{BAR}^{\text{F}}_4]^-$ (see below).

Synthesis of Rhenium Neopentyl/Neopentylidene/Neopentylidyne Complexes. $\text{W}(\text{C-}t\text{-Bu})(\text{CH}_2\text{-}t\text{-Bu})_3$ is known to react with excess PMe_3 or dmpe under forcing conditions (100–110 °C) to form $\text{W}(\text{C-}t\text{-Bu})(\text{CH-}t\text{-Bu})(\text{CH}_2\text{-}t\text{-Bu})(\text{L})_2$ (L = PMe_3 , $1/2$ dmpe).²⁴ We hoped that $\text{Re}(\text{C-}t\text{-Bu})(\text{CH}_2\text{-}t\text{-Bu})_3\text{X}$ would react with coordinating ligands to form neopentane and $\text{Re}(\text{C-}t\text{-Bu})(\text{CH-}t\text{-Bu})(\text{CH}_2\text{-}t\text{-Bu})(\text{L})_n\text{X}$. Such α -hydrogen abstraction reactions had not been observed for $\text{Re}(\text{C-}t\text{-Bu})(\text{CH}_2\text{-}t\text{-Bu})_3\text{Cl}$.²¹ α -Hydrogen abstraction reactions generally are more facile in cationic systems or systems in which the metal is relatively electrophilic.²⁵ Thus it might be expected that $\text{Re}(\text{C-}t\text{-Bu})(\text{CH}_2\text{-}t\text{-Bu})_3\text{X}$ (X = OTf, BF_4) and $[\text{Re}(\text{C-}t\text{-Bu})(\text{CH}_2\text{-}t\text{-Bu})_3(\text{H}_2\text{O})_n]_x^+[\text{BAR}^{\text{F}}_4]^-$ ($n = 0, 1$) would be more likely to undergo α -hydrogen abstraction reactions than $\text{Re}(\text{C-}t\text{-Bu})(\text{CH}_2\text{-}t\text{-Bu})_3\text{Cl}$.

(23) Hauptman, E.; Brookhart, M.; Fagan, P.; Calabrese, J. C. *Organometallics* **1994**, *13*, 774.

(24) Clark, D. N.; Schrock, R. R. *J. Am. Chem. Soc.* **1978**, *100*, 6774.

(25) Schrock, R. R. In *Reactions of Coordinated Ligands*; Braterman, P. R., Ed.; Plenum: New York, 1986.

(15) Blosch, L. L.; Gamble, A. S.; Abboud, K.; Boncella, J. M. *Organometallics* **1992**, *11*, 2963.

(16) Gamble, A. S.; Boncella, J. M. *Organometallics* **1993**, *12*, 2814.

(17) Murdzek, J. S.; Schrock, R. R. In *Carbyne Complexes*; VCH: New York, 1988.

(18) Klaui, W. *Angew. Chem., Int. Ed. Engl.* **1990**, *29*, 627.

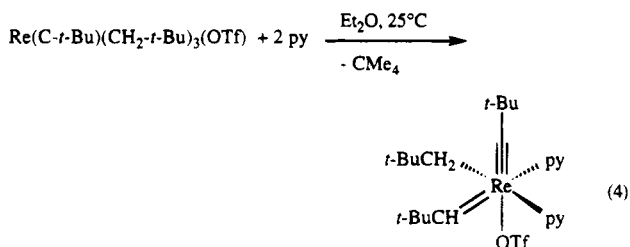
(19) Lawrence, G. A. *Chem. Rev.* **1986**, *86*, 17.

(20) Edwards, D. S.; Biondi, L. V.; Ziller, J. W.; Churchill, M. R.; Schrock, R. R. *Organometallics* **1993**, *2*, 1505.

(21) Edwards, D. S. Ph.D. Thesis, Massachusetts Institute of Technology, Cambridge, MA, 1983.

(22) Savage, P. D.; Wilkinson, G.; Motevalli, M.; Hursthouse, M. B. *Polyhedron* **1987**, *6*, 1599.

Re(C-*t*-Bu)(CH₂-*t*-Bu)₃(OTf) reacts rapidly with 2–3 equiv of pyridine in ether to form neopentane and colorless Re(C-*t*-Bu)(CH-*t*-Bu)(CH₂-*t*-Bu)(py)₂(OTf), which precipitates from the reaction mixture virtually quantitatively. The structure shown in eq 4 is based on NMR



data as well as by analogy with several structurally characterized six-coordinate rhenium neopentylidene/neopentylidyne complexes, all of which have several common features. The most important feature is that alkylidene and alkylidyne ligands are oriented *cis* to each other, and the remaining anionic ligands often are *cis* to the alkylidene and alkylidyne ligands.^{7,8,20} Rapid exchange on the NMR time scale is observed when pyridine is added to a sample of Re(C-*t*-Bu)(CH-*t*-Bu)(CH₂-*t*-Bu)(py)₂(OTf) at 25 °C in CD₂Cl₂. Only one rotamer is present, which we presume is the *syn* rotamer in which the *tert*-butyl group points toward the neopentylidyne ligand.

The reaction between Re(CMe₂Ph)(CH₂CMe₂Ph)₃(OTf) and excess pyridine in ether results in formation of pink Re(CMe₂Ph)(CHCMe₂Ph)(CH₂CMe₂Ph)(py)₂(OTf), which is similar to Re(C-*t*-Bu)(CH-*t*-Bu)(CH₂-*t*-Bu)(py)₂(OTf), according to NMR studies, but is much more soluble in ether and benzene.

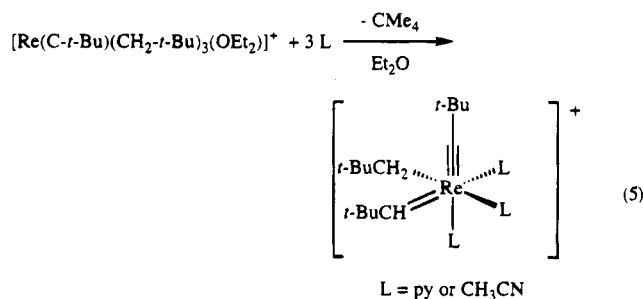
The reaction between Re(C-*t*-Bu)(CH₂-*t*-Bu)₃(OTf) and excess acetonitrile in ether results in formation of neopentane and Re(C-*t*-Bu)(CH-*t*-Bu)(CH₂-*t*-Bu)(CH₃CN)(OTf) as a beige powder. Re(C-*t*-Bu)(CH-*t*-Bu)(CH₂-*t*-Bu)(CH₃CN)_n(OTf) (*n* = 2 or 3, according to proton NMR spectra) is formed initially as crystals in the crude reaction mixture, but CH₃CN is readily lost upon isolation of the crystals to yield Re(C-*t*-Bu)(CH-*t*-Bu)(CH₂-*t*-Bu)(CH₃CN)(OTf). When excess CH₃CN (6 equiv) is added to a C₆D₆ solution of Re(C-*t*-Bu)(CH-*t*-Bu)(CH₂-*t*-Bu)(CH₃CN)(OTf), a spectrum analogous to that observed for "Re(C-*t*-Bu)(CH-*t*-Bu)(CH₂-*t*-Bu)(CH₃CN)_n(OTf)" is obtained (as evidenced by shifts of all of the observed resonances), although only one CH₃CN resonance is found, consistent with rapid exchange of acetonitrile on the NMR time scale at 25 °C. The structure of Re(C-*t*-Bu)(CH-*t*-Bu)(CH₂-*t*-Bu)(CH₃CN)(OTf) is not known, and attempts to grow crystals suitable for X-ray diffraction were unsuccessful. At this stage we assume that it is a neutral five-coordinate trigonal bipyramidal species.

Re(C-*t*-Bu)(CH₂-*t*-Bu)₃(OTf) eliminates neopentane when it is dissolved in CD₃OD, and resonances consistent with formation of Re(C-*t*-Bu)(CH-*t*-Bu)(CH₂-*t*-Bu)(CD₃OD)_n(OTf) (*n* = 1–3) are observed by proton NMR. Attempts to isolate Re(C-*t*-Bu)(CH-*t*-Bu)(CH₂-*t*-Bu)(CD₃OD)_n(OTf) have not been successful, even though Re(C-*t*-Bu)(CH-*t*-Bu)(CH₂-*t*-Bu)(CD₃OD)_n(OTf) appears to be stable for several hours in solution. Addition of pyridine to CD₃OD solutions of Re(C-*t*-Bu)(CH-*t*-Bu)(CH₂-*t*-Bu)(CD₃OD)_n(OTf) yields Re(C-*t*-Bu)(CH-*t*-Bu)(CH₂-*t*-Bu)(py)₂(OTf). Re(C-*t*-Bu)(CH₂-*t*-Bu)₃(OTf) re-

acts slowly with neat THF-*d*₈ to form neopentane and Re(C-*t*-Bu)(CH-*t*-Bu)(CH₂-*t*-Bu)(THF)_n(OTf), according to NMR studies, but again no crystalline product could be isolated.

Re(C-*t*-Bu)(CH₂-*t*-Bu)₃(BF₄) reacts with excess acetonitrile to yield colorless crystals of Re(C-*t*-Bu)(CH-*t*-Bu)(CH₂-*t*-Bu)(CH₃CN)₂(BF₄) in 70–80% yield. However, analogous complexes containing coordinating ligands other than CH₃CN could not be isolated, even though Re(C-*t*-Bu)(CH-*t*-Bu)(CH₂-*t*-Bu)(L)_n(BF₄) (L = CD₃OD, THF-*d*₈) and neopentane are formed when Re(C-*t*-Bu)(CH₂-*t*-Bu)₃(BF₄) is dissolved in CD₃OD or THF-*d*₈, according to NMR spectra. The reaction between Re(C-*t*-Bu)(CH₂-*t*-Bu)₃(BF₄) and 3 equiv of pyridine in C₆D₆ proceeded cleanly to yield a compound whose ¹H NMR spectrum is consistent with the formulation Re(C-*t*-Bu)(CH-*t*-Bu)(CH₂-*t*-Bu)(py)₂(X), but no product could be isolated, and it is not known whether X = BF₄ or F.

[Re(C-*t*-Bu)(CH₂-*t*-Bu)₃(Et₂O)]⁺[BAR^F₄]⁻ reacts with pyridine or acetonitrile in ether to yield [Re(C-*t*-Bu)(CH-*t*-Bu)(CH₂-*t*-Bu)(L)₃]⁺[BAR^F₄]⁻ (L = py, CH₃CN)



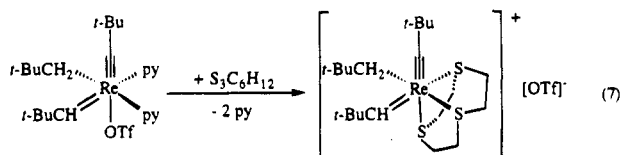
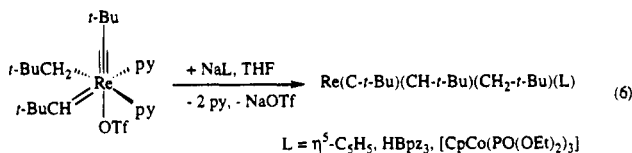
virtually quantitatively. Lower yields (70%) are obtained if [Re(C-*t*-Bu)(CH₂-*t*-Bu)₃(Et₂O)]⁺[BAR^F₄]⁻ is generated *in situ* and pyridine or acetonitrile is added, although this procedure reduces the problem of contamination by water.

[Re(C-*t*-Bu)(CH₂-*t*-Bu)₃(H₂O)(Et₂O)]⁺[BAR^F₄]⁻ reacts with 3 equiv of pyridine in ether to yield peach-colored cubes of [Re(C-*t*-Bu)(CH-*t*-Bu)(CH₂-*t*-Bu)(py)₂(pyH₂O)]⁺[BAR^F₄]⁻. The water molecule could not be observed by IR or NMR spectroscopy. Crystals of [Re(C-*t*-Bu)(CH-*t*-Bu)(CH₂-*t*-Bu)(py)₃(H₂O)]⁺[BAR^F₄]⁻ suitable for X-ray diffraction were grown from ether/pentane (3/1 v/v) solution at –40 °C, and the structure was determined by X-ray crystallography. Unfortunately, disorder in the CF₃ groups and the large number of atoms in the molecule prevented satisfactory refinement. Nonetheless, connectivity could be established in the cationic fragment. The water molecule was observed to be coordinated to rhenium *trans* to the neopentylidyne ligand, and a molecule of pyridine was located within hydrogen-bonding distance of the water molecule.

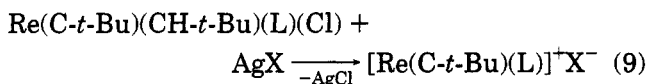
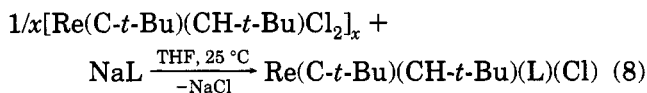
All of the rhenium neopentyl/neopentylidene/neopentylidyne complexes described in this section were stable in C₆D₆, CD₂Cl₂, pyridine-*d*₅, or THF-*d*₈ in the presence of water, but they were essentially insoluble in water itself.

Synthesis of Re(C-*t*-Bu)(CH-*t*-Bu)(CH₂-*t*-Bu)(L) (L = Cp, HBpz₃, LOEt). Re(C-*t*-Bu)(CH-*t*-Bu)(CH₂-*t*-Bu)(py)₂(OTf) reacts with NaL (L = Cp, HBpz₃, [CpCo(PO(OEt)₂)₃]⁻["LOEt"]) in THF to cleanly produce complexes of the type Re(C-*t*-Bu)(CH-*t*-Bu)(CH₂-*t*-Bu)(L) in 80–95% yield (eq 6) and with 1,4,7-trithiacyclononane in dichloromethane to yield colorless crystals of [Re(C-

t-Bu)(CH-*t*-Bu)(CH₂-*t*-Bu)(S₃C₆H₁₂)[OTf] quantitatively (eq 7). Re(C-*t*-Bu)(CH-*t*-Bu)(CH₂-*t*-Bu)(L) and [Re(C-*t*-Bu)(CH-*t*-Bu)(CH₂-*t*-Bu)(S₃C₆H₁₂)[OTf] are thermally stable, 18-electron compounds.

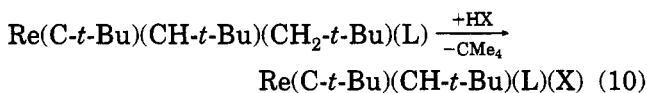


Reaction of Re(C-*t*-Bu)(CH-*t*-Bu)(CH₂-*t*-Bu)(L) and [Re(C-*t*-Bu)(CH-*t*-Bu)(CH₂-*t*-Bu)(η³-S₃C₆H₁₂)]⁺[OTf]⁻ with Acids. A possible route to complexes that contain the [Re(C-*t*-Bu)(CH-*t*-Bu)(L)]⁺ core is shown in eqs 8 and 9. Complexes of the type Re(C-*t*-Bu)(CH-*t*-Bu)(L)Cl are readily synthesized from [Re(C-*t*-Bu)(CH-*t*-Bu)Cl]₂ and 1 equiv of NaL (L = Cp,⁷ L_{OEt}). Unfortunately, however, all attempts to abstract chloride ion with silver or thallium salts were unsuccessful.



Therefore an indirect route to [Re(C-*t*-Bu)(CH-*t*-Bu)(L)]⁺ complexes was developed that employs a combination of protonation and α-hydrogen abstraction reactions similar to that used to synthesize the Re(C-*t*-Bu)(CH-*t*-Bu)(CH₂-*t*-Bu)(L)_nX species.

Reaction between Re(C-*t*-Bu)(CH-*t*-Bu)(CH₂-*t*-Bu)(L) (L = Cp, [CpCo(PO(OEt)₂)₃]) and triflic acid in ether yields Re(C-*t*-Bu)(CH-*t*-Bu)(L)(OTf) complexes in 50–80% yields (eq 10). We speculate that this reaction



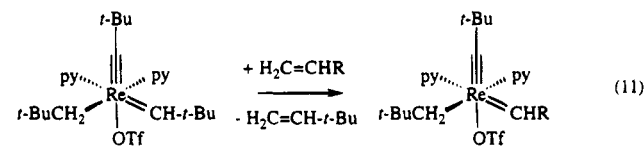
proceeds via initial protonation of C_α of the alkylidene ligand to form Re(C-*t*-Bu)(CH₂-*t*-Bu)₂(L)(OTf), followed by α-hydrogen abstraction to form neopentane and Re(C-*t*-Bu)(CH-*t*-Bu)(L)(OTf). It should be noted that, in the d² manifold, the neutral osmium complexes, Os(C-*t*-Bu)(CH₂-*t*-Bu)₂(L) (L = Cp, L_{OEt}, HBPz₃), show no evidence of α-hydrogen abstraction.^{26,27} Re(C-*t*-Bu)(CH-*t*-Bu)(L_{OEt})(OTf) is thermally stable, but Re(C-*t*-Bu)(CH-*t*-Bu)Cp(OTf) decomposes slowly in the solid state at -40 °C to form an insoluble unidentified blue material. The C-H coupling constant in the alkylidene ligand in the cyclopentadienyl complex is only 90 Hz, a value that is 25–40 Hz lower than is typically observed for complexes containing the Re(C-*t*-Bu)(CH-*t*-Bu) core,

including Re(C-*t*-Bu)(CH-*t*-Bu)(L_{OEt})(OTf) (121 Hz). Low J_{CH_α} values have been attributed to an agostic interaction involving H_α in the alkylidene ligand.^{25,28} If Re(C-*t*-Bu)(CH-*t*-Bu)(Cp)(OTf) is a neutral species, it is nominally a six-coordinate, 18-electron species in which an agostic interaction is not possible. On the other hand, an agostic interaction is possible if it exists as the cationic species, [Re(C-*t*-Bu)(CH-*t*-Bu)(Cp)]⁺[OTf]⁻. Re(C-*t*-Bu)(CH-*t*-Bu)(Cp)(OTf) reacts readily with pyridine to form stable [Re(C-*t*-Bu)(CH-*t*-Bu)(Cp)(py)]⁺[OTf]⁻, which can also be synthesized in a one-pot reaction from Re(C-*t*-Bu)(CH-*t*-Bu)(CH₂-*t*-Bu)(Cp) and pyHOTf in CH₂Cl₂. As expected, J_{CH_α} in [Re(C-*t*-Bu)(CH-*t*-Bu)(Cp)(py)]⁺[OTf]⁻ is 125 Hz, consistent with no agostic interaction being present. Therefore we suspect that Re(C-*t*-Bu)(CH-*t*-Bu)(Cp)(OTf) exists as the cationic complex [Re(C-*t*-Bu)(CH-*t*-Bu)(Cp)]⁺[OTf]⁻ in which there is an agostic Re=CH_α interaction.

The reaction between Re(C-*t*-Bu)(CH-*t*-Bu)(CH₂-*t*-Bu)(L_{OEt}) and [H(OEt)₂]⁺[BAR^F₄]⁻ in ether at -40 °C proceeds cleanly to yield yellow, crystalline [Re(C-*t*-Bu)(CH-*t*-Bu)(L_{OEt})(Et₂O)]⁺[BAR^F₄]⁻. The presence of the tridentate ligand L_{OEt} requires that the neutral ether ligand be located *cis* to the neopentylidene and neopentylidyne ligands, although this is not normally the preferred site for a neutral donor ligand in six-coordinate alkylidene/alkylidyne complexes.

The reaction between [Re(C-*t*-Bu)(CH-*t*-Bu)(CH₂-*t*-Bu)(S₃C₆H₁₂)]⁺[OTf]⁻ and triflic acid in dichloromethane proceeds cleanly to yield [Re(C-*t*-Bu)(CH-*t*-Bu)(S₃C₆H₁₂)(OTf)]⁺[OTf]⁻. However, the reaction between Re(C-*t*-Bu)(CH-*t*-Bu)(CH₂-*t*-Bu)(Cp) and [H(OEt)₂]⁺[BAR^F₄]⁻ or [pyH]⁺[BAR^F₄]⁻ in CH₂Cl₂ or ether failed to yield any isolable products. Likewise, reactions between Re(C-*t*-Bu)(CH-*t*-Bu)(CH₂-*t*-Bu)(HBPz₃) and triflic acid or [H(OEt)₂]⁺[BAR^F₄]⁻ did not yield any characterizable products cleanly.

Reactions of the Neopentylidene/Neopentylidyne Complexes with Terminal Olefins. Re(C-*t*-Bu)(CH-*t*-Bu)(CH₂-*t*-Bu)(py)₂(OTf) reacts with H₂C=CHR (R = OCH₂CH₃, C₆H₅) in benzene or dichloromethane to yield neohexene and the new alkylidene complexes, Re(C-*t*-Bu)(CHR)(CH₂-*t*-Bu)(py)₂(OTf) (eq 11). No evi-



dence for formation of the methylidene complex, Re(C-*t*-Bu)(CH₂)(CH₂-*t*-Bu)(py)₂(OTf), is seen. The ethoxymethylene complex is isolated as a thermally stable pink powder. It shows no evidence of bimolecular decomposition in solution at 25 °C. The two bound pyridine molecules are inequivalent on the NMR time scale at 25 °C in CDCl₃, and exchange with added pyridine does not occur on the NMR time scale under these conditions. Re(C-*t*-Bu)(CHC₆H₅)(CH₂-*t*-Bu)(py)₂(OTf) is isolated as beige crystals. The two bound pyridine ligands are inequivalent on the NMR time scale.

Hydrogen scrambling between the alkyl, alkylidene, and alkylidyne ligands in these complexes cannot be

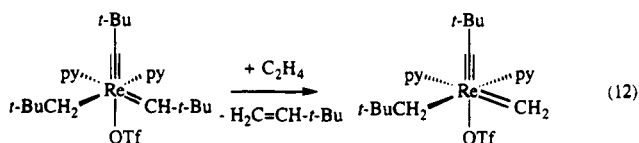
(26) LaPointe, A. M.; Schrock, R. R. *Organometallics* **1993**, *13*, 3379.

(27) LaPointe, A. M.; Schrock, R. R.; Davis, W. M. *J. Am. Chem. Soc.*, in press.

(28) Oskam, J. H.; Schrock, R. R. *J. Am. Chem. Soc.* **1993**, *115*, 11831.

totally ruled out without a crystal structure determination. However, in d^0 systems, hydrogen scrambling among alkyl and alkylidene²⁹ or alkylidyne³⁰ ligands has been found to be a relatively high energy process. $\text{Re}(\text{C}-t\text{-Bu})(\text{CHF}_c)[\text{OCMe}(\text{CF}_3)_2]_2$ ($\text{Fc} = (\text{C}_5\text{H}_4)\text{FeCp}$) and $\text{Re}(\text{C}-t\text{-Bu})(\text{CH}-\text{OEt})[\text{OCMe}(\text{CF}_3)_2]_2(\text{THF})_2$ were prepared by the reaction of $\text{Re}(\text{C}-t\text{-Bu})(\text{CH}-t\text{-Bu})[\text{OCMe}(\text{CF}_3)_2]_2$ with vinylferrocene or ethyl (vinyl) ether, respectively; X-ray structure determinations revealed that no scrambling of H_α had occurred between the carbene and neopentylidyne ligands.⁸ Likewise, we found that $\text{Re}(\text{C}-t\text{-Bu})(\text{CH}-t\text{-Bu})(\text{CD}_2-t\text{-Bu})_2$ shows no evidence for H/D scrambling among the neopentyl and neopentylidene ligands at 80 °C in toluene- d_8 . On the basis of these results, we believe that scrambling of H_α does not occur in the alkyl/alkylidene/alkylidyne systems and that the complexes can be described by the formula $\text{Re}(\text{C}-t\text{-Bu})(\text{CHR})(\text{CH}_2-t\text{-Bu})(\text{py})_2(\text{OTf})$.

The reaction of $\text{Re}(\text{C}-t\text{-Bu})(\text{CH}-t\text{-Bu})(\text{CH}_2-t\text{-Bu})(\text{py})_2(\text{OTf})$ with 3–5 equiv of ethylene in C_6D_6 or CD_2Cl_2 initially yields neohexene and $\text{Re}(\text{C}-t\text{-Bu})(\text{CH}_2)(\text{CH}_2-t\text{-Bu})(\text{py})_2(\text{OTf})$ (eq 12). However, the methyldene com-

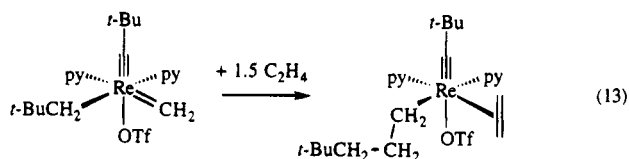


plex is unstable at 25 °C in C_6D_6 , even in the presence of 2–5 equiv of pyridine. Upon isolation it decomposes to $\text{Re}(\text{C}-t\text{-Bu})[(\text{CH}_2)_3-t\text{-Bu}](\text{C}_2\text{H}_4)(\text{py})_2(\text{OTf})$ (see below) and unidentified products. However, addition of bipyridyl to solutions containing freshly prepared $\text{Re}(\text{C}-t\text{-Bu})(\text{CH}_2)(\text{CH}_2-t\text{-Bu})(\text{py})_2(\text{OTf})$ yields red $\text{Re}(\text{C}-t\text{-Bu})(\text{CH}_2)(\text{CH}_2-t\text{-Bu})(\text{bpy})(\text{OTf})$, which can be recrystallized from toluene/ether mixtures at –40 °C. Unfortunately, $\text{Re}(\text{C}-t\text{-Bu})(\text{CH}_2)(\text{CH}_2-t\text{-Bu})(\text{bpy})(\text{OTf})$ is thermally unstable and for this reason has been characterized only by ^1H NMR and partially by ^{13}C NMR. In the proton NMR spectrum, two doublets ($J_{\text{HH}} = 3$ Hz) corresponding to H_α protons of the methylene ligand are observed at 14.05 ($J_{\text{CH}} = 135$ Hz) and 13.49 ppm ($J_{\text{CH}} = 150$ Hz).

The reaction between $\text{Re}(\text{C}-t\text{-Bu})(\text{CH}-t\text{-Bu})(\text{CH}_2-t\text{-Bu})(\text{py})_2(\text{OTf})$ and excess ethylene in benzene or dichloromethane yields a colorless microcrystalline solid whose proton NMR spectrum contained two inequivalent *tert*-butyl groups, two inequivalent bound pyridines, and a series of complex multiplets corresponding to five sets of inequivalent methylene groups. Because of the complexity of the spectrum and the fact that some of the resonances overlapped, it was impossible to assign the methylene portion of the spectrum. ^{19}F NMR confirmed the presence of the triflate anion, and elemental analysis confirmed the formulation $\text{ReC}_{25}\text{H}_{38}\text{N}_2\text{F}_3\text{O}_3\text{S}$. The reaction of $\text{Re}(\text{C}-t\text{-Bu})(\text{CH}-t\text{-Bu})(\text{CH}_2-t\text{-Bu})(\text{py})_2(\text{OTf})$ with $^{13}\text{CH}_2^{13}\text{CH}_2$ produced a product that contained three isotopically enriched peaks, a singlet at 20 ppm ($J_{\text{CH}} = 123$ Hz) with twice the intensity of the other two doublets ($J_{\text{CC}} = 36$ Hz) at 52 ppm ($J_{\text{CH}} = 153$ Hz) and 46 ppm ($J_{\text{CH}} = 156$ Hz). These results suggest that 1 equiv of ethylene was incorpo-

rated in a manner that rendered its two carbon atoms inequivalent and the other equivalent of ethylene was incorporated so that its two carbon atoms are equivalent. The reaction of $\text{Re}(\text{C}-t\text{-Bu})(\text{CH}-t\text{-Bu})(\text{CH}_2-t\text{-Bu})(\text{py})_2(\text{OTf})$ with excess C_2D_4 yields a complex with a greatly simplified ^1H NMR. Two peaks that had been complex multiplets in the unlabeled complex appeared as doublets in the labeled complex and therefore were assigned as the methylene protons in the original neopentyl ligand. These labeling experiments suggested that one of the molecules of ethylene had coordinated to the metal and the other had inserted into the metal–carbon single bond to yield $\text{Re}(\text{C}-t\text{-Bu})[(\text{CH}_2)_3-t\text{-Bu}](\text{C}_2\text{H}_4)(\text{py})_2(\text{OTf})$. No further reaction with ethylene is observed at 1 atm and 25 °C in C_6H_6 .

In the reaction of $\text{Re}(\text{C}-t\text{-Bu})(\text{CH}-t\text{-Bu})(\text{CH}_2-t\text{-Bu})(\text{py})_2(\text{OTf})$ with an excess of ethylene, the only observed byproduct is neohexene (formed in the initial metathesis reaction) and the only observed intermediate is $\text{Re}(\text{C}-t\text{-Bu})(\text{CH}_2)(\text{CH}_2-t\text{-Bu})(\text{py})_2(\text{OTf})$. There was no evidence for formation of any other organic product (such as propylene or cyclopropane). Therefore we speculate that $\text{Re}(\text{C}-t\text{-Bu})(\text{CH}_2)(\text{CH}_2-t\text{-Bu})(\text{py})_2(\text{OTf})$ decomposes to “ $\text{Re}(\text{C}-t\text{-Bu})(\text{CH}_2-t\text{-Bu})(\text{py})_2(\text{OTf})$ ” in a bimolecular process and that subsequent reaction of transient “ $\text{Re}(\text{C}-t\text{-Bu})(\text{CH}_2-t\text{-Bu})(\text{py})_2(\text{OTf})$ ” with ethylene yields $\text{Re}(\text{C}-t\text{-Bu})[(\text{CH}_2)_3-t\text{-Bu}](\text{C}_2\text{H}_4)(\text{py})_2(\text{OTf})$ (eq 13).



Benzene solutions of $\text{Re}(\text{C}-t\text{-Bu})(\text{CH}-t\text{-Bu})(\text{CH}_2-t\text{-Bu})(\text{CH}_3\text{CN})_2(\text{BF}_4)$ become green when terminal olefins such as styrene or ethyl vinyl ether are added, and no evidence of productive metathesis is observed by NMR. The six-coordinate, cationic complexes $[\text{Re}(\text{C}-t\text{-Bu})(\text{CH}-t\text{-Bu})(\text{CH}_2-t\text{-Bu})(\text{L})_3]^+[\text{BAR}^F_4]^-$ ($\text{L} = \text{py}, \text{CH}_3\text{CN}$) do not react with styrene, ethyl vinyl ether, or ethylene in ether. Likewise, none of the neutral or cationic complexes containing a tridentate ligand reacts with terminal olefins such as styrene or ethylene. It is likely that at least one coordination site must be free for coordination of olefin to occur. Thus, under identical conditions (C_6D_6 , 25 °C, 5–10 equiv olefin), $\text{Re}(\text{C}-t\text{-Bu})(\text{CH}-t\text{-Bu})(\text{CH}_2-t\text{-Bu})(\text{py})_2(\text{OTf})$ reacts rapidly with terminal olefins but $\text{Re}(\text{C}-t\text{-Bu})(\text{CH}-t\text{-Bu})(\text{CH}_2-t\text{-Bu})(\text{bpy})(\text{OTf})$ does not react.

Reaction of the Neopentylidene/Neopentylidyne Complexes with Unstrained Internal Olefins. $\text{Re}(\text{C}-t\text{-Bu})(\text{CH}-t\text{-Bu})(\text{CH}_2-t\text{-Bu})(\text{CH}_3\text{CN})(\text{OTf})$ reacts rapidly with 5–10 equiv of *cis*-3-hexene in C_6D_6 to yield a new propylidene complex that decomposes within 1 h at 25 °C. Similar results were obtained in reactions between $\text{Re}(\text{C}-t\text{-Bu})(\text{CH}-t\text{-Bu})(\text{CH}_2-t\text{-Bu})(\text{CH}_3\text{CN})(\text{OTf})$ and methyl oleate or oleic acid. When the reaction between $\text{Re}(\text{C}-t\text{-Bu})(\text{CH}-t\text{-Bu})(\text{CH}_2-t\text{-Bu})(\text{CH}_3\text{CN})_n(\text{OTf})$ and 5–10 equiv of *cis*-3-hexene in C_6D_6 is conducted in the presence of 5–10 equiv of CH_3CN , “ $\text{Re}(\text{C}-t\text{-Bu})(\text{CHCH}_2\text{CH}_3)(\text{CH}_2-t\text{-Bu})(\text{CH}_3\text{CN})_n(\text{OTf})$ ” forms within 10 min, but still largely decomposes within 4 h in C_6D_6 at 25 °C. In neat CD_3CN , $\text{Re}(\text{C}-t\text{-Bu})(\text{CH}-t\text{-Bu})(\text{CH}_2-t\text{-Bu})(\text{CH}_3\text{CN})_n(\text{OTf})$ does not react with 5 equiv of *cis*-3-hexene at 25 °C. At

(29) Schrock, R. R.; Fellmann, J. D. *J. Am. Chem. Soc.* **1978**, *100*, 3359.

(30) Caulton, K. G.; Chisholm, M. H.; Streib, W. E.; Xue, Z. *J. Am. Chem. Soc.* **1991**, *113*, 6082.

60 °C the reaction proceeds slowly (2/1 propylidene/neopentylidene after 1 h); in CD₃CN, Re(C-*t*-Bu)(CHCH₂-CH₃)(CH₂-*t*-Bu)(CH₃CN)_n(OTf) is stable for 24 h at 25 °C. Upon addition of excess 2,2,2-trimethyl-3-hexene to a CD₃CN solution of Re(C-*t*-Bu)(CHCH₂-CH₃)(CH₂-*t*-Bu)(CH₃CN)_n(OTf) at 25 °C, no metathesis was observed at room temperature in 24 h. Therefore, in acetonitrile, Re(C-*t*-Bu)(CHCH₂-CH₃)(CH₂-*t*-Bu)(CH₃CN)_n(OTf) is not much more reactive than the analogous neopentylidene complex.

Upon addition of 100 equiv of *cis*-2-pentene to Re(C-*t*-Bu)(CH-*t*-Bu)(CH₂-*t*-Bu)(CH₃CN)_n(OTf) at 25 °C in benzene, an equilibrium mixture of butenes, pentenes, and hexenes was reached in ~5 min. However, no further metathesis occurred when another 100 equiv of *cis*-2-pentene was added 1 h later.

The reaction of Re(C-*t*-Bu)(CH-*t*-Bu)(CH₂-*t*-Bu)(CD₃OD)_n(OTf) with 5–10 equiv of *cis*-3-hexene in CD₃OD occurs within 30 min at 25 °C. Re(C-*t*-Bu)(CHCH₂-CH₃)(CH₂-*t*-Bu)(CD₃OD)(OTf) is stable for several hours at 25 °C in CD₃OD. However, very little (<5%) metathesis was observed in the reaction of Re(C-*t*-Bu)(CH-*t*-Bu)(CH₂-*t*-Bu)(CH₃OH)_n(OTf) with 100 equiv of *cis*-2-heptene in CH₃OH.

None of the other rhenium alkylidene complexes described here reacts with unstrained internal olefins. Low reactivity can be traced to the fact that the neutral donor ligands and/or multidentate ligands L (L = Cp, HBpz₃, L_{OEt}, S₃C₆H₁₂) are not sufficiently labile, so no coordination sites are available to bind the olefin.

Discussion

A wide variety of coordinating ligands was found to induce α-hydrogen abstraction reactions in Re(C-*t*-Bu)(CH₂-*t*-Bu)₃(X) (X = OTf, BF₄, BAr^F₄) species. The finding that acetonitrile and methanol can induce α-hydrogen abstraction reactions is particularly interesting; these ligands are frequently incompatible with alkylidene complexes of tantalum, molybdenum, and tungsten. This result is a nice example of the greater tolerance of rhenium–carbon multiple bonds for a variety of organic functional groups. It should be noted that the coordinating ligands must be nucleophilic but not especially basic. For example, the reaction of Re(C-*t*-Bu)(CH₂-*t*-Bu)₃(OTf) with quinuclidine or *tert*-butylamine results in deprotonation at C_α to form Re(C-*t*-Bu)(CH-*t*-Bu)(CH₂-*t*-Bu)₂. Similar results have been observed in the case of Re(C-*t*-Bu)(CH₂-*t*-Bu)₃Cl.^{20,21}

Although quantitative experiments were not possible, α-hydrogen abstraction was significantly faster in the systems where cationic intermediates could form. Thus, for a given ligand, α-hydrogen abstraction reactions of Re(C-*t*-Bu)(CH₂-*t*-Bu)₃(X) were much faster when X = OTf, BAr^F₄ than when X = Cl, OC₆F₅. For instance, the reaction of Re(C-*t*-Bu)(CH₂-*t*-Bu)₃(OTf) with 3 equiv of pyridine in ether or pentane was complete within 10 min at 25 °C, while the reaction of Re(C-*t*-Bu)(CH₂-*t*-Bu)₃Cl with neat pyridine-*d*₅ required 24 h. These observations are consistent with earlier findings that demonstrated that α-hydrogen elimination reactions are faster in systems that are cationic or strongly polarized.²⁵

The synthesis of a large number of complexes containing the rhenium neopentyl/neopentylidene/neopentylidyne core suggests that this system can support a

wide range of ligand environments. Once formed, complexes containing the Re(C-*t*-Bu)(CH-*t*-Bu)(CH₂-*t*-Bu) core are quite stable. All of the complexes described here that contain the Re(C-*t*-Bu)(CH-*t*-Bu)(CH₂-*t*-Bu) core are thermally stable, in the solid state they are moderately stable to air and water, and in solution they are stable to water at 25 °C. For instance, a solid sample of Re(C-*t*-Bu)(CH-*t*-Bu)(CH₂-*t*-Bu)(HBpz₃) showed no decomposition after a month of exposure to moist air. The tradeoff is that the complexes described here are not especially active for the metathesis of olefins, or, if they are, activity is short-lived as a consequence of (presumably) bimolecular decomposition reactions involving relatively small alkylidenes. An interesting result to note is the extremely low reactivity of the tetra-(aryl)borate complexes. Since these systems are truly cationic, they might be expected to be more reactive than the triflate derivatives. However, the extreme electrophilicity of the metal center causes the coordinated pyridine, acetonitrile, or ether to be bound quite tightly to the metal, and no reactivity with olefins is observed. The most desirable anion would be one that is so weakly coordinated that it is readily displaced by an incoming olefin, but coordinated strongly enough to prevent decomposition of the “naked” cation.

In an attempt to surmount the problems of ligand dissociation and bimolecular decomposition, the complexes containing tridentate ligands such as Cp, HBpz₃, L_{OEt}, and 1,4,7-trithiacyclononane were synthesized and their reactivity with olefins was investigated. However, cationic “[Re(C-*t*-Bu)(CH-*t*-Bu)(L)]⁺” is already a five-coordinate, 16-electron species, and dissociation of part of the tridentate ligand (to yield a more reactive intermediate) would be expected to be quite difficult. Furthermore, the Re(C-*t*-Bu)(CH-*t*-Bu)(L) fragment typically binds another ligand (triflate, pyridine, ether) to form exceedingly unreactive species. It should be noted that cationic tungsten alkylidene complexes containing a hydridotris(pyrazolyl)borate ligand do not react with olefins in the absence of a Lewis acid cocatalyst,^{9,15,16} nor does five-coordinate Re(NAr)(CH-*t*-Bu)[OCMe(CF₃)₂]₃¹¹ or six-coordinate ReO(CHCHCPh₂)[OCMe(CF₃)₂]₃(THF).¹⁰ These results reaffirm the proposal that in a long-lived olefin metathesis catalyst, four coordination sites *must* be filled by nonlabile, ionic ligands which provide a large amount of steric protection. If additional neutral donor ligands are present, they must be quite labile. According to these general requirements, complexes such as [Re(NAr)(CHR)(OR')₂]⁺ and Re(N·BPh₃)(CHR)(OR')₂ (if they could be synthesized) might be relatively reactive toward olefins, but relatively stable thermally.

A variety of reduction pathways for transition metal alkylidenes and alkylidyne have been discovered. These include bimolecular coupling to form an olefin and a reduced metal complex, intramolecular coupling with another metal–ligand multiple bond (e.g., in the reduction of Os(CH-*t*-Bu)₂(CH₂-*t*-Bu)₂ to Os(PMe₃)₃(*t*-Bu-CC-*t*-Bu)),²⁷ and a formally “3 + 2” addition of ethylene to a rhenium alkylidene/alkylidyne to form a metallacyclopentene complex.³¹ In the “3 + 2” reaction, the “supporting” neopentylidyne ligand is involved; this illustrates one potential pitfall in the design of transi-

(31) Vaughan, G. A.; Toreki, R.; Schrock, R. R.; Davis, W. M. *J. Am. Chem. Soc.* **1993**, *115*, 2980.

tion metal catalysts. The reduction of $\text{Re}(\text{C-}t\text{-Bu})(\text{CH-}t\text{-Bu})(\text{CH}_2\text{-}t\text{-Bu})(\text{py})_2(\text{OTf})$ to $\text{Re}(\text{C-}t\text{-Bu})(\text{CH}_2\text{-}t\text{-Bu})(\text{py})_2(\text{OTf})$ provides another example of involvement of the supporting ligands, in this case, insertion of ethylene into the metal-carbon single bond.

Experimental Section

General Details. All experiments were performed under a nitrogen atmosphere in a Vacuum Atmospheres HE-43 drybox or using standard Schlenk techniques unless otherwise specified. Pentane was washed with sulfuric/nitric acid (95/5 v/v), aqueous sodium bicarbonate solution, and then water, stored over CaCl_2 , and then distilled from sodium benzophenone ketyl. Ether, tetrahydrofuran, benzene, and 1,2-dimethoxyethane were distilled from sodium benzophenone ketyl under nitrogen or argon. Toluene was distilled from molten sodium under nitrogen or argon, and dichloromethane, acetonitrile, and pyridine were distilled from calcium hydride under nitrogen or argon. All deuterated NMR solvents were purchased from Cambridge Isotope Laboratories. Tetrahydrofuran- d_8 was vacuum transferred from sodium benzophenone ketyl. C_6D_6 , CD_2Cl_2 , CDCl_3 , CD_3CN , and pyridine- d_5 were stored over activated molecular sieves in the drybox. CD_3OD was used as received.

Neopentyl chloride was purchased from Strem and purified by literature methods.³² $t\text{-BuCH}_2\text{MgCl}$ was prepared by the published procedure.³² Rhenium heptoxide (99.99%) was purchased from Aesar. $[\text{Re}(\text{C-}t\text{-Bu})(\text{CH-}t\text{-Bu})\text{Cl}_2]_7$ and $[\text{Re}(\text{C-}t\text{-Bu})(\text{CH-}t\text{-Bu})(t\text{-BuNH}_2)\text{Cl}_2]_{20}$ were prepared by literature methods, and $\text{Re}(\text{C-}t\text{-Bu})(\text{CH-}t\text{-Bu})(\text{CH}_2\text{-}t\text{-Bu})_2$ was prepared by the published procedure²⁰ or from $[\text{Re}(\text{C-}t\text{-Bu})(\text{CH-}t\text{-Bu})\text{Cl}_2]_k$ and $t\text{-BuCH}_2\text{MgCl}$ in THF at -40°C . $[\text{H}(\text{OEt}_2)_2]^+[\text{BAR}^F_4]^-$ was prepared by literature methods.¹⁴ $\text{Na}[\text{CpCo}(\text{PO}(\text{OEt})_2)_3]$ ¹⁸ was a gift from Dr. Robert D. Simpson. Ethylene (polymer grade) was purchased from Matheson and used as received. $^{13}\text{C}_2\text{H}_4$ and C_2D_4 were purchased from Cambridge Isotope Laboratories. Pyridine and acetonitrile were distilled from calcium hydride. All other reagents were purchased from Aldrich and used as received.

NMR spectra were recorded on either a Bruker WM-250, Varian XL-300, or Varian UNITY-300 spectrometer. ^1H and ^{13}C data are listed in parts per million downfield from tetramethylsilane and were referenced by the residual solvent proton peak. ^{19}F data are listed in parts per million downfield from CF_2Cl_2 and were externally referenced. Coupling constants are listed in hertz. Obvious multiplicities and routine coupling constants are usually not listed. IR spectra were recorded in a Mattson spectrometer. Elemental analyses were performed on a Perkin-Elmer 2400 CHN analyzer in our laboratories.

$\text{Re}(\text{C-}t\text{-Bu})(\text{CH}_2\text{-}t\text{-Bu})_3(\text{OTf})$. $\text{Re}(\text{C-}t\text{-Bu})(\text{CH-}t\text{-Bu})(\text{CH}_2\text{-}t\text{-Bu})_2$ (1.07 g, 2.28 mmol) was dissolved in 15 mL of ether, and the solution was cooled to -40°C . Triflic acid (200 μL , 2.28 mmol) was added, and the solution was allowed to warm to room temperature and stir for 1 h. Ether was removed *in vacuo*, leaving a yellow-brown solid, which was extracted with pentane (50 mL). The solution was filtered through Celite, and the filtrate was concentrated to 10 mL and then cooled to -40°C . Yellow, microcrystalline $\text{Re}(\text{C-}t\text{-Bu})(\text{CH}_2\text{-}t\text{-Bu})_3(\text{OTf})$ was isolated, washed with cold pentane, and dried; yield 1.00 g (71%). The spectral data for the compound prepared in this manner matched those reported.^{20,21}

$[\text{Re}(\text{C-}t\text{-Bu})(\text{CH}_2\text{-}t\text{-Bu})_3(\text{Et}_2\text{O})]^+[\text{BAR}^F_4]^-$. $\text{Re}(\text{C-}t\text{-Bu})(\text{CH-}t\text{-Bu})(\text{CH}_2\text{-}t\text{-Bu})_2$ (230 mg, 0.49 mmol) was dissolved in 5 mL of ether, and solid $[\text{H}(\text{OEt}_2)_2]^+[\text{BAR}^F_4]^-$ (489 mg, 0.49 mmol) was added. After stirring the solution for 30 min at room temperature, the volume was reduced to 2 mL and the solution was stored at -40°C overnight. Bright yellow crystals were

collected and washed with cold ether; yield 506 mg (73%): ^1H NMR (CD_2Cl_2) δ 7.7 (s, 8, Ar), 7.6 (s, 4, Ar), 3.55 (q, 4, $\text{OCH}_2\text{-CH}_3$), 2.65 (s, 6, $\text{ReCH}_2\text{-}t\text{-Bu}$), 1.65 (s, 9, $\text{ReC-}t\text{-Bu}$), 1.20 (t, 6, OCH_2CH_3), 1.14 (s, 27, $\text{CH}_2\text{-}t\text{-Bu}$).

$[\text{Re}(\text{C-}t\text{-Bu})(\text{CH}_2\text{-}t\text{-Bu})_3(\text{Et}_2\text{O})(\text{H}_2\text{O})]^+[\text{BAR}^F_4]^-$. $[\text{Re}(\text{C-}t\text{-Bu})(\text{CH}_2\text{-}t\text{-Bu})_3(\text{Et}_2\text{O})(\text{H}_2\text{O})]^+[\text{BAR}^F_4]^-$ was prepared in a fashion identical to $[\text{Re}(\text{C-}t\text{-Bu})(\text{CH}_2\text{-}t\text{-Bu})_3(\text{Et}_2\text{O})]^+[\text{BAR}^F_4]^-$ except that 1 equiv of water was added by syringe prior to recrystallization from ether: ^1H NMR (CD_2Cl_2) δ 7.75 (s, 8, Ar), 7.6 (s, 4, Ar), 7.0 (s, 2, OH_2), 3.56 (q, 4, $\text{O}(\text{CH}_2\text{CH}_3)_2$), 2.56 (s, 6, $\text{CH}_2\text{-}t\text{-Bu}$), 1.65 (s, 9, $\text{C-}t\text{-Bu}$), 1.14 (s, 27, $\text{CH}_2\text{-}t\text{-Bu}$); ^{13}C NMR (CD_2Cl_2) δ 307.0 ($\text{ReC-}t\text{-Bu}$), 162.3 (q, CF_3 , $J_{\text{CF}} = 50$ Hz), 135.3, 126.9, 123.3, 117.9 (C_{aryl}), 86.0 ($\text{CH}_2\text{-}t\text{-Bu}$), 66.2 ($\text{O}(\text{CH}_2\text{CH}_3)_2$), 55.6 (CCMe_3), 37.7 (CH_2CMe_3), 32.9 (CH_2CMe_3), 27.7 (CCMe_3), 15.4 ($\text{O}(\text{CH}_2\text{CH}_3)_2$); ^{19}F NMR (CD_2Cl_2) δ -62.3 ; IR (Nujol) cm^{-1} 3640 (O-H). Anal. Calcd for $\text{C}_{66}\text{H}_{66}\text{BF}_4\text{O}_2$: C, 47.23; H, 4.67. Found: C, 47.53; H, 4.76.

$[\text{Re}(\text{C-}t\text{-Bu})(\text{CH}_2\text{-}t\text{-Bu})_3]^+[\text{BF}_4]^-$. $\text{Re}(\text{C-}t\text{-Bu})(\text{CH-}t\text{-Bu})(\text{CH}_2\text{-}t\text{-Bu})_2$ (445 mg, 0.95 mmol) was dissolved in 8 mL of ether, and the solution was cooled to -40°C . An 85% solution of $\text{HBF}_4\cdot\text{Et}_2\text{O}$ (190 mg, 1.0 mmol) was added, and a yellow precipitate formed immediately. The mixture was allowed to warm to room temperature and was stirred for 30 min. The precipitate was collected, washed with pentane, and determined to be $>95\%$ pure by ^1H NMR; yield 305 mg (58%): ^1H NMR (CD_2Cl_2) δ 2.75 (s, 6, $\text{CH}_2\text{-}t\text{-Bu}$), 1.62 (s, 9, $\text{C-}t\text{-Bu}$), 1.13 (s, 27, $\text{CH}_2\text{-}t\text{-Bu}$); ^{13}C NMR (CD_2Cl_2) δ 300.9 ($\text{C-}t\text{-Bu}$), 85.2 ($\text{CH}_2\text{-}t\text{-Bu}$), 54.8 (CCMe_3), 37.5 (CH_2CMe_3), 32.7 (CH_2CMe_3), 27.5 (CCMe_3); ^{19}F NMR (CD_2Cl_2) δ -141 . Anal. Calcd for $\text{ReC}_{20}\text{H}_{24}\text{BF}_4$: C, 43.24; H, 7.62. Found: C, 43.37; H, 7.56.

$\text{Re}(\text{C-}t\text{-Bu})(\text{CH}_2\text{-}t\text{-Bu})_3(\text{OC}_6\text{F}_5)$. $\text{Re}(\text{C-}t\text{-Bu})(\text{CH}_2\text{-}t\text{-Bu})_3(\text{OC}_6\text{F}_5)$ was prepared in a manner similar to that employed to synthesize $\text{Re}(\text{C-}t\text{-Bu})(\text{CH}_2\text{-}t\text{-Bu})_3(\text{OTf})$: ^1H NMR (C_6D_6) δ 2.75 (s, 6, $\text{ReCH}_2\text{-}t\text{-Bu}$), 1.29 (s, 9, $\text{ReC-}t\text{-Bu}$), 1.04 (s, 27, $\text{ReCH}_2\text{-}t\text{-Bu}$). Anal. Calcd for $\text{ReC}_{26}\text{H}_{42}\text{F}_5\text{O}$: C, 47.91; H, 6.49. Found: C, 47.84; H, 6.75.

$\text{Re}(\text{C-}t\text{-Bu})(\text{CH-}t\text{-Bu})(\text{CH}_2\text{-}t\text{-Bu})(\text{py})_2(\text{O}_3\text{SCF}_3)$. $\text{Re}(\text{C-}t\text{-Bu})(\text{CH}_2\text{-}t\text{-Bu})_3(\text{O}_3\text{SCF}_3)$ (106 mg, 0.172 mmol) was dissolved in 4 mL of ether. Pyridine (57 μL , 0.72 mmol) was added, and a white precipitate formed after several minutes. After 3 h the precipitate was collected, washed with pentane, and dried *in vacuo* to yield 108 mg (89%) of a white powder that was pure $\text{Re}(\text{C-}t\text{-Bu})(\text{CH-}t\text{-Bu})(\text{CH}_2\text{-}t\text{-Bu})(\text{py})_2(\text{O}_3\text{SCF}_3)$ by NMR and elemental analysis: ^1H NMR (CD_2Cl_2) δ 13.73 (s, 1, $\text{CH-}t\text{-Bu}$), 8.65, 8.6 (d, 2 each, py), 7.9, 7.8 (t, 1 each, py), 7.5, 7.3 (t, 2 each, py), 2.38 (d, 2, $\text{CH}_a\text{H}_b\text{-}t\text{-Bu}$, $J_{\text{HH}} = 12$), 1.84 (d, 2, $\text{CH}_a\text{H}_b\text{-}t\text{-Bu}$, $J_{\text{HH}} = 12$), 1.34, 1.22, 0.93 (s, 9 each, $t\text{-Bu}$); ^{13}C NMR (CD_2Cl_2) δ 289.1 ($J_{\text{CH}} = 128$, $\text{CH-}t\text{-Bu}$), 287 ($\text{C-}t\text{-Bu}$), 155.3, 151.4 (py *ortho*), 139.1, 139.0 (py *meta*), 125.3, 125.0 (py *para*), 55.9, 48.3 (CMe_3 , third resonance obscured by solvent peak), 34.1 ($\text{CH}_2\text{-}t\text{-Bu}$), 33.9, 30.8, 29.1 (CMe_3); ^{19}F NMR (CD_2Cl_2) δ -78.3 . Anal. Calcd for $\text{ReC}_{26}\text{H}_{40}\text{F}_3\text{N}_2\text{O}_3\text{S}$: C, 44.37; H, 5.73; N, 3.98. Found: C, 44.15; H, 5.70; N, 3.94.

$\text{Re}(\text{CCMe}_2\text{Ph})(\text{CHCMe}_2\text{Ph})(\text{CH}_2\text{CMe}_2\text{Ph})(\text{py})_2(\text{O}_3\text{SCF}_3)$. $\text{Re}(\text{CCMe}_2\text{Ph})(\text{CHCMe}_2\text{Ph})(\text{CH}_2\text{CMe}_2\text{Ph})(\text{py})_2(\text{O}_3\text{SCF}_3)$ was prepared in a manner analogous to that used to prepare $\text{Re}(\text{C-}t\text{-Bu})(\text{CH-}t\text{-Bu})(\text{CH}_2\text{-}t\text{-Bu})(\text{py})_2(\text{O}_3\text{SCF}_3)$ from crude $\text{Re}(\text{CCMe}_2\text{Ph})(\text{CH}_2\text{CMe}_2\text{Ph})_3(\text{O}_3\text{SCF}_3)$ and excess pyridine in ether. A pink powder was obtained, which could be recrystallized from ether to yield analytically pure purplish-pink microcrystals: ^1H NMR (pyr- d_5) δ 14.0 (s, 1, $\text{CHCMe}_2\text{-Ph}$), 7.66 (m, 3, H_{aryl}), 7.1 (m, 6, H_{aryl}), 3.15 (d, 1, $J_{\text{HH}} = 12$, $\text{CH}_a\text{H}_b\text{CMe}_2\text{Ph}$), 2.25 (br d, 1, $\text{CH}_a\text{H}_b\text{CMe}_2\text{Ph}$), 1.98, 1.88, 1.84, 1.67, 1.58, 1.57 (s, 3 each, CH_3). Anal. Calcd for $\text{C}_{41}\text{H}_{46}\text{F}_3\text{N}_2\text{O}_3\text{SRe}$: C, 55.33; H, 5.21; N, 3.15. Found: C, 55.23; H, 5.39; N, 3.15.

$\text{Re}(\text{C-}t\text{-Bu})(\text{CH-}t\text{-Bu})(\text{CH}_2\text{-}t\text{-Bu})(\text{CH}_3\text{CN})(\text{O}_3\text{SCF}_3)$. $\text{Re}(\text{C-}t\text{-Bu})(\text{CH}_2\text{-}t\text{-Bu})_3(\text{O}_3\text{SCF}_3)$ (196 mg, 0.32 mmol) was dissolved in 3 mL of ether, and 1 mL of acetonitrile was added. The solution was stirred at room temperature for an hour, and then the solvent was removed *in vacuo*. The resulting beige solid was washed with pentane (180 mg, 96%): ^1H NMR

(CD₃CN) δ 13.24 (s, 1, CH-*t*-Bu), 2.22 (d, 1, CH_aH_b-*t*-Bu, $J_{\text{HH}} = 12$), 1.34 (d, 1, CH_aH_b-*t*-Bu, $J_{\text{HH}} = 12$), 1.26, 1.14, 0.78 (s, 9 each, *t*-Bu); ¹³C NMR (CD₃CN) δ 294.8 (C-*t*-Bu), 291.8 (CH-*t*-Bu, $J_{\text{CH}} = 116$), 53.5, 50.1, 48.1 (CMe₃), 33.5 (CH₂-*t*-Bu), 33.8, 30.4, 28.5 (CMe₃). Anal. Calcd for ReC₁₈H₃₃F₃NO₃S: C, 36.85; H, 5.67; N, 2.39. Found: C, 36.65; H, 5.63; N, 2.29.

[Re(C-*t*-Bu)(CH-*t*-Bu)(CH₂-*t*-Bu)(py)₃]⁺[BAR^F₄]⁻. Re(C-*t*-Bu)(CH-*t*-Bu)(CH₂-*t*-Bu)₂ (160 mg, 0.34 mmol) was dissolved in 5 mL of ether, solid [H(OEt)₂]⁺[BAR^F₄]⁻ (344 mg, 0.34 mmol) was added, and the mixture was stirred for 45 min. Pyridine (110 μ L, 1.39 mmol) was added, and the resulting red solution was allowed to stir for an additional 30 min. The volume of the solution was reduced to 3 mL and cooled to -40 °C overnight to yield orange-pink microcrystals (370 mg, 73%), which were washed with pentane and dried: ¹H NMR (py-*d*₅) δ 13.78 (s, 1, CH-*t*-Bu), 8.41 (s, 8, H_{aryl}), 7.81 (s, 4, H_{aryl}), 2.81 (d, 1, CH_aH_b-*t*-Bu, $J_{\text{HH}} = 12$), 1.82 (d, 1, CH_aH_b-*t*-Bu, $J_{\text{HH}} = 12$), 1.33, 1.24, 1.12 (9 each, *t*-Bu); ¹³C NMR (py-*d*₅) δ 289.9 (C-*t*-Bu), 288.5 (CH-*t*-Bu, $J_{\text{CH}} = 120$), 163 (CF₃, $J_{\text{C-F}} = 49$), 155, 127.1, 120, 118.5 (C_{aryl}), 54.5, 53.4, 48.6 (CMe₃), 34.6 (CH₂-*t*-Bu), 34.2, 30.8, 28.9 (CMe₃). Anal. Calcd for ReC₂₂H₅₇BF₂₄N₃: C, 49.74; H, 3.83; N, 2.94. Found: C, 49.74; H, 4.13; N, 2.90.

[Re(C-*t*-Bu)(CH-*t*-Bu)(CH₂-*t*-Bu)(py)₂(py·H₂O)]⁺[BAR^F₄]⁻. [Re(C-*t*-Bu)(CH-*t*-Bu)(CH₂-*t*-Bu)(py)₂(py·H₂O)]⁺[BAR^F₄]⁻ was prepared from [Re(C-*t*-Bu)(CH₂-*t*-Bu)₃(OH₂)]⁺[BAR^F₄]⁻ and 3 equiv of pyridine in ether and was recrystallized from 2/1 ether/pentane at -40 °C. Orange cubes formed and were collected and dried. Spectral data matched those for [Re(C-*t*-Bu)(CH-*t*-Bu)(CH₂-*t*-Bu)(py)₃]⁺[BAR^F₄]⁻ in pyridine-*d*₅. These complexes are insoluble in C₆D₆ and toluene-*d*₈ and decompose in CD₂Cl₂ and CDCl₃.

[Re(C-*t*-Bu)(CH-*t*-Bu)(CH₂-*t*-Bu)(CH₃CN)₃][BAR^F₄]. Re(C-*t*-Bu)(CH-*t*-Bu)(CH₂-*t*-Bu)₂ (340 mg, 0.72 mmol) was dissolved in 5 mL of ether, solid [H(OEt)₂]⁺[BAR^F₄]⁻ (700 mg, 0.70 mmol) was added, and the mixture was stirred for 20 min. CH₃CN (1 mL) was added, and the solution was stirred for 45 min. The solvent was removed *in vacuo*, and the resulting beige powder was washed with pentane until the washings were colorless. An analytical sample was recrystallized from ether/pentane: ¹H NMR (C₆D₆) δ 13.38 (s, 1, ReCH-*t*-Bu), 8.25 (s, 8, H_{aryl}), 7.53 (s, 4, H_{aryl}), 2.47 (d, 1, ReCH_aH_b-*t*-Bu, $J_{\text{HH}} = 12$), 1.56 (d, 1, ReCH_aH_b-*t*-Bu, $J_{\text{HH}} = 12$), 1.21, 1.15, 1.07 (s, 9 each, *t*-Bu), 0.78 (br s, 9, CH₃CN); ¹³C NMR (CD₃CN) δ 298 (C-*t*-Bu), 292.1 (CH-*t*-Bu), 163 (q, CF₃, $J_{\text{C-F}} = 48$), 130.9, 127.6, 124.0, 120.4 (C_{aryl}), 54.0, 49.2, 33.8 (CMe₃), 48.5 (CH₂-*t*-Bu), 34.0, 30.6, 28.7 (CMe₃). Anal. Calcd for C₅₃H₅₁BF₂₄N₃Re: C, 46.03; H, 3.72; N, 3.04. Found: C, 45.70; H, 3.99; N, 2.79.

Re(C-*t*-Bu)(CH-*t*-Bu)(CH₂-*t*-Bu)(CH₃CN)₂(BF₄). Re(C-*t*-Bu)(CH₂-*t*-Bu)₃(BF₄) (43 mg, 0.078 mmol) was dissolved in 1 mL of ether, and 1 mL of CH₃CN was added. The solution immediately became colorless and was stirred for 1 h at room temperature. The solvents were removed *in vacuo*, and the resulting solid was washed with pentane to yield 35 mg (74%) of pale yellow Re(C-*t*-Bu)(CH-*t*-Bu)(CH₂-*t*-Bu)(CH₃CN)₂(BF₄): ¹H NMR (C₆D₆) δ 13.59 (s, 1, CH-*t*-Bu), 2.68 (d, 1, $J_{\text{HH}} = 12$, CH_aH_b-*t*-Bu), 1.95 (d, 1, $J_{\text{HH}} = 12$, CH_aH_b-*t*-Bu), 1.80 (br s, 3, CH₃CN), 1.51 (br s, 6, CH₃CN), 1.32, 1.28, 1.19 (s, 9 each, *t*-Bu); ¹³C NMR (CD₃CN) δ 296.1 (ReCCMe₃), 291.5 (ReCH-*t*-Bu, $J_{\text{CH}} = 122$), 53.6, 48.7, 48.1 (CMe₃), 33.6, 30.2, 28.3 (CMe₃), 33.4 (CH₂-*t*-Bu); ¹⁹F NMR (C₆D₆) δ -151.3. Anal. Calcd for ReC₁₉H₃₆N₂BF₄: C, 40.35; H, 6.42; N, 4.95. Found: C, 40.30; H, 6.45; N, 4.82.

Re(C-*t*-Bu)(CH-*t*-Bu)(CH₂-*t*-Bu)(CD₃OD)_n(O₃SCF₃). Re(C-*t*-Bu)(CH₂-*t*-Bu)₃(O₃SCF₃) (15 mg) was transferred to an NMR tube which was capped with a septum cap and brought out of the drybox. CD₃OD (1 mL) was added by syringe to yield a yellow solution of Re(C-*t*-Bu)(CH-*t*-Bu)(CH₂-*t*-Bu)(CD₃OD)_n(O₃SCF₃). Experiments employing an internal standard showed that Re(C-*t*-Bu)(CH-*t*-Bu)(CH₂-*t*-Bu)(CD₃OD)_n(O₃SCF₃) is formed in >90% yield: ¹H NMR (CD₃OD) δ 13.00 (s, 1, CH-

t-Bu), 2.82 (d, 1, CH_aH_b-*t*-Bu, $J_{\text{HH}} = 12$), 2.39 (d, 1, CH_aH_b-*t*-Bu, $J_{\text{HH}} = 12$), 1.36, 1.26, 1.15 (s, 9 each, *t*-Bu).

Re(C-*t*-Bu)(CH-*t*-Bu)(CH₂-*t*-Bu)(THF-*d*₈)_n(O₃SCF₃). Re(C-*t*-Bu)(CH-*t*-Bu)(CH₂-*t*-Bu)(THF-*d*₈)_n(O₃SCF₃) was prepared in the same manner as Re(C-*t*-Bu)(CH-*t*-Bu)(CH₂-*t*-Bu)(CD₃OD)_n(O₃SCF₃) in THF-*d*₈, although it took 2 h for Re(C-*t*-Bu)(CH₂-*t*-Bu)₃(O₃SCF₃) to react completely: ¹H NMR (THF-*d*₈) δ 13.08 (s, 1, CH-*t*-Bu), 2.50 (d, 1, CH_aH_b-*t*-Bu, $J_{\text{HH}} = 12$), 1.48 (d, 1, CH_aH_b-*t*-Bu, $J_{\text{HH}} = 12$), 1.36, 1.27, 0.94 (s, 9 each, *t*-Bu).

ReCl(L_{OR})(C-*t*-Bu)(CH-*t*-Bu). Solid [Re(C-*t*-Bu)(CH-*t*-Bu)Cl₂]_k (44 mg, 0.11 mmol) and NaL_{OR} (55 mg, 0.10 mmol) were combined, and 3 mL of THF was added. The orange-red mixture was stirred for 1.5 h, and the THF was then removed *in vacuo* to yield an orange-pink solid, which was extracted with ether. Ether was then removed *in vacuo* to yield a pink film (85 mg, 95%). An analytical sample was recrystallized from ether/pentane at -40 °C: ¹H NMR (C₆D₆) δ 13.95 (s, 1, ReCH-*t*-Bu), 4.89 (s, 5, Cp), 3.8–4.6 (m, 12 total, POCH₂CH₃), 1.62, 1.54 (s, 9 each, *t*-Bu), 1.0–1.4 (m, 18 total, POCH₂CH₃). Anal. Calcd for ReCoC₂₇H₅₄ClO₉P₃: C, 36.18; H, 6.07. Found: C, 35.94; H, 5.92.

Re(η^5 -C₅H₅)(C-*t*-Bu)(CH-*t*-Bu)(CH₂-*t*-Bu). Re(C-*t*-Bu)(CH-*t*-Bu)(CH₂-*t*-Bu)(py)₂(O₃SCF₃) (100 mg, 0.14 mmol) was dissolved in 5 mL THF, and a THF solution of NaCp (0.15 mmol) was added. The resulting orange mixture was stirred for 1 h, and the volatile components were removed *in vacuo*. The resulting beige solid was extracted with pentane (10 mL), and solvent was removed *in vacuo* to yield a beige oil (62 mg, 96%) that was pure by ¹H NMR: ¹H NMR (C₆D₆) δ 12.67 (s, 1, ReCH-*t*-Bu), 5.32 (s, 5, η^5 -C₅H₅), 2.52 (d, 1, $J_{\text{HH}} = 12$, ReCH_aH_b-*t*-Bu), 2.36 (d, 1, $J_{\text{HH}} = 12$, ReCH_aH_b-*t*-Bu), 1.34, 1.12, 1.11 (s, 9 each, *t*-Bu); ¹³C NMR (C₆D₆) δ 285.7 (ReC-*t*-Bu), 265.6 (ReCH-*t*-Bu, $J_{\text{CH}} = 116$), 97.6 (C₅H₅), 52.9, 47.6, 33.0 (CMe₃), 34.2, 31.9, 29.4 (CMe₃), 17.4 (ReCH₂-*t*-Bu). Anal. Calcd for ReC₂₀H₃₆: C, 52.03; H, 7.64. Found: C, 52.54; H, 7.75.

Re(L_{OR})(C-*t*-Bu)(CH-*t*-Bu)(CH₂-*t*-Bu). Re(C-*t*-Bu)(CH-*t*-Bu)(CH₂-*t*-Bu)(py)₂(O₃SCF₃) (78 mg, 1.10 mmol) was dissolved in 5 mL of THF, and solid NaL_{OR} was added. The mixture was stirred for 1.5 h, and then the THF was removed *in vacuo* to yield a yellow solid. The solid was extracted with 2 mL of ether, and the ether was removed *in vacuo* to yield pure Re(L_{OR})(C-*t*-Bu)(CH-*t*-Bu)(CH₂-*t*-Bu) as a pale yellow solid (97 mg, 94%): ¹H NMR (C₆D₆) δ 13.02 (s, 1, ReCH-*t*-Bu), 4.90 (s, 5, η^5 -C₅H₅), 3.8–4.4 (m, 12 total, POCH₂CH₃), 2.73 (d, 2, $J_{\text{HH}} = 12$, ReCH_aH_b-*t*-Bu), 1.79 (d, 2, $J_{\text{HH}} = 12$, ReCH_aH_b-*t*-Bu), 1.59, 1.52, 1.39 (s, 9 each, *t*-Bu), 1.0–1.3 (m, 18 total, POCH₂CH₃); ¹³C NMR (C₆D₆) δ 281.6 (ReC-*t*-Bu), 275.7 (ReCH-*t*-Bu, $J_{\text{CH}} = 125$), 89.5 (η^5 -C₅H₅), 61.1 (POCH₂CH₃), 54.8 (ReCH₂-*t*-Bu), 51.7, 46.3, 34.2 (CMe₃), 34.7, 32.5, 29.7 (CMe₃), 17.3 (POCH₂CH₃). Anal. Calcd for CoOsC₃₂H₆₅O₉P₃: C, 41.24; H, 7.03. Found: C, 40.93; H, 6.86.

Re(HBpz₃)(C-*t*-Bu)(CH-*t*-Bu)(CH₂-*t*-Bu). Re(C-*t*-Bu)(CH-*t*-Bu)(CH₂-*t*-Bu)(py)₂(O₃SCF₃) (90 mg, 0.128 mmol) was dissolved in 3 mL of THF, and solid NaHBpz₃ (30 mg, 0.127 mmol) was added. The resulting solution was allowed to stir for 1 h, and then the THF was removed *in vacuo*. The residue was extracted with ether, the resulting solution was filtered through Celite, and the ether was removed *in vacuo* to yield a white solid; yield 67 mg (0.110 mmol, 86%): ¹H NMR (C₆D₆) δ 13.22 (s, 1, ReCH-*t*-Bu), 8.34, 8.09, 7.79 (s, 1 each, pz), 7.34, 7.32, 7.28 (s, 1 each, pz), 5.97, 5.88, 5.80 (s, 1 each, pz), 2.74 (d, 2, $J_{\text{HH}} = 12$, ReCH_aH_b-*t*-Bu), 1.74 (d, 2, $J_{\text{HH}} = 12$, ReCH_aH_b-*t*-Bu), 1.40, 1.35, 1.24 (s, 9 each, *t*-Bu); ¹³C NMR (C₆D₆) δ 289.3 (ReC-*t*-Bu), 282.7 (ReCH-*t*-Bu), 148.1, 144.3, 141.7, 135.0, 134.5, 134.0, 105.9, 105.4, 105.2 (pz), 53.0 (ReCH₂-*t*-Bu), 52.3, 47.7, 34.3 (CMe₃), 34.7, 31.3, 29.1 (CMe₃). Anal. Calcd for ReC₂₄H₄₀N₆: C, 47.28; H, 6.61; N, 13.79. Found: C, 47.53; H, 6.18; N, 13.85.

Re(C-*t*-Bu)(CH-*t*-Bu)(CH₂-*t*-Bu)(C₆H₁₂S₃)(O₃SCF₃). Re(C-*t*-Bu)(CH-*t*-Bu)(CH₂-*t*-Bu)(py)₂(O₃SCF₃) (183 mg, 0.26 mmol) was dissolved in 5 mL of dichloromethane, and solid S₃C₆H₁₂ (70 mg, 0.39 mmol) was added. The solution was stirred for 2

h, and then the dichloromethane was removed *in vacuo* to yield a colorless solid, which was recrystallized from dichloromethane/pentane at $-40\text{ }^{\circ}\text{C}$; yield 180 mg (95%): $^1\text{H NMR}$ (CD_2Cl_2) δ 12.91 (s, 1, ReC-t-Bu), 2.95–3.9 (m, 12 total, $\text{S}_3\text{C}_6\text{H}_{12}$), 2.59 (d, 1, $\text{ReCH}_a\text{H}_b\text{-t-Bu}$, $J_{\text{HH}} = 12$), 1.54 (d, 1, $\text{ReCH}_a\text{H}_b\text{-t-Bu}$, $J_{\text{HH}} = 12$), 1.27, 1.17, 0.92 (s, 9 each, *t-Bu*); $^{13}\text{C NMR}$ (CD_2Cl_2) δ 294.9 (ReC-t-Bu), 283.5 (ReCH-t-Bu), 53.6 ($\text{ReCH}_2\text{-t-Bu}$), 49.5, 40.3, 40.2, 38.7, 36.6, 36.3 ($\text{S}_3\text{C}_6\text{H}_{12}$), 35.2, 33.2, 32.1 (CMe_3), 33.6, 29.6, 28.2 (CMe_3). Anal. Calcd for $\text{ReC}_{22}\text{H}_{42}\text{O}_3\text{S}_4\text{F}_3$: C, 36.39; H, 5.83. Found: C, 36.17; H, 5.40.

$\text{Re}(\eta^5\text{-C}_5\text{H}_5)(\text{C-t-Bu})(\text{CH-t-Bu})(\text{O}_3\text{SCF}_3)$. $\text{Re}(\eta^5\text{-C}_5\text{H}_5)(\text{C-t-Bu})(\text{CH-t-Bu})(\text{CH}_2\text{-t-Bu})$ (110 mg, 0.23 mmol) was dissolved in 5 mL of ether, and the mixture was cooled to $-40\text{ }^{\circ}\text{C}$. Triflic acid (20 μL , 0.22 mmol) was added, and the mixture was warmed to room temperature and stirred for 10 min. Ether was then removed *in vacuo*, and the solid was extracted with pentane (10 mL). Pentane was removed *in vacuo* from the filtrate, and a microcrystalline colorless solid was collected; yield 104 mg (84%): $^1\text{H NMR}$ (C_6D_6) δ 13.72 (s, 1, ReCH-t-Bu), 5.27 (s, 5, $\eta^5\text{-C}_5\text{H}_5$), 1.29, 1.14 (s, 9 each, *t-Bu*); $^{13}\text{C NMR}$ (C_6D_6) δ 306.5 (ReC-t-Bu), 298.6 (ReCH-t-Bu , $J_{\text{CH}} = 90$), 98.5 (C_5H_5), 54.4, 48.8 (CMe_3), 31.7, 29.4 (CMe_3); $^{19}\text{F NMR}$ (C_6D_6) δ -75.5 . $\text{Re}(\eta^5\text{-C}_5\text{H}_5)(\text{C-t-Bu})(\text{CH-t-Bu})(\text{O}_3\text{SCF}_3)$ is too unstable in the solid state for elemental analysis.

$[\text{Re}(\eta^5\text{-C}_5\text{H}_5)(\text{C-t-Bu})(\text{CH-t-Bu})(\text{py})]^+[\text{OTf}]^-$. $\text{Re}(\text{Cp})(\text{C-t-Bu})(\text{CH-t-Bu})(\text{CH}_2\text{-t-Bu})$ (65 mg, 0.141 mmol) was dissolved in 5 mL of CH_2Cl_2 , and the solution was cooled to $-40\text{ }^{\circ}\text{C}$. Solid pyHOTf (31 mg, 0.135 mmol) was added, and the solution became yellow. The mixture was allowed to warm to room temperature and was stirred for 1 h. Dichloromethane was removed *in vacuo*, and a pale yellow solid was isolated, washed with pentane, and crystallized from a CH_2Cl_2 /ether mixture at $-40\text{ }^{\circ}\text{C}$; yield 50 mg (60%): $^1\text{H NMR}$ (C_6D_6) δ 14.33 (s, 1, ReCH-t-Bu), 8.60 (d, 2, *py*), 7.13 (t, 1, *py*), 7.00 (t, 2, *py*), 5.76 (s, 5, C_5H_5), 1.08, 1.00 (s, 9 each, *t-Bu*); $^{13}\text{C NMR}$ (CDCl_3) δ 311.4 (ReC-t-Bu), 295.8 (ReCH-t-Bu , $J_{\text{CH}} = 125$), 161.5, 140.4, 127.3 (*py*), 99.3 (*Cp*), 55.1, 50.4 (CMe_3), 30.6, 28.8 (CMe_3). Anal. Calcd for $\text{ReC}_{21}\text{H}_{29}\text{NF}_3\text{O}_3\text{S}$: C, 40.77; H, 4.72; N, 2.26. Found: C, 41.02; H, 4.67; N, 2.20.

$\text{Re}(\text{LOEt})(\text{C-t-Bu})(\text{CH-t-Bu})(\text{O}_3\text{SCF}_3)$. $\text{Re}(\text{LOEt})(\text{C-t-Bu})(\text{CH-t-Bu})(\text{CH}_2\text{-t-Bu})$ (100 mg, 0.11 mmol) was dissolved in 5 mL of ether, and the solution was cooled to $-40\text{ }^{\circ}\text{C}$. Triflic acid (10 μL , 0.11 mmol) was added, and the yellow mixture was warmed to room temperature and stirred for 45 min. Ether was then removed *in vacuo*, and the sticky yellow solid was recrystallized from ether/pentane at $-40\text{ }^{\circ}\text{C}$ to yield yellow prisms; yield 63 mg (59%): $^1\text{H NMR}$ (CD_2Cl_2) δ 13.77 (s, 1, ReCH-t-Bu), 5.13 (s, 5, $\eta^5\text{-C}_5\text{H}_5$), 3.4–4.2 (br m, 12 total, POCH_2CH_3), 1.34, 1.33 (s, 9 each, *t-Bu*), 1.16 (br m, 18, POCH_2CH_3); $^{13}\text{C NMR}$ (CD_2Cl_2) δ 300.8 (ReCH-t-Bu , $J_{\text{CH}} = 121$), 298.0 (ReC-t-Bu), 90.1 (C_5H_5), 61.9 (br, POCH_2CH_3), 46.9 (CMe_3 , other CMe_3 peak obscured by the solvent peak), 32.9, 29.5 (CMe_3), 16.7 (POCH_2CH_3); $^{19}\text{F NMR}$ (CD_2Cl_2) δ -78.1 . Anal. Calcd for $\text{CoReC}_{28}\text{H}_{54}\text{F}_3\text{O}_{12}\text{P}_3\text{S}$: C, 33.30; H, 5.39. Found: C, 32.92; H, 5.10.

$[\text{Re}(\text{LOEt})(\text{C-t-Bu})(\text{CH-t-Bu})(\text{Et}_2\text{O})]^+[\text{BAR}^{\text{F}}_4]^-$. $\text{Re}(\text{LOEt})(\text{C-t-Bu})(\text{CH-t-Bu})(\text{CH}_2\text{-t-Bu})$ (140 mg, 0.15 mmol) was dissolved in 5 mL of ether, and the solution was cooled to $-40\text{ }^{\circ}\text{C}$. Solid $[\text{H}(\text{OEt})_2][\text{BAR}^{\text{F}}_4]$ (149 mg, 0.15 mmol) was added and the yellow solution was allowed to warm to room temperature and stirred for 1.5 h. Ether was removed *in vacuo* and the yellow-tan solid was recrystallized from ether/pentane at $-40\text{ }^{\circ}\text{C}$ overnight; yield 140 mg (50%): $^1\text{H NMR}$ (CD_2Cl_2) δ 13.78 (s, 1, ReCH-t-Bu), 7.72 (s, 8, Ar^{F}), 7.56 (s, 4, Ar^{F}), 5.32 (s, 5, *Cp*), 3.8–5.2 (m, 12, OCH_2CH_3), 3.40 (br q, 4, OCH_2CH_3), 1.33, 1.31 (s, 9 each, *t-Bu*), 1.0–1.3 (m, 24 total, OCH_2CH_3); $^{13}\text{C NMR}$ (CDCl_3) δ 302.9 (ReCH-t-Bu , $J_{\text{CH}} = 124$), 299.0 (ReC-t-Bu), 163.0 (q, CF_3 , $J_{\text{C-F}} = 48$), 135.0, 130.0, 126.6, 123.0 (C_{aryl}), 90.1 (*Cp*), 61.8 (OCH_2CH_3), 61.5 (OCH_2CH_3), 32.7, 29.3 (CMe_3), 53.0, 46.9 (CMe_3), 16.5 (OCH_2CH_3), 12.6 (OCH_2CH_3). Anal. Calcd for $\text{ReCoC}_{63}\text{H}_{76}\text{BF}_{24}\text{O}_{10}\text{P}_3$: C, 42.08; H, 4.26. Found: C, 42.39; H, 4.23.

$[\text{Re}(\text{S}_3\text{C}_6\text{H}_{12})(\text{C-t-Bu})(\text{CH-t-Bu})(\text{O}_3\text{SCF}_3)]^+[\text{O}_3\text{SCF}_3]^-$. $[\text{Re}(\text{S}_3\text{C}_6\text{H}_{12})(\text{C-t-Bu})(\text{CH-t-Bu})(\text{CH}_2\text{-t-Bu})]^+[\text{O}_3\text{SCF}_3]^-$ (60 mg, 0.083 mmol) was dissolved in 5 mL of CH_2Cl_2 , and the solution was cooled to $-40\text{ }^{\circ}\text{C}$. Triflic acid (8 μL , 0.09 mmol) was added, and the resulting pale pink mixture was warmed to room temperature and stirred for 45 min. CH_2Cl_2 was then removed *in vacuo*, and the resulting microcrystalline pale pink solid was washed with pentane and dried; yield 40 mg (60%): $^1\text{H NMR}$ (CD_2Cl_2) δ 14.56 (s, 1, ReCH-t-Bu), 3.1–4.2 (overlapping multiplets, 12 total, $\text{S}_3\text{C}_6\text{H}_{12}$), 1.43, 1.32 (s, 9 each, *t-Bu*); $^{13}\text{C NMR}$ (CD_2Cl_2) δ 306.4 (ReCH-t-Bu , $J_{\text{CH}} = 116$), 304.6 (ReC-t-Bu), 55.2, 51.6 (CMe_3), 43.7, 41.9, 36.5, 34.0, 32.9, 30.1 ($\text{S}_3\text{C}_6\text{H}_{12}$), 29.7, 28.5 (CMe_3); $^{19}\text{F NMR}$ (CD_2Cl_2) δ -75.6 , -78.6 . Anal. Calcd for $\text{ReC}_{18}\text{H}_{31}\text{F}_6\text{O}_6\text{S}_6$: C, 26.89; H, 3.89. Found: C, 26.96; H, 3.74.

$\text{Re}(\text{C-t-Bu})(\text{CHC}_6\text{H}_5)(\text{CH}_2\text{-t-Bu})(\text{py})_2(\text{OTf})$. $\text{Re}(\text{C-t-Bu})(\text{CH-t-Bu})(\text{CH}_2\text{-t-Bu})(\text{py})_2(\text{OTf})$ (49 mg, 0.26 mmol) was dissolved in 3 mL of CH_2Cl_2 . Styrene (36 μL , 0.315 mmol) was added, and the resulting orange solution was allowed to stir at room temperature for 1.5 h. The volatiles were removed *in vacuo* to yield a beige powder, which was washed with pentane (10 mL) and recrystallized from CH_2Cl_2 /ether to yield beige microcrystals: $^1\text{H NMR}$ (CD_2Cl_2) δ 14.35 (s, 1, ReCHC_6H_5), 8.76, 8.46 (d, 2 each, *py ortho*), 8.00, 7.80 (br t, 1 each, *py meta*), 7.76 (d, 2, $J_{\text{HH}} = 9$, *phenyl ortho*), 7.55, 7.38 (t, 2 each, *py meta*), 7.25 (m, 3, *phenyl meta and para*), 2.52 (d, 2, $J_{\text{HH}} = 12$, $\text{ReCH}_a\text{H}_b\text{CMe}_3$), 2.07 (d, 2, $J_{\text{HH}} = 12$, $\text{ReCH}_a\text{H}_b\text{CMe}_3$), 1.33, 0.86 (s, 9 each, *t-Bu*); $^{13}\text{C NMR}$ (CD_2Cl_2) δ 290.4 (ReC-t-Bu), 270.3 (ReCHC_6H_5 , $J_{\text{CH}} = 128\text{ Hz}$), 155.2, 153.2, 152.2, 139.6, 139.4, 129.7, 128.7, 128.4, 125.6 (*py and phenyl*), 57.6 ($\text{ReCH}_2\text{C}_6\text{H}_5$), 36.1 (CMe_3), 34.0, 28.5 (CMe_3). Anal. Calcd for $\text{C}_{28}\text{H}_{36}\text{N}_2\text{F}_3\text{O}_3\text{SR}$: C, 46.46; H, 5.01; N, 3.87. Found: C, 46.16; H, 5.04; N, 3.63.

$\text{Re}(\text{C-t-Bu})(\text{CHOEt})(\text{CH}_2\text{-t-Bu})(\text{py})_2(\text{OTf})$. $\text{Re}(\text{C-t-Bu})(\text{CHOEt})(\text{CH}_2\text{-t-Bu})(\text{py})_2(\text{OTf})$ was prepared from $\text{Re}(\text{C-t-Bu})(\text{CH-t-Bu})(\text{CH}_2\text{-t-Bu})(\text{py})_2(\text{OTf})$ and ethyl vinyl ether in a manner similar to that used in the preparation of $\text{Re}(\text{C-t-Bu})(\text{CHC}_6\text{H}_5)(\text{CH}_2\text{-t-Bu})(\text{py})_2(\text{OTf})$. A pink solid was obtained after dichloromethane was removed *in vacuo*; this was washed with ether and dried; yield 60%: $^1\text{H NMR}$ (CDCl_3) δ 12.89 (ReCH-t-Bu), 8.76, 8.45 (d, 2 each, *py*), 7.83, 7.70 (t, 1 each, *py*), 7.40, 7.20 (d, 2 each, *py*), 4.07 (q, 2, OCH_2CH_3), 2.03 (d, 1, $\text{ReCH}_a\text{H}_b\text{-t-Bu}$), 1.38 (d, 1, $\text{ReCH}_a\text{H}_b\text{-t-Bu}$), 1.31 (t, 3, OCH_2CH_3), 1.20, 0.94 (s, 9 each, *t-Bu*); $^{13}\text{C NMR}$ (CDCl_3) δ 288.1 (ReCHOEt), 280.3 (ReC-t-Bu), 154.6, 153.1, 138.6, 138.2, 125.4, 124.8 (*py*), 75.4 (OCH_2CH_3), 50.6, 35.0 (CMe_3), 33.8, 27.9 (CMe_3), 16.1 (OCH_2CH_3).

$\text{Re}(\text{C-t-Bu})(\text{CH}_2)(\text{CH}_2\text{-t-Bu})(\text{bpy})(\text{OTf})$. $^1\text{H NMR}$ (C_6D_6) δ 14.03 (d, 1, ReCH_aH_b , $J_{\text{HH}} = 3$, $J_{\text{CH}} = 135$), 13.50 (d, 1, ReCH_aH_b , $J_{\text{HH}} = 3$, $J_{\text{CH}} = 150$), 6.4–9 (m, 8 total, *bpy*), 2.79 (d, 1, $\text{ReCH}_a\text{H}_b\text{-t-Bu}$), 1.86 (d, 1, $\text{ReCH}_a\text{H}_b\text{-t-Bu}$), 1.39, 0.86 (s, 9 each, *t-Bu*); ^{13}C (partial) δ 258 (ReCH_2). Due to the instability of $\text{Re}(\text{C-t-Bu})(\text{CH}_2)(\text{CH}_2\text{-t-Bu})(\text{bpy})(\text{OTf})$ at $-40\text{ }^{\circ}\text{C}$, a pure sample could not be prepared, and neither elemental analysis nor a complete set of $^{13}\text{C NMR}$ data could be obtained. The ^{13}C data were obtained by preparing a sample of $\text{Re}(\text{C-t-Bu})(^{13}\text{CH}_2)(\text{CH}_2\text{-t-Bu})(\text{bpy})(\text{OTf})$.

$\text{Re}(\text{C-t-Bu})(\text{CH}_2)_3\text{-t-Bu}(\text{C}_2\text{H}_4)(\text{py})_2(\text{O}_3\text{SCF}_3)$. $\text{Re}(\text{C-t-Bu})(\text{CH-t-Bu})(\text{CH}_2\text{-t-Bu})(\text{py})_2(\text{O}_3\text{SCF}_3)$ (176 mg, 0.25 mmol) was dissolved in 10 mL of benzene and stirred under an atmosphere of ethylene for 45 min. The brown-orange solution was then reduced in volume to 2 mL, and 5 mL of pentane was added to precipitate a beige powder, which was then washed with 15 mL of pentane and dried to yield a beige solid; yield 135 mg (78%). An analytical sample was recrystallized from ether at $-40\text{ }^{\circ}\text{C}$: $^1\text{H NMR}$ (C_6D_6) δ 8.9, 8.7 (d, 2 each, *py ortho*), 6.65 (br m, 2, *py meta*), 6.45 (br m, 4, *py para*), 3.5 (br m, 4, C_2H_4), 3.15 (m, 1, ReCH_2), 2.51 (m, 1, ReCH_2), 2.42 (overlapping multiplets, 2 total, $\text{ReCH}_2\text{CH}_a\text{H}_b$ and $\text{Re}(\text{CH}_2)_2\text{CH}_a\text{H}_b$, partial assignment by C_2D_4 labeling experiment), 2.04 (m, 1, $\text{ReCH}_2\text{CH}_a\text{H}_b$), 1.80 (m, 1, $\text{Re}(\text{CH}_2)_2\text{CH}_a\text{H}_b$), 1.16, 0.80 (s, 9 each, *t-Bu*); $^{13}\text{C NMR}$ (C_6D_6) δ 248.2 (ReC-t-

Bu), 153.9, 153.7 (py *ortho*), 138.4, 137.6 (py *meta*), 125.4, 125.1 (py *para*), 53.9 (ReCH₂CH₂-, $J_{\text{CH}} = 153$, $J_{\text{C-C}} = 36$), 53.0, 50.6 (CMe₃), 51.2 (Re(CH₂)₂CH₂-), 46.6 (ReCH₂CH₂-, $J_{\text{CH}} = 156$, $J_{\text{C-C}} = 36$), 29.9, 25.8 (CMe₃), 20.7 (C₂H₄, $J_{\text{CH}} = 123$); ¹⁹F NMR (C₆D₆) δ -78.7. Anal. Calcd for ReC₂₅H₃₈N₂F₃O₃SRe: C, 43.53; H, 5.55; N, 4.02. Found: C, 43.71; H, 5.76; N, 4.02.

Observation of Re(C-*t*-Bu)(CH₂Et)(CH₂-*t*-Bu)(CD₃CN)_n-(OTf). A 2:1 mixture of Re(C-*t*-Bu)(CH₂Et)(CH₂-*t*-Bu)(CD₃CN)_n-(OTf) and Re(C-*t*-Bu)(CH-*t*-Bu)(CH₂-*t*-Bu)(CD₃CN)_n-(OTf) was generated by heating a CD₃CN solution of Re(C-*t*-Bu)(CH-*t*-Bu)(CH₂-*t*-Bu)(CD₃CN)(OTf) (12 mg, 0.02 mmol) and *cis*-3-hexene (10 μ L, 0.08 mmol) at 60 °C for 1 h. Partial ¹H NMR

(CD₃CN) δ 13.53 (t, 1, ReCH₂Et), 3.5 (d of m, 2 total, ReCHCH₂-CH₃), 2.2 (d, 1, ReCH₂H-*t*-Bu), 1.25, 0.9 (s, 9 each, *t*-Bu). The remaining resonances could not be assigned due to overlap with the resonances associated with *cis*-3-hexene.

Acknowledgment. R.R.S. thanks the National Science Foundation (Grant CHE 91 22827) for research support, and A.M.L. thanks Dr. R. D. Simpson for a gift of NaL_OEt.

OM940949S

Interaction of Acyclic Tetraenes and Trienes with Transition Metals: Organoiron Compounds

P. W. Jolly,* C. Kopiske, C. Krüger, and A. Limberg

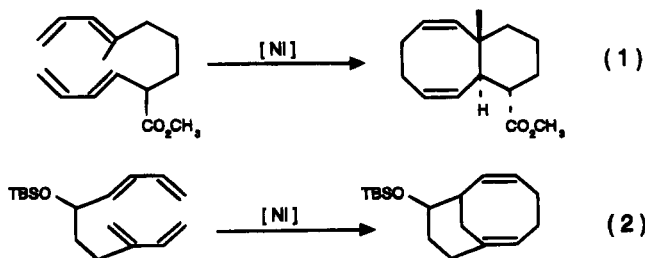
Max-Planck-Institut für Kohlenforschung, D-45466 Mülheim an der Ruhr, Germany

Received December 13, 1994[®]

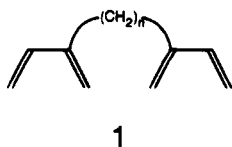
The tetraene 3,6-dimethylene-1,7-octadiene (DMOD) reacts with zerovalent $[\text{FePR}_3]$ species (prepared by reduction of $\text{FeCl}_2 \cdot n\text{THF}$ with active Mg in the presence of the donor ligand) to give $(\eta^4, \eta^4\text{-DMOD})\text{FePR}_3$ compounds. The crystal structure of the PPh_3 -stabilized derivative (space group $R\bar{3}$, $a = b = c = 20.290(9)$ Å, $\alpha = \beta = \gamma = 117.47(3)^\circ$, $Z = 6$, $R = 0.048$, $R_w = 0.052$) confirms that the iron atom lies at the center of a square pyramid with the P atom at the apex and the two 1,3-diene fragments forming the base. That the products of the reaction of the trienes 3-methylene-1,6-heptadiene (MHD) and 3-methylene-1,7-octadiene (MOD) with zerovalent $[\text{Fe}(\text{Pr}^i_2\text{P}(\text{CH}_2)_n\text{PPr}^i_2)]$ species ($n = 1, 2, 3$) contain a triene molecule bonded in an η^2, η^4 -manner to the metal atom has been confirmed by X-ray diffraction for $(\eta^2, \eta^4\text{-MHD})\text{Fe}(\text{Pr}^i_2\text{PC}_2\text{H}_4\text{PPr}^i_2)$ (space group $P2_1/c$, $a = 11.831(1)$ Å, $b = 9.744(1)$ Å, $c = 20.917(2)$ Å, $\beta = 104.87(1)^\circ$, $Z = 4$, $R = 0.042$, $R_w = 0.039$). Warming a red ethereal solution of $(\eta^2, \eta^4\text{-MOD})\text{Fe}(\text{Pr}^i_2\text{PC}_3\text{H}_6\text{PPr}^i_2)$ to room temperature causes dissociation of the nonconjugated double bond of the triene to give the green, paramagnetic compound $(\eta^4\text{-MOD})\text{Fe}(\text{Pr}^i_2\text{PC}_3\text{H}_6\text{PPr}^i_2)$ which reacts with CO to give the yellow, diamagnetic compound $(\eta^4\text{-MOD})\text{Fe}(\text{CO})(\text{Pr}^i_2\text{PC}_3\text{H}_6\text{PPr}^i_2)$.

Introduction

The transition metal catalyzed reactions of 1,3-dienes have been investigated intensively for over 30 years, and in particular those involving 1,3-butadiene form the basis of a number of industrial processes.¹ In contrast, the reactions of substrates containing two 1,3-diene fragments have received much less attention and are confined to the nickel-catalyzed [4 + 4] cycloaddition of a few 1,1'- and 1,2'-bridged species which have been studied by Wender et al.² Two representative reactions are shown in eqs 1 and 2 and are of particular interest in view of recent attempts to construct the taxane skeleton.

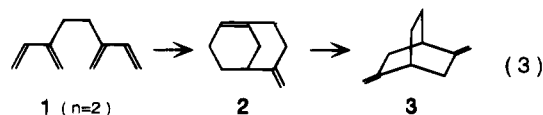


Analogous reactions involving the 2,2'-bridged species **1** have not, as far as we are aware, been reported and



are the subject of our current research. At least on paper, the intermolecular dimerization through a double

[4 + 4] cycloaddition reaction should lead to bridged 1,5-cyclooctadiene derivatives while intramolecular cycloaddition could give bicyclic products. Since it was anticipated that ring strain in the products of the reactions involving the methylene-bridged species **1** ($n = 1$) would hinder their formation or isolation, we initially turned our attention to the reactions of 3,6-dimethylene-1,7-octadiene (**1**, $n = 2$; DMOD) particularly since it has been reported that DMOD can be converted into the intramolecular Diels–Alder product **2** by a gas-phase thermolysis at 400 °C.³ As expected, **2** rearranges to the bicyclooctane derivative **3** (eq 3).⁴ It is a moot point whether the presence of transition metal species would catalyze the formation of **2** at lower temperatures or whether they would instead catalyze the further reaction.



In this and the following publication, we describe the stoichiometric reactions of **1** ($n = 2$) with zerovalent metal compounds, and the catalytic reactions and the extension to other tetraenes will be presented later. The following discussion describes the reactions of zerovalent

(1) Parshall, G. W.; Ittel, S. D. In *Homogeneous Catalysis*; Wiley: New York, 1992.

(2) (a) Wender, P. A.; Ihle, N. C. *J. Am. Chem. Soc.* **1986**, *108*, 4678. (b) Wender, P. A.; Snapper, M. L. *Tetrahedron Lett.* **1987**, *28*, 2221. (c) Wender, P. A.; Ihle, N. C. *Tetrahedron Lett.* **1987**, *28*, 2451. (d) Wender, P. A.; Ihle, N. C.; Correia, C. R. D. *J. Am. Chem. Soc.* **1988**, *110*, 5904. (e) Wender, P. A.; Tebbe, M. *J. Synthesis* **1991**, 1089.

(3) Wise, S.; Shea, K. J. *J. Am. Chem. Soc.* **1978**, *100*, 6519.

(4) (a) Limberg, A. Diploma Thesis, Ruhr-Universität, Bochum, 1991. (b) Limberg, A.; Roth, W. R. Unpublished results.

* To whom correspondence should be addressed.

[®] Abstract published in *Advance ACS Abstracts*, March 15, 1995.

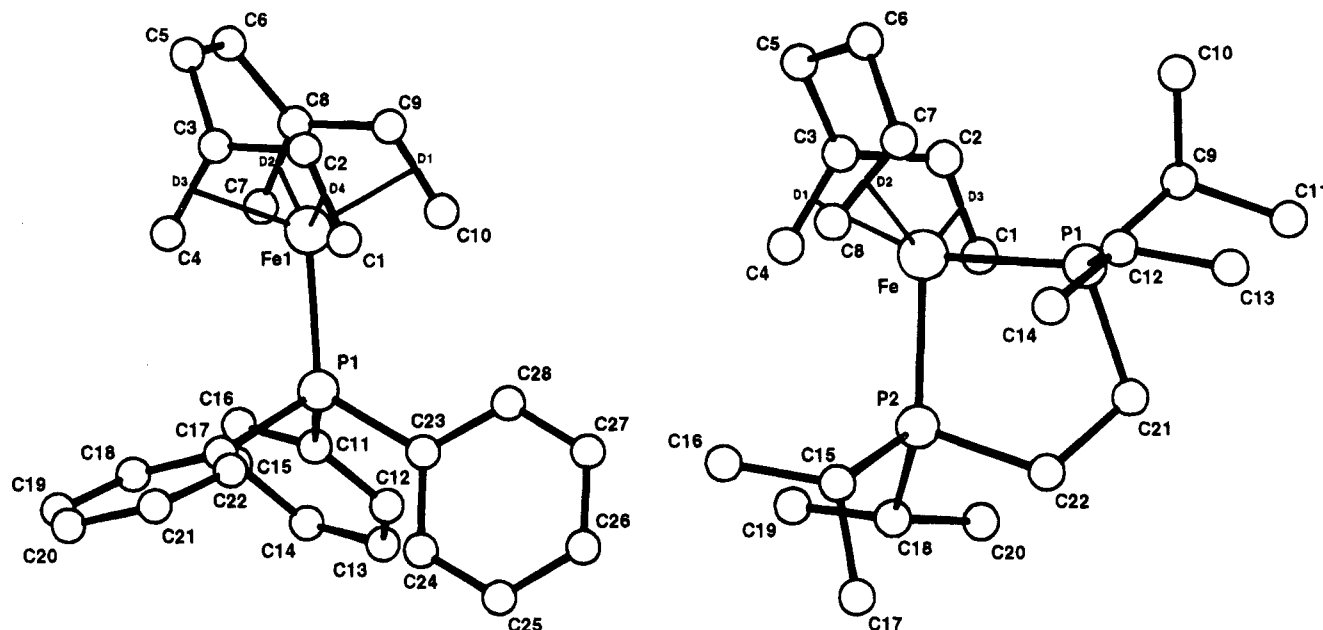
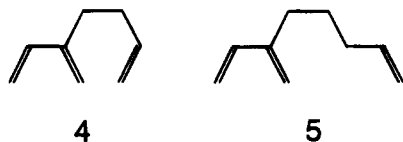


Figure 1. Molecular structure of (left) $(\eta^4, \eta^4\text{-DMOD})\text{FePPh}_3$ (**8**) and (right) $(\eta^2, \eta^4\text{-MHD})\text{Fe}(\text{Pr}^i_2\text{PC}_2\text{H}_4\text{PPr}^i_2)$ (**13**).

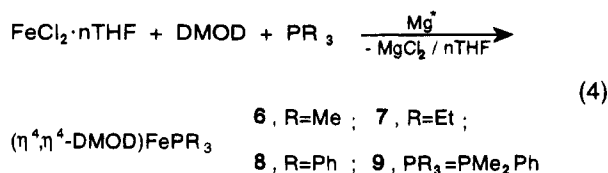
iron species with DMOD and with the related trienes 3-methylene-1,6-heptadiene (**4**, MHD) and 3-methylene-1,7-octadiene (**5**, MOD).



Results and Discussion

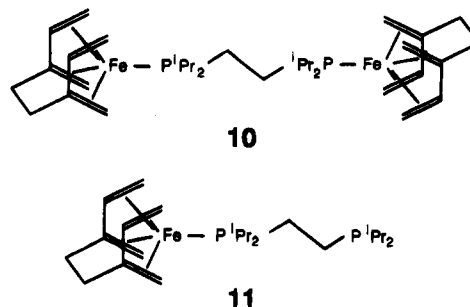
Reactions of 3,6-Dimethylene-1,7-octadiene (DMOD). Bis(1,3-butadiene)metal complexes of chromium,⁵ manganese,⁶ and iron⁷ stabilized by monodentate P-donor ligands have been prepared by reducing the appropriate metal dichloride in the presence of the diene and ligand. These results have been extended to DMOD by using active Mg powder (prepared by thermolysis of MgH_2 ⁸) as the reducing agent. Although in the case of Cr and Mn it proved possible to isolate PMe_3 -stabilized derivatives, the Cr compound was isolated as a green oil and could not be obtained analytically pure while the Mn compound was only formed in traces—possibly because of the low solubility of MnCl_2 in THF. Furthermore, both compounds were paramagnetic.

In contrast, the product of analogous reactions between iron dichloride and DMOD led to the formation in high yield of orange, stable compounds (**6–9**) which are moreover diamagnetic and crystalline (eq 4). At-



tempts to prepare a compound in which only three of

the four double bonds of the tetraene are complexed to the metal atom by reacting $\text{Pr}^i_2\text{PC}_2\text{H}_4\text{PPr}^i_2$ were unsuccessful: a 5:1 mixture of **10** and **11** is formed indicating that the chelating property of the tetraene is stronger than that of the bidentate ligand.



The molecular structure has been confirmed by a crystal structure determination of the PPh_3 -stabilized derivative **8** (Figure 1), and selected bond lengths and angles are listed in Table 1. The iron atom in **8** lies at the center of a square pyramid with the P-atom at the apex and is positioned 0.7 Å above the plane defined by the centers of the four double bonds (D1–D4). The two halves of the tetraene are bonded symmetrically to the metal atom, and within each diene fragment the bonds are identical in length. The crystal structure of $(\eta^4\text{-1,3-C}_4\text{H}_6)_2\text{FePMe}_3$ (**12**) had been determined previously,⁹ and a comparison of the two structures indicates that the ethano bridge in **8** forces the terminal diene C-atoms (C1, C4, C7, C10) to occupy positions slightly farther from the metal atom than in **12** (Fe–C = 2.101(5)–2.112(7) Å for **8** and 2.080(4)–2.090(4) Å for **12**), while

(7) Hoberg, H.; Jenni, K.; Raabe, E.; Krüger, C.; Schroth, G. *J. Organomet. Chem.* **1987**, *320*, 325.

(8) Bogdanovic', B. *Acc. Chem. Res.* **1988**, *21*, 261.

(9) McCall, J. M.; Morton, J. R.; Page, Y. Le; Preston, K. F. *Organometallics* **1984**, *3*, 1299.

(5) Jolly, P. W.; Zakrzewski, U. *Polyhedron* **1991**, *10*, 1427.

(6) Harlow, R. L.; Krusic, P. J.; McKinney, R. J.; Wreford, S. S. *Organometallics* **1982**, *1*, 1506.

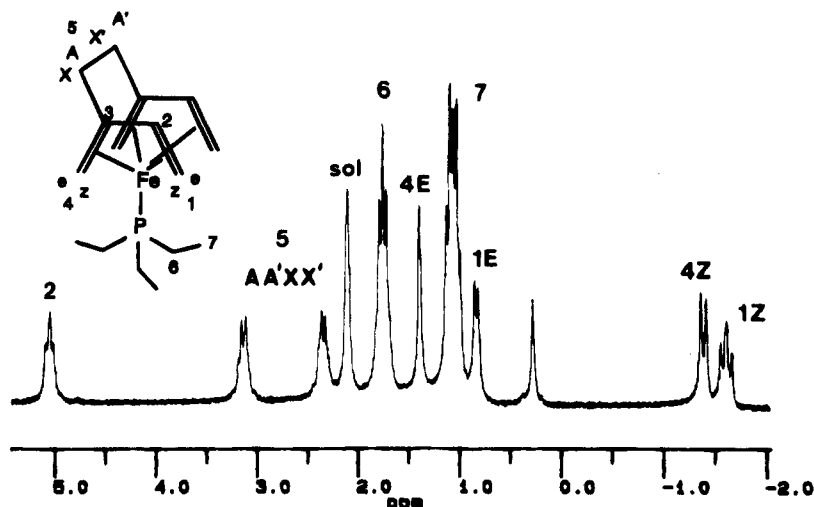


Figure 2. $^1\text{H-NMR}$ spectrum of $(\eta^4,\eta^4\text{-DMOD})\text{FePET}_3$ (**7**) (d_8 -toluene, 300 K, 200.1 MHz).

Table 1. Selected Structural Parameters for $(\eta^4,\eta^4\text{-DMOD})\text{FePPh}_3$ (**8**)

bond lengths (Å)		bond angles (deg)	
Fe-P	2.246(1)	C1-Fe-C2/C10-Fe-C9	39.8(2)/39.3(3)
Fe-C1/C10	2.101(5)/2.112(7)	C2-Fe-C3/C9-Fe-C8	40.7(2)/40.4(3)
Fe-C2/C9	2.021(5)/2.022(8)	C3-Fe-C4/C8-Fe-C7	39.8(2)/39.1(2)
Fe-C3/C8	2.021(6)/2.026(5)	C1-C2-C3/C10-C9-C8	119.7(5)/120.1(6)
Fe-C4/C7	2.104(6)/2.106(4)	C2-C3-C4/C9-C8-C7	117.8(5)/116.4(6)
C1-C2/C10-C9	1.407(7)/1.39(1)	C2-C3-C5/C9-C8-C6	118.6(6)/119.6(5)
C2-C3/C9-C8	1.407(8)/1.398(9)	C4-C3-C5/C7-C8-C6	121.8(5)/122.2(6)
C3-C4/C8-C7	1.405(9)/1.386(8)	C3-C5-C6/C8-C6-C5	113.7(7)/115.3(6)
C3-C5/C8-C6	1.517(9)/1.51(1)	P-Fe-D4/P-Fe-D1	106.6/111.3
C5-C6	1.41(1)	P-Fe-D3/P-Fe-D2	111.1/116.1
Fe-D1/D4	1.946/1.937	D4-Fe-D3/D1-Fe-D2	65.0/63.7
Fe-D2/D3	1.946/1.939	D3-Fe-D1/D4-Fe-D2	137.5/137.2

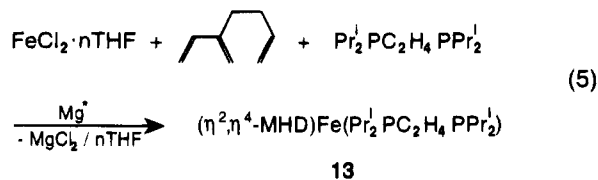
the angle formed by the two diene planes to each other increases from 10.6° in **12**¹⁰ to 21.4° in **8**.

The NMR spectra of compounds **6**–**11** confirm the symmetrical arrangement of the DMOD molecule. The $^1\text{H-NMR}$ spectra are typical for $(\eta^4\text{-1,3-diene})\text{iron}$ species, and that for the PET_3 -stabilized compound **7** is shown in Figure 2. The proton at C-2 is relatively uninfluenced by the complexation of the tetraene to the metal atom whereas those bonded to the terminal C-atoms (C1–C4) experience the familiar high-field shift whereby those for H-1Z and H-4Z, which are directly influenced by the iron atom, are unusually large. Similar effects have been discussed previously for $(\eta^4\text{-1,3-butadiene})_2\text{FePR}_3$ complexes.¹¹ The protons of the ethano bridge form an AA'XX' spin system. The ^1H - and the ^{13}C -NMR data are collected together in Tables 2 and 3.

Attempts to prepare complexes in which only three of the four double bonds in the DMOD molecule interact with the metal atom were unsuccessful: in the presence of $\text{Pr}^i_2\text{PC}_2\text{H}_4\text{PPr}^i_2$, **10** and **11** are formed (see above) while a pentane solution of **7** does not react with CO at atmospheric pressure. We were, however, able to prepare triene-iron compounds by reaction of 3-methylene-1,6-heptadiene (MHD) and 3-methylene-1,7-octadiene (MOD), and these results are discussed below.

Reactions of 3-Methylene-1,6-heptadiene (MHD) and 3-Methylene-1,7-octadiene (MOD). The product of the reaction between MHD and the zerovalent $[\text{Fe}$ -

$(\text{Pr}^i_2\text{PC}_2\text{H}_4\text{PPr}^i_2)]$ species is the expected $(\eta^2,\eta^4\text{-MHD})\text{-Fe}$ compound **13** (eq 5) as an orange crystalline solid



which is stable at room temperature. The NMR spectra of **13** (Tables 2 and 3) indicate that all three double bonds interact with the metal atom, and this has been confirmed by a crystal structure determination. The molecular structure is shown in Figure 1, and selected structural parameters are listed in Table 4. The arrangement of the three double bonds and the two P-atoms around the metal atom can be described either as a distorted tetragonal pyramid (with P2 at the apex; Figure 1) or alternatively as a distorted trigonal bipyramid (with P1 and the methylene group C3/C4 at the apices). The main distortions in the tetragonal pyramidal description are the displacement of the metal atom (0.7964 \AA) and P1 (0.9613 \AA) out of the plane formed by the center of three of the double bonds, while, in the trigonal bipyramidal description, the angle between the two apical groups (P1 and D1) is decreased from an ideal value of 180° to 154° . In the latter case, the metal atom, P2, and the centers of the two remaining double bonds (D2 and D3) lie in the same plane.

(10) Allen, F. H. *Acta Crystallogr. B*, **1979**, *35*, 2331; Cambridge Crystallographic data file.

(11) Benn, R.; Rufinska, A. *J. Organomet. Chem.* **1987**, *323*, 305.

Table 2. ¹H-NMR Spectroscopic Data

compd,(L)	solvent (T, °C)	δ(H-n)							J (Hz)	misc
		1Z	1E	2	4Z	4E	5			
6 ^a (PMe ₃)	<i>d</i> ₈ -toluene (27)	-1.52 (ddd)	0.75 (ddd)	5.00 (dd)	-1.26 (d, br)	1.34 (d, br)	3.08/2.31 (m)	<i>J</i> (1Z,2) 9.2, <i>J</i> (1Z,P) 13.7, <i>J</i> (1Z,1E) 1.7, <i>J</i> (1E,2) 7.0, <i>J</i> (1E,P) 0.9, <i>J</i> (4Z,P) 11.4, <i>J</i> (4E,P) 1.2	1.43 (Me), <i>J</i> (Me,P) 7.5	
7 ^a (PEt ₃)	<i>d</i> ₈ -toluene (-30)	-1.60 (dd)	0.85 (d)	5.06 (dd)	-1.40 (d)	1.40 (s)	3.11/2.33 (m)	<i>J</i> (1Z,2) 9.2, <i>J</i> (1Z,P), 12.4, <i>J</i> (1E,2) 6.8, <i>J</i> (4Z,P) 10.1, <i>J</i> (5,5') 12.1/6.1, ~-16.9/~2.9 (AA'XX')	1.65/1.01 (Et)	
8 ^a (PPh ₃)	<i>d</i> ₈ -THF (27)	-1.90 (ddd)	1.08 (ddd)	4.44 (dd)	-2.18 (d)	1.44 (s)	3.23/2.23 (m)	<i>J</i> (1Z,2) 9.7, <i>J</i> (1Z,P) 13.3, <i>J</i> (1Z,1E) 1.8, <i>J</i> (1E,2), 7.2, <i>J</i> (1E,P) 0.9, <i>J</i> (2,1E) ~8, <i>J</i> (4Z,P) 10.7, <i>J</i> (4E,P) 1.2	7.70/7.30 (Ph)	
9 ^a (PMe ₂ Ph)	<i>d</i> ₈ -toluene (27)	-1.65 (m)	0.75 (m)	5.02 (m)	-1.50 (m)	1.32 (s)	3.02/2.25 (m)	signals broad	7.43/7.10 (Ph), 1.72 (Me)	
10 ^{a,b} (Pr ₂ PC ₂ H ₄ PPr ₂)	<i>d</i> ₈ -toluene (27)	-1.38 (ddd)	0.86 (d, br)	5.35 (dd)	-1.18 (d)	2.50 (s)	3.13/2.32 (m)	<i>J</i> (1Z,2) 9.6, <i>J</i> (1Z,P) 11.3, <i>J</i> (1Z,1E) 1.6, <i>J</i> (1E,2) 6.9, <i>J</i> (4Z,P) 9.6	2.58/1.42-1.16 (Pr ₂ PC ₂ H ₄ PPr ₂)	
11 ^a (Pr ₂ PC ₂ H ₄ PPr ₂)	<i>d</i> ₈ -toluene (27)	-1.35 (ddd)	0.85 (d, br)						2.55/1.42-1.22 (Pr ₂ PC ₂ H ₄ PPr ₂)	
13 ^{c,d} (Pr ₂ PC ₂ H ₄ PPr ₂)	<i>d</i> ₈ -toluene (27)	-1.49 (m)		5.37 (m)	-0.46(d)			<i>J</i> (4Z,P) 9.7	2.52-0.40 (Pr ₂ PC ₂ H ₄ PPr ₂)	
14 ^{c,d} (Pr ₂ PCH ₂ PPr ₂)	<i>d</i> ₈ -toluene (-30)	-0.49 (m)		5.80 (m)	-1.10 (d)	-0.70 (s)		<i>J</i> (4Z,P) 10.5	3.1-0.7 (Pr ₂ PCH ₂ PPr ₂)	
15 ^{c,e} (Pr ₂ PC ₂ H ₄ PPr ₂)	<i>d</i> ₈ -THF (-20)	-1.54 (4d)	0.63 (3d)	4.91 (t)	-1.04 (dt)	-0.76 (s)	2.21/2.04 (m)	<i>J</i> (1Z,2) 6.9, <i>J</i> (1Z,1E) 2.0, <i>J</i> (1Z,P) 14.0/6.0, <i>J</i> (1E,2) 6.1, <i>J</i> (1E,P) 8.1, <i>J</i> (4Z,E) 1.5, <i>J</i> (4Z,P) 11.0/1.5	2.91-1.51/1.7-0.6 (Pr ₂ PC ₂ H ₄ PPr ₂)	
16 ^c (Pr ₂ PC ₃ H ₆ PPr ₂)	<i>d</i> ₈ -THF (-20)	-1.16 (dt)		5.17 (t)	-1.73 (d)	-0.72 (s)		<i>J</i> (1Z,2) 7, <i>J</i> (1Z,P) 7/11, <i>J</i> (4Z,P) 10	2.74/2.57/2.4-0.8 (Pr ₂ PC ₃ H ₆ PPr ₂)	
17 ^{c,h} (Pr ₂ PC ₃ H ₆ PPr ₂ /CO)	<i>d</i> ₈ -toluene (27)	-0.91 (m)		4.92 (m)	-0.49 (d)			<i>J</i> (4Z,P) 9.4	2.8-0.7 (Pr ₂ PC ₃ H ₆ PPr ₂)	

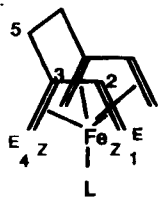
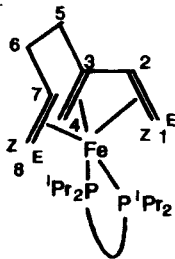
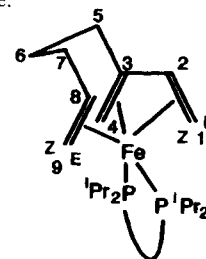
^a Numbering scheme:^b Dinuclear compound. ^c Numbering scheme:^d δ 3.05/2.78/2.08/1.80. ^e Numbering scheme:^f δ 1.55/1.20/0.90/0.70/-0.70. ^g δ 1.64/1.25 (6), 1.92/1.39 (7), 2.39 (m, 8), 0.78 (dd 9Z), 0.98 (dd, 9E) *J*(9Z,8) 11.6, *J*(9Z,P) 1.7/1.7, *J*(9E,8) 8.9, *J*(9E,P) 14.3. ^h δ 5.90 (ddt, 8), 5.09 (br, d, 9Z), 4.99 (br, d, 9E), *J*(8,7) 6.6, *J*(8,9Z) 16.9, *J*(8,9E) 10.3.

Table 3. ^{13}C -NMR Spectroscopic Data

compd (L)	solvent (T, °C)	1	2	3	4	5	6	7	8	9	misc
7 ^a (PEt ₃)	<i>d</i> ₈ -toluene (-30)	34.38 (11.0)	85.47 (2.0)	101.93 (1.4)	44.84 (9.0)	37.52 (~0)					18.78/8.01 (Et)
8 ^a (PPh ₃)	<i>d</i> ₈ -THF (27)	36.6 (9.5)	86.3	103.4	50.5 (6.7)	36.4					139.4-126.7 (Ph)
13 ^b (Pr ₂ PC ₃ H ₄ PPr ₂)	<i>d</i> ₈ -toluene (27)	36.8 ^c (7.9)	71.9	108.1	46.5 (9.0)	37.8 ^c	32.9 ^f	56.5 (7.1/2.7)	31.5 ^e (9.6)		32.5-19.3 (Pr ₂ PC ₃ H ₄ PPr ₂)
15 ^c (Pr ₂ PC ₃ H ₄ PPr ₂)	<i>d</i> ₈ -THF (-20)	30.9 (7.6/13.1)	76.2	97.1	29.7 (9.2/10.8)	33.0	25.7 (3.0)	31.2 (2.3)	43.9 (3.0/15.6)	35.2 (1.4/10.6)	31.4-19.4 (Pr ₂ PC ₃ H ₄ PPr ₂)
16 ^c (Pr ₂ PC ₃ H ₆ PPr ₂)	<i>d</i> ₈ -THF (-20)	33.6 (7.2/12.7)	77.9	92.4	34.4 (9/11)	31.7	23.4 (~0)	29.8 (2.2)	41.2 (2.0/7.2)	36.4 (12.7)	32.3-19.3 (Pr ₂ PC ₃ H ₆ PPr ₂)
17 ^{c,d} (Pr ₂ PC ₃ H ₆ PPr ₂ /CO)	<i>d</i> ₈ -toluene (27)		79.1	96.9				114.4	139.5	114.4	219.5 (CO) (J(C,P) 8.0/28.0)

^a Numbering scheme:

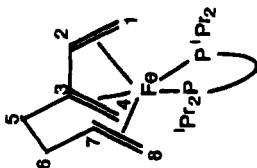
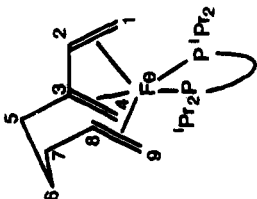
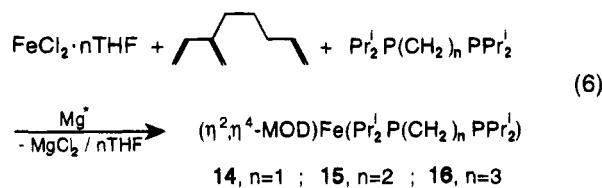
^b Numbering scheme:

^c Numbering scheme:

^d δ 39.0-18.0 (Pr₂PC₃H₆PPr₂). ^{e,f} Assignment could be reversed.

 Table 4. Selected Structural Parameters for (η^2, η^4 -MHD)Fe(Pr₂PC₂H₄PPr₂) (13)

bond lengths (Å)		bond angles (deg)	
Fe-P1	2.232(1)	P1-Fe-P2	86.1(1)
Fe-P2	2.237(1)	C1-Fe-C2	40.1(1)
Fe-C1	2.092(3)	C2-Fe-C3	41.0(1)
Fe-C2	2.014(3)	C3-Fe-C4	39.0(1)
Fe-C3	2.045(3)	C7-Fe-C8	38.7(1)
Fe-C4	2.142(3)	C1-C2-C3	116.3(2)
Fe-C7	2.100(3)	C2-C3-C4	115.6(2)
Fe-C8	2.086(3)	C2-C3-C5	121.6(2)
C1-C2	1.409(4)	C4-C3-C5	121.5(2)
C2-C3	1.420(3)	C3-C5-C6	109.1(2)
C3-C4	1.402(4)	C5-C6-C7	110.3(2)
C3-C5	1.504(4)	C6-C7-C8	122.9(2)
C5-C6	1.490(5)	D1-Fe-D2	90.3
C6-C7	1.524(4)	D1-Fe-D3	62.8
C7-C8	1.388(4)	D2-Fe-D3	131.1
Fe-D1	1.973	P1-Fe-D1	154.0
Fe-D2	1.974	P1-Fe-D2	97.3
Fe-D3	1.928	P1-Fe-D3	94.2

The 3-methylene-1,7-octadiene (MOD) compounds 14-16 have been prepared similarly (eq 6). These

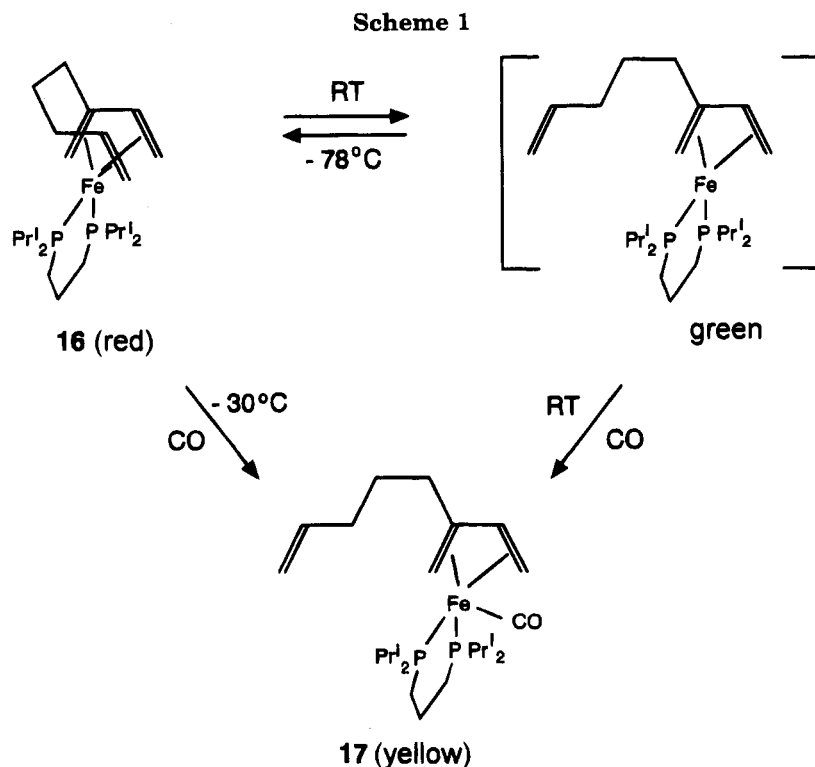


compounds have a lower thermal stability than the MHD compound 13 and decompose above -30 °C. Isomers are possible depending upon the position adopted by the terminal alkene with respect to the 1,3-diene fragment and the conformation of the propane chain, and since we could not obtain crystals of a quality suitable for an X-ray diffraction study, the arrangement of the triene and bidentate ligand around the metal atom remains undecided. One possibility is indicated in Scheme 1. The ¹H-NMR spectra (Table 2) show the characteristic high field shifts for both H-1Z and H-4Z. A third signal at ca. -0.7 ppm is assigned to H-4E on the basis of extensive correlation measurements.

The reaction of the bis(diisopropylphosphino)propane-stabilized compound 16 with CO has been studied in detail (Scheme 1). Reaction in diethyl ether occurs at -30 °C to give the yellow compound 17 in which the presence of an uncomplexed double bond and a CO molecule have been confirmed spectroscopically. The same compound can be prepared by allowing a solution of 16 to warm to room temperature and then treating the resulting green solution with CO. The color change from red to green is reversible, and it is presumably the result of dissociation of the terminal alkene to give a paramagnetic (16e) species. In agreement with this interpretation; the signals in the NMR spectra of 16 at -30 °C are extremely broad while related paramagnetic compounds, e.g. (η^4 -isoprene)Fe(Pr₂PC₃H₆PPr₂), have been isolated and are also green.¹²

Experimental Section

All of the experiments described below were carried out under argon using oxygen-free dried solvents. NMR spectro-



scopic samples were prepared under argon, and the spectra were recorded using the following Bruker instruments: WH 300, WM 300, AM 200, and AC 200. Infrared spectra were recorded as KBr disks using a Nicolet FT-7199 instrument. Mass spectra were recorded with a Finnegan MAT 311A spectrometer using 70 eV ionization energy. Elemental analyses were carried out by the microanalytical firm of Dornis and Kolbe, Mülheim an der Ruhr, Germany. The active Mg used was prepared from MgH_2 .⁸ $\text{FeCl}_2 \cdot n\text{THF}$ was prepared by extracting anhydrous FeCl_2 with THF in a Soxhlet apparatus and dried for 48 h under high vacuum: the composition was determined by elemental analysis before use.

3,6-Dimethylene-1,7-octadiene (1, $n = 2$, DMOD). The following synthesis is a modification of the published procedure.¹³ A solution of 2-(bromomethyl)-1,3-butadiene (50 g, 0.34 mol)¹⁴ in diethyl ether (400 mL) was added at room temperature over 3 h to iodine-activated Mg shavings (4.1 g, 0.17 mol). Gentle refluxing took place, and the mixture was stirred for a further 2 h and then carefully hydrolyzed with ammonium chloride (50 g) in water (400 mL). The ether phase was separated, washed with water (3 \times 150 mL), and then dried with magnesium sulfate. The compound was isolated by fractional distillation (bp 50 °C/10 mbar). Yield: 14.7 g (64.7%).

3-Methylene-1,6-heptadiene (4, MHD).¹⁵ 2-(Bromomethyl)-1,3-butadiene (22 g, 0.15 mol)¹⁴ in diethyl ether (200 mL) was added to (1-propen-3-yl)magnesium bromide (150 mL of a 1.0 M solution) in diethyl ether at 0 °C over 2 h. The reaction mixture was stirred for a further 2 h and the product isolated as described above (bp 52 °C/90 mbar). Yield: 10.7 g (66.7%).

3-Methylene-1,7-octadiene (5, MOD).¹⁶ **5** was prepared as described above by reaction of (1-buten-4-yl)magnesium bromide (bp 43 °C/25 mbar). Yield: 73.3%.

(DMOD)CrPMe₃. $\text{CrCl}_2 \cdot 1.85\text{THF}$ (1.57 g, 6.12 mmol) was suspended in THF (80 mL) and treated at -78 °C with PMe_3 (0.63 mL, 6.09 mmol), DMOD (1.00 mL, 5.88 mmol), and active

Mg (0.29 g, 11.93 mmol). The reaction mixture was stirred for 24 h at -30 °C and evaporated to dryness, and the resulting green residue was extracted with precooled hexane at -30 °C. The resulting extract was evaporated to give a green oil. Yield: 0.61 g (38.1%). Satisfactory analytical data could not be obtained. IR (KBr): 2970 (s), 2900 (s), 950 (s), 1100 (s), 1060 (s) cm^{-1} . MS (85 °C): m/e 262 (M^+ , 34%), 186 ($\text{M}^+ - \text{PMe}_3$, 13%), 128 ($\text{M}^+ - \text{DMOD}$, 95%).

(DMOD)MnPMe₃ was prepared as described above by reaction of MnCl_2 at room temperature as a brown crystalline solid in 6% yield. Anal. Calcd for $\text{C}_{13}\text{H}_{23}\text{MnP}$: C, 58.9; H, 8.7; Mn, 20.7; P, 11.7. Found: C, 58.8; H, 8.8; Mn, 20.8; P, 11.6. IR (KBr): 2820 (s), 940 (s), 670 (s) cm^{-1} . MS (15 °C): m/e 265 (M^+ , 47%), 189 ($\text{M}^+ - \text{PMe}_3$, 27%), 131 ($\text{M}^+ - \text{DMOD}$, 31%).

(η^4, η^4 -DMOD)FePMe₃ (6) was prepared as described below in 45.4% yield as red-orange crystals by reaction of excess PMe_3 at -30 °C. Anal. Calcd for $\text{C}_{13}\text{H}_{23}\text{FeP}$: C, 58.7; H, 8.7; Fe, 21.0; P, 11.6. Found: C, 58.6; H, 8.9; Fe, 21.1; P, 11.5. IR (KBr): 1420 (s), 1275 (s), 950 (s), 710 (s) cm^{-1} . MS (18 °C): m/e 266 (M^+ , 100%), 190 ($\text{M}^+ - \text{PMe}_3$, 44%), 162 (33%), 132 (9%). ³¹P NMR (d_8 -toluene): δ 30.0. ¹H-NMR: see Table 2.

(η^4, η^4 -DMOD)FePEt₃ (7). $\text{FeCl}_2 \cdot n\text{THF}$ ($n = 1.32$, 0.83 g, 3.73 mmol) was suspended in THF (50 mL) and treated with PEt_3 (0.55 mL, 3.73 mmol), DMOD (0.63 mL, 3.73 mmol), and active Mg (95 mg, 3.90 mmol). The reaction mixture was stirred at room temperature for 15 h and evaporated to dryness, and the residue was extracted with pentane. The orange-red pentane extract was concentrated to 20 mL and cooled to -78 °C to give the compound as red crystals which were washed with a little precooled pentane at -78 °C and dried under high vacuum. Yield: 0.60 g (52.3%). Anal. Calcd for $\text{C}_{16}\text{H}_{29}\text{FeP}$: C, 62.4; H, 9.5; Fe, 18.1; P, 10.1. Found: C, 62.3; H, 9.6; Fe, 18.1; P, 10.1. IR (KBr): 2920 (s), 1035 (s), 760 (s), 710 (s) cm^{-1} . MS (60 °C): m/e 308 (M^+ , 27%), 190 ($\text{M}^+ - \text{PEt}_3$, 20%), 174 ($\text{M}^+ - \text{DMOD}$, 14%), 118 (30%). ³¹P NMR (d_8 -toluene, -30 °C): δ 57.3. ¹H- and ¹³C-NMR: see Figure 2 and Tables 2 and 3.

(η^4, η^4 -DMOD)FePPh₃ (8) was prepared as described above in 4.8% yield as ruby-red crystals by reaction of PPh_3 . Anal. Calcd for $\text{C}_{28}\text{H}_{29}\text{FeP}$: C, 74.4; H, 6.5; Fe, 12.4; P, 6.9. Found: C, 74.3; H, 6.6; Fe, 12.3; P, 6.6. IR (KBr): 2920 (s), 1475 (s),

(13) Butler, G. B.; Raymond, M. A. *J. Org. Chem.* **1965**, *30*, 2410.

(14) Krug, R. C.; Yen, T. F. *J. Org. Chem.* **1956**, *21*, 1082.

(15) Kawamura, T.; Matsunaga, M.; Yonezawa, T. *J. Am. Chem. Soc.* **1978**, *100*, 92.

(16) Shea, K. J.; Kim, J.-S. *J. Am. Chem. Soc.* **1992**, *114*, 3044.

Table 5. Crystallographic Data for 8 and 13

	8	13
formula	C ₂₈ H ₂₉ FeP	C ₂₂ H ₄₄ FeP ₂
mol wt	452.4	426.4
cryst size, mm	0.42 × 0.53 × 0.46	0.21 × 0.28 × 0.39
V, Å ³	3397.1	2330.6
D _c , g cm ⁻³	1.33	1.22
T, °C	20	20
λ(Mo), Å	0.710 69	0.710 69
Z	6	4
μ _{abs} , cm ⁻¹	7.46	7.85
reflms measd	20 351 (±h, ±k, +l)	16 637 (±h, ±k, +l)
ind reflms	6602	8086
obsd reflms	5356	4733
no. of variables	271	358
space group (No.)	R $\bar{3}$ (148)	P2 ₁ /c (14)
a, b, c, Å	20.290(9)	11.831(1), 9.744(1), 20.917(2)
α, β, γ, deg	117.47(3)	90.0, 104.87(1), 90.0
R	0.048	0.042
R _w	0.052	0.039
res electron density, e Å ⁻³	0.45	0.30

Table 6. Final Coordinates and Equivalent Isotropic Thermal Parameters (Å²) of the Non-Hydrogen Atoms for 8

atom	x	y	z	U _{eq} ^a
Fe1	0.9040(1)	0.6856(1)	0.6134(1)	0.033(1)
P1	1.0075(1)	0.7621(1)	0.5970(1)	0.030(2)
C1	0.7074(3)	0.4894(3)	0.3876(3)	0.056(8)
C2	0.6905(2)	0.5079(3)	0.4506(3)	0.052(8)
C3	0.7554(3)	0.6324(3)	0.5512(3)	0.05(1)
C4	0.8322(3)	0.7326(3)	0.5817(3)	0.05(1)
C5	0.7716(4)	0.6706(4)	0.6475(4)	0.08(2)
C6	0.8898(5)	0.7395(6)	0.7661(5)	0.13(2)
C7	1.0867(3)	0.8789(3)	0.8387(3)	0.057(9)
C8	0.9776(3)	0.7615(3)	0.7756(3)	0.06(1)
C9	0.9288(3)	0.6471(4)	0.6906(4)	0.07(1)
C10	0.9859(4)	0.6529(4)	0.6690(3)	0.08(1)
C11	1.2062(2)	0.9331(2)	0.7642(2)	0.032(7)
C12	1.2867(2)	0.9446(3)	0.7797(3)	0.042(8)
C13	1.4364(3)	1.0751(3)	0.9099(3)	0.05(1)
C14	1.5066(3)	1.1942(3)	1.0244(3)	0.052(8)
C15	1.4296(3)	1.1853(3)	1.0125(2)	0.049(8)
C16	1.2807(2)	1.0560(2)	0.8842(2)	0.040(7)
C17	0.9562(2)	0.7916(2)	0.5275(2)	0.033(7)
C18	1.0287(3)	0.9211(3)	0.6168(2)	0.044(8)
C19	0.9776(3)	0.9344(3)	0.5607(3)	0.05(1)
C20	0.8532(3)	0.8197(3)	0.4150(3)	0.06(1)
C21	0.7799(3)	0.6905(3)	0.3238(3)	0.050(9)
C22	0.8307(2)	0.6763(2)	0.3793(2)	0.042(8)
C23	0.9697(2)	0.6468(2)	0.4753(2)	0.039(7)
C24	1.0016(3)	0.6735(3)	0.4356(3)	0.06(1)
C25	0.9779(4)	0.5914(4)	0.3489(4)	0.07(2)
C26	0.9213(3)	0.4798(3)	0.2996(3)	0.08(1)
C27	0.8904(3)	0.4523(3)	0.3381(4)	0.07(1)
C28	0.9130(3)	0.5344(3)	0.4250(3)	0.052(9)

$$^a U_{eq} = 1/3 \sum_i U_{ij} a_i^* a_j^* \bar{a}_i \bar{a}_j.$$

1435 (s), 1085 (s), 690 (s), 530 (s) cm⁻¹. MS (130 °C): the sample decomposed. ³¹P NMR (*d*₈-THF): δ 88.5. ¹H- and ¹³C-NMR: see Tables 2 and 3. Crystal structure: see Figure 1 and Table 1.

(η^4, η^4 -DMOD)FePMe₂Ph (9) was prepared as described above in 16.5% yield by reaction of PMe₂Ph. Anal. Calcd for C₁₈H₂₅FeP: C, 65.9; H, 7.7; Fe, 17.0; P, 9.4. Found: C, 65.8; H, 7.7; Fe, 17.1; P, 9.3. IR (KBr): 3040 (s), 3005–2800 (s), 950–870 (s), 745 (s), 700 (s), 675 (s), 575 (s), 495 (s), 480 (s) cm⁻¹. MS (70 °C): *m/e* 328 (M⁺, 100%), 194 (M⁺ – DMOD, 4.7%), 190 (M⁺ – PMe₂Ph, 72.7%). ³¹P NMR (*d*₈-toluene, –30 °C): δ 45.6. ¹H-NMR: see Table 2.

[(η^4, η^4 -DMOD)Fe]₂(Pr¹₂PC₂H₄PPPr¹₂) (10) and (η^4, η^4 -DMOD)FePPPr¹₂C₂H₄PPPr¹₂ (11) were prepared as a mixture (5:1 10:11) in a total yield of 40% by reaction of Pr¹₂PC₂H₄PPPr¹₂ at –30 °C. IR (KBr): 3000–2840 (s), 1455 (s), 1435 (s), 640 (s), 620 (s) cm⁻¹. MS (11, 100 °C): *m/e* 452 (M⁺, 42%), 318 (M⁺ – DMOD, 13%). MS (10, 155 °C): *m/e* 642 (M⁺, 0.5%), 508 (M⁺ – DMOD, 29%), 452 (41%), 318 (11%). ³¹P NMR

Table 7. Final Coordinates and Equivalent Isotropic Thermal Parameters (Å²) of the Non-Hydrogen Atoms for 13

atom	x	y	z	U _{eq} ^a
Fe	0.2635(1)	0.0758(1)	0.1470(1)	0.036(1)
P1	0.3572(1)	0.2169(1)	0.0941(1)	0.038(1)
P2	0.1435(1)	0.2523(1)	0.1487(1)	0.042(1)
C1	0.3860(2)	0.1259(3)	0.2354(1)	0.050(2)
C2	0.4020(2)	–0.0069(3)	0.2127(1)	0.049(1)
C3	0.3050(2)	–0.0974(2)	0.2033(1)	0.056(2)
C4	0.2054(3)	–0.0432(3)	0.2186(2)	0.063(2)
C5	0.3003(3)	–0.2298(3)	0.1658(2)	0.075(2)
C6	0.3201(3)	–0.2004(3)	0.0997(2)	0.072(2)
C7	0.2585(2)	–0.0679(2)	0.0716(1)	0.051(1)
C8	0.1456(2)	–0.0359(3)	0.0743(1)	0.053(2)
C9	0.5202(2)	0.2050(3)	0.1193(1)	0.050(1)
C10	0.5631(3)	0.0872(4)	0.0841(2)	0.069(2)
C11	0.5907(3)	0.3348(4)	0.1184(2)	0.075(2)
C12	0.3244(2)	0.2230(3)	0.0016(1)	0.052(2)
C13	0.3855(4)	0.3332(5)	–0.0283(2)	0.096(3)
C14	0.1951(3)	0.2269(4)	–0.0326(2)	0.074(2)
C15	–0.0100(2)	0.2449(3)	0.0964(1)	0.054(2)
C16	–0.0821(2)	0.1321(4)	0.1159(2)	0.072(2)
C17	–0.0778(3)	0.3799(4)	0.0864(2)	0.087(3)
C18	0.1224(2)	0.3318(4)	0.2264(1)	0.068(2)
C19	0.0775(3)	0.2387(5)	0.2709(2)	0.098(3)
C20	0.2310(4)	0.4080(4)	0.2656(2)	0.095(3)
C21	0.3267(2)	0.3929(2)	0.1167(2)	0.056(2)
C22	0.1969(2)	0.4040(2)	0.1120(2)	0.058(2)

$$^a U_{eq} = 1/3 \sum_i U_{ij} a_i^* a_j^* \bar{a}_i \bar{a}_j.$$

(*d*₈-toluene): δ 70.6 (10); 68.3, 11.4, *J*(P,P) 23.2 Hz (11). ¹H-NMR: see Table 2.

(η^2, η^4 -MHD)Fe(Pr¹₂PC₂H₄PPPr¹₂) (13) was prepared as described above in 54% yield as bright red crystals by reaction of MHD and Pr¹₂PC₂H₄PPPr¹₂ at –30 °C. Anal. Calcd for C₂₂H₄₄FeP₂: C, 62.0; H, 10.4; Fe, 13.1; P, 14.5. Found: C, 61.8; H, 10.4; Fe, 13.1; P, 14.7. IR (KBr): 3080 (s), 3020–2860 (s), 2820 (s), 1455 (s), 1080 (s), 885 (s), 800 (s), 690 (s) cm⁻¹. MS (110 °C): *m/e* 426 (M⁺, 100%), 318 (M⁺ – MHD, 16%), 276 (96%), 234 (88%), 192 (47%), 150 (22%). ³¹P NMR (*d*₈-toluene): δ 100.7, 92.5, *J*(P,P) 6.8 Hz. ¹H- and ¹³C-NMR: see Tables 2 and 3. Crystal structure: see Figure 1 and Table 4.

(η^2, η^4 -MOD)Fe(Pr¹₂PCH₂PPPr¹₂) (14) was prepared as described above in 52% yield as a red crystalline solid by reaction of MOD and Pr¹₂PCH₂PPPr¹₂ at –30 °C. Anal. Calcd for C₂₂H₄₄FeP₂: C, 62.0; H, 10.4; Fe, 13.1; P, 14.5. Found: C, 62.1; H, 10.3; Fe, 13.2; P, 14.4. IR (KBr): 3060–2800 (s), 1460 (s), 1365 (s), 1090 (s), 1055 (s), 880 (s), 745 (s), 700 (s), 595 (s) cm⁻¹. MS (110 °C): *m/e* 426 (M⁺, 40%), 304 (M⁺ – MOD, 8%), 262 (65%), 220 (63%), 205 (100%). ³¹P NMR (*d*₈-toluene, –80 °C): δ 53.7, 41.5. ¹H-NMR: see Table 2.

(η^2, η^4 -MOD)Fe(Pr¹₂PC₂H₄PPPr¹₂) (15) was prepared as described above in 86% yield as a red crystalline solid by reaction of Pr¹₂PC₂H₄PPPr¹₂ at –30 °C. Anal. Calcd for C₂₃H₄₆FeP₂: C, 62.7; H, 10.5; Fe, 12.7; P, 14.1. Found: C, 62.8; H, 10.5; Fe, 12.8; P, 14.1. IR (KBr): 2960–2840 (s), 1455 (s), 1360 (s), 880 (s), 805 (s), 685 (s), 660 (s), 630 (s), 595 (s), 510 (s) cm⁻¹. MS (90 °C): *m/e* 440 (M⁺, 62%), 318 (M⁺ – MOD, 23%), 276 (88%), 234 (100%). ³¹P NMR (*d*₈-THF, –20 °C): δ 95.0, 86.8, *J*(P,P) 2.0 Hz. ¹H- and ¹³C-NMR: see Tables 2 and 3.

(η^2, η^4 -MOD)Fe(Pr¹₂PC₃H₆PPPr¹₂) (16) was prepared as described above in 66% yield by reaction of Pr¹₂PC₃H₆PPPr¹₂ at –30 °C. Anal. Calcd for C₂₄H₄₈FeP₂: C, 63.4; H, 10.7; Fe, 12.3; P, 13.6. Found: C, 63.6; H, 10.8; Fe, 12.2; P, 13.5. IR (KBr): 3000–2800 (s), 1460 (s), 965 (s), 880 (s), 835 (s), 785 (s), 665 (s), 620 (s), 580 (s), 510 (s) cm⁻¹. MS (90 °C): *m/e* 454 (M⁺, 2.7%), 332 (M⁺ – MOD, 1.5%), 296 (6.7%), 248 (12%), 233 (100%). ³¹P NMR (*d*₈-THF, –20 °C): δ 52.6, 44.0, *J*(P,P) 20.5 Hz. ¹H- and ¹³C-NMR: see Tables 2 and 3.

(η^4 -MOD)Fe(CO)(Pr¹₂PC₃H₆PPPr¹₂) (17). 16 (0.62 g, 1.36 mmol) was dissolved in diethyl ether (200 mL) and exposed to CO at –30 °C for 30 min. The color of the reaction mixture changed from bright red to yellow. The resulting solution was

filtered through avicel and evaporated to dryness. The residue was dissolved in pentane (15 mL) and the solution filtered and cooled to $-78\text{ }^{\circ}\text{C}$ to give the compound as pale yellow needles which were washed at $-78\text{ }^{\circ}\text{C}$ with a little precooled pentane and dried under high vacuum. Yield: 0.58 g (88.2%). Anal. Calcd for $\text{C}_{25}\text{H}_{49}\text{FeP}_2\text{O}$: C, 62.1; H, 10.2; Fe, 11.6; P, 12.8. Found: C, 62.1; H, 10.0; Fe, 11.7; P, 12.8. IR (KBr): 1860 (CO), 1640 (m, C:C); 3080–2840 (s), 1460 (s), 670 (s), 625 (s), 585 (s), 560 (s). MS (110 $^{\circ}\text{C}$): m/e 482 (M^+ , 10%), 360 ($\text{M}^+ - \text{MOD}$, 58%), 332 ($\text{M}^+ - \text{MOD}/\text{CO}$), 290 (100%), 248 (76%), 233 (57%). ^{31}P NMR (d_8 -toluene): δ 62.3, 57.4, $J(\text{P},\text{P})$ 13.0 Hz. ^1H - and ^{13}C -NMR: see Tables 2 and 3.

Single-Crystal X-ray Diffraction Studies of 8 and 13.

The crystal structure analyses were carried out with an Enraf-Nonius CAD-4 diffractometer. Crystallographic data and

details of the refinement are listed in Table 5, and final coordinates and equivalent isotropic thermal parameters, in Tables 6 and 7. Further details are to be found in the supplementary material.

Supplementary Material Available: Detailed information on the crystal structure determinations of **8** and **13** including tables of data collection parameters, final atomic positional parameters, final thermal parameters, and interatomic distances and angles and an ORTEP diagram (17 pages). Ordering information is given on any current masthead page.

OM9409478

Interaction of Acyclic Tetraenes and Trienes with Transition Metals: Organonickel Compounds

E. Dreher, B. Gabor, P. W. Jolly,* C. Kopiske, C. Krüger, A. Limberg, and R. Mynott

Max-Planck-Institut für Kohlenforschung, D-45466 Mülheim an der Ruhr, Germany

Received December 13, 1994[®]

The tetraene 3,6-dimethylene-1,7-octadiene (DMOD) reacts with zerovalent $[\text{NiPR}_3]$ species to give $(\eta^2, \eta^2\text{-DMOD})\text{NiPR}_3$ in which the methylene group of one 1,3-diene fragment and the vinyl group of the second interact with the metal atom. This unsymmetrical complexation of the tetraene has been confirmed by X-ray diffraction for the $\text{P}(\text{OC}_6\text{H}_4\text{-}o\text{-Ph})_3$ -stabilized derivative (space group $P2_1/c$, $a = 10.057(1) \text{ \AA}$, $b = 36.196(1) \text{ \AA}$, $c = 10.944(1) \text{ \AA}$, $\alpha = \gamma = 90^\circ$, $\beta = 105.76(1)^\circ$, $Z = 4$, $R = 0.056$, $R_w = 0.071$) and is the result of the preferred coordination of a 1,6-heptadiene chain to the metal atom. The NMR spectra indicate that the molecule is fluxional with a pairwise exchange of the methylene groups and of the vinyl groups. The structure of the product formed in the presence of the bidentate ligands $\text{Pr}_2\text{P}(\text{CH}_2)_n\text{PPr}_2$ ($n = 1, 2, 3$) is dependent upon the length of the chain bridging the two P-atoms, and compounds have been isolated having the composition $(\eta^2, \eta^2, \eta^2, \eta^2\text{-DMOD})\text{Ni}_2(\text{Pr}_2\text{-PCH}_2\text{PPr}_2)$, $(\eta^4, \eta^4\text{-DMOD})[\text{Ni}(\text{Pr}_2\text{PC}_2\text{H}_4\text{PPr}_2)]_2$, and $(\eta^2, \eta^2\text{-DMOD})[\text{Ni}(\text{Pr}_2\text{PC}_3\text{H}_6\text{PPr}_2)]_2$. The molecular structure of the bis(diisopropylphosphino)ethane-containing compound has been established by X-ray diffraction (space group $C2/c$, $a = 17.535(2) \text{ \AA}$, $b = 24.152(1) \text{ \AA}$, $c = 11.767(1) \text{ \AA}$, $\alpha = \gamma = 90^\circ$, $\beta = 120.65(1)^\circ$, $Z = 4$, $R = 0.034$, $R_w = 0.035$) and confirms that the two 1,3-diene fragments of the tetraene interact with $[\text{Ni}(\text{Pr}_2\text{PC}_2\text{H}_4\text{PPr}_2)]$ moieties. The trienes 3-methylene-1,6-heptadiene and 3-methylene-1,7-octadiene react with $[\text{NiPPr}_3]$ species to give $(\eta^2, \eta^2\text{-triene})\text{NiPPr}_3$ compounds in which a 1,6-heptadiene chain is complexed to the metal atom.

Introduction

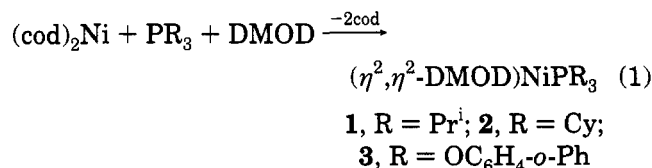
In the preceding publication,¹ we have shown that the tetraene 3,6-dimethylene-1,7-octadiene (DMOD) interacts with zerovalent $[\text{FePR}_3]$ species in an η^4, η^4 -manner whereas 3-methylene-1,6-heptadiene (MHD) and 3-methylene-1,7-octadiene (MOD) form compounds containing an η^2, η^4 -bonded triene molecule. Interesting as these compounds may be, their predictive value as model intermediates for potential zerovalent iron-catalyzed reactions is limited by the paucity of reactions involving this metal. The situation in the case of nickel is, however, completely different, and a gamut of catalytic reactions involving 1,3-dienes have been reported² suggesting that a study of the stoichiometric behavior of DMOD would be of considerable interest.

Although the nickel-catalyzed cyclooligomerization and cyclo-cooligomerization of 1,3-butadiene has been extended to methyl-substituted 1,3-dienes such as isoprene and piperylene,² the investigation of substrates containing two 1,3-diene fragments is limited to the 1,1'- and 1,2'-bridged tetraenes discussed in the Introduction of the preceding paper¹ and, as far as we are

aware, reactions involving 2,2'-bridged species such as DMOD have not been reported. Here we describe the stoichiometric reactions between DMOD and ligand-modified zerovalent nickel species and the extension to the trienes MHD and MOD.

Results and Discussion

Reactions of 3,6-Dimethylene-1,7-octadiene (DMOD). Zerovalent nickel complexes such as $(\text{cod})_2\text{Ni}$ ($\text{cod} = 1,5,9\text{-cyclododecatriene}$, $\text{cod} = 1,5\text{-cyclooctadiene}$) react with DMOD at -10°C in diethyl ether with decomposition and formation of a nickel mirror. In contrast, in the presence of a monodentate P-donor ligand, $(\text{cod})_2\text{Ni}$ reacts readily to give the yellow compounds 1–3 in high yield (eq 1). The phosphite-stabilized derivative is stable at room temperature whereas the trialkylphosphine derivatives should be stored at -30°C .



The IR spectra of 1–3 indicate the presence of uncomplexed double bonds ($\nu(\text{C}=\text{C})$ ca. 1600 cm^{-1}), and this is confirmed by the NMR spectroscopic results discussed below. The DMOD molecule could complex to the $[\text{NiPR}_3]$ fragment in an η^2, η^4 -manner to give an 18-electron system or in an η^4 - or η^2, η^2 -manner to give a 16-electron system. Both electronic configurations

* To whom correspondence should be addressed.

[®] Abstract published in *Advance ACS Abstracts*, March 15, 1995.

(1) Jolly, P. W.; Kopiske, C.; Krüger, C.; Limberg, A. *Organometallics* 1995, 14, xxx.

(2) (a) Jolly, P. W. In *Comprehensive Organometallic Chemistry*; Wilkinson, G., Stone, F. G. A., Abel, E. W., Eds.; Pergamon Press: Oxford, U.K., 1982; Vol. 8, p 251. (b) Keim, W. *Angew. Chem.* 1990, 102, 251.

(3) (a) Bogdanović, B.; Kröner, M.; Wilke, G. *Justus Liebig's Ann. Chem.* 1966, 699, 1. (b) Jolly, P. W. In *Comprehensive Organometallic Chemistry*; Wilkinson, G., Stone, F. G. A., Abel, E. W., Eds.; Pergamon Press: Oxford, U.K., 1982; Vol. 8, p 101.

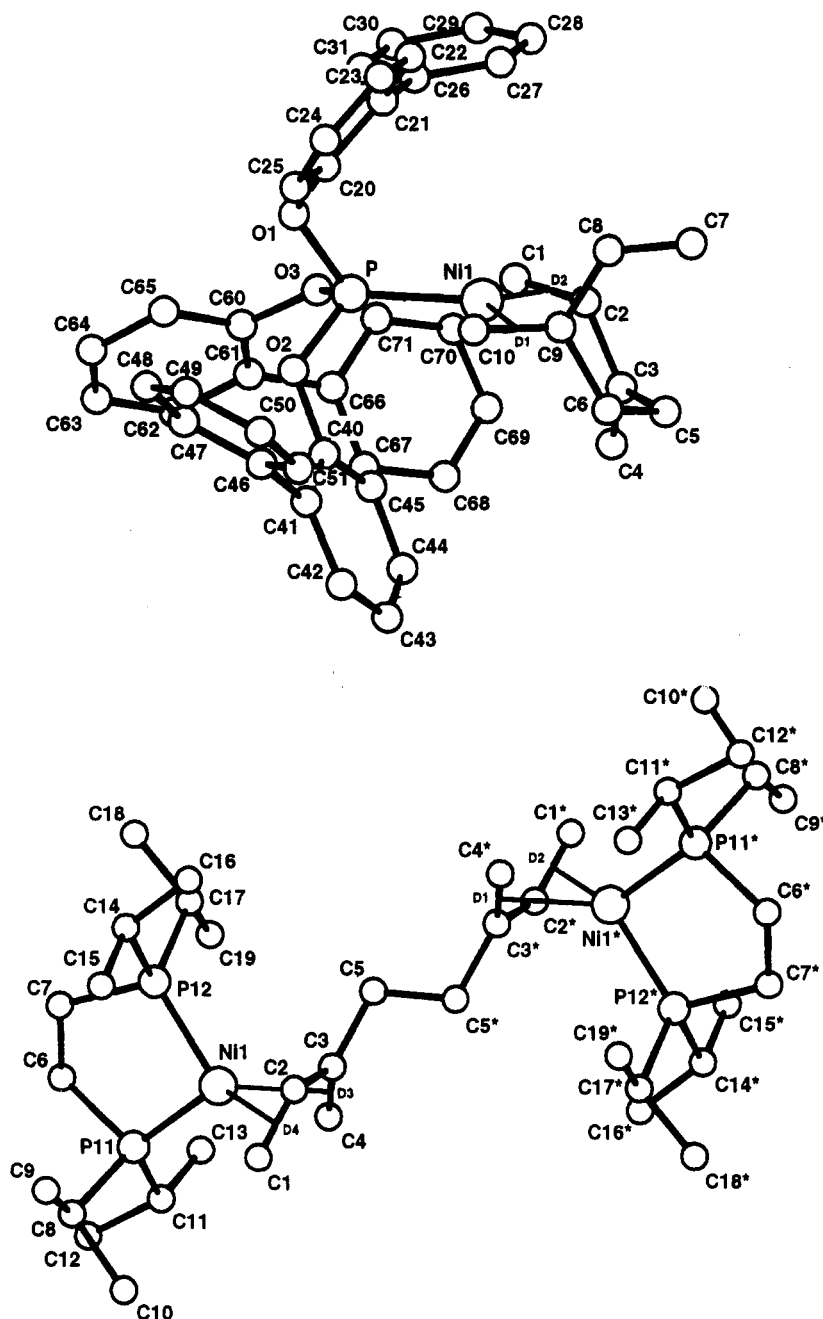


Figure 1. Molecular structures of (top) $(\eta^2, \eta^2\text{-DMOD})\text{NiP}(\text{OC}_6\text{H}_4\text{-}o\text{-Ph})_3$ (**3**) and (bottom) $(\eta^4, \eta^4\text{-DMOD})[\text{Ni}(\text{Pr}^2\text{PC}_2\text{H}_4\text{-PPR}^2)_2]$ (**4**).

have been observed in relevant examples, e.g. (cdt)- NiPR_3 and (1,5-hexadiene) NiPR_3 .^{4,5} The crystal structure of the tris(*o*-phenylphenyl)phosphite derivative **3** has been determined by X-ray diffraction and establishes the η^2, η^2 -complexation of the DMOD molecule.

The molecular structure of **3** is shown in Figure 1, and selected structural parameters are listed in Table 1. The nickel atom lies in a trigonal environment and is bonded to the P-atom of the phosphite as well as to the methylene group (C9–C10) of one 1,3-diene fragment and to the vinyl group (C1–C2) of the second. The maximum deviation of these atoms from the plane formed by these atoms and the Ni-atom is 0.075 Å. The

Table 1. Selected Structural Parameters for $(\eta^2, \eta^2\text{-DMOD})\text{NiP}(\text{OC}_6\text{H}_4\text{-}o\text{-Ph})_3$ (**3**)

bond lengths (Å)		bond angles (deg)	
Ni–P	2.090(1)	C1–Ni–C2	39.9(1)
Ni–C1	2.015(3)	C9–Ni–C10	40.5(1)
Ni–C2	2.017(3)	C1–C2–C3	124.7(3)
Ni–C9	2.060(3)	C2–C3–C5	116.8(3)
Ni–C10	1.997(3)	C2–C3–C4	122.2(4)
C1–C2	1.376(5)	C3–C5–C6	113.3(3)
C9–C10	1.406(5)	C4–C3–C5	120.9(4)
C2–C3	1.464(5)	C5–C6–C9	116.5(3)
C3–C4	1.335(6)	C6–C9–C8	118.8(3)
C3–C5	1.485(6)	C6–C9–C10	119.6(3)
C5–C6	1.517(5)	C9–C8–C7	128.5(3)
C6–C9	1.509(5)	Ni–P–O1	121.5(1)
C9–C8	1.456(5)	Ni–P–O2	116.5(1)
C7–C8	1.317(5)	Ni–P–O3	118.1(1)
Ni–D1	1.902	P–Ni–D1	116.3
Ni–D2	1.894	P–Ni–D2	115.1
		D1–Ni–D2	128.2

(4) Henc, B.; Jolly, P. W.; Salz, R.; Stobbe, S.; Wilke, G.; Benn, R.; Mynott, R.; Seevogel, R.; Goddard, R.; Krüger, C. *J. Organomet. Chem.* **1980**, *191*, 449.

(5) Michaelis, S. Doctoral Thesis, Ruhr-Universität Bochum, 1991.

Ni-bonded 1,6-heptadiene chain adopts a chair conformation. The uncomplexed methylene group (C3-C4) is *cis* to the complexed vinyl group (C1-C2) with a dihedral angle between C1/C2/C3/C4 of 27° whereas the uncomplexed vinyl group (C7-C8) is *trans* to the methylene group (C9-C10) with a dihedral angle between C7/C8/C9/C10 of 102°. The encapsulation of the Ni-atom by the biphenyl groups can be clearly seen in Figure 1 and will account in part for the stability of the compound in comparison with the trialkylphosphine derivatives **1** and **2**. The distance between the Ni-atom and the center of the closest phenyl ring, however, is 4.16 Å, so that it is unlikely that a direct interaction occurs between the metal atom and π -electrons of the ring. The preferred unsymmetrical complexation of the tetraene to the Ni-atom has its origin in the observation by Pörschke et al. that the η^2, η^2 -complexation of 1,6-heptadiene to zerovalent nickel is more favorable than that of 1,5-hexadiene^{5,6} or of 1,7-octadiene which fails to form complexes.⁷ This stability is associated with the strain-free, chair conformation adopted by the 1,5-heptadiene fragment and the resulting planar arrangement of the Ni-atom and alkene groups. Moreover, the angle of 128.2° between the midpoints of the double bonds and the nickel atom (D1-Ni-D2) is similar to that observed in (CH₂:CH₂)₂NiPCy₃.⁸

The NMR spectroscopic data for **1-3** (Tables 2 and 3) indicate that the complexes have the same structure in solution as in the crystal. For example, the ¹³C-NMR data for **1** and **2** at -70 °C show the expected magnetic inequivalence of the ten C-atoms of the tetraene and confirm that one methylene group and one vinyl group interact with the metal atom. At higher temperatures, the molecules are fluxional and a simplification of the spectra occurs. For example, the ¹H-NMR spectrum of **3** at room temperature contains only 6 signals for the 14 H-atoms of the tetraene, none of which have chemical shifts typical for an uncomplexed double bond: H-2 which is found at 6.3 ppm in the free tetraene is shifted to 4.2 ppm, while H-1 and H-4 which are found at ca. 5 ppm in the free tetraene are shifted to 3.5-3.1 ppm (Table 2). Extensive correlation and NOESY experiments show that the fluxionality arises from the pairwise exchange of the two methylene groups and of the two vinyl groups. This could proceed by a stepwise, intramolecular exchange of the alkene groups, and a simplified sequence involving the intermediate formation of 18-electron species is shown as Scheme 1.

An indication that relatively stable intermediates are involved in this process is obtained from the low-temperature ³¹P-NMR spectra of **3**: at -80 °C two signals are observed at 165.1 and 152.5 ppm (ratio 1:5). Unfortunately, the ¹H- and ¹³C-NMR spectra of **3** are relatively uninformative and are broad even at -100 °C.

The reaction of DMOD with zerovalent nickel in the presence of a bidentate phosphine takes a completely different course. Initially, the behavior of bis(diisopropylphosphino)ethane was investigated and since (cod)₂Ni forms a stable complex with this ligand, use was made of the more reactive (cdt)Ni. The reaction with DMOD (eq 2) led to the formation of a red compound **4** in high yield. The compound is surprisingly stable and melts

(6) Proft, B.; Pörschke, K.-R.; Lutz, F.; Krüger, C. *Chem. Ber.* **1991**, *124*, 2667.

(7) Pörschke, K.-R. Private communication, 1994.

(8) Krüger, C.; Tsay, Y.-H. *J. Organomet. Chem.* **1972**, *34*, 387.

Table 2. ¹H-NMR Spectroscopic Data for the (DMOD)Ni Compounds^a

	δ (H ₂ O) (J, Hz)					
	(1) ^b (η^2, η^2 -DMOD)NiPPt ₃	(2) ^b (η^2, η^2 -DMOD)NiPCy ₃	(3) ^{c,d} (η^2, η^2 -DMOD)NiP(C ₆ H ₄ - <i>o</i> -Ph) ₂	(4) ^e (η^2, η^2 -DMOD)Ni(Pt ₂ PC ₂ H ₄ PPt ₂) ₂	(5) ^e (η^2, η^2 -DMOD)Ni(Pt ₂ PC ₃ H ₆ PPt ₂) ₂	(6) ^e ($\eta^2, \eta^2, \eta^2, \eta^2$ -DMOD)Ni ₂ (Pt ₂ PCH ₃ PPt ₂) ₂
1Z	2.49 dd (1Z,2 12.9; 1Z,P 9.2)	~1.90	3.46 dd (1Z,2 15.3; 1Z,P 3.9)	2.23 dq (1Z,2 12.0; 1Z,1E 1.7)	2.35 dbr (1Z,2 12.0)	
1E	1.95 dd (1E,2 8.8; 1E,P 2)	~1.90	3.09 dq (1E,2 9.9; 1E,P -)	2.48 dq (1E,2 8.5; 1E,P 1.7)	2.05 dbr (1E,2 9.7)	
2	3.39 ddd (2,P 5.0)	~3.36	4.24 ddd (2,P 1.7)	4.63 dd	3.81 dd	5.27 dbr
4Z	4.21 s	4.21 s	3.04 d (4Z,P 5.9)	3.30 s	4.73 sbr ^g	
4E	4.44 s	4.42 s	3.34 s (4E,P 2.2)	3.61 sbr	4.63 sbr ^g	
5a/5b	3.02 dt/2.15 dd (5a,5b 13.0) ^f	3.02 dt/2.14	2.05 br	2.70 s	2.59 s	
6a/6b	2.83 dt/1.22 (6a,6b 14.2; 6a,P 5.0)	2.84/1.24				
7E	4.94 d (7Z,8 17.5)	4.93 d (7Z,8 17.3)				
7Z	4.73 d (7E,8 10.9)	4.72 d (7E,8 10.9)				
8	5.53 dd	5.51 dd				
10Z	2.13 d (10Z,P 4.8)	2.05				
10E	2.26 d (10E,P 9.5)	2.05				
Misc.	2.33/1.20 (Ph)	2.14/1.80-1.29 (Cy)	7.41-6.74 (Ar)	2.70-0.86 (Pt ₂ PC ₂ H ₄ PPt ₂)	1.95-0.80 (Pt ₂ PC ₃ H ₆ PPt ₂)	1.57 v/1.35-1.00 m (Pt ₂ PCH ₃ PPt ₂)

^a d_g-THF, -70 °C. ^c d_g-toluene, 27 °C. ^d d_g-toluene, 60 °C. ^e d_g-THF, 27 °C. ^f J(5a, 6a) 5.0, J(5b, 6a) 0, J(5b, 6b) 4.2. ^g Assignment could be reversed. ^h Unassigned abs at δ 3.45-3.20 m, 2.83 d, 2.68 m, 2.45 s, 2.27 m, 2.05-1.80 m, 2.05-1.80 m. ⁱ Molecule fluxional.

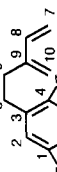
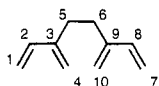


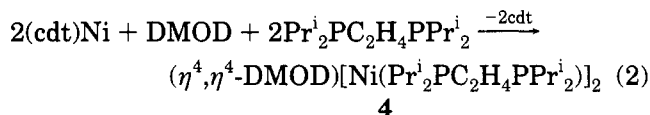
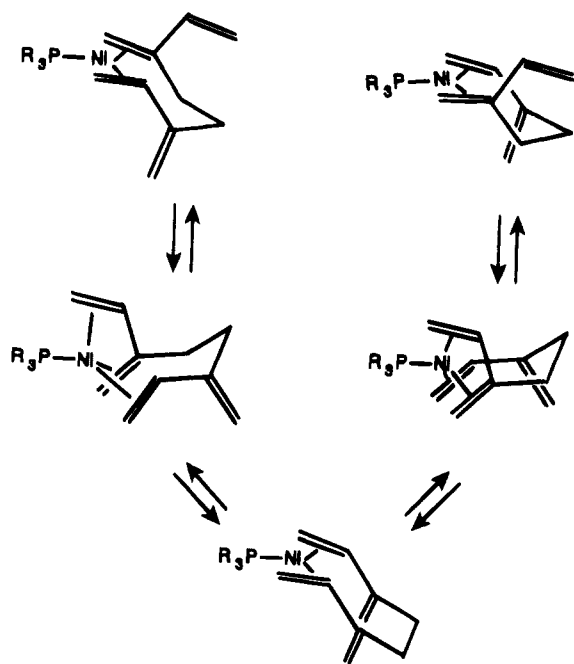
Table 3. ^{13}C -NMR Spectroscopic Data for the (DMOD)Ni Compounds^a

	$\delta(\text{C}_i)$ (J(C,P) Hz)			
	$(\eta^2, \eta^2\text{-DMOD})\text{NiPPr}^i_3$ (1) ^b	$(\eta^2, \eta^2\text{-DMOD})\text{NiPCy}_3$ (2) ^b	$(\eta^4, \eta^4\text{-DMOD})[\text{Ni}(\text{Pr}^i_2\text{PC}_2\text{H}_4\text{PPr}^i_2)]_2$ (4) ^c	$(\eta^2, \eta^2, \eta^2, \eta^2\text{-DMOD})\text{Ni}_2(\text{Pr}^i_2\text{PCH}_2\text{PPr}^i_2)$ (6) ^c
1	44.4	44.3	41.8 (6.2)	<i>d</i>
2	76.4 (7.9)	76.5 (6.7)	74.5	80.9 (10.5)
3	152.2 (3.7)	152.2 (3.6)		100.0 (10.5/2.5)
4	100.3	100.0	66.7	<i>d</i>
5	37.9 (4.2)	37.8	43.2	<i>d</i>
6	39.4 (2.2)	39.3		
7	104.8 (2.2)	104.6		
8	144.8 (4.0)	144.2 (3.7)		
9	77.7 (9.6)	77.9		
10	58.0	58.0		
Misc.	26.2/20.2 (Pr ⁱ)	37.6–27.6 (Cy)	26.3–18.2 (Pr ⁱ ₂ PC ₂ H ₄ PPr ⁱ ₂)	27.4–14.2 (Pr ⁱ ₂ PCH ₂ PPr ⁱ ₂)

^a ^b *d*₈-THF, -70 °C. ^c *d*₈-THF, 27 °C. ^d Unassigned abs for C₁/C₄/C₅ at 43.3(3.0)/44.1(2.0)/54.5.



Scheme 1



at 140 °C without decomposition. The elemental analysis and mass spectrum indicated that a binuclear species has been formed. The IR and NMR spectra suggest that all four double bonds of the tetraene interact with the metal atoms, while the NMR spectra suggest that the molecule is symmetrical. Repeated recrystallization from toluene led to the isolation of red needles (in addition to an amorphous powder) suitable for an X-ray diffraction study, and the crystal structure determination established the $\mu\text{-}\eta^4, \eta^4$ -complexation of the tetraene to the two nickel atoms.

The molecular structure of **4** is shown in Figure 1, and selected structural parameters are listed in Table 4. The nickel atom lies at the center of a distorted tetrahedron and is bonded to the P-atoms of the bidentate ligand and to one of the 1,3-diene fragments. The molecule has a center of inversion at the middle point of C5–C5*.

Table 4. Selected Structural Parameters for $(\eta^4, \eta^4\text{-DMOD})[\text{Ni}(\text{Pr}^i_2\text{PC}_2\text{H}_4\text{PPr}^i_2)]_2$ (**4**)

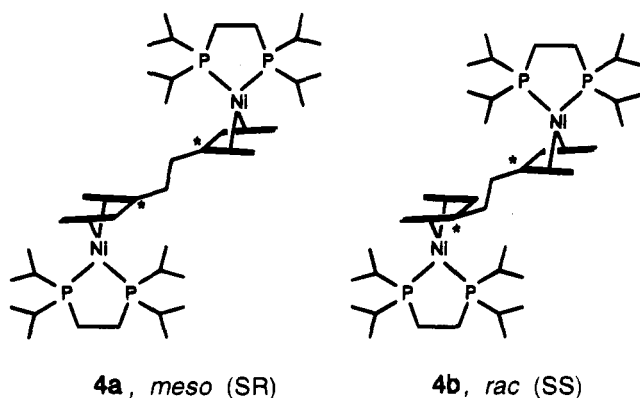
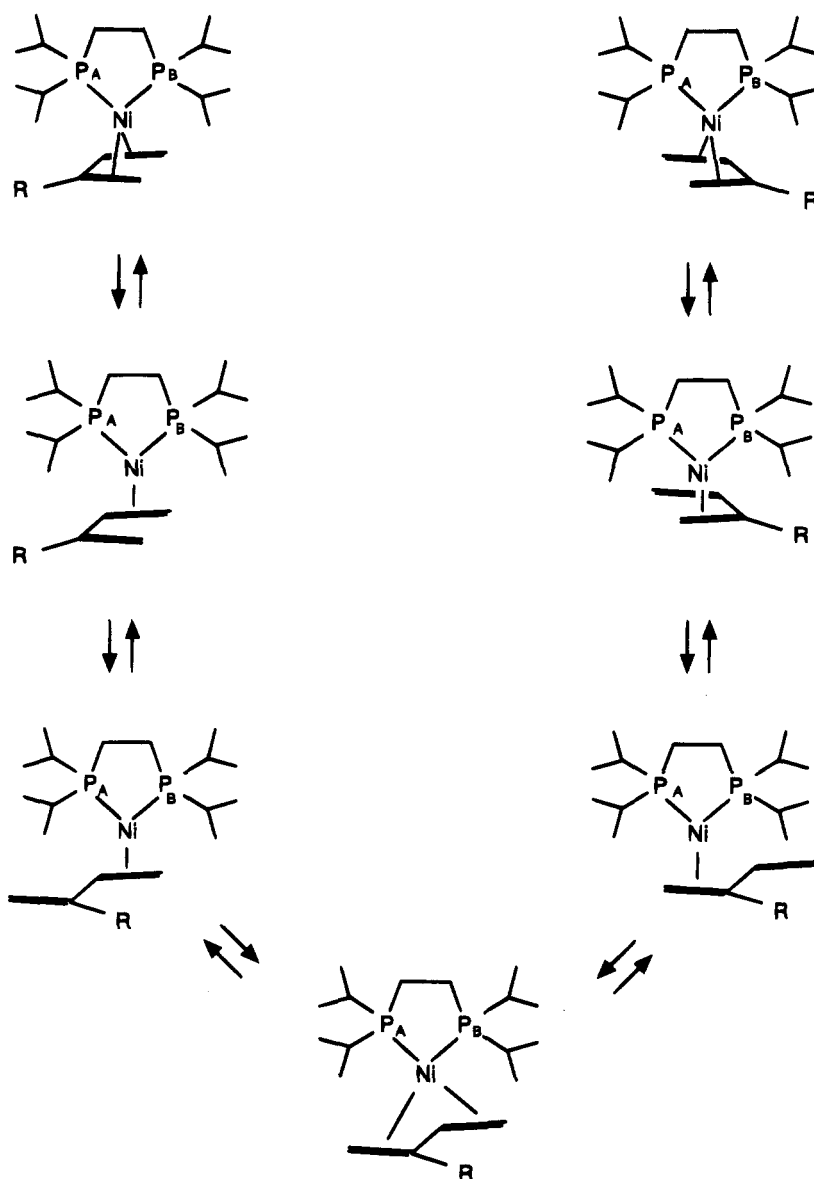
	bond lengths (Å)		bond angles (deg)	
Ni–P1	2.128(1)	C1–C2–C3	122.0(3)	
Ni–P2	2.156(1)	C2–C3–C4	118.7(3)	
Ni–C1	2.155(3)	C2–C3–C5	119.6(2)	
Ni–C2	2.025(2)	C4–C3–C5	121.8(3)	
Ni–C3	2.068(2)	C3–C5–C5*	112.2(2)	
Ni–C4	2.183(3)	P1–Ni–P2	92.8(1)	
C1–C2	1.379(5)	D1–Ni–D2	64.6	
C2–C3	1.434(4)	D1–Ni–P1	126.2	
C3–C4	1.377(4)	D1–Ni–P2	125.8	
C3–C5	1.503(4)	D2–Ni–P1	126.8	
C5–C5*	1.531(3)	D2–Ni–P2	123.8	
Ni–D1	1.974			
Ni–D2	2.012			

Although the presence of an inversion center can be expected to lead to a simplification of the NMR spectra, that for the ^{31}P nuclei is unexpectedly complex and consists at -80 °C of an apparent triplet at ca. 98.0 ppm and a double doublet at ca. 54.8 ppm. This spectrum arises from the overlap of two AB-spin systems having very similar chemical shifts and identical coupling constants and intensities and suggests that the molecule is formed as diastereomers. These could be associated either with the arrangement of the ethano bridge in the bidentate ligand with respect to the 1,3-diene fragment or alternatively be the result of the presence of two chiral centers (C3/C3*) in the molecule. The first possibility has been discussed for $(\eta^4\text{-1,3-butadiene})\text{Ni}(\text{Cy}_2\text{PC}_2\text{H}_4\text{PCy}_2)$ ⁹ and has been shown to exist in the crystal but is not maintained in solution. The crystal structure of **4** is of the meso-form (**4a**; *RS/SR*), but in addition a racemic form is possible (**4b**; *RR/SS*; only the *SS*-form is shown) which differs only in the mode of complexation of a 1,3-diene fragment. It is possible that the choice of a crystal having the meso structure was accidental or that the racemic form did not form suitable crystals and precipitated as an amorphous powder (see above).

The ^{31}P NMR spectra of **4** are temperature dependent: the two overlapping AB-systems observed at -80 °C coalesce at room temperature to become two broad signals at room temperature and one sharp signal at +90 °C. This process, which is reversible, suggests that two consecutive processes occur: initially the P-atoms

(9) Benn, R.; Betz, P.; Goddard, R.; Jolly, P. W.; Kokel, N.; Krüger, C.; Topalović, I. *Z. Naturforsch.* **1991**, *46b*, 1395.

Scheme 2



exchange and this is followed by diastereomer exchange. Any mechanism explaining these effects must involve side exchange of the metal atom at the 1,3-diene fragment. A possibility which accounts for both effects is shown as Scheme 2 and involves the intermediate formation of an η^2 -bonded diene fragment followed by isomerization from the *cis* to a *trans* configuration. This mechanism, which has precedence in the literature,⁶ avoids the previously favored¹⁰ rotation of the η^2 -bonded

diene fragment about the Ni-alkene axis which is now believed to be energetically unlikely in these systems. An alternative mechanism involving the isomerization of the (η^4 -1,3-diene)Ni fragment to a nickel cyclopentene ring followed by ring inversion can be envisaged and has been invoked for Zr-containing species¹¹ but is without precedence in organonickel chemistry. Unfortunately, further information could not be obtained from the ¹H- and ¹³C-NMR spectra since the relative insolubility of the compound precluded the measurement of low-temperature spectra.

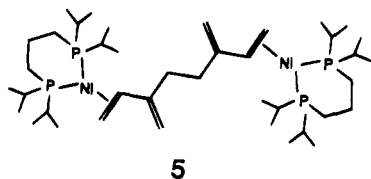
Changing the length of the chain between the two phosphorus atoms in the bidentate ligand has a remarkable effect upon the course of the reaction between DMOD and zerovalent nickel.

The product of the reaction in the presence of bis-(diisopropylphosphino)propane is a yellow compound (5) whose mass spectrum indicates the composition (DMOD)-

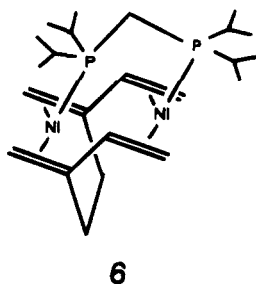
(10) Benn, R.; Jolly, P. W.; Joswig, T.; Mynott, R.; Schick, K. P. *Z. Naturforsch.* **1986**, *41b*, 680.

(11) (a) Erker, G.; Wicher, J.; Engel, K.; Rosenfeldt, F.; Dietrich, W.; Krüger, C. *J. Am. Chem. Soc.* **1980**, *102*, 6344. (b) Erker, G.; Engel, K.; Krüger, C.; Chiang, A.-P. *Chem. Ber.* **1982**, *115*, 3311. (c) Erker, G.; Krüger, C.; Müller, G. *Adv. Organomet. Chem.* **1985**, *24*, 1.

$[\text{Ni}(\text{Pr}^i_2\text{PC}_3\text{H}_6\text{PPr}^i_2)]_2$. However, in contrast to **4** the IR spectrum suggests the presence of uncomplexed double bonds ($\nu(\text{C}=\text{C})$ 1590, 885 cm^{-1}), and this is supported by the ^1H -NMR spectrum in which signals at 4.6 and 4.7 ppm are assigned to the protons of the uncomplexed methylene groups (these are observed at 5.25 and 5.04 ppm in DMOD). On the basis of this evidence, a possible structure for **5** is shown in which the Ni-atoms are complexed to the vinyl groups and lie in a 16-electron, trigonal planar environment:



In the presence of bis(diisopropylphosphino)methane, a completely different reaction occurs: the product of the reaction between $(\text{cdt})\text{Ni}$, the bidentate ligand, and DMOD is a dark violet compound (**6**) which is stable at room temperature and whose mass spectrum and elemental analysis indicate the composition $(\text{DMOD})\text{-Ni}_2(\text{Pr}^i_2\text{PCH}_2\text{PPr}^i_2)$. The ^{31}P -NMR spectrum is that of an AB-spin system suggesting that the two P-atoms lie in different environments. The ^{13}C -NMR spectrum contains 5 signals attributable to the 10 C-atoms of the DMOD molecule indicating that the tetraene is bonded in a symmetrical manner to the two metal atoms. In addition, the ^{13}C -NMR spectrum contains a signal at 14.2 ppm which is assigned to the methylene C-atom of the bidentate ligand and is typical for systems in which the ligand bridges two metal atoms. This signal is shifted to lower field in species in which the ligand is acting in a chelating manner and, for example, appears at 33.5 ppm in $(\eta^3\text{-C}_3\text{H}_5)_2\text{Fe}(\text{Pr}^i_2\text{PCH}_2\text{PPr}^i_2)$,¹² while it absorbs at 14.7 ppm in the free ligand. A structure which unites all these observations is shown below:



Popular prejudice would attribute the dark color of **6** to a metal-metal interaction similar to that observed for $[(\text{cyclooctatetraene})\text{Ni}]_2$ ¹³ or $[\text{Pd}(\text{Pr}^i_2\text{PCH}_2\text{PPr}^i_2)]_2$,¹⁴ however, this must remain speculation since we were unable to grow crystals of a quality sufficient for an X-ray diffraction study.

The difference in behavior between the ethano- and propano-bridged bidentate ligands is presumably associated with the difference in their space-filling properties: models suggest that the Ni-atom in **3** is less

(12) Gabor, B.; Holle, S.; Jolly, P. W.; Mynott, R. *J. Organomet. Chem.* **1994**, *466*, 201.

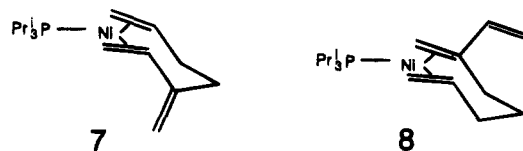
(13) (a) Brauer, D. J.; Krüger, C. *J. Organomet. Chem.* **1976**, *122*, 139. (b) Brauer, D. J.; Krüger, C. *Angew. Chem.* **1969**, *81*, 708.

(14) Döhring, A.; Goddard, R.; Hopp, G.; Jolly, P. W.; Kokel, N.; Krüger, C. *Inorg. Chim. Acta* **1994**, *222*, 179.

shielded by the P-bonded isopropyl groups than in **5**. The behavior of the methano-bridged bidentate ligand is certainly a result of the unfavorable bite angle in this ligand which leads to a destabilization of a chelating arrangement.

Reaction of 3-Methylene-1,6-heptadiene and 3-Methylene-1,7-octadiene with Zerovalent Nickel.

In the hope of obtaining additional information on the mechanism of the rearrangement of the $(\text{DMOD})\text{NiPr}_3$ species shown in Scheme 1, we prepared the complexes **7** and **8** by reacting $(\text{cod})_2\text{Ni}$ with PPr^i_3 and the trienes



3-methylene-1,6-heptadiene and 3-methylene-1,7-octadiene. In both cases, the NMR spectroscopic results (see Experimental Section) indicate that a 1,6-heptadiene chain is complexed in an η^2, η^2 -manner to the metal atom. This is attained by the complexation of the terminal olefin and the vinyl group, in the case of **7**, or the methylene group, in the case of **8**, and underlines once again the special stability associated with the 1,6-heptadiene chain.

Both **7** and **8** are more stable than the corresponding DMOD-containing species, but unfortunately, the NMR spectra of neither compound show any temperature-dependent effect between -80 and $+60$ $^\circ\text{C}$.

Experimental Section

The general experimental conditions and instrumentation have been described in the preceding publication.¹ $(\text{Cod})_2\text{Ni}$ and $(\text{cdt})\text{Ni}$ were prepared according to published procedures.³ $(\eta^2, \eta^2\text{-DMOD})\text{NiPr}^i_3$ (**1**). DMOD (0.99 mL, 5.83 mmol) and PPr^i_3 (1.12 mL, 5.80 mmol) was added to a suspension of $(\text{cod})_2\text{Ni}$ (1.60 g, 5.82 mmol) in diethyl ether (200 mL) cooled to -78 $^\circ\text{C}$. The mixture was warmed to -30 $^\circ\text{C}$ and stirred for 48 h. The resulting dark yellow solution was filtered through a pad of avicel at -30 $^\circ\text{C}$ in order to remove traces of precipitated nickel and concentrated to 50 mL. The solution was held at -78 $^\circ\text{C}$ for 1 week to give the compound as a bright yellow crystalline solid which was washed at -78 $^\circ\text{C}$ with precooled pentane (2×10 mL). The compound decomposes at room temperature and should be stored at -30 $^\circ\text{C}$. Yield: 1.46 g (4.13 mmol, 71%). Anal. Calcd for $\text{C}_{19}\text{H}_{35}\text{NiP}$: C, 64.6; H, 10.0; Ni, 16.6; P, 8.8. Found: C, 64.7; H, 10.1; Ni, 16.5; P, 8.7. IR (KBr): 2930 (s), 1610 (s), 1460 (s), 880 (s), 860 (s), 650 (s) cm^{-1} . MS (90 $^\circ\text{C}$): m/e 352 (M^+ , 66%), 218 ($\text{M}^+ - \text{DMOD}$, 18%), 192 ($\text{M}^+ - \text{PPr}^i_3$, 59%), 176 (100%). ^{31}P -NMR (d_8 -THF, -70 $^\circ\text{C}$): δ 52.7. ^1H - and ^{13}C -NMR spectroscopic data: see Tables 2 and 3.

$(\eta^2, \eta^2\text{-DMOD})\text{NiPCy}_3$ (**2**) was prepared as described above by reacting PCy_3 as a yellow solid in 66% yield. Anal. Calcd for $\text{C}_{28}\text{H}_{47}\text{NiP}$: C, 71.1; H, 10.0; Ni 12.4; P, 6.5. Found: C, 71.0; H, 9.9; Ni, 12.3; P, 6.6. IR (KBr): 2920 (s), 1610 (s), 1490 (s) cm^{-1} . MS (80 $^\circ\text{C}$): m/e 472 (M^+ , 0.4%) (the compound decomposed during measurement). ^{31}P -NMR (d_8 -THF, -70 $^\circ\text{C}$): δ 42.0. ^1H - and ^{13}C -NMR spectroscopic data: see Tables 2 and 3.

$(\eta^2, \eta^2\text{-DMOD})\text{NiP}(\text{OC}_6\text{H}_4\text{-}o\text{-Ph})_3$ (**3**) was prepared as described above by reacting $\text{P}(\text{OC}_6\text{H}_4\text{-}o\text{-Ph})_3$ as a pale yellow crystalline solid in 41% yield. Anal. Calcd for $\text{C}_{46}\text{H}_{41}\text{O}_3\text{NiP}$: C, 75.5; H, 5.7; Ni, 8.0; P, 4.2. Found: C, 75.7; H, 5.8; Ni, 7.9; P, 4.2. IR (KBr): 1475 (s), 1430 (s), 1190 (s), 1110 (s), 910 (s), 880 (s), 755 (s), 700 (s). MS (180 $^\circ\text{C}$): m/e 730 (M^+ , 0.2%)

Table 5. Crystallographic Data for 3 and 4

	3	4
formula	C ₄₆ H ₄₁ NiO ₃ P	C ₃₈ H ₇₈ Ni ₂ P ₄
mol wt	731.5	776.4
cryst size, mm	0.39 × 0.35 × 0.42	0.53 × 0.35 × 0.25
V, Å ³	3834.1	4287.2
D _c , g cm ⁻³	1.27	1.20
T, °C	20	20
λ(Cu), Å	1.541 78	1.541 78
Z	4	4
μ _{abs} , cm ⁻¹	5.86	26.75
reflms measd	9483 (±h,±k,+l)	13 927 (±h,±k,+l)
ind reflms	7600	4410
obsd reflms	6325	3972
no. of variables	460	355
space group (No.)	P2 ₁ /c (14)	C2/c (15)
a, b, c, Å	10.057(1), 36.196(1), 10.944(1)	17.535(2), 24.152(1), 11.767(1)
α, β, γ, deg	90.0, 105.76(1), 90.0	90.0, 120.65(1), 90.0
R	0.056	0.034
R _w	0.071	0.035
res electron density, e Å ⁻³	0.24	0.30

(the compound decomposed during the measurement). ³¹P-NMR (*d*₈-toluene): 27 °C, δ 152.0; -80 °C, 152.5, 165.1 (ratio 5:1). ¹H-NMR spectroscopic data: see Table 2. Crystal structure: see Figure 1 and Tables 1 and 5.

(η^4, η^4 -DMOD)[Ni(Prⁱ₂PC₂H₄PPPrⁱ₂)₂] (4). DMOD (0.56 mL, 3.30 mmol) and Prⁱ₂PC₂H₄PPPrⁱ₂ (1.03 mL, 3.30 mmol) were added to a suspension of (cdt)Ni (0.83 g, 3.31 mmol) in diethyl ether (200 mL) cooled to -78 °C. The reaction mixture was allowed to warm to room temperature over 5 h. A yellow solid precipitated and then dissolved to give a red solution. The reaction mixture was stirred for 2 d, filtered through a pad of avicel, and evaporated to dryness. The residue was dissolved in toluene (50 mL) at 50 °C and filtered. Cooling the filtrate to -78 °C gave the compound as red needles which were washed with precooled pentane (10 mL) at -78 °C and dried in high vacuum. Yield: 1.09 g (1.40 mmol, 85%). Anal. Calcd for C₃₈H₇₈Ni₂P₄: Ni, 15.1; P, 16.0. Found: Ni, 14.7; P, 15.4 (satisfactory analytical data could not be obtained despite repeated recrystallization, however, in all cases the values correspond to a Ni:chelate phosphine:olefin ratio of 2:2:1). IR (KBr): 2980–2860 (s), 2460 (s), 1025 (s), 880 (s), 670 (s), 645 (s), 620 (s). MS (130 °C): *m/e* 774 (M⁺, 0.1%). ³¹P-NMR (*d*₈-toluene): 90 °C, δ 73.0; -80 °C, δ 98.3 (*J*(P,P) ca. 40 Hz), 97.8 (*J*(P,P) ca. 40 Hz), 55.0 (*J*(P,P) 41.5 Hz), 54.8 (*J*(P,P) 40.5 Hz) (the spectrum consists of two AB-spin systems in the ratio 1:1 which could not be assigned). ¹H- and ¹³C-NMR spectroscopic data: see Tables 2 and 3. Crystal structure: see Figure 1 and Tables 4 and 5.

(η^2, η^2 -DMOD)[Ni(Prⁱ₂PC₃H₆PPPrⁱ₂)₂] (5) was prepared as described above by reacting Prⁱ₂PC₃H₆PPPrⁱ₂ as a yellow powder in 53% yield. The substance could not be obtained analytically pure. IR (KBr): 2980–2860 (s), 1460 (s), 1025 (s), 885 (s). MS (180 °C): *m/e* 802 (M⁺, 5.8%). ³¹P-NMR (*d*₈-toluene): 27 °C, δ 30.7; -80 °C, 30.5, 24.6 both as broad doublets. ¹H-NMR spectroscopic data: see Table 2.

($\eta^2, \eta^2, \eta^2, \eta^2$ -DMOD)Ni₂(Prⁱ₂PCH₂PPPrⁱ₂) (6). DMOD (0.17 mL, 1.00 mmol) and Prⁱ₂PCH₂PPPrⁱ₂ (0.55 mL, 1.84 mmol) were added to a suspension of (cdt)Ni (0.46 g, 1.83 mmol) in diethyl ether (200 mL) cooled to -78 °C. The reaction mixture was allowed to warm to room temperature over 5 h and the resulting dark red solution stirred for a further 2 d. The solution was filtered through a pad of avicel and evaporated to dryness, and the residue was dissolved in pentane (20 mL). The pentane solution was filtered and held at -78 °C for 5 d to give the compound as a dark-violet to black solid which was dried under high vacuum. Yield: 0.34 g (0.68 mmol, 74%). Anal. Calcd for C₂₃H₄₄Ni₂P₂: C, 55.3; H, 8.9; Ni, 23.5; P, 12.4. Found: C, 54.3; H, 8.6; Ni, 24.1; P, 12.9 (although the analytical results are not completely satisfactory, the Ni:P ratio is 1:1). IR (KBr): 2980–2840 (s), 1465 (s), 1385 (s), 1360 (s)

Table 6. Final Coordinates and Equivalent Isotropic Thermal Parameters (Å²) of the Non-Hydrogen Atoms for 3^a

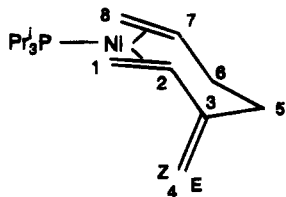
atom	x	y	z	U _{eq}
Ni1	0.0386(1)	0.1525(1)	0.4529(1)	0.048(1)
P	-0.0719(1)	0.1086(1)	0.3486(1)	0.045(1)
O1	-0.0880(2)	0.0696(1)	0.4149(2)	0.053(1)
O2	-0.0122(2)	0.0917(1)	0.2367(2)	0.055(1)
O3	-0.2317(2)	0.1152(1)	0.2746(2)	0.050(1)
C1	-0.1275(3)	0.1853(1)	0.4368(3)	0.066(2)
C2	-0.0083(3)	0.2048(1)	0.4907(3)	0.060(2)
C3	0.0607(4)	0.2292(1)	0.4207(3)	0.076(2)
C4	-0.0074(5)	0.2463(1)	0.3126(4)	0.115(4)
C5	0.2130(4)	0.2331(1)	0.4710(4)	0.083(3)
C6	0.2883(3)	0.1964(1)	0.4696(3)	0.070(2)
C7	0.3345(3)	0.1919(1)	0.7521(3)	0.071(2)
C8	0.2696(3)	0.1659(1)	0.6737(3)	0.059(2)
C9	0.2433(3)	0.1644(1)	0.5368(3)	0.052(2)
C10	0.2254(3)	0.1294(1)	0.4798(3)	0.068(2)
C20	0.0048(3)	0.0602(1)	0.5311(3)	0.057(2)
C21	-0.0136(3)	0.0741(1)	0.6437(3)	0.062(2)
C22	0.0831(4)	0.0634(1)	0.7541(4)	0.090(3)
C23	0.1914(5)	0.0407(1)	0.7524(6)	0.120(4)
C24	0.2069(4)	0.0277(1)	0.6434(7)	0.111(4)
C25	0.1128(4)	0.0371(1)	0.5278(4)	0.081(3)
C26	-0.1294(3)	0.0988(1)	0.6487(3)	0.066(2)
C27	-0.1057(5)	0.1296(1)	0.7257(4)	0.095(3)
C28	-0.2126(7)	0.1527(1)	0.7329(6)	0.125(5)
C29	-0.3431(7)	0.1447(2)	0.6677(6)	0.123(5)
C30	-0.3697(4)	0.1148(2)	0.5898(5)	0.103(4)
C31	-0.2632(3)	0.0916(1)	0.5804(4)	0.076(2)
C40	0.0503(3)	0.1144(1)	0.1655(3)	0.056(2)
C41	0.1678(3)	0.1007(1)	0.1369(3)	0.066(2)
C42	0.2307(4)	0.1240(1)	0.0689(4)	0.086(3)
C43	0.1810(5)	0.1586(1)	0.0317(4)	0.101(4)
C44	0.0646(5)	0.1715(1)	0.0609(4)	0.091(3)
C45	-0.0015(3)	0.1489(1)	0.1277(3)	0.070(2)
C46	0.2290(4)	0.0648(1)	0.1857(4)	0.078(3)
C47	0.1550(5)	0.0323(1)	0.1699(5)	0.103(4)
C48	0.2156(7)	-0.0008(1)	0.2166(6)	0.126(5)
C49	0.3536(8)	-0.0008(2)	0.2838(7)	0.149(7)
C50	0.4278(6)	0.0304(2)	0.3014(7)	0.138(5)
C51	0.3680(4)	0.0628(1)	0.2529(5)	0.104(4)
C60	-0.3050(3)	0.0996(1)	0.1590(3)	0.050(2)
C61	-0.3813(3)	0.1239(1)	0.0683(3)	0.057(2)
C62	-0.4495(3)	0.1091(1)	-0.0492(3)	0.072(2)
C63	-0.4440(4)	0.0718(1)	-0.0729(4)	0.087(3)
C64	-0.3696(4)	0.0485(1)	0.0181(4)	0.086(3)
C65	-0.2993(3)	0.0623(1)	0.1363(3)	0.065(2)
C66	-0.3894(3)	0.1641(1)	0.0934(3)	0.061(2)
C67	-0.3455(4)	0.1902(1)	0.0212(4)	0.083(3)
C68	-0.3533(5)	0.2276(1)	0.0474(6)	0.108(4)
C69	-0.4056(5)	0.2387(1)	0.1396(7)	0.117(4)
C70	-0.4536(4)	0.2139(1)	0.2120(5)	0.097(3)
C71	-0.4436(3)	0.1767(1)	0.1902(4)	0.074(2)

$$^a U_{eq} = 1/3 \sum_i \sum_j U_{ij} a_i^* a_j^* \bar{a}_i \bar{a}_j.$$

cm⁻¹. MS (120 °C): *m/e* 498 (M⁺, 0.6%), 364 (M⁺ - DMOD, 0.1%) (the sample decomposed during the measurement). ³¹P-NMR (*d*₈-THF, 27 °C): δ 67.9, 72.0, *J*(P,P) 176.5. ¹H- and ¹³C-NMR spectroscopic data: see Tables 2 and 3.

(η^2, η^2 -MHD)NiPPPrⁱ₃ (7). MHD (0.47 mL, 2.95 mmol) and PPPrⁱ₃ (0.56 mL, 2.90 mmol) were added to a suspension of (cod)₂Ni (0.80 g, 2.91 mmol) in diethyl ether (80 mL) cooled to -78 °C. The reaction mixture was stirred at -30 °C for 4 d to give a red solution which was filtered through a pad of avicel at -30 °C and concentrated to ca. 20 mL. The solution was cooled to -78 °C for 14 d to give the compound as a yellow crystalline solid which was washed with precooled pentane (2 × 10 mL) at -78 °C and dried under high vacuum. The compound is stable at room temperature. Yield: 0.64 g (1.96 mmol, 67%). Anal. Calcd for C₁₇H₃₃NiP: C, 62.4; H, 10.2; Ni, 17.9; P, 9.5. Found: C, 62.3; H, 10.2; Ni, 18.0; P, 9.4. IR (KBr): 3005–2870 (s), 1465 (s), 1180 (s), 885 (s), 655 (s). MS (80 °C): *m/e* 326 (M⁺, 45%), 218 (M⁺ - MHD, 20%), 176 (60%), 134 (100%). ³¹P-NMR (*d*₈-toluene, 60 °C): 56.7. ¹H-NMR (*d*₈-toluene, -30 °C): δ 4.95 (s, H-4E), 4.63 (s, H-4Z), 4.15 (ddd,

H-2, $J(2, 1Z)$ ca. 13.2 Hz, $J(2, 1E)$ ca. 8.7 Hz, $J(2, P)$ ca. 5.1 Hz, 3.56 (m, H-7), 2.90–2.30/2.05–1.95 (m, H-1/5/6/8), 1.90/0.94 (Prⁱ). ¹³C-NMR (d_8 -THF, 27 °C): δ 153.2 (C-3), 100.9 (C-4, $J(C,P)$ 2.8), 70.6/66.9 (C-2/7, $J(C,P)$ 9.4/8.5 Hz), 51.6 (C-1, $J(C,P)$ 4.7 Hz), 41.0 (C-8, $J(C,P)$ 5.1 Hz), 39.0/38.6 (C-5/6) 6, $J(C,P)$ 5.3/2.8 Hz), 26.4/20.5 (Prⁱ). The numbering scheme is shown below:



(η^2, η^2 -MOD)NiPPrⁱ₃ (**8**) was prepared in 64% yield as described above as a yellow-brown solid by reacting MOD. Anal. Calcd for C₁₈H₃₅NiP: C, 63.4; H, 10.3; Ni 17.2; P, 9.1. Found: C, 63.3; H, 10.4; Ni, 17.1; P, 9.2. IR (KBr): 3000–2800 (s), 1610 (s), 1455 (s), 650 (s), 530 (s). MS (80 °C): m/e 340 (M⁺, 87%), 218 (M⁺ – MOD, 29%), 180 (M⁺ – PPrⁱ₃, 30%), 176 (100%). ³¹P-NMR (d_8 -toluene, –30%): δ 53.1. ¹H-NMR (d_8 -toluene, 60 °C): δ 5.77 (dd, H-2), 4.96 (dt, H-1Z), 4.77 (dt, H-1E), 1.99/1.01/1.02 (Prⁱ), $J(1Z, 2)$ 17.4 Hz, $J(1Z, 5)$ 1.8 Hz, $J(1E, 2)$ 10.9 Hz; additional unassigned absorptions at δ 3.01/2.74/2.51–2.32/1.71/0.95–0.55. ¹³C-NMR (d_8 -toluene, –30 °C): δ 144.1 (C-2, $J(C,P)$ 3.6 Hz), 104.8 (C-1, $J(C,P)$ ca. 2.7 Hz), 77.5 (C-8, $J(C,P)$ 9.0 Hz), 73.9 (C-3, $J(C,P)$ 10.2 Hz), 52.3/51.4 (C-4/9, $J(C,P)$ 5.7/4.6 Hz), 34.1/32.5/28.8 (C-5/6/7, $J(C,P)$ ca. 0/ca. 2.2/6.1 Hz), 25.5/10.9 (Prⁱ). The numbering scheme is shown below:

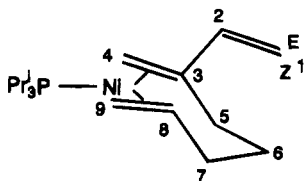


Table 7. Final Coordinates and Equivalent Isotropic Thermal Parameters (Å²) of the Non-Hydrogen Atoms for 4^a

atom	x	y	z	U _{eq}
Ni	0.2853(1)	0.4203(1)	0.2728(1)	0.032(1)
P1	0.1972(1)	0.3760(1)	0.0977(1)	0.038(1)
P2	0.3143(1)	0.3480(1)	0.3955(1)	0.036(1)
C1	0.2256(2)	0.4993(1)	0.2646(4)	0.061(3)
C2	0.3098(2)	0.4927(1)	0.3720(2)	0.045(2)
C3	0.3841(2)	0.4794(1)	0.3576(2)	0.039(2)
C4	0.3703(2)	0.4725(1)	0.2323(3)	0.053(2)
C5	0.4743(2)	0.4727(1)	0.4786(3)	0.044(2)
C6	0.2060(2)	0.3019(1)	0.1427(3)	0.052(2)
C7	0.2373(2)	0.2930(1)	0.2872(3)	0.055(2)
C8	0.2153(2)	0.3748(1)	–0.0450(3)	0.053(2)
C9	0.3099(2)	0.3590(2)	–0.0020(4)	0.068(3)
C10	0.1506(3)	0.3393(2)	–0.1615(4)	0.083(3)
C11	0.0759(2)	0.3898(1)	0.0136(3)	0.053(2)
C12	0.0446(2)	0.3881(2)	0.1141(5)	0.085(4)
C13	0.0532(3)	0.4447(2)	–0.0591(4)	0.085(3)
C14	0.2929(2)	0.3456(1)	0.5359(3)	0.052(2)
C15	0.3665(3)	0.3723(2)	0.6590(3)	0.072(3)
C16	0.2051(3)	0.3735(2)	0.4957(4)	0.073(3)
C17	0.4263(2)	0.3151(1)	0.4707(3)	0.050(2)
C18	0.4531(2)	0.3091(2)	0.3664(4)	0.069(3)
C19	0.4379(3)	0.2603(2)	0.5413(5)	0.083(4)

$$^a U_{eq} = 1/3 \sum_i \sum_j U_{ij} a_i^* a_j^* \bar{a}_i \bar{a}_j$$

Single-Crystal X-ray Diffraction Studies of 3 and 4.

The crystal structure analyses were carried out using an Enraf-Nonius CAD-4 diffractometer. Crystallographic data and details of the refinements are listed in Table 5, and final coordinates and equivalent isotropic thermal parameters are in Tables 6 and 7. Further details are to be found in the supplementary material.

Supplementary Material Available: Detailed information on the crystal structure determination of **3** and **4** including tables of data collection parameters, final atomic positional parameters, final thermal parameters, and interatomic distances and angles and ORTEP diagrams (19 pages). Ordering information is given on any current masthead page.

OM9409480

Synthesis and Dynamic Behavior of (Pentamethylcyclopentadienyl)azatantalacyclopropane Complexes. Crystal Structures of TaCp*Cl₄[C(Me)(NHR)] and TaCp*Me₂(η²-Me₂CNR)

Mikhail V. Galakhov, Manuel Gómez, Gerardo Jiménez, and Pascual Royo*

*Departamento de Química Inorgánica, Universidad de Alcalá de Henares,
Campus Universitario, E-28871 Alcalá de Henares, Spain*

Maria Angela Pellinghelli and Antonio Tiripicchio

*Dipartimento di Chimica Generale ed Inorganica, Chimica Analitica, Chimica Fisica,
Università di Parma, Centro di Studio per la Strutturistica Diffattometrica del CNR,
Viale delle Scienze 78, I-43100 Parma, Italy*

Received June 24, 1994*

The amino carbene adducts TaCp*Cl₄[C(Me)NHR] (R = 2,6-Me₂C₆H₃, **1a**; 2,4,6-Me₃C₆H₂, **1b**) have been prepared by reaction with HCl of solutions containing the acylimidoyl complexes TaCp*Cl₃(η²-MeC=NR) prepared by addition of isocyanides CNR to TaCp*Cl₃Me. Solutions of pure acylimidoyl derivatives can be prepared and characterized in sealed tubes or in a drybox, as they are very easily hydrolyzed in the presence of traces of water. Reaction of TaCp*Cl₂Me₂ with 1 equiv of isocyanides takes place with double migration of methyl, leading to the formation of azatantalacyclopropane complexes TaCp*Cl₂(η²-Me₂CNR) (R = 2,6-Me₂C₆H₃, **2a**; 2,4,6-Me₃C₆H₂, **2b**). Complexes **2** are easily protonated by HCl to give aryl isopropyl amido derivatives TaCp*Cl₃(NⁱPrR) (R = 2,6-Me₂C₆H₃, **3a**; 2,4,6-Me₃C₆H₂, **3b**), which decompose at 120 °C with evolution of isopropyl chloride to give the imido complexes TaCp*Cl₂(NR) (R = 2,6-Me₂C₆H₃, **4a**; 2,4,6-Me₃C₆H₂, **4b**). Methylation of **2a** with 2 equiv of LiMe gives TaCp*Me₂[η²-Me₂CN(2,6-Me₂C₆H₃)] (**5a**), which alternatively can be obtained by reaction of **3a** with 3 equiv of MgClMe with evolution of methane. All the complexes isolated were studied by IR and ¹H, ¹³C NMR spectroscopy. The dynamic behavior of **2a** and **5a** was studied in solution between 203 and 303 K, and kinetic parameters were determined. The crystal structures of **1a** and **5a** were determined by X-ray diffraction methods. Crystals of the benzene solvate of **1a** are triclinic, space group *P*-1 with *Z* = 2 in a unit cell of dimensions *a* = 8.381(4) Å, *b* = 8.977(4) Å, *c* = 18.316(9) Å, α = 100.17(2)°, β = 97.83(2)°, and γ = 105.04(2)°. Crystals of **5a** are monoclinic, space group *P*2₁/*n* with *Z* = 4 in a unit cell of dimensions *a* = 10.515(6) Å, *b* = 14.615(9) Å, *c* = 14.594(8) Å, and β = 100.66(2)°. Both structures were solved from diffractometer data by Patterson and Fourier methods and refined by full-matrix least-squares fit on the basis of 3218 (**1a**·¹/₂C₆H₆) and 3786 (**5a**) observed reflections to *R* and *R*_w values of 0.0432 and 0.0534 (**1a**·¹/₂C₆H₆) and 0.0299 and 0.0316 (**5a**), respectively.

Introduction

Migratory insertion of carbon monoxide into metal-alkyl bonds and the reactivity of the resulting metal-acyl function is one of the most important organometallic reactions, leading to different products through stoichiometric or catalytic processes.¹ The isoelectronic isocyanide ligands can be attacked at the nucleophilic nitrogen atom by hard electrophiles to give aminocarbene complexes² or can be transformed into formimidoyl and acylimidoyl functions by migratory insertion of hydride³ and alkyl groups.⁴ In comparison with the acyl ligands, the reactivity of these iminoacyl groups is even

more versatile. They can participate in reactions such as the following: (a) isomerization to the vinylamide⁵ and η³-1-azaallyl⁶ complexes; (b) alkyl migration to the carbon atom to give coordinated imines;⁷ (c) deprotonation followed by C=C coupling;⁸ (d) coupling with coordinated alkynes;⁹ (e) insertion of a second isocyanide leading to dihapto-coordinated 1,4-diaza-3-alkylbutadien-2-yl heterometallacycles;⁶ (f) multiple insertion.¹⁰ The chemistry of related amido and imido derivatives is receiving increasing interest, but to date these types of complexes have not proved readily available for group

(3) (a) Wolczanski, P. T.; Bercaw, J. E. *J. Am. Chem. Soc.* **1979**, *101*, 6450. (b) Evans, W. J.; Meadows, J. H.; Hunter, W. E.; Atwood, J. L. *Organometallics* **1983**, *2*, 1252. (c) Evans, W. J.; Hanusa, T. P.; Meadows, J. H.; Hunter, W. E.; Atwood, J. L. *Organometallics* **1987**, *6*, 295.

(4) Durfee, L. D.; Rothwell, I. P. *Chem. Rev.* **1988**, *88*, 1059.

(5) Beshouri, S. M.; Fanwick, P. E.; Rothwell, I. P.; Huffman, J. C. *Organometallics* **1987**, *6*, 891.

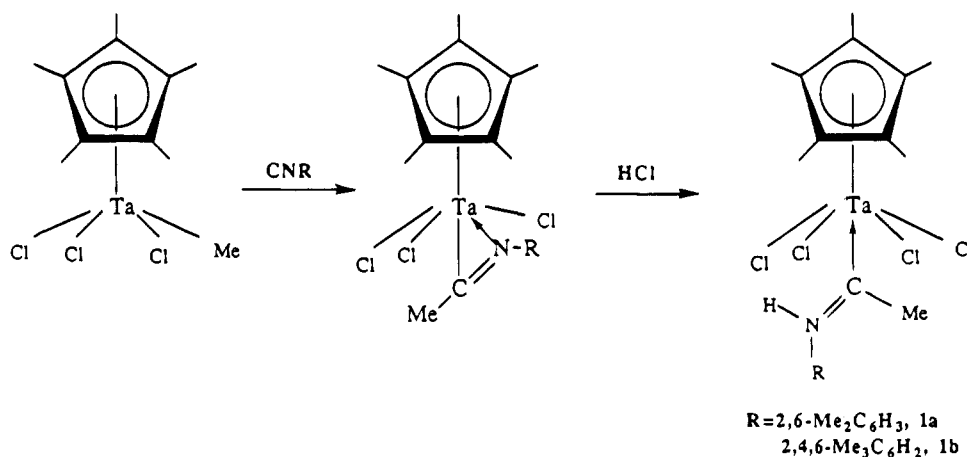
(6) (a) Filippou, A. C.; Grünleitner, W.; Völkl, C.; Kiprof, P. *J. Organomet. Chem.* **1991**, *413*, 181. (b) Filippou, A. C.; Völkl, C.; Kiprof, P. *J. Organomet. Chem.* **1991**, *415*, 375.

* Abstract published in *Advance ACS Abstracts*, March 15, 1995.

(1) Wolczanski, P. T.; Bercaw, J. E. *Acc. Chem. Res.* **1980**, *13*, 121.

(2) (a) Filippou, A. C.; Fischer, E. O.; Grünleitner, W. *J. Organomet. Chem.* **1990**, *386*, 333. (b) Filippou, A. C.; Grünleitner, W. *J. Organomet. Chem.* **1990**, *398*, 99; **1991**, *407*, 61. (c) Filippou, A. C.; Grünleitner, W.; Fischer, E. O.; Imhof, W.; Huttner, G. *J. Organomet. Chem.* **1991**, *413*, 165.

Scheme 1



5 metals^{7e,11} and the chemistry of their isocyanide derivatives has not been particularly well developed.^{7f,7i,9,12}

We report herein the insertion and intramolecular rearrangement processes^{13a} observed when isocyanides, CNR (R = 2,6-Me₂C₆H₃, 2,4,6-Me₃C₆H₂), are reacted with chloromethyl(pentamethylcyclopentadienyl)tantalum complexes, of the type TaCp*Cl_nMe_{4-n} (Cp* = η⁵-C₅Me₅, n = 2, 3).^{13b} All compounds were fully characterized. In addition, some of the complexes were studied by X-ray diffraction methods.

Results and Discussion

Reactions with Ta(η⁵-C₅Me₅)Cl₃Me. Ta(η⁵-C₅Me₅)Cl₄ easily reacts with isocyanides¹⁴ to give stable ad-

ducts of the type Ta(η⁵-C₅Me₅)Cl₄(CNR), (R = ^tBu; 2,6-Me₂C₆H₃) containing the isocyanide ligand trans to the cyclopentadienyl ring. In spite of the lower acidity of the chloromethyl derivatives, Ta(η⁵-C₅Me₅)Cl_nMe_{4-n} (n = 2, 3), whose isocyanide adducts cannot be isolated, the coordination of the isocyanide can be reasonably assumed as the first step in subsequent reactions. When isocyanides are added to toluene suspensions of yellow Ta(η⁵-C₅Me₅)Cl₃Me, an instantaneous insertion reaction takes place to give the iminoacyl derivatives Ta(η⁵-C₅Me₅)Cl₃(η²-MeC=NR) (Scheme 1). These compounds are extremely sensitive to moisture, evolving HCl in the presence of water, which then reacts with the iminoacyl complexes to give the carbene complexes Ta(η⁵-C₅Me₅)Cl₄[CMe=N(H)R] (Scheme 1).

The formation of the intermediate iminoacyl complexes is confirmed by ¹H NMR of the reaction solution, which along with the resonances due to the presence of a small amount of the carbene complex **1a** show one singlet at δ 1.90 (6H, Me₂C₆H₃), one singlet at δ 2.06 (15H, C₅Me₅) and one singlet at δ 2.55 (3H, RN=CMe) as for the iminoacyl complex Ta(η⁵-C₅Me₅)Cl₃[η²-MeC=N-(2,6-Me₂C₆H₃)]. Solutions containing only the iminoacyl complex can be prepared when the reaction is carried out in a sealed tube, but all attempts to recover the pure complex by working up the solution always resulted in its transformation into the aminocarbene complex. The latter is quantitatively formed when solutions of the iminoacyl complexes are treated with HCl.

The resulting pseudooctahedral 16-electron species are air-stable and do not react with additional isocyanide. NMR data are in full agreement with the proposed structure for **1a** and **1b** (see Experimental Section), the methyl protons being observed at δ 2.93 and 3.00, respectively, and the amino proton being observed as a broad signal at δ 12.20 for both complexes. In both complexes, the presence of the amino proton causes the ¹H methyl carbene signal to appear as a doublet (⁴J_{H(Me)-H(N)} = 0.9 Hz). This is also consistent with the spin-spin coupling between the methyl carbene carbon and the NH proton observed in the ¹³C NMR spectra (³J_{C-H} = 9.1 Hz) of these compounds. The}}

(7) (a) Wilkins, J. D. *J. Organomet. Chem.* **1974**, *67*, 269. (b) Takahashi, Y.; Onoyama, N.; Ishikawa, Y.; Motojirna, S.; Sugiyama, K. *Chem. Lett.* **1978**, 525. (c) Chiu, W. K.; Jones, R. A.; Wilkinson, G.; Galas, A. M. R.; Hursthouse, M. B. *J. Am. Chem. Soc.* **1980**, *102*, 7978. (d) Chiu, W. K.; Jones, R. A.; Wilkinson, G.; Galas, A. M. R.; Hursthouse, M. B. *J. Chem. Soc., Dalton Trans.* **1981**, 2088. (e) Mayer, J. M.; Curtis, C. J.; Bercaw, J. E. *J. Am. Chem. Soc.* **1983**, *105*, 2651. (f) Chamberlain, L. R.; Rothwell, I. P.; Huffman, J. C. *J. Chem. Soc., Chem. Commun.* **1986**, 1203. (g) Brunner, H.; Wachter, J.; Schmidbauer, J. *Organometallics* **1986**, *5*, 2212. (h) Durfee, L. D.; Fanwick, P. E.; Rothwell, I. P. *J. Am. Chem. Soc.* **1987**, *109*, 472. (i) Chamberlain, L. R.; Steffey, B. D.; Rothwell, I. P.; Huffman, J. C. *Polyhedron* **1989**, *8*, 341. (j) Durfee, L. D.; Hill, J. E.; Fanwick, P. E.; Rothwell, I. P. *Organometallics* **1990**, *9*, 75.

(8) Martín, A.; Mena, M.; Pellinghelli, M. A.; Royo, P.; Serrano, R.; Tiripicchio, A. *J. Chem. Soc., Dalton Trans.* **1993**, 2117.

(9) (a) Curtis, M. D.; Real, J. *J. Am. Chem. Soc.* **1986**, *108*, 4668. (b) Curtis, M. D.; Real, J.; Hirpo, W.; Butler, W. M. *Organometallics* **1990**, *9*, 66.

(10) Carmona, E.; Marín, J. M.; Palma, P.; Poveda, P. L. *J. Organomet. Chem.* **1989**, *377*, 157, and references therein.

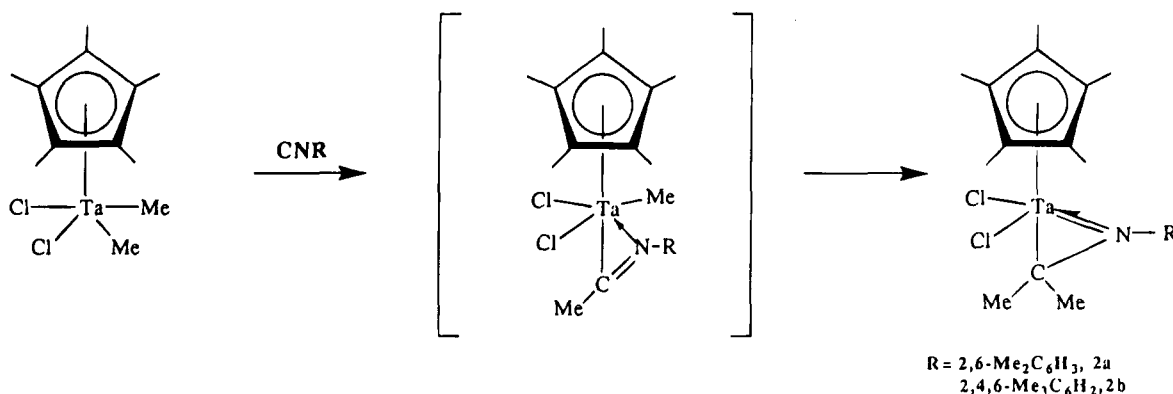
(11) (a) Nugent, W. A.; Haymore, B. L. *Coord. Chem. Rev.* **1980**, *31*, 123. (b) Parkin, G.; van Asselt, A.; Leahy, D. J.; Whinnery, LeRoy; Hua, N. G.; Quan, R. W.; Henling, L. M.; Schaefer, W. P.; Santarsiero, B. D.; Bercaw, J. E. *Inorg. Chem.* **1992**, *31*, 82. (c) Rocklage, S. M.; Schrock, R. R. *J. Am. Chem. Soc.* **1982**, *104*, 3077. (d) Bradley, D. C.; Hursthouse, M. B.; Abdul Malik, K. M.; Nielson, A. J.; Chota Vuru, G. B. *J. Chem. Soc., Dalton Trans.* **1984**, 1069. (e) Williams, D. N.; Mitchell, J. P.; Poole, A. D.; Siemeling, U.; Clegg, W.; Hockless, D. C. R.; O'Neil, P. A.; Gibson, V. N. *J. Chem. Soc., Dalton Trans.* **1992**, 739. (f) Bradley, D. C.; Hursthouse, M. B.; Howes, A. J.; N. de M. Jelfs, A.; Runnacles, J. D.; Thornton-Pett, M. *J. Chem. Soc., Dalton Trans.* **1991**, 841. (g) Cockroft, J. K.; Gibson, V. C.; Howard, J. A. K.; Poole, A. D.; Siemeling, U.; Wilson, C. *J. Chem. Soc., Chem. Commun.* **1992**, 1668. (h) Siemeling, U.; Gibson, V. C. *J. Chem. Soc., Chem. Commun.* **1992**, 1670. (i) Poole, A. D.; Gibson, V. C.; Clegg, W. *J. Chem. Soc., Chem. Commun.* **1992**, 237. (j) Siemeling, U.; Gibson, V. C. *J. Organomet. Chem.* **1992**, *426*, C25. (k) Jolly, M.; Mitchell, J. P.; Gibson, V. C. *J. Chem. Soc., Dalton Trans.* **1992**, 1331.

(12) Chamberlain, L. R.; Durfee, L. D.; Fanwick, P. E.; Kobriger, L.; Latesky, S. L.; McMullen, A. K.; Rothwell, I. P.; Folting, K.; Huffman, J. C.; Streib, W. E.; Wang, R. *J. Am. Chem. Soc.* **1987**, *109*, 390.

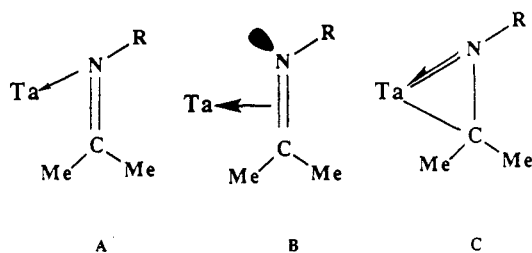
(13) (a) Galakhov, M. V.; Gómez, M.; Jiménez, G.; Pellinghelli, M. A.; Royo, P.; Tiripicchio, A. *Organometallics* **1994**, *13*, 1564. (b) Gómez, M.; Jiménez, G.; Royo, P.; Selas, J. M.; Raithby, P. R. *J. Organomet. Chem.* **1992**, *439*, 147.

(14) Gómez, M.; Gómez-Sal, P.; Royo, P.; Nicolás, P. *J. Organomet. Chem.*, in press.

Scheme 2



Scheme 3



chemical shifts observed in the ¹H spectra for the amino NH proton and in the ¹³C spectra for the carbene carbon atom ($\delta \sim 261$) are consistent with those reported^{2c,15} for other aminocarbene ligands. The IR spectra show a characteristic $\nu(\text{N-H})$ absorption at $\sim 3240 \text{ cm}^{-1}$.

The X-ray crystal structure of complex **1a** confirms the location of the carbene ligand in the axial position trans to the Cp* ligand. This suggests that the reaction leading to **1a** and **1b** involves the coordination of isocyanide at the axial position, followed by migration of the equatorial methyl group to the isocyanide carbon with coordination of the resulting iminoacyl nitrogen to the tantalum center, and finally protonation of the η^2 -iminoacyl ligand with HCl.

Reactions with Ta(η^5 -C₅Me₅)Cl₂Me₂. When the dimethyl complex is used, the sequence of reactions represented in Scheme 2 is observed. By addition of 1 equiv of the isocyanides to toluene solutions of the dimethyl derivative under rigorously anhydrous conditions (drybox or sealed NMR tube), red solutions are obtained, which after evaporation of the solvent afford complexes **2** as red crystals (Scheme 2).

Formation of these compounds can be explained as the result of two consecutive steps. The first step involves migration of one methyl group to the electrophilic isocyanide carbon atom, giving an iminoacyl intermediate. Although many stable alkyl iminoacyl complexes have been isolated,^{3a,7f-h-j,12} in the present case, further reaction takes place in the presence of the second methyl group, which easily migrates to the iminoacyl carbon atom to give an η^2 -imine ligand. Three limiting structures have been proposed^{7e-j} to describe the bonding of this ligand as represented in Scheme 3.

At room temperature, the equivalency of both methyl groups, as evidenced by the ¹H and ¹³C{¹H} NMR spectra of **2a** and **2b**, argue against an η^1 -imine (A) binding mode, suggesting either an η^2 -imine group (B)

or an azatantalacyclopropane structure (C) with the plane of the metallacycle being perpendicular to the Cp* ring plane. Unfortunately, we were not able to obtain crystals adequate for X-ray diffraction, but the structure must be presumably the same as that described below for the analogous dimethyl derivative. Similar azatantalacyclopropane species have been proposed^{7f} as intermediates in the transformation of alkyl bis(iminoacyl) complexes into imidoamidotantalum derivatives and their structures confirmed by X-ray diffraction in the case of Ti(OAr-2,6-ⁱPr₂)₂[η^2 -^tBuNC(CH₂Ph)₂](py-4-Ph)^{7j} and two tungsten derivatives.^{7c,d} More recently, new azazirconacyclopropane derivatives have been isolated¹⁶ by orthometalation of 2,6-diethylpyridine with the cationic complex [ZrCp₂Me(THF)]⁺.

When the same reactions are carried out in the presence of traces of water (under not rigorously dry argon), hydrolysis takes place and the evolved HCl reacts with the metallacycles to give, after protonation of the carbon atom, the dialkylamido derivatives **3a** and **3b**, in 50% yield. However, complexes **3a** and **3b** are obtained in almost quantitative yield when **2a** and **2b** are treated with a stoichiometric amount of HCl. Their formulation as dialkylamide complexes is consistent with the IR spectra showing an absorption at 599 cm^{-1} , which is tentatively assigned to the $\nu(\text{Ta-N})$ stretching frequency^{11d,f} and a characteristic isopropyl absorption at 1168 and 1112 cm^{-1} [$\nu(\text{CH}_3)$]. The ¹H NMR spectra show characteristic resonances for the isopropyl group and one singlet at $\delta 2.26$ (**3a**) and 2.20 (**3b**) for the equivalent methyl substituents of the phenyl group. This behavior is also consistent with the observed ¹³C{¹H} spectra (see Experimental Section). Complexes **3** are very soluble in aromatic hydrocarbons and moderately soluble in hexane. Their toluene solutions are slowly hydrolyzed in air to give, after elimination of the appropriate arylisopropyl ammonium chloride, the reported¹⁷ μ -oxohydroxo dimer [TaCp*Cl₂(OH)]₂(μ -O).

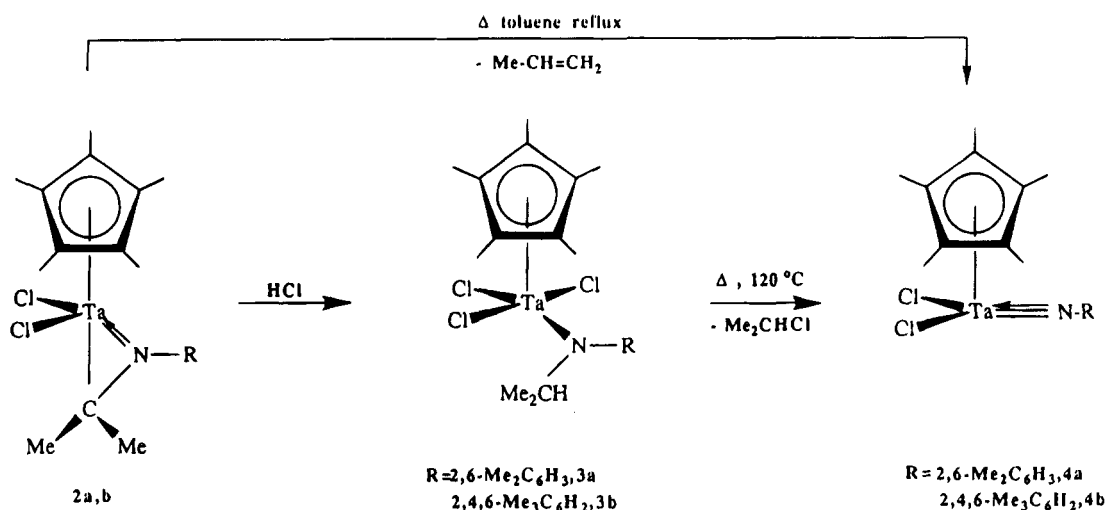
The amido complexes **3** are transformed by heating at 120°C into the imido derivatives **4a** and **4b**. These reactions are accompanied by the evolution of 2-chloropropane, as proved by the ¹H NMR spectrum of the resulting reaction solutions.¹⁸ The same compounds can be also obtained by thermal decomposition^{7b} of the azatantalacyclopropane complexes, **2a** and **2b**, in re-

(16) Guram, A. S.; Swenson, D. C.; Jordan, R. F. *J. Am. Chem. Soc.* **1992**, *114*, 8991.

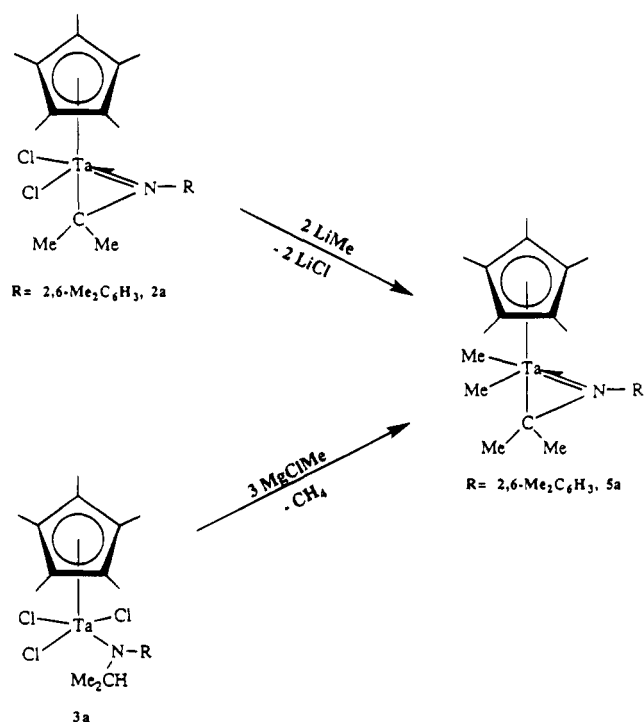
(17) Jernakoff, P.; de Meric de Bellefon, C.; Geoffroy, G. L.; Rheingold, A. L.; Geib, S. J. *Organometallics* **1987**, *6*, 1362.

(15) Filippou, A. C.; Fischer, E. O. *J. Organomet. Chem.* **1990**, *382*, 143; **1990**, *383*, 179.

Scheme 4



Scheme 5



fluxing toluene. Propene is liberated in these reactions. The two new imido complexes show a $\nu(\text{Ta}=\text{N})^{11e,f}$ IR absorption at $\sim 1323 \text{ cm}^{-1}$. In addition, one singlet is observed for the equivalent *o*-methyl(phenyl) protons and carbons in the ^1H and ^{13}C NMR spectra (see Experimental Section). The X-ray crystal structure of complex **4a**^{13a} confirms a pseudotetrahedral structure. Similar imidotantalum complexes have been obtained^{11c} by reacting alkylidene derivatives with $\text{RN}=\text{CHR}'$ in a metathesis-like reaction or by reacting the tetrachloro complexes $\text{Ta}(\eta^5\text{-C}_5\text{R}_5)\text{Cl}_4$ ($\text{R} = \text{H}$ or Me) with trimethylsilylamines.^{11e}

The dimethylazatantalacyclopropane complex **5** can be obtained by two alternative methods, as shown in Scheme 5.

Addition of 2 equiv of MeLi to a toluene solution of **2a** leads to an orange solution from which pure **5a** can

be isolated as an orange oil after extraction with pentane and evaporation of the solvent. Similarly, alkylation of the amido derivative **3a** with 3 equiv of MgClMe takes place with evolution of methane to give **5a**. This behavior can be explained as the result of the β -hydrogen elimination in the intermediate trimethyl-amido complex.

Dynamic Behavior of Azatantalacyclopropane Complexes. The ^{13}C CP MAS NMR spectra of **2a** and **5a** (see Table 1) show the presence of only one isomer with inequivalent pairs of methyl groups. Both complexes show inequivalent methyl groups bound to tantalum (Ta-Me_2 , **5a**), to the metallacycle carbon (CMe_2), and to the phenyl ring ($\text{NC}_6\text{H}_3\text{Me}_2$). The ortho and meta phenyl ring carbon atoms are also inequivalent, as shown in Figures 3 and 4.

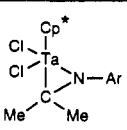
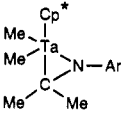
The resonance corresponding to the ipso carbon atom appears as a doublet due to interaction with the ^{14}N quadrupolar moment, with coupling constants that increase for decreasing positive charge on the nitrogen atom [$J = 68$ (**5a**), 50 Hz (**2a**)]. Broad signals are observed for metal-bonded methyl groups and for the metallacycle carbon atom, probably due to the interaction with tantalum and nitrogen quadrupolar moments.

However, at room temperature, in CDCl_3 solution, complex **5a** shows pairs of equivalent methyl groups, in agreement with the existence of a plane of symmetry defined by the tantalum, nitrogen, and carbon atoms, which is perpendicular to the C_5Me_5 ring plane. Solutions of **5a** show a dynamic behavior at variable temperature, as shown in Figure 1.

At 293 K, a broad signal ($\Delta\Delta\nu = 1.2$ Hz) is observed for the methyl groups bonded to the tantalacycle carbon, which broadens and shifts to high field (**2a**) as the temperature decreases. The other signal, **2b**, is accidentally coincident with resonance due to the Cp^* ligand. At temperatures lower than 213 K, two new signals are observed, which narrow and appear at 203 K as two new resonances, **1b** and **3b**, at $\delta -0.02$ and 1.8. The values of spin-lattice relaxation times (T_1) measured at 203 K and the results of saturation transfer at 213 K show that the two new resonances correspond to methyl tantalum and Cp^* , respectively. When the solution is diluted 10 times, the ratio does not change, indicating that the transformation is an intramolecular

(18) ^1H NMR spectrum of 2-chloropropane: δ 1.13 (d, $^2J_{\text{H-H}} = 6.5$ Hz, 6H, Me), 3.67 (sept, $^2J_{\text{H-H}} = 6.5$ Hz, 1H, CHCl).

Table 1. ¹³C Chemical Shifts for Complexes 2a and 5a in Solution at Variable Temperature and in Solid

complex	conditions	chemical shifts, ppm								
		Cp*	Me-Ta	C-Me ₂	C-Me ₂	C _{ipso}	C _{ortho}	C _{meta}	C _{para}	Me
 2a	293 K, CDCl ₃	10.8, 122.1		93.5	28.8	150.5	133.5	128.9	125.3	20.5
	208 K, CDCl ₃	10.8, 121.6		94.4	28.7	149.9	132.8	128.7	125.2	20.3
	solid, 293 K	10.6, 115.5		95.6 (br)	29.6, 27.1	150.6 ^a	134.1, 133.2	129.0	127	22.0, 21.5
 5a	293 K, CDCl ₃	10.6, 115.5	52.9	82.9	27.6	152.3	134.4	128.4	123.4	20.4
	203 K, CDCl ₃	10.9, 114.8	50.0	81.4	26.8	152.4	135.5	127.8	123.3	20.3
		10.2, 115.2	55.8	87.2	28.5	152.0	132.8			
	solid, 293 K	11.5, 115.7	53.5	86.7 (br)	29.7, 27.6	152.1 ^b	135.3, 134.3	129.7, 129.4	125.6	22.4, 21.5

^a J = 50 Hz. ^b J = 68 Hz.

dynamic process. This behavior indicates the existence of two stereoisomers in an approximate ratio 3/1, the major component corresponding to that observed in the solid. Both isomers contain the N and C azatantalacyclopropane atoms interchanging their mutual positions. The ¹³C{¹H} spectrum at 203 K (Table 1) also shows two groups of signals belonging to two different isomers. Complex 2a also shows the same dynamic behavior, but the ratio of the two isomers is ~7/1. So, from these results is possible to conclude that an intramolecular isomerization process takes place.

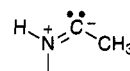
Kinetic parameters were evaluated (see Table 2) by using ¹H D NMR data.¹⁹ Values of log A confirm the intramolecular nature of the process, and the negative values of ΔS[‡] suggest that the transition state is characterized by a high polarization. Two different activated species could be proposed, as shown in Scheme 6.

The transition state species **A** is a tantalum(III) complex containing the alkylideneamine group coordinated by a metal-olefin-type bond, whereas **B** is the result of the Ta-C bond breaking to give a tantalum(V) amido complex. Formulation of species **B** would be in good agreement with the chemical behavior described above, which reveals the nucleophilic character of the carbon atom, whereas **A** seems to fit better the low values found for the free activation energy and the displacement by ligands of the alkylideneamine reported^{7j} for similar titanium derivatives. The isomerization activation energy *E_a* depends on the charge separation in the ground state, as observed in Table 2 for relative values measured for chloro (2a) and methyl (5a) derivatives and is also in agreement with relative values of the quadrupole coupling constants between ¹⁴N and the ipso phenyl carbon, observed in the ¹³C CP MAS spectra.

X-ray Crystal Structures of 1a^{1/2}C₆H₆ and 5a. In the crystals of TaCp*Cl₄[C(Me)(NHR)] (R = 2,6-Me₂C₆H₃) (1a), 0.5 mol of C₆H₆ solvate is present. A view of the complex 1a is shown in Figure 2 together with the atom numbering scheme. Selected bond distances and angles are given in Table 3. The pentamethylcyclopentadienyl ring is bound to the Ta atom in a nearly symmetric η⁵-fashion [the Ta-C distances range from 2.466(14) to 2.527(10) Å] with the distance between the metal and the centroid of the ring being 2.184(13) Å. The Ta atom is bound also to four Cl atoms with the Ta-Cl bond

lengths ranging from 2.384(4) to 2.418(4) Å. The coordination around the Ta atom is completed by the carbenic C(11) atom from the aminocarbene ligand [Ta-C(11) = 2.321(12) Å]. The complex can be described as pseudooctahedral if the centroid of the Cp* ring is considered as occupying one coordination site. The Ta atom is displaced by 0.551(1) Å from the equatorial plane containing the four Cl atoms toward the Cp* ring and the carbenic atom C(11) is positioned trans to the Cp* ring.

The NC(11)C(12)C(13) moiety of the aminocarbene ligand is perfectly planar, the aminocarbene plane including the Ta atom and being perpendicular to the phenyl ring [dihedral angle 89.2(6)°]. The N-C(11), N-C(13), and C(11)-C(12) bond distances, 1.279(15), 1.468(15), and 1.512(17) Å, respectively, agree with the following bonding system



confirming the carbenic nature of the C(11) atom. Also, the Ta-C(11) bond length of 2.321(12) Å is comparable to those found in TaCp*Cl₄[CH₂PMePh₂] [2.35(3) Å],²⁰ and in TaCp*Cl₃[(CH₂)₂PPh₂] [2.347(12) Å]²¹ in which the carbon atom is also in the trans position with respect to the Cp* centroid and is bound to the Ta atom through a σ bond.

The N-bound hydrogen of the carbene ligand is involved in an intramolecular bifurcated hydrogen bond with two of the coordinated Cl atoms. The N···Cl(1) and N···Cl(2) distances of 3.036(9) and 3.105(11) Å, as well as the H···Cl(1) and H···Cl(2) distances of 2.63(12) and 2.45(14) Å, respectively, suggest such an interaction.

A view of the complex TaCp*Me₂(η²-Me₂CNR) (R = 2,6-Me₂C₆H₃, 5a) is shown in Figure 3 together with the atom numbering scheme. Selected bond distances and angles are given in Table 4. The pentamethylcyclopentadienyl ring is bound to the Ta atom in a nearly symmetric η⁵-fashion [the Ta-C distances range from 2.451(5) to 2.525(6) Å], with the distance between the metal and the centroid of the ring being 2.172(5) Å. This distance is only slightly shorter than that of 1a. The Ta atom is also bound to two C atoms of the methyl

(20) Fandos, R.; Gómez, M.; Royo, P.; Garcia-Blanco, S.; Martínez-Carrera, S.; Sanz-Aparicio, J. *Organometallics* **1987**, *6*, 1581.

(21) Gómez, M.; Jiménez, G.; Royo, P.; Pellinghelli, M. A.; Tiripicchio, A. *J. Organomet. Chem.* **1992**, *439*, 309.

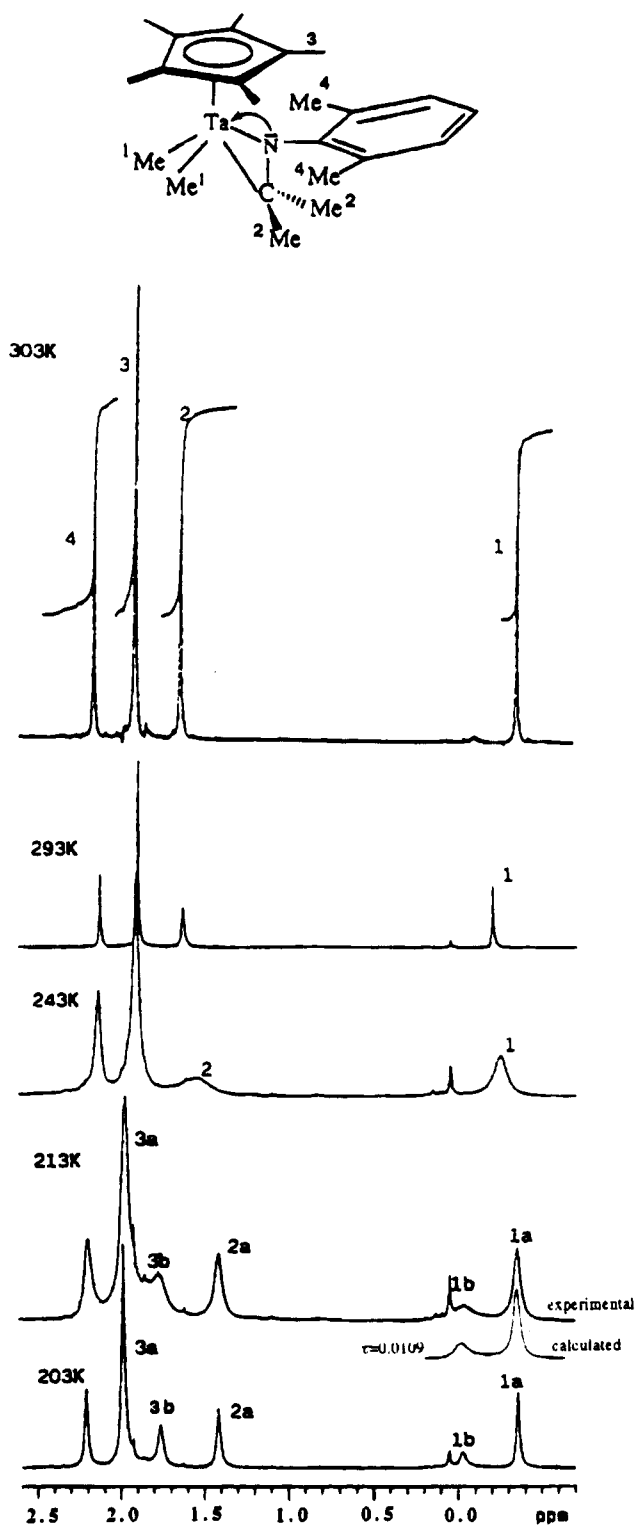


Figure 1. ^1H NMR variable-temperature spectra of $5\text{a}\text{-CD}_2\text{Cl}_2$: $T_1(4) = 0.439$ s; $T_1(3) = 0.604$ s (3a), 0.614 s (3b); $T_1(2\text{a}) = 0.133$ s; $T_1(1) = 0.410$ s (1a), 0.411 s (1b).

groups [Ta–C(11) = 2.179(7) Å, Ta–C(12) = 2.178(7) Å]. The CMe_2NR ligand is coordinated to the Ta atom in a η^2 -fashion with the N and C(13) atoms forming an azatantalacyclopropane system. The Ta–C(13) bond distance, 2.209(6) Å, is only slightly longer than those of the tantalum-bonded methyl groups and is comparable to those found for other Ta alkyls.²² The value of

the Ta–N bond length, 1.930(4) Å, is comparable to those found in tantalum dialkylamido derivatives²³ and denotes a certain degree of double-bond character. Finally, the value of the N–C(13) bond length, 1.467(7) Å, is consistent with a single bond. The azatantalacyclopropane ring is perpendicular to the cyclopentadienyl ring, to the TaC(11)C(12) plane, and to the aryl group, the dihedral angles being 89.7(3)°, 89.5(2)°, and 89.6(2)°, respectively. It bisects the C(11)–Ta–C(12) angle and is simultaneously the pseudomirror plane of the molecule (Figure 4). The coordination of the Ta atom can be therefore considered as a distorted trigonal bipyramid [the distortion being mainly due to the very narrow N–Ta–C(13) angle], with the C(11), C(12), and N atoms occupying the equatorial positions and the centroid of the Cp* ring and the C(13) atom the apical sites.

Experimental Section

All manipulations were performed under an inert atmosphere of argon using standard Schlenk techniques or a glovebox. Solvents used were previously dried and freshly distilled from *n*-hexane (Na/K alloy) and toluene (sodium). Reagent grade HCl (1 M in OEt_2), LiMe (1.6 M in OEt_2), and MgClMe (3 M in THF) were purchased from Aldrich Chemical Co. and were used without further purification. Isocyanides²⁴ RNC (R = 2,6- $\text{Me}_2\text{C}_6\text{H}_3$, 2,4,6- $\text{Me}_3\text{C}_6\text{H}_2$) and the starting materials $\text{TaCp}^*\text{Cl}_n\text{Me}_{4-n}$ ($n = 2, 3$)¹¹ were prepared as described previously.

Infrared spectra were recorded on a Perkin-Elmer 583 spectrophotometer (4000–200 cm^{-1}) as Nujol mulls between CsI or as polyethylene pellets. ^1H and ^{13}C NMR spectra were recorded on a Varian VXR-300 Unity instrument. ^1H and ^{13}C NMR shifts were measured relative to residual ^1H and ^{13}C resonances in the deuterated solvents: C_6D_6 (δ 7.15), CDCl_3 (δ 7.24) and C_6D_6 (δ 128), CDCl_3 (δ 77), respectively. C_6D_6 and CDCl_3 were purchased from Fluorochem Limited.

A DNMR5 program²⁵ was used for evaluation of kinetic parameters. Mass spectra were recorded on a HP 5988A instrument. C, H, and N analyses were carried out with a Perkin-Elmer 240 C microanalyzer.

TaCp*Cl₄{C(Me)(NHR)} (1a,b). A solution of CNR (1.44 mmol) in 10 mL of toluene was slowly added at room temperature to a stirred freshly prepared suspension of $\text{TaCp}^*\text{Cl}_3\text{Me}$ (0.63 g, 1.44 mmol) in 50 mL of toluene. The reaction mixture was treated with ethyl ether solution of HCl (1.44 mmol) and stirred for 2 h. The solvent was evaporated to dryness and the residue extracted with *n*-hexane (3 × 15 mL). The resulting yellow solution was concentrated to ~30 mL and subsequently cooled at –40 °C to give 1a (R = 2,6- $\text{Me}_2\text{C}_6\text{H}_3$) or 1b (R = 2,4,6- $\text{Me}_3\text{C}_6\text{H}_2$) as yellow crystals. The data for 1a follows. Yield: 0.37 g (85%). IR (Nujol mull, ν cm^{-1}): 3242 (m), 1555 (s), 1020 (m) 778 (s), 354 (s), 323 (s), 300 (s). ^1H NMR (δ ppm, in C_6D_6): 12.20 [br, 1H, $\text{CMe}(\text{NHR})$], 6.75 (t, 1H, $^3J_{\text{H-H}} = 7.3$ Hz, *p*- $\text{H}_3\text{C}_6\text{Me}_2$), 6.60 (d, 2H, $^3J_{\text{H-H}} = 7.3$ Hz, *m*- $\text{H}_3\text{C}_6\text{Me}_2$), 2.93 [d, 3H, $^4J_{\text{H-H}} = 0.9$ Hz, $\text{CMe}(\text{NHR})$], 2.35 (s, 15H, C_5Me_5), 2.05 (s, 6H, 2,6- $\text{Me}_2\text{C}_6\text{H}_3$). ^{13}C NMR (δ ppm, in C_6D_6): 261.1 [q, $^2J_{\text{C-H}} = 6.1$ Hz, $\text{CMe}(\text{NHR})$], 138.2 (m, *i*- $\text{C}_6\text{H}_3\text{Me}_2$), 133.8 (m, *o*- $\text{C}_6\text{H}_3\text{Me}_2$), 131.5 (m, C_5Me_5), 129.0 (d, $^1J_{\text{C-H}} = 158.7$ Hz, *p*- $\text{C}_6\text{H}_3\text{Me}_2$), 128.9 (d, $^1J_{\text{C-H}} = 159.1$ Hz, *m*- $\text{C}_6\text{H}_3\text{Me}_2$), 29.6 (qd, $^1J_{\text{C-H}} = 129.3$ Hz, $^3J_{\text{C-H}} = 4.9$ Hz, 2,6- $\text{Me}_2\text{C}_6\text{H}_3$), 17.8 [qd, $^1J_{\text{C-H}} = 127.6$ Hz, $^3J_{\text{C-H}} = 9.1$ Hz, $\text{CMe}(\text{NHR})$], 12.8 (q, $^1J_{\text{C-H}} = 128.1$ Hz, C_5Me_5). MS (EI, 70 eV): *m/e* 470 (10), 323 (3), 288 (4), 147 (86), 135 (45), 132 (100),

(23) Profflet, R. D.; Fanwick, P. E.; Rothwell, I. P. *Polyhedron* **1992**, *12*, 1559.

(24) Weber, A. P.; Gokel, G. W.; Ugi, I. K. *Angew. Chem., Int. Ed. Engl.* **1972**, *11*, 530.

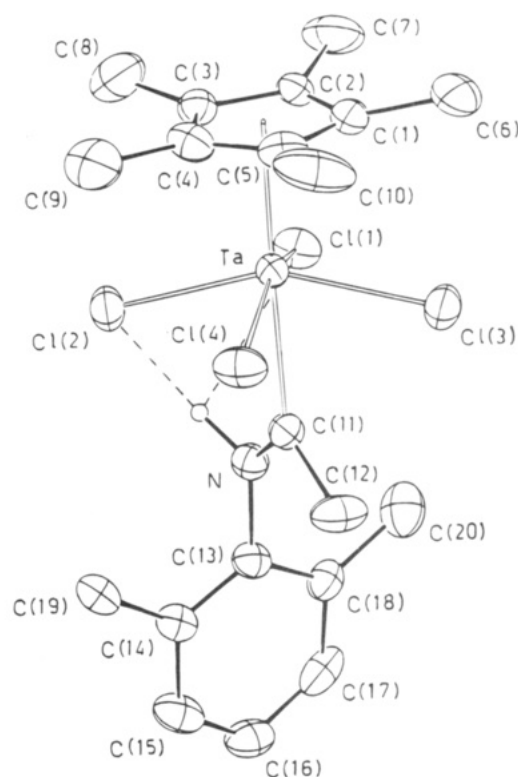
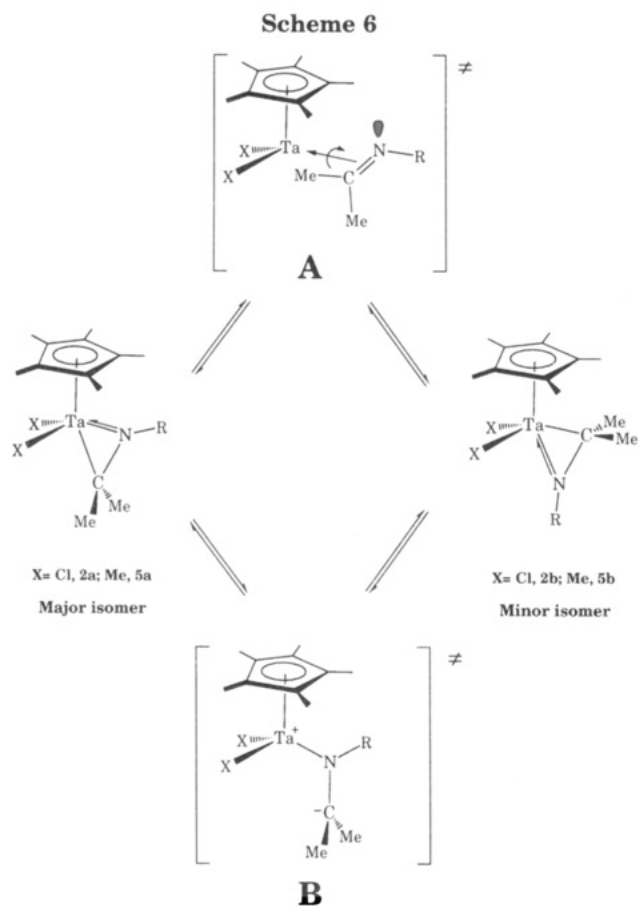
(25) Stephenson, D. S.; Binsch, G. *QCPE* **1978**, *11*, 365.

(22) Churchill, M. R.; Youngs, W. J. *J. Am. Chem. Soc.* **1979**, *101*, 6462.

Table 2. Kinetic Parameters for Isomerization of Complexes **2a** ⇌ **2b** and **5a** ⇌ **5b** Obtained from ¹H DNMR Data by Using Arrhenius and Eyring Equations

temp range, K	lifetime range τ, s	E _a , kcal/mol	log A	ΔH [‡] , kcal/mol	ΔS [‡] , eu	ΔG ^{‡298K} , kcal/mol	
2^a	208–273	0.00017–0.0020	9.2 ± 0.15 <i>r</i> = 0.9984	11.3 ± 0.4	7.6 ± 0.3 <i>r</i> = 0.9988	-13.2 ± 1.2	11.5
5^a	203–253	0.00060–0.025	7.6 ± 0.15 <i>r</i> = 0.9986	11.5 ± 1.0	7.1 ± 0.7 <i>r</i> = 0.9991	-15.1 ± 1.4	11.6

^a For seven experimental points and 0.95 confidence limit.

**Figure 2.** ORTEP view of the molecular structure of TaCp*Cl₄[C(Me)(NHR)] (R = 2,6-Me₂C₆H₃, **1a**) with the atom numbering scheme. The thermal ellipsoids are drawn at the 30% probability level.**Table 3.** Selected Bond Distances (Å) and Angles (deg) with ESDs in Parentheses for **1a**·1/2C₆H₆^a

Bond Distances					
Ta–CE(1)	2.184(13)	Ta–Cl(3)	2.384(4)	N–C(11)	1.279(15)
Ta–Cl(1)	2.417(3)	Ta–Cl(4)	2.393(3)	N–C(13)	1.468(15)
Ta–Cl(2)	2.418(4)	Ta–C(11)	2.321(12)	C(11)–C(12)	1.512(17)
Bond Angles					
CE(1)–Ta–Cl(1)	102.7(3)	Cl(2)–Ta–Cl(4)		85.3(1)	
CE(1)–Ta–Cl(2)	103.7(3)	Cl(2)–Ta–C(11)		77.9(3)	
CE(1)–Ta–Cl(3)	103.2(3)	Cl(3)–Ta–Cl(4)		90.3(1)	
CE(1)–Ta–Cl(4)	103.5(3)	Cl(3)–Ta–C(11)		75.2(3)	
CE(1)–Ta–C(11)	178.1(4)	Cl(4)–Ta–C(11)		75.6(3)	
Cl(1)–Ta–Cl(2)	84.6(1)	C(11)–N–C(13)		130.2(9)	
Cl(1)–Ta–Cl(3)	87.7(1)	Ta–C(11)–N		123.0(8)	
Cl(1)–Ta–Cl(4)	153.5(1)	Ta–C(11)–C(12)		125.9(9)	
Cl(1)–Ta–C(11)	78.3(3)	N–C(11)–C(12)		111.1(10)	
Cl(2)–Ta–Cl(3)	153.0(1)				

^a CE(1) is the centroid of the C(1)–C(5) cyclopentadienyl ring.

105 (48). Anal. Calcd for C₂₀H₂₈Cl₄NTa: C, 39.70; H, 4.66; N, 2.31. Found: C, 39.68; H, 4.62; N, 2.27. The data for **1b** follow. Yield: 0.27 g (80%). IR (Nujol mull, ν cm⁻¹): 3235 (m), 1550 (s), 1025 (m), 780 (s), 354 (s), 321 (s), 305 (m). ¹H NMR (δ ppm, in C₆D₆): 12.20 [br, 1H, CMe(NHR)], 6.42 (s, 2H, *m*-H₂C₆Me₃), 3.00 [d, 3H, ⁴J_{H-H} = 0.9 Hz, CMe(NHR)], 2.36 (s, 15H, C₅Me₅), 2.05 (s, 6H, 2,4,6-Me₃C₆H₂), 1.94 (s, 3H, 2,4,6-Me₃C₆H₂). ¹³C{¹H} NMR (δ ppm, in C₆D₆): 261.3 [s, CMe(NHR)], 138.6 (s), 136.0 (s), 133.7 (s), 129.7 (s, C_i, C_p, C_o, C_m, C₆H₂Me₃), 131.5 (s, C₅Me₅), 29.6 [s, CMe(NHR)], 20.8 (s, 2,4,6-Me₃C₆H₂), 17.7 (s, 2,4,6-Me₃C₆H₂), 12.8 (s, C₅Me₅). Anal. Calcd for C₂₁H₃₀Cl₄NTa: C, 40.79; H, 4.88; N, 2.26. Found: C, 40.36; H, 4.77; N, 2.30.

TaCp*Cl₂(η²-Me₂CNR) (2a,b). A stirred yellow-green solution of TaCp*Cl₂Me₂ (0.97 g, 2.32 mmol) in toluene (60 mL) was treated with CNR (2.32 mmol) under rigorously anhydrous conditions for 30 min. During this time, the color of the mixture changed to dark red. Subsequently, the solution was concentrated to ~10 mL, *n*-hexane (15 mL) was added, and the mixture cooled to -40 °C to give **2a** (R = 2,6-Me₂C₆H₃) or **2b** (R = 2,4,6-Me₃C₆H₂). The data for **2a** follow. Yield: 1.16 g (91%). IR (Nujol mull, ν cm⁻¹): 1259 (m), 1105 (w), 1024 (m), 803 (m), 768 (m), 347 (s). ¹H NMR (δ ppm, in C₆D₆): 7.02 (t, 1H, ³J_{H-H} = 7.5 Hz, *p*-H₃C₆Me₂), 6.94 (d, 2H, ³J_{H-H} = 7.5 Hz, *m*-H₃C₆Me₂), 2.44 (s, 6H, 2,6-Me₂C₆H₃), 2.11 (s, 6H, Me₂CNR), 1.74 (s, 15H, C₅Me₅). ¹³C NMR (δ ppm, in C₆D₆): 150.5 (m, *i*-C₆H₃Me₂), 133.5 (m, *o*-C₆H₃Me₂), 128.9 (dm, ¹J_{C-H} = 157.8 Hz, *m*-C₆H₃Me₂), 125.3 (d, ¹J_{C-H} = 159.8 Hz, *p*-C₆H₃-

Me₂), 122.1 (m, C₅Me₅), 93.5 (spt, ²J_{C-H} = 8.6 Hz, Me₂CNR), 28.8 (qq, ¹J_{C-H} = 124.0 Hz, ³J_{C-H} = 4.1 Hz, Me₂CNR), 20.5 (qd, ¹J_{C-H} = 126.8 Hz, ³J_{C-H} = 5.1 Hz, 2,6-Me₂C₆H₃), 10.8 (q, ¹J_{C-H} = 128.2 Hz, C₅Me₅). Anal. Calcd for C₂₁H₃₀Cl₂NTa: C, 45.99; H, 5.51; N, 2.55. Found: C, 46.23; H, 5.62; N, 2.47. The data for **2b** follow. Yield: 1.15 g (95%). IR (Nujol mull, ν cm⁻¹): 1259 (m), 1227 (m), 1102 (w), 1024 (m), 803 (m), 768 (m), 346 (s). ¹H NMR (δ ppm, in C₆D₆): 6.80 (s, 2H, H₂C₆-Me₃), 2.50 (s, 6H, 2,4,6-Me₃C₆H₂), 2.17 (s, 3H, 2,4,6-Me₃C₆H₂), 2.08 (s, 6H, Me₂CNR), 1.76 (s, C₅Me₅). ¹³C{¹H} NMR (δ ppm,

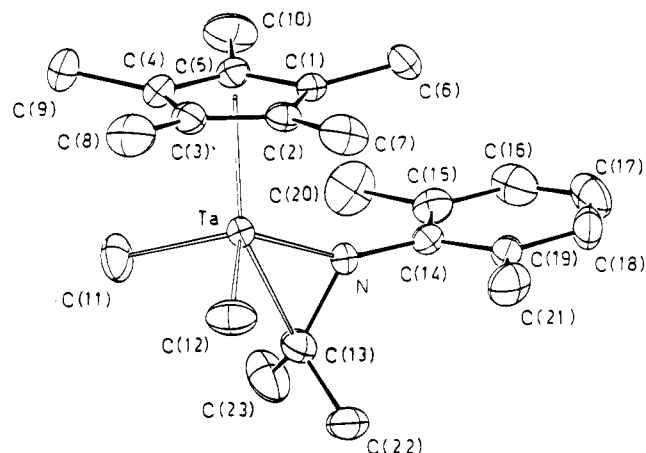


Figure 3. ORTEP view of the molecular structure of $\text{TaCp}^*\text{Me}_2(\eta^2\text{-Me}_2\text{CNR})$ ($\text{R} = 2,6\text{-Me}_2\text{C}_6\text{H}_3$, **5a**) with the atom numbering scheme. The thermal ellipsoids are drawn at the 30% probability level.

Table 4. Selected Bond Distances (Å) and Angles (deg) with ESDs in Parentheses for **5a**^a

Bond Distances			
Ta-CE(1)	2.172(5)	Ta-C(12)	2.178(7)
Ta-N	1.930(4)	Ta-C(13)	2.209(6)
Ta-C(11)	2.179(7)	N-C(13)	1.467(7)
		N-C(14)	1.426(7)
		C(13)-C(22)	1.534(9)
		C(13)-C(23)	1.530(9)
Bond Angles			
CE(1)-Ta-N	115.0(2)	Ta-N-C(13)	79.9(3)
CE(1)-Ta-C(11)	107.3(2)	Ta-N-C(14)	154.3(3)
CE(1)-Ta-C(12)	106.0(2)	C(13)-N-C(14)	125.8(4)
CE(1)-Ta-C(13)	155.8(2)	Ta-C(13)-N	59.3(3)
N-Ta-C(11)	112.1(2)	Ta-C(13)-C(22)	123.9(4)
N-Ta-C(12)	111.9(2)	Ta-C(13)-C(23)	124.2(4)
N-Ta-C(13)	40.8(2)	N-C(13)-C(22)	115.9(5)
C(11)-Ta-C(12)	103.8(3)	N-C(13)-C(23)	114.8(5)
C(11)-Ta-C(13)	87.4(2)	C(22)-C(13)-C(23)	108.6(6)
C(12)-Ta-C(13)	88.3(2)		

^a CE(1) is the centroid of the C(1)···C(5) cyclopentadienyl ring.

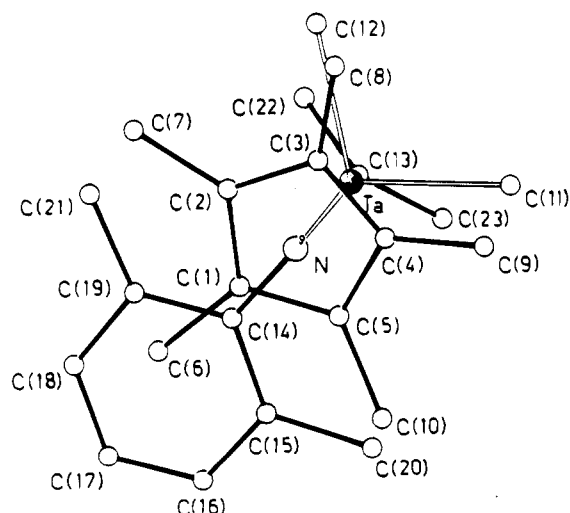


Figure 4. Projection of the structure of **5a** on the $\text{TaC}(11)\text{C}(12)$ plane showing the pseudomirror (excepting for the Cp^* ring) and the azatantalacyclopropane ring perpendicular to it.

in C_6D_6 : 147.8 (s), 134.4 (s), 133.1 (s), 129.7 (s, C_i , C_p , C_o , C_m , $\text{C}_6\text{H}_2\text{Me}_3$), 122.1 (s, C_5Me_5), 93.2 (s, Me_2CNR), 28.9 (s, $\text{Me}_2\text{-CNR}$), 20.7 (s, 2,4,6- $\text{Me}_3\text{C}_6\text{H}_2$), 20.4 (s, 2,4,6- $\text{Me}_3\text{C}_6\text{H}_2$), 10.8 (s, C_5Me_5). Anal. Calcd for $\text{C}_{22}\text{H}_{32}\text{Cl}_2\text{NTa}$: C, 46.98; H, 5.73; N, 2.49. Found: C, 46.86; H, 5.68; N, 2.42.

TaCp*Cl₃[N(CHMe₂)₂R] (3a,b). A solution of HCl 1 M in OEt_2 (0.24 mL, 0.42 mmol) was added at -78°C to a solution

of **2a** or **2b** (0.42 mmol) in toluene (50 mL) and stirred for 5 min. The color of the mixture changed quickly from red to pale yellow. The mixture was then warmed to room temperature, the solvent evaporated to dryness, and the resulting pale yellow solid washed with cold *n*-hexane (2×5 mL) and dried in vacuo. The data for **3a** follow. Yield: 0.23 g (92%). IR (Nujol mull, ν cm^{-1}): 1206 (m), 1168 (m), 1112 (m), 1091 (m), 1023 (m), 804 (m), 787 (m), 373 (m), 319 (m), 295 (m). ^1H NMR (δ ppm, in C_6D_6): 6.80 (m, 3H, $\text{H}_3\text{C}_6\text{Me}_2$), 4.57 (spt, 1H, $^3J_{\text{H-H}} = 4.6$ Hz, Me_2CH), 2.91 (s, 15H, C_5Me_5), 2.26 (s, 6H, 2,6- $\text{Me}_2\text{C}_6\text{H}_3$), 1.12 (d, 6H, Me_2CH). ^{13}C NMR (δ ppm, in C_6D_6): 143.3 (m, *i*- $\text{C}_6\text{H}_3\text{Me}_2$), 139.9 (m, *o*- $\text{C}_6\text{H}_3\text{Me}_2$), 129.3 (dm, $^1J_{\text{C-H}} = 160.3$ Hz, *m*- $\text{C}_6\text{H}_3\text{Me}_2$), 126.8 (d, $^1J_{\text{C-H}} = 160.2$ Hz, *p*- $\text{C}_6\text{H}_3\text{Me}_2$), 126.0 (m, C_5Me_5), 46.9 (d, $^1J_{\text{C-H}} = 113$ Hz, Me_2CH), 21.1 (q, $^1J_{\text{C-H}} = 125.7$ Hz, 2,6- $\text{Me}_2\text{C}_6\text{H}_3$), 16.4 (qm, $^1J_{\text{C-H}} = 134.5$ Hz, Me_2CH), 12.6 (q, $^1J_{\text{C-H}} = 129.3$ Hz, C_5Me_5). MS (EI, 70 eV): *m/e* 547 (3), 505 (100), 386 (26), 135 (31), 119 (68). Anal. Calcd for $\text{C}_{21}\text{H}_{31}\text{Cl}_3\text{NTa}$: C, 43.17; H, 5.35; N, 2.40. Found: C, 42.97; H, 5.28; N, 2.44. The data for **3b** follow. Yield: 0.24 g (95%). IR (Nujol mull, ν cm^{-1}): 1225 (m), 1156 (m), 1089 (m), 1025 (m), 790 (m), 380 (m), 305 (m), 290 (m). ^1H NMR (δ ppm, in C_6D_6): 6.60 (s, 2H, *m*- $\text{H}_2\text{C}_6\text{H}_3$), 4.60 (spt, 1H, $^3J_{\text{H-H}} = 5.1$ Hz, Me_2CH), 2.20 (s, 6H, 2,4,6- $\text{Me}_3\text{C}_6\text{H}_2$), 2.10 (s, 3H, 2,4,6- $\text{Me}_3\text{C}_6\text{H}_2$), 1.94 (s, 15H, C_5Me_5), 1.12 (d, 6H, $^3J_{\text{H-H}} = 5.1$ Hz, Me_2CH). $^{13}\text{C}\{^1\text{H}\}$ NMR (δ ppm, in C_6D_6): 141.2 (s), 139.1 (s), 136.4 (s), 130.3 (s, C_i , C_o , C_p , C_m , $\text{C}_6\text{H}_2\text{Me}_3$), 126.3 (s, C_5Me_5), 47.0 (s, Me_2CH), 21.4 (s, 2,4,6- $\text{Me}_3\text{C}_6\text{H}_2$), 20.7 (s, 2,4,6- $\text{Me}_3\text{C}_6\text{H}_2$), 16.8 (s, Me_2CH), 12.9 (s, C_5Me_5). Anal. Calcd for $\text{C}_{22}\text{H}_{33}\text{Cl}_3\text{NTa}$: C, 44.12; H, 5.55; N, 2.34. Found: C, 44.10; H, 5.45; N, 2.22.

TaCp*Cl₂(NR) (4a,b). Method A. A C_6D_6 solution of **3** (0.205 mmol) was heated at 120°C for 4–5 days in a sealed NMR tube. The reaction was monitored by ^1H NMR spectroscopy until total conversion of **3** to **4** was observed with simultaneous appearance of isopropyl chloride.

Method B. Toluene (50 mL) solutions of **2a,b** (1.82 mmol) were heated under reflux for 4 days. The resulting red solutions were evaporated to dryness and the residues extracted with *n*-hexane (2×30 mL). The solutions were concentrated to ~ 20 mL and cooled to -40°C to give microcrystalline red solids identified as **4a** [$\text{R} = 2,6\text{-Me}_2\text{C}_6\text{H}_3$; yield 0.53 g (62%)] or **4b** [$\text{R} = 2,4,6\text{-Me}_3\text{C}_6\text{H}_2$; yield 0.49 g (56%)]. When the same reaction was carried out in a sealed NMR tube and monitored by ^1H NMR spectroscopy, the presence of free propene was detected. The data for **4a** follow. IR (Nujol mull, ν cm^{-1}): 1323 (s), 1158 (w), 1095 (m), 1024 (m), 981 (w), 915 (w), 758 (s), 395 (w), 348 (s). ^1H NMR (δ ppm, in C_6D_6): 6.96 (d, 2H, $^3J_{\text{H-H}} = 7.5$ Hz, *m*- $\text{H}_3\text{C}_6\text{Me}_2$), 6.66 (t, 1H, $^3J_{\text{H-H}} = 7.5$ Hz, *p*- $\text{H}_3\text{C}_6\text{Me}_2$), 2.45 (s, 6H, 2,6- $\text{Me}_2\text{C}_6\text{H}_3$), 1.83 (s, 15H, C_5Me_5). $^{13}\text{C}\{^1\text{H}\}$ NMR (δ ppm, in C_6D_6): 151.1 (s), 135.1 (s), 127.3 (s), 124.1 (s, C_i , C_o , C_p , C_m , $\text{C}_6\text{H}_2\text{Me}_3$), 121.3 (s, C_5Me_5), 18.8 (s, 2,6- $\text{Me}_2\text{C}_6\text{H}_3$), 11.2 (s, C_5Me_5). MS (EI, 70 eV): *m/e* 505 (M^+ , 75), 386 (28), 351 (11), 135 (29), 119 (96). Anal. Calcd for $\text{C}_{18}\text{H}_{24}\text{Cl}_2\text{NTa}$: C, 42.70; H, 4.28; N, 2.77. Found: C, 43.02; H, 4.31; N, 2.75. The data for **4b** follow. IR (Nujol mull, ν cm^{-1}): 1320 (s), 1145 (w), 1022 (m), 965 (w), 775 (s), 375 (m). ^1H NMR (δ ppm, in C_6D_6): 6.77 (s, 2H, *m*- $\text{H}_2\text{C}_6\text{Me}_3$), 2.47 (s, 6H, 2,4,6- $\text{Me}_3\text{C}_6\text{H}_2$), 2.25 (s, 3H, 2,4,6- $\text{Me}_3\text{C}_6\text{H}_2$), 1.85 (s, C_5Me_5). $^{13}\text{C}\{^1\text{H}\}$ NMR (δ ppm, in C_6D_6): 151.0 (s), 134.8 (s), 132.3 (s), 129.8 (s, C_i , C_o , C_p , C_m , $\text{C}_6\text{H}_2\text{Me}_3$), 121.2 (s, C_5Me_5), 20.7 (s, 2,4,6- $\text{Me}_3\text{C}_6\text{H}_2$), 18.8 (s, 2,4,6- $\text{Me}_3\text{C}_6\text{H}_2$), 11.3 (s, C_5Me_5). Anal. Calcd for $\text{C}_{19}\text{H}_{26}\text{Cl}_2\text{NTa}$: C, 43.86; H, 5.04; N, 2.69. Found: C, 44.13; H, 5.02; N, 2.76.

TaCp*Me₂[η^2 -Me₂CN($\text{C}_6\text{H}_3\text{Me}_2$)] (5a). Method A. **2a** (0.41 g, 0.74 mmol) was dissolved in 40 mL of toluene, and 0.93 mL of a 1.6 M solution of LiMe (1.48 mmol) in OEt_2 was added at -78°C . After 30 min, the reaction mixture was warmed to room temperature and stirred for a further 2-h period. The suspension was evaporated to dryness and the orange residue extracted with *n*-hexane (2×20 mL). The solution was filtered, concentrated to ~ 10 mL, and cooled to -40°C to give **5a** as orange crystals. Yield 0.17 g (52%).

Table 5. Experimental Data for the X-ray Diffraction Studies

	1a ^{1/2} C ₆ H ₆	5a
mol formula	C ₂₀ H ₂₈ Cl ₄ NTa ^{1/2} C ₆ H ₆	C ₂₃ H ₃₆ NTa
mol wt	644.26	507.49
cryst system	triclinic	monoclinic
space group	P $\bar{1}$	P ₂ /n
radiatn	Nb-filtered	graphite-monochromated
	(Mo K α , $\bar{\lambda}$ = 0.710 73 Å)	
a, Å	8.381(4)	10.515(6)
b, Å	8.977(4)	14.615(9)
c, Å	18.316(9)	14.594(8)
α , deg	100.17(2)	
β , deg	97.83(2)	100.66(2)
γ , deg	105.04(2)	
V, Å ³	1286(1)	2204(2)
Z	2	4
D _{calcd} , g/cm ³	1.664	1.529
F(000)	634	1016
cryst dimens, mm	0.24 × 0.30 × 0.35	0.22 × 0.27 × 0.38
μ (Mo K α), cm ⁻¹	47.00	49.92
diffractometer	Siemens AED	Phillips PW 1100
2 θ range, deg	6–50	6–60
reflectns measd	$h, \pm k, \pm l$	$\pm h, k, l$
no. of unique total reflectns	4531	6419
no. of unique obsd reflectns	3218 [$I \geq 2\sigma(I)$]	3786 [$I \geq 2\sigma(I)$]
R	0.0432	0.0299
R _w	0.0534	0.0316

Method B. A sample of **3a** (0.17 g, 0.294 mmol) was dissolved in toluene (15 mL), and 0.3 mL of a 3 M solution of MgClMe (0.88 mmol) in THF was added at -78 °C. After 30 min, the reaction mixture was allowed to warm to room temperature and stirred for a further 4-h period. Evolution of methane was observed. The orange suspension was evaporated to dryness and the residue extracted with *n*-hexane (2 × 15 mL). After removal of the solvent, 0.08 g of an orange solid identified as **5a** was obtained. Yield 50%. The data for **5a** follow. IR (Nujol mull, ν cm⁻¹): 1262 (s), 1231 (s), 1105 (m), 1025 (m), 973 (w), 789 (m), 767 (s), 424 (m). ¹H NMR (δ ppm, in C₆D₆): 7.21 (d, 2H, ³J_{H-H} = 7.5 Hz, *m*-H₃C₆Me₂), 7.05 (t, 1H, ³J_{H-H} = 7.5 Hz, *p*-H₃C₆Me₂), 2.31 (s, 6H, 2,6-Me₂C₆H₃), 1.98 (s, 6H, CMe₂), 1.72 (s, 15H, C₅Me₅), -0.17 (s, 6H, Me₂Ta). ¹³C NMR (δ ppm, in C₆D₆): 152.3 (m, *i*-C₆H₃Me₂), 134.4 (qd, ²J_{C-H} = ³J_{C-H} = 5.4 Hz, *o*-C₆H₃Me₂), 128.4 (dm, ¹J_{C-H} = 157 Hz, *m*-C₆H₃Me₂), 123.4 (d, ¹J_{C-H} = 159.4 Hz, *p*-C₆H₃Me₂), 115.5 (m, C₅Me₅), 82.9 (spt, ²J_{C-H} = 7.8 Hz, CMe₂), 52.9 (q, ¹J_{C-H} = 118.9 Hz, Me₂Ta), 27.6 (qq, ¹J_{C-H} = 123.6 Hz, ³J_{C-H} = 4.5 Hz, CMe₂), 18.8 (qd, ¹J_{C-H} = 126.3 Hz, ³J_{C-H} = 5.05 Hz, 2,6-Me₂C₆H₃), 10.6 (q, ¹J_{C-H} = 127.3 Hz, C₅Me₅). Anal. Calcd for C₂₃H₃₆NTa: C, 54.43; H, 7.15; N, 2.76. Found: C, 54.33; H, 7.22; N, 2.80.

X-ray Data Collection, Structure Determination, and Refinement for Compounds 1a^{1/2}C₆H₆ and 5a. Crystals suitable for the X-ray analyses were obtained by recrystallization from benzene solutions. The crystallographic data for both compounds are summarized in Table 5. Data were collected at room temperature (22 °C) on a Siemens AED diffractometer (1a^{1/2}C₆H₆, using the niobium-filtered Mo K α radiation) and on a Phillips PW 1100 (5a, using the graphite-monochromated Mo K α radiation) and the $\theta/2\theta$ scan type. The reflections for both compounds were collected with a variable-scan speed of 3–12° min⁻¹ and a scan width (deg) of 1.20 + 0.346 tan θ . One standard reflection was monitored every 100 measurements; no significant decay was noticed over the time of data collection. The individual profiles have been analyzed following Lehmann and Larsen.²⁶ Intensities were corrected for Lorentz and polarization effects. A correction for absorption was applied (maximum and minimum values for the transmission factors were 1.235 and 1.051 (1a^{1/2}C₆H₆) and

Table 6. Atomic Coordinates ($\times 10^4$) and Isotropic Thermal Parameters ($\text{\AA}^2 \times 10^4$) with ESDs in Parentheses for the Non-Hydrogen Atoms of 1a^{1/2}C₆H₆

atom	<i>x/a</i>	<i>y/b</i>	<i>z/c</i>	<i>U</i>
Ta	2405(1)	3940(1)	2626(1)	365(2) ^a
Cl(1)	723(4)	3217(4)	1366(2)	570(11) ^a
Cl(2)	4169(4)	2511(4)	2059(2)	621(13) ^a
Cl(3)	1335(4)	6159(4)	2858(2)	652(13) ^a
Cl(4)	4887(4)	5341(4)	3555(2)	687(13) ^a
N	4149(10)	5419(11)	1362(5)	448(34) ^a
C(1)	117(15)	3158(14)	3365(7)	565(49) ^a
C(2)	-271(12)	1928(13)	2704(7)	531(46) ^a
C(3)	1035(13)	1213(13)	2725(7)	500(43) ^a
C(4)	2189(14)	1962(16)	3414(7)	580(49) ^a
C(5)	1663(15)	3168(14)	3797(6)	559(47) ^a
C(6)	-1107(21)	4023(19)	3585(11)	1066(87) ^a
C(7)	-1908(18)	1313(19)	2144(10)	981(77) ^a
C(8)	984(24)	-227(18)	2179(11)	1073(93) ^a
C(9)	3741(20)	1438(21)	3673(10)	1052(90) ^a
C(10)	2286(24)	4147(25)	4563(9)	1249(98) ^a
C(11)	3949(13)	5767(13)	2045(6)	463(43) ^a
C(12)	4833(2)	7490(18)	2402(8)	720(60) ^a
C(13)	5076(13)	6410(12)	910(6)	470(41) ^a
C(14)	6716(13)	6459(13)	919(6)	471(40) ^a
C(15)	7519(17)	7339(16)	462(7)	617(51) ^a
C(16)	6716(18)	8094(15)	17(7)	634(55) ^a
C(17)	5046(21)	7967(14)	11(8)	673(60) ^a
C(18)	4175(15)	7134(13)	464(6)	488(43) ^a
C(19)	7582(16)	5624(19)	1402(9)	684(59) ^a
C(20)	2410(20)	7000(21)	459(9)	762(66) ^a
C(1B)	-32(42)	-932(39)	4468(13)	1186(215)
C(2B)	1467(42)	-1018(39)	4870(13)	1323(139)
C(3B)	2099(42)	-119(39)	5606(13)	1010(102)
C(4B)	1231(42)	865(39)	5939(13)	1273(136)
C(5B)	-268(42)	951(39)	5536(13)	918(178)
C(6B)	-900(42)	52(39)	4801(13)	1264(134)

^a Equivalent isotropic *U* defined as one-third of the trace of the orthogonalized U_{ij} tensor.

Table 7. Atomic Coordinates ($\times 10^4$) and Isotropic Thermal Parameters ($\text{\AA}^2 \times 10^4$) with ESDs in Parentheses for the Non-Hydrogen Atoms of 5a

atom	<i>x/a</i>	<i>y/b</i>	<i>z/c</i>	<i>U</i> ^a
Ta	453(1)	2377(1)	1899(1)	333(1)
N	-560(4)	2297(3)	2872(3)	368(12)
C(1)	455(5)	697(3)	1924(3)	374(14)
C(2)	1752(5)	961(3)	1937(4)	414(16)
C(3)	1824(5)	1371(3)	1063(4)	478(19)
C(4)	583(6)	1375(4)	523(4)	504(20)
C(5)	-276(5)	969(3)	1047(4)	446(18)
C(6)	2(6)	99(3)	2637(4)	592(22)
C(7)	2887(5)	753(4)	2705(4)	707(25)
C(8)	3044(6)	1654(5)	731(5)	792(29)
C(9)	219(8)	1622(5)	-502(4)	971(37)
C(10)	-1693(6)	756(4)	689(5)	829(29)
C(11)	-454(7)	3251(5)	753(5)	692(27)
C(12)	2323(6)	3022(5)	2387(5)	684(26)
C(13)	-376(6)	3291(4)	2841(4)	582(23)
C(14)	-1217(5)	1821(3)	3499(3)	397(16)
C(15)	-2543(5)	1631(4)	3257(4)	526(20)
C(16)	-3151(7)	1140(4)	3861(5)	729(29)
C(17)	-2476(8)	845(4)	4698(6)	874(36)
C(18)	-1200(8)	1027(4)	4944(4)	734(29)
C(19)	-526(6)	1525(3)	4364(4)	503(19)
C(20)	-3346(6)	1905(6)	2312(5)	920(33)
C(21)	904(6)	1668(4)	4684(4)	723(26)
C(22)	414(8)	3725(4)	3723(5)	898(33)
C(23)	-1622(7)	3842(4)	2549(5)	945(35)

^a Equivalent isotropic *U* defined as one-third of the trace of the orthogonalized U_{ij} tensor.

1.103 and 0.887 (**5a**).²⁷ Only the observed reflections were used in the structure solutions and refinements.

Both structures were solved by Patterson and Fourier methods and refined by full-matrix least-squares fits first with isotropic thermal parameters and then with anisotropic ther-

mal parameters for the non-hydrogen atoms, excepting the carbons of the solvent for $1\mathbf{a}^{1/2}\text{C}_6\text{H}_6$. All hydrogen atoms of $1\mathbf{a}^{1/2}\text{C}_6\text{H}_6$, except those of the methyl groups of the Cp* ring which were placed at their geometrically calculated positions (C-H = 0.96 Å) and refined "riding" on the corresponding carbon atoms (with isotropic thermal parameters) and those of the benzene molecule which were not calculated, were clearly localized in the final ΔF map and refined isotropically. All hydrogen atoms of $5\mathbf{a}$, except those of the methyl groups at C(11) and C(12) which were clearly localized in the final ΔF map and refined isotropically, were placed at their geometrically calculated positions (C-H = 0.96 Å) and refined "riding" on the corresponding carbon atoms (with isotropic thermal parameters). The final cycles of refinement were carried out on the basis of 291 ($1\mathbf{a}^{1/2}\text{C}_6\text{H}_6$) and 249 ($5\mathbf{a}$) variables; after the last cycles, no parameters shifted by more than 0.88 ($1\mathbf{a}^{1/2}\text{C}_6\text{H}_6$) and 0.92 ($5\mathbf{a}$) ESD. The highest remaining peak in the final difference map was equivalent to 1.09 ($1\mathbf{a}^{1/2}\text{C}_6\text{H}_6$) and 0.75 ($5\mathbf{a}$) $e/\text{Å}^3$. In the final cycles of refinement a weighting scheme $w = K[\sigma^2(F_o) + gF_o^2]^{-1}$ was used; at convergence, the K and g values were 0.638 and 0.0035 ($1\mathbf{a}^{1/2}\text{C}_6\text{H}_6$) and 1.137 and 0.0004 ($5\mathbf{a}$), respectively. The analytical scattering factors, corrected for the real and imaginary parts of anomalous dispersion, were taken from ref 28. All calculations were carried out on the GOULD POWER-

NODE 6040 and ENCORE 91 computers of the "Centro di Studio per la Strutturistica Diffattometrica" del CNR, Parma, using the SHELX-76 and SHELXS-86 systems of crystallographic computer programs.²⁹ The final atomic coordinates for the non-hydrogen atoms are given in Table 6 ($1\mathbf{a}^{1/2}\text{C}_6\text{H}_6$) and Table 7 ($5\mathbf{a}$). The atomic coordinates of the hydrogen atoms are given in Tables SI ($1\mathbf{a}^{1/2}\text{C}_6\text{H}_6$) and SII ($5\mathbf{a}$), the thermal parameters in Tables SIII ($1\mathbf{a}^{1/2}\text{C}_6\text{H}_6$) and SIV ($5\mathbf{a}$) of the supplementary material.

Acknowledgment. We are grateful to DGICYT (Project PB-92-0178-C) and Consiglio Nazionale delle Ricerche, Rome, for financial supports.

Supplementary Material Available: Tables of hydrogen atom coordinates (Tables SI, SII), thermal parameters (Tables SIII, SIV), and complete bond distances and angles (Tables SV, SVI), variable-temperature ^1H NMR spectra of complexes 2 and 5 , and Eyring plots of the kinetics of isomerization of $2\mathbf{a}$ and $5\mathbf{a}$ (27 pages). Ordering information is given on any current masthead page.

OM940497J

(28) *International Tables for X-Ray Crystallography*; Kynoch Press: Birmingham, England, 1974; Vol. IV.

(29) Sheldrick, G. M. SHELX-76 Program for crystal structure determination, University of Cambridge, England, 1976; SHELXS-86 Program for the solution of crystal structures, University of Göttingen, 1986.

(27) Walker, N.; Stuart, D. *Acta Crystallogr., Sect A* **1983**, *39*, 158. Ugozzoli, F. *Comput. Chem.* **1987**, *11*, 109.

Hybrid Diborolyl/Tricarbadeboranyl Triple-Deckers: (η^5 -Cyclopentadienyl)cobalt-(μ - η^5 -1,3-Diborolyl)metal-(η^6 - and η^4 -Tricarbadeboranyl) Complexes (M = Fe, Co, Ni). Triple-Decker Complexes with Open Cage Distortions

Wolfgang Weinmann, Andreas Wolf, Hans Pritzkow, and Walter Siebert*

Anorganisch-Chemisches Institut der Universität, Im Neuenheimer Feld 270,
69120 Heidelberg, Germany

Beverly A. Barnum, Patrick J. Carroll, and Larry G. Sneddon*

Department of Chemistry, University of Pennsylvania, Philadelphia, Pennsylvania 19104-6323

Received November 14, 1994[®]

The reaction of a mixture of the $[(\eta^5\text{-C}_5\text{H}_5)\text{Co}(\eta^5\text{-MeEt}_4\text{C}_3\text{B}_2)]^{1-}$ and *nido*-6-Me-5,6,9-C₃B₇H₉¹⁻ anions with MX₂ (M = Fe (**1**), Co (**2**), Ni, (**3**)) yields the new hybrid diborolyl/tricarbadeboranyl triple-decker complexes $(\eta^5\text{-C}_5\text{H}_5)\text{Co}(\mu\text{-}\eta^5\text{-MeEt}_4\text{C}_3\text{B}_2)\text{M}(\text{MeC}_3\text{B}_7\text{H}_9)$, containing 30 (M = Fe), 31 (M = Co), and 30 (M = Ni) valence electrons, respectively. An X-ray structural study of **1** confirmed that the FeC₃B₇ fragment has a *closo* geometry, consistent both with its 24-skeletal-electron count and with the cage structure previously confirmed for *closo*-1-($\eta^5\text{-C}_5\text{H}_5$)Fe-(5-Me-2,3,5-C₃B₇H₉). Structural studies of **2** and **3** confirmed that their MC₃B₇ fragments have open cage distortions consistent with higher skeletal-electron counts. These complexes are the first triple-decker complexes in which the terminal cage ligands have open cage structures. As predicted on the basis of its 25-skeletal-electron count, in **2** the observed CoC₃B₇ cage structure is intermediate between those expected for 11-vertex *closo* (24-electron) and *nido* (26-electron) frameworks. This open cage structure is likewise consistent with that found for 1-($\eta^5\text{-C}_5\text{H}_5$)Co-(2-Me-2,3,5-C₃B₇H₉) (**4**). In complexes **1** and **2**, the MeC₃B₇H₉ ligand is functioning as a cyclopentadienyl analog, but electrochemical studies show that the tricarbadeboranyl ligand is much more electron-withdrawing than the cyclopentadienyl ligand and can thus stabilize the formation of anionic species. If, as in **1** and **2**, the MeC₃B₇H₉ cage in **3** is functioning as a 5-electron ligand, then **3** should be a paramagnetic 32-valence-electron system. However, **3** is diamagnetic and the structural and spectroscopic data suggest 30 valence electrons, with the MeC₃B₇H₉ ligand functioning as only an η^4 , 3-electron ligand similar to an η^3 π -allyl. This conclusion is also supported by structural studies of 1-($\eta^3\text{-C}_3\text{H}_5$)Ni-(η^6 -2-Me-2,3,5-C₃B₇H₉) (**5a**), 1-(η^3 -2-MeC₃H₄)Ni-(η^6 -2-Me-2,3,5-C₃B₇H₉) (**5b**), and 9-($\eta^5\text{-C}_5\text{H}_5$)Ni-(η^4 -8-Me-7,8,10-C₃B₇H₉) (**6**), which show that, in **5a** and **5b**, the NiC₃B₇H₉ cages have *closo*-type structures (i.e. 24-skeletal-electrons) consistent with 5-electron donation to the nickel atom, whereas in **3** and **6** the NiC₃B₇H₉ cages have *nido*-type structures (i.e. 26-skeletal-electrons), suggesting only 3 electrons are donated to the nickel atom.

Introduction

The designed synthesis of a wide range of hybrid complexes containing either the dicarba C₂B₄ or C₂B₉ carboranes and the C₃B₂ diborole ring, including double-, triple-, and quadruple-decker compounds, has been accomplished.^{1–6} Owing to the limited number of tricarbaborane clusters, there are, however, far fewer

examples of complexes containing both tricarbaborane and diborole ligands. The first examples of such diborole/tricarbaborane complexes were based on the *nido*-R₆C₃B₃¹⁻ tricarbahaexaboranyl ligand and include, as shown in Figure 1, (η^5 -2,3,5-tricarbahaexaboranyl)nickel-(η^5 -1,3-diborolyl) (**A**), the bis[(η^5 -2,3,5-tricarbahaexaboranyl)nickel]-(μ - η^5 -1,3-diborolyl) triple-decker complex **B**, and the (η^5 -2,3,5-tricarbahaexaboranyl)nickel-(μ - η^5 -1,3-diborolyl)nickel-(η^5 -cyclopentadienyl) triple-decker complex **C**, as well as a series of oligodecker complexes $[(2,3,4\text{-R}_6\text{C}_3\text{B}_3)\text{Ni}]_2(\text{R}_5\text{C}_3\text{B}_2)_n\text{Ni}_{n-1}$ ($n = 2\text{--}8$).^{7,8}

Recently, an efficient synthetic route for the preparation of the *nido*-tricarbadeboranyl anion *nido*-6-Me-

[®] Abstract published in *Advance ACS Abstracts*, March 15, 1995.

(1) Attwood, M. D.; Fonda, K. K.; Grimes, R. N.; Brodt, G.; Hu, D.; Zenneck, U.; Siebert, W. *Organometallics* **1989**, *8*, 1300–1303.

(2) (a) Fessenbecker, A.; Attwood, M. D.; Bryan, R. F.; Grimes, R. N.; Woode, M. K.; Stephan, M.; Zenneck, U.; Siebert, W. *Inorg. Chem.* **1990**, *29*, 5157–5163. (b) Fessenbecker, A.; Attwood, M. D.; Grimes, R. N.; Stephan, M.; Pritzkow, H.; Zenneck, U.; Siebert, W. *Inorg. Chem.* **1990**, *29*, 5164–5168.

(3) Siebert, W.; Hetttrich, R.; Pritzkow, H. *Angew. Chem.* **1994**, *106*, 215–216; *Angew. Chem., Int. Ed. Engl.* **1994**, *33*, 203–204.

(4) Edwin, J.; Bochmann, M.; Böhm, M. C.; Brennan, D. E.; Geiger, W. E.; Krüger, C.; Pebler, J.; Pritzkow, H.; Siebert, W.; Swiridoff, W.; Wadepohl, H.; Weiss, J.; Zenneck, U. *J. Am. Chem. Soc.* **1983**, *105*, 2582–2598.

(5) Forward, J. M.; Mingos, D. M. P.; Siebert, W.; Hauss, J.; Powell, H. R. *J. Chem. Soc., Dalton Trans.* **1993**, 1783–1788.

(6) (a) Siebert, W. *Adv. Organomet. Chem.* **1993**, *35*, 187–210. (b) Siebert, W. In *Transition Metal Chemistry*; Müller, A.; Diemann, E., Eds.; Verlag Chemie: Weinheim, Germany, 1981; p 157. (c) Siebert, W. *Angew. Chem.* **1985**, *97*, 924–939; *Angew. Chem., Int. Ed. Engl.* **1985**, *24*, 943–958.

(7) (a) Siebert, W.; Bochmann, M. *Angew. Chem.* **1977**, *89*, 483–484; *Angew. Chem., Int. Ed. Engl.* **1977**, *16*, 468. (b) Kuhlmann, T. Ph.D. Dissertation, Universität Heidelberg, 1985.

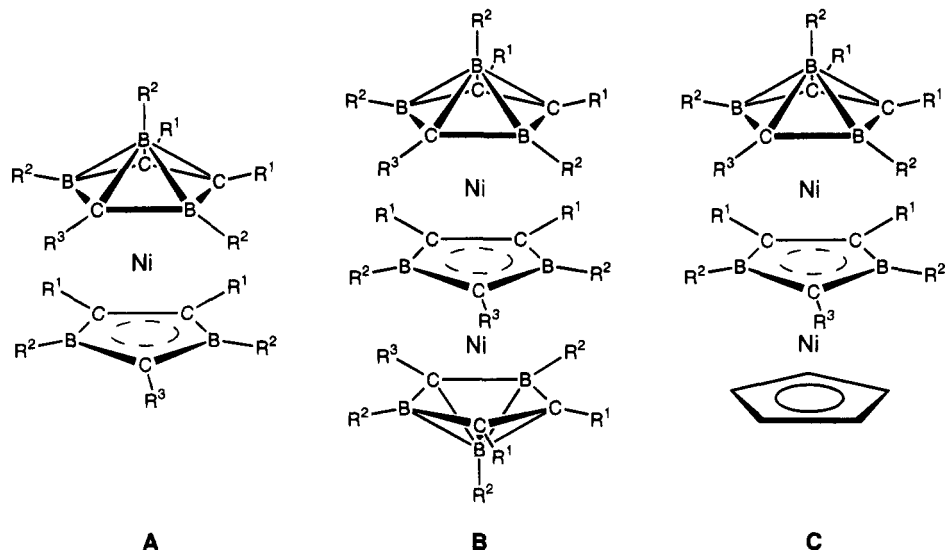


Figure 1. $(\eta^5\text{-}2,3,5\text{-tricarbahehexaboranyl})\text{nickel}-(\eta^5\text{-}1,3\text{-diboroly})$ (A), bis $[(\eta^5\text{-}2,3,5\text{-tricarbahehexaboranyl})\text{nickel}]-(\mu\text{-}\eta^5\text{-}1,3\text{-diboroly})$ triple-decker B, and $(\eta^5\text{-}2,3,5\text{-tricarbahehexaboranyl})\text{nickel}-(\mu\text{-}\eta^5\text{-}1,3\text{-diboroly})\text{nickel}-(\eta^5\text{-cyclopentadienyl})$ triple-decker C.

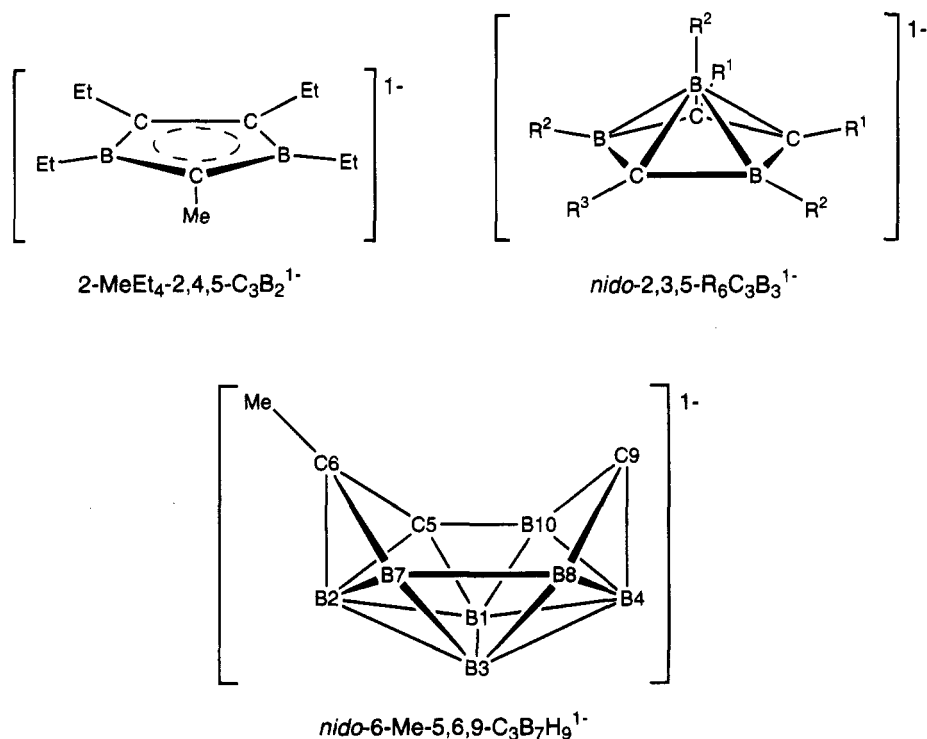


Figure 2. Diboroly ($\text{R}_5\text{C}_3\text{B}_2^-$), tricarbahehexaboranyl ($\text{nido-R}_6\text{C}_3\text{B}_3^-$), and tricarbadeboranyl ($\text{nido-6-Me-5,6,9-C}_3\text{B}_7\text{H}_9^-$) anions.

$5,6,9\text{-C}_3\text{B}_7\text{H}_9^{1-}$ was developed that is now allowing systematic explorations of the metal coordination properties of intermediate-sized tricarbaboranes.⁹ As shown in Figure 2, the diboroly ($\text{R}_5\text{C}_3\text{B}_2^{1-}$), the tricarbahehexaboranyl ($\text{nido-R}_6\text{C}_3\text{B}_3^{1-}$), and the tricarbadeboranyl ($\text{nido-6-Me-5,6,9-C}_3\text{B}_7\text{H}_9^{1-}$) ligands might be expected to show related metal coordination properties,

but due to the differences in the size (six- versus five-membered) and structure (puckered versus planar) of its open face, the $\text{nido-6-Me-5,6,9-C}_3\text{B}_7\text{H}_9^{1-}$ anion should exhibit more complex structures.

This work describes our joint efforts to use the $\text{nido-6-Me-5,6,9-C}_3\text{B}_7\text{H}_9^{1-}$ and the $(\eta^5\text{-C}_5\text{H}_5)\text{Co}(\eta^5\text{-MeEt}_4\text{-C}_3\text{B}_2)^{1-}$ anions for the construction of mixed-ligand triple-decker complexes.

Results and Discussion

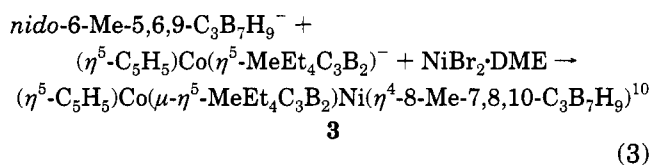
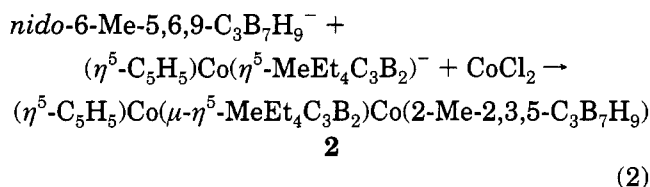
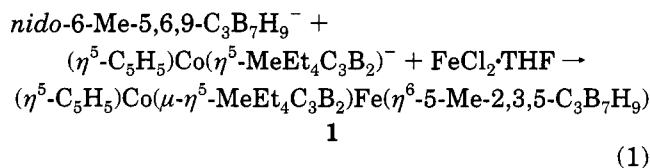
The new triple-decker complexes 1–3 are obtained by the reaction of a mixture of the $(\eta^5\text{-C}_5\text{H}_5)\text{Co}(\eta^5\text{-}$

(8) (a) Kuhlmann, T.; Pritzkow, H.; Zenneck, U.; Siebert, W. *Angew. Chem.* **1984**, *96*, 994–995; *Angew. Chem., Int. Ed. Engl.* **1984**, *12*, 965–966. (b) Zwecker, J.; Kuhlmann, T.; Pritzkow, H.; Siebert, W.; Zenneck, U. *Organometallics* **1988**, *7*, 2316–2324. (c) Zwecker, J.; Pritzkow, H.; Zenneck, U.; Siebert, W. *Angew. Chem.* **1986**, *98*, 1129–1130; *Angew. Chem., Int. Ed. Engl.* **1986**, *12*, 1099–1100.

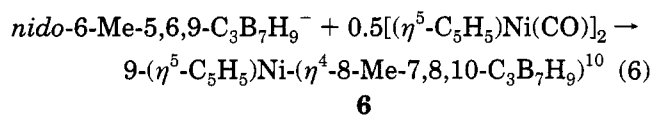
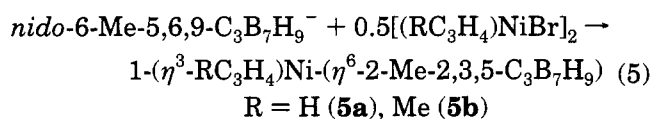
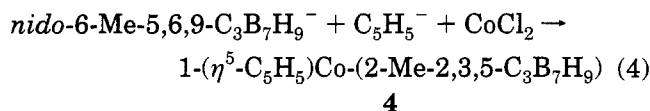
(9) (a) Plumb, C. A.; Carroll, P. J.; Sneddon, L. G. *Organometallics* **1992**, *11*, 1665–1671. (b) Plumb, C. A.; Carroll, P. J.; Sneddon, L. G. *Organometallics* **1992**, *11*, 1672–1680. (c) Plumb, C. A.; Sneddon, L. G. *Organometallics* **1992**, *11*, 1681–1685. (d) Barnum, B. A.; Carroll, P. J.; Sneddon, L. G. Manuscript in preparation.

(10) For 1, 2, 4, 5a, and 5b, the cage numbering is based on a closo cage geometry. For 3 and 6, the cage numbering is based on a nido cage geometry.¹¹

$\text{MeEt}_4\text{C}_3\text{B}_2)^{1-}$ and $nido\text{-}6\text{-Me-}5,6,9\text{-C}_3\text{B}_7\text{H}_9^{1-}$ anions with the corresponding metal halides.



After removal of solvent, the crude reaction products were chromatographed on Al_2O_3 and the compounds were recrystallized from pentane/dichloromethane. Complexes **1** (brown) and **3** (brown) are diamagnetic, while **2** (dark green) is paramagnetic. For structural comparisons, the complexes **4**, **5a,b**, and **6** were also synthesized in a straightforward manner by the reactions given in eqs 4–6.



4, **5a,b**, and **6** were each isolated as air-stable crystalline compounds. Elemental analyses or/and exact mass determinations on all compounds are consistent with their proposed compositions, and in each case, their structures were established by single-crystal X-ray studies.

$(\eta^5\text{-C}_5\text{H}_5)\text{Co}(\mu\text{-}\eta^5\text{-MeEt}_4\text{C}_3\text{B}_2)\text{Fe}(\eta^6\text{-}5\text{-Me-}2,3,5\text{-C}_3\text{B}_7\text{H}_9)$ (**1**). The X-ray determination of **1** established the triple-decker structure shown in Figure 3, containing a cobalt-iron bridging diborolyl deck and terminal cyclopentadienyl and tricarbaboranyl ligands. The $\eta^5\text{-C}_5\text{H}_5$ ring is almost coplanar with the 1,3-diborolyl ligand, and the bond distances and angles in the $(\eta^5\text{-C}_5\text{H}_5)\text{Co}(\eta^5\text{-MeEt}_4\text{C}_3\text{B}_2)$ fragment of the complex appear to be normal and to be in the ranges observed for other triple-decker complexes containing this unit.^{1,2a,4,5} Ac-

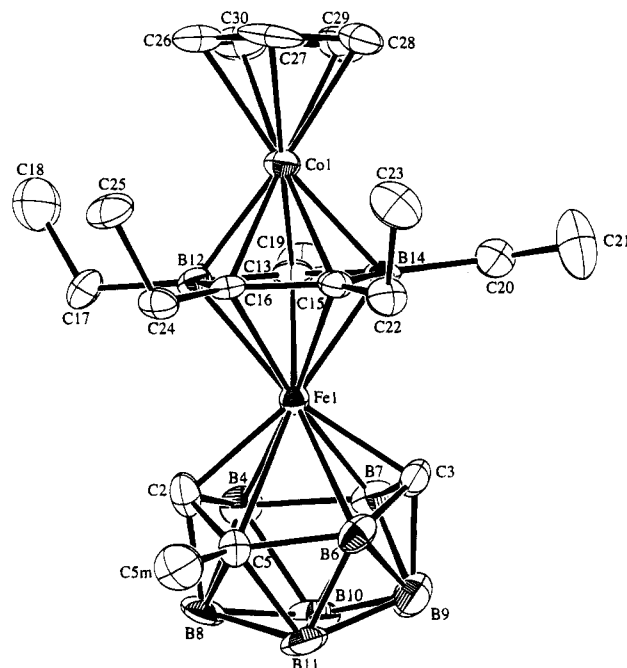


Figure 3. ORTEP drawing of $(\eta^5\text{-C}_5\text{H}_5)\text{Co}(\mu\text{-}\eta^5\text{-MeEt}_4\text{C}_3\text{B}_2)\text{Fe}(\eta^6\text{-}5\text{-Me-}2,3,5\text{-C}_3\text{B}_7\text{H}_9)$ (**1**).

Table 1. Selected Intramolecular Bond Distances (Å)

	Iron and Cobalt Complexes			
	1	<i>closo</i> -1-CpFe-(5-MeC ₃ B ₇ H ₉) ^{9a}	2	4
M–C2	1.979(9)	1.935(5)	2.047(6)	1.978(4)
M–C3	1.962(8)	1.944(4)	1.960(6)	1.922(5)
M–B4	2.190(11)	2.204(5)	2.201(7)	2.243(6)
M–B7	2.221(11)	2.236(5)	2.201(7)	2.258(5)
M–C5	2.408(9)	2.282(4)	2.673(8)	2.549(6)
M–B6	2.342(11)	2.274(5)	2.586(9)	2.456(7)
Nickel Complexes				
	3	5a	5b	6
Ni–C2(C8) ^a	2.075(2)	1.997(3)	1.998(2)	2.019(5)
Ni–C3(C10) ^a	2.003(2)	1.945(3)	1.963(3)	1.991(6)
Ni–B4(B4) ^a	2.133(3)	2.188(3)	2.153(3)	2.093(6)
Ni–B7(B5) ^a	2.142(3)	2.248(3)	2.226(3)	2.108(7)
Ni–C5(C7) ^a	2.875(3)	2.515(3)	2.588(2)	2.880(5)
Ni–B6(B11) ^a	2.844(3)	2.397(3)	2.500(3)	2.871(7)

^a Nido geometry numbering of corresponding atoms for **3** and **6** given in parentheses.

ording to skeletal-electron-counting rules^{11a,b} and cluster structural patterns,^{11c–f} the FeC_3B_7 cluster fragment in **1** would have 24-skeletal-electrons and thus should adopt a *closo* cage geometry based on an octadecahedron. As shown in Figure 3, the observed cluster framework is consistent with this prediction and is quite similar to that found in *closo*-1-($\eta^5\text{-C}_5\text{H}_5$)Fe-(5- CH_3 -2,3,5- $\text{C}_3\text{B}_7\text{H}_9$)^{9a} (Table 1). The iron atom occupies a six-coordinate position in the tricarbaborane cage with the strongest bonding interactions at the C2 and C3 carbons. The Fe–C2 and Fe–C3 distances are similar to those between the iron and carbon atoms of the diborolyl ring, but due to the puckered ring structure of the C_3B_7 cage the Fe–B4, –B6, –B7, and –C5 distances are

(11) (a) Wade, K. *Adv. Inorg. Chem. Radiochem.* **1976**, *18*, 1–66. (b) Rudolph, R. W. *Acc. Chem. Res.* **1976**, *9*, 446–452. (c) Williams, R. E. *Adv. Inorg. Chem. Radiochem.* **1976**, *18*, 67–142. (d) Williams, R. E. *Inorg. Chem.* **1971**, *10*, 210–214. (e) Williams, R. E. In *Electron Deficient Boron and Carbon Clusters*; Olah, G. A., Wade, K., Williams, R. E., Eds.; Wiley: New York, 1991; pp 11–93. (f) Williams, R. E. *Chem. Rev.* **1992**, *92*, 177–207.

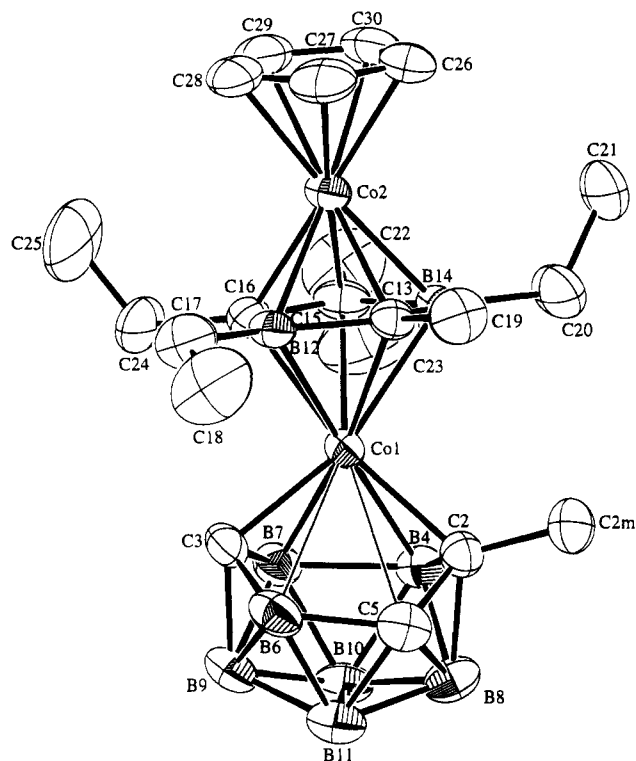


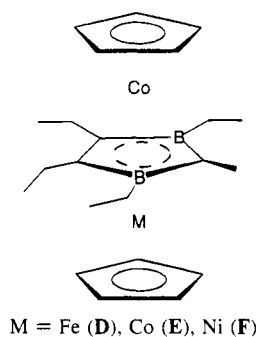
Figure 4. ORTEP drawing of $(\eta^5\text{-C}_5\text{H}_5)\text{Co}(\mu\text{-}\eta^5\text{-MeEt}_4\text{C}_3\text{B}_2)\text{Co}(2\text{-Me-2,3,5-C}_3\text{B}_7\text{H}_9)$ (**2**).

much longer. As found previously for *closo*-1- $(\eta^5\text{-C}_5\text{H}_5)\text{-Fe}(5\text{-CH}_3\text{-2,3,5-C}_3\text{B}_7\text{H}_9)$, the iron atom is somewhat closer to the B4–B7 edge than to the C5–B6 edge of the face.

It should also be noted that on basis of the the position of the methyl group in the starting *nido*-6-Me-5,6,9- $\text{C}_3\text{B}_7\text{H}_9^{1-}$ anion, methyl substitution at the C2 carbon in **1** would be expected. Instead, the methyl group is observed at the C5 position. This result is similar to the previously observed structural rearrangement that converts *closo*-1- $(\eta^5\text{-C}_5\text{H}_5)\text{Fe}(2\text{-CH}_3\text{-2,3,5-C}_3\text{B}_7\text{H}_9)$ to *closo*-1- $(\eta^5\text{-C}_5\text{H}_5)\text{Fe}(5\text{-CH}_3\text{-2,3,5-C}_3\text{B}_7\text{H}_9)$ and again illustrates the ease of structural rearrangements in 11-vertex clusters.¹² The possible mechanisms by which these rearrangements may occur have been discussed.^{9c}

$(\eta^5\text{-C}_5\text{H}_5)\text{Co}(\mu\text{-}\eta^5\text{-MeEt}_4\text{C}_3\text{B}_2)\text{Co}(2\text{-Me-2,3,5-C}_3\text{B}_7\text{H}_9)$, (**2**). The green 31-VE "CoCo" complex is paramagnetic. Electrochemical studies (Table 2) show that the electron-withdrawing tricarbaborane ligand shifts the redox potentials to significantly more positive values compared to the values of the related triple-decker complexes $(\eta^5\text{-C}_5\text{H}_5)\text{Co}(\mu\text{-}\eta^5\text{-MeEt}_4\text{C}_3\text{B}_2)\text{Fe}(\eta^5\text{-C}_5\text{H}_5)$ (**D**), $(\eta^5\text{-C}_5\text{H}_5)\text{Co}(\mu\text{-}\eta^5\text{-MeEt}_4\text{C}_3\text{B}_2)\text{Co}(\eta^5\text{-C}_5\text{H}_5)$ (**E**), and $(\eta^5\text{-C}_5\text{H}_5)\text{Co}(\mu\text{-}\eta^5\text{-MeEt}_4\text{C}_3\text{B}_2)\text{Ni}(\eta^5\text{-C}_5\text{H}_5)$ (**F**).⁴ This is consistent with the observed air stability of **1**–**3**. Other 19-VE monocobalt complexes containing the $\text{MeC}_3\text{B}_7\text{H}_9$ ligand, such as *commo*- $\text{Co}-(1\text{-Co-2-Me-2,3,5-C}_3\text{B}_7\text{H}_9)_2$ ^{9b} and $1\text{-}(\eta^5\text{-C}_5\text{H}_5)\text{Co}-(2\text{-Me-2,3,5-C}_3\text{B}_7\text{H}_9)$, (**4**; *vide infra*), show similar oxidative stabilities versus their cyclopentadienyl analogs. An electrochemical comparison of the sandwich complexes **4**, **6**, and $(\eta^5\text{-C}_5\text{H}_5)\text{Fe}(2\text{-Me-2,3,5-C}_3\text{B}_7\text{H}_9)$ ^{9a} (**G**) with the triple-decker

Table 2. Redox Potentials (V)



	"Fe"			"Co"			"Ni"		
	D	1	G ^{9a}	E	2	4	F	3	6
2+/+		+1.66 ^a		+1.74 ^a			+1.08		
+0	-0.06	+0.61	+0.79	-0.57	+0.66	+0.52	+0.06	+0.96	+1.23
0/-	-1.77	-0.84		-0.53	-0.59	-0.57	-1.63	-0.49	-0.67 ^a
-2-		-2.03		-2.56 ^a	-1.98			-2.19	

^a Irreversible.

complexes **1**–**3** reveals that the 1,3-diborolyl–cobalt unit has only a slight influence on the first redox potentials but enables an additional reversible redox state.

In principle, the additional electron in **2** could occupy either a metal- or cage-localized orbital. Previous studies of 31-VE triple-deckers have concluded that metal-centered orbitals were favored^{5,13} and, as a result, no cage distortions that would result from a higher cage skeletal electron count are observed. Thus, for example, the MC_2B_9 cage fragments in both the 30-VE $(\eta^5\text{-C}_5\text{H}_5)\text{-Co}(\mu\text{-}\eta^5\text{-MeEt}_4\text{C}_3\text{B}_2)\text{Co}(\text{C}_2\text{B}_9\text{H}_{11})$ and 31-VE $(\eta^5\text{-C}_5\text{H}_5)\text{-Co}(\mu\text{-}\eta^5\text{-MeEt}_4\text{C}_3\text{B}_2)\text{Ni}(\text{C}_2\text{B}_9\text{H}_{11})$ clusters show *closo*-icosahedral structures.⁵ On the other hand, the structural (Table 2) and spectroscopic evidence for **2** and **3** suggests that the additional electrons occupy cage-localized orbitals leading to cage opening, as normally expected in metallocarborane complexes.¹⁴ Thus, in **2**, a CoC_3B_7 distorted cage structure (Figure 4), consistent with a 25-skeletal-electron count, is observed that is intermediate between those expected for 11-vertex *closo* (24-electron) and *nido* (26-electron) frameworks. Structural studies of *commo*- $\text{Co}-(1\text{-Co-2-Me-2,3,5-C}_3\text{B}_7\text{H}_9)_2$ ^{9b} and the new complex $1\text{-}(\eta^5\text{-C}_5\text{H}_5)\text{Co}-(2\text{-Me-2,3,5-C}_3\text{B}_7\text{H}_9)$ (**4**; Figure 6) have shown similar types of cage structures. Again, as in **1**, the strongest cage interactions of Co1 in both **2** and **4** are with the C2 and C3 carbons, but the Co1–C5 and Co1–B6 distances are significantly longer than the Co1–B4 and Co1–B7 distances, leading to a puckered Co1–C2–C5–B6–C3 open face.

$(\eta^5\text{-C}_5\text{H}_5)\text{Co}(\mu\text{-}\eta^5\text{-MeEt}_4\text{C}_3\text{B}_2)\text{Ni}(\eta^4\text{-8-Me-7,8,10-C}_3\text{B}_7\text{H}_9)$ (**3**). If, as in **1** and **2**, the $\text{MeC}_3\text{B}_7\text{H}_9$ cage in **3** is functioning as a 5-electron ligand, then **3** should be a paramagnetic 32-valence-electron system. However, **3** is diamagnetic and the spectroscopic and structural data (Figure 5, Table 1) suggest 30 valence electrons, with the $\text{MeC}_3\text{B}_7\text{H}_9$ cage functioning as only a η^4 3-electron ligand similar to a η^3 π -allyl. This conclusion is also supported by structural studies of $1\text{-}(\eta^3\text{-C}_3\text{H}_5)\text{-}$

(12) (a) Williams, R. E. *Prog. Boron Chem.* **1970**, *2*, 37–118. (b) Williams, R. E. In *Electron Deficient Boron and Carbon Clusters*; Olah, G. A., Wade, K., Williams, R. E., Eds.; Wiley: New York, 1991; pp 67–68. (c) Dustin, D. F.; Evans, W. J.; Jones, C. J.; Wiersma, R. J.; Gong, H.; Chan, S.; Hawthorne, M. F. *J. Am. Chem. Soc.* **1974**, *96*, 3085–3090.

(13) (a) Lauher, J. W.; Elian, M.; Summerville, R. H.; Hoffmann, R. *J. Am. Chem. Soc.* **1976**, *98*, 3219–3224. (b) Werner, H. *Angew. Chem.* **1977**, *89*, 1–9; *Angew. Chem., Int. Ed. Engl.* **1977**, *16*, 1–9.

(14) Grimes, R. N. In *Comprehensive Organometallic Chemistry*; Wilkinson, G., Stone, F. G. A., Abel, E., Eds.; Pergamon Press: Oxford, England, 1982; Chapter 5.5, pp 459–542.

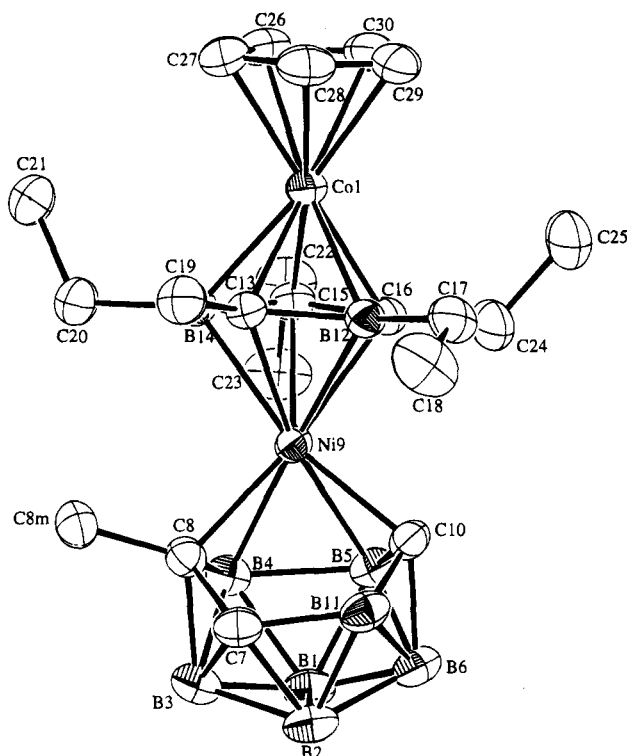


Figure 5. ORTEP drawing of $(\eta^5\text{-C}_5\text{H}_5)\text{Co}(\mu\text{-}\eta^5\text{-MeEt}_4\text{C}_3\text{B}_2\text{)-Ni}(\eta^4\text{-8-Me-7,8,10-C}_3\text{B}_7\text{H}_9)$ (**3**).

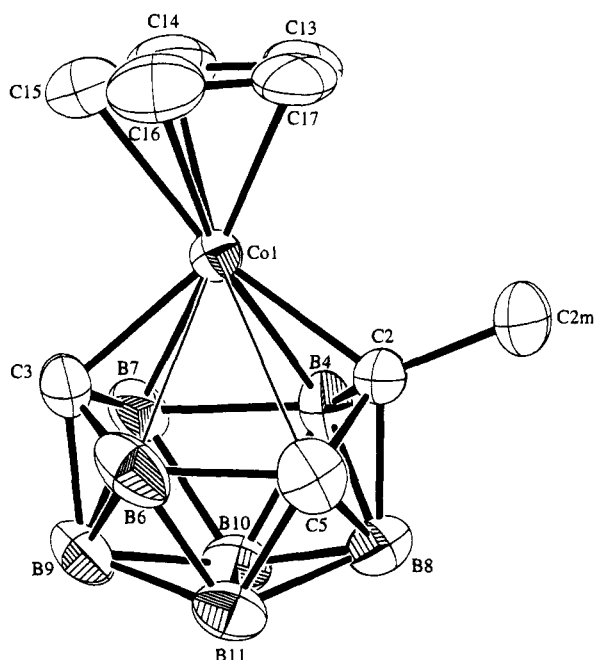
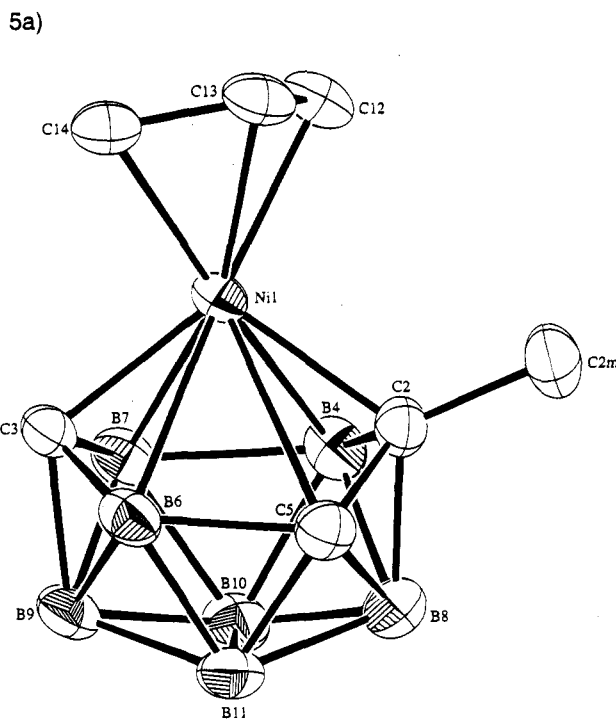


Figure 6. ORTEP drawing of $1\text{-}(\eta^5\text{-C}_5\text{H}_5)\text{Co}\text{-}(2\text{-Me-2,3,5-C}_3\text{B}_7\text{H}_9)$ (**4**).

$\text{Ni}(\eta^6\text{-2-Me-2,3,5-C}_3\text{B}_7\text{H}_9)$ (**5a**), $1\text{-}(\eta^3\text{-2-MeC}_3\text{H}_4)\text{Ni}\text{-}(\eta^6\text{-2-Me-2,3,5-C}_3\text{B}_7\text{H}_9)$ (**5b**) (Figure 7) and $9\text{-}(\eta^5\text{-C}_5\text{H}_5)\text{Ni}\text{-}(\eta^4\text{-8-Me-7,8,10-C}_3\text{B}_7\text{H}_9)$ (**6**) (Figure 8), which show that, in **5a** and **5b**, the $\text{NiC}_3\text{B}_7\text{H}_9$ cages have closo-type structures (i.e. 24-skeletal-electrons) consistent with 5-electron donation to the nickel atom, whereas in **3** and **6** the $\text{NiC}_3\text{B}_7\text{H}_9$ cages have nido-type structures (i.e. 26-skeletal-electrons), suggesting that only 3 electrons are donated to the nickel. Thus, as can be seen in Table 1, in **5a** and **5b** the nickel atom occupies a six-coordinate cage position which (as observed in **1** and *closo*- $1\text{-}(\eta^5\text{-C}_5\text{H}_5)\text{Fe}\text{-}(5\text{-Me-2,3,5-C}_3\text{B}_7\text{H}_9)$) is only slightly shifted away from the B6–C5 edge toward the B4–B7 edge.



5a)

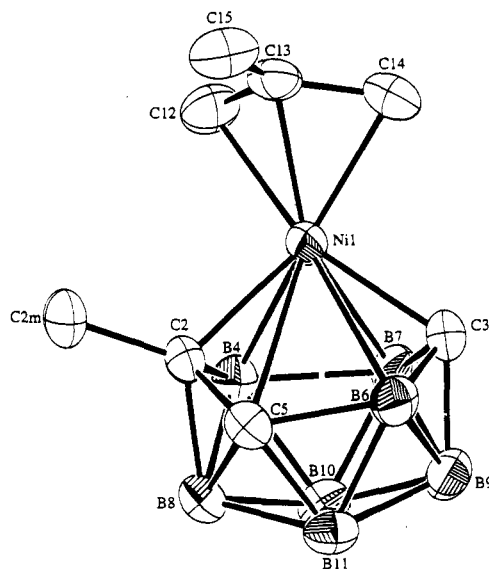


Figure 7. ORTEP drawings of $1\text{-}(\eta^3\text{-C}_3\text{H}_5)\text{Ni}\text{-}(\eta^6\text{-2-Me-2,3,5-C}_3\text{B}_7\text{H}_9)$ (**5a**) and $1\text{-}(\eta^3\text{-2-MeC}_3\text{H}_4)\text{Ni}\text{-}(\eta^6\text{-2-Me-2,3,5-C}_3\text{B}_7\text{H}_9)$ (**5b**).

On the other hand, in **3** and **6**, the nickel atom is clearly in only a four-coordinate cage position, showing normal bond distances in the range of $\sim 1.99\text{--}2.14$ Å to C8, C10, B4, and B5 but greatly increased distances to C7 (**3**, 2.875(3) Å; **6**, 2.880(5) Å) and B11 (**3**, 2.844(3) Å; **6**, 2.871(7) Å). This has the effect of forming an open five-membered ring composed of the Ni–C8–C7–B11–C10 atoms in both **3** and **6**. Such a geometry is based on an icosahedron missing one vertex and is typical of those exhibited by 11-vertex, 26-skeletal-electron complexes.^{14,15} Therefore, **3** is a diamagnetic 30-VE complex and the isolobal *nido*- $9\text{-}(\eta^5\text{-C}_5\text{H}_5)\text{Ni}\text{-}(\eta^4\text{-8-Me-7,8,10-C}_3\text{B}_7\text{H}_9)$ (**6**) is an 18-VE sandwich complex.

(15) Onak, T. In *Comprehensive Organometallic Chemistry*; Wilkinson, G., Stone, F. G. A., Abel, E., Eds.; Pergamon Press: Oxford, England, 1982; Chapter 5.4, pp 411–458.

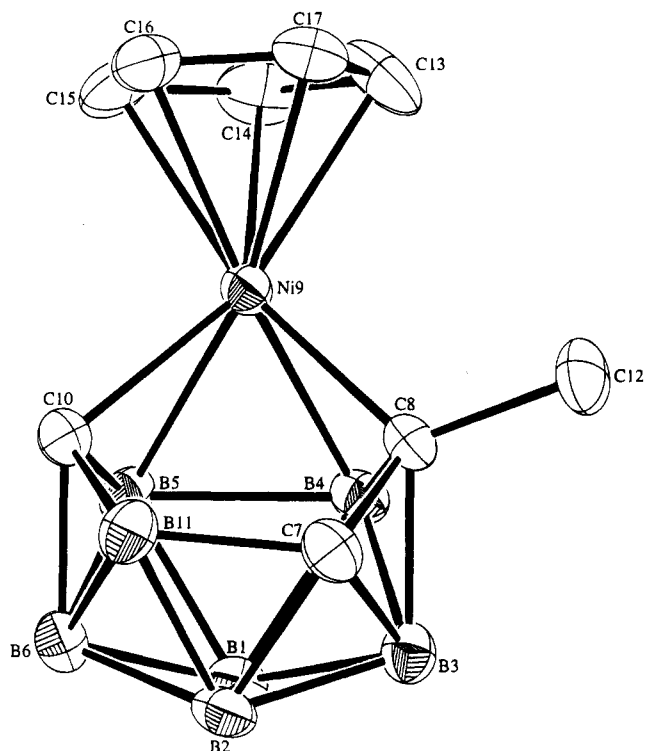


Figure 8. ORTEP drawing of 9-(η^5 -C₅H₅)Ni-(η^4 -8-Me-7,8,10-C₃B₇H₉) (**6**).

The geometric and electronic structures observed for **3** and **6** contrast sharply with those found for the related diborolyl/tricarbahexaboranyl nickel complexes **A–C** (Figure 1) and with the bis(tricarbahexaboranyl) complex (η^5 -R₆C₃B₃)₂Ni.^{6c} In these complexes, the tricarbhexaboranyl ligand is clearly functioning as a 5-electron donor to the nickel atoms resulting in 18-VE (**A**) and 20-VE ((η^5 -R₆C₃B₃)₂Ni) complexes and 33-VE triple-deckers (**B** and **C**). In spite of their higher electron counts, the NiC₃B₃ cages in **B**, **C**, and (η^5 -R₆C₃B₃)₂Ni show normal pentagonal-bipyramidal *closo* geometries similar to that of **A**. Apparently, in these complexes the η^5 -C₃B₃ (5-electron) bonding mode is strongly favored with additional electrons localizing at the metal, whereas in complexes containing the MeC₃B₇H₉ ligand, cage distortions leading to open cage geometries and an η^6 to η^4 metal coordination are favored.

The above results indicate that the *nido*-6-Me-5,6,9-C₃B₇H₉¹⁻ ligand can donate a different number of electrons to the metal, depending upon its coordination geometry. This variable electron-donating ability suggests that this ligand may be able to undergo reversible $\eta^6 \rightarrow \eta^4$ coordination similar to the $\eta^5 \rightarrow \eta^3$ ring-slippage process proposed for Cp-metal complexes.¹⁶

In summary, the syntheses of double-decker and triple-decker systems with the MeC₃B₇H₉ ligand described herein clearly show the close relationship of the tricarbdecaboranyl and cyclopentadienyl ligands. However, in contrast to the case for C₅H₅, the MeC₃B₇H₉ ligand easily changes its hapticity. As expected, **1** is a diamagnetic 30-VE species with a *closo* cage geometry whereas **3**, which is also a 30 VE triple-decker complex, has a *nido* cage geometry due to an $\eta^6 \rightarrow \eta^4$ cage distortion. The electrochemical and structural studies show that the additional electrons in **2** and **3** seem to be localized in the electron-withdrawing tricarbdecabo-

boranyl ligand. These results are supported by the electronic and structural characteristics of the metal complexes **4**, **5a**, **5b**, and **6**.

Experimental Section

General Procedures. Unless otherwise noted, all reactions and manipulations were performed in dry glassware under a nitrogen atmosphere using standard Schlenk techniques. Solvents were distilled from appropriate drying agents under nitrogen before use. Na⁺(*nido*-6-Me-5,6,9-C₃B₇H₉)⁻,^{9a,17} Li⁺[(η^5 -C₅H₅)Co(η^5 -MeEt₄C₃B₂)]⁻,¹⁸ [(RC(CH₂)₂)NiBr]₂ (R = H, CH₃)^{2,19} and *nido*-9-(η^5 -C₅H₅)Ni-(8-Me-7,8,10-C₃B₇H₉)^{9a} were prepared by previously described methods. FeCl₂·2THF was extracted with THF before use.²⁰ CoCl₂ was dried for 15 h at 120 °C in vacuo and stored under a nitrogen atmosphere until used. NiBr₂·DME was prepared as previously described.^{6a,21}

The NMR spectra were recorded in C₆D₆ solution on Jeol FX-90Q or Bruker 200 instruments. Mass spectrometry analyses were obtained on Varian MAT CH7, Finnigan MAT 8230, or VG-ZAB-E high-resolution spectrometers. Elemental analyses were obtained on a C,H,N,O-Rapid Heraeus or from Robertson Microlit Labs, Inc., NJ.

Cyclic voltammetry was conducted on samples in dimethylformamide using tetra-*n*-butylammonium hexafluorophosphate (Bu₄NPF₆) as the supporting electrolyte. Voltammetric experiments were performed using a Princeton Applied Research Model 173 potentiostat, a Model 179 digital coulometer, and a Model 175 function generator. The data were recorded on a Hewlett-Packard 7001A X-Y plotter. All potentials were referenced to an aqueous saturated calomel electrode (SCE) and checked by using a Keithley digital voltmeter.

Syntheses of Triple-Decker (Cyclopentadienyl)cobalt-(μ - η^5 -1,3-Diborolyl)metal-Tricarbadecaboranyl Complexes: M = Fe (1**), Co (**2**), Ni (**3**). (η^5 -C₅H₅)Co(μ - η^5 -MeEt₄C₃B₂)Fe(η^6 -5-Me-2,3,5-C₃B₇H₉) (**1**). In a 100-mL Schlenk flask under N₂, a stirred mixture of Li⁺[(η^5 -C₅H₅)Co(η^5 -MeEt₄C₃B₂)]⁻ (0.180 g, 0.56 mmol) and Na⁺(6-Me-5,6,9-C₃B₇H₉)⁻ (0.94 g, 0.59 mmol) in THF (20 mL) was maintained at -90 °C, while a THF suspension of FeCl₂·2THF (0.172 g, 0.64 mmol) was added dropwise. The solution was warmed gradually to room temperature, with a color change to dark brown occurring at -40 °C. After 15 h at room temperature, the solvent was vacuum-evaporated. The oily brown residue was chromatographed on alumina with pentane-toluene (2:1) to yield 0.21 g (0.42 mmol, 7.4%) of **1**: mp 109 °C; ¹H NMR (C₆D₆, 200 MHz) δ 7.08 (br, 1H, C3H-carb), 5.95 (br, 1H, C2H-carb), 3.92 (s, 5H, C₅H₅), 3.15–2.90 (m, 2H, CH₂CH₃), 2.63–2.21 (m, 4H, CH₂CH₃), 2.12–2.03 (m, 2H, CH₂CH₃), 1.72–1.50 (m, 6H, CH₂CH₃), 1.28 (s, 3H, CH₃ of C₃B₂), 1.10 (s, 3H, CH₃-carb), 1.08–0.95 (m, 6H, CH₂CH₃); ¹¹B NMR (C₆D₆, 64.2 MHz) δ 18.7 (2B), 1.7 (1B), -4.1 (1B), -6.2 (1B), -8.1 (1B), -21.0 (2B), -33.4 (1B); MS (EI) *m/z* 505 [M⁺], 313 [M⁺ - MeC₃B₇H₉-Fe]; HRMS calcd for ¹²C₂₁¹¹H₄₀¹¹B₉⁵⁹Co⁵⁵Fe 505.2701, found 505.2671.**

(η^5 -C₅H₅)Co(μ - η^5 -MeEt₄C₃B₂)Co(2-Me-2,3,5-C₃B₇H₉) (**2**). In a procedure similar to that used to synthesize **1**, a stirred mixture of Li⁺[(η^5 -C₅H₅)Co(η^5 -MeEt₄C₃B₂)]⁻ (0.116 g, 0.37 mmol) and Na⁺(6-Me-5,6,9-C₃B₇H₉)⁻ (0.067 g, 0.42 mmol) in THF (20 mL) was maintained at -90 °C, while a THF

(17) Kang, S. O.; Furst, G. T.; Sneddon, L. G. *Inorg. Chem.* **1989**, *28*, 2339–2347.

(18) (a) Siebert, W.; Edwin, J.; Pritzkow, H. *Angew. Chem., Int. Ed. Engl.* **1982**, *21*, 148–149. (b) Edwin, J.; Böhn, M. C.; Chester, N.; Hoffman, D. M.; Hoffmann, R.; Pritzkow, H.; Siebert, W.; Stumpf, K.; Wade, P. H. *Organometallics* **1983**, *2*, 1666–1674.

(19) (a) Corey, E. J.; Semmelhack, M. F. *J. Am. Chem. Soc.* **1967**, *89*, 2755–2757. (b) Fischer, E. O.; Bürger, G. *Z. Naturforsch.* **1961**, *16B*, 77. (c) Wilke, G.; Bogdanovic, B.; Hardt, P.; Heimback, P.; Keim, W.; Kröner, M.; Oberkirch, W.; Tanaka, K.; Steinbrüche, E.; Walter, D.; Zimmermann, H. *Angew. Chem.* **1966**, *78*, 157–170.

(20) LeVanda, C.; Bechgaard, K.; Cowan, D. O.; Mueller-Westerhoff, U. T.; Eilbracht, P.; Candela, G. A.; Collins, R. L. *J. Am. Chem. Soc.* **1976**, *98*, 3181–3187.

(21) (a) King, R. B. *Organomet. Synth.* **1965**, *1*, pp 71–73. (b) Rettig, M. R.; Drago, R. S. *J. Am. Chem. Soc.* **1969**, *91*, 1361–1370.

Table 3. Crystallographic Data Collection and Structure Refinement Information

	1	2	3	
formula	C ₂₁ H ₄₀ B ₉ CoFe	C ₂₁ H ₄₀ B ₉ Co ₂	C ₂₁ H ₄₀ B ₉ CoNi	
fw	504.60	507.68	507.46	
space group	P2 ₁ 2 ₁ 2 ₁	P2 ₁ /n	P2 ₁ /n	
Z	4	4	4	
cell constants				
<i>a</i> , Å	12.158(8)	11.444(10)	11.389(2)	
<i>b</i> , Å	14.297(10)	14.582(13)	14.458(2)	
<i>c</i> , Å	14.713(10)	15.408(14)	15.474(2)	
β, deg		95.30(7)	96.62(1)	
<i>V</i> , Å ³	2557.5(30)	2560.2(40)	2531.0(7)	
μ, cm ⁻¹	12.24	13.04	14.08	
cryst size, mm	0.3 × 0.5 × 0.5	0.2 × 0.5 × 0.7	0.2 × 0.4 × 0.5	
<i>D</i> _{calcd} , g/cm ⁻³	1.311	1.317	1.332	
radiation (λ, Å)	Mo K _α (0.710 70)	Mo K _α (0.710 70)	Mo K _α (0.710 70)	
θ range, deg	2.0–28.0	1.93–25.00	1.93–29.09	
<i>h,k,l</i> collected	±16,±18,±19	±13,±17,+18	+14,+18,±21	
no. of rflns measd	4877	4808	6331	
no. of unique rflns	4455	4513	5813	
no. of obsd rflns	2643 ^a	2682 ^a	4879 ^a	
no. of params	336	346	395	
R1	0.064 ^c	0.056 ^c	0.037 ^c	
wR2	0.134 ^d	0.155 ^d	0.102 ^d	
	4	5a	5b	6
formula	C ₉ B ₇ H ₁₇ Co	C ₇ H ₁₇ B ₇ Ni	C ₈ H ₁₉ B ₇ Ni	C ₉ B ₇ H ₁₇ Ni
fw	259.84	235.59	249.61	259.60
space group	I2/a (No. 15)	P2 ₁ /n	P2 ₁ /n	P2 ₁
Z	8	4	4	2
cell constants				
<i>a</i> , Å	14.4637(7)	7.874(1)	6.577(4)	8.6982(4)
<i>b</i> , Å	7.9481(7)	11.984(2)	15.104(10)	10.0330(5)
<i>c</i> , Å	22.689(2)	13.189(2)	13.395(9)	8.0877(3)
β, deg	94.027(4)	104.61(1)	99.26(5)	117.017(2)
<i>V</i> , Å ³	2601.9(3)	1204.4(3)	1313.3(15)	628.78(5)
μ, cm ⁻¹	12.83	15.63	14.38	15.05
cryst size, mm	0.36 × 0.12 × 0.01	0.4 × 0.4 × 0.6	0.3 × 0.5 × 0.8	0.22 × 0.22 × 0.10
<i>D</i> _{calcd} , g cm ⁻³	1.327	1.299	1.262	1.371
radiation (λ, Å)	Mo K _α (0.710 70)	Mo K _α (0.710 70)	Mo K _α (0.710 70)	Mo K _α (0.710 70)
θ range, deg	2.0–25.0	2.3–26.46	2.05–28.50	2.0–25.0
<i>h,k,l</i> collected	±16,±19,±26	+9,±14,±16	±8,+20,+17	±10,±11,±9
no. of rflns measd	11429	4249	3453	6075
no. of unique rflns	3237 (<i>R</i> _{merge} = 5.04)	2150	3323	1086 (<i>R</i> _{merge} = 5.34)
no. of obsd rflns	1047 ^b	1763 ^a	2480 ^a	1637 ^b
no. of params	154	204	219	154
R1	0.046 ^c	0.033 ^c	0.035 ^c	0.030 ^c
wR2		0.083 ^d	0.097 ^d	
R2	0.061 ^c			0.042 ^c

^a $I > 2\sigma$. ^b $I > 3.0\sigma$. ^c $R_1 = \sum ||F_o| - |F_c|| / \sum |F_o|$. ^d $wR_2 = [\sum [w(F_o^2 - F_c^2)^2] / \sum w(F_o^2)^2]^{1/2}$. ^e $R_2 = (\sum w(|F_o| - |F_c|)^2 / \sum w|F_o|^2)^{1/2}$.

suspension of CoCl₂ (0.055 g, 0.42 mmol) was added dropwise. After removal of the solvent, the product was isolated by chromatography on alumina with hexane–CH₂Cl₂ (3:1) to yield 0.63 g of crude **2**. Recrystallization from pentane–CH₂Cl₂ (10:1) gave 0.48 g (0.95 mmol, 27%) of pure **2**: mp 158 °C; paramagnetic; MS (EI) *m/z* 508 [M⁺], 313 [M⁺ – MeC₃B₇H₉Co]; HRMS calcd for ¹²C₂₁¹H₄₀¹¹B₉⁵⁹Co 508.2682, found 508.2686.

(η^5 -C₅H₅)Co(μ - η^5 -MeEt₄C₃B₂)Ni(η^4 -8-Me-7,8,10-C₃B₇H₉) (**3**). Using a procedure similar to that for the synthesis of **1**, a stirred mixture of Li⁺[(η^5 -C₅H₅)Co(η^5 -MeEt₄C₃B₂)]⁻ (0.194 g, 0.61 mmol) and Na⁺(6-Me-5,6,9-C₃B₇H₉)⁻ (0.102 g, 0.64 mmol) in THF (20 mL) was maintained at –80 °C, and a THF suspension of NiBr₂·DME (0.225 g, 0.73 mmol) was added dropwise. The mixture was warmed to room temperature and stirred for 14 h. Chromatography on alumina with pentane–toluene (2:1) yielded, after crystallization from pentane–CH₂Cl₂ (10:1) at –30 °C, 0.62 g (1.22 mmol, 20%) of pure **3**: mp 178 °C; ¹H NMR (C₆D₆, 200 MHz) δ 3.93 (s, 5H, C₅H₅), 2.71 (s, 3H, CH₃ of C₃B₂), 2.55–2.26 (m, 4H, CH₂CH₃), 2.40 (m, 1H, CH-carb), 1.92–1.42 (m, 4H, CH₂CH₃), 1.55 (t, 3H, CH₂CH₃), 1.29 (t, 3H, CH₂CH₃), 1.14 (t, 3H, CH₂CH₃), 0.94 (s, 3H, CH₃-carb), 0.75 (t, 3H, CH₂CH₃);²² ¹¹B NMR (C₆D₆, 64.2 MHz) δ 14.1 (2B), 9.7 (1B), 5.3 (1B), 2.0 (1B),

–7.7 (1B), –9.6 (1B), –17.3 (1B), –19.7 (1B); MS (EI) *m/z* 507 [M⁺], 313 [M⁺ – CH₃C₃B₇H₉Ni]; HRMS calcd for ¹²C₂₁¹H₄₀¹¹B₉⁵⁹Co⁵⁵Ni 507.2707, found 507.2708; Anal. Calcd for C₂₁H₄₀B₉CoNi: C, 49.69; H, 7.96. Found: C, 47.57; H, 8.03.

Synthesis of 1-(η^5 -C₅H₅)Co-(2-Me-2,3,5-C₃B₇H₉) (4). A solution of Na⁺(6-Me-5,6,9-C₃B₇H₉)⁻ (4.0 mL of a 0.36 M solution, 1.4 mmol) in THF was added dropwise while a solution of Na⁺C₅H₅⁻ (0.7 mL of a 2.0 M solution, 1.4 mmol) in THF was concurrently added dropwise to a stirred solution of CoCl₂ (0.18 g, 1.4 mmol) in THF, resulting in a color change from bright blue to dark green. After the mixture was stirred for 15 h at room temperature, the solvent was vacuum-evaporated. The oily green residue was dissolved in CH₂Cl₂ and filtered through a 2 cm plug of Florisil. The solvent was vacuum-evaporated, and the dark residue was chromatographed (SiO₂:4:1 hexane–CH₂Cl₂) to give 0.260 g (0.78 mmol, 56%) of *commo*-Co-(1-Co-2-Me-2,3,5-C₃B₇H₉)₂^{9b} and 0.122 g (0.47 mmol, 34%) of dark red **4**: mp 143 °C dec; paramagnetic; HRMS calcd for ¹²C₉¹H₁₇¹¹B₇⁵⁹Co 261.1314, found 261.1326. Anal. Calcd for C₉H₁₇B₇Co: C, 41.60; H, 6.59. Found: C, 40.66; H, 6.98.

Synthesis of 1-(η^3 -C₃H₅)Ni-(η^6 -2-Me-2,3,5-C₃B₇H₉) (5a). A solution of Na⁺(6-Me-5,6,9-C₃B₇H₉)⁻ (0.122 g, 0.77 mmol) in THF (10 mL) was maintained at 0 °C, while a THF solution of [(HC(CH₂)₂)NiBr]₂ (0.18 g, 0.49 mmol) was added dropwise. The solution was stirred for 3 h at room temperature and then

(22) One CH hydrogen was not found in the ¹H NMR for **3** but is suspected to be obscured by the four triplet systems.

Table 4. Refined Positional Parameters for $(\eta^5\text{-C}_5\text{H}_5)\text{Co}(\mu\text{-}\eta^5\text{-MeEt}_4\text{C}_3\text{B}_2)\text{Fe}(\eta^6\text{-5-Me-2,3,5-C}_3\text{B}_7\text{H}_9) \mathbf{1}$

atom	x	y	z	$B_{\text{eq}}, \text{\AA}^2$
Co1	-0.04513(9)	0.58786(8)	1.11975(7)	3.01(5)
Fe1	-0.00289(9)	0.42711(8)	0.96834(7)	2.39(4)
C2	-0.1097(8)	0.3359(6)	0.9188(7)	3.8(4)
C3	0.1394(7)	0.3963(6)	0.9130(6)	3.7(4)
C5	-0.0289(7)	0.2633(6)	0.9371(6)	3.6(4)
C5m	-0.0625(9)	0.1818(6)	0.9987(7)	5.6(4)
C13	-0.0447(7)	0.5689(6)	0.9817(5)	2.9(4)
C15	0.0492(8)	0.4692(5)	1.0957(5)	2.8(4)
C16	-0.0702(7)	0.4471(5)	1.0972(5)	2.5(4)
C17	-0.2643(7)	0.5005(7)	1.0022(7)	4.6(4)
C18	-0.3391(8)	0.576(1)	1.0278(9)	9.0(4)
C19	-0.0625(9)	0.6418(6)	0.9082(6)	4.8(4)
C20	0.1826(8)	0.6046(6)	0.9979(7)	5.0(4)
C21	0.2875(8)	0.591(1)	1.0495(8)	8.7(4)
C22	0.1323(7)	0.4148(7)	1.1531(5)	3.7(4)
C23	0.1461(9)	0.4465(7)	1.2516(6)	5.6(4)
C24	-0.1204(8)	0.3690(5)	1.1557(6)	3.3(4)
C25	-0.1762(8)	0.4039(7)	1.2420(6)	4.8(4)
C26	-0.151(1)	0.6515(8)	1.2101(9)	5.9(4)
C27	-0.054(1)	0.6311(7)	1.2531(7)	6.3(4)
C28	0.032(1)	0.6774(8)	1.2085(9)	5.8(4)
C29	-0.015(1)	0.7272(6)	1.1364(8)	5.3(4)
C30	-0.129(1)	0.7106(7)	1.1388(8)	5.1(4)
B4	-0.0745(9)	0.4002(9)	0.8343(8)	4.0(4)
B6	0.106(1)	0.2944(8)	0.9439(8)	3.7(4)
B7	0.069(1)	0.4336(9)	0.8298(8)	4.1(4)
B8	-0.083(1)	0.2755(9)	0.8240(9)	4.5(4)
B9	0.146(1)	0.325(1)	0.826(1)	5.3(4)
B10	0.022(1)	0.3315(8)	0.7696(7)	4.8(4)
B11	0.048(1)	0.2366(9)	0.8451(8)	4.7(4)
B12	-0.1358(8)	0.5077(6)	1.0256(7)	2.7(4)
B14	0.0717(8)	0.5492(6)	1.0239(6)	2.8(4)

$B_{\text{eq}} = \frac{8}{3}[U_{11}(aa^*)^2 + U_{22}(bb^*)^2 + U_{33}(cc^*)^2 + 2U_{12}aa^*bb^*(\cos \gamma) + 2U_{13}aa^*cc^*(\cos \beta) + 2U_{23}bb^*cc^*(\cos \alpha)]$.

Table 5. Refined Positional Parameters for $(\eta^5\text{-C}_5\text{H}_5)\text{Co}(\mu\text{-}\eta^5\text{-MeEt}_4\text{C}_3\text{B}_2)\text{Co}(2\text{-Me-2,3,5-C}_3\text{B}_7\text{H}_9) \mathbf{2}$

atom	x	y	z	$B_{\text{eq}}, \text{\AA}^2$
Co1	0.25479(6)	0.31778(5)	-0.02882(5)	3.61(3)
Co2	0.24658(7)	0.16178(5)	0.12712(5)	4.32(4)
C2	0.2462(5)	0.4580(4)	-0.0320(4)	4.6(4)
C2m	0.236(1)	0.5177(6)	0.0480(6)	6.6(4)
C3	0.3192(6)	0.2978(5)	-0.1408(4)	5.2(4)
C5	0.3536(6)	0.4730(5)	-0.0784(4)	5.4(4)
C13	0.3159(5)	0.2879(4)	0.1043(3)	4.0(4)
C15	0.1377(5)	0.2169(4)	0.0290(4)	4.9(4)
C16	0.2377(6)	0.1748(4)	-0.0048(4)	4.6(4)
C17	0.4867(6)	0.1788(5)	0.0247(6)	7.7(4)
C18	0.5877(7)	0.2358(7)	0.0435(8)	12.7(4)
C19	0.3939(6)	0.3435(5)	0.1710(5)	6.7(4)
C20	0.0982(7)	0.3593(6)	0.1493(5)	8.1(4)
C21	0.0407(8)	0.3266(6)	0.2233(6)	9.4(4)
C22	0.0094(8)	0.1820(8)	0.0087(7)	11.4(4)
C23	-0.062(1)	0.2285(8)	-0.0466(9)	15.2(4)
C24	0.2289(9)	0.1009(5)	-0.0769(5)	8.1(4)
C25	0.245(2)	0.0092(7)	-0.0558(7)	19.4(4)
C26	0.2456(9)	0.1454(6)	0.2589(5)	6.8(4)
C27	0.3505(8)	0.1107(7)	0.2317(6)	7.4(4)
C28	0.320(1)	0.0415(6)	0.1723(6)	8.0(4)
C29	0.1981(9)	0.0329(5)	0.1632(5)	7.3(4)
C30	0.1515(8)	0.0974(6)	0.2171(5)	6.8(4)
B4	0.1422(6)	0.4213(5)	-0.0988(5)	4.5(4)
B6	0.4046(7)	0.3820(6)	-0.1288(5)	5.7(4)
B7	0.1871(7)	0.3254(5)	-0.1671(5)	5.0(4)
B8	0.2265(7)	0.5181(6)	-0.1267(5)	5.6(4)
B9	0.3020(8)	0.3681(7)	-0.2260(5)	5.9(4)
B10	0.1836(7)	0.4385(6)	-0.2068(5)	5.3(4)
B11	0.3353(7)	0.4757(6)	-0.1870(5)	5.7(4)
B12	0.3598(6)	0.2150(5)	0.0416(4)	4.2(4)
B14	0.1787(6)	0.2943(5)	0.0962(4)	4.4(4)

^aSee footnote a in Table 4.

heated for 1 h at 50 °C. The solvent was then removed in vacuo. The oily brown residue was chromatographed on alumina with toluene to yield crude **5a**. Recrystallization from pentane gave 0.116 g (0.49 mmol, 64%) of pure **5a**; mp 76 °C;

Table 6. Refined Positional Parameters for $(\eta^5\text{-C}_5\text{H}_5)\text{Co}(\mu\text{-}\eta^5\text{-MeEt}_4\text{C}_3\text{B}_2)\text{Ni}(\eta^4\text{-8-Me-7,8,10-C}_3\text{B}_7\text{H}_9) \mathbf{3}$

atom	x	y	z	$B_{\text{eq}}, \text{\AA}^2$
Ni9	0.25561(2)	0.18412(2)	0.02632(2)	3.27(1)
Co1	0.25783(3)	0.34458(2)	-0.12771(2)	3.66(2)
C7	0.1426(2)	0.0183(2)	0.0781(2)	4.26(4)
C8m	0.2581(3)	-0.0145(2)	-0.0503(2)	5.07(4)
C8	0.2478(2)	0.0409(2)	0.0316(2)	3.91(4)
C10	0.1690(2)	0.1947(2)	0.1314(2)	4.17(4)
C13	0.1855(2)	0.2182(2)	-0.105(1)	3.55(4)
C15	0.3726(2)	0.2876(2)	-0.0336(2)	3.86(4)
C16	0.2766(2)	0.3284(2)	0.0053(2)	3.81(4)
C17	0.0227(3)	0.3295(2)	-0.0220(2)	5.37(4)
C18	-0.0814(3)	0.2656(3)	-0.0375(3)	8.52(4)
C19	0.1038(3)	0.1648(2)	-0.1718(2)	5.12(4)
C20	0.4004(3)	0.1409(2)	-0.1532(2)	5.36(4)
C21	0.4593(4)	0.1791(3)	-0.2271(3)	7.16(4)
C22	0.5014(3)	0.3170(3)	-0.0152(2)	5.83(4)
C23	0.5726(3)	0.2683(3)	0.0578(2)	7.05(4)
C24	0.2930(4)	0.4000(2)	0.0773(2)	5.99(4)
C25	0.2495(5)	0.4953(3)	0.0569(3)	8.74(4)
C26	0.3516(3)	0.4116(2)	-0.2152(2)	5.44(4)
C27	0.2566(3)	0.3629(3)	-0.2584(2)	5.60(4)
C28	0.1515(3)	0.3969(3)	-0.2320(2)	5.93(4)
C29	0.1813(4)	0.4664(3)	-0.1718(2)	6.31(4)
C30	0.3060(3)	0.4764(2)	-0.1606(2)	5.82(4)
B1	0.3171(3)	0.0618(2)	0.2056(2)	4.68(4)
B2	0.1675(3)	0.0168(2)	0.1885(2)	4.86(4)
B3	0.2763(3)	-0.0214(2)	0.1252(2)	4.60(4)
B4	0.3562(2)	0.0785(2)	0.0970(2)	4.07(4)
B5	0.3063(3)	0.1759(2)	0.1638(2)	4.19(4)
B6	0.1931(3)	0.1290(3)	0.2217(2)	4.76(4)
B11	0.0869(3)	0.1071(2)	0.1280(2)	4.56(4)
B12	0.1485(2)	0.2904(2)	-0.0401(2)	3.73(4)
B14	0.3256(2)	0.2086(2)	-0.0993(2)	3.71(4)

^aSee footnote a in Table 4.

¹H NMR (C_6D_6 , 200 MHz) δ 5.95 (sept, $J = 6.6$ Hz, 1H, CH -allyl), 4.36 (br s, 1H, C3H -carb), 4.22 (dd, $^3J = 6.8$ Hz, 1H, CH_2 -allyl), 3.83 (dd, $^2J = 2.8$ Hz, $^4J = 6.6$ Hz, 1H, CH_2 -allyl), 2.91 (br s, 1H, C5H -carb), 2.70 (d, $^4J = 13.9$ Hz, 1H, CH_2 -allyl), 2.61 (d, $^4J = 13.4$ Hz, 1H, CH_2 -allyl), 2.07 (s, 3H, CH_3 -carb); ¹¹B NMR (C_6D_6 , 28.75 MHz) δ 6.5 (1B), -1.2 (1B), -9.8 (2B), -15.1 (2B), -20.4 (1B); ¹³C NMR (C_6D_6 , 50.3 MHz) δ 106.6 (CH -allyl), 84 (br, C2 -carb), 73 (br, C3(5) -carb), 69.5 (CH_2 -allyl), 63.2 (CH_2 -allyl), 57 (br, C5(3) -carb), 28.2 (CH_3 -C2carb); ²³MS (EI) m/z 235 [M^+], 193 [$\text{M}^+ - \text{C}_3\text{H}_6$]. Anal. Calcd for $\text{C}_7\text{H}_{17}\text{B}_7\text{Ni}$: C, 35.68; H, 7.29. Found: C, 35.60; H, 7.02.

Synthesis of 1-($\eta^3\text{-2-MeC}_3\text{H}_4$)Ni-($\eta^6\text{-2-Me-2,3,5-C}_3\text{B}_7\text{H}_9$) (5b**).** The procedure used in the preparation of **5a** was used for the reaction of $\text{Na}^+(\text{6-Me-5,6,9-C}_3\text{B}_7\text{H}_9)^-$ (0.108 g, 0.68 mmol) with $[(\text{Me}(\text{CH}_2)_2)\text{NiBr}]_2$ (0.165 g, 0.43 mmol) in 20 mL of THF. The same workup was used to yield 0.114 g (0.46 mmol, 67%) of pure **5b**; mp 85 °C; ¹H NMR (C_6D_6 , 200 MHz) δ 4.08 (br s, 1H, C3H -carb), 3.94 (dd, $^2J = 1.1$ Hz, $^4J = 3.4$ Hz, 1H, CH_2 -allyl), 3.79 (d, $^4J = 3.5$ Hz, 1H, CH_2 -allyl), 3.03 (br s, 1H, C5H -carb), 2.86 (s, 1H, CH_2 -allyl), 2.53 (s, 1H, CH_2 -allyl), 2.25 (s, 3H, CH_3 -allyl), 2.18 (s, 3H, CH_3 -carb); ¹¹B NMR (C_6D_6 , 28.75 MHz) δ 7.5 (1B), 0.7 (1B), -9.5 (2B), -15.9 (2B), -18.7 (1B); ¹³C NMR (C_6D_6 , 50.3 MHz) δ 123.3 (CCH_3 -allyl), 85 (br, C2 -carb), 71.7 (CH_2 -allyl), 69 (br, C3(5) -carb), 63.7 (CH_2 -allyl), 58 (br, C5(3) -carb), 29.8 (CH_3 -C2carb), 22.4 (CH_3 -allyl); ²³MS (EI) m/z 249 [M^+], 193 [$\text{M}^+ - \text{C}_4\text{H}_8$]. Anal. Calcd for $\text{C}_8\text{H}_{19}\text{B}_7\text{Ni}$: C, 38.49; H, 7.69. Found: C, 39.53; H, 7.97. CV: +/0, +1.33 V (irrev); 0/-, -1.36 V (irrev).

Synthesis of 9-($\eta^5\text{-C}_5\text{H}_5$)Ni-($\eta^4\text{-8-Me-7,8,10-C}_3\text{B}_7\text{H}_9$) (6**).** Using a procedure similar to that previously reported,^{9a} a 0.189 g (0.62 mmol) sample of $[(\eta\text{-C}_5\text{H}_5)\text{Ni}(\text{CO})]_2$ in 20 mL of THF was stirred at room temperature while a solution of $\text{Na}^+(\text{6-Me-5,6,9-C}_3\text{B}_7\text{H}_9)^-$ (2.9 mL of 0.435 M, 1.6 mmol) was added.

(23) Due to carbon-boron scalar coupling, the resulting signals for the carbon atoms adjacent to boron atoms are very broad in the ¹³C NMR. See: (a) Wrackmeyer, B. *Prog. NMR Spectrosc.* **1979**, *12*, 227-259. (b) Gragg, B. R.; Layton, W. J.; Niedenzu, K. *J. Organomet. Chem.* **1977**, *132*, 29-36.

Table 7. Refined Positional Parameters for 1-(η^5 -C₅H₅)Co-(2-Me-2,3,5-C₃B₇H₉) (4)

atom	x	y	z	$B_{eq.}^a \text{ \AA}^2$
Co1	0.51102(4)	0.20473(7)	0.88473(3)	3.97(3)
C2	0.3912(3)	0.1333(6)	0.84521(22)	4.4(2)
C2m	0.3792(4)	-0.0367(7)	0.8161(3)	8.2(4)
C3	0.4800(4)	0.4103(7)	0.9234(3)	6.1(3)
C5	0.3383(4)	0.1762(6)	0.8984(3)	5.9(3)
C13	0.6047(5)	0.0624(14)	0.8411(4)	9.2(5)
C14	0.6496(5)	0.2043(11)	0.8609(6)	9.1(5)
C15	0.6470(5)	0.2118(11)	0.9199(5)	9.3(5)
C16	0.6079(6)	0.0703(13)	0.9398(4)	9.1(5)
C17	0.5778(4)	-0.0256(8)	0.8916(6)	9.5(5)
B4	0.4119(4)	0.2984(7)	0.81158(24)	4.5(2)
B6	0.3939(6)	0.3198(9)	0.9469(3)	7.0(4)
B7	0.4659(4)	0.4666(6)	0.8569(3)	5.3(3)
B8	0.2994(4)	0.2641(8)	0.8332(3)	5.2(3)
B9	0.3833(5)	0.5202(8)	0.9088(3)	5.8(3)
B10	0.3457(4)	0.4672(7)	0.8366(3)	5.0(3)
B11	0.2938(4)	0.3730(8)	0.8987(3)	5.6(3)

^aSee footnote a in Table 4.

Table 8. Refined Positional Parameters for closo-1-(η^3 -C₃H₅)Ni-(η^6 -2-Me-2,3,5-C₃B₇H₉) (5a)

atom	x	y	z	$B_{eq.}^a \text{ \AA}^2$
Ni1	0.21252(4)	0.66851(3)	0.53578(2)	3.07(1)
C2	0.2212(3)	0.8345(2)	0.5245(2)	3.7(1)
C2m	0.1841(6)	0.9075(3)	0.6105(3)	5.4(1)
C3	0.3228(4)	0.6099(3)	0.4305(2)	3.8(1)
C5	0.4038(4)	0.8296(3)	0.5126(2)	4.0(1)
C12	0.0296(4)	0.6541(3)	0.6202(3)	4.7(1)
C13	0.1942(4)	0.6218(3)	0.6759(2)	4.4(1)
C14	0.2764(5)	0.5358(3)	0.6355(2)	4.7(1)
B4	0.0868(4)	0.7934(3)	0.4200(2)	4.1(1)
B6	0.4715(4)	0.6998(3)	0.4757(2)	4.1(1)
B7	0.1515(5)	0.6605(3)	0.3600(2)	4.1(1)
B8	0.2510(5)	0.8965(3)	0.4143(3)	4.8(1)
B9	0.3632(5)	0.6891(3)	0.3366(3)	4.5(1)
B10	0.2006(5)	0.7954(4)	0.3170(3)	4.6(1)
B11	0.4266(5)	0.8195(3)	0.3891(3)	4.7(1)

^aSee footnote a in Table 4.

The bright red solution was stirred at room temperature for 15 h; then the solvent was vacuum-evaporated. The reaction mixture was opened to the air and dissolved in CH₂Cl₂, the solution was filtered, and the dark solution was evaporated to dryness. Chromatography on silica gel yielded **6**. Spectroscopic and characterization data were similar to those previously reported.^{9a}

Crystallographic Data for 1-6. Single crystals were grown by slow evaporation in air of methylene chloride or pentane solutions.

Collection and Reduction of the Data. X-ray intensity data for **1-3**, **5a**, and **5b** were collected on a Syntex R3 and Siemens-STOE-AED2 diffractometer employing graphite-monochromated Mo K α radiation ($\lambda = 0.71073 \text{ \AA}$) and using the ω -scan technique. The intensity data were corrected for Lorentz, polarization, and absorption effects. X-ray intensity data for **4** and **6** were collected on an MSC/RAXIS area detector employing graphite-monochromated Mo K α radiation ($\lambda = 0.7107 \text{ \AA}$). The intensity data were corrected for Lorentz and polarization effects but not for absorption.

Solution and Refinement of the Structures. X-ray data for **1-3**, **5a**, and **5b** were processed and the structures were solved by direct methods using the SHELXS-86²⁴ structure package on a PC. Refinement was by full-matrix least-squares techniques of all reflections based on F^2 (SHELX 93²⁴). Non-

Table 9. Refined Positional Parameters for closo-1-(η^3 -MeC₃H₄)Ni-(η^6 -2-Me-2,3,5-C₃B₇H₉) (5b)

atom	x	y	z	$B_{eq.}^a \text{ \AA}^2$
Ni1	0.08745(5)	0.21547(2)	0.35241(2)	3.90(2)
C2	0.0795(3)	0.3108(2)	0.4552(2)	3.82(4)
C2m	0.0043(6)	0.2880(3)	0.5534(2)	5.69(4)
C3	0.1106(5)	0.2836(2)	0.2300(2)	5.07(4)
C5	-0.0446(3)	0.3724(2)	0.3853(2)	4.01(4)
C12	0.1199(6)	0.1083(2)	0.4445(3)	5.93(4)
C13	-0.0552(5)	0.0990(2)	0.3722(2)	5.21(4)
C14	-0.0220(8)	0.1067(2)	0.2718(3)	6.59(4)
C15	-0.2669(6)	0.0979(2)	0.3980(3)	6.97(4)
B4	0.3091(4)	0.3058(2)	0.4324(2)	3.95(4)
B7	0.3301(5)	0.2937(2)	0.2941(2)	4.78(4)
B8	0.1887(4)	0.4111(2)	0.4453(2)	4.24(4)
B9	0.1971(5)	0.3858(2)	0.2319(2)	4.94(4)
B10	0.3463(4)	0.3990(2)	0.3527(2)	4.41(4)
B6	-0.0532(5)	0.3503(2)	0.2572(2)	4.71(4)
B11	0.0853(4)	0.4433(2)	0.3216(2)	4.61(4)

^aSee footnote a in Table 4.

Table 10. Refined Positional Parameters for 9-(η^5 -C₅H₅)Ni-(η^4 -8-Me-7,8,10-C₃B₇H₉) (6)

atom	x	y	z	$B_{eq.}^a \text{ \AA}^2$
Ni9	-0.06384(6)	-0.00763	-0.78609(6)	2.81(3)
C7	0.2664(7)	-0.0827(6)	-0.4906(8)	3.5(2)
C8	0.1292(7)	0.0226(5)	-0.5284(7)	3.5(2)
C10	0.0916(7)	-0.1058(6)	-0.8637(8)	3.0(2)
C12	0.0794(8)	0.0463(6)	-0.3720(8)	4.5(2)
C13	-0.2829(10)	0.0577(8)	-0.7637(13)	4.8(3)
C14	-0.3092(9)	0.0953(8)	-0.9438(13)	5.4(3)
C15	-0.2995(7)	-0.0260(9)	-1.0291(7)	4.7(3)
C16	-0.2755(9)	-0.1316(7)	-0.9069(11)	4.6(3)
C17	-0.2657(10)	-0.0833(7)	-0.7423(13)	4.3(3)
B1	0.3139(7)	0.1031(6)	-0.7097(8)	3.2(2)
B2	0.4072(7)	-0.0467(6)	-0.5782(9)	3.6(2)
B3	0.3263(9)	0.0805(6)	-0.4887(9)	3.5(2)
B4	0.1304(9)	0.1364(5)	-0.6713(9)	3.3(2)
B5	0.1092(9)	0.0511(7)	-0.8891(10)	3.1(2)
B6	0.2921(7)	-0.0533(6)	-0.8148(8)	3.3(2)
B11	0.2406(9)	-0.1674(6)	-0.6778(9)	3.7(2)

^aSee footnote a in Table 4.

hydrogen atoms were refined anisotropically. For **1** and **2**, only the hydrogen atoms of the carborane ligand were refined isotropically, all others were included in a calculated position or as part of a rigid group (CH₃). For **3**, **5a**, and **5b**, all hydrogen atoms were refined isotropically, excluding the methyl hydrogen atoms. X-ray data for **4** and **6** were processed and the structure was solved and refined using the Molecular Structure Corp. teXsan²⁵ package on a Silicon Graphics Indigo R4000 computer. The structure for **4** was solved by direct methods (SIR92²⁶). The structure for **6** was solved by standard heavy-atom Patterson techniques followed by weighted Fourier synthesis. Refinement was by full-matrix least-squares techniques based on F to minimize the quantity $\sum w(|F_o| - |F_c|)^2$ with $w = 1/\sigma^2(F)$. Non-hydrogen atoms were refined anisotropically, and hydrogen atoms were included as constant contributions to the structure factors and were not refined.

Data collection and refinement information are given in Table 3. Final positional parameters are given in Tables 4-10. Selected intramolecular bond distances are presented in Table 1.

Acknowledgment. At the University of Heidelberg we thank the Deutsche Forschungsgemeinschaft (Grant No. SFB 247). At the University of Pennsylvania we thank the National Science Foundation for the support of this research.

Supplementary Material Available: Tables giving complete sets of bond distances and angles, hydrogen atom coordinates, thermal parameters, and least-squares planes for **1-6** (70 pages). Ordering information is given on any current masthead page.

OM940858V

(24) Sheldrick, G. M. SHELX 86, Program for Crystal Structure Solution; University of Göttingen, Göttingen, Germany, 1986. Sheldrick, G. M. SHELX 93, Program for Crystal Structure Determination; University of Göttingen, Göttingen, Germany, 1993.

(25) teXsan: Crystal Structure Analysis Package; Molecular Structure Corp., The Woodlands, TX, 1985 and 1992.

(26) Burla, M. D.; Camalli, M.; Cascarano, G.; Giacovazzo, D.; Polidori, G.; Spagna, R.; Viterbo, D. *J. Appl. Crystallogr.* **1989**, *72*, 389.

Metal Centers Connected by Conjugated Bridges. A Theoretical Evaluation of Delocalization Effects

Michael B. Sponsler

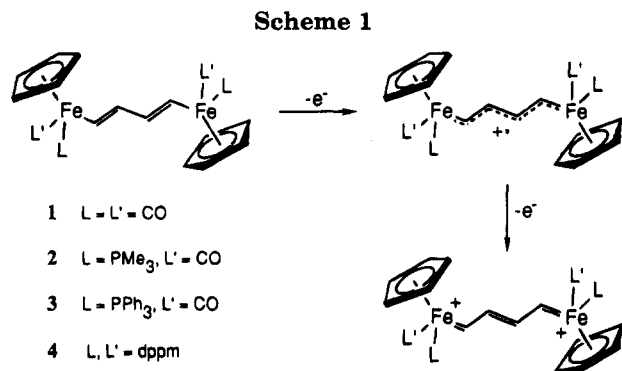
Department of Chemistry and W. M. Keck Center for Molecular Electronics, Syracuse University, Syracuse, New York 13244-4100

Received August 30, 1994[®]

A series of diiron complexes, in which the Fe atoms are linked by a conjugated bridge, have been investigated through Fenske–Hall molecular orbital calculations. The complexes studied were $[\text{CpFeL}_2]_2[\mu\text{-(X)}_m]^{n+}$, where $\text{Cp} = \eta^5\text{-C}_5\text{H}_5$, $\text{L}_2 = (\text{CO})_2$ or $\eta^2\text{-H}_2\text{PCH}_2\text{PH}_2$, $\text{X} = \text{-CHCHCHCH-}$, -CCCC- , $p\text{-C}_6\text{H}_4$, or -NCHCHN- , $m = 1$ or 2 , and $n = 0, 1$, or 2 (in selected combinations). For $\text{L} = \text{CO}$, the neutral complexes exhibit only weak delocalization, but the radical cationic and dicationic species show relatively strong π delocalization, as measured by population analysis and effective coupling parameter (V_{ab}) for the mixed-valence cations. All bridges studied participate in π delocalization, with the polyenediyl bridges promoting delocalization most effectively. The property of the bridges that most strongly affects the conjugating ability in the cationic and dicationic complexes is the energy of its highest π orbital relative to the metal π_{d} orbital, while the property that most strongly effects the conjugating ability in the neutrals is the energy of the lowest π^* orbital. For $\text{L}_2 = \text{H}_2\text{PCH}_2\text{PH}_2$, delocalization in the neutrals is increased, but the extent of additional delocalization upon oxidation is decreased. In the mononuclear complexes $[\text{CpFe}(\text{CO})_2(\text{CHCH})_m\text{H}]^{n+}$, where $m = 1$ or 2 and $n = 0$ or 1 , π delocalization is less extensive than in the dinuclear complexes, but not dramatically so.

Conjugated organometallic complexes have captured the interest of many research groups in the last several years,¹ driven in part by potential applications as materials for nonlinear optics, electrooptics, and molecular electronics. A large number of dinuclear complexes with conjugated bridges have been reported, and the extent of delocalization between metal centers has been debated on the basis of experimental and theoretical evidence. In this contribution, Fenske–Hall molecular orbital calculations² on bridged diiron complexes are used to address several issues pertaining to delocalization, such as the importance of π vs σ interactions and the effects of structural modifications, including the identity of the bridge, the orientation of the bridge, the nature of the other ligands, and the number of metal centers. Some general conclusions that extend beyond the CpFe ($\text{Cp} = \eta^5\text{-C}_5\text{H}_5$) systems studied have been made.

Recent reports from my laboratories have described a series of butadienediyl-bridged diiron complexes $[\text{CpFe}(\text{L})(\text{L}')_2]_2[\mu\text{-CH=CHCH=CH}]$ (**1–4**; Scheme 1) that have been chemically and electrochemically oxidized to produce the corresponding radical cation and dication species.³ Cyclic voltammetry showed two reversible oxidation waves for **2–4**, suggesting that the monocations are delocalized.⁴ Spectroscopic data supporting



ground-state delocalization of these mixed-valence radical cations were presented for **2+** (EPR), **3+** (EPR, IR), and **4+** (near-IR absorption). An X-ray crystal structure of **4²⁺** showed bond length alternation in the bridge that was consistent with the bis(carbene) formulation in Scheme 1. Fenske–Hall calculations were used to help interpret some of the experimental observations, such as the EPR spectrum of **4+** and the bond distances of **4²⁺**.^{3b}

The mixed-valence radical cations **1+–4+** may be classified as $(N + 1)\pi$ polymethines with $N = 6$,⁵ and complexes **1–4** are the first organometallic examples of the multistage redox systems first described by Deuchert and Hünig,⁶ which have the general formula XCH=CHCH=CHX . However, a large body of experimental and theoretical work has been published con-

[®] Abstract published in *Advance ACS Abstracts*, March 1, 1995.

(1) (a) Chisholm, M. H. *Angew. Chem., Int. Ed. Engl.* **1991**, *30*, 673–674. (b) Biswas, M.; Mukherjee, A. *Adv. Polym. Sci.* **1994**, *115*, 89–123.

(2) (a) Hall, M. B.; Fenske, R. F. *Inorg. Chem.* **1972**, *11*, 768–775. (b) Bursten, B. E. *Pure Appl. Chem.* **1991**, *63*, 839–844.

(3) (a) Etzenhouser, B. A.; Cavanaugh, M. D.; Spurgeon, H. N.; Sponsler, M. B. *J. Am. Chem. Soc.* **1994**, *116*, 2221–2222. (b) Etzenhouser, B. A.; Chen, Q.; Sponsler, M. B. *Organometallics* **1994**, *13*, 4176–4178. (c) Compound **1** was previously known: Sanders, A.; Giering, W. P. *J. Organomet. Chem.* **1976**, *104*, 67–78.

(4) Compound **1** showed an irreversible oxidation wave at 0 °C, suggesting that **1+** undergoes rapid decomposition at this temperature. At –78 °C, this wave becomes quasi-reversible; an EPR spectrum for **1+** has also been obtained at this temperature.^{3a}

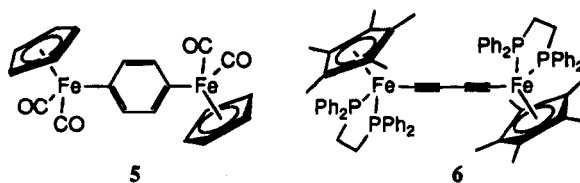
(5) Fabian, J.; Hartmann, H. *J. Mol. Struct.* **1975**, *27*, 67–78.

(6) Deuchert, K.; Hünig, S. *Angew. Chem., Int. Ed. Engl.* **1978**, *17*, 875–886.

cerning dinuclear complexes with other conjugating bridges, with special attention devoted to experimental and theoretical evaluation of the extent of delocalization in the mixed-valence species.⁷ The most common bridges are those bound through nitrogen, including pyrazine, as found in the Creutz-Taube ion,⁸ 4,4'-bipyridine,⁹ bipyridines incorporating additional conjugated linkers,¹⁰ and related heteroaromatic groups.¹¹ Conjugated hydrocarbon bridges in di- and polynuclear complexes include (CH)_n analogues with odd or even *n*,¹² C_n (polyyne) or cumulene,¹³ cyclopentadienyl,¹⁴ and fulvalene and other Cp-X-Cp species.¹⁵ Other bridge types include bis(diketonato),¹⁶ linked porphyrins,¹⁷ linked cyclams,¹⁸ and dinitrogen.¹⁹ This list is not intended to be exhaustive.

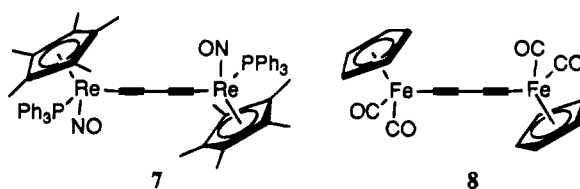
A complex closely related to 1 that has been studied experimentally and theoretically with respect to delo-

calization effects is the *p*-phenylene-bridged complex $\text{FpC}_6\text{H}_4\text{Fp}$ (5; $\text{Fp} = \text{CpFe}(\text{CO})_2$). Hunter has reported



a variety of spectroscopic evidence in support of delocalization occurring through the participation of a quinoidal resonance contributor in the neutral complex.²⁰ This evidence includes spectral data (NMR, IR), electrochemical data, and X-ray structural data. However, the interpretation of these data has been questioned by Richardson and Hall,²¹ who used Fenske-Hall calculations on 5 and several organic models to support their assertion that π delocalization effects are unimportant in 5. They further argued that small delocalization effects in this complex, if they exist, are better described as σ effects.

Another related bridge that has received considerable recent attention is the butadienediyl bridge. Le Narvor and Lapinte^{13a} have reported the diiron complex 6, and Gladysz and co-workers^{13b,c} have reported the dirhenium complex 7, each of which contains the C₄ bridge. In both cases, oxidation of the neutral complex provided the radical cation and dication species, which were isolated. Strong evidence was presented in both cases for ground-state delocalization in the radical cations. The neutral complex 8, which is included in the present study, has also been prepared.²²



An extensive amount of experimental and theoretical work has been reported on complexes with mixed alkyne/phenylene bridges, such as $-\text{C}\equiv\text{CC}_6\text{H}_4\text{C}\equiv\text{C}-$. Takahashi and co-workers first described a series of group 10 polymers that exhibit liquid crystallinity,²³ and some of these polymers have been found to display strong nonlinear optical effects.²⁴ A wide variety of mono-, di-, and polynuclear complexes have been prepared by Lewis,²⁵ Marder,²⁶ and Field²⁷ and their co-workers. Lewis and co-workers have used Fenske-Hall calculations to investigate electronic structure.^{25c} Frapper and Kertesz have reported extended Hückel calculations on a series of related complexes of Fe and Pt with

(20) Richter-Addo, G. B.; Hunter, A. D. *Inorg. Chem.* **1989**, *28*, 4063-4065.

(21) Richardson, N. A.; Hall, M. B. *Organometallics* **1993**, *12*, 1338-1343.

(22) (a) Wong, A.; Kang, P. C. W.; Tagge, C. D.; Leon, D. R. *Organometallics* **1990**, *9*, 1992-1994. (b) Crescenzi, R.; Sterzo, C. L. *Organometallics* **1992**, *11*, 4301-4305.

(23) (a) Takahashi, S.; Morimoto, H.; Murata, E.; Kataoka, S.; Sonogashira, K.; Hagihara, N. *J. Polym. Sci., Polym. Chem. Ed.* **1982**, *20*, 565-573. (b) Kaharu, T.; Matsubara, H.; Takahashi, S. *J. Mater. Chem.* **1991**, *1*, 145-146. (c) Abe, A.; Kimura, N.; Tabata, S. *Macromolecules* **1991**, *24*, 6238-6243.

(24) Porter, P. L.; Guha, S.; Kang, K.; Frazier, C. C. *Polymer* **1991**, *32*, 1756-1760.

(7) (a) Robin, M. B.; Day, P. *Adv. Inorg. Chem. Radiochem.* **1967**, *10*, 247-422. (b) Hush, N. S. *Prog. Inorg. Chem.* **1967**, *8*, 391-444. (c) Creutz, C. *Prog. Inorg. Chem.* **1983**, *30*, 1-73. (d) *Mixed Valency Systems: Applications in Chemistry, Physics, and Biology*; Prassides, K., Ed.; Kluwer: Dordrecht, The Netherlands, 1991.

(8) Experimental: (a) Creutz, C.; Taube, H. *J. Am. Chem. Soc.* **1973**, *95*, 1086-1094. (b) Fürholz, U.; Bürgi, H.-B.; Wagner, F. E.; Stebler, A.; Ammeter, J. H.; Krausz, E.; Clark, R. J. H.; Stead, M. J.; Ludi, A. *J. Am. Chem. Soc.* **1984**, *106*, 121-123. Theoretical: (c) Zhang, L.-T.; Ko, J.; Ondrechen, M. *J. Am. Chem. Soc.* **1987**, *109*, 1666-1671. (d) Piepho, S. B. *J. Am. Chem. Soc.* **1990**, *112*, 4197-4206.

(9) Woitellier, S.; Launay, J. P.; Joachim, C. *Chem. Phys.* **1989**, *131*, 481-488.

(10) (a) Woitellier, S.; Launay, J. P.; Spangler, C. W. *Inorg. Chem.* **1989**, *28*, 758-762. (b) Joachim, C.; Launay, J. P.; Woitellier, S. *Chem. Phys.* **1990**, *147*, 131-141. (c) Reimers, J. R.; Hush, N. S. *Inorg. Chem.* **1990**, *29*, 4510-4513. (d) Thomas, J. A.; Jones, C. J.; McCleverty, J. A.; Collison, D.; Mabbs, F. E.; Harding, C. J.; Hutchings, M. G. *J. Chem. Soc., Chem. Commun.* **1992**, 1796-1798.

(11) (a) Kaim, W.; Olbrich-Deussner, B. In *Organometallic Radical Processes*; Troglor, W. C., Ed.; J. Organomet. Chem. Libr. 22; Elsevier: New York, 1990; pp 173-200. (b) Boyde, S.; Strouse, G. F.; Jones, W. E., Jr.; Meyer, T. J. *J. Am. Chem. Soc.* **1990**, *112*, 7395-7396.

(12) (a) Davison, A.; Solar, J. P. *J. Organomet. Chem.* **1978**, *155*, C8-C12. (b) Kolobova, N. Y.; Skripkin, V. V.; Alexandrov, G. G.; Struchkov, Y. T. *J. Organomet. Chem.* **1979**, *169*, 293-300. (c) Schaefer, W. P.; Spotts, J. M.; Marder, S. R. *Acta Crystallogr.* **1992**, *C48*, 811-814. (d) Lemke, F. R.; Szalda, D. J.; Bullock, R. M. *J. Am. Chem. Soc.* **1991**, *113*, 8466-8477. (e) O'Connor, J. M.; Uhrhammer, R.; Rheingold, A. L.; Roddick, D. M. *J. Am. Chem. Soc.* **1991**, *113*, 4530-4544.

(13) (a) Le Narvor, N.; Lapinte, C. *J. Chem. Soc., Chem. Commun.* **1993**, 357-359. (b) Seyler, J. W.; Weng, W.; Zhou, Y.; Gladysz, J. A. *Organometallics* **1993**, *12*, 3802-3804. (c) Zhou, Y.; Seyler, J. W.; Weng, W.; Arif, A. M.; Gladysz, J. A. *J. Am. Chem. Soc.* **1993**, *115*, 8509-8510. (d) Bruce, M. I.; Hintending, P.; Tiekink, E. R. T.; Skelton, B. W.; White, A. H. *J. Organomet. Chem.* **1993**, *450*, 209-218. (e) Rappert, T.; Nürnberg, O.; Werner, H. *Organometallics* **1993**, *12*, 1359-1364. (f) Lang, H. *Angew. Chem., Int. Ed. Engl.* **1994**, *33*, 547-550. (g) Weng, W.; Bartik, T.; Gladysz, J. A. *Angew. Chem., Int. Ed. Engl.* **1994**, *33*, 2199-2202. (h) Brady, M.; Weng, W.; Gladysz, J. A. *J. Chem. Soc., Chem. Commun.* **1994**, 2655-2656.

(14) Schneider, J. J.; Goddard, R.; Werner, S.; Krüger, C. *Angew. Chem., Int. Ed. Engl.* **1991**, *30*, 1124-1126.

(15) (a) Sterzo, C. L. *Organometallics* **1990**, *9*, 3185-3188. (b) Stephan, M.; Davis, J. H., Jr.; Meng, X.; Chase, K. J.; Hauss, J.; Zenneck, U.; Pritzkow, H.; Siebert, W.; Grimes, R. N. *J. Am. Chem. Soc.* **1992**, *114*, 5214-5221. (c) Webb, R. J.; Hagen, P. M.; Wittebort, R. J.; Sorai, M.; Hendrickson, D. N. *Inorg. Chem.* **1992**, *31*, 1791-1801. (d) Delville, M.-H.; Rittinger, S.; Astruc, D. *J. Chem. Soc., Chem. Commun.* **1992**, 519-520. (e) Hudeczek, P.; Köhler, F. H. *Organometallics* **1992**, *11*, 1773-1775. (f) Dong, T.-Y.; Huang, C.-H.; Chang, C.-K.; Wen, Y.-S.; Lee, S.-L.; Chen, J.-A.; Yeh, W.-A.; Yeh, A. J. *J. Am. Chem. Soc.* **1993**, *115*, 6357-6368. (g) Atwood, C. G.; Geiger, W. E.; Rheingold, A. L. *J. Am. Chem. Soc.* **1993**, *115*, 5310-5311. (h) Gilbert, A. M.; Katz, T. J.; Geiger, W. E.; Robben, M. P.; Rheingold, A. L. *J. Am. Chem. Soc.* **1993**, *115*, 3199-3211.

(16) Kasahara, Y.; Hoshino, Y.; Kajitani, M.; Shimizu, K.; Satō, G. *P. Organometallics* **1992**, *11*, 1968-1971.

(17) Arnold, D. P.; Heath, G. A. *J. Am. Chem. Soc.* **1993**, *115*, 12197-12198, and references cited therein.

(18) (a) McAuley, A.; Xu, C. *Inorg. Chem.* **1992**, *31*, 5549-5554. (b) Mountford, H. S.; Spreer, L. O.; Otvos, J. W.; Calvin, M.; Brewer, K. J.; Richter, M.; Scott, B. *Inorg. Chem.* **1992**, *31*, 717-718. (c) Spreer, L. O.; Allan, C. B.; MacQueen, D. B.; Otvos, J. W.; Calvin, M. *J. Am. Chem. Soc.* **1994**, *116*, 2187-2188.

(19) Powell, C. B.; Hall, M. B. *Inorg. Chem.* **1984**, *23*, 4619-4627.

variations in bridge structure and analysis of band structure in the polymers.²⁸

Conjugated mononuclear complexes have been studied both experimentally and theoretically. Radical cations of the form $CpFeL_2(C\equiv CR)^+$ have been isolated as PF_6^- salts and characterized spectroscopically.²⁹ Lichtenberger and co-workers³⁰ have recorded photoelectron spectra of several alkynyl Fp complexes and correlated the results with Fenske–Hall calculations. The vinyl complex $CpFe(PH_3)_2CH=CH_2$ ³¹ and the carbene complex $Fp=CH_2^+$ ³² have also been calculated with the Fenske–Hall method. The results are consistent with relatively strong Fe–C π bonding for the carbene and weak π antibonding interactions for the alkynyl and vinyl complexes.

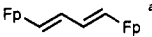
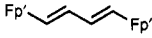
The goals of the present theoretical study included the following: (1) to compare some of the bridges mentioned above, along with longer versions of them, in their ability to promote interaction between metal centers, (2) to investigate the bonding changes induced by oxidation to radical cation and dication complexes, (3) to investigate the effects of ancillary ligands, (4) to compare mono- and dinuclear complexes, in order to evaluate the possibility of synergism in the metal–bridge interactions, and (5) to assign any delocalization effects as π or σ effects. These goals were addressed by comparing calculations for several Fp complexes, along with one diphosphine analog.

Theoretical Methods

The Fenske–Hall program, version 5.1, was used for all calculations. The standard basis functions included with the program were used. The exponent was 2.0 for the 4s and 4p orbitals of Fe.

The geometry of the Fp fragment was taken from the structure of 1,4-FpC₆F₄Fp,³³ idealized to C_s symmetry. The geometry of Fp' ($CpFe(\eta^2-H_2PCH_2PH_2)$) was also idealized to C_s symmetry on the basis of the structure of $[CpFe(dppm)]_2(\mu-CHCHCHCH)^{2+}(PF_6^-)_2$.^{3b} Bridge geometries were idealized from X-ray crystal structures of appropriate neutral models: $FpCH=CHCH=CHFp$ ³⁴ for butadienediyl and diazabutadienediyl, and 7^{3c} (for C–C bond lengths: 1.20, 1.39 Å) and $FpC\equiv CPh$ ³⁵ (for the Fe–C bond length: 1.92 Å) for butadiynediyl. For phenylene bridges, C–C bond lengths were 1.39 Å, the Fe–C bond length was 1.987 Å (the same as for butadienediyl), and bond angles were 120°. All C–H bond lengths were 1.08 Å. The geometry used for cation and

Table 1. Fragment π -Orbital Energy Gaps and Populations: Variation of Ligand, Charge, and Geometry

	charge	energy gap, eV		Mulliken population		
		$\pi-\pi_d$	$\pi^*-\pi_d$	π	π^*	
						
C_{2h} , neutral geometry	1	0	2.1	9.0	2.00	0.13
		+	2.2	9.0	1.73	0.13
		2+	2.2	9.0	1.48	0.14
						
C_{2h} , neutral geometry	4h	0	5.1	5.8	2.00	0.20
		+	4.3	6.7	1.90	0.17
		2+	3.8	7.3	1.73	0.17
C_{2h} , cation geometry	4h1	+	3.9	5.7	1.84	0.26
C_{2h} , dication geometry	4h2	2+	3.3	5.1	1.52	0.36
C_2 , X-ray geometry	4hx	2+	3.1 ^c	5.0	1.50 ^c	0.38

^a Fp = $CpFe(CO)_2$. ^b Fp' = $CpFe(\eta^2-H_2PCH_2PH_2)$. ^c Subject to a small uncertainty due to $\sigma-\pi$ mixing.

dication complexes was generally the same as that of the neutral. The different geometries of 4h have different compound labels (4h, 4h1, 4h2, 4hx).

The results in Table 4 (effective coupling parameter and HOMO–LUMO gaps) were obtained from calculations with output in the atomic basis, as were overlap populations given in text. Transformed-basis calculations were performed in order to obtain the results in Tables 1 and 2 (fragment orbital energy gaps and populations) and 3 (organic fragment π orbital energy gaps and overlaps with π_d). In the transformed-basis calculations, Mulliken population analysis³⁶ was done with respect to the orbitals of two fragments: (1) the bridge and (2) the Fe centers with their other ligands. Fragment orbitals were obtained from calculations of the charged fragments $[Fp]_2^{2+}$ or $[Fp']_2^{2+}$ and $[bridge]^{2-}$. Energies of the fragment orbitals were obtained from the corresponding diagonal element of the self-consistent field matrix from a transformed-basis calculation of the entire molecule and, therefore, may differ somewhat from the energies of the same fragment orbitals in a different molecule. In other words, the fragment orbitals are “prepared” for bonding with the other fragments, and the energies reflect the bonding environment of the complete molecule.^{2a,21}

Results and Discussion

FpCHCHCHCHFp (1). The results from this study are summarized in Tables 1–4 regarding the different bridges and oxidation levels. Before these results are analyzed, the molecular orbital (MO) diagram for $FpCH=CHCHCHFp$ (1) will be presented as a basis for the comparisons that follow. The Fe–C bonding in 1 was analyzed in terms of fragment orbitals, the most important of which are shown in Figure 1. The bridge orbitals that interact significantly with the Fp_2 orbitals are the nonbonding symmetric (n (a_g)), and antisymmetric (n (b_u)), orbitals, which consist primarily of lone pairs on C_1 and C_4 , and the frontier π orbitals, π (b_g) and the π^* (a_u). (Symmetry labels are from the C_{2h} point group.) The Fp_2 orbitals³² come in degenerate pairs, since the Fp groups are too far apart to interact directly. Four of the frontier orbital pairs are composed mainly of d orbital combinations: d_{z^2} , which has σ symmetry with respect to the bridge, d_{xz} and d_{yz} , which have π symmetry, and $d_{x^2-y^2}$, which has δ symmetry. The fifth d orbital pair, d_{xy} (δ symmetry), lies at much higher energy due to σ donation from the carbonyl ligands.

(35) Goddard, R.; Howard, J.; Woodward, P. *J. Chem. Soc., Dalton Trans.* **1974**, 2025–2027.

(36) Mulliken, R. S. *J. Chem. Phys.* **1955**, *23*, 1833–1840. Mulliken, R. S. *J. Chem. Phys.* **1955**, *23*, 1841–1846.

(25) (a) Khan, M. S.; Davies, S. J.; Kakkar, A. K.; Schwartz, D.; Lin, B.; Johnson, B. F. G.; Lewis, J. *J. Organomet. Chem.* **1992**, *424*, 87–97. (b) Atherton, Z.; Faulkner, C. W.; Ingham, S. L.; Kakkar, A. K.; Khan, M. S.; Lewis, J.; Long, N. J.; Raithby, P. R. *J. Organomet. Chem.* **1993**, *462*, 265–270. (c) Khan, M. S.; Kakkar, A. K.; Ingham, S. L.; Raithby, P. R.; Lewis, J.; Spencer, B.; Wittmann, F.; Friend, R. H. *J. Organomet. Chem.* **1994**, *472*, 247–255.

(26) Fyfe, H. B.; Mlekuz, M.; Zargarian, D.; Taylor, N. J.; Marder, T. B. *J. Chem. Soc., Chem. Commun.* **1991**, 188–190.

(27) (a) Field, L. D.; George, A. V.; Laschi, F.; Malouf, E. Y.; Zanello, P. *J. Organomet. Chem.* **1992**, *435*, 347–356. (b) Field, L. D.; George, A. V.; Hamby, T. W.; Malouf, E. Y.; Young, D. J. *J. Chem. Soc., Chem. Commun.* **1990**, 931–933.

(28) Frapper, G.; Kertesz, M. *Inorg. Chem.* **1993**, *32*, 732–740.

(29) Connolly, N. G.; Gamasa, M. P.; Gimeno, J.; Lapinte, C.; Lastra, E.; Maher, J. P.; Le Narvor, N.; Rieger, A. L.; Rieger, P. H. *J. Chem. Soc., Dalton Trans.* **1993**, 2575–2578.

(30) Lichtenberger, D. L.; Renshaw, S. K.; Bullock, R. M. *J. Am. Chem. Soc.* **1993**, *115*, 3276–3285.

(31) Kostic, N. M.; Fenske, R. F. *Organometallics* **1982**, *1*, 974–982.

(32) Schilling, B. E. R.; Hoffmann, R.; Lichtenberger, D. L. *J. Am. Chem. Soc.* **1979**, *101*, 585–591.

(33) Chukwu, R.; Hunter, A. D.; Santarsiero, B. D.; Bott, S. G.; Atwood, J. L.; Chassignac, J. *Organometallics* **1992**, *11*, 589–597.

(34) C=C = 1.34 Å, C–C = 1.45 Å, Fe–C = 1.987 Å, Fe–C–C = 131.8°. Churchill, M. R.; Wormald, J. *Inorg. Chem.* **1969**, *8*, 1936–1941.

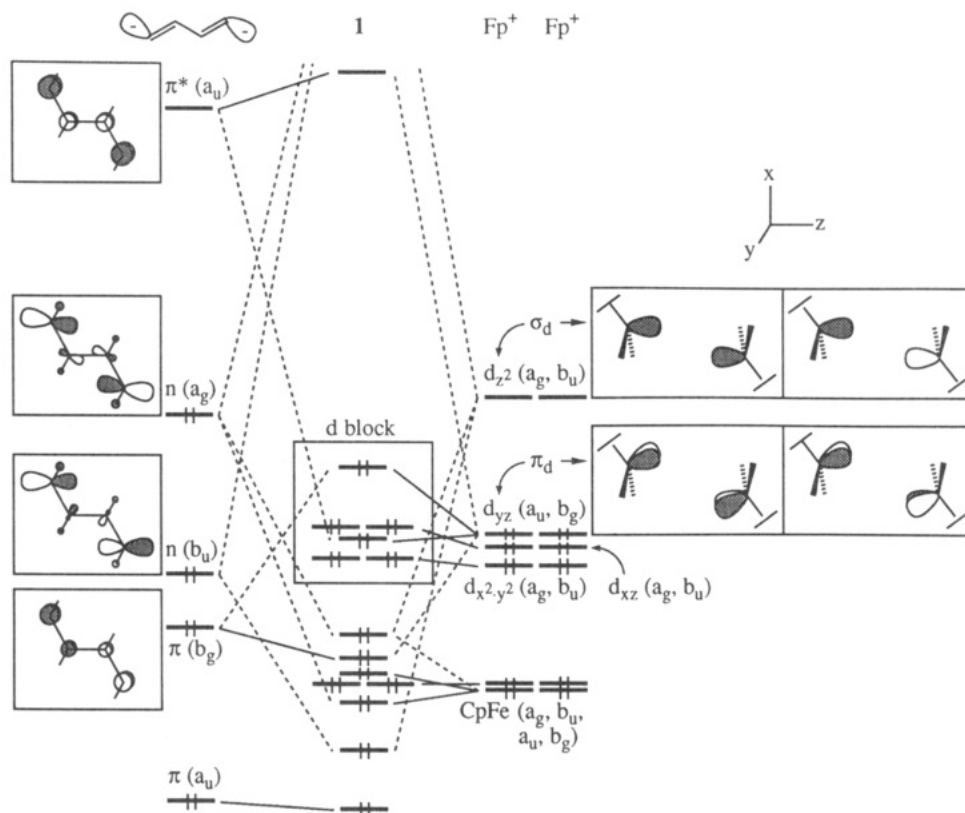


Figure 1. Partial molecular orbital mixing diagram for **1**, with fragment orbitals of $(\text{CH})_4^{2-}$ on the left and $(\text{Fp}^+)_2$ on the right. A solid line indicates that the fragment orbital contributes at least 50% to the resulting MO, and a dashed line indicates a contribution of less than 50%. Energy spacings shown are proportional to the relative orbital energies from the calculation.

Table 2. Fragment π -Orbital Energy Gaps and Populations: Bridge Variation

		energy gap, eV		Mulliken population π^*
		$\pi-\pi_d$	$\pi^*-\pi_d$	
	1	2.1	9.0	0.13
	1r	2.0	9.1	0.10
	8	2.4	12.4	0.11
	5	3.5	11.3	0.10
	9	1.8	6.9	0.13
	10	3.8	11.9	0.07
	11	2.5	9.0	0.09

In Figure 1, the MO energy levels of **1** are shown in the center, the fragment orbital levels for the butadienediyl bridge are on the left, and the fragment orbital levels for Fp are on the right. The bridge orbitals participate in two σ and two π interactions with the Fp orbitals. The nonbonding (lone pair) orbitals each interact with a Fp_2 σ orbital, which is principally a d_{z^2} combination with the appropriate symmetry, to form σ bonding and antibonding orbitals. (The a_g bonding combination also has a contribution from a Fp_2 orbital that is principally a Cp-Fe bonding orbital. The σ antibonding orbitals do not appear in the figure due to their high energy.) Two π interactions are also present: a filled-filled interaction between the $\pi(b_g)$ bridge orbital and a Fp_2 π_d orbital, consisting primarily of the b_g combination of d_{yz} orbitals, and an empty-filled interaction between the $\pi^*(a_u)$ bridge orbital

Table 3. Organic Fragment π -Orbital Energy Gaps and Overlaps with π_d

		energy gap, eV		overlap with π_d	
		$\pi-\pi^*$		π	π^*
	1	11.0		0.15	0.14
	8	14.8		0.15	0.15
	5	14.8		0.15	0.13
	9	8.6		0.13	0.11
	10	15.7		0.12	0.12
	11	11.5		0.11	0.10
	4h	10.9		0.13	0.12

^a $\text{Fp}' = \text{CpFe}(\eta^2\text{-H}_2\text{PCH}_2\text{PH}_2)$.

and the $\pi_d(a_u)$ orbital. The filled-filled interaction is stronger, because the $\pi-\pi_d$ energy gap, 2.1 eV, is much smaller than the $\pi^*-\pi_d$ gap, 9.0 eV. (One should be cautious about drawing conclusions from the magnitudes of these numbers or any others given by the calculations, but *trends* in the values are more meaningful.) The overlaps between these pairs of orbitals are similar (0.15 and 0.14, respectively; see Table 3).

The MOs that result from these interactions (middle of Figure 1) follow the expected pattern for a d^6 , pseudooctahedral complex. The nonbonding d block contains six MOs that are all filled (*i.e.*, the t_{2g} -like set), with the somewhat antibonding $\pi-\pi_d$ orbital appearing higher than the rest as the highest occupied MO (HOMO). The lowest unoccupied MO (LUMO) is composed primarily of the bridge π^* orbital, mixed with

Table 4. Effective Coupling Parameters (V_{ab}) and HOMO-LUMO Energy Gaps^a

	<i>n</i>	label	V_{ab} , eV cation	HOMO-LUMO gap, eV		
				neutral	cation	dication
	1	1	0.74	8.4	8.5	1.2
	2	1a	0.60	6.3	6.2	1.2
	1	8	0.68	8.9	9.4	0.6
	2	8a	0.44	8.7	8.8	0.5
	1	5	0.60	8.9	9.3	0.7
	2	5a	0.45	8.2	8.4	0.9
		10		9.7	10.4	
		11		8.7	9.4	
		4h	0.48	6.3	7.0	0.7

^a The geometries were identical for each oxidation level. ^b Fp' = CpFe(η^2 -H₂PCH₂PH₂).

small amounts of the π_d (a_u) and a few high-lying Fp orbitals (not shown). The primary features of this diagram are common to all of the complexes studied, with differences occurring in the relative energies of the orbitals.

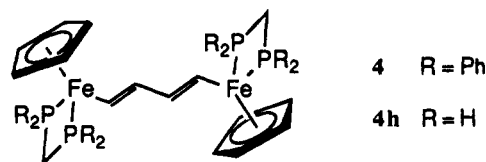
Mulliken's population analysis is valuable in determining the importance of these interactions (Table 1). In **1**, the bridge π^* orbital is populated by 0.13 electron, indicating that its interaction with the π_d (a_u) orbital is relatively weak. Since the π orbital interacts with another filled orbital, its population remains 2.00 electrons, even though the interaction is stronger. The nonbonding bridge orbitals, which form the C-Fe σ bonds, are depopulated to the level of 1.23 and 1.09 electrons, reflecting the formation of C-Fe bonds which are largely covalent but are polarized toward C.

Overlap populations between appropriate atomic orbitals are also informative as a measure of bond orders.³⁶ The overlap population between the C₁ p_π (i.e., p_y) orbital and the adjacent Fe d_π orbital³⁷ is -0.01, indicating that the interaction is slightly antibonding. Thus, the filled-filled interaction dominates the filled-empty interaction. The p_π - p_π overlap populations for C₁-C₂ and C₂-C₃ are 0.49 and 0.11, respectively, which are virtually identical with the corresponding values for 1,3-butadiene³⁸ of 0.49 and 0.10.

The σ overlap populations (obtained by summing all s , p_x , and p_z contributions) are 0.87 and 0.79 for C₁-C₂ and C₂-C₃, while the corresponding values for 1,3-butadiene are 0.82 and 0.80. The C₁-C₂ difference reflects, in part, changes in electron density at C₁. This effect is very localized and does not indicate that σ delocalization between Fe centers exists. This is more apparent from calculations on related complexes with longer bridges, Fp₂(μ -(CH)_{*n*}), n = 8 or 12. In these cases, an identical effect is observed for C₁-C₂ (and C_{*n*-1}-C_{*n*}), while no differences in σ overlap population are observed for any other C-C bonds with respect to the corresponding polyene.

These results are in line with Richardson and Hall's calculations for **5**.²¹ In both **1** and **5**, π interactions between Fe and C have little effect on the total energy of the complexes. This is not true, however, for oxidized forms of these complexes (see below).

Fp'CHCHCHCHFP' (**4h**). Because phosphine derivatives of **1** have been studied experimentally, calculations were also done for Fp'CHCHCHCHFP' (**4h**; Fp' = CpFe(η^2 -H₂PCH₂PH₂)). The diphosphine is a more effective donor than the carbonyls, and the energies of the Fp'₂ orbitals are therefore higher relative to the bridge orbitals. The π - π_d energy gap is thus increased to 5.1 eV in **4h**, while the π^* - π_d gap is reduced to 5.8 eV (see Table 1). This leads to a weakening of the filled-filled interaction and a strengthening of the filled-empty interaction, and the p_π - d_π overlap population is now 0.0, corresponding to a nonbonding interaction.³⁹ As expected, the π^* bridge orbital becomes populated to a larger extent, 0.20 electron, and the p_π - p_π overlap populations for C₁-C₂ and C₂-C₃, 0.47 and 0.13, show a slightly increased delocalization of π bonding. The σ overlap populations for C₁-C₂ and C₂-C₃ are 0.86 and 0.80.



The MO diagram of Figure 1 makes clear that the HOMO of **1** (and of **4h**) has a significant amount of Fe-C π antibonding character. Removal of electrons from these compounds should therefore provide radical cation and dication species that show significantly enhanced π bonding. Indeed, calculations for **4h**⁺ and **4h**²⁺ (at the same geometry as **4h**) do show positive p_π - d_π overlap populations (0.03 and 0.07) and changed π overlap populations for C₁-C₂ and C₂-C₃ (0.45 and 0.15 for **4h**⁺, 0.41 and 0.18 for **4h**²⁺). The changes, as expected, are related mainly to the π - π_d interaction. Thus, the C-C σ overlap populations remain unchanged. The population of the π^* orbital drops to 0.17 electron in both species due to increases in the π^* - π_d energy gap (6.7 eV in **4h**⁺ and 7.3 eV in **4h**²⁺).

The effects of oxidation upon bonding are markedly attenuated from reality if one holds the bond lengths constant, as was done for the calculations above. Since the X-ray crystal structure of **4**²⁺ is known,^{3b} a better indication of the actual magnitude of these bonding effects was obtained by using the crystal structure geometry for **4**²⁺ (designated **4hx**²⁺). The X-ray geometry has only C₂ symmetry, but it is not far from C_{2h}. The Fe-C-C-C-Fe π system is bent somewhat from planarity: the Fe-C-C-C dihedral angle is 161.8°. Most importantly, the C-C bond distances in the bridge show a long-short-long alternation (1.418 Å for C₁-C₂ and 1.366 Å for C₂-C₃), which is opposite to the alternation in **1**. The Fe-C bond distance is 1.841 Å, considerably shorter than in **1** (and **4h**: 1.987 Å).

The results of a calculation for **4hx**²⁺ show the expected changes with respect to **4h**²⁺, given the structural differences noted above. The p_π - d_π overlap population is doubled to 0.15 due to the shorter Fe-C distance. The π^* orbital is 2.3 eV lower in energy due to the changes in the C-C bond lengths, and the population of the π^* orbital is almost doubled to 0.38 electron. Consistent with the C-C distances, the p_π -

(37) The p_π - d_π overlap population was taken as the sum of the contributions from C1 p_y -Fe d_π and C1 p_y -Fe p_y . In other words, the d_π orbital is actually a d - p mixture (mostly d).

(38) Calculated with the same bond distances used for **1**.

(39) The same bond lengths were used for **1** and **4h**; therefore, the population analysis probably underestimates the differences between the two complexes.

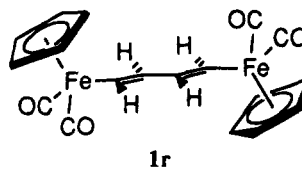
p_π overlap populations also show a reversed alternation with respect to **4h**: 0.27 for C_1-C_2 and 0.31 for C_2-C_3 . The reduced symmetry leads to strong mixing between the bridge π orbital and the b_u -like nonbonding orbital, complicating interpretation.

In order to provide a cleaner evaluation of the bond distance changes through the bridge, the bond distances were varied while C_{2h} symmetry was kept. **4h2²⁺** has the same geometry as **4h**, except that the Fe- C_1 , C_1-C_2 , and C_2-C_3 bond distances were taken from the X-ray structure of **4²⁺**. For **4h1⁺**, the bridge bond distances of **4h** and **4h2²⁺** were averaged. From Table 1, one can see that the differences between **4hx²⁺** and **4h2²⁺** are very small, indicating that the effects of the bond distance changes outweigh those of the loss of symmetry in **4²⁺**. Also, **4h1⁺** gives results that are between those for **4h** and **4h2²⁺**, as expected. This series is almost certainly closer to reality than the one with a constant geometry.⁴⁰

These results demonstrate that adjusting the bridge bond lengths is very important if one wishes to correlate properties with experimental data. However, for most of the calculations in this paper, bond lengths have been held constant, because experimental structural models are unavailable for the bridges studied in the different oxidation levels. When the geometry is held constant for all oxidation levels, the bonding changes are attenuated but still display trends that can be used to make comparisons.

Conformational Analysis. Several previous studies have dealt with the rotational preference of unsaturated ligands coordinated to Fp.^{31,32} In the case of σ -bound vinyl and phenyl groups, the rotational preference is driven by the repulsive $\pi-\pi_d$ interaction. This results in a slight preference for the conformation in which the plane of the organic group is perpendicular to the Fp symmetry plane, because a slightly weaker π interaction occurs in this conformation.^{31,32} For carbene and other ligands in which the π interaction is bonding, the plane of the ligand coincides with the Fp symmetry plane, and the rotation barrier is larger. These preferences are in agreement with several experimental structures, including the X-ray structure for **4²⁺**.^{3b} This dication has a bonding π interaction, as shown by the calculation for **4hx²⁺**, and the experimental structure has near- C_{2h} symmetry, with the bridge plane approximately bisecting the Cp ring.

In this study, comparisons between bridges and oxidation levels in this work were made in the C_{2h} geometry, similar to that found for **4²⁺**. The similarity of the Fp $\pi_d(d_{yz})$ and $\pi_d(d_{xz})$ orbitals for π bonding suggests that similar results would have been obtained had the bridges all been rotated by 90°. In order to verify this idea, calculations of **1** and its oxidized forms were repeated for the conformation in which the bridge has been rotated 90° into the "horizontal" yz plane (**1r**; C_i symmetry). As shown in Table 2, the π energy gaps and π^* Mulliken population are very similar in the two conformations. The most significant difference is a 0.03 electron reduction in the π^* population. Therefore, the same trends among bridges and oxidation levels would almost certainly be observed for either conformation.



Comparisons between Bridges. For purposes of evaluating the ability of different bridges to promote delocalization, calculations were performed on Fp-X-Fp, with X = -CHCHCHCH- (**1**), -CCCC- (**8**), and p -C₆H₄ (**5**), along with their oxidized forms. These complexes show some significant differences, and these differences can be primarily attributed to variations in relative orbital energies, since the overlaps are very similar (Table 3). The π orbital energy gaps (Table 2) show that all of the Fp complexes have considerably smaller gaps for $\pi-\pi_d$ than for $\pi^*-\pi_d$. The $\pi-\pi_d$ gaps are similar for **1** (2.1 eV) and **8** (2.4 eV), but the gap is a bit higher for the phenylene case (3.5 eV). As a result, the complexes show comparable extents of π delocalization upon oxidation, as measured by populations and overlap populations, with a somewhat smaller effect for the phenylene case. Thus, for example, the population of the bridge π orbital drops by 0.52 electron upon oxidation of **1** to **1²⁺**, by 0.47 electron upon oxidation of **8** to **8²⁺**, and by 0.39 electron upon oxidation of **5** to **5²⁺**. Similarly, the Fe-C π overlap populations increase by 0.10 for **1** to **1²⁺**, by 0.10 for **8** to **8²⁺**, and by 0.08 for **5** to **5²⁺**.

The $\pi^*-\pi_d$ energy gaps also vary, with **1** having a smaller gap (9.0 eV) than **8** (12.4 eV) or **5** (11.3 eV). These differences are manifested in the $\pi^*-\pi_d$ bonding interactions, with π^* populations of 0.13 electron for **1**, 0.11 electron for **8**, and 0.10 electron for **5**. These populations remain nearly constant in all three oxidation levels.

The interactions involving the π and π^* bridge orbitals are simultaneously described by the quantity V_{ab} , known as the effective coupling parameter for mixed-valence complexes.⁴¹ V_{ab} , which can also be thought of as the resonance stabilization energy, represents half of the intervalence transition energy for delocalized mixed-valence complexes.^{7c} It was simply obtained by using the "dimer splitting" method,^{9,42} which sets V_{ab} equal to half of the energy difference between the two MOs that are primarily $\pi_d(d_{yz})$ in character. Values of V_{ab} for the various cations, shown in Table 4, are all greater than 0.4 eV, indicating that strong coupling persists even when the bridge length is doubled. The order is the same as that identified above, with the extent of coupling decreasing from **1⁺** to **8⁺** to **5⁺**. The double-length octatetraenediyl bridge (**1a⁺**) promotes coupling with equal effectiveness as the single-length phenylene bridge (**5⁺**).

As noted above for **1**, σ effects appear to be unimportant for delocalization in any of the bridges. In **1** and **5**, the C_1-C_2 σ overlap populations are increased relative to the corresponding organic compound (with H replacing Fp),⁴³ while for **8**, no change is found with respect to the hydrocarbon. In every case, the σ overlap

(41) Also denoted in the literature as H_{AB} , C_{eff} , ϵ , etc. See ref 7c for a general discussion.

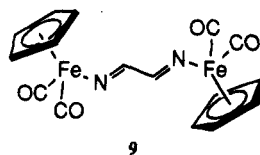
(42) Caution is advised in the direct comparison of these values to others in the literature, due to differences in method (e.g., Fenske-Hall vs extended Hückel theory) and in geometry conventions.

(43) This result contradicts the report of Richardson and Hall,²¹ possibly due to differences in basis sets.

(40) This series probably slightly exaggerates the differences between oxidation states, since the bridge geometry for **4h** was taken from the X-ray structure for **1**. The actual bond lengths in **4h** probably show less alternation, due to the delocalizing effect of the phosphines.

populations are unaffected by oxidation. In the case of the butadienyldiyl complex (**8**), the "in-plane" (xz) π overlap populations are also invariant with oxidation; the only changes that occur are in the yz π system.

Since many conjugated dinuclear transition-metal complexes are known in which the bridge is attached through nitrogen atoms,⁸⁻¹¹ calculation of the diaza-butadienyldiyl complex **9** was also done. This complex

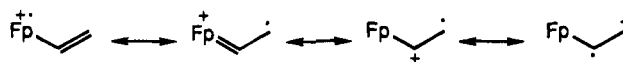


exhibits lower energy gaps for both $\pi-\pi_d$ (1.8 eV) and $\pi^*-\pi_d$ (6.9 eV). However, the overlaps for these orbital pairs are also reduced (see Table 3), due to the more contracted p_y orbital on N. As a result of these competing effects, the π^* population is the same as that for **1** at 0.13 electron, but V_{ab} is considerably reduced to 0.55 eV.⁴⁴ A complicating feature of **9** is that the N lone pair orbitals lie at higher energy than the π orbital, so that upon oxidation electrons are removed from the lone pairs instead of the π system.⁴⁵ This complication does not exist in most of the known complexes with N-containing bridges such as pyrazine, since the nitrogen centers have no free lone pairs. Nonetheless, the results show that replacement of CH with N somewhat reduces the bridge's ability to promote delocalization.

By comparing the $\pi-\pi^*$ energy gaps and the $\pi-\pi_d$ and $\pi^*-\pi_d$ overlaps of the Fp complexes for the different bridges (Table 3), one may estimate the relative conjugating abilities of the bridges for any choice of metal and ligands. As discussed above, the π and π^* orbitals play somewhat different roles in delocalization, at least with respect to oxidation of the Fp complexes, but decreases in the $\pi-\pi^*$ gap tend to enhance delocalization by increasing the interaction involving one or both of the orbitals with the metal centers. While differences in overlaps among the bridges will depend on the metal/ligand environment, the trends established in the table are likely to remain, since the differences mostly reflect the coefficients and diffuseness of the p_y orbital on the atom attached to the metal. The values in Table 3 show that the four conjugated bridges studied show minor to moderate differences in overlap and energy matching as discussed above. The table also shows that phosphine substitution leads to a small decrease in overlap.

Examination of the mononuclear vinyl and butadienyldiyl complexes **10** and **11** allows evaluation of the possibility of synergism in the interaction between metal centers. Both complexes have smaller π interactions than **1**, as measured by population of π^* (Table 2) and depopulation of π in the cations (to 1.83 electrons in **10**⁺ and 1.66 electrons in **11**⁺). For **10**, the organic fragment $\pi-\pi^*$ gap is considerably larger and the overlap is smaller than that for **1**. For **11**, the $\pi-\pi^*$ gap is similar to that for **1**, but the overlap is lower. The reduction in the number of Fe-C interactions contributes to the decrease in overlap, and to this degree the delocalization in **1** and

Scheme 2



its oxidized forms can be considered synergistic. Nonetheless, the cationic mononuclear complexes are both significantly delocalized.

A different measure of a bridge's effectiveness at promoting delocalization is the HOMO-LUMO gap of the dinuclear complex. As the molecules are extended to polymers, this becomes the band gap, which relates directly to electrical and electrooptic properties. Analyses of HOMO-LUMO gaps and band gaps have been presented for a number of transition-metal alkynyl polymers.^{25c,28} HOMO-LUMO gaps for the complexes studied herein are presented in Table 4. The gaps for **1**, **8**, and **5** are within the narrow range 8.4-8.9 eV, as is the gap for the mononuclear **11**. The vinyl complex **10** has a larger gap of 9.7 eV, due mainly to a lower energy HOMO. Phosphine coordination in **4h** destabilizes both frontier orbitals but primarily the more Fe-based HOMO, resulting in a markedly lower gap of 6.3 eV. A similar effect was noted for the alkynyl complexes.^{25c}

Doubling the length of the bridge has the effect of lowering the HOMO-LUMO gap. Both orbitals are stabilized, but the LUMO is affected more strongly, since it is more localized on the bridge. This effect is much more significant for the octatetraenyldiyl complex **1a**, with a 25% reduction, than it is for the octatetraenyldiyl (**8a**) and biphenylene (**5a**) complexes, with reductions of 2% and 6%, respectively.

Only minor changes in the HOMO-LUMO gaps were found upon removal of one electron to give the radical cations. However, with removal of a second electron, the HOMO becomes the LUMO, and the HOMO-LUMO gaps are very small for the dications. This suggests the possibility of open-shell states in the dinuclear cations and very small band gap materials for oxidized polymers. For the butadienyldiyl complex (**8**²⁺), the HOMO and LUMO are very similar antibonding $\pi-\pi_d$ orbitals: the former in the xz plane and the latter in the yz plane. While the orbital energies are not accurate enough to make predictions about spin states in particular cases, they do suggest that open-shell ground states might be observed in some of these dications.

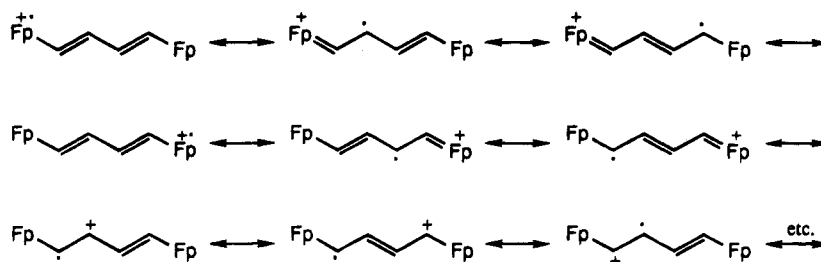
As a practical matter, one should consider that butadienyldiyl has the advantage that its interactions with the metal center are unaffected by rotations of the bridge with respect to the metal fragments. However, with d^6 metal fragments such as Fp, the effect of rotation of the other bridges is less important than it might be with fragments that do not have two similar d orbitals with π symmetry. In the absence of steric hindrances, the planar bridges can rotate in order to maximize the π -bonding interactions.

Delocalization of Spin. Examination of the singly occupied HOMOs of the radical cations **1**⁺, **10**⁺, and **11**⁺ reveals a trend that is consistent with simple valence-bond resonance ideas. Resonance structures for **10**⁺ (Scheme 2) and **11**⁺ are suggestive of higher spin densities on alternant atoms (*i.e.*, Fe and β - and δ -C atoms), in analogy to the organic allyl and pentadienyldiyl radicals. The α - and γ -C atoms in the radical cations can gain some spin density through resonance structures that have both spin and charge on the ligand (*e.g.*,

(44) Computed for **9**⁺ by using the MOs with d_{xz} character, even though the singly occupied orbital had d_{yz} character. See text.

(45) In **9**²⁺, the lone pair and $\pi-\pi_d$ antibonding orbitals are nearly degenerate, and the program was unable to converge.

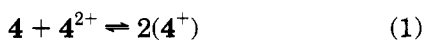
Scheme 3



the last structure in Scheme 2), but these structures should be relatively disfavored. The calculated singly occupied orbitals indeed show an alternation in spin densities for both 10^+ (Fe 0.59, α 0.03, β 0.15) and 11^+ (Fe 0.50, α 0.07, β 0.12, γ 0.02, δ 0.13).⁴⁶

In contrast, the situation is much different for 1^+ , in which the C atom α to one Fe atom is also δ to the other. Thus, each C atom is separated from Fe atoms by both an odd and even number of bonds, resulting in efficient delocalization of spin to each C atom (Scheme 3). Due to the 2-fold symmetry, alternation cannot occur, and a more even distribution of spin densities is observed for 1^+ (Fe 0.28, C_1 0.08, C_2 0.06, C_3 0.06, C_4 0.08, Fe 0.28). Uniform spin densities have been predicted as a general phenomenon for radical polymethines,⁵ of which **1** is an example. In fact, spin densities were found to be relatively evenly distributed for all of the dinuclear cations in this study.

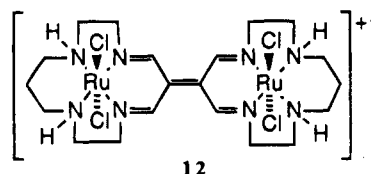
An important question concerning the mixed-valence complexes is whether they are spin-delocalized (class III) or spin-trapped (class II).⁷ The large V_{ab} values in Table 4 indicate that all of the mixed-valence species examined are potentially delocalized. Experimental evidence also favors a delocalized structure for 4^+ ,^{3b} and the V_{ab} value of 0.48 eV calculated for $4h^+$ is fortuitously identical⁴⁷ with the experimental V_{ab} value obtained for 4^+ from its near-IR intervalence transition and is also close to the comproportionation energy of 0.44 eV obtained for eq 1 from cyclic voltammetry.⁴⁸



Conclusions

This study allows a number of conclusions to be drawn. (1) All of the conjugated bridges promote significant delocalization in the cations and dication, while delocalization effects are minimized in the neutral complexes. (2) Delocalization in the oxidized species is dominated by π interactions. Changes in σ bonding are small in comparison. (3) Among the hydrocarbon bridges, the polyenediyl bridges most effectively promote delocalization, due mainly to better energy matching of π orbitals. Among the bridges studied, the polyenediyls

promote by far the strongest reduction in HOMO-LUMO gap as the bridge is lengthened. (4) Replacement of the α -CH groups in butadienediyl with N atoms somewhat reduces the ability of the bridge to promote delocalization. (5) Phosphine substituents have the expected effect of increasing the energy of the π_d orbitals, which leads to a stronger $\pi^*-\pi_d$ interaction and a weaker $\pi-\pi_d$ interaction. This translates into stronger delocalization in the neutral complex but a weaker additional effect upon oxidation. This also leads to a reduced effective coupling parameter (V_{ab}). (6) Mononuclear polyenyl complexes also show appreciable delocalization when oxidized, suggesting that synergistic effects between metal centers are relatively minor. (7) The dinuclear dication has very small HOMO-LUMO gaps, suggesting that some of these species might have open-shell ground states. Very low band gap materials might be realized in the polymeric forms of these dication. (8) The "weak link" in intermetal communication is the M-C interaction, which suffers from low overlap relative to the C-C interactions. This is probably the reason that Spreer's diruthenium mixed-valence complex **12**, having twice as many M-C inter-



12

actions, shows such strong intermetal communication.^{18c} This complex has the highest reported comproportionation constant for any mixed-valence compound at 3.5×10^{15} .

Finally, the approach taken in this study of holding bond lengths constant for different oxidation levels has utility in identifying trends among the levels and among different complexes. However, the actual bonding changes that take place upon oxidation are undoubtedly much greater than those represented in most of the tables presented herein, as shown by the calculational comparison of **4h** and several alternate geometries and by the experimental (X-ray structure) comparison of **1** and 4^{2+} .

Acknowledgment is made to the Camille and Henry Dreyfus Foundation New Faculty Award Program for partial support of this work.

OM9406916

(46) These spin densities should be viewed as highly approximate, given the problematic nature of open-shell calculations.

(47) The value of V_{ab} obtained depends strongly on geometry. For example, a value of 0.75 eV was obtained for $4h1^+$.

(48) The comproportionation energy was taken as the separation between E° values (0.44 V) times the charge of one electron.^{7c}

First Stereochemical Characterization of Configurationally Stable Diastereomers of Hypervalent Stiboranes (10-Sb-5) and Acceleration of Intramolecular Permutation by Donor Solvents

Satoshi Kojima, Yasutaka Doi, Manabu Okuda, and Kin-ya Akiba*

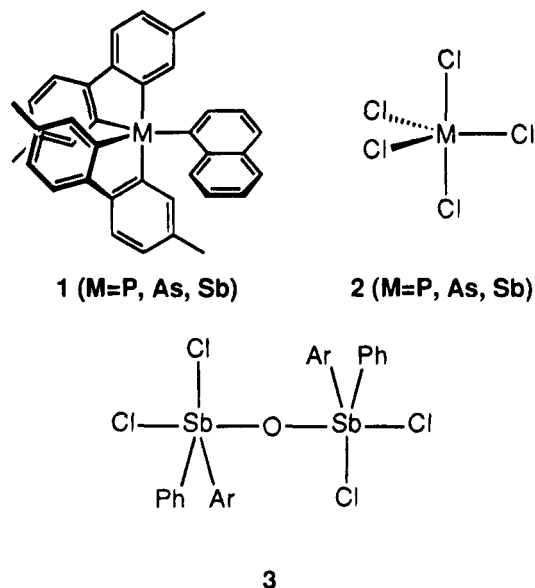
Department of Chemistry, Faculty of Science, Hiroshima University,
1-3-1 Kagamiyama, Higashi-Hiroshima 739, Japan

Received December 20, 1994[®]

The first stereochemical characterization of a pair of configurationally stable diastereomeric 10-Sb-5 compounds (*o*-O(CF₃)(CH₃)C*₆H₄)(*o*-O(CF₃)₂C₆H₄)Sb*(*p*-C₆H₄CH₃) with an asymmetric antimony atom was accomplished by NOE differential spectra and confirmed by the X-ray analysis of the major diastereomer **6a**. Kinetic measurements of the interconversion between the major diastereomer **6a** and the minor diastereomer **6b** were carried out in 10 different solvents, and it was found that the process was intramolecular and protonation was not an essential factor. The rates were accelerated in polar solvents, and the activation enthalpy (ΔH^\ddagger) decreased from 26.1 to 23.5 kcal mol⁻¹ changing the E_T^N values from 0.012 (*n*-octane) to 0.327 (1,2-dichloroethane) while the donor numbers DN^N were kept to almost zero. Larger acceleration of the rates was observed in donor solvents, and this is apparent by comparing the ΔH^\ddagger values of pairs of solvents with different DN^N values and similar E_T^N values, i.e., ethyl propionate (21.3) and *o*-dichlorobenzene (24.9); pyridine (17.3) and 1,2-dichloroethane (23.5). This is rationalized by invoking a hexacoordinate transition state.

The permutation process of pentacoordinate species has been well documented, especially for compounds with phosphorus as the central atom.¹ In the case of phosphorus the barrier of permutation has been successfully altered to allow the isolation of configurationally stable diastereomers¹ or optically active species² with phosphorus as a center of asymmetry. Assuming that the Berry pseudorotation mechanism,³ which has its foundation upon vibrational bending motions, is operative, the strength of the bonds about the pentacoordinate atom would reflect the barrier to permutation. Thus, pentacoordinate compounds of elements of lower rows on the periodic table having weaker bonds would naturally be expected to have smaller permutation barriers compared with phosphorus, therefore making it difficult to obtain configurationally stable diastereomers. In fact, there is experimental evidence that is in good accordance with this assumption. For example, for compound **1** with M = P, As, and Sb the barriers for a multistep permutation process between rapidly interconverting enantiomers have been determined by variable temperature NMR techniques to be 15.8, 15.4, and 11.6 kcal/mol,⁴ respectively. On the other hand, for compound **2** both measurements (3.6, 2.8, and 1.6 kcal/mol, respectively)⁵ and theoretical calculations (4.78, 2.80, and 1.98 kcal/mol, respectively)⁶

for a single-step permutation process which exchanges the apical and equatorial substituents support this tendency. In the case of antimony, Doak et al. have reported that compound **3** could be observed as two



separate diastereomeric species by NMR,⁷ but to our knowledge there have been no reports on the isolation of such compounds as configurationally stable species. Martin et al. have successfully prepared a number of hypervalent compounds of extraordinary thermal and

[®] Abstract published in *Advance ACS Abstracts*, March 15, 1995.

(1) For example: Holmes, R. R. *Pentacoordinated Phosphorus—Structure and Spectroscopy*; ACS Monograph 175; American Chemical Society: Washington, DC, 1980; Vol. 1.

(2) (a) Kojima, S.; Kajiyama, K.; Akiba, K.-y. *Tetrahedron Lett.* **1994**, *35*, 7037. (b) McClure, C. K.; Grote, C. W.; Lockett, B. A. *J. Org. Chem.* **1992**, *57*, 5195. (c) Moriarty, R. M.; Hiratake, J.; Liu, K.; Wendler, A.; Awasthi, A. K.; Gilardi, R. *J. Am. Chem. Soc.* **1991**, *113*, 9374 and references cited therein.

(3) Berry, R. S. *J. Chem. Phys.* **1960**, *32*, 933.

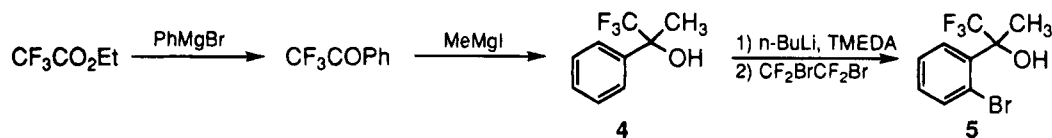
(4) (a) Hellwinkel, D.; Knaebe, B. *Phosphorus* **1972**, *2*, 129. (b) Hellwinkel, D.; Bach, M. *Naturwissenschaften* **1969**, *56*, 214. (c) Hellwinkel, D.; Lindner, W. *Chem. Ber.* **1976**, *109*, 1497.

(5) Ivashkevich, L. S.; Ishchenko, A. A.; Spiridonov, V. P.; Strand, T. G.; Ivanov, A. A.; Nikolaev, A. N. *Russ. J. Struct. Chem.* **1982**, *23*, 295.

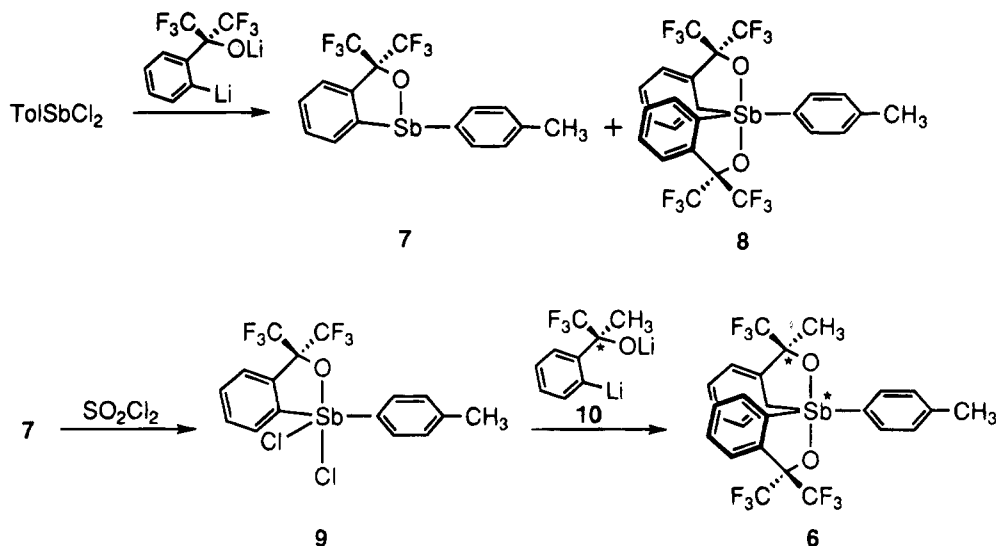
(6) Breidung, J.; Thiel, W. *J. Comput. Chem.* **1992**, *13*, 165.

(7) Doak, G. O.; Summy, J. M. *J. Organomet. Chem.* **1973**, *55*, 143.

Scheme 1



Scheme 2



kinetic stability by incorporating bidentate ligands derived from hexafluorocumyl alcohol.⁸ With pentavalent phosphoranes,^{2a,8c,d} and silicates^{8d} it has also been found that the barrier to permutation was very high. By utilizing this bidentate ligand and a modified ligand with a methyl group instead of one of the trifluoromethyl groups, we have succeeded in preparing and stereochemically characterizing the first configurationally stable diastereomeric 10-Sb-5⁹ stiborane, and herein we report the details. Kinetics of the interconversion process of the diastereomers have also been examined, and it has been found that the process was very sensitive to the nature of the solvent and additives.

Preparation of Stiborane 6. The ligand possessing the asymmetric carbon was prepared according to Scheme 1. Trifluoromethyl phenyl ketone was prepared in 60% yield from ethyl trifluoroacetate and phenyl Grignard reagent according to a reported procedure.¹⁰ Treating the ketone with methyl Grignard reagent gave alcohol 4. Treatment of 4 with *n*-BuLi in the presence of tetramethylethylenediamine in THF followed by the addition of 1,2-dibromo-1,1,2,2-tetrafluoroethane gave bromide 5 in 62% yield. The diastereomeric stiborane 6 was synthesized according to Scheme 2. 2-Phenyl-1,1,1,3,3,3-hexafluoro-2-propanol dilithiated by the procedure reported by Martin et al.^{8b} was added to a THF solution of (4-methylphenyl)antimony dichloride¹¹ to give monocyclic compound 7 in 78% yield along with a small amount of spiro compound 8 (7%). The tricoor-

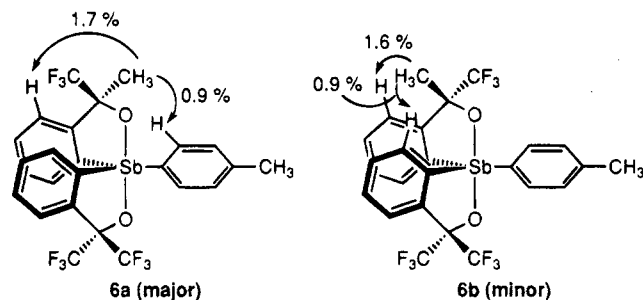


Figure 1. ¹H NMR NOE of diastereomers **6a** and **6b** by irradiation of the methyl group of bidentate ligand **10**.

dinate compound 7 was oxidized with sulfuryl chloride in dichloromethane to yield moisture sensitive pentacoordinate compound 9. Compound 9 was treated with dilithiated 2-phenyl-1,1,1-trifluoro-2-propanol (**10**) generated from the bromide 5 in ether to furnish compound 6 as a 6:4 diastereomeric mixture. Attempts to prepare 6 by the direct use of 4 met with failure and gave only trace amounts of the desired product.

Determination of Stereochemistry by NOE. To determine the relative stereochemistry of the diastereomers, differential NOE spectra were taken with a mixture of diastereomers 6 in C₆D₆. Proton irradiation of the major methyl group (δ 1.73) of the bidentate ligand resulted in intensity enhancement of signals of the ortho protons of the *p*-tolyl group (δ 8.17) and of the proton ortho to the 2-propoxy group (δ 7.31) of the bidentate ligand **10** (**6a**, drawing on the left), whereas proton irradiation of the minor methyl group (δ 1.59) led to the intensity enhancement of the proton ortho (δ 8.21) to the antimony of the symmetric bidentate ligand and to the proton ortho to the 2-propoxy group (δ 7.32) of the bidentate ligand **10** (**6b**, drawing on the right). Thus, as shown in Figure 1 the major diastereomer could be assigned as the compound with the methyl group of the bidentate ligand facing the *p*-tolyl group

(8) For example: (a) Perozzi, E. F.; Martin, J. C. *J. Am. Chem. Soc.* **1972**, *94*, 5519. (b) Perozzi, E. F.; Michalak, R. S.; Figuly, G. D.; Stevenson, W. H., III; Dess, D. B.; Ross, M. R.; Martin, J. C. *J. Org. Chem.* **1981**, *46*, 1049. (c) Granoth, I.; Martin, J. C. *J. Am. Chem. Soc.* **1979**, *101*, 4618, 4623. (d) Stevenson, W. H., III; Wilson, S.; Martin, J. C.; Farnham, W. B. *J. Am. Chem. Soc.* **1985**, *107*, 6340.

(9) For designation: Perkins, C. W.; Martin, J. C.; Arduengo, A. J.; Lau, W.; Alegria, A.; Kochi, J. K. *J. Am. Chem. Soc.* **1980**, *102*, 7753.

(10) Creary, X. *J. Org. Chem.* **1987**, *52*, 5026.
(11) Nunn, M.; Sowerby, D. B.; Wesolok, D. M. *J. Organomet. Chem.* **1983**, *251*, C45.

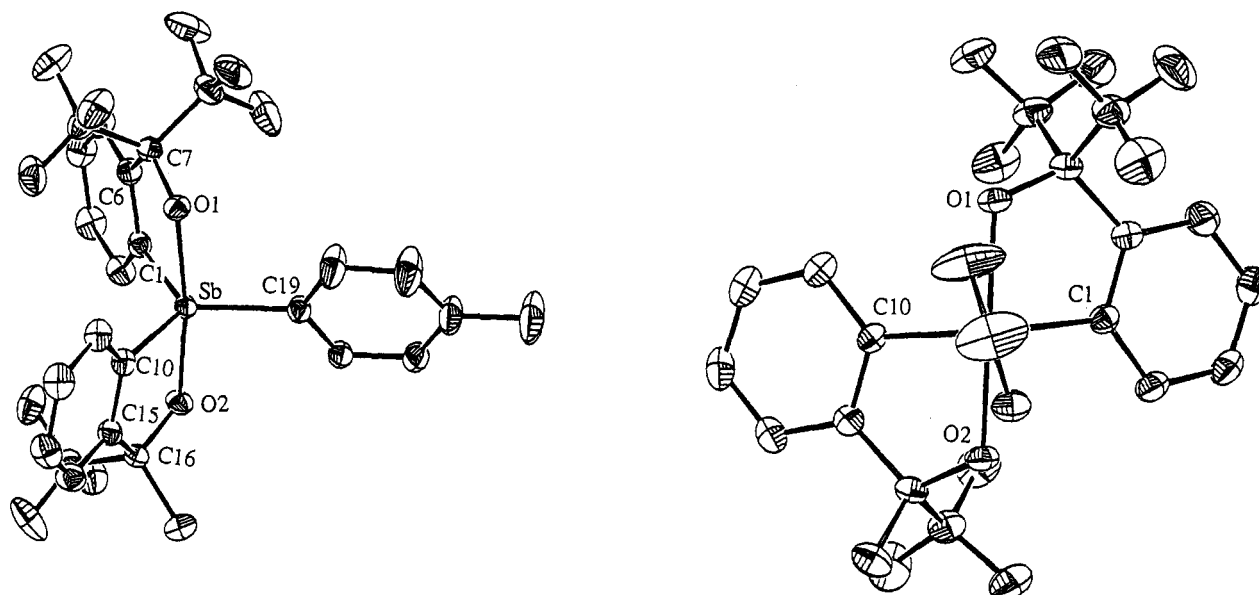


Figure 2. ORTEP drawing of **6a** showing the thermal ellipsoids at the 30% probability level. The figure on the right is a view from the direction along the axis between Sb and the methyl group of the *p*-tolyl group.

and could be designated (S_C, S_{Sb})¹² and (R_C, R_{Sb}), while the minor could be assigned as the compound with the methyl group of the bidentate ligand **10** facing the other bidentate and designated (R_C, S_{Sb}) and (S_C, R_{Sb}).

As with other spiro compounds containing Martin's ligand, a significant low field shift for the protons (6-H) of the bidentate ligand benzene ring ortho to antimony and opposite to the 2-propoxy substituent could be observed at δ 8.38 and 8.32 for **6a** and at δ 8.33 and 8.21 for **6b**. From the NOE measurements the signal at δ 8.21 could be assigned to the sole proton facing a methyl group; the other three all face trifluoromethyl groups. Thus, in this case besides the low field shift caused by electrostatic repulsion by the polarized apical bond, a secondary differentiation has occurred by the change from a trifluoromethyl group to a methyl group. The fact that the chemical shift of the proton facing the trifluoromethyl group of ligand **10** in the major diastereomer is slightly shifted more downfield (δ 8.38) than the other two protons (δ 8.33 and 8.32) is in accord with the fact that the ¹⁹F NMR spectrum of this trifluoromethyl group is more upfield (δ -80.0 in C₆D₆) than those of the symmetry Martin's ligand (δ -76.5 and -75.1 in C₆D₆), corresponding to larger electron density upon the fluorines in ligand **10**.

X-ray Structural Analysis of 6a and 8. Separation of the diastereomers was initially carried out by preparative TLC (hexane-CH₂Cl₂ (3:1)/SiO₂; major, R_f 0.24; minor, R_f 0.26). However, due to the closeness of the R_f value and facile permutation of the compounds under the separation conditions, workup usually afforded samples enriched up to only about 4:1 of either diastereomer. Other sources of gel (alumina and Florisil) and gel permeation chromatography were even less effective. Fortunately, it was later found that careful recrystallization of the diastereomeric mixture from acetonitrile afforded the major diastereomer **6a** as the sole product in crystals sufficient for X-ray structural analysis. Examination of the filtrate showed the presence of the

Table 1. Selected Crystallographic Data for **6a** and **8**

	6a	8
Bond Lengths (Å)		
Sb-O1	2.053(2)	2.042(3)
Sb-O2	2.019(2)	2.035(2)
Sb-C1	2.090(3)	2.094(4)
Sb-C10	2.083(3)	2.089(4)
Sb-C19	2.098(3)	2.094(4)
O1-C7	1.379(4)	1.377(5)
O2-C16	1.409(3)	1.384(4)
C1-C6	1.380(4)	1.385(6)
C10-C15	1.385(4)	1.382(5)
C6-C7	1.540(4)	1.546(6)
C15-C16	1.538(4)	1.533(6)
Bond Angles (deg)		
O1-Sb-O2	172.43(8)	170.6(1)
C1-Sb-C10	123.0(1)	121.5(1)
C1-Sb-C19	119.2(1)	118.7(2)
C10-Sb-C19	117.7(1)	119.8(2)
O1-Sb-C1	80.9(1)	81.2(1)
O2-Sb-C10	82.4(1)	81.5(1)
O1-C7-C6	112.6(2)	112.8(3)
O2-C16-C15	111.4(2)	112.8(3)
Sb-O1-C7	116.6(2)	116.8(2)
Sb-O2-C16	116.3(2)	116.4(2)
Sb-C1-C6	113.1(2)	112.8(3)
Sb-C10-C15	111.7(2)	112.4(3)
C1-C6-C7	116.6(2)	116.3(4)
C10-C15-C16	117.7(2)	116.8(3)
Torsion Angles (deg)		
O1-Sb-C19-C20	19.19	21.60
O1-Sb-C19-C24	18.39	21.39
O2-Sb-C19-C20	18.94	21.84
O2-Sb-C19-C24	18.14	21.64
av	18.89	21.62

diastereomers as a near equilibrium mixture, thus implying that isomerization of the diastereomers had occurred to give the more crystallizable major diastereomer during the recrystallization. The ORTEP drawings of **6a** are depicted in Figure 2, and selected structural parameters and crystal parameters are listed in Tables 1 and 2, respectively.

To make a comparison, X-ray structural analysis of pentacoordinate compound **8**, which has two identical bidentate ligands, was also carried out. The compound could also be obtained according to a procedure previ-

(12) Martin, J. C.; Balthazor, T. M. *J. Am. Chem. Soc.* **1977**, *99*, 152.

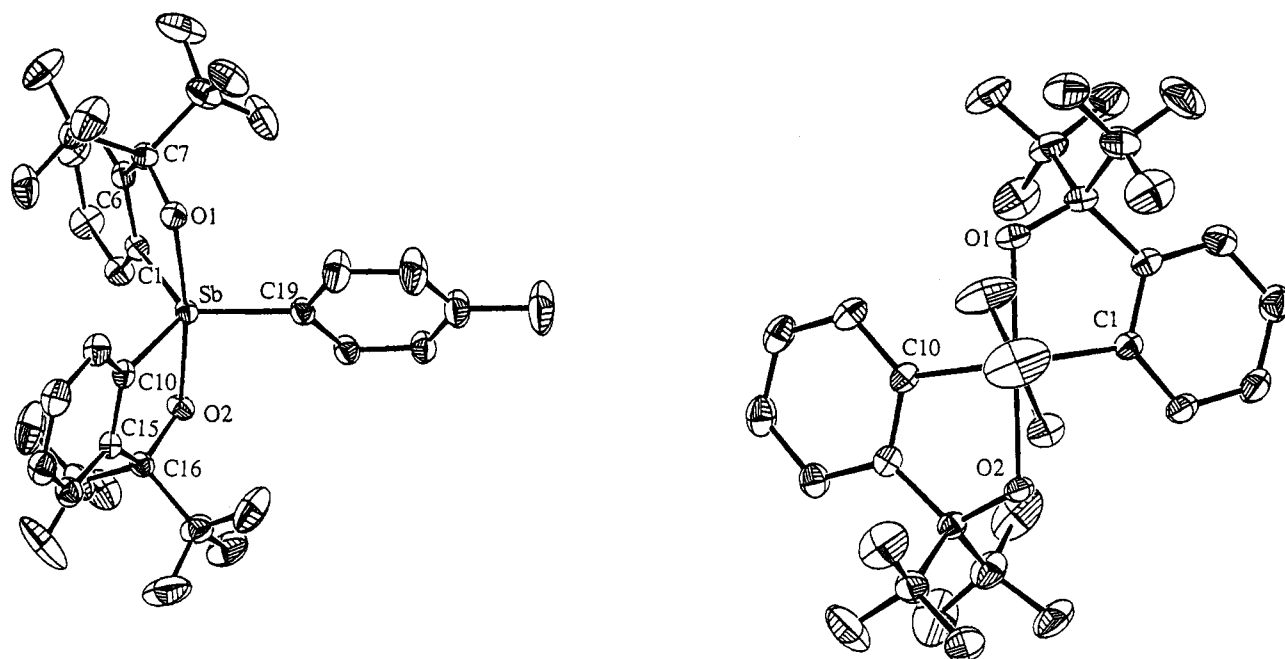


Figure 3. ORTEP drawing of **8** showing the thermal ellipsoids at the 30% probability level. The figure on the right is a view from the direction along the axis between Sb and the methyl group of the *p*-tolyl group.

Table 2. Crystal Data for **6a**, **8**, and **11**

	6a	8	11
formula	C ₂₅ H ₁₈ F ₉ O ₂ Sb	C ₂₅ H ₁₅ F ₁₂ O ₂ Sb	C ₃₃ H ₃₅ F ₁₃ NO ₂ Sb
mol wt	643.2	697.1	846.40
cryst syst	monoclinic	monoclinic	orthorhombic
space group	<i>P</i> 2 ₁ / <i>n</i>	<i>P</i> 2 ₁ / <i>n</i>	<i>P</i> n2 ₁ <i>a</i>
cryst dimens, mm	0.60 × 0.50 × 0.30	0.60 × 0.60 × 0.40	0.50 × 0.40 × 0.25
<i>a</i> , Å	17.700(3)	18.064(2)	17.323(5)
<i>b</i> , Å	9.272(2)	9.238(1)	19.928(5)
<i>c</i> , Å	15.219(2)	15.514(2)	10.054(3)
α, deg	90	90	90
β, deg	93.99(1)	96.32(1)	90
γ, deg	90	90	90
<i>V</i> , Å ³	2491.7(7)	2573.3(6)	3471(2)
<i>Z</i>	4	4	4
<i>D</i> _{calcd} , g cm ⁻³	1.71	1.80	1.62
abs coeff (<i>ν</i>), cm ⁻¹	10.84	10.69	8.04
<i>F</i> (000)	1264	1360	1696
radiation; λ, Å	Mo Kα, 0.71073	Mo Kα, 0.71073	Mo Kα, 0.71073
temp, °C	23 ± 1	23 ± 1	23 ± 1
2θ _{max} , deg	55.0	50.0	55.0
scan rate, deg/min	10.0	10.0	6.0
linear decay, %			
data collected	+ <i>h</i> , - <i>k</i> , ± <i>l</i>	± <i>h</i> , + <i>k</i> , + <i>l</i>	+ <i>h</i> , - <i>k</i> , + <i>l</i>
total no. of data collected, unique, obsd	6331, 5719, 4806 (<i>I</i> > 3σ(<i>I</i>))	6583, 5921, 5193 (<i>I</i> > 3σ(<i>I</i>))	4532, 4092, 3545 (<i>I</i> > 3σ(<i>I</i>))
<i>R</i> _{int}	0.03	0.01	0.00
no. of params refined	394	407	456
<i>R</i> , <i>R</i> _w , <i>S</i>	0.028, 0.046, 0.95	0.036, 0.045, 3.23	0.036, 0.044, 1.45
max shift in final cycle	0.35	0.24	0.44
final diff map, max, e/Å ³	0.59	2.03	0.99

ously reported.¹³ The ORTEP drawings of **8** are shown in Figure 3 while selected structural parameters and crystal parameters are listed alongside those of **6a** in Tables 1 and 2.

Both molecules have pseudotrigonal bipyramidal structures with the two oxygen atoms in the apical positions and three carbon atoms in the equatorial positions. The average dihedral angle between the plane of the *p*-tolyl group and the apical axis was found to be ca. 19° for compound **6a** and ca. 22° for compound **8** in the direction of the open space between the two

bidentate ligands as shown on the right-side drawing in Figures 2 and 3. From the electronic viewpoint, this conformation corresponds to one in which the apical bonds and the *p* orbitals of the aromatic ring have aligned nearly perpendicularly to avoid unfavorable orbital overlap. This observation implies that the apical bonds upon the antimony atom are of energy levels rather close to the highest occupied π energy level in the benzene ring and are not effectively stabilized by the benzene π* orbital. The deviation of the angle from 0° is probably due to steric repulsion between the ortho H of the *p*-tolyl group and the oxygens of the bidentate ligands. The only notable difference between the two

(13) Akiba, K.-y.; Nakata, H.; Yamamoto, Y.; Kojima, S. *Chem. Lett.* **1992**, 1559.

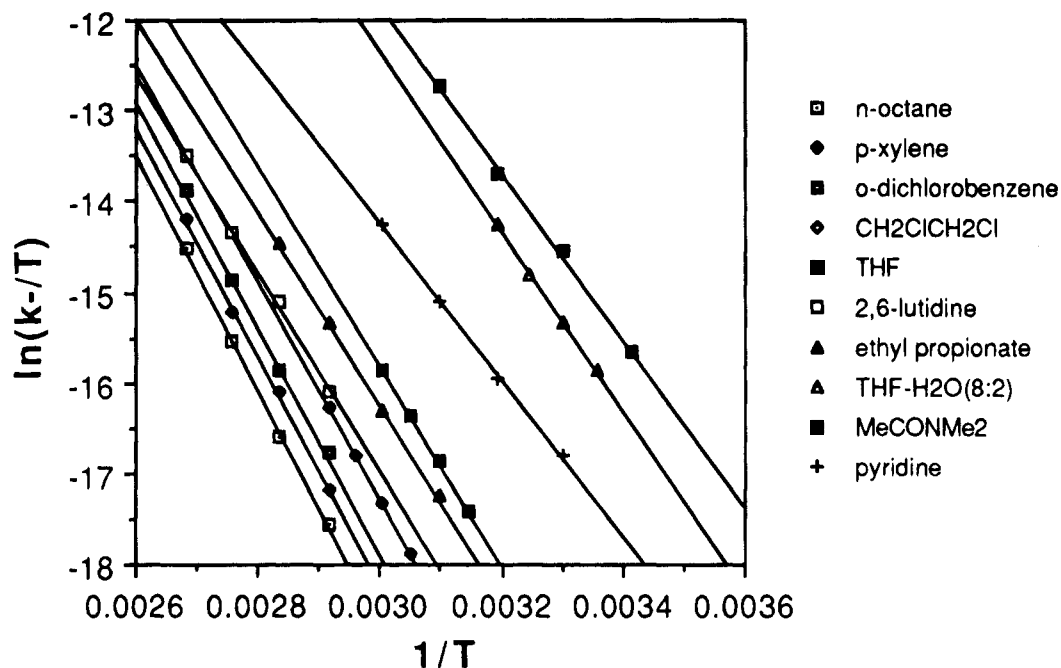


Figure 4. Eyring plot of the rates of conversion of minor **6b** to major **6a** determined in various solvents.

compounds is the bond length between the two apical bonds. In compound **6a** the bond of ligand **10** (Sb–O2, 2.019 Å) was observed to be shorter than that of the symmetric ligand (Sb–O1, 2.053 Å) by 0.034 Å, whereas little difference (0.007 Å) was observed in compound **8** (2.035 and 2.042 Å), while the sum of the two Sb–O bond lengths remains the same for **6a** and **8** (4.072 and 4.077 Å, respectively). This implies that the bond strength is nearly equal in the symmetric compound while it has been perturbed in compound **6a** to give a slightly stronger Sb–O bond for the ligand **10** moiety. The methyl group of ligand **10** in compound **6a** was found to be facing toward the *p*-tolyl group, thus confirming the relative stereochemistry established by NMR techniques. It is also evident from the acute bond angles (ca. 81°) of the rings that ring strain already exists in the ground state structure.

Permutation in Solvents of Various Donor Abilities. Initially, it was found that permutation took place rather rapidly at room temperature in deuterated solvents, especially in CDCl₃, with equilibrium attained within a few hours or much less with no reproducibility in rates. However, by using freshly purified benzene, it was found that the rate could be reduced dramatically. Therefore, to determine the magnitude of the permutation barrier and also deduce solvent effects on the rates, we performed measurements in various solvents freshly distilled.

Kinetic measurements of the permutation process were carried out by using samples highly enriched with the major diastereomer **6a** and monitoring the relative amount of the ¹⁹F NMR signals due to the trifluoromethyl group of ligand **10** of **6a** (δ –80) and **6b** (δ –79). Ten different solvents having various polarities and donor abilities were utilized, and the rates were measured at four different temperatures each. A THF–H₂O (8:2 by weight) mixture prepared from freshly distilled THF and deionized water was also included in the 10 solvents as a substitute for pure water, which could serve not only as a highly polar and donating solvent but also as a proton source. The equilibrium ratios of

6a (major) to **6b** (minor) were in the range 60.0–66.7:40.0–33.3, depending on the solvents and temperatures. By assuming that the process follows reversible pseudo-first-order kinetics, $\ln\{(x_e - x_0)/(x_e - x)\}$ (x = percentage of minor diastereomer, x_0 = initial percentage, x_e = percentage at equilibrium) was plotted against time. In all cases, the plots showed good linear relationship. (See supplementary material for rate constants and equilibrium ratios). *p*-Xylene, in which we measured, first of all, a sample with a concentration about 5-fold that of other samples, was also measured at 343 K, since there existed the slight possibility that the process might include some intermolecular process. If a second-order intermolecular process were operative, a rate increase of up to 5 times could have occurred. However, the rates measured at this temperature (for minor **6b** to major **6a**, $(1.17 \pm 0.01) \times 10^{-5}$ and $(1.19 \pm 0.02) \times 10^{-5}$; for major **6a** to minor **6b**, $(7.70 \pm 0.07) \times 10^{-6}$ and $(7.84 \pm 0.13) \times 10^{-6}$) turned out to be essentially the same. Therefore, it could be concluded that the process was intramolecular, and thereafter the measurements were primarily made with only one concentration. Since the observed rates of samples using dimethylacetamide (DMA) distilled from CaH₂ turned out to be unexpectedly large (for minor **6b** to major **6a**, $(1.47 \pm 0.04) \times 10^{-4}$; for major **6a** to minor **6b**, $(7.48 \pm 0.18) \times 10^{-5}$ at 303 K), we suspected that there could be the presence of liberated amine generated during the distillation process. A measurement at 303 K using DMA distilled from CaSO₄ gave a similar result (for minor **6b** to major **6a**, $(1.41 \pm 0.02) \times 10^{-4}$; for major **6a** to minor **6b**, $(7.21 \pm 0.12) \times 10^{-5}$), and thus this concern was dismissed.

The Eyring plot of these rate constants shown in Figure 4 also showed good correlation, and from it activation parameters were calculated as given in Table 3 along with reported values of E_T^N (polarity)¹⁴ and DN^N (normalized donor number).¹⁵ The reported estimated donor numbers for *p*-xylene and *o*-dichlorobenzene are

(14) Reichardt, C. *Solvents and Solvent Effects in Organic Chemistry*, 2nd ed.; VCH Publishers: Weinheim, Germany, 1988.

(15) Marcus, Y. *J. Solution Chem.* **1984**, *13*, 599.

Table 3. Activation Parameters in Various Solvents^a

solvent	E_T^N ^b	DN ^c	minor 6b to major 6a			major 6a to minor 6b		
			ΔH^\ddagger (kcal mol ⁻¹)	ΔS^\ddagger (eu)	ΔG^\ddagger_{298} (kcal mol ⁻¹)	ΔH^\ddagger (kcal mol ⁻¹)	ΔS^\ddagger (eu)	ΔG^\ddagger_{298} (kcal mol ⁻¹)
<i>n</i> -octane	0.012	0.00	26.0 ± 2.0	-6.3 ± 5.6	27.9	26.1 ± 2.1	-6.9 ± 5.9	28.2
<i>p</i> -xylene	0.074	(0.13) ^d	25.0 ± 1.0	-8.3 ± 2.9	27.7	25.1 ± 0.9	-8.9 ± 2.6	27.8
<i>o</i> -dichlorobenzene	0.225	(0.08) ^d	24.7 ± 2.2	-8.8 ± 6.2	27.3	25.0 ± 2.2	-8.8 ± 6.3	27.6
1,2-dichloroethane	0.327	0.00	23.5 ± 0.5	-11.1 ± 1.5	26.8	23.5 ± 0.6	-11.9 ± 1.8	27.1
THF	0.207	0.52	21.8 ± 0.9	-13.4 ± 2.8	25.7	21.9 ± 0.7	-13.8 ± 2.2	26.0
2,6-lutidine	0.191		21.7 ± 1.7	-15.8 ± 4.8	26.4	21.9 ± 1.7	-16.1 ± 4.6	26.7
ethyl propionate	0.228	0.44	21.1 ± 0.6	-16.2 ± 1.6	25.9	21.4 ± 0.6	-16.4 ± 1.8	26.2
THF-H ₂ O (8:2)	0.563 ^e	0.51 ^f	19.8 ± 0.8	-12.4 ± 2.6	23.5	19.8 ± 0.8	-13.5 ± 2.5	23.8
dimethylacetamide	0.401	0.72	18.1 ± 1.3	-16.4 ± 4.1	23.0	18.4 ± 1.3	-16.9 ± 4.3	23.4
pyridine	0.302	0.85	17.1 ± 1.0	-24.1 ± 3.1	24.3	17.4 ± 1.1	-24.3 ± 3.5	24.6

^a Error estimated at 90% confidence level. ^b Cited from ref 15. ^c Cited from ref 16. ^d Estimated values in ref 16. ^e Measured by us. ^f Weighted value between THF (0.52) and H₂O (0.46).

shown in parentheses; however, since aromatic π electrons do not coordinate to the antimony of **6**, we can regard the DN^N values to be 0 for these solvents. The E_T^N for the THF-H₂O mixture, of which we used a mixture by weight, was measured to be 0.563. Since enthalpy would be the basis of determining the stability of the transition state, the solvents have been listed in the order of activation enthalpy. A comparison of the activation enthalpies in solvents of no donor ability clearly shows that as the E_T^N value of the solvent increases, i.e., 0.012 (*n*-octane), 0.074 (*p*-xylene), 0.225 (*o*-dichlorobenzene), and 0.327 (1,2-dichloroethane), the enthalpies decrease accordingly, i.e., 26.1, 25.1, 24.9, and 23.5 kcal mol⁻¹, respectively. THF ($E_T^N = 0.207$) and THF-H₂O ($E_T^N = 0.563$), which have about the same donor ability, show a similar trend, with the ΔH^\ddagger values being 21.9 and 19.8 kcal mol⁻¹, respectively. Thus, it is quite evident that the polarity of the solvent serves to stabilize the transition state. This implies that the transition state is more polarized than the ground state. When we compare pairs of solvents of similar polarity and of differing donor ability such as *o*-dichlorobenzene ($E_T^N = 0.225$, DN^N = 0.00) and ethyl propionate ($E_T^N = 0.228$, DN^N = 0.44) and pyridine ($E_T^N = 0.302$, DN^N = 0.85) and 1,2-dichloroethane ($E_T^N = 0.327$, DN^N = 0.00), it is quite clear that the solvent with the larger donor number stabilizes the transition state to a much larger extent. The reduction of donor ability by virtue of steric hindrance in 2,6-lutidine brought about by the methyl groups in the vicinity of the nucleophilic center clearly led to a quite significant decrease in rates compared with pyridine, and the activation parameters showed a consistent trend; i.e., the average activation enthalpy and activation entropy were 21.8 kcal mol⁻¹ and -16.0 eu for 2,6-lutidine and 17.3 kcal mol⁻¹ and -24.2 eu for pyridine, respectively. The role of THF-H₂O as a proton source turned out to be insignificant.

The value of activation entropy was found to be negative for all solvents measured, even for those solvents that do not possess donative character. Since *n*-octane also gave a negative value of significance, the value cannot be attributed to the realignment of solvent such that could be supposed for aromatic or polar solvents. We are not sure of the origin, but it could be due to the structural change on going from the trigonal bipyramidal structure in the ground state to the unfavorable trigonal bipyramidal structure where the *p*-tolyl group should be at an apical position or square pyramidal structure in the transition state, which is more congested. Solvents having donor abilities showed larger negative values, and the values corresponded well

with the nature of the coordinating group, i.e., THF (-13.6) and THF-H₂O (-13.0) having single-bonded oxygen atoms and ethyl propionate (-16.3) and dimethylacetamide (-16.7) having carbonyl oxygens. This probably indicates that these pairs share similar degrees of freedom or, in other words, similar structure in the transition state. The large negative value for pyridine compared with the others suggests a highly congested hexacoordinate transition state compared with the pentacoordinate ground state.

Although the data clearly show that the effect of donor ability is more significant than the polarity, we decided to evaluate the two in quantitative terms by applying multiregression analysis, using the normalized E_T^N and DN^N as variants of the nine solvents (2,6-lutidine was omitted) of which both values have been determined.¹⁶ The following equation was thus derived.

$$\Delta H^\ddagger = 25.83 - 5.00E_T^N - 7.42DN^N \quad (1)$$

The equation showed a very good fit of $R = 0.984$. The fact that the coefficient of DN^N turned out to be larger than that of E_T^N implies that it has a larger role in stabilizing the transition state.

Although there was a strong dependence of the rate upon the solvent, there was no appreciable change in the relative difference of ¹⁹F NMR chemical shifts among the three trifluoromethyl groups in either diastereomer no matter which solvent was used, thus implying that there was little if any stabilization by coordination of solvent in the ground state even when pyridine was used as solvent, whereas solvent effect was substantial in chemical shift difference in stiboranes in which the *p*-tolyl group in **8** was replaced with halogen atoms.¹⁷ The temperature dependence of the chemical shift was also examined in the temperature range 20–100 °C, and the shift showed practically no change in this case either. Therefore, it could be concluded that there is little perturbation, if any, in the ground state and its contribution need not be considered for the observed solvent effects.

Our observations lead us to the following mechanistic interpretation of the permutation. In solvents of no donor ability the pentacoordinate compounds probably undergo a permutation that can be illustrated by the usual Berry pseudorotation mechanism, having a transition state of high ring strain brought about by the five-

(16) Krygowski, T. M.; Fawcett, W. R. *J. Am. Chem. Soc.* **1975**, *97*, 2143.

(17) Kojima, S.; Nakata, H.; Takagi, R.; Yamamoto, Y.; Akiba, K.-y. Unpublished results.

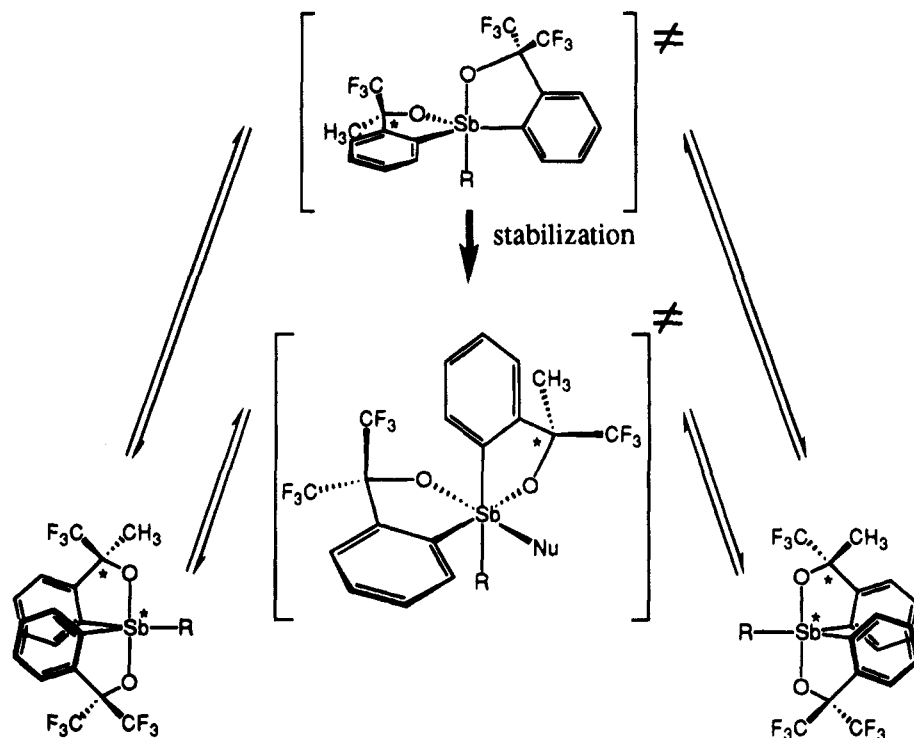


Figure 5. Possible transition state structures in the absence and presence of donative species.

membered bidentate in an unfavorable and inevitable equatorial–equatorial disposition, whereas the least ring strain is expected in the ground state structure in which the bidentate occupies apical–equatorial positions in a nearly ideal 90° angle. Whether or not the transition state of highest energy in this multistep transformation is actually the trigonal bipyramid shown in Figure 5 is not known for certain, and it could be that the transition state is more of a square pyramidal structure. Whichever it may be, the presence of high ring strain does not diminish to a large extent and does not change the essence of the transition state. However, when solvents of donating nature are used, it can relieve the ring strain by interacting with the antimony atom and thus creating a pseudooctahedral species in which the bond angles upon antimony become close to the ideal value of 90° , thereby lowering the energy of the transition state. This explanation is consistent with the fact that solvents with small donor numbers would give a weakly coordinate species resembling more of a penta-coordinate species, while those of larger donor numbers would give tighter coordination to form pseudooctahedral species, leading to larger stabilization in the transition state. This stabilization effect was absent in the case of corresponding pentacoordinate phosphorus compounds.¹⁸

Permutation in the Presence of Acid. To look into other possible factors, we next carried out measurements in the presence of acid to see whether protonation of the pentacoordinate antimony compound could be the key factor for the rapid permutation observed in unpurified CDCl_3 .

The THF– H_2O mixture can be considered a weakly acidic solvent; however, we found no effect (*vide supra*). Therefore, we considered examination with a strong acid, namely trifluoroacetic acid. The results of mea-

Table 4. Rates of Equilibration in the Presence of Trifluoroacetic Acid at 293 K^a

concn (mol L ⁻¹)	rates ^b (s ⁻¹)	
	minor to major	major to minor
none	$(4.0 \pm 0.2) \times 10^{-7}$ ^c	$(2.0 \pm 0.1) \times 10^{-7}$ ^c
8.33×10^{-3}	$(1.25 \pm 0.13) \times 10^{-6}$	$(7.54 \pm 0.80) \times 10^{-7}$
1.90×10^{-1}	$(1.78 \pm 0.06) \times 10^{-5}$	$(1.07 \pm 0.03) \times 10^{-5}$

^a THF was used as solvent. ^b Error estimated at 90% confidence level. ^c Extrapolated from data in Table 3.

surements of THF solutions with 0.35 and 7.4 equiv of trifluoroacetic acid (TFA) at 293 K are shown in Table 4 along with the rate in THF without the presence of TFA at this temperature derived by extrapolating the plotted data in Figure 4. Assuming that the observed data follow reversible pseudo-first-order kinetics as before, the observed rate could be analyzed according to the equation $k_{\text{obsd}} = k_1 + k_2[\text{TFA}]$ (k_{obsd} = observed rate, k_1 = rate constant first order on **6**, k_2 = rate constant first order on both **6** and TFA and second order overall). From this we obtained $k_1 = (4.99 \pm 0.44) \times 10^{-7} \text{ s}^{-1}$ and $k_2 = (9.21 \pm 0.60) \times 10^{-5} \text{ s}^{-1} \text{ mol}^{-1} \text{ L}$.¹⁹ When k_1 and the effective molar rate constant of k_2 are compared, even the order of magnitude is enough to conclude that a significant acceleration is caused by the addition of acid. However, the magnitude of acceleration was not as drastic as would have been expected if protonation was the cause, judging from the large amount of the strong acid in the acidic samples as compared with the trace amount expected in nonpurified CDCl_3 in which in some cases equilibrium was attained within half an hour at ambient temperature. Therefore, we can conclude that although proton concentration could be a factor, its contribution is relatively small, and it is rather the nucleophilicity (or donor ability) of the conjugate base of the acid that is the predominant factor in this case.

(18) Kojima, S.; Nakamoto, M.; Kajiyama, K.; Akiba, K.-y. Unpublished results.

(19) Error estimated at 90% confidence level.

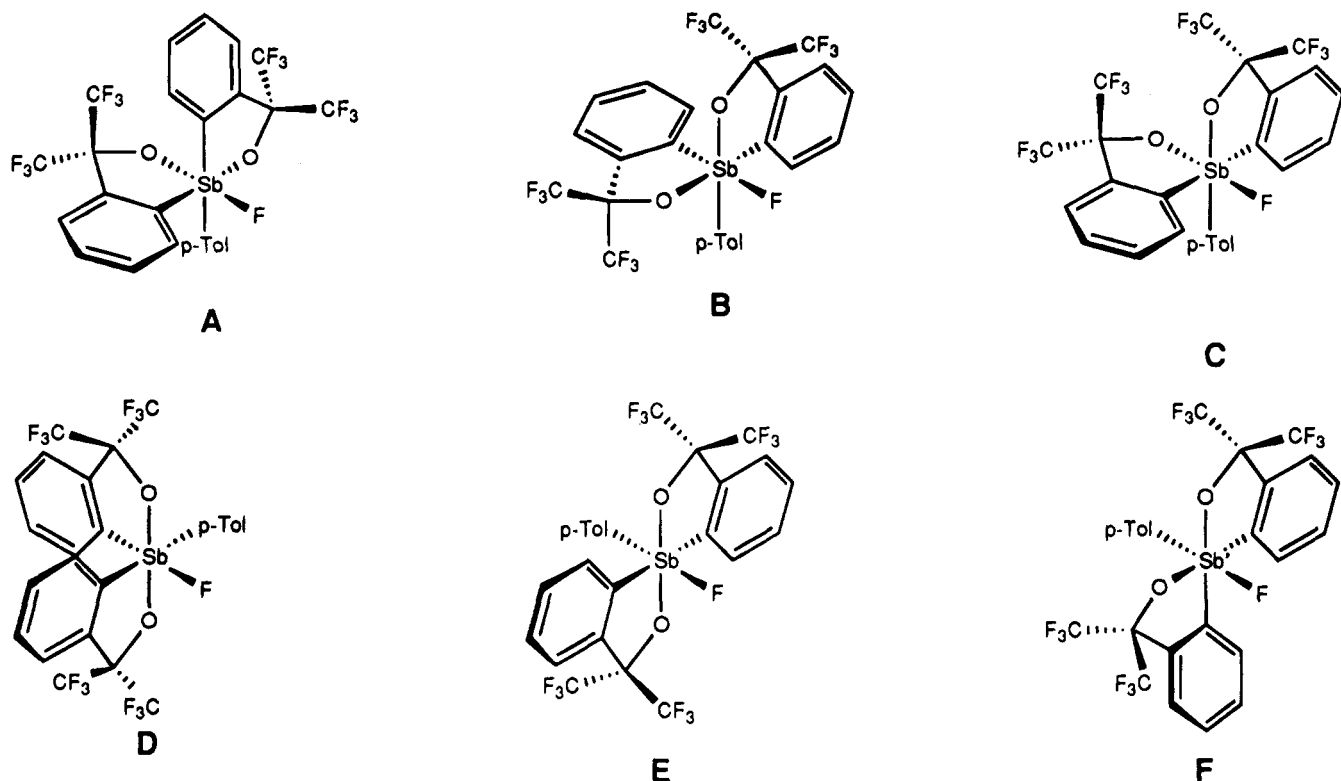


Figure 6. Probable configurational isomers of **11**.

Permutation in the Presence of Anionic Nucleophiles. To make the role of nucleophiles clear, we next attempted to examine the rates in the presence of very strong nucleophiles. NMR samples with less than ca. 0.1 equiv ("less than" meaning that 0.1 equiv of the nucleophile was mixed but most of it was left undissolved) of Et_4NF or MeONa present in THF were measured within 10 min of their preparation. The spectra indicated that equilibration had already taken place in both cases. Therefore, we can conclude that there is a strong influence of nucleophiles on the rate. Thus, the great acceleration observed in unpurified CDCl_3 could be explained according to these results. That is, the nucleophilic nature of the trace amount of liberated chloride anion should be the cause of the acceleration, and the varying rates can be attributed to the actual amount of the chloride anion present in the solvent. We attempted to examine rates in the presence of Bu_4NCl to verify this assumption. As a whole, the rates were in measurable range and acceleration was obvious. However, the rate values were not reproducible.

Formation and Structure of Hexacoordinate Species. Close examination of the ^{19}F NMR spectra of the mixture with a small amount of Et_4NF revealed the presence of small peaks other than those of the pentacoordinate diastereomers. Since there were no broad peaks that could be assigned to a free fluoride anion, it could be assumed that the peaks were those of hexacoordinate ate complexes formed by the coordination of the fluoride anion. Since it was possible that these ate complexes could be intermediates or catalysts for the acceleration, we next attempted the isolation of the hexacoordinate adduct. To simplify matters, we utilized compound **8** instead of **6**. By dissolving compound **8** and an excess amount of tetraethylammonium fluoride in acetone and allowing the solution to stand, we obtained

the desired compound as cubic crystals. ^1H and ^{19}F NMR spectra of the compound in acetone- d_6 measured at room temperature were complex with mostly broad signals; however, a measurement at -40°C revealed the presence of three sets of signals, none of which could be assigned to pentacoordinate **8**. Thus, at least three different configurational isomers of the six geometrically possible, as shown in Figure 6, are present in solution. When this solution was treated with water, the pentacoordinate starting material **8** could be recovered, quantitatively. This implies that an equilibrium between the pentacoordinate and the hexacoordinate species exists, in which the hexacoordinate species is highly favored thermodynamically. The presence of a fast equilibration process between the penta- and hexacoordinate species implies that the interconversion among the hexacoordinate isomers is a very rapid process. However, assignment of the isomers could not be carried out because of the complexity of the spectra and lack of data with which to compare. Among the three compounds we believe that two are **A** and **C** on the basis of the solid state structure of **11** which had an oxygen and the fluorine in an anti relationship (vide infra).

X-ray structural analysis on **11** was carried out, and the ORTEP drawing is depicted in Figure 7, with structural parameters in Table 5 and crystal parameters listed along with those of **6a** and **8** in Table 2. The fluoride was found to be attached anti to one of the oxygen atoms of the bidentate. All of the bonds in the original pentacoordinate compound are elongated because of the incoming fluoride. The ring angles about the antimony atom are very close to those of **6a** and **8**, with a slight contraction in line with the elongation of the Sb-element bonds. Thus, the ring strain in **11** should not be too different from that in **6a** and **8**. The configuration about the antimony atom turned out to

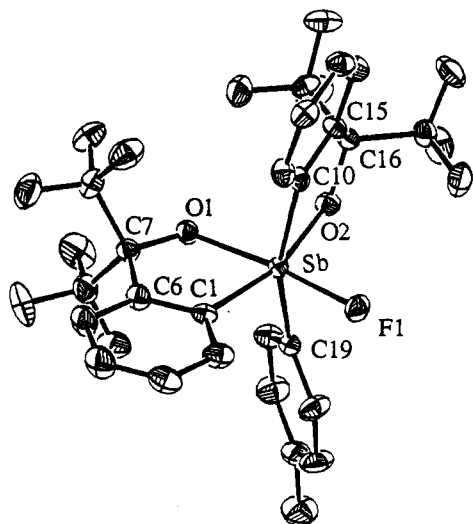
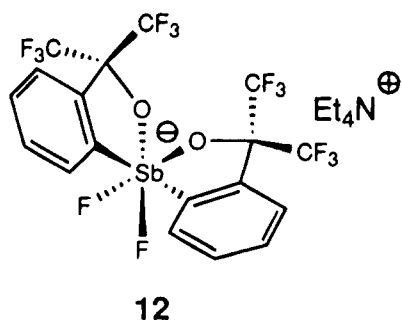


Figure 7. ORTEP drawing of **11** showing the thermal ellipsoids at the 30% probability level. The tetraethylammonium cation has been omitted for clarity.

Table 5. Selected Crystallographic Data for **11**

Bond Lengths (Å)			
Sb—O1	2.066(4)	Sb—O2	2.107(4)
Sb—C1	2.148(7)	Sb—C10	2.116(7)
Sb—C19	2.124(6)	Sb—F1	1.999(4)
O1—C7	1.360(8)	O2—C16	1.378(7)
C1—O6	1.36(1)	C10—C15	1.368(9)
C6—C7	1.56(1)	C15—C16	1.543(9)
Bond Angles (deg)			
O1—Sb—F1	172.0(2)	O2—Sb—C1	164.8(2)
C10—Sb—C19	159.6(2)	O1—Sb—C1	79.2(2)
O2—Sb—C10	77.5(2)	O1—Sb—O2	86.5(2)
C1—Sb—C10	98.7(3)	Cl—Sb—C19	100.6(2)
O1—C7—C6	112.6(5)	O2—C16—C15	111.9(5)
Sb—O1—C7	118.5(4)	Sb—O2—C16	118.4(4)
Sb—C1—C6	113.5(5)	Sb—C10—C15	116.7(5)
C1—C6—C7	116.2(6)	C10—C15—C16	115.1(6)

be that of **A** and not **C** which can be considered an analog of **12**¹⁷ having a fluorine in the place of the *p*-tolyl



group. The main reason for adopting the configuration **A** can be explained on steric grounds. Configuration **A** seems to be less structurally hindered than **C** because the two sets of trifluoromethyl groups are further apart. The distance between the two CF₃ carbons facing each other is 5.018 Å in **11**, while it is 4.561 Å in ate complex **12**. Since **12** turned out to assume a structure like **C** with two pairings of anti fluorine and oxygen atoms, it seems that the electronic preference for fluorine and oxygen to assume an anti relationship prevails over repulsion of the trifluoromethyl groups. A point to note is that the anti relationship of one oxygen and the fluorine of the X-ray structure resembles the stereo-

chemical relationship of one oxygen and the nucleophilic species in the transition state structure we proposed for the permutation in the presence of nucleophilic species (Figure 5 and **A** in Figure 6). Thus, this X-ray structure is highly indicative that hexacoordination is facile to attain especially with coordination of a nucleophilic species to the pentacoordinate compound anti to an oxygen atom. The same should apply for the strongly nucleophilic alkoxide anion and also nucleophilic solvents.

In conclusion, we have succeeded in stereochemically characterizing the first configurationally stable 10-Sb-5 stiborane, and through kinetic investigations we have found that the permutation of the compound was strongly accelerated by electron donating species, apparently by the formation of transient or stable hexacoordinate species. To gain further insight into this process, we are currently examining substituent effects from the steric and electronic standpoints by introducing other groups in the place of the *p*-tolyl group. The results will be reported in due course.

Experimental Section

Melting points were measured with a Yanagimoto micro melting point apparatus and are uncorrected. ¹H NMR (400 MHz) and ¹⁹F (376 MHz) spectra were recorded on a JEOL EX-400 spectrometer or routinely on a Hitachi R-90H spectrometer. ¹H NMR chemical shifts (δ) are given in parts per million downfield from internal Me₄Si or from residual chloroform (δ 7.26) or benzene (δ 7.2). ¹⁹F NMR chemical shifts (δ) are given in parts per million downfield from internal CFC1₃. Elemental analyses were performed on a Perkin-Elmer 2400CHN elemental analyzer.

All reactions were carried out under N₂ except where noted otherwise. THF and Et₂O were freshly distilled from sodium benzophenone. Dimethylacetamide was distilled from either CaH₂ or CaSO₄. All other solvents and liquid reagents were distilled from CaH₂. Trifluoromethyl phenyl ketone¹⁰ and dichloro(4-methylphenyl)stibine¹¹ were prepared according to published procedures. Column chromatography was carried out with Merck silica gel 60 (70–230 mesh). Preparative thin layer chromatography was carried out on plates of Merck silica gel 60 GF₂₅₄.

1,1,1-Trifluoro-2-phenyl-2-propanol (4). To an ether (130 mL) solution of MeMgI prepared from magnesium (10.4 g, 0.43 mol) and iodomethane (26.6 mL, 0.43 mol) was added trifluoromethyl phenyl ketone (40.0 mL, 0.29 mol) in ether (40 mL) at 0 °C. After the mixture was stirred overnight at room temperature the solution was quenched with aqueous NH₄Cl, extracted with ether, dried with MgSO₄, and concentrated in vacuo. Distillation under reduced pressure from CaH₂ gave the product (48.4 g, 89%) as a colorless liquid: bp 83–85 °C/15 mmHg; ¹H NMR (CDCl₃) δ 7.26–7.64 (m, 5 H), 2.47 (bs, 1 H), 1.79 (q, *J*_{H-F} = 1.1 Hz, 3 H); ¹⁹F NMR (CDCl₃) δ -81.5 (s).

1,1,1-Trifluoro-(2-bromophenyl)-2-propanol (5). To a THF (15 mL) solution of *n*-BuLi (c 1.65 M in hexane, 203 mL, 0.34 mol) and tetramethylethylenediamine (50.6 mL, 0.34 mol) was added alcohol **2** (28.98 g, 0.152 mol) at 0 °C, and the solution was stirred for 2 h. To this solution was added 1,2-dibromo-1,1,2,2-tetrafluoroethane (23.7 mL, 0.20 mol) at -78 °C. After the solution was allowed to warm to room temperature, it was additionally stirred for 2 h and then quenched with aqueous NH₄Cl. Extraction with ether, drying with MgSO₄, and removal of solvent followed by distillation under reduced pressure yielded the product as a colorless liquid (25.4 g, 62%): bp 84–85 °C/0.9 mmHg; ¹H NMR (CDCl₃) δ 7.17–7.70 (m, 5 H), 4.04 (s, 1 H), 1.92 (q, *J*_{H-F} = 1.1 Hz, 3 H); ¹⁹F NMR (CDCl₃) δ -79.3 (s).

3,3-Bis(trifluoromethyl)-1-(4-methylphenyl)-3*H*-2,1-benzoxastibole (7). To *n*-BuLi (c 1.6 M in hexane, 52 mL, 83 mmol) was added tetramethylethylenediamine (1.21 mL, 7.81 mmol), and the solution was stirred for a few minutes to allow the formation of a suspension. After THF (3 mL) was added to dissolve the precipitation, 1,1,1,3,3,3-hexafluoro-2-phenyl-2-propanol (6.68 mL, 40.0 mmol) was added dropwise at 0 °C. After the solution was stirred overnight at room temperature, THF (100 mL) was added to dissolve the newly formed precipitate followed by the dropwise addition of **3** (11.28 g, 40.0 mmol) in THF (100 mL) at -78 °C. The solution was quenched with aqueous NH₄Cl after stirring overnight. Extraction was done with ether followed by usual workup. Chromatography (*n*-hexane-ethyl acetate = 10:1 on SiO₂) furnished **7** (14.19 g, 78%) as a colorless solid along with a small amount of spiro compound **8** (2.87 g, 7%). Compound **7**: mp 113.5–115 °C; ¹H NMR (CDCl₃) δ 7.05–7.54 (m, 4 H), 2.25 (s, 3 H); ¹⁹F NMR (CDCl₃) δ -75.1 (q, *J* = 9.3 Hz, 3F), -77.3 (q, *J* = 9.3 Hz, 3F). Anal. Calcd for C₁₆H₁₁F₆OSb: C, 42.24; H, 2.44. Found: C, 42.39; H, 2.51. Compound **8**: mp 135.5–136 °C; ¹H NMR (CDCl₃) δ 8.0–8.2 (m, 2H), 7.92 (d, *J* = 7.9 Hz, 2H), 7.5–7.9 (m, 6H), 7.32 (d, *J* = 7.9 Hz, 2H), 2.33 (s, 3H); ¹⁹F NMR (CDCl₃) δ -74.2 (q, *J* = 8.3 Hz, 3F), -73.0 (q, *J* = 8.3 Hz, 3F).

1,1-Dichloro-3,3-bis(trifluoromethyl)-1-(4-methylphenyl)-3*H*-2,1-benzoxastibole (9) and 3,3,3'-Tris(trifluoromethyl)-3'-methyl-1-(4-methylphenyl)-1,1'-spirobi(3*H*-2,1-benzoxastibole) (6). To compound **7** (0.553 g, 1.22 mmol) dissolved in CH₂Cl₂ (10 mL) was added SO₂Cl₂ (0.20 mL, 2.5 mmol) at 0 °C. After 1 h of stirring at room temperature, the solvent and excess SO₂Cl₂ were removed under reduced pressure to give the dichloride quantitatively as a white solid sensitive to moisture. This product was subsequently used without further purification. ¹H NMR (CDCl₃) δ 7.05–7.54 (m, 4 H), 2.25 (s, 3 H); ¹⁹F NMR (CDCl₃) δ -75.1 (q, *J* = 9.3 Hz, 3 F), -77.3 (q, *J* = 9.3 Hz, 3 F).

To 1,1,1-trifluoro-2-(2-bromophenyl)-2-propanol (0.352 g, 1.31 mmol) in ether (10 mL) was added *n*-BuLi (c 1.65 M, 1.7 mL, 2.80 mmol) at -78 °C, and the resulting solution was stirred overnight at room temperature, during which time the gradual formation of a white mass was observed. THF (10 mL) was added to the mixture to make a homogeneous solution of lithium 1,1,1-trifluoro-2-(2-lithiophenyl)-2-propoxide (**10**).

The solution of **10** was added dropwise to a THF (10 mL) solution of the dichloride **9** at -78 °C. After the solution was stirred at this low temperature for 1 h, the solution was allowed to warm to room temperature. The solution was treated with aqueous NH₄Cl followed by extraction with CH₂Cl₂. Usual workup and subsequent chromatography (*n*-hexane-CH₂Cl₂ = 2:1) yielded a diastereomeric mixture of **6** (0.182 g, 23%) as a colorless oil. Slow recrystallization from CH₃CN gave the major diastereomer (0.141 g, 18%) as colorless crystals. The filtrate was found to have an equilibrium mixture of the diastereomers. Separation by TLC could give the minor diastereomer in up to only 80% purity due to the facile permutation under the separation procedure. **6a (major)**: mp 152–153 °C; ¹H NMR (C₆D₆) δ 8.38 (d, *J* = 7.3 Hz, 1 H), 8.32 (d, *J* = 7.3 Hz, 1 H), 8.17 (d, *J* = 6.8 Hz, 2 H), 7.81 (d, *J* = 7.8 Hz, 1 H), 7.31 (d, *J* = 6.3 Hz, 1H), 6.99–7.11 (m, 4 H), 6.93 (d, *J* = 7.3 Hz, 2 H), 1.93 (s, 3 H), 1.73 (s, 3 H); ¹⁹F NMR (C₆D₆) δ -74.0 (q, *J* = 9.3 Hz, 3 F), -76.5 (q, *J* = 9.3 Hz, 3 F), -80.0 (s, 3 F). Anal. Calcd for C₂₃H₁₈F₉O₂Sb: C, 46.69; H, 2.82. Found: C, 46.50; H, 2.71. **6b (minor)**: ¹H NMR (C₆D₆) δ 8.33 (d, *J* = 6.8 Hz, 1 H), 8.28 (d, *J* = 8.4 Hz, 2 H), 8.21 (d, *J* = 8.0 Hz, 1 H), 7.84 (d, *J* = 9.6 Hz, 1 H), 7.32 (d, *J* = 10.8 Hz, 1H), 6.99–7.12 (m, 4 H), 6.93 (d, *J* = 7.3 Hz,

2 H), 1.83 (s, 3 H), 1.59 (s, 3 H); ¹⁹F NMR (C₆D₆) δ -74.2 (q, *J* = 9.3 Hz, 3 F), -75.1 (q, *J* = 9.3 Hz, 3 F), -78.7 (s, 3 F).

Tetraethylammonium Fluorobis[α,α-bis(trifluoromethyl)benzenemethanolato(2-)-C²,O](4-methylphenyl)antimonate(1-)] (11). 3,3,3',3'-Tetrakis(trifluoromethyl)-1-(4-methylphenyl)spirobi(3*H*-2,1-benzoxastibole) (105 mg, 0.150 mmol) and tetraethylammonium fluoride (64 mg, 0.43 mmol) were dissolved in acetone in the open air, and the solution was left standing overnight. The resulting colorless crystals (92 mg, 73%) were collected. They were found to be suitable crystals for X-ray analysis. mp 226–228 °C. Anal. Calcd for C₃₃H₃₅F₁₃NO₂Sb: C, 46.83; H, 4.17; N, 1.65. Found: C, 46.75; H, 4.08; N, 1.59.

Kinetic Measurements. Samples enriched with **6a** (ca. 8.5–10 mg in 0.5–0.6 mL of solvent unless noted otherwise) dissolved in freshly distilled solvents were sealed in NMR tubes under N₂. Measurements for the kinetic runs were carried out with a JEOL EX-400 spectrometer in a variable temperature mode, and the specified temperatures were maintained throughout each set of measurements (error within ±1 °C). The observed temperatures were calibrated with the ¹H NMR chemical shift difference of signals of neat MeOH (low temperature region) and neat 1,3-propanediol (high temperature region). The composition of the diastereomers was monitored by integration of ¹⁹F NMR signals. The data were analyzed by assuming reversible first-order kinetics using the equation ln{(x_e - x₀)/(x_e - x)} = k(K + 1)t, in which x_e = ratio at equilibrium, x₀ = ratio observed at t = 0, x = ratio observed at arbitrary intervals, k = rate constant to be determined, and K = equilibrium ratio. The equilibrium ratios were determined by heating the measured sample in a silicon oil bath at the specified temperature (±2 °C) for at least 5 lifetimes.

Crystallographic Studies. Crystal Structures of 6a, 8, and 11. Crystal data and numerical details of the structural determinations are given in Table 3. Crystals were mounted on a Mac Science MXC3 diffractometer and irradiated with graphite-monochromated Mo Kα radiation (λ = 0.71073 Å) for data collection. Lattice parameters were determined by least-squares fitting of 24 reflections for **6a** and 31 reflections for **8** and **11** in the range 31° < 2θ < 35°. Data were collected with the 2θ/ω scan mode. Data for **6a** were corrected for absorption.²⁰ The structures were solved by a direct method with the Shelx 86 program. Refinement of *F* was carried out by the full-matrix least-squares method. All non-hydrogen atoms were refined with anisotropic thermal parameters. The hydrogen atoms in **11** were included in the refinement at calculated positions (C-H = 1.0 Å) riding on their carrier atom with isotropic thermal parameters. All computations were carried out on a Titan 750 computer.

Acknowledgment. We thank Central Glass Co. for supplying us with hexafluorocumyl alcohol. Part of this work was supported by Grant-in-Aids for Scientific Research on Priority Area of Organic Unusual Valency (03233104 and 04217105) from the Ministry of Education, Science, and Culture, Japan.

Supplementary Material Available: Tables of positional and thermal parameters and complete interatomic distances and angles for **6a**, **8**, and **11** and a table of observed rates and equilibrium ratios for the permutation of **6** (47 pages). Ordering information is given on any current masthead page.

OM940975Q

Activation of Prop-2-yn-1-ols by Metal Carbonyls: Synthesis of (Alkoxyalkenylcarbene)- and (Aminoalkenylcarbene)chromium and -tungsten Complexes

Christophe Cosset, Ignacio Del Rio, and Hubert Le Bozec

Organometallics, 1995, 14 (4), 1938-1944 • DOI: 10.1021/om00004a054 • Publication Date (Web): 01 May 2002

Downloaded from <http://pubs.acs.org> on March 9, 2009

More About This Article

The permalink <http://dx.doi.org/10.1021/om00004a054> provides access to:

- Links to articles and content related to this article
- Copyright permission to reproduce figures and/or text from this article



Activation of Prop-2-yn-1-ols by Metal Carbonyls: Synthesis of (Alkoxyalkenylcarbene)- and (Aminoalkenylcarbene)chromium and -tungsten Complexes

Christophe Cosset, Ignacio Del Rio, and Hubert Le Bozec*

Laboratoire de Chimie de Coordination Organique, URA CNRS 415, Campus de Beaulieu, Université de Rennes, 35042 Rennes, France

Received December 12, 1994[®]

Fischer type methoxyalkenylcarbene complexes $(\text{CO})_5\text{M}=\text{C}(\text{OMe})(\text{CH}=\text{CRR}')$ have been prepared in one step by photolysis of $\text{M}(\text{CO})_6$ [$\text{M} = \text{Cr}, \text{W}$] in tetrahydrofuran-methanol, in the presence of prop-2-yn-1-ol derivatives $\text{HC}\equiv\text{CC}(\text{OH})(\text{R})(\text{R}')$ [$\text{R}, \text{R}' = \text{Me}; \text{R} = \text{H}, \text{R}' = \text{Me}, \text{Ph}, \text{C}_6\text{H}_4\text{-}p\text{-NMe}_2$]. Photolysis of a tetrahydrofuran-methanol solution of $\text{M}(\text{CO})_6$ with $\text{HC}\equiv\text{CC}(\text{OH})(\text{H})\{(\text{CH}=\text{CH})_n\text{CH}=\text{CRR}'\}$ [$n = 0 \text{ R}, \text{R}' = \text{Me}; \text{R} = \text{H}, \text{R}' = \text{H}, \text{Me}, \text{Ph}, \text{C}_6\text{H}_4\text{-}p\text{-NMe}_2, \text{C}_5\text{H}_{11}; n = 1 \text{ R} = \text{H}, \text{R}' = \text{Me}$] provides the new dienyl- and trienylcarbene complexes $(\text{CO})_5\text{W}=\text{C}(\text{OMe})(\text{CH}=\text{CHCH}=\text{CRR}')$ and $(\text{CO})_5\text{M}=\text{C}(\text{OMe})(\text{CH}=\text{CHCH}=\text{CHCH}=\text{CHMe})$ in 30–70% yields. Alkoxyalkenylcarbene complexes $(\text{CO})_5\text{M}=\text{C}(\text{OCH}_2\text{Z})(\text{CH}=\text{CRR}')$ are prepared analogously by using other primary alcohols ZCH_2OH [$\text{Z} = \text{CH}_2\text{CH}(\text{Me})(\text{Et}), \text{CH}_2\text{-CH}_2\text{C}\equiv\text{CMe}, \text{CH}_2\text{CH}_2\text{CH}=\text{CH}_2, \text{CH}_2\text{CH}_2\text{C}(\text{Me})=\text{CH}_2$]. [(Alkenyloxy)alkenylcarbene]tungsten complexes undergo smooth thermal intramolecular cyclopropanation reactions leading to 1-alkenyl-2-oxabicyclo[3.1.0]hexane compounds. Finally, a series of aminodienylcarbene complexes $(\text{CO})_5\text{W}=\text{C}(\text{NHR}')(\text{CH}=\text{CHCH}=\text{CHR})$ [$\text{R} = \text{Ph}, \text{C}_5\text{H}_{11}; \text{R}' = \text{CHMe}_2, \text{CMe}_3, \text{CH}_2\text{-CH}=\text{CH}_2, \text{CH}_2\text{CHMe}_2$] have been synthesized by aminolysis of the corresponding methoxydienyl carbenes.

Introduction

Fischer type alkenylcarbene complexes of group 6 metals have attracted interest as useful reagents for organic synthesis. Most extensively studied are the annelation,^{1–3} cyclopropanation,^{4,5} and Diels–Alder reactions.^{6,7} They are also precursors to new functional organometallic compounds such as bis(carbene)dimetal complexes^{8,9} and organometallic polymers.¹⁰ Alkenyl-

carbene complexes are normally prepared by the Fischer procedure which involves the nucleophilic addition of vinylolithium reagents to a group 6 metal hexacarbonyl followed by O-alkylation of the acylmetalate salts.^{11–14} This method has some limitations and is restricted to alkenyl groups which are available from organolithium reagents. An alternative multistep, but more general, procedure requires the synthesis of a methoxymethylcarbene complex and the condensation of an aldehyde,¹⁵ ketone,¹⁶ or enol ether¹⁷ with the corresponding conjugated base $(\text{CO})_5\text{M}=\text{C}(\text{OMe})\text{CH}_2^-$. Several other specific methods for the preparation of alkoxyalkenylcarbene complexes, such as the nucleophilic attack of the pentacarbonylchromate dianion on alkenyl acid chlorides followed by alkylation on oxygen,¹⁸ or the insertion of ethoxyacetylene into a metal carbene bond,¹⁹ have been reported.

Another attractive and convenient way to produce metal carbene complexes involves the activation of terminal alkynes by transition metal complexes.²⁰ This one pot reaction, based on the nucleophilic addition of alcohols to vinylidene species, has been used by Rudler²¹

[®] Abstract published in *Advance ACS Abstracts*, March 15, 1995.

(1) (a) Dötz, K. H.; Dietz, R. *Chem. Ber.* **1978**, *111*, 2517. (b) Dötz, K. H.; Kuhn, W. *Angew. Chem., Int. Ed. Engl.* **1983**, *22*, 732. (c) Dötz, K. H.; Popall, M.; Müller, G.; Ackermann, K. *Angew. Chem., Int. Ed. Engl.* **1986**, *25*, 911.

(2) (a) Tang, P.-C.; Wulff, W. D. *J. Am. Chem. Soc.* **1984**, *106*, 1132. (b) Wulff, W. D.; Chan, K.-S.; Tan, P.-C. *J. Org. Chem.* **1984**, *49*, 2293. (c) Wulff, W. D.; Tang, P.-C.; Chan, K.-S.; Mc Callum, J. S.; Yang, D. C.; Gilbertson, S. R. *Tetrahedron* **1985**, *41*, 5813. (d) Gilbertson, S. R.; Wulff, W. D. *Synlett* **1989**, *1*, 47.

(3) King, J.; Quayle, P.; Malone, J. F. *Tetrahedron Lett.* **1990**, *31*, 5221.

(4) Wienand, A.; Reissig, H.-U. *Chem. Ber.* **1991**, *124*, 957.

(5) (a) Wulff, W. D.; Yang, D. C.; Murray, C. K. *J. Am. Chem. Soc.* **1988**, *110*, 2653. (b) Murray, C. K.; Yang, D. C.; Wulff, W. D. *J. Am. Chem. Soc.* **1990**, *112*, 5660.

(6) (a) Wulff, W. D.; Bauta, W. E.; Kaesler, R. W.; Langford, P. J.; Miller, R. A.; Murray, C. K.; Yang, D. C. *J. Am. Chem. Soc.* **1990**, *112*, 3642. (b) Anderson, B. A.; Wulff, W. D.; Powers, T. S.; Tribitt, S.; Rheingold, A. L. *J. Am. Chem. Soc.* **1992**, *114*, 10784. (c) Wulff, W. D.; Powers, T. S. *J. Org. Chem.* **1993**, *58*, 2381.

(7) (a) Dötz, K. H.; Kuhn, W.; Müller, G.; Huber, B.; Alt, H. G. *Angew. Chem., Int. Ed. Engl.* **1986**, *25*, 812. (b) Dötz, K. H.; Noack, R.; Müller, G. *J. Chem. Soc., Chem. Commun.* **1988**, 302. (c) Dötz, K. H.; Noack, R.; Harms, K.; Müller, G. *Tetrahedron* **1990**, *46*, 1235.

(8) Alvarez-Toledano, C.; Parlier, A.; Rose-Munch, F.; Rudler, H.; Daran, J. C.; Knobber, C.; Jeannin, V. *J. Organomet. Chem.* **1987**, *323*, 371.

(9) (a) Macomber, D. W.; Liang, M.; Rogers, R. D. *Organometallics* **1988**, *7*, 416. (b) Macomber, D. W.; Hung, M.-H.; Mahukar, P.; Liang, M.; Rogers, R. D. *Organometallics* **1991**, *10*, 737.

(10) Macomber, D. W.; Hung, M.-H.; Liang, M.; Verma, A. G.; Madhukar, P. *Macromolecules* **1988**, *21*, 1189.

(11) Connor, J. A.; Jones, E. M. *J. Chem. Soc. A* **1971**, 1974.

(12) Wilson, J. W.; Fischer, E. O. *J. Organomet. Chem.* **1973**, *57*, C63.

(13) See: Fischer, H. In *Transition Metal Carbene Complexes*; Verlag Chemie GmbH: Weinheim, 1984; pp 1–68.

(14) Hoye, T. R.; Chen, K.; Vyvyan, J. R. *Organometallics* **1993**, *12*, 2806.

(15) (a) Casey, C. P.; Brunsvold, W. R. *J. Organomet. Chem.* **1974**, *77*, 345. (b) Aumann, R.; Heiner, H. *Chem. Ber.* **1987**, *120*, 537.

(16) Wulff, W. D.; Gilbertson, S. R. *J. Am. Chem. Soc.* **1985**, *107*, 503.

(17) Rudler-Chauvin, M.; Rudler, H. *J. Organomet. Chem.* **1981**, *212*, 203.

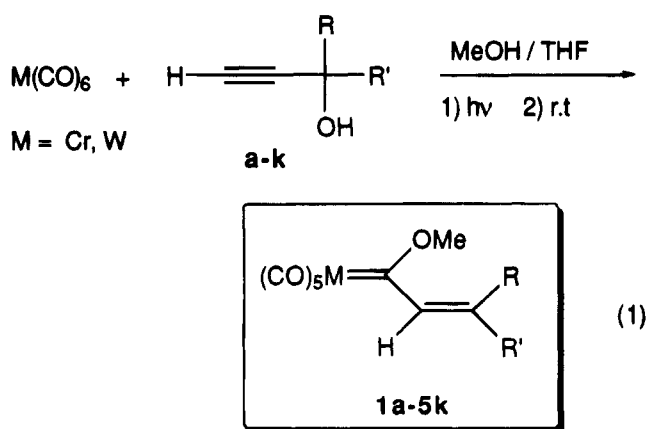
(18) Semmelhack, M. F.; Lee, G. R. *Organometallics* **1987**, *6*, 1839.

(19) Casey, C. P.; Polichnowski, S. W.; Shusterman, A. J.; Jones, C. R. *J. Am. Chem. Soc.* **1979**, *101*, 7282.

and Dötz²² to prepare some (alkoxyalkylcarbene)chromium and -tungsten carbene complexes. Our interest in the activation of terminal alkynes with (arene)-ruthenium(II) complexes has already produced evidence for the formation of very reactive vinylidene intermediate precursors of carbene.²³ Furthermore, we have recently reported an easy one step synthesis of novel alkenylcarbene ruthenium cations, *via* allenylidene ruthenium intermediates, by dehydration of propargylic alcohol derivatives.²⁴ We sought to apply this strategy for the preparation of α,β -unsaturated carbene complexes of group 6 metals. Here we report the results of our studies on the activation of prop-2-yn-1-ols by chromium and tungsten hexacarbonyl in the presence of alcohol nucleophiles. We show that this reaction opens the route to new alkoxyalkenylcarbene complexes. The aminolysis reactions of several methoxydienylcarbenes will also be described. A preliminary account of part of this work has appeared.²⁵

Results and Discussion

Our initial experiments were directed toward the synthesis of the known methoxypropenyl-,²⁶ methoxystyryl-,¹⁵ and methoxyisobutenylcarbene¹⁷ complexes **1a**, **2b**, and **1c**. Photolysis of a 1:2 methanol:tetrahydrofuran solution of $W(CO)_6$ or $Cr(CO)_6$ for 2–3 h at room temperature with a 2-fold excess of prop-2-yn-1-ols **a–c** resulted, after further 16 h of stirring, in the formation of complexes **1a**, **2b**, and **1c** in 24–40% yields (eq 1; Table 1, entries 1, 2, and 4). Complex **1a** was

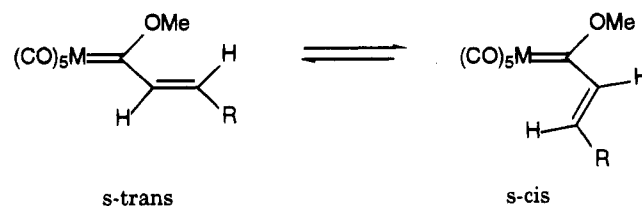


- a** [R : H ; R' : Me]
b [R : H ; R' : Ph]
c [R, R' : Me]
d [R : H ; R' : 4-Me₂NC₆H₄]
e [R : H ; R' : CH=CH₂]
f [R : H ; R' : CH=CHMe]
g [R : H ; R' : CH=CHPh]
h [R : H ; R' : CH=CH(4-Me₂NC₆H₄)]
i [R : H ; R' : CH=CH(C₅H₁₁)]
j [R : H ; R' : CH=CMe₂]
k [R : H ; R' : CH=CHCH=CHMe]

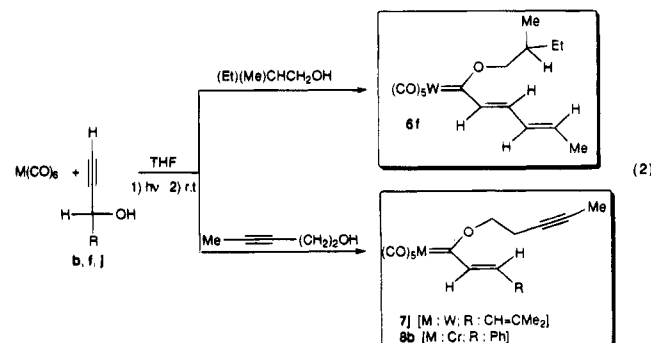
also produced in 60% yield by treatment at room temperature of the photogenerated $W(CO)_5(THF)$ with

a methanol solution of **a**. When alkyne **d** was irradiated with $M(CO)_6$ (M = Cr and W), the new deep red 4-(dimethylamino)styryl carbene complexes **1d** and **2d** were obtained in *ca.* 50% yield (entries 3 and 5). The synthetic sequence outlined for the preparation of methoxyalkenylcarbene complexes was successfully applied to the synthesis of polyenylcarbene complexes from the readily available alkenyl- and dienyl propargylic alcohol derivatives **e–k**.²⁴ After chromatographic purification (methoxydienylcarbene)tungsten complexes **3e–j** and methoxyoctatrienylcarbene complexes **4k** and **5k** were isolated in good yields (entries 6–13).

These compounds were easily characterized on the basis of their IR and ¹H, ¹³C, and ¹H–¹³C correlated NMR spectra (Table 2). The reaction is completely stereoselective, giving exclusively the *all-trans* isomers for the alkenyl, dienyl, and trienyl substituents, according to the strong vicinal coupling constants (³J_{HH} ≈ 15 Hz). Difference NOE experiments were conducted with complexes **1d** and **2b**, in order to establish the conformation of the metal–alkenyl moiety: irradiation of the methoxy protons led to the enhancement of the vinyl H²C signal [**2b**, 4%; **1d**, 8%] as well as of the H³C signal [**2b**, 2.5%; **1d**, 4%], consistent with an *s-cis* → *s-trans* equilibrium. This equilibrium has also been suggested by Aumann in the case of the (CO)₅Cr=C(OEt)-(CH=CHPh) complex.^{15b}



(Alkenyloxy)- and (alkynyloxy)carbene complexes have found useful applications in organic synthesis such as intramolecular cyclopropanation,^{27,28} annelation²⁹ and Diels–Alder reactions.^{7c} They are generally made either by base-catalyzed reaction of ethylene alcohols with methoxycarbene complexes,²⁷ alcoholysis of (acyloxy)carbene complexes,^{28,29} or alkylation of acylmetalates.¹⁴ The success of our strategy to prepare methoxyalkenylcarbene complexes has prompted us to examine the generalization of this simple procedure by using more sophisticated alcohols in place of methanol (eq 2). The chiral [(2-methyl-1-butoxy)pentadienylcar-



(20) Bruce, M. J.; Swincer, A. G. *Adv. Organomet. Chem.* **1983**, *22*, 59.

(21) Parlier, A.; Rudler, H. *J. Chem. Soc., Chem. Commun.* **1986**, 514.

(22) Dötz, K. H.; Sturm, W.; Alt, H. G. *Organometallics* **1987**, *6*, 1424.

(23) Le Bozec, H.; Ouzzine, K.; Dixneuf, P. H. *Organometallics* **1991**, *10*, 2768.

Table 1. Yields of Alkoxyalkenylcarbene Complexes $(\text{CO})_5\text{M}=\text{C}(\text{OCH}_2\text{Z})(\text{CH}=\text{CRR}')$

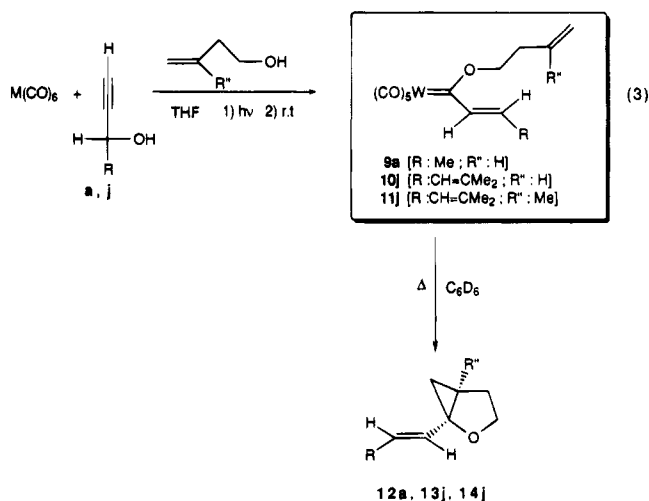
entry	M	CH_2Z	$\text{CH}=\text{C}(\text{R})(\text{R}')$	complex	% yield
1	W	Me	$\text{CH}=\text{CH}(\text{Me})$	1a	30 (60 ^a)
2	W	Me	$\text{CH}=\text{C}(\text{Me})_2$	1c	24
3	W	Me	$\text{CH}=\text{CH}(\text{C}_6\text{H}_4\text{-}p\text{-NMe}_2)$	1d	55
4	Cr	Me	$\text{CH}=\text{CH}(\text{Ph})$	2b	40
5	Cr	Me	$\text{CH}=\text{CH}(\text{C}_6\text{H}_4\text{-}p\text{-NMe}_2)$	2d	50
6	W	Me	$\text{CH}=\text{CHCH}=\text{CH}_2$	3e	50
7	W	Me	$\text{CH}=\text{CHCH}=\text{CH}(\text{Me})$	3f	62
8	W	Me	$\text{CH}=\text{CHCH}=\text{CH}(\text{Ph})$	3g	73
9	W	Me	$\text{CH}=\text{CHCH}=\text{CH}(\text{C}_6\text{H}_4\text{-}p\text{-NMe}_2)$	3h	30
10	W	Me	$\text{CH}=\text{CHCH}=\text{CH}(\text{C}_5\text{H}_{11})$	3i	47
11	W	Me	$\text{CH}=\text{CHCH}=\text{C}(\text{Me})_2$	3j	63
12	W	Me	$(\text{CH}=\text{CH})_3\text{Me}$	4k	53
13	Cr	Me	$(\text{CH}=\text{CH})_3\text{Me}$	5k	46
14	W	$\text{CH}_2\text{CH}(\text{Me})(\text{Et})$	$\text{CH}=\text{CHCH}=\text{CH}(\text{Me})$	6f	50
15	W	$\text{CH}_2\text{CH}_2\text{C}\equiv\text{CMe}$	$\text{CH}=\text{CHCH}=\text{C}(\text{Me})_2$	7j	22
16	Cr	$\text{CH}_2\text{CH}_2\text{C}\equiv\text{CMe}$	$\text{CH}=\text{CH}(\text{Ph})$	8b	15
17	W	$\text{CH}_2\text{CH}_2\text{CH}=\text{CH}_2$	$\text{CH}=\text{CH}(\text{Me})$	9a	59
18	W	$\text{CH}_2\text{CH}_2\text{CH}=\text{CH}_2$	$\text{CH}=\text{CHCH}=\text{CMe}_2$	10j	69
19	W	$\text{CH}_2\text{CH}_2\text{CMe}=\text{CH}_2$	$\text{CH}=\text{CHCH}=\text{CMe}_2$	11j	24

^a From $\text{W}(\text{CO})_5(\text{THF})$.

benzene]tungsten **6f** was obtained in 50% yield from alkyne **f** and 2-methyl-1-butanol (entry 14). Similarly, the reaction of $\text{M}(\text{CO})_6$ with pent-3-yn-1-ol (25 equiv) and alkynes **b** and **j** gave the new (pent-3-yn-1-oxy)alkenylcarbenes **7j** and **8b** in 15–22% yields (entries 15–16).

We have extended this simple reaction to synthesize the first (alkenyloxy)alkenylcarbene complexes; [(but-3-en-1-oxy)alkenylcarbene]tungsten complexes **9a** and **10j** were produced in good isolated yields (59 and 69%, respectively) from but-3-en-1-ol in large excess (3 mL) and the propargylic alcohol derivatives **a** and **j** (entries 17 and 18).

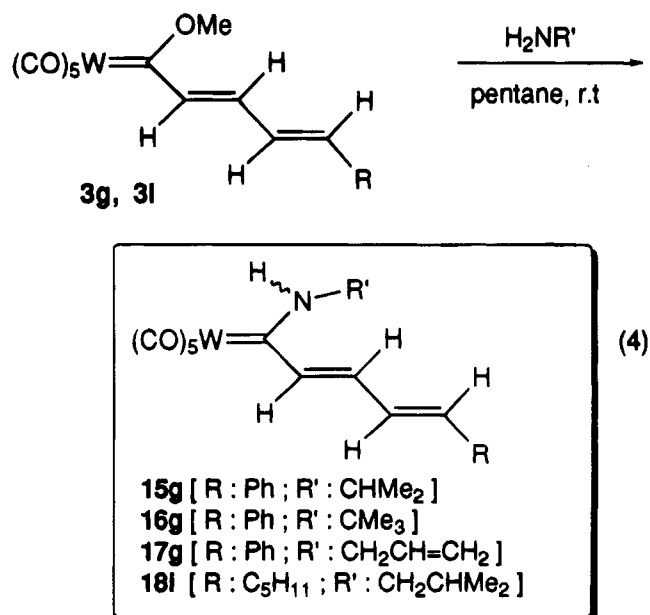
The complexes **9a** and **10j** underwent intramolecular cyclopropanation reactions similar to those previously described for [(alkenyloxy)aryl]tungsten²⁷ and -chromium²⁸ complexes. The thermolysis, performed at 70 °C for 2 h in benzene-*d*₆, gave exclusively and quantitatively (NMR yield) the vinylcyclopropanes 1-propenyl-2-oxabicyclo[3.1.0]hexane and 1-(3-methylpentadienyl)-2-oxabicyclo[3.1.0]hexane (**12a** and **13j**), respectively (eq 3). Use of 3-methylbut-3-en-1-ol produced the corre-



sponding carbene complex **11j** in low yield (entry 19). Unlike **9a** and **10j**, which are stable in solution at room temperature, **11j** was readily converted to the cyclopropane derivative **14j** in C₆D₆ at 25 °C. This inherent thermal instability has also been observed by Soderberg

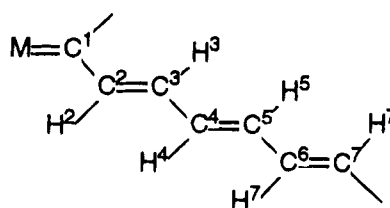
and Hegedus for [(3-methylbut-3-en-1-oxy)arylcarbene]-chromium complexes.²⁸ This reaction appears to be a straightforward entry to bicyclic alkenylcyclopropanes.

Aminoalkenylcarbene complexes are also well-known useful reagents for organic synthesis.^{7,30–33} Thus we sought to prepare them by following the same methodology, but with amines as nucleophiles. Our attempts with *tert*-butylamine failed, and the reaction resulted only in the formation of a pentacarbonyltungsten *tert*-butylamine complex, $(\text{CO})_5\text{W}(\text{H}_2\text{N}^t\text{Bu})$. These compounds, however, could be easily obtained by the standard aminolysis method^{7,33,34} from the readily available methoxyalkenylcarbene complexes synthesized. For example, addition of a variety of primary amines to **3g** and **3i** at room temperature led to the isolation of the aminodienylcarbene complexes **15g–17g** and **18i** in high yields as 1:1 mixtures of *E* and *Z* isomers (eq 4).



These isomers could be easily distinguished by means

(24) (a) Pilette, D.; Ouzzine, K.; Le Bozec, H.; Dixneuf, P.; Rickard, C. E. F.; Roper, W. R. *Organometallics* **1992**, *11*, 809. (b) Pilette, D.; Le Bozec, H.; Romero, A.; Dixneuf, P. H. *J. Chem. Soc., Chem. Commun.* **1992**, 1220.

Table 2. Selected ^1H and ^{13}C NMR Data (ppm) for Alkoxyalkenylcarbene Complexes

complex	C ¹	C ² (H ²)	C ³ (H ³)	C ⁴ (H ⁴)	C ⁵ (H ⁵)	C ⁶ (H ⁶)	C ⁷ (H ⁷)
1a ^a	309.8	149.3 (7.25)	137.1 (6.58)				
1c ^a	311.7	145.2 (7.35)	146.4				
1d ^a	299.5	140.8 (7.70)	138.4 (7.40)				
2b ^b	333.7	139.6 (7.89)	130.9 (6.89)				
2d ^a	324.1	137.6 (7.72)	134.7 (7.43)				
3e ^a	308.9	147.9 (7.31)	134.8 (6.79)	129.7 (6.40)	136.2 (5.81–5.74)		
3f ^a	307.2	145.7 (7.21)	137.1 (6.88)	131.2 (6.15)	145.6 (6.78)		
3g ^b	305.4	147.0 (7.42)	135.2 (7.05)	127.3 (6.83)	145.0 (7.12)		
3h ^a	300.7	148.0 (7.31)	140.4 (7.20)	122.5 (6.68)	144.4 (7.10)		
3i ^a	307.1	151.3 (7.22)	137.3 (6.88)	129.8 (6.15)	145.7 (6.41)		
3j ^b	306.0	144.9 (7.13)	134.8 (7.29)	125.3 (5.98)	153.3		
4k ^a	305.0	146.8 (7.26)	137.2 (6.95)	129.1 (6.16)	146.4 (6.78)	132.4 (6.23)	137.9 (6.08)
5k ^a	330.6	147.9 (7.42)	138.4 (6.99)	129.6 (6.35)	142.6 (6.99)	132.9 (6.35)	142.1 (6.14)
6f ^a	304.8	145.4 (7.20)	136.1 (6.85)	131.0 (6.85)	144.6 (6.41)		
7j ^a	303.6	144.9 (7.15)	135.0 (7.36)	125.3 (5.99)	153.5		
8b ^b	332.3	140.0 (7.97)	131.3 (7.04)				
9a ^c	307.4	149.8 (7.10)	138.2 (6.28)				
10j ^c	303.7	144.8 (7.10)	134.6 (7.32)	125.1 (5.55)	153.2		

^a Recorded in CD₂Cl₂. ^b Recorded in CDCl₃. ^c Recorded in C₆D₆.

Table 3. Selected ^1H and ^{13}C NMR Data (ppm) for Aminoalkenylcarbene Complexes^a

complex	C ¹	NH	H ²	H ³	H ⁴	H ⁵
15g (Z)	239.0	8.16	6.88	6.43	6.82	6.83
(E)	243.4	8.08	6.68	7.18	6.89	6.94
16g (Z)	244.4	8.90	7.13	5.76	6.68	6.72
(E)	249.4	8.48	6.93	7.08	6.86	6.86
17g (Z)	247.1	8.26	6.83	6.48	6.75	6.77
(E)	249.3	8.26	6.59	7.18	6.87	6.88
18i (Z)	245.9	8.26	6.65	6.28	6.02	6.02
(E)	247.0	8.18	6.44	7.09	6.20	6.20
19a ^b (Z)	247.0	8.50	6.75	5.90		
(E)	249.3	8.36	6.48	6.67		

^a In CDCl₃. ^b Reference 33.

of their ^1H and ^{13}C NMR chemical shifts (Table 3), which are in good agreement with those recently reported by Wulff for (CO)₅W=C(NHMe)(CH=CHMe) (19a).³³

A plausible mechanism that can account for the formation of alkoxyalkenylcarbene complexes 1a–11j is presented in Scheme 1. We suggest that photolysis promotes the elimination of one CO ligand to give, *via* a metal carbonyl solvent adduct, the η^2 -alkyne intermediate **A**. Then, the mechanism involves the rear-

angement of **A** to its η^1 -hydroxyvinylidene isomer **B** which readily loses water to afford the allenylidene intermediate **C**.³⁵ The last step is likely to be the nucleophilic addition of the alcohol. Indeed, several disubstituted allenylidene chromium and tungsten complexes, stabilized by electron-donating groups, have recently been generated by dehydration of 1,1-diaryprop-2-yn-1-ols³⁶ or by a multistep reaction between dianions LiC≡CCR₂OLi (R = aryl) and M(CO)₆.³⁷ Other stable (3-aminoallenylidene)chromium and -tungsten complexes are known; they have been prepared either by acid-catalyzed alcohol elimination from ethoxy(2-aminoalkenyl)carbene complexes,³⁸ *via* a process that is actually the reverse of the **C** → **D** reaction, or by reactions of amines with ethoxyalkynylcarbene complexes.³⁹

In summary we have developed a simple route which allows the preparation of alkoxyalkenyl and polyenylcarbene complexes by direct activation of readily available propargylic alcohol derivatives. Moreover this methodology has been extended to a variety of carbene complexes containing "functional" alkoxy groups such as (alkenyloxy)alkenylcarbenes which undergo facile intramolecular cyclopropanation reactions. Finally, aminoalkenylcarbene complexes can be easily obtained by a traditional aminolysis route, thus in two steps from W(CO)₆.

(25) Le Bozec, H.; Cosset, C.; Dixneuf, P. H. *J. Chem. Soc., Chem. Commun.* **1991**, 881.

(26) Parlier, A.; Rudler, M.; Rudler, H.; Daran, J. C. *J. Organomet. Chem.* **1987**, *323*, 353.

(27) Casey, C. P.; Shusterman, A. J. *Organometallics* **1985**, *4*, 736.

(28) Söderberg, B. C.; Hegedus, L. S. *Organometallics* **1990**, *9*, 3113.

(29) Semmelhack, M. L.; Bozell, J. J. *Tetrahedron Lett.* **1982**, *23*, 2931.

(30) (a) Dötz, K. H.; Neugebauer, D. *Angew. Chem., Int. Ed. Engl.* **1978**, *17*, 851. (b) Dötz, K. H.; Pruskil, I. *Chem. Ber.* **1978**, *111*, 2059.

(c) Dötz, K. H.; Grotjahn, D.; Harms, K. *Angew. Chem., Int. Ed. Engl.* **1989**, *28*, 1384.

(31) (a) Merlic, C. A.; Burns, E. E.; Xu, D.; Chen, S. Y. *J. Am. Chem. Soc.* **1992**, *114*, 8722. (b) Merlic, C. A.; Xu, D.; Gladstone, B. G. *J. Org. Chem.* **1993**, *58*, 538.

(32) (a) Merlic, C. A.; Burns, E. E.; Xu, D.; Chen, S. Y. *J. Am. Chem. Soc.* **1992**, *114*, 8722. (b) Merlic, C. A.; Xu, D.; Gladstone, B. G. *J. Org. Chem.* **1993**, *58*, 538.

(33) Anderson, B. A.; Wulff, W. D.; Powers, T. S.; Tribitt, S.; Rheingold, A. L. *J. Am. Chem. Soc.* **1992**, *114*, 10784.

(34) Klabunde, U.; Fischer, E. O. *J. Am. Chem. Soc.* **1967**, *89*, 7141.

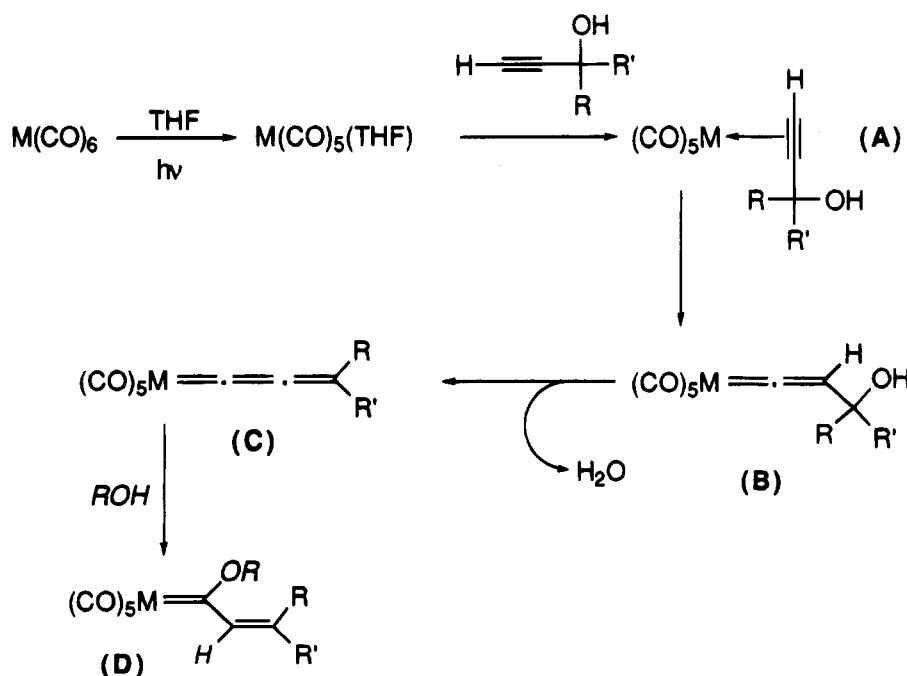
(35) Although a similar mechanism has been clearly established to explain the formation of alkenylcarbene ruthenium complexes,^{24a} we cannot rule out an alternative mechanism involving the addition of the alcohol to **B** followed by elimination of H₂O. We thank one of the reviewers for suggesting this alternative mechanism.

(36) Fischer, H.; Roth, G.; Reindl, D.; Troll, C. *J. Organomet. Chem.* **1993**, *454*, 133.

(37) (a) Berke, H.; Härter, P.; Huttner, G.; Van Seyerl, J. J. *Organomet. Chem.* **1981**, *219*, 317. (b) Berke, H.; Härter, P.; Huttner, G.; Zsolnai, L. *Chem. Ber.* **1992**, *115*, 695.

(38) Fischer, E. O.; Kalder, H. J.; Frank, A.; Köhler, F. H.; Huttner, G. *Angew. Chem., Int. Ed. Engl.* **1976**, *15*, 623.

Scheme 1



Experimental Section

General Data. All reactions were conducted under an inert argon or nitrogen atmosphere. The solvents were dried by standard methods. Infrared spectra were recorded on a Nicolet 205 FT-IR spectrometer. ^1H (300.13 MHz) and ^{13}C (75.47 MHz) NMR spectra were recorded on a Bruker AM 300 spectrometer at 297 K and referenced to TMS. Elemental analyses were performed by the Service Central de Microanalyses du CNRS at Lyon, France. High-resolution mass spectra were obtained on a Varian MAT 311 at CRMPO, University of Rennes. Propargylic alcohols were prepared according to literature procedures.^{40,41}

General Procedure for the Synthesis of Methoxyalkenylcarbene Complexes 1–5. A solution of 3 mmol of metal carbonyl [Cr(CO)_6 or W(CO)_6] and 6 mmol of propyn-1-ol derivatives in 75 mL of a 2/1 mixture of tetrahydrofuran/methanol was irradiated for 2–4 h at room temperature by using a Rayonet photochemical reactor and a Pyrex photochemical cell. The solution was then transferred into a Schlenk flask and stirred for 18 h at room temperature. After evaporation of the solvent under vacuum, the residue was chromatographed on silica gel. Elution with dichloromethane/pentane (1/9) followed by evaporation of the solvent gave complexes 1–5 as red solids or oils.

(CO)₅W=C(OMe)(CH=CHMe), 1a: yield 0.37 g (30%); IR (Nujol) 2068, 1942, 1610 cm^{-1} ; ^1H NMR (CD_2Cl_2) δ 7.25 (dq, 1H, CH=, $^3J = 15.0$ Hz, $^4J = 1.5$ Hz), 6.58 (dq, 1H, CH=, $^3J = 15.0$ and 7 Hz), 4.57 (3H, OMe), 1.82 (dd, 3H, Me, $^3J = 7.0$ Hz, $^4J = 1.5$ Hz); ^{13}C NMR (CD_2Cl_2) δ 309.8 (W=C), 203.6 (CO), 197.6 (CO), 149.3 (HC=), 137.1 (HC=), 69.0 (OMe), 18.5 (Me). Anal. Calcd for $\text{C}_{10}\text{H}_8\text{O}_6\text{W}$: C, 30.01; H, 1.97. Found: C, 29.44; H, 1.97.

(CO)₅W=C(OMe)(CH=CMe₂), 1c: yield 0.31 g (24%); IR (Nujol) 2067, 1939, 1610 cm^{-1} ; ^1H NMR (CD_2Cl_2) δ 7.35 (m, 1H, CH=), 4.59 (3H, OMe), 1.90 (d, 3H, Me, $^4J = 1.0$ Hz), 1.86 (d, 3H, Me, $^4J = 1.0$ Hz); ^{13}C NMR (CD_2Cl_2) δ 311.7 (W=C), 204.6 (CO), 198.3 (CO), 146.4 (CMe₂), 145.2 (HC=), 69.7 (OMe), 28.6 and 22.6 (Me). Anal. Calcd for $\text{C}_{11}\text{H}_{10}\text{O}_6\text{W}$: C, 31.30; H, 2.39. Found: C, 31.01; H, 2.34.

(CO)₅W=C(OMe)[CH=C(H)(*p*-C₆H₄NMe₂)], 1d: yield 0.85 g (55%); IR (Nujol) 2061, 1937 cm^{-1} ; ^1H NMR (CD_2Cl_2) δ 7.70 (d, 1H, CH=, $^3J = 15.0$ Hz), 7.54 (d, 2H, C₆H₄-, $^3J = 9.0$ Hz), 7.40 (d, 1H, CH=, $^3J = 15.0$ Hz), 6.67 (d, 2H, C₆H₄-, $^3J = 9.0$ Hz), 4.51 (3H, OMe), 3.03 (6H, NMe₂); ^{13}C NMR (CD_2Cl_2) δ 299.5 (W=C), 204.7 (CO), 198.8 (CO), 153.5 (C₆H₄-), 140.8 (CH=), 138.4 (CH=), 132.6, 121.8, 112.5 (C₆H₄-), 68.4 (OMe), 40.3 (NMe₂). Anal. Calcd for $\text{C}_{17}\text{H}_{16}\text{NO}_6\text{W}$: C, 39.79; H, 2.95. Found: C, 39.92; H, 3.30.

(CO)₅Cr=C(OMe)(CH=CHPh), 2b: yield 0.29 g (40%); IR (Nujol) 2058, 1946 cm^{-1} ; ^1H NMR (CDCl_3) δ 7.82 (d, 1H, CH, $^3J = 15.2$ Hz), 7.51–7.10 (m, 5H, C₆H₅), 6.89 (d, 1H, CH=, $^3J = 15.2$ Hz), 4.75 (3H, OMe); ^{13}C NMR (CDCl_3) δ 333.7 (Cr=C), 224.3 (CO), 216.7 (CO), 139.6 (CH=), 134.4 (C₆H₅), 130.9 (CH=), 129.7, 129.5, 129.1 (C₆H₅), 66.5 (OMe).

(CO)₅Cr=C(OMe)[CH=C(H)(*p*-C₆H₄NMe₂)], 2d: yield 0.33 g (50%); IR (Nujol) 2053, 1940 cm^{-1} ; ^1H NMR (CD_2Cl_2) δ 7.72 (d, 1H, CH=, $^3J = 15.0$ Hz), 7.52 (d, 2H, C₆H₄-, $^3J = 9.0$ Hz), 7.43 (d, 1H, CH=, $^3J = 15.0$ Hz), 6.67 (d, 2H, C₆H₄-, $^3J = 9.0$ Hz), 4.62 (3H, OMe), 3.03 (6H, NMe₂); ^{13}C NMR (CD_2Cl_2) δ 324.1 (Cr=C), 225.2 (CO), 218.1 (CO), 167.1 (C₆H₄-), 137.6 (CH=), 134.7 (CH=), 132.6, 121.6, 112.4 (C₆H₄-), 65.7 (OMe), 40.3 (NMe₂). HRMS M^+ Calcd for $\text{C}_{17}\text{H}_{15}\text{NO}_6\text{Cr}$: 381.0304. Found: 381.0307.

(CO)₅W=C(OMe)(CH=CHCH=CH₂), 3e: yield 0.63 g (50%); IR (Nujol) 2066, 1941, 1633, 1572 cm^{-1} ; ^1H NMR (CD_2Cl_2) δ 7.31 (dd, 1H, CH=, $^3J = 14.9$ Hz, $^4J = 0.4$ Hz), 6.79 (m, 1H, CH=, $^3J = 14.8$ and 11.0 Hz), 6.40 (m, 1H, CH=), 5.81 (m, 1H, =CH₂, $^3J = 16.9$ Hz), 5.74 (m, 1H, =CH₂, $^3J = 9.9$ Hz), 4.55 (OMe); ^{13}C NMR (CD_2Cl_2) δ 308.9 (W=C), 203.6 (CO), 197.6 (CO), 147.9 (CH=), 136.2 (CH₂), 134.8 (CH=), 129.7 (CH=), 69.6 (OMe). HRMS M^+ Calcd for $\text{C}_{11}\text{H}_8\text{O}_6\text{W}^{182}$: 417.9819. Found: 417.9802.

(CO)₅W=C(OMe)(CH=CHCH=CHMe), 3f: yield 0.81 g (62%); IR (Nujol) 2066, 1941, 1610, 1571 cm^{-1} ; ^1H NMR (CD_2Cl_2) δ 7.21 (d, 1H, CH=, $^3J = 14.8$ Hz), 6.88 (dd, 1H, CH=, $^3J = 14.8$ and 10.9 Hz), 6.78 (dq, 1H, CH=, $^3J = 14.9$ and 7.0 Hz), 6.15 (ddq, 1H, CH=, $^3J = 14.7$ and 10.9 Hz, $^4J = 1.5$ Hz), 4.53 (3H, OMe), 1.83 (d, 3H, Me, $^3J = 7.0$ Hz); ^{13}C NMR (CD_2Cl_2) δ 307.2 (W=C), 204.6 (CO), 198.2 (CO), 145.7 (CH=), 145.6 (CH=), 137.1 (CH=), 131.2 (CH=), 69.3 (OMe), 19.8 (Me). Anal. Calcd for $\text{C}_{12}\text{H}_{10}\text{O}_6\text{W}$: C, 33.21; H, 2.31. Found: C, 33.12; H, 2.52.

(39) Stein, F.; Duetsch, M.; Pohl, E.; Herbst-Irmer, R.; De Meijere, A. *Organometallics* **1993**, *12*, 2556.

(40) Midland, M. M. *J. Org. Chem.* **1975**, *40*, 2659.

(41) Pilette, D. Thesis, Université de Rennes, 1992.

(CO)₅W=C(OMe)(CH=CHCH=CHPh), **3g**: yield 1.09 g (73%); IR (Nujol) 2065, 1942, 1610 cm⁻¹; ¹H NMR (CDCl₃) δ 7.42 (d, 1H, CH=, ³J = 14.6 Hz), 7.53–7.34 (m, 5H, C₆H₅), 7.12 (d, 1H, CH=, ³J = 15.4 Hz), 7.05 (dd, 1H, CH=, ³J = 14.6 and 11.1 Hz), 6.83 (dd, 1H, CH=, ³J = 15.4 and 11.1 Hz), 4.59 (3H, OMe); ¹³C NMR (CDCl₃) δ 305.4 (W=C), 204.0 (CO), 197.7 (CO), 147.0 (CH=), 145.0 (CH=), 136.3 (C₆H₅), 130.2 (CH=), 129.7, 129.0, 127.5, 127.3 (C₆H₅), 68.8 (OMe). HRMS M⁺ Calcd for C₁₇H₁₂O₆W¹⁸⁶: 498.0175. Found: 498.0173.

(CO)₅W=C(OMe)[CH=CHCH=C(H)(p-C₆H₄NMe₂)], **3h**: yield 0.49 g (30%); IR (Nujol) 2061, 1938, 1595, 1552 cm⁻¹; ¹H NMR (CD₂Cl₂) δ 7.41 (d, 2H, C₆H₄-, ³J = 9.0 Hz), 7.31 (d, 1H, CH=, ³J = 14.3 Hz), 7.20 (dd, 1H, CH=, ³J = 14.3 and 10.8 Hz), 7.10 (d, 1H, CH=, ³J = 15.1 Hz), 6.68 (dd, 1H, CH=, ³J = 15.1 and 10.8 Hz), 6.65 (d, 2H, C₆H₄-, ³J = 9.0 Hz), 4.50 (3H, OMe), 3.00 (6H, NMe₂); ¹³C NMR (CD₂Cl₂) δ 300.7 (W=C), 204.8 (CO), 198.7 (CO), 152.2 (C₆H₄), 148.0 (CH=), 144.4 (CH=), 140.4 (CH=), 130.0, 124.6 (C₆H₄-), 122.5 (CH=), 112.3 (C₆H₄-), 68.7 (OMe), 40.4 (NMe₂). Anal. Calcd for C₁₉H₁₇NO₆W: C, 42.32; H, 3.18; N, 2.60. Found: C, 41.02; H, 3.26; N, 2.59.

(CO)₅W=C(OMe)[CH=CHCH=C(H)(C₆H₁₁)], **3i**: yield 0.81 g (47%); IR (Nujol) 2065, 1942, 1628, 1571 cm⁻¹; ¹H NMR (CD₂Cl₂) δ 7.22 (d, 1H, CH=, ³J = 14.7 Hz), 6.88 (dd, 1H, CH=, ³J = 14.7 and 10.9 Hz), 6.41 (dt, 1H, CH=, ³J = 15.0 and 7.0 Hz), 6.15 (ddt, 1H, CH=, ³J = 15.0 and 10.9 Hz, ⁴J = 1.0 Hz), 4.53 (3H, OMe), 2.15 (m, 2H, CH₂-), 1.43 (m, 2H, CH₂-), 1.33–1.22 (m, 4H, CH₂-), 0.86 (t, 3H, Me, ³J = 7.0 Hz); ¹³C NMR (CD₂Cl₂) δ 307.1 (W=C), 204.6 (CO), 198.3 (CO), 151.3 (CH=), 145.7 (CH=), 137.3 (CH=), 129.8 (CH=), 69.3 (OMe), 34.2, 31.8, 28.6, 22.9 (CH₂-), 14.2 (Me).

(CO)₅W=C(OMe)(CH=CHCH=CMe₂), **3j**: yield 0.85 g (63%); IR (Nujol) 2065, 1939, 1622, 1559 cm⁻¹; ¹H NMR (CDCl₃) δ 7.29 (dd, 1H, CH=, ³J = 14.6 and 11.3 Hz), 7.13 (d, 1H, CH=, ³J = 14.6 Hz), 5.98 (m, 1H, CH=), 4.53 (3H, OMe), 1.90 (3H, Me), 1.88 (3H, Me); ¹³C NMR (CDCl₃) δ 306.0 (W=C), 203.9 (CO), 197.8 (CO), 153.3 (=CMe₂), 144.9 (CH=), 134.8 (CH=), 125.3 (CH=), 68.6 (OMe), 27.5 (Me), 19.6 (Me). Anal. Calcd for C₁₃H₁₂O₆W: C, 34.85; H, 2.70. Found: C, 35.06; H, 3.02.

(CO)₅W=C(OMe)(CH=CHCH=CHCH=CHMe), **4k**: yield 0.73 g (53%); IR (Nujol) 2065, 1941, 1594, 1556 cm⁻¹; ¹H NMR (CD₂Cl₂) δ 7.26 (d, 1H, CH=, ³J = 14.6 Hz), 6.95 (dd, 1H, CH=, ³J = 14.6 and 11.4 Hz), 6.78 (dd, 1H, CH=, ³J = 14.8 and 10.6 Hz), 6.23 (m, 1H, CH=, ³J = 15.0 and 10.5 Hz, ⁴J = 1.4 and 0.5 Hz), 6.16 (ddd, 1H, CH=, ³J = 14.8 and 11.4 Hz, ⁴J = 0.5 Hz), 6.08 (dq, 1H, CH=, ³J = 15.0 and 6.8 Hz), 4.53 (3H, OMe), 1.78 (d, 3H, Me, ³J = 6.7 Hz); ¹³C NMR (CD₂Cl₂) δ 305.0 (W=C), 204.7 (CO), 198.3 (CO), 146.8 (CH=), 146.4 (CH=), 137.9 (CH=), 137.2 (CH=), 137.4 (CH=), 129.1 (CH=), 69.2 (OMe), 19.1 (Me). Anal. Calcd for C₁₄H₁₂O₆W: C, 36.55; H, 2.63. Found: C, 36.57; H, 2.49.

(CO)₅Cr=C(OMe)(CH=CHCH=CHCH=CHMe), **5k**: yield 0.44 g (46%); IR (Nujol) 2055, 1944, 1594, 1556 cm⁻¹; ¹H NMR (CD₂Cl₂) δ 7.42 (d, 1H, CH=, ³J = 14.3 Hz), 6.99 (m, 2H, CH=), 6.35 (m, 2H, CH), 6.14 (dq, 1H, CH=, ³J = 14.5 and 6.9 Hz), 4.75 (3H, OMe), 1.85 (d, 3H, Me, ³J = 6.9 Hz); ¹³C NMR (CD₂Cl₂) δ 330.6 (Cr=C), 225.7 (CO), 218.0 (CO), 147.9 (CH=), 142.6 (CH=), 142.1 (CH=), 138.4 (CH=), 132.9 (CH=), 129.6 (CH=), 66.8 (OMe), 18.9 (Me).

General Procedure for the Synthesis of Alkoxyalkenylcarbene Complexes 6–11. A solution of 2–3 mmol of metal hexacarbonyl, 6–9 mmol of propyn-1-ol derivatives, and 3 mL of the appropriate alcohol in 60 mL of tetrahydrofuran was irradiated for 6–9 h at room temperature. The solution was then transferred into a Schlenk flask and stirred for 18 h at room temperature. After evaporation of the solvent under vacuum, the residue was chromatographed on silica gel. Elution with dichloromethane/pentane (1/9) followed by evaporation of the solvent gave complexes **6–11** as red oils.

(CO)₅W=C[OCH₂CH(Me)(Et)][CH=CHCH=CHMe], **6f**: yield 0.74 g (50%) from 1.06 g (3 mmol) of W(CO)₆, 0.57 g (6

mmol) of **f**, and 3 mL of 2-methyl-1-butanol; IR (Nujol) 2064, 1937, 1632, 1572 cm⁻¹; ¹H NMR (CD₂Cl₂) δ 7.20 (d, 1H, CH=, ³J = 14.8 Hz), 6.85 (dd, 1H, CH=, ³J = 14.8 and 10.9 Hz), 6.41 (ddq, 1H, CH=, ³J = 15.0 and 10.9 Hz, ⁴J = 1.4 Hz), 4.60 (dd, 1H, OCH₂, ²J = 10.3 Hz, ³J = 5.6 Hz), 4.50 (dd, 1H, OCH₂, ²J = 10.3 Hz, ³J = 5.6 Hz), 1.98 (m, 1H, -CH-), 1.83 (dd, 3H, Me, ³J = 7.0 Hz, ⁴J = 1.4 Hz) 1.50 (m, 1H, CH₂-), 1.32 (m, 1H, CH₂-), 1.02 (d, 3H, Me, ³J = 6.8 Hz), 0.96 (d, 3H, Me, ³J = 7.4 Hz); ¹³C NMR (CD₂Cl₂) δ 304.8 (W=C), 204.1 (CO), 197.8 (CO), 145.4 (CH=), 144.6 (CH=), 136.1 (CH=), 131.0 (CH=), 87.1 (OCH₂), 35.4 (-CH-), 26.3 (CH₂-), 19.6 (Me), 16.8 (Me), 11.3 (Me). HRMS M⁺ Calcd for C₁₆H₁₈O₆W¹⁸²: 488.0585. Found: 488.0591.

(CO)₅W=C(OCH₂CH₂C=CMe)(CH=CHCH=CMe₂), **7j**: yield 0.22 g (22%) from 0.70 g (2 mmol) of W(CO)₆, 0.66 g (6 mmol) of **j**, and 2.5 mL of 3-pentyn-1-ol; IR (Nujol) 2064, 1940, 1623, 1562 cm⁻¹; ¹H NMR (CD₂Cl₂) δ 7.36 (dd, 1H, CH=, ³J = 14.5 and 11.6 Hz), 7.15 (d, 1H, CH=, ³J = 14.5 Hz), 5.99 (dm, 1H, CH=, ³J = 11.6 Hz), 4.78 (t, 2H, OCH₂-, ³J = 6.5 Hz), 2.76 (m, 2H, CH₂-), 1.90 (3H, Me), 1.88 (3H, Me), 1.77 (t, 3H, Me, ⁵J = 2.5 Hz); ¹³C NMR (CD₂Cl₂) δ 303.6 (W=C), 203.8 (CO), 197.8 (CO), 153.5 (=C), 144.9 (CH=), 135.0 (CH=), 125.3 (CH=), 79.6 (OCH₂), 77.2 (C≡), 74.3 (C≡), 29.7 (CH₂), 27.5 (Me), 20.1 (Me), 19.5 (Me). Anal. Calcd for C₁₆H₁₃O₆W: C, 40.82; H, 3.22. Found: C, 40.41; H, 3.51.

(CO)₅Cr=C(OCH₂CH₂C=CMe)(CH=CHPh), **8b**: yield 0.16 g (15%) from 0.66 g (3 mmol) of Cr(CO)₆, 0.40 g (3 mmol) of **b**, and 3.0 mL of 3-pentyn-1-ol; IR (Nujol) 2057, 1946, 1595 cm⁻¹; ¹H NMR (CDCl₃) δ 7.97 (d, 1H, CH=, ³J = 15.3 Hz), 7.62–7.41 (m, 5H, C₆H₅), 7.04 (d, 1H, CH=, ³J = 15.3 Hz), 5.08 (t, 2H, OCH₂-, ³J = 6.5 Hz), 2.88 (m, 2H, CH₂-), 1.80 (t, 3H, Me, ⁵J = 2.5 Hz); ¹³C NMR (CDCl₃) δ 332.3 (Cr=C), 225.0 (CO), 217.2 (CO), 140.0 (CH=), 134.9 (C₆H₅), 131.3 (C₆H₅), 130.9, 129.9, 129.5 (C₆H₅), 78.4 (OCH₂), 74.5 (C≡), 71.6 (C≡), 29.8 (CH₂-), 20.6 (Me). Anal. Calcd for C₁₉H₁₄O₆Cr: C, 58.47; H, 3.62. Found: C, 58.33; H, 3.72.

(CO)₅W=C(OCH₂CH₂CH=CH₂)(HC=CHMe), **9a**: yield 1.06 g (59%) from 1.06 g (3 mmol) of W(CO)₆, 0.42 g (6 mmol) of **a**, and 2.5 mL of 3-buten-1-ol; IR (Nujol) 2067, 1942, 1611 cm⁻¹; ¹H NMR (C₆D₆) δ 7.10 (dq, 1H, CH=, ³J = 15.0 Hz, ⁴J = 1.5 Hz), 6.28 (dq, 1H, CH=, ³J = 15.0 Hz, ⁴J = 7.0 Hz), 5.55 (m, 1H, CH=), 4.96 (m, 2H, =CH₂), 4.49 (t, 2H, OCH₂, ³J = 6.5 Hz), 2.16 (m, 2H, CH₂), 1.23 (dd, 3H, CH₃, ³J = 7.0 Hz, ⁴J = 1.5 Hz); ¹³C NMR (C₆D₆) δ 307.4 (W=C), 204.2 (CO), 198.4 (CO), 149.8 (CH=), 138.2 (CH=), 134.0 (CH=), 118.3 (CH=), 82.2 (OCH₂), 33.9 (CH₂), 18.4 (CH₃). HRMS M⁺ Calcd for C₁₃H₁₂O₆W¹⁸²: 446.0124. Found: 446.0115.

(CO)₅W=C(OCH₂CH₂CH=CH₂)(HC=CHHC=CHMe₂), **10j**: yield 0.68 g (69%) from 0.70 g (2 mmol) of W(CO)₆, 0.66 g (6 mmol) of **j**, and 2.5 mL of 3-buten-1-ol; IR (Nujol) 2064, 1940, 1623, 1560 cm⁻¹; ¹H NMR (C₆D₆) δ 7.32 (dd, 1H, CH=, ³J = 14.5 and 11.6 Hz), 7.10 (d, 1H, CH=, ³J = 14.5 Hz), 5.57 (m, 1H, CH=), 5.55 (dm, 1H, CH=, ³J = 11.6 Hz) 4.98 (m, 2H, =CH₂), 4.48 (t, 2H, OCH₂, ³J = 6.3 Hz), 2.12 (m, 2H, CH₂), 1.47 (3H, CH₃), 1.38 (3H, CH₃); ¹³C NMR (C₆D₆) δ 303.7 (W=C), 203.9 (CO), 197.9 (CO), 153.2 (=CMe₂), 144.8 (CH=), 134.6 (CH=), 133.7 (CH=), 125.1 (CH=), 117.9 (=CH₂), 80.7 (OCH₂), 33.9 (CH₂), 27.4 (CH₃), 19.5 (CH₃). Anal. Calcd for WC₁₆H₁₆O₆: C, 39.74; H, 3.25. Found: C, 39.37; H, 3.30. HRMS M⁺ calcd for C₁₆O₆H₁₆W¹⁸⁴: 488.04546. Found: 488.04526.

(CO)₅W=C[OCH₂CH₂C(Me)=CH₂][CH=CHHC=CMe₂], **11j**: yield 0.48 g (24%) from 1.41 g (4 mmol) of W(CO)₆, 1.32 g (12 mmol) of **j**, and 4 mL of 3-methyl-3-buten-1-ol; IR (Nujol) 2064, 1939, 1620, 1560 cm⁻¹. HRMS M⁺ calcd for C₁₇H₁₈O₆W¹⁸²: 500.05849. Found: 500.0585. **11j** decomposes to **14j** at 25 °C in C₆D₆.

Thermolysis of 9a, 10j, and 11j. The thermolyses were carried out in NMR tubes. A solution of 25 mg of **9a** and **10j** in 0.6 mL of C₆D₆ was heated at 60–70 °C for 2 h. The red solution gradually darkened. The ¹H NMR spectra of the

samples showed total conversion of **9a** and **10j** to **12a** and **13j**, respectively. The conversion of **11j** to **14j** was obtained at 25 °C in C₆D₆.

12a: ¹H NMR (C₆D₆) δ 5.64 (dq, 1H, CH=, ³J = 15.2 Hz, ³J = 6.4 Hz), 5.45 (dq, 1H, CH=, ³J = 15.2 Hz, ⁴J = 1.5 Hz), 4.00 (ddd, 1H, OCH₂-, ²J = 9.1 Hz, ³J = 9.1 Hz, ³J = 2.3 Hz), 3.48 (ddd, 1H, OCH₂-, ²J = 9.1 Hz, ³J = 9.1 Hz, ³J = 7.3 Hz), 2.06 (m, 1H, CH₂-), 1.87 (ddd, 1H, CH₂-, ³J = 9.1 Hz, ³J = 7.3 Hz, ³J = 2.3 Hz), 1.67 (dd, 3H, CH₃, ³J = 6.4 Hz, ⁴J = 1.5 Hz), 1.39 (m, 1H, -CH-), 1.0 (dd, 1H, CH₂ cyclopropyl, ²J = 5.6 Hz, ³J = 5.6 Hz), 0.68 (dd, 1H, CH₂ cyclopropyl, ³J = 8.9 Hz, ³J = 5.6 Hz).

13j: ¹H NMR (C₆D₆) δ 6.99 (dd, 1H, CH=, ³J = 15.1 Hz, ³J = 11.2 Hz), 5.99 (d, 1H, CH=, ³J = 11.2 Hz), 5.50 (d, 1H, CH=, ³J = 15.1 Hz), 3.89 (ddd, 1H, OCH₂-, ²J = 9.0 Hz, ³J = 9.0 Hz, ³J = 2.3 Hz), 3.31 (ddd, 1H, OCH₂-, ²J = 9.0 Hz, ³J = 9.0 Hz, ³J = 7.3 Hz), 1.75 (m, 1H, CH₂-), 1.65 (3H, CH₃), 1.63 (3H, CH₃), 1.48 (m, 1H, CH₂-), 1.20 (m, 1H, -CH-), 0.99 (dd, 1H, CH₂ cyclopropyl, ²J = 6.0 Hz, ³J = 6.0 Hz), 0.60 (ddd, 1H, CH₂ cyclopropyl, ³J = 8.9 Hz, ²J = 6.0 Hz, ⁴J = 0.3 Hz).

14j: ¹H NMR (C₆D₆) δ 7.00 (dd, 1H, CH=, ³J = 15.1 Hz, ³J = 11.1 Hz), 5.99 (dm, 1H, CH=, ³J = 11.1 Hz), 5.53 (d, 1H, CH=, ³J = 15.1 Hz), 3.83 (ddd, 1H, OCH₂-, ²J = 9.0 Hz, ³J = 9.0 Hz, ³J = 2.5 Hz), 3.26 (ddd, 1H, OCH₂-, ²J = 10.2 Hz, ²J = 9.0 Hz, ³J = 7.5 Hz), 1.66 (m, 1H, CH₂-), 1.65 (d, 3H, CH₃, ⁴J = 0.5 Hz), 1.63 (d, 3H, CH₃, ⁴J = 1.0 Hz), 1.60 (m, 1H, CH₂-), 1.15 (d, 1H, CH₂ cyclopropyl, ²J = 6.1 Hz), 1.01 (3H, CH₃), 0.43 (dd, 1H, CH₂ cyclopropyl, ²J = 6.1 Hz, ⁴J = 1.4 Hz).

General Procedure for the Aminolysis of (Methoxyalkenylcarbene)tungsten Complexes. A solution of 1 mmol of complex **3g** or **3i** in 50 mL of pentane was treated with 0.5 mL of amine (5–7 equiv) at room temperature. The color rapidly changed from red to orange. After stirring for 1 h (the reaction was slower with *tert*-butylamine and needed 18 h of stirring), the solvent was removed and the crude product was chromatographed on silica gel using pentane/dichloromethane (1/1) as eluent. Evaporation of the solvent gave complexes **15–18** as orange solids.

(OC)₅W=C(NHCHMe₂)(CH=CHCH=CHPh), 15g: yield 0.45 g (86%) from 0.5 g (1 mmol) of **3g** and 0.5 mL (5.8 mmol) of isopropylamine; IR (Nujol) 2061, 1925, 1614, 1590 cm⁻¹. Anal. Calcd for WC₁₉H₁₇NO₅: C, 43.59; H, 3.28; N, 2.68. Found: C, 43.56; H, 3.30; N, 2.67. (Z): ¹H NMR (CDCl₃) δ 8.16 (s broad, 1H, NH), 7.46–7.27 (m, 5H, C₆H₅), 6.88 (d, 1H, CH=, ³J = 15.0 Hz), 6.83 (d, 1H, CH=, ³J = 15.7 Hz), 6.82 (dd, 1H, CH=, ³J = 15.7 Hz, ³J = 10.1 Hz), 6.43 (m, 1H, CH=), 4.60 (m, 1H, N-CH), 1.42 (d, 6H, CH₃, ³J = 6.5 Hz); ¹³C NMR (CDCl₃) δ 239.0 (W=C), 203.3 (CO), 196.7 (CO), 145.2 (CH=), 138.9 (CH=), 136.3 (C₆H₅), 131.6 (CH=), 128.8 (CH=), 128.8, 126.9, 126.8 (C₆H₅), 57.3 (N-C), 21.1 (CH₃). (E): ¹H NMR (CDCl₃) δ 8.08 (s broad, 1H, NH), 7.46–7.27 (m, 5H, C₆H₅), 7.18 (m, 1H, CH=), 6.94 (d, 1H, CH=, ³J = 15.5 Hz), 6.89 (dd, 1H, CH=, ³J = 15.5 Hz, ³J = 12.0 Hz), 6.68 (d, 1H, CH=, ³J = 14.2 Hz), 4.07 (m, 1H, N-CH), 1.28 (d, 6H, CH₃, ³J = 6.5 Hz); ¹³C NMR (CDCl₃) δ 243.4 (W=C), 201.5 (CO), 197.8 (CO), 49.2 (N-C), 21.2 (CH₃).

(OC)₅W=C(NHCHMe₃)(CH=CHHC=CHPh), 16g: yield 0.32 g (60%) from 0.5 g (1 mmol) of **3g** and 0.5 mL (4.8 mmol)

of *tert*-butylamine; IR (Nujol) 2061, 1933, 1618, 1590 cm⁻¹. Anal. Calcd for WC₂₀O₅H₁₉N: C, 44.72; H, 3.56; N, 2.61. Found: C, 44.90; H, 3.81; N, 2.54. (Z): ¹H NMR (CDCl₃) δ 8.90 (s broad, 1H, NH), 7.46–7.27 (m, 5H, C₆H₅), 7.13 (d, 1H, CH=, ³J = 14.7 Hz), 6.72 (d, 1H, CH=, ³J = 15.5 Hz), 6.68 (dd, 1H, CH=, ³J = 15.5 Hz, ³J = 12.0 Hz), 5.76 (m, 1H, CH=), 1.57 (9H, CH₃); ¹³C NMR (CDCl₃) δ 244.4 (W=C), 203.4 (CO), 198.7 (CO), 58.1 (N-C), 30.3 (CH₃). (E): ¹H NMR (CDCl₃) δ 8.48 (s broad, 1H, NH), 7.46–7.27 (m, 5H, C₆H₅), 7.08 (m, 1H, CH=), 6.93 (d, 1H, CH=, ³J = 14.6 Hz), 6.86 (m, 1H, CH=), 6.86 (m, 1H, CH=), 1.45 (9H, CH₃); NMR ¹³C{¹H} (CDCl₃) δ 249.4 (W=C), 203.0 (CO), 199.4 (CO), 60.7 (N-C), 30.6 (CH₃).

(OC)₅W=C(NHCH₂CH=CH₂)(HC=CHHC=CHPh), 17g: yield 0.41 g (82%) from 0.5 g (1 mmol) of **3g** and 0.5 mL (6.7 mmol) of allylamine; IR (Nujol) 2061, 1927, 1612, 1590 cm⁻¹. (Z): ¹H NMR (CDCl₃) δ 8.26 (s broad, 1H, NH), 7.46–7.27 (m, 5H, C₆H₅), 6.83 (d, 1H, CH=, ³J = 15.0 Hz), 6.77 (m, 1H, CH=), 6.75 (m, 1H, CH=), 6.48 (m, 1H, CH=), 5.93 (m, 1H, CH=), 5.28 (m, 2H, =CH₂), 4.44 (m, 2H, NCH₂); ¹³C NMR (CDCl₃) δ 247.1 (W=C), 203.0 (CO), 198.2 (CO), 57.1 (-CH₂N). (E): ¹H NMR (CDCl₃) δ 8.26 (s broad, 1H, NH), 7.46–7.27 (m, 5H, C₆H₅), 7.18 (m, 1H, CH=), 6.87 (m, 1H, CH=), 6.88 (m, 1H, CH=), 6.59 (d, 1H, CH=, ³J = 14.7 Hz), 5.82 (m, 1H, CH=), 5.28 (m, 2H, =CH₂), 4.01 (m, 2H, NCH₂); ¹³C NMR (CDCl₃) δ 249.3 (W=C), 203.3 (CO), 199.1 (CO), 51.3 (-CH₂N).

(OC)₅W=C(NHCH₂CHMe₂)(HC=CHHC=CHC₅H₁₁), 18i: yield 0.49 g (92%) from 0.49 g (1 mmol) of **3i** and 0.5 mL (5.9 mmol) of isopropylamine; IR (Nujol) 2060, 1926, 1636, 1596 cm⁻¹. Anal. Calcd for C₁₉H₁₅NO₅W: C, 42.96; H, 4.74. Found: C, 41.56; H, 4.38. (Z): ¹H NMR (CDCl₃) δ 8.26 (s broad, 1H, NH), 6.65 (d, 1H, CH=, ³J = 14.9 Hz), 6.28 (m, 1H, CH=), 6.02 (m, 1H, CH=), 6.02 (m, 1H, CH=) 3.63 (m, 2H, N-CH₂), 2.12 (m, 2H, CH₂), 1.92 (sept, 1H, -CH-, ³J = 6.7 Hz), 1.38 (2H, CH₂, ³J = 7.2 Hz, ³J = 7.2 Hz), 1.29–1.18 (m, 4H, CH₂), 1.00 (d, 6H, CH₃, ³J = 6.7 Hz), 0.82 (t, 3H, CH₃, ³J = 6.9 Hz); ¹³C NMR (CDCl₃) δ 245.9 (W=C), 203.3 (CO), 198.4 (CO), 143.6 (HC=), 143.4 (HC=), 133.1 (HC=), 128.7 (HC=), 62.1 (CH₂), 33.1 (CH₂), 31.4 (CH₂), 28.7 (CH), 28.4 (CH₂), 22.5 (CH₂), 20.1 (CH₃), 14.0 (CH₃). (E): ¹H NMR (CDCl₃) δ 8.18 (s broad, 1H, NH), 7.09 (dd, 1H, CH=, ³J = 14.8 Hz, ³J = 9.5 Hz), 6.44 (d, 1H, CH=, ³J = 14.8 Hz), 6.20 (m, 1H, CH=), 6.20 (m, 1H, CH=), 3.20 (m, 2H, N-CH₂), 2.12 (m, 2H, CH₂), 1.92 (sept, 1H, CH, ³J = 6.7 Hz), 1.38 (tt, 2H, CH₂, ³J = 7.2 Hz, ³J = 7.2 Hz), 1.29–1.18 (m, 4H, CH₂), 0.96 (d, 6H, CH₃, ³J = 6.7 Hz), 0.83 (t, 3H, CH₃, ³J = 6.9 Hz); ¹³C NMR (CDCl₃) δ 247.0 (W=C), 202.8 (CO), 199.3 (CO), 152.5 (HC=), 145.6 (CH=), 133.1 (CH=), 129.7 (CH=), 56.2 (CH₂), 33.2 (CH₂), 31.4 (CH₂), 28.7 (CH), 28.4 (CH₂), 22.5 (CH₂), 20.0 (CH₃), 14.0 (CH₃).

Acknowledgment. This work was supported by the CNRS. We thank J. P. Guégan for NMR technical assistance, the European ERASMUS program for a grant to I.D.R., the University of Oviedo (Spain), and the European Union (CHM program, contract CHRXCT 940501) for financial support.

OM9409433

Nucleophilic and Electrophilic Allylation Reactions. Synthesis, Structure, and Ambiphilic Reactivity of (η^3 -Allyl)ruthenium(II) Complexes

Teruyuki Kondo,* Hiroyuki Ono, Nobuya Satake, Take-aki Mitsudo, and Yoshihisa Watanabe*

Division of Energy and Hydrocarbon Chemistry, Graduate School of Engineering, Kyoto University, Sakyo-ku, Kyoto 606-01, Japan

Received November 3, 1994[®]

Several (η^3 -allyl)ruthenium(II) complexes bearing carbon monoxide ligands can function as both a nucleophile and an electrophile, *i.e.*, as an ambiphile. Namely, they smoothly react with both aldehydes and $\text{NaCH}(\text{COOMe})_2$ under extremely mild reaction conditions to give the corresponding allylated products in good to high yields. The higher valent (η^3 -allyl)ruthenium(IV) complex, $\text{Cp}^*\text{RuCl}_2(\eta^3\text{-allyl})$ (Cp^* = pentamethylcyclopentadienyl), is only electrophilic and unusually high regioselectivity of allylation of carbon and nitrogen nucleophiles can be attained.

Introduction

Interest in η^3 -allyl transition-metal chemistry, particularly that of (η^3 -allyl)palladium, has undergone incredible growth over the last decade,¹ and a large number of η^3 -allyl transition-metal complexes have been prepared. However, the essence of (η^3 -allyl)palladium-mediated functionalization is the activation of an allylic system to be attacked by only nucleophilic compounds. On the other hand, several η^3 -allyl transition-metal complexes such as Ni,² Ti,³ and Mo⁴ show nucleophilic reactivity and react with electrophiles such as aldehydes and ketones, while other Mo complexes show electrophilic reactivity.⁵ Some η^3 -allyl Ni⁶ and Fe⁷ complexes are reported to react with both nucleophiles such as alkenyltin^{6a} or malonate⁷ and electrophiles such as alkyl halides.^{6b,7} The reaction of alkyl halides with the allylic compounds, however, proceeds via alkylation of the metallic centers forming (alkyl)(allyl)metal complexes, and successive reductive elimination gives the products.^{6,7} Thus, the allyl ligands are not attacked by the electrophiles during the reaction. Consequently, no η^3 -

allyl ligand exhibits both electrophilic and nucleophilic behavior. If a η^3 -allyl ligand in a transition-metal complex can be applied not only as an electrophile but also as a nucleophile, the chemistry of η^3 -allyl complexes could be further developed in organic syntheses. In the last decade, palladium-catalyzed allylation of carbonyl compounds has been achieved, but the use of low-valent metals is essential for the transformation of allylic compounds to allylic metal compounds.^{8,9}

In the course of our studies on ruthenium catalysis,¹⁰ we have succeeded in developing several novel ruthenium-catalyzed allylation reactions as illustrated in Scheme 1.¹¹ They were classified as a nucleophilic allylation and an electrophilic allylation. Thus, there exists the possibility that (η^3 -allyl)ruthenium complexes can alternately function as a nucleophile and an electrophile, *i.e.*, as an ambiphile, depending on the reactivity of the substrates. In order to investigate this novel reactivity of (η^3 -allyl)ruthenium complexes, we have tried to synthesize several (η^3 -allyl)ruthenium(II) and

[®] Abstract published in *Advance ACS Abstracts*, March 15, 1995.

(1) (a) Trost, B. M. *Acc. Chem. Res.* **1980**, *13*, 385. (b) Trost, B. M.; Verhoeven, T. R. In *Comprehensive Organometallic Chemistry*; Wilkinson, G., Stone, F. G. A., Abel, E. W., Eds.; Pergamon Press: Oxford, UK, 1982; Vol. 8, p 799. (c) Tsuji, J. *Organic Synthesis with Palladium Compounds*; Springer-Verlag: New York, 1980. (d) Heck, R. F. In *Palladium Reagents in Organic Syntheses*; Katritzky, A. R., Meth-Cohn, O., Rees, C. W., Eds.; Academic Press: London, 1985; Chapter 5, p 117. (e) Godleski, S. A. In *Comprehensive Organic Synthesis*; Trost, B. M., Fleming, I., Eds.; Pergamon Press: Oxford, UK, 1991; Vol. 4, p 585.

(2) (a) Corey, E. J.; Semmelhack, M. F. *J. Am. Chem. Soc.* **1967**, *89*, 2755. (b) Hegedus, L. S.; Wagner, S. D.; Waterman, E. L.; S.-Hansen, K. *J. Org. Chem.* **1975**, *40*, 593.

(3) Collins, S.; Dean, W. P.; Ward, D. G. *Organometallics* **1988**, *7*, 2289.

(4) (a) Faller, J. W.; Linebarrier, D. L. *J. Am. Chem. Soc.* **1989**, *111*, 1937. (b) Faller, J. W.; John, J. A.; Mazzieri, M. R. *Tetrahedron Lett.* **1989**, *30*, 1769.

(5) (a) Faller, J. W.; Lambert, C.; Mazzieri, M. R. *J. Organomet. Chem.* **1990**, *383*, 161. (b) Trost, B. M.; Merlic, C. A. *J. Am. Chem. Soc.* **1990**, *112*, 9590.

(6) (a) Grisso, B. A.; Johnson, J. R.; Mackenzie, P. B. *J. Am. Chem. Soc.* **1992**, *114*, 5160. (b) Johnson, J. R.; Tully, P. S.; Mackenzie, P. B.; Sabat, M. *J. Am. Chem. Soc.* **1991**, *113*, 6172.

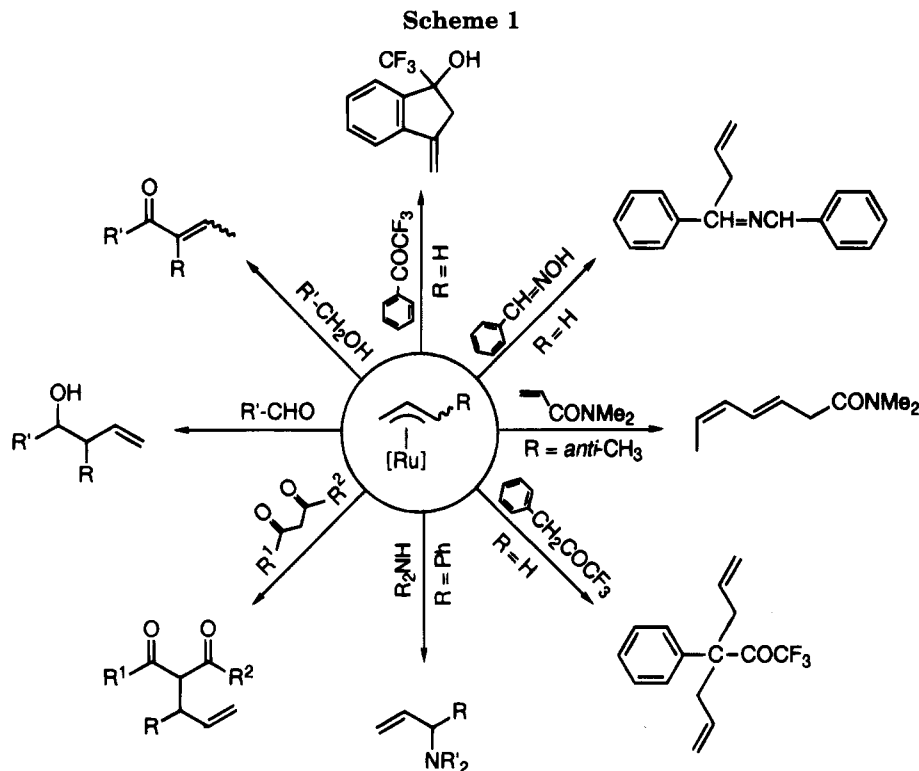
(7) Itoh, K.; Nakanishi, S.; Ohtsui, Y. *J. Organomet. Chem.*, **1994**, *473*, 215.

(8) (a) Trost, B. M.; Herndon, J. W. *J. Am. Chem. Soc.* **1984**, *106*, 5835. (b) Matsubara, S.; Wakamatsu, K.; Morizawa, Y.; Tsuboniwa, N.; Oshima, K.; Nozaki, H. *Bull. Chem. Soc. Jpn.* **1985**, *58*, 1196. (c) Tabuchi, T.; Inanaga, J.; Yamaguchi, M. *Tetrahedron Lett.* **1986**, *27*, 1195. (d) Tabuchi, T.; Inanaga, J.; Yamaguchi, M. *Tetrahedron Lett.* **1987**, *28*, 215. (e) Masuyama, Y.; Kinugawa, N.; Kurusu, Y. *J. Org. Chem.* **1987**, *52*, 3702. (f) Masuyama, Y.; Hayashi, R.; Otake, K.; Kurusu, Y. *J. Chem. Soc., Chem. Commun.* **1988**, *44*. (g) Takahara, J. P.; Masuyama, Y.; Kurusu, Y. *J. Am. Chem. Soc.* **1992**, *114*, 2577. (h) Qiu, W.; Wang, Z. *J. Chem. Soc., Chem. Commun.* **1989**, 356. (i) Zhang, P.; Zhang, W.; Zhang, T.; Wang, Z.; Zhou, W. *J. Chem. Soc., Chem. Commun.* **1991**, 491.

(9) Only one example showing that (π -allyl)palladium intermediate serves as a nucleophile rather than its normal reactivity as an electrophile without low-valent metal reductant was reported by Trost et al. in the reductive cleavage of enediacarbonates: Trost, B. M.; Tometzki, G. B. *J. Org. Chem.* **1988**, *53*, 915.

(10) (a) Mitsudo, T.; Hori, Y.; Watanabe, Y. *J. Organomet. Chem.* **1987**, *334*, 157, and references cited therein. (b) Tsuji, Y.; Kotachi, S.; Huh, K.-T.; Watanabe, Y. *J. Org. Chem.* **1990**, *55*, 580, and references cited therein. (c) Kondo, T.; Akazome, M.; Tsuji, Y.; Watanabe, Y. *J. Org. Chem.* **1990**, *55*, 1286, and references cited therein.

(11) (a) Tsuji, Y.; Mukai, T.; Kondo, T.; Watanabe, Y. *J. Organomet. Chem.* **1989**, *369*, C51. (b) Kondo, T.; Mukai, T.; Watanabe, Y. *J. Org. Chem.* **1991**, *56*, 487. (c) Mitsudo, T.; Zhang, Z.-W.; Kondo, T.; Watanabe, Y. *Tetrahedron Lett.* **1992**, *33*, 341. (d) Mitsudo, T.; Zhang, S.-W.; Satake, N.; Kondo, T.; Watanabe, Y. *Tetrahedron Lett.* **1992**, *33*, 5533. (e) Zhang, S.-W.; Mitsudo, T.; Kondo, T.; Watanabe, Y. *J. Organomet. Chem.* **1993**, *450*, 197. (f) Allylation reactions of trifluoromethyl ketones and aldoximes are our unpublished results.

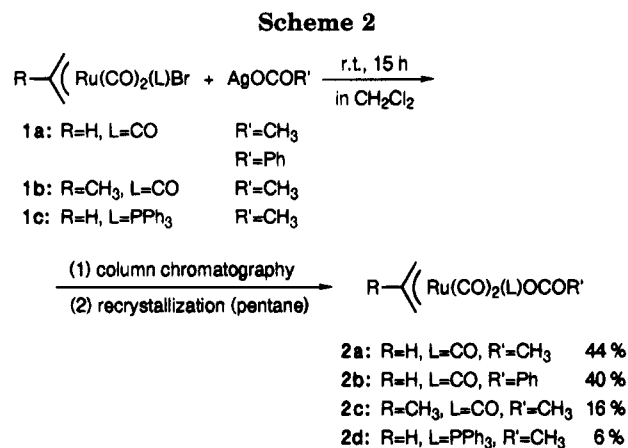


(IV) complexes which seem to be the most plausible key intermediates in our previously reported ruthenium-catalyzed allylation reactions.^{11a,e} In this paper, we present details of the synthesis, structure, and ambiphilic reactivity of $(\eta^3\text{-allyl})\text{Ru}(\text{CO})_3\text{X}$. In addition, a higher valent $(\eta^3\text{-allyl})$ ruthenium(IV) complex reacted with only nucleophiles and an unusually high regioselectivity of allylation of both carbon and nitrogen nucleophiles was attained.

Results and Discussion

Synthesis of $(\eta^3\text{-allyl})\text{RuL}_3\text{X}$ ($\text{L} = \text{CO}$ or PPh_3 , $\text{X} = \text{OCOR}$ or OTf). First, we tried to synthesize novel ruthenium complexes bearing both $\eta^3\text{-allyl}$ and carboxylate ligands by direct oxidative addition of allyl carboxylates to low-valent ruthenium complexes such as $\text{Ru}_3(\text{CO})_{12}$ and $\text{Ru}(\text{COD})(\text{COT})$ [$(\eta^4\text{-1,5-cyclooctadiene})(\eta^6\text{-1,3,5-cyclooctatriene})$ ruthenium]. However, the reaction did not proceed even in refluxing toluene. Then, we employed the reaction of ruthenium halide with NaOAc .¹² Fortunately, Pino et al. already reported the synthesis of $(\eta^3\text{-C}_3\text{H}_5)\text{Ru}(\text{CO})_3\text{Br}$ (**1a**) from the reaction of $\text{Ru}_3(\text{CO})_{12}$ with allyl bromide.¹³ Although the complex **1a** did not react with NaOAc , the treatment of **1a** with AgOAc in dry CH_2Cl_2 at room temperature for 15 h under an argon atmosphere in the dark afforded $(\eta^3\text{-C}_3\text{H}_5)\text{Ru}(\text{CO})_3\text{OAc}$ (**2a**) as white needles in 44% yield (after purification by column chromatography (Al_2O_3 , CH_2Cl_2) and recrystallization from *n*-pentane). Similarly, $(\eta^3\text{-C}_3\text{H}_5)\text{Ru}(\text{CO})_3\text{OCOPh}$ (**2b**) (40% yield), $(\eta^3\text{-2-methylallyl})\text{Ru}(\text{CO})_3\text{OAc}$ (**2c**) (16% yield), and $(\eta^3\text{-C}_3\text{H}_5)\text{Ru}(\text{CO})_2(\text{PPh}_3)\text{OAc}$ (**2d**) (6%) were synthesized (Scheme 2).

Furthermore, $[(\eta^3\text{-C}_3\text{H}_5)\text{Ru}(\text{CO})_3]^+(\text{OTf})^-$ (**2e**) was obtained in 47% yield from the reaction of **1a** with



AgOTf . The complex **2e** is a coordinatively unsaturated 16-electron complex which was fully characterized by ^1H NMR, ^{13}C NMR, IR, and elemental analysis. However, during recrystallization, **2e** was converted into a cationic complex, $[(\eta^3\text{-C}_3\text{H}_5)\text{Ru}(\text{CO})_3(\text{H}_2\text{O})]^+(\text{OTf})^-$ (**2f**). The results of the X-ray analysis of **2f** are shown in Figure 1 and Tables 1–3. Although Pino et al. reported the synthesis of these types of octahedral $(\eta^3\text{-allyl})$ -ruthenium(II) complexes¹³ and spectroscopic investigation of the conformation of $\eta^3\text{-allyl}$ ligands was performed by Wu and Wrighton,¹⁴ the exact crystal structure of these complexes has not yet been reported.

On the other hand, we could not prepare single crystals of the complexes **2a–d**, but the structure of these complexes was confirmed by the following spectral data and elemental analyses (Experimental Section). In the IR spectra, the three terminal $\nu(\text{M}-\text{CO})$ absorptions of **2a–d** were found at $2110\text{--}2000\text{ cm}^{-1}$, while those of **2e** were shifted to 2128 cm^{-1} , due to the cationic character of this complex. The $\nu(\text{C}=\text{O})$ absorptions of the acetato ligand in **2a** were found at 1619 cm^{-1} ($\nu_{\text{asym}}(\text{COO})$)

(12) For example, see: Young, R.; Wilkinson, G. *Inorg. Synth.* **1977**, *17*, 79.

(13) Sbrana, G.; Braca, G.; Piacenti, F.; Pino, P. *J. Organomet. Chem.* **1968**, *13*, 240.

(14) Wu, Y.-M.; Wrighton, M. S. *Organometallics* **1988**, *7*, 1839.

Table 1. Crystal and Intensity Collection Data for 2f and 3a

	$[(\eta^3\text{-C}_3\text{H}_5)\text{Ru}(\text{CO})_3(\text{H}_2\text{O})]^+(\text{OTf})^-$ (2f)	$\text{Cp}^*\text{RuCl}_2(\text{CH}_2\text{CHCHPh})$ (3a)
composition	$\text{C}_7\text{F}_3\text{H}_7\text{O}_7\text{RuS}$	$\text{C}_{19}\text{Cl}_2\text{H}_{24}\text{Ru}$
fw	393.25	424.37
cryst color	colorless, prismatic	orange, plate
cryst dimens (mm)	$0.10 \times 0.10 \times 0.20$	$0.20 \times 0.20 \times 0.05$
cryst syst	triclinic	orthorhombic
space group	$P\bar{1}$ (No. 2)	$Pna2_1$ (No. 33)
cell const		
a, Å	8.143(3)	17.560(1)
b, Å	10.556(3)	12.604(1)
c, Å	8.100(3)	8.347(1)
α , deg	97.30(3)	90.0
β , deg	97.65(3)	90.0
γ , deg	102.55(3)	90.0
V, Å ³	664.8(4)	1847.3(5)
Z	2	4
diffractometer	Rigaku AFC7R	Rigaku AFC7R
radiation, (λ , Å)	Mo K α av = 0.710 69	Mo K α av = 0.710 69
ρ (calcd), g/cm ³	1.964	1.526
μ (Mo K α), cm ⁻¹	13.96	11.32
2 θ_{max} (deg)	59.9	60.0
no. of collected rflns	4132	3081
no. of unique rflns	2666 ($I > 3.00\sigma(I)$)	1516 ($I > 3.00\sigma(I)$)
goodness of fit	1.43	1.84
R^a	0.039	0.051
R_w^b	0.040	0.052

$$^a R = \sum ||F_o| - |F_c|| / \sum |F_o|. \quad ^b R_w = [\sum w(|F_o| - |F_c|)^2 / \sum w F_o^2]^{1/2}.$$

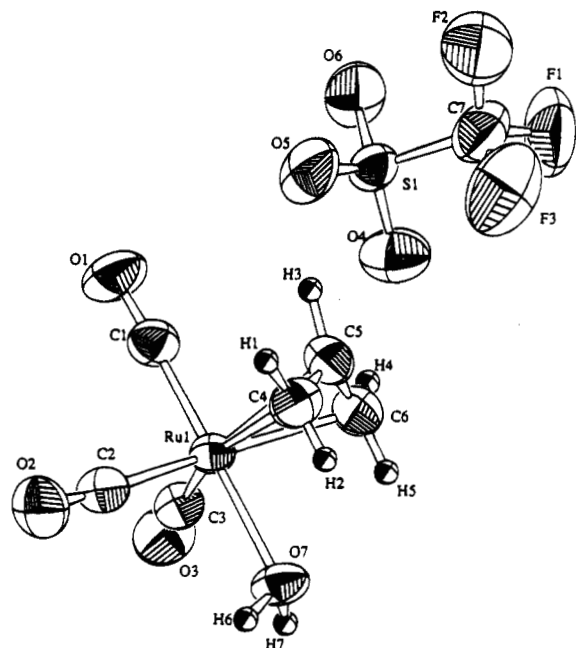


Figure 1. Molecular structure and labeling scheme for 2f.

Table 2. Bond Lengths (Å) for 2a

Ru(1)-O(7)	2.167(3)	O(7)-H(7)	0.949(3)	F(1)-C(7)	1.337(7)
Ru(1)-C(2)	1.953(5)	C(4)-H(1)	1.028(5)	F(3)-C(7)	1.312(7)
Ru(1)-C(4)	2.232(4)	C(5)-C(6)	1.392(7)	O(2)-C(2)	1.125(5)
Ru(1)-C(6)	2.237(5)	C(6)-H(4)	1.014(5)	O(7)-H(6)	0.946(3)
S(1)-O(5)	1.433(4)	Ru(1)-C(1)	1.866(4)	C(4)-C(5)	1.391(7)
S(1)-C(7)	1.805(6)	Ru(1)-C(3)	1.961(5)	C(4)-H(2)	0.950(5)
F(2)-C(7)	1.291(7)	Ru(1)-C(5)	2.226(4)	C(5)-H(3)	1.048(5)
O(1)-C(1)	1.133(5)	S(1)-O(4)	1.422(4)	C(6)-H(5)	0.976(5)
O(3)-C(3)	1.130(5)	S(1)-O(6)	1.411(3)		

and 1321 cm^{-1} ($\nu_{\text{sym}}(\text{COO})$) (KBr). The position and value of $\Delta\nu$ ($\nu_{\text{asym}}(\text{COO}) - \nu_{\text{sym}}(\text{COO})$)^{12,15} is quite large (298 cm^{-1}), revealing an unsymmetrical monodentate (η^1) coordination mode of the acetato ligand to ruthenium.¹⁶ Furthermore, in the ¹³C NMR spectra, chemical shift values

(15) (a) Nakamoto, K. *Infrared and Raman Spectra of Inorganic and Coordination Compounds*; John Wiley & Sons: New York, 1978; p 232. (b) Dobson, A.; Robinson, S. D.; Uttley, M. *Inorg. Synth.* **1977**, *17*, 124.

Table 3. Bond Angles (deg) for 2a

O(7)-Ru(1)-C(1)	179.0(2)	Ru(1)-C(2)-O(2)	176.6(4)
O(7)-Ru(1)-C(4)	82.2(1)	Ru(1)-C(4)-H(1)	120.5(3)
C(1)-Ru(1)-C(2)	89.8(2)	C(5)-C(4)-H(2)	115.8(5)
C(1)-Ru(1)-C(5)	83.4(2)	Ru(1)-C(5)-C(6)	72.3(3)
C(2)-Ru(1)-C(4)	95.6(2)	C(4)-C(5)-H(3)	115.4(5)
C(3)-Ru(1)-C(4)	161.4(2)	Ru(1)-C(6)-H(4)	117.5(4)
C(4)-Ru(1)-C(5)	36.4(2)	C(5)-C(6)-H(5)	125.2(5)
O(4)-S(1)-O(5)	114.1(2)	S(1)-C(7)-F(2)	112.2(4)
O(5)-S(1)-O(6)	113.2(2)	F(1)-C(7)-F(3)	107.8(5)
Ru(1)-O(7)-H(6)	112.1(2)	O(7)-Ru(1)-C(3)	89.0(2)
Ru(1)-C(1)-O(1)	177.1(4)	O(7)-Ru(1)-C(6)	82.6(1)
Ru(1)-C(4)-C(5)	71.6(3)	C(1)-Ru(1)-C(4)	98.7(2)
C(5)-C(4)-H(1)	117.5(4)	C(2)-Ru(1)-C(3)	100.9(2)
Ru(1)-C(5)-C(4)	72.1(3)	C(2)-Ru(1)-C(6)	161.0(2)
C(4)-C(5)-C(6)	122.0(4)	C(3)-Ru(1)-C(6)	96.7(2)
Ru(1)-C(6)-C(5)	71.4(3)	C(5)-Ru(1)-C(6)	36.4(2)
C(5)-C(6)-H(4)	122.8(5)	O(4)-S(1)-C(7)	103.8(3)
S(1)-C(7)-F(1)	109.3(4)	O(6)-S(1)-C(7)	103.8(3)
F(1)-C(7)-F(2)	106.6(6)	H(6)-O(7)-H(7)	105.1(3)
O(7)-Ru(1)-C(2)	90.5(2)	Ru(1)-C(3)-O(3)	177.1(4)
O(7)-Ru(1)-C(5)	97.1(1)	Ru(1)-C(4)-H(2)	98.2(3)
C(1)-Ru(1)-C(3)	90.0(2)	H(1)-C(4)-H(2)	121.2(5)
C(1)-Ru(1)-C(6)	97.4(2)	Ru(1)-C(5)-H(3)	111.0(3)
C(2)-Ru(1)-C(5)	128.4(2)	C(6)-C(5)-H(3)	119.5(5)
C(3)-Ru(1)-C(5)	130.0(2)	Ru(1)-C(6)-H(5)	97.9(3)
C(4)-Ru(1)-C(6)	66.0(2)	H(4)-C(6)-H(5)	109.9(5)
O(4)-S(1)-O(6)	116.9(3)	S(1)-C(7)-F(3)	110.8(5)
O(5)-S(1)-C(7)	102.8(3)	F(2)-C(7)-F(3)	110.0(6)
Ru(1)-O(7)-H(7)	111.2(2)		

of the carbonyl carbon of carboxylato ligand of **2a-d** were at ~ 170 ppm, which are higher than those of bidentate (η^2) chelate carboxylato ligands.¹⁷

As for the ¹H NMR of **2a**, central, *syn*- and *anti*-H of η^3 -allyl ligand were observed at δ 5.19, 4.02, and 2.38 ppm, respectively. It has already been reported that ($\eta^3\text{-C}_3\text{H}_5$)M(CO)₃Br (M = Fe or Ru) exists in solution in a conformational equilibrium between endo and exo

(16) For bidentate chelate (carboxylato)ruthenium complexes, see: (a) RuH(PPh₃)₃(OAc), $\Delta\nu = 75 \text{ cm}^{-1}$. Rose, D.; Gilbert, J. D.; Richardson, R. P.; Wilkinson, G. *J. Chem. Soc. A* **1969**, 2610. (b) Ru[(S)-BINAP](OAc)₂, $\Delta\nu = 66 \text{ cm}^{-1}$. Ohta, T.; Takaya, H.; Noyori, R. *Inorg. Chem.* **1988**, *27*, 566. For monodentate (carboxylato)ruthenium complexes, see: (c) Ru(CO)₂(PPh₃)₂(OAc)₂, $\Delta\nu = 289 \text{ cm}^{-1}$. Robinson, S. D.; Uttley, M. F. *J. Chem. Soc., Dalton Trans.* **1973**, 1912.

(17) For example, the chemical shift value (¹³C NMR) of CH₃COO in Ru[(S)-BINAP](OAc)₂ is δ 188.1 ppm.^{13b}

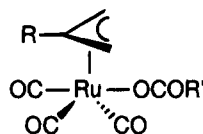
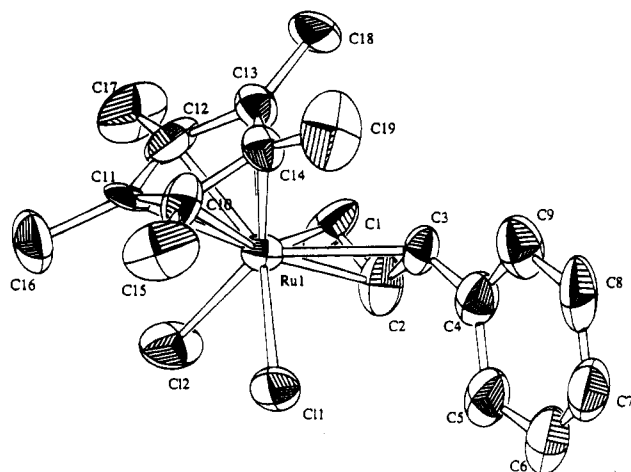
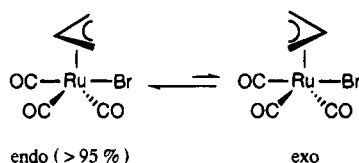


Figure 2.

Figure 3. Molecular structure and labeling scheme for **3a**.

Scheme 3



isomers differing principally in the orientation of the allyl group (Scheme 3).^{14,18} At room temperature, the two isomers interconvert slowly ($t_{1/2} > 10$ min) and the endo isomer predominates (>95%). So, on the basis of ¹H NMR spectra and the structure of **2f**, we confirmed that the present η^3 -allylruthenium complexes (**2a–d**) exist as the endo isomers. Consequently, the structure of these novel η^3 -allylruthenium carboxylate complexes (**2a–d**) is depicted as Figure 2.

Synthesis of Cp*RuCl₂(η^3 -CH₂CHCHPh). We have already reported Ru(COD)(COT)-catalyzed regioselective allylation of carbon nucleophiles.^{10e} Recently, we found that the regioselective allylation of nitrogen nucleophiles was more effectively promoted by Cp*Ru catalysts at 0 °C within 1 h (Scheme 4).¹⁹ These products are obtained by selective γ -attack of a nitrogen nucleophile to the (η^3 -allyl)ruthenium(IV) intermediate.

Here, we synthesized a model complex of the reaction intermediate Cp*RuCl₂(η^3 -CH₂CHCHPh) (**3a**) by direct oxidative addition of cinnamyl chloride to Cp*RuCl(COD). The complex **3a** was obtained as red-brown crystals in 69% yield after recrystallization from CHCl₃–Et₂O (Scheme 5).

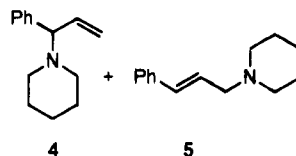
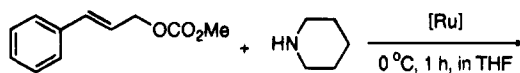
The results of X-ray diffraction analysis for **3a** are shown in Figure 3 and Tables 1, 4 and 5. The complex **3a** has a square-pyramidal structure with two chlorine atoms and the terminal carbons of the *endo*- η^3 -allyl ligand at basal positions, similar to the reported Cp*RuBr₂(η^3 -C₃H₅).²⁰

Reactivity of (η^3 -C₃H₅)Ru(CO)₃X (1a, 2a, 2e). (i) Nucleophilic Allylation of Aldehydes with (η^3 -

(18) For M = Fe: Simon, F. E.; Lauher, J. W. *Inorg. Chem.* **1980**, *19*, 2338.

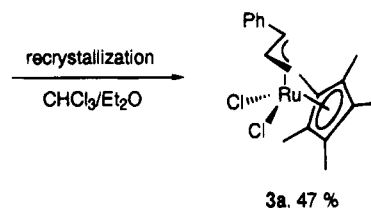
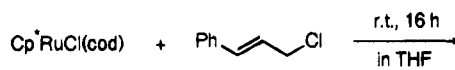
(19) Mitsudo, T.; Satake, N.; Kondo, T.; Watanabe, Y., unpublished results.

Scheme 4



[Ru] = Cp*RuCl(COD)	84	:	16	overall yield: 99%
Cp*RuBr(COD)	84	:	16	99%
[Cp*RuOMe] ₂	83	:	17	99%
[Cp*RuCl ₂] ₂	83	:	17	99%

Scheme 5

Table 4. Bond Lengths (Å) for **3a**

Ru(1)–Cl(1)	2.398(3)	C(10)–C(14)	1.45(2)	C(2)–C(3)	1.43(2)
Ru(1)–C(1)	2.18(1)	C(11)–C(12)	1.41(2)	C(4)–C(5)	1.48(2)
Ru(1)–C(3)	2.35(2)	C(12)–C(13)	1.46(2)	C(5)–C(6)	1.43(2)
Ru(1)–C(11)	2.25(1)	C(13)–C(14)	1.45(2)	C(7)–C(8)	1.43(3)
Ru(1)–C(13)	2.20(1)	C(14)–C(19)	1.48(2)	C(10)–C(11)	1.46(2)
C(1)–C(2)	1.38(2)	Ru(1)–Cl(2)	2.423(4)	C(10)–C(15)	1.48(2)
C(3)–C(4)	1.49(2)	Ru(1)–C(2)	2.14(2)	C(11)–C(16)	1.53(2)
C(4)–C(9)	1.38(2)	Ru(1)–C(10)	2.32(1)	C(12)–C(17)	1.56(2)
C(6)–C(7)	1.39(3)	Ru(1)–C(12)	2.16(1)	C(13)–C(18)	1.50(2)
C(8)–C(9)	1.45(2)	Ru(1)–C(14)	2.25(1)		

C₃H₅Ru(CO)₃X. Since the complexes **1a** and **2a** are thought to be the most plausible key intermediates in ruthenium-catalyzed allylation reactions of aldehydes with allylic acetates^{11a} and allylic bromides, the reactivity of the complexes (**1a**, **2a**, **2e**) toward several aldehydes was investigated. These complexes smoothly reacted with both aromatic and aliphatic aldehydes in the presence of Et₃N in CHCl₃ at room temperature for 48–72 h under an argon atmosphere, affording the corresponding homoallyl alcohols in 46–70% yields (Scheme 6). Carbon monoxide, which was essential for the catalytic allylation of aldehyde,^{11a} was not crucial for the present stoichiometric reaction. In the reaction with aliphatic aldehydes such as 1-hexanal and cyclohexanecarboxaldehyde, better results were obtained from **2a** than from **1a**.

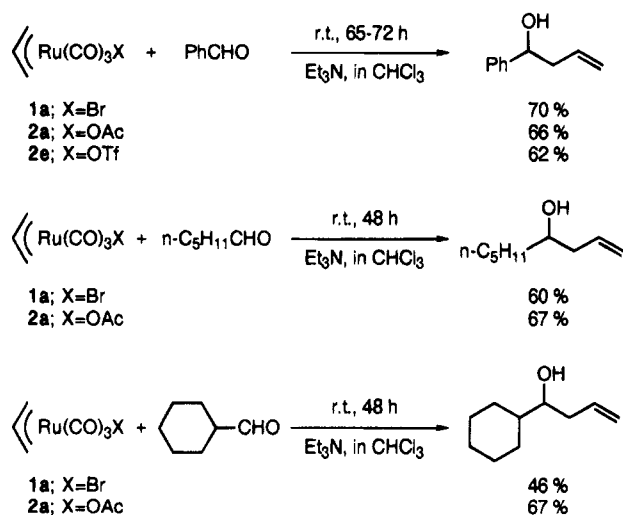
In both the catalytic and stoichiometric allylation of aldehydes, addition of amines such as Et₃N is essential for both high catalytic activity and high yields of the products. It is considered that the added amine operates as an hydrogen source as well as a suitable ligand for an active ruthenium intermediate. Without Et₃N, the yield of 1-phenyl-3-buten-1-ol from the reaction of **1a** with benzaldehyde drastically decreased to 28%, together with the generation of a considerable amount of a yellow precipitate. This yellow solid would be the

(20) Nagashima, H.; Mukai, K.; Shiota, Y.; Yamaguchi, K.; Ara, K.; Fukahori, T.; Suzuki, H.; Akita, M.; Moro-oka, Y.; Itoh, K. *Organometallics* **1990**, *9*, 799.

Table 5. Bond Angles (deg) for 3a

Cl(1)–Ru(1)–Cl(2)	83.9(1)	Ru(1)–C(2)–C(1)	73.2(10)
Cl(1)–Ru(1)–C(3)	84.9(4)	Ru(1)–C(3)–C(2)	63(1)
Cl(1)–Ru(1)–C(12)	140.5(6)	C(3)–C(4)–C(5)	118(1)
Cl(2)–Ru(1)–C(1)	80.2(5)	C(4)–C(5)–C(6)	116(1)
Cl(2)–Ru(1)–C(10)	112.8(4)	C(7)–C(8)–C(9)	119(1)
Cl(2)–Ru(1)–C(13)	128.4(3)	Ru(1)–C(10)–C(14)	68.8(7)
C(1)–Ru(1)–C(3)	64.1(5)	C(11)–C(10)–C(15)	127(1)
C(1)–Ru(1)–C(12)	92.0(7)	Ru(1)–C(11)–C(12)	67.8(8)
C(2)–Ru(1)–C(3)	36.7(6)	C(10)–C(11)–C(16)	123(1)
C(2)–Ru(1)–C(12)	127.8(8)	Ru(1)–C(12)–C(13)	72.0(8)
C(3)–Ru(1)–C(10)	118.8(5)	C(11)–C(12)–C(17)	124(1)
C(3)–Ru(1)–C(13)	91.6(5)	Ru(1)–C(13)–C(14)	72.7(7)
C(10)–Ru(1)–C(12)	62.0(7)	C(12)–C(13)–C(18)	127(1)
C(11)–Ru(1)–C(12)	37.1(6)	Ru(1)–C(14)–C(13)	69.2(7)
C(12)–Ru(1)–C(13)	39.2(5)	C(10)–C(14)–C(19)	123(1)
Ru(1)–C(1)–C(2)	69.6(9)	Cl(1)–Ru(1)–C(2)	91.6(5)
Cl(1)–C(2)–C(3)	118(1)	Cl(1)–Ru(1)–C(11)	103.3(3)
C(2)–C(3)–C(4)	129(1)	Cl(1)–Ru(1)–C(14)	101.4(4)
C(5)–C(4)–C(9)	123(1)	Cl(2)–Ru(1)–C(3)	125.4(4)
C(6)–C(7)–C(8)	121(1)	Cl(2)–Ru(1)–C(12)	91.0(5)
Ru(1)–C(10)–C(11)	68.9(7)	C(1)–Ru(1)–C(2)	37.2(6)
C(11)–C(10)–C(14)	107(1)	C(1)–Ru(1)–C(11)	126.0(5)
Ru(1)–C(11)–C(10)	74.0(7)	C(1)–Ru(1)–C(14)	120.0(5)
C(10)–C(11)–C(12)	107(1)	C(2)–Ru(1)–C(11)	163.3(6)
Ru(1)–C(12)–C(11)	75.1(9)	C(2)–Ru(1)–C(14)	122.1(6)
C(11)–C(12)–C(13)	110(1)	C(3)–Ru(1)–C(12)	127.9(6)
Ru(1)–C(13)–C(12)	68.8(7)	C(10)–Ru(1)–C(11)	37.1(5)
C(12)–C(13)–C(14)	105(1)	C(10)–Ru(1)–C(14)	36.9(5)
Ru(1)–C(14)–C(10)	74.3(8)	C(11)–Ru(1)–C(14)	62.8(4)
C(10)–C(14)–C(13)	108(1)	C(13)–Ru(1)–C(14)	38.1(5)
Cl(1)–Ru(1)–C(1)	125.3(4)	Ru(1)–C(2)–C(3)	79(1)
Cl(1)–Ru(1)–C(10)	83.9(4)	Ru(1)–C(3)–C(4)	124.9(10)
Cl(1)–Ru(1)–C(13)	139.5(4)	C(3)–C(4)–C(9)	117(1)
Cl(2)–Ru(1)–C(2)	90.5(5)	C(5)–C(6)–C(7)	120(1)
Cl(2)–Ru(1)–C(11)	83.7(3)	C(4)–C(9)–C(8)	117(1)
Cl(2)–Ru(1)–C(14)	146.4(3)	Ru(1)–C(10)–C(15)	127(1)
C(1)–Ru(1)–C(10)	150.0(5)	C(14)–C(10)–C(15)	124(1)
C(1)–Ru(1)–C(13)	88.0(5)	Ru(1)–C(11)–C(16)	127.7(9)
C(2)–Ru(1)–C(10)	155.5(6)	C(12)–C(11)–C(16)	128(1)
C(2)–Ru(1)–C(13)	109.3(6)	Ru(1)–C(12)–C(17)	123(1)
C(3)–Ru(1)–C(11)	150.7(5)	C(13)–C(12)–C(17)	125(1)
C(3)–Ru(1)–C(14)	88.2(5)	Ru(1)–C(13)–C(18)	131.0(9)
C(10)–Ru(1)–C(13)	62.6(5)	C(14)–C(13)–C(18)	125(1)
C(11)–Ru(1)–C(13)	63.7(4)	Ru(1)–C(14)–C(19)	129(1)
C(12)–Ru(1)–C(14)	63.7(6)	C(13)–C(14)–C(19)	127(1)

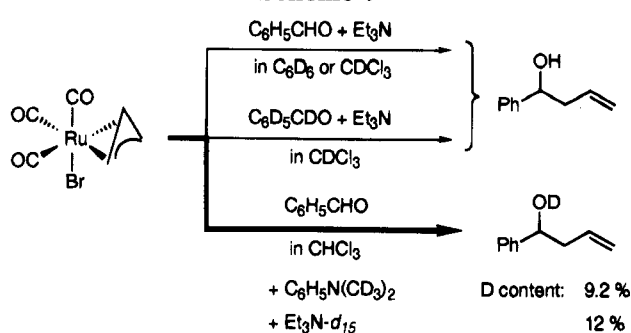
Scheme 6



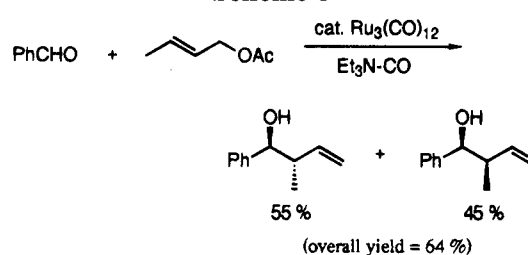
halogen-bridged (homoallylalkoxy)ruthenium cluster,²¹ since the hydrogen source for the generation of the homoallyl alcohol is extremely deficient. Other hydrogen sources such as methanol were also examined in the reaction, but the yield of the homoallyl alcohol did

(21) ¹³C NMR of this complex (THF-*d*₆): δ 44.35 (CH₂), 73.27 (CH), 78.51 (C), 115.62 (=CH₂), 125.74–128.53 (=CH and phenyl), 145.99 (phenyl C₁), 183.50, 184.36, 189.28 (M – CO).

Scheme 7



Scheme 8



not increase (~40%). So, we examined the following deuterium-labeled experiments in the stoichiometric allylation of benzaldehyde with **1a** (Scheme 7). In C₆D₆ or CDCl₃, no deuterium was detected in the homoallyl alcohol. Even with the use of C₆H₅CDO or C₆D₅CDO, no deuterium was incorporated into the hydroxy group of the product, but when C₆H₅N(CD₃)₂ or Et₃N-*d*₁₅ was used in place of Et₃N in CHCl₃, deuterium was incorporated into the hydroxy group of the generated homoallyl alcohol at 9.2% and 12%, respectively. These results strongly suggest that the hydrogen source of the homoallyl alcohol is not the solvent (or aldehyde), but the amine. It is well-known that ruthenium complexes showed high catalytic activity for the transalkylation reaction between tertiary amines.²² In the present reaction, a similar hydride abstraction from tertiary amines by the ruthenium complex would occur via a metallazaacyclopropane or an iminium ion intermediate.

As for **1a**, dynamic π - σ (η^3 - η^1) equilibrium of the allyl ligand could not be observed by ¹H NMR (room temperature to 80 °C in toluene-*d*₆). The reaction of **1a** with benzaldehyde was monitored by ¹H NMR. During the reaction, such π - σ isomerization could not be observed and direct insertion of the carbonyl group into the η^3 -allyl-Ru bond occurred. In consideration of these results, the possibility that π - σ isomerization of the allyl ligand in **1a** causes the high nucleophilicity of **1a** toward aldehydes was excluded.²³ In addition, it is suggested by preliminary MO calculation that the conversion of π to σ of the allyl ligand in ruthenium is thermodynamically more unfavorable than that of palladium.²⁴

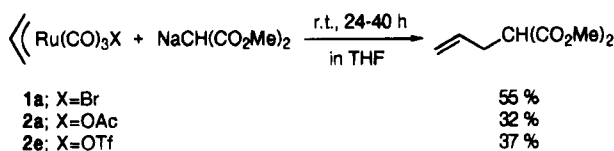
Thus, on the basis of the results mentioned above, we present the most plausible pathway to homoallyl alco-

(22) Wilson, R. B.; Laine, R. M. *J. Am. Chem. Soc.* **1985**, *107*, 361.

(23) If the present reaction proceeds via a (σ -allyl)ruthenium intermediate, high diastereoselectivity (anti selectivity) of the allylation reaction using crotyl (or 1-methylallyl) acetate can be expected through a six-membered cyclic transition state.^{3,5g} However, under the catalytic reaction conditions, low diastereoselectivity was observed (Scheme 8).

(24) The energy gap between the model complexes, [Ru(NH₃)(CO)₃-(η^3 -C₃H₅)]⁺ and [Ru(NH₃)(CO)₃-(η^1 -C₃H₅)], was calculated as ~26 kcal/mol by an ab initio MO/MP4 (SDQ) method, which is larger than that between Pd(CO)₂(η^3 -C₃H₅) and Pd(CO)₂(η^1 -C₃H₅) (~23 kcal/mol): Satake, S., unpublished result.

Scheme 9



hols by the reaction of η^3 -allylruthenium(II) complexes with aldehydes in the presence of amines. Direct insertion of the carbonyl group of an aldehyde to the η^3 -allyl-ruthenium bond (not through a η^1 -allylruthenium complex) gives a (homoallylalkoxy)ruthenium intermediate. We now suggest that α -hydride transfer from amine to the ruthenium produces a (homoallylalkoxy)(hydrido)ruthenium complex, which then undergoes reductive elimination of the observed homoallyl alcohol product.

(ii) **Electrophilic Allylation of $\text{NaCH}(\text{CO}_2\text{Me})_2$ with (η^3 -allyl) $\text{Ru}(\text{CO})_3\text{X}$ (1a, 2a, 2e).** As mentioned previously, we had found that several ruthenium complexes showed high catalytic activity for regioselective allylation of carbon nucleophiles.^{11e} Therefore we investigated the reactivity of (η^3 -allyl) $\text{Ru}(\text{CO})_3\text{X}$ (1a, 2a, 2e) toward a representative carbon nucleophile, $\text{NaCH}(\text{CO}_2\text{Me})_2$.

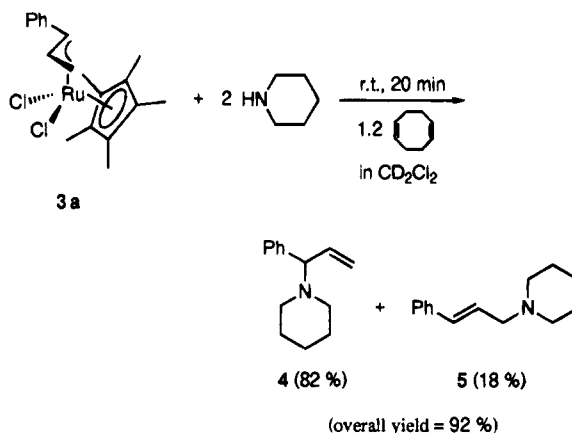
Results are shown in Scheme 9. (η^3 -Allyl) $\text{Ru}(\text{CO})_3\text{X}$, 1a, 2a and 2e, smoothly reacted with $\text{NaCH}(\text{COOMe})_2$ in THF at room temperature for 24–40 h under an argon atmosphere to give the corresponding allylated products in 32%–55% yields. It is noteworthy that the same complex showed *reverse* reactivity, depending on the reactivity of the opposing substrates.

The role of the carbonyl ligand is highly important, and the ambiphilic reactivity is realized only in ruthenium complexes bearing carbon monoxide ligands. Since we discovered the ambiphilic reactivity of (η^3 -allyl)ruthenium(II) complexes,²⁵ several research groups in Japan prepared phosphine-coordinated (η^3 -allyl)ruthenium(II) complexes. However, these ruthenium complexes, such as (η^3 - C_3H_5) $\text{Ru}(\text{PMe}_3)\text{Br}$ ²⁶ and (η^3 - C_3H_5) $\text{Ru}(\text{PEt}_3)\text{OCOCF}_3$,²⁷ could not react with $\text{NaCH}(\text{CO}_2\text{Me})_2$, while they reacted with benzaldehyde only at elevated temperature (50–80 °C) to give the corresponding homoallyl alcohol.

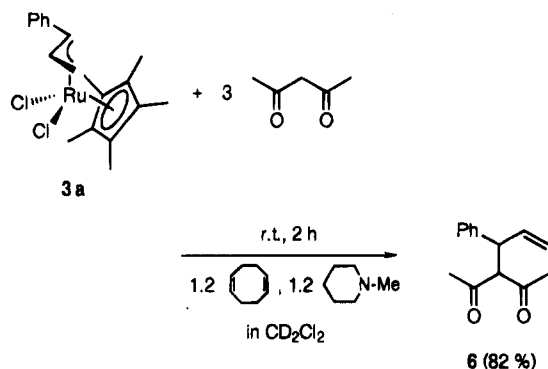
(iii) **Regioselective Electrophilic Allylation of Carbon and Nitrogen Nucleophiles with Cp^*RuCl_2 (η^3 -allyl).** The reaction of $\text{Cp}^*\text{RuCl}_2(\eta^3\text{-CH}_2\text{CHCHPh})$ (3a) with 2 equiv of piperidine in the presence of 1.2 equiv of 1,5-cyclooctadiene in CD_2Cl_2 at room temperature was monitored by ^1H NMR. The complex 3a was completely consumed in 20 min to give the corresponding allylamines 4 and 5 (the ratio was 82:18) in total 92% yield (Scheme 10). Without 1,5-cyclooctadiene, the ratio of 4 and 5 was 62:38 under the same reaction conditions after 10 min. Furthermore, complete isomerization of 4 to 5 proceeded and only linear allylamine 5 was obtained after 2 h. Thus, 1,5-cyclooctadiene plays the role of the ligand that suppresses the isomerization of 4 to 5.

We examined the reaction of 3a with 3 equiv of acetylacetone in the presence of 1.2 equiv of 1,5-cyclo-

Scheme 10



Scheme 11



octadiene and *N*-methylpiperidine. The complete conversion of the complex 3a required 2 h, and only branched product 6 was obtained selectively in 82% yield (Scheme 11). The present reaction did not proceed in the absence of *N*-methylpiperidine, and such base is required for the elimination of HCl from acetylacetone and 3a.

The results of these stoichiometric reactions are in accord with those of the catalytic reactions depicted in Scheme 4. In addition, complex 3a showed high catalytic activity in the allylation of both carbon and nitrogen nucleophiles. Hence, it appears that the active intermediate in the Cp^*Ru complex-catalyzed allylation of nucleophiles has configuration analogous to complex 3a. Although Åkermark et al. reported the regiocontrol of alkylation²⁸ and amination²⁹ of η^3 -allylpalladium systems, the regioselectivity is not always high. Further, addition of phosphine^{28a,29} or other specific ligand^{28b} is necessary to promote their reactions.

In addition, $\text{Cp}^*\text{RuCl}(\text{COD})$ -catalyzed allylation of piperidine with other allylic carbonates also afforded the branched *N*-allylamines as a major product (Table 6).

The reaction mechanism is not clear yet, but at this stage, we consider that it is difficult for secondary amine to preferentially attack the more sterically hindered allyl carbon directly. In consideration of the result that the ruthenium complexes also catalyze the isomerization of the generated branched amine 4 to the linear amine 5 (vide supra), the amine nucleophilically sub-

(25) Kondo, T.; Ono, H.; Mitsudo, T.; Watanabe, Y. The 39th Symposium on Organometallic Chemistry, Japan: Tokyo (Japan), October 1992; Abstr. p 199.

(26) Maruyama, Y.; Shimizu, I.; Yamamoto, A. *Chem. Lett.* **1994**, 1041.

(27) Komiya, S.; Kabasawa, T.; Yamashita, K.; Hirano, M.; Fukuoka, A. *J. Organomet. Chem.* **1994**, 471, C6.

(28) (a) Åkermark, B.; Hansson, S.; Krakenberger, B.; Vitagliano, A.; Zetterberg, K. *Organometallics* **1984**, 3, 679. (b) Sjögren, M. P. T.; Hansson, S.; Åkermark, B. *Organometallics* **1994**, 13, 1963, and references cited therein.

(29) Åkermark, B.; Åkermark, G.; Hegedus, L. S.; Zetterberg, K. *J. Am. Chem. Soc.* **1981**, 103, 3037.

Table 6. Cp**RuCl(COD)*-Catalyzed Allylation of Piperidine with Allylic Methyl Carbonates^a

entry	allylic carbonate	yield ^b (%)	products ^b (ratio)
1		99	 (84:16)
2		98	(90:10)
3		74	 (74:26)
4		91	(56:44)

^a Standard conditions: Cp**RuCl(COD)* (0.10 mmol), allylic carbonate (2.5 mmol), piperidine (2.5 mmol), and THF (5.0 mL) at 0°C for 1 h under Ar. ^b Determined by GLC.

stitutes the chlorine ligand to give the intermediates **7** and **8** (Scheme 12). A cis-reductive elimination from the intermediate **7** would give **4**, while **5** would be generated from **8**. We suggest two reasons for the kinetic advantage on the formation of the intermediate **7**: (1) A nucleophile is liable to substitute Cl(1) compared with Cl(2) on the basis of the distances between atoms in **3a** (C(3)–Cl(1)(3.21 Å) > C(1)–Cl(2)(2.97 Å) and/or Ru–C(3)(2.35 Å) > Ru–C(1)–(2.18 Å)). (2) The elimination of Cl(1) from **3a** is accelerated more than that of Cl(2) by the steric hindrance of hydrogen atoms on the phenyl group. Hence, in the present reaction, the intermediate **7** is predominantly generated to give the branched product **4**, selectively.³⁰

Conclusion

Although "ambiphilic" reagents are useful for reactions involving the sequential formation of two bonds and several efficient carbocycle-forming reactions have been developed, ambiphilic reagents so far reported are zwitterionic and they are usually employed in the two-step cyclization reactions—first as a nucleophile and then as an electrophile.³¹

We have now succeeded in the synthesis of the first (η^3 -allyl)ruthenium(II) carboxylates and triflate and disclosed that η^3 -allyl ligands in these complexes as well as (η^3 -C₃H₅)Ru(CO)₃Br show a real ambiphilic reactivity. Namely, η^3 -allyl ligands of the present (η^3 -allyl)-ruthenium(II) complexes can function as both a nucleophile and an electrophile in the individual reactions, depending on the reactivity of the opposing substrates.³²

(30) In considering the regioselectivity, several contributing factors must be weighed. These factors include (1) the steric hindrance of the regioisomeric alkylation sites, (2) the reactivity of the nucleophile, (3) the steric hindrance of the nucleophile, (4) the charge distribution in the η^3 -allyl complex, and (5) the relative stability of the two possible metal–olefin complexes. If the three carbons of the allylic fragment and the substituent are approximately in a single plane so that the steric hindrance to attack at the more substituted allylic carbon is minimized, charge effects dominate. In the present reaction, this charge control may be expected to give the kinetic product **4** whereas equilibration may be expected to give the thermodynamically preferred, less hindered, more fully conjugated product **5**.

(31) Hegedus, L. S.; Holden, M. S. *J. Org. Chem.* **1985**, *50*, 3920, and references cited therein.

(32) Ambiphilic behavior in (CO)₅W=NPh has been recently reported: Arndtsen, B. A.; Sleiman, H. F.; Chang, A. K.; McElwee-White, L. *J. Am. Chem. Soc.* **1991**, *113*, 4871.

Further, we succeeded in developing the regioselective allylation of nucleophiles which is characteristic of Cp**Ru* catalysts. We anticipate that this novel reactivity of (η^3 -allyl)ruthenium complexes will be applicable as a useful reagent and catalyst to synthetic organic chemistry.

Experimental Section

General Considerations. All manipulations were performed using a Schlenk technique. ¹H (270.05 MHz) and ¹³C NMR spectra (67.80 MHz) were measured on a JEOL GSX-270 spectrometer. Samples were dissolved in CDCl₃ or THF-*d*₈, and the chemical shift values were expressed relative to Me₄Si as an internal standard. IR spectra were recorded on a Shimadzu FT-IR 8100 spectrophotometer. GLC analyses were carried out on a Shimadzu GC-14A chromatograph equipped with capillary columns (Shimadzu capillary column: 3 mm i.d. × 50 m; CBP10-S25-050 (polarity similar to OV-1701) and CBP20-S25-050 (polarity similar to PEG-20M)). Mass spectra (MS) were obtained on a Shimadzu QP-2000 spectrometer. Melting points of the ruthenium complexes were measured on a Yanagimoto micro-melting-point apparatus. Elemental analyses were carried out at the Microanalytical Center of Kyoto University. Authentic samples of 1-phenyl-3-buten-1-ol, 1-nonen-4-ol, and 1-cyclohexyl-3-buten-1-ol were synthesized by the method in the literature³³ and distilled (>98% purity by GC). Dimethyl 2-propenylmalonate was synthesized by palladium-catalyzed allylation of dimethyl malonate with allyl methyl carbonate.³⁴

Materials. Solvents were distilled from suitable drying reagents under an argon atmosphere just before use. Silver acetate, silver benzoate and silver triflate were purchased from Aldrich Chemical Co. and used without further purification. Ru₃(CO)₁₂ was purchased from Strem Chemicals and used without further purification. (η^3 -C₃H₅)Ru(CO)₃Br (**1a**)¹³ and (η^3 -C₃H₅)Ru(CO)₂(PPh₃)Br (**1c**)³⁵ were prepared by the methods in the literatures. 2-Methallyl bromide used in the preparation of (η^3 -2-methallyl)Ru(CO)₃Br (**1b**) was prepared by halogen exchange reaction of 2-methallyl chloride with LiBr³⁶ and used after distillation (>90% purity by GC). PhN(CD₃)₂ was prepared by ruthenium-catalyzed N-alkylation of aniline with CD₃OD.³⁷ Et₃N-*d*₁₅ (D, 98%) was purchased from Cambridge Isotope Laboratories and used without purification. Cp**RuCl(COD)*,³⁸ Cp**RuBr(COD)*,³⁹ [Cp**RuOMe*]₂,⁴⁰ and [Cp**RuCl*]₂³⁸ were prepared according to the literature methods.

Preparation of (η^3 -2-Methallyl)Ru(CO)₃Br (1b**).** The complex **1b** was prepared from Ru₃(CO)₁₂ and 2-methallyl bromide by a procedure similar to that for **1a**.¹³ mp: 107–110 °C. Anal. Calcd for C₇H₇O₃BrRu: C, 26.27; H, 2.20. Found: C, 25.77; H, 2.16. ¹H NMR (CDCl₃): δ 2.08 (3H, s, CH₃), 3.05 (2H, s, CHH (anti)), 3.93 (2H, s, CHH (syn)). ¹³C NMR (CDCl₃): δ 25.59 (CH₃), 59.16 (CH₂), 128.60 ((CH₂)-C(CH₃)), 188.96 and 191.10 (M – CO).

Preparation of (η^3 -Allyl)RuL₃X. Treatment of the complex **1a** (605 mg, 1.98 mmol) with silver acetate (331 mg, 1.98 mmol) in CH₂Cl₂ (30 mL) at room temperature for 15 h under an argon atmosphere in the dark affords a colorless solution and brown precipitate. The colorless solution was chromat-

(33) (a) Mukaiyama, T.; Harada, T. *Chem. Lett.* **1981**, 1527. (b) Nokami, J.; Otera, J.; Sudo, T.; Okawara, R. *Organometallics* **1983**, *2*, 191.

(34) Tsuji, J.; Shimizu, I.; Minami, I.; Ohashi, Y.; Sugita, T.; Takahashi, K. *J. Org. Chem.* **1985**, *50*, 1523.

(35) Sbrana, G.; Braca, G.; Benedetti, E. *J. Chem. Soc., Dalton Trans.* **1975**, 754.

(36) Semmelhack, F.; Helquist, P. M. *Organic Syntheses*; Wiley: New York, 1988; Collect. Vol. VI, p 722.

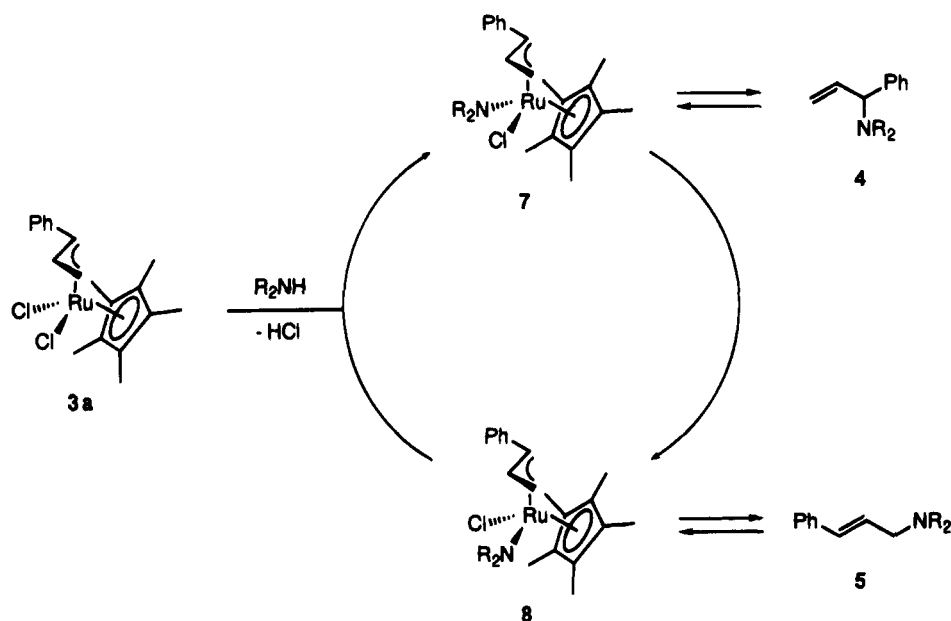
(37) Huh, K.-T.; Tsuji, Y.; Kobayashi, M.; Okuda, F.; Watanabe, Y. *Chem. Lett.* **1988**, 449.

(38) Oshima, N.; Suzuki, H.; Moro-oka, Y. *Chem. Lett.* **1984**, 1161.

(39) Albers, A. O.; Robinson, J. D.; Shaver, A.; Singleton, E. *Organometallics* **1986**, *5*, 2199.

(40) Koelle, U.; Kossakowski, J. *J. Organomet. Chem.* **1989**, *362*, 383.

Scheme 12



graphed on neutral Al_2O_3 (2 cm i.d. \times 2 cm; eluent CH_2Cl_2), and solvent was removed under vacuum. The resulting white solid was dissolved in a small amount of *n*-pentane and cooled at -40 °C for recrystallization. White needles of **2a** were obtained (247 mg, 44%). mp: 33–35 °C. Anal. Calcd for $\text{C}_8\text{H}_8\text{O}_5\text{Ru}$: C, 33.68; H, 2.83. Found: C, 33.61; H, 2.85. IR data (KBr): 2110, 2062, 2014 (ν_{CO}), 1619 ($\nu_{\text{COO(asy)}}$) and 1321 ($\nu_{\text{COO(sym)}}$) cm^{-1} . ^1H NMR (CDCl_3): δ 1.79 (3H, s, CH_3), 2.38 (2H, d, $J = 12.86$ Hz, CHH (anti)), 4.02 (2H, d, $J = 7.92$ Hz, CHH (syn)), 5.19 (1H, m, CH). ^{13}C NMR (CDCl_3): δ 22.63 (CH_3), 60.73 (CH_2), 108.20 (CH), 176.00 (CH_3COO), 190.00 and 192.40 (M – CO).

Complex **2b** was obtained by the reaction of **1a** (605 mg, 1.98 mmol) with silver benzoate (457 mg, 2.00 mmol) in CH_2Cl_2 (30 mL) at room temperature for 24 h, as a white powder, 275 mg (40%). IR data (in CH_2Cl_2): 2112, 2062, 2019 (ν_{CO}), 1614 ($\nu_{\text{COO(asy)}}$), 1350 ($\nu_{\text{COO(sym)}}$) cm^{-1} . ^1H NMR (CDCl_3): δ 2.52 (2H, d, CHH (anti)), 4.06 (2H, d, CHH (syn)), 5.18 (1H, m, CH), 7.19–7.30 (3H, m, phenyl), 7.76–7.80 (2H, m, phenyl). ^{13}C NMR (CDCl_3): δ 60.9 (CH_2), 108.2 (CH), 127.7, 129.4, 130.8, 133.7 (phenyl), 170.7 (PhCOO), 189.8 and 192.1 (M – CO).

Complex **2c** was obtained by a procedure similar to that for **1a** from the reaction of (η^3 -2-methylallyl)Ru(CO) $_3$ Br (357 mg, 1.12 mmol) with silver acetate (189 mg, 1.13 mmol), as white needles, 55 mg (16%). mp: 52–55 °C. Anal. Calcd for $\text{C}_9\text{H}_{10}\text{O}_5\text{Ru}$: C, 36.12; H, 3.37. Found: C, 35.61; H, 3.24. IR data (in *n*-pentane): 2109, 2060, 2008 (ν_{CO}), 1638 ($\nu_{\text{COO(asy)}}$) cm^{-1} . ^1H NMR (CDCl_3): δ 1.80 (3H, s, CH_3COO), 2.03 (3H, s, CH_3 (2-methylallyl)), 2.30 (2H, s, CHH (anti)), 3.85 (2H, s, CHH (syn)). ^{13}C NMR (CDCl_3): δ 22.62 (CH_3COO), 26.54 (CH_3 (2-methylallyl)), 60.72 (CH_2), 128.25 ($(\text{CH}_2)_2\text{C}(\text{CH}_3)$), 175.65 (CH_3COO), 190.06 and 193.65 (M – CO).

Similarly, complex **2d** was synthesized from (η^3 - C_3H_5)Ru(CO) $_2$ (PPh_3)Br (332 mg, 0.598 mmol) and silver acetate (154 mg, 0.598 mmol), as white microneedle crystals, 20 mg (6%). mp: 37–39 °C. Anal. Calcd for $\text{C}_{25}\text{H}_{23}\text{O}_4\text{PRu}$: C, 57.80; H, 4.46. Found: C, 57.51; H, 4.51. ^1H NMR (CDCl_3): δ 1.22 (3H, s, CH_3), 2.02 (1H, m, CH_2 (anti)), 2.38 (1H, d, $J = 13.35$ Hz, CH_2 (anti)), 3.61 (1H, d, $J = 7.91$ Hz, CH_2 (syn)), 3.88 (1H, m, CH_2 (syn)), 5.15 (1H, m, CH), 7.30–7.49 (15H, m, 3 C_6H_5). ^{13}C NMR (CDCl_3): δ 22.98 (CH_3), 56.45, 56.76 (CH_2), 62.77 (CH_2), 106.06 (CH), 128.29–133.88 (phenyl, CH), 175.13 (CH_3COO), 197.2 and 198.4 (M – CO).

Preparation of [(η^3 - C_3H_5)Ru(CO) $_3$] $^+$ (OTf) $^-$ (2e**).** Treatment of complex **1a** (501 mg, 1.64 mmol) with silver acetate (422 mg, 1.64 mmol) in CH_2Cl_2 (30 mL) at room temperature for 15 h under an argon atmosphere in the dark affords a

colorless solution and a yellow precipitate. The colorless solution was chromatographed on neutral Al_2O_3 (2 cm i.d. \times 2 cm; eluent CH_2Cl_2), and solvent was removed under vacuum. The resulting white powder was washed with *n*-pentane and dried under vacuum. Recrystallization was performed from CHCl_3 –*n*-pentane; yield 290 mg (47%). mp: 84–85 °C. Anal. Calcd for $\text{C}_7\text{H}_8\text{F}_3\text{O}_6\text{SRu}$: C, 22.41; H, 1.34; F, 15.19. Found: C, 22.67; H, 1.43; F, 15.37. IR data (in CH_2Cl_2): 2128, 2078, 2037 (ν_{CO}) cm^{-1} . ^1H NMR (CDCl_3): δ 2.64 (2H, d, $J = 13.36$ Hz, CHH (anti)), 4.35 (2H, d, $J = 7.42$ Hz, CHH (syn)), 5.37 (1H, m, CH). ^{13}C NMR (CDCl_3): δ 60.33 (CH_2), 109.07 (CH), 118.64 (CF_3 , q, $J = 318$ Hz), 187.23 and 190.13 (M – CO).

Preparation of Cp*RuCl $_2$ (η^3 -CH $_2$ CHCHPh) (3a**).** A mixture of Cp*RuCl(COD) (509 mg, 1.34 mmol), cinnamyl chloride (0.373 mL, 2.68 mmol), and THF (20 mL) was placed in a two-necked 50-mL Pyrex flask equipped with a magnetic stirring bar under an argon atmosphere, and the mixture was stirred at room temperature for 15 h. The color of the solution changed from orange to deep red gradually, the solvent was evaporated, and the residue was washed with two portions of *n*-pentane (2 mL). The supernatant was removed, and the crude crystal was dried under vacuum and recrystallized from the CH_2Cl_2 – Et_2O by cooling at -78 °C to give **3a** in 69% yield (393 mg; red-brown powder). mp: 192–193 °C dec. IR data (KBr): 758, 695 cm^{-1} . ^1H NMR (CDCl_3): δ 1.55 (15H, s, 5 Cp CH_3), 2.50 (1H, d, $J = 9.3$ Hz, CHH (anti)), 4.09 (1H, d, $J = 10.7$ Hz, CHPh), 4.11 (1H, d, $J = 6.4$ Hz, CHH (syn)), 5.54 (1H, ddd, $J = 6.4, 9.3, 10.7$ Hz, CH_2CH), 7.26–7.30 (5H, m, Ph). ^{13}C NMR (CDCl_3): δ 9.7 (Cp CH_3), 62.9 (CH_2), 90.4 (CHPh), 92.8 (CHCH_2), 104.0 (Cp), 127.8, 129.3, 131.3, and 135.4 (phenyl C3, C4, C2, C1).

X-ray Structure Determination of [(η^3 - C_3H_5)Ru(CO) $_3$ (H_2O)] $^+$ (OTf) $^-$ (2f**).** Crystal data, data collection, and refinement parameters of [(η^3 - C_3H_5)Ru(CO) $_3$ (H_2O)] $^+$ (OTf) $^-$ are summarized in Table 1. A single crystal of [(η^3 - C_3H_5)Ru(CO) $_3$ (H_2O)] $^+$ (OTf) $^-$ was mounted and placed on a Rigaku AFC-7R diffractometer. The unit cell was determined by the automatic indexing of 25 centered reflections and confirmed by examination of the axial photographs. Intensity data were collected using graphite-monochromated Mo K α X-radiation ($\lambda = 0.71069$ Å). Check reflections were measured every 100 reflections, and the data were scaled accordingly and corrected for Lorentz, polarization, and absorption effects. The structure was solved using Patterson and standard difference map techniques on a IRIS computer using SAPI91.³⁹ Systematic absences were consistent uniquely with the space group $\text{P}\bar{1}$ (No. 2). Bond

Table 7. Atomic Coordinates and B_{iso}/B_{eq} for **2f**

atom	x	y	z	B_{eq}
Ru(1)	0.34655(4)	0.24869(3)	0.15664(4)	3.175(7)
S(1)	0.2371(1)	-0.2660(1)	0.2191(2)	4.30(3)
F(1)	-0.0083(5)	-0.3964(5)	0.3455(6)	10.5(1)
F(2)	0.2265(6)	-0.3380(5)	0.5116(5)	11.0(1)
F(3)	0.0851(6)	-0.1951(5)	0.4625(5)	11.1(2)
O(1)	0.6175(5)	0.0965(4)	0.1686(5)	6.24(10)
O(2)	0.6296(5)	0.5003(3)	0.1842(5)	5.96(9)
O(3)	0.2470(5)	0.1561(4)	-0.2284(4)	5.89(9)
O(4)	0.1091(5)	-0.2377(4)	0.1017(5)	6.9(1)
O(5)	0.3749(5)	-0.1549(3)	0.2903(6)	7.4(1)
O(6)	0.2919(5)	-0.3816(3)	0.1731(6)	7.2(1)
O(7)	0.1526(4)	0.3604(3)	0.1423(4)	4.61(7)
C(1)	0.5123(6)	0.1512(4)	0.1649(6)	4.3(1)
C(2)	0.5241(6)	0.4089(4)	0.1693(6)	4.2(1)
C(3)	0.2873(6)	0.1922(4)	-0.0884(6)	4.1(1)
C(4)	0.3262(6)	0.2780(5)	0.4303(6)	4.7(1)
C(5)	0.2669(6)	0.1448(5)	0.3660(6)	4.8(1)
C(6)	0.1382(6)	0.0990(5)	0.2262(7)	5.0(1)
C(7)	0.1320(7)	-0.2991(7)	0.3970(8)	6.6(2)
H(1)	0.4342	0.3057	0.5207	6(1)
H(2)	0.2430	0.3287	0.4252	4.5(9)
H(3)	0.3494	0.0854	0.3999	5.9(10)
H(4)	0.1119	0.0061	0.1618	5.7(10)
H(5)	0.0442	0.1400	0.1963	3.3(8)
H(6)	0.2004	0.4520	0.1576	9.4(10)
H(7)	0.0834	0.3399	0.0341	11.3(8)

Table 8. Atomic Coordinates and B_{iso}/B_{eq} for **3a**

atom	x	y	z	B_{eq}
Ru(1)	0.20907(5)	0.31955(6)	0.2653	2.77(1)
Cl(1)	0.2608(2)	0.4772(2)	0.1468(5)	4.20(8)
Cl(2)	0.1820(2)	0.4354(3)	0.4898(5)	5.8(1)
C(1)	0.2619(8)	0.229(1)	0.458(2)	4.9(4)
C(2)	0.317(1)	0.279(2)	0.368(2)	4.7(4)
C(3)	0.3282(9)	0.244(1)	0.207(2)	3.5(3)
C(4)	0.3823(8)	0.285(1)	0.084(2)	4.7(4)
C(5)	0.4262(8)	0.382(1)	0.120(2)	5.4(4)
C(6)	0.4821(9)	0.413(1)	0.005(2)	6.1(5)
C(7)	0.4898(9)	0.358(2)	-0.138(3)	6.6(5)
C(8)	0.4472(9)	0.263(2)	-0.170(2)	6.9(5)
C(9)	0.3916(10)	0.226(1)	-0.054(2)	5.7(5)
C(10)	0.1194(7)	0.333(1)	0.062(2)	4.3(3)
C(11)	0.0832(7)	0.3346(9)	0.219(2)	3.8(3)
C(12)	0.1016(8)	0.239(1)	0.297(2)	5.8(5)
C(13)	0.1494(8)	0.173(1)	0.193(2)	3.6(3)
C(14)	0.1623(8)	0.235(1)	0.049(2)	3.4(3)
C(15)	0.114(1)	0.415(1)	-0.065(2)	7.2(5)
C(16)	0.0295(7)	0.423(1)	0.275(4)	7.0(4)
C(17)	0.069(1)	0.205(1)	0.463(2)	7.1(5)
C(18)	0.1699(8)	0.0591(9)	0.216(2)	4.7(4)
C(19)	0.202(1)	0.202(2)	-0.099(2)	7.4(5)

lengths and angles for $[(\eta^3\text{-C}_3\text{H}_5)\text{Ru}(\text{CO})_3(\text{H}_2\text{O})]^+(\text{OTf})^-$ are given in Tables 2 and 3. Atomic coordinates and B_{iso}/B_{eq} are given in Table 7.

X-ray Structure Determination of $\text{Cp}^*\text{RuCl}_2(\eta^3\text{-CH}_2\text{CHCHPh})$ (3a**).** Crystal data, data collection, and refinement parameters are summarized in Table 1, and general procedure is as described for $[(\eta^3\text{-C}_3\text{H}_5)\text{Ru}(\text{CO})_3(\text{H}_2\text{O})]^+(\text{OTf})^-$ (using SHELX86⁴²). Systematic absences were consistent uniquely with the space group $Pna2_1$ (No. 33). Bond lengths and angles are listed in Tables 4 and 5. Atomic coordinates and B_{iso}/B_{eq} are given in Table 8.

Reaction of **1a, **2a**, and **2e** with Aldehydes.** In a typical procedure, a mixture of the complex **2a** (9.8 mg, 0.034 mmol), benzaldehyde (29 mg, 0.27 mmol), and Et_3N (78 mg, 0.77 mmol) in CHCl_3 was stirred at room temperature for 48–72 h under an argon atmosphere. The resulting orange-brown solution was analyzed by GLC and GC–MS.

Reaction of **1a, **2a**, and **2e** with $\text{NaCH}(\text{CO}_2\text{Me})_2$.** In a typical procedure, THF solution of $\text{NaCH}(\text{CO}_2\text{Me})_2$ (~0.6 mM), which was prepared from dimethyl malonate and NaH in oil, was added to the THF solution (1.0 mL) of the complexes (**1a**, **2a**, **2e**) (0.10 mmol) at room temperature under an argon atmosphere, and the mixture was stirred for 24–40 h. The resulting yellow solution containing yellow powder was analyzed by GLC and GC–MS.

Reaction of **3a with Nucleophiles.** A mixture of $\text{Cp}^*\text{RuCl}_2(\eta^3\text{-CH}_2\text{CHCHPh})$ (**3a**; 0.20 mmol), 1,5-cyclooctadiene (0.24 mmol), and CD_2Cl_2 (0.50 mL) was placed in an NMR measurement tube (5 mm i.d.) under an argon atmosphere and dissolved completely. Then, piperidine (0.40 mmol) was added. The reaction was carried out at room temperature and observed by ^1H NMR. Yield of the product was determined by ^1H NMR based on the phenyl proton. In the case of carbon nucleophile, employing 3 equiv of acetylacetone (0.60 mmol) and *N*-methylpiperidine (0.24 mmol), the reaction was performed similarly.

1-(1-Phenyl-2-propenyl)piperidine (4**).** Colorless liquid. Kugelrohr distillation (bp 65 °C, 0.5 mmHg) from the reaction illustrated in Scheme 4. Anal. Calcd for $\text{C}_{14}\text{H}_{19}\text{N}$: C, 83.53; H, 9.51; N, 6.96. Found: C, 83.23; H, 9.51; N, 6.94, for a 93:7 mixture of **4** and **5**. MS: m/z 201 (M^+). IR data (neat): 1638, 994, 918, 756, 700 cm^{-1} . ^1H NMR (CDCl_3): δ 1.28–1.36 (2H, m, CH_2), 1.43–1.54 (4H, m, CH_2), 2.16–2.24 (2H, m, CH_2N), 2.32–2.36 (2H, m, CH_2N), 3.56 (1H, d, $J = 8.8$ Hz, NCHPh), 4.99 (1H, dd, $J = 1.7, 10.0$ Hz, (*E*)- $\text{CH}_2=$), 5.09 (1H, ddd, $J = 1.0, 1.7, 17.1$ Hz, (*Z*)- $\text{CH}_2=$), 5.87 (1H, ddd, $J = 8.6, 10.0, 17.1$ Hz, $\text{CH}=\text{}$), 7.08–7.30 (5H, m, *Ph*). ^{13}C NMR (CDCl_3): δ 24.6 (CH_2), 26.0 (CH_2), 52.4 (CH_2N), 75.4 (NCHPh), 115.8 ($=\text{CH}_2$), 140.3 ($\text{CH}=\text{}$), 126.8, 127.9, 128.3, 142.3 (*phenyl* C-4, C-2, C-3, C-1).

(E)-1-(3-Phenyl-2-propenyl)piperidine (5**).** Colorless liquid. Kugelrohr distillation (bp 75 °C, 0.5 mmHg) from the reaction illustrated in Scheme 4. MS, m/z 201 (M^+). IR data (neat): 1653, 965, 739, 693 cm^{-1} . ^1H NMR (CDCl_3): δ 1.44–1.46 (2H, m, CH_2), 1.56–1.64 (4H, m, CH_2), 2.43 (4H, br, CH_2N), 3.11 (2H, d, $J = 6.4$ Hz, $\text{CH}_2\text{CH}=\text{}$), 6.30 (1H, dt, $^2J = 15.6$ Hz, $^3J = 6.8$ Hz, $\text{CH}=\text{CHPh}$), 6.49 (1H, d, $J = 15.6$ Hz, $=\text{CHPh}$), 7.18–7.38 (5H, m, *Ph*). ^{13}C NMR (CDCl_3): δ 24.3 (CH_2), 26.0 (CH_2), 54.6 (CH_2N), 61.9 ($\text{CH}_2\text{CH}=\text{}$), 127.2 ($\text{CH}=\text{CHPh}$), 132.5 ($=\text{CHPh}$), 126.2, 127.3, 128.5, 137.0 (*phenyl* C-2, C-4, C-3, C-1).

3-Acetyl-4-phenyl-5-hexen-2-one (6**).** White solid. Kugelrohr distillation (bp 95 °C, 0.5 mmHg). mp: 35.0–36.0 °C. Anal. Calcd for $\text{C}_{14}\text{H}_{16}\text{O}_2$: C, 77.74; H, 7.46. Found: C, 77.66; H, 7.35. MS: m/z 216 (M^+). IR data (KBr): 1738–1696, 1640, 992, 930, 754, 702 cm^{-1} . ^1H NMR (CDCl_3): δ 1.86 (3H, s, CH_3), 2.23 (3H, s, CH_3), 4.17 (1H, dd, $J = 7.3, 11.5$ Hz, CHPh), 4.28 (1H, d, $J = 11.5$ Hz, CHCHPh), 5.04 (1H, d, $J = 10.3$ Hz, (*E*)- $\text{CH}_2=$), 5.06 (1H, d, $J = 17.1$ Hz, (*Z*)- $\text{CH}_2=$), 5.86 (1H, ddd, $J = 7.3, 10.3, 17.1$ Hz, $\text{CH}=\text{}$), 7.08–7.30 (5H, m, *Ph*). ^{13}C NMR (CDCl_3): δ 29.3 (CH_3), 29.8 (CH_3), 49.5 (CHCHPh), 73.8 (CHCHPh), 116.2 ($=\text{CH}_2$), 137.9 ($\text{CH}=\text{}$), 126.9, 127.7, 128.6, 139.6 (*Phenyl* C-4, C-2, C-3, C-1), 202.3 ($\text{C}=\text{O}$), 202.4 ($\text{C}=\text{O}$).

Acknowledgment. We are very grateful to Professor Shigeyoshi Sakaki of Kumamoto University for his helpful discussion and MO calculation. This work was partly supported by a Grant-in-Aid for Scientific Research from the Japanese Ministry of Education, Science and Culture. Portions of this work have been reported previously: Kondo, T.; Ono, H.; Mitsudo, T.; Watanabe, Y. *Abstracts of Papers*, The 63th Annual Meeting of Chemical Society of Japan; Osaka, Japan, March 1992.

(41) Hai-Fu, F. *Structure Analysis Programs with Intelligent Control*; Rigaku Corp.: Tokyo, 1991.

(42) Sheldrick, G. M. In *Crystallographic Computing 3*; Sheldrick, G. M., Kruger, C., Goddard, R., Eds.; Oxford University Press: New York, 1985; p 175.

Supplementary Material Available: Lists of complete crystallographic data of **2f** and **3a** (30 pages). Ordering information is given on any current masthead page.

OM9408369

Reactivity of Germa- and Stannaphosphenes with *o*-Quinones and α -Diketones

A. Kandri-Rodi,[†] J.-P. Declercq,[‡] A. Dubourg,[§] H. Ranaivonjatovo,[†] and J. Escudié*,[†]

Laboratoire de Chimie des Organominéraux, URA 477, Université P. Sabatier, 118 route de Narbonne, 31062 Toulouse Cedex, France, Laboratoire de Chimie Physique et de Cristallographie, Université Catholique de Louvain, Place Pasteur 1, B-1348 Louvain-La-Neuve, Belgium, and Groupe de Biochimie Structurale, URA 1111, Faculté de Pharmacie, 15 Avenue Charles Flahaut, 34060 Montpellier, France

Received November 15, 1994[®]

Stable germaphosphene **1** (germylidene phosphine) and stannaphosphene **2** (stannylidene phosphine) react with *o*-quinones (tetrachloro-*o*-benzoquinone, 3,5-di-*tert*-butyl-*o*-benzoquinone, and 1,2-naphthoquinone) to afford six-membered-ring heterocycles **3**–**8**. Depending on the steric hindrance, one (from germaphosphene) or two (from stannaphosphene) regioisomers are formed. The structure of regioisomer **5a** is unambiguously proved by an X-ray study; **5a** crystallizes in the triclinic space group $P\bar{1}$ with $Z = 2$. Lattice constants were $a = 10.102(1) \text{ \AA}$, $b = 13.619(1) \text{ \AA}$, $c = 18.820(2) \text{ \AA}$, $\alpha = 106.57(1)^\circ$, $\beta = 102.58(1)^\circ$, and $\gamma = 97.47(1)^\circ$. The main feature is the folding of the six-membered ring GePO(1)C(1)C(2)O(2) along the O(1)O(2) direction with an angle of 55° between the two planes O(1)PGeO(2) and O(1)C(1)C(2)O(2). **1** and **2** undergo $[2 + 4]$ cycloaddition with an α -diketone such as benzil, whereas an ene reaction is observed with biacetyl, leading to germylphosphine **11**.

Introduction

Intensive studies on the chemical behavior of the stable doubly bonded derivatives $M=X$ ($M = \text{Si, Ge, Sn}$; $X = \text{C, M, N, P, As, ...}$) have been performed over the last 10 years. The reactivity of various types of carbonyl compounds has been systematically investigated: aldehydes, ketones, α,β -unsaturated aldehydes and ketones with doubly bonded silicon (transient^{1,2a-d} or stable^{2e-1}) and germanium compounds,³⁻⁵ stannanimines⁶ and stannaphosphenes,⁷ acid chlorides with disilenes,⁸ ketenes with silenes⁹ and disilenes,⁸ esters with silenes,^{10a} and acylsilanes with silenes.^{10b}

However, the chemical behavior of quinones and α -diketones toward low-coordinate main-group derivatives is less well known, since reactions of quinones only with germanimines,¹¹ phosphalkenes¹² and phosphinimines¹³ and of α -diketones with phosphinimines¹³ have been studied.

We describe here the reactions of doubly bonded $>M=P-$ compounds, the germaphosphene (germylidene phosphine) **1** ($M = \text{Ge}$) and the stannaphosphene (stannylidene phosphine) **2** ($M = \text{Sn}$), with three *o*-quinones (tetrachloro-*o*-benzoquinone, 3,5-di-*tert*-butyl-*o*-benzoquinone, and 1,2-naphthoquinone), as well as with an enolizable (biacetyl) or nonenolizable (benzil) diketone.

[†] Université P. Sabatier.

[‡] Université Catholique de Louvain.

[§] URA 1111, Faculté de Pharmacie.

[®] Abstract published in *Advance ACS Abstracts*, March 15, 1995.

(1) For reviews, see: (a) Raabe, G.; Michl, J. *Chem. Rev.* **1985**, *85*, 419. *The Chemistry of Organosilicon Compounds*; Patai, S., Rappoport, Z., Eds.; Wiley: Chichester, U.K., 1989; Part 2, p 1015. (b) West, R. *Angew. Chem., Int. Ed. Engl.* **1987**, *26*, 1201. (c) Brook, A. G.; Baines, K. M. *Adv. Organomet. Chem.* **1986**, *25*, 1. (d) Weidenbruch, M. *Coord. Chem. Rev.* **1994**, *130*, 275.

(2) (a) Schäfer, A.; Weidenbruch, M.; Pohl, S. *J. Organomet. Chem.* **1985**, *282*, 331. (b) Auner, N.; Seidenschwarz, C. *Z. Naturforsch.* **1990**, *45B*, 909. (c) Ishikawa, M.; Nishimura, Y.; Sakamoto, H. *Organometallics* **1991**, *10*, 2701. (d) Sekiguchi, A.; Ando, W. *Organometallics* **1987**, *6*, 1857. (e) Fanta, A. D.; De Young, D. J.; Belzner, J.; West, R. *Organometallics* **1991**, *10*, 3466. (f) Vollbrecht, S.; Klingebiel, U.; Schmidt-Baese, D. *Z. Naturforsch.* **1991**, *46B*, 709. (g) Brook, A. G.; Hu, S. S.; Chatterton, W. J.; Lough, A. J. *Organometallics* **1991**, *10*, 2752. (h) Märkl, G.; Horn, M. *Tetrahedron Lett.* **1983**, *24*, 1477. (i) Wiberg, N.; Wagner, G. *Angew. Chem., Int. Ed. Engl.* **1983**, *22*, 1005. (j) Wiberg, N.; Preiner, G.; Schurz, K.; Fischer, G. *Z. Naturforsch.* **1988**, *43B*, 1468. (k) Wiberg, N.; Schurz, K.; Müller, G.; Riede, J. *Angew. Chem., Int. Ed. Engl.* **1988**, *27*, 935. (l) Brook, A. G.; Chatterton, W. J.; Sawyer, J. F.; Hughes, D. W.; Vorspohl, K. *Organometallics* **1987**, *6*, 1246.

(3) For reviews, see: (a) Barrau, J.; Escudié, J.; Satgé, J. *Chem. Rev.* **1990**, *90*, 283. (b) Escudié, J.; Couret, C.; Ranaivonjatovo, H.; Satgé, J. *Coord. Chem. Rev.* **1994**, *130*, 427. (c) Satgé, J. *J. Organomet. Chem.* **1990**, *400*, 121.

(4) Ranaivonjatovo, H.; Escudié, J.; Couret, C.; Declercq, J.-P.; Dubourg, A.; Satgé, J. *Organometallics* **1993**, *12*, 1674.

(5) (a) Lazraq, M.; Couret, C.; Escudié, J.; Satgé, J.; Dräger, M. *Organometallics* **1991**, *10*, 1771. (b) Rivière, P.; Castel, A.; Satgé, J. *J. Am. Chem. Soc.* **1980**, *102*, 541. (c) Wiberg, N.; Kim, C. K. *Chem. Ber.* **1986**, *119*, 2980. (d) Wiberg, N.; Preiner, G.; Karamatses, P.; Kim, C. K.; Schurz, K. *Chem. Ber.* **1987**, *120*, 1357. (e) Batcheller, S. A.; Masamune, S. *Tetrahedron Lett.* **1988**, *29*, 3383. (f) Rivière-Baudet, M.; Satgé, J.; Morère, A. *J. Organomet. Chem.* **1990**, *386*, C7. (g) Lazraq, M.; Escudié, J.; Couret, C.; Satgé, J.; Soufiaoui, M. *Organometallics* **1992**, *11*, 555. (h) Ranaivonjatovo, H.; Escudié, J.; Couret, C.; Satgé, J. *J. Organomet. Chem.* **1991**, *415*, 327.

(6) Ossig, G.; Meller, A.; Freitag, S.; Herbst-Irmer, R.; Sheldrick, G. M. *Chem. Ber.* **1993**, *126*, 2247.

(7) Kandri-Rodi, A.; Ranaivonjatovo, H.; Escudié, J. *Organometallics* **1994**, *13*, 2787.

(8) Fanta, A. D.; Belzner, J.; Powell, R. D.; West, R. *Organometallics* **1993**, *12*, 2177.

(9) Brook, A. G.; Baumegger, A. *J. Organomet. Chem.* **1993**, *446*, C9.

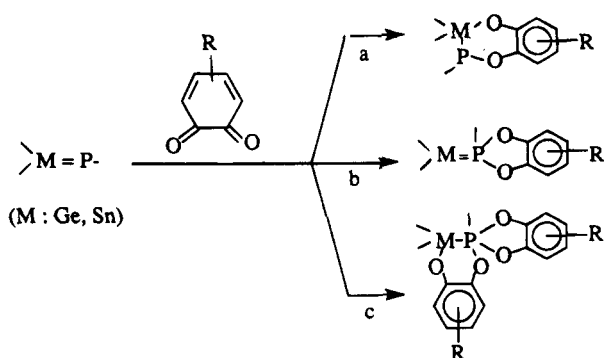
(10) (a) Brook, A. G.; Hu, S. S.; Saxena, A. K.; Lough, A. J. *Organometallics* **1991**, *10*, 2758. (b) Brook, A. G.; Kumarathasan, R.; Chatterton, W. *Organometallics* **1993**, *12*, 4085.

(11) Rivière-Baudet, M.; Morère, A. *J. Organomet. Chem.* **1992**, *431*, 17.

(12) (a) Van der Knaap, Th. A.; Bickelhaupt, F. *Tetrahedron* **1983**, *39*, 3189. (b) Heinicke, J.; Tzschach, A. *Tetrahedron Lett.* **1983**, *24*, 5481. (c) Zurmühlen, F.; Rösch, W.; Regitz, M. *Z. Naturforsch.* **1985**, *40B*, 1077.

(13) Diallo, O.; Boisdon, M. T.; Malavaud, C.; Lopez, L.; Haddad, M.; Barrans, J. *Tetrahedron Lett.* **1984**, *25*, 5521.

Scheme 1



Results and Discussion

Quinones. Various types of reactions are, in principle, possible between metallaphosphenes and quinones (Scheme 1): a formal [2 + 4] reaction leading to a six-membered-ring compound, as occurs with $>Ge=N$ and $-P=C$ derivatives (route a); a [1 + 4] cycloaddition involving phosphorus, as in the case of phosphinimines¹³ (route b); both reactions, finally leading to a pentacoordinated phosphorus, as was observed in the reactions of phosphoranes with excess quinone¹² (route c).

Addition of solutions of tetrachloro-*o*-benzoquinone, 3,5-di-*tert*-butyl-*o*-benzoquinone, and 1,2-naphthoquinone in pentane or Et₂O to solutions of germaphosphene **1** or stannaphosphene **2** in the same solvent resulted in an immediate green, blue, or brown coloration, depending on the quinone used (see Experimental Section). A ³¹P NMR study showed the disappearance of starting **1** and **2** and the formation of compounds **3–8** (Scheme 2). All these heterocycles, which have a Ge–P–O linkage, are very stable, in contrast to their isologs with a Ge–N–O linkage (obtained by reaction between germinimines and quinones¹¹), which easily eliminate a nitrene and cannot be isolated.

From **1** only one regioisomer was obtained in all cases. However, from **2**, two regioisomers were formed with 3,5-di-*tert*-butyl-*o*-benzoquinone (ratio **6a/6b** 60/40) and with 1,2-naphthoquinone (85/15 or 15/85 **8a/8b**, see below). In both cases only the major isomer could be isolated as a pure compound.

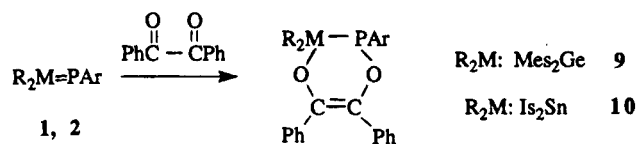
ESR studies performed during the course of all the reactions showed signals indicative of the intermediate formation of radicals of various multiplicities (singlets, doublets with coupling constants of 5.5 G ($g = 2.0036$), 100 G ($g = 2.0050$), ...) whose provenance was difficult to establish.

For steric reasons, we observed the exclusive formation (in the limit of precision of NMR) of **5a** in the reaction between **1** and 3,5-di-*tert*-butyl-*o*-benzoquinone. That **5a** rather than **5b** is formed is supported by the ¹H NMR spectrum of the product and unambiguously proved by the X-ray study (see below). The same regiochemistry, involving the formation of the analogous isomer, also was observed in the reaction of germinimines with 3,5-di-*tert*-butyl-*o*-benzoquinone.¹¹ The formation of the two regioisomers **6a/6b** and **8a/8b** in reactions of the stannaphosphene **2** with 3,5-di-*tert*-butyl-*o*-benzoquinone and naphthoquinone, respectively, is surprising since for steric reasons only one regioisomer was expected (as was found in the germanium

series). This result could be explained in terms of lesser steric hindrance due to the longer Sn–O, Sn–C, and Sn–P bonds compared with Ge–O, Ge–C, and Ge–P.

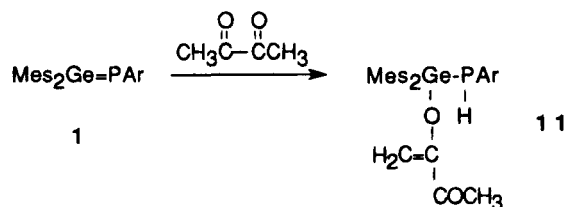
The regiochemistry observed in the reactions between **1** and **2** and 3,5-di-*tert*-butyl-*o*-benzoquinone is, as expected, opposite to the one observed in reactions between phosphoranes and the same quinone:^{12a} in the latter it is the phosphorus atom and not the group 14 element which is bonded to the less encumbered oxygen. This is a consequence of the first step of the reaction, which involves in the case of phosphoranes ($P^{\delta+}=C^{\delta-}$) the formation of a P–O bond and with metallaphosphenes ($M^{\delta+}=P^{\delta-}$) the formation of a M–O bond.

α -Diketones. **1** and **2** react with α -diketones such as benzil to give the corresponding six-membered-ring compounds **9** and **10** in nearly quantitative yield.



Only the reaction with the conjugated system occurs. A [2 + 2] cycloaddition with an isolated C=O bond has not been observed.

A very different reaction was observed with biacetyl. Only an ene reaction occurs, corresponding to the reaction of **1** with the enolic form of the diketone:

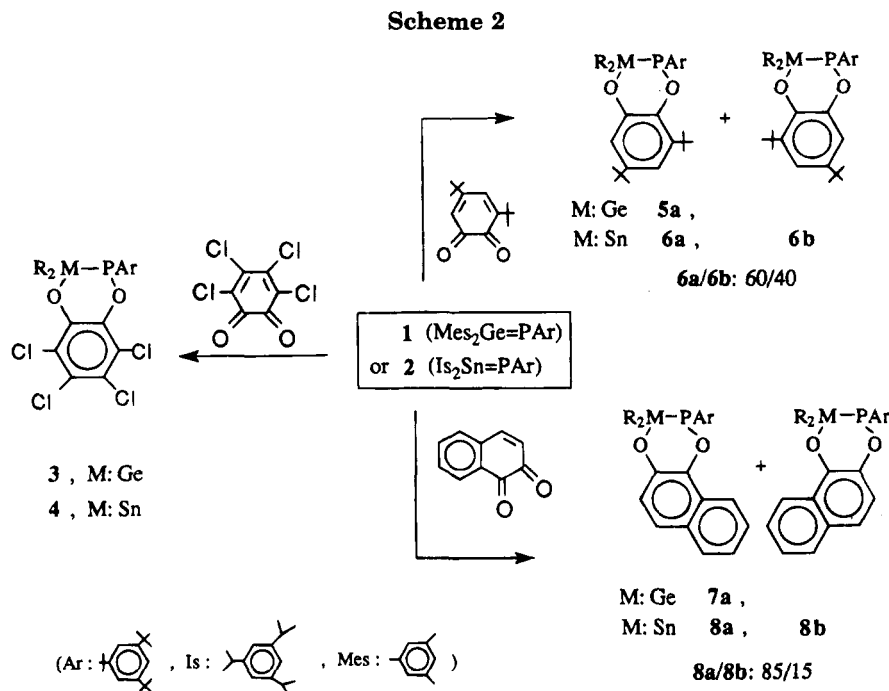


In the reaction of **1** with biacetyl in a 1:1 molar ratio, only **11** was obtained, rather than a product resulting from the reaction of both carbonyl groups. The formation of **11**, instead of a [2 + 4] cycloadduct as in the reaction of **1** and benzil, is not surprising since compounds with a CH₃CO moiety, such as acetone, react with polar double bonds, for example, $>Ge=C$ ^{3b} or $>Si=C$ ^{1a} in a similar ene reaction.

NMR Data. ³¹P and ¹¹⁹Sn NMR (see Table 1). NMR spectroscopy is a good tool in the structure determination of derivatives **3–11**. In the ³¹P NMR spectra of the germanium compounds **3**, **5**, **7**, and **9**, signals between 110.8 and 122.4 ppm were observed, and for the tin cycloadducts **4**, **6**, **8**, and **10**, signals between 133.9 and 147.1 ppm occurred. These are in the normal range for a phosphorus atom bonded to an oxygen atom,¹⁴ a germanium, or a tin. $\delta(^{31}P)$ for the ene product **11** (–96.6 ppm) lies also in the normal range for a germylphosphine.¹⁴

In the ¹¹⁹Sn NMR spectra of **4**, **6**, **8**, and **10**, all signals (from –58.6 to –95.2 ppm) appear as doublets with Sn–P coupling constants between 1533 and 1673 Hz. These large coupling constants are greater than those

(14) Fluck, E.; Heckmann, G. Phosphorus-31 NMR Spectroscopy in Stereochemical Analysis. In *Methods in Stereochemical Analysis*; Verkade, J. G., Quin, L. D., Eds.; VCH: Weinheim, Germany, 1987; Vol. 8, pp 108–113.

**Table 1.** ^{31}P and ^{119}Sn NMR Spectra of 3–11^a

	3	4	5	6a (60%)	6b (40%)	7	8a (85%)	8b (15%)	9	10	11
^{31}P	111.6	133.9	122.4	147.1	141.1	110.8	137.5	139.9	117.4	139.4	-96.6 ^b
^{119}Sn		-63.8		-95.2	-58.6		-66.6	-67.0		-75.5	
$^1J_{\text{P}^{119}\text{Sn}}$		1467		1599	1598		1547			1550	
$^1J_{\text{P}^{119}\text{Sn}}$		1533		1673	1673		1618	1604		1622	

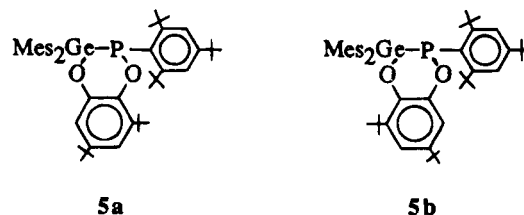
^a In units of δ (J in Hz); solvent CDCl_3 . ^b $^1J_{\text{PH}} = 220.9$ Hz.

generally observed in the case of phosphorus–tin single bonds (usually around 1000 Hz¹⁵).

^1H NMR. In compounds **3**, **5**, **7**, **9**, and **11**, the two mesityl groups on germanium are, as expected, inequivalent due to the presence of the chiral phosphorus atoms. In tin compounds **4**, **6**, **8**, and **10**, the triisopropylphenyl groups on tin also are inequivalent but generally result in very complex signals. Theoretically eight doublets are expected, since methyl groups Me and Me' of CHMeMe' groups are diastereotopic. As, moreover, some of the doublets are sometimes broad, due to slow rotation, it has not been possible to determine all the signals.

In contrast to cycloadducts $\text{R}_2\text{M}-\text{P}(\text{Ar})-\text{CH}_2-\text{CH}=\text{CH}-\text{O}$ (**12**; $\text{R}_2\text{M} = \text{Mes}_2\text{Ge}$,⁴ Is_2Sn ⁷), in which the phosphorus inversion was generally observed at room temperature, such inversion does not occur, as expected, in compounds **3**–**10**. If the steric hindrance (main factor in the decreasing of the phosphorus inversion barrier) in **3**–**10** and in **12** is about the same, the electronegativity of the atoms bonded to phosphorus (another important factor in phosphorus inversion) is higher in **3**–**10** (oxygen) than in **12** (carbon), which explains a higher inversion barrier.

Whereas only one singlet is observed for the two equivalent *o*-*t*-Bu groups of the 2,4,6-tri-*tert*-butylphenyl group in the ^1H NMR spectra of **3**, **4**, and **6**–**11**, two singlets are observed in the spectrum of compound **5**. This is due to the slow rotation of the Ar group in this compound, caused by the severe steric hindrance, and

Chart 1

this is further evidence in favor of structure **5a** instead of **5b** (Chart 1).

In the tin heterocycle **6** the coupling constants between the aromatic hydrogens and the phosphorus atom are similar (as had been found in the case of **5a**), so we can postulate that the major isomer of product **6** is **6a**.

The determination of the regiochemistry for **7** has not been possible on the basis of its ^1H and ^{13}C NMR spectra. In the ^{13}C NMR spectrum, the two carbons C(3) and C(4) joining the aromatic rings could not be unambiguously identified and, consequently, it was impossible to examine their coupling with phosphorus. In the ^1H NMR spectrum the two hydrogens H(1) and H(2) of the quinonic heterocycle give two doublets (AX spectrum) with no coupling with phosphorus. This result favors structure **7a**, in which coupling between H(1) or H(2) and P should not be observed (6J and 5J). In contrast, in **7b**, proton H(1) should exhibit coupling with phosphorus, although it can be very small (see Chart 2). Thus, from NMR arguments and from mechanistic considerations (as in the case of **5a**), we favor structure **7a**. In the case of the reactions of the tin compounds with 1,2-naphthoquinone, **8a** should be the major regioisomer.

(15) Wrackmeyer, B. *Annu. Rep. NMR Spectrosc.* **1985**, *16*, 73.

(16) Wiberg, N.; Wagner, G. *Chem. Ber.* **1986**, *119*, 1467.

Chart 2

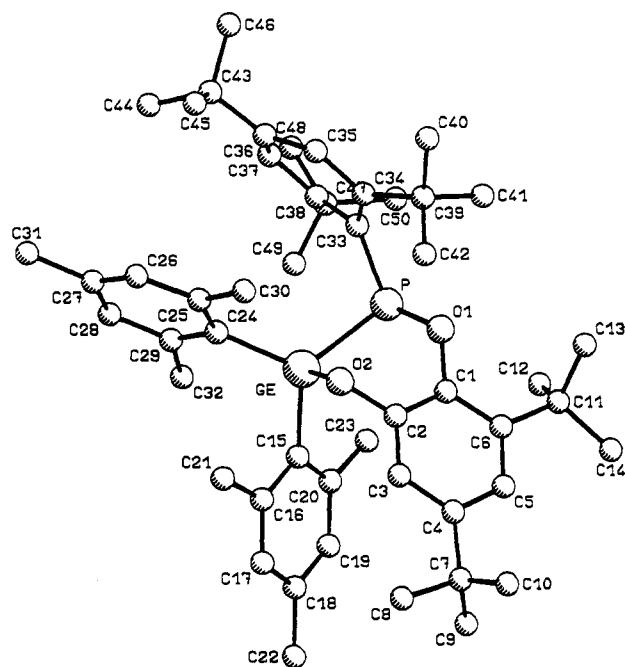
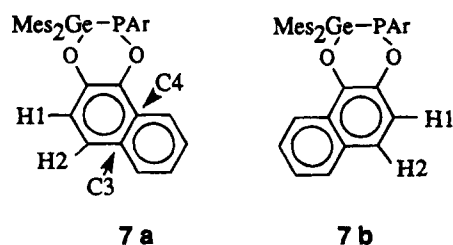
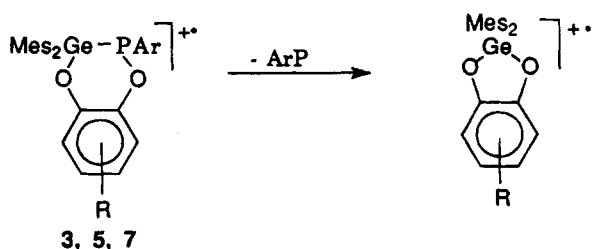


Figure 1. Crystal structure of 5a.

Mass Spectroscopy. The molecular peak was observed for all products. In the case of the germanium compounds, the most abundant fragment corresponded to the elimination of ArP, leading to a more symmetric five-membered-ring derivative with two Ge–O bonds:



A similar fragmentation was observed for 9. **X-ray Structural Determination** (see Tables 2–4 and Figure 1). Although the NMR gives valuable information about the structure of 5 (*tert*-butyl groups on carbons 4 and 6 instead of 3 and 5 (see Figure 1)), an X-ray analysis was necessary to confirm this structure.

O(1), P, Ge, and O(2) are approximately in a plane; the longest distance from one of these atoms to the mean plane is less than 0.15 Å. O(1), C(1), C(2), and O(2) also are nearly in a plane; the longest distance from one of the atoms to the mean plane is 0.03 Å. Thus, the six-membered ring Ge–P–O(1)–C(1)–C(2)–O(2) is folded along the O(1)–O(2) direction with a fold angle of 55° between the two planes O(1)–P–Ge–O(2) and O(1)–

C(1)–C(2)–O(2). Due to the large steric hindrance, the Ge–P bond is slightly longer than the standard Ge–P bonds: 2.401 Å instead of generally 2.33–2.35 Å.¹⁷ All other bond lengths and bond angles lie in the normal range. The sum of angles on phosphorus (302.1°) is much less than in other six-membered-ring compounds with similar bulky groups on phosphorus (Mes₂Ge and Ar) such as Mes₂Ge–P(Ar)–CH(Me)CH=CH–O (13; 323.2°) (obtained by reaction between 1 and crotonaldehyde).⁴ This probably is due to the substitution in 5a of phosphorus by an electronegative oxygen.

Experimental Section

As the compounds are usually highly air- and moisture sensitive, their synthesis and handling require high-vacuum techniques and the use of carefully deoxygenated solvents which must be freshly distilled from sodium benzophenone.

¹H NMR spectra were recorded on Bruker AC 80, AC 200, and AC 250 instruments at 80.1, 200.1, and 250.1 MHz, respectively; ¹³C NMR spectra were recorded on Bruker AC 200 and AC 250 instruments at 50.3 and 62.9 MHz (reference TMS), respectively. ³¹P NMR spectra were recorded on a Bruker AC 80 and AC 200 at 32.4 and 81.0 MHz (reference H₃PO₄), respectively. ¹¹⁹Sn NMR spectra were recorded on a Bruker AC 200 at 74.6 MHz (reference Me₄Sn). The NMR solvent is always CDCl₃, except for 8a in ¹³C NMR (C₆D₆).

IR spectra were recorded on a Perkin-Elmer 1600 FT instrument. Mass spectra were measured on a Hewlett-Packard 5989 A spectrometer by EI at 70 eV and on a Nermag R 1010 spectrometer by DCI with CH₄. Fragments are calculated in relation to ⁷⁴Ge and ¹²⁰Sn. Melting points were determined on a Leitz microscope heating stage 350.

Elemental analyses were performed by the Service de Microanalyse de l'École de Chimie de Toulouse (Toulouse, France).

Orange crystals of 1 were prepared as previously described.¹⁷ Crude solutions of 2 in Et₂O were obtained from I₂Sn(F)P(H)Ar and 1 molar equiv of *t*-BuLi 1.6 M in pentane and were used without further purification.¹⁹

Synthesis of 3. To an orange solution of 1 (0.87 g, 1.48 mmol) in Et₂O (10 mL) was added at room temperature a red solution of tetrachloro-*o*-benzoquinone (0.36 g, 1.48 mmol) in Et₂O (6 mL). Immediate reaction occurred, as shown by the blue color which appeared. The reaction mixture was stirred for 1 h. After removal of Et₂O, crude 3 was recrystallized from pentane to afford white crystals (mp 146 °C; 0.65 g, 53%). ¹H NMR: δ 1.30 (s, 9H, *p*-*t*-Bu), 1.34 (s, 18H, *o*-*t*-Bu), 1.90 (s, 6H, *o*-Me), 2.03 (s, 6H, *o*-Me), 2.17 (s, 3H, *p*-Me), 2.22 (s, 3H, *p*-Me), 6.68 (s, 4H, arom H Mes), 7.33 (d, ⁴J_{PH} = 2.6 Hz, 2H, arom H Ar). ¹³C NMR: δ 21.02 and 21.10 (*p*-Me), 23.92 (*o*-Me), 24.13 (d, ⁴J_{CP} = 6.7 Hz, *o*-Me), 31.22 (*p*-Me₃C), 33.83 (d, ⁴J_{CP} = 6.1 Hz, *o*-Me₃C), 35.03 (*p*-Me₃C), 39.91 (d, ³J_{CP} = 5.9 Hz, *o*-Me₃C), 122.44 (d, ³J_{CP} = 9.5 Hz, *m*-C Ar), 122.05, 124.36, 124.73 (*J*_{CP} = 2.2 Hz) and 127.09 (CCl), 125.99 (d, ¹J_{CP} = 59.1 Hz, ipso-C Ar), 129.05 and 129.43 (*m*-C Mes), 136.54 (d, *J*_{CP} = 10.3 Hz), 137.94 (d, *J*_{CP} = 4.1 Hz), and 146.91 (d, *J*_{CP} = 7.7 Hz) (OCO and ipso-C Mes), 139.69 and 139.72 (*p*-C Mes), 142.57 and 142.96 (*o*-C Mes), 153.28 (d, ⁴J_{CP} = 2.8 Hz, *p*-C Ar), 161.20 (d, ²J_{CP} = 17.4 Hz, *o*-C Ar). MS (EI): *m/z* 833 (M + 1, 1), 798 (M + 1 – Cl, 1), 587 (Mes₂GePAr – 1, 1), 556 (M – ArP, 100), 522 (M – ArP – Cl + 1, 6), 436 (M – ArP – Mes – 1, 11), 311 (Mes₂Ge – 1, 24), 276 (ArP, 40), 220 (ArP – *t*-Bu + 1, 58).

(17) Dräger, M.; Escudié, J.; Couret, C.; Ranaivonjatovo, H.; Satgé, J. *Organometallics* **1988**, 7, 1010 (and references cited therein).

(18) (a) Escudié, J.; Couret, C.; Satgé, J.; Andrianarison, M.; Andriamizaka, J. D. *J. Am. Chem. Soc.* **1985**, 107, 3378. (b) Escudié, J.; Couret, C.; Andrianarison, M.; Satgé, J. *J. Am. Chem. Soc.* **1987**, 109, 386.

(19) Ranaivonjatovo, H.; Escudié, J.; Couret, C.; Satgé, J. *J. Chem. Soc., Chem. Commun.* **1992**, 1047.

Anal. Calcd for $C_{42}H_{51}Cl_4GeO_2P$: C, 60.54; H, 6.17. Found: C, 60.70; H, 6.47.

Synthesis of 4. To a red solution of **2** (1.38 mmol) in Et_2O (20 mL) was added 1 molar equiv of tetrachloro-*o*-benzoquinone (0.38 g) in Et_2O solution (6 mL). The reaction mixture turned green immediately with formation, after a few minutes, of a yellow precipitate. After 1 h of stirring, Et_2O was added to dissolve the yellow compound, and LiF was removed by filtration; **4** was crystallized from a mixture of Et_2O and pentane and isolated in the form of yellow crystals (mp 146–147 °C; 0.46 g, 32%). 1H NMR: δ 0.75–1.15 (m, 24 H, *o*- Me_2 -CH), 1.25 (d, $^3J_{HH} = 6.8$ Hz, 6H, *p*- Me_2 CH), 1.30 (d, $^3J_{HH} = 6.8$ Hz, 6 H, *p*- Me_2 CH), 1.34 (s, 9 H, *p*-*t*-Bu), 1.51 (broad s, 18 H, *o*-*t*-Bu), 2.48–2.70 (m, 4H, *o*- Me_2 CH), 2.82 (sept, 2 H, *p*- Me_2 CH), 6.89 and 6.91 (s, 2 \times 2 H, arom H Is), 7.50 (d, $^4J_{CP} = 2.8$ Hz, 2 H, arom H Ar). ^{13}C NMR: δ 23.89 (*p*- Me_2 CH), 24.75, 25.16, 25.58 (*o*- Me_2 CH), 31.30 (*p*- $CMes_3$), 34.51 (*o*- $CMes_3$), 35.17 (*p*- $CMes_3$), 38.1, 38.8 (*o*-CHIs), 39.40 (d, $^3J_{CP} = 4.7$ Hz, *o*- $CMes_3$), 122.30, 122.38, and 123.13 (*m*-C Ar and Is), 124.90 (d, $J_{CP} = 2.0$ Hz), 125.16 and 129.92 (CCl), 127.80 (d, $^1J_{CP} = 67.1$ Hz, ipso-C Ar), 143.41 (d, $J_{CP} = 4.4$ Hz), 146.14 (d, $J_{CP} = 6.3$ Hz), and 149.20 (d, $J_{CP} = 5.3$ Hz) (OCCO and ipso-C Is), 150.98 (d, $^4J_{CP} = 3.0$ Hz, *p*-C Ar), 153.47 and 153.61 (*p*-C Is), 154.93 ($^2J_{CSn} = 63.9$ Hz, *o*-C Is), 155.16 ($^2J_{CSn} = 46$ Hz, *o*-C Is), 157.64 (d, $^2J_{CP} = 17.7$ Hz, *o*-C Ar). MS (EI): *m/z* 772 (M - ArP, 67), 736 (M - ArP - Cl - 1, 5), 525 (Is₂Sn - 1, 15), 523 (M - Is₂Sn + 1, 16), 482 (M - ArPO - 2Cl - Is - 1, 29). Anal. Calcd for $C_{54}H_{75}Cl_4O_2Psn$: C, 61.90; H, 7.21. Found: C, 61.54; H, 6.92.

Synthesis of 5a. A solution of 3,5-di-*tert*-butyl-*o*-benzoquinone (0.32 g, 1.48 mmol) in Et_2O (10 mL) is added to an orange solution of **1** (0.87 g, 1.48 mmol) in Et_2O (20 mL). The reaction mixture immediately turned green and was stirred for 2 h. Recrystallization from pentane afforded yellow crystals (0.30 g, 25%). A second slow recrystallization afforded 0.45 g (total yield: 62%). Mp: 167 °C. 1H NMR: δ 1.14 (s, 9 H, *t*-Bu quinone), 1.23 and 1.47 (2s, 2 \times 9 H, *p*-*t*-Bu and *t*-Bu quinone), 1.36 and 1.56 (2 broad s, 2 \times 9 H, *o*-*t*-Bu), 1.99 (s, 6 H, *o*-Me), 2.13 (s, 3 H, *p*-Me), 2.18 (s, 9 H, *o*-Me and *p*-Me), 6.52 (dd, $^4J_{HH} = 2.4$ Hz, $^3J_{PH} = 6.5$ Hz, 1H, OCCCH), 6.55 and 6.62 (2s, 2 \times 2 H, arom H Mes), 6.85 (dd, $^4J_{HH} = 2.4$ Hz, $^5J_{PH} = 6.6$ Hz, 1H, OCCCH), 7.14 (broad s, 2 H, arom H Ar). ^{13}C NMR: δ 20.78 and 20.96 (*p*-Me), 23.87 (*o*-Me), 24.95 (d, $^4J_{CP} = 10.9$ Hz, *o*-Me), 31.18, 31.32, and 33.59 (*p*- Me_3 C Ar, Me_3 C quinone), 34.29, 34.83, and 35.13 (*p*- Me_3 C Ar and Me_3 C quinone), 35.10 (d, $^4J_{CP} = 3.2$ Hz, *o*- Me_3 C), 38.91 (*o*- Me_3 C), 39.60 (d, $^3J_{CP} = 8.6$ Hz, *o*- Me_3 C), 115.55 and 118.07 (O-C-CH-*t*-Bu)-CH), 121.87 (*m*-C Ar), 122.77 (d, $^3J_{CP} = 13.6$ Hz, *m*-C Ar), 128.65 and 128.68 (*m*-C Mes), 132.71 (d, $^1J_{CP} = 74.4$ Hz, ipso-C Ar), 137.43 (d, $J_{CP} = 8.1$ Hz) and 141.64 (d, $J_{CP} = 3.2$ Hz) (OCCO), 138.40 and 138.65 (*p*-C Mes), 142.44 and 143.26 (*o*-C Mes), 142.78 (ipso-C Mes), 145.62 (*t*-BuC-C-C-O), 150.66 (d, $^4J_{CP} = 1.9$ Hz, *p*-C Ar), 150.86 (d, $^3J_{CP} = 7.2$ Hz, *t*-BuC-C-O), 155.92 (d, $^2J_{CP} = 37.2$ Hz, *o*-C Ar), 159.01 (d, $^2J_{CP} = 4.8$ Hz, *o*-C Ar). MS (EI): *m/z* 809 (M + 1, 1), 752 (M + 1 - *t*-Bu, 56), 533 (M + 1 - ArP, 100), 517 (M + 1 - ArPO, 26), 497 (M - Mes₂Ge, 5), 312 (Mes₂Ge, 12), 275 (ArP - 1, 31), 192 (MesGe - 1, 32). Anal. Calcd for $C_{50}H_{71}GeO_2P$: C, 74.35; H, 8.86. Found: C, 74.10; H, 8.77.

Single-Crystal X-ray Diffraction Analysis for 5a. Single crystals of **5a** were obtained by slow recrystallization from pentane at room temperature for 2–3 days. Data were collected on a Huber diffractometer with graphite-monochromated Mo K α ($\lambda = 0.71069$ Å) radiation. Accurate lattice parameters were obtained from the centering of 30 reflections ($10 < \tau < 35^\circ$). A standard reflection (1, -1, 7) measured every 50 reflections showed no significant variation. The structure was solved by using SHELXS-86. The least-squares refinement was performed by using SHELX-76 (using *F*). Carbon, phosphorus, oxygen, and germanium were refined anisotropically, while hydrogens were located in calculated positions. A strong thermal agitation was observed for C(8), C(9), and C(10).

Table 2. Crystal Structure Data for **5a**

formula	$C_{50}H_{71}GeO_2P$
<i>M_r</i> (g)	807.6
cryst dimens, mm ³	0.3 \times 0.3 \times 0.7
cryst syst	triclinic
space group	$P\bar{1}$
<i>a</i> , Å	10.102(1)
<i>b</i> , Å	13.619(1)
<i>c</i> , Å	18.820(2)
α , deg	106.57(1)
β , deg	102.58(1)
γ , deg	97.47(1)
<i>V</i> , Å ³	2370.4(5)
<i>Z</i>	2
<i>d</i> (calcd), g/cm ³	1.13
μ (Mo K α), mm ⁻¹	0.72
<i>F</i> (000)	868
<i>T</i> , °C	room temp
<i>hkl</i> range	0–12, -16 to +16, -23 to +22
no. of rflns	
measd	9272
obsd (> 2.5 σ (<i>I</i>))	5969
<i>s</i> (goodness of fit)	1.34
$\Delta\sigma$ max	< 1
<i>R</i> (final)	0.067
<i>R_w</i>	0.085
$\Delta\rho$ (final) (min/max), e/Å ³	-0.66/+0.77

Table 3. Selected Bond Distances (Å), Bond Angles (deg), and Torsion Angles (deg) for **5a**

Ge-P	2.401(2)	C(1)-O(1)	1.406(7)
Ge-O(2)	1.838(4)	Ge-C(24)	1.959(5)
P-O(1)	1.671(4)	Ge-C(15)	1.969(5)
O(2)-C(2)	1.374(5)	P-C(33)	1.870(4)
C(2)-C(1)	1.389(8)		
O(2)-Ge-P	93.7(1)	C(33)-P-Ge	99.6(2)
C(15)-Ge-P	118.1(2)	O(1)-P-C(33)	106.9(2)
C(15)-Ge-O(2)	99.8(2)	P-O(1)-C(1)	123.8(2)
C(24)-Ge-P	119.5(2)	Ge-O(2)-C(2)	109.8(3)
C(24)-Ge-O(2)	110.1(2)	C(2)-C(1)-O(1)	117.9(4)
C(24)-Ge-C(15)	111.6(2)	C(1)-C(2)-O(2)	120.5(5)
O(1)-P-Ge	95.6(2)		
Ge-P-O(1)-C(1)	37.6(3)	P-O(1)-C(1)-C(2)	-64.2(5)
P-Ge-O(2)-C(2)	-65.7(3)	Ge-O(2)-C(2)-C(1)	63.7(5)
O(1)-P-Ge-O(2)	19.1(2)	O(1)-C(1)-C(2)-O(2)	5.7(6)

angle between the two mean planes O(1)-C(1)-C(2)-O(2) and O(2)-Ge-P-O(1): 55°

Synthesis of 6. A 0.35 g amount of 3,5-di-*tert*-butyl-*o*-benzoquinone (1.59 mmol) in Et_2O (10 mL) was added to a red solution of **2** (1.59 mmol) in Et_2O (20 mL). The reaction mixture turned blue-green. ^{31}P and ^{119}Sn NMR spectra of the crude mixture showed the formation of **6a/6b** in the ratio 60/40 in greater than 80% yield. After removal of Et_2O in vacuo, crystallization from pentane afforded pure **6a** as yellow crystals (0.17 g, yield 10%). **6b** could not be obtained in a pure state. **6a**: mp 162 °C; 1H NMR δ 0.55 (d, $^3J_{HH} = 6.4$ Hz, *p*- Me_2 -CH), 0.92 (broad s), 1.12 and 1.14 (2d, $^3J_{HH} = 6.4$ Hz), and 1.23–1.28 (m) (all signals Me_2 CH), 0.91, 1.11, 1.58, and 1.65 (*t*-Bu), 2.80 (sept, $^3J_{HH} = 6.4$ Hz, *o*- Me_2 CH), 3.05 (sept, $^3J_{HH} = 6.4$ Hz, *p*- Me_2 CH), 6.41 and 6.79 (2d, $^4J_{HH} = 2.7$ and 2.2 Hz, arom H quinone), 6.79 and 6.86 (s, arom H Is), 7.31 (d, $^4J_{HH} = 2.6$ Hz, arom H Ar).

Synthesis of 7. A suspension of 1,2-naphthoquinone (0.17 g, 1.07 mmol) in Et_2O was added to an orange solution of **1** (0.63 g, 1.07 mmol) in Et_2O (15 mL). The reaction mixture turned brown. After 1 h of stirring, a brown precipitate was formed. Filtration gave 0.16 g (20%) of **7**, which was washed with pentane. A 0.40 g amount of **7** was obtained by crystallization from cold pentane (total yield: 70%). Mp: 159–160 °C. 1H NMR (250 MHz): δ 1.40 (s, 9 H, *p*-*t*-Bu), 1.46 (s, 18 H, *o*-*t*-Bu), 2.03 (broad s, 6 H, *o*-Me (Mes cis to Ar)), 2.15 (s, 6 H, *o*-Me), 2.28 and 2.32 (2s, 2 \times 3 H, *p*-Me), 6.74 (s, 4 H, arom H Mes), 7.19 (d, $^4J_{HP} = 2.4$ Hz, 2 H, arom H Ar), 7.21–7.54

Table 4. Fractional Atomic Coordinates ($\times 10^4$) and Isotropic Temperature Factors for **5a**

	<i>x/a</i>	<i>y/b</i>	<i>z/c</i>	<i>B</i> _{eq.} , Å ²
Ge	252(1)	5819(0)	7335(0)	3.13
P	1273(1)	5026(1)	8249(1)	2.90
O(1)	2903(3)	5389(3)	8225(2)	3.48
O(2)	1764(4)	5893(3)	6943(2)	3.69
C(1)	3439(5)	6360(4)	8166(3)	3.24
C(2)	2886(6)	6572(4)	7496(3)	3.34
C(3)	3436(6)	7480(4)	7380(4)	4.48
C(4)	4542(7)	8194(5)	7932(4)	4.77
C(5)	5081(6)	7961(4)	8595(4)	4.63
C(6)	4553(6)	7057(4)	8740(3)	3.80
C(7)	5168(8)	9237(5)	7851(5)	6.40
C(8)	4435(14)	9343(8)	7077(7)	15.00
C(9)	5004(15)	10097(6)	8415(7)	19.00
C(10)	6567(11)	9264(8)	7783(8)	14.86
C(11)	5224(6)	6861(4)	9495(3)	4.37
C(12)	4145(8)	6715(6)	9938(4)	7.11
C(13)	5854(8)	5887(5)	9309(4)	6.91
C(14)	6383(8)	7762(6)	10030(4)	7.90
C(15)	216(6)	7318(4)	7714(3)	3.51
C(16)	55(6)	7848(4)	7163(3)	4.18
C(17)	151(6)	8918(5)	7396(4)	5.14
C(18)	375(7)	9515(5)	8160(4)	5.48
C(19)	509(7)	8994(4)	8695(4)	5.09
C(20)	422(6)	7914(4)	8492(3)	4.25
C(21)	-242(8)	7288(5)	6305(4)	6.03
C(22)	463(9)	10687(5)	8400(5)	8.23
C(23)	541(8)	7437(5)	9126(4)	6.05
C(24)	-1415(6)	5033(4)	6511(3)	3.78
C(25)	-1335(7)	4330(4)	5814(3)	4.90
C(26)	-2558(9)	3817(5)	5239(4)	6.10
C(27)	-3847(9)	3945(6)	5325(5)	6.80
C(28)	-3911(7)	4651(5)	6010(5)	5.93
C(29)	-2714(6)	5206(5)	6607(4)	4.49
C(30)	19(8)	4128(5)	5656(3)	5.49
C(31)	-5163(9)	3333(6)	4703(5)	9.55
C(32)	-2925(7)	5992(5)	7301(4)	5.65
C(33)	673(5)	3616(4)	7647(3)	2.85
C(34)	1238(5)	2964(4)	7097(3)	3.32
C(35)	318(6)	2132(4)	6505(3)	3.81
C(36)	-1083(6)	1883(4)	6437(3)	3.90
C(37)	-1508(6)	2375(4)	7077(3)	3.92
C(38)	-651(5)	3192(4)	7701(3)	3.17
C(39)	2799(6)	3017(4)	7176(3)	3.98
C(40)	3073(7)	1952(5)	6719(4)	6.20
C(41)	3548(6)	3212(4)	8025(4)	4.67
C(42)	3465(7)	3823(5)	6864(4)	5.22
C(43)	-2077(7)	1021(5)	5740(4)	5.24
C(44)	-3560(8)	1220(6)	5615(5)	8.65
C(45)	-1673(9)	999(6)	5005(4)	8.38
C(46)	-2062(9)	-21(5)	5865(4)	8.83
C(47)	-1158(6)	3511(4)	8450(3)	3.98
C(48)	-2350(7)	2635(5)	8409(4)	6.57
C(49)	-1768(7)	4507(5)	8545(4)	5.85
C(50)	5(7)	3613(5)	9159(3)	5.20

(m, 4 H, arom H, naphth ring), 7.79 (d, $^3J_{\text{HH}} = 7.9$ Hz, OCCH, 1 H), 8.17 (d, $^3J_{\text{HH}} = 7.9$ Hz, OCCCH, 1 H). ^{13}C NMR: δ 21.00 and 21.10 (*p*-Me), 24.02 (*o*-Me), 24.67 (d, $^4J_{\text{CP}} = 7.6$ Hz, *o*-Me), 31.34 (*p*-Me₃C), 33.92 (d, $^4J_{\text{CP}} = 6.9$ Hz, *o*-Me₃C), 35.07 (*p*-Me₃C), 39.79 (d, $^3J_{\text{CP}} = 5.4$ Hz, *o*-Me₃C), 122.33 (d, $^3J_{\text{CP}} = 8.6$ Hz, *m*-C Ar), 121.16, 123.23, 123.76, 123.91, 125.67, and 127.64 (CH naphth), 128.55 (d, $^1J_{\text{CP}} = 63.2$ Hz, ipso-C Ar), 129.02 (*m*-C Mes), 137.62 (d, $^2J_{\text{CP}} = 10.6$ Hz) and 146.25 (d, $^3J_{\text{CP}} = 9.1$ Hz) (OCCO), 139.03 and 139.14 (*p*-C Mes), 142.90 and 143.18 (*o*-C Mes), 152.20 (d, $^4J_{\text{CP}} = 2.4$ Hz, *p*-C Ar), 160.06 (d, $^2J_{\text{CP}} = 16.9$ Hz, *o*-C Ar). MS (EI): *m/z* 747 (M + 1, 1), 690 (M + 1 - *t*-Bu, 1) 501 (M - Ar, 2), 470 (M - ArP, 100), 434 (M - Mes₂Ge, 1), 351 (M - ArP - Mes - H, 1), 329 (Mes₂GeO + 1, 1), 311 (Mes₂Ge - 1, 6). Anal. Calcd for C₄₆H₅₇GeO₂P: C, 74.10; H, 7.70. Found: C, 73.81; H, 7.64.

Synthesis of 8a. To a red solution of **2** (1.31 mmol) in Et₂O (15 mL) was added 1 molar equiv of 1,2-naphthoquinone (0.21 g) in pentane at room temperature. The reaction mixture became blue. After 1 h of stirring, LiF was removed by

filtration; ^{119}Sn and ^{31}P NMR spectroscopy showed the formation of an **8a/8b** mixture in an 85/15 ratio. **8a** was recrystallized from pentane as a brown powder: 0.19 g, yield 15%; mp 158–159 °C; ^1H NMR (250 MHz) δ 0.58, 0.86, 0.90 (3d, $^3J_{\text{HH}} = 6.5$ Hz, 18 H, *o*-Me₂CH), 0.77 (very broad s, 6H, *o*-Me₂CH), 1.05, 1.07 (2d, $^3J_{\text{HH}} = 5.3$ Hz, 12 H, *p*-Me₂CH), 1.18 (s, 9H, *p*-*t*-Bu), 1.48 (s, 18 H, *o*-*t*-Bu), 2.70–2.95 (m, 6 H, *o*- and *p*-Me₂CH), 6.79 and 6.83 (2s, 2 × 2H, arom H Is), 6.90–7.56 (m, 6H, arom H Ar and arom H naphth), 7.60 (d, $^3J_{\text{HH}} = 8.1$ Hz, 1 H, OCCH), 7.94 (d, $^3J_{\text{HH}} = 8.1$ Hz, 1 H, OCCCH); ^{13}C NMR (C₆D₆) δ 24.16 (*p*-Me₂CH), 25.28, 25.42, 25.53, 26.46 (*o*-Me₂CH), 31.30 (*p*-Me₃C), 34.22 (d, $^4J_{\text{CP}} = 8.3$ Hz, *o*-Me₃C), 35.04 (*p*-Me₃C), 38.45 and 39.00 (*o*-Me₂CH), 39.59 (*o*-Me₃C), 121.30, 122.47, 122.59, 122.92, 123.10, 124.59, 126.08, 127.86, 128.35 (*m*-C Ar and Is, arom CH), 132.54 (d, $^1J_{\text{CP}} = 73.0$ Hz, ipso-C Ar), 145.40 (d, $J_{\text{CP}} = 4.0$ Hz), 147.07 (d, $J_{\text{CP}} = 7.8$ Hz), and 149.18 (d, $J_{\text{CP}} = 6.8$ Hz) (O–C–C–O and ipso-C Is), 150.74 and 150.95 (*p*-C Is), 151.60 (*p*-C Ar), 154.50 (*o*-C Is), 155.53 ($^2J_{\text{CSn}} = 45.6$ Hz, *o*-C Is), 157.5 (broad s, *o*-C Ar); MS (EI, 70 eV, ^{120}Sn) *m/z* 802 (Is₂Sn=PAR, 1), 684 (M - ArP, 5), 526 (Is₂Sn, 9), 434 (M - Is₂Sn, 15), 322 (Is₂Sn - 1, 100), 275 (ArP - 1, 99), 219 (ArP - *t*-Bu - 1, 11). Anal. Calcd for C₅₈H₈₁O₂SnP: C, 72.57; H, 8.51. Found: C, 72.17; H, 8.35.

Synthesis of 9. To a solution of **1** (0.60 g, 1.02 mmol) in Et₂O (10 mL) was added 1 molar equiv of benzil (0.21 g) dissolved in Et₂O (10 mL), at room temperature. The solution turned from orange to brown. After 1 h of stirring, Et₂O was removed in vacuo, and crude **9** was recrystallized from hexane/Et₂O to afford yellow crystals (0.31 g, 38%, first batch); a second recrystallization afforded 0.20 g (total yield 62%). Mp: 146 °C. ^1H NMR: δ 1.31 (s, 9H, *p*-*t*-Bu), 1.35 (s, 18H, *o*-*t*-Bu), 1.96 (broad s, 6H, *o*-Me, Mes cis to Ar), 2.17 (s, 3H, *p*-Me), 2.23 (broad s, 9H, *p*-Me and *o*-Me trans to Ar), 6.64 and 6.67 (2s, 2 × 2H, arom H Mes), 6.95–7.23 (m, 10H, Ph), 7.24 (d, $^4J_{\text{HP}} = 2.5$ Hz, 2H, arom H Ar). ^{13}C NMR: δ 21.04 and 21.14 (*p*-Me), 23.60 (*o*-Me), 24.90 (d, $^4J_{\text{CP}} = 8.6$ Hz, *o*-Me), 31.41 (*p*-Me₃C), 33.90 (d, $^4J_{\text{CP}} = 7.8$ Hz, *o*-Me₃C), 34.88 (*p*-Me₃C), 39.57 (d, $^3J_{\text{CP}} = 3.7$ Hz, *o*-Me₃C), 122.23 (d, $^3J_{\text{CP}} = 6.4$ Hz, *m*-C Ar), 126.58 and 127.04 (*p*-C Ph), 127.52, 127.65, 129.00, 129.05, 129.52, and 129.68 (*o*- and *m*-C Ph, *m*-C Mes), 130.77 (d, $^1J_{\text{CP}} = 68.1$ Hz, ipso-C Ar), 135.31, 137.27 (d, $J_{\text{CP}} = 2.5$ Hz), and 138.90 (ipso-C Ph, ipso-C Mes), 137.70 (d, $J_{\text{CP}} = 8.4$ Hz) and 138.64 (d, $J_{\text{CP}} = 6.0$ Hz) (O–C=C–O), 138.74 and 139.02 (*p*-C Mes), 143.40 (broad) and 143.45 (*o*-C Mes), 150.98 (*p*-C Ar), 158.50 (d, $^2J_{\text{CP}} = 14.5$ Hz, *o*-C Ar). MS (EI): *m/z* 799 (M + 1, 3), 742 (M + 1 - *t*-Bu, 1), 589 (Mes₂Ge=PAR + 1, 1), 553 (M - Ar, 4), 522 (M - ArP, 100), 486 (M - Mes₂Ge, 1), 375 (Mes₂GeOPO, 6), 311 (Mes₂Ge - 1, 13), 192 (MesGe - 1, 27). Anal. Calcd for C₅₀H₆₁GeO₂P: C, 75.29; H, 7.71. Found: C, 74.74; H, 7.58.

Synthesis of 10. A solution of benzil (0.29 g, 1.38 mmol) in Et₂O (6 mL) was added to a solution of **2** (1 molar equiv) in Et₂O (25 mL). The reaction mixture turned from red to dark red, then brown, and finally dark brown. After elimination of LiF by filtration and removal of a part of the solvent, crystallization from Et₂O afforded yellow crystals of **10** (mp 49–50 °C; 0.35 g, 31%). ^1H NMR: δ 0.75 (d, $^3J_{\text{HH}} = 6.7$ Hz, 12H, *o*-Me₂CH), 0.86 (d, $^3J_{\text{HH}} = 6.4$ Hz, 12H, *o*-Me₂CH), 1.17 (d, $^3J_{\text{HH}} = 7.0$ Hz, 12H, *p*-Me₂CH), 1.20 (s, 9H, *p*-*t*-Bu), 1.59 (s, 18H, *o*-*t*-Bu), 2.70–3.20 (m, 6H, *o*- and *p*-Me₂CH), 6.84 and 6.89 (2s, 2 × 2H, arom H Is), 7.07–7.30 (m, 10H, Ph), 7.33 (d, $^4J_{\text{HP}} = 2.4$ Hz, 2H, arom H Ar). ^{13}C NMR: δ 24.00, 24.10, 24.49, 25.15, and 25.58 (*p*- and *o*-Me₂CH), 31.11 (*p*-Me₃C), 34.06 (d, $^4J_{\text{CP}} = 8.3$ Hz, *o*-Me₃C), 34.23 (*p*-Me₂CH), 34.73 (*p*-Me₃C), 38.0 (*o*-Me₂CH), 39.09 (d, $^3J_{\text{CP}} = 3.5$ Hz, *o*-Me₃C), 122.03, 122.33, 122.45, and 122.63 (*m*-C Is and Ar), 125.56 and 126.80 (*p*-C Ph), 127.31, 127.36, 128.66, and 129.89 (*o*- and *m*-C, Ph), 134.41 (d, $^1J_{\text{CP}} = 74.5$ Hz, ipso-C Ar), 140.18 and 145.75 (ipso-C Is), 146.2 (d, $J_{\text{CP}} = 8.3$ Hz) and 146.74 (d, $J_{\text{CP}} = 7.4$ Hz, O–C=C–O), 150.11 (*p*-C Ar), 150.20 (*p*-C Is), 153.58 and 154.33 (*o*-C Is), 156.41 (broad signal, *o*-C Ar). MS: *m/z* 738 (M - ArP, 3), 486 (M - Is₂Sn, 14), 322 (IsSn - 1, 21), 276

(ArP, 54), 241 (PhCOC(Ph)OP, 77), 220 (ArPH - *t*-Bu, 82), 161 (IsH - *i*-Pr, 53), 105 (PhC=O, 100). Anal. Calcd for C₆₂H₈₅O₂PSn: C, 73.58; H, 8.46. Found: C, 73.07; H, 8.09.

Synthesis of 11. Biacetyl (0.13 g, 1.48 mmol) was added via syringe to a solution of **1** (0.87 g, 1.48 mmol) in Et₂O (20 mL) at room temperature. The color slowly turned from orange to light yellow during the course of 2 h. After removal of Et₂O, recrystallization from pentane afforded a white, air-sensitive compound: 0.32 g, 32%; mp 143 °C. ¹H NMR: δ 1.29 (s, 9H, *p-t*-Bu), 1.36 (s, 18H, *o-t*-Bu), 1.93, 2.06, and 2.18 (3s, 3 × 6H, *o*- and *p*-Me), 2.41 (s, 3H, COCH₃), 4.14 and 4.91 (2d, ²J_{HH} = 1.7 Hz, 2 × 1H, C=CH₂), 5.37 (d, ¹J_{HP} = 218.2 Hz, 1H, PH), 6.62 (s, 4H, arom H Mes), 7.14 (d, ⁴J_{HP} = 2.6 Hz, 2H, arom H Ar). ¹³C NMR: δ 20.98 (*p*-Me), 24.20 (d, ⁴J_{CP} = 4.6 Hz, *o*-Me), 24.45 (d, ⁴J_{CP} = 8.0 Hz, *o*-Me), 26.40 (CH₃CO), 32.45

(*p*-Me₃C), 33.70 (broad s, *o*-Me₃C), 34.75 (*p*-Me₃C), 38.44 (*o*-Me₃C), 97.98 (CH₂), 122.16 (*m*-C Ar), 129.04 and 129.12 (*m*-C Mes), 135.61 and 136.42 (ipso-C Mes), 138.95 and 139.04 (*p*-C Mes), 142.61 and 142.98 (*o*-C Mes), 148.79 (*p*-C Ar), 156.08 (*o*-C Ar), 198.31 (C=O). IR: ν(PH) 2365.9 cm⁻¹, ν(CO) 1689.3 cm⁻¹. MS (EI): *m/z* 674 (M, 1), 605 (Mes₂Ge(O)PAr, 1), 588 (Mes₂Ge=PAR, 1), 397 (M - ArP - 1, 100), 329 (Mes₂GeO, 41), 311 (Mes₂Ge - 1, 27), 277 (ArPH, 60).

Supplementary Material Available: Tables of bond lengths, bond angles, torsion angles, and thermal parameters and an ORTEP plot for **5a** (7 pages). Ordering information is given on any current masthead page.

OM940865J

Structure and Metal Coordination of the Diphosphine 2,2'-Bis((diphenylphosphino)methyl)-1,1'-binaphthyl (NAPHOS)

Wolfgang A. Herrmann,* Rochus Schmid, Christian W. Kohlpaintner,[†] and
Thomas Priermeier

Anorganisch-chemisches Institut der Technischen Universität München, Lichtenbergstrasse 4,
D-85747 Garching, Germany

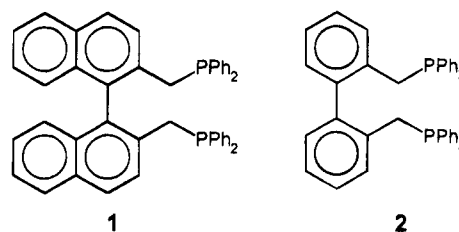
Received November 29, 1994[®]

The crystal structure of the diphosphine 2,2'-bis((diphenylphosphino)methyl)-1,1'-binaphthyl (**1**, NAPHOS) has been determined by means of an X-ray diffraction study. The compound crystallizes in the triclinic space group $P\bar{1}$ with $a = 10.568(1) \text{ \AA}$, $b = 10.737(1) \text{ \AA}$, $c = 15.986(1) \text{ \AA}$, $\alpha = 81.63(1)^\circ$, $\beta = 86.42(1)^\circ$, $\gamma = 81.47(1)^\circ$, $V = 1773 \text{ \AA}^3$, and $Z = 2$. The metal complex $\text{Mo}(\text{CO})_4(\text{NAPHOS})$ (**4**) crystallizes in the space group $P2_1/c$ with $a = 11.064(3) \text{ \AA}$, $b = 15.931(2) \text{ \AA}$, $c = 28.462(8) \text{ \AA}$, $\beta = 100.67(1)^\circ$, $V = 4930 \text{ \AA}^3$, and $Z = 4$. Molecular mechanics (MM) calculations for both $\text{Mo}(\text{CO})_4(\text{NAPHOS})$ (**4**) and $\text{Mo}(\text{CO})_4(\text{BISBI})$ (**5**) show an excellent match with the experimentally determined structures. A molecular dynamics (MD) simulation is demonstrated to be an efficient tool to sample over the accessible conformational space in order to cope with the "global minimum problem". The dynamic behavior of these compounds in solution is also explainable on this basis.

Introduction

Tertiary phosphines represent the major class of ligands used in homogeneous catalysis to stabilize metal centers in low formal oxidation states. Chelating ligands such as diphosphines often show improved activities and selectivities for a given catalytic reaction.¹ Recent developments in the field of hydroformylation clearly show that the activity of rhodium catalysts is improved by orders of magnitude upon replacement of multidentate for monodentate phosphines as ligands.² Moreover, the selectivity for linear aldehydes is improved by enlargement of the ligand's "bite angle".³ In our ongoing work on water-soluble catalysts⁴ and hydroformylation⁵ we became interested in diphosphines with large bite angles, with NAPHOS (**1**) and BISBI (**2**) being typical examples. They both exhibit high activity and n/iso selectivity in the rhodium-catalyzed hydroformylation,³ especially as sulfonated derivatives in two-phase processes.⁶

As an experimental basis of further investigations in this field we present in this paper the crystal structures



of the free and metal-coordinated ligand NAPHOS. $\text{Mo}(\text{CO})_4(\text{NAPHOS})$ (**4**) is the first structurally characterized complex of NAPHOS and can be compared with several similar complexes of diphosphine ligands. Thus, it serves as a model to study the coordination behavior of NAPHOS.

In order to predict the coordination chemistry and the behavior of phosphines in catalytic systems, it is necessary to quantify their steric requirements, their conformational flexibility, and their electronic properties. These correlations are based mainly on experimental results such as the so-called "cone angle" and "electronic factor", as defined by Tolman for monodentate phosphines.⁷ Recently, the determination of steric requirements of phosphines was extended by means of MM calculations,⁸ since their structure cannot be considered to be rigid. This approach accounts for deformations upon coordination and dynamic effects in a quantitative way. For diphosphines Casey et al. introduced the so-called "natural bite angle", which is also determined by MM calculations;⁹ it gives an estimate of the bidentate ligands' steric requirements.

The consideration of the coordination mode of ligands alone describes the behavior in catalysis only insuf-

* Present address: HOECHST Celanese, Technical Center, 1901 Clarkwood Rd., Corpus Christi, TX 78469.

[®] Abstract published in *Advance ACS Abstracts*, March 1, 1995.

(1) Pignolet, L. H. *Homogeneous Catalysis with Metal Phosphine Complexes*; Plenum Press: New York, 1983.

(2) (a) Broussard, M. E.; Juma, R.; Train, S. G.; Peng, W. J.; Laneman, S. A.; Stanley, G. G. *Science* **1993**, *260*, 1784. (b) Süß-Fink, G. *Angew. Chem.* **1994**, *106*, 71; *Angew. Chem., Int. Ed. Engl.* **1994**, *33*, 67.

(3) Devon, T. J.; Phillips, G. W.; Puckette, T. A.; Stavinoha, J. L.; Vanderbilt, J. J. *WO* 87/07600; Dec 17, 1987.

(4) Recent review: Herrmann, W. A.; Kohlpaintner, C. W. *Angew. Chem.* **1993**, *105*, 1588; *Angew. Chem., Int. Ed. Engl.* **1993**, *32*, 1524.

(5) (a) Herrmann, W. A.; Kulpe, J. A.; Kellner, J.; Riepl, H.; Bahrmann, H.; Konkol, W. *Angew. Chem.* **1990**, *102*, 408; *Angew. Chem., Int. Ed. Engl.* **1990**, *29*, 391. (b) Herrmann, W. A.; Kulpe, J. A.; Bahrmann, H.; Konkol, W. *J. Organomet. Chem.* **1990**, *389*, 85. (c) Herrmann, W. A.; Kulpe, J. A.; Kellner, J.; Riepl, H. *J. Organomet. Chem.* **1990**, *389*, 103.

(6) (a) Herrmann, W. A.; Kohlpaintner, C. W.; Bahrmann, H.; Konkol, W. *J. Mol. Catal.* **1992**, *73*, 191. (b) Herrmann, W. A.; Kohlpaintner, C. W.; Manetsberger, R. B.; Kottmann, G.; Bahrmann, H. *J. Mol. Catal.*, in press.

(7) Tolman, C. A. *Chem. Rev.* **1977**, *77*, 313.

(8) (a) Caffery, M. L.; Brown, T. L. *Inorg. Chem.* **1991**, *30*, 3907. (b) Lee, K. J.; Brown, T. L. *Inorg. Chem.* **1992**, *31*, 289. (c) Brown, T. L. *Inorg. Chem.* **1992**, *31*, 1286. (d) Choi, M. G.; Brown, T. L. *Inorg. Chem.* **1993**, *32*, 5603. (e) Chin, M.; Durst, G. L.; Head, S. R.; Bock, P. L.; Mosbo, J. A. *J. Organomet. Chem.* **1994**, *470*, 73. (f) Woo, T. K.; Ziegler, T. *Inorg. Chem.* **1994**, *33*, 1857.

ficiently. For example, the correlation of the natural bite angle of ligands $R_2P-X-PR_2$ with the *n*/*iso* selectivity in the (Rh^I -catalyzed) hydroformylation of 1-hexene is limited to diphosphines with equal substituents R at phosphorus. More reliable strategies to estimate the selectivity of a given ligand in a catalytic cycle should include ligand–ligand interactions in the transition state(s). Since the structures of the latter are not known with certainty, reasonable model structures must be used. This approach has been successful, for example, in modeling the isospecific polymerization of propylene by means of substituted *ansa*-metallocenes.¹⁰

Recent methodical developments in the area of molecular mechanics calculations have established that this empirical approach can be elaborated to treat transition-metal complexes. Landis et al. introduced a scheme to describe π -bonding¹¹ and extended the analytical expressions of angular potential energy terms according to angular overlap considerations.¹² The problem of parametrization has been tackled by Rappé et al. in an elegant way: parameters are generated by rules based on atomic values.¹³ Nevertheless, "conventional" calculations can also give reasonable insight into the coordination behavior of (organic) ligands.¹⁴

In this context, empirical force field calculations are demonstrated to be able to predict conformational changes induced upon coordination of diphosphine ligands. This validates the method on experimental results as a useful tool in catalysis-related applications.

Results and Discussion

A. Crystal Structure of the Diphosphine NAPHOS. NAPHOS (1) was first described in 1977 by Kumada et al.¹⁵ Single crystals were grown from a CH_2Cl_2/n -hexane solution (1/3 v/v). The compound crystallizes in the triclinic space group $P\bar{1}$ with $a = 10.568(1)$ Å, $b = 10.737(1)$ Å, $c = 15.986(1)$ Å, $\alpha = 81.63(1)^\circ$, $\beta = 86.42(1)^\circ$, $\gamma = 81.47(1)^\circ$, $V = 1773$ Å³, and $Z = 2$. Figure 1 shows a PLATON plot of NAPHOS (1). The coordination geometry of phosphorus is as expected for sp^3 hybridization including an electron lone pair, with the sum of bond angles C–P–C amounting to 301.6° and 304.9°. The bond distances are in the normal range of P–C(aliphatic) and P–C(aromatic) single bonds (Table 1). Although the interplanar angle of the binaphthyl structure is almost the same as in one of the two

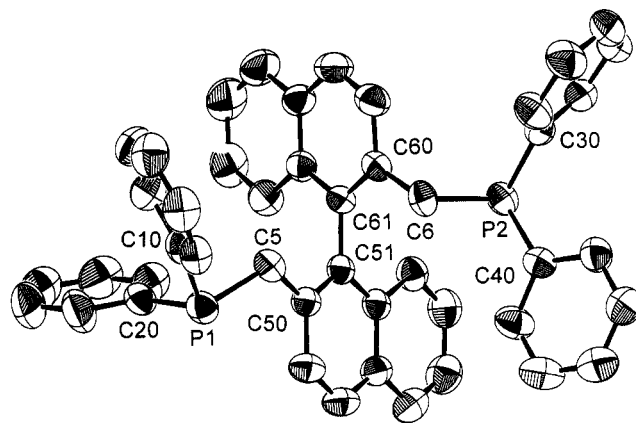
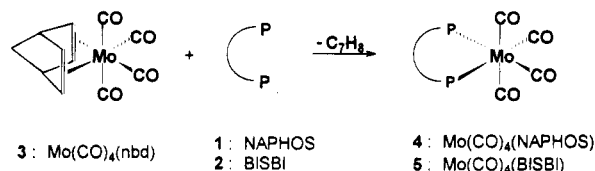


Figure 1. PLATON view of NAPHOS (1) with 50% probability ellipsoids. Hydrogen atoms are omitted for clarity.

Table 1. Selected Bond Lengths (Å) and Angles (deg) for NAPHOS (1)

P1–C5	1.859(1)	P2–C6	1.868(1)
P1–C10	1.820(2)	P2–C30	1.821(1)
P1–C20	1.824(2)	P2–C40	1.844(1)
C5–P1–C10	97.89(7)	C6–P2–C30	103.41(7)
C5–P1–C20	102.96(7)	C6–P2–C40	99.94(7)
C10–P1–C20	100.78(8)	C30–P2–C40	101.51(7)

Scheme 1. Preparation of $Mo(CO)_4(NAPHOS)$ (4) and $Mo(CO)_4(BISBI)$ (5) from the Norbornadiene Complex 3



crystallographically observed structures of BISBI (2) (76.8 vs 77.0°) the (nonbonding) distance of the two P atoms is somewhat longer than in 2 (7.01 vs 6.86 Å).¹⁶ This result is due to the conformationally flexible Ar–CH₂–P chain (Ar = aryl). In the solid state the two phosphine fragments of 1 adopt different rotational conformations. The lone pair of atom P2 is almost *parallel* to the C_2 axis of the binaphthyl moiety, whereas that of P1 is *perpendicular* to this axis, pointing away from the molecule.

B. Synthesis and Crystal Structure of $Mo(CO)_4(NAPHOS)$. If NAPHOS is treated with the norbornadiene complex 3 (as a traditional source of $Mo(CO)_4$ fragments) in refluxing toluene, the complex $Mo(CO)_4(NAPHOS)$ (4) forms as a yellow, air-stable solid (61% yield) according to Scheme 1.

Single crystals of 4 were grown from an NMR sample ($CDCl_3$) at room temperature. Figure 2 shows a PLATON plot, and Table 2 gives selected bond lengths and angles. The Mo atom is the center of an octahedral coordination sphere with a *cis* arrangement of the phosphorus atoms. The P–Mo–P bite angle in 4 amounts to 100.0(1)°; the P–Mo bond lengths average 2.559 Å. The corresponding values for $Mo(CO)_4(BISBI)$ (5) are 103.54(2)° and 2.566 Å, respectively. The least-squares planes of the two naphthyl systems C50–C59 and C60–C69 are tilted toward each other by 94.3° (obtuse angle), whereas the corresponding interplanar

(16) Herrmann, W. A.; Kohlpaintner, C. W.; Herdtweck, E.; Kiprof, P. *Inorg. Chem.* **1991**, *30*, 4271.

(9) (a) Casey, C. P.; Whiteker, G. T.; Melville, M. G.; Petrovich, L. M.; Gavney, J. A., Jr.; Powell, D. R. *J. Am. Chem. Soc.* **1992**, *114*, 5535. (b) Casey, C. P.; Whiteker, G. T.; Campana, C. F.; Powell, D. R. *Inorg. Chem.* **1990**, *29*, 3376. (c) Casey, C. P.; Whiteker, G. T. *Isr. J. Chem.* **1990**, *30*, 299.

(10) (a) Castonguay, L. A.; Rappé, A. K. *J. Am. Chem. Soc.* **1992**, *114*, 5832. (b) Hart, J. R.; Rappé, A. K. *J. Am. Chem. Soc.* **1993**, *115*, 6159. (c) Klein, R. *International Symposium "40 Years Ziegler Catalysis"*; Freiburg, Germany, 1993. (d) Herrmann, W. A.; Behm, J.; Schmid, R. Unpublished results.

(11) Doman, T. N.; Landis, C. R.; Bosnich, B. *J. Am. Chem. Soc.* **1992**, *114*, 7264.

(12) (a) Allured, V. S.; Kelly, C. M.; Landis, C. R. *J. Am. Chem. Soc.* **1991**, *113*, 1. (b) Root, D. M.; Landis, C. R.; Cleveland, T. J. *Am. Chem. Soc.* **1993**, *115*, 4201.

(13) (a) Rappé, A. K.; Casewit, C. J.; Colwell, K. S.; Goddard, W. A., III; Skiff, W. M. *J. Am. Chem. Soc.* **1992**, *114*, 10024. (b) Casewit, C. J.; Colwell, K. S.; Rappé, A. K. *J. Am. Chem. Soc.* **1992**, *114*, 10035. (c) Casewit, C. J.; Colwell, K. S.; Rappé, A. K. *J. Am. Chem. Soc.* **1992**, *114*, 10046. (d) Rappé, A. K.; Colwell, K. S.; Casewit, C. J. *Inorg. Chem.* **1993**, *32*, 3438.

(14) (a) Ferguson, D. M.; Raber, D. J. *J. Comput. Chem.* **1990**, *11*, 1061. (b) Castonguay, L. A.; Rappé, A. K.; Casewit, C. J. *J. Am. Chem. Soc.* **1991**, *113*, 7177.

(15) Tamao, K.; Yamamoto, H.; Matsumoto, H.; Miyake, N.; Hayashi, T.; Kumada, M. *Tetrahedron Lett.* **1977**, *16*, 1389.

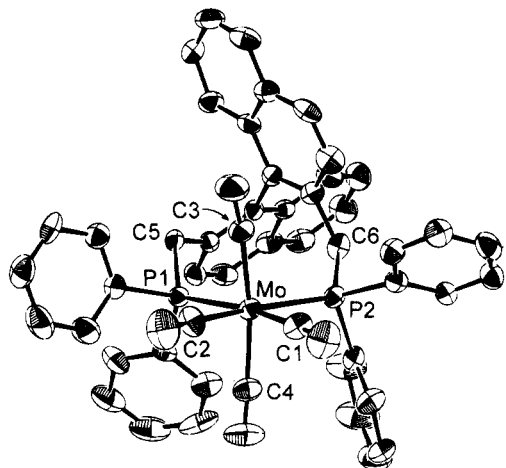


Figure 2. PLATON view of $\text{Mo}(\text{CO})_4(\text{NAPHOS})$ (**4**) with 50% probability ellipsoids. Hydrogen atoms are omitted for clarity.

Table 2. Selected Bond Lengths (Å) and Angles (deg) for $\text{Mo}(\text{CO})_4(\text{NAPHOS})$ (**4**)

P1-C5	1.883(7)	Mo-P1	2.570(2)
P1-C10	1.820(7)	Mo-P2	2.547(2)
P1-C20	1.827(7)	Mo-C1	1.976(8)
P2-C6	1.844(7)	Mo-C2	1.986(8)
P2-C30	1.830(7)	Mo-C3	2.037(7)
P2-C40	1.855(7)	Mo-C4	2.035(8)
C5-P1-C10	99.2(3)	P1-Mo-P2	100.0(1)
C5-P1-C20	99.7(3)	C3-Mo-C4	171.4(3)
C10-P1-C20	103.5(3)	P1-Mo-C1	172.2(2)
C6-P2-C30	102.4(3)	P1-Mo-C2	89.5(2)
C6-P2-C40	100.0(3)	P1-Mo-C3	88.1(2)
C30-P2-C40	101.6(3)	P1-Mo-C4	89.7(2)
Mo-P1-C5	126.2(2)	P2-Mo-C2	170.5(2)
Mo-P1-C10	118.8(2)	P2-Mo-C1	86.2(2)
Mo-P1-C20	106.1(2)	P2-Mo-C3	94.5(2)
Mo-P2-C6	121.9(2)	P2-Mo-C4	94.0(2)
Mo-P2-C30	112.3(3)	C1-Mo-C2	84.3(3)
Mo-P2-C40	115.9(2)	C1-Mo-C3	96.2(3)
		C1-Mo-C4	85.0(3)
		C2-Mo-C3	86.4(3)
		C2-Mo-C4	85.2(2)

angle of the biphenyl system of **5** is 117.7°. The average metal-carbon distance (1.981 Å) of the carbonyl groups *trans* to phosphorus (C1 and C2) shows the expected shortening as compared with the (average) metal-carbon bond length of 2.036 Å for the apical positions C3 and C4. The average phosphorus-phenyl carbon distance of 1.833 Å and the average C-P-C angle of 102.6° show no significant difference from the values for NAPHOS (**1**) at 1.827 Å and 101.1°, respectively. This is in full accord with the result of a systematic structure analysis of triphenylphosphine fragments by Orpen et al., which confirmed that there is no structural deformation upon coordination on low-valent metals.¹⁷ This allows the utilization of parameters derived for free phosphines in empirical force field calculations on metal-coordinated phosphines.

The asymmetric unit of **4** contains two additional disordered molecules of CDCl_3 . The occupation factor of one molecule with a disordered carbon atom is 1.0, the other CDCl_3 position is 76% occupied. Due to packing effects in the solid state and the presence of solvent molecules, a detailed comparison of **4** and **5** concerning the conformation of the phenyl rings is not possible.

(17) Dunne, B. J.; Morris, R. B.; Orpen, A. G. *J. Chem. Soc., Dalton Trans.* **1991**, 653.

The molecular symmetry of **4** in the solid state is C_1 . The two inequivalent phosphorus atoms should therefore give rise to two separate signals in the $^{31}\text{P}\{^1\text{H}\}$ NMR spectra. However, only a singlet is observed, even at temperatures as low as -80°C . The *solid-state* ^{31}P CP/MAS NMR spectrum shows *two* signals with a line separation of 2.67 ppm, being in full accord with the C_1 symmetry seen in the crystal structure.

At room temperature the ^1H NMR shows the expected coupling of the diastereotopic methylene protons. This double doublet is further complicated by coupling to the phosphorus nuclei: because of the different magnitudes of the $^2J(\text{PH})$ coupling constants, only one doublet is split up into a tripletlike pattern. The $^{13}\text{C}\{^1\text{H}\}$ NMR spectrum exhibits one broad signal for the methylene carbons and one multiplet each (due to coupling with phosphorus) for the *trans* and for the *cis* carbonyls. The rather complex aromatic regions of the ^1H and $^{13}\text{C}\{^1\text{H}\}$ NMR spectra have been elucidated by 2D ^1H - ^{13}C correlated NMR experiments with *inverse detection* (^1H - ^{13}C HMBC¹⁸ and ^1H - ^{13}C HMQC¹⁹). All carbon and hydrogen resonances of the naphthyl systems could thus be assigned unambiguously under the assumption of C_2 symmetry. The remaining ^1H - ^{13}C cross-peaks in the HMBC spectrum are the six expected couplings in the two diastereotopic but freely rotating phenyl systems. ^1H and ^{13}C NMR spectra hence support C_2 symmetry for the molecule under the given conditions of observation.

There are two possible explanations for this phenomenon: (i) the diphosphine ligand changes the coordination mode in solution or (ii) a dynamic process faster than the NMR time scale equilibrates inequivalent positions. For the latter possibility, the signals in the $^{31}\text{P}\{^1\text{H}\}$ NMR should split at sufficiently low temperatures; this is not seen, however, down to -80°C .

C. Molecular Mechanics Calculations on $\text{Mo}(\text{CO})_4(\text{NAPHOS})$ and $\text{Mo}(\text{CO})_4(\text{BISBI})$. The commercially available force field *cff91* of BIOSYM²⁰ utilizes a potential energy expression similar to that of MM2.²¹ A set of "cross-terms" is parametrized for pure hydrocarbon interactions:

$$E = \sum E_{\text{bond}} + \sum E_{\text{angle}} + \sum E_{\text{torsion}} + \sum E_{\text{out of plane}} + \sum E_{\text{nonbonded}} + \sum E_{\text{electrostatic}} + (\sum E_{\text{cross}})$$

$$E_{\text{bond}} = k_2(r - r_0)^2 + k_3(r - r_0)^3 + k_4(r - r_0)^4$$

$$E_{\text{angle}} = h_2(\varphi - \varphi_0)^2 + h_3(\varphi - \varphi_0)^3 + h_4(\varphi - \varphi_0)^4$$

$$E_{\text{torsion}} = V_1\{1 + \cos[\phi - \phi_0]\} + V_2\{1 + \cos[2(\phi - \phi_0)]\} + V_3\{1 + \cos[3(\phi - \phi_0)]\}$$

$$E_{\text{out of plane}} = k_\chi(\chi - \chi_0)^2$$

$$E_{\text{nonbonded}} = \epsilon_{ij} \left[2 \left(\frac{r_{\text{vdW},ij}}{r} \right)^9 - 3 \left(\frac{r_{\text{vdW},ij}}{r} \right)^6 \right]$$

(18) Bax, A.; Summers, M. F. *J. Am. Chem. Soc.* **1986**, *108*, 2093.

(19) Sanders, J. K. M.; Hunter, B. K. *Modern NMR Spectroscopy*, 2nd ed.; Oxford University Press: Oxford, England, 1993.

(20) (a) Maple, J. R.; Dinur, U.; Hagler, A. T. *Proc. Natl. Acad. Sci. U.S.A.* **1988**, *85*, 5350. (b) Maple, J. R.; Thacher, T. S.; Dinur, U.; Hagler, A. T. *Chemical Design Automation News* **1990**, *5*(9), 5.

(21) Allinger, N. L. *J. Am. Chem. Soc.* **1977**, *99*, 8127.

$$r_{\text{vdW},ij} = \sqrt{\frac{r_{\text{vdW},i}^6 + r_{\text{vdW},j}^6}{2}}$$

$$\epsilon_{ij} = 2 \sqrt{\epsilon_i \epsilon_j \left[\frac{(r_{\text{vdW},i})^3 (r_{\text{vdW},j})^3}{r_{\text{vdW},i}^6 + r_{\text{vdW},j}^6} \right]}$$

$$E_{\text{electrostatic}} = \frac{1}{4\pi\epsilon} \frac{q_1 q_2}{r}$$

We extended the force field by a set of parameters for phosphines adapted from the values published for MM2²² to reproduce structure and vibrational frequencies of model compounds (aryl and alkyl phosphines) in the given framework of *cff91*. These parameters are given in Table 5.²³

Because of the conventional force field used in this study with its lack of metal–ligand interaction parameters and the inability to treat octahedral coordination,^{12a} we introduced some simplifications in our model of complexes **4** and **5**. On the other hand, we incorporated only parameters already known from a general analysis of the given class of compounds and did not use any specific data from the crystal structure analysis of **4** and **5**.

(1) The carbonyl ligands were placed in octahedral positions with bond lengths typical for such complexes (Mo–C, 2.00 Å; C–O, 1.14 Å²⁴).

(2) The resulting Mo(CO)₄ fragment was kept invariable in all calculations.

(3) The phosphine-to-molybdenum interactions were described as follows: (i) the Mo–P distance was restrained to 2.55 Å, which quantity results from the X-ray structure analysis; (ii) the phosphorus atoms were forced into a tetrahedral geometry to ensure that the lone pairs point toward the metal atom. No P–Mo–P or P–Mo–C_{CO} bending interactions hold the phosphine fragments in octahedral sites with respect to the carbonyls. Therefore, the description is reminiscent of the “point on a sphere model” often referred to in coordination chemistry. In this model only *nonbonding interactions* determine the details of coordination geometry around the metal atom.²⁵

(4) Electrostatic interactions were excluded in all calculations.

Since the *nine*-membered rings in the structures of **4** and **5** should allow for a plethora of conformations, we used a simple “simulated annealing” sequence known from structure determinations of biopolymers.²⁶ For both compounds a molecular dynamics (MD) simulation at high temperature (1000 K) for 170 picoseconds (ps) was performed.²⁷ Every 1 ps a structure was retained which gave a set of perturbed structures out of the accessible conformational space. A subsequent energy minimization resulted in six different conformers in the range of 5 kcal/mol above the global minimum. Figure 3 shows the minimized steric energy vs the duration of

the MD simulation. The conformation of the nine-membered-ring structure can be described by a total of seven dihedral angles defined by the ring bonds, because two dihedral angles of the binaphthyl moiety vary only slightly around 0°.

A comparison of all calculated conformers shows that some of them adopt the same ring conformation but differ in the orientation of the phenyl rings. Three different types of ring conformations were found for both **4** and **5**. The lowest energy conformers of these are **a**, **b**, and **e** for **4** and **a**, **b**, and **d** for **5** (see Figure 4).

Tables 3 and 4 show the dihedral angles of the conformers of **4** and **5**. The axial chirality of the biaryl structure excludes a mirror plane. For conformers **e** of **4** and **d** of **5** the C₂ axis of the ligand is equivalent with the C₂ axis of the metal fragment. These conformers show an overall C₂ symmetry, whereas all others lack any symmetry elements (C₁). The C₂-symmetrical coordination with respect to the P–M–P moiety is also found in the crystal structure of Fe(CO)₃(BISBI) where the ligand occupies two *trans*-spanning basal positions in a square pyramid with the very large P–Fe–P angle of 152.0°. The tendency of large bite angles in the C₂-symmetric coordination—and *vice versa*—is also manifested in the systematically large P–M–P angles for these conformers of **4** and **5**. These findings support the view that the flexibility introduced by the methylene groups between the phosphine and the biaryl fragments is the source of the ligands' ability to adopt to a wide range of bite angles.

Conformers **a** and **b** are different by rotation of one phosphine fragment around the Mo–P2 bond axis (Figure 5).

Superposition of the X-ray structure with the global minimum structure **a** shows that both belong to the same type of ring conformation (Figure 6). Especially for compound **5**, the experimental and the calculated structures are virtually identical, even with regard to the rotational conformation of the phenyl rings. In the case of the crystal structure, the geometric perturbations by the solvent molecules are to be taken into consideration. The calculated minimum energy structures **a** show the same deviation with respect to the crystal structures: the biaryl moiety is slightly tilted, together with a rotation of the Mo–P1 bond (difference in C5–P1–Mo–P2: 15.7° in **4** and 7.6° in **5**). Obviously there is a steric repulsion between one of the aromatic systems of the biaryl fragment and the axial carbonyl ligand, the latter being severely distorted off the octahedral position in the experimental structure. These differences between experimental and calculated structures thus could be due to the fixation of the carbonyl ligands in the molecular mechanics model.

Since the calculated structure (gas-phase conditions) and the crystal structure (solid state) are closely related, it seems reasonable to assume a C₁ symmetry for both compounds in solution and a dynamic process that equilibrates the chemical environment of the two phosphorus atoms. Due to the rigidity of the biaryl moiety, the methylene carbon atoms remain fixed with a through-space distance of ~4.4 Å. This reduces the structure to a virtual five-membered ring in an envelope conformation as drawn in Figure 7. The phosphorus atoms are inequivalent as a result of axial (biaryl) chirality. P_A and P_B will change their environment by a flip of the molybdenum tetracarbonyl fragment (tip

(22) Bowen, J. P.; Allinger, N. L. *J. Org. Chem.* **1987**, *52*, 2937.

(23) Schmid, R. Diploma Thesis, Technische Universität München, München, Germany, 1993.

(24) Approximate mean values from several crystal structures of the complexes *cis*-L₂Mo(CO)₄ (L = phosphine) as found from a CSD search (e.g. BEGMUV, BILMEO, BILMIS, BILMOY).

(25) Hay, B. P. *Coord. Chem. Rev.* **1993**, *126*, 177.

(26) Van Gunsteren, W. F.; Berendsen, H. J. C. *Angew. Chem.* **1990**, *102*, 1020; *Angew. Chem., Int. Ed. Engl.* **1990**, *29*, 992.

(27) Since we did not intend a physically meaningful simulation but a simple generation of various starting structures, an equilibration period was not included in the MD calculation.

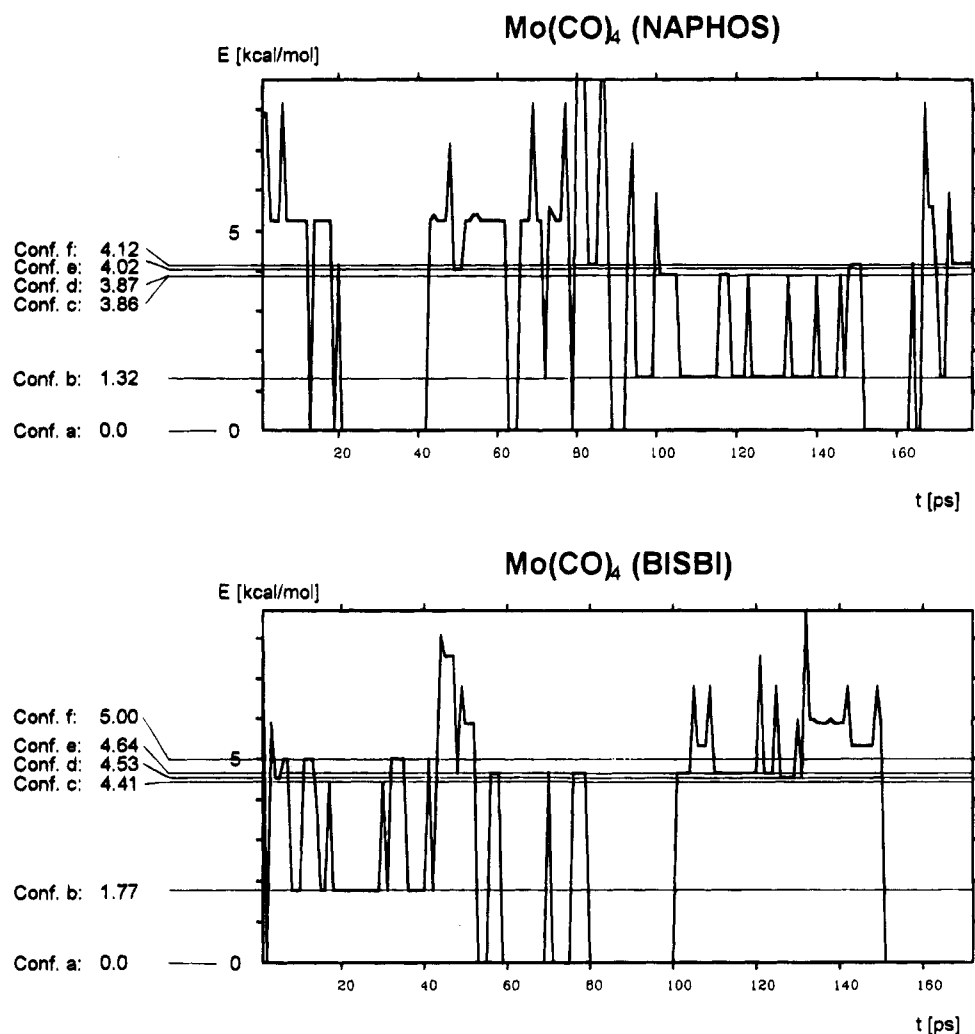


Figure 3.

Table 3. Relative Steric Energies and Structural Data for the Six Lowest Energy Conformers of $\text{Mo}(\text{CO})_4(\text{NAPHOS})$ (4) in Comparison with the Experimental Values (Crystal Structure)

	conformer						exptl
	a	b	c	d	e	f	
ΔE (kcal/mol)	0.00	1.32	3.86	3.87	4.02	4.12	
P1-Mo-P2 (deg)	105.0	106.6	106.5	105.5	113.4	102.3	100.0
C50-C51-C61-C60 (deg)	107.2	107.6	108.0	108.6	106.9	97.1	99.0
P2-Mo-P1-C5 (deg)	-66.1	-42.0	-40.7	-39.1	35.9	-57.7	-50.3
Mo-P1-C5-C50 (deg)	101.5	67.2	65.9	58.7	-8.5	104.9	81.2
P1-C5-C50-C51 (deg)	-101.0	-110.1	-109.7	-105.0	-81.9	-112.0	-105.0
P1-Mo-P2-C6 (deg)	32.3	73.5	77.2	76.5	35.9	28.7	39.5
Mo-P2-C6-C60 (deg)	54.2	-10.0	-18.4	-12.3	-8.5	55.3	39.5
P2-C6-C60-C61 (deg)	-116.2	-83.5	-77.1	-81.4	-81.9	-120.6	-119.0

of the envelope) to the other side of the ring plane, as indicated by the arrow in Figure 7. This process occurred accidentally in the MD simulation of 4.

This mechanism is supported by the C_2 -symmetric structure of the conformers e of 4 and d of 5. They resemble a *twist* conformation of the virtual five-membered ring. If the activation barrier between a and e for $\text{Mo}(\text{CO})_4(\text{NAPHOS})$ and a and d for $\text{Mo}(\text{CO})_4(\text{BISBI})$ is small, this should be a facile process for both these compounds. It could also explain the equivalence of the two phosphorus atoms on the NMR time scale.

Conclusion

Our study reveals that the diphosphine ligand NAPHOS exhibits the same structural flexibility as BISBI. In spite of the higher steric demands of the binaphthyl

fragment, NAPHOS is able to coordinate to metals with the relatively small P-M-P angle of only 100.0° . The structural similarities of the molybdenum complexes $\text{Mo}(\text{CO})_4(\text{BISBI})$ and $\text{Mo}(\text{CO})_4(\text{NAPHOS})$ lend support to this assessment. As a matter of fact, NAPHOS-type diphosphines have become outstanding ligands in rhodium-catalyzed CC-coupling reactions.^{6,28}

The MM calculations reproduce the experimental structure in terms of a reasonable description of conformational changes induced upon coordination of the ligands, despite the simplified model used in this study. The necessity of a systematic screening of the conformational space to find the global minimum conformation is demonstrated. The high-temperature MD simulation

(28) Kohlpaintner, C. W. Ph.D. Thesis, Technische Universität München, München, Germany, 1992.

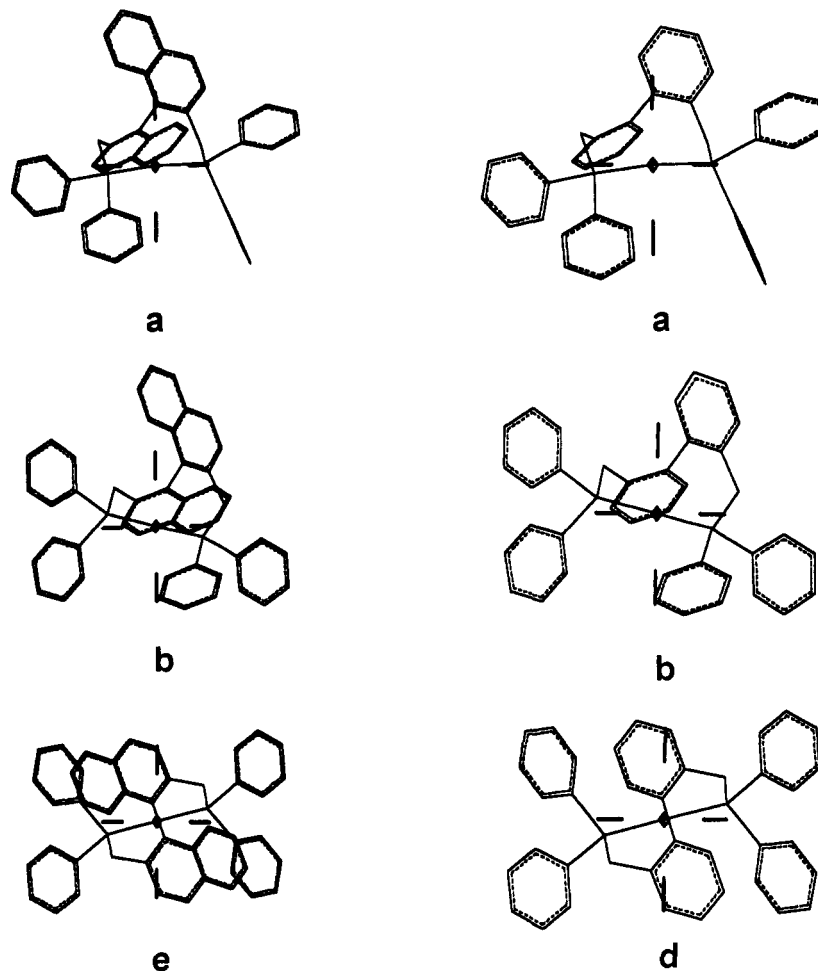


Figure 4.

Table 4. Relative Steric Energies and Structural Data for the Six Lowest Energy Conformers of $\text{Mo}(\text{CO})_4(\text{BISBI})$ (5) in Comparison with the Experimental Values (Crystal Structure)

	conformer						exptl
	a	b	c	d	e	f	
ΔE (kcal/mol)	0.00	1.77	4.41	4.53	4.64	5.00	
P1-Mo-P2 (deg)	106.0	108.5	108.5	116.5	102.9	108.5	103.5
C50-C51-C61-C60 (deg)	110.9	114.0	114.3	114.7	96.6	122.8	117.8
P2-Mo-P1-C5 (deg)	-67.9	-43.1	-41.9	35.6	-57.5	-33.2	-60.3
Mo-P1-C5-C50 (deg)	100.7	66.2	64.6	-6.7	105.4	48.5	87.4
P1-C5-C50-C51 (deg)	-96.9	-104.6	-104.0	-77.9	111.2	-87.9	-93.0
P1-Mo-P2-C6 (deg)	32.5	73.8	77.6	35.6	26.8	74.2	37.0
Mo-P2-C6-C60 (deg)	53.9	-9.1	-17.1	-6.7	57.3	-12.7	44.4
P2-C6-C60-C61 (deg)	-113.0	-79.50	-73.9	-77.9	-119.7	-73.4	-106.2

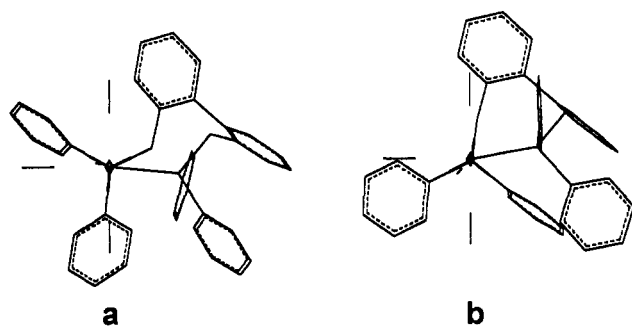


Figure 5.

has proven very efficient to give a sufficiently broad set of starting structures that cover all relevant conformations of ligands of a given size.

The force field predicts conformational changes of the diphosphine geometry resulting from steric interactions

with other ligands. Assuming a reasonable transition-state model for a reaction step in the catalytic cycle, a complete description of the steric interactions seems possible in the future merely on the basis of theoretical calculations. Work in this field is in progress.

Experimental Part

Computational Details. All molecular mechanics calculations were performed on a Silicon Graphics "Personal Iris" 4D25 with the INSIGHT/DISCOVER program of Biosym Technologies.²⁹ The "consistent forcefield 1991" *cff91*³⁰ was extended by a set of parameters that properly describe tertiary aryl- and alkylphosphines (see Table 5).

The $\text{Mo}(\text{CO})_4$ fragment was fixed in an ideal octahedral geometry with a Mo-C distance of 2.00 Å and a C-O distance

(29) *InsightII User Guide*, Version 2.1; Biosym Technologies: San Diego, CA, 1992.

(30) *Discover User Guide*, Version 2.8; Biosym Technologies: San Diego, CA, 1992.

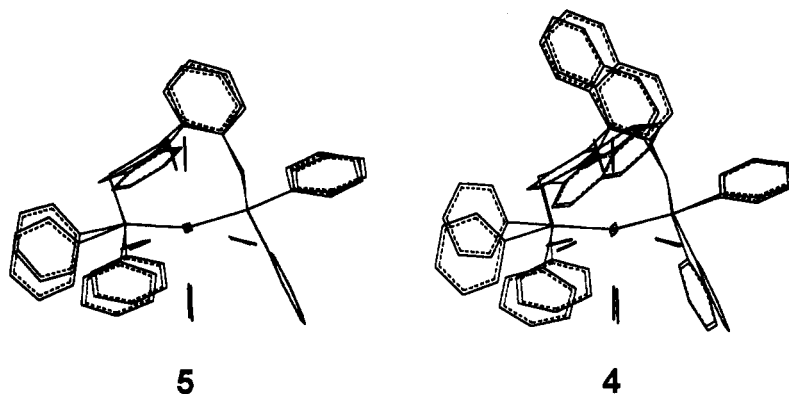


Figure 6.

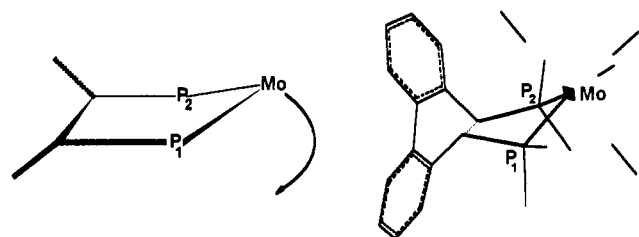


Figure 7.

Table 5. *cff91* Force Field Parameters for Phosphines^a

bond	r_0 (Å)	k_2 (kcal/(mol·Å ²))	k_3 (kcal/(mol·Å ³))	k_4 (kcal/(mol·Å ⁴))
p-c	1.84	205	0	0
p-cp	1.82	205	0	0
angle	φ_0 (rad)	h_2 (kcal/(mol·rad ²))	h_3 (kcal/(mol·rad ³))	h_4 (kcal/(mol·rad ⁴))
cp-p-cp	92.2	39.0	0	0
c-p-c	96.0	45.0	0	0
c-p-cp	92.5	41.0	0	0
p-cp-cp	120.0	27.4	0	0
p-c-cp	110.5	46.6	0	0
p-c-h	111.0	40.0	0	0
torsion angle	ϕ_0 (deg)	V_2 (kcal/mol)	V_3 (kcal/mol)	V_4 (kcal/mol)
c-p-cp-cp	0	0.000	0.000	0.200
cp-p-cp-cp	0	0.000	0.000	0.170
cp-p-c-h	0	0.025	0.000	0.100
cp-p-c-cp	0	-0.025	0.050	0.150
cp-cp-cp-p	0	0.000	4.400	0.000
h-cp-cp-p	0	0.000	1.560	0.000
cp-cp-c-p	0	0.122	0.051	-0.223
out of plane	χ_0 (deg)	k_z (kcal/(mol·rad ²))		
cp-cp-cp-p	0	8.0		
nonbond	r_{vdW} (Å)	ϵ (kcal/mol)		
p	4.2	0.15		

^a The atom types are defined as follows: p, general phosphorus atom; c, sp³ carbon atom; cp, sp² aromatic carbon (six-membered ring); h, hydrogen.

of 1.14 Å. The bond order between molybdenum and the carbonyl carbon atoms was set to zero. Thus, the van der Waals 1,3-interactions around the metal atom are included in the calculation as is done in MMX.³¹ The Mo-P distances were constrained to 2.55 Å by a force constant of 1000 kcal/(mol·Å²). The *cff91* atom types c' and o' were used for the carbonyl ligands that are used in the standard *cff91* to describe organic carbonyl functions. Because of the fixation of the carbon and oxygen atoms, only the nonbonding interactions

Table 6. Force Field Parameters for the Metal-Phosphine Interaction

M-P	$r_0 = 2.55$ Å, $k = 1000$ kcal/(mol·Å ²)
M-P-C	$\varphi_0 = 109.5^\circ$, $k = 70$ kcal/(mol·rad ²)
P-M-P-C	$k = 0$ kcal/(mol·rad ²)
M-P-C-C	$k = 0$ kcal/(mol·rad ²)
M _{vdW}	$r_{vdW} = 0$ Å, $\epsilon = 0$ kcal/mol

were active in the calculation. All nonbonding interactions to the metal atom were set to zero. The metal-related parameters are summarized in Table 6.

The standard Verlet integration algorithm³² of *discover 2.8* with a time step of 1 fs was used in the molecular dynamics simulations. The temperature was held at 1000 K. Every 1 ps a structure was retained and minimized with a pseudo-Newton-Raphson minimizer (VA09A) until each degree of freedom had a derivative of less than 0.1 kcal/(mol·Å²). The resulting structures were partitioned in groups of equal steric energy and checked for their conformations. One representative was then minimized until each degree of freedom had a derivative of less than 0.001 kcal/(mol·Å²).

General Procedures. ¹H NMR spectra and ¹³C{¹H} NMR spectra were measured on a JEOL JMN-GX 400 spectrometer (¹³C NMR, 100.5 MHz). The 2D ¹H-¹³C HMBC and 2D ¹H-¹³C HMQC of Mo(CO)₄(NAPHOS) (4) were recorded on a Bruker AMX 500 spectrometer (¹³C NMR, 125.8 MHz). Hydrogen and carbon resonances of 4 were assigned by the 2D heteronuclear correlation experiments. Multiplicities and coupling constants are given only when it was possible to derive them from the 1D NMR spectra.

³¹P{¹H} NMR spectra were measured at room temperature and at -80 °C on a JEOL JMN-GX 400 spectrometer (161.8 MHz) and referenced to external H₃PO₄ (85%). The ³¹P CP/MAS NMR spectra were measured on a Bruker MSL 300 P spectrometer (121.5 MHz) with NH₄[H₂PO₄] as an external standard which was also used to match the Hartmann-Hahn condition. Infrared spectra were obtained on a Nicolet 5-DX FT-IR spectrometer. Mass spectra were determined on a Finnigan MAT-90 instrument. Elemental analyses were performed in the Microanalytical Laboratories of our institute (M. Barth). Air-sensitive materials were manipulated under an inert-gas atmosphere using Schlenk techniques. Solvents were dried in the usual way.

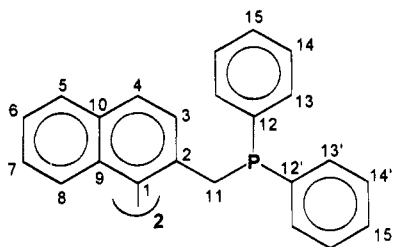
Synthesis and Spectroscopy. The labeling scheme of NAPHOS shown in Chart 1 has been used.

(1) 2,2'-Bis((diphenylphosphino)methyl)-1,1'-binaphthyl (1) was synthesized according to ref 28; mp 148 °C. Spectroscopic data: ¹H NMR (*d*₆-acetone) δ 3.26 (dd, ²J(HH) = 14.3 Hz, ²J(PH) = 1.5 Hz, CH_aH_b, 2H), 3.36 (d, ²J(HH) = 14.6 Hz, CH_aH_b, 2H), 7.01-7.40 (m, 28H); ¹³C{¹H} NMR (*d*₆-acetone) δ 35.20 (d, ¹J(PC) = 18.3 Hz, C₁₁), 126.24 (s, C₈), 127.05 (s, C₆), 127.23 (s, C₇), 128.55 (s, C₅), 128.80 (s, C₄), 128.89-129.34 (m, C_{14,14'}, C_{15,15'} [meta/para]), 129.63 (s, C₃),

(31) (a) Mackie, S. C.; Baird, M. C. *Organometallics* **1992**, *11*, 3712. (b) Polowin, J.; Mackie, S. C.; Baird, M. C. *Organometallics* **1992**, *11*, 3724.

(32) Verlet, L. *Phys. Rev.* **1967**, *159*, 98.

(33) Prince, E. *Mathematical Techniques in Crystallography*; Springer-Verlag: Berlin, Germany, 1982.

Chart 1. Labeling of the Ligand in the NMR Spectroscopic Results

133.35 (s, C₉), 133.38 (d, ²J(PC) = 19.8 Hz, C₁₃ [ortho]), 133.84 (d, ²J(PC) = 19.8 Hz, C_{13'} [ortho]), 133.89 (s, C₁₀), 135.67 (s, C₁), 136.30 (d, ²J(PC) = 10.7 Hz, C₂), 139.60 (d, ¹J(PC) = 17.3 Hz, C₁₂ [ipso]), 139.69 (d, ¹J(PC) = 17.3 Hz, C_{12'} [ipso]); ³¹P{¹H} NMR (CD₂Cl₂) δ -14.03 (s); IR (KBr, cm⁻¹) ν(aryl-H) 2923 (st), 2853 (m), 743 (st), 696 (vs), ν(C-H) 3070 (m), 1479 (w); MS (EI) *m/e* 651 ([MH]⁺), 466 ([MH - PPh₂]⁺). Anal. Calcd for C₄₆H₃₆P₂: C, 84.90; H, 5.58; P, 9.52. Found: C, 84.52; H, 5.54; P, 9.16.

(2) [2,2'-Bis((diphenylphosphino)methyl)-1,1'-binaphthyl]tetracarbonylmolybdenum (4). A 566 mg (0.87 mmol) amount of **1** in 20 mL of toluene was added dropwise at room temperature to a solution of (bicyclo[2.2.1]hepta-2,5-diene)-tetracarbonylmolybdenum (**3**; 262 mg, 0.87 mmol) in 10 mL of toluene. The solution was then heated for 15 min to reflux and subsequently cooled to ambient temperature. After evaporation of the solvent *in vacuo*, the resulting solid was dissolved in a minimum amount of methylene chloride and then overlaid with 15 mL of *n*-hexane. Crystallization at -20 °C yielded 453 mg (0.53 mmol) of a yellow, crystalline powder (61% yield); mp 198 °C dec. Spectroscopic data: ¹H NMR (CD₂Cl₂) δ 3.64 (d, ²J(HH) = 13 Hz, CH₂H₅), 3.80 ("tr", CH₂H₅), 6.43 (d, ³J(HH) = 8.5 Hz, H₃), 6.86 (d, ³J(HH) = 8.5 Hz, H₃), 7.20 (H₇), 7.31 (H_{phenyl}), 7.32 (H_{phenyl}), 7.35 (H_{phenyl}), 7.37 (H_{phenyl}), 7.42 (H₆), 7.47 (H_{phenyl}), 7.51 (H₄), 7.56 (H_{phenyl}), 7.83 (d, ³J(HH) = 8.5 Hz, H₅); ¹³C{¹H} NMR (CD₂Cl₂) δ 39.55 (bs, C₁₁), 125.7 (s, C₈), 126.1 (s, C₆), 126.9 (s, C₇), 127.8 (s, C₄), 128.3 (C₃), 128.3 (C_{phenyl}), 128.4 (C₅), 128.5 (C_{phenyl}), 129.0 (C_{phenyl}), 130.7 (d, *J*(PC) = 5 Hz, C_{phenyl}), 130.8 (d, *J*(PC) = 5 Hz, C_{phenyl}), 132.9 (s, C₉), 133.0 (s, C₁₀), 133.5 (s, C₂), 135.8 (s, C₁), 135.9 (d, *J*(PC) = 6 Hz, C_{phenyl}), 136.5 ("qua", *N* = 30.6 Hz, C_{12/12'}), 208.4 (t, ²J(PC) = 9 Hz, CO [trans]), 214.1 ("qui", *N* = 18.3 Hz, CO [cis]); ³¹P{¹H} NMR (CD₂Cl₂) δ 30.74 (s); ³¹P-CP/MAS NMR δ 25.00, 27.67; IR (KBr, cm⁻¹) ν(CO) 2024 (st), 1913 (vst), 1875 (vst), ν(aryl-H) 3060 (s), 740 (m), 694 (m), ν(C-H) 3070 (m), 1479 (w); MS (EI) *m/e* 804 ([M - 2CO]⁺), 776 ([M - 3CO]⁺), 748 ([M - 4CO]⁺), 541 ([NAPHOS]⁺), 573 ([NAPHOS - Ph]⁺), 465 ([NAPHOS - PPh₂]⁺). Anal. Calcd for C₅₀H₃₆MoO₄P₂: C, 69.94; H, 4.23; Mo, 11.17; O, 7.45; P, 7.21. Found: C, 69.11; H, 4.26; Mo, 11.33; O, 8.31; P, 7.30.

X-ray Crystallography. Crystals of compounds **1** and **4** were grown by standard techniques at room temperature from a CH₂Cl₂/*n*-hexane mixture (1/3 v/v) and from a deuteriochloroform solution, respectively. Preliminary examination and data collection were carried out on an Enraf-Nonius CAD4 diffractometer with Cu Kα radiation (λ = 151.18 pm) for **1** and Mo Kα radiation (λ = 71.07 pm) for **4**. Final cell constants were obtained by least-squares analysis of 25 automatically centered reflections (**1**, 79.8° < 2θ < 88.7°; **4**, 30.1° < 2θ < 40.0°). Data were collected by a ω/2θ scan mode for **1** (*h*, -12 to +12; *k*, -12 to +12; *l*, -18 to 0) and with a ω scan mode in the case of **4** (*h*, -13 to +13; *k*, 0 to 18; *l*, 0 to 33). Orientation control reflections were monitored every 200th reflection, and the intensities of 3 reflections were checked every 3600 s for both crystals. Changes in intensities were not corrected. Crystal data and intensity collection parameters together with details of the refinements are summarized in Table 7.

Table 7. Crystallographic Data, Summary of Data Collection, and Refinement Parameters for NAPHOS (1) and Mo(CO)₄(NAPHOS) (4)

	1	4
formula	C ₄₆ H ₃₆ P ₂	C ₅₀ H ₃₆ MoO ₄ P ₂ plus ca. 1.8 CDCl ₃
fw	650.75	858.72 (without solvent)
cryst syst	triclinic	monoclinic
space group	P $\bar{1}$ (No. 2)	P2 ₁ /c (No. 14)
temp, K	293	223
<i>a</i> , Å	10.568(1)	11.064(3)
<i>b</i> , Å	10.737(1)	15.931(2)
<i>c</i> , Å	15.986(2)	28.462(8)
α, deg	81.63(1)	90
β, deg	86.42(1)	100.67(1)
γ, deg	81.47(1)	90
Z	2	4
<i>V</i> , Å ³	1773	4930
λ, Å	1.5418 (Cu Kα)	0.7107 (Mo Kα)
<i>d</i> _{calc} , g·cm ⁻³	1.219	1.1577 (without CDCl ₃) ^d
<i>μ</i> , cm ⁻¹	13.4	3.6 (without CDCl ₃) ^d
<i>R</i> ₁ , %	6	7.1
<i>R</i> _w , %	4.8 ^b	6.7 ^c

^a $R = \sum(|F_o| - |F_c|) / \sum |F_o|$. ^b $R_w = [\sum w(|F_o| - |F_c|)^2 / \sum w |F_o|^2]^{1/2}$ with weighting scheme 1/*σ*². ^c Weighting scheme according to ref 33 with five refined parameters: *p*(1) = 0.736, *p*(2) = -0.137, *p*(3) = 0.483, *p*(4) = -0.112, *p*(5) = 0.113. ^d Solvent molecules in the crystal structure; see text.

The structures were solved by direct methods³⁴ (**1**) and Patterson methods³⁴ (**4**) followed by subsequent difference Fourier techniques. Full-matrix least-squares refinements were carried out, minimizing $\sum w(|F_o| - |F_c|)^2$. Hydrogen atoms were included at their calculated positions (*d*_{C-H} = 96 pm) and were not refined in both cases. Anomalous dispersion was considered. The refinement stopped at shift/error < 0.001, and final difference Fourier maps showed no significant features. All calculations were performed on a MicroVax 3100 computer and a DEC Station 5000/25 using the program CRYSTALS³⁵ and the STRUX-IV³⁶ system, including the programs PLATON,³⁷ SDP,³⁸ and SHELXS-86.³⁴

Acknowledgment. This work was supported by the Bundesministerium für Forschung und Technologie (Bonn, Germany) and Hoechst AG (Frankfurt am Main, Germany). We are grateful to Dr. Joachim Behm for the crystal structure determination of NAPHOS and Dr. Janet Blümel for the solid-state NMR spectra. Matthias Eberstadt and Franz-Robert Klingan are acknowledged for the 2D-NMR experiments, and Robert Eckl is thanked for experimental assistance.

Supplementary Material Available: For both **1** and **4**, tables of atom positions, anisotropic displacement parameters, and bond distances and angles for all atoms (20 pages). Ordering information is given on any current masthead page.

OM940914S

(34) Sheldrick, G. M. SHELX-86; Universität Göttingen: Göttingen, Germany, 1986.

(35) Watkin, D. J.; Betteridge, P. W.; Carruthers, J. R. *CRYSTALS User Manual*; Oxford University Computing Laboratory: Oxford, England, 1986.

(36) Scherer, W.; Kiprof, P.; Herdtweck, E.; Schmidt, R. E.; Birkhahn, M.; Massa, W. *STRUX-IV, ein Programmsystem zur Verarbeitung von Röntgenstrahlung*; Technische Universität München and Universität Marburg: München and Marburg, Germany, 1985/1990.

(37) Spek, A. L. The "EUCLID" Package. In *Computational Crystallography*; Sayre, D., Ed.; Clarendon Press: Oxford, England, 1982; p 528.

(38) Frenz, B. A. The ENRAF-Nonius CAD4 SDP System. In *Computing in Crystallography*; Delft University Press: Delft, Holland, 1978.

Thermal and Photochemical Disproportionation of the Oxo-Bridged Dimer $[\{W^V(\eta^5-C_5H_5)_2(CH_3)\}_2(\mu-O)](PF_6)_2$

Robert L. Thompson, Michael D. Hopkins, and N. John Cooper*

Department of Chemistry and Materials Research Center, University of Pittsburgh,
Pittsburgh, Pennsylvania 15260

Samkeun Lee

Department of Chemistry, Taejon University, 96-3 Young-dong Tong-gu, S. Korea

Received November 15, 1994[®]

The diamagnetic d^1-d^1 oxo-bridged dimer $[\{W^V(\eta^5-C_5H_5)_2(CH_3)\}_2(\mu-O)]^{2+}$ (1^{2+}) undergoes a thermal disproportionation reaction in CD_3CN to give the d^0 monomer $[W^{VI}(\eta^5-C_5H_5)_2(O)(CH_3)]^+$ (4^+) and the acetonitrile-trapped d^2 monomer $[W^{IV}(\eta^5-C_5H_5)_2(CH_3)(NCCD_3)]^+$ (5^+-d^3). The reaction is first order in 1^{2+} , and 1H NMR kinetic studies between 54 and 72 °C have established that there is a large enthalpic barrier to disproportionation with $\Delta H^\ddagger = 33.7 \pm 1.7$ kcal mol⁻¹ and a significant positive entropy of activation for this dissociative process ($\Delta S^\ddagger = 25.1 \pm 5.2$ cal K⁻¹ mol⁻¹), corresponding to $\Delta G^\ddagger = 26.2$ kcal mol⁻¹ at 25 °C. The dimer 1^{2+} is also subject to photodisproportionation, and the barrier to thermal disproportionation of 1^{2+} is sufficiently large to allow determination of the quantum yield for photodisproportionation of 1^{2+} to 4^+ and 5^+ in CH_3CN . The reaction was readily monitored by electronic spectroscopy, since the only visible absorptions in electronic spectra of 4^+ and 5^+ are the tails of UV absorptions at 330 ($\epsilon = 525$ L mol⁻¹ cm⁻¹) and 400 nm ($\epsilon = 400$ L mol⁻¹ cm⁻¹), respectively, while 1^{2+} has a strong absorption at 525 nm ($\epsilon = 23\,600$ L mol⁻¹ cm⁻¹) in the region characteristic of d^1-d^1 oxo-bridged dimers. Quantum yield determinations established that 1^{2+} photodisproportionates when irradiated in the UV ($\Phi_{310} = 0.082$) and when irradiated in the principal visible absorption band ($\Phi_{530} = 0.014$).

Introduction

We recently determined that ferrocenium oxidation of $[W^{IV}(\eta^5-C_5H_5)_2(CH_3)(OCH_3)]$ in methyl ethyl ketone (MEK) led to formation of a W(V) dimer $[\{W^V(\eta^5-C_5H_5)_2(CH_3)\}_2(\mu-O)](PF_6)_2$ (1^{2+}), established crystallographically to have a linear oxo bridge between the two metal centers.¹ This material is diamagnetic both in solution and in the solid state, despite the formal d^1-d^1 electron count, and this can be attributed to π -interactions between the frontier orbitals of the metal centers and a filled p-orbital of the bridging oxygen atom.^{2,3}

The best known class of molecules in which a linear oxo bridge spin pairs two d^1 centers are the Mo(V) oxo complexes in which a $[Mo^V_2O_3]^{4+}$ core,³ containing two mutually syn or anti terminal oxo ligands perpendicular to the Mo–O–Mo axis, is complexed by four bis-chelate dithiocarbamate ligands such as xanthate ($[S_2COR]^-$),^{4,5} dithiocarbamate ($[S_2CNR_2]^-$),^{5,6} or dithiophosphate ($[S_2P(OR)_2]^-$).^{7,8} It is well established that many of these $[Mo^V_2O_3(S_2EX_n)_4]$ complexes are in thermal equi-

librium with their Mo(IV) and Mo(VI) disproportionation products $[Mo^{IV}O(S_2EX_n)_2]$ and $[Mo^{VI}O_2(S_2EX_n)_2]$,^{9–11} and we recently reported that in the dithiocarbamate system such equilibria can be photodriven to give rise to marked photochromic behavior, as established in the specific cases of $[Mo^V_2O_3\{S_2CN(CH_2Ph)_2\}_4]$ (**2**) and the isologous complex $[W^V_2O_3\{S_2CN(CH_2Ph)_2\}_4]$ (**3**).¹² We suggested¹² that this new class of photochromic transition metal complexes might find useful technical applications in the areas of optical memory systems and photoresists,¹³ but determining the quantitative characteristics of the photochromic behavior was difficult in the dithiocarbamate systems because of the rapidity of the thermal recombination reactions.

Our initial reactivity studies readily established that 1^{2+} , like **2** and **3**, undergoes facile photodisproportionation.¹ In the presence of CD_3CN as a trapping agent, this results (Scheme 1) in clean photolysis to give $[W^{VI}(\eta^5-C_5H_5)_2(O)(CH_3)]^+$ (4^+) and $[W^{IV}(\eta^5-C_5H_5)_2(CH_3)(NCCD_3)]^+$ (5^+-d^3), but in sharp contrast with the cases of **2** and **3**, this occurs under conditions where thermal

[®] Abstract published in *Advance ACS Abstracts*, January 15, 1995.
(1) Jernakoff, P.; Fox, J. R.; Hayes, J. C.; Lee, S.; Foxman, B. M.; Cooper, N. J. *Organometallics*, in press.

(2) Dunitz, J. D.; Orgel, L. E. *J. Chem. Soc.* **1953**, 2594.

(3) Holm, R. H. *Chem. Rev.* **1987**, *87*, 1401.

(4) Blake, A. B.; Cotton, F. A.; Wood, J. S. *J. Am. Chem. Soc.* **1964**, *86*, 3024.

(5) Thompson, R. L.; Lee, S.; Geib, S. J.; Cooper, N. J. *Inorg. Chem.* **1993**, *32*, 6067.

(6) (a) Ricard, L.; Estienne, J.; Karagiannidis, P.; Toledano, O.; Fischer, J.; Mitschler, A.; Weiss, R. *J. Coord. Chem.* **1974**, *3*, 227. (b) Garner, C. D.; Howlader, N. C.; Mabbs, F. E.; McPhail, A. T.; Onan, K. D. *J. Chem. Soc., Dalton Trans.* **1979**, 962.

(7) (a) Knox, J. R.; Prout, C. K. *Acta Crystallogr. B.* **1969**, *B25*, 2281. (b) Aliev, Z. G.; Atoumyan, L. O.; Tkachev, V. V. *Zh. Strukt. Khim.* **1975**, *16*, 694.

(8) Thompson, R. L.; Geib, S. J.; Cooper, N. J. *Inorg. Chem.* **1993**, *32*, 6076.

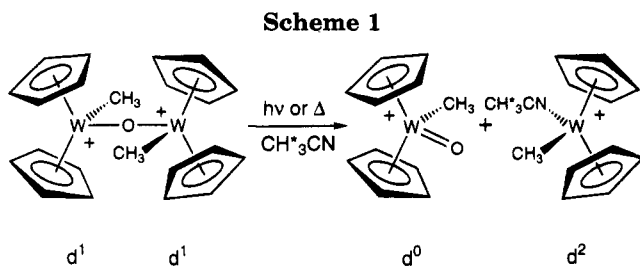
(9) Barral, R.; Bocard, C.; Séré de Roch, I.; Sajus, L. *Tetrahedron Lett.* **1972**, 1693.

(10) Chen, G. J. J.; McDonald, J. W.; Newton, W. E. *Inorg. Chem.* **1976**, *15*, 2612.

(11) (a) Matsuda, T.; Tanaka, K.; Tanaka, T. *Inorg. Chem.* **1979**, *18*, 454. (b) Tanaka, T.; Tanaka, K.; Matsuda, T.; Hashi, K. In *Molybdenum Chemistry of Biological Significance*; Newton, W. E., Otsuka, K., Eds.; Plenum Press: New York, 1980; p 361.

(12) Lee, S.; Staley, D. L.; Rheingold, A. L.; Cooper, N. J. *Inorg. Chem.* **1990**, *29*, 4391.

(13) (a) *Photochromism—Molecules and Systems*; Durr, H., Bouas-Laurent, H., Eds.; Elsevier: Amsterdam, 1990. (b) Emmelius, M.; Pawlowski, G.; Vollman, H. W. *Angew. Chem., Int. Ed. Engl.* **1989**, *28*, 1445.



disproportionation is slow. This meant that 1^{2+} provided the first case in which it was feasible to study independently the photochemical and thermal disproportionation of a d^1-d^1 dimer with a linear oxo bridge, and we now report quantum yields for the photodisproportionation of 1^{2+} in CH_3CN and kinetic parameters for the thermal disproportionation of 1^{2+} in CD_3CN .

Experimental Section

General Procedures. All manipulations were carried out under a dry, oxygen-free nitrogen atmosphere by means of drybox or standard Schlenk techniques. Acetonitrile was distilled from CaH_2 before use. Deuterated acetonitrile (CD_3CN , 99.5% D, Aldrich), and deuterated nitromethane (CD_3NO_2 , 99% D, 1% (v/v) TMS, Aldrich) were degassed by dry nitrogen purge before use. Ethylene glycol was used as received from Aldrich Chemical Co. Electronic spectra were recorded on an IBM 9430 UV-Vis spectrometer, fitted with thermostated cell holders, while the solution temperature within the cells was kept constant by means of a circulating bath of 50% aqueous ethylene glycol. ^1H NMR spectra were recorded on a Bruker AF 300 spectrometer at 300 MHz; spectra were recorded using the solvent signal as an internal standard. Photolyses were performed using an Oriel 200 W mercury-xenon arc lamp as a light source, and Oriel interference filters were used as monochromators.

The compounds $\{[\text{W}^{\text{VI}}(\eta^5\text{-C}_5\text{H}_5)_2(\text{CH}_3)_2(\mu\text{-O})][\text{PF}_6]_2$ ($1[\text{PF}_6]_2$), $[\text{W}^{\text{VI}}(\eta^5\text{-C}_5\text{H}_5)_2(\text{O})(\text{CH}_3)]\text{PF}_6$ (4PF_6), and $[\text{W}^{\text{IV}}(\eta^5\text{-C}_5\text{H}_5)_2(\text{CH}_3)_2(\text{NCCCH}_3)]\text{PF}_6$ (5PF_6) were all prepared as reported elsewhere.¹

Variable-Temperature ^1H NMR Studies. ^1H NMR spectra were recorded on a Bruker AF 300 spectrometer at 300 MHz. Temperatures within the NMR probe were controlled by a Bruker variable-temperature unit, which was calibrated against boiling and freezing distilled H_2O , and were monitored before and after each trial by monitoring the chemical shifts of ethylene glycol resonances.¹⁴ A typical trial involved the loading of a sample of $1[\text{PF}_6]_2$ (~5 mg, 0.005 mmol) and 0.5 mL of CD_3CN into an NMR tube in a darkened room. The tube was maintained at -78°C in the dark until the NMR probe had been brought to temperature. Just prior to loading into the probe, the sample tube was shaken several times to effect dissolution of $1[\text{PF}_6]_2$.

The rate of thermal disproportionation of 1^{2+} in CD_3CN was measured by quantitatively monitoring the disappearance of the cyclopentadienyl resonance of 1^{2+} via integration. To obtain quantitative information from the NMR spectra, the long proton translational relaxation time (T_1) of the cyclopentadienyl protons in 1^{2+} ($T_1 = 2.13$ s as measured by the inversion-recovery method and analyzed by Bruker AF300 software) required that a long pulse delay be employed to ensure full relaxation between pulses; for this reason, a pulse delay of $>5T_1$ was used. Five sequential summed free-induction decays were used to generate the spectrum for each point in the kinetic analysis; the time at which the third FID was accumulated was taken to be the time at which the observed spectrum had been recorded. This process allowed approximately 10–30 time points to be collected during the 1–5 h experiment duration at each temperature.

The first-order rate constants (k_1) for the thermal disproportionation of 1^{2+} in CD_3CN were obtained from the slopes of plots of $\ln([1^{2+}]_0/[1^{2+}]_t)$ vs time (t) at nine different temperatures. The $\ln([1^{2+}]_0/[1^{2+}]_t)$ vs t plots were all linear for at least 3 half-lives. The free energies of activation (ΔG^\ddagger) for the disproportionation at each temperature were then calculated from the k_1 values by means of the Eyring equation,^{15a} taking the transmission coefficient $\kappa = 1$ as is usual in dynamic NMR studies.^{15b} The activation enthalpies and entropies (ΔH^\ddagger and ΔS^\ddagger) were calculated from the intercept and slope of plots of ΔG^\ddagger vs temperature (T).

The reported errors in k_1 and temperature represent one standard deviation from the least-squares fit of the experimental data, whereas the uncertainties in ΔG^\ddagger were calculated according to the equation derived by Binsch.¹⁶ Uncertainties in ΔH^\ddagger and ΔS^\ddagger were estimated from extreme least-squares fits for ΔG^\ddagger vs T plots.

Quantum Yield Determinations. Quantum yields were determined in a manner similar to that reported by Wegner and Adamson for the measurement of the photoaquation of Reinecke's salt.¹⁷ An air-cooled 200 W Oriel mercury-xenon arc lamp was used as the light source, and the light was collimated to give a beam of ~ 1 cm² in area that was passed through a water filter, an iris, and appropriate interference filters (Oriel; 10 nm band width; 310 and 530 nm). The collimated, monochromatic light beam was passed through sample cells in a brass thermostated cell holder, the temperature of which was controlled to $\pm 0.2^\circ\text{C}$ using a circulating bath of 50% ethylene glycol- H_2O . The temperature within the cell holder was monitored by a Fluke K-type thermocouple. Absorbances of irradiated samples were measured by rapidly transferring the cells to an IBM 9430 spectrometer fitted with a second thermostated cell holder, which was connected to the same circulating bath as the irradiation cell holder through glass T-joints and insulated rubber tubing. The lamp output was determined immediately before each quantum yield measurement by means of an Aberchrome 540 chemical actinometer. This consisted of a toluene solution of the heterocyclic fulgide (*E*)- α -(2,5-dimethyl-3-furylethylidene)(isopropylidene)succinic anhydride¹⁸ of known concentration and volume sealed inside a 1 cm quartz cell under vacuum. Aberchrome 540 undergoes a highly reversible conrotatory ring-closure reaction to give deep red 7,7a-dihydro-2,4,7,7,7a-pentamethylbenzo[*b*]furan-5,6-dicarboxylic anhydride, and the known quantum yields for the forward and reverse reactions¹⁹ were used to measure intensities in the 310–370 nm and 436–545 nm ranges, respectively, from plots of the absorbance increase or decrease at 494 nm vs time and application of the relations $I = (V/\Phi_A \epsilon_A l)(\Delta A/t)$, where I is the flux in einstein s⁻¹, V is the solution volume (3.00×10^{-3} L), Φ_A is the forward (0.20) or reverse (0.0508 at 530 nm - Φ_A for the reverse reaction exhibits some wavelength dependence, while the Φ_A for the forward reaction does not^{19b}) quantum yield for Aberchrome 540 photolysis, ϵ_A is the extinction coefficient for Aberchrome 540 at 494 nm (8200 L mol⁻¹ cm⁻¹), l is the cell length (1.00 cm), and $\Delta A/t$ is the slope from the absorbance vs time plot (s⁻¹).

After the lamp intensity measurement, sample solutions of known volume were allowed to equilibrate thermally in the dark for at least 10 min and were then irradiated for periods such that the absorbance at 525 nm decayed no more than 10–15% from the absorbance at $t = t_0$. Concentrations of

(15) (a) Glasstone, S.; Laidler, K. J.; Eyring, H. *The Theory of Rate Processes*; McGraw Hill: New York, 1941; p 195. (b) Binsch, G. *Top. Stereochem.* **1968**, 3, 97.

(16) Binsch, G. In *Dynamic Nuclear Magnetic Resonance Spectroscopy*; Jackman, L. M., Cotton, F. A., Eds.; Academic Press: New York, 1975; Chapter 3, eq 111.

(17) Wegner, E. E.; Adamson, A. W. *J. Am. Chem. Soc.* **1966**, 88, 394.

(18) Davey, P. J.; Heller, H. G.; Strydom, P. J.; Whittall, J. *Chem. Soc., Perkin Trans. 2* **1981**, 202.

(19) (a) Heller, H. G.; Langan, J. R. *J. Chem. Soc., Perkin Trans 2* **1981**, 341. (b) Wintgens, V.; Johnston, L. J.; Scaiano, J. C. *J. Am. Chem. Soc.* **1988**, 110, 511.

Table 1. Summary of ^1H NMR Spectra for Complexes 1^{2+} , 4^+ , and 5^+ in CD_3CN

compound	chemical shift (δ)
$\{[\text{W}(\eta^5\text{-C}_5\text{H}_5)_2(\text{CH}_3)_2(\mu\text{-O})][\text{PF}_6]_2 (1[\text{PF}_6]_2)$	6.09 (s, 20 H, 4 C_5H_5), 0.88 (s, 6 H, 2 CH_3)
$[\text{W}(\eta^5\text{-C}_5\text{H}_5)_2(\text{O})(\text{CH}_3)]\text{PF}_6 (4\text{PF}_6)$	6.58 (s, 10 H, 2 C_5H_5), 1.28 (s, 3 H, CH_3)
$[\text{W}(\eta^5\text{-C}_5\text{H}_5)_2(\text{CH}_3)(\text{NCCD}_3)]\text{PF}_6 (5\text{PF}_6)$	5.16 (s, 10 H, 2 C_5H_5), 0.22 (s, 3 H, CH_3)

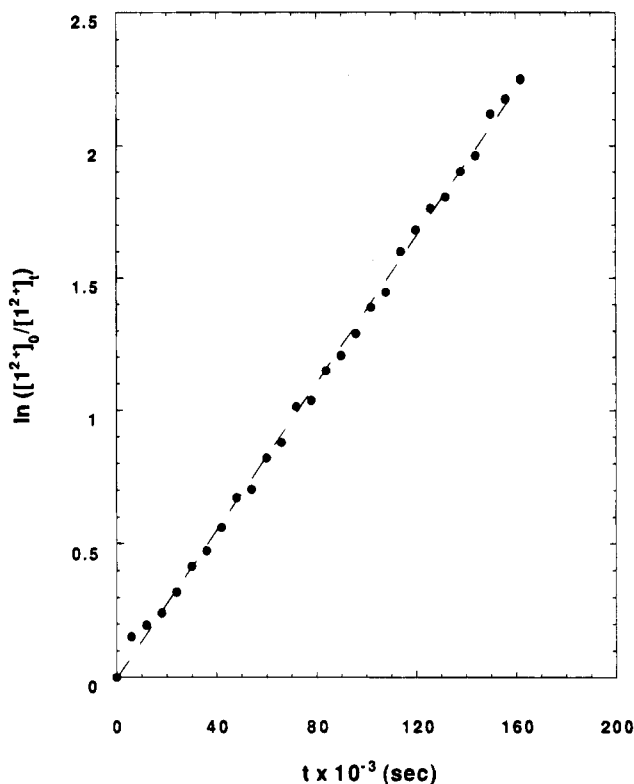
sample solutions were chosen such that the absorbance at the irradiation wavelength was >1.7 absorbance unit ($>98\%$ incident intensity absorption) and that the absorbance at the measuring wavelength (525 nm) was no larger than 2.2–2.3 absorbance units to ensure readability. Quantum yields Φ were determined from the slope of plots of ΔA at 525 nm vs t by means of a relationship analogous to that above. Each quantum yield reported at a particular wavelength is the average of three values obtained in independent runs.

Results and Discussion

Thermal Disproportionation of $1[\text{PF}_6]_2$. The ^1H NMR spectrum of 1^{2+} in CD_3CN is straightforward and contains a large singlet at δ 6.09 assigned to the cyclopentadienyl rings and a singlet at δ 0.88 (with 2.4 Hz ^{183}W satellites) assigned to the methyl group. The absence of other signals establishes that 1^{2+} is the only cyclopentadienyl-containing complex present in solution and that 1^{2+} is therefore kinetically or thermodynamically stable with respect to disproportionation in CD_3CN at room temperature. At higher temperatures, however, new cyclopentadienyl signals appear at δ 5.16 and 6.58 and new methyl signals appear at δ 0.22 and 1.28 in the ^1H NMR spectrum of a sample of 1^{2+} in CD_3CN . The new cyclopentadienyl signals are of equal intensity and are located on either side of the original cyclopentadienyl signal of 1^{2+} , and the new methyl signals are similarly of equal intensity and on either side of the original methyl signal. Comparison of the new signals with those of authentic samples¹ permitted unambiguous assignment to the disproportionation products 4^+ and 5^+ , produced as per Scheme 1 (NMR data are summarized in Table 1).

We have determined the kinetics of the thermal disproportionation reaction by ^1H NMR spectroscopy at temperatures from 54 to 72 °C using solutions that were $\sim 3 \text{ mmol L}^{-1}$ 1^{2+} in CD_3CN (see Experimental Section for details of sample preparation and spectrum acquisition). The reaction is remarkably clean, and the disappearance of 1^{2+} was followed by monitoring the change in the integration of the cyclopentadienyl signal of 1^{2+} relative to the solvent signal. It was assumed that the integration is directly proportional to the concentration of 1^{2+} ($[1^{2+}]$). Data were plotted by assuming first-order kinetics in $[1^{2+}]$ (as confirmed by the linearity of the plots to three half-lives) and a representative plot of $\ln([1^{2+}]_0/[1^{2+}]_t)$ vs time is shown in Figure 1. The slopes of these plots were used to obtain the first-order rate constants, k_1 and, hence, the free energies of activation, ΔG^\ddagger , as summarized in Table 2.

The free energy of activation varied linearly with temperature as expected from the relationship $\Delta G^\ddagger = \Delta H^\ddagger - T\Delta S^\ddagger$, and separation of ΔG^\ddagger into its enthalpic and entropic components allowed us to determine that there is a large enthalpic barrier to disproportionation of 1^{2+} ($\Delta H^\ddagger = 33.7 \pm 1.7 \text{ kcal mol}^{-1}$) but that formation of the transition state is entropically favored with a positive entropy of activation ($\Delta S^\ddagger = 25.1 \pm 5.2 \text{ cal K}^{-1}$

**Figure 1.** Representative first-order kinetics plot for the thermal disproportionation of $[\{\text{W}^{\text{V}}(\eta^5\text{-C}_5\text{H}_5)_2(\text{CH}_3)_2(\mu\text{-O})\}[\text{PF}_6]_2 (1[\text{PF}_6]_2)$ in CD_3CN at 331.5 K.**Table 2.** First-Order Rate Constants (k_1) and Free Energies of Activation (ΔG^\ddagger) for Disproportionation of $[\{\text{W}^{\text{V}}(\eta^5\text{-C}_5\text{H}_5)_2(\text{CH}_3)_2(\mu\text{-O})\}[\text{PF}_6]_2$ in CD_3CN at Various Temperatures (T)

T (K)	$k_1 \times 10^5$ (s^{-1})	ΔG^\ddagger (kcal mol^{-1})	T (K)	$k_1 \times 10^5$ (s^{-1})	ΔG^\ddagger (kcal mol^{-1})
327 ± 0.3	7.78 ± 0.35	25.4 ± 0.1	340 ± 0.3	43.1 ± 2.0	25.3 ± 0.1
330 ± 0.3	8.47 ± 0.40	25.6 ± 0.1	342 ± 0.3	68.9 ± 3.6	25.1 ± 0.1
332 ± 0.3	13.8 ± 6.2	25.4 ± 0.1	343 ± 0.3	79.3 ± 4.0	25.1 ± 0.1
337 ± 0.3	31.2 ± 1.5	25.3 ± 0.1	345 ± 0.3	112 ± 6	25.0 ± 0.1
338 ± 0.3	32.6 ± 1.6	25.3 ± 0.1			

mol^{-1}). This value is reasonable for a dissociative reaction, although the significance of the value is limited by the uncertainty in its determination and by the possibility that solvent molecules may be involved in the transition state (see below).²⁰

It is appropriate to compare the activation parameters obtained by us with the values reported by Tanaka et al. for the disproportionation of $[\text{Mo}^{\text{V}}_2\text{O}_3(\text{S}_2\text{EX}_n)_4] (\text{S}_2\text{-EX}_n = \text{S}_2\text{CNET}_2, \text{S}_2\text{P}(\text{OEt})_2, \text{S}_2\text{PPh}_2)$ in 1,2-dichloroethane on the basis of concentration-jump kinetics experiments.¹¹ The ΔG^\ddagger values for 1^{2+} are 7–8 kcal mol^{-1} larger than those for the molybdenum complexes, in reasonable agreement with the increased kinetic stability of 1^{2+} , but it is difficult to see why the

(20) The ambiguity with respect to the potential involvement of the CH_3CN solvent in the transition state led us to examine the possibility of using the Arrhenius activation energy E_a (as defined by $k_1 = Ae^{-E_a/RT}$) to quantify the dependence of k_1 on temperature. A plot of $\ln k_1$ vs $1/T$ confirmed the anticipated linear relationship ($R = 0.99$), and a value of $35.3 \text{ kcal mol}^{-1}$ for E_a was derived from the slope. This is, within the error limits, the same as the value of $34.4 \text{ kcal mol}^{-1}$ predicted for E_a at 340 K on the basis of the gas phase relation $\Delta E_a = \Delta H^\ddagger + RT$.²¹ This observation supports the validity of separating ΔG^\ddagger into enthalpic and entropic components, and we have chosen to retain this approach to presentation of the data.

(21) Sun, Y.-P.; Saltiel, J.; Park, N. S.; Hoburg, E. A.; Waldeck, D. H. *J. Phys. Chem.* **1991**, *95*, 10336.

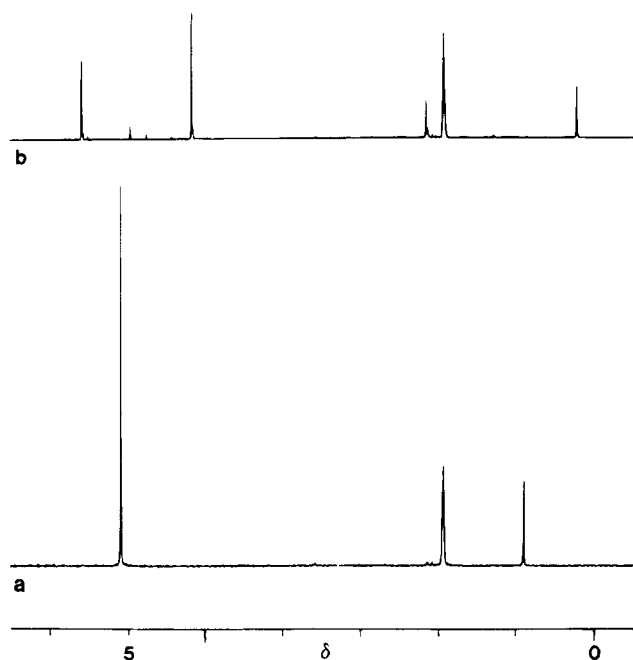


Figure 2. ^1H NMR spectrum of a solution of $[\{\text{W}^{\text{V}}(\eta^5\text{-C}_5\text{H}_5)_2(\text{CH}_3)_2(\mu\text{-O})\}][\text{PF}_6]_2$ ($1[\text{PF}_6]_2$) in CD_3CN : (a) before and (b) after photolysis.

molybdenum complexes should have negligible entropies of activation for dissociation as reported. If this is correct, it implies that ΔH^\ddagger values for the molybdenum systems are only half that which we have observed for 1^{2+} .

Photodisproportionation of $1[\text{PF}_6]_2$ in CH_3CN .

We have previously reported that solutions of $1[\text{PF}_6]_2$ in CD_3CN exhibit marked photosensitivity, decolorizing in bright sunlight to give a mixture of $[\text{W}^{\text{VI}}(\eta^5\text{-C}_5\text{H}_5)_2(\text{O})(\text{CH}_3)]^+$ (4^+) and the trapped W(IV) photodisproportionation product $[\text{W}^{\text{IV}}(\eta^5\text{-C}_5\text{H}_5)_2(\text{CH}_3)(\text{NCCD}_3)]^+$ (5^+ , d^3).¹ This reaction is remarkably clean (see Figure 2), and this, together with the anticipation on the basis of the thermal disproportionation studies that disproportionation is not kinetically accessible at room temperature ($t_{1/2} = 33$ d at 25°C), suggested that photolysis of 1^{2+} in acetonitrile would be suitable for quantum yield determinations. A Beer's law plot of the visible maximum in the electronic spectrum of 1^{2+} in CH_3CN at 28°C was linear ($R^2 = 1.00$) from concentrations of 2.49×10^{-5} to 8.30×10^{-5} mol L^{-1} and allowed determination of the extinction coefficient at 525 nm as $23\,600$ $\text{L mol}^{-1} \text{cm}^{-1}$.

The strong visible absorption of 1^{2+} at 525 nm (see Figure 3 and Table 3) offered an obvious approach to monitoring the photolysis by use of the decrease in absorbance at this wavelength, and inspection of the electronic spectra of the photolysis products 4^+ and 5^+ (Figure 4 and Table 3) established that this would be straightforward experimentally since neither of the products has electronic absorptions in this region. Monitoring at 525 nm allowed determination of the quantum yields for photodisproportionation of 1^{2+} in CH_3CN following irradiation at 310 and 530 nm as described in the Experimental Section and reported in Table 4.

The quantum yields for photodisproportionation of 1^{2+} are moderate in both the UV and visible regions of the spectrum but show marked wavelength dependence

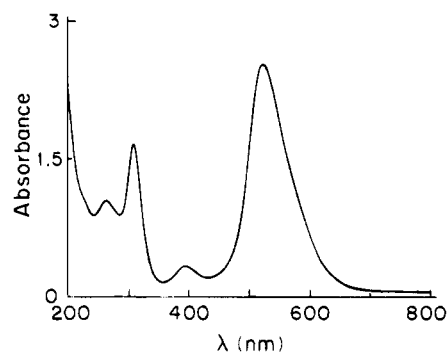


Figure 3. Electronic spectrum of a 1.10×10^{-4} mol L^{-1} solution of $[\{\text{W}^{\text{V}}(\eta^5\text{-C}_5\text{H}_5)_2(\text{CH}_3)_2(\mu\text{-O})\}][\text{PF}_6]_2$ ($1[\text{PF}_6]_2$) in CH_3CN .

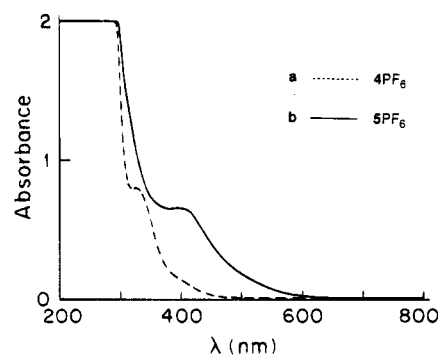


Figure 4. Electronic spectra in CH_3CN of (a) a 1.53×10^{-3} mol L^{-1} solution of $[\text{W}^{\text{VI}}(\eta^5\text{-C}_5\text{H}_5)_2(\text{O})(\text{CH}_3)]\text{PF}_6$ (4PF_6) and (b) a 1.66×10^{-3} mol L^{-1} solution of $[\text{W}^{\text{IV}}(\eta^5\text{-C}_5\text{H}_5)_2(\text{CH}_3)(\text{NCCCH}_3)]\text{PF}_6$ (5PF_6).

Table 3. Electronic Absorption Bands of Complexes 1^{2+} , 4^+ , and 5^+ in CH_3CN

compound	absorp max, $\text{cm}^{-1} \times 10^{-3}$ (ϵ , $\text{L mol}^{-1} \text{cm}^{-1}$)
$[\{\text{W}^{\text{V}}(\eta^5\text{-C}_5\text{H}_5)_2(\text{CH}_3)_2(\mu\text{-O})\}][\text{PF}_6]_2$ ($1[\text{PF}_6]_2$)	19.0 (23 600), 25.4 (3120), 32.3 (15 700), 37.9 (9810)
$[\text{W}^{\text{VI}}(\eta^5\text{-C}_5\text{H}_5)_2(\text{O})(\text{CH}_3)]\text{PF}_6$ (4PF_6)	30.3 (520)
$[\text{W}^{\text{IV}}(\eta^5\text{-C}_5\text{H}_5)_2(\text{CH}_3)(\text{NCCCH}_3)]\text{PF}_6$ (5PF_6)	25.0 (400)

Table 4. Disappearance Quantum Yields for the 525 nm Band of $[\{\text{W}^{\text{V}}(\eta^5\text{-C}_5\text{H}_5)_2(\text{CH}_3)_2(\mu\text{-O})\}][\text{PF}_6]_2$ in CH_3CN at 28.0°C

λ (nm)	conc $\times 10^5$ (mol L^{-1})	intensity $\times 10^9$ (einstein s^{-1})	$\Delta A/t \times 10^4$ (s^{-1})	quantum yield, Φ
310	8.31	1.69	10.4	0.078
		1.61	10.6	0.084
		1.61	10.8	0.085
		8.03	52.6	0.083
		8.45	54.7	0.082
		8.45	54.1	0.081
			av	0.082
530	10.4	1.39	1.57	0.014
			1.60	0.015
			1.52	0.014
			av	0.014

($\Phi_{310}:\Phi_{530} = 6$). Irradiation at two different intensities (Table 4) established that the quantum yield at 310 nm does not depend significantly on the intensity. The observation of photochemistry upon irradiation of the main visible absorption suggests that its energy is above the threshold for disproportionation, but we have no evidence that the excited state associated with this band is responsible for photodisproportionation. The dissociative state may be formed by thermal population or

internal conversion from this initial state and may be more efficiently formed from higher lying excited states such as that associated with the 310 nm band.²² The uncertainty in interpretation of the mechanism of the photodisproportionation is reinforced by our observation that, although an intense visible absorption at ~500 nm is an almost universal characteristic of d¹-d¹ linear oxo-bridged dimers,²³ this absorption is photoactive with respect to disproportionation in some systems (such as 1²⁺ and the dithiocarbamate complexes **2** and **3**) but is photoinactive in other systems (such as the dithiophosphate complexes [Mo₂^VO₃{S₂P(OR)₂]₄ (R = Et, Ph, Me)).⁸

Acetonitrile is an effective trapping reagent in this system, but it was unclear whether CH₃CN plays a significant role in driving the photodisproportionation reaction. This is a particularly important point to address in light of Tyler's elegant demonstration that photodisproportionation of [Mo(η⁵-C₅H₅)(CO)₃]₂ and related dimers involves initial homolysis followed by coordination of a donor ligand to form a 19-electron species from which the electron transfer step occurs.²⁴

The range of potential alternative solvents was limited by the need for a highly polar solvent to dissolve dicationic 1²⁺, but we were able to probe the importance of the solvent by photolyzing 1[PF₆]₂ in the less coordinating solvent CH₃NO₂. This clearly established that the presence of CH₃CN was not necessary to photodisproportionate 1²⁺, since solutions of 1²⁺ in CH₃NO₂ did change from purple to yellow in color following photolysis. Monitoring of this reaction by ¹H NMR in CD₃NO₂ revealed, however, that the reaction had generated the pure W(VI) complex 4⁺; no signals could be observed from a W(IV) solvato complex such as [W(η⁵-C₅H₅)₂(CD₃-NO₂)CH₃]⁺. This suggests that photodisproportionation is occurring but that the W(IV) fragment formed is sufficiently reactive to abstract an oxygen atom from CD₃NO₂. We have, therefore, been unable to eliminate the possibility that the solvent plays an important role

in the photolysis reaction, although we have also established that the presence of a nitrile trapping reagent is not required.

Although these experiments leave the exact mechanism of the photodisproportionation step undetermined, the reaction does require a metal to metal charge transfer at some stage, and it is tempting to speculate that the excited state that leads to dissociation is intrinsically ionic in character. In particular, the ¹(ππ*) states of these species should be susceptible to the sudden polarization effect.²⁵ Experiments to probe these and related questions are underway in this laboratory.

Conclusions

The diamagnetic d¹-d¹ oxo-bridged [W(η⁵-C₅H₅)₂(CH₃)₂(μ-O)]²⁺ (1²⁺) undergoes first-order thermal disproportionation at moderately elevated temperatures in CD₃CN to give the d⁰ oxo complex [W(η⁵-C₅H₅)₂(O)(CH₃)]⁺ (4⁺) and the d³ acetonitrile-trapped d² complex [W(η⁵-C₅H₅)₂(CH₃)(NCCD₃)]⁺ (5⁺-d³). The large enthalpy of activation and favorable entropy of activation are consistent with a dissociative transition state in which an enthalpically expensive charge transfer is well advanced. The resulting half-life of 33 d at 25 °C is sufficient to allow independent study of the analogous photodisproportionation of 1²⁺. This gives an equimolar mixture of 4⁺ and 5⁺, and the modest quantum yield for irradiation in the visible region (Φ₅₃₀ = 0.014) suggests that the lowest photoexcited state does not lead directly to disproportionation but that this occurs from a derived excited state that can be more efficiently accessed by UV irradiation (Φ₃₁₀ = 0.082).

Acknowledgment. This work was supported in part by the Office of Naval Research. We thank Dr. Cecilia Philbin and Professor David Waldeck for helpful conversations and Professor Greg Geoffroy for the gift of a sample of Aberchrome 540.

OM9408674

(22) (a) Adamson, A. W.; Fleischauer, P. D. *Concepts in Inorganic Photochemistry*; Krieger: Malabar, FL, 1984. (b) Ferraudi, G. J. *Elements of Inorganic Photochemistry*; Wiley: New York, 1988.

(23) Craig, J. A.; Harlan, E. W.; Snyder, B. S.; Whitener, M. A.; Holm, R. H. *Inorg. Chem.* **1989**, *28*, 2082.

(24) Tyler, D. R. *Acc. Chem. Res.* **1991**, *24*, 325.

(25) (a) Dauben, W. G.; Ritscher, J. S. *J. Am. Chem. Soc.* **1970**, *92*, 2925. (b) Wulfman, C. E.; Kumei, S. E. *Science* **1971**, *172*, 1061. (c) Salem, L. *Acc. Chem. Res.* **1979**, *12*, 87. (d) Michl, J.; Bonacic-Koutecky, V. *Electronic Aspects of Organic Photochemistry*; Wiley: New York, 1990.

Two-Electron and One-Electron Reduction of the Indenyl Complex $[\text{Mn}(\eta^5\text{-C}_9\text{H}_7)(\text{CO})_3]$ and Reversible Counterion-Controlled Comproportionation of $[\text{Mn}(\eta^5\text{-C}_9\text{H}_7)(\text{CO})_3]$ and $[\text{Mn}(\eta^3\text{-C}_9\text{H}_7)(\text{CO})_3]^{2-}$ To Give $[\text{Mn}(\eta^5\text{-C}_9\text{H}_7)(\text{CO})_3]^-$

Sijoon Lee, Sherri R. Lovelace, and N. John Cooper*

Department of Chemistry, University of Pittsburgh, Pittsburgh, Pennsylvania 15260

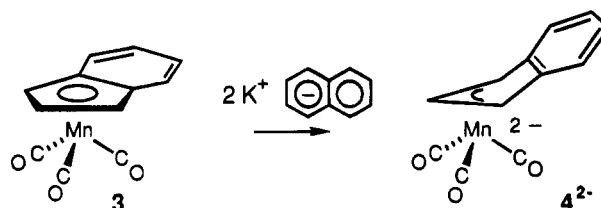
Received December 28, 1994[®]

Two-electron reduction of $[\text{Mn}(\eta^5\text{-C}_9\text{H}_7)(\text{CO})_3]$ (**3**) gives a dianion formulated as the ring-slipped indenyl complex $[\text{Mn}(\eta^3\text{-C}_9\text{H}_7)(\text{CO})_3]^{2-}$ (**4²⁻**), and protonation of the activated indenyl ligand in **4²⁻** in the presence of naphthalene yields the η^4 -naphthalene complex $[\text{Mn}(\eta^4\text{-C}_{10}\text{H}_8)(\text{CO})_3]^-$ (**6⁻**). One-electron reduction of **3** leads to a mixture of **3**, **4²⁻**, and the monoanionic species $[\text{Mn}(\eta^5\text{-C}_9\text{H}_7)(\text{CO})_3]^-$ (**5⁻**). Subsequent addition of 18-crown-6 (18-C-6) gives a solution of **5⁻** alone (IR), and we propose that 18-C-6 complexation of K^+ perturbs solution ion pairing, which would be expected to stabilize **4²⁻**, sufficiently to induce **3** and **4²⁻** to comproportionate to **5⁻**. This equilibrium can be shifted back toward **3** and **4²⁻** by addition of 10 equiv of NaPF_6 to induce disproportionation of **5⁻**. The formulation of **5⁻** as $[\text{Mn}(\eta^5\text{-C}_9\text{H}_7)(\text{CO})_3]^-$ is supported by EPR spectra (a symmetrical sextet, $\langle g \rangle = 1.986$, $\langle a \rangle(^{55}\text{Mn}) = 31$ G) and susceptibility measurements. The importance of disproportionation of **5⁻** in its chemistry is demonstrated by the reaction of $[\text{K}(18\text{-C-6})]\mathbf{5}$ with Bu_3SnH to give $[\text{K}(18\text{-C-6})][\text{Mn}(\eta^5\text{-C}_9\text{H}_7)(\text{CO})_2(\text{SnBu}_3)]$ ($[\text{K}(18\text{-C-6})]\mathbf{7}$) in 34% yield together with **3** (41%). Equimolar formation of **7⁻** and **3** suggests that **5⁻** disproportionates in this reaction to **3** and **4²⁻** and that **4²⁻** then reacts with Bu_3SnH to form **7⁻**. Independent experiments establish that Bu_3SnH reacts with **4²⁻** to give **7⁻** (60% by IR). Treatment of **3** with excess $[\text{K}(18\text{-C-6})][\text{SnBu}_3]$ gives $[\text{K}(18\text{-C-6})]\mathbf{7}$ in 35% yield, establishing that **7⁻** could be formed from **4²⁻** via **3**. Treatment of **5⁻** with O_2 , CO_2 , the trityl dimer, or H_2O_2 gives **3** quantitatively. Cyclic voltammograms of **3** in THF exhibit two successive one-electron reductions (as confirmed by chronocoulometry) at $(E_a + E_c)/2 = -1.95$ and -2.20 V vs SCE. The small difference between these potentials suggests marked stabilization of the final reduction product **4²⁻** by an $\eta^5 \rightarrow \eta^3$ hapticity shift concomitant with the second reduction and also supports η^5 -indenyl ligation in the first reduction product **5⁻**.

Introduction

We recently reported that $[\text{Mn}(\eta^5\text{-C}_5\text{H}_4\text{Me})(\text{CO})_3]$ (cymantrene, **1**) undergoes a two-electron alkali reduction to give a highly reduced complex formulated as $[\text{Mn}(\eta^3\text{-C}_5\text{H}_4\text{CH}_3)(\text{CO})_3]^{2-}$ (**2²⁻**).¹ The unusual nature of the proposed reductively induced $\eta^5 \rightarrow \eta^3$ hapticity shift of the cyclopentadienyl ligand² in **1** has led us to search for complementary systems in which the two-electron reduction product might be isolable and, hence, to an examination of the reduction of the indenyl complex $[\text{Mn}(\eta^5\text{-C}_9\text{H}_7)(\text{CO})_3]$ (**3**). We anticipated that, as a consequence of the well-established propensity of indenyl ligands to adopt η^3 conformations more readily than their cyclopentadienyl analogs,³ the two-electron reduction product $[\text{Mn}(\eta^3\text{-C}_9\text{H}_7)(\text{CO})_3]^{2-}$ (**4²⁻**) might be isolable (Scheme 1), as is the isoelectronic complex $[\text{Fe}(\eta^3\text{-C}_9\text{H}_7)(\text{CO})_3]^-$ structurally characterized by Cutler and co-workers.⁴ We now report that the dianion **4²⁻** is only accessible as a reactive intermediate but that the 19-electron monoanion $[\text{Mn}(\eta^5\text{-C}_9\text{H}_7)(\text{CO})_3]^-$ (**5⁻**) is surprisingly stable; we also show that the disproportionation equilibrium between **5⁻**, **3**, and **4²⁻** is directly observable. Most interestingly, however, the disproportionation equilibrium between **5⁻**, **3**, and **4²⁻** can be controlled through counterion ion-pairing effects.

Scheme 1



tionation equilibrium between **5⁻**, **3**, and **4²⁻** is directly observable. Most interestingly, however, the disproportionation equilibrium between **5⁻**, **3**, and **4²⁻** can be controlled through counterion ion-pairing effects.

Experimental Section

General Data. All reactions and manipulations were carried out under an atmosphere of dry, oxygen-free nitrogen using standard Schlenk techniques or a Vacuum Atmospheres drybox unless otherwise stated. Glassware was soaked in KOH-saturated 2-propanol for ca. 12 h and washed with distilled water and acetone before use. Glass reaction vessels were oven-dried and flamed under vacuum before use.

Solvents and Reagents. All solvents were freshly distilled and deoxygenated before use. Tetrahydrofuran (THF) and diethyl ether (Et_2O) were predried over sodium ribbon and

[®] Abstract published in *Advance ACS Abstracts*, February 15, 1995.

(1) Lee, S.; Cooper, N. J. *J. Am. Chem. Soc.* **1991**, *113*, 716.

(2) O'Connor, J. M.; Casey, C. P. *Chem. Rev.* **1987**, *87*, 307.

freshly distilled from potassium/benzophenone ketyl. *n*-Pentane was stirred over concentrated H₂SO₄ for more than 24 h, neutralized with K₂CO₃, and distilled under nitrogen from CaH₂. Bis(triphenylphosphoranylidene)ammonium chloride ([PPN]Cl) was dried in an Abderhalden drying pistol with P₄O₁₀ at 140 °C. 18-Crown-6 (18-C-6) and NaPF₆ were recrystallized from acetonitrile and dried under vacuum. Matheson "bone dry" CO₂ was used as supplied without further purification. Matheson "extra dry" O₂ was used after passage through a CaSO₄-packed column. Tri-*n*-butylstannyl hydride (Bu₃SnH) was purchased from Aldrich Chemicals. Trityl dimer (Ph₃C-C₆H₄=CPh₂) was prepared as described in the literature⁵ using "molecular" silver reductant prepared as described by Brauer.⁶ [K(18-C-6)][SnBu₃] was synthesized by the stoichiometric reaction of KH with Bu₃SnH⁷ followed by addition of 1.0 equiv of 18-C-6 in THF at room temperature. The mixture was washed with *n*-pentane and Et₂O and then dried under vacuum. [Mn(η⁵-C₉H₇)(CO)₃] (3) was prepared by the method of Efraty and King.⁸ Potassium naphthalenide (K(Nap)) was prepared by dissolution of freshly cut potassium metal in a solution of naphthalene (1.2 equiv) in THF. The mixture was then stirred overnight under an N₂ atmosphere at room temperature. Potassium naphthalenide solutions were stored under N₂ in glass-capped Schlenk vessels at -80 °C. Sodium naphthalenide (Na(Nap)) was obtained by a similar procedure. Tetrabutylammonium perchlorate (TBAP) was recrystallized from ethanol and dried for 24 h under vacuum over phosphorus pentoxide.

Physical Measurements. Infrared spectra were recorded on a Perkin-Elmer Model 783 spectrophotometer. Solution spectra were recorded with samples in Teflon-sealed solution cells fitted with Suba Seals and thoroughly purged with nitrogen before use. Polystyrene was used as an external standard (1601 cm⁻¹ peak). ¹H NMR spectra were recorded on a Bruker AF300 spectrometer at 300 MHz or a Bruker AF500 spectrometer at 500 MHz. ¹³C{¹H} and ¹³C ¹H-gated decoupled spectra were recorded on a Bruker AF300 spectrometer at 74.5 MHz or a Bruker AF500 spectrometer at 125 MHz. EPR spectra were recorded on a Varian E-4 spectrometer in a quartz tube which had been sealed by means of a graded quartz/Pyrex seal. Elemental analyses were performed by Dornis und Kolbe Mikroanalytisches Laboratorium in Mülheim am Ruhr, Germany. Solution magnetic susceptibili-

ties were determined by the Evans method^{9,10}—in a typical experiment the paramagnetic sample was dissolved in THF-d₃ at -78 °C and a portion of this solution was transferred through a cannula into an NMR tube. A 30 μL portion of protio THF was added, and a sealed capillary tube containing 40 μL of protio THF was added to the NMR tube. The mass susceptibility, χ_g, of the complex was determined by means of an expression appropriate for a longitudinal magnet/sample geometry:

$$\chi_g = \frac{3\Delta f}{4\pi f m} + \chi_0$$

where Δ*f* is the frequency separation between the shifted and unshifted THF signals, *f* is the spectrometer frequency, *m* is the mass of the complex in 1 mL of solution, and χ₀ is the mass susceptibility of the solvent. The molar susceptibility, χ_M, was then calculated, and a correction for the diamagnetic contribution of the complex was applied.¹¹ The effective magnetic moment, μ_{eff}, was determined from the relation μ_{eff} = 2.84(χ_M^{corr}T)^{1/2}.

Electrochemistry. Cyclic voltammetry was performed in THF at room temperature under argon with a Bioanalytical Systems BAS 100 electrochemical analyzer. The solutions contained 0.1 M TBAP as the supporting electrolyte. Voltammograms were recorded at 1.0 × 10⁻³ M L⁻¹ for both the substrate and the internal standard. A three-electrode cell was used with a silver/silver chloride (Ag/AgCl) reference electrode, a glassy-carbon working electrode, and a platinum-wire auxiliary electrode. Ferrocene served as the internal standard, and potentials are reported versus the saturated calomel electrode (SCE) using a value of 500 mV for the ferrocene/ferrocenium reduction potential. Experimentally, the ferrocene/ferrocenium reduction potential was constant to ±5 mV under these conditions and exhibited *i_a/i_c* = 1.0 at 100 mV s⁻¹. The presence of a standard did not affect the electrochemical behavior of [Mn(η⁵-C₉H₇)(CO)₃]. Under the same experimental conditions the reduction potential of an external ferrocene/ferrocenium solution was 480 mV at 100 mV s⁻¹ with a peak separation of 80 mV. Over a range of scan rates from 25 to 1000 mV s⁻¹ the peak separation increased from 60 to 100 mV, presumably as a consequence of uncompensated resistance.

Protonation of K₂[Mn(η³-C₉H₇)(CO)₃] and Isolation of [PPN][Mn(η⁴-C₁₀H₈)(CO)₃] ([PPN]6). A solution of 0.3 g (1.18 mmol) of [Mn(η⁵-C₉H₇)(CO)₃] in THF (20 mL) was cooled to -78 °C. Dropwise addition of 6.2 mL of 0.4 M K(Nap) (2.1 equiv) resulted in color changes from yellow to orange-red and then through greenish blue just before the dark green of K(Nap) persisted. After 10 min at -78 °C 1.0 equiv of H₂O was added to the mixture. The solution was stirred for 30 min at -78 °C and was then warmed to room temperature and stirred for a further 1 h. A slurry of 1.0 equiv of [PPN]Cl in 15 mL of THF was cannulated into this solution. After 1 h the mixture was filtered through Celite 545 and the solvent was removed to give a red oil. Addition of Et₂O (100 mL) gave a sticky solid together with a dark red solution, which was removed by decantation. The residue was redissolved in THF and concentrated to a volume of about 5 mL. Crystals were obtained by slow diffusive mixing of the THF solution with a layer of 80 mL of Et₂O to give red-orange crystals of [PPN]-[Mn(η⁴-C₁₀H₈)(CO)₃] (0.48 g, 0.60 mmol, 51%), which were washed with Et₂O and dried under vacuum.

(3) (a) Baker, R. T.; Tulip, T. H. *Organometallics* **1986**, *5*, 839. (b) Habib, A.; Tauke, R.; Holt, E. M.; Crabtree, R. H. *Organometallics* **1989**, *8*, 1225. (c) Turaki, N. N.; Huggins, J. M.; Lebiada, L. *Inorg. Chem.* **1988**, *27*, 424. (d) Kakkar, A. K.; Taylor, N. J.; Marder, T. B. *Organometallics* **1989**, *8*, 1765. (e) Carl, R. T.; Hughes, R. P.; Rheingold, A. L.; Marder, T. B.; Taylor, N. J. *Organometallics* **1988**, *7*, 1613. (f) Kakkar, A. K.; Taylor, N. J.; Calabrese, J. C.; Nugent, W. A.; Roe, D. C.; Conaway, E. A.; Marder, T. B. *J. Chem. Soc., Chem. Commun.* **1989**, 990. (g) Westcott, S. A.; Kakkar, A. K.; Stringer, G.; Taylor, N. J.; Marder, T. B. *J. Organomet. Chem.* **1990**, *394*, 777. (h) Pannell, K. H.; Lin, S.-H.; Kapoor, R. N.; Cervantes-Lee, F.; Pinon, M.; Parkanyi, L. *Organometallics* **1990**, *9*, 2454. (i) Ma, L.; Szajek, L. P.; Shapley, J. R. *Organometallics* **1991**, *10*, 1662. (j) Szajek, L. P.; Lawson, R. J.; Shapley, J. R. *Organometallics* **1991**, *10*, 357. (k) Ahmed, H.; Brown, D. A.; Fitzpatrick, N. J.; Glass, W. K. *J. Organomet. Chem.* **1991**, *418*, C14. (l) Foo, T.; Bergman, R. G. *Organometallics* **1992**, *11*, 1801. (m) Foo, T.; Bergman, R. G. *Organometallics* **1992**, *11*, 1811. (n) Bartsch, R.; Hitchcock, P. B.; Nixon, J. F. *J. Chem. Soc., Chem. Commun.* **1990**, 472. (o) Kakkar, A. K.; Jones, S. F.; Taylor, N. J.; Collins, S.; Marder, T. B. *J. Chem. Soc., Chem. Commun.* **1989**, 1454. (p) Kowaleski, R. M.; Rheingold, A. L.; Troglor, W. C.; Basolo, F. *J. Am. Chem. Soc.* **1986**, *108*, 2460. (q) For most references prior to 1988 see ref 2.

(4) Forschner, T. C.; Cutler, A. R.; Kullnig, R. K. *Organometallics* **1987**, *6*, 889.

(5) (a) Copenhauer, J. W.; Roy, M. F.; Marvel, C. S. *J. Am. Chem. Soc.* **1935**, *57*, 1311. (b) McBride, J. M. *Tetrahedron* **1974**, *30*, 2009 and references therein.

(6) Brauer, G. *Handbook of Preparative Inorganic Chemistry*, 2nd ed.; Academic: New York, 1965; Vol. II, p 1623.

(7) Corrin, R.; Guerin, C.; Kolani, B. In *Inorganic Syntheses*; Allcock, H. R., Ed.; Wiley: New York, 1989; Vol. 25, p 110.

(8) King, R. B.; Efraty, A. *J. Organomet. Chem.* **1970**, *23*, 527.

(9) Evans, D. F. *J. Chem. Soc.* **1959**, 2003.

(10) (a) Becker, E. D. *High Resolution NMR: Theory and Chemical Applications*; Academic: New York, 1980. (b) Bartle, K. D.; Jones, D. W.; Maricic, S. *Croat. Chem. Acta* **1968**, *40*, 227. (c) Line, D. H.; Chan, S. I. *Anal. Chem.* **1970**, *42*, 791.

(11) Mulay, L. N. *Magnetic Susceptibility*; Wiley: New York, 1963; Chapter IID.

Protonation of $K_2[Mn(\eta^5-C_9H_7)(CO)_3]$ and Isolation of $[K(18-C-6)][Mn(\eta^4-C_{10}H_8)(CO)_3]$ (6**).** A solution of $[Mn(\eta^5-C_9H_7)(CO)_3]$ (0.30 g, 1.18 mmol) in THF (20 mL) was reduced with 2.1 equiv of $K(Nap)$ (6.2 mL of a 0.4 M solution) in a manner similar to that described above. After addition of H_2O (1 equiv) at $-78^\circ C$ the solution was stirred for 30 min at $-78^\circ C$, warmed to room temperature, and stirred for a further 1 hour. A solution of 18-C-6 (0.31 g, 1.18 mmol) in THF (15 mL) was then added and $[K(18-C-6)][Mn(\eta^4-C_{10}H_8)(CO)_3]$ (0.47 g, 0.82 mmol, 70%) isolated by a procedure similar to that used to isolate $[PPN][Mn(\eta^4-C_{10}H_8)(CO)_3]$.

Preparation of $[K(18-C-6)][Mn(\eta^5-C_9H_7)(CO)_3]$ (5**).** Dropwise addition of 2.2 mL of 0.2 M $K(Nap)$ (1.1 equiv) to a cold ($-78^\circ C$) stirred solution of 0.1 g (0.39 mmol) of $[Mn(\eta^5-C_9H_7)(CO)_3]$ in 20 mL of THF resulted in a color change from yellow to greenish blue. Addition of 1.0 equiv of 18-C-6 to this mixture at $-78^\circ C$ gave a deep blue solution. The solution was warmed to room temperature and stirred for 10 min before it was concentrated to a volume of 20 mL and mixed with 10 mL of *n*-pentane. The mixture was cooled to $-78^\circ C$ to give deep blue needles of a crystalline product. This product was washed with 5×10 mL of cold ($-78^\circ C$) *n*-pentane and vacuum-dried at $-78^\circ C$ to give 0.21 g (95% yield) of crystalline but thermally unstable $[K(18-C-6)][Mn(\eta^5-C_9H_7)(CO)_3]$. $\mu_{eff}(THF) = 1.72 \pm 0.03$. The material used in reactivity studies was stored at $-80^\circ C$ under N_2 and was indefinitely stable under these conditions.

Reaction of $[K(18-C-6)][Mn(\eta^5-C_9H_7)(CO)_3]$ with Bu_3SnH and Isolation of $[Mn(\eta^5-C_9H_7)(CO)_3]$ and of $[K(18-C-6)][Mn(\eta^5-C_9H_7)(CO)_2(SnBu_3)]$ (7**).** Addition of 0.24 mL (2.5 equiv) of Bu_3SnH to a solution of 0.20 g (0.36 mmol) of $[K(18-C-6)][Mn(\eta^5-C_9H_7)(CO)_3]$ in THF (10 mL) at room temperature resulted in a slow color change to red-brown. The mixture was stirred for 12 h until there was no further color change. The solvent was removed under vacuum, and the mixture was extracted into Et_2O (3×20 mL). The solvent was removed under vacuum. The solid was washed with 3×20 mL of *n*-pentane, and 0.037 g (0.15 mmol, 41% yield) of spectroscopically pure $[Mn(\eta^5-C_9H_7)(CO)_3]$ (IR, 1H NMR) was isolated from this *n*-pentane solution. The pentane-insoluble material was redissolved in Et_2O , and the solution was filtered. Red-orange crystals of $[K(18-C-6)][Mn(\eta^5-C_9H_7)(CO)_2(SnBu_3)]$ were obtained by crystallization from a 1:2 mixture of Et_2O and *n*-pentane at $-10^\circ C$ (0.1 g, 0.12 mmol, 34% yield based on $[K(18-C-6)][Mn(\eta^5-C_9H_7)(CO)_3]$). IR ($\nu_{C=O}$ only, THF): 1863 (s), 1798 (s) cm^{-1} . 1H NMR (500 MHz, CD_3CN): δ 0.62 (t, 6H, $J = 8.1$ Hz, $SnCH_2-$), 0.87 (t, 9H, $J = 7.3$ Hz, $-CH_3$), 1.28 (sextet, 6H, $J = 7.3$ Hz, $-CH_2CH_3$), 1.46 (pent, 6H, $J = 7.5$ Hz, $-CH_2CH_2CH_2-$), 4.50 (d, 2H, $J = 2.5$ Hz, $H_{2,2'}$), 4.72 (t, 1H, $J = 2.5$ Hz, H_1), 6.72 (m, 2H, $H_{3,3'}$), 7.35 (m, 2H, $H_{4,4'}$). ^{13}C NMR (125 MHz, CD_3CN): δ 13.5 (t, 3C, $J = 123$ Hz, $SnCH_2-$), 14.3 (q, 3C, $J = 124$ Hz, $-CH_3$), 28.9 (t, 3C, $J = 123$ Hz, $SnCH_2CH_2-$), 31.7 (t, 3C, $J = 123$ Hz, $-CH_2CH_2CH_3$), 68.4 (d, 2C, $J = 175$ Hz, $C_{2,2'}$), 84.8 (d, 1C, $J = 163$ Hz, C_1), 101.6 (s, 2C, $C_{5,5'}$), 121.2 (d of d, 2C, $J = 158$ Hz, 7.7 Hz, $C_{4,4'}$), 127.0 (d, 2C, $J = 157$ Hz, $C_{3,3'}$), 237.5 (s, CO). Anal. Calcd for $C_{35}H_{58}O_8KMnSn$: C, 51.29; H, 7.13. Found: C, 50.98; H, 7.30.

Reaction of $[Mn(\eta^5-C_9H_7)(CO)_3]$ with $[K(18-C-6)][SnBu_3]$. Addition of a 10-fold excess of $[K(18-C-6)][SnBu_3]$ in THF to a solution of 0.15 g (0.59 mmol) of $[Mn(\eta^5-C_9H_7)(CO)_3]$ in THF (20 mL) at room temperature resulted in an immediate color change to orange. The solution was stirred for 12 h, and the solvent was then removed under vacuum. The residue was washed with 3×20 mL of *n*-pentane, and the mixture was extracted into 3×20 mL of Et_2O . Spectroscopically pure $[K(18-C-6)][Mn(\eta^5-C_9H_7)(CO)_2(SnBu_3)]$ was obtained (IR, 1H NMR) by triple recrystallization as red-orange crystals (0.17 g, 0.21 mmol; 35% yield) from a 1:2 mixture of Et_2O and *n*-pentane at $-10^\circ C$.

Reaction of $[K(18-C-6)][Mn(\eta^5-C_9H_7)(CO)_3]$ with CO_2 . Addition of excess CO_2 to a solution of 0.3 g (0.54 mmol) of $[K(18-C-6)][Mn(\eta^5-C_9H_7)(CO)_3]$ in THF (10 mL) at room tem-

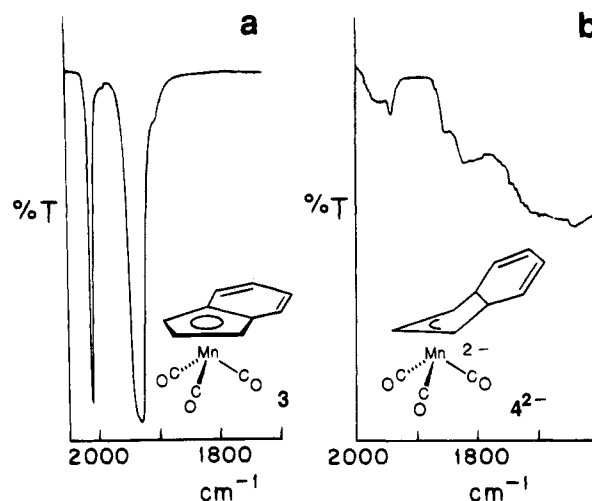


Figure 1. IR spectra of $[Mn(\eta^5-C_9H_7)(CO)_3]$ and its two-electron-reduction product in THF: (a) $[Mn(\eta^5-C_9H_7)(CO)_3]$ in THF; (b) $K_2[Mn(\eta^5-C_9H_7)(CO)_3]$ prepared by two-electron naphthalenide reduction of $[Mn(\eta^5-C_9H_7)(CO)_3]$ in THF.

perature resulted in a slow color change from deep blue to yellow-orange. Solution IR spectra established that the CO absorptions at 1920 (s) and 1820 (vs) cm^{-1} of $[K(18-C-6)][Mn(\eta^5-C_9H_7)(CO)_3]$ had completely disappeared and had been replaced by bands at 2025 (s) and 1930 (vs) cm^{-1} characteristic of $[Mn(\eta^5-C_9H_7)(CO)_3]$. Only traces of other carbonyl complexes could be observed by IR. The mixture was stirred for 1 h, and the solvent was removed under vacuum. The neutral species were extracted with *n*-pentane (3×20 mL). Flash chromatography (silica gel, *n*-pentane eluent) provided a yellow fraction which was concentrated to a volume of 5 mL and stored at $-80^\circ C$. After 1 day, orange-yellow solids had formed. These were collected and washed with 3×10 mL of cold ($-78^\circ C$) *n*-pentane to give 0.123 g (0.48 mmol, 90% yield) of $[Mn(\eta^5-C_9H_7)(CO)_3]$ (IR, 1H NMR).

Reaction of $[K(18-C-6)][Mn(\eta^5-C_9H_7)(CO)_3]$ with O_2 . The reaction of $[K(18-C-6)][Mn(\eta^5-C_9H_7)(CO)_3]$ with excess O_2 was carried out in a manner similar to the reaction with CO_2 . The course of the reaction was visually and spectroscopically similar, and an analogous workup gave $[Mn(\eta^5-C_9H_7)(CO)_3]$ in 95% yield.

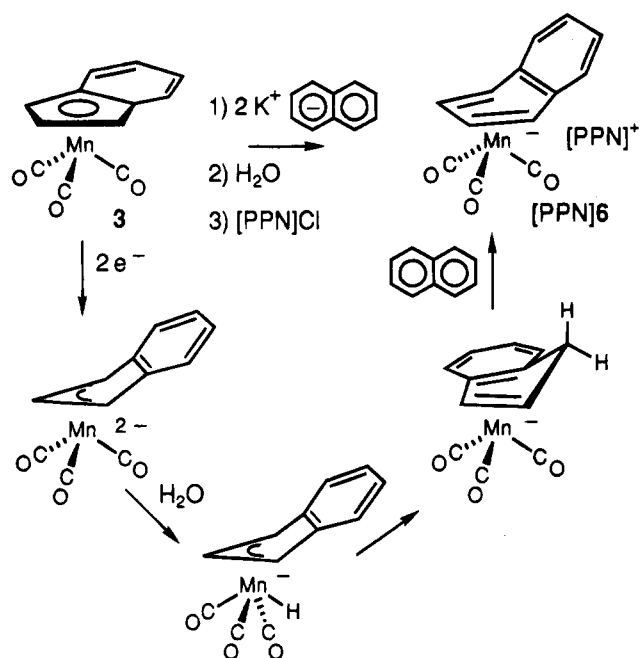
Reaction of $[K(18-C-6)][Mn(\eta^5-C_9H_7)(CO)_3]$ with Trityl Dimer. The reaction of $[K(18-C-6)][Mn(\eta^5-C_9H_7)(CO)_3]$ with 5 equiv of trityl dimer ($Ph_3CC_6H_4=CPh_2$) was carried out in a manner similar to the reaction with CO_2 . The course of the reaction was visually and spectroscopically similar, and an analogous workup gave $[Mn(\eta^5-C_9H_7)(CO)_3]$ in 93% yield.

Reaction of $[K(18-C-6)][Mn(\eta^5-C_9H_7)(CO)_3]$ with H_2O_2 . The reaction of $[K(18-C-6)][Mn(\eta^5-C_9H_7)(CO)_3]$ with 0.5 equiv of H_2O_2 was carried out in a manner similar to the reaction with CO_2 . The course of the reaction was visually and spectroscopically similar, and analogous workup gave $[Mn(\eta^5-C_9H_7)(CO)_3]$ in 98% yield.

Results and Discussion

Two-Electron Reduction of $[Mn(\eta^5-C_9H_7)(CO)_3]$. Reduction of $[Mn(\eta^5-C_9H_7)(CO)_3]$ (**3**) in tetrahydrofuran (THF) with 2.1 equiv of potassium naphthalenide ($K(Nap)$) is visually similar to alkali reduction of $[Mn(\eta^5-C_5H_4Me)(CO)_3]^1$ and results in consumption of the neutral starting material (as indicated by the loss of CO stretching absorptions at 2025 (s) and 1930 (vs) cm^{-1} ; Figure 1a) and concomitant formation of a highly reduced species characterized by a single, broad, very strong absorption at ca. 1670 cm^{-1} (Figure 1b). Although less well defined, this spectrum is similar to that

Scheme 2



assigned previously¹ to $[\text{Mn}(\eta^3\text{-C}_5\text{H}_4\text{Me})(\text{CO})_3]^{2-}$ and we propose (Scheme 1) that this spectrum indicates, as anticipated, formation of the ring-slipped indenyl complex $[\text{Mn}(\eta^3\text{-C}_9\text{H}_7)(\text{CO})_3]^{2-}$ (**4**²⁻). Consistent with this hypothesis, the indenyl ligand in **4**²⁻ is activated toward electrophiles, as established by protonation with H_2O (1 equiv) and subsequent $[\text{PPN}]\text{Cl}$ ($[\text{PPN}]^+ = [\text{Ph}_3\text{PNPPH}_3]^+$) metathesis to give the η^4 -naphthalene complex $[\text{PPN}][\text{Mn}(\eta^4\text{-C}_{10}\text{H}_8)(\text{CO})_3]$ (**6**), which we have previously characterized crystallographically¹² in 51% recrystallized yield. We propose that this sequence involves protonation of the indenyl ligand (probably metal mediated) followed by naphthalene substitution of the indene ligand (Scheme 2).

Although the IR spectrum assigned to **K**₂**4** contains only broad, rather ill-defined absorptions, we do not believe that this reflects formation of a complex mixture of transition-metal products but rather the influence of ion pairing on the spectrum of this dianion. The **K**₂**4** salt probably exists as multiple tight ion pairs in THF solution, and the observed IR spectrum would be expected to be the sum of the IR absorption spectra of the various ion pairs.^{13a}

Relatively clean reduction of **3** to **4**²⁻ is supported by the electrochemical studies discussed below and by our ability to improve the yield of **6**⁻ by an alternate procedure in which the alkali-metal counterion is complexed with 18-crown-6 (18-C-6). The η^4 -naphthalene complex is then isolated as $[\text{K}(18\text{-C-6})]\text{6}$ in 70% recrystallized yield, establishing good intrinsic yields for both the reduction and protonation steps.

One-Electron Reduction of $[\text{Mn}(\eta^5\text{-C}_9\text{H}_7)(\text{CO})_3]$ and Formation of $[\text{Mn}(\eta^5\text{-C}_9\text{H}_7)(\text{CO})_3]^-$ by Comproportionation of **3 and **4**²⁻.** In the course of two-electron reduction of **3** we observed intermediate color changes which led us to explore one-electron reduction by addition of 1 equiv of potassium naphthalenide to a

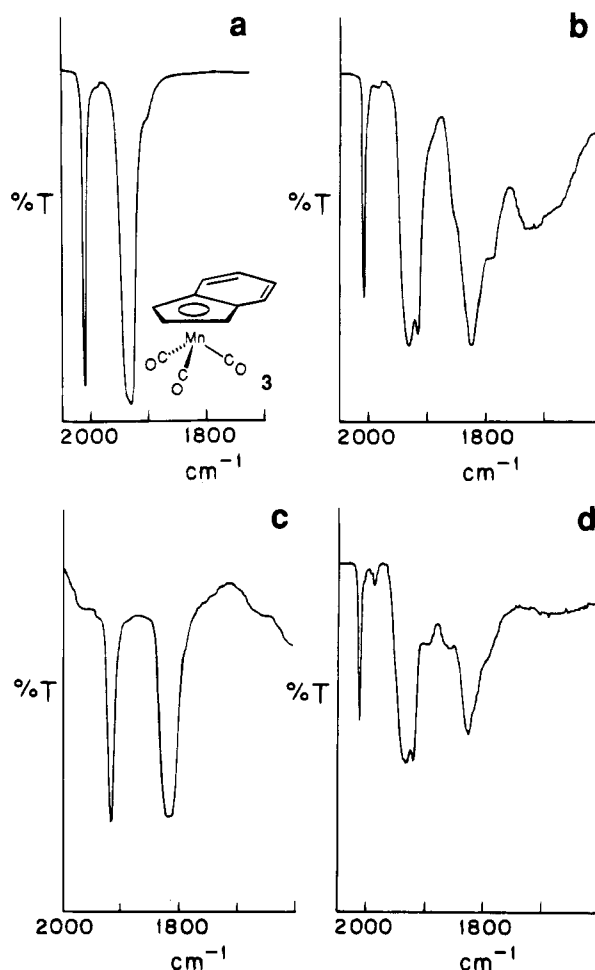


Figure 2. IR spectra of $[\text{Mn}(\eta^5\text{-C}_9\text{H}_7)(\text{CO})_3]$ and its one-electron-reduction products in THF: (a) $[\text{Mn}(\eta^5\text{-C}_9\text{H}_7)(\text{CO})_3]$ in THF; (b) solution obtained following one-electron naphthalenide reduction of $[\text{Mn}(\eta^5\text{-C}_9\text{H}_7)(\text{CO})_3]$ in THF; (c) solution obtained following 18-C-6 addition to one-electron-reduction mixture in b; (d) solution obtained following NaPF_6 addition to solution of $[\text{K}(18\text{-C-6})][\text{Mn}(\eta^5\text{-C}_9\text{H}_7)(\text{CO})_3]$ in c.

solution of **3** in THF at -78°C . Infrared spectra (Figure 2b) indicated that the resulting solution contained a mixture of three products: unreacted **3**, a highly reduced species with a broad absorption at ca. 1730 cm^{-1} assumed to be **4**²⁻,¹⁴ and what appears to be a monoanionic species with absorptions at 1920 (s) and 1820 (vs) cm^{-1} .

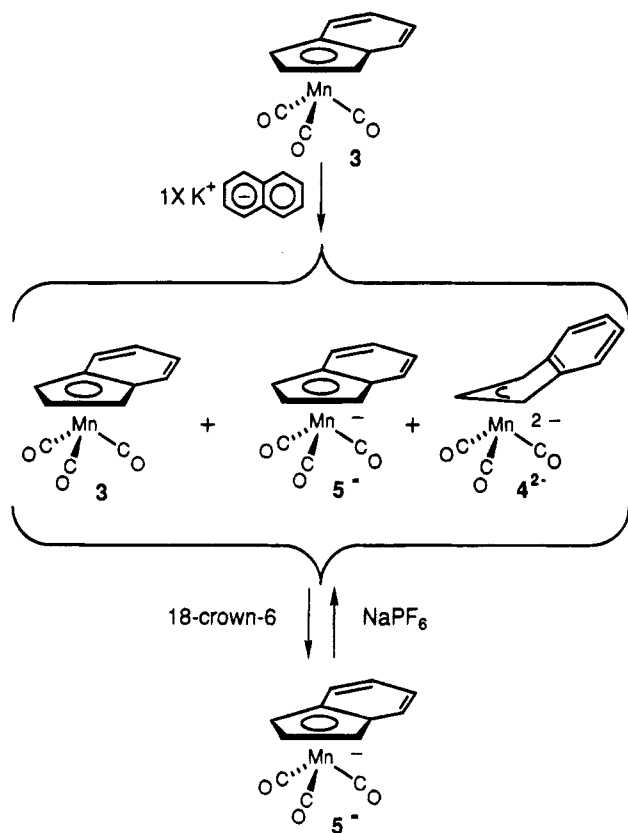
Addition of 1 equiv of 18-C-6 to this solution produced a remarkable transformation. The solution became deep blue, and IR absorptions assigned to **3** and **4**²⁻ disappeared while the monoanion absorptions increased markedly in intensity (Figure 2c). The monoanionic material is stable in solution at room temperature (>12 h by IR), and a blue crystalline product could be obtained by a procedure in which the solution was concentrated, the polarity reduced by addition of pentane (2:1 THF/pentane), and the mixture cooled to -78°C . The crystalline product is, however, thermally

(14) The differences between the positions of the maxima of the IR absorptions assigned to **4**²⁻ in Figure 1b and Figure 2b is not believed to be significant, given the ill-defined nature of the absorption in Figure 1b, the high probability that the IR spectra of **4**²⁻ will be markedly dependent on changes in ion pairing effects,^{13a} and the fact that the species in Figures 1b and 2b are generated under differing conditions which are likely to lead to the presence of different ion pairs.

(12) Thompson, R. L.; Lee, S.; Rheingold, A. L.; Cooper, N. J. *Organometallics* **1991**, *10*, 1657.

(13) (a) Darensbourg, M. Y. *Prog. Inorg. Chem.* **1985**, *33*, 221. (b) Kochi, J. K.; Bockman, T. M. *Adv. Organomet. Chem.* **1991**, *33*, 51.

Scheme 3



unstable above -20°C , and this instability has precluded characterization by combustion analysis or by X-ray diffraction (despite several attempts to carry out low-temperature diffraction studies).

The most obvious interpretation of the effect of the added 18-C-6 is that it perturbs solution ion pairing effects, by complexation of the K^+ counterion, to the point at which 3 and 4^{2-} comproportionate to form the 19-electron radical anion $[\text{Mn}(\eta^5\text{-C}_9\text{H}_7)(\text{CO})_3]^-$ (5⁻; Scheme 3). This would imply, as is reasonable, that ion pairing significantly stabilizes 4^{2-} , but this should not be taken as implying that $[\text{K}(18\text{-C-6})]5$ is not ion paired in THF; the most reasonable interpretation of the intense blue color of $[\text{K}(18\text{-C-6})]5$ is that it arises from a charge-transfer absorption of the $[\text{K}(18\text{-C-6})]5$ contact ion pair, and such an assignment would account nicely for the counterion dependence in the color of 5⁻.^{13b}

The formation of a radical following 18-C-6 addition is supported by EPR spectra of the solution, which exhibit a single resonance, $\langle g \rangle = 1.986$, split into a sextet with equal-intensity components as a consequence of coupling ($\langle a \rangle = 31 \text{ G}$) with ^{55}Mn ($I = 5/2$).

The magnitude of this coupling is reasonable for an electron located primarily in a Mn 3d orbital in 5⁻.¹⁵ In paramagnetic Mn complexes in which the bonding is primarily ionic, spin polarization of inner s electrons typically gives rise to isotropic couplings to ^{55}Mn of ca. -90 G ; any occupation of the 4s orbital, a natural corollary of the degree of covalence which would be anticipated in a low-valent organometallic complex such as 5⁻, should make a positive contribution to $\langle a \rangle$ and hence reduce its magnitude.

The d^7 radical $[\text{Mn}(\text{CO})_5]$ provides the only obvious, albeit highly approximate, electronic model for 5⁻, and an authoritative report and interpretation of the controversial EPR literature on $[\text{Mn}(\text{CO})_5]$ concludes, on the basis of anisotropic spectra recorded in an Ar matrix, that a_{\parallel} and a_{\perp} have opposite signs and magnitudes such that $\langle a \rangle$ is negligible.¹⁶ This is reasonable and suggests that positive contributions to $\langle a \rangle$ arising from ca. 8% occupancy of the Mn 4s orbital effectively counterbalance the negative $\langle a \rangle$ arising from spin polarization.

Comparison of these data with those for 5⁻, which should have at least as large a covalent contribution to its electronic structure, raises the intriguing question as to whether 4s occupation has become the dominant source of coupling with 5⁻, giving rise to a positive hyperfine coupling constant. Available data do not address this, and although we do observe an anisotropic spectrum for 5⁻ in a 2-MeTHF glass at 15 K (as is reasonable for a low-symmetry radical), the quality of the spectra obtained has not yet permitted the detailed analysis which would resolve this question.

We have independently confirmed the presence of approximately one unpaired electron per metal center in solutions of 5⁻ by an Evans method susceptibility measurement^{9,10} which gave a molar susceptibility of $(1.24 \pm 0.04) \times 10^{-3}$ for 5⁻, corresponding to $\mu_{\text{eff}} = 1.72 \pm 0.03 \mu_B$ on the assumption that all of the initial 3 has been converted to the monoanion.

If formation of $[\text{Mn}(\eta^5\text{-C}_9\text{H}_7)(\text{CO})_3]^-$ does indeed reflect ion pairing effects on comproportionation of 3 and 4^{2-} , we ought to be able to disproportionate 5⁻ by addition of a coordinating counterion. This has been confirmed by the addition of a solution containing 10 equiv of NaPF_6 in THF (KPF_6 is insoluble in THF) to a solution of 5⁻ at -78°C . When the solution was warmed to room temperature, IR spectra (Figure 2d) indicated re-formation of 3 (with bands at 2025 (s) and 1930 (vs) cm^{-1}) and of 4^{2-} (Scheme 3). Although the intensity of the low-energy band assigned to 4^{2-} is less in Figure 2d than in Figure 2b, this is consistent with the independently established thermal instability of 4^{2-} —the dianion decomposes with a half-life of ca. 5 min at room temperature to an unidentified product with absorptions at 1895 and 1865 cm^{-1} , and the disproportionation conditions are such that extensive decomposition would be anticipated.

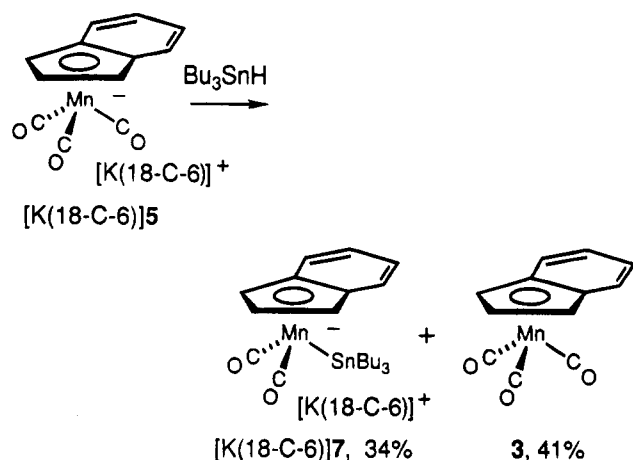
Chemical Evidence for Facile Disproportionation of $[\text{Mn}(\eta^5\text{-C}_9\text{H}_7)(\text{CO})_3]^-$: Reaction of 5⁻ with Bu_3SnH . Indirect chemical evidence that disproportionation of 5⁻ is kinetically facile comes from the reaction of 5⁻ with Bu_3SnH . This was examined during a survey of reagents which might exhibit radical-like reactivity with 5⁻, and initial studies established that $[\text{K}(18\text{-C-6})][\text{Mn}(\eta^5\text{-C}_9\text{H}_7)(\text{CO})_3]$ reacts with Bu_3SnH in a few hours at room temperature to give a solution from which the tributyltin complex $[\text{K}(18\text{-C-6})][\text{Mn}(\eta^5\text{-C}_9\text{H}_7)(\text{CO})_2(\text{SnBu}_3)]$ ($[\text{K}(18\text{-C-6})]7$) was isolated in 34% recrystallized yield. This complex has been fully characterized spectroscopically and analytically (see Experimental Section).

It was initially tempting to assume that 7⁻ was formed by a radical addition pathway, but this is inconsistent with the observation that the other principal product of this reaction sequence is the neutral

(15) Symons, M. *Chemical and Biochemical Aspects of Electron-Spin Resonance Spectroscopy*; Wiley: New York, 1978.

(16) Symons, M. C. R.; Sweany, R. L. *Organometallics* 1982, 1, 834.

Scheme 4



parent complex $[\text{Mn}(\eta^5\text{-C}_9\text{H}_7)(\text{CO})_3]$ (**3**), isolated from the reaction mixture in 41% yield (Scheme 4). The formation of roughly equimolar quantities of **3** and **7**—following addition of Bu_3SnH suggests (Scheme 5) that disproportionation of 5^- generates a small standing concentration of 4^{2-} which reacts with Bu_3SnH . This would imply that the tin hydride is acting as a Lewis acid and that formation of 7^- involves bis protonation of 4^{2-} to give $[\text{Mn}(\eta^3\text{-C}_9\text{H}_7)(\text{CO})_3\text{H}_2]$ (**8**), or some other manganese dihydride, followed by H_2 elimination, tributyltin anion coordination (before or after H_2 loss), and eventual loss of CO to give the observed product.

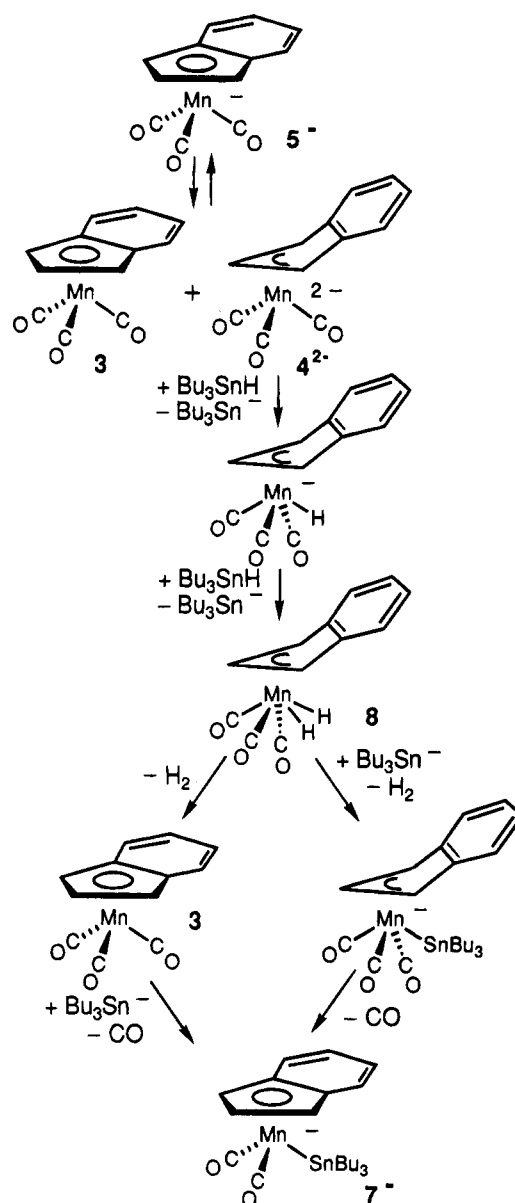
One implication of this hypothesis is that Bu_3SnH is a strong enough Brønsted acid to protonate $[\text{Mn}(\eta^3\text{-C}_9\text{H}_7)(\text{CO})_3]^{2-}$ (4^{2-}), and this has been confirmed by the preparation of 7^- by direct reaction of 4^{2-} with Bu_3SnH (Scheme 6). Separation problems (arising from the presence of naphthalene in the solution of $[\text{Mn}(\eta^3\text{-C}_9\text{H}_7)(\text{CO})_3]^{2-}$ (4^{2-}), precluded the determination of isolated yields of 7^- from this reaction, but we have used quantitative IR to confirm the formation of a 60% spectroscopic yield of $[\text{Mn}(\eta^5\text{-C}_9\text{H}_7)(\text{CO})_2(\text{SnBu}_3)]^-$.

The mechanism proposed in Scheme 5 for the reaction of 4^{2-} with Bu_3SnH involves the same monohydride intermediate $[\text{Mn}(\eta^3\text{-C}_9\text{H}_7)(\text{CO})_3\text{H}]^-$ as that invoked in Scheme 2 to account for the hydrolysis of 4^{2-} to give the naphthalene complex $[\text{Mn}(\eta^4\text{-C}_{10}\text{H}_8)(\text{CO})_3]^-$ (**6**), and it is reassuring to note that the reaction of 4^{2-} with Bu_3SnH does indeed give **6** as a byproduct, isolated as [PPN]**6** in 9% yield from the reaction of 4^{2-} with 1 equiv of Bu_3SnH and in 22% yield from the reaction of 4^{2-} with 2 equiv of Bu_3SnH .

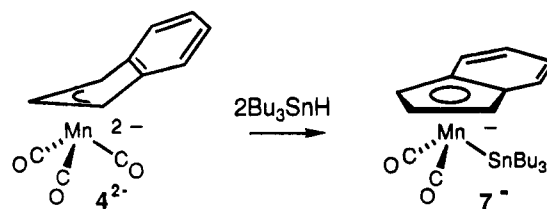
A surprising implication of the mechanism in Scheme 5 is that $[\text{Bu}_3\text{Sn}]^-$ is a good enough nucleophile to displace either CO from **3** or H_2 from **8**. In an attempt to discriminate between these possibilities, we examined the reactivity of **3** with $[\text{K}(\text{18-C-6})][\text{SnBu}_3]$, anticipating no reaction, and were surprised to discover (Scheme 7) that, under these conditions, Bu_3Sn^- is a sufficiently powerful nucleophile to displace CO from **3** in THF, presumably because 18-C-6 complexation of the K^+ counterion makes $[\text{Bu}_3\text{Sn}]^-$ a strong nucleophile. The isolated yield of $[\text{K}(\text{18-C-6})]7$ was ca 35% from a reaction utilizing a 10-fold excess of $[\text{K}(\text{18-C-6})][\text{SnBu}_3]$, and the generation of 7^- from 5^- may therefore involve either or both of the pathways in Scheme 5.

It should be noted that the stoichiometry of Scheme 5 would imply the generation of one intermediate

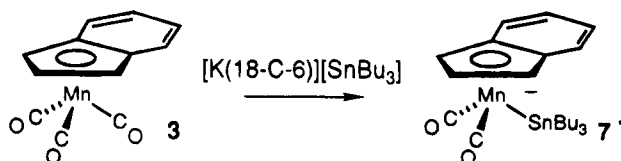
Scheme 5



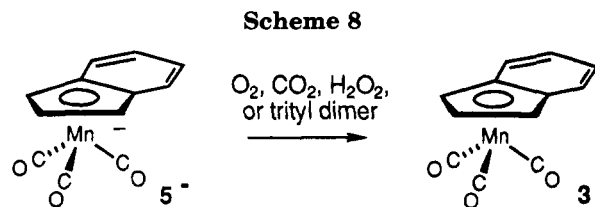
Scheme 6



Scheme 7



$[\text{SnBu}_3]^-$ anion per Mn center, and this raises the question of why we are able to isolate *any* **3** from the reaction of **5** with $[\text{SnBu}_3]^-$ —if Scheme 5 provided a complete description of the reaction, all the initial 5^- should be converted to 7^- . It would appear, however,



that Scheme 5 is incomplete because the reaction of **3** with $[\text{SnBu}_3]^-$ is more complex than suggested in Scheme 7—if **3** is reacted with 2 molar equiv of $[\text{SnBu}_3]^-$, a ca. 1:1 mixture of **3** and **7**⁻ is generated (IR), implying that more than 1 equiv of $[\text{SnBu}_3]^-$ is required to form **7**⁻. We have been unable to date to establish why this should be so, but this observation does explain the persistence of **3** following the reaction of **5**⁻ with $[\text{Bu}_3\text{SnH}]$. We have also noted that the reaction of **3** with a 10-fold excess of $[\text{K}(18\text{-C-6})][\text{SnBu}_3]$ results in the formation (in addition to **7**⁻) of a new (probably monoanionic) Mn complex characterized by bands at 1973 (s) and 1890 (vs) cm^{-1} which we have been unable to purify or characterize further to date.

Reactions of $[\text{K}(18\text{-C-6})][\text{Mn}(\eta^5\text{-C}_9\text{H}_7)(\text{CO})_3]$ with O_2 , CO_2 , Trityl Dimer, and H_2O_2 . Other reactivity studies to date indicate that **5**⁻ behaves primarily as a one-electron reducing agent (Scheme 8). Thus, treatment with reagents ranging from oxidants such as O_2 to Lewis acids such as CO_2 result, in general, in regeneration of the neutral starting material **3**, frequently in excellent recovered yield (95% and 90%, respectively, in these cases). Even a reagent such as the trityl radical,⁵ which might be expected to exhibit radical-like behavior with this metal-centered radical, reoxidized **5**⁻ to **3** (93% recovered yield). Similar results were obtained with hydrogen peroxide, which might have participated in oxidative addition reactions analogous to the classical addition of H_2O_2 to $[\text{Co}(\text{CN})_5]^{3-}$.¹⁷ The result was again, however, reoxidation to **3** (98% yield).

Electrochemical Reduction of $[\text{Mn}(\eta^5\text{-C}_9\text{H}_7)(\text{CO})_3]$. The accessibility of both the one- and two-electron reduction products of **3** has been confirmed by voltammetric studies. Cyclic voltammetry in THF using tetrabutylammonium perchlorate (TBAP) supporting electrolyte resulted in the observation of two successive one-electron reductions at $(E_a + E_c)/2 = -1.95$ and -2.20 V vs SCE at scan rates between 10 and 1000 mV s^{-1} , as illustrated by the voltammogram in Figure 3. The two charge transfers are quasi-reversible processes with midpoint potentials independent of voltage sweep rate.

Chronocoulometry¹⁸ confirmed that the first electron transfer was a one-electron reduction, presumably to give **5**⁻, and the similar i_a and i_c values at equivalent scan rates then confirmed that the second electron transfer was also a one-electron reduction, presumably to give **4**²⁻.

The electrochemical conditions approximate those of the synthetic reduction in the presence of 18-C-6, in that the supporting electrolyte does not provide a coordinating counterion which might stabilize **4**²⁻. These are therefore conditions under which **5**⁻ should be stable

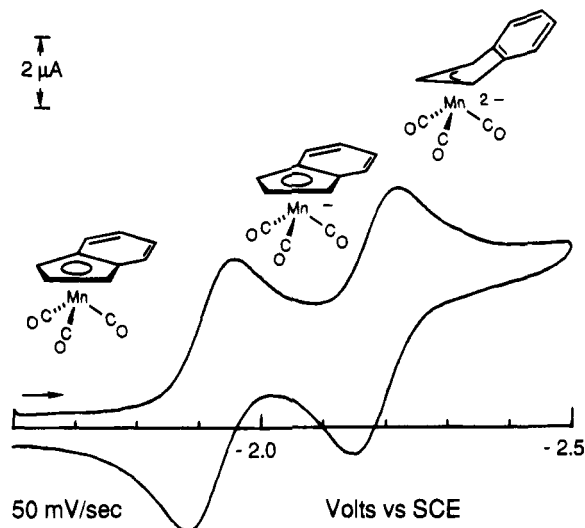


Figure 3. Cyclic voltammogram of $[\text{Mn}(\eta^5\text{-C}_9\text{H}_7)(\text{CO})_3]$ at 50 mV s^{-1} with 0.1 M TBAP in THF.

with respect to disproportionation, and we would anticipate the observation of two discrete one-electron steps in the reduction of **3**, as observed experimentally.

The IR evidence that addition of NaPF_6 dramatically changed the disproportionation constant for **5**⁻ raised the intriguing possibility that addition of NaPF_6 might affect the voltammetric reduction of **3**. We have examined the CV of **3** in the presence of variable amounts of added NaPF_6 , but the only effect which we have observed is a marked passivation of the electrode surface which renders the CV featureless after the addition of ca. 10 equiv of NaPF_6 . This experiment does not provide additional support for our proposal that disproportionation of **5**⁻ is favored by coordinating counterions, but it also does not argue against this proposal, since the electrochemical reduction is occurring under nonequilibrium conditions and is subject to surface effects, adsorption effects, and electrolyte effects.

Hapticity Changes Associated with One- and Two-Electron Reduction of $[\text{Mn}(\eta^5\text{-C}_9\text{H}_7)(\text{CO})_3]$. Our studies of the reduction of **3** were initiated in the hope that the established ability of indenyl ligands to adopt η^3 conformations in which the C_6 ring remains aromatic would stabilize the η^3 dianion **4**²⁻. Our IR and electrochemical results establish that two-electron reduction of **3** does give a relatively stable dianion which retains the indenyl ligand (since **4**²⁻ can be reoxidized to **3**), but we have been unable to explore the indenyl coordination mode crystallographically since attempts to obtain crystalline salts of **4**²⁻ from samples prepared by $\text{K}(\text{Nap})$ reduction have been unsuccessful. Approaches attempted have included counterion metathesis to give a tetraalkylammonium or PPN^+ ($[\text{Ph}_3\text{PNPPH}_3]^+$) salt and complexation of the K^+ counterion with a crown ether, and their failure to date probably reflects the instability of the dianion in the absence of ion pair stabilization (see above).

Despite our inability to explore crystallographically the geometry of **4**²⁻, our hypothesis that the indenyl ligand in **4**²⁻ adopts an η^3 conformation is supported by comparison with the literature—the isoelectronic monoanion $[\text{Fe}(\eta^3\text{-C}_9\text{H}_7)(\text{CO})_3]^-$ is a close analog of **4**²⁻, and crystallography has established that this contains an η^3 -indenyl ligand.⁴

(17) Halpern, J. *Acc. Chem. Res.* **1970**, *3*, 386.

(18) Bard, A. J.; Faulkner, L. R. *Electrochemical Methods*, Wiley: New York, 1980.

If the indenyl ligand in 4^{2-} does exhibit η^3 coordination, the observation that reduction can be stopped following formation of the initial one-electron-reduction product 5^- , together with the relative stability of this species in solution, allows us to pose an intriguing further question as to the point at which the hapticity shift occurs. The crystallographic precedents on this point are not clear-cut—comparison with some 19-electron complexes of 3d metals with cyclic diene ligands such as $[\text{Fe}(\eta^5\text{-C}_6\text{Me}_6)(\eta^5\text{-C}_5\text{H}_5)]^{19}$ would suggest that the indenyl conformation in 5^- probably approximates that of an η^5 planar ligand (although even then the ligand geometry might be deformed from the ideal as in the reported X-ray structure of 19-electron $[\text{Co}(\eta^5\text{-C}_9\text{H}_7)_2]^{20}$, while other literature precedents would favor an η^3 coordination mode. It has, for example, been established crystallographically that the paramagnetic indenyl complex $[\text{V}(\text{C}_9\text{H}_7)_2(\text{CO})_2]$ is not a 19-electron complex with two η^5 -indenyl ligands but is instead a 17-electron complex $[\text{V}(\eta^5\text{-C}_9\text{H}_7)(\eta^3\text{-C}_9\text{H}_7)(\text{CO})_2]$ in which one of the ligands adopts an η^3 coordination mode.^{3p}

We do, however, have one piece of experimental information which argues in favor of an essentially η^5 -indenyl ligand in 5^- and an η^3 -indenyl ligand in 4^{2-} , and that is the small difference ΔE of -0.25 V between the potentials at which **3** and 5^- are reduced. This ΔE value is consistent with marked stabilization of the final reduction product 4^{2-} by an appropriate hapticity shift concomitant with reduction of 5^- and is remarkably similar to the ΔE values of -0.37 and -0.26 V reported for $[\text{Rh}(\eta^5\text{-C}_5\text{Me}_5)(\eta\text{-C}_6\text{Me}_6)]^{2+/+0}$ ²⁰ and $[\text{Ru}(\eta\text{-C}_6\text{-Me}_6)_2]^{2+/+0}$,²¹ respectively—in both of these systems the second reduction is associated with an $\eta^6 \rightarrow \eta^4$ hapticity shift of the arene, and we would speculate that the hapticity shift must take place concurrently with addition of the second electron (EE mechanism) or immediately after addition of the second electron (EEC mechanism). We note also that the ΔE value is markedly smaller than the values of -1.1 and -1.0 V reported for the cyclopentadienyl systems $[\text{Co}(\eta^5\text{-C}_5\text{H}_5)_2]^{+/0-}$ ²³ and $[\text{Co}(\eta^5\text{-C}_5\text{H}_5)(\eta^6\text{-C}_6\text{Me}_6)]^{2+/+0}$.²⁴ The aromatic ligands in these systems are believed to retain planar configurations through the d^6 , d^7 , and d^8 electron configurations,²³ and it was the contrast between the large ΔE values for these cobalt complexes and the -0.37 V ΔE for the $[\text{Rh}(\eta^5\text{-C}_5\text{Me}_5)(\eta\text{-C}_6\text{Me}_6)]^{2+/+0}$ system which originally led Bowyer and Geiger to propose that the arene $\eta^6 \rightarrow \eta^4$ ring slippage in the rhodium system occurred concomitant with the second reduction.²⁰ Comparison of the $[\text{Mn}(\eta\text{-C}_9\text{H}_7)(\text{CO})_3]^{0/-2-}$ data with the

cobalt data similarly provides support for both η^5 -indenyl ligation in 5^- and η^3 -indenyl ligation in 4^{2-} . Although establishing these coordination modes definitively would require X-ray or NMR confirmation, our argument is also consistent with the elegant report by Astruc on four closely related binuclear complexes in which stabilizing structural rearrangements during the second of two sequential one-electron reductions resulted in small (0.13 and ca. 0 V) ΔE values for one pair of complexes while the absence of such rearrangements resulted in larger (0.32 and 0.48 V) ΔE values for the other pair ("large" ΔE values are of course smaller in a binuclear system than in a mononuclear system because of reduced electrostatic repulsion).²⁵

Summary

The indenyl complex $[\text{Mn}(\eta^5\text{-C}_9\text{H}_7)(\text{CO})_3]$ represents a significant addition to the class of molecules containing unsaturated hydrocarbon ligands which can undergo two successive one-electron reductions without ligand dissociation. In a few cases of similar reduction sequences (such as the cobaltocenium/cobaltocene/cobaltocene anion system²³) the reductions occur without apparent ligand distortion, but in the case of $[\text{Mn}(\eta^5\text{-C}_9\text{H}_7)(\text{CO})_3]$ the electrochemical data suggest that the two-electron-reduction product is stabilized by an hapticity shift, similar to the $\eta^6 \rightarrow \eta^4$ arene hapticity shifts studied by Geiger and others,^{20,21,23,26} to give $[\text{Mn}(\eta^3\text{-C}_9\text{H}_7)(\text{CO})_3]^{2-}$ (4^{2-}).

Both the one-electron-reduction product $[\text{Mn}(\eta^5\text{-C}_9\text{H}_7)(\text{CO})_3]^-$ (5^-) and the two-electron-reduction product 4^{2-} can be observed by electrochemical means and by IR, and the disproportionation equilibrium between 5^- , the neutral molecule $[\text{Mn}(\eta^5\text{-C}_9\text{H}_7)(\text{CO})_3]$ (**3**), and 4^{2-} is kinetically facile. The accessibility of this equilibrium dominates the reactivity of the 19-electron anion 5^- , and we have been unable to find conditions under which 5^- reacts as an organometallic radical— 5^- either acts as a one-electron reductant or as a source, via disproportionation, of highly reactive 4^{2-} .

Organo-transition-metal anions are typically extensively ion paired in mildly polar solvents such as THF,¹³ and in the case of the model dianionic system offered by Collman's reagent it has, for example, been specifically demonstrated that $\text{Na}_2[\text{Fe}(\text{CO})_4]$ is largely ion paired in THF.²⁷ This background would lead us to anticipate significant ion pairing in solutions of **K₂4** in THF, and this does appear to be the case as suggested by the effect of added 18-C-6 on the equilibrium between **3**, 5^- , and 4^{2-} . IR spectra established that this leads to comproportionation of **3** and 4^{2-} to form 5^- , suggesting that contact ion pairing in solutions of **K₂4** stabilizes 4^{2-} markedly relative to the 4^{2-} in solutions of $[\text{K}(18\text{-C-6})]_2\text{4}$.

Contact ion pair stabilization of organic dianions is well established, particularly by the work of Szwarc and others on polyaromatic hydrocarbons and related unsaturated organic molecules subject to one- and two-electron reduction.^{28,29} This work includes examples of hydrocarbon/radical anion/dianion disproportionation equilibria subject to marked counterion effects qualita-

(19) (a) Astruc, D. *Tetrahedron* **1983**, *39*, 4027. (b) Astruc, D.; Hamon, J.-R.; Althoff, G.; Roman, E.; Batail, P.; Michaud, P.; Mariot, J.-P.; Varret, F.; Cozak, D. *J. Am. Chem. Soc.* **1979**, *101*, 5445. (c) Hamon, J.-R.; Astruc, D.; Michaud, P. *J. Am. Chem. Soc.* **1981**, *103*, 758. (d) Astruc, D. *Acc. Chem. Res.* **1986**, *19*, 377.

(20) Bowyer, W. J.; Geiger, W. E. *J. Am. Chem. Soc.* **1985**, *107*, 5657.

(21) (a) Finke, R. G.; Voegeli, R. H.; Laganis, E. D.; Boekelheide, V. *Organometallics* **1983**, *2*, 347. (b) Merkert, J.; Nielson, R. M.; Weaver, M. J.; Geiger, W. E. *J. Am. Chem. Soc.* **1989**, *111*, 7084.

(22) Values quoted are in CH_2Cl_2 —in more polar solutions such as CH_3CN the magnitude of ΔE decreases, presumably as a consequence of CH_3CN stabilization of the 2+ cations, to -0.25 and <0 V respectively.²¹

(23) (a) Holloway, J. D. L.; Geiger, W. E. *J. Am. Chem. Soc.* **1979**, *101*, 2038. (b) Geiger, W. E.; Bowden, W. L.; El Murr, N. *Inorg. Chem.* **1979**, *18*, 2358.

(24) (a) Koelle, U.; Fuss, B.; Rajasekharan, M. V.; Ramakrishna, B. L.; Ammeter, J. H.; Böhm, M. C. *J. Am. Chem. Soc.* **1984**, *106*, 4152. (b) Jonas, K.; Deffense, E.; Habermann, D. *Angew. Chem., Int. Ed. Engl.* **1983**, *22*, 716.

(25) Astruc, D.; Lacoste, M.; Toupet, L. *J. Chem. Soc., Chem. Commun.* **1990**, 558.

(26) Geiger, W. E. *Prog. Inorg. Chem.* **1985**, *33*, 275.

(27) Collman, J. P.; Finke, P. G.; Cawse, J. N.; Brauman, J. I. *J. Am. Chem. Soc.* **1977**, *99*, 2515.

tively similar to those which we observe in the 3, 5⁻, and 4²⁻ system and corresponding quantitatively to disproportionation constant changes of up to 10¹¹.^{28e} More recently, the magnitude of ion-pairing effects on the potentials of organic reductions has led to the development of a large and rapidly expanding area of research focused on the development and application of electroactive crown ethers and cryptands.³⁰

The literature on contact ion pairing effects on the stabilization of inorganic and organometallic anions is more recent and includes examples of effects on the spectroscopy of the anions,¹³ on reactivity factors such as the nucleophilicity of organometallic anions,²⁷ on the promotion of CO bond scission in clusters,³¹ and on the stability of highly reduced carbonylmetalates.³² There has also been an elegant recent report³³ on the kinetic and thermodynamic effect of added Na[PF₆] on disproportionation of neutral 19-electron organometallic radicals of the type [Fe(η^5 -C₅H₅)(arene)], which is part of a growing body of work on salt effects in organometallic chemistry and, in particular, on the ability of double ion-pair exchange reactions to control the course of reactions both stoichiometrically and catalytically.³⁴

Vleck and other contributors to the polarographic

literature have discussed the ability of ion pairs to facilitate the transport of anions to negatively charged electrodes,³⁵ and there have been some reports of cation effects on the potentials for reduction of monomeric inorganic anions. These include a series of papers on the [Fe(CN)₆]⁴⁻/[Fe(CN)₆]³⁻ couple³⁶ and recent work by Lintvedt on binuclear bis(1,3,5-triketonato)dicopper(II) complexes, in which he observed that the potential of the second reduction of these neutral, dimeric complexes is so sensitive to added alkali-metal cations that their reductive behavior switches from a simple one-electron transfer to the sequential, reversible transfer of two electrons at very nearly the same potential.³⁷ Analogous counteranion effects have also been reported for the reduction of cationic transition-metal-centered dimers and monomers.³⁸

The spectra in Figure 2 provide an interesting example of how dramatically ion pairing can affect the stability of highly reduced organo-transition-metal complexes and suggest again that increased attention should be paid to the importance of counterions in such systems.

Acknowledgment. We thank the National Science Foundation for financial support through Grant No. CHE-9113808, Mr. Greg Meisner for assistance with the EPR spectroscopy, and Professors Adrian Michael, Steve Weber, and Johannes Coetzee for helpful discussions.

OM940989W

(28) (a) Szwarc, M.; Jagur-Grodzinski, J. In *Ions and Ion Pairs in Organic Reactions*; Szwarc, M., Ed.; Wiley: New York, 1974; Vol. 2, Chapter 1. (b) Hogen-Esch, T. E. *Adv. Phys.-Org. Chem.* **1977**, *15*, 154. (c) Szwarc, M.; Levin, G. In *Protons and Ions Involved in Fast Dynamic Phenomena*; Laszlo, P., Ed.; Elsevier: Amsterdam, 1978; p 229. (d) Szwarc, M. *Acc. Chem. Res.* **1972**, *5*, 169. (e) Szwarc, M. *Pure Appl. Chem.* **1976**, *48*, 247.

(29) (a) Strauss, H. L.; Katz, T. J.; Fraenkel, G. K. *J. Am. Chem. Soc.* **1963**, *85*, 2360. (b) Smid, J.; Chan, L. L. *J. Am. Chem. Soc.* **1968**, *90*, 4654. (c) Cox, R. H.; Harrison, L. W.; Austin, W. K. *J. Phys. Chem.* **1973**, *77*, 200.

(30) (a) Beer, P. D. *Chem. Soc. Rev.* **1989**, *18*, 409. (b) Medina, J. C.; Goodnow, T. T.; Rojas, M. T.; Atwood, J. L.; Lynn, B. C.; Kaifer, A. E.; Gokel, G. W. *J. Am. Chem. Soc.* **1992**, *114*, 10583 and references therein. (c) Delgado, M.; Wolf, R. E.; Hartman, J. R.; McCafferty, G.; Yagbusan, R.; Rawle, S. C.; Watkin, D. J.; Cooper, S. R. *J. Am. Chem. Soc.* **1992**, *114*, 8983 and references therein. (d) Miller, S. M.; Gustowski, D. A.; Chen, Z.; Gokel, G. W.; Echegoyen, L.; Kaifer, A. E. *Anal. Chem.* **1988**, *60*, 2021 and references therein. (e) Bock, H.; Herrmann, H.-F. *New J. Chem.* **1992**, *16*, 29.

(31) Horowitz, C. P.; Schriver, D. P. *Adv. Organomet. Chem.* **1984**, *23*, 219.

(32) Ellis, J. E. *Adv. Organomet. Chem.* **1990**, *31*, 1.

(33) Ruiz, J.; Lacoste, M.; Astruc, D. *J. Am. Chem. Soc.* **1990**, *112*, 5471.

(34) (a) Loupy, A.; Tchoubar, B. *Salt Effects in Organic and Organometallic Chemistry*; VCH: Weinheim, Germany, 1992. (b) Loupy, A.; Tchoubar, B.; Astruc, D. *Chem. Rev.* **1992**, *92*, 1141.

(35) (a) Vleck, A. A. *Prog. Inorg. Chem.* **1963**, *5*, 211. (b) Frumkin, A. N.; Nikolaeva-Fedorovich, N. *Prog. Polarogr.* **1962**, *1*, 223.

(36) (a) Koltoff, I. M.; Tomsicek, W. J. *J. Phys. Chem.* **1935**, *39*, 945. (b) Halianah, G. I. H.; Irvine, D. H.; Eaton, W. A.; George, P. *J. Phys. Chem.* **1967**, *71*, 2022. (c) Peter, L. M.; Durr, W.; Bondre, P.; Gerisher, H. *J. Electroanal. Chem. Interfacial Electrochem.* **1976**, *71*, 31.

(37) (a) Lintvedt, R. L.; Kramer, L. S. *Inorg. Chem.* **1983**, *22*, 796. (b) Lintvedt, R. L.; Ranger, G.; Schoenfelner, B. A. *Inorg. Chem.* **1984**, *23*, 688. (c) Lintvedt, R. L.; Schoenfelner, B. A.; Rupp, K. A. *Inorg. Chem.* **1986**, *25*, 2704.

(38) (a) Bohling, D. A.; Evans, J. F.; Mann, K. R. *Inorg. Chem.* **1982**, *21*, 3546. (b) Hill, M. G.; Mann, K. R. *Inorg. Chem.* **1991**, *30*, 1429. (c) Hill, M. G.; Lammanna, W. M.; Mann, K. R. *Inorg. Chem.* **1991**, *30*, 4687.

Synthesis and Coordination Chemistry of a Novel Phosphinimine Phosphine

Chung-Yuan Liu, Der-Yi Chen, Ming-Chu Cheng, Shie-Ming Peng, and Shiuh-Tzung Liu*

Department of Chemistry, National Taiwan University, Taipei, Taiwan 106, Republic of China

Received November 16, 1994[®]

The incorporation of a phosphinimino moiety into phosphine ligands to form a new bidentate $\text{Ph}_3\text{P}=\text{N}(\text{CH}_2)_3\text{PPh}_2$ (**1**) is reported. Compound **1** can act as a σ -N and σ -P donor ligand or react with metal carbonyls to form isocyanide complexes. Complexes of $(\text{CO})_4\text{M}-(1-P,N)$ [$\text{M} = \text{Mo}$ (**2**), W (**3**)] were prepared from the reaction of $\text{Et}_4\text{N}[\text{M}(\text{CO})_5\text{Br}]$ with **1** in refluxing THF solution, whereas the isocyanide complexes of $(\text{CO})_5\text{MCN}(\text{CH}_2)_3\text{PPh}_2$ [$\text{M} = \text{Cr}$ (**4**), Mo (**5**), W (**6**)] are obtained from the reaction of $\text{M}(\text{CO})_6$ with **1** at 25 °C. The deoxygenation nature is also shown in the reaction of $\text{CpFe}(\text{CO})_2\text{I}$, $\text{CpRu}(\text{CO})_2\text{I}$, $\text{Re}(\text{CO})_5\text{Br}$, and $\text{Re}_2(\text{CO})_{10}$ with **1** to form the corresponding isocyanide complexes $[\text{CpFe}(\text{CO})\{\text{CN}(\text{CH}_2)_3\text{PPh}_2-C,P\}]\text{I}$ (**7**), $\text{CpRu}(\text{CO})\{\text{CN}(\text{CH}_2)_3\text{PPh}_2-C\}$ (**10**), $\text{BrRe}(\text{CO})_{5-n}\{\text{CN}(\text{CH}_2)_3\text{PPh}_2-C\}_n$ [$n = 1$ (**12**), 2 (**14**)], and $\text{Re}_2(\text{CO})_9\{\text{CN}(\text{CH}_2)_3\text{PPh}_2-C\}$ (**15**), respectively. The free phosphine of **10** underwent exchange with one triphenylphosphine ligand in $\text{CpRu}(\text{PPh}_3)_2\text{Cl}$ to yield the binuclear species $[\text{CpRu}(\text{PPh}_3)\text{Cl}\{\text{P}(\text{Ph}_2)(\text{CH}_2)_3\text{NC}\}\text{Ru}(\text{CO})\text{CpI}]$ (**11**), whereas intramolecular ligand substitution occurred in both **12** and **15** to give $\text{Br}(\text{CO})_3\text{Re}\{\text{CN}(\text{CH}_2)_3\text{PPh}_2-C,P\}$ (**13**) and $\{\mu-\text{CN}(\text{CH}_2)_3\text{PPh}_2\}\text{Re}_2(\text{CO})_8$ (**16**). Reaction of $(\text{COD})\text{PdCl}_2$ with **1** produced the complex $(1-P,N)\text{PdCl}_2$ (**18**), in which **1** acts as a σ -N, σ -P bidentate ligand. X-ray crystal structural analysis of $[\text{CpFe}(\text{CO})\{\text{CN}(\text{CH}_2)_3\text{PPh}_2-C,P\}]\text{PF}_6$ (**7a**) and **18** confirmed the formulation of both complexes. The $\text{C}\equiv\text{N}$ bond distance [$1.20(3)$ Å] of **7a** is greater than those in the related iron–isocyanide complexes; the angle $\text{C}-\text{N}-\text{C}$ [$141(2)^\circ$] deviates from 180° , indicating that the resonance contribution of $\text{Fe}=\text{C}=\text{N}-$ is more important than that of $\text{Fe}-\text{C}\equiv\text{N}-$. These observations are consistent with spectral data, the smaller infrared stretching wavenumber (2089 cm^{-1}), and the greater shift (^{13}C NMR δ 183.7 ppm) of the isocyanide moiety of **7**.

Introduction

The nature of the highly polar P–N bond in phosphinimine makes a ligand of this kind versatile in both coordination and organometallic chemistry.^{1–14} The nitrogen atom of phosphinimine is able to act as a two-

electron donor for complexation with various metal ions^{2,3} and as a four-electron donor (bridging mode) in $\text{Mo}_2(\text{CO})_6(\text{Ph}_3\text{PNH})_3$.⁴ Furthermore, phosphinimines can react with metal carbonyl complexes⁶ and metal oxides⁷ to produce isocyanide and nitrene functions, respectively, by elimination of phosphine oxide.

Incorporation of a phosphinimino moiety with other donor atoms to form a chelate bidentate has been reported for $9,10\text{-H}_2\text{NC}_{14}\text{H}_8\text{N}=\text{PPh}_3$,⁸ $o\text{-(HO)C}_6\text{H}_4\text{N}=\text{PPh}_3$,⁹ $8\text{-(Ph}_3\text{P}=\text{N}-\text{C}_9\text{H}_6\text{N})$,¹⁰ $(\eta^1\text{-C}_5\text{Me}_5)\text{P}=\text{N}(t\text{-Bu})$,¹¹ $\text{Ph}_3\text{P}=\text{NC}_6\text{H}_4\text{N}=\text{PPh}_3$,^{7b,12} $\text{Ph}_2\text{P}(=\text{NR})\text{CH}_2\text{PPh}_2(=\text{NR})$,¹³ and $\text{PhN}=\text{P}(\text{Ph}_2)\text{CH}=\text{CH}(p\text{-Tol})(\text{NH}_2)$.¹⁴ Among these bidentate ligands, only one phosphine–phosphinimine, $\text{Ph}_2\text{PCH}_2\text{PPh}_2(=\text{NSiMe}_3)$, is reported,¹⁵ for which the coordination mode toward metal ions is confined due to the short carbon chain. We recently showed that the phosphinimine function is stable toward the phosphide nucleophile, which allows us to prepare the potential bidentate phosphino–phosphinimine ligands **1**.¹⁶ Analogous to $\text{Ph}_2\text{PCH}_2\text{PPh}_2(=\text{NSiMe}_3)$, one expects compound **1** to be able to coordinate in a σ -N and σ -P chelate mode toward metal ions and that compound **1** would react

[®] Abstract published in *Advance ACS Abstracts*, March 15, 1995.

(1) Dehnicke, K.; Strahle, J. *Polyhedron* **1989**, *8*, 707.
 (2) Choukroun, R.; Gervais, D.; Dilworth, J. R. *Transition Met. Chem.* **1979**, *4*, 249.
 (3) (a) Sleiman, H. F.; Mercer, S.; McElwee-White, L. *J. Am. Chem. Soc.* **1989**, *111*, 8007. (b) Briggs, E. M.; Brown, G. W.; Jiricny, J. *J. Inorg. Nucl. Chem.* **1979**, *41*, 667.
 (4) Miller, J. S.; Visscher, M. O.; Caulton, K. G. *Inorg. Chem.* **1974**, *13*, 1632.
 (5) Roesky, H. W.; Munzenberg, J.; Bohra, R.; Noltemeyer, M. *J. Organomet. Chem.* **1991**, *418*, 339.
 (6) (a) Alper, H.; Partis, R. A. *J. Organomet. Chem.* **1972**, *35*, C40. (b) Mirkin, C. A.; Lu, K.-L.; Geoffroy, G. L. *J. Am. Chem. Soc.* **1989**, *111*, 7279. (c) Lin, Y.-W.; Gau, H.-M.; Wen, Y.-S.; Lu, K.-L. *Organometallics* **1992**, *11*, 1445.
 (7) (a) Maatta, E. A.; Haymore, B. L.; Wentworth, R. A. *D. Inorg. Chem.* **1980**, *19*, 1055. (b) Maatta, E. A.; Kim, C. *Inorg. Chem.* **1989**, *28*, 623. (c) Chatt, J.; Rowe, G. A. *J. Chem. Soc. A* **1969**, 2288. (d) Chong, A. O.; Oshima, K.; Sharpless, K. B. *J. Am. Chem. Soc.* **1977**, *99*, 3420.
 (8) Dapporto, P.; Denti, G.; Dolcetti, G.; Ghedini, M. *J. Chem. Soc., Dalton Trans.* **1983**, 779.
 (9) Charalambous, J.; Kensett, M. J.; Jenkins, J. M. *J. Chem. Res., Synop.* **1982**, 306.
 (10) Saravanamuthu, A.; Ho, D. M.; Kerr, M. E.; Fitzgerald, C.; Bruce, M. R. M.; Bruce, A. E. *Inorg. Chem.* **1993**, *32*, 2202.
 (11) Gudat, D.; Niecke, E.; Krebs, B.; Dartmann, M. *Organometallics* **1986**, *5*, 2376.
 (12) Herring, D. L. *J. Org. Chem.* **1961**, *26*, 3998.
 (13) Imhoff, P.; van Asselt, R.; Elsevier, C. J.; Zoutberg, M. C.; Stam, C. H. *Inorg. Chim. Acta* **1991**, *184*, 73.

(14) Fernandez, M. J.; Del Val, J. J.; Oro, L. A.; Palacios, F.; Barluenga, J. *Polyhedron* **1987**, *6*, 1999.

(15) (a) Katti, K. V.; Cavell, R. G. *Organometallics* **1988**, *7*, 2236. (b) Katti, K. V.; Cavell, R. G. *Inorg. Chem.* **1989**, *28*, 413. (c) Katti, K. V.; Cavell, R. G. *Inorg. Chem.* **1989**, *28*, 3033. (d) Katti, K. V.; Cavell, R. G. *Organometallics* **1989**, *8*, 2147. (e) Katti, K. V.; Batchelor, R. J.; Einstein, F. W. B.; Cavell, R. G. *Inorg. Chem.* **1990**, *29*, 808. (f) Katti, K. V.; Cavell, R. G. *Organometallics* **1991**, *10*, 539.
 (16) Liu, S.-T.; Liu, C.-Y. *J. Org. Chem.* **1992**, *57*, 6079.

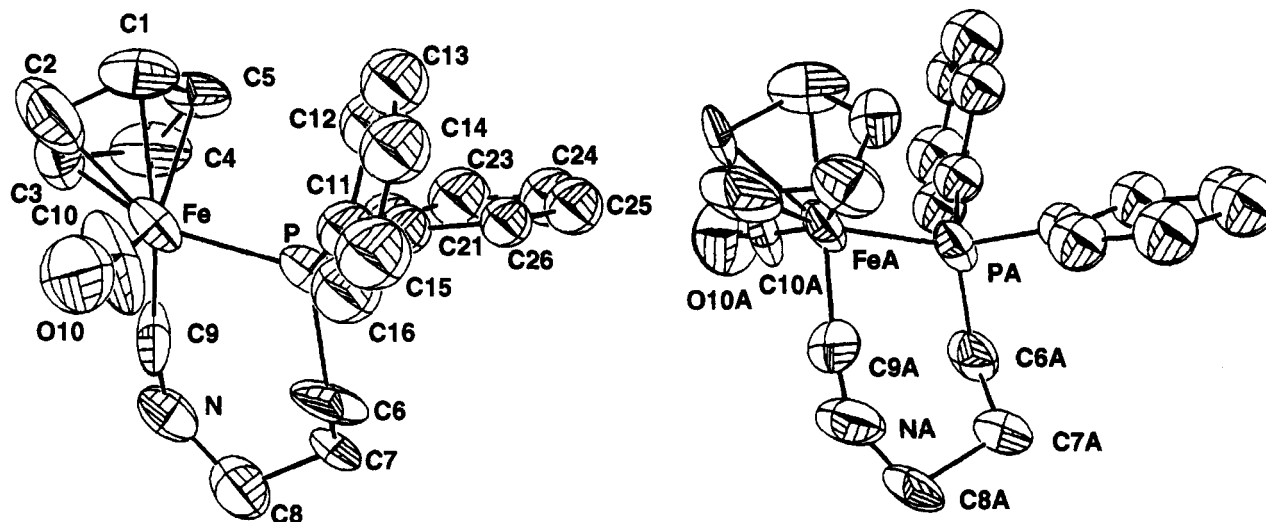
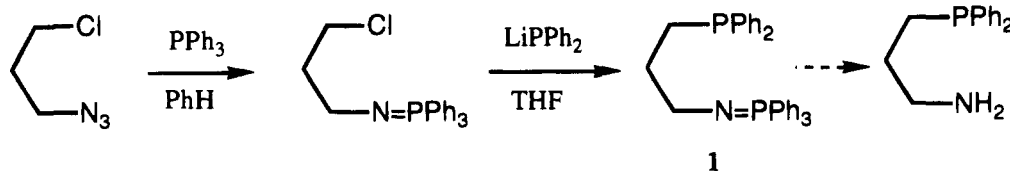
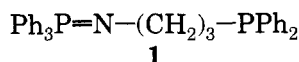


Figure 1. ORTEP view of the cation of complex **7a** showing 50% probability thermal ellipsoids. Two independent molecules exist in the unit cell.

Scheme 1



with a metal–carbonyl ligand to form a new ligand $\text{CN}(\text{CH}_2)_3\text{PPh}_2$ of bidentate type in either a bridging or a chelating mode. Here we report the results of coordination chemistry of **1** toward various metal complexes.



Results and Discussion

The ligand $\text{Ph}_3\text{P}=\text{N}(\text{CH}_2)_3\text{PPh}_2$ was obtained after isolation of the intermediate in the synthesis of $\text{H}_2\text{N}(\text{CH}_2)_3\text{PPh}_2$ (Scheme 1).¹⁶ This phosphino–phosphinimine **1** is stable in air but sensitive to moisture. The ^{31}P NMR spectrum of the new ligand displays two singlets at -16.0 and 4.3 ppm in benzene- d_6 for diphenylphosphino and iminophosphorane moieties, respectively. The ^{31}P chemical shift corresponding to the moiety of $\text{Ph}_3\text{P}=\text{N}-$ is varied from nonpolar solvent to polar solvent. Thus the chemical shift of the phosphinimino moiety is 12.1 ppm in CDCl_3 , indicating the polar nature of the P–N bond.

Addition of **1** to a stirred tetrahydrofuran solution of $\text{NEt}_4[\text{M}(\text{CO})_5\text{Br}]$ ($\text{M} = \text{Mo}, \text{W}$) at refluxing temperature results in the formation of chelate complexes $(\text{CO})_4\text{M}-(1-P,N)$ [**2**, $\text{M} = \text{Mo}$; **3**, $\text{M} = \text{W}$]. Both complexes were isolated as solids stable in air and characterized by spectral methods. The carbonyl stretching wavenumbers of the complexes occur in the 2010 – 1900 cm^{-1} region, which is in accord with a tetracarbonyl species. The ^{31}P NMR spectrum displays two sets of doublets [39.4 (d, $J = 14$ Hz), 16.3 (d, $J = 14$ Hz) ppm for **2** and 37.9 (d, $J = 18$ Hz), 2.67 (dt, $J_{\text{P-P}} = 18$ Hz, $J_{\text{P-W}} = 224$ Hz) ppm for **3**] due to phosphorus atoms of two kinds coupled to each other. Both the coordination chemical shifts and long range phosphorus–phosphorus couplings verify the existence of the $\text{Ph}_3\text{P}=\text{N}-$ moiety in the complexes. The infrared spectra of both **2** and **3** exhibit

Table 1. Infrared Absorptions and ^{13}C NMR Chemical Shifts of Isocyanide Complexes^a

complex	$\nu_{\text{CN}}, \text{cm}^{-1}$	^{13}C NMR, ppm	ref
4	2173	162.5	this work
5	2173	153.4	this work
6	2175	143.0	this work
7	2089	183.7 (d, $J_{\text{P-C}} = 35$ Hz)	this work
$[\text{CpFe}(\text{PPh}_3)(\text{CO})(\text{CNCH}_3)]\text{BF}_4$	2194		20
10	2170	145.1	this work
11	2170	144.9, 144.8 ^c	this work
12	2222	129.2	this work
$\text{ReBr}(\text{CO})_4(\text{CNPr})$	2221	129.4	21
13	2138	163(d, $J_{\text{P-C}} = 6.8$ Hz)	this work
<i>fac</i> - $\text{Re}(\text{CO})_3(\text{CN}^i\text{Bu})(\text{PPh}_2\text{Me})\text{Br}$	2186		23
<i>fac</i> - $\text{Re}(\text{CO})_3(\text{CN}^i\text{Bu})(\text{PPh}_3)\text{Br}$	2181		23
14	2219, 2192	134.3	this work
$\text{ReBr}(\text{CO})_3(\text{CNPr})_2$	2219, 2197	134.5	21
15	2187	134.5	this work
$\text{Re}_2(\text{CO})_9(\text{CN}^i\text{Bu})$	2173 ^d		22
16	2156 ^b	178.9	this work
17	2221	130.7	this work

^a Recorded in CH_2Cl_2 for IR and in CDCl_3 for ^{13}C NMR, unless otherwise noted. ^b KBr. ^c Diastereomers. ^d In hexane.

no band that could be assigned to $\text{C}\equiv\text{N}-$ modes, in agreement with the structural formulation. Apparently, compound **1** acts as a simple chelate ligand (a σ -N and σ -P chelate mode) in $\text{Mo}(0)$ and $\text{W}(0)$ complexes.

Deoxygenation of the carbonyl group took place in the reaction of **1** with $\text{M}(\text{CO})_6$ at room temperature to yield the corresponding isocyanide complex $(\text{CO})_5\text{M}[\text{CN}(\text{CH}_2)_3\text{PPh}_2\text{-C}]$ [**4**, $\text{M} = \text{Cr}$; **5**, $\text{M} = \text{Mo}$; **6**, $\text{M} = \text{W}$]. The structural determination of **4**–**6** was confirmed by infrared and NMR spectra. Infrared spectra of these series complexes exhibit characteristic absorptions at ca. 2174 cm^{-1} for the coordinated isocyanide group and

Table 2. Atomic Parameters and Thermal Parameters of **7a**

	<i>x</i>	<i>y</i>	<i>z</i>	<i>B</i> _{eq} , Å ²
Fe	0.8039(4)	0.10504(21)	0.3151(3)	4.74(20)
FeA	-0.2101(4)	0.60450(21)	0.1790(3)	4.93(21)
P	0.9299(8)	0.0482(4)	0.2060(5)	4.5(4)
PA	-0.0815(8)	0.5491(4)	0.2933(5)	4.5(4)
C1	0.693(3)	0.0222(15)	0.3925(16)	5.8(15)
C2	0.644(3)	0.0930(17)	0.4132(22)	9.4(22)
C3	0.764(3)	0.1324(15)	0.4491(18)	6.3(16)
C4	0.891(3)	0.0897(16)	0.4446(17)	6.7(16)
C5	0.8376(25)	0.0201(14)	0.4105(15)	5.0(14)
C6	1.000(3)	0.1108(13)	0.1170(16)	6.4(17)
C7	1.138(3)	0.1578(13)	0.1465(18)	7.1(17)
C8	1.106(3)	0.2374(15)	0.1836(18)	6.6(18)
N	0.9989(22)	0.2295(10)	0.2562(13)	5.6(12)
C9	0.9133(25)	0.1844(14)	0.2854(18)	5.6(15)
C10	0.668(3)	0.1222(15)	0.2373(23)	9.4(21)
O10	0.5616(20)	0.1276(12)	0.1930(13)	9.1(13)
C11	0.818(3)	-0.0158(14)	0.1395(15)	4.9(6)
C12	0.778(3)	-0.0877(15)	0.1793(16)	5.7(7)
C13	0.678(3)	-0.1348(15)	0.1320(16)	5.9(7)
C14	0.622(3)	-0.1131(15)	0.0470(16)	5.9(7)
C15	0.659(3)	-0.0480(16)	0.0074(18)	6.9(8)
C16	0.753(3)	0.0006(15)	0.0554(17)	6.4(7)
C21	1.0888(24)	-0.0072(13)	0.2416(14)	4.1(6)
C22	1.176(3)	0.0137(14)	0.3150(16)	5.5(7)
C23	1.301(3)	-0.0266(15)	0.3377(17)	6.5(7)
C24	1.346(3)	-0.0803(15)	0.2771(16)	5.9(7)
C25	1.265(3)	-0.1006(14)	0.2047(15)	5.3(7)
C26	1.1355(24)	-0.0681(13)	0.1824(14)	3.9(6)
C1A	-0.109(3)	0.5891(15)	0.0512(17)	6.6(16)
C2A	-0.246(4)	0.6364(15)	0.0397(19)	8.5(20)
C3A	-0.364(3)	0.5954(15)	0.0664(19)	7.5(17)
C4A	-0.307(3)	0.5193(15)	0.0988(16)	6.5(16)
C5A	-0.162(3)	0.5223(14)	0.0827(14)	4.5(14)
C6A	-0.009(3)	0.6139(14)	0.3840(16)	5.3(15)
C7A	0.124(3)	0.6643(14)	0.3626(18)	6.1(16)
C8A	0.074(3)	0.7477(14)	0.3228(19)	6.9(18)
NA	-0.029(3)	0.7323(11)	0.2462(13)	7.1(14)
C9A	-0.104(3)	0.6870(14)	0.2157(16)	6.3(16)
C10A	-0.350(3)	0.6229(14)	0.2482(17)	5.2(14)
O10A	-0.4500(20)	0.6329(12)	0.2949(12)	8.7(13)
C11A	-0.1901(25)	0.4821(13)	0.3532(15)	4.6(6)
C12A	-0.252(3)	0.4972(15)	0.4341(16)	5.6(7)
C13A	-0.344(3)	0.4453(17)	0.4784(19)	8.1(8)
C14A	-0.369(3)	0.3783(16)	0.4340(18)	7.1(8)
C15A	-0.319(3)	0.3588(16)	0.3554(18)	7.6(8)
C16A	-0.222(3)	0.4086(14)	0.3099(16)	5.6(7)
C21A	0.0803(24)	0.4988(13)	0.2652(14)	3.9(6)
C22A	0.129(3)	0.4378(15)	0.3219(16)	5.7(7)
C23A	0.268(3)	0.4053(15)	0.3038(16)	5.8(7)
C24A	0.344(3)	0.4237(16)	0.2312(17)	6.6(7)
C25A	0.297(3)	0.4861(16)	0.1718(17)	6.7(7)
C26A	0.165(3)	0.5195(15)	0.1943(16)	5.5(7)
P1	0.2762(10)	0.7122(5)	-0.0048(6)	7.3(5)
F1	0.373(3)	0.7305(10)	0.0772(15)	15.7(16)
F2	0.189(3)	0.6917(14)	-0.0872(16)	19.2(20)
F3	0.2680(23)	0.6285(9)	0.0263(13)	12.4(14)
F4	0.2832(24)	0.7966(12)	-0.0284(18)	18.1(20)
F5	0.1334(22)	0.7286(12)	0.0395(17)	15.5(17)
F6	0.4217(23)	0.6960(13)	-0.0516(14)	15.4(16)
P2	0.6984(10)	0.7900(5)	0.4896(6)	7.0(5)
F7	0.643(3)	0.7798(10)	0.5868(12)	13.4(15)
F8	0.752(3)	0.8018(12)	0.3930(12)	15.2(16)
F9	0.703(3)	0.8747(9)	0.5146(15)	14.8(16)
F10	0.6975(23)	0.7042(10)	0.4713(15)	13.5(15)
F11	0.8552(20)	0.7828(12)	0.5213(15)	14.3(16)
F12	0.5378(21)	0.7955(12)	0.4558(13)	13.4(14)

at ca. 2070 and 1955 cm⁻¹ for the pentacarbonylmetal moiety. The ¹³C NMR shifts of the isocyanide carbon appear at 162.5 ppm for **4**, 153.4 ppm for **5**, and 143.0 ppm for **6**, respectively. Both IR and NMR data indicate the existence of an isocyanide function. The formation of isocyanide complex is presumably preceded by the nucleophilic attack of iminophosphorane at the carbonyl ligand followed by the elimination of triphenylphosphine

Table 3. Selected Bond Distances (Å) and Bond Angles (deg)

Complex 7a			
Fe-P	2.229(9)	FeA-PA	2.229(9)
Fe-C9	1.77(2)	FeA-C9A	1.80(2)
Fe-C10	1.67(3)	FeA-C10A	1.69(2)
C9-N	1.20(3)	C9A-NA	1.12(3)
N-C8	1.47(3)	NA-C8A	1.45(3)
C10-O10	1.16(3)	C10A-O10A	1.17(3)
C10-Fe-P	90(1)	C10A-FeA-PA	92.2(8)
C10-Fe-C9	96(1)	C10A-FeA-C9A	95(1)
C9-Fe-P	82.0(8)	C9A-FeA-PA	82.7(8)
Fe-C9-N	169(2)	FeA-C9A-NA	171(2)
C9-N-C8	141(2)	C9A-NA-C8A	142(2)
Fe-C10-O10	169(3)	FeA-C10A-O10A	177(2)
Complex 18			
Pd-Cl1	2.371(2)	Pd-N	2.067(5)
Pd-Cl2	2.277(2)	P2-N	1.575(6)
Pd-P1	2.203(2)		
Cl1-Pd-Cl2	91.17(8)	P1-Pd-N	83.5(2)
Cl2-Pd-P1	92.19(8)	P2-N-C8	119.4(4)
Cl2-Pd-N	175.1(2)	P2-N-Pd	125.6(3)
Cl1-Pd-P1	171.17(8)	C8-N-Pd	112.8(4)
Cl1-Pd-N	93.4(2)		

oxide.⁶ It appears that the carbonyl ligand of M(CO)₆ is more reactive toward nucleophilic attack by the iminophosphorane than that of [M(CO)₅Br]⁻. Such a difference is believed due to the poorer M-C back-bonding of M(CO)₆ compared with that of [M(CO)₅Br]⁻.

Reaction of phosphine-phosphinimine **1** with CpFe(CO)₂I [Cp = η⁵-C₅H₅] in toluene at 25 °C yielded a yellow precipitate {CpFe(CO)[CNCH₂CH₂CH₂PPh₂-P,C]}I (**7**) and triphenylphosphine oxide; the desired complex was purified by extraction of Ph₃P=O with toluene from the reaction mixture. Anionic metathesis of **7** with NH₄PF₆ gave {CpFe(CO)[CNCH₂CH₂CH₂-PPh₂-P,C]}PF₆ (**7a**) as a crystalline solid upon recrystallization. The phosphinimine function of **1** acts as a deoxygenating agent, which reacts with the carbonyl ligand to form an isocyanide moiety. In the infrared spectrum of **7**, the stretching wavenumbers corresponding to isocyanide (2089 cm⁻¹) and carbonyl (1998 cm⁻¹) were observed, clearly indicating the existence of both moieties around the metal center. An ORTEP plot of the cation of **7a** is illustrated in Figure 1. Atomic coordinates and selected bond distances and angles are listed in Tables 2 and 3, respectively. The iron atom displays a slightly distorted octahedral geometry with one face occupied by the cyclopentadienyl moiety. The Fe-C9 distance [1.77(2) Å] is smaller and the C9-N distance [1.20(3) Å] is larger than the average bond distance of Fe-C (1.84 Å) and C-N (1.17 Å) in complexes of Fe(*t*-BuNC)₅,¹⁷ Fe(C₆H₅)(CO)₂(EtNC),¹⁸ and Fe₂(EtNC)₉,¹⁹ respectively. The angle C9-N-C8 [141-(2)°] is much deviated from 180°. All this information indicates that the nitrogen atom is no longer restrained in a linear environment, which implies that the reso-

(17) Bassett, J.-M.; Berry, D. E.; Barker, G. K.; Green, M.; Howard, J. A. K.; Stone, F. G. A. *J. Chem. Soc., Dalton Trans.* **1979**, 1003.

(18) Yamamoto, Y. *Coord. Chem. Rev.* **1980**, *32*, 193.

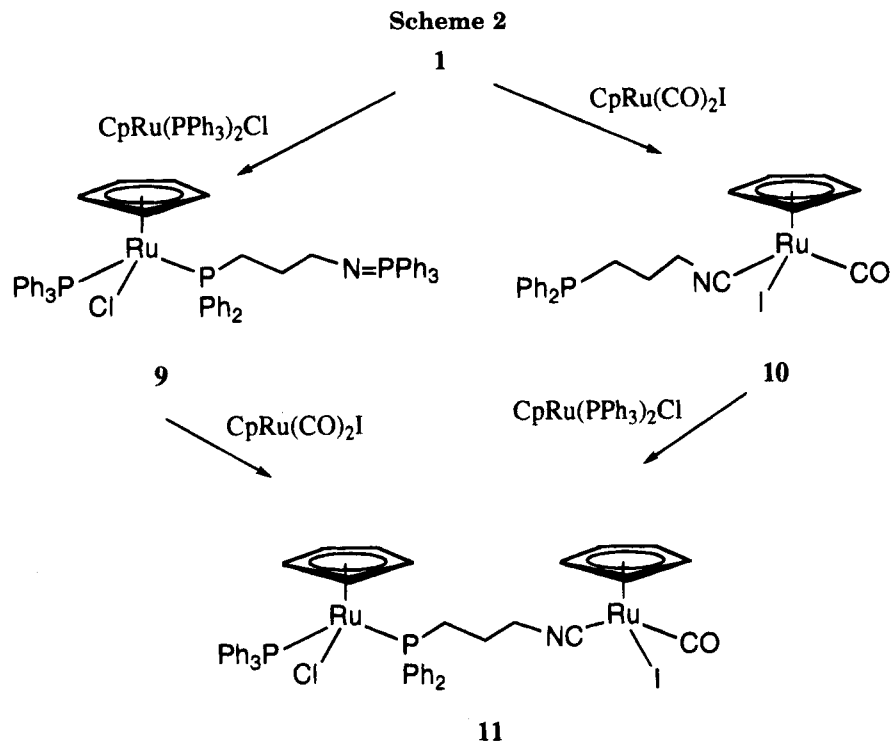
(19) Bassett, J.-M.; Barker, G. K.; Green, M.; Howard, J. A. K.; Stone, F. G. A.; Wolsey, W. C. *J. Chem. Soc., Dalton Trans.* **1981**, 219.

(20) Angelici, R. J.; Christian, P. A.; Dombek, B. D.; Pfeffer, G. A. *J. Organomet. Chem.* **1974**, *67*, 287.

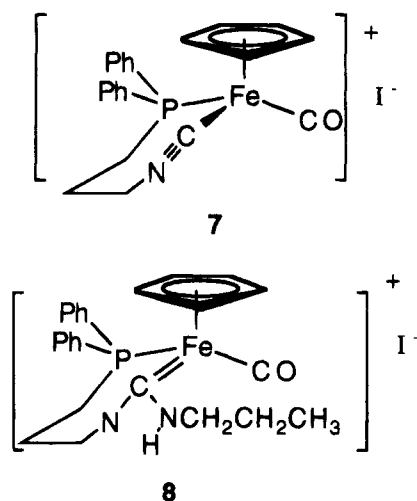
(21) Chen, L.-C.; Chen, M.-Y.; Chen, J.-H.; Wen, Y.-S.; Lu, K.-L. *J. Organomet. Chem.* **1992**, *425*, 99.

(22) Harris, G. W.; Coville, N. J. *Organometallics* **1985**, *4*, 908.

(23) Leins, A. E.; Coville, N. J. *J. Organomet. Chem.* **1994**, *464*, 183.



nance form $\text{Fe}=\text{C}=\text{N}-$ in the coordinated isocyanide group is much more important than $\text{Fe}-\text{C}\equiv\text{N}-$. This observation is also consistent with the smaller stretching wavenumber of isocyanide (2089 cm^{-1}) in **7** (Table 1) compared with $[\text{CpFe}(\text{PPh}_3)(\text{CO})(\text{CNCH}_3)]\text{BF}_4$ (2194 cm^{-1}). Complex **7** readily reacted with propylamine to give carbene complex **8**. The structure of this carbene metal complex was determined by spectral and elemental analyses (Experimental Section).

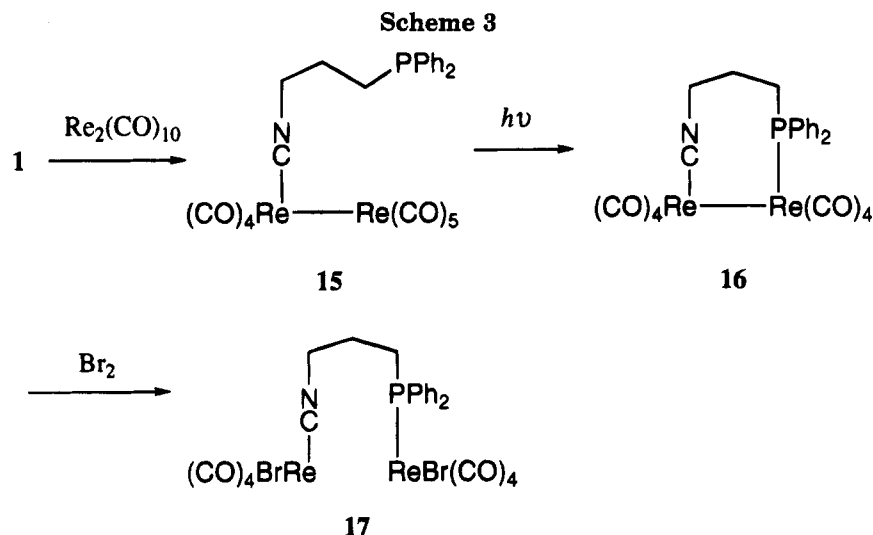


The chemistry of **1** toward ruthenium(II) complexes is summarized in Scheme 2. As expected, the ligand substitution reaction of $\text{CpRu}(\text{PPh}_3)_2\text{Cl}$ by the phosphino site of **1** took place immediately to yield the simple substituted complex **9**, but further substitution to form a $\sigma\text{-N}$ and $\sigma\text{-P}$ chelate complex did not occur, even under severe reaction conditions. Reaction of **1** with $\text{CpRu}(\text{CO})_2\text{I}$ produced isocyanide complex **10** accompanied by formation of triphenylphosphine oxide. Unlike the iron complex, the diphenylalkylphosphine moiety in **10** remained as a free donor. Attempts to prepare a chelating mode of $\text{CN}(\text{CH}_2)_3\text{PPh}_2$ complex, like the iron

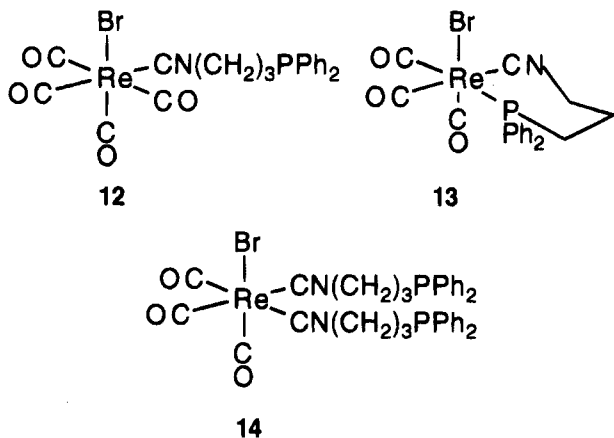
analog, failed. Nevertheless, the uncoordinating donors in both **9** and **10** become an advantage in preparation of a binuclear species. Thus reaction of either complex **9** with $\text{CpRu}(\text{CO})_2\text{I}$ or complex **10** with $\text{CpRu}(\text{PPh}_3)_2\text{Cl}$ yielded a bridging diruthenium complex **11**. As both ruthenium centers are chiral, the diastereomeric pair of complexes **11** were observed in ^{31}P NMR spectrum: one is 44.1 and 35.7 ppm; the other is 44.0 and 35.8 ppm. All these absorptions appear as doublets with phosphorus-phosphorus coupling constant 41 Hz. Attempts to separate these isomers by chromatography and recrystallization were unsuccessful.

The ruthenium complexes were characterized by spectral and elemental analyses. The ^{31}P NMR spectrum of complex **9** shows three sets of resonances: 44.1 (d, $J = 41\text{ Hz}$, PPh_3); 36.8 (d, $J = 41\text{ Hz}$, $-\text{PPh}_2$), and 13.0 (br, $-\text{N}=\text{PPh}_3$) ppm, in which the broad peak at 13.0 ppm corresponds to the free phosphinimine site. The naturally abundant ratio of ^{35}Cl and ^{37}Cl in the FAB mass spectrum of **9** indicates that the chloride is a coordinated ligand around the metal ion. The ^{31}P NMR spectrum of complex **10** shows only a signal due to a free diphenylalkylphosphine at $\delta -17.3\text{ ppm}$, thus indicating that the phosphine moiety did not coordinate to the metal center and the phosphinimine function disappeared. Both infrared and ^{13}C NMR spectra of **10** show the presence of a coordinated isocyanide (2107 cm^{-1}) and a carbonyl ligand [IR 2107 cm^{-1} (NC) and 1973 cm^{-1} (CO); ^{13}C NMR δ 145.1 ppm (CN) and 199.5 ppm (CO)]. On this basis with elemental analysis the ruthenium complexes **10** and **11** were assigned as formulated.

When $\text{Re}(\text{CO})_5\text{Br}$ reacted with **1** under thermal conditions, deoxygenation at the carbonyl ligand occurred in dichloromethane solution to form an isocyanide complex **12**. The phosphine site of **1** in complex **12** remained a free donor, but it underwent further substitution with carbonyl ligands to give **13**. Treatment of **12** with **1** in a further equimolar quantity provided the diisocyanide



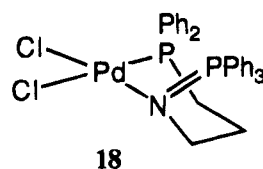
species **14** that has two free phosphine donors away from the metal center. The structures of **12–14** were confirmed by their spectral properties (see Experimental Section). The infrared stretching wavenumber of the isocyanide moiety (2138 cm^{-1}) in **13** is smaller than that of the other $\text{Re}-\text{CN}$ species and the ^{13}C NMR shift of isocyanide carbon (δ 163 ppm) is also greater than those of related species (Table 1), similar to complex **7** due to ring strain.



Reaction of phosphino-phosphinimine **1** with dirhenium decacarbonyl also yielded isocyanide complex **15** in which the phosphino site stays uncoordinated. On irradiation of **15** in chloroform with light, the phosphine exchanged a carbonyl ligand to form a bridging binuclear complex **16** (Scheme 3). Because of the ring strain of **16**, the properties of the coordinated isocyanide ligand in both infrared and ^{13}C NMR spectra show the same trend as in complexes **7** and **13**: a smaller wavenumber of the infrared stretching mode of $\text{CN}-$ and a considerable downfield chemical shift of ^{13}C NMR of $\text{CN}-$. The lack of phosphorus-carbon coupling of the isocyanide carbon supports assignment of a structure in which $\text{CN}(\text{CH}_2)_3\text{PPh}_2$ binds in a bridging mode, not a chelating one. Upon treatment of **16** with bromine, the cleavage of the metal-metal bond of **16** occurred to yield $\text{Br}(\text{CO})_4\text{Re}\{\mu_2-\text{CNCH}_2\text{CH}_2\text{CH}_2\text{PPh}_2-C,P\}\text{Re}(\text{CO})_4\text{Br}$ (**17**). As the ring strain lessens, the spectral data for the coordinated isocyanide ligand of **17** exhibit the normal features; i.e. both the infrared absorption and ^{13}C NMR chemical shift of the isocyanide group are similar to those of non-chelate complexes (Table 1).

Addition of (cyclooctadiene) PdCl_2 to $\text{Ph}_3\text{P}=\text{N}(\text{CH}_2)_3\text{PPh}_2$ (**1**) in dichloromethane resulted in formation of palladium complex **18** as a yellow solid. This compound is stable, even in the presence of moisture. Complex **18** in chloroform- d_1 solution exhibited a pair of doublets in the ^{31}P NMR spectrum at 17.2 and 40.5 ppm with a coupling constant of 3.3 Hz, clearly indicating that both phosphinimine and phosphine are coordinated at the metal center. The formulation of **18** is further confirmed with X-ray structural analysis.

The results of an X-ray structural analysis of **18** are depicted in Figure 2 and in Tables 3 and 4. The coordination environment about the metal center in **18** is slightly distorted square-planar with the two chloride ligands situated in a *cis* fashion. All bond distances and bond angles in **18** are in the normal range. The $\text{Pd}-\text{Cl}(1)$ bond [2.371(2) Å] is notably longer than $\text{Pd}-\text{Cl}(2)$ [2.277(2) Å] which is an indication of the *trans* influence of phosphorus versus nitrogen donors. Attempts to prepare nickel and platinum analogs of **18** were unsuccessful.



Summary

We have demonstrated various reactions of the phosphinimine-phosphine $\text{Ph}_3\text{P}=\text{N}(\text{CH}_2)_3\text{PPh}_2$ (**1**) toward metal complexes. For coordination of phosphinimine, compound **1** acts as a $\sigma\text{-P}$ donor (**I**), or in a $\sigma\text{-N}$ and $\sigma\text{-P}$ chelate fashion (**II**) (Chart 1). For deoxygenation of carbonyl, compound **1** becomes an isocyanide-phosphine ligand $\text{CN}(\text{CH}_2)_3\text{PPh}_2$, which acts as a $\sigma\text{-C}$ donor (**III**), a $\sigma\text{-C}$ and $\sigma\text{-P}$ chelate (**IV**), a $\sigma\text{-C}$ and $\sigma\text{-P}$ bridging mode with a metal-metal bond (**V**), and a $\sigma\text{-C}$ and $\sigma\text{-P}$ bridging mode without a metal-metal bond (**VI**).

Experimental Section

General Information. Nuclear magnetic resonance spectra were recorded on either a Bruker AC-E 200 or a AM-300 spectrometer. For ^{31}P NMR spectra, the chemical shifts are given in parts per million (δ) relative to 85% H_3PO_4 . Infrared spectra were measured on a Biorad FT-30 instruments. The

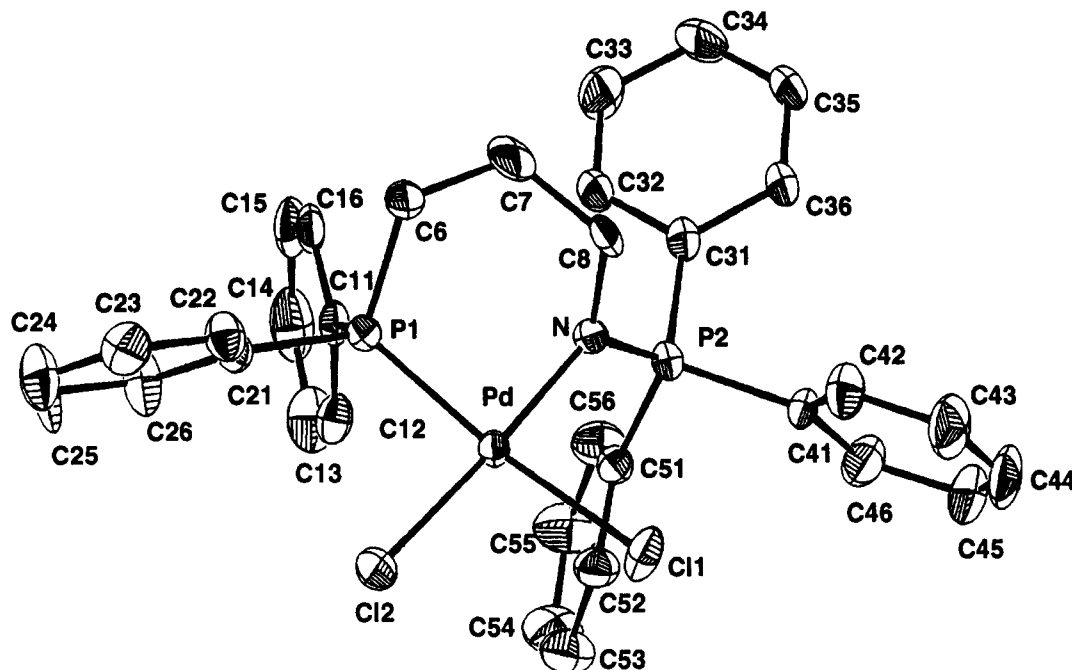


Figure 2. ORTEP diagram of palladium complex 18 showing 50% probability thermal ellipsoids.

Table 4. Atomic Coordinates and Thermal Parameters of 18

	x	y	z	$B_{eq}, \text{\AA}^2$
Pd	0.40595(5)	0.76395(4)	0.05976(3)	2.54(3)
C11	0.22543(19)	0.70733(15)	-0.01970(10)	4.61(11)
C12	0.52498(20)	0.78297(15)	-0.02029(10)	4.66(11)
P1	0.55445(19)	0.83510(14)	0.13482(10)	2.83(10)
P2	0.26680(19)	0.65156(15)	0.16298(10)	2.98(10)
N	0.3129(5)	0.7467(4)	0.13834(24)	2.7(3)
C6	0.4730(7)	0.9220(5)	0.1750(4)	4.2(5)
C7	0.3599(8)	0.8910(6)	0.2035(5)	6.4(6)
C8	0.2576(7)	0.8336(5)	0.1581(4)	4.1(4)
C12	0.6423(6)	0.7590(5)	0.1982(3)	3.1(4)
C12	0.6773(7)	0.6732(5)	0.1780(4)	3.8(4)
C13	0.7457(8)	0.6116(6)	0.2223(4)	5.9(5)
C14	0.7754(8)	0.6339(7)	0.2878(4)	6.5(6)
C15	0.7430(7)	0.7182(6)	0.3104(4)	5.3(5)
C16	0.6774(6)	0.7817(6)	0.2640(4)	4.1(4)
C21	0.6784(7)	0.9023(5)	0.1059(4)	3.2(4)
C22	0.6451(7)	0.9803(5)	0.0694(4)	4.1(4)
C23	0.7382(8)	1.0339(6)	0.0477(4)	5.0(5)
C24	0.8623(8)	1.0063(6)	0.0621(5)	6.2(6)
C25	0.8989(8)	0.9304(7)	0.0984(5)	7.6(7)
C26	0.8097(7)	0.8747(6)	0.1205(5)	5.5(5)
C31	0.2620(7)	0.6629(5)	0.2483(4)	3.3(4)
C32	0.3749(7)	0.6830(6)	0.2937(4)	4.1(4)
C33	0.3779(8)	0.6959(6)	0.3611(4)	5.6(5)
C34	0.2595(8)	0.6904(6)	0.3828(4)	6.2(6)
C35	0.1490(7)	0.6709(6)	0.3386(4)	5.4(5)
C36	0.1471(7)	0.6569(6)	0.2726(4)	4.2(4)
C41	0.1064(7)	0.6102(5)	0.1214(4)	3.3(4)
C42	0.0163(7)	0.6708(6)	0.0862(4)	5.0(5)
C43	-0.1067(8)	0.6372(7)	0.0561(5)	6.6(6)
C44	-0.1337(8)	0.5477(7)	0.0619(5)	7.0(6)
C45	-0.0493(9)	0.4863(7)	0.0963(5)	7.1(6)
C46	0.0748(8)	0.5175(6)	0.1261(4)	5.1(5)
C51	0.3744(7)	0.5580(5)	0.1530(4)	3.1(4)
C52	0.3928(7)	0.5353(5)	0.0915(4)	3.9(4)
C53	0.4628(8)	0.4583(6)	0.0823(4)	5.3(5)
C54	0.5183(9)	0.4064(6)	0.1359(5)	6.2(5)
C55	0.5056(9)	0.4280(6)	0.1981(4)	6.2(6)
C56	0.4333(8)	0.5045(6)	0.2078(4)	4.9(5)

Table 5. Crystal Data for Complexes 7a and 18

	7a	18
formula	$C_{22}H_{21}F_6NOP_2Fe$	$C_{33}H_{31}Cl_2NP_2Pd$
fw	547.2	680.75
cryst syst	triclinic	monoclinic
space group	$P\bar{1}$	$P2_1/n$
temp, K	298	298
a, \AA	9.175(13)	10.460(3)
b, \AA	17.514(9)	14.440(5)
c, \AA	14.481(25)	20.558(8)
α , deg	90.51(8)	
β , deg	92.28(12)	101.99(3)
γ , deg	90.61(8)	
V, \AA ³	2325(5)	3038(2)
2 θ range, deg	18.68–26.30	19.28–24.84
F(000)	1112	1384
Z	4	4
D_{calcd} , g cm ⁻³	1.563	1.489
μ , cm ⁻¹	8.440	9.757
scan width	$\omega-2\theta$	$\omega-2\theta$
radiation	Mo K α	Mo K α
cryst dimens, mm	0.20 \times 0.30 \times 0.35	0.30 \times 0.30 \times 0.35
scan width	2(1.00 + 0.35 tan θ)	2(0.90 + 0.35 tan θ)
transm range	0.551, 1.00	0.913, 1.00
2 θ_{max} , deg	45.0	45.0
no. of unique reflns	6055	3962
no. of reflns obsd ^a	1868	2821
computation	NRCS DP-VAX	NRCS DP-VAX
soln method	heavy atom	heavy atom
no. of params	475	352
R	0.089	0.044
R_w	0.084	0.033
S	2.67	2.51

^a $I > 2\sigma(I)$. ^b $R = \sum |F_o - F_c| / \sum (F_o)$; $R_w = [\sum w(F_o - F_c)^2 / \sum w(F_o)^2]^{1/2}$; $S = [\sum w(F_o - F_c)^2 / (\text{no. of reflns} - \text{no. of params})]$.

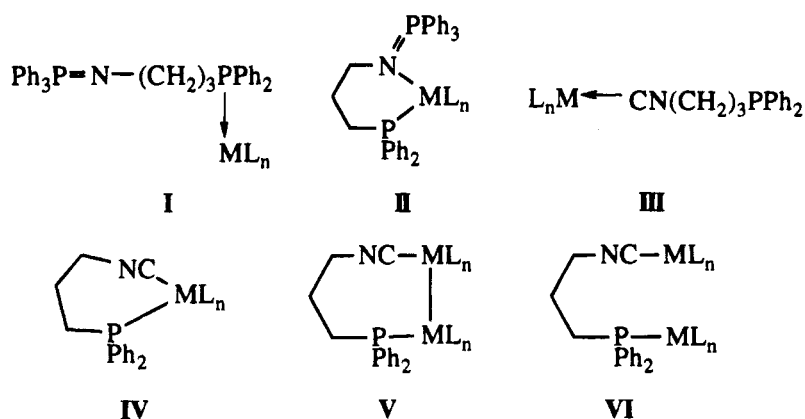
photochemical apparatus was a 450 W Conrad-Hanovia medium-pressure mercury lamp (Ace Glass).

All of the reaction, manipulation, and purification steps involving phosphines were performed under a dry nitrogen atmosphere. Tetrahydrofuran was distilled under nitrogen

from sodium benzophenone ketyl. Benzene and toluene were distilled from sodium under nitrogen. Dichloromethane was dried by CaH_2 and then distilled under nitrogen. Other chemicals and solvents were used from commercial sources without further purification.

N-(3-(Diphenylphosphino)propyl)triphenylphosphinimine, 1. To a benzene solution of 3-azidopropyl chloride (4.74 g, 39.6 mmol) was added a benzene solution of triphenylphosphine (10.4 g, 39.6 mmol). The resulting solution was stirred for 8 h, and the solvent was removed under reduced pressure. A white solid of (3-chloropropyl)tri-

Chart 1



phenylphosphinimine (15.14 g, 100%) was obtained, which was characterized by spectral methods: ^1H NMR δ 7.70–7.25 (m, 15 H, Ar H), 3.67 (t, $J = 6.6$ Hz, 2 H, $-\text{CH}_2\text{Cl}$), 3.20 (dt, $J = 16, 6.4$ Hz, 2 H, $-\text{CH}_2\text{NP}-$), 1.95 (dtt, $J = 1.2, 6.4, 6.4$ Hz, 2 H, $-\text{CH}_2-$); ^{13}C NMR δ (aliphatic carbon) 43.6 ($-\text{CCl}$), 42.1 (d, $J_{\text{P-C}} = 4.4$ Hz, $-\text{CN}=\text{P}$), 37.8 (d, $J_{\text{P-C}} = 18.7$ Hz, $-\text{CH}_2-$); ^{31}P NMR δ 12.4.

A solution of diphenylphosphide anion was prepared by the addition of a 1.6 M hexane solution of *n*-butyllithium (25 mL, 40 mmol) to a THF solution (100 mL) of diphenylphosphine (7.4 g, 39.7 mmol). This anion solution was then added to a solution of (3-chloropropyl)triphenylphosphinimine (15.4 g) in THF (100 mL) with stirring. The resulting mixture was kept stirred for 4 h, and solvents were removed under reduced pressure. The residue was dissolved in benzene and filtered. The filtrate was concentrated and recrystallized from acetonitrile to give the desired compound 1 as a white solid (13.2 g, 66%), which is quite sensitive to moisture: mp 120–122 °C; ^1H NMR (C_6D_6) δ 7.80–7.50 (m, 12 H, Ar H), 7.15–6.95 (m, 13 H, Ar H), 3.50 (dt, $J = 16, 6.4$ Hz, 2 H, $-\text{CH}_2\text{N}$), 2.41 (m, 2 H, $-\text{CH}_2\text{P}-$), 2.08 (m, 2 H, $-\text{CH}_2-$); ^{13}C NMR δ (aliphatic carbon) 46.8 (dd, $J = 14.4, 4.6$ Hz, $-\text{CNP}-$), 32.7 (dd, $J = 20.9, 14.8$ Hz, $-\text{CPh}_2$), 26.4 (d, $J = 11.5$ Hz, $-\text{CH}_2-$); ^{31}P NMR (C_6D_6) δ 4.3, -16.0 ; ^{31}P NMR (CDCl_3) δ 12.1 (br), -15.0 . HRMS Calcd for $\text{C}_{33}\text{H}_{31}\text{NP}_2$: m/z 503.1932. Found: $m/z = 503.1933$. Anal. Calcd for $\text{C}_{33}\text{H}_{31}\text{NP}_2$: C, 78.71; H, 6.21; N, 2.78. Found: C, 78.52; H, 6.26; N, 2.75.

{Ph₂P(CH₂)₃NPPh₃-P,N}Mo(CO)₄ (2). A mixture of 1 (201 mg, 0.40 mmol) and Et₄N[Mo(CO)₅Br] (175 mg, 0.38 mmol) in THF (10 mL) was heated to reflux for 8 h. The reaction mixture was filtered, and the filtrate was concentrated to give the desired complex 2 as a yellow solid (175 mg, 66%): mp 125–138 °C dec; IR (THF) ν_{CO} 2004, 1891, 1875, 1843 cm^{-1} ; ^1H NMR (CDCl_3) δ 7.71–7.20 (m, 25 H, Ar H), 3.47 (dm, $J_{\text{P-H}} = 20.7$ Hz, 2 H, $-\text{CH}_2\text{NP}-$), 2.62 (m, 2 H, $-\text{CH}_2\text{P}-$), 1.64 (m, 2 H, $-\text{CH}_2-$); ^{13}C NMR δ (aliphatic) 54.8 (d, $J = 5.1$ Hz, $-\text{CH}_2-\text{NP}-$), 29.3 (d, $J = 15.1$ Hz, $-\text{CPh}_2$), 28.0 (d, $J = 8.6$ Hz, $-\text{CH}_2-$); ^{31}P NMR δ 39.4 (d, $J = 14$ Hz), 16.3 (d, $J = 14$ Hz). Anal. Calcd for $\text{C}_{37}\text{H}_{31}\text{NO}_4\text{P}_2\text{Mo}$: C, 62.46; H, 4.39; N, 1.97. Found: C, 62.00; H, 4.80; N, 1.86.

{Ph₂P(CH₂)₃NPPh₃-P,N}W(CO)₄ (3). The preparation of 3 was similar to the procedure described for 2. Complex 3 is a yellow solid: mp 179–186 °C dec; IR (THF) ν_{CO} 1998, 1881, 1863, 1838 cm^{-1} ; ^1H NMR (CDCl_3) δ 7.22–7.40 (m, 25 H, Ar H), 3.67 (dm, $J_{\text{P-H}} = 19.5$ Hz, 2 H, $-\text{CH}_2\text{NP}-$), 2.77 (m, 2 H, $-\text{CH}_2\text{P}-$), 1.67 (m, 2 H, $-\text{CH}_2-$); ^{13}C NMR δ (aliphatic) 56.1 (d, $J = 5.7$ Hz, $-\text{CNP}-$), 29.4 (d, $J = 18.5$ Hz, $-\text{CPh}_2$), 27.8 (d, $J = 8.3$ Hz, $-\text{CH}_2-$); ^{31}P NMR δ 37.9 (d, $J = 18$ Hz), 2.67 (dt, $J_{\text{P-P}} = 18$ Hz, $J_{\text{P-W}} = 224$ Hz). Anal. Calcd for $\text{C}_{37}\text{H}_{31}\text{NO}_4\text{P}_2\text{W}$: C, 55.59; H, 3.91; N, 1.75. Found: C, 55.20; H, 3.90; N, 2.10.

General Procedure for Preparation of M(CO)₅(CNCH₂-CH₂CH₂PPh₂-C) [M = Cr, Mo, W]. A mixture of M(CO)₅ and 1 in equimolar quantity in THF was stirred at 25 °C for 40 h.

The reaction mixture was concentrated, and the residue was chromatographed on silica gel with elution of dichloromethane. A yellow band was collected and concentrated to give the desired product.

{Ph₂P(CH₂)₃NC-C}Cr(CO)₅ (4). A yellow liquid (46% yield): IR (CH_2Cl_2) ν_{CN} 2173 cm^{-1} , ν_{CO} 2066, 1955 cm^{-1} ; ^1H NMR δ 7.47–7.32 (m, 10 H, Ar H), 3.65 (t, $J = 6.4$ Hz, 2 H, $-\text{NCH}_2-$), 2.18 (m, 2 H, $-\text{CH}_2\text{P}-$), 1.85 (m, 2 H, $-\text{CH}_2-$); ^{13}C NMR δ 216.9, 214.9, 162.5 (CN-), 137.5 (d, $J = 11$ Hz), 132.6 (d, $J = 19$ Hz), 129.0, 128.7 (d, $J = 5.8$ Hz), 45.3 (d, $J = 14.3$ Hz), 26.1 (d, $J = 19.3$ Hz, $-\text{CH}_2\text{P}-$), 25.0 (d, $J = 12.7$ Hz, $-\text{CH}_2-$); ^{31}P NMR δ -17.66. Anal. Calcd for $\text{C}_{21}\text{H}_{16}\text{NO}_5\text{PCr}$: C, 56.64; H, 3.62; N, 3.15. Found: C, 56.60; H, 3.10; N, 2.94.

{Ph₂P(CH₂)₃NC-C}Mo(CO)₅ (5). A yellow liquid (50%): IR (CH_2Cl_2) ν_{CN} 2173 cm^{-1} , ν_{CO} 2071, 1952 cm^{-1} ; ^1H NMR δ 7.51–7.33 (m, 10 H, Ar H), 3.67 (t, $J = 6.5$ Hz, 2 H, $-\text{NCH}_2-$), 2.21 (m, 2 H, $-\text{CH}_2\text{PPh}_2$), 1.89 (m, 2 H, $-\text{CH}_2-$); ^{13}C NMR δ 206.7, 203.8, 153.4 (CN-), 137.4 (d, $J = 12.5$ Hz), 132.5 (d, $J = 19$ Hz), 129.0, 128.6 (d, $J = 6.8$ Hz), 44.8 (d, $J = 14.3$ Hz), 25.9 (d, $J = 18.2$ Hz), 24.9 (d, $J = 13.7$ Hz); ^{31}P NMR δ -17.71. Anal. Calcd for $\text{C}_{21}\text{H}_{16}\text{NO}_5\text{PMo}$: C, 51.55; H, 3.30; N, 2.80. Found: C, 51.52; H, 3.40; N, 2.83.

{Ph₂P(CH₂)₃NC-C}W(CO)₅ (6). A yellow liquid (67%): IR (CH_2Cl_2) ν_{CN} 2175 cm^{-1} , ν_{CO} 2068, 1956 cm^{-1} ; ^1H NMR δ 7.47–7.32 (m, 10 H, Ar H), 3.72 (t, $J = 6.5$ Hz, 2 H, $-\text{NCH}_2-$), 2.19 (m, 2 H, $-\text{CH}_2\text{P}-$), 1.89 (m, 2 H, $-\text{CH}_2-$); ^{13}C NMR δ 196.1, 194.3, 143.0, 137.4 (d, $J = 12.3$ Hz), 132.6 (d, $J = 18.2$ Hz), 129.0, 128.7 (d, $J = 6.9$ Hz), 45.0 (d, $J = 14.2$ Hz), 26.10 (d, $J = 18.3$ Hz), 25.0 (d, $J = 12.9$ Hz); ^{31}P NMR δ -17.75. Anal. Calcd for $\text{C}_{21}\text{H}_{16}\text{NO}_5\text{PW}$: C, 43.70; H, 2.79; N, 2.43. Found: C, 43.77; H, 2.76; N, 2.44.

[[Ph₂P(CH₂)₃NC-P,C]Fe(CO)] (7). A solution of CpFe(CO)₂I (75.9 mg, 0.25 mmol) and 1 (126 mg, 0.25 mmol) in toluene (20 mL) was stirred at room temperature for 4 h. A yellow precipitate formed during the reaction was collected by filtration. The yellow solid was washed with toluene and hexane to give the pure complex 7 (110 mg, 83%): mp 165–169 °C dec; IR (CHCl_3) 2089 (ν_{CN}), 1998 cm^{-1} (ν_{CO}); ^1H NMR (CDCl_3) δ 7.64–7.13 (m, 10 H), 4.97 (s, 5 H), 4.57–4.48 (m, 1 H), 3.67–3.56 (m, 1 H), 3.50–3.42 (m, 1 H), 2.74–2.62 (m, 1 H), 2.30–2.20 (m, 1 H), 2.20–2.05 (m, 1 H); ^{13}C NMR (CDCl_3) δ 213.0 (d, $J = 22.3$ Hz, $-\text{CO}$), 183.7 (d, $J = 35.1$ Hz, $-\text{NC}$), 133.9, 128.1 (m), 48.9, 32.0 (d, $J = 31$ Hz), 28.8 (d, $J = 4.8$ Hz); ^{31}P NMR (CDCl_3) δ 54.0; FAB $m/z = 402$. Anal. Calcd for $\text{C}_{22}\text{H}_{21}\text{INPOFe}$: C, 49.94; H, 4.00; N, 2.65. Found: C, 49.59; H, 4.05; N, 2.53.

[[Ph₂P(CH₂)₃NC-P,C]Fe(CO)]PF₆ (7a). A solution of 7 and excess NH_4PF_6 in acetone was stirred for 4 h. The reaction mixture was filtered and concentrated, and the residue was recrystallized from a mixed solvent (hexane/ CH_2Cl_2) to give 7a as a yellow solid quantitatively: mp 175–180 °C dec; IR (KBr) 2098 (ν_{CN}), 2011 cm^{-1} (ν_{CO}); ^1H NMR (CDCl_3) δ 7.64–7.13 (m, 10 H, Ar H), 4.87 (s, 5 H, Cp H), 4.03 (m, 1 H), 3.50

(m, 1 H), 2.96 (m, 1 H), 2.60 (m, 1 H), 2.20 (m, 1 H), 2.00 (m, 1 H); ^{31}P NMR (CDCl_3) δ 54.0, -143.6 (PF_6).

[$\text{Ph}_2\text{P}(\text{CH}_2)_3\text{NH}(n\text{-PrNH})\text{C}=\text{Fe}(\text{CO})\text{I}$] (8**).** A mixture of *n*-propylamine (5 mL) and **7** (450 mg, 0.166 mmol) in dichloromethane (20 mL) was stirred at 25 °C for 1 h. On removal of the solvent, the residue was crystallized from chloroform and pentane to give **8** as a yellow crystalline solid (435 mg, 87%): mp 185–190 °C dec; IR (CH_2Cl_2) $\nu(\text{CO})$ 1949 cm^{-1} ; ^1H NMR (CDCl_3) δ 8.31 (br, 1 H), 7.49–7.12 (m, 10 H), 6.40 (br, 1 H), 4.53 (s, 5 H), 4.35 (m, 1 H), 3.60 (m, 2 H), 3.50 (m, 1 H), 2.79 (m, 2 H), 2.17 (m, 1 H), 2.11 (m, 2 H), 1.30 (m, 1 H), 1.11 (t, $J = 7$ Hz, 3 H); ^{13}C NMR (CDCl_3) δ 218.6 (d, $J = 31.8$ Hz), 209.8 (d, $J = 25.6$ Hz), 139.2 (d, $J = 48.3$ Hz), 132.9 (d, $J = 47$ Hz), 132.8 (d, $J = 9.4$ Hz), 131.02 (d, $J = 1.9$ Hz), 130.2 (d, $J = 1.7$ Hz), 130.0 (d, $J = 8.6$ Hz), 129.0 (d, $J = 9.5$ Hz), 128.6 (d, $J = 9.8$ Hz), 84.7, 48.2, 45.5, 35.5 (d, $J = 22$ Hz), 24.8, 21.9, 11.6; ^{31}P NMR (CDCl_3) δ 56.5. Anal. Calcd for $\text{C}_{25}\text{H}_{30}\text{IN}_2\text{POFe}$: C, 51.05; H, 5.14; N, 4.76. Found: C, 52.12; H, 5.07; N, 4.84.

[$\text{CpRu}(\text{Ph}_2\text{P}(\text{CH}_2)_3\text{NPPH}_3\text{-P})(\text{PPh}_3)\text{Cl}$] (9**).** A mixture of $\text{CpRu}(\text{PPh}_3)_2\text{Cl}$ (634 mg, 0.873 mmol) and **1** (440 mg, 0.873 mmol) in benzene (40 mL) was heated to reflux for 4 h. The benzene solvent was replaced by ether, and a yellow precipitate was formed and collected. The precipitate was subsequently washed with ether (20 mL \times 2) to give complex **5** as a yellow solid (570 mg, 68%): mp 122–125 °C dec; ^1H NMR (CDCl_3) δ 7.80–6.95 (m, 40 H), 4.03 (s, 5 H), 2.61 (dt, $J = 20$, 7.8 Hz, 2 H), 2.21–2.11 (m, 1 H), 1.38–1.20 (m, 1 H), 0.80–0.60 (m, 2 H); ^{13}C NMR δ (aliphatic) 80.5, 43.0 (d, $J = 11.6$ Hz), 28.4 (d, $J = 8.9$ Hz), 18.9 (dd, $J = 38.7$, 20 Hz); ^{31}P NMR δ 44.1 (d, $J = 41.4$ Hz), 36.8 (d, $J = 41.4$ Hz), 13.0 (br); FAB ($m + 1$)/ $z = 968$. Anal. Calcd for $\text{C}_{66}\text{H}_{51}\text{NP}_3\text{RuCl}$: C, 69.52; H, 5.31; N, 1.45. Found: C, 69.31; H, 5.24; N, 1.57.

[$\text{CpRu}(\text{Ph}_2\text{P}(\text{CH}_2)_3\text{NC-C})(\text{CO})\text{I}$] (10**).** To a solution of $\text{CpRu}(\text{CO})_2\text{I}$ (200 mg, 0.57 mmol) in dichloromethane was added compound **1** (302 mg, 0.60 mmol); the resulting mixture was stirred at room temperature for 10 h. Removal of solvent yielded a liquid residue, which was chromatographed on alumina (10 g) with elution with dichloromethane. A red band eluate was collected and concentrated to give the complex **6** as a red liquid (272 mg, 83%): IR (CH_2Cl_2) $\nu(-\text{NC})$ 2170, $\nu(-\text{CO})$ 1973 cm^{-1} ; ^1H NMR δ 7.46–7.24 (m, 10 H), 5.14 (s, 5 H), 3.82 (t, $J = 6.4$ Hz, 2 H), 2.25–2.19 (m, 2 H), 1.92–1.79 (m, 2 H); ^{13}C NMR δ 199.5 (–CO), 145.1 (CN–), 137.5–128.6 (Ar C), 84.4 (Cp–), 45.7 (d, $J = 14.5$ Hz), 26.3 (d, $J = 18.1$ Hz), 24.8 (d, $J = 11.9$ Hz); ^{31}P NMR δ –17.3. Anal. Calcd for $\text{C}_{22}\text{H}_{21}\text{INOPRu}$: C, 46.01; H, 3.69; N, 2.44. Found: C, 45.78; H, 3.69; N, 2.46.

[$\text{Cp}(\text{PPh}_3)\text{ClRu}(\mu\text{-Ph}_2\text{P}(\text{CH}_2)_3\text{NC-P,C})\text{RuCp}(\text{CO})\text{I}$] (11**).** **Method 1.** A mixture of **9** (140 mg, 0.144 mmol) and $\text{CpRu}(\text{CO})_2\text{I}$ (50.4 mg, 0.144 mmol) in toluene (10 mL) was stirred at room temperature for 10 h. Concentration of the reaction mixture gave the crude product as a red solid, which was purified by chromatography on alumina with elution of dichloromethane. Recrystallization from CHCl_3 /pentane at –20 °C provided the desired complex **11** as an orange crystalline solid (107 mg, 72%).

Method 2. A benzene solution of **10** (60 mg, 0.104 mmol) and $\text{CpRu}(\text{PPh}_3)_2\text{Cl}$ (75.8 mg, 0.104 mmol) was heated to reflux for 4 h. Replacement of benzene with ether solvent yielded a red precipitate solid, which was washed with ether (20 mL, \times 2) to provide pure **11** as an orange-red solid (63 mg, 58%).

Both methods provided formation of diastereomeric pairs of **11**, which could not be separated at present. IR (CH_2Cl_2): $\nu(-\text{NC})$ 2170, $\nu(-\text{CO})$ 1970 cm^{-1} . ^1H NMR: δ 7.90–7.88 (m, 2 H), 7.50–7.04 (m, 23 H), 5.14 (s, 5 H), 4.13 (s, 5 H), 3.31–3.13 (m, 2 H), 2.31–2.22 (m, 1 H), 1.29–1.21 (m, 1 H), 1.10–1.00 (m, 1 H), 0.88–0.74 (m, 1 H). ^{31}P NMR: δ 44.12 (d, $J = 41.4$ Hz), 35.74 (d, $J = 41.4$ Hz) as one pair of diastereomers; δ 44.05 (d, $J = 41.4$ Hz), 35.78 (d, $J = 41.4$ Hz). Anal. Calcd for $\text{C}_{45}\text{H}_{41}\text{ClINOP}_2\text{Ru}_2\cdot 0.5\text{CHCl}_3$: C, 49.77; H, 3.81; N, 1.24. Found: C, 49.28; H, 3.74; N, 1.24.

$\text{Br}(\text{CO})_4\text{Re}(\text{CNCH}_2\text{CH}_2\text{PPh}_2\text{-C})$ (12**).** A mixture of $\text{Re}(\text{CO})_5\text{Br}$ (73 mg, 0.18 mmol) and **1** (90.5 mg, 0.18 mmol) in CH_2Cl_2 (10 mL) was heated to reflux for 2 h. After removal of solvent, the residue was chromatographed on silica gel with dichloromethane as the eluent. The eluate was collected and concentrated to give the desired complex **12** as a colorless liquid (75 mg, 66%): IR (CH_2Cl_2) ν_{CN} 2222 cm^{-1} , ν_{CO} 2112, 2020, 1958 cm^{-1} ; ^1H NMR δ 7.47–7.30 (m, 10 H, Ar H), 3.87 (t, $J = 6.5$ Hz, 2 H, – NCH_2 –), 2.22 (m, 2 H, – PCH_2 –), 1.93 (m, 2 H, – CH_2 –); ^{13}C NMR δ 182.3, 181.1, 180.1 (–CO), 137.2 (d, $J = 11.2$ Hz), 132.6 (d, $J = 19.2$ Hz), 129.0, 128.6 (d, $J = 6.8$ Hz) (Ar C), 129.2 (–CN), 45.4 (d, $J = 15.1$ Hz, – NCH_2 –), 25.6 (d, $J = 18.7$ Hz, – PCH_2 –), 24.7 (d, $J = 13.2$, – CH_2 –); ^{31}P NMR δ –17.83. Anal. Calcd for $\text{C}_{20}\text{H}_{16}\text{BrNPO}_4\text{Re}$: C, 38.04; H, 2.22; N, 2.55. Found: C, 37.95; H, 2.31; N, 2.52.

$\text{Br}(\text{CO})_3\text{Re}(\text{CNCH}_2\text{CH}_2\text{CH}_2\text{PPh}_2\text{-P,C})$ (13**).** A solution of **12** (50 mg, 0.08 mmol) in benzene (10 mL) was heated to reflux for 4 h. The reaction mixture was chromatographed on silica gel (5 g) with elution with CH_2Cl_2 . The eluate was collected and concentrated to give **13** as a clear colorless liquid (35 mg, 73%): IR ν_{CN} 2137 cm^{-1} , ν_{CO} 2039, 1975, 1917 cm^{-1} ; ^1H NMR δ 7.68–7.36 (m, 10 H), 4.00 (m, 1 H), 3.44 (m, 2 H), 2.76 (m, 1 H), 2.07 (m, 2 H); ^{13}C NMR δ 190.2 (d, $J = 8.9$ Hz), 187.83 (d, $J = 58.5$ Hz), 187.78 (d, $J = 6.2$ Hz) (–CO), 163.0 (d, $J = 6.8$ Hz, –CN), 134.3–128.0 (Ar C), 47.2, 28.7 (d, $J = 2.7$ Hz), 27.7 (d, $J = 28$ Hz); ^{31}P NMR δ –4.33. Anal. Calcd for $\text{C}_{19}\text{H}_{16}\text{NPO}_3\text{ReBr}$: C, 37.82; H, 2.67; N, 2.32. Found: C, 37.57; H, 2.73; N, 2.30.

$(\text{CO})_3\text{BrRe}(\text{CNCH}_2\text{CH}_2\text{CH}_2\text{PPh}_2\text{-C})_2$ (14**).** A mixture of **1** (920 mg, 1.827 mmol) and $\text{BrRe}(\text{CO})_5$ (370 mg, 0.911 mmol) in benzene (40 mL) was stirred at 25 °C for 10 h. After concentration of the reaction mixture, the residue was chromatographed on silica gel with dichloromethane as the eluent. The eluate was concentrated to give **14** as a colorless liquid (565 mg, 73%): IR (CHCl_3) 2219 (ν_{CN}), 2041, 1981, 1926 cm^{-1} (ν_{CO}); ^1H NMR δ 7.47–7.31 (m, 20 H, Ar H), 3.68 (t, $J = 6.4$ Hz, 4 H, CNCH_2 –), 2.17 (m, 4 H, – CH_2PPh_2), 1.83 (m, 4 H, – CH_2 –); ^{13}C NMR δ 186.1, 183.8, 137.1 (d, $J = 8.6$ Hz), 137.0 (d, $J = 8.9$ Hz), 134.3 (–CN), 132.4 (d, $J = 6.8$ Hz), 132.2 (d, $J = 6.6$ Hz), 128.7, 128.6, 128.3 (d, $J = 6.6$ Hz), 44.6 (d, $J = 14.5$ Hz), 25.3 (d, $J = 18.5$ Hz), 24.2 (d, $J = 13.1$ Hz); ^{31}P NMR δ –17.80; FABMS ($m + 1$)/ $z = 857.0$. Anal. Calcd for $\text{C}_{35}\text{H}_{32}\text{N}_2\text{P}_2\text{O}_3\text{ReBr}$: C, 49.07; H, 3.76; N, 3.27. Found: C, 49.01; H, 3.80; N, 3.26.

$(\text{CO})_9\text{Re}_2(\text{CNCH}_2\text{CH}_2\text{CH}_2\text{PPh}_2\text{-C})$ (15**).** A solution of **1** (42 mg, 0.083 mmol) and $\text{Re}_2(\text{CO})_{10}$ (54 mg, 0.083 mmol) in toluene (10 mL) was stirred at 25 °C for 10 h. The reaction mixture was chromatographed on silica gel with dichloromethane as the eluent. Upon concentration of the eluate, the desired product was obtained as a colorless liquid (67 mg, 92%): IR 2187 (ν_{CN}), 2099, 2074, 2046, 2008, 1994, 1968, 1942 cm^{-1} (ν_{CO}); ^1H NMR δ 7.50–7.33 (m, 10 H), 3.85 (t, $J = 6.7$ Hz, 2 H), 2.12 (m, 2 H), 1.85 (m, 2 H); ^{13}C NMR δ 194.6, 192.0, 184.6 (–CO), 134.5 (–CN), 137.3 (d, $J = 12$ Hz), 132.6 (d, $J = 19.3$ Hz), 129.0, 128.7 (d, $J = 7.6$ Hz) (Ar C), 45.6 (d, $J = 14.4$ Hz), 25.8 (d, $J = 19.5$ Hz), 25.0 (d, $J = 13.9$ Hz); ^{31}P NMR δ –17.5. Anal. Calcd for $\text{C}_{25}\text{H}_{16}\text{NO}_9\text{Re}_2$: C, 34.21; H, 1.84; N, 1.60. Found: C, 34.32; H, 1.80; N, 1.59.

$(\text{CO})_4\text{Re}(\mu_2\text{-CNCH}_2\text{CH}_2\text{CH}_2\text{PPh}_2\text{-P,C})\text{Re}(\text{CO})_4$ (16**).** A solution of **15** (640 mg, 0.729 mmol) in chloroform was irradiated with light for 2 h. After concentration, the residue was chromatographed on silica gel with dichloromethane as eluent. The eluate was concentrated to give the desired product **16** as a white solid (450 mg, 73%): mp 165–185 °C dec; IR (KBr) ν 2156 (–CN), 2081, 2062, 2034, 1973, 1958 cm^{-1} (–CO); ^1H NMR δ 7.64–7.47 (m, 10 H), 3.86 (t, $J = 6$ Hz, 2 H), 2.92 (m, 2 H), 1.83 (m, 2 H); ^{13}C NMR δ 185.4 (d, $J = 9$ Hz), 183.5, 183.3 (d, $J = 7$ Hz), 182.8, 182.1, 180.6, 178.9 (CN–), 132.3, 132.2 (d, $J = 10.5$ Hz), 131.5 (d, $J = 2$ Hz), 129.4 (d, $J = 9.7$ Hz), 45.2 (d, $J = 17$ Hz), 23.5, 22.9 (d, $J = 30$ Hz); ^{31}P NMR δ –0.3. Anal. Calcd for $\text{C}_{24}\text{H}_{16}\text{NO}_8\text{Re}_2$: C, 35.21; H, 1.97; N, 1.71. Found: C, 34.93; H, 2.05; N, 1.69.

Br(CO)₄Re{μ₂-CNCH₂CH₂CH₂PPh₂-P,C}Re(CO)₄Br (17). Bromine (31 mg, 0.194 mmol) was added to a solution of **16** (140 mg, 0.166 mmol) in dichloromethane (100 mL) at room temperature. After stirring for 3 h, the reaction mixture was concentrated and the residue was chromatographed on silica gel with ethyl acetate and hexane (1/4) as the eluent. The eluate was collected and concentrated to give **17** as a clear, colorless liquid (125 mg, 75%): IR (CH₂Cl₂) 2221 cm⁻¹ (-CN), 2110, 2021, 1954 cm⁻¹ (-CO); ¹H NMR δ 7.62–7.47 (m, 10 H), 3.88 (t, *J* = 6 Hz, 2 H), 3.02 (m, 2 H), 1.80 (m, 2 H); ¹³C NMR δ 184.2 (d, *J* = 9.2 Hz), 182.5 (d, *J* = 6.6 Hz), 182.3, 181.7, 181.0, 179.9, 132.0 (d, *J* = 10.6 Hz), 131.4, 131.3, 130.7, 129.1 (d, *J* = 9.8 Hz), 44.8 (d, *J* = 17 Hz), 24.1 (d, *J* = 31.3 Hz), 23.2; ³¹P NMR δ -5.12. Anal. Calcd for C₂₄H₁₆Br₂NO₈-Re₂: C, 29.46; H, 1.65; N, 1.43. Found: C, 29.31; H, 1.75; N, 1.42.

Cl₂Pd(Ph₂PCH₂CH₂CH₂NPPh₃-P,N) (18). A mixture of **1** (106 mg, 0.21 mmol) and Pd(COD)Cl₂ (60 mg, 0.21 mmol) in dichloromethane (15 mL) was stirred at 25 °C for 8 h. On removal of solvents, the residue was dissolved in chloroform and pentane and the desired complex **18** crystallized as a yellow-orange solid (136 mg, 95%): mp 154–158 °C dec; ¹H NMR δ 7.67–7.33 (m, 25 H), 3.21 (m, 2 H), 2.05 (m, 2 H), 1.86 (m, 2 H); ¹³C NMR δ (aliphatic) 45.5 (d, *J* = 2.9 Hz), 25.3 (d, *J* = 9.5 Hz), 22.5 (d, *J* = 33.5 Hz); ³¹P NMR δ 40.5 (d, *J* = 3.3

Hz), 17.2 (d, *J* = 3.3 Hz). Anal. Calcd for C₃₃H₃₁Cl₂NP₂Pd: C, 58.21; H, 4.59; N, 2.06. Found: C, 58.19; H, 4.84; N, 1.81.

X-ray Crystallography. Single crystals suitable for X-ray analysis of complexes **7a** and **18** were obtained in each case by slow evaporation of a chloroform/pentane solution under air. Cell parameters were determined on a CAD-4 diffractometer at 298 K by a least-squares treatment. Atomic scattering factors were taken from ref 24. The NRCC SDP VAX program was used for calculation.²⁵ Crystal data of these complexes are summarized in Table 5, and their non-hydrogen atomic coordinates are listed in Tables 2 and 4, respectively.

Acknowledgment. We thank the National Science Council of the Republic of China for grant support (NSC84-2113-M002-018).

Supplementary Material Available: Anisotropic thermal parameters and complete bond distances and bond angles for **7a** and **18** (7 pages). Ordering information is given on any current masthead page.

OM940875K

(24) *International Tables for X-ray Crystallography*; Kynoch Press: Birmingham, U.K., 1974; Vol. IV.

(25) Gabe, E. J.; Lee, F. L. *Acta Crystallogr.* **1981**, A37, S339.

Intramolecular and Intermolecular Bonding in $\text{Ru}_3(\text{CO})_{12}$, $\text{Ru}_3(\text{CO})_9(\mu_3\text{-}\eta^2\text{:}\eta^2\text{:}\eta^2\text{-C}_6\text{H}_6)$, and $\text{Ru}_3(\text{CO})_6(\mu\text{-CO})_3(\mu_3\text{-S}_3\text{C}_3\text{H}_6)$

Dario Braga* and Fabrizia Grepioni

Dipartimento di Chimica G. Ciamician, Università di Bologna, Via Selmi 2,
40126 Bologna, Italy

Maria José Calhorda*

Instituto de Tecnologia Química e Biológica, R. da Quinta Grande 6,
2780 Oeiras, Portugal and IST, Lisboa, Portugal

Luis F. Veiros

Instituto Superior Técnico, Departamento de Engenharia Química,
1096 Lisboa Codex, Portugal

Received October 24, 1994[®]

The relationship between molecular and crystal structures of $\text{Ru}_3(\text{CO})_{12}$ (**1**), of the benzene derivative $\text{Ru}_3(\text{CO})_9(\mu_3\text{-}\eta^2\text{:}\eta^2\text{:}\eta^2\text{-C}_6\text{H}_6)$ (**2**), and of the 1,3,5-trithiacyclohexane derivative $\text{Ru}_3(\text{CO})_6(\mu\text{-CO})_3(\mu_3\text{-S}_3\text{C}_3\text{H}_6)$ (**3**) has been investigated by a combined use of extended Hückel molecular orbital calculations, empirical atom–atom pairwise packing potential energy calculations and computer graphics. The presence of CO bridges has been related to the capabilities of the “facial” ligand (C_6H_6 and $\text{S}_3\text{C}_3\text{H}_6$) as a π -acceptor or a π -donor. Bridging carbonyl groups in the equatorial plane are more effective in competing with the facial ligand for back-donation, and thus they stabilize π -donors. In $\text{Ru}_3(\text{CO})_{12}$, three carbonyls replace C_6H_6 as π -acceptors. Hydrogen-bonding networks of the C–H...O type involving the carbonyl oxygen atoms have been detected in crystalline **2** and **3**. Bridging CO's are observed to form preferential interactions with respect to terminal ligands.

Introduction

There is an increasing interest in the chemistry of transition metal clusters as chemical materials.¹ The properties of the solids formed by organometallic complexes and clusters are a bridge between those of typical molecular solids formed by organic molecules and those of inorganic materials.² These properties all depend on the relationship between the characteristics of the individual molecular entity (intramolecular bonds and steric interactions, size, shape, charge, etc.) and those resulting from the collection of identical molecules present in the crystal (intermolecular bonds, interactions between ions, inclusion, clathration, segregation, phase transitions, conductive and magnetic properties, etc.).³

The relationship between the molecule and crystal becomes especially intriguing when dealing with flexible molecules whose molecular structure can be conditioned

by the need for a simultaneous optimization of intramolecular and intermolecular bonding. We have recently investigated several such cases in the organometallic chemistry field. The intra/intermolecular dualism has been tackled essentially via a combination of extended Hückel theoretical calculations (to address specific bonding problems) and packing potential energy calculations and packing analysis (to study the intermolecular bonding). With the aid of these tools we have recently reported on the relationship between the structure of penta- and hexaruthenium cluster isomers containing benzene ligands bound in facial and/or apical bonding modes and the respective crystals,⁴ as well as on the relationship between the presence of intermolecular hydrogen bonds and the conformation and the bending of C–H bonds in bis(arene) complexes of the type [(arene)₂Ru₂Cl₃]⁺ (arene = benzene, toluene).⁵

In this paper we focus our attention on the relationship between molecular and crystal structures of three closely related complexes, namely $\text{Ru}_3(\text{CO})_{12}$ (**1**),⁶ the benzene derivative $\text{Ru}_3(\text{CO})_9(\mu_3\text{-}\eta^2\text{:}\eta^2\text{:}\eta^2\text{-C}_6\text{H}_6)$ (**2**),⁷ and

[®] Abstract published in *Advance ACS Abstracts*, March 15, 1995.

(1) (a) Mingos, D. M. P.; Wales, D. J. In *Introduction to Cluster Chemistry*; Grimes, Russell N., Ed.; Prentice-Hall International Editions: Englewood Cliffs, NJ, 1990. (b) *Physics and Chemistry of Finite Systems: From Clusters to Crystals*; Jena, P., Khanna, S. N., Rao, B. K., Eds.; NATO ASI Series; Kluwer: Dordrecht, The Netherlands, 1989. (c) *Metal-Metal Bonds and Clusters in Chemistry and Catalysis*; Fackler, P., Jr., Ed.; Plenum Press, NY, 1989. (d) *The Chemistry of Metal Cluster Complexes*; Shriver, D. F., Kaesz, H. D., Adams, R. D., Eds.; VCH: NY, 1990.

(2) (a) Desiraju, G. R. *Crystal Engineering, The Design of Organic Solids*; Elsevier: Amsterdam, 1989; p 47. (b) *Inorganic Materials*; Bruce, D. W., O'Hare, Dermot, Eds.; John Wiley & Sons: Chichester, U.K., 1992.

(3) Braga, D.; Grepioni, F. *Acc. Chem. Res.* **1994**, *27*, 51.

(4) Braga, D.; Dyson, P. J.; Grepioni, F.; Johnson, B. F. G.; Calhorda, M. J. *Inorg. Chem.* **1994**, *33*, 3218.

(5) Braga, D.; Calhorda, M. J.; Dyson, P.; Grepioni, F.; Johnson, B. F. G.; Veiros, L. *Organometallics*, in press.

(6) Churchill, M. R.; Hollander, F. J.; Hutchinson, J. P. *Inorg. Chem.* **1977**, *16*, 2655.

(7) Braga, D.; Grepioni, F.; Johnson, B. F. G.; Lewis, J.; Housecroft, C. E.; Martinelli, M. *Organometallics* **1991**, *10*, 1260.

(8) (a) Hoferkamp, L.; Rheinwald, G.; Stoeckli-Evans, H.; Süß-Fink, G. *Helv. Chim. Acta* **1992**, *75*, 2227. (b) Rossi, S.; Kallinen, K.; Pursiainen, J.; Pakkanen, T. T.; Pakkanen, T. A. *J. Organomet. Chem.* **1992**, *440*, 367.

the 1,3,5-trithiacyclohexane (TTC, hereafter) derivative Ru₃(CO)₆(μ-CO)₃(μ₃-S₃C₃H₆) (**3**).⁸

The reasons for this choice are manifold and reside in the structural differences at the molecular level and in the differences in intermolecular interactions that the three complexes present in their respective crystals. Upon substitution of benzene for three axial CO's the distribution of CO ligands present in Ru₃(CO)₁₂ is preserved in **2**, *viz.* each Ru atom bears two radial and one axial CO's in the terminal bonding mode. In **3**, on the contrary, substitution of the TTC ligand for the three axial CO's leads to a new distribution of CO ligands, uncommon in Ru₃ structural chemistry, with three edge-bridging CO's spanning the Ru–Ru bonds and six ligands terminally bound on each Ru atom. This leads to the following questions: why a bridged structure for **3**, and an all-terminal structure for **2**? What is the *relative* stability of the bridged and unbridged isomers for these molecules?

In terms of intermolecular interactions we also face an interesting situation. The TTC ligand in **3** has been shown to participate in the formation of hydrogen bonds of the C–H···O(CO) type. Interactions of this type were detected for example in crystals of the two isomers Ir₄(CO)₆(μ-CO)₃(μ₃-S₃C₃H₆) and Ir₄(CO)₉(μ₃-S₃C₃H₆).⁹ It was shown that, in the case of the bridged isomer, the bridging CO ligands are preferentially involved in short C–H···O interactions. This observation is in keeping with the higher Lewis basicity usually attributed to bridging CO's with respect to terminal ones.¹⁰ Such a behavior has been recently substantiated through a systematic study of C–H···O interactions in organometallic crystals containing metal-bound CO ligands.¹¹ As a result of this study, it has become apparent that also arene hydrogens are involved in C–H···O interactions with CO ligands and that CO cannot compete in hydrogen bond formation when stronger hydrogen-acceptor groups are present in the same crystal structure.¹²

On this premise it should be of interest to study molecular assembly and intermolecular interactions in the crystals of benzene and TTC derivatives **2** and **3**. This study brings about new questions: is the presence of bridging ligands in the structure of **3** related to the formation of a stronger intermolecular hydrogen bonding network? Secondly, what is the role of C–H···O interactions in the stabilization of crystalline **2**?

We will approach these problems from two different sides: the molecular structures of **1–3** and the relative stability of their possible isomeric forms will be investigated by extended Hückel molecular orbital calculations. The crystal structures will be studied with the aid of empirical atom–atom pairwise packing potential energy calculations and computer graphics. When used together, the two tools afford complementary information, providing valuable insights into the structural and solid state chemistry of organometallic complexes and clusters.

(9) Braga, D.; Grepioni, F. *J. Chem. Soc., Dalton Trans.* **1993**, 1223.

(10) Horwitz, C. P.; Shriver, D. F. *Adv. Organomet. Chem.* **1984**, 23, 218.

(11) Braga, D.; Biradha, K.; Grepioni, F.; Pedireddi, V. R.; Desiraju, G. R. *J. Am. Chem. Soc.*, in press. For a more general reference on C–H···O interactions see also: Desiraju, G. R. *Acc. Chem. Res.* **1991**, 24, 290.

(12) Braga, D.; Grepioni, F.; Sabatino, P.; Desiraju, G. R. *Organometallics* **1994**, 13, 3532.

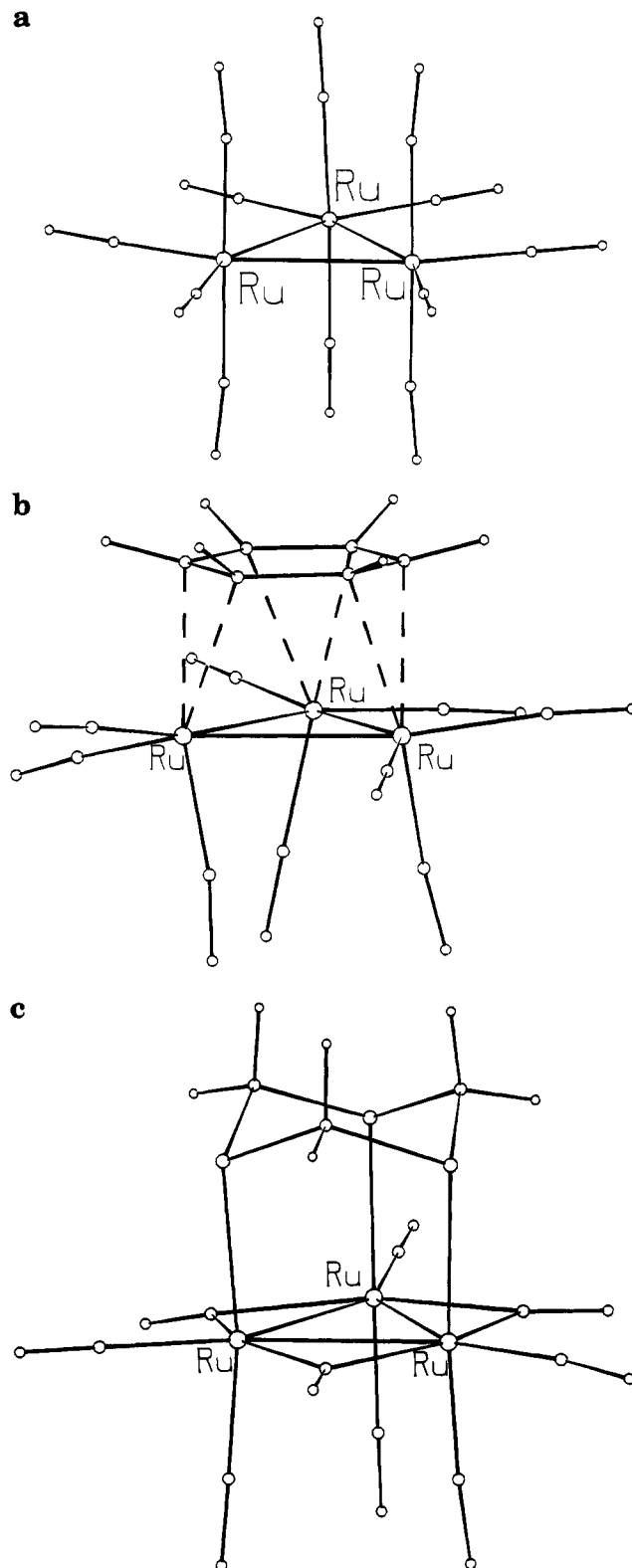


Figure 1. The solid state structures of (a) Ru₃(CO)₁₂ (**1**), (b) Ru₃(CO)₉(μ₃-η²:η²:η²-C₆H₆) (**2**), and (c) Ru₃(CO)₆(μ-CO)₃(μ₃-S₃C₃H₆) (**3**).

Molecular Structures in the Solid State

The most relevant structural features of Ru₃(CO)₁₂ (**1**), Ru₃(CO)₉(μ₃-η²:η²:η²-C₆H₆) (**2**), and Ru₃(CO)₆(μ-CO)₃(μ₃-S₃C₃H₆) (**3**) as determined from X-ray diffraction studies will now be briefly summarized. Sketches of the three molecules are given in Figure 1; relevant structural parameters, as obtained from the original papers, are reported in Table 1.

Table 1. Comparison of Relevant Structural Parameters for 1–3

	Ru ₃ (CO) ₁₂	Ru ₃ (CO) ₉ (μ ₃ :η ² :η ² :η ² -C ₆ H ₆) 193 K	Ru ₃ (CO) ₆ (μ-CO) ₃ (μ ₃ -S ₃ C ₃ H ₆)
M–M _{range}	2.851–2.859(1)	2.827–2.855(1)	2.838–2.868(1)
M–M _{av}	2.855(1)	2.837(1)	
M–CO _{eq}	1.92(1)	1.91(1)	1.90(1)
M–CO _{ax}	1.94(1)	1.88(1)	1.88(1)
C–O _{eq}	1.13(1)	1.15(1)	
C–O _{ax}	1.13(1)	1.15(1)	
M–X		C 2.331(4)	S 2.428(2)
M–CO _{br}			2.14(1)

Ru₃(CO)₁₂ possesses the well-known “all terminal” structure with each ruthenium atom carrying four CO ligands (see Figure 1a). Six ligands are radially bound and lie roughly in the plane of the triruthenium cluster, whereas the other six ligands are axially bound three above and three below the cluster plane. The overall idealized molecular symmetry is *D*_{3h}. The Ru–Ru bonds, however, are not equivalent, with one “long” and two “short” bonds [2.8595(4) versus 2.8521(4) and 2.8518(4) Å, respectively]. This small but significant difference has been shown to have an intermolecular origin. The most relevant (in terms of intermolecular cohesion) packing motif in crystalline Ru₃(CO)₁₂ is based on the insertion of one axial CO of one molecule into the tetracarbonyl unit generated by two axial and two radial CO's on a next neighboring molecule (the so-called “key–keyhole” interaction).¹³ The same feature is present in the isomorphous crystals of the isostructural species Os₃(CO)₁₂.¹⁴

The structure of Ru₃(CO)₉(μ₃:η²:η²:η²-C₆H₆) (**2**) has been determined at room temperature and 193 K (see Figure 1b). The species is almost isostructural with the osmium analogue Os₃(CO)₉(μ₃:η²:η²:η²-C₆H₆).¹⁵ In the ruthenium species the H atoms bend out-of-plane with respect to the ruthenium atoms. The average bending with respect to the C₆ plane is 21.1 and 21.5° at room temperature and at 193 K, respectively. The benzene and Ru₃ planes are almost parallel. This is a common feature in μ₃-arene clusters carrying facial ligands.¹⁶

The solid state molecular structure of the trithiane derivative Ru₃(CO)₆(μ-CO)₃(μ₃-S₃C₃H₆) (**3**) has been determined in the same crystalline form independently by two groups of scientists⁸ and is very much related to that of the benzene cluster. The trithiane ligand binds the three Ru atoms *via* the interaction of one lone pair on each sulfur atom (see Figure 1c), as has been observed, for example, for the two isomers of Ir₄(CO)₉(μ₃-S₃C₃H₆) mentioned above.

The most remarkable feature about the structure of **3** is the presence of three bridging CO ligands coplanar with the Ru₃ triangle and spanning the three edges. The Ru–Ru bonds are slightly shorter than in **1** and present the same pattern, *viz.* two “short” [2.8378(9) and 2.8306-

(13) Å] and one “long” bond [2.8687(8) Å]. All μ-CO groups are nearly symmetric.

Molecular Orbital Calculations

The M₃ triangular clusters have been the subject of many theoretical studies, done at several levels.^{17,18} In a recent one, the Os₃(CO)₉(μ₃:η²:η²:η²-C₆H₆) cluster was addressed and the bonding between the benzene molecule and the Os₃(CO)₉ fragment discussed in detail.¹⁹ The benzene–M₃ interaction can be described according to the general scheme through which electrons are donated from benzene (the low lying a_{2u} and 1e π orbitals), while the metals back-donate to the high-lying benzene π orbitals, especially to the e_{2u} set. The bonding is favored by the bending back of the hydrogens, and this distortion is found wherever benzene coordinates a M₃ metallic cluster. Also typical of such a coordination is the distortion of benzene toward cyclohexatriene upon coordination, the difference between short and long C–C bonds in benzene depending, for instance, upon the nature of the metal. In the pair of similar M₃(CO)₉(μ₃:η²:η²:η²-C₆H₆) molecules, C–C bonds range from 1.41 to 1.56 Å when M = Os and from 1.37 to 1.45 Å when M = Ru. It is induced by the mixing of the e_{1g} and e_{2u} levels of benzene taking place in this coordination mode.

Theoretical studies of M₃(CO)₁₂ clusters are extremely abundant for M = Fe, but not so much for the heavier metal derivatives.^{17a,c,20} The cluster containing the sulfur donor ligand 1,3,5-trithiacyclohexane, TTC, has not yet been theoretically studied, as far as we know.

We will now investigate the reason for the presence of three bridging carbonyls in the Ru₃ plane for Ru₃(CO)₆(μ-CO)₃(μ₃-S₃C₃H₆) while in the other clusters all carbonyls are terminal. The study of the bonding between the TTC ligand and the cluster, using the extended Hückel method,²¹ will be the starting point.

In the observed geometry, TTC binds to the Ru₃(CO)₆(μ₂-CO)₃ fragment using three linear combinations of sulfur lone pairs of a₁ and e symmetry pointing toward the metal atoms. Electrons are donated to three empty z, z² ruthenium orbitals, forming the three Ru–S σ bonds. The other sulfur lone pairs are approximately parallel to the Ru₃ triangle and their interaction with

(13) Braga, D.; Grepioni, F. *Organometallics* **1991**, *10*, 1254.

(14) Churchill, M. R.; DeBoer, B. G. *Inorg. Chem.* **1977**, *16*, 878.

(15) Gomez-Sal, M. P.; Johnson, B. F. G.; Lewis, J.; Raithby, P. R.; Wright, A. H. *J. Chem. Soc., Chem. Commun.* **1985**, 1682.

(16) Braga, D.; Grepioni, F.; Dyson, P. J.; Johnson, B. F. G. *Chem. Rev.* **1994**, *94*, 1585.

(17) (a) Schilling, B. E. R.; Hoffmann, R. *J. Am. Chem. Soc.* **1979**, *101*, 3456. (b) Pinhas, A. R.; Albright, T. A.; Hoffmann, P.; Hoffmann, R. *Helv. Chim. Acta* **1980**, *63*, 29. (c) Delley, B.; Manning, M. C.; Ellis, D. E.; Berkowitz, J.; Trogler, W. C. *Inorg. Chem.* **1982**, *21*, 2247. (d) Chesky, P. T.; Hall, M. B. *Inorg. Chem.* **1983**, *22*, 2998. (e) Halet, J.-F.; Saillard, J.-Y.; Lissillour, R.; McGlinchey, M. J.; Jaouen, G. *Inorg. Chem.* **1985**, *24*, 218.

(18) (a) Mealli, C. *J. Am. Chem. Soc.* **1985**, *107*, 2245. (b) Barreto, R. D.; Fehlner, T. P.; Hsu, L.-Y.; Shore, S. G. *Inorg. Chem.* **1986**, *25*, 3572. (c) Griewe, G. L.; Hall, M. B. *Inorg. Chem.* **1988**, *27*, 2250. (d) Cotton, F. A.; Feng, X. *Inorg. Chem.* **1991**, *30*, 3666. (e) Gallop, M. A.; Gomez-Sal, M. P.; Housecroft, C. E.; Johnson, B. F. G.; Lewis, J.; Owen, S. M.; Raithby, P. R.; Wright, A. H. *J. Am. Chem. Soc.* **1992**, *114*, 2502.

(19) Riehl, J.-F.; Koga, N.; Morokuma, K. *Organometallics* **1993**, *12*, 4788.

(20) (a) Baerends, E. J.; Rosa, A. *New J. Chem.* **1991**, *15*, 815. (b) Li, J.; Jug, K. *Inorg. Chim. Acta* **1992**, *196*, 89.

(21) (a) Hoffmann, R. *J. Chem. Phys.* **1963**, *39*, 1397. (b) Hoffmann, R.; Lipscomb, W. N. *J. Chem. Phys.* **1962**, *36*, 2179, 3489.

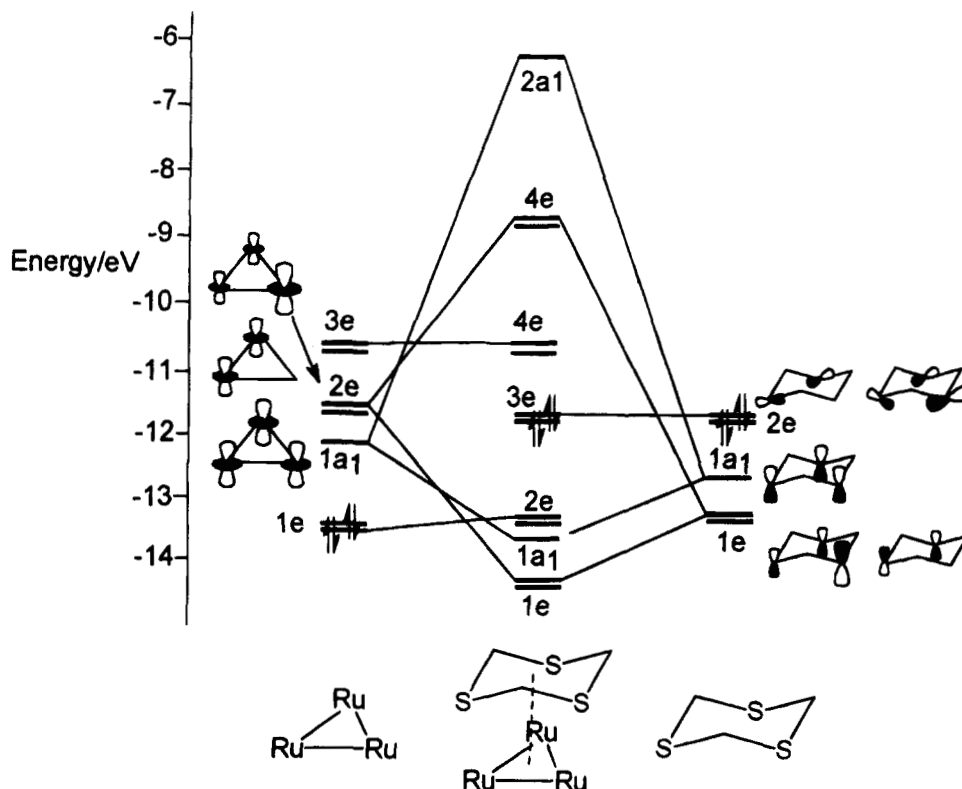


Figure 2. Bonding between TTC and the fragment Ru₃(CO)₆(μ₂-CO)₃ in **3**.

Table 2. Relative Energies, Interaction Energies, and Overlap Populations between Fragments for the Four Clusters Containing Benzene or TTC and Ru₃(CO)₆(μ-CO)₃ or Ru₃(CO)₉

ligand	benzene		TTC	
	Ru ₃ (CO) ₆ (μ-CO) ₃	Ru ₃ (CO) ₉	Ru ₃ (CO) ₆ (μ-CO) ₃	Ru ₃ (CO) ₉
energy ^a	0.17	0	0	1.05
ΔE ^b	-2.52	-3.04	-8.72	-8.02
OP	0.98	1.05	1.41	1.41

^a Relative energy (eV). ^b ΔE = E_{molecule} - (E_{ligand} + E_{Ru₃ fragment}).

metal orbitals is negligible. This is shown schematically in Figure 2.

Knowing the bonding modes of the facial ligands, benzene and TTC, to the rest of the molecules, the effect of the bridging carbonyls can be analyzed. This problem has been briefly addressed for the binuclear system M₂(CO)₈, where the interaction of two bridging or two terminal carbonyls with M₂(CO)₆ was studied and compared.²² Using for the two Ru₃(CO)₉ fragments the geometries they exhibit in each complex, the energies of the four possible clusters were determined. They agree with the molecular structures observed in the crystals, as can be seen from their values in Table 2.

The relative energies indicate which geometry should be more stable: benzene prefers to bind to the all-terminal Ru₃(CO)₉ fragment, while the TTC cluster is stabilized by the fragment containing bridging carbonyls. The interaction energy, ΔE, given by the difference between the energy of a molecule and the sum of the energies of its fragments when not interacting, makes allowance for the different energies of the two Ru₃ groups [Ru₃(CO)₆(μ-CO)₃ has a lower energy than Ru₃(CO)₉]. Finally, the overlap population between fragments, on the last row, reflects the strength of the bond

between the ligand, benzene or TTC, and the rest of the cluster. It suggests that the local bond to TTC does not depend much on the nature of the metallic moiety, while benzene can form stronger bonds to Ru₃(CO)₉ when all CO groups are terminal.

The interaction diagram for the bonding of benzene to both metal fragments is shown in Figure 3, with the benzene π orbitals in the center, those of Ru₃(CO)₆(μ-CO)₃ on the left, and those of Ru₃(CO)₉ on the right, while the orbitals of the possible clusters occupy the areas in between. The orbitals of a triangular M₃(CO)₉ cluster with terminal carbonyls have been described earlier^{17a} and can be derived from those of the well-known M(CO)₃ half-octahedron.²³ There are three cluster orbitals which are mainly responsible for the energy difference between the two structures, namely the 2a₁ orbital (HOMO of the cluster with terminal carbonyls; at lower energy in the other) and the 1e set. The other levels have comparable energies.

The 1e and 2e sets of benzene π orbitals are allowed to mix under C_{3v} symmetry. In the free undistorted molecule they were the e_{1g} (occupied) and the e_{2u} (empty) levels. On the other hand, each of the Ru₃-based fragments has two sets of e symmetry at an appropriate energy, one full, 1e, one empty, 2e. They seem to fulfill the conditions for strong interaction. What can be seen, however, is that the complete interaction is only taking place when there are no bridging CO ligands, as both levels are pushed down by it (right side). Conversely, in the case of Ru₃(CO)₆(μ-CO)₃, the energy of the lower 1e set remains the same. It does not interact with the corresponding empty π orbital of benzene and, because of this, there is practically no back-donation. These

(22) Thorn, D. L.; Hoffmann, R. *Inorg. Chem.* **1978**, *17*, 126.

(23) Albright, T. A.; Whangbo, M.-H.; Burdett, J. K. *Orbital Interactions in Chemistry*; John Wiley & Sons, New York, 1985.

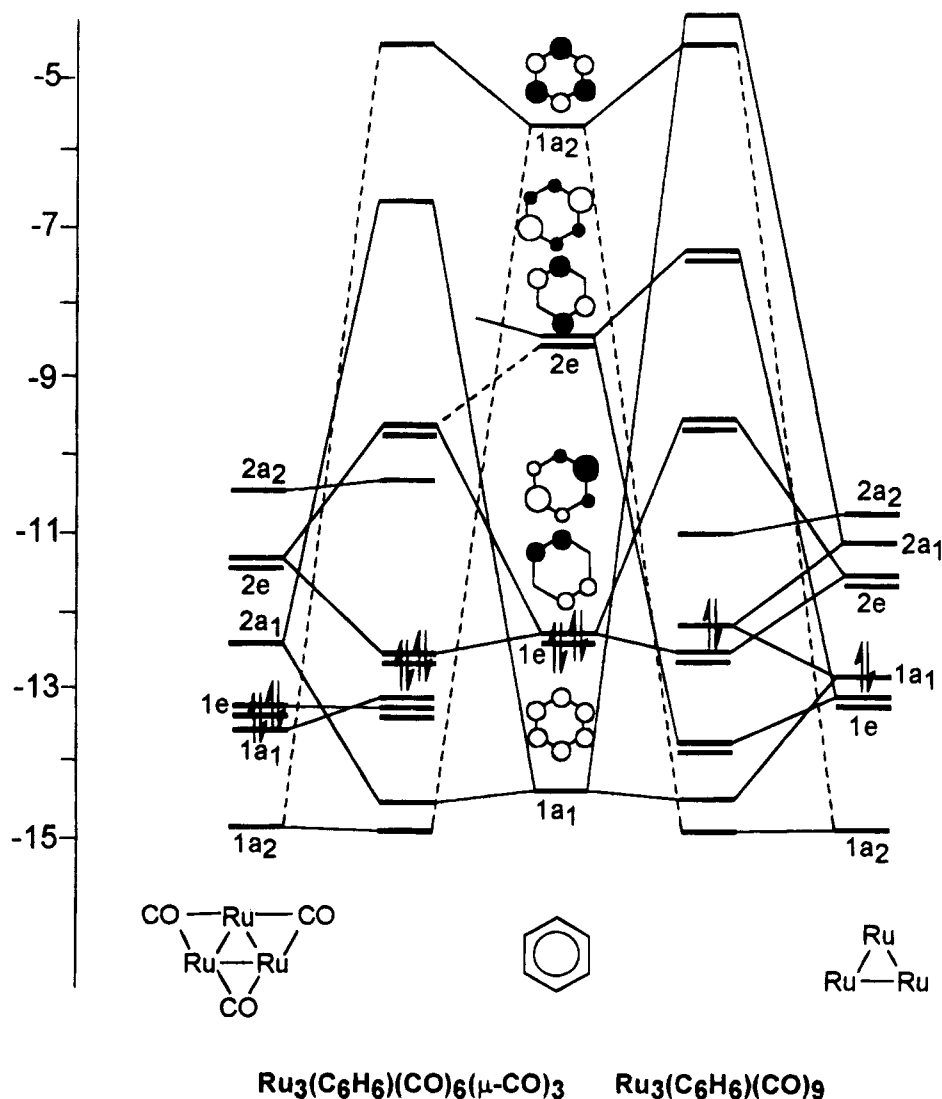


Figure 3. Interaction diagram for the bonding between the benzene fragment and the two fragments, $\text{Ru}_3(\text{CO})_6(\mu_2\text{-CO})_3$ on the left (3) and $\text{Ru}_3(\text{CO})_9$ on the right (2). The more important orbitals of the metallic fragments are shown in Figures 4 and 5.

interactions only are shown in Figure 4 for a better comparison.

The main reason why there is practically no back-donation from $\text{Ru}_3(\text{CO})_6(\mu\text{-CO})_3$ is that the lower energy set, 1e, of this fragment is involved in an interaction with carbonyl π^* orbitals. It is therefore much less localized in the ruthenium atoms than the corresponding 1e set in the nonbridged fragment, and overlap with the benzene empty 2e orbitals is smaller. It can be said, in a different way, that there is a competition between back-donation from $\text{Ru}_3(\text{CO})_6$ to benzene and to the bridging carbonyls. As carbonyls are strong π acceptors, back-donation to benzene becomes less important and the bonding of benzene weaker, as mentioned earlier. We can see that back-donation has indeed decreased, when there are CO bridges, from the smaller population of the $e_2(e_{2u})$ level (0.158 vs. 0.179). Notice that mixing of all e levels, allowed by C_{3v} symmetry, slightly obscures this picture.

The extra stabilization due to back-donation is partly lost from the destabilization of one a_1 level. The lowest π orbital of benzene is a_1 under C_{3v} symmetry and can therefore interact with a_1 Ru_3 orbitals. Their overlap will be better when the z , z^2 (out-of-plane) character

increases (compared with in-plane $x^2 - y^2$, for instance). For the $\text{Ru}_3(\text{CO})_6(\mu\text{-CO})_3$ fragment, such an orbital is empty, the low-energy $1a_1$ orbital being the one mainly in the plane. On the other hand, for $\text{Ru}_3(\text{CO})_9$, $1a_1$ has z^2 character and is occupied, giving rise to a four-electron destabilizing interaction. The resulting antibonding orbital has this character decreased by mixing in a bonding way of the high-energy empty $2a_1$, essentially z , but it has two electrons. This interaction is schematically depicted in Figure 5.

The previous effect is obviously less important than the one discussed earlier concerning back-donation to benzene 2e orbitals.

In order to check for the reliability of this explanation, we tried to find other examples of clusters. The only one available seems to be $\text{Ru}_3(\text{CO})_{12}$, whose structure was discussed above. Indeed, the three carbonyl groups on one face of the ruthenium triangle can be considered as replacing benzene and they are also π acceptor ligands. The structure has no bridges. As $\text{Ru}_3(\text{CO})_6(\mu\text{-CO})_3$ and $\text{Ru}_3(\text{CO})_6$ fragments have the geometry found in the benzene and TTC clusters, and no attempt at optimizing them in this case was done, the energies are not good indicators. But, if one takes the overlap

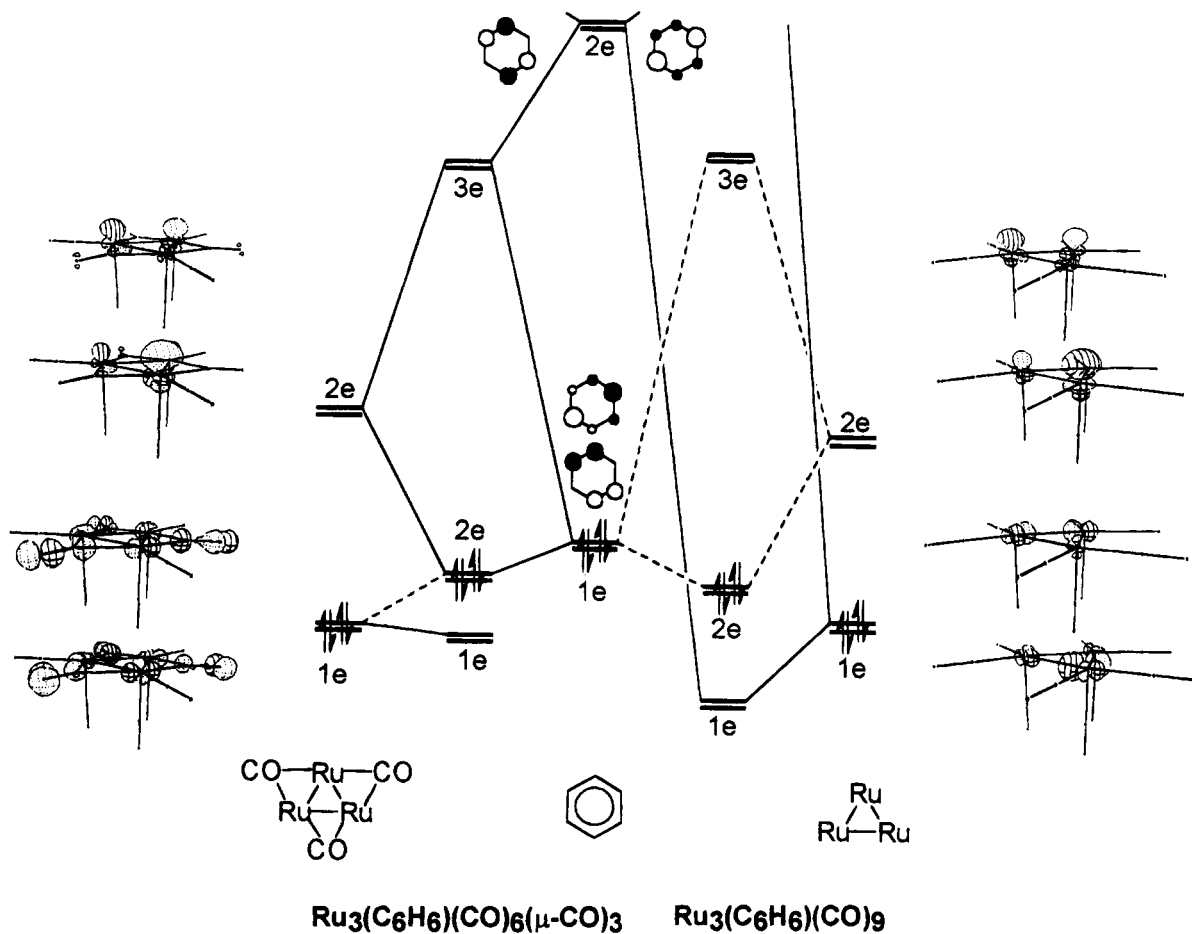


Figure 4. Comparison between the interactions of benzene 2e orbitals with the two $Ru_3(CO)_9$ fragments.

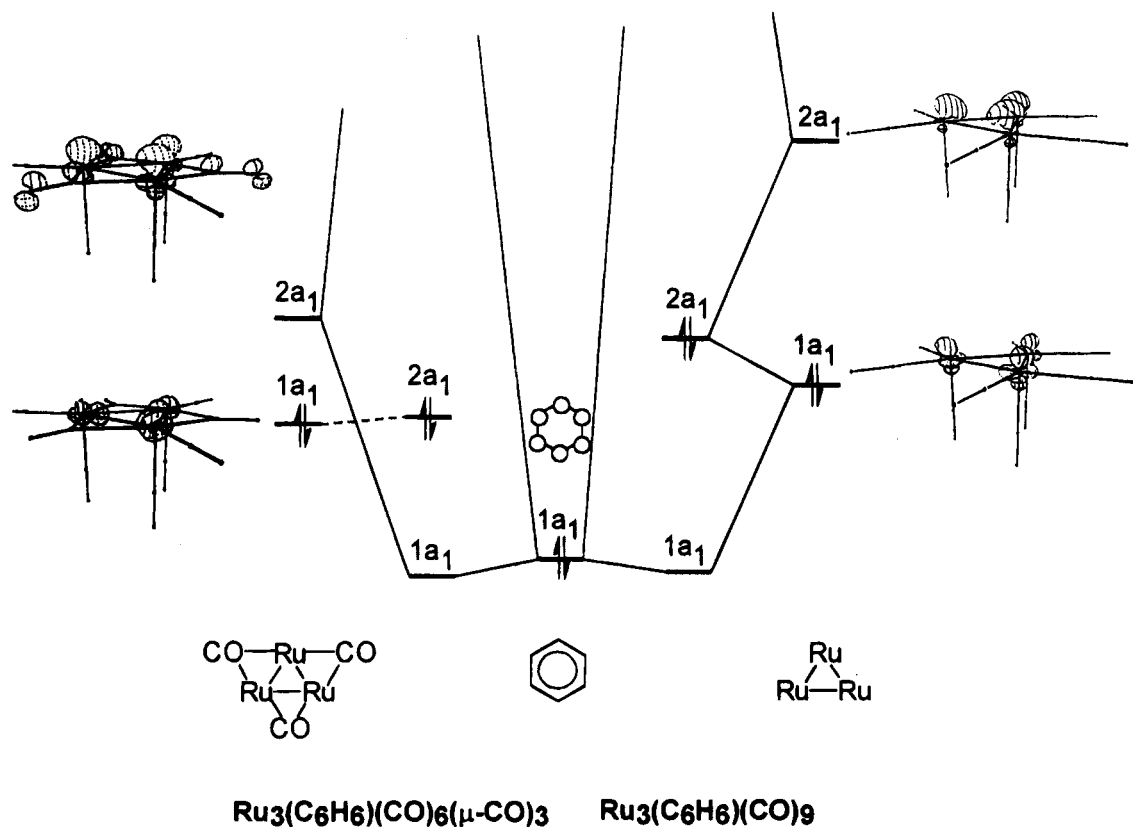


Figure 5. Comparison between the interactions of the benzene $1a_1$ orbital with the two $Ru_3(CO)_9$ fragments.

population between fragments, one fragment now being the group of three facial carbonyls, it decreases from

2.32 to 2.24 with introduction of three equatorial bridges. The pattern is the same. The bridging carbo-

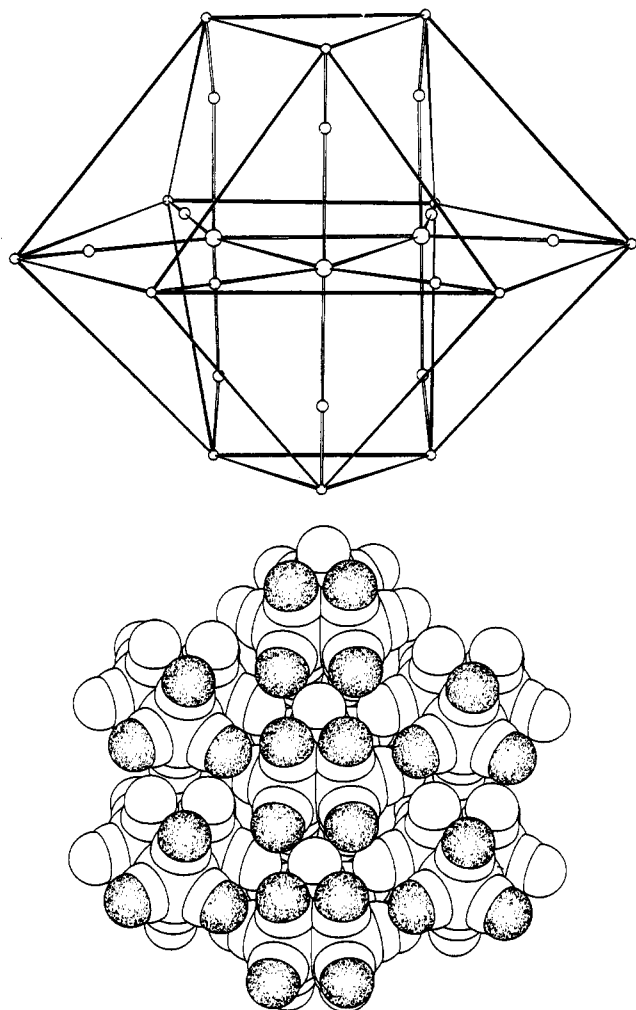


Figure 6. (a) *Anti*-cuboctahedral ligand polyhedron of $\text{Ru}_3(\text{CO})_{12}$ possessing only triangular and rectangular faces formed by sets of three and four terminal CO ligands. (b) Two-dimensional crystal of $\text{Ru}_3(\text{CO})_{12}$ molecules. Note how the outermost packing motif is made up of groups of three and four terminal CO's.

nyls compete more efficiently for back-donation from the metals than terminal ones.

Crystal Structures

We will now proceed by investigating the way molecules assemble in crystals of the three species with a focus on the intermolecular interactions established by the CO ligands in terminal and bridging bonding modes with the surrounding atoms. In terms of molecular shape, $\text{Ru}_3(\text{CO})_{12}$ can be described as an *anti*-cuboctahedron. This polyhedron is delimited by triangular and rectangular faces, which, in the case of $\text{Ru}_3(\text{CO})_{12}$, are formed by groups of three and four terminal CO's, respectively (see Figure 6a). The overall idealized molecular symmetry is D_{3h} . As discussed previously,¹⁴ the most relevant packing motif in crystalline $\text{Ru}_3(\text{CO})_{12}$ is the "key-keyhole" interaction attained *via* insertion of one axial CO of one molecule into the tetracarbonyl unit generated by two axial and two radial CO's on a next neighboring molecule. Molecules linked in such a way form a molecular row of $\text{Ru}_3(\text{CO})_{12}$ molecules. Once the packing pattern has been *decoded*, one can reconstruct the experimental crystal structure in the follow-

Table 3. Hydrogen Bonding Interactions in Crystalline **2** and **3**

donor-H...acceptor	D...A (Å)	H...A (Å)	D-H...A (deg)
$\text{Ru}_3(\text{CO})_9(\mu_3\text{-}\eta^2\text{:}\eta^2\text{:}\eta^2\text{-C}_6\text{H}_6)$ (2) at Room Temperature			
C(11)-H(2)...O(1)	3.363	2.573	129.3
C(12)-H(3)...O(5)	3.306	2.416	138.9
C(14)-H(5)...O(2)	3.207	2.372	133.0
C(15)-H(6)...O(9)	3.463	2.597	136.7
$\text{Ru}_3(\text{CO})_9(\mu_3\text{-}\eta^2\text{:}\eta^2\text{:}\eta^2\text{-C}_6\text{H}_6)$ (2) at 193 K			
C(11)-H(2)...O(1)	3.318	2.582	124.7
C(12)-H(3)...O(5)	3.263	2.287	149.3
C(14)-H(5)...O(2)	3.156	2.334	131.6
C(15)-H(6)...O(9)	3.435	2.470	148.2
C(10)-H(1)...O(4)	3.501	2.549	146.6
$\text{Ru}_3(\text{CO})_9(\mu_3\text{-S}_3\text{C}_3\text{H}_6)$ (3) at Room Temperature			
C(120)-H(120)...O(13)	3.328	2.369	148.3
C(120)-H(121)...O(23)	3.146	2.330	131.7
C(120)-H(121)...O(5)	3.307	2.547	127.3
C(230)-H(230)...O(13)	3.246	2.262	152.1
C(230)-H(230)...O(1)	3.141	2.559	113.3
C(230)-H(231)...O(12)	3.340	2.538	131.0

ing (hypothetical) process of molecule deposition and crystal nucleation. A molecular layer is obtained by placing molecular rows side by side, leaving groups of three and four terminal CO's protruding from the surface of the layer (see Figure 6b). Such a surface pattern affords "Velcro-like" units for incoming molecules to cling to in order to generate the stacking of molecular layers and the tridimensional structure.

Although $\text{Ru}_3(\text{CO})_9(\mu_3\text{-}\eta^2\text{:}\eta^2\text{:}\eta^2\text{-C}_6\text{H}_6)$ and $\text{Os}_3(\text{CO})_9(\mu_3\text{-}\eta^2\text{:}\eta^2\text{:}\eta^2\text{-C}_6\text{H}_6)$ are *almost* isostructural in the solid state, their crystals differ substantially in terms of intermolecular organization. $\text{Ru}_3(\text{CO})_9(\mu_3\text{-}\eta^2\text{:}\eta^2\text{:}\eta^2\text{-C}_6\text{H}_6)$ crystallizes in the space group $P2_1$ with $Z = 2$. The "enclosure shell" (*viz.* the molecules in the immediate neighborhood of the one chosen for reference) consists of 12 molecules distributed in *anti*-cuboctahedral arrangement (A/B/A sequence of layers). In spite of the structural similarity, the osmium analogue $\text{Os}_3(\text{CO})_9(\mu_3\text{-}\eta^2\text{:}\eta^2\text{:}\eta^2\text{-C}_6\text{H}_6)$ possesses a different crystal structure.¹⁵ Because of the presence of two independent molecules, the "enclosure shell" is formed by two groups of 12 molecules both organized in cuboctahedral fashion (A/B/C sequence of layers).¹³

We have discussed previously that the differences in structure and packing between $\text{Ru}_3(\text{CO})_9(\mu_3\text{-}\eta^2\text{:}\eta^2\text{:}\eta^2\text{-C}_6\text{H}_6)$ and $\text{Os}_3(\text{CO})_9(\mu_3\text{-}\eta^2\text{:}\eta^2\text{:}\eta^2\text{-C}_6\text{H}_6)$ can be explained by assuming that the two crystal structures represent two *alternative solutions* to the minimization of the "global" energy (*i.e.* inter- and intramolecular energy) of the molecule-crystal system. The crystals of the two benzene clusters can thus be regarded as a sort of polymorphic modification, whose existence might be due to the difference in intermolecular cohesion caused by substitution of Ru for Os.

Our findings on the participation of C-H...O(CO) interactions in the stabilization of organometallic crystals¹¹ have prompted us to re-investigate the crystal structure of **2**. We have indeed discovered the existence in crystalline **2** of an intricate network of intermolecular bonds between the facially bound benzene ligands and the CO ligands. Donor-acceptor separations, as well as H...O distances, and C-H...O angles for the hydrogen bonds are given in Table 3. The comparison

(24) (a) Green, R. D. *Hydrogen Bonding by C-H Groups*; Wiley: New York, 1974. (b) Taylor, R.; Kennard, O. *J. Am. Chem. Soc.* **1982**, *104*, 5063.

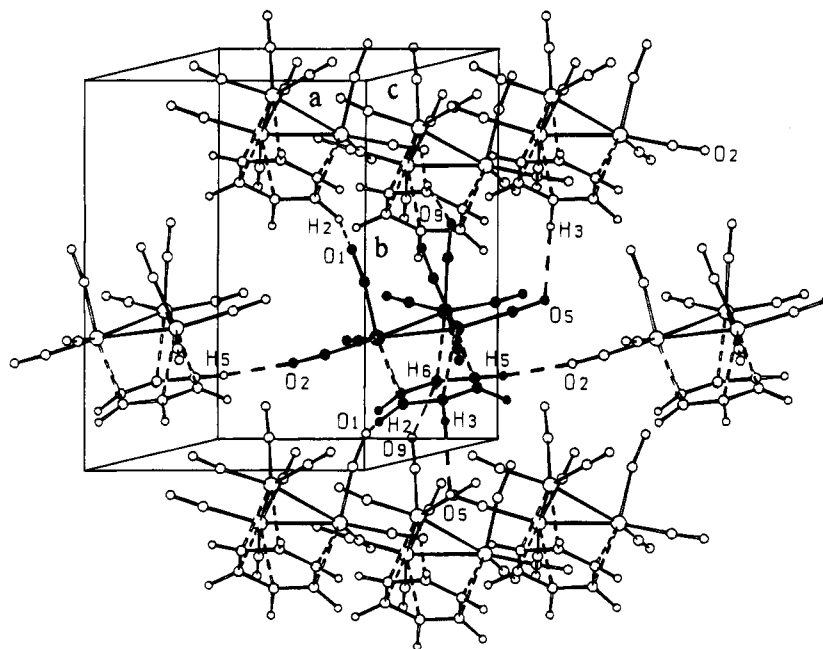


Figure 7. C–H···O hydrogen bonds between a reference molecule and the first neighboring molecules in crystalline **2**.

between the data at room temperature and at 193 K allows one to see the effect of the temperature on these interactions. The H-bond network is shown in Figure 7.

Four of the six benzene hydrogens participate in interactions that are shorter than 2.6 Å (*i.e.* shorter than the sum of the van der Waals radii: 1.20 and 1.50 Å, respectively). Two of these are short [H(3)···O(5) 2.416, H(5)···O(2) 2.372 Å] and fall toward the lower limits for C–H···O interactions in organic and organometallic crystals.¹¹ It is important to recall in this context that C–H···O interactions, being mainly electrostatic in nature, decrease much more slowly with distance and contribute to crystal cohesion at distances which can be even longer than those of the van der Waals interactions.²⁴ Another important criterion is the C–H···O angle, since it has been observed that the shortest H···O separations involving CO ligands are associated with C–H···O angles usually in the range 120–140°.^{11a} Indeed, the C–H···O angles in crystalline **2** span the narrow range 129.3–138.9° at room temperature, and 124.7–149.3° at 193 K (see Table 3). On the basis of these observations it seems possible to conclude that C–H···O interactions in crystalline **2** participate in the stabilization of the crystalline edifice and should be taken into account in evaluating the effect of crystal structure optimization on the molecular features. We had previously pointed out that the deviation from idealized *C*_{3v} symmetry (caused by the tilt of the benzene ligand away from exact eclipsing of the C=C bond midpoints over the Ru atom and by the rotation of the tricarbonyl units around the 3-fold axes) appears to have an essential intermolecular origin. Since (CO)₃ torsion accompanied by benzene tilting costs little to the bonding in **2**, the interpenetration of the molecular units at the expense of small deformations of the molecular structure allows a high efficiency of packing. We can now add that the benzene H atoms in **2** appear to be sufficiently acidic so as to establish hydrogen bonds with the carbonyl oxygens.

Let us now discuss the molecular arrangement in crystalline **3**, which not only possesses both terminal and bridging CO ligands but also carries the TTC ligand. We have previously observed, in the study of the crystals of the two isomers Ir₄(CO)₆(μ-CO)₃(μ₃-S₃C₃H₆) and Ir₄(CO)₉(μ₃-S₃C₃H₆),⁹ that the H atoms of the CH₂ units are sufficiently acidic to participate in C–H···O hydrogen-bonding networks and that bridging CO ligands are preferentially involved in short C–H···O interactions.

The first neighboring molecules are distributed in cuboctahedral fashion in crystalline **3**. A network of C–H···O interactions is clearly detectable in this crystal. Relevant geometrical features are listed in Table 3. The shortest interactions are those established by the bridging CO ligands. Carbonyl CO(13), in particular, appears to be involved in a bifurcated interaction [O(13)···H(120) 2.369, O(13)···H(230) 2.262 Å]; CO(23) and CO(12) are instead in close proximity of only one H atom [O(23)···H(121) 2.330, O(12)···H(231) 2.538 Å], but these two interactions are present twice in the same molecule because of symmetry relationships with the first neighboring molecules (see Figure 8a). C–H···O bonds are not confined to these ligands, though. Two interactions involve two terminal CO's *trans* to the S atoms, as shown in Figure 8b. These interactions, however, are appreciably longer than those involving the bridging ligands (see Table 3). A further point of interest arises from the participation of the lone pairs of a S atom in an interaction with an H atom. The separation S(2)···H(131) is 2.924 Å, *viz.* appreciably shorter than the sum of the van der Waals radii of hydrogen and sulfur (1.20 and 1.85 Å, respectively).²⁵

Conclusions

With this paper we have addressed the dualism between molecular structure in the solid state and crystal structure for three closely related cluster com-

(25) (a) Bondi, A. *J. Phys. Chem.* **1964**, *68*, 441. (b) Gavezzotti, A. *Nouv. J. Chim.* **1982**, *6*, 443.

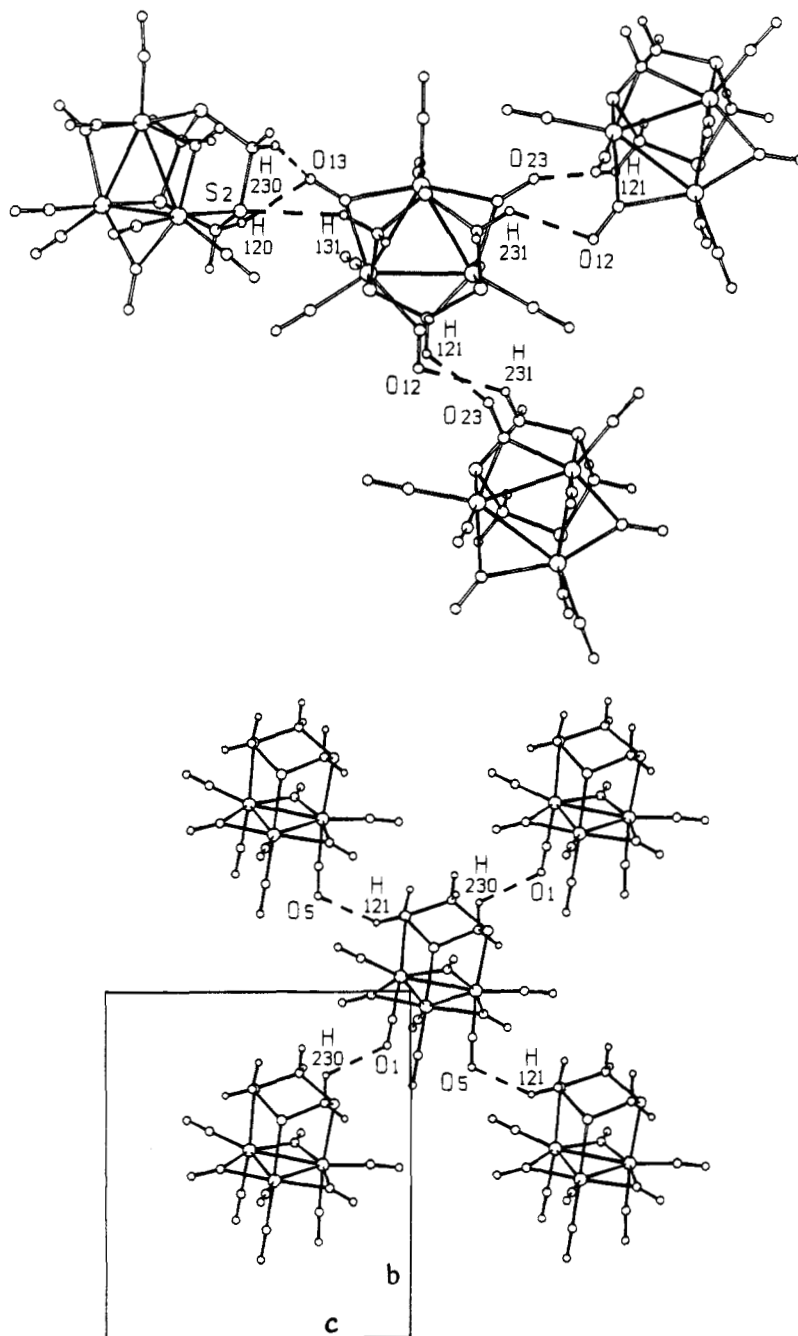


Figure 8. (a) C-H \cdots O hydrogen bonds involving bridging CO ligands in crystalline **3**. The interaction between a H(CH) atom and a S atom is also shown. (b) C-H \cdots O interactions involving two terminal CO's *trans* to the S atoms.

plexes of ruthenium. Our observations can be summarized as follows:

(i) Extended Hückel calculations have shown that, since bridging CO's are more efficient π -acceptors than terminal CO's, their presence in **3** is required in order to compensate for the substitution of the σ -donor ligand TTC for three axial ligands in the structure of Ru₃(CO)₁₂.

(ii) This is not so in **2** where the facial C₆H₆ ligand takes the place of the axial CO's as π -acceptor and stabilizes the all-terminal structure.

(iii) Whereas **1** forms a van der Waals solid based on the interlocking of CO ligands, hydrogen-bonding networks of the C-H \cdots O type involving the carbonyl oxygen atoms stabilize the crystal structures of **2** and **3**.

(iv) Although the terminal ligands participate in C-H \cdots O bonding in both **2** and **3**, the shortest interactions are observed between the TTC hydrogen atoms and the bridging CO's in **3**. This is in keeping with the charge distribution obtained from the extended Hückel calculations, which assigns a slightly more positive charge to the TTC hydrogens with respect to those of benzene (+0.03 *vs* +0.02) and a slightly more negative charge to the oxygen atoms of the bridging ligands (-0.70 *vs* -0.63 and -0.62 for the terminal ligands in **2** and in **3**, respectively).

(v) As the calculations show, each cluster is present in its solid state structure as the isomeric form which optimizes the bonding, i.e. with only terminal CO's for **1** and **2** and with bridging CO's for **3**.

Methodology

All the molecular orbital calculations were done using the extended Hückel method²¹ with modified H_{ij} 's.²⁶ The basis set for the metal atom consisted of ns , np , and $(n-1)d$ orbitals. Only 3s and 3p orbitals were considered for sulfur. The s and p orbitals were described by single Slater-type wave functions, and the d orbitals were taken as contracted linear combinations of two Slater-type wave functions. Standard parameters were used for H, C, O, and S, while those for Ru were the following (H_{ij}/eV , ζ): 5s, -10.40, 2.078; 5p, -6.89, 2.043; 4d, -14.90, 5.378, 2.303 (ζ_2), 0.5340 (C_1), 0.6365 (C_2). Three-dimensional representations of orbitals were drawn using the program CACAO.²⁷

Idealized models having C_{3v} symmetry were used for the clusters studied. The two metallic fragments Ru₃(CO)₆(μ -CO)₃ and Ru₃(CO)₉ are based on the geometries they exhibit on the respective benzene and TTC clusters.^{7,8} The following distances (Å) were used: Ru-Ru 2.85, Ru-C(terminal) 1.90, Ru-C(bridging) 2.14, C-O 1.15, Ru-C(benzene) 2.33, Ru-S 2.42, C-C 1.40, C-S 1.80, C-H 1.09. The benzene hydrogen atoms were considered as bent back from the metal atoms by 20°.

Crystal structure analysis was carried out with the aid of the computer program OPEC,^{29a} which allows the calculation of packing potential energies as well as of molecular volumes and packing coefficients. Partition-

ing of the packing potential energy among the molecules forming the enclosure shell allows recognition of most relevant packing motifs and crystal structure decoding. In particular, when atom-atom potential parameters for purely van der Waals interactions are used,²⁸ the interaction between the oxygen acceptor and the hydrogen atom participating in a hydrogen bond gives rise to a substantial repulsion because the distance between the atoms is below that of a van der Waals contact. This repulsion in the crystal is overcome by the electrostatic attraction between the two atoms involved in the hydrogen bond. Therefore, strongly repulsive O...H interactions in the list of intermolecular interactions can be taken as diagnostically indicative of the presence of a hydrogen bond. In the present study no attempt was made to evaluate the energy contribution to packing cohesion of the C-H...O interactions. The geometric features of the intermolecular hydrogen-bonding networks were investigated by using the graphic program SCHAKAL92^{29b} and the suite of programs PLATON.^{29c} Atomic coordinates and crystal data were obtained from the Cambridge Crystallographic Database.³⁰ The available coordinates for the hydrogen atoms were normalized by extending the C-H distances along the C-H vectors to the typical neutron-derived value of 1.08 Å.³¹

Acknowledgment. D.B., F.G., M.J.C., and L.F.V. acknowledge CNR (Italy) and JNICT (Portugal) for joint financial support.

OM940815E

(26) Ammeter, J. H.; Bürgi, H.-B.; Thibeault, J. C.; Hoffmann, R. *J. Am. Chem. Soc.* **1978**, *100*, 3686.

(27) Mealli, C.; Proserpio, D. M. *J. Chem. Educ.* **1990**, *67*, 39.

(28) (a) Filippini, G.; Gavezzotti, A. *Acta Crystallogr.* **1993**, *B49*, 868. (b) Gavezzotti, A.; Filippini, G. *J. Phys. Chem.* **1994**, *98*, 4831.

(29) (a) Gavezzotti, A. OPEC, Organic Packing Potential Energy Calculations, University of Milano, Italy. See also: Gavezzotti, A. *J. Am. Chem. Soc.* **1983**, *105*, 5220. (b) Keller, E. SCHAKAL92, University of Freiburg, Germany, 1992. (c) Spek, A. L. PLATON. *Acta Crystallogr., Sect A* **1990**, *46*, C31.

(30) Allen, F. H.; Davies, J. E.; Galloy, J. J.; Johnson, O.; Kennard, O.; Macrae, C. F.; Watson, D. G. *J. Chem. Inf. Comput. Sci.* **1991**, *31*, 204.

(31) Murray-Rust, P.; Glusker, J. P. *J. Am. Chem. Soc.* **1984**, *106*, 1018.

Structure of (2,2'-Biallylene)hexacarbonyldiiron

Robert C. Kerber,* M. Jawad Miran, and Brian Waldbaum

Department of Chemistry, SUNY at Stony Brook, Long Island, New York 11794-3400

Arnold L. Rheingold

Department of Chemistry, University of Delaware, Newark, Delaware 19716

Received October 11, 1994[®]

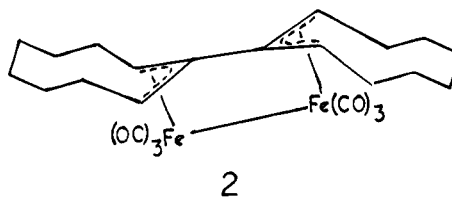
The crystal structures of the title compound [$C_{12}H_8Fe_2O_6$, orthorhombic, *Iba*2 (No. 45), $a = 22.762(15)$ Å, $b = 12.229(11)$ Å, $c = 9.615(8)$ Å, $Z = 8$] and its triphenylphosphine substitution product [$C_{29}H_{13}Fe_2O_5P$, triclinic, $P\bar{1}$ (No. 2), $a = 10.7506(20)$ Å, $b = 13.3657(23)$ Å, $c = 9.5827(16)$ Å, $\alpha = 92.803(11)$, $\beta = 94.022(11)$, $\gamma = 73.444(14)^\circ$, $Z = 2$] are reported. They show systematic deviations from C_{2v} symmetry, with the biallylene ligand being nonplanar due to pyramidalization and internal rotation about its central C–C bond; also, the Fe–Fe and central C–C axes are not parallel, being twisted by 11° relative to each other. Low-temperature NMR studies at -95° indicate similar distortions in solution, with very low activation energy for interconversion of equivalent lower-symmetry forms. In the crystal structures, these distortions of the biallylene ligand are accompanied by relief of eclipsing interactions among the equatorial carbonyl ligands of the $Fe_2(CO)_5L$ fragment. Pyramidalization is found in all published (2,2'-biallylene)diiron structures, but the twisting and rotation are not, consistent with the small energy change which accompanies these latter deformations.

The unstable organic fragment 2,2'-biallylene¹ [sometimes called tetramethyleneethane; systematic name: 2,3-bis(methylene)-1,4-butanediyl] should constitute an excellent ligand for formation of bimetallic complexes, on the basis of the ready formation of stable allyl complexes of many metals and the proximity of the two allyl groups. Current interest in bimetallic complexes, especially fulvalene complexes, as potential exemplars of cooperative reactivity² would lead one to expect many studies of (biallylene)bimetallics, but there have been surprisingly few.

In fact, the only known metal–metal-bonded biallylene complexes are the diiron complexes, first reported in 1965.³ These complexes have most commonly been prepared by *in situ* dimerization of allenes during reaction with various iron carbonyls.^{3–9} The parent

(C_6H_8) $Fe_2(CO)_6$, **1**, has also been prepared by reaction of 2,3-bis(bromomethyl)-1,3-butadiene or 2,3-bis(bromomethyl)-1,4-dibromo-2-butene with diiron nonacarbonyl.⁹ Derivatives having the biallylene moiety incorporated in rings have also been formed in *o*-xylylene-derived systems^{10,11} and from polycyclic hydrocarbons such as anthracene¹² and naphthalene.¹³

Early discussion³ of parallel vs perpendicular isomers of **1** (Scheme 1) was effectively resolved by means of extended Hückel calculations by Thorn and Hoffmann,¹⁴ which indicated a substantial energetic preference (1.7 eV) for the parallel, C_{2v} form, and by a partial crystal structure ($R = 0.12$, the result of "multiple twinning") of the product, **2**, from reaction of 1,2-cyclonadiene with $Fe_2(CO)_9$.⁵ However, the crystal structure showed only C_2 symmetry for **2**, which, together with reduced



symmetry apparent in low-temperature NMR studies of **1** and **2**, led to a further suggestion of equilibrating

(8) Song, J.-S.; Han, S.-H.; Nguyen, S. T.; Geoffroy, G. L.; Rheingold, A. L. *Organometallics* **1990**, *9*, 2386–95. Structure TACFOS in Cambridge Structural Database.

(9) Gaoni, Y.; Sadeh, S. *J. Org. Chem.* **1980**, *45*, 870–81.

(10) Victor, R.; Ben-Shoshan, R. *J. Organomet. Chem.* **1974**, *80*, C1–4. Boschi, T.; Vogel, P.; Roulet, R. *J. Organomet. Chem.* **1977**, *133*, C36–8.

(11) Girard, L.; Decken, A.; Blecking, A.; McGlinchey, M. J. *J. Am. Chem. Soc.* **1994**, *116*, 6427–8.

(12) Begley, M. J.; Puntambekar, S. G.; Wright, A. H. *J. Chem. Soc., Chem. Commun.* **1987**, 1251–2. Structure FIVJUP in Cambridge Structural Database, but with numbering inconsistent with published structure.

[®] Abstract published in *Advance ACS Abstracts*, March 15, 1995.

(1) Experimental study: Dowd, P.; Chang, W.; Paik, Y. H. *J. Am. Chem. Soc.* **1986**, *108*, 7416–7. Recent theoretical studies: Nachtigall, P.; Jordan, K. D. *J. Am. Chem. Soc.* **1993**, *115*, 270–1. Pranata, J. *J. Am. Chem. Soc.* **1992**, *114*, 10537–41. Chakrabarti, A.; Albert, I. D. L.; Ramasesha, S.; Lalitha, S.; Chandrasekhar, J. *Proc. Indian Acad. Sci., Chem. Sci.* **1993**, *105*, 53–62.

(2) (a) Tilset, M.; Vollhardt, K. P. C.; Boese, R. *Organometallics* **1994**, *13*, 3146–69 and previous papers, cited therein, from the Vollhardt group. (b) Beck, W.; Niemer, B.; Wieser, M. *Angew. Chem., Int. Ed. Engl.* **1993**, *32*, 923–49. (c) Scott, P.; Rief, U.; Diebold, J.; Brintzinger, H. H. *Organometallics* **1993**, *12*, 3094–3101. (d) Delville, M.-H.; Lacoste, M.; Astruc, D. *J. Am. Chem. Soc.* **1992**, *114*, 8310–1.

(3) (a) Nakamura, A.; Hagihara, N. *J. Organomet. Chem.* **1965**, *3*, 480–1. (b) Nakamura, A.; Kim, P.-J.; Hagihara, N. *J. Organomet. Chem.* **1965**, *3*, 7–15. (c) Nakamura, A. *Bull. Chem. Soc. Jpn.* **1966**, *39*, 543–7. (d) Otsuka, S.; Nakamura, A.; Tani, K. *J. Chem. Soc. A* **1968**, 2248–53.

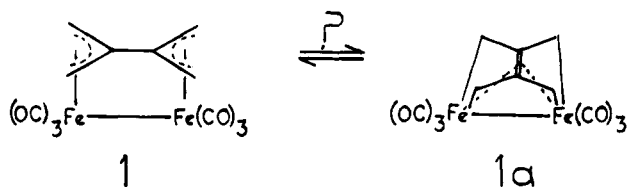
(4) King, R. B.; Harmon, C. A. *J. Organomet. Chem.* **1975**, *86*, 239.

(5) Howell, J. A. S.; Lewis, J.; Matheson, T. W.; Russell, D. R. *J. Organomet. Chem.* **1975**, *99*, C55–8.

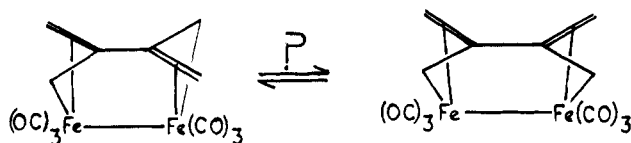
(6) Aumann, R.; Melchers, H.-D.; Weidenhaupt, H.-J. *Chem. Ber.* **1990**, *123*, 351–6.

(7) Seyferth, D.; Anderson, L. L.; Davis, W. B.; Cowie, M. *Organometallics* **1992**, *11*, 3736–44. Structure YAJWAH in Cambridge Structural Database.

Scheme 1



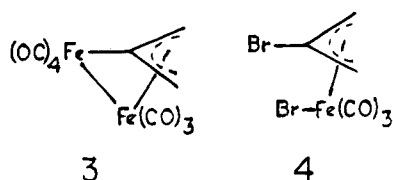
Scheme 2



nonequivalent σ,π structures in solution (Scheme 2). Attempts to secure a crystal structure of **1** were apparently unsuccessful.^{3d} Crystal structures of some di- or tetrasubstituted derivatives of **1**^{7,8,11,12} have been published more recently, and all show more or less parallel structures; however, the possible effects of reduced symmetry due to substituents or of structural rigidity imposed by polycyclic frameworks make unclear to what extent these may reflect the structure of the unperturbed parent complex, **1**. We therefore sought to establish the structures of complexes of unsubstituted 2,2-biallylene, which we report here.

Experimental Section

(2,2'-Biallylene)hexacarbonyldiiron, 1.³ Allene was condensed into a dry ice-cooled graduated cylinder (4.0 mL, *ca.* 90 mmol), diluted with 60 mL of hexane, and transferred to a small stainless steel autoclave. Nonacarbonyldiiron (28.56 g, 73 mmol) was added to the hexane solution, and the autoclave was sealed and heated in an oil bath at 60–70 °C for 23 h. The apparatus was cooled to room temperature, the autoclave was opened, and the mixture was filtered. Evaporation of the filtrate left 4.18 g of dark green-brown oil. Chromatography on silica, eluting with hexane, gave 66 mg (2%) of a product identified by IR and NMR spectra as $(C_3H_4)Fe_2(CO)_7$, **3**,^{6,16}



followed by 2.38 g (18%) of **1**. Pure **1** was obtained by slow cooling of hexane solutions to -80 °C, giving red crystals, mp 84–6 °C (lit.^{3,9} mp 88–9 °C). IR: (hexane, cm^{-1}) 2066 s, 2046 w, 2025 s, 1998 s, 1976 m, 1952 w ($^{13}CO?$); (CCl_4) 2064 s, 2046 w, 2024 s, 1995 s, 1972 m. Room-temperature 300 MHz 1H NMR: ($CDCl_3$) δ 1.68 (s), 1.75 (s); (acetone- d_6) δ 1.91 (s), 2.03 (s). Variable-temperature NMR spectra were measured at 250 MHz. The crystal structure of **1** is described below. Also produced, but not fully purified and identified, was a product which appeared by mass spectrometry to have the composition $(C_3H_4)_3Fe_3(CO)_7$; its proton NMR spectrum showed peaks at δ 2.26, 2.44, 6.21, and 6.43 in a ratio of 2:2:1:1. The ^{13}C NMR

(13) Bauer, R. A.; Fischer, E. O.; Kreiter, C. G. *J. Organomet. Chem.* **1970**, *24*, 737–51.

(14) Thorn, D. L.; Hoffmann, R. *Inorg. Chem.* **1978**, *17*, 126–40.

(15) Murdoch, H. D.; Weiss, E. *Helv. Chim. Acta* **1962**, *45*, 1927–33. Nesmeyanov, A. N.; Kritskaya, I. I.; Fedin, E. I. *Dokl. Akad. Nauk SSSR* **1965**, *164*, 1058–61.

(16) Ben-Shoshan, R.; Pettit, R. *Chem. Commun.* **1968**, 247–8. Kritskaya, I. I. *Russ. Chem. Rev. (Engl. Transl.)* **1972**, *41*, 1027–45.

Table 1. Crystallographic Data for $(\eta^6-C_6H_8)Fe_2(CO)_6$, **1**, and $(\eta^6-C_6H_8)Fe_2(CO)_5PPh_3$, **5**

Crystal Data		
formula	$C_{12}H_8Fe_2O_6$	$C_{29}H_{23}Fe_2O_5P$
formula wt	359.9	594.1
cryst color and habit	orange plate	brown prism
cryst size, mm	$0.04 \times 0.48 \times 0.68$	$0.2 \times 0.3 \times 0.35$
cryst syst	orthorhombic	triclinic
space group	<i>Iba</i> 2 (No. 45)	<i>P</i> 1 (No. 2)
<i>a</i> , Å	22.762(15)	10.751(2)
<i>b</i> , Å	12.229(11)	13.366(2)
<i>c</i> , Å	9.615(8)	9.583(2)
α , deg	90	92.80(1)
β , deg	90	94.02(1)
γ , deg	90	73.44(1)
<i>V</i> , Å ³	2676(3)	1315.9(4)
<i>Z</i>	8	2
<i>D</i> (calcd), $g\ cm^{-3}$	1.786	1.499
μ (Mo $K\alpha$), cm^{-1}	21.9	11.975
Data Collection		
diffractometer	Siemens P4	Enraf-Nonius CAD4
rflns collected	1575 (max $2\theta = 50^\circ$)	6671 (max $2\theta = 54^\circ$)
independent rflns	1378	6339
obsd rflns	1222 (4.5 σ (<i>F</i>))	3855 (3 σ (<i>F</i>))
min/max transmission	0.53/0.94	0.92/1.03
Refinement		
<i>R</i> (<i>F</i>), <i>R</i> (<i>wF</i>), %	3.12, 3.47	3.29, 3.62
data/param	6.7	11.5
Δ (max), $e\ \text{\AA}^{-3}$	0.36	0.25
goodness of fit	0.89	1.25

showed peaks at δ 212.6, 149.3, 112.5, 38.0, 31.9, and 19.4. Attempted reaction of allene with pentacarbonyliron in the autoclave at 120 °C gave predominantly oligo(allene) products rather than iron carbonyl products.

2,3-Dibromopropene (10.7 mL, 20.7 g, 0.103 mol) was stirred for 2.5 h at 40 °C under a nitrogen atmosphere with 36.5 g (0.10 mol) of nonacarbonyldiiron in 50 mL of hexanes. The solution was filtered, and the solid was washed with hexane; evaporation of the filtrate left a yellow-brown solid product, which was predominantly (2-bromoallyl)tricarbonyliron bromide, **4**; recrystallization from hexanes yielded 2.31 g of **4**.¹⁵ A similar reaction run under reflux conditions produced predominantly **3** and small amounts of **1**, as indicated by NMR.

Stirring 0.633 g (1.87 mmol) of **4** with 0.152 g (2.32 mmol) of zinc powder in 25 mL of ether under nitrogen for 15 h gave a complex mixture of products, in which little or no **1** was detectable by NMR.

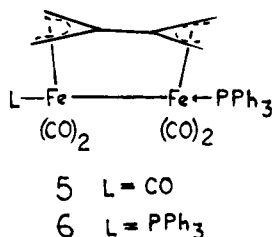
X-ray Crystallographic Structure Determination of 1.

Crystallographic data are collected in Table 1. Structural studies were done on very brittle crystals with an extremely thin plate-like habit. Most cements distorted and cracked specimens as they hardened, and immobilization within a capillary was impossible due to the extreme fragility. Crystals were ultimately affixed to a fine glass fiber with a very small amount of an alkyd varnish. High esd's associated with the unit cell parameters are likely the result of crystal flexing due to air currents within the diffractometer chamber. A laminar correction for absorption was applied to the diffraction data, with data making a glancing angle $\leq 3^\circ$ discarded.

Systematic absences in the diffraction data indicated either of the orthorhombic space groups *Iba*2 or *Ibam*. Since *Z* = 8 and the molecule does not possess mirror-plane symmetry, processing was confined to the noncentrosymmetric alternative. The Fe atoms were located from a Patterson synthesis. All non-hydrogen atoms were refined anisotropically, and all hydrogen atoms were located and successfully refined isotropically. All computations used SHELXLT software (version 4.2, G. Sheldrick, Siemens XRD, Madison, WI).

(2,2'-Biallylene)pentacarbonyl(triphenylphosphine)diiron, 5. Triphenylphosphine (291 mg, 1.11 mmol) and **1** (200 mg, 0.556 mmol) were refluxed for 16 h under nitrogen in 10 mL of benzene. Filtration and evaporation of the filtrate left a solid residue, which was chromatographed on silica.

Elution with hexanes yielded some unreacted **1**. Elution with 10% ethyl acetate/hexanes yielded 235 mg of substitution product **5**, contaminated by some unreacted triphenylphosphine.



phine. Pure **5** (100 mg, 37%) was obtained by recrystallization from ethyl acetate/hexanes or ethyl acetate/methanol as brown-black crystals, mp 150 °C dec. IR (KBr, cm⁻¹): 2026 s, 1977 s, 1961 s, 1948 m sh, 1911 m. ¹H NMR (CDCl₃): δ 7.5–7.3 (complex m, 15H), 1.72 (s, 2H), 1.51 (s, 2H), 1.35 (s, 2H), 0.60 (d, 2H, ³J_{PH} = 10.5 Hz). MS (direct inlet) (*m/z*, intensity, assignment): 594, 0.2, P; 566, 1.0, P–CO; 538, 0.7, P–2CO; 510, 3.2, P–3CO; 482, 2.6, P–4CO; 454, 14, P–5CO; 398, 6.0, P–Fe(CO)₅; 318, 6.5, FePPh₃; 262, 100, PPh₃; 183, 93, C₁₂H₈P; 108, 42, PPh; 56, 31, Fe. Anal. Found: C, 59.30; H, 4.32; Fe, 18.22; P, 5.10. Calcd for C₂₅H₂₃Fe₂O₅P: C, 58.62; H, 3.90; Fe, 18.80; P, 5.21.

Repetition of the reaction using the same quantities of reactants, but refluxing for 45 h, gave 476 mg of crude product. Chromatography of the hexane-soluble portion of this material gave some recovered **1**, triphenylphosphine, and an unidentified product, not completely separable from **5**, which showed two multiplets of equal size in the ¹H NMR at δ 1.3 and 0.9, along with phenyl absorptions at δ 7.6–7.2, and infrared absorptions at 2033, 1975, and 1968 cm⁻¹. Recrystallization of the hexane-insoluble portion of the crude product (226 mg) from ethyl acetate left a ruby-red product, mp 160 °C dec, which appeared to be a bis(triphenylphosphine) substitution product, (C₆H₅)Fe₂(CO)₄(PPh₃)₂, **6**. IR (KBr, cm⁻¹): 1984 s, 1940 s, 1901 m. ¹H NMR (CD₂Cl₂): δ 7.6–7.3 (complex m, 30H), 1.70 (s, 4H), 0.43 (d, 4H, ³J_{PH} = 11.4 Hz). MS (direct inlet) (*m/z*, intensity, assignment): 482, 0.5, (C₆H₅)Fe₂(CO)PPh₃; 454, 3.1, (C₆H₅)Fe₂PPh₃; 400, 8.8; 398, 8.0, (C₆H₅)FePPh₃; 318, 11.5, FePPh₃; 262, 45, PPh₃; 183, 81, C₁₂H₈P; 108, 54, PPh; 107, 47, C₆H₄P; 77, 46, C₆H₅; 51, 100, C₄H₃. The mother liquor contained principally **5**.

X-ray Crystallographic Structure Determination of 5. Suitable crystals of **5** were obtained by slow cooling of a toluene solution to –80 °C, using an insulating container. A dark brown crystal (ca. 0.2 × 0.3 × 0.35 mm³) was mounted on a glass fiber using epoxy resin. Data were collected at 23 °C on an Enraf-Nonius CAD-4 diffractometer and processed using the TEXSAN suite of programs. A random search at low θ yielded 25 reflections, which were indexed to give an initial cell. An accurate cell was obtained using higher angle (θ = 10–12°) reflections. The structure was solved by direct methods using the SHELXS program, which revealed the irons, phosphorus, and most of the carbons and oxygens. A difference Fourier map then yielded the remaining heavy atoms. After partial refinement, hydrogen atom positions were calculated assuming sp² hybridization, and the structure was subject to full anisotropic refinement of the heavy atoms and isotropic refinement of the hydrogen atoms, after applying an absorption correction using the program DIFABS.

Extended Hückel Calculations. Calculations were run on a VAX cluster using program FORTICON 8 (No. 517 from the Quantum Chemistry Program Exchange, Bloomington IN), slightly modified for more convenient data input and output. The atomic parameters used were identical to those of Thorn and Hoffman.¹⁴ For modeling the biallylene fragment, C–C, C–CH₂, and C–H distances used were 1.47, 1.41, and 1.07 Å, respectively. The Fe–Fe bond distance used was 3.00 Å, and the OC_{eq}–Fe–CO_{eq} angle was 100°. All Fe–CO bond distances

were set at 1.77 Å, and all C–O at 1.16 Å. Pyramidalization of the biallylene ligand, keeping Fe–C distances of 2.04 Å while leaving the C₂H₄ fragments planar, did not result in stabilization of the structure, even though the Fe–CH₂ distances became more realistic as they decreased from 2.25 to 2.09 Å. It was necessary to rotate the CH₂ groups of the pyramidalized ligand so that the axial (*anti*) hydrogens moved away from the irons and the equatorial (*syn*) hydrogens moved toward the irons in order to observe stabilization relative to the planar combination. The best such structure had 0.15 Å pyramidalization (i.e., the central C's lay 0.15 Å above the plane of the four CH₂ carbons) and 26° rotation of the CH₂ groups; its energy was 0.63 eV lower than the all-planar model. Extended Hückel calculations using the actual coordinates of **1**, **5** (with the triphenylphosphine replaced by a CO), and **9** (with the phenylthio groups replaced by hydrogens) gave still lower energies, however. The energies of **1** and modified **5** were almost identical, indicating net bonding of 6.99 and 7.00 eV relative to the separated C₆H₅ and Fe₂(CO)₆ fragments. The corresponding bonding energy using modified **9** was 7.51 eV. The HOMO–LUMO gap was greatest (1.83 eV) for **1**. Most of the energy differences arose from changes in the levels of the three highest filled MO's, which in C_{2v} symmetry have a₂, b₁, and b₂ symmetry. These have been pictured and discussed by Thorn and Hoffmann.¹⁴

Results

Compound **1** was conveniently prepared by reaction of allene with Fe₂(CO)₉ in hexane at 70 °C.¹ It was also produced, but only in trace amounts, by reaction of 2,3-dibromopropene with Fe₂(CO)₉; the major product of the latter reaction was (2-bromoallyl)tricarbonyliron bromide, **4**.¹⁵ Reaction of this dibromo product with zinc dust did not produce **1** in significant amounts, although such a coupling reaction was claimed for the corresponding dichloride.¹⁶

The infrared spectrum of **1** in hexane or carbon tetrachloride solution shows four strong carbonyl peaks rather than the five allowed for a Fe₂(CO)₆ species with C_{2v} symmetry or the six allowed with C₂ symmetry. In the absence of a total vibrational analysis, including isotopic labeling studies, vibrational degeneracies in **1** will apparently prevent assignment of the symmetry of the species present in solution.

The proton NMR spectrum of **1** at room temperature showed two closely spaced resonances,^{3c,6} whose chemical shifts were unusually solvent sensitive, ranging from δ 1.68 and 1.75 in CDCl₃ to 1.91 and 2.03 in acetone-*d*₆. Nakamura^{3c} reported that, on cooling a carbon tetrachloride solution of **1**, the two peaks coalesced into a singlet at –10 °C; *three* broad peaks were reported at –55 °C in chloroform. We also find gradual merger of the two room-temperature proton resonances upon cooling a CD₂Cl₂ solution of **1**, the result of the high-field peak (δ 1.73 at 25 °C) drifting downfield to merge with the low-field peak (δ 1.79 at 25 °C) to form a single, slightly broad peak at δ 1.80 at –80 °C. No evidence of decoalescence was observed at 250 MHz and –85 °C. In toluene-*d*₈, the two proton resonances (δ 1.18 and 1.10 at 25 °C) merged upon cooling by moving upfield (δ 0.79 at –63 °C). The merger of the peaks upon cooling was solvent dependent, however, and therefore does not seem to correspond to any process resulting in chemical equivalence. In 1:1 acetone-*d*₆–chloroform-*d*, both peaks drifted downfield and broadened at comparable rates upon cooling. At –98 °C, two broad peaks, at δ 1.98 and 2.13, were seen. Decoalescence into

Table 2. Atomic Coordinates ($\times 10^4$) and $U(\text{eq})$ ($\text{\AA}^2 \times 10^3$) for **1**

atom	x	y	z	$U(\text{eq})^a$
Fe1	1444.6(6)	2029.6(9)	0	32(1)
Fe2	1061.8(5)	2578.5(9)	2821.2(5)	33(1)
O1	2580(3)	1176(6)	931(10)	74(3)
O2	1685(4)	1427(8)	-2871(10)	72(4)
O3	699(3)	97(6)	313(10)	69(3)
O4	-32(4)	1331(5)	2548(11)	68(3)
O5	837(4)	3182(8)	5711(9)	79(4)
O6	1878(3)	844(6)	3636(10)	56(2)
C1	2133(4)	1484(8)	656(11)	44(3)
C2	1590(5)	1682(8)	-1759(12)	46(4)
C3	979(4)	856(7)	242(11)	44(3)
C4	398(4)	1769(7)	2621(11)	41(3)
C5	922(5)	2934(9)	4600(11)	52(4)
C6	1576(5)	1516(8)	3258(10)	40(3)
C7	808(5)	3186(9)	-597(12)	49(4)
C8	1256(4)	3651(7)	210(12)	41(3)
C9	1827(5)	3588(7)	-371(12)	50(4)
C10	630(4)	4060(7)	2256(12)	46(3)
C11	1183(4)	3957(6)	1672(10)	36(3)
C12	1656(4)	3897(8)	2645(14)	48(4)

^a Equivalent isotropic U defined as one-third of the trace of the orthogonalized U_{ij} tensor.

the four peaks expected of a species of C_2 symmetry was not observed at this lowest obtainable temperature.

The room-temperature ^{13}C NMR spectrum of **1** showed four carbon resonances, two for the equatorial and axial carbonyl groups and two for the biallylene ligand, at δ 38.6 and 87.9. On cooling, the high-field methylene resonance ($^1J_{\text{CH}} = 158.3$ Hz) broadened somewhat relative to the others, but did not decoalesce even at -98 °C. Similarly, in toluene- d_8 at -79 °C, the width of the methylene carbon resonance was five times that of the central carbons, which was essentially the same as that of TMS.

The low-temperature line broadening observed for the methylene groups in the ^1H and ^{13}C NMR spectra is consistent with equilibration of unsymmetrical forms, but limiting spectra which would allow more complete characterization of those forms could not be obtained. No broadening of the equatorial carbonyl resonance was discernible, even at the lowest accessible temperatures.

Heating **1** with triphenylphosphine in benzene solution resulted in formation of the displacement product **5**, $(\text{C}_6\text{H}_5)_2\text{Fe}_2(\text{CO})_5\text{PPh}_3$. The proton NMR data showed four equally intense sets of proton resonances, indicating maintenance of a plane of symmetry. This requires the phosphine to occupy an axial position in the $\text{Fe}_2(\text{CO})_5\text{L}$ "sawhorse" moiety. Only the most highly shielded pair of hydrogens, at δ 0.60, showed coupling to the phosphorus ($J_{\text{PH}} = 11$ Hz); both the shielding and the coupling suggest that these are the axial hydrogens *syn* to the phosphine group. The crystal structure (*vide infra*) clearly shows these hydrogens in the face of a phenyl ring of the triphenylphosphine. Further reaction with triphenylphosphine gave a disubstitution product **6**, $(\text{C}_6\text{H}_5)_2\text{Fe}_2(\text{CO})_4(\text{PPh}_3)_2$, whose spectroscopic data likewise indicated a diaxial substitution pattern. The preference for axial orientation of the bulky triphenylphosphine substituents is probably steric in origin.

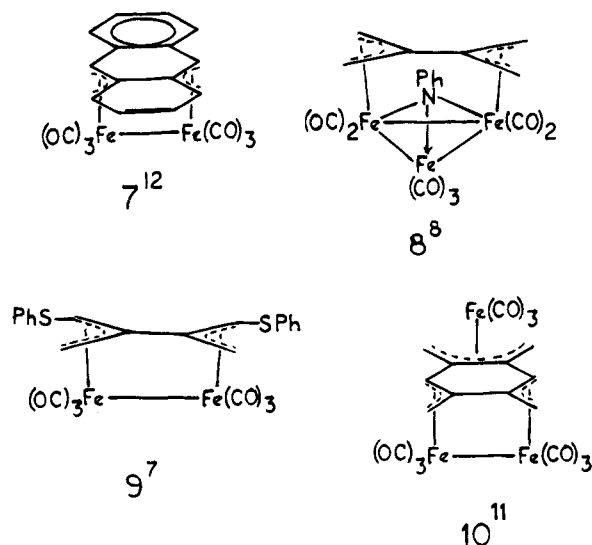
Crystal structures have been obtained for both **1** and **5**. Details of data collection are given in Table 1; coordinates for **1** and **5** are given in Tables 2 and 3, respectively. Significant bond distances and angles for both compounds are given in Tables 4 and 5. Pictures of the structures of **1** and **5** are shown in Figures 1 and

Table 3. Atomic Coordinates ($\times 10^4$) and $U(\text{eq})$ ($\text{\AA}^2 \times 10^3$) for **5**

atom	x	y	z	$U(\text{eq})^a$
Fe1	230.8(4)	7024.8(3)	2920.4(4)	31.0(2)
Fe2	2920.0(4)	5575.9(3)	2737.8(5)	40.8(2)
P1	-1726.2(7)	8212.1(6)	3116.3(7)	32.0(5)
O1	1472(2)	8702(2)	3106(3)	70(2)
O2	4016(3)	7171(2)	4086(3)	86(2)
O3	-236(2)	6892(2)	-109(2)	71(2)
O4	5486(2)	4100(2)	2464(3)	82(2)
O5	2607(3)	6049(3)	-223(3)	95(2)
C1	-2377(3)	8403(2)	4847(3)	34(1)
C2	-1651(3)	8717(3)	5969(3)	46(2)
C3	-2075(4)	8826(3)	7306(3)	56(2)
C4	-3211(4)	8607(3)	7559(4)	60(2)
C5	-3939(3)	8297(3)	6477(4)	57(2)
C6	-3534(3)	8192(2)	5122(3)	44(2)
C7	-3106(3)	8036(2)	1985(3)	37(1)
C8	-3092(3)	7078(2)	1355(3)	46(2)
C9	-4161(3)	6952(3)	550(4)	58(2)
C10	-5253(3)	7789(3)	371(4)	60(2)
C11	-5280(3)	8735(3)	970(4)	62(2)
C12	-4212(3)	8870(3)	1780(4)	52(2)
C13	-1755(3)	9536(2)	2662(3)	35(1)
C14	-2113(3)	10403(2)	3556(3)	49(2)
C15	-2087(4)	11375(3)	3141(4)	62(2)
C16	-1716(3)	11499(3)	1835(4)	56(2)
C17	-1397(3)	10654(3)	930(4)	58(2)
C18	-1406(3)	9672(2)	1329(3)	48(2)
C19	1018(3)	8024(2)	3048(3)	43(2)
C20	-24(3)	6938(3)	1074(3)	43(2)
C21	4479(3)	4682(3)	2553(4)	56(2)
C22	2670(3)	5914(3)	950(4)	58(2)
C23	3537(3)	6588(3)	3539(4)	57(2)
C24	556(3)	5748(2)	4121(3)	38(1)
C25	1770(3)	4953(2)	3809(3)	42(2)
C26	-595(3)	5803(2)	3298(3)	46(2)
C27	514(3)	6606(3)	5033(3)	46(2)
C28	2909(3)	4863(3)	4681(4)	52(2)
C29	1961(3)	4400(2)	2508(4)	51(2)

^a Equivalent isotropic U ($\text{\AA}^2 \times 10^3$) defined as one-third of the trace of the orthogonalized U_{ij} tensor.

2, respectively. The phosphine substitution in **5** does increase the Fe-Fe bond length by 0.07 Å, but it does not induce qualitatively significant changes in the metrics or conformation of the biallylene ligand, and so the structures of both will be discussed together in this section. Comparisons will also be made to the reported structures of related compounds **7-10**. (The reported



structure of **2**,⁵ while qualitatively consistent with the others, is of too low precision to justify discussion.)

Table 4. Important Intramolecular Bond Distances (Å) in Biallylene Complexes 1 and 5

type	1		5	
	atoms	distance	atoms	distance
Fe-Fe	Fe1-Fe2	2.927(3)	Fe1-Fe2	2.998(1)
Fe-CH ₂	Fe1-C7	2.104(11)	Fe1-C27	2.105(3)
(short)	Fe2-C12	2.112(10)	Fe2-C29	2.108(3)
Fe-CH ₂	Fe1-C9	2.125(10)	Fe1-C26	2.125(3)
(long)	Fe2-C10	2.131(10)	Fe2-C28	2.135(3)
Fe-C	Fe1-C8	2.039(8)	Fe1-C24	2.038(3)
	Fe2-C11	2.035(9)	Fe2-C25	2.031(3)
C-CH ₂	C7-C8	1.402(15)	C24-C27	1.399(4)
	C8-C9	1.417(15)	C24-C26	1.406(4)
	C10-C11	1.385(14)	C25-C28	1.412(4)
	C11-C12	1.428(15)	C25-C29	1.416(4)
C-C	C8-C11	1.464(15)	C24-C25	1.468(4)
Fe-CO (ax)	Fe1-C2	1.775(11)	Fe2-C21	1.775(4)
	Fe2-C5	1.793(11)		
Fe-CO (eq)	Fe1-C1	1.817(10)	Fe1-C19	1.769(3)
	Fe1-C3	1.800(9)	Fe1-C20	1.775(3)
	Fe2-C4	1.818(9)	Fe2-C23	1.788(4)
	Fe2-C6	1.798(11)	Fe2-C22	1.776(4)
C-O (ax)	average	1.131(14)	C21-O4	1.144(4)
C-O (eq)	average	1.123(13)	average	1.142(4)
Fe-P			Fe1-P1	2.259(1)

The iron-iron bond lengths in these biallylene complexes are very long; only the (allyl)tricarbonyliron dimer, with Fe-Fe distance 3.138(3) Å,¹⁷ shows a longer Fe-Fe bond. Compounds **7**,¹² **9**,⁷ and **10**¹¹ show similarly long bonds, the range being from 2.872(1) to 2.977(1) Å. In the cluster compound **8**,⁸ the iron-iron bond distance is only 2.566(1) Å, but bonding to the 2,2'-biallylene unit remains intact. A normal, unbridged Fe-Fe single-bond length has been estimated to be 2.76 Å,¹⁸ and the range of values in several salts of Fe₂(CO)₈²⁻ is 2.787(2)-2.841(1) Å.¹⁹ From this perspective, the bond length in the biallylene complexes appears to be increased from a normal value by the constraints imposed by the ligand. Indeed, the metal-metal distance which would result from normal metal-allyl bonding to the two ends of a fully coplanar 2,2'-biallylene ligand would be well in excess of 3 Å. In the actual structures of **1** and **5**, the Fe-CH₂ and Fe-C distances average 2.12 and 2.04 Å, similar to those in many allyliron complexes.²⁰ Given the Fe-Fe bond distance of almost 3 Å, these distances can only be achieved by systematic distortion of the biallylene ligand from coplanarity. The distortions seen involve (1) pyramidalization of the central carbons, and (2) rotation about the central C-C bond of the ligand such that one transoid C₄ portion of the unit (C9-C8-C11-C10 in **1**, C26-C24-C25-C28 in **5**) is nearly coplanar, with the remaining two CH₂ groups bent down toward the irons.

(17) Putnik, C. F.; Welter, J. J.; Stucky, G. D.; D'Aniello, M. J., Jr.; Sosinsky, B. A.; Kirner, J. F.; Muettterties, E. L. *J. Am. Chem. Soc.* **1978**, *100*, 4107-16.

(18) Chini, P. (*Compounds with Iron-Metal Bonds and Clusters*.) In *The Organic Chemistry of Iron*; Koerner von Gustorf, E. A., Grevels, F.-W., Fischler, I., Eds.; Academic Press: New York, 1981; Vol. 2, 189-282.

(19) (a) Chin, H. B.; Smith, M. B.; Wilson, R. D.; Bau, R. *J. Am. Chem. Soc.* **1974**, *96*, 5285-7. (b) Bhattacharya, N. K.; Coffy, T. J.; Quintana, W.; Salupo, T. J.; Bricker, J. C.; Shay, T. B.; Payne, M.; Shore, S. G. *Organometallics* **1990**, *9*, 2368-74. (c) Deng, H.; Shore, S. G. *Inorg. Chem.* **1992**, *31*, 2289-91. (d) Cassidy, J. M.; Whitmire, K. H.; Long, G. J. *J. Organomet. Chem.* **1992**, *427*, 355-62.

(20) Deeming, A. J. Mononuclear Iron Compounds with η²-η⁶ Hydrocarbon Ligands. In *Comprehensive Organometallic Chemistry*; Wilkinson, G., Stone, F. G. A., Abel, E. A., Eds.; Pergamon Press: New York, 1982; Vol. 4, p 414. (b) Kerber, R. C. Mononuclear Iron Compounds with η¹-η⁶ Hydrocarbon Ligands. In *Comprehensive Organometallic Chemistry II*; Abel, E. A., Stone, F. G. A., Wilkinson, G., Eds.; Pergamon Press: New York, in press.

Table 5. Important Intramolecular Bond Angles (deg) in Biallylene Complexes 1 and 5

type	1		5	
	atoms	distance	atoms	distance
CH ₂ -C-CH ₂	C7-C8-C9	115(1)	C26-C24-C27	115.3(3)
	C10-C11-C12	115(1)	C28-C25-C29	115.1(3)
CH ₂ -C-C	C7-C8-C11	123.5(9)	C27-C24-C25	123.0(3)
	C8-C11-C10	121.1(9)	C24-C25-C28	120.5(3)
	C9-C8-C11	119.8(9)	C26-C24-C25	120.6(3)
	C8-C11-C12	122.0(9)	C24-C25-C29	123.0(3)
CH ₂ -Fe-CH ₂	C7-Fe1-C9	68.5(4)	C26-Fe1-C27	68.1(1)
	C10-Fe2-C11	68.0(4)	C28-Fe2-C29	68.4(1)
Fe-Fe-CH ₂	Fe2-Fe1-C7	93.9(3)	Fe2-Fe1-C27	83.1(1)
	Fe2-Fe1-C9	94.1(3)	Fe2-Fe1-C26	93.5(1)
	Fe1-Fe2-C10	95.5(3)	Fe1-Fe2-C28	94.5(1)
	Fe1-Fe2-C12	84.8(4)	Fe1-Fe2-C29	84.3(1)
CH ₂ -Fe-ax	C7-Fe1-C2	91.7(5)	C27-Fe1-P1	96.4(1)
	C9-Fe1-C2	88.8(4)	C26-Fe1-P1	90.3(1)
	C10-Fe2-C5	87.4(5)	C28-Fe2-C21	86.7(1)
	C12-Fe2-C5	90.3(5)	C29-Fe2-C21	93.4(1)
	C1-Fe1-C2	94.7(5)	C19-Fe1-P1	91.0(1)
OC _{eq} -Fe-ax	C3-Fe1-C2	92.4(5)	C20-Fe1-P1	91.6(1)
	C4-Fe2-P5	94.9(5)	C23-Fe2-C21	94.5(2)
	C6-Fe2-C5	93.9(5)	C22-Fe2-C21	95.1(2)
	C1-Fe1-C3	99.8(4)	C19-Fe1-C20	99.4(1)
	C4-Fe2-C6	99.9(4)	C22-Fe2-C23	102.9(2)

This results in diagonally opposed Fe-CH₂ distances averaging 2.129(6) Å to the coplanar CH₂ groups and 2.107(5) Å to the downward-bent CH₂ groups. The relative twisting of the two pyramidalized allyl units is accompanied by a comparable twisting of the Fe-Fe axis relative to the C-C axis, giving Fe-Fe-C-C torsion angles of 11-12° in **1** and **5**; the twisting motion is equivalent to rotation of the two iron octahedra (each composed of the three CO groups, the two CH₂ groups, and the other iron) about the Fe-Fe bond, and is illustrated in Figure 3. This rotation results in loss of the eclipsing of the equatorial carbonyl groups, which necessarily occurs when a "sawhorse" Fe₂(CO)₆ unit is bound to an untwisted 2,2'-biallylene unit. The torsion angles between neighboring equatorial CO groups in **1** and **5** average 21(3)°. This pyramidal-twist distortion reduces the symmetry of the (C₆H₈)Fe₂(CO)₆ complex from the idealized C_{2v} to C₂ and is consistent with the line broadening of the CH₂ groups observed in the low-temperature NMR spectra of **1**.

To what extent are analogous distortions found in the previously studied compounds **7-10**? In **7** and **10**, four carbons of the biallylene units are incorporated into benzenoid rings, whose tendency to maintain coplanarity tends to resist pyramidalization and (especially) twisting. The least pyramidalized structure is accordingly that of the tricyclic **7**,¹² in which the central carbons of the biallylene unit lie only 0.11 Å above the mean plane of the four peripheral carbons. The most highly pyramidalized is **8**,⁸ with the central carbons 0.19 Å out of the plane, clearly the result of accommodation of the biallylene unit to the much shorter Fe-Fe bond distance in **8**. Compounds **9** and **10** show intermediate degrees of pyramidalization, the central carbons being 0.15 and 0.14 Å out of the plane, respectively. It thus appears that significant pyramidalization is the norm for these biallylene complexes, being observed in all six known examples.

There is, however, little twisting in **7-10**, with the torsion angles Fe-Fe-C-C and OC_{eq}-Fe-Fe-CO_{eq} being less than 5° in all cases. The relationship between these distortions is indicated in Table 6. It will be seen

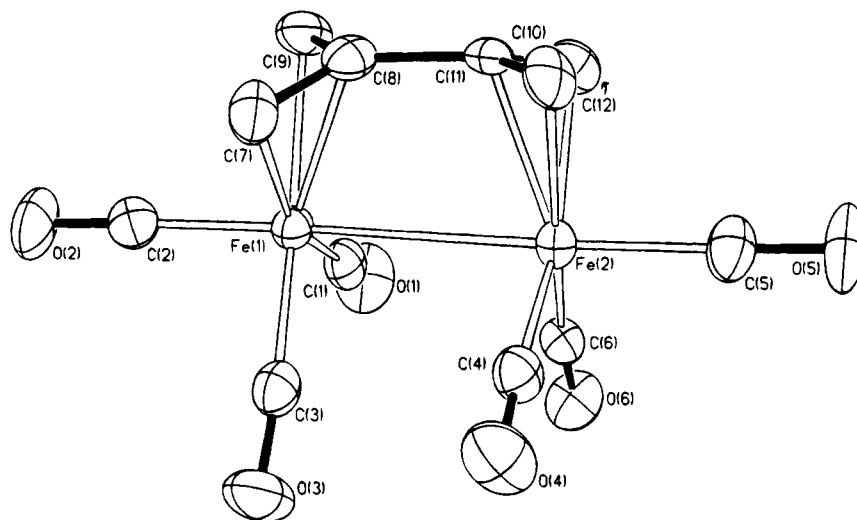


Figure 1. ORTEP drawing of **1** showing the labeling scheme. Atoms are represented by thermal ellipsoids at the 50% level. Hydrogen atoms are omitted.

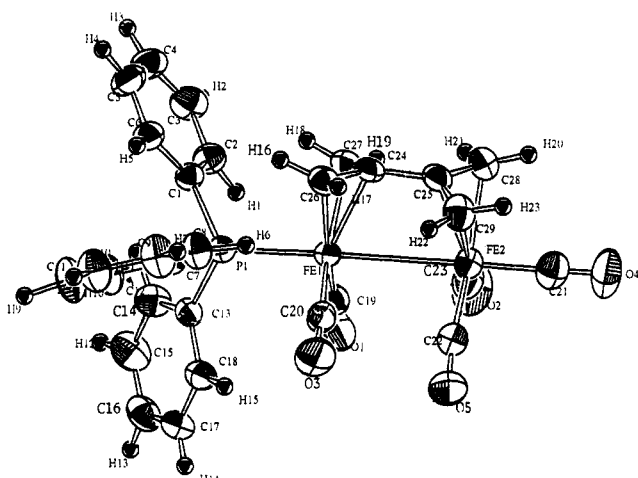


Figure 2. ORTEP drawing of **5** showing the labeling scheme. Atoms are represented by thermal ellipsoids at the 50% level.

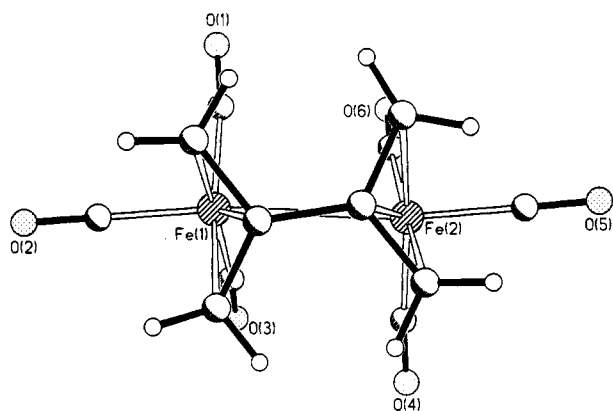


Figure 3. PLUTO drawing of **1** showing the effects of intramolecular rotation about the Fe-Fe bond, with concomitant twisting of the biallylene ligand.

that in **7-10** the pairs of trans $\text{CH}_2\text{-C-C-CH}_2$ torsion angles within the biallylene ligand are similar. The value around 166° indicates the pyramidalization of the two central carbons, and the similarity of the two values indicates the lack of rotation around the central C-C bond. Similarly in these compounds, the very small Fe-Fe-C-C torsion angles indicate the parallelism of the

Fe-Fe and central C-C axes, and the equatorial carbonyl groups are nearly eclipsed. In **1** and **5**, the degree of pyramidalization is very similar to the other compounds, but in addition rotation and twisting generate substantial inequality in the $\text{CH}_2\text{-C-C-CH}_2$ torsion angles, large Fe-Fe-C-C torsion angles, and reduced equatorial carbonyl eclipsing. While structural constraints in **7, 8**, and **10** would clearly hinder rotation and twisting, it remains unclear why the unconstrained **9** does not manifest these distortions to a greater extent. Its nearly idealized C_{2v} structure (except for the phenylthio substituents) is consistent, however, with the low barrier indicated in the variable-temperature NMR studies of **1** for interconversion of the two C_2 forms through the C_{2v} intermediate. Given the low energy difference between the C_2 and C_{2v} forms, the packing energies of the crystals may play a decisive role in defining which is observed.

High-level theoretical studies of free 2,2'-biallylene, as either the singlet or triplet, show no preference for the planar form, rotation about the central C-C bond being favored.¹ Extended Hückel calculations give the same result. Pyramidalization of the central carbons in the free ligand is not favored, costing 0.22 eV (extended Hückel result) for removal of the central C's 0.2 Å out of plane, leaving the individual C_3H_4 allyl units coplanar. However, binding of a planar 2,2'-biallylene unit to a $\text{Fe}_2(\text{CO})_6$ "sawhorse", even one having a Fe-Fe bond distance as long as 3.0 Å, results in rather long Fe- CH_2 distances of 2.25 Å. Most of the ligand-metal bonding in these complexes results from interaction of the a_2 and b_1 orbitals of the $\text{Fe}_2(\text{CO})_6$ and 2,2'-biallylene moieties,¹⁴ the ligand orbitals involving only the CH_2 carbons. Hence, optimum bonding appears to require pyramidalization of the ligand in order to achieve satisfactory overlap. The range of Fe- CH_2 bond lengths observed in **1, 5, 7, 9**, and **10** is 2.10–2.15 Å, achieved in all cases by pyramidalization. Unless prevented by a cyclic structure, rotation of the two pyramidalized allyl units, with concomitant twisting of the "sawhorse," appears to require little energy, being found in **1** and **5**, but not in **9**. Twisting appears to be favored by the reduced eclipsing of the equatorial carbonyl groups. [Note that unconstrained $\text{Fe}_2(\text{CO})_6^{2-}$ is found only in the staggered, D_{3d} , form in the crystal

Table 6. Torsional Angles (deg) In Biallylene Complexes

compd	Fe-Fe-C-C	CH ₂ -C-C-CH ₂		OC _{eq} -Fe-Fe-CO _{eq}	ref no.
		trans	cis		
7	0.1	169.3, 169.8	0.2, 0.7	3.5, 3.7	12
10	0.4	165.6, 167.6	0.5, 1.6	1.8, 3.7	11
8	1.7	159.7, 164.2	1.1, 3.4	4.9	8
9	2.2	162.4, 168.3	2.4, 3.5	1.8, 3.8	7
5	11.2	149.3, 176.6	16.7, 17.5	17.2, 21.0	this paper
1	11.5	148, 178	16, 18	23.8, 23.9	this paper

structures of four different salts;¹⁹ the staggered form is favored by molecular mechanics calculations²¹ and by extended Hückel calculations.] Twisting may be opposed, however, by the loss of δ -bonding interactions between the two iron atoms. In the balance, there appears to be little energy difference between twisted C₂ and untwisted C_{2v} structures.

Given that all extant (2,2'-biallylene)Fe₂(CO)₆-derived structures show pyramidalization, we were initially somewhat perplexed when extended Hückel calculations on model structures having planar C₃H₄ units and Fe-Fe and Fe-C bond lengths of 3.00 and 2.04 Å failed to indicate stabilization upon pyramidalization, even though the Fe-CH₂ distances went from 2.25 Å down to 2.09 Å in the process. In order to manifest such stabilization, it is necessary also to rotate the CH₂ groups within the pyramidal structure so that the axial (*anti*) H's move away from the iron and the equatorial (*syn*) H's toward the iron. With a degree of pyramidalization of 0.15 Å (typical for these structures), the amount of such CH₂ group rotation necessary to achieve optimum stabilization is about 20–30°. Seyferth et al.⁷ have previously noted this curious positioning of the axial substituents in discussing the structure of **9**, attributing it to steric interactions with the axial carbonyl groups; the calculations suggest that optimum orbital alignment is also significant.

At the extended Hückel level, the structure of **9** (with hydrogens replacing the phenylthio substituents), which had its C-C and Fe-Fe axes nearly parallel, was slightly more stable than the twisted structures of **1** and **5** (with a CO replacing the phosphine); the latter were almost identical energetically despite the 0.07 Å difference in Fe-Fe bond lengths.

Finally, we may note that a recent structure of a related "sawhorse" complex, ($\mu, \eta^5: \eta^5$ -C₅H₄-C₅H₄)Mo₂(CO)₄(PMe₃)₂, showed distortions very analogous to those of **1** and **5**: pyramidalization of the carbons joining the two rings and twisting about the metal-metal axis.^{2a,22} The corresponding hexacarbonyl showed similar pyramidalization but no twisting,²³ as was also the

case for the fulvalene-W₂(CO)₆²⁴ and -Ru₂(CO)₄²⁵ complexes. Some twisting was observed, however, in the bimetallic ($\mu, \eta^5: \eta^5$ -fulvalene)RhW(CO)₄(COMe)²⁶ and in a carbenoid derivative of (fulvalene)Mo₂(CO)₆.²³ The presence of lengthened metal-metal bonds and analogous distortions from planarity (consistent pyramidalization and variable twisting) in these fulvalene-based systems and in the 2,2'-biallylene-based systems described here confirms the similarities between them. One difference which may deserve note is that bis-(trimethylphosphine) substitution into the (fulvalene)-Mo₂(CO)₆ system resulted in shortening of the Mo-Mo bond by 0.15 Å,^{2a,22,23} whereas our introduction of a triphenylphosphine substituent into **1** resulted in the Fe-Fe bond lengthening by 0.07 Å.

We expect to undertake studies of the chemical consequences of the long and presumably weak Fe-Fe bonds in the 2,2'-biallylene species in the near future. Preparation of biallylene complexes with a wider range of metals will also be a goal of future work.

Acknowledgment. We wish to thank Mr. Ian Becker for running some of the extended Hückel calculations during his tenure as a Simons Fellow during Summer 1994 and Mr. David Nellis for crystallographic assistance with **5**. We are also grateful to Dr. Luc Girard and Prof. M. J. McGlinchey for supplying crystallographic coordinates for **10**.

Supplementary Material Available: Tables of hydrogen parameters and anisotropic temperature factors for compounds **1** and **5** (3 pages). Ordering information is given on any current masthead page.

OM940785F

(22) Kretchmar, S. A.; Cass, M. E.; Turowski, P. N. *Acta Crystallogr.* **1987**, C43, 435.

(23) Drage, J. S.; Vollhardt, K. P. C. *Organometallics* **1986**, 5, 280–97.

(24) Abrahamson, H. B.; Heeg, M. A. *Inorg. Chem.* **1984**, 23, 2281–86.

(25) Vollhardt, K. P. C.; Weidman, T. W. *J. Am. Chem. Soc.* **1983**, 105, 1676–7.

(26) Kahn, A. P.; Boese, R.; Blümel, J.; Vollhardt, K. P. C. *J. Organomet. Chem.* **1994**, 472, 149–62.

(21) Lauher, J. W. *J. Am. Chem. Soc.* **1986**, 108, 1521–31.

Reactions of Hydrosilsesquioxanes and Chlorosilsesquioxanes with Phosphoranes

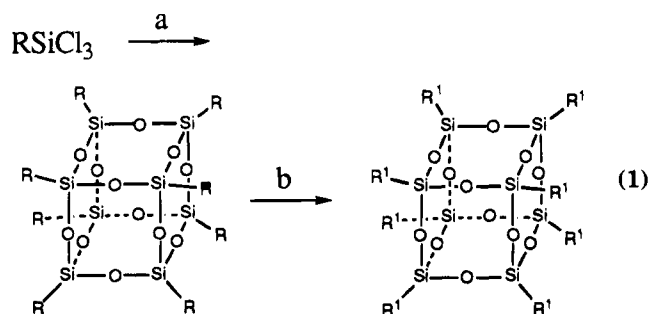
Frank J. Feher,* Keith J. Weller, and Joseph J. Schwab

Department of Chemistry, University of California, Irvine, California 92717

Received October 11, 1994[®]

Monofunctional hydro- and chloro-silsesquioxanes react with phosphoranes to give high yields of phosphorane-substituted frameworks. The reaction of [(c-C₆H₁₁)₇Si₈O₁₂(H)] (**1a**) with Me₃PCH₂ (2 equiv) produces Me₃P, methane, and high yields of [(c-C₆H₁₁)₇Si₈O₁₂(CHPMe₃)] (**2a**), which can also be obtained from the reaction of Me₃PCH₂ (2 equiv) with [(c-C₆H₁₁)₇Si₈O₁₂(Cl)] (**1c**). Mechanisms are suggested for both transformations. Hydrosilsesquioxane **1a** does not react with Ph₃PCH₂, but **1c** reacts with Ph₃PCH₂ to afford high yields of [(c-C₆H₁₁)₇Si₈O₁₂(CHPh₃)] (**2b**). Both **2a** and **2b** react as Wittig reagents with a variety of aldehydes to afford high yields of the corresponding olefination products.

Functionalized silsesquioxanes and spherosilicates offer interesting possibilities as building blocks for siliceous materials,^{1–4} and numerous examples have been reported over the past 50 years.⁵ Most silsesquioxanes and spherosilicates are synthesized via the hydrolytic condensation of trifunctional organosilicon monomers (reaction 1, step a). The most common products are cube-octameric clusters (i.e., R₈Si₈O₁₂), but in some cases it is possible to obtain high yields of other clusters, including incompletely-condensed frameworks.⁶



In principle, the currently available pool of known polyhedral oligosilsesquioxanes and spherosilicates could be synthetically manipulated to provide a large variety of useful compounds (reaction 1, step b). In practice,

however, it is often very difficult to synthetically manipulate or displace the substituents on silsesquioxanes and spherosilicates without compromising their structural integrity. Even seemingly trivial functional group transformations can present formidable synthetic challenges because of the susceptibility of Si/O frameworks to destructive polymerization by nucleophilic reagents.

During a recent effort to synthesize homogeneous models for aluminosilicates, we discovered that phosphorus ylides could be used to assemble well-defined Si/O frameworks.^{1d} Even when used in large excess, these strongly basic, potentially powerful nucleophiles do not initiate the polymerization of silsesquioxane frameworks. With an eye toward developing a general methodology for the synthesis of functionalized silsesquioxanes, we have examined the reactivity of phosphorus ylides Me₃PCH₂ and Ph₃PCH₂ with readily available hydrosilsesquioxanes and chlorosilsesquioxanes. In this paper we report the results from this work.

Results and Discussion

Reactions of Hydrosilsesquioxanes with Phosphoranes (Me₃PCH₂ and Ph₃PCH₂). In an attempt to produce anions via the deprotonation of hydrosilsesquioxanes, **1a** was reacted with an excess of Me₃PCH₂ (C₆D₆, 25 °C). Instead of obtaining the desired anion, multinuclear NMR spectra indicated that this reaction produced a new silsesquioxane possessing a C₃-symmetric framework. Repeated attempts to crystallize the silsesquioxane product were unsuccessful because it is extremely soluble in all common solvents with which it

[®] Abstract published in *Advance ACS Abstracts*, March 15, 1995.

(1) (a) Feher, F. J.; Weller, K. J. *Chem. Mater.* **1994**, *6*, 7–9. (b) Feher, F. J.; Weller, K. J.; *Inorg. Chem.* **1991**, *30*, 880–882. (c) Feher, F. J.; Budzichowski, T. A. *J. Organomet. Chem.* **1989**, *379*, 33–40. (d) Feher, F. J.; Weller, K. J.; Ziller, J. W. *J. Am. Chem. Soc.* **1992**, *114*, 9686–9688.

(2) (a) Lichtenhan, J. D.; Vu, N. G.; Carter, J. A.; Gilman, J. W.; Feher, F. J. *Macromolecules* **1993**, *26*, 2141–2142. (b) Lichtenhan, J. D.; Mantz, R. A.; Jones, P. F.; Carr, M. J. *Polym. Prepr. (Am. Chem. Soc., Div. Polym. Chem.)* **1994**, *35*, 523–524. (c) Gilman, J. W.; Schlitzer, D. S.; Lichtenhan, J. D. *J. Appl. Polym. Sci.*, submitted for publication. (d) Lichtenhan, J. D. *Silsesquioxane-Based Polymers*. In *The Polymeric Materials Encyclopedia: Synthesis, Properties and Applications*; CRC Press: Boca Raton, FL, in press.

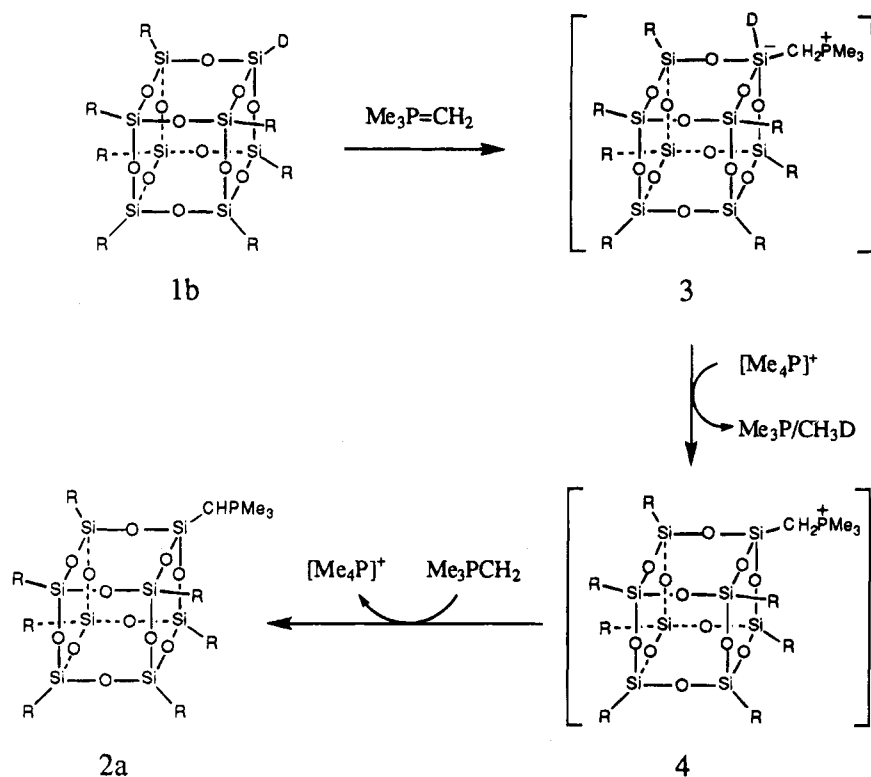
(3) (a) Desu, S. B.; Peng, C. H.; Agaskar, P. A. *J. Electrochem. Soc.* **1992**, *139*, 2682–2685. (b) Agaskar, P. A. *J. Chem. Soc., Chem. Commun.* **1992**, 1024–1026. (c) Agaskar, P. A. *Colloids Surf.* **1992**, *63*, 131–138. (d) Brevett, C. S.; Cagle, P. C.; Klemperer, W. G.; Millar, D. M.; Ruben, G. C. *J. Inorg. Organomet. Polym.* **1991**, *1*, 335–342. (e) Agaskar, P. A. *Synth. React. Inorg. Met.-Org. Chem.* **1990**, *20*, 483–493. (f) Agaskar, P. A. *Inorg. Chem.* **1990**, *29*, 1603. (g) Agaskar, P. A. *J. Am. Chem. Soc.* **1989**, *111*, 6858–6859. (h) Agaskar, P. A.; Day, V. W.; Klemperer, W. G. *J. Am. Chem. Soc.* **1987**, *109*, 5554–5556. (i) Day, V. W.; Klemperer, W. G.; Mainz, V. V.; Millar, D. M. *J. Am. Chem. Soc.* **1985**, *107*, 8262–8264.

(4) (a) Martynova, T. N.; Korshkov, V. P.; Semyannikov, P. P. *J. Organometal. Chem.* **1983**, *258*, 277–282. (b) Korshkov, V. P.; Martynova, T. N.; Danilovich, V. S. *Thin Solid Films* **1983**, *101*, 369–372.

(5) Reviews concerning silsesquioxanes and spherosilicates: (a) Voronkov, M. G.; Lavrent'yev, V. I. *Top. Curr. Chem.* **1982**, *102*, 199–236. (b) Burgy, H.; Calzaferri, G.; Herren, D.; Zhdanov, A. *Chimia* **1991**, *45*, 3–8.

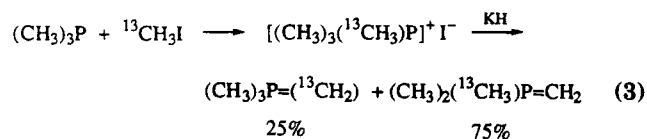
(6) (a) Feher, F. J.; Newman, D. A.; Walzer, J. F. *J. Am. Chem. Soc.* **1989**, *111*, 1741–1748. (b) Feher, F. J.; Budzichowski, T. A.; Blanski, R. L.; Weller, K. J.; Ziller, J. W. *Organometallics* **1991**, *10*, 2526–2528. (c) Hambley, T. W.; Maschmeyer, T.; Masters, A. F. *Appl. Organomet. Chem.* **1992**, *6*, 253–60. (d) Brown, J. F.; Vogt, L. H. *J. Am. Chem. Soc.* **1965**, *87*, 4313–4317. (e) Brown, J. F. *J. Am. Chem. Soc.* **1965**, *87*, 4317–24.

Scheme 1



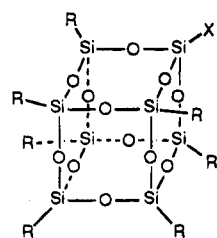
does not react (e.g., alkanes, arenes, chlorocarbons, ethers), but on the basis of ^1H , ^{13}C , ^{29}Si , and ^{31}P NMR spectroscopy, this compound was identified as **2a**. This assignment was eventually confirmed by the preparation of **2a** via a more conventional pathway, namely the reaction of **1c** with Me_3PCH_2 (vide infra).

formed in the reaction (i.e., CH_4 and Me_3P), was greatly facilitated by performing the reaction with ^{13}C -labeled Me_3PCH_2 , which was prepared from Me_3P and $^{13}\text{CH}_3\text{I}$:

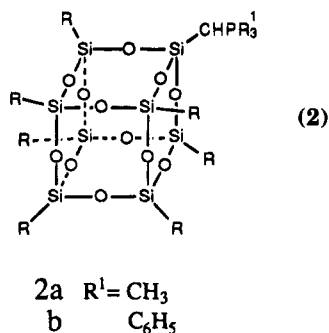


From the standpoint of elucidating the mechanism by which **2a** is formed, little could be gleaned from the ^{13}C labeling experiments. However, the reactions of Me_3PCH_2 with ^2H -labeled **1a** (i.e., **1b**) provided a number of important mechanistic clues. Of particular mechanistic relevance was the reaction of **1b** with two equiv of Me_3PCH_2 , which occurs rapidly upon mixing to afford methane, trimethylphosphine, and **2a**. Examination of the product mixture by ^1H , ^{13}C , and ^{31}P NMR spectroscopy established that there was no significant D incorporation into the Me_3P and indicated that the methane was present as CH_3D and CH_4 in a 4:1 ratio. (The small amount of CH_4 results from the reaction of $\text{Me}_3\text{P}=\text{CH}_2$ with traces of H_2O , because Me_3PO is observed in the ^{31}P NMR spectrum.) When **1a** and **1b** (1:1) were allowed to compete for 1 equiv of Me_3PCH_2 , CH_3D and CH_4 were obtained in a ratio of approximately 2:3, indicating that there is little (if any) primary kinetic isotope effect associated with breaking the Si-H(D) bond. Any mechanism involving proton or H-atom abstraction from Si-H(D) prior to or during the rate-limiting step can therefore be eliminated.

One possible mechanism that would be consistent with our results is illustrated in Scheme 1 for the reaction of **1b** with Me_3PCH_2 . The first step in this mechanism involves rate-limiting nucleophilic addition to the hydrosilsesquioxane to produce a five-coordinate



- 1a X = H R = $\text{c-C}_6\text{H}_{11}$
 b D
 c Cl

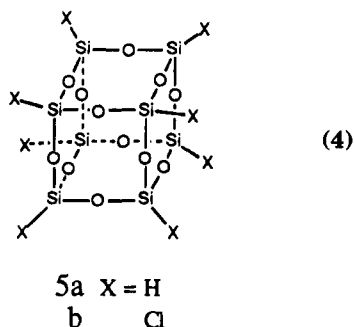


The ^1H and ^{13}C NMR spectra of silsesquioxanes contain many resonances, which often complicates the identification of unexpected reaction products. The initial identification of **2a**, as well as the other products

Si center (i.e., **3**). Structurally similar pentacoordinate Si centers are frequently invoked as hydride donors in a number of silane-based reducing agents;⁷ therefore, **3** should be a potent reducing agent. Net transfer of hydride to a catalytic amount of $[\text{Me}_4\text{P}]^+$, which is expected to be present from side reactions of Me_3PCH_2 with traces of water or other impurities in the system, should produce Me_3P and CH_4 ,⁸ as well as the silyl-substituted phosphonium ion **4**. Subsequent deprotonation of **4** by the more basic starting ylide (i.e., Me_3PCH_2) would produce **2a** and regenerate $[\text{Me}_4\text{P}]^+$.^{8b}

It is difficult to test this mechanism, because the reaction occurs so rapidly without added $[\text{Me}_4\text{P}]^+$ that any rate enhancement would be difficult to detect. In addition, Me_3PCH_2 is extremely reactive toward a variety of potential proton donors; therefore, it is virtually impossible to eliminate traces of $[\text{Me}_4\text{P}]^+$ from the system.

Attempts to expand the utility of this reaction were unsuccessful. Hydrosilsesquioxane **1a** does not react with readily available Ph_3PCH_2 , even after 12 h at 80 °C and the addition of a phosphonium salt (e.g., $[\text{Me}_4\text{P}]\text{-Cl}$). It appears that the less reactive triphenylphosphorane does not have the nucleophilicity necessary to attack the Si-H group. In the case of multifunctional silsesquioxanes such as $\text{H}_8\text{Si}_8\text{O}_{12}$ (**5a**), which can be

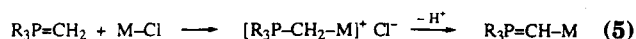


several orders of magnitude more reactive than **1a** toward nucleophilic reagents,^{1b} the addition of Me_3PCH_2 (2 equiv/SiH) completely consumes the hydrosilsesquioxane to produce a very complex mixture of products, including Me_3P and methane. There is no evidence for the formation of an octafunctional ylide analogous to **2a**; the resulting silsesquioxane product appears to be a phosphorane-substituted "T-resin".

When the same reaction was attempted using the less reactive Ph_3PCH_2 , the hydrosilsesquioxane was again consumed to produce a T-resin, but little (if any) of the phosphorane was consumed in the reaction. It therefore

appears that both Me_3PCH_2 and Ph_3PCH_2 (or impurities in these reagents) are capable of initiating the polymerization of $\text{H}_8\text{Si}_8\text{O}_{12}$. In the case of Me_3PCH_2 , polymerization is accompanied by functionalization of the Si-H groups via the mechanism suggested in Scheme 1.

Reactions of Chlorosilsesquioxanes with Phosphoranes (Me_3PCH_2 and Ph_3PCH_2). The reactions of phosphoranes with chlorosilanes,⁹ bromosilanes,^{9d,10} and a variety of other electrophilic metal and main-group halide compounds^{10,11} have been reported. In most cases, the first step in these reactions involves net displacement of halide. This is often followed by deprotonation of the resulting phosphonium complex:



The reaction of **1c** with Me_3PCH_2 (2 equiv) in benzene at 25 °C appears to follow the same course. It is complete within a few minutes of mixing at 25 °C, and the only products observable by ¹H, ¹³C, and ³¹P NMR spectroscopy are $[\text{Me}_4\text{P}]\text{Cl}$ and **2a**, which is obtained in quantitative (NMR) yield. Ph_3PCH_2 reacts similarly to produce $[\text{Ph}_3\text{PMe}]\text{Cl}$ and **2b**. Like **2a**, **2b** is extremely soluble in all common solvents with which it does not react (e.g., alkanes, arenes, chlorocarbons, ethers), and all attempts to recrystallize it were unsuccessful. However, a product which is pure by ¹H, ¹³C, and ³¹P NMR spectroscopy can be obtained by removing the volatiles from the reaction mixture, extracting the residue with hexane, and evaporating the solvent.

One of the more attractive mechanisms for the reaction of **1c** with Me_3PCH_2 (and Ph_3PCH_2) involves nucleophilic attack of the chlorosilsesquioxane by the ylide (Scheme 2). Expulsion of chloride from the resulting five-coordinate silicate (**6**) would produce a silyl-substituted phosphonium ion (**4**), which should be rapidly deprotonated by the more basic starting ylide to produce the observed products.^{8b,12}

This mechanism is very reasonable, but we strongly suspect that some other mechanism may be operative because neither Me_3PCH_2 nor Ph_3PCH_2 reacts with $\text{Cl}_8\text{-Si}_8\text{O}_{12}$ (**5b**) under similar conditions. (Oxidized silsesquioxane or spherosilicate frameworks are normally more susceptible to nucleophilic attack than alkyl-substituted silsesquioxanes,^{1b} and we know of no other case where **1c** is more reactive than $\text{Cl}_8\text{-Si}_8\text{O}_{12}$ toward a potential nucleophile.)

Another attractive mechanism for the reaction of **1c** with R_3PCH_2 involves initial electron-transfer, as illustrated in Scheme 3.

Somewhat surprisingly, there appear to be no reports of electrochemical phosphorane oxidation potentials in

(7) (a) Corriu, R. J. P.; Perez, R.; Reye, C. *Tetrahedron* **1983**, *39*, 999–1009. (b) Boyer, J.; Corriu, R. J. P.; Perez, R.; Reye, C. *Tetrahedron* **1981**, *37*, 2165–71. (c) Chuit, C.; Corriu, R. J. P.; Reye, C. *Synthesis* **1982**, 981–984. (d) Kohoro, S.; Hayashida, H.; Tominga, Y.; Hosomi, H. *Tetrahedron Lett.* **1988**, *29*, 89–92. (e) Hajdasz, D. J.; Ho, Y.; Squires, R. R. *J. Am. Chem. Soc.* **1994**, *116*, 10751–10760.

(8) (a) The mechanism by which methane is produced is not clear, but traces of phosphonium salts are often invoked to explain the chemistry of phosphoranes,^{8b} and the hydride reduction of $[\text{R}_4\text{P}]^+$ to R_3P is well-established.^{8c,d} (b) Bestmann, H. J.; Liberda, H. G.; Snyder, J. P. *J. Am. Chem. Soc.* **1968**, *90*, 2963–2964. (c) Gilheany, D. G.; Mitchell, C. M. in *The Chemistry of Functional Groups: The Chemistry of Organophosphorus Compounds*; Hartley, F. R., Ed.; Wiley & Sons: New York, 1990; Vol. 1, Chapter 7, and references cited therein. (d) Cristau, H. J.; Plenat, F. in *The Chemistry of Functional Groups: The Chemistry of Organophosphorus Compounds, Phosphonium Salts, Ylides and Phosphoranes*; Hartley, F. R., Ed.; Wiley: New York, 1994, pp 138–140, and references cited therein.

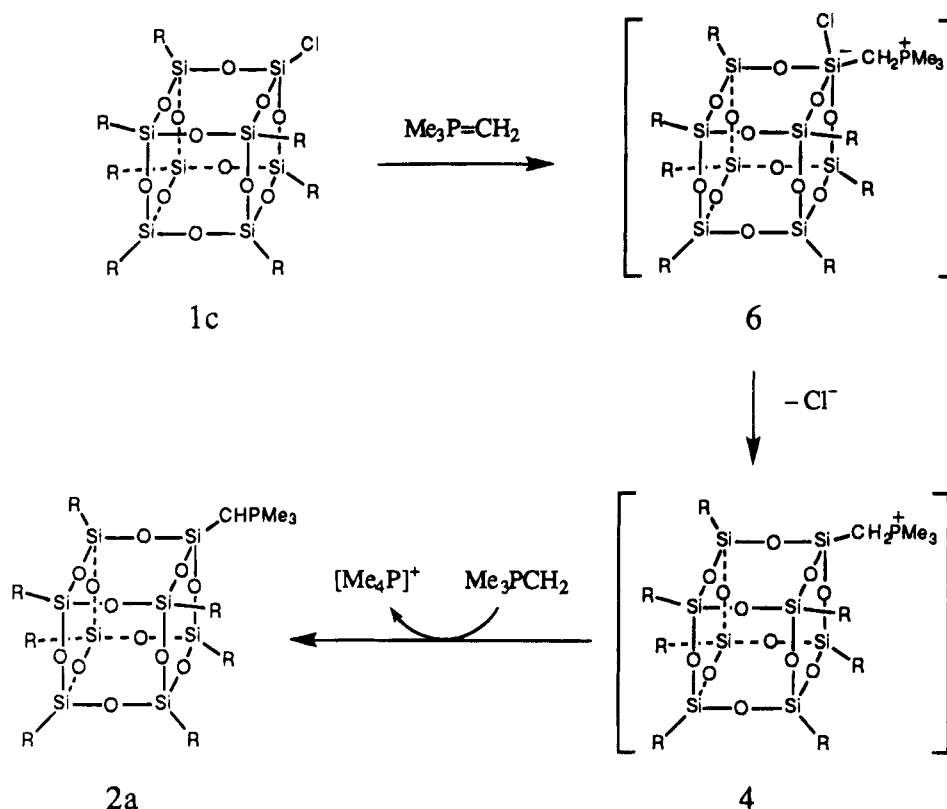
(9) (a) Schmidbauer, H.; Malisch, W. *Angew. Chem., Int. Ed. Engl.* **1970**, *9*, 77–78. (b) Schmidbauer, H.; Vornberger, W. *Angew. Chem., Int. Ed. Engl.* **1970**, *9*, 737–8. (c) Schmidbauer, H.; Malisch, W. *Chem. Ber.* **1969**, *102*, 83–89. (d) Schmidbauer, H.; Malisch, W. *Chem. Ber.* **1971**, *104*, 150–159.

(10) Seyferth, D.; Grim, S. O. *J. Am. Chem. Soc.* **1961**, *83*, 1610–1613.

(11) (a) Johnson, A. W. *Ylides and Imines of Phosphorus*; Wiley-Interscience: New York, 1993; pp 158–165 and references cited therein. (b) Mathiason, D. R.; Miller, N. E. *Inorg. Chem.* **1968**, *7*, 709–714.

(12) (a) Schmidbauer, H.; Malisch, W. *Angew. Chem. Int. Ed. Engl.* **1969**, *8*, 372–373. (b) Schmidbauer, H.; Malisch, W. *Chem. Ber.* **1970**, *103*, 3007–3018. (c) Miller, N. E. *Inorg. Chem.* **1965**, *4*, 1458–1463.

Scheme 2



the literature.¹³ Nevertheless, it is reasonable to expect¹⁴ that Me_3PCH_2 and Ph_3PCH_2 should be able to reduce **1c**, which exhibits an irreversible cyclic voltammetry reduction wave at 1.20 V. Electron transfer from R_3PCH_2 to **1c** and dissociation of chloride from the resulting radical anion could produce silyl radical **8**, which might be rapidly trapped within the solvent cage by oxidized phosphorane (i.e., $[\text{R}_3\text{PCH}_2]^{+\bullet}$) to afford **4** directly. Alternatively, **8** might react with another molecule of phosphorane to produce a new radical (**9**), which could transfer an electron to **1c** to propagate a radical-chain process analogous to the $\text{S}_{\text{RN}}1$ reaction.¹⁵ In either case, deprotonation of **4** by Me_3PCH_2 should rapidly afford **2a**.

It is not obvious why this mechanism would not be available to reactions of phosphoranes with $\text{Cl}_3\text{Si}_8\text{O}_{12}$. Electrochemical measurements are ambiguous, but it seems highly probable that the reduction potential of $\text{Cl}_3\text{Si}_8\text{O}_{12}$ is less than the reduction potential of **1c**.¹⁶ Initial electron transfer from the phosphorane should therefore be easier to the completely chlorinated framework. However, the seven electron-withdrawing chlo-

rine atoms on the framework might strongly discourage dissociation of chloride by simultaneously stabilizing the initial radical anion and destabilizing the expected silyl radical. We have no evidence to support this hypothesis, but it is interesting to note that $\text{S}_{\text{RN}}1$ reactions of aromatic hydrocarbons occur much less readily when the aromatic nucleus is substituted with electron-withdrawing groups (which tend to destabilize phenyl radicals).¹⁵

Silsesquioxane-Substituted Phosphoranes as Wittig Reagents: Reactions of 2a and 2b with Aldehydes and Ketones. The Wittig reaction is a very general reaction for the preparation of olefins from aldehydes or ketones and a phosphorus ylide.¹⁷ The ready availability of **2a** and **2b** therefore provides a potentially general route to silsesquioxanes with a wide variety of tether groups. Bulky α -silyl substituents on the phosphorane can lead to undesirable reactions,¹⁸ but in the case of **2a** and **2b**, Wittig methodology works quite well when aldehydes are used to attach the tether group. Ketones fail to react under conditions which do not destroy the Si/O frameworks.

The reaction of **2a** with benzaldehyde occurs rapidly at room temperature to afford *trans*-**10** and Me_3PO in quantitative NMR yields. The large (19 Hz) coupling constant for the two vinylic protons clearly indicates a mutually *trans* relationship, and the absence of any other significant olefinic resonances in the ^1H NMR spectrum indicates that selectivity for the *trans* isomer is greater than 98%. Somewhat surprisingly, *trans*-**10** decomposes upon standing in solution over several days

(13) (a) Photoelectron spectra^{13b} suggest that Me_3PCH_2 is easily oxidized, but it is difficult to extrapolate the reported ionization potential (6.78 eV) to a solution oxidation potential. (b) Starzewski, K. A. O.; Dieck, H. T.; Bock, H. *J. Organometal. Chem.* **1974**, *65*, 311–25.

(14) Me_3PCH_2 is a very reactive molecule.^{21a} We have not been able to measure its oxidation potential, but we have observed that its reactions with benzylic iodides produce bibenzyls and free iodine. This suggests that Me_3PCH_2 should be capable of effecting the one-electron reduction of **1c**.

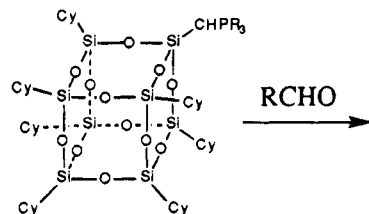
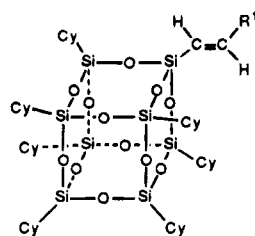
(15) Bunnett, J. F. *Acc. Chem. Res.* **1978**, *11*, 413–420.

(16) $\text{Cl}_3\text{Si}_8\text{O}_{12}$ (**5b**) is poorly soluble in most organic solvents, especially electrolyte solutions commonly used for electrochemical studies. Cyclic voltammograms of **5b** exhibit poorly defined, irreversible reduction waves at potentials less than those observed for **1c**, but we are not entirely confident that these waves correspond to the true reduction potential of **5b**.

(17) (a) March, J. *Advanced Organic Chemistry*, 4th ed.; Wiley-Interscience: New York, 1992; pp 956–963, and references cited therein. (b) Reference 11, Chapter 8.

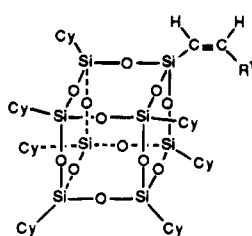
(18) Reference 11a, pp 243–244, and references cited therein.

at 25 °C. Analytically pure product can be obtained by recrystallization from C₆H₆/EtOH. The corresponding reaction of **2b** with benzaldehyde also occurs within 1 min of mixing at 25 °C. The yield is quantitative by ¹H NMR spectroscopy, but the selectivity for *trans* olefination decreases from >98:2 to 71:29. By using this methodology, we have successfully prepared silsesquioxanes containing a variety of functionalized tether groups (e.g., **10–15**). It appears that the reaction is quite

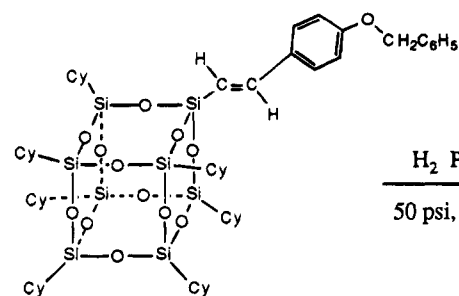
2a R = CH₃trans-10 R¹ = C₆H₅

- | | |
|----|--|
| 11 | C(CH ₃)CH ₂ |
| 12 | (CH ₂) ₈ CHCH ₂ |
| 13 | <i>p</i> -C ₆ H ₄ OCH ₂ C ₆ H ₅ |
| 14 | <i>p</i> -C ₆ H ₄ OC(O)C(CH ₃)CH ₂ |
| 15 | <i>p</i> -C ₆ H ₄ Br |

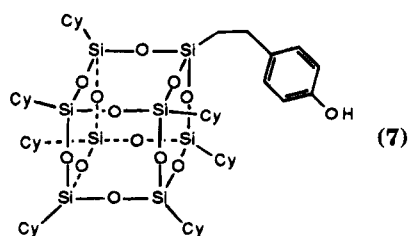
(6)

cis-10 R¹ = C₆H₅

general for aldehydes. It also appears that the olefinic group formed via the Wittig reaction can be easily hydrogenated. For example, the product derived from **2a** and *p*-(PhCH₂O)C₆H₄CHO affords **16** in high yield after hydrogenation with Pd/C (50 psi, 25 °C, 12 h).



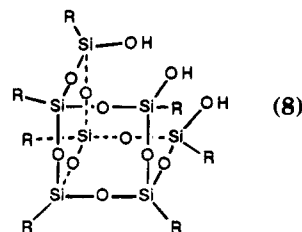
trans-13



16

In summary, we have demonstrated that monofunctional hydro- and chlorosilsesquioxanes react with phos-

phoranes to give high yields of phosphorane-substituted frameworks, which can be used as Wittig reagents to synthesize a variety of monofunctionalized silsesquioxanes. This methodology represents an important alternative to the traditional methods for synthesizing these compounds, which are based on "corner-capping reactions" of incompletely condensed silsesquioxanes^{5a,6a,d} (e.g., **17**) or hydrosilylation reactions of hydridosilsesquioxanes (e.g., **1a** or **5a**).¹⁹



- | | |
|-----|---|
| 17a | R = <i>c</i> -C ₅ H ₉ |
| b | <i>c</i> -C ₆ H ₁₁ |
| c | <i>c</i> -C ₇ H ₁₃ |

Experimental Section

General Considerations. Unless otherwise noted, all manipulations were performed under an atmosphere of dry nitrogen using either standard Schlenk techniques or a Vacuum Atmospheres Corp. Dri-Lab.

Tetrahydrofuran (THF) and diethyl ether were distilled from dark purple solutions of potassium benzophenone ketyl under nitrogen. Aliphatic and aromatic hydrocarbon solvents were distilled from dark purple solutions of potassium benzophenone ketyl containing tetraglyme. Before distillation, aliphatic hydrocarbon solvents were stirred for 48 h over two portions of concentrated H₂SO₄, washed successively with KMnO₄ in 10% H₂SO₄, three portions of H₂O, and one portion of saturated Na₂CO₃, and dried over CaCl₂. Dichloromethane, chloroform, pyridine, acetonitrile, and triethylamine were distilled from CaH₂ under nitrogen immediately before use. CDCl₃ was vacuum-distilled (25 °C, 0.1 Torr) from CaH₂, while C₆D₆ was vacuum-distilled (25 °C, 0.1 Torr) from sodium benzophenone ketyl. Triethylamine (Aldrich) was stirred over CaH₂ for 12 h and distilled prior to use.

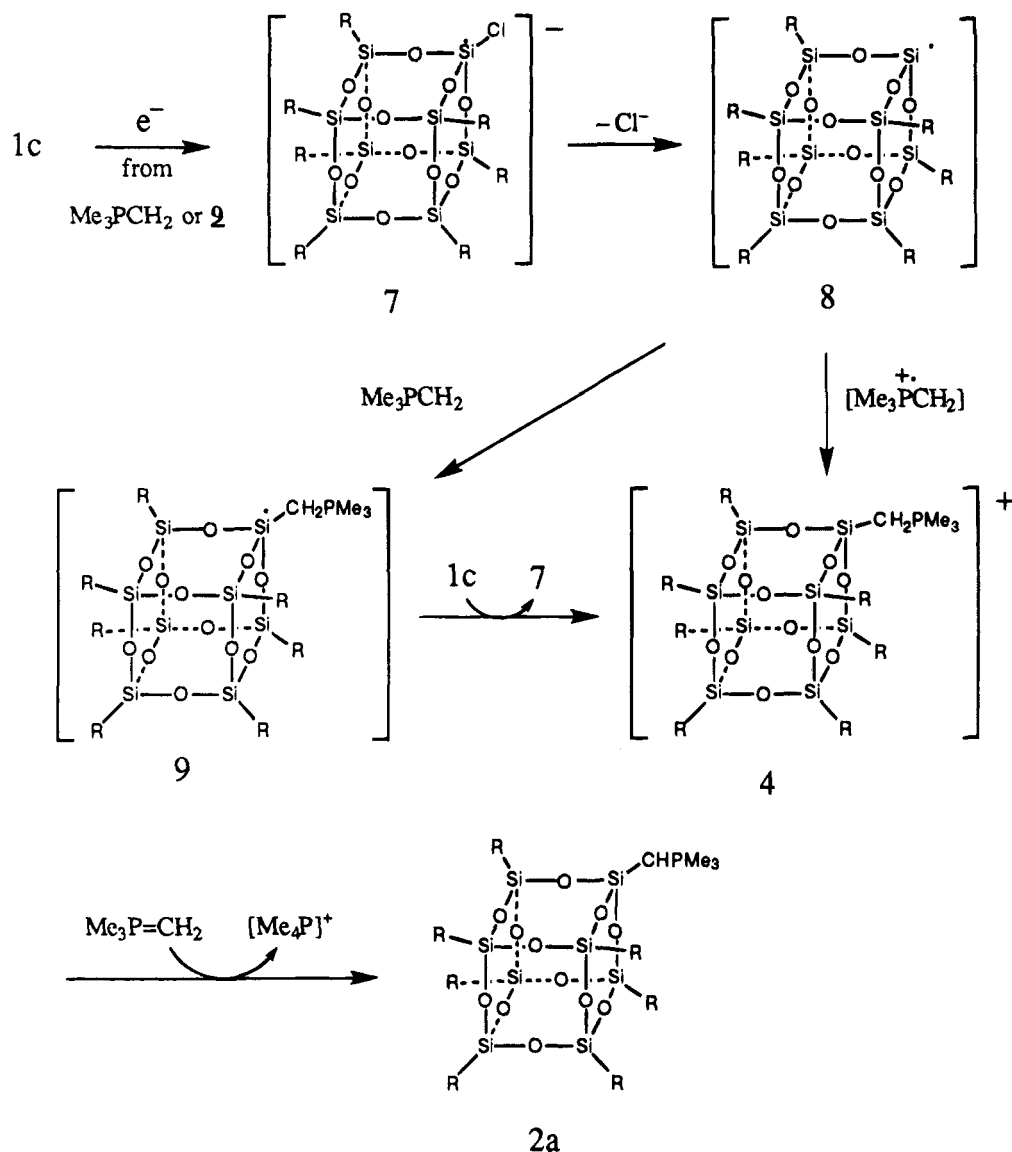
NMR spectra were recorded on Bruker WM-250 (¹H, 250.1 MHz; ¹³C, 62.5 MHz; ²⁹Si, 49.7 MHz) and General Electric QE-300 (¹H, 300.15 MHz; ¹³C, 75.04 MHz), GN-500 (¹H, 500.1 MHz; ¹³C, 125.03 MHz; ²⁹Si, 99.36 MHz; ³¹P, 202 MHz; ¹⁷O, 67 MHz; ¹¹⁹Sn, 186.45 MHz), or Omega-500 (¹H, 500.1 MHz; ¹³C, 125.03 MHz; ²⁹Si, 99.36 MHz; ³¹P, 202 MHz; ¹⁷O, 67 MHz; ¹¹⁹Sn, 186.45 MHz) spectrometers. Most ²⁹Si spectra were recorded with inverse-gated proton decoupling in order to minimize nuclear Overhauser effects. Electron impact mass spectral analyses were conducted on a VG 7070e high-resolution mass spectrometer. Combustion analyses (C, H, Cl, P) were performed by either Desert Analytics Microanalytical Laboratories (Tucson, AZ) or Galbraith Laboratories, Inc. (Knoxville, TN). Melting points were measured in sealed capillaries under dry nitrogen with a Mel-Temp melting point apparatus and are uncorrected.

Me₃P=CH₂ was prepared by the literature method²⁰ and distilled immediately before using. Ph₃P=CH₂ was prepared

(19) (a) Calzaferri, G.; Herren, D.; Imhof, R. *Helv. Chim. Acta* **1991**, *74*, 1278–1280. (b) Calzaferri, G.; Imhof, R. *J. Chem. Soc., Dalton Trans.* **1992**, 3391–3392. (c) Calzaferri, G.; Imhof, R.; Tornroos, K. W. *J. Chem. Soc., Dalton Trans.* **1993**, 3741–3748.

(20) (a) Schmidbauer, H.; Tronich, W. *Chem. Ber.* **1968**, *101*, 595–603. (b) Koster, R.; Simic, D.; Grassberger, M. *A. Inorg. Synth.* **1978**, *18*, 138–139.

Scheme 3



by the literature method,²¹ using KH instead of NaNH_2 , and was recrystallized from hexanes prior to use. Methyl iodide (99.4% ^{13}C labeled) was obtained from MSD Isotopes, dried over molecular sieves, and vacuum-distilled (25 °C) on a high-vacuum line prior to use. Unless specified otherwise, all other reagents were obtained from commercial vendors; most solids were used without further purification, but liquids were normally distilled prior to use.

Electrochemical measurements were performed under a nitrogen atmosphere in a glovebag using a BAS 100 electrochemical analyzer. Measurements were taken on approximately 0.01 M CH_2Cl_2 solutions of material using 0.1 M $[\text{NBu}_4][\text{PF}_6]$ as the supporting electrolyte. The working and auxiliary electrodes were glassy carbon and platinum wire, respectively, while the reference electrode was a Ag/AgCl microelectrode.

Synthesis of [(c-C₆H₁₁)₇Si₈O₁₂(H)] (1a). Freshly distilled HSiCl_3 (0.995 g, 7.35 mmol) was added to a solution of (c-C₆H₁₁)₇Si₇O₉(OH)₃^{6a} (7.155 g, 7.35 mmol) and Et_3N (2.41 g, 23.25 mmol) in ether (35 mL). The mixture was stirred overnight and then filtered to remove Et_3NHCl . Evaporation of the volatiles (~25 °C, 0.01 Torr) gave 6.50 g (88%) of **1a**. The product obtained in this fashion is spectroscopically pure (^1H , ^{13}C , ^{29}Si NMR), but it can be recrystallized in high yields

(>90%) from $\text{C}_6\text{H}_6/\text{MeCN}$. For **1a**: ^1H NMR (500.1 MHz, C_6D_6 , 25 °C) δ 4.689 (s, 1 H), 2.09–1.99 (complex m, 14 H), 1.75–1.57 (complex m, 35 H), 1.26–1.20 (complex m, 21 H), 0.950 (m, 7 H); $^{13}\text{C}\{^1\text{H}\}$ NMR (125.03 MHz, C_6D_6 , 25 °C) δ 27.73, 27.68, 27.28, 27.26, 27.21, 27.07 (CH_2); 23.78, 23.53 (4:3 for CH); $^{29}\text{Si}\{^1\text{H}\}$ NMR (99.35 MHz, C_6D_6 , 25 °C): δ -68.05, -68.12, -68.15, -83.16 (3:1:3:1); mass spectrum (20 eV, 200 °C; relative intensity) m/e 998 (M^+ , 10%), 915 ($\text{M}^+ - \text{C}_6\text{H}_{11}$, 100%), 833 ($\text{M}^+ - 2 \text{C}_6\text{H}_{11}$, 20%). Anal. Calcd (found) for $\text{C}_{42}\text{H}_{78}\text{O}_{12}\text{Si}_8$: C, 50.46 (49.90); H, 7.86 (7.77). Mp: >400 °C (dec).

Synthesis of [(c-C₆H₁₁)₇Si₈O₁₂(D)] (1b). The method used to prepare **1b** is analogous to the procedure described by Calzaferri²² for the preparation of $\text{D}_8\text{Si}_8\text{O}_{12}$ from $\text{H}_8\text{Si}_8\text{O}_{12}$. Hydrosilsesquioxane **1a** (0.325 g, 0.325 mmol) was placed into a Fischer–Porter bottle containing a suspension of 10% Pd/C (0.050 g) in hexanes (40 mL). A magnetic stirring bar was added, the bottle was pressurized to 25 psi with 99.7% D_2 gas, and the solution was stirred for 3 h. The bottle was vented and repressurized, then the solution was again stirred for 3 h under D_2 . After the bottle was vented the solution was filtered and the volatiles were removed in vacuo to afford 140 mg of a white powder (43%). The product obtained in this fashion is spectroscopically pure (^1H , ^{13}C , ^{29}Si NMR), but it can be recrystallized in high yields (>90%) from $\text{C}_6\text{H}_6/\text{MeCN}$. A ^1H

(21) Koster, R.; Simic, D.; Grassberger, M. A. *Justus Liebig's Ann. Chem.* **1970**, 739, 211–219.

(22) Burgy, H.; Calzaferri, G. *Helv. Chim. Acta* **1990**, 73, 698–699.

NMR spectrum of the product indicated that it contained >97% D on the unique Si atom. All other aspects of the ^1H and ^{13}C NMR spectra were identical with spectra observed for **1a**.

Synthesis of [(c-C₆H₁₁)₇Si₈O₁₂(Cl)] (1c). Freshly distilled SiCl₄ (0.773 g, 4.548 mmol) was added to a solution of (c-C₆H₁₁)₇Si₇O₉(OH)₃ (4.428 g, 4.458 mmol) and Et₃N (1.343 g, 13.280 mmol) in ether (100 mL). The mixture was stirred overnight and then filtered to remove Et₃NHCl. Evaporation of the volatiles (~25 °C, 0.01 Torr) gave 4.05 g (86%) of **1c**. Large colorless crystals (2.78 g, 60%) were obtained by allowing MeCN to slowly diffuse into a saturated C₆H₆ solution of **1c**. For **1c**: ^1H NMR (500.1 MHz, C₆D₆, 25 °C) δ 2.07–1.98 (complex m, 14 H), 1.75–1.56 (complex m, 34 H), 1.25–1.02 (complex m, 29 H); $^{13}\text{C}\{^1\text{H}\}$ NMR (125.03 MHz, C₆D₆, 25 °C) δ 27.69, 27.55, 27.20, 26.98, 26.88 (CH₂), 23.69, 23.65, 23.20 (1:3:3 for CH); $^{29}\text{Si}\{^1\text{H}\}$ NMR (99.35 MHz, C₆D₆, 25 °C) δ -67.34, -68.03 -68.07, -88.54 (3:3:1:1); mass spectrum (FAB+, *m*-nitrobenzyl alcohol; relative intensity) *m/e* 1032 (M + H⁺, 6%), 949 (M⁺ - C₆H₁₁, 100%). Anal. Calcd (found) for C₄₂H₇₇O₁₂Si₈Cl: C, 48.78 (47.90); H, 7.50 (7.08). Mp: 372–275 °C.

Synthesis of ^{13}C -Labeled Me₃P=CH₂. Methyl iodide (99.4% ^{13}C labeled, 1.98 g, 0.014 mmol) was slowly added to a solution of PMe₃ (1.28 g, 0.017 mol) in dry diethyl ether (40 mL). After the mixture was stirred for 12 h at room temperature, the [Me₄P]I was collected by vacuum filtration, washed with diethyl ether (3 × 50 mL), and dried *in vacuo* (~25 °C, 0.01 Torr, 2 h). The yield of ^{13}C -labeled [Me₄P]I was 3.00 g (99%).

KH (0.95 g, 0.024 mmol) was added to a suspension of [Me₄P]I (3.00 g, 0.014 mmol) in diethyl ether (20 mL). The solution was stirred for 24 h; then the low-boiling volatiles (<80 °C) were removed by distillation at ~1 atm. The remaining liquid was vacuum-distilled on a high-vacuum line (25 °C) to afford 150 mg (18%) of ^{13}C -labeled Me₃P=CH₂. The label is randomly distributed; therefore, the product is a 3:1 mixture of (^{13}C CH₃)(CH₂)₂PCH₂ and (CH₃)₃P(^{13}C CH₂). ^1H NMR (500.1 MHz, C₆D₆, 25 °C): δ 0.90 (br m, (CH₃)₃P=CH₂), 0.11 (br m, (CH₃)₃P=CH₂). $^{13}\text{C}\{^1\text{H}\}$ NMR (125.03 MHz, C₆D₆, 25 °C): δ 19.04 (d, (CH₃)₃P=CH₂, *J* = 56.2 Hz), -2.81 (br d, (CH₃)₃P=CH₂, *J* = 87.2 Hz). $^{31}\text{P}\{^1\text{H}\}$ NMR (202 MHz, C₆D₆, 25 °C): δ -2.58 (d, *J* = 39.8 Hz) versus 85% orthophosphoric acid (0.0 ppm).

Reactions of 1a with Me₃P=CH₂ (NMR-Tube Reactions). Me₃P=CH₂ (8 μL , ~0.09 mmol) was added to a solution of **1a** (26 mg, 0.026 mmol) in C₆D₆ (0.5 mL) in a 5-mm NMR tube. The tube was shaken briefly to mix the reagents, then a series of ^1H , ^{13}C , and ^{31}P NMR spectra were recorded. In addition to resonances for **2a** and excess, unreacted Me₃P=CH₂, the only other resonances in the spectrum were those attributable to Me₃P and CH₄. After the volatiles were evaporated (25 °C, 10⁻³ Torr, 3 h) and the residue was redissolved in C₆D₆, the resonances for CH₄, Me₃P, and Me₃P=CH₂ were gone, and only resonances for **2a** were observed. The yield is quantitative by NMR spectroscopy, but all attempts to recrystallize the residue failed; **2a** is extremely soluble in all common solvents with which it does not react (e.g., alkanes, arenes, chlorocarbons, ethers). For Me₃PCH₂: ^1H NMR (500.1 MHz, C₆D₆, 25 °C) δ 0.84 (d, (CH₃)₃P=CH₂, *J* = 12.5 Hz), -0.17 (d, (CH₃)₃P=CH₂, *J* = 12.8 Hz); $^{31}\text{P}\{^1\text{H}\}$ NMR (202 MHz, C₆D₆, 25 °C) δ -2.18 versus 85% orthophosphoric acid (0.0 ppm). For Me₃P: ^1H NMR (500.1 MHz, C₆D₆, 25 °C) δ 0.79 (d, *J* = 2.7 Hz); $^{31}\text{P}\{^1\text{H}\}$ NMR (202 MHz, C₆D₆, 25 °C) δ -62.02 versus 85% orthophosphoric acid (0.0 ppm). For CH₄: ^1H NMR (500.1 MHz, C₆D₆, 25 °C) δ 0.15. For **2a**: ^1H NMR (500.1 MHz, C₆D₆, 25 °C): δ 2.32–2.01 (complex m, 14 H), 1.90–1.51 (complex m, 35 H), 1.40–1.15 (complex m, 21 H), 1.14–0.80 (complex m, 7H), 0.987 (d, *J*_{HP} = 12 Hz, 9 H), -0.175 (d, *J*_{HP} = 8 Hz, 1 H); $^{13}\text{C}\{^1\text{H}\}$ NMR (125.03 MHz, C₆D₆, 25 °C) δ 27.95, 27.86, 27.49, 27.43, 27.38, 27.32, 27.06 (CH₂), 24.27, 24.02, 23.95 (3:3:1 for CH), 18.44 (d, *J*_{CP} = 56 Hz), -3.14 (d, *J*_{CP} = 98 Hz); $^{29}\text{Si}\{^1\text{H}\}$ NMR (99.35 MHz, C₆D₆, 25 °C) δ -67.31 (d,

$J_{\text{SiP}} = 31$ Hz), -67.60, -68.79 (1.4:3). $^{31}\text{P}\{^1\text{H}\}$ NMR (202 MHz, C₆D₆, 25 °C) δ 3.83 versus 85% orthophosphoric acid (0.0 ppm).

When the reaction was performed using an excess of ^{13}C -labeled Me₃P=CH₂, ^{13}C -labeled Me₃P and CH₄ (δ 0.21, d, *J* = 60 Hz) were observed in the NMR spectra of the reaction mixture, as well as resonances for ^{13}C -labeled **2a**.

Reaction of 1b with Me₃P=CH₂ (NMR Tube Reaction). Me₃P=CH₂ (7 mg, 0.078 mmol) was added to a solution of **1b** (33 mg, 0.033 mmol) in 0.5 mL of C₆D₆ in a 5-mm NMR tube. Examination of the ^1H NMR spectrum showed the formation of **2a** and Me₃P, as well as CH₃D (δ 0.14, t, 1:1:1, *J* = 3 Hz) and CH₄ (δ 0.15) in a 4:1 ratio. (CH₄ is produced by the reaction of Me₃P=CH₂ with traces of water.) A ^{31}P NMR spectrum showed no evidence for deuterium incorporation into Me₃P, but a resonance attributable to Me₃PO was observed.

Competitive Reaction of 1a and 1b (1:1) with Me₃P=CH₂ (NMR-Tube Reaction). A 1:1 mixture of **1a** and **1b** (~0.03 mmol) in ~0.5 mL of C₆D₆ in a 5-mm NMR tube was reacted with half of the stoichiometrically required amount of Me₃P=CH₂. A ^1H NMR spectrum of the reaction mixture recorded within a few minutes of mixing revealed the presence of CH₄ and CH₃D in a ratio of ~3:2.

Reaction of 1a with Ph₃P=CH₂. Ph₃P=CH₂ (29 mg, 0.105 mmol) was added to a solution of **1a** (52 mg, 0.052 mmol) in 0.5 mL of C₆D₆ in a 5-mm NMR tube. The solution was heated at 80 °C for 12 h. Examination of the ^1H and ^{13}C NMR spectra revealed only unreacted starting material and slight decomposition of Ph₃P=CH₂.

Reaction of 1c with Me₃P=CH₂. Me₃P=CH₂ (110 μL , 1.00 mmol) was added to a solution of **1c** (510 mg, 0.493 mmol) in C₆H₆ (15 mL). The mixture was stirred for 30 min and the solvent removed *in vacuo* (~25 °C, 0.01 Torr) to afford a white semisolid. Extraction with hexane, filtration to remove [Me₄P]Cl, and evaporation *in vacuo* (~25 °C, 0.01 Torr) afford a material which was identical in all respects to a sample of **2a** prepared by the reaction of **1a** with Me₃P=CH₂.

Reaction of 1c with Ph₃P=CH₂. Ph₃P=CH₂ (32 mg, 0.116 mmol) was added to a solution of **1c** (57 mg, 0.055 mmol) in 0.5 mL of C₆D₆ in a 5-mm NMR tube. A white precipitate of Ph₃PCH₂Cl formed immediately. Examination of the ^1H and ^{13}C NMR spectra revealed the formation of **2b**. For **2b**: ^1H NMR (500.1 MHz, C₆D₆, 25 °C) δ 7.80–7.60 (m, 9 H), 7.20–7.00 (m, 6 H), 2.25–1.85 (complex m, 14 H), 1.82–1.00 (complex m, 56 H), 0.80–0.72 (complex m, 7 H), 0.54 (d, *J*_{HP} = 8 Hz); $^{13}\text{C}\{^1\text{H}\}$ NMR (125.03 MHz, C₆D₆, 25 °C) δ 133.71 (d, *J*_{CP} = 89 Hz), 133.03 (d, *J*_{CP} = 7 Hz), 131.07 (d, *J*_{CP} = 29 Hz), 128.42 (d, *J*_{CP} = 11 Hz), 27.92, 27.74, 27.43, 27.33, 27.26 (CH₂), 23.99, 23.91 (4:3 for CH), -5.51 (d, *J*_{CP} = 106 Hz); $^{29}\text{Si}\{^1\text{H}\}$ NMR (99.35 MHz, C₆D₆, 25 °C) δ -67.69, -68.29 (d, *J*_{SIP} = 33 Hz), -68.74 (4:1:3).

Reaction of 2a with Benzaldehyde. Benzaldehyde (53 mg, 0.499 mmol) was added to a solution of **2a** (628 mg, 0.493 mmol) in 15 mL of C₆H₆. The mixture was stirred for 30 min, and the volatiles removed *in vacuo* (~25 °C, 0.01 Torr). The solid was redissolved in 10 mL of C₆H₆ and filtered through a pad of basic alumina on the benchtop. The clear solution was placed in a large test tube, and EtOH was carefully layered on top. After 2 days a precipitate had formed at the bottom of the tube. The solution was carefully decanted and the solvent removed *in vacuo* to yield 135 mg (24%) of pure product. The material appears to be somewhat unstable in solution over long periods (>48 h). For *trans*-**10**: ^1H NMR (500.1 MHz, C₆D₆, 25 °C) δ 7.59 (d, 19 Hz, 1 H), 7.34 (d, 8 Hz, 2 H), 7.04–7.02 (m, 3 H), 6.49 (d, 19 Hz, 1 H), 2.25–2.00 (complex m, 14 H), 1.84–1.50 (complex m, 35 H), 1.40–1.15 (complex m, 21 H), 1.15–0.95 (complex m, 7 H); $^{13}\text{C}\{^1\text{H}\}$ NMR (125.03 MHz, C₆D₆, 25 °C) δ 149.47, 137.74, 129.05, 128.85, 127.18, 118.52, 27.77, 27.71, 27.34, 27.26, 27.17, 27.08 (CH₂), 23.86, 23.73 (4:3 for CH); $^{29}\text{Si}\{^1\text{H}\}$ NMR (99.35 MHz, C₆D₆, 25 °C) δ -67.34, -67.95, -68.10, -68.20 (1:1:3:3); mass spectrum (FAB+, *m*-nitrobenzyl alcohol; relative intensity): *m/e* 1023 (M⁺ - C₆H₅, 100%). Anal. Calcd (found) for C₅₀H₈₅O₁₂Si₈: C,

54.50 (52.82); H, 7.68 (7.62). Mp: >400 °C dec. The ^1H NMR resonance for the product of cis olefination (i.e., *cis*-**10**) is barely observable at δ 5.86 (d, J = 15 Hz).

Reaction of 2b with Benzaldehyde. Benzaldehyde (7 mg, 0.066 mmol) was added to a solution of **2b** prepared by the addition of Ph_3PCH_2 (32 mg, 0.116 mmol) to **1c** (57 mg, 0.055 mmol) in C_6D_6 (0.5 mL). The solution was mixed for approximately 1 min; then the volatiles were removed *in vacuo* (~25 °C, 0.01 Torr) to afford a white solid. Examination of the ^1H NMR spectrum (C_6D_6) revealed the formation of both *cis*-**10** and *trans*-**10** in a 29:71 ratio.

Reaction of 2a with $\text{HC}(\text{O})\text{C}(\text{Me})=\text{CH}_2$. A solution of $\text{CH}_2=\text{PMe}_3$ (87.0 mg, 106 μL , 0.97 mmol, 2 equiv) in benzene (3 mL) was added to a solution of **1c** (500 mg, 0.48 mmol) in benzene (30 mL). The reaction mixture was stirred for 4.5 h and filtered through Celite and the benzene removed under reduced pressure. The resulting white solid was dissolved in benzene (20 mL) and methacrolein (32 mg, 42.0 μL , 0.46 mmol) added by syringe. The reaction mixture was stirred for 16 h, after which the benzene was removed under reduced pressure. The residue was dissolved in Et_2O and cooled to -30 °C. The $\text{O}=\text{PMe}_3$ precipitated as fine needle like crystals which were collected by vacuum filtration. The Et_2O was removed from the filtrate to give 400 mg (75% based on **1c**) of *trans*-**11**. Recrystallization from $\text{Et}_2\text{O}/\text{CH}_3\text{CN}$ affords *cis*-**11** as large blocks. ^1H NMR (500.1 MHz, CDCl_3 , 22 °C): δ 6.93 (d, 1H, J = 19 Hz, $\text{SiCH}=\text{CH}_2$), 5.54 (d, 1H, J = 19 Hz, $\text{SiCH}=\text{CH}_2$), 5.15 (s, 1H, $\text{C}(\text{Me})=\text{CH}_2$), 5.09 (s, 2H, $\text{C}(\text{Me})=\text{CH}_2$), 1.87 (s, 3H, $\text{C}(\text{CH}_3)=\text{CH}_2$), 1.75 (m, 35H, cyclohexyl CH_2), 1.24 (m, 35H, cyclohexyl CH_2), 0.78 (m, 7H, cyclohexyl CH). ^{13}C NMR (125.03, CDCl_3 , 22 °C) δ 150.83 ($\text{SiCH}=\text{CH}_2$), 143.09 ($\text{SiCH}=\text{CH}_2$), 119.02 ($\text{SiCH}=\text{CH}_2$), 118.65 ($\text{C}(\text{Me})=\text{CH}_2$), 27.51, 27.47, 26.90, 26.86, 26.63, 26.44 (cyclohexyl CH_2), 23.15, 23.13, 22.84 (cyclohexyl CH , 1:3:3), 17.70 ($\text{C}(\text{CH}_3)=\text{CH}_2$).

Reaction of 2a with $\text{HC}(\text{O})(\text{CH}_2)_8\text{CH}=\text{CH}_2$. A solution of $\text{CH}_2=\text{PMe}_3$ (349 mg, 425 μL , 3.87 mmol, 2 equiv) in benzene (3 mL) was added to a solution of **1c** (2.00 g, 1.93 mmol) in benzene (30 mL). The reaction mixture was stirred for 4.5 h and filtered through Celite. A solution of undecylenic aldehyde (325 mg, 402 μL , 1.93 mmol) in benzene (3 mL) was added dropwise to the solution of **2a**. The reaction mixture was stirred for 33 h, after which the benzene was removed under reduced pressure. The solid was removed from the drybox and the residue stirred with EtOH (5 mL), filtered, washed with EtOH (5 mL), and dried to afford 1.714 g (76% based on **1c**) of *trans*-**12**. ^1H NMR (500.1 MHz, CDCl_3 , 22 °C): δ 6.39 (dt, 1H, J = 6.2, 18.6 Hz, $\text{SiCH}=\text{CH}_2$), 5.82 (m, 1H, $\text{CH}=\text{CH}_2$), 5.39 (d, 1H, J = 18.6, $\text{SiCH}=\text{CH}_2$), 4.99 (dd, J = 1.5, 17.2 Hz, $\text{CH}=\text{CH}_2$), 4.93 (d, J = 9.54 Hz, $\text{CH}=\text{CH}_2$), 2.13 (m, 2H, $\text{SiCH}=\text{CH}_2$), 2.04 (m, 2H, $\text{CH}=\text{CH}_2$), 1.75 (m, 35H, cyclohexyl CH_2), 1.23 (m, 35H, cyclohexyl CH_2), 0.76 (m, 7H, cyclohexyl CH). ^{13}C NMR (125.03 MHz, CDCl_3 , 22 °C) δ 152.52 ($\text{SiCH}=\text{CH}_2$), 139.20 ($\text{CH}=\text{CH}_2$), 119.98 ($\text{SiCH}=\text{CH}_2$), 114.09 ($\text{CH}=\text{CH}_2$), 36.27, 33.80, 29.48, 29.45, 29.15, 29.08, 28.94, 28.28 ($\text{SiCH}=\text{CH}(\text{CH}_2)_8$), 27.51, 27.46, 26.90, 26.85, 26.63, 26.44 (cyclohexyl CH_2), 23.16, 23.13, 22.84 (cyclohexyl CH , 1:3:3). Anal. Calcd (found) for $\text{C}_{54}\text{H}_{98}\text{O}_{12}\text{Si}_8$: C, 55.72 (55.88); H, 8.49 (8.36).

Reaction of 2a with $\text{HC}(\text{O})\text{C}_6\text{H}_5\text{OCH}_2\text{C}_6\text{H}_5$. A solution of $\text{CH}_2=\text{PMe}_3$ (34.8 mg, 43 μL , 0.39 mmol) in benzene (3 mL) was added to a solution of **1c** (1.00 g, 0.967 mmol) in benzene (3 mL). The reaction mixture was stirred for 15 min. A solution of $\text{HC}(\text{O})\text{C}_6\text{H}_5\text{OCH}_2\text{C}_6\text{H}_5$ (205.2 mg, 0.967 mmol) in benzene (3 mL) was added to the solution of **2a**. The reaction mixture was stirred for 10 h. The benzene was removed under reduced pressure, and the off-white residue was removed from the drybox and stirred with EtOH (20 mL), filtered, washed with EtOH (10 mL), and dried to afford 0.849 g (72% based on **1c**) of *trans*-**13**. ^1H NMR (500.1 MHz, CDCl_3 , 20 °C) δ 7.41 (m, 7H, H-3 of C_6H_4 and C_6H_5), 7.16 (d, 1H, $\text{SiCH}=\text{CH}$, J = 19.1 Hz), 6.97 (d, 1H, H-2 of C_6H_4 , J = 8.8 Hz), 6.00 (d, 2H,

$\text{SiCH}=\text{CH}$, J = 19.1 Hz), 5.10 (s, 2H, OCH_2), 1.74 (m, 35H, cyclohexyl CH_2), 1.26 (m, 35H, cyclohexyl CH_2), 0.81 (m, 7H, cyclohexyl CH). ^{13}C NMR (125.03 MHz, CDCl_3 , 20 °C): δ 159.23 (C-1 of C_6H_4), 147.35 ($\text{SiCH}=\text{CH}$), 136.79 (C-1 of C_6H_5), 130.83 (C-4 of C_6H_4), 128.61 (C-3,5 of C_6H_4), 128.13 (C-3,5 of C_6H_5), 128.01 (C-4 of C_6H_5), 127.44 (C-2,6 of C_6H_5), 116.08 ($\text{SiCH}=\text{CH}$), 114.89 (2,6 of C_6H_4), 70.00 (OCH_2), 27.47, 26.88, 26.63 (cyclohexyl CH_2), 23.14, 23.10 (4:3 cyclohexyl CH_2). Anal. Calcd (found) for $\text{C}_{57}\text{H}_{90}\text{Si}_8\text{O}_{12}$: C, 56.67 (56.78); H, 7.51 (7.58).

Reaction of 2a with $\text{HC}(\text{O})\text{C}_6\text{H}_4\text{OC}(\text{O})\text{C}(\text{CH}_3)=\text{CH}_2$. A solution of $\text{CH}_2=\text{PMe}_3$ (35 mg, 43 μL , 0.39 mmol) in benzene (3 mL) was added to a solution of **1c** (200 mg, 0.193 mmol) in benzene (20 mL). The reaction mixture was stirred for 15 min. A solution of $\text{HC}(\text{O})\text{C}_6\text{H}_4\text{OC}(\text{O})\text{C}(\text{CH}_3)=\text{CH}_2$ (37 mg, 0.193 mmol) in benzene (2 mL) was added to the reaction mixture. The mixture was stirred for 15 min and the benzene removed under reduced pressure to give an off-white residue, which was stirred with EtOH (10 mL). The resulting suspension was filtered and the white solid washed with EtOH (10 mL) to provide 125 mg (55% based on **1c**) of *trans*-**14**. ^1H NMR (500.1 MHz, CDCl_3 , 20 °C): δ 7.49 (d, 2H, H-3,5 of C_6H_4 , J = 8.4 Hz), 7.18 (d, 1H, $\text{SiCH}=\text{CH}$, J = 19 Hz), 7.12 (d, 2H, H-2,6 of C_6H_4 , J = 8.4 Hz), 6.36 (s, 1H, $\text{C}(\text{CH}_3)=\text{CH}_{\text{cis}}\text{H}$), 6.11 (d, 1H, $\text{SiCH}=\text{CH}$, J = 19 Hz), 5.76 (s, 1H, $\text{C}(\text{CH}_3)=\text{CH}_{\text{trans}}\text{H}$), 2.07 (s, 3H, $\text{C}(\text{CH}_3)=\text{CH}_2$), 1.73 (m, 35H, cyclohexyl CH_2), 1.25 (m, 35H, cyclohexyl CH_2), 0.80 (m, 7H, cyclohexyl CH). ^{13}C NMR (125.03 MHz, CDCl_3 , 20 °C): δ 165.75 ($\text{OC}=\text{O}$), 151.11 (C-1 of C_6H_4), 146.88 ($\text{SiCH}=\text{CH}$), 135.81 ($\text{C}(\text{CH}_3)=\text{CH}_2$), 135.38 (C-4 of C_6H_4), 127.79 (C-3,5 of C_6H_4), 127.36 ($\text{C}(\text{CH}_3)=\text{CH}_2$), 121.72 (C-2,6 of C_6H_4), 119.01 ($\text{SiCH}=\text{CH}$), 27.46, 26.88, 26.86, 26.62 (cyclohexyl CH_2), 23.09, 23.12 (cyclohexyl CH , 4:3), 18.39 ($\text{C}(\text{CH}_3)=\text{CH}_2$). Anal. Calcd (found) for $\text{C}_{54}\text{H}_{88}\text{Si}_8\text{O}_{14}$: C, 54.69 (54.12); H, 7.48 (7.61).

Reaction of 2a with $\text{HC}(\text{O})\text{C}_6\text{H}_4\text{Br}$. A solution of $\text{CH}_2=\text{PMe}_3$ (87 mg, 106 μL , 0.97 mmol) in benzene (3 mL) was added to a solution of **1c** (500 mg, 0.48 mmol) in benzene (25 mL). The reaction mixture was stirred for 15 min. A solution of *p*-bromobenzaldehyde (89 mg, 0.48 mmol) in benzene (3 mL) was added to the reaction mixture. The mixture was stirred for 1 h and taken out of the drybox and the benzene removed under reduced pressure to give an off-white residue. The residue was stirred with EtOH (30 mL) for 30 min. The resulting suspension was filtered and the white solid washed with EtOH (10 mL) and dried under vacuum to give 412 mg (72% based on **1c**) of *trans*-**15**. ^1H NMR (500.1 MHz, CDCl_3 , 20 °C): δ 7.48 (d, 2H, H-2,6 of $\text{C}_6\text{H}_4\text{-Br}$, J = 8.43 Hz), 7.32 (d, 2H, H-3,5 of $\text{C}_6\text{H}_4\text{-Br}$, J = 8.43 Hz), 7.12 (d, 1H, $\text{CH}=\text{CH}$, J = 19.07 Hz), 6.14 (d, 1H, $\text{CH}=\text{CH}$, J = 19.06 Hz), 1.73 (m, 35H, cyclohexyl CH_2), 1.24 (m, 35H, cyclohexyl CH_2), 0.78 (m, 7H, cyclohexyl CH). ^{13}C NMR (125.03 MHz, CDCl_3 , 20 °C): δ 146.58 ($\text{CH}=\text{CHC}$), 136.58 (C-4 of $\text{C}_6\text{H}_4\text{-Br}$), 131.69 (C-2,6 of $\text{C}_6\text{H}_4\text{-Br}$), 128.30 (C-3,5 of $\text{C}_6\text{H}_4\text{-Br}$), 122.58 ($\text{CH}=\text{CHC}$), 119.84 (C-1 of $\text{C}_6\text{H}_4\text{-Br}$), 27.46, 26.88, 26.64 (cyclohexyl CH_2), 23.12, 23.09 (4:3 cyclohexyl CH). Anal. Calcd (found) for $\text{C}_{50}\text{H}_{83}\text{BrSi}_8\text{O}_{14}$: C, 50.86 (50.77); H, 7.09 (7.41).

Reaction of 2a with Benzophenone. A solution of **2a** (50 mg, 0.04 mmol) in C_6D_6 (0.7 mL) was prepared and placed in a 5-mm NMR tube. A sample of benzophenone (8 mg, 0.04 mmol) was added to the NMR tube and the reaction mixture thoroughly mixed. The reaction was checked by ^1H , ^{13}C , and ^{31}P NMR spectroscopy. No reaction was observed.

Reaction of 2a with 2-Butanone. A solution of **2a** (57 mg, 0.05 mmol) in C_6D_6 (0.7 mL) was prepared and placed in a 5-mm NMR tube. A sample of 2-butanone (4 mg, 5 μL , 0.5 mmol) was added to the NMR tube and the reaction mixture thoroughly mixed. The reaction was then checked by ^1H , ^{13}C , and ^{31}P NMR spectroscopy. No reaction was observed.

Hydrogenation of *trans*-13**.** A solution of *trans*-**13** (130 mg, 0.108 mmol) in EtOAc (30 mL) was placed in a Fischer-

Porter bottle along with 10% Pd/C (50 mg). The bottle was pressurized with H_2 (50 psi) and the reaction mixture stirred for 12 h. The reaction mixture was filtered through Celite and the EtOAc removed under reduced pressure to provide a quantitative yield of **16**. 1H NMR (500.1 MHz, $CDCl_3$, 18 °C): δ 7.08 (d, 2H, H-3,5 of C_6H_4OH , $J = 8.43$ Hz), 6.75 (d, 2H, H-2,6 of C_6H_4OH , $J = 8.43$ Hz), 4.69 (br s, 1H, $C_2C_6H_4OH$), 2.67 (m, 2H, $SiCH_2CH_2C$), 1.73 (m, 35H, cyclohexyl CH_2), 1.24 (m, 35H, cyclohexyl CH_2), 0.93 (m, 2H, $SiCH_2$), 0.77 (m, 7H, cyclohexyl CH_2). ^{13}C NMR (125.03 MHz, $CDCl_3$, 18 °C): δ 153.44 (C-1 of C_6H_4OH), 136.87 (C-4 of C_6H_4OH), 128.84 (C-3,5 of C_6H_4OH), 115.06 (C-2,6 of C_6H_4OH), 28.19 ($SiCH_2CH_2$), 27.48, 26.88, 26.78, 26.64, 26.50 (cyclohexyl CH_2), 23.14, 23.09 (4:3 cyclohexyl CH), 14.40 ($CH_2CH_2C_6H_4OH$). The compound

appears to be both air- and light-sensitive, but pure sample can be obtained by recrystallization from hexane/ Et_2O .

Acknowledgment. We are grateful to Michael T. Hay and Jeremy Way (University of Illinois, Champaign-Urbana, IL) for performing the electrochemical studies. These studies were supported by the National Science Foundation and Phillips Laboratory (Edwards AFB). Acknowledgment is also made to the donors of the Petroleum Research Fund, administered by the American Chemical Society, for partial support of this work.

OM940783V

A Density Functional Study of Ethylene Insertion into the M–CH₃ Bond of the Constrained Geometry Catalysts [(SiH₂–C₅H₄–NH)MCH₃]⁺ (M = Ti, Zr, Hf) and (SiH₂–C₅H₄–NH)TiCH₃

Liangyou Fan,^{*,†} Daryll Harrison,[†] Tom K. Woo,[‡] and Tom Ziegler^{*,‡}

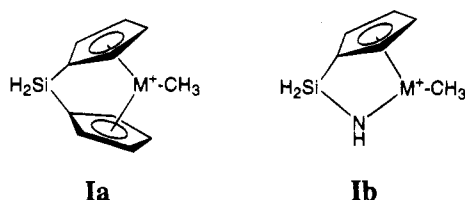
Novacor Research & Technology Corporation, 2928-16 Street N.E.,
Calgary, Alberta, Canada T2E 7K7, and Department of Chemistry, University of Calgary,
Calgary, Alberta, Canada T2N 1N4

Received August 24, 1994[®]

The chain propagation mechanism of the constrained geometry catalysts (CGC) (SiH₂–C₅H₄–NH)MCH₃⁺ (M = Ti, **1**, Zr, **3**, Hf, **4**) and (SiH₂–C₅H₄–NH)TiCH₃, **2**, has been studied theoretically by density functional theory (DFT) and molecular mechanics. DFT energy profiles have been determined for the insertion of ethylene into the M–CH₃ bonds of the aforementioned CGCs (L₂M–CH₃ + CH₂=CH₂ → L₂M–CH₂–CH₂–CH₃). One of the objectives of the study was to compare the insertion process involving the cationic Ti(IV) CGC, **1**, and its neutral Ti(III) counterpart, **2**. The insertion process for both oxidation states was found to be quite feasible with the Ti(IV) and Ti(III) complexes possessing modest insertion barriers of 3.8 and 3.3 kcal/mol, respectively. The insertion process for the Ti(IV)-, Zr(IV)-, and Hf(IV)-based CGCs were compared, and it was found that the insertion barriers increased in the order Ti < Zr ≈ Hf. The calculated insertion barriers were calculated to be 3.8, 5.1, and 5.8 kcal/mol for the Ti, Zr, and Hf complexes, respectively. A possible chain rearrangement mechanism involving the rotation of the M–C_α bond was also examined by molecular mechanics. The results suggest that this process is sterically unhindered for the half-sandwich constrained geometry catalysts whereas it is significantly more hindered for the full sandwich bis-Cp metallocenes.

Introduction

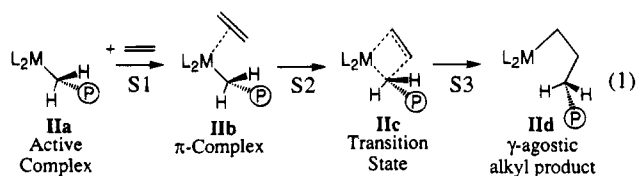
There is currently considerable interest in metallocenes as alternatives to traditional Ziegler–Natta catalysts in olefin polymerization. Kaminsky and Brintzinger^{1c} have pioneered a new generation of bridged cationic metallocenes with group-4 metals, **Ia**, that can



be used to produce high-density polyethylenes and both isotactic and syndiotactic α -olefins. Uniformity of the active site in these metallocene-based systems leads to greater uniformity of the polymer microstructure, allows for incorporation of comonomers with higher regularity, and produces plastic with molecular weight distributions which are narrower than those produced by traditional heterogeneous Ziegler–Natta catalysts. Most

recently, half-sandwich metallocenes, **Ib**, or constrained geometry catalysts (CGC) first recognized by Bercaw^{2e} *et al.* are reported² to produce polymers with side branches well beyond the traditional C₃ to C₈ α -olefins. This long chain branching, as it is termed, along with the narrow molecular weight distributions characteristic of metallocenes allows CGC plastics to break the rules of the structure–property–processibility relationships. In other words the CGC products possess very desirable performance properties while still allowing for acceptable processibility.

The most widely accepted mechanism for olefin polymerization by heterogeneous Ziegler–Natta systems as well as the homogeneous metallocene catalysts is due to Cossee.³ This propagation mechanism is shown for the metallocene systems in eq 1.



The active species **IIa** of eq 1 coordinates an olefin to form the π -complex, **IIb**, followed by the formation of

(2) (a) Stevens, J. C.; Timmers, F. J.; Wilson, D. R.; Schmidt, G. F.; Nickias, P. N.; Rosen, R. K.; Knight, G. W.; Lai, S. European Patent Application EP-416-815-A2, March 13, 1991. (b) Canich, J. A. PCT Application WO 91/04257, April 4, 1991. (c) Devore, D. D. European Patent Application EP-514-828-A1, November 25, 1992. (d) Lai, S. Y.; Wilson, J. R.; Collier, R.; Knight, G. W.; Stevens, J. C. PCT Application WO93/08221, April 29, 1993. (e) Shapiro, P. J.; Bunel, E.; Schaefer, W. P.; Bercaw, J. E. *Organometallics* **1990**, *9*, 867.

[†] Novacor Research & Technology Corp.

[‡] University of Calgary.

[®] Abstract published in *Advance ACS Abstracts*, February 1, 1995.

(1) (a) Ewen, J. A. *J. Am. Chem. Soc.* **1984**, *106*, 6355. (b) Ewen, J. A.; Jones, R. L.; Razavi, A.; Ferrara, J. D. *J. Am. Chem. Soc.* **1988**, *110*, 6255. (c) Kaminsky, W.; Kulper, K.; Brintzinger, H. H.; Wild, F. R. W. P. *Angew. Chem., Int. Ed. Engl.* **1985**, *24*, 507. (d) Kaminsky, W.; Steiger, R. *Polyhedron*, **1988**, *7*, 2375. (e) Spaleck, W.; Küber, F.; Winter, A.; Rohrmann, J.; Bachmann, B.; Antberg, M.; Dolle, V.; Paulus, E. F. *Organometallics* **1994**, *13*, 954. (f) Stehling, U.; Diebold, J.; Kirsten, R.; Röhl, W.; Brintzinger, H. H. *Organometallics* **1994**, *13*, 964.

the transition state **Ic** and the product **IId** in which the chain has been increased by two carbon units. There have been a number of experimental^{1a,4} studies aimed at providing a more detailed picture of the scheme outlined in eq 1.

Molecular modeling has also been used extensively in studies of the steps involved in olefin polymerization. Molecular mechanics simulations have so far focused on the stereoregularity of polyolefins by analyzing the steric repulsion at the assumed transition state, **Ic**, of the olefin insertion step in the Cossee mechanism.^{5,6,7d} A number of *ab initio*,⁷ semi-empirical,⁸ and density functional theory^{7g,9} (DFT) methods have been employed in studies of the electronic factors of importance in the Cossee mechanism. The active catalytic species in the electronic studies were assumed to be unsaturated cations, L₂MR⁺, where M is a group IV transition metal, and the growing chain R is represented by CH₃ whereas L₂ varies from Cl₂ and bis(cyclopentadienyl) (Cp) to bridged bis-Cp's. The possible influence of the solvent and the counterion (cocatalyst) was ignored in those calculations.

We present here a DFT-based study of the CGC system **Ib** and its possible role as a catalyst in olefin polymerization according to eq 1. In our calculations the growing chain is presented by a methyl group, and any influence from the solvent or the counterion has been neglected. The zirconium-based CGC has been studied briefly in a previous general study on metallocene based homogeneous Ziegler-Natta catalysts.^{9a,b,d} Here, we provide a more comprehensive study of Ti-, Hf-, and Zr-based constrained geometry catalytic systems.

The first point of interest is concerned with the potential performance of a neutral group-4 catalyst in which a single electron has been added to the cationic CGC system **Ib** so as to produce a d¹ CGC catalyst. We shall specifically deal with M = Ti since titanium d¹ system on occasion have been invoked as Ziegler-Natta catalysts.¹⁰

The second objective of our investigation is related to the role of the metal. We shall study how the stability and structure of the π -complex, **Ib**, the geometry and energy of the transition state **Ic**, and the relative energy of the product **IId** varies among the group 4-elements titanium, zirconium, and hafnium.

Finally, we have briefly examined the freedom of the polymer chain in the half-sandwich constrained geometry catalysts, **Ib**, and compared it to that in the full sandwich bis-Cp metallocenes, **Ia**.

Computational Details

The calculations reported here were carried out by using the density functional package, ADF, developed by Baerends *et al.*^{11 a,b} and vectorized by Ravenek.^{10c} The adopted numerical integration scheme was that developed by te Velde *et al.*¹² A set of uncontracted triple- ζ Slater-type orbitals (STO) was employed for the *ns*, *np*, *nd*, (*n* + 1)*s*, and (*n* + 1)*p* valence orbitals of the transition metal atoms.¹³ For the 2s and 2p orbitals of carbon and nitrogen, use was made of a double- ζ basis augmented by an extra 3d polarization function.¹² The inner core shells were treated by the frozen-core approximation.^{9a} A set of auxiliary s, p, d, f, and g STO functions, centered on all nuclei, was introduced to fit the molecular density and to represent Coulomb and exchange potentials accurately.¹⁴ All molecular geometries were optimized according to the analytic energy gradient method implemented by Versluis and Ziegler¹⁵ at the local density approximation (LDA) level.¹⁶ Nonlocal corrections based on Beckes's functional^{17 a} for exchange and Perdew's functional^{15b} for correlation were added as a perturbation (LDA/NL-P). The transition states were located by the algorithm due to Baker.¹⁸

For the molecular mechanics calculations the POLYGRAF²⁴ package by Molecular Simulations Inc. was utilized. The catalyst backbone was fixed in this model, since no force field parameters were available at the time. The L₂M-C_n fragment of the catalysts was held rigid with the structure of the backbones taken from the DFT-optimized γ -agostic propyl structures. The POLYGRAF implementation of Allinger's

(3) (a) Cossee, P. *J. Catal.* **1964**, *3*, 80. (b) Arlman, E. J.; Cossee, P. *J. Catal.* **1964**, *3*, 99.

(4) (a) Fink, G.; Rottler, R. *Angew. Makromol. Chem.* **1984**, *94*, 25. (b) Brookhart, M.; Green, M. L. H. *J. Organomet. Chem.* **1983**, *250*, 395. (c) Soto, J.; Steigerwald, M. L.; Grubbs, R. H. *J. Am. Chem. Soc.* **1982**, *104*, 4479.

(5) (a) Corradini, P.; Guerra, G.; Vacatello, M.; Villana, V. *Gazz. Chim. Ital.* **1988**, *118*, 173. (b) Cavallo, L.; Guerra, G.; Oliva, L.; Vacatello, M.; Corradini, P. *Poly. Commun.* **1989**, *30*, 16. (c) Cavallo, L.; Corradini, P.; Guerra, G.; Vacatello, M. *Polymer* **1991**, *32*, 1329. (d) Cavallo, L.; Guerra, G.; Vacatello, M.; Corradini, P. *Chirality* **1991**, *3*, 299. (e) Cavallo, L.; Guerra, G.; Corradini, P. *Macromolecules* **1993**, *26*, 260.

(6) (a) Castonguay, L. A.; Rappe, A. K. *J. Am. Chem. Soc.* **1992**, *114*, 5832. (b) Hart, J. R.; Rappe, A. K. *J. Am. Chem. Soc.* **1993**, *115*, 6159.

(7) (a) Novaro, O.; Blaisten-Barojas, E.; Clementi, E.; Giunchi, G.; Ruiz-Vizcaya, M. E. *J. Chem. Phys.* **1978**, *68*, 2337. (b) Fujimoto, H.; Yamasaki, T.; Mizutani, H.; Koga, N. *J. Am. Chem. Soc.* **1985**, *107*, 6157. (c) Kawamura-Kuribayashi, H.; Koga, N.; Morokuma, K. *J. Am. Chem. Soc.* **1992**, *114*, 2359. (d) Kawamura-Kuribayashi, H.; Koga, N.; Morokuma, K. *J. Am. Chem. Soc.* **1992**, *114*, 8687. (e) Koga, N.; Yoshida, T.; Morokuma, K. *Organometallics* **1993**, *12*, 2777. (f) Siegbahn, P. E. M. *Chem. Phys. Lett.* **1993**, *205*, 290. (g) Weiss, H.; Ehrig, M.; Ahlrichs, R. *J. Am. Chem. Soc.* **1994**, *116*, 4919. (h) Bierwagen, E. P.; Bercaw, J. E.; Goddard, W. A., III. *J. Am. Chem. Soc.* **1994**, *116*, 1481. (i) Koga, N.; Yoshida, T.; Morokuma, K. *International Symposium: 40 years of Ziegler Catalysts*. Freiburg, Germany, Sep 1-3, 1993; Springer-Verlag: Berlin, in press.

(8) (a) Armstrong, D. R.; Pekins, P. G.; Stewart, J. J. P. *J. Chem. Soc., Dalton Trans.* **1972**, 9172. (b) Cassoux, P.; Crasnifer, F.; Labarre, J.-F. *J. Organomet. Chem.* **1979**, *165*, 303. (c) McKinney, R. J. *J. Chem. Soc., Chem. Commun.* **1980**, 490. (d) Balazs, A. C.; Johnson, K. H. *J. Chem. Phys.* **1982**, *77*, 3148. (e) Shiga, A.; Kawamura, H.; Ebara, T.; Sasaki, T. *J. Organomet. Chem.* **1989**, *266*, 95. (f) Prosenec, M.-H.; Janiak, C.; Brintzinger, H.-H. *Organometallics* **1992**, *11*, 4036.

(9) (a) Woo, T. K.; Fan, L.; Ziegler, T. *Organometallics* **1994**, *13*, 432. (b) Woo, T. K.; Fan, L.; Ziegler, T. *Organometallics* **1994**, *13*, 2252. (c) Meier, R. J.; van Doremale, G. H. J.; Iarlori, S.; Buda, F. *J. Am. Chem. Soc.*, submitted for publication. (d) Woo, T. K.; Fan, L.; Ziegler, T. *International Symposium: 40 years of Ziegler Catalysts*. Freiburg, Germany, Sep 1-3, 1993; Springer-Verlag: Berlin, in press.

(10) Rosen, R. K.; Nickias, P. N.; Devore, D. D.; Stevens, J. C.; Timmers, F. J. International Patent Application WO93/19104, Sep 30, 1993. Luinstra, G. A.; ten Cate, L. C.; Heeres, H. J.; Pattiasina, J. W.; Meetsma, A.; Teuben, J. H. *Organometallics* **1991**, *10*, 3227. Eish, J. J.; Boleslawski, M. P. *J. Organomet. Chem.* **1987**, *334*, C1.

(11) (a) Baerends, E. J.; Ellis, D. E.; Ros, P. *Chem. Phys.* **1973**, *2*, 41. (b) Baerends, E. J. Ph.D. Thesis, Vrije Universiteit, Amsterdam, 1975. (c) Ravenek, W. In *Algorithms and Applications on Vector and Parallel Computers*; te Riele, H. J. J., Dekker, Th. J., van de Vorst, H. A., Eds.; Elsevier: Amsterdam, 1987.

(12) (a) Boerrigter, P. M.; te Velde, G.; Baerends, E. J. *Int. J. Quant. Chem.* **1988**, *33*, 87. (b) te Velde, G.; Baerends, E. J. *J. Comput. Phys.* **1992**, *99*, 84.

(13) (a) Snijders, J. G.; Baerends, E. J.; Vernooijs, P. *At. Nucl. Data Tables* **1982**, *26*, 483. (b) Vernooijs, P.; Snijders, J. G.; Baerends, E. J. Slater type basis functions for the whole periodic system; Internal report; Free University of Amsterdam, The Netherlands, 1981.

(14) Krijn, J.; Baerends, E. J. Fit functions in the HFS-method; Internal report (in Dutch); Free University of Amsterdam, The Netherlands, 1984.

(15) Versluis, L.; Ziegler, T. *J. Chem. Phys.* **1988**, *88*, 322.

(16) Vosko, S. H.; Wilk, L.; Nusair, M. *Can. J. Phys.* **1980**, *58*, 1200.

(17) (a) Becke, A. D. *Phys. Rev.* **1988**, *A38*, 3098. (b) Perdew, J. P. *Phys. Rev.* **1986**, *B33*, 8822.

(18) Baker, J. J. *Comput. Chem.* **1986**, *7*, 385.

MM2¹⁹ force field was used as a starting point with all unknown parameters approximated as follows. All torsions involving the metal center were assumed to have no barrier. The force constant for the M–C(sp³)–C(sp³) bend was approximated to be the same as the MM2 C(sp³)–C(sp³)–C(sp³) force constant of $k_b = 64.75$ kcal/mol. The average M–C_α–C_β bond angle from a number of DFT-optimized γ -agostic propyl zirconocenes and titanocenes of 84° was used as the equilibrium angle for this bend. The C(sp³)–C(sp³)–H MM2 parameters were used for the M–C(sp³)–H bending parameters ($k_b = 51.8$ kcal/mol and $\theta_o = 109.4^\circ$). To allow for the short M–C and M–H nonbonded distances that are observed, the metal van der Waals interactions were turned off. Including the metal van der Waals interactions caused the growing chain to be unnaturally far away from the metal center. Removal of the metal van der Waals interactions resulted in geometries which were more indicative of those observed in **1d**, **3d**, and **4d**. Other interactions prevented the growing chain from collapsing onto the metal center such as the M–C(sp³)–C(sp³) bend and the steric interactions between the growing chain and the catalyst backbone. It should be noted that the exclusion of the metal van der Waals interactions did not actually effect the rotation profiles shown in Figure 6 significantly compared to the profiles with the van der Waals interactions included. In this model electrostatic interactions were also neglected.

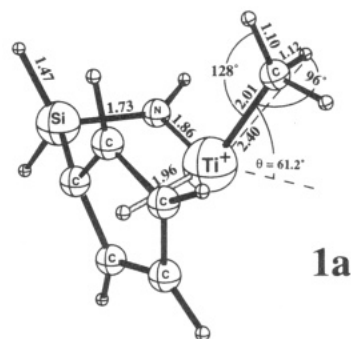
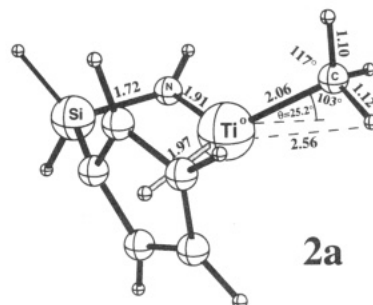
In these calculations the ω dihedral was fixed by increasing the cen-Zr–C_α–C_β dihedral barrier to 1000 kcal/mol (This is the standard method in POLYGRAF for constraining particular internal coordinates). With ω constrained and the L₂M–C_α backbone fixed, the growing chain was fully optimized for each 10° interval from $\omega = -180^\circ$ to $+180^\circ$. For each ω , the global minimum was searched for, which involved minimizing several different chain conformations. The lowest energy conformations are represented in Figure 6.

Results and Discussion

We shall here present the results from our DFT calculations on the constrained geometry catalysts [SiH₂–C₅H₄–NHMCH₃]^x, where M = Ti, Zr, and Hf for $x = +1$ and M = Ti for $x = 0$. The positively charged species correspond to a formal oxidation state of IV for the metal center. It will be referred to as M(IV) for the sake of simplicity. Similarly, the neutral species will be referred to as Ti(III) in the following discussion. We shall start with a comparison of the Ti(VI)- and Ti(III)-based systems.

Comparison of Ti(VI) and Ti(III). The optimized structure of the Ti(IV) catalyst [SiH₂–C₅H₄–NHTiCH₃]⁺ is shown in **1a** whereas the corresponding neutral Ti(III) species is given in **2a**. In both, the Si atom is nearly coplanar (within 1°) with the plane defined by the centroid of the Cp ring, Ti, and the N atom, while the Ti–methyl bond is bent out of this plane as defined by the angle θ . The charged species **1a** displays a large bending angle of $\theta = 61^\circ$ whereas the bending angle for **2a** is much smaller at 25°. A similar difference in the degree of bending between neutral and cationic species has also been calculated by Bierwagen^{7h} *et al.* The bending mode is soft, and less than 3 kcal/mol is required to move the methyl group from the in-plane to the out-of-plane position.

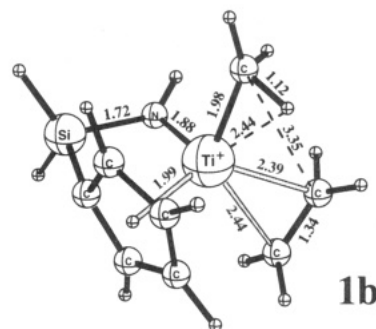
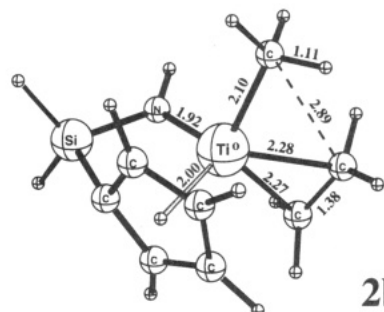
The metal–ligand bond distances are generally reduced in going from Ti(III) to Ti(IV). The reduction

**1a****2a**

amounts to 0.05 Å for the Ti–N and Ti–CH₃ bonds and 0.02 Å for the Ti–Cp distance. The shortening of the metal–ligand bond distances is in keeping with the smaller radius of Ti(IV) as well as its stronger ability to accept electron density.

Structure **1a** is stabilized by an agostic interaction between the methyl hydrogen and the Ti center. An angle of 96° between the C–H and Ti–C bonds as well as a slightly elongated C–H bond of 1.12 Å are both indicative of such an interaction. The agostic interaction in the neutral species **2a** is less pronounced with a H–C–Ti angle of 103°, a C–H bond length of 1.12 Å, and a Ti–H distance of 2.56 Å.

The coordination by ethylene to the vacant site of the titanium center in **1a** leads to a π -complex **1b**. The

**1b****2b**

bending angle θ in **1b** has slightly increased by 3° compared to **1a**. Also, the ethylene coordination to **1a**

(19) (a) Allinger, N. L.; Yuh, Y. H.; Lii, J. H. *J. Amer. Chem. Soc.* **1989**, *111*, 8551. (b) Spargue, J. T.; Tai, J. C.; Yuh, Y.; Allinger, N. L. *J. Comput. Chem.* **1987**, *8*, 581.

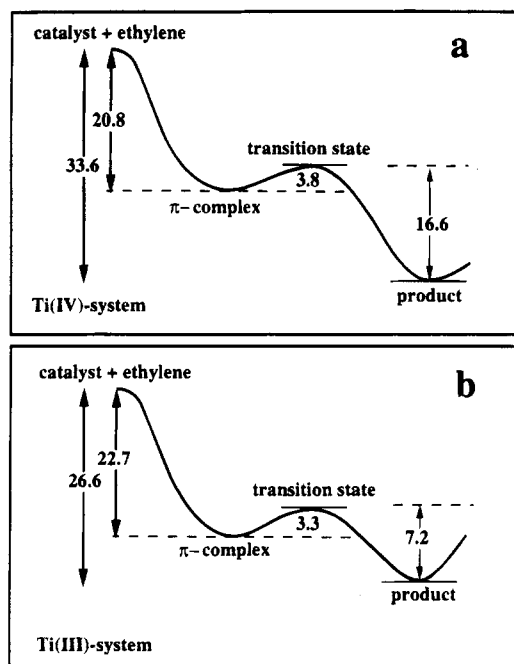


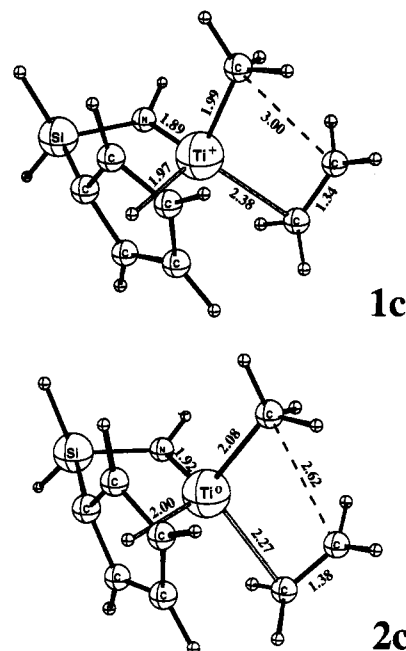
Figure 1. Reaction profile for the insertion of ethylene into the M-CH₃ bond: (a) M = Ti(IV), (b) M = Ti(III).

results in an elongation of the Ti-Cp and Ti-N bonds by 0.03 and 0.02 Å, respectively. The Ti-CH₃ bond is, on the other hand, contracted by 0.03 Å. The coordination of ethylene to **1a** is exothermic by 20.8 kcal/mol, as indicated by the reaction profile shown in Figure 1a.

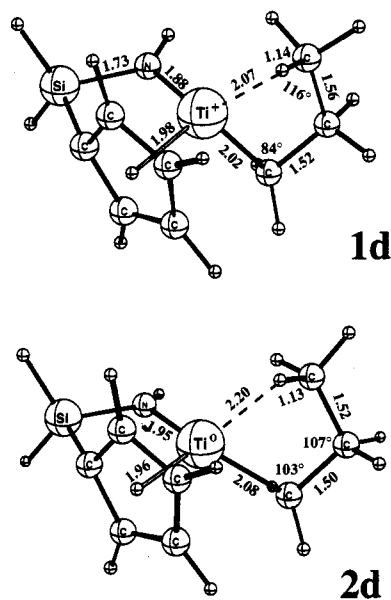
The π -complex with the neutral Ti(III) species **2a** was optimized as **2b**. The methyl group of **2a** has undergone a considerable movement out of the Ti-N-Si plane in order for the metal center to accommodate the incoming ethylene. The bending angles of the methyl group are quite similar in **1b** and **2b**. The coordination of ethylene to **2a** is exothermic by 22.7 kcal/mol, Figure 1b.

There is a considerable difference between the charged Ti(IV) species **1b** and the neutral Ti(III) complex **2b** with regard to the structure of the coordinated ethylene and the way in which it is bound to the metal center. The bonding between ethylene and the d⁰ metal center in the Ti(IV) species **1b** is basically established by an electrostatic stabilization of the ethylene π -electrons due to the positively charged metal center. The ethylene double bond distance in **1b** remains essentially the same as in the free molecule (1.34 Å), and the Ti-C distances of 2.39 and 2.44 Å, respectively, are rather long. The ethylene double bond in the neutral Ti(III) species **2b** is on the other hand elongated to 1.38 Å. This elongation stems from a delocalization of the single d-electron on titanium into the π^* orbital of ethylene. The Ti(III)-C distances to the two carbon atoms of the ethylene at 2.29 and 2.27 Å, respectively, are in addition noticeably shorter than those in **1b**. Thus, **2b** can be characterized as a real π -complex in which both donation and back-donation are important.

We have carried out a full transition state optimization for the insertion processes involving the Ti(III) and Ti(IV) species. The optimized transition state for the Ti(IV) system is given in **1c** whereas **2c** represents the transition state for the neutral Ti(III) system. The two transition states **1c** and **2c** were confirmed to have a single imaginary frequency.



The Ti(IV) transition state **1c** is seen to be much closer in geometry to the π -complex **1b** than the propyl product **1d**. Thus, **1c** must be characterized as an early



transition state. The distance between the methyl and ethylene carbon atoms is shortened from 3.35 Å in **1b** to 3.00 Å in **1c**, but it is still not close enough for the two atoms to be bonded at this stage of reaction. The double bond of ethylene remains unchanged at 1.34 Å in **1c**. The Ti-methyl distance is 0.01 Å longer in **1c** than in the π -complex **1b**, while the Ti-C(ethylene) distance is shortened by 0.06 Å. The metal to ethylene interaction in the transition state **1c** is thus similar to that found in the π -complex **1b**. It should also be noted that the local C₃-axis of the methyl group is pointed toward the metal center rather than the approaching ethylene carbon. The calculated barrier for the insertion step **1b** \rightarrow **1c** \rightarrow **1d** is modest and amounts to 3.8 kcal/mol. We have previously^{9a,b,d} calculated an even smaller barrier of less than 1 kcal/mol for the insertion process involving bis-Cp systems such as **1a** suggesting

that some bis-Cp systems may undergo insertion without a barrier.^{7e}

The Ti(III) transition state **2c** is also quite similar to the corresponding π -complex **2b**. The only significant difference between **2c** and **2b** is that the methyl-ethylene distance is 0.27 Å closer in **2c**; all other changes are minor. The calculated barrier for the insertion, **2b** \rightarrow **2c** \rightarrow **2d**, is only 3.3 kcal/mol, Figure 1b. Thus it would seem that the neutral Ti catalyst should be as active as the positively charged Ti(IV) species.

The kinetic product from the insertion process, eq 1, is a γ -agostic propyl complex. The optimized structure of the propyl complex is shown as **1d** for the Ti(IV) system and as **2d** for the neutral Ti(III) system. Structure **1d** displays a clear agostic interaction between Ti and the γ -hydrogens. The β -carbon in **1d** is twisted out of the C_α -Ti- C_γ plane so that the hydrogens are in a staggered positions. The kinetic product **1d** was found to be a very stable conformation with an energy that is 12.8 kcal/mol lower than the π -complex **1b**. The γ -agostic structure **1d** is not likely to be the most stable conformation for the propyl chain. Previous calculations^{9a,b} on bis-Cp systems gave a β -agostic structure as the most stable, and we expect the same to be the case for the present system.

Compared to **1d**, the neutral species **2d** displays a weaker agostic interaction as the Ti(III) metal center is less electron deficient. The closest γ -hydrogen contact to the titanium center is 2.20 Å. The Ti- C_α bond is 0.06 Å longer in **2d** than in **1d**, which is comparable to the difference in the Ti- C_α (methyl) distance for the two corresponding methyl compounds **1a** and **2a**. The variation can be explained by the difference between the radius of Ti(III) and Ti(IV). Further, the Ti-alkyl bond in the neutral systems is weakened by the three-electron two-orbital interaction between the odd electron on the metal center and the electron pair in the Ti-alkyl bonding orbital. The Ti(III) propyl product **2d** is only 4.2 kcal/mol more stable than the corresponding Ti(III) π -complex **2b**. Thus, the neutral system might exhibit an equilibrium between **2d** and **2b**. The greater stability of the Ti(IV)-based system results in a larger overall insertion enthalpy of -33.6 kcal/mol compared to the insertion enthalpy of -26.6 kcal/mol for the Ti(III) system. These values are in good agreement with the intrinsic enthalpy of inserting an olefin into the M-C bond (the energy gain from breaking one C-C double bond and forming a C-C single bond during the insertion). An indication of the intrinsic insertion enthalpy is given by the exothermicities of the general reaction $\cdot\text{CH}_3 + \text{C}_n\text{H}_m \rightarrow \cdot\text{C}_{n+1}\text{H}_{m+3}$, ΔH° ²⁰ (this is assuming that the M-Me and M-R bond dissociation enthalpies are roughly equivalent). For ethylene ΔH° is determined experimentally²⁰ to be 23.5 kcal/mol. The difference between the the intrinsic enthalpy and the calculated enthalpy of insertion can be used to estimate the energy gained due to the additional agostic interactions in the γ -agostic propyl complex, **1d**, as compared to the methyl complex **1a**. The experimental value of ΔH° suggests that, for the Ti(III) system, the agostic

interactions amount to about 3 kcal/mol²¹ whereas for the cationic Ti(IV) system the additional interactions amount to about 10 kcal/mol.

The calculated energetics for the two insertion processes involving either Ti(IV) or Ti(III) is summarized in Figure 1. The formation of the π -complex, **S1** of eq 1, is exothermic for both systems. However, the ethylene complexation energy of the neutral π -complex **2b** is larger by 2 kcal/mol due to the more effective titanium to olefin back-donation. The two calculated activation energies of 3.8 kcal/mol, Ti(IV), and 3.3 kcal/mol, Ti(III), are modest and quite similar. Thus, by consideration of electronic effects, the insertion process involving either Ti(III) or Ti(IV) should be kinetically quite feasible in the gas-phase.

We would also expect the insertion process involving the neutral Ti(III) system to be feasible in solution, perhaps even more so than the cationic Ti(IV) system. In solution, there should be a barrier to the formation of the π -complex, **11b**, due to the displacement of weakly coordinated solvent molecules.^{7h} For the cationic Ti(IV) system, the coordination of the solvent to the metal center is based on an electrostatic interaction equivalent to that in the olefin π -complex. Therefore, we would expect the complexation of the solvent to be of comparable strength to the complexation of the olefin. In contrast to this, the neutral Ti(III) CGC is expected to form a much weaker complex with the solvent than with the olefin. The reason for this is that the olefin-Ti(III) complex enjoys the stabilization due to back-donation, whereas the solvent complex would not normally possess any significant back-donation. In addition to this, the electrostatic stabilization of the neutral Ti(III)-solvent complex would not be nearly as strong as electrostatic stabilization enjoyed by the cationic Ti(IV)-solvent complex. Therefore, the displacement of the solvent from the Ti(III) complex is expected to possess a small barrier compared with the analogous displacement from its Ti(IV) counterpart. Figure 2 illustrates schematically the expected differences in the energy profile between the insertion in the gas-phase and in solution for both the neutral Ti(III) and cationic Ti(IV) systems. We expect the effect of solvation on the energy profile of the neutral Ti(III) system to be much less dramatic than that of its cationic Ti(IV) analogue. Furthermore, we also expect the Ti(III) system to more readily form the olefin π -complex than the Ti(IV) complex because the neutral system will have a much smaller displacement barrier.

(21) The zero-point energy contributions will for the most part cancel out except for those due to the agostic interactions. If one included zero-point energy corrections (zpe) in our estimates of the strength of the agostic interactions, the estimate would be slightly smaller than stated since the calculated enthalpies of insertion for the Ti(III) and Ti(IV) complexes do not include zpe corrections. However, the contribution to the zpe correction due to the agostic interactions are expected to be very small, less than 1 kcal/mol.

(22) Longer chains have also been modeled (up to C_6) and been shown to produce similar results. Trends and the basic behavior of the profile are expected to be the same for both long and short chain models.

(23) This is somewhat of a surprise that the bis-Cp titanocene has roughly the same profile up to $\pm 80^\circ$ as its larger more open zirconocene counterpart. The titanocene is more sterically constrained, but when the energies are normalized with the zero energy set equal to the energy at $\omega = 0^\circ$, this fact is somewhat obscured.

(24) POLYGRAF version 3.0 (17/2/1992) of Molecular Simulations Inc. (MSI), 16 New England Executive Park, Burlington, MA, 1-800-756-4647. POLYGRAF is a commercial molecular mechanics, molecular dynamics program system.

(20) (a) Christ, C. S.; Eyley, J. R.; Richardson, D. E. *J. Am. Chem. Soc.* **1988**, *110*, 4038. Christ, C. S.; Eyley, J. R.; Richardson, D. E. *J. Am. Chem. Soc.* **1990**, *112*, 596.

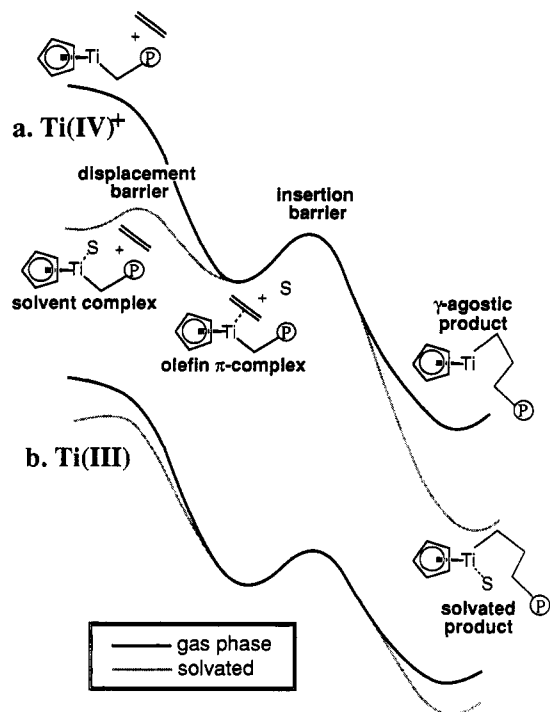


Figure 2. Approximate gas-phase and solution-phase profiles for the insertion of olefin into an L_2M-R bond.

These results suggest that, for the insertion step, the neutral Ti(III)-based systems are likely as good or better constrained geometry catalysts as the cationic Ti(IV) systems. On the other hand, there are many other factors which influence a systems polymerization rate. First, the insertion step is only one step in the overall propagation process and perhaps not the rate-limiting step. Previous theoretical studies⁹ of the bis-Cp systems suggest that the rate-limiting step in the chain propagation is not the insertion step but possibly a process involving the rearrangement of the γ -agostic kinetic product. This may also be true for the constrained geometry catalysts. If this is the case, then the observed differences in reactivities of Ti(III) and Ti(IV) systems may have its origins in the rearrangement process. Furthermore, Ti(III) complexes are probably not stable as monomers and are likely to dimerize much in the same way neutral scandium CGCs are observed to dimerize.²⁵ Dimerization may then result in a decreased number of active centers. Similarly, as with the neutral Sc CGC systems²⁵ the Ti(III) active chain propagation species is expected to be a monomeric complex whereas the cationic Ti(IV) active species exists as an ion pair with the cocatalyst or counteranion. The cocatalyst may play a fundamental role in the overall propagation process which would again differentiate the Ti(III) and Ti(IV) systems.

Comparison of Reactivities of Ti, Zr, and Hf.

Studies on the original cationic group-4 metallocenes with two Cp ligands, **1a**, seem to indicate that the catalytic activity in olefin polymerization increases in going from titanium to zirconium. This trend can be rationalized by observing that the active site is more crowded for titanium with the shorter M-Cp distance.

For the CGC type catalysts, **1b**, steric crowding might not be so important, and experiments seem to indicate that the titanium homologue in this case is the most active. We report here a DFT-based study on the trend in activity of the CGC systems, **1b**, along the triad Ti, Zr, and Hf.

Some of the more important structural parameters from the optimized geometries of the zirconium-, **3a**, and hafnium-based, **4a**, CGC active complexes are compared with those of the titanium homologue in Figure 3a. Here the parameters for titanium are given in parentheses (), those of hafnium are given without enclosures. The length of the metal-methyl bond increases in the order Ti << Zr ~ Hf, in accordance with what one might expect from the relative sizes of the metal atoms. The distances from the metal to the centroid of the Cp ring as well as the metal-N bond length increases in the same order. The deformation of the methyl group caused by the agostic interaction is most significant for Ti, presumably due to the shorter Ti-C distance.

The structures of the π -complexes are compared in Figure 3b. The ethylene double bonds in all of the three cases are essentially unchanged, with a length of 1.34 Å. The metal-ethylene interaction is thus not sensitive to the size of the metal but is closely related to the oxidation state as discussed earlier. The C _{α} (methyl)-C _{β} (ethylene) distances are 3.35, 3.72, and 3.80 Å for Ti, Zr, and Hf, respectively. The exothermicities for the ethylene coordination are 24.2 kcal/mol for zirconium (Figure 4a), and 25.7 kcal/mol for hafnium (Figure 4b), as compared to 20.8 kcal/mol (Figure 1a) in the case of titanium. The difference in the relative stabilities of the three π -complexes may be attributed to steric factors. Thus, the steric repulsion between the coordinating ethylene and the coligands on the metal center is likely to be largest for titanium with the shortest metal-ligand bond distances. The titanium system forms, as a consequence, the weakest π -complex. The largest steric contribution in the titanium system is likely to come from the interaction between ethylene and the methyl group.

The transition state structures, **4c** and **5c**, were optimized by the same standard algorithm as the titanium homologue. The key parameters are summarized in Figure 3c. A feature common to all three structures is an increase in the metal-C _{α} (ethylene) distance in going from the π -complex **b** to the transition state **c**, while the metal-C _{α} (methyl) distance at the same time is increased. No notable variation is observed in the ethylene double bond distance between **b** and **c**. The most significant modification is in the C _{α} (methyl)-C _{β} (ethylene) distance, which is nearly the same in all three transition state structures. The distance has changed considerably from the π -complex in the case of zirconium ($\Delta R = 0.62$ Å) and hafnium ($\Delta R = 0.74$ Å) whereas the change is much more modest in the titanium species with $\Delta R = 0.35$ Å. The energy barriers for Ti, Zr, and Hf increase in the order of 3.8 kcal/mol (Figure 1a), 5.1 kcal/mol (Figure 4a), and 5.7 kcal/mol (Figure 4b). We suggest that the higher barrier associated with the **4d** and **5d** systems can be explained by a larger increase in the steric interaction between ethylene and the methyl group associated with the greater change in the C _{α} (methyl)-C _{β} (ethylene) distance.

(25) (a) Shapiro, P. J.; Bunel, E.; Schaefer, W. P.; Bercaw, J. E. *Organometallics* **1990**, *9*, 4623. (b) Shapiro, P. J.; Cotter, W. D.; Schaefer, W. P.; Labinger, J. A.; Bercaw, J. E. *J. Am. Chem. Soc.* **1994**, *116*, 4623.

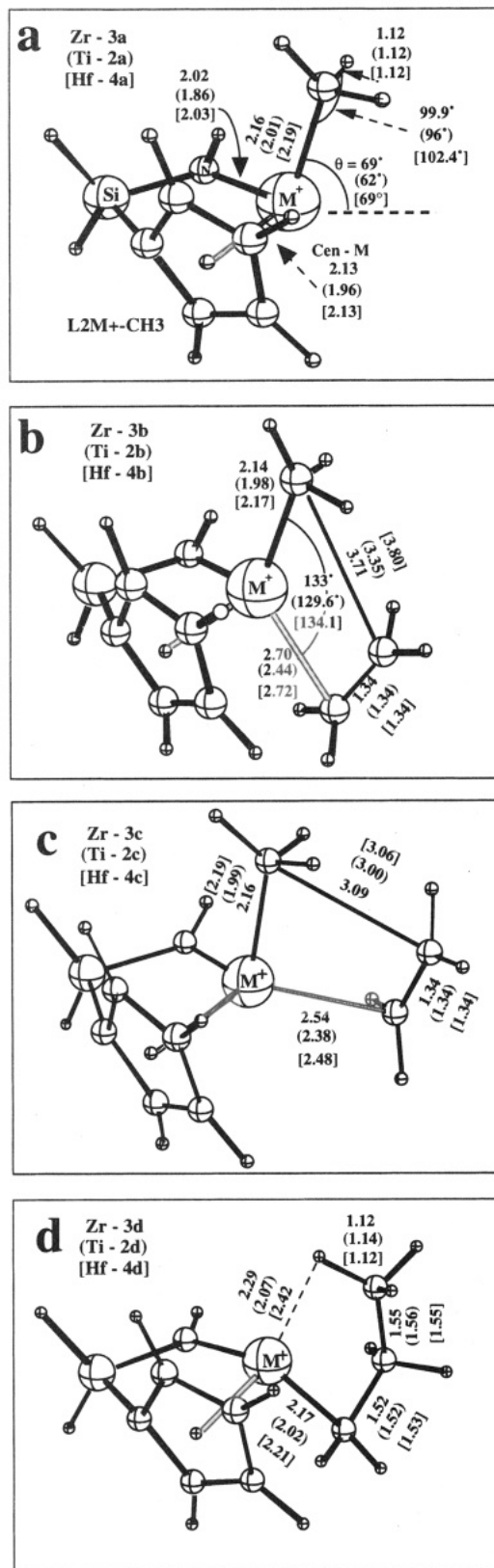


Figure 3. LDA-optimized structures of titanium, zirconium, and hafnium analogues of (a) **IIa**, (b) **IIb**, (c) **IIc**, and (d) **IIId**. Various geometric parameters are given in parentheses () for the titanium CGC, no enclosures for the zirconium CGC, brackets [] for the hafnium CGC.

In other words, the lower activation barrier for the Ti CGC can be largely explained by the formation of a weaker π -complex than the analogous Zr and Hf complexes. It should be noted that our previous esti-

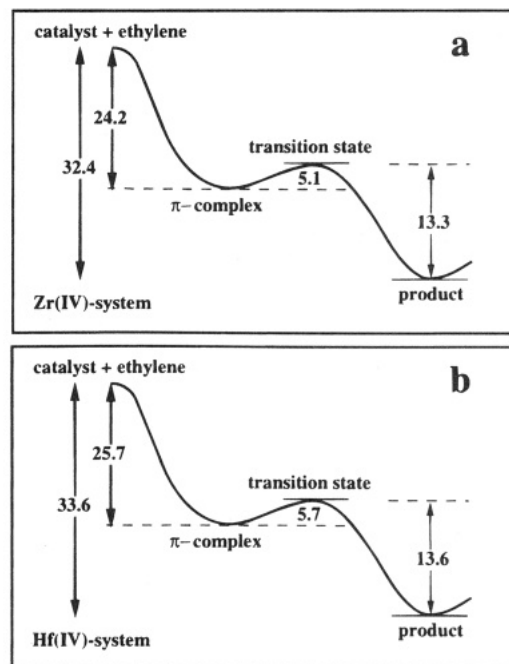


Figure 4. Reaction profile for the insertion of ethylene into the M-CH₃ bond: (a) M = Zr(IV); (b) M = Hf(IV).

mation^{9a,b} of the insertion barrier for the Zr CGC was determined to be 6.5 kcal/mol. The discrepancy in the two results is due to the fact that the earlier estimate is based on a linear transit calculation, while these results are based on a "true" transition state optimization. Additionally, a larger basis set was used in this work.

The γ -agostic propyl complex generated as a kinetic product in the ethylene insertion process, eq 1, is shown in Figure 3d. Again, the elongation of the C-H bonds due to the agostic interaction is more significant for titanium, $R(\text{C-H}) = 1.14 \text{ \AA}$, than for zirconium and hafnium, $R(\text{C-H}) = 1.12 \text{ \AA}$. For titanium the γ -agostic propyl complex is 12.8 kcal/mol lower in energy than the corresponding π -complex, Figure 1a, compared to 8.2 and 7.9 kcal/mol for zirconium and hafnium, respectively, Figure 4. The energy gap between the products, **d**, and the catalysts, **a**, plus a free ethylene is 33.8 kcal/mol for Ti, 32.4 kcal/mol for Zr, and 33.6 kcal/mol for Hf (see Figures 1a and 4). Again, the calculated overall insertion enthalpies and the intrinsic insertion enthalpies can be used to estimate the energy gained due to the additional agostic interactions in the γ -agostic propyl complex as compared to the methyl complex. The gain in the agostic interactions, ΔH_{ag} , for the series Ti(IV), Ti(III), Zr(IV), and Hf(IV) is 10.1, 3.1, 8.9, and 10.1 kcal/mol respectively. The trend in the gain in agostic interactions Ti(IV) \approx Hf(IV) > Zr(IV) > Ti(III) is somewhat surprising because one would normally expect the trend Ti(IV) > Zr(IV) \approx Hf(IV) > Ti(III).

As noted earlier, the insertion is only one step of the overall propagation mechanism. With the bis-Cp metallocenes our studies suggest that the insertion step is not the rate-limiting step. Instead, the rate-limiting step likely involves the rearrangement of the γ -agostic kinetic product, **IIId** (eq 1). During the insertion of the olefin molecule into the M-C bond, the coordination site of this M-C bond is vacated allowing for the complexation of the olefin and the next insertion. Initially, however, this coordination site is partially blocked by

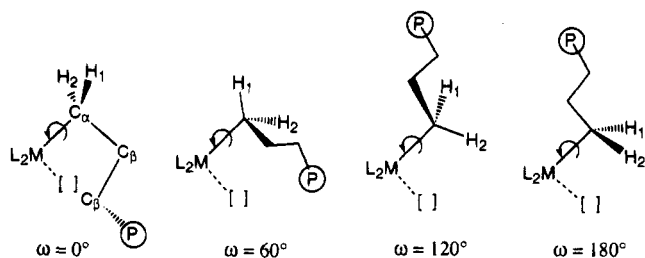


Figure 5. Rotation about the M-C_α bond for $\omega = 0^\circ$, 60° , 120° , and 180° . [] represents a vacant coordination site.

the γ -agostic interactions of the growing chain (eq 1 and Figure 3d). To accommodate the next monomer unit, this chain must vacate the coordination site by rotating about the M-C_α bond. The rotation of the polymer chain can be characterized by the VAC-M-C_α-C_β dihedral angle ω shown in Figure 5, where VAC represents the bond vector of the vacant coordination site. One can consider the VAC bond vector to be the bond vector of the M-C bond vacated during the previous insertion. For the γ -agostic product ω is roughly zero, where VAC, M, C_α, and C_β lie in the same plane. A rotation of $\omega = 60^\circ$, which would place one of the hydrogens (H₁ of Figure 5) into the coordination plane, would be enough to vacate the site and be appropriate for the eclipsed insertion of olefin. Other conformations are also depicted in Figure 5.

In this study we have attempted to model the rotation process with a gas-phase molecular mechanics simulation where the M-C_α bond vector is fixed. Although, the θ angle bending mode is calculated to be soft (3 kcal/mol barrier to cross the cen-M-N plane), such fluctuation along with full rotation about the M-C_α bond would result in inversion of the metal center between monomer insertions. If the Cossee-Arman mechanism is assumed, rapid inversion of the metal center between insertions has consequences in syndiospecific α -olefin polymerization²⁶ that would ultimately lead to atactic polymerization. In solution the M-C_α rotation may be a concerted process whereby the rearrangement is assisted by complexation of solvent or monomer to the metal. In fact, such assistance may be necessary since the rotation about the M-C_α bond breaks favorable agostic interactions in both the γ -agostic product and the most stable product conformer,^{9b} the β -agostic complex.

In this simple model the polymer chain was modeled with a propyl group²² and the force field used only accounted for structural differences between catalysts and not subtle electronic differences. The molecular mechanics rotation profiles for $\omega = -180^\circ$ to $+180^\circ$ of Ti/Zr bis-Cp and CGC metallocenes are shown in Figure 6 with the zero energy set equal to the molecular mechanics energy at $\omega = 0^\circ$. The energy profiles for the hafnium analogues were not shown because they were virtually identical to the profiles for the zirconocenes. The reason for this is that the hafnium complexes are almost identical in structure to their zirconium counterparts.

The M-C_α rotation profiles for the bis Cp titanocene and zirconocene are very similar.²³ The rotation profiles of the bis Cp complexes are symmetric about $\omega = 0^\circ$

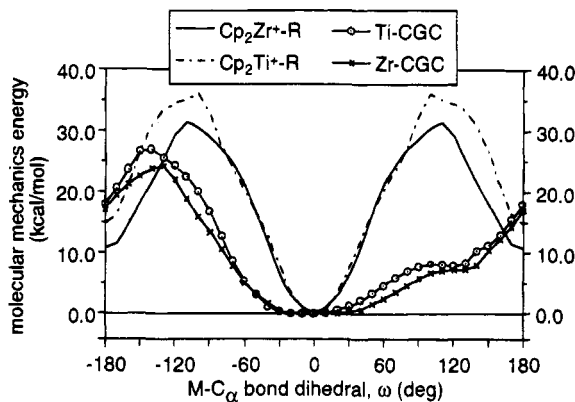


Figure 6. Normalized molecular mechanics energy profile for the rotation of the M-C_α bond for the half-sandwich constrained geometry catalysts and the full sandwich bis-Cp metallocenes. The energies are relative to the molecular mechanics energy at $\omega = 0^\circ$, which represents the zero energy.

with a global minimum at $\omega = 0^\circ$ and another minimum at 180° . The maximas for the two complexes occur at roughly $\omega = 100^\circ$. Figure 6 shows that the bis-Cp complexes possess a barrier of between 20 kcal/mol for a rotation of $\omega = 60^\circ$. These barriers are exaggerated because of the nature of the force field used (the catalyst backbone was held rigid). Although the absolute values of the energies presented may be poor, the calculations are expected to give the general behavior of the steric requirements as the M-C_α bond is rotated through 360° .

As Figure 5 shows, a $\pm 120^\circ$ rotation is severely hindered with a calculated barrier of between 30 and 40 kcal/mol. The 180° rotation of the growing chain is also unlikely because although $\omega = \pm 180^\circ$ is a minimum, the chain must overcome the large steric barrier at $\sim 100^\circ$. This is not to say that the conformation with $\omega = \pm 180^\circ$ is unlikely; it means that this conformation will not be achieved by the M-C_α bond rotation that was simulated. (This conformation can be attained by the bending of the angle θ through 0° which was determined to have a barrier less than 3.5 kcal/mol.)

The energy profiles of Figure 6 suggest that the rotation of the polymer chain in the constrained geometry catalysts is much less hindered than in the bis-Cp metallocenes. The 60° rotation for the CGCs is calculated to be less than 5 kcal/mol compared to 20 kcal/mol for the bis Cp systems. Additionally, rotation of the M-C_α bond to $\omega = +120^\circ$ (positive being toward the amido group) is also relatively unhindered with a calculated barrier of roughly 7 kcal/mol. Thus when only steric factors are considered, the growing chain of the CGCs have much more freedom than their corresponding bis-Cp analogues.

The point here is that the overall chain propagation mechanism for the bis-Cp systems and the constrained geometry catalysts may be quite distinct from one another and may even have different rate determining steps. Our DFT calculations^{9a,b,d} show that the bis-Cp zirconocenes possess an electronic insertion barrier of less than 1 kcal/mol, while the molecular mechanics rotation profile of Figure 6 suggests that they may have a large rearrangement barrier. On the other hand, its CGC counterpart, **3**, has an electronic insertion barrier of over 5 kcal/mol and potentially a small rearrangement barrier.

(26) Ewan, J. A.; Jones, R. L.; Razavi, A.; Ferrara, J. D. *J. Am. Chem. Soc.* **1988**, *110*, 6255.

Conclusions

The reactivities of the Ti(III)-, Ti(IV)-, Zr(IV)-, and Hf(IV)-based constrained geometry catalysts have been studied by calculating the structures and relative stabilities of the species **IIa–d** in eq 1. Although the active catalysts are generally assumed to be the positively charged methyl complexes of group IV elements with a formal oxidation state of IV, the neutral species of oxidation state III of titanium has been found to be as reactive as Ti(IV) in terms of reaction energies of ethylene insertion. The much stronger π -complex of Ti(III) is the major difference between Ti(III) and Ti(IV), which facilitate the followed insertion step.

In comparison of the insertion process for the Ti(IV)-, Zr(IV)-, and Hf(IV)-based catalysts, the reaction exothermicity for the insertion process was found to be quite similar for the three species. On the other hand, the activation barrier for ethylene insertion was found to increase in the order Ti < Zr ~ Hf. The differences between the zirconium- and hafnium-based catalysts are minor with regard to the structure of the catalysts, the π -complexes, the transition states, the propyl products, and the relative energies. The titanium-based catalyst was found to possess the smallest insertion barrier of the three. The higher activity of the titanium-based CGC is related to a lower stability of the corresponding π -complex due to steric repulsions between ethylene and the coligands on the metal center, notably the methyl group.

The insertion process is only one step in the overall chain propagation mechanism. After the insertion of

the olefin into the M–C bond, the growing chain must rearrange to allow for the insertion of the next monomer unit. Our molecular mechanics simulations of one possible rearrangement process, the rotation of the M–C $_{\alpha}$ bond, suggest that this process is not sterically hindered for the constrained geometry catalysts. However, for their full sandwich metallocene counterparts there is significantly more hindrance to the process. Previous calculations^{7g,9a-d} suggest that there is virtually no insertion barrier for bis-Cp metallocenes while our studies show that the insertion barriers for the constrained geometry catalysts are between 3.8 and 5.8 kcal/mol. Thus, we suggest that the overall chain propagation mechanisms for the half-sandwich constrained geometry catalysts and the full sandwich bis-Cp metallocenes may be distinctly different, possibly possessing different rate determining steps.

Acknowledgment. This investigation was supported by the Natural Sciences and Engineering Research Council of Canada (NSERC). We gratefully acknowledge the donors of the Petroleum Research Fund, administered by the American Chemical Society (ACS-PRF No. 27023-AC3). Dr. J. McMeeking of Novacor Research & Technology is thanked for many useful discussions.

Supplementary Material Available: Tables of Cartesian coordinates of DFT-optimized structures **1a–d**, **2a–d**, **3a–d**, and **4a–d** (11 pages). Ordering information is given on any current masthead page.

OM940680C

Nucleophilic Aromatic Substitutions: Hydrodealkoxylation, Hydrodehalogenation, and Hydrodeamination of Alkoxy, Halogeno, and Amino (η^6 -Arene)tricarboxylchromium Complexes

Jean-Pierre Djukic, Françoise Rose-Munch, Eric Rose,* and Frederic Simon

Laboratoire de Chimie Organique, URA 408, Université Pierre et Marie Curie, Case 181,
4, place Jussieu, 75252 Paris Cedex 05, France

Yves Dromzee

Laboratoire de Chimie des Métaux de Transition, Université Pierre et Marie Curie,
Batiment F, 4, place Jussieu, 75252 Paris Cedex 05, France

Received July 28, 1994[®]

Hydrodealkoxylation, -dehalogenation, and -deamination, occur while lithium triethylborohydride is added to [η^6 -alkoxy-, halogeno-, and -(dimethylamino)benzene]tricarboxylchromium complexes. In the case of (η^6 -benzene)tricarboxylchromium, addition of deuteride to the benzene ring gives reversibly an anionic tricarboxyl(η^5 -cyclohexadienyl)chromium complex which can be trapped by triphenyltin chloride to yield the neutral binuclear complex (η^5 -C₆H₅D)(CO)₃Cr–Sn(C₆H₅)₃. The latter complex molecular structure has been confirmed by single-crystal X-ray diffraction analysis. Empirical formula C₂₇H₂₁DCrO₃Sn: triclinic system, space group P1, $z = 2$, $a = 8.961(4)$ Å, $b = 10.853(5)$ Å, $c = 12.713(2)$ Å, $\alpha = 85.15(3)^\circ$, $\beta = 86.26(2)^\circ$, $\gamma = 72.40(4)^\circ$, $R = 0.033$, $R_w = 0.037$ (unit weight).

Introduction

(η^6 -Arene)tricarboxylchromium complexes play an important role in organometallic chemistry, which stems from their particular reactivity as it has been described in numerous reviews.¹ Their easy preparation has promoted series of studies of their ability to form stabilized benzylic anions^{2–4} and cations,³ to react in various ways with nucleophiles,⁴ to be easily metalated,⁵ and to be active catalysts in hydrogenation reactions.⁶

Our research is mainly oriented toward the application of these π -arene–metal complexes in organic synthesis as well as in the mechanistic study of their reactions with nucleophiles and electrophiles. For instance, in the case of chiral complexes, we have recently described the asymmetric formation and the resolution of ortho-substituted (η^6 -benzaldehyde)tricarboxylchromium complexes,⁷ and in the case of alkoxy and halogeno (η^6 -arene)tricarboxylchromium complexes, we have described the cleavage of aromatic carbon–oxygen⁸ and carbon–halogen^{9,10} bonds by carbon nucleophiles via ipso, cine,^{9a} and tele^{8b} nucleophilic aromatic substitutions (S_NAr). We decided to undertake the complete study of the

[®] Abstract published in *Advance ACS Abstracts*, February 1, 1995.

(1) (a) Silverthorn, W. E. *Adv. Organomet. Chem.* **1975**, *13*, 48. (b) Jaouen, G. *Ann. N.Y. Acad. Sci.* **1977**, *295*, 59. (c) Semmelhack, M. F. *Ann. N.Y. Acad. Sci.* **1977**, *295*, 36. (d) Jaouen, G. In *Transition Metal Organometallics in Organic Synthesis*; Alper, H., Ed.; Academic Press: New York, 1978; Vol. 2, p 65. (e) Davies, S. G. In *Organotransition Metal Chemistry, Applications to Organic Syntheses*; Pergamon Press: Oxford, U.K., 1982; p 166. (f) Watts, W. E. In *Comprehensive Organometallic Chemistry*; Pergamon Press: Oxford, U.K., 1982; Vol. 8, p 1013. (g) Solladie-Cavallo, A. *Polyhedron* **1985**, *4*, 901. (h) Kündig, E. P. *Pure Appl. Chem.* **1985**, *57*, 1855. (i) Kalinin, V. N. *Russ. Chem. Rev.* **1987**, *56*, 682. (j) Collman, J. P.; Hegedus, L. S.; Norton, J. R.; Finke, R. G. *Principles and Applications of Organotransition Metal Chemistry*; University Science Books; Mill Valley, CA, 1987; Vol. 20, p 921. (k) Balas, L.; Jhurry, D.; Latxaoue, L.; Grelier, S.; Morel, Y.; Handani, M.; Ardoin, N.; Astruc, D. *Bull. Soc. Chim. Fr.* **1990**, *127*, 401. (l) Mc Quillin, F. J.; Parker, D. G. N.; Stephenson, G. R. *Transition Metal in Organic Synthesis*; Cambridge University Press: New York, 1991; p 182. (m) Semmelhack, M. F. In *Comprehensive Organic Synthesis*; Trost, B. M., Ed.; Pergamon Press: Oxford, U.K., 1991; Vol. 4, p 517. (n) Rose-Munch, F.; Rose, E. *Trends in Organometallic Chemistry*; in press.

(2) (a) Trahanovsky, W. S.; Card, R. J. *J. Am. Chem. Soc.* **1972**, *94*, 2897. (b) Jaouen, G.; Top, S.; Mc Glinchley, M. J. *J. Organomet. Chem.* **1980**, *195*, C5. (c) Lebib, J.; Pelinski, L.; Maciejewski, L.; Brocard, J. *Tetrahedron* **1990**, *46*, 6011. (d) Davies, S. G.; Coote, S. J.; Goodfellow, C. L. *Advances in Metal–Organic Chemistry*; JAI Press Ltd: London, 1991; Vol. 2, p 1. (e) Senechal-Tocquer, M. C.; Senechal, D.; Le Bihan, J. Y.; Gentric, D.; Caro, B. *Bull. Soc. Chim. Fr.* **1992**, *129*, 121.

(3) (a) Holmes, J. D.; Jones, D. A.; Pettit, R. *J. Organomet. Chem.* **1965**, *4*, 324. (b) Trahanovsky, W. S.; Wells, D. K. *J. Am. Chem. Soc.* **1969**, *91*, 5870. (c) Top, S.; Jaouen, G. *J. Org. Chem.* **1981**, *46*, 78. (d) Reetz, M. T.; Sauerwald, M. *Tetrahedron Lett.* **1983**, *24*, 2837. (e) Davies, S. G.; Donohoe, T. J. *Synlett* **1993**, 323.

(4) See, for example: (a) Semmelhack, M. F.; Hall, H. T.; Farina, R.; Yoshifuji, M.; Clark, G.; Bargar, T.; Hirotsu, K. *J. Am. Chem. Soc.* **1979**, *101*, 3535. (b) Semmelhack, M. F.; Hall, H. T.; Yoshifuji, M.; Clark, G. *J. Am. Chem. Soc.* **1975**, *97*, 1247. (c) Semmelhack, M. F.; Hall, H. T.; Yoshifuji, M. *J. Am. Chem. Soc.* **1976**, *98*, 6387. (d) Kündig, E. P.; Desobry, V.; Simmons, D. P.; Wenger, E. *J. Am. Chem. Soc.* **1989**, *111*, 1804. (e) Kündig, E. P.; Ripa, A.; Liu, R.; Amurrio, D.; Bernardinelli, G. *Organometallics* **1993**, *12*, 3724.

(5) (a) Nesmeyanov, A. N.; Kolobova, N. E.; Anisimov, K. N.; Makarov, Yu. V. *Izv. Akad. Nauk. SSSR, Ser. Chim.* **1968**, 2665. (b) Semmelhack, M. F.; Bisaha, J.; Czarny, M. *J. Am. Chem. Soc.* **1979**, *101*, 768. (c) Ghavshou, M.; Widdowson, D. A. *J. Chem. Soc., Perkin Trans. 1* **1983**, 3065. (d) Kündig, E. P.; Grivet, C.; Spichiger, S. *J. Organomet. Chem.* **1987**, *332*, C13. (e) Lotz, S.; Schindehutte, M.; van Royen, P. H. *Organometallics* **1992**, *11*, 629. (f) van Royen, P. H.; Schindehutte, M.; Lotz, S. *Organometallics* **1992**, *11*, 1104.

(6) For a review, see: Sodeoka, M.; Shibasaki, M. *Synthesis* **1993**, 643.

(7) Alexakis, A.; Mangeney, P.; Marek, I.; Rose-Munch, F.; Rose, E.; Semra, A.; Robert, F. *J. Am. Chem. Soc.* **1992**, *114*, 8288.

(8) The term "tele substitution" is used in accordance with IUPAC recommendations to denote reactions in which the entering group takes up a position more than one atom away from the atom to which the leaving group is attached: Glossary of Terms used in Physical Organic Chemistry. Gold, V. Ed. *Pure Appl. Chem.* **1979**, *51*, 1725. (9) Boutonnet, J. C.; Rose-Munch, F.; Rose, E. *Tetrahedron Lett.* **1985**, *26*, 3989. (b) Rose-Munch, F.; Rose, E.; Semra, A. *J. Chem. Soc., Chem. Commun.* **1986**, 1108. (c) Boutonnet, J. C.; Rose-Munch, F.; Rose, E.; Semra, A. *Bull. Soc. Chim. Fr.* **1987**, 640.

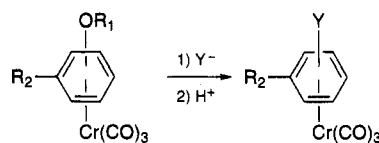
reactivity of (η^6 -arene)tricarbonylchromium complexes vs noncarbanionic nucleophiles such as H^- in order to shed light on the mechanism of the hydride nucleophilic aromatic substitution reaction (S_NAr).

Hydride addition to cationic π -arene-metal complexes occurs readily in the case of complexes such as $[(\eta^6\text{-arene})M(\text{CO})_3]^+$ ($M = \text{Mn},^{11a-e} \text{Re}^{11f,g}$), $[(\eta^6\text{-arene})\text{Mn}(\text{CO})_2\text{L}]^+$,¹² ($L = \text{CH}_3\text{CN}, \text{PR}_3$), $[(\eta^6\text{-arene})(\eta^5\text{-cyclopentadienyl})\text{Fe}]^+$,¹³ $[(\eta^6\text{-arene})\text{V}(\text{CO})_4]^+$,¹⁴ $[(\eta^6\text{-arene})\text{Cr}(\text{CO})_2\text{NO}]^+$,¹⁵ $[(\eta^6\text{-arene})_2\text{M}]^{2+}$ ($M = \text{Fe},^{16a,b} \text{Ru}^{16a,c,d}$), and $[(\eta^6\text{-arene})(\eta^5\text{-pentamethylcyclopentadienyl})\text{Ir}]^{2+}$,¹⁷ the major products obtained being neutral or monocationic η^5 -cyclohexadienyl complexes. In the case of chromium derivatives, we recently reported that hydrides such as LiEt_3BH react with alkoxy,^{18a,d} halogeno,^{18b} and dimethylamino^{18c} arenetricarbonylchromium complexes via ipso, cine, and tele nucleophilic aromatic substitution. Herein, we report the full details of this study¹⁹ along with further explorations of the chemistry of tricarbonyl- (η^5 -cyclohexadienyl)chromium complexes.

Results and Discussion

Preparation of Complexes. (η^6 -Arene)tricarbonylchromium complexes were synthesized by using the standard procedure of thermolysis of $\text{Cr}(\text{CO})_6$ in presence of the free arenes.²⁰ Purification by flash chromatography and recrystallization afforded air-stable yellow

Table 1. Products Obtained by Addition of a Hydride to Alkoxy- or Methoxyarene Tricarbonylchromium Complexes



(a) LiEt_3BH ; (b) LiEt_3BD ; (c) HCl ; (d) $\text{CF}_3\text{CO}_2\text{H}-\text{THF}$; (e) H_2O

substrate	OR ₁	R ₂	Y ⁻	H ⁺	products	Y	yield (%)	entry
1	<i>m</i> -OMe	Et	a	e or f	2a	H	100	1
1	<i>m</i> -OMe	Et	b	e or f	2b	<i>m</i> -D	100	2
3a	<i>o</i> -OMe	SiMe ₃	a	f	4	H	71	3
3b	<i>o</i> -OPh	SiMe ₃	a	f	4	H	76	4
3a	<i>o</i> -OMe	SiMe ₃	b	f	4- <i>p</i>	<i>p</i> -D	71	5
3b	<i>o</i> -OPh	SiMe ₃	b	f	4- <i>p</i>	<i>p</i> -D, <i>o</i> -D	76	6
5	<i>o</i> -OPh	Me	a	f	6	H	55	7
7a	<i>o</i> -OMe	‘Bu	a	h	8	H	34	8
7b	<i>m</i> -OMe	‘Bu	a	h	8	H	66	9
7c	<i>p</i> -OMe	‘Bu	a	h	8	H	83	10
7a	<i>o</i> -OMe	‘Bu	b	f or h	8- <i>o</i>	<i>o</i> -D	34	11
7b	<i>m</i> -OMe	‘Bu	b	f	8- <i>m</i> , 8- <i>p</i>	<i>m</i> -D, <i>p</i> -D	77 (84:16)	12
7c	<i>p</i> -OMe	‘Bu	b	f or h	8- <i>p</i>	<i>p</i> -D	83	13

crystals of complexes **1**, **7a**, **7b**, **7c**, **9**, **13**, **14**, **15**, **16**, **18**,^{8c} and **23**.^{9d} Complexes **3a**, **3b**, **5**,^{8c} **20**, **22**, and **29**^{9f} were obtained by lithiation of [η^6 -chloro-, -fluoro-, -phenoxy- or -(*N,N*-dimethylamino)benzene]tricarbonylchromium with *n*-BuLi followed by treatment with an electrophile (Me_3SiCl , (*i*-Pr)₃SiCl, MeI).

¹H and ¹³C NMR Spectra.²¹ The ¹H and ¹³C NMR spectra of the new complexes showed the usual upfield shift of the aromatic proton and carbon resonances with respect to those of the corresponding free arenes. Spectra were assigned through a combination of peak multiplicities, chemical shifts, coupling constants analyses, and ¹³C-¹H two-dimensional correlation experiments. Complete data are reported in the experimental section.

Addition of Lithium Triethylborohydride to Alkoxy and Aryloxy Arenetricarbonylchromium Complexes. LiEt_3BH was added to a refluxing THF solution of (η^6 -3-ethylanisole) $\text{Cr}(\text{CO})_3$ (**1**). After refluxing the reaction mixture for 2 h and treating the solution with aqueous HCl, (η^6 -ethylbenzene) $\text{Cr}(\text{CO})_3$ (**2a**) was recovered quantitatively (Table 1, entry 1). In order to determine the regioselectivity of the addition of this hydride to the arene ring, we undertook the same experiment with LiEt_3BD . Thus, complex **1** yielded quantitatively (η^6 -3-(deuterioethyl)benzene) $\text{Cr}(\text{CO})_3$, complex **2b** (Table 1, entry 2).

Knowing that cine^{9a} and/or tele⁸ nucleophilic aromatic substitution could occur by adding a carbon nucleophile to a chromium complex, the last experiment (Table 1, entry 1) could not ascertain whether the hydride added on the carbon bearing the methoxy group (ipso addition) or on the carbon meta to the methoxy group (tele-meta addition).^{8a} Consequently, we undertook the study of the reaction of complex **1** with LiEt_3BD by ¹H NMR spectroscopy. Addition of a THF-*d*₈ solution of LiEt_3BD (2 equiv) to complex **1** at room temperature led, without any acidic treatment, to the slow in situ formation of the deuterated ethylbenzene complex. This proves that the displacement of the methoxy group occurred via an ipso S_NAr process. These results provide relevant information about the capability of

(21) Van Meurs, F.; Van der Toorn, J. M.; Van Bekkum, M. J. *Organomet. Chem.* **1976**, *113*, 341.

(9) The term "cine substitution" is used in accordance with IUPAC recommendations to denote reactions in which the entering group takes up a position ortho to the leaving group: (a) Rose-Munch, F.; Rose, E.; Semra, A. *J. Chem. Soc., Chem. Commun.* **1986**, 1551. (b) Rose-Munch, F.; Rose, E.; Semra, A. *J. Chem. Soc., Chem. Commun.* **1987**, 942. (c) Rose-Munch, F.; Rose, E.; Semra, A.; Jeannin, Y.; Robert, F. *J. Organomet. Chem.* **1988**, *353*, 53. (d) Rose-Munch, F.; Rose, E.; Semra, A.; Bois, C. *J. Organomet. Chem.* **1989**, *363*, 103. (e) Rose-Munch, F.; Rose, E.; Semra, A.; Philoche, A. *J. Organomet. Chem.* **1989**, *363*, 123. (f) Rose-Munch, F.; Rose, E.; Semra, A.; Mignon, L.; Garcia-Orcaiza, J.; Knobler, C. *J. Organomet. Chem.* **1989**, *363*, 297. (g) Rose-Munch, F.; Rose, E.; Semra, A. *J. Organomet. Chem.* **1989**, *377*, C9.

(10) (a) Khourzom, R.; Rose-Munch, F.; Rose, E. *Tetrahedron Lett.* **1990**, *31*, 2011. (b) Rose-Munch, F.; Aniss, K.; Rose, E. *J. Organomet. Chem.* **1990**, *385*, C1. (c) Rose-Munch, F.; Aniss, K.; Vaisserman, J. *J. Organomet. Chem.* **1991**, *415*, 223. (d) Rose-Munch, F.; Khourzom, R.; Djukic, J.-P.; Rose, E. *J. Organomet. Chem.* **1993**, *456*, C8. (e) Rose-Munch, F.; Khourzom, R.; Djukic, J. P.; Perrotey, A.; Rose, E.; Brocard, J. *J. Organomet. Chem.* **1994**, *467*, 195.

(11) (a) Winkhaus, G.; Pratt, L.; Wilkinson, G. *J. Chem. Soc.* **1961**, 3807. (b) Khand, I. U.; Pauson, P. L.; Watts, W. E. *J. Chem. Soc. C* **1969**, 116. (c) Pauson, P. L.; Segal, J. A. *J. Chem. Soc., Dalton Trans.* **1975**, 1683. (d) Sweigart, D. A. *Synlett* **1991**, 369. (e) Morken, A. M.; Eyman, D. P.; Wolff, M. A.; Schauer, S. J. *Organometallics* **1993**, *12*, 725. (f) Bird, P. H.; Churchill, M. R. *J. Chem. Soc., Chem. Commun.* **1967**, 777. (g) Pike, R. D.; Ryan, W. J.; Lennhoff, N. S.; Epp, J. N.; Sweigart, D. *J. Am. Chem. Soc.* **1990**, *112*, 4798.

(12) (a) Pike, R. D.; Carpenter, G. B. *Organometallics* **1993**, *12*, 1416. (b) Synder, D. B.; Schauer, S. J.; Eyman, D. P.; Moler, J. L.; Weers, J. *J. Am. Chem. Soc.* **1993**, *115*, 6718.

(13) (a) Khand, I. U.; Pauson, P. L.; Watts, W. E. *J. Chem. Soc. C* **1969**, 2024. (b) Astruc, D. *Tetrahedron* **1983**, *39*, 4027.

(14) Calderazzo, F. *Inorg. Chem.* **1966**, *5*, 429.

(15) Connelly, N. G.; Kelly, R. L. *J. Chem. Soc., Dalton Trans.* **1974**, 2334.

(16) (a) Munro, G. A. M.; Pauson, P. L. *Z. Anorg. Allg. Chem.* **1979**, *458*, 211. (b) Madonik, A. M.; Mandon, D.; Michaud, P.; Lapinte, C.; Astruc, D. *J. Am. Chem. Soc.* **1984**, *106*, 3381. (c) Elsegood, M. R. J.; Steed, J. W.; Tocher, D. A. *J. Chem. Soc., Dalton Trans.* **1992**, 1797. (d) Steed, J. W.; Tocher, D. A. *J. Chem. Soc. Dalton Trans* **1993**, 3187.

(17) Hackett, S. C.; Angelici, R. *J. Organometallics* **1988**, *7*, 1491.

(18) (a) Rose-Munch, F.; Djukic, J.-P.; Rose, E. *Tetrahedron Lett.* **1990**, *31*, 2589. (b) Djukic, J.-P.; Geysersmans, P.; Rose-Munch, F.; Rose, E. *Tetrahedron Lett.* **1991**, *32*, 6703. (c) Djukic, J. P.; Rose-Munch, F.; Rose, E. *J. Chem. Soc., Chem. Commun.* **1991**, 1634. (d) For other dealkoxylation reactions using LiAlH_4 , see: Persson, M.; Hackzell, V.; Csoregh, I. *J. Chem. Soc., Perkin Trans.* **1991**, 1453.

(19) Djukic, J.-P.; Rose-Munch, F.; Rose, E.; Dromzee, Y. *J. Am. Chem. Soc.* **1993**, *115*, 6434.

(20) Mahaffy, C. A. L.; Pauson, P. L. *Inorg. Synth.* **1979**, *19*, 154.

hydride to add at a substituted position of the complexed arene although it is strongly disfavored by steric and electronic interactions.

We decided to carry out further investigations on the regioselectivity of the hydride addition in the case of ortho-disubstituted complexes. $[\eta^6\text{-2-(Trimethylsilyl)anisole}]\text{Cr}(\text{CO})_3$ (**3a**) was chosen. Treatment of **3a** with LiEt_3BD , followed by acidification of the reaction medium yielded $[\eta^6\text{-4-deuterio(trimethylsilyl)benzene}]\text{Cr}(\text{CO})_3$ (**4-p**; 71% yield) (Table 1, entry 5). In order to see whether this reaction could occur in the case of phenoxy-substituted derivatives, we carried out the same experiment with $(\eta^6\text{-2-methylphenoxybenzene})\text{Cr}(\text{CO})_3$ (**5**) and we obtained $(\eta^6\text{-toluene})\text{Cr}(\text{CO})_3$ (**6**; 55% yield) (Table 1, entry 7). $[\eta^6\text{-2-(Trimethylsilyl)phenoxybenzene}]\text{Cr}(\text{CO})_3$ (**3b**) reacted with LiEt_3BH at 67 °C for 24 h to yield, after $\text{CF}_3\text{CO}_2\text{H}$ treatment, the (trimethylsilyl)benzene derivative **4** (76% yield) (Table 1, entry 4). When a deuteride source was used, the ratio between the deuterio isomers was easy to determine by ^1H NMR spectroscopy; in all cases the para-deuterated isomer **4-p** (tele-meta $\text{S}_{\text{N}}\text{Ar}$ product) was the major product even though contaminated with the ortho-deuterated isomer **4-o** (15-25%) (Table 1, entry 6). $(\eta^6\text{-tert-Butylanisole})\text{Cr}(\text{CO})_3$ (**7a**) reacted with LiEt_3BD (2 equiv) in THF at 67 °C for 18 h and yielded, after $\text{CF}_3\text{CO}_2\text{H}$ treatment or hydrolysis, the ortho-deuterated *tert*-butylbenzene derivative **8-o** (34% yield) along with the starting complex (60% recovered) (Table 1, entry 11). With the meta isomer **7b**, using similar experimental procedures, complexes **8-m** and **8-p** were obtained in a ratio of 84:16 (77% overall yield) after CF_3COOH treatment (entry 12). With the para isomer **7c**, the reaction with LiEt_3BD followed by a CF_3COOH treatment or hydrolysis led to the complex **8-p** only (83% yield) (entry 13).

It is worth noting that if complex **7c** is treated at room temperature for 1 h with LiEt_3BD and the resulting medium with $\text{CF}_3\text{CO}_2\text{H}$ (5 equiv), the major product is the ortho-deuterated *tert*-butylbenzene derivative **8-o**, the starting complex **7c** being recovered in large amounts (**8-o**:**8-p**:**7c** = 21:7:72). After 6 h at room temperature, the ratio **8-o**:**8-p**:**7c** is 8:40:52. This clearly indicates the reversible character of the hydride addition and means that formation of the para isomer is favored at longer reaction times vs that of the ortho isomer. The evolution of the reaction medium composition was easy to follow by ^1H NMR, after treatment of aliquots with $\text{CF}_3\text{CO}_2\text{H}$, since the aromatic protons of the *tert*-butylbenzene derivative produced resonate at very different fields. These results are reproduced in Figure 1. If LiEt_3BD (2 equiv) and $\text{CF}_3\text{CO}_2\text{H}$ (5 equiv) are used, **8-p** is obtained in 83% yield (Table 1, entry 13).

Scheme 1 displays a mechanism for the reversible addition of hydride to an unsubstituted position at the complexed ring. Compound **8-o**, which is favored early in the reaction, results from the protonation of an anionic η^5 -cyclohexadienyl intermediate formed from the reversible addition of deuteride at the meta position with respect to the methoxy group. The latter evolves by successive isomerizations involving putative fluxional chromium-hydride species^{16d,22} that give ultimately, after MeOH elimination, the rearomatization product **8-o**. As proposed elsewhere, the rearomatization process can be the driving step of this process that allows

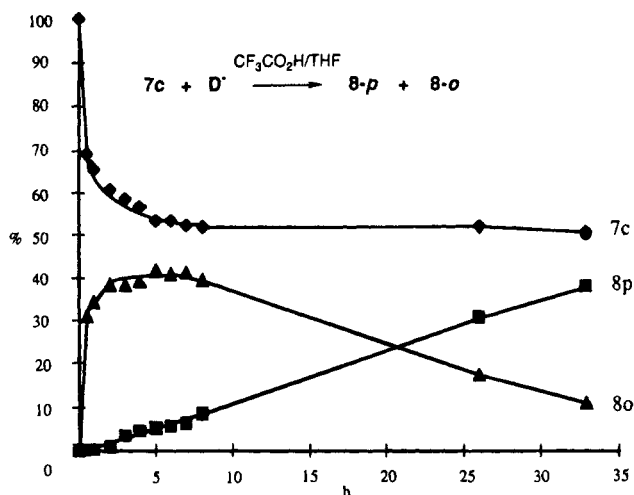
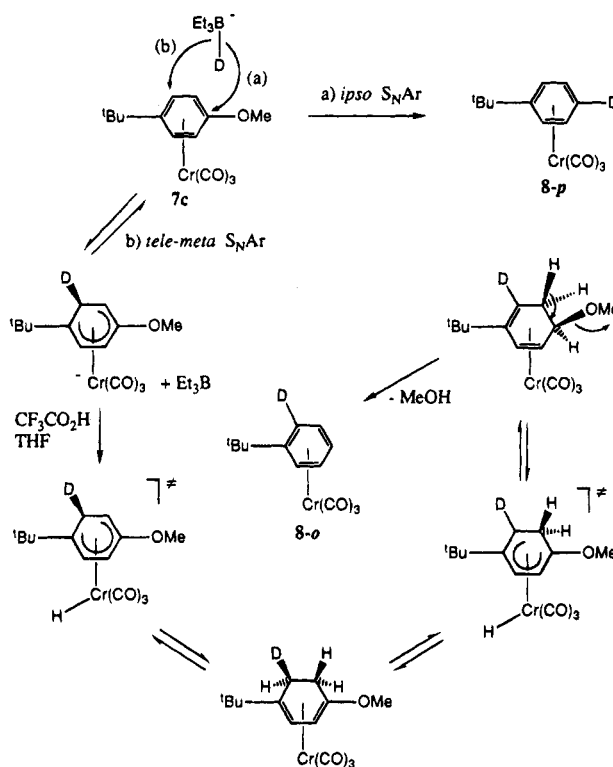


Figure 1. Addition of LiEt_3BD to **7c** (1:1): evolution of the reaction medium composition (molar percent) after quenching with $\text{CF}_3\text{CO}_2\text{H}$ vs time.

Scheme 1



the recovery of an arene-chromium complex without loss of the tricarbonylchromium moiety.^{8c} Several groups^{4d,23-25} noticed that under kinetic control the electronic effects of the arene substituents can influence the regiochemistry of nucleophilic additions. But we have proposed^{25a} that the conformation of the $\text{Cr}(\text{CO})_3$ tripod can control the regiochemistry of the nucleophilic

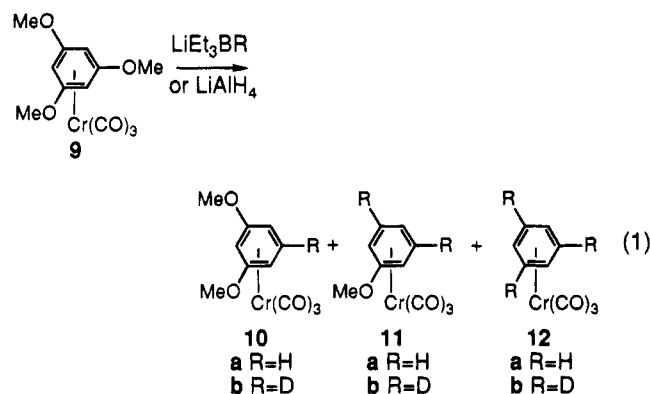
(22) Several examples of such fluxional organometallic complexes have been reported previously; for key references, see: (a) Brookhart, M.; Lamanna, W.; Humphrey, M. B. *J. Am. Chem. Soc.* **1982**, *104*, 2117. (b) Brookhart, M.; Lamanna, W.; Pinhas, A. R. *Organometallics* **1983**, *2*, 638. (c) Brookhart, M.; Lukacs, A. *Organometallics* **1983**, *2*, 649. (d) Swann, R. T.; Hanson, A. W.; Boekelheide, V. *J. Am. Chem. Soc.* **1986**, *108*, 3324. (e) Kreiter, C. G. *Adv. Organomet. Chem.* **1986**, *26*, 297. (f) Kündig, E. P.; Amurrio, D.; Bernardinelli, G.; Chowdhury, R. *Organometallics* **1993**, *12*, 4275.

(23) Semmelhack, M. F.; Clark, G.; Farina, R.; Saeman, M. *J. Am. Chem. Soc.* **1979**, *101*, 217.

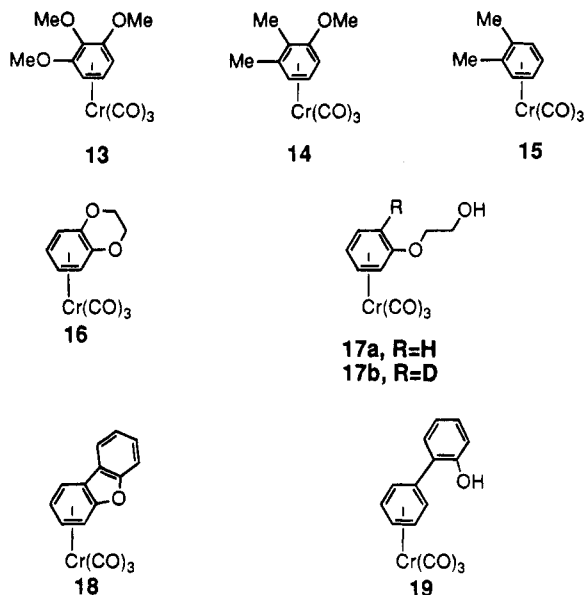
(24) Albright, T. A.; Carpenter, B. K. *Inorg. Chem.* **1980**, *19*, 3092.

attack so that Cr-CO bond eclipsed positions at the arene ring are favored. Thus, in the case of complex **7c**, it is reasonable to define the anionic η^5 -cyclohexadienyl adduct as the kinetic product of the addition of D^- as well as the precursor of **8-o**, which is created by the subsequent protonation-elimination reaction. Under similar experimental conditions, the three complexes **7a**, **7b**, and **7c** yielded only the ipso S_NAr products **8-o** (34% yield), **8-m** (66% yield) and **8-p** (83% yield) along with the corresponding starting complexes when the reaction media were hydrolyzed with acidic water rather than treated with a solution of trifluoroacetic acid in tetrahydrofuran (Table 1, entries 8-10).

We decided to study these alkoxy and aryloxy group displacement reactions with different trisubstituted complexes and particularly with trimethoxyarene derivatives. In the case of (η^6 -1,3,5-trimethoxybenzene)- $Cr(CO)_3$ (**9**), it was not necessary to heat the reaction mixture. Even at room temperature, it was possible to monodemethoxylate the arene ring, the major product being (η^6 -1,3-dimethoxybenzene) $Cr(CO)_3$ (**10a**) (**10b** for the 5-deuterio analog of **10a**, 73% yield, eq 1). Of course, heating the reaction mixture with an excess of hydride yielded quantitatively (η^6 -benzene) $Cr(CO)_3$ (**12**) (this reaction occurs with $LiAlH_4$ as well).

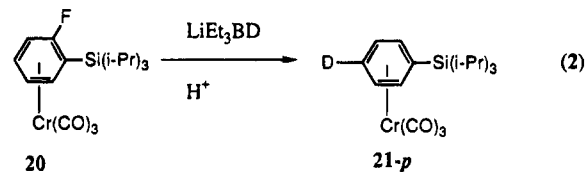


In the case of the trisubstituted trimethoxyarene complex **13**, the major product can be the anisole derivative **11a**. Indeed, treatment of (η^6 -1,2,3-trimethoxybenzene) $Cr(CO)_3$ (**13**) with an excess of $LiEt_3BD$ yielded as major products the dideuterated anisole derivatives respectively deuterated at the 2, 6 and 2, 3 positions. Similarly, treatment of (η^6 -2,3-dimethylanisole) $Cr(CO)_3$ (**14**) with $LiEt_3BH$ yielded the *o*-xylene complex **15** (47% yield). Complexed phenyl-substituted oxygenated heterocycles were studied in order to verify the possibility of ring-opening reactions by a hydride treatment. For instance, (η^6 -benzodioxane) $Cr(CO)_3$ (**16**) underwent ring opening when treated with $LiEt_3BH$, yielding a mixture of **17a** (33% yield) and **12a** (10% yield). $LiEt_3BD$ treatment afforded, via an ipso S_NAr , the complex **17b** deuterated at the position ortho to the ether group. In addition, we noticed that no nucleophilic addition oc-



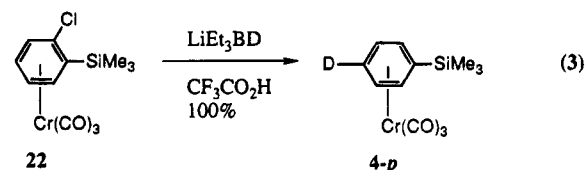
curred on the ethylene fragment. Another example was obtained with the dibenzofuran complex **18**. Using the same experimental procedure, we isolated complex **19** (75% yield).

Addition of Lithium Triethylborohydride to (η^6 -Halogenoarene) $Cr(CO)_3$ Complexes. Addition of deuteride to [η^6 -2-fluoro(triisopropylsilyl)benzene] $Cr(CO)_3$ (**20**) at $-78^\circ C$ followed by CF_3CO_2H treatment gave a red solution which slowly became yellow (eq 2).



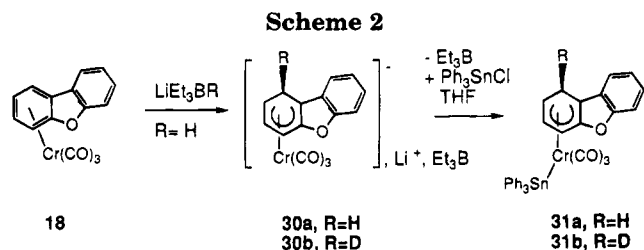
After recrystallization, [η^6 -4-deuterio(triisopropylsilyl)benzene] $Cr(CO)_3$ (**21-p**) was obtained via a tele-meta S_NAr reaction (86% yield). When water was used instead of CF_3CO_2H , complex **21-p** was recovered in 60% yield. Similar experiments carried out with the trimethylsilyl analog of **20** yielded not only the hydrodefluorination product but also some benzene complex resulting from the displacement of both the fluoride and trimethylsilyl groups induced by the CF_3CO_2H treatment.

We undertook the study of the behavior of hydrides toward [η^6 -2-chloro(trimethylsilyl)benzene] $Cr(CO)_3$ (**22**); trimethylsilylbenzene derivative **4-p**, deuterated at the para position via a tele-meta S_NAr was obtained quantitatively (eq 3). In the case of *p*-chlorotoluene



derivative **23**, $LiAlD_4$ reacted at room temperature to yield quantitatively, after CF_3CO_2H treatment, toluene derivatives **6-o** and **6-m** respectively deuterated at the ortho and meta positions (34:66) according to NMR spectra, via cine and tele-meta S_NAr (Table 2, entry 1). Using $LiEt_3BD$ instead of $LiAlD_4$ (Table 2, entry 2),

(25) (a) Boutonnet, J. C.; Mordenti, L.; Rose, E.; Le Martret, O.; Precigoux, G. *J. Organomet. Chem.* **1981**, *221*, 147. (b) Uemura, M.; Minami, T.; Shinoda, Y.; Nishimura, H.; Shiro, M.; Hayashi, Y. *J. Organomet. Chem.* **1991**, *406*, 371. (c) The protons meta to the amino group resonate at the lowest field 5.69 ppm in $CDCl_3$ and the anti eclipsed ortho protons resonate at higher field (4.68 ppm in $CDCl_3$). The ortho and meta protons of the corresponding free arene resonate respectively at 6.73 and 7.27 ppm in $CDCl_3$; it is worth noting the relatively stronger shielding of the noneclipsed aromatic protons (2.05 ppm) vs that of the eclipsed protons (1.58 ppm).



studied the reaction using LiEt₃BD and CF₃CO₂D and obtained, as expected, the 3,4-dideuterated trimethylsilylbenzene derivative, **4-m, p** (entry 6).

Tricarbonyl(η^5 -cyclohexadienyl)chromium Complexes. Although the parameters that drive the kinetic control of nucleophilic attack on (η^6 -arene)tricarbonylchromium complexes are rather well understood, there is a lack of data for the factors determining thermodynamically controlled reactions. These latter reactions are mainly driven by the stability of the adducts, e.g., the anionic tricarbonyl(η^5 -cyclohexadienyl)chromium complexes.^{26,28a,28c} The stability of such intermediates is likely to be determined by the electronic distribution and steric interactions. We were interested in investigating a few (η^5 -cyclohexadienyl) complexes in order to understand their properties.

We reported previously that the addition of LiEt₃BR on (η^6 -dibenzofuran)Cr(CO)₃ yielded, after the removal of both Et₃B and solvents, the anionic adducts **30a** and **30b** as yellow amorphous powders (Scheme 2).¹⁹ The same reaction carried out for 48 h afforded, after hydrolysis, the biphenyl derivative **19** resulting from the cleavage of the C_{Ar}-O bond via an ipso S_NAr reaction. The anionic intermediates **30** trapped with Ph₃SnCl gave the bimetallic complexes **31**; single-crystal X-ray diffraction of **31a** provided the first molecular structure of a hetero-disubstituted tricarbonyl(η^5 -cyclohexadienyl)triphenyltinchromium(II) (Sn-Cr) complex.¹⁹

The ¹³C NMR (CDCl₃, 50 MHz) spectrum, performed at room temperature, showed a large unresolved signal in the carbonyl resonance zone at approximately 231 ppm.¹⁹ At low temperature (213 K), a ¹³C NMR experiment (75 MHz) carried out in the same solvent revealed three well-defined resonances at 238.87, 230.73 and 223.76 ppm, accounting for the three differentiated carbonyl ligands. This indicates that, on the NMR time scale at this temperature, the triphenyltintricarbonylchromium moiety rotates very slowly. Unfortunately, we were not able to observe the coalescence of these signals at higher temperatures in part because of an important line-broadening effect and mainly because of decomposition. Variable-temperature ¹H NMR experiments monitored from 213 to 343 K did not show any significant temperature-related shifts of the resonances of the main complex **31**.

The formation of complex **30a** is the result of the reversible addition of hydride on complex **18**. Indeed, it undergoes an isomerization at longer reaction times that leads to C_{Ar}-O bond ipso cleavage and the formation of complex **19**. This isomerization is likely to be caused by the triethylborane released from the reaction of LiEt₃BH with the starting complex **18**. A further evidence of the reversibility of the hydride addition is given by the hydride transfer reaction occurring stoichiometrically between the pure anionic complex **32a** and the cationic (η^6 -benzene)tricarbonylmanganese com-

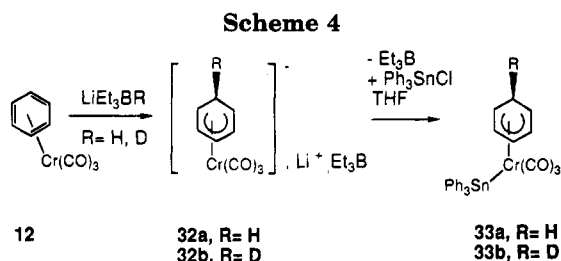
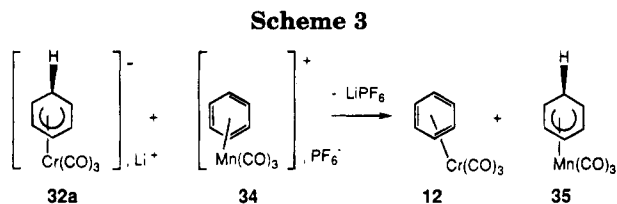


Table 4. ¹H NMR Data of Anionic Complexes **30a** and **32a** and of Bimetallic Complexes **31a** and **33a** (Chemical Shifts Expressed in δ (ppm))

	H _{1exo}	H _{1endo}	H ₂	H ₃	H ₄	H ₅	H ₆
30a ^a	2.76	3.59	2.63	4.57	5.63		
32a ^a	2.58 ^d	2.85 ^e	2.53	4.74	5.43	4.74	2.53
31a ^b	2.80	4.06	3.42	3.88	6.71		
33a ^c	1.60 ^f	2.43 ^g	2.60 ^h	3.72 ⁱ	6.06 ^j	3.72	2.60

^a THF-*d*₈. ^b C₆D₆. ^c CDCl₃. ^d d, *J*_{gem} = 11 Hz. ^e dt, *J*_{gem} = 11 Hz, ³*J* = 6 Hz. ^f d, *J*_{gem} = 13 Hz. ^g dt, *J*_{gem} = 13 Hz, ³*J* = 6 Hz. ^h t, ³*J* = 6 Hz. ⁱ t, ³*J* = 5 Hz. ^j t, ³*J* = 5 Hz.

plex **34** (Scheme 3).²⁹ A 50:50 mixture of complex **12** and neutral tricarbonyl(η^5 -cyclohexadienyl)manganese (**35**) is obtained as a result of hydride transfer from complex **32a** to the electrophilic complex **34**.¹⁹

Treatment of (η^6 -benzene)Cr(CO)₃ (**12**) with LiEt₃BR (R = H, D) in THF gave the lithium salts of the anionic tricarbonyl(η^5 -cyclohexadienyl)chromium complexes **32a** (R = H) and **32b** (R = D) (Scheme 4). Trapping the anionic complexes **32a** and **32b** with Ph₃SnCl yielded the neutral bimetallic complexes **33a** and **33b**. Selected ¹H NMR data of anionic complexes **30** and **32** and those of bimetallic complexes **31** and **33** are reported in Table 4.

¹H and ¹³C NMR data confirm that the nucleophilic addition of hydride or deuteride occurred on the exo side of the complexed arene, for example the H_{1exo} resonance at 1.60 ppm of the deuterated complex **32a** is absent and the C1 resonance at 25.8 ppm is a relatively weak triplet with a ¹J_{C-D} coupling constant of 20 Hz.

X-ray Single-Crystal Structure Analysis of **33b.** Figures 2 and 3 show ORTEP diagrams of complex **33b** molecular structure with the atom-numbering scheme. Relevant bond lengths and angles are listed in Table 5.

Complex **33b** has the usual η^5 -bonded cyclohexadienyl structure described for other complexes that have been published^{19,4a,30} (Figure 4). The bimetallic moiety Ph₃SnCr(CO)₃ is approximately symmetrically oriented with respect to a plane perpendicular to and bisecting the cyclohexadienyl ligand through C4 and C1. The five cyclohexadienyl sp² carbons are contained in a mean plane (maximum deviation of 0.023 Å). The interplanar

(29) A series of anionic tricarbonyl(η^5 -cyclohexadienyl)chromium complexes have been prepared and their reactivities studied with various electrophiles; see Reference 4a.

(30) One similar neutral complex, **36**, has been isolated and characterized by X-ray diffraction analysis: Kündig, E. P.; Cunningham, A. F.; Paglia, P.; Simmons, D. P.; Bernardinelli, G. *Helv. Chim. Acta* **1990**, *73*, 386.

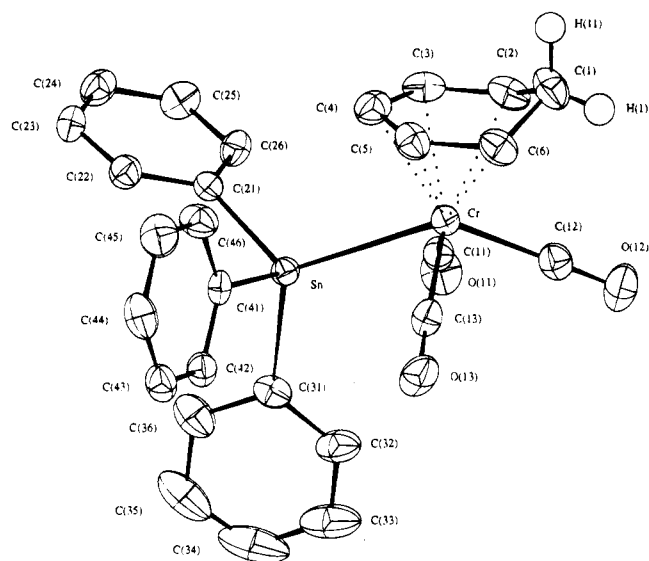


Figure 2. ORTEP diagram of the molecular structure of complex **33b** and the atom numbering.

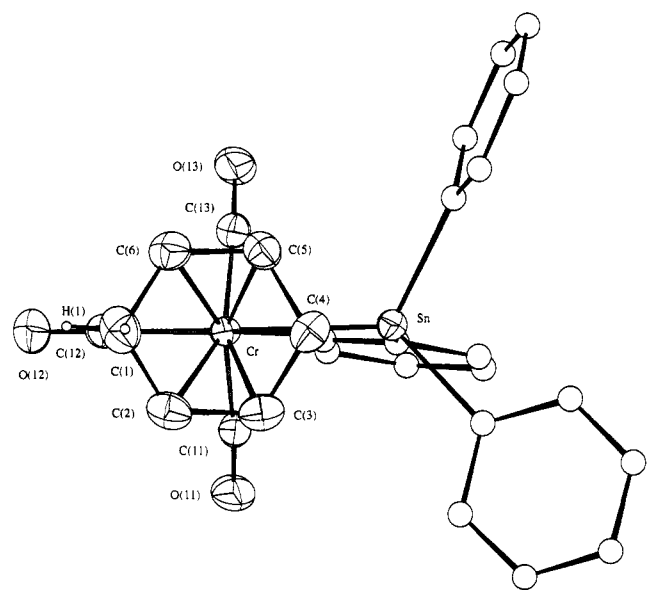


Figure 3. Projection of the cyclohexadienyl ring of **33b** on the plane formed by the three carbonyl oxygen atoms.

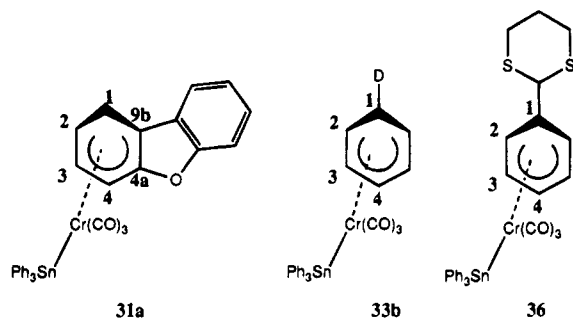


Figure 4. Developed formulas of reported substituted neutral $(\eta^5\text{-cyclohexadienyl})(\text{CO})_3\text{Cr-Sn}(\text{C}_6\text{H}_5)_3$ complexes.

angle between the five cyclohexadienyl carbons and the C1–C2–C3 plane is 39.2° in the range of values observed for other $\eta^5\text{-cyclohexadienyl}$ complexes but slightly more open than for **31a** ($32.5(5)^\circ$) and **36**³⁰ (35.1°). Metal–ligand bond lengths can be compared to the two other structures **36** and **31a**¹⁹ described in the literature (Figure 4).

Table 5. Selected Structural Data for Complexes **33b**, **36**, and **31b**

	33b	36 ^a	31b
Bond Distances (Å)			
Cr–(C2)	2.276(6)	2.278(10)	2.28(1)
Cr–(C3)	2.191(6)	2.187(9)	2.20(1)
Cr–(C4)	2.193(6)	2.179(9)	2.18(1)
Cr–(C5)	2.187(6)	2.194(10)	
Cr–(C6)	2.280(6)	2.304(9)	
Cr–Sn	2.713(1)	2.719(2)	2.722(2)
Cr–(C4a)			2.249(9)
Cr–(C9b)			2.41(1)
Cr–CO	1.87	1.85	1.83
(C1)–(C2)	1.51(1)	1.507(12)	1.50(2)
(C1)–(C9b)			1.50(2)
(C2)–(C3)	1.37(1)	1.400(14)	1.38(2)
(C3)–(C4)	1.397(9)	1.409(15)	1.46(2)
(C4)–(C4a)			1.39(1)
(C4a)–(C9b)			1.40(1)
(C1)–(C6)	1.51(1)	1.507(14)	
(C4)–(C5)	1.407(9)	1.411(13)	
(C5)–(C6)	1.370(9)	1.407(15)	
Bond Angles (deg)			
(C2)–(C1)–(C6)	102.7(5)	104.0(8)	
(C2)–(C1)–(C9b)			104.5(9)

^a See ref 30.

Table 5 shows a comparison of selected data of the three complexes. The average of Cr–CO distances in **31a** (1.83 Å) is slightly smaller than in **36** (1.85 Å) and **33b** (1.87 Å). Indeed, the average distance between the Cr atom and C2, C3, C4, and C4a carbons is 2.23 Å and that to C9b is 2.41 Å. This latter longer Cr–C9b distance can be attributed to the disubstituted nature of the $\eta^5\text{-cyclohexadienyl}$ ligand in **31a** and reflects the steric strain between the organic and the bimetallic fragments. Indeed, in the case of complexes **36** and **33b**, the average distance between the chromium atom and the five pentadienyl-like carbons is 2.23 Å. The longest and the shortest Cr–C distances for **33b** are 2.30 (Cr–C6) and 2.18 (Cr–C4) Å.

Concluding Remarks

In conclusion, these results show that nucleophilic aromatic substitutions of alkoxy, aryloxy, halogeno, and dimethylamino groups by hydride occur if the corresponding substituted arenetricarbonylchromium complexes are treated with lithium triethylborohydride followed by treatment with acid. Depending on the nature of the substituted arene complex, hydrides can displace these various groups via ipso, cine, and tele nucleophilic aromatic substitution pathways. Usually these reactions are performed by stepwise addition of a hydride and an acid. In some cases, water is acidic enough to protonate the anionic $\eta^5\text{-cyclohexadienyl}$ intermediates. The unprecedented carbon–nitrogen and carbon–oxygen bond cleavage reactions can be of interest in organic synthesis. The reversibility of the addition of hydrides has been clearly demonstrated in the case of the dibenzofuran complex as well as in the case of a *p*-methoxy-*tert*-butylbenzene complex. The carbon–halogen bond cleavage that occurs readily under different conditions is also of interest for the regioselective synthesis of deuterated aromatic compounds and the use of the latter as labeled substrates in biochemistry. Finally, in two cases, the anionic $\eta^5\text{-cyclohexadienyl}$ complexes have been trapped by Ph_3SnCl giving rise to bimetallic air-stable complexes. Further study of their reactivity and structural properties is underway and will be the subject of a subsequent article.

Experimental Section

All reactions were carried out under a dry nitrogen atmosphere. All experiments involving (η^6 -arene)tricarbonylchromium complexes were always protected from exposure to light and oxygen. All air-sensitive tricarbonyl(η^6 -cyclohexadienyl)chromium complexes were handled inside a glovebox under a continuous flow of dry and purified nitrogen. Solvents used for these very reactive complexes were distilled over sodium-benzophenone ketyl anion and degassed by three freeze-pump-thaw cycles. Tetrahydrofuran (THF) and di-*n*-butyl ether (DBE) were dried over sodium-benzophenone ketyl anion under dry nitrogen atmosphere and distilled just before use. Deuterated solvents and sample tubes were purged with dry nitrogen to remove oxygen. (η^6 -3-Ethylanisole)tricarbonylchromium (**1**), (η^6 -anisole)tricarbonylchromium (**11**), complex **16**, tricarbonyl(η^6 -diphenyl ether)chromium, tricarbonyl(η^6 -2-methylphenyl phenyl ether)chromium (**5**), tricarbonyl(η^6 -dibenzofuran)chromium (**18**), tricarbonyl(η^6 -4-chlorotoluene)chromium (**23**), tricarbonyl(η^6 -4-fluorotoluene)chromium (**24**), tricarbonyl(η^6 -chlorobenzene)chromium, and tricarbonyl(η^6 -fluorobenzene)chromium were prepared according to standard procedures. (*N,N*-Dimethylamino)arenes, giving complexes **25**, **27**, **28**, and **29** after complexation, were obtained from aniline using a direct method of *N*-dimethylation with trimethyl phosphate.

Products were separated by flash chromatography on silica gel column (15 or 60 μ m) under a dry atmosphere nitrogen pressure (1 atm). Diethyl ether and petroleum ether (PE) were used as solvent for elution. Triethylborohydride and triethylborodeuteride THF solutions were purchased from Aldrich Chemical Co.

^1H and ^{13}C NMR spectra were acquired on a Brücker AC 200 (resonance frequencies: 200 MHz for ^1H and 50 MHz for ^{13}C) spectrometer and chemical shifts are reported in parts per million (ppm) downfield of Me_4Si . All 2D NMR experiments were performed on a Jeol GSX 400 (resonance frequencies: 400 MHz for ^1H and 100 MHz for ^{13}C) spectrometer. ^1H NMR spectra were referenced against the residual ^1H impurity of the deuterated solvent (δ (ppm) 7.15 (C_6D_6); 7.24 (CDCl_3); 2.05 ($(\text{CD}_3)_2\text{CO}$); 1.73, 3.58 ($\text{C}_4\text{D}_8\text{O}$)), and ^{13}C NMR spectra were referenced against the ^{13}C resonance of the solvent (δ 128.0 (C_6D_6); 77.1 (CDCl_3); 29.8, 206.0 ($(\text{CD}_3)_2\text{CO}$); 25.3, 67.4 ($\text{C}_4\text{D}_8\text{O}$)). Variable-temperature experiments were performed on a Brücker AC 300 using flame-sealed NMR sample tubes under a 10^{-2} Torr vacuum. Infrared spectra (reported in cm^{-1}) were performed on Perkin-Elmer 1420 and Brücker FT spectrometers. Mass spectra were obtained on a Nermag R 30-40 spectrometer, with a direct insert source, using electronic impact (EI) and chemical ionization (CI) methods. Elemental analyses (reported in percent mass) were performed by Le Service de Microanalyses de l'Université P. et M. Curie and the Service Central d'Analyse du CNRS at Vernaison, France. Melting points were measured on a Reichert apparatus. Crystal structures were determined at the Laboratoire de Chimie des Métaux de Transition, Université P. et M. Curie.

Single-Crystal X-ray Diffraction of Complex 33b. The selected crystal was set up on an Enraf Nonius CAD4F diffractometer. Accurate unit cell dimensions and crystal orientation matrice together with their estimated standard deviations were obtained from least-squares refinements of the setting angles of 25 reflections. Two standard reflections were monitored periodically; no intensity decay occurred during the data collections. Corrections were made for Lorentz and polarization effects. Empirical absorption corrections were applied (Difabs).³¹ Crystallographic data and other pertinent informations are summarized in Table 6.

Structure Solution and Refinement. Computations were performed by using CRYSTALS³² adapted on a Microvax

Table 6. X-ray Diffraction Acquisition and Calculation Data for Complex 33b

empirical formula	$\text{C}_{27}\text{H}_{21}\text{DCrO}_3\text{Sn}$
MW ($\text{g}\cdot\text{mol}^{-1}$)	566.2
cryst dims (mm)	$0.18 \times 0.25 \times 0.62$
cryst syst	triclinic
space group	$P\bar{1}$
<i>a</i> (Å)	8.961(4)
<i>b</i> (Å)	10.853(5)
<i>c</i> (Å)	12.713(2)
α (deg)	85.15(3)
β (deg)	86.26(2)
γ (deg)	72.40(4)
<i>V</i> (Å ³)	1173(15)
<i>Z</i>	2
ρ ($\text{g}\cdot\text{cm}^{-3}$)	1.600
<i>T</i> (K)	293
monochromator	graphite
λ (Mo K α) (Å)	0.71069
μ (Mo K α) (cm^{-1})	15.45
2θ range (deg)	$3 < 2\theta < 50$
no. of reflectns collected	4310
no. of unique reflectns	4107
merging <i>R</i> factor	0.045
no. of reflections with $I > 3\sigma(I)$	2905
absorption corrected by	Difabs ^c
transm coeff	0.89, 1.15
<i>R</i> ^a	0.33, <i>S</i> = 1.55
<i>R</i> _w ^b	0.037 (unit weight)
no. of variables	289

^a $R = \sum(|F_o| - |F_c|)/\sum|F_o|$. ^b $R_w = [\sum w(|F_o| - |F_c|)^2/\sum w(F_c)^2]^{1/2}$. ^c See ref 31.

II computer. Atomic factor for neutral Cr, Sn, C, O, and H were taken from ref 33. Anomalous dispersion was taken into account. The structure was solved by interpretation of the Patterson maps, which clearly indicated Cr and Sn atom positions. All remaining non-hydrogen atoms were found by successive electron density map calculations. Their atomic coordinates were refined together with anisotropic temperature factors. At this stage, hydrogen atoms were located on a difference electron density map; their coordinates were refined with an overall isotropic temperature factor. Least-squares refinements were carried out by minimizing the function $\sum w(F_o - F_c)^2$, where F_o and F_c are the observed and calculated structure factors. The models reached convergence with *R* and *R*_w having the values listed in Table 6. The criteria for a satisfactory complete analysis were the ratios of the root-mean-square shift to standard deviation being less than 0.1 and no significant features in the final difference maps.

Atomic coordinates are given in Table 7; selected bond distances and bond angles are given in Table 8. The molecular geometry and the numbering scheme are shown in Figures 2 and 3.

Preparations of (η^6 -Arene)tricarbonylchromium Complexes. Tricarbonyl[η^6 -2-methoxy(trimethylsilyl)benzene]chromium (3a**).** To a solution of complex **11** (732 mg, 3 mmol) in THF (10 mL) was added a hexane solution of *n*-BuLi (1.5 M, 2 mL, 3 mmol) at -78°C . The resulting solution was stirred for 30 min, and chlorotrimethylsilane (0.5 mL, 3 mmol) was added dropwise. The solution was warmed and extracted at room temperature with Et_2O , washed with water, dried over MgSO_4 , and filtered through a Celite column, and solvents were removed under reduced pressure to give a yellow residue. Separation of the products by flash chromatography affords the disilylated product ($\text{Et}_2\text{O}:\text{PE} = 2:98$) and the complex **3a** ($\text{Et}_2\text{O}:\text{PE} = 3:97$) which was recrystallized from pentane to give 280 mg (0.88 mmol) in 30% yield, mp 110°C . MS (CI) (NH_3): *m/e* 334 ($\text{M} + \text{H} + \text{NH}_3$)⁺, 317 ($\text{M} + \text{H}$)⁺. Anal. Calcd

(32) Watkin, D. J.; Carruthers, J. R.; Betteridge, P. W. *Crystals in Advanced Crystallographic Program System*; Chemical Crystallography Laboratory, University of Oxford: Oxford, England, 1988.

(33) *International Tables for X-ray Crystallography*; Kynoch Press; Birmingham, England, 1974; Vol. IV.

(31) Walker, N.; Stuart, D. *Acta Crystallogr.* **1983**, *A39*, 158.

Table 7. Fractional Atomic Coordinates for the Molecular Structure of 33b

atom	<i>x/a</i>	<i>y/b</i>	<i>z/c</i>	U_{eq}^a
Sn	0.13371(5)	0.20336(4)	0.26635(3)	0.0359
Cr	-0.1298(1)	0.40864(9)	0.26841(7)	0.0379
C(1)	-0.4387(8)	0.5079(8)	0.3534(6)	0.0655
C(2)	-0.3866(8)	0.4177(8)	0.2547(5)	0.0561
C(3)	-0.2939(8)	0.2934(7)	0.2841(5)	0.0535
C(4)	-0.1996(8)	0.2614(6)	0.3716(5)	0.0536
C(5)	-0.1944(7)	0.3623(7)	0.4326(5)	0.0507
C(6)	-0.2890(8)	0.4859(7)	0.4105(5)	0.0574
C(11)	-0.0809(7)	0.3726(6)	0.1273(5)	0.0453
O(11)	-0.0634(6)	0.3581(5)	0.0392(3)	0.0625
C(12)	-0.2028(7)	0.5810(7)	0.2132(5)	0.0506
O(12)	-0.2445(6)	0.6842(5)	0.1788(4)	0.0719
C(13)	0.0360(8)	0.4599(6)	0.3113(5)	0.0483
O(13)	0.1304(6)	0.4971(4)	0.3414(4)	0.0609
C(21)	0.0992(6)	0.0226(5)	0.2364(4)	0.0389
C(22)	0.1793(7)	-0.0904(6)	0.2936(5)	0.0491
C(23)	0.1711(8)	-0.2104(6)	0.2697(5)	0.0509
C(24)	0.0826(8)	-0.2209(6)	0.1889(5)	0.0522
C(25)	0.0016(8)	-0.1108(6)	0.1319(5)	0.0518
C(26)	0.0076(7)	0.0106(6)	0.1556(5)	0.0461
C(31)	0.3153(7)	0.2258(6)	0.1530(4)	0.0455
C(32)	0.3108(9)	0.3413(8)	0.0995(5)	0.0607
C(33)	0.424(1)	0.355(1)	0.0271(7)	0.0801
C(34)	0.547(1)	0.250(2)	0.0074(7)	0.0878
C(35)	0.560(1)	0.132(1)	0.0575(8)	0.0871
C(36)	0.4399(9)	0.1189(8)	0.1327(6)	0.0693
C(41)	0.2432(6)	0.1682(5)	0.4163(4)	0.0361
C(42)	0.3828(7)	0.1976(6)	0.4241(5)	0.0440
C(43)	0.4547(7)	0.1797(6)	0.5195(5)	0.0521
C(44)	0.3879(8)	0.1358(7)	0.6091(5)	0.0566
C(45)	0.2502(8)	0.1072(7)	0.6057(5)	0.0597
C(46)	0.1763(8)	0.1238(7)	0.5083(5)	0.0550

^a $U_{eq} = (U_1U_2U_3)^{1/3}$, where U_1, U_2, U_3 are the eigenvalues of the U_{ij} matrix.

for $C_{13}H_{16}CrO_4Si$: C, 49.37; H, 5.15. Found: C, 49.67; H, 5.06. IR (neat): $\nu(C=O)$ 1954, 1878 cm^{-1} . ¹H NMR ($CDCl_3$): δ 5.67 (td, H_4 , $^3J = 6.5$ Hz, $^4J = 1.5$ Hz), 5.58 (dd, H_6 , $^3J = 6.5$ Hz, $^4J = 1.5$ Hz), 4.97 (d, H_3 , $^3J = 6.5$ Hz), 4.77 (t, H_5 , $^3J = 6.5$ Hz), 3.67 (s, CH_3O), 1.25 (s, $(CH_3)_3Si$). ¹³C NMR ($CDCl_3$): δ 0.3 (CH_3Si), 55.5 (CH_3O), 73.6–88.1–96.0–101.0 ($C_{3,4,5,6}$), 108.0 (C_2), 123.2 (C_1), 233.1 (CO).

Tricarboxyl[η^6 -2-phenoxy(trimethylsilyl)benzene]chromium (3b): phenoxybenzenetricarboxylchromium (3.06 g, 10 mmol), THF (25 mL), *n*-BuLi (1.6 M, 6.25 mL), $T = -78$ °C, $ClSi(CH_3)_3$ (1.3 mL, 10 mmol); stirring 30 min. Complex **3b** (2.1 g, 5.5 mmol, 55% yield), mp 107 °C. MS (CI) (NH_3): m/e 379 ($M + H$)⁺, 351 ($M + H - CO$)⁺, 243 ($M + H - Cr(CO)_3$)⁺. Anal. Calcd for $C_{18}H_{12}CrO_4Si$: C, 57.14; H, 4.82. Found: C, 57.06; H, 4.76. IR (neat): $\nu(C=O)$ 1962, 1878 cm^{-1} . ¹H NMR ($CDCl_3$): δ 7.28 (m, 5H, OPh), 5.64 (d, H_6 , $^3J = 5.0$ Hz), 5.55 (t, H_4 , $^3J = 7.0$ Hz), 4.68 (m, $H_{5,3}$), 0.39 (s, $(CH_3)_3Si$).

Tricarboxyl[η^6 -2-*tert*-butylanisole]chromium (7a): 2-*tert*-butylanisole (3.3 g, 20 mmol), $Cr(CO)_6$ (4.6 g, 20 mmol), THF (10 mL), and DBE (90 mL); reflux 5 days. Complex **7a** (45% yield, 2.5 g), mp 140 °C. Anal. Calcd for $C_{14}H_{16}CrO_4$: C, 56.00; H, 5.37. Found: C, 55.87; H, 5.35. IR (CH_2Cl_2): $\nu(C=O)$ 1960, 1875 cm^{-1} . ¹H NMR ($CDCl_3$): δ 5.78 (d, H_3 , $^3J = 7$ Hz), 5.59 (t, H_5 , $^3J = 7$ Hz), 5.00 (d, H_6 , $^3J = 7$ Hz), 4.73 (t, H_4 , $^3J = 7$ Hz), 3.79 (s, MeO), 1.35 (s, $(CH_3)_3C$). ¹³C NMR ($CDCl_3$): δ 30.8 (CH_3-C), 34.8 (CH_3-C), 55.4 (CH_3-O), 73.9–96.8 ($C_{3,4,5,6}$), 110.7 (C_2), 143.4 (C_1), 234.0 (CO). For **7b**, **7c**, **9**, **13**, and **16**, see supplementary material except for NMR. For **7b**. ¹H NMR ($CDCl_3$): δ 5.51 (t, H_5 , $^3J = 6.6$ Hz), 5.25 (s, H_2 , $^3J = 6.6$ Hz), 5.08 (d, H_4 , $^3J = 6.6$ Hz), 4.98 (d, H_6 , $^2J = 6.6$ Hz), 3.71 (s, MeO), 1.32 (s, $(CH_3)_3C$). ¹³C NMR ($CDCl_3$): δ 30.9 (CH_3-C), 34.4 (CH_3-C), 55.7 (CH_3O), 76.7–93.8 ($C_{2,4,5,6}$), 126.4 (C_3), 143.3 (C_1), 233.8 (CO). For **7c**. ¹H NMR ($CDCl_3$): δ 5.66 (d, $H_{3,5}$, $^3J = 7.2$ Hz), 5.02 (d, $H_{2,6}$, $^3J = 7.2$ Hz), 3.70 (s, MeO), 1.24 (s, $(CH_3)_3C$). ¹³C NMR ($CDCl_3$): δ 30.7 (CH_3C), 34.8 (CH_3C), 55.4 (CH_3O), 76.6 ($C_{3,5}$), 93.8 ($C_{2,6}$), 116.2 (C_4), 143.4 (C_1), 233.8 (CO). For **9**. ¹H NMR ($(CD_3)_2CO$): δ 5.27 (s, 3H,

Table 8. Selected Bond Distances (Å) and Bond Angles (deg) for $Cr(C_6H_7)(CO)_3-Sn(C_6H_5)_3$

Bond Distances			
Cr–Sn	2.713(1)		
Cr–C(2)	2.276(6)	C(1)–C(2)	1.51(1)
Cr–C(3)	2.191(6)	C(2)–C(3)	1.37(1)
Cr–C(4)	2.193(6)	C(3)–C(4)	1.397(9)
Cr–C(5)	2.187(6)	C(4)–C(5)	1.407(9)
Cr–C(6)	2.280(6)	C(5)–C(6)	1.370(9)
Cr–C(11)	1.864(6)	C(6)–C(1)	1.51(1)
Cr–C(12)	1.875(7)	C(11)–O(11)	1.138(7)
Cr–C(13)	1.863(7)	C(12)–O(12)	1.128(7)
Sn–C(21)	2.145(6)	C(13)–O(13)	1.141(7)
Sn–C(41)	2.153(5)	Sn–C(31)	2.158(6)
Bond Angles			
C(1)–C(2)–C(3)	120.5(6)	C(4)–C(5)–C(6)	120.2(6)
C(2)–C(3)–C(4)	119.9(6)	C(5)–C(6)–C(1)	119.9(6)
C(3)–C(4)–C(5)	118.0(6)	C(6)–C(1)–C(2)	102.7(5)
Cr–C(11)–O(11)	174.0(6)	C(11)–Cr–C(12)	84.1(3)
Cr–C(12)–O(12)	178.8(6)	C(11)–Cr–C(13)	105.1(3)
Cr–C(13)–O(13)	175.5(6)	C(12)–Cr–C(13)	83.8(3)
C(2)–Cr–C(11)	95.7(3)	C(5)–Cr–C(11)	154.0(3)
C(2)–Cr–C(12)	83.3(3)	C(5)–Cr–C(12)	118.5(3)
C(2)–Cr–C(13)	154.1(3)	C(5)–Cr–C(13)	91.0(3)
C(3)–Cr–C(11)	92.0(3)	C(6)–Cr–C(11)	156.0(3)
C(3)–Cr–C(12)	118.2(3)	C(6)–Cr–C(12)	83.5(3)
C(3)–Cr–C(13)	153.8(3)	C(6)–Cr–C(13)	93.8(3)
C(4)–Cr–C(12)	142.5(3)		
C(4)–Cr–C(11)	116.6(2)		
C(4)–Cr–C(13)	116.7(3)		
Sn–Cr–C(2)	130.7(2)	Sn–Cr–C(3)	95.7(2)
Sn–Cr–C(4)	77.5(2)	Sn–Cr–C(5)	93.3(2)
Sn–Cr–C(6)	127.7(2)		
Sn–Cr–C(11)	73.5(2)	Sn–Cr–C(12)	140.0(2)
Sn–Cr–C(12)	73.5(2)		
Cr–Sn–C(21)	115.2(1)	C(21)–Sn–C(31)	105.0(2)
Cr–Sn–C(31)	114.9(2)	C(21)–Sn–C(41)	105.0(2)
Cr–Sn–C(41)	111.3(1)	C(31)–Sn–C(41)	104.5(2)

H-Ar), 3.83 (s, 9H, OCH_3). ¹³C NMR ($(CD_3)_2CO$): δ 56.5 (OCH_3), 66.3 ($C_{2,4,6}$), 144.6 ($C_{1,3,5}$), 233.0 (CO). For **13**. ¹H NMR ($(CD_3)_2CO$): δ 5.72 (t, H_5 , $J = 6.5$ Hz), 5.20 (d, $H_{4,6}$, $J = 6.5$ Hz), 3.86 (s, 6H, OCH_3), 3.82 (s, 3H, OCH_3). ¹³C NMR ($(CD_3)_2CO$): δ 56.9 (OCH_3), 65.7 (OCH_3), 71.5 ($C_{4,6}$), 91.6 (C_5), 141.6 ($C_{1,2,3}$), 235.3 (CO). For **16**. ¹H NMR ($CDCl_3$): δ 5.43 (dd, $H_{5,8}$, $^3J = 5.0$ Hz, $^4J = 3.0$ Hz), 5.02 (dd, $H_{6,7}$, $^3J = 5.0$ Hz, $^4J = 3.0$ Hz), 4.24 (s, CH_2CH_2). ¹³C NMR ($CDCl_3$): δ 64.8 ($C_{2,3}$), 83.5–87.8 ($C_{5,6,7}$), 126.4 ($C_{4,1}$), 233.8 (CO).

Tricarboxyl[η^6 -2-fluoro(triisopropylsilyl)benzene]chromium (20): THF (15 mL), tricarboxyl(η^6 -fluorobenzene)chromium (1.16 g, 5 mmol), *n*-BuLi (1.6 M, 3.13 mL, 5 mmol), -78 °C. The resulting solution was stirred for 30 min and $ClSi(i\text{-}Pr)_3$ (0.70 mL, 5.5 mmol) was added. The resulting mixture was extracted with Et_2O , washed with water and brine, filtered through a Celite column, and dried over $MgSO_4$; solvents were removed under reduced pressure. The crude product was purified by flash chromatography on silica gel to give **20** (1.03 g, 2.7 mmol, 54% yield), mp 105 °C (dec). Anal. Calcd for $C_{18}H_{25}CrFO_3Si$: C, 55.67; H, 6.44. Found: C, 55.48; H, 6.54. IR (neat): $\nu(C=O)$ 1970, 1892 cm^{-1} . ¹H NMR ($CDCl_3$): δ 5.66 (m, H_4), 5.52 (m, H_6), 5.21 (t, H_5 , $^3J = 6$ Hz), 4.78 (m, H_3), 1.78 (sept, $CHCH_3$, $^3J = 7$ Hz), 1.17 (d, $CHCH_3$, $^3J = 7$ Hz). For complex **22**, see supplementary material except for NMR data. For **22**. ¹H NMR ($CDCl_3$): δ 5.59 (t, H_4 , $^3J = 6.5$ Hz), 5.52 (dd, H_6 , $^3J = 6.5$ Hz), 5.32 (d, H_3 , $^3J = 6.5$ Hz), 4.89 (t, H_5 , $^3J = 6.5$ Hz), 0.41 ($Si(CH_3)_3$).

Tricarboxyl [η^6 -2-(*N,N*-dimethylamino)(trimethylsilyl)benzene]chromium (29a) and Tricarboxyl[η^6 -3-(*N,N*-dimethylamino)(trimethylsilyl)benzene]chromium (29b). To a THF solution (10 mL) of 2,2,6,6-tetramethylpiperidine (678 mg, 0.81 mL, 4.8 mmol) was added dropwise a solution

of *n*-BuLi (1.6 M, 3.0 mL, 4.8 mmol) in hexane, at $-78\text{ }^{\circ}\text{C}$. The resulting solution was stirred for 10 min, and a solution of (η^6 -*N,N*-dimethylaniline)Cr(CO)₃ (1.01 g, 4. mmol) in THF (10 mL) was added. The solution was stirred again for 30 min at $-78\text{ }^{\circ}\text{C}$, and Me₃SiCl (1.3 g, 1.53 mL, 12 mmol) was added dropwise. The resulting mixture was allowed to warm to room temperature and extracted with Et₂O. The organic phase was washed with water and brine, dried over MgSO₄, and filtered through a Celite column; solvents were removed under reduced pressure. The yellow residue was purified by flash chromatography on silica gel to give the starting complex, (η^6 -*N,N*-dimethylaniline)Cr(CO)₃, (PE 100%), complex **29a** (Et₂O:PE = 10:90), and complex **29b** (Et₂O:PE = 20:80). After recrystallization in pentane, complexes **29a** (200 mg, 0.61 mmol, 15% yield) and **29b** (739 mg, 2.25 mmol, 57% yield) were obtained as pure yellow crystals. For complex **29a**, mp $78\text{ }^{\circ}\text{C}$. Anal. Calcd for C₁₄H₁₉CrNO₃Si: C, 51.05; H, 5.81; N, 4.25. Found: C, 51.31; H, 5.85; N, 4.28. MS (CI) (NH₃): *m/e* 330 (M + H)⁺, 302 (M + H - CO)⁺, 194 (M + H - Cr(CO)₃)⁺. IR (neat): ν (CO) 1956, 1872 cm⁻¹. ¹H NMR (CDCl₃): δ 5.60 (td, H₄, ³J = 6.5 Hz, ⁴J = 1.5 Hz), 5.49 (dd, H₆, ³J = 6.0 Hz, ⁴J = 1.5 Hz), 4.96 (t, H₅, ³J = 6.0 Hz), 4.94 (d, H₃, ³J = 6.5 Hz), 2.63 (s, 6H, CH₃N), 0.36 (s, 9H, CH₃Si). ¹³C NMR (CDCl₃): δ 0.7 (CH₃Si), 45.6 (CH₃N), 79.9–88.4–95.2–101.5 (C_{3,4,5,6}), 98.9 (C₁), 141.0 (C₂), 233.8 (CO). For complex **29b**, mp $97\text{ }^{\circ}\text{C}$. Anal. Calcd for C₁₄H₁₉CrNO₃Si: C, 51.05; H, 5.81; N, 4.25. Found: C, 51.13; H, 5.78; N, 4.14. MS (CI) (NH₃): *m/e* 330 (M + H)⁺, 302 (M + H - CO)⁺, 194 (M + H - Cr(CO)₃)⁺. IR (neat): ν (CO) 1944, 1852 cm⁻¹. ¹H NMR (CDCl₃): δ 5.55 (t, H₅, ³J = 6.5 Hz), 4.95 (dd, H₆, ³J = 6.5 Hz, ⁴J = 2 Hz), 4.81 (d, H₄, ³J = 6.0 Hz), 4.72 (s, H₂), 2.87 (s, 6H, CH₃N), 0.30 (s, 9H, CH₃Si). ¹³C NMR (CDCl₃): δ 0.6 (CH₃Si), 41.0 (CH₃N), 76.5 (C₂), 79.5 (C₆), 89.3 (C₄), 97.5 (C₅), 99.3 (C₁), 135.5 (C₃), 233.2 (CO). ¹³C NMR signals were assigned according to a ¹³C–¹H correlation 2D NMR experiment.

Reaction of Lithium Triethylborohydride with (η^6 -Alkoxyarene)Cr(CO)₃ and (η^6 -Aryloxyarene)Cr(CO)₃ Complexes. *Ips*o Aromatic Nucleophilic Substitutions. **Tricarbonyl(η^6 -ethylbenzene)chromium (2a): **1** (272 mg, 1 mmol), THF (15 mL), LiEt₃BH (1 M, 2 mL, 2 mmol). The resulting solution was refluxed for 2 h and treated with a diluted solution of chlorhydric acid or trifluoroacetic acid. The mixture was extracted with Et₂O, washed with a saturated solution of Na₂CO₃ and with brine, dried over Na₂SO₄, and filtered through a Celite column. Solvents were removed under reduced pressure. The yellow residue was recrystallized in a mixture of hexane and acetone to give pure yellow crystals of complex **2a** (241 mg, 0.995 mmol, 100% yield). Spectroscopic and analytical data were in agreement with a standard sample. For **2b**, see supplementary material.**

Tricarbonyl(η^6 -*tert*-butylbenzene)chromium (8): **7c** (150 mg, 0.5 mmol), THF (20 mL), LiEt₃BH (1 M, 2 mL, 2 mmol), reflux 24 h; hydrolysis. For complex **8** (110 mg, 0.4 mmol, 80% yield). ¹H NMR (CDCl₃): δ 5.52 (d, H_{2,6}, ³J = 7 Hz), 5.38 (t, H₄, ³J = 7 Hz), 5.22 (t, H_{3,5}, ³J = 7 Hz), 1.28 (s, (CH₃)₃C). ¹³C NMR (CDCl₃): δ 31.1 (CH₃C), 34.1 (CH₃C), 90.8 (C_{2,6}), 92.2 (C₄), 92.6 (C_{3,5}), 126.4 (C₁), 233.6 (CO). For **8-p**, **8-m**, and **8-o**, see supplementary material.

Tricarbonyl(η^6 -benzene)chromium (12a): **9** (471 mg, 1.5 mmol), THF (10 mL), LiAlH₄ (118 mg, 3.1 mmol) in THF (5 mL), reflux 24 h; hydrolysis. For complex **12a** data (320 mg, 1.5 mmol, 100% yield, see supplementary material).

Tricarbonyl(η^6 -1,3-dimethoxybenzene)chromium (10a): **9** (155.2 mg, 0.51 mmol), THF (20 mL), LiEt₃BH (1 M, 2.2 mL, 2.2 mmol), stirring 20 min, room temperature. The composition of the residue was obtained by ¹H NMR spectroscopy and based on comparison with ¹H NMR spectra from reference samples. According to ¹H NMR spectra, the composition (molality) was as follows: **10a**, 73%; **11**, 13%; starting complex, 14%. For **10b**, see supplementary material.

(η^6 -Anisole)tricarbonylchromium (11): **13** (155.2 mg, 0.51 mmol), THF (15 mL), LiEt₃BH (1 M, 0.8 mL, 0.8 mmol),

CF₃CO₂H (0.5 mL). The composition of the residue was obtained by ¹H NMR spectroscopy and based on comparison with ¹H NMR spectra of reference samples. According to ¹H NMR spectra, the composition (molality) was as follows: **11**, 36%; (η^6 -1,2-dimethoxybenzene)Cr(CO)₃, 30%; **12**, 5%; starting complex **13**, 29%.

2-[Tricarbonyl(η^6 -phenoxy)chromium]ethanol (17a): **16** (272 mg, 1 mmol), THF (30 mL), HMPA (0.2 mL), LiEt₃BH (1 M, 1.5 mL, 1.5 mmol), reflux 23 h; hydrolysis. The yellow residue was chromatographed on silica gel to give the starting complex **16** and **12** (Et₂O:PE = 50:50, 10% (molality) of **12** and **17a** (100% Et₂O)). **17a** was recrystallized in a mixture of pentane and Et₂O and was obtained pure (91 mg as yellow needles, 0.33 mmol, 33% yield). Anal. Calcd for C₁₁H₉CrO₅: C, 48.17; H, 3.65. Found: C, 47.91; H, 3.67. MS (CI) (NH₃): *m/e* 292 (M + H + NH₃)⁺, 275 (M + H)⁺, 139 (M + H - Cr(CO)₃)⁺. IR (Nujol): ν (C=O) 1975, 1900 cm⁻¹. ¹H NMR (CDCl₃): δ 5.54 (t, H_{3,5}, ³J = 6.0 Hz), 5.13 (d, H_{2,6}, ³J = 6.0 Hz), 4.88 (t, H₄, ³J = 6.0 Hz), 3.96 (m, CH₂CH₂), 1.60 (s, OH). ¹³C NMR (CDCl₃): δ 61.0 (CH₂OAr), 70.1 (CH₂OH), 78.7 (C_{2,6}), 85.6 (C₄), 95.0 (C_{3,5}), 120.0 (C₁), 233.1 (CO). ¹³C NMR signals were assigned according to a ¹³C–¹H correlation 2D NMR experiment.

2-[Tricarbonyl(η^6 -2'-deuteriophenoxy)chromium]ethanol (17b): **16** (272 mg, 1 mmol), THF (30 mL), LiEt₃BD (1 M, 1.5 mL, 1.5 mmol), complex **17b** (60 mg, 0.22 mmol, 22% yield), mp $94\text{ }^{\circ}\text{C}$. MS (CI) (NH₃): *m/e* 293 (M + H + NH₃)⁺, 276 (M + H)⁺, 140 (M + H - Cr(CO)₃)⁺. ¹³C NMR (CDCl₃): δ 61.0 (CH₂OAr), 70.1 (CH₂OH), 78.5 (t, C₂, ¹J_{C-D} = 27.0 Hz), 78.8 (C₆), 85.6 (C₄), 95.0 (C_{3,5}), 120.0 (C₁), 233.1 (CO).

2-[Tricarbonyl(η^6 -phenyl)chromium]phenol (19): **18** (1g, 3.28 mmol), THF (100 mL), LiEt₃BH (1 M, 6.56 mL, 6.56 mmol), reflux 48 h; HCl treatment. Complex **19** (753 mg, 2.46 mmol, 75% yield). Anal. Calcd for C₁₅H₁₀CrO₄: C, 58.82; H, 3.26. Found: C, 58.68; H, 3.31. MS (CI) (NH₃): *m/e* 324 (M + H + NH₃)⁺, 307 (M + H)⁺, 171 (M + H - Cr(CO)₃)⁺. IR (CHCl₃): ν (O–H) 3560, ν (C=O) 1975, 1980, 1905 cm⁻¹. ¹H NMR ((CD₃)₂CO): δ 8.35 (s, OH), 6.96 (m, 4H, HAr), 6.06 (m, H_{3,5}, ArCr), 5.70 (m, H_{2,4,6}, ArCr). ¹³C NMR (CDCl₃): δ 92.1–92.3–95.0 (C_{2,6,3,5,4}, ArCr), 106.5 (C₁, ArCr), 116.9 (C₆, Ar), 121.3 (C₄, Ar), 130.5 (C_{3,5}, Ar), 132.0 (C₂, Ar), 152.5 (C₁, Ar), 233.0 (CO).

¹H NMR Study of Deuteride Addition to Tricarbonyl(η^6 -3-ethylanisole)chromium. To a solution of LiEt₃BD (0.11 mmol, 0.11 mol·dm⁻³) in THF-*d*₈ (1 mL) was added the complex **1** (16 mg, 5.88 × 10⁻² mmol, 0.0588 mol·dm⁻³). The solution was stirred for 1 min. A small quantity of the previous solution (0.5 mL) was injected into a NMR sample tube via a syringe. The resulting solution was frozen at $-180\text{ }^{\circ}\text{C}$ under N₂ and the sample tube was sealed under vacuum. ¹H NMR experiments were carried out at room temperature and at $80\text{ }^{\circ}\text{C}$. For Et₃BdLi. ¹H NMR (C₄D₈O): δ 0.63 (m, BCH₂CH₃), -0.14 (m, BCH₂CH₃). As the reaction proceeded, the amount of complex **1** decreased. A major new compound, (η^6 -3-deuterioethylbenzene)Cr(CO)₃ (**2b**), was detected after several hours of reaction in the NMR probe along with uncharacterized products.

¹H NMR Study of Hydride Addition to Complex 9. To a solution of complex **9** (10 mg, 0.033 mmol) in THF-*d*₈ (2 mL) was added a solution of LiEt₃BH (1 M, 6.6 μ L, 0.066 mmol) in THF-*d*₈. The solution of LiEt₃BH in THF-*d*₈ was obtained from the commercial solution by removing THF under vacuum and adding the same volume of deuterated solvent. The dark red solution was stirred for 1 min and quickly cooled at $-40\text{ }^{\circ}\text{C}$. A small quantity of the previous solution (0.25 mL) was injected under N₂ in a NMR sample tube via a syringe and diluted with THF-*d*₈ (0.75 mL). The resulting dark red solution was frozen and the sample tube was sealed under dry N₂. All NMR experiments were carried out at room temperature. For complex **9**. ¹H NMR (C₄D₈O): δ 5.23 (s, H_{2,4,6}), 3.78 (s, CH₃O). For complex **10**. ¹H NMR (C₄D₈O): δ 5.78 (t, H₅, ³J = 6.7 Hz),

5.44 (d, H₂, ⁴J = 2 Hz), 5.07 (dd, H_{4,6}, ³J = 6.7 Hz, ⁴J = 2 Hz), 3.75 (s, CH₃O).

Cine and Tele-Meta Aromatic Nucleophilic Substitutions. Tricarbonyl($\eta^6\text{-toluene}$)chromium (6). To a solution of **5** (320 mg, 1 mmol) in THF (40 mL) was added a solution of LiEt₃BH (1 M, 4 mL, 4 mmol) in THF. The resulting solution was refluxed for 48 h and added to a solution of CF₃CO₂H (8 mL) in THF (7 mL). The solution was neutralized with a concentrated aqueous solution of NaOH and extracted with Et₂O. The organic phase was washed with water and brine, dried over MgSO₄, and filtered through a Celite column; solvents were removed under reduced pressure. The crude product was recrystallized in a mixture of pentane and Et₂O to give 78 mg of pure complex **6** (0.55 mmol, 55% yield). Spectrometric and analytical data were in agreement with those published in the literature.²¹ IR (neat): $\nu(\text{C}=\text{O})$ 1982, 1868 cm⁻¹. ¹H NMR (CDCl₃): δ 5.40 (t, H_{3,5}, ³J = 6.0 Hz), 5.14 (m, H_{2,4,6}, ³J = 6.0 Hz), 2.16 (s, CH₃). ¹³C NMR (C₆D₆): δ 20.2 (CH₃), 89.3 (C₄), 92.5 (C_{2,6}), 94.0 (C_{3,5}), 109.8 (C₁), 233.8 (CO). ¹³C NMR signals were assigned according to ¹³C-¹H correlation 2D NMR and selective heteronuclear irradiation experiments. For **6-o**, see supplementary material.

Tricarbonyl($\eta^6\text{-(trimethylsilyl)benzene}$)chromium (4): **3b (189 mg, 0.5 mmol), THF (15 mL), LiEt₃BH (1 M, 2 mL, 2 mmol), refluxed 24 h, CF₃CO₂H (2 mL), THF (4 mL). Complex **4** (101 mg, 0.35 mmol, 71% yield), mp 99 °C. MS (CI) (NH₃): *m/e* 287 (M + H)⁺, 259 (M + H - CO)⁺, 153 (M + H - Cr(CO)₃)⁺. IR (neat): $\nu(\text{C}=\text{O})$ 1944, 1864 cm⁻¹. ¹H NMR data were in agreement with a standard sample. For **4-p**, see supplementary material.**

Kinetic Study of Hydride Addition to Tricarbonyl($\eta^6\text{-}p\text{-tert-butylanisole}$)chromium (7c). To a solution of **7c** in THF was added a solution of LiEt₃BD in THF at 20 °C. Aliquots of the reaction medium were removed every 30 min for 1 h and every hour for 7 h. Two aliquots were removed after 26 and 33 h of reaction. All samples were injected in THF solutions of trifluoroacetic acid in excess. Resulting mixtures were extracted with diethyl ether and washed with a diluted solution of NaOH and with brine. Organic phases were dried over MgSO₄ and filtered through Celite. Solvents were removed under reduced pressure to afford crude solvent-free oily residues that were weighed and analyzed by ¹H NMR.

Reaction of Lithium Triethylborohydride with Tricarbonyl($\eta^6\text{-halogenoarene}$)Chromium Complexes. Hydrodechlorination. Tricarbonyl($\eta^6\text{-monodeuteriotoluene}$)chromium (6-m**, **6-o**): **23** (262.5 mg, 1 mmol), THF (10 mL), LiAlD₄ (155.9 mg, 3.7 mmol), THF (5 mL), room temperature, stirring 5 h, CF₃CO₂H (2 mL), THF (5 mL); **6-m** and **6-o** (228 mg, 0.995 mmol, 100% yield). The composition of the mixture was obtained by analysis of ¹H NMR signal integration values (*I*) of H_{3,5} and H_{2,4,6} and according to ¹³C NMR spectra for the position of deuterium on the aromatic ring. Values were as follows: *I* = 5.5 (H_{3,5}), *I* = 10.6 (H_{2,4,6}). Consequently, the composition (molality) was 0.66 **6-m** and 0.34 **6-o**.**

Tricarbonyl($\eta^6\text{-3-deuteriotoluene}$)chromium (6-m): **23 (262.5 mg, 1 mmol), THF (20 mL), LiEt₃BD (1 M, 4.5 mL, 4.5 mmol), room temperature, stirring for 1 day.**

An initial amount (10 mL) was added dropwise to a solution of CF₃CO₂H (1 mL) in THF (5 mL) under N₂ atmosphere. The resulting red solution turns to yellow after a few seconds. This solution was then extracted with Et₂O, washed twice with a concentrated aqueous NaOH solution and with brine, dried over MgSO₄, and filtered through a Celite column; solvents were removed under reduced pressure. The crude product was recrystallized in PE and the pure isomer **6-m** was obtained (114 mg, 0.497 mmol, 100% yield). ¹H NMR (C₆D₆): δ 4.47 (t, H₅, ³J = 6 Hz), 4.19 (s + d, H_{2,4,6}, ³J = 6 Hz), 1.50 (CH₃).

The second part of the initial reaction medium was treated similarly with CF₃CO₂D (99.5% D, 1 mL), in THF (5 mL). After extraction and purification the complex **6-o**, -*m* deuterated at the 2 and 3 positions was obtained, 98% yield (113 mg, 0.49

mmol). ¹H NMR (C₆D₆): δ 4.47 (t + d, H₅, 1H, ³J = 6 Hz), 4.19 (m, H_{2,4,6}, 2H, ³J = 6 Hz), 1.50 (CH₃).

Tricarbonyl($\eta^6\text{-4-deuterio(trimethylsilyl)benzene}$)chromium (4-p): **22 (160 mg, 0.5 mmol), THF (7.5 mL), LiEt₃BD (1 M, 2.5 mL, 2.5 mmol), stirring 50 min at -78 °C, CF₃CO₂H (2 mL), THF (3 mL); complex **4-p** (143 mg, 0.5 mmol, 100% yield). Spectroscopic and analytical data were in agreement with those obtained previously.**

Hydrodefluorination. Tricarbonyl($\eta^6\text{-toluene}$)chromium (6): **24 (246 mg, 1 mmol), THF (20 mL), LiEt₃BH (1 M, 2.2 mL, 2.2 mmol); complex **6** (161 mg, 0.70 mmol, 70% yield). Spectrometric and analytical data were in agreement with a standard sample.**

Tricarbonyl($\eta^6\text{-4-deuteriotoluene}$)chromium (6-p): **24 (246 mg, 1 mmol), THF (20 mL), LiEt₃BD (1 M, 2 mL, 2 mmol), stirring 20 h, hydrolysis; complex **6-p** (163 mg, 0.71 mmol, 71% yield).**

Tricarbonyl($\eta^6\text{-2-deuteriotoluene}$)chromium (6-o): ($\eta^6\text{-2-Fluorotoluene}$)Cr(CO)₃ (123 mg, 0.5 mmol), THF (15 mL), LiEt₃BD (1 M, 2 mL, 2 mmol) in THF, stirring 20 h; hydrolysis; complex **6-o was obtained (80 mg, 0.35 mmol, 70% yield).**

Tricarbonyl($\eta^6\text{-4-deuterio(triisopropylsilyl)benzene}$)chromium (21-p), Treatment with CF₃CO₂H-THF: **20 (194 mg, 0.5 mmol), THF (7.5 mL), LiEt₃BD (1 M, 2.5 mL, 2.5 mmol), stirring 3 h at 20 °C, CF₃CO₂H (2 mL), THF (3 mL); complex **21-p** (160 mg, 0.43 mmol, 86% yield). ¹H NMR (CDCl₃): δ 5.49 (d, H_{2,6}, 2H, ³J = 6.5 Hz), 5.14 (d, H_{3,5}, 2H, ³J = 6.5 Hz), 1.30 (sept, CHCH₃, 3H), 1.15 (d, CHCH₃, 18H, ³J = 6.5 Hz).**

Tricarbonyl($\eta^6\text{-4-deuterio(triisopropylsilyl)benzene}$)chromium (21-p), Treatment with Water: **20 (194 mg, 0.5 mmol), THF (7.5 mL), LiEt₃BD (1 M, 2.5 mL, 2.5 mmol), stirring 3 h at 20 °C, hydrolysis; complex **21-p** (112 mg, 0.3 mmol, 60% yield). The same results were obtained when the initial solution of **20** and LiEt₃BD was stirred for 50 min at -78 °C before acid treatment.**

Reaction of Lithium Triethylborohydride with [$\eta^6\text{-(}N,N\text{-Dimethylamino)arene}$]tricarbonylchromium Complexes. Tricarbonyl($\eta^6\text{-4-deuterio-(}N,N\text{-dimethylamino)benzene}$)chromium (26b). To a solution of **25 (287 mg, 1 mmol) in THF (40 mL) was added a solution of LiEt₃BD (1 M, 4 mL, 4 mmol) in THF. The resulting mixture was refluxed for 18 h and treated with a diluted hydrochloric aqueous solution. The mixture was extracted with Et₂O, and the organic phase was washed with water and brine, dried over MgSO₄, and filtered through a Celite column; solvents were removed under reduced pressure. The residue was chromatographed on silica gel to give **26b** (Et₂O:PE = 90:10) and the starting complex **25**. After recrystallization in pentane complex, **26b** (111.2 mg, 0.43 mmol, 43% yield) was obtained as a pure yellow powder. Anal. Calcd for C₁₁H₁₀DCrNO₃; C, 51.16; H + ^{1/2}D, 4.26; N, 5.42. Found: C, 51.63; H + ^{1/2}D, 4.27; N, 5.13. MS (CI) (NH₃): cm⁻¹ 259 (M + H)⁺, 123 (M + H - Cr(CO)₃)⁺. ¹H NMR (CDCl₃) δ 5.58 (d, H_{3,5}, ³J = 6.5 Hz), 4.77 (d, H_{2,6}, ³J = 6.5 Hz).**

Tricarbonyl($\eta^6\text{-(}N,N\text{-dimethylamino)benzene}$)chromium (26a): **25 (287 mg, 1 mmol), THF (40 mL), LiEt₃BH (1 M, 4 mL, 4 mmol), reflux 1 day, hydrolysis; complex **26a** (115.1 mg, 0.45 mmol, 45% yield). Spectrometric and analytical data were in agreement with those obtained with a standard sample. MS (CI) (NH₃): *m/e* 258 (M + H)⁺, 122 (M + H - Cr(CO)₃)⁺.**

($\eta^6\text{-Anisole}$)tricarbonylchromium (11) and ($\eta^6\text{-}N,N\text{-dimethylaniline}$)Cr(CO)₃ (26a): **25 (143.5 mg, 0.5 mmol), THF (10 mL), LiEt₃BH (1 M, 2.5 mL, 2.5 mmol), stirring 3 h at room temperature, CF₃CO₂H (2 mL), THF (2 mL). The composition of the yellow residue (133.3 mg) was obtained by ¹H NMR spectroscopy and based on comparison with reference sample ¹H NMR spectra. According to ¹H NMR spectra respective yields were as follows: **11**, 34% (41.8 mg, 0.17 mmol); **26a**, 24% (30.8 mg, 0.12 mmol).**

General Procedure for Hydrodeamination Reactions.

To a solution of (η^6 -N,N-dimethylaminoarene)tricarbonylchromium in THF was added a solution of LiEt₃BR (R = H or D) in THF. The resulting mixture was stirred for several hours at room temperature and injected via a syringe to a solution of CF₃CO₂H in THF. During the injection an exothermic reaction occurs that turns the solution to deep red and after a few seconds to yellow. To the resulting solution was added a concentrated aqueous solution of NaOH. The mixture was extracted with Et₂O, and the organic phase was washed with water and brine, dried over Na₂SO₄ and KOH pellets, and filtered through a Celite column; solvents were removed under reduced pressure. The residue was chromatographed on silica gel.

Tricarbonyl(η^6 -monodeuteriobenzene)chromium (12-D): (η^6 -N,N-dimethylaniline)Cr(CO)₃ (126.4 mg, 0.5 mmol), THF (9 mL), LiEt₃BD (1 M, 3 mL, 3 mmol), stirring 24 h. CF₃CO₂H (1.5 mL), THF (1 mL); complex **12-D** (25 mg, 0.12 mmol, 24% yield). Anal. Calcd for C₉H₅DCrO₃: C, 50.16; H + ^{1/2}D, 2.80. Found: C, 50.06; H, 2.90. MS (CI) (NH₃): *m/e* 233 (M + H + NH₃)⁺, 216 (M + H)⁺.

Tricarbonyl(η^6 -monodeuteriotoluene)chromium (6-o, 6-m): **27a** (271 mg, 1 mmol), THF (15 mL), LiEt₃BD (1 M, 3 mL, 3 mmol), stirring 25 h at room temperature, CF₃CO₂H (2.5 mL), THF (1 mL); complexes **6-o** and **6-m** (52 mg, 0.23 mmol, 23% yield). The composition of the mixture was obtained by analysis of ¹H NMR signals integration values (*I*) of H_{3,5} and H_{2,4,6} and according to ¹³C NMR spectra for the position of deuterium in the aromatic cycle. Values were as follows: *I* = 3.0 (H_{3,5}), *I* = 4.6 (H_{2,4,6}). Consequently, the composition (molality) was 40% **6-m** and 60% **6-o**.

Tricarbonyl(η^6 -monodeuteriotoluene)chromium (6-o, 6-m) with CF₃SO₃H acid step: **27a** (271 mg, 1 mmol), THF (10 mL), LiEt₃BD (1 M, 3 mL, 3 mmol), stirring 20 h at room temperature, CF₃SO₃H (3 mL), THF (1 mL); complexes **6-o** and **6-m** (52 mg, 0.23 mmol, 23% yield). The composition was 40% **6-m** and 60% **6-o**.

Tricarbonyl(η^6 -monodeuteriotoluene)chromium (6-o or 6-p and 6-m): **27b** (271 mg, 1 mmol), THF (10 mL), LiEt₃BD (1 M, 3 mL, 3 mmol), stirring 21 h at room temperature, CF₃CO₂H (2 mL), THF (1 mL); complexes **6-o** or **6-p** and **6-m** (18 mg, 0.078 mmol, 8% yield). The composition was 75% **6-m** and 25% **6-o** or **6-p**.

Tricarbonyl(η^6 -monodeuterio-*tert*-butylbenzene)chromium (8-o, 8-m): **28** (313 mg, 1 mmol), THF (10 mL), LiEt₃BD (1 M, 5 mL, 5 mmol), stirring 24 h at room temperature, CF₃CO₂H (3 mL), THF (1 mL); complexes **8-o** and **8-m** (22 mg, 0.08 mmol, 8% yield). Anal. Calcd for C₁₃H₁₃DCrO₃: C, 57.56; H, 5.20. Found: C, 57.60; H, 5.19. ¹H NMR (CDCl₃): δ 5.52 (dd + d, H_{2,6}, ³*J* = 6.5 Hz, ⁴*J* = 1.0 Hz), 5.38 (t, H₄, ³*J* = 6.0 Hz, ⁴*J* = 1.0 Hz), 5.22 (td + dd, H_{3,5}, ³*J* = 6.0 Hz, ⁴*J* = 1.0 Hz), 1.30 (s, 9H, CH₃C). The composition was 6% **8-m** and 94% **8-o**.

Tricarbonyl(η^6 -deuterio(trimethylsilyl)benzene)chromium (4-p, 4-o): **29a** (281 mg, 0.8 mmol), THF (20 mL), LiEt₃BD (1 M, 1.2 mL, 1.2 mmol), stirring 20 h at room temperature, CF₃CO₂H (10 mL), THF (1 mL); complexes **4-p** and **4-o** (115 mg, 0.4 mmol, 47% yield). ¹H NMR (CDCl₃): δ 5.51 (t, H₄, ³*J* = 6.5 Hz), 5.41 (d, H_{2,6}, ³*J* = 6.5 Hz), 5.16 (d + t, H_{3,5}, ³*J* = 6.5 Hz), 0.28 (s, (CH₃)₃Si). The composition was 16% **4-p** and 84% **4-o**.

Tricarbonyl(η^6 -4-deuterio(trimethylsilyl)benzene)chromium (4-p): **29b** (164 mg, 0.5 mmol), THF (15 mL), LiEt₃D

(1 M, 2.5 mL, 2.5 mmol), stirring 4.5 h at room temperature, CF₃CO₂H (3 mL), THF (1 mL); complex **4-p** (87 mg, 0.30 mmol, 61% yield).

Synthesis of Tricarbonyl(η^5 -cyclohexadienyl)chromium Complexes.³⁵ General Procedure for the Preparation of Lithium Tricarbonyl(η^5 -cyclohexadienyl)chromium(0) Complexes. To a solution of (η^6 -arene)tricarbonylchromium was added a solution of LiEt₃BR (R = D or H) in THF. The resulting solution was refluxed for 30 min and cooled in liquid nitrogen; a mixture of toluene (10 mL) and *n*-hexane (25 mL) was added to induce the formation of two liquid phases. The upper phase was removed, and additional *n*-hexane was added to wash the lower phase that became rapidly a brown-yellow oil. Solvents were removed under 0.1 Torr vacuum to give an oily residue that was washed with dry benzene, and the resulting lithium salt precipitated as a pale yellow amorphous and pyrophoric powder when exposed as it was to air. Elemental analyses and mass spectroscopy failed to provide useful information given the high reactivity of these complexes.

Li[(η^5 -C₆H₇)Cr(CO)₃] (32a): complex **12** (1.26 g, 6 mmol), THF (4 mL), LiEt₃BH (6 mL, 6 mmol); complex **32a** (1.3 g, 5.8 mmol, 97% yield).

Li[(η^5 -C₆H₆D)Cr(CO)₃] (32b): complex **12** (1.26 g, 6 mmol), THF (4 mL), LiEt₃BD (6 mL, 6 mmol); complex **32b** (1.30 g, 5.8 mmol, 97% yield).

Li[(η^5 -1-*exo*-C₁₂H₉O)Cr(CO)₃] (30a): complex **18** (1.21 g, 4 mmol), THF (4 mL), LiEt₃BH (4 mL, 4 mmol); complex **30a** (0.69 g, 2.21 mmol, 55% yield).

Preparation of tricarbonyl(η^5 -cyclohexadienyl)(triphenyltin)chromium(II) (Sn-Cr) complexes. [(η^5 -C₆H₇)(CO)₃Cr-Sn(C₆H₅)₃] (**33a**): THF (6 mL), **32a** (304.8 mg, 1.4 mmol), -78 °C, THF (5 mL), Ph₃SnCl (580.9 mg, 1.5 mmol), stirring for 1 h at -78 °C; complex **33a** (418 mg, 0.74 mmol, 53% yield). MS (EI): *m/e* 566, 564, 562 (M (¹²⁰Sn, ¹¹⁸Sn, ¹¹⁶Sn))⁺, 481 (M - 3CO)⁺, 403-401 (Cr-SnPh₃)⁺, 351 (¹²⁰Sn-Ph₃)⁺.

[(η^5 -C₆H₆D)(CO)₃Cr-Sn(C₆H₅)₃] (**33b**): THF (6 mL), **32b** (304.8 mg, 1.4 mmol), -78 °C, saturated THF solution (5 mL) of Ph₃SnCl (580.9 mg, 1.5 mmol); complex **33b** (418 mg, 0.74 mmol, 53% yield).

[(η^5 -1-*exo*-C₁₂H₉O)(CO)₃Cr-Sn(C₆H₅)₃] (**31**): THF (4 mL), complex **30** (280 mg, 0.89 mmol), -78 °C, THF (4 mL), Ph₃SnCl (385.5 mg, 1 mmol); complex **31** (68.1 mg, 0.104 mmol, 11.6% yield). MS (EI): *m/e* 655, 653, 651 (M (¹²⁰Sn, ¹¹⁸Sn, ¹¹⁶Sn)).

Acknowledgment. The CNRS and the Ministry of Research and Technology (J.-P.D.) are gratefully acknowledged for financial support. We thank Pascale Geysersmans for her participation to this work.

Supplementary Material Available: Additional experimental data, all bond distances and all bond angles, anisotropic temperature factors, hydrogen atom positions, and important least-squares planes (9 pages). Ordering information is given on any current masthead page.

OM940602P

(35) For complete analytical data, see: Reference 19.

Kinetics and Mechanism of the Reductive Elimination of Cyclic Titanocene Iminoaclys

Juan Cámpora and Stephen L. Buchwald*

Department of Chemistry, Massachusetts Institute of Technology,
Cambridge, Massachusetts 02139

Enrique Gutiérrez-Puebla* and Angeles Monge

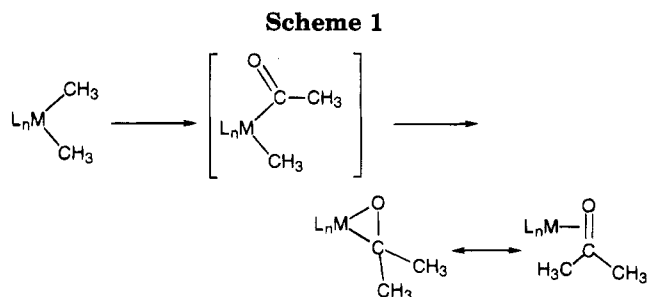
Instituto de Ciencia de Materiales, Sede D, CSIC, Serrano 113, 28006 Madrid, and
Facultad de Ciencias Químicas, Universidad Complutense, 28040 Madrid, Spain

Received November 30, 1994*

1,1-Dicyclopentadienyltitanaindan (**1**) reacts with isocyanides (RNC) to give cyclic iminoacyl complexes **2** (R = *t*-Bu) and **5a–e** (R = *p*-R'C₆H₄, R' = Et₂N, MeO, Me, H, and Cl) where the isocyanide has inserted into the Ti–CH₂ bond. The X-ray crystal structure of **2** has been determined. Complex **2** crystallizes in a monoclinic space group *P*2₁ with *a* = 14.353(1), *b* = 8.556(2), *c* = 15.652(2) Å; β = 88.95(5); and *Z* = 4. Compounds **2** and **5a–e** decompose in solution with formation of imines and paramagnetic Ti species. The decomposition follows first-order kinetics, with Δ*G*[‡] = 24.5 ± 0.2 Kcal mol, Δ*H*[‡] = 24.3 ± 0.2 Kcal mol, and Δ*S*[‡] = –0.4 ± 2 eu in the case of **2**. The rate of imine elimination depends on the nature of the substituent on the nitrogen atom, higher rates are observed for electron-withdrawing substituents (Hammett ρ = +1.59 ± 0.04 for **5a–e**), and the rate is little affected by the solvent or by the presence of PMe₃. These results are consistent with a concerted reductive elimination mechanism that initially leads to an unstable η¹-imine complex which subsequently converts to the observed products.

Introduction

Reductive elimination reactions of metal bis(σ-hydrocarbyl) derivatives have a central role in many stoichiometric and catalytic processes of interest in organic synthesis,¹ since they lead to the formation of new carbon–carbon bonds. Examples of these reactions are known for virtually all transition metals.² Late transition metal dialkyl or metallacyclic complexes frequently decompose by reductive elimination.³ For their early transition metal counterparts, however, processes such as hydrogen abstraction from the ligands^{4a–d} or metal–carbon bond homolysis are more common.^{4d–h} Thus, while reductive coupling of aryl ligands is well documented for group 10 biaryls,³ the analogous process on biaryl zirconocene derivatives can only be induced under photochemical conditions,^{4f} and a radical decomposition seems to be preferred when diaryltitanocenes are



irradiated.^{4d,e} One-electron oxidation of titanacyclobutanes also induces Ti–C bond homolysis, leading to cyclopropanes.^{4h} Yet, reductive elimination is still a feasible process involving complexes of group 4 σ-hydrocarbyl derivatives. The most commonly observed carbon–carbon reductive elimination process involving complexes of group 4 metals is the coupling of an alkyl and an acyl ligand to yield a ketone, free or complexed to the metallocene moiety.⁵ The formation of a strong metal–oxygen bond in the intermediate ketone complex (e.g. Scheme 1) has been invoked to explain the occurrence of this kind of process. More recently, examples of related alkyl–iminoacyl couplings have also been observed.⁶ These coupling reactions are valuable tools

* Abstract published in *Advance ACS Abstracts*, February 1, 1995.

(1) (a) Davies, S. *Organotransition Metal Chemistry: Applications to Organic Synthesis*; Pergamon Press: Oxford, 1982. (b) *The Chemistry of the Metal-Carbon Bond*; Hartley, F. R., Patai, S., Eds.; J. Wiley & Sons: Chichester, 1985; Vol. 3 (Carbon-Carbon bond formation using Organometallic Compounds).

(2) Collman, P.; Hegedus, L. S.; Norton, J. R.; Finke, R. G. *Principles and Applications of Organotransition Metal Chemistry*, 2nd ed.; University Science Books: Mill Valley, CA, 1987.

(3) (a) Yamamoto, A. *Organotransition Metal Chemistry. Fundamental Concepts and Applications*; J. Wiley & Sons: Toronto, 1986. (b) Merwin, P. K.; Schanbel, R. C.; Koola, J. D.; Roddick, D. H. *Organometallics* **1992**, *11*, 2972 and references therein.

(4) (a) Erker, G.; Kropp, K. *J. Am. Chem. Soc.* **1979**, *101*, 3659. (b) Kropp, K.; Erker, G. *Organometallics* **1982**, *1*, 1246. (c) Buchwald, S. L.; Watson, B. T. *J. Am. Chem. Soc.* **1986**, *108*, 7411. (d) Rausch, M. D.; Boon, W. H.; Mintz, E. A. *J. Organomet. Chem.* **1978**, *160*, 81. (e) Tumas, W.; Wheeler, D. R.; Grubbs, R. H. *J. Am. Chem. Soc.* **1987**, *109*, 6182. (f) Erker, G. *J. Organomet. Chem.* **1977**, *134*, 189. (g) Buchwald, S. L.; Nielsen, R. B. *J. Am. Chem. Soc.* **1988**, *110*, 3171 and references therein. (h) Burk, M. J.; Tumas, W.; Ward, M. D.; Wheeler, D. R. *J. Am. Chem. Soc.* **1990**, *112*, 6133.

(5) (a) Fachinetti, G.; Floriani, C. *J. Chem. Soc., Chem. Commun.* **1972**, 654. (b) Wilson, M. E.; McDermott, J. X.; Whitesides, G. M. *J. Am. Chem. Soc.* **1976**, *98*, 6529. (c) Erker, G.; Kropp, K. *J. Organomet. Chem.* **1980**, *194*, 45. (d) Erker, G. *Acc. Chem. Res.* **1984**, *17*, 103. (e) Erker, G.; Rosenfeldt, F. *J. Organomet. Chem.* **1982**, *224*, 29. (f) Negishi, E.; Holmes, S. J.; Tour, J. M.; Miller, J. A.; Cederbaum, F. E.; Swanson, D. R.; Takahashi, T. *J. Am. Chem. Soc.* **1989**, *111*, 3336. (g) Grossman, R. B.; Buchwald, S. L. *J. Org. Chem.* **1992**, *57*, 5803. (h) Fang, Q. Ph.D. dissertation, Massachusetts Institute of Technology, 1990. (i) Cardin, D. J.; Lappert, M. F.; Raston, C. L. *Chemistry of Organo-Zirconium and -Hafnium Compounds*; Ellis Horwood: Chichester, 1986; pp 304–306.

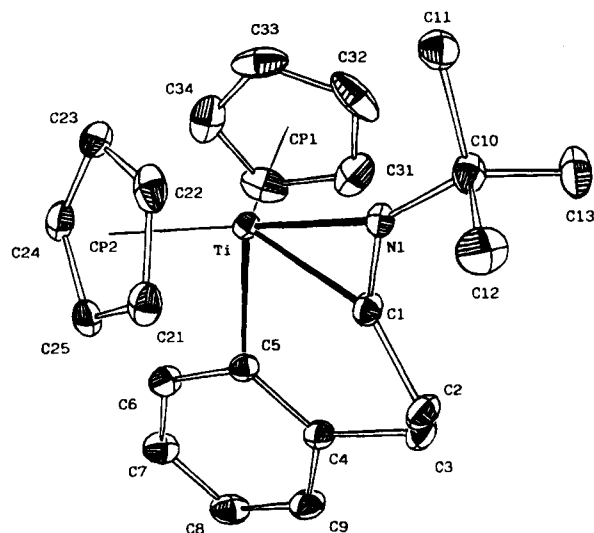


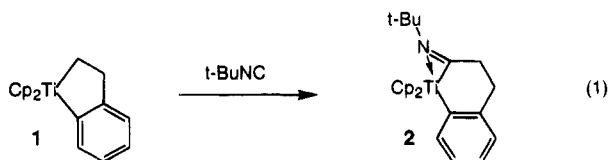
Figure 1. Crystal structure of compound **2**.

for ring formation, in view of the ready availability of metallacyclic compounds of group 4 metals,⁷ although, in some instances, the carbonylation-reductive elimination sequence with titanium or zirconium metallacycles is complicated by side reactions.^{5c,d}

We are currently investigating the chemistry and possible synthetic applications of titanaindanes and other related metallacycles.⁸ As a result of this research, we have discovered that the titanium metallacycles of the type **2**, which can be readily prepared by reaction of dicyclopentadienyltitanaindan (**1**) with a suitable isocyanide, cleanly undergo reductive elimination, providing the corresponding imines as the only observed organic product. In order to gain a deeper understanding of the reductive elimination reaction in these iminoacyls and the related acyl complexes, we have studied this process in detail. The results of this study are reported herein.

Results

Treatment of diethyl ether solutions of red dicyclopentadienyltitanaindan (**1**) with *tert*-butyl isocyanide at room temperature causes an immediate color change to pale yellow. Concentration and cooling of the reaction mixture affords yellow crystals of the iminoacyl product **2** in high yield (eq 1). The ¹H NMR spectrum of **2**



displays a single resonance at δ 0.91 that integrates for nine hydrogens, indicating that only 1 equiv of isocya-

(6) (a) Durfee, L. D.; Fanwick, P. E.; Rothwell, I. P. *Organometallics* **1990**, *9*, 75. (b) Chamberlain, L. R.; Staffey, B. D.; Rothwell, I. P. *Polyhedron* **1984**, *8*, 351. (c) Hessen, B.; Blenkins, J.; Teuben, J. H.; Helgesson, G.; Jagner, S. *Organometallics* **1989**, *8*, 830. (d) Berk, S. C.; Grossman, R. B.; Buchwald, S. L. *J. Am. Chem. Soc.* **1993**, *115*, 4912. (e) Davis, J. M.; Whitby, J. M.; Jexa-Chamiec, A. *Tetrahedron Lett.* **1992**, *33*, 5655.

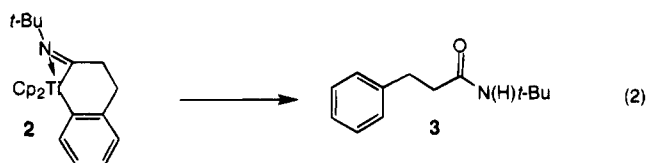
(7) (a) Buchwald, S. L.; Nielsen, R. B. *Chem. Rev.* **1988**, *88*, 1047. (b) RajanBabu, T. V.; Nugent, W. A.; Taber, D. F.; Fagan, P. J. *J. Am. Chem. Soc.* **1988**, *111*, 7128. (c) Knight, K. S.; Waymouth, R. M. *J. Am. Chem. Soc.* **1991**, *113*, 6268 and references therein.

(8) Cámpora, J.; Buchwald, S. L. *Organometallics* **1993**, *12*, 4182.

Table 1. Selected Bond Distances (Å) and Angles (deg) of Complex **2**

Ti-N1	2.148(2)	C1-C2	1.483(3)
Ti-C1	2.056(2)	C2-C3	1.521(4)
Ti-C5	2.229(2)	C3-C4	1.520(3)
N1-C1	1.241(3)	C4-C5	1.410(3)
N1-C10	1.496(3)		
C1-Ti-C5	77.8(1)	C1-N1-C10	131.4(2)
N1-Ti-C5	111.7(1)	N1-C1-C2	139.1(2)
N1-Ti-C1	34.3(1)	Cp1-Ti-Cp2	131.7(1)
Ti-C1-C2	143.8(2)	Ti-N1-C10	159.7(1)

nide has been incorporated. An absorption at 1725 cm^{-1} in the IR spectrum and a signal for an imino carbon atom at δ 219.2 ppm in the ¹³C NMR spectrum are characteristic of the iminoacyl group.¹⁰⁻¹² In **1**, ¹H NMR signals for the methylene groups appear at δ 3.23 (t, 2H) and δ 1.45 (t, 2H). The corresponding methylene groups in **2** give rise to signals at δ 2.76 (t, 2H) and δ 2.53 (t, 2H). The chemical shifts for the corresponding methylene ¹³C NMR resonances for **2** (δ 37.4 and 58.6, respectively) are also very similar to those for **1** (δ 38.8 and 60.1). These data do not allow the unambiguous demonstration of the regiochemistry of the isocyanide insertion in **1**. This was determined by treatment of compound **2** with methanesulfonic acid, followed by 30% aqueous hydrogen peroxide to afford the amide **3** in 85% isolated yield. This result proves that the isocyanide insertion has taken place into the Ti-CH₂ bond (eq 2).



We have also addressed the question of whether the iminoacyl group coordinates to the metal in a dihapto (η^2) or monohapto (η^1) fashion. Although the spectroscopic features of the iminoacyl fragment can be used to ascertain the coordination mode within a particular class of compounds,^{10a} there is not a generally applicable set of criteria^{10,11} to unambiguously make this determination. Therefore, an X-ray structure determination was undertaken in order to complete the characterization of **2**. Figure 1 shows an ORTEP diagram for **2**, which clearly indicates that the iminoacyl ligand is bound in a η^2 fashion. The Ti-C, Ti-N, and C=N distances (Table 1) in **2** are very similar to those found for $[\text{Cp}_2\text{Ti}(\eta^2\text{-C(=N}t\text{Bu}^i)\text{Me})(\text{C}\equiv\text{N}t\text{Bu}^i)]^+[\text{BPh}_4]^-$.¹¹ The cyclic nature of complex **2** forces the nitrogen group to adopt a "N-outside" coordination mode, which is disfavored in open-chain metallocene acyl and iminoacyl complexes.¹³

When a benzene solution of **2** is allowed to stand at room temperature for 2 days or is gently heated, its color changes to dark brown. From these solutions it is possible to isolate imine **4**. If this transformation is monitored by ¹H NMR, the gradual disappearance of

(9) Erker, G.; Korek, U.; Petrenz, P.; Rheingold, A. L. *J. Organomet. Chem.* **1991**, *421*, 215.

(10) Carmona, E.; Palma, P.; Paneque, M.; Poveda, M. L. *Organometallics* **1990**, *9*, 583.

(11) Bochmann, M.; Wilson, L. M.; Hursthouse, M. B.; Short, R. *Organometallics* **1987**, *6*, 2556.

(12) Durfee, L. D.; Rothwell, I. P. *Chem. Rev.* **1988**, *88*, 1059.

(13) Tatsumi, K.; Nakamura, A.; Hofmann, P.; Stauffert, P.; Hoffmann, R. *J. Am. Chem. Soc.* **1985**, *107*, 4440.

Table 2. Crystal and Refinement Data

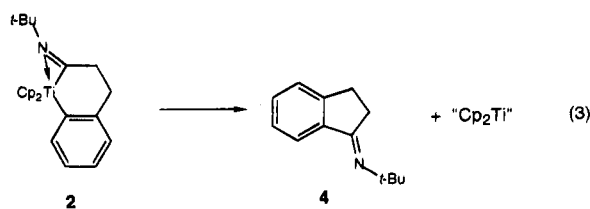
formula	TiC ₂₃ H ₂₇ N ₁
M _r	365.37
crystal system	monoclinic
space group	P2 ₁ /c
a, Å	14.353(1)
b, Å	8.556(2)
c, Å	15.652(2)
β	88.95(5)
V, Å ³	1921.8(5)
Z	4
F(000)	776
ρ (calcd), g cm ⁻³	1.26
temp, °C	21
μ, cm ⁻¹	4.43
cryst dims, mm	0.2 × 0.2 × 0.2
diffractometer	Enraf-Nonius CAD4
radiation	graphite-monochromatic Mo Kα (λ = 0.71069 Å)
scan technique	Ω/2θ
data collected	1 < 30° θ; (-20,0,0) to (20,12,22)
unique data	5580
unique data (I) ≥ 3σ(I)	4072
R(int), %	1.0
std rflns	3/78 rflns
variables	222
R _F , %	3.8
R _{wF} , % (unit weights)	4.2
average shift/error	0.008

Table 3. Atomic Parameters for TiC₂₃H₂₇N^a

atom	X/a	Y/b	Z/c	U _{eq}
Ti	0.29399(2)	0.37505(4)	0.79171(2)	301(1)
N1	0.27993(12)	0.53660(20)	0.89619(10)	356(5)
C1	0.20900(15)	0.45484(26)	0.88951(13)	397(6)
C2	0.11907(18)	0.42746(33)	0.93534(16)	552(8)
C3	0.10739(19)	0.25133(35)	0.94302(16)	566(9)
C4	0.10973(15)	0.16489(27)	0.85812(14)	418(7)
C5	0.17410(14)	0.19694(25)	0.79123(13)	368(6)
C6	0.16741(17)	0.09798(29)	0.71974(16)	487(8)
C7	0.10495(18)	-0.02442(32)	0.71372(18)	568(9)
C8	0.04296(18)	-0.05284(34)	0.77970(20)	616(10)
C9	0.04539(17)	0.04172(34)	0.85068(18)	562(9)
C10	0.30448(17)	0.66153(27)	0.95879(14)	449(7)
C11	0.35369(24)	0.58563(36)	1.04653(16)	695(11)
C12	0.22824(22)	0.78550(34)	0.95903(22)	708(20)
C13	0.39759(19)	0.73378(32)	0.93147(17)	558(9)
C21	0.20688(19)	0.57174(30)	0.71466(16)	517(8)
C22	0.29990(21)	0.62365(31)	0.71849(15)	563(9)
C23	0.35571(18)	0.52109(35)	0.67163(16)	556(9)
C24	0.29748(19)	0.40424(32)	0.63863(14)	518(8)
C25	0.20602(17)	0.43655(31)	0.66459(14)	472(7)
C31	0.36288(23)	0.18109(46)	0.88678(21)	791(13)
C32	0.42336(27)	0.30510(44)	0.88305(27)	921(25)
C33	0.45657(19)	0.31741(41)	0.80122(30)	826(22)
C34	0.41917(25)	0.19822(48)	0.75490(20)	819(13)
C35	0.36219(20)	0.11596(33)	0.80752(25)	691(19)

^a Coordinates and thermal parameters are defined as $U_{eq} = \frac{1}{3} \sum_i U_{ij} a_i^* a_j^* a_i a_j \times 10^4$.

the signals for **2** occurs, concomitant with the appearance of new resonances for **4** (eq 3). No new cyclopen-



tadienyl signals are observed; any "titanocene" species which are presumably formed could not be isolated.¹⁴

(14) Bercaw, J. E.; Marvich, R. H.; Bell, L. G.; Britzinger, H. H. *J. Am. Chem. Soc.* **1972**, *94*, 1219.

If the reaction is run in the presence of Me₂S₂, however, Cp₂Ti(SME)₂¹⁵ is formed in high yield, without affecting the rate of the elimination reaction.

In order to study the rate of this reductive elimination reaction, compound **2** was generated *in situ* in an NMR tube, and its conversion to **4** was monitored by ¹H NMR. The reaction follows first-order kinetics for > 3 half-lives. Additionally, the rate constant does not change appreciably when the initial concentration of iminoacyl complex was varied from 0.07 to 0.3 M (in benzene, $k = (1.1 \pm 0.1) \times 10^{-3} \text{ s}^{-1}$ at 65.7 °C).

The solvent dependence of this transformation has also been investigated. A small solvent effect was found when the reaction rate was measured in four different solvents (benzene, chloroform, tetrahydrofuran, and acetonitrile) at 65 °C; the elimination being somewhat slower in polar solvents ($k(\text{benzene}) = (1.14 \pm 0.02) \times 10^{-3} \text{ s}^{-1}$, $k(\text{acetonitrile}) = (4.48 \pm 0.05) \times 10^{-4} \text{ s}^{-1}$, see Experimental Section for details).

To ascertain whether the transformation of **2** to **4** was an example of a ligand-induced reductive elimination,^{3a,6a} the reaction was run in the presence of added PMe₃. A small decrease in the rate was observed in the presence of this ligand. For example, the rate constant for the reaction in benzene at 59.7 °C was $(4.5 \pm 0.1) \times 10^{-4} \text{ s}^{-1}$. Addition of a 2- or a 5-fold excess of PMe₃ had almost no effect, and a 10-fold excess (ca. 1.43 M) caused a very small rate decrease ($k = (3.2 \pm 0.1) \times 10^{-4} \text{ s}^{-1}$). Thus, there is little or no effect in the reductive elimination process by added ligand in this system.

Figure 2a shows one set of measurements of the temperature dependence of the elimination rate of compound **2**. Activation parameters deduced from an Eyring plot (Figure 2b, rates averaged from three runs) are $\Delta G^\ddagger = 24.5 \pm 0.2 \text{ Kcal/mol}$, $\Delta H^\ddagger = 24.3 \pm 0.2 \text{ Kcal/mol}$, and $\Delta S^\ddagger = -0.4 \pm 2 \text{ eu}$. Rate measurements were made at temperatures from 311.5 K (38.5 °C) to 354 K (81 °C). Our interpretation of these results will be discussed in a later section of this paper.

As previously mentioned, the reductive elimination of some bis(σ -hydrocarbyl) group **4** derivatives can be photochemically induced. Since all the kinetic measurements described herein were performed in the dark, in an NMR probe, we decided to qualitatively determine whether there is any influence of light on the reductive elimination of **2**. Two NMR tubes containing samples of a solution of **2** in benzene were placed in a water bath at 20 °C. One of these was covered with aluminum foil and the other exposed to the light of a sun lamp. In both cases the progress of the reaction was monitored by ¹H NMR. The rate of reductive elimination observed for the sample exposed to the light ($t_{1/2}$ ca. 11 h) was approximately twice that of the foil-covered sample ($t_{1/2}$ ca. 20 h). This shows that, under these conditions, photochemical and thermal elimination reactions proceed at roughly comparable rates.

In order to evaluate the influence of electronic factors, we have prepared and spectroscopically characterized a series of iminoacyl complexes (**5a–e**) derived from the reaction of **1** with five different para-substituted phenyl isocyanides (Scheme 2). The spectroscopic features of these complexes are similar to those of **2** (see Experimental Section), except for the chemical shifts of the ¹³C resonances of one of the methylene groups. Thus,

(15) Abel, E. W.; Jenkins, C. R. *J. Organomet. Chem.* **1968**, *14*, 285.

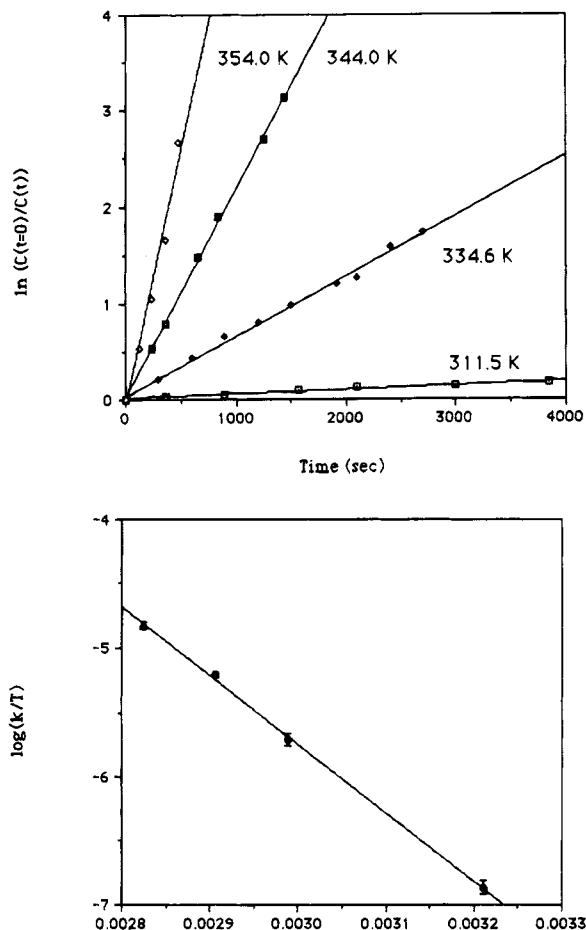
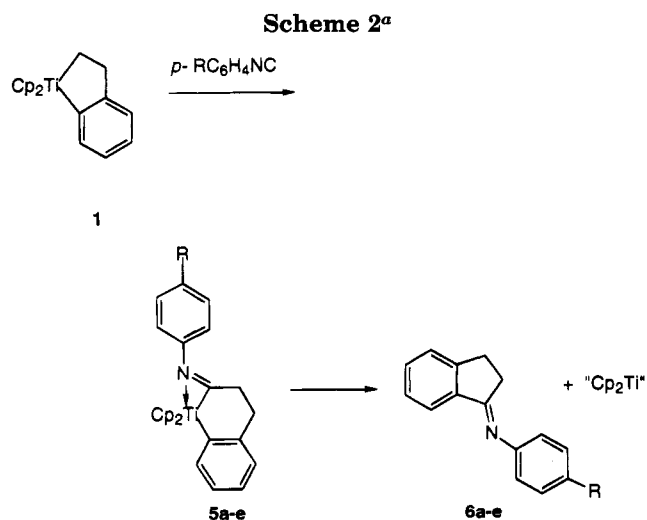


Figure 2. Reaction rates for the reductive elimination of **3** at different temperatures (a) and the resulting Eyring plot (b).



^a Legend: **a**, R = Et₂N; **b**, R = MeO; **c**, R = Me; **d**, R = H; **e**, R = Cl.

while the signal for one methylene carbon appears at 37 ppm in **2** and in **5a-e**, the other methylene signal shifts from 58.6 ppm in **2** to ca. 29 ppm in **5a-e**.

Although all other features, including the chemical shifts of the NMR signals of the phenylene group remain unchanged on passing from **2** to **5a-e**, we chose to confirm the regiochemistry of aryl isocyanide insertion. Therefore, the structure of one of these compounds, **5b**, was unequivocally established by a procedure analogous to the one used for **2**. In this manner, *N*-(4 methox-

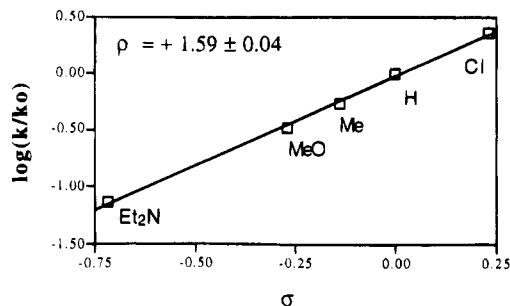


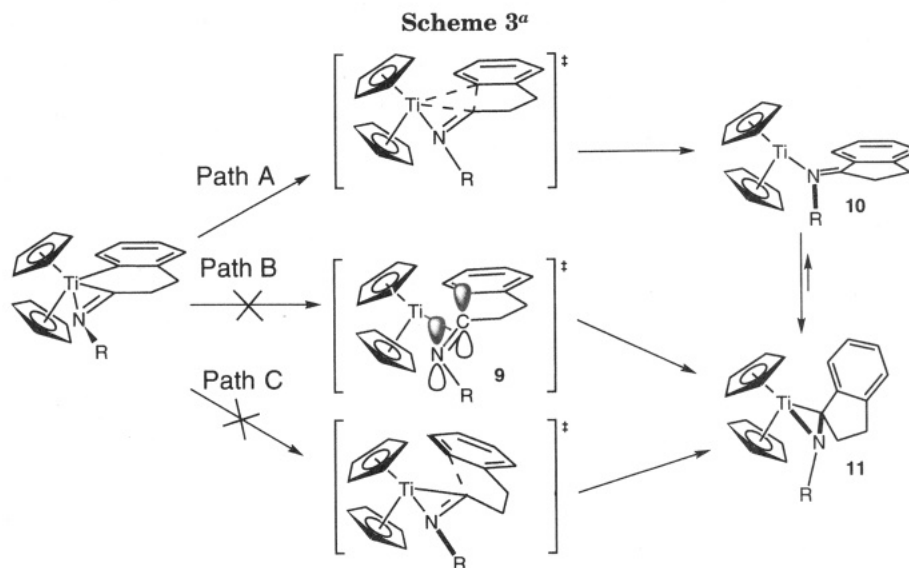
Figure 3. Hammett plot of the rates of reductive elimination of **5a-e**.

phenyl)-3-phenylpropionamide (**7**) was formed from **5b**. On the basis of the spectroscopic similarity of the series **5a-e** and the analogous IR and ¹³C features of the iminoacyl group of **5a-e** and **2**, we conclude that all these cyclic iminoacyl complexes must be structurally similar.

The rates of the reductive elimination reactions of the (*N*-arylimino)acyl complexes are appreciably faster than those for **2**. This instability prevented the isolation of these compounds in an analytically pure form. They were, however, all characterized by ¹H and ¹³C NMR and IR spectroscopy. Fortunately, the reaction of **1** with the corresponding isocyanides is still fast as compared to the reductive elimination of **5a-e**. Samples of pale-yellow **5a-e** of purity higher than 90% (as deduced from their ¹H NMR spectra using ferrocene as an internal standard) can be prepared by reacting cold (-40 °C) solutions of **1** in diethyl ether with the isocyanide, collecting the precipitated compound and washing it with cold hexane. The general features of the decomposition of **5a-e** are similar to those seen for **2**. In all cases they react by a process which exhibits first-order kinetics for at least 3 half-lives. No significant differences were found when the decomposition of **5c** was monitored starting with different initial concentrations (0.14, 0.28, and 0.7 M). Although the formation of the imine is apparently not quantitative in benzene-*d*₆ (presumably due to complexation or reaction with some paramagnetic titanium species), quantitative yields of imine, as determined by ¹H NMR, were observed to form when the reaction was carried out in CD₂Cl₂ or CD₃CN, even when no new ¹H NMR signals attributable to the cyclopentadienyl group of diamagnetic titanium products could be observed. For this reason, CD₂Cl₂ was the solvent used for quantitative runs. When **5c** was allowed to decompose in benzene-*d*₆ in the presence of Me₂S₂, quantitative production of Cp₂Ti(SMe)₂ and the imine was observed. Figure 3 is a Hammett plot of the elimination rate (averaged over duplicate runs) of **5a-e** at 23.5 °C. As can be seen, the transformation is slowed by electron-releasing substituents (**5a,b**) and accelerated by electron-withdrawing substituents (**5e**). A ρ value of $+1.59 \pm 0.04$ was found.

Discussion

Reductive elimination appears to be a relatively disfavored process for early transition metal bis(σ -hydrocarbyls).^{2b} However, reductive elimination reactions of early transition metal acyl-alkyl or iminoacyl-alkyl complexes are more common.^{5,6} Nearly all known examples of well-characterized acyl and iminoacyl de-

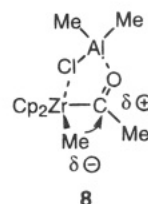


^a Legend: path A, “in-plane” reductive elimination to η^1 -imine complex; path B, “in-plane” reductive elimination to η^2 -imine complex (note: π -system of the imine is orthogonal to the LUMO of the titanocene fragment); path C, reductive elimination via nucleophilic attack.

rivatives of group 4 and other early transition metals display η^2 -type coordination.¹² Therefore, we have first considered whether the special reactivity associated with this ligand combination could partially explain the facile elimination that occurs in acyl- or iminoacyl-alkyl complexes. It is known that the product of the elimination from a number of titanium and zirconium acyl- and iminoacyl-hydrocarbyl derivatives is the corresponding ketone^{5d-f} or imine^{6a-c} either free or coordinated to the metal (Scheme 1). On this basis, Erker has proposed that, in the case of the acyl derivatives, the stability gained by the formation of a strong metal-oxygen bond may overcome the unfavorable energetic contribution of the reduction of the metallic center by two units.^{5d} It should be noted that in this process only a formal reduction of the zirconium center takes place, since these ketone and imine complexes are better described as metallaioxiranes^{5j} or metallaaziridines,^{6,16b} than as π -complexes. We have not been able to detect imine complexes during the decomposition of **2** or **5a-e** even when the reaction was run in the presence of ligands (PMe_3)¹⁶ or trapping agents (MeCN, MeOH), probably due to the low stability of such complexes. In contrast, reductive elimination of aryl-oxide-supported (iminoacyl)alkyltitanium complexes has been observed by Rothwell,^{6a-d} and Whitby has reported the generation and *in situ* trapping of zirconocene complexes of imines formed by reductive elimination processes.^{6e}

Formation of an η^2 -ketone ligand from Zr-acyl complexes has been shown to be promoted by aluminum alkyls.¹⁷ Grubbs has attributed this to the increase in the electrophilic character of the carbon atom induced upon coordination of the acyl oxygen to aluminum, which facilitates the migration of the alkyl to the acyl group. In this case the carbon-carbon bond-forming

process can best be described as a nucleophilic attack of the methyl group at the carbon atom of the electrophilic carbonyl. Here, the intermediate **8** should be flexible enough to allow for attack to occur in a stereo-electronically favorable manner.¹⁹



In contrast to **8**, the rigidly planar structure of complexes **2** and **5a-e** renders an analogous attack stereo-electronically unfavorable (Scheme 3, path C). A concerted, “in-plane”, reductive elimination appears to more feasible. Such a process is consistent with the near-zero value for ΔS^\ddagger . Although the meaning of ΔS^\ddagger values is often unclear, the simplicity of this system, in particular the absence of ligand or solvent binding processes (i.e., association or dissociation) makes the interpretation of this number for ΔS^\ddagger less ambiguous. Thus, we can surmise that there is a small degree of structural change on going from the ground state to the transition state (Scheme 3, path A) in these reactions of **2** and **5a-e**. Since the ligand is generated in a position in which the π -(C=N) orbitals of the imine are orthogonal to the LUMO of the Cp_2Ti fragment, intermediate **9** should be of high energy. As a consequence, we postulate that the initial product of the reductive elimination should be an η^1 -imine complex (**10**). The fate of **10** depends on the conditions under which it is generated: it could either react (e.g., with Me_2S_2) or rearrange to the more stable complex **11**.

(16) (a) Buchwald, S. L.; Wannamaker, M. W.; Watson, B. T. *J. Am. Chem. Soc.* **1989**, *111*, 776. (b) Buchwald, S. L.; Watson, B. T.; Wannamaker, M. W.; Dewan, J. C. *J. Am. Chem. Soc.* **1989**, *111*, 4486. (c) Coles, R. J.; Whitby, R. J.; Blagg, J. *Synlett* **1989**, 4486. (d) Coles, R. J.; Harris, M. C. J.; Whitby, R. J.; Blagg, J. *Organometallics* **1994**, *13*, 190.

(17) Waymouth, R. M.; Grubbs, R. H. *Organometallics* **1988**, *7*, 1631.

(18) While there is no effect on the reaction rate by the addition of ligands such as PMe_3 (**2** and **5a-e** are 18-electron complexes), the electronically less saturated species $(\text{ArO})_2\text{Ti}(\eta^2\text{-C(=N-}t\text{-Bu)CH}_2\text{Ph})(\text{CH}_2\text{Ph})$ undergoes a ligand-induced reductive elimination to give $(\text{ArO})_2\text{Ti}(\eta^2\text{-C(=N-}t\text{-Bu)(CH}_2\text{Ph)}_2)(\text{L})$.^{6a} In the absence of added ligand, no reductive elimination is seen.

(19) Deslongschamps, P. *Stereoelectronic Effects in Organic Chemistry*; Pergamon: Oxford, 1983.

Since a nucleophilic attack on the iminoacyl carbon is not likely in our system, the accelerating effect of electron-withdrawing substituents is not easily explainable on the basis of the increase of the electrophilic character of the iminoacyl carbon. In order to explain the observed reaction rates, it is necessary to consider both ground-state and transition-state effects. In the ground state, X = electron-donating substituent should be stabilizing, causing enhanced interaction of the nitrogen of the η^2 -iminoacyl to the titanium center. Thus, the order of stability would be **5a** > **5b** > **5c** > **5d** > **5e**. Therefore, ground-state effects should tend to accelerate the rate of reductive elimination when electron-withdrawing substituents are present.

In the transition state, there are two opposing effects. Electron-withdrawing substituents can stabilize the nascent Ti(II) center by decreasing the electron density of the complex. Thus, an enhanced reaction rate would be expected. In contrast, the 14-electron Cp₂Ti fragment is being stabilized by the η^1 -imine ligand,¹⁸ and for this reason, better electron-donor substituents should be stabilizing and contribute to lower the energy of the transition state. These two factors oppose one to another and might be expected to cancel each other to some extent. If this is the case, ground-state effects would be expected to dominate.

Conclusions

Cyclic titanocene iminoacyl complexes **2** and **5a–e** readily undergo reductive elimination to yield the corresponding imines. The reaction rate is controlled by the nature of the substituents on the nitrogen atom, probably due to ground-state factors. In contrast with the reductive elimination in related Zr complexes induced by aluminum alkyls, we believe that the reaction takes place in a concerted manner, giving rise to a transient η^1 -imine complex which subsequently converts to the observed products. Stereoelectronic considerations lead us to believe that this result is relevant to the carbonylation of zircona and titanacycles to ketones.^{5,20} Here an η^1 -ketone complex may be a transient intermediate prior to the formation of a more stable η^2 complex.

Experimental Section

All manipulations were performed using either standard Schlenk techniques under argon or a Vacuum Atmospheres dry box under N₂, unless stated otherwise. Argon used in the Schlenk work was purified by passage through columns of BASF-RS-11 (Chemalog) and Linde 4 Å molecular sieves. Nuclear magnetic resonance (NMR) spectra were recorded on a Varian XL-300 spectrometer. Infrared (IR) spectra were recorded on a Mattson Cygnus Starlab 100 Fourier transform spectrometer. Only significant IR bands are reported. Electron-impact high-resolution mass determinations (HRMS) were recorded on a Finnegan MAT system 8200 spectrometer. Elemental analyses were performed by Desert Analytics, Tucson, AZ. Spinning plate chromatography was performed with a Harrison Research Chromatotron using 2 and 4 mm thick plates poured with Merck Kieselgel 60 PF25A silica gel.

Tetrahydrofuran, benzene, and diethyl ether were dried and deoxygenated by refluxing over sodium/benzophenone ketyl followed by distillation under argon or nitrogen. Hexane was

deoxygenated by standard procedures and then stored over CaH₂. The deoxygenated hexane thus obtained was dried and deoxygenated by refluxing over sodium/benzophenone ketyl followed by distillation under nitrogen. Toluene was dried over sodium followed by distillation under nitrogen. Dichloromethane was dried by distillation from CaH₂ under nitrogen. Deuterated solvents were purchased from Cambridge Isotopes Co. Benzene-*d*₆ and THF-*d*₆ were vacuum transferred from sodium/benzophenone ketyl. CDCl₃ and CD₂Cl₂ were vacuum transferred from CaH₂. CD₃CN was vacuum transferred without further purification.

tert-Butyl isocyanide was purchased from Aldrich and used as received. 1,1-Dicyclopentadienyl-1-titanaindane (**1**),⁹ *p*-(diethylamino)phenyl, *p*-methoxyphenyl, *p*-methylphenyl, phenyl, and *p*-chlorophenyl isocyanide were prepared according published procedures.²¹

Preparation of Iminoacyl 2. A solution of compound **1** (282 mg, 1 mmol) in diethyl ether (30 mL) was treated with *tert*-butyl isocyanide (0.11 mL, 1 mmol). The color of the solution immediately changed from red to bright yellow. Concentration *in vacuo* to ca. 5–10 mL and cooling to –20 °C yielded 230 mg of yellow crystals of **2** which were collected by filtration and washed with cold hexane. The mother liquor was concentrated to ca. 3 mL and was mixed with an equal volume of hexane. This solution was cooled to –20 °C overnight, to yield an additional 50 mg of compound **2** which was isolated by filtration and washed with cold hexane. Overall yield, 280 mg (77%). IR (Nujol mull) 1725 cm⁻¹ (ν (C=N)). ¹H NMR (300 MHz, C₆D₆, 20 °C) δ 0.91 (s, 9H, C(CH₃)₃), 2.53 (m, 2H, CH₂), 2.76 (m, 2H, CH₂), 5.26 (s, 10H, Cp), 7.18 (m, 2H, CH_{arom}), 7.31 (m, 1H, CH_{arom}), 7.51 (m, 1H, CH_{arom}). ¹³C {¹H} (75 MHz, C₆D₆, 20 °C) δ 29.3 (C(CH₃)₃), 29.6 (C(CH₃)₃), 37.4 (CH₂), 58.6 (CH₂), 106.6 (Cp), 122.0, 123.1, 129.8, 144.4 (CH_{arom}), 145.2, 175.7 (C_{quat arom}), 219.2 (C=N). Anal. Calcd for C₂₃H₂₇NTi: C, 75.61; H, 7.45. Found: C, 75.44; H, 7.35.

Conversion of Iminoacyl 2 to *N-tert*-Butyl-3-phenylpropionamide (3). A solution of **1** (282 mg, 1 mmol) in 30 mL of THF was treated with *t*-BuNC (0.11 mL, 1 mmol) at room temperature. After 5 min, MsOH (96 mg, 1 mmol) was added. The mixture was allowed to stir for 5 min and 35% aqueous H₂O₂ (0.25 mL) was added. After 10 min, a yellow precipitate had formed. The mixture was concentrated *in vacuo* and filtered through a pad of silica gel. Purification by spinning plate chromatography using a 4:6 diethyl ether/pentane mixture yielded 144 mg (83%) of the title compound. IR (Nujol mull) 3311 (ν (N–H)), 1639 (amide I), 1548 (amide II). ¹H NMR (300 MHz, CDCl₃, 20 °C) δ 1.24 (s, 9H, C(CH₃)₃), 2.34 (t, *J* = 7.8 Hz, 2H, CH₂), 2.89 (t, *J* = 7.8 Hz, 2H, CH₂), 5.05 (bs, 1H, NH), 7.20 (m, 5H, CH_{arom}). ¹³C {¹H} (75 MHz, CDCl₃, 20 °C) δ 29.1 (C(CH₃)₃), 32.2 (CH₂), 32.6 (CH₂), 51.4 (C(CH₃)₃), 126.5 (CH_{arom}), 128.8 (4 overlapping CH_{arom}), 141.5 (C_{quat arom}), 171.8 (C=O). HRMS calcd for C₁₃H₁₉NO 205.1466, found 205.1465.

Conversion of 2 to *N-tert*-Butyl-1-indanimine 4. A solution of compound **1** (601 mg, 1 mmol) in THF (20 mL) was treated with *tert*-butyl isocyanide (0.24 mL, 2.13 mmol), and the resulting solution of **2** was heated at 60 °C for 2 h. The solvent was evaporated *in vacuo* and the residue treated with chloroform (10 mL). The resulting red solution was evaporated and the residue was extracted with 2 × 15 mL of hexane. The solution was filtrated and evaporated and the residue extracted again with hexane (2 × 15 mL) in order to eliminate as much titanium-containing solids as possible. After removal of the hexane, the residue was distilled using a Kugelrohr apparatus. The colorless liquid thus obtained was a mixture of **4** and its enamine tautomer **4'** in an 2:1 ratio. Yield, 213 mg (53%). IR (liquid film) 1715 (ν (C=N)). Imine **4**: ¹H NMR (300 MHz, C₆D₆, 20 °C) δ 1.42 (s, 9H, C(CH₃)₃), 2.78 (m, 2H, CH₂), 3.35 (m, 2H, CH₂), 7.2–7.5 (m, 3H, CH_{arom}), 7.83 (d, *J* =

(20) Swanson, D. R.; Rousset, C. J.; Negishi, E.; Takahashi, T.; Seki, T.; Saburi, M.; Uchida, Y. *J. Org. Chem.* **1989**, *54*, 3521.

(21) Ugi, I.; Meyr, P. *Chem. Ber.* **1960**, *93*, 239.

7.4 Hz, CH_{arom}). ^{13}C { 1H } (75 MHz, C_6D_6 , 20 °C) δ 2.89 (CH_2), 29.9 ($C(CH_3)_3$), 30.1 (CH_2), 55.3 ($C(CH_3)_3$), 122.4 (CH_{arom}), 125.0 (CH_{arom}), 126.6 (CH_{arom}), 130.4 (CH_{arom}), 141.9 ($C_{quat\ arom}$), 147.7 ($C_{quat\ arom}$), 168.9 ($C=N$). Enamine 4': 1H NMR (300 MHz, C_6D_6 , 20 °C) δ 1.23 (s, 9H, $C(CH_3)_3$), 3.4 (d, $J = 2.0$ Hz, 2H, CH_2), 5.21 (t, $J = 2.0$ Hz, 1H, $=CH$), 7.2–7.5 (m, 3H, CH_{arom}). ^{13}C { 1H } (75 MHz, C_6D_6 , 20 °C) δ 29.9 ($C(CH_3)_3$), 36.1 (CH_2), 50.6 ($C(CH_3)_3$), 98.2 (CH), 115.8 (CH_{arom}), 123.5 (CH_{arom}), 124.6 (CH_{arom}), 125.4 (CH_{arom}), 142.0 (C_{quat}), 142.4 (C_{quat}), 143.3 (C_{quat}). HRMS M^+ calcd for $C_{13}H_{19}N$ 187.1360, found 187.1359.

Preparation of 5a–e. A solution of 1 (282 mg, 1 mmol) in diethyl ether (20–30 mL), cooled to -40 °C, was treated with a solution of 1 mmol of the corresponding isocyanide in diethyl ether (10 mL). After stirring for 5–15 min at -40 °C, a yellow precipitate of the iminoacyl complex had formed. In the case of **5d**, precipitation was accomplished by addition of 35 mL of hexane and cooling the resulting solution to -80 °C overnight. The compounds thus obtained have moderate thermal stability in the solid state, their color darkening upon standing at room temperature for several hours. The purity of the samples was higher than 90% as estimated by 1H NMR, using an internal standard of ferrocene. Yields: **5a**, 323 mg, 71%; **5b**, 212 mg, 51%; **5c**, 260 mg, 65%; **5d**, 196 mg, 20%; **5e**, 260 mg, 62%.

5a: IR (Nujol mull) 1703 cm^{-1} (ν ($C=N$)). 1H NMR (300 MHz, CD_2Cl_2 , -20 °C) δ 1.20 (t, $J = 7.0$, 6H, NCH_2CH_3), 2.99 (m, 2H, CH_2), 3.07 (m, 2H, CH_2), 3.42 (q, $J = 7.0$, 4H, NCH_2CH_3), 5.42 (s, 10H, Cp), 6.75 (m, 2H, CH_{arom}), 6.86 (m, 2H, CH_{arom}), 7.50 (m, 1H, CH_{arom}), 7.38 (m, 2H, CH_{arom}), 7.46 (m, 1H, CH_{arom}). ^{13}C { 1H } (75 MHz, $CDCl_3$, -20 °C) δ 12.2 (NCH_2CH_3), 28.8 (CH_2), 37.2 (CH_2), 44.2 (NCH_2CH_3), 106.0 (Cp), 110.1 (2 CH_{arom}), 121.4 (CH_{arom}), 122.1 (CH_{arom}), 124.6 (2 CH_{arom}), 127.2 (CH_{arom}), 130.0 ($C_{quat\ arom}$), 144.2 (CH_{arom}), 145.0 ($C_{quat\ arom}$), 146.1 ($C_{quat\ arom}$), 175.6 ($C_{quat\ arom}$), 218.8 ($C=N$).

5b: IR (Nujol mull) 1717 cm^{-1} (ν ($C=N$)). 1H NMR (300 MHz, CD_2Cl_2 , -20 °C) δ 3.02 (m, 2H, CH_2), 3.09 (m, 2H, CH_2), 3.87 (s, 3H, OCH_3), 5.42 (s, 10H, Cp), 6.84 (m, 1H, CH_{arom}), 7.05 (m, 2H, CH_{arom}), 7.20 (m, 1H, CH_{arom}), 7.63 (m, 1H, CH_{arom}), 7.82 (m, 3H, CH_{arom}). ^{13}C { 1H } (75 MHz, $CDCl_3$, -20 °C) δ 28.9 (CH_2), 37.0 (CH_2), 55.2 (OCH_3), 106.0 (Cp), 114.1 (2 CH_{arom}), 121.4 (CH_{arom}), 122.1 (CH_{arom}), 124.1 (2 CH_{arom}), 129.1 (CH_{arom}), 135.1 ($C_{quat\ arom}$), 144.1 (CH_{arom}), 144.7 ($C_{quat\ arom}$), 158.1 ($C_{quat\ arom}$), 175.1 ($C_{quat\ arom}$), 225.6 ($C=N$).

5c: IR (Nujol mull) 1712 cm^{-1} (ν ($C=N$)); 1H NMR (300 MHz, CD_2Cl_2 , -20 °C) δ 2.44 (s, 3H, CH_3), 3.02 (m, 2H, CH_2), 3.08 (m, 2H, CH_2), 5.45 (s, 10H, Cp), 6.87 (m, 2H, CH_{arom}), 7.12 (m, 1H, CH_{arom}), 7.34 (m, 4H, CH_{arom}), 7.80 (m, 1H, CH_{arom}). ^{13}C { 1H } (75 MHz, $CDCl_3$, -20 °C) δ 21.1 (CH_3), 29.3 (CH_2), 37.1 (CH_2), 106.1 (Cp), 121.5 (CH_{arom}), 122.3 (CH_{arom}), 122.7 (2 CH_{arom}), 129.4 (CH_{arom}), 129.9 (2 CH_{arom}), 137.2 ($C_{quat\ arom}$), 139.3 ($C_{quat\ arom}$), 144.2 (CH_{arom}), 144.8 ($C_{quat\ arom}$), 175.2 ($C_{quat\ arom}$), 228.5 ($C=N$).

5d: IR (Nujol mull) 1712 cm^{-1} (ν ($C=N$)). 1H NMR (300 MHz, CD_2Cl_2 , -20 °C) δ 3.01 (m, 2H, CH_2), 3.10 (m, 2H, CH_2), 5.46 (s, 10 H, Cp), 6.86 (m, 2H, CH_{arom}), 7.11 (m, 1H, CH_{arom}), 7.39 (m, 4H, CH_{arom}), 7.54 (m, 2H, CH_{arom}). ^{13}C { 1H } (75 MHz, $CDCl_3$, -20 °C) δ 29.4 (CH_2), 37.1 (CH_2), 106.2 (Cp), 121.5 (CH_{arom}), 122.4 (CH_{arom}), 122.8 (2 CH_{arom}), 127.2 (CH_{arom}), 129.2 (CH_{arom}), 129.4 (2 CH_{arom}), 144.1 (CH_{arom}), 141.7 ($C_{quat\ arom}$), 144.8 ($C_{quat\ arom}$), 175.8 ($C_{quat\ arom}$), 230.8 ($C=N$).

5e: IR (Nujol mull) 1699 cm^{-1} (ν ($C=N$)). 1H NMR (300 MHz, CD_2Cl_2 , -20 °C) δ 3.00 (m, 2H, CH_2), 3.06 (m, 2H, CH_2), 5.45 (s, 10 H, Cp), 6.85 (m, 2H, CH_{arom}), 7.10 (m, 1H, CH_{arom}), 7.34 (m, 3H, CH_{arom}), 7.50 (m, 2H, CH_{arom}). ^{13}C { 1H } (75 MHz, $CDCl_3$, -20 °C): δ 29.4 (CH_2), 36.9 (CH_2), 106.3 (Cp), 121.5 (CH_{arom}), 122.4 (CH_{arom}), 123.9 (2 CH_{arom}), 129.4 (2 CH_{arom}), 132.4 (CH_{arom}), 140.2 ($C_{quat\ arom}$), 141.8 ($C_{quat\ arom}$), 144.0 (CH_{arom}), 144.5 ($C_{quat\ arom}$), 174.8 ($C_{quat\ arom}$), 233.0 ($C=N$).

N-Aryl-1-indanimines (Aryl = *p*-(Diethylamino)phenyl, **6a; *p*-Methoxyphenyl, **6b**; *p*-Tolyl, **6c**; Phenyl, **6d**; *p*-Chlorophenyl, **6e**).** A solution of 1 (282 mg, 1 mmol) in methylene chloride (20 mL) at -20 °C was treated with the

corresponding isocyanide (1 mmol). The mixture was allowed to stir at room temperature for 14 h, the volume was reduced to ca. 1 mL, and the solution was eluted through a column of silica gel using a mixture of hexane/triethylamine (1:1). The solvent was removed, and the residue was purified by spinning plate chromatography using hexane/ NET_3 mixtures as the eluent. Yields: **6a**, 203 mg, 73%; **6b**, 185 mg, 77%; **6c**, 65 mg, 29%; **6d**, 200 mg, 97%; **6e**, 184 mg, 77%.

6a: IR (Nujol mull) 1636 cm^{-1} (ν ($C=N$)). 1H NMR (300 MHz, $CDCl_3$, 20 °C) δ 1.15 (t, $J = 7.0$, 6 H, NCH_2CH_3), 3.32 (m, 2H, CH_2), 3.06 (m, 2H, CH_2), 3.32 (q, $J = 7.0$, 4H, NCH_2CH_3), 6.71 (m, 2H, CH_{arom}), 6.98 (m, 2H, CH_{arom}), 7.35 (m, 2H, CH_{arom}), 7.41 (m, 1H, CH_{arom}), 7.93 (d, $J = 7.6$, 1H, CH_{arom}). ^{13}C { 1H } (75 MHz, $CDCl_3$, 20 °C) δ 12.5 (NCH_2CH_3), 28.3 (CH_2), 30.1 (CH_2), 44.5 (NCH_2CH_3), 112.6 (2 CH_{arom}), 122.2 (2 CH_{arom}), 122.5 (CH_{arom}), 125.4 (CH_{arom}), 126.8 (CH_{arom}), 131.1 (CH_{arom}), 140.3 ($C_{quat\ arom}$), 140.5 ($C_{quat\ arom}$), 144.9 ($C_{quat\ arom}$), 149.4 ($C_{quat\ arom}$), 172.6 ($C=N$). HRMS M^+ calcd for $C_{19}H_{22}N_2$ 278.1783, found 278.1781.

6b: IR (Nujol mull) 1643 cm^{-1} (ν ($C=N$)). 1H NMR (300 MHz, $CDCl_3$, 20 °C) δ 2.68 (m, 2H, CH_2), 3.01 (m, 2H, CH_2), 3.78 (s, 3H, OCH_3), 6.90 (m, 4H, CH_{arom}), 7.32 (m, 2H, CH_{arom}), 7.40 (m, 1H, CH_{arom}), 7.94 (d, $J = 7.4$, 1H, CH_{arom}). ^{13}C { 1H } (75 MHz, $CDCl_3$, 20 °C) δ 28.0 (CH_2), 29.5 (CH_2), 55.2 (OCH_3), 114.1 (2 CH_{arom}), 121.1 (2 CH_{arom}), 122.6 (CH_{arom}), 125.5 (CH_{arom}), 126.9 (CH_{arom}), 131.5 (CH_{arom}), 139.6 ($C_{quat\ arom}$), 145.2 ($C_{quat\ arom}$), 150.0 ($C_{quat\ arom}$), 156.0 ($C_{quat\ arom}$), 174.6 ($C=N$). HRMS M^+ calcd for $C_{16}H_{15}NO$ 237.1154, found 237.1152.

6c: IR (Nujol mull) 1652 cm^{-1} (ν ($C=N$)). 1H NMR (300 MHz, $CDCl_3$, 20 °C) δ 2.35 (s, 3H, CH_3), 2.68 (m, 2H, CH_2), 3.01 (m, 2H, CH_2), 6.83 (m, 2H, CH_{arom}), 7.15 (m, 2H, CH_{arom}), 7.37 (m, 2H, CH_{arom}), 7.43 (d, $J = 6.7$, 1H, CH_{arom}), 7.94 (d, $J = 7.6$, 1H, CH_{arom}). ^{13}C { 1H } (75 MHz, $CDCl_3$, 20 °C) δ 20.9 (CH_3), 28.1 (CH_2), 29.4 (CH_2), 119.7 (2 CH_{arom}), 125.6 (CH_{arom}), 127.1 (CH_{arom}), 128.9 (CH_{arom}), 131.8 (2 overlapping CH_{arom}), 131.8 (CH_{arom}), 132.9 ($C_{quat\ arom}$), 139.5 ($C_{quat\ arom}$), 149.7 ($C_{quat\ arom}$), 150.3 ($C_{quat\ arom}$), 175.0 ($C=N$). HRMS M^+ calcd for $C_{16}H_{15}N$ 221.1204, found 221.1203.

6d: IR (Nujol mull) 1640 cm^{-1} (ν ($C=N$)). 1H NMR (300 MHz, $CDCl_3$, 20 °C) δ 2.67 (m, 2H, CH_2), 3.06 (m, 2H, CH_2), 6.92 (m, 2H, CH_{arom}), 7.10 (m, 1H, CH_{arom}), 7.36 (m, 4H, CH_{arom}), 7.47 (m, 1H, CH_{arom}), 7.94 (d, $J = 8.0$ Hz, 1H, CH_{arom}). ^{13}C { 1H } (75 MHz, $CDCl_3$, 20 °C) δ 28.0 (CH_2), 29.2 (CH_2), 119.6 (2 CH_{arom}), 122.8 (CH_{arom}), 123.1 (CH_{arom}), 125.6 (CH_{arom}), 127.0 (CH_{arom}), 128.9 (2 CH_{arom}), 131.8 (CH_{arom}), 174.9 ($C=N$). HRMS M^+ calcd for $C_{15}H_{13}N$ 207.1048, found 207.1047.

6e: IR (Nujol mull) 1652 cm^{-1} (ν ($C=N$)). 1H NMR (300 MHz, $CDCl_3$, 20 °C) δ 2.64 (m, 2H, CH_2), 3.07 (m, 2H, CH_2), 6.85 (m, 2H, CH_{arom}), 7.31 (m, 2H, CH_{arom}), 7.38 (m, 1H, CH_{arom}), 7.45 (m, 1H, CH_{arom}), 7.92 (m, 1H, CH_{arom}). ^{13}C { 1H } (75 MHz, $CDCl_3$, 20 °C): δ 28.0 (CH_2), 29.3 (CH_2), 121.0 (2 CH_{arom}), 122.8 (CH_{arom}), 125.6 (CH_{arom}), 127.0 (CH_{arom}), 128.9 (2 CH_{arom}), 132.0 (CH_{arom}), 129.0 ($C_{quat\ arom}$), 139.1 ($C_{quat\ arom}$), 150.4 ($C_{quat\ arom}$), 150.8 ($C_{quat\ arom}$), 175.5 ($C=N$). HRMS M^+ calcd for $C_{15}H_{12}NCl$ 241.0658, found 241.0656.

Conversion of 5b to *N*-(4-Methoxyphenyl)-3-phenylpropionamide (7). A solution of 1 (400 mg, 1.4 mmol) in THF (30 mL) was cooled to -80 °C and treated with a solution of *p*-methoxyphenyl isocyanide (190 mg, 1.4 mmol) in THF (5 mL). The cooling bath was removed, and the mixture was allowed to warm to 0 °C. The resulting yellow mixture was cooled again to -80 °C and treated with 15 mL of a 0.1 M solution of HCl in THF. The resulting mixture was allowed to warm to -5 °C, and 35% H_2O_2 (2 mL) was added. The mixture was stirred at room temperature for 30 min and was concentrated to approximately 5–10 mL. The solution was filtered through a pad of silica gel, which was washed with a 1:1 mixture of hexane and ethyl acetate and the filtrate was concentrated *in vacuo*. The product was purified by spinning plate chromatography to yield 110 mg (0.43 mmol, 28%) of 7. IR (Nujol mull) 3295 (ν (NH)), 1616 (amide I), 1548 (amide II).

Table 4

substituent	σ	$k(1), \text{s}^{-1}$	$k(2), \text{s}^{-1}$
<i>p</i> -C ₆ H ₄ -NEt ₂	-0.72	$(1.13 \pm 0.01) \times 10^{-4}$	$(1.21 \pm 0.01) \times 10^{-4}$
<i>p</i> -C ₆ H ₄ -OMe	-0.27	$(4.36 \pm 0.03) \times 10^{-4}$	$(3.95 \pm 0.03) \times 10^{-4}$
<i>p</i> -C ₆ H ₄ -Me	-0.17	$(7.8 \pm 0.1) \times 10^{-4}$	$(7.9 \pm 0.1) \times 10^{-4}$
C ₆ H ₅	0	$(12.2 \pm 0.2) \times 10^{-4}$	$(12.8 \pm 0.3) \times 10^{-4}$
<i>p</i> -C ₆ H ₄ -Cl	0.23	$(26.2 \pm 0.6) \times 10^{-4}$	$(23.4 \pm 0.6) \times 10^{-4}$

¹H NMR (300 MHz, CDCl₃, 20 °C) δ 2.59 (t, $J = 8.0$ Hz, 2H, CH₂), 3.01 (t, $J = 8.0$ Hz, 2H, CH₂), 3.54 (s, 3H, OCH₃), 6.77–7.31 (m, 10H, CH_{arom} and NH). ¹³C{¹H} (75 MHz, CDCl₃, 20 °C) δ 31.6 (CH₂), 39.1 (CH₂), 55.4 (OCH₃), 114.4 (2 CH_{arom}), 121.9 (2 CH_{arom}), 126.2 (CH_{arom}), 128.3 (2 CH_{arom}), 128.5 (2 CH_{arom}), 130.8 (C_{quat} arom), 140.7 (C_{quat} arom), 156.3 (C_{quat} arom), 170.3 (C=O). HRMS calcd for C₁₆H₁₇NO₂ 255.12592, found 255.1268.

X-Ray Structure Determination of 2. A crystal was mounted on the diffractometer and the cell dimensions were refined by the least-squares fitting the θ values of 25 reflections. The crystal data and the parameters used during the collection and refinement of the diffraction data are summarized in Table 2.

Three reflections were monitored periodically during data collection and revealed no crystal decomposition. The intensities were corrected for the Lorentz and polarization effects. Scattering factors for neutral atoms and anomalous dispersion correction for the Ti atom was taken from the *International Tables for X-Ray Crystallography*.²²

The structure was solved by Patterson and Fourier methods. An empirical absorption correction was applied at the end of the isotropic temperature factors and positions for the H atoms.^{23a}

The calculations were carried out with X-RAY80.^{23b}

General Procedure for the Determination of the Rate of Reductive Elimination of Compound 2. Samples of 2 at the specified concentrations containing an internal standard of ferrocene were prepared *in situ* from solutions of 1 prepared by dissolving this compound and ferrocene (equimolecular amounts) in 0.7 mL of the deuterated solvent (C₆D₆ unless otherwise indicated). The solutions of 1 were placed in 5 mm NMR tubes and were treated with a equimolecular amount of *tert*-butyl isocyanide. Conversion of 1 to 2 was clean and quantitative under these conditions. A sample was placed in a NMR probe at a temperature determined by using a sample of neat methanol, and the progress of the reaction monitored by ¹H NMR. The rate was determined from the ratio of the cyclopentadienyl signal of 2 to the signal of ferrocene.

Determination of the Rate of Reductive Elimination of 2 at Different Concentrations. Two sets of solutions of 2 at a concentration 0.07, 0.14, and 0.29 M, containing ferrocene as an internal standard were prepared as described before. The elimination rate measurements were carried at 69 °C. The rate constant was found to be the same in all cases within the experimental error ($k = (1.1 \pm 0.2) \times 10^{-3} \text{ s}^{-1}$).

Determination of the Activation Parameters for the Reductive Elimination of 2. The elimination rate of samples of 2 at a concentration of 0.14 M was determined three times at each temperature, and the average values of the rate

constants obtained from these measurements were used in the calculation of the activation parameters. Averaged rate constants: $T = 311.5 \text{ K}$, $k = (4.2 \pm 0.5) \times 10^{-5} \text{ s}^{-1}$; $T = 334.6 \text{ K}$, $k = (6.5 \pm 0.8) \times 10^{-4} \text{ s}^{-1}$; $T = 344.0 \text{ K}$, $k = (2.1 \pm 0.1) \times 10^{-3} \text{ s}^{-1}$; $T = 354.0 \text{ K}$; $k = (5.2 \pm 0.3) \times 10^{-3} \text{ s}^{-1}$.

Determination of the Rate of Reductive Elimination of 2 in Different Solvents. The rate of reductive elimination was measured at 338 K for two sets of samples of 2 of concentration 0.14 M prepared as described in C₆D₆, CDCl₃, THF-*d*₈, and CD₃CN. C₆D₆: $k(1) = (1.14 \pm 0.02) \times 10^{-3} \text{ s}^{-1}$, $k(2) = (9.0 \pm 0.3) \times 10^{-4} \text{ s}^{-1}$. CDCl₃: $k(1) = (8.8 \pm 0.2) \times 10^{-4} \text{ s}^{-1}$, $k(2) = (7.6 \pm 0.3) \times 10^{-4} \text{ s}^{-1}$. THF-*d*₈: $k(1) = (7.5 \pm 0.4) \times 10^{-4} \text{ s}^{-1}$, $k(2) = (6.0 \pm 0.2) \times 10^{-4} \text{ s}^{-1}$. CD₃CN: $k(1) = (4.48 \pm 0.05) \times 10^{-4} \text{ s}^{-1}$, $k(2) = (4.7 \pm 0.1) \times 10^{-4} \text{ s}^{-1}$.

Determination of the Rate of Reductive Elimination of 2 in the Presence of Trimethylphosphine and Dimethyl Disulfide. Samples of compound 2 (0.14 M), prepared as described, were treated with trimethylphosphine (20, 50, and 100 μL), and the rate of reductive elimination reaction was determined at 333 K for each concentration of trimethylphosphine (0.28, 0.71, and 1.43 M, respectively). The rate in the two first cases ($k([\text{PMe}_3]=0.28\text{M}) = (4.9 \pm 0.1) \times 10^{-4} \text{ s}^{-1}$; $k([\text{PMe}_3]=0.71\text{M}) = (4.6 \pm 0.1) \times 10^{-4} \text{ s}^{-1}$) was very similar to the value found in the absence of phosphine ($k = (4.5 \pm 0.1) \times 10^{-4} \text{ s}^{-1}$). A small decrease of the rate ($k([\text{PMe}_3]=1.43\text{M}) = (3.2 \pm 0.1) \times 10^{-4} \text{ s}^{-1}$) was observed in the last case. By following a similar procedure, a solution of 2 was treated with 17 μL (0.2 mmol) of dimethyl disulfide and the reaction rate determined at the same temperature ($k = (4.1 \pm 0.1) \times 10^{-4} \text{ s}^{-1}$).

Determination of Hammett ρ for Compounds 5a–e. The corresponding compound (0.1 mmol) and ferrocene (18 mg, 0.1 mmol) were placed in a 5 mm NMR tube. The tube was cooled at -80 °C and CD₂Cl₂ (0.7 mL) was slowly added. The mixture was shaken for several seconds and quickly returned to the cooling bath. This operation was repeated until a clear solution was obtained. The sample was then stored in a bath between -10 and -20 °C. Samples were allowed to stand 5 min in a NMR probe at 23.5 °C before the starting rate measurement, in order to stabilize the temperature of the sample. It was previously determined that the temperature of a methanol standard is equilibrated under the same conditions. The value of the rate constants (Table 4) were averaged from two sets of measurements. The values of the σ constants was obtained from ref 24.

Acknowledgment. We thank the National Science Foundation for support of this work. S.L.B. acknowledges additional support as an Alfred P. Sloan Fellow and a Camille & Henry Dreyfus Teacher–Scholar. J.C. thanks the Ministerio de Educación y Ciencia (Spain) and the Fulbright Foundation for a postdoctoral fellowship. We acknowledge helpful discussions with Professors Robert H. Grubbs and Christopher Cummins as well as B. P. Warner and C. A. Willoughby.

Supplementary Material Available: Tables of complete bond distances and angles, H atom coordinates, and thermal parameters (7 pages). Ordering information is given on any current masthead page.

OM940916C

(22) *International Tables for X-Ray Crystallography*; Kynoch Press: Birmingham, U.K., 1974.

(23) (a) Stewart, J. H. *The X-RAY80 System*; Computer Science Center, University of Maryland: College Park, MD, 1985. (b) Walker, N.; Stuart, D. *Acta Crystallogr.* **1983**, *A39*, 158.

(24) Hansch, C.; Leo, A.; Taft, W. R. *Chem. Rev.* **1991**, *91*, 165.

Organometallic Chemistry of Diphosphazanes.

11.¹ Reactions of *fac*-[Mo(CO)₃(MeCN){η²-Ph₂PN(Prⁱ)PPh(DMP)}] (DMP = 3,5-Dimethyl-1-pyrazolyl) with Diphosphazanes and Diphosphinoalkanes and Oxidative Addition with Iodine

Ruppa P. K. Babu, Setharampattu S. Krishnamurthy,* and Munirathinam Nethaji

Department of Inorganic and Physical Chemistry, Indian Institute of Science, Bangalore 560 012, India

Received June 21, 1994[⊗]

The use of *fac*-[Mo(CO)₃(MeCN)(η²-L¹)] (**1a**) {L¹ = Ph₂PN(Prⁱ)PPh(DMP)}² as a precursor to metalloligands and bimetallic, heterotrimetallic, and heptacoordinated complexes is reported. The reaction of **1a** with diphosphazane, dppa, or a diphosphinoalkane such as dpmm or dppe yields the *fac*-η¹-diphosphine substituted metalloligands, *fac*-[Mo(CO)₃(η²-L¹)(η¹-PXP)] {PXP = dppa (**2**), dpmm (**3**), and dppe (**4**)}. These undergo isomerization to yield the corresponding *mer*-diphosphine complexes (**5**–**7**). Oxidation of the uncoordinated phosphorus atom of the *mer*-η¹-dpmm-substituted complex eventually provides *mer*-[Mo(CO)₃(η²-L¹){η¹-Ph₂PCH₂P(O)Ph₂}] (**8**). The structure of the latter complex has been confirmed by single crystal X-ray diffraction {triclinic system, *P* $\bar{1}$; *a* = 11.994(3), *b* = 14.807(2), *c* = 15.855(3) Å; α = 114.24(1), β = 91.35(2), and γ = 98.95(1)°; *Z* = 2, 4014 data (*F*_o > 5σ(*F*_o)), *R* = 0.066, *R*_w = 0.069}. Treatment of the dppe metalloligand **7** with [PtCl₂(COD)] yields the heterotrimetallic complex *cis*-[PtCl₂{*mer*-[Mo(CO)₃(η²-L¹)(η¹-dppe)]₂] (**9**). Attempts to prepare a related trimetallic complex with the dpmm-containing metalloligand were unsuccessful; only the tetracarbonyl complex *cis*-[Mo(CO)₄(η²-L¹)] (**1b**) and *cis*-[PtCl₂(η²-dpmm)] were obtained. Reaction of **1a** with dppe in the ratio 2:1 yields the *mer-mer* dinuclear complex [{*mer*-[Mo(CO)₃(η²-L¹)]₂(μ-dppe)] (**10**) bridged by dppe. Oxidation of **1a** with iodine yields the Mo(II) heptacoordinated complex [MoI₂(CO)₂(η³-L¹)] (**11**) with tridentate PPN coordination. The same Mo(II) complex **11** is also obtained by the direct oxidation of the tetracarbonyl complex *cis*-[Mo(CO)₄(η²-L¹)] (**1b**) with iodine. The structure of **11** has been confirmed by X-ray diffraction studies {monoclinic system, *Cc*; *a* = 10.471(2), *b* = 19.305(3), *c* = 17.325(3) Å; β = 95.47(2)°; *Z* = 4, 3153 data (*F*_o > 5σ(*F*_o)), *R* = 0.049, *R*_w = 0.051}. This complex exhibits an unusual capped-trigonal prismatic geometry around the metal. A similar heptacoordinated complex **12** with a chiral diphosphazane ligand {L³ = (*S,R*)-Ph₂PN-(*CHMePh)*PPh(DMP)} has also been synthesized.

Introduction

Heterofunctional ligands containing soft and hard donor sites is of considerable current interest in connection with the development of novel homogeneous catalysts.³ Organotransition metal chemistry of symmetrically substituted diphosphazanes have been investigated extensively over the past three decades⁴ whereas studies on unsymmetrically substituted diphosphazanes are sparse.⁵ Unsymmetrically substituted diphosphazanes offer an advantage in that the ²J_{PP} coupling constant can be obtained directly from their ³¹P NMR spectra. The facile synthetic route for diphosphazanes can be gainfully employed to prepare various

unsymmetrical ligands.⁵ We have synthesized a series of unsymmetrically substituted diphosphazanes possessing heterofunctional donor sites and also a few chiral diphosphazanes.^{6,7} We have recently reported the synthesis of a molybdenum tricarbonyl complex of a heterofunctional diphosphazane Ph₂PN(Prⁱ)PPh(DMP) (L¹) *viz.*, *fac*-[Mo(CO)₃(MeCN)(η²-L¹)] (**1a**) that contains a labile acetonitrile ligand and its substitution reactions with monophosphines.⁸ In this paper, we report the syntheses of metalloligands and polymetallic complexes starting from **1a** and also a Mo(II) heptacoordinated complex in which the heterofunctional diphosphazane

[⊗] Abstract published in *Advance ACS Abstracts*, February 15, 1995.

(1) For Part 10, see: Reddy, V. S.; Krishnamurthy, S. S.; Nethaji, M. *J. Chem. Soc., Dalton Trans.* **1994**, 2661.

(2) Abbreviations used: DMP = 3,5-dimethyl-1-pyrazolyl; dppa = bis(diphenylphosphino)amine; dpmm = bis(diphenylphosphino)methane; dpmo = bis(diphenylphosphino)methane monoxide; dppe = bis(diphenylphosphino)ethane; COD = cycloocta-1,5-diene.

(3) Bader, A.; Lindner, E. *Coord. Chem. Rev.* **1991**, *108*, 27.

(4) (a) Balakrishna, M. S.; Reddy, V. S.; Krishnamurthy, S. S.; Nixon, J. F.; Burckett St. Laurent, J. C. T. R. *Coord. Chem. Rev.* **1994**, *129*, 1. (b) King, R. B. *Acc. Chem. Res.* **1980**, *13*, 243.

(5) (a) Cross, R. J.; Green, T. H.; Keat, R. *J. Chem. Soc., Dalton Trans.* **1976**, 1424. (b) Colquhoun, I. J.; McFarlane, W. *J. Chem. Soc., Dalton Trans.* **1977**, 1674. (c) Prout, T. R.; Imiolezyk, T. W.; Haltiwanger, R. C.; Hill, T. G.; Norman, A. D. *Inorg. Chem.* **1992**, *31*, 215.

(6) (a) Babu, R. P. K.; Krishnamurthy, S. S.; Nethaji, M. *Heteroatom Chem.* **1991**, *2*, 477. (b) Babu, R. P. K.; Krishnamurthy, S. S. *Proc. Indian Acad. Sci. (Chem. Sci.)* **1994**, *106*, 37.

(7) (a) Babu, R. P. K.; Aparna, K.; Krishnamurthy, S. S.; Nethaji, M. *Phosphorus, Sulfur, Silicon*, in press. (b) Babu, R. P. K.; Krishnamurthy, S. S.; Nethaji, M. *Tetrahedron: Asymmetry*, in press.

(8) Babu, R. P. K.; Krishnamurthy, S. S.; Nethaji, M. *J. Organomet. Chem.* **1993**, *454*, 157.

Table 1. Infrared^a and ¹H NMR^b Spectroscopic Data for the Diphosphine-Substituted Molybdenum Diphosphazane Complexes (5–8 and 10)

compd	IR ν_{CO} (cm ⁻¹)	¹ H NMR δ (ppm)
<i>mer</i> -[Mo(CO) ₃ (η^2 -L ¹)(η^1 -dppa)] (5)	1983, 1876, 1835	5.98 (s, 1H, CH of DMP), 3.85 (m, 1H, CH of Pr ⁱ), 3.05 (dd, ² J _{PH} = 17.0, 8.5 Hz, 1H, NH), 2.39 (s, 3H, CH ₃ of DMP), 2.21 (s, 3H, CH ₃ of DMP), 1.11 (d, 3H, CH ₃ of Pr ⁱ), -0.15 (d, 3H, CH ₃ of Pr ⁱ)
<i>mer</i> -[Mo(CO) ₃ (η^2 -L ¹)(η^1 -dppm)] (6)	1972, 1868 (br) ^c	5.92 (s, 1H, CH of DMP), 4.2 (m, 1H, CH of Pr ⁱ), 3.45 (m, 2H, CH ₂ of dppm), 2.47 (s, 6H, CH ₃ of DMP), 1.30 (d, 3H, CH ₃ of Pr ⁱ), 0.04 (d, 3H, CH ₃ of Pr ⁱ)
<i>mer</i> -[Mo(CO) ₃ (η^2 -L ¹)(η^1 -dppe)] (7)	1980, 1866, 1833	5.99 (s, 1H, CH of DMP), 3.8 (m, 1H, CH of Pr ⁱ), 2.39 (s, 3H, CH ₃ of DMP), 2.24 (s, 3H, CH ₃ of DMP), 2.2 (m, 2H, CH ₂ of dppe), 1.9 (m, 2H, CH ₂ of dppe), 1.07 (d, 3H, CH ₃ of Pr ⁱ), -0.19 (d, 3H, CH ₃ of Pr ⁱ)
<i>mer</i> -[Mo(CO) ₃ (η^2 -L ¹)(η^1 -dppmo)] (8)	1970, 1867 (br) ^c	5.98 (s, 1H, CH of DMP), 3.85 (m, 1H, CH of Pr ⁱ), 2.96 (m, 2H, CH ₂ of dppmo), 2.39 (s, 3H, CH ₃ of DMP), 2.23 (s, 3H, CH ₃ of DMP), 1.08 (d, 3H, CH ₃ of Pr ⁱ), -0.20 (d, 3H, CH ₃ of Pr ⁱ)
[{ <i>mer</i> -Mo(CO) ₃ (η^2 -L ¹)} ₂ (μ -dppe)] (10)	1980, 1869, 1851	5.95 (s, 1H, CH-DMP), 3.85 (m, 1H, CH-Pr ⁱ), 2.35 (s, 3H, CH ₃ of DMP), 2.18 (s, 3H, CH ₃ of DMP), 2.12 (m, 4H, CH ₂ of dppe), 1.04 (d, 3H, CH ₃ of Pr ⁱ), -0.24 (d, 3H, CH ₃ of Pr ⁱ)

^a Nujol mull. ^b Recorded at 200 MHz in CDCl₃ solvent; methyl (Prⁱ) resonances are doublets with ³J_{HH} ≈ 7 Hz; aryl proton resonances are multiplets in the region 8.5–6.5 ppm. ^c br = broad.

Table 2. Phosphorus-31 NMR Data^a for the Diphosphine-Substituted Mo(0) Diphosphazane Complexes (2–8,10) and Mo(II) Heptacoordinated Diphosphazane Complexes (11,12)

compd	d (ppm)								J (Hz)			
	δ_A	$\Delta\delta$	δ_M	$\Delta\delta$	δ_R	$\Delta\delta$	δ_X	$\Delta\delta$	AM	AR	MR	RX
<i>fac</i> -[Mo(CO) ₃ (η^2 -L ¹)(η^1 -dppa)] (2)	112.3	40.7	88.5	44.7	81.3	39.3	27.2	-14.8	25	25	25	9
<i>mer</i> -[Mo(CO) ₃ (η^2 -L ¹)(η^1 -dppa)] (5)	125.7	54.1	81.6	37.8	97.8	55.8	26.7	-15.3	9	94	29	13
<i>fac</i> -[Mo(CO) ₃ (η^2 -L ¹)(η^1 -dppm)] (3)	113.8	42.2	88.5	44.7	27.0	50.6	-25.8	-2.2	27	27	27	18
<i>mer</i> -[Mo(CO) ₃ (η^2 -L ¹)(η^1 -dppm)] (6)	127.0	55.4	80.8	37.0	42.6	66.2	-26.5	-2.9	12	89	26	67
<i>fac</i> -[Mo(CO) ₃ (η^2 -L ¹)(η^1 -dppe)] (4)	113.7	42.1	87.9	44.1	29.7	42.2	-13.8	-1.3	26	26	26	29
<i>mer</i> -[Mo(CO) ₃ (η^2 -L ¹)(η^1 -dppe)] (7)	126.3	54.7	80.5	36.7	45.6	58.1	-12.8	-0.3	12	87	26	37
<i>mer</i> -[Mo(CO) ₃ (η^2 -L ¹)(η^1 -dppmo)] (8)	126.9	55.3	80.2	36.4	42.8	71.2	21.9	-5.8	12	91	25	24
[{ <i>mer</i> -Mo(CO) ₃ (η^2 -L ¹)} ₂ (μ -dppe)] (10)	126.2	54.6	80.4	36.6	45.5	58.0			12	87	br ^b	
[MoI ₂ (CO) ₂ (η^3 -L ³)] (11) ^{c,d}	113.2	41.6	74.7	30.9					161			
[MoI ₂ (CO) ₂ (η^3 -L ³)] (12) ^{c,d}	120.2	52.7	81.3	34.1					167			

^a Recorded at 81 MHz in toluene solvent; $\Delta\delta = \delta_{\text{complex}} - \delta_{\text{ligand}}$; A = PPh(DMP); M = PPh₂-L¹ or L³; R = η^1 -PPh₂(PXP); X = uncoordinated PPh₂(PXP) or P(O)Ph₂ of dppmo. ^b br = broad. ^c Recorded in CH₂Cl₂. ^d The ³¹P chemical shifts for L³ are 67.5 (d) and 47.2 (d) with ²J_{PP} = 32 Hz.

L¹ behaves as a PPN tridentate ligand. A similar heptacoordinated complex with a chiral heterofunctional ligand, (*S,R*)-Ph₂PN(*CHMePh)*PPh(DMP) (L³)^{7b,9} is also reported in this paper.

Experimental Section

Apparatus and Chemicals. All experimental manipulations were performed under an atmosphere of dry nitrogen in a vacuum system or in Schlenk apparatus.¹⁰ Petroleum ether (60–80 °C), benzene, toluene, dichloromethane, and acetonitrile were purified by conventional procedures and freshly distilled prior to use.¹¹ The diphosphazane ligand Ph₂PN(Prⁱ)-PPh(DMP) (L¹) was prepared by the reported procedure.⁸ The other diphosphazane ligands Ph₂PN(Prⁱ)PPh(OC₆H₄Me-4) (L²)^{7a} and (*S,R*)-Ph₂PN(*CHMePh)*PPh(DMP) (L³)^{7b} were prepared by a similar procedure {for L³ starting from Ph₂P{NH((*S*)-*CHMePh)} instead of Ph₂P(NHPrⁱ)⁹}. Syntheses of these ligands will be reported separately.^{7a,b} The complex *fac*-[Mo(CO)₃(MeCN){ η^2 -Ph₂PN(Prⁱ)PPh(DMP)}] (1a)⁸ and the organometallic precursor complexes, *fac*-[Mo(CO)₃(MeCN)₃]¹² and *cis*-[PtCl₂(COD)],¹³ were prepared and purified by published procedures.

The ¹H and ³¹P NMR spectra were recorded using a Bruker ACF-200 or a Bruker AMX-400 spectrometer with (CH₃)₄Si as

an internal standard for ¹H NMR measurements and 85% H₃PO₄ as an external standard for ³¹P NMR measurements. Chemical shifts downfield from the standard are assigned positive values. Infrared spectra were recorded using a BIO-RAD FTIR Model FTS-7 or a Perkin-Elmer Model 457 spectrometer. C, H, N analyses were performed on a Heraeus CHN-O-Rapid elemental analyzer. Melting points were determined on a Reichert-Kofler microheating stage fitted with a polarizing microscope and were uncorrected.

***fac*-[Mo(CO)₃(η^2 -L¹)(η^1 -PXP)] {PXP = dppa (2), dppm (3), dppe (4) and *mer*-[Mo(CO)₃(η^2 -L¹)(η^1 -PXP)] {PXP = dppa (5), dppm (6), dppe (7)}.** A mixture of *fac*-[Mo(CO)₃(MeCN)(η^2 -L¹)] (1a) (0.240 g, 3.6 × 10⁻⁴ mol) and the diphosphine ligand (0.143 g of dppa or 0.142 g of dppm or 0.147 g of dppe; 3.7 × 10⁻⁴ mol) was dissolved in 25 mL of toluene, and the solution was stirred for 12 h at room temperature. The resultant solution was passed through a short silica gel column and eluted with 20 mL of toluene. Solvent was removed *in vacuo* to obtain a yellow oil. Dissolution of the oil in toluene/petroleum ether (1:1) and cooling the solution at 0 °C afforded crystals of the *mer* complexes 5–7. The *fac* isomers (2–4) were observed only by ³¹P NMR spectra of the reaction mixtures immediately after dissolution of the reactants. Attempts to isolate these complexes in a pure state were unsuccessful as these complexes isomerized rapidly in solution to the corresponding *mer* complexes (5–7). The yield, melting point, microanalyses, and IR spectral data for these complexes are given below. The ¹H and ³¹P NMR data are given in Tables 1 and 2, respectively.

***mer*-[Mo(CO)₃(η^2 -L¹)(η^1 -(Ph₂P)NH)] (5).** Yield: 0.320 g, 88%. Mp: 190 °C. IR (Nujol, cm⁻¹): 3337 (w), 1983 (s), 1876

(9) Data for L²: mp 160 °C. Anal. Calcd for C₃₁H₃₁N₃P₂: C, 73.35; H, 6.17; N, 8.28. Found: C, 73.72; H, 5.78; N, 8.10.

(10) Shriver, D. F.; Drezdson, M. A. *The Manipulation of Air-sensitive Compounds*, 2nd ed.; Wiley-Interscience: New York, 1986.

(11) Perrin, D. D.; Armarego, W. L. F. *Purification of Laboratory Chemicals*, 3rd ed.; Pergamon Press: Oxford, U.K., 1988.

(12) Tate, D. P.; Knipple, W. R.; Augl, J. M. *Inorg. Chem.* **1962**, *1*, 433.

(13) Drew, D.; Doyle, J. R. *Inorg. Synth.* **1972**, *13*, 52.

(s), 1835 (s), 1436 (s), 1309 (w), 1245 (w), 1135 (w), 1092 (w), 1036 (w), 885 (m), 862 (w), 743 (m), 720 (m), 694 (s), 609 (m), 583 (m), 526 (s), 456 (m). Anal. Calcd for $C_{53}H_{50}MoN_4O_3P_4$: C, 62.97; H, 5.00; N, 5.54. Found: C, 63.61; H, 5.23; N, 5.90.

mer-[Mo(CO)₃(η^2 -L¹)(η^1 -dppm)] (6). Yield: 0.313 g, 86%. Mp: 180 °C. IR (Nujol, cm^{-1}): 1972 (m), 1868 (s, br), 1552 (w), 1481 (w), 1433 (m), 1307 (w), 1123 (m), 1093 (m), 1035 (m), 865 (m), 741 (m), 695 (s), 608 (m). Anal. Calcd for $C_{54}H_{51}MoN_3O_3P_4$: C, 64.22; H, 5.10; N, 4.16. Found: C, 63.89; H, 4.82; N, 4.28.

mer-[Mo(CO)₃(η^2 -L¹)(η^1 -dppe)] (7). Yield: 0.332 g, 90%. Mp: 163 °C. IR (Nujol, cm^{-1}): 1980 (s), 1866 (s), 1833 (s), 1548 (w), 1437 (s), 1311 (w), 1122 (w), 1092 (m), 1032 (m), 870 (m), 732 (w), 696 (m). Anal. Calcd for $C_{55}H_{53}MoN_3O_3P_4$: C, 64.51; H, 5.23; N, 4.10. Found: C, 64.10; H, 4.89; N, 3.92.

Reaction of [Mo(CO)₃(MeCN)(η^2 -L¹)] (1a) with Ph₂PN-(Prⁱ)PPhY' {Y' = DMP (L¹), OC₆H₄Me-4 (L²)}. A mixture of *fac*-[Mo(CO)₃(MeCN)(η^2 -L¹)] (1a) (0.240 g, 3.6×10^{-4} mol) and the diphosphazane ligand L¹ or L² (0.165 g of L¹ or 0.169 g of L²; 3.7×10^{-4} mol) was dissolved in 20 mL of toluene, and the solution was stirred for 12 h at room temperature. The solution turned dark brown and was found to contain *cis*-[Mo(CO)₄(η^2 -L¹)] (1b) or *cis*-[Mo(CO)₄(η^2 -L²)] (1c) along with their respective free ligands L¹ or L², as revealed by ³¹P NMR spectroscopy.^{6b}

Isolation of mer-[Mo(CO)₃(η^2 -L¹)(η^1 -dppmo)] (8). Slow crystallization of 6 from a diethyl ether/toluene (1:1) mixture yields 6 along with minor amounts of 8 owing to oxidation by atmospheric air. Crystals of compound 8 were separated by hand-picking them under a microscope. Mp: 183 °C. IR (ν_{CO} ; Nujol, cm^{-1}): 1970 (m), 1867 (s, br). The ¹H and ³¹P-¹H NMR data for this complex are given in Tables 1 and 2 respectively.

cis-[PtCl₂{mer-[Mo(CO)₃(η^2 -L¹)(η^1 -dppe)]₂ (9). A mixture of *cis*-[PtCl₂(COD)] (0.036 g, 9.76×10^{-5} mol) and the metalloligand 7 (0.200 g, 1.95×10^{-4} mol) was dissolved in 30 mL of dichloromethane, and the solution was stirred for 10 min. Evaporation of the solvent *in vacuo* yields an oily residue which was washed twice with hot petroleum ether to remove cyclooctadiene. The resultant crude yellowish solid was crystallized from a CH₂Cl₂/petroleum ether (4:1) mixture. Yield: 0.147 g, 65%. IR (Nujol, cm^{-1}): 1969 (s), 1933 (s), 1863 (br (s), 1557 (w), 1435 (s), 1306 (w), 1171 (w), 1138 (w), 1124 (w), 1096 (m), 1033 (m), 865 (m), 804 (w), 744 (m), 695 (s), 609 (m), 586 (w), 533 (m), 517 (m), 491 (m), 423 (w), 278 (w). ³¹P NMR (CH₂Cl₂, ppm): 125.2 (dd, P_A), 79.2 (dd, P_M), 46.2 (m, P_R), 6.1 (d, ¹J_{PXPt} = 3631 Hz, P_X); ²J_{AM} = 12.5 Hz, ²J_{AR} = 86.5 Hz, ²J_{MR} = 26.2 Hz, ²J_{RX} = 31.1 Hz.

Elemental analyses and the ¹H NMR spectrum were not obtained, as this complex could not be isolated in a pure state; invariably, this complex was associated with some tetracarbonyl impurity, *cis*-[Mo(CO)₄(η^2 -L¹)] (1b).

Reaction of 6 with cis-[PtCl₂(COD)]. A mixture of *cis*-[PtCl₂(COD)] (0.036 g, 9.76×10^{-5} mol) and the metalloligand 6 (0.20 g, 1.95×10^{-4} mol) was dissolved in 10 mL of dichloromethane, and the solution was stirred. After 20 min the ³¹P NMR spectrum of the reaction mixture was recorded, which revealed the presence of *cis*-[Mo(CO)₄(η^2 -L¹)] (1b) and *cis*-[PtCl₂(η^2 -dppm)] as the major products of the reaction.

{mer-[Mo(CO)₃(η^2 -L¹)]₂(μ -dppe)} (10). A mixture of *fac*-[Mo(CO)₃(MeCN)(η^2 -L¹)] (1a) (0.353 g, 5.3×10^{-4} mol) and dppe (0.100 g, 2.5×10^{-4} mol) was dissolved in 30 mL of benzene, and the solution was stirred for 24 h. The resultant pale yellow solution was passed through a short silica gel column and eluted with benzene (20 mL). Evaporation of the solvent, followed by crystallization of the residue from a dichloromethane/petroleum ether mixture (1:1), yielded 10 as a deep yellow solid. (Yield: 0.297 g, 72%). Mp: 195 °C dec. IR (Nujol, cm^{-1}): 1980 (s), 1869 (s), 1851 (s), 1554 (w), 1308 (w), 1122 (w), 1092 (m), 1032 (m), 855 (m), 696 (m), 609 (m). Anal. Calcd for $C_{34}H_{32}Mo_2N_6O_6P_6$: C, 61.16; H, 5.02; N, 5.10. Found: C, 60.58; H, 4.82; N, 4.84.

Table 3. Crystal Data and Intensity Collection Parameters for mer-[Mo(CO)₃(η^2 -L¹)(η^1 -dppmo)] (8) and [MoI₂(CO)₂(η^3 -L¹)] (11)

param	8	11
cryst color	pale yellow	deep red
cryst morphology	rectangular plates	parallelepipeds
cryst size, mm	0.15 × 0.20 × 0.1	0.15 × 0.30 × 0.7
solvent used for crystallization	diethyl ether/toluene (1:1)	dichloromethane
formula	C ₅₄ H ₅₁ MoN ₃ O ₄ P ₄	C ₂₉ H ₃₁ Cl ₂ I ₂ MoN ₃ O ₂ P ₂
MW	1025.9	936.2
cryst syst	triclinic	monoclinic
ocants syst collectd	+h,+k,±l	+h,+k,±l
space group	P $\bar{1}$	Cc
Z	2	4
a, Å	11.994(3)	10.471(2)
b, Å	14.807(2)	19.305(3)
c, Å	15.855(3)	17.325(3)
α , deg	114.24(1)	
β , deg	91.35(2)	95.47(2)
γ , deg	98.95(1)	
V, Å ³	2524.2	3486.3
d _c , g cm ⁻³	1.35	1.59
no. of params	596	368
radiation (graphite monochromator); λ , Å	Mo K α : 0.710 69	Mo K α : 0.710 69
linear abs coeff (μ), cm ⁻¹	3.86	23.95
temp, °C	20	20
scan technique	$\omega/2\theta$	$\omega/2\theta$
2 θ range	2–42	2–50
total no. of reflns	5939	4679
no. of unique reflns	5388	3235
no. of observed reflns	4014 ($F_o > 5\sigma(F_o)$)	3153 ($F_o > 5\sigma(F_o)$)
% decay	<1	<1
R ^a	0.066	0.049
R _w ^b	0.069	0.051
w	1.0000/($\sigma^2(F) + 0.010449F^2$)	10.1837/($\sigma^2(F) + 0.0000F^2$)
Residual peak in final diff map, e/Å ³	0.88	1.44
(Δ/σ) _{max}	0.061	0.069

$$^a R = \sum(|F_o| - |F_c|)/\sum|F_o|. \quad ^b R_w = (\sum w(|F_o| - |F_c|)^2/\sum w|F_o|)^{1/2}.$$

[MoI₂(CO)₂(η^3 -L¹)]-CH₂Cl₂ (11). A mixture of *fac*-[Mo(CO)₃(MeCN)(η^2 -L¹)] (1a) (0.200 g, 3×10^{-4} mol) or *cis*-[Mo(CO)₄(η^2 -L¹)] (1b) (0.196 g, 3×10^{-4} mol) and molecular iodine (0.079 g, 3.1×10^{-4} mol) was dissolved in 30 mL of benzene, and the solution was stirred for 3 h. During this period, a yellowish orange solid was precipitated. The product was filtered off and recrystallized from CH₂Cl₂. The compound crystallized as a solvate containing one molecule of CH₂Cl₂. Yield: 0.225 g, 80%. Mp: 183 °C. IR (Nujol, cm^{-1}): 1962 (s), 1890 (s), 1297 (m), 1130 (m), 1106 (m), 1052 (s), 853 (m), 737 (s), 717 (w), 572 (w), 530 (w), 500 (w), 472 (w), 444 (w), 360 (w). ¹H NMR (CDCl₃, ppm): 7.9–7.2 (m, 15H, aryl protons), 6.19 (s, 1H, CH of DMP), 5.30 (s, 2H, CH₂ of dichloromethane), 3.8 (m, 1H, CH of Prⁱ), 2.81 (s, 3H, CH₃ of DMP), 2.14 (s, 3H, CH₃ of DMP), 1.19 (d, ³J_{HH} = 6.1 Hz, 3H, CH₃ of Prⁱ), 0.33 (d, ³J_{HH} = 6.1 Hz, 3H, CH₃ of Prⁱ). ³¹P NMR (CH₂Cl₂, ppm): 113.2 {d, PPh(DMP)}, 74.7 (d, PPh₂), ²J_{PP} = 161 Hz. Anal. Calcd for C₂₅H₃₁Cl₂I₂MoN₃O₂P₂: C, 37.20; H, 3.34; N, 4.49. Found: 36.91; H, 3.12; N, 4.18.

[MoI₂(CO)₂(η^3 -L³)] (12). Analogous to the preparation of the Mo complex 1a,⁸ the acetonitrile complex *fac*-[Mo(CO)₃(MeCN)(η^2 -L³)] (1d) was prepared from *fac*-[Mo(CO)₃(MeCN)₃] {generated *in situ* by heating Mo(CO)₆ (0.050 g, 1.9×10^{-4} mol) in 15 mL of MeCN for 24 h} and the diphosphazane ligand L³ (0.102 g, 2.0×10^{-4} mol) in acetonitrile solvent. Solvent was removed *in vacuo* to obtain an air-sensitive oily compound.

Molecular iodine (0.056 g, 2.2×10^{-4} mol) was added to this oily product, the mixture was dissolved in 25 mL of benzene, and the solution was stirred for 3 h. Solvent was removed *in vacuo* to obtain a brown solid which was dissolved in CH₂Cl₂ and the solution cooled at 0 °C to obtain the title compound

Table 4. Non-Hydrogen Atomic Coordinates and Equivalent Thermal Parameters ($10^{-4}U_{eq}$, Å²) for *mer*-[Mo(CO)₃(η²-L¹)(η¹-dppmo)] (8)

atom	<i>x/a</i>	<i>y/b</i>	<i>z/c</i>	<i>U</i> _{eq} ^a
Mo1	0.13352(5)	0.25866(4)	0.23743(4)	254(3)
P1	0.2237(2)	0.1449(1)	0.2919(1)	296(8)
N1	0.1040(5)	0.1132(4)	0.3401(4)	338(28)
P2	0.0167(2)	0.1842(1)	0.3225(1)	309(9)
P3	0.2878(2)	0.3307(1)	0.1694(1)	310(8)
C54	0.3124(8)	0.4693(6)	0.2316(6)	427(36)
P4	0.3881(2)	0.5564(2)	0.1899(1)	354(8)
N2	-0.0111(5)	0.2627(5)	0.4365(4)	364(27)
N3	0.0387(6)	0.2522(5)	0.5110(5)	476(34)
O1	-0.0267(7)	0.3913(6)	0.2086(5)	846(47)
O2	0.2271(6)	0.4446(4)	0.4260(4)	569(28)
O3	0.0376(7)	0.1064(5)	0.0318(4)	883(38)
O4	0.5018(5)	0.5378(4)	0.1631(4)	508(29)
C1	0.0321(8)	0.3402(7)	0.2175(6)	470(44)
C2	0.1934(7)	0.3750(6)	0.3581(5)	336(35)
C3	0.0749(8)	0.1584(6)	0.1090(6)	457(41)
C4	0.2655(7)	0.0256(6)	0.2213(6)	387(43)
C5	0.2160(9)	-0.0274(7)	0.1289(7)	581(52)
C6	0.2381(13)	-0.1214(9)	0.0742(9)	918(65)
C7	0.3118(13)	-0.1629(9)	0.1084(11)	857(78)
C8	0.3586(10)	-0.1151(9)	0.1966(10)	686(56)
C9	0.3380(8)	-0.0192(7)	0.2524(7)	501(48)
C10	0.3406(8)	0.2112(7)	0.3817(6)	415(43)
C11	0.3175(8)	0.2783(7)	0.4714(6)	442(44)
C12	0.4057(13)	0.3475(9)	0.5340(7)	735(58)
C13	0.5150(14)	0.3503(11)	0.5068(11)	960(85)
C14	0.5375(9)	0.2852(12)	0.4230(10)	829(77)
C15	0.4494(8)	0.2156(9)	0.3604(7)	596(55)
C16	-0.1207(7)	0.1017(6)	0.2794(6)	383(41)
C17	-0.1382(8)	0.0374(7)	0.1874(7)	528(48)
C18	-0.2415(10)	-0.0278(9)	0.1488(8)	717(59)
C19	-0.3295(10)	-0.0259(9)	0.2043(10)	819(70)
C20	-0.3153(9)	0.0399(9)	0.2941(10)	766(73)
C21	-0.2086(9)	0.1016(8)	0.3349(7)	642(50)
C22	0.0095(8)	0.3264(7)	0.5846(6)	460(42)
C23	-0.0554(9)	0.3821(7)	0.5591(6)	491(49)
C24	-0.0678(8)	0.3406(7)	0.4652(6)	406(42)
C25	0.0498(12)	0.3405(9)	0.6812(8)	838(65)
C26	-0.1293(9)	0.3688(8)	0.3985(7)	572(47)
C27	0.0748(8)	0.0405(6)	0.3825(7)	460(44)
C28	0.1649(11)	0.0520(8)	0.4554(7)	666(61)
C29	0.0428(10)	-0.0657(8)	0.3090(8)	670(53)
C30	0.2690(8)	0.3101(6)	0.0460(5)	359(38)
C31	0.3618(8)	0.3051(7)	-0.0058(6)	465(46)
C32	0.3470(10)	0.2904(7)	-0.0969(7)	534(48)
C33	0.2410(11)	0.2806(8)	-0.1377(7)	603(56)
C34	0.1487(10)	0.2853(8)	-0.0869(7)	605(48)
C35	0.1641(8)	0.3018(7)	0.0048(6)	455(49)
C36	0.4262(8)	0.2946(7)	0.1740(6)	396(40)
C37	0.5241(9)	0.3605(8)	0.2224(7)	563(56)
C38	0.6257(11)	0.3258(12)	0.2216(11)	801(79)
C39	0.6285(12)	0.2274(19)	0.1737(11)	1078(125)
C40	0.5324(14)	0.1585(12)	0.1257(9)	899(78)
C41	0.4276(9)	0.1902(8)	0.1267(7)	586(51)
C42	0.2999(8)	0.5601(6)	0.0986(6)	370(36)
C43	0.3439(8)	0.5507(6)	0.0179(6)	424(39)
C44	0.2844(11)	0.5556(8)	-0.0536(7)	632(57)
C45	0.1770(12)	0.5726(9)	-0.0453(9)	737(57)
C46	0.1275(10)	0.5829(10)	0.0362(10)	878(74)
C47	0.1861(9)	0.5742(9)	0.1067(7)	628(58)
C48	0.3947(9)	0.6783(6)	0.2873(6)	404(44)
C49	0.3033(10)	0.7122(7)	0.3324(7)	603(49)
C50	0.3106(14)	0.8018(10)	0.4059(9)	902(75)
C51	0.4138(18)	0.8637(10)	0.4365(9)	1023(76)
C52	0.5102(15)	0.8362(10)	0.3925(9)	987(83)
C53	0.4997(10)	0.7410(7)	0.3171(7)	574(51)

$$^a U_{eq} = \frac{1}{3} \sum_i \sum_j (U_{ij} a_i^* a_j^* \vec{a}_i \cdot \vec{a}_j)$$

as a reddish orange powder. Yield: 0.104 g, 60%. Mp: 170 °C. IR (Nujol, cm⁻¹): 1961 (s), 1894 (s). ¹H NMR (CDCl₃, ppm): 8.0–6.9 (m, 20H, aryl protons), 6.15 (s, 1H, CH of DMP), 4.7 (m, 1H, CH of *CHMePh), 2.79 (s, 3H, CH₃ of DMP), 2.25 (s, 3H, CH₃ of DMP), 0.8 (d, ³J_{HH} = 7.4 Hz, 3H, CH₃ of *CHMePh). ³¹P NMR (CH₂Cl₂, ppm): 120.2 {d, PPh(DMP)},

Table 5. Non-Hydrogen Atomic Coordinates and Equivalent Thermal Parameters ($10^{-4}U_{eq}$, Å²) for [MoI₂(CO)₂(η³-L¹)] (11)

atom	<i>x/a</i>	<i>y/b</i>	<i>z/c</i>	<i>U</i> _{eq} ^a
Mo1	0.12360	0.18045(4)	-0.13970	280(2)
I1	0.32838(10)	0.23265(4)	-0.03248(7)	490(2)
I2	-0.00522(10)	0.15368(4)	-0.00518(6)	435(2)
P1	0.1452(3)	0.1194(1)	-0.2567(2)	331(7)
N1	-0.0026(9)	0.0953(4)	-0.2854(5)	333(25)
C3	-0.0478(15)	0.0439(7)	-0.3475(8)	545(43)
C4	-0.0536(17)	-0.0298(7)	-0.3163(9)	424(50)
C5	-0.1738(20)	0.0657(10)	-0.3911(9)	787(64)
P2	-0.0732(2)	0.1251(1)	-0.2048(2)	303(8)
C1	0.2323(11)	0.2402(7)	-0.2014(7)	428(40)
O1	0.2882(10)	0.2784(5)	-0.2353(6)	572(30)
C2	0.0221(11)	0.2647(5)	-0.1555(6)	339(32)
O2	-0.0361(10)	0.3139(4)	-0.1642(7)	565(33)
N11	0.2335(9)	0.0551(5)	-0.2044(6)	399(29)
N12	0.2298(8)	0.0735(4)	-0.1284(6)	353(26)
C13	0.2791(11)	0.0234(6)	-0.0862(7)	416(33)
C14	0.3131(13)	-0.0310(6)	-0.1349(8)	513(42)
C15	0.2844(13)	-0.0094(7)	-0.2095(7)	463(37)
C16	0.2921(17)	0.0241(8)	0.0010(8)	606(47)
C17	0.3008(16)	-0.0439(8)	-0.2857(10)	630(51)
C21	0.2293(14)	0.1334(6)	-0.3405(8)	514(38)
C22	0.3662(16)	0.1288(9)	-0.3348(11)	682(59)
C23	0.4242(23)	0.1508(11)	-0.4052(17)	1017(101)
C24	0.3574(38)	0.1696(10)	-0.4681(12)	1055(125)
C25	0.2264(33)	0.1732(8)	-0.4705(11)	958(99)
C26	0.1651(19)	0.1612(8)	-0.4104(9)	644(58)
C31	-0.2039(12)	0.1822(6)	-0.2344(7)	411(36)
C32	-0.2074(12)	0.2204(7)	-0.3022(8)	477(39)
C33	-0.3033(16)	0.2689(7)	-0.3217(10)	598(49)
C34	-0.3955(14)	0.2813(8)	-0.2695(11)	618(50)
C35	-0.3915(13)	0.2449(8)	-0.1994(9)	538(44)
C36	-0.2946(11)	0.1960(7)	-0.1825(8)	475(41)
C41	-0.1462(11)	0.0476(5)	-0.1665(7)	392(35)
C42	-0.2736(12)	0.0312(7)	-0.1878(9)	532(42)
C43	-0.3237(15)	-0.0306(8)	-0.1677(10)	638(52)
C44	-0.2448(14)	-0.0771(7)	-0.1212(11)	628(55)
C45	-0.1186(14)	-0.0605(6)	-0.1002(9)	547(45)
C46	-0.0704(12)	0.0015(7)	-0.1245(8)	479(39)
CI1	0.6296(7)	0.0763(4)	-0.0044(5)	1183(28)
C50	0.6453(23)	0.1435(16)	0.0639(18)	1110(110)
CI2	0.5743(11)	0.1285(10)	0.1448(5)	2288(81)

81.3 (d, PPh₂), ²J_{PP} = 167 Hz. Anal. Calcd for C₃₃H₃₁I₂MoN₃O₂P₂: C, 43.39; H, 3.43; N, 4.60. Found C, 43.10; H, 3.19; N, 4.84.

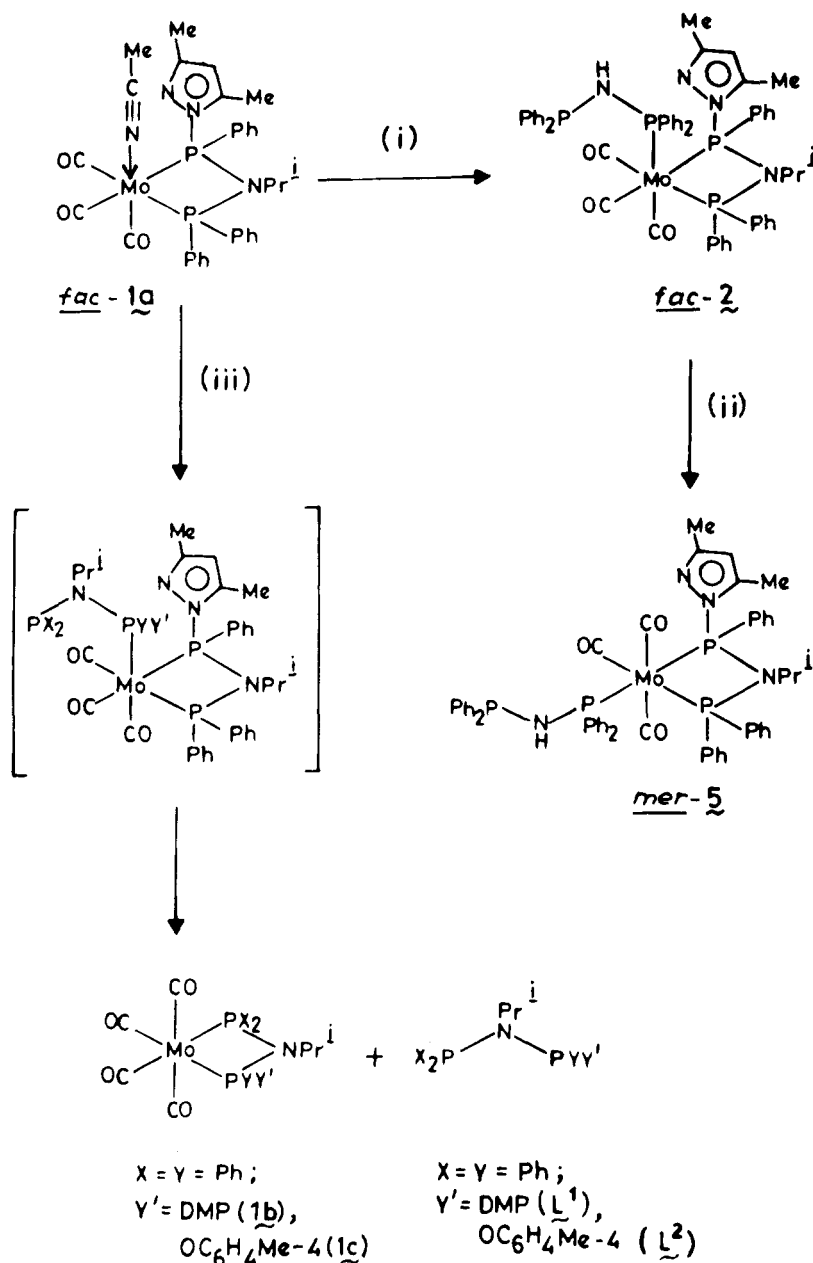
X-ray Structure Determinations of *mer*-[Mo(CO)₃(η²-L¹){η¹-Ph₂PCH₂P(O)Ph₂}] (8) and [MoI₂(CO)₂(η³-L¹)] (11). The crystal in each case was coated with paraffin oil to protect it from atmospheric air and moisture. Intensity data were collected on an Enraf-Nonius CAD-4 diffractometer using graphite-monochromated Mo Kα radiation as described in our previous publication.⁸ The structures were solved by the Patterson method using SHELXS-86¹⁴ and refinements were carried out by SHELX-76.¹⁵ An empirical absorption correction was applied for **11** using the DIFABS programme.¹⁶ Hydrogen atoms for **8** were located from difference Fourier maps; all non-hydrogen atoms were refined anisotropically and hydrogen atoms refined isotropically. For **11** all non-hydrogen atoms except those of the lattice held solvent (CH₂Cl₂) were refined anisotropically; the solvent molecule showed disorder and hence was refined only isotropically. The hydrogen atoms were not located for **11**. Crystal data and details pertinent to each structure determination are given in Table 3. The final atomic coordinates with equivalent isotropic thermal parameters are listed in Tables 4 and 5. Other data are included as supplementary material.

(14) Sheldrick, G. M. *SHELXS86*, Program for crystal structure solution; University of Göttingen: Göttingen, Germany 1986.

(15) Sheldrick, G. M. *SHELX76*, Program for crystal structure refinement; University of Cambridge: Cambridge, U.K., 1976.

(16) Walker, N.; Stuart, D. *Acta Crystallogr.* **1982**, A39, 158.

Scheme 1



^a (i) (Ph₂P)₂NH/toluene/25 °C; (ii) isomerization; (iii) X₂PN(Prⁱ)PYY'/toluene/25 °C.

Results and Discussion

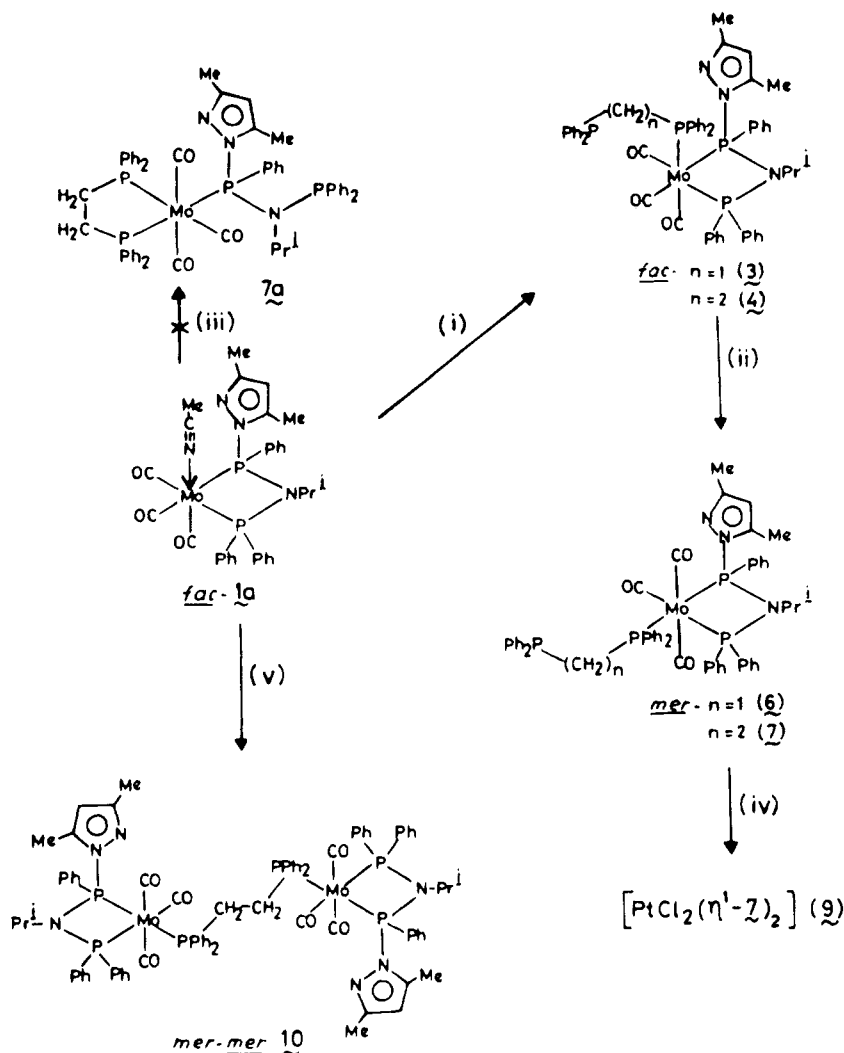
Syntheses of *fac*-[Mo(CO)₃(η²-L¹)(η¹-PXP)] {PXP = *dppa* (2), *dppm* (3), *dppe* (4)} and *mer*-[Mo(CO)₃(η²-L¹)(η¹-PXP)] {PXP = *dppa* (5), *dppm* (6), *dppe* (7)}. Treatment of the Mo(0) acetonitrile complex *fac*-[Mo(CO)₃(MeCN)(η²-L¹)] (**1a**) with the diphosphazane, *dppa*, or diphosphinoalkane such as *dppm* or *dppe* in the ratio 1:1 immediately gives the complexes *fac*-[Mo(CO)₃(η²-L¹)(η¹-PXP)] (**2–4**). These complexes rapidly isomerize to give *mer*-[Mo(CO)₃(η²-L¹)(η¹-PXP)] (**5–7**) (Schemes 1 and 2). The rate of isomerization is faster for the *dppe* complex (completed in 4 h at 25 °C) than for the *dppa* or *dppm* complex (completed in 6 h). In all these cases, the yield of the final product (*mer* isomers **5–7**) is high (>80%); minor quantities of the tetracarbonyl complex *cis*-[Mo(CO)₄(η²-L¹)] (**1b**) and the free diphosphazane ligand L¹ are also present in the reaction mixture. The *fac* complexes are identified only

by ³¹P NMR spectroscopy and could not be isolated in a pure form. The *mer* complexes are purified by column chromatography, followed by crystallization.

The reaction of **1a** with *dppe* follows a course different from that observed for the reaction of the complex *fac*-[Mo(CO)₃(MeCN)(η²-*dppm*)] with *dppe*.¹⁷ The product obtained in the latter reaction, *viz.*, *fac*-[Mo(CO)₃(η²-*dppe*)(η¹-*dppm*)] contains a five-membered chelate ring formed by *dppe* and a η¹-coordinated *dppm*. The four-membered chelate ring of *dppm* is opened up to leave a η¹-coordinated *dppm* while a more stable η² five-membered chelate ring is formed by *dppe*. In the present study, the reaction of **1a** with *dppe* does not give a product of the type **7a** (Scheme 2); only *mer*-[Mo(CO)₃(η²-L¹)(η¹-*dppe*)] (**7**) in which the four-membered diphosphazane chelate ring is retained and *dppe* is coordinated in the η¹-mode is obtained. The preference of the

(17) Schenk, W. A.; Hilpert, G. H. *J. Chem. Ber.* **1991**, *124*, 433.

Scheme 2



^a (i) $\text{Ph}_2\text{P}(\text{CH}_2)_n\text{PPh}_2/\text{toluene}/25^\circ\text{C}$; (ii) isomerization; (iii) $\text{dppe}/\text{toluene}/25^\circ\text{C}$; (iv) $[\text{PtCl}_2(\text{COD})]/\text{dichloromethane}/25^\circ\text{C}$; (v) $\text{dppe}(1:2 \text{ L/Mo ratio})/\text{benzene}/25^\circ\text{C}$.

diphosphazane to form a chelate ring is clearly evident from this result.

In the process of crystallization of $\text{mer-}[\text{Mo}(\text{CO})_3(\eta^2\text{-L}^1)(\eta^1\text{-dppm})]$ (**6**) from a diethyl ether/toluene mixture, the uncoordinated phosphorus is oxidized to give $\text{mer-}[\text{Mo}(\text{CO})_3(\eta^2\text{-L}^1)\{\eta^1\text{-Ph}_2\text{PCH}_2\text{P}(\text{O})\text{Ph}_2\}]$ (**8**). Darensbourg and co-workers¹⁸ have reported a similar result during the crystallization of $\text{fac-}[\text{W}(\text{CO})_3(\eta^2\text{-dppm})(\eta^1\text{-dppm})]$ from tetrahydrofuran; isomerization and oxidation of the uncoordinated phosphorus occurs to yield $\text{mer-}[\text{W}(\text{CO})_3(\eta^2\text{-dppm})(\eta^1\text{-Ph}_2\text{PCH}_2\text{P}(\text{O})\text{Ph}_2)]$.

The reaction of **1a** with the diphosphazanes $\text{Ph}_2\text{PN}(\text{Pr}^i)\text{PPh}(\text{DMP})$ (L^1) or $\text{Ph}_2\text{PN}(\text{Pr}^i)\text{PPh}(\text{OC}_6\text{H}_4\text{Me-4})$ (L^2) does not give a η^1 -coordinated product analogous to **2**, as shown by the ³¹P NMR spectrum of the reaction mixture. In the case of L^2 , after 10 min, the spectrum shows four pairs of doublets which can be assigned to the tetracarbonyl Mo(0) complexes, $\text{cis-}[\text{Mo}(\text{CO})_4(\eta^2\text{-L}^1)]$ (**1b**) and $\text{cis-}[\text{Mo}(\text{CO})_4(\eta^2\text{-L}^2)]$ (**1c**) and the free ligands L^1 and L^2 (Scheme 1). In addition, some unidentified decomposition products are also present. Presumably, the η^1 -coordinated complex $\text{fac-}[\text{Mo}(\text{CO})_3(\eta^2\text{-L}^1)(\eta^1\text{-L}^2)]$ is formed as a transient species which undergoes

disproportionation to yield the molybdenum tetracarbonyl complexes of the individual ligands L^1 and L^2 . The isolation of a η^1 -complex of dppa (**5**) clearly demonstrates the operation of steric factors in determining the stability of a η^1 -coordinated complex such as **2**.

Spectroscopic Data for fac and mer Complexes (2–7). The title complexes have been characterized by elemental analyses, IR, and ¹H and ³¹P NMR spectroscopic data. The IR (ν_{CO}) and ¹H NMR data are listed in Table 1. The NH stretching vibration for **5** is observed at 3337 cm^{-1} . The ν_{CO} absorptions occur in the region $1983\text{--}1833 \text{ cm}^{-1}$, and the values are close to those in the spectra of $\text{mer-}[\text{Mo}(\text{CO})_3(\eta^2\text{-L}^1)(\text{PPh}_3)]$ ⁸ which contains a monophosphine ligand. The ¹H NMR spectra show two doublets for the methyl groups of the isopropyl substituent, as these are diastereotopic (Table 1). One of these resonances is strongly shielded compared to the other, as observed in the case of $\text{mer-}[\text{Mo}(\text{CO})_3(\eta^2\text{-L}^1)(\text{PR}_3)]$ ($\text{R} = \text{Ph}$ or OPh).⁸ The η^1 -substituted dppa , dppm , or dppe show the expected multiplet signals for NH or methylene protons. The ³¹P NMR spectra of these complexes are much more informative. They contain four nonequivalent phosphorus nuclei, and an AMRX type spectrum is observed in each case. A typical spectrum is shown in Figure 1. The data are listed in

(18) Darensbourg, D. J.; Zalewski, D. J.; Plepys, C.; Campana, C. *Inorg. Chem.* **1987**, *26*, 3727.

Table 2. The *fac* and *mer* isomers show clear differences in their spectra. The P–P coupling constants indicate that the η^1 -coordinated phosphorus is *trans* to the P(Ph)(DMP) phosphorus of the chelated diphosphazane.

The ^{31}P NMR spectrum of the reaction mixture obtained by the treatment of *dppa* with **1a** is shown in Figure 2. After 10 min, the spectrum shows the presence of *fac* isomer **2** along with a minor amount of the *mer* complex **5**; the signals of the starting material are also observed. After 100 min, the *fac* and the *mer* complexes are present in almost equal quantities; after 6 h, conversion to the *mer* complex is nearly complete. The same type of transformation is observed for the *dppm* complex **3** but in the case of *dppe* complex **4**, the conversion is faster and is complete within 4 h. After 10 min, equal amounts of *fac* and *mer* complexes are seen and after 30 min, the *mer* complex is the major component. The $^{31}\text{P}\{^1\text{H}\}$ NMR spectrum of *mer*-[Mo(CO) $_3$ (η^2 -L 1)(η^1 -Ph $_2$ PCH $_2$ P(O)Ph $_2$)] (**8**) shows multiplets similar to those observed for **6**.

Crystal Structure of *mer*-[Mo(CO) $_3$ (η^2 -L 1)(η^1 -Ph $_2$ PCH $_2$ P(O)Ph $_2$)] (8**).** The structure of **8** has been determined by X-ray diffraction. A perspective view of the molecule is shown in Figure 3. Selected bond angles and bond distances are listed in Table 6. The coordination geometry of the complex is that of a regular octahedron. The diphosphazane ligand Ph $_2$ PN(Pr i)PPh(DMP) (L 1) is coordinated to molybdenum in a η^2 -fashion (chelate mode) whereas the heterofunctional bis(diphenylphosphinomethane) monooxide (Ph $_2$ PCH $_2$ P(O)Ph $_2$; *dppmo*) is coordinated in an η^1 -mode. The PPh(DMP) of the diphosphazane ligand is *trans* to the PPh $_2$ of *dppm* monooxide.

The three M–P distances are different; that involving the pyrazole-substituted phosphorus is shorter (2.414 Å) than the other M–P distances (2.544, 2.480 Å) presumably because of the electron-withdrawing nature of the dimethylpyrazolyl group. The η^1 -Ph $_2$ P(*dppmo*) M–P distance is shorter than the diphosphazane chelate PPh $_2$ M–P distance because of the presence of CO *trans* to the latter. Correspondingly, this M–CO distance (1.947 Å) is shorter than the other M–CO distances (mean 1.996 Å) in the molecule. The diphosphazane bite angle is 64.5°, which is shorter than the *dppm* bite angle (67.2°) in the complex *mer*-[W(CO) $_3$ (η^2 -*dppm*)(η^1 -*dppmo*)].¹⁸ The P–N–P angle is 101.5° and the geometry around the nitrogen (N1) is planar ($\Sigma\tilde{N} = 360^\circ$).

Synthesis and Characterization of *cis*-[PtCl $_2$ -{*mer*-[Mo(CO) $_3$ (η^2 -L 1)(η^1 -*dppe*)] $_2$] (9**).** The uncoordinated phosphorus in the complexes **5–7** can be utilized suitably for coordination to other transition metals to build polymetallic complexes. Thus the reaction of **7** with the Pt $^{2+}$ complex *cis*-[PtCl $_2$ (COD)] gives a trimetallic complex (**9**), as shown in Scheme 2. Complex **9** contains two independent *mer*-metallo-ligands (complex **7**) coordinated to the PtCl $_2$ moiety in a *cis* fashion. The IR spectrum of this complex shows three strong ν_{CO} absorptions in the region 1863–1969 cm^{-1} analogous to that of the η^1 -coordinated complex **7**. As there is no difference in the ^{31}P chemical shifts and the P–P coupling constants in the metalloligand moiety of complex **9** and those of **7**, it is likely that the *mer* geometry around molybdenum is retained in this trimetallic complex **9**. The resonance of the uncoordi-

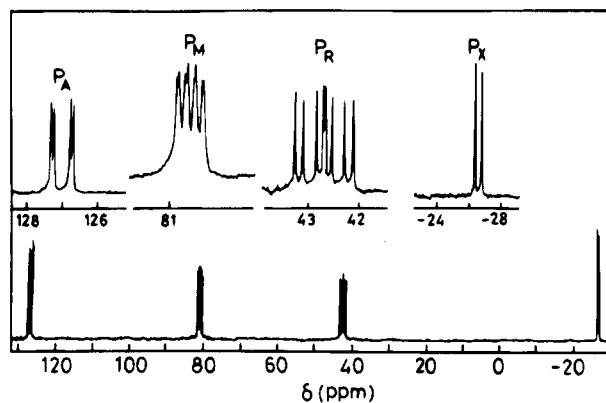


Figure 1. $^{31}\text{P}\{^1\text{H}\}$ NMR spectrum of *mer*-[Mo(CO) $_3$ { η^2 -Ph $_2$ -PN(Pr i)PPh(DMP)}(η^1 -*dppm*)] (**6**).

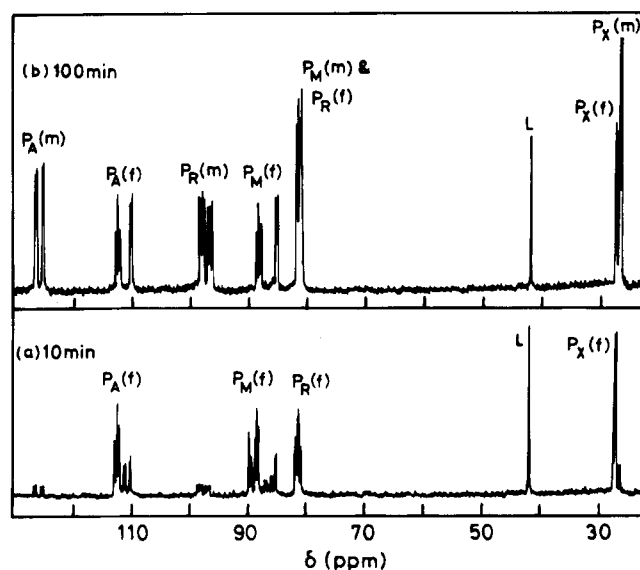


Figure 2. $^{31}\text{P}\{^1\text{H}\}$ NMR spectra of the products of the reaction of *fac*-[Mo(CO) $_3$ (MeCN){ η^2 -Ph $_2$ PN(Pr i)PPh(DMP)}] (**1a**) with *dppa* in benzene: (a) after 10 min; (b) after 100 min (f = facial, m = meridional). For assignment of the observed resonances, see Table 2.

nated phosphorus (P $_X$) of the η^1 -*dpe* complex (**7**) is shifted downfield upon coordination to platinum; this resonance appears as a doublet at 6.1 ppm ($^2J_{\text{PP}} = 31.1$ Hz) with platinum satellites. The $^1J_{\text{PtP}}$ coupling (3631 Hz) is much higher than that observed for a *trans* η^1 -*dppm* Pt $^{2+}$ complex, *trans*-[Pt(CN) $_2$ (η^1 -*dppm*) $_2$] (2274 Hz).¹⁹

The reaction of the η^1 -*dppm* complex **6** with *cis*-[PtCl $_2$ (COD)] leads to the decomposition of complex **6** to yield the stable chelate complexes *cis*-[PtCl $_2$ (η^2 -*dppm*)] and *cis*-[Mo(CO) $_4$ (η^2 -L 1)] (**1b**) in addition to the liberation of the free ligand (L 1). From these results, it is clear that a two carbon spacer between the two phosphorus atoms is required to build polymetallic complexes when a diphosphazane is chelated to a metal carbonyl moiety. This is in contrast to the observation with the η^1 -*dppm* complex *fac*- or *mer*-[Mo(CO) $_3$ (η^2 -*dppm*)(η^1 -*dppm*)] which readily reacts with [PdCl $_2$ (COD)] to give a heterobimetallic complex with a bridging *dppm* ligand.¹⁷

Synthesis and Characterization of [mer-[Mo(CO) $_3$ (η^2 -L 1)] $_2$ (μ -*dppe*)] (10**).** The reaction of **1a** with

(19) Pringle, P. G.; Shaw, B. L. *J. Chem. Soc., Chem. Commun.* **1982**, 956.

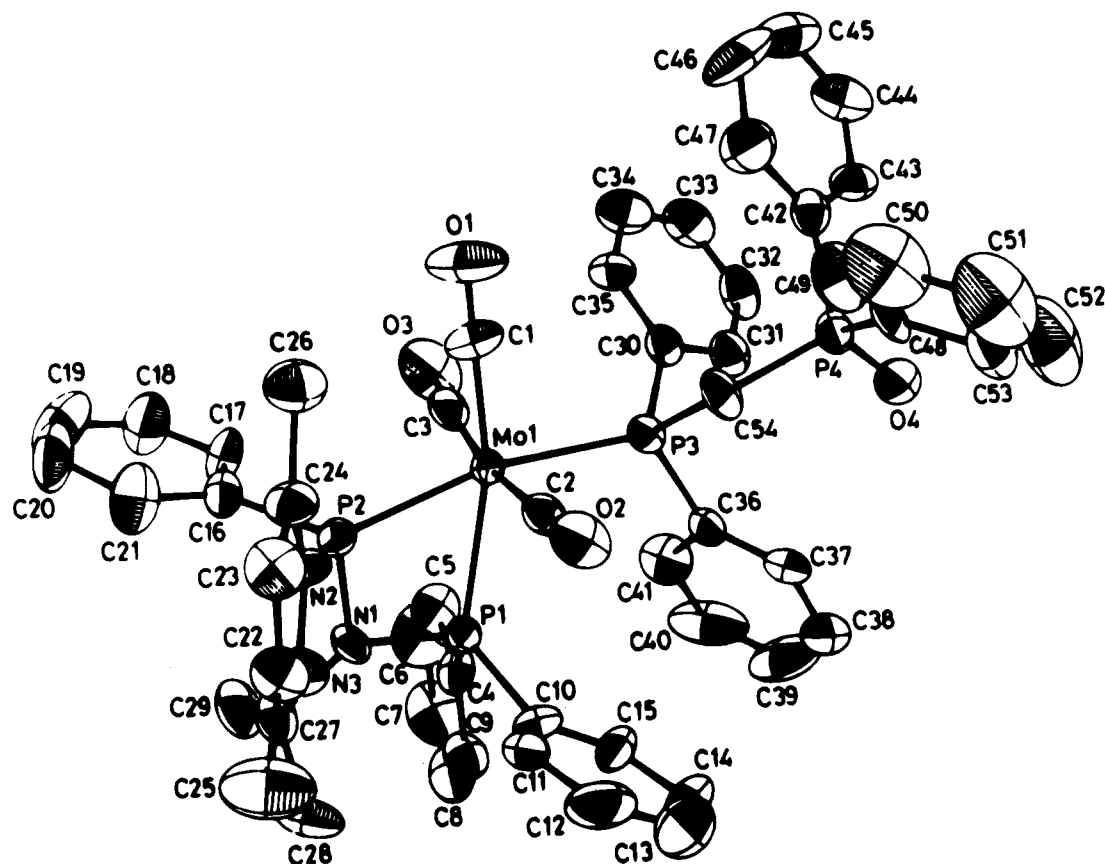


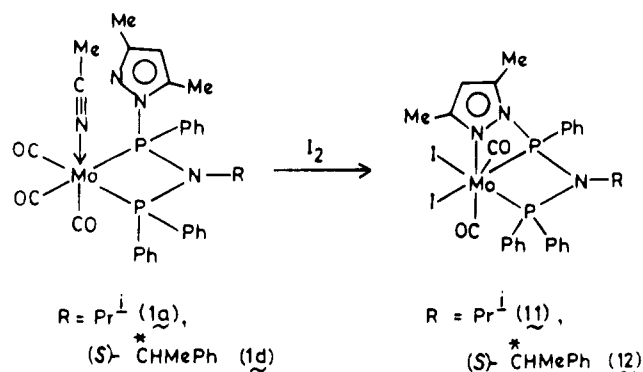
Figure 3. ORTEP plot of a perspective view of *mer*-[Mo(CO)₃{η²-Ph₂PN(Prⁱ)PPh(DMP)}{η¹-Ph₂PCH₂P(O)Ph₂}] (**8**). Thermal ellipsoids are drawn at the 50% probability level.

Table 6. Selected Bond Distances (Å) and Bond Angles (deg) in *mer*-[Mo(CO)₃(η²-L¹)(η¹-dppmo)] (**8**)

(a) bond distances		(b) bond angles	
Mo1-P1	2.544(2)	C2-Mo1-C3	171.1(4)
Mo1-P2	2.414(2)	P1-Mo1-C1	163.9(4)
Mo1-P3	2.480(2)	P1-Mo1-P3	104.3(4)
Mo1-C1	1.947(11)	P1-Mo1-P2	64.5(4)
Mo1-C2	1.997(6)	P1-N1-C27	132.7(4)
Mo1-C3	1.993(8)	P1-N1-P2	101.5(4)
P1-N1	1.733(7)	P2-N1-C27	125.8(4)
N1-P2	1.688(7)	P3-C54-P4	125.3(4)
P2-N2	1.776(6)	P2-N2-C24	129.7(4)
P3-C54	1.846(8)	P2-N2-N3	118.5(4)
C54-P4	1.814(11)	N3-N2-C24	111.6(4)
P4-O4	1.471(7)		
N2-N3	1.387(11)		
O1-C1	1.157(15)		
O2-C2	1.150(8)		
O3-C3	1.177(10)		

dpppe in the ratio 2:1 in benzene yields a bimetallic dppe-bridged complex [*mer*-[Mo(CO)₃(η²-L¹)]₂(μ-dpppe)] (**10**) (Scheme 2). Attempts to obtain an analogous complex of dppm were unsuccessful. The ³¹P{¹H} NMR spectrum of **10** shows an AMR pattern, as expected, and the chemical shift values are in the same region as observed for the coordinated phosphorus centers in *mer*-[Mo(CO)₃(η²-L¹)(η¹-dpppe)] (**7**). Only the P_A {PPh(DMP)} resonance is resolved as a doublet of doublets at 126.2 ppm (²J_{PP} = 87 and 12 Hz); the other two resonances P_M (PPh₂ of L¹, 80.4 ppm) and P_R (PPh₂ of dppe, 45.5 ppm) are broad multiplets. The high P_A-P coupling (*J*_{AR} = 87 Hz) comparable to the magnitude of the *trans* coupling in *mer* complexes of **5**-**7** indicates that in this bimetallic complex, two *mer* centers are bridged by the dppe ligand.

Scheme 3



Heptacoordinated Complexes of Mo(II), [Mo₂(CO)₂{η³-Ph₂PN(R)PPh(DMP)}] (R = Prⁱ (11**), (S)-*CHMePh (**12**)).** Oxidative addition of iodine to *fac*-[Mo(CO)₃(MeCN)(η²-L¹)] (**1a**) or *cis*-[Mo(CO)₄(η²-L¹)] (**1b**) in benzene yields the heptacoordinated complex [Mo₂(CO)₂(η³-L¹)] (**11**). The corresponding Mo(II) complex with the chiral diphosphazane [Mo₂(CO)₂{η³-(S,R)-Ph₂PN(*CHMePh)*PPh(DMP)}] (**12**) is prepared in the same way, but in this case the intermediate complex *fac*-[Mo(CO)₃(MeCN)(η²-(S,R)-Ph₂PN(*CHMePh)*PPh(DMP))] (**1d**) is not isolated and is directly oxidized with iodine (Scheme 3). These Mo(II) complexes are air-stable and can be crystallized from a dichloromethane/petroleum ether mixture.

Structural Assignments for [Mo₂(CO)₂{η³-Ph₂PN(R)PPh(DMP)}] (R = Prⁱ (11**), (S)-*CHMePh (**12**)).** The elucidation of the structures of the seven-coordinated complexes **11** and **12** in which the diphosphazane

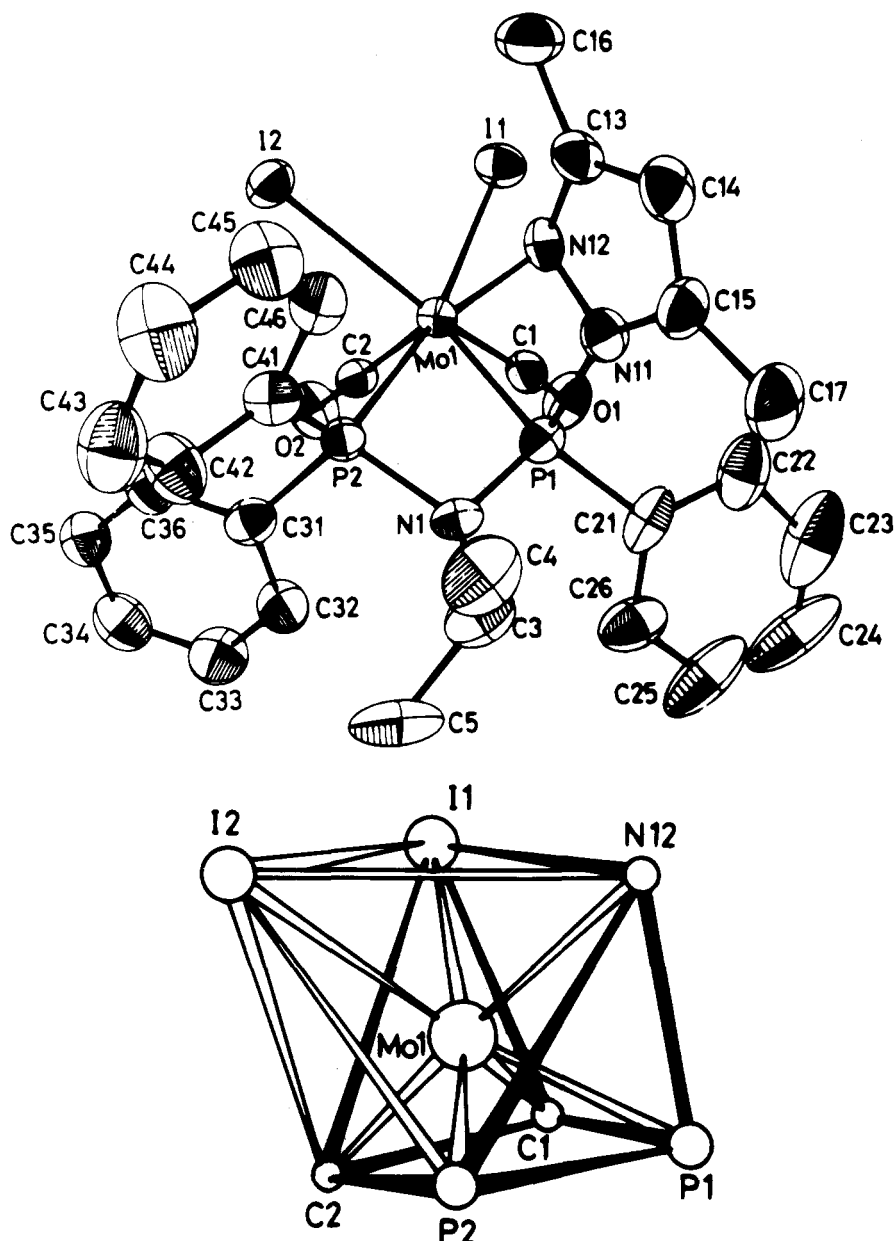


Figure 4. (a, top) ORTEP plot of a perspective view of $[\text{MoI}_2(\text{CO})_2\{\eta^3\text{-Ph}_2\text{PN}(\text{Pr})\text{PPh}(\text{DMP})\}]$ (**11**). Thermal ellipsoids are drawn at the 50% probability level. (b, bottom) coordination polyhedron of **11**.

Table 7. Selected Bond Distances (Å) and Bond Angles (deg) in $[\text{MoI}_2(\text{CO})_2(\eta^3\text{-L}^1)]$ (**11**)

(a) bond distances		(b) bond angles	
MoI-I1	2.882(1)	C2-MoI-N12	174.4(4)
MoI-I2	2.849(1)	C1-MoI-C2	76.9(5)
MoI-P1	2.374(3)	P2-MoI-N12	91.5(2)
MoI-P2	2.493(2)	P1-MoI-N12	63.3(2)
MoI-C1	2.000(13)	P1-MoI-P2	62.8(1)
MoI-C2	1.948(10)	I1-MoI-I2	85.3(1)
MoI-N12	2.344(8)	P1-N1-P2	97.1(5)
P1-N1	1.647(9)	P1-N1-C3	128.6(8)
P1-N11	1.748(10)	C3-N1-P2	131.5(8)
N1-P2	1.739(10)	P1-N11-C15	143.8(9)
C1-O1	1.139(17)	P1-N11-N12	104.6(7)
C2-O2	1.131(13)	N12-N11-C15	110.0(1)

acts as a tridentate ligand is based on IR and NMR spectroscopic data and also a single crystal X-ray study of **11**.

The infrared spectra of **11** and **12** show two strong carbonyl absorption bands at ~ 1960 and 1890 cm^{-1} . The CO stretching vibrations for the heptacoordinated diphos-

phazane complexes $[\text{MI}_2(\text{CO})_3\{\eta^2\text{-(PX)}_2\text{NR}\}]$ (R = Me or Ph, X = OPh, Ph; M = Mo or W) in which two phosphorus atoms are coordinated to the metal are observed in the region $2070\text{--}1940\text{ cm}^{-1}$.^{20,21} The weak 1890 cm^{-1} band observed for **11** and **12** is consistent with the coordination of a strong σ -donor but a weak π -acceptor nitrogen in addition to coordination of two phosphorus atoms. The ^1H NMR spectrum of **11** shows considerable deshielding of the protons of one of the methyl groups of the dimethylpyrazole which resonates at 2.81 ppm; the other methyl group resonates at 2.14 ppm. The difference in the chemical shifts of these methyl groups is about 0.67 ppm. The unusual deshielding of one of the pyrazolyl methyl protons is presumably because of the close approach of this group to an iodine atom as revealed by X-ray crystallography (nonbonded I \cdots C distance is 3.97 Å; see below). The ^1H NMR

(20) Prakasha, T. K.; Krishnamurthy, S. S. Unpublished results.

(21) Balakrishna, M. S.; Krishnamurthy, S. S.; Manohar, H. *Organometallics* **1991**, *10*, 2522.

spectrum of **12** also shows a similar deshielding of the pyrazolyl methyl protons whose resonances are observed at 2.79 and 2.25 ppm.

The ^{31}P NMR spectra of **11** and **12** show an AX pattern. Both the phosphorus resonances are shifted downfield when compared with the chemical shift for the free ligand. The coordination shift ($\Delta\delta = \delta_{\text{complex}} - \delta_{\text{ligand}}$) (Table 2) is comparable to that (24.8) noted for $[\text{MoI}_2(\text{CO})_3\{\eta^2\text{-}(\text{Ph}_2\text{P})_2\text{NPr}^i\}]$;²⁰ in contrast, similar diphosphazane complexes with phosphite substituents, $[\text{MoI}_2(\text{CO})_3\{\eta^2\text{-}(\text{PX}_2)_2\text{NR}\}]$ ²¹ (R = Me or Ph, X = OPh) show an upfield shift of 30 ppm. Cotton and Matusz²² have reported similar upfield shift for the Mo(II) complex, $[\text{MoI}_2(\text{CO})_2(\eta^2\text{-dppm})(\eta^1\text{-dppm})]$.

X-ray Crystal Structure of $[\text{MoI}_2(\text{CO})_2\{\eta^3\text{-Ph}_2\text{PN}(\text{Pr}^i)\text{PPh}(\text{DMP})\}]\cdot\text{CH}_2\text{Cl}_2$ (11**).** A perspective view of the molecule is shown in Figure 4a, and the selected structural parameters are listed in Table 7. The molybdenum atom in **11** is seven coordinated with a capped trigonal prismatic geometry (Figure 4b).²³ The tridentate PPN ligand occupies one face of the trigonal prism; the other face is filled with two carbonyl groups and an iodine atom (I1), while the other iodine (I2) is the capping atom of the C2–P2–N12–I1 rectangular face. The ligand forms two adjacent strained four-membered rings. Both the four-membered rings retain their planarity and form an open booklike structure. The geometry around the nitrogen of the P–N–P framework and the pyrazolyl nitrogen connected to the phosphorus atom is planar.

The bond angles P1–Mo–P2 and P1–Mo1–N12 are acute (62.8 and 63.3°, respectively). The PNP bond angle is 97.1° and is slightly shorter than that (97.6°)

(22) Cotton, F. A.; Matusz, M. *Polyhedron* **1987**, *6*, 261.

(23) Capped octahedral geometry is the most common stereochemistry observed for complexes of the type $[\text{MX}_2(\text{CO})_3(\eta^2\text{-L-L})]$.^{24,25} Below a "normalised bite" of 1.1 for the bidentate ligand (L-L), a pentagonal bipyramidal geometry is observed, as in $[\text{WI}_2(\text{CO})_3(\eta^2\text{-dppm})]$.²⁶ $[\text{WI}_2(\text{CO})_3\{\eta^2\text{-}((\text{PhO})_2\text{P})_2\text{NPh}\}]$,²¹ and $[\text{MoBr}_2(\text{CO})(\text{bipy})(\eta^2\text{-dppm})]$.²⁷ Seven-coordinated complexes of the type $[\text{MX}_4(\eta^3\text{-L})]$ (where L contains NNN, OSO, ONO, or ONN donor sites) also display a pentagonal bipyramidal geometry.²⁵

(24) Kepert, D. L. *Prog. Inorg. Chem.* **1979**, *25*, 41.

(25) Drew, M. G. B. *Prog. Inorg. Chem.* **1977**, *23*, 67.

observed for the tungsten diphosphazane complex $[\text{WI}_2(\text{CO})_3\{\eta^2\text{-}((\text{PhO})_2\text{P})_2\text{NPh}\}]$.²¹ Two different P–N bond lengths are observed due to the unsymmetrical nature of the diphosphazane and also because of the involvement of the pyrazolyl nitrogen in coordination. The P–N distance involving the phosphorus atom (P1) bearing the pyrazolyl substituent is much shorter (1.647 Å) than the other P–N bond length (1.739 Å). The Mo–P{PPh(DMP)} bond distance (2.374 Å) is also shorter than the Mo–P(PPh₂) bond distance (2.493 Å). The two iodine atoms are at the expected distances from Mo(II) (≈ 2.86 Å). The Mo–N distance is slightly longer (2.344 Å) than that observed (2.25 Å) in seven-coordinated Mo(II) complex $[\text{Mo}(\text{CO})_2(\eta^2\text{-}(\text{S,S}))(\eta^3\text{-Tp})]$ $\{(\text{S,S})^- = \text{dithiocarbamate, Tp} = \text{tris(pyrazolyl)borate}\}$ where three nitrogens of the tris(pyrazolyl)borate are coordinated along with a dithiocarbamate ligand.²⁸ The Mo–C2 bond distance (1.948 Å) on the rectangular face is slightly shorter than the Mo–C1 bond distance (2.000 Å) (see Figure 4b).

Conclusions. The results reported here bring out the differences in the reactivity between diphosphazanes and diphosphinoalkanes toward group 6 metal carbonyl moieties. The unsymmetrical diphosphazane complex *fac*- $[\text{Mo}(\text{CO})_3(\text{MeCN})\{\eta^2\text{-Ph}_2\text{PN}(\text{Pr}^i)\text{PPh}(\text{DMP})\}]$ (**1a**) is a useful synthon for various metalloligands and poly-metallic complexes as well as a heptacoordinated complex.

Acknowledgment. We thank the Department of Science and Technology, New Delhi, India, for support.

Supplementary Material Available: Tables of anisotropic thermal parameters, bond distances and angles, and H atom coordinates for **8** and **11** (12 pages). Ordering information is given on any current masthead page.

OM940487I

(26) Foy, R. M.; Kepert, D. L.; Raston, C. L.; White, A. H. *J. Chem. Soc., Dalton Trans.* **1980**, 440.

(27) Arnaiz, F. J.; Garcia, G.; Riera, V.; Dromzée, Y.; Jeannin, Y. *J. Chem. Soc., Dalton Trans.* **1987**, 819.

(28) Shiu, K. B.; Lee, J. Y.; Wang, Y.; Cheng, M. C. *Inorg. Chem.* **1993**, *32*, 3565.

Synthesis, Characterization, and Reactivity of Heterodinuclear RuM (M = Cu(I), Ag(I), Au(I), Rh(I), and Ir(I)) and Heterotrinnuclear RuAg₂ and RuRhAg Compounds Derived from the Metal-Complex Ligand Bis(pyrazolato)(*p*-cymene)(pyrazole)ruthenium(II)

Daniel Carmona,* Joaquina Ferrer, Reinaldo Atencio, Fernando J. Lahoz, and Luis A. Oro*

Departamento de Química Inorgánica, Instituto de Ciencia de Materiales de Aragón, Universidad de Zaragoza-Consejo Superior de Investigaciones Científicas, 50009 Zaragoza, Spain

María Pilar Lamata

Departamento de Química Inorgánica, Escuela Universitaria de Ingeniería Técnica Industrial, Instituto de Ciencia de Materiales de Aragón, Universidad de Zaragoza-Consejo Superior de Investigaciones Científicas, Corona de Aragón 35, 50009 Zaragoza, Spain

Received July 5, 1994[®]

The reaction of the mononuclear ruthenium *p*-cymene pyrazolate complex [(η^6 -*p*-cymene)-Ru(pz)₂(Hpz)] (**1**) (*p*-cymene = *p*-isopropylmethylbenzene; Hpz = pyrazole, C₃H₄N₂) with the halide triphenylphosphine complexes [MCl(PPh₃)₃]_x and KOH led to the corresponding heterodinuclear compounds [(η^6 -*p*-cymene)Ru(pz)₃M(PPh₃)₃] (M = Cu (**2**), Ag (**3**), Au (**4**)). In solution, complexes **2–4** showed a dynamic behavior consisting of exchange between terminal and bridging pyrazolate groups accompanied by dissociation of the phosphine ligand. Complex **3** reacted with AgBF₄ and PPh₃ to yield the heterotrinnuclear RuAg₂ complex [(η^6 -*p*-cymene)Ru(μ -pz)₃{Ag(PPh₃)₂}₂]BF₄ (**5**) which was also fluxional. Heterodinuclear derivatives of formula [(η^6 -*p*-cymene)(pz)Ru(μ -pz)₂ML₂] (M = Rh; L₂ = 1,5-cyclooctadiene (COD) (**6**), (CO)₂ (**7**); M = Ir; L₂ = (CO)₂ (**8**)) have been prepared by treating complex **1** with the appropriate [M(acac)L₂] (acac = acetylacetonate) compounds. The carbonyl complexes **7** and **8** reacted with mono- or diphosphines, rendering [(η^6 -*p*-cymene)(pz)Ru(μ -pz)₂ML₂] (M = Rh; L₂ = CO, PPh₃ (**9**), CO, P(OMe)₃ (**10**), CO, bis(diphenylphosphino)methane (dppm) (**11**), dppm (**14**), 1,2-bis(diphenylphosphino)ethane (dppe) (**15**), *cis*-1,2-bis(diphenylphosphino)ethylene (dppen) (**16**), (*R*)-(+)-1,2-bis(diphenylphosphino)propane (*R*-prophos) (**17a,b**); M = Ir; L₂ = CO, PPh₃ (**12**), CO, dppm (**13**), dppe (**18**)). Protonation of **6–9** and **12** with HBF₄ afforded the corresponding cationic complexes [(η^6 -*p*-cymene)(Hpz)Ru(μ -pz)₂ML₂]BF₄ (M = Rh; L₂ = COD (**19**), (CO)₂ (**20**), CO, PPh₃ (**21**); M = Ir; L₂ = (CO)₂ (**22**), CO, PPh₃ (**23**)). The molecular structure of complex **22** has been determined by X-ray diffraction methods. Crystals are monoclinic, space group *P*2₁/*c*, with cell parameters *a* = 7.9909(6) Å, *b* = 17.0590(9) Å, *c* = 19.083(2) Å, β = 93.94(1)°, and *Z* = 4. The molecule exhibits two bridging pyrazolate groups between the metals. No direct intermetallic interaction is observed, the Ru···Ir distance being 3.6770(6) Å. In the solid state, a clear hydrogen bond is present between one fluorine atom of the tetrafluoroborate anion and the pyrazole ligand. The heterotrinnuclear RuRhAg cationic derivatives [(η^6 -*p*-cymene)Ru{(μ -pz)Ag(PPh₃)₂}{(μ -pz)₂RhL₂}]BF₄ (L₂ = COD (**24**), CO, PPh₃ (**25**)) have been prepared on the addition of equimolar amounts of AgBF₄ and PPh₃ to complexes **6** and **9**, respectively.

Introduction

A large area of coordination and organometallic chemistry has been developed around polypyrazolylborate anions which includes most transition-metal ions.¹ These anions usually function as tridentate or bidentate ligands and, in solution, often undergo rapid exchange of the coordinated and uncoordinated pyrazolate groups.² Very recently the activation of C–H bonds by pyra-

zolyborate complexes of rhodium and iridium has received particular attention.^{2e,3} On the other hand, the site of protonation of tripyrazolylborates of rhodium and iridium can not be previously determined. Thus, while protonation of the rhodium complex [HB(Me₂pz)₃Rh(CO)₂] by HBF₄ takes place at a pyrazolate nitrogen,

(2) See, for example: (a) Cocivera, M.; Desmond, T. J.; Ferguson, G.; Kaitner, B.; Lalor, F. J.; O'Sullivan, D. J. *Organometallics* **1982**, *1*, 1125. (b) Cocivera, M.; Ferguson, G. F.; Lalor, J.; Szczecinski, P. *Organometallics* **1982**, *1*, 1139. (c) Schubert, D. M.; Knobler, C. B.; Trofimenko, S.; Hawthorne, M. F. *Inorg. Chem.* **1990**, *29*, 2346. (d) Bovens, M.; Gerfin, T.; Gramlich, V.; Petter, W.; Venanzi, L. M.; Haward, M. T.; Jackson, S. A.; Eisenstein, O. *New J. Chem.* **1992**, *16*, 337. (e) Bloyce, P. E.; Mascetti, J.; Rest, A. J. *J. Organomet. Chem.* **1993**, *444*, 223.

[®] Abstract published in *Advance ACS Abstracts*, December 1, 1994.
(1) (a) Trofimenko, S. *Acc. Chem. Res.* **1971**, *4*, 17. (b) Trofimenko, S. *Chem. Rev.* **1972**, *72*, 497. (c) Trofimenko, S. *Prog. Inorg. Chem.* **1986**, *34*, 115. (d) Trofimenko, S. *Chem. Rev.* **1993**, *93*, 943.

Table 1. ^1H and ^{31}P NMR Data^a for Complexes 2–5

complex	^1H							^{31}P	
	<i>p</i> -cymene			pyrazolate ^b				293 K	213 K
	Me	<i>i</i> -Pr	H _{AA} /H _{BB} ^c	H _{3/5}	H _{5/3}	H ₄	PPh ₃		
2	1.51 (s)	1.00 (d, <i>J</i> = 7.0) 2.25 (sp)	5.20, 5.53 (<i>J</i> = 6.0)	6.61 (bs)	<i>c</i>	6.05 (bs)	7.5 (m)	1.5 (bs)	0–2 (bs)
3	1.46 (s)	0.97 (d, <i>J</i> = 6.9) 2.17 (sp)	5.26, 5.59 (<i>J</i> = 6.1)	6.61 (bs)	<i>c</i>	6.08 (bs)	7.5 (m)	15 (bs)	15.8 (d, <i>J</i> (¹⁰⁷ AgP) = 565, <i>J</i> (¹⁰⁹ AgP) = 653)
4	1.62 (s)	0.94 (d, <i>J</i> = 6.8) 2.50 (sp)	5.29, 5.62 (<i>J</i> = 6.0)	6.60 (bs)	<i>c</i>	6.03 (bs)	7.5 (m)	31.3 (s)	
5	1.39 (s)	0.93 (d, <i>J</i> = 6.8) 2.50 (sp)	5.23, 5.39 (<i>J</i> = 6.0)	<i>c</i>	<i>c</i>	6.25 (bs)	7.5 (m)	17.4 (d) <i>J</i> (AgP) = 640	15.8 (d, <i>J</i> (¹⁰⁷ AgP) = 573, <i>J</i> (¹⁰⁹ AgP) = 661), 19.1 (d, <i>J</i> (¹⁰⁷ AgP) = 641, <i>J</i> (¹⁰⁹ AgP) = 740)

^a Measured in CDCl₃ at room temperature (^1H) or in CDCl₃/CHCl₃ (1/1, v/v) at 293 or 213 K (^{31}P). Chemical shifts in ppm from TMS (^1H) or from 85% H₃PO₄ in D₂O (^{31}P) as external standards. *J* values in hertz. Abbreviations: s, singlet; bs, broad singlet; d, doublet; t, triplet; q, quartet; sp, septet; m, multiplet; bm, broad multiplet. ^b *J*(H₃H₄) ≈ *J*(H₄H₅). ^c Obscured by the PPh₃ protons.

leading to the cationic compound [HB(Me₂pz)₂(Me₂pzH)-Rh(CO)₂]₂BF₄, protonation of the homologous iridium complex [HB(Me₂pz)₃Ir(CO)₂], by the same acid, affords the iridium(III) cationic hydride [HB(Me₂pz)₃IrH(CO)₂]-BF₄.⁴ Nevertheless, the iridium complex [HB(Me₂pz)₃Ir(COD)] (COD = 1,5-cyclooctadiene) is protonated by CF₃SO₃H at a pyrazolate nitrogen, rendering [HB(Me₂pz)₂(Me₂pzH)Ir(COD)]CF₃SO₃.^{2d}

We have recently described the preparation and characterization of the bis(pyrazolato)pyrazole complexes [(η^5 -C₅Me₅)Ir(pz)₂(Hpz)]⁵ and (η^6 -*p*-cymene)Ru(pz)₂(Hpz) (*p*-cymene = *p*-isopropylmethylbenzene) (1).⁶ From a coordination point of view, these compounds are comparable to protonated tripyrazolylborates and, in fact, we have shown that the iridium anion [(η^5 -C₅Me₅)Ir(pz)₃]⁻ (the deprotonated form of [(η^5 -C₅Me₅)Ir(pz)₂(Hpz)]) can act as metalloligand toward a variety of metallic fragments showing η^2 or η^3 coordination modes.⁷

In this paper we describe the synthesis and characterization of heterodinuclear RuM (M = Cu(I), Ag(I), Au(I), Rh(I), Ir(I)) complexes in which the [(η^6 -*p*-cymene)Ru(pz)₃]⁻ anion is acting as metal-complex ligand. Their general formulae are [(η^6 -*p*-cymene)Ru(pz)₃M(PPh₃)] (M = Cu (2), Ag (3), Au (4)) and [(η^6 -*p*-cymene)(pz)Ru(μ -pz)₂ML₂] (M = Rh, L₂ = COD (6); (CO)₂ (7); CO, PPh₃ (9); CO, P(OMe)₃ (10); CO, bis(diphenylphosphino)methane (dppm) (11); dppm (14); 1,2-bis(diphenylphosphino)ethane (dppe) (15); *cis*-1,2-bis(diphenylphosphino)ethylene (dppen) (16); (*R*)-(+)-1,2-bis(diphenylphosphino)propane (*R*-prophos) (17a,b). M = Ir, L₂ = (CO)₂ (8); CO, PPh₃ (12); CO, dppm (13); dppe (18)). Taking into account the different possibilities of protonation of these compounds, we also report the reactivity of some of them with HBF₄ to give the cationic complexes [(η^6 -*p*-cymene)(Hpz)Ru(μ -pz)₂ML₂]-BF₄ (M = Rh, L₂ = COD (19); (CO)₂ (20); CO, PPh₃ (21); M = Ir, L₂ = (CO)₂ (22); CO, PPh₃ (23)) as well as the preparation of the trinuclear cationic derivatives [(η^6 -*p*-cymene)Ru(μ -pz)₃[Ag(PPh₃)₂]₂BF₄ (5) and [(η^6 -*p*-cymene)Ru(μ -pz)Ag(PPh₃)]₂[(μ -pz)₂RhL₂]₂BF₄ (L₂ = COD (24); CO, PPh₃ (25)). The molecular structure of the RuIr complex [(η^6 -*p*-cymene)(Hpz)Ru(μ -pz)₂Ir(CO)₂]₂BF₄ (22) is also described.

Results and Discussion

Heterometallic Complexes [(η^6 -*p*-Cymene)Ru(pz)₃M(PPh₃)] (M = Cu, Ag, Au) and [(η^6 -*p*-Cy-

mene)Ru(μ -pz)₃[Ag(PPh₃)₂]₂BF₄. The reaction in acetone or methanol of the mononuclear ruthenium complex [(η^6 -*p*-cymene)Ru(pz)₂(Hpz)] (1)⁶ with the chloride compounds [MCl(PPh₃)_x] (x = 4, M = Cu,⁸ Ag;⁹ x = 1, M = Au¹⁰) and equimolar amounts of KOH afforded the heterobinuclear complexes [(η^6 -*p*-cymene)Ru(pz)₃M(PPh₃)] (M = Cu (2), Ag (3), Au (4)) in yield ranging from 75 to 89%. The new compounds have been characterized by elemental analyses¹¹ (see Experimental Section) and IR and NMR spectroscopy. In particular, the IR spectra showed the characteristic bands of the pyrazolate (ca. 1050 cm⁻¹)¹² and triphenylphosphine (ca. 500 cm⁻¹)¹³ ligands and the absence of the N–H vibration of the starting material. ^1H and $^{31}\text{P}\{^1\text{H}\}$ NMR data are recorded in Table 1. The ^1H NMR spectra, in CDCl₃ at room temperature, showed the expected resonances for the protons of the *p*-cymene, pyrazolate, and PPh₃ ligands and indicated the presence of only one type of pyrazolate group. On cooling to 213 K, two pyrazolate environments in a 2/1 ratio were observed but the slow-exchange limiting spectra were not achieved

(3) (a) Ghosh, C. K.; Graham, W. A. G. *J. Am. Chem. Soc.* **1987**, *109*, 4726. (b) Ghosh, C. K.; Rodgers, D. P. S.; Graham, W. A. G. *J. Chem. Soc., Dalton Trans.* **1988**, 1511. (c) Ghosh, C. K.; Graham, W. A. G. *J. Am. Chem. Soc.* **1989**, *111*, 375. (d) Ghosh, C. K.; Hoyano, J. K.; Krentz, R.; Graham, W. A. G. *J. Am. Chem. Soc.* **1989**, *111*, 5480. (e) Fernández, M. J.; Rodríguez, M. J.; Oro, L. A.; Lahoz, F. J. *J. Chem. Soc., Dalton Trans.* **1989**, 2073. (f) Tanke, R.; Crabtree, R. H. *Inorg. Chem.* **1989**, *28*, 3444. (g) Jones, W. D.; Duttweiler, R. P.; Feher, F. J.; Hessel, E. T. *New J. Chem.* **1989**, *13*, 725. (h) Barrientos, C.; Ghosh, C. K.; Graham, W. A. G.; Thomas, M. J. *J. Organomet. Chem.* **1990**, *394*, C31. (i) Pérez, P. J.; Poveda, M. L.; Carmona, E. *J. Chem. Soc., Chem. Commun.* **1992**, 8. (j) Boutry, O.; Gutiérrez, E.; Monge, A.; Nicasio, M. C.; Pérez, P. J.; Carmona, E. *J. Am. Chem. Soc.* **1992**, *114*, 7288. (k) Gutiérrez, E.; Monge, A.; Nicasio, M. C.; Poveda, M. L.; Carmona, E. *J. Am. Chem. Soc.* **1994**, *116*, 791.

(4) Ball, R. G.; Ghosh, C. K.; Hoyano, J. K.; McMaster, A. D.; Graham, W. A. G. *J. Chem. Soc., Chem. Commun.* **1989**, 341.

(5) Carmona, D.; Oro, L. A.; Lamata, M. P.; Elguero, J.; Apreda, M. C.; Foces-Foces, C.; Cano, F. H. *Angew. Chem., Int. Ed. Engl.* **1986**, *25*, 1114.

(6) Carmona, D.; Ferrer, J.; Oro, L. A.; Apreda, M. C.; Foces-Foces, C.; Cano, F. H.; Elguero, J.; Jimeno, M. L. *J. Chem. Soc., Dalton Trans.* **1990**, 1463.

(7) (a) Carmona, D.; Lahoz, F. J.; Oro, L. A.; Lamata, M. P.; Buzarra, S. *Organometallics* **1991**, *10*, 3123. (b) Carmona, D.; Lamata, M. P.; Ferrer, J.; Modrego, M.; Perales, M.; Lahoz, F. J.; Atencio, R.; Oro, L. A. *J. Chem. Soc., Chem. Commun.* **1994**, 575.

(8) Churchill, M. R.; Kalra, K. L. *Inorg. Chem.* **1974**, *13*, 1065.

(9) Teo, B.-K.; Calabrese, J. C. *J. Am. Chem. Soc.* **1975**, *97*, 1256.

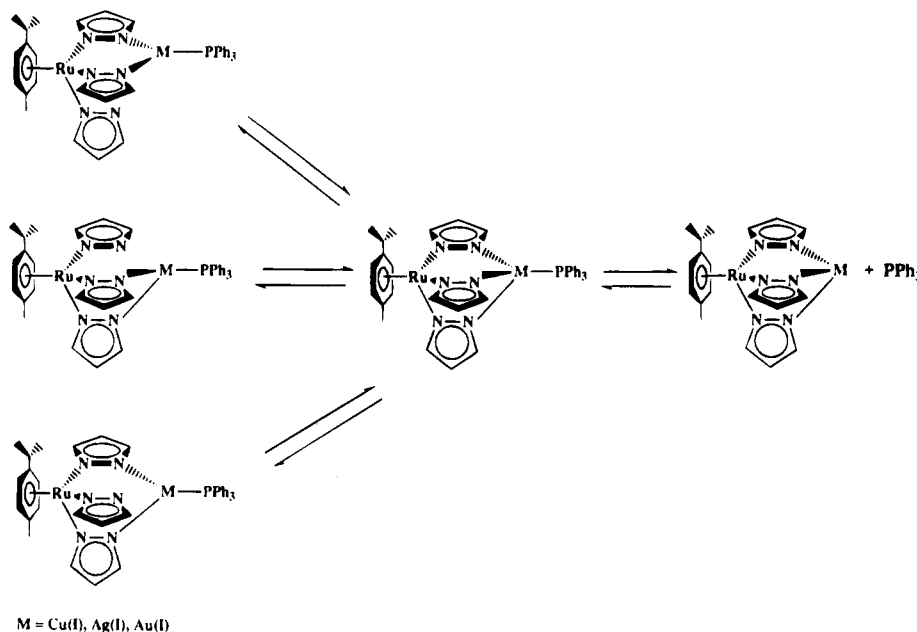
(10) Malvaho, L. *Atti. Acad. Naz. Lincei, Cl. Sci. Fis., Mat. Nat., Rend.* **1908**, *17*, 857.

(11) We have not been able to obtain satisfactory analyses for 2, probably due to the presence of traces of Cu(II) oxidation products.

(12) Usón, R.; Oro, L. A.; Esteban, M.; Cuadro, A. M.; Navarro, P.; Elguero, J. *Transition Met. Chem.* **1982**, *7*, 234.

(13) Bellamy, L. J. *The Infrared Spectra of Complex Molecules*; Chapman and Hall: London, 1975; Vol. 1, p 358.

Scheme 1. Proposed Mechanism for the Fluxional Processes of 2–4



in any case. Their $^{31}\text{P}\{^1\text{H}\}$ spectra showed, at room temperature, broad signals centered at 1.5 and 15 ppm for **2** and **3**, respectively, and a sharp singlet at 31.3 ppm for **4**. At 213 K the spectrum of complex **2** was similar to that registered at ambient temperature and showed a broad signal in the 0–2 ppm region. However, the spectrum of complex **3** consisted of two doublets of similar intensity centered at 15.8 ppm ($^1J(^{107}\text{AgP}) = 565$, $^1J(^{109}\text{AgP}) = 653$ Hz) consistent with direct Ag–P bonding.¹⁴ The spectrum of the RuAu complex **4** did not show significant changes on varying the temperature from 293 to 213 K.

We have recently determined the molecular structure of the related IrAg complex $[(\eta^5\text{-C}_5\text{Me}_5)\text{Ir}(\text{pz})_3\text{Ag}(\text{PPh}_3)]$ by single-crystal X-ray analysis. In this molecule two pyrazolate groups bridge the iridium and silver atoms and the third pyrazolate is terminal and only coordinates to iridium.^{7a} Interestingly, the spectroscopic data of $[(\eta^5\text{-C}_5\text{Me}_5)\text{Ir}(\text{pz})_3\text{Ag}(\text{PPh}_3)]$ are comparable to those of **3** and, therefore, both compounds probably adopt similar structures. The spectroscopic observations can be accounted for by assuming that, at room temperature, there is a rapid equilibrium between structures which exchange bridging and terminal pyrazolate groups through an intermediate in which M is tetracoordinate as depicted in Scheme 1. Additionally, an equilibrium of dissociation of the triphenylphosphine must be invoked to account for the observed $^{31}\text{P}\{^1\text{H}\}$ NMR spectra. In fact, the $^{31}\text{P}\{^1\text{H}\}$ NMR spectrum of **3**, at room temperature, in the presence of 1 equiv of PPh_3 , consisted of a peak at 4.8 ppm without coupling to silver, indicative of a fast exchange between free and coordinated PPh_3 . Fluxional processes involving exchanges between free and coordinated pyrazolate groups have been observed in polypyrazolylborate complexes of Cu(I)¹⁵ and Ag(I),^{15c} and lability of PR_3 groups is a phenomenon commonly observed.¹⁶ The activation energies for the rupture of P–Ag bonds are in the zone of barriers that can be

measured by NMR spectroscopy, and, very recently, we have determined by a complete NMR line shape analysis that the rupture activation energy in complex **3** is 46 kJ mol^{-1} , comparable to those determined for other phosphorus–metal bonds.¹⁷

As commented above, complexes **2–4** contain one pyrazolate ligand in which one nitrogen atom is capable of subsequent coordination. In order to probe this capacity, we performed the reaction of $[(\eta^6\text{-p-cymene})\text{Ru}(\text{pz})_3\text{Ag}(\text{PPh}_3)]$ with AgBF_4 and PPh_3 . When **3** was treated with equimolar amounts of AgBF_4 and PPh_3 , a yellow solid characterized as the trinuclear complex $[(\eta^6\text{-p-cymene})\text{Ru}(\mu\text{-pz})_3\{\text{Ag}(\text{PPh}_3)_2\}]\text{BF}_4$ (**5**) was obtained in 77% isolated yield. Subsequent addition of AgBF_4 and PPh_3 to **5** did not produce the corresponding reaction, and complex **5** remained unchanged. At room temperature, the ^1H NMR spectrum of complex **5** (Table 1) showed a unique environment for the pyrazolate groups. The $^{31}\text{P}\{^1\text{H}\}$ NMR spectrum of **5**, at room temperature, showed two very broad signals centered at 17.4 ppm and separated by ca. 640 Hz, which we assigned to directly bound to silver PPh_3 groups. At 213 K the ^1H NMR showed a slight broadening of the pyrazolate signal, whereas the $^{31}\text{P}\{^1\text{H}\}$ spectrum consisted of four doublets. Two were centered at 15.8 ppm, with coupling constants $^1J(^{107}\text{AgP}) = 573$ and $^1J(^{109}\text{AgP}) = 661$ Hz, and the other two at 19.1 ppm, with $^1J(^{107}\text{AgP}) = 641$ and $^1J(^{109}\text{AgP}) = 740$ Hz. These spectral data could be explained by assuming that a fluxional process consisting of the rotation of the two AgPPh_3 groups of molecule **5** around the three free

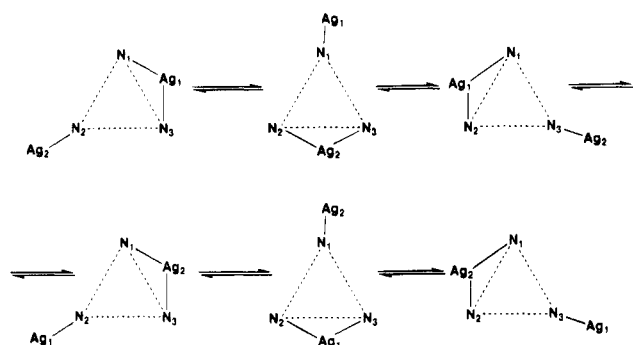
(15) (a) Bruce, M. I.; Ostazewski, A. P. *J. Chem. Soc., Dalton Trans.* **1973**, 2433. (b) Churchill, M. R.; DeBoer, B. G.; Rotella, F. J.; Abu Salah, O. M.; Bruce, M. I. *Inorg. Chem.* **1975**, *14*, 2051. (c) Abu Salah, O. M.; Bruce, M. I. *J. Organomet. Chem.* **1975**, *87*, C15.

(16) (a) Muetterties, E. L.; Alegrianti, C. W. *J. Am. Chem. Soc.* **1972**, *94*, 6386. (b) Huffman, J. C.; Roth, R. S.; Siedle, A. R. *J. Am. Chem. Soc.* **1976**, *98*, 4340. (c) Green, M.; Orpen, A. G.; Salter, I. D.; Stone, F. J. A. *J. Chem. Soc., Dalton Trans.* **1984**, 2497. (d) Brice, R. A.; Pearce, S. C.; Salter, I. D.; Henrick, K. *J. Chem. Soc., Dalton Trans.* **1986**, 2181. (e) Freeman, M. J.; Orpen, A. G.; Salter, I. D. *J. Chem. Soc., Dalton Trans.* **1987**, 379.

(17) Carmona, D.; Ferrer, J.; Lamata, M. P.; Oro, L. A.; Limbach, H.-H.; Scherer, G.; Elguero, J.; Jimeno, M. L. *J. Organomet. Chem.* **1994**, *470*, 271.

(14) Pregosin, P. S.; Kunz, R. W. *Phosphorus-31 and Carbon-13 Nuclear Magnetic Resonance Studies of Transition Metal Complexes Containing Phosphorus Ligands*; Springer-Verlag: New York, 1979; pp 107–109.

Scheme 2. Proposed Mechanism for the Fluxional Processes of Complex 5. Ag₁ and Ag₂ Represent the Two AgPPh₃ Groups of the Cation and N₁, N₂, and N₃ the Three Pyrazolate Nitrogen Atoms Not Coordinated to Ruthenium (See Text)



nitrogen atoms of the (η^6 -*p*-cymene)Ru(pz)₃ moiety was occurring in a concerted way as it is schematically represented in Scheme 2. So, the static structure proposed for **5** consists of a trigonal silver atom coordinated to two bridging pyrazolates and one PPh₃ group and one digonal Ag atom bound to one bridging pyrazolate group and one PPh₃ ligand (Figure 1). The chemical shifts and the coupling constants of the two phosphorus nuclei of **5** in the low-temperature limiting spectrum have been assigned by comparison with those of the precursor **3** at the same conditions.

Heterometallic Complexes [(η^6 -*p*-Cymene)-(pz)Ru(μ -pz)₂ML₂] (M = Rh, Ir). The ruthenium complex [(η^6 -*p*-cymene)Ru(pz)₂(Hpz)] (**1**) reacted with equimolar amounts of [M(acac)L₂] (M = Rh; L₂ = COD,¹⁸ (CO)₂.¹⁹ M = Ir; L₂ = (CO)₂²⁰) to give the corresponding heterodinuclear complexes [(η^6 -*p*-cymene)(pz)Ru(μ -pz)₂ML₂] (M = Rh; L₂ = COD (**6**), (CO)₂ (**7**). M = Ir; L₂ = (CO)₂ (**8**)). With [Ir(acac)(COD)],²¹ the above reaction led to a mixture of [Ir(μ -pz)(COD)]₂²² and unidentified *p*-cymene-ruthenium products, which were probably formed by fragmentation of the unstable dinuclear intermediate [(η^6 -*p*-cymene)(pz)Ru(μ -pz)₂Ir(COD)]. The dicarbonyl RuRh derivative **7** could also be prepared upon bubbling CO through dichloromethane or tetrahydrofuran solutions of complex **6**. The very high solubility of complex **8**, even in hydrocarbon solvents, precluded its isolation. Its formation was inferred from IR solution data and from its chemical reactivity. The structures of **6** and **7** were assigned on the basis of elemental microanalyses and IR and NMR spectroscopic measurements. In the IR spectra the absence of the bands corresponding to the acac group²³ and to the ν -(NH)¹² vibration of the starting materials was observed. Furthermore, complexes **7** and **8** showed the characteristic *cis*-dicarbonyl bands²⁴ at ca. 2000 and 2080 cm⁻¹.

(18) Chatt, J.; Venanzi, L. M. *J. Chem. Soc.* **1957**, 4735.

(19) Varshavskii, Yu. S.; Cherkasova, T. G. *Russ. J. Inorg. Chem.* **1967**, 599.

(20) [Ir(acac)(CO)₂] can be prepared by bubbling CO at atmospheric pressure through *n*-hexane solutions of [Ir(acac)(COD)]. The starting yellow solutions became dark in a few seconds, and a brown-blue solid began to precipitate which, after filtering and drying, is characterized as the dichroic [Ir(acac)(CO)₂]. Yield: 90%. Ir (Nujol) ν (CO) 2050 (vs), 1990 (vs) cm⁻¹. Anal. Calcd for C₇H₇IrO₄: C, 24.20; H, 2.03. Found: C, 24.12; H, 1.95. ¹H NMR (CDCl₃, δ): 5.76 (s, 1H), 2.09 (s, 6H).

(21) Robinson, S. D.; Shaw, B. L. *J. Chem. Soc.* **1965**, 4997.

(22) Coleman, A. W.; Eadie, D. T.; Stobart, S. R.; Zaworotko, M. J.; Atwood, J. L. *J. Am. Chem. Soc.* **1982**, *104*, 922.

(23) Rigby, W.; Lee, H.-B.; Bailey, P. M.; McCleverty, J. A.; Maitlis, P. M. *J. Chem. Soc., Dalton Trans.* **1979**, 387.

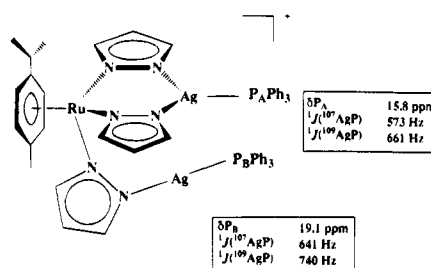


Figure 1. Schematic structure of complex **5** with ³¹P{¹H} NMR data assignments.

The ¹H NMR spectra of complexes **6** and **7**, in CDCl₃ at room temperature, showed, besides the expected resonances of the *p*-cymene and diolefin ligands, two sets of pyrazolate signals in a 2/1 ratio. As the temperature was increased, a slight broadening of the signals was observed although, until 363 K in toluene-*d*₈, the fast exchange limiting spectra were not achieved. These data indicated that in solution a dynamic equilibrium between structures that slowly exchange the two types of chemically inequivalent pyrazolates was taking place above room temperature. Three static structures (excluding the uncommon one with a tricoordinate rhodium atom) are compatible with the spectral data (Figure 2). In structure **A** two pyrazolates are bridging the two metals while the third pyrazolate is only coordinated to ruthenium. In structures **B** and **C** a triple pyrazolate bridge connects the two metals, rendering M five-coordinated and displaying square-pyramidal (**B**) or trigonal-bipyramidal (**C**) geometries. In the first case, an exchange between free and coordinated pyrazolate groups can be postulated to explain the fluxional process, whereas an exchange between axial and equatorial nitrogen atoms would account for the spectral data in the case of structures **B** and **C**. Both types of dynamic processes have been reported for the related complexes [B(pz)₄Rh(diolefin)],^{2b} exchange between axial and equatorial sites occurring faster than that involving mono- and bidentate ligands. In our case, as the dynamic processes involving complexes **6** and **7** were still slow at 363 K, we propose they adopt structure **A** with the M atom being four-coordinated. This proposal was also supported by the shift to higher field observed for the resonance of the H₅ proton of the terminal pyrazolate ring in **6** and **7** (Table 2). Most probably this shielding is produced by the electronic ring current of the bridging pyrazolates^{5,7} which is only possible in structure **A**. In fact, the molecular structure of the related complex [(η^6 -*p*-cymene)(Hpz)Ru(μ -pz)₂Ir(CO)₂]-BF₄ (**22**) (see below) exhibits an azolate ligand disposition comparable to that of **A**. Finally, the reactivity shown by complexes **6**–**8** also corroborates the proposed structure.

Reactivity of Complexes [(η^6 -*p*-Cymene)(pz)Ru(μ -pz)₂M(CO)₂]. (a) With Mono- or Bidentate Phosphorus Donor Ligands. The dicarbonyl complexes **7** and **8** reacted with monodentate phosphorus donor ligands or dppm to give the monocarbonyl dinuclear complexes [(η^6 -*p*-cymene)(pz)Ru(μ -pz)₂M(CO)L] (M = Rh; L = PPh₃ (**9**), P(OMe)₃ (**10**), dppm (**11**). M = Ir; L

(24) (a) Usón, R.; Oro, L. A.; Claver, C.; Garralda, M. A. *J. Organomet. Chem.* **1976**, *105*, 365. (b) Usón, R.; Oro, L. A.; Artigas, J.; Sariego, R. *J. Organomet. Chem.* **1979**, *179*, 65. (c) Bonati, F.; Wilkinson, G. *J. Chem. Soc.* **1964**, 3156.

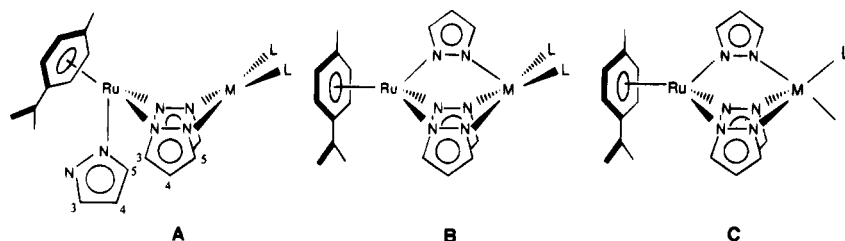


Figure 2. Possible static structures for complexes 6–8.

Table 2. ¹H NMR Data^a for Complexes 6–25

complex	<i>p</i> -cymene			terminal pz ^b			bridging pz ^b			others
	Me	<i>i</i> -Pr	H _{AA'} /H _{BB'} ^c	H ₃	H ₅	H ₄	H ₃	H ₅	H ₄	
6	1.71 (s)	1.11 (d, <i>J</i> = 6.9) 2.32 (sp)	5.97, 6.12 (<i>J</i> = 5.8)	7.61 (d)	5.56 (d)	5.86 (t, <i>J</i> = 1.5)	7.41 (d)	6.56 (d)	6.00 (t, <i>J</i> = 1.8)	4.43 (m), 3.95 (m), 2.66 (m), 2.00 (m) (COD)
7	1.70 (s)	1.08 (d, <i>J</i> = 7.0) 2.40 (sp)	5.70, 5.89 (<i>J</i> = 5.9)	7.64 (bs)	5.83 (d)	5.92 (t, <i>J</i> = 1.8)	7.54 (d)	6.68 (d)	6.13 (t, <i>J</i> = 2.1)	
9 ^c	1.71 (s)	1.03 (d, <i>J</i> = 6.8) 1.14 (d, <i>J</i> = 6.8) 2.52 (sp)	5.22 (t) ^d 6.22, 6.38 (<i>J</i> = 5.7)	7.63 (d)	5.61 (d)	5.86 (t, <i>J</i> = 1.7)	7.68 (d) 6.73 (d)	6.66 (t) 6.60 (d)	6.11 (q, <i>J</i> = 2.0 ^e) 5.76 (t, <i>J</i> = 1.8)	7.4 (m, PPh ₃)
10 ^c	1.68 (s)	1.07 (d, <i>J</i> = 6.8) 2.38 (sp)	5.68, 5.83 (<i>J</i> = 6.0) 5.17, 6.20 (<i>J</i> = 6.0)	7.63 (bs)	5.82 (bs)	5.99 (t, <i>J</i> = 1.8)	7.63 (s) 7.44 (bs)	6.73 (t) 6.53 (bs)	6.12 (q, <i>J</i> = 1.9 ^e) 5.91 (bs)	3.79 (d, <i>J</i> (PH) = 12.0, OMe)
11 ^c	1.61 (s)	0.93 (d, <i>J</i> = 7.0) 1.08 (d, <i>J</i> = 6.9) 2.40 (sp)	5.17, 6.32 (<i>J</i> = 6.0) <i>f</i>		5.60 (d)	5.85 (t, <i>J</i> = 1.9)	<i>f</i>	6.64 (bs) <i>f</i>	6.10 (bs) 5.81 (t, <i>J</i> = 1.9)	3.5 (m), 7–8 (m, dppm)
12 ^c	1.70 (s)	1.01 (d, <i>J</i> = 6.8) 1.11 (d, <i>J</i> = 6.8) 2.50 (sp)	5.19, <i>f</i> (<i>J</i> = 5.8) 6.16, 6.31 (<i>J</i> = 6.0)	7.59 (d)	5.74 (d)	5.83 (t, <i>J</i> = 1.9)	7.77 (d) 6.80 (d)	6.68 (t) 6.58 (d)	6.11 (q, <i>J</i> = 2.1 ^e) 5.55 (t, <i>J</i> = 1.9)	7.4 (m, PPh ₃)
13 ^c	1.61 (s)	0.93 (d, <i>J</i> = 6.8) 1.05 (d, <i>J</i> = 6.9) 2.43 (sp)	5.14, 6.27 (<i>J</i> = 6.0) <i>f</i>		5.54 (d)	5.82 (t, <i>J</i> = 1.9)	<i>f</i>	6.65 (bs) 6.54 (d)	6.10 (bs) 5.81 (t)	3.4 (m), 4.2 (m), 7–8 (m) (dppm)
14	1.18 (s)	0.91 (d, <i>J</i> = 6.6) 1.97 (sp)	5.59, 5.94 (<i>J</i> = 6.0) <i>f</i>		5.59 (d)	5.89 (bm)	<i>f</i>	6.54 (d)	5.89 (bm)	3.5 (m), 4.3 (m), 7–8 (bm, dppm)
15	0.79 (s)	0.90 (d, <i>J</i> = 6.8) 2.12 (sp)	5.32 (t) ^d	<i>f</i>	5.63 (d)	5.81 (t, <i>J</i> = 1.5)	<i>f</i>	6.47 (d)	5.89 (t, <i>J</i> = 1.9)	1.8 (m), 2.1 (m), 7–8 (bm) (dppe)
16	0.58 (s)	0.85 (d, <i>J</i> = 6.8) 1.67 (sp)	5.16 (bm) ^d	<i>f</i>	5.69 (d)	5.82 (t, <i>J</i> = 1.5)	<i>f</i>	6.47 (d)	5.84 (t, <i>J</i> = 1.9)	1.7 (m), 2.7 (m), 7–8 (bm) (dppen)
18 ^e	0.82 (s)	0.90 (d, <i>J</i> = 6.8) 2.70 (sp)	5.26, 5.30 (<i>J</i> = 6.2) <i>f</i>		5.63 (d)	5.81 (t, <i>J</i> = 1.5)	<i>f</i>	6.47 (d)	5.84 (t, <i>J</i> = 1.9)	1.8 (m), 2.5 (m), 7–8 (bm) (dppe)
19	1.76 (s)	1.12 (d, <i>J</i> = 6.8) 2.25 (sp)	6.28 (s) ^d	7.87 (d)	5.85 (d)	6.08 (t, <i>J</i> = 1.8)	7.44 (d)	6.51 (d)	6.08 (t, <i>J</i> = 2.1)	1.9 (m), 2.6 (m), 3.9 (m), 4.4 (m) (COD), 12.1 (bs, NH)
20	1.74 (s)	1.11 (d, <i>J</i> = 6.9) 2.25 (sp)	6.00, 6.11 (<i>J</i> = 6.2)	7.98 (d)	5.96 (d)	6.16 (t, <i>J</i> = 1.9)	7.60 (d)	6.67 (d)	6.24 (t, <i>J</i> = 2.2)	12.4 (bs, NH)
21 ^c	1.68 (s)	1.05 (d, <i>J</i> = 6.9) 1.10 (d, <i>J</i> = 6.8) 2.20 (sp)	5.46, 6.35 (<i>J</i> = 6.1) 5.66, 6.40 (<i>J</i> = 5.9)	7.89 (d)	5.80 (bs)	6.10 (t, <i>J</i> = 2.5)	7.70 (d) 6.81 (d)	6.51 (t) 6.58 (d)	6.18 (q, <i>J</i> = 2.1 ^e) 5.87 (t, <i>J</i> = 2.2)	12.2 (bs, NH), 7.5 (m, PPh ₃)
22	1.77 (s)	1.12 (d, <i>J</i> = 6.9) 2.33 (sp)	6.08, 6.17 (<i>J</i> = 5.9)	8.04 (s)	5.87 (d)	6.14 (d)	7.75 (d)	6.75 (d)	6.29 (t, <i>J</i> = 1.9)	12.4 (bs, NH)
23 ^c	1.68 (s)	1.03 (d, <i>J</i> = 6.9) 1.07 (d, <i>J</i> = 6.8) 2.20 (sp)	5.46, 6.35 (<i>J</i> = 6.1) 5.66, 6.40 (<i>J</i> = 5.9)	7.80 (s)	5.66 (bs)	6.07 (t, <i>J</i> = 2.5)	7.90 (d) 6.88 (d)	6.58 (t) 6.54 (d)	6.19 (q, <i>J</i> = 2.1 ^e) 5.86 (t, <i>J</i> = 2.2)	12.2 (bs, NH), 7.5 (m, PPh ₃)

complex	<i>p</i> -cymene			Ru–pz–Ag ^b			Ru–pz–Rh ^b			others
	Me	<i>i</i> -Pr	H _{AA'} /H _{BB'} ^c	H ₃	H ₅	H ₄	H ₃	H ₅	H ₄	
25 ^c	1.68 (s)	1.05 (d, <i>J</i> = 6.9) 1.10 (d, <i>J</i> = 6.8) 2.20 (sp)	5.47, 6.36 (<i>J</i> = 5.9) 5.67, 6.41 (<i>J</i> = 6.4)	7.93 (t)	5.76 (t)	6.10 (q, <i>J</i> = 1.9 ^e)	7.70 (d) 6.81 (d)	6.51 (t) 6.59 (d)	6.19 (q, <i>J</i> = 2.0 ^e) 5.87 (t, <i>J</i> = 2.1)	7.5 (m, PPh ₃)

^a All conditions as stated in footnote *a* in Table 1. ^b For labeling of pyrazolate protons, see Figure 2. *J*(H₃H₄) ≈ *J*(H₄H₅). ^c Pyrazolate protons assigned through selective decoupling experiments. The first set of bridging pyrazolate resonances corresponds to the pyrazolate group *trans* to the phosphorus ligand. ^d Four aromatic protons. ^e *J*(HP) ≈ *J*(H₃H₄) ≈ *J*(H₄H₅). ^f Obscured by the phosphorus ligand protons. ^g In (CD₃)₂CO.

= PPh₃ (**12**), dpmm (**13**). The non-carbonyl-containing derivatives [(η⁶-*p*-cymene)(pz)Ru(μ-pz)₂M(LL)] (M = Rh; LL = dpmm (**14**), dppe (**15**), dppen (**16**), *R*-prophos (**17a,b**), M = Ir; LL = dppe (**18**)) were obtained by treating **7** and **8** with the appropriate diphosphine ligand. Complexes **14**–**18** were most probably formed via the monocarbonyl intermediates [(η⁶-*p*-cymene)(pz)-Ru(μ-pz)₂M(CO)(LL)], which we have been able to isolate in the case of the dpmm derivatives **11** and **13**.

Monocarbonyl complexes **9**–**13** have been characterized by microanalyses (see Experimental Section) and IR and ¹H and ³¹P{¹H} NMR spectroscopies (Table 2). The IR spectra showed a strong ν(CO) band in the 1950–2000 cm⁻¹ region, characteristic of four-coordinated square-planar monocarbonyl rhodium or iridium(I) complexes. Moreover, their ¹H NMR spectra, at room temperature, showed three different AMX systems corresponding to the three pyrazolate groups. The

chemical shifts and the relative intensities of the signals were in accord with a structure containing two bridging and one terminal pyrazolate ligand, the rhodium or iridium atoms being four-coordinated. The $^{31}\text{P}\{^1\text{H}\}$ NMR spectra of the dppm complexes **11** and **13** showed one high-field doublet (at -25.7 ppm) and one doublet of doublets for the RuRh complex **11** and two doublets (one of them at -26.3 ppm) for the RuIr complex **13**, which unequivocally established the monodentate coordination of the diphosphine.

The ^1H NMR spectra of complexes **14**–**18** showed two sets of signals, in a 2/1 ratio, assigned to two bridging and one terminal pyrazolate. The $^{31}\text{P}\{^1\text{H}\}$ spectra showed the equivalence of both phosphorus nuclei and consisted of one doublet with characteristic phosphorus–rhodium coupling constants (complexes **14**–**16**) or one singlet (compound **18**). The ruthenium atom in the monocarbonyl complexes **9**–**13** and in the *R*-prophos derivative **17** is a chiral center. Thus, we have prepared complexes **9**–**13** as racemic mixtures of the two possible enantiomers. In the case of the chiral *R*-prophos ligand, the two diastereomers $R_{\text{Ru}}R_{\text{C}}$ and $S_{\text{Ru}}R_{\text{C}}$ (**17a,b**) were stereoselectively formed, the diastereomeric excess being 33%.

All the data described so far allowed assignment of dinuclear structures of the **A** type (see Figure 2) to complexes **9**–**18**.

(b) With Tetrafluoroboric Acid. Complexes **6**–**18** could potentially be protonated either at nitrogen of the terminal pyrazolate group or at M metal. Both types of processes have been reported in the polypyrazolylborate chemistry of these metals.⁴ In order to determine where protonation occurs in these complexes, we have reacted some of them with HBF_4 . When complexes $[(\eta^6\text{-}p\text{-cymene})(\text{pz})\text{Ru}(\mu\text{-pz})_2\text{ML}_2]$ ($\text{M} = \text{Rh}$; $\text{L}_2 = \text{COD}$ (**6**), $(\text{CO})_2$ (**7**), CO , PPh_3 (**9**), $\text{M} = \text{Ir}$; $\text{L}_2 = (\text{CO})_2$ (**8**), CO , PPh_3 (**12**)) in THF or diethyl ether were treated with equimolar amounts of HBF_4 , the cationic derivatives $[(\eta^6\text{-}p\text{-cymene})(\text{Hpz})\text{Ru}(\mu\text{-pz})_2\text{ML}_2]\text{BF}_4$ ($\text{M} = \text{Rh}$; $\text{L}_2 = \text{COD}$ (**19**), $(\text{CO})_2$ (**20**), CO , PPh_3 (**21**), $\text{M} = \text{Ir}$; $\text{L}_2 = (\text{CO})_2$ (**22**), CO , PPh_3 (**23**)) were obtained. The IR spectra of complexes **19**–**23** showed broad bands in the region of 3300 cm^{-1} assigned to $\nu(\text{NH})$ stretching vibrations as well as the characteristic bands due to the BF_4 anion under T_d symmetry.²⁵ The frequencies of their $\nu(\text{CO})$ bands were very similar to those found for their corresponding precursors, and the values of the resonances and coupling constants of the phosphorus nuclei of complexes **21** and **23** were comparable to those of their respective parents **9** and **12** (see Experimental Section). The ^1H NMR spectra of **19**–**23** showed a broad resonance at low field but nothing below the TMS signal. The AMX systems of the pyrazolate protons appeared slightly more withdrawn than the respective protons in the neutral precursors. All these spectroscopic observations strongly support the fact that protonation occurs at the uncoordinated nitrogen atom of the terminal pyrazolate as confirmed by the determination of the molecular structure of compound **22** by X-ray diffraction methods (see below). Interestingly, protonation takes place on the pyrazolate group even in the iridium complexes **8** and **12**. This behavior contrasted with that found in the related tripyrazolylborate complexes $[\text{HB-}$

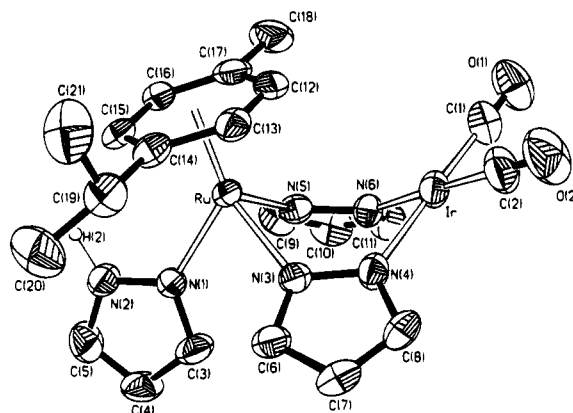


Figure 3. ORTEP view of the cation of the complex $[(\eta^6\text{-}p\text{-cymene})(\text{Hpz})\text{Ru}(\mu\text{-pz})_2\text{Ir}(\text{CO})_2]\text{BF}_4$ (**22**).

Table 3. Atomic Coordinates ($\times 10^4$; $\times 10^5$ for Ir and Ru Atoms) and Equivalent Isotropic Displacement Coefficients ($\text{\AA}^2 \times 10^3$) for **22**

atom	<i>x/a</i>	<i>y/b</i>	<i>z/c</i>	<i>U(eq)^a</i>
Ir	13608(3)	8714(1)	11255(1)	58(1)
Ru	27432(5)	28992(3)	14706(2)	41(1)
O(1)	2849(9)	-164(3)	70(3)	108(3)
O(2)	1591(9)	-393(4)	2203(4)	121(3)
N(1)	1165(5)	3859(3)	1224(3)	53(2)
N(2)	1681(6)	4601(3)	1145(3)	67(2)
N(3)	646(5)	2391(3)	1889(2)	47(2)
N(4)	267(6)	1616(3)	1813(2)	54(2)
N(5)	1731(6)	2492(3)	500(2)	50(2)
N(6)	1157(6)	1751(3)	387(2)	54(2)
C(1)	2297(10)	225(4)	470(4)	77(3)
C(2)	1504(11)	87(5)	1795(5)	88(3)
C(3)	-491(8)	3886(4)	1095(4)	75(3)
C(4)	-1018(8)	4649(4)	945(4)	80(3)
C(5)	378(10)	5079(4)	996(4)	81(3)
C(6)	-304(7)	2680(4)	2381(3)	58(2)
C(7)	-1324(7)	2098(4)	2617(3)	64(2)
C(8)	-916(8)	1444(4)	2259(3)	65(2)
C(9)	1513(9)	2881(4)	-105(3)	67(2)
C(10)	798(10)	2416(5)	-611(3)	83(3)
C(11)	607(9)	1708(5)	-296(4)	78(3)
C(12)	4734(7)	2037(4)	1729(4)	60(2)
C(13)	4211(7)	2376(4)	2358(3)	55(2)
C(14)	4256(7)	3200(4)	2460(3)	55(2)
C(15)	4776(6)	3667(3)	1897(3)	49(2)
C(16)	5279(7)	3331(4)	1270(3)	53(2)
C(17)	5267(7)	2512(4)	1189(3)	60(2)
C(18)	5766(10)	2137(5)	526(4)	91(3)
C(19)	3749(9)	3540(5)	3134(3)	72(3)
C(20)	3086(12)	4372(6)	3088(4)	102(4)
C(21)	5201(12)	3478(5)	3691(4)	104(4)
B	4965(15)	5908(6)	1169(6)	93(3)
F(1a) ^b	4784(16)	5233(8)	686(8)	110(4)
F(2a) ^b	4678(17)	5675(7)	1910(6)	114(4)
F(3a) ^b	6311(13)	6302(7)	1115(7)	98(3)
F(4a) ^b	3703(16)	6419(8)	1067(8)	133(5)
F(1b) ^b	4951(12)	5152(6)	923(6)	66(3)
F(2b) ^b	3886(21)	5884(8)	1657(8)	119(5)
F(3b) ^b	6664(14)	6132(7)	1405(7)	85(4)
F(4b) ^b	4003(22)	6389(11)	594(12)	172(8)

^a Equivalent isotropic *U* defined as one-third of the trace of the orthogonalized U_{ij} tensor. ^b This group of atoms, involved in disorder, were refined with isotropic displacement parameters. The refined occupancy factors were 0.54(2) for a-labeled atoms and 0.46(2) for b-labeled ones.

$(\text{dmpz})_3\text{M}(\text{CO})_2]$ ($\text{M} = \text{Rh}, \text{Ir}$). While protonation of the rhodium complex takes place at the nitrogen of the free pyrazolate group, protonation of the iridium complex occurs at the metal.⁴

Molecular Structure of $[(\eta^6\text{-}p\text{-Cymene})(\text{Hpz})\text{Ru}(\mu\text{-pz})_2\text{Ir}(\text{CO})_2]\text{BF}_4$ (22**).** Figure 3 shows a view of the cationic complex, together with the atom labeling used.

(25) Nakamoto, K. *Infrared Spectra of Inorganic and Coordination Compounds*, 2nd ed.; John Wiley and Sons: 1970; p 110.

Table 4. Selected Bond Distances (Å) and Angles (deg) for **22**

Ir-C(1)	1.862(8)	Ru-N(1)	2.101(5)
Ir-C(2)	1.849(8)	Ru-N(3)	2.093(5)
Ir-N(4)	2.062(5)	Ru-N(5)	2.088(4)
Ir-N(6)	2.058(5)	Ru-G ^a	1.697(5)
C(1)-O(1)	1.125(10)	C(2)-O(2)	1.128(11)
N(1)-N(2)	1.343(7)	N(3)-N(4)	1.362(7)
N(1)-C(3)	1.330(7)	N(3)-C(6)	1.341(8)
N(2)-C(5)	1.337(9)	N(4)-C(8)	1.346(8)
C(3)-C(4)	1.391(11)	C(6)-C(7)	1.379(9)
C(4)-C(5)	1.333(10)	C(7)-C(8)	1.360(10)
N(5)-N(6)	1.357(7)	N(5)-C(9)	1.332(8)
N(6)-C(11)	1.348(8)	C(9)-C(10)	1.347(10)
C(10)-C(11)	1.362(11)		
C(1)-Ir-C(2)	91.5(3)	N(1)-Ru-N(3)	85.7(2)
C(1)-Ir-N(4)	177.3(3)	N(1)-Ru-N(5)	82.5(2)
C(1)-Ir-N(6)	89.3(3)	N(3)-Ru-N(5)	85.9(2)
C(2)-Ir-N(4)	90.8(3)	N(1)-Ru-G ^a	131.4(3)
C(2)-Ir-N(6)	178.9(3)	N(3)-Ru-G ^a	126.4(3)
N(4)-Ir-N(6)	88.3(2)	N(5)-Ru-G ^a	129.0(2)

^a G represents the centroid of the *p*-cymene ring.

Atomic positional parameters and selected bond lengths and angles are presented in Tables 3 and 4, respectively. The cation consists of one ruthenium and one iridium atom bridged by two pyrazolate groups. The ruthenium atom completes its pseudooctahedral coordination through bonding to an η^6 -*p*-cymene ring and to a terminal pyrazole ligand. The Ru-*p*-cymene bond distance, 1.697(5) Å, falls in the upper range of those found in *p*-cymene-ruthenium complexes with pyrazolate ligands.^{6,26,27} Two carbon monoxide terminal groups complete the square-planar coordination of the iridium, angles around it adding 359.9°. The six-membered RuN₄Ir cyclic core is bent into a boat conformation, which brings the two metals to 3.6770(6) Å from one another. This intermetallic separation excludes any significant metal-metal interaction. The Ru-N(3) and Ru-N(5) (mean 2.090(4) Å) and Ir-N bond distances (mean 2.060(4) Å) compare well with the averaged bond distances found in related compounds of these metals with pyrazolate bridging ligands such as $[(\eta^6\text{-}p\text{-cymene})\text{ClRu}(\mu\text{-pz})_2\text{M}(\text{CO})_2]$ (M = Ir; Ru-N = 2.083(3) Å, Ir-N = 2.062(3) Å. M = Rh; Ru-N = 2.086(2) Å,²⁶ $[(\eta^6\text{-}p\text{-cymene})\text{Ru}]_2(\mu\text{-pz})_2(\mu\text{-OH})\text{BPh}_4$ (Ru-N = 2.086(2) Å),²⁷ $[(\eta^6\text{-benzene})\text{Ru}]_2(\mu\text{-pz})_2(\mu\text{-Cl})\text{Cl}$ (Ru-N = 2.083(3) Å),²⁸ $[\text{Ir}(\mu\text{-pz})(\text{CO})(\text{PPh}_3)]_2$ (Ir-N = 2.07(1) Å),²⁹ $[\text{Ir}(\mu\text{-pz})(\text{COD})]_2$ (Ir-N = 2.081(8) Å).³⁰ Complex **22** has been prepared by protonation of the neutral compound $[(\eta^6\text{-}p\text{-cymene})(\text{pz})\text{Ru}(\mu\text{-pz})_2\text{Ir}(\text{CO})_2]$ with HBF₄. The N(2)···F(1b) separation, 2.836(11) Å, is indicative of the existence of a N-H···F interaction. Furthermore, the C-C bond distances (1.333(10) vs 1.391(10) Å) within the terminal pyrazole ring suggest a partial localization of the electronic density toward a N=C-C=C-NH bond distribution as expected for a protonated pyrazole. These structural data along with the spectroscopic data, reported above, strongly sup-

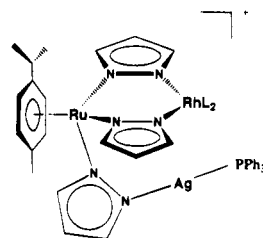
(26) Carmona, D.; Ferrer, J.; Mendoza, A.; Lahoz, F. J.; Reyes, J.; Oro, L. A. *Angew. Chem., Int. Ed. Engl.* **1991**, *30*, 1171.

(27) Oro, L. A.; Garcia, M. P.; Carmona, D.; Foces-Foces, C.; Cano, F. H. *Inorg. Chim. Acta* **1985**, *96*, L21.

(28) Sheldrick, W. S.; Hagen-Eckhard, H.-S.; *J. Organomet. Chem.* **1991**, *410*, 73.

(29) Atwood, J. L.; Beveridge, K. A.; Bushnell, G. W.; Dixon, K. R.; Eadie, D. T.; Stobart, S. R.; Zaworotko, M. J. *Inorg. Chem.* **1984**, *23*, 4050.

(30) Beveridge, K. A.; Bushnell, G. W.; Stobart, S. R.; Atwood, J. L.; Zaworotko, M. J. *Organometallics* **1983**, *2*, 1447.

**Figure 4.** Schematic structure proposed for complexes **24** and **25**.

ported the fact that the free nitrogen of the terminal pyrazole of the parent complex has been protonated in the reaction. However, although from the crystallographic data a N-H···F interaction is evident, no significant shift to lower energies of the $\nu(\text{NH})$ stretching frequency (3320 cm⁻¹, Nujol mull) has been observed.

(c) **With AgBF₄ and PPh₃.** The free nitrogen atom of the neutral complexes $[(\eta^6\text{-}p\text{-cymene})(\text{pz})\text{Ru}(\mu\text{-pz})_2\text{-ML}_2]$ could be coordinated to unsaturated metallic fragments as, for example, the cationic moiety AgPPh_3^+ . Thus, addition of equimolar amounts of AgBF₄ and PPh₃ to THF solutions of **6** (M = Rh, L₂ = COD) or **9** (M = Rh, L₂ = (CO), PPh₃) afforded the cationic heterotrimeric complexes $[(\eta^6\text{-}p\text{-cymene})\text{Ru}\{(\mu\text{-pz})\text{Ag}(\text{PPh}_3)\}\{(\mu\text{-pz})_2\text{RhL}_2\}]\text{BF}_4$ (M = Rh, L₂ = COD (**24**); CO, PPh₃ (**25**)). Adequate analyses and ¹H NMR data were not obtained for complex **24** because it was impurified by small amounts of the dimer $[\text{Rh}(\mu\text{-pz})(\text{COD})]_2$ and other *p*-cymene-containing unidentified products which we were not able to efficiently separate. Its ³¹P{¹H} NMR spectrum consisted of two doublets centered at 18.2 ppm with characteristic phosphorus-silver coupling constants, ¹J(¹⁰⁷AgP) = 639 and ¹J(¹⁰⁹AgP) = 736 Hz. Complex **25** has been completely characterized by elemental analyses and spectroscopic means (Table 2). Its IR spectrum indicated its ionic character (BF₄⁻ absorptions) and showed, along with the characteristic bands of the PPh₃ ligand, a very strong absorption at 1990 cm⁻¹ corresponding to the $\nu(\text{CO})$ stretching vibration of the terminal carbonyl group. The ¹H NMR spectrum showed two doublets and two AB systems for the isopropyl methyl and aromatic protons of the *p*-cymene, respectively, which demonstrated that the ruthenium atom was linked to three chemically different pyrazolates.³¹ Accordingly, nine resonances corresponding to nine different pyrazolate protons were also observed. Finally, the ³¹P{¹H} NMR spectrum of **25** consisted of a doublet at 41.2 ppm with ¹J(RhP) = 152 Hz and two doublets centered at 17.4 ppm with coupling constants ¹J(¹⁰⁷AgP) = 640 Hz and ¹J(¹⁰⁹AgP) = 738 Hz, according to the proposed structure drawn in Figure 4. As expected, the values of the coupling constants ¹J(AgP) in **24** and **25** are comparable to those found for the phosphorus atom bound to digonal silver in complex $[(\eta^6\text{-}p\text{-cymene})\text{Ru}(\mu\text{-pz})_3\{\text{Ag}(\text{PPh}_3)\}_2]\text{BF}_4$ (**5**), supporting a similar coordination mode for the silver in all three complexes.

(31) (a) Bennett, M. A.; Ennett, J. P. *Organometallics* **1984**, *3*, 1365. (b) Esteban, M.; Pequerul, A.; Carmona, D.; Lahoz, F. J.; Martin, A.; Oro, L. A. *J. Organomet. Chem.* **1991**, *404*, 421. (c) Carmona, D.; Ferrer, J.; Reyes, J.; Oro, L. A. *Organometallics* **1993**, *12*, 4241.

Conclusions

The bis(pyrazolato)(pyrazole) complex **1** has successfully been used to build heteropolynuclear compounds of transition-metal ions of the 9 and 11 groups. Its deprotonated form $[(\eta^6\text{-}p\text{-cymene})\text{Ru}(\text{pz})_3]^-$ behaves as the tripyrazolylborate anion in some respects. Thus, coordinates $\text{M}(\text{PPh}_3)$ ($\text{M} = \text{Cu}, \text{Ag}, \text{Au}$) and the resulting heterodinuclear compounds showed exchange between terminal and bridging pyrazolate groups. The RuAg complex incorporates a second $\text{Ag}(\text{PPh}_3)$ moiety, and in the new complex the two $\text{Ag}(\text{PPh}_3)$ groups rotate in a concerted way around the three nitrogen atoms of the $[(\eta^6\text{-}p\text{-cymene})\text{Ru}(\text{pz})_3]^-$ anion. This type of fluxionality involving changes in the hapticity is characteristic of polypyrazolylborate ligands. In the heterodinuclear derivatives $[(\eta^6\text{-}p\text{-cymene})(\text{pz})\text{Ru}(\mu\text{-pz})_2\text{ML}_2]$ ($\text{M} = \text{Rh}, \text{Ir}$), the $[(\eta^6\text{-}p\text{-cymene})\text{Ru}(\text{pz})_3]^-$ ligand is bidentate in the ground state and the exchange between coordinated and uncoordinated pyrazolate groups is slow even at 363 K in toluene- d_8 . The CO groups in $[(\eta^6\text{-}p\text{-cymene})(\text{pz})\text{Ru}(\mu\text{-pz})_2\text{M}(\text{CO})_2]$ can be partially or completely removed by mono- and ditertiary phosphines and electrophiles such as H^+ or $\text{Ag}(\text{PPh}_3)^+$ attack the lone pair of the uncoordinated nitrogen of the terminal pyrazolate, rendering the corresponding cationic products. Protonation occurs at nitrogen even in the RuIr complexes as it has been unequivocally demonstrated by spectroscopic and crystallographic methods.

Experimental Section

Infrared spectra were recorded on a Perkin-Elmer 783 spectrophotometer (range 4000–200 cm^{-1}) using Nujol mulls between polyethylene sheets or dichloromethane solutions between NaCl plates. Proton and $^{31}\text{P}\{^1\text{H}\}$ NMR spectra were recorded on a Varian Unity 300 spectrometer (300.0 (^1H) and 121.4 (^{31}P) MHz). The C, H, and N analyses were carried out with a Perkin-Elmer 240C microanalyzer. All solvents were dried and distilled before use.

Preparation of $[(\eta^6\text{-}p\text{-Cymene})\text{Ru}(\text{pz})_3\text{Cu}(\text{PPh}_3)]$ (2**).** Under nitrogen, to a solution of **1** (0.140 g, 0.32 mmol) in acetone (25 mL) were added $[\text{CuCl}(\text{PPh}_3)_4]$ (0.116 g, 0.08 mmol) and KOH (2.0 mL, 0.16 N, 0.32 mmol) in MeOH. After stirring for 30 min, the solution was vacuum-evaporated to 0.5 mL. Slow addition of hexane led to the precipitation of a yellow solid which was filtered off, washed with hexane, and dried under vacuum. Yield: 83%. Anal.¹¹ Calcd for $\text{C}_{37}\text{H}_{38}\text{N}_6\text{CuPRu}$: C, 58.68; H, 5.03; N, 11.05. Found: C, 56.63; H, 5.11; N, 10.82.

Complexes **3** and **4** were prepared similarly in MeOH as solvent. **3**. Yield: 75%. Anal. Calcd for $\text{C}_{37}\text{H}_{38}\text{N}_6\text{AgPRu}$: C, 55.11; H, 4.83; N, 10.45. Found: C, 55.63; H, 5.12; N, 10.00. **4**. Yield: 89%. Anal. Calcd for $\text{C}_{37}\text{H}_{38}\text{N}_6\text{AuPRu}$: C, 49.62; H, 4.33; N, 9.41. Found: C, 48.93; H, 4.21; N, 8.93.

Preparation of $[(\eta^6\text{-}p\text{-Cymene})\text{Ru}(\text{pz})_3\{\text{Ag}(\text{PPh}_3)\}_2]\text{BF}_4$ (5**).** Under nitrogen, to a solution of complex $[(\eta^6\text{-}p\text{-cymene})\text{Ru}(\text{pz})_3\text{Ag}(\text{PPh}_3)]$ (0.133 g, 0.16 mmol) in acetone (40 mL) were added PPh_3 (0.043 g, 0.16 mmol) and AgBF_4 (0.032 g, 0.16 mmol). After stirring for 1 h, the solution was filtered to remove any remaining solid. The filtrate was concentrated under reduced pressure, and the addition of hexane led to the precipitation of a pale yellow solid which was filtered off, washed with hexane, and dried under vacuum. Yield: 77%. Anal. Calcd for $\text{C}_{55}\text{H}_{53}\text{N}_6\text{Ag}_2\text{BF}_4\text{P}_2\text{Ru}$: C, 52.31; H, 4.23; N, 6.62. Found: C, 52.72; H, 4.32; N, 6.30.

Preparation of $[(\eta^6\text{-}p\text{-Cymene})(\text{pz})\text{Ru}(\mu\text{-pz})_2\text{Rh}(\text{COD})]$ (6**).** Under nitrogen, to a solution of **1** (0.564 g, 1.29 mmol) in acetone (40 mL) was added $[\text{Rh}(\text{acac})(\text{COD})]$ (0.400 g, 1.29 mmol). The starting yellow solution became yellow-brown and

after stirring for 15 min was concentrated until dryness. Addition of MeOH (20 mL) gave a yellow solid which was filtered off, washed with MeOH and cold hexane, and dried under vacuum. Yield: 70%. Anal. Calcd for $\text{C}_{27}\text{H}_{36}\text{N}_6\text{RhRu}$: C, 50.11; H, 5.43; N, 13.01. Found: C, 49.64; H, 5.63; N, 12.67.

Preparation of $[(\eta^6\text{-}p\text{-Cymene})(\text{pz})\text{Ru}(\mu\text{-pz})_2\text{Rh}(\text{CO})_2]$ (7**).** **Method 1.** Under nitrogen, to a solution of **1** (0.700 g, 1.60 mmol) in THF (50 mL) was added $[\text{Rh}(\text{acac})(\text{CO})_2]$ (0.413 g, 1.60 mmol). The starting yellow solution became yellow-brown. The isolation of solid **7** by addition of different precipitants failed due to its great solubility. So, the compound could be isolated by concentrating the solutions until dryness. The residue was then dried under vacuum during 24 h. **Method 2.** Bubbling of carbon monoxide (atmospheric pressure, room temperature) for 1 h through CH_2Cl_2 or THF solutions (20 mL) of compound **6** (1.000 g, 1.54 mmol) led to a yellow solution. Complex **7** was obtained by workup as above. Yield: 85%. IR (CH_2Cl_2): $\nu(\text{CO})$ 2070 (vs), 2010 (vs) cm^{-1} . Anal. Calcd for $\text{C}_{21}\text{H}_{23}\text{N}_6\text{O}_2\text{RhRu}$: C, 42.51; H, 3.91; N, 14.12. Found: C, 43.11; H, 4.33; N, 14.50.

Preparation of $[(\eta^6\text{-}p\text{-Cymene})(\text{pz})\text{Ru}(\mu\text{-pz})_2\text{Rh}(\text{CO})(\text{PPh}_3)]$ (9**).** To a suspension of the dicarbonyl complex **7** (0.173 g, 0.29 mmol) in diethyl ether (30 mL) prepared *in situ* by method **2** was added solid PPh_3 (0.076 g, 0.29 mmol). From the resulting solution, the precipitation of a yellow solid was observed, and after stirring for 12 h, the compound was filtered off, washed with diethyl ether, and vacuum-dried. Yield: 70%. IR (CH_2Cl_2): $\nu(\text{CO})$ 1985 (vs) cm^{-1} . Anal. Calcd for $\text{C}_{38}\text{H}_{38}\text{N}_6\text{OPRhRu}$: C, 55.03; H, 4.60; N, 10.12. Found: C, 55.43; H, 4.95; N, 9.90. $^{31}\text{P}\{^1\text{H}\}$ NMR ($\text{CDCl}_3/\text{CHCl}_3$, 1/1, v/v, δ): 41.5 (d, $J_{\text{RHP}} = 153$ Hz).

Preparation of Complexes 10–13 and 15–18. Complexes **10**, **11**, and **15–17** were similarly prepared by using the appropriate phosphorus ligand. The RuIr complexes **12**, **13**, and **18** were prepared by the same method, starting from solutions of **8**.

Complex 10. Yield: 51%. IR (CH_2Cl_2): $\nu(\text{CO})$ 1995 (vs) cm^{-1} . Anal. Calcd for $\text{C}_{23}\text{H}_{32}\text{N}_6\text{OPRhRu}$: C, 39.93; H, 4.70; N, 12.13. Found: C, 39.23; H, 4.75; N, 11.60. $^{31}\text{P}\{^1\text{H}\}$ NMR ($\text{CDCl}_3/\text{CHCl}_3$, 1/1, v/v, δ): 137.5 (d, $J_{\text{RHP}} = 242$ Hz).

Complex 11. Yield: 69%. IR (CH_2Cl_2): $\nu(\text{CO})$ 1985 (vs) cm^{-1} . Anal. Calcd for $\text{C}_{45}\text{H}_{45}\text{N}_6\text{OP}_2\text{RhRu}$: C, 56.83; H, 4.82; N, 8.82. Found: C, 56.64; H, 5.05; N, 8.56. $^{31}\text{P}\{^1\text{H}\}$ NMR ($\text{CDCl}_3/\text{CHCl}_3$, 1/1, v/v, δ): 35.9 (dd, $J_{\text{RHP}} = 152$ Hz), -25.7 (d, $J_{\text{PP}} = 75$ Hz). **Complex 12.** Yield: 75%. IR (CH_2Cl_2): $\nu(\text{CO})$ 1980 (vs) cm^{-1} . Anal. Calcd for $\text{C}_{38}\text{H}_{38}\text{N}_6\text{IrOPRu}$: C, 49.63; H, 4.17; N, 9.12. Found: C, 49.04; H, 4.22; N, 9.03. $^{31}\text{P}\{^1\text{H}\}$ NMR ($\text{CDCl}_3/\text{CHCl}_3$, 1/1, v/v, δ): 16.5 (s). **Complex 13.** Yield: 82%. IR (CH_2Cl_2): $\nu(\text{CO})$ 1975 (vs) cm^{-1} . Anal. Calcd for $\text{C}_{45}\text{H}_{45}\text{N}_6\text{IrOP}_2\text{Ru}$: C, 51.93; H, 4.44; N, 8.13. Found: C, 51.90; H, 5.25; N, 8.06. $^{31}\text{P}\{^1\text{H}\}$ NMR ($\text{CDCl}_3/\text{CHCl}_3$, 1/1, v/v, δ): 8.2 (d, $J_{\text{PP}} = 70$ Hz), -26.3 (d). **Complex 15.** Yield: 75%. Anal. Calcd for $\text{C}_{45}\text{H}_{47}\text{N}_6\text{P}_2\text{RhRu}$: C, 57.62; H, 5.12; N, 8.93. Found: C, 57.14; H, 5.15; N, 8.66. $^{31}\text{P}\{^1\text{H}\}$ NMR ($\text{CDCl}_3/\text{CHCl}_3$, 1/1, v/v, δ): 71.7 (d, $J_{\text{RHP}} = 170$ Hz). **Complex 16.** Yield: 74%. Anal. Calcd for $\text{C}_{45}\text{H}_{45}\text{N}_6\text{P}_2\text{RhRu}$: C, 57.73; H, 4.92; N, 9.02. Found: C, 56.94; H, 5.00; N, 8.76. $^{31}\text{P}\{^1\text{H}\}$ NMR ($\text{CDCl}_3/\text{CHCl}_3$, 1/1, v/v, δ): 77.5 (d, $J_{\text{RHP}} = 170$ Hz). **Complex 17.** Yield: 72%. Anal. Calcd for $\text{C}_{46}\text{H}_{49}\text{N}_6\text{P}_2\text{RhRu}$: C, 58.03; H, 5.22; N, 8.83. Found: C, 57.67; H, 5.35; N, 8.75. ^1H NMR (CDCl_3 , δ): major isomer 7.76 (d), 6.77 (d), 6.30 (t, $J_{\text{HH}} = 2.3$ Hz), 6.05, 5.99 (AB system, $J_{\text{AB}} = 6.4$ Hz), 2.34 (sp), 1.83 (s), 1.12 (d, $J_{\text{HH}} = 6.8$). $^{31}\text{P}\{^1\text{H}\}$ NMR ($\text{CDCl}_3/\text{CHCl}_3$, 1/1, v/v, δ): major isomer 78.7 (dd, $J_{\text{RHP}} = 168$, $J_{\text{PP}} = 45$ Hz), 61.1 (dd, $J_{\text{RHP}} = 169$ Hz); minor isomer 78.4 (dd, $J_{\text{RHP}} = 170$, $J_{\text{PP}} = 44$ Hz), 56.5 (dd, $J_{\text{RHP}} = 167$ Hz). **Complex 18.** Yield: 79%. Anal. Calcd for $\text{C}_{45}\text{H}_{47}\text{N}_6\text{P}_2\text{IrRu}$: C, 52.63; H, 4.62; N, 8.23. Found: C, 52.14; H, 4.65; N, 7.81. $^{31}\text{P}\{^1\text{H}\}$ NMR ($(\text{CD}_3)_2\text{CO}$, δ): 43.1 s.

Preparation of $[(\eta^6\text{-}p\text{-Cymene})(\text{pz})\text{Ru}(\mu\text{-pz})_2\text{Rh}(\text{dppm})]$ (14**).** A THF solution (50 mL) of complex **7** (0.173 g, 0.29 mmol) was heated under reflux for 1 h after adding dppm

(0.115 g, 0.29 mmol). The resulting solution was evaporated to ca. 2 mL, and the slow addition of hexane led to the precipitation of a yellow solid which was filtered off, washed with the precipitant, and vacuum-dried. Yield: 58%. Anal. Calcd for $C_{44}H_{45}N_6P_2RhRu$: C, 56.71; H, 4.92; N, 9.12. Found: C, 57.24; H, 4.75; N, 8.85. $^{31}P\{^1H\}$ NMR ($CDCl_3/CHCl_3$, 1/1, v/v, δ): -19.6 (d, $J_{RhP} = 144$ Hz).

Preparation of $[(\eta^6-p\text{-Cymene})(Hpz)Ru(\mu\text{-pz})_2Rh(CO)_2]BF_4$ (20). To a solution of the dicarbonyl complex **7** (ca. 0.29 mmol) in THF (30 mL) prepared *in situ* by method 2 was added HBF_4 in diethyl ether (40.6 μ L, 54% w/w, 0.29 mmol). The solution was concentrated to ca. 2 mL, and the slow addition of diethyl ether led to the precipitation of a yellow solid which was separated by filtration, washed with the precipitant and dried under vacuum. Yield: 87%. IR (Nujol) $\nu(NH)$ 3300 (br), $\nu(CO)$ 2070 (vs), 2010 (vs) cm^{-1} . Anal. Calcd for $C_{21}H_{24}N_6BF_4O_2RhRu$: C, 36.93; H, 3.49; N, 12.28. Found: C, 37.52; H, 3.55; N, 12.31.

Complexes **19** and **22** were similarly prepared starting from **6** and solutions of **8**, respectively. **Complex 19.** Yield: 75%. IR (Nujol): $\nu(NH)$ 3320 (br) cm^{-1} . Anal. Calcd for $C_{27}H_{36}N_6BF_4RhRu$: C, 44.09; H, 4.91; N, 11.37. Found: C, 44.13; H, 5.03; N, 11.52. **Complex 22.** Yield: 53%. IR (Nujol): $\nu(NH)$ 3320 (br), $\nu(CO)$ 2070 (vs), 2010 (vs) cm^{-1} . Anal. Calcd for $C_{21}H_{24}N_6BF_4IrO_2Ru$: C, 32.72; H, 3.12; N, 10.90. Found: C, 33.23; H, 3.13; N, 10.88.

Preparation of $[(\eta^6-p\text{-Cymene})(Hpz)Ru(\mu\text{-pz})_2Rh(CO)(PPh_3)]BF_4$ (21). Under nitrogen, 21 μ L of a solution of HBF_4 in diethyl ether (54% w/w, 0.15 mmol) was added to a solution of $[(\eta^6-p\text{-cymene})(pz)Ru(\mu\text{-pz})_2Rh(CO)(PPh_3)]$ (**9**) (0.124 g, 0.15 mmol) in THF (20 mL). After 15 min of stirring, the solution was concentrated to ca. 2 mL and the slow addition of diethyl ether led to the precipitation of a yellow solid which was separated by filtration, washed with the precipitant, and dried under vacuum. Yield: 80%. IR (Nujol): $\nu(NH)$ 3330 (br), $\nu(CH_2Cl_2)$ 1985 (vs) cm^{-1} . Anal. Calcd for $C_{38}H_{39}N_6BF_4OPRhRu$: C, 49.72; H, 4.33; N, 9.1. Found: C, 49.01; H, 4.75; N, 8.54. $^{31}P\{^1H\}$ NMR ($CDCl_3/CHCl_3$, 1/1, v/v, δ): 41.2 (d, $J_{RhP} = 153$ Hz).

Complex 23 was similarly obtained from **12**. Yield: 53%. IR (Nujol): $\nu(NH)$ 3350 (br), $\nu(CO)$ 1995 (vs) cm^{-1} . Anal. Calcd for $C_{38}H_{39}N_6BF_4IrOPRhRu$: C, 45.32; H, 3.91; N, 8.29. Found: C, 45.03; H, 3.87; N, 7.92. $^{31}P\{^1H\}$ NMR ($CDCl_3/CHCl_3$, 1/1, v/v, δ): 16.7 (s).

Preparation of $[(\eta^6-p\text{-Cymene})Ru(\mu\text{-pz})Ag(PPh_3)]\{(\mu\text{-pz})_2Rh(CO)(PPh_3)\}BF_4$ (25). Under nitrogen and in the absence of light, PPh_3 (0.029 g, 0.11 mmol) and $AgBF_4$ (0.021 g, 0.11 mmol) were added to a solution of $[(\eta^6-p\text{-cymene})(pz)Ru(\mu\text{-pz})_2Rh(CO)(PPh_3)]$ (**9**) (0.090 g, 0.11 mmol) in THF (25 mL). The resulting solution was stirred for 15 min and then was vacuum-evaporated to ca. 2 mL. Addition of hexane afforded a yellow powder which was filtered off, washed with hexane, and vacuum-dried. Yield: 85%. IR (Nujol): $\nu(CO)$ 1990 (vs) cm^{-1} . Anal. Calcd for $C_{56}H_{53}N_6AgBF_4OP_2RhRu$: C, 52.26; H, 4.12; N, 6.52. Found: C, 52.42; H, 4.54; N, 6.53. $^{31}P\{^1H\}$ NMR ($CDCl_3/CHCl_3$, 1/1, v/v, δ): 41.1 (d, $J_{RhP} = 152$ Hz), 17.4 (d, $J^{107}AgP = 640$ Hz, $J^{109}AgP = 738$ Hz).

Complex **24** was similarly prepared starting from **6**. $^{31}P\{^1H\}$ NMR ($CDCl_3/CHCl_3$, 1/1, v/v, δ): 18.2 (d, $J^{107}AgP = 640$ Hz, $J^{109}AgP = 736$ Hz).

X-ray Measurements and Structure Determination for 22. An irregular crystal of dimension $0.236 \times 0.188 \times 0.603$ mm was glued to the end of a glass fiber. It was mounted on

Table 5. Crystal Data and Refinement Details for 22

formula	$C_{21}H_{24}BF_4IrN_6O_2Ru$
fw	772.5
symmetry	monoclinic, $P2_1/c$
a (\AA)	7.9909(6)
b (\AA)	17.0590(9)
c (\AA)	19.083(2)
β (deg)	93.94(1)
V (\AA^3), Z	2595.2(4), 4
radiation	Mo K α ($\lambda = 0.71073$ \AA)
method of collcn	$\omega/2\theta$ scan
scan range (deg)	$(3 \leq 2\theta \leq 50)$
no. of reflns:	8528 ($h = -9$ to $k = -17$ to $l = 22$)
obsd	3652 ($F_o \geq 4.0\sigma(F_o)$)
μ (cm^{-1})	57.3
largest difference peaks	0.66 e/ \AA^3 , close to BF_4
R^a , R_w^b	0.0316, 0.0342
S^c (goodness-of-fit)	1.15
data-to-parameter ratio	11.5:1

$^a R = \sum ||F_o| - |F_c|| / \sum |F_o|$. $^b R_w = \{ \sum w(|F_o| - |F_c|)^2 / \sum w|F_o|^2 \}^{1/2}$, $w^{-1} = \sigma^2(F) + 0.000423F^2$. $^c S = \{ \sum w(|F_o| - |F_c|)^2 / (M - N) \}^{1/2}$, where M and N denote the number of data and variables, respectively.

a four-circle Siemens AED diffractometer working with graphite-monochromated Mo K α radiation. Selected crystallographic data are collected in Table 5. Precise lattice parameters were determined by least-squares fit to 54 reflections ($20 \leq 2\theta \leq 45^\circ$). Three standard reflections were monitored every hour to check crystal and instrument stability. There were no significant fluctuations of the intensities. Data were corrected for Lorentz and polarization effects, and a semiempirical absorption correction³² based on ψ scans was also applied (min and max trans fact. 0.150 and 0.261). The structure was solved by the heavy-atom method followed by difference Fourier calculations using the SHELXTL-PLUS package.³³ All non H-atoms of the cation were anisotropically refined. The tetrafluoroborate anion was isotropically refined with two orientations as disorder model. Hydrogen atoms were included in the last cycles in calculated and found positions. The hydrogen bonded to the azolate nitrogen N(2) was clearly observed in the difference Fourier map and included in the observed position. All H-atoms were refined with a common thermal parameter using the riding method. The scattering factors, with anomalous dispersion correction for heavy atoms, were taken from ref 34. All calculations were carried out on a μ -VAX 3400 computer.

Acknowledgment. We thank the Direcció General de Investigaci6n Científica y T6cnica for financial support (Grant PB92/19). R.A. is grateful to the CONICIT for a grant.

Supplementary Material Available: Full details of crystallographic and experimental data, hydrogen positional parameters, and anisotropic displacement parameters (4 pages). Ordering information is given on any current mast-head page.

OM940522L

(32) North, A. C. T.; Phillips, D. C.; Mathews, F. S. *Acta Crystallogr.* **1968**, *A24*, 351.

(33) Sheldrick, G. M. SHELXTL-PLUS, Siemens Analytical X-ray Instruments, Madison, WI, 1990.

(34) *International Tables For Crystallography*; Kynoch Press: Birmingham, England, 1974; Vol. IV.

Heterobi- and Heterotetranuclear RuRh and RuIr Complexes with 2,2'-Biimidazolate and 2,2'-Bibenzimidazolate Anions as Bridging Ligands

Daniel Carmona,* Joaquina Ferrer, Ana Mendoza, Fernando J. Lahoz, and Luis A. Oro*

Departamento de Química Inorgánica, Instituto de Ciencia de Materiales de Aragón, Universidad de Zaragoza-Consejo Superior de Investigaciones Científicas, 50009 Zaragoza, Spain

Fernando Viguri

Departamento de Química Inorgánica, Escuela Universitaria de Ingeniería Técnica Industrial, Instituto de Ciencia de Materiales de Aragón, Universidad de Zaragoza-Consejo Superior de Investigaciones Científicas, Corona de Aragón 35, 50009 Zaragoza, Spain

Josefa Reyes

Departamento de Química Inorgánica, Centro Politécnico Superior de Ingenieros, Universidad de Zaragoza, María Zambrano s/n, 50015 Zaragoza, Spain

Received August 3, 1994[⊗]

The reaction of the dimer $[(\eta^6\text{-}p\text{-cymene})\text{RuCl}]_2(\mu\text{-Cl})_2$ (*p*-cymene = *p*-isopropylmethylbenzene) with 2,2'-biimidazole (H_2Bim) afforded the chloride complex $[(\eta^6\text{-}p\text{-cymene})\text{Ru}(\text{H}_2\text{Bim})\text{Cl}]\text{Cl}$ (**1**) which has also been isolated as the tetrafluoroborate salt $[(\eta^6\text{-}p\text{-cymene})\text{Ru}(\text{H}_2\text{Bim})\text{Cl}]\text{BF}_4$ (**2**) by metathesis with NaBF_4 . Complex **1** underwent reaction with $[\text{M}(\text{acac})\text{L}_2]$ yielding the corresponding heterobinuclear species $[(\eta^6\text{-}p\text{-cymene})\text{ClRu}(\mu\text{-HBim})\text{MClL}_2]$ ($\text{M} = \text{Rh}$; $\text{L}_2 = \text{cis,cis-1,5-cyclooctadiene (COD)}$ (**3**), $(\text{CO})_2$ (**4**); $\text{M} = \text{Ir}$, $\text{L}_2 = \text{COD}$ (**5**)). Complexes **3–5** exhibit a dynamic behavior which equilibrates the two imidazole rings of the HBim bridging ligand. The reaction of **4** with KOH led to two tetranuclear isomers $[(\eta^6\text{-}p\text{-cymene})\text{ClRu}(\mu\text{-Bim})\text{Rh}(\text{CO})_2]_2$ (**6**) which in solution reached an equilibrium with a *K* value for the process $\mathbf{6b} \rightleftharpoons \mathbf{6a} \leq 0.11$. Reaction of $[(\eta^6\text{-}p\text{-cymene})\text{Ru}(\text{acac})\text{Cl}]$ with $[\text{Rh}(\text{HBim})(\text{COD})]$ afforded the heterobinuclear complex $[(\eta^6\text{-}p\text{-cymene})\text{Ru}(\text{acac})(\mu\text{-HBim})\text{Rh}(\text{COD})]\text{A}$ ($\text{A} = \text{Cl}$ (**7**), BF_4 (**8**)). At room temperature the $\text{Rh}(\text{HBim})(\text{COD})$ moiety of complexes **7** and **8** rotates rapidly around the Ru-N bond, but this process stops at 223 K. $[(\eta^6\text{-}p\text{-cymene})\text{Ru}(\text{acac})\text{Cl}]$ and $[(\eta^6\text{-}p\text{-cymene})\text{Ru}(\text{acac})(\text{PPh}_3)]\text{BF}_4$ reacted with 2,2'-bibenzimidazole (H_2Bbzim) rendering $[(\eta^6\text{-}p\text{-cymene})\text{Ru}(\text{HBbzim})\text{Cl}]$ (**9**) and $[(\eta^6\text{-}p\text{-cymene})\text{Ru}(\text{HBbzim})(\text{PPh}_3)]\text{BF}_4$ (**10**), respectively. Complex **9** undergoes reaction with $[\text{M}(\text{acac})\text{L}_2]$ yielding $[(\eta^6\text{-}p\text{-cymene})\text{ClRu}(\mu\text{-Bbzim})\text{ML}_2]_n$ ($\text{M} = \text{Rh}$; $\text{L}_2 = \text{COD}$ ($n = 1$) (**11**), norborna-2,5-diene (NBD) ($n = 2$) (**12**), $(\text{CO})_2$ ($n = 2$) (**13**); $\text{M} = \text{Ir}$; $\text{L}_2 = \text{COD}$ ($n = 1$) (**14**)). The molecular structure of complex **12** has been determined. Crystals are triclinic, space group $P\bar{1}$, with cell parameters $a = 12.998(1)$ Å, $b = 14.035(1)$ Å, $c = 18.081(2)$ Å, $\alpha = 79.864(4)^\circ$, $\beta = 78.046(5)^\circ$, $\gamma = 73.326(7)^\circ$, and $Z = 2$. The compound is tetranuclear with two Bbzim^{2-} ligands bridging the metal atoms. Each Bbzim^{2-} coordinates to the metals in an unsymmetrical tetradentate manner through its four nitrogen atoms, chelated to the Ru atoms and bonded in a unidentate manner to the two Rh atoms. The cationic complex **10** undergoes reaction with the acetylacetonates $[\text{M}(\text{acac})\text{L}_2]$ yielding the cationic binuclear complexes $[(\eta^6\text{-}p\text{-cymene})(\text{PPh}_3)\text{Ru}(\mu\text{-Bbzim})\text{ML}_2]\text{BF}_4$ ($\text{M} = \text{Rh}$; $\text{L}_2 = \text{COD}$ (**15**), NBD (**16**), $(\text{CO})_2$ (**17**); $\text{M} = \text{Ir}$; $\text{L}_2 = \text{COD}$ (**18**)). Carbonylation of **18** afforded $[(\eta^6\text{-}p\text{-cymene})(\text{PPh}_3)\text{Ru}(\mu\text{-Bbzim})\text{Ir}(\text{CO})_2]\text{BF}_4$ (**19**) and complex **17** could analogously be obtained from complexes **15** or **16**. The molecular structure of complex **19** has been determined by diffractometric methods. Crystals are monoclinic, space group $P2_1/c$, with cell parameters $a = 11.586(2)$ Å, $b = 20.489(2)$ Å, $c = 17.225(1)$ Å, $\beta = 95.34(1)^\circ$, and $Z = 4$. In the solid state, two complex cations $[(\eta^6\text{-}p\text{-cymene})(\text{PPh}_3)\text{Ru}(\mu\text{-Bbzim})\text{Ir}(\text{CO})_2]$ related by an inversion center are joined by an intermetallic Ir–Ir interaction (3.0808(5) Å). The cation consists of a Ru and an Ir atom connected by a Bbzim^{2-} anion that chelates both metals through four nitrogen atoms. Complexes **11**, **14**, and **15–19** are active catalysts for the homogeneous hydrogenation of cyclohexene. Kinetic studies showed that the reduction catalyzed by **14** is first-order in catalyst concentration and second-order in hydrogen concentration.

Introduction

The coordination of 2,2'-biimidazole (H_2Bim), 2,2'-bibenzimidazole (H_2Bbzim), and their related anions to

transition metal ions has attracted much attention since Rasmussen et al. published the first examples of binuclear complexes containing the tetracoordinate dianion Bim^{2-} .¹ The presence of an imidazole moiety in important biological molecules has encouraged the

[⊗] Abstract published in *Advance ACS Abstracts*, December 1, 1994.

preparative studies of discrete H₂Bim- and H₂Bbzim-containing transition metal complexes. Thus, for example, H₂Bim has been used as ligand in pentacoordinate zinc complexes relevant for the discussion of the active sites in enzymes such as carboxypeptidase.² Several chelates resulting from the reaction of H₂Bim and H₂Bbzim with a variety of ferrous salts have been synthesized and studied owing to the interest of such ferrous complexes as models of the ferrous ion of mononuclear non-heme-containing proteins.³

Haga and co-workers have extensively studied the synthesis, electrochemical, and spectral properties of mono- and binuclear complexes of Ru, Os, Co, and Ni in various oxidation states with H₂Bim and H₂Bbzim or their derived mono- and dianions as ligands.⁴ In particular, the spectroscopic and electrochemical properties of multimetallic ruthenium(II) complexes containing H₂Bim and H₂Bbzim in their protonated and deprotonated forms have been investigated with the ultimate goal of effecting multiple-electron-transfer events from excited-state species.⁵ Anionic bridging ligands derived from 2,2'-biimidazole have been employed in order to prepare bimetallic ruthenium complexes for use in solar energy utilization studies.⁶ Very recently, the molecular structure and photophysical properties of di- and tetranuclear gold(I) complexes with the Bbzim²⁻ anion acting as bridging ligand have been described.⁷ Indirect cooperative effects leading to synergism in bimetallic homogeneous hydrogenation reactions have been found for Ru-Ir based catalysts containing Bim²⁻ as bridging ligand.⁸

However, 2,2'-biimidazole and 2,2'-bibenziimidazole and their derived anions have unique properties as coordinating ligands. They can complex as bidentate chelates. The dianions can also act as bis-bidentate-chelate toward a pair of metal ions. Additionally, mono- and bidentate nonchelate coordination modes can be achieved through the uncoordinated remaining nitrogens. Furthermore, the resulting complexes can be homo- or heterometallic, increasing the synthetic possibilities of this type of ligands. Compounds belonging to most of these coordination types have been described.^{4d,7,9}

Pursuing our work in the study of the chemistry of transition metal ions with azole ligands,⁸⁻¹⁰ we now report the preparation and characterization of several RuRh and RuIr complexes, with the mono- and dianions

derived from H₂Bim and H₂Bbzim as bridging ligands, of stoichiometries [(η⁶-*p*-cymene)ClRu(μ-HBim)MClL₂] (M = Rh; L₂ = COD (3), (CO)₂ (4). M = Ir; L₂ = COD (5)), [(η⁶-*p*-cymene)ClRu(μ-Bim)Rh(CO)₂]₂ (6), [(η⁶-*p*-cymene)Ru(acac)(μ-HBim)Rh(COD)]A (A = Cl, (7) BF₄ (8)), [(η⁶-*p*-cymene)ClRu(μ-Bbzim)ML₂]_n (M = Rh; L₂ = COD (n = 1) (11), NBD (n = 2) (12), (CO)₂ (n = 2) (13). M = Ir; L₂ = COD (n = 1) (14)) and [(η⁶-*p*-cymene)-(PPh₃)Ru(μ-Bbzim)ML₂]BF₄ (M = Rh; L₂ = COD (15), NBD (16), (CO)₂ (17). M = Ir; L₂ = COD (18), (CO)₂ (19)). The fluxional behavior in solution of complexes 3-5, 7, and 8 is studied as well as an unexpected isomerization process that exhibits the carbonyl compound 6. The molecular structures of [(η⁶-*p*-cymene)ClRu(μ-Bbzim)Rh(NBD)]₂·2CH₂Cl₂ ((12)·2CH₂Cl₂) and [(η⁶-*p*-cymene)(PPh₃)Ru(μ-Bbzim)]Ir(CO)₂]BF₄ (19) are also reported.

Results and Discussion

Complexes with 2,2'-Biimidazole. Reaction of the binuclear complex¹¹ [(η⁶-*p*-cymene)RuCl]₂(μ-Cl)₂ with 1 equiv of 2,2'-biimidazole (H₂Bim) afforded the yellow mononuclear compound [(η⁶-*p*-cymene)Ru(H₂Bim)Cl]Cl (1). The tetrafluoroborate derivative [(η⁶-*p*-cymene)Ru(H₂Bim)Cl]BF₄ (2) can be prepared by adding equimolar amounts of NaBF₄ to 1 in methanol. Both complexes have been characterized by elemental analyses and spectroscopic methods (see Experimental Section). Their IR spectra showed (i) a strong and very broad ν(NH) band in the 3650-2250 cm⁻¹ region which suggested that a strong N-H-X association is operating,^{10c,f,k} (ii) a band at ca. 300 cm⁻¹ attributable to the stretching vibration ν(RuCl)¹² and, (iii) bands of the H₂Bim ligand.^{3,13} Complex 2 showed two bands at ca. 1100 and 520 cm⁻¹ characteristic of the uncoordinated BF₄⁻ anion.¹⁴ The molar conductivity of 1 in methanol, that corresponds to 1:1 electrolytes,¹⁵ along with the easy displacement of one chlorine atom by NaBF₄ strongly indicated that one of the chlorines in 1 is not covalently bonded to the ruthenium. Consequently, the FAB mass

(1) (a) Kaiser, S. W.; Saillant, R. B.; Rasmussen, P. G. *J. Am. Chem. Soc.* **1975**, *97*, 425. (b) Kaiser, S. W.; Saillant, R. B.; Butler, W. M.; Rasmussen, P. G. *Inorg. Chem.* **1976**, *15*, 2681. (c) Kaiser, S. W.; Saillant, R. B.; Butler, W. M.; Rasmussen, P. G. *Inorg. Chem.* **1976**, *15*, 2688.

(2) Kirchner, C.; Krebs, B. *Inorg. Chem.* **1987**, *26*, 3569.

(3) Boinnard, D.; Cassoux, P.; Petrouleas, V.; Savariault, J.-M.; Tuchagues, J.-P. *Inorg. Chem.* **1990**, *29*, 4114.

(4) (a) Haga, M. *Inorg. Chim. Acta* **1980**, *45*, L183. (b) Haga, M. *Inorg. Chim. Acta* **1983**, *75*, 29. (c) Bond, A. M.; Haga, M. *Inorg. Chem.* **1986**, *25*, 4507. (d) Haga, M.; Matsumura-Inoue, T.; Yamabe, S. *Inorg. Chem.* **1987**, *26*, 4148.

(5) Rillema, D. P.; Sahai, R.; Matthews, Ph.; Edwards, A. K.; Shaver, R. J.; Morgan, L. *Inorg. Chem.* **1990**, *29*, 167.

(6) Sahai, R.; Murphy Jr., W. R.; Petersen, J. D. *Inorg. Chim. Acta* **1986**, *114*, 137.

(7) Tzeng, B.-C.; Li, D.; Peng, S.-M.; Che, C.-M. *J. Chem. Soc., Dalton Trans.* **1993**, 2365.

(8) (a) García, M. P.; López, A. M.; Esteruelas, M. A.; Lahoz, F. J.; Oro, L. A. *J. Chem. Soc., Dalton Trans.* **1990**, 3465. (b) Esteruelas, M. A.; García, M. P.; López, A. M.; Oro, L. A. *Organometallics* **1991**, *10*, 127.

(9) Usón, R.; Oro, L. A.; Gimeno, J.; Ciriano, M. A.; Cabeza, J. A.; Tiripicchio, A.; Tiripicchio-Camellini, M. *J. Chem. Soc., Dalton Trans.* **1983**, 323 and references therein.

(10) (a) Usón, R.; Gimeno, J.; Oro, L. A.; Martínez de Ilarduya, J. M.; Cabeza, J. A.; Tiripicchio, A.; Tiripicchio-Camellini, M. *J. Chem. Soc., Dalton Trans.* **1983**, 1729. (b) Usón, R.; Oro, L. A.; Ciriano, M. A.; Naval, M. M.; Aprea, M. C.; Foces-Foces, C.; Cano, F. H.; García-Blanco, S. *J. Organomet. Chem.* **1983**, *256*, 331. (c) Oro, L. A.; Carmona, D.; Lamata, M. P.; Tiripicchio, A.; Lahoz, F. J. *J. Chem. Soc., Dalton Trans.* **1986**, 15. (d) Carmona, D.; Oro, L. A.; Lamata, M. P.; Elguero, J.; Aprea, M. C.; Foces-Foces, C.; Cano, F. H. *Angew. Chem. Int. Ed. Engl.* **1986**, *25*, 1114. (e) Carmona, D.; Oro, L. A.; Lamata, M. P.; Puebla, M. P.; Ruiz, J.; Maitlis, P. M. *J. Chem. Soc., Dalton Trans.* **1987**, 639 and references therein. (f) Carmona, D.; Ferrer, J.; Oro, L. A.; Aprea, M. C.; Foces-Foces, C.; Cano, F. H.; Elguero, J.; Jimeno, M. L. *J. Chem. Soc., Dalton Trans.* **1990**, 1463. (g) Carmona, D.; Oro, L. A.; Lamata, M. P.; Buzarra, S. *Organometallics* **1991**, *10*, 3123. (h) Carmona, D.; Ferrer, J.; Lahoz, F. J.; Oro, L. A.; Reyes, J.; Esteban, M. *J. Chem. Soc., Dalton Trans.* **1991**, 2811 and references therein. (i) Carmona, D.; Ferrer, J.; Mendoza, A.; Lahoz, F. J.; Reyes, J.; Oro, L. A. *Angew. Chem. Int. Ed. Engl.* **1991**, *30*, 1171. (j) Carmona, D.; Ferrer, J.; Reyes, J.; Oro, L. A. *Organometallics* **1993**, *12*, 4241. (k) Carmona, D.; Ferrer, J.; Marzal, I. M.; Oro, L. A.; Trofimenko, S. *Gazz. Chim. Ital.* **1994**, *124*, 35. (l) Carmona, D.; Ferrer, J.; Lamata, M. P.; Oro, L. A.; Limbach, H.-H.; Scherer, G.; Elguero, J.; Jimeno, M. L. *J. Organomet. Chem.* **1994**, *470*, 271. (m) Carmona, D.; Lamata, M. P.; Ferrer, J.; Modrego, J.; Perales, M.; Lahoz, F. J.; Atencio, R.; Oro, L. A. *J. Chem. Soc., Chem. Commun.* **1994**, 575. (n) Carmona, D.; Oro, L. A.; Lamata, M. P.; Jimeno, M. L.; Elguero, J.; Belguise, A.; Lux, Ph. *Inorg. Chem.* **1994**, *33*, 2196.

(11) Bennet, M. A.; Smith, A. K. *J. Chem. Soc., Dalton Trans.* **1974**, 233.

(12) (a) Zelonka, R. A.; Baird, M. C. *J. Organomet. Chem.* **1972**, *35*, C43. (b) *Ibid.* **1972**, *44*, 383.

(13) (a) Reedijk, J. *Recl. Trav. Chim. Pays Bas* **1969**, *88*, 1451. (b) Usón, R.; Gimeno, J.; Forníés, J.; Martínez, F. *Inorg. Chim. Acta* **1981**, *50*, 173.

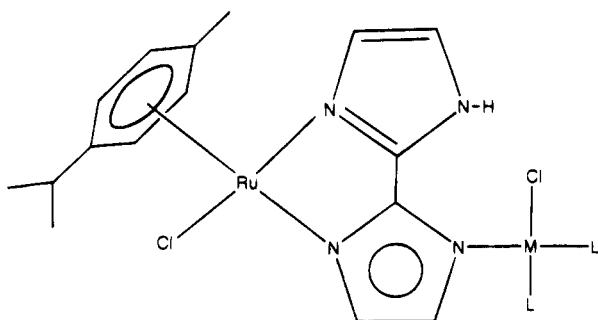


Figure 1. Proposed static structure for complexes 3–5.

spectrum showed a peak at m/z 405 with an isotopic distribution that matches the calculated for the $[(\eta^6\text{-}p\text{-cymene})\text{Ru}(\text{H}_2\text{Bim})\text{Cl}]^+$ fragment. The ^1H spectra were consistent with the proposed formulations. They showed two signals at 7.15 and 7.41 ppm for **1**, and at 7.17 and 7.45 ppm for **2** corresponding to the CH protons of the 2,2'-biimidazole¹⁶ and the *p*-cymene and NH resonances with the expected relative intensities and multiplicities.

Attempts to prepare the neutral complex $[(\eta^6\text{-}p\text{-cymene})\text{Ru}(\text{HBim})\text{Cl}]$ from the reaction of **1** with a base (KOH, NEt_3 or $^t\text{BuOK}$) have been unsuccessful. The reactions gave complex mixtures of *p*-cymene-containing complexes that we have not been able to resolve. Similar mixtures were obtained when the acetylacetonate complex $[(\eta^6\text{-}p\text{-cymene})\text{Ru}(\text{acac})\text{Cl}]$ ^{10f} was allowed to react with 2,2'-biimidazole.

Complex **1** has two NH groups that, potentially, could be used in ulterior coordination to afford bi- or polynuclear complexes. Thus, **1** reacted with $[\text{M}(\text{acac})\text{L}_2]$ ($\text{M} = \text{Rh}$; $\text{L}_2 = \text{COD}$,¹⁷ $(\text{CO})_2$,¹⁸ $\text{M} = \text{Ir}$; $\text{L}_2 = \text{COD}$ ¹⁹) yielding the corresponding yellow heterobinuclear complexes $[(\eta^6\text{-}p\text{-cymene})\text{ClRu}(\mu\text{-HBim})\text{MClL}_2]$ ($\text{M} = \text{Rh}$; $\text{L}_2 = \text{COD}$ (**3**), $(\text{CO})_2$ (**4**). $\text{M} = \text{Ir}$; $\text{L}_2 = \text{COD}$ (**5**)). Complex **4** could also be prepared by bubbling carbon monoxide through dichloromethane solutions of **3**. The new heterobinuclear complexes **3–5** were characterized on the basis of elemental analyses, IR and NMR spectroscopies (see Experimental Section). Their IR spectra in Nujol showed vibration bands at ca. 3300 and 300 cm^{-1} attributable to N–H and M–Cl bonds, respectively, and the disappearance of the acac vibrations. The

carbonyl complex **4** showed two strong $\nu(\text{CO})$ bands characteristic of a *cis*-dicarbonyl structure.²⁰ The proposed structure for these complexes is schematically drawn in Figure 1. However, their ^1H NMR spectra at room temperature showed less bands than expected for a static structure as the proposed. The spectra exhibited only one doublet and one AB system assigned to the isopropyl methyl and aromatic protons of the *p*-cymene ligand, respectively. These data indicated that a fluxional process was occurring. In particular, the spectrum of **3** (Table 1), only showed two signals at 7.20 and 7.55 ppm for the CH protons of the biimidazole ligand. By lowering the temperature to 193 K, four sharp separate singlets at 7.02, 7.39, 7.54 and 7.72 ppm appeared, and the broadening of the doublet and the AB system of the *p*-cymene ligand was observed. Consistently, while the $^{13}\text{C}\{^1\text{H}\}$ NMR spectrum of **3** at room temperature (Table 2) only exhibited one signal for the 2 and 2' carbons and a broad resonance for the 4, 4', 5, and 5' carbon nuclei of the biimidazole ligand, at 223 K there were six separate signals for these nuclei. Furthermore, at this temperature, it showed several overlapped signals for the diolefinic carbon nuclei of the cyclooctadiene ligand, while at room temperature only two broad resonances centered at 79.9 and 30.0 ppm were observed for this group.

All these observations were consistent with the existence, at low temperature, of the static structure shown in Figure 1. When the temperature was increased, a fluxional process operated, which rendered equivalent the two halves of the biimidazole ligand and the two L groups. For this process, we suggest a dissociative mechanism via deprotonation of the NH group, loss of the chlorine atom attached to M, and formation of a new M–N bond to give the symmetric intermediate $[(\eta^6\text{-}p\text{-cymene})\text{ClRu}(\mu\text{-Bim})\text{ML}_2]$ followed by rupture of the former M–N bond and recoordination of the chloride and proton. A comparable mechanism has been previously reported by Dixon et al. for the palladium complex *cis*- $[\text{PdCl}(\text{PET}_3)_2(4\text{-Br-3,5-Me}_2\text{Hpz})]\text{ClO}_4$.²¹ Interestingly, the estimated energy barrier ΔG^\ddagger for the fluxional process in complex **3**, according to the coalescence temperature of the biimidazole protons, is 54 kJ

Table 1. ^1H NMR Spectroscopic Data^a at Different Temperatures for Complexes 3, 7, and 8

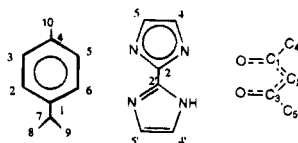
complex (T, K)	<i>p</i> -cymene			NH	HBim		COD		acetylacetonate	
	Me	ⁱ Pr	AA'BB'		CH	vinylc	aliphatic	Me	H	
3 ^b (293)	2.14 (s)	1.06 (d, $J = 7.0$)	5.62 (d, $J = 6.1$) 5.83 (d, $J = 6.1$)	—	7.55 (s), 7.20 (br s)	3.93 (m), 3.01 (m)	2.33 (m), 1.75 (m)	—	—	—
	(193)	2.20 (br s)	1.02 (br)	5.75 (br), 5.86 (br)	12.20 (s)	7.72 (s), 7.54 (s), 7.39 (s), 7.02 (s)	4.25 (m), 3.60 (m)	2.20 (m), 1.80 (m)	—	—
7 (323)	1.74 (s)	1.19 (d, $J = 7.0$), 2.81 (sp)	5.55 (br s)	—	7.75 (s), 6.67 (s), 6.46 (s), 6.44 (s)	4.41 (m)	2.46 (m), 1.93 (m)	1.87 (s)	4.97 (s)	—
	(293)	1.71 (s)	1.17 (br d), 2.79 (sp, $J = 6.4$)	5.21 (br s), 5.55 (br s), 5.77 (br s), 6.65 (br s)	11.76 (br s)	7.71 (s), 6.66 (s), 6.45 (s), 6.43 (s)	4.38 (m)	2.43 (m), 1.94 (m)	1.85 (s)	4.95 (s)
	(223)	1.68 (s)	1.18 (d, $J = 6.4$), 1.11 (d, $J = 6.2$), 2.82 (sp)	5.17 (d, $J = 5.9$), 5.19 (d, $J = 5.9$), 5.65 (d, $J = 6.0$), 6.60 (d, $J = 6.0$)	11.70 (s)	7.67 (s), 6.63 (s), 6.44 (s), 6.42 (s)	4.49 (m), 4.38 (m)	2.45 (m), 1.95 (m)	1.82 (s), 1.80 (s)	4.29 (s)
8 (323)	1.70 (s)	1.21 (d, $J = 6.8$), 2.73 (sp)	5.1–6.3 (br)	11.42 (br s)	7.49 (s), 6.70 (s), 6.50 (s), 6.48 (s)	4.43 (m)	2.47 (m), 1.96 (m)	1.89 (s)	5.02 (s)	—
	(293)	1.69 (s)	1.20 (br s), 2.75 (sp)	5.12 (br s), 5.43 (br s), 5.54 (br s), 6.16 (br s)	11.45 (br s)	7.47 (s), 6.69 (s), 6.50 (s), 6.47 (s)	4.41 (m)	2.46 (m), 1.95 (m)	1.88 (s)	5.01 (s)
	(223)	1.67 (s)	1.14 (d, $J = 6.8$), 1.19 (d, $J = 6.8$), 2.73 (sp)	5.12 (d, $J = 5.8$), 5.32 (d, $J = 5.8$), 5.51 (d, $J = 5.9$), 6.12 (d, $J = 5.9$)	11.44 (s)	7.43 (s), 6.66 (s), 6.49 (s), 6.46 (s)	4.51 (m), 4.41 (m)	2.45 (m), 1.90 (m)	1.87 (s), 1.84 (s)	4.98 (s)

^a Measured in CDCl_3 ; J in hertz; d = doublet, sp = septet, m = multiplet; br = broad. ^b In CD_3COCD_3 .

Table 2. $^{13}\text{C}\{\text{H}\}$ NMR Spectroscopic Data^a at Different Temperatures for Complexes 3 and 7

complex (T, K)	<i>p</i> -cymene ^b					HBim ^b			COD		acetylacetonate		
	C _{1/4}	C _{2,6/3,5}	C ₇	C _{8/9}	C ₁₀	C _{2/2'}	C _{4/4'}	C _{5/5'}	C(sp ³)	C(sp ²)	C _{1/3}	C ₂	C _{4/5}
3 ^c (293)	102.2, 99.8	83.6, 81.8	—	22.0	18.6	145.1	130.9	—	30.0	79.9	—	—	—
(223)	101.8, 99.0	<i>d</i>	—	22.1	18.5	143.6	131.8, 129.9, 129.6, 118.6	—	32.4, 31.4, 31.0	76.9 (d, <i>J</i> = 14.2), 76.3 (d, <i>J</i> = 13.5) ^d	—	—	—
7 ^e (293)	102.0, 100.0	86.7	30.6	22.4	18.0	—	129.8, 125.7	123.7, 120.8	30.6	79.8	187.0	99.4	27.0
(223)	101.5, 99.3	86.1, 84.9, 78.3, 78.0	30.1	22.4	17.9	147.1	129.4, 125.5, 142.9	123.6, 120.0	30.7, 30.6, 29.8	79.3 (d, <i>J</i> = 11.0), 78.8 (d, <i>J</i> = 12.0), 80.6	187.1, 186.1	99.0	27.1, 26.7

^a *J* in hertz; d = doublet. ^b The *p*-cymene and biimidazolate carbon atoms are numbered as follows:



^c In CD_3COCD_3 . ^d There are five resonances at 84.1, 84.0, 83.9, 82.8, and 82.0 ppm for the two remaining sp^2 diolefinic carbon atoms and for the $\text{C}_{2,6/3,5}$ carbons of the *p*-cymene ligand. ^e In CDCl_3 .

mol^{-1} , similar to the ΔG^\ddagger value of 60 kJ mol^{-1} found in the above mentioned palladium complex.²¹

The formation of the heterobinuclear complexes **3–5** containing the monoanion HBim[−] coordinated as a bridging tridentate ligand could be considered as an intermediate step in the preparation of $[(\eta^6\text{-}p\text{-cymene})\text{ClRu}(\mu\text{-Bim})\text{ML}_2]_n$ complexes, in which the tetradentate dianion Bim^{2−} is present. Thus, the reaction of **4** with stoichiometric amounts of KOH in methanol led to the formation of the new neutral red-orange complex $[(\eta^6\text{-}p\text{-cymene})\text{ClRu}(\mu\text{-Bim})\text{Rh}(\text{CO})_2]_n$ (**6**). Nevertheless, starting from the diolefinic complexes **3** and **5**, untreatable mixtures of reaction products were obtained. The IR spectrum of **6** in dichloromethane showed three strong $\nu(\text{CO})$ bands at 2080, 2060, and 2010 cm^{-1} , a characteristic pattern for folded binuclear structures with four carbonyl groups coordinated to two adjacent metals.^{1c,10b,22} The mass spectrum showed an envelope of peaks at m/z 1124 with the isotopic distribution calculated for the tetranuclear $[(\eta^6\text{-}p\text{-cymene})\text{ClRu}(\mu\text{-Bim})\text{Rh}(\text{CO})_2]_2^+$ fragment. These data were consistent with a tetranuclear formulation $[(\eta^6\text{-}p\text{-cymene})\text{ClRu}(\mu\text{-Bim})\text{Rh}(\text{CO})_2]_2$ for complex **6**. A similar increment of the nuclearity in biimidazolate complexes was found in the carbonylation of the binuclear complexes $[\text{Rh}_2(\mu\text{-Bim})(\text{COD})_2]^{1c}$ and $[\text{Rh}_2(\mu\text{-TcBim})(\text{COD})_2]$ (TcBim = 4,4',5,5'-tetracyano-2,2'-biimidazolate)²³ to give the tetranuclear species $[\text{Rh}_4(\mu\text{-tetraazolate})(\text{CO})_8]$. Although we have only observed the above-mentioned three- $\nu(\text{CO})$ -band pattern, analytical and ^1H NMR data showed the presence of two isomers in solution which were obtained in different ratios from one preparation to another. One isomer had only one type of *p*-cymene ligand and only two proton NMR signals were observed for its two biimidazolate ligands, while the other showed two different kind of *p*-cymene ligands and four biimidazolate proton resonances (**6a–c**) are schematically shown in Figure 2. Assuming free rotation of the *p*-cymene groups around the Ru–arene axis, the spectrum with only one type of *p*-cymene had to be assigned to **6a** or **6c**, rigid tetranuclear structures with C_{2v} symmetry. The other spectrum was attributed to the C_s isomer **6b**. We could not conclude

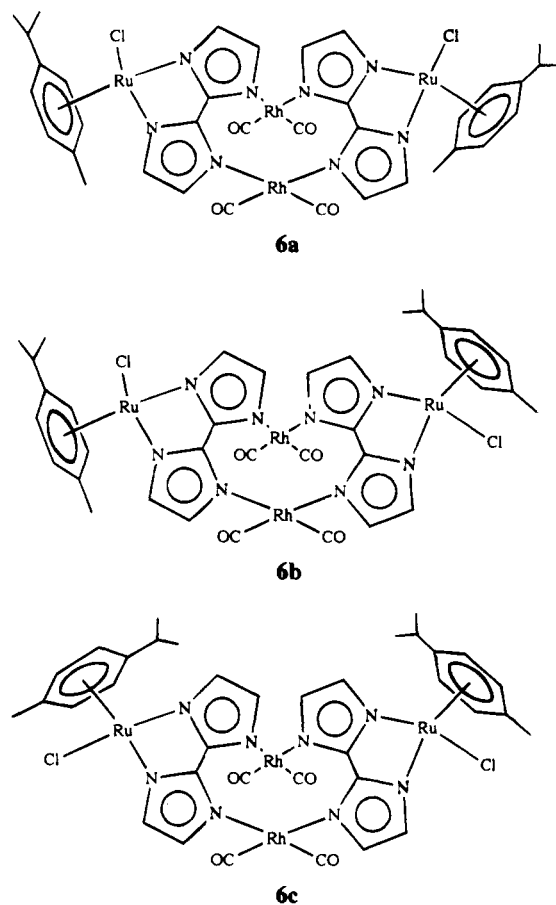


Figure 2. Possible structures for the isomers of complex **6**.

if the obtained isomer was **6a** or **6c**, but only one of them was detected. Furthermore, we have been able to isolate isomer **6a** or **6c** pure and establish that an isomerization process between **6a** or **6c** and **6b** takes place. This process was monitored by ^1H NMR spectroscopy in CDCl_3 at room temperature. Starting from a solution mixture 40/60 of **6b/6a** (or **6c**), the ratio was 90/10 after 4 h and remained constant (within the ± 2 error limit) over a 4-day period. Consequently, the equilibrium constant $\text{6b} \rightleftharpoons \text{6a}$ (or **6c**) will be ≤ 0.11 .

Looking for an alternative route to prepare polynuclear compounds with the Bim^{2−} anion, the neutral acetylacetonate complex $[(\eta^6\text{-}p\text{-cymene})\text{Ru}(\text{acac})\text{Cl}]^{10f}$ was allowed to react with the mononuclear rhodium(I)

(14) See for example: Lehner, H.; Matt, D.; Togni, A.; Thouvenot, R.; Venanzi, L. M.; Albinati, A. *Inorg. Chem.* **1984**, *23*, 4254.

(15) Geary, J. *Coord. Chem. Rev.* **1981**, *7*, 81.

(16) Kirchner, C.; Krebs, B. *Inorg. Chem.* **1987**, *26*, 3569.

complexes and found that the constant corresponding to the bibenzimidazole system is about 2 orders of magnitude greater.^{4a,b}

The synthesis of bi- or polynuclear bibenzimidazolate complexes was attempted by alternative routes. The reaction of the acetylacetonate complex $[(\eta^6\text{-}p\text{-cymene})\text{Ru}(\text{acac})\text{Cl}]^{10f}$ with H_2Bbzim led to the neutral complex $[(\eta^6\text{-}p\text{-cymene})\text{Ru}(\text{HBbzim})\text{Cl}]$ (**9**). Similarly, the acetylacetonate group can be removed from the cationic compound $[(\eta^6\text{-}p\text{-cymene})\text{Ru}(\text{acac})(\text{PPh}_3)]\text{BF}_4^{10f}$ by reaction with H_2Bbzim yielding $[(\eta^6\text{-}p\text{-cymene})\text{Ru}(\text{HBbzim})(\text{PPh}_3)]\text{BF}_4$ (**10**). Long reaction times, 24 h and 7 days, respectively, were necessary to achieve greater than 70% yields, most probably due to the coordinative saturation of the parent ruthenium(II) complexes. An alternative route to **10** was the reaction of **9** with stoichiometric amounts of AgBF_4 and PPh_3 . Both compounds have been characterized by elemental analyses and spectroscopic methods (see Experimental Section). Their IR spectra, in the solid state, showed a strong and very broad absorption in the 3200–2200 cm^{-1} region, a band at 290 cm^{-1} attributable to $\nu(\text{RuCl})$ for **9**, and the characteristic bands of the tetrafluoroborate anion and of the PPh_3 ligand for **10**. These observations indicated the presence of a remaining N–H bond in the coordinated heterocycle and suggested a strong N–H–X association in the solid state. The ^1H NMR data were as expected for an endobidentate coordination of the HBbzim^- anion and, interestingly, showed only one type of p -cymene ligand in the molecule. These spectroscopic observations could be accounted for by assuming that, at room temperature, a prototropic exchange of the remaining NH proton between the two uncoordinated nitrogens is operating fast in the ^1H NMR time-scale. Related prototropic processes have been recently described for pyrazolate ligands.^{10d,f,k}

Furthermore, this NH group is capable of ulterior coordination rendering polynuclear compounds. Thus, **9** reacted with $[\text{Rh}(\text{acac})\text{L}_2]$ ($\text{L}_2 = \text{COD}$, NBD ,²⁵ $(\text{CO})_2$) in methanol with displacement of the acetylacetonate group and formation of the corresponding complexes $[(\eta^6\text{-}p\text{-cymene})\text{ClRu}(\mu\text{-Bbzim})\text{RhL}_2]_n$ ($\text{L}_2 = \text{COD}$ (**11**), NBD (**12**), $(\text{CO})_2$ (**13**)). The related RuIr complex $[(\eta^6\text{-}p\text{-cymene})\text{ClRu}(\mu\text{-Bbzim})\text{Ir}(\text{COD})]_n$ (**14**) was similarly prepared but in acetone because in methanol a mixture of the homobinuclear complexes $[(\eta^6\text{-}p\text{-cymene})\text{ClRu}]_2(\mu\text{-Bbzim})$ and $[\text{Ir}_2(\mu\text{-Bbzim})(\text{COD})_2]$ was obtained. Again, in this process, the acidic character of coordinated HBbzim^- groups was manifested. Thus, they displaced acac coordinated anions while related HBim^- compounds did not. Carbonylation of **11** readily gave **13**.

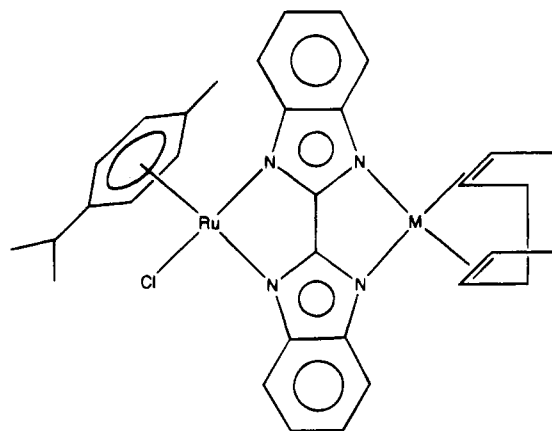


Figure 4. Proposed structure for complexes **11** and **14**.

The IR spectra of these complexes showed the characteristic bands of the bibenzimidazolate anion^{3,13} and one band in the 285–300 cm^{-1} region assignable to $\nu(\text{RuCl})$.¹² The mass spectra of **11** and **14** showed molecular ions at m/z 714 and 804, respectively, and the peaks corresponding to the loss of the chlorine ligand from them. These values pointed to a binuclear formulation for these complexes ($n = 1$). The ^1H NMR data (see Experimental Section) showed one type of p -cymene and 2,2'-bibenzimidazolate ligand in a 1/1 ratio. From these data, we propose for complexes **11** and **14** a binuclear structure with the Bbzim^{2-} anion acting as a tetradentate bis-chelate bridging ligand between two $(\eta^6\text{-}p\text{-cymene})\text{ClRu}$ fragments (Figure 4).

However, the IR spectrum of **13** in a dichloromethane solution showed three strong absorptions due to $\nu(\text{CO})$ at 2090, 2070, and 2020 cm^{-1} , characteristic of four carbonyl groups coordinated to two adjacent metals.^{1c,10b,22} Its mass spectrum showed peaks at m/z 1324 and 1289 that we assign to the molecular ion and to the loss of one chlorine ligand from a tetranuclear structure ($n = 2$). The spectroscopic data of the bibenzimidazolate complex **13**, closely resembled those previously found for the C_{2v} biimidazolate isomers **6a** or **6c**, but no isomerization was detected in this case. According to all these spectroscopic data, we propose a tetranuclear C_{2v} structure of the **6a** or **6c** type for complex **13**.

The ^1H NMR spectrum of **12** (Experimental Section) showed the expected signals for one p -cymene ligand that has lost its plane of symmetry,^{10j,26} eight signals for eight inequivalent CH bibenzimidazolate protons and eight resonances for the protons of the NBD (C_7H_8) ligand.²⁷ These experimental data exclude structural assignment of **12** according to related heteronuclear compounds previously described in this paper: a binuclear geometry with a tetradentate azolate anion (complexes **11** and **14**) or a tetranuclear structure with C_{2v} or C_s symmetries (compounds **6** and **13**). Thus, in order to ascertain the molecular structure of complex **12**, an X-ray diffraction study was undertaken.

Molecular Structure of $[(\eta^6\text{-}p\text{-Cymene})\text{ClRu}(\mu\text{-Bbzim})\text{Rh}(\text{NBD})]_2\text{2CH}_2\text{Cl}_2$ (12**· $2\text{CH}_2\text{Cl}_2$).** Figure 5 shows a view of the complex, together with the atom

(17) Chatt, J.; Venanzi, L. M. *J. Chem. Soc.* **1957**, 4735.

(18) Varsharvskii, Y. S.; Cherkasova, T. G. *Russ. J. Inorg. Chem.* **1967**, 599.

(19) Robinson, S. D.; Shaw, B. L. *J. Chem. Soc.* **1965**, 4997.

(20) (a) Oro, L. A.; Carmona, D.; Reyes, J.; Foces-Foces, C.; Cano, F. H. *J. Chem. Soc., Dalton Trans.* **1986**, 31. (b) Usón, R.; Oro, L. A.; Garralda, M. A. *J. Organomet. Chem.* **1976**, 105, 365. (c) Usón, R.; Oro, L. A.; Artigas, J.; Sariego, R. *J. Organomet. Chem.* **1979**, 179, 65.

(21) Bushnell, G. W.; Dixon, K. R.; Eadie, D. T.; Stobart, S. R. *Inorg. Chem.* **1981**, 1545.

(22) Crooks, G. R.; Johnson, B. F. G.; Lewis, J.; Williams, I. G.; Gamlen, G. J. *J. Chem. Soc. (A)* **1969**, 2761.

(23) Rasmussen, P. G.; Bailey, O. H.; Bayón, J. C. *Inorg. Chem.* **1984**, 23, 338.

(24) Kotake, S.; Sei, T.; Miki, K.; Kai, Y.; Yasuoka, N.; Kasai, N. *Bull. Chem. Soc. Jpn.* **1980**, 53, 10.

(25) Bonati, F.; Wilkinson, G. *J. Chem. Soc.* **1964**, 3156.

(26) (a) Bennett, M. A.; Ennett, J. P. *Organometallics* **1984**, 3, 1365.

(b) Esteban, M.; Pequerul, A.; Carmona, D.; Lahoz, F. J.; Martín, A.; Oro, L. A. *J. Organomet. Chem.* **1991**, 404, 421.

(27) Solutions of **12** spontaneously evolved to the homobinuclear species $[(\eta^6\text{-}p\text{-cymene})\text{ClRu}]_2(\mu\text{-Bbzim})$ and $[\text{Rh}_2(\mu\text{-Bbzim})(\text{NBD})_2]$ which precludes to take more time demanding spectroscopic measurements. An authentic sample of the later was prepared by reacting H_2Bbzim with $[\text{Rh}(\text{acac})(\text{NBD})]$ in methanol.

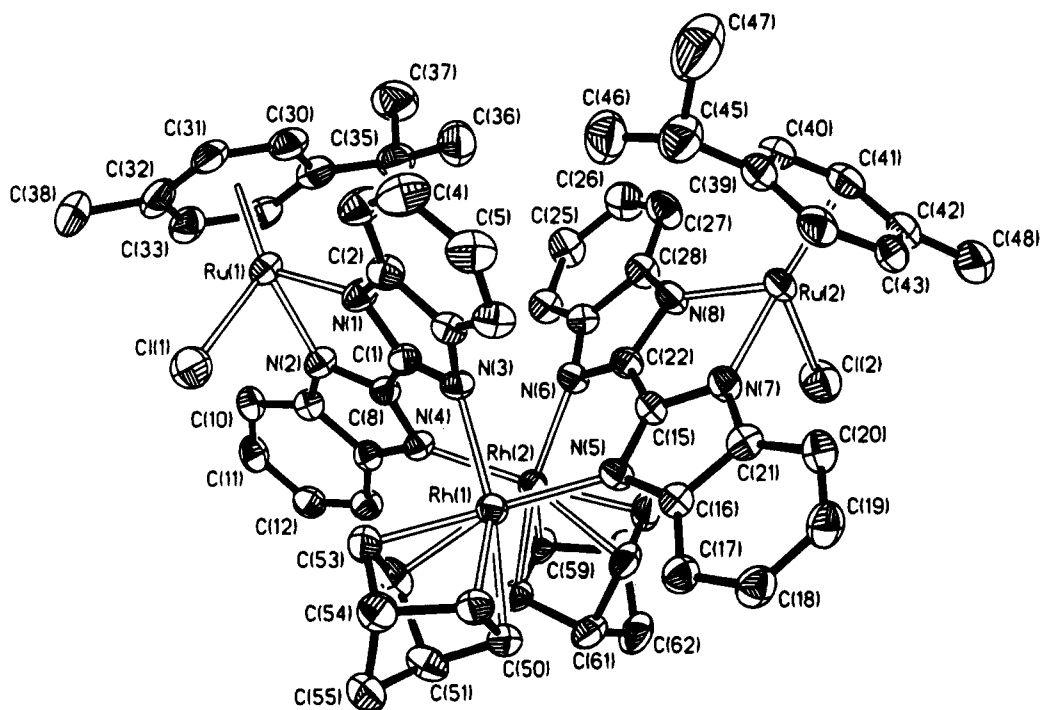


Figure 5. ORTEP view of the molecule $[(\eta^6\text{-}p\text{-cymene})\text{ClRu}(\mu\text{-Bbzim})\text{Rh}(\text{NBD})]_2$ (**12**) showing the atom-labeling scheme.

Table 3. Atomic Coordinates ($\times 10^4$; $\times 10^5$ for Rh and Ru Atoms) and Equivalent Isotropic Displacement Coefficients ($\text{\AA}^2 \times 10^4$) for $[(\eta^6\text{-}p\text{-Cymene})\text{ClRu}(\mu\text{-Bbzim})\text{Rh}(\text{NBD})]_2 \cdot 2\text{CH}_2\text{Cl}_2$

atom	<i>x/a</i>	<i>x/b</i>	<i>y/z</i>	U_{eq}^a	atom	<i>x/a</i>	<i>x/b</i>	<i>y/z</i>	U_{eq}^a
Rh(1)	58069(3)	18277(3)	38249(2)	272(1)	C(30)	6076(4)	714(4)	16(3)	416(21)
Rh(2)	56191(3)	40250(3)	28460(2)	276(1)	C(31)	7004(4)	-104(4)	-41(3)	423(21)
Ru(1)	72052(3)	9674(3)	6293(2)	316(1)	C(32)	8043(5)	58(4)	-326(3)	458(22)
Ru(2)	11003(3)	36271(3)	35130(2)	312(1)	C(33)	8130(4)	1055(4)	-545(3)	437(21)
Cl(1)	8480(1)	-79(1)	1423(1)	509(5)	C(34)	7188(4)	1864(4)	-462(3)	396(20)
Cl(2)	1310(1)	5157(1)	3815(1)	530(6)	C(35)	5146(4)	2613(4)	-130(3)	471(22)
N(1)	6083(3)	1021(3)	1627(2)	320(15)	C(36)	4160(5)	2399(5)	432(4)	596(26)
N(2)	7363(3)	2146(3)	1114(2)	287(14)	C(37)	4855(5)	3049(5)	-921(4)	675(29)
N(3)	5466(3)	1569(3)	2787(2)	272(13)	C(38)	9025(5)	-816(4)	-359(3)	575(25)
N(4)	6777(3)	3208(3)	2016(2)	269(13)	C(39)	596(4)	2434(4)	3149(3)	399(20)
N(5)	4130(3)	2389(3)	4238(2)	285(14)	C(40)	287(4)	3345(4)	2671(3)	415(20)
N(6)	4307(3)	3631(3)	2564(2)	279(13)	C(41)	-341(4)	4242(4)	2961(3)	435(21)
N(7)	2334(3)	2928(3)	4145(2)	320(14)	C(42)	-693(4)	4261(4)	3756(3)	458(22)
N(8)	2519(3)	3658(3)	2740(2)	328(14)	C(43)	-393(4)	3373(4)	4245(3)	424(21)
C(1)	6042(3)	1693(3)	2091(3)	285(16)	C(44)	263(4)	2472(4)	3949(3)	416(20)
C(2)	5455(4)	416(3)	2052(3)	335(18)	C(45)	1240(5)	1474(5)	2833(3)	560(25)
C(3)	5192(4)	-417(4)	1889(3)	424(21)	C(46)	2125(5)	1600(5)	2152(4)	697(30)
C(4)	4508(5)	-858(4)	2441(3)	505(24)	C(47)	482(6)	958(7)	2619(5)	1117(48)
C(5)	4084(4)	-489(4)	3139(3)	452(22)	C(48)	-1309(5)	5213(5)	4071(4)	664(28)
C(6)	4357(4)	317(4)	3316(3)	359(18)	C(49)	6357(4)	970(4)	4807(3)	343(18)
C(7)	5056(3)	767(3)	2766(3)	300(17)	C(50)	6432(4)	1941(4)	4787(3)	340(18)
C(8)	6687(3)	2395(3)	1760(2)	260(16)	C(51)	7592(4)	1949(4)	4371(3)	411(20)
C(9)	8001(3)	2815(3)	945(2)	279(16)	C(52)	7501(4)	1819(4)	3567(3)	390(19)
C(10)	8900(3)	2865(3)	363(3)	321(17)	C(53)	7407(4)	851(4)	3607(3)	389(19)
C(11)	9438(4)	3576(4)	371(3)	374(18)	C(54)	7457(4)	375(4)	4431(3)	394(19)
C(12)	9097(4)	4225(4)	924(3)	370(19)	C(55)	8224(4)	879(4)	4648(3)	464(21)
C(13)	8214(4)	4183(4)	1491(3)	332(18)	C(56)	4933(4)	4486(4)	3945(3)	374(19)
C(14)	7656(3)	3469(3)	1506(2)	285(16)	C(57)	4468(4)	5213(4)	3401(3)	420(20)
C(15)	3372(3)	2856(3)	3801(2)	277(16)	C(58)	5166(4)	5965(4)	3183(3)	456(21)
C(16)	3516(3)	2182(3)	4951(3)	288(16)	C(59)	6199(4)	5309(4)	2754(3)	381(19)
C(17)	3826(4)	1773(4)	5660(3)	357(18)	C(60)	6687(4)	4573(4)	3300(3)	342(18)
C(18)	3015(4)	1677(4)	6277(3)	392(19)	C(61)	5939(4)	4783(4)	4066(3)	395(20)
C(19)	1913(4)	1982(4)	6210(3)	412(20)	C(62)	5533(5)	5928(4)	3944(3)	505(23)
C(20)	1590(4)	2412(4)	5515(3)	373(18)	Cl(1S)	8324(6)	7421(5)	1863(4)	768(33)
C(21)	2404(4)	2503(3)	4893(2)	309(17)	Cl(3)	9737(2)	6882(2)	1785(1)	1002(11)
C(22)	3468(3)	3355(3)	3028(3)	282(16)	Cl(4)	7785(2)	7080(2)	1181(1)	954(10)
C(23)	3882(4)	4135(3)	1918(3)	290(16)	Cl(2Sa) ^b	1416(8)	7477(10)	3069(5)	518(32)
C(24)	4378(4)	4579(4)	1248(3)	362(18)	Cl(5a) ^b	2458(5)	7173(6)	2326(3)	1189(22)
C(25)	3751(4)	5044(4)	697(3)	421(20)	Cl(6a) ^b	2018(6)	7639(5)	3808(3)	1247(25)
C(26)	2642(4)	5079(4)	815(3)	468(21)	C(2Sb) ^b	1052(10)	7977(18)	2886(7)	1269(74)
C(27)	2131(4)	4648(4)	1477(3)	437(20)	Cl(5b) ^b	1166(5)	8204(5)	3778(3)	1299(25)
C(28)	2774(4)	4158(4)	2034(3)	333(17)	Cl(6b) ^b	2341(5)	7788(6)	2371(3)	1351(23)
C(29)	6139(4)	1723(4)	-198(3)	409(20)					

^a Equivalent isotropic U defined as one-third of the trace of the orthogonalized U_{ij} tensor. ^b These groups of atoms, involved in disorder, were refined with isotropic displacement parameters. The refined occupancy factors were 0.485(7) for a-labeled atoms and 0.515(7) for b-labeled ones.

Table 4. Selected Bond Distances (Å) and Angles (deg) for the Complex $[(\eta^6\text{-}p\text{-Cymene})\text{ClRu}(\mu\text{-Bbzim})\text{Rh}(\text{NBD})]_2\cdot 2\text{CH}_2\text{Cl}_2^a$

Ru(1)–N(1)	2.069(3)	Ru(2)–N(7)	2.074(4)
Ru(1)–N(2)	2.080(4)	Ru(2)–N(8)	2.077(3)
Ru(1)–Cl(1)	2.411(2)	Ru(2)–Cl(2)	2.406(2)
Ru(1)–G(1)	1.669(6)	Ru(2)–G(2)	1.669(6)
Ru(1)–C(29)	2.177(5)	Ru(2)–C(39)	2.205(7)
Ru(1)–C(30)	2.151(6)	Ru(1)–C(40)	2.171(6)
Ru(1)–C(31)	2.191(6)	Ru(2)–C(41)	2.190(5)
Ru(1)–C(32)	2.236(5)	Ru(2)–C(42)	2.222(5)
Ru(1)–C(33)	2.214(5)	Ru(1)–C(43)	2.194(5)
Ru(1)–C(34)	2.147(5)	Ru(2)–C(44)	2.155(6)
Rh(1)–Rh(2)	3.2448(6)		
Rh(1)–N(3)	2.128(4)	Rh(2)–N(4)	2.124(3)
Rh(1)–N(5)	2.116(3)	Rh(2)–N(6)	2.115(4)
Rh(1)–G(3)	1.988(5)	Rh(2)–G(5)	2.019(5)
Rh(1)–G(4)	2.030(4)	Rh(2)–G(6)	1.997(6)
Rh(1)–C(49)	2.097(5)	Rh(2)–C(56)	2.133(5)
Rh(1)–C(50)	2.114(5)	Rh(2)–C(57)	2.135(5)
Rh(1)–C(52)	2.151(5)	Rh(2)–C(59)	2.113(6)
Rh(1)–C(53)	2.139(4)	Rh(2)–C(60)	2.121(6)
N(1)–Ru(1)–N(2)	75.6(2)	N(7)–Ru(2)–N(8)	76.0(2)
N(1)–Ru(1)–Cl(1)	84.8(1)	N(7)–Ru(2)–Cl(2)	84.8(1)
N(2)–Ru(1)–Cl(1)	85.2(1)	N(8)–Ru(2)–Cl(2)	83.4(1)
N(1)–Ru(1)–G(1)	131.4(2)	N(7)–Ru(2)–G(2)	132.5(2)
N(2)–Ru(1)–G(1)	131.1(2)	N(8)–Ru(2)–G(2)	132.8(2)
Cl(1)–Ru(1)–G(1)	129.8(2)	Cl(2)–Ru(2)–G(2)	128.2(2)
N(3)–Rh(1)–N(5)	91.6(2)	N(4)–Rh(2)–N(6)	92.9(2)
N(3)–Rh(1)–G(4)	97.5(2)	N(4)–Rh(2)–G(6)	100.7(2)
G(3)–Rh(1)–G(4)	71.1(2)	G(5)–Rh(2)–G(6)	71.7(2)
N(5)–Rh(1)–G(3)	100.5(2)	N(6)–Rh(2)–G(5)	95.3(2)

^a G1 and G2 represent the centroids of the Ru(1) and Ru(2) *p*-cymene rings, respectively, and G3, G4, G5, and G6 the midpoints of the olefinic bonds C49–C50, C52–C53, C56–C57, and C59–C60, respectively.

labeling used. Atomic positional parameters and selected bond lengths and angles are presented in Tables 3 and 4, respectively. The molecule consists of two independent $(\eta^6\text{-}p\text{-cymene})\text{ClRu}(\mu\text{-Bbzim})\text{Rh}(\text{NBD})$ units related to each other by a *pseudo* C_2 axis which accounts for the observed ^1H NMR data. Each Bbzim^{2-} anion coordinates to the metals in an unsymmetrical quadridentate manner through the four nitrogen atoms of the two imidazolate rings, chelating to one Ru atom through two nitrogens and bonding in a unidentate manner to the two rhodiums through the other two nitrogens. The ruthenium atoms complete their pseudooctahedral coordination by an $\eta^6\text{-}p\text{-cymene}$ ligand and a chloride anion. The chelate N–Ru–N angles (N(1)–Ru(1)–N(2) 75.6(2), N(7)–Ru(2)–N(8) 76.0(2)°) compare well with those found in the related tetranuclear biimidazolate complex $[(\eta^5\text{-C}_5\text{Me}_5)\{\text{P}(\text{OEt})_3\}\text{Rh}(\mu\text{-Bim})\text{Rh}(\text{NBD})]_2[\text{ClO}_4]_2$ in which the Ru(III) atom also displays a pseudooctahedral coordination,^{10c} and the Bim^{2-} anion coordinates in a similar way to Bbzim^{2-} in **12**. However, these values are slightly lower than the N–Ru–N bond angle found in the RuIr complex $[(\eta^6\text{-}p\text{-cymene})(\text{PPh}_3)\text{Ru}(\mu\text{-Bbzim})\text{Ir}(\text{CO})_2]_2[\text{BF}_4]_2$ (**19**) in which, although the Ru atom is also pseudooctahedral, the Bbzim^{2-} anion chelates both metals (see below).

As a consequence of the asymmetry of coordination about the metal, both *p*-cymene rings show significantly different Ru–C bond distances ranging from 2.147(5) to 2.236(5) Å. The two distances of the Ru metals to the least-squares plane through the six-membered carbocyclic ring are 1.669(4) Å comparable to those found in related *p*-cymene ruthenium complexes with azolate-type ligands.^{10f,i,28} The Ru–N bond distances (mean value 2.075(2) Å) are significantly shorter than those found in the related bibenzimidazolate complex **19** (mean value 2.163(2) Å) (see below) and in the binuclear

biimidazolate complex $[(\text{Ph}_3\text{P})_2(\text{CO})\text{HRu}(\mu\text{-Bim})\text{Rh}(\text{COD})]$, 2.283(5) and 2.180(5) Å.^{8a} The Ru–Cl distances 2.411(2) and 2.406(2) Å are in the range of usual Ru(II)–Cl bond distances.²⁹

The coordination of the rhodiums, besides the two N atoms from the two Bbzim^{2-} ligands, involves a NBD molecule interacting through the two double bonds. The geometry around the rhodiums is approximately square planar with the plane defined by the two N atoms and the midpoints of the two olefinic bonds of the norborna-2,5-diene ligand. The rhodium atoms are out of these planes by +0.1803(5) (Rh(1)) and –0.1599(5) (Rh(2)) Å. These slight deviations of the metals from square planar coordination toward the other metal suggest some interaction between them, in spite of the relatively long Rh(1)–Rh(2) separation (3.2448(6) Å). The Rh–N bond distances (mean value 2.121(2) Å) are comparable to those found in related biimidazolate complexes in which the Bim^{2-} anion displays the same type of coordination.^{10c} The two $\text{C}_7\text{H}_4\text{N}_2$ moieties of each Bbzim^{2-} ligand are essentially planar, making dihedral angles of 14.8(1)° and 14.6(1)° with each other. This twist is probably due to the ligand behaving as both chelating and bridging. Consequently, in Bim^{2-} and Bbzim^{2-} compounds with this type of coordination dihedral angles ranging from 4.0 to 17.6° have been found.^{1c,9,10a,c}

The cationic complex **10** underwent reaction with the acetylacetonates $[\text{M}(\text{acac})\text{L}_2]$ ($\text{M} = \text{Rh}$; $\text{L}_2 = \text{COD}$, NBD, $(\text{CO})_2$. $\text{M} = \text{Ir}$; $\text{L}_2 = \text{COD}$) yielding the cationic polynuclear complexes $[(\eta^6\text{-}p\text{-cymene})(\text{PPh}_3)\text{Ru}(\mu\text{-Bbzim})\text{ML}_2]_n[\text{BF}_4]_n$ ($\text{M} = \text{Rh}$; $\text{L}_2 = \text{COD}$ (**15**), NBD (**16**), $(\text{CO})_2$ (**17**). $\text{M} = \text{Ir}$; $\text{L}_2 = \text{COD}$ (**18**)). Carbonylation of **18** afforded $[(\eta^6\text{-}p\text{-cymene})(\text{PPh}_3)\text{Ru}(\mu\text{-Bbzim})\text{Ir}(\text{CO})_2]_n[\text{BF}_4]_n$ (**19**) and, analogously, complex **17** could be obtained by carbonylation of complexes **15** or **16** (Scheme 2). Compounds **15–19** have been characterized by elemental analyses, IR, and ^1H and $^{31}\text{P}\{^1\text{H}\}$ NMR spectroscopies (see Experimental Section). All these complexes showed, in the IR spectra bands assignable to the Bbzim^{2-} ligand, BF_4^- anion under T_d symmetry and the triphenylphosphine group. The FAB mass spectra for complexes **15**, **16**, and **18** showed peaks assignable to the dinuclear $[(\eta^6\text{-}p\text{-cymene})(\text{PPh}_3)\text{Ru}(\mu\text{-Bbzim})\text{M}(\text{diolefin})]^+$ fragment and their NMR data were consistent with a binuclear structure ($n = 1$). Analogously, solution IR spectra for the carbonylated compounds **17** and **19** exhibited two $\nu(\text{CO})$ bands in the 2080–2000 cm^{-1} region characteristic of *cis*-dicarbonyl species, suggesting a binuclear structure. Interestingly, solid **19** is violet but it gives yellow solutions. This behavior could be indicative of important structural differences between the solid state and solution, and in order to unequivocally know the crystal structure of **19**, an X-ray diffraction study was undertaken.

Molecular Structure of $[(\eta^6\text{-}p\text{-Cymene})(\text{PPh}_3)\text{Ru}(\mu\text{-Bbzim})\text{Ir}(\text{CO})_2]_2[\text{BF}_4]$ (19**).** A view of the complex cation is shown in Figure 6 and atomic positional parameters and selected bond lengths and angles are presented in Tables 5 and 6, respectively. The cation is binuclear with a tetradentate bridging Bbzim ligand. In the solid state, a clear intermetallic interaction is established between two adjacent, symmetry related

(28) Oro, L. A.; García, M. P.; Carmona, D.; Foces-Foces, C.; Cano, F. H. *Inorg. Chim. Acta* **1985**, *96*, L21.

(29) Oro, L. A.; Carmona, D.; García, M. P.; Lahoz, F. J.; Reyes, J.; Foces-Foces, C.; Cano, F. H. *J. Organomet. Chem.* **1985**, *296*, C43 and references therein.

Table 5. Atomic Coordinates ($\times 10^4$; $\times 10^5$ for Ir and Ru Atoms) and Equivalent Isotropic Displacement Coefficients ($\text{\AA}^2 \times 10^3$; $\times 10^4$ for Ir, Ru, and P atoms) for $[(\eta^6\text{-}p\text{-Cymene})(\text{PPh}_3)\text{Ru}(\mu\text{-Bbzim})\text{Ir}(\text{CO})_2]\text{BF}_4$

atom	<i>x/a</i>	<i>y/b</i>	<i>z/c</i>	<i>U_{eq}^a</i>
Ir(1)	-6553(2)	51156(2)	41920(2)	387(1)
Ru(1)	31836(1)	43818(3)	26951(3)	312(2)
P	1980(2)	4682(1)	1562(1)	351(7)
N(1)	83(5)	4268(3)	3737(3)	37(2)
N(2)	1672(5)	3965(3)	3135(3)	33(2)
N(3)	910(5)	5529(3)	3862(3)	35(2)
N(4)	2487(4)	5238(3)	3235(3)	31(2)
O(1)	-1559(5)	6373(3)	4755(4)	64(2)
O(2)	-2833(5)	4416(3)	4471(4)	70(3)
C(1)	-1200(7)	5898(5)	4536(5)	48(3)
C(2)	-1999(8)	4691(5)	4374(5)	51(3)
C(3)	1105(6)	4420(3)	3488(4)	33(3)
C(4)	-52(6)	3620(4)	3524(4)	39(3)
C(5)	-959(7)	3185(4)	3607(5)	50(3)
C(6)	-870(8)	2576(5)	3314(6)	68(4)
C(7)	90(8)	2386(4)	2932(5)	56(3)
C(8)	1001(7)	2800(4)	2849(5)	46(3)
C(9)	919(6)	3424(3)	3140(4)	35(3)
C(10)	1528(6)	5066(3)	3555(4)	34(3)
C(11)	1530(6)	6097(4)	3756(4)	35(3)
C(12)	1335(7)	6730(4)	3960(4)	48(3)
C(13)	2123(8)	7189(4)	3761(5)	57(4)
C(14)	3127(7)	7021(4)	3399(5)	55(3)
C(15)	3339(7)	6388(4)	3207(4)	43(3)
C(16)	2527(6)	5915(3)	3380(4)	32(3)
C(17)	4377(6)	3848(4)	3598(5)	38(3)
C(18)	4066(6)	3457(4)	2923(5)	43(3)
C(19)	4280(6)	3654(4)	2180(5)	47(3)
C(20)	4779(6)	4268(4)	2042(5)	46(3)
C(21)	5016(6)	4682(4)	2695(5)	44(3)
C(22)	4829(6)	4465(4)	3453(5)	39(3)
C(23)	4165(7)	3595(4)	4385(5)	51(3)
C(24)	5007(8)	3027(5)	4621(6)	73(4)
C(25)	4247(7)	4113(5)	5012(5)	66(4)
C(26)	5075(7)	4457(5)	1240(5)	71(4)
C(27)	2289(7)	5466(4)	1129(4)	40(3)
C(28)	1488(7)	5750(4)	562(5)	51(3)
C(29)	1764(8)	6344(4)	241(5)	59(4)
C(30)	2802(8)	6652(4)	452(5)	61(4)
C(31)	3558(9)	6385(4)	1008(5)	67(4)
C(32)	3315(7)	5796(4)	1360(5)	53(3)
C(33)	2020(6)	4080(4)	786(5)	42(3)
C(34)	2217(8)	4246(5)	21(5)	62(4)
C(35)	2304(10)	3759(6)	-512(5)	92(5)
C(36)	2166(11)	3121(6)	-327(7)	100(6)
C(37)	1971(9)	2954(5)	424(7)	85(5)
C(38)	1918(7)	3432(4)	964(6)	58(4)
C(39)	443(6)	4767(4)	1724(4)	37(3)
C(40)	-320(7)	4243(4)	1624(5)	51(3)
C(41)	-1448(7)	4319(5)	1814(6)	63(4)
C(42)	-1812(8)	4892(6)	2102(6)	73(4)
C(43)	-1061(7)	5413(5)	2195(5)	58(3)
C(44)	73(6)	5350(4)	2010(4)	46(3)
B	3505(9)	1655(6)	2233(8)	64(5)
F(1)	2345(6)	1688(3)	2028(5)	125(4)
F(2)	3832(6)	1050(3)	2131(6)	163(5)
F(3)	4048(6)	2076(3)	1816(5)	128(4)
F(4)	3623(8)	1844(5)	2964(4)	167(5)

^a Equivalent isotropic *U* defined as one-third of the trace of the orthogonalized *U_{ij}* tensor.

bond distances (2.118(6) and 2.126(6) Å) are of the same order as those found in the Ir(III) complex $[(\eta^5\text{-C}_5\text{-Me}_5)\text{Ir}(\text{H}_2\text{Bim})\text{Cl}]\text{Cl}$,³² although slightly longer bonds lengths might be anticipated for Ir(I)-N due to the larger Ir(I) ionic radius. The geometry about the *cis*-Ir(CO)₂ moiety closely resembles that found in related *cis*-dicarbonyl azolate iridium complexes.^{10i,33}

Catalytic Hydrogenation. The homogeneous catalytic activity of the heteronuclear complexes **11**, **14**, and **15-19** for the hydrogenation of cyclohexene with molecular hydrogen was explored. Preliminary hydrogenation runs were performed in methanol at different H₂

Table 6. Selected Bond Distances (Å) and Angles (deg) for the Complex $[(\eta^6\text{-}p\text{-Cymene})(\text{PPh}_3)\text{Ru}(\mu\text{-Bbzim})\text{Ir}(\text{CO})_2]\text{BF}_4$

Ir(1)-Ir(1')	3.081(1)	Ir(1)-N(1)	2.118(6)
Ir(1)-N(3)	2.126(6)	Ir(1)-C(1)	1.841(9)
Ir(1)-C(2)	1.836(9)	O(1)-C(1)	1.137(11)
O(2)-C(2)	1.144(11)	Ru(1)-N(4)	2.175(6)
Ru(1)-N(2)	2.150(6)	Ru(1)-P	2.371(2)
Ru(1)-C(17)	2.263(7)	Ru(1)-C(18)	2.172(8)
Ru(1)-C(19)	2.198(8)	Ru(1)-C(20)	2.264(8)
Ru(1)-C(21)	2.210(7)	Ru(1)-C(22)	2.215(7)
Ru(1)-G	1.716(7)		
N(1)-Ir(1)-N(3)	81.0(2)	N(3)-Ir(1)-C(1)	93.8(3)
N(1)-Ir(1)-C(2)	93.0(3)	C(1)-Ir(1)-C(2)	92.1(4)
P-Ru(1)-N(2)	87.6(2)	P-Ru(1)-N(4)	86.0(1)
N(2)-Ru(1)-N(4)	79.8(2)	P-Ru(1)-G	131.7(3)
N(2)-Ru(1)-G	125.7(3)	N(4)-Ru(1)-G	129.3(3)
N(1)-Ir(1)-Ir(1')	91.5(2)	N(3)-Ir(1)-Ir(1')	86.7(1)
C(1)-Ir(1)-Ir(1')	89.9(2)	C(2)-Ir(1)-Ir(1')	97.3(3)

^a G represents the centroid of the *p*-cymene ring.

Table 7. Catalytic Hydrogenation of Cyclohexene^a

catalyst	<i>P</i> (H ₂) (atm)	<i>T</i> (K)	time (min)	% cyclohexane
$[(\eta^6\text{-}p\text{-cymene})\text{CIRu}(\mu\text{-Bbzim})\text{Rh}(\text{COD})]$ (11)	2	313	105	98.0
	2.5	293	105	36.2
	3	313	90	100.0
$[(\eta^6\text{-}p\text{-cymene})\text{CIRu}(\mu\text{-Bbzim})\text{Ir}(\text{COD})]$ (14)	3	323	25	100.0
	2	293	90	37.4
	2	313	90	100.0
$[(\eta^6\text{-}p\text{-cymene})(\text{PPh}_3)\text{Ru}(\mu\text{-Bbzim})\text{Rh}(\text{COD})]\text{BF}_4$ (15)	3	313	30	70.0
	2	293	75	14.9
	2.6	293	120	5.1
$[(\eta^6\text{-}p\text{-cymene})(\text{PPh}_3)\text{Ru}(\mu\text{-Bbzim})\text{Rh}(\text{NBD})]\text{BF}_4$ (16)	3	313	90	19.0
	3	323	120	62.3
	2.5	293	105	8.5
$[(\eta^6\text{-}p\text{-cymene})(\text{PPh}_3)\text{Ru}(\mu\text{-Bbzim})\text{Ir}(\text{COD})]\text{BF}_4$ (17)	2	293	90	7.6
	3	313	60	8.0
	3	323	120	43.0
$[(\eta^6\text{-}p\text{-cymene})(\text{PPh}_3)\text{Ru}(\mu\text{-Bbzim})\text{Ir}(\text{CO})_2]\text{BF}_4$ (19)	2	293	2400	67.9

^a [catalyst] = 5.6 $\times 10^{-4}$ M; [cyclohexene]/[catalyst] = 100; preactivation period: 30 min.

pressure and temperature and the data are collected in Table 7. No reduction of cyclohexene was observed either at atmospheric pressure, or under a N₂ atmosphere, the last fact showing that hydrogen transfer from methanol does not represent an important mechanistic pathway in the processes. According to the data of Table 7, the neutral compounds **11** and **14** are more active than the cationic complexes **15-19**, the best results being obtained with complex **14**. We then studied the catalytic activity of **14** in some detail.

The reaction shows an induction period that disappears by treating the solution of **14** with hydrogen during 30 min at 313 K. The reaction profiles do not change significantly when this period is increased from 30 to 90 min. Figure 7 summarizes the course of a typical reaction catalyzed by hydrogen-pretreated **14** at different hydrogen pressures (see Experimental Section).

The reaction was followed by measuring the cyclohexane formed as a function of time. Although no deactivation was observed up to ca. 70-80% conversion, the data correspond to cyclohexane percentages below 30% in order to perform a kinetic analysis based on the initial rates method. Values for initial rates under different reaction conditions are collected in Table 8. The results of varying the concentration of the substrate

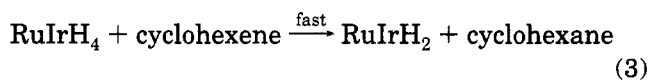
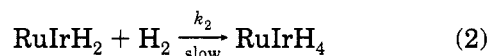
while all the other concentrations were kept constant showed that the rate of the catalytic process is independent of the substrate concentration. However, plots of the $\log(-d[\text{cyclohexene}]/dt)$ versus $\log[14]$ and $\log[\text{H}_2]$ yielded straight lines of slope 0.95 and 1.96, respectively, showing that the reduction of cyclohexene is first-order in catalyst concentration and second-order in hydrogen pressure. The catalytic rate law therefore is

$$-d[\text{cyclohexene}]/dt = k_{\text{cat}}[14][\text{H}_2]^2$$

The value of the catalytic rate constant at 313 K was calculated from this rate law as $2.3 \pm 0.2 \text{ s}^{-1} \text{ M}^{-2}$.

We also proved that in the presence of variable concentrations of chloride ions the hydrogenation rate does not change significantly. The effect of temperature on the rate constant was studied in the range 313–333 K for concentrations of cyclohexene at $5.6 \times 10^{-2} \text{ M}$, catalyst at $5.6 \times 10^{-4} \text{ M}$, and at 2 atm of hydrogen pressure. Within the range of temperatures used, the variation of the hydrogen solubility in methanol is negligible.³⁴ An Arrhenius plot allowed us to evaluate the activation energy E_a , 59.8 kJ/mol, and the values of ΔH^\ddagger , 58.5 kJ/mol, and ΔS^\ddagger , -3.1 eu, and free energy of activation, ΔG^\ddagger , 62.7 kJ/mol.

The ^1H NMR spectrum in CD_3OD of a sample of **14** treated with hydrogen (2 atm, 313 K, 30 min) showed the presence of hydrogenated *p*-cymene and COD groups, and no high field NMR signals were detected from 213 K (the limiting solubility temperature) to room temperature. Thus, during the preactivation period the *p*-cymene and COD ligands are hydrogenated and displaced from the coordination sphere of the metals rendering quantitatively unsaturated species without chloride dissociation (RuIr). Most probably, these species reacted with hydrogen leading to the true catalyst (RuIrH_2). The fact that the rate of hydrogenation is independent of the cyclohexene concentration indicates that the olefin is not involved in either the rate-determining step of the catalytic cycle or in a previous step. Consequently, we propose the reaction with hydrogen as the initial step of the catalytic cycle. From these considerations, the following set of reactions could be operating in the catalytic cycle:



If the rate-determining step of the catalytic cycle is reaction 2, the rate of formation of cyclohexane will be

$$d[\text{cyclohexane}]/dt = d[\text{RuIrH}_4]/dt = k_2[\text{RuIrH}_2][\text{H}_2]$$

$$d[\text{cyclohexane}]/dt = k_2 K_1 [14][\text{H}_2]^2$$

in good agreement with the kinetic measurements.

Very recently, one of us has reported that the bimidozolate bridged RuIr compound $[\text{H}(\text{CO})(\text{PPh}_3)_2\text{Ru}(\mu\text{-Bim})\text{Ir}(\text{COD})]$ catalyzes the reduction of cyclohexene by molecular hydrogen and, on the basis of kinetic and spectroscopic data, it has been proposed that the reduc-

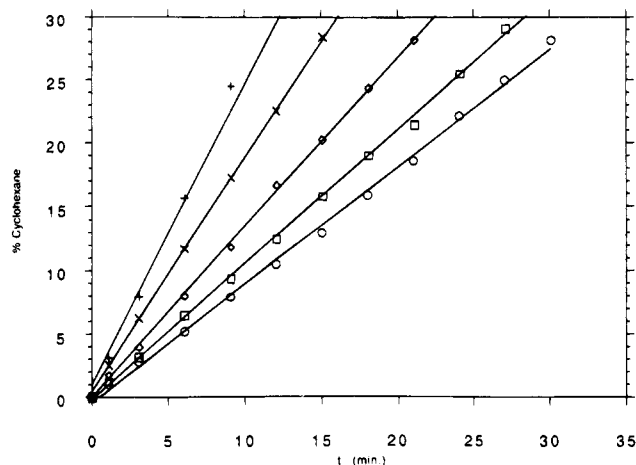


Figure 7. Hydrogenation of cyclohexene by complex **14** at different pressures: (○) 1.8 atm, (□) 2.0 atm, (◇) 2.2 atm, (×) 2.6 atm, (+) 3.0 atm. $[14] = 5.6 \times 10^{-4} \text{ M}$. $[\text{Cyclohexene}] = 5.6 \times 10^{-2} \text{ M}$. Solvent: methanol. $V_{\text{tot}} = 15 \text{ mL}$. $T = 313 \text{ K}$.

Table 8. Kinetic Data for the Hydrogenation of Cyclohexene Catalyzed by $[(\eta^6\text{-}p\text{-cymene})\text{CIRu}(\mu\text{-Bzim})\text{Ir}(\text{COD})]$ (**14**)^a

$10^4[14]$ (M)	$10^2[\text{cyclohexene}]$ (M)	$10^3[\text{H}_2]$ (M)	$P(\text{H}_2)$ (atm)	$10^3[\text{Cl}^-]$ (M)	$10^7 r_i$ (M s^{-1})	T (K)
5.6	5.6	8.5	2.0	—	0.98	313
8.3	5.6	8.5	2.0	—	1.39	313
9.7	5.6	8.5	2.0	—	1.62	313
11.1	5.6	8.5	2.0	—	1.93	313
5.6	5.6	7.7	1.8	—	0.84	313
5.6	5.6	9.4	2.2	—	1.23	313
5.6	5.6	11.1	2.6	—	1.70	313
5.6	5.6	12.7	3.0	—	2.25	313
5.6	11.1	8.5	2.0	—	0.81	313
5.6	16.6	8.5	2.0	—	1.01	313
5.6	22.2	8.5	2.0	—	0.85	313
5.6	11.1	12.7	3.0	—	2.19	313
5.6	16.6	12.7	3.0	—	2.41	313
5.6	22.2	12.7	3.0	—	2.02	313
5.6	5.6	8.5	2.0	0.17	0.85	313
5.6	5.6	8.5	2.0	0.33	0.83	313
5.6	5.6	8.5	2.0	0.50	0.94	313
5.6	5.6	8.5	2.0	1.20	0.98	313
5.6	5.6	8.7	2.0	—	1.43	318
5.6	5.6	9.0	2.0	—	2.28	323
5.6	5.6	9.4	2.0	—	4.49	333

^a r_i = initial rates.

tion mainly proceeds via the ruthenium atom, while the same process catalyzed by $[\text{H}(\text{CO})(\text{PPh}_3)_2\text{Ru}(\mu\text{-pz})_2\text{Ir}(\text{TfB})]$ (TfB = tetrafluoro[5.6]bicyclo[2.2.2]octan-2,5,7-triene), under similar conditions, operates through the iridium.^{8b} Interestingly, the results that we now report

(30) (a) Angoletta, M.; Ciani, G.; Manassero, M.; Sansoni, M. *J. Chem. Soc., Chem. Commun.* **1973**, 789. (b) Demartin, F.; Manassero, M.; Sansoni, M.; Garlaschelli, L.; Raimondi, C.; Martinengo, S. *J. Chem. Soc., Chem. Commun.* **1981**, 528. (c) Rasmussen, P. G.; Anderson, J. E.; Bailey, O. H.; Tamres, M.; Bayón, J. C. *J. Am. Chem. Soc.* **1985**, *107*, 279. (d) Ciriano, M. A.; Sebastián, S.; Oro, L. A.; Tiripicchio, A.; Tiripicchio Camellini, M.; Lahoz, F. *J. Angew. Chem. Int. Ed. Engl.* **1988**, *27*, 402. (e) Einstein, F. W. B.; Jones, R. H.; Zhang, X.; Yan, X.; Nagelkerke, R.; Sutton, D. *J. Chem. Soc., Chem. Commun.* **1989**, 1424. (f) Beringhelli, T.; Ciani, G.; D'Alfonso, G.; Garlaschelli, L.; Moret, M.; Sironi, A. *J. Chem. Soc., Dalton Trans.* **1992**, 1865.

(31) (a) Haddad, M. S.; Duesler, E. N.; Hendrickson, D. N. *Inorg. Chem.* **1979**, *18*, 141. (b) Usón, R.; Oro, L. A.; Gimeno, J.; Ciriano, M. A.; Cabeza, J. A.; Tiripicchio, A.; Tiripicchio-Camellini, M. *J. Chem. Soc., Dalton Trans.* **1983**, 323.

(32) Ziessel, R.; Youinou, M.-T.; Balegroune, F.; Grandjean, D. *J. Organomet. Chem.* **1992**, *441*, 143.

(33) (a) Rasmussen, P. G.; Bailey, O. H.; Bayón, J. C.; Butler, W. M. *Inorg. Chem.* **1984**, *23*, 343. (b) Nussbaum, S.; Rettig, S. J.; Storr, A.; Trotter, J. *Can. J. Chem.* **1985**, *63*, 692.

(34) Katayama, T.; Nitta, T. *J. Chem. Eng. Data* **1976**, *21*, 2.

are indicative that in the RuIr complex **14** both metals could be active for the hydrogenation process. In this context, it is therefore of interest to mention that the parent complexes $[(\eta^6\text{-}p\text{-cymene})\text{RuCl}(\text{HBzim})]$ and $[\text{Ir}(\text{HBzim})(\text{COD})]$ are inactive for the hydrogenation of cyclohexene even under forcing conditions.

Conclusions

In this paper we report the preparation and characterization of a family of bi- and tetranuclear RuRh or RuIr complexes with biimidazolate or bibenzimidazolate anions, as bridging ligands. We have isolated and elucidated the structure of the heterobinuclear species $[(\eta^6\text{-}p\text{-cymene})\text{ClRu}(\mu\text{-HBim})\text{MClL}_2]$ (**3–5**) and $[(\eta^6\text{-}p\text{-cymene})\text{Ru}(\text{acac})(\mu\text{-HBim})\text{Rh}(\text{COD})]^+$ (**7, 8**) that could be considered as intermediates in the synthesis of $\mu\text{-Bim}^{2-}$ derivatives as has been demonstrated by preparing **6** from **4**. Complexes **3–5** showed a dynamic behavior for which we suggest a dissociative mechanism via deprotonation of the NH group and loss of the chlorine atom attached to M. From NMR measurements, we have calculated the energy barrier for this process, 54 kJ mol⁻¹, for complex **3**. We have spectroscopically characterized two isomers of the tetracarbonyl complex **6** and studied an isomerization process between them, unprecedented in the chemistry of biimidazolate complexes. In solution, at room temperature, the Rh-(HBim)(COD) unit of complexes **7** and **8** rotates fast around the Ru–N bond but this process collapses at 223 K. It is remarkable that H₂Bim and H₂Bzim (free or coordinated) react differently with (*p*-cymene)Ru compounds. The greater acidity of H₂Bzim or its derivatives accounts for the observed results. The factors that govern the nuclearity of heteronuclear bi- or bibenzimidazolate compounds remain unclear. Even, in some cases, intermetallic interactions could be responsible for the increase in nuclearity, in the solid state, as has been observed in complex **19**. Finally, complexes **11, 14**, and **15–19** are active catalysts for the homogeneous hydrogenation of cyclohexene by molecular hydrogen at low pressures. Kinetic and spectroscopic studies conclude that the hydrogenation catalyzed by complex **14** operates through the hydride route and follows the kinetic rate law: $-d[\text{cyclohexene}]/dt = k_{\text{cat}}[\mathbf{14}][\text{H}_2]^2$.

Experimental Section

General Considerations. All solvents were dried over appropriate drying agents, distilled under nitrogen, and degassed prior to use. All preparations have been carried out under nitrogen. Cyclohexene (Merck) was passed through an alumina column.

Physical Measurements. ¹H, ¹³C, and ³¹P NMR spectra were recorded on a Varian UNITY 300 (299.949 (1H), 75.4 (13C) and 121.421 (31P) MHz) and a Varian XL-200 (200.0 (1H), 50.3 (13C) and 80.9 (31P) MHz) using SiMe₄ (1H, ¹³C) and 85% H₃PO₄ in D₂O (31P) as external standards. Chemical shifts are expressed in ppm up field from SiMe₄ (1H, ¹³C) or H₃PO₄ (31P).

Preparation of $[(\eta^6\text{-}p\text{-Cymene})\text{Ru}(\text{H}_2\text{Bim})\text{Cl}]\text{Cl}$ (1**).** To a red suspension of $[(\eta^6\text{-}p\text{-cymene})\text{RuCl}_2(\mu\text{-Cl})_2]$ (306.2 mg, 0.50 mmol) in acetone (30 mL) was added H₂Bim (134.2 mg, 1.00 mmol). The resulting yellow solution was stirred during 4 h and then vacuum-concentrated to 5 mL. The slow precipitation of a yellow solid was observed. The precipitation was completed by addition of diethyl ether (20 mL). The solid was collected, washed with diethyl ether, and dried under vacuum. Yield: 94%. $\Lambda_{\text{M}}(\text{CH}_3\text{COCH}_3) = 2.15 \text{ ohm}^{-1} \text{ cm}^2 \text{ mol}^{-1}$, $\Lambda_{\text{M}}(\text{MeOH}) = 87.2 \text{ ohm}^{-1} \text{ cm}^2 \text{ mol}^{-1}$. IR (Nujol): $\nu(\text{NH})$

3300–2250 (br); $\nu(\text{RuCl})$ 300(m) cm⁻¹. Anal. Calcd for C₁₆H₂₀N₄Cl₂Ru: C, 43.6; H, 4.5; N, 12.7. Found: C, 43.7; H, 4.6; N, 12.85. ¹H NMR (CD₃COCD₃, δ) 13.89 (2H, br s, NH), 7.41, 7.15 (2H each, s, CH's of H₂bim), 5.64, 5.46 (AA'BB' system of *p*-cymene, $J_{\text{AB}} = J_{\text{A'B'}} = 6.1 \text{ Hz}$), 2.69 (1H, sp, ³J_{HH} = 6.8 Hz, CH of ¹Pr), 2.15 (3H, s, Me), 1.08 (6H, d, Me of ¹Pr). ¹³C NMR (CD₃COCD₃, δ) 138.8 (t, $J_{\text{CH}} = 8.0 \text{ Hz}$, C_{2/2'} of H₂-Bim), 130.3 (ddd, ¹J_{CH} = 194.7 Hz, ²J_{CH} = 10.8 Hz, ³J_{CH} = 4.8 Hz, C_{4/4'} of H₂Bim), 119.7 (dd, ¹J_{CH} = 197.2 Hz, ²J_{CH} = 13.5 Hz, C_{5/5'} of H₂Bim), 103.0, 100.0 (s, C_{1/4} of *p*-cymene), 82.9 (d, ¹J_{CH} = 173.1 Hz, C_{2/6} or C_{3/5} of *p*-cymene), 81.2 (d, ¹J_{CH} = 167.5 Hz, C_{3/5} or C_{2/6} of *p*-cymene), 31.0 (d, ¹J_{CH} = 130.7 Hz, C₇ of *p*-cymene), 22.1 (q, ¹J_{CH} = 127.9 Hz, C_{8/9} of *p*-cymene), 18.9 (q, ¹J_{CH} = 130.1 Hz, C₁₀ of *p*-cymene). FAB MS *m/z* (*m*-nitrobenzyl alcohol) 405 (M⁺, 30%), 369 (M⁺ – Cl, 100%).}}}}}}}}}}}

Preparation of $[(\eta^6\text{-}p\text{-Cymene})\text{Ru}(\text{H}_2\text{Bim})\text{Cl}]\text{BF}_4$ (2**).** To a solution of **1** (174.0 mg, 0.39 mmol) in methanol (30 mL) was added NaBF₄ (93.3 mg, 0.78 mmol). The solution was stirred during 13 h and then evaporated to dryness. The residue was dissolved in dichloromethane (3 × 20 mL) and filtered. The filtrate was concentrated under reduced pressure to ca. 2 mL and the slow addition of diethyl ether gave a yellow solid, which was filtered off, washed with diethyl ether, and dried under vacuum. Yield 85%. $\Lambda_{\text{M}}(\text{CH}_3\text{COCH}_3) = 58.2 \text{ ohm}^{-1} \text{ cm}^2 \text{ mol}^{-1}$, $\Lambda_{\text{M}}(\text{MeOH}) = 79.0 \text{ ohm}^{-1} \text{ cm}^2 \text{ mol}^{-1}$. IR (Nujol): $\nu(\text{NH})$ 3650–2450 (br); $\nu(\text{RuCl})$ 300 (m); BF₄⁻ 1100 (vs), 520 (s) cm⁻¹. Anal. Calcd for C₁₆H₂₀N₄BF₄ClRu: C, 39.1; H, 4.1; N, 11.4. Found: C, 39.9; H, 4.5; N, 11.6. ¹H NMR (CD₃COCD₃, δ) 7.45, 7.17 (2H each, s, CH's of H₂bim), 6–8 (2H, br, NH), 5.68, 5.46 (AA'BB' system of *p*-cymene, $J_{\text{AB}} = J_{\text{A'B'}} = 6.0 \text{ Hz}$), 2.71 (1H, sp, ³J_{HH} = 6.9 Hz, CH of ¹Pr), 2.16 (3H, s, Me), 1.10 (6H, d, Me of ¹Pr).}

Preparation of $[(\eta^6\text{-}p\text{-Cymene})\text{ClRu}(\mu\text{-HBim})\text{RhCl}(\text{COD})]$ (3**).** To a solution of **1** (150.0 mg, 0.34 mmol) in methanol (30 mL) was added [Rh(acac)(COD)] (106.0 mg, 0.34 mmol). The resulting yellow solution was stirred during 4 h. The precipitation of a yellow solid was completed by addition of diethyl ether. The solid was filtered off, washed with diethyl ether, and dried under vacuum. Yield 87%. $\Lambda_{\text{M}}(\text{CH}_3\text{COCH}_3) = 4.45 \text{ ohm}^{-1} \text{ cm}^2 \text{ mol}^{-1}$. IR (Nujol): $\nu(\text{NH})$ 3350 (s); $\nu(\text{MCl})$ 280 (m); cm⁻¹. Anal. Calcd for C₂₄H₃₁N₄Cl₂RhRu: C, 44.4; H, 4.8; N, 8.6. Found: C, 44.1; H, 4.8; N, 8.6.

Complexes **4** and **5** were similarly prepared. Complex **4**: Yellow-orange solid, yield: 69%. $\Lambda_{\text{M}}(\text{CH}_3\text{COCH}_3) = 2.54 \text{ ohm}^{-1} \text{ cm}^2 \text{ mol}^{-1}$. IR (Nujol): $\nu(\text{NH})$ 3220 (s); $\nu(\text{MCl})$ 290 (m), 320 (m); $\nu(\text{CO})$ (CH₂Cl₂) 2075 (s), 2001 (s) cm⁻¹. Anal. Calcd for C₁₈H₁₉N₄Cl₂O₂RhRu: C, 36.1; H, 3.2; N, 9.4. Found: C, 35.8; H, 3.1; N, 9.1. ¹H NMR (CDCl₃, δ) 7.40, 7.35, 7.18, 7.04 (1H each, br s, CH's of HBim), 5.58, 5.38 (AA'BB' system of *p*-cymene, $J_{\text{AB}} = J_{\text{A'B'}} = 6.1 \text{ Hz}$), 2.74 (1H, sp, ³J_{HH} = 6.8 Hz, CH of ¹Pr), 2.19 (3H, s, Me), 1.14 (6H, d, Me of ¹Pr).}

Compound **4** can be alternatively prepared by bubbling carbon monoxide for 2 h through dichloromethane solutions of **3**. The resulting solution was filtered and then concentrated under reduced pressure to ca. 2 mL. Slow addition of diethyl ether gave the yellow-orange solid **4**. Yield: 60%.

Complex **5**: yellow solid, yield: 79%. $\Lambda_{\text{M}}(\text{CH}_3\text{COCH}_3) = 17.95 \text{ ohm}^{-1} \text{ cm}^2 \text{ mol}^{-1}$. IR (Nujol): $\nu(\text{NH})$ 3330 (s); $\nu(\text{MCl})$ 285 (m) cm⁻¹. Anal. Calcd for C₂₄H₃₁N₄Cl₂IrRu: C, 39.0; H, 4.2; N, 7.6. Found: C, 38.2; H, 4.1; N, 7.6. ¹H NMR (CD₃COCD₃, δ) 11.52 (1H, br, NH), 7.63, 7.2, 7.1 (4H, br, CH's of HBim), 5.83, 5.62 (AA'BB' system of *p*-cymene, $J_{\text{AB}} = J_{\text{A'B'}} = 6.4 \text{ Hz}$), 2.64 (1H, sp, ³J_{HH} = 6.9 Hz, CH of ¹Pr), 2.15 (3H, s, Me), 1.06 (6H, d, Me of ¹Pr).}

Preparation of $[(\eta^6\text{-}p\text{-Cymene})\text{ClRu}(\mu\text{-Bim})\text{Rh}(\text{CO})_2]$ (6**).** To a suspension of **4** (200.0 mg, 0.33 mmol) in methanol (30 mL) was added KOH (1.18 mL, 0.286 mol L⁻¹, 0.33 mmol). Within a few seconds the suspension became a red solution which was stirred for 30 min and vacuum evaporated to dryness. The residue was extracted with dichloromethane (3 × 20 mL) and then filtered. The filtrate was concentrated under reduced pressure to ca. 2 mL. Addition of diethyl ether

led to the precipitation of a red-orange solid which was filtered off, washed with diethyl ether, and vacuum dried. Yield: 82%. IR (CH₂Cl₂): $\nu(\text{CO})$ 2080 (s), 2060 (s), 2010 (s) cm⁻¹. Anal. Calcd for C₁₈H₁₈N₄ClO₂RhRu: C, 38.5; H, 3.2; N, 10.0. Found: C, 38.4; H, 3.2; N, 10.2. ¹H NMR (CDCl₃, δ) **6a** or **6c**: 7.24, 6.85 (4H each, s, CH's of Bim), 5.39, 5.25 (4H each, AA'BB' system of *p*-cymene, $J_{AB} = J_{A'B'} = 5.9$ Hz), 2.55 (2H, sp, ³J_{HH} = 7.0 Hz, CH of ⁱPr), 2.08 (6H, s, Me), 0.94 (12H, d, Me of ⁱPr). **6b**: 7.21, 7.19, 6.86, 6.80 (2H each, s, CH's of Bim), 5.43, 5.37, 5.29, 5.15, (two AA'BB' systems of *p*-cymene, $J_{AB} = J_{A'B'} = 6.8$ Hz), 2.78, 2.59 (1H each, sp, ³J_{HH} = 6.8 Hz, CH of ⁱPr), 2.19, 1.65 (3H each, s, Me), 1.11, 1.02 (6H each, d, Me of ⁱPr). FAB MS *m/z* (*m*-nitrobenzyl alcohol) 1124 (M⁺, 10%), 1088 (M⁺ - Cl, 95%), 527 (¹/₂M⁺ - Cl, 100%), 471 (¹/₂M⁺ - Cl - 2CO, 50%).

Preparation of [(η^6 -*p*-Cymene)Ru(acac)(μ -HBim)Rh(COD)]Cl (7**).** To a suspension of [(η^6 -*p*-cymene)Ru(acac)Cl] (150.0 mg, 0.40 mmol) in methanol (30 mL) was added [Rh(HBim)(COD)] (140.0 mg, 0.40 mmol). The resulting yellow solution was stirred during 3 h and then filtered. The filtrate was worked up as above and a yellow solid was collected. Yield: 75%. $\Lambda_M(\text{CH}_3\text{COCH}_3) = 90.7$ ohm⁻¹ cm² mol⁻¹. IR (Nujol): $\nu(\text{NH})$ 3320 (ν br); $\nu(\text{CO})$ 1580 (s), 1520 (s) cm⁻¹. Anal. Calcd for C₂₉H₃₈N₄ClO₂RhRu: C, 48.8; H, 5.4; N, 7.9. Found: C, 48.1; H, 6.2; N, 7.7. FAB MS *m/z* (*m*-nitrobenzyl alcohol) 679 (M⁺, 55%), 335 (M⁺ - COD - Rh - Bim, 100%).

Preparation of [(η^6 -*p*-Cymene)Ru(acac)(μ -HBim)Rh(COD)]BF₄ (8**).** To a solution of **7** (125.0 mg, 0.17 mmol) in methanol (30 mL) was added NaBF₄ (62.0 mg, 0.51 mmol). The solution was stirred during 17 h and vacuum evaporated to dryness. The residue was extracted with dichloromethane (3 \times 20 mL), filtered, and worked up as above and a yellow solid was collected. Yield: 56%. $\Lambda_M(\text{CH}_3\text{COCH}_3) = 129.8$ ohm⁻¹ cm² mol⁻¹. IR (Nujol): $\nu(\text{NH})$ 3280 (ν br); $\nu(\text{CO})$ 1575 (s), 1520 (s); BF₄⁻ 1100 (ν s), 520 (s) cm⁻¹. Anal. Calcd for C₂₉H₃₈N₄O₂BF₄RhRu: C, 45.5; H, 5.0; N, 7.3. Found: C, 45.7; H, 4.9; N, 7.3. FAB MS *m/z* (*m*-nitrobenzyl alcohol) 679 (M⁺, 100%).

Preparation of [(η^6 -*p*-Cymene)Ru(HBbzim)Cl] (9**).** To a red suspension of [(η^6 -*p*-cymene)Ru(acac)Cl] (200.0 mg, 0.53 mmol) in acetone was added H₂Bbzim (126.8 mg, 0.53 mmol). After stirring for 24 h the solvent was vacuum-evaporated to dryness. The residue was extracted with chloroform and filtered. The filtrate was worked up as above and an orange solid was collected. Yield: 89%. IR (Nujol): $\nu(\text{NH})$ 3200–2200 (ν br); $\nu(\text{RuCl})$ 290 (m) cm⁻¹. Anal. Calcd for C₂₄H₂₃N₄ClRu: C, 57.2; H, 4.6; N, 11.1. Found: C, 56.7; H, 4.5; N, 11.2. ¹H NMR (CDCl₃, δ) 7.78 pd, 7.60 pd, 7.39 pt, 7.29 pt (2H each, CH's of HBbzim), 6.03, 5.86 (AA'BB' system of *p*-cymene, $J_{AB} = J_{A'B'} = 4.8$ Hz), 5.8–4.6 (1H, br, NH), 2.42 (1H, sp, ³J_{HH} = 6.6 Hz, CH of ⁱPr), 2.33 (3H, s, Me), 0.87 (6H, d, Me of ⁱPr).

Preparation of [(η^6 -*p*-Cymene)Ru(HBbzim)(PPh₃)]BF₄ (10**).** **Method A.** To a solution of [(η^6 -*p*-cymene)Ru(acac)(PPh₃)]BF₄ (273.4 mg, 0.40 mmol) in methanol (30 mL) H₂Bbzim (187.4 mg, 0.80 mmol) was added. The orange mixture became yellow after stirring for a week. Excess H₂Bbzim was filtered off, and the resulting solution was concentrated at reduced pressure to ca. 2 mL. Addition of Et₂O completed the precipitation of a yellow solid which was filtered off, washed with Et₂O, and vacuum-dried. Yield: 73%.

Method B. To a suspension of **9** (206.0 mg, 0.40 mmol) in methanol (30 mL) was added AgBF₄ (79.5 mg, 0.40 mmol). The mixture was stirred during 1 h and the AgCl formed filtered off. Solid PPh₃ (107.2 mg, 0.40 mmol) was added to the red solution which was stirred during 24 h. The resulting yellow solution was worked up as above and a yellow solid was collected. Yield: 81%. IR (Nujol): $\nu(\text{OH})$ 3610 (m), 3440 (m); $\nu(\text{NH})$ 3150–2300 (br); $\nu(\text{RuCl})$ 290 (m) cm⁻¹. Anal. Calcd for C₄₂H₃₈N₄BF₄PRu: C, 61.7; H, 4.7; N, 6.85. Found: C, 60.0; H, 4.75; N, 6.9. ³¹P{¹H} NMR (CDCl₃, δ) 41.3 (s). ¹H NMR

(CDCl₃, δ) 8.04 pd, 7.62 pt (2H each, CH's of HBbzim), 7.5–6.9 m (4H, CH's of HBbzim and 15H of PPh₃), 6.64, 6.25 (AA'BB' system of *p*-cymene, $J_{AB} = J_{A'B'} = 6.2$ Hz), 3.8–2.6 (1H, br, NH), 2.14 (1H, sp, ³J_{HH} = 6.6 Hz, CH of ⁱPr), 1.68 (3H, s, Me), 0.55 (6H, d, Me of ⁱPr).

Preparation of [(η^6 -*p*-Cymene)ClRu(μ -Bbzim)Rh(COD)] (11**).** To a suspension of **9** (100.8 mg, 0.20 mmol) in methanol (30 mL) was added [Rh(acac)(COD)] (62.0 mg, 0.20 mmol). Within a few seconds, the suspension became a yellow solution, and after 30 min the precipitation of a yellow solid was observed. The mixture was stirred during 4 h and then vacuum-concentrated to ca. 2 mL. Addition of Et₂O completed the precipitation of the yellow solid which was filtered off, washed with Et₂O, and dried under vacuum. Yield: 71%. IR (Nujol): $\nu(\text{RuCl})$ 295 (m) cm⁻¹. Anal. Calcd for C₃₂H₃₄N₄ClRhRu: C, 53.8; H, 4.8; N, 7.85. Found: C, 53.7; H, 5.0; N, 8.0. ¹H NMR (CDCl₃, δ) 7.59 (2H, pd, 2CH's of Bbzim), 7.26–7.14 (6H, m, 6CH's of Bbzim), 5.86, 5.70 (AA'BB' system of *p*-cymene, $J_{AB} = J_{A'B'} = 5.6$ Hz), 4.96 (4H, m, vinylic CH of COD), 2.78 (1H, sp, ³J_{HH} = 6.9 Hz, CH of ⁱPr), 2.49, 1.87 (4H each, m, aliphatic CH₂ of COD), 2.21 (3H, s, Me), 1.12 (6H, d, Me of ⁱPr). FAB MS *m/z* (*m*-nitrobenzyl alcohol) 714 (M⁺, 20%), 679 (M⁺ - Cl, 65%), 469 (M⁺ - Cl - COD - Rh, 100%).

Complexes **12** and **13** were similarly prepared. Complex **12**: red solid, yield: 50%. Anal. Calcd for C₆₂H₆₀N₈Cl₂Rh₂Ru₂: C, 53.3; H, 4.3; N, 8.0. Found: C, 53.5; H, 4.2; N, 8.3. ¹H NMR (CDCl₃, δ) 7.62, 7.4–7.2, 7.14, 6.99, and 6.82 (16H, CH's of Bbzim), 5.87, 5.83, 5.67, 5.28 (two AA'BB' systems of *p*-cymene, $J_{AB} = J_{A'B'} = 5.8$ Hz), 5.59, 4.82, 4.76, 4.32 (8H, vinylic CH of NBD), 3.62, 2.71, 1.36, 1.13 (8H, aliphatic CH of NBD), 1.95 (2H, sp, ³J_{HH} = 6.8 Hz, CH of ⁱPr), 1.55 (6H, s, 2Me), 0.77, 0.23 (6H each, d, Me of ⁱPr).

Complex **13**: yellow solid, yield: 76%. IR (Nujol): $\nu(\text{RuCl})$ 300 (m); (CH₂Cl₂): $\nu(\text{CO})$ 2090 (s), 2070 (s) 2020 (s) cm⁻¹. Anal. Calcd for C₅₂H₄₄N₈Cl₂O₄Rh₂Ru₂: C, 47.2; H, 3.3; N, 8.5. Found: C, 47.15; H, 3.5; N, 8.45. ¹H NMR (CDCl₃, δ) 7.26–7.12 (16H, m, 16CH's of Bbzim), 5.80, 5.58 (two AA'BB' systems of *p*-cymene, $J_{AB} = J_{A'B'} = 5.8$ Hz), 1.86 (6H, s, Me), 1.82 (2H, sp, ³J_{HH} = 6.7 Hz, CH of ⁱPr), 0.26 (12H, d, Me of ⁱPr). FAB MS *m/z* (*m*-nitrobenzyl alcohol) 1324 (M⁺, 30%), 1289 (M⁺ - Cl, 95%).

Compound **13** can be alternatively prepared by bubbling carbon monoxide for 2 h through yellow dichloromethane solutions of **11**. The resulting orange solution was filtered and then concentrated under reduced pressure to ca. 2 mL. Slow addition of *n*-hexane gave an orange solid, which was collected, washed with *n*-hexane, and dried under vacuum. Yield: 69%.

Complex **14** was prepared as complex **11** but in acetone: yellow solid, yield 70%. IR (Nujol): $\nu(\text{RuCl})$ 285 (m) cm⁻¹. Anal. Calcd for C₃₂H₃₄N₄ClIrRu: C, 47.8; H, 4.3; N, 7.0. Found: C, 47.7; H, 4.4; N, 7.1. ¹H NMR (CDCl₃, δ) 7.61–7.06 (8H, m, CH's of Bbzim), 5.85, 5.69 (AA'BB' system of *p*-cymene, $J_{AB} = J_{A'B'} = 5.5$ Hz), 4.72 (4H, m, vinylic CH of COD), 2.82 (1H, sp, ³J_{HH} = 6.9 Hz, CH of ⁱPr), 2.30, 1.56 (4H each, m, aliphatic CH₂ of COD), 2.18 (3H, s, Me), 1.16 (6H, d, Me of ⁱPr). FAB MS *m/z* (*m*-nitrobenzyl alcohol) 804 (M⁺, 20%), 769 (M⁺ - Cl, 45%), 469 (M⁺ - Cl - COD - Ir, 100%).

Preparation of [(η^6 -*p*-Cymene)(PPh₃)Ru(μ -Bbzim)Rh(COD)]BF₄ (15**).** The same procedure described for **11**, but starting from **10** (163.5 mg, 0.20 mmol) and [Rh(acac)(COD)] (62.0 mg, 0.20 mmol) gave **15** as an orange solid. Yield: 72%. Anal. Calcd for C₅₀H₄₉N₄BF₄PRhRu: C, 58.4; H, 4.8; N, 5.5. Found: C, 57.6; H, 4.8; N, 5.4. ³¹P{¹H} NMR (CDCl₃, δ) 42.6 (s). ¹H NMR (CDCl₃, δ) 7.82 (2H, pd, 2CH's of Bbzim), 7.5–6.9 (6H, 6CH's of Bbzim and 15H of PPh₃), 6.42, 5.89 (AA'BB' system of *p*-cymene, $J_{AB} = J_{A'B'} = 5.8$ Hz), 4.85, 4.65 (2H each, m, vinylic CH of COD), 2.49, 1.84 (4H each, m, aliphatic CH₂ of COD), 2.28 (1H, sp, ³J_{HH} = 6.8 Hz, CH of ⁱPr), 1.65 (3H, s, Me), 0.76 (6H, d, Me of ⁱPr), FAB MS *m/z* (*m*-nitrobenzyl alcohol) 941 (M⁺, 20%), 731 (M⁺ - COD - Rh, 60%).

Complexes **16**–**18** were similarly prepared. Complex **16**: yellow solid, yield: 78%. Anal. Calcd for C₄₉H₄₆N₄BF₄PRhRu: C, 58.2; H, 4.5; N, 5.5. Found: C, 57.9; H, 4.5; N,

Table 9. Crystal Data and Refinement Details for $[(\eta^6\text{-}p\text{-Cymene})\text{CIRu}(\mu\text{-Bbzim})\text{Rh}(\text{NBD})]_2$ (12**) and $[(\eta^6\text{-}p\text{-Cymene})(\text{PPh}_3)\text{Ru}(\mu\text{-Bbzim})\text{Ir}(\text{CO})_2]\text{BF}_4$ (**19**)**

complex	12 : $2\text{C}_2\text{H}_2\text{Cl}_2$	19
formula	$\text{C}_{62}\text{H}_{60}\text{Cl}_2\text{N}_8\text{Rh}_2\text{Ru}_2 \cdot 2\text{C}_2\text{H}_2\text{Cl}_2$	$\text{C}_{44}\text{H}_{37}\text{BF}_4\text{IrN}_4\text{O}_2\text{PRu}$
fw	1565.9	1064.9
symmetry	triclinic, $P\bar{1}$	monoclinic, $P2_1/c$
a (Å)	12.998(1)	11.586(2)
b (Å)	14.035(1)	20.489(2)
c (Å)	18.081(2)	17.225(1)
α (deg)	79.864(4)	—
β (deg)	78.046(5)	95.34(1)
γ (deg)	73.326(7)	—
V (Å ³), Z	3067.3(5), 2	4071.2(9), 4
D (calcd), g cm ⁻³	1.695	1.737
radiation	Mo K_α ($\lambda = 0.71073$ Å)	Mo K_α ($\lambda = 0.71073$ Å)
method of collcn	$\omega/2\theta$ scan	$\omega/2\theta$ scan
scan range (deg)	($3 \leq 2\theta \leq 50^\circ$)	($3 \leq 2\theta \leq 45^\circ$)
no. of reflns:	12264 (h : -15 15; k : -1 16; l : -21 21)	6745 (h : -12 12; k : 0.22; l : -18 3)
observed	8941 ($F_o \geq 4.0 \sigma(F_o)$)	4242 ($F_o \geq 4.0 \sigma(F_o)$)
μ (cm ⁻¹)	13.0	37.2
largest difference peaks	1.66 e/Å ³ , close to disordered solvent	0.73 e/Å ³ , close to the BF ₄ anion
R_w^a, R_u^b	0.0375, 0.0434	0.0359, 0.0388
S^c (goodness-of-fit)	1.61	1.16
data-to-parameter ratio	12.1:1	8.1:1

^a $R = \sum |F_o| - |F_c| / \sum |F_o|$. ^b $R_w = \{\sum w(|F_o| - |F_c|)^2 / \sum w|F_o|^2\}^{1/2}$, $w^{-1} = \sigma^2(F) + 0.0002F^2$ (**12**), $w^{-1} = \sigma^2(F) + 0.0003F^2$ (**19**). ^c $S = \{\sum w(|F_o| - |F_c|)^2 / (M - N)\}^{1/2}$, where M and N denote the number of data and variables, respectively.

5.5. ³¹P{¹H} NMR (CDCl₃, δ) 42.5 (s). ¹H NMR (CDCl₃, δ) 7.74 pd, 7.55 pt, 7.10 pt, 6.86 pd (2H each, CH's of Bbzim), 7.5–6.9 (15H, m, PPh₃), 6.38, 5.85 (AA'BB' system of *p*-cymene, $J_{AB} = J_{A'B'} = 6.2$ Hz), 4.32, 4.18 (2H each, m, vinylic CH of NBD), 4.01, 1.29 (2H each, m, aliphatic CH of NBD), 2.28 (1H, sp, ³J_{HH} = 6.8 Hz, CH of ⁱPr), 1.61 (3H, s, Me), 0.73 (6H, d, Me of ⁱPr). FAB MS m/z (*m*-nitrobenzyl alcohol) 925 (M⁺, 10%), 731 (M⁺ - NBD - Rh, 60%), 469 (M⁺ - NBD - Rh - PPh₃, 100%).

Complex **17**: orange solid, yield: 79%. IR (CH₂Cl₂): $\nu(\text{CO})$ 2080 (s), 2020 (s) cm⁻¹. Anal. Calcd for C₄₄H₃₇N₄BF₄O₂-PRhRu: C, 54.2; H, 3.8; N, 5.7. Found: C, 53.65; H, 3.6; N, 5.6. ³¹P{¹H} NMR (CDCl₃, δ) 42.7 (s). ¹H NMR (CDCl₃, δ) 7.78 (2H, pd, 2CH of Bbzim), 7.5–6.9 (6H, 6CH's of Bbzim and 15H of PPh₃), 6.39, 5.72 (AA'BB' system of *p*-cymene, $J_{AB} = J_{A'B'} = 6.0$ Hz), 2.35 (1H, sp, ³J_{HH} = 7.0 Hz, CH of ⁱPr), 1.67 (3H, s, Me), 0.74 (6H, d, Me of ⁱPr).

Complex **17** was also prepared by bubbling carbon monoxide during 2 h through dichloromethane solutions of **15** or **16**. The resulting orange solution was worked up as above and an orange solid was collected. Yield: 69%.

Complex **18**: yellow solid, yield: 82%. Anal. Calcd for C₅₀H₄₈N₄BF₄IrPRu: C, 53.8; H, 4.4; N, 5.0. Found: C, 53.8; H, 4.7; N, 5.1. ³¹P{¹H} NMR (CDCl₃, δ) 42.6 (s). ¹H NMR (CDCl₃, δ) 7.87 (2H, pd, 2CH of Bbzim), 7.5–6.9 (6H, 6CH's of Bbzim and 15H of PPh₃), 6.45, 5.89 (AA'BB' system of *p*-cymene, $J_{AB} = J_{A'B'} = 6.1$ Hz), 4.63, 4.47 (2H each, m, vinylic CH of COD), 2.28 (5H, m, CH of ⁱPr and aliphatic CH₂ of COD), 1.66 (3H, s, Me), 1.58, 1.52 (2H each, m, aliphatic CH₂ of COD), 0.79 (6H, d, ³J_{HH} = 6.8 Hz, Me of ⁱPr). FAB MS m/z (*m*-nitrobenzyl alcohol) 1031 (M⁺, 30%), 769 (M⁺ - PPh₃, 30%), 731 (M⁺ - COD - Ir, 70%), 469 (M⁺ - COD - Ir - PPh₃, 100%).

Preparation of $[(\eta^6\text{-}p\text{-Cymene})(\text{PPh}_3)\text{Ru}(\mu\text{-Bbzim})\text{Ir}(\text{CO})_2]\text{BF}_4$ (19**).** Carbon monoxide was bubbled through a solution of **18** in dichloromethane (40 mL) during 30 min. The resulting yellow solution was filtered and vacuum-concentrated to ca. 2 mL. The slow addition of Et₂O (10 mL) gave a dark violet solid which was filtered off, washed with Et₂O, and vacuum-dried. Yield: 86%. IR (CH₂Cl₂): $\nu(\text{CO})$ 2070 (s), 2000 (s) cm⁻¹. Anal. Calcd for C₄₄H₃₇N₄BF₄O₂PIrRu: C, 49.6; H, 3.5; N, 5.3. Found: C, 50.0; H, 3.7; N, 5.1. ³¹P{¹H} NMR (CD₃-COCD₃/CH₃COCH₃, 1/4 v/v, δ) 42.9 (s). ¹H NMR (CD₂Cl₂, δ) 7.87 (2H, pd, 2CH's of Bbzim), 7.53–6.90 (6H, 6CH's of Bbzim

and 15H of PPh₃), 6.46, 5.88 (AA'BB' system of *p*-cymene, $J_{AB} = J_{A'B'} = 6.1$ Hz), 2.32 (1H, sp, ³J_{HH} = 7.1 Hz, CH of ⁱPr), 1.67 (3H, s, Me), 0.76 (6H, Me of ⁱPr).

Catalytic Reactions. In a typical experiment, a degassed solution of the catalyst in methanol (10 mL) was placed into a 100 mL flask attached to a hydrogen reservoir through a three-way valve. The system was evacuated and flushed with hydrogen four times and then hydrogen was admitted to the system at the desired pressure. The flask was then immersed in a thermostated bath, at a preestablished temperature and, prior to the introduction of the substrate dissolved in methanol (5 mL), it was shaken for 30 min. Solutions of tetrabutylammonium chloride in methanol were added with the substrate for the study of the influence of the chloride anions. The reaction was followed by measuring, by GC, the percentage of the formed cyclohexane as a function of time. Starting time corresponds to the addition of the substrate. All straight lines were fitted by use of conventional linear regression software to $r^2 > 0.98$. Concentrations of dissolved hydrogen were calculated using solubility data reported by Katayama et al.³⁴

X-ray Measurements and Structure Determinations for $12\text{-}2\text{C}_2\text{H}_2\text{Cl}_2$ and **19.** Red crystals of $12\text{-}2\text{C}_2\text{H}_2\text{Cl}_2$ and dark red crystals of **19** were grown by slow diffusion of Et₂O into solutions of **12** and **19** in CH₂Cl₂. Prismatic blocks of dimensions 0.20 × 0.14 × 0.48 mm ($12\text{-}2\text{C}_2\text{H}_2\text{Cl}_2$) and 0.17 × 0.23 × 0.34 mm (**19**) were glued to the end of glass fibers. In each case, it was mounted on a four-circle Siemens AED diffractometer working with graphite-monochromated Mo K_α radiation and operating at 230 K for $12\text{-}2\text{C}_2\text{H}_2\text{Cl}_2$ or 273 K for **19**. Selected crystallographic data are collected in Table 9. Precise lattice parameters were determined by least-squares fit from 68 ($12\text{-}2\text{C}_2\text{H}_2\text{Cl}_2$) and 58 (**19**) centered reflections in the region $20 \leq 2\theta \leq 42^\circ$. Three standard reflections were monitored every 55 min to check crystal and instrument stability. There were no significant fluctuations of the intensities. Data were corrected for Lorentz and polarization effects, and a semiempirical absorption correction³⁵ based on ψ scans was also applied (min and max trans. fact. 0.156 and 0.186 for $12\text{-}2\text{C}_2\text{H}_2\text{Cl}_2$ and 0.725 and 0.777 for **19**). The structures were solved by the heavy-atom method followed by difference Fourier calculations using the SHELXTL-PLUS package.³⁶ All non-

(35) North, A. C. T.; Phillips, D. C.; Mathews, F. S. *Acta Crystallogr.* **1968**, A24, 351.

(36) Sheldrick, G. M. SHELXTL-PLUS, Siemens Analytical X-ray Instruments, Madison, WI, 1990.

(37) *International Tables For Crystallography*; Kynoch Press: Birmingham, England, 1974; Vol. IV.

H-atoms were anisotropically refined except those of the disordered CH₂Cl₂ solvent molecule of compound **12** which were refined with isotropic displacement parameters. This disorder was modeled with two molecules each of them with a refined occupancy factor of ca. 1/2. Hydrogen atoms were included in the last cycles in calculated (for **12**·2CH₂Cl₂) and found (for **19**) positions. All H-atoms were refined with a common thermal parameter using the riding method. The scattering factors, with anomalous dispersion correction for heavy-atoms, were taken from ref 37. All calculations were carried out on a μ -VAX 3400 computer.

Acknowledgment. We thank the Dirección General de Investigación Científica y Técnica for financial support (Grant PB92/19).

Supplementary Material Available: Tables SI–SVI with full details of crystallographic and experimental data, hydrogen positional parameters, anisotropic displacement parameters, and a full list of bond distances and angles for **12**·2CH₂Cl₂ and **19**, respectively (11 pages). Ordering information is given on any current masthead page.

OM940614A

Fast Atom Bombardment Tandem Mass Spectrometry of Organometallic Palladium Complexes Containing Terdentate Nitrogen Ligands

Kai A. N. Verkerk,^{†,‡} Chris G. de Koster,^{*,§,||} Bertus A. Markies,[‡] Jaap Boersma,[‡] Gerard van Koten,[‡] Wigger Heerma,^{||} and Johan Haverkamp^{||}

Bijvoet Center for Biomolecular Research, Mass Spectrometry, Utrecht University, P.O. Box 80083, 3508 TB Utrecht, The Netherlands, and The Debye Institute, Department of Metal-Mediated Synthesis, Utrecht University, Padualaan 8, 3584 CH Utrecht, The Netherlands

Received April 29, 1994[®]

Fast atom bombardment and collisional-induced dissociation tandem mass spectrometry were used to analyze 12 cationic organometallic palladium [Pd(L)(R)](OTf) complexes containing three different terdentate nitrogen ligands (L), an organic group (R) attached in the σ bonding mode, and a trifluoromethanesulfonate anion (OTf is CF_3SO_3^-) using *m*-nitrobenzyl alcohol as a matrix. FAB ionization gives abundant Pd(L)(R) cations and some fragment ions. Tandem mass spectrometry of collisionally activated monoisotopic $^{108}\text{Pd(L)(R)}$ cations affords additional information on fragmentation mechanisms and enables discrimination between isomeric complexes. The MS/MS experiments also provided evidence for the occurrence of an abundant gas-phase cyclopalladation reaction of the $^{108}\text{Pd(L)(R)}$ cations by activation of a sp^3 C–H bond according to an oxidative addition/reductive elimination or a multicentered pathway.

Introduction

The unique catalytic properties of many transition-metal complexes have led to an increased interest in the structures of the active species and prompted numerous studies concerning the influences of different ligand environments.^{1,2} In the past mass spectrometric techniques were of a limited value since many coordination complexes and organometallic compounds are prone to thermal decomposition, which hampered a detailed structural study. However, with the development of soft ionization techniques the possibility of analyzing involatile and thermally labile compounds was provided. Where other soft ionization techniques as field desorption (FD)^{3,4} and laser desorption (LD) have found application in this field, fast atom bombardment mass spectrometry (FAB-MS)^{6,7} has proven throughout the years to be a versatile and sensitive method for the

analysis of organometallics.⁸ With this technique parent ion molecular weight information as well as further structurally informative ions can be obtained. Together with the applicability of FAB mass spectrometry to organometallic compounds, new matrices for the (organometallic) samples were also investigated. In particular *m*-nitrobenzyl alcohol (NBA) gave good results for many compounds and has also successfully been applied in this study.^{8,9}

The recent availability of four sector instruments adds a new dimension to the analysis of organometallic compounds. In tandem mass spectrometry (MS/MS) the ion of interest is selected in the first mass spectrometer (MS-1) at unit resolution. The mass-selected ions collide with an inert gas such as helium in a collision cell located in the field-free region between MS-1 and the second mass spectrometer (MS-2). Upon collision, part of the translation energy of the ion (10 keV) is converted into internal energy. The internal energy acquired is sufficient to induce rapid fragmentations (10^{-13} – 10^{-5} s) of the collisionally activated ions. The product ions are analyzed at unit resolution in the second mass spectrometer.

An interesting advantage of studying reactions in the field-free region of the mass spectrometer by MS/MS techniques is that the selected ions are isolated species. Therefore, mass spectra obtained in such a way reflect the intrinsic properties of isolated reaction systems. The reactions are not affected by extraneous and variable phenomena such as participation of solvent molecules and/or counterions, which are superimposed upon factors determining the activation energy barrier, the stability of reactants, and the reaction products. Only unimolecular reaction product ions which are the result

* To whom correspondence should be addressed.

[†] Present address: Institut für Technische Chemie und Petrolchemie der Rhein.-Westf. Technische Hochschule, Worringerweg 1, 52074 Aachen, Germany.

[‡] Debye Institute.

[§] Present address: FOM Institute for Atomic and Molecular Physics, Kruislaan 407, 1098 SJ Amsterdam, The Netherlands.

^{||} Bijvoet Center for Biomolecular Research, Mass Spectrometry Group.

[®] Abstract published in *Advance ACS Abstracts*, February 15, 1995.

(1) Davies, S. G. *Organotransition Metal Chemistry: Applications to Organic Synthesis*; Pergamon Press: Oxford, U.K., 1982.

(2) Omae, I. J. *Organomet. Chem. Libr.* **1986**, 18, 9.

(3) Beckey, H. D. *Principles of Field Ionization and Field Desorption Mass Spectrometry*; Pergamon Press: Oxford, U.K., 1977.

(4) Staal, H. J.; Van Koten, G.; Fokkens, R. H.; Nibbering, N. M. *Inorg. Chim. Acta* **1981**, 50, 205.

(5) Weller, R. R.; MacMahon, T. J.; Freiser, B. S. In *Lasers and Mass Spectrometry*; Lubman, D. M., Ed.; Oxford Series on Optical Sciences; Oxford University Press: Oxford, U.K., 1990; p 249.

(6) Surman, D. W.; Vickerman, J. C. *J. Chem. Soc., Chem. Commun.* **1981**, 324.

(7) Barber, M.; Bordoli, R. S.; Sedgwick, R. D.; Tyler, A. N. *J. Chem. Soc., Chem. Commun.* **1981**, 325, 325.

(8) Miller, J. M. *Mass Spectrom. Rev.* **1989**, 9, 319.

(9) Barber, M.; Bell, D. J.; Eckersley, M.; Morris, M.; Tetler, L. W. *Rapid Commun. Mass Spectrom.* **1988**, 2, 18.

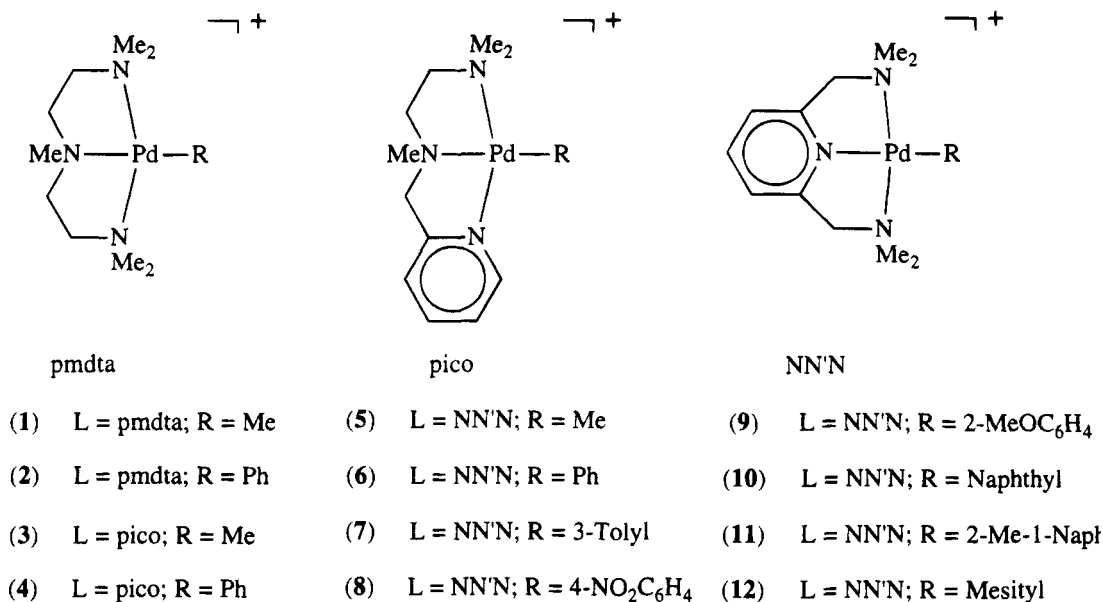


Figure 1. Structures of the complexes $[\text{Pd}(\text{L})(\text{R})]^+\text{OTf}^-$: pmdeta = *N,N,N',N',N''*-pentamethyldiethylenetriamine; pico = *N,N,N'*-trimethyl-(2-picolyl)ethylenediamine; NN'N = 2,6-bis[(dimethylamino)methyl]pyridine; OTf = CF_3SO_3^- (trifluoromethanesulfonate); mesityl = 1,3,5-trimethylbenzene.¹⁰

of intramolecular isomerization and/or fragmentation in a solvent-free environment are collected on the detector of MS-2.

In this report the gas-phase ion chemistry of several organometallic palladium(II) complexes under FAB conditions is studied. Our results center around ionic complexes $[\text{Pd}(\text{L})(\text{R})\text{OTf}]^+$ where the cation consists of a neutral terdentate nitrogen ligand (L) coordinated to the dicationic palladium metal center with an anionic organic group (R) attached in the σ bonding mode. A noncoordinating triflate (OTf) is serving as anion.¹⁰ The used ligands (L) and organic groups (R) are depicted in Figure 1 with their adopted numbering. In addition to the structural information obtained by FAB-MS additional collision-induced dissociation MS/MS experiments have been carried out to enable unambiguous identification of the structures. A second subject of research is the applicability of MS/MS techniques as a tool to study the gas-phase chemistry of intramolecular C–H bond activation (cyclometalation) by transition-metal complexes.^{11–16} For this purpose the unimolecular loss of RH from mass-selected $[\text{Pd}(\text{L})(\text{R})]^+$ cations in the field-free region of the mass spectrometer is used as a model reaction.

Experimental Section

Positive FAB mass spectra and collisional-induced dissociation (CID) spectra were obtained with a JEOL JMS-SX102/102A four sector instrument of $\text{B}_1\text{E}_1-\text{B}_2\text{E}_2$ geometry (B = magnet, E = electrostatic analyzer). FAB mass spectra were obtained with MS-1. Tandem mass spectra were acquired by selecting the desired precursor ion with MS-1 and colliding

the selected ion at 10 keV translational energy in a collision cell operated at ground potential and located in the third field-free region of the instrument. The resulting fragment ions were determined by linked scanning of MS-2. The CID spectra were recorded at a main beam attenuation of 50% with helium as the collision gas. The resolution was 1000 $(\text{m}/\text{dm})_{10\%}$ for MS-1 as well as for MS-2. Xenon was used as the FAB gas; the gun was operated at 6 kV and a 5 mA discharge current.

Samples were dissolved in methanol *pa* [Westburg] at a concentration of 0.1 $\text{mol}\cdot\text{L}^{-1}$. Aliquots (1 μL) were transferred by syringe and mixed with 1 μL of *m*-nitrobenzyl alcohol (NBA) [Fluka] on the stainless steel FAB probe tip.

The details of the synthesis of the complexes including $[\text{Pd}(\text{NN}'\text{N})(\text{CD}_3)\text{OTf}]^+$ were described elsewhere in combination with the structural confirmation deduced by spectroscopic methods such as $^1\text{H-NMR}$, $^{13}\text{C-NMR}$, IR, and elemental analysis. Several complexes were subjected to a crystallographic study.¹⁰

Results and Discussion

FAB Mass Spectra. The positive FAB mass spectra of the methyl compounds (R = CH_3) 1, 3 and 5¹⁰ are presented in Figure 2a–c, respectively. Partial positive ion FAB mass spectra of these and the other compounds are given in Table 1. $[\text{Pd}(\text{L})(\text{R})]^+$ cations form a cluster of very abundant peaks in the FAB mass spectra of all compounds. In all cases there is a good similarity between the calculated and observed isotope distribution (data not shown). Formation of $[\text{Pd}(\text{L})(\text{R})\text{OTf}]^{2+}$ ions was not observed.

The fragmentation pattern was dominated by $[\text{Pd}(\text{L})(\text{R})-\text{RH}]^+$ cations yielding peaks at m/z 278 (^{106}Pd) for the pmdta complexes (1, 2), whereas for the isomeric pico (3, 4) and NN'N complexes (5–12) signals at m/z 300 (^{106}Pd) were found. The abundant loss of RH is the result of a cyclometalation reaction^{11–15} of the $[\text{Pd}(\text{L})(\text{R})]^+$ cation involving metal–carbon σ -bond formation by the ligand with concomitant loss of RH. The occurrence of cyclometalation reactions has also been observed for other FAB-ionized organometallics in the ion source of the mass spectrometer. For example,

(10) Markies, B. A.; Wijkens, P.; Boersma, J.; Kooijman, H.; Veldman, N.; Spek, A. L.; van Koten, G. *Organometallics* **1990**, *13*, 3244.

(11) Dehand, J.; Pfeffer, M. *Coord. Chem. Rev.* **1976**, *18*, 327.

(12) Bruce, M. I. *Angew. Chem.* **1977**, *89*, 75.

(13) Constable, E. C. *Polyhedron* **1984**, *3*, 1037.

(14) Newkome, G. R.; Puckett, W. E.; Gupta, V. K.; Kiefer, G. E. *Chem. Rev.* **1986**, *86*, 451.

(15) Evans, D. W.; Baker, G. R.; Newkome, G. R. *Coord. Chem. Rev.* **1989**, *93*, 155.

(16) Ryabov, A. D. *Chem. Rev.* **1990**, *90*, 403.

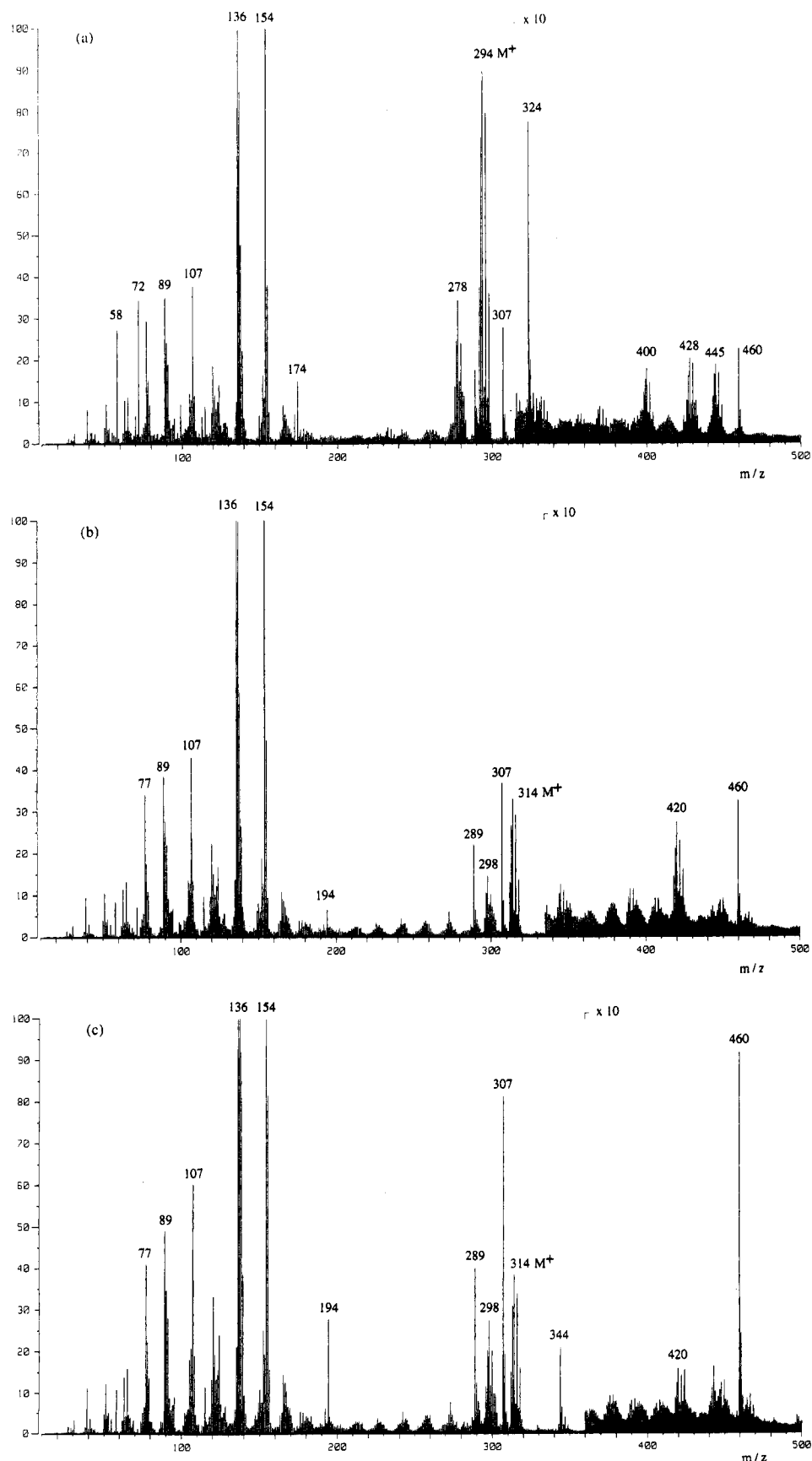


Figure 2. Positive ion FAB mass spectra of (a) Pd(pmdeta)(Me)OTf, (b) Pd(pico)(Me)OTf, and (c) Pd(NN'N)(Me)OTf.

Cerny et al. studied the fragmentations of bis(2,2'-bipyridyl) complexes of Ru(II) and Os(II) containing η^2 -alkene, carbonyl, and alkyl ligands by FAB-MS.¹⁷ They observed $[M(\text{bpy})_2 - \text{H}]^+$ ($M = \text{Os}, \text{Ru}$) fragments which

were ascribed to the formation of cyclometalated ions, in which one of the bipyridine ligands is bound to the metal center through a nitrogen and a carbon atom. So far similar ions have been reported to be present in the

Table 1. Abundant Ions in the FAB Mass Spectra of Complexes 1–12 (Relative Abundances in Parentheses)

cation	1	2	3	4	5	6	7	8	9	10	11	12
[M + NBA] ⁺		509 (7)		529 (10)		529 (14)	543 (9)	574 (19)	559 (12)			571 (13)
[M + NBA - H ₂] ⁺	445 (21)		465 (20)		465 (29)							
[M + Pd - H ₂] ⁺	400 (18)		420 (79)	482 (21)	420 (43)	482 (12)	496 (9)	527 (12)	512 (9)			
[M] ⁺	294 (1000)	356 (1000)	314 (1000)	376 (1000)	314 (1000)	376 (1000)	390 (1000)	421 (1000)	406 (1000)	426 (1000)	440 (1000)	418 (1000)
[M - RH] ⁺	278 (302)	278 (197)	298 (351)	298 (217)	298 (678)	298 (578)	298 (651)	298 (551)	298 (581)	298 (589)	298 (546)	298 (1076)
[L + H] ⁺	174 (185)		194 (219)			194 (232)	194 (172)	194 (201)				
[L - H] ⁺	172 (89)					192 (142)	192 (126)	192 (150)	192 (123)	192 (243)	192 (297)	192 (203)
[M - RH + NBA - 3H] ⁺	428 (24)		448 (31)	448 (14)	448 (38)	448 (21)	448 (26)	448 (26)				
344	(101)				(637)	(156)	(109)	(240)	(78)	(79)	(69)	
72	(433)	(298)	(248)	(141)								
58	(342)	(250)	(335)	(161)	(320)	(211)	(273)	(171)	(199)	(207)	(363)	(290)

^a *m/z* values based on ¹⁰⁶Pd. ^b M corresponds to Pd(L)(R).

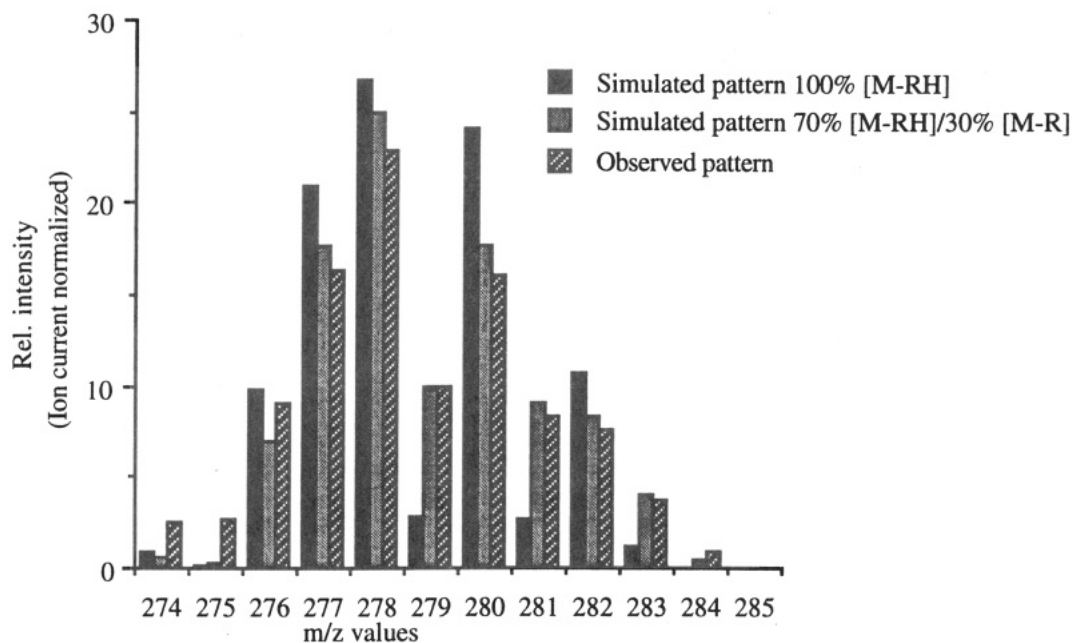


Figure 3. Comparison of the theoretical isotope distribution for formation of 100% [Pd(L)(R) - RH]⁺, 70% [Pd(L)(R) - RH]⁺/30% [Pd(L)(R) - R]⁺ cations and the observed isotope distribution; L = pmdeta, R = CH₃.

FAB mass spectra of several other organometallic complexes.^{18–24} However, these observations do not label cyclometalation as a common process; the structure of the ligand is of great influence,^{19,22,24,25} as was demonstrated by comparing several ligand systems. For example in the FAB mass spectra of neutral methanide and ionic carbene platinum(II) derivatives with dppe as a chelating ligand [Pt(dppe) - H]⁺ was found as the most abundant ion,¹⁹ whereas in contrast with this observation a study of platinum(II) and palladium(II) complexes containing dpmp and dpmp, respectively, as bi- and terdentate phosphine ligands, revealed that

(17) Cerny, R. L.; Sullivan, B. P.; Bursey, M. M.; Meyer, T. J. *Inorg. Chem.* **1985**, *24*, 397.

(18) Bandini, A. L.; Banditelli, G.; Minghetti, G.; Vettori, U.; Traldi, P. *Inorg. Chim. Acta* **1988**, *142*, 101.

(19) Cetini, G.; Operti, L.; Vaglio, G. A.; Bandini, A. L.; Banditelli, G.; Minghetti, G. *Org. Mass Spectrom.* **1989**, *24*, 479.

(20) Cinellu, M. A.; Minghetti, G.; Banditelli, G.; Bandini, A. L.; Pelli, B.; Traldi, P. *Inorg. Chim. Acta* **1989**, *161*, 57.

(21) Divisia-Blohorn, B.; Kyriakou, G.; Ulrich, J. *Org. Mass Spectrom.* **1985**, *20*, 463.

(22) Kowalski, M. H.; Sharp, T. S.; Stang, P. J. *Org. Mass Spectrom.* **1987**, *22*, 642.

(23) Bertani, R.; Diversi, P.; Ingrosso, G.; Lucherini, A.; Marchetti, F.; Adovasio, V.; Nardelli, M.; Pucci, S. *J. Chem. Soc. Dalton Trans.* **1988**, 2983.

(24) Bruce, M. I.; Humphrey, M. G.; Liddell, M. J. *Organomet. Chem.* **1987**, *321*, 91.

(25) Asker, K. A.; Greenway, A. M.; Seddon, K. R.; Shimran, A. A. *J. Organomet. Chem.* **1988**, *354*, 257.

cyclometalated species were totally absent in these cases.²⁵ [dppe = 1,2-bis(diphenylphosphino)ethane; dpmp = 1,1-bis(diphenylphosphino)methane; dpmp = bis(diphenylphosphinomethyl)phenylphosphine.]

A comparison between the theoretical and experimental isotope distribution (Figure 3) for the *m/z* 278 [Pd(L)(R) - RH]⁺ fragment ion of compound 1 indicates that homolytic dissociation of the Pd-R bond also occurred. The experimental values clearly show a deviating isotopic pattern compared with the cluster expected for 100% RH loss from the [Pd(pmdeta)(CH₃)]⁺ cation 1. Calculating the isotope pattern for the product ions of both fragmentations in a ratio of 70% [Pd(pmdeta)(CH₃) - CH₄]⁺ and 30% [Pd(pmdeta)(CH₃) - CH₃]⁺ results in a modeled isotope distribution which is quite consistent with the observed cluster (Figure 3). Formation of [Pd(L)]⁺ by loss of R[•] formally involves a reduction of Pd(II) to Pd(I). As demonstrated by this example, a decisive assignment of fragmentation reactions based on fitting calculated isotope distributions is rather elaborate.

Interactions between compound and matrix frequently occur,^{26,27} and these were also observed in the FAB mass spectra (Table 1) of the investigated palladium complexes, giving rise to small signals of ions corresponding to [Pd(L)(R) + (NBA)]⁺. Surprisingly, in

Table 2. CID Spectra of the [Pd(L)(M)]⁺ Cations of Compounds 1–12. (Relative Abundances in Parentheses)

1, <i>m/z</i> 296	281 (10), 280 (100), 278 (13), 266 (2), 264 (2), 249 (1), 235 (10), 223 (2), 178 (2), 165 (2), 141 (3), 139 (3), 127 (3), 72 (5), 58 (4)
2, <i>m/z</i> 358	343 (1), 300 (1), 281 (14), 280 (100), 279 (2), 278 (10), 264 (3), 235 (10), 72 (5), 58 (3)
3, <i>m/z</i> 316	315 (7), 301 (7), 300 (100), 299 (3), 298 (2), 285 (2), 257 (5), 256 (2), 243 (2), 242 (2), 229 (2), 228 (2), 200 (5), 149 (5), 135 (3), 121 (3), 91 (2), 72 (2), 58 (2)
4, <i>m/z</i> 378	360 (2), 301 (15), 300 (100), 299 (4), 286 (2), 285 (2), 284 (2), 257 (5), 256 (4), 243 (2), 242 (2), 229 (3), 228 (2), 200 (5), 149 (5), 135 (4), 92 (2), 72 (2), 58 (2)
5, <i>m/z</i> 316	301 (3), 300 (100), 299 (3), 298 (8), 284 (2), 268 (1), 258 (1), 255 (2), 241 (2), 214 (3), 149 (4), 147 (2), 58 (1)
6, <i>m/z</i> 378	334 (1), 301 (32), 300 (100), 299 (7), 298 (8), 284 (5), 268 (2), 258 (3), 255 (2), 242 (2), 241 (25), 225 (2), 214 (3), 213 (1), 149 (5), 147 (3), 135 (1), 105 (1), 95 (2), 58 (2)
7, <i>m/z</i> 392	377 (1), 374 (1), 348 (1), 305 (1), 301 (7), 300 (100), 299 (7), 298 (10), 284 (3), 268 (2), 258 (3), 255 (3), 242 (2), 241 (2), 214 (3), 192 (1), 149 (5), 147 (3), 135 (1), 105 (1), 95 (1), 91 (1), 58 (1)
8, <i>m/z</i> 423	406 (1), 405 (1), 379 (1), 377 (1), 301 (10), 300 (100), 299 (8), 298 (13), 284 (7), 268 (3), 258 (4), 255 (4), 242 (3), 241 (4), 214 (5), 192 (13), 149 (6), 147 (4), 105 (3), 95 (2), 58 (1)
9, <i>m/z</i> 408	393 (1), 390 (1), 364 (1), 301 (9), 300 (100), 299 (7), 298 (10), 284 (5), 268 (2), 258 (3), 255 (3), 242 (2), 241 (3), 214 (4), 192 (2), 185 (2), 149 (5), 147 (3), 134 (1), 105 (2), 95 (1), 58 (1)
10, <i>m/z</i> 428	410 (1), 384 (1), 341 (1), 301 (7), 300 (100), 299 (9), 298 (11), 284 (6), 275 (4), 268 (2), 258 (4), 255 (3), 242 (2), 241 (3), 235 (2), 214 (4), 192 (1), 149 (6), 147 (3), 105 (2), 95 (1), 58 (1)
11, <i>m/z</i> 442	424 (29), 301 (4), 300 (100), 299 (8), 298 (9), 289 (41), 288 (4), 287 (2), 284 (5), 271 (3), 268 (2), 258 (2), 255 (2), 242 (2), 241 (2), 214 (2), 192 (1), 154 (3), 149 (4), 147 (2), 140 (2), 105 (2), 90 (1), 89 (1), 58 (1)
12, <i>m/z</i> 420	405 (2), 376 (1), 301 (4), 300 (100), 299 (7), 298 (8), 284 (5), 268 (3), 258 (3), 255 (3), 242 (2), 241 (3), 214 (4), 192 (1), 149 (4), 147 (2), 105 (1), 58 (1)

all cases where R = Me this peak was found 2 *m/z* units lower pointing to a formal loss of H₂ from this [Pd(L)-(R) + (NBA)]⁺ complex. It is not clear whether these hydrogen atoms arise from NBA or the organopalladium complex, neither which mechanism accounts for the observed difference.

In the lower mass region(s) of the FAB mass spectra (Table 1) peaks were found at *m/z* 172 and 174 for the pmdta-containing derivatives and at *m/z* 192 and 194 for the pico- and NN'N-containing complexes. These peaks can be assigned to the intact ligands (L) and correspond to [L - H]⁺ and [L + H]⁺, respectively. Additionally, ligand fragment ion peaks were observed at *m/z* 58 and 72 which are assigned to the [(CH₂=NMe₂)⁺ and [CH₃CH=NMe₂]⁺ cations, respectively. The *m/z* 72 [CH₃CH=NMe₂]⁺ cation which is not observed in the spectra of NN'N-bound complexes (Table 1) in principle could allow discrimination between the isomeric pico and NN'N ligands because this structural fragment is not part of the NN'N ligand. However, the observation and assignment of peaks at *m/z* 58 and 72 in the FAB mass spectra is complicated by the fact that these ions are present in the lower mass range of the mass spectrum, which contains a lot of chemical background originating from matrix ions thus hampering conclusive discrimination of isomeric ligands.

Reduction processes occurring in the matrix can be held responsible for the presence of multiple metal ions of the composition [Pd(L)(R) + Pd - H₂]⁺. In other studies ions of this type were also found for [M(PPh₃)₄]⁺ (M = Pd,²⁸ Pt²⁹). In contrast with the earlier described

NBA-containing fragment ions, loss of H₂ was now found in all cases, the observed ions for **1a**, **2a**, and **3a** (R = CH₃) being more abundant than those of the other compounds. This could suggest that hydrogen dissociation is being favored by a small R group. However, within the limits of the present investigation this process could not be studied in further detail.

CID Spectra. The fragmentation patterns of complexes containing different ligands were compared by using CID to discriminate between the various ligand systems and to study the gas-phase ion chemistry of collisionally activated [Pd(L)(R)]⁺ cations. The CID spectra of the [Pd(L)(R)]⁺ cations were recorded by selecting the ¹⁰⁸Pd isotope. This isotope was chosen in order to prevent a ¹³C contribution from the preceding isotope. In each case the ligand structure was found to exert a significant influence on the obtained spectra. The relevant ions (abundance >1%) are summarized in Table 2. The spectra of the isomeric *m/z* 316 [Pd(pico)-(CH₃)]⁺ (**3**) and [Pd(NN'N)(CH₃)]⁺ (**5**) cations are presented in Figures 4 and 5, respectively.

The most important collisional-induced fragmentation of the [Pd(L)(R)]⁺ cations is loss of RH, producing peaks at *m/z* 280 (¹⁰⁸Pd) for the pmdta derivatives and at *m/z* 300 (¹⁰⁸Pd) for the pico- and NN'N-containing complexes. The abundant loss of RH is, as discussed above, the result of a cyclometalation reaction¹⁰⁻¹⁴ of the [Pd(L)-(R)]⁺ cation. In contrast with ion-source reactions, the occurrence of a cyclometalation reaction in the field-free region of the mass spectrometer offers the possibility of further mechanistic conclusions.

The mechanism of ion formation in the ion source under conditions of FAB has received considerable

(26) Barber, M.; Bell, D. J.; Morris, M.; Tetler, L. W.; Woods, M. D.; Monaghan, J. J.; Morden, W. E. *Rapid Commun. Mass Spectrom.* **1988**, *2*, 181.

(27) Bowen, R. D.; Danks, T. N.; Mitchell, D.; Thomas, S. E. *Org. Mass Spectrom.* **1988**, *23*, 674.

(28) Mallis, L. M.; Scott, W. J. *Org. Mass Spectrom.* **1990**, *25*, 415.

(29) Davies, R.; Groves, I. F.; Durrant, J. L. A.; Brooks, P.; Lewis, I. J. *Organomet. Chem.* **1983**, *241*, C27.

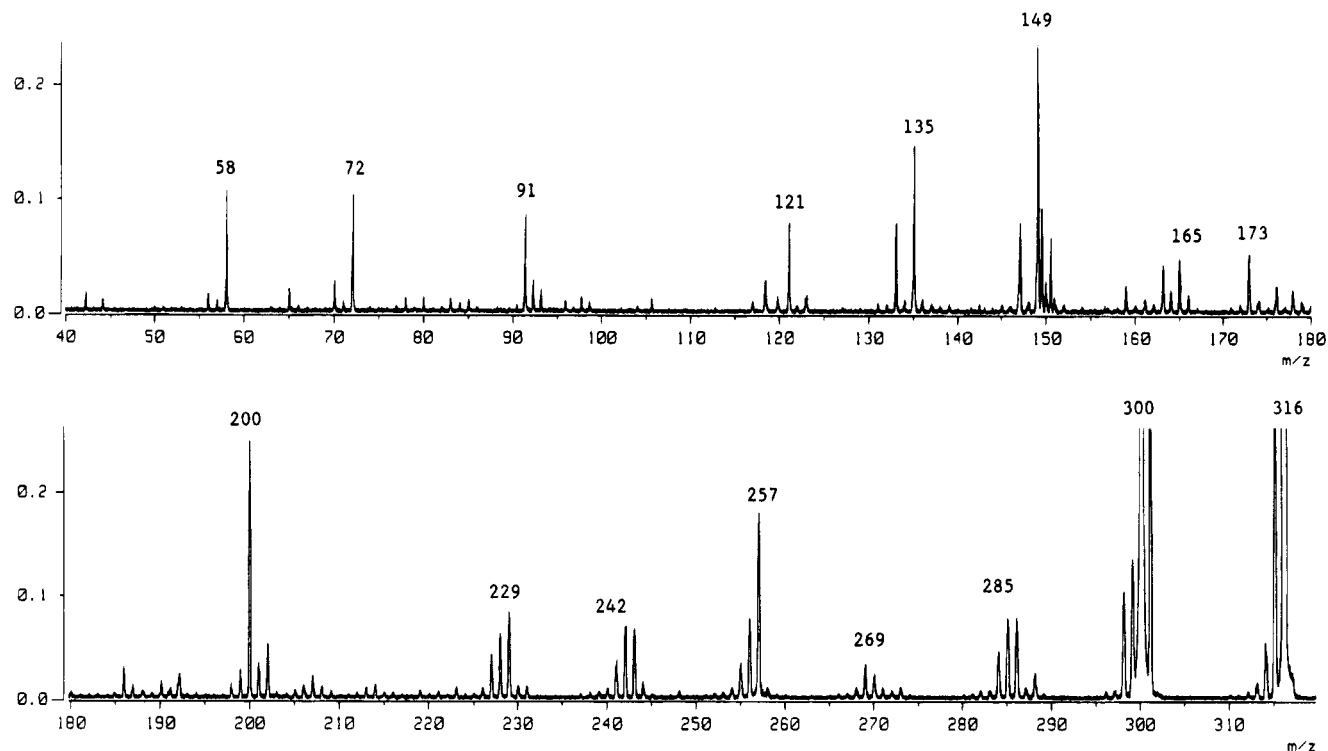


Figure 4. CID spectrum of the m/z 316 $[\text{Pd}(\text{L})(\text{R})]^+$ cation; L = pico, R = CH_3 .

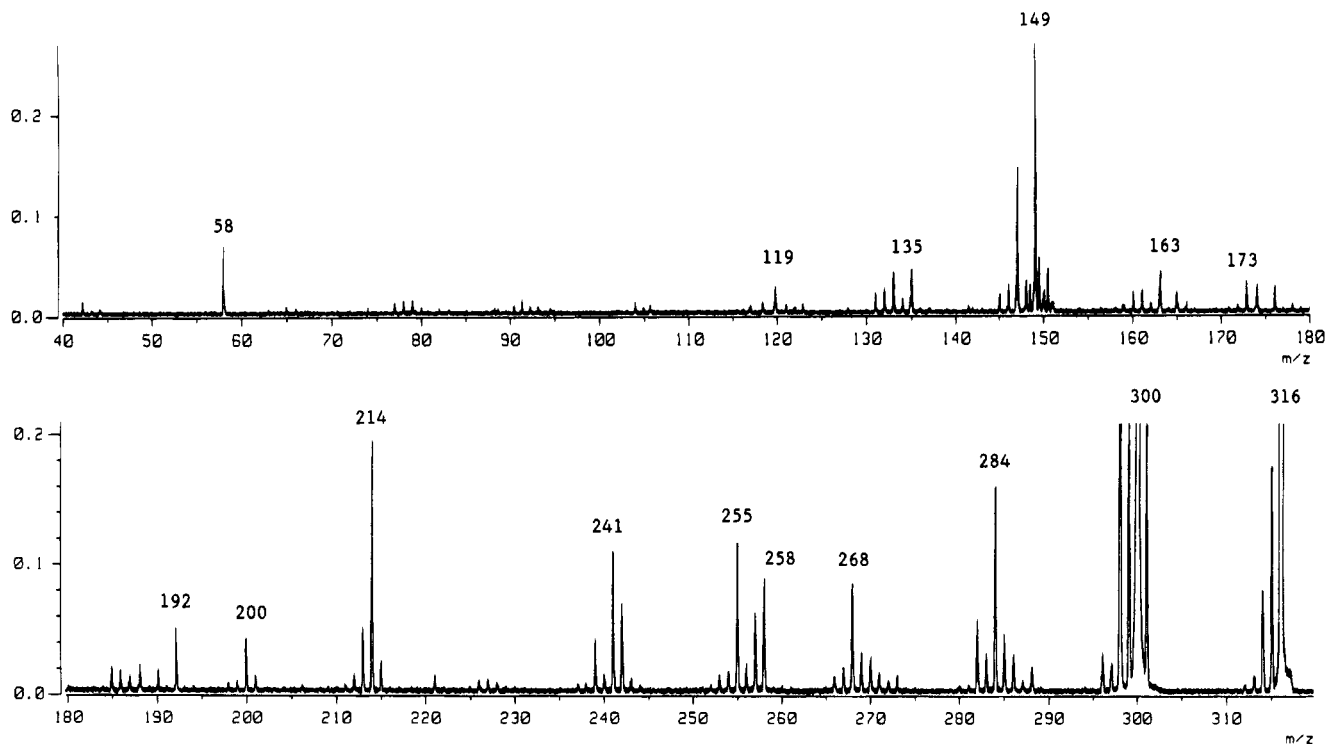


Figure 5. CID spectrum of the m/z 316 $[\text{Pd}(\text{L})(\text{R})]^+$ cation; L = NN'N, R = CH_3 .

attention.^{30,31} The ions detected in FAB mass spectra can be either preformed in solution before bombardment or produced during the energy dissipation process of the primary beam. The incoming atoms cause some ions to be formed in a collision cascade. As a result of the energy released, a cavity (selvedge region) is formed, filled with a high-pressure gas mainly consisting of

matrix molecules but also of matrix and analyte ions released as a result of the sputtering action of the primary beam. Under these chemical ionization-like conditions, reactive collisions governed by well-known gas-phase chemistry rules will occur.³²⁻³⁶ Therefore, the formation of $[\text{M} - \text{RH}]^+$ fragment ions by cyclo-

(32) Pachuta, G.; Cooks, R. G. *Chem. Rev.* **1987**, *87*, 647.

(33) Campana, J. E.; Ross, M. M.; Callhan, J. H. *Int. J. Mass Spectrom. Ion Processes* **1987**, *78*, 195.

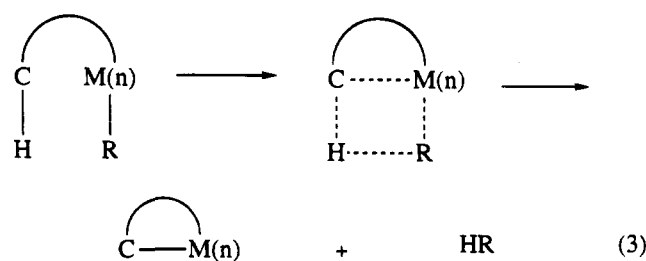
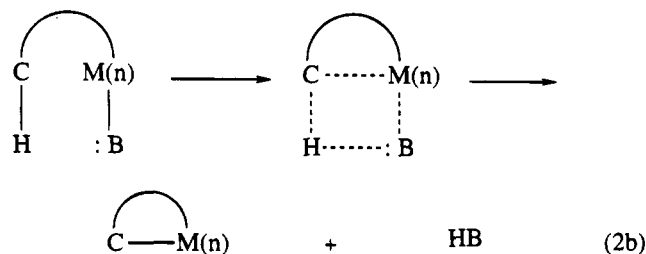
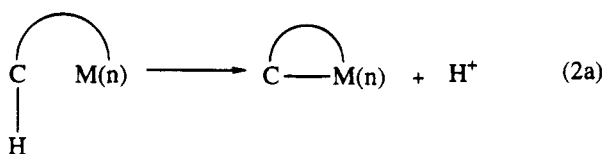
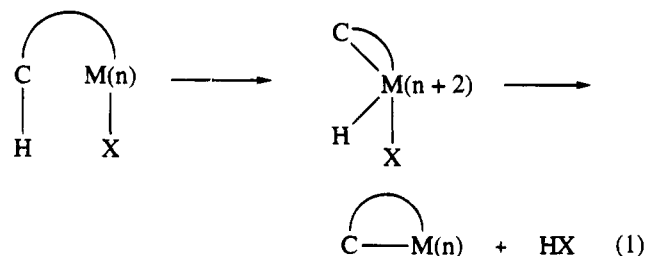
(34) Shiea, J. T.; Sunner, J. *Int. J. Mass Spectrom. Ion Processes* **1990**, *96*, 243.

(30) De Pauw, E. *Mass Spectrom. Rev.* **1986**, *5*, 191.

(31) De Pauw, E.; Agnello, A.; Derwa, F. *Mass Spectrom. Rev.* **1991**, *10*, 283.

metalation in the ion source of the mass spectrometer under conditions of FAB ionization precludes unambiguous, i.e. decisive, conclusions about the occurrence of solvent-assisted mechanisms.

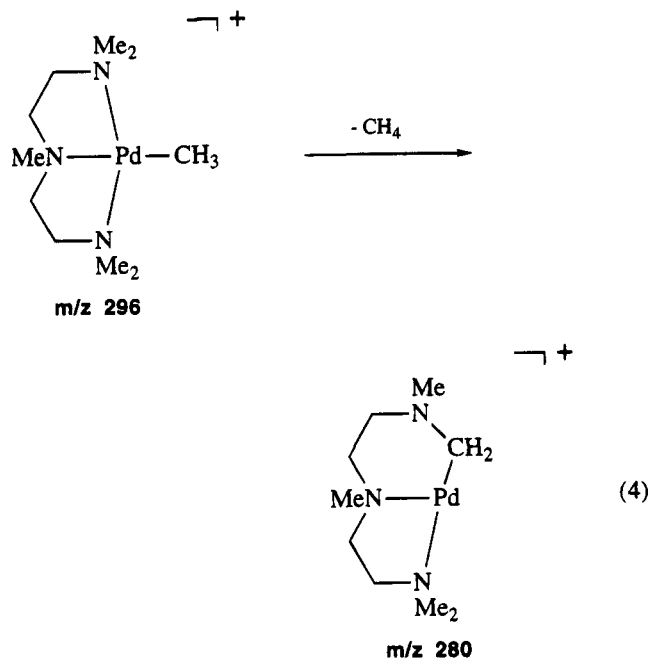
The unimolecular loss of RH from $[Pd(L)(R)]^+$ cations may be considered as a gas-phase analogue of a condensed-phase intramolecular cyclometalation reaction.¹⁰⁻¹⁴ In condensed phase chemistry cyclometalation reactions involving metal-carbon σ -bond formation occur for many reagents.¹³ There are three generally accepted mechanisms for C-H cleavage:¹⁵ oxidative addition (eq 1), electrophilic substitution (eq 2a,b), and



a multicentered pathway (eq 3). In an oxidative addition the C-H bond formally receives two electrons from the metal atom and the oxidation state of the metal $M(n)$ increases by two units ($M(n+2)$). In an oxidative addition the hydride remains in the coordination sphere. Subsequent reductive elimination of the hydride with a suitable ligand X is possible. In an electrophilic mechanism metal hydrides are not formed, the metal ion does not change its oxidation number, and the hydrogen dissociates as a free (eq 2a) or bound proton (eq 2b). Electrophilic reactions are often nucleophilically assisted by coordinated (eq 2b) or free bases which accept the leaving proton. The discrimination between the mechanistic pathways, oxidative addition/reductive elimination or electrophilic substitution, appears to be

complicated.^{15,37,38} A multicentered pathway (eq 3) may be formally considered as an electrophilic one which is nucleophilically assisted; i.e. the metal center is the electrophile which is assisted by the metal-bonded group R acting as a "base". The principal difference is that alkyl, benzyl, or phenyl groups (R) must be present instead of the base B (eq 3).

In condensed phase chemistry cyclopalladation reactions are well recognized. Electrophilic displacement mechanisms (eq 2a) and (eq 2b) are proposed to be operative in cyclopalladation chemistry. It has been shown for orthopalladation of ring-substituted *N,N*-dimethylbenzylamines that the kinetics of the cyclometalation reaction are solvent dependent.³⁹ The loss of RH in the field-free region of the mass spectrometer, however, can only be the result of an intramolecular isomerization reaction followed by a dissociation without the participation of the solvent or other reactants in the transition state. The amine methyl groups are the most likely sources of hydrogen in the $Pd(L)(R)$ cations. Additional support for this proposal is the observation that only CHD_3 neutrals are lost upon collisional activation of $[Pd(NN'N)(CD_3)]^+$ cations. It is assumed that the palladium-nitrogen bond is broken and a six-membered ring is formed *via* a carbon atom of the amine methyl group, as visualized for $Pd(pmdta)(CH_3)$ in eq 4. In condensed phase chemistry a five-membered ring



size of the cyclometalated species is reported to have the most ideal geometry.¹³ However, an X-ray structure of a six-membered ring in a Pd complex with relatively strain-free bond angles and lengths was described.⁴⁰ Another premise for an electrophilic mechanism like in eq 2b is the presence of base with an n-donor electron pair as a leaving group. In the model compounds

(37) Jawad, J. K.; Puddephatt, R. J. *J. Chem. Soc., Chem. Commun.* 1977, 892.

(38) Jawad, J. K.; Puddephatt, R. J.; Stalteri, M. A. *Inorg. Chem.* 1982, 21, 332.

(39) Ryabov, A. D.; Sakodinskaya, I. K.; Yatsimirsky, A. K. *J. Chem. Soc., Dalton Trans.* 1985, 2629.

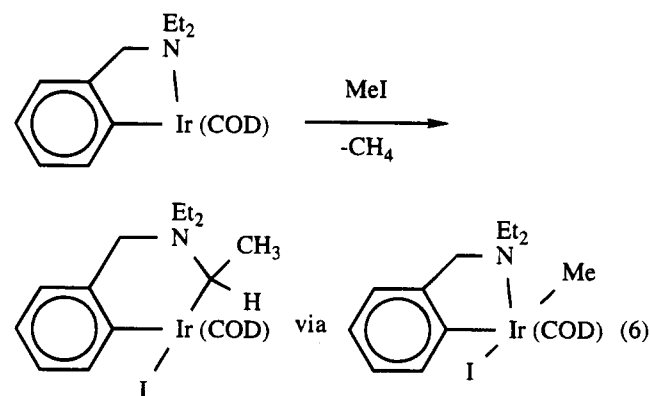
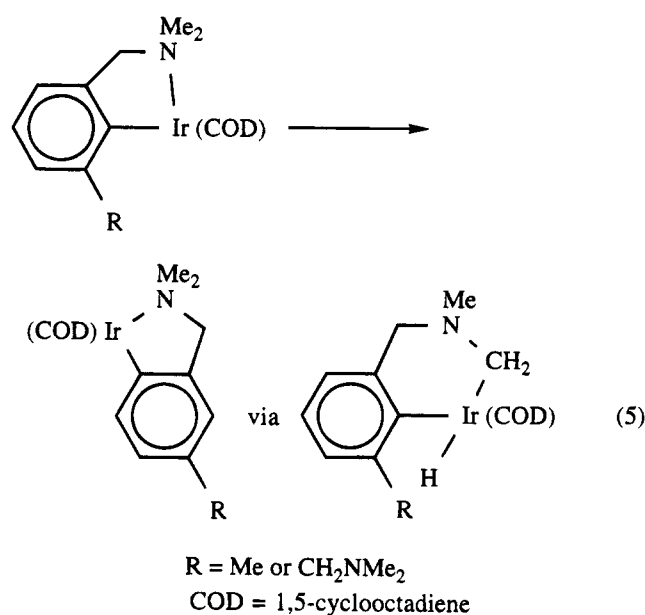
(40) Newkome, G. R.; Puckett, W. E.; Gupta, V. K.; Fronzeck, F. R. *Organometallics* 1983, 2, 1247.

(35) Sunner, J.; Morales, A.; Kebarle, P. *Anal. Chem.* 1987, 59, 1378.

(36) Sunner, J.; Morales, A.; Kebarle, P. *Int. J. Mass Spectrom. Ion Processes* 1989, 87, 287.

(Figure 1) used in this study a covalent bonded R group is lost as RH. This result points in contrast with solution chemistry, to a cyclometalation mechanism (1) or (3) for the unimolecular loss of RH from collisionally activated Pd(L)(R)^+ cations. Furthermore, an interesting aspect in the case of $\text{Pd}(\text{pmdta})(\text{CH}_3)$ is that a cyclopalladation reaction of a tertiary amine occurs by activation of an sp^3 C–H bond. Generally, in condensed phase chemistry of orthopalladated compounds, direct activation of C–H bonds by Pd(II) is the most feasible in the case of tertiary amines,⁴¹ whereas primary and secondary amines are usually not reactive toward such activation, and in cyclometalation sp^2 C–H bonds are more easily activated than sp^3 C–H bonds.^{42,43}

It must be noted that also in solution chemistry this unimolecular pathway is operative. An example where C–H bond cleavage and re-formation occurs is the quantitative skeletal rearrangement of $\text{Ir}(\text{C}_6\text{H}_3\text{CH}_2\text{NMe}_2\text{-2-R-6})(\text{COD})$ ($\text{R} = \text{Me}$ or CH_2NMe_2) to $\text{Ir}(\text{C}_6\text{H}_3\text{-CH}_2\text{NMe}_2\text{-2-R-4})(\text{COD})$ shown in eq 5. The formation



of a coordinative unsaturated, three-coordinate Ir^{I} species through prior Ir–N bond dissociation is followed by intramolecular C–H bond cleavage and concomitant formation of an Ir^{III} intermediate. The latter intermedi-

ate reacts further by aryl C–H (forward reaction) or alkyl C–H (backward reaction) bond formation; cf. Scheme 1 in ref 44. The second example (eq 6) involves the generation of an Ir^{III} oxidative addition intermediate in the reaction of $\text{Ir}(\text{C}_6\text{H}_4\text{CH}_2\text{NEt}_2\text{-2})(\text{COD})$ with MeI .⁴⁵ This intermediate reacts further under CH_4 elimination to form a six-membered ring compound comprising the N center and the Ir^{III} center. This structural motif is encountered in fragment ions m/z 300 (Schemes 1 and 2), which are both generated by unimolecular CH_4 loss. The reaction shown in eq 6 most likely involves a multicenter pathway (cf. eq 3) which so far is rare for C–H bond activation in late transition metal chemistry but recently has been shown to be operative for H–H bond activation.

Fragment ions $[\text{M} - \text{R}]^+$ caused by homolytic bond dissociation of Pd–R were also present, as the isotope clusters in the FAB mass spectra already indicated. The latter process where the σ -bound ligand is lost as a radical is a common fragmentation pathway for FAB-ionized organometallics. It represents a formal redox reaction involving reduction of Pd(II) to Pd(I). Kowalski²² found a similar behavior for $[(\text{PPh}_3)_3\text{PtR}]^+$ complexes ($\text{R} = \text{alkyl, vinyl}$), where fragment ions corresponding to $[\text{M} - \text{R}]^+$ were observed. Such observations reflect known solution properties: fragmentations taking place at the metal–ligand bonds and not within the ligands. Moreover, an analogous behavior is found for complexes bearing π -bound ligands where loss of the intact ligand occurs, as is predicted by their thermal displacement chemistry.^{17,23,46}

Abundant fragmentations of the *pmdta* derivatives 1 and 2 are losses of CH_4 and C_6H_6 . A fairly abundant signal is also found at m/z 278, which is assigned to the loss of H_2 from m/z 280. Subsequent elimination of azapropene ($\text{CH}_2=\text{N}-\text{CH}_3$) leads to the formation m/z 235 cations.

The CID spectra of the m/z 316 *pico* and *NN'N* cations (Table 2) show several collisional-induced fragmentation reactions of the nitrogen ligand, giving various peaks in the CID spectra. The isomeric *pico* and *NN'N* cations are easily differentiated by their CID spectra (Figures 4 and 5). The CID spectrum of m/z 316 Pd(*pico*)(CH_3) cations contains ions at m/z 72, 91, 200, and 229 whereas these ions are not present in the spectrum of m/z 316 Pd(*NN'N*)(CH_3) cations. The CID spectrum of m/z 316 *NN'N* cations shows ions at m/z 284, 258, 255, and 241 which are less abundant or absent in the spectrum of the m/z 316 *pico* cations. The fragmentation pathways leading to the generation of these ions are rationalized in Schemes 1 and 2. The mechanistic proposals are based on permutations of (consecutive/concerted) losses of H_2 , CH_4 , C_2H_4 , $\text{CH}_2=\text{N}-\text{CH}_3$, and CH_3N molecules and a CH_3^{\cdot} radical. It is plausible that several other pathways which are not depicted in Schemes 1 and 2 lead to similar product ions, as neutrals may be lost in different sequences.

The first collisional-induced fragmentation reaction step is loss of CH_4 or CH_3^{\cdot} , yielding cations at m/z 300

(44) van der Zeijden, A. A. H.; van Koten, G.; Luijk, R.; Nordemann, R. A. *Organometallics* **1988**, *7*, 1549.

(45) Wehman-Ooyevaar, I. C. M. *Organometallic Complexes of rhodium, iridium and platinum: steric and electronic effects of chelating nitrogen ligands*. Ph.D. thesis, Utrecht university, 1992.

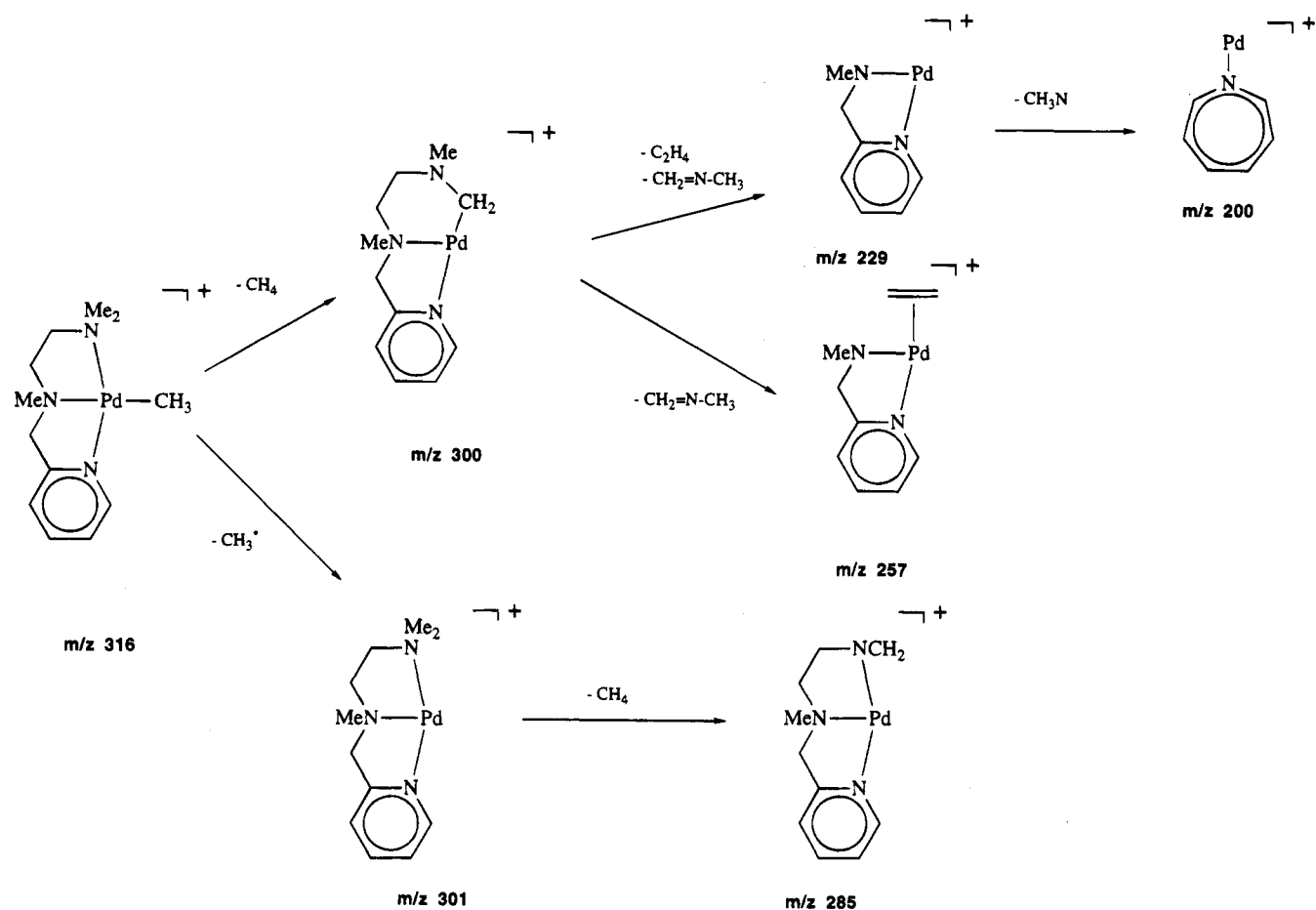
(46) Sharp, T. R.; White, M. W.; Davis, J. F.; Stang, P. J. *Org. Mass Spectrom.* **1984**, *19*, 107.

(41) Alsters, P. L.; Engel, P. F.; Hogerheide, M. P.; Copijn, M.; Spek, A. L.; van Koten, G. *Organometallics* **1993**, *12*, 1831.

(42) Jones, W. D.; Feher, F. J. *J. Am. Chem. Soc.* **1982**, *104*, 4240.

(43) Jones, W. D.; Feher, F. J. *J. Am. Chem. Soc.* **1984**, *106*, 1650.

Scheme 1



and 301, respectively. The second fragmentation of m/z 300 is elimination of H_2 , $\text{CH}_2=\text{N}-\text{CH}_3$, or CH_4 for the NN'N compounds and C_2H_4 or $\text{CH}_2=\text{N}-\text{CH}_3$ for the pico compounds. In the case of the pico ligand no abundant peak was found at m/z 298 corresponding to H_2 dissociating from the $[\text{M} - \text{RH}]^+$ cation. The pico ligand contains only one dimethylamino group, indicating that the hydrogen atoms involved in the initial CH_4 and subsequent H_2 loss from m/z 316 NN'N Pd(L)(R) cations are most likely originating from the dimethylamino group. The m/z 255 ion, resulting from expulsion of $\text{CH}_2=\text{N}-\text{CH}_3$ from m/z 298 pico cations is an azabenzyl cation (Pd(0)) which most likely ring-expands to a seven-membered ring with concomitant σ -bond formation between Pd and the azacycloheptatrienium N atom. In such a mechanism the oxidation state of Pd(II) remains unaltered. Ring expansion of azabenzyl cations to seven-membered ring azatropylium ions and methylpyridine molecular ions to azacycloheptatriene ions is a facile rearrangement reaction in gas-phase ion chemistry.⁴⁷ As H_2 loss of the m/z 300 cations is not a feasible process for the pico compounds, abundant formation of m/z 255 cations by subsequent loss of $\text{CH}_2=\text{N}-\text{CH}_3$ is not expected. The peak at m/z 255 present in Figure 5 is of minor importance in Figure 4. Formation of fragment ions at m/z 229 or 257 (present in Figure 4, absent in Figure 5) by loss of CH_4 , C_2H_4 , and $\text{CH}_2=\text{N}-\text{CH}_3$ or CH_4 and $\text{CH}_2=\text{N}-\text{CH}_3$, respec-

tively, requires a saturated six-membered ring intermediate which can only be formed by cyclometalation of the m/z 316 pico cations (Scheme 1). Another discriminating reaction channel of collisionally induced m/z 316 pico and NN'N cations is formation of m/z 284. This m/z 284 ion is the result of cyclometalation of m/z 316, yielding m/z 300, followed by loss of CH_4 . This process requires the presence of two dimethylamino groups. Loss of CH_4 from dimethylamino compounds is well recognized in the organic mass spectrometry of nitrogen compounds.^{48,49}

Conclusions

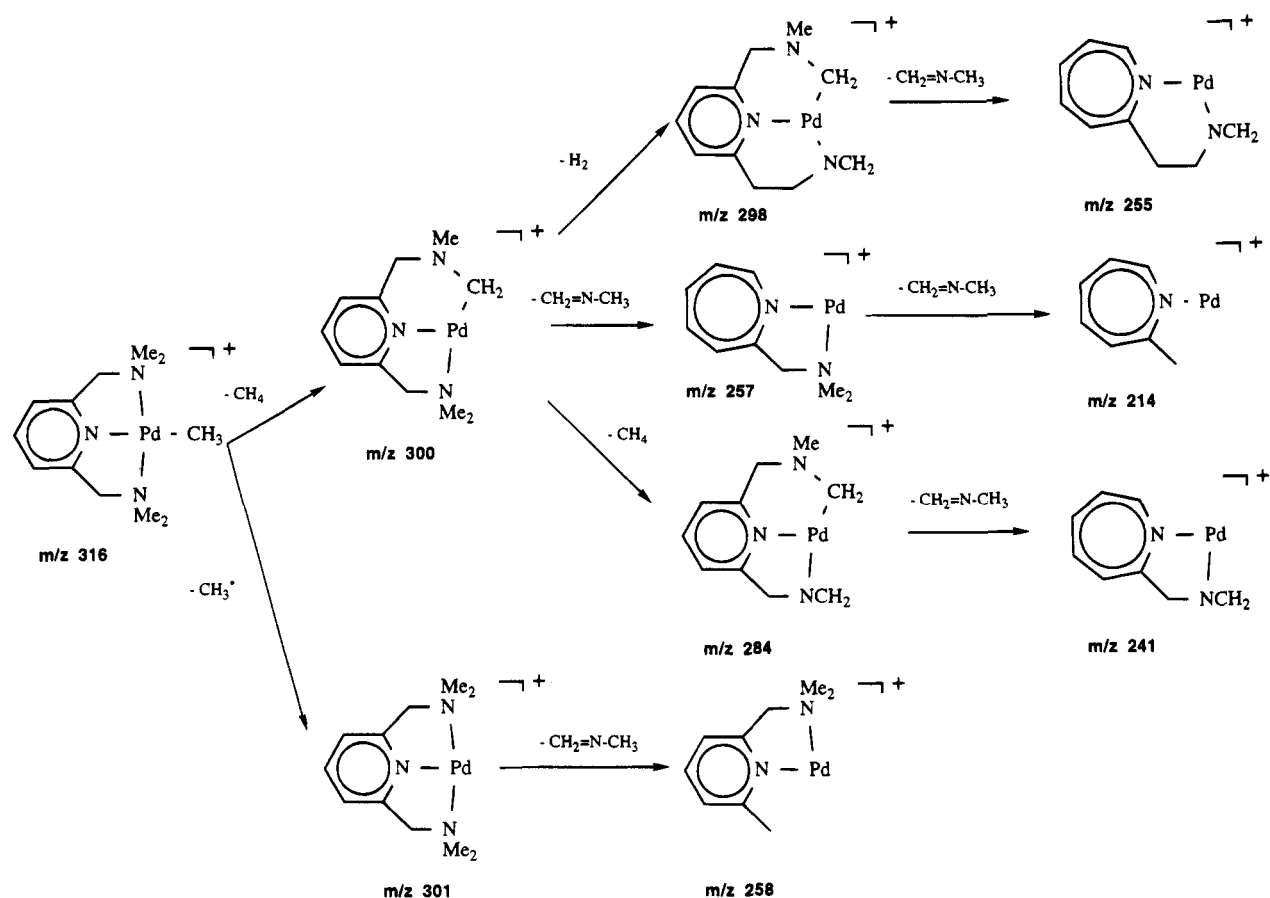
FAB-MS is a valuable technique for the structural characterization of organometallic palladium complexes containing terdentate nitrogen ligands. However, solely FAB-MS has its limitations. FAB ionization of the Pd(L)(R)(OTf) compounds with *m*-nitrobenzyl alcohol as a matrix gives abundant Pd(L)(R) cations. The Pd isotope distribution of their m/z values provides molecular mass information of the compounds. Structural information is present to a lesser extent in the FAB mass spectra, and correct assignment of a particular fragment ion, i.e. the identity of the neutral lost, is obscured by the interference of fragmentation reactions of higher and lower Pd isotopomers leading to isobaric fragment ions. Moreover, diagnostic fragment ions of

(47) Porter, Q. N.; Baldas, J. *Mass spectrometry of heterocyclic compounds*; General Heterocyclic Chemistry; ed. Taylor, E. C., Weissberger, A., Eds.; Wiley & Sons, Inc.: New York, 1971.

(48) Ballard, J. M.; Betowski, L. D. *Org. Mass Spectrom.* **1986**, *21*, 575.

(49) Burinsky, D. J.; Dilliplane, R. L.; DiDonato, G. C.; Busch, K. L. *Org. Mass Spectrom.* **1988**, *23*, 231.

Scheme 2



the ligand system are hidden in the chemical background originating from matrix ions.

FAB-MS/MS offers excellent possibilities to overcome such problems. In MS/MS experiments only the fragment ions from collisionally activated mass-selected monoisotopic ^{108}Pd cations are detected at unit mass resolution with MS-2. The MS/MS spectra contain a variety of ligand characteristic fragment ions, allowing discrimination of the isomeric terdentate pica and NNN nitrogen ligands. In addition to the structural analysis and elucidation of the fragmentation pathways of the $\text{Pd}(\text{L})(\text{R})$ cations to rationalize the formation of the structurally characteristic fragment ions, MS/MS was

also used to study cyclopalladation of the organopalladium compounds in a solvent-free system. Our MS/MS results clearly show, without the need of kinetic experiments with isotopically labeled molecules and/or solvents as required for condensed phase mechanistic studies, that a cyclopalladation reaction mode of the $\text{Pd}(\text{L})(\text{R})$ cations by activation of an sp^3 C-H bond is operative, which invokes an oxidative addition/reductive elimination or a multicentered pathway mechanism instead of a solvent or n -donor ligand assisted electrophilic substitution.

OM940324U

Generation of (2,3- η)-Naphthalene–Nickel(0) Complexes and Their Reactions with Unsaturated Molecules

Martin A. Bennett,* David C. R. Hockless, and Eric Wenger

Research School of Chemistry, Australian National University, Canberra, ACT 0200, Australia

Received November 2, 1994[⊗]

Sodium-amalgam reduction of the (3-bromonaphthyl)nickel(II) complexes NiBr(3-Br-2-C₁₀H₆)L₂ gives the first monomeric nickel(0) complexes of 2,3-naphthalene, Ni(η^2 -C₁₀H₆)L₂ (2 L = 2 PEt₃ (**2**), dcpe (**5**); dcpe = 1,2-bis(dicyclohexylphosphino)ethane, Cy₂PCH₂CH₂PCy₂). Complex **2** undergoes double-insertion reactions with dimethyl acetylenedicarboxylate (DMAD) or diphenylacetylene to give 1,2,3,4-tetrasubstituted anthracenes, C₁₄H₆R₄ (R = CO₂Me (**8**), Ph (**9**)). Complex **5** reacts with CO₂ and with C₂F₄ to give isolable products of monoinsertion into the naphthalene–nickel(0) bond, Ni(3-C₁₀H₆COO-2)(dcpe) (**6**) and Ni(3-C₁₀H₆CF₂CF₂-2)(dcpe) (**7**), respectively, and **7** undergoes further insertion with DMAD to give Ni{3-C(CO₂Me)=C(CO₂Me)C₁₀H₆CF₂CF₂-2}(dcpe) (**10**). The structures of **6**, **7**, and **10** have been solved by heavy-atom methods and refined by least-squares methods. Crystal data: **6**, space group P2₁/n (No. 14), *a* = 14.714(2) Å, *b* = 17.100(1) Å, *c* = 15.990(2) Å, β = 110.244(9)°, *Z* = 4, 2997 observed reflections (*I* > 3 σ (*I*)) with *R* = 4.1 and *R*_w = 2.8; **7**, space group P2₁/c (No. 14), *a* = 11.139(2) Å, *b* = 19.557(2) Å, *c* = 16.809(2) Å, β = 92.927(9)°, *Z* = 4, 3872 observed reflections (*I* > 3 σ (*I*)) with *R* = 3.5 and *R*_w = 2.9; **10**, space group P $\bar{1}$ (No. 2), *a* = 9.415(3) Å, *b* = 11.759(2) Å, *c* = 20.218(3) Å, α = 93.94(1)°, β = 94.77(2)°, γ = 108.90(2)°, *Z* = 2, 4432 observed reflections (*I* > 3 σ (*I*)) with *R* = 3.6 and *R*_w = 3.0.

Introduction

We have shown that monomeric nickel(0)–benzyne complexes Ni(4,5-R₂-(1,2- η)-C₆H₂)L₂ (R = H, F; 2 L = 2 PEt₃, dcpe),¹ which can be prepared by alkali-metal reduction of the corresponding (2-halogenoaryl)nickel(II) complexes NiX(2-X-4,5-R₂C₆H₂)L₂,^{2–4} react with various alkynes to form substituted naphthalenes.⁴ In this reaction the alkyne is believed to undergo double insertion into the nickel–benzyne bond to form an undetected benzonickelacycloheptatriene, which reductively eliminates the naphthalene and forms NiL₂ (Scheme 1). For some unsymmetrical acetylenes, e.g. *t*-BuC₂H and MeC₂CO₂Me, good regioselectivity was observed, as a possible consequence of control by steric and electronic effects, respectively, on the sequential insertions.⁴ In this paper we show that 2,3-naphthalene complexes of nickel(0) can be generated similarly to their benzyne analogues and make some preliminary observations on their reactivity. Free 2,3-naphthalene has been generated previously by the action of phenyllithium on 2,3-dibromonaphthalene and trapped by cycloaddition with 2-methylisindole and with furan.⁵

Results and Discussion

The syntheses of the (2,3- η)-naphthalene complexes are outlined in Scheme 2. Oxidative addition of 2,3-dibromonaphthalene to Ni(COD)₂ in the presence of triethylphosphine (2 equiv) gave a good yield of the (3-bromonaphthyl)nickel(II) complex NiBr(3-Br-2-C₁₀H₆)-(PEt₃)₂ (**1**), which, in contrast with the (2-bromophenyl)nickel(II) complexes,⁴ was not reactive toward lithium. Reduction of **1** with 1% Na/Hg gave the required (2,3- η)-naphthalene complex Ni(η^2 -C₁₀H₆)(PEt₃)₂ (**2**), which was isolated in 90% yield as a highly air-sensitive, oily, yellow solid from hexane at –78 °C. The FAB mass spectrum of **2** in tetraglyme shows the compound to be monomeric, and the IR spectrum contains a strong band at 1585 cm⁻¹, which, like the corresponding band in the benzyne–nickel(0) complexes,^{2,3} is assigned tentatively to ν (C=C) modified by coordination. In addition to the signals due to PEt₃, there are three two-proton resonances in the ¹H NMR spectrum: a pair of AA'BB' multiplets due to H^{6,7} and H^{5,8} and a singlet due to H^{1,4} whose chemical shifts are close to those of free naphthalene. Thus, the aromatic ring is not greatly affected by the presence of the coordinated triple bond, consistent with the presence of a weak additional bond perpendicular to the π -system.^{6–8} In agreement, the ¹³C NMR spectrum shows four resonances in the usual aromatic region together with a singlet at δ 142.52, which is assigned to the bound carbon atoms (C^{2,3}) of the naphthalene. As in the case of the corresponding

(6) Hoffmann, R. W. *Dehydrobenzenes and Cycloalkynes*; Academic Press: New York, 1967.

(7) Hoffmann, R. W. In *Chemistry of Acetylenes*; Viehe, H. G., Ed.; Marcel Dekker: New York, 1969; Chapter 16, p 1063.

(8) Gilchrist, J. L. In *The Chemistry of Functional Groups*; Patai, S., Rapoport, Z., Eds.; Wiley: New York, 1983; Suppl. C, part 1, p 383.

[⊗] Abstract published in *Advance ACS Abstracts*, March 1, 1995.

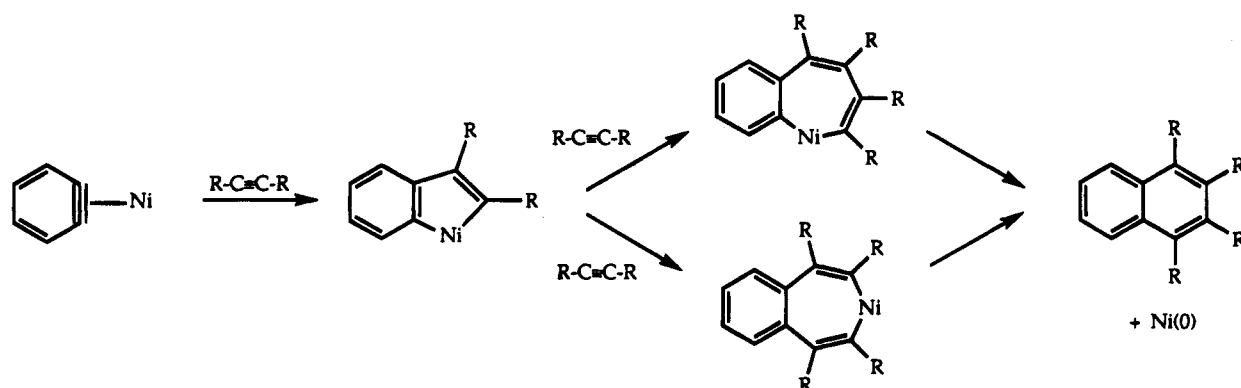
(1) Abbreviations: dcpe = 1,2-bis(dicyclohexylphosphino)ethane, Cy₂PCH₂CH₂PCy₂; COD = 1,5-cyclooctadiene, C₈H₁₂; dppe = 1,2-bis(diphenylphosphino)ethane; DMAD = dimethyl acetylenedicarboxylate, C₂(CO₂Me)₂; AIBN = azobisisobutyronitrile, C₈H₁₂N₄.

(2) Bennett, M. A.; Hambley, T. W.; Roberts, N. K.; Robertson, G. B. *Organometallics* **1985**, *4*, 1992.

(3) Bennett, M. A.; Griffiths, K. D.; Okano, T.; Parthasarathi, V.; Robertson, G. B. *J. Am. Chem. Soc.* **1990**, *112*, 7047.

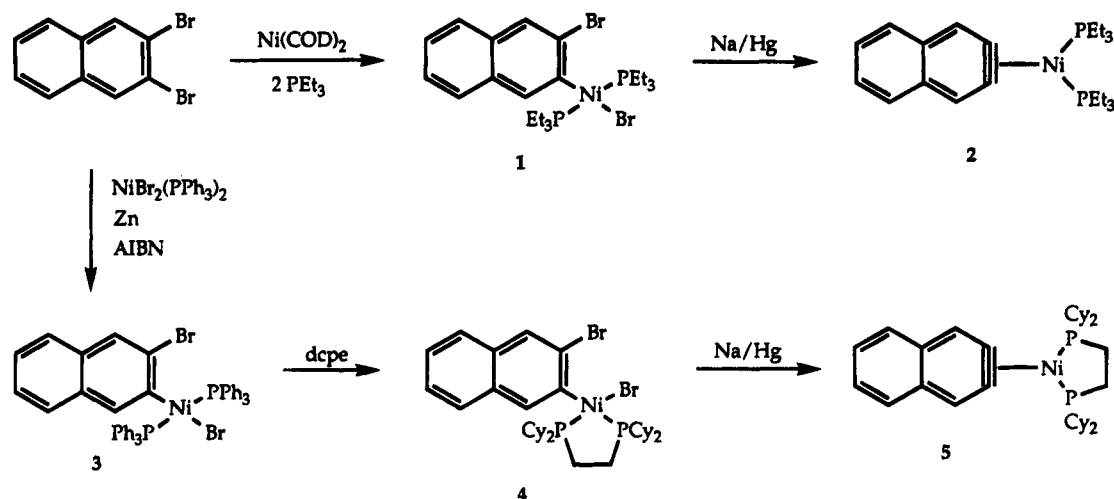
(4) Bennett, M. A.; Wenger, E. *Organometallics*, in press.

(5) LeHoullier, C. S.; Gribble, G. W. *J. Org. Chem.* **1983**, *48*, 2364.

Scheme 1^a

^a Phosphine ligands omitted for clarity.

Scheme 2



$Ni(\eta^2\text{-benzynes})(PEt_3)_2$ complexes, the last resonance shows no ^{31}P coupling at room temperature, owing to rapid intermolecular exchange with traces of residual PEt_3 . Chemical evidence for the formulation of **2** as a (2,3- η)-naphthalene complex is provided by the reaction with DCl , which gives $NiCl_2(PEt_3)_2$ and 2,3-dideuterio-naphthalene quantitatively. The latter was the only isomer present, as shown by GC-MS and NMR (1H , ^{13}C) spectroscopy. The ^{13}C resonances belonging to carbon atoms C^1 and C^4 showed a typical isotropic shift (0.2 ppm);⁹ hence, the deuterium atoms must be attached to carbon atoms C^2 and C^3 .

The reaction of 2,3-dibromonaphthalene with $NiBr_2(PPh_3)_2$ in the presence of zinc that had been sonicated gave the (3-bromonaphthyl)nickel(II) complex $NiBr(3\text{-Br-}2\text{-}C_{10}H_6)(PPh_3)_2$ (**3**), which when heated with $dcpe$ gave $NiBr(3\text{-Br-}2\text{-}C_{10}H_6)(dcpe)$ (**4**) in 64% yield. Like **1**, **4** was unaffected by lithium but was reduced by 1% Na/Hg , giving the (2,3- η)-naphthalene complex $Ni(\eta^2\text{-}C_{10}H_6)(dcpe)$ (**5**) as a beige-yellow, air-sensitive solid in 44% yield. The chemical shifts of the aromatic protons and of the carbon atoms in **5** are similar to those of **2**; the bound carbon atoms $C^{2,3}$ appear at δ 144.4–144.9 as a poorly resolved AAX multiplet similar to that observed in $Ni(\eta^2\text{-}C_6H_4)(dcpe)$.² In the $^{31}P\{^1H\}$ NMR spectrum there is a sharp singlet at δ 77.3 (cf. δ 77.6 in $Ni(\eta^2\text{-}C_6H_4)(dcpe)$).²

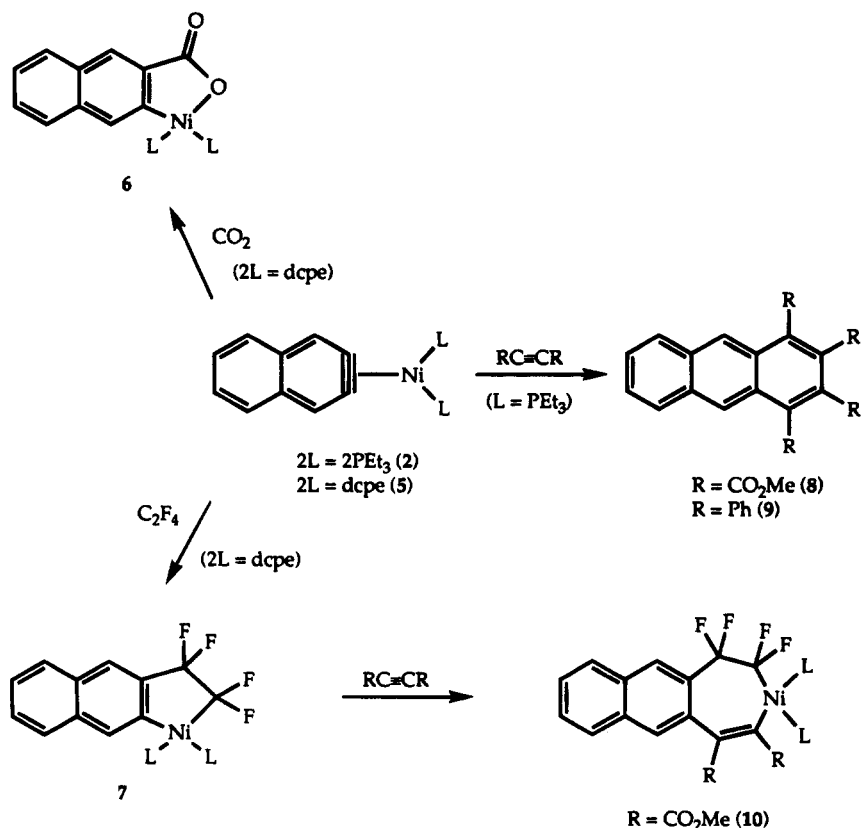
The naphthalene complexes have been characterized further by their insertion reactions with small molecules (Scheme 3). Complex **5** reacted with CO_2 to give $Ni(3\text{-}C_{10}H_6COO\text{-}2)(dcpe)$ (**6**), which was isolated in 25% yield as a yellow solid. It shows a parent ion in its FAB mass spectrum and characteristic carboxylate bands at 1632 and 1615 cm^{-1} in its IR spectrum; similar bands have been observed in the IR spectra of $Ni(C_6H_4COO)(dcpe)^2$ and $Ti(C_6H_4COO)(\eta^5\text{-}C_5H_5)_2$.¹⁰ The $^{31}P\{^1H\}$ NMR spectrum consists of an AB quartet ($^2J_{PP} = 25.0$ Hz) arising from cis-inequivalent phosphorus atoms, and the ^{13}C NMR spectrum contains a doublet of doublets at δ 150.24 assigned to the σ -bonded carbon atom C^2 , which is coupled to the two phosphorus atoms. There are also resonances assignable to the remaining aromatic carbon atoms and to the CH and CH_2 groups of coordinated $dcpe$, but the carbonyl ^{13}C resonance could not be located.

A similar insertion product, $Ni(3\text{-}C_{10}H_6CF_2CF_2\text{-}2)(dcpe)$ (**7**), was obtained in 75% yield by reaction of **5** with tetrafluoroethylene at $-60^\circ C$ with subsequent warming to room temperature. These conditions are considerably milder than those necessary for the cor-

(9) Günther, H. *NMR Spectroscopy, An Introduction*; Wiley: New York, 1980; pp 361–363.

(10) (a) Kolomnikov, I. S.; Lobeveva, T. S.; Gorbachevskaya, V. V.; Aleksandrov, G. G.; Struchkov, Yu. T.; Vol'pin, M. E. *J. Chem. Soc. D* **1971**, 972. (b) Kolomnikov, I. S.; Lobeveva, T. S.; Vol'pin, M. E. *J. Gen. Chem. USSR (Engl. Transl.)* **1972**, 42, 2229.

Scheme 3



responding insertion of the less electrophilic olefin ethylene with $\text{Ni}(\eta^2\text{-C}_6\text{H}_4)(\text{dcpe})$ (3 bar, 80 °C).² The $^{31}\text{P}\{^1\text{H}\}$ NMR spectrum shows a pair of multiplets arising from P–F coupling: one phosphorus atom is coupled to all the fluorine atoms; the other is coupled only to the fluorine atoms of the Ni–CF₂ group. The P–P coupling constant of 14.5 Hz confirms that the phosphorus atoms are mutually cis. Correspondingly, the ^{19}F NMR spectrum of **7** shows a broad signal and a multiplet of equal intensity in the region $\delta_{\text{F}} - 100$ corresponding to the two different CF₂ groups.

The structures assigned to **6** and **7** have been confirmed by single-crystal X-ray structural analyses (see below).

Dimethyl acetylenedicarboxylate (DMAD) reacted with **2** at –30 °C to give a 16% isolated yield of tetramethyl 1,2,3,4-anthracenetetracarboxylate, C₁₄H₆(CO₂Me)₄ (**8**), together with a small amount of hexamethyl benzenehexacarboxylate, C₆(CO₂Me)₆, arising from cyclotrimerization. The former is probably formed by a double-insertion sequence similar to that shown in Scheme 1 for $\text{Ni}(\eta^2\text{-C}_6\text{H}_4)\text{L}_2$, and the $^{31}\text{P}\{^1\text{H}\}$ NMR spectrum of the reaction mixture showed a peak at δ 26.6, which may be due to $\text{Ni}(\eta^2\text{-DMAD})(\text{PEt}_3)_2$ formed after reductive elimination of **8** from the coordination sphere. A similar reaction occurred, though much more slowly, on treatment of **2** with diphenylacetylene. After 6 days at 60 °C, 1,2,3,4-tetraphenylanthracene (**9**) was obtained in 17% isolated yield. In neither case could intermediate monoinsertion complexes analogous to those formed from $\text{Ni}(\eta^2\text{-C}_6\text{H}_4)(\text{dcpe})$ or $\text{Ni}(4,5\text{-F}_2\text{-1,2}\eta\text{-C}_6\text{H}_2)(\text{dcpe})$ and DMAD be detected.

Dimethyl acetylenedicarboxylate also reacted with the C₂F₄ insertion product **7** in refluxing THF to give the

seven-membered nickelacycle $\text{Ni}\{3\text{-C}(\text{CO}_2\text{Me})=\text{C}(\text{CO}_2\text{Me})\text{C}_{10}\text{H}_6\text{CF}_2\text{CF}_2\text{-2}\}(\text{dcpe})$ (**10**) as a yellow solid in 37% isolated yield. No organic products arising from reductive elimination or possible multiple insertion followed by reductive elimination were detected. In addition to the usual aromatic and dcpe resonances, the ^1H NMR spectrum of **10** shows a pair of singlets at δ 3.58 and 3.74 due to the inequivalent CO₂Me groups. In the ^{19}F NMR spectrum there are four ^{19}F - and ^{31}P -coupled resonances in the region $\delta -120$ to -70 , which indicate that all four fluorine atoms are inequivalent and suggest that the chelate ring is not planar, in agreement with the structure determined by X-ray crystallography (see below). The $^{31}\text{P}\{^1\text{H}\}$ NMR spectrum consists of a pair of ^{19}F -coupled multiplets with $^2J_{\text{PP}} = 27.0$ Hz, showing that the complex, like its precursor, has cis-phosphorus atoms. The existence of strong P–F coupling is in accord with the proposed structure and rules out the alternative derived by insertion of DMAD into the Ni–CF₂ bond.

Molecular Structures of $\text{Ni}\{3\text{-C}(\text{CO}_2\text{Me})=\text{C}(\text{CO}_2\text{Me})\text{C}_{10}\text{H}_6\text{CF}_2\text{CF}_2\text{-2}\}(\text{dcpe})$ (**6**), $\text{Ni}\{3\text{-C}(\text{CO}_2\text{Me})=\text{C}(\text{CO}_2\text{Me})\text{C}_{10}\text{H}_6\text{CF}_2\text{CF}_2\text{-2}\}(\text{dcpe})$ (**7**), and $\text{Ni}\{3\text{-C}(\text{CO}_2\text{Me})=\text{C}(\text{CO}_2\text{Me})\text{C}_{10}\text{H}_6\text{CF}_2\text{CF}_2\text{-2}\}(\text{dcpe})$ (**10**).

These are shown in Figures 1–3, respectively; the respective atomic coordinates are in Tables 1–3, and selected bond lengths and interbond angles are given in Tables 4–6, respectively. In all cases the coordination geometry about nickel is close to square planar. In **6** the σ -bonded aryl carbon atom C2 and the oxygen atom O2 of the five-membered chelate ring are twisted slightly out of the coordination plane by 0.214 and –0.125 Å, respectively. The Ni–O distance (1.900(3) Å) is similar to the corre-

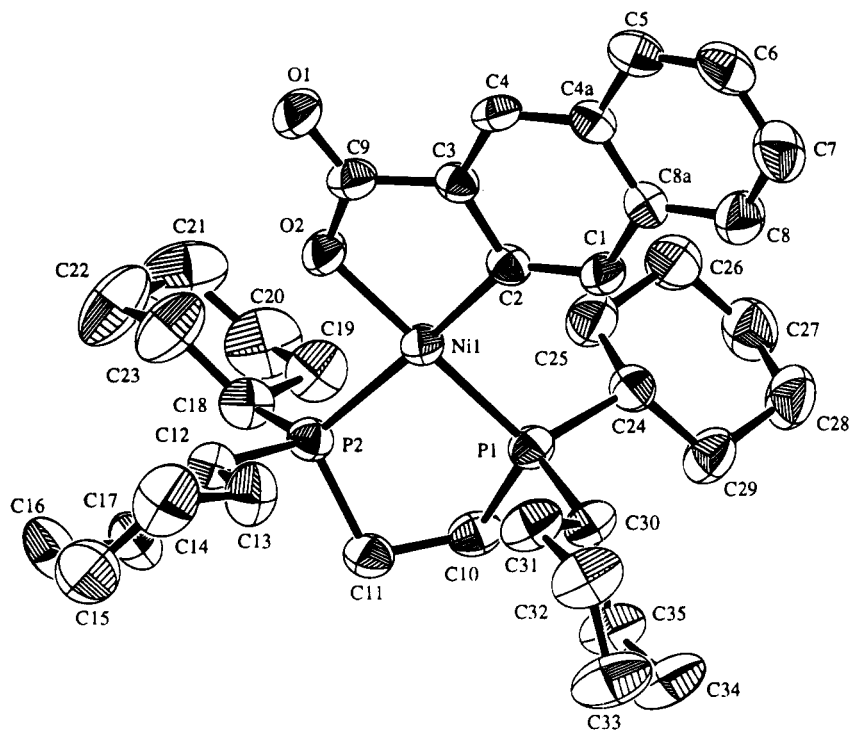


Figure 1. ORTEP diagram for **6** with atom labeling and with 50% probability ellipsoids. Hydrogen atoms have been omitted for clarity.

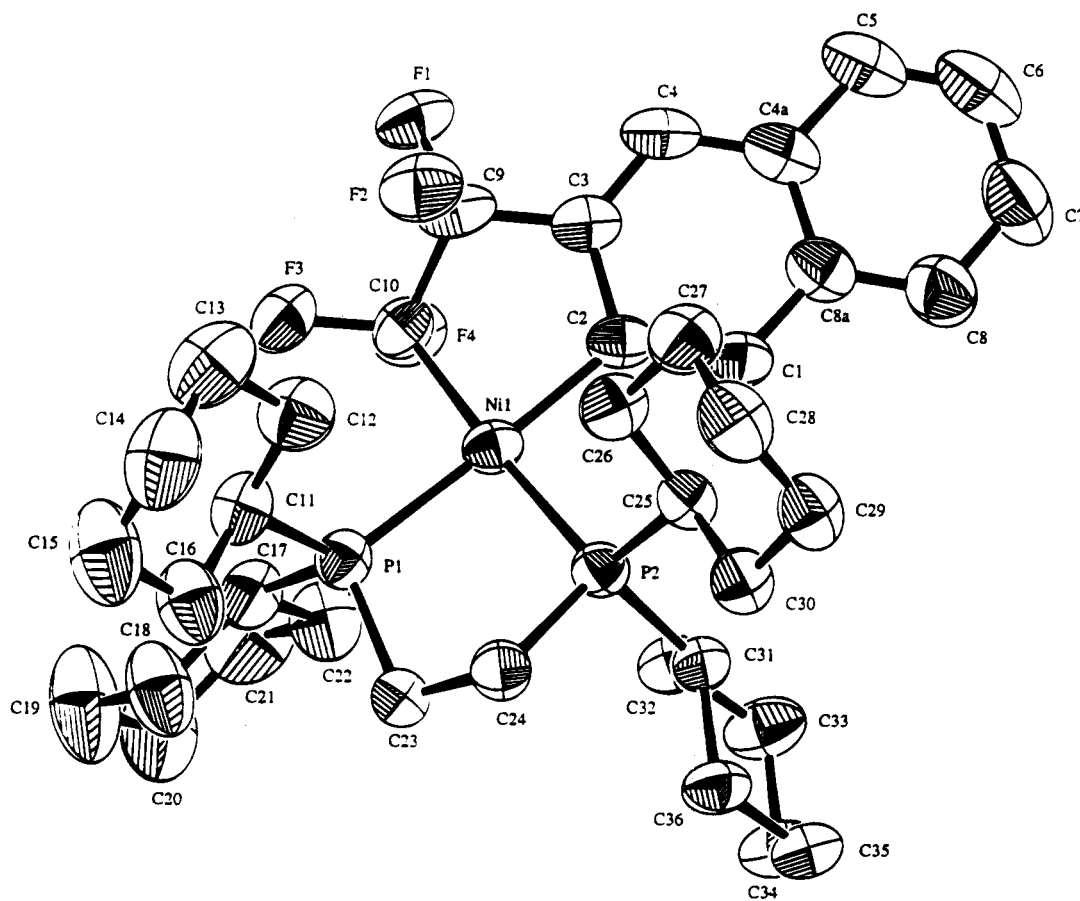


Figure 2. ORTEP diagram for **7** with atom labeling and with 50% probability ellipsoids. Hydrogen atoms have been omitted for clarity.

sponding value of 1.877(9) Å found in the seven-membered-ring nickelacycle $\text{Ni}(\text{CH}_2\text{CMe}_2\text{C}_6\text{H}_4\text{COO}-2)(\text{PMe}_3)_2$ ¹¹ and to the distances observed in

$\text{NiMe}(\text{acac})(\text{PCy}_3)$ (1.881, 1.896 Å)¹² and in $\text{NiEt}(\text{acac})(\text{PPh}_3)$ (1.909(9), 1.913(9) Å).¹³ The C=O distance of 1.235(5) Å (*cf.* 1.222(16) Å in $\text{Ni}(\text{CH}_2\text{CMe}_2-$

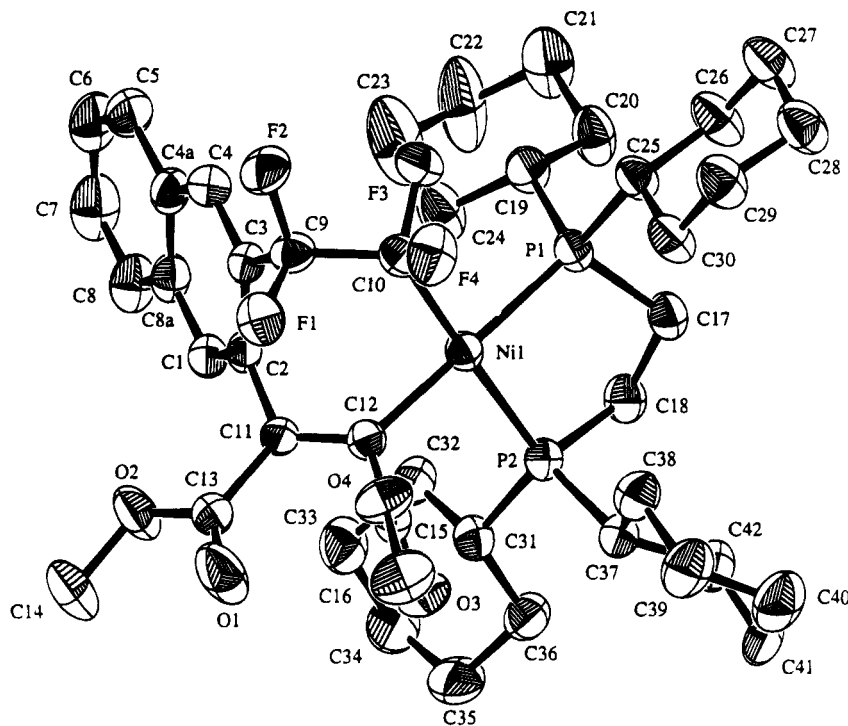


Figure 3. ORTEP diagram for **10** with atom labeling and with 50% probability ellipsoids. Hydrogen atoms have been omitted for clarity.

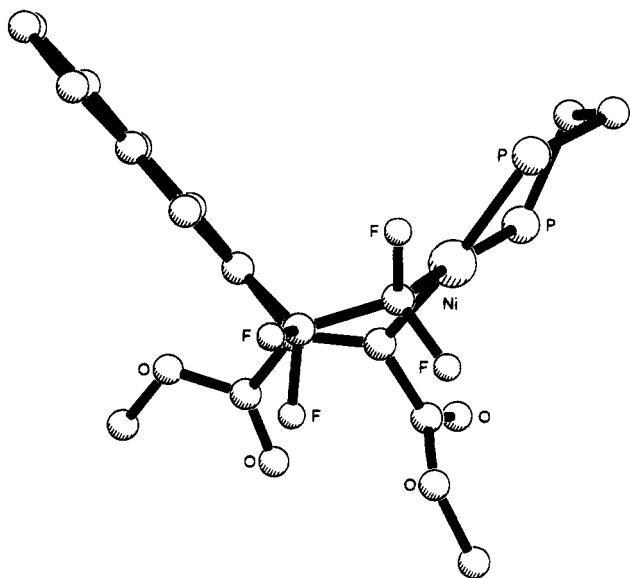


Figure 4. Side view of complex **10** showing the boat conformation of the metallacycle. Hydrogen atoms and cyclohexyl groups of the dcpe ligand have been omitted for clarity.

$\text{C}_6\text{H}_4\text{COO-2})(\text{PMe}_3)_2$ ¹¹ is slightly greater than the typical values for an uncoordinated aryl ester (1.202 Å) or for a γ -lactone (1.198 Å),¹⁴ whereas the O–CO bond length (1.307(5) Å) appears to be significantly less than those in aryl esters and lactones (1.337 Å and 1.350 Å, respectively).¹⁴ These trends may be a consequence of

(11) (a) Carmona, E.; Palma, P.; Paneque, M.; Poveda, M. L.; Gutiérrez-Puebla, E.; Monge, A. *J. Am. Chem. Soc.* **1986**, *108*, 6424. (b) Carmona, E.; Gutiérrez-Puebla, E.; Marín, J. M.; Monge, A.; Paneque, M.; Poveda, M. L.; Ruiz, C. *J. Am. Chem. Soc.* **1989**, *111*, 2883.

(12) Barnett, B. L.; Krüger, C. *J. Organomet. Chem.* **1972**, *42*, 169.

(13) Cotton, F. A.; Frenz, B. A.; Hunter, D. L. *J. Am. Chem. Soc.* **1974**, *96*, 4820.

electron donation from the phosphorus atoms via the nickel atom to the C–O π^* -orbital of the ester group.

Complex **7** contains an envelope-shaped five-membered metallacycle derived by insertion of C_2F_4 into the nickel–benzyne bond of **5**; the nickel atom is 0.750 Å out of the plane formed by C2–C3–C9–C10. Complex **10** contains a boat-shaped seven-membered metallacycle derived by insertion of DMAD into the nickel–aryl bond of **7**, the angle between the planes formed by Ni–C10–C12 and C9–C10–C11–C12 being 38.5°, as illustrated in Figure 4. This geometry renders the four fluorine atoms chemically inequivalent, in agreement with the NMR results (see above). A similar conformation has been reported for the seven-membered nickelacycle Ni-

$(\text{CH}_2\text{CMe}_2\text{C}_6\text{H}_4\text{COO-2})(\text{PMe}_3)_2$.¹¹ The Ni–CF₂ bond lengths in **7** and **10**, 1.926(3) and 1.955(4) Å, respectively, are close to the value of 1.948(6) Å reported for the five-membered nickelacycle $\text{Ni}\{\text{CF}_2(\text{CF}_2)_2\text{CF}_2\}-$ $(\text{PEt}_3)_2$ ¹⁵ and are somewhat less than the Ni–CH₂ separations in $\text{Ni}(\text{C}_6\text{H}_4\text{CH}_2\text{CH}_2-2)(\text{dcpe})$ (1.988(12) Å)² and $\text{Ni}(\text{C}_6\text{H}_4\text{CMe}_2\text{CH}_2-2)(\text{PMe}_3)_2$ (1.97(1) Å);¹¹ this trend has been observed previously in comparable alkyl- and perfluoroalkyl-transition-metal complexes.¹⁶ The nickel–aryl bond lengths in **6**, **7**, and **10** fall in the range 1.93–1.95 Å and are similar to that in $\text{Ni}(\text{C}_6\text{H}_4\text{-CMe}_2\text{CH}_2)(\text{PMe}_3)_2$.^{11b} The Ni–P distances trans to the various σ -bonded carbon atoms in **6**, **7**, and **10** are in the range 2.17–2.21 Å (cf. 2.218(2) Å in $\text{Ni}\{\text{CF}_2-$

(14) Schweizer, W. B.; Dunitz, J. D. *Helv. Chim. Acta* **1982**, *65*, 1547.

(15) Burch, R. R.; Calabrese, J. C.; Ittel, S. D. *Organometallics* **1988**, *7*, 1642.

(16) Hughes, R. P. *Adv. Organomet. Chem.* **1990**, *31*, 183 and references cited therein.

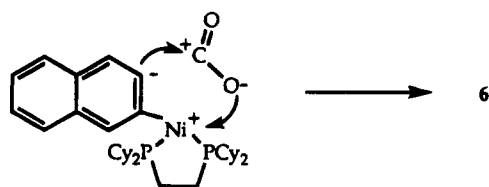
Table 1. Atomic Coordinates for
Ni(3-C₁₀H₅COO-2)(dcpe) (6)

atom	x	y	z
Ni1	0.77099(6)	0.24022(5)	0.18495(5)
Cl(1)	0.6145(2)	0.3572(1)	0.4300(2)
Cl(2)	0.4384(1)	0.2759(1)	0.3464(2)
P1	0.87131(10)	0.16905(8)	0.14850(9)
P2	0.80959(10)	0.17296(8)	0.31155(9)
O1	0.5708(3)	0.3951(2)	0.1754(2)
O2	0.6762(2)	0.2958(2)	0.2170(2)
C0	0.5206(5)	0.3416(5)	0.3332(5)
C1	0.7826(3)	0.3275(3)	0.0207(3)
C2	0.7428(3)	0.3121(3)	0.0857(3)
C3	0.6681(3)	0.3640(3)	0.0871(3)
C4a	0.6736(4)	0.4384(3)	-0.0391(3)
C4	0.6335(3)	0.4230(3)	0.0277(3)
C5	0.6418(4)	0.5012(3)	-0.1009(4)
C6	0.6875(4)	0.5177(3)	-0.1591(4)
C7	0.7659(5)	0.4711(4)	-0.1608(4)
C8	0.7965(4)	0.4094(3)	-0.1031(4)
C8a	0.7514(4)	0.3912(3)	-0.0408(3)
C9	0.6333(4)	0.3530(3)	0.1636(3)
C10	0.9076(4)	0.0860(3)	0.2267(3)
C11	0.9160(4)	0.1122(3)	0.3210(3)
C12	0.8439(3)	0.2404(3)	0.4064(3)
C13	0.9127(4)	0.3046(3)	0.3985(4)
C14	0.9265(5)	0.3655(4)	0.4718(5)
C15	0.9637(5)	0.3290(5)	0.5635(5)
C16	0.9008(5)	0.2638(4)	0.5725(4)
C17	0.8843(4)	0.2020(3)	0.4985(4)
C18	0.7248(4)	0.1044(3)	0.3343(4)
C19	0.6813(4)	0.0461(3)	0.2584(4)
C20	0.6119(5)	-0.0121(4)	0.2783(5)
C21	0.5369(5)	0.0282(4)	0.3056(6)
C22	0.5804(5)	0.0843(4)	0.3811(5)
C23	0.6456(4)	0.1447(4)	0.3569(5)
C24	0.8150(4)	0.1253(3)	0.0372(3)
C25	0.7167(4)	0.0895(3)	0.0281(4)
C26	0.6635(4)	0.0594(4)	-0.0662(4)
C27	0.7252(5)	0.0015(4)	-0.0951(4)
C28	0.8225(5)	0.0371(4)	-0.0865(4)
C29	0.8772(4)	0.0680(3)	0.0082(4)
C30	0.9855(4)	0.2151(3)	0.1481(3)
C31	1.0085(4)	0.2912(3)	0.2011(4)
C32	1.0960(4)	0.3326(3)	0.1907(4)
C33	1.1839(4)	0.2807(4)	0.2200(5)
C34	1.1638(4)	0.2044(4)	0.1694(5)
C35	1.0757(4)	0.1618(3)	0.1804(4)

Table 2. Atomic Coordinates for
Ni(3-C₁₀H₆CF₂CF₂-2)(dcpe) (7)

atom	x	y	z
Ni1	0.10269(5)	0.23883(3)	0.29766(3)
P1	0.24452(8)	0.17264(4)	0.25315(5)
P2	-0.01045(7)	0.20780(4)	0.19228(5)
F1	0.2151(2)	0.37990(9)	0.4631(1)
F2	0.2224(2)	0.38502(9)	0.3344(1)
F3	0.3270(2)	0.27225(10)	0.3852(1)
F4	0.1777(2)	0.24493(9)	0.45874(10)
C1	-0.1416(3)	0.2991(2)	0.3335(2)
C2	-0.0170(3)	0.2993(1)	0.3399(2)
C3	0.0333(3)	0.3554(2)	0.3849(2)
C4	-0.0323(4)	0.4066(2)	0.4162(2)
C4a	-0.1590(4)	0.4063(2)	0.4069(2)
C5	-0.2327(4)	0.4582(2)	0.4379(2)
C6	-0.3539(5)	0.4549(2)	0.4290(3)
C7	-0.4094(4)	0.3994(2)	0.3900(3)
C8	-0.3415(4)	0.3483(2)	0.3596(2)
C8a	-0.2142(3)	0.3503(2)	0.3665(2)
C9	0.1674(3)	0.3502(2)	0.3938(2)
C10	0.2007(3)	0.2749(2)	0.3856(2)
C11	0.3709(3)	0.2157(2)	0.2048(2)
C12	0.3392(3)	0.2885(2)	0.1817(2)
C13	0.4443(4)	0.3268(2)	0.1464(3)
C14	0.4906(4)	0.2892(3)	0.0764(3)
C15	0.5256(4)	0.2169(3)	0.0990(3)
C16	0.4204(3)	0.1786(2)	0.1338(2)
C17	0.3162(3)	0.1155(2)	0.3281(2)
C18	0.3968(3)	0.0600(2)	0.2972(3)
C19	0.4554(4)	0.0186(2)	0.3666(3)
C20	0.3622(4)	-0.0121(2)	0.4177(3)
C21	0.2818(4)	0.0427(2)	0.4489(2)
C22	0.2225(3)	0.0842(2)	0.3803(2)
C23	0.1734(3)	0.1174(2)	0.1763(2)
C24	0.0865(3)	0.1619(2)	0.1245(2)
C25	-0.0728(3)	0.2804(2)	0.1342(2)
C26	0.0234(3)	0.3360(2)	0.1291(2)
C27	-0.0267(3)	0.4000(2)	0.0874(2)
C28	-0.0775(3)	0.3820(2)	0.0045(2)
C29	-0.1748(3)	0.3282(2)	0.0093(2)
C30	-0.1278(3)	0.2636(2)	0.0508(2)
C31	-0.1383(3)	0.1489(2)	0.2091(2)
C32	-0.1259(3)	0.1158(2)	0.2915(2)
C33	-0.2388(3)	0.0754(2)	0.3091(2)
C34	-0.2649(3)	0.0215(2)	0.2457(2)
C35	-0.2760(3)	0.0527(2)	0.1635(2)
C36	-0.1652(3)	0.0944(2)	0.1452(2)

Scheme 4



(CF₂)₂CF₂}(PEt₃)₂¹⁵ and 2.291(4) Å in Ni(C₆H₄CM_e₂CH₂-2)(PMe₃)₂,¹¹ whereas the Ni-P distance trans to the carboxylate oxygen atom of **6** is considerably less (2.144(2) Å; cf. 2.143(4) Å in Ni(CH₂CM_e₂C₆H₄COO-2)(PMe₃)₂¹¹), consistent with the expected low trans influence of the oxygen donor.

Discussion

(2,3-η)-Naphthalene-nickel(0) complexes Ni(η²-C₁₀H₆-L₂) can be generated similarly to their benzyne analogues, and they undergo similar reactions. The insertion of CO₂ into the nickel-naphthalene bond of **5** can be regarded as a nucleophilic attack by coordinated naphthalene on the electrophilic carbon atom of CO₂; addition of the negatively charged oxygen atom of CO₂

to the positively charged nickel atom then forms the metallacycle (Scheme 4). Similar mechanisms probably apply also to the reaction of **5** with C₂F₄ and of **2** with acetylenes. In contrast with CO₂, C₂H₄, and C₂F₄, the alkynes undergo double insertion with both the η²-naphthalene and η²-benzyne complexes, especially those containing PEt₃. This may be driven by the dissociation of one of the PEt₃ ligands and by the formation of a new aromatic ring. The insertion of DMAD into the nickel-aryl bond of **7** requires more vigorous conditions than the corresponding reactions of DMAD with Ni{C₆H₄C(CO₂Me)=C(CO₂Me)-2}(dcpe) or Ni{4,5-F₂C₆H₂C(CO₂Me)=C(CO₂Me)-2}(dcpe).⁴ Moreover, in contrast with these reactions and with the reaction of alkynes with

Ni(C₆H₄CM_e₂CH₂-2)(PMe₃)₂ leading to 1,2-dihydronaphthalenes,¹¹ this insertion is not accompanied by reductive elimination leading to an organic product. It seems likely that reductive elimination occurs more easily in complexes containing monodentate ligands such as PMe₃ or PEt₃. For example, the rates of reductive elimination of ethane from *cis*-PdMe₂L₂ decrease in the order PPh₃ > PMePh₂ > dppe, which can be correlated

Table 3. Atomic Coordinates for

Ni{3-C(CO ₂ Me)=C(CO ₂ Me)C ₁₀ H ₆ CF ₂ CF ₂ -2}(dcpe) (10)			
atom	x	y	z
Ni1	-0.35724(6)	-0.13854(5)	-0.25815(3)
P1	-0.2423(1)	-0.11625(8)	-0.35093(4)
P2	-0.1240(1)	-0.07326(8)	-0.20327(4)
F1	-0.7491(2)	-0.2413(2)	-0.23308(10)
F2	-0.8138(2)	-0.3194(2)	-0.33536(10)
F3	-0.5619(2)	-0.2338(2)	-0.37438(9)
F4	-0.6078(2)	-0.0897(2)	-0.3149(1)
O1	-0.5727(4)	-0.2197(2)	-0.0532(1)
O2	-0.6026(3)	-0.4112(2)	-0.0757(1)
O3	-0.3153(3)	-0.0234(2)	-0.0842(1)
O4	-0.5281(3)	-0.0153(2)	-0.1378(1)
C1	-0.5179(4)	-0.4907(3)	-0.1981(2)
C2	-0.5609(4)	-0.3925(3)	-0.2089(2)
C3	-0.6551(4)	-0.3967(3)	-0.2690(2)
C4	-7.033(4)	-0.4989(3)	-0.3132(2)
C4a	-0.6611(4)	-0.6018(3)	-0.3018(2)
C5	-0.7118(5)	-0.7104(3)	-0.3463(2)
C6	-0.6665(5)	-0.8055(3)	-0.3328(2)
C7	-0.5708(5)	-0.8000(3)	-0.2758(2)
C8	-0.5203(4)	-0.6984(3)	-0.2318(2)
C8a	-0.5650(4)	-0.5968(3)	-0.2433(2)
C9	-0.6942(4)	-0.2869(3)	-0.2855(2)
C10	-0.5588(4)	-0.1874(3)	-0.3074(2)
C11	-0.5158(4)	-0.2832(3)	-0.1590(2)
C12	-0.4447(4)	-0.1714(3)	-0.1759(2)
C13	-0.5638(4)	-0.2988(3)	-0.0912(2)
C14	-0.6452(5)	-0.4287(4)	-0.0093(2)
C15	-0.4208(4)	-0.0653(3)	-0.1266(2)
C16	-0.5202(5)	-0.0838(3)	-0.0895(2)
C17	-0.0389(4)	-0.0410(3)	-0.3282(2)
C18	0.0096(4)	-0.0834(3)	-0.2630(2)
C19	-0.2588(4)	-0.2645(3)	-0.3965(2)
C20 ^a	-0.1319(5)	-0.2714(4)	-0.4348(2)
C20 ^b	-0.351(3)	-0.300(2)	-0.458(1)
C21 ^a	-0.1707(7)	-0.3956(4)	-0.4744(3)
C21 ^b	-0.326(3)	-0.414(2)	-0.493(1)
C22 ^a	-0.2032(8)	-0.4924(4)	-0.4274(4)
C22 ^b	-0.354(4)	-0.513(2)	-0.448(1)
C23	-0.3248(8)	-0.4889(4)	-0.3876(3)
C24	-0.2923(5)	-0.3641(3)	-0.3495(2)
C25	-0.2927(4)	-0.0249(3)	-0.4140(2)
C26	-0.1968(5)	-0.0038(3)	-0.4719(2)
C27	-0.2410(5)	0.0763(3)	-0.5201(2)
C28	-0.2349(5)	0.1952(3)	-0.4842(2)
C29	-0.3369(5)	0.1740(3)	-0.4289(2)
C30	-0.2922(4)	0.0957(3)	-0.3796(2)
C31	-0.0902(4)	-0.1598(3)	-0.1350(2)
C32	-0.1290(4)	-0.2935(3)	-0.1609(2)
C33	-0.1292(5)	-0.3686(3)	-0.1018(2)
C34	0.0229(5)	-0.3237(4)	-0.0600(2)
C35	0.0692(5)	-0.1900(4)	-0.0368(2)
C36	0.0663(4)	-0.1134(3)	-0.0950(2)
C37	-0.0591(4)	0.0874(3)	-0.1674(2)
C38	-0.1529(4)	0.1594(3)	-0.1978(2)
C39	-0.1102(5)	0.2853(3)	-0.1596(2)
C40	0.0568(5)	0.3540(3)	-0.1577(2)
C41	0.1518(4)	0.2826(3)	-0.1297(2)
C42	0.1095(4)	0.1575(3)	-0.1685(2)

^a Populations 0.844(4). ^b Population 0.156(4).

with the ease of dissociation of a P-donor from the coordination sphere.¹⁷

Experimental Section

General Procedures. All experiments were performed under an inert atmosphere using standard Schlenk techniques,¹⁸ and all solvents were dried and degassed prior to use. All reactions with benzyne complexes were carried out under argon. NMR spectra were recorded on the following instru-

Table 4. Selected Bond Lengths (Å) and Interbond Angles (deg) for Ni(3-C₁₀H₆COO-2)(dcpe) (6)

Bond Lengths			
Ni1-P1	2.144(2)	Ni1-P2	2.224(2)
Ni1-O2	1.900(3)	Ni1-C2	1.936(4)
P1-C10	1.844(5)	P2-C11	1.840(5)
P1-C24	1.842(5)	P1-C30	1.858(5)
P2-C12	1.832(5)	P2-C18	1.839(5)
O1-C9	1.235(5)	O2-C9	1.307(5)
C1-C2	1.383(6)	C1-C8a	1.433(6)
C2-C3	1.419(6)	C3-C4	1.358(6)
C3-C9	1.492(6)	C4-C4a	1.414(6)
C4a-C5	1.423(6)	C4a-C8a	1.408(6)
C5-C6	1.352(7)	C6-C7	1.410(8)
C7-C8	1.372(7)	C8-C8a	1.409(6)
C10-C11	1.537(6)	C12-C13	1.528(7)
C12-C17	1.532(7)	C13-C14	1.527(7)
C14-C15	1.512(9)	C15-C16	1.487(9)
C16-C17	1.542(8)	C18-C19	1.530(7)
C18-C23	1.502(7)	C19-C20	1.535(8)
C20-C21	1.489(9)	C21-C22	1.500(9)
C22-C23	1.547(8)	C24-C25	1.530(7)
C24-C29	1.520(6)	C25-C26	1.527(7)
C26-C27	1.520(8)	C27-C28	1.518(8)
C28-C29	1.541(7)	C30-C31	1.526(6)
C30-C35	1.544(7)	C31-C32	1.530(7)
C32-C33	1.503(8)	C33-C34	1.511(8)
C34-C35	1.549(8)		
Bond Angles			
P1-Ni1-P2	88.33(6)	P1-Ni1-O2	175.4(1)
P1-Ni-C2	96.3(1)	P2-Ni1-O2	89.6(1)
P2-Ni1-C2	171.7(1)	O2-Ni1-C2	86.3(2)
Ni1-P1-C10	108.5(2)	Ni1-P1-C24	111.8(2)
Ni1-P1-C30	118.0(2)	C10-P1-C24	105.7(2)
C10-P1-C30	106.2(2)	C24-P1-C30	105.9(2)
Ni1-P2-C11	108.0(2)	Ni1-P2-C12	109.8(2)
Ni1-P2-C18	122.2(2)	C11-P2-C12	107.7(2)
C11-P2-C18	103.9(2)	C12-P2-C18	104.4(2)
Ni1-O2-C9	115.5(3)	C2-C1-C8a	122.8(4)
Ni1-C2-C1	135.3(4)	Ni1-C2-C3	109.4(3)
C1-C2-C3	115.1(4)	C2-C3-C4	124.0(5)
C2-C3-C9	114.9(4)	C4-C3-C9	121.0(4)
C4-C4a-C5	122.8(5)	C4-C4a-C8a	117.6(5)
C5-C4a-C8a	119.6(5)	C3-C4-C4a	120.9(4)
C4a-C5-C6	120.8(5)	C5-C6-C7	120.1(5)
C6-C7-C8	120.1(5)	C7-C8-C8a	121.3(5)
C1-C8a-C4a	119.5(5)	C1-C8a-C8	122.4(5)
C5a-C8a-C8	118.1(5)	O1-C9-O2	123.5(5)
O1-C9-C3	122.5(5)	O2-C9-C3	114.0(4)

ments: Varian XL-200E (¹H at 200 MHz, ¹³C at 50.3 MHz, ¹⁹F at 188.1 MHz, and ³¹P at 80.96 MHz), Varian Gemini-300 BB (¹H at 300 MHz and ¹³C at 75.4 MHz), or Varian VXR-300 (¹H at 300 MHz and ¹³C at 75.4 MHz). The chemical shifts (δ) for ¹H and ¹³C are given in ppm relative to residual signals of the solvent, to external 85% H₃PO₄ for ³¹P, and to internal CFCl₃ for ¹⁹F. The spectra of all nuclei (except ¹H and ¹⁹F) were ¹H-decoupled. Coupling constants (*J*) are given in Hz. Infrared spectra were measured in solution (KBr cells) on a Perkin-Elmer 683 instrument. Mass spectra of the complexes were obtained on a VG ZAB2-SEQ spectrometer by means of the fast-atom bombardment (FAB) technique. Solutions of the samples were prepared with dry THF (for naphthalene complexes) or CH₂Cl₂ and added to a matrix of glycerol, 3-nitrobenzyl alcohol, *o*-nitrophenyl octyl ether, or degassed tetraglyme (for naphthalene complexes). Mass spectra of organic compounds were obtained by the electron impact method (EI) on a VG Micromass 7070F spectrometer. Bis-(1,5-cyclooctadiene)nickel(0) was prepared by reduction of anhydrous Ni(acac)₂¹⁹ with Et₃Al in the presence of COD and a trace of butadiene.²⁰ 2,3-Dibromonaphthalene was prepared by the Diels-Alder reaction of furan with 4,5-dibromobenzyne

(17) Gillie, A.; Stille, J. K. *J. Am. Chem. Soc.* **1980**, *102*, 4933.

(18) Shriver, D. F.; Drezdson, M. A. *The Manipulation of Air-Sensitive Compounds*, 2nd ed.; Wiley: New York, 1986.

(19) Charles, R. G.; Pawlikowski, M. A. *J. Phys. Chem.* **1958**, *62*, 440.

(20) Schunn, R. A. *Inorg. Synth.* **1974**, *15*, 5.

Table 5. Selected Bond Lengths (Å) and Interbond Angles (deg) for Ni(3-C₁₀H₆CF₂CF₂)(dcpe) (7)

Bond Lengths			
Ni-IP1	2.203(1)	Ni1-P2	2.2058(9)
Ni1-C2	1.944(3)	Ni1-C10	1.926(3)
P1-C11	1.862(3)	P1-C17	1.836(3)
P1-C23	1.833(3)	P2-C24	1.843(3)
P2-C25	1.839(3)	P2-C31	1.864(3)
F1-C9	1.383(3)	F2-C9	1.377(3)
F3-C10	1.409(3)	F4-C10	1.397(3)
C1-C2	1.386(4)	C1-C8a	1.418(4)
C2-C3	1.429(4)	C3-C4	1.362(4)
C3-C9	1.498(4)	C4-C4a	1.412(4)
C4a-C6	1.421(4)	C4a-C8a	1.414(4)
C5-C5	1.352(5)	C6-C7	1.395(5)
C7-C8	1.368(5)	C8-C8a	1.416(4)
C9-C10	1.527(4)	C11-C12	1.513(4)
C11-C16	1.524(4)	C12-C13	1.534(5)
C13-C14	1.502(6)	C14-C15	1.511(6)
C15-C16	1.531(5)	C17-C18	1.516(5)
C17-C22	1.525(4)	C18-C19	1.538(5)
C19-C20	1.506(5)	C20-C21	1.507(6)
C21-C22	1.533(5)	C23-C24	1.538(4)
C25-C26	1.533(4)	C25-C30	1.535(4)
C26-C27	1.527(4)	C27-C28	1.518(5)
C28-C29	1.516(5)	C29-C30	1.522(4)
C31-C32	1.528(4)	C31-C36	1.532(4)
C32-C33	1.528(4)	C33-C34	1.517(4)
C34-C35	1.510(5)	C35-C36	1.524(4)
Bond Angles			
P1-Ni1-P2	87.48(4)	P1-Ni1-C2	177.45(10)
P1-Ni1-C10	95.0(1)	P2-Ni1-C2	94.95(10)
P2-Ni1-C10	174.4(1)	C2-Ni1-C10	82.5(1)
Ni1-P1-C11	117.0(1)	Ni1-P1-C17	114.8(1)
Ni1-P1-C23	107.1(1)	C11-P1-C17	105.2(1)
C11-P1-C23	105.6(2)	C17-P1-C23	106.4(1)
Ni1-P2-C24	107.6(1)	Ni1-P2-C25	113.5(1)
Ni1-P2-C31	117.2(1)	C24-P2-C25	105.4(1)
C24-P2-C31	105.6(1)	C25-P2-C31	106.7(1)
C2-C1-C8a	123.8(3)	Ni1-C2-C1	132.2(2)
Ni1-C2-C3	113.7(2)	C1-C2-C3	114.1(3)
C2-C3-C4	124.4(3)	C2-C3-C9	111.3(3)
C4-C3-C9	124.2(3)	C3-C4-C4a	120.5(3)
C4-C4a-C5	123.4(4)	C4-C4a-C8a	117.6(3)
C5-C4a-C8a	118.9(4)	C4a-C5-C6	121.2(4)
C5-C6-C7	120.4(4)	C6-C7-C8	120.2(4)
C7-C8-C8a	121.3(4)	C1-C8a-C4a	119.5(3)
C1-C8a-C8	122.5(3)	C4a-C8a-C8	118.0(3)
F1-C9-F2	103.8(2)	F1-C9-C3	113.2(3)
F1-C9-C10	113.3(3)	F2-C9-C3	111.9(3)
F2-C9-C10	107.0(3)	C3-C9-C10	107.5(3)
Ni1-C10-F3	120.7(2)	Ni1-C10-F4	113.5(2)
Ni1-C10-C9	107.0(2)	F3-C10-F4	102.5(2)
F3-C10-C9	106.4(3)	F4-C10-C9	105.7(3)

generated by the action of *n*-BuLi on 1,2,4,5-tetrabromobenzene; the resulting epoxide was deoxygenated by treatment with Zn/TiCl₄.²¹ Microanalyses were done in-house.

Preparation of NiBr(3-Br-2-C₁₀H₆)(PEt₃)₂ (1). A suspension of Ni(COD)₂ (2.63 g, 9.6 mmol) in *n*-hexane (60 mL) was treated successively with PEt₃ (3.6 mL, 24.2 mmol) and solid 2,3-dibromonaphthalene (3.9 g, 13.6 mmol). The mixture was stirred for 35 min at room temperature, for 1 h under reflux, and again for 16 h at room temperature. The solution was filtered through Celite, and the residue was washed with toluene (4 × 5 mL). The solution was evaporated to dryness, and the brown oil was crystallized from MeOH/toluene (40 mL/15 mL) to yield **1** as a brown solid (4.87 g, 83%). IR (CH₂Cl₂): 3045 (w), 2975 (s), 2945 (m), 2920 (m), 2890 (m), 1578 (w), 1560 (w), 1487 (m), 1460 (m), 1418 (m), 1402 (m), 1195 (w), 1137 (w), 1105 (w), 1065 (m), 1040 (vs), 945 (m), 880 (s) cm⁻¹. ¹H NMR (200 MHz, C₆D₆): δ 0.99 (quint, 18H, ³J = 7.5, CH₃),

(21) (a) Hart, H.; Lai, C.; Chukuemeka, G.; Shamouilian, S. *Tetrahedron* **1987**, *43*, 5203. (b) Hart, H.; Bashir-Hashemi, A.; Luo, J.; Meador, M. A. *Tetrahedron* **1986**, *42*, 1641. (c) Akula, M. R. *Org. Prep. Proced. Int.* **1990**, *22*, 102.

Table 6. Selected Bond Lengths (Å) and Interbond Angles (deg) for Ni{3-C(CO₂Me)=C(CO₂Me)C₁₀H₆CF₂CF₂}(dcpe) (10)

Bond Lengths			
Ni1-P1	2.231(1)	Ni1-P2	2.243(1)
Ni1-C10	1.955(4)	Ni1-C12	1.924(3)
P1-C17	1.833(4)	P1-C19	1.869(3)
P1-C25	1.850(3)	P2-C18	1.839(3)
P2-C31	1.837(3)	P2-C37	1.860(3)
F1-C9	1.367(4)	F2-C9	1.382(4)
F3-C10	1.419(4)	F4-C10	1.382(3)
O1-C13	1.194(4)	O2-C13	1.320(4)
O2-C14	1.441(4)	O3-C15	1.203(4)
O4-C15	1.334(4)	O4-C16	1.447(4)
C1-C2	1.368(4)	C1-C8a	1.416(4)
C2-C3	1.432(4)	C2-C11	1.499(4)
C3-C4	1.372(4)	C3-C9	1.503(4)
C4-C4a	1.418(4)	C4a-C5	1.430(4)
C4a-C8a	1.414(5)	C5-C6	1.355(5)
C6-C7	1.388(6)	C7-C8	1.364(5)
C8-C8a	1.416(4)	C9-C10	1.546(4)
C11-C12	1.350(4)	C11-C13	1.484(4)
C12-C15	1.488(4)	C17-C18	1.527(4)
C19-C20	1.497(5)	C19-C24	1.530(4)
C20-C21	1.534(6)	C21-C22	1.505(7)
C22-C23	1.462(7)	C23-C24	1.535(5)
C25-C26	1.523(4)	C25-C30	1.534(4)
C26-C27	1.523(5)	C27-C28	1.513(5)
C28-C29	1.514(5)	C29-C30	1.525(4)
C31-C32	1.537(4)	C31-C36	1.530(4)
C32-C33	1.533(4)	C33-C34	1.515(5)
C34-C35	1.517(5)	C35-C36	1.534(5)
C37-C38	1.530(4)	C37-C42	1.537(4)
C38-C39	1.535(5)	C39-C40	1.513(5)
C40-C41	1.514(6)	C41-C42	1.532(5)
Bond Angles			
P1-Ni1-P2	85.84(4)	P1-Ni1-C10	93.1(1)
P1-Ni1-C12	173.24(10)	P2-Ni1-C10	177.1(1)
P2-Ni1-C12	90.88(10)	C10-Ni1-C12	90.4(1)
Ni1-P1-C17	109.0(1)	Ni1-P1-C19	112.3(1)
Ni1-P1-C25	119.4(1)	C17-P1-C19	104.8(2)
C17-P1-C25	103.8(2)	C19-P1-C25	106.4(2)
Ni1-P2-C18	108.1(1)	Ni1-P2-C31	116.2(1)
Ni1-P2-C37	114.5(1)	C18-P2-C31	105.6(2)
C18-P2-C37	105.8(2)	C31-P2-C37	105.9(2)
C13-O2-C14	115.5(3)	C15-O4-C16	115.1(3)
C2-C1-C8a	122.7(3)	C1-C2-C3	118.4(3)
C1-C2-C11	121.9(3)	C3-C2-C11	119.6(3)
C2-C3-C4	119.9(3)	C2-C3-C9	120.0(3)
C4-C3-C9	120.0(3)	C3-C4-C4a	121.9(3)
C4-C4a-C5	123.2(4)	C4-C4a-C8a	118.3(3)
C5-C4a-C8a	118.5(3)	C4a-C5-C6	120.3(4)
C5-C6-C7	121.1(4)	C6-C7-C8	120.5(4)
C7-C8-C8a	120.7(4)	C1-C8a-C4a	118.8(3)
C1-C8a-C8	122.4(4)	C4a-C8a-C8	118.8(3)
F1-C9-F2	103.5(3)	F1-C9-C3	111.3(3)
F1-C9-C10	110.1(3)	F2-C9-C3	109.7(3)
F2-C9-C10	109.6(3)	C3-C9-C10	112.3(3)
Ni1-C10-F3	112.7(2)	Ni1-C10-F4	111.7(2)
Ni1-C10-C9	121.9(2)	F3-C10-F4	102.7(2)
F3-C10-C9	100.4(3)	F4-C10-C9	105.4(3)
C2-C11-C12	121.7(3)	C2-C11-C13	118.2(3)
C12-C11-C13	119.9(3)	Ni1-C12-C11	124.4(2)
Ni1-C12-C15	116.4(2)	C11-C12-C15	119.0(3)
O1-C13-O2	120.9(3)	O1-C13-C11	124.8(3)
O2-C13-C11	114.3(3)	O3-C15-O4	122.9(3)
O3-C15-C12	125.9(3)	O4-C15-C12	111.0(3)
P1-C17-C18	109.4(2)	P2-C18-C17	107.8(2)

1.22–1.57 (m, 12H, CH₂), 7.05 (t, 1H, ³J = 7, H⁶ or H⁷), 7.18 (t, 1H, ³J = 7, H⁷ or H⁶), 7.39 (d, 1H, ³J = 8, H⁵ or H⁸), 7.46 (d, 1H, ³J = 8, H⁵ or H⁸), 7.70 (s, 1H, H¹ or H⁴), 7.77 (s, 1H, H⁴ or H¹). ¹³C{¹H} NMR (75.4 MHz, C₆D₆): δ 8.38 (CH₃), 14.88 (t, J_{CP} = 12.6, CH₂), 124.21 (CH), 125.82 (CH), 125.93 (CH), 127.02 (CH), 127.18 (CH), 131.47 (C^{4a} or C^{8a}), 132.20 (C^{8a} or C^{4a}), 133.07 (br s, C³), 137.42 (t, J_{CP} = 4.4, C¹-H), 157.99 (t, J_{CP} = 34, C²). ³¹P{¹H} NMR (80.96 MHz, C₆D₆): δ 9.8 (s). FAB-

MS (tetraglyme, $C_{22}H_{36}Br_2NiP_2$): m/z 501 (18, 2-Br- $C_{10}H_6Ni$ -(PEt_3)₂), 325 (95), 323 (100, 2-Br-3- $PEt_3C_{10}H_6$), 295 (27), 294 (37), 293 (47, $Ni(PEt_3)_2$); the molecular ion at m/z 578 was not observed. Anal. Calcd for $C_{22}H_{36}Br_2NiP_2$: C, 45.48; H, 6.25; P, 10.66; Br, 27.51. Found: C, 45.12; H, 6.37; P, 10.41; Br, 27.16.

Preparation of Ni((2,3- η)- $C_{10}H_6$)(PEt_3)₂ (2). A 1% sodium amalgam (494 mg of Na, 3.6 mL of Hg) suspended in THF (30 mL) was cooled to 0 °C and treated with **1** (646 mg, 1.11 mmol). The mixture was stirred at room temperature for 3.5 h and decanted into a flask kept at -30 °C. The solvent was evaporated at 0 °C, the residue was extracted with hexane (6 \times 10 mL), and the extract was filtered through Celite into a flask kept at -78 °C. The volume of solvent was reduced to about half. The complex was crystallized at -78 °C to yield **2** as a yellow oily solid (464 mg, 90%). IR (hexane): 3030 (w), 1585 (s, C=C), 1505 (m), 1250 (m), 1192 (m), 1178 (m), 1030 (s), 838 (s), 760 (vs), 725 (vs) cm^{-1} . 1H NMR (200 MHz, C_6D_6): δ 0.85–1.05 ($[A_3B_2X]$ m, 18H, $J = 7.5$, CH_3), 1.45–1.65 ($[A_3B_2X]$ m, 12H, $J = 7.5$, CH_2), 7.37–7.44 ($[AA'BB']$ m, 2H, $H^{6,7}$), 8.04 (s, 2H, $H^{1,4}$), 8.05–8.15 ($[AA'BB']$ m, 2H, $H^{5,8}$). ^{13}C - $\{^1H\}$ NMR (75.4 MHz, C_6D_6): δ 9.00 (CH_3), 19.94 (d, $J_{CP} = 20.7$, CH_2), 118.14 (CH), 123.64 (CH), 128.17 (CH), 137.72 ($C^{4a,8a}$), 142.52 ($C^{2,3}$). $^{31}P\{^1H\}$ NMR (80.96 MHz, C_6D_6): δ 27.0 (br s). FAB-MS (tetraglyme, $C_{22}H_{36}NiP_2$): m/z 420 (100, M), 393 (43), 391 (68, M - Et), 296 (46), 294 (92, $Ni(PEt_3)_2$).

Preparation of NiBr(3-Br-2- $C_{10}H_6$)(PPh_3)₂ (3). A suspension of Zn (0.43 g, 6.5 mmol) in THF (5 mL) that had been activated by ultrasound for 40 min at room temperature was treated successively with a solution of 2,3-dibromonaphthalene (1.6 g, 5.6 mmol) in THF (7 mL), $NiBr_2(PPh_3)_2$ (3.5 g, 4.7 mmol), AIBN (56 mg), and THF (10 mL). The green solution was stirred for 2.5 h at 25 °C to give a brown suspension. The solvent was removed by evaporation, the residue was extracted with CH_2Cl_2 , and the solution was filtered through Celite. The volume of filtrate was reduced to 20 mL under reduced pressure. On addition of hexane (20 mL) and cooling to -78 °C, complex **3** crystallized. The yield was 3.58 g (88%). 1H NMR (200 MHz, CD_2Cl_2): δ 7.00–7.80 (m, 36H). $^{31}P\{^1H\}$ NMR (80.96 MHz, CD_2Cl_2): δ 22.2 (s).

Preparation of NiBr(3-Br-2- $C_{10}H_6$)(dcpe) (4). A solution containing **3** (3.58 g, 4.1 mmol) and dcpe (1.9 g, 4.51 mmol) in toluene (70 mL) was stirred for 3 h at 60 °C. The solution was filtered through Celite, and the solid formed during the reaction was extracted with CH_2Cl_2 . The solvent was removed by evaporation, and the compound was purified by column chromatography (silica gel, CH_2Cl_2). The yield of **4** was 2 g (64%). 1H NMR (200 MHz, CD_2Cl_2): δ 1.15–2.60 (m, 48H, CH_2 and C_6H_{11}), 7.14–7.39 (m, 3H, H^{arom}), 7.49–7.63 (m, 2H, H^{arom}), 7.74 (br s, 1H, H^{arom}). ^{13}C NMR (75.4 MHz, CD_2Cl_2): δ 19.30 (dd, $J_{CP} = 20.8$, $J_{CP} = 10.9$, CH_2), 23.92 (t, $J_{CP} = 20.9$, CH_2), 25.94–28.13 (m, CH_2), 28.50, 29.28, 29.49, 30.32, 32.38 (CH_2), 32.60 (d, $J_{CP} = 24$), 33.71 (d, $J_{CP} = 20.9$), 35.52 (d, $J_{CP} = 19.8$), 36.99 (d, $J_{CP} = 24.1$, CH of C_6H_{11}), 123.94, 125.21, 126.43, 126.84, 127.83 (CH), 131.87, 132.41, 135.03 (C), 136.72 (CH), 159.35 (dd, $J_{CP} = 86.0$, $J_{CP} = 33.9$, C^2). $^{31}P\{^1H\}$ NMR (80.96 MHz, CD_2Cl_2): δ 65.3, 68.0 ([AB] q, $^2J = 28.2$). FAB-MS (3-nitrobenzyl alcohol, $C_{36}H_{54}Br_2NiP_2$): m/z 766 (23, M), 687 (100 M - Br). Anal. Calcd for $C_{36}H_{54}Br_2NiP_2$: C, 56.35; H, 7.09; P, 8.07. Found: C, 57.07; H, 7.89; P, 7.80.

Preparation of Ni((2,3- η)- $C_{10}H_6$)(dcpe) (5). A 1% sodium amalgam (572 mg of Na, 4 mL of Hg) suspended in THF (60 mL) was cooled to 0 °C and treated with **4** (2.86 g, 3.76 mmol). The mixture was stirred for 3 h at 25 °C. At this stage, ^{31}P NMR spectroscopy showed that **5** had been formed quantitatively. The solution was decanted, the solvent was removed by evaporation, and the residue was extracted with toluene. The extract was filtered through Celite and pumped to dryness under a vacuum. The brown oil was washed with hexane and dissolved in THF, and the product was precipitated as a yellow-beige powder by adding hexane at -20 °C. The yield of **5** was 1 g (44%). 1H NMR (300 MHz, C_6D_6): δ 0.80–2.25 (m, 48H,

CH_2 and C_6H_{11}), 7.37–7.40 ($[AA'BB']$ m, 2H, $H^{6,7}$), 8.11–8.14 ($[AA'BB']$ m, 2H, $H^{5,8}$), 8.42 (s, 2H, $H^{1,4}$). $^{13}C\{^1H\}$ NMR (75.4 MHz, C_6D_6): δ 22.31 (t, $J_{CP} = 19$, CH_2), 26.25 (t, $J_{CP} = 19$, CH_2), 26.41, 26.92, 27.53, 29.67, 30.01 (CH_2 of C_6H_{11}), 35.16 (t, $J_{CP} = 10.5$, CH of C_6H_{11}), 121.62, 123.58 (CH), 138.51 ($C^{4a,8a}$), 144.4–144.9 (m, $C^{2,3}$) (one naphthalenic CH signal hidden by C_6D_6). $^{31}P\{^1H\}$ NMR (80.96 MHz, C_6D_6): δ 77.3 (s). FAB-MS (tetraglyme, $C_{36}H_{54}NiP_2$): m/z 607 (M + 1).

Reaction of 5 with CO_2 . A sample of the crude naphthalene complex **5** (prepared by 1% Na/Hg reduction of **4** (0.575 g, 0.75 mmol) in THF) was exposed at -78 °C to 1 atm of CO_2 .

The yellow monoinsertion complex $Ni(3-C_{10}H_6COO-2)(dcpe)$ (**6**) was isolated (123 mg, 25% based on **4**) and purified by crystallization from CH_2Cl_2 . IR (CH_2Cl_2): 2935 (s), 2870 (m), 1632 (s), 1615 (m), 1450 (w), 1325 (m), 1285 (w) cm^{-1} . 1H NMR (200 MHz, CD_2Cl_2): δ 1.10–2.20 (m, 48H, CH_2 and C_6H_{11}), 7.37 (quint, 2H, $^3J = 7.5$, $H^{6,7}$), 7.58 (d, 1H, $J_{HP} = 6.4$, H^1), 7.71 (d, 1H, $^3J = 7.5$, $H^{5\text{ or }8}$), 7.81 (d, 1H, $J = 7.5$, $H^{8\text{ or }5}$), 7.87 (s, 1H, H^4). ^{13}C NMR (75.4 MHz, CD_2Cl_2): δ 26.31 (t, $J_{CP} = 11.0$, CH_2), 27.08–28.99 (m, CH_2), 29.19, 29.92 (CH_2), 32.06 (d, $J_{CP} = 3.3$, CH_2 of C_6H_{11}), 34.01 (d, $J_{CP} = 16.5$, CH of C_6H_{11}), 36.58 (d, $J_{CP} = 22.0$, CH of C_6H_{11}), 124.67, 126.12, 126.24, 127.50, 129.03 (CH), 131.74 (C^{4a}), 135.29 (dd, $J_{CP} = 6.6$, $J_{CP} = 3.2$, C^1-H), 135.63 (d, $J_{CP} = 7.5$, C^{8a}), 142.06 (C^3), 150.24 (dd, $J_{CP} = 80.1$, $J_{CP} = 27.5$, C^2); the CO_2 carbon was not visible. $^{31}P\{^1H\}$ NMR (80.96 MHz, CD_2Cl_2): δ 68.7, 76.1 ([AB] q, $^2J_{PP} = 25.0$). FAB-MS (3-nitrobenzyl alcohol, $C_{37}H_{54}NiO_2P_2$): m/z 651 (100, M + 1). Anal. Calcd for $C_{37}H_{54}NiO_2P_2$: C, 68.22; H, 8.35; P, 9.51. Found: C, 67.74; H, 8.69; P, 8.51.

Reaction of 5 with C_2F_4 . A solution of **5** (prepared by reduction of **4** (0.85 g, 1.11 mmol) with 1% Na/Hg) in THF (20 mL) was placed under 1 atm of C_2F_4 at -60 °C and stirred for 16 h while the solution was warmed to room temperature. The solution was filtered through silica gel, the solvent was removed by evaporation, and the residual solid was washed

with hexane to give $Ni(3-C_{10}H_6CF_2CF_2-2)(dcpe)$ (**7**; 590 mg, 75% based on **4**). Crystals suitable for X-ray analysis were obtained from $CH_2Cl_2/EtOH$. 1H NMR (200 MHz, CD_2Cl_2): δ 1.00–2.30 (m, 48H, CH_2 and C_6H_{11}), 7.32–7.49 (m, 2H, $H^{6,7}$), 7.72 (d, 1H, $^3J = 7.7$, $H^{5\text{ or }8}$), 7.78–7.92 (m, 3H, $H^{8\text{ or }5}$, $H^{1,4}$). ^{13}C NMR (75.4 MHz, CD_2Cl_2): δ 19.98 (dd, $J_{CP} = 21.9$, $J_{CP} = 16.4$, CH_2), 20.72 (dd, $J_{CP} = 23.0$, $J_{CP} = 16.4$, CH_2), 26.42, 26.58, 27.53, 27.65, 27.82, 27.92, 28.00, 28.11 (CH_2), 29.53 (d, $J_{CP} = 3.3$), 29.65 (d, $J_{CP} = 3.3$), 30.72 (d, $J_{CP} = 4.4$), 31.50 (d, $J_{CP} = 5.4$, CH_2 of C_6H_{11}), 35.67 (d, $J_{CP} = 25.3$, CH of C_6H_{11}), 35.91 (d, $J_{CP} = 26.3$, CH of C_6H_{11}), 121.23, 124.67, 125.98, 127.62, 128.44 (CH), 131.76, 133.84 ($C^{4a,8a}$), 137.74 (d, $J_{CP} = 6.6$, C^1-H), 142.73 (t, $J_{CF} = 20.4$, C^3), 156.6–157.6 (m, C^2); CF_2 not visible. ^{19}F NMR (188.1 MHz, CD_2Cl_2): δ -106.06 (br s, 2F), -96.28 (ddt, 2F, $J_{FP} = 31.4$, $J_{FP} = 19.8$, $J_{FF} = 10.7$). $^{31}P\{^1H\}$ NMR (80.96 MHz, CD_2Cl_2): δ 65.1 (dtt, $J_{PP} = 14.5$, $^3J_{FP} = 31.3$, $^4J_{FP} = 4.4$), 69.4 (dt, $J_{PP} = 14.5$, $^3J_{FP} = 19.7$). FAB-MS (3-nitrophenyl octyl ether, $C_{38}H_{54}F_4NiP_2$): m/z 706 (15, M), 687 (14, M - F), 499 (87), 480 (100). Anal. Calcd for $C_{38}H_{54}F_4NiP_2$: C, 64.51; H, 7.69; P, 8.76. Found: C, 63.63; H, 7.90; P, 8.43.

Reaction of 2 with DCl. A few drops of 35% DCl/ D_2O were added to a solution of **2** (50 mg) in C_6D_6 in a 5 mm NMR tube. After 5 min at room temperature, the reaction was complete (^{31}P NMR) to quantitatively form $NiCl_2(PEt_3)_2$ (δ 11.6) and 2,3-dideuterionaphthalene. The solution was dissolved in ether (10 mL), washed with water (3 \times 10 mL), and dried over $MgSO_4$. The solvent was removed, and 2,3- $D_2-C_{10}H_6$ was purified by sublimation. 1H NMR (200 MHz, CD_2Cl_2): δ 7.44–7.50 ($AA'BB'$, 2H, $H^{6,7}$), 7.81–7.88 ($AA'BB'$, 2H, $H^{5,8}$), 7.84 (s, 2H, $H^{1,4}$). $^{13}C\{^1H\}$ NMR (50.3 MHz, CD_2Cl_2): δ 126.15 (C^6-H and C^7-H), 128.01 (C^1-H and C^4-H) (isotopic shift), 128.13 (C^5-H and C^8-H), 133.80 ($C^{4a,8a}$); the resonance due to $C^{2,3}$ was not located. GC-MS ($C_{10}H_6D_2$): m/z 130 (100, M), 129 (30), 128 (10); retention time 6 min (column BPI 12.5 m, initial temperature 50 °C, final temperature 180 °C, $\Delta T = 10$ °C/

Table 7. Crystal and Structure Refinement Data for Compounds 6, 7, and 10

	Ni(3-C ₁₀ H ₆ COO-2)(dcpe) (6)	Ni(3-C ₁₀ H ₆ CF ₂ CF ₂ -2)(dcpe) (7)	Ni{3-C(CO ₂ Me)=C(CO ₂ Me)C ₁₀ H ₆ CF ₂ CF ₂ -2}(dcpe) (10)
	(a) Crystal Data		
chem formula	C ₃₇ H ₅₄ NiO ₂ P ₂ ·CH ₂ Cl ₂	C ₃₈ H ₅₄ F ₄ NiP ₂	C ₄₄ H ₆₀ F ₄ NiO ₄ P ₂
fw	736.41	707.49	849.60
cryst syst	monoclinic	monoclinic	triclinic
unit cell dimens			
<i>a</i> (Å)	14.714(2)	11.139(2)	9.415(3)
<i>b</i> (Å)	17.100(1)	19.557(2)	11.759(2)
<i>c</i> (Å)	15.990(2)	16.809(2)	20.218(3)
α (deg)			93.94(1)
β (deg)	110.244(9)	92.927(9)	94.77(2)
γ (deg)			108.90(2)
<i>V</i> (deg) (Å ³)	3774.8(7)	3657.1(6)	2099.3(8)
space group	<i>P</i> 2 ₁ / <i>n</i> (No. 14)	<i>P</i> 2 ₁ / <i>c</i> (No. 14)	<i>P</i> 1 (No. 2)
<i>D</i> _c (g cm ⁻³)	1.296	1.285	1.344
<i>Z</i>	4	4	2
<i>F</i> (000)	1568	1504	900
color, habit	yellow, block	yellow, block	pale yellow, plate
cryst dimens	0.08 × 0.11 × 0.21	0.28 × 0.10 × 0.06	0.24 × 0.10 × 0.03
<i>μ</i> (cm ⁻¹)	30.80 (Cu Kα)	19.65 (Cu Kα)	18.80 (Cu Kα)
	(b) Data Collection and Processing		
diffractometer	Rigaku AFC 6R	Rigaku AFC 6R	Rigaku AFC 6R
X-radiation	Cu Kα (graphite monochromated)	Cu Kα (graphite monochromated)	Cu Kα (graphite monochromated)
scan mode	<i>ω</i> -2θ	<i>ω</i> -2θ	<i>ω</i> -2θ
<i>ω</i> -scan width	1.42 + 0.30 tan θ	1.10 + 0.30 tan θ	1.20 + 0.30 tan θ
2θ limits (deg)	120.0	120.3	120.3
data collected (<i>hkl</i>)	(-17,0,0) to (17,19,18)	(0,0,-19) to (12,22,19)	(-11,-13,-23) to (0,13,23)
no. of rflns			
total	6058	5833	6672
unique (<i>R</i> _{int} /%)	5825 (3.75)	5621 (2.0)	6231 (1.7)
obsd	2997 (<i>I</i> > 3σ(<i>I</i>))	3872 (<i>I</i> > 3σ(<i>I</i>))	4432 (<i>I</i> > 3σ(<i>I</i>))
abs cor (transmission factors)	azimuthal scans (0.43-1.00)	azimuthal scans (0.90-1.00)	azimuthal scans (0.88-1.00)
secondary extinction cor coeff	[1.5(4)] × 10 ⁻⁸	[3(2)] × 10 ⁻⁸	
	(c) Structure Analysis and Refinement ^a		
structure soln	direct methods (SAPI91 ²² DIRDIF92 ²³)	Patterson methods (PATTY, DIRDIF92) ²³	Patterson methods (PATTY, DIRDIF92) ²³
refinement	full-matrix least squares	full-matrix least squares	full-matrix least squares
no. of params	407	407	509
weighting scheme	4 <i>F</i> _o ² /[σ ² (<i>F</i> _o ²) + (0.001 <i>F</i> _o ²) ²]	4 <i>F</i> _o ² /[σ ² (<i>F</i> _o ²) + (0.005 <i>F</i> _o ²) ²]	4 <i>F</i> _o ² /[σ ² (<i>F</i> _o ²) + (0.004 <i>F</i> _o ²) ²]
<i>R</i> (obsd data) (%)	4.1	3.5	3.6
<i>R</i> _w (obsd data) (%)	2.8	2.9	3.0

^a All calculations were performed using teXsan²⁴ with neutral atom scattering factors from Cromer and Waber,²⁵ Δ*f* and Δ*f*' values from ref 26, and mass attenuation coefficients from ref 27. Anomalous dispersion effects were included in *F*_{calc}.²⁸

min, injector temperature 200 °C); for comparison, the retention time of naphthalene is 6 min.

Reaction of 2 with Dimethyl Acetylenedicarboxylate (DMAD). Addition of DMAD (0.1 mL, 0.74 mmol) in THF (2 mL) to a solution of 2 (260 mg, 0.62 mmol) in THF (20 mL) at -50 °C gave a black solution. The mixture was stirred for 3 h at -30 °C, and the solvent was evaporated to give a red oil which showed a peak at δ 26.6 in the ³¹P NMR spectrum, probably due to Ni(*η*²-DMAD)(PEt₃)₂. The organic compounds were separated by column chromatography (silica gel, ether) to give tetramethyl anthracene-1,2,3,4-tetracarboxylate (8; 40 mg, 16%) together with a trace of hexamethyl benzenehexacarboxylate. 1,2,3,4-(CO₂Me)₄-C₁₄H₆ (8): IR (CHCl₃) 2960 (w), 1740 (s), 1445 (m), 1365 (w), 1305 (w) cm⁻¹; ¹H NMR (200 MHz, CDCl₃) δ 3.92 (s, 6H, OCH₃), 4.07 (s, 6H, OCH₃), 7.55-7.63 (AA'BB', 2H, H^{7,8}), 7.97-8.05 (AA'BB', 2H, H^{6,9}), 8.62 (s, 2H, H^{5,10}); ¹³C{¹H} NMR (75.4 MHz, CDCl₃) δ 53.07 (OCH₃), 53.17 (OCH₃), 126.06 (CH), 126.26 (C^{4a,10a} or C^{5a,9a}), 126.55 (C^{5a,9a} or C^{4a,10a}), 127.82 (CH), 128.49 (CH), 133.17 (C^{2,3}), 134.57 (C^{1,4}), 166.76 (C=O), 167.41 (C=O); EI-MS (C₂₂H₁₈O₈) *m/z* 410 (100, M), 379 (54), 176 (26).

Reaction of 2 with Diphenylacetylene. A solution of 2 (260 mg, 0.62 mmol) in THF (20 mL) at -30 °C was treated with a solution of diphenylacetylene (132 mg, 0.74 mmol) in THF (2 mL). After 70 h at room temperature no reaction was observed (³¹P NMR). After 6 days at 60 °C, the only phosphorus-containing material was OPET₃. The solvent was removed

by evaporation. The residue was dissolved in ether, washed with water, dried over MgSO₄, and filtered through Celite. The product was crystallized from ether to give 1,2,3,4-tetraphenylanthracene (9; 50 mg, 17%). ¹H NMR (200 MHz, CDCl₃): δ 6.86 (s, 10H, C₆H₅), 7.27 (s, 10H, C₆H₅), 7.32-7.40 (AA'BB', 2H, H^{7,8}), 7.76-7.88 (AA'BB', 2H, H^{6,9}), 8.18 (s, 2H, H^{5,10}). ¹³C{¹H} NMR (75.4 MHz, CDCl₃): δ 125.26 (CH), 125.36 (CH), 125.89 (CH), 126.50 [CH(phenyl) + CH], 127.58 [CH(phenyl)], 128.26 (CH), 130.84 (C), 131.23 [CH(phenyl)], 131.38 [CH(phenyl)], 131.54 (C), 138.04 (C), 138.42 (C), 139.66 (C), 140.52 (C) (all quaternary carbons were identified by APT experiments). EI-MS (C₃₈H₂₆): *m/z* 482 (100, M), 405 (7).

Reaction of 7 with DMAD. A solution of 7 (215 mg, 0.3 mmol) in THF (15 mL) was refluxed with DMAD (2 mL) for 16 h. The solvent was pumped off, and the red oil was washed with ether (3 × 20 mL). The residue was purified by preparative TLC (ether/hexane 1:1), and the double-insertion complex 10 was isolated as a yellow solid (94 mg, 37%). Crystals suitable for X-ray analysis were obtained from CH₂Cl₂. ¹H NMR (200 MHz, CD₂Cl₂): δ 1.10-2.45 (m, 48H, CH₂ and C₆H₁₁), 3.58 (s, 3H, OCH₃), 3.74 (s, 3H, OCH₃), 7.43-7.51 (m, 2H, H^{6,7}), 7.76-7.88 (m, 2H, H^{5,8}), 7.89 (br s, 1H, H^{1 or 4}), 8.07 (br s, 1H, H^{4 or 1}). ¹⁹F NMR (188.1 MHz, CD₂Cl₂): δ -124.26 (d, ²*J*_{FF} = 228.9), -96.53 (dd, ²*J*_{FF} = 228.5, ³*J*_{FF} = 13.9), -92.58 (ddd, ²*J*_{FF} = 273.7, ³*J*_{FF} = 12.1, ³*J*_{FP} = 25), -77.97 (dddd, ²*J*_{FF} = 273.5, ³*J*_{FF} = 11.9, ³*J*_{FP} = 99.2, ³*J*_{FP} = 32.3), ³¹P{¹H} NMR (80.96 MHz, CD₂Cl₂): δ 57.9 (ddt, ²*J*_{PP} = 27.0, ³*J*_{FP} = 9.4, ³*J*_{FP}

= 26.9), 66.9 (dd, $^2J_{PP} = 27.0$, $^3J_{FP} = 97.6$). FAB-MS (*o*-nitrophenyl octyl ether, $C_{44}H_{60}F_4NiO_4P_2$): m/z 849 (5, $M + 1$), 829 (6, $M - F$), 789 (18, $M - CO_2Me$), 499 (100, $NiF(dcpe)$), 480 (88, $Ni(dcpe)$). Anal. Calcd for $C_{44}H_{60}F_4NiO_4P_2$: C, 62.20; H, 7.12. Found: C, 61.21; H, 7.53.

X-ray Crystallography of Complexes 6, 7, and 10. Crystal data, details of data collection, data processing, structure analysis, and structure refinement are given in Table 7. Structure **6** was solved by direct methods (SAPI91),²² whereas **7** and **10** were solved using Patterson methods (PATTY),²³ and all were expanded using Fourier techniques (DIRDIF92).²³ All non-hydrogen atoms were refined anisotropically (except for the minor component of a disordered Cy group in **10**) by full-matrix least squares. Hydrogen atoms were included at calculated positions ($C-H = 0.95 \text{ \AA}$) and held fixed. All calculations were performed using the teXsan Structure Analysis Software of Molecular Structure Corp.²⁴

Acknowledgment. We thank the Swiss National Science Foundation for the award of a fellowship (E.W.) (Grant No 8220-033162).

Supplementary Material Available: For complexes **6**, **7**, and **10**, tables of atomic coordinates with isotropic displacement parameters, bond lengths, bond angles, torsion angles, and anisotropic displacement parameters (46 pages). Ordering information is given on any current masthead page.

OM940833W

(22) Hai-Fu, F. *Structure Analysis Programs with Intelligent Control*; Rigaku Corp.: Tokyo, Japan, 1991.

(23) Beurskens, P. T.; Admiraal, G.; Beurskens, G.; Bosman, W. P.; Garcia-Granda, S.; Gould, R. O.; Smits, J. M. M.; Smykalla, C. *The DIRDIF Program System, Technical Report of the Crystallographic Laboratory*; University of Nijmegen: Nijmegen, The Netherlands, 1992.

(24) teXsan: Single Crystal Structure Analysis Software, Version 1.6c (1993); Molecular Structure Corp., The Woodlands, TX 77381.

(25) Cromer, D. T.; Waber, J. T. *International Tables for X-Ray Crystallography*; Kynoch Press: Birmingham, England, 1974; Vol. IV, Table 2.2A.

(26) Creagh, D. C.; McAuley, W. J. In *International Tables for Crystallography*; Wilson, A. J. C., Ed.; Kluwer Academic: Boston, MA, 1992; Vol. C, Table 4.2.6.8, pp 219–222.

(27) Creagh, D. C.; Hubbell, J. H. In ref 26, Vol. C, Table 4.2.4.3, pp 200–206.

(28) Ibers, J. A.; Hamilton, W. C. *Acta Crystallogr.* **1964**, *17*, 781.

Notes

Synthesis and Structural Characterization of a Diiridium μ -Acyl ComplexJoseph M. O'Connor^{*,1} and Richard Merwin

Departments of Chemistry, University of California, San Diego, La Jolla, California 92093-0358, and University of Nevada, Reno, Nevada 89557

Arnold L. Rheingold* and Melanie L. Adams

Department of Chemistry, University of Delaware, Newark, Delaware 19716

Received December 16, 1994[®]

Summary: The metallacyclopentadiene chloride complex

$\text{Ir}(\text{CR}=\text{CRCR}=\text{CR})(\text{AsPh}_3)_2\text{Cl}$ (**3**, $\text{R} = \text{CO}_2\text{CH}_3$) undergoes reaction with 3-butyn-1-ol at room temperature to give the metallacycle-carbene complex

$\text{Ir}(\text{CR}=\text{CRCR}=\text{CR})[\text{C}(\text{CH}_2)_3\text{O}](\text{AsPh}_3)_2\text{Cl}$ (**1-AsPh**₃, $\text{R} = \text{CO}_2\text{CH}_3$). Thermolysis of **1-AsPh**₃ at 75 °C leads to a 73% isolated yield of the diiridium μ - η^2 -(C,O)-acyl complex

$\{[\text{Ir}(\text{CR}=\text{CRCR}=\text{CR})(\text{AsPh}_3)](\mu\text{-Cl})_2[\mu\text{-C}(\text{O})(\text{CH}_2)_3\text{AsPh}_3]\}[\text{Ir}(\text{CR}=\text{CRCR}=\text{CR})(\text{AsPh}_3)](\mu\text{-Cl})_2[\mu\text{-C}(\text{O})(\text{CH}_2)_3\text{AsPh}_3]\}[\text{Ir}(\text{CR}=\text{CRCR}=\text{CR})\text{-}(\text{C}(\text{CH}_2)_3\text{O})]$ (**4**, $\text{R} = \text{CO}_2\text{CH}_3$).

We previously reported the quantitative conversion of the iridacyclopentadiene-carbene complex

$\text{Ir}(\text{CR}=\text{CRCR}=\text{CR})[\text{C}(\text{CH}_2)_3\text{O}](\text{PPh}_3)_2\text{Cl}$ (**1-PPh**₃, $\text{R} = \text{CO}_2\text{CH}_3$) to iridacyclobutene **2** upon thermolysis of **1-PPh**₃ at 72 °C in chloroform solution (Scheme 1).² On the basis of phosphine inhibition studies, we proposed an initial loss of PPh₃ from **1-PPh**₃. Subsequent steps would then include insertion of the carbene ligand into the iridium-carbon bond of the metallacycle and ring contraction of the metallacyclohexadiene intermediate (**I**). In the hope of facilitating this unprecedented insertion reaction we prepared the triphenylarsine analogue of **1-PPh**₃ and report herein that thermolysis of the arsine derivative leads not to a metallacyclobutene but rather to the first homodinuclear μ - η^2 -(C,O)-acyl complex of the cobalt triad metals.

Results and Discussion

The bis(triphenylarsine) complex $\text{Ir}(\text{CR}=\text{CRCR}=\text{CR})(\text{AsPh}_3)_2\text{Cl}$ (**3**, $\text{R} = \text{CO}_2\text{CH}_3$) was prepared from $\text{Ir}(\text{AsPh}_3)_2(\text{CO})\text{Cl}$,³ furoyl azide, and dimethyl acetylenedicarboxylate by a modification of Collman's procedure

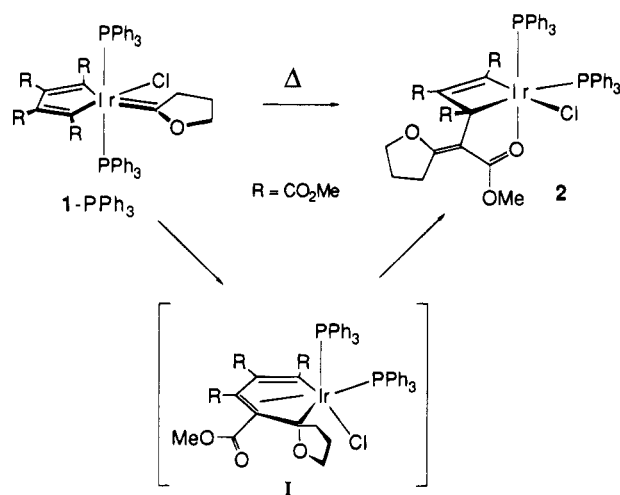
[®] Abstract published in *Advance ACS Abstracts*, March 15, 1995.

(1) Address correspondence to this author at the University of California.

(2) O'Connor, J. M.; Pu, L.; Woolard, S.; Chadha, R. K. *J. Am. Chem. Soc.* **1990**, *112*, 6731.

(3) Kubota, M.; Kiefer, G. W.; Ishikawa, R. M.; Bencala, K. E. *Inorg. Chim. Acta* **1973**, *7*, 195.

Scheme 1

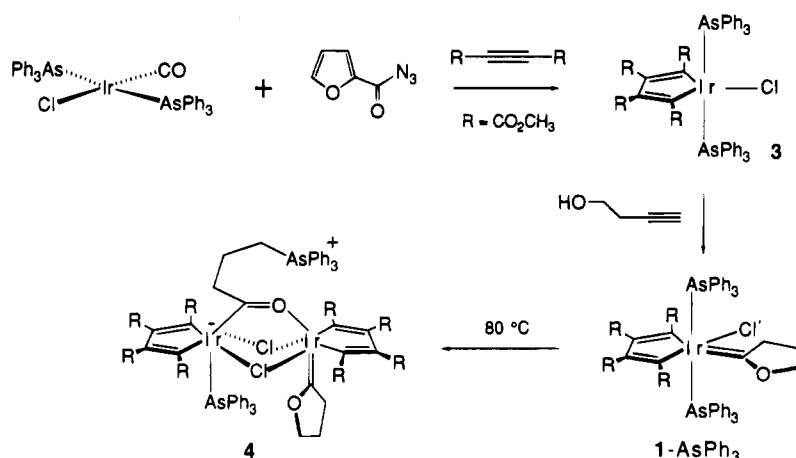


for the synthesis of the triphenylphosphine analogue.⁴ In the solid state, brick red **3** rapidly and reversibly turned yellow upon exposure to air. At room temperature **3** underwent reaction with 3-butyn-1-ol to give the metallacycle-carbene complex $\text{Ir}(\text{CR}=\text{CRCR}=\text{CR})[\text{C}(\text{CH}_2)_3\text{O}](\text{AsPh}_3)_2\text{Cl}$ (**1-AsPh**₃, $\text{R} = \text{CO}_2\text{CH}_3$) in 82% isolated yield. The physical and spectroscopic properties of **1-AsPh**₃ are similar to those of the triphenylphosphine analogue **1-PPh**₃. Both complexes are faint yellow, air-stable solids which exhibit similar melting point behavior (162–164 °C for **1-AsPh**₃, 168–170 °C for **1-PPh**₃). In the ¹³C{¹H} NMR spectra both complexes exhibit a signal at 286.2 ppm, assigned to the carbene carbon.

When a methylene chloride solution of **1-AsPh**₃ (0.36 mmol, 36 mM) was heated at 75 °C for 18 h the color darkened to a yellow-orange. Reduction of the solution volume and addition of diethyl ether led to precipitation of **4** as an air-stable, yellow-orange, analytically pure powder in 73% yield (Scheme 2). The ¹H NMR spectrum (CDCl₃) of **4** exhibits four singlets integrating for 6 H's each at δ 3.52, 3.50, 3.48, and 3.46, which are assigned to the methyl groups of the methoxycarbonyl metallacycle substituents. These signals are consistent with

(4) Collman, J. P.; Kang, J. W.; Little, W. F.; Sullivan, M. F. *Inorg. Chem.* **1968**, *7*, 1298.

Scheme 2



two equivalent 1,4-butadiendiyl ligands, each with four methoxycarbonyl environments, or two nonequivalent 1,4-butadiendiyl ligands, each with two methoxycarbonyl environments. Six two-proton multiplets are also observed in the ^1H NMR spectrum at δ 4.60 (t, $J_{\text{HH}} = 7.2$ Hz), 3.33 (m), 2.73 (t, $J_{\text{HH}} = 5.1$ Hz), 2.10 (t, $J_{\text{HH}} = 7.8$ Hz), 1.70 (m), and 1.59 (t, $J_{\text{HH}} = 7.8$ Hz), consistent with two unique $-\text{CH}_2\text{CH}_2\text{CH}_2-$ fragments. For comparison, the methylene hydrogens in the oxacyclopentylidene ligand of **1-AsPh₃** are observed in the ^1H NMR spectrum (CDCl_3) at δ 4.28 (t, $J_{\text{HH}} = 7.95$ Hz), 2.75 (t, $J_{\text{HH}} = 7.95$ Hz), and 0.93 (m). Thus, on the basis of the ^1H NMR spectroscopic data only one oxacyclopentylidene ligand remains intact in **4**. In the $^{13}\text{C}\{^1\text{H}\}$ NMR spectrum (CDCl_3) of **4**, two downfield singlets are observed at 256.2 and 253.4 ppm. These resonances are at somewhat high field for carbene carbons but downfield of where an η^1 -acyl carbon is typically observed.

Ultimately we resorted to a single-crystal X-ray diffraction study to determine the structure of **4** (Tables 1 and 2). An orange crystal of **4** was obtained by recrystallization from THF/hexanes. Refinement gave the structure shown in Figure 1. Bond distances and bond angles are summarized in Table 2. The structure consists of two iridium atoms bridged by two chloride ligands and a μ - η^2 -(C,O)-acyl ligand. The iridium-iridium distance of 3.44 Å is well beyond the upper limit of 3.2 Å for an iridium-iridium single bond.⁵ The average iridium-chloride bond distance is 0.032 Å longer to iridium(1) than to iridium(2). For comparison, the iridium-chloride bond distances in the symmetric dimer $[\text{IrCl}_2\text{Me}(\text{CO})_2]_2$ are 2.52 and 2.38 Å.⁶ In solution, rapid rotation about the Ir(2)-C(25) double bond would account for the plane of symmetry required by the ^1H NMR data. In addition to the μ -acyl ligand, two unusual structural features of **4** are the presence of 1,4-butadiendiyl ligands which do not bridge the metals and the facial arrangement of the carbene and butadiendiyl ligands on iridium(2). The only other stable metallacycle-carbene complexes reported to date have a meridional arrangement of these ligands.⁷

The formation of the acyl ligand in **4** is the result of triphenylarsine-induced ring opening of the oxacyclo-

Table 1. Crystallographic Data for $\text{C}_{68}\text{H}_{66}\text{As}_2\text{Cl}_2\text{Ir}_2\text{O}_{18}$ (**4**)

(a) Crystal Parameters	
formula	$\text{C}_{68}\text{H}_{66}\text{As}_2\text{Cl}_2\text{Ir}_2\text{O}_{18}$
fw	1777.4
cryst system	monoclinic
space group	$P2_1/n$
<i>a</i> , Å	15.614(3)
<i>b</i> , Å	13.722(4)
<i>c</i> , Å	31.564(8)
α , deg	
β , deg	94.15(2)
γ , deg	
<i>V</i> , Å ³	6745(2)
<i>Z</i>	4
cryst dimens, mm	0.07 × 0.22 × 0.36
cryst color	orange
<i>D</i> (calc), g cm ⁻³	1.750
μ (Mo K α), cm ⁻¹	50.65
temp, K	298
<i>T</i> (max)/ <i>T</i> (min)	N/A
(b) Data Collection	
diffractometer	Siemens P4
monochromator	graphite
radiation	Mo K α ($\lambda = 0.71073$ Å)
2θ scan range, deg	4–45
data collcd (<i>h,k,l</i>)	±16, ±14, ±33
rflns collcd	9447
indpt rflns	8812
<i>R</i> (merg), %	10.61
indpt obsvd rflns with, $F_o \geq n\sigma(F_o)$ ($n = 4$)	5311
std rflns	3 std/197 rflns
(c) Refinement	
<i>R</i> (<i>F</i>), %	7.86
<i>R</i> (<i>wF</i>), %	9.34
Δ/σ (max)	0.015
Δ/ρ , e Å ⁻³	3.12
<i>N</i> _o / <i>N</i> _v	9.5
GO _F	1.22

pentylidene ligand. We previously observed this type of a transformation in the reaction of cationic metallacycle-carbene **5** with pyridine and PPh₃ to give the mononuclear acyls **6-L**.⁷ For η^2 -acyl **4** the carbene Ir(2)-C(25) double bond distance of 1.79 Å is 0.22 Å shorter than the acyl Ir(1)-C(29) distance of 2.01 Å and the C(29)-O(18) distance is 1.305(26) Å. For comparison, the η^1 -acyl ligand in **6-pyr** has Ir-C and C=O bond distances of 2.136(4) and 1.212(5) Å, respectively. These structural comparisons indicate that the bridging acyl ligand of **4** is appropriately described by resonance structures **II** and **III**, with **II** as the major contributor to the ground state structure.

A search of the Cambridge Crystallographic Data Base failed to locate a structurally characterized ex-

(5) Arif, A. M.; Heaton, D. E.; Jones, R. A.; Kidd, K. B.; Wright, T. C.; Whittlesey, B. R.; Atwood, J. L.; Hunter, W. E.; Zhang, H. *Inorg. Chem.* **1987**, *26*, 4065.

(6) Bailey, N. A.; Jones, C. J.; Shaw, B. L.; Singleton, E. *J. Chem. Soc., Chem. Commun.* **1967**, 1051.

(7) O'Connor, J. M.; Pu, L.; Rheingold, A. L. *J. Am. Chem. Soc.* **1990**, *112*, 6232.

Table 2. Selected Bond Distances (Å) and Angles (deg) for 4

Ir(1)–Cl(1)	2.495(6)	Ir(1)–Cl(2)	2.492(6)
Ir(1)–As(2)	2.561(3)	Ir(1)–C(1)	2.044(22)
Ir(1)–C(4)	1.984(27)	Ir(1)–C(29)	2.010(20)
Ir(2)–Cl(1)	2.464(6)	Ir(2)–Cl(2)	2.461(6)
Ir(2)–O(18)	2.177(16)	Ir(2)–C(13)	2.020(22)
Ir(2)–C(16)	2.001(21)	Ir(2)–C(25)	1.786(34)
Cl(1)–Ir(1)–Cl(2)	81.8(2)	Cl(1)–Ir(1)–As(2)	88.2(2)
Cl(2)–Ir(1)–As(2)	95.3(2)	Cl(1)–Ir(1)–C(1)	103.7(6)
Cl(2)–Ir(1)–C(1)	171.0(6)	As(2)–Ir(1)–C(1)	92.0(6)
Cl(1)–Ir(1)–C(4)	177.6(8)	Cl(2)–Ir(1)–C(4)	95.8(8)
As(2)–Ir(1)–C(4)	92.6(8)	C(1)–Ir(1)–C(4)	78.6(10)
Cl(1)–Ir(1)–C(29)	86.6(6)	Cl(2)–Ir(1)–C(29)	85.3(6)
As(2)–Ir(1)–C(29)	174.6(6)	C(1)–Ir(1)–C(29)	87.9(9)
C(4)–Ir(1)–C(29)	92.6(10)	C(13)–Ir(2)–C(16)	82.6(9)
Cl(1)–Ir(2)–Cl(2)	83.1(1)	O(18)–Ir(2)–C(13)	94.6(8)
Cl(1)–Ir(2)–O(18)	82.7(4)	Cl(2)–Ir(2)–O(18)	81.4(5)
Cl(1)–Ir(2)–C(13)	96.2(7)	Cl(2)–Ir(2)–C(13)	176.0(7)
Cl(1)–Ir(2)–C(16)	173.3(6)	Cl(2)–Ir(2)–C(16)	97.6(6)
O(18)–Ir(2)–C(16)	90.8(7)	O(18)–Ir(2)–C(25)	173.8(9)
Cl(1)–Ir(2)–C(25)	95.6(8)	Cl(2)–Ir(2)–C(25)	92.5(8)
C(13)–Ir(2)–C(25)	91.5(10)	C(16)–Ir(2)–C(25)	91.0(10)

ample of a homodinuclear μ -acyl complex within the cobalt triad. Kaesz et al. have structurally characterized the heterodinuclear (μ -acyl)iridium(III) complex **7** which exhibits iridium–carbon bond distances of 1.983–(10) and 2.008(9) Å for the benzoyl and acetyl ligands, respectively.^{8,9}

The mechanism for conversion of **1-AsPh₃** to **4** is clearly a complicated one which involves dissociation of three triphenylarsine ligands, isomerization of a meridional metallacycle–carbene to a facial geometry, oxacyclopentylidene ligand ring opening, and the formation of three bridging ligands. We believe that the remarkable contrast in the thermal behavior of **1-PPh₃** and **1-AsPh₃** is primarily related to the greater lability of triphenylarsine as compared to triphenylphosphine. Wovkulich and Atwood have measured the rate of **AsPh₃** dissociation from **Cr(CO)₅L** to be 120 times faster than for **L = PPh₃**.¹⁰ Manzer and Tolman have also established that the displacement energy for group 15 ligands from **Pt(II)** complexes decreases in the order **PPh₃ > AsPh₃ > SbPh₃**.¹¹ Thus, the open coordination sites necessary for establishment of ligand bridges are more readily generated in the case of **1-AsPh₃** than for **1-PPh₃**.

Experimental Section

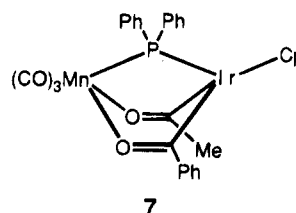
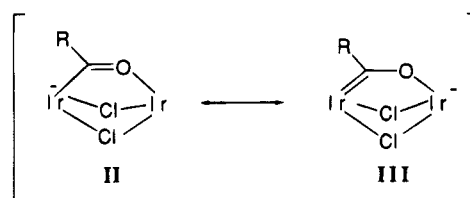
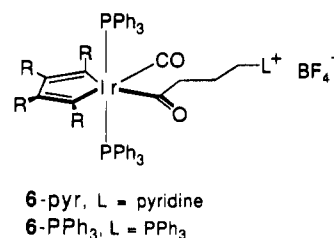
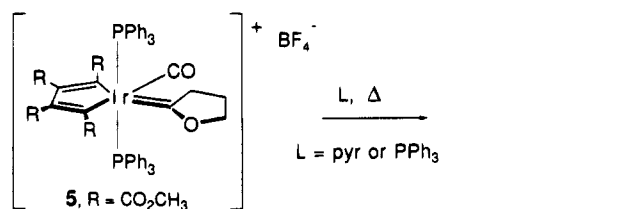
General Information. Commercially available reagents were used as received. Solvents were distilled and dried by standard procedures. All reactions were carried out under a

(8) Blickensderfer, J. R.; Knobler, C. B.; Kaesz, H. D. *J. Am. Chem. Soc.* **1975**, *97*, 2681.

(9) Examples of structurally characterized homodinuclear μ -acyl complexes: (a) Pysnograeva, N. I.; Setkina, V. N.; Andrianov, V. G.; Struchkov, Yu. T.; Kursanov, D. N. *J. Organomet. Chem.* **1981**, *206*, 169. (b) Mott, G. N.; Granby, R.; MacLaughlin, S. A.; Taylor, N. J.; Carty, A. *J. Organometallics* **1983**, *2*, 189. (c) Lindley, P. F.; Mills, O. S. *J. Chem. Soc. A* **1969**, 1279. (d) Henrick, K.; McPartlin, M.; Iggo, J. A.; Kamball, A. C.; Mays, M. J.; Raithby, P. R. *J. Chem. Soc., Dalton Trans.* **1987**, 2669. (e) Henrick, K.; Iggo, J. A.; Mays, M. J.; Raithby, P. R. *J. Chem. Soc., Chem. Commun.* **1984**, 209. (f) Kampe, C. E.; Boag, N. M.; Kaesz, H. D. *J. Mol. Catal.* **1983**, *21*, 297. (g) Kreiter, C. G.; Franzreb, K. H.; Sheldrick, W. S. *J. Organomet. Chem.* **1984**, *270*, 71. (h) Hoke, J. B.; Dewan, J. C.; Seyferth, D. *Organometallics* **1987**, *6*, 1816. (i) Boag, N. M.; Sieber, W. J.; Kampe, C. E.; Knobler, C. B.; Kaesz, H. D. *J. Organomet. Chem.* **1988**, *355*, 385. (j) Chisholm, M. H.; Ho, D.; Huffman, J. C.; Marchant, N. S. *Organometallics* **1989**, *8*, 1626. (k) Schweiger, M. J.; Nagel, U.; Beck, W. *J. Organomet. Chem.* **1988**, *355*, 289. (l) Fässler, Th.; Huttner, G. *J. Organomet. Chem.* **1989**, *376*, 367.

(10) Wovkulich, M. J.; Atwood, J. D. *J. Organomet. Chem.* **1979**, *184*, 77.

(11) Manzer, L. E.; Tolman, C. A. *J. Am. Chem. Soc.* **1975**, *97*, 1955.



dry nitrogen atmosphere. Melting points were determined on an Electrothermal melting point apparatus and are uncorrected. Elemental analyses were performed by Galbraith Laboratories, Knoxville, TN. Infrared spectra were obtained on a Perkin-Elmer 599 spectrometer. ¹H and ¹³C{¹H} NMR spectra were recorded at 300 and 75 MHz, respectively, on a GE GN-300 spectrometer. Proton and carbon chemical shifts are relative to the residual protio solvent resonance and solvent carbon resonance, respectively.

Ir(CR=CRCR=CR)(AsPh₃)₂Cl (**3**, **R = CO₂CH₃**). To a stirred methylene chloride solution (25 mL) of **Ir(AsPh₃)₂(CO)Cl** (1.27 g, 1.4 mmol) at room temperature was added an excess of dimethyl acetylenedicarboxylate (0.523 g, 3.68 mmol) by syringe. The mixture was degassed by N₂-purge and stirred until homogenous, after which time a 25 mL methylene chloride solution of furoyl azide (0.282 g, 2.0 mmol) was added by cannula. The solution was stirred overnight at room temperature, and the volatiles were removed under vacuum. The residue was washed with methanol and recrystallized from methylene chloride/methanol to give **3** as a red solid in 78% yield (1.29 g): mp (sealed cap) 241–243 °C; ¹H NMR (CDCl₃) δ 7.6–7.5 (m, 12H), 7.4–7.3 (m, 18H), 3.44 (s, 6H), 3.25 (s, 6H); ¹³C{¹H} NMR (CDCl₃) δ 169.4, 164.7, 150.7, 140.9, 135.1, 134.1, 130.0, 129.6, 128.4, 128.1, 51.2, 51.0; IR (Nujol) 1705 (vs), 1721 (vs), 1260 (s), 1220 (vs), 1170 (s) cm⁻¹. Anal. Calcd for C₄₈H₄₂As₂ClIrO₈: C, 51.27; H, 3.76; Cl, 3.15. Found: C, 51.16; H, 3.70; Cl, 3.21.

Ir(CR=CRCR=CR)[=C(CH₂)₃O](AsPh₃)₂Cl (**1-AsPh₃**, **R = CO₂CH₃**). To a stirred methylene chloride solution of **3** (0.5 g, 0.44 mmol) at –78 °C was added a slight excess of 3-butyn-1-ol (0.034 g, 0.48 mmol) by syringe. The mixture was degassed by N₂-purge and allowed to warm to room temperature. The reaction was stirred for 1.5 h, the solution volume reduced under vacuum, and diethyl ether added to give **1-AsPh₃** as a faint yellow powder (0.437 g) in 82% yield: mp (sealed cap) 241–243 °C; ¹H NMR (CDCl₃) δ 7.6 (m, 12H) 7.3

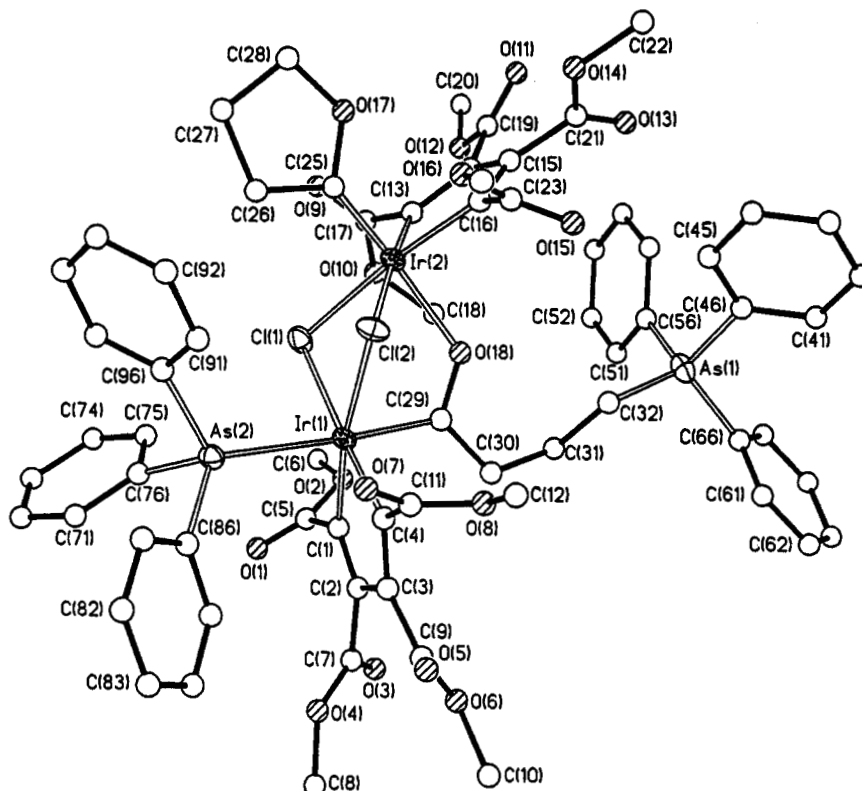


Figure 1. Molecular structure and numbering scheme for **4** with thermal ellipsoids drawn at the 35% level.

(m, 18H), 4.28 (t, $J = 7.95$ Hz, 2H), 3.90 (s, 3H), 3.63 (s, 3H), 3.46 (s, 3H), 3.24 (s, 3H), 2.75 (t, $J = 7.95$ Hz, 2H), 0.93 (m, 2H); $^{13}\text{C}\{^1\text{H}\}$ NMR (CDCl_3) δ 287.0, 176.4, 166.1, 164.1, 153.6, 149.2, 149.7, 145.7, 134.8, 132.0, 129.4, 127.6, 87.1, 57.4, 50.5, 50.3, 50.0, 19.0; IR (Nujol) 1710 (s), 1380 (m), 1330 (w), 1205 (s) 1160 (m) cm^{-1} . Anal. Calcd for $\text{C}_{52}\text{H}_{48}\text{As}_2\text{ClIrO}_9$: C, 52.29; H, 4.34; Cl, 2.97. Found: C, 52.37; H, 4.20; Cl, 3.17.

$\{[\text{Ir}(\eta^2\text{-C}_4\text{R}_4)(\text{AsPh}_3)](\mu\text{-Cl})_2[\mu\text{-C}(=\text{O})(\text{CH}_2)_3(\text{AsPh}_3)]\}_2[\text{Ir}(\eta^2\text{-C}_4\text{R}_4)[\text{C}(\text{CH}_2)_3\text{O}]]$ (**4**, $\text{R} = \text{CO}_2\text{CH}_3$). A methylene chloride solution of 1- AsPh_3 (0.44 g, 0.36 mmol) was heated in a sealed tube under a nitrogen atmosphere for 18 h. The solution volume was reduced under vacuum and diethyl ether added to give **4** as a faint yellow-orange powder (0.236 g) in 73% yield: mp 214–216 °C; ^1H NMR (CDCl_3) δ 7.6 (m, 20H) 7.3 (m, 10H), 4.60 (t, $J = 7.2$ Hz, 2H), 3.52 (s, 6H), 3.50 (s, 6H), 3.48 (s, 6H), 3.46 (s, 6H), 3.33 (m, 2H), 2.73 (t, $J = 5.1$ Hz, 2H), 2.10 (t, $J = 7.8$ Hz, 2H), 1.70 (m, 2H), 1.59 (t, $J = 7.8$ Hz, 2H); $^{13}\text{C}\{^1\text{H}\}$ NMR (CDCl_3) δ 256.2, 253.4, 174.5, 174.4, 165.6, 164.7, 154.6, 154.0, 143.4, 148.1, 134.6, 133.8, 133.1, 132.6, 130.8, 128.6, 127.5, 121.4, 83.1, 55.2, 50.9, 50.5, 50.2, 48.2, 23.6, 21.4, 18.5; IR (Nujol) 1730 (vs), 1705 (vs), 1550 (w), 1380 (m), 1330 (m), 1205 (vs) 1070 (m) cm^{-1} . Anal. Calcd for $\text{C}_{68}\text{H}_{66}\text{As}_2\text{Cl}_2\text{Ir}_2\text{O}_{18}$: C, 45.97; H, 3.74; Cl, 3.99. Found: C, 46.00; H, 3.75; Cl, 4.09.

X-ray Structure of 4. Crystallographic data for **4** are collected in Table 1. Cell constants and orientation matrices were determined by the least squares refinement of 25 high-angle reflections. No absorption correction was required; the max/min transmission ratio was less than 1.1. The crystal diffracted weakly and broadly leading to a decrease in the overall quality of the structural characterization. The structure was solved by direct methods. All non-hydrogen atoms were anisotropically refined, and the phenyl rings were fixed as rigid hexagons. All computer programs used for data collection and structure refinement are from the P4 and SHELXTL (G. Sheldrick, Siemens, Madison, WI) program libraries.

Acknowledgment. Partial support by the National Science Foundation is gratefully acknowledged. We are grateful to Johnson Matthey for a generous loan of precious metals.

Supplementary Material Available: Tables of bond lengths, bond angles, anisotropic thermal parameters, and atomic coordinates and thermal parameters (8 pages). Ordering information is given on any current masthead page.

OM940962C

(*N,N'*-Dimethyl-*p*-toluamidinato)trichlorotitanium: Synthesis, Structure, and Polymerization Catalysis

Juan C. Flores, James C. W. Chien, and Marvin D. Rausch*

Department of Chemistry and Department of Polymer Science & Engineering, University of Massachusetts, Amherst, Massachusetts 01003

Received November 15, 1994[®]

Summary: A reaction between *N*-(trimethylsilyl)-*N,N'*-dimethyl-*p*-toluamidine and TiCl_4 in CH_2Cl_2 produces (*N,N'*-dimethyl-*p*-toluamidinato)trichlorotitanium, which is formulated as a dimer with two chloro bridges. The new complex is moderately active in the polymerization of both styrene and ethylene when activated with methylaluminoxane.

Amidinato-transition methyl compounds have recently aroused much interest and expectation since the amidinate ligand has been considered as an alternative to the well-known cyclopentadienyl ligand.¹ In fact, an extensive variety of metal complexes of this type has been reported in the past few years,^{1,2} including group 4 mono(benzamidinate) $\{[\eta\text{-C}_6\text{H}_5\text{C}(\text{NSiMe}_3)_2]\text{MCl}_3\}_2$ (M = Ti, Zr)³ and bis(benzamidinate) $[\eta\text{-C}_6\text{H}_5\text{C}(\text{NSiMe}_3)_2]_2\text{MCl}_2$ (M = Ti, Zr)⁴ complexes. More recently, the mixed-ligand compounds $\{(\eta^5\text{-C}_5\text{R}_5)[\eta\text{-C}_6\text{H}_5\text{C}(\text{NSiMe}_3)_2]\text{MX}_2\}$ (R = H, Me; M = Ti, Zr, Hf; X = Cl, alkyl)⁵ have been found to be active for the polymerization of ethylene and propylene. We have recently demonstrated that mono- $[\text{N,N}'\text{-bis}(\text{trimethylsilyl})\text{benzamidinato}]$ titanium complexes polymerize styrene with methylaluminoxane (MAO) as cocatalyst in a highly syndiospecific process,⁶ although the reaction rates are lower than those achieved with CpTiCl_3 or IndTiCl_3 .⁷

Here we report the preparation of *N*-trimethylsilyl-*N,N'*-dimethyl-*p*-toluamidine (**1**) and (*N,N'*-dimethyl-*p*-toluamidinato)trichlorotitanium (**2**), together with the application of the latter as a precursor in the catalytic polymerization of styrene and ethylene.

Following the procedure described by Boeré,⁸ $\{p\text{-MeC}_6\text{H}_4\text{C}(\text{NMe})\text{N}[\text{Me}(\text{SiMe}_3)]\}$ (**1**) was obtained in 52%

yield from a reaction of *p*-tolunitrile and lithium dimethylamide and subsequent reaction with chlorotrimethylsilane (Scheme 1). The ¹H NMR spectrum of **1** showed the aromatic protons of the tolyl group as an apparent doublet of doublets (δ 7.08 ppm) due to an AA'BB' splitting pattern characteristic in para unsymmetrically disubstituted benzenes.⁹ The two methyl groups attached to the nitrogens were recorded as a broad singlet (\sim 16 Hz) at 2.88 ppm. The equivalence of these methyl groups is the consequence of the fluxional behavior of the trimethylsilyl group along the NCN-amidinate framework and is in complete agreement with earlier findings for $\text{PhC}(\text{NMe})\text{N}[\text{Me}(\text{SiMe}_3)]$ and $\text{PhC}(\text{NSiMe}_3)\text{N}(\text{SiMe}_3)_2$.^{8b} Both the trimethylsilyl group and the methyl group of the *p*-tolyl fragment appeared as singlets at -0.22 and 2.36 ppm, respectively. Compared to analogous resonances for *p*- $\text{MeC}_6\text{H}_4\text{C}(\text{NSiMe}_3)\text{N}(\text{SiMe}_3)_2$ (δ 0.09 and 2.37 ppm)^{8a} in the same deuterated solvent, almost the same chemical shift is observed for the methyl protons in the para position, but the SiMe_3 signal in **1** is shifted ca. 0.3 ppm to higher field. This shift is understandable considering that, in **1**, two of the SiMe_3 groups linked to the nitrogens are replaced by stronger electron-donating groups.

A reaction between **1** and TiCl_4 in CH_2Cl_2 solution at room temperature produced $\{[p\text{-MeC}_6\text{H}_4\text{C}(\text{NMe})_2]\text{TiCl}_2\}_2$ (**2**) in 69% yield (Scheme 1). The ¹H NMR spectrum of **2** showed the AA'BB' splitting pattern for the protons on the aromatic ring and a singlet for the methyl protons on the tolyl group. Interesting, in either chloroform-*d*₁, benzene-*d*₆, or toluene-*d*₈, the two methyls attached to the nitrogens were magnetically nonequivalent. This result was unexpected considering that, in $\{[\eta\text{-PhC}(\text{NSiMe}_3)_2]\text{TiCl}_3\}_2$, the protons of the SiMe_3 groups were found to be equivalent by ¹H NMR.³ An example of nonequivalent SiMe_3 groups in the same benzimidinate ligand has been reported for $[\eta\text{-PhC}(\text{NSiMe}_3)_2]_3\text{UMe}$.^{2c} In this case, X-ray crystal structure and variable-temperature ¹H NMR (VT ¹H NMR) studies indicated that the geometry of this uranium molecule is responsible for such a behavior.

The compound $\{[\eta\text{-PhC}(\text{NSiMe}_3)_2]\text{TiCl}_3\}_2$ is known to exist as a dimer with two chloro bridges that complete a distorted octahedral environment around the titanium atoms.³ At each metal center, one nitrogen atom of the amidinato group is located in a cis position to the chloro bridges and the other trans to one chloro bridge, with two different titanium-nitrogen bond lengths (2.07 Å, cis; 1.99 Å, trans) in the solid state. By analogy with this structure, we propose **2** to be a dimeric molecule with the same cis and trans disposition of the nitrogens

* To whom correspondence should be addressed at the Department of Chemistry.

[®] Abstract published in *Advance ACS Abstracts*, March 1, 1995.

(1) (a) Wedler, M.; Knösel, F.; Noltemeyer, M.; Edelmann, F. T. *J. Organomet. Chem.* **1990**, *388*, 21. (b) Duchateau, R.; van Wee, C. T.; Meetsma, A.; Teuben, J. H. *J. Am. Chem. Soc.* **1993**, *115*, 4931.

(2) (a) Dehnicke, K.; Ergezinger, C.; Hartmann, E.; Zinn, A.; Höslter, K. *J. Organomet. Chem.* **1988**, *352*, C1. (b) Buijink, J.-K.; Noltemeyer, M.; Edelmann, F. T. *Z. Naturforsch.* **1991**, *46b*, 1328. (c) Wedler, M.; Knösel, F.; Edelmann, F. T.; Behrens, U. *Chem. Ber.* **1992**, *125*, 1313. (d) Wedler, M.; Recknagel, A.; Gilje, J. W.; Noltemeyer, M.; Edelmann, F. T. *J. Organomet. Chem.* **1992**, *426*, 295. (e) Kilimann, V.; Noltemeyer, M.; Edelmann, F. T. *J. Organomet. Chem.* **1993**, *443*, 35. (f) Edelmann, F. T.; Ziegler, W.; Behrens, U. *J. Organomet. Chem.* **1992**, *426*, 261.

(3) Fenske, D.; Hartmann, E.; Dehnicke, K. *Z. Naturforsch.* **1988**, *43b*, 1611.

(4) Roesky, H. W.; Meller, B.; Noltemeyer, M.; Schmidt, H.-G.; Scholz, V.; Sheldrick, G. M. *Chem. Ber.* **1988**, *121*, 1403.

(5) Chernega, A. N.; Gómez, R.; Green, M. L. H. *J. Chem. Soc., Chem. Commun.* **1993**, 1415.

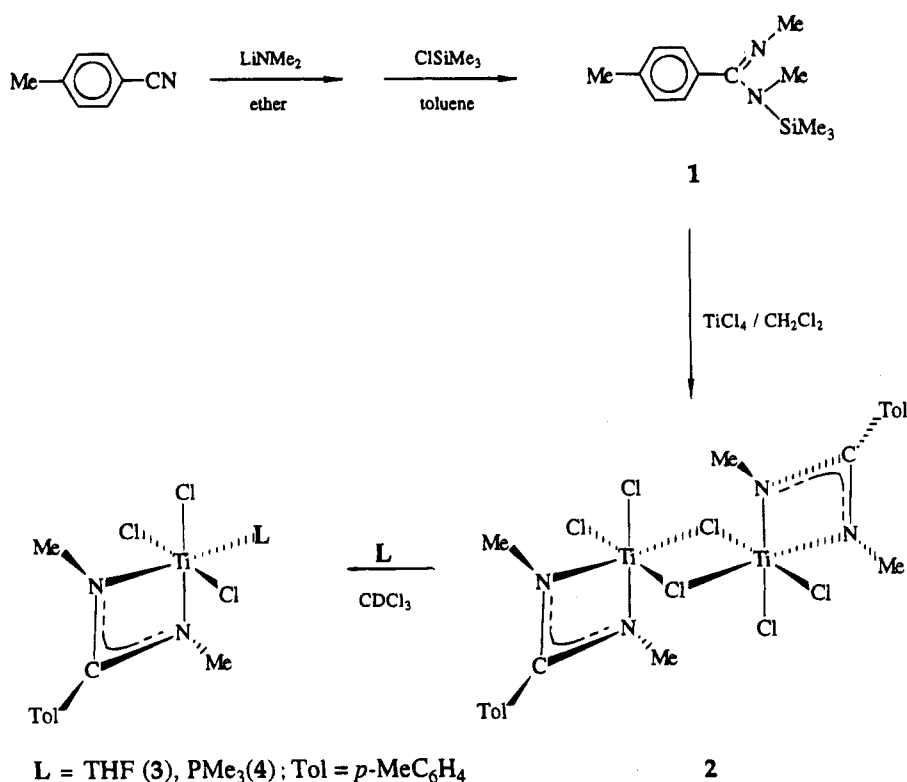
(6) Flores, J. C.; Chien, J. C. W.; Rausch, M. D. *Organometallics*, in press.

(7) (a) Ready, T. E.; Day, R. O.; Chien, J. C. W.; Rausch, M. D. *Macromolecules* **1993**, *26*, 5822. (b) Ishihara, N.; Kuramoto, M.; Voi, M. *Macromolecules* **1988**, *21*, 3356.

(8) (a) Boeré, R. T.; Oakley, R. T.; Reed, R. W. *J. Organomet. Chem.* **1987**, *331*, 161. (b) Sanger, A. R. *Inorg. Nucl. Chem. Lett.* **1973**, *9*, 351.

(9) Günther, H. *NMR Spectroscopy*; John Wiley and Sons: New York, 1987.

Scheme 1

Table 1. VT ^1H NMR Spectral Data for **2** in Toluene- d_8

	T (K)					
	263	298	313	333	363	373
$\delta(N\text{-Me})$ (trans)	2.72	2.76	2.79	2.82	2.87	2.89
$\delta(N\text{-Me})$ (cis)	1.91	1.98	2.03	2.09	2.17	2.20
gap (ppm)	0.81	0.78	0.76	0.73	0.70	0.69

of the *p*-toluamidinate ligand.¹⁰ In **2**, a stronger interaction of the nitrogens with titanium could be expected because of the more efficient electron-donating nature of the methyl substituents. Furthermore, these methyl groups are linked directly to nitrogen, whereas in $\{[\eta\text{-PhC}(\text{NSiMe}_3)_2]\text{TiCl}_3\}_2$ there is an additional bond through the silicon atom. Considering these arguments, the dimeric structure of **2** has to be rigid enough in solution to make the amidinato methyls nonequivalent in the ^1H NMR spectrum, differentiating the cis and trans positions relative to the chloro bridges.

In order to test the strength of such a conformation, a VT ^1H -NMR experiment was carried out in toluene- d_8 (see Table 1). Increasing the temperature from -10 to 100 $^\circ\text{C}$ failed to coalesce the two amidinato methyl signals. Instead, both resonances broadened and the chemical shift difference between them decreased significantly. It can be estimated that the two methyl resonances will collapse to a singlet at temperatures considerably above 100 $^\circ\text{C}$. After this VT ^1H -NMR experiment and over the course of several days at 25 $^\circ\text{C}$, the spectrum of this sample was unchanged, indicating a high thermal stability for **2**.

As observed for $\{[\eta\text{-PhC}(\text{NSiMe}_3)_2]\text{TiCl}_3\}_2$, the dimer **2** is easily broken by using electron-donor solvents or

(10) The stability provided by the Cl bridges to mono(benzamidinato)titanium complexes has already been demonstrated.⁶ For example, in contrast to the thermal stabilities of **2** and $\{[\eta\text{-PhC}(\text{NSiMe}_3)_2]\text{TiCl}_3\}_2$, $[\eta\text{-PhC}(\text{NSiMe}_3)_2]\text{TiMe}_3$ could not be isolated because it was readily converted to $[\eta\text{-PhC}(\text{NSiMe}_3)_2]\text{TiMe}_2$, and $[\eta\text{-PhC}(\text{NSiMe}_3)_2]\text{Ti}(\text{O-Pr-}i)_3$ underwent thermolysis under mild conditions.

ligands (Scheme 1).⁶ In an NMR-tube scale experiment, a solution of **2** in CDCl_3 was treated with an excess of THF (8:1) and the spectrum was recorded. The volatiles were then carefully removed, keeping the sample under vacuum overnight. The spectrum was again recorded by redissolving the solid in CDCl_3 . The ^1H NMR spectrum of this solid was identical to the previous one, except that one molecule of THF was present per amidinate ligand, indicating the formation of $[\eta\text{-MeC}_6\text{H}_4\text{C}(\text{NMe}_2)_2]\text{TiCl}_3\cdot\text{THF}$ (**3**).¹¹ The same experiment conducted with PMe_3 instead of THF led to the formation of the corresponding phosphine adduct $[\eta\text{-MeC}_6\text{H}_4\text{C}(\text{NMe}_3)_2]\text{TiCl}_3\cdot\text{PMe}_3$ (**4**).¹²

Complex **2** was found to be active in the polymerization of both styrene and ethylene when activated with MAO, but **2**/MAO does not polymerize propylene. Table 2 summarizes some representative results.¹³

Previously, we have shown that $\{[\eta\text{-PhC}(\text{NSiMe}_3)_2]\text{TiCl}_3\}_2$ (**5**)/MAO polymerized styrene under the above conditions with very high syndiotactic yield (SY = % *s*-PS); 94% of the product remained after extraction with refluxing 2-butanone.⁶ Instead, the syndiospecificity of **2**/MAO was similar to that of CpTiCl_3 /MAO, whereas the syndiospecificity of **5**/MAO was comparable to IndTiCl_3 /MAO.^{7a} The difference may be explained by

(11) ^1H NMR spectrum of $[\eta\text{-MeC}_6\text{H}_4\text{C}(\text{NMe}_2)_2]\text{TiCl}_3\cdot\text{THF}$ in CDCl_3 : $\delta_{\text{AA}'}$ 7.63 (2 H, C_6H_4 , $J_{\text{AB}} + J_{\text{AB}'} = 8$ Hz); $\delta_{\text{BB}'}$ 7.30 (2 H, C_6H_4 , $J_{\text{AB}} + J_{\text{AB}'} = 8$ Hz); 4.08 (m, 4 H, THF); 3.81 (s, 3 H, trans *N*-Me); 3.16 (s, 3 H, cis *N*-Me); 2.43 (s, 3 H, Me); 1.89 (m, 4 H, THF) (trans and cis refer to the THF position).

(12) ^1H NMR spectrum of $[\eta\text{-MeC}_6\text{H}_4\text{C}(\text{NMe}_3)_2]\text{TiCl}_3\cdot\text{PMe}_3$ in CDCl_3 : $\delta_{\text{AA}'}$ 7.43 (2 H, C_6H_4 , $J_{\text{AB}} + J_{\text{AB}'} = 8$ Hz); $\delta_{\text{BB}'}$ 7.30 (2 H, C_6H_4 , $J_{\text{AB}} + J_{\text{AB}'} = 8$ Hz); 3.54 (s, 3 H, trans *N*-Me); 3.07 (s, 3 H, cis *N*-Me); 2.39 (s, 3 H, Me); 1.28 (d, 9 H, PMe_3 , $J_{\text{P-H}} = 14$ Hz) (trans and cis refer to the PMe_3 position).

(13) The procedure used to polymerize styrene has been given in detail in ref 7a, and the procedure to polymerize ethylene is given in: (a) Chien, J. C. W.; Tsai, W.-M.; Rausch, M. D. *J. Am. Chem. Soc.* **1991**, *113*, 8570. (b) Tsai, W.-M.; Rausch, M. D.; Chien, J. C. W. *Appl. Organomet. Chem.* **1993**, *7*, 71.

Table 2. Olefin Polymerization by 2/MAO^a

run	monomer ^b	[Ti] (μ M)	Al/Ti	yield (mg)	activity ^c	% <i>s</i> -PS ^d	$10^{-5} M_w$
1	S	25	4000	53	5.0×10^5	77	
2	S	50	4000	59	3.6×10^5	68	
3	S	50	2000	77	4.7×10^5	84	
4	E	25	4000	40	5.7×10^4		0.96
5	E	50	4000	115	8.3×10^4		0.78
6	E	50	2000	97	7.0×10^4		1.03

^a Polymerization conditions: volume = 50 mL of toluene, $T_p = 20^\circ\text{C}$, $t_p = 1.5$ h. ^b S = 43.49 mmol of styrene; E = ethylene at 15 psig ($[\text{C}_2\text{H}_4] = 0.37$ M). ^c For styrene, g of polymer/(mol of Ti \cdot mol of styrene \cdot h); for ethylene, g of polymer/(mol of Ti \cdot [C_2H_4] \cdot h). ^d % *s*-PS = (g of 2-butanone insoluble polymer/g of bulk polymer) \times 100.

the smaller bulkiness of the *N*-methyl substituents in **2** compared to the *N*-trimethylsilyl substituents in **5**. Therefore, stereochemical control is greater in the latter than in the former, both in the conformational arrangement of the growing polymer chains and in the approaching fashion of the incoming monomer.

The two amidinate systems have very similar styrene polymerization activity, with 2/MAO slightly superior. This difference may be due to the better electron-donor character of the *N*-substituents in **2** and in agreement with the results observed with the effects of substituents in indenyl- and cyclopentadienyltrichlorotitanium complexes.¹⁴

In the polymerization of ethylene, 2/MAO also showed a slightly higher activity (*i.e.* 7.0×10^4 g of PE/(mol of Ti \cdot [C_2H_4] \cdot h)) than 5/MAO (5.5×10^4). These activities are nevertheless low as compared to high-activity ethylene polymerization catalysts systems such as $\text{Cp}_2\text{ZrCl}_2/\text{MAO}$.¹⁵

Experimental Section

Reactions were carried out under an argon atmosphere using standard Schlenk techniques. Methylaluminoxane (MAO) was purchased from Akzo, and all other reagents were from

(14) Ready, T. E.; Chien, J. C. W.; Rausch, M. D. Unpublished studies.

(15) (a) Sinn, H.; Kaminsky, W. *Adv. Organomet. Chem.* **1980**, *18*, 99. (b) Chien, J. C. W.; Wang, B.-P. *J. Polym. Sci., Part A* **1990**, *28*, 15.

Aldrich. Toluene, diethyl ether, and tetrahydrofuran (THF) were distilled with Na/K alloy under argon, whereas CH_2Cl_2 and styrene were distilled from CaH_2 . ^1H NMR spectra were recorded on a Varian XL-200 spectrometer. Elemental analyses were performed by the Microanalytical Laboratory, University of Massachusetts, Amherst, MA.

Synthesis of *N*-(Trimethylsilyl)-*N,N*-dimethyl-*p*-toluamidine (1). Utilizing a literature procedure,⁸ a large scale stepwise reaction of *p*-tolunitrile (35.14 g, 0.30 mol) with lithium dimethylamide (15.31 g, 0.30 mol) was carried out in diethyl ether (250 mL) at room temperature. Replacement of the solvent by toluene, subsequent reaction with chlorotrimethylsilane (88.1 mL, 0.30 mol), and workup of the reaction mixture afforded **1** as a yellow oil. Fractional high vacuum distillation of this crude product (85°C , 2×10^{-3} mmHg) allowed the isolation of pure **1** (36.37 g, 52%) as a low-melting, colorless crystalline solid, mp 28°C .

Anal. Calcd for $\text{C}_{13}\text{H}_{22}\text{N}_2\text{Si}$: C, 66.61; H, 9.46; N, 11.95. Found: C, 66.81; H, 9.59; N, 11.88. ^1H NMR (CDCl_3): $\delta_{\text{AA}'}$ 7.14 (2 H, C_6H_4 , $J_{\text{AB}} + J_{\text{AB}'} = 8$ Hz); $\delta_{\text{BB}'}$ 7.03 (2 H, C_6H_4 , $J_{\text{AB}} + J_{\text{AB}'} = 8$ Hz); 2.88 (br s, 16 Hz, 6 H, NMe); 2.36 (s, 3 H, Me); -0.22 (s, 9 H, SiMe_3).

Synthesis of *N,N*-Dimethyl-*p*-toluamidinato)trichlorotitanium (2). Slow addition of **1** (5.58 g, 23.8 mmol) to a solution of TiCl_4 (4.52 g, 23.8 mmol) in CH_2Cl_2 (30 mL) at room temperature, followed by stirring for 1 h and removal of the solvent, led to the dimer **2**. Compound **2** was obtained as a fine yellow-orange powder and was recrystallized from CH_2Cl_2 , affording it analytically pure as a moisture-sensitive orange powder (5.21 g, 69%).

Anal. Calcd for $\text{C}_{10}\text{H}_{13}\text{N}_2\text{Cl}_3\text{Ti}$: C, 38.07; H, 4.15; N, 8.88. Found: C, 37.97; H, 4.28; N, 8.39. ^1H NMR (CDCl_3): $\delta_{\text{AA}'}$ 7.51 (2H, C_6H_4 , $J_{\text{AB}} + J_{\text{AB}'} = 8$ Hz); $\delta_{\text{BB}'}$ 7.31 (2 H, C_6H_4 , $J_{\text{AB}} + J_{\text{AB}'} = 8$ Hz); 3.60 (s, 3 H, trans *N*-Me); 3.23 (s, 3 H, cis *N*-Me); 2.43 (s, 3 H, Me). ^1H NMR (benzene- d_6): $\delta_{\text{AA}'}$ 7.09 (2 H, C_6H_4 , $J_{\text{AA}'} + J_{\text{AB}'} = 8$ Hz); $\delta_{\text{BB}'}$ 6.76 (2 H, C_6H_4 , $J_{\text{AA}'} + J_{\text{AB}'} = 8$ Hz); 2.70 (s, 3 H, trans *N*-Me); 1.93 (s, 3 H, cis *N*-Me); 1.88 (s, 3 H, Me). ^1H NMR (toluene- d_8): $\delta_{\text{AA}'}$ 7.10 (2 H, C_6H_4 , $J_{\text{AB}} + J_{\text{AB}'} = 8$ Hz); $\delta_{\text{BB}'}$ 6.76 (2 H, C_6H_4 , $J_{\text{AB}} + J_{\text{AB}'} = 8$ Hz); 2.76 (s, 3 H, trans *N*-Me); 1.98 (s, 3 H, cis *N*-Me); 1.96 (s, 3 H, Me) (trans and cis refer to the chloro bridges).

Acknowledgment. J.C.F. is indebted to the MEC (Spain) for a postdoctoral fellowship.

OM9408690

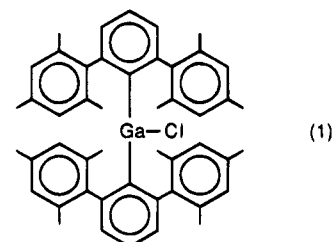
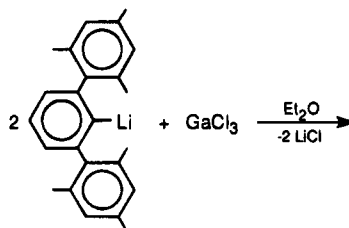
Synthesis and Molecular Structure of Bis(2,6-dimesitylphenyl)gallium Chloride, $(\text{Mes}_2\text{C}_6\text{H}_3)_2\text{GaCl}$ (Mes = 2,4,6- $\text{Me}_3\text{C}_6\text{H}_2$): A T-Shaped Tricoordinate Molecule

Xiao-Wang Li, William T. Pennington, and Gregory H. Robinson*

Howard L. Hunter Chemistry Laboratory, Department of Chemistry, Clemson University, Clemson, South Carolina 29634-1905

Received December 13, 1994[®]

Summary: Bis(2,6-dimesitylphenyl)gallium chloride, $(\text{Mes}_2\text{C}_6\text{H}_3)_2\text{GaCl}$ (Mes = 2,4,6- $\text{Me}_3\text{C}_6\text{H}_2$), has been prepared by reaction of (2,6-dimesitylphenyl)lithium, $\text{Mes}_2\text{C}_6\text{H}_3\text{Li}$, with gallium chloride in diethyl ether. The title compound crystallizes in the monoclinic space group $P2_1/n$ (No. 14) with unit cell parameters $a = 12.256(3)$ Å, $b = 20.644(4)$ Å, $c = 16.361(4)$ Å, $\beta = 100.96(2)^\circ$, $D_{\text{calc}} = 1.20 \text{ g cm}^{-3}$, and $V = 4064 \text{ Å}^3$ for $Z = 4$. Refinement, based on 1454 observed reflections, converged at $R = 0.069$ and $R_w = 0.066$. The Ga–Cl bond distance is $2.177(5)$ Å, while the Ga–C bond distances are $1.956(16)$ Å and $2.000(6)$ Å. The steric demands associated with the two bulky 2,6-dimesitylphenyl ligands are manifested most prominently in the coordination about the gallium atom as it is sufficiently distorted from the expected trigonal planar geometry so as to approach that of the rare T-shaped configuration.



Introduction

Although the quest for advanced materials has resulted in a number of seminal discoveries in organogallium chemistry over the last decade,¹ fundamental advances in structure and bonding in organogallium chemistry are also significant. The syntheses of low-coordination number organogallium complexes, principally *via* the utilization of sterically demanding ligands, provides an illustrative example.² In an effort to assess the extremes of steric loading in organogallium chemistry, we sought to examine the feasibility of incorporating the exceedingly bulky ligand 2,6-dimesitylphenyl, $\text{Mes}_2\text{C}_6\text{H}_3$ (Mes = 2,4,6- $\text{Me}_3\text{C}_6\text{H}_2$), into an organogallium compound and to appraise its effects on the coordination environment about the gallium center. Herein, we report the synthesis and molecular structure of bis(2,6-dimesitylphenyl)gallium chloride, $(\text{Mes}_2\text{C}_6\text{H}_3)_2\text{GaCl}$ (**I**), prepared by reaction of $(\text{Mes}_2\text{C}_6\text{H}_3)\text{Li}$ with GaCl_3 in diethyl ether (eq 1).

The environment about the gallium atom sufficiently deviates from trigonal planar so as to approach that of an exceedingly rare coordination for a three-coordinate gallium atom—T-shape geometry. The title compound is sufficiently crowded about the metal center so as to preclude diethyl ether association.

Experimental Section

General Comments. Standard Schlenk techniques were employed in conjunction with an inert-atmosphere drybox (Vacuum Atmospheres HE-43 Dri-Lab). Solvents were distilled from sodium benzophenone under an atmosphere of argon prior to use. NMR spectra were recorded on a Bruker AC300 FT-NMR spectrometer. X-ray diffraction data were collected on a Nicolet R3mV single-crystal diffractometer, while IR data were collected on a Perkin-Elmer 1310 spectrometer. Gallium chloride was purchased from Strem Chemical Co. and used as received. Elemental analyses were performed by E + R Microanalytical Laboratories (Corona, NY).

Synthesis of $(\text{Mes}_2\text{C}_6\text{H}_3)_2\text{GaCl}$ (I**).** Both 2,6-dimesityl-1-iodobenzene, $(\text{Mes}_2\text{C}_6\text{H}_3)\text{I}$,³ and its lithium salt, $(\text{Mes}_2\text{C}_6\text{H}_3)\text{Li}$,⁴ were prepared using published procedures. Inside the drybox a reaction vessel was charged with Et_2O (50 mL) and $(\text{Mes}_2\text{C}_6\text{H}_3)\text{Li}$ (1.92 g, 6 mmol). At 0 °C the $(\text{Mes}_2\text{C}_6\text{H}_3)\text{Li}$ - Et_2O solution was added to GaCl_3 (0.53 g, 3 mmol) in Et_2O (30 mL). After 1 h of stirring at 0 °C and 2 days at room temperature the solution was filtered, leaving behind a precipitate (LiCl). The filtrate was collected, and its solvent was removed in vacuo. The residue was extracted with pentane (80 mL). Concentration of the solution and cooling for several days afforded colorless crystals of **I** (1.58 g, 2.16 mmol) in 72% yield; mp 170 °C. ¹H NMR (300 MHz, 297 K, C_6D_6 (nonprimed positions refer to the phenyl ring bonded to gallium, while primed positions refer to the mesityl substituents)): δ 6.98–7.01 (m, 4H, *m*-H), 6.86 (s, 4H, *m'*-H), 6.84 (s, 4H, *m'*-H), 6.63 (t, 2H, *p*-H), 2.24 (s, 6H, *p'*-H), 2.21 (s, 6H, *p'*-H), 2.07 (s, 12H, *m'*-CH₃), 1.83 (s, 12H, *m'*-CH₃). ¹³C NMR

(3) Du, C.-J. F.; Hart, H.; Ng, K.-K. D. *J. Org. Chem.* **1986**, *51*, 3162.

(4) Ruhland-Senge, K.; Ellison, J. J.; Wehmschulte, R. J.; Pauer, F.; Power, P. P. *J. Chem. Soc.* **1993**, *115*, 11353.

[®] Abstract published in *Advance ACS Abstracts*, March 15, 1995.
 (1) (a) Cowley, A. H.; Benac, B. L.; Ekerdt, J. G.; Jones, R. A.; Kidd, K. B.; Lee, J. Y.; Miller, J. E. *J. Am. Chem. Soc.* **1988**, *110*, 6248. (b) Cowley, A. H.; Jones, R. A. *Angew. Chem., Int. Ed. Engl.* **1989**, *28*, 1208. (c) Russell, D. K. *Coord. Chem. Res.* **1992**, *112*, 131.
 (2) Petrie, M. A.; Power, P. P.; Dias, H. V. R.; Ruhlandt-Senge, K.; Waggoner, K. M.; Wehmschulte, R. J. *Organometallics* **1993**, *12*, 1086.

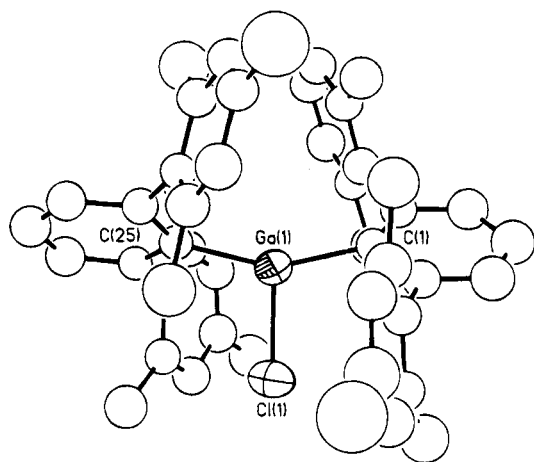


Figure 1. Molecular structure of $(\text{Mes}_2\text{C}_6\text{H}_3)_2\text{GaCl}$ (**I**) (thermal ellipsoids are shown at 35% probability levels). Selected bond distances (\AA) and angles (deg): Ga–Cl(1), 2.177(5); Ga–C(1), 2.001(16); Ga–C(25), 1.956(16); C(1)–Ga–C(25), 153.5(5); Cl–Ga–C(1), 103.2(4); Cl–Ga–C(25), 103.4(4).

Table 1. Crystallographic Data for $(\text{Mes}_2\text{C}_6\text{H}_3)_2\text{GaCl}$ (**I**)

Crystal Data	
empirical formula	$\text{C}_{48}\text{H}_{50}\text{ClGa}$
fw	732.05
color; habit	colorless; parallelepiped
size (mm)	$0.18 \times 0.26 \times 0.33$
space group	monoclinic, $P2_1/n$ (No. 14)
unit cell dimens	
a (\AA)	12.256(3)
b (\AA)	20.644(4)
c (\AA)	16.361(4)
β (deg)	100.96(2)
formula units/cell	4
V (\AA^3)	4064(2)
D_{calc} (g/cm^3)	1.20
$F(000)$	1544
Data Collection	
unit cell reflns	45 ($15.44 < 2\theta < 27.33^\circ$)
2θ range (deg)	$3.5\text{--}45.0^\circ$
scan type	$\omega/2\theta$
scan speed (deg/min)	2.09
no. of rflns collected	5544
no. of unique rflns (R_{int})	5255 (0.027)
indices	$(14, 23, \pm 10)$
cryst dec	linear (38%)
abs coeff (mm^{-1})	0.77
min/max transmissn	0.89/1.00
Refinement	
final residuals	$R = 0.069$; $R_w = 0.066$
goodness of fit	$S = 1.11$
largest Δ/σ	0.0008
no. of obs rflns ($I > 2\sigma(I)$)	1454
no. of params refined	212
data-to-param ratio	6.86:1
max/min diff peaks ($e/\text{\AA}^3$)	$+0.43/-0.37$

(300 MHz, 297 K, C_6D_6): δ 20.94 (p' - CH_3), 21.10 (p' - CH_3), 21.28 (o' - CH_3), 21.93 (o' - CH_3); aromatic carbon atoms δ 128.45, 128.82, 129.08, 135.73, 136.77, 137.03, 137.49, 139.44, 141.09, 141.93, 147.48, 148.52. IR (Nujol mull) 680 (w), 710 (m), 720 (m), 736 (m), 796 (s), 845 (s), 970 (m), 1010 (s), 1063 (s), 1080 (s), 1150 (w), 1215 (w), 1225 (w), 1360 (m), 1525 (w), 1560 (m), 1605 (m), 1750 (w), 2720 (w), 2862 (s) cm^{-1} . Anal. Calcd (Found) for $\text{C}_{48}\text{H}_{50}\text{GaCl}$: C, 78.80 (80.48); H, 6.90 (7.58).

Crystal Structure Determination. A colorless parallelepiped crystal of $(\text{Mes}_2\text{C}_6\text{H}_3)_2\text{GaCl}$ was mounted in a glass capillary under an atmosphere of argon. X-ray intensity data were collected on a Nicolet R3mV diffractometer, with graphite-monochromated Mo K α radiation ($\lambda = 0.71073 \text{ \AA}$) at 21 $^\circ\text{C}$,

Table 2. Atomic Coordinates ($\times 10^4$) and Equivalent Isotropic Displacement Coefficients ($\text{\AA}^2 \times 10^3$) for $(\text{Mes}_2\text{C}_6\text{H}_3)_2\text{GaCl}$ (**I**)

	x	y	z	U_{eq}^a
Ga(1)	22(2)	2208(1)	8604(1)	57(1)
Cl(1)	1191(4)	1966(3)	9739(3)	105(3)
C(1)	607(13)	1715(7)	7727(9)	45(5)
C(2)	1747(15)	1762(8)	7678(9)	55(5)
C(3)	2226(16)	1309(8)	7226(9)	76(6)
C(4)	1567(16)	817(9)	6796(10)	79(6)
C(5)	478(15)	791(8)	6797(10)	72(6)
C(6)	-23(15)	1247(8)	7258(9)	55(5)
C(7)	2497(13)	2306(9)	8045(9)	53(5)
C(8)	3385(13)	2249(9)	8700(9)	54(5)
C(9)	4051(15)	2768(10)	8934(10)	81(6)
C(10)	3891(18)	3369(10)	8497(12)	95(7)
C(11)	3041(15)	3404(9)	7839(10)	75(6)
C(12)	2350(15)	2896(9)	7573(10)	72(5)
C(13)	3620(14)	1617(7)	9152(9)	87(6)
C(14)	4670(17)	3919(9)	8807(11)	143(9)
C(15)	1492(14)	2957(8)	6785(9)	88(6)
C(16)	-1260(15)	1177(8)	7117(9)	60(5)
C(17)	-1933(15)	1589(8)	6536(10)	61(5)
C(18)	-3065(15)	1483(8)	6357(9)	64(5)
C(19)	-3566(16)	996(9)	6675(10)	69(6)
C(20)	-2914(15)	577(8)	7236(10)	72(6)
C(21)	-1782(15)	668(8)	7444(9)	56(5)
C(22)	-1374(13)	2103(7)	6105(9)	75(6)
C(23)	-4807(15)	879(8)	6452(11)	100(7)
C(24)	-1108(14)	198(7)	8046(9)	76(6)
C(25)	-1034(11)	2788(8)	8993(8)	46(4)
C(26)	-1625(13)	2611(8)	9593(9)	48(5)
C(27)	-2235(14)	3051(8)	9987(9)	66(6)
C(28)	-2267(14)	3697(8)	9756(9)	66(5)
C(29)	-1732(13)	3903(8)	9148(9)	59(5)
C(30)	-1170(13)	3450(8)	8742(9)	50(5)
C(31)	-1696(14)	1916(8)	9853(9)	48(5)
C(32)	-2435(15)	1502(8)	9337(10)	60(5)
C(33)	-2499(14)	847(8)	9518(10)	70(6)
C(34)	-1809(16)	613(9)	10233(11)	72(6)
C(35)	-1132(14)	1014(8)	10776(10)	69(6)
C(36)	-1084(14)	1668(8)	10601(10)	58(5)
C(37)	-3223(14)	1766(8)	8610(10)	82(6)
C(38)	-1790(15)	-120(8)	10411(9)	94(7)
C(39)	-412(13)	2103(7)	11244(9)	80(6)
C(40)	-661(13)	3733(7)	8057(9)	45(5)
C(41)	-1305(14)	3772(7)	7242(10)	58(5)
C(42)	-917(14)	4075(7)	6616(10)	61(5)
C(43)	68(15)	4391(8)	6789(10)	57(5)
C(44)	745(15)	4387(7)	7570(10)	67(5)
C(45)	342(14)	4049(8)	8201(10)	64(5)
C(46)	-2429(15)	3447(8)	7088(10)	101(7)
C(47)	517(17)	4752(9)	6100(11)	132(9)
C(48)	1086(14)	4032(8)	9073(9)	92(7)

^a Equivalent isotropic U , defined as one-third of the trace of the orthogonalized U_{ij} tensor.

using the ω - 2θ scan technique to a maximum 2θ value of 45° . The structure was solved by direct methods using the TEXSAN⁵ and SHELXTL⁶ package of computer programs. The gallium and chlorine atoms were refined using anisotropic thermal parameters, while the carbon atoms were refined isotropically. Hydrogen atoms were located by standard difference Fourier techniques, included in the structure factor calculation at idealized positions ($d_{\text{C-H}} = 0.96 \text{ \AA}$), and allowed to ride on the atoms to which they were bonded. An isotropic group thermal parameter ($U_{\text{iso}} = 0.0998(8) \text{ \AA}^2$) was refined for all of the hydrogen atoms. The final cycle of full-matrix least-squares refinement was based on 1454 observed reflections ($I > 2\sigma(I)$). Refinement converged at $R = 0.069$ and $R_w = 0.066$. The X-ray crystal structure of $(\text{Mes}_2\text{C}_6\text{H}_3)_2\text{GaCl}$ is given in Figure 1. Table 1 provides a summary of crystallographic

(5) Swepston, P. N. TEXSAN: Structure Analysis Software; Molecular Structure Corp., The Woodlands, TX, 1993.

(6) Sheldrick, G. M. SHELXTL, Crystallographic Computing System; Nicolet Instruments Division, Madison, WI, 1986.

Table 3. Comparison of Bond Angles (deg) and Distances (Å) in Sterically Demanding Monomeric Ar_{3-n}GaX_n Complexes

compd	C-Ga-C	C-Ga-X	Ga-C	Ga-X
Ph ₃ Ga	118.9(4) 120.6(2)		1.946(7) 1.968(5)	
Mes ₃ Ga (Mes = 2,4,6-Me ₃ C ₆ H ₂)	119.93(16)		1.968(4)	
Trip ₃ Ga (Trip = 2,4,6- <i>i</i> -Pr ₃ C ₆ H ₂)	116.6(5) 121.4(5) 121.9(5)		1.972(11)	
Mes ^(f) ₃ Ga (Mes ^(f) = 2,4,6-(CF ₃) ₃ C ₆ H ₂)	115.9(2) 121.8(2) 122.3(2)		1.998(5) 2.001(5) 2.004(5)	
Trip ₂ GaCl	133.8(7)	113.1(22)	1.954(16)	2.220(5)
Trip ₂ GaBr	135.5(4)	112.2(15)	1.955(12)	2.324(2)
sMes ₂ GaCl (sMes = 2,4,6- <i>t</i> -Bu ₃ C ₆ H ₂)	135.6(2)	103.1(1)	1.970(5)	2.231(1)
(Mes ₂ C ₆ H ₃) ₂ GaCl	153.5(5)	103.2(4) 103.4(4)	1.956(16) 2.001(16)	2.177(5)

data, data collection, and structural refinement, while atomic coordinates are given in Table 2.

Results and Discussion

A number of sterically demanding gallium aryls and arylgallium halides, Ar_{3-n}GaX_n, have been reported. Unassociated compounds which possess three-coordinate gallium centers are particularly interesting in this regard. These compounds, generally substituted derivatives of triphenylgallium, Ph₃Ga,⁷ include Mes₃Ga (Mes = 2,4,6-Me₃C₆H₂),⁸ Trip₂GaX (X = Cl, Br), and Trip₃Ga (Trip = 2,4,6-*i*-Pr₃C₆H₂).⁹ The fluoro derivative of mesityl, 2,4,6-tris(trifluoromethyl)phenyl, Mes^(f), has recently been utilized to prepare Mes^(f)₃Ga,¹⁰ and the tri-*tert*-butyl-substituted mesityl derivative, the so-called *super*-mesityl ligand, has been used to prepare sMes₂GaCl (sMes = 2,4,6-*t*-Bu₃C₆H₂).¹¹ Table 3 provides a comparison of these arylgallium compounds.

Although somewhat distorted in some cases, while nearly idealized in others, the coordination of the gallium atoms in the Ar_{3-n}GaX_n complexes in Table 3 may be described as trigonal planar.

Valence shell electron repulsion (VSEPR) theory¹² predicts that when the coordination number is 3, with no lone electron pairs on the central atom, trigonal-planar geometry should be observed.

The coordination of the gallium atom in **I** stands in notable contrast to the other previously reported Ar_{3-n}GaX_n trigonal-planar compounds in Table 3. The Ga-Cl bond distance of 2.177(5) Å in **I** is noticeably

shorter than the values reported for the other two Ar₂-GaCl compounds, while the Ga-C bond distances are in good agreement. The two Ga-Ph phenyl rings in **I** are rotated with respect to each other at an angle of 54.6°. The most intriguing metrical values, however, are found in the bond angles about the gallium center in **I**. The C-Ga-C bond angle of 153.5(5)° is a substantial 33.5° beyond the 120° expected for a trigonal-planar geometry. Furthermore, the C-Ga-Cl bond angles of 103.2(4)° and 103.4(5)° are closer to 90° than they are to 120°. The C-Ga-C bond angle of 153.5(5)° in **I** approaches the 150° mean of trigonal planar (120°) and T-shaped (180°). Indeed, the mean C-Ga-Cl bond angle of 103.3° in **I** correspondingly approaches the 105° mean of trigonal planar (120°) and T-shaped (90°). Thus, perhaps it is most reasonable to categorize the coordination of **I** as being *along the transition from trigonal planar to T-shaped*—indeed, a bit closer to the latter than the former. Relative to the ligand itself, it is interesting that the lithium salt of 2,6-dimesitylphenyl is dimeric ({Li(2,6-Mes₂C₆H₃)₂)₂) in the solid state.⁴ The fact that the title compound does not form an adduct with Et₂O is a likely consequence of the steric bulk about the metal center.

The utilization of aryl-substituted phenyl ligands such as 2,6-dimesitylphenyl affords a unique dimension to the concept of steric loading in contemporary organogallium chemistry. Forthcoming studies will address the reactivity of this compound.

Acknowledgment. We are grateful to the National Science Foundation (Grant No. CHE-9100518) and to the donors of The Petroleum Research Fund, administered by the American Chemical Society, for support of this work. We also thank Professor Arne Haaland for useful discussions.

Supplementary Material Available: A textual summary of data collection and refinement and tables of crystal data, bond distances and angles, final fractional coordinates for H atoms, and thermal parameters (9 pages). Ordering information is given on any current masthead page.

OM940950R

(7) Malone, M. F.; McDonald, W. S. *J. Chem. Soc. (A)* **1970**, 3262.
(8) Beachley, O. T., Jr.; Churchill, M. R.; Pazik, J. C.; Ziller, J. W. *Organometallics* **1985**, *5*, 1814.

(9) Petrie, M. A.; Power, P. P.; Dias, H. V. R.; Ruhlandt-Senge, K.; Waggoner, K. M.; Wehmschulte, R. J. *Organometallics* **1993**, *12*, 1086.

(10) Schluter, R. D.; Isom, H. S.; Cowley, A. H.; Atwood, D. A.; Jones, R. A.; Olbrich, F.; Corbelin, S.; Lagow, R. J. *Organometallics* **1994**, *13*, 4058.

(11) Meller, A.; Pusch, S.; Pohl, E.; Häming, L.; Herbst-Irmer, R. *Chem. Ber.* **1993**, *126*, 2255.

(12) (a) Gillespie, R. J.; Nyholm, R. S. *Q. Rev. Chem. Soc.* **1957**, *11*, 339. (b) Gillespie, R. J. *J. Chem. Educ.* **1963**, *40*, 295. (c) Gillespie, R. J. *J. Chem. Educ.* **1970**, *47*, 18. (d) Gillespie, R. J. *J. Chem. Soc. Rev.* **1992**, 59.

Synthesis and Structure of a Diiron Complex with a Highly Bent Dithiolene Bridge, $\text{Cp}^*_2\text{Fe}_2(\text{CO})\{\text{S}_2\text{C}_2(\text{CO}_2\text{Me})_2\}$ ($\text{Cp}^* = \eta^5\text{-C}_5\text{Me}_5$)

Shinji Inomata, Hidehiro Takano, Kunimasa Hiyama, Hiromi Tobita, and Hiroshi Ogino

Organometallics, 1995, 14 (4), 2112-2114 • DOI: 10.1021/om00004a075 • Publication Date (Web): 01 May 2002

Downloaded from <http://pubs.acs.org> on March 9, 2009

More About This Article

The permalink <http://dx.doi.org/10.1021/om00004a075> provides access to:

- Links to articles and content related to this article
- Copyright permission to reproduce figures and/or text from this article



ACS Publications
High quality. High impact.

Synthesis and Structure of a Diiron Complex with a Highly Bent Dithiolene Bridge, $\text{Cp}^*_2\text{Fe}_2(\text{CO})\{\text{S}_2\text{C}_2(\text{CO}_2\text{Me})_2\}$ ($\text{Cp}^* = \eta^5\text{-C}_5\text{Me}_5$)

Shinji Inomata,* Hidehiro Takano, Kunimasa Hiyama, Hiromi Tobita, and Hiroshi Ogino*

Department of Chemistry, Faculty of Science, Tohoku University, Sendai 980-77, Japan

Received January 4, 1995[⊗]

Summary: A novel dithiolene-bridged diiron complex $\text{Cp}^*_2\text{Fe}_2(\text{CO})\{\text{S}_2\text{C}_2(\text{CO}_2\text{Me})_2\}$ (**1**) was synthesized by the reaction of $\text{Cp}^*_2\text{Fe}_2(\text{CO})_4$ with elemental sulfur and dimethyl acetylenedicarboxylate in refluxing xylene. X-ray crystal structure analysis reveals that the dithiolene ligand in **1** bridges the Cp^*Fe and $\text{Cp}^*\text{Fe}(\text{CO})$ fragments unsymmetrically and that the dithiolene chelate ring is highly bent along the S-S axis.

Introduction

A number of dithiolene complexes have been synthesized and structurally characterized in which the dithiolene ligands adopt a variety of coordination modes. In most of these, the dithiolene chelate rings are completely planar.^{1,2} Only three monomeric titanium complexes, $\text{Cp}_2\text{Ti}(\text{S}_2\text{C}_2\text{H}_2)$,³ $(\text{MeC}_5\text{H}_4)_2\text{Ti}\{\text{S}_2\text{C}_2(\text{CO}_2\text{Me})_2\}$,⁴ and $\text{Cp}_2\text{Ti}(\text{S}_2\text{C}_6\text{H}_4)$ ⁵ are known as complexes containing nonplanar dithiolene chelate rings, in which π donation from the dithiolene to the titanium atom causes the distortion of the chelate rings.

Recently, we found that the reaction of $\text{Cp}^*_2\text{Fe}_2(\text{CO})_4$ with S_8 and $\text{PhC}\equiv\text{CPh}$ affords the mixed-ligand tetrairon-sulfur clusters $\text{Cp}^*_2(\text{Ph}_2\text{C}_2\text{S}_2)_2\text{Fe}_4\text{S}_4$ and $\text{Cp}^*_3(\text{Ph}_2\text{C}_2\text{S}_2)\text{Fe}_4\text{S}_5$.⁶⁻⁸ In order to extend the chemistry, similar syntheses using various alkynes other than $\text{PhC}\equiv\text{CPh}$ have been carried out. When dimethyl acetylenedicarboxylate (DMAD) was used as one of the alkynes, an unexpected dimeric complex was obtained along with tetrairon-sulfur clusters analogous to the products obtained in the $\text{PhC}\equiv\text{CPh}$ system.

We now report the synthesis and structure of the first example of a dinuclear dithiolene-bridged complex in which the dithiolene chelate ring is highly bent and bridges the two iron atoms unsymmetrically.

Experimental Section

General Procedures. Ether and hexane were distilled over sodium benzophenone ketyl. Toluene and xylene were distilled over sodium. NMR spectra were recorded on Varian XL-200 and Bruker ARX300 spectrometers. IR spectra were

recorded on a JASCO IR810 spectrometer. Mass spectra were recorded on a JEOL JMS-HX110 spectrometer.

Synthesis of $\text{Cp}^*_2\text{Fe}_2(\text{CO})\{\text{S}_2\text{C}_2(\text{CO}_2\text{Me})_2\}$ (1**).** A solution containing $\text{Cp}^*_2\text{Fe}_2(\text{CO})_4$ (249 mg, 0.504 mmol) with elemental sulfur (66 mg, 0.26 mmol) and dimethyl acetylenedicarboxylate (DMAD) (145 mg, 1.02 mmol) in xylene (30 mL) was refluxed for 2 h under a dinitrogen atmosphere. After removal of the solvent under reduced pressure, the residue was subjected to silica gel chromatography. The first and second bands were eluted by toluene/ether (3:1). Evaporation of the solvent from the first fraction afforded $\text{Cp}^*_2\text{Fe}_2(\text{CO})\{\text{S}_2\text{C}_2(\text{CO}_2\text{Me})_2\}$ (**1**) as a dark green oil which was crystallized from hexane. Yield: 49 mg (16%). After removal of the solvent from the second fraction, the cluster $\text{Cp}^*_3\{(\text{MeO}_2\text{C})_2\text{C}_2\text{S}_2\}\text{Fe}_4\text{S}_5$ (**2**) was obtained as a brown powder.⁹ Yield: 27 mg (11%). The last fraction was eluted with toluene/ether (1:1). The evaporation of the solvent afforded the cluster $\text{Cp}^*_2\{(\text{MeO}_2\text{C})_2\text{C}_2\text{S}_2\}_2\text{Fe}_4\text{S}_4$ (**3**) as a black powder.⁹ Yield: 31 mg (12%). Data for **1**: ¹H NMR (200 MHz, C_6D_6) δ 1.33 and 1.46 (s, 15 H \times 2, C_5Me_5), 3.66 (s, 6 H, CO_2Me); ¹³C NMR (50 MHz, C_6D_6) δ 8.9 and 9.8 ($\text{C}_5\text{Me}_5 \times 2$), 52.7 (CO_2Me), 89.2 and 90.3 ($\text{C}_5\text{Me}_5 \times 2$), 99.3 ($\text{S}_2\text{C}_2(\text{CO}_2\text{Me})_2$), 173.6 (CO_2Me), 224.2 (CO ligand); IR (KBr pellet, ν_{CO}) 1913 (s) cm^{-1} ; mass (FAB, *m*-nitrobenzyl alcohol matrix, Xe) *m/z* 616 (51, M⁺), 588 (100, M⁺ - CO). Anal. Calcd for $\text{C}_{27}\text{H}_{36}\text{Fe}_2\text{O}_8\text{S}_2$: C, 52.61; H, 5.89. Found: C, 52.49; H 5.89.

X-ray Crystal Structural Determination of $\text{Cp}^*_2\text{Fe}_2(\text{CO})\{\text{S}_2\text{C}_2(\text{CO}_2\text{Me})_2\}$ (1**).** Diffraction data were collected on a Rigaku AFC-6A four-circle diffractometer with graphite-monochromated Mo K α radiation using the ω - 2θ scan technique. The reflection data were corrected for Lorentz and polarization factors. No correction was applied for absorption. The unit cell dimensions were determined by the least-squares method using 85 reflections in the range $25 < 2\theta < 30^\circ$.

The crystal structure was solved by direct methods (RANTAN81),¹⁰ which afforded the positions of the two iron atoms and two sulfur atoms. All remaining non-hydrogen atoms were refined by the block-diagonal least-squares method with anisotropic thermal parameters. None of the hydrogen atoms was found from the difference Fourier map.

Values for the atomic scattering factors of non-hydrogen atoms were those in ref 11. Calculations were performed on a Nippon Electric Co. ACOS-2000 computer at Tohoku University Computer Center using the Universal Computation Program System UNICS III.¹² Crystallographic data for **1** are listed in Table 1.

[⊗] Abstract published in *Advance ACS Abstracts*, March 1, 1995.

(1) Müller-Westerhoff, U. T.; Vance, B. In *Comprehensive Coordination Chemistry*; Wilkinson, G., Gilland, R. D., McCleverty, J. A., Eds.; Pergamon: Oxford, U.K., 1988; Vol. 2, p 595.

(2) Eisenberg, R. *Prog. Inorg. Chem.* **1970**, *12*, 295.

(3) Kutoglu, A. *Acta Crystallogr.* **1973**, *B29*, 2891.

(4) Bolinger, C. M.; Rauchfuss, T. B. *Inorg. Chem.* **1982**, *21*, 3947.

(5) Kutoglu, A. *Z. Anorg. Allg. Chem.* **1972**, *390*, 195.

(6) Inomata, S.; Tobita, H.; Ogino, H. *J. Am. Chem. Soc.* **1990**, *112*, 6145.

(7) Inomata, S.; Tobita, H.; Ogino, H. *Inorg. Chem.* **1992**, *31*, 722.

(8) Inomata, S.; Hiyama, K.; Tobita, H.; Ogino, H. *Inorg. Chem.* **1994**, *33*, 5337.

(9) Formation of **2** and **3** was confirmed by mass spectral measurements, which showed the molecular ion peaks (995 for **2** and 1034 for **3**) and fragmentation patterns characteristic of $\text{Cp}^*_3(\text{dithiolene})\text{Fe}_4\text{S}_5$ and $\text{Cp}^*_2(\text{dithiolene})_2\text{Fe}_4\text{S}_4$.⁶⁻⁸

(10) (a) Jia-xing, Y. *Acta Crystallogr.* **1981**, *A37*, 642. (b) Jia-xing, Y. *Acta Crystallogr.* **1983**, *A39*, 39.

(11) Sakurai, T.; Kobayashi, K. *Rikagaku Kenkyusho Hokoku* **1979**, *55*, 69.

(12) *International Tables for X-ray Crystallography*; Kynoch: Birmingham, England, 1974; Vol. IV, Table 2.2A, pp 72-98, and Table 2.3.1, pp 149-150.

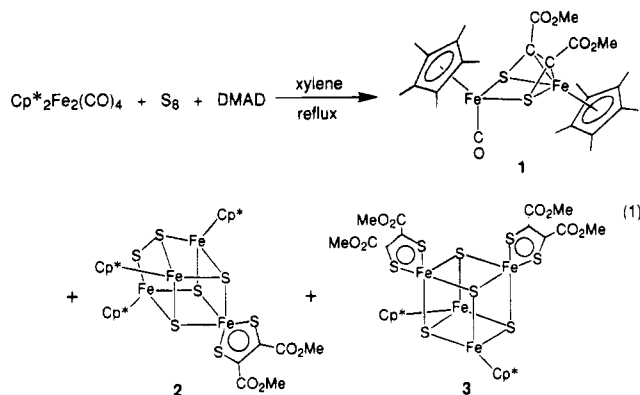
Table 1. Crystallographic Data for $\text{Cp}^*_2\text{Fe}_2(\text{CO})\{\text{S}_2\text{C}_2(\text{CO}_2\text{Me})_2\}$ (1)

formula	$\text{C}_{27}\text{H}_{36}\text{Fe}_2\text{O}_5\text{S}_2$
fw	616.41
cryst syst	monoclinic
space group	$P2_1/a$ (variant of No. 14)
a , Å	15.995(2)
b , Å	17.434(2)
c , Å	10.386(1)
β , deg	102.11(1)
V , Å ³	2831.7(5)
Z	4
d_{calcd} , g cm ⁻³	1.45
$\mu(\text{Mo K}\alpha)$, cm ⁻¹	12.3
temp, °C	20
reflcs measd	$\pm h, k, l$
2θ range, deg	3–65
no. of data used with $ F_o > 3\sigma(F_o)$	6941
no. of params refined	326
R^a	0.061
R_w^b	0.098

^a $R = \sum ||F_o| - |F_c|| / \sum |F_o|$. ^b $R_w = [\sum w(|F_o| - |F_c|)^2 / \sum w|F_o|^2]^{1/2}$; $w = [\sigma^2(|F_o|) + aF_o^2]^{-1}$, where $a = 0.009$.

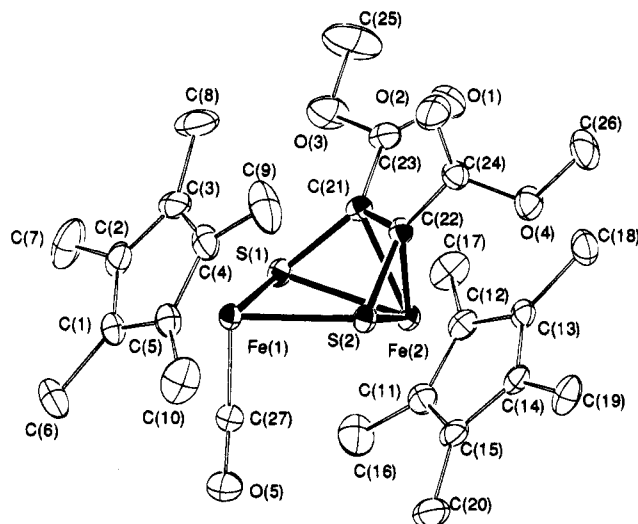
Results and Discussion

Refluxing a xylene solution containing $\text{Cp}^*_2\text{Fe}_2(\text{CO})_4$, S_8 , and DMAD in a 1:0.5:2 molar ratio afforded a dithiolene-bridged diiron complex $\text{Cp}^*_2\text{Fe}_2(\text{CO})\{\text{S}_2\text{C}_2(\text{CO}_2\text{Me})_2\}$ (1) together with two mixed-ligand tetrairon-sulfur clusters $\text{Cp}^*_3\{(\text{MeO}_2\text{C})_2\text{C}_2\text{S}_2\}_2\text{Fe}_4\text{S}_5$ (2) and $\text{Cp}^*_2\{(\text{MeO}_2\text{C})_2\text{C}_2\text{S}_2\}_2\text{Fe}_4\text{S}_4$ (3) (eq 1). Compound 1 was characterized extensively by spectroscopic methods, elemental analysis, and X-ray structure analysis.



The structure of 1 is shown in Figure 1. Final atomic coordinates and selected interatomic distances and angles are listed in Tables 2 and 3, respectively. One iron atom (Fe(1)) bears carbonyl and Cp* ligands, while the other (Fe(2)) bears a Cp* ligand. The dithiolene ligand in 1 bridges the Cp*Fe(CO) and Cp*Fe fragments unsymmetrically. Each of the two sulfur atoms (S(1) and S(2)) in the ligand is coordinated to the two iron atoms. On the other hand, the two carbon atoms (C(21) and C(22)) in the ligand are coordinated to Fe(2) only. The coordination of the carbon atoms was confirmed by the short Fe–C distances (1.996(4) and 1.991(3) Å). This is reflected in the elongation of the C(21)–C(22) distance (1.423(5) Å), which is longer by ca. 0.1 Å than that in most dithiolene complexes.^{1,2} The two C–S bond lengths are normal (1.759(3) and 1.753(3) Å). The interatomic distance of Fe(1)–Fe(2) is 3.398(1) Å indicating no Fe–Fe bond.

The dithiolene chelate ring consisting of Fe(1), S(1), S(2), C(21), and C(22) is highly bent along the S(1)–

**Figure 1.** ORTEP diagram of $\text{Cp}^*_2\text{Fe}_2(\text{CO})\{\text{S}_2\text{C}_2(\text{CO}_2\text{Me})_2\}$ (1).**Table 2. Final Atomic Coordinates ($\times 10^4$) and Equivalent Isotropic Temperature Factors for $\text{Cp}^*_2\text{Fe}_2(\text{CO})\{\text{S}_2\text{C}_2(\text{CO}_2\text{Me})_2\}$ (1)**

atom	x	y	z	B_{eq}^a , Å ²
Fe(1)	3245.4(3)	1874.9(3)	3506.7(4)	2.4
Fe(2)	3255.1(3)	3015.3(3)	857.1(4)	2.2
S(1)	2289(1)	2514(1)	1958(1)	2.6
S(2)	4134.9(5)	2709.7(5)	2805(1)	2.4
C(1)	3088(3)	1042(2)	4869(4)	3.1
C(2)	2414(3)	1573(3)	4726(4)	3.7
C(3)	2763(4)	2308(3)	5124(4)	4.4
C(4)	3673(3)	2225(2)	5513(4)	4.1
C(5)	3884(3)	1439(2)	5331(4)	3.3
C(6)	2998(4)	178(3)	4691(5)	5.0
C(7)	1480(3)	1376(4)	4304(7)	6.7
C(8)	2266(6)	3033(4)	5176(7)	8.4
C(9)	4310(6)	2846(4)	6053(5)	7.6
C(10)	4758(3)	1083(4)	5649(6)	5.9
C(11)	2845(3)	2541(2)	-1039(3)	3.5
C(12)	2602(2)	3326(2)	-1016(3)	3.1
C(13)	3370(2)	3776(2)	-635(3)	2.8
C(14)	4081(2)	3261(2)	-363(3)	3.1
C(15)	3756(3)	2490(2)	-626(4)	3.5
C(16)	2249(4)	1868(3)	-1430(5)	5.7
C(17)	1716(3)	3634(3)	-1401(4)	4.7
C(18)	3412(3)	4635(3)	-592(5)	4.3
C(19)	5017(3)	3460(3)	74(5)	4.6
C(20)	4292(4)	1773(3)	-553(5)	5.5
C(21)	2642(2)	3471(2)	2162(3)	2.5
C(22)	3542(2)	3563(2)	2576(3)	2.4
C(23)	2074(3)	4151(2)	1915(4)	3.4
C(24)	3939(3)	4301(2)	3097(4)	3.1
C(25)	679(4)	4620(4)	1599(9)	8.1
C(26)	4908(4)	5295(3)	2941(5)	5.3
C(27)	3422(3)	1161(2)	2425(4)	3.5
O(1)	2322(2)	4796(2)	1799(4)	5.2
O(2)	3793(3)	4597(2)	4064(3)	5.5
O(3)	1256(2)	3965(2)	1868(4)	5.2
O(4)	4505(2)	4569(2)	2455(3)	3.9
O(5)	3544(3)	651(2)	1774(4)	5.7

^a The equivalent isotropic temperature factors for non-hydrogen atoms were computed using the following expression: $B_{\text{eq}} = \frac{1}{3}(B_{11}a^2 + B_{22}b^2 + B_{33}c^2 + B_{13}ac \cos \beta)$. The B_{ij} 's are defined by $\exp[-(h^2B_{11} + k^2B_{22} + l^2B_{33} + 2hkB_{12} + 2hlB_{13} + 2klB_{23})]$.

S(2) axis. The dihedral angle between the plane of S(1)–Fe(1)–S(2) and the least squares plane of S(1)–C(21)–C(22)–S(2) is 43.2°, a value comparable with those in the monomeric dithiolene complexes, $\text{Cp}_2\text{Ti}(\text{S}_2\text{C}_2\text{H}_2)$ (46.1°),³ $(\text{MeC}_5\text{H}_4)_2\text{Ti}\{\text{S}_2\text{C}_2(\text{CO}_2\text{Me})_2\}$ (44°),⁴ and $\text{Cp}_2\text{Ti}(\text{S}_2\text{C}_6\text{H}_4)$ (46°).⁵

Table 3. Selected Interatomic Distances (Å) and Angles (deg) for Cp*₂Fe₂(CO){S₂C₂(CO₂Me)₂} (1)

Distances			
Fe(1)–S(1)	2.266(1)	Fe(1)–S(2)	2.260(1)
Fe(2)–S(1)	2.280(1)	Fe(2)–S(2)	2.272(1)
Fe(1)···C(21)	3.171(3)	Fe(1)···C(22)	3.164(3)
Fe(2)–C(21)	1.996(4)	Fe(2)–C(22)	1.991(3)
S(1)–C(21)	1.759(3)	S(2)–C(22)	1.753(3)
C(21)–C(22)	1.423(5)	Fe(1)···Fe(2)	3.398(1)
Angles			
S(1)–Fe(1)–S(2)	80.27(4)	S(1)–Fe(2)–S(2)	79.74(4)
Fe(1)–S(1)–Fe(2)	96.74(3)	Fe(1)–S(2)–Fe(2)	97.12(3)
Fe(1)–S(1)–C(21)	103.26(11)	Fe(2)–S(1)–C(21)	57.54(11)
Fe(1)–S(2)–C(22)	103.36(11)	Fe(2)–S(2)–C(22)	57.58(11)
S(1)–C(21)–C(22)	115.0(2)	S(2)–C(22)–C(21)	115.4(2)

Although there are several examples of dinuclear complexes containing a bridging dithiolene ligand, the coordination modes of the dithiolene ligands are different from that in **1**: The most closely related complexes to **1** are (C₅Me₄Et)₂Ru₂(S₂C₂Ph₂)¹³ and (OC)₆Mn₂(S₂C₂Ph₂)¹⁴. Although the dithiolene in each of these complexes acts as an η²-ligand for M(1) and as an η⁴-ligand for M(2), the chelate rings are completely planar, and also, each complex has a metal–metal bond, which is different from **1**. In the other dinuclear complexes (OC)₆Fe₂(S₂C₂Ph₂)¹⁵, Cp₂V₂(S₂){S₂C₂(CF₃)₂}¹⁶, Cp₂Mo₂{S₂C₂(CF₃)₂}₂¹⁷ and (MeC₅H₄)₂Mo₂(S₂CH₂)(S₂C₂H₂)¹⁸ each dithiolene ligand bridges the two metal atoms symmetrically.

(13) Rauchfuss, T. B.; Rodgers, D. P. S.; Wilson, S. R. *J. Am. Chem. Soc.* **1986**, *108*, 3114.

(14) Lindner, E.; Butz, I. P.; Hoehne, S.; Hiller, W.; Fawzi, R. *J. Organomet. Chem.* **1983**, *259*, 99.

(15) Weber, H. P.; Bryan, R. F. *J. Chem. Soc. A* **1967**, 182.

(16) Bolinger, C. M.; Rauchfuss, T. B.; Rheingold, A. L. *J. Am. Chem. Soc.* **1983**, *105*, 6321.

(17) Roesselet, K.; Doan, K. E.; Johnson, S. D.; Nicholls, P.; Miessler, G. L.; Kroeker, R.; Wheeler, S. H. *Organometallics* **1987**, *6*, 480.

(18) McKenna, M.; Wright, L. L.; Miller, D. J.; Tanner, L.; Haltiwanger, R. C.; DuBois, M. R. *J. Am. Chem. Soc.* **1983**, *105*, 5329.

The ¹H NMR spectrum of **1** in C₆D₆ solution shows two signals assignable to nonequivalent Cp* ligands and a single signal assignable to two equivalent methoxy carbonyl groups. This result is consistent with that of the X-ray structure analysis of **1**. The ¹³C NMR spectrum of **1** also supports this. The most notable feature of the spectrum is that the signal assignable to the chelate ring carbon atoms in the dithiolene ligand (99.3 ppm) appears at a much higher field than the corresponding signals reported for other dithiolene complexes (130–180 ppm).^{4,6,8,19} This indicates enhanced sp³ character of the carbon atoms in the dithiolene chelate ring of **1**.

Acknowledgment. This work was supported by a Grant-in-Aid for Scientific Research on Priority Area of Reactive Organometallics No. 06227205 from the Ministry of Education, Science and Culture of Japan.

Supplementary Material Available: Tables of crystal data, anisotropic thermal parameters, and bond distances and angles for **1** (8 pages). Ordering information is given on any current masthead page.

OM9500073

(19) For example, see: (a) Seyferth, D.; Henderson, R. S. *J. Organomet. Chem.* **1979**, *182*, C39. (b) Seyferth, D.; Womack, G. B.; Song, L.-C. *Organometallics* **1983**, *2*, 776. (c) Carty, A. J.; Dixneuf, P. H.; Gorgues, A.; Hartstock, F.; Le Bozec, H.; Taylor, N. *J. Inorg. Chem.* **1981**, *20*, 3929. (d) Ushijima, H.; Kajitani, M.; Shimizu, K.; Satō, G. P.; Akiyama, T.; Sugimori, A. *J. Electroanal. Chem.* **1991**, *303*, 199. (e) Kajitani, M.; Suetsugu, T.; Wakabayashi, R.; Igarashi, A.; Akiyama, T.; Sugimori, A. *J. Organomet. Chem.* **1985**, *293*, C15. (f) Vollhardt, K. P. C.; Walborsky, E. C. *J. Am. Chem. Soc.* **1983**, *105*, 5507. (g) Kajitani, M.; Ochiai, R.; Kikuchi, R.; Okubo, M.; Akiyama, T.; Sugimori, A. *Polyhedron* **1990**, *9*, 1123. (h) Mazid, M. A.; Razi, M. T.; Sadler, P. *J. Inorg. Chem.* **1981**, *20*, 2872. (i) Lowe, N. D.; Garner, C. D. *J. Chem. Soc., Dalton Trans.* **1993**, 2197. (j) Herberhold, M.; Jin, G.-X.; Milius, W. *Z. Anorg. Allg. Chem.* **1994**, *620*, 1295.

Synthesis and Structural Characterization of the Heterometallic Clusters $\text{CpCoFe}_2(\mu_3\text{-Se})_2(\text{CO})_6$ and $\text{CpCoFe}_2(\mu_3\text{-S})(\mu_3\text{-Se})(\text{CO})_6$

Pradeep Mathur,^{*,1a} P. Sekar,^{1a} and C. V. V. Satyanarayana^{1b}

Chemistry Department and Regional Sophisticated Instrumentation Center, Indian Institute of Technology, Powai, Bombay 400 076, India

Mary F. Mahon

School of Chemistry, University of Bath, Claverton Down, Bath BA2 7AY, U.K.

Received November 17, 1994[®]

Summary: The heterometallic clusters $\text{CpCoFe}_2(\mu_3\text{-Se})_2(\text{CO})_6$ (**1**) and $\text{CpCoFe}_2(\mu_3\text{-S})(\mu_3\text{-Se})(\text{CO})_6$ (**2**) were prepared in moderate yield from the room-temperature reaction of the mixed-chalcogenide compound $(\text{CO})_6\text{Fe}_2(\mu\text{-SSe})$ with freshly prepared $\text{CpCo}(\text{CO})_2$. Both clusters were characterized by elemental analysis, IR, and ^1H , ^{13}C , and ^{77}Se NMR as well as X-ray diffraction analysis. Compound **1** crystallized in the triclinic space group $P\bar{1}$, with $a = 6.638(1)$ Å, $b = 14.675(4)$ Å, $c = 17.844(7)$ Å, $\alpha = 111.37(3)^\circ$, $\beta = 100.80(2)^\circ$, $\gamma = 89.88(2)^\circ$, $V = 1585.9$ Å³, $Z = 4$, $D_c = 2.35$ g cm⁻³, $R = 3.85\%$, and $R_w = 3.12\%$. Compound **2** crystallized in the monoclinic space group $C2/c$, with $a = 34.994(10)$ Å, $b = 6.599(2)$ Å, $c = 14.766(5)$ Å, $\beta = 111.95(3)^\circ$, $V = 3162.7$ Å³, $Z = 8$, $D_c = 2.16$ g cm⁻³, $R = 3.51\%$, and $R_w = 3.26\%$. Both clusters consist of square pyramidal cores of Fe_2CoSe_2 and Fe_2CoSSe , respectively, and in each case the Co atom occupies the apical site of the square pyramid.

Introduction

The use of single-atom ligands derived from the main groups of the periodic table for the synthesis of cluster compounds has met with considerable success.² Of the group 16 elements, the sulfido ligand has been the most extensively used.³ In recent years, however the use of Se and Te in cluster synthesis has led to the isolation of several new clusters.⁴ A convenient starting material for the synthesis of chalcogen-bridged clusters is the class of compounds $\text{Fe}_2(\text{CO})_6(\mu\text{-E}_2)$, where E = S, Se, or Te.⁵ A characteristic feature of these compounds is the presence of a reactive E–E bond across which addition of organic and inorganic moieties occur readily. Also, base-induced reductions generate anionic species to which electrophiles can add.⁶ In both types of reactions,

the chalcogen atoms serve to bridge the $\text{Fe}_2(\text{CO})_6$ unit with the adding moiety. We have previously reported the synthesis of the mixed-chalcogenide compounds $\text{Fe}_2(\text{CO})_6(\mu\text{-SeTe})$ and $\text{Fe}_2(\text{CO})_6(\mu\text{-STe})$ and their reactions with coordinatively unsaturated metal carbonyl species to yield new mixed-metal, mixed-chalcogenide clusters.⁷ Here, we report on the synthesis of $\text{Fe}_2(\text{CO})_6(\mu\text{-SSe})$, its reaction with $\text{CpCo}(\text{CO})_2$, and characterization of the two products isolated.

Experimental Section

General Procedures. Reactions and manipulations were carried out under an inert atmosphere of nitrogen by means of standard Schlenk techniques. Solvents were deoxygenated immediately prior to use. $\text{CpCo}(\text{CO})_2$ was prepared as described in the literature.⁸ Infrared spectra were recorded on a Nicolet Impact 400 FT infrared spectrometer in NaCl cells of 0.1 mm path length as hexane solutions. NMR (^1H , ^{13}C , and ^{77}Se) spectra were obtained on a Varian XL-300 NMR spectrometer in CDCl_3 solutions using appropriate references at 25 °C. The ^{77}Se NMR spectra were referenced to an external

(4) (a) Flomer, W. A.; O'Neal, S. C.; Kolis, J. W.; Jeter, D.; Cordes, A. W. *Inorg. Chem.* **1988**, *27*, 969. (b) O'Neal, S. C.; Pennington, W. T.; Kolis, J. W. *Can. J. Chem.* **1989**, *67*, 1980. (c) O'Neal, S. C.; Pennington, W. T.; Kolis, J. W. *Inorg. Chem.* **1990**, *29*, 3134. (d) Roof, L. C.; Pennington, W. T.; Kolis, J. W. *J. Am. Chem. Soc.* **1990**, *112*, 8172. (e) Kolis, J. W. *Coord. Chem. Rev.* **1990**, *105*, 195. (f) Roof, L. C.; Pennington, W. T.; Kolis, J. W. *Angew. Chem., Int. Ed. Engl.* **1992**, *31*, 913. (g) Huang, S.-P.; Kanatzidis, M. G. *Inorg. Chem.* **1993**, *32*, 821. (h) Linford, L.; Raubenheimer, H. G. *Adv. Organomet. Chem.* **1991**, *32*, 1. (i) Mathur, P.; Chakrabarty, D.; Mavunkal, I. J. *J. Cluster Sci.* **1993**, *4*, 351. (j) Mathur, P.; Thimmappa, B. H. S.; Rheingold, A. L. *Inorg. Chem.* **1990**, *29*, 4658. (k) Mathur, P.; Mavunkal, I. J.; Rugmini, V.; Mahon, M. F. *Inorg. Chem.* **1990**, *29*, 4838.

(5) (a) Mathur, P.; Mavunkal, I. J.; Rheingold, A. L. *J. Chem. Soc., Chem. Commun.* **1989**, 382. (b) Mathur, P.; Mavunkal, I. J.; Rugmini, V. *Inorg. Chem.* **1989**, *28*, 3616. (c) Day, V. W.; Lesch, D. A.; Rauchfuss, T. B. *J. Am. Chem. Soc.* **1982**, *104*, 1290. (d) Bogan, L. E.; Rauchfuss, T. B.; Rheingold, A. L. *J. Am. Chem. Soc.* **1985**, *107*, 3843. (e) Lesch, D. A.; Rauchfuss, T. B. *Inorg. Chem.* **1983**, *22*, 1854. (f) Bogan, L. E., Jr.; Lesch, D. A.; Rauchfuss, T. B. *J. Organomet. Chem.* **1983**, *250*, 429.

(6) (a) Seyferth, D.; Henderson, R. S.; Gallagher, M. K. *J. Organomet. Chem.* **1980**, *193*, C75. (b) Seyferth, D.; Henderson, R. S.; Song, L.-C. *J. Organomet. Chem.* **1980**, *192*, C1. (c) Seyferth, D.; Henderson, R. S.; Song, L.-C. *Organometallics* **1982**, *1*, 125. (d) Seyferth, D.; Womack, G. B.; Henderson, R. S.; Cowie, M.; Hames, B. W. *Organometallics* **1986**, *5*, 1568. (e) Seyferth, D.; Womack, G. B. *Organometallics* **1986**, *5*, 2360. (f) Seyferth, D.; Womack, G. B.; Song, L.-C. *Organometallics* **1983**, *2*, 776. (g) Seyferth, D.; Womack, G. B.; Gallagher, M. K.; Cowie, M.; Hames, B. W.; Fackler, J. P., Jr.; Mazany, A. M. *Organometallics* **1987**, *6*, 283. (h) Seyferth, D.; Kiwan, A. M. *J. Organomet. Chem.* **1985**, *286*, 219. (i) Seyferth, D.; Henderson, R. S.; Song, L.-C. *J. Organomet. Chem.* **1985**, *292*, 9.

(7) (a) Mathur, P.; Chakrabarty, D.; Hossain, Md. M. *J. Organomet. Chem.* **1991**, *401*, 167. (b) Chakrabarty, D.; Hossain, Md. M.; Kumar, R. K.; Mathur, P. *J. Organomet. Chem.* **1991**, *410*, 143. (c) Mathur, P.; Chakrabarty, D.; Hossain, Md. M. *J. Organomet. Chem.* **1991**, *418*, 415. (d) Mathur, P.; Chakrabarty, D.; Hossain, Md. M.; Rashid, R. S. *J. Organomet. Chem.* **1991**, *420*, 79.

(8) Rausch, M. D.; Genetti, R. A. *J. Org. Chem.* **1970**, *35*, 3888.

[®] Abstract published in *Advance ACS Abstracts*, March 1, 1995.

(1) (a) Chemistry Department. (b) Regional Sophisticated Instrumentation Center.

(2) (a) Whitmire, K. H. *J. Coord. Chem.* **1988**, *17*, 95. (b) Compton, N. A.; Errington, R. J.; Norman, N. C. *Adv. Organomet. Chem.* **1990**, *31*, 91. (c) Roof, L. C.; Kolis, J. W. *Chem. Rev.* **1993**, *93*, 1037. (d) Wachter, *J. Angew. Chem., Int. Ed. Engl.* **1989**, *28*, 1613. (e) Müller, A. *Polyhedron* **1986**, *5*, 323. (f) Wachter, J. *J. Coord. Chem.* **1988**, *15*, 219. (g) Ansari, M. A.; Ibers, J. A. *Coord. Chem. Rev.* **1990**, *100*, 223. (h) Tatsumi, K.; Kawaguchi, H.; Tani, K. *Angew. Chem., Int. Ed. Engl.* **1993**, *32*, 591.

(3) (a) Adams, R. D. *Polyhedron* **1985**, *4*, 2003. (b) Adams, R. D.; Babin, J. E.; Mathur, P.; Natarajan, K.; Wang, J. W. *Inorg. Chem.* **1989**, *28*, 1440. (c) Adams, R. D.; Babin, J. E.; Wang, J.-G.; Wu, W. *Inorg. Chem.* **1989**, *28*, 703. (d) Adams, R. D.; Wang, J.-G. *Polyhedron* **1989**, *8*, 1437. (e) Adams, R. D.; Babin, J. E.; Estrada, J. W.; Wang, J.-G.; Hall, M. B.; Low, A. A. *Polyhedron* **1989**, *8*, 1885. (f) Mathur, P.; Mavunkal, I. J.; Rugmini, V. *J. Organomet. Chem.* **1989**, *367*, 243. Shaowu, D.; Nianyong, Z.; Pengcheng, C.; Xintao, W.; Jaixi, L. *J. Chem. Soc., Dalton Trans.* **1992**, 339.

standard of Me_2Se ($\delta = 0$), and the spectra were obtained at the operating frequency of 57.23 MHz; 90° pulses were used with 1.0 s delay and 1.0 s acquisition time.

Preparation of $\text{Fe}_2(\text{CO})_6(\mu\text{-SSe})$. A solution of Na_2SO_3 (1 g, 7.94 mmol) and Na_2SeO_3 (1.5 g, 8.67 mmol) in 35 mL of H_2O was added to a flask containing an ice-cooled solution prepared from 5 mL (17.11 mmol) of $\text{Fe}(\text{CO})_5$, 12 mL of 50% aqueous KOH, and 40 mL of CH_3OH . After being stirred for 0.5 h, the reaction mixture was cooled to 0 °C and acidified with 6 M HCl. The resulting black precipitate was filtered off in air, washed with distilled water, and dried in vacuo. The solid was then extracted with four 25 mL portions of CH_2Cl_2 , and the combined extracts were filtered and evaporated to dryness. The solid residue containing the mixture of $\text{Fe}_3(\text{CO})_9(\mu_3\text{-S})(\mu_3\text{-Se})$, $\text{Fe}_3(\text{CO})_9(\mu_3\text{-S})_2$, and $\text{Fe}_3(\text{CO})_9(\mu_3\text{-Se})_2$ (1.8 g) was added to a solution of NaOMe (9 g of Na in 400 mL MeOH), and the mixture was stirred at room temperature until complete dissolution had taken place. The solution was diluted with hexane (150 mL) and water (100 mL) and acidified with 6 M HCl. After separation of the layers, the aqueous phase was further extracted with hexane and the combined organic extracts were washed with H_2O and dried over anhydrous Na_2SO_4 . The organic fraction was concentrated and subjected to chromatography on a silica column. Using hexane as eluant, in order of elution, the following compounds were obtained: $\text{Fe}_2(\text{CO})_6(\mu\text{-S})_2$ (12%); $\text{Fe}_2(\text{CO})_6(\mu\text{-SSe})$ (15%) [IR ($\nu(\text{CO})$, cm^{-1}) 2081 (m), 2040 (vs), 2004 (vs)]; $\text{Fe}_2(\text{CO})_6(\mu\text{-Se}_2)$ (13%).

Preparation of $\text{CpCoFe}_2(\mu_3\text{-Se})_2(\text{CO})_6$ (1) and $\text{CpCoFe}_2(\mu_3\text{-S})(\mu_3\text{-Se})(\text{CO})_6$ (2). A hexane solution (75 mL) of $\text{Fe}_2(\text{CO})_6(\mu\text{-SSe})$ (0.25 g, 0.64 mmol) and $\text{CpCo}(\text{CO})_2$ (0.6 mL) was stirred at room temperature under N_2 for 10 h. The solvent was removed in vacuo, and the residue was chromatographed on a silica gel column using hexane as eluent. In order of elution the following compounds were isolated: dark red 1 [yield 0.09 g (25%); IR ($\nu(\text{CO})$, cm^{-1}) 2060 (m), 2036 (vs), 2030 (sh), 1994 (s), 1983 (vs), 1955 (w), 1947 (w); ^1H NMR 5.85 ppm (s, C_5H_5); ^{13}C NMR 207.4 (s, CO), 82.4 ppm (s, C_5H_5); ^{77}Se NMR 796.4 ppm (s); mp 143–145 °C. Anal. Calcd for 1: C, 23.5; H, 0.89. Found: C, 23.6; H, 1.17]; dark red 2 [yield 0.11 g (34%); IR ($\nu(\text{CO})$, cm^{-1}) 2063 (m), 2039 (vs), 2032 (sh), 1997 (s), 1986 (vs), 1957 (w), 1951 (w); ^1H NMR 5.84 ppm (s, C_5H_5); ^{13}C NMR 206.6 (s, CO), 83.4 ppm (s, C_5H_5); ^{77}Se NMR 737.8 ppm (s); mp 148–150 °C. Anal. Calcd for 2: C, 25.7; H, 0.09. Found: C, 26.1; H, 1.17].

Crystal Structure Determination of $\text{CpCoFe}_2(\mu_3\text{-Se})_2(\text{CO})_6$ (1). Black crystals of 1 were grown from a hexane/dichloromethane solution by slow evaporation of solvent at –5 °C. A crystal of approximate dimensions $0.3 \times 0.3 \times 0.15 \text{ mm}^3$ was selected for the X-ray diffraction study. Crystallographic data are summarized in Table 1. The data were measured at room temperature on a CAD4 automatic four-circle diffractometer in the range $2^\circ \leq \theta \leq 24^\circ$; 5460 reflections were collected of which 2888 were unique with $I \geq 2\sigma(I)$. Data were corrected for Lorentz and polarization effects, a linear crystal decay of 11.8% (based on the standard reflection intensities) during data collection, and absorption.⁹ The structure was solved by direct methods and refined using the SHELX¹⁰ suite of programs. In the final least squares cycles all atoms were allowed to vibrate anisotropically. Hydrogen atoms were included at calculated positions. Final residuals after 12 cycles of blocked-matrix least squares refinement were $R = 0.0385$ and $R_w = 0.0312$, for a weighting scheme of $w = 2.7018/[\sigma^2(F) + 0.000190(F)^2]$. The maximum final shift/esd was 0.001. The maximum and minimum residual densities were 0.47 and –0.43 $\text{e} \text{ \AA}^{-3}$, respectively. Final fractional atomic coordinates

Table 1. Crystallographic Data for 1 and 2

	compound	
	1	2
formula	$\text{C}_{11}\text{H}_5\text{CoFe}_2\text{Se}_2\text{O}_6$	$\text{C}_{11}\text{H}_5\text{CoFe}_2\text{SSeO}_6$
fw	561.7	514.8
cryst syst	triclinic	monoclinic
space group	$P\bar{1}$	$C2/c$
<i>a</i> , Å	6.638(1)	34.994(10)
<i>b</i> , Å	14.675(4)	6.599(2)
<i>c</i> , Å	17.844(7)	14.766(5)
α , deg	111.37(3)	
β , deg	100.80(2)	111.95(3)
γ , deg	89.88(2)	
<i>V</i> , Å ³	1585.9	3162.7
<i>Z</i>	4	8
<i>D</i> (calc), g cm^{-3}	2.35	2.16
$\mu(\text{Mo K}\alpha)$, cm^{-1}	72.5	52.7
<i>F</i> (000)	1064	1984
$2\theta_{\text{max}}$, deg	48	48
<i>T</i> , K	298	298
no. of reflns collcd	5460	2776
no. of obsd reflns	2888	1626
weighting scheme	$w = 2.7018/[\sigma^2(F) + 0.000190(F)^2]$	$w = 2.7640/[\sigma^2(F) + 0.000498(F)^2]$
final <i>F</i> indices, %	$R = 3.85, R_w = 3.12$	$R = 3.51, R_w = 3.26$
$\Delta\rho_{\text{max}}, \Delta\rho_{\text{min}}$, $\text{e} \text{ \AA}^{-3}$	0.47, –0.43	0.27, –0.28
max. min abs corrs	0.863, 0.600	0.371, 0.914

Table 2. Selected Bond Distances and Angles for $\text{CpCoFe}_2(\mu_3\text{-Se})_2(\text{CO})_6$ (1)

(a) Bond Distances (Å)			
Fe(1)–Se(1)	2.364(3)	Co(1)–Fe(1)	2.565(5)
Fe(1)–Se(2)	2.359(3)	Co(1)–Fe(2)	2.551(4)
Fe(2)–Se(1)	2.364(3)	Co(1)–Se(1)	2.284(4)
Fe(2)–Se(2)	2.365(3)	Co(1)–Se(2)	2.291(3)
Se(2)–Se(1)	3.106(4)		
(b) Bond Angles (deg)			
Fe(1)–Co(1)–Se(1)	58.0(0)	Co(1)–Fe(1)–Se(1)	55.0(0)
Fe(1)–Co(1)–Se(2)	57.8(0)	Co(1)–Fe(1)–Se(2)	55.3(0)
Fe(2)–Co(1)–Se(1)	58.2(0)	Co(1)–Fe(2)–Se(2)	55.4(0)
Fe(2)–Co(1)–Se(2)	58.2(0)	Co(1)–Se(1)–Fe(1)	67.0(2)
Fe(1)–Se(1)–Se(2)	48.8(0)	Co(1)–Se(1)–Fe(2)	66.5(0)
Fe(1)–Se(2)–Se(1)	49.0(0)	Co(1)–Se(2)–Fe(1)	66.9(0)
Fe(2)–Se(2)–Se(1)	48.9(0)	Co(1)–Se(2)–Fe(2)	66.4(0)
Fe(2)–Se(1)–Fe(1)	97.2(0)	Co(1)–Se(1)–Se(2)	47.3(0)
Fe(2)–Se(2)–Fe(1)	97.3(0)	Co(1)–Se(2)–Se(1)	47.2(0)
Fe(2)–Co(1)–Fe(1)	87.8(2)	Se(2)–Co(1)–Se(1)	85.5(2)
Se(2)–Fe(1)–Se(1)	82.2(0)	Se(2)–Fe(2)–Se(1)	82.1(0)

and isotropic thermal parameters are given in the supplementary material; bond distances and bond angles are given in Table 2.

Crystal Structure Determination of $\text{CpCoFe}_2(\mu_3\text{-S})(\mu_3\text{-Se})(\text{CO})_6$ (2). Black crystals of 2 were grown from a hexane/dichloromethane solution by slow evaporation of solvent at –5 °C. A crystal of approximate dimensions $0.15 \times 0.15 \times 0.2 \text{ mm}^3$ was selected for the X-ray diffraction study. Crystallographic data are summarized in Table 1. The data were measured at room temperature on a CAD4 automatic four-circle diffractometer in the range $2^\circ \leq \theta \leq 24^\circ$; 2776 reflections were collected of which 1626 were unique with $I \geq 2\sigma(I)$. Data were corrected for Lorentz and polarization and also absorption.⁹ The structure was solved by direct methods and refined using the SHELX¹⁰ suite of programs. Early convergence revealed that the Se(1) and S(1) positions were disordered in the ratio of 67:33 with their primed analogues. This disorder is not depicted in the ORTEP plot, where only the position of the unprimed atoms is illustrated. The very proximate disordered moieties are indicated by bracketed labels. In the final least squares cycles all atoms except for the partial occupiers Se(1') and S(1') were allowed to vibrate anisotropically. Hydrogen atoms were included at calculated positions. Final residuals after 10 cycles of least squares were $R = 0.0351$ and $R_w = 0.0326$, for a weighting scheme of $w = 2.7640/[\sigma^2(F) + 0.000498(F)^2]$. The maximum final shift/esd was 0.001. The

(9) Walker, N.; Stewart, D. *Acta Crystallogr., Sect. A* **1983**, *39*, 158.

(10) (a) Sheldrick, G. M. SHELX86, a computer program for crystal structure determination, University of Göttingen, 1986. (b) Sheldrick, G. M. SHELX76, a computer program for crystal structure determination, University of Cambridge, 1976.

Table 3. Selected Bond Distances and Angles for CpCoFe₂(μ₃-S)(μ₃-Se)(CO)₆ (2)

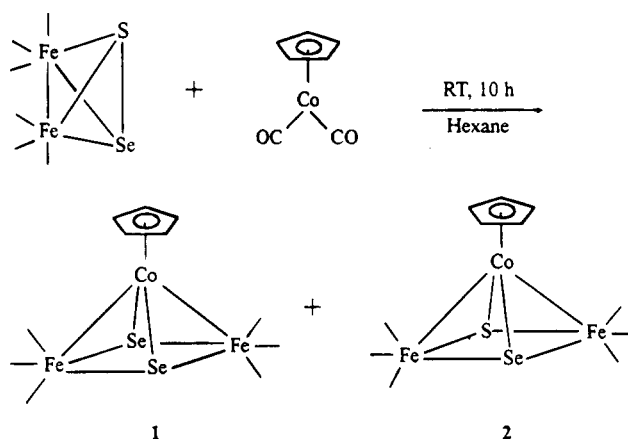
(a) Bond Distances (Å)			
Fe(1)–Co(1)	2.538(4)	Se(1)–Fe(1)	2.345(7)
Fe(2)–Co(1)	2.521(4)	Se(1)–Fe(2)	2.334(7)
Se(1)–Co(1)	2.291(7)	S(1)–Fe(1)	2.311(11)
S(1)–Co(1)	2.298(16)	S(1)–Fe(2)	2.326(13)
(b) Bond Angles (deg)			
Fe(2)–Co(1)–Fe(1)	86.7(4)	S(1)–Co(1)–Fe(1)	56.8(3)
Fe(2)–S(1)–Fe(1)	97.0(6)	S(1)–Co(1)–Fe(2)	57.5(4)
Fe(2)–Se(1)–Fe(1)	95.8(3)	S(1)–Co(1)–Se(1)	84.7(4)
S(1)–Fe(1)–Se(1)	83.2(4)	Se(1)–Co(1)–Fe(1)	57.8(2)
S(1)–Fe(2)–Se(1)	83.1(4)	Se(1)–Co(1)–Fe(2)	57.8(2)

maximum and minimum residual densities were 0.27 and $-0.28 \text{ e}\text{\AA}^{-3}$, respectively. Final fractional atomic coordinates and isotropic thermal parameters are given in the supplementary material; bond distances and bond angles are given in Table 3.

Results and Discussion

Synthesis of Fe₂(CO)₆(μ-SSe). The mixed-chalcogenide Fe₂(CO)₆(μ-SSe) was obtained by a method similar to that used for the preparation of Fe₂(CO)₆(μ-Se₂).^{11,12} An aqueous solution of a mixture of Na₂SO₃ and Na₂SeO₃ was added to a methanol solution containing Fe(CO)₅ and KOH. After room-temperature stirring and workup, Fe₂(CO)₆(μ-SSe) was separated by column chromatography from the other products formed in the reaction, Fe₂(CO)₆(μ-S₂) and Fe₂(CO)₆(μ-Se₂). An optimum yield of 15% of Fe₂(CO)₆(μ-SSe) was obtained when a 8:9 molar ratio of Na₂SO₃ and Na₂SeO₃ was used. Like Fe₂(CO)₆(μ-Te₂), Fe₂(CO)₆(μ-SSe) decomposes rapidly in the solid form, but in solution it can be stored at 0 °C for several days. The IR spectrum of Fe₂(CO)₆(μ-SSe) shows carbonyl stretching frequencies which are almost the exact mean of the corresponding frequencies observed in the spectra of Fe₂(CO)₆(μ-S₂) and Fe₂(CO)₆(μ-Se₂).

Synthesis and Characterization of CpCoFe₂(μ₃-Se)₂(CO)₆ (1) and CpCoFe₂(μ₃-S)(μ₃-Se)(CO)₆ (2). When a hexane solution containing Fe₂(CO)₆(μ-SSe) and CpCo(CO)₂ was stirred for 10 h, after chromatographic workup, two products were obtained and characterized as CpCoFe₂(μ₃-Se)₂(CO)₆ (1) and CpCoFe₂(μ₃-S)(μ₃-Se)(CO)₆ (2) (Scheme 1). Formation of 1 from an Fe₂(CO)₆(μ-Se₂) impurity is unlikely on account of the following. FT-IR spectroscopy confirmed that Fe₂(CO)₆(μ-SSe) did not contain any Fe₂(CO)₆(μ-Se₂) impurity. In solution, Fe₂(CO)₆(μ-SSe) converts very slowly to Fe₂(CO)₆(μ-Se₂) (after 24 h, there is less than 5% conversion), and this would not account for formation of 1 in 25% yield. Compound 1 has previously been prepared in 56% yield from the room-temperature reaction of Fe₂(CO)₆(μ-Se₂) and CpCo(CO)₂ in THF solvent and has been spectroscopically characterized.¹¹ The related compound (η⁵-C₅Me₅)Co(μ₃-S)₂Fe₂(CO)₆ has been similarly obtained and structurally characterized by X-ray analysis.¹³ The infrared spectra of 1 and 2 display identical CO stretching pattern, with the stretching frequencies observed for 1 being 2–4 cm⁻¹ lower than the corresponding

Scheme 1. Formation of 1 and 2

frequencies observed for 2. ¹H and ¹³C NMR spectra confirm the presence of Cp ligands in 1 and 2. The ⁷⁷Se NMR spectra of 1 and 2 showed a single peak in each case. Comparison with the ⁷⁷Se NMR spectra of Fe₃(CO)₉(μ₃-Se)₂ and Fe₃(CO)₉(μ₃-S)(μ₃-Se) shows the replacement of a Fe(CO)₃ group by a CpCo group shifts the signal downfield by 18 and 59 ppm, respectively.¹⁴

Molecular Structures of 1 and 2. ORTEP drawings of compounds 1 and 2 are shown in Figures 1 and 2, respectively. Both molecules exhibit a heavy atom square pyramidal geometry with the Co atom occupying the apical site. Overall, the core structure is similar to that of (η⁵-C₅Me₅)Co(μ₃-S)₂Fe₂(CO)₆.¹³ The average Co–Fe bond distances in 1 (2.558 Å) and 2 (2.529 Å) are similar to the average Co–Fe distance of 2.539 Å in (η⁵-C₅Me₅)Co(μ₃-S)₂Fe₂(CO)₆ but are shorter than the average Co–Fe bond distances reported for FeCo₂(CO)₉(μ₃-Se) (2.581 Å)¹⁵ and other Fe–Co mixed-metal clusters Fe₂Co₂(CO)₁₁(μ₄-S)₂ (2.58 Å),¹⁶ Fe₂Co₂(CO)₁₁(μ₄-PPh)₂ (2.62 Å),¹⁶ and H(Cp)MoCoFe(CO)₈(μ₃-Ge^tBu)¹⁷ (2.684 Å). In 1, the two Co–Se bond distances are almost identical (Co–Se(1) = 2.284(4) Å and Co–Se(2) = 2.291(4) Å) which indicates that the Co atom lies on the perpendicular bisector of the Fe(1)–Fe(2) segment. Although in 2 the Co atom is bonded to different chalcogen atoms, the almost equal bond distances of Co–S (2.298(16) Å) and Co–Se (2.291(7) Å) indicate that, in 2 also, the disposition of the Co atom in the square pyramidal core is as symmetric as in compound 1. The average Fe–Se bond distance in 1 (2.363 Å) is longer than the average Fe–Se bond distance in 2 (2.323 Å) but comparable to the average Fe–Se bond distances in Fe₃(CO)₉(μ₃-Se)₂¹⁸ (2.35 Å) and in Fe₃(CO)₉(μ₃-S)(μ₃-Se)¹⁹ (2.351 Å). It is shorter than the average Fe–Se bond distance of 2.437 Å reported for Fe₃(CO)₉(μ₃-Se)(μ₃-Te).¹⁹ The Fe–Co–Fe angles in both 1 and 2 are similar (87.8(2) and 86.7(4)°, respectively).

Assuming that the S and Se atoms act as 4-electron donors, both 1 and 2 are 50-electron clusters, and the formal application of the 18-electron rule would predict two metal–metal bonds as observed. According to the

(14) Unpublished results for ⁷⁷Se NMR data: Fe₃(CO)₉(μ₃-Se)₂, δ 778.5; Fe₃(CO)₉(μ₃-S)(μ₃-Se), δ 679.7.

(15) Strouse, C. E.; Dahl, L. F. *J. Am. Chem. Soc.* **1971**, *93*, 6032.

(16) Vahrenkamp, H.; Wucherer, E. *J. Angew. Chem., Int. Ed. Engl.* **1981**, *20*, 680.

(17) Gusbeth, P.; Vahrenkamp, H. *Chem. Ber.* **1985**, *118*, 1770.

(18) Dahl, L. F.; Sutton, P. W. *Inorg. Chem.* **1963**, *2*, 1067.

(19) Gervasio, G. *J. Organomet. Chem.* **1993**, *445*, 147.

(11) Seyferth, D.; Henderson, R. S. *J. Organomet. Chem.* **1981**, *204*, 333.

(12) Mathur, P.; Chakrabarty, D.; Hossain, Md. M.; Rashid, R. S.; Rugmini, V.; Rheingold, A. L. *Inorg. Chem.* **1992**, *31*, 1106.

(13) Cowie, M.; DeKock, R. L.; Wagenmaker, T. R.; Seyferth, D.; Henderson, R. S.; Gallagher, M. K. *Organometallics* **1989**, *8*, 119.

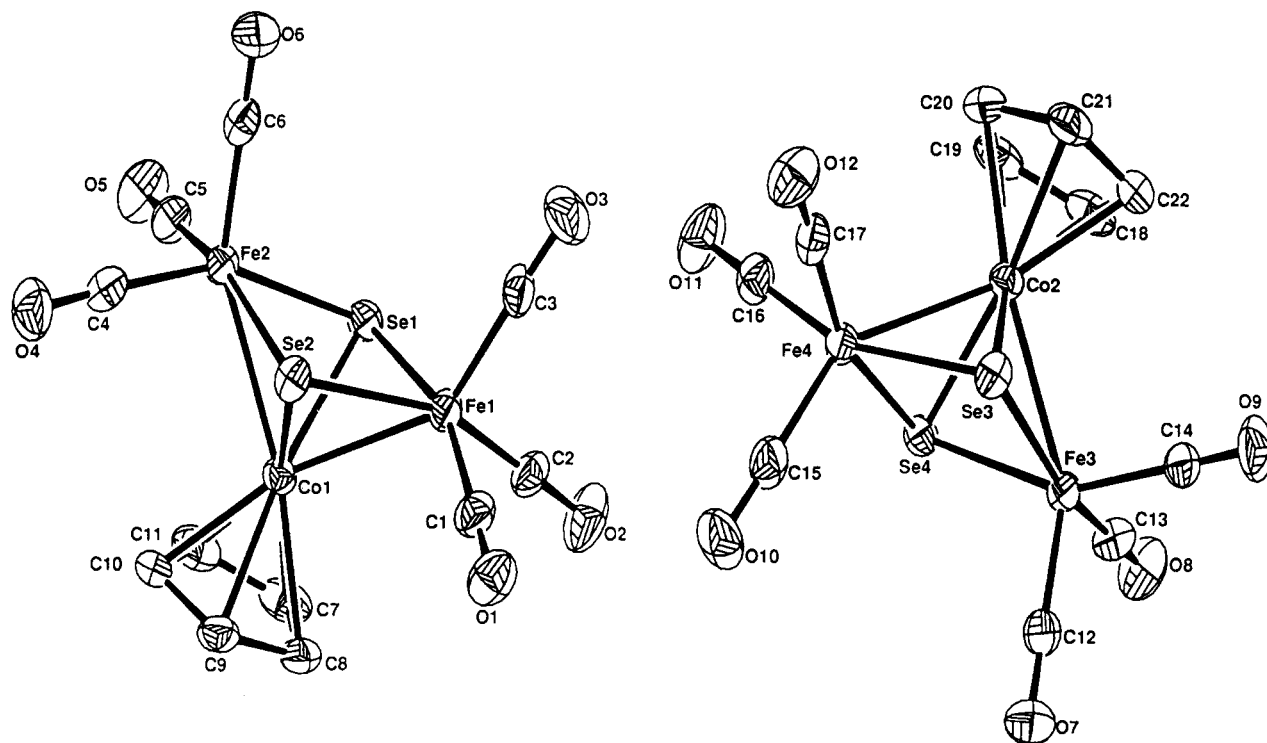


Figure 1. Molecular structure of **1** with the atom-labeling scheme.

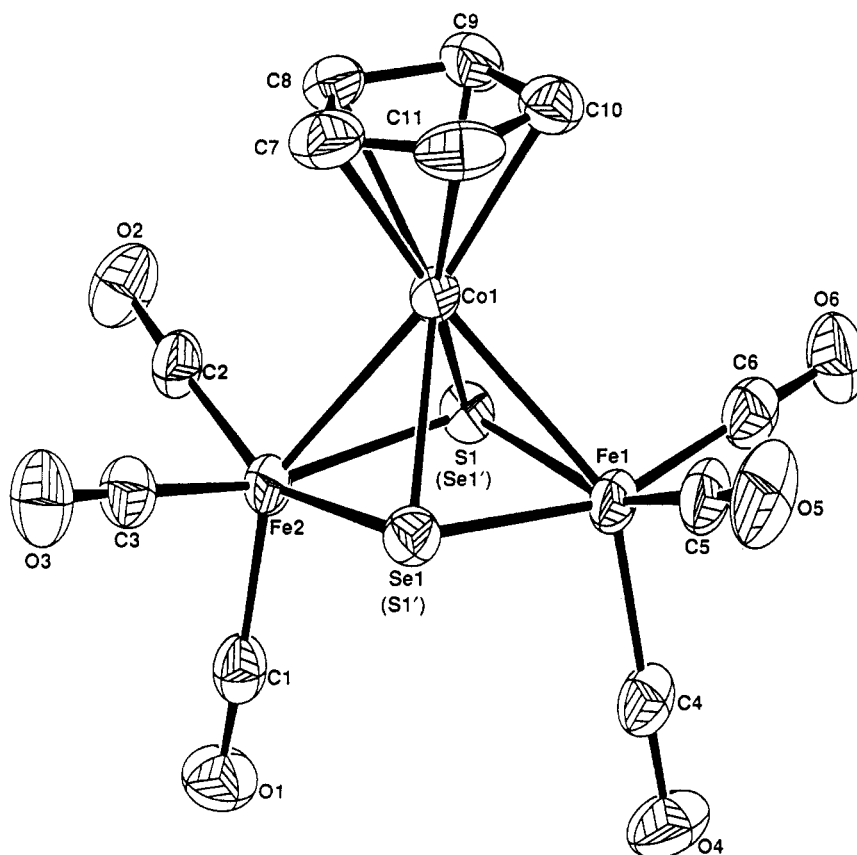


Figure 2. Molecular structure of **2** with the atom-labeling scheme.

PSEP theory, the presence of 7 skeletal electron pairs in each cluster correctly predicts the nido octahedral structure.

Acknowledgment. We thank the Department of Science & Technology, Government of India, for support of this work.

Supplementary Material Available: Tables of complete bond lengths and angles, nonbonded distances, fractional atomic coordinates, and isotropic and anisotropic thermal parameters (23 pages). Ordering information is given on any current masthead page.

OM9408775

{1,2-[(η^5 -C₅Me₅)Ir]₂B₅H₅}: Isolation and Structural Characterization of a *Closo*-Polyhedral Metallaborane Cluster with a Capping BH Group

Jonathan Bould, Nigam P. Rath, and Lawrence Barton*

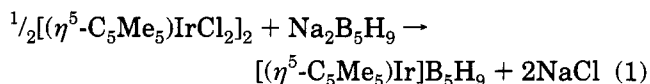
Department of Chemistry, University of Missouri—St. Louis, St. Louis, Missouri 63121

Received November 28, 1994[⊗]

Summary: The synthesis and characterization of the novel *pileo*-cluster [(η^5 -C₅Me₅)₂Ir₂B₅H₅], **1**, are reported. Compound **1** is formed as yellow crystals in very low yield from the reaction between [(η^5 -C₅Me₅)IrCl₂]₂ and Na₂[B₅H₉] in tetrahydrofuran. It is characterized by ¹H and ¹¹B NMR spectra, elemental analysis, a mass spectrum, and a crystal structure determination. The structure of **1** is that of an octahedral cluster containing four BH groups and two adjacent [(η^5 -C₅Me₅)Ir] groups. A fifth BH group caps a B–Ir–Ir triangular face. The *pileo*-cluster, **1**, is related to the known system [(η^5 -C₅Me₅)₂Co₂B₅H₅] for which a similar structure is proposed and [(η^5 -C₅Me₅)Co]₃B₄H₄, the known structure of which also indicates the presence of a capping BH group, this one involving a [(η^5 -C₅Me₅)Co]₃ face.

We are interested in the preparation of homo- and heterobimetalaboranes based on borane templates containing 5 and 6 boron atoms. A recent success was the preparation of Cu[Ph₃P]₂B₅H₉Fe(CO)₄,¹ a system in which the two metals are “pseudo-protons” in that they occupy positions which may be replaced by protons. A related system, prepared several years ago by Shore et al.,² is Cu[Ph₃P]₂B₅H₈Fe(CO)₃ in which the Fe atom is a true vertex. Related to this are the species {(PPh₃)₂(CO)Os[Ph(Me)₂P]ClHPtB₅H₇}³ and [(PPh₃)₂COHr(PMe₂Ph)ClPtB₅H₆]⁴ prepared from the readily accessible and relatively stable metallahexaboranes (PPh₃)₂(CO)OsB₅H₉⁵ and (PPh₃)₂(CO)IrB₅H₈.⁶ We have found that, in using the latter reagents, the Os species, which contains four bridging hydrogen atoms, is easily deprotonated with KH or C₄H₉Li but the Ir species, with one fewer bridging H atom, is much more difficult to deprotonate. We therefore made some attempts to prepare an iridahexaborane analogue with four bridging hydrogen atoms, and herein we report the result of one such attempt. The synthetic strategy followed the precept that, whereas (PPh₃)₂(CO)IrB₅H₈ is formed in high yield from a simple metathesis between Na[B₅H₈] and IrCl(CO)(PPh₃)₂,⁶ it might be possible to form the desired product from a similar metathetical reaction between the recently reported⁷ *arachno*-pentaborane

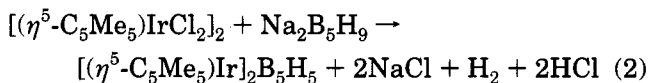
anion [B₅H₉]²⁻ and [(η^5 -C₅Me₅)IrCl₂]₂ as follows:



On the other hand, since the *nido*-bimetalheptaborane analogue (η^5 -C₅Me₅)₂Co₂B₅H₉ is reported by Venable and Grimes to form from the reaction between [B₅H₈]⁻, CoCl₂, and (η^5 -C₅Me₅)⁻,⁸ an alternative product of reaction 1 might be the the iridium analogue of the bicobaltaheptaborane (η^5 -C₅Me₅)₂Co₂B₅H₉. Indeed this could represent a rational process to the formation of [(η^5 -C₅Me₅)Ir]₂B₅H₉, since the species [B₅H₉]²⁻ presumably contains two basic B–B bonds and thus the [(η^5 -C₅Me₅)IrCl₂]₂ moiety could possibly insert into the borane anion. This note reports that the only isolable product of this reaction containing five boron atoms, completely characterized by analytical, spectral, and crystallographic methods, is the novel *pileo*-cluster [(η^5 -C₅Me₅)₂Ir₂B₅H₅], **1**, which consists of an octahedral Ir₂B₄ cluster with an additional BH group capping a BIr₂ triangle.

Results and Discussion

The addition of 1.25 mmol of [(η^5 -C₅Me₅)IrCl₂]₂ to a stirred solution of 2.5 mmol of Na₂B₅H₉ at –78 °C followed by slow warming to room temperature and isolation of the products by thin layer chromatography gave low yields of a number of metallaborane products one of which has been fully characterized as *pileo*-1,2-[(η^5 -C₅Me₅)Ir]₂B₅H₅ (compound **1**, 1% yield) by elemental analysis, ¹¹B and ¹H NMR, IR, and FAB mass spectrometry, according to



A second product was partially characterized as *nido*-{2-[(η^5 -C₅Me₅)Ir]B₄H_{3}} by ¹¹B and ¹H NMR spectra (see Experimental Section).}

NMR data for **1** are listed in Table 1 together with those for the closely related cobalt analogue [(η^5 -C₅Me₅)Co]₂B₅H₅, **2**.⁸ On the basis of NMR data and the polyhedral skeletal electron pair theory,⁹ the cobaltaborane **2** is proposed to have a capped-*closo* (or *pileo*)¹⁰ structure, although no structural data were reported. The structure of the trimetalla analogue [(η^5 -C₅Me₅)Co]₃B₄H₄, **3**, which also has a capping BH group, but involving a Co₃ face,¹¹ and the [(η^5 -C₅H₅)Co]₃ analogue

[⊗] Abstract published in *Advance ACS Abstracts*, February 15, 1995.

(1) Barton, L.; Srivastava, D. K. *Organometallics* **1991**, *10*, 2982.
(2) Mangion, M.; Ragaini, J. D.; Schmitkoms, T. A.; Shore, S. G. *J. Am. Chem. Soc.* **1979**, *101*, 754.

(3) Bould, J.; Crook, J. E.; Greenwood, N. N.; Kennedy, J. D. *J. Chem. Soc., Chem. Commun.* **1983**, 951. (b) Kennedy, J. D. *Prog. Inorg. Chem.* **1986**, *34*, 211. (c) Kennedy, J. D. *Main Group Chem.*, **1989**, *12*, 149. (d) Bould, J.; Crook, J. E.; Greenwood, N. N.; Kennedy, J. D. *J. Chem. Soc., Dalton Trans.* **1991**, 185.

(4) Bould, J.; Barton, L. *Abstracts of Papers*; Fourth BUSA Workshop, Syracuse, NY, July 1994; No. 45.

(5) Bould, J.; Greenwood, N. N.; Kennedy, J. D. *J. Organomet. Chem.* **1983**, *249*, 11.

(6) Greenwood, N. N.; Kennedy, J. D.; McDonald, W. S.; Reed, D.; Staves, J. *J. Chem. Soc., Dalton Trans* **1979**, 117.

(7) Wermer, J. R.; Shore, S. G. *Inorg. Chem.* **1987**, *26*, 1644.

(8) Venable, T. L. and Grimes, R. N. *Inorg. Chem.* **1982**, *21*, 887.

(9) Williams, R. E. *Inorg. Chem.* **1971**, *10*, 210. (b) Wade, K. *Adv. Inorg. Chem. Radiochem.* **1971**, *13*, 1. (c) Mingos, D. M. P. *Acc. Chem. Res.* **1984**, *17*, 311.

(10) For a definition of *pileo*, see ref 3b, p 523.

Table 1. ^{11}B and ^1H NMR Data for $[(\eta^5\text{-C}_5\text{Me}_5)_2\text{Ir}_2\text{B}_5\text{H}_5]$, **1**, in CDCl_3 Solution at 25 °C with Data for $[(\eta^5\text{-C}_5\text{Me}_5)_2\text{Co}_2\text{B}_5\text{H}_5]$ ^d **2** (CDCl_3 Solution), for Comparison

tentative assgnt	compd 1 ^{a,b}		compd 2 ^{a,c,d}	
	$\delta(^{11}\text{B})$	$\delta(^1\text{H})$	$\delta(^{11}\text{B})$	$\delta(^1\text{H})$
(7)	+103.0 (169) ^e	+11.28	+135.6 (140)	+10.1
(4,6)	+52.6 (144 \pm 20) ^f	+9.15	+76.6 (140)	+7.0
(5)	+52.3 (130 \pm 20) ^f	+6.75	+96.3 (140)	+8.4
(3)	-17.3 (136) ^e	+3.68	+2.9 (128)	-0.8
(C ₅ (CH ₃) ₅)		+2.03		+1.71

^a Referenced to low field of $\text{BF}_3\cdot\text{OEt}_2$ for ^{11}B and to low field of $\text{Si}(\text{CH}_3)_4$ for ^1H . Coupling constants in parentheses. ^b ^{11}B and ^1H resonances related by ^{11}B - ^1H HETCOR experiments. ^c Related ^{11}B and ^1H resonances ordered by relative chemical shift values only. ^d Data from ref 8. ^e $\delta(^{11}\text{B})$ (xylene/ C_6D_6 , 125 °C, relative intensities in parentheses): 102.3 (1), 101.8 (2), 101.3 (1), and -14.9 (1), -15.3(1), -15.5(1) ppm. Resonances at 52.6 and 52.3 unaffected by temperature change. See text for discussion. ^f Overlapping resonances.

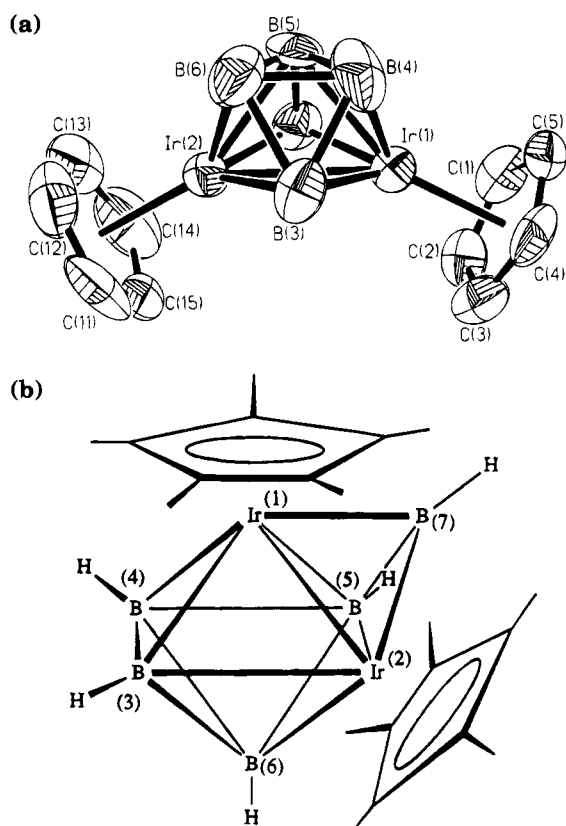


Figure 1. (a) A projection view of **1**. The thermal ellipsoids are drawn at the 50% probability level, and the $[\text{C}_5\text{Me}_5]$ methyl groups have been omitted for clarity. (b) Alternative representation of **1**.

4,¹² have been reported. The similarity of the NMR data for the iridaborane, **1**, and the cobaltaborane, **2**, suggested that they must have similar structures, and as the only *pileo*-metallaboranes reported in the literature in which a boron vertex caps the triangular face of a closed cluster are **2**,⁸ **3**,¹¹ and **4**¹² plus the most recently reported system **2,3,4**- $[(\eta^5\text{-C}_5\text{Me}_5)\text{Co}]_3\text{B}_2\text{H}_4$,¹³ **5**, we carried out a single crystal X-ray diffraction study of **1**. A projection of the molecule, with the methyl groups omitted for clarity, is given in Figure 1a, and a line drawing of **1** is given in Figure 1b. Table 2 lists selected interatomic distances and angles.

(11) Venable, T. L.; Sinn, E.; Grimes, R. N. *Inorg. Chem.* **1982**, *21*, 904.

(12) Pipal, T. R.; Grimes, R. N. *Inorg. Chem.* **1977**, *16*, 3255.

(13) Nishihara, Y. N.; Deck, K. J.; Shang, M.; Fehner, T. P.; Hagerty, B. S.; Rheingold, A. L. *Organometallics* **1994**, *13*, 4510.

Table 2. Selected Bond Lengths (Å) and Angles (deg) for **1**

Ir(1)-B(7)	2.05(2)	Ir(2)-B(5)	2.21(2)
Ir(1)-B(5)	2.23(2)	Ir(2)-C(13)	2.243(10)
Ir(1)-C(1)	2.269(8)	B(3)-B(4)	1.71(3)
Ir(1)-Ir(2)	2.7079(10)	B(4)-B(5)	1.77(3)
Ir(2)-B(3)	2.17(2)	Ir(1)-B(3)	2.16(2)
Ir(2)-C(11)	2.229(11)	Ir(1)-C(4)	2.238(8)
Ir(2)-C(14)	2.284(12)	Ir(1)-C(2)	2.295(9)
B(4)-B(6)	1.62(3)	Ir(2)-B(6)	2.16(2)
B(5)-B(7)	1.80(3)	Ir(2)-C(12)	2.208(11)
Ir(1)-B(4)	2.13(2)	Ir(2)-C(15)	2.276(11)
Ir(1)-C(5)	2.234(8)	B(3)-B(6)	1.74(3)
Ir(1)-C(3)	2.276(8)	B(5)-B(6)	1.74(3)
Ir(2)-B(7)	2.01(2)		
B(7)-Ir(1)-B(4)	96.9(9)	B(7)-Ir(1)-B(3)	97.0(8)
B(4)-Ir(1)-B(3)	47.1(9)	B(7)-Ir(1)-B(5)	49.6(8)
B(4)-Ir(1)-B(5)	47.9(9)	B(3)-Ir(1)-B(5)	69.8(9)
B(7)-Ir(1)-Ir(2)	47.6(6)	B(4)-Ir(1)-Ir(2)	75.5(6)
B(3)-Ir(1)-Ir(2)	51.4(5)	B(5)-Ir(1)-Ir(2)	52.1(5)
B(7)-Ir(2)-B(3)	97.8(7)	B(6)-Ir(2)-B(3)	47.5(8)
B(7)-Ir(2)-B(5)	50.3(9)	B(6)-Ir(2)-B(5)	46.8(9)
B(3)-Ir(2)-B(5)	70.1(8)	B(7)-Ir(2)-Ir(1)	48.7(5)
B(6)-Ir(2)-Ir(1)	75.0(6)	B(3)-Ir(2)-Ir(1)	51.1(5)
B(5)-Ir(2)-Ir(1)	52.9(6)	Ir(2)-B(7)-Ir(1)	83.6(7)
B(4)-B(3)-B(6)	55.8(13)	B(4)-B(3)-Ir(1)	65.5(10)
B(6)-B(3)-Ir(1)	99.9(12)	B(4)-B(3)-Ir(2)	100.5(12)
B(6)-B(3)-Ir(2)	66.1(10)	Ir(1)-B(3)-Ir(2)	77.6(6)
B(6)-B(4)-B(3)	63.0(13)	B(6)-B(4)-B(5)	61.4(14)
B(3)-B(4)-B(5)	92.3(13)	B(6)-B(4)-Ir(1)	105.4(13)
B(3)-B(4)-Ir(1)	67.4(10)	B(5)-B(4)-Ir(1)	69.2(10)
B(6)-B(5)-B(4)	54.8(13)	B(6)-B(5)-B(7)	123(2)
B(4)-B(5)-B(7)	122(2)	B(6)-B(5)-Ir(2)	65.0(10)
B(4)-B(5)-Ir(2)	96.8(13)	B(7)-B(5)-Ir(2)	59.1(9)
B(6)-B(5)-Ir(1)	97.1(12)	B(4)-B(5)-Ir(1)	62.9(10)
B(7)-B(5)-Ir(1)	59.8(8)	Ir(2)-B(5)-Ir(1)	75.1(6)
B(4)-B(6)-B(5)	63.8(14)	B(4)-B(6)-B(3)	61.2(14)
B(5)-B(6)-B(3)	92.6(14)	B(4)-B(6)-Ir(2)	104.1(13)
B(5)-B(6)-Ir(2)	68.1(10)	B(3)-B(6)-Ir(2)	66.5(10)
B(5)-B(7)-Ir(2)	70.5(10)	B(5)-B(7)-Ir(1)	70.5(10)
B(7)-Ir(2)-B(6)	96.5(9)		

The structure of **1** is that of a closed octahedral ($\eta^5\text{-C}_5\text{Me}_5$)₂Ir₂B₄H₄ cluster with a fifth BH group capping one face occupied by the two metal atoms and one boron atom. It is related to the structure of the octahedral, doubly *ortho*-cycloboronated, *closo*-diiridahexaborane

$[(\text{CO})_3(\text{PPh}_3)(\text{Ph}_2\text{PC}_6\text{H}_4)_2(\text{Ir}_2\text{B}_4\text{H}_2)]$, isolated from the degradation of $[\text{B}_{10}\text{H}_{10}]^{2-}$ with *trans*- $[\text{Ir}(\text{CO})\text{Cl}(\text{PPh}_3)_2]$.¹⁴ All iridium-boron distances in **1** are similar to those of other structurally characterized metallaboranes containing the $[(\eta^5\text{-C}_5\text{Me}_5)\text{Ir}]$ group¹⁵ with the exception of the distances to the capping atom B(7) of 2.01(2) and 2.05(2) Å which, as might be expected for such a low coordinate boron vertex, are extremely short. These latter distances are very low and close to the lowest Ir-B distances known.¹⁶ The Ir-Ir distance of 2.7079(10) Å is *ca.* 0.2 Å longer than the Co-Co distance of 1.954(3) Å in **3**, in line with the greater covalent radius of iridium versus cobalt (1.36 *vs.* 1.24 Å). The interboron distances range from 1.62(3) to 1.80(3) Å but the large estimated standard deviations preclude too much comment on these values although the longer distance B(7)-B(5) of 1.80(3) Å may be due to the influence of the two iridium atoms. On the other hand, the angle of the vector from the center of the Ir(1)Ir(2)B(5) triangle to

(14) Crook, J. E.; Greenwood, N. N.; Kennedy, J. D.; McDonald, W. S. *J. Chem. Soc., Chem. Commun.* **1982**, 383.

(15) Nestor, K.; Fontaine, X. L. R.; Greenwood, N. N.; Kennedy, J. D.; Thornton-Pett, M. *J. Chem. Soc., Dalton Trans.* **1989**, 1465. (b) Nestor, K.; Fontaine, X. L. R.; Greenwood, N. N.; Kennedy, J. D.; Thornton-Pett, M. *J. Chem. Soc., Dalton Trans.* **1991**, 2657. (c) Fontaine, X. L. R.; Greenwood, N. N.; Kennedy, J. D.; Nestor, K.; Thornton-Pett, M.; Hermanek, S.; Jelinek, T. J.; Stibr, B. *J. Chem. Soc., Dalton Trans.* **1990**, 661. (d) Nestor, K.; Fontaine, X. L. R.; Greenwood, N. N.; Kennedy, J. D.; Thornton-Pett, M. *J. Chem. Soc., Chem. Commun.* **1989**, 455.

B(7) is within 1° of being perpendicular to the centroid of the Ir₂B plane suggesting that the capping B atom is not distorted toward the metal atoms.

NMR spectra suggest mirror symmetry in solution, but this is not maintained in the solid state probably due to the crystal packing constraints imposed by the bulky disordered (η^5 -C₅Me₅) ligands. The assignments of the ¹¹B and ¹H NMR resonances in compound **1** were made by a consideration of the symmetry of the molecule in addition to [¹¹B-¹H] HETCOR and [¹¹B-¹H] COSY experiments. All the assignments given in Table 1 were confirmed, but a correlation between B(5) and B(7) was not observed, possibly due to the length of the bond or lack of spectral resolution. The ¹¹B{¹H} NMR spectrum of a xylene solution of **1** at 100 °C indicates that some sort of fluxional process occurs, as the resonance at δ -(¹¹B) +103 ppm due to the capping vertex B(7) separates into three peaks of approximate relative intensity 1:2:1. Similarly the resonance assigned to B(3) at -17 ppm shows signs of separating into three resonances of unit intensity. These apparent triplets coalesce to singlets on cooling to ambient temperature, ruling out decomposition. The reasons for these observations are not clear.

The electron count for the molecule clearly conforms to polyhedral skeletal electron pair theory for a capped-closed octahedron containing 14 skeletal electrons and 7 vertices in which the two 18-electron [(η^5 -C₅Me₅)Ir] moieties contribute 3-orbitals and 2-electrons each to the cluster and the five BH vertices contribute a total of 10 electrons to the cluster electron count.^{9,17} The low yield of compound **1** precludes too much useful comment about the mechanism of the reaction. Although the presence of two [(η^5 -C₅Me₅)Ir] moieties in both the starting metal complex and the metallaborane product might suggest that bimetallic group inserts directly into the cluster, this is not necessarily so as we have isolated a similar *pileo* heterobimetalloheptaborane cluster [(PPh₃(CO)H)IrB₅H₅Os(CO)(PPh₃)₂], **6**, from the reaction of IrCl(CO)(PPh₃)₂ with Li[(PPh₃)₂(CO)OsB₅H₈]¹⁸ suggesting that the reaction could proceed *via* a mono-metallo species which then incorporates a further [(η^5 -C₅Me₅)Ir] moiety. Reaction *via* a [B₅H₈]⁻ impurity may also be a possibility. On the other hand, the formation of the analogous species [(η^5 -C₅Me₅)Co]₂B₅H₅, **2**,⁸ does not form directly from [B₅H₈]⁻ but proceeds via the thermolysis of a precursor [(η^5 -C₅Me₅)Co]₂B₅H₇ for 17 h at 225 °C so the process described previously may have some merit.

Capped transition metal clusters have been known for some time,¹⁹ but **1**, to our knowledge, is the first

structurally characterized example of a BH group capping a cluster face which contains a boron atom. There are examples involving BH groups capping trimetal faces including **2-4** and **6** described above, and another, [Co₅(CO)₁₃(-CO)B₂H], **7**,²⁰ in which a (CO)₃Co group caps a Co₂B face, but our structure appears to be unique. We expect that our studies will reveal further examples of capped borane clusters, and we expect to report fully on the system **6**, described briefly above, very soon.

Experimental Section

Materials. B₅H₉ was obtained from laboratory stock and distilled on the vacuum line before use. [(η^5 -C₅Me₅)IrCl₂]₂ was prepared according to the literature method²¹ as was Na₂[B₅H₉].⁷ THF was dried over LiAlH₄ followed by Na/benzophenone ketyl and stored over molecular sieves. CH₂Cl₂ was dried and distilled over P₂O₅. Pentane was dried over CaH₂, distilled from Na/benzophenone, and stored over molecular sieves. All solvents were reagent grade and were dried and distilled prior to use and stored in Pyrex vessels with Teflon stopcocks.

Apparatus. Standard high-vacuum line and drybox techniques were employed in this work.²² Thin layer chromatography (TLC) of the products was performed in air using 20 x 20 cm glass plates coated with 0.1 cm of silica gel (Aldrich, TLC standard grade with gypsum binder and fluorescent indicator). NMR spectroscopy was carried out on a Bruker ARX-500 spectrometer at 500.1 MHz for proton and 160.5 MHz for boron-11. ¹¹B chemical shifts are reported in ppm, positive signs denoting a shift at a lower field with respect to (C₂H₅)₂O·BF₃ reference (0.0 ppm). The mass spectrum was recorded using FAB on a VG Autospec mass spectrometer. IR spectra were run on a Perkin-Elmer 1604 FT-IR spectrometer using 3M disposable IR cards, and elemental analyses were performed by Atlantic Microlabs Inc.

Preparation of {1,2-[(η^5 -C₅Me₅)Ir]₂B₅H₅}. Under a nitrogen atmosphere a THF solution of sodium naphthalide (11.4 mL, 5.02 mmol) was syringed through a septum into a 50 mL, 3-neck round bottom flask connected to vacuum line and containing a magnetic stir-bar. The flask was frozen in liquid N₂ and evacuated and B₅H₉ (2.51 mmol) condensed in. The reaction flask was allowed to warm slowly to room temperature over a 1 h period during which time the solution changed from green to reddish-brown. The flask was then cooled to -78 °C and [(C₅Me₅)IrCl₂]₂ (1.0 g, 1.25 mmol) added via a tipper tube which was attached to the third arm of the flask. The mixture was allowed to warm, with stirring, to room temperature. As the solution warmed, effervescence was observed to occur. After stirring of the solution at room temperature for 10 m in, the solvent was removed under vacuum, 2 mL of CH₂Cl₂ was condensed into the vessel, and then 30 mL pentane was added to effect precipitation of a flocculant solid. The precipitate was filtered off in air, washed with pentane, and redissolved in CH₂Cl₂, and the mixture was filtered through silica gel. The filtrate was reduced in volume on a rotary evaporator, applied to a preparative TLC plate, and developed using CH₂Cl₂/pentane (1:1) as the mobile phase. A number of bands were evident under visible and UV light of which two have been identified after repeated chromatography to remove traces of naphthalene. One, a yellow band at R_f 0.7, was tentatively identified by ¹¹B and ¹H NMR spectroscopy as [*nido*-(C₅Me₅)IrB₄H₈] (<1% yield). NMR (δ in ppm) [¹¹B (¹H in parentheses),

(19) For example see: (a) Albano, V. G.; Bellon, P. L.; Ciani, G. F. *J. Chem. Soc. D* **1969**, 1024. (b) Eady, C. R.; Johnson, B. F. G.; Lewis, J. J. *J. Chem. Soc., Dalton Trans.* **1975**, 2606. (c) Mingos, D. M. P.; Wales, D. J. *Introduction to Cluster Chemistry*; Prentice Hall: New York, 1990.

(20) Jun, C. S.; Fehlner, T. P.; Rheingold, A. L. *J. Am. Chem. Soc.* **1993**, *115*, 4393.

(21) Ball, R. G.; Graham, W. A. G.; Heineky, D. M.; Hoyars, J. K.; McMaster, A. D.; Mattson, B. M.; Michel, S. T. *Inorg. Chem.* **1990**, *29*, 2023.

(22) Shriver, D. F.; Drezdon, M. A. *The Manipulation of Air-Sensitive Compounds*; John Wiley: New York, 1986.

(16) Ir-B distances, obtained through a Cambridge Data Base search of values less than 2.1 Å, include the following. 2.093 Å in [IrH₂(9-BBN)(PMe₃)₃]; Baker, R. T.; Ovenall, D. W.; Calabrese, J. C.; Westcott, S. A.; Taylor, N. J.; Williams, I. D.; Marder, T. B. *J. Am. Chem. Soc.* **1990**, *112*, 9399. 2.087 Å in [(PPh₃)₂(H)IrC₂B₉H₁₀]; Nestor, K.; Fontaine, X. L. R.; Greenwood, N. N.; Kennedy, J. D.; Plessek, J.; Stibr, B.; Thornton-Pett, M. *Inorg. Chem.* **1989**, *28*, 2219. 2.076 Å in [1-(PPh₃)-2-H-2,2-(PPh₃)₂-2,10-IrC₂B₉H₈]; Alcock, N. W.; Taylor, J. G.; Wallbridge, M. G. H. *J. Chem. Soc., Chem. Commun.* **1983**, 1168. 2.071 Å in 2-[IrBr₂(CO)(PMe₃)₂]B₅H₈; Churchill, M. R.; Hackbarth, J. J.; Davison, A.; Traficante, D. D.; Wreford, S. S. *J. Am. Chem. Soc.* **1974**, *96*, 4041. 2.052 Å in [(3-OEt)-4,9-(PPh₃)₂-7-Cl-(*o*-C₆H₄)PPH₂-7-IrB₉H₅-8]; Bould, J.; Brint, P.; Kennedy, J. D.; Thornton-Pett, M. *Acta Crystallogr.* **1990**, *46C*, 1010. 2.03 Å in [IrAuH(μ - σ , η -C₂B₅H₈Me₂)-(PPh₃)₃] and 2.022 Å in *mer*-Ir(H)(BO₂C₆H₄)(Cl)(PMe₃)₃.

(17) (a) Mason, R.; Thomas, K. M.; Mingos, D. M. P. *J. Am. Chem. Soc.* **1973**, *95*, 3802. (b) Mingos, D. M. P.; Forsyth, M. I. *J. Chem. Soc., Dalton Trans.* **1977**, *610*. (c) Johnson, R. L.; Mingos, D. M. P. *J. Chem. Soc., Dalton Trans.* **1987**, 1445.

(18) Bould, J.; Rath, N. P.; Barton, L. Unpublished observations, 1994.

Table 3. Crystal Data and Structure Refinement for 1

empirical formula	C ₂₀ H ₃₅ B ₅ Ir ₂
fw	713.93
temp	298(2) K
wavelength	0.710 73 Å
cryst system	triclinic
space group	<i>P</i> $\bar{1}$
unit cell dimens	<i>a</i> = 8.891(2) Å, <i>b</i> = 8.950(2) Å, <i>c</i> = 15.709(4) Å, α = 101.61(2)°, β = 94.49(2)°, γ = 99.63(2)°
<i>V</i>	1199.1(5) Å ³
<i>Z</i>	2
<i>D</i> (calcd)	1.977 Mg/m ³
abs coeff	11.089 mm ⁻¹
<i>F</i> (000)	668
cryst size	0.30 × 0.20 × 0.05 mm
θ range for data colln	2.34–22.50°
index ranges	–1 ≤ <i>h</i> ≤ 9, –9 ≤ <i>k</i> ≤ 9, –16 ≤ <i>l</i> ≤ 16
reflcs collcd	3718
independent reflcs	3108 (<i>R</i> _{int} = 0.0868)
refinement method	full-matrix least-squares on <i>F</i> ²
Data/restraints/parameters	3106/0/148
Goodness-of-fit on <i>F</i> ²	1.080
final <i>R</i> indices [<i>I</i> > 2σ(<i>I</i>)]	<i>R</i> ₁ = 0.0449, <i>wR</i> ₂ = 0.1117
<i>R</i> indices (all data)	<i>R</i> ₁ = 0.0775, <i>wR</i> ₂ = 0.1292
largest diff peak and hole	2.185 and –1.282 e Å ⁻³

CDCl₃, 25 °C): 7.1 (+7.10), *J*_{BH} = 136 Hz, 1B; 13.3 (+2.37), *J*_{BH} = 136 Hz, 2B; –28.7 (–0.06) *J*_{BH} = 156 Hz, 1B; δ(¹H)_{bridging}, –2.46 (2H), –12.72 (2H), δ(¹H)_{C₅Me₅} 2.15 (15H).

A second orange band at *R*_f 0.4 was rechromatographed in 35:65 CH₂Cl₂/pentane solution giving a broad, pale yellow band observed under UV light at *R*_f 0.1–0.3. The band was crystallized by slow evaporation at room temperature, under a nitrogen atmosphere, from a CH₂Cl₂/hexane solution (1:3) to give pale yellow crystalline clumps from which a crystal suitable for single crystal X-ray diffraction was excised. The band was identified as the title compound [1,2-[(η⁵-C₅Me₅)-Ir]₂B₅H₅] (compound 1) [17 mg, 25 μmol, 1% yield. Anal. Found (calcd): C, 33.76 (33.64); H, 4.94 (4.89)]. The FAB mass spectrum revealed an envelope with a cutoff at *m/z* = 716 corresponding to ¹²C₂₀¹H₃₅¹¹B₅¹⁹³Ir₂ (716.246). The data were as follows [(*m/z*) relative intensities]: obsd (710) 30, (711) 49, (712) 73, (713) 96, (714) 100, (715) 80, (716) 56, (717) 19; calcd (710) 12, (711) 32, (712) 61, (713) 87, (714) 100, (715) 76, (716) 60, (717) 12. The infrared spectrum gave data as follows [*ν*(BH) (cm⁻¹): 2454 (m), 2488 (sh).

X-ray Structure Determination. A pale yellow colored rectangular shaped crystal of dimensions 0.3 × 0.2 × 0.05 mm was obtained as described above and mounted on a glass fiber in random orientation. Preliminary examination and data collection were performed using a Siemens P4RA automated single crystal X-ray diffractometer using graphite monochromated Mo Kα radiation (*λ* = 0.710 73 Å) at 25 °C. Autoindexing of 12 centered reflections from the rotation photograph indicated a triclinic lattice. Equivalent reflections were checked to confirm the Laue symmetry, and a fractional index search was conducted to confirm the cell lengths.²³ Final cell constants and orientation matrix for data collection were calculated by least squares refinement of the setting angles for 44 reflections (12° < 2θ < 58°). Intensity data were collected using ω–2θ scans with variable scan speed. Three representative reflections measured every 97 reflections showed <25% variation during data collection. Crystal data and intensity data collection parameters are listed in Table 3. 1 crystallizes in the triclinic space group *P* $\bar{1}$, with *a* = 8.891(2) Å, *b* = 8.950(2) Å, *c* = 15.709(4) Å, α = 101.61(2)°, β = 94.49(2)°, γ = 99.63(2)°, and *Z* = 2.

Data reduction was carried out using XSCANS, and the structure solution was carried out using the SHELXTL-PLUS (VMS) software package.²⁴ An empirical absorption correction was applied to the data using equivalent reflections

Table 4. Atomic Coordinates (×10⁴) and Equivalent Isotropic Displacement Parameters (Å² × 10³) for 1^a

	<i>x</i>	<i>y</i>	<i>z</i>	<i>U</i> (eq)
Ir(1)	2411(1)	366(1)	3092(1)	45(1)
Ir(2)	3519(1)	2481(1)	1740(1)	47(1)
B(3)	4718(20)	2480(25)	2994(13)	54(5)
B(4)	4497(28)	525(31)	2942(16)	78(7)
B(5)	3307(30)	76(23)	1929(14)	69(6)
B(6)	5165(27)	1150(29)	2125(14)	70(6)
B(7)	1626(24)	927(24)	1789(12)	57(5)
C(1)	162(10)	526(10)	3589(6)	69(6)
C(2)	291(10)	2141(10)	3654(5)	63(5)
C(3)	1610(10)	2903(10)	4239(5)	66(5)
C(4)	2297(10)	1758(10)	4536(5)	64(5)
C(5)	1402(10)	289(10)	4134(5)	63(5)
C(6)	–1075(15)	–721(15)	3037(9)	114(9)
C(7)	–786(15)	2914(15)	3183(9)	112(8)
C(8)	2181(15)	4627(14)	4500(9)	98(7)
C(9)	3727(15)	2052(15)	5169(8)	115(8)
C(10)	1714(16)	–1254(14)	4264(9)	119(9)
C(11)	4417(17)	4844(13)	1532(8)	95(9)
C(12)	4768(16)	3745(15)	859(8)	93(8)
C(13)	3403(17)	2917(15)	382(7)	92(8)
C(14)	2208(17)	3505(15)	759(9)	108(9)
C(15)	2834(18)	4696(14)	1470(8)	107(10)
C(16)	5530(25)	5972(22)	2196(13)	249(23)
C(17)	6321(22)	3499(25)	683(14)	217(19)
C(18)	3250(26)	1638(23)	–391(12)	192(16)
C(19)	561(23)	2960(25)	457(14)	258(24)
C(20)	1970(27)	5639(23)	2056(13)	224(20)

^a *U*(eq) is defined as one-third of the trace of the orthogonalized *U*_{ij} tensor.

(SHELXA).²⁵ The structure was solved by the Patterson Method and refined successfully in the space group *P* $\bar{1}$.

Least-squares refinement was achieved by using SHELXL-93.²⁴ Full matrix least-squares refinement was carried out by minimizing $\sum w(F_o^2 - F_c^2)^2$. All the non-hydrogen atoms were refined anisotropically to convergence, except the (C₅Me₅) methyl carbons. The (C₅Me₅) rings were refined as rigid body. Due to large thermal vibrations of the terminal CH₃ groups of the C₅(CH₃)₅ rings, the C atoms were refined isotropically. Several disorder models were tried, but the disorder could not be resolved due to the resulting unstable refinement. All hydrogen atoms of the boron cage were located from difference Fourier synthesis but could not be refined. These hydrogens were included in the final refinement and were held fixed. Only H(5) could be refined using a riding model. The hydrogen atoms of the CH₃ groups were calculated using a riding model in the rigid group. The final residual values for 1 were: *R*(*F*) = 4.49 for reflections *I* > 2σ(*I*), *wR*(*F*²) = 11.17%, and *s* = 1.080.

Structure refinement parameters are listed in Table 3. The atomic coordinates for the non-hydrogen atoms and selected bond distances and angles are listed in Tables 4 and 2, respectively. A projection view of the molecule showing non-hydrogen atoms represented by 50% probability ellipsoids and showing the atom labeling is presented in Figure 1. The C₅-Me₅ ligands have been omitted for clarity.

Acknowledgment. We thank Dr. J. D. Kennedy and Dr. B. Watson at the University of Leeds for mass spectra, the National Science Foundation, the Missouri Research Board, a UM–St. Louis Research Incentive Award, and the University of Missouri–St. Louis for the financial support of this work, and the Johnson Matthey Co. for a loan of IrCl₃·3H₂O.

Supplementary Material Available: Tables of bond distances and angles, anisotropic displacement parameters, and hydrogen coordinates and isotropic displacement parameters (4 pages). Ordering information is given on any current masthead page.

OM940904R

(23) XSCANS, Siemens Analytical Instruments, Madison, WI, 1994.
(24) Sheldrick, G. M. SHELXL-93. Structure refinement package, Universität Göttingen, Germany, 1993.

(25) Sheldrick, G. M. SHELXL-93. Empirical correction programme, Universität Göttingen, Germany, 1993.

Synthesis and Characterization of (Me₃SiCH₂)₃M·E(SiMe₃)₃ (M = Ga, E = P or As; M = In, E = P). X-ray Crystal Structures of (Me₃SiCH₂)₃Ga·P(SiMe₃)₃ and (Me₃SiCH₂)₃In·P(SiMe₃)₃

Richard L. Wells* and Ryan A. Baldwin

Department of Chemistry, Paul M. Gross Chemical Laboratory, Duke University,
Durham, North Carolina 27708

Peter S. White

Department of Chemistry, University of North Carolina at Chapel Hill,
Chapel Hill, North Carolina 27514

Received December 15, 1994[®]

Summary: The reaction of (Me₃SiCH₂)₃Ga with P(SiMe₃)₃ or As(SiMe₃)₃ in a 1:1 mole ratio affords the simple adducts (Me₃SiCH₂)₃Ga·P(SiMe₃)₃ (**1**) and (Me₃SiCH₂)₃Ga·As(SiMe₃)₃ (**2**), respectively. Combining (Me₃SiCH₂)₃In with P(SiMe₃)₃ in a 1:1 mole ratio yields the adduct (Me₃SiCH₂)₃In·P(SiMe₃)₃ (**3**), in a nearly quantitative yield. The solid-state structures of **1** and **3** were established by X-ray crystallography. Isomorphous **1** and **3** crystallize in the trigonal system, space group P3₁, with *a* = 16.027(3) Å, *c* = 11.9928(18) Å, *V* = 2667.9(7) Å³, *Z* = 3, and *D*_{calc} = 1.087 g cm⁻³ for **1** and *a* = 16.061(8) Å, *c* = 12.0913(19) Å, *V* = 2701.0(13) Å³, *Z* = 3, and *D*_{calc} = 1.156 g cm⁻³ for **3**. Full-matrix least-squares refinement based on 3397 (**1**) and 4156 (**3**) reflections with *I* > 2.5σ converged at *R* = 0.059 (*R*_w = 0.062) and *R* = 0.039 (*R*_w = 0.044), respectively. Metal–pnictogen bond lengths were found to be as follows: Ga–P = 2.646 Å and In–P = 2.771 Å. The thermal decomposition behavior of **1–3** was examined by TGA–DTA. These studies indicated that compounds **1** and **2** eliminated their organic ligands in a stepwise manner, while compound **3** decomposed in a single-step process.

Introduction

Recent investigations in our laboratory have centered on the facile formation of the 13–15 bond by reactions of organo-group 13 reagents with either the silylpnictogen compounds E(SiMe₃)₃ (E = P or As) or their monolithium salts in solution.¹ As a result of our efforts, we have isolated several new compounds containing the 13–15 covalent bond. Included in our results are compounds which exhibit dimeric structures in the solid state² and those in which two group 13 centers are bridged by a halogen atom and a group 15 atom.² In addition, adducts of the type R₃M·E(SiMe₃)₃ (R = Me₃SiCH₂, M = In, E = As,³ R = Ph³ or C₆F₅,⁴ M = Ga, E = As or P) have been isolated in our laboratory. Adducts of this type may find utility as potential single-

source precursors to binary 13–15 semiconductors;⁵ however, a review of the literature finds limited structural and thermal analysis data for adducts of this type. We report herein the synthesis, characterization, and thermal analysis of three new main group adducts, (Me₃SiCH₂)₃Ga·P(SiMe₃)₃ (**1**), (Me₃SiCH₂)₃Ga·As(SiMe₃)₃ (**2**), and (Me₃SiCH₂)₃In·P(SiMe₃)₃ (**3**).

Experimental Section

General Considerations. All manipulations of air- and moisture-sensitive materials were performed in a Vacuum Atmospheres HE-493 Dri-Lab containing an argon atmosphere or by general Schlenk techniques. Pentane was distilled over LiAlH₄ under dry dinitrogen. Literature procedures were used to prepare and purify P(SiMe₃)₃,⁶ As(SiMe₃)₃,⁷ (Me₃SiCH₂)₃Ga,⁸ and (Me₃SiCH₂)₃In.⁹ The integrity of all materials used was confirmed via ¹H NMR spectra. ¹H, ¹³C{¹H}, and ³¹P{¹H} NMR spectra were recorded on a Varian XL-300 spectrometer operating at 300, 75.4, and 121.4 MHz, respectively and a Varian Unity 500 spectrometer operating at 500, 125.7, and 202.3 MHz, respectively. ¹H and ¹³C{¹H} spectra were referenced to TMS by using the residual protons or carbons of deuterated benzene at δ 7.15 or 128 ppm. ³¹P{¹H} spectra were referenced externally to H₃PO₄ at δ 0.00 ppm. All NMR samples were prepared in 5-mm tubes which were septum-sealed under argon. All melting points (uncorrected) were obtained on a Thomas-Hoover Uni-melt apparatus, and the melting point capillaries were flame-sealed under argon. Thermo-gravimetric analysis/differential thermal analysis data were collected on a TA Instruments SDT 2960 simultaneous TGA–DTA instrument. Elemental analyses were performed by E+R Microanalytical Laboratory, Inc., Corona, NY. X-ray crystallographic analyses were conducted in the Single Crystal X-ray Structure Center at the University of North Carolina at Chapel Hill.

Preparation of (Me₃SiCH₂)₃Ga·P(SiMe₃)₃ (1**).** Inside the drybox, a one-necked 250 mL round-bottomed flask equipped with a Teflon valve was charged with pentane (30 mL) and (Me₃SiCH₂)₃Ga (0.331 g, 0.999 mmol) furnishing a clear solution to which was added dropwise P(SiMe₃)₃ (0.250 g, 0.998 mmol) in pentane (30 mL). The resulting clear solution was stirred outside of the drybox for 48 h at room temperature. Following removal of the volatiles *in vacuo*, the crude crystal-

* Author for correspondence.

[®] Abstract published in *Advance ACS Abstracts*, March 1, 1995.

(1) For example, see the following and references therein: Wells, R. L. *Coord. Chem. Rev.* **1992**, *112*, 273.

(2) Wells, R. L.; McPhail, A. T.; Self, M. F. *Organometallics* **1992**, *11*, 221.

(3) Wells, R. L.; McPhail, A. T.; Jones, L. J., III; Self, M. F.; Butcher, R. J. *Organometallics* **1992**, *11*, 2694.

(4) Wells, R. L.; McPhail, A. T.; Hallock, R. B.; Johansen, J. D. J. *Organomet. Chem.*, unpublished results.

(5) Cowley, A. H.; Jones, R. A. *Angew. Chem., Int. Ed. Engl.* **1989**, *28*, 1208.

(6) Becker, G.; Hoelderich, W. *Chem. Ber.* **1975**, *108*, 2484.

(7) Becker, G.; Gutekunst, G.; Wessely, H. J. *Z. Anorg. Allg. Chem.* **1980**, *462*, 113.

(8) Beachley, O. T., Jr.; Simmons, R. G. *Inorg. Chem.* **1980**, *19*, 1021.

(9) Beachley, O. T., Jr.; Rusinko, R. N. *Inorg. Chem.* **1979**, *18*, 1966.

Table 1. Crystallographic Data and Measurements for (Me₃SiCH₂)₃Ga-P(SiMe₃)₃ (1) and (Me₃SiCH₂)₃In-P(SiMe₃)₃ (3)

	1	3
molecular formula	C ₂₁ H ₆₀ GaPSi ₆	C ₂₁ H ₆₀ InPSi ₆
fw	581.91	627.01
cryst system	trigonal	trigonal
space group	P3 ₁	P3 ₁
a, Å	16.027(3)	16.061(8)
c, Å	11.9928(18)	12.0913(2)
V, Å ³	2667.8(7)	2701.0(1)
Z	3	3
radiation (λ, Å)	Mo Kα (0.710 73)	Mo Kα (0.710 73)
μ, cm ⁻¹	10.2	8.9
temp, °C	-135	-135
D _{calcd} , g cm ⁻³	1.087	1.156
cryst dimens, mm	0.40 × 0.30 × 0.25	0.38 × 0.32 × 0.25
T _{max} , T _{min}	0.782; 0.626	0.804; 0.727
scan type	ω	ω
scan width, deg	1.00	1.00
θ _{max} , deg	50	60
no. of rflns rec	5284	5466
no. of nonequiv rflns rec	5284	5224
no. of rflns retained, I > 2.5σ(I)	3397	4156
no. of params refined	261	262
R; R _w ^a	0.059; 0.062	0.039; 0.044
goodness-of-fit ^b	1.32	1.08
max shift/esd in final least-squares cycle	0.013	0.001
final max, min Δρ, e/Å ⁻³	0.830, -0.780	0.890, -0.760

^a R = Σ(|F_o| - |F_c|)/Σ|F_o|; R_w = [Σw(|F_o| - |F_c|)²/Σw|F_o|²]^{1/2}.
^b Goodness-of-fit = [ΣwΔ²/(N_{observns} - N_{params})]^{1/2}.

line product was dissolved in warm pentane (5 mL). Upon cooling to -15 °C for several days, colorless, air-sensitive crystals of **1** formed: 0.564 g, 97% yield; mp 48–53 °C. Anal. Calcd for C₂₁H₆₀GaPSi₆: C, 43.34; H, 10.39. Found: C, 43.02; H, 10.23. ¹H NMR: δ 0.272 [d, SiMe₃ (J_{P-H} = 4.5 Hz)], 0.078 (s, CH₂), 0.109 (s, C-SiMe₃). ¹³C{¹H} NMR: δ 4.066 [d, SiMe₃ (J_{P-C} = 10.9 Hz)], 2.543 (s, CH₂), 12.247 (s, Me₃). ³¹P{¹H} NMR: δ -248.98 (s).

Preparation of (Me₃SiCH₂)₃Ga-As(SiMe₃)₃ (2). [Compound **2** was synthesized in the manner described for **1**.] Reactants: (Me₃SiCH₂)₃Ga (0.331 g, 0.999 mmol), As(SiMe₃)₃ (0.294 g, 0.998 mmol). Product: 0.501 g, 80% yield, mp 43–50 °C. Anal. Calcd for C₂₁H₆₀GaAsSi₆: C, 40.30; H, 9.66. Found: C, 39.91; H, 9.54. ¹H NMR: δ 0.343 (s, SiMe₃), 0.120 (s, CH₂), 0.132 (s, C-SiMe₃). ¹³C{¹H} NMR: δ 4.066 (s, SiMe₃), 2.543 (s, CH₂), 12.247 (s, Me₃).

Preparation of (Me₃SiCH₂)₃In-P(SiMe₃)₃ (3). [Compound **3** was synthesized in the manner described for **1**.] Reactants: (Me₃SiCH₂)₃In (0.376 g, 0.999 mmol), P(SiMe₃)₃ (0.250 g, 0.998 mmol). Product: 0.613 g, 98% yield, mp 125–127 °C. Anal. Calcd for C₂₁H₆₀InPSi₆: C, 40.23; H, 9.65. Found: C, 39.97; H, 9.43. ¹H NMR: δ 0.244 [d, SiMe₃ (J_{P-H} = 5.0 Hz)], -0.112 (s, CH₂), 0.295 (s, C-SiMe₃). ¹³C{¹H} NMR: δ 3.538 [d, SiMe₃ (J_{P-C} = 9.1 Hz)], 3.239 (s, CH₂), 5.235 (s, Me₃). ³¹P{¹H} NMR: δ -241.80 (s).

X-ray Structural Solution and Refinement. Crystallographic data are summarized in Table 1. Colorless crystals of **1** and **3** were mounted on a glass fiber with a viscous oil under a stream of cold dinitrogen. X-ray intensity data were recorded at -135 °C on a Rigaku AFC6/S diffractometer utilizing graphite-monochromated Mo Kα radiation (λ = 0.710 73 Å), and the structures were solved by direct methods. Full-matrix least-squares refinement with weights based upon counting-statistics was performed. Hydrogen atoms were incorporated at their calculated positions using a riding model in the later iterations of refinement which converged at R = 0.059 (R_w = 0.062) for **1** and R = 0.039 (R_w = 0.044) for **3**. A final difference-Fourier synthesis revealed no unusual features. Crystallographic calculations were performed using the NRCVAX¹⁰ suite of structure determination programs. For all structure-factor calculations, neutral atom scattering factors and their anomalous dispersion corrections were taken

Table 2. Selected Bond Distances (Å) and Bond Angles (deg) for 1, with Estimated Standard Deviations in Parentheses

Bond Lengths			
Ga1-P(1)	2.646(3)	Ga1-C(31)	2.019(15)
Ga1-C(11)	2.014(14)	P(1)-Si(5)	2.284(5)
Ga1-C(21)	2.025(14)		
Bond Angles			
P(1)-Ga(1)-C(11)	98.4(4)	C(11)-Ga(1)-C(31)	116.5(6)
Ga(1)-P(1)-Si(5)	113.54(19)	Si(4)-P(1)-Si(5)	106.25(21)
P(1)-Si(4)-C(42)	109.8(5)	C(11)-Si(1)-C(14)	112.9(7)
C(13)-Si(1)-C(14)	108.0(8)	Ga(1)-C(31)-Si(3)	119.7(8)

Table 3. Selected Bond Distances (Å) and Bond Angles (deg) for 3, with Estimated Standard Deviations in Parentheses

Bond Lengths			
In1-P(1)	2.7713(15)	In1-C(31)	2.207(6)
In1-C(11)	2.206(6)	P(1)-Si(5)	2.2809(23)
In1-C(21)	2.218(6)		
Bond Angles			
P(1)-In(1)-C(11)	98.45(16)	P(1)-Si(4)-C(42)	109.39(20)
C(11)-In(1)-C(31)	117.53(22)	C(11)-Si(1)-C(14)	111.1(3)
In(1)-P(1)-Si(5)	112.73(7)	C(13)-Si(1)-C(14)	108.6(3)
Si(4)-P(1)-Si(5)	107.56(8)	In(1)-C(31)-Si(3)	117.7(3)

Table 4. Non-Hydrogen Atom Fractional Coordinates and Equivalent Isotropic Thermal Parameters for 1, with Estimated Standard Deviations in Parentheses

atom	x	y	z	B _{iso} (Å ²) ^a
Ga	-0.32356(11)	-0.33654(13)	-0.82776(-)	0.93(8)
P	-0.3380(3)	-0.3255(3)	-0.6091(3)	1.11(18)
Si(1)	-0.0930(3)	-0.2016(3)	-0.9218(4)	1.58(21)
Si(2)	-0.4372(3)	-0.2556(3)	-0.9888(4)	2.05(23)
Si(3)	-0.4041(3)	-0.5558(3)	-0.9407(4)	1.82(23)
Si(4)	-0.3518(3)	-0.1957(3)	-0.5596(4)	1.56(22)
Si(5)	-0.2086(3)	-0.3119(3)	-0.5133(4)	1.50(22)
Si(6)	-0.4678(3)	-0.4539(3)	-0.5306(4)	1.70(21)
C(11)	-0.1992(10)	-0.2119(10)	-0.8509(12)	1.4(8)
C(12)	-0.0401(10)	-0.2621(11)	-0.8364(14)	2.3(8)
C(13)	-0.0009(11)	-0.0717(13)	-0.9359(15)	3.0(9)
C(14)	-0.1205(12)	-0.2559(13)	-1.0637(14)	3.0(10)
C(21)	-0.4449(10)	-0.3378(10)	-0.8774(12)	1.4(7)
C(22)	-0.3938(11)	-0.1348(13)	-0.9304(14)	2.7(10)
C(23)	-0.3510(13)	-0.2428(12)	-1.1022(14)	3.6(11)
C(24)	-0.5578(10)	-0.2968(10)	-1.0546(13)	1.5(7)
C(31)	-0.3178(10)	-0.4589(10)	-0.8449(13)	1.8(8)
C(32)	-0.4099(14)	-0.5104(13)	-1.0815(17)	4.1(11)
C(33)	-0.3708(12)	-0.6522(11)	-0.9636(14)	2.7(9)
C(34)	-0.5307(12)	-0.6203(12)	-0.8830(15)	3.0(10)
C(41)	-0.3321(10)	-0.1678(11)	-0.4105(12)	2.0(8)
C(42)	-0.2620(11)	-0.0869(10)	-0.6387(13)	2.0(8)
C(43)	-0.4776(12)	-0.2216(12)	-0.5921(14)	2.8(9)
C(51)	-0.1050(11)	-0.1871(11)	-0.5340(13)	2.2(8)
C(52)	-0.2311(10)	-0.3360(10)	-0.3609(12)	1.4(7)
C(53)	-0.1787(12)	-0.3994(12)	-0.5727(14)	2.8(9)
C(61)	-0.5752(11)	-0.4870(11)	-0.6195(16)	2.8(9)
C(62)	-0.4466(11)	-0.5566(11)	-0.5258(15)	3.1(9)
C(63)	-0.4927(11)	-0.4288(13)	-0.3851(16)	3.7(10)

^a B_{iso} = the mean of the principal axes of the thermal ellipsoid.

from ref 11. Interatomic distances and angles and atomic coordinates are given in Tables 2–5. ORTEP¹² diagrams showing the solid-state conformations and atom-numbering schemes of **1** and **3** are presented in Figures 1 and 2. Full information concerning conditions for crystallographic data collection and structure refinement, atomic coordinates, thermal and positional parameters, and observed and calculated

(10) Gabe, E. J.; Page, Y. L.; Charland, J. P.; Lee, F. L.; White, P. S. *J. Appl. Crystallogr.* **1989**, *22*, 384.

(11) *International Tables for X-ray Crystallography*; The Kynoch Press: Birmingham, England, 1974; Vol. IV.

(12) Johnson, C. K. ORTEP-A Fortran Thermal Ellipsoid Plot Program, Technical Report ORNL-5138, Oak Ridge, TN, 1976.

Table 5. Non-Hydrogen Atom Fractional Coordinates and Equivalent Isotropic Thermal Parameters for 3, with Estimated Standard Deviations in Parentheses

atom	x	y	z	$B_{\text{iso}} (\text{\AA}^2)^{\text{e}}$
In	0.32963(3)	0.31798(2)	0.20454(-)	0.985(2)
P	0.34260(1)	0.34696(1)	0.43129(1)	1.01(6)
Si(1)	0.47458(1)	0.22386(1)	0.11329(1)	1.41(8)
Si(2)	0.40727(1)	0.51762(1)	0.03687(2)	1.60(8)
Si(3)	0.10208(1)	0.17049(1)	0.09229(2)	1.60(7)
Si(4)	0.47110(1)	0.49332(1)	0.47400(1)	1.29(7)
Si(5)	0.36011(1)	0.23342(1)	0.52505(1)	1.32(7)
Si(6)	0.21244(1)	0.34570(1)	0.50542(2)	1.51(8)
C(11)	0.4689(4)	0.3251(4)	0.1779(5)	1.40(2)
C(12)	0.4101(5)	0.1120(5)	0.1983(6)	2.0(3)
C(13)	0.6034(5)	0.2539(5)	0.1005(6)	2.3(3)
C(14)	0.4189(5)	0.1969(5)	-0.0285(6)	2.3(3)
C(21)	0.3187(4)	0.4424(4)	0.1435(5)	1.5(3)
C(22)	0.5293(5)	0.5930(5)	0.0995(7)	2.1(3)
C(23)	0.4172(5)	0.4410(5)	-0.0740(5)	2.5(3)
C(24)	0.3711(5)	0.5996(6)	-0.0317(6)	2.9(4)
C(31)	0.1981(4)	0.1769(4)	0.1842(5)	1.7(3)
C(32)	0.1512(5)	0.2247(6)	-0.0456(6)	2.8(3)
C(33)	0.0048(5)	0.0423(5)	0.0687(6)	2.1(3)
C(34)	0.0422(5)	0.2339(5)	0.1564(7)	2.8(4)
C(41)	0.4416(5)	0.5876(5)	0.4350(6)	2.4(3)
C(42)	0.5783(4)	0.5116(5)	0.3936(5)	1.8(3)
C(43)	0.5004(5)	0.5065(5)	0.6243(5)	2.1(3)
C(51)	0.4848(5)	0.2575(5)	0.5019(6)	2.0(3)
C(52)	0.3392(5)	0.2346(5)	0.6760(6)	2.3(3)
C(53)	0.2719(5)	0.1128(5)	0.4659(6)	2.0(3)
C(61)	0.2352(5)	0.3948(6)	0.6498(6)	2.7(4)
C(62)	0.1107(5)	0.2188(5)	0.5081(7)	2.6(3)
C(63)	0.1782(5)	0.4177(5)	0.4149(6)	2.2(3)

^e B_{iso} = the mean of the principal axes of the thermal ellipsoid.

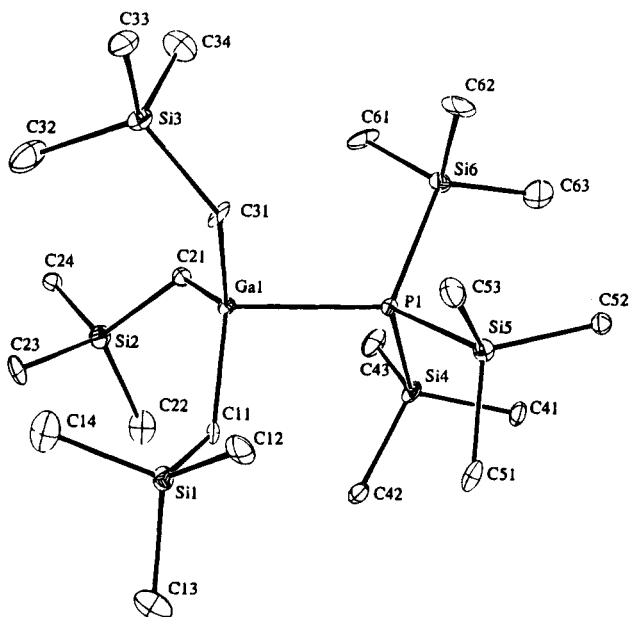


Figure 1. ORTEP diagram (30% probability ellipsoids) showing the solid-state structure and atom-numbering scheme of 1. Hydrogen atoms are omitted for clarity.

structure factors has been deposited with the Cambridge Crystallographic Data Centre.

Results and Discussion

The 1:1 mole ratio reaction of $(\text{Me}_3\text{SiCH}_2)_3\text{Ga}$ with $\text{E}(\text{SiMe}_3)_3$ ($\text{E} = \text{P}$ or As) at room temperature affords the simple adducts 1 and 2 in high yields. Similarly, compound 3 results from the 1:1 mole reaction of $(\text{Me}_3\text{SiCH}_2)_3\text{In}$ and $\text{P}(\text{SiMe}_3)_3$ in pentane solution. Compounds 1 and 3 are white crystalline materials which

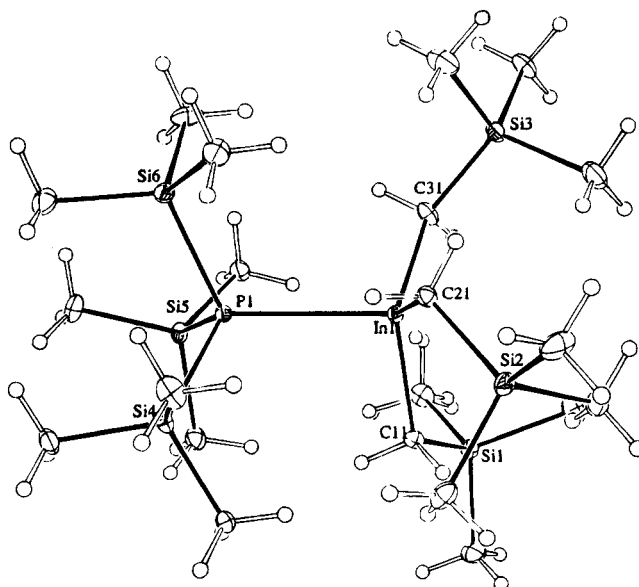


Figure 2. ORTEP diagram (30% probability ellipsoids) showing the solid-state structure and atom-numbering scheme of 3. Hydrogen atoms are represented by small circles.

are stable over long periods of time under inert atmosphere. Compound 2, however, decomposes from a white crystalline solid to an orange liquid upon long standing. All three compounds are extremely sensitive to air and moisture and decompose rapidly upon exposure. The ^1H and ^{13}C NMR spectra of 1-3 confirm that these compounds do not dissociate in solution at room temperature and are pure prior to recrystallization.

The solid-state structures of 1 and 3 were determined by single-crystal X-ray analysis. The inability to isolate a suitable crystal of 2 precluded its structural determination. Compound 1 is one of a few crystallographically characterized 1:1 Ga-P adducts. Those whose structures have been determined are $(\text{Me}_3\text{CCH}_2)_3\text{Ga}\cdot\text{P}(\text{H})\text{Ph}_2$ (4),¹³ $\text{Ph}_3\text{Ga}\cdot\text{P}(\text{SiMe}_3)_3$ (5),¹⁴ $\text{Ph}_2(\text{Cl})\text{Ga}\cdot\text{P}(\text{SiMe}_3)_3$ (6),¹⁴ $\text{Me}_2(\text{Cl})\text{Ga}\cdot\text{PPh}_2\text{CH}_2\text{PPh}_2$ (7),¹⁵ $\text{Cl}_3\text{Ga}\cdot\text{PMe}_3$ (8),¹⁶ and $\text{I}_3\text{Ga}\cdot\text{PPh}_3$ (9).¹⁷ In addition, the 2:1 complex $(\text{Me}_3\text{Ga})_2\cdot(\text{PPh}_2\text{CH}_2)_2$ (10)¹⁸ was also characterized in this manner. The Ga-P bond length of 2.646 Å in 1 is within the established range of lengths previously observed [the shortest being 2.353(2) Å in 8 and the longest being 2.6853(5) Å in 4]. The elongated bond length in 1 is most likely due to the steric repulsions between the trimethylsilyl groups and the bulky (trimethylsilyl)methyl ligands. These repulsions are also evidenced by the staggered conformation between the Me_3SiCH_2 and Me_3Si moieties. The coordination geometry about the gallium center is that of a distorted tetrahedron with a mean C-Ga-C angle of 116.7° and a mean C-Ga-P angle of 100.3°. Mean bond angles at the P atom [$\text{Ga-P-Si} = 113.4^\circ > \text{Si-P-Si} = 105.3^\circ$]

(13) Banks, M. A.; Beachley, O. T., Jr.; Maloney, J. D. *Polyhedron* 1990, 9, 335.

(14) Wells, R. L.; Aubuchon, S. R.; Self, M. F.; Jasinski, J. P.; Woudenberg, R. C.; Butcher, R. J. *Organometallics* 1992, 11, 3370.

(15) Schmidbaur, H.; Lauteschlager, S.; Muller, G. *J. Organomet. Chem.* 1985, 281, 25.

(16) Carter, J.; Jugie, G.; Enjalbert, R.; Galy, J. *Inorg. Chem.* 1978, 17, 1248.

(17) Taylor, M. J. Private communication, 1994.

(18) Bradley, D. C.; Chudzynska, H.; Faktor, M. M.; Frigo, D. M.; Hursthouse, M. B.; Hussain, B.; Smith, L. M. *Polyhedron* 1988, 7, 1289.

reflect the relayed effect of the steric compressions resulting from the angular deformations around Ga.

Crystallographic information on simple organoindium–phosphorus adducts is scant and is limited to $(\text{Me}_3\text{CCH}_2)_3\text{In}\cdot\text{P}(\text{SiMe}_3)_3$ (**11**),¹⁹ $\text{Me}(\text{Me}_3\text{CCH}_2)_2\text{In}\cdot\text{P}(\text{SiMe}_3)_3$ (**12**),¹⁹ and $(\text{Me}_3\text{In})_2(\text{PPh}_2\text{CH}_2)_2$ (**13**).¹⁸ The unit cell in **3** consists of discrete monomeric units with the In–P bond length being 2.771 Å. This is within range of the lengths previously observed in compounds **11–13** [the shortest being 2.755(4) Å in **13** and the longest being 2.944(4) Å in **11**]. The mean P–Si and In–C bond lengths at 2.276 and 2.210 Å, respectively, in **3** are nearly identical to the average P–Si (2.271 Å) and In–C (2.213 Å) in **11**, whereas the angles around the In atoms (P–In–C = 101.43°, C–In–C = 116.18° for the mean values in **3**; P–In–C = 95.5°, C–In–C = 119.1° in **11**) differ significantly. These observed bond angle variations may be directly related to the fact that the C–C distances in Me_3CCH_2 groups are substantially shorter than Si–C bonds in Me_3SiCH_2 moieties thereby increasing the severity of the steric crowding in **11** vs **3**; although, the bond lengths should reflect this steric difference as well.

The potential for compounds **1–3** to serve as single-source precursors to 13–15 semiconductor materials motivated our study of their thermal decomposition behavior. Ideally, we desired that these adducts would

completely eliminate their organic substituents at moderate thermal conditions (<450 °C) with the resultant formation of the desired 13–15 material. Subsequently, we performed thermo-gravimetric analysis studies on milligram quantities of **1–3**. Samples were heated at a rate of 5 °C/min under a stream of nitrogen. The resulting TGA–DTA plots for each adduct **1–3** are given in the supplementary material. From these data, we concluded that compounds **1** and **2** undergo stepwise elimination of the organic ligands, while compound **3** decomposes in a single-step process. For each decomposition, it is important to note that weight percentages corresponding to GaP, GaAs, and InP, respectively, were observed for the remaining decomposition residues; however, no further analysis was done to characterize these residues.

Acknowledgment. We thank the Office of Naval Research, the AT&T Bell Laboratories Cooperative Research Fellowship Program, and the Duke Endowment Graduate Fellowship Program for their financial support. We also wish to acknowledge Dr. Steven R. Aubuchon for his contributions to the TGA–DTA studies.

Supplementary Material Available: Tables of bond distances and angles, anisotropic thermal parameters, and hydrogen coordinates and thermal parameters and figures showing thermogravimetric analysis data (16 pages). Ordering information is given on any current masthead page.

OM940960S

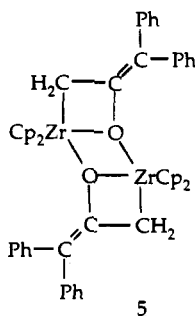
(19) Self, M. F.; McPhail, A. T.; Jones III, L. J.; Wells, R. L. *Polyhedron* **1994**, *13*, 625.

Additions and Corrections

1994, Volume 13

Dietmar Seyferth,* Tao Wang, and William M. Davis: Organometallic Chemistry of Ambident Dianions. Reactions of Acetone Dianions as C,O Dinucleophiles with Group 4 Metallocene Dichlorides.

Pages 4135 and 4136. Formula 5 on these pages should be



OM940964X

reflect the relayed effect of the steric compressions resulting from the angular deformations around Ga.

Crystallographic information on simple organoindium–phosphorus adducts is scant and is limited to $(\text{Me}_3\text{CCH}_2)_3\text{In}\cdot\text{P}(\text{SiMe}_3)_3$ (**11**),¹⁹ $\text{Me}(\text{Me}_3\text{CCH}_2)_2\text{In}\cdot\text{P}(\text{SiMe}_3)_3$ (**12**),¹⁹ and $(\text{Me}_3\text{In})_2(\text{PPh}_2\text{CH}_2)_2$ (**13**).¹⁸ The unit cell in **3** consists of discrete monomeric units with the In–P bond length being 2.771 Å. This is within range of the lengths previously observed in compounds **11–13** [the shortest being 2.755(4) Å in **13** and the longest being 2.944(4) Å in **11**]. The mean P–Si and In–C bond lengths at 2.276 and 2.210 Å, respectively, in **3** are nearly identical to the average P–Si (2.271 Å) and In–C (2.213 Å) in **11**, whereas the angles around the In atoms (P–In–C = 101.43°, C–In–C = 116.18° for the mean values in **3**; P–In–C = 95.5°, C–In–C = 119.1° in **11**) differ significantly. These observed bond angle variations may be directly related to the fact that the C–C distances in Me_3CCH_2 groups are substantially shorter than Si–C bonds in Me_3SiCH_2 moieties thereby increasing the severity of the steric crowding in **11** vs **3**; although, the bond lengths should reflect this steric difference as well.

The potential for compounds **1–3** to serve as single-source precursors to 13–15 semiconductor materials motivated our study of their thermal decomposition behavior. Ideally, we desired that these adducts would

completely eliminate their organic substituents at moderate thermal conditions (<450 °C) with the resultant formation of the desired 13–15 material. Subsequently, we performed thermo-gravimetric analysis studies on milligram quantities of **1–3**. Samples were heated at a rate of 5 °C/min under a stream of nitrogen. The resulting TGA–DTA plots for each adduct **1–3** are given in the supplementary material. From these data, we concluded that compounds **1** and **2** undergo stepwise elimination of the organic ligands, while compound **3** decomposes in a single-step process. For each decomposition, it is important to note that weight percentages corresponding to GaP, GaAs, and InP, respectively, were observed for the remaining decomposition residues; however, no further analysis was done to characterize these residues.

Acknowledgment. We thank the Office of Naval Research, the AT&T Bell Laboratories Cooperative Research Fellowship Program, and the Duke Endowment Graduate Fellowship Program for their financial support. We also wish to acknowledge Dr. Steven R. Aubuchon for his contributions to the TGA–DTA studies.

Supplementary Material Available: Tables of bond distances and angles, anisotropic thermal parameters, and hydrogen coordinates and thermal parameters and figures showing thermogravimetric analysis data (16 pages). Ordering information is given on any current masthead page.

OM940960S

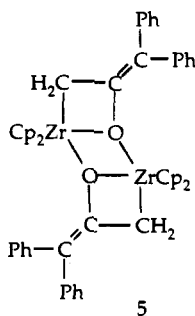
(19) Self, M. F.; McPhail, A. T.; Jones III, L. J.; Wells, R. L. *Polyhedron* **1994**, *13*, 625.

Additions and Corrections

1994, Volume 13

Dietmar Seyferth,* Tao Wang, and William M. Davis: Organometallic Chemistry of Ambident Dianions. Reactions of Acetone Dianions as C,O Dinucleophiles with Group 4 Metallocene Dichlorides.

Pages 4135 and 4136. Formula 5 on these pages should be



OM940964X